

Review article

Recent advances in the determination of the platinum group elements and gold

R.R. Barefoot *, J.C. Van Loon

Department of Geology, University of Toronto, Toronto, ON, Canada M5S 3B1

Received 21 July 1998; accepted 15 October 1998

Abstract

Accurate determinations of the platinum group elements (PGEs) and gold, known as the precious metals, have always been difficult tasks. The metals are often present at trace levels in sample types of complex composition. This situation has improved recently due to developments of instrumental methods and their applications to analyses of the precious metals in a variety of matrices. Attention has been given to determinations of traces of precious metals in biological, clinical and environmental samples. Foremost in importance is inductively coupled plasma mass spectrometry (ICP-MS) which has provided a sensitive means of simultaneous determination of traces of PGEs and gold. Important extensions and improvements in atomic absorption spectrometry (AAS), nuclear and electrochemical methods have been reported also. More research on sample treatments, especially fire assays, applied to PGEs has been carried out. Chlorination has proven to be a viable alternative to fire assays for preconcentration of PGEs and gold in analyses of geological materials. In addition, the recent availability of some additional reference materials will be of great assistance in research work on precious metals. © 1999 Elsevier Science B.V. All rights reserved.

Keywords: Platinum group elements; Gold; Instrumental methods; Inductively coupled plasma mass spectrometry

1. Introduction

A large amount of research has been conducted on methods for accurate determinations of traces of platinum group elements (PGEs) and gold (Au) contained in a variety of sample types or matrices. PGEs comprise a group of six elements, namely platinum (Pt), palladium (Pd), rhodium (Rh), irid-

ium (Ir), ruthenium, (Ru) and osmium (Os). The PGEs and Au are known as the precious metals. This term reflects their economic value as well as the rare occurrences of the metals. This review covers the period mainly from 1990 to 1998. A selection has been made from the many publications in this subject area. It includes significant research contributions in the fields of sample preparation, and of preconcentration of the precious metals prior to their determinations. Several instrumental methods of analysis are reviewed. In

* Corresponding author. Tel.: +1-416-978-3022; fax: +1-416-978-3938.

Table 1
Fire assay preconcentration.

Sample	Elements	Collector	Procedure	Detection limits ^a	Ref.
Rocks, soils, sediments 10–30 g	Pt, Pd, Au	Pb	Ag prill dissolved; ICP-MS	0.1 (Pt)–2.0 (Au)	[2]
Rocks, RMs	PGEs, Au	NiS (0.5 g Ni)	Residue PGEs & Au; INAA.	–	[4]
RMs	Pt, Pd, Rh, Ir, Ru	NiS (1.9 g Ni)	PGEs dissolved; GFAAS.	–	[6]
RMs (chromites)	Pt, Pd, Rh, Ir, Ru	NiS (17 g Ni)	Flux contained 1:1 mixture of Na and Li tetra-borates; PGEs dissolved; GFAAS	–	[8]
RMs (kimberlites) 50 g	PGEs, Au	NiS (5 g Ni)	Flux contained SiO ₂ borax; PGEs & Au dissolved; INAA.	0.002 (Au)–3.8 (Pt)	[9]
SARM-7, rocks 15 g	PGEs, Au	NiS (5 g Ni)	Collector, analytes dissolved in bombs; ICP-MS	0.06 (Ir)–1.4 (Au)	[11]

^a Method detection limits, ng g⁻¹.

atomic absorption spectrometry (AAS), both flame (FAAS) and electrothermal (GFAAS) have been used extensively in many laboratories. Of the newer techniques, inductively coupled plasma mass spectrometry (ICP-MS) is the most important, and many reports of applications of ICP-MS have been published. The review includes descriptions of several recently-available reference materials (RMs) for precious metals.

2. Sample treatment and preconcentration

2.1. Fire assay

In the analysis of geological materials, the most important method used for the preconcentration and of PGEs and Au and for their separation from base metals and silicates is the fire assay (FA). Although FA have been used for the preconcentration of Au for many years, and have been called the ‘classical’ method of collection, applications of FA to the collection of PGEs are of more recent origin. New research on FA methods have resulted in valuable information on treatments of some types of samples that have not yielded readily to usual procedures. In addition, better accuracy and precision, and lower limits of detection are needed for analyses of samples containing very small (ng g⁻¹) concentrations of

precious metals. Two collectors are currently in general use in FA. These are lead and nickel sulfide [1]. Lead fire assays (Pb-FA) are used for the collection of Au, Pt, Pd and Rh. Silver is collected also, and there must be sufficient silver present for the cupellation of the lead button. Au, Pt and Pd are concentrated in the resulting silver bead. Rh (and Ir) is retained quantitatively in a gold bead. Nickel sulfide fire assays (NiS-FA) are capable of collecting all of the PGEs, but the results for the collection of Au are usually too low. NiS beads are heated in HCl in order to dissolve all of the NiS and leave PGEs and Au as a residue. Precious metals in the residue can be determined directly by instrumental neutron activation analysis (INAA), or the residue can be dissolved in acids. The acidic solutions are analyzed by spectrometric methods such as GFAAS, inductively coupled plasma atomic emission spectrometry (ICP-AES) and ICP-MS. In some procedures, precious metals in solution are concentrated and separated from matrix elements before spectrometric determinations.

A simple and effective Pb-FA has been described for determinations of low levels of Au, Pt and Pd in rocks, soils, sediments and humus [2]. Solutions of the silver assay beads were analyzed by ICP-MS (Table 1). The combined cost of the assay and instrumental analysis was in the range of \$8–16 (Cdn) per sample as compared with the

cost of about \$115 (Cdn) per sample for a corresponding NiS-FA and analysis. Pb-FA and NiS-FA methods were compared with an acid dissolution method for the determination of PGEs and Au in rocks and RMs [3]. The best recoveries of all the analytes were obtained by the NiS-FA method. Method detection limits ranged from 0.09 (Ir) to 2.1 ng g⁻¹ (Ru). Aqua regia (AR) leaches of samples did not yield accurate results for the precious metals. The recoveries were too low. See also Section 2.3.

One of the disadvantages of fire assays of samples containing very low levels of PGEs and Au is the problem of relatively large reagent blanks which result from the presence of precious metals in the chemicals required for fluxes and sample preparation. More than 10 g of nickel are used to make the NiS beads in most of the NiS-FA procedures. Reagent blanks for PGEs and Au were reduced significantly when a much smaller quantity (0.5 g) of nickel was used [4]. Recoveries of the precious metals ranged from 76 to 85% of the known values (Table 1). Recoveries of PGEs and Au from a Pt ore grade sample ($\mu\text{g g}^{-1}$ precious metal concentration) were independent of collector mass for NiS masses of 1, 3.3 and 5 g [5]. However, recoveries of Pt, Pd, Rh and Ru from komatiite sample (ng g⁻¹ precious metal concentration) were dependent on the collector mass. Partition coefficients (K_d values) were up to 103-fold larger for the ore grade sample as for komatiite. Thus, significant biases may occur in determinations of very low levels of precious metals in other sample types.

In research on fusion charge compositions for NiS-FA, two parameters were defined as being useful in characterizing the melts [6]. The first was the extraction ratio E , the ratio of the combined weights of sample + flux to the weight of the collector (Ni + S). The second was the sulfur content S_c , the percentage (wt.) of sulfur in the collector. Compromise conditions based upon these parameters, namely $E = 15$ and $S_c = 45\text{--}48\%$ proved to be satisfactory in analyses of several RMs.

Analyses of samples containing chromite have been studied because of difficulties in establishing conditions for the complete fusion of all chromite

grains. A number of modified NiS-FA procedures have been reported. Additional sodium hydroxide in the flux composition and heating at 1200°C, together with additions of more flux after a fusion period of 1 h, produced a thinner melt free of chromium oxide crystals [7]. The effects of lithium tetraborate and/or sodium tetraborate in flux compositions were investigated by analyzing three chromitite RMs [8]. The best results were obtained when a 1:1 mixture of the tetraborates was a constituent of the composition.

Problems have been encountered also because of incomplete fusion's of some South African kimberlites with some compositions rich in magnesium (> 30% magnesium oxide and < 40% silica), and others rich in carbonate (> 15% carbonate and < 25% silica) [9]. The difficulties were overcome by the additions of more silica and borax to the usual flux composition for NiS-FA. The same report described the results of investigations of observed losses of Pt, Pd and Au during acid dissolutions of NiS buttons. Losses were minimized by maintaining a reducing (sulfide) atmosphere inside the reaction flasks, and then by filtering the residual precious metals as soon as possible after the dissolution of NiS. PGEs and Au were determined by INAA. The limits of detection (Table 1) of this procedure were significantly better than those of others based upon INAA.

In many procedures, NiS buttons are crushed or pulverized before treatment with acid. However, some workers have expressed concern that appreciable losses of NiS together with precious metals can occur during this operation. Boisvert et al. [10] reported that crushing buttons in a shatter-box resulted in losses of up to 20% of the buttons. Assuming uniform distributions of precious metals in the buttons, corresponding large losses of precious metals would result. A crusher was designed so that NiS buttons could be reduced to large particles. In this manner, mechanical losses were well below 1% of the collector. In other work, they were contained in plastic bags while they were cracked with a hammer [9]. Sun et al. [11] dissolved NiS buttons in heated screw-capped Teflon bombs so no crushing was necessary. In addition, Teflon bombs were used also in

the dissolutions of precious metals recovered by coprecipitation with Te. Recoveries of precious metals from SARM-7 were good except for Au and Os whose recoveries averaged 90% and 60%, respectively. A special flux composition was recommended for chromitites.

2.2. Chlorination

Dry chlorination of geological samples was developed as an alternative to FA as a means of preconcentration for the determination of very low concentrations of PGEs and Au [12]. In this method, PGEs and Au present in the forms of native metals, natural alloys and as PGE- (or Au-) bearing sulfide minerals were converted to their respective water-soluble sodium salts. Powdered samples were mixed with small amounts of sodium chloride; mixtures were treated with chlorine gas in tubular furnaces heated to 580°C. The salts were dissolved in weak HCl and were separated from chlorination-resistant and water-insoluble materials by filtration. Determinations of PGEs and Au were carried out by ICP-MS. Samples as large as 250 g were analyzed [13]. The capability of handling large samples is important because small concentrations of precious metals are not distributed uniformly in rocks. Even sample weights of 20–30 g of non-ores may not be representative. Results of analyses of RMs were comparable to or better than results from FA procedures. Method detection limits ranged from 0.06 (Rh) to 0.28 (Pt) ng g⁻¹. Another important advantage of dry chlorination was extremely low reagent blanks.

As stated previously, chlorinating is a means of preconcentration of the metallic fraction of a geological material, i.e. the fraction of a sample containing precious metals in the forms of native metals, natural alloys and sulfide group minerals. The chlorination resistant, non-metallic fraction of a sample may contain precious metals also. Chlorination residues (or non-metallic fractions) were dissolved in acids by microwave digestions and analyzed for PGEs and Au by ICP-MS [14]. The research provided a means of investigating PGE depletions in layered mafic intrusions which host PGEs deposits. Drill core samples of the Fox

River Sill (Canada) were analyzed [15]. The PGE and Au in chlorination-resistant (or non-metallic) fractions of samples collected from mineralized layers were significantly depleted relative to the contents of precious metals in silicate fractions of samples collected from a non-mineralized layer.

2.3. Acid dissolution

Digestion in acids has been used extensively for sample preparation. Extractions of PGEs and Au by acids have been investigated as more rapid and economical alternatives to FA. Usually, additional purification and preconcentration steps are needed prior to determination of the analytes after acid dissolution. A number of reports are listed in Table 3. Sample weights in the range of 0.5–5 g are the most convenient, much smaller than those taken for FA or chlorination. However, an acid dissolution procedure accommodated samples of up to 40 g [16]. RMs have been used for investigations of new or modified procedures. Because RMs have been finely ground and well mixed, the accuracy and precision of the results for small sample weights can be expected to be superior to those obtained from an average geological sample. The efficiency of extraction of Au from geological samples continues to be important. Acid extraction procedures are used in many laboratories for analyses of large numbers of samples from field surveys. Efficiency of extraction has been a function of type of sample as well as the experimental conditions. When Au was extracted from RMs and geological materials with AR and with HBr containing 5% Br₂, the results for some samples were 20–40% too low [17]. A change in the ratio of the weight of sample to the volume of the extractant, i.e. 1 g of sample to 24 ml of acid instead of 10 g of sample to 24 ml of acid yielded satisfactory results. Also, AR combined with HF yielded better results for Au than AR alone [18]. In another investigation, PGEs and Au were extracted from RMs and samples by AR, and the extracts were analyzed by ICP-MS [19]. A sample of 10 g of sample was treated with 20 ml of acid. Au and Pd were recovered efficiently from a few of the standards. However, results for the other elements were far below the

Table 2
Acid dissolution

Sample	Elements	Procedure	Detection limits ^a	Ref.
RMs 0.5–2 g	Au	AR & HF; solvent extr. GFAAS.	–	[24]
RMs 40 g	Au	HCl-Br ₂ ; Te coprecip.; FAAS	–	[16]
Rocks 5 g	Au	H ₃ PO ₄ & HClO ₄ ; HBr-Br ₂ ; solvent extr.; GFAAS.	1	[21]
RMs, rocks, 5–10 g	Au	AR & Br ₂ ; adsorption; FAAS.	0.1	[25]
RMs 0.5–2 g	Pd, Pt	AR & HF; solvent extr.; GFAAS.	0.2 (Pd); 0.5 (Pt)	[26]
RMs 5 g	PGEs, Au	AR & HF; ion ex.; GFAAS.	–	[27]
RMS 2–5 g	PGEs, Au	AR & HF; Te coprecip.; GFAAS.	–	[28]
RMs	PGEs, Au	AR & HF microwave digest; alk. fusion; cat. ex; ICP-MS.	1.3 (Rh)–11 (Pd) ^b	[22]

^a Method detection limits, ng g⁻¹;

^b lower quantitation limits, ng g⁻¹.

expected values. Extractions of PGEs and Au from RMs and geological samples were compared with results obtained when the materials were subjected to FA [3]. The conclusion was that AR extractions were not quantitative for all types of geological samples, and that the results were usually too low. Therefore, AR extraction should only be used for preliminary studies when rapid results are required rapidly.

A partial dissolution method was used for extractions and subsequent measurements of weakly-bound Au in humus [20]. Samples of 3 g of humus were treated with 1.2 M HCl to yield solution concentrations of usually less than 1 ng g⁻¹ Au. The solutions were analyzed by ICP-MS. This method distinguished the indigenous Au fraction derived from underlying bedrock mineralization by biological mechanisms from Au transported to the site with the overburden. (The transported Au fraction bore no relationship to the concentration of Au in the underlying bedrock)

A method was outlined for the determination of Au in large numbers of geological samples at low cost by acid extraction [21]. Samples (5 g) were treated with solutions of H₃PO₄ and HClO₄ and then with HBr-Br₂ in order to dissolve all of the Au. Comparative studies showed that when samples contained Au which was occluded in silicate or refractory materials, up to 50% of the Au content of these samples was not extracted by either AR or HBr-Br₂. PGEs in RMs were deter-

mined by ICP-MS after microwave heating and digestion in AR and HF within sealed vessels [22]. Insoluble residues were attacked by alkali fusions, and matrix elements were separated from the sample solutions by cation-exchange chromatography.

Total dissolutions in acids, mainly HNO₃, HCl and HClO₄, has been used frequently in analyses of precious metals in biological and environmental samples. Tolg [23] reported on the determination of very low concentrations of Pt in environmental samples. The acid dissolution procedures included: (i) open wet digestion; (ii) high-pressure digestion; and (iii) open wet digestion for samples containing appreciable proportions of siliceous materials. Details of additional reports are listed in Table 2.

2.4. Fusion

Fusions of samples in small crucibles, as distinct from the fusion step in a fire assay, provide a means of decomposition which results in the formation of water soluble salts of the precious metals. Either Na₂O₂ alone or combined with NaOH has been used most frequently for this purpose. Many radiochemical neutron activation analysis (RNAA) procedures incorporate fusions of irradiated samples. Disadvantages and limitations of fusions include small sample weights, large concentrations of sodium salts in sample solutions and the introduction of contaminants

Table 3
Fusion

Sample	Elements	Procedure	Detection limits ^a	Ref.
RMs, ores 0.5–1 g	PGEs Au	Na ₂ O ₂ ; dilution; ICP-MS	–	[29]
RMs 0.5 g C	Pt, Pd, Rh, Ir	Na ₂ O ₂ ; Te coprecip.; ICP-MS	0.3(Ir)–2(Pt)	[30]
RMs 0.25 g	Pt, Pd, Ir, Au	Na ₂ O ₂ ; Te coprecip.; RNAA	0.1(Au)–2(Pt)	[31]
RMs, rocks 0.4 g	Pt, Pd, Ir, Au	Na ₂ O ₂ ; Te coprecip.; RNAA	0.01(Ir)–2(Pt)	[32]
Silicate rocks	PGEs, Au	Fe-Ni alloy; Sraffion NMRR; RNAA	0.004(Au)–2(Pt)	[33]

^a Method detection limits, ng g⁻¹.

from the salts as well as from any attack on the walls of the crucibles by the flux. Consequently, most procedures include purification and preconcentration steps. However, dilution of the aqueous solutions was sufficient preparation for the determination of PGEs and Au in SARM-7 and ores by ICP-MS [29]. Coprecipitation with Te, solvent extraction and ion exchange have been used to purify and concentrate precious metals prior to determinations in RNAA and ICP-MS procedures. Summaries of a number of reports appear in Table 3. For determinations of precious metals in silicate rocks, samples were fused in an iron-nickel alloy at 1600°C under a reducing atmosphere [33]. Then, the metallic phase containing the precious metals was dissolved in acid.

2.5. Solvent extraction

Au and PGEs in solution can be separated from other elements and concentrated by means of liquid–liquid extractions. For Au, the most common method is the extraction of Au(III) by methyl isobutyl ketone (MIBK) from aqueous solutions of HCl or HBr [17,24,34,36]. Au has been extracted from HBr solution by amyl acetate [21,35], and from HCl solution with dibutylsulfide dissolved in di-isobutyl ketone [37]. Pt and Pd were extracted with dibutylsulfide also [38], and by MIBK in the presence of potassium iodide [26]. Dithizone in CCl₄ has been used to extract Pt [23]. Subsequent determinations of the analytes have been carried out mostly by FAAS and GFAAS. Additional information is found in Tables 2 and 3.

2.6. Sorption and ion exchange

A number of sorbents and resins have been applied to the preconcentration of the precious metals. Pt and Pd in natural water [39], and Au in thiourea leaching solution [40] have been concentrated on charcoal. Other sorbents reported for Au include polyurethane foam [41], Cellex T, i.e. cellulose absorbent with triethylamino functional groups [42] thiol-cotton fiber [43] and sulfhydryl cotton [44,45]. The work described in refs. [42,44,45] was adapted to flow injection and on-line trace enrichment. Pt in natural water was determined by FAAS after preconcentration on a microcolumn of alumina [46] with flow injection and on-line operation.

Preconcentration of Au from natural water [34], and on an anion exchange resin has been described. A procedure was developed for the determination by ICP-MS of Pt, Pd, Ru and Au using an anion-exchange resin for samples containing concentrations of precious metals greater than 1 µg g⁻¹ [47]. In addition, the procedure was recommended for Ir determinations over a range of concentrations. Anion exchange resins were applied also for preconcentration of Pt and separation of matrix elements for the determination of Pt in airborne particulate matter by ICP-MS [48,49]. Detection limits were about 5 ng g⁻¹. Other work has involved applications of XAD-4 resin for the retention of Pt, Pd and Rh as chelates [50], XAD-7 resin for Au [25] and Sraffion NMRR resin to concentrate PGEs and Au [33]. In the last application, the elements were determined by INAA.

Table 4
Applications of atomic absorption spectrometry

Sample	Elements	Procedure	Detection limits ^a	Ref.
Natural water 15 ml	Pt	Microcolumn of alumina.	0.02 mg l ⁻¹ ; FAAS 0.03 µg l ⁻¹ ; GFAAS	[46]
Natural water 2 l	Au	Anion ex.; GFAAS	0.4 ng l ⁻¹	[34]
Environ., biotic 0.1–2 g	Pt	Acid digestion, PTFE bomb; electrodepos.; GFAAS.	0.3 ng	[52]

^a Method detection limits.

2.7. Coprecipitation and electrodeposition

Coprecipitation of the PGEs and Au with a carrier such as Te has been employed in many analytical procedures for their recovery from dilute solutions, and for their separation from other elements prior to their determinations. This pre-concentration step is of particular importance and value in analyses of geological materials. Te is the most popular precipitant, and examples of Te coprecipitation are found in several reports including refs. [16,30–32,51]. Tables 2 and 3 contain additional information.

In the determination of Pt in biotic and environmental samples, Pt was concentrated on a graphite tube prior to its determination by GFAAS [52]. The limit of detection was 0.3 ng of Pt. Au in biological samples was separated from other elements and concentrated on a niobium cathode for its subsequent determination by RNAA [53].

3. Instrumental methods

3.1. Atomic absorption spectrometry

For many years, both FAAS and GFAAS have been popular instrumental methods for determinations of elements. Some important new applications have been noted in other sections of this report. Work involving FAAS include the determination of Au in geological materials [16,25,35], and of Pt in natural water [46]. GFAAS has been used for determinations of precious metals in RMs [6,8,26–28], Au in RMs and rocks [21,24],

Pt, Pd and Au in vegetation [65], Au in natural water [34], and Pt in environmental samples [54] and water [46]. Tables 1, 2 and 4 contain information about these procedures. Recently, simultaneous multielement GFAAS has been adapted and applied to determinations of the Pt, Pd, Rh, Ir, Ru and Au contents of geological RMs [27]. This was a distinct advantage over the single-element determinations. Samples of 5 g were decomposed in acids, and the analytes were purified and concentrated by means of ion exchange. Pt, Rh, Ir and Ru were determined simultaneously in one aliquot of the solution, and Pd and Au in a second aliquot.

3.2. Inductively coupled plasmas

Instruments based upon inductively coupled plasmas as atomization and ionization sources for analytes have been applied to the determinations of precious metals in a variety of matrices. ICP-AES has been used for many years, while applications of ICP-MS are of more recent origin. Both techniques have provided accurate results rapidly when employed for simultaneous multielement measurements. ICP-MS has become a popular technique for precious metals because of its sensitivity which is comparable to that of GFAAS [55]. In addition, ICP-MS has been used for measurements of isotope ratios also. A number of applications of ICP-MS are listed in Tables 1–3 and 5. ICP-AES was used to measure Au in sludge and soil [43] and water [44], and PGEs in polluted biological materials after preconcentration steps.

Although samples are introduced to plasma spectrometers as solutions in most procedures,

Table 5
Applications of ICP-MS

Sample	Elements	Procedure	Detection limits ^a	Ref.
RMs, rocks	PGEs, Au	NiS-FA; Te coprecip.	0.1 (Ir)–8.7 (Au)	[51]
RMs	PGEs,	Slurry	0.04 (Rh)–0.2 (Au) ^b	[57]
Plasma, tissue	Pt	Acid digestion	0.01 $\mu\text{g kg}^{-1}$ (tissue)	[59]
Serum, liquids	Pt	Dilution	0.06 ng g^{-1}	[60]
Cells	Pt	Aqueous dispersion; acid digestion	1 ng g^{-1}	[61]
Natural water 2 l	Au	Solvent extr.	0.2 ng l^{-1}	[34]
Natural water 49 ml	Au	Sulfhydryl cotton fiber column; FI.	0.2 ng l^{-1}	[45]
Seawater 4 l	Au	Anion ex.	10 fM	[62]
Natural water	Pt, Pd	Charcoal adsorption	0.3–0.8 ng l^{-1}	[39]
Humus 3 g	Au	HCl partial extr.	<1	[20]
Twigs	Au	Ash at 875°C;	0.02	[63]
Organic 1 g ash	Au	Ash at 450°C	–	[64]
Organic 2 g ash	Pt, Pd, Au	Ash at 870°C	0.5 (Au)–2 (Pt)	[72]

^a Method detection limits, ng g^{-1} , unless noted;

^b Quantitation limits, $\mu\text{g g}^{-1}$.

laser ablation (LA) is an alternative means of introduction that does not require extensive use of chemicals for sample preparation. Interferences from polyatomic ions in the plasma are reduced because aqueous sample solutions are not used. Quantitative data were obtained for Pt, Pd and other trace elements in high purity Au and Ag, and in 14-carat Au–Ag alloys by LA-ICP-MS [56]. Concentration ranges for Pt and Pd were 4–111 and 7–188 $\mu\text{g g}^{-1}$, respectively. Concentrations of Pt in ferromanganese nodules were measured by LA-ICP-MS [58]. In this investigation, Pt concentrations ranged from 150 to 500 ng g^{-1} . Pt, Pd, Rh and Au in Ag and Au cupellation beads were determined by means of a spark source connected to the inlet of an ICP-mass spectrometer [66]. Detection limits for the analytes ranged from 0.6 (Pt) to 1.2 $\mu\text{g g}^{-1}$ (Pd).

The rhenium-osmium decay scheme, viz. $^{187}\text{Re} \rightarrow ^{187}\text{Os}$, $t_{1/2} = 4.56 \times 10^{10}$ y, has contributed to the dating of several types of geological materials including ore deposits. Os has seven naturally occurring isotopes and Re has two. Os and Re are among the least abundant naturally occurring stable elements in crustal rocks. ^{187}Os comprises only 1–2% of total Os. Thus, preconcentration and separation techniques are usually required in the preparation of samples for isotope analysis. The

generation of OsO_4 vapor as the means of Os separation and the introduction of the vapor to the mass spectrometer has been used in most of the work [67–69]. Os is oxidized readily to OsO_4 whose boiling point is lower than most Re compounds. In this manner, Os can be separated from ^{187}Re . Any losses of Os during sample preparation were minimized by combining the powdered sample with a Re–Os isotopic spike prior to any chemical treatment [68]. Accuracy of 0.1–0.2% and precision as good as 0.3% (2 s) have been reported in measurements of Os isotopes [69].

3.3. Nuclear methods

Nuclear methods continue to be important in determinations of trace quantities of precious metals in many types of samples, but particularly in geological materials. Recent reports have described determinations of PGEs and Au in RMs and rocks [31–33], environmental materials [41] and of Pt and Au in biological samples [53]. Summaries of RNAA and INAA determinations are found in Tables 1 and 3. A procedure for the determination of gold in sulfides by direct neutron activation with a low-flux reactor has been developed [70]. Concentrations of Au down to 50 ng g^{-1} in sulfide minerals separates were measured using samples of less than 10 mg.

3.4. *Electrometric methods*

Although a number of different electrometric techniques have been used over the years for determinations of the precious metals, voltammetric methods have become more important recently. Sensitive voltammetric methods have been adapted and applied to determinations of Pt at baseline levels in biotic and environmental materials [71], in human body fluids [72], in airborne particulate matter [73], and in chromatographic effluents [74]. Samples were digested in a high-pressure asher. The apparatus was cleaned carefully and conditioned in order to reduce Pt contamination. The method involved the accumulation of a Pt complex (a condensation product of formaldehyde and hydrazine, or 'formazone'), at the surface of a hanging mercury drop electrode. The electrochemically-active metal complex lowered the hydrogen overpotential at the mercury electrode, and produced a very sensitive catalytic current. The current was measured in a differential pulse mode. The detection limit was 2 pg of Pt. Baseline levels of Pt in persons who had not been exposed to Pt compounds, and had not been treated with Pt drugs were 0.8–6.9 ng l⁻¹ (blood and blood products), and 0.5–15 ng l⁻¹ (urine) [72]. Concentrations of Pt in road dust and in particulate matter varied with particle size. The largest Pt concentrations, 3.0–8.9 ng g⁻¹, occurred in the fraction containing the smallest particle sizes [73]. Information on 'soluble platinum' in dust, i.e. the proportion of total Pt dissolved in dilute HCl, was included also.

Methods have been developed for the determination of Au in geological materials (rocks, soils, sediments) by means of a field portable anodic stripping voltammeter. The portable instrument was a battery-operated and microprocessor controlled voltammeter, model PDV-2000, manufactured by Chemtronics (Bentley, Western Australia). For the determination of Au in geological materials, one procedure involved the dissolution of Au from crushed solids, its extraction into ethyl acetate and then its re-extraction into a final electrolytic solution. A detection limit of 10 ng g⁻¹ for Au was obtained using a sample weight of 10 g and a 2-min plating period [75]. In

another procedure [76], Au was extracted from a sample of 100 g by alkaline cyanide solution, and then concentrated by extraction into ethyl acetate or diethyl ether. The solvent was evaporated, and Au was redissolved in the electrolyte. Comparisons of results of field methods with those obtained in laboratories by well-established techniques demonstrated good accuracy of the voltammetric measurements.

3.5. *Other methods*

Accelerator mass spectrometry (AMS) is a technique which originated in particle accelerator technology of nuclear physics. Applications of AMS to earth sciences began during the 1980s. A review of AMS in environmental geoscience described the importance of this technique [77]. 'In situ' analyses of precious metals at ng g⁻¹ levels in polished mineral samples and sulfide 'standards' [78] and in iron meteorites [79] by AMS have been reported. Under the designated experimental conditions, there was essentially zero background. Sensitivities for monatomic negative ions ranged from 0.1 (Au) to less than 600 ng g⁻¹ (Os).

The development of 'in situ' microbeam techniques for determinations of PGEs and Au is of great interest to the minerals industry. Determinations of Au in arsenian pyrite using proton microprobe and ion microprobe techniques were compared [80]. Detection limits for Au using particle induced X-ray excitation (PIXE) and proton microprobe (micro-PIXE) were 21–26 µg g⁻¹. The corresponding detection limit using secondary ion mass spectrometry (SIMS), or ion microprobe was 0.4 µg g⁻¹. The volumes analyzed were different, namely, 5000 µm³ for PIXE, and 2400 µm³ for SIMS. The geometries of the volumes were different, also: a parallelepiped (micro-PIXE), and a thin disc (SIMS). Thus, results of analyses of the same grains by the two instruments were not readily comparable because of the heterogeneous distribution of Au at the ng g⁻¹ levels in pyrite. The complementary nature of micro-PIXE and ion microprobe techniques was emphasized in analyses of PGEs from placer deposits [81]. PIXE proved to be more useful as an

exploratory tool in rapid areal analyses of complex minerals. A method for calibrating an ion microprobe for quantitative determinations of traces of Pt, Pd, Rh, Ir and Au in common sulfide and sulfarsenide minerals was described [82].

Ru concentrations in the range 3–33 $\mu\text{g g}^{-1}$ found in metallic FeNi minerals in iron meteorites were measured [83]. The technique used was X-ray fluorescence with synchrotron orbital radiation. The X-ray beam sizes ranged from 0.5×0.5 to 0.25×0.25 mm squares. Calibration curves were constructed from standard FeNi alloys doped with Ru.

3.6. Speciation

Compounds of Pt and Au have been administered in treatments of some forms of cancer and of rheumatoid arthritis, respectively. The detection and determination of very low concentrations of chemical forms of Pt and Au in clinical samples often provides important information on the active species, and the modes of operation and extents of utilization of the drugs. Of the platinum-based drugs, cis-diamminedichloroplatinum(II), or cisplatin, is used widely in cancer chemotherapy and has contributed to successful treatments of some forms of cancerous tumors. In many studies, total and ultrafilterable or 'free Pt' concentrations were measured in blood serum or plasma. 'Free Pt' is defined as Pt not bound to proteins. Samples were analyzed by ICP-MS [84]. Total Pt concentrations were in the range of 100–1000 $\mu\text{g l}^{-1}$, and 'free Pt' concentrations were 3–7% of the total Pt.

Separations of cisplatin and some Pt metabolites from other species were carried out by HPLC [85]. An anion-exchange column was connected to a post-column reactor and a UV-spectrophotometer for measurements of cisplatin in plasma and urine. The detection limit was 20 nM. Modes of action of cisplatin in cancer treatments have been studied [86]. In the presence of fluid media containing low concentrations of chloride ions, the mono- and dihydrated-complexes of cisplatin are formed. The monohydrated complex is said to be the most important cytotoxic species. Cisplatin and its hydrated complexes in plasma samples

were separated on a strong cation-exchange column. The outlet of the chromatograph was coupled directly to an ICP-mass spectrometer so that Pt compounds in the effluent could be detected on-line.

The main gold-containing drugs used in treatments of arthritis are: (1) auranofin or triethylphosphinegold (I) teraacetylthioglucose; and (2) myochrisine or sodium gold(I) thiomalate. Anion-exchange columns were used in studies of auranofin and its metabolites [87], and reversed-phase columns were used to separate auranofin, myochrisine and their respective metabolites. The columns were coupled to an ICP-mass spectrometer. In another study, two Au-containing drugs and their metabolites were separated by ion pair chromatography [88]. The detection limit of myochrisine using ICP-MS was 0.3 ng, and the recovery of the Au-containing species was above 90%. A more detailed description of research on the determination of Pt and Au species in drugs and metabolites is available [89].

The catalytic treatment of exhaust gases from motor vehicles has resulted in environmental contamination by airborne particulate material, or dust, from the deterioration of the catalysts. The dust contains precious metals, mainly Pt, together with Pd and Rh. Information on Pt-containing species in vegetation, soils and sediments is needed so that the biotransformations and modes of transport of Pt and its compounds in the environment may be understood. Pt species in grass treated with a Pt salt were separated by GPC, and the Pt-containing fractions of effluent were subjected to isotachopheresis [90]. Sharp peaks of Pt-containing species were detected in this work, but more information on their chemical compositions is required. A clay-like humic soil treated with Pt-containing dust (from catalysts) and with Pt model compounds was investigated in order to detect biotransformation products [91]. Extracts of the soil were analyzed by means of HPLC-ICP-MS using reversed phase columns. Capillary electrophoresis-ICP-MS was used in parallel to study Pt speciation. Detection limits were about 25 ng l^{-1} for HPLC and $1\mu\text{g l}^{-1}$ for electrophoresis, both expressed as Pt. Additional information on speciation is found in ref. [54].

Table 6
RMs for PGE and Au concentrations, $\mu\text{g g}^{-1}$

	TDB-1	UMT-1	WGB-1	WMG-1	WMS-1	WPR-1	WITS-1
Pt	0.0058	0.129	0.0061	0.731	1.741	0.285	0.0110 ^a
Pd	0.0224	0.106	0.0139	0.382	1.185	0.235	0.0079 ^a
Rh	0.0007	0.0095	0.00032 ^b	0.026	0.225	0.0134	0.0013 ^a
Ir	0.00015 ^b	0.0088	0.00033 ^b	0.046	0.235	0.0135	0.0016 ^a
Ru	–	0.0109	–	0.035	0.099	0.022	0.0051 ^a
Os	–	0.008 ^b	–	0.24 ^b	0.119 ^b	0.013 ^b	0.0010–0.0015 ^a
Au	0.0063	0.048	0.0029	0.11	0.279	0.042	0.0056 ^a
Diabase rock	Ultramafic ore tailing	Gabbro rock	Mineralized gabbro	Massive sulfide	Peridotite rock	Komatite	

^a Certified values except recommended values.

^b Certified values except values for information.

4. Reference materials

Reference materials are of great importance in research programs. In projects and investigations involving analyses of geological samples, there has been a need for additional RMs containing very low concentrations of PGEs and Au. The well-known SARM-7 has been used extensively in studies of new, as well as established analytical methods. Recently, other RMs have been prepared for distribution. The precious metals in some of these are listed in Tables 6 and 7. In keeping with the nomenclature adopted in the special issue of the Geostandards Newsletter [92], the term ‘working values’ is used in this report to cover expressions such as certified values, recommended values, usable values, etc. In this review, the terms certified, recommended, provisional and working are those used in the citations.

Six new RMs listed in Table 6 have been issued by the Canadian Certified Reference Materials Project (CCRMP) in association with the Minerals Resources Division of the Geological Survey of Canada. The source of the materials is the Wellgreen Complex, YK, Canada, with the exceptions of TDB-1 and UMT-1. The source of the former material is Trembley Lake, SK, Canada and of the latter is Giant Mascot, Hope, BC, Canada. WMS-1 is a massive sulfide matrix material, while the others are all siliceous matrices. WITS 1 is a silicified komatite from the Barberton area, South Africa [93].

CHR-Pt + and CHR-Bkg, listed in Table 7, are chromatite samples from the Isles of Shetland, (North Scotland). They have been issued by the Centre de Recherches Petrographiques et Geochimiques (CRPG), France, in cooperation with The Open University, UK [94]. Although these RMs have the same type of matrix as SARM-7, CHR-Pt + is enriched in precious metal content while CHR-Bkg is depleted relative to SARM-7. The three RMs offer the possibility of studies of instrumental analytical methods for the determinations of precious metals in chromitite matrices over a range of concentrations. Data for an ultramafic rock standard, DZΣ-2, from the Peoples Republic of China (PRC) is included in Table 7 [95].

SRM 886 is a refractory gold ore available from the National Institute of Standards and Technology (NIST). It contains $8.25 \mu\text{g g}^{-1}$ of Au finely disseminated in a siliceous matrix. (Table 7). Eleven Au reference samples, GAu8-18, which include granites, soils, stream sediments and ores, have been prepared by the Institute for Geophysical and Geochemical Exploration, PRC [96]. Certified values for Au range from 0.5 ng g^{-1} to $10 \mu\text{g g}^{-1}$ in this group of standards. In addition, the Ministry of Geology, PRC, has prepared a set of Au standards designated GBW(E) 070018-070023. The certified Au concentrations range from 0.27 to $3.6 \mu\text{g g}^{-1}$ [97].

Two new SRMs, 2556 and 2557, from NIST are used auto catalysts in the form of powders (75

Table 7

RMs for PGE and Au concentrations, $\mu\text{g g}^{-1}$

	CHR-Pt+	CHR-Bkg	DZE-2	SRM 886	SRM 2556	SRM 2557
Au	4.3	0.028 ^b	–	8.25 ^a	–	–
Pt	58.0	0.05 ^b	0.006	–	697.4 ^a	1131 ^a
Pd	80.8	0.07 ^b	0.002	–	326.0 ^a	233.2 ^a
Rh	4.7	0.009 ^b	0.012	–	51.2 ^a	135.1 ^a
Ir	6.2	0.028 ^b	0.003	–	–	–
Os	1.9 ^b	0.027 ^b	0.006	–	–	–
Ru	9.2	0.067 ^b	0.009	–	–	–
	Chromitite enriched PGE	Chromitite	Ultramafic rock	Gold ore	Used catalyst	Used catalyst

^a Certified values.^b provisional values; others are recommended or working values.

μm ; Table 7). They are intended for use in the evaluation of methods for the determination of Pt, Pd, Rh and lead in catalysts. SRM 2556 is recycled pellet and SRM 2557 is recycled monolith. RMs for Pt in three environmental matrices are available. They are tunnel dust (13.0 ng g^{-1}), corn leaves (585 ng g^{-1}) and cordierite (50 ng g^{-1}). More information on these RMs is found in ref. [54].

5. Conclusions

Many research reports on determinations of the precious metals have appeared recently. A number of the most important and significant have been cited in this review. Instrumental techniques, especially ICP-MS, have yielded more reliable data in determinations of traces of PGEs and Au in a variety of matrices. Improvements in sample treatments and preconcentration steps in order to enhance recoveries of the analytes, and to reduce contamination from chemicals and equipment, have assisted in the achievement of better results. Both the availability of new RMs, and their use in the development and verification of analytical methods have been important.

References

- [1] J.C. Van Loon, R.R. Barefoot, *Determination of the Precious Metals*, Wiley, New York, 1991, p. 106.
- [2] G.E.M. Hall, J.C. Pelchat, *Chem. Geol.* 115 (1994) 61.
- [3] R. Juvonen, E. Kallio, T. Lakomaa, *Analyst* 119 (1994) 617.
- [4] M. Asif, S.J. Parry, H. Malik, *Analyst* 117 (1992) 1351.
- [5] A. Frimpong, B.J. Fryer, H.P. Longrich, Z. Chen, S.E. Jackson, *Analyst* 120 (1995) 1675.
- [6] T. Paukert, I. Rubeska, *Anal. Chim. Acta* 278 (1993) 125.
- [7] M. Asif, S.J. Parry, *Analyst* 116 (1991) 1071.
- [8] F. Zereini, B. Skerstupp, H. Urban, *Geostand. Newslett.* 18 (1994) 105.
- [9] I. McDonald, R.J. Hart, M. Tredoux, *Anal. Chim. Acta* 289 (1994) 237.
- [10] R. Boisvert, M. Bergeron, J. Turcotte, *Anal. Chim. Acta* 246 (1991) 365.
- [11] M. Sun, J. Jain, M. Zhou, R. Kerrich, *Can. J. Appl. Spectrosc.* 38 (1993) 103.
- [12] B.J. Perry, J.C. Van Loon, D.V. Speller, *J. Anal. At. Spectrom.* 7 (1992) 883.
- [13] B.J. Perry, D.V. Speller, R.R. Barefoot, J.C. Van Loon, *Can. J. Appl. Spectrosc.* 38 (1993) 131.
- [14] B.J. Perry, R.R. Barefoot, J.C. Van Loon, A.J. Naldrett, D.V. Speller, in: G. Holland, A.N. Eaton (Eds.), *Applications of Plasma Source Mass Spectrometry II*, The Royal Society of Chemistry, Cambridge, UK, 1993, p. 91.
- [15] B.J. Perry, D.V. Speller, R.R. Barefoot, J.C. Van Loon, *Chem. Geol.* 124 (1995) 47.
- [16] G.S. Reddi, S. Ganesh, C.R.M. Rao, V. Ramanan, *Anal. Chim. Acta* 260 (1992) 131.
- [17] J.B. McHugh, R.M. O' Leary, *J. Geochem. Explor.* 42 (1992) 387.
- [18] G.E.M. Hall, J.E. Vaive, J.A. Coope, E.F. Weiland, *J. Geochem. Explor.* 34 (1989) 157.
- [19] C.J.B. Gowing, P.J. Potts, *Analyst* 116 (1991) 773.
- [20] B.J. Perry, J.C. Van Loon, in: G. Holland, A.N. Eaton (Eds.), *Applications of Plasma Source Mass Spectrometry*, The Royal Society of Chemistry, Cambridge, UK, 1991, p. 38.
- [21] J.M. Vermeulen, *J. Anal. At. Spectrom.* 4 (1989) 77.
- [22] I. Jarvis, M.M. Totland, K.E. Jarvis, *Chem. Geol.* 143 (1997) 1.
- [23] G. Tolg, *Anal. Chim. Acta* 283 (1993) 3.

- [24] S. Terashima, S. Itoh, A. Ando, *Geostand. Newslett.* 16 (1992) 9.
- [25] A. Rivoldini, T. Haile, *At. Spectrosc.* 10 (1989) 89.
- [26] S. Terashima, *Geostand. Newslett.* 15 (1991) 125.
- [27] J.G. Sen Gupta, *Talanta* 40 (1993) 791.
- [28] J.G. Sen Gupta, *Talanta* 36 (1989) 651.
- [29] J. Godfrey, E.M. McCurdy, in: G. Holland, A.N. Eaton (Eds.), *Applications of Plasma Source Mass Spectrometry II*, The Royal Society of Chemistry, Cambridge, UK, 1993, p. 64.
- [30] J.ENZWEILER, P.J. POTTS, K.E. JARVIS, *Analyst* 120 (1995) 1391.
- [31] C.A. Nogueira, M.G. Figueiredo, *Analyst* 120 (1995) 1441.
- [32] W.E. Stone, J.H. Crockett, *Chem. Geol.* 106 (1993) 219.
- [33] G.E. Brugmann, M.P. Gorton, R.G.V. Hancock, *J. Geochem. Explor.* 37 (1990) 25.
- [34] R. Cidu, L. Fanfani, P. Shand, W.M. Edmunds, L. Van't dack, R. Gijbels, *Anal. Chim. Acta* 296 (1994) 295.
- [35] R.A. Davidson, *At. Spectrosc.* 13 (1992) 199.
- [36] P. Noras, in: E. Kontas (Ed.), *Analytical Methods for Determining Gold in Geological Samples*, Report of Investigation 114, Geological Survey of Finland 1993, p. 17.
- [37] U. Penttinen, *ibid.*, E. Kontas (Ed.), *Analytical Methods for Determining Gold in Geological Samples*, Report of Investigation 114, Geological Survey of Finland 1993.
- [38] E. Ojaniemi, *ibid.*, E. Kontas (Ed.), *Analytical Methods for Determining Gold in Geological Samples*, Report of Investigation 114, Geological Survey of Finland 1993.
- [39] G.E.M. Hall, J.C. Pelchat, *J. Anal. At. Spectrom.* 8 (1993) 1059.
- [40] S. Peraniemi, J. Parkkinen, K. Smolander, H. Mustalahti, M. Ahlgren, *Fresenius J. Anal. Chem.* 343 (1992) 292.
- [41] V. Krivan, D. Wildhagen, *Anal. Chim. Acta* 274 (1993) 257.
- [42] K. Pyrznska, *J. Anal. At. Spectrom.* 9 (1994) 801.
- [43] L. Xu, P. Schramel, *Fresenius J. Anal. Chem.* 342 (1992) 179.
- [44] M.M. Gomez, C.W. McLeod, *J. Anal. At. Spectrom.* 8 (1993) 461.
- [45] M.M. Gomez, C.W. McLeod, *J. Anal. At. Spectrom.* 10 (1995) 89.
- [46] A. Cantarero, M.M. Gomez, C. Camara, M.A. Palacios, *Anal. Chim. Acta* 296 (1994) 205.
- [47] I. Jarvis, M.M. Totland, K.E. Jarvis, *Analyst* 122 (1997) 19.
- [48] H. Mukai, Y. Ambe, M. Morita, *J. Anal. At. Spectrom.* 5 (1990) 75.
- [49] K. Akatsuka, S. Hoshi, J.W. McLaren, S.S. Berman, *Bunseki Kagaku* 43 (1994) 67.
- [50] M.L. Lee, G. Tolg, E. Beinrohr, P. Tschopel, *Anal. Chim. Acta* 272 (1993) 193.
- [51] S.E. Jackson, B.J. Fryer, W. Gosse, D.C. Healy, H.P. Longrich, D.F. Strong, *Chem. Geol.* 83 (1990) 119.
- [52] E. Beinrohr, M.L. Lee, P. Tschopel, G. Tolg, *Fresenius J. Anal. Chem.* 34 (1993) 689.
- [53] B. Rietz, K. Heydorn, *J. Radioanal. Nucl. Chem.* 174 (1993) 49.
- [54] R.R. Barefoot, *Environ. Sci. Technol.* 31 (1997) 309.
- [55] B.J. Perry, R.R. Barefoot, J.C. Van Loon, *Trends Anal. Chem.* 14 (1995) 388.
- [56] V.V. Kogan, M.W. Hinds, G.I. Ramendik, *Spectrochim. Acta Part B* 49B (1994) 333.
- [57] M. Totland, I. Jarvis, K.E. Jarvis, *Chem. Geol.* 104 (1993) 175.
- [58] C.-D. Garbe-Schonberg, G.M. McMurtry, *Fresenius J. Anal. Chem.* 350 (1994) 264.
- [59] P. Tothill, L.M. Matheson, J.F. Smyth, K. McKay, *J. Anal. At. Spectrom.* 5 (1990) 619.
- [60] B. Casetta, M. Roncadin, G. Montanari, M. Furlanutt, *At. Spectrosc.* 12 (1991) 81.
- [61] B.J. Perry, R.E. Balazs, *Anal. Proc.* 31 (1994) 269.
- [62] K.K. Falkner, J.M. Edmond, *Anal. Chem.* 62 (1990) 1477.
- [63] G.E.M. Hall, A.M. Rencz, A.I. Maclaurin, *J. Geochem. Explor.* 41 (1991) 291.
- [64] C.A. Williams, F.R. Abou-Shakra, N.I. Ward, *Analyst* 120 (1995) 341.
- [65] G.E.M. Hall, J.C. Pelchat, C.E. Dunn, *J. Geochem. Explor.* 37 (1990) 1.
- [66] R.L. Van Hoven, S.-H. Nam, A. Montaser, M.W. Doughten, A.F. Dorzappf Jr., *Spectrochim. Acta Part B* 50B (1995) 549.
- [67] G.P. Russ III, J.M. Bazan, *Spectrochim. Acta Part B* 42B (1987) 49.
- [68] J.M. Richardson, A.P. Dickin, R.H. McNutt, J.I. McAndrew, S.B. Beneteau, *J. Anal. At. Spectrom.* 4 (1989) 465.
- [69] A.P. Dickin, R.H. McNutt, J.I. McAndrew, *J. Anal. At. Spectrom.* 3 (1988) 337.
- [70] M.D. Hannington, M.P. Gorton, *Geostand. Newslett.* 15 (1991) 145.
- [71] K. Hoppstock, F. Alt, K. Cammann, G. Weber, *Fresenius J. Anal. Chem.* 335 (1989) 813.
- [72] J. Messerschmidt, F. Alt, G. Tolg, J. Angerer, K.H. Schaller, *Fresenius J. Anal. Chem.* 343 (1992) 391.
- [73] F. Alt, A. Bambauer, K. Hoppstock, B. Mergler, G. Tolg, *Fresenius J. Anal. Chem.* 346 (1993) 693.
- [74] J. Messerschmidt, F. Alt, G. Tolg, *Anal. Chim. Acta* 291 (1994) 161.
- [75] G.E. M. Hall, J.E. Vaive, *Chem. Geol.* 102 (1992) 41.
- [76] M.J. Lintern, A.W. Mann, G.D. Longman, *J. Geochem. Explor.* 43 (1992) 233.
- [77] J.C. Rucklidge, *Analyst* 120 (1995) 1283.
- [78] G.C. Wilson, L.R. Kilius, J.C. Rucklidge, *Geochim. Cosmochim. Acta* 55 (1991) 2241.
- [79] G.C. Wilson, J.C. Rucklidge, R.L. Kilius, G.-J. Ding, R.G. Cresswell, *Nucl. Instrum. Methods Phys. Res. Sect. B* 123 (1997) 583.
- [80] L.J. Cabri, S.L. Chryssoulis, J.L. Campbell, W.J. Teesdale, *Appl. Geochem.* 6 (1991) 225.
- [81] A.J. Criddle, H. Tamana, J. Spratt, K.J. Reeson, D. Vaughan, G. Grime, *Nucl. Instrum. Methods Phys. Res. Sect. B* 77 (1993) 444.

- [82] S.L. Chrystoulis, L.J. Cabri, W. Lennard, *Econ. Geol.* 84 (1989) 1684.
- [83] J. Saito, T. Nakamura, A. Yamaguchi, K. Saiki, H. Takeda, *Mineral. J.* 16 (1993) 258.
- [84] P. Allain, S. Berre, Y. Mauras, A. Le Bouil, *Biol. Mass Spectrom.* 21 (1992) 141.
- [85] R. Kizu, T. Yamamoto, T. Yokoyama, M. Tanaka, M. Miyazuki, *Chem. Pharm. Bull.* 43 (1995) 108.
- [86] A. Andersson, H. Ehrsson, *J. Pharm. Biomed. Anal.* 13 (1995) 639.
- [87] S.G. Matz, R.C. Elder, K. Tepperman, *J. Anal. At. Spectrom.* 4 (1989) 767.
- [88] Z. Zhao, W.B. Jones, K. Tepperman, J.G. Dorsey, R.C. Elder, *J. Pharm. Biomed. Anal.* 10 (1992) 279.
- [89] R.R. Barefoot, J.C. Van Loon, *Anal. Chim. Acta* 334 (1996) 5.
- [90] J. Messerschmidt, F. Alt, G. Tolg, *Electrophoresis* 16 (1996) 800.
- [91] S. Lustig, B. Michalke, W. Beck, P. Schramel, *Fresenius J. Anal. Chem.* 360 (1998) 18.
- [92] K. Govindaraju, *Geostand. Newslett.* 18 (1994) 1.
- [93] M. Tredoux, I. McDonald, *Geostand. Newslett.* 20 (1996) 267.
- [94] P.J. Potts, C.J.B. Gowing, K. Govindaraju, *Geostand. Newslett.* 16 (1992) 81.
- [95] X. Li, C. Tong, *J. Radioanal. Nucl. Chem.* 196 (1995) 11.
- [96] M. Yan, C. Wang, Q. Cao, T. Gu, Q. Chi, *Geostand. Newslett.* 19 (1995) 125.
- [97] W.-m. Yang, Z.-m. Ni, *Spectrochim. Acta Part B* 51B (1996) 65.

Comparison of conventional filtration and a denuder-based methodology for sampling of particulate-phase mercury in ambient air

Julia Y. Lu, William H. Schroeder *

Atmospheric Environment Service, Environment Canada, 4905 Dufferin Street, Toronto, Ont. M3H 5T4, Canada

Received 30 July 1998; received in revised form 9 October 1998; accepted 12 October 1998

Abstract

This paper compares the results of total atmospheric particulate-phase mercury determinations using samples collected by two methods. The conventional filtration method (FM) collects airborne particulate matter first, whereas the denuder-based method (DM) removes gaseous-phase mercury prior to particulate matter collection. In each case, particulate-phase mercury (PM) is collected on a quartz fiber disc held in a miniaturized device and is analyzed using a pyrolysis/gold amalgamation/thermal desorption/cold vapor atomic fluorescence spectrometry (CVAFS) technique. The results show that the concentrations of PM determined using the samples collected by DM are higher than those determined using the samples collected by FM. Evidence presented shows that the higher results are due to mercury-bearing gold particles flaking off from the gold-coated denuder surfaces in the denuder-based sampling system. © 1999 Elsevier Science B.V. All rights reserved.

Keywords: Denuder; Particulate-phase mercury; Ambient air

1. Introduction

Atmospheric particulate-phase mercury (typically at $\sim 1\text{--}100\text{ pg m}^{-3}$ levels) has long been neglected by the scientific community because it generally accounts for only a few percent of the total Hg in ambient air, most of which exists in the gaseous phase. A value as high as 100 ng m^{-3} for PM, however, has been reported in the Amazon Basin, Brazil [1]. In recent studies in the

Arctic [2–4], elevated levels of PM concentrations ($\sim 40\%$ of the total atmospheric mercury) have occasionally been observed (during mercury vapor depletion episodes in the springtime [5,6]). Since airborne particles containing Hg can be readily deposited to the earth's surface, through rain- and wash-out processes [7,8], particulate-phase mercury, under certain conditions, can be a very important form of atmospheric Hg, and can significantly affect the cycling and distribution of this element in the atmosphere [4,9].

Traditionally, particulate matter in ambient air is collected by filtration of the air through filters

* Corresponding author. Fax: +1-416-739-4318.

E-mail address: bill.schroeder@ec.gc.ca (W.H. Schroeder)

having diameters of 47 mm or larger. Different materials, such as quartz fiber [10,11], cellulose [12,13] and polypropylene [14], have been used as collection media for the determination of PM in ambient air. The major advantages of using commercially available filter media for sampling particulate matter in air are that these media have specified pore sizes, are easy to use and are cost efficient. To avoid contamination due to handling and transfer of the sample during sample collection and sample preparation (e.g. acid digestion/extraction), ultra-clean sampling techniques and a clean room facility are necessary [15].

Particulate traps containing quartz wool plugs [16–18] have the advantage of being easy to use. No direct handling of the filter medium nor sample transfer are involved when pyrolysis is used for sample preparation/analysis. A major drawback of using quartz wool plugs is that it is difficult, if even possible, to pack the quartz wool uniformly from one sampler/trap to the next. The efficiency for collecting particles, therefore, varies from plug to plug. Schroeder et al. [19] compared two sampling methods: (1) glass-fiber filters in Teflon filter cassettes at a nominal flow rate of 30 l min^{-1} and (2) traps consisting of quartz-wool plugs contained in quartz tubes (6 mm o.d., 4 mm i.d.) at a flow rate of $300\text{--}500 \text{ ml min}^{-1}$. The results of this intercomparison showed that the values obtained by method (1) were much lower than those obtained by method (2), in one case by as much as a factor of 10. It has been suggested that the higher values might result from adsorption of gaseous species of Hg (possibly Hg^0) by the quartz wool [20].

A miniaturized device has been developed by Lu et al. [3] for sampling and analysis of particulate-phase mercury in ambient air. This device combines the inherent advantages of the quartz fiber filter and the quartz wool plug technologies, and serves as both particulate trap (during sampling) and pyrolyzer (during analysis) for airborne particulate-phase mercury species. It has been used in combination with amalgamation/thermal desorption/CVAFS detection of elemental mercury vapor for the determination of PM associated with atmospheric aerosols.

When sampling airborne particulate matter using FM as described above, possible sampling artifacts include: (i) interactions among particles retained, the filter materials and vapor-phase Hg species; (ii) condensation of vapor-phase Hg onto the particles retained; and/or (iii) release of weakly-bound volatile Hg species from the particles into the vapor phase. Hence, the results obtained by this method may be uncertain. To overcome these potential problems, a denuder-based method (DM), which separates and removes gaseous mercury prior to collection of the particulate matter, has been developed and applied to sampling of particulate matter in ambient air [20,21]. The results, however, were 2–16% higher than those obtained from samples collected simultaneously using FM [22].

In a recent study [23], four different techniques (three filtration-based and one denuder-based) used by different laboratories were intercompared for sampling and analysis of PM in ambient air. The results show that the values obtained by the denuder-based system were always the highest. Since these four techniques differ in sampling methods as well as sample preparation techniques, it is difficult to explain the discrepancy.

This paper presents the values for PM concentrations in ambient air, determined using samples collected by FM and DM. The discrepancy of the results obtained from the two sampling methods has been experimentally demonstrated and explained. Scanning electron microscopy (SEM) has been widely used for characterizing particles [24,25] and is used in this work for obtaining experimental evidence to support interpretation of our empirical observations on gold-coated denuders.

2. Experimental

2.1. Materials

2.1.1. Particulate traps

The particulate traps used in both sampling methods were developed by Lu et al. [3]. Each trap consists of a quartz fiber filter disc (diameter, 6 mm; pore size, $0.2\text{--}10 \mu\text{m}$; Gelman) held in a

quartz tube (6 mm i.d.; 8 mm o.d.). The traps were cleaned by firing twice at 470°C for 5 min with a ‘zero air’ (dry air with $[Hg] < 0.1 \text{ ng m}^{-3}$) flow at a rate of 100 ml min^{-1} .

2.1.2. Gold-coated denuders

The denuders (URG, Chapel Hill, NC) were made by coating quartz tubes (62 cm long with an inner diameter of 4 mm) with gold solution. The denuders were cleaned by firing them five times at 650°C with zero air flow at a rate of 1 l min^{-1} . A series of tests under different experimental conditions have been carried out to characterize the gold-coated denuders.

2.1.2.1. Collection efficiency as a function of time. Air flowed through the gold-coated denuders at a rate of 1.5 l min^{-1} for times ranging from 1.25 to 33 h, and the air downstream of the gold-coated denuders was monitored using an automated Mercury Vapor Analyzer (Tekran, Model 2537A) at 5-min sampling intervals. Two types of air, ambient air and a stream of dry air containing a constant concentration of Hg^0 , which was generated from a permeation–dilution system, were used for this type of test. When ambient air was used, two Mercury Vapor Analyzers were operating side by side: one was used for monitoring the total gaseous mercury (TGM) concentration in the ambient air, the other was used to monitor the TGM concentration in the effluent from the gold-coated denuder.

2.1.2.2. Collection efficiency as a function of air flow rate. Ambient air at flow rates of 0.5, 1.0 and 1.5 l min^{-1} was pulled through the gold-coated denuders. The mercury concentrations in the air upstream and downstream of the denuders were determined using the aforementioned Mercury Vapor Analyzers.

2.1.2.3. Comparison of the collection efficiencies of a single denuder and a set of two denuders in series. A stream of ambient air at a flow rate of 1.0 l min^{-1} was directed through a single and a pair of denuders in series, respectively. The mercury concentrations upstream and downstream of the denuder(s) were monitored using the Mercury Vapor Analyzers.

2.2. Off-line sampling and analysis of PM in ambient air

2.2.1. Sampling

2.2.1.1. Conventional filtration method. Ambient air was pulled through the particulate trap using two types of air pumps: single-stage (contained in the Tekran Model 2537A Mercury Vapor Analyzer) and dual-stage (Model DAA-V110-GB, GAST, Benton Harbor, MI). The sampling flow rate was measured by a mass flow meter (Hastings, Hampton, VA).

2.2.1.2. Denuder-based method. A single denuder or a pair of gold-coated denuders in series was added upstream of the particulate trap for removal of gaseous mercury species prior to airborne particulate matter collection.

2.2.2. Determination of mercury

The samples collected with each sampling system were taken into the laboratory and connected to an analytical train, Fig. 1, for analysis of their Hg content. The analytical train consists of a converter/pyrolyzer, a pre-focusing (‘analytical’) gold trap and a CVAFS detector (Tekran, Model 2500). The converter/pyrolyzer consists of a quartz tube containing granular MgO (0.5–1 mm, light form, J. T. Baker, Phillipsburg, NJ) and is maintained at 900°C by an external nickel–chromium alloy resistance heating ribbon. The purpose of using MgO in the converter is 2-fold: (i) to reduce/eliminate the effect of acidic gases;

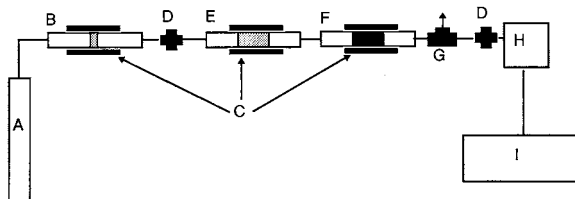


Fig. 1. Experimental set-up for sample analysis. (A) Compressed Ar cylinder; (B) particulate trap; (C) heaters; (D) injection ports; (E) converter (consisting of a quartz tube containing MgO); (F) analytical gold trap; (G) three-way solenoid valve; (H) CVAFS detector; (I) computer (for process automation, data acquisition/display and report generation).

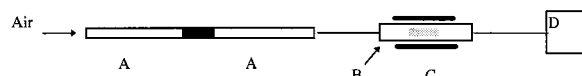


Fig. 2. Experimental set-up for in-line sampling and analysis of particulate-phase mercury in ambient air. (A) Dual stage gold-coated denuder; (B) pyrolyzer consisting of a quartz tube containing granular MgO; (C) heater; (D) Mercury Vapor Analyzer (Tekran, Model 2537A).

(ii) to increase the turbulence and the total residence time of the gaseous Hg species in the high temperature zone so as to achieve a more complete conversion of Hg compounds into the elemental form [3]. The particulate trap containing the sample is heated at 900°C for 5 min. The released Hg species are carried, by a stream of argon gas at a flow rate of 200 ml min⁻¹, to the converter/pyrolyzer, to convert all Hg compounds to the elemental form [21,22,26], and the resulting Hg⁰ is pre-concentrated on the analytical Au-trap downstream. The analyte is then thermally desorbed from the Au-trap at 500°C and detected by the CVAFS detector.

Calibration of the analytical system is achieved by injecting a known volume of air saturated with Hg⁰ vapor at a pre-determined temperature.

2.3. In-line sampling and analysis of PM in ambient air

Fig. 2 shows the experimental set-up for in-line sampling and analysis of PM in ambient air. This set-up is duplicated during the measurements. The Mercury Vapor Analyzer, Fig. 2, D, is equipped with two gold cartridges for mercury pre-concentration, a mass flow meter for measuring sampling flow and an air pump. The entire procedure, from sampling to analysis has been fully automated. When air flows through the denuders, the gaseous mercury species in the air are removed by the gold-coated denuders [27] and the mercury species associated with airborne particulate matter pass through the denuders and into the pyrolyzer. The pyrolyzer consists of a quartz tube (6 mm o.d., 4 mm i.d.) containing granular MgO (0.5–1 mm). The MgO was held in place in the quartz tube by quartz wool plugs. The lengths of the MgO plugs in the quartz tube were about 3 cm.

Mercury associated with airborne particulate matter was collected and analyzed using the following two approaches:

2.3.1. *In situ* pyrolysis

With the pyrolyzer temperature maintained at 900°C, mercury species associated with airborne particulate matter, which is retained by MgO, are thermally decomposed to the elemental form while the air is pulled through the pyrolyzer. The elemental mercury is carried downstream by air and is pre-concentrated on a gold trap in the Mercury Vapor Analyzer. After 4 h, the sampling line was switched off and the mercury collected on the gold trap was thermally desorbed and analyzed by the CVAFS detector in the analyzer. Considering that the gaseous mercury species may not be 100% removed by the dual stage denuder, the concentration of mercury determined in this way can be defined as the sum of PM and gaseous mercury not collected by the tandem denuder (i.e. PM + Hg denuder break-through).

2.3.2. *In-line collection and pyrolysis*

With the heater off at the pyrolyzer during the sampling process, the mercury species associated with airborne particulate matter are retained by the granular MgO in the pyrolyzer. What the Mercury Vapor Analyzer measures during the sampling period is the sum of the gaseous mercury species break-through from the second stage of the denuder and the mercury species ‘blow-off’ (desorbed/volatilized) from the particulate matter retained by the granular MgO (Hg denuder break-through + PM blow-off). After 4 h, the heater was turned on for 10 min to raise the temperature of the pyrolyzer to 900°C so as to thermally decompose all the mercury species associated with the airborne particles which were retained by the granular MgO in the pyrolyzer during the sampling step. The mercury thus released was analyzed by the Tekran Analyzer. The results obtained from this step can be defined as PM – (PM blow-off).

The break-through of gaseous mercury species from the paired gold denuders was determined with a Mercury Vapor Analyzer before and after the PM measurements.

Table 1

Efficiency of the gold-coated denuders for removing gaseous species of mercury in dry and ambient air at a sampling flow rate of 1.5 l min^{-1}

Denuder	Air type	Total passage time (min)	$[\text{Hg}]_{\text{in}} \pm 0.1 \text{ (ng m}^{-3}\text{)}$	$[\text{Hg}]_{\text{out}} \text{ (ng m}^{-3}\text{)}$	$([\text{Hg}]_{\text{in}} - [\text{Hg}]_{\text{out}}) / [\text{Hg}]_{\text{in}} \text{ (%)}$	Mean \pm S.D. (%)
1	Dry	60	5.0	0.19 ± 0.06	96	98 ± 1
2				0.14 ± 0.03	97	
3				0.008 ± 0.003	100	
5				0.074 ± 0.010	98	
7				0.089 ± 0.010	98	
1	Dry	600	5.0	0.14 ± 0.04	97	98 ± 1
2				0.12 ± 0.02	98	
3				0.017 ± 0.005	100	
2	Dry	1980	5.0	0.13 ± 0.02	97	89 ± 11
3		1140		0.035 ± 0.007	99	
2	Ambient	60	2.0	0.60 ± 0.008	70	89 ± 11
3				0.07 ± 0.002	96	
4				0.10 ± 0.003	95	
8				0.13 ± 0.004	94	
2				0.48 ± 0.006	75	
3	Ambient	600	2.0	0.12 ± 0.004	94	89 ± 8
4				0.13 ± 0.003	94	
8				0.13 ± 0.004	94	

2.4. Scanning electron microscopy (SEM)

The filter disc, along with the airborne particulate matter collected, was mounted onto glass slides with double-sided carbon tape, then coated with carbon. X-ray microanalysis was performed with a Link eXL, LZ-4 system (Oxford Analysis Instrumentation, Oxford, UK), using the Be-window at 20 kV, 39 mm working distance and probe current set at 0.8 nA with a Faraday cup. Spectra were collected for 100 s live time. Quantitation was carried out using the Link ZAF program.

3. Results and discussion

3.1. Characterization of the gold-coated denuders

Table 1 lists the concentrations of gaseous mercury species in the air downstream of specific (single) denuders. When a stream of dry air was used, the collection efficiency of the five denuders tested ranged from 96.2 to 99.8%. Statistically, there was no significant decrease in the efficiency when the passage time increased from 1 to 10 h.

No significant decrease was observed even when the passage time increased to 19 h for denuder 3 and 33 h for denuder 2. Calculations based on a simplified form of the Gormly–Kennedy equation [28] predict that denuders of the same dimensions as those used in this study are capable of removing $>99.55\%$ of the gaseous Hg at an air flow rate of 1 l min^{-1} . An efficiency of $>99.9\%$ was observed in laboratory tests [20]. The lower removal efficiency observed in this study is probably due to the higher flow rate, i.e. 1.5 rather than 1.0 l min^{-1} .

With the same experimental conditions, but using ambient air with lower concentration of mercury instead of dry air, the removal efficiency dropped significantly (from 98 to 89%) and the magnitude of the decrease differed from denuder to denuder. However, the removal efficiency of the denuders remained essentially unchanged when the passage time increased to 10 h. The observed decrease in the removal efficiency may be due to the presence of moisture and/or chemical species in ambient air, which react with or are adsorbed onto the gold and thus inhibit quantitative sampling of mercury [29].

Table 2

Effect of flow rate on the efficiency of the gold-coated denuders for removing gaseous mercury species in ambient air: total passage time, 1 h

Denuder	Flow rate (l min ⁻¹)	[Hg] _{in} (ng m ⁻³)	[Hg] _{out} ^a (ng m ⁻³)	([Hg] _{in} - [Hg] _{out})/[Hg] _{in} (%)
2	1.5	2.0 ± 0.1	0.24 ± 0.05	88
	1.0		0.15 ± 0.03	93
	0.5		0.16 ± 0.04	92
4	1.5	2.0 ± 0.1	0.38 ± 0.09	81
	1.0		0.20 ± 0.05	90
	0.5		0.10 ± 0.02	95

^a [Hg]_{out} was measured every 5 min using a Tekran Mercury Vapor Analyzer.

Table 2 shows the effect of flow rate on the efficiency of the denuders for removing gaseous species of mercury in ambient air. In general, the higher the flow rate, the lower the removal efficiency. But even at a flow rate of only 0.5 l min⁻¹, the two denuders tested removed only 92–95% of the total gaseous mercury from the ambient air. The concentration of gaseous mercury in the air downstream of the denuder is, therefore, at least equivalent to or, in most cases, higher than that of PM in ambient air. From a consideration of the removal efficiency of the gold-coated denuders tested and the air volume to be sampled, a flow rate of 1.0 l min⁻¹ was chosen for further studies.

To further reduce the residual gaseous Hg from the denuder, two denuders in series were tested. Table 3 compares the efficiencies of four single and two pairs of gold-coated denuders in series for removing gaseous Hg species from ambient air. A slight enhancement in the removal efficiency was observed when two denuders were used in series, but the residual gaseous mercury concentration is still higher than desired (i.e. it is equivalent to or higher than typical PM concentrations in ambient air!). Nevertheless, further study using the denuder-based sampling method is still worthwhile because of a reduction of more than 90% in TGM by the denuder(s) possible interactions among the filter materials, filter-retained particulate matter and vapor-phase mercury species may be significantly less and the degree of condensation/adsorption of the vapor-phase mercury onto the material surface/particles retained may be reduced. By comparing the re-

sults obtained from two sampling methods (FM and DM), some of the possible gas–surface interactions may be identified.

3.2. Results from in-line sampling and analysis of PM

Table 4 shows the results from in-line sampling and analysis (in duplicate) of PM using the denuder-based sampling method. Mercury breakthrough accounts for about 8% of TGM in ambient air from the denuder in duplicate 1, about 6% from the denuder in duplicate 2. PM blow-off during the sampling period, observed from duplicate 2 was twice that observed from duplicate 1, and the values themselves seem to be quite high (ranging from 0.15 to 0.28 ng m⁻³). The concentrations of PM obtained from the two parallel set-ups and from two different approaches, as shown in Table 4, do not agree well. The values of PM calculated from the measured parameters are 0.19 and 1.48 ng m⁻³ from the *in situ* pyrolysis approach, 0.27 and 0.56 ng m⁻³ from the in-line pyrolysis approach. All these values are much higher than those (<0.1 ng m⁻³) reported in the literature for Toronto [3] and for the Great Lakes Region [30], even though there is a possibility that the collection efficiency of the MgO plugs may not be as high as that of quartz fiber filters used in the quoted references.

3.3. Results from off-line sampling and analysis of PM

Table 5 lists the concentrations of PM determined using the samples collected by FM and

Table 3

Comparison of the efficiencies of single gold-coated denuders, and a group of two denuders in series, for removing gaseous mercury species in ambient air at a flow rate of 1.0 l min^{-1}

Denuder	Total passage time (h)	$[\text{Hg}]_{\text{in}} \pm 0.1 \text{ (ng m}^{-3}\text{)}$	$[\text{Hg}]_{\text{out}} \text{ (ng m}^{-3}\text{)}$	$([\text{Hg}]_{\text{in}} - [\text{Hg}]_{\text{out}}) / [\text{Hg}]_{\text{in}} \text{ (\%)}$
4	18	3.0	0.20 ± 0.02	93
5	18	2.5	0.44 ± 0.03	82
6	3	3.0	0.45 ± 0.02	85
8	20	2.4	0.22 ± 0.03	91
5+8	20	2.5	0.14 ± 0.03	94
	52		0.19 ± 0.06	92
4+6	20	2.5	0.084 ± 0.03	97
	52		0.12 ± 0.02	95

DM, determined off-line. The values obtained from FM range from 0.0064 to 0.050 ng m^{-3} and are within the range (0 – 0.1 ng m^{-3}) of those reported in the literature for Toronto [3] and for the Great Lakes Region [30]. The values obtained by the DM range from 0.012 to 0.36 ng m^{-3} and are all higher than those obtained from the samples collected by FM at the same time. This situation is similar to that observed in a study where four sampling methods used by four laboratories were compared for the determination of PM in ambient air [23].

The consistently higher values obtained with the DM, using both in-line and off-line determinations, led us to suspect that there might exist a sampling artifact when using gold-coated denuders. For the denuders used in this study, we surmised that the gold-coating might be flaking off from the interior surface of the denuders during sampling. Because these gold flakes would be retained by the particulate filter (situated downstream of the denuder), any gaseous mercury species previously adsorbed by the gold flakes would be thermally released during the pyrolysis process and consequently be (erroneously) determined as particulate-phase mercury, thus resulting in erroneously high PM values.

3.4. Experimental evidence of gold flaking off from the denuders

To obtain direct evidence of the presence (or absence) of gold flakes in air exiting these denud-

ers, a batch of four samples (two by FM and two by DM), plus a procedural blank were collected and analyzed for their Hg content following the procedure previously described in this paper. After this analysis, the filters were sent to another laboratory for SEM analysis. One might expect that gold flakes from the denuder would remain on the filter after pyrolysis at 900°C and their presence should be detected by SEM. The initial results, however, showed no evidence of gold flakes on the particulate filters. After reflecting on the possible reason(s) for the higher values of PM concentrations obtained from the DM, we still believed that flaking-off of the gold-coating might be the problem. Considering the procedure used in coating the denuder, the thickness of the gold coating should be in the range of a few μm or even less. The size of the flakes should, therefore, be in a similar range. Such tiny flakes of gold may conceivably be vaporized during pyrolysis at a temperature of 900°C , leaving nothing to be ‘seen’ by SEM. Therefore, another batch of four samples (one using FM, one using DM with a single denuder, two using DM with a pair denuders in series), plus a blank, were collected and this time sent out for SEM analysis without prior pyrolysis. Fig. 3 shows a portion of the SEM image for sample F16, which was collected downstream of a pair of denuders in series. The light spots were identified, by elemental analysis, to be gold flakes. This image also shows that these gold flakes are different in size and shape. Irregular size and

Table 4

Mercury denuder break-through, particulate-phase mercury (PM) blow-off and PM (ng m^{-3}), in duplicate, obtained from the in situ and in-line pyrolysis procedures: sampling flow rate, 1.0 l min^{-1}

	In situ pyrolysis ^a	In-line pyrolysis ^b		
Hg denuder break-through ^c	0.21	0.16	0.21	0.16
PM + (Hg denuder break-through)	0.40	1.64		
(Hg denuder break-through) + (PM blow-off) ^d			0.36	0.44
PM - (PM blow-off)			0.12	0.28
PM (calculated)	0.19	1.48	0.27	0.56

^a Mercury associated with particulate matter was converted to Hg^0 in the trap (900°C) while the air flows through.

^b Mercury associated with particulate matter was collected on the trap (the heater at the trap is off during sampling process) and pyrolyzed at the end of each sampling period.

^c Mercury concentration measured downstream of the gold denuders.

^d Mercury desorbed/volatilized from the particulate matter retained on the filter during sampling period.

shape support our hypothesis that gold is flaking off from the denuder. The results of the elemental analysis for all the samples are listed in Table 6. For each sample, at least 14 points (representing different locations on the filter) have been analyzed. The relative amount of gold on the blank filter and the filter with airborne particulate matter collected using FM was below the limit of detection ($< 1000 \text{ ppm}$) for all the determinations. Gold flakes were detected in all the samples collected using DM. With a single denuder, fewer flakes were detected (3/14), while a greater number of flakes was observed when pairs of denuders in series were used (7/20 and 11/20, respectively). The results also indicate that the size of the gold flakes varies, since the size of the laser beam ($1\text{--}2 \mu\text{m}$) and the depth the laser beam can penetrate are the same for all the analyses, the relative amount of gold in each determination will there-

fore indicate the size of the flakes. These tiny flakes of gold, not visible to the naked eye, are released ('eroded') from the interior gold surface of a denuder during the sampling step and end up on the particulate filter situated downstream of the denuder. Such specks of gold would have gaseous-phase Hg species (mainly Hg^0) amalgamated to them and would bias the PM determination, which is based on chemical analysis of all materials on the filter located downstream of the denuder. These observations provide a plausible explanation of why the DM tends to give results which are higher than those obtained with the FM. For the denuder-based systems described in Ebinghaus et al. [23] and Xiao et al. [20] for the determination of PM in ambient air, gaseous mercury breaking through the denuder may also contribute to the high values of PM, because it was assumed that the denuder can remove 99.9% of

Table 5

Comparison of particulate-phase mercury (PM) concentrations determined using samples (duplicates from each method) collected by the conventional filtration method (FM) and the denuder-based method (DM)^a

Date 1997	Denuder	Sampling time (h)	Flow rate (l min^{-1})	PM by FM (ng m^{-3})	PM by DM (ng m^{-3})
Jan. 25	3, 8	16	1.4–1.9	0.0084 ± 0.0043	0.012 ± 0.006
Jan. 30	2, 6	16.5	1.4–2.4	0.0064 ± 0.0024	0.027 ± 0.002
Jan. 31	4, 5	15	1.2–2.7	0.044 ± 0.005	$0.092 \pm ?$
Feb. 1	4, 5	27.8	1.2–3.3	0.041 ± 0.022	0.062 ± 0.010
Mar. 28	2, 6	21	2.1–5.4	0.050 ± 0.009	0.36 ± 0.063
Mar. 29	1&8, 3&6 in series	26	1.3–3.4	0.032 ± 0.004	0.26 ± 0.047

^a Values after \pm signs are the difference from the mean value.

Table 6

Gold content in samples of airborne particulate matter collected with and without front-end gold-coated denuders

Sample ID	Sample description	<i>n</i> ^a	Au content in each measurement (%) ^b
F0	Blank	15	<L.O.D. ^c
F15	Sample collected without a gold-coated denuder	16	<L.O.D.
F17	Sample collected downstream of one gold-coated denuder	14	84.7, 81.4, 77.4. Others <L.O.D.
F6	Sample collected downstream of two gold-coated denuders in series	20	10.2, 23.9, 61.1, 94.0, 91.1, 92.7, 21.3. Others <L.O.D.
F16	Sample collected downstream of two gold-coated denuders in series	20	91.1, 43.4, 87.7, 64.5, 26.6, 41.6, 92.3, 8.0, 66.6, 25.3, 87.4. Others <L.O.D.

^a Total number of determinations on one filter sample.

^b $\text{Au}/(\text{Si} + \text{Al} + \text{Ti} + \text{Cr} + \text{Fe} + \text{Mg} + \text{Mn} + \text{K} + \text{Ca} + \text{Na} + \text{Cl} + \text{Ni} + \text{Zn} + \text{P} + \text{S} + \text{Cu} + \text{Au} + \text{Ba} + \text{Pb} + \text{'C'}) \times 100$.

^c L.O.D., limit of detection, 1000 ppm.

the TGM even under ambient conditions, and gold traps located downstream of the denuders were employed as particulate collectors. Our results (Table 1) indicate a general decrease in the removal efficiency of denuders when ambient air is used instead of purified dry air. The resulting increased concentration of gaseous mercury in the effluent air from the denuder will be collected on the gold trap situated downstream of the denuder and consequently be determined as particulate-phase mercury, thus leading to erroneously high PM values.

It should be kept in mind that our work involved gold-coated denuders from one supplier, and hence should be independently verified by

others who use Au-coated denuders for the determination of particulate-phase mercury. Nevertheless, gold flaking off from the denuder, if it is a general phenomenon, will bias (high) the determination of PM and this problem must be resolved before attempting to use DM for sampling particulate matter in ambient air for the purpose of PM determination. In addition, gaseous mercury break-through from the denuder must be checked under field conditions. Therefore, use of in situ pyrolysis with a gold trap downstream of a gold-coated denuder is not recommended for sampling and analysis of PM in ambient air. A system using gold tubing (instead of gold-coated quartz tubing) combined with a miniaturized particle collection device is being developed in our laboratory for unambiguous sampling and analysis of particulate-phase mercury in ambient air.



Fig. 3. Image of scanning electron microscopy for sample F16, showing gold flakes (light spots) of different sizes.

Acknowledgements

We thank Dr Cheng Huang at Carleton University, Ottawa, Canada for performing the SEM analysis.

References

- [1] S. Hacon, P. Artaxo, F. Gerab, M.A. Yamasoe, R.C. Campos, L.F. Conti, L.D. De Lacerda, *Water Air Soil Pollut.* 80 (1995) 273.

- [2] J.Y. Lu, W.H. Schroeder, A. Steffen, AMAP International Symposium on Environmental Pollution in the Arctic (Extended abstracts), Tromsø, Norway, 1997, pp. 352–353.
- [3] J.Y. Lu, W.H. Schroeder, T. Berg, J. Munthe, D. Schneeberger, F. Schaedlich, *Anal. Chem.* 70 (1998) 2403.
- [4] W.H. Schroeder, K. Anlauf, L.A. Barrie, T. Berg, J.Y. Lu, D. Schneeberger, Paper presented at the International Symposium on Atmospheric Chemistry and Future Global Environment, Nagoya, Japan, 11–13 November 1997.
- [5] W.H. Schroeder, K. Anlauf, L.A. Barrie, J.Y. Lu, A. Steffen, D. Schneeberger, T. Berg, *Nature* 394 (1998) 331.
- [6] W.H. Schroeder, L.A. Barrie, International Global Atmospheric Chemistry (IGAC) Newsletter, Issue # 14, September 1998, pp. 7–8.
- [7] D.H. Matheson, in: J.O. Nriagu (Ed.), *The Biogeochemistry of Mercury in the Environment*, Elsevier, North-Holland, Amsterdam, 1979.
- [8] C.H. Lamborg, W.F. Fitzgerald, G.M. Vandal, K.R. Rolfhus, *Water Air Soil Pollut.* 80 (1995) 189.
- [9] W.F. Fitzgerald, R.P. Mason, G.M. Vandal, F. Dulac, Air-water cycling of mercury in lakes, in: C.J. Watras, J. Huckabee (Eds.), *Mercury Pollution-Integration and Synthesis*, Lewis Publishers, Boca Raton, FL, 1994, pp. 203–220.
- [10] G.J. Keeler, G. Glinsorn, N. Pirrone, *Water Air Soil Pollut.* 80 (1995) 159.
- [11] N. Fukuzaki, R. Tamura, Y. Hirano, Y. Mizushima, *Atmos. Environ.* 20 (1986) 2291.
- [12] G.E. Millward, J.H. Griffin, *Sci. Total Environ.* 16 (1980) 239.
- [13] A. Brzezinska-Paudyn, J.C. Van Loon, M.R. Balicki, *Water Air Soil Pollut.* 27 (1986) 45.
- [14] C. Pollman, G. Gill, W.M. Landing, J.L. Guentzel, D. Bare, D. Porcella, E. Zillioux, T. Atkeson, *Water Air Soil Pollut.* 80 (1995) 285.
- [15] G.J. Keeler, M.E. Hoyer, C. Lamborg, Measurements of Atmospheric Mercury in the Great Lakes Basin, in: C.J. Watras, J. Huckabee (Eds.), *Mercury Pollution-Integration and Synthesis*, Lewis Publishers, Boca Raton, FL, 1994, pp. 231–250.
- [16] W.F. Fitzgerald, R.P. Mason, G.M. Vandal, *Water Air Soil Pollut.* 56 (1991) 745.
- [17] C. Brosset, E. Lord, *Water Air Soil Pollut.* 56 (1991) 493.
- [18] R. Ebinghaus, H.H. Kock, S.G. Jennings, P. McCartin, M.J. Orren, *Atmos. Environ.* 29 (1995) 3333.
- [19] W.H. Schroeder, G. Keeler, H.H. Kock, P. Roussel, D. Schneeberger, F. Schaedlich, *Water Air Soil Pollut.* 80 (1995) 611.
- [20] Z.F. Xiao, J. Munthe, O. Lindqvist, *Water Air Soil Pollut.* 56 (1991) 141.
- [21] K. Kvietkus, Z. Xiao, O. Lindqvist, *Water Air Soil Pollut.* 80 (1995) 1209.
- [22] J. Munthe, The Redox Cycling of Mercury in the Atmosphere, Ph.D. Thesis, Department of Inorganic Chemistry, University of Göteborg, 1991, p. 9.
- [23] R. Ebinghaus, S.G. Jennings, W.H. Schroeder, T. Berg, T. Donaghy, R. Ferrara, J. Guentzel, C. Kenny, H.H. Kock, K. Kvietkus, W. Landing, B. Mazzolai, T. Muhleck, J. Munthe, E.M. Prestbo, D. Schneeberger, F. Slemr, J. Sommar, A. Urba, D. Wallschläger, Z. Xiao, *Atmos. Environ.* (1999) in press.
- [24] A. Hunt, D.L. Johnson, *Scanning Microsc.* 10 (1996) 69.
- [25] J.L. Abraham, A. Hunt, *Environ. Res.* 69 (1995) 67.
- [26] W.H. Schroeder, R.A. Jackson, *Int. J. Environ. Anal. Chem.* 22 (1985) 1.
- [27] J. Munthe, W.H. Schroeder, Z. Xiao, O. Lindqvist, *Atmos. Environ.* 24A (1990) 2271.
- [28] M. Ferm, *Atmos. Environ.* 13 (1979) 1385.
- [29] W.H. Schroeder, M.C. Hamilton, S.R. Stobart, *Rev. Anal. Chem.* 8 (1985) 179.
- [30] G. Keeler, *UMAQL Newsletter*, Issue 1, The University of Michigan, Ann Arbor, MI, 1996.

Association constants for the NaSO_4^- ion pair in concentrated cesium chloride solutions

S.G. Capewell, G.T. Hefter *, P.M. May

Department of Chemistry, Murdoch University, Murdoch, WA 6150, Australia

Received 10 August 1998; accepted 15 October 1998

Abstract

Values of the association constant, $\beta_{\text{NaSO}_4^-}$, for the weak ion-pair formed by sodium and sulfate ions in aqueous solution have been determined at 25°C by high precision sodium ion-selective electrode potentiometry in solutions of ionic strength ranging from 0.50 to 7.00 M in CsCl media and in 1.00 M Me_4NCl . The data in CsCl media were fitted to an extended form of the Debye–Hückel equation which yielded $\log \beta_{\text{NaSO}_4^-}^0 = 0.834 \pm 0.005$ at infinite dilution. Evidence is also presented for the formation of very weak ion-pairs between Cs^+ and SO_4^{2-} . © 1999 Elsevier Science B.V. All rights reserved.

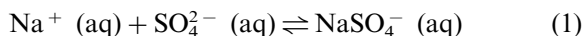
Keywords: Sulfate ion; Sodium ion; Ion-pairing; Cesium chloride

1. Introduction

Knowledge of thermodynamic parameters for sulfate equilibria in concentrated electrolyte solutions are of great importance in a variety of chemical systems of oceanographic, geochemical, hydrothermal and industrial interest. These thermodynamic data are a prerequisite for developing computerised chemical speciation models of such systems, which are valid over a wide range of conditions. Modelling of sulfate equilibria is of particular interest for understanding the behaviour of the highly concentrated alkaline sodium aluminate solutions which are used in the

refining of aluminium hydroxide from bauxite ores [1], as sulfate is a major inorganic impurity in many of these so-called ‘Bayer liquors’. Despite the large body of thermodynamic data in the literature describing aqueous sulfate equilibria, little quantitative information is available for the association of sulfate with alkali metal ions such as sodium. Although such complexes are extremely weak they can have a profound effect on the chemical speciation, particularly in concentrated solutions.

The interaction of SO_4^{2-} (aq) with Na^+ (aq),



for which the corresponding association constant, $\beta_{\text{NaSO}_4^-}$, is defined as

* Corresponding author. Tel.: +61-8-9360-2226; fax: +61-8-9310-1711.

E-mail address: hefter@chem.murdoch.edu.au (G.T. Hefter)

Table 1

Literature values of $\log \beta_{\text{NaSO}_4^-}$ (M scale) under various conditions at 25.0°C

Method	Medium	<i>I</i> (M)	$\log \beta_{\text{NaSO}_4^-}$ ^a	Reference
Calorimetry	–	0	0.65	[3]
Conductivity	–	0	0.72	[4]
Calculation	–	0	0.82 (5)	[5]
Dielectric relaxation spectroscopy	–	0	0.82 (2)	[6]
Conductivity	–	0	1.10	[7]
Na ISE potentiometry	NaCl	0.50	0.40 (3)	[8]
Na ISE potentiometry	NaCl/Na ₂ SO ₄	0.61	0.301	[9]
Na ISE potentiometry	NaCl/Na ₂ SO ₄	0.69	0.305 (6)	[10]
		Variable	$\beta = 2.73 - 2.58I + 2.28I^2$	
Calculation	Seawater	0.72	0.41	[11]
Na ISE potentiometry	NaClO ₄	1.0	0.61 (4)	[12]
Na ISE potentiometry	Me ₄ NCl	1.89	0.40 (9) ^b	
		2.67	0.43 (8)	[13]

^a Numbers in parentheses are the estimated errors (*E*) in the last decimal place of $\beta_{\text{NaSO}_4^-}$ given by the original authors and, where appropriate, were converted to the log scale using the formula $E(\log \beta) = \log_e (1/\beta \cdot E(\beta))$.

^b Data also available at 55 and 80°C in the same medium.

$$\beta_{\text{NaSO}_4^-} = \frac{[\text{NaSO}_4^-]}{[\text{Na}^+][\text{SO}_4^-]} \quad (2)$$

is significantly weaker than the interaction with alkaline earth or transition metal ions [2]. This makes these ion-pairs difficult to detect quantitatively, which may explain the lack of data in the literature. Previous investigations and theoretical treatments of this system have been largely confined to solutions of low ionic strengths or those approximating the composition of sea water (Table 1). The lack of reliable data for this important system is highlighted in Table 1 which shows that major disparities exist between $\log \beta_{\text{NaSO}_4^-}$ values obtained by different authors under similar conditions. For example, the equilibrium constant at infinite dilution, $\log \beta_{\text{NaSO}_4^-}^0$, ranges from 0.65 [3] to 1.10 [7] at 25°C. Such uncertainties are most unsatisfactory for the reliable calculation of chemical speciation in complex mixtures.

The purpose of the current paper is therefore to accurately determine the association constant for the NaSO₄[−] ion-pair over a wide range of ionic strength at 25°C. The technique employed was Na⁺ ion-selective glass electrode (Na ISE) potentiometry which has previously been shown to produce highly precise and reliable results for other weakly bound sodium complexes [14,15].

CsCl was chosen as the background electrolyte due to its relative ‘inertness’, high solubility (ca. 7.1 M at 25°C) [16] and because it does not interfere with the operation of the Na ISE. For comparison, measurements were also made at *I* = 1.00 M in Me₄NCl; measurements at higher Me₄NCl concentrations are precluded because the Na ISE response becomes erratic [15,17].

2. Experimental

2.1. Materials

All reagents were of analytical grade and were used without further purification, except for tetramethylammonium chloride (Aldrich, 97%) which was twice recrystallised from AR grade ethanol and dried in vacuo at room temperature [18]. Cesium chloride (Ajax, Australia, > 99.5 mol%) was dried in a vacuum oven at 70°C and ca. 100 Pa for 24 h and was stored over silica gel in a desiccator under reduced pressure prior to use. The trace Na⁺-impurities in the CsCl and Me₄NCl were determined by inductively coupled plasma atomic emission (ICP) spectrometry. Typical values were 5.6×10^{-4} M in 1.0 M CsCl and 9.2×10^{-6} M in 1.0 M Me₄NCl which were quan-

tatively consistent with the performance of the Na ISE at low $[\text{Na}^+]$ as described elsewhere [15]. These values were incorporated into the data analysis. All solutions were prepared using high purity Millipore Milli-Q water, which had been made carbonate-free by simultaneously boiling and purging with high purity nitrogen for 20 min. The ionic strength of all solutions for potentiometric purposes was adjusted by addition of the appropriate amounts of the required salt.

Cesium hydroxide solutions were prepared from AR grade pellets (Aldrich, '99.0%'). AR grade tetramethylammonium hydroxide (Me_4NOH) was obtained as an aqueous solution (Aldrich, 25% w/w). The carbonate content of the Me_4NOH solutions was minimised by adding 0.5 g solid CaO (Ajax, AR grade) to 250 ml of solution, agitating for at least 48 h and then filtering on a supported membrane filter (0.45 μm) [18]. Analysis of this solution with standard HCl using the Gran method [19,20] indicated a typical CO_3^{2-} concentration of < 0.2% of the total alkalinity. As the addition of solid CaO has been found to be unsatisfactory in removing carbonate from CsOH solutions, it was treated with barium hydroxide reducing the carbonate content to ~ 0.3% [21]. Care was taken to avoid contamination by atmospheric CO_2 and all base solutions were used within one week of preparation.

Cesium sulfate solutions were prepared from crystalline Cs_2SO_4 (Fluka, anhydrous, > 99.5 mol%), which had been dried over silica gel in a desiccator under reduced pressure for at least 24 h before use. Tetramethylammonium sulfate solutions were prepared by neutralising sulfuric acid (BDH 'Convol' Concentrated Volumetric Standard) with Me_4NOH in 1.00 M Me_4NCl .

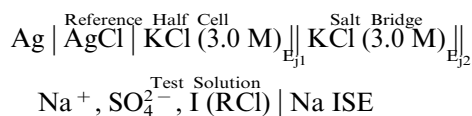
2.2. Apparatus and procedure

Values of $\beta_{\text{NaSO}_4^-}$ were determined by potentiometric titration of an accurately known NaCl solution dissolved in the appropriate concentration of CsCl or Me_4NCl with freshly prepared Cs_2SO_4 or $(\text{Me}_4\text{N})_2\text{SO}_4$ solution in the same medium. Measurements were carried out over the ionic strength range of $0.50 \leq I \leq 7.00\text{M}$ in CsCl media and at $I = 1.00\text{M}$ in Me_4NCl .

As the detection of weak M'L complexes with an M'^+ -responsive electrode is best achieved when $[\text{L}] \gg [\text{M}']$ [17], it is desirable to use very low concentrations of M' so as to maximise the $[\text{L}]/[\text{M}']$ ratio with minimal replacement of the ionic medium. This is essential for maintaining reasonable constancy of activity coefficients and liquid junction potentials (LJPs). Minimising the replacement level is especially important in the present system where L is the doubly charged SO_4^{2-} (aq). Consequently, four different groups of titrations were carried out at each ionic strength, viz., using a titrant solution containing 100 or 200 mM SO_4^{2-} with $[\text{Na}^+]_{\text{initial}} = 5$ or 10 mM in the cell, resulting in $[\text{SO}_4^{2-}]/[\text{Na}^+]$ ratios of up to 120.

The potentiometric titrations were made using our usual high precision titration system [22]. An inert atmosphere was maintained in the titration cell with high purity nitrogen, pre-humidified by bubbling through a solution containing the same ionic medium as in the measurement cell. The cell was maintained at $25.0 \pm 0.01^\circ\text{C}$ using a Haake N3 circulator-thermostat which itself was cooled by a Neslab refrigerated circulator-thermostat set at $22 \pm 0.5^\circ\text{C}$. The cell temperature was monitored using a thermistor calibrated to an accuracy of 0.01 K against a NIST-traceable quartz crystal thermometer (Hewlett Packard, Model HP2804A).

The cells used in the present study can be represented as:



where R denotes the cation of the background electrolyte (i.e. Cs^+ or Me_4N^+), $I(\text{RCl})$ indicates the solution was held at constant ionic strength I ($= 1/2 \sum c_i z_i^2$) with appropriate amounts of RCl, Na ISE denotes the Na^+ -ion selective glass electrode and E_{j1} and E_{j2} are LJPs. The Na ISE (Metrohm, model 6.0501.100) was conditioned and stored in 0.1 M NaCl/(RCl). No loss in performance was observed for the Na ISE, even

Table 2

Present values of $\log \beta_{\text{NaSO}_4^-}$ at 25.0°C in Me_4NCl and CsCl media determined by Na ISE potentiometry

Medium	I (M)	$\log \beta_{\text{NaSO}_4^-}$ (S.D.) ^a	No. titrations/No. data points	OBJE ($\times 10^4$) ^b
Me_4NCl	1.0	0.0927 (15)	8/352	3.26
CsCl	0.0	0.834(5) ^c	—	—
	0.5	0.0108 (38)	4/172	12.03
	1.0	-0.1497 (35)	5/190	11.44
	2.0	-0.2610 (31)	4/166	4.59
	3.0	-0.3169 (33)	5/261	5.71
	5.0	-0.3316 (31)	4/167	12.10
	7.0	-0.3164 (32)	4/165	13.63

^a Numbers in parentheses refer to the standard deviation in the last decimal place quoted.^b Unweighted objective function calculated with respect to difference in electrode potentials [27].^c Extrapolated value, with estimated maximum error (see text).

at the highest [CsCl]. However, as already noted, the Na ISE response becomes erratic at $[\text{Me}_4\text{NCl}] > 1.00$ M. All potentials were measured relative to Ag/AgCl reference electrodes, consisting of silver wire in contact with solid silver chloride [23]. The reference electrode filling solution was 3.0 M KCl, employed in conjunction with a salt bridge also containing 3.0 M KCl.

Assuming that throughout the course of a titration activity coefficients and LJPs are constant and thus may be incorporated in the formal cell potential E^0 , it is readily shown by the usual methods of electrochemical thermodynamics that the relationship between the observed cell potential E_{obs} and the sodium ion concentration is [24]

$$E_{\text{obs}} = E^0 + k \log[\text{Na}^+] \quad (3)$$

where k is the electrode slope.

Electrode calibrations [15] gave linear plots of E_{obs} vs. $\log[\text{Na}^+]$ with slopes close to Nernstian (59.16 mV at 25°C) and E^0 constant to within 0.2 mV between titrations in each medium at $12 \leq \text{pH} \leq 6$. At lower pH values the curve deviates significantly as the Na ISE responds to H^+ . Accordingly, all titration solutions were buffered to pH 12.5 with Me_4NOH or CsOH and a slope of 59.16 was assumed.

Least squares analyses of the data from the potentiometric titrations were performed using the equilibrium simulation for titration analysis (ESTA) suite of programs [25,26].

3. Results and discussion

The details of the titrations and the corresponding ESTA optimisations are summarised in Table 2. The numbers in parentheses are the standard deviations produced by the computational analysis; real errors can be up to an order of magnitude greater [27]. The present results obtained in CsCl media for $\log \beta_{\text{NaSO}_4^-}$ are plotted along with selected literature data in Fig. 1. It is interesting to note that the latter suggest there is almost no change in the association constant as a function

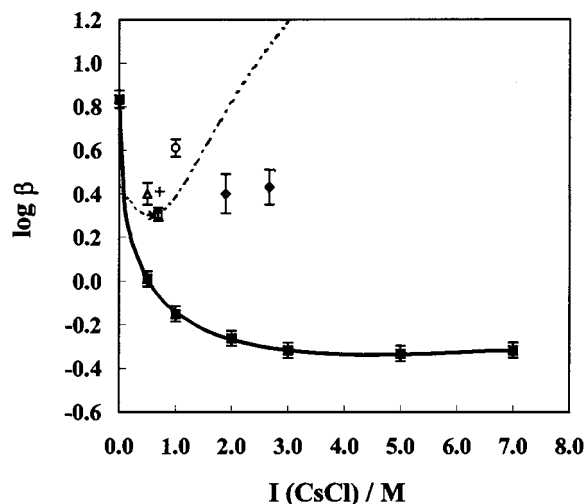


Fig. 1. Values of $\log \beta_{\text{NaSO}_4^-}$ at 25°C: ■, present results, with the solid curve corresponding to Eq. (4) where $A = 2.046$ and $B = 0.0487$; △, [8]; ×, [9]; □, [10]; +, [11]; ○, [12]; ◇, [13].

of ionic strength in the range $0.5 \leq I \leq 3.0$. This is very unlikely, and contrasts with the present results which display the more usual dependence on I .

The dotted curve in Fig. 1 is from Pytkowicz and Kester [10], and is based on their Na ISE measurements in NaCl/Na₂SO₄ solutions. Their curve predicts much stronger NaSO₄⁻ ion-pairing and a much sharper increase with I than is observed in the present study. Even allowing for differences in background electrolyte, the values predicted by this equation appear unrealistic when compared with the present results. Furthermore, the infinite dilution value of $\log \beta_{\text{NaSO}_4^-}^0 = 0.44$ [10] is very much lower than the present value (see below) and lies well outside the generally accepted range for this constant [2].

The present result at $I = 1.00$ M in Me₄NCl ($\log \beta_{\text{NaSO}_4^-} = 0.0927$) is much lower than that reported by Sapieszko et al. [13] in the same medium at $I = 1.89$ and 2.67 M also obtained by Na ISE potentiometry ($\log \beta_{\text{NaSO}_4^-} = 0.40$ and 0.43, respectively). It is noteworthy that the authors report, without elaboration [13], that they experienced difficulties with the Na ISE in this medium which they used to justify the rather large uncertainties ($\pm 20\%$) in their measured constants. This is consistent with our previous findings [15,17] that the response of the glass Na ISE becomes erratic at $I > 1.0$ M in Me₄NCl, and suggests that the $\log \beta_{\text{NaSO}_4^-}$ values of Sapieszko et al. are almost certainly unreliable.

3.1. Determination of $\log \beta_{\text{NaSO}_4^-}^0$ at $I = 0$

Although the present measurements were not designed for this purpose (being restricted to $I \geq 0.50$ M), it is instructive to use the present data to estimate the standard state (infinite dilution) value of $\log \beta_{\text{NaSO}_4^-}^0$. This is probably best done using one of the more recent activity coefficient models such as that of Pitzer [28]. However, for the present purpose it is sufficient to use a simple extended form of the Debye–Hückel equation [29]. This gives

$$\log \beta_i = \log \beta_i^0 - A \left(\frac{\sqrt{I}}{1 + \sqrt{I}} \right) + BI \quad (4)$$

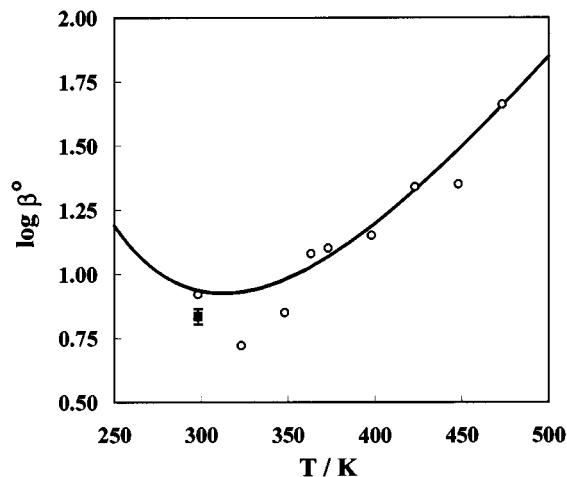


Fig. 2. Values of $\log \beta_{\text{NaSO}_4^-}^0$ as a function of temperature: ○, [30], with the solid curve corresponding to the authors modified HKF equation (see text); ■, present result at 298.15 K.

for the equilibrium defined in Eq. (1), where the Debye–Hückel constant A has the value of 2.046 at 25°C and the empirical parameter B was found to be 0.0487 for these data. The value of $\log \beta_{\text{NaSO}_4^-}^0 = 0.834 \pm 0.005$ is in excellent agreement with that of Reardon [5] calculated from activity coefficient data, and with a recent value from these laboratories determined by dielectric relaxation spectroscopy [6] (Table 1).

It is also interesting to compare the present $\log \beta_{\text{NaSO}_4^-}^0$ value with the recent data of Pokrovski et al. [30] (Fig. 2), which were obtained with a new type of ceramic Na ISE designed for high temperature operation and fitted to a revised HKF (Helgeson–Kirkham–Flowers) equation. Although there is considerable scatter in the data at lower temperatures (where the behaviour of the ceramic Na ISE becomes unreliable) the present value at 298.15 K is clearly in good agreement with the general trend of Pokrovski et al.'s data and the HKF model.

3.2. Estimation of the CsSO₄⁻ association constant

The general shape of the $\log \beta_{\text{NaSO}_4^-}$ versus I (CsCl) curve in Fig. 1, as expressed in the small

value of the empirical constant B in Eq. (4), suggests there may be a weak interaction between Cs^+ (aq) and SO_4^{2-} (aq) [31]. Further evidence for this hypothesis is the significant increase in $\log \beta_{\text{NaSO}_4^-}$ when reaction (1) is transferred from CsCl to Me_4NCl media at $I = 1.00\text{M}$ (Table 2). If all the difference in $\log \beta_{\text{NaSO}_4^-}$ in these two media is ascribed to Cs^+ binding and it is further assumed that higher order $(\text{Na}(\text{SO}_4)_n^{(1-2n)+})$, with $n > 1$ and protonated $(\text{Na}(\text{HSO}_4)_m^{(1-m)+})$ complexes, activity coefficient changes, and $\text{Me}_4\text{N}^+ - \text{SO}_4^{2-}$ interactions are all negligible, it can be shown [31] that

$$\begin{aligned} & (\beta_{\text{NaSO}_4^-})_{\text{Me}_4\text{NCl}} \\ & \approx (\beta_{\text{NaSO}_4^-})_{\text{CsCl}} \{1 + \beta_{\text{CsSO}_4^-} [\text{Cs}^+]_T\} \end{aligned} \quad (5)$$

Substituting in the appropriate values from Table 2 gives $\log \beta_{\text{CsSO}_4^-} = -0.10$ in 1.00 M Me_4NCl . This constant can also be determined directly from the titration data by the ESTA optimisation program, which gives a value of $\log \beta_{\text{CsSO}_4^-} = -0.13 \pm 0.05$, in good agreement with the value obtained by Eq. (5). This appears to be the first reported estimate of the CsSO_4^- association constant. However, in view of the weakness of the association and the uncertainty of the various assumptions involved, the value must be treated with caution.

Acknowledgements

The authors wish to acknowledge the support of the Australian Government and Worsley Alumina in the form of an Australian Postgraduate Award (Industry) scholarship for S.G.C.

References

- [1] T.G. Pearson, The Chemical Background of the Aluminium Industry, Royal Institute of Chemistry, London, 1955.
- [2] L.G. Sillen and A.E. Martell, Stability Constants of Metal-Ion Complexes, Special Publications Nos.17 and 25, Chemical Society, London, 1964, 1971.
- [3] R.M. Izatt, D. Eatough, J.J. Christensen, C.H. Bartholomew, J. Chem. Soc. (A) (1969) 45.
- [4] I.L. Jenkins, C.B. Monk, J. Am. Chem. Soc. 72 (1950) 2695.
- [5] E.J. Reardon, J. Phys. Chem. 79 (1975) 422.
- [6] R. Buchner, S.G. Capewell, G.T. Hefter, P.M. May, J. Phys. Chem. (B) in press.
- [7] F.H. Fisher, A.P. Fox, J. Solution Chem. 4 (1975) 225.
- [8] M. Manuela Santos, J.R.F. Guedes de Carvalho, R.A. Guedes de Carvalho, J. Solution Chem. 4 (1975) 25.
- [9] D.R. Kester, R.M. Pytkowicz, Geochim. Cosmochim. Acta 34 (1970) 1039.
- [10] R.M. Pytkowicz, D.R. Kester, Am. J. Sci. 267 (1969) 217.
- [11] D. Dyrssen, I. Hansson, Marine Chem. 1 (1972) 137.
- [12] P. Luts, J.L.C. Vanhees, J.H.E. Yperman, J.M.A. Mullens, L.C. Van Poucke, J. Solution Chem. 21 (1992) 375.
- [13] R.S. Sapieszko, R.C. Patel, E. Matijevic, J. Phys. Chem. 81 (1977) 1061.
- [14] S.G. Capewell, G.T. Hefter, P. Sipos, P.M. May, J. Solution Chem. 26 (1997) 957.
- [15] S.G. Capewell, G.T. Hefter, P.M. May, J. Solution Chem. 27 (1998) 865.
- [16] W.F. Linke (Ed.), Solubilities of Inorganic and Metal-Organic Compounds, 4th Edn., American Chemical Society, Washington, 1965.
- [17] S.G. Capewell, Honours Thesis, Murdoch University, Western Australia, 1996.
- [18] P. Sipos, I. Bodi, P.M. May, G.T. Hefter, Talanta 44 (1997) 617.
- [19] G. Gran, Anal. Chim. Acta 206 (1988) 111.
- [20] G. Gran, Analyst 77 (1952) 661.
- [21] P. Sipos, G.T. Hefter, P.M. May, Unpublished results.
- [22] P. Verhoeven, G.T. Hefter, P.M. May, Miner. Metal. Proc. 5 (1990) 185.
- [23] G.T. Hefter, J. Electroanal. Chem. 39 (1972) 345.
- [24] A.S. Feiner, A.J. McEnvoy, J. Chem. Educ. 71 (1994) 493.
- [25] P.M. May, K. Murray, D.R. Williams, Talanta 32 (1985) 483.
- [26] P.M. May, K. Murray, D.R. Williams, Talanta 35 (1988) 825.
- [27] P.M. May, K. Murray, Talanta 35 (1988) 933.
- [28] K.S. Pitzer (Ed.), Activity Coefficients in Electrolyte Solutions, 2nd Edn., CRC Press, Boca Raton, FL, 1991.
- [29] G.H. Nancollas, Interactions in Electrolyte Solutions, Elsevier, New York, 1966.
- [30] G.S. Pokrovski, J. Schott, A.S. Sergeev, Chem. Geol. 124 (1995) 253.
- [31] G.T. Hefter, J. Solution Chem. 13 (1984) 179.

Cathodic adsorptive stripping voltammetric determination of uranium with potassium hydrogen phthalate

Othman A. Farghaly ^{a,*}, Mahmoud A. Ghandour ^b

^a Chemistry Department, Faculty of Science (Qena), South Valley University, Qena, Egypt

^b Chemistry Department, Faculty of Science, Assiut University, Assiut, 71516, Egypt

Received 9 June 1998; received in revised form 15 October 1998; accepted 16 October 1998

Abstract

The adsorption properties of dioxouranium (II)-Phthalate complexes onto hanging mercury drop electrode are exploited in developing a highly sensitive and selective stripping voltammetric procedure for the determination of uranium (VI). The reduction current of adsorbed complex ions of U(VI) was measured by both linear sweep (LSCSV) and differential pulse cathodic stripping voltammetry (DPCSV), preceded by a period of preconcentration onto the electrode surface. As low as 2×10^{-9} mol dm⁻³ (0.5 µg/l) and 2×10^{-8} mol dm⁻³ (4.8 µg/l) with accumulation time 240 and 120 s using DPCSV and LSCSV, respectively, have been determined successfully. The relative standard deviation of 2.2% at the 5 ppm level was obtained. The interferences of some metal ions and anions were studied. The application of this method was tested in the determination of uranium in superphosphate fertilizer. © 1999 Elsevier Science B.V. All rights reserved.

Keywords: Uranium determination as phthalate complex; Cyclic voltammetry; Linear sweep and differential pulse stripping voltammetry; Super-phosphate fertilizer

1. Introduction

The geographical distribution of uranium is of interest because the element is used in the production of energy in nuclear reactors. It is of geochemical interest because it belongs to the actinide group, the geochemical pathways of which have

not been studied as rigorously as those of some of the transition metals [1]. Several techniques have been developed for the determination of U(VI) in different environmental samples including α -spectrometry [2], neutron activation [3,4], spectrophotometry [5], molecular fluorescence spectrometry [6], compleximetric titration [7], pulse polarography [8,9], gas chromatography [10–12], radioactivation [13,14] and inductively coupled plasma emission spectrometry [15]. These techniques are not sufficiently sensitive for the direct determina-

* Corresponding author. Tel.: +20-96-211-274; fax: +20-96-211-274.

E-mail address: sci@svalley.u.jwnet.eun.eg (O.A. Farghaly)

tion of U(VI), so that a pre-concentration stage is necessary. The use of stripping analysis has been expanded greatly during this decade, owing to the growing needs for on-site environmental monitoring or clinical testing of trace metals [16,17]. However adsorptive stripping voltammetry is a powerful technique useful for uranium trace analysis. Adsorption voltammetry is a technique in which the analyte is preconcentrated first by adsorption onto a working electrode surface followed by voltammetric measurements of the electroactive species. This method has been applied to the stripping voltammetric determination of uranium in the absence [18,19] and in the presence of various complexing reagents [20–38].

In order to determine uranium more sensitively and selectively, potassium hydrogen phthalate has been found to form a uranium complex, which was more stable than those of other metal ions [39,40].

2. Experimental

2.1. Instrumentation

Stripping and cyclic voltammograms were recorded by polarographic Analyzer stripping voltammeter Model 264 A (EG&G, Princeton Applied Research; Princeton, NJ, USA), coupled with a PAR 303 A Static Mercury Drop Electrode (SMDE; drop size: medium, area of the drop: 0.014 cm^2). The polarographic cell bottom (PAR Model K 0060) was fitted with a saturated Ag/AgCl, reference electrode, and platinum wire used as a counter electrode. A PAR 305 stirrer was connected to the 303 SMDE. A PAR Model RE 0089 X-Y recorder was used for recording the voltammograms.

2.2. Chemicals

The following reagents were prepared. A 0.01-mol dm^{-3} aqueous stock solution of U(VI) was prepared by diluting appropriate volume from uranyl perchlorate (prepared in our laboratory) [41]. A 0.01-mol dm^{-3} solution of the ligand; potassium hydrogen phthalate (Merck) was pre-

pared by dissolving the appropriate amount in bidistilled water. The solution was used for few days only to avoid the bacterial effects. Solutions of 0.1 mol dm^{-3} sodium perchlorate, potassium nitrate, potassium chloride and 0.2 mol dm^{-3} sodium dihydrogen phosphate were used as supporting electrolytes. Sodium hydroxide solution (0.1 mol dm^{-3}) was used to adjust the pH of the supporting electrolytes using an Orion 601 A precision Research Ionanalyzer digital pH meter.

2.3. Procedure

A known volume (10 ml) of 0.01 mol dm^{-3} sodium perchlorate ($\text{pH} \approx 7$) as supporting electrolyte was deaerated with nitrogen for 16 min then for 30 s before each adsorptive stripping cycle. The preconcentration potential of $+0.1 \text{ V}$ (vs. Ag/AgCl); was applied to the electrode for a period of time, while the solution was stirred at 400 rpm. The stirring was then stopped as controlled by the microprocessor and after 15 s (equilibrium time) the voltammogram with negative potential scan was recorded. The scan rate was 100 mVs^{-1} for direct current stripping (DCSV) and 5 mVs^{-1} for differential pulse stripping voltammetry (DPSV) with 50 mV pulse amplitude and pulse duration of 1 s. The same procedure was repeated after spiking the ligand and uranyl perchlorate. All data were obtained at room temperature ($25 \pm 1^\circ\text{C}$).

3. Results and discussion

3.1. Cyclic voltammetry

At low pH and in a non complexing perchlorate solution the U(VI)–U(V) reversible reduction wave is located at -0.175 V (vs. SCE) [42]. The reduction wave is shifted in a negative direction, with increasing pH and becomes irreversible due to the relatively slow hydroxide complex formation of U(VI) [20]. Cyclic voltammetry of $1.5 \times 10^{-6} \text{ mol dm}^{-3}$ UO_2^{2+} preceded by quiescent period of 15 s (without preconcentration time) at deposition potential $+0.1 \text{ V}$ in the presence of $10^{-5} \text{ mol dm}^{-3}$ potassium hydrogen phthalate at

pH \approx 7, 0.01 mol dm⁻³ sodium perchlorate shows that the U(VI)–U(V) reduction peak is located at -0.6 V Fig. 1. There is a 0.31 V difference in the cathodic and anodic peak potentials. The peak heights of scan 1, 2, 3 are almost the same, whereas subsequent cycles shows an increase in the peak signal. Thus, reduction of this complex is irreversible as demonstrated by cyclic voltammetry Fig. 1. Complex ions of U(VI) are reduced to U(V), which is oxidized initially to the free uranyl ion, followed by relatively slow complex reformation. Then, some of the U(VI) formed by reoxidation remained on or near the electrode surface and was reduced again in the next cathodic scan. This behavior illustrate the increase of the cathodic peak height. As well as, some part of U(V) formed in cathodic scan is reoxidized to U(VI), this may be leads to a very small anodic peak appears in the opposite scan (anodic) direction. This mechanism was confirmed by van Den Berg and Huang. [20].

3.2. Effect of pH

The pH of the solution affects the U(VI) determination because of changes in the distribution of the complex ions with potassium hydrogen phthalate. The pH was varied by adding dilute perchloric acid or sodium hydroxide. The voltammograms of 1×10^{-6} mol dm⁻³ uranyl ion in the presence of 1×10^{-4} mol dm⁻³ potassium hydrogen phthalate and 0.01 mol dm⁻³ sodium perchlorate as supporting electrolyte at different pHs viz. 4.4, 5.1, 6.35, 7.2, 7.7 and 8.5 were studied. It was observed that the height of the reduction peak increases on increasing the pH of the medium. This due to increase of the deprotonated ligand which give more complexed uranyl species adsorbable onto electrode surface. Also, the peak potential is shifted to more negative potential in the same manner. This means that hydrogen ions are participated in the reduction step. The peak height reached its maximum at pH

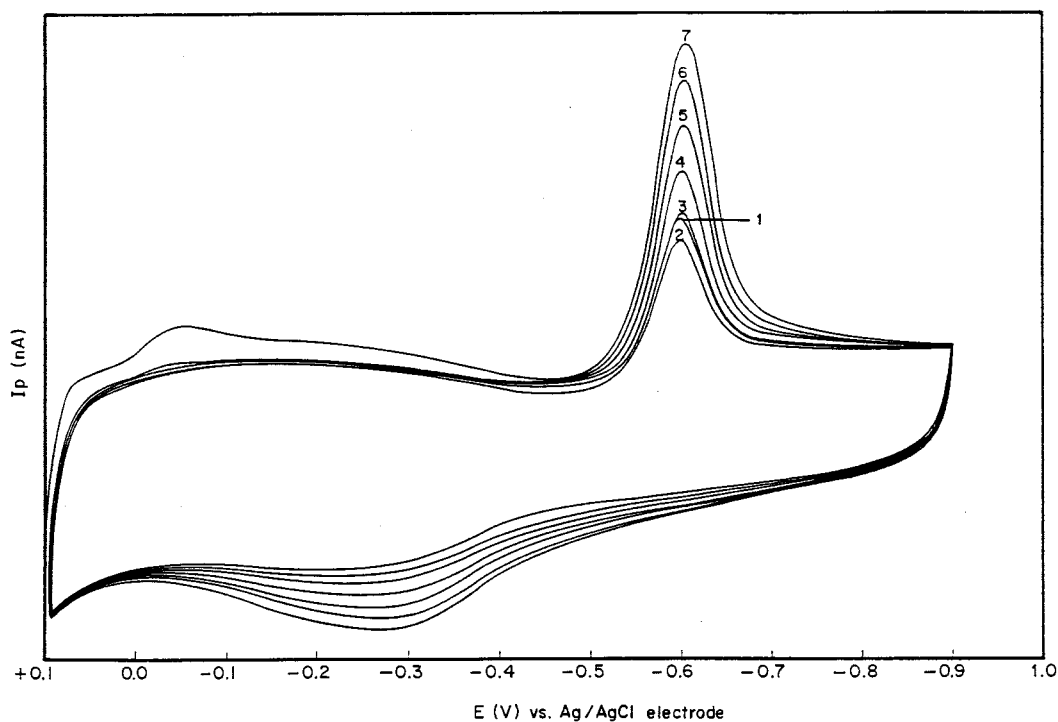


Fig. 1. Cyclic voltammograms of 1.5×10^{-6} mol dm⁻³ UO₂(II), 0.01 mol dm⁻³ NaClO₄, 10^{-5} mol dm⁻³ Potassium Hydrogen phthalate (pH = 7.2).

ranged from 6.3 to 7.2 at $E_p = -0.61$ V. At $pH = 7.7$ the reduction peak splits into two peaks. Furthermore, at higher $pH = 8.5$, the height of reduction peak decreases. This decrease in current is due to competitive formation of hydroxo complexes. It means that the optimum pH to carry out all experiments ranged from 6.3 to 7.2.

3.3. Effect of supporting electrolyte

A series of supporting electrolytes were tested (sodium perchlorate, potassium nitrate, potassium chloride and sodium dihydrogen phosphate). Both the peak height and the peak shape were taken into consideration when choosing the supporting electrolyte. However, 0.01 mol dm^{-3} of NaClO_4 , KCl and KNO_3 ($pH = 7$), as well as 0.01 mol dm^{-3} sodium dihydrogen phosphate ($pH \approx 5$), with $2 \times 10^{-6} \text{ mol dm}^{-3}$ potassium hydrogen phthalate and $2 \times 10^{-8} \text{ mol dm}^{-3}$ UO_2^{2+} were investigated using linear sweep (LSCSV) and differential pulse cathodic stripping voltammetry (DPCSV) methods. The results indicate that the highest signal peak current was obtained in the presence of sodium perchlorate medium. Furthermore, different concentrations of NaClO_4 ranged from 0.01 to 0.1 mol dm^{-3} were tested at constant uranyl ion concentration $1 \times 10^{-7} \text{ mol dm}^{-3}$ and potassium hydrogen phthalate $1 \times 10^{-3} \text{ mol dm}^{-3}$. At 0.01 mol dm^{-3} NaClO_4 gave the highest signals of reduction peak, then by increasing the ionic strength the peak height decreased. Therefore, the optimum ionic strength for studying is 0.01 mol dm^{-3} sodium perchlorate.

3.4. Effect of initial potential and scan rate

The effect of the accumulation potential on the cathodic stripping peak current was examined over the range $+0.15 - -0.4$ V after a preconcentration time of 60 s. On plotting the peak current obtained as a function of preconcentration potential, the graph indicates that the current is very high and almost constant at the range of $0.00 - +0.15$ V and exhibits a sudden decrease on going towards more electronegative potential. The effect of scan rate was studied by varying it from 10 to 200 mvs^{-1} . It was found that the peak current increased and

the peak potential shifted to more negative values with increasing scan rate. For subsequent work 100 mvs^{-1} was selected in LSCSV. The plot of $\log i$ versus $\log v$ (scan rate) gives a straight line with a slope of 1.0. This value is expected for ideal reaction of surface species [43]. A $70 - \text{mv}$ negative shift in the peak potential was observed upon increasing the scan rate in the range given. The plot of E_p versus $\log v$ is also linear. This is another evidence for the irreversible and adsorption phenomena of the reduction process [44].

3.5. Effect of ligand concentration

Different concentrations of potassium hydrogen phthalate ranged from 2×10^{-5} to $1 \times 10^{-4} \text{ mol dm}^{-3}$ in the presence of $1 \times 10^{-6} \text{ mol dm}^{-3}$ UO_2^{2+} ion and 0.01 mol dm^{-3} sodium perchlorate as supporting electrolyte ($pH \approx 7$) were studied. It was noticed that the peak height decreased as the concentration of the ligand increased. Since phthalate anion is adsorbed onto mercury electrode surface, then its concentration must be adjusted in a manner that it will not hindered the adsorption of the UO_2^{2+} phthalate complex itself [45]. Consequently, less electrode surface is available for the adsorption of the metal complex in case of increasing ligand as shown in Fig. 2. However, the optimum concentration range for ligand was $2 \times 10^{-5} - 1 \times 10^{-4} \text{ mol dm}^{-3}$ with $1 \times 10^{-6} \text{ mol dm}^{-3}$ uranyl ion and $2 \times 10^{-7} - 2 \times 10^{-6} \text{ mol dm}^{-3}$, in the presence of lower concentration of uranium viz. 10^{-9} and $10^{-8} \text{ mol dm}^{-3}$, respectively. Also, the concentration range of uranium was $2 \times 10^{-8} - 1 \times 10^{-7} \text{ mol dm}^{-3}$, with $2 \times 10^{-6} \text{ mol dm}^{-3}$ ligand using LSCSV and from 2×10^{-9} to 1.4×10^{-8} of uranium, in the presence of $2 \times 10^{-7} \text{ mol dm}^{-3}$ ligand, using DPCSV. Thus, lower concentrations of uranyl ion viz. 10^{-8} and $10^{-9} \text{ mol dm}^{-3}$ were determined at concentrations of 10^{-6} and $10^{-7} \text{ mol dm}^{-3}$ potassium hydrogen phthalate, respectively.

3.6. Effect of preconcentration time

The effect of the accumulation time on the stripping peak current was examined for 2×10^{-8} and $2 \times 10^{-7} \text{ mol dm}^{-3}$ uranyl ion, in the pres-

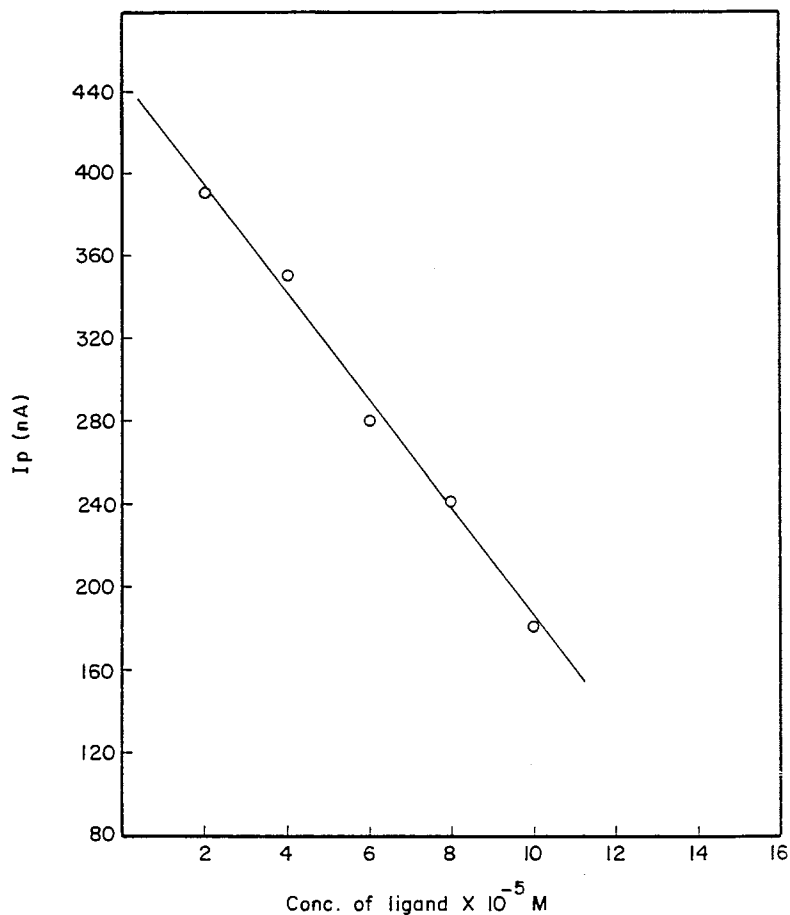


Fig. 2. Plot of I_p versus ligand concentration, at 1×10^{-6} mol dm $^{-3}$ UO $_2$ (II), in the presence of 0.01 mol dm $^{-3}$ NaClO $_4$, (pH = 7.0) and accumulation time 60 s.

ence of 2×10^{-6} and 2×10^{-5} mol dm $^{-3}$ potassium hydrogen phthalate (pH \approx 7), respectively. The peak current increased linearly with preconcentration time. The surface coverage occurs at 180 and 120 s, for 2×10^{-8} and 2×10^{-7} mol dm $^{-3}$ uranyl ion, respectively.

3.7. Effect of uranyl ion concentration

It is found that the reduction peak current increases with increasing uranyl ion concentration. On plotting the peak currents against uranyl ion concentration gives straight lines as shown in Fig. 3. Generally, the peak height increases with increasing uranyl ion concentration and accumulation time.

Using (2–10) 10^{-7} mol dm $^{-3}$ UO $_2^{2+}$ and preconcentration time of 60 s, with 2×10^{-5} mol dm $^{-3}$ potassium hydrogen phthalate the linear sweep voltammograms are taken, where the well defined peak is observed at $E_p = -0.61$ V. From the current-concentration plot, it can be seen that 6×10^{-7} mol dm $^{-3}$ is the concentration of UO $_2^{2+}$ required to obtain the surface coverage as shown in Fig. 3a. The slope of this straight line is 33.3 nA/ 10^{-7} mol dm $^{-3}$. Further trials were made to investigate more lower concentration of uranium. Thus starting from 2×10^{-8} mol dm $^{-3}$ at 120 and 180 s, with 2×10^{-5} mol dm $^{-3}$ potassium hydrogen phthalate a straight line was observed covering the range from 2×10^{-8} to

1×10^{-7} mol dm $^{-3}$ with the slope equal to 4.7 and 6.15 nA/10 $^{-8}$ mol dm $^{-3}$, respectively as shown in Fig. 3b and c. The use of the lower concentration (2×10^{-8} mol dm $^{-3}$) brings about 2.2% in standard deviation (ten replicates). Also, if we use a lower concentration of phthalate (2×10^{-6} mol dm $^{-3}$) the same result can be obtained with 120 s accumulation time as shown in Fig. 3d with a slope equal to 100 nA/10 $^{-8}$ mol dm $^{-3}$ uranyl ion.

On testing the differential pulse cathodic stripping voltammetric technique, a well defined peak is observed with $E_p = -0.58$ V in three different media (0.01 mol dm $^{-3}$ of NaClO $_4$, KCl, and KNO $_3$) pH \approx 7, with 2×10^{-7} mol dm $^{-3}$ potassium hydrogen phthalate and accumulation times

of 240, 120 and 420 s, respectively. Plotting the peak current against uranyl ion concentration gives straight line in each case viz., a, b and c as shown in Fig. 4 with a slope equal to 0.5, 0.8 and 1.0 nA/10 $^{-9}$ mol dm $^{-3}$ respectively. A straight line was observed covering the range from 2×10^{-9} to 1.4×10^{-8} mol dm $^{-3}$ UO $_2^{2+}$ with 240 s (preconcentration time) in 0.01 mol dm $^{-3}$ NaClO $_4$ (pH \approx 7). However, as low as 2×10^{-8} mol dm $^{-3}$ (4.8 ppb) at 120 s and 2×10^{-9} mol dm $^{-3}$ (0.5 ppb) at 240 s, in the presence of 0.01 mol dm $^{-3}$ NaClO $_4$ (pH \approx 7), with 2×10^{-6} and 2×10^{-7} mol dm $^{-3}$ potassium hydrogen phthalate, using LSCSV and DPSCV techniques, respectively, have been determined successfully. The relative standard deviation (RSD) was 2.2 (ten

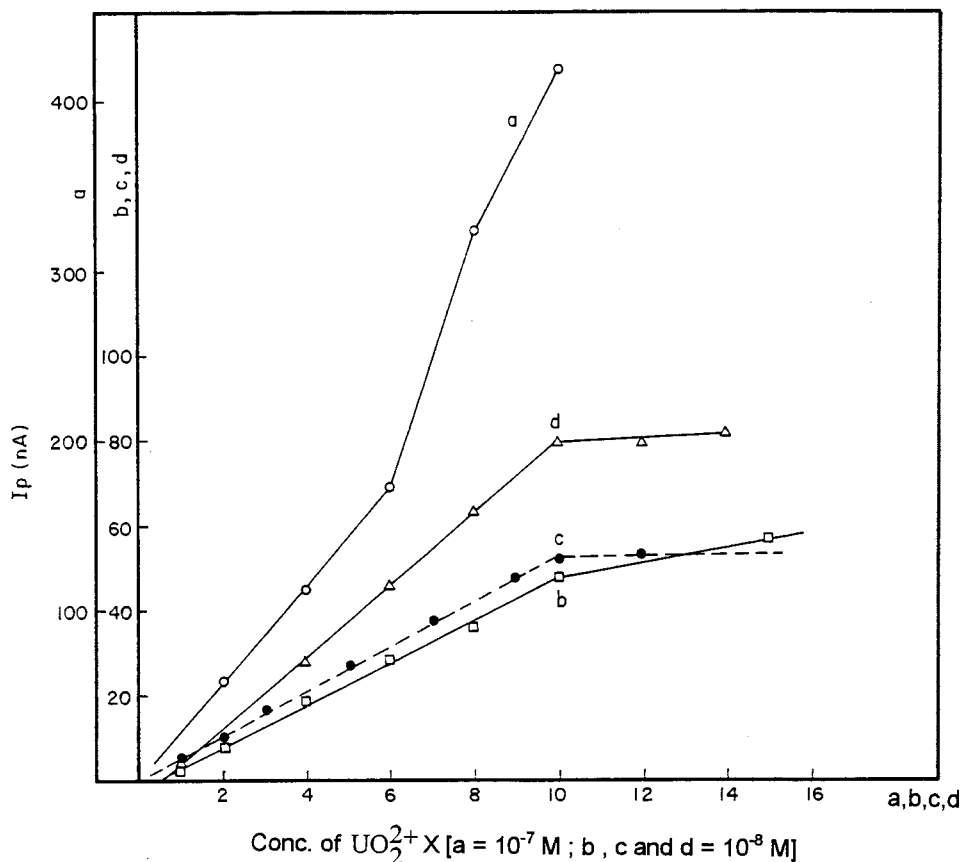


Fig. 3. Current-concentration graphs in presence of 0.01 mol dm $^{-3}$ NaClO $_4$ (pH = 7): a: 2×10^{-5} mol dm $^{-3}$ phthalate and 60 s accumulation time; b: 2×10^{-5} mol dm $^{-3}$ phthalate and 120 s accumulation time; c: 2×10^{-5} mol dm $^{-3}$ phthalate and 180 s accumulation time; and d: 2×10^{-6} mol dm $^{-3}$ phthalate and 120 s accumulation time.

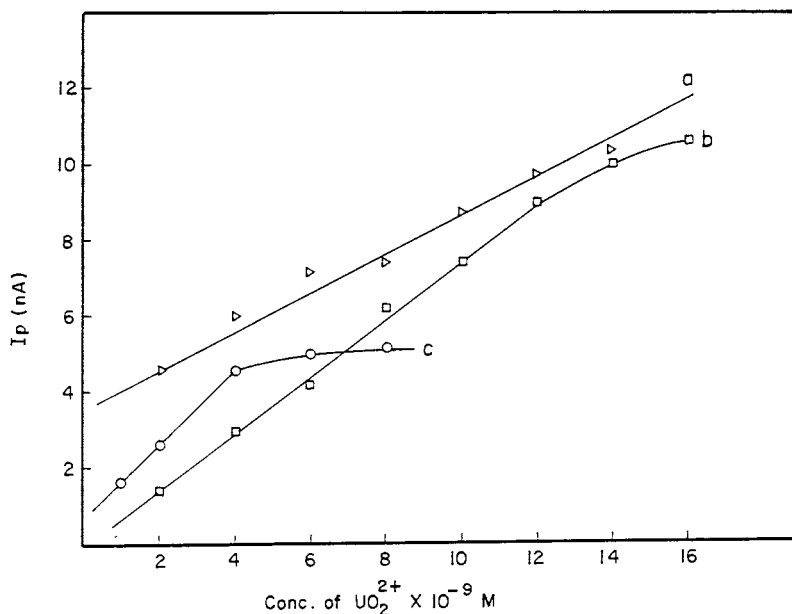


Fig. 4. Plot of I_p vs. uranyl ion concentration with $2 \times 10^{-7} \text{ mol dm}^{-3}$ phthalate ($\text{pH} = 7$) using differential pulse cathodic stripping voltammetry: a: $(2\text{--}12) \times 10^{-9} \text{ mol dm}^{-3} \text{ UO}_2(\text{II})$ and $0.01 \text{ mol dm}^{-3} \text{ NaClO}_4$, accumulation time = 240 s; b: $(2\text{--}14) \times 10^{-9} \text{ mol dm}^{-3} \text{ UO}_2(\text{II})$ and $0.01 \text{ mol dm}^{-3} \text{ KCl}$, accumulation time = 120 s; c: $(1\text{--}8) \times 10^{-9} \text{ mol dm}^{-3} \text{ UO}_2(\text{II})$ and $0.01 \text{ mol dm}^{-3} \text{ NaNO}_3$, accumulation time = 420 s.

replicates), with 0.9989 correlation coefficient. The accuracy of the method was investigated by determining the recovery ($99.98 \pm 2\%$) of the standard addition of U(VI) [$(2\text{--}10 \times 10^{-8}) \text{ mol dm}^{-3}$] to a definite concentration $4.8 \mu\text{g/l}$ ($2 \times 10^{-8} \text{ mol dm}^{-3}$) of U(VI) level.

3.8. Application

Trials were made to apply the present method for quantitation of UO_2^{2+} in matrix samples. Superphosphate fertilizer is chosen to such type of analysis. One gram of the sample from Assiut plant (Sebaeia Ore) was leached by 100 ml bidistilled water. The solution was filtered through sintered glass G_4 . Five milliliters of the sample solution were added to 5 ml of bidistilled water containing supporting electrolyte ($0.01 \text{ mol dm}^{-3} \text{ NaClO}_4$, $\text{pH} = 3.95$) without addition of the ligand. The second experiment was carried out in the presence of $10^{-4} \text{ mol dm}^{-3}$ potassium hydrogen phthalate. In both experiments, uranium was determined by means of standard addition method.

However, two peaks are observed from the sample solution Fig. 5a, on addition of UO_2^{2+} to the sample solution the second peak increases whereas the first one being constant (figure is not shown). On adding $1 \times 10^{-4} \text{ mol dm}^{-3}$ potassium hydrogen phthalate the second peak is vitiated whereas the first one is improved as shown in Fig. 5b. On addition of uranyl ion concentration the first peak is increased (Fig. 5a–h). This complicated behavior may be attributed to the existence of more than one complexed species of uranium with the phosphate in the original sample solution. In the presence of phthalate, the complex of uranium with phthalate is predominating, therefore, the single (first) peak is increased on increasing analyte concentration. However, the highest signal obtained at $\text{pH} \approx 4$ compared with $\text{pH} \approx 7$ in synthetic solution may be due to high selectivity of adsorption of the uranyl ion complexes onto the electrode surface. This phenomena may be attributed to the species of the ligands (Potassium hydrogen phthalate and phosphate). In addition to the presence of several

foreign cations and anions as impurities in the super-phosphate fertilizer samples.

On plotting the peak current against the concentration of uranium added, a straight line is obtained in each case. From its intersection with horizontal axis in negative direction, the determination of uranium in the sample is found to be $1 \times 10^{-7} \text{ mol dm}^{-3}$ (4.8 ppm), the same results has been obtained using maleic acid as a ligand [26] in the analysis of the same sample. The reduction current of the uranyl ion in the fertilizer sample alone is lower than that obtained in presence of phthalate. This may be due to the preference of complex formation in the sample between

uranyl ion and phthalate which leads to the accumulation of uranyl phthalate species onto the electrode surface. However, the standard addition method gives the same original concentration of uranium in synthetic solutions containing different cations (Cu(II), Zn(II), Pb(II), Cd(II), Fe(III), Ni(II), Mn(II) and Bi(III)) and anions (NO_3^- , PO_4^{3-} , ClO_4^- and Cl^-). The precision of the method is satisfactory with $\text{RSD} = 2.5$ and correlation coefficients ($r = 0.998$) obtained for ten replicate analyses. The standard addition method gives the same original concentration of uranium in the sample (superphosphate fertilizer) in the absence or presence of phthalate and foreign metal ions. This conclusion is drawn from the results of some experiments done in the addition of some cations and anions to the original sample as will be mentioned later.

In the absence of phthalate ligand, the adsorption of uranium phosphate species on to the electrode surface was studied by increasing the accumulation (preconcentration) time, whereby an increase in the current was observed. However, addition of phthalate ligand brought about a further increase in the current due to the formation of a more strong complex.

3.9. Interferences

The promising results hitherto obtained in the selective determination of uranium in phosphate sample encourage us to investigate the role played by the possible existing foreign ions in the matrix by adding foreign ions to the sample directly. In the presence of $1 \times 10^{-4} \text{ mol dm}^{-3}$ potassium hydrogen phthalate and fertilizer phosphate sample solution in $0.01 \text{ mol dm}^{-3} \text{ NaClO}_4$ ($\text{pH} \approx 3.95$), 1×10^{-7} and $1 \times 10^{-6} \text{ mol dm}^{-3}$ of each metal ions viz; Cu(II), Pb(II), Cd(II), Zn(II), Ni(II) and Mn(II) ions (individually and in one mixture) were added to the sample solution. Slight decrease in the current signal were observed. However, in the case of $1 \times 10^{-6} \text{ mol dm}^{-3}$ Bi(III) decreases the peak height of uranium ion by about one-sixth of its value.

Since fluoride ions are normally existing in the original phosphate minerals, experiments were performed by adding small increments of sodium

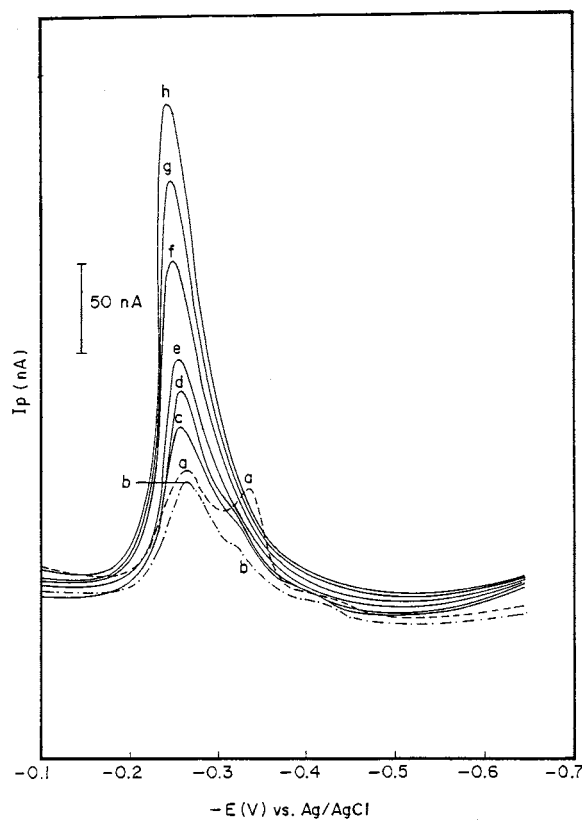


Fig. 5. LSSV of the fertilizer sample solution in $0.01 \text{ mol dm}^{-3} \text{ NaClO}_4$ and 30 s (accumulation time): a: without ligand; b: with $1 \times 10^{-4} \text{ mol dm}^{-3}$ phthalate; c: $b + 5 \times 10^{-8} \text{ mol dm}^{-3} \text{ UO}_2(\text{II})$; d: $b + 8 \times 10^{-8} \text{ mol dm}^{-3} \text{ UO}_2(\text{II})$; e: $b + 1 \times 10^{-7} \text{ mol dm}^{-3} \text{ UO}_2(\text{II})$; f: $b + 1.5 \times 10^{-7} \text{ mol dm}^{-3} \text{ UO}_2(\text{II})$; g: $b + 2.5 \times 10^{-7} \text{ mol dm}^{-3} \text{ UO}_2(\text{II})$; and h: $b + 3 \times 10^{-7} \text{ mol dm}^{-3} \text{ UO}_2(\text{II})$ ion.

fluoride solution to the polarographic cell followed by measurements. It has been noticed that up to 5×10^{-4} mol dm⁻³ fluoride ions concentration, no change in the current signal of the sample was observed. Therefore, the original fluoride content of the sample solution has no effect on the precision of the method. However, a series interferences has been observed if the concentration of fluoride added to the superphosphate fertilizer sample exceed 1×10^{-3} mol dm⁻³, where a diminution of the current was noticed and eventually vitiated at concentration 8×10^{-3} mol dm⁻³ fluoride ions.

However, in the case of a synthetic solution 1×10^{-3} mol dm⁻³ potassium hydrogen phthalate and 1×10^{-6} mol dm⁻³ uranyl ion with 0.01 mol dm⁻³ NaClO₄ (pH ≈ 7), up to five-fold concentration of Pb(II), Cu(II), Ni(II), Zn(II), and Fe(III) were examined, where no change in the current signal was observed. Furthermore 20-fold Cd(II) concentration had also no effect on the determination of uranium. However, the half concentration of Bi(III) decreases the peak height of uranyl complex to half its value. On the other hand up to 2000 fold of PO₄³⁻, ClO₄⁻, NO₃⁻, Cl⁻ and 1000 of F⁻ anions concentration do not interfere. Irrespective of a slight decrease in the current has been observed in the presence of 2×10^{-3} mol dm⁻³ fluoride ions concentration, the standard addition methods gave the same original concentration of uranium.

It has been reported that interferences of some metal ions had some effects on the determination of uranium using oxine as a ligand [35]. However, in using pyrocatechol [20] which is known as a wide-band complexing agent, the uranium signal is interfered with by numerous elements and organic compounds. On using mordant blue, Wang and Zadeii [37] mentioned that the mixture of uranium and some other metal ions in a ratios 1:1 (w/w) and 5:1 metal:uranium had no interference in some cases, e.g. Cu(II), Zn(II), Pb(II), Cd(II) and Sb(III). The voltammetric and polarographic determination of uranium in the presence of chloranilic acid is highly selective and sensitive. Only molybdenum, antimony, tin, vanadium and tungsten also form adsorbable complexes with this agent. Because of differences in their peak

potentials, these metals do not interfere with the determination of uranium [30]. Furthermore, chloranilic acid has been reported to be a suitable ligand in direct determination of uranium in natural water without any pretreatment of the sample [21].

In the present work, as high as 10:1 metal:uranium ratio had no effect providing the use of standard addition method.

It is concluded that the use of phthalate as ligand in cathodic adsorptive stripping voltammetric determination of uranium is superior to other ligands formerly used such as oxine [35], or pyrocatechol [20]. The interferences of other metal ions (Pb(II), Cd(II), Cu(II), Ni(II), Fe(III), Mn(II), Zn(II) ions) is less pronounced in our experimental conditions. This is because the phthalato complexes of uranyl ion are more stable [39,40] than those of other metal ions.

References

- [1] D. Langmuir, *Geochim. Cosmochim. Acta* 42 (1978) 547.
- [2] T.L. Ku, K.G. Knaus, G.G. Mathieu, *Deep-Sea Res.* 24 (1977) 1005.
- [3] J. Holzbecher, D.E. Ryan, *Anal. Chim. Acta* 119 (1980) 405.
- [4] M.A. El-Khatib, M. Bassiouny, I.A. Arslan, A.M. Fawzy, *Bull. Fac. Sci. Alexandria Univ.* 36 (1996) 67.
- [5] T.M. Florence, Y. Farrer, *Anal. Chem.* 35 (1963) 1613.
- [6] W.C. Li, D.M. Victor, C.L. Chakrabarti, *Anal. Chem.* 52 (1980) 520.
- [7] S.F. Marsh, M.R. Betts, J.E. Rein, *Anal. Chim. Acta* 119 (1980) 401.
- [8] G.W.C. Milner, J.D. Wilson, G.A. Barnett, A.A. Smales, *J. Electroanal. Chem.* 2 (1961) 25.
- [9] S.K. Das, A.V. Kulkarni, R.G. Dhaneshwar, *Analyst* 118 (1993) 1153.
- [10] R.F. Sieck, J.J. Richard, K. Iverson, C.V. Barks, *Anal. Chem.* 43 (1971) 913.
- [11] F. Hao, B. Paull, R.P. Haddad, *Chromatographia* 42 (1996) 690.
- [12] K. Oguma, T. Shimizu, R. Kuroda, *Bunseki Kagaku* 44 (1995) 1.
- [13] M. Garcia-Leon, A. Martinez-Aguirre, R. Perianez, J.P. Bolivar, R. Garcia-Tenorio, *J. Radioanal. Nucl. Chem.* 197 (1995) 173.
- [14] T.B. Florin, I. Miu, D. Razvan, P. Eugen, *Sci. Technol. Environ. Prot.* 1 (1994) 1.
- [15] O.A. Zaror, R.S. Juarez, L. Zeiller, R. Zeisler, *Fresenius J. Anal. Chem.* 355 (1996) 694.

- [16] J. Wang, *Analyst* 119 (1994) 763.
- [17] D. Noble, *Anal. Chem.* 265A (1993) 65.
- [18] R. Djogic, M. Branica, *Analyst* 120 (1995) 1989.
- [19] R.L. Sawant, K.P. Kalsi, V. Kulkarni, S. Vaidyanathan, *J. Radioanal. Nucl. Chem.* 207 (1996) 39.
- [20] C.M.G. Van Den Berg, Z.Q. Huang, *Anal. Chim. Acta* 164 (1984) 209.
- [21] S. Sander, W. Wagner, G. Henze, *Anal. Chim. Acta* 305 (1995) 154.
- [22] J.Y. Wang, J. Wang, B. Tian, M. Jiang, *Anal. Chem.* 69 (1997) 1657.
- [23] S. Sander, G. Henze, *GIT Fachz. Lab.* 40 (1996) 1232.
- [24] J.T.V. Elteron, C.M.G. Van den Berg, H. Zhang, T.D. Martin, E.P. Achterberg, *Anal. Chem.* 67 (1995) 3903.
- [25] A.M.M. Ali, M.A. Ghandour, M. Khodari, *Analyst* 120 (1995) 1065.
- [26] R. Elshiekh, M.A.F. Elmosalamy, A.M.M. Ali, M.A. Abd El-Fattah, M.A. Ghandour, *Bull. Fac. Sci. Assiut Univ.* 23 (1994) 13.
- [27] J. Wang, J. Lu, D.D. Larson, K. Olsen, *Electroanalysis* 7 (1995) 247.
- [28] J. Wang, T. Baomin, R. Setiadji, *Electroanalysis* 6 (1994) 317.
- [29] M. Paneli, H. Ouguenoune, F. David, A. Bolyos, *Anal. Chim. Acta* 304 (1995) 177.
- [30] S. Sander, G. Henze, *Fresenius J. Anal. Chem.* 349 (1994) 654.
- [31] J.Y. Wang, J. Wang, J.M. Lu, K. Olsen, *Anal. Chim. Acta* 292 (1994) 91.
- [32] M. Mlakar, M. Branica, *Mar. Chem.* 46 (1994) 61.
- [33] N. Verma, K.S. Pitre, *Analyst* 118 (1993) 65.
- [34] W. Wagner, G. Henze, *GIT Labor-Fachz.* 41 (1997) 287.
- [35] C.M.G. Van Den Berg, M. Nimmo, *Anal. Chem.* 59 (1987) 924.
- [36] P. Li, Z. Zhao, X. Cai, *Talanta* 34 (1987) 813.
- [37] J. Wang, J.M. Zadeii, *Talanta* 34 (1987) 247.
- [38] M.H. Pournaghi-Azar, J. Ordoukhanian, *Talanta* 38 (1991) 1469.
- [39] A.E. Martell. *Stability Constants of Metal Ion Complexes*. The Chemical Society, Supplement No. 1, Special Publication No. 25. London, 1971.
- [40] D.D. Perrin. *Stability Constants of Metal Ion Complexes*. Organic ligands IUPAC Chemical data, series No. 22. Pergamon Press, London, 1979.
- [41] M.A. Ghandour, R.A. Abo-Doma, R.E. Gomaa, *Electrochim. Acta* 27 (1982) 157.
- [42] L. Sipos, L.J. Jeftic, M.J. Branica, *Electroanal. Chem. Interfacial Electrochem.* 32 (1971) 35.
- [43] J. Wang, P. Tuzhi, M.S. Lin, T. Tapia, *Talanta* 33 (1986) 707.
- [44] A.M. Bond, *Modern Polarographic Methods in Analytical Chemistry*, Marcel Dekker, New York, 1980, pp. 195–197.
- [45] M.A. Ghandour, H.A. Azab, A.M.M. Aly, *Bull. Fac. Sci. Assiut Univ.* 17 (1988) 119.

Determination of carbidic carbon in steels

K.K. Gupta ^{a,*}, Dolly Ghosh ^a, A.N. Bhagat ^b, Jhumki Biswas ^a,
S. Chakravarty ^a, S. Ranganathan ^a

^a National Metallurgical Laboratory, Jamshedpur, 831007, India

^b Research and Development Laboratory, Tata Steel, Jamshedpur, 831001, India

Received 1 July 1998; received in revised form 25 October 1998; accepted 6 November 1998

Abstract

An attempt has been made to develop a simple analytical technique that can readily be used in an industrial laboratory to isolate and quantify the precipitated carbides in steel samples. Attempt has also been made to correlate this value with the thermodynamically predicted values. There is good agreement between the predicted and experimental results. More work is in progress to develop this technique for the preparation of Certified Reference Materials with dissolved and precipitated carbon in steels. © 1999 Elsevier Science B.V. All rights reserved.

Keywords: Carbidic carbon; Precipitation; Steel

1. Introduction

Steels used in special applications contain alloying elements at significant levels along with C and N which may precipitate as carbide, nitride or carbonitrides. These steels are used in applications where the temperatures are high (about 500–700 C) such as steam boilers, pipes conveying petrochemicals, etc. Precipitation influences the mechanical properties of the steel such as creep resistance, and determines the life of the components. The precipitates usually have a complex chemistry containing more than one alloying element in the cationic as well as the anionic sub-lattice. It is essential to understand the type of

precipitate formed for an intelligent design of these alloys for structural applications and also to predict the life of the components.

High strength low alloy (HSLA) steels contain microalloying additions such as Ti, Nb, V, etc. (about 0.04%). They form fine precipitates of carbonitrides and strengthen the alloy through grain refinement. These alloys are developed for structural applications where the strength-to-weight ratio is a crucial factor, such as in defence structures. Intelligent design of the alloys and the thermomechanical processing of the same are needed for application of these alloys in these structures. This again requires a thorough understanding of the nature of the complex precipitates formed in these alloys.

The mass fraction of the precipitates; their types and chemical compositions are the crucial

* Corresponding author. Fax: +91-657-426527.

E-mail address: kkg@csnml.ren.nic.in (K.K. Gupta)

information required for establishing the solubility relations in steels. Several techniques have been used for analysing these precipitates. For in situ analysis of the precipitates, SEM and TEM along with energy dispersive analysis of X-rays; electron probe micro analysis (EPMA); electron energy loss spectroscopy (EELS) and XRD have been widely used [1–8].

In HSLA steels, the carbonitrides of alloying elements such as niobium, titanium, vanadium, etc. are predominately precipitated. They are usually very small in size, the cross-section of the precipitates measuring a few hundred nanometres, typically. The chemical analysis of these precipitates employing the instruments mentioned above is prone to significant errors and sometimes even impossible due to interference from the matrix in which the precipitates are embedded. Further, to adopt these instrumental techniques, suitable standards are required by comparing with which the instruments can be calibrated. Analysis of the isolated precipitates will lead to more reliable results and help in establishing the equilibrium relations between the precipitates and the matrix. This will help in developing suitable standards for calibration of instruments also. Hence, considerable efforts are expended in many laboratories of the world to isolate the precipitates through suitable wet chemical techniques.

Efforts have been made in many laboratories to develop suitable techniques to isolate these precipitates for further analysis [9–16]. It was appreciated that a simple technique will find immediate application in industries for assessment of remaining life of the structures; for routine evaluation of the impact of thermomechanical processing and for analysis of failure of structures and components in service. Therefore, studies were made to develop a suitable technique to isolate carbides in steel. The study initially focussed on synthetic mixtures of carbides and iron. The technique developed could isolate the carbides from the mixture, quantitatively. This method was then extended to some steels. The carbides could be isolated quantitatively, in this case also. Results obtained have been compared with the thermodynamically predicted values. The following sections discuss the technique and the studies carried out.

2. Experimental

2.1. Reagents: HCl (AR grade), de-ionised water, specpure materials

A dissolution method was developed for the separation of metal carbides from the steel matrix. Attempts were made with various acid mixtures on synthetically prepared carbide and pure iron mixtures. Best results were obtained with 30 ml of 1:10 HCl and heating the sample slowly for 3–5 h.

2.2. Sample dissolution

The experimental part was divided into various parts. In the first phase it was decided to try out different acid mixtures on synthetically prepared samples. A host of synthetic samples were prepared by mixing specpure materials from Jhonson Mathey. Three grams of sample along with 30 ml of 1:10 HCl was used to dissolve the matrix. The sample was digested for 3–5 h at 60–80 C on a hot plate. The matrix dissolved out along with Fe₃C leaving behind carbidic carbon and graphitic carbon as residue. The solution was filtered through a pad prepared from 0.5 g of burnt asbestos. The asbestos used was previously burnt at 950 C for 5 h in a muffle furnace. The presence of carbon in the burnt asbestos was checked by LECO and was found to be nearly 0.04%. For each experiment a blank of 0.5 g of burnt asbestos was run and necessary corrections made to compute the amount of carbon present in the sample. The alloying element present in the filtrate as shown in Table 5 were analysed using GBC 908 Atomic Absorption Spectrophotometry. The analytical conditions are presented: wavelength of Cr: 357.9 nm, Mo: 313.3 nm, reducing flame of air acetylene in the ratio of 1:1.

2.3. Residue analysis:

The residue along with the entire pad was then subjected to analysis on a LECO CS 444 apparatus for the carbon estimation. Initial experiments were carried out with only binary mixtures, i.e. Fe and a carbide. The results of the analysis along

Table 1
Carbide carbon estimated in iron and carbide binary mixtures

Sl.No.	Sample	Percent carbon	
		Originally taken	Obtained by LECO ^a
1.	Iron + Graphite	0.11	0.12 ± 0.01
2.	Iron + Graphite	0.10	0.095 ± 0.01
3.	Iron + SiC	0.12	0.11 ± 0.01
4.	Iron + TiC	0.168	0.156 ± 0.02
5.	Iron + TiC	0.027	0.03 ± 0.007
6.	Iron + TiC	0.045	0.051 ± 0.005
7.	Iron + TiC	0.10	0.11 ± 0.012
8.	Iron + TiC	0.07	0.075 ± 0.006
9.	Iron + TiC	0.05	0.04 ± 0.005
10.	Iron + NbC	0.026	0.027 ± 0.003

^a Average ± 2σ for a measurement of five replicates.

with the expected values for the synthetically prepared mixtures are presented in Table 1.

After ascertaining the dissolution technique on the binary mixtures, attempts were made on synthetically prepared ternary mixtures. The results are presented in Table 2

In the third part of the experiment, the analysis was carried out on actual steel samples. The steels (the compositions are given in Table 3) were subjected to suitable heat treatment for precipitating out the carbon as carbides.

Attempts have also been made to analyse the alloying elements in the filtrate after the carbide separation to vindicate a model developed to

Table 2
Carbide carbon estimated in iron and carbide ternary mixtures

Sl.No.	Sample	Percent carbon	
		Originally taken	Obtained by LECO ^a
1.	Iron + TiC + Graphite	0.0176	0.016 ± 0.004
2.	Iron + TiC + Graphite	0.03	0.033 ± 0.005
3.	Iron + TiC + Graphite	0.05	0.047 ± 0.005
4.	Iron + TiC + Graphite	0.05	0.05 ± 0.006
5.	Iron + SiC + Graphite	0.0009	0.0011 ± 0.0008
6.	Iron + SiC + Graphite	0.054	0.053 ± 0.005
7.	Iron + SiC + Graphite	0.16	0.16 ± 0.02

^a Average ± 2σ for a measurement of three replicates.

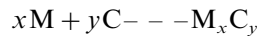
Table 3
Compositions of steels studied (wt.%)

	Steel-1	Steel-2
C	0.10	0.17
Cr	8.42	7.5
Mo	0.92	0.72
Mn	0.37	0.25
P	0.023	0.024
S	0.026	0.019
Si	0.24	0.23
Ni	0.12	—
N	0.008	0.0075

quantify and predict the carbide precipitation (presented in the following section). The results are presented in Table 5.

2.4. Prediction of carbide precipitation in steels

Considering the formation of carbide M_xC_y , where M is an alloying element,



$$\Delta G^0 = -RT \ln K \quad (1)$$

$$K = a_{M_xC_y} / (a_x)^x \cdot (a_c)^y \quad (2)$$

ΔG^0 is the standard free energy of formation of the carbide; K the equilibrium constant and a_i is the activity of the element i in solid solution. The activity of the carbide is taken as unity. The activity a_i is related to the mole fraction X_i , by $a_i = X_i \gamma_i$ where γ_i is the activity coefficient. The

activity coefficient is evaluated using Wagner's interaction parameters [17].

Austenite is the solid phase stable at the temperatures employed in the investigations reported here [18]. From Eqs. (1) and (2), it is possible to estimate the mass of the carbide formed and the amounts of the alloying elements and carbon in the solid solution at equilibrium with the carbide. The alloying elements such as Cr, Mo and Mn in these steels can form more than one type of carbide. For example, chromium can form the carbides Cr_{23}C_6 , Cr_{27}C_3 , Cr_3C_2 [19]. The type of carbide formed depends on the composition of the steel and the temperature of equilibrium. Also several alloying elements such as Nb, Cr, Mo and Mn can form carbides. It is necessary to predict the type of carbide formed and the quantity of the same. These are predicted using the technique of successive partial equilibration [20,21]. The carbides formed are complex in nature. The cationic sub-lattice contains more than one alloying element. For example, both Cr and Mo are likely to be present in a carbide precipitated in a steel containing these elements. The free energy of formation of the complex carbide depends on the proportion of the different alloying elements present in the cationic sub-lattice. When nitrogen is at significant levels in the steels, carbonitrides are precipitated. Two types of steels were considered in this investigation to estimate the carbidic carbon. In these steels, Cr and Mo precipitate essentially as carbides since the relative amount of nitrogen is low compared to the levels of Cr, Mo and C in these steels. The relevant data for the prediction of the amount of carbidic carbon precipitated were obtained from literature [22–26].

3. Results and discussions

Literature shows [27] that cementite, Fe_3C is decomposed by dilute hydrochloric acid. The carbides of other alloying elements such as Cr, Mo, V, Nb, etc. are unaffected by this acid. Studies were made with synthetic mixtures of a carbide and iron powder. TiC and SiC were chosen as the carbides to evaluate the technique adopted for estimating the carbidic carbon. The amounts of

carbide and iron were so adjusted as to give different levels of carbidic carbon in the mixtures. The estimated and expected levels of carbidic carbon (in percentages) are reported in Table 1. The first two samples of this table used electrolytic iron containing 0.06% C. Graphite was added to bring the total carbon in the sample to about 0.1%. The results show that the technique could isolate graphitic carbon and the carbon in iron was removed. As seen from Table 1, the estimated percentages of carbidic carbon in the synthetic samples are in good agreement with the theoretical values.

In the next step, carbide, iron and graphite were mixed to produce various synthetic samples containing different levels of carbidic plus graphitic carbon. The estimated and expected percentages of this carbon are reported in Table 2. There is good agreement between these figures.

In the next step of investigations, steel samples were used to estimate the carbidic carbon. The compositions of these steels are reported in Table 3. The percentages of carbon in these steels precipitated as carbidic carbon were predicted as already described.

Steel 1 of Table 3 precipitates a complex carbide containing both Cr and Mo in the cationic sub-lattice. A piece of this steel was encapsulated in quartz under vacuum and maintained at 1200 C for 3 h. At this temperature all the carbides dissolve in the solid solution phase [28]. The sample was quenched in water. It was again encapsulated in quartz and maintained at 850 C for 3 h to ensure attainment of equilibrium between the carbide and the solid solution phase. It was quenched in water. Three grams of this was analysed for estimating the carbidic carbon. One piece of steel 2 of Table 3 was similarly quenched from 800 C

Table 4
Predicted and estimated carbidic carbon in steels

S.No.	Steel	% C precipitated	
		Predicted	Estimated
1.	Steel 1	43.45	40.0
2.	Steel 2-1	44.83	46.67
3.	Steel 2-2	45.57	47.0

Table 5
Analysis of filtrate of Steel 2-2 (wt.%)

Chromium		Molybdenum	
Predicted	Estimated	Predicted	Estimated ^a
6.558	6.78 ± 0.13	0.513	0.429 ± 0.04

^a Average ± 2σ, for a measurement of three replicates.

after initial solutionising treatment at 1200 C. Another piece of this steel was treated at 850 C and quenched. The carbidic carbon in these samples were estimated. The percentage of carbon precipitated as the carbide was also predicted. The predicted and estimated values are compared in Table 4 under the categories steel 1 and steel 2-1 and steel 2-2, respectively. The percentage of carbon estimated to be precipitated is in excellent agreement with the predicted value in each case.

In the case of steel 2-2 the filtrate collected after isolating the carbide was analysed for chromium and molybdenum levels. The predicted and evaluated levels are compared in Table 5. There is good agreement between these two. This observation enhances the confidence in the analytical technique developed for estimating the carbidic carbon.

Acknowledgements

The authors are grateful to the Office of Naval Research, Washington, USA, for financial support to carry out this work under Grant No. N-00014-95-1-0015.

References

- [1] K. Tsubota, *Tetsu-To-Hagane* 69 (7) (1983) 853–860.
- [2] D. Henriot, P. De Gelis, R. Berneron, *Meon. Etud. Sci. Rev. Metall* 80 (2) (1983) 73–77.
- [3] Mokhuenko, A.N., Potapora, M.S., Medvedev, V.V., Kryuchkov, L.A., *Izv.V.U.Z. Chernaya Metall.* (1982) 111–114.
- [4] S.P. Duckworth, Conference Proceedings, Modern Metallurgy in Metallurgy Conference and Exhibition, Cambridge, UK, 6–8 September 1982, The Metals Society, 1 Carlton House Tenace, London SW1Y, 5DB, UK.
- [5] M. Niset, R. Demuzere, A. van Bemst, Proceedings of the International Conference on Cobalt, Metallurgy and Uses, vol. 2, Brussels, Belgium, 10–13 Nov.1981, Benelux Metallurgie, 50 ave. F.D. Rossevelt, Belgium, 1981.
- [6] J. Ruste, M. Bouchaourt, F. Thevenot, *J. Less Common Metals* 59 (2) (1978) 131–138.
- [7] L. Aggour, E. Fitzer, W. Weisweilu, *High Temp. High Pressures* 6 (1) (1974) 73–84.
- [8] J.E. Feruguson, F.W. Pastma, Jr, *Am. Ceram. Soc. Bull.* 52 (12) (1973) 876–878.
- [9] R. Kannan, S.R. Rajagopalan, *Trans. Ind. Inst. Met.* 35 (6) (1982) 568–573.
- [10] K. Narita, *Tetsu-to-Hagane* 66 (14) (1980) 2119–2138.
- [11] T.P.S. Gill, J.B. Gnanamoorthy, *J. Mater. Sci.* 17 (5) (1982) 1513–1518.
- [12] K. Narita, A.T. Miyamoto, H. Iwakiri, *Trans. Iron Steel Inst, Japan* 16 (3) (1976) 168–179.
- [13] H. Berns, J. Kettel, *Arch. Eisenhüttenwes* 47 (6) (1976) 391–393.
- [14] K. Narita, H. Hara, A.T. Miyamoto, H. Iwakiri, *Testsu-To-Hagane* 60 (13) (1979) 1962–1979.
- [15] K. Kawanura, S. Watanabe, T. Suzuki, *Tetsu-To-Hagane* 58 (14) (1972) 2067–2077.
- [16] S. Read, R.K. Gobbs, B.A. Parker, *Mater. Forum* 14 (1990) 304–307.
- [17] C. Wagner, *Thermodynamics of Alloys*, Addison Wesley, MA, 1952.
- [18] W.C. Leslie, *The Physical Metallurgy of Steels*, McGraw-Hill, London, 1981, p. 257.
- [19] R. Hultgren, P.D. Desai, D.T. Hawkins, M. Gleiser, K.K. Kelly, *Selected Values of Thermodynamic Properties of Binary Alloys*, American Society For Metals, Metals Park, Ohio, 1973.
- [20] S. Ranganathan, *Calphad* 20 (4) (1996) 461–470.
- [21] S. Ranganathan, *Calphad* 21 (4) (1997) 453–461.
- [22] M.W. Chase, Jr, C.A. Davies, J.R. Downey Jr, D.J. Fruip, R.A. McDonald, A.N. Syverud, *JANAF Thermochemical Tables*, 3rd edition, American Chemical Society and the American Institute of Physics, 1986.
- [23] O. Knack, O. Kubaschewski, K. Hesselmann, *Thermo Chemical Properties of Inorganic Substances*, 2nd edition, Springer-Verlag, Berlin, 1991.
- [24] H.J. Eckstein, M. Fennert, J. Osher, *Steel Res.* 64 (3) (1993) 143–147.
- [25] H. Adrian, Proceedings of the Conference on Microalloying '95, Iron and Steel Society, Pittsburg, PA, June 1995, pp. 285–305.
- [26] R.C. Sharma, V.K. Lakshmanan, J.S. Kirkaldy, *Metall. Trans. A* 15A (1984) 545–553.
- [27] J.W. Mellor, *A Comprehensive Treatise on Inorganic and Theoretical Chemistry*, vol. V, 2nd edition, Griffin, High Wycombe, UK, 1938, p. 897.
- [28] S. Pathak, S. Ranganathan, S. Das, S.K. Das, *Scr. Mater.* 39 (2) (1998) 253–259.

Determination of fosfomycin by indirect spectrophotometric method

Yu-Ling Hu, Yu-Qi Feng, Qing-He Zhang, Shi-Lu Da *

Department of Chemistry, Wuhan University, Wuhan, 430072, People's Republic of China

Received 21 July 1998; received in revised form 26 October 1998; accepted 6 November 1998

Abstract

2-(5-Bromo-2-pyridylazo)-5-diethylaminophenol (5-Br-PADAP) is a sensitive photometric reagent for determination of zirconium, when fosfomycin is added, it can quantitatively replace 5-Br-PADAP by complexing with zirconium, thus, an indirect spectrophotometric method based on ligand exchange has been established. The detection wavelength is at 605 nm, and the apparent molar absorption coefficient was found to be $4.59 \times 10^4 \text{ l mol}^{-1} \text{ cm}^{-1}$. Beer's law is obeyed in the range of $0-28 \times 10^{-6} \text{ M}$. The composition and stability constant of zirconium with 5-Br-PADAP and with fosfomycin has also been estimated. The proposed method is simple and reproducible, it was applicable to the analysis of fosfomycin from pharmaceutical manufacture. © 1999 Elsevier Science B.V. All rights reserved.

Keywords: 5-Br-PADAP; Fosfomycin; Indirect spectrophotometry; Zirconium

1. Introduction

Fosfomycin, the sodium salt of *cis*-(3-methylxiranyl)phosphonic acid (Fig. 1), is a promising broad-spectrum antibiotic. It has been found to be effective against both Gram-positive and Gram-negative infections because of its ability to inhibit bacterial cell wall synthesis. Fosfomycin has a low molecular mass, no UV absorption and can not give fluorescence. These characters led to difficulties in its analysis. Up to now, few methods have been published concerning the determination

of fosfomycin in biological fluids or pharmaceutical forms, it also appears interesting for the determination in aqueous forms. The methods reported for determination of fosfomycin include gas chromatography after derivation [1], ion chromatography [2], reversed-phase liquid chromatography [3] and capillary electrophoresis [4,5] using indirect UV detection. Photometric analysis is a classical method known for its convenience and cheapness. Jimenez [6] reported a colorimetric method for analysis of fosfomycin after the rupture of C–P bond by oxidation followed by formation of $\text{PO}_4(\text{NH}_4)_3\text{12MoO}_3$. It was also mentioned to analyze fosfomycin by fluorometry after derivation [7], however, these photometric methods are all time-consuming.

* Corresponding author. Fax: +86-27-8764617.

E-mail address: yqfeng@public.wh.hb.cn (S.-L. Da)

Indirect spectrophotometry by decoloration has been widely investigated in the past few years [8–10]. It has been reported that the detected substance usually accelerates the decoloring reaction resulting from the oxidation of chromogenic reagent, the degree of decoloration has linear relationship with the concentration of the detected substance in a limited concentration range. However, very few investigations on indirect spectrophotometry based on ligand-exchange have been mentioned.

2-(5-Bromo-2-pyridylazo)-5-diethylaminophenol (5-Br-PADAP) is a chelating reagent known for its ability to form stable complexes with various metal ions, including Fe, Ni, Co, Nb, Sc. Colorimetric methods based on these complexing reaction have been thoroughly studied [11–13]. 5-Br-PADAP is also a sensitive reagent for Zr, based on which, the spectrophotometric methods for determination of Zr have been proposed [14–16]. Zirconium is known for its hard lewis acid character, while fosfomycin is a hard lewis base due to its phosphonic structure, therefore fosfomycin is expected to form a stronger complex with Zr than 5-Br-PADAP. In the present work, we found that fosfomycin, being added to the Zr-5-Br-PADAP solution, could quantitatively replace 5-Br-PADAP from the chromophoric complex. Thus an indirect spectrophotometric method based on ligand-exchange for determination of fosfomycin is established. The composition and stability constant of zirconium with 5-Br-PADAP and fosfomycin were estimated, which provided a cogent theoretical evidence for the experimental phenomena.

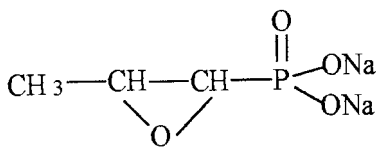


Fig. 1. Structure of fosfomycin.

2. Experimental

2.1. Apparatus

A UV-1601 spectrophotometer (Shimadzu, Japan) was used with 1-cm light-path cuvettes.

2.2. Reagents

Fosfomycin (F), 1×10^{-2} M and 1×10^{-3} M; Zirconium (Zr), 1×10^{-2} M and 1×10^{-3} M, dissolved in 0.4 M HCl solution; 5-Br-PADAP (L), 1×10^{-2} M.

Fosfomycin is provided by Northeast Pharmaceutical Factory (China), other reagents are of analytical grade. Distilled water was used throughout.

2.3. Procedure

In a 25-ml tube, 2 ml of 1×10^{-3} M Zr and a certain amount of fosfomycin were mixed for 8 min, then 0.6 ml of 1×10^{-2} M 5-Br-PADAP was added and the solution was diluted with distilled water. After 10 min, place the solution with fosfomycin in the reference cuvette and the solution without fosfomycin in the sample cuvette. The absorbance was measured at 605 nm.

3. Result and discussion

3.1. Optimization of conditions

In 0.032 M HCl medium, Zr forms purplish blue complex with 5-Br-PADAP, the maximal absorption is at 605 nm where reagent itself exhibits poor absorption. When fosfomycin is added, the position of peak is not changed but the intensity of absorption decreased linearly with different concentration of fosfomycin (Fig. 2), so 605 nm is selected for the following experiments.

To establish the optimal conditions for determination of fosfomycin, we studied the influence of the acidity, concentration of zirconium and 5-Br-PADAP on the degree of decoloration.

The sensitivity for determination of fosfomycin reaches maximum when the concentration of Zr is

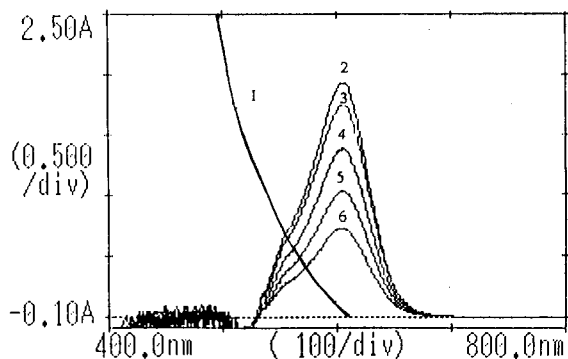


Fig. 2. Absorption spectra. 1: L; 2: Zr + L; 3, 4, 5, 6: 4, 12, 20, 28×10^{-6} M F + Zr + L. $C_{Zr} = 8 \times 10^{-5}$ M; $C_L = 2.4 \times 10^{-4}$ M; $C_{HCl} = 0.032$ M.

over 5.6×10^{-5} M (Fig. 3). In the experiment, we choose concentration of Zr as 8×10^{-5} M which provides high sensitivity for determination of fosfomycin and reduces analytical deviation.

The acidity of the solution is also important condition. Fig. 4 shows the effect of the concentration of hydrochloric acid on the degree of decoloration of Zr-5-Br-PADAP in the presence of 1×10^{-5} M fosfomycin. It can be found that the degree of the decoloration (difference in absorption between sample and reference) increases

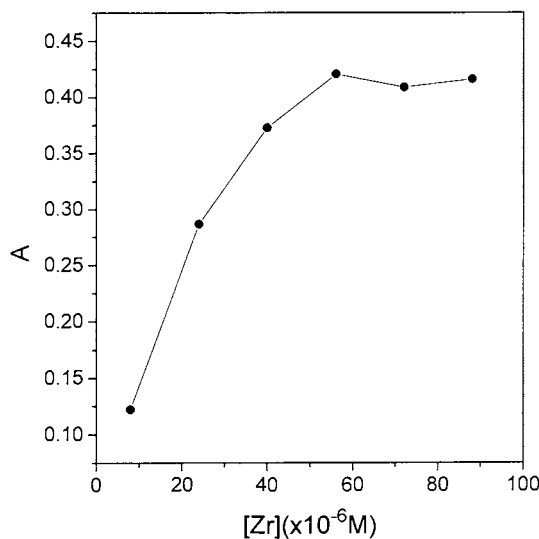


Fig. 3. Dependence of the absorbance on the concentration of Zr. $C_F = 1 \times 10^{-5}$ M; $C_L = 2.8 \times 10^{-4}$ M; $C_{HCl} = 0.032$ M.

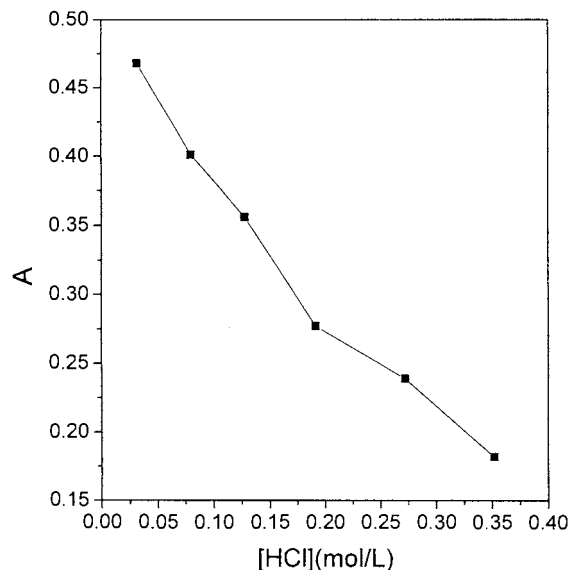


Fig. 4. Dependence of the absorbance on the acidity. $C_F = 1 \times 10^{-5}$ M; $C_{Zr} = 8 \times 10^{-5}$ M; $C_L = 2.8 \times 10^{-4}$ M.

with the decrease of the concentration of hydrochloric acid. Unfortunately, when the pH of the solution is over 3, precipitate appears. Therefore, 0.032 M HCl medium was chosen in the experiment.

5-Br-PADAP is a competitive complexing reagent for Zr in solution. The effect of the concentration of 5-Br-PADAP on the intensity of determination for fosfomycin was also investigated. It was found that the intensity reached maximum at the concentration of 5-Br-PADAP between 1.6×10^{-4} and 3.2×10^{-4} M (Fig. 5).

Fig. 6 shows the change of Zr-5-Br-PADAP complex in light-absorption with incubation time in the presence and absence of fosfomycin, respectively. For comparison, reagent blank was utilized as reference solution. Curve B shows the variety of absorbance with the incubation time in the case that there was no fosfomycin added. The solution reached the maximal absorption in 12 min and remained stable for at least 70 min. Curve C shows the decoloration of Zr-5-Br-PADAP in the presence of fosfomycin with incubation time. In this case, Zr and 5-Br-PADAP was mixed and kept for 15 min in order to form a stable Zr-5-Br-PADAP complex, soon after the addition of fos-

fomycin, the absorbance was measured in sequence. It can be seen from Curve C that the absorbance decreased rapidly first and became stable after 30 min. For the curve D, the adding order of reagent was reversed, that is mixing Zr and fosfomycin first, and kept for 8 min, then 5-Br-PADAP was added. The result is opposite to curve C, the absorbance increased first and became stable after 10 min. It is worth mentioning that both curves C and D reached almost the same absorbance when the solution system reached equilibrium at the same concentration of reagent. This phenomenon proved the ligand-exchange reaction is an interconversion course. The absorbance was stable for at least 70 min in both cases, suitable for quantitative analysis.

3.2. Interference

On the determination of 4×10^{-7} mol fosfomycin, different element and substance was added to solution to examine interference. At least following amount of substance did not interfere, the unit of the number in brackets is 10^{-6} M: Cl^- (800), Br^- (140), HCO_3^- (100), Ac^- (200),

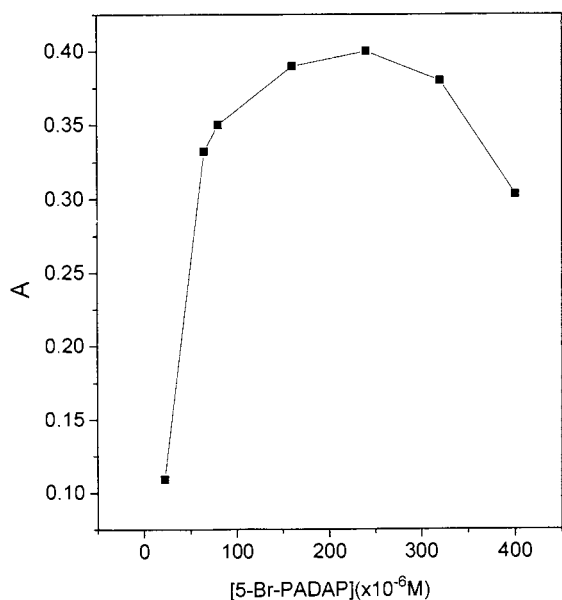


Fig. 5. Dependence of the absorbance on the concentration of 5-Br-PADAP. $C_F = 1 \times 10^{-5}$ M; $C_{Zr} = 8 \times 10^{-5}$ M; $C_{HCl} = 0.032$ M.

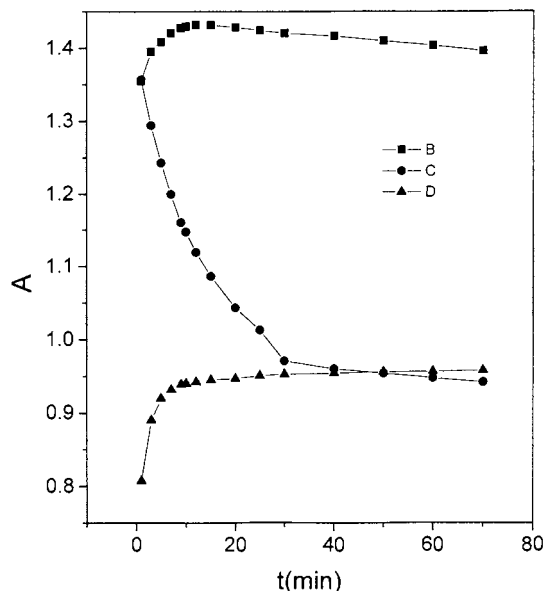


Fig. 6. Dependence of the absorbance on time. B: Zr-5-Br-PADAP solution; C: Addition of fosfomycin into Zr-5-Br-PADAP solution; D: Addition of 5-Br-PADAP into Zr and fosfomycin solution. $C_F = 1 \times 10^{-5}$ M; $C_{Zr} = 8 \times 10^{-5}$ M; $C_L = 2.8 \times 10^{-4}$ M; $C_{HCl} = 0.032$ M.

α -phenylethylamine (38), F^- (3.8), SO_4^{2-} (2.4), H_2PO_4^- (0.063), Na^+ (400), K^+ (400). The result shows that the method can be free from interferences of most anions. However, being strong complexing anions for Zr, SO_4^{2-} , H_2PO_4^- and F^- interfere severely. Fortunately, for product analysis of fosfomycin in the experiment, the amount of these anions is rather small, and they can also be removed by recrystallization with ethanol. Phenylethylamine that is of a great quantity in the intermediary product does not interfere.

3.3. Linearity, reproducibility and detectability

In optimized condition, the correlation of absorbance with concentration of fosfomycin is linear in the range of $0-28 \times 10^{-6}$ M. The correlation coefficient is 0.99949. The indirect molar absorption coefficient was found to be $4.59 \times 10^4 \text{ l mol}^{-1} \text{ cm}^{-1}$.

The relative standard deviation was 1.25% on determination of 4×10^{-7} mol fosfomycin. The detectability was 5×10^{-7} M.

Table 1
Result of sample analysis

Sample	Fosfomycin determined (%)			Average (%)	RSD (%)
(–)Fosfomycin-phenylethylamine	97.5	95.8	94.2	95.8	1.72
(+)Fosfomycin-phenylethylamine	97.6	93.9	96.4	95.3	1.33
(±)Fosfomycin-phenylethylamine	75.2	74.6	74.6	74.8	0.46

3.4. Sample analysis

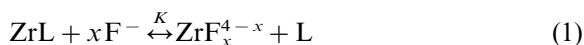
Fosfomycin-phenylethylamine is the intermediary product of the terminal medicine fosfomycin-disodium. The present method was successfully applied to the determination of fosfomycin in this intermediary product of Northeast Pharmaceutical Factory. All the samples were not pretreated and were dissolved in distilled water directly. The results are given in Table 1. The recovery was evaluated by spiking sample with various amount of standard fosfomycin. Average recovery was 102.7%. The analysis results are satisfactory. Moreover, the method is simple and rapid for product assay.

3.5. Mechanism of decolouration

Stronger complexing ability of fosfomycin with Zr than 5-Br-PADAP is supposed to be the direct reason for decolouration. In order to confirm this hypothesis, the composition and stability constant of Zr with 5-Br-PADAP and fosfomycin was estimated, respectively.

The composition of the Zr-5-Br-PADAP complex in the medium of 0.032 M HCl was determined by molar ratio and Job's methods, and found to be 1:1. The result is in agreement with earlier report in 0.2 M HNO₃ medium [14]. The stability constant of Zr-5-Br-PADAP complex, K_{ZrL} , was found to be 2.69×10^5 in the current experimental condition.

The composition of Zr–fosfomycin complex is expected to be ZrF_x , accordingly, the interconversion reaction in solution can be expressed as:



The equilibrium constant, K , of the Reaction 1 is given by

$$\begin{aligned} K &= \frac{[ZrF_x^{4-x}][L]}{[ZrL][F^-]^x} \\ &= \frac{([ZrL_0] - [ZrL])[L]}{[ZrL] \left(C_F \frac{K_{a1}}{K_{a1} + [H^+]} \right)^x} \\ &= \frac{(A_0 - A)[L](K_{a1} + [H^+])^x}{A C_F^x K_{a1}^x} \end{aligned} \quad (2)$$

Where, A_0 , A is the absorbance of initial Zr-5-Br-PADAP solution and the solution with fosfomycin, respectively; K_{a1} is the first grade acid dissociation constant of fosfomycin, it has been reported to be $1 \times 10^{-1.5}$ [2]; and C_F stands for the whole concentration of fosfomycin added to the solution.

$$C_F = [F] + [F^-]$$

Since the concentration of L in solution is much excessive compared to Zr and F, it can be conceived as a constant.

Eq. (2) can be rewritten as:

$$\log\left(\frac{1}{A} - \frac{1}{A_0}\right) = x \log C_F + \log \frac{K_{a1}^x K}{A_0 [L] (K_{a1} + [H^+])^x} \quad (3)$$

Eq. (3) indicates that the plot of $\log(1/A - 1/A_0)$ vs $\log C_F$ should give a straight line with the slope of x . Fig. 7 shows plot of the $\log(1/A - 1/A_0)$ vs $\log C_F$, which gives a straight line with the slope of 1.6. So the composition of Zr and fosfomycin complex was calculated to be 2:3, while the equilibrium constant of the ligand-exchange reaction, K , was 2.063×10^4 . Based on the above results, the stability constant of the Zr_2F_3 , $K_{Zr_2F_3}$, was obtained as 5.55×10^9 .

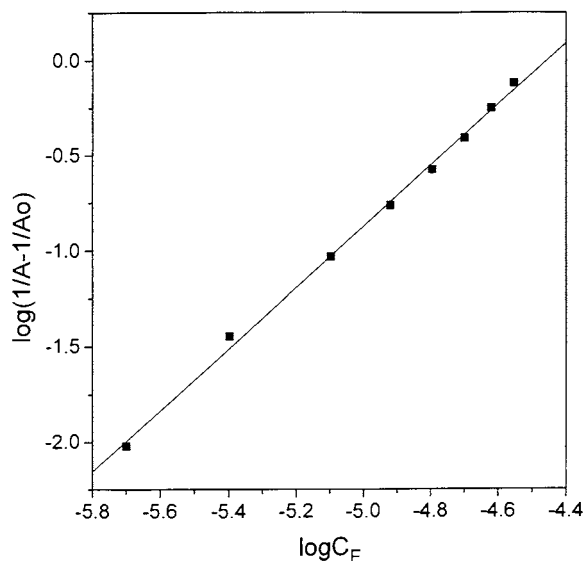


Fig. 7. Plot of $\log(1/A - 1/A_0) \sim \log C_F$.

As discussed above, the stability constant of Zr_2F_3 is much larger than ZrL , so it can replace 5-Br-PADAP from the original complex, which leads to decolouration of the solution.

References

- [1] M.C. Dessalles, J. Levieux, M. Souleau, G. Mahuzier, *Pathol. Biol.* 35 (1987) 200.
- [2] G.A. Pianetti, L.M. Moreira de Campos, P. Chaminade, A. Baillet, D. Baylocq-Ferrier, G. Mahuzier, *Anal. Chim. Acta* 284 (1993) 291.
- [3] Y.L. Hu, S.L. Da, Y.Q. Feng, Q.H. Zhang, *Sepu (Chin. J. Chromatogr.)* (1999) in press.
- [4] D. Leveque, C. Gallion, E. Tarral, H. Monteil, F. Jehl, *J. Chromatogr. B* 655 (1994) 320.
- [5] A. Baillet, G.A. Pianetti, M. Taverna, G. Mahuzier, D. Baylocq-Ferrier, *J. Chromatogr. Biomed. Appl.* 616 (1993) 311.
- [6] H. Jimenez, M. Vidal, *Ann. R. Acad. Farm* 52 (1986) 687.
- [7] S. Takitani, M. Suzuki, *Iyakuhi Kenkyu* 16 (1985) 1142.
- [8] G.S. Cheng, Y. Song, X.L. Gong, *Fenxi Huaxue* 16 (1988) 144.
- [9] F. Li, S.L. Cheng, *Fenxi Xuaxue* 19 (1991) 921.
- [10] J.Y. Gao, J.L. Zhao, *Fenxi Huaxue* 19 (1991) 1329.
- [11] G.S. Cheng, X.D. Nie, X.Y. Yan, *Fenxi Huaxue* 17 (1989) 548.
- [12] H.M. Shi, X.W. He, G.Z. Zhang, *Chem. J. Chin. Univ.* 1 (1980) 44.
- [13] X.K. Wang, *Fenxi Huaxue* 19 (1991) 297.
- [14] H.M. Li, H.X. Sheng, *Huaxue Shiji* 8 (1986) 63.
- [15] Z.L. Li, J.X. Cheng, L.M. Shi, *Huaxue Shiji* 7 (1985) 330.
- [16] D.R. Zhang, H.M. Shi, X.W. He, *Fenxi Huaxue* 18 (1990) 504.

Polarographic determination of deltamethrin

K. Samatha, N.Y. Sreedhar *

Department of Chemistry, Sri Venkateswara University, Tirupati, 517 502, Andhra Pradesh, India

Received 18 August 1998; received in revised form 26 October 1998; accepted 6 November 1998

Abstract

The electrochemical characteristics of deltamethrin have been determined by means of electrochemical techniques such as d.c. polarography, cyclic voltammetry and differential pulse polarography over a wide range of pH from 2.0–12.0. The title compound exhibits a single well defined peak due to the reduction of the $-C=C-$ moiety present in deltamethrin. The overall reduction process is diffusion-controlled and adsorption free in nature. The variation of half-wave potential with the pH, concentration of the title compound, and other experimental conditions is described. A possible mechanism for the reduction is suggested. The number of electrons involved in the electrode reduction is two. Investigation was also undertaken for the determination of deltamethrin in vegetables and in storage bags of rice and wheat under FCI's storage system. © 1999 Elsevier Science B.V. All rights reserved.

Keywords: Deltamethrin; Polarography; Vegetables; Storage bags; Wheat; Rice.

1. Introduction

deltamethrin [cyano(3-phenoxyphenyl) methyl 3-(2,2-dichloro ethenyl)-2,2-dimethyl cyclopropane carboxylate] (I) is a systemic, granular pyrethroid insecticide for the control of pests of rice, sorghum, barley, maize, cotton, vegetables, fruits etc., Today it is widely used because of its low persistence and high effectiveness. Its widespread use as an effective pesticide has created a demand for a quick, easy, and reliable method for its determination.

Wybieralski et al. [1]. proposed the quantitative

determination of deltamethrin in aqueous solutions by gas chromatography. Darwish [2] has described the use of HPLC for the determination of deltamethrin in wool. deltamethrin and its residues have been determined by a spectrophotometric method in insecticidal formulations and in water [3]. Furthermore, deltamethrin has also been determined by different techniques of which TLC [4], photochemical–spectrofluorometric [5], and NMR [6] are dominant.

The purpose of the present investigation was to elucidate the electrochemical reduction mechanism and electrode kinetics by employing advanced electrochemical techniques and to develop analytical procedures for the quantitative estimation of deltamethrin in vegetables and in storage bags of wheat and rice.

* Corresponding author: Fax: +91-8574-27499.

E-mail address: svuni@ao.nic.in (N.Y. Sreedhar)

2. Experimental

A detailed description of the instrumentation and experimental conditions has been reported earlier [7]. All the experiments were performed at $25 \pm 1^\circ\text{C}$. pH measurements were carried out with a Elico digital pH meter. Dissolved air was removed from the solution by degassing with oxygen-free nitrogen for 10–15 min. prior to each run.

deltamethrin was supplied by 'Hoechst schering Agr Evo', Mumbai. The purity of the compound was tested by boiling point and by TLC experiments. A stock solution was prepared by dissolution of the required amount of pesticide in dimethylformamide. Universal buffers of pH 2.0–12.0 were prepared from 0.2 M boric acid, 0.05 M citric acid, and 0.1 M trisodium orthophosphate [8]. All the chemicals used were of Analar grade.

3. Results and discussion

The electrochemical behaviour of deltamethrin was examined over the pH range 2.0–12.0. Typical polarograms are given in Figs. 1 and 2. In all the cases, a single well defined peak is observed at

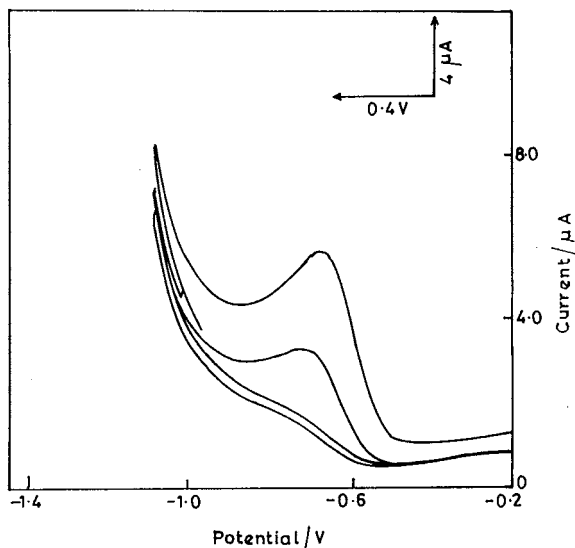


Fig. 1. cyclic voltammogram of deltamethrin at pH 2.0. Concentration, 0.5 mM; drop time, 2 s; scan rate, 40 mV s^{-1} .

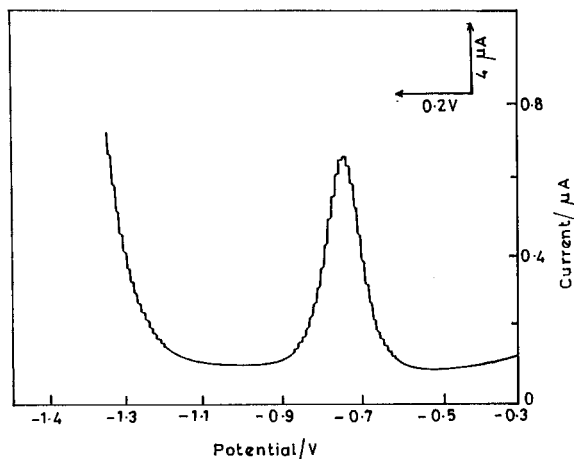


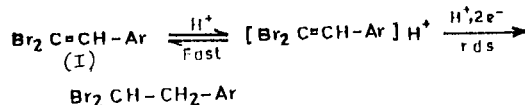
Fig. 2. differential pulse polarogram of deltamethrin at pH 4.0. Concentration, 0.5 mM; drop time, 2 s; pulse amplitude, 50 mV.

a potential around -0.7 V . In the case of cyclic voltammetry, no anodic peak is observed in the reverse scan.

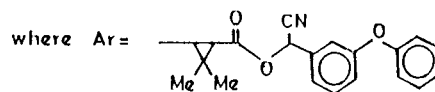
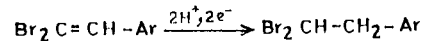
From the polarograms, it was concluded that the peak current increases as the concentration increases. The above facts suggest that the electrochemical reduction is irreversible and involves diffusion-controlled electron transfer. Irreversibility is also indicated by the variation of peak potential (E_p) with scan rate in cyclic voltammetry.

The number of electrons was determined by millicoulometry at -0.65 V . The n value was found to be two. On the basis of the above results, the following mechanism may be pro-

In acidic medium:



In alkaline medium:



Scheme 1.

Table 1
 Typical kinetic data of deltamethrin, concentration: 0.5 mM

Supporting elec- trolyte of pH	d.c. polarography			Cyclic voltammetry			Differential pulse polarography		
	$-E_{1/2}$ (V)	$D \times 10^5$ (cm ² s ⁻¹)	$K_{i,h}^0$ (cm s ⁻¹)	$-E_p$ (V)	$D \times 10^5$ (Cm ² S ⁻¹)	$K_{i,h}^0$ (CmS ⁻¹)	$-E_m$ (V)	$D \times 10^5$ (cm ² s ⁻¹)	$K_{i,h}^0$ (cm s ⁻¹)
2.0	0.68	6.52	8.71×10^{-9}	0.67	6.41	7.98×10^{-9}	0.65	6.65	2.86×10^{-9}
4.0	0.71	6.55	1.08×10^{-11}	0.73	6.35	2.31×10^{-11}	0.71	6.64	4.45×10^{-11}
6.0	0.84	6.02	3.32×10^{-12}	0.89	5.91	6.81×10^{-12}	0.81	6.31	8.56×10^{-12}
8.0	1.18	6.85	1.70×10^{-17}	1.20	5.95	2.21×10^{-16}	1.13	6.98	4.10×10^{-16}
10.0	1.21	6.65	8.91×10^{-18}	1.22	5.88	8.98×10^{-18}	1.20	6.72	9.19×10^{-18}
12.0	1.27	6.50	3.65×10^{-19}	1.31	5.61	2.11×10^{-20}	1.29	6.58	8.72×10^{-19}

Table 2

Determination of deltamethrin in formulations by differential pulse polarography at pH 4.0

Deltamethrin formulation	Labelled amount (mg)	Average amount found (mg) ^a	Average recovery
Decis	5.0	4.82	96.4
	10.0	9.59	95.9
K-othrin	5.0	4.76	95.2
	15.0	14.30	95.3
Mixed formulation (deltamethrin + heptenophos)	10.0	9.49	94.9

^a Each value is an average of three determinations.

posed (Scheme 1). Controlled potential electrolysis (CPE) was carried out at pH 4.0 at -0.82 V vs. SCE to identify the product, and it was further confirmed by I.R. spectral studies.

Kinetic data obtained with different techniques are summarised in Table 1. The diffusion coefficient values evaluated from all techniques are in good agreement. This is particularly evident because no adsorption complications are involved in the electrode process. The slight decrease in D -values with an increase in pH may be attributed to the lower availability of protons with an increase in pH 2.

The rate constants [$K_{f,h}^0$] obtained for the reduction of the $>C=C<$ group are high in acidic media for all techniques, indicating that the rate of reaction is fast since in the acidic solutions proton involvement is high which makes the reduction process easier. But in basic media, the reduction process is not easily facilitated owing to the lower availability of protons. Hence, $E_{1/2}$, E_p , and E_m values in basic media are observed to shift to more negative potentials. Consequently, lower values are obtained for rate constants in basic media in contrast to acidic media.

The DPP wave obtained in the pH range from 2 to 6 is well resolved and is highly reproducible, and it was therefore chosen for the analysis of deltamethrin in vegetables and rice and wheat under FCI's storage system.

3.1. Recommended analytical procedure

A stock solution (1.0×10^{-5} M) is prepared by

dissolution of the appropriate amount of the electroactive species in dimethylformamide. Standard solution, 1 ml, is transferred into a polarographic cell and diluted with 9 ml of supporting electrolyte and then deoxygenated with nitrogen gas for 10 min. After the polarogram is recorded, small increments (0.2 ml) of standard solution are added and a polarogram is recorded after each addition under similar conditions. In the present study, the best precision was obtained at pH 4.0, with a drop time of 2 s, a pulse amplitude of 50 mV, and an applied potential of -0.7 V.

3.2. Analysis of formulations

The required quantity of formulation corresponding to a 1.0×10^{-3} M stock solution was accurately measured and transferred into a 50-ml volumetric flask containing 50 ml of dimethylformamide. A solution of approximately 1.0×10^{-5} M was prepared by dilution of this stock solution with universal buffer. Assay results for deltamethrin in formulations at pH 4.0 are given in Table 2. Attempts were made to apply the proposed method to the determination of deltamethrin in mixed formulation (deltamethrin + heptenophos). The latter insecticide does not give a reduction wave and hence it was believed to be a non-interfering substance. Therefore, the proposed method has been employed for the assay of deltamethrin in mixed formulations, and these results are incorporated in Table 2.

Table 3
Recovery of deltamethrin from fortified samples using DPP

Deltamethrin Formulation	Labelled amount (mg)	Amount found (mg) ^a		Average recovery	
		Cabbage	Tomato	Cabbage	Tomato
Decis	2.0	1.90	1.88	95.0	94.0
	6.0	5.68	5.65	94.6	94.1
	10.0	9.40	9.52	94.0	95.2
K-othrin	15.0	14.15	14.09	94.3	93.9
	20.0	18.98	18.92	94.9	94.6

^a Each value is an average of three determinations.

3.3. Analysis of deltamethrin in vegetables

In the present investigation, vegetables such as cabbage and tomato have been chosen for the analysis of deltamethrin. Known amounts of deltamethrin (decis, K-othrin) were sprayed on cabbage and tomato crops and left for 1–2 h. The extracts were prepared by the treatment of a crushed sample with 100 ml of acetone. Then the extract was allowed to dry. The residue of deltamethrin was dissolved in DMF and transferred into a 50-ml volumetric flask. Then the polarograms were recorded in the same manner as described earlier. The results obtained using the DPP method are shown in Table 3.

To ascertain the practical limit of determination of the method, 25-g portions of potatoes were fortified at the 0.01 mg kg⁻¹ level for deltamethrin. It could be determined at this level by the proposed DPP method. The levels detected are below the Food and Agricultural Organisation and World Health Organisation maximum residue limit for deltamethrin on cabbage and tomato of 2 mg kg⁻¹ when calculated [9].

Recovery of deltamethrin ranging from 93.9 to 95.2% was found, which indicates the high accuracy and reproducibility of the proposed differential pulse polarographic method.

3.4. Analysis of deltamethrin in wheat and rice under FCI's storage system

Rice and wheat stacks of usual dimension and capacity were selected in the Food Corporation of

India godowns at palamaner. Small jute bags of 4 kg capacity were chosen for these studies. The jute bags were filled with wheat and rice and properly stitched. The dosages used were 1.0 and 1.5 g m⁻² of a.i. of deltamethrin (Decis). The quantity required of deltamethrin was dissolved in 50 ml of acetone and spraying was done on the jute bags with the help of a small hand sprayer. Every care was taken to prevent loss of deltamethrin during spraying and to see that there was uniform deposit over the bag surface.

The observations of residual toxicity were recorded on the first day and after 15 days. The samples for analysis of residues of deltamethrin were drawn 1 h after mixing and after 15 days. At each sampling the stitching of the bags was undone, the grains poured over a tray and thoroughly mixed. Each sample comprised a bag of 50 g of wheat and rice. The samples of wheat and rice were ground to a powder in an electrically operated grinder. The samples were extracted with acetone and the extract was filtered through a Büchner funnel. Then the extract was allowed to dry. The residue of deltamethrin was dissolved in DMF and transferred to a 50-ml volumetric flask. The residues of deltamethrin in wheat and rice in jute bags were estimated by DPP and the results are presented in Table 4.

It is clear from the data that the residues of deltamethrin on the wheat were 1.02, and 1.34 ppm, and on the rice were be 0.99 and 1.30 ppm just after spraying of deltamethrin 1.0 and 1.5 g m⁻² a.i., respectively. The residues of deltamethrin on wheat in samples collected 15

Table 4

Persistence of residues of deltamethrin on wheat and rice penetrated during spraying on jute bags

Sample	Period after treatment	Deltamethrin dose							
		1.0 g				1.5 g			
		R_1	R_2	R_3	Mean	R_1	R_2	R_3	Mean
Wheat	1 h	1.68	0.86	0.34	0.96	1.91	0.97	1.45	1.44
	15 days	0.44	0.60	0.55	0.53	0.96	0.78	0.50	0.75
Rice	1 h	1.62	0.84	0.52	0.99	1.75	0.82	1.34	1.30
	15 days	0.52	0.46	0.32	0.43	0.96	0.75	0.51	0.77

days after of spraying were 0.55 and 0.75 ppm. Similarly, on rice they were 0.43 and 0.77 ppm. Thus the residues of deltamethrin penetrated during the spraying on jute bags were below the tolerance limit of FAO [10]. These results suggest that, even after 15 days of application, of the deltamethrin fell within the detection limit. Hence in the light of above data, the use of deltamethrin at dosages of 1.0 and 1.5g m⁻² a.i treatments for the control of storage pests is without any health hazard whatsoever to the consumers.

The proposed method is free from interferences due to ingredients present in deltamethrin and also other constituents present in vegetables and storage bags of rice and wheat. Therefore the proposed method is simple, inexpensive, rapid, reliable, and sensitive. The proposed method does not involve the elaborate cleanup procedures required with the other methods. The method can also be extended for the study of the efficacy of deltamethrin against insect infestation in various stored samples.

References

- [1] J. Wybieralski, G. Dabrowska, H. Siwek, *Zesz. Nauk-Akad. Roln. Szczecinie* 159 (56) (1993) 4–562.
- [2] A. Darwish, *J. Liq. Chromatogr.* 17 (19) (1994) 4215–4228.
- [3] R.V. Prabhakara Raju, R. Raghava Naidu, *J. AOAC Int.* 77 (3) (1994) 748–751.
- [4] A. Coly, J.J. Aaron, *Analyst* 119 (6) (1994) 1205–1209.
- [5] K.M. Appaiah, M.A. Sreenivasa, K.V. Nagaraja, *Indian Food Packer* 47 (5) (1993) 61–63.
- [6] R. Cong, Z. Zhou, Y. Liu, D.-X. Xiamen, *Ziran Kexueban* 31 (6) (1992) 708–710.
- [7] N.Y. Sreedhar, P.R.K. Reddy, S. Jayarama Reddy, *Bull. Electrochem.* 13 (1) (1997) 88.
- [8] D.D. Perrin, D. Boyd (Eds.), *Buffers for pH and Metal Ion Control*, Chapman and Hall, London, 1974, p. 156.
- [9] Anon, *Pesticide residues in food*, report of the joint FAO/WHO meeting, FAO Agricultural Series, No. 88, 1972.
- [10] Anon, F.A.O, *Pesticide residues in Food report of the 1974 joint FAO/WHO meeting held in Geneva*, Nov. 24–Dec. 3, 1980.

Square-wave anodic stripping voltammetric determination of thallium(I) at a Nafion/mercury film modified electrode

Tsai-Hwa Lu, Hao-Yun Yang, I. Wen Sun *

Department of Chemistry, National Cheng Kung University, Tainan, 70101, Taiwan ROC

Received 15 July 1998; received in revised form 29 October 1998; accepted 9 November 1998

Abstract

A Nafion/mercury film electrode (NMFE) was used for the determination of trace thallium(I) in aqueous solutions. Thallium(I) was preconcentrated onto the NMFE from the sample solution containing 0.01 M ethylenediaminetetraacetate (EDTA), and determined by square-wave anodic stripping voltammetry (SWASV). Various factors influencing the determination of thallium(I) were thoroughly investigated. This modified electrode exhibits good resistance to interferences from surface-active compounds. The presence of EDTA effectively eliminated the interferences from metal ions, such as lead(II) and cadmium(II), which are generally considered as the major interferences in the determination of thallium at a mercury electrode. With 2-min preconcentration, linear calibration graphs were obtained over the range 0.05–100 ppb of thallium(I). An even lower detection limit, 0.01 ppb, were achieved with 5-min accumulation. The electrode is easy to prepare and can be readily renewed after each stripping experiment. Applicability of this procedure to various water samples is illustrated. © 1999 Elsevier Science B.V. All rights reserved.

Keywords: Mercury film electrode; Nafion; Square-wave voltammetry; Stripping analysis; Thallium

1. Introduction

The high toxicity of thallium and its compounds has made the determination of traces of thallium in various samples important. While spectrometric methods including atomic absorption spectrometry [1], spectrophotometry [2], emission spectrophotometry [3] have been em-

ployed in such determination, anodic stripping voltammetry (ASV) is also very suitable for trace measurement of thallium due to its remarkable sensitivity. However, conventional voltammetric stripping methods for thallium determination are usually complicated by the interference from neighboring peaks associated with the stripping of coexisting metal ions [4,5]. Extensive efforts have thus been devoted to overcome such interference through the addition of certain adsorptive agents, or the use of chemically modified electrode [6–10].

* Corresponding author. Fax: +886-6-2740552.

E-mail address: iwsun@mail.ncku.edu.tw (I.W. Sun)

These methods, however, could be interfered by ions which are also capable of forming complexes with the adsorptive agents. Furthermore, these methods may suffer from interferences due to organic surfactants adsorption on the electrode.

This article describes a square-wave stripping voltammetric (SWSV) procedure for the determination of traces of cationic thallium(I) by using a Nafion/mercury film coated glassy carbon disk electrode (NMFE) with the presence of ethylenediaminetetraacetate (EDTA) in the sample solution. In this way, significant advantages come into effect: the cation-exchange and preconcentration feature of Nafion [11], the remarkable accumulation effect of the mercury film for thallium [12], and the high sensitivity of the SWSV [13]. In addition, the extraordinary chelating agent EDTA chelates to interfering metal ions forming bulky complexes that are excluded from the Nafion film. This simple procedure yields good sensitivity for thallium(I) and displays good resistance to the interference from common ions such as cadmium and lead as well as the interference from surface-active compounds such as sodium dodecyl sulfate (SDS) and Triton X-100.

2. Experimental

2.1. Apparatus

All electrochemical experiments were performed with a Bioanalytical Systems BAS CV-50W electrochemical analyzer in conjunction with a BAS model C-2 electrochemical cell. The three-electrode system consisted of a glassy carbon disk working electrode (BAS, 3 mm diameter) coated with Nafion and mercury, an Ag/AgCl reference electrode, and a platinum spiral auxiliary electrode. All glassware was cleaned with 8 N nitric acid and rinsed with deionized water.

2.2. Chemicals and reagents

Nafion perfluorinated ion-exchange powder, 5% *m/v* solution in a mixture of lower aliphatic alcohols and 10% water, was obtained from Aldrich. Sodium perchlorate, sodium nitrate and nitric

acid were of analytical grade from Riedel de Haen (RDH). Standard metal solutions (1000 ppm) of Mg(II), Ni(II), Fe(III), Zn(II), Cr(VI), Cu(II), and Cd(II) were from Fisher. Standard solutions (1000 ppm) of Mo(VI), Se(IV), and Au(III) were from Mallinckrodt. Hg(II) standard solution (1000 ppm) was from Merck. Anionic surfactant sodium dodecyl sulphate (SDS) was received from RDH and nonionic surfactant Triton X-100 was received from Lancaster. Thallium(I) stock solutions (1000 ppm) were prepared by dissolving thallium(I) chloride (99.999%, Stream) in nitric acid. All the preparation and dilution of solutions were made with deionized water.

2.3. Preparation of Nafion mercury film electrode (NMFE) and sample solution

After polished with a polishing cloth to a shiny surface, the glassy carbon electrode (GCE) was rinsed with deionized water and then cleaned ultrasonically in 1 + 1 nitric acid and deionized water. Then, 4 μ l of Nafion coating solution was spin-coated onto the GCE at a spin rate of 3000 rpm. A uniform thin film was formed by evaporating the solvent at room temperature after about 3 min of spinning.

Mercury was electrodeposited on the Nafion coated GCE from 5 ml of 10 ppm mercury(II) solution containing 0.1 M sodium perchlorate at an applied potential of -0.8 V vs Ag/AgCl for 4 min with stirring.

The sample solution medium contained thallium(I), 0.01 M EDTA to reduce the concentration of interfering metal ions and proper amount of 0.1 M nitric acid to adjust the solution pH, and 0.1 M sodium nitrate as the supporting electrolyte for all electrochemical experiments.

2.4. Procedure

The freshly prepared NMFE was dipped into the stirred analyte solution containing Tl(I) and kept at -0.9 V vs Ag/AgCl for the time required for preconcentration (the optimized time was 2 min). Quantitative determinations were then performed in the SWSV mode. The potential was scanned in the anodic direction from -1.0 to

–0.4 V vs Ag/AgCl. A medium containing 0.01 M EDTA, 0.1 M sodium nitrate (pH = 4.5) was used in the electrochemical experiments. Solutions and samples were analyzed with 3 min deoxygenation. After recording the voltammogram, the electrode was regenerated by immersing the electrode in 1 M nitric acid at –0.4 V vs Ag/AgCl for 30 s. The renewed electrode was then checked in the supporting electrolyte before the next measurement to ensure that it did not show any peak within the potential range. Tap water, ground water, and rain water were collected and stored in precleaned polyethylene bottles after filtration. The standard addition method was used to evaluate the content of Tl(I) in the water samples.

3. Results and discussion

3.1. Electrochemical behavior of Tl(I) at the various electrodes

The cyclic voltammograms for a solution containing 10 ppm thallium(I), 0.1 M NaNO₃, and 0.01 M EDTA at a bare GCE and a NMFE are shown in Fig. 1. At the bare GCE (Fig. 1a), a cathodic peak which can be assigned to the cathodic deposition of thallium(I) to elemental thallium, and an anodic stripping peak corresponding to the reoxidation of thallium to thallium(I) are observed. The peak potential separation of these two peaks is fairly wide, indicative of a quasi-reversible electrochemical reaction. On the other hand, the cathodic deposition peak and the anodic stripping peak observed for the thallium(I)/(0) redox couple at the NMFE (Fig. 1b) are fairly symmetric in shape. This behavior is typical for an electrochemical reaction occurring in a film at the electrode surface. Furthermore, the peak potential separation observed for thallium(I)/(0) redox reaction on the NMFE is much smaller than that observed on the bare GCE, indicating that the NMFE is more suitable than the bare GCE for the determination of thallium(I) by SWSV [14,15]. The advantage of using the NMFE in the determination of thallium(I) is further demonstrated in Fig. 2. This figure shows the responses of 10 ppb thallium(I) on different electrodes in the same

supporting electrolyte. As can be seen in Fig. 2a, no voltammetric response at all was detected on the bare GCE at this low thallium(I) concentration while a distinguishable oxidation peak of thallium at –0.70 and –0.61 V was observed on the Nafion film coated GCE (NFE)(Fig. 2b) and the mercury film electrode (MFE)(Fig. 2c), respectively. The results indicate that the preconcentration efficiency of the electrode could be enhanced by the ion-exchange property of Nafion or the good solubility of thallium in mercury. When the NMFE was used, a well-defined oxidation peak of thallium(I) at about –0.66 V was observed (Fig. 2d). As can be seen, the peak height for NMFE is much higher than that of the NFE and MFE under the same experimental conditions. This confirms that remarkable improvement on the voltammetric detection of thallium(I) is achieved by combining the effect of Nafion film and mercury film.

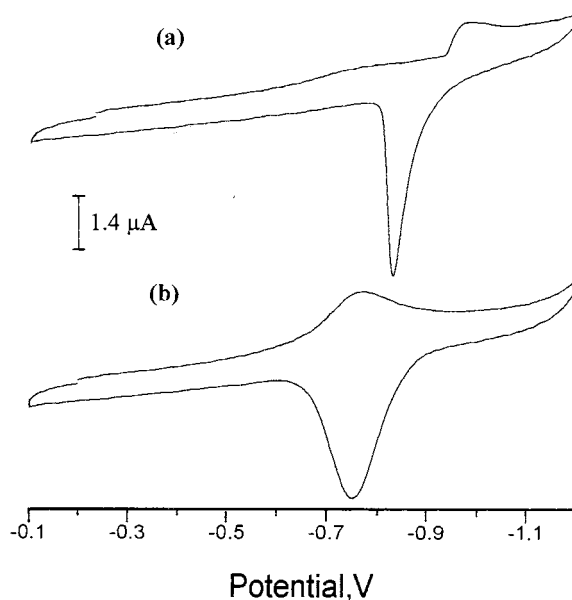


Fig. 1. Cyclic voltammograms for a 10 ppm thallium(I) solution containing 0.1 M NaNO₃ and 0.01 M EDTA: (a) at a glassy carbon electrode (GCE); (b) at the NMFE. Potential was scanned from about –0.2 to about –1.2 V and reversed to –0.1 V vs Ag/AgCl. Scan rate 100 mV s⁻¹.

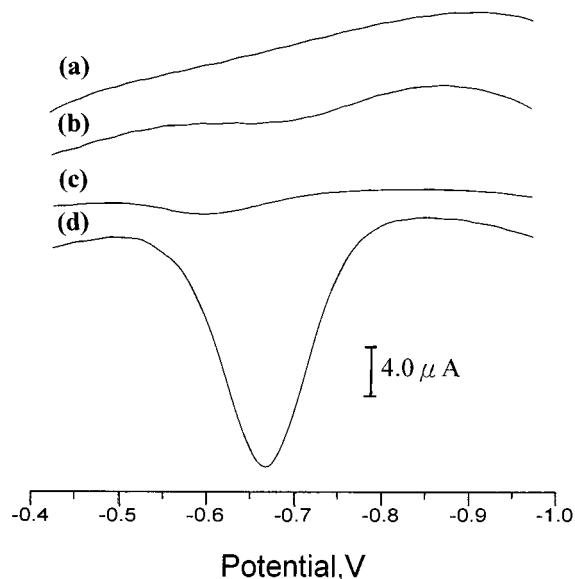


Fig. 2. SWSV for 10 ppb thallium(I) in the 0.1 M NaNO_3 + 0.01 M EDTA (pH = 4.5) solution: (a) on the bare GCE, (b) on the Nafion film coated GCE, (c) on the mercury film coated GCE and (d) on the Nafion/mercury film coated GCE. Pre-concentration potential, E_p , was -0.9V vs Ag/AgCl, and pre-concentration time, t_p , was 2 min. The SWSV was scanned from -1.0 to -0.4 V. SWSV parameter: modulation pulse height 50 mV, modulation frequency 200 Hz, effective scan rate 800 mV s^{-1} .

3.2. Effect of pH

For the NMFE, the optimum condition for thallium(I) accumulation was observed when the sample solution was slightly acidic (pH 4.5), as shown in Fig. 3. In the more acidic solutions, the SO_3^- sites of Nafion attract more proton ions and hold them inside the polymer matrix, and this would reduce its preconcentration ability for the thallium(I) cations. In the more basic solutions, however, the response of thallium(I) declines. Therefore, solutions of pH 4.5 were used in subsequent experiments.

3.3. Effect of preconcentration potential

The effect of preconcentration potential on the SWSV response for thallium(I) on the NMFE is shown in Fig. 4. This figure shows that between -0.6 and -0.9 V vs Ag/AgCl, the peak current

increases as the preconcentration potential becomes more negative. This behavior is not unexpected because thallium(I) bears a positive charge, and as a result the accumulation of thallium(I) is favored at more negative potentials. In addition, more negative potentials result in more complete reduction of the accumulated Tl(I), which may not be completely converted at less negative potentials. However, the peak current drops as the potential becomes more negative than -0.9 V. A preconcentration potential of -0.9V was therefore chosen in all subsequent work.

3.4. Effect of preconcentration time

The dependence of the thallium stripping peak current on the preconcentration time was studied with solutions of various thallium(I) concentration and the results are shown in Fig. 5. For higher concentration of thallium(I), (100 ppb), the peak current increase as the preconcentration time increases and starts to level off around 3 min. For a lower concentration of thallium(I) (10 ppb), it takes about 5 min for the current to level off. At even lower concentrations of thallium(I), (1 ppb), it takes more than 6 min for the peak current to level off. Apparently, the rate of thallium(I) uptake is dependent on concentration; higher concentration gradient enhances the diffusion of thallium(I) toward the NMFE during the accumulation and, thus, reaches the equilibrium state faster.

The relation between the peak current and the thallium(I) concentration with preconcentration time of 1 and 2 min, respectively, was also studied. For both cases, good linear relationship between the peak current and the thallium(I) concentration are obtained between 1 and 100 ppb of thallium(I). Since a longer preconcentration time give a better sensitivity, the preconcentration time of 2 min was chosen in all the subsequent work.

3.5. Effect of square-wave parameters

The square-wave parameters that were investigated were the frequency and the pulse height. These parameters together affect the peak shape

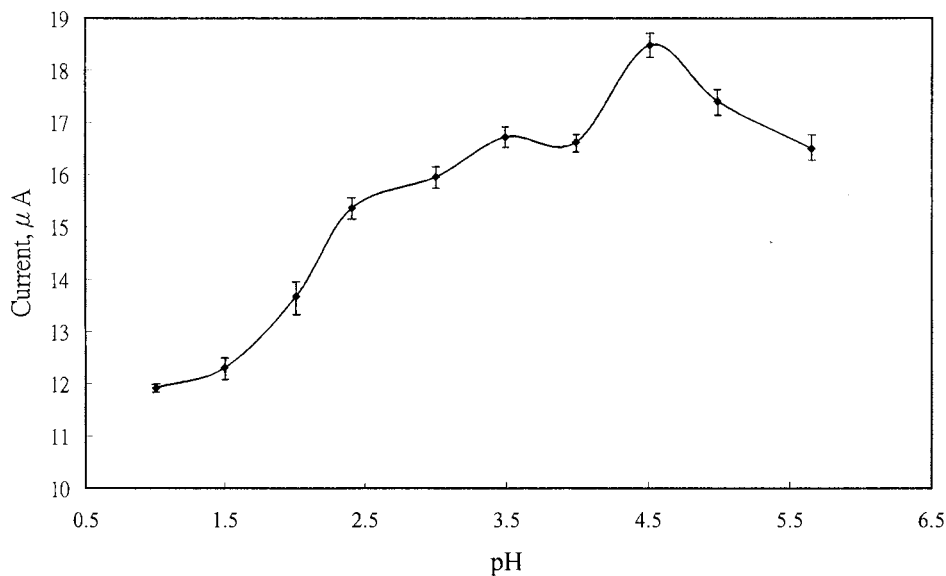


Fig. 3. Dependence of square-wave stripping peak height of 10 ppb thallium(I) (in 0.1 M NaNO_3 supporting electrolyte) on pH for Tl(I) determination obtained on NMFE. $E_p = -0.9$ V, $t_p = 1$ min. SWSV parameter: modulation pulse height 75 mV, modulation frequency 200 Hz, effective scan rate 800 mV s^{-1} .

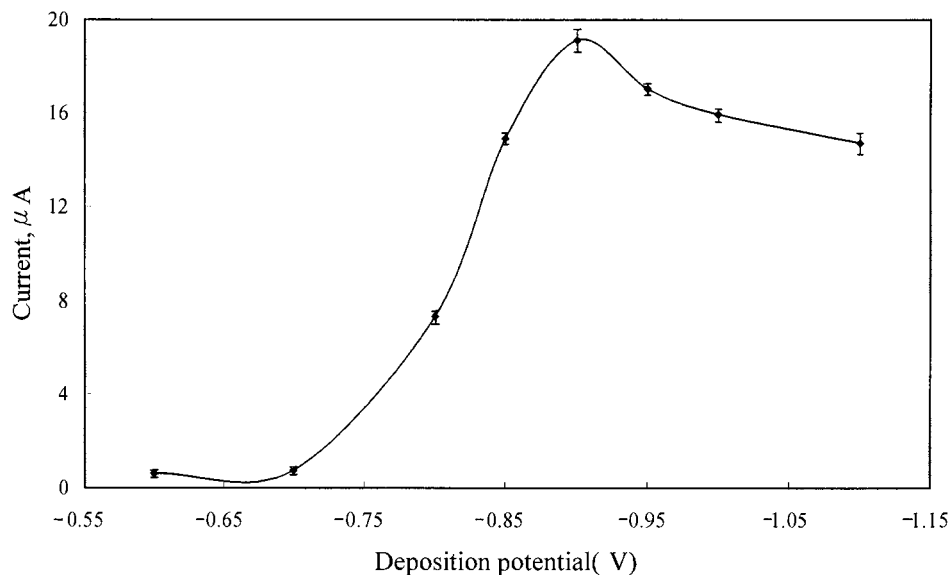


Fig. 4. Relation between the preconcentration potential (E_p) and the square-wave stripping peak height of 10 ppb thallium(I) recorded on the NMFE. Supporting electrolyte: 0.1 M NaNO_3 . The pH of the solution was 4.5 and $t_p = 1$ min. SWSV parameters as in Fig. 3.

and peak current of the thallium response. It is found that the response for thallium increases with increasing SWSV frequency up to 200 Hz,

which is the limit of the instrument. An increase in the pulse height up to 50 mV causes an increase in the thallium peak. When the pulse height is

higher than 65 mV the peak starts to broaden and finally peak split occurs when the pulse height reaches 100 mV. Overall, the best signal-to-background current characteristic can be obtained with the following instrumental settings: pulse height, 50 mV; frequency, 200 Hz, and effective scan rate 800 mV s^{-1} .

3.6. Effect of EDTA

The function of EDTA in this procedure is to reduce the interference from metal ions by taking advantage of its reaction with most interfering metal ions to form complexes that can not diffuse

onto the electrode surface. Fig. 6A shows the square wave stripping voltammograms for a solution containing 10 ppb thallium(I) and 1 ppm lead(II) before and after the addition of 0.01 M EDTA. Without EDTA, lead(II) produces a stripping peak at ca. -0.54 V which partially overlaps with the thallium(I) stripping peak. When EDTA is added to this solution, the lead(II) stripping peak is clearly removed. The efficacy of EDTA on reducing the interference from metal ion is further demonstrated in Fig. 6B with a 10 ppb thallium(I) solution containing 1 ppm of cadmium(II). This figure clearly shows that the thallium peak is completely buried in the cadmium peak when EDTA is not present in the solution. However, with the presence of EDTA, interference from the cadmium(II) is effectively suppressed while the thallium peak remains unaffected.

Although EDTA is an effective reagent for masking interfering metal ions, too much EDTA may cause the formation of EDTA–thallium chelate, and this would reduce the effective concentration of thallium(I) that can be detected by the NMFE. Thus, the effect of EDTA concentration on the response for thallium(I) was studied. The results showed that for a 10 ppb thallium(I) solution, EDTA does not cause any significant depression in the thallium peak current unless the EDTA concentration is higher than 0.01 M. At EDTA concentration higher than this value the thallium stripping peak current drops rapidly. Consequently, 0.01 M EDTA was used in this procedure.

3.7. Calibration

Calibration data were obtained under optimum experimental conditions mentioned above. Fig. 7 presents some of the typical SWSV voltammograms for the NMFE after have been in contact with thallium(I) for 2 min preconcentration time at concentrations of 0.05, 0.2, 0.5, 2, 5, and 10 ppb, respectively. In all cases a stripping response was observed at a potential in the vicinity of -0.75 V vs Ag/AgCl. A calibration graph was then constructed from the observed peak currents. The graph shows a very linear behavior with a slope (sensitivity) of $2.75 \mu\text{A ppb}^{-1}$, and a corre-

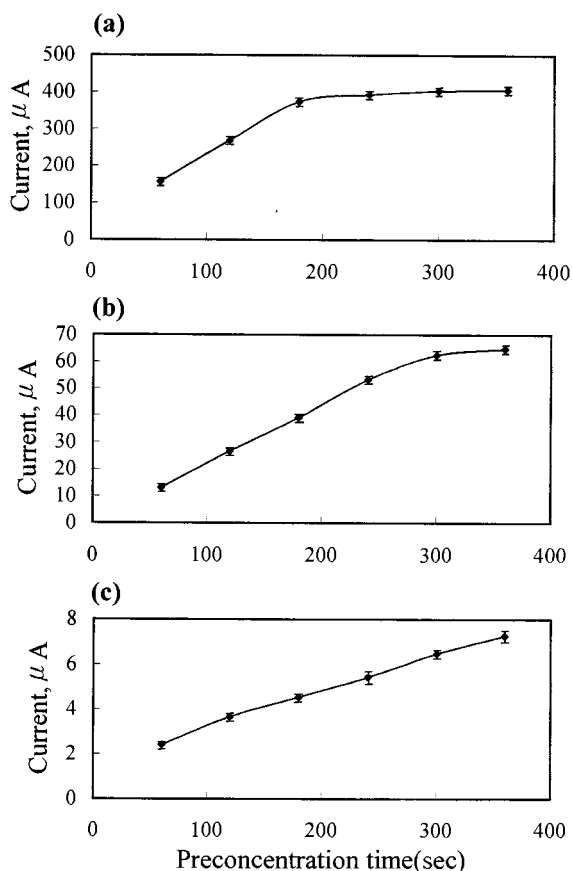


Fig. 5. Effect of preconcentration time on the square-wave stripping peak height of: (a) 100, (b) 10, (c) 1 ppb thallium(I) at the NMFE. The pH of the solution was 4.5 and $E_p = -0.9 \text{ V}$. Supporting electrolyte: 0.1 M NaNO_3 , SWSV parameters as in Fig. 2.

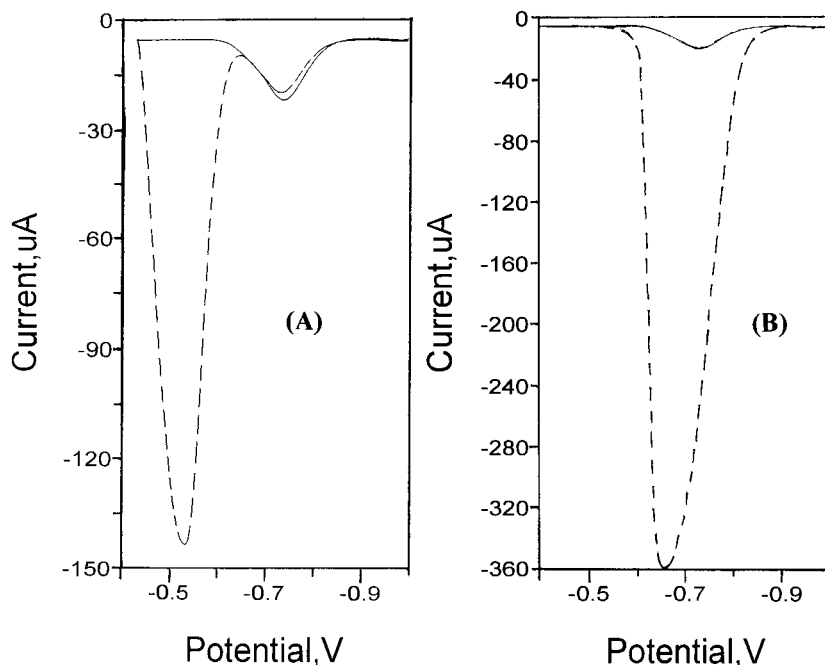


Fig. 6. Square-wave stripping voltammograms obtained at the NMFE for a 10 ppb thallium(I) + 0.1 M NaNO₃ solution containing (A) 1 ppm lead(II), and (B) 1 ppm cadmium(II). (---) without EDTA, (—) with 0.01 M EDTA. The pH of the solution was 4.5, $E_p = -0.9$ V, and $t_p = 2$ min, and SWSV parameters as in Fig. 2.

lation coefficient of 0.995. The linear range is between 0.05 and 100 ppb thallium(I). Peak current due to thallium(I) with a concentration as low as 0.05 ppb can be actually distinguished from the background current. This detection limit is comparable to or better than the detection limits offered by previous reports on voltammetric determination of thallium [6–10]. An even lower detection limit could be achieved for thallium(I) provided that the preconcentration time is longer than 2 min. For example, 0.01 ppb (5×10^{-11} M) thallium(I) can be detected with a preconcentration time of 5-min.

3.8. Interferences

Various ions were examined regarding their interference in the determination of thallium(I). For a bare MFE, any metal ions that can be reduced on the MFE and subsequently stripped at a potential close to that of the thallium(I) ion are likely interferents. However, the use of a NMFE

with the presence of EDTA in the sample solution successively minimizes such interferences. For 10 ppb thallium(I), the results showed that over 1000-fold excess concentration of germanium(IV), molybdenum(VI), magnesium(II), nickel(II), iron(III), zinc(II), selenium(IV), chromium(VI) and over 100-fold excess concentration of gold(III), copper(II), lead(II), and cadmium(II) can be tolerated (Table 1). Note that lead(II) and cadmium(II) are generally considered as the major interference in the determination of thallium on a bare mercury electrode. However, this problem can actually be greatly improved by the proposed procedure as indicated above.

The interference from surface-active compounds in stripping analysis using bare mercury electrode are well recognized. These compounds may adsorb on the electrode surface and reduces the analytical response of the analyte. Such interferences can be overcome by coating the electrode with Nafion. One of the function of the Nafion membrane coating on the mercury film electrode

is to prevent the organic interferences from reaching the interface at which the deposition and stripping takes place. In this study, the nonionic surfactant Triton X-100 and anionic surfactant SDS were used to simulate the effect of typical surfactants. Fig. 8 shows how the 10 ppb thallium(I) stripping peak current is affected by different concentration of Triton X-100 and SDS. As can be seen, the detection can tolerate the presence of both surfactants for at least up to 10 ppm with the NMFE (solid lines). Compared to the same experiments performed with a bare mercury electrode (dashed lines), the tolerance was greatly improved.

3.9. Electrode renewal

After each stripping analysis, the NMFE was renewed by immersing the electrode in 1 M nitric acid and regenerated at a potential of -0.4 V vs

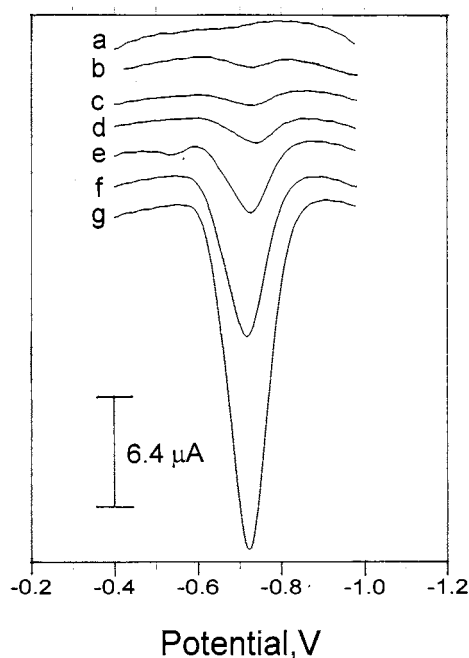


Fig. 7. Square-wave stripping voltammograms for increasing thallium(I) concentration of (a) 0, (b) 0.05, (c) 0.2, (d) 0.5, (e) 2, (f) 5 and (g) 10 ppb, respectively. The thallium(I) was preconcentrated at -0.9 V for 2 min in pH = 4.5 solutions. Supporting electrolyte: 0.1 M NaNO_3 and 0.01 M EDTA. SWSV parameters as in Fig. 2.

Table 1
Influence of other ions on the response of Tl(I)^a

Ions	Concentration excess over Tl(I)	Contribution (%) [$i_{\text{Tl(I)}} = 100\%$]
Ge(IV)	1000 ×	0.76
Mo(VI)	1000 ×	-4.15
Mg(II)	1000 ×	2.03
Ni(II)	1000 ×	-8.59
Fe(III)	1000 ×	-2.30
Zn(II)	1000 ×	-1.12
Se(IV)	1000 ×	3.43
Cr(VI)	1000 ×	0.16
Au(III)	500 ×	-2.66
Cu(II)	100 ×	-4.38
Cd(II)	100 ×	-3.33
Pb(II)	100 ×	1.39
SDS	1000 ×	-14.52
Triton X-100	1000 ×	-3.82

^a [Tl(I)] = 10 ppb

(Ag/AgCl) for about 30 s with stirring. This method showed an excellent reproducibility of the measurements, usually around 2.7% in terms of percent relative standard deviation for eight repetitive preconcentration/stripping/renewal experiments. Apparently, during this cleaning procedure, the residual thallium(I) from preceding deposition is removed from the NMFE by ion-exchange with the excess amount of proton.

3.10. Determination of thallium in real water samples

The analytical utility of the NMFE for the determination of thallium(I) was assessed by applying it to the determination of thallium(I) in tap water, ground water and rain water samples. No thallium was detected in all the three original water samples so they were spiked with appropriate amounts of thallium(I). The results collected in Table 2 are those for the original and spiked water samples. As can be seen, the recovery of the spiked thallium(I) is very good for all the three water samples, indicating that the proposed procedure is feasible for the determination of thallium(I) in different water samples. Note that the amount of thallium(I) in natural water is typically very low, and this is indeed the case in this study.

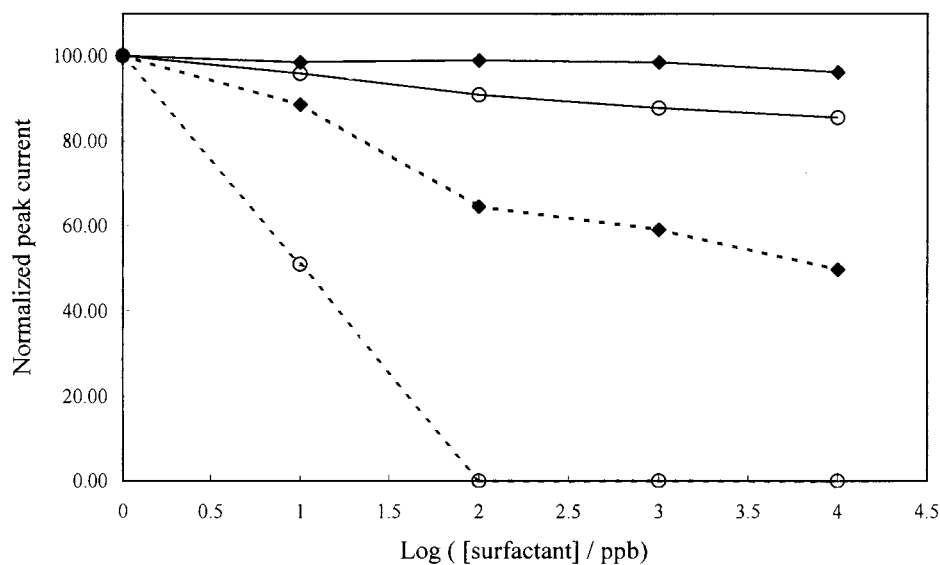


Fig. 8. Effect of the surfactants Triton X-100 (◆) and SDS (○) at different concentrations on the SWSV response for 10 ppb thallium(I) with the NMFE (—) and MFE (---). The thallium(I) was preconcentrated at -0.9 V for 2 min in $\text{pH} = 4.5$ solutions. Supporting electrolyte contains 0.1 M NaNO_3 and 0.01 M EDTA. SWSV parameters as in Fig. 2. Peak currents are given relative to those obtained with no added surfactants.

Table 2

Determination of Tl(I) in tap water, rain water and ground water samples^a

	Tap water	Rain water	Ground water
Detected value original	ND	ND	ND
Spiked (ppb)	0.3	1.0	1.0
Detected value after spike(ppb)	0.29 ± 0.02	0.98 ± 0.01	0.99 ± 0.04
Recovery (%)	97	98	99

^a Number of samples assayed = 4.

Consequently, the amount of thallium(I) in the original water samples assayed in this study can not be detected by the proposed procedure with 2 min preconcentration time. Nevertheless, it was found that the spiked 0.05 ppb thallium stripping peak could be actually seen for these samples with 5 min of preconcentration time, and the amount of thallium(I) in these original water samples was therefore believed to be well below 0.05 ppb.

Note that Nafion has unusually large selectivity coefficients for hydrophobic cations [16]. In real samples, such as biological materials, this may be a problem if these cations are not too bulky and will therefore be preferentially exchanged over Tl(I). Thus, the effect of such cations on the

determination of Tl(I) with the NMFE will be further studied.

4. Conclusions

The results show that the anodic SWSV determination of trace thallium(I) based on the preconcentration and subsequent stripping of thallium on a NMFE in the presence of EDTA is simple and effective. The proposed procedure not only yields good sensitivity with a short preconcentration time but also offers improved resistance to metal ions and organic surfactants interferences than a bare MFE. These advantages result mainly

from the ion-exchange property of Nafion, the good solubility of thallium in mercury, the good sensitivity of the square-wave voltammetry, and the chelating property of EDTA. The modified electrode is easily prepared and can be readily regenerated.

Acknowledgements

The authors gratefully acknowledge the financial support of the National Science Council of the Republic of China (Taiwan) under Grants NSC87-2815-C-006-073M.

References

- [1] J.P. Riley, S.A. Siddiqui, *Anal. Chim. Acta* 181 (1986) 117.
- [2] G. Jialong, G. Gang, L. Xilin, C. Tongyueic, *Talanta* 32 (1985) 1072.
- [3] C.M. Elson, C.A.R. Albuquerque, *Anal. Chim. Acta* 134 (1982) 393.
- [4] G.E. Batley, T.M. Florence, *J. Electroanal. Chem.* 61 (1975) 205.
- [5] J.E. Bonelli, H.E. Talyor, R.K. Skogerboe, *Anal. Chim. Acta* 118 (1980) 243.
- [6] J. Wang, J. Lu, *Anal. Chim. Acta* 282 (1993) 329.
- [7] I. Svancara, P. Ostapczuk, J. Arunachalam, H. Emons, K. Vytras, *Electroanalysis* 9 (1997) 26.
- [8] W. Diewald, K. Kalcher, C. Neuhold, X. Cai, R.J. Magee, *Anal. Chim. Acta* 273 (1993) 237.
- [9] Q. Cai, S.B. Khoo, *Analyst* 120 (1995) 1047.
- [10] Q. Cai, S.B. Khoo, *Electroanalysis* 7 (1995) 379.
- [11] B. Hoyer, T.M. Florence, *Anal. Chem.* 59 (1987) 2839.
- [12] T.R. Copeland, R.K. Skogerboe, *Anal. Chem.* 46 (1974) 1257A.
- [13] J. Wang, *Analytical Electrochemistry*, VCH, New York, 38 pp., 1994.
- [14] M. Lovric, M. Branica, *J. Electroanal. Chem.* 226 (1987) 239.
- [15] M. Lovric, S. Komorsky-Lovric, *J. Electroanal. Chem.* 248 (1988) 239.
- [16] M.W. Espenscheid, A.R. Ghatak-Roy, R.B. Moore III, R.M. Penner, M.N. Szentirmay, C.R. Martin, *J. Chem. Soc. Faraday Trans. 1* (82) (1986) 1051.

Lead selective lipophilic acyclic diionizable polyethers

Jong Seung Kim ^{a,*}, Moon Hwan Cho ^b, Sang Chul Lee ^b, Jin Hyun Pang ^a,
Joung Hae Lee ^c, Akira Ohki ^d

^a Department of Chemistry, Konyang University, Nonsan 320-711, South Korea

^b Department of Chemistry, Kangwon National University, Chuncheon 200-701, South Korea

^c Korea Research Institute of Standards and Science, Taejeon 305-606, South Korea

^d Department of Applied Chemistry & Chemical Engineering, Faculty of Engineering, Kagoshima University, Kagoshima 890, Japan

Received 29 July 1998; received in revised form 28 October 1998; accepted 9 November 1998

Abstract

A structural series of acyclic polyether dicarboxylic acids with *n*-butyl and *n*-tetradecyl alkyl side chains at the α -position of the carboxylic acid units, as well as varying lengths of the ethylene glycol ether linkage connecting two benzo units were prepared. In terms of stability constants, competitive solvent extraction and cation transport experiment by bulk liquid membrane toward transition metal ions, ligand **3** with a monoethylene glycol unit and *n*-butyl side chains provide the best selectivity for the lead ion. © 1999 Elsevier Science B.V. All rights reserved.

Keywords: Liquid membrane; Podand; Selective complexation; Solvent extraction

1. Introduction

Acyclic polyether (podand) chemistry has received a great deal of attention for many years, and various types of compounds have been synthesized [1–5]. Several studies have focused on determination of the selectivity and efficiency of the podand-mediated extraction or transport of metal ions through an organic medium into an aqueous receiving phase [6]. The complexation ability was markedly enhanced by the attachment of proton-ionizable groups, such as carboxylic,

phosphonic, and sulfonic acids functions, onto the crown ether backbone [7,8]. Metal ion extraction by such chelating agents does not require concomitant transfer of one or more aqueous phase anions into the organic medium. This factor is of immense importance for potential applications in which hard aqueous phase anions (chloride, nitrate, and sulfate) would be involved.

The development of chelating materials for the separation of toxic heavy metal ions from waste and processing solutions is also an important area of endeavor [9]. Especially, selective removal of Pb(II) in the treatment of acute and chronic lead poisoning has been regarded as one of the most urgent problems we have to solve [10–12]. For conventional chelating reagents, Cu(II) exhibits

* Corresponding author. Tel.: +82-461-730-5240; fax: +82-461-736-4078.

E-mail address: jongskim@kytis.konyang.ac.kr (J. Seung Kim)

the highest complexation in the Irving–Williams order [13]. However, a polymeric resin prepared from an acyclic dicarboxylic acid monomer was reported to give efficient and selective sorption of Pb(II) from aqueous solutions containing other heavy metal ions [14]. Recently, the Pb(II)-sensing ionophore **1** with hexyl side arms to increase the lipophilicity of the ligand at the aqueous surface was reported to show a good selectivity for Pb(II) over Cu(II) in a bulk liquid membrane transport experiment [15].

Based upon studies cited above, we have been interested in finding an optimum organic structure to selectively complex Pb(II). We have synthesized a series of acyclic polyethers dicarboxylic acids with varying **2–9** lengths of the ether linkage and lipophilicity to elucidate the extent to which the individual building blocks control the selectivity of complex formation with cations.

2. Experimental

2.1. Instrumentation and materials

Melting points were measured with a Mel-Temp or Fisher-Johns melting point apparatus without correction. IR spectra were obtained with a Perkin-Elmer 1600 Series FT-IR spectrophotometer using potassium bromide pellets and are recorded in reciprocal centimeters. ^1H NMR spectra were recorded with a 400 MHz (Bruker ARX-400) spectrometer, and the chemical shifts (δ) are reported downfield from the internal standard, tetramethylsilane. Unless specified otherwise, reagent grade reactants and solvents were obtained from chemical suppliers and used as received. Tetrahydrofuran was freshly distilled from sodium metal ribbon or chunks. Dichloromethane was freshly distilled from lithium aluminum hydride. A series of bisphenols are starting materials prepared by the reported methods [16]. Compounds **2** and **5** are known [17].

2.2. General preparation method

After removal of the protecting mineral oil

from NaH (50% dispersion in mineral oil, 6.00 g, 0.34 mol) by washing with pentane under nitrogen, a solution of the bisphenol (34.4 mmol) in 150 ml of dry THF was added. The mixture was stirred for 2 h at room temperature. The 2-bromoalkanoic acid (86.2 mmol) in 20 ml of dry THF was added dropwise at room temperature during a period of 2 h. Upon completion of the addition, the reaction mixture was allowed to stir for additional 10 h at room temperature. Careful addition of water to the reaction mixture in an ice bath to destroy the unreacted excess NaH, gave a homogeneous solution. The THF was removed in vacuo leaving an aqueous mixture. Into this basic solution was poured 100 ml of ethyl acetate to extract the unreacted bisphenol and organic impurities. The aqueous layer was washed with ethyl acetate (2×50 ml). Upon acidification with conc. HCl to pH 1, the crude product was extracted with methylene chloride (3×50 ml). The methylene chloride solution was dried over MgSO_4 and evaporated in vacuo to provide a colorless oil which was recrystallized from 100 ml of diethyl ether to give white crystals.

2.2.1. 1,2-Bis[2-(2'-carboxybutyloxy)-phenoxy]ethane (**3**)

Yield 92%. Mp 127–130°C. ^1H NMR (CDCl_3) δ 0.86 (t, 6H), 1.10–1.60 (m, 8H), 2.80–2.11 (m, 4H), 4.36 (s, 4H), 4.57 (t, 2H), 6.91 (s, 8H). IR (KBr, cm^{-1}) 3455 (O–H), 1711 (C=O).

2.2.2. 1,2-Bis[2-(2'-carboxytetradecyloxy)-phenoxy]ethane (**4**)

Yield 95%. Mp 108–110°C. ^1H NMR (CDCl_3) δ 0.77–1.00 (t, 6H), 1.10–2.00 (br s, 48H), 2.12–2.40 (m, 4H), 4.36 (s, 4H), 4.57 (t, 2H), 6.87–7.07 (m, 8H). IR (KBr, cm^{-1}) 3445 (O–H), 1713 (C=O).

2.2.3. 1,5-Bis[2-(2'-carboxybutyloxy)-phenoxy]-3-oxapentane (**6**)

Yield 90%. Mp 158–162°C. ^1H NMR (CDCl_3) δ 0.90 (t, 6H), 1.20–1.80 (m, 8H), 1.80–2.10 (m, 4H), 3.80–4.20 (m, 8H), 4.55 (t, 2H), 6.94 (s, 8H). IR (KBr, cm^{-1}) 3389 (O–H), 1703 (C=O).

2.2.4. 1,5-Bis[2-(2'-carboxytetradecyloxy)-phenoxy]-3-oxapentane (7)

Yield 93%. Mp 92–93°C. $^1\text{H NMR}$ (CDCl_3) δ 0.77 (t, 6H), 1.10–1.77 (m, 48H), 2.10–2.40 (m, 4H), 3.96 (m, 4H), 4.15–4.23 (m, 4H), 4.47 (t, 2H), 6.87–7.07 (m, 8H). IR (KBr, cm^{-1}) 3450 (O–H), 1710 (C=O), 1110 (C–O).

2.2.5. 1,8-Bis[2-(2'-carboxybutyloxy)-phenoxy]-3,6-dioxaoctane (8)

Yield 91%. Mp 97–99°C. $^1\text{H NMR}$ (CDCl_3) δ 0.93 (t, 6H), 1.20–1.71 (m, 8H), 1.77–1.88 (m, 4H), 3.57–4.50 (m, 14H), 6.85–7.12 (m, 8H). IR (KBr, cm^{-1}) 3430 (O–H), 1715 (C=O), 1106 (C–O).

2.2.6. 1,8-Bis[2-(2'-carboxytetradecyloxy)-phenoxy]-3,6-dioxaoctane (9)

Yield 90%. Mp 72–73°C. $^1\text{H NMR}$ (CDCl_3) δ 0.79 (t, 6H), 1.11–1.90 (m, 48H), 2.10–2.40 (m, 4H), 3.96 (m, 4H), 4.15–4.23 (m, 4H), 4.30–4.41 (m, 4H), 4.47 (t, 2H), 6.87–7.07 (m, 8H). IR (KBr, cm^{-1}) 3429 (O–H), 1710 (C=O), 1107 (C–O).

2.3. Potentiometric titration

Measurements of pH were made with an Orion Model 701A pH meter which could be read by 0.001 pH unit. The pH meter was standardized against oxalate buffer solution before each titration. For the sample solution, the ionic strength was adjusted to 0.10 M with tetramethylammonium perchlorate with the temperature at $25.0 \pm 0.1^\circ\text{C}$. Into a thermostat titration vessel equipped with a magnetic stirring bar, a glass combination electrode, and a microburet with 5.0 ml capacity, 50 ml of a 1.0 mM solution of the ligand in 90% methanol–10% water (by volume) was introduced. The tetramethylammonium hydroxide titrant concentration was 20.3 mM. A nitrogen atmosphere was maintained over the solution during the titration. Titrations were conducted in triplicate. Protonation and stability constants were calculated by the program Best [18].

2.4. Solvent extraction

The solvent extraction procedure was developed from that reported by Bartsch and co-workers [6]. For competitive extraction of transition metal nitrate solutions, a micro-extraction technique was used. An aqueous solution of transition metal nitrate (2.00 ml, 0.125 M with 0.2 M cesium hydroxide for pH adjustment) and 2.00 ml of 0.01 M organic ligand in chloroform in a 10-ml centrifuge tube were mixed with a vortex mixer for 5 min. After centrifuging, the equilibrium pH of the upper aqueous layer was measured. Then a 1.00-ml sample of the chloroform layer was taken and stripped with 1.00 ml of 0.1 M HCl solution. The concentration of metal ion extracted into an aqueous phase was determined by atomic absorption spectrophotometer.

2.5. Bulk liquid membrane transport

Membrane transport experiments were carried out at 25°C using a bulk liquid membrane cell based on the concept of the Schulman bridge [19,20]. The bottom half of the beaker was filled with 3.0 ml of 1.0 mM solution of the lipophilic acyclic polyether dicarboxylic acids in chloroform and a glass tube was inserted. The interior of the tube above the organic medium was filled with the source phase composed of 0.8 ml of a solution which was 0.010 M in metal acetate ($\text{M}^{2+}(\text{CH}_3\text{CO}_2)_2$) and 0.090 M in the transition metal nitrate. The outer cylinder is filled with 5.0 ml of 2.0 mM HNO_3 solution as the receiving phase. The details of the transport conditions are summarized in the footnotes for the single ion and competitive transport data listed in Tables 3 and 4, respectively. The receiving phase was sampled stirring for 24 h with 120 rpm at 25°C . The cation concentration in the receiving phase was determined with a Perkin-Elmer 2380 atomic absorption spectrophotometer.

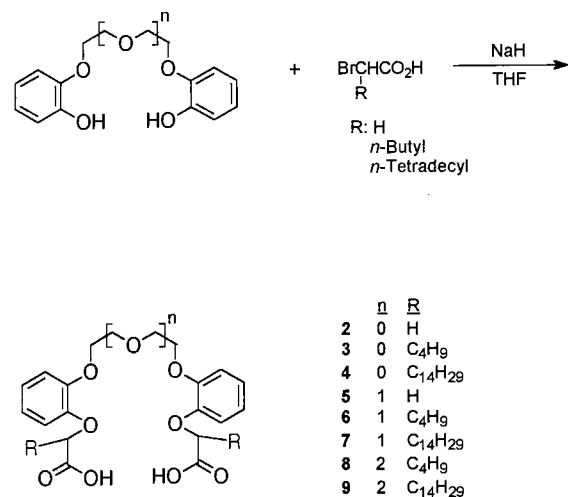
3. Results and discussion

3.1. Synthesis

The synthetic route for the preparation of acyclic polyether dicarboxylic acids is shown in Scheme 1. Bisphenols prepared from the reported method were used as starting materials [16]. Reaction of the bisphenol with 2.5 equivalents of 2-bromoalkanoic acid in the presence of 5 equivalents of sodium hydride as a base provided the crude acyclic polyether dicarboxylic acid. Recrystallization from diethyl ether gave the desired products as white solids in over 90% yields.

3.2. Complexation with transition metal ions

When a ligating agent complexes with a specific metal ion, the major factors which influence the stability constant are the radius of the metal ion, the oxidation state of the metal ion, the identity of the donor atoms, the solvation effect, the anion effect, and the dipolar interaction between the organic ligand and the metal ion [4]. For use in calculating the stability constant, protonation constants ($\log \beta_{\text{HL}}$) were measured and are presented in Table 1. Due to their high lipophilicity, the acyclic polyether dicarboxylic acids are not soluble in water. So, the protonation constant was



Scheme 1. Synthetic route for preparation acyclic polyether dicarboxylic acids 2–9.

Table 1

Protonation constants for acyclic polyether dicarboxylic acid in 90% (by volume) methanol–water mixture at 25°C and $\mu = 0.10$ M

Ligand	Log $\beta_{\text{HL}}^{\text{a}}$	Log $\beta_{\text{H2L}}^{\text{b}}$
2	4.51 ± 0.01	8.19 ± 0.02
3	4.92 ± 0.03	8.48 ± 0.02
5	4.63 ± 0.01	8.13 ± 0.02
6	5.63 ± 0.02	9.34 ± 0.01
7	5.68 ± 0.02	9.23 ± 0.04
8	5.98 ± 0.01	9.60 ± 0.04

^a Log β_{HL} is for the equilibrium: $\text{L}^{2-} + \text{H}^+ \leftrightarrow \text{HL}^-$.

^b Log β_{H2L} is for the equilibrium: $\text{HL}^- + \text{H}^+ \leftrightarrow \text{H}_2\text{L}$.

determined in 90% methanol–10% water (vol.%) at 25°C with $\mu = 0.10$ M. The obtained protonation constants are similar for the series of compounds. Variation of the length of the bridging unit which joins the two benzo units and the introduction of a butyl or side chains at the α -position of the carboxylic acid groups do not significantly affect the acidity.

Stability constants ($\log \beta_{\text{ML}}$) for the complexation of divalent transition metal cations by **2** and **5** were measured and are listed in Table 2. These ligands were chosen to evaluate the effect of the ring size of pseudocavity in the absence of lipophilic side groups. Both compounds show high stability constants for Pb(II) over the other transition metal ions. Interestingly, **2**, in which a monoethylene glycol unit connects the two benzo groups, has a higher stability constant than does **5** with a diethylene glycol bridging which shows that an acyclic polyether dicarboxylic acid with a monoethylene glycol unit provides a proper match with Pb(II). The order of stability constants is Pb(II) > Cu(II) > Zn(II) > Cd(II) \approx Mn(II) > Ni(II) > Co(II). The Pb(II) selectivity indicates that in a pseudo-cyclic conformation of the organic ligand, the monoethylene glycol unit fits Pb(II) to give maximized ion–dipolar and electrostatic interactions.

To further probe the influence of the lipophilicity and the polyether length in the organic ligand on metal ion complexation, competitive solvent extraction experiments of Cd(II), Cu(II), Pb(II) and Zn(II) were conducted with **3**, **4**, **6**, and **7**

Table 2

Stability constant for acyclic polyether dicarboxylic acids (**2** and **5**) with transition metal cations in 90% (v/v) methanol–water mixture at 25°C and $\mu = 0.1$ M

Compound	Log β_{ML}^a						
	Pb ²⁺	Cu ²⁺	Cd ²⁺	Zn ²⁺	Mn ²⁺	Co ²⁺	Ni ²⁺
2	7.35 ± 0.10	6.69 ± 0.08	4.70 ± 0.01	6.37 ± 0.05	4.83 ± 0.08	1.89 ± 0.05	3.67 ± 0.01
5	6.57 ± 0.04	5.49 ± 0.05	4.18 ± 0.04	4.45 ± 0.06	3.82 ± 0.02	3.10 ± 0.05	3.67 ± 0.02

^a Log β_{ML} is for the equilibrium: $M^{2+} + L^{2-} \leftrightarrow ML$.

which possess *n*-butyl or *n*-tetrabutyl lipophilic side groups. Solvent extractions with **2** and **5** which do not contain lipophilic side chains could not be conducted because of poor solubility of the ligand–metal complex in chloroform. The concentrations of extracted metal ions in competitive extraction usually increase with higher pH as shown in Fig. 1. The data presented in Table 3 shows a selectivity order of extracted metal ions by $Pb^{2+} > Cu^{2+} > Cd^{2+} > Zn^{2+}$ with total metal ion loadings exceeding 90% in all cases. Among the four ionophores, **3** which contains the monoethylene glycol bridging unit and *n*-butyl side chains, exhibits the highest Pb(II) selectivity. As the connecting ethereal linkage lengthens for **3** → **6**, the Pb(II)/Cu(II) selectivity decreases from 6.8 to 3.4. For **4** → **7**, the Pb(II)/Cu(II) selectivity decreases from 5.8 to 2.9. The high Pb(II)/Zn(II) noted for **3** and **4** decreases markedly for **6** and **7**. The Pb(II) extraction selectivity indicates that the

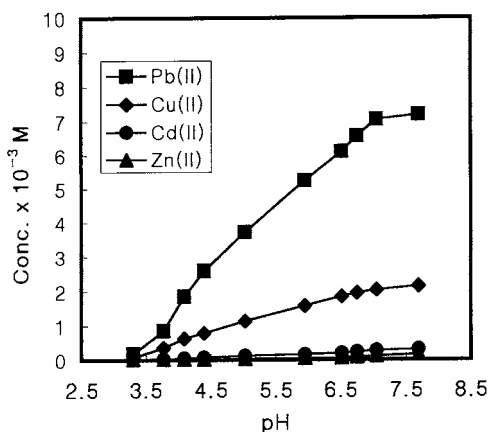


Fig. 1. Profiles for pH dependence of competitive solvent extraction using ligand **3**.

monoethylene glycol unit fits Pb(II) in a *wrapping around fashion* and two *n*-butyl side chains are lipophilic enough to make the ligand–metal complexes soluble in the organic layer. The more lipophilic compound **4** which has *n*-tetradecyl side chains exhibits diminished Pb(II) selectivity presumably because the side chains are too large and hinder metal ion complexation due to an unfavorable entropy effect [6].

To further study the influence of structural variation of acyclic polyethers with carboxylic acid groups on metal ion complexation, we have used a bulk liquid membrane system to transport metal ions an aqueous source phase into a receiving phase through an organic medium. The results of single ion transport experiments are shown in Table 4. For pH adjustment, LiOH has been used

Table 3

Selectivity and efficiency for competitive solvent extraction of transition metal cations from aqueous solution into chloroform by acyclic polyether dicarboxylic acids

Ligand	Selectivity order and selectivity coefficients ^a	Total loading (%) ^b
3	Pb(II) > Cu(II) > Cd(II) > Zn(II) 6.8 29.3 164	97.4
4	Pb(II) > Cu(II) > Cd(II) > Zn(II) 5.8 29.7 154	93.5
6	Pb(II) > Cu(II) > Cd(II) > Zn(II) 3.4 23.2 30	97.4
7	Pb(II) > Cu(II) > Cd(II) > Zn(II) 2.9 23.7 40	98.8

^a Mol ratio of extracted Pb(II)/transition metal cations at pH 7.5.

^b (Total loaded metal ion concentration)/(Ligand concentration) × 100(%).

Table 4

Transport rate of single transition metal cations by bulk liquid membrane^a containing acyclic polyether dicarboxylic acids

M ²⁺ Transport rate ($\times 10^{-8}$ mol s ⁻¹ m ⁻²) ^b	3	4	6	7	8	9
Pb ²⁺	246	218	194	127	127	114
Cd ²⁺	124	101	53	87	75	84
Cu ²⁺	81	71	84	87	75	69
Zn ²⁺	64	80	59	66	68	56
Mn ²⁺	46	41	21	38	– ^c	– ^c
Ni ²⁺	77	13	17	18	– ^c	– ^c
Co ²⁺	52	29	25	49	21	27

^a Transport condition: source phase (aqueous solution of metal nitrate, 0.8 ml) [M²⁺(NO₃)₂] 0.09 M + M²⁺(CH₃COO)₂ 0.01 M; membrane phase (CHCl₃ saturated with water, 3 ml), [carrier] = 1.0 mM; receiving phase (2.0 mM HNO₃ in water, 5.0 ml).

^b Reproducibility of the values is $\pm 10\%$ or better.

^c No transport was observed.

previously due to the low extractability of Li⁺ from aqueous solutions into chloroform by acyclic polyether dicarboxylic acid [6,7]. However, in this study, precipitation of a ligand–lithium ion complex took place on the surface of the membrane to give poor transport behavior. Therefore, transition metal acetates were used in the transport studies.

In control experiments carried out without an acyclic polyether dicarboxylic acids in chloroform layer, it was confirmed that no metal ion transport was observed in the absence of carrier. In all cases, Pb(II) was selectively transported over other transition metal ions. Considering the ethereal linkage length, as the polyether unit is lengthened from **3** to **6** to **8**, the Pb(II) transport rates gradually decrease, indicating that **3** with a monoethylene glycol with gives the best fit for the Pb(II). The same trends of decreasing transport rate were observed for compounds **4**, **7**, and **9** with two tetradecyl side chains. An influence of the lipophilicity of the organic ligand on metal ion complexation is also evident. In most cases, ligands with a shorter lipophilic tail (*n*-C₄H₉) exhibit more rapid transport of metal ions than do those with a longer tail (*n*-C₁₄H₂₉). The slow transport rate observed for carrier with tetradecyl side chains might be due to an unfavorable entropy effect as mentioned previously for the solvent extraction experiments [6].

The competitive transport experiment exhibits more interesting results as shown in Table 5. For example, with acyclic polyether dicarboxylic acid **3** and only a single divalent metal ion species present in the aqueous source phase, the transport rates for Pb(II) and Cd(II) were 247 and 124 (see Table 4), respectively, resulting in a Pb(II)/Cd(II) selectivity of 2. However, when both Pb(II) and Cd(II) ions are present in the aqueous phase (competitive experiment), Pb(II) gave almost same flux value, but the Cd(II) transport rate was markedly diminished, resulting in a Pb(II)/Cd(II) selectivity of nearly 200. For most combinations of ligand and metal ions, the selectivity for competitive transport is much higher than that for single ion transport experiment, although the selectivity order for Pb(II) in single and competitive experiments are not consistent.

These results suggest that acyclic polyether dicarboxylic acids have a potential for practical application in the removal of Pb(II) from industrial waste which may contain a variety of toxic, heavy and transition metal ions.

4. Conclusion

A series of acyclic polyether dicarboxylic acids in which the length of the ethereal linkage connecting the two benzo moieties is varied to contain mono-, di-, and triethylene glycol units and

Table 5

Competitive transport of Pb^{2+} and M^{2+} simultaneously by bulk liquid membrane^a containing acyclic polyether dicarboxylic acids

$\text{Pb}^{2+}/\text{M}^{2+}$	Transport rate ($\times 10^{-8} \text{ mol s}^{-1} \text{ m}^{-2}$) ^b					
	3	4	6	7	8	9
$\text{Pb}^{2+}/\text{Cd}^{2+}$	243/1.2	387/1.4	239/2.0	111/– ^c	164/0.4	195/0.9
$\text{Pb}^{2+}/\text{Cu}^{2+}$	180/19.3	349/10.4	177/42.9	124/5.8	164/20.5	175/16.7
$\text{Pb}^{2+}/\text{Zn}^{2+}$	199/0.8	415/0.3	219/1.8	139/0.2	162/0.22	199/0.28
$\text{Pb}^{2+}/\text{Mn}^{2+}$	206/0.6	419/5.2	234/– ^c	134/– ^c	199/– ^c	171/– ^c
$\text{Pb}^{2+}/\text{Ni}^{2+}$	199/0.8	399/– ^c	222/– ^c	131/– ^c	186/– ^c	179/– ^c
$\text{Pb}^{2+}/\text{Co}^{2+}$	250/1.1	454/– ^c	240/– ^c	137/– ^c	218/– ^c	183/– ^c

^a Transport condition: source phase (aqueous solution of metal nitrate, 0.8 ml) ($\text{Pb}(\text{NO}_3)_2$ 0.09 M + $\text{Pb}(\text{CH}_3\text{COO})_2$ 0.01 M) + ($\text{M}^{2+}(\text{NO}_3)_2$ 0.09 M + $\text{M}^{2+}(\text{CH}_3\text{COO})_2$ 0.01 M); membrane phase (CHCl_3 saturated with water, 3 ml), [carrier] = 1.0 mM; receiving phase (2.0 mM HN_3 in water, 5.0 ml).

^b Reproducibility of the values is $\pm 10\%$ or better.

^c No transport was observed.

α -groups of hydrogen, *n*-butyl, and *n*-tetradecyl were synthesized. In solution calorimetric titration, competitive solvent extraction, and single species and competitive ion transport across bulk liquid membranes, the acyclic polyether dicarboxylic acids show $\text{Pb}(\text{II})$ selectivity over other transition metal ions. Compound **3** with a monoethylene glycol unit and *n*-butyl side groups provides the best selectivity for $\text{Pb}(\text{II})$. The high $\text{Pb}(\text{II})$ selectivity and efficiency appear to arise from a unique combination of lipophilic group, number of polyether oxygens, and carboxylic end groups.

Acknowledgements

This study was fully supported by the academic research fund of Ministry of Education in South Korea.

References

- [1] D.J. Cram, N.K. Trueblood, Host guest complex chemistry, in: F. Vögtle, E. Weber (Eds.), *Macrocycles. Synthesis, Structures, and Applications*, Springer, New York, 1985.
- [2] B. Dietrich, P. Viout, J.-M. Lehn, *Macrocyclic Chemistry*, VCH, New York, 1993.
- [3] Y. Inoue, G.W. Gokel, *Cation Binding by Macrocycles. Complexation of Cationic Species by Crown Ethers*, Marcel Dekker, New York, 1990.
- [4] K. Hiratani, K. Taguchi, H. Sugihara, *J. Membr. Sci.* 56 (1991) 153.
- [5] F. Vögtle, E. Weber, *Angew. Chem. Int. Ed. Engl.* 18 (1979) 753.
- [6] W. Walkowiak, G.M. Ndip, D.H. Desai, H.K. Lee, R.A. Bartsch, *Anal. Chem.* 64 (1992) 1685.
- [7] R.A. Bartsch, G.S. Heo, S.I. Kang, Y. Liu, J. Strzelbick, *J. Org. Chem.* 47 (1982) 457.
- [8] R.A. Bartsch, I.W. Yang, E.G. Jeon, W. Walkowiak, W.A. Charewicz, *J. Coord. Chem.* 27 (1992) 75.
- [9] C. Kantipully, S. Katragadda, A. Chow, H.D. Gesser, *Talanta* 37 (1990) 491.
- [10] R.M. Izatt, J.S. Bradshaw, S.A. Nielsen, J.D. Lamb, J.J. Christensen, D. Sen, *Chem. Rev.* 85 (1985) 271.
- [11] R.D. Hancock, *Pure Appl. Chem.* 58 (1986) 1445.
- [12] K.V. Damu, M.S. Shaikjee, J.P. Michael, A.S. Howard, R.D. Hancock, *Inorg. Chem.* 25 (1986) 3879.
- [13] H. Irving, R.J.P. Williams, *J. Chem. Soc.* (1953) 3129.
- [14] K. Hiratani, H. Sugihara, K. Kasuga, K. Fujiwara, T. Hayashita, R.A. Bartsch, *J. Chem. Soc. Chem. Commun.* (1994) 319.
- [15] T. Hayashita, T. Husimoto, Y. Morita, R.A. Bartsch, *Chem. Lett.* (1994) 2385.
- [16] G.S. Hoe, Ph.D. Dissertation, Department of Chemistry and Biochemistry, Texas Tech University, TX, 1983.
- [17] J.S. Kim, M.H. Cho, S.C. Lee, Y. -I. Lee, W. Sim, N.S. Cho, *Microchem. J.* 55 (1997) 115.
- [18] A.E. Martell, R.J. Motekaitis, *Determination and use of stability constant*, VCH Publishers, New York, 1988, pp. 21–23.
- [19] G. Gokel, *Crown Ethers and Cryptands*, The Royal Society of Chemistry, London, 1991, p. 81.
- [20] S.S. Lee, J.H. Jung, S.H. Yu, M.H. Cho, *Thermochim. Acta* 259 (1995) 133.

Photochemical fluorescence enhancement of the terbium–lomefloxacin complex and its application

Zhang Tieli, Zhao Huichun *, Jin Linpei

Department of Chemistry, Beijing Normal University, P.O. Box 55, Beijing, 100875, PR China

Received 30 July 1998; received in revised form 27 October 1998; accepted 9 November 1998

Abstract

The sensitized fluorescence intensity of the terbium ion (Tb^{3+}) can be notably enhanced after the Tb^{3+} –lomefloxacin(LFLX) complex system was irradiated by 365nm ultraviolet light. A photochemical reaction occurs to the irradiated Tb^{3+} –LFLX complex. A new Tb^{3+} system with intense fluorescence is obtained. On this basis a new sensitive and selective photochemical fluorimetry for the determination of LFLX was established. Under the optimal experimental conditions, the linear range of the determination is 2.0 – 500×10^{-8} mol l^{-1} for LFLX, and the detection limit is 6.0×10^{-9} mol l^{-1} . Without any pre-treatment the recoveries of LFLX in human urine and serum were determined. © 1999 Elsevier Science B.V. All rights reserved.

Keywords: Terbium complex; Lomefloxacin; Photochemical fluorimetry; Body fluids

1. Introduction

Lomefloxacin (LFLX) is one of the synthetic antibacterial fluoroquinolone agents of the third generation (its chemical structure shown in Fig. 1.), which exhibits high activity against a broad spectrum of gram-negative and gram-positive bacteria. In consequence, it is of great importance to determine its contents in various biological samples, such as blood, urine and tissues.

At the moment, the detection of LFLX in biological fluids is usually performed by liquid chromatography method [1–3] and microbiologi-

cal assay method [4], which either needs an expensive equipment or is too time-consuming. Because the fluoroquinolone nucleus has the α -keto carboxylic skeleton, we attempted to explore the chelate formation between LFLX and lanthanides to give the narrow and intense fluorescence of the lanthanide ions [5,6] with the aim of improving the sensitivity and specificity by fluorimetric method. Of the lanthanide complexes with LFLX giving the native fluorescence of Ln^{3+} , the Tb^{3+} –LFLX complex can enhance the characteristic fluorescence of the Tb^{3+} . On investigating the sensitized fluorescence of the Tb^{3+} –LFLX complex, we surprisingly found that the sensitized fluorescence intensity of the Tb^{3+} was enhanced with the excitation time going on. This is because a photochemical reaction in the Tb^{3+} –LFLX

* Corresponding author. Tel. +86-10-6220-0567.

complex system takes place and the new fluorescent terbium complex formed facilitates energy transfer. On this basis, a new method—photochemical fluorimetry of lanthanide complexes was proposed for the determination of LFLX. The method has the advantages of both sensitized fluorescence of lanthanide ions and photochemical fluorimetry, with high selectivity and sensitivity. In this paper, detailed study of the appropriate conditions has been conducted for the determination of LFLX by this method, and satisfaction with the recoveries of LFLX in urine and serum samples was obtained.

2. Experimental

2.1. Apparatus

Fluorescence spectra were recorded with a Hitachi-850 spectrofluorimeter (Japan) equipped with a 150W xenon lamp. Absorption spectra were recorded on a Shimadzu-UV250 spectrophotometer, Japan. The pH measurements were made with a pH-2 meter, Shanghai. A ZF-1 Ultraviolet analytical meter (Shanghai) was used as the light source for irradiation.

2.2. Reagents

All of the reagents used were of analytical grade and distilled, de-ionized water was used throughout.

Stock standard solution ($1.00 \times 10^{-3} \text{ mol l}^{-1}$) of LFLX (Institute of Medical Biotechnology, Beijing) was prepared by dissolving 38.8 mg LFLX in an appropriate amount of water containing three drops of 0.1 mol l^{-1} NaOH solution and diluting to 100 ml with water, kept at 4°C and protected from light. The working standard solutions were obtained by appropriate dilution of the stock standard solution with water.

Stock standard solution of the Tb^{3+} ($1.00 \times 10^{-2} \text{ mol l}^{-1}$) was prepared by dissolving 186.9 mg Tb_4O_7 (purity, 99.99%) in hot (75°C) 1:1 HCl and evaporating the solution to be almost dry before diluting to 100 ml with water, stored in a plastic bottle, kept at 4°C . It was diluted to the desired concentration when used.

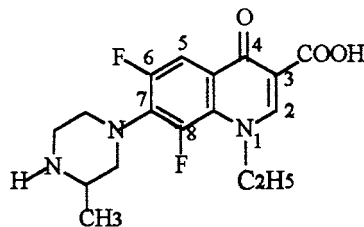


Fig. 1. Chemical structure of lomefloxacin.

0.2 mol l^{-1} acetic acid–sodium acetate buffer solution was prepared for pH 3.5–6.5, and pH 6.5–8.5 was obtained by buffering with 0.2 mol l^{-1} ammonium acetate–ammonia.

2.3. Procedure

Add a proper amount of standard LFLX solution, 0.40 ml of $1.00 \times 10^{-2} \text{ mol l}^{-1}$ standard Tb^{3+} solution and 5.0 ml of $\text{NH}_4\text{Ac-NH}_3$ (pH = 7.0) buffer solution to a 10 ml calibrated tube with a stopper, then dilute up to the mark with water before shaking. After the sample was irradiated for 30 min under a ultraviolet lamp at 365 nm with the irradiation intensity of 30 mw cm^{-2} , the difference of fluorescence intensities ΔI_F between sample and blank was determined using an excitation wavelength of 320 nm and monitored at the emission wavelength of 545 nm , with excitation and emission slits of 6 and 8 nm in width, respectively.

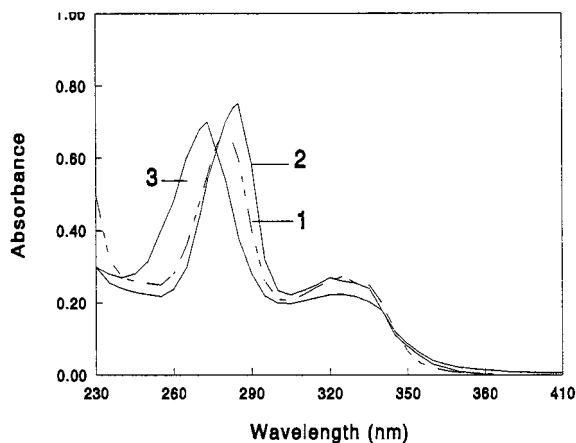


Fig. 2. Absorption spectra of LFLX and Tb^{3+} –LFLX systems in the ultraviolet region.

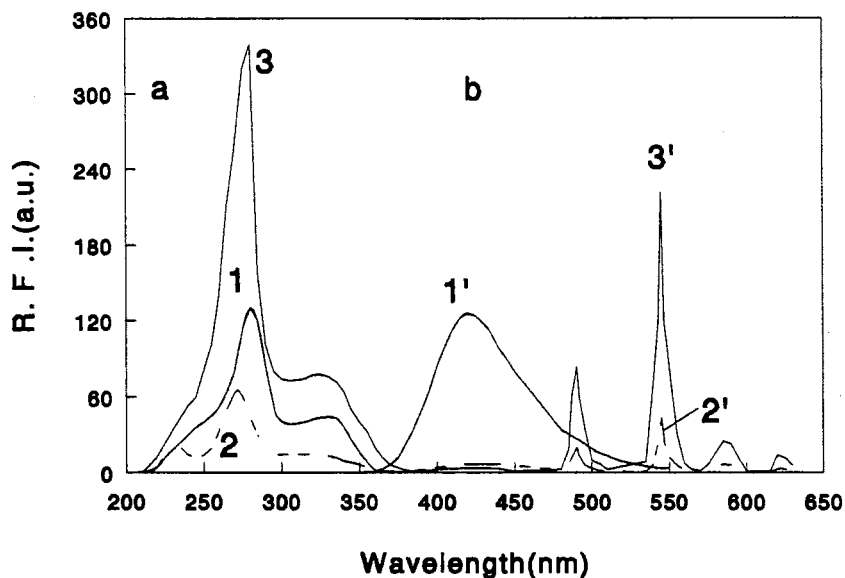


Fig. 3. Fluorescence excitation (a) and emission (b) spectra of LFLX and the Tb^{3+} -LFLX systems.

3. Results and discussion

3.1. Spectroscopic characteristics

The absorption spectra of LFLX and Tb^{3+} -LFLX systems with and without irradiation are shown in Fig. 2. From the curves 1 and 2, it can be seen that there are two absorption bands for each of them, but the absorption peak position has a slight red shift, from 280 nm of LFLX to 283 nm of the Tb^{3+} -LFLX, and the intensity of the latter increases. This suggests that the complexation of the Tb^{3+} and LFLX has occurred. From the curve 3, we can see that two absorption bands of the irradiated Tb^{3+} -LFLX system at 273 and 324 nm are observed, which are different from that of the non-irradiated Tb^{3+} -LFLX system. It implies that the absorption property of the Tb^{3+} -LFLX complex has been changed after it is irradiated by 365 nm ultraviolet light, i.e. the complex may have undergone photochemical reactions and some new absorption substances may have been produced in the process.

Fig. 3. shows the fluorescence excitation and emission spectra of LFLX and the Tb^{3+} -LFLX systems with and without irradiation. It can be

seen from the excitation spectra that the maximum excitation wavelengths are in the range of 270–280 nm for the three systems. But in order to avoid the direct excitation of the Tb^{3+} and the disturbance of the scattered excitation light at these wavelengths, the excitation was performed at the shoulder of the main excitation band, i.e. at 320 nm [7]. The emission spectra show that the native fluorescence emission wavelength of LFLX is 420 nm. After the Tb^{3+} -LFLX complex is formed, the band is red-shifted to 430 nm and this broad emission band decreases in intensity greatly while the narrow emission bands of the Tb^{3+} appear at 490, 545, 585 and 620 nm, corresponding to the transitions of the Tb^{3+} $^5D_4 \rightarrow ^7F_6$, $^5D_4 \rightarrow ^7F_5$, $^5D_4 \rightarrow ^7F_4$ and $^5D_4 \rightarrow ^7F_3$, respectively. Therefore, it can be concluded that the intramolecular energy transfer has occurred between LFLX and the Tb^{3+} . From the curve 3', it can be seen that in the irradiated Tb^{3+} -LFLX system the broad emission band at 420 nm arising from the ligand is further decreased and the sensitized fluorescence emission of the terbium ion is enhanced notably. This suggests that the new Tb^{3+} complex, the photoproduct, has a higher energy transfer effi-

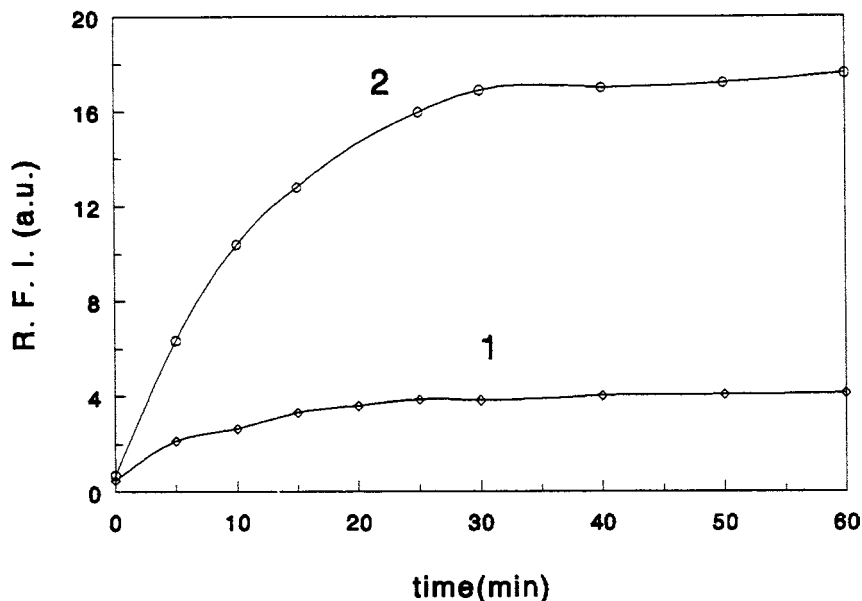


Fig. 4. Influence of irradiation time on the fluorescence intensity.

ciency than the Tb^{3+} -LFLX complex, i.e. the photoproduct is more favorable to intramolecular energy transfer. The further research is in progress. The detailed discussion will be reported in another paper.

3.2. Experimental conditions

Through our experiments it was found that the sensitized fluorescence intensity of the Tb^{3+} was increasing with lengthening the excitation time. In order to get the highest I_F value, the following factors were tested and the best experimental conditions were obtained.

3.2.1. The irradiation wavelength

Under the same conditions, the two wavelengths of the ultraviolet lamp, 254 and 365 nm, were tested as the irradiation wavelengths. It was found that the I_F value of the latter was about three times as high as the former. So 365 nm was selected as the irradiation wavelength in this work.

3.2.2. Influence of irradiation time

Fig. 4. Shows the influence of irradiation time

on I_F value. Irradiation intensity was set to 30 mw cm^{-2} . As shown in Fig. 4, the I_F value is increased notably with the irradiation time at the beginning, then slowly and becomes almost constant after 20–30 min. Two different concentrations of LFLX were tested. It was found that a little longer time was required when the concentration was higher. 30 min was selected as the irradiation time in this work.

3.2.3. Influence of pH and medium

Fig. 5. gives the relationship between the fluorescence intensity of the irradiated Tb^{3+} -LFLX complex and pH value. As shown, the maximum emission intensity was observed in the pH range of 7.0–7.5. At $\text{pH} > 8.0$, the sensitized fluorescence of the Tb^{3+} decreases, probably owing to the precipitation of terbium hydroxide[8]. And we also tested the effect of the following buffer solution media on the fluorescence intensity, NH_4Ac-NH_3 , Tris-HCl and $(CH_2)_6N_4-HCl$. It was found that the sensitivity in the NH_4Ac-NH_3 medium is the highest. Therefore, 5.0 ml of $0.2 \text{ mol l}^{-1} NH_4Ac-NH_3$ of pH 7.0 buffer solution was chosen.

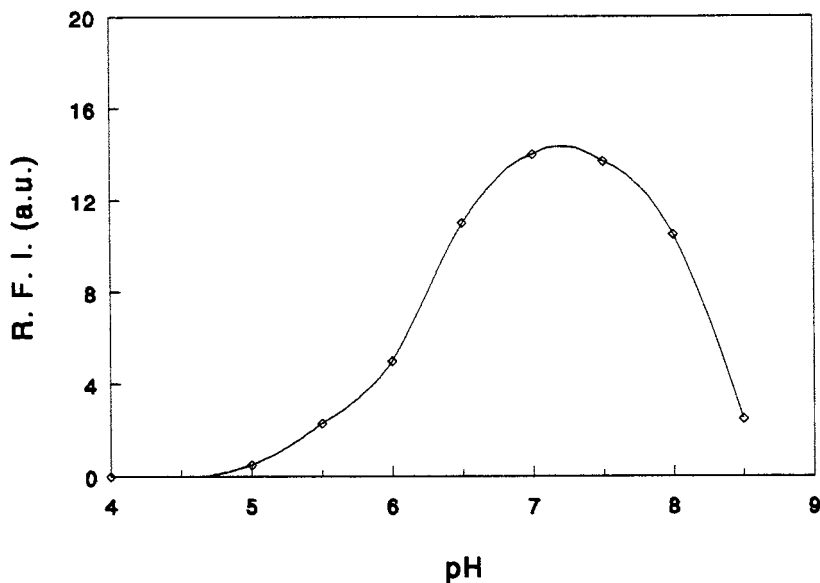


Fig. 5. Influence of pH on the fluorescence intensity.

3.2.4. Influence of the terbium concentration

Fig. 6. Shows the influence of the mole ratio of the terbium ion to LFLX on the fluorescence intensity. As we can see, the sensitized fluorescence intensity of the terbium ion is related to the mole ratio. The intensity increases with the increasing of the mole ratio and tends to be constant at a certain ratio (≥ 200). When the

concentration of LFLX is different, the ratio to get the maximum intensity is different, too. The lower the concentration of LFLX is, the higher the ratio required. For a fixed $2.00 \times 10^{-6} \text{ mol l}^{-1}$ LFLX concentration, $4.00 \times 10^{-4} \text{ mol l}^{-1}$ solution of the terbium ion gives an optimal emission. It was used in the calibration curve drawing.

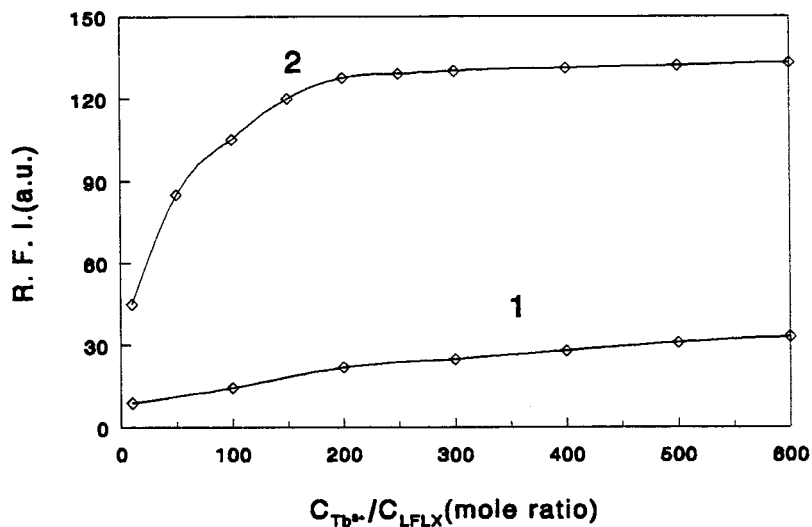


Fig. 6. Influence of Tb^{3+} concentration on the fluorescence intensity.

Table 1
Recovery of lomefloxacin added to urine and serum samples

Samples	LFLX added (mol l ⁻¹ , × 10 ⁻⁶)	LFLX found (mol l ⁻¹ , × 10 ⁻⁶)	Mean recovery (%)	R.S.D. (%)
Urine 1	0.40	0.383 ^a	95.8	3.4
Urine 2	0.80	0.777 ^a	97.2	3.2
Serum	0.020	0.0203 ^b	101.3	5.3

^a Average of nine experiments.

^b Average of five experiments.

3.3. Calibration curve and detection limit

According to the experimental method described above, values of ΔI_F were determined and the calibration curve was drawn, within the range of 2.00×10^{-8} – 5.00×10^{-6} mol l⁻¹ a linear relation was found between ΔI_F value and the LFLX concentration. The linear equation obtained by the least-square analysis was found to be $\Delta I_F = 0.0545 + 1.773 \times 10^6 C_{\text{LFLX}}$ (mol l⁻¹), with correlation coefficient $r = 0.9996$. The detection limit for LFLX was calculated from the standard deviation of the blank (the reagent blank without LFLX, $n = 19$) (3σ) as 6.0×10^{-9} mol l⁻¹LFLX.

3.4. Sample determination

After an oral administration of 400 mg of LFLX within 24 h the average concentrations of LFLX in the urine and serum samples were in the ranges of 332–41 and 3.98–0.20 mg l⁻¹ [9], i.e. 8.6 – 1.1×10^{-4} mol l⁻¹ and 100.0 – 5.1×10^{-7} mol l⁻¹, respectively. In order to make the sample concentrations of the drug within the linear range of determination, urine and serum samples were diluted 500-fold and 50-fold, respectively, and the recoveries of artificially synthetic urine and serum samples containing LFLX were determined by calibration curve method and standard addition method, respectively, and the spectral calibration was made to eliminate the background emission of the serum. The results obtained are shown in Table 1.

4. Conclusion

A new photochemical fluorimetric method for determination of LFLX has been established. Because of its high sensitivity, selectivity, accuracy and good repeatability, it has been successfully used in the determination of LFLX in urine and serum samples without any pre-handling but only by appropriate dilution of the samples. It is a simple and rapid method for determination of LFLX in body fluids.

Acknowledgements

The authors thank the National Natural Science Foundation of China for the financial support of this research.

References

- [1] A.M. Shibli, A.F. Tawfik, S. El-Houfy, F.J. Al-Shammary, *J. Clin. Pharm. Ther.* 16 (1991) 353.
- [2] G. Carlucci, A. Cilli, M. Liberato, P. Mazzeo, *J. Pharm. Biomed. Anal.* 11 (1993) 1105.
- [3] Y. Huang, Zh.W. Li, Zh. Hong, *Chin. Pharm. J.* 31 (1996) 417.
- [4] J.S. Lou, J.L. Zhang, C.L. Zhang, *Chin. J. Antibiotics* 19 (1994) 253.
- [5] T. Moeller, D.F. Martin, L.C. Thompson, R. Ferrus, G.I. Feistel, W.J. Rendall, *Chem. Rev.* 62 (1965) 1.
- [6] S. Schreurs, J.P.C. Vissers, C. Gooijer, N.H. Velthorst, *Anal. Chim. Acta* 262 (1992) 201.
- [7] A. Rieutord, L. Vazquez, M. Soursac, P. Prognon, J. Blais, Ph. Bourget, G. Mahuzier, *Anal. Chim. Acta* 290 (1994) 215.
- [8] J.X. Duggan, *J. Liq. Chromatogr.* 14 (1991) 2499.
- [9] Y.G. Shi, Y.J. Cao, L. Wang, Q.J. Zhang, Y.Y. Zhang, *Chin. J. Antibiotics* 19 (1994) 248.

A new selenite selective membrane electrode and its application

Güler Ekmekçi, Güler Somer *

Gazi Üniversitesi, Fen-Edebiyat Fakültesi, Kimya Bölümü, 06500, Ankara, Turkey

Received 24 June 1998; received in revised form 23 October 1998; accepted 10 November 1998

Abstract

A new membrane ion selective electrode sensitive to selenite ion has been developed. The electrode consisted of 1,2-phenylenediamine selen complex PIS (piaselenol) as the active material, PVC or SR (silicon rubber) as membrane matrix and DBF (dibutylphthalate) as plasticizer. This electrode showed linear response for selenite ion in the 10^{-5} – 10^{-1} M concentration range. The slope of the linear portion was 21 mV/10-fold change in selenite concentration. The effect of membrane composition and membrane thickness on electrode response was studied and the electrode which contains 2% PIS, 49% PVC and 49% DBF was found to be the most sensitive one to selenite. The slope of the electrode did not change for 2 months and the pH change did not affect the response of the electrode in pH range of 3–9. The interferences of SO_4^{2-} , SO_3^{2-} , S^{2-} , HPO_4^{2-} , Cl^- , Br^- , and I^- are investigated and while no interference was observed for SO_4^{2-} , SO_3^{2-} , S^{2-} and I^- , a very small interference was observed for Cl^- and Br^- . The selenium present in anodic slime is determined using this electrode. © 1999 Elsevier Science B.V. All rights reserved.

Keywords: Ion-selective membrane electrodes; Selenium; Anodic slime; Standard addition method

1. Introduction

Investigations about ion selective electrodes are steadily increasing. The rapid development of these electrodes reflect the extent to which these devices meet the need for accurate, cheap and

rapid analytical and control techniques. These electrodes are being used in clinical analysis and in routine control analysis of some cations and anions [1,2]. When porous material such as polyvinylchloride (PVC) or silicon rubber (SR) is impregnated with suitable substances, it forms the basis of a membrane for an ion selective electrode. Pungor successfully developed silicon rubber membrane as selective electrodes for halogenides and sulfide ions [3]. Silicon rubber membranes are reviewed by Pungor et al. [4]. Using PVC as the polymer matrix, electrodes sensitive for K^+ , Ca^{2+} and NH_4^+ ions are also developed [5–7].

* Corresponding author. Tel.: +90-312-212-6030; fax: +90-312-212-2279.

E-mail address: gsomer@quark.fef.gazi.edu.tr (G. Somer)

There are only a few investigations about selenite ion selective electrodes. Using picrate selective electrode, selenite could be determined indirectly [8–11]. This method is based on the catalytic effect of selenium on the reaction between picrate and sulphide. In another study a liquid membrane is prepared with the solution of 3,3-diaminobenzidine in hexane and selenite could be determined using this membrane [12]. The detection limit of this electrode was larger than 10^{-4} M for Se and the life time was shorter than 1 day. The measurements with liquid membrane electrodes are usually not easy, since the electrode potentials are easily affected by mechanical stirring and pressure changes. With a membrane electrode composed of 4,6-dibromopiaselenole as active material, PVC as a membrane matrix and DBF as plasticizer, a linear response was observed for selenite in 10^{-1} – 10^{-5} M concentration range. However the life-span of the electrode was only 1 week.

The present paper describes the development of selenite selective electrode using 1,2-phenylendiamin–Se complex as the active membrane constituent, PVC and silicon rubber (SR) as the membrane matrix. Interference studies have been made and it has been used for the determination of selenium in anodic slime.

2. Experimental

2.1. Apparatus and reagents

For the potentiometric measurements JENWAY 3030 Ion Analyzer was used. A double junction Ag/AgCl electrode 924036, was used as the outer reference electrode. As the inner reference home made Ag/AgCl electrode [13] is prepared. For the pH measurements the ion analyzer with 924005 combined pH electrode is used. All measurements were done in a 10-ml glass cell prepared for this purpose. A magnetic stirrer was used throughout the experiments. All reagents used were of analytical reagent grade (Merck) Triply distilled water was used for the preparation of solutions. The stock solution of 0.1 M Se IV was prepared by dissolving 2.63 g $\text{Na}_2\text{SeO}_3 \cdot 5\text{H}_2\text{O}$ in 100 ml of water.

2.2. Preparation of piaselelol (PIS) complex

In a 50.0 ml beaker, 0.6 ml 0.1 M Se IV solution and 5.0 ml of 0.5% (v/v) phenylenediamine are mixed (phenylenediamine is prepared in 1:1 ethanol–water solution). 40 ml of formate buffer (pH = 2.5) is added and the solution was heated at 50°C on a water bath. It is cooled down to room temperature and the complex is extracted in a separating funnel with 1.0 ml of toluene two times. The complex is washed with 15 ml of 2 M HCl two times. The solvent is evaporated at room temperature, the PIS crystals are formed in the bottom of the beaker.

2.3. Preparation of the electrode

2.3.1. PVC membrane electrodes

In a 50-ml beaker, with a diameter of 4.2 cm, 8–10 mg of PIS complex, 100–200 mg PVC dissolved in 5 ml THF (tetrahydrofuran) and 0.2–0.3 ml of DBF are mixed and stirred. The solvent is then allowed to evaporate at room temperature for about 24 h. The membrane formed as a film in the bottom is taken out carefully using a teflon forceps. This film membrane is cemented to the flat end of a PVC tube (1cm diameter) with an adhesive of PVC dissolved in THF. 1 day after, the excess membrane is cut and the tube is filled with 0.1 M Na_2SeO_3 and 0.1 M NaCl solution. Ag/AgCl electrode is immersed as the inner reference. The membrane electrode is immersed into a 10^{-5} M Na_2SeO_3 solution for about 2 days in order to condition the electrode.

2.3.2. Silicon rubber membrane electrode

For this purpose 10 ml beakers with flat and 2-cm diameter bottoms are used. First 4–16 mg of PIS complex and 170–350 mg siloprene K-1000 are mixed until PIS complex was homogeneously dispersed. Then 30–40 mg of cross-linking agent, Silopren K-11, is added. The solvent is allowed to evaporate for about 3 h at room temperature. The membrane is taken out carefully as a film from the beaker and is mounted on the end of glass tube with a silicon rubber sealant. After about $\frac{1}{2}$ h the excess membrane is cut from the edges of tubing and after about 1–2 h it is filled with 0.1

M Na_2SeO_3 and 0.1M NaCl solution and Ag/AgCl electrode is immersed as a inner reference electrode. The electrode has to wait for about 24 h in 10^{-5} M Na_2SeO_3 solution so that steady potentials can be obtained.

3. Results and discussion

3.1. Effect of matrix material

Calibration curves for PIS–PVC and PIS–SR electrodes in a concentration range of 10^{-6} – 10^{-1} M are prepared. For a fixed ionic strength all measurements were made in 0.1 M NaNO_3 solution. Potential readings obtained for two different electrodes at various selenite concentrations are plotted. As can be seen from Fig. 1, the slope obtained for the electrode prepared with PVC is smaller. While the slope between 10^{-5} – 10^{-2} M selenite concentration was 13.7 mV for PVC electrode, it was 20.7 for SR electrode. There were also sealing and splitting problems with PVC electrodes. Thus SR electrodes were preferred and used throughout the investigations.

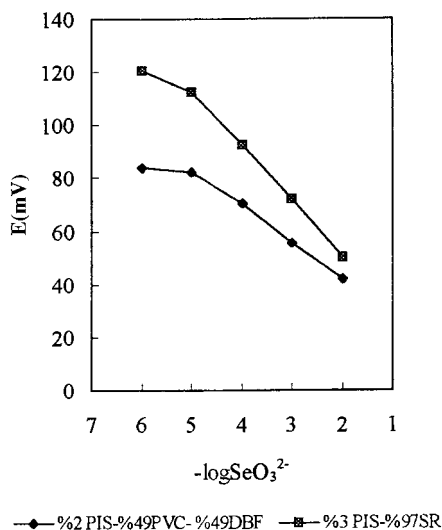


Fig. 1. Calibration curves of PIS–PVC and PIS–SR electrodes.

3.2. Effect of membrane composition and thickness

When membrane mixtures in different weight quantities were used in the same size beakers the thickness of membranes were also different. Membranes in 3% PIS, 97% SR composition but at different masses were prepared and they were used as the electrode material. For each electrode the potential responses were measured at different selenite concentrations. It was found that the electrode with a total mass of 0.2 g has the highest slope, the membrane thickness affects the response time of the electrode and thin membranes have shorter response times. It is not possible to obtain very thin membranes with every kind of matrix material. However SR material has good mechanical properties and very thin membranes could be prepared with no problems of splitting and breaking.

In order to investigate the effect of composition, electrodes in 0.2 g weight were prepared in different active material ratios. The responses of these electrodes and of the electrodes at different weights are summarized in Table 1. As can be seen the electrode with 3% of active material has better response than the others.

3.3. Effect of pH

Effect of pH on the potential readings at various selenite concentrations are also investigated. For this purpose 10^{-3} , 10^{-4} and 10^{-5} M selenite solutions are prepared and the pH is adjusted to certain values by the addition of HCl or NaOH using a pH meter. For each selenite concentration measured potentials at each pH values are plotted against pH. The potential readings remained unchanged within the pH range about 3–9 at various concentrations of selenite. There is a slight effect at higher and lower pH values.

3.4. The response time of the electrodes

The response time of the electrode in 3% PIS, 97% SR composition, is measured for different selenite concentrations. When the selenite concentration was increased from 10^{-3} to 10^{-2} it was

Table 1

Effect of membrane thickness and composition on the response of the electrode (Potentials are measured against Ag/AgCl reference electrode)

SeO ₃ ²⁻ (M)	0.2 g			%3 PIS 0.3 g E (mV)	%3 PIS 0.4 g E (mV)
	% 1 PIS E (mV)	% 3 PIS E (mV)	% 5 PIS E (mV)		
1.0 × 10 ⁻⁶	95.4	120.8	108.8	66.8	52.5
1.0 × 10 ⁻⁵	93.2	112.6	104.3	62.5	48.3
1.0 × 10 ⁻⁴	81.8	92.5	90.3	45.0	34.5
1.0 × 10 ⁻³	65.8	72.2	75.8	28.3	19.5
9.0 × 10 ⁻³ (~10 ⁻²)	55.9	50.3	59.3	11.4	6.7
10 ⁻⁶ –10 ⁻² M slope	10.6	18.1	12.8	14.5	12.0
10 ⁻⁵ –10 ⁻² M slope	12.8	20.7	14.9	17.0	13.9

about 3 min. When it changed from 10⁻⁴ to 10⁻³ it was 3 min and 15 s, for a change from 10⁻⁵ to 10⁻⁴ it was 4 min 30 s. The larger the change in concentration the larger is the response time, e.g. for a change from 10⁻⁵ to 10⁻² it is 7 min. The change of potential with time by the selenite ion additions at different concentrations are given in Fig. 2. As the stirring rate or temperature is increased, the response time will be shorter. This work is done at 20 ± 2°C at room temperature.

3.5. The lifetime of the electrode

The membrane surface loses its sensitivity because of the effect of interfering ions or some other ruining effect, such as mechanical rubbing. The membrane surfaces are cleaned by washing with distilled water or by waiting in 10⁻⁵ M SeO₃²⁻ solution for about 24 h. The lifetime of the electrode is found to be about 2 months when it is immersed into a 10⁻⁵ M SeO₃²⁻ solution for about 30 min after each measurement. The sensitivity of the electrode decreases after 2 months.

3.6. Interference studies

For the determination of selectivity coefficient separate solution methods and mixed solution methods can be used. However mixed solution

method is preferred as it usually corresponds more closely to the situation in samples. Here solutions are prepared with a constant activity of the main ion and varying activity of interfering ion. In this work interference studies are made for

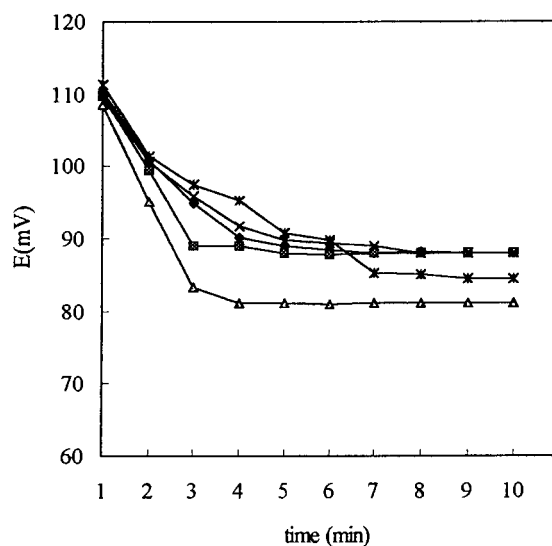


Fig. 2. The dependence of response time on the change of concentration.

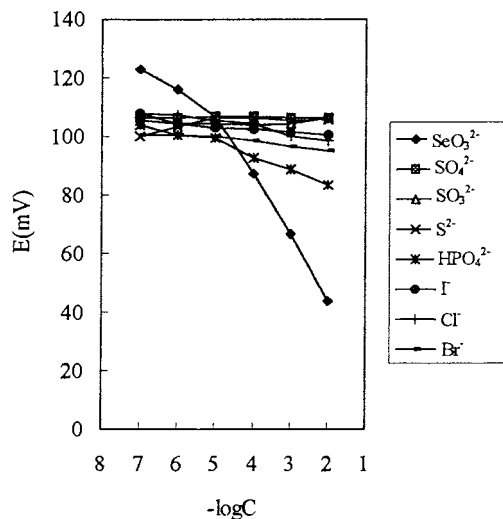


Fig. 3. The response of electrode against some anions.

SO_4^{2-} , SO_3^{2-} , S^{2-} and HPO_4^{2-} divalent anions and for Cl^- , Br^- and I^- monovalent ions. For this purpose the interfering ion in different concentrations is added to 10^{-5} M selenite ion solution and the change of potential for each addition is recorded. The results obtained are given in Fig. 3. As can be seen no interference is observed for SO_4^{2-} , SO_3^{2-} , S^{2-} and I^- but a very small interference is observed for Cl^- and Br^- ions. Mixed solution method is used [14] for the calculation of the selectivity coefficient in the presence of 10^{-5} M selenite ion. The equation used for this purpose can be given as

$$k_{A,B}^{\text{pot}} a_B^{n_A/n_B} = a_A \left\{ \text{antilog} \left[\frac{E_1 - E_2}{S} \right] \right\} - a_A \quad (1)$$

where $S = 2.303RT/n_A F$ (the slope of selenite electrode) a_A is the activity of the primary ion, a_B is the activity of the interfering ion, E_1 is the potential measured when only A is present, E_2 is the potential responsive to the primary ion in the

presence of interfering ion, $k_{A,B}$ is the selectivity coefficient and n_A , n_B the charges of A and B.

For the determination of the selectivity coefficient first the potential of 1×10^{-5} M selenite solution is measured (E_1), then in the presence of 10^{-5} M, 10^{-4} M, 10^{-3} and 10^{-2} M of interfering ions the potential values are once more recorded (E_2). The $a_B^{n_A/n_B}$ values are plotted against the right hand side of Eq. (1) and the slope will be equal to the selectivity coefficient of the interfering ion. The results are summarized in Table 2.

3.7. Determination of selenium of anodic slime

Anodic slime is an important source for selenium. During the electrolytic purification of copper it is collected at the bottom of anode compartment. Anodic slime contains Se, Te, Cu, Au, Pb, As and Sb. The level of selenium in anodic slimes is between 8 and 20%, copper is between 20 and 40% and Ag, Ni, Pb and Te in much smaller quantities, 0.3–3%. The newly developed membrane electrode is applied to some samples prepared from anodic slime. For this purpose about 1.0 g of anodic slime sample is dissolved in $\text{HCl} + \text{HNO}_3(1 + 3)$ mixture [15]. The acids are then evaporated nearly to dryness and it is diluted to 50.0 ml with distilled water. About the same amount of sample was dissolved only in HNO_3 to see the effect of solvent. From the sample solution prepared in HNO_3 0.05 ml is taken, 5 ml of 0.1M $\text{NH}_3\text{-NH}_4\text{Cl}$ buffer (pH = 8) and 1 ml NaNO_3 is added and it is diluted to 10.0 ml. The potential of this solution is measured using the new selenite selective electrode (3% PIS, 97% SR) against Ag/AgCl reference electrode. Then standard additions are made and the potential changes are recorded. From these potential values the quantity of selenium in the anodic

Table 2

Selectivity coefficients ($k_{A,B}^{\text{pot}}$) for the selenite electrode in mixed solutions (in the presence of 10^{-5} M SeO_3^{2-})^a

B	SO_4^{2-}	SO_3^{2-}	S^{2-}	HPO_4^{2-}	I^-	Cl^-	Br^-
$k_{A,B}^{\text{pot}}$	-2.7×10^{-5}	-2.5×10^{-4}	-3.4×10^{-4}	1.5×10^{-2}	6.3×10^{-2}	1.6×10^{-1}	1.6×10^{-1}

^a B, interfering ion; A, selenite ion in pH = 8–9.

Table 3

Determination of selenium in anodic slime using standard addition method (electrode: 3% PIS-97% SR)^a

Sample	$\Delta E_{\text{ave.}}$ (mV)	Calculated ave. $C_{\text{SeO}_3^-}$ (M)	Average % Se	$S = \sqrt{\frac{\sum(\bar{x} - x_i)^2}{N-1}}$	$CI^* = \bar{x} \pm \frac{t \cdot S}{\sqrt{N}}$
Digested in HNO ₃ (NH ₃ -NH ₄ Cl, pH = 8)	16.2	1.37×10^{-4}	10.8	0.7	10.8 ± 0.8
Digested in HCl+HNO ₃ (NH ₃ -NH ₄ Cl, pH = 8)	16.1	1.38×10^{-4}	10.9	1.1	10.9 ± 1.2
Digested in HNO ₃ (NaOH, pH = 6.5)	17.1	1.23×10^{-4}	9.4	0.4	9.4 ± 0.5

^a Number of samples, $N = 5$.

* 95% confidence interval.

Table 4

Percentage of selenium in anodic slime determined by four different methods

Method used	Weight percentage of selenium in slime
This work	10 ± 1
Volumetric [15]	10 ± 1
Spektrophotometric [16,17]	10 ± 1
Polarographic [18]	10 ± 1

slime is calculated. To check the pH effect the same solution is adjusted to pH = 6 with NaOH and again selenite concentration in the sample is determined.

The same experiment is repeated using the sample solution obtained by digestion with HCl + HNO₃. The selenite content is determined by standard additions. The results are given in Table 3, together with their standard deviations and 95% confidence interval. Each set is the mean of at least five determinations. As can be seen there is a good agreement with the results obtained for different digestion procedures and pH values. To check the validity of the results obtained with this electrode the same anodic slime was analyzed by volumetric [15], spectrophotometric [16,17] and polarographic [18] methods and the results are given in Table 4.

The electrode developed enables the determination of selenium in complex matrices such as anodic slime, it exhibits fairly good selectivity for

selenium IV over other ions, its lifetime is quite long if compared with the electrodes reported earlier. It can be used directly, there is no need for long and tedious separation procedures and there is no need for expensive instruments.

Acknowledgements

This investigation was supported by Gazi University Research Fund.

References

- [1] J. Wang, *Electroanalytical Techniques in Clinical Chemistry and Laboratory Medicine*, VCH, New York, 1988.
- [2] G.A. Junter (Ed.), *Electrochemical Detection Techniques in the Applied Biosciences*, Ellis Horwood, Chichester, UK, 1998.
- [3] E. Pungor, *Anal. Chem.* 39 (13) (1967) A28.
- [4] E. Pungor, K. Toth, *Pure Appl. Chem.*, Rev. 34 (1973) 105.
- [5] T. Satchwill, D.J. Harrison, *J. Electrochem.* 202 (1986) 75.
- [6] D.J. Harrison, L.I. Cunningham, X. Li, A. Teclemariam, D. Permann, *J. Electrochem. Soc.* 135 (1988) 2473.
- [7] S.C. Ma, N.A. Chaniotakis, M.E. Meyerhoff, *Anal. Chem.* 60 (1988) 2293.
- [8] E.D. Diamandis, T.P. Hadjiioannou, *Anal. Chim. Acta* 123 (1981) 143.
- [9] E.D. Diamandis, M.A. Koupparis, T.P. Hadjiioannou, *Microchem. J.* 22 (1977) 498.
- [10] W. Li, W. Shi, Q. Cai, *Huaxue Chuangang (China)* 1 (1985) 49.
- [11] W. Li, W. Shi, Q. Cai, *J. Huazhong Univ. Sci. Technol. (China)* 2 (1986) 269.

- [12] T.L. Malone, G.D. Christian, *Anal. Lett.* 7 (1974) 33.
- [13] G. Ekmekçi, Ph.D. Thesis, 1997.
- [14] K. Srinivasan, G.A. Rechnitz, *Anal. Chem.* 41 (1969) 1203.
- [15] H. Aydın, G. Somer, *Talanta* 36 (1989) 723–726.
- [16] G. Somer, G. Ekmekçi, *Anal. Sci.* 13 (1997) 205–208.
- [17] G. Somer, N. Kutay, *Can. J. Chem.* 71 (1993) 834–835.
- [18] E. Hasdemir, G. Somer, *Analyst* 115 (1990) 238.

Preparation and properties of solid state selenite ion selective electrodes and their applications

Güler Ekmekçi, Güler Somer *

Gazi Üniversitesi, Fen Edebiyat Fakültesi, Kimya Bölümü, 06500, Ankara, Turkey

Received 24 June 1998; received in revised form 23 October 1998; accepted 10 November 1998

Abstract

A new selenite ion selective electrode using solid salts of Ag_2Se and Cu_2S has been developed. Detailed information is provided concerning the composition, working pH and conditioning of the electrode. The change of potential with concentration is found to be linear in the range of 10^{-5} – 10^{-2} M, the slope of the linear portion is 28 mV/10-fold change in selenite concentration. The effect of other ions on selenite response is evaluated and selenium content of anodic slime is determined. © 1999 Elsevier Science B.V. All rights reserved.

Keywords: Ion-selective membrane electrodes; solid state membrane; selenium; anodic slime

1. Introduction

The use of ion selective electrodes has gained importance because of their ease of handling and their selectivities on specific ions. Silver salts of spare solubility are used mostly for their preparation. It was found that solid state electrodes prepared from silver halogenides were sensitive to halogenides, however these electrodes could also be used for the determination of some cations such as mercury [1,2] indirectly. Pungor et al. [3] could determine iodide ion in the presence of chloride ion using an electrode prepared from silver iodide and paraffin. It was found that the

electrodes made from two sulfide salts such as Ag_2S – PbS and Ag_2S – CdS were sensitive to lead and cadmium ions respectively [4]. The correlation found between the crystalline structure of the sensing material and the potentiometric response made possible the controlled preparation of several precipitate based electrodes such as cadmium, lead and copper selective electrodes [5–7]. The mixtures of less soluble salts such as Ag_2S , PbS , PbSO_4 and Cu_2S in different combinations when prepared as solid state pellet electrodes responded well against sulfate ion [8] and it was possible to determine 10^{-5} M sulfide. The response of the sulfide-selective electrode to sulfide, iodide and cyanide was investigated [9] and the slopes were found to be 57 mV for I^- , 28 mV for S^{2-} and 115 mV for CN^- . Linear responses were observed down to ca. 10^{-7} M solutions of these

* Corresponding author. Tel.: +90-312-212-6030; fax: +90-312-212-2279.

E-mail address: gsomer@quark.fef.gazi.edu.tr (G. Somer)

ions. Halide and sulfide selective electrodes were prepared using a slightly soluble silver salt together with silicon rubber [10] and linear relationship was observed in the range of 10^{-1} – 10^{-4} M with a slope of 30 mV per activity decade.

Although there are many investigations about pellet electrodes prepared from solid salts, non of these were subject for selenite ion determination. In this study we used Ag_2S , Ag_2Se , Ag_2SeO_3 and Cu_2S salts in different combinations in order to prepare a selenium sensitive electrode. These electrodes were investigated for their potentiometric response and selectivity to the selenite ion. In addition their optimum working conditions were studied. The selenite ion selective electrode is used for the determination of selenium content in anodic slime.

2. Experimental

2.1. Apparatus and reagents

Potential measurements were made with a HANNA HI 8521 pH meter. All potential values reported are taken with respect to an HI 5412 saturated calomel electrode which was hold in a Luggin–Haber capillary. Reagent grade chemicals were used without further purification. All solutions were prepared with triple distilled water. Stock 0.1 M solution of selenium was prepared by dissolving 2.63 g of $\text{Na}_2\text{SeO}_3 \cdot 5\text{H}_2\text{O}$ (Merck pro analysi) in 100.0 ml of distilled water.

pH 4 buffer: To 50.0 ml of 0.1 M potassium hydrogen phtalate, 0.1 M HCl is added until the pH was 4 and then it was diluted into 100.0 ml with distilled water.

pH 4 buffer: To 50.0 ml of 0.1 M sodium acetate 0.1 M acetic acid is added until the pH was 4 and then it was diluted into 100.0 ml with distilled water.

pH 6.5 buffer: To 50.0 ml of 0.1 M potassium hydrogen phosphate, 0.1 M NaOH is added until the pH was 6.5 and then it was diluted into 100.0 ml with distilled water.

pH 8.0 buffer: To 50.0 ml of 0.025 M borax solution 0.1 M HCl is added until the pH was 8.0 and then it was diluted into 100.0 ml with distilled water.

pH 8.0 buffer: To 50.0 ml of 0.1 M NH_4Cl , 0.1 M NH_3 is added until the pH was 8.0 and then it was diluted into 100.0 ml with distilled water.

2.2. Preparation of the electrodes

The solid salts used in the electrode composition, such as Cu_2S , Ag_2Se , Ag_2SeO_3 and Ag_2S , were prepared using analytical grade substances. Precipitated solid salts were dried and then mixed in different compositions. A certain amount of the salt or salt mixture (10–15 mg) was taken and pellets were made by holding first under a pressure of 5000 kg cm^{-2} for 5 min and then under a pressure of 8000 kg cm^{-2} for 10 min. The pellets of 7 mm diameter and 0.1–0.3 mm thickness were sealed with epoxy resin (0.7 g epoxy + 0.9 g hardener). To obtain a good sealing the epoxy resin on the edge of the tubing had to wait for about 10 min and then the pellet was sealed. One day after the pellet was sealed a silver wire is connected. For this purpose the inside of the glass tube was filled to about 1cm with a mixture of 0.5 g graphite powder and epoxy resin.

The electrode prepared had to wait for about 2 days so that the resin can get dry. The surface of the electrode is washed and then polished with a soft paper. These electrodes should wait in air and in a dark place when they are not in use. The lifetime of these electrodes can be at least 2 years, when they are used two times a day.

3. Results and discussion

3.1. Calibration curves of the electrodes

The potentiometric response of electrodes prepared in different compositions are investigated against selenite ion concentration. For this purpose appropriate spikes of 0.1 M selenite was introduced to the cell and corresponding potentials were recorded. For a fixed ionic strength all measurements were made in 0.1 M NaNO_3 solution. The potential readings were plotted against $-\log$ of selenite concentration. The slope of the electrode did not change for 6 months.

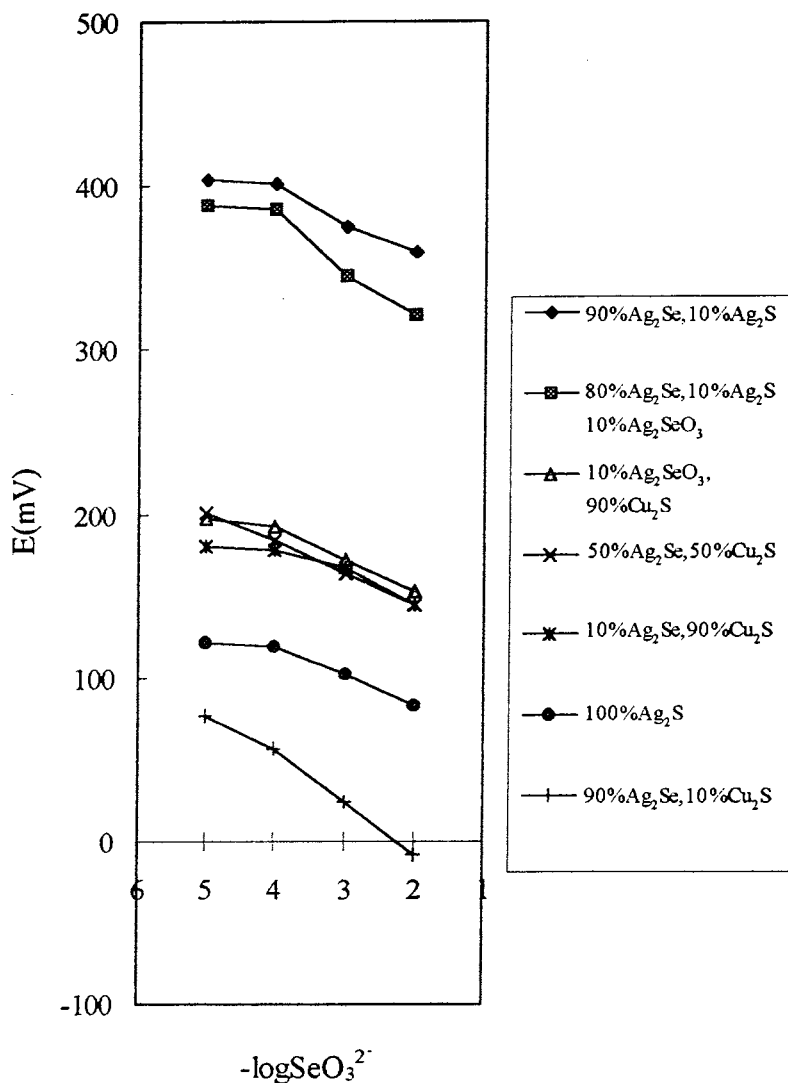


Fig. 1. Calibration curves for electrodes in different compositions. Potential measured vs. SCE (sat.) electrode with KNO₃ salt bridge.

3.2. Effect of electrode composition

The principal components of the electrode were Ag₂Se, Ag₂SeO₃ and Ag₂S. However it was important to incorporate Cu₂S to improve its dynamic properties [11,12]. It is known that the detection limit, selectivity and the maintenance of the electrode depends on its composition. In this study electrodes in different compositions were prepared and their potential responses were mea-

sured in the range of 10⁻⁶–10⁻² M selenite concentration for each ten times of concentration change. The calibration curves for various electrodes are given in Fig. 1. A linear relationship is obtained in the 10⁻¹–10⁻⁴ M concentration range. Because of practical reasons 10⁻¹ M selenite concentration is not included.

For each composition five electrodes were prepared and their responses were measured, their slopes as mV per activity decade are given in

Table 1
Calculated slopes for electrodes in different compositions

% Composition	10^{-5} – 10^{-2} M average slope	$S = \sqrt{\frac{\sum(\bar{x} - x_i)^2}{N-1}}$	$CI^* = \bar{x} \mp \frac{t \cdot S}{\sqrt{N}}$
%90 Ag ₂ Se,%10 Cu ₂ S	27.8	1.17	27.8 ± 1.4
%50 Ag ₂ Se,%50 Cu ₂ S	16.4	0.36	16.4 ± 0.4
%10 Ag ₂ Se,%90 Cu ₂ S	10.1	1.04	10.1 ± 1.3
%10 Ag ₂ SeO ₃ ,%90 Cu ₂ S	14.5	0.56	14.5 ± 0.7
%10 Ag ₂ S,%90 Ag ₂ Se	15.3	0.90	15.3 ± 1.1
%10 Ag ₂ S,%80 Ag ₂ Se,%10 Ag ₂ SeO ₃	21.5	2.11	21.5 ± 2.6
%100 Ag ₂ S	9.1	2.56	9.1 ± 3.1

* Five electrodes for each composition, $N = 5$; %95 confidence interval.

Table 1. As can be seen two of these electrodes one in 90% Ag₂Se, 10% Cu₂S composition and the other in 80% Ag₂Se, 10% Ag₂SeO₃, 10% Ag₂S composition showed the highest slope against selenite ion. The slopes obtained for only seven electrodes in different compositions could be given in Table 1. Although more different compositions were used for the electrodes some of them could not be used since they were easily breakable. These were mostly electrodes with higher percentage of Ag₂SeO₃ such as 90% Ag₂SeO₃, 10% Cu₂S and 33% Ag₂SeO₃, 33% Ag₂Se, 33% Cu₂S. It was found that when Ag₂SeO₃ ratio was higher than 10% the pellets were breakable.

To obtain better conductivity Cu₂S or Ag₂S is mostly used in pellet electrodes, it is also known

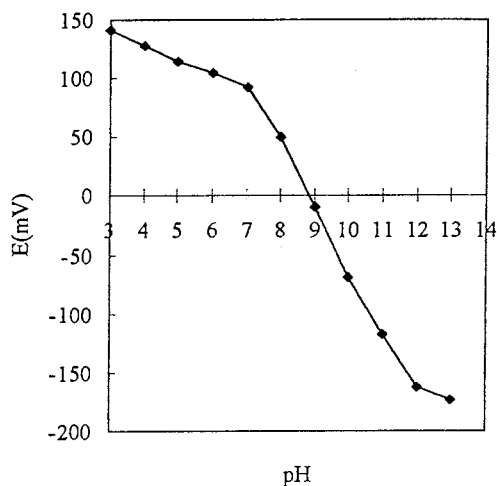


Fig. 2. pH dependence of 90% Ag₂Se, 10% Cu₂S electrode.

that Cu₂S enhances the dynamic properties [11] of these kind of electrodes. According to our investigations electrodes without Cu₂S and Ag₂S are not stable mechanically. In our further studies such as the effect of pH interference of some ions we used the electrode in 90% Ag₂Se and 10% Cu₂S since it had the highest slope.

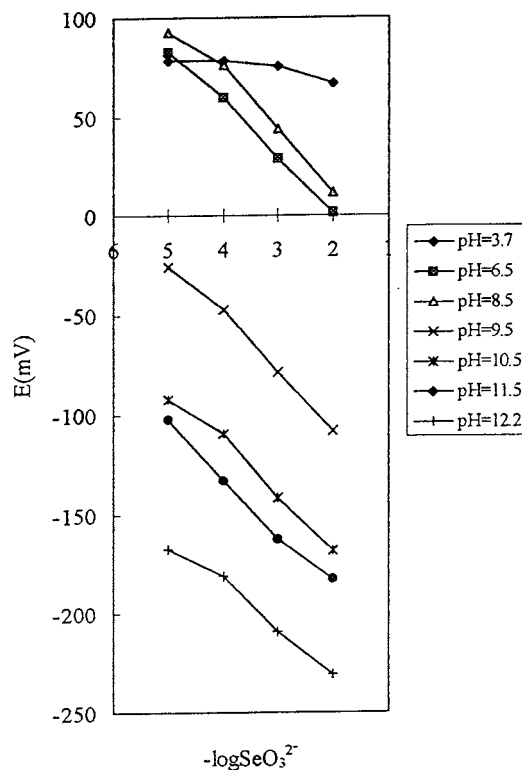


Fig. 3. The change of potential with selenite concentration at various pH values (Electrode: 90% Ag₂Se, 10% Cu₂S).

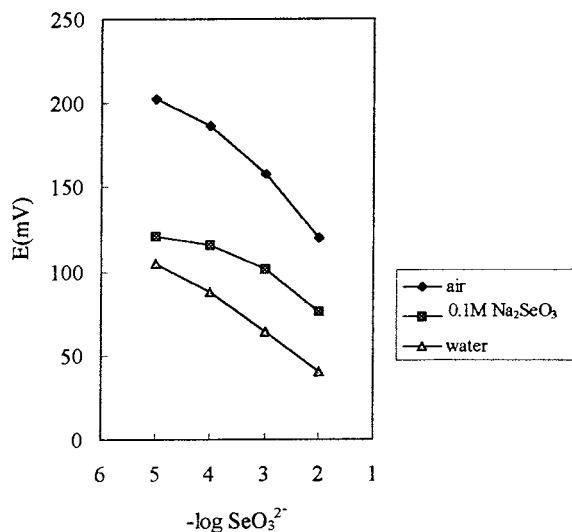


Fig. 4. The effect of medium on the slope of the electrode.

3.3. Effect of pH

In order to study the effect of pH on the response of the electrode, solutions at different pH values (measured with a pH meter) were prepared. The pH was adjusted by the addition of HCl or NaOH to distilled water which contained 0.1 M NaNO₃. The potential of the electrode is measured against saturated calomel electrode. The results obtained for different pH values are given in Fig. 2.

As it is observed this electrode is sensitive to OH⁻ ions. Between the pH values of 7 and 13 there is a linear relationship between the OH⁻ concentration and potential values with a slope of 53 mV. The response of the electrode to OH⁻ ions is also investigated in different fixed selenite concentrations. The same slope was observed for OH⁻ ion at selenite concentrations changing from 10⁻² to 10⁻⁴M. Since with ordinary glass electrodes measurement of high pH values bring alkaline error, this electrode may be used for the measurement of high pH values also.

The response of the electrode against selenite concentration is measured at different pH values. Mostly pH buffers are used for this purpose. The pH was adjusted to 3.7 using phtalic acid–phtalate buffer, pH 6.5 was obtained with potassium

dihydrogen phosphate, pH 8 could be fixed by borax or NH₃/NH₄Cl buffers and pH values higher than 9 was obtained with NaOH. The variation of potential against selenite concentration at different pH values are given in Fig. 3. Each point on the curve is at least a mean of 5 measurements. The slope was the smallest for pH 3.7. However, in the pH range of 7–13, the slope was changing from 26 to 28 mV (10⁻²–10⁻⁵ M selenite) with correlation coefficients changing from $r = 0.9934$ to 0.9987. Since at these pH values the electrode was also sensitive to OH⁻ ion the response of the electrode has to be measured at fixed pH values.

3.4. Conditioning of the electrode

The electrodes in 90% Ag₂Se and 10% Cu₂S composition were left in air (in dark), in distilled water and in 0.1 M Na₂SeO₃ solution under same

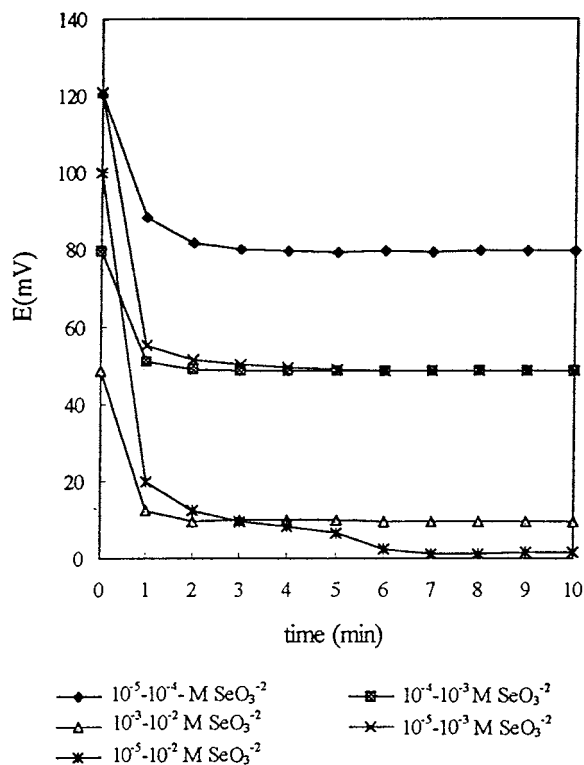


Fig. 5. The dependence of response time of the electrode on the change of concentration.

Table 2

Change of potential with the concentration of interfering ion for the selenite electrode measured in the presence 10^{-5} M selenite

C_B (M)	Potentials of interfering ions (C_B) (mV)						SeO_3^{2-} potentials in the absence of C_B (mV)
	Cl^-	Br^-	I^-	S^{2-}	SO_3^{2-}	SO_4^{2-}	
1.0×10^{-5}	78.6	80.7	76.9	45.8	73.7	79.5	76.5
1.0×10^{-4}	78.2	80.2	76.3	16.5	70.6	79.3	56.0
1.0×10^{-3}	75.6	77.6	70.8	-15.5	68.4	78.1	23.8
9.0×10^{-3} ($\sim 10^{-2}$)	67.0	65.3	56.2	-48.3	33.4	70.5	-6.5
10^{-5} – 10^{-2} M slope	3.7	4.8	6.7	31.4	12.4	2.8	28.1
10^{-3} – 10^{-2} M slope	8.6	2.6	14.6	32.8	35.0	7.6	30.3

Table 3

Selectivity coefficients ($k_{A,B}^{\text{pot}}$) for the selenite electrode in mixed solutions^a

B	Cl^-	Br^-	I^-	S^{2-}	SO_3^{2-}	SO_4^{2-}
$k_{A,B}^{\text{pot}}$	1.5×10^{-1}	4.3×10^{-1}	4.1×10^{-1}	28.9	3.4×10^{-2}	8.5×10^{-4}

^a B, interfering ion; A, selenite ion in pH = 8–9

duration of time and then their responses to selenite ion were measured. As can be seen from Fig. 4 the electrodes left under air had higher slopes.

3.5. The response time of the electrodes

The response time of the electrode depends to the concentration change. If the concentration of SeO_3^{2-} was changed from 10^{-5} to 10^{-4} M by standard addition, the response time was about 2 min and 15 s. For a change of concentration from 10^{-4} to 10^{-3} M response time was 1 min and 15 s and from 10^{-3} to 10^{-2} M the response time was only 1 min. The responses of the electrode for different concentration changes are shown in Fig. 5. All these measurements were made at constant temperature.

3.6. Interference studies

Possible interferences by a number of monovalent (Cl^- , Br^- , I^-), divalent (S^{2-} , SO_3^{2-} , SO_4^{2-}) ions and some cations (Cu^{2+} , Ag^+) were studied. For this purpose the potential readings of these ions at different concentrations in the presence of 10^{-5} M selenite were recorded. The slopes per activity decade are given in Table 2. As it can be

observed Cl^- and Br^- ions show nearly no sensitivity when they are in 10^{-5} – 10^{-2} M concentration range. The selectivity constants are determined by using the mixed solutions method [13] in the presence of 10^{-5} M SeO_3^{2-} ion. The equation used for this purpose can be given as

$$k_{A,B}^{\text{pot}} a_B^{n_A/n_B} = a_A \left\{ \text{antilog} \left[\frac{E_1 - E_2}{S} \right] \right\} - a_A \quad (1)$$

where $S = 2.303RT/n_A F$ (the slope of selenite electrode) a_A is the activity of the primary ion, a_B is the activity of the interfering ion, E_1 is the potential measured when only A is present, E_2 is the potential responsive to the primary ion in the presence of interfering ion, $k_{A,B}^{\text{pot}}$ is the selectivity constant and n_A , n_B the charges of A and B.

For the determination of the selectivity constants first the potential of 1×10^{-5} M selenite solution is measured (E_1), then in the presence of 10^{-5} M, 10^{-4} M, 10^{-3} and 10^{-2} M of interfering ions the potential values are once more recorded (E_2). The $a_B^{n_A/n_B}$ values are plotted against the right hand side of Eq. (1) and the slope will be equal to the selectivity coefficient of the interfering ion.

The selectivity coefficients obtained for some anions are given in Table 3. They are all measured

Table 4

Determination of selenium in anodic slime using standard addition method (Electrode:%90 Ag₂Se, %10 Cu₂S)^a

Sample	$\Delta E_{\text{ave.}}$ (mV)	Calculated ave. $C_{\text{SeO}_3^-}$ (M)	average% Se	$S = \sqrt{\frac{\sum(\bar{x} - x_i)^2}{N-1}}$	$CI^* = \bar{x} \pm \frac{t \cdot S}{\sqrt{N}}$
Digested in HNO ₃ pH 8 (NH ₃ -NH ₄ Cl)	23.5	1.57×10^{-4}	12.4	1.28	12.4 ± 1.4
Digested in HCl+HNO ₃ pH 8 (NH ₃ -NH ₄ Cl)	21.6	1.88×10^{-4}	14.8	2.04	14.8 ± 2.3
Digested in HNO ₃ pH 6.5 (NaOH)	25.4	1.32×10^{-4}	10.5	1.35	10.5 ± 1.5

^a Number of samples, $N = 5$; %95 confidence interval.

at pH 8 and 9 and no difference was observed. Since Table 3 summarizes the results of measurements carried out in mixed solutions it probably corresponds more realistically to practical samples where mixtures of ions are often present. As can be seen the selenite electrode is relatively insensitive to SO_3^{2-} , SO_4^{2-} and halides, but is strongly sensitive to S^{2-} ion. However in most solutions S^{2-} is easily oxidized either during digestion of the sample or by air oxygen to SO_4^{2-} , which is insensitive.

The cationic interferences are also investigated and it is found that this electrode responds well to Ag^+ and Cu^{2+} ions as expected. The slope for copper was about 30.0 mV without buffer but in buffer solution such as HAC-Ac, NH₃-NH₄Cl and with NaOH (pH 6.5) because of complex formation the slope was found to be very small. The results are given in Table 4. At higher copper concentration the concentration of acetate buffer was not enough to complex copper ion.

3.7. Application to anodic slime

Anodic slime is an important source for selenium production, which is obtained during the electrolytic purification of copper. It is known to contain 8–12% of selenium and 20–40% Cu and in much smaller quantities 0.3–3% Ag, Ni, Pb and Te. Since Ag₂Se, Cu₂S electrode was sensitive to copper ion, the interference has to be eliminated by working at pH 6.5 [14] or in acetate or ammonium buffer medium (Table 4). The anodic slime sample is dried first for 2 h at 110°C, about 1.0 g of it was digested in HCl and HNO₃[15]. The solution was filtered and washed with water. Nitric acid was removed by urea and the solution was diluted into 50.0 ml. The same digestion procedure was applied to another sample by using HNO₃ in order to avoid the Cl⁻ interference. An aliquot of 0.05 ml solution from each of the digested sample solution is taken, 5.0 ml of 0.1M NH₃-NH₄Cl buffer (pH 8) 1.0 ml of 1 M NaNO₃ is added and it is diluted into 10.0 ml. The potential of this solution is measured against saturated calomel electrode while the solution was stirring at a constant speed. To the same cell 1.0 ml of 10^{-2} M selenite solution is added and the change in potential is measured. The same standard addition method is applied to the solution of pH = 6.5, adjusted with NaOH. The calculations are made using the below given equation.

$$C_x = \frac{C_s V_s}{(V_x + V_s)10^{\Delta E/S} - V_x} \quad (2)$$

Table 5

Percentage of selenium in anodic slime determined by four different methods

Method used	Weight percentage of selenium in slime
This work	10 ± 1
Spectrophotometric [14,15]	10 ± 1
Volumetric [16]	10 ± 1
Polarographic [17]	10 ± 1

Where C_s and V_s are the concentration and volume of standard solution respectively, S is the slope of the mentioned electrode (The slope has to be determined before each work) which was determined as 28.5 mV per activity decade of selenite ion. The results obtained for different digesting solutions are given in Table 4. As can be seen from Table 4, the best result was obtained with the solution digested with HNO_3 . Because of chloride interference the selenium content obtained was higher than expected for solutions containing high amounts of chloride ion. To check the validity of the method, the same anodic slime was analyzed by spectrophotometric [14,15] volumetric [16] and polarographic [17] methods (Table 5). It can be seen that the results obtained with this new electrode are consistent with those given by other methods.

References

- [1] R.F. Overman, *Anal. Chem.* 43 (1971) 616–617.
- [2] G. Somer, *Anal. Chem.* 53 (1981) 2144–2146.
- [3] E. Pungor, Hollos-Rokosingi, *Acta Chim. Acad. Sci. Hung.* 27 (1961) 63.
- [4] G.A. Rechnitz, *Anal. Chem.* 41 (1969) 12–109.
- [5] F. Pal, K. Toth, E. Pungor, M. Farkas-Jhanke, H. Ebel, M.F. Ebel, *Anal. Chim. Acta* 180 (1986) 313.
- [6] M. Farkas-Jahnke, F. Pal, K. Toth, E. Pungor, in: E. Pungor, et al. (Eds.), *Ion-Selective Electrodes*, vol. 4, Akademiai Kiado, Budapest, 1985, p. 373.
- [7] E.G. Harsanyi, K. Toth, E. Pungor, M.F. Ebel, *Mikrochim. Acta* 194 (1987) 163.
- [8] M.S. Mohan, G.A. Rechnitz, *Anal. Chem.* 45 (1973) 1323–1326.
- [9] I. Sekerka, J.F. Lechner, *Anal. Chim. Acta* 93 (1977) 139–144.
- [10] E. Pungor, *Anal. Chem.* 39 (1967) 28A.
- [11] H. Hirata, K. Higashyma, *Bull. Chem. Jpn.* 44 (1971) 2420.
- [12] T.L. Malone, G.D. Christian, *Anal. Lett.* 7 (1974) 33.
- [13] K. Srinivasan, G.A. Rechnitz, *Anal. Chem.* 41 (1969) 1203.
- [14] G. Somer, G. Ekmekçi, *Anal. Sci.* 13 (1997) 205–208.
- [15] G. Somer, N. Kutay, *Can. J. Chem.* 71 (1993) 834.
- [16] H. Aydın, G. Somer, *Talanta* 36 (1989) 723–726.
- [17] E. Hasdemir, G. Somer, *Analyst* 115 (1990) 297.

UV–Vis spectroscopic and chemometric study on the aggregation of ionic dyes in water

L. Antonov^{a,*}, G. Gergov^b, V. Petrov^c, M. Kubista^d, J. Nygren^d

^a Department of Ecology, National Forestry University, Sofia 1756, Bulgaria

^b Faculty of Pharmacy, Medical University, Sofia 1000, Bulgaria

^c Institute of Organic Chemistry, Bulgarian Academy of Science, Sofia 1113, Bulgaria

^d Department of Biochemistry and Biophysics, Chalmers university of technology, SE-413 90 Gothenburg, Sweden

Received 8 July 1998; received in revised form 3 November 1998; accepted 10 November 1998

Abstract

The monomer–dimer equilibrium in several ionic dyes (Methylene Blue, Acridine Orange, Nile Blue A, Neutral Red, Rhodamine 6G and Safranin O) has been investigated by means of UV–Vis spectroscopy. The data have been processed by a recently developed method for quantitative analysis of undefined mixtures, based on simultaneous resolution of the overlapping bands in the whole set of absorption spectra. In the cases of Acridine Orange a second chemometric approach has been used as a reference. It is based on a decomposition of the recorded spectra into a product of target and projection matrices using non iterative partial least squares (NIPALS). The matrices are then rotated to give the correct concentrations, spectral profiles of the components and the equilibrium constant. The dimeric constants determined by the two methods were in excellent agreement, evidencing the accuracy of the analysis. From the calculated dimeric constant and monomer and dimer spectra, the structures of the dimeric forms of the studied dyes are estimated. © 1999 Elsevier Science B.V. All rights reserved.

Keywords: Aggregation; Chemometrics; UV–Vis spectroscopy; Ionic dyes

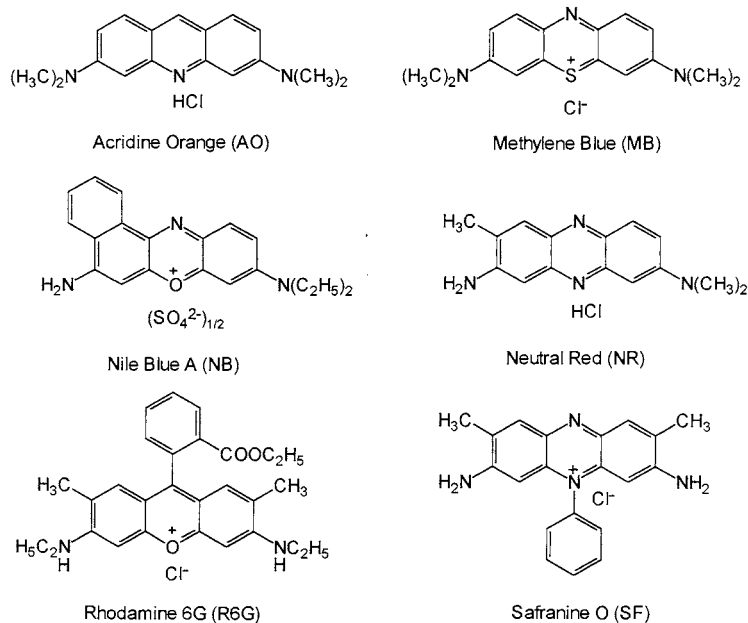
1. Introduction

Aggregation is one of the features of dyes in solution [1–7], affecting their colouristic and photophysical properties and therefore being of special interest. It is well known that the ionic dyes [8,9] tend to aggregate in diluted solutions, lead-

ing to dimer formation, and sometimes even higher order aggregates. In such a case the molecular nature of dye is strongly affected by, and therefore related to such parameters as dye concentration and structure, ionic strength, temperature and presence of organic solvents [10]. Although dyes are very individualistic as structure and, of course behaviour, certain broad rules are well established regarding the aggregation in general. It may increase with an increase of dye concentration or ionic strength; it will decrease

* Corresponding author. Tel.: + 359-2-91907; fax: + 359-2-622830.

E-mail address: lantonov@l.acad.bg; <http://www.orgchm.bas.bg/~lantonov> (L. Antonov)



Scheme 1.

with temperature rising or organic solvents adding; addition to the dye structure of ionic solubilizing groups (as sulphonate group) will decrease aggregation, whereas the inclusion of long alkyl chains [11] increases aggregation because of higher hydrophobic interaction in solution.

The absorption UV–Vis spectroscopy is one of the most suitable methods for quantitative studying the aggregation properties of dyes as function of concentration, since in the concentration range used (10^{-3} – 10^{-6} M) mainly monomer-dimer equilibrium exists.



There are numerous UV–Vis spectroscopy studies on the aggregation, but surprisingly their results are frequently inconsistent and sometimes contradictory [10,12], particularly for studies carried out on the same dye. For example the value of dimeric constant of Methylene Blue varies from 1500 to 55 600 or in orders [12]. This unsatisfactory situation arises from two main reasons, ill defined experimental conditions (the purified or commercial dye is used) and numerous assumptions made in the processing of the spectral data

[2,3,13–17]. The latter is a consequence of that the individual spectra of the components (monomer and dimer) cannot be measured experimentally, which renders classical spectrophotometry impossible.

Therefore the aim of the present paper is to apply the recently developed approach for quantitative analysis [18] to study the monomer–dimer equilibrium in the case of several wide used ionic dyes (Scheme 1) and to confirm the results by processing the same data by an independent chemometric approach based on matrix calculations [19].

2. Experimental part

The investigated dyes (for microscopy grade) were purchased from Fluka and Aldrich and were studied without additional purification (except SF). The experiment was carried out in distilled water, keeping the cell thickness (l) and total dye concentration (c^*) so that $l \cdot c^* = \text{constant}$. The absorption spectra were measured on a PE Lambda 5 UV–Vis spectrophotometer. The data

for each dye were stored in spectral files as matrices of size m (wavelengths) and p (concentrations) and then processed by using MULTIRES [18] and DATAN [19,20] packages.

3. Theoretical part

The analysis of monomer–dimer equilibria consists of two consecutive steps: (i) estimation of the dimeric constant (which provides information about aggregation-dye structure relation); and (ii) studying the dimer structure (which depends on the electronic interaction between the two dye molecules in the dimer).

3.1. Estimation of the dimeric constant

The basic relations describing a monomer (M)–dimer (D) equilibrium as a function of the dye concentration are:

Beer's law:

$$A_{i,j}^* = \varepsilon_j^M \cdot c_i^M \cdot l_i + \varepsilon_j^D \cdot c_i^D \cdot l_i = A_j^M \cdot x_i^M + A_j^D \cdot x_i^D, \quad (1)$$

Mass balance:

$$c_i^M + 2c_i^D = c_i^* \quad (2)$$

$$\text{or, } x_i^M + x_i^D = 1 \quad (3)$$

Dimeric constant:

$$K_D = \frac{c_i^D}{(c_i^M)^2} = \frac{x_i^D}{2c_i^* (x_i^M)^2} \quad (4)$$

where: i ($i = 1 - p$) and j ($j = 1 - m$) denote i^{th} concentration and j^{th} wavelength, A^* is the measured absorbance, ε^M and ε^D are the molar absorptivities of monomer and dimer, respectively, c^M and c^D are the concentrations of monomer and dimer, respectively.

The molar fractions (x) and partial absorbances (A) are defined according to Eqs. (5)–(8):

$$x_i^M = \frac{c_i^M}{c_i^*} \quad (5)$$

$$x_i^D = \frac{2c_i^D}{c_i^*} \quad (6)$$

$$A_j^M = \varepsilon_j^M \cdot c_i^* \cdot l_i \quad (7)$$

$$A_j^D = \frac{\varepsilon_j^D}{2} \cdot c_i^* \cdot l_i \quad (8)$$

If the individual spectra of M and D are known it would be easy to calculate the molar fractions and dimeric constant. However the individual spectrum of the dimer cannot be obtained experimentally because the increase of c^* causes formation of higher order aggregates. Further, the spectrum of the monomer could in principle be measured in a highly diluted solution, but such a spectrum is often very noisy leading to considerable uncertainty in the analysis [3]. For these reasons the quantitative analysis of monomer–dimer equilibria represents a case of analysis of undefined mixtures, which cannot be solved by the methods of classical spectrophotometry.

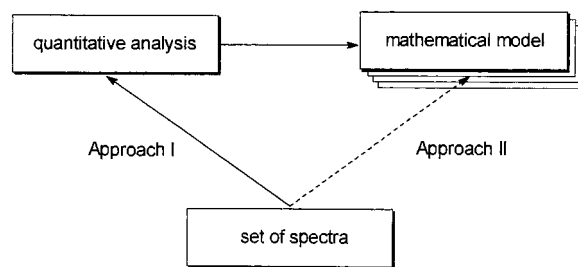
The two possible ways for analysis of such mixtures without a priori assumptions are shown in Scheme 2. The first one is directed primary to quantitative analysis (i.e. calculation of the molar fractions and then the individual spectra) without any model assumptions of the system investigated. That could be done using:

- additional spectral information as finding individual areas of absorbance,
- resolution of overlapping bands [18,21,22],
- derivative spectroscopy [23].

After performing the quantitative analysis, the molar fractions are used for adopting a suitable model (from several existing) of the system.

The second approach starts by choosing a mathematical model and, using the experimental data, fitting the spectral responses [19,20,24,25].

Both approaches have their advantages and disadvantages, but (and most important) if no assumptions have been made when fitting Eq. (1),



Scheme 2.

the results of the approaches should be identical in the frame of some computational errors.

In the present study the two methods were used to treat the same data to allow stringent comparison.

3.1.1. Method 1

It is well known that each UV–Vis absorption spectrum could be presented as superposition of Gauss functions (F) describing its individual bands [26,27]. In such a case the individual spectra of M and D can be expressed as:

$$A_j^M = \sum_{k=1}^{n_M} F(\lambda_j, A_{\max_k}^M, \lambda_{\max_k}^M, \Delta v_{1/2_k}^M) \quad (9)$$

$$A_j^D = \sum_{s=1}^{n_D} F(\lambda_j, A_{\max_s}^D, \lambda_{\max_s}^D, \Delta v_{1/2_s}^D) \quad (10)$$

where n_M and n_D are numbers of individual bands composing the individual spectrum of M and D, respectively ($n_M + n_D = n$), A_{\max} , λ_{\max} , $\Delta v_{1/2}$ are the three basic spectral parameters (intensity, position and band width) describing the definite individual band.

According to Eqs. (3), (9) and (10) the Eq. (1) can be written as follows:

$$A_{i,j} = x_i^M \cdot \left\{ \sum_{k=1}^{n_M} F(\lambda_j, A_{\max_k}^M, \lambda_{\max_k}^M, \Delta v_{1/2_k}^M) - \sum_{s=1}^{n_D} F(\lambda_j, A_{\max_s}^D, \lambda_{\max_s}^D, \Delta v_{1/2_s}^D) \right\} + \sum_{s=1}^{n_D} F(\lambda_j, A_{\max_s}^D, \lambda_{\max_s}^D, \Delta v_{1/2_s}^D) \quad (11)$$

Eq. (11) correctly (from both mathematical and physical point of view) describes the real measured spectrum and allows an optimisation function, characterised by $3n + p$ optimisation parameters ($3n$ basic parameters for the individual bands and p unknown monomer molar fractions) and pm experimental points, to be defined:

$$S_1^2 = \frac{\sum_{i=1}^p \sum_{j=1}^m (A_{i,j}^* - A_{i,j})^2}{p \cdot m} \quad (12)$$

where A^* is the measured absorbance, while A is the calculated one according to Eq. (11).

The values of the individual bands basic parameters (and the individual spectra of M and D according to Eqs. (9) and (10)) and monomer molar fractions in each solution can be obtained after minimization of Eq. (12) using two step optimization procedure [18]. Note that the minimization procedure, which is implemented in the program MULTIRES [18], is valid for any two components mixture; that the components are involved in a monomer–dimer equilibrium is not used as criterion (i.e. no model assumptions are made).

Then the molar fractions obtained could be plotted versus c^* in the linear equation (where log denotes base 10 logarithm):

$$\log c_i^* = \log \frac{1 - x_i^M}{2(x_i^M)^2} - \log K_D \quad (13)$$

which results from Eqs. (4) and (3).

The slope of the curve, which has to tend to 1, is used as a criterion of adopting monomer–dimer model.

3.1.2. Method 2

A chemometric approach for quantitative analysis, based on decomposition of the matrix A^* into a product of target and projection matrices [19] was used for comparison. Its application for analysis of monomer–dimer equilibria has been described in details previously and the approach is implemented in the program DATAN [19]. DATAN uses matrix A^* and calculates the value of K_D (optimised stepwise), the individual spectra and molar fractions of both species.

As a fitting function the Eq. (14) is used:

$$S_2^2 = \frac{\sum_{i=1}^p \sum_{j=1}^m \left(A_{i,j}^* - \frac{\sqrt{1 + 8c_i^* \cdot K_D} - 1}{4c_i^* \cdot K_D} \cdot (A_j^M - A_j^D) - A_j^D \right)^2}{p \cdot m} \quad (14)$$

3.2. Estimation of dimer structure

The spectral changes observed upon dimer formation are caused by electronic interactions between the dye molecules in the dimer. Identical

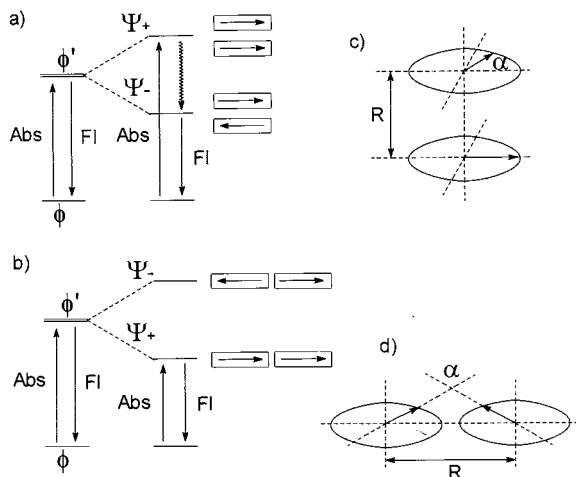


Fig. 1. Energy graphs and structure of 'sandwich' (a and c) and 'head to tail' (b and d) dimers.

dye molecules with ground state wavefunctions ϕ_1 and ϕ_2 and singlet excited state wavefunctions ϕ'_1 and ϕ'_2 , have in dimeric state the ground state wavefunction:

$$\Psi_0 = \phi_1 \cdot \phi_2 \quad (15)$$

In the excited state the dimer wavefunctions are split into symmetric and asymmetric combinations:

$$\Psi_+ = \frac{1}{\sqrt{2}} \cdot (\phi'_1 \cdot \phi_2 + \phi_1 \cdot \phi'_2) \quad (16)$$

$$\Psi_- = \frac{1}{\sqrt{2}} \cdot (\phi'_1 \cdot \phi_2 - \phi_1 \cdot \phi'_2) \quad (17)$$

The energies of these two states are consequently different.

According to the molecular exciton theory [28,29] there are two ideal cases of dimer structure:

1. 'Sandwich' dimer (Fig. 1a)—the transition moments of both monomer molecules are one direction parallel in the higher energy state Ψ_+ , which means that the intensity (and oscillator strength) of the transition $\Psi_0 \rightarrow \Psi_+$ is substantial. The opposite is true for the lower energy transition. As a result in the absorption spectrum of dimer a band (called 'H-band'), shifted hypsochromic in respect of pure monomer one, appears.

2. 'Head to tail' dimer (Fig. 1b). The transition $\Psi_0 \rightarrow \Psi_-$ is forbidden, because of the opposite directions of the transition moments. However the lower energy transition is permitted and a bathochromic band ('J-band') appears in the dimer spectrum.

In general the both cases of the dimer are idealistic and in the reality the transition moments are neither parallel or anti-parallel, which leads to appearance of both H- and J-bands in the dimer spectrum (Fig. 1c, d) with energy difference between them:

$$\Delta v = v_H - v_J \quad (18)$$

Their relative intensities depend on the angle α between the transition moments, which is defined as:

$$\alpha = 2 \arctan \frac{\sqrt{v_H \cdot f_J}}{\sqrt{v_J \cdot f_H}} \quad (19)$$

where v is the position (in cm^{-1}) and f is the oscillator strength of the corresponding transition. The distance (R in Å) between the monomers in the dimer could be find by the expression:

$$R = \sqrt[3]{\frac{2 \cdot 14 \times 10^{10} \cdot \cos \alpha \cdot f_M}{\Delta v \cdot v_M}} \quad (20)$$

where M denotes the oscillator strength and energy of the transition in the pure monomer.

Of course this theoretical model is too simplified description of the interactions in the dimer and the crude physical basis of Eq. (20) has to be taken into account. While comparison of related dyes is rather straight forward, one should interpret the absolute values of R with concern.

4. Results and discussion

The absorption spectra of AO recorded as a function of the dye concentration are shown in Fig. 2a. Increasing total dye concentration leads to a decrease in the intensity of the monomer band at 490 nm and a new maximum at 460 nm appears signifying the formation of dimer.

The set of spectra was analysed by method 1 and the most suitable fit of Eq. (12) ($S_1^2 = 1.191 \cdot 10^{-4}$) was obtained when the spectra of M

and D have been described by 6 ($n_M = 6$) and 5 ($n_D = 5$) individual bands respectively. The general calculational conditions of resolution procedure were described previously [18,26,27]. The spectra of both species, reconstructed according to Eqs. (9) and (10) are presented in Fig. 2b. It should be noted especially that the calculated spectrum of the dimer predicts both H- and J-bands according to the theory discussed above. The values of the monomer molar fractions calculated in the optimization procedure are collected in Table 1 as a function of the dye concentration. The plot of Eq. (13) showed good correlation (0.998) with a slope 0.88. The deviation from 1, which is expected for a monomer dimer equilibrium, might result from the experimental noise in the recorded spectra and also from errors in the nonlinear optimization procedure when calculat-

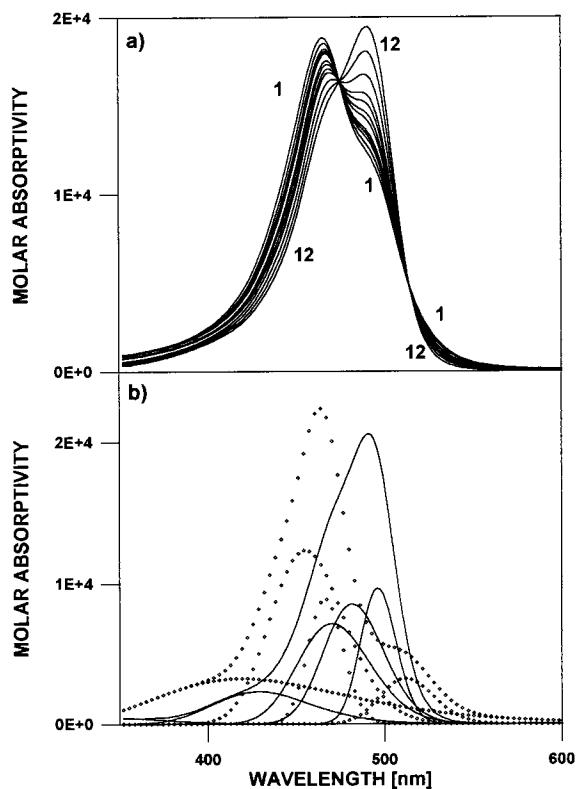


Fig. 2. (a) Absorption spectra of AO in water recorded as different concentrations (see Table 1); (b) calculated individual spectra ε^M (solid line) and $\varepsilon^D/2$ (dots) with their composing individual bands.

Table 1

Calculated molar fractions (%) of the monomer

i	$c_i^* \cdot 10^4$ (mol l ⁻¹)	Method 1	Method 2
1	11.01	43.4	43.2
2	7.200	48.0	50.1
3	6.372	51.6	52.1
4	5.740	53.5	53.9
5	5.031	55.2	56.1
6	4.320	61.1	58.7
7	3.600	63.8	61.9
8	2.880	67.9	65.6
9	2.160	71.8	70.4
10	1.440	79.3	76.6
11	0.720	87.3	85.4
12	0.288	95.4	93.1

ing the molar fractions. The values of $\log K_D$ were calculated for each solution using Eq. (4) and the final mean result was estimated as 3.10 ± 0.06 .

The same raw data (Fig. 2a) were processed by method 2 and after stepwise optimization of $\log K_D$ (Fig. 3) the best fit ($S_2^2 = 1.583.10^{-4}$) was found at $\log K_D = 3.14$. The calculated monomer molar ratios are very close to those obtained from the first analysis (Table 1). The calculated monomer and dimer spectra were essentially identical to those from the first analysis depicted in Fig. 2b.

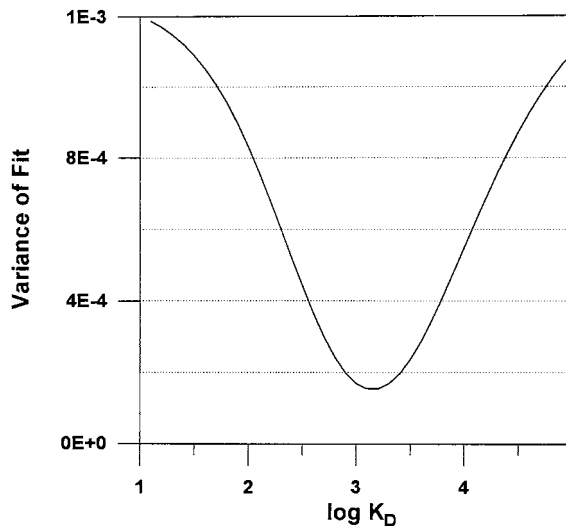


Fig. 3. Stepwise optimization of $\log K_D$ of AO in water.

Table 2
Dimeric constants and structure parameters of the dimer calculated by method 1

	Dye					
	AO	MB	NR	NB	R6G	SF
$\log K_D$	3.10	3.6	3.27	3.09	3.50	4.3
SD	0.06	0.1	0.03	0.05	0.06	0.1
Monomer						
ν_M (cm ⁻¹)	20 370	15 060	18 660	15 750	18 980	19 050
f_M	0.182	0.502	0.268	0.377	0.604	0.431
Dimer						
ν_H (cm ⁻¹)	21 550	16 530	19 800	17 180	20 080	20 160
ν_J (cm ⁻¹)	19 530	14770	17 300	14 680	18 830	19 460
f_H	0.356	1.028	0.764	2.334	1.086	0.583
f_J	0.041	0.159	0.094	0.334	0.074	0.166
$\Delta\nu$ (cm ⁻¹)	2020	1760	2500	2500	1250	700
α (°)	39	45	41	45	30	57
R (Å)	4.2	6.6	4.5	5.3	7.8	7.2

The calculated $\log K_D$ values by the two methods are essentially the same, even though they use quite different approaches. This confirms their reliability and evidences that they both are appropriate for analysing monomer-dimer equilibria.

Knowing the spectra of the monomer and dimer it is possible to make conclusions about the dimer structure. Usually a detailed analysis requires the dimer spectrum to be resolved into the H- and J-bands, but this is not necessary here because these parameters were obtained already in the optimisation procedure (Fig. 2b). The positions, intensities and band widths of the individual bands were determined, which makes it possible to calculate energies and oscillator strengths of the electronic transitions involved [27].

The values for the $\log K_D$ as well as the structural parameters of the corresponding dimers for the investigated ionic dyes, obtained according to the present approach are collected in Table 2. The differences in the calculated structural parameters for the different dyes are rather small, suggesting that they all have similar structures. This is reasonable in view of that they all have a core of three fused aromatic rings, with a central heteroatom. The calculated monomer–monomer distances are 4–8 Å, excluding end-to-end

arrangement. The angles between the dye transition moments are 30–60°, suggesting that the two monomer dyes stack on top of each other, being significantly rotated. The dyes' permanent dipole moment should, for some of them owing to symmetry reasons and for the other owing to the heteroatoms, be directed essentially along the molecular short axis. The dyes should therefore stack in opposite direction (i.e. top to bottom) for the dipoles to interact attractively. The dyes are also expected to be highly polarizable owing to their large aromatic systems, and the polarizability tensor should have the largest component along the molecular long axis. This is probably the reason for the monomers to be twisted, since that may optimize the permanent dipole–induced-dipole interactions.

5. Conclusions

A new approach for analysis of monomer–dimer equilibria, based on the simultaneous resolution of individual bands in a set of spectra, is proposed. It determines the monomer molar ratios in the samples, as well as the monomer and dimer spectra with high accuracy, as evidenced by comparison with the DATAN approach. The re-

sults of the analysis can be used to extract information about electronic interactions of the dye monomers in the dimer, from which the dimer structure can be deduced.

Acknowledgements

The comments of the unknown reviewers is greatly helpful. Financial support from the National Science Found and Eureka Foundation is gratefully acknowledged (LA).

References

- [1] S.E. Cheppard, Proc. R. Soc. 82A (1909) 256.
- [2] A.R. Monahan, D.F. Brossey, J. Phys. Chem. 74 (1970) 1970.
- [3] W. West, S. Pearce, J. Phys. Chem. 69 (1965) 1894.
- [4] K. Bergmann, C. O'Konski, J. Phys. Chem. 69 (1965) 1884.
- [5] W. Stork, G. Lippits, M. Mandel, J. Phys. Chem. 76 (1972) 1772.
- [6] B. Craven, A. Datyner, JSDC 79 (1963) 515.
- [7] A.R. Monahan, J.A. Brado, A.F. Delura, J. Phys. Chem. 76 (1972) 1972, 1994.
- [8] J. Georges, Spectrochim. Acta 51A (1995) 985.
- [9] T. Stoyanova, L. Antonov, D. Dimitrov, S. Stoyanov, Ann. Univ. Sofia 87 (1995) 55 (Bulg.), Chem. Abstr. 125:316864j.
- [10] B.C. Burdett, Aggregation of dyes, in: Studies in Physical and Theoretical Chemistry, vol. 28, Elsevier, 1983, p. 241.
- [11] T. Iijima, E. Jojima, L. Antonov, S. Stoyanov, T. Stoyanova, Dyes Pigm. 37 (1998) 81 (and references cited therein).
- [12] Some results for the dimer constant of Methylene Blue: 1500, A.K. Busenbaev, L.B. Zouaou, A.M. Saletskii, Zh. Prikl. Spekt. 52 (1989) 424; 8900, reference 9; 9600, C. Lee, Y.W. Sung, J.W. Park, Anal. Sci. 13 (1997) 167; 55600, Suzuki, K. Tsuchiya, M. Bull. Chem. Soc. Jpn. 44 (1971) 967.
- [13] K.K. Rohatgi, J. Mol. Struct. 27 (1968) 545.
- [14] J. Lavorel, J. Phys. Chem. 61 (1957) 1000.
- [15] I.L. Arbeloa, J. Chem. Soc. Faraday Trans. 2 (77) (1981) 1725.
- [16] F. Lopez, Y. Liebana, E.C. Fernandez, I.L. Arbeloa, Spectrochim. Acta 45A (1989) 1201.
- [17] S. Stoyanov, T. Deligeorgiev, D. Simov, J. Mol. Struct. 115 (1984) 363.
- [18] L. Antonov, D. Nedeltcheva, Anal. Lett. 29 (1996) 2055.
- [19] M. Kubista, R. Sjoback, B. Albinson, Anal. Chem. 65 (1993) 994.
- [20] I. Scarmino, M. Kubista, Anal. Chem. 65 (1993) 409.
- [21] L. Antonov, S. Stoyanov, Anal. Chim. Acta 314 (1995) 225.
- [22] M.C. Argoni, M. Arca, G. Crisponi, V.M. Nurchi, Anal. Chim. Acta 316 (1995) 195.
- [23] N. Mateeva, L. Antonov, M. Mitewa, S. Miteva, Talanta 43 (1996) 275.
- [24] J.F. Rusling, Crit. Rev. Anal. Chem. 21 (1989) 49.
- [25] F. Peral, J. Mol. Struct. 266 (1992) 373.
- [26] L. Antonov, S. Stoyanov, Appl. Spectrosc. 47 (1993) 1030.
- [27] L. Antonov, Trends Anal. Chem. 16 (1997) 536.
- [28] M. Kasha, H.R. Rawls, M.A. El-Bayomi, Pure Appl. Chem. 11 (1965) 371.
- [29] S.F. Mason, JSDC 84 (1968) 604.

Photochemically-induced fluorescence determination of sulfonylurea herbicides using micellar media

Atanasse Coly¹, Jean-Jacques Aaron*

Institut de Topologie et de Dynamique des Systèmes de l'Université Denis-Diderot-Paris 7, Laboratoire Associé au CNRS, 1, rue Guy de la Brosse, 75005 Paris, France

Received 10 July 1998; received in revised form 3 November 1998; accepted 10 November 1998

Abstract

An analytical method based on the use of UV irradiation to produce fluorescent derivatives from four non-fluorescent sulfonylurea herbicides, including chlorsulfuron, metsulfuron methyl, 3-rimsulfuron and sulfometuron methyl is described. Their photochemically-induced fluorescence (PIF) properties in several solvents (water, dimethyl sulfoxide (DMSO), dimethyl formamide (DMF), acetonitrile, methanol, ethanol, propan-2-ol and their binary mixtures with water) and micellar solutions of sodium dodecyl sulfate (SDS), and cetyltrimethylammonium chloride (CTAC) are reported. Physicochemical variable influencing the sensitivity of the method have been optimized. A PIF method is developed for the determination of the four herbicides under study. Micellar media are found to provide the best analytical figures of merits. Linear dynamic ranges are established over about two orders of magnitude. The limit of detection (LOD) range from 0.2 to 6 ng ml⁻¹ according to the compound, with relative standard deviation (RSD) between 1.2 and 3.9%. Examples of applications to the analysis of these herbicides in spiked river water samples are given. The mean recoveries range from 80 to 104%. © 1999 Elsevier Science B.V. All rights reserved.

Keywords: Sulfonylurea herbicides; Photochemically-induced fluorescence; Micellar effect; River water analysis

1. Introduction

Sulfonylurea herbicides were developed in the mid-1970s for the control of weeds in crops [1,2]. They are characterized by a high herbicidal activ-

ity resulting in low application doses (usually 2–75 g of active ingredient per hectare) that are 100–1000 times smaller than those of conventional herbicides [1]. It provides marked environmental advantages, but as a consequence the determination of these compounds in water, soil and crop samples is difficult, since low residue levels can be expected. Therefore, very sensitive methods are needed for residue analysis of these compounds. A variety of techniques and detectors

* Corresponding author. Fax: +33-1-44276814.

E-mail address: aaron@paris7.jussieu.fr (J.-J. Aaron)

¹ On leave from the Faculté des Sciences et Techniques, Département de Chimie, Université Cheikh Anta DIOP, Dakar, Sénégal.

have already been used for determining sulfonyurea herbicides in various matrices. Because of their thermal instability and low volatility, high performance liquid chromatography (HPLC) is preferred to gas chromatography (GC) for these herbicides. The rather poor sensitivity of HPLC-UV detection [3–7] has been partly overcome by using photoconductivity [8–13] or mass spectrometry [14–19] detectors. Direct GC is unfeasible because these herbicides are non-volatile, thermally unstable and polar, and derivatization prior to detection is needed [20–27]. Other available methods include bioassay [28–37], enzyme immunoassay [38–43], and capillary electrophoresis (CE) [44]. To the best of our knowledge, fluorimetric detection has not been applied to the determination of sulfonyurea herbicides except a paper of Patel et al. [45]. These authors investigated the flow injection analysis (FIA) post-column photolysis formation of fluorophores from chlorsulfuron, chlorimuron ethyl, metsulfuron methyl and sulfometuron methyl in water and methanol/water (1:1, v/v). Fluorescence improvement defined as the ratio of fluorescence intensity of photolyzed herbicides to fluorescence intensity of untreated compounds ranged from 3.7 to 48.3, but no analytical application was reported [45].

In this work, we have developed a photochemically-induced fluorescence (PIF) method for residue analysis of four sulfonyurea herbicides,

including chlorsulfuron, metsulfuron methyl, 3-rimsulfuron and sulfometuron methyl, in river water samples. After an extensive investigation of the effect of various physicochemical parameters, including solvent system, pH, micellar concentration and UV irradiation time, a PIF method was carried out for the analysis of the four herbicides. The applicability of the method to spiked river water samples was studied. The performances of the PIF method in terms of simplicity, sensitivity, rapidity and reliability are compared to literature data obtained with other techniques.

2. Experimental

2.1. Reagent

Chlorsulfuron (99.2%, m/m), metsulfuron methyl (97.4%, m/m), 3-rimsulfuron (99.1%, m/m) and sulfometuron methyl (99.2%, m/m) were a generous gift from E.I. DuPont de Nemours and Company, Inc. (Wilmington, DE). Their molecular structures are presented in Fig. 1. Spectroscopic-grade solvents including methanol, ethanol, propan-2-ol (Merck, Darmstadt, Germany), dimethyl sulfoxide (DMSO), dimethyl formamide (DMF) and acetonitrile (Aldrich, Milwaukee, WI) were utilized. Cetyltrimethylammonium chloride (CTAC), 25% wt. solution in water (Aldrich) and sodium dodecyl sulfate (SDS,

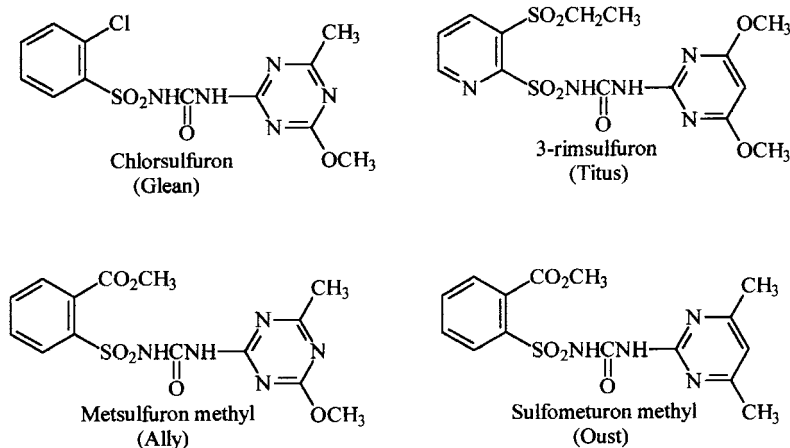


Fig. 1. Structure of the sulfonyurea herbicides under study (trade name).

Table 1
PIF spectroscopic and analytical parameters for sulfonylurea herbicides in various media

Compound ^a	Medium	Optimal NaOH concentration (M) or buffer pH*	$\lambda_{\text{ex}}/\lambda_{\text{em}}$ (nm) ^b	I_r^c	$t_{\text{irr}}^{\text{opt}}$ (s) ^d
Chlorsulfuron (4×10^{-6} M)	H ₂ O	0.01	312/398	1.9	300
	CTAC	0.01	314/380	5.9	150
	SDS	0.01	312/398	2.2	250
	DMSO	0.01	369/423	2.2	90
	DMF	0.01	324/358	3.0	60
	2-PrOH	0.01	317/395	1.9	90
	MeOH/H ₂ O (1:1, v/v)	0.01	314/392	1.0	600
	EtOH/H ₂ O (1:1, v/v)	0.01	314/390	1.9	600
	2-PrOH/H ₂ O (1:1, v/v)	0.01	314/391	2.4	600
Metsulfuron methyl (4×10^{-6} M)	CTAC	0.01	308/418	2.2	160
	SDS	0.01	322/378	27.0	60
	DMSO	0.01	378/441	4.9	80
	MeOH	0.1	322/378	10.6	80
	EtOH	0.01	321/375	4.6	100
	2-PrOH	0.01	316/415	1.0	100
	MeOH/H ₂ O (1:1, v/v)	0.01	318/385	5.6	60
	EtOH/H ₂ O (1:1, v/v)	0.01	319/380	10.6	60
	2-PrOH/H ₂ O (1:1, v/v)	0.01	321/377	8.4	60
3-rimsulfuron (10^{-6} M)	H ₂ O	7*	317/365	3.2	300
	CTAC	7*	317/365	3.9	150
	SDS	7*	318/364	3.0	250
	DMSO	0.01	371/425	16.9	100
	MeCN	10^{-7}	327/366	2.8	200
	MeOH	10^{-7}	325/368	2.9	100
	EtOH	10^{-7}	322/360	1.3	60
	2-PrOH	10^{-7}	323/360	1.0	60
	MeOH/H ₂ O (1:1, v/v)	7*	322/365	3.2	150
Sulfometuron methyl (10^{-5} M)	H ₂ O	9*	291/343	4.2	600
	CTAC	9*	290/341	6.1	150
	SDS	9*	291/341	5.8	150
	DMSO	0.01	360/420	5.0	100
	DMF	0.01	358/420	5.6	300
	MeCN	2×10^{-4}	337/408	4.1	100
	MeOH	2×10^{-4}	325/400	2.6	200
	EtOH	2×10^{-4}	335/408	2.1	50
	2-PrOH	2×10^{-4}	333/400	1.0	50

^a Surfactant concentration: [CTAC] = 7.8×10^{-3} M; [SDS] = 5×10^{-2} M.

^b Analytical PIF excitation and emission wavelengths.

^c Relative maximum PIF intensity, corrected for the solvent (blank) signal and normalized to the lowest PIF intensity for each compound.

^d Optimum irradiation time, corresponding to the maximum PIF intensity (I_F).

99%, m/m) analytical-reagent grade (Acros Organics, Geel, Belgium) were used as received. Distilled water was utilized for preparing binary mixtures of organic solvents with water and micellar aqueous solution. 20%, v/v buffer solutions of pH 2–11 were used for pH studies (Acros Organics, Aldrich, Fluka and Merck). Very alkaline solutions (pH > 11) were prepared with NaOH convenient concentrations (0.004–0.1 M). For analytical applications, natural water samples were freshly collected in plastic flasks from the Seine river at Chatou (near Paris), and stored at room temperature. The samples were spiked and analysed within 3 days of their collection.

2.2. Apparatus

All PIF measurements were performed at room

temperature on a Kontron SFM-25 spectrofluorimeter controlled by a Geocom microcomputer Model CPD 1420E. Uncorrected fluorescence spectra were acquired and processed using a Kontron SFM-25 data control and acquisition program. An unfiltered Osram 200 W HBO high pressure mercury lamp with an Oriel Model 8500 power supply was utilized for photolysis reactions. The photochemical set-up included a light-box consisting of a fan, the mercury lamp and a quartz lens. A standard Hellma (Mullheim, Germany) 1-cm pathlength quartz fluorescence cuvette was placed on an optical bench at 30 cm from the mercury lamp. During photolysis, the quartz cuvette solution was stirred magnetically. pH measurements were performed with a Schott Geraete pH-meter Model CG 832.

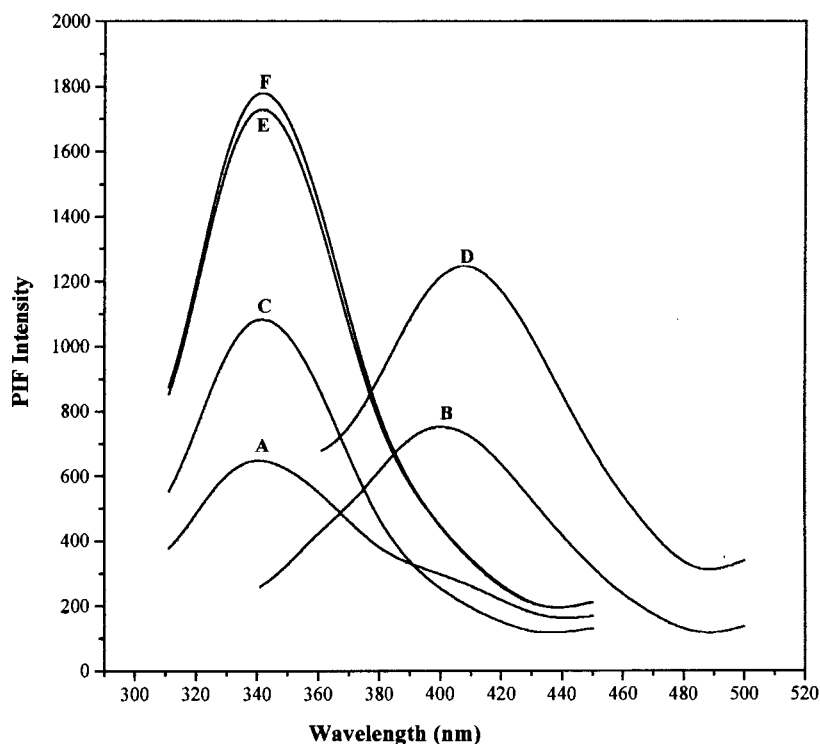


Fig. 2. PIF emission spectra of sulfometuron methyl (10^{-5} M) under optimal pH condition in (A) DMSO/water (1:1, v/v), ($\lambda_{\text{ex}} = 295$ nm, $\lambda_{\text{em}} = 338$ nm); (B) MeOH ($\lambda_{\text{ex}} = 325$ nm, $\lambda_{\text{em}} = 400$ nm); (C) water ($\lambda_{\text{ex}} = 291$ nm, $\lambda_{\text{em}} = 343$ nm); (D) MeCN ($\lambda_{\text{ex}} = 337$ nm, $\lambda_{\text{em}} = 408$ nm); (E) 5×10^{-2} M SDS ($\lambda_{\text{ex}} = 291$ nm, $\lambda_{\text{em}} = 341$ nm); (F) 7.8×10^{-3} M CTAC ($\lambda_{\text{ex}} = 290$ nm, $\lambda_{\text{em}} = 341$ nm). All spectra were recorded with an irradiation time of 150 s.

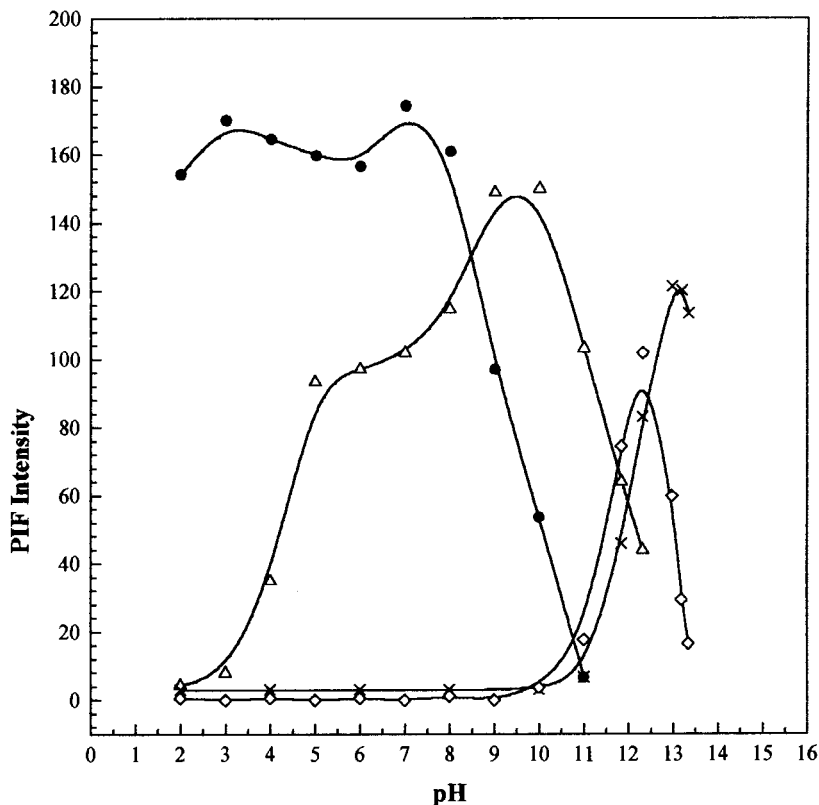


Fig. 3. Effect of pH on the PIF intensity of (×) chlorsulfuron ($C = 4 \times 10^{-6}$ M, $\lambda_{\text{ex}} = 312$ nm, $\lambda_{\text{em}} = 398$ nm, $t_{\text{irr}} = 150$ s); (◇) metsulfuron methyl ($C = 4 \times 10^{-6}$ M, $\lambda_{\text{ex}} = 315$ nm, $\lambda_{\text{em}} = 392$ nm, $t_{\text{irr}} = 40$ s); (●) 3-rimsulfuron ($C = 10^{-6}$ M, $\lambda_{\text{ex}} = 317$ nm, $\lambda_{\text{em}} = 365$ nm, $t_{\text{irr}} = 150$ s); (△) sulfometuron methyl ($C = 10^{-5}$ M, $\lambda_{\text{ex}} = 291$ nm, $\lambda_{\text{em}} = 343$ nm, $t_{\text{irr}} = 200$ s).

2.3. Procedure

2.3.1. Solution preparation

Stock solutions of herbicides (10^{-3} M) were freshly prepared by dissolving the compound in methanol. Serial dilutions were performed to obtain working standard solutions. All solutions were protected against light with aluminium foil and stored in a refrigerator. Stock solutions of both SDS and CTAC (0.1 M) were prepared with distilled water, and serial dilutions were made from these stock solutions. Micellar solutions of the herbicides were prepared by transferring 10–50 μl aliquots of the methanolic working standard solutions into a 5-ml volumetric flask and adjusting to marker with the micelle solution required volume, 1 ml of the optimal pH buffer solution and distilled water. The solutions were then

shaken vigorously before irradiation and analytical measurements. All working aqueous and micellar aqueous solutions contained less than 1% (v/v) methanol.

2.3.2. Photolysis reactions and analytical measurements

An aliquot of the herbicide solution was placed in a quartz cuvette and irradiated for a fixed time at room temperature. Curves of PIF intensity (I_{F}) versus UV irradiation time (t_{irr}) were constructed at the analytical excitation (λ_{ex}) and emission (λ_{em}) wavelengths of the herbicide photoproduct, using 2–5-min time intervals according to the herbicide. Linear calibration curves were obtained at these λ_{ex} and λ_{em} values by measuring the PIF signal corresponding to the optimum t_{irr} ($(t_{\text{irr}}^{\text{opt}})$). All PIF intensities measurements were corrected

for the background signal with the appropriate blanks. To optimize analytical conditions, PIF measurements were carried out in triplicate and the results were expressed as mean values. Microcal Origin 4.00, application software was used for the statistical treatment of the data.

2.3.3. River water samples analysis

Seine river water was filtered with Whatman No. 1 filter paper in order to eliminate the suspended organic matter. A pH value of 7.83 was found for this sample. Volumes of 10-ml of the natural water were spiked with 36.0, 3.84, 4.32 and 36.4 $\mu\text{g ml}^{-1}$ of chlorsulfuron, metsulfuron methyl, 3-rimsulfuron and sulfometuron methyl, respectively, and the solutions were then stirred ultrasonically for 15 min before being kept in the dark and used as the stock standard solutions of natural water. Aliquots of six concentrations levels of the spiked stock standard solutions of river water were introduced in six 5-ml volumetric flasks in which the convenient volume of micelle solution, 1 ml of the optimal pH buffer solution and the required amount of distilled water were added before irradiation and analytical measurements. No residue of the four herbicides was found in river water. However, it was detected the presence of a fluorescent organic species with maximum wavelength values ($\lambda_{\text{ex}} = 361 \text{ nm}$, $\lambda_{\text{em}} = 433 \text{ nm}$) relatively far from those of the herbicides in the analytical solvents (SDS and CTAC). The standard addition procedure was used for the recovery experiments.

3. Results and discussion

3.1. PIF characteristics

The PIF excitation (λ_{ex}) and emission (λ_{em}) wavelengths, optimum irradiation times ($t_{\text{irr}}^{\text{opt}}$) and relative PIF intensities (I_{F}) of the four herbicides in various media are reported in Table 1. These herbicides were found to be naturally non-fluorescent in all solvents under study, whereas an intense fluorescence band appeared upon UV irradiation. Consequently, the PIF excitation and emission spectra were obtained after irradiating the solution for a period of time that depended on the herbicide structure and the solvent used (Fig. 2).

Sulfonylurea herbicides present very similar structure, including three parts, i.e. a substituted benzene or pyridine ring, a sulfonylurea bridge and a nitrogen-containing heterocycle derived from triazine or pyrimidine (Fig. 1). The bridge portion is quite labile and can be cleaved thermally [18,21], hydrolytically [1,18,25] and photochemically [12] on both sides of the carbonyl, yielding an aryl sulfonamide and an amino heterocycle. The heterocyclic product is non-fluorescent [46] which implies that the observed PIF emission is probably due to the aryl sulfonamide moiety. However, further investigation is necessary to characterize the structure of breakdown fluorescent photoproduct(s).

3.2. Optimization of pH conditions

We investigated the effect of pH on the PIF intensity of sulfonylurea herbicides in aqueous and non aqueous media.

Table 2
PIF optimal analytical conditions

Compound	Medium	pH	$\lambda_{\text{ex}}/\lambda_{\text{em}}$ (nm)	$t_{\text{irr}}^{\text{opt}}$ (s)
Chlorsulfuron	[CTAC], $2 \times 10^{-3} \text{ M}$	12.1*	314/380	150
Metsulfuron methyl	[SDS], $6 \times 10^{-2} \text{ M}$	12.1*	322/378	60
3-rimsulfuron	[CTAC], $2 \times 10^{-3} \text{ M}$	7	317/365	150
Sulfometuron methyl	[CTAC], $2 \times 10^{-3} \text{ M}$	9	290/341	150

* Value corresponding to $[\text{NaOH}] = 0.01 \text{ M}$.

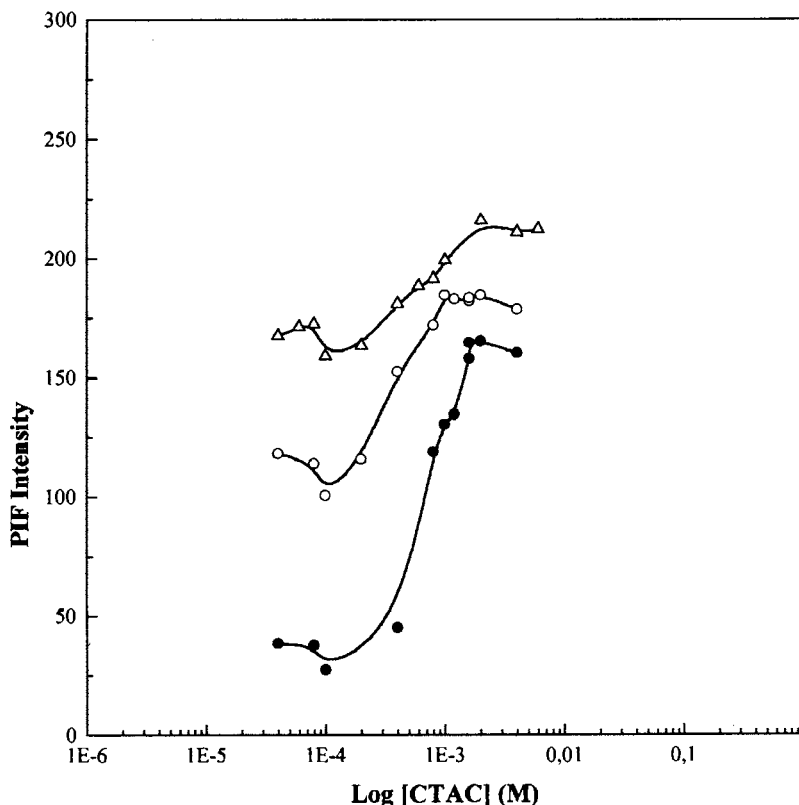


Fig. 4. Influence of CTAC concentrations on the PIF intensity of the herbicides under study; (●) chlorsulfuron ($C = 2 \times 10^{-6}$ M, $\lambda_{\text{ex}} = 314$ nm, $\lambda_{\text{em}} = 380$ nm, $t_{\text{irr}} = 150$ s, $[\text{NaOH}] = 10^{-2}$ M); (Δ) 3-rimsulfuron ($C = 10^{-6}$ M, $\lambda_{\text{ex}} = 317$ nm, $\lambda_{\text{em}} = 365$ nm, $t_{\text{irr}} = 150$ s, $\text{pH} = 7$); (\circ) sulfometuron methyl ($C = 10^{-5}$ M, $\lambda_{\text{ex}} = 290$ nm, $\lambda_{\text{em}} = 341$ nm, $t_{\text{irr}} = 150$ s, $\text{pH} = 9$).

The results obtained in aqueous buffer solutions show that the curves of the PIF signal versus the pH present different patterns according to the herbicide structure (Fig. 3). Indeed, the triazine-based herbicides (chlorsulfuron and metsulfuron methyl) exhibit only a PIF signal for pH values between 12 and 13, whereas the pyrimidine-based compounds present strong PIF intensities for a large pH scale, ranging between 2 and 8 for 3-rimsulfuron and 5 and 11 for sulfometuron methyl. For the latter compounds, intense PIF signal, were also obtained in non-buffered solutions. In the case of chlorsulfuron and metsulfuron methyl, a 0.01 M NaOH aqueous solution was selected for all analytical measurements, while for 3-rimsulfuron and sulfometuron methyl, we have chosen pH 7 and 9 buffer solutions, respectively, as optimal analytical media.

A previous study performed on aromatic pesticides in organic solvents demonstrated that the nature of the solvent provoked a significant change in the fluorescence and PIF intensities of these compounds [47,48]. Therefore, we also investigated the influence of organic solvents on the PIF signal of sulfonylurea herbicides (Section 3.3). The effect of sodium hydroxyde concentration added to these organic solvents (with a constant percentage of water 1%, v/v) was found to play an important role in these media. The curves of PIF signal versus NaOH concentration drawn in the various solvents indicated that the optimal NaOH concentration is 0.01 M in DMSO and DMF for all compounds. In the other organic solvents, chlorsulfuron and metsulfuron methyl exhibit a maximum PIF signal at a NaOH concentration of 0.01 M, whereas the two other her-

bicides give maximum PIF intensities for NaOH concentrations ranging, respectively between 10^{-7} and 5×10^{-5} M for 3-rimsulfuron and 10^{-3} and 6×10^{-2} M for sulfometuron methyl. The optimal NaOH concentrations are displayed in Table 1.

3.3. Solvent effect

We studied the effect of several protic, aprotic solvents, their binary aqueous mixtures and aqueous micellar solutions on the PIF spectral properties of the sulfonylurea herbicides under optimal pH and NaOH concentration conditions. As can be seen in Table 1, no significant shift of the excitation and emission wavelengths occurred on changing the polarity of the protic solvent, whereas a red-shift of both excitation and emission bands (~ 55 nm) took place when DMSO or DMF was used instead of protic solvents, with a more marked effect for DMSO. In contrast, the optimum irradiation time and PIF intensity values exhibited important variations with the solvent polarity and its protic or aprotic character. A significant enhancement of the PIF signal was observed for all compounds in aqueous micellar solution, which appears to be, for most sulfonylurea, the convenient medium for analytical purposes (Fig. 2). This behaviour is in agreement with previous literature data showing that the analyte solubilities and fluorescence signals were generally increased in micellar media [49]. Selected analytical parameters are

summarized in Table 2. For practical reasons, we chose the medium which gave the shortest optimum irradiation time and largest PIF signal. However, in the case of 3-rimsulfuron, although the signal of DMSO is about four times greater than that of CTAC, analytical measurements were conducted in the latter medium because the former solvent was characterized by a high blank signal.

3.4. Surfactant concentration effect

As previously observed [49], the surfactant concentration has a marked influence on analyte PIF intensity. The plots of PIF intensity versus the logarithm of surfactant concentration present shapes similar to those found for other aromatic insecticides in the presence of SDS [49], i.e. an increase of PIF signal with increasing the surfactant concentration close to the critical micellar concentration (cmc) value until saturation is reached (Fig. 4). For the herbicides under study, we selected surfactant concentrations (larger than the cmc) of 2×10^{-3} and 6×10^{-2} M for CTAC and SDS, respectively.

3.5. UV photolysis effect

To evaluate the fluorophore formation kinetics, we investigated the evolution of PIF intensity with irradiation time, in micellar aqueous media, organic solvents and aqueous binary mixtures.

Table 3
Analytical figures of merit for the determination of sulfonylurea herbicides

Compound	Medium	$\lambda_{\text{ex}}/\lambda_{\text{em}}$ (nm)	Concentration range (ng ml ⁻¹)	Slope ^a	r^b	LOD ^c (ng ml ⁻¹)	ALOD ^d (ng)	$t_{\text{irr}}^{\text{opt}}$ (s)	RSD ^e (%)
Chlorsulfuron	CTAC	314/380	1–720	0.90	0.998	0.5	1.7	150	3.9
Metsulfuron-Me	SDS	322/378	0.2–192	0.82	0.997	0.2	0.6	60	1.2
3-rimsulfuron	CTAC	317/365	2–303	1.08	0.994	0.8	2.7	150	2.8
	DMSO	343/375	8–173	1.20	0.995	7	25	100	2.9
Sulfometuron-Me	CTAC	290/341	14–2912	1.02	0.998	6	21	150	1.5

^a Slope of the log–log calibration curves.

^b Correlation coefficient.

^c Limits of detection (LOD) was defined as the amount of analyte giving a signal-to-noise ratio of 3.

^d Absolute limits of detection (ALOD) calculated with a 3.5 ml volume solution.

^e Relative standard deviation, ($n = 4$).

Table 4
Determination of sulfonylurea herbicides in spiked river water samples

Compound	Concentration (ng ml ⁻¹)		Recovery (%)	
	Added	Found*		
Chlorsulfuron	299.3	265.2 ± 3.4	88.6	
	313.7	290.5 ± 4.5	92.6	
	356.9	370.8 ± 2.6	103.9	(95.2 ± 4.9)
	428.9	409.1 ± 2.6	95.4	
	500.9	491.1 ± 2.7	98.0	
	572.9	529.6 ± 0.9	92.5	
Metsulfuron methyl	38.0	39.6 ± 0.9	104.2	
	44.2	41.4 ± 0.8	93.7	
	74.9	71.7 ± 0.3	95.7	
	113.3	116.4 ± 0.7	102.7	(99.7 ± 3.8)
	151.7	151.6 ± 0.9	99.9	
	228.5	232.8 ± 1.3	101.9	
3-rimsulfuron	63.5	61.7 ± 0.7	97.2	
	80.8	67.0 ± 1.3	82.9	
	98.1	78.4 ± 0.3	80.0	(90.4 ± 6.8)
	227.7	204.7 ± 2.0	89.9	
	270.9	258.9 ± 1.9	95.6	
	314.1	302.6 ± 1.6	96.4	
Sulfometuron methyl	824.5	804.3 ± 2.8	97.6	
	1042.9	995.9 ± 11.3	95.5	
	1479.7	1473.4 ± 13.6	99.6	(96.0 ± 2.3)
	1843.7	1753.3 ± 7.1	95.1	
	2935.7	2705.7 ± 19.3	92.2	
	3663.7	3510.1 ± 25.4	95.8	

* Mean ± standard deviation of three replicates.

These kinetics performed in the different solvent systems are similar to those previously described for several aromatic insecticides [48,49]. For all compounds, a two-step mechanism was found, i.e. the PIF intensity initially increased with increasing irradiation time, then reached a maximum value and, finally decreased continuously. The optimum irradiation time ($t_{\text{irr}}^{\text{opt}}$), defined as the irradiation time corresponding to the maximum PIF intensity ranged from 50 to 600 s according to the compounds. Metsulfuron methyl photo-product was found to be unstable in water and aqueous binary mixtures with DMSO and acetonitrile, resulting into short and poorly reproducible $t_{\text{irr}}^{\text{opt}}$ values in these media. For the remaining pesticides, $t_{\text{irr}}^{\text{opt}}$ present larger values in water than in the other solvent systems (Table 1). An interesting feature is that the analytical $t_{\text{irr}}^{\text{opt}}$

values found for these herbicides in micellar media allow their determination within a relatively short time (Table 2).

3.6. Analytical figures of merit

To evaluate the usefulness of our method, we determined the analytical figures of merit in micellar media and under the optimal conditions given in Table 2. Calibration graphs were found to be linear over about two orders of magnitude (Table 3). Regression analysis of the data indicated a satisfactory precision of the linear plots, with correlation coefficients larger than 0.99. Limits of detection (LOD) (signal-to-noise ratio of 3) ranged from 0.2 to 6 ng ml⁻¹ according to the compound. Absolute LOD values were comprised between 0.6 and 21 ng. The reproducibility was

1.2–3.9%. The low LOD obtained show that PIF detection is convenient for determining the herbicides in natural water. However, for agricultural runoff water where lower herbicide concentrations ($\leq 0.05 \text{ ng ml}^{-1}$) may be found [20], a preconcentration and/or a purification step is needed before analysis. These LODs compare favourably with those reported for chlorsulfuron by more sophisticated methods such as HPLC-PCD (photoconductivity detector) in soil (0.2 ng ml^{-1}) [8], GC-ECD (electron capture detection) in soil (1 ng ml^{-1}) [22], enzyme-linked immunosorbent assay (ELISA) in soil (0.4 ng ml^{-1}) [38], and for both chlorsulfuron and metsulfuron methyl by capillary electrophoresis (CE) in tap water (0.1 ng ml^{-1}) [44]. Our LODs are significantly lower than those obtained for chlorsulfuron by HPLC-PCD in plant tissue ($10\text{--}50 \text{ ng ml}^{-1}$) [9]. However, our LOD values are higher than those found by GC-ECD in water for chlorsulfuron (0.025 ng ml^{-1}) [20] and metsulfuron methyl (0.01 ng ml^{-1}) [25].

3.7. Analytical applications

The proposed method was applied to the determination of the sulfonylurea herbicides under study in natural water. Validation data were obtained with spiked river water samples by adding a known herbicide amount to the samples, and determining the concentration by means of the standard addition procedure (Table 4). Each sample was analyzed twice. The average recoveries for all compounds over six concentrations were between 90 and 100%. Representative standard addition and calibration curves demonstrate the linear response of the method over the concentration range under study; moreover, no interference was noticeable from the matrix since their slopes are close. In most instances, the accuracy was satisfactory for real samples.

3.8. Analytical advantages of the PIF method

The results obtained by our PIF approach for sulfonylurea herbicides determination present several analytical advantages over other methods described in the literature. For instance, HPLC-UV detection [3–7] is not suitable because of the

high sensitivity required for herbicide residue measurements. The photoconductivity detectors [8–13] need extensive sample preparation and laborious clean-up steps. Due to the polar nature of sulfonylureas, a chemical derivatization is necessary for GC analysis prior to detection, which increases their analysis time [20–27]. Current bioassay techniques [28–37] are able to detect sulfonylurea herbicides in the low ng range; however, these techniques are non-selective and time-consuming, since they require several weeks to conduct the analyses. Enzyme immunoassays [38–43] reduce sample preparation and analysis time (7.5 min for incubation of the reagents [42]), but are relatively expensive. Capillary electrophoresis (CE) [44] with UV detector decreases the time of analysis, but lacks specificity and is costly. Our PIF method is simple (besides the low cost equipment, no complicated sample pretreatment and no isolation of the fluorescent photoproduct are needed), rather sensitive (LOD in the low ng range), rapid ($t_{\text{irr}}^{\text{opt}}$ in 60–150 s) and reproducible. Another interesting analytical aspect of the PIF method is that it might be used to resolve sulfonylurea herbicide mixtures without applying separation technique such as HPLC, GC or CE. This might be accomplished either by using different $t_{\text{irr}}^{\text{opt}}$ values or by applying specific techniques such as derivative PIF spectra, synchronous fluorimetry and/or partial least square (PLS) multivariate method.

4. Conclusion

We have demonstrated in this work that UV irradiation of the sulfonylurea herbicides in micellar media during 150 s or less yields strongly fluorescent photoproducts. Using this photochemical approach, we have developed a simple, efficient and reproducible photochemically-induced fluorescence (PIF) method suitable for residue analysis of these herbicides in spiked river water samples. A combination of PIF detection with flow injection analysis (FIA) and on-line fluorogenic labelling may be also considered in the future for improving the determination of sulfonylurea herbicides in drainage and runoff waters.

Acknowledgements

We thank Dupont de Nemours and Co., Inc., (Wilmington, DE) for the kind gift of herbicide samples. Dr A. Coly wishes to thank the University of Paris 7 for financial support during his stay in Paris.

References

- [1] H.M. Brown, *Pestic. Sci.* 29 (1990) 263.
- [2] J. Tekel, J. Kovacicova, *J. Chromatogr.* 643 (1993) 298.
- [3] M.J.M. Wells, J.L. Kovacicova, *J. Chromatogr.* 643 (1993) 298.
- [4] G. Nilvé, R. Stebbins, *Chromatographia* 32 (1991) 269.
- [5] A.L. Howard, L.T. Taylor, *J. Chromatogr. Sci.* 30 (1992) 374.
- [6] A.L. Howard, W.J. Yoo, L.T. Taylor, *J. Chromatogr. Sci.* 31 (1993) 401.
- [7] G. Nilvé, M. Knutsson, J.A. Joensson, *J. Chromatogr.* 688A (1994) 75.
- [8] E.W. Zahnow, *J. Agric. Food Chem.* 30 (1982) 854.
- [9] R.V. Slates, *J. Agric. Food Chem.* 31 (1983) 113.
- [10] E.W. Zahnow, *J. Agric. Food Chem.* 33 (1985) 479.
- [11] E.W. Zahnow, *J. Agric. Food Chem.* 33 (1985) 1206.
- [12] J.L. Prince, R.A. Guinivan, *J. Agric. Food Chem.* 36 (1988) 63.
- [13] R.V. Slates, *J. Agric. Food Chem.* 36 (1988) 1207.
- [14] L.M. Shalaby, *Biomed. Mass Spectrom.* 12 (1985) 261.
- [15] A.C. Barefoot, R.W. Reiser, *J. Chromatogr.* 398 (1987) 217.
- [16] A.C. Barefoot, R.W. Reiser, S.A. Cousins, *J. Chromatogr.* 474 (1989) 39.
- [17] A.C. Barefoot, R.W. Reiser, *Biomed. Environ. Mass Spectrom.* 18 (1989) 77.
- [18] R.W. Reiser, A.C. Barefoot, R.F. Dietrich, A.J. Fogiel, W.R. Johnson, M.T. Scott, *J. Chromatogr.* 554 (1991) 91.
- [19] L.M. Shalaby, F.Q. Bramble Jr., P.W. Lee, *J. Agric. Food Chem.* 40 (1992) 513.
- [20] I. Ahmad, *J. Assoc. Off. Anal. Chem.* 70 (1987) 745.
- [21] A.R. Long, L.C. Hsieh, M.S. Malbrough, C.R. Short, S.A. Barker, *J. Assoc. Off. Anal. Chem.* 72 (1989) 813.
- [22] I. Ahmad, G. Crawford, *J. Agric. Food Chem.* 38 (1990) 138.
- [23] G.C. Galletti, G. Chiavari, F.A. Mellon, K. Parlsey, *J. Anal. Appl. Pyrolysis* 21 (1991) 239.
- [24] E.G. Cotterill, *Pestic. Sci.* 34 (1992) 291.
- [25] D.G. Thompson, L.M. MacDonald, *J. AOAC Int.* 75 (1992) 1084.
- [26] P. Klaffenbach, P.T. Holland, *J. Agric. Food Chem.* 41 (1993) 396.
- [27] P. Klaffenbach, P.T. Holland, *Biol. Mass Spectrom.* 22 (1993) 565.
- [28] A.I. Hsiao, A.E. Smith, *Weed Res.* 23 (1983) 231.
- [29] A. Walker, P.A. Brown, *Bull. Environ. Contam. Toxicol.* 30 (1983) 365.
- [30] H. Nilsson, *Weeds Weed Control* 25 (1984) 76.
- [31] D.W. Morishita, D.C. Thill, D.G. Flom, T.C. Campbell, G.A. Lee, *Weed Sci.* 33 (1985) 420.
- [32] W. Mersie, C.L. Foy, *Weed Sci.* 33 (1985) 564.
- [33] A.E. Smith, A.I. Hsiao, *Weed Sci.* 33 (1985) 555.
- [34] W. Iwanzick, H. Egli, *Proc. Brighton Crop Prot. Conf. Weeds* 3 (1989) 1145.
- [35] P. Gunther, A. Rahman, W. Pestemer, *Weed Res.* 29 (1989) 141.
- [36] D. Gomez de Barreda, E. Lorenzo, *Proc. Brighton Crop Prot. Conf. Weeds* 2 (1991) 515.
- [37] S.L. Sunderland, P.W. Santelmann, T.A. Baughman, *Weed Sci.* 39 (1991) 296.
- [38] M.M. Kelley, E.W. Zahnow, W.C. Petersen, S.T. Toy, *J. Agric. Food Chem.* 33 (1985) 962.
- [39] M. Nord-Christerson, L. Bergstrom, *Proc. Brighton Crop Prot. Conf. Weeds* 3 (1989) 1127.
- [40] J.C. Hall, R.J.A. Deschamps, M.R. Mc Dermott, *Weed Technol.* 4 (1990) 226.
- [41] J.-M.A. Schlaeppi, W. Meyer, K. Ramsteiner, *J. Agric. Food Chem.* 40 (1992) 1093.
- [42] J.-M.A. Schlaeppi, A. Kessler, W. Foery, *J. Agric. Food Chem.* 42 (1994) 1914.
- [43] J.F. Brady, J. Turner, D.H. Skinner, *J. Agric. Food Chem.* 43 (1995) 2542.
- [44] G. Dinelli, A. Vicari, P. Catizone, *J. Agric. Food Chem.* 41 (1993) 742.
- [45] B.M. Patel, H.A. Moye, R. Weinberger, *Talanta* 38 (1991) 913.
- [46] M.C. Mahedero, J.-J. Aaron, *Analisis* 20 (1992) 53.
- [47] A. Coly, J.-J. Aaron, *Talanta* 41 (1994) 1475.
- [48] A. Coly, J.-J. Aaron, *Analyst* 119 (1994) 1205.
- [49] J.-J. Aaron, A. Coly, *Analyst* 121 (1996) 1545.

Solid-phase extraction and spectrophotometric determination of trace amounts of copper in water samples

Yadollah Yamini ^{a,*}, Atefeh Tamaddon ^b

^a *Department of Chemistry Tarbiat Modarres University, Tehran, Iran*

^b *Department of Chemistry Shahid Beheshti University, Tehran, Iran*

Received 14 July 1998; received in revised form 4 November 1998; accepted 10 November 1998

Abstract

A simple method for rapid and selective extraction, preconcentration and determination of copper as its neocuproine complex by using octadecylsilica membrane disks and spectrophotometry is presented. Extraction efficiency and the influence of flow rates of sample solution and eluent, pH, amount of neocuproine and hydroxylamine hydrochloride, type and least amount of eluent for elution of copper complex from disks, break through volume and limit of detection were evaluated. Also the effects of various cationic interferences on percent recovery of copper were studied. Extraction efficiencies > 99% were obtained by elution of the disks with minimal amount of solvent. The limit of detection of the proposed method is 0.12 ppb. The method was applied to the recovery and determination of copper in different water samples. © 1999 Elsevier Science B.V. All rights reserved.

Keywords: Copper(I); Neocuproine; Octadecylsilica membrane disks; SPE

1. Introduction

Copper is both vital and toxic for many biological systems [1,2]. Thus the determination of trace amounts of Cu is becoming increasingly important because of the increased interest in environmental pollution. Flame and graphite furnace atomic absorption spectrometry [3] and spectrophotometric methods [4–7] are the most common methods, but their sensitivity is usually insufficient for the low concentrations in environmental samples. Consequently, a preconcentration and matrix elimination step is usually required.

The most widely used techniques for the separation and preconcentration of trace amounts of Cu are liquid–liquid extraction (LLE) [4,5], precipitation and cation exchange resins [4]. In LLE copper(II) or copper(I) form a stable complex with proper chelating agents, and are then extracted into nonpolar or intermediately polar solvents, such as CCl₄, CHCl₃, isopentyl alcohol, etc. [4,9]. Classical methods of extraction (LLE using a chelating agent) are usually time consuming and labor intensive; the other main disadvantages of the technique are the use of large amounts of high-purity solvents for extraction and the subsequent disposal of the solvent, which creates another environmental problem. Nevertheless,

* Corresponding author. Fax: +98-21-8006544.

several other techniques for the preconcentration of copper have been proposed, including adsorption of its diethyldithiocarbamate chelates on microcrystalline naphthalene [8], and preconcentration on C₆₀–C₇₀ fullerenes [9], activated carbon [10], as well as solid-phase extraction [11–15].

Solid-phase extraction (SPE) is an attractive technique that reduces solvent usage and exposure, disposal costs, and extraction time for sample preparation [16]. The basic principle behind the SPE involves passing the water sample through a cartridge or a tube containing an adsorbent that retains the analytes. After the sample has been passed through the tube or cartridge, the analytes are eluted from the adsorbent using a suitable solvent. However, there are also a number of problems with SPE cartridges and tubes [17]. Columns with a narrow internal diameter limit usable flow rates to a range (1–10 ml/min) that necessitates long trace-enrichment times for large sample volumes. Samples with particulate matter will plug the cartridge, and channeling may occur. However, the use of flat disks with high cross-sectional area (SPE disks) may largely prevent these problems. The decreased back pressure encountered with these devices makes much higher flow rates possible, and their wide bed decreases the chance of plugging. In addition new technology for embedding the stationary phase into a disk format prevents channeling and improves mass transfer, especially when 8- μ m dp microparticulates packing are used. In recent years the SPE disks and cartridges have been successfully used for the separation and sensitive determination of metal ions [18–25].

The present work describes the application of SPE disks for the selective extraction, concentration and determination of trace amount of copper as its neocuproine complex spectrophotometrically. Different experimental conditions, e.g. the type and volume of eluting solvent, the effect of pH, the effect of sample and eluent flow rates, the amount of neocuproine and hydroxylamine hydrochloride, on the extraction efficiency and break through volume, limit of detection and maximum capacity of disks for Cu²⁺ ion recovery has been studied.

2. Experimental

2.1. Chemicals and reagents

High-purity methanol, ethanol, chloroform, isopentyl alcohol, hydrochloric acid, acetic acid and ammonia solution (all from Merck) were used without any further purification. Reagent-grade neocuproine (Merck) was used as received. Analytical-grade cupric sulphate, mercuric chloride, sodium tungstate, sodium molybdate, sodium acetate, hydroxylamine hydrochloride and nitrate salts of lithium, sodium, potassium, beryllium, magnesium, calcium, barium, strontium, manganese, iron, lead, cobalt and nickel (all from Merck) were of the highest purity available and used without any further purification. Doubly distilled deionized water was used throughout. The standard stock solution of copper was prepared by dissolving an appropriate amount of CuSO₄·5H₂O in deionized water. Working solutions were prepared by appropriate dilution of the stock solution.

2.2. Apparatus

All absorbance measurements were obtained using a Shimadzu UV-2100 spectrophotometer. An inductively coupled plasma (ICP) model Varian Liberty 150AX Turbo was used for copper concentration determination in river water. A model 624 digital Metrohm pH meter equipped with a combined glass–calomel electrode was used for the pH adjustments.

2.3. Sample extraction

Extraction were performed with 47 × 0.5 mm (diameter × thickness), Empore membrane disks containing octadecyl-bonded silica (8- μ m particles, 60-Å pore size) from J. T. Baker. The disks were used in conjunction with standard Millipore 47-mm filtration apparatus. In order to eliminate small suspended particles, before extraction water samples were filtered through 0.45- μ m pore size nylon filters (Millipore). After each filtration the residue in the filter was washed with 10 ml deionized water.

Table 1
Effect of type and amount of eluent on extraction efficiency

Eluent ^a	Volume (ml)	% Recovery				
		1.0	2.5	5.0	7.5	10.0
Isopentyl alcohol		75.0	80.0	100.0	100.0	100.0
CHCl ₃ /EtOH (4/1)		70.0	94.0	100.0	99.0	100.0

^a Absorbance measurement was performed at $\lambda = 454$ nm for isopentyl alcohol and $\lambda = 457$ nm for chloroform–ethanol mixture.

Before extraction each membrane was washed with 5 ml eluting solvent. After placing the membrane in the filtration apparatus, solvent (5 ml) was introduced to the reservoir of the apparatus and drawn slowly through the disk by applying a slight vacuum. After the disk had been completely dried by drawing air through it for a few minutes, another 10 ml of methanol were again drawn through.

With a thin layer of methanol remaining on the disk, it was washed twice with 10 ml of deionized water. It is important to also note that the surface of the disk did not become dry from the time that methanol was added until the extraction was completed. Then the sample solution containing Cu²⁺, neocuproine, hydroxylamine hydrochloride and buffer was passed through the membrane. After the extraction, the disk was dried completely by passing air through it for a few minutes. The extracted complex was stripped from the membrane disk using appropriate amounts of a suitable solvent. Then the copper neocuproine complex concentration was determined by spectrophotometry at $\lambda = 454$ nm.

3. Results and discussion

Some preliminary experiments were carried out in order to investigate quantitative retention of Cu²⁺ ions by the octadecyl silica membrane disk in the absence and presence of neocuproine. It was found that while the membrane disk does not show any tendency for copper ions, it is capable of retaining copper neocuproine complex in the sample solutions quantitatively (the test solution used contained 15 μ g copper and 5 mg neocuproine in 50 and 250 ml water).

3.1. Choice of eluent

In order to choose a proper eluent for the retained copper complex, after its extraction from water, the complex was stripped with varying volumes of isopentyl alcohol and chloroform–ethanol (mixture) (the molar absorptivity of the complex in these solvents is large [26,27]). From the data given in Table 1, it is obvious that 5 ml of both solvents can accomplish the quantitative elution of the complex from the disk. Subsequent elutions of the complex were carried out with 5 ml isopentyl alcohol.

3.2. Effect of amount of ligand and reducing agent

In order to investigate the optimum amount of neocuproine on the quantitative extraction of copper by the membrane disk, copper ion extraction was conducted by varying the amount of ligand from 0 to 10 mg (Fig. 1). The extraction of copper was found to be quantitative using above 3 mg of the ligand. Hence, subsequent extraction experiments were carried out with 5 mg of the ligand. In these experiments Cu²⁺ were reduced to Cu⁺ ions by using hydroxylamine hydrochloride, and formed a very stable complex with neocuproine. Fig. 2 shows that for quantitative extraction of copper ions more than 0.1 g of hydroxylamine hydrochloride is needed, thus 0.2 g of the reducing agent was used in experiments.

3.3. Effect of pH and flow rate

The influence of pH on the SPE of copper ions was studied in the range of 3–6 and 6–10 using

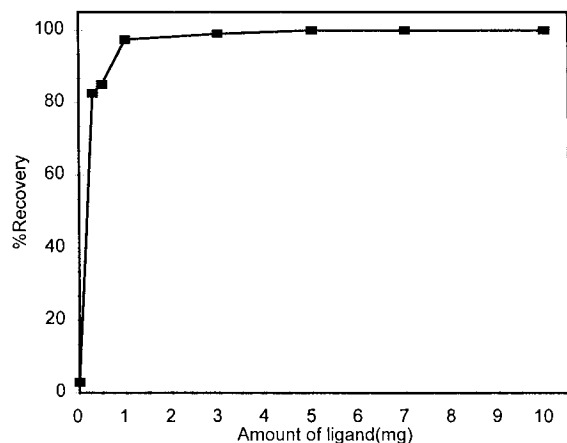


Fig. 1. Effect of the amount of ligand on extraction efficiency.

acetic acid (2 M)/sodium acetate (2 M) and ammonia (1 M)/HCl (1 M) for pH adjustment, respectively (Fig. 3).

The percent recovery depended on the pH of the solution, which was nearly constant in the pH range of 4–8.5. At pH values higher than 8.5, however, the percent recovery decreased. Most probably due to the competition of NH_3 with neocuproine and formation of a non-retained $\text{Cu}(\text{NH}_3)_4^{2+}$ complex, percent recovery decreased. In this study, a buffer solution of 5.0 was adopted.

The effect of flow rates of the sample and stripping solutions from the membrane disk on

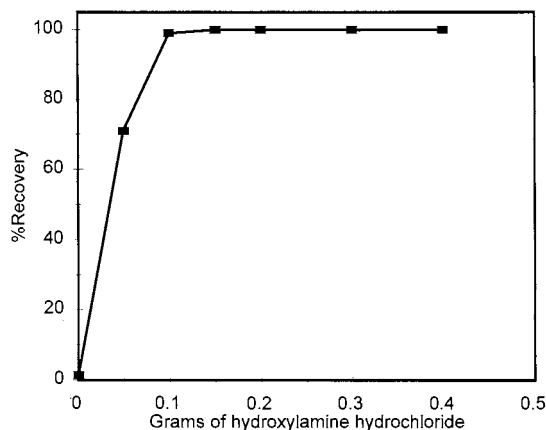


Fig. 2. Effect of the amount of hydroxylamine hydrochloride on extraction efficiency.

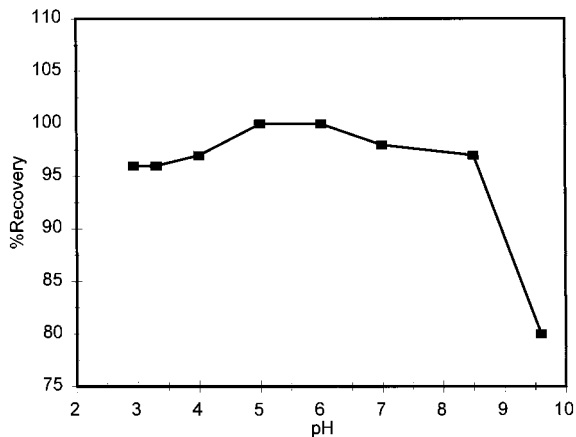


Fig. 3. Effect of pH of sample solution on extraction efficiency.

the retention and recovery of copper ions was investigated. It was found that, in the range of 5–50 ml/min, the retention of the copper complex by the membrane disk was not considerably affected by the sample solution flow rate. Similar results for the extraction of organic materials and cations by octadecyl silica membrane disks have already been reported [25,28,29]. On the other hand, quantitative stripping of the copper complex from the disk was achieved in a flow range of 1–6.5 ml/min, using 5 ml of isopentyl alcohol.

3.4. Analytical performance

The break-through volume of sample solution was tested by dissolving 15 μg of copper in 50, 100, 250, 325, 400 and 500 ml water and the recommended procedure was followed. In all cases, the extraction by membrane disk was found to be quantitative. Thus the break-through volume for the method should be greater than 500 ml. The limit of detection (LOD) of the proposed method for the determination of copper was studied under the optimal experimental conditions. The LOD obtained from $C_{\text{LOD}} = k_b S_b \text{ m}^{-1}$ [30,31] for a numerical factor $k_b = 3$ is 0.12 ppb (for 500 ml of sample solution).

The maximum capacity of the membrane disk was determined by passing 50-ml portions of an aqueous solution containing 1000 μg copper fol-

lowed by washing the disk with 25 ml deionized water and determination of retained metal ions spectrophotometrically. The maximum capacity of the disk was found to be 940 μg of Cu^{+2} ions. In order to investigate the selective separation and determination of Cu^{+2} ion from its binary mixtures with diverse metal ions, an aliquot of aqueous solution (250 ml) containing 15 μg Cu^{+2} and milligram amounts of other cations was taken and the recommended procedure was followed. The results are summarized in Table 2. The results show that the copper(II) ions in the binary mixtures are retained almost completely by the membrane disk, even in the presence of up to about 15 mg of the diverse ions.

In order to assess the applicability of the method to real samples with different matrices containing varying amounts of a variety of diverse ions, it was applied to the separation and extraction of copper(II) ions from 250 ml of three different water samples (i.e. distilled water, tap water and spring water).

Table 3 shows the extraction of 15 μg of added copper ions from 250 ml of different water samples. As seen, the results of three analysis of each sample show that the copper recovery was almost

Table 2
Determination of copper from binary mixtures^a

Foreign ion	Amount taken (mg) ^b	% Recovery
Li^+	15.0	102.0
Na^+	15.0	99.0
K^+	15.0	98.0
Be^{2+}	0.2	101.3
Mg^{2+}	15.0	98.0
Ca^{2+}	15.0	100.0
Ba^{2+}	15.0	100.0
Sr^{2+}	15.0	99.0
Mn^{2+}	15.0	99.0
Fe^{2+}	15.0	101.0
Pb^{2+}	15.0	98.0
Co^{2+}	7.5	99.0
Ni^{2+}	7.5	99.0
Hg^{2+}	0.2	98.0
MoO_4^{2-}	0.3	99.3
WO_4^{2-}	0.3	98.0

^a Amount of copper taken is 15 μg .

^b Fifteen milligrams is the maximum amount of cation that was tested.

Table 3
Recovery of 15 μg copper added to 250 ml of the water samples

Sample	Cu^{2+} found	% Recovery	% RSD
Distilled water	15.0	100.0	0.7
Tap water	14.9	99.7	0.8
Spring water	15.0	100.4	0.6

quantitative. Table 4 shows the concentration of copper at three stations on the Sarcheshmeh river (Kerman, Iran). This river is located next to Sarcheshmeh copper mines and the samples were collected from distances of 1, 20 and 30 km from the mine. As seen, the results of three analyses of each sample obtained by the proposed method and ICP are in satisfactory agreement.

It is noteworthy that, due to its strong tendency for copper ions, the neutral neocuproine used is able to completely retain the copper ions even in the presence of sulfate ions as a counter ion of relatively low lipophilic character.

4. Conclusions

The proposed method has the following advantages. The method is rapid as compared with previously reported procedures for the separation and determination of copper [4,5]. The time taken for the separation and analysis of copper in a 500-ml water sample is at most 12 min. It can selectively separate copper ions from other associated metal ions, even at a much higher concentration. The use of organic solvents in the proposed

Table 4
Determination of copper in Sarcheshmeh river

Sample ^a	Cu conc. (ppm) (SPE)	Cu concn. (ppm) (ICP)	% Error
1	22.57(0.23) ^b	22.00(0.3)	2.59
2	0.23 ₂ (0.59)	0.23 ₅ (1.2)	-1.28
3	0.09 ₄₃ (2.20)	0.09 ₄₀ (0.5)	0.32

^a Samples were collected from the river at distances of 1, 20 and 30 km from copper mines.

^b % RSD based on three replicate analysis.

method is much lower than those consumed in the liquid–liquid extraction methods. The method can be successfully applied to the separation and determination of copper in real samples. It is a simple, highly selective and reproducible method for the separation of copper(II). The reproducibility of procedure is at the most 2%. It is interesting to note that, by combination of the SPE procedure proposed with other copper determination methods, such as flameless AAS, the detection limit of the system can be lowered by a factor of about 100.

References

- [1] I.H. Scheinberg, A.G. Morell, Ceruloplasmin, in: G.L. Eichhorn (Ed.), *Inorganic Biochemistry*, vol. 1, Elsevier, New York, 1973, pp. 306–343.
- [2] N.N. Greenwood, A. Earnshaw, *Chemistry of Elements*, Pergamon, New York, 1984.
- [3] B. Welz, *Atomic Absorption Spectroscopy*, VCH, Amsterdam, 1985.
- [4] Z. Marczenko, *Separation and Spectrophotometric Determination of Elements*, Ellis Horwood, London, 1986.
- [5] *Standard Methods for Examination of Water and Waste Water*, 19th ed., American Public Health Assoc., Washington, DC, 1995, pp. 3–63.
- [6] I. Mori, T. Fujimoto, Y. Fujita, T. Matsuo, *Talanta* 42 (1995) 77.
- [7] M.P. San Andres, M.L. Marina, S. Vera, *Analyst* 120 (1995) 255.
- [8] S.A. Wasay, B.K. Puri, I. Haq, *Int. J. Environ. Studies* 36 (1990) 191.
- [9] Y.P. de Pena, M. Gallego, M. Valcarcel, *Anal. Chem.* 67 (1995) 2524.
- [10] R. Devi, G.R.K. Naidu, *Analyst* 115 (1990) 1469.
- [11] S. Hutchinson, G.A. Kearney, E. Horne, B. Lynch, J.D. Glennon, M.A. Mckervey, S.J. Harris, *Anal. Chim. Acta* 291 (1994) 269.
- [12] P. Lessi, N.L. Dias Filho, J.C. Moreira, J.T.S. Campos, *Anal. Chim. Acta* 327 (1996) 183.
- [13] V. Cuculic, M. Mlakar, M. Branica, *Anal. Chim. Acta* 339 (1997) 181.
- [14] B.S. Garg, J.S. Bist, R.K. Sharma, N. Bhojak, *Talanta* 43 (1996) 2093.
- [15] V. Porta, E. Mentasti, C. Sarzanini, M.C. Gennaro, *Talanta* 35 (1998) 167.
- [16] R. Majors, *LC-GC* 4 (1986) 972.
- [17] C. Markell, D.F. Hagen, V.A. Bunnelle, *LC-GC* 9 (1990) 332.
- [18] R. Lima, K.C. Leandro, R.E. Santelli, *Talanta* 43 (1996) 977.
- [19] M. Groschner, P. Appriou, *Anal. Chim. Acta* 297 (1994) 369.
- [20] R. Compano, M. Granados, C. Leal, M.D. Prat, *Anal. Chim. Acta* 283 (1993) 272.
- [21] M.F. Garcia, R.P. Garcia, N.B. Garcia, A. Sanz-Medel, *Talanta* 41 (1994) 1833.
- [22] M.B. Shabani, T. Akagi, A. Masuda, *Anal. Chem.* 64 (1992) 737.
- [23] Z.S. Liu, S.D. Huang, *Anal. Chim. Acta* 267 (1992) 31.
- [24] Y. Yamini, N. Alizadeh, M. Shamsipur, *Sep. Sic. Technol.* 32 (1997) 2079.
- [25] Y. Yamini, N. Alizadeh, M. Shamsipur, *Anal. Chim. Acta* 355 (1997) 69.
- [26] A.R. Gahler, *Anal. Chem.* 26 (1954) 577.
- [27] G.F. Smith, W.H. McCurdy, *Anal. Chem.* 24 (1952) 371.
- [28] Y. Yamini, M. Ashraf-Khorasani, *J. High Resolut. Chromatogr.* 17 (1994) 634.
- [29] Y. Yamini, M. Shamsipur, *Talanta* 43 (1996) 2117.
- [30] ACS Committee on Environment Improvement, *Anal. Chem.* 52 (1980) 2242.
- [31] J.D. Ingle, S.R. Crouch, *Spectrochemical Analysis*, Prentice Hall, Englewood Cliffs, NJ, 1988.

A low consumption air-segmented sequential injection vapor generation system for the determination of mercury by atomic absorption spectrometry

Hong-Bing Ma^a, Zhao-Lun Fang^{a,*}, Jin-Feng Wu^b, Shu-Sheng Liu^b

^a *Research Center for Analytical Sciences, Box 332, Northeastern University, Shenyang, 110006, China*

^b *Department of Communications Engineering, Northeastern University, Shenyang, 110006, China*

Received 9 September 1998; accepted 10 November 1998

Abstract

A sequential injection system for the determination of mercury by vapor generation atomic absorption spectrometry (VGAAS) using tetrahydroborate reductant was developed, characterized by prevention of sample and reagent mixing in the holding coil using small air segments and initiation of the vapor generation in a flow-through gas–liquid separator. Extremely small volumes of reductant of 15–30 μl (0.2–1.0% NaBH_4) and sample acidity as low as 0.05 mol l^{-1} HCl were sufficient for achieving performance similar to flow injection (FI) VGAAS systems. A sample throughput of 90 h^{-1} was achieved with 400 μl samples with a precision of 2.0% RSD at 10 $\mu\text{g l}^{-1}$ Hg, and a detection limit of 0.1 $\mu\text{g l}^{-1}$ (3σ). Reagent consumption was reduced by a factor of 25 in comparison to the FI-VGAAS system. Good agreement with the certified value was obtained for the determination of mercury in seawater in a standard reference sample © 1999 Elsevier Science B.V. All rights reserved.

Keywords: Sequential injection; Flow injection; Vapor generation; Atomic absorption spectrometry; Mercury.

1. Introduction

In recent years flow injection (FI) vapor generation (VG) techniques for atomic absorption spectrometry (AAS) have enjoyed increasing popularity owing to their outstanding performance compared to the earlier batch-wise operated systems. The merits of FI-VGAAS are convincing and well documented [1], including decreased sample and

reagent consumption, stronger tolerance to interferences, higher sample throughput, and better precision. In addition to fully automated hydride and cold vapor generation AAS determinations, the FI systems also provide easy adaptation of on-line separation systems with sorption columns [1–3] and in situ trapping of hydrides in graphite furnaces [4,5] to further enhance the selectivity and sensitivity, and even adaptation to on-line oxidation of organo analyte species [6,7]. Therefore, it is not surprising that FI-VGAAS has become the first commercialized FI system for AAS.

* Corresponding author. Fax: +86-24-2389-0448.

E-mail address: fangzl@mail.neu.edu.cn (Z.-L. Fang)

However, the FI-VGAAS system is not entirely without limitations, although some are associated with those of FI instrumentation itself. The majority of FI-VGAAS systems, including the commercialized version, are equipped with peristaltic pumps as liquid drives. The aging of pump tubes is rather high owing to the relatively high carrier and waste flow rates (and therefore high pump rotation speeds) often employed in such systems. Frequent re-calibration of flow rates is required for optimum performance, and consumption of pump tubes is relatively high. In spite of that reagent consumptions of FI-VGAAS systems are about an order of magnitude lower than batch systems, further reduction of the tetrahydroborate reductant should be desirable and feasible owing to the fact that the duration of the vapor generation reaction phase constitutes to less than one-third of the total analytical cycle, during which tetrahydroborate reagents are usually delivered continuously. Reduction of acid concentration in the sample and carrier is also desired not only for decreasing the acid consumption, but also for maintaining a better laboratory environment both for the operator and the FI/AAS instruments. Although the merging zones approach has been considered as a means for saving expensive reagents in FI systems, in order to compensate for small flow-rate drifts in the two merging channels, the volume of the reagent should usually be larger than that of the sample, which generally falls in the range of 200–500 μl for FI-VGAAS systems [1]. A reagent volume of at least 300–600 μl should therefore be required, making the saving quite marginal. Moreover, more frequent calibration of the flow rate of the two merging channels should be required to ensure synchronous merging of the two zones, making the procedure less robust.

Recently, the sequential injection (SI) approach [8], usually based on equipment composed of a computer controlled syringe pump and multiposition valve, has been used in a number of applications to substitute FI procedures in combination with various detectors. Often the purpose of this transformation is for

simplifying the operations associated with the manipulation of peristaltic pumps and/or the saving of reagents, which both may be of help in overcoming some of the limitations of FI-VGAAS systems. However, in the case of VG systems, the transformation of FI to SI appears not that straightforward or even optimistic. The reason is that VG is often associated with a violent gas-forming reaction involving the use of tetrahydroborate reductants. On contact of the acidified sample and reagent, when sequentially introducing them into the storage tube, partial initiation of the hydrogen forming reaction would interfere with the solution metering process and seriously deteriorate the precision. At least for the cold vapor determination of mercury, this was avoided by using weaker reactions with stannous chloride reductant without hydrogen evolution, as reported by Brindle and Zheng [9] and more recently by Bauza de Mirabo et al. [10] in the first SI systems used for that purpose. Brindel and Zheng gave no details on the manifold design and performance of the system in their technical note which was mainly aimed at comparing the various designs of gas-liquid separators used in that application. However, in the work reported by Bauza de Mrabo et al. a sampling frequency of 30 h^{-1} was obtained, which was much lower than those (typically 100 h^{-1}) achievable with FI cold vapor systems using tetrahydroborate reductants. This might be, at least partially, the result of the weaker reaction with stannous chloride, which took 30 s to complete. The stannous chloride reductant excludes the direct determination of organic mercury species such as methylmercury [11], and also restricts the extension of the SI system to other elements requiring stronger reducing conditions for vapor generation.

This work was aimed at finding the appropriate conditions to perform automated VGAAS determinations using the SI approach with tetrahydroborate reductant. This resulted in a system which not only maintained all the advantages of FI-VGAAS, but also with enhanced ruggedness and significant reduction in reagent consumption.

2. Experimental

2.1. Apparatus

A Perkin-Elmer Model 2100 atomic absorption spectrometer with deuterium-arc background corrector was used with the Model FIAS-200 flow-injection system and hydride generation accessories with a detachable gas-liquid separator equipped with membrane filter for removal of liquid droplets. Mercury hollow cathode lamp was used at 253.7 nm wavelength, and operated at 7.0 mA. The temperature of the quartz atomizer cell was set to 200°C, and the argon carrier flow was set at 200 ml min⁻¹. The gas-liquid separator and the quartz atomizer were connected with a 100-cm, 1.0-mm i.d. PTFE tubing. The injection valve of the FI instrument was not used in this study. A single pump channel was run continuously for withdrawal of reaction waste from the gas-liquid separator at 18 ml min⁻¹. The 15-s readout time was programmed and controlled by the spectrometer computer. The signals were processed with a time constant of 0.5 s in the peak height mode and recordings from the graphic screen were printed out by a Model FX-850 printer.

The SI system was constructed from a Hamilton Model ML-511C syringe pump (Hamilton, Reno) and a Valco Model E10-220 10-position stepper motor operated selector valve. The pump was equipped with a two-way valve, connected to a 5.0 ml syringe, and programmable in 1000 steps. The operation of the syringe pump and valve were synchronously controlled from a computer program written in VISUAL BASIC. The pump and central port of the valve were connected by a holding coil made from 240-cm, 1.0-mm i.d. PTFE tubing. All other transport lines were made using 0.7-mm i.d. PTFE tubing, including that from the valve outlet to the gas-liquid separator, which was 40 cm in length. Argon gas was introduced from a three-way connector into this latter line 1 cm upstream of the connection to the gas-liquid separator

2.2. Reagents and solutions

Mercury working standards were prepared

through two-stage dilutions of a 1000 mg l⁻¹ stock solution (in 1 mol l⁻¹ HCl) by the appropriate acid of the sample matrix used in each individual study.

Sodium tetrahydroborate reagents were freshly prepared daily by dissolving the appropriate amount of NaBH₄ (China Pharmaceutical, Beijing Branch, Beijing) in 0.2 mol l⁻¹ sodium hydroxide solution.

Hydrochloric acid was of ultra-pure reagent grade, all other chemicals were of analytical reagent grade and demineralized water was used throughout. Water carrier was de-gassed before use.

2.3. Procedures

The flow manifold and optimized sequence of operation are shown in Fig. 1 and Table 1 respectively. The syringe steps travelled during sequences 4, 6, and 7 were varied during system optimization to introduce different sample and reagent volumes.

In the pre-stage, required only for starting-up the system (not shown in Table 1), demineralized water carrier was fully aspirated into the syringe with valve V2 in left position, and with valve V2 turned to right position, water was discharged into the holding coil and thence to waste with selector valve in position 5, removing any air bubbles trapped in the syringe. In sequence 1,

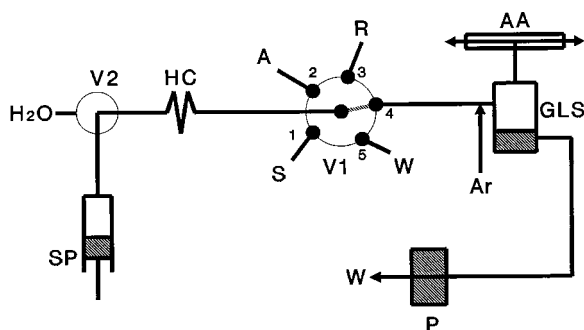


Fig. 1. diagram of the SI-VGAAS system. SP, syringe pump; P, peristaltic pump; AA, atomic absorption quartz atomizer cell; V1, selector valve; V2, syringe valve; HC, holding coil; GLS, gas-liquid separator; S, acidified sample; R, NaBH₄ reagent; A, air; H₂O, washing (carrier) water; W, waste.

Table 1
Sequence of operation of the SI-VGAAS system

Sequence No.	Valve V1 position	Valve V2 position	Syringe steps moved	Volume processed (μl)	Time duration (s)	Function
1	No change	Left	80	400	6	Wash water aspiration
2	2, Air	Right	5	25	5	Air aspiration
3	1, Sample	Right	80 ^a	400	9	Sample aspiration
4	2, Air	Right	5	25	5	Air aspiration
5	3, Reagent	Right	6 ^b	30	5	Reagent aspiration
6	4, Separator	Right	–176 ^c	1350	6	Injection of reagent/sample
7	1, Sample	Right	20	100	5	Aspiration of next sample
8	5, Waste	Right	–20	100	5	Discharge of sample to waste
			Steps 1–6	Total time	25	

^a Steps moved for 400 μl sample.

^b Steps moved for 30 μl reagent.

^c Steps moved for 400 μl sample and 30 μl reagent.

with V2 in left position and V1 remaining in the original position from the end of the previous cycle, 600 μl water was aspirated into the syringe; in sequence 2, with V2 in right position and V1 in 2 position, 25 μl air was aspirated into the holding coil; in sequence 3, with V2 in right position and V1 in 1 position, 200–1000 μl sample was aspirated into the holding coil; in sequence 4, with V2 in right position and V1 in 2 position, 25 μl air was again aspirated into the holding coil; in sequence 5, with V2 in right position and V1 in 4 position, 15–30 μl tetrahydroborate reagent was aspirated into the holding coil; in sequence 6, with V2 in right position and V1 in 4 position the aspirated contents in the holding coil were pushed into the gas–liquid separator at about 13 ml min^{-1} flow rate. The readout was initiated at the beginning of sequence 6 with a readout period of 15 s. The next analytical cycle was activated before the termination of readout and printout of results, and a sampling frequency of 90 h^{-1} was achieved with 400 μl sample volume. The sequences 7 and 8 were required only when a new sample was introduced to flush out the previous sample in the sampling probe capillary to waste at valve position 5, and could be operated in parallel with the readout of the previous sample. Short probes of < 15 cm, 0.7 mm i.d. PTFE tubing are preferred for easy flushing and minimum carry-over. The waste solution exiting the gas–liquid separator was drawn out continuously by the peristaltic pump at a flow rate of 18 ml min^{-1} , which was about 5 ml min^{-1} higher than the inflow rate.

2.4. Method development

The chemical and SI parameters were optimized mainly using an univariate approach, based on conditions adopted in FI-VGAAS systems [1], taking sensitivity expressed in peak height as the principle figure of merit, but with concurrent considerations on precision, throughput and selectivity. The variables studied included sample volume and acidity, reagent volume and concentration. The flow rates of the reaction mixture, waste withdrawal, and carrier (stripping) gas were mainly adopted from FI-VGAAS systems, and

checked in preliminary experiments to be adaptable to the SI system. a 20.0 $\mu\text{g l}^{-1}$ Hg standard solution was used for the studies.

3. Results and discussion

3.1. Considerations in system design

In general, SI systems are characterized by simple manifolds with a single reaction line, functioning as an extension of the holding coil during the reaction/detection sequence of operation. Owing to penetration of neighboring zones of sample and reagent not only in the reactor, but already in the holding coil, the reactions are usually initiated even in the sample and reagent aspirating (metering) stage. Since the entire procedure is computer controlled and highly reproducible, this feature usually does not deteriorate the performance of SI systems, and in fact even be desirable for shortening the reaction time and increasing the throughput. However, such expectations are no more valid when the reactions involve gas evolution, such as hydride generation. Partial penetration and mixing of sample and reagent zones result in gas formation already in the aspiration stage, and inevitably interfere with the precise metering of at least one of the solutions. The subsequent delivery of the contents in the holding coil is also disturbed seriously, owing to the compressibility of large gas segments in the conduits. Such behavior, observed in our preliminary studies, persuaded us to produce a barrier between neighboring zones of reactive solutions which could avoid their mutual penetration before reaching the reactor. Intercalated water zones may serve the purpose, but owing to dispersion in the holding coil, relatively large zones of a few hundred microliters were required in our studies in order to completely avoid the contact of reactive zones, and such measures significantly decreased the sampling frequency of the procedure. Small air segments were therefore introduced to form the barrier. Despite the compressibility of air, previous experiences in FI systems [12,13] show that small segments in the order of a few tens of microliters introduced in 0.5–1 mm i.d. conduits, will not affect the flow

rate noticeably, while dispersion between neighboring zones are completely hindered. Air segments have been used also in a SI solvent extraction system to aid the formation of liquid films on the walls of the extraction walls [14]. Air segmentation was adopted in the design of the present system not only to avoid the premature initiation of the vapor generation reaction but also to limit the dispersion between the sample and washing (water) solutions. Owing to the relatively large sample volumes of usually a few hundred microliters involved in FI-VGAAS systems, which should be also generally applicable to SI-VGAAS, a washing solution is definitely required in the latter to substitute the function of the carrier solution in FI systems in order to avoid carryover between samples. A small air segment between the sample and wash solution avoids dispersion and improves the efficiency of the washing significantly.

Although air segmentation was successful in preventing reaction during the aspiration stage, this measure also obliterated the possibility of initiating the reaction within the tubular reactor, as practised in FI-VGAAS systems. Therefore such attempts were given up completely, and the vapor generation reaction was designed to initiate within the gas-liquid separator, which in this case also functioned as the reactor. Based on Brindel and Zheng's observations, the commercialized Perkin-Elmer gas-liquid separator (version 2) was used for most of the work in this study, but with the membrane filter loaded in place. Preliminarily, in view of the small capacity (about 2.5 ml below the membrane filter) of the gas-liquid separator, and the large waste withdrawal rate required for preventing transport of liquid phase into the atomizer, it was doubted that such a reactor could provide sufficient mixing of sample and reagent as well as reaction time for the resulting mixture. In fact under continuous withdrawal of waste, the liquid volume retained in the reactor (including the liquid film formed on its walls) was no more than 30 μl . However, the efficiency of the mixing happened to be surprisingly high, as demonstrated by the performance discussed in Section 3.3, probably owing to the intensive mixing of solutions caused by strong gas evolution.

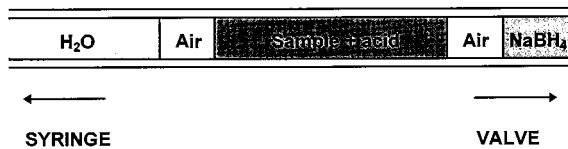


Fig. 2. Schematic diagram of the sequence of zones in the holding coil before injection into the gas-liquid separator through the selector valve.

Based on these considerations, the train of solutions aspirated into the holding coil before being sequentially injected into the reactor was arranged as shown in Fig. 2. In this sequence, the reductant was introduced into the reactor first, preceding the acidified sample; this being the only choice considering the relatively large sample volume and small reactor capacity. With sample introduced first, the majority of the sample would have been drawn to waste before coming into contact with the reagent. In earlier studies, a format involving the introduction of more than one reagent zones intercalated within the sample zone (also with air segment barrier) was also tested with the aim of providing better mixing. This inevitably decreased the throughput of the procedure; however, no favorable effects were observed, while a peak broadening, often accompanied by other complications of the peak profile, was encountered. The simplest design in the train sequence was therefore adopted for further optimization.

3.2. Optimization of chemical variables and SI parameters

The optimization was conducted as described under Section 2.4. Owing to the small capacity of the gas-liquid separator for liquid retention, the testing of reagent volumes above 30 μl was considered meaningless. Volumes of 15 and 30 μl of different concentrations of reductant in the range 0.2–1.0% (w/v) NaBH₄ were studied for their effects on peak height absorbance and reproducibility against different HCl concentrations for different sample volumes. The effect was insignificant for all sample volumes studied (200–1000 μl) at a low sample acidity of 0.05 mol l⁻¹, and on the average only about 5 and 7% lower for the 15 μl volume at 0.3 and 1.0 mol l⁻¹ HCl,

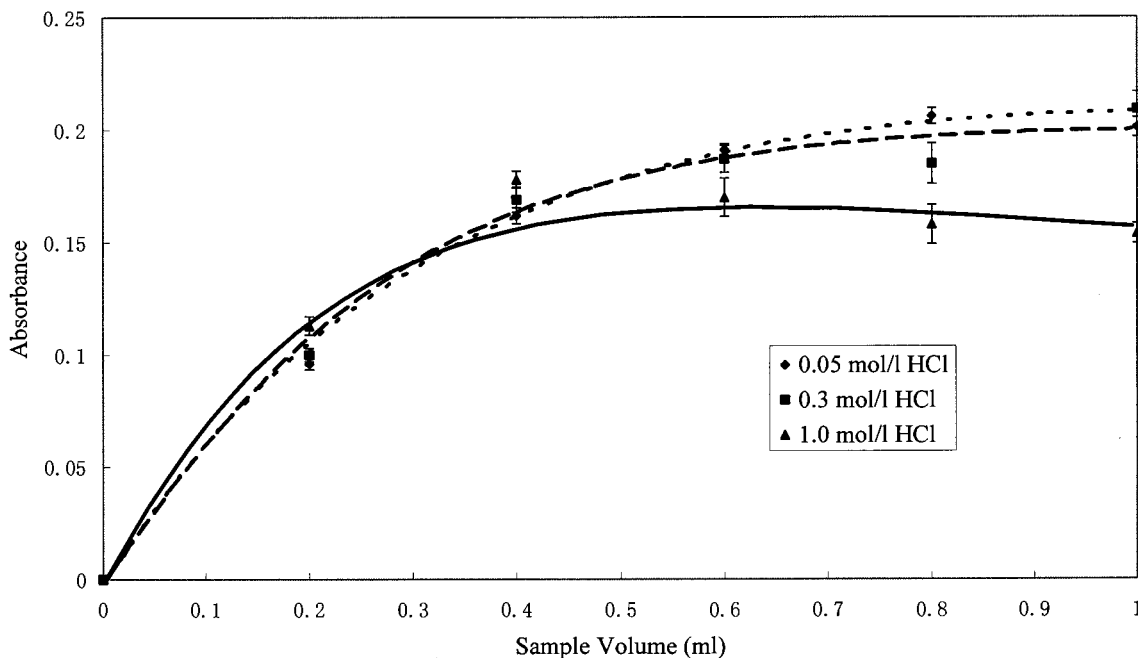


Fig. 3. Effect of sample volume and acidity on peak height response of $20 \mu\text{g l}^{-1}$ Hg using $30 \mu\text{l}$ 0.2% NaBH_4 ; 13 ml min^{-1} injection flow rate; 18 ml min^{-1} out flow.; 200 ml min^{-1} Ar flow rate.

respectively. The effect of reductant concentration (0.2–1.0%) on sensitivity was also generally insignificant in the various combinations of sample volume, acidity, and reductant volume ranges studied. Based on these results, $30 \mu\text{l}$ 0.2% NaBH_4 was adopted to save reagent, which implies a low consumption of 0.06 mg NaBH_4 for each determination, an amount lower than the FI-VGAAS procedure by a factor of 25.

The effects of sample volume and acidity were studied in the range $200\text{--}1000 \mu\text{l}$ and $0.05\text{--}1.0 \text{ mol l}^{-1}$ HCl. The results presented in Fig. 3 showed sharp increases in peak absorbance below $400 \mu\text{l}$ in the entire acid concentration range, above which the response levelled significantly, an observation quite similar to those reported in FI-VGAAS systems. The maximum absorbance reached tend to decrease at higher acidity. Thus the maximum peak height attained at 0.05 mol l^{-1} was more than 20% greater than that at 1.0 mol l^{-1} . This may be explained by the more intensive consumption of the reductant at higher acidity and/or the more intensive generation of hydrogen gas, resulting in larger dilution of the

evolved analyte species. The higher intensity of the reaction resulted in larger peak heights. The close proximity of the 0.05 and 0.3 mol l^{-1} HCl curves, and of all curves below $400 \mu\text{l}$ sample volume imply good ruggedness on acidity requirements, particularly at lower sample volumes. Sensitivities were found to remain more or less constant within a sample volume range of $400\text{--}1000 \mu\text{l}$ for all sample acidity studied. It is noteworthy that, despite continuous forced outflow of reaction mixture, the small volume of reductant ($15\text{--}30 \mu\text{l}$) retained in the reactor (gas-liquid separator) at the beginning of the reaction was in fact sufficient for maintaining the vapor generation reaction up till a sample volume of at least $600 \mu\text{l}$. However, particularly at higher sample acidity (e.g. 1.0 mol l^{-1}), the smoothness of the falling slope of the peak profile was disturbed at sample volumes above $800 \mu\text{l}$, resulting in irregular peak shoulders on the slope, with degradation of precision in peak maximum readout. Apparently, this is a result of reagent depletion at the further end of the sample bolus. Therefore sample volumes of $400\text{--}500 \mu\text{l}$ are recommended for bet-

ter ruggedness and higher throughput. The precision of the data points, illustrated by the error bars, representing S.D. of seven replicate measurements, shows a degradation at higher acidity, with an average of 2.0, 3.5, and 4.0% RSD for sample acidity of 0.05, 0.3 and 1.0 mol l⁻¹ HCl, respectively. Therefore, for better precision, lower sample acidity are recommended.

3.3. Performance of the SI-VGAAS system

The figures of merit of the SI-VGAAS system with 400 µl sample in 1.0 mol l⁻¹ HCl, 30 µl 0.5% NaBH₄ reagent are shown in Table 2. The detection limit obtained could have been further improved by reducing the blank value, which was about 1 µg l⁻¹ Hg. In this study, sources of contamination were tracked to impurities in the hydrochloric acid and argon gas. However, improving the detection limit was not the main objective of this study, and no special attempts were made to lower the blank values.

An outstanding advantage of FI-VGAAS methods is their often dramatically improved tolerance to interferences, the mechanism of which has been discussed in great detail [1]. Whether such features are inherited in the SI-VGAAS system requires serious consideration, although the extremely short residence of the reaction mixture was expected to be beneficial for reducing interferences. Nickel was taken as a model interferent for the study. The results show a similar behavior to the FI-VGAAS system with tolerance of Ni up to a high concentration of 300 mg l⁻¹ (90% recovery) in a 1 mol l⁻¹ HCl sample matrix. At the lower acidity recommended in this work, the tolerance was somewhat degraded (50 mg l⁻¹ Ni tolerated), but still better than the batch procedure by a factor of 50, and sufficient for most applications.

Table 2
Figures of merit on the performance of the SI-VGAAS system

Sampling frequency	90 h ⁻¹
Regression equation (0–20.0 µg l ⁻¹ Hg)	$A = 0.0148C + 0.0044$ ($r^2 = 0.9984$, $n = 7$)
Precision	2.0% RSD (20 µg l ⁻¹ Hg, $n = 10$)
Detection limit (3σ)	0.1 µg l ⁻¹ Hg

The tolerance to other hydride forming elements was studied by testing the tolerated concentrations of Se(IV) and As(III). Up to 10 mg l⁻¹ As(III) and Se(IV) were tolerated (90% recovery) at a sample acidity of 1.0 mol l⁻¹ HCl, and 5 mg l⁻¹ As(III), 0.5 mg l⁻¹ Se(IV) was tolerated at 0.05 mol l⁻¹ HCl.

The method was tested using a standard reference sea water GBW(E)080042 (Institute of Oceanology, Hangzhou) with a certified mercury content of 1.00 ± 0.06 µg l⁻¹. The sample was acidified to contain 1.0 mol l⁻¹ HCl before injection, and corrected for the dilution following readout. The result obtained was 1.00 ± 0.04 µg l⁻¹ ($n = 3$), which was in excellent agreement with the certified value.

4. Conclusions

To our best knowledge, this is the first report of successfully applying the SI technique to a VG atomic spectrometric system using the tetrahydroborate reductant. The system developed in this work for the determination of mercury by VGAAS demonstrated distinct advantages over the now widely accepted FI-VGAAS procedure, overcoming some of its limitations, particularly in achieving large savings in reagent consumption, with reduction by a factor of 25, and improvement in the robustness of the procedure, while maintaining the high throughput, precision, selectivity and low detection level of FI-VGAAS procedures. The principles of design, characterized by air-segmentation between sample and reagent zones and reaction in the gas–liquid separator, should as well be applicable to other VG atomic spectrometric systems, in particular hydride generation systems. In fact, further attempts at adaptation of the system, with exactly the same SI hardware, to the determination of bismuth to achieve similar effects as for mercury, has proved to be fairly simple. However, the extremely short residence time of the reaction mixture within the reactor may limit its use only to fast vapor generation reactions. Nevertheless, it is believed that most vapor generation reactions may be fast enough to achieve sensitivities sufficient for a large number of applications.

Acknowledgements

This work is partially supported by a research grant from the State Natural Science Foundations of China. The authors express their thanks to Bodenseewerk Perkin-Elmer for the loan of the atomic absorption spectrometer, for the donation of the syringe pump, and for partial financial support.

References

- [1] Z.-L. Fang, Flow Injection Atomic Absorption Spectrometry, Wiley, Chichester, UK, 1995.
- [2] S.-C. Zhang, S.-K. Xu, Z.-L. Fang, Guangpuxue yu Guangpu Fenxi 8/6 (1988) 39.
- [3] S.-C. Zhang, S.-K. Xu, Z.-L. Fang, Quim. Anal. 8 (1989) 191.
- [4] G.-H. Tao, Z.-L. Fang, J. Anal. At. Spectrom. 8 (1993) 577.
- [5] P. Bermajo-Barrera, J. Moreda-Pineiro, A. Moreda-Pineiro, J. Anal. At. Spectrom. 12 (1997) 317.
- [6] T.-Z. Guo, J. Baasner, M. Gradl, A. Kristner, Anal. Chim. Acta 320 (1996) 171.
- [7] C.P. Hanna, J.F. Tyson, S. McIntosh, Anal. Chem. 65 (1993) 653.
- [8] J. Ruzicka, G.D. Marshall, Anal. Chim. Acta 237 (1990) 329.
- [9] I.D. Brindel, S. Zheng, Spectrochim. Acta B 51 (1996) 1777.
- [10] F.M. Bauza de Mirabo, A.Ch. Thomas, E. Rubi, R. Forteza, V. Cerda, Anal. Chim. Acta 355 (1997) 203.
- [11] C.E. Oda, J.D. Ingle, Anal. Chem. 53 (1981) 2305.
- [12] B.F. Reis, M.A.Z. Arruda, E.A.G. Zagatto, J.R. Ferreira, Anal. Chim. Acta 206 (1988) 253.
- [13] S.-K. Xu, M. Sperling, B. Welz, Fresenius J. Anal. Chem. 344 (1992) 535.
- [14] Y. Luo, R. Al-Othman, J. Ruzicka, G.D. Christian, Analyst 121 (1996) 601.

Direct determination of bismuth, indium and lead in sea water by Zeeman ETAAS using molybdenum containing chemical modifiers

Orhan Acar ^a, A. Rehber Türker ^{b,*}, Ziya Kılıç ^c

^a TAEA, Ankara Nükleer Araştırma ve Eğitim Merkezi, 06983, Ankara, Turkey

^b Gazi Üniversitesi, Fen Edebiyat Fakültesi, 06500, Ankara, Turkey

^c Gazi Üniversitesi, Gazi Eğitim Fakültesi, 06500, Ankara, Turkey

Received 9 July 1998; received in revised form 20 October 1998; accepted 12 November 1998

Abstract

Direct determination of Bi, In and Pb in sea water samples has been carried out by ETAAS with Zeeman background correction using molybdenum containing chemical modifiers and tartaric acid as a reducing agent. Maximum pyrolysis temperatures and the effect of mass ratios of the mixed modifier components on analytes have been investigated. Mo + Pd + TA or Mo + Pt + TA mixture was found to be powerful for the determination of 50 µg l⁻¹ of Bi, In and Pb spiked into synthetic and real sea waters. The accuracy and precision of the determination were thereby enhanced. The recoveries of analytes spiked were 94–103% with Mo + Pd + TA or Mo + Pt + TA and they are only 49–61% without modifier. © 1999 Elsevier Science B.V. All rights reserved.

Keywords: ETAAS–Zeeman background correction; Bismuth; Indium; Lead; Sea water; Chemical modifiers

1. Introduction

In recent years, determination of volatile elements such as bismuth, indium and lead in sea water samples has become increasingly important in order to monitor the pollution of this environment. Owing to its high sensitivity and specificity, electrothermal atomic absorption spectrometry (ETAAS) with Zeeman background correction is

one of the most promising methods for the direct determination of trace elements in water samples [1–3]. However, the high salt contents of sea water matrix and very low concentrations of volatile elements cause considerable difficulty in the direct analysis. During the determination of volatile elements by ETAAS, chemical interferences and significant background absorbance often occur in graphite furnace due to covolatilization of the analyte with the matrix [2,3].

To overcome most of the matrix interferences and to increase the accuracy of determination in

* Corresponding author. Tel.: +90-312-212-2900; fax: +90-312-212-2279.

E-mail address: rrturker@quark.fef.gazi.edu.tr (A.R. Türker)

ETAAS, the application of chemical modification for the stabilization of volatile elements during pyrolysis stage is one of the methods that has met with reasonable success for analyte elements [1]. For this purpose many metal salts, their mixtures and some organic substances have been recommended and used as chemical modifiers [2–11]. The aim of matrix modification is to permit the pyrolysis temperature to be high enough to remove the bulk of the interfering substances during the pyrolysis stage without loss of analyte before atomization stage. In our previous works [10,11], the effects of tungsten, palladium and molybdenum containing chemical modifiers as well as tartaric acid (TA) for the thermal stabilization of Bi, In and Pb have been investigated systematically and applied to the determination of Bi and Pb in geological samples. Several matrix modifiers and organic substances have been recommended and used to determine lead in water samples [7,8].

The aim of presented work is to determine Bi, In and Pb in synthetic and real sea water samples by using molybdenum containing chemical modifiers. Tartaric acid (TA) was added as chemical reductant to the sample solutions together with the mixed modifiers to provide higher thermal pre-treatment temperatures of analytes, to modify the form of modifier and help to reduce chemical interferences. Tartaric acid produces reductants such as C, CO and H₂ by thermal decomposition, similar to ascorbic acid or oxalic acid used by Byrne et al. [12]. Addition of tartaric acid should assure an early reduction of modifiers and analytes to highly dispersed metallic forms in the temperature programme and elimination of chlorides as HCl (g). Efficient reductants produced from TA at the surface of the tube might react with the chlorides in the aqueous matrices to form HCl (g) which is removed at low temperatures [13], thus preventing the loss of analyte as chloride. Therefore, Mo + Pd + TA and Mo + Pt + TA mixed modifiers that provided the higher pre-treatment temperatures for the analytes [11] were applied to the direct determination of spiked Bi, In and Pb in synthetic and real sea water samples by ETAAS with Zeeman background correction system.

2. Experimental

2.1. Instrumentation

A Hitachi Model 180/80 flame and graphite furnace atomic absorption spectrometer equipped with a Zeeman effect background corrector, autosampler (P/N-170/126) and an automatic data processor was used for all measurements. Details about the AAS equipment, thermal stabilizing studies and optimized graphite furnace temperature programme for wall atomization is given in previous works [10,11]. The operating parameters were set as recommended by the manufacturer except that a spectral band pass of 1.3 nm and alternate wavelength was used for Bi (306.8 nm). The light sources are single-element hollow cathode lamps. A Varian model 9176 recorder was connected to AAS to obtain atomization profiles of analytes in a 20 mV/FS spans. Hitachi pyrolytically coated graphite tubes (P/N-180/7444) were used for atomization throughout. All absorbance values were obtained by using integrated mode. Argon served as a carrier gas in 300 ml min⁻¹ flow rate.

2.2. Reagents

All solutions were prepared by dissolving analytical grade reagents in deionized water distilled in an Elgastat type C114 distillation unit. Stock standard solutions (2000 µg ml⁻¹) of Pd and Pt were prepared according to [9]. 0.4% (m/v) of Mo (VI) was prepared from H₂MoO₄ (Merck) dissolved in 1% (v/v) ammonia solution. All modifier solutions were diluted as required. 4% (m/v) tartaric acid (TA) solution was prepared daily. 1000 µg ml⁻¹ of Bi, In and Pb standard solutions (BDH chemicals) were used. Working standard solutions were freshly prepared by successive dilution to the desired concentrations using 0.2% HNO₃.

2.3. Procedure

Synthetic sea water was prepared according to Cantle [14]. 2.67 g of NaCl, 0.54 g of MgCl₂, 0.11 g of CaCl₂ and 0.08 g of KCl salts were dissolved

in a teflon beaker with deionized water. 1 ml of each Bi, In and Pb standard solutions ($20 \mu\text{g ml}^{-1}$) were spiked into it and this solution was transferred into a 100 ml glass calibrated flask. The Teflon beaker was washed two times with 0.2% (v/v) nitric acid. 600 μl of conc. nitric acid was also added to final solution to avoid the absorption of analytes onto glass walls and diluted to the mark with deionized water. Sea water sample was collected from the surface water of the Marmara sea coast in Türkiye in a 2 l polyethylene bottle. A sample portion was transferred into 100 ml volumetric flasks and immediately acidified with 1 ml of conc. nitric acid. 1 ml of each Bi, In and Pb standard solutions ($20 \mu\text{g ml}^{-1}$) were spiked into these flasks because of natural contents of the analytes are below the detection limits. All of the flasks were filled with sample (sea water) to the mark.

Synthetic or Marmara sea water sample containing $200 \mu\text{g l}^{-1}$ analytes was diluted by a factor 4 (0.5 ml of sample + 1.5 ml of deionized water) in order to decrease interferences in the absence of modifier. In the presence of modifier, 0.5 ml of sample solution and 0.5 ml of water were added to 1 ml of modifier solution ($20\,000 \mu\text{g ml}^{-1}$ of TA, $2000 \mu\text{g ml}^{-1}$ of Mo, $400 \mu\text{g ml}^{-1}$ of Pd or Pt, $2000 \mu\text{g ml}^{-1}$ of Mo + $20\,000 \mu\text{g ml}^{-1}$ of TA, $400 \mu\text{g ml}^{-1}$ of Pd or Pt). 0.5 ml of sample solution and 0.5 ml of TA (4% (m/v)) stock solution instead of water were added to 1 ml of modifier solution ($2000 \mu\text{g ml}^{-1}$ of Mo + $400 \mu\text{g ml}^{-1}$ of Pd or Pt) for the triple modifier mixtures such as Mo + Pd + TA. 20 μl of the sample solution (analyte concentration $50 \mu\text{g l}^{-1}$) prepared in the presence or absence of single or mixed modifiers were injected into the graphite tube.

The optimized graphite furnace temperature programme for wall atomization is given in Ref. [11]. The optimum modifier mass and mass ratio of the mixed modifier components were found to be 20 μg of Mo, 4 μg of Pd and Pt, and 20/4 ($\mu\text{g}/\mu\text{g}$) of Mo/Pd and Mo/Pt. 200 μg of TA was used together with the mixed modifiers [11].

3. Results and discussion

3.1. Stabilizing effects of modifiers on analytes

In order to remove the high contents of salts in sea water, higher pyrolysis temperatures for analytes may be preferable. A chemical modifier has been recommended for a long time to increase maximum permissible temperature and to minimize interferences in the determination of volatile elements in ETAAS [2]. Maximum pyrolysis temperatures (T_{max}) of the analytes studied and the optimum mass ratios of the mixed modifier components were found in our previous work [11]. Obtained pyrolysis temperatures are approximately in agreement with Tsalev's results [13,15]. When Mo + Pd + TA was used, higher pyrolysis temperatures were obtained than the other modifier mixtures studied by Havezov et al. [16].

In this study, thermal pre-treatment curves for analytes with TA, Pd + TA and Pt + TA modifiers were also studied and lower pyrolysis temperatures were obtained. The addition of TA to Pd and Pt did not increase the pyrolysis temperature, but it increased the formation of analyte atoms at lower temperatures [12]. The effect of tartaric acid on atomic absorption signal of analyte can be explained primarily by reaction that occur between gaseous analyte-containing molecules such as PbO (g) and the reducing gases produced by pyrolysis of tartaric acid during the atomization temperature ramp [12].

When the Mo + Pd + TA or Mo + Pt + TA was added to the solution, the pyrolysis temperatures could be increased up to 1350–1400°C for Bi and In and 1250–1300°C for Pb to remove much of sample matrix without the risk of analyte loss [11]. The mechanism of increased thermal stability can be explained from the reaction between analyte and modifier elements. Shan and Wang from X-ray photoelectron spectra, suggested the formation of Pb–Pd and Bi–Pd intermetallic bonds on graphite furnace [17].

3.2. Effect of modifiers on the atomization profiles of analytes

One advantage of chemical modification is that

the atomization signals become fairly symmetrical and shifted to higher pre-treatment temperatures and appearance times [18]. Welz et al. [4] demonstrated this behaviour by comparing the shapes of atomization signals of various elements in both the absence and presence of a Pd–Mg modifier. In order to demonstrate how the Mo, Mo + Pd + TA and other Mo-based modifiers affect the atomization and background profiles of analytes, a comparative study was conducted. Fig. 1 shows that the analyte and background atomization

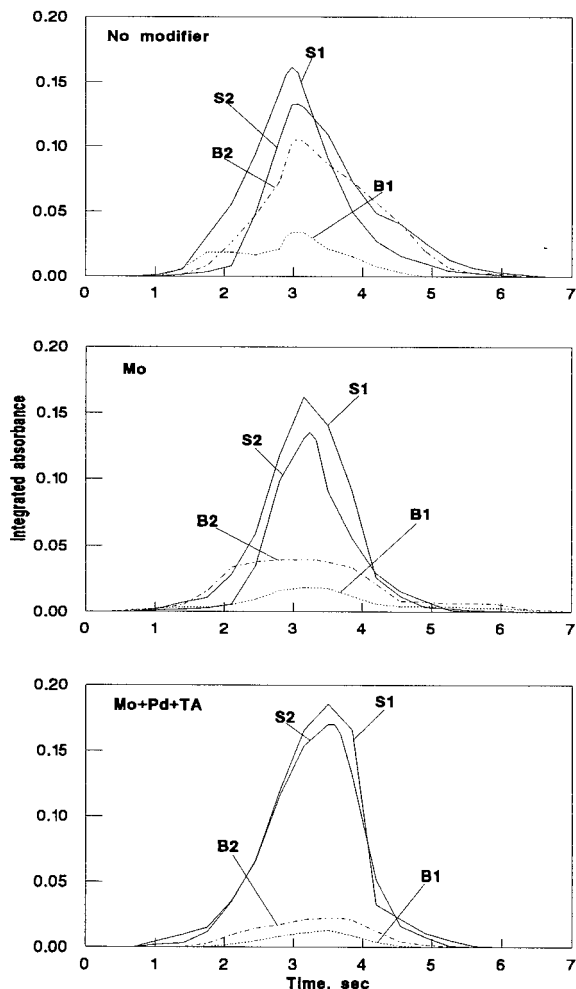


Fig. 1. Atomization profiles of Pb in aqueous standard and in sea water sample; where S1, standard ($50 \mu\text{g l}^{-1}$); S2, sample ($50 \mu\text{g l}^{-1}$); B1 and B2, background absorption profiles of Pb in standard and sample respectively.

profiles of sea water spiked with $50 \mu\text{g l}^{-1}$ of lead as an example. The atomization and background absorption profiles of spiked Pb for sea water and for aqueous Pb standard solution obtained with and without modifiers were compared. As can be seen in Fig. 1, although similar symmetrical atomization signal shapes were obtained for Pb in sea water, both in the absence and presence of chemical modifiers, the atomic signals appeared at an earlier time in the absence of a modifier mixture than in its presence. The appearance times of the peaks were identical for sea water and for aqueous standard. However, the maximum peak times of Pb in sample were slightly later than those in the aqueous Pb standard. When Mo + Pd + TA mixture has been used, the appearance time of atomization signal for Pb in sample and in aqueous standard was shifted to a later time while increasing pyrolysis temperature and no reduction in atomic absorption signal was observed up to a maximum pyrolysis temperature above 1200°C . It may be due to early reduction of analyte and modifiers to reactive metallic forms. Thermal stability of these compounds is higher and the corresponding inter-metallic compounds (or alloys between them) [17] are formed when Mo + Pd + TA is used. With no modifier was used, small analyte signal and higher background absorbance were obtained for Pb in sample even when the solution was diluted by a factor of 1 + 3. When Mo + Pd + TA was used, it was observed that analyte signal increased while the background absorption decreased. As can be seen in Fig. 1, higher signal/noise ratios of Pb was obtained in the presence of Mo + Pd + TA than this obtained in the absence of modifier. The reason for this is attributed to the behavior of mixed chemical modifier. Tartaric acid may reduce the modifiers and analytes to their free reactive metals at pyrolysis temperatures less than 800°C [18] and therefore the stabilizing effect of modifier is increased. It can be seen in Fig. 1 that under these conditions the background absorbance from the matrix is perfectly corrected using Zeeman corrector which allows direct determination of sea water into furnace for the determination of analytes.

Table 1

Detection limits (LOD, 3 σ -criterion) and characteristic masses (m_0) for Bi, In and Pb determination using some modifiers

Matrix modifiers	Analytes ^a					
	Bi		In		Pb	
	LOD, $\mu\text{g l}^{-1}$	m_0 , pg	LOD, $\mu\text{g l}^{-1}$	m_0 , pg	LOD, $\mu\text{g l}^{-1}$	m_0 , pg
No modifier	22.69	175.0	15.79	111.4	6.26	43.0
TA	18.43	168.4	13.21	94.4	5.44	37.2
Mo	17.03	161.9	10.15	81.1	5.07	31.1
Mo+TA	15.57	131.6	8.74	78.2	4.83	30.2
Pd+TA	14.64	120.6	7.99	76.4	4.77	28.9
Mo+Pd	10.26	105.3	5.44	65.9	2.25	27.1
Mo+Pd+TA	7.03	51.6	3.68	33.2	0.97	23.5

^a Analytical range: 20–400 $\mu\text{g l}^{-1}$ for Bi and In; 5–80 $\mu\text{g l}^{-1}$ for Pb with or without of single or mixed modifier mixtures. Sample volume: 20 μl .

3.3. Analytical conditions and calibration

The determination of Bi, In and Pb in sample solutions were performed with and without Mo-based modifiers by using the calibration on the base of single element solutions in nitric acid for comparison. Calibration against standard solutions in the presence or absence of modifiers was performed for analytes by using optimum parameters such as furnace temperature programme, modifier mass and mass ratios of the mixed modifiers as described in [11]. To obtain calibration graph, working standard solutions of analytes in analytical ranges given in Table 1 were added to the modifier solutions as described in Section 2.3. All calibration graphs were linear and correlation coefficients were about > 0.999 .

Detection limits (LOD, 3 σ -criterion) and characteristic mass (m_0) of Bi, In and Pb spiked to sea water (20 $\mu\text{g l}^{-1}$ of each analyte) were determined in the presence or absence of some modifiers and given in Table 1. As can be seen in Table 1, the lowest detection limits and characteristic masses of analytes were obtained by using Mo + Pd + TA mixed modifier.

3.4. Application

For new modifiers, they are particularly important that their stabilizing powers for analyte elements persist also in the presence of complex

matrix and of high salt concentrations. Therefore, Mo + Pd + TA and Mo + Pt + TA mixed modifiers providing higher pyrolysis temperatures for the analytes and their components providing lower pyrolysis temperatures were applied to the determination of Bi, In and Pb in synthetic and real sea water samples. Results were given in Tables 2 and 3. The determination of analytes in sample solutions were performed with and without modifier by using calibration graph method and seven parallel sample solutions. As can be seen in Tables 2 and 3, a good accuracy was obtained by using mixed modifiers containing TA. When higher chloride concentrations are to be expected in samples such as sea water, the chloride interferences are to be important to determine volatile elements. As can be seen in Tables 2 and 3, Mo + Pd + TA or Mo + Pt + TA mixed modifiers could be used for the determination of Bi, In and Pb in sea water with about 5% relative error. Tartaric acid acts on the chloride interference in the matrix. It can be plausibly concluded that tartaric acid is a valid modifier for reducing the chloride ions in samples [13]. The products of TA can be convert chloride ions to HCl (g) and high contents of chloride ions vaporize at low temperatures in the pyrolysis stage. Especially Mo + Pd + TA and Mo + Pt + TA mixtures were efficient to allow the use of pyrolysis temperatures in the range of 1350–1400°C for Bi and In and 1250–1300°C for Pb. These temperatures could be

Table 2

Recovery tests performed for bismuth, indium and lead determination in synthetic sea water

Element determined	Modifier	Pyrolysis temperature (°C)	Concentrations		Recovery (%)
			Spiked ($\mu\text{g l}^{-1}$)	Found ^a	
Bi	No modifier	800	50.0	24.4 \pm 4.6	49
	TA	750	50.0	29.1 \pm 3.7	58
	Mo	1000	50.0	36.1 \pm 2.4	72
	Pd	1200	50.0	41.2 \pm 2.5	82
	Pd + TA	1150	50.0	42.5 \pm 2.1	85
	Pt	1100	50.0	39.7 \pm 2.2	79
	Pt + TA	1100	50.0	41.9 \pm 2.0	84
	Mo + Pd	1300	50.0	40.7 \pm 1.9	81
	Mo + Pd + TA	1400	50.0	47.2 \pm 1.8	94
	Mo + Pt	1300	50.0	43.9 \pm 1.9	88
Mo + Pt + TA	1350	50.0	48.4 \pm 1.5	97	
In	No modifier	1000	50.0	28.9 \pm 2.5	58
	TA	850	50.0	31.5 \pm 2.3	63
	Mo	1100	50.0	36.4 \pm 2.1	73
	Pd	1250	50.0	39.6 \pm 2.1	79
	Pd + TA	1150	50.0	41.9 \pm 1.9	84
	Pt	1200	50.0	38.3 \pm 2.4	77
	Pt + TA	1150	50.0	39.3 \pm 2.0	79
	Mo + Pd	1400	50.0	42.5 \pm 1.8	85
	Mo + Pd + TA	1350	50.0	48.3 \pm 1.5	97
	Mo + Pt	1300	50.0	43.4 \pm 1.9	87
Mo + Pt + TA	1350	50.0	48.2 \pm 1.5	96	
Pb	No modifier	800	50.0	24.3 \pm 2.6	49
	TA	750	50.0	31.9 \pm 2.5	64
	Mo	1000	50.0	35.6 \pm 2.2	71
	Pd	1100	50.0	38.4 \pm 2.1	77
	Pd + TA	1150	50.0	40.1 \pm 1.8	80
	Pt	1050	50.0	37.9 \pm 1.9	76
	Pt + TA	1100	50.0	39.2 \pm 2.0	78
	Mo + Pd	1250	50.0	45.3 \pm 2.1	91
	Mo + Pd + TA	1300	50.0	47.5 \pm 1.6	95
	Mo + Pt	1200	50.0	42.9 \pm 1.9	86
Mo + Pt + TA	1250	50.0	51.4 \pm 1.5	103	

^a Mean of seven replicate measurements with 95% confidence level.

sufficient to volatilize many matrix constituents without loss of analyte elements. When no modifier is used, the error is very high because of matrix interferences. Such effects are negligible when Mo + Pd + TA or Mo + Pt + TA is present and accuracy and precision are satisfactory. It can be expected, therefore, that the recommended chemical modifiers are applicable to the determination of Bi, In and Pb in sea water samples.

4. Conclusion

Direct determination of volatile elements such as Bi, In and Pb in sea water by ETAAS using Mo-based modifiers were examined. In general terms, the analytical problems arising from the sample matrix can be controlled only with dilution and using Mo + Pd + TA or Mo + Pt + TA mixed modifier and Zeeman background correc-

Table 3
Recovery tests performed for bismuth, indium and lead determination in Marmara sea water

Element determined	Modifier	Pyrolysis temperature (°C)	Concentrations		Recovery (%)
			Spiked ($\mu\text{g l}^{-1}$)	Found ^a	
Bi	No modifier	800	50	30.6 ± 4.4	61
	TA	750	50	32.7 ± 3.4	65
	Mo	1000	50	36.4 ± 2.6	73
	Mo+TA	1050	50	37.6 ± 2.5	75
	Pd+TA	1150	50	40.5 ± 2.3	81
	Pt+TA	1100	50	39.2 ± 2.4	78
	Mo+Pd	1300	50	43.8 ± 2.1	88
	Mo+Pd+TA	1400	50	48.8 ± 1.6	98
	Mo+Pt	1300	50	41.9 ± 2.3	84
	Mo+Pt+TA	1350	50	47.1 ± 1.8	94
In	No modifier	1000	50	30.7 ± 4.2	61
	TA	850	50	32.5 ± 3.7	65
	Mo	1100	50	35.4 ± 2.9	71
	Mo+TA	1150	50	37.2 ± 2.2	74
	Pd+TA	1150	50	41.2 ± 2.6	82
	Pt+TA	1150	50	39.8 ± 2.3	80
	Mo+Pd	1350	50	42.8 ± 2.0	86
	Mo+Pd+TA	1400	50	49.0 ± 1.4	98
	Mo+Pt	1300	50	45.3 ± 2.3	91
	Mo+Pt+TA	1350	50	47.5 ± 1.6	95
Pb	No modifier	800	50	28.3 ± 4.1	57
	TA	750	50	32.8 ± 3.7	66
	Mo	1000	50	35.2 ± 3.2	70
	Mo+TA	1050	50	37.4 ± 2.6	75
	Pd+TA	1150	50	39.1 ± 2.4	78
	Pt+TA	1100	50	38.3 ± 2.5	77
	Mo+Pd	1250	50	41.5 ± 2.3	83
	Mo+Pd+TA	1300	50	50.3 ± 1.4	101
	Mo+Pt	1200	50	41.1 ± 2.4	82
	Mo+Pt+TA	1250	50	47.5 ± 1.7	95

^a The mean of seven replicate measurements with 95% confidence level.

tion. Recoveries of analytes spiked to water samples were 94–103% with Mo + Pd + TA or Mo + Pt + TA. The recoveries of analytes are only 49–61% without modifier.

Acknowledgements

The supports of Turkish Atomic Energy Authority and Gazi University Research Found are gratefully acknowledged.

References

- [1] A.L. Garcia, E.B. Gonzalez, A. Sanz-Medel, *Microchim. Acta* 112 (1993) 19.
- [2] Y.-Z. Liang, M. Li, Z. Rao, *Fresenius J. Anal. Chem.* 357 (1997) 112.
- [3] H. Shan-Da, L. Wen-Rong, S. Kun-Yauh, *Spectrochim. Acta* 50 (1995) 1237.
- [4] B. Welz, G. Schlemmer, J.R. Mudakavi, *J. Anal. At. Spectrom.* 7 (1992) 1257.
- [5] B. He, Z.-M. Ni, *J. Anal. At. Spectrom.* 11 (1996) 165.
- [6] D.L. Tsalev, V.I. Slaveykova, *J. Anal. At. Spectrom.* 7 (1992) 147.

- [7] S. Sachsenberg, T. Klenke, W.E. Krumbein, H.J. Schellhuber, E. Zeeck, *Anal. Chim. Acta* 279 (1993) 241.
- [8] I. Sekerka, J.F. Lechner, *Anal. Chim. Acta* 254 (1991) 99.
- [9] S. Imai, N. Hasegawa, Y. Nishiyama, Y. Hayashi, K. Saito, *J. Anal. At. Spectrom.* 11 (1996) 601.
- [10] O. Acar, A.R. Türker, Z. Kılıç, *Fresenius J. Anal. Chem.* 357 (1997) 656.
- [11] O. Acar, A.R. Türker, Z. Kılıç, *Fresenius J. Anal. Chem.* 360 (1998) 645.
- [12] J.P. Byrne, C.L. Chakrabarti, G.F.R. Gilchrist, M.M. Lamoureux, P. Bertels, *Anal. Chem.* 65 (1993) 1267.
- [13] D.L. Tsalev, V.I. Slaveykova, *Spectrosc. Lett.* 25 (1992) 221.
- [14] J.E. Cantle, *Atomic Absorption Spectrometry*, Elsevier, New York, 1982.
- [15] V.I. Slaveykova, D.L. Tsalev, in: D.L. Tsalev (Ed.), XXVI CSI, July 2–9 Selected papers, vol. 7, 1989, p. 85.
- [16] I. Havezov, A. Detcheva, J. Rendl, *Mikrochim. Acta* 119 (1995) 147.
- [17] X.-Q. Shan, D.X. Wang, *Anal. Chim. Acta* 173 (1985) 315.
- [18] X.-Q. Shan, B. Wen, *J. Anal. At. Spectrom.* 10 (1995) 791.

Simultaneous kinetic spectrophotometric determination of spironolactone and canrenone in urine using partial least-squares regression

E. Martín, A.I. Jiménez, O. Hernández, F. Jiménez, J.J. Arias *

Departamento de Química Analítica, Nutrición y Bromatología, Facultad de Química, Universidad de La Laguna, E-38204, La Laguna, Tenerife, Spain

Received 10 July 1998; received in revised form 10 November 1998; accepted 12 November 1998

Abstract

A method is proposed for the simultaneous determination of spironolactone and canrenone in urine based on the different rates at which they react with sulphuric acid to yield a trienone. Kinetic spectrophotometric data are processed by partial least-squares (PLS) regression. The optimum sulphuric acid concentration and temperature are determined from response surfaces, using PLS methodology to relate both variables to the relative square error of prediction (RSEP, the parameter to be minimized). The relative errors made in the quantitation of each diuretic by the proposed method are less than 5% and the overall error, as RSEP, ranges from 1.06 and 1.44%. © 1999 Elsevier Science B.V. All rights reserved.

Keywords: Canrenone; Spironolactone; Kinetics; PLS

1. Introduction

The quantitation of multiple analytes in the same sample (i.e. multicomponent analysis) has long been one of the most interesting fields of chemical analysis. In this respect, differential kinetic methods [1–3] have enabled the simultaneous determination of two or more sample components reacting with a common reagent at appreciably different rates. The analytical poten-

tial of kinetic methods has grown markedly in the last few years for various reasons prominent among which are (a) the extensive use of computers in the laboratory, (b) the development of diode array spectrophotometers and (c) the high automatability of these methods, which results in more efficient control of the experimental variables on which the reaction rate depends [4].

The methods most widely used lately for processing kinetic spectrophotometric data include curve fitting and linear Kalman filtering [5–9]. Both require fulfillment of very strict conditions (viz. the kinetics concerned must be first- or pseudo first-order, the analytes should exhibit no

* Corresponding author. Tel.: +34-922-318-076; fax +34-922-318-003.

E-mail address: jjarias@ull.es (J.J. Arias)

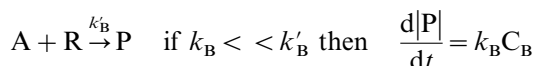
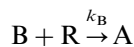
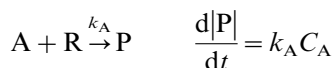
mutual interactions and their rate constants should not vary with the experimental conditions); as a result, effective usage of these methodologies entails an exhaustive knowledge of the system concerned. Multivariate calibration based on powerful algorithms has also been used in this context [10]. Thus, Schechter et al. [11,12] developed an algorithm based on non-linear least-squares regression to solve the problems encountered when the order or the rate constant for a reaction is known only approximately. Other authors have used factor analysis [13,14] and principal component regression (PCR) [15] for the simultaneous determination of several analytes. However, judging by late trends in this field, the best results are provided by methods based on partial least-squares (PLS) regression [16–20] and artificial neural networks [21–23]. The latter are less restrictive as regards the reaction conditions and have the sole pitfall that accurate definition of the system entails processing a large number of calibration samples. In addition to being applicable to non-linear systems, PLS methodology requires no prior knowledge of the rate constants involved since calibration and prediction can be done from a whole kinetic profile obtained at one or more different wavelengths.

Spironolactone is a potassium-saving diuretic that is excreted unaltered in a 30% and metabolized to canrenone in a 60% [24,25]. There are spectrophotometric [26–28] and chromatographic methods [29–31] for the individual and simultaneous determination of both the drug and its major metabolite.

In this work, a new method for the simultaneous determination of spironolactone and canrenone in urine was developed. The method is based on the different rate at which the two analytes react with hot sulphuric acid to form the corresponding trienone. The reaction is monitored by recording the spectrum for the trienone, using a diode array spectrophotometer, the data thus obtained being subsequently processed by partial least-squares regression. The results obtained were contrasted with those provided by HPLC method for urine samples.

2. Theoretical background

Consider two analytes A and B that react with a common reagent to give the same absorbing specie, P, according to the following scheme:



where, k_A , k_B and k'_B ($k_A = k'_B$) are the rate constants for A and B, respectively.

The product formed, P, can be monitored by recording its absorption spectrum as a function of the time or by measuring the absorbance at a fixed wavelength.

As can be seen, from the above scheme, two different processes should be considered, according to the type of reaction involved: simple reaction, and multistage reaction (above).

It has been assumed that the reactions involved in both processes to follow a first or pseudo-first-order kinetic with respect to the analyte concentrations, and in the multistage process the rate-determination step is the first one.

If the absorbance is assumed to be proportional to the amount of product formed, then, in the absence of interactions between the kinetics of both analytes, it will be given by

$$A_T = A_{P_A} + A_{P_B} \quad (1)$$

where A_{P_A} and A_{P_B} are the absorbencies for the reaction product of analyte A and B, respectively.

Eq. (1) can be rewritten as

$$A_{(\lambda, t)} = \sum_i E_{(i, \lambda, t)} C_i^0 \quad (2)$$

where, C_i^0 is the initial concentration of the specie i to be quantified, for first-order reactions, $E_{(i, \lambda, t)} = \varepsilon_i [1 - \exp(-kt)]$, and for reactions of order than one, $E_{(i, \lambda, t)}$ depends on the same variables (viz. species i , wavelength λ and time t) but in a different way.

By analogy between $E_{(i, \lambda, t)}$ and molar absorptivity in the Lambert–Beer law in spectrophotometric determinations, the variation of the

absorbance as a function of time at a given wavelength can be used to construct a ‘temporal spectrum’, $A_{t_1}, A_{t_2} \dots A_{t_n}$ at times $t_1, t_2 \dots t_n$. If the kinetics is monitored at several wavelengths, then these are used to construct a chain of spectra in the sequence

$$(A_{\lambda_1}, A_{\lambda_2} \dots A_{\lambda_n})_{t_1}, (A_{\lambda_1}, A_{\lambda_2} \dots A_{\lambda_n})_{t_2}$$

... $(A_{\lambda_1}, A_{\lambda_2} \dots A_{\lambda_n})_{t_n}$ for wavelengths $\lambda_1, \lambda_2 \dots \lambda_n$.

Eq. (2) can be expressed in matrix form as

$$\mathbf{A} = \mathbf{E}\mathbf{C} \quad (3)$$

where \mathbf{A} and \mathbf{C} are the absorbance and concentration matrix, respectively. For a kinetic system being monitored at a single wavelength, the dimensions of \mathbf{A} and \mathbf{E} are $(N_m \times N_t)$ and $(N_p \times N_t)$, respectively, where N_t is the number of time values at which the absorbance is measured and N_m that of solutions containing known concentrations of N_p components used. For a kinetic system that is monitored at N_λ wavelengths, the dimensions of \mathbf{A} and \mathbf{E} will be $N_m \times (N_t \times N_\lambda)$ and $N_p \times (N_t \times N_\lambda)$, respectively. On the other hand, the dimensions of matrix \mathbf{C} will be $N_m \times N_p$ in both cases.

$$\begin{bmatrix} (A_{1\lambda_1} \dots A_{1\lambda_n})_{t_1} & \dots & (A_{\lambda_1} \dots A_{\lambda_n})_{t_n} \\ (A_{2\lambda_1} \dots A_{2\lambda_n})_{t_1} & \dots & (A_{\lambda_1} \dots A_{\lambda_n})_{t_n} \\ \vdots & \vdots & \vdots \\ (A_{m\lambda_1} \dots A_{m\lambda_n})_{t_1} & \dots & (A_{\lambda_1} \dots A_{\lambda_n})_{t_n} \end{bmatrix} = \begin{bmatrix} (E_{1\lambda_1} \dots E_{1\lambda_n})_{t_1} & \dots & (E_{1\lambda_1} \dots E_{1\lambda_n})_{t_n} \\ \vdots & \vdots & \vdots \\ (E_{p\lambda_1} \dots E_{p\lambda_n})_{t_1} & \dots & (E_{p\lambda_1} \dots E_{p\lambda_n})_{t_n} \end{bmatrix} \times \begin{bmatrix} C_{11} & \dots & C_{1p} \\ C_{21} & \dots & C_{2p} \\ \vdots & \vdots & \vdots \\ C_{m1} & \dots & C_{mp} \end{bmatrix}$$

This procedure allows one to resolve kinetic systems without the need to know the underlying reaction mechanism since multivariate PLS calibration relates the signal produced by each analyte to its concentration via absorbance–time data pairs for the whole kinetic curve. This methodology often uses a number of factors greater than that of analytes in order to account for absorbance–time variations not directly related to the analyte concentrations (e.g. those resulting from interactions between analytes).

3. Experimental

3.1. Apparatus

A Hewlett Packard HP 8452A diode array spectrophotometer furnished with quartz cells of 1 cm path length and connected to a Vectra ES computer, also from Hewlett Packard, via an RS232C interface, was used to record spectra.

The HPLC measurements were made on an HPLC system consisting in: a Waters 600E liquid chromatograph, equipped with a Waters 996 diode array detector, both of which were governed by a NEC Power Mate 433 computer. Determinations were all carried out by using a Nova-Pack column C₁₈ (150 mm × 3.9 mm i.d.) with a particle size of 4 μm. Manual injections were carried out using a Rheodyne injection valve and a 20 μl sample loop.

pH measurements were made with a Radiometer PHM84 digital pH meter equipped with a dual glass–saturated calomel electrode. The meter was calibrated with at least two buffer solutions of pH 4.02 and 7.00.

Solution temperatures were controlled to within ± 0.1°C by using a Lauda MS6 thermostat.

Solutions were homogenized by using an Ika–Werk HS 500 mechanical agitator and centrifuged in a Hettich EBA 3S apparatus.

3.2. Hardware and software

UNSCRAMBLER II v. 5.0 [32], a software package for calibration, prediction and experimental design was used to process acquired data, which were converted to ASCII format using WordPerfect 6.0 for Windows prior to importing.

The chromatographic system was controlled using the software package Millennium 2010 from Water [33].

Data processing were done on a PC/AT 486 DX-2 66-MHz and an NEC Power Mate 433 computers.

3.3. Reagents

Standard solutions containing 100 $\mu\text{g ml}^{-1}$ spironolactone or canrenone were prepared by direct weighing of the required amounts of each, which were dissolved and made to the desired volumes with ethanol. Spironolactone was purchased from Sigma, whereas canrenone, a γ -lactone, was synthesized from canrenoic acid (Sigma) in an acid medium [12] and purified prior to use.

Working-strength solutions of both analytes were made from the stocks by exact dilution and stored at room temperature in the dark.

An $\text{H}_3\text{PO}_4/\text{NaH}_2\text{PO}_4$ buffer of pH 3.3 ($C_T = 0.5$ M) and a 10 mM $\text{NaH}_2\text{PO}_4/\text{Na}_2\text{HPO}_4$ buffers of pH 6.0 were used for pH adjustment.

All chemicals and solvents used were analytical reagent-grade and Millipore Milli-Q de-ionized water was used throughout.

3.4. Procedures

3.4.1. Preparation of samples

Samples were prepared by following the procedure of Sheppard et al. [34] as describe below. Thus, an appropriate aliquot of ethanolic solutions of spironolactone and/or canrenone, containing between 2 and 20 μg , were placed in an empty centrifuge tubes and dried in vacuo at 50°C. The dry extracts were supplied with 5 ml of urine and, after agitation, with 1 ml of $\text{H}_3\text{PO}_4/\text{H}_2\text{PO}_4^-$ buffer at pH 3.3 and 5 ml of ethyl acetate. After homogenizing in the mechanical agitator for 10 min, the mixture was centrifuged at 3500 ppm for 10 min. Finally, a volume of 4.5 ml of the organic phase was dried in vacuo at 50°C, the sample thus being made ready for analysis.

3.4.2. Recording of reaction kinetics

Once the tubes containing the dry sample extract, the sulphuric acid solution and the spec-

trophotometric cell were thermostated at the desired temperature, a volume of 3 ml of sulphuric acid was placed in each tube, which was agitated, and spectra were recorded over the 400–520 nm wavelength range at 30 s intervals for 10 min, using an integration time of 0.4 s.

3.4.3. Experimental optimal condition for the simultaneous determination of spironolactone and canrenone.

The dry residue samples, the sulphuric acid solution and the spectrophotometer cell were thermostated at 48.5°C. A volume of 3 ml of H_2SO_4 50%, is added to the dry residue and the formed solution is shaken and homogenized. The chronometer was simultaneously set on. The solution was transferred in the thermostated 1.0 cm quartz spectrophotometer cell, and the spectra were recorded over the 400–520 nm wavelength range at 30-s intervals during 10 min, an integration time being 0.4 s.

3.4.4. Calibration

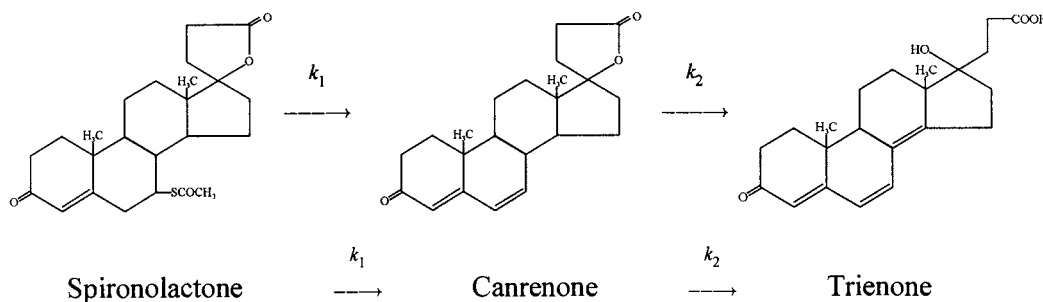
The calibration matrix was constructed from dry extracts of samples to which urine was added, using a 2ⁿ design including a central point, and amounts of spironolactone and canrenone from 2 to 20 μg . Each sample was prepared in triplicate and its reaction kinetics recorded as described in the previous section.

3.4.5. Prediction

An overall 12 samples containing amounts of spironolactone and canrenone between 2 and 20 μg were prepared in various specimens.

3.4.6. Validation of the proposed method by HPLC

Determinations were all carried out by using 150 mm long \times 3.9 mm ID Nova-Pack column C_{18} (with a particle size of 4 μm) and a mobile phase consisting of 63:37 methanol–10 mM $\text{NaH}_2\text{PO}_4/\text{Na}_2\text{HPO}_4$ (pH 6.0), that was filtered and degassed before use. The flow rate was 1.0 ml min^{-1} . Detection was spectrophotometric and involved measuring the area under the chromatogram at 238 and 288 nm for spironolactone and canrenone, respectively. The measurements were made at ambient temperature.



Scheme 1.

4. Results and discussion

Spirolactone and canrenone react with sulphuric acid to give the same product: a trienone. However, their reaction rates are different since, in both cases, the trienone is formed from canrenone according to Scheme 1 [25,35].

The first step is the rate-determining one in the reaction of spiro lactone (the second is common to both analytes and $k_1 < k_2$).

Fig. 1 shows the temporal variation of the absorption spectra for the reactions of spiro lactone and canrenone under identical conditions. As can be seen, canrenone reaches virtual equilibrium within about 10 min, whereas spiro lactone takes more than 30 min.

4.1. Optimization of the extraction conditions

One of the goals of this work was the simultaneous determination of spiro lactone and canrenone in urine, which may be interfered by various species; this requires the prior extraction of one of the analytes. In this work, we used the procedure of Sheppard et al. [34] for this purpose.

Of the different solvents tested (viz. chloroform, carbon tetrachloride, *n*-hexane, ethyl acetate and diethyl ether), ethyl acetate resulted in the highest extraction yield (> 99%).

In order to optimize the conditions for extracting both analytes, the influence of the pH and ionic strength of the urine samples was studied. The extraction of spiro lactone was found not to be affected by pH over the range studied (3.0–8.5); on the other hand, the extraction of

canrenone was less efficient above pH 5.5. Thus a pH 3.3 was chosen for the simultaneous extraction of both analytes. At this pH, the ionic strength of the medium, adjusted with NaCl, had no effect on the extraction of either analyte. The pH was adjusted with $\text{H}_3\text{PO}_4/\text{H}_2\text{PO}_4^-$ buffer of $C_T = 0.5$ M.

4.2. Optimization of the temperature and sulphuric acid concentration

Fig. 2 shows the kinetics for the two analytes as recorded at different temperatures by measuring the absorbance at 486 nm (the maximum absorption wavelength for the trienone formed). As can be seen, the kinetics of spiro lactone exhibits an initial induction period, consistent with the above reaction scheme.

The variation of the kinetics of spiro lactone and canrenone as a function of the sulphuric acid concentration (Fig. 3) suggests that the reaction rate increases with increasing H_2SO_4 concentration; however, at high acid concentrations—lower for canrenone than for spiro lactone—the resulting trienone is decomposed.

Because the kinetics of spiro lactone and canrenone were both dependent on temperature and the sulphuric acid concentration, the working conditions must be optimized in such a way as to ensure the best possible results in the simultaneous quantitation of the two analytes, with due provisions for potential mutual interactions. The optimization procedure used was response surface methodology and experiments were selected following a three-level Box Behnken factor design

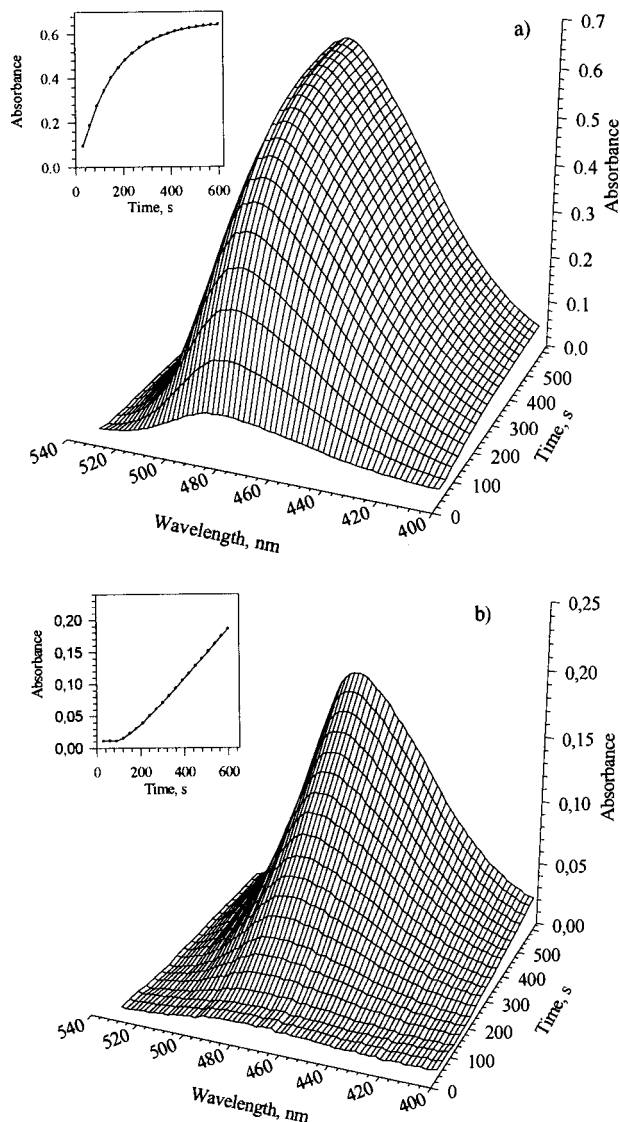


Fig. 1. Spectra as a function of the time of the trienone formed by the reaction of 50 µg of (a) canrenone and (b) spironolactone with 50% sulphuric acid at 50°C. Measurements made every 30 s.

[36]. This type of design requires at least three variables; because we were to optimize only two, a third, imaginary one, was included. The extreme values for the variables to be optimized were 40–60°C and 50–65% for temperature and sulphuric acid concentration, respectively. Table 1 shows the experiments required. The response adopted was the relative square error of prediction, defined as

$$100 \times \sqrt{\frac{\sum (C_{\text{found}} - C_{\text{added}})^2}{\sum (C_{\text{added}})^2}}$$

In order to calculate it, a calibration matrix was constructed by using a $2^n + 1$ experimental design, with minimum and maximum amounts of analyte of 2 and 20 µg, respectively, and a set of prediction samples containing randomly chosen analyte

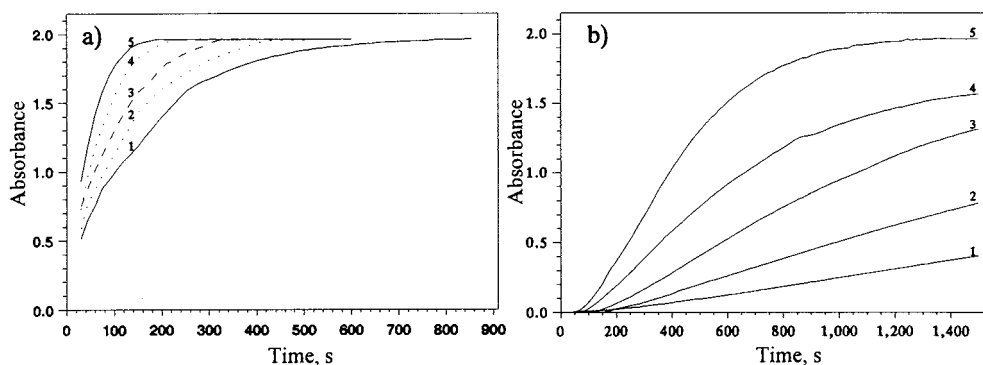


Fig. 2. Absorbance of trienone formed at 486 nm vs. time as a function of temperature for 50 µg: (a) canrenone and (b) spironolactone with 65% sulphuric acid at: (1) 30, (2) 35 (3)40, (4) 45 and (5) 50°C.

amounts within the studied range (Table 2), the spectra for which were recorded under the conditions summarized in Table 1. Once the different models were constructed, the response of each sample (RSEP) was predicted.

Fig. 4 shows the response surface obtained; as can be seen, the minimum appeared at a temperature of 47–51°C and a sulphuric acid concentration of 50%. Conditions of 48.5°C and 50% H₂SO₄ being adopted as optimal for subsequent work.

4.3. Calibration

In order to simplify the procedure for determining spironolactone and canrenone by PLS regression, we assayed calibration in water and in urine. The calibration matrices were constructed using the above-described design, the optimum temperature (48.5°C) and sulphuric acid concentration (50%), and kinetic data for whole spectra recorded over the 400–520 nm wavelength range.

The results thus obtained were grouped by

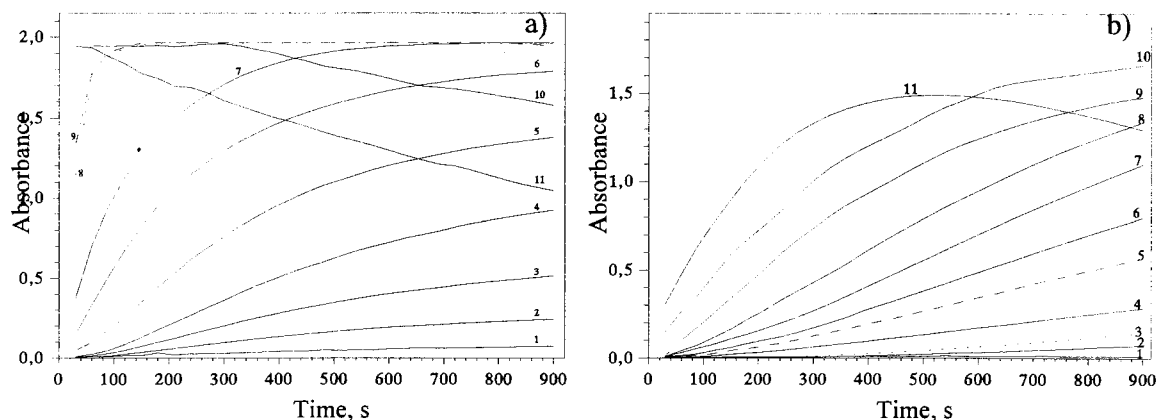


Fig. 3. Absorbance of trienone formed at 486 nm vs. time as a function of sulphuric acid concentration for 50 µg: (a) canrenone and (b) spironolactone at 50°C sulphuric acid concentration (1) 30, (2) 35, (3) 40, (4) 45, (5) 50, (6) 55, (7) 60, (8) 65, (9) 70 (10) 75 and (11) 80%.

Table 1
Experimental from Box–Bhenken design

Experiment ^a	Sulphuric acid (%)	Temperature (°C)	Imaginary variable
1	50.0	60.0	2.0
2	65.0	50.0	3.0
3	65.0	40.0	2.0
4	57.5	40.0	1.0
5	57.5	40.0	3.0
6	57.5	50.0	2.0
7	50.0	40.0	2.0
8	50.0	50.0	1.0
9	57.5	60.0	1.0
10	57.5	60.0	3.0
11	57.5	50.0	2.0
12	50.0	50.0	3.0
13	57.5	50.0	2.0
14	65.0	60.0	2.0
15	65.0	50.0	1.0

^a Experiment 4 = 5, 2 = 15, 8 = 12, and 9 = 10.

placing the spectra recorded every 30 s next to each other. These then were used to construct a chain of spectra, as can be seen in Fig. 5.

Two PLS components were found to account for 99% of the variance in the calibrations with water and urine. This suggests that the matrices behave similarly, as confirmed by plotting score 1 against score 2 (Fig. 6). As can be seen, each analyte influences both scores identically in both matrices; thus, score 1 depends largely (and directly) on canrenone and only slightly on spironolactone, whereas score 2 is directly related to spironolactone and slightly (and indirectly) to canrenone. Based on these results, the calibration does not depend sig-

nificantly on the medium used to prepare the samples (urine or water).

Calibration at 486 nm (the maximum absorption wavelength for the trienone formed) led to identical results.

4.4. Simultaneous determination of spironolactone and canrenone in urine

The proposed method was applied to the determination of spironolactone and canrenone in synthetic urine samples (with a composition as similar as possible to actual ones), other than those used to construct the calibration matrix. The content of each analyte in each sample was predicted from calibration matrices consisting of water and urine samples containing the analytes within 2–20 µg range; these amounts are lower than those excreted during 24 h interval by a person having treatment with spironolactone (average dose 50–100 mg day⁻¹ and normal volume of excretion 800–1600 ml day⁻¹) [37]. Simultaneously with their kinetic–spectrophotometric determination, the proposed method was validated by HPLC technique. Table 3 shows the results obtained for each analyte, using both the proposed method and the HPLC. As can be seen, these were no significant differences between the results provided by the two methods. The relative errors made in quantifying both analytes, for each method, were always less than 7% and

Table 2
Calibration matrix and prediction set employed in the optimization process

Sample	Added (µg)			
	Calibration		Prediction	
	CAN	SP	CAN	SP
1	20.00	20.00	4.00	4.00
2	20.00	2.00	7.00	15.00
3	2.00	20.00	8.00	7.00
4	2.00	2.00	16.00	8.00
5	11.00	11.00	15.00	20.00

Table 3

Simultaneous determination of canrenone and spironolactone in urine by applying PLS method to the kinetic–spectrophotometric signal and validation by HPLC

Sample	Added (μg)		Urine ^a				Water ^b				HPLC			
			Found (μg)		Relative error (%)		Found (μg)		Relative error (%)		Found (μg)		Relative error (%)	
	CAN	SP	CAN	SP	CAN	SP	CAN	SP	CAN	SP	CAN	SP	CAN	SP
1	4.00	4.00	3.85	4.18	−3.75	4.50	4.08	4.18	2.00	4.50	3.82	4.06	−4.50	1.50
2	7.00	15.00	7.04	15.15	0.57	1.00	7.04	15.15	0.57	1.00	7.28	14.94	4.00	−0.40
3	8.00	8.00	8.33	7.87	4.13	−1.62	8.33	8.07	4.13	0.88	8.08	8.04	1.00	0.50
4	16.00	8.00	15.95	7.81	−0.31	−2.38	16.10	8.01	0.63	0.12	15.83	7.83	−1.06	−2.13
5	15.00	13.00	14.95	12.93	−0.33	−0.54	15.04	13.03	0.27	0.23	14.87	12.89	−0.87	−0.85
6	11.00	11.00	10.86	11.09	−1.27	0.82	11.10	11.09	0.91	0.82	10.66	11.09	−3.09	0.82
7	11.00	11.00	10.91	10.99	−0.82	−0.09	11.10	11.10	0.91	0.91	10.35	10.54	−5.91	−4.18
8	11.00	11.00	11.04	10.97	0.36	−0.27	11.14	11.20	1.27	1.82	11.36	10.66	3.27	−3.09
9	11.00	11.00	10.96	10.92	−0.36	−0.73	11.15	11.05	1.36	0.45	10.62	10.66	−3.45	−3.09
10	11.00	11.00	11.18	10.88	1.64	−1.09	11.28	11.15	2.55	1.36	11.46	11.20	4.18	1.82
11	11.00	11.00	10.94	10.97	−0.55	−0.27	11.09	11.21	0.82	1.91	10.24	11.07	−6.91	0.64
RSEP					1.24	1.06			1.44	1.22			3.63	2.08

^a Calibration with urine solutions.^b Calibration with water solutions.

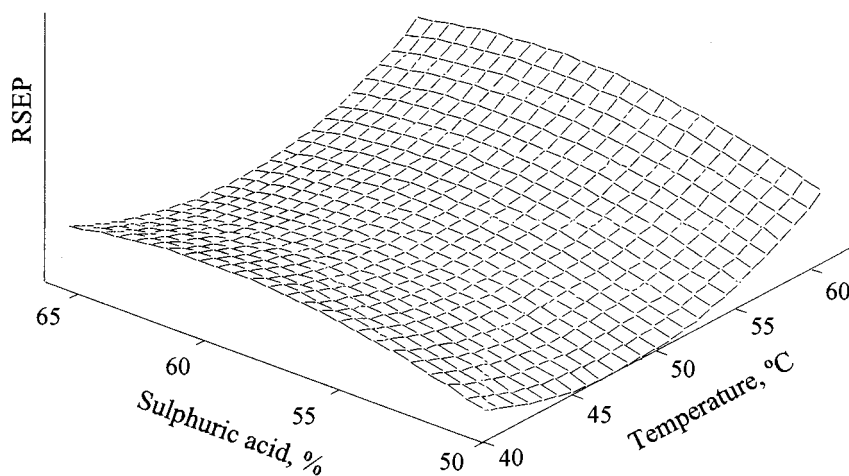


Fig. 4. Response surface for RSEP vs. sulphuric acid concentration and temperature.

overall error for the body of samples, as 1.06–1.44% and 2.08–3.63% for the proposed method and HPLC, respectively.

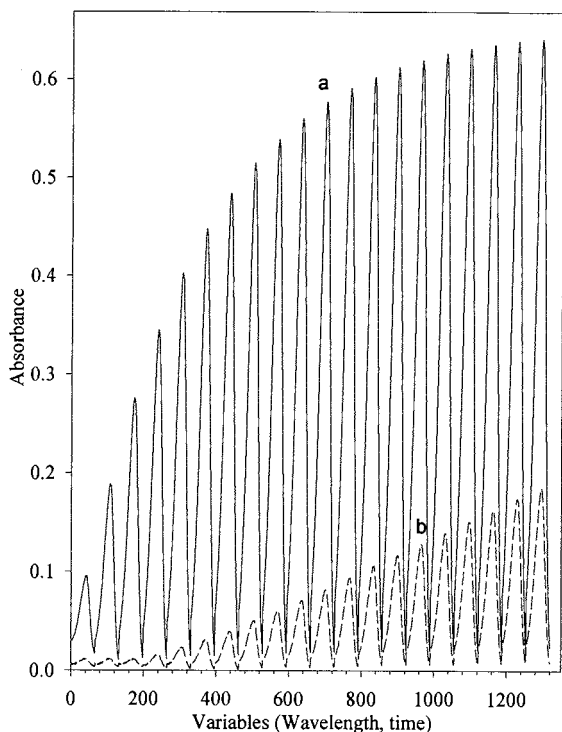


Fig. 5. Graph of data obtained for reaction of 50 µg (a) canrenone and (b) spironolactone with 50% sulphuric acid at 50°C measured 20 times in the wavelength 400–530 nm.

Because RSEP is only a measure of the overall precision of the method, the goodness of individual predictions of each analyte was assessed by plotting added amounts against found amounts for both in all the samples studied. The results obtained in this regression (using the data of the calibrations in water and urine) are shown in Table 4. The high correlation coefficient obtained in both cases ($r > 0.999$) suggests the absence of random errors; also, the near-unity slopes confirm the high consistency between the amounts added and found. On the other hand, the fact that the intercepts obtained with the two matrices were different can be ascribed to a potential effect of the matrix.

The accuracy of the proposed method was evaluated by using the confidence region test for the slope and intercept, developed by Mandel and Linning [38], at $\alpha = 0.05$. The method was found to be subject to no systematic errors when using urine samples; on the other hand, the water samples were subject to systematic errors probably arising from differences in the background signal or a matrix effect—which was minimized in the calibration with urine samples.

Finally, the proposed method presents high versatility because it permits working at different sensitivity ranges, depending on the needs of the analysis. So, in order to obtain a higher sensitivity levels, further samples should be required.

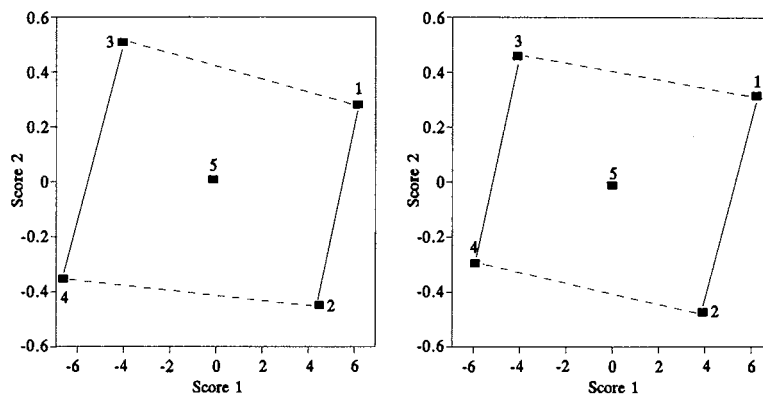


Fig. 6. Scores plot for the calibration sets, where each number appears according to solutions on Table 2; (a) calibration in water and (b) calibration in urine.

Table 4

Parameters of the regression lines (added amount vs. found amount) in the simultaneous determination of canrenone and spironolactone in urine

Parameter	Urine		Water	
	CAN	SP	CAN	SP
Correlation coefficient, r	0.9991	0.9992	0.9996	0.9997
Slope	0.9952	0.9999	0.9965	0.9994
Slope standard deviation	0.0141	0.0136	0.0091	0.0080
Interception	0.0519	-0.0227	0.1684	0.1191
Interception standard deviation	0.1555	0.1463	0.1008	0.0862

5. Conclusions

As shown in this work, PLS regression is an effective choice for the kinetic quantitation of several analytes even if they yield the same reaction product. Once again, the applicability of PLS to kinetic data is shown not to require the prior knowledge of the reaction order or the individual rate constant for each analyte. Also, in the case studied, the results are independent of the working wavelength used since the reaction product is the same for both analytes and the signals obtained at different wavelengths are linear combinations of one another. On the other hand, this is a simple, inexpensive, and sensitive method for the simultaneous determination of spironolactone and canrenone. It takes the advantages of both the spectrophotometric technique and partial least regression methodology.

Acknowledgements

The authors wish to acknowledge the financial support of this work by the Board of Education of the Government of the Canary Islands, research project no. PI1997/059

References

- [1] M.D. Pérez, M. Valcarcel (Eds.), *Métodos Cinéticos de Análisis*, Caja de Ahorros de Córdoba y Universidad de Córdoba, Córdoba, 1984.
- [2] H.A. Mottola (Ed.), *Kinetic Aspects of Analytical Chemistry*, Wiley, New York, 1988.
- [3] D. Pérez-Bendito, M. Silva (Eds.), *Kinetic Methods in Analytical Chemistry*, Ellis Horwood, London, 1988.
- [4] B.M. Quencer, S.R. Crouch, *Crit. Rev. Anal. Chem.* 24 (1993) 243.
- [5] Y.L. Xie, J.J. Baeza-Baeza, G. Ramis-Ramos, *Anal. Chim. Acta* 321 (1996) 75.

- [6] S.C. Rutan, S.D. Brown, *Anal. Chim. Acta* 167 (1985) 23.
- [7] M.D. Pérez-Bendito, *Analyst* 115 (1990) 689.
- [8] M. Otto, *Analyst* 115 (1990) 685.
- [9] A. Velasco, X. Riu, M. Silva, D. Pérez-Bendito, *Talanta* 40 (1993) 1505.
- [10] K.R. Beebe, B.R. Kowalski, *Anal. Chem.* 59 (1987) 1007A.
- [11] I. Schechter, H. Schröder, *Anal. Chem.* 64 (1992) 325.
- [12] I. Schechter, *Anal. Chem.* 64 (1992) 729.
- [13] A. Cladera, E. Gómez, J.M. Estela, V. Cerdá, *Anal. Chem.* 65 (1993) 707.
- [14] A. Cladera, E. Gómez, J.M. Estela, V. Cerdá, *Anal. Chim. Acta* 272 (1993) 339.
- [15] M. Blanco, J. Coello, H. Iturriaga, S. MasPOCH, J. Riva, E. Rovina, *Talanta* 40 (1993) 261.
- [16] J. Havel, F. Jiménez, R.D. Bautista, J.J. Arias, *Analyst* 118 (1993) 1355.
- [17] J.M. García, A.I. Jimenez, J.J. Arias, K. Khalaf, A. Morales-Rubio, M. de la Guardia, *Analyst* 120 (1995) 307.
- [18] M. Blanco, J. Coello, H. Iturriaga, S. MasPOCH, J. Riva, *Anal. Chem.* 66 (1994) 2905.
- [19] A. Espinosa-Mansilla, A. Muñoz de la Peña, F. Salinas, A. Zamora, *Quim. Anal.* 13 (1994) 106.
- [20] G. López-Cueto, S. MasPOCH, J. Rodríguez-Medina, C. Ubide, *Analyst* 121 (1996) 407.
- [21] S. Ventura, M. Silva, D. Pérez-Bendito, *Anal. Chem.* 67 (1995) 4458.
- [22] M. Blanco, J. Coello, H. Iturriaga, S. MasPOCH, M. Redón, *Anal. Chem.* 67 (1995) 4477.
- [23] M. Blanco, J. Coello, H. Iturriaga, S. MasPOCH, M. Redón, Villegas, *Analyst* 121 (1996) 395.
- [24] N. Gochman, C.L. Gantt, *J. Pharmacol. Exp. Ther.* 185 (1975) 686.
- [25] W. Sadee, M. Dagcioglu, R. Shroder, *J. Pharmacol. Exp. Ther.* 61 (1972) 1126.
- [26] B.A. Lodge, M. Lanoutle, *Can. J. Pharm. Sci.* 14 (1979) 53.
- [27] C.S. Sastry, T.N. Prasad, E.V. Rao, *Indian J. Pharma. Sci.* 47 (1985) 190.
- [28] A.M. Wahbi, M.S. Mahrous, Y.A. Beltegy, A.S. Issa, A.M. Limora, *Spectrosc. Lett.* 25 (1992) 721.
- [29] L. Jacson, J. Stafford, *J. Chromatog. Biomed. Appl.* 428 (1988) 377.
- [30] E. Bonet, M. Medina, M.C. García, *J. Pharm. Biomed. Anal.* 11 (1993) 711.
- [31] F. Belal, *Mickrocim. Acta* 107 (1992) 11.
- [32] UNSCAMBLER-Ex (version 5.0), Computer-Aided Modelling A/S, Thondheim, Norway, 1993.
- [33] MILENNIUM (version 2.10), Millipore Corp., 1993.
- [34] H. Sheppard, T.F. Mowles, J.A. Plumer, *J. Am. Pharm. Sci.* 49 (1960) 722.
- [35] W. Sadee, S. Riegelman, L.F. Johnson, *Steroids* 17 (1971) 599.
- [36] D.C. Montgomery, *Diseño y Análisis de Experimentos*, in: P. Nicolás Grepe (Ed.), Grupo Editorial, Iberoamericana, Mexico, 1991, p. 490.
- [37] Anon, *Catálogo de Especialidades Farmacéuticas*, Consejo General de Colegios Oficiales de Farmacéuticos, Madrid, 1996.
- [38] J. Mandel, F.J. Lining, *Anal. Chem.* 29 (1957) 743.

A chemometric study of the simultaneous determination of calcium and magnesium in natural waters

F. Blasco Gómez, F. Bosch Reig, P. Campíns Falcó *

Departament de Química Analítica, Facultat de Química, Universitat de València, C/ Doctor Moliner 50. Burjassot, Valencia, E-46100, Spain

Received 29 July 1998; received in revised form 23 October 1998; accepted 12 November 1998

Abstract

A method for the simultaneous spectrophotometric determination of calcium and magnesium in mineral waters with an FIA system is tested. The method is based on the reaction between the analytes and arsenazo(III) at pH 8.5. The calculations of the amounts of both analytes in the samples are carried out with the H-point standard addition method (HPSAM) for ternary mixtures, and with a partial least squares (PLS) model after a proper variable selection. The results obtained for the determination of calcium were comparable using both methods. The employment of the HPSAM brings to our attention the influence of the calcium concentration in the sample to the development of the reaction between magnesium and arsenazo(III). HPSAM also permits to estimate the concentration of magnesium in the samples. © 1999 Elsevier Science B.V. All rights reserved.

Keywords: H-point standard addition; Partial least-squares regression; Calcium; Magnesium; Simultaneous determination; Arsenazo(III)

1. Introduction

The control of the concentrations of magnesium and calcium in waters is important, as they are the responsible for water hardness and their presence at high concentrations lowers the quality of drinking waters. From a physiological point of view, calcium and magnesium, along with sodium and potassium, are the most important ions affecting cardiology, owing to their role in nervous impulse conduction and cell contraction.

Titrimetry, spectrophotometry and atomic spectrometry are the most frequently used techniques for such determinations [1]. The traditional method in quality control of calcium and magnesium in water and waste water is complexometry using EDTA as titrant. By the other side this technique is time consuming since the determination of both cations is not simultaneous, otherwise sequential. In order to obtain a higher sampling rate several flow injection (FI) assemblies have been designed [2,3] making use of EDTA and the usual indicators. These complexometric methods cannot be applied when Ca and Mg are present at concentrations lower than ap-

* Corresponding author. Tel.: + 34-96-398-3002; fax: + 34-96-386-4436.

E-mail address: pilar.campins@uv.es (P. Campíns Falcó)

proximately 20 ppm (total hardness) owing to their lack of sensitivity. Several attempts have been made to develop suitable spectrophotometric methods for the determination of Ca(II) and Mg(II) [4–6].

Several reagents have been proposed to carry out the spectrophotometric determination of those cations, some of them are: 4-(2-pyridylazo)-resorcinol (PAR) [7–10], arsenazo(I) [11], arsenazo(III) [12–15], emodin [16], chlorphosphonazo(I) [17], chlorphosphonazo(III) [18], 3,3'-bis[*N,N*-bis(carboximethyl)aminomethyl]

-*o*-cresolphthalein [19], *o,o'*-dihydroxyazo-compounds [20], beryllon(II) [21], methylthymol blue [22], *o*-cresolphthalein [23], alizarin red S [24], azochromotropic acid [25] and PA-FPNS [26].

Ca(II) and Mg(II) react with the proposed reagents yielding to similar spectra. To allow the analyst the assessment of one cation in presence of the other one, by using a single reagent, several strategies have been developed. Some of them are a change in the pH value [18,27], avoiding the formation of the complex of one cation, and the use of masking agents [19] with a great difference between the log *K* value for the complex of one cation and the log *K* value for the complex of the other one. In that cases the determination of calcium and magnesium should be described as sequential not as simultaneous, since two consecutive measurements are required while the simultaneous determination should be related to the determination of more than one parameter per measurement.

Simultaneous determinations are among the major issues of analytical chemistry as they avoid the need to separate a mixture of components by using one of the many techniques available for this purpose [28] making use of simpler, faster and cheaper techniques such as UV/VIS spectrophotometry. On the other hand, the main drawback of UV/VIS spectrophotometry is its lack of selectivity.

Sometimes multivariate analysis of data permits the treatment of the non-specific data obtained with UV/VIS detectors. This strategy allows the simultaneous determination of calcium and magnesium avoiding a previous separation or a mod-

ification of the experimental conditions. Multiple linear regression (MLR) [8,9,12], partial least squares regression (PLS) [7,13,22,28] or H-point standard additions method (HPSAM) [14,15], have been proposed for the simultaneous determination of Ca(II) and Mg(II) in waters by spectrophotometry. PAR and arsenazo(III) are generally the most employed reagents for the simultaneous determination of both ions. PAR presents a too high molar absorptivity in relation to that of the Ca(II) and Mg(II) complexes in the working wavelength range, and it offers a narrow spectral window from a multivariate perspective.

In this paper, an FIA method for the simultaneous spectrophotometric determination of calcium and magnesium, in mineral waters, with arsenazo(III) at pH 8.5 is chemometrically studied from the point of view of the model used for the calibration and from the point of view of the prediction. The usefulness of the method for the prediction of the concentration of calcium and magnesium in commercial waters is discussed.

2. Experimental

2.1. Apparatus and software

A detection system consisting of a Hewlett Packard HP8453 UV–Visible spectrophotometer was used. The spectrophotometer was interfaced to a Hewlett Packard Vectra XM 5/90 personal computer, furnished with the G1115AA software.

The FI assembly (Fig. 1) was built using a peristaltic pump (Minipuls 3, Gilson, Middleton, WI, USA), an injection valve (Model 5020, Rheodyne, Cotati, CA, USA), a 10-mm path length

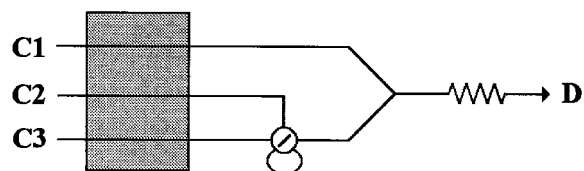


Fig. 1. FI assembly employed for the determination of Ca^{2+} and Mg^{2+} . C1: arsenazo(III), C2: sample/standard, C3: carrier, D: detector.

flow cell (Model 178.712-QS, Hellma, Mülheim/Baden, Germany) and 0.5mm i.d. PTFE tubes. FI conditions were: flow rate 1.75 ml min^{-1} , sample volume $50 \mu\text{l}$ and a 100-cm length reactor coil.

The pH was measured using a Crison micropH 2000 pH-meter.

HPSAM calculations were carried out with MICROSOFTEXCEL[®]. PLS calculations were done with Parvus 1.3 (ISBN: 0-444-43012-1).

2.2. Reagents and standards

Individual stock solutions of Ca(II) and Mg(II) 0.125M of each metal were made by dissolving the appropriate amounts of CaCl_2 (Probus S.A., Badalona (Barcelona), Spain) and $\text{MgCl}_2 \times 6\text{H}_2\text{O}$ (Probus) respectively. The reagent solution was 0.245 g l^{-1} in arsenazo(III) (BDH Chemicals, Poole, UK) and 0.1 M in $\text{NH}_3/\text{NH}_4^+$ (pH = 8.5). A stock solution of $\text{NH}_3/\text{NH}_4^+$ buffer 10 M at pH = 10 from NH_3 (Probus) and NH_4Cl (Probus); NaOH (Probus) and HCl (Panreac, Barcelona, Spain). Ethylenediaminetetraacetic acid disodium salt, EDTA (Probus); Eriochrome black T and murexide (Probus, used as solid reagents diluted in NaCl (Probus)). Water was distilled and then deionized using a Sybron/Barnstead (IZASA, Madrid, Spain) Nanopure II purification system, including a filtration system (Hollow Fibre Filter 0.2 m (Barnstead D3750)).

2.3. Procedures

2.3.1. Spectrophotometric determination.

Calibration sets

The spectrophotometric determination of Ca(II) and Mg(II) was done with the FI system shown in Fig. 1 using as carrier $\text{NH}_3/\text{NH}_4^+$ pH = 8.5, 0.1 M, and as reagent arsenazo(III), the spectra were recorded each second from 0 to 60 s, and each nanometer from 200 to 800 nm every 1 nm. The spectra at the time which gave the maximum signal were selected.

A calibration set consisting of 25 standards was used, a code with a number and a letter was assigned to each standard. The first one refers to the Ca(II) concentration and the second to the Mg(II) concentration, their concentrations are

Table 1

Calibration set concentrations for the determination of calcium and magnesium

Magnesium (ppm)	Calcium (ppm)				
	0	3.09	6.19	9.27	12.36
0	1A	2A	3A	4A	5A
1.82	1B	2B	3B	4B	5B
3.65	1C	2C	3C	4C	5C
5.47	1D	2D	3D	4D	5D
7.30	1E	2E	3E	4E	5E

shown in Table 1. The samples of commercial waters were diluted with $\text{NH}_3/\text{NH}_4^+$ pH = 8.5 buffer to give concentrations of Ca(II) and Mg(II) included in the calibration set.

2.3.2. Titrimetric determination

The total hardness of the waters by using EDTA titration was measured at pH = 10, buffered with $\text{NH}_3/\text{NH}_4^+$ buffer; Eriochrome black T was used as indicator. Ca(II) determination by using EDTA titration was performed at pH > 12, and murexide was used as indicator. The Mg(II) concentration was then obtained by difference. The titrations were made three times a day for 3 consecutive days.

3. Results and discussion

3.1. H-point standard additions method

As it was explained in the Experimental section the calibration set consisted on 25 standards that contained different concentrations of both cations. The aim of the employment of the HPSAM for ternary mixtures is to find couples of wavelengths that allow the building of calibration curves that only respond to one analyte in the sample. It is then necessary to find pairs of wavelengths which accomplish the condition expressed in the Eq. (1) of the appendix, which means that both species considered as interferents present the same relationship of absorbances at the two selected wavelengths. A possible way to locate these couples of wavelengths is to plot the quotient

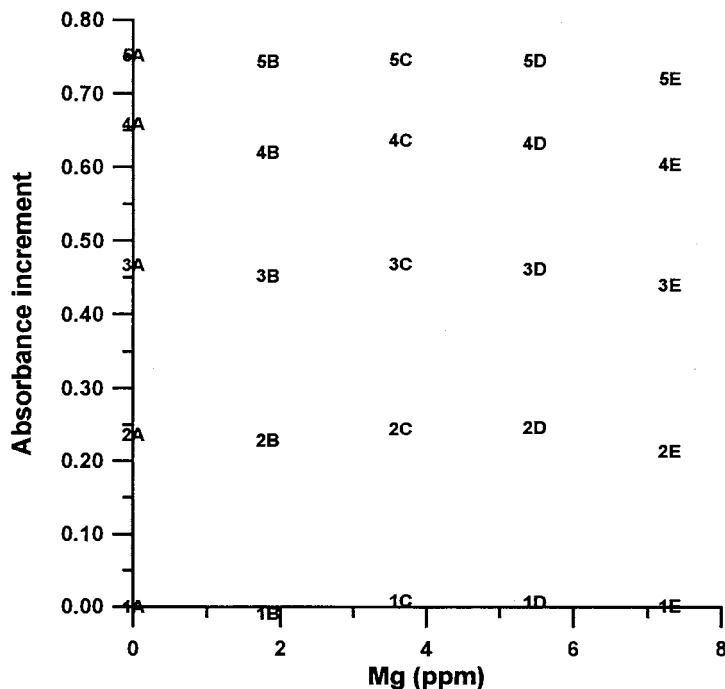


Fig. 2. Isolation of the signal of Calcium. Absorbance increment: $A_{655} - r_{YZ} A_{688}$, being Y = Mg and Z = Arsenazo(III).

spectra of the interferents (the reagent and the other cation considered as interferent). So to determine the amount of Ca(II) in the sample we should plot the quotient spectra between arsenazo(III) and Mg(II) complex and select couples of wavelengths with the same quotient value. We considered that two wavelengths had the same quotient value when the difference between their values was lower than 5%.

There are always several pairs of wavelengths which meet that condition, the best results in prediction of the analyte concentration will be provided by those increments with the highest slope in the calibration equation for the analyte. For the determination of Ca(II) (Mg(II) and arsenazo(III) considered as interferents) the selected pairs of wavelengths were those with the highest slope in the calibration line for Ca(II) and a correlation coefficient equal or higher than 0.995. Those pairs of wavelengths were 655–684, 655–685, 655–686, 655–687 and 655–688. The calibration graphs best fitted to a two order polynomial, no dependence of the signals for

Ca(II) on the Mg(II) concentration in the sample was observed (i.e. for the increment $A_{655} - r_{YZ} A_{688}$ the curve equation was $y = -0.0022x^2 + 0.0877x - 0.0053$, $r^2 = 0.997$, $n = 25$). As can be observed in Fig. 2, the absorbance increment does not depend on the amount of Mg(II), but only on the concentration of Ca(II). 1A-1E series corresponds to a calibration plot of Mg(II), where Ca(II) is not present, and as it can be seen the analytical signal is equal to zero. So, accurate results could be obtained by the method regardless of the Mg(II) content in the sample. Six samples were tested, one of them was a synthetic water and the rest were commercially available waters for consumption. The results, summarized in Table 2, were compared with those reported by the complexometric titration with EDTA. As can be seen the HPSAM provides accurate results, the precision is also good, with relative standard deviations lower than 5%.

To determine the amount of Mg(II) it is necessary to proceed in the same way as previously, so the first step is to plot the quotient spectra be-

Table 2

Results of the prediction of calcium and magnesium in commercial and synthetic waters, with different calibration methods^a

Method/results (ppm)	Font vella	Lanjaron	Synthetic	Solan de cabras	Solares	Viladrau
EDTA						
Ca	38 ± 1	23.0 ± 0.6	80 ± 5	52 ± 3	71 ± 2	16 ± 0.5
Mg	9.0 ± 0.1	8.9 ± 0.7	33.7 ± 0.7	26.1 ± 0.9	13.0 ± 2.0	3.9 ± 0.2
HPSAM						
Ca	39. ± 1	25.1 ± 0.8	84 ± 4.3	52.0 ± 2	76 ± 3	19.6 ± 0.7
Mg	11 ± 2	9.6 ± 0.9	33 ± 9	26 ± 7	20 ± 5	4.5 ± 0.6
PLS						
Ca	39 ± 1	26 ± 1	97 ± 3	50 ± 2	75 ± 3	20.1 ± 0.8
Mg	—	—	—	—	—	—
PLS^b						
Ca	36 ± 1	25.2 ± 0.7	79 ± 4	—	70 ± 3	19.8 ± 0.6
Mg	—	—	—	—	—	—

^a Mean of nine samples ± S.D.^b PLS model without the standards with Ca(II) concentration higher than 6.2 ppm. Bold: relative error in absolute value lower than 10%.

tween arsenazo(III) and Ca(II) complex. 597–627, 599–630, 604–631, 609–630 and 611–626 increments were selected among all the increments that accomplished the condition established in Eq. (1) of the appendix. Those increments presented the highest value of the slope in the calibration lines and a correlation coefficient equal or higher than 0.99. Using those increments it was possible to isolate the signal due to the Mg(II) in the sample [12], but five calibration curves were found instead of only one, this is due to the influence of Ca(II) in the formation of the Mg(II) complex. The analytical signal provided by Mg(II) decreases as the Ca(II) present in the sample increases, therefore, a different calibration equation is obtained depending on the amount of Ca(II) in the sample. Even so the intercept of every curve was equal to zero, this means that the signal only depend on the Mg(II) concentration in the sample.

The resolution of Mg(II) concentration as a ternary mixture is not a good form, because the slopes of the calibration curves obtained were very low, but it is possible to work in another way. To solve the problem we followed the HP-SAM for binary mixtures selecting wavelengths that cancel the signal of arsenazo(III). Once the wavelengths have been selected, the absorbance due to the amount of Ca(II) in the standards at

those wavelengths was subtracted. The result was a signal that only depended on the amount of Mg(II) since the influence of arsenazo(III) and Ca(II) had been eliminated. The absorbance increments used to cancel the signal of arsenazo(III) were 622–478, 621–479, 618–484, 621–478 and 624–475. In the Fig. 3 can be seen the calibration curves obtained for the absorbance increment $A_{622}-A_{478}$, after the subtraction of the calcium signal. It can be seen that when there is no Mg(II) in the standard the analytical signal is zero value, so the isolation of the Mg(II) signal was achieved successfully. Fig. 3 shows the importance of the amount of Ca(II) in the sample for the Mg(II) complex formation (the same concentration of Mg(II) gives a higher analytical signal when Ca(II) is absent), so depending on the concentration of Ca(II) in the sample a different calibration equation for determining Mg(II) must be used. There is a linear relationship between the amount of Ca(II) in the sample and the analytical signal of Mg(II), so once the amount of Ca(II) in a sample is known, it is possible to calculate the equation that will allow the calculation of Mg(II) concentration in the sample. This is very important because the results obtained for the Mg(II) will depend on the accuracy of the Ca(II) prediction.

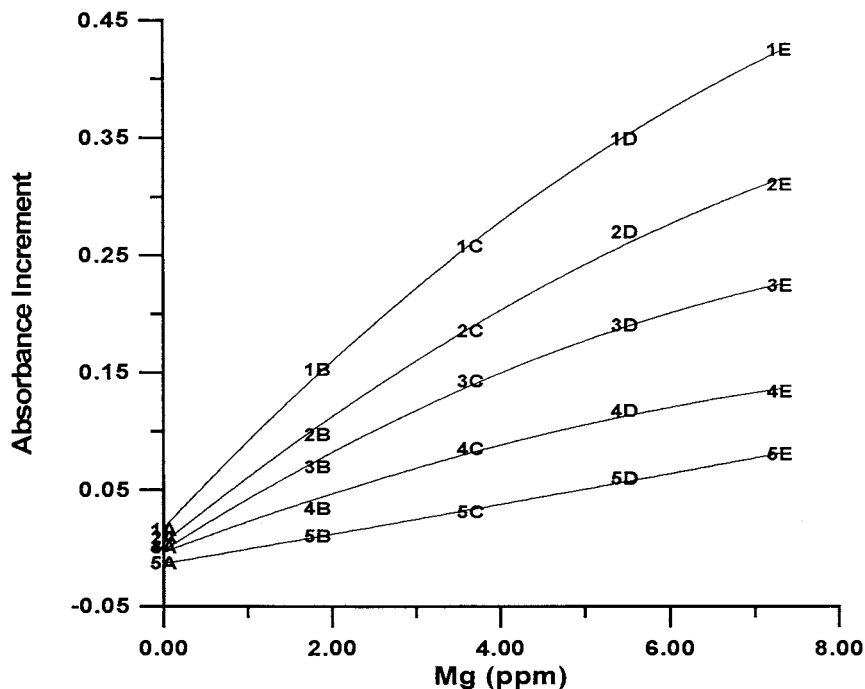


Fig. 3. Calibration curves for the determination of Mg(II) in presence of different amounts of Ca(II). Absorbance increment: $A_{622} - A_{478}$.

The results obtained are given in Table 2 and show that the accuracy and precision of the predictions of both analytes are suitable for almost all the samples.

3.2. Analysis of PLS models

The data was also treated with a PLS algorithm (PLS-1). For this purpose the concentration of the standards were used as the **Y**-block in combination with the **X**-block data. For the first model studied, the **X**-block consisted on the full centered spectra from 250 to 798 nm every 4 nm, so 138 spectral variables were introduced. This model gave a percentage of explained variance in cross-validation (%EVCV) of 99.2% for Ca(II) and 86.5% for Mg(II), with 5 factors for both of them. The first factor was clearly related with the Ca(II) concentration (it explained 95.1% of variance in cross-validation for Ca(II) while 0.8% for Mg(II)), and the second one was related with Mg(II) concentration (it only raised an additional 0.4% of the total *Y* variance of the calibration for Ca(II)

while for Mg(II) it raised 49.5%). In order to select the relevant spectral information the **B**-coefficients corresponding to the equation $Y = B_0 + BX$ for each analyte were studied. The magnitude of the **B**-coefficients (in absolute values) should be related to the importance of the original variables in the prediction of the analytes.

Fig. 4 shows the **B**-coefficients versus the original variables corresponding to the model built with one and two factors. It can be seen that the range 580–680 nm is the most important for the prediction of both analytes. A new PLS model was tested, it used as **X**-block data the absorbances of the standards in the range 580–680 nm. The %EVCV was 99.4 and 96.7% for Ca(II) and Mg(II) respectively, using four factors for both of them, so a great improvement, specially for Mg(II), was achieved reducing the number of spectral variables. Several models with the absorbances at different spectral windows within the range 580–680 nm were assayed. The best results were those provided by the model built with the absorbances in the range 600–680 nm, with

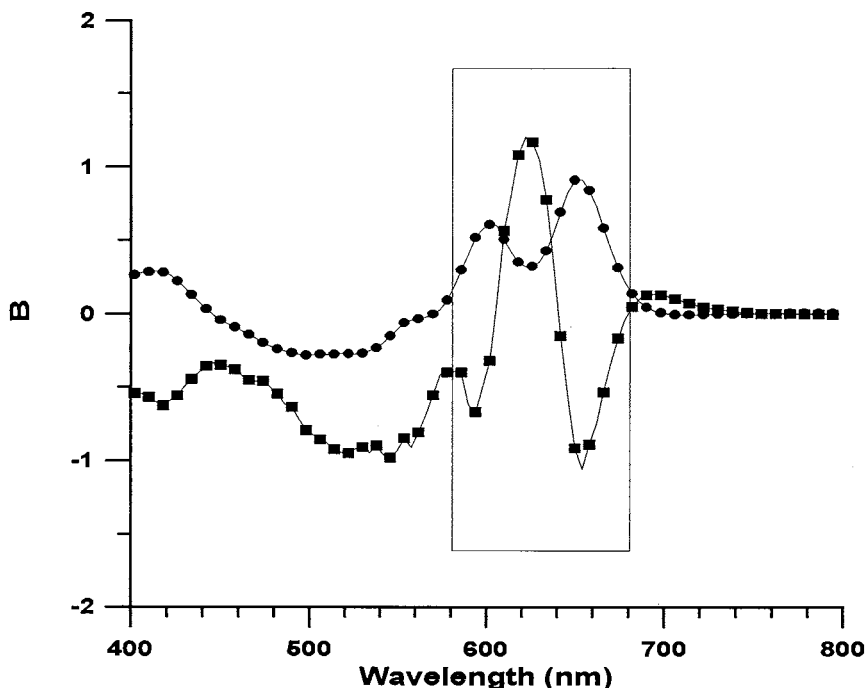


Fig. 4. Regression coefficients **B** versus the original wavelengths. PLS models built with one (●) and two (■) factors.

%EVCVs of 99.6 and 97.0% for Ca(II) and Mg(II) respectively with four factors for both of them. As can be seen in Table 2 the prediction of Ca(II) in the samples was appropriate for almost all of them.

The wrong prediction of the amount of Ca(II) in some samples may be due to non-linearities of the signals at high concentrations of Ca(II), in order to test that fact a new PLS model was constructed, with the same spectral window (600–680 nm) but without the standards with a concentration higher than 6.2 ppm of Ca(II). With this new model, the %EVCVs obtained were 99.5 and 97.7% with two and four factors for Ca(II) and Mg(II) respectively. The amount of Ca(II) in all samples was suitably predicted except for Viladrau. The content of Ca(II) in Solan de Cabras is not given since this water was out of the calibration.

In spite of having high values of %EVCVs for Mg(II), the prediction of this analyte in the

samples was wrong with both models, this means that though the models are able to predict the concentration of Mg(II) in the standards, they are not able to do it in the samples. A calibration set consisting on real samples may result in better predictions for Mg(II) concentration, as it was found by Ruisánchez et al. [11]. They reported a methodology for the automatic, simultaneous determination of Ca(II) and Mg(II) in natural waters based on a Sinusoidal Injection Analysis (SIA) system with diode array spectrophotometric detection. They measured the complex formed by both cations with arsenazo(III), using as calibration set samples of natural water fit for human consumption. The amount of Ca(II) and Mg(II) in the samples was previously determined by atomic absorption spectrometry. This model, built with real samples, provided a mean square error (MSE) in prediction lower for Mg(II) than for Ca(II) using four and two factors respectively.

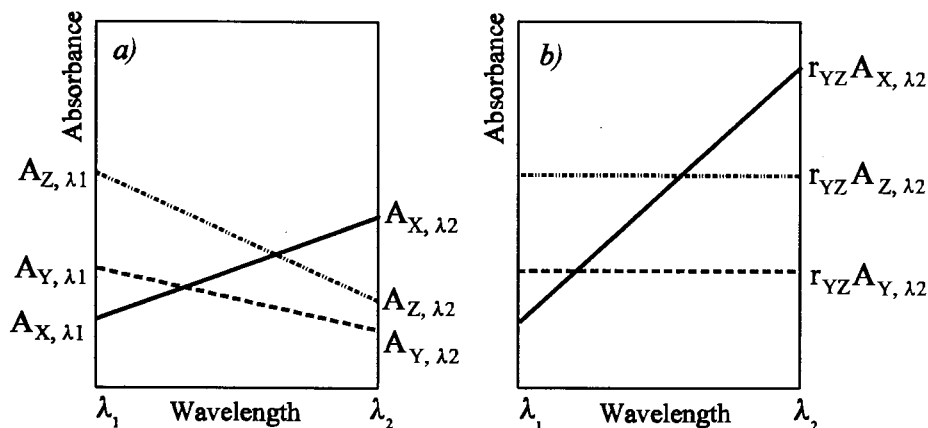


Fig. 5. Signals of the three components of the sample (X, Y and Z) at the wavelengths λ_1 and λ_2 before the employment of the correction r_{YZ} factor (a) and final signals after using the r_{YZ} factor (b). Since the r_{YZ} factor operate in λ_2 , A_{X, λ_1} , A_{Y, λ_1} and A_{Z, λ_1} have the same value in a and b cases.

4. Conclusions

It has been proved the ability of the HPSAM and PLS methods to calculate the amount of an analyte in presence of an interference and in presence of the reagent, when the three compounds absorb the UV/VIS radiation in the same spectral range, and the overlap is severe.

The results obtained for Ca(II) with the PLS models are suitable if a variable selection is done properly, it has been shown a possible way to make the variable selection.

Ca(II) determination is easier than Mg(II) determination since its signal is much larger than the Mg(II) signal. By the other side the determination of Mg(II) is conditioned by the presence of Ca(II) in the sample. This fact became evident upon isolating the Mg(II) signal with the HPSAM method.

The prediction of Mg(II) in the standards is successfully achieved by the PLS model, but it was not able to predict this cation in the samples, so the use of real samples (i.e. mineral water) to build the calibration set may give more robust and reliable models for the prediction of Mg(II) content in commercial waters.

Acknowledgements

The authors are grateful to the DGICYT (Project No. PB 94-0984) for its financial support.

Appendix A. Fundamentals of the HPSAM for ternary samples

If we consider a sample in which X and Y are the analytes to be determined with Z reagent [29], the concentration of X can be calculated by finding pairs of wavelengths which satisfy the following equation

$$\frac{A_{Y, \lambda_1}}{A_{Y, \lambda_2}} = \frac{A_{Z, \lambda_1}}{A_{Z, \lambda_2}} = r_{y,z} \quad (1)$$

Only one spectrum of the species Y and another of the species Z are needed. Although this relationship depends on the concentration of Y and Z, it will be equal at the two selected wavelengths, regardless of the concentrations chosen. There are generally several pairs of wavelengths to choose from.

The $r_{Y, Z}$ factor transforms the original situation (a) into (b), as can be seen in Fig. 5. Since the

signals of Y and Z are the same at both wavelengths after the correction made using the $r_{Y,Z}$ factor, the absorbance increment calculated depends only on the concentration of X.

If we consider that the response variable (absorbance increment) follows the Beer-Lambert law, the concentration of X ($-C_{H(X)}$) can be calculated from the equation:

$$-C_{H(X)} = \frac{A_{S,\lambda_1} - r_{Y,Z}A_{S,\lambda_2}}{r_{Y,Z}M_{X,\lambda_2} - M_{X,\lambda_1}} = \frac{A_{X,\lambda_1}^0 - r_{Y,Z}A_{X,\lambda_2}^0}{r_{Y,Z}M_{X,\lambda_2} - M_{X,\lambda_1}} \quad (2)$$

where A_{S,λ_1} and A_{S,λ_2} are the absorbance values measured for the sample at the two chosen wavelengths, M_{X,λ_1} and M_{X,λ_2} are the slopes of the standard additions method for X or, if the matrix effect is known not to be present, the molar absorption coefficients for the species X at the two wavelengths. A_{X,λ_1}^0 and A_{X,λ_2}^0 are the absorbance values of the species X in the sample. Therefore, the calculated concentration corresponds to compound X.

Similar equations can be described for resolving species Y from $r_{X,Z}$ factor.

References

- [1] M.A.H. Franson, Standard Methods for the Examination of Water and Wastewater, 18th edn, American Public Health Association and Water Pollution Control Federation, Washington, DC, 1992.
- [2] F. Cañete, A. Ríos, M.D. Luque de Castro, M. Valcárcel, Analyst 112 (1987) 267.
- [3] Y.A. Zolotov, E.I. Morosanova, S.V. Zhalovannaya, S.S. Dyukarev, Anal. Chim. Acta 308 (1–3) (1995) 386.
- [4] G. Robisch, A. Rericha, Anal. Chim. Acta 153 (1983) 281.
- [5] M.A. Belo López, M. Callejón Mochón, J.L. Gómez Ariza, A. Guiraúm Pérez, Analyst 111 (1986) 429.
- [6] C.G. Halliday, M.A. Leonard, Analyst 112 (1987) 83.
- [7] O. Hernández, F. Jiménez, A.I. Jimenez, J.J. Arias, J. Havel, Anal. Chim. Acta 320 (1996) 177.
- [8] E. Gómez, C. Tomás, A. Cladera, J.M. Estela, V. Cerdá, Analyst 120 (1995) 1181.
- [9] E. Gómez, J.M. Estela, V. Cerdá, Anal. Chim. Acta 249 (1991) 513.
- [10] E. Engstrom, B. Karlberg, J. Chemometrics 10 (5–6) (1996) 509.
- [11] D.L. Smith, J.S. Fritz, Anal. Chim. Acta 204 (1–2) (1988) 87.
- [12] M. Blanco, J. Coello, J. Gené, H. Iturriaga, S. Maspocho, Anal. Chim. Acta 224 (1989) 23.
- [13] I. Ruisánchez, A. Rius, M.S. Larrechi, M.P. Callao, F.X. Rius, Chemom. Intell. Lab. Syst. 24 (1994) 55.
- [14] P. Campíns Falcó, J. Verdú Andrés, F. Bosch Reig, Anal. Chim. Acta 348 (1997) 39.
- [15] P. Campíns Falco, F. Blasco Gómez, F. Bosch Reig, Talanta 47 (1998) 193.
- [16] P. Tarasankar, R.J. Nikhil, Analyst 118 (1993) 1337.
- [17] X.C. Qiu, Y.Q. Zhu, Mikrochim. Acta 3 (1–2) (1983) 1.
- [18] J. Marcos, A. Ríos, M. Valcárcel, Analyst 117 (1992) 1629.
- [19] T. Yamane, E. Goto, Talanta 38 (2) (1991) 139–143.
- [20] H. Wada, G. Nakagawa, K. Ohshita, Anal. Chim. Acta 159 (1984) 289.
- [21] X.C. Qiu, Y.Q. Zhu, Anal. Chim. Acta 149 (1983) 375.
- [22] F. Blasco, M.J. Medina Hernández, S. Sagrado, F.M. Fernández, Analyst 122 (1997) 639.
- [23] K. Wrobel, K. Wrobel, P.L. Lopez de Alba, L. Lopez Martinez, Anal. Lett. 30 (4) (1997) 717.
- [24] M.E. Khalifa, Chem. Analityczna 41 (3) (1996) 357.
- [25] D.P.S. Rathore, M. Kumar, P.K. Bhargava, Chem. Analityczna 42 (5) (1996) 725.
- [26] H.M. Ma, Y.X. Huang, S.C. Liang, Talanta 43 (1) (1996) 21.
- [27] M.E. Díez-Dorado, M.L. Álvarez-Bartolomé, R. Morogarcía, An-Quim. 86 (6) (1990) 649.
- [28] B. Paull, M. Macka, P.R.J. Haddad, Chromatography A 348 (1–3) (1997) 113.
- [29] J. Verdú Andrés, F. Bosch Reig, P. Campíns Falcó, Analyst 120 (1995) 299.

Source apportionment of inorganic ions in airborne urban particles from Coruña city (N.W. of Spain) using positive matrix factorization

P. Prendes, J.M. Andrade, P. López-Mahía *, D. Prada

Department of Analytical Chemistry, University of A Coruña, Campus da Zapateira S/N, E-15071, A Coruña, Spain

Received 28 May 1998; received in revised form 13 November 1998; accepted 16 November 1998

Abstract

Water-soluble atmospheric particulate matter was analyzed for pH, conductivity and inorganic ions: Mg^{2+} , Ca^{2+} , K^+ , Na^+ , NH_4^+ , Cl^- , NO_3^- and SO_4^{2-} by ion-chromatography. In order to get a deeper insight on the atmospheric data and assess the 'optimal' number of pollution sources, principal component analysis and cluster analysis were applied. After that, the second objective was to apply a recently developed chemometric technique (positive matrix factorization) to perform source apportionment and get ion balances. Four pollution patterns were identified, namely, marine, industrial, urban and building-related source pollutants. Ion balances were also made in a straightforward manner. © 1999 Elsevier Science B.V. All rights reserved.

Keywords: Airborne particles; Urban environment; Source apportionment

1. Introduction

One of the current objectives in many studies focused on the urban environment is to model atmospheric aerosols with particular reference to aerosol sources and their corresponding intensity of emissions. Aerosols greatly influence the chemical characteristics of the atmosphere and troposphere, the condensation characteristics of water vapour and general visibility.

Aerosols (so, airborne particles) may contain a great number of potentially interesting analytes (e.g. heavy metals, volatile organic compounds, polycyclic aromatic hydrocarbons, NO_x , SO_x , etc.) although this work has relied upon analyzing water-soluble major ions which, according to Ali [1] can account up to 60–70% of the total mass of the aerosol. Though this figure greatly depends on the amount of crustal materials retained by the filters, this seemed a reasonable value for the present work since no large amounts of crustal particles were expected. Instead, two main sources for soluble ions were expected a priori because of the geographic characteristics of the city, namely, marine- and industry-related ions. This working

* Corresponding author. Tel.: +34-981167000; fax: +34-981167065.

E-mail address: purmahia@udc.es (P. López-Mahía)

hypothesis became confirmed after this study (being the ‘industry-related’ factor split between an ‘urban’- and an ‘industry’-related sources, this was considered in Sections 4 and 4.4).

Airborne particulate matter is a mixture of naturally generated substances, materials introduced directly into the air masses by human activities, and products of gas-to-particle conversion processes into the atmosphere (having both natural and anthropogenic origins). Human-based air pollutants are mostly emitted by high temperature processes such as road traffic (cars and trucks), oil combustion, domestic heating, building activities, etc.

The main requirement to instigate protective and political decisions is to assess, first, which are the main pollution sources (i.e. how many) and, second, to what extent each eventual source is responsible for the air pollution (i.e. how much). In this respect, source apportionment methods have an important role to extract the number of (main) pollution sources and, then, model their relative contribution to the total amount of air pollutants. Accordingly, in chemical atmospheric studies it is a common practice to model the system by applying source apportionment techniques. Without doubt, any developed model should exhibit two important characteristics:

1. It should be as accurate as possible. Within the limits of the data set, such data should not be incoherent, redundant or biased. There is a fundamental problem in most atmospheric studies, namely, the availability of samplers. They are expensive (many university departments can not afford several samplers but one) and they may only be deployed in specific secure locations. One of the most common sampling locations is at the roof top of the faculty or any other practical site. This, without doubt, have advantages. The main disadvantage is that some assumptions are needed to generalize the final results to the overall surrounding area. It is thought that the results presented here may be adequate to explain the airborne characteristics of A Coruña city thanks to the advantageous situation of the sampling location.

2. Models intended to discover atmospheric patterns should focus on the main patterns defined by the data rather than making attempts to explain all the initial variance in the data set, statistical factors, principal components, etc.

The classical chemical mass balance models (CMB) [2] have two starting points, namely:

1. a number of aerosol sources have to be assumed in advance (maybe, rather subjectively).
2. the ‘source profiles’ needed to perform the multivariate regressions in which many CMB methods rely are too specific since they were usually obtained from common data bases, results from published papers, etc. Therefore, they might be not adequate everywhere. This is a crucial problem since, e.g. the emissions of a refinery will differ from those caused by another one. Unfortunately, it is not simple to obtain ‘pure profiles’ from industries, fugative sources, etc [3]. Despite these problems, at last, such uncertain source compositions have to be used to make CMB models.

Different source apportionment studies have been presented following the original algorithms of Thurston and Spengler in which absolute principal component scores are defined [4]. This is a useful technique since it uses the idea of ‘only the main patterns into the data set’, and it does not make initial assumptions regarding the number of pollution sources. Limitations to this approach are:

1. It is not obvious how to perform the ‘weighted regressions’, which, in turn, are needed at several steps (e.g. to regress absolute principal scores against the total mass of particles and to estimate the content of a particular analyte in each source).
2. The presence of negative regression coefficients may cause distortion of the factors since negative masses or concentrations do not exist. Frequently, the presence of such coefficients suggest too many factors. Before dropping such factor, new runs have to be made to discover suspicious data and to recalculate the coefficients. If this is not successful, omitting a factor is recommended. Sometimes, however, negative coefficients can not be avoided and they have to be presented with caution [5].

Remembering that one of the main objectives of any source apportionment technique is to seek out the contribution of each main source to the concentration of each analyte in the sampled airborne particles, any attempt to treat and, hope-

fully, avoid negative regression coefficients is not trivial. In our opinion, the main problem of the Thurston and Spengler's approach is that it defines the total concentration of each analyte by using weighted multiple linear regression against

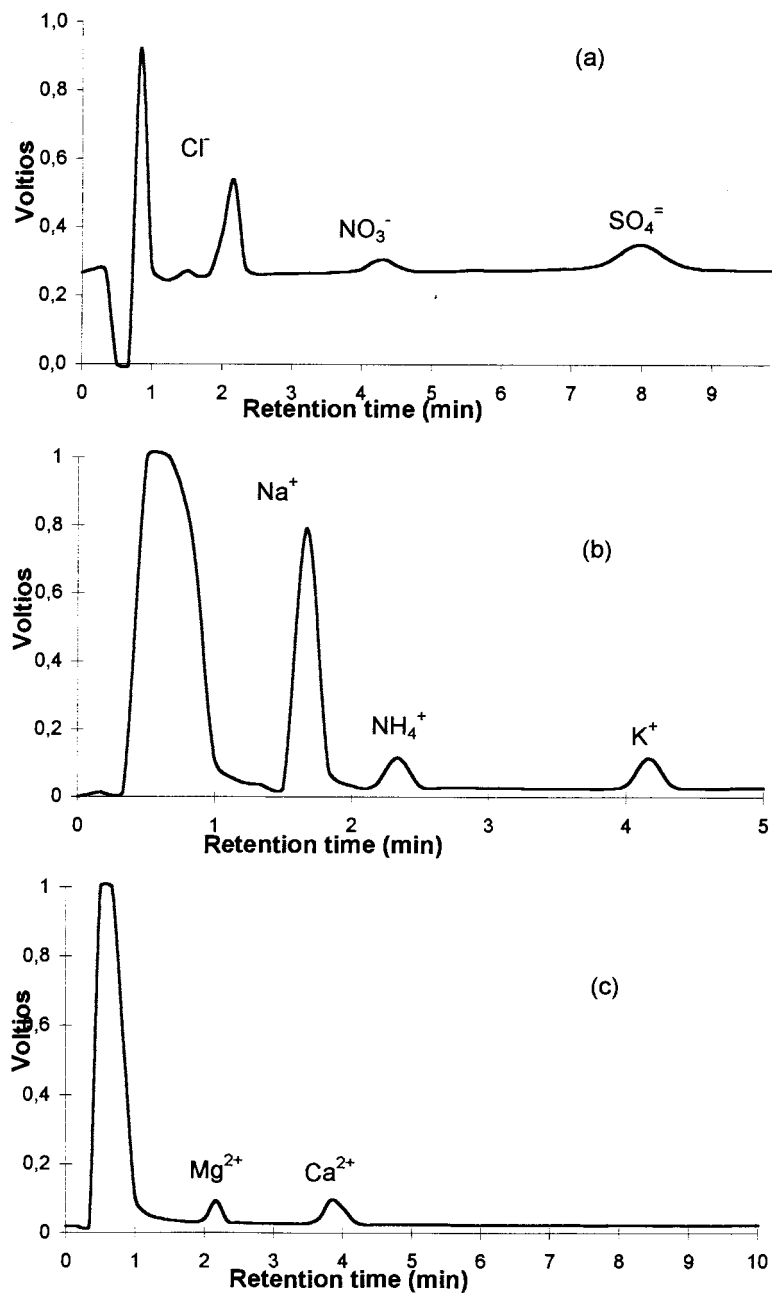


Fig. 1. Examples of chromatograms for one representative sample (a) anions (b) monovalent cations (c) divalent cations.

Table 1

Univariate descriptors for the overall the data ($\mu\text{g m}^{-3}$ for all variables excepting pH—pH units and conductivity— $\mu\text{S cm}^{-1}$)

Variable	Mean	SD	Minimum	Maximum
Mg	0.18	0.17	0.03	0.83
Ca	0.71	0.34	0.29	2.13
K	1.13	0.84	0.44	3.37
NH ₄	1.88	2.02	0.09	8.60
NO ₃	2.24	3.13	0.33	14.72
Na	5.07	2.55	0.68	11.10
Cl	5.37	5.23	0.32	19.52
pH	6.26	0.57	4.18	7.16
SO ₄	7.04	5.59	1.01	19.22
Conductivity	52.64	21.71	23.20	94.80

all the selected pollution sources. The multiple regression techniques indeed regress all the factors against each analyte and, so, all the factors will participate in the regression equations. This might provoke ‘artifacts’ to increase the correlation coefficient (which is usually high) or, simply, to minimize the sum of squares. Accordingly, the study of such coefficients and source apportionment model could be difficult tasks.

Another reported problem for the Thurston and Spengler’s—based apportionment approaches is that the absolute PCA techniques suffer from an inherent bias, which is extended to the concentration apportionments [6].

Some of the above problems have been addressed using the effective variance weighting for least squares calculations for the chemical mass

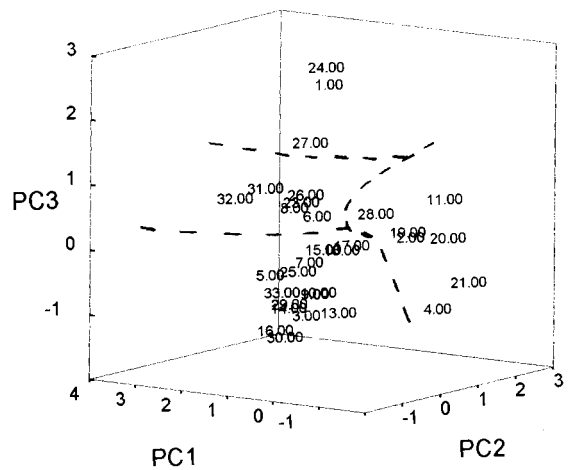


Fig. 2. PC1 PC2 PC3 score subspace, autoscaled data, Varimax rotated.

balance (CMB) method [7]. In the Watson’s work [7] realistic estimates of the uncertainties of the receptor concentrations and source compositions are known (which, unfortunately, is not always the case for most routine applications). Despite these problems, this approach is still in use because it is one of the source apportionment methods accepted by the US-EPA [2].

Different solutions have been tried to improve receptor models. For example, Hopke [3] has focused onto target transformation factor analysis, Wang and Hopke [8] have used constrained least-squares in an attempt to correct the negative values from CMB. As a general rule of thumb, it can be said that some prior knowledge about the

Table 2

Loadings encountered for the first principal components (autoscaled data, Varimax-rotated)

Variable	PC1	PC2	PC3	PC4
Ca	−0.265	−0.063	0.705	−0.651
Cl	0.904	0.260	0.181	0.064
K	−0.084	−0.149	0.770	0.484
Mg	0.842	0.303	0.168	0.055
Na	0.741	0.523	0.110	−0.136
NH ₄	−0.401	0.822	−0.104	−0.069
NO ₃	−0.520	0.283	0.362	0.206
SO ₄	−0.594	0.725	−0.019	0.093
Explained variance (%)	36.7	21.8	16.3	9.3
Total (%)	36.7	58.5	74.9	84.1

particular problem at hand is highly recommended before performing source apportionment (for instance, by means of previous principal component analysis, factor analysis, etc.).

In this paper, a rather recently proposed approach to source apportionment of environmental data, named positive matrix factorization, will be applied. In the authors opinion, this is an appealing way either to avoid the use of previous subjective assumptions about the number of sources and to skip most problems linked to classical regression techniques. It is not intended to present here all the theoretical background or to fully compare this new approach with the existing ones, instead, a conceptual overview will be given and the fundamental works are referred to.

2. Positive matrix factorization

Consider a final data table from any environmental study, say $\mathbf{X}_{(n \times p)}$, where n is the number of samples and p is the number of variables or analytes. This table comprises all the available data regarding the system under study so it collects almost all the (hidden) information regarding the pollution parameters and pollution sources which characterize the atmospheric airborne particles from the sampling site and its surroundings. The main objective of positive matrix factorization (PMF) [9] is to decompose \mathbf{X} into two new matrices, named $\mathbf{Z}_{(n \times k)}$ and $\mathbf{C}_{(k \times p)}$ is such a way that \mathbf{ZC} collects almost all the important variation in \mathbf{X} but leaves out the noise [say, $\mathbf{E}_{(n \times p)}$, and

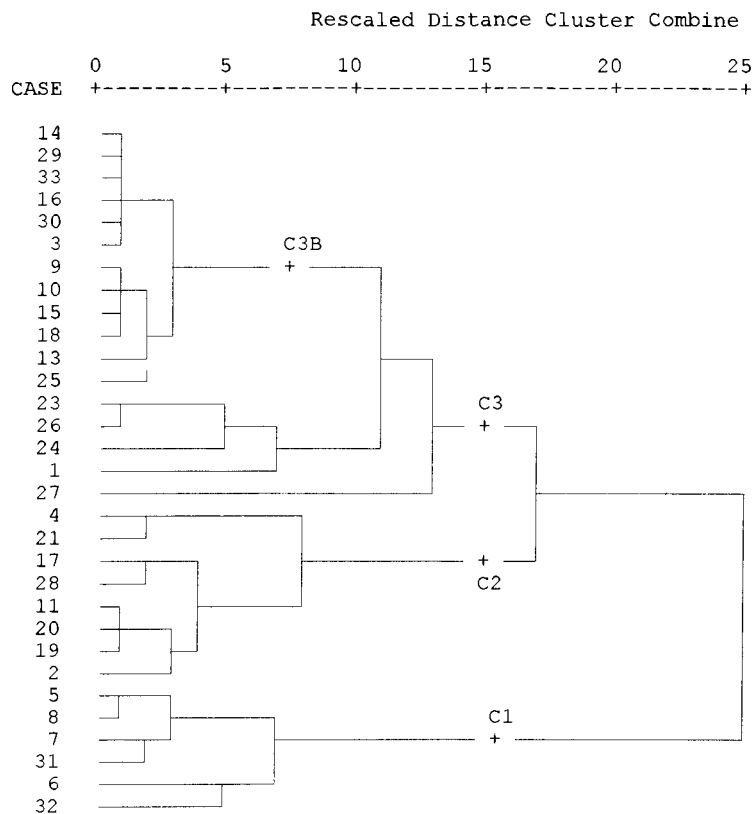


Fig. 3. Dendrogram obtained after cluster analysis, autoscaled data, squared euclidean distance, complete linkage. Clusters C1, C2, C3 and C3B are explained into the text.

Table 3

Error estimation for each variable before performing source apportionment (pH and conductivity were not included in these studies, see text for details). X means X_{ij} , i.e. the analytical concentration for each sample (i) and each variable (j)

Variable	Reproducibility ($\mu\text{g m}^{-3}$)	Proportionality factor	Special events where $3 \times$ estimated error was considered
Mg	0.0230	$0.05 \times X$	$X_{1,1}$ $X_{1,4}$ $X_{1,8}$
Ca	0.0230	$0.05 \times X$	$X_{2,7}$
K	0.0022	$0.05 \times X$	$X_{6,6}$
NH ₄	0.0004	$0.05 \times X$	$X_{7,4}$ $X_{7,7}$
NO ₃	0.0649	$0.05 \times X$	$X_{12,2}$
Na	0.0032	$0.05 \times X$	$X_{17,6}$
Cl	0.0246	$0.05 \times X$	$X_{22,2}$ $X_{22,5}$
SO ₄	0.1527	$0.05 \times X$	$X_{27,3}$ $X_{27,5}$

$\mathbf{X} = \mathbf{ZC} + \mathbf{E}$. In PMF, the matrix \mathbf{X} is not centred so each row of \mathbf{C} represents a single source of pollutants (which can be called, source profile) where each value in the row represents the mean concentration of the analyte for this source. Each column in \mathbf{Z} represents how much pollutant from each of the p th source was collected on each sample (n th sample), in the present work this corresponds to different days.

One of the differences with PCA is that while in PCA the least-squares sum of the residuals is minimized, PMF (by definition) attempts to decompose \mathbf{X} so that $\mathbf{Z}_{ik} \geq 0$ and, also, $\mathbf{C}_{kj} \geq 0$ ($i = 1, \dots, n$; $j = 1, \dots, p$; $k = 1, \dots, k$, which is called constrained weighted least-squares) [10] and, therefore, a function has to be iteratively minimized, say Q (Eq. (1)):

$$Q = \frac{E_{ij}^2}{\sigma_{ij}^2} \quad (1)$$

where, σ_{ij} is the standard deviation of x_{ij} . Q minimises the sum of squares of the residuals weighted inversely with the standard deviation of the data points. This is a key feature of PMF and it allows great flexibility in treating below detection limit, outliers and missing data. PMF does have options for non-negative constraints which are added as a penalty function added to σ_{ij} . One important advantage arising from this decomposition is that \mathbf{C} and \mathbf{Z} are given directly in the same units as \mathbf{X} , excepting for a scaling step performed on \mathbf{C} that it will be considered later on. The \mathbf{C} factors are not orthogonal nor orthonormal as typical principal components. In this respect,

strictly speaking the word ‘factor’ could be mathematically inadequate and ‘pollution pattern’ or ‘source profile’ might be more correct, despite this the more simple word ‘factor’ will be maintained.

In order to restrict the possible solutions available from the rotational space and get a ‘unique’ solution Antilla et al. [11] have adopted the normalization that \mathbf{Z} is dimensionless and $\text{Mean}_i(z_{ik}) = 1$ ($k = 1, \dots, k$) was adopted. The columns of the \mathbf{C} matrix are scaled in order to see the relative importance of each analyte across each factor as well as to assess the importance of each factor in explaining the variations of different analytes. Therefore, the total explained weighted variation of analyte j (say, EV_j) can be calculated as in Eq. (2):

$$EV_j = \frac{1 - \sum_{i=1}^n \frac{E_{ij}^2}{\sigma_{ij}^2}}{\sum_{i=1}^n \frac{X_{ij}^2}{\sigma_{ij}^2}} \quad (2)$$

Each column of \mathbf{C} is scaled so that the column sum = EV_j . Accordingly, a scaled matrix with elements EV_{kj} is obtained, see Eq. (3):

$$EV_{kj} = \frac{EV_j * C_{kj}}{\sum_{k=1}^k C_{kj}} \quad (3)$$

In this way, the columns of the new scaled- \mathbf{C} are analogous to the loading vectors in the PCA studies. A weakness of this technique is that a sound and careful selection of initial estimates for the errors associated to each value (σ_{ij}) has to be decided. A general-purpose way is applied in the

experimental section which is rooted on the mathematical background discussed by Paatero and Tapper [10].

In this paper, two studies are to be presented. First, a classical one (PCA, Varimax rotations and cluster analysis) to gain insight on variable associations and sample groups. Second, a source apportionment study using PMF. This approach implies that the interpretation of the source apportionment results can be made easier. This approach agree quite well with the recent paper of Gleser [12] where it is said that multivariate analyses of airborne particles (e.g. PCA) need many extra-information in order to fully interpret them. Therefore, applying typical multivariate techniques before PMF try to gain knowledge before the ‘final’ apportionment.

3. Experimental

3.1. Sampling

The city of A Coruña is located at the upper

NW of Spain on the Iberian Peninsula, in South Europe ($8^{\circ} - 8^{\circ}30'$ and $43^{\circ} - 43^{\circ}30'$), looking towards the Atlantic Ocean. The city ($\approx 250\,000$ inhabitants) is placed in a peninsular area whose isthmus is formed by a smooth hill area (about 300 m height). One of the Campuses of the University of A Coruña was built at one of these hills, about 200 m height, facing the city. The prevailing wind directions are from the NE in summer and from the SW in winter. The area has very good natural mixing throughout all the year and the average wind speed is about 25 km h^{-1} [13], nevertheless, there are on average 90 days (during fall and winter) when wind speeds average 60 km h^{-1} .

The Northern quadrant (from NW to NE) is dominated by the urban and marine sources, the NE–SE quadrant is dominated by rural and marine sources, the SE–SW quadrant corresponds to rural areas, the SW–NW directions correspond to an industrial area (which has several industries, including a refinery, truck garages, building companies, etc.). The city centre and industrial area are located 4 and 3 km away from

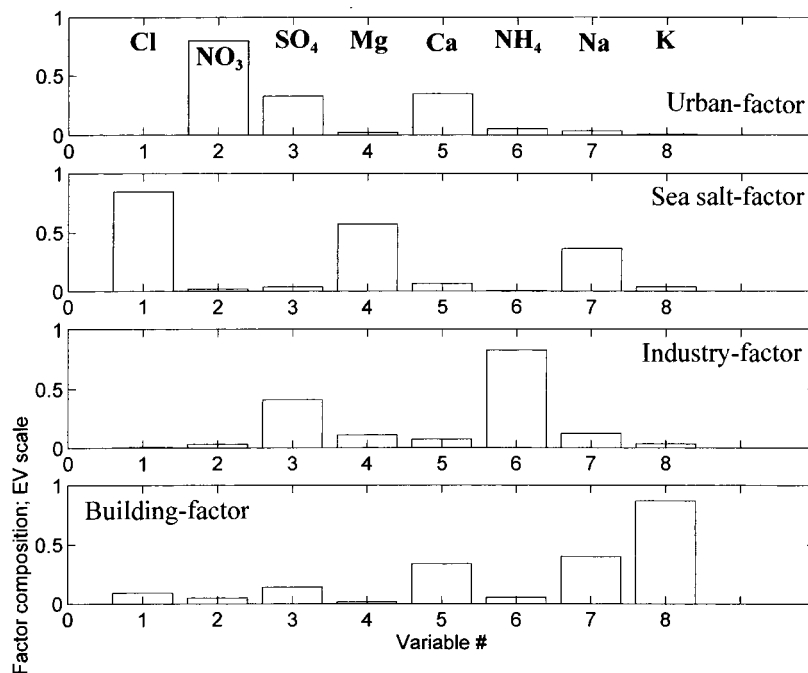


Fig. 4. Explained weighted variation for each variable in each factor. The general label for each factor agrees with the most important variables dominating each factor.

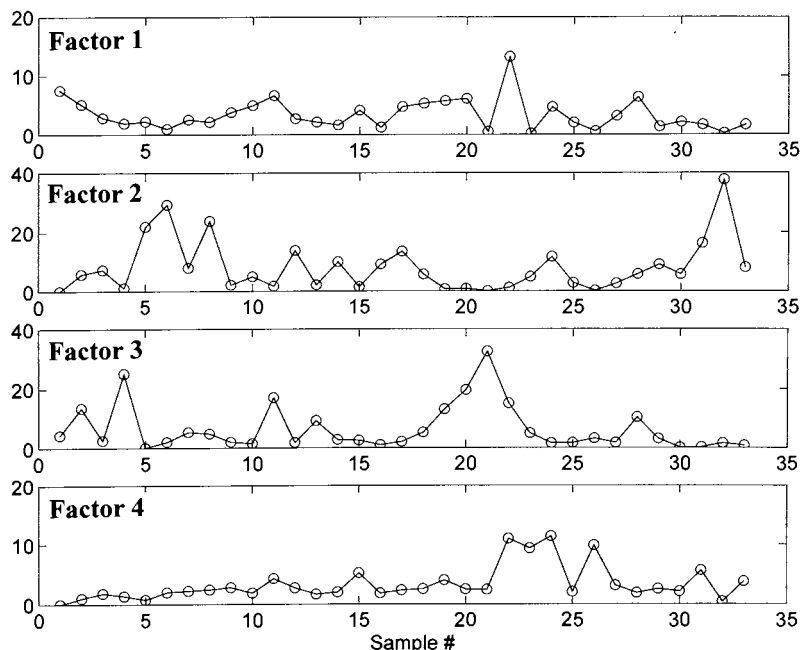


Fig. 5. Time series concentration ($\mu\text{g m}^{-3}$) calculated for each factor. The axis is normalized so that the mean value over the whole series is unity.

the sampling point, respectively. The sampling season was from March to September, 1994 and 33 24-hourly samples were taken. The total number of samples is not as large as it would be desirable and the reason is that the project supporting this work was intended to study the characteristics of the particulate matter included in A Coruña aerosols during spring and, mostly, summer. Fall and winter are rainy in this region so this study (the first in our city) was intended to apportion aerosol particles during the weather conditions, presumably, most unfavourable for the pollution characteristics of this area (higher amounts of particles, highest levels of pollutants, etc).

Aerosols were collected by air filtration with a high-volume sampler (MCV, mod. CAV-A/HF) equipped with Whatman GF/A glass fiber filters (20.3×25.4 cm). The sampling period was 24 h and the air flow was $60 \text{ m}^3 \text{ h}^{-1}$. Before and after the sampling, filters were kept for 48 h in a desiccator. Then, total suspended particulate (TSP) matter was determined by weighting them on a microbalance (Sartorius, model A200S). Ac-

cordingly, all the studies were carried out considering the TSP airborne particles.

3.2. Ion analysis

Here, the major water-soluble inorganic ions Mg^{2+} , Ca^{2+} , K^+ , Na^+ , NH_4^+ , Cl^- , NO_3^- , SO_4^{2-} collected by the glass fiber filters were analyzed as well as pH and conductivity. The filter portions employed in all the ion analyses were extracted in aqueous solution. All the ions were determined by a Waters ion chromatography device, equipped with a Waters pump 501LC and a Waters conductivity detector Mod. 431 and a Rheodyne injector (and a $20 \mu\text{l}$ loop) and IC-Pack-ATM (4.6×50 mm) column for anions or a IC-Pack-CTM (4.6×50 mm) column for cations. The compositions of the mobile phases were: for anions a borate-gluconate solution [2% (v/v) borate/gluconate, 20% (v/v) acetonitrile, 0.8% (v/v) *n*-butanol], for monovalent cations an ethylenediaminetetraacetic acid–nitric acid solution [0.05 mM EDTA, 0.003% HNO_3 (65%)] and for divalent cations an ethylenediamine–nitric acid mix-

ture [0.0035% (v/v) of EDA, 0.65% (v/v) HNO₃ (2% v/v)]. Fig. 1 shows one example of the chromatograms where good separations can be observed.

It was verified that the matrix did not interfere because all the recoveries were close to 100% when spiked samples were used. The recoveries found were 101.5% for Cl⁻, 99.5% for NO₃⁻, 101.5% for SO₄²⁻, 99.2% for Na⁺, 103.0% for NH₄⁺, 101.1% for K⁺, 96.2% for Ca²⁺, and 95.3% for Mg²⁺. Additionally, precision figures, calibration linearity, limits of detection and quantification were calculated in order to establish the analytical figures of merit (results not included in this work).

4. Results and discussion

The basic univariate statistics are resumed in Table 1. The overall raw data matrix consisted of ten analytical variables and 33 samples. All the multivariate studies presented below were made

using this matrix although scaling and outlier treatments differ in each particular application.

4.1. Principal component analysis

A preliminary principal component analysis (PCA) was performed using autoscaled data and outliers were looked for. Two samples (# 12 and 22) presented a quite clear outlying behaviour since they had by far the highest values for all the variables. They were located far away from the swarm of points formed by the remaining samples and they corresponded with samples taken from westerly winds, i.e. from the refinery/industrial area without any rain events. In order to avoid their negative effect on the statistical studies, they were discarded and the PCA repeated.

Considering the correlation matrix, two variables, namely pH and conductivity, were poorly correlated with all the remaining ones. Particularly, conductivity had low correlations (0.6 with NH₄⁺ and 0.5 with SO₄²⁻ and Mg²⁺) and also pH showed very low correlations (0.3 with NH₄⁺ and

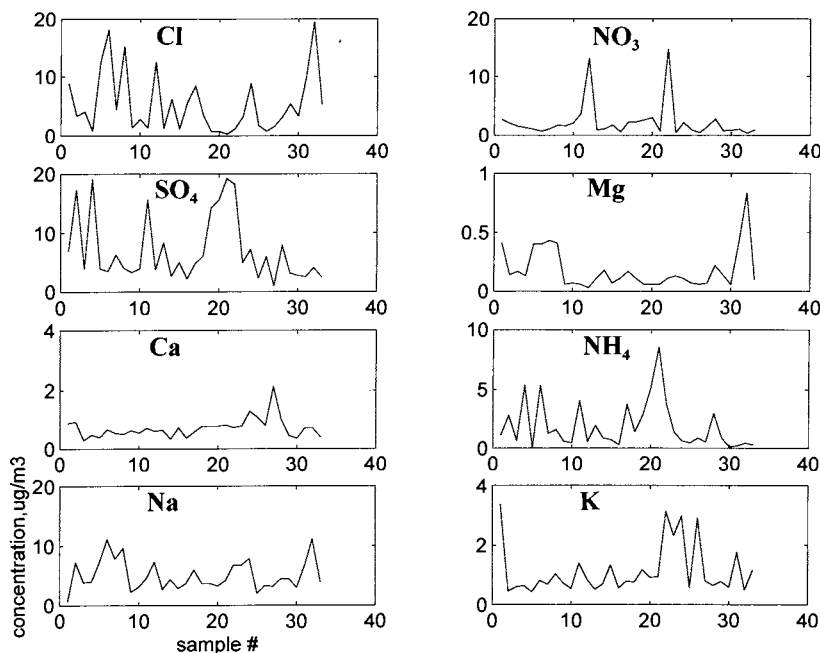


Fig. 6. Time series concentration ($\mu\text{g m}^{-3}$) for each original variable. Note the excellent agreement between the NO₃⁻, Cl⁻, SO₄²⁻ and K⁺ profiles and those time series for factors 1–4, respectively (normalized time series).

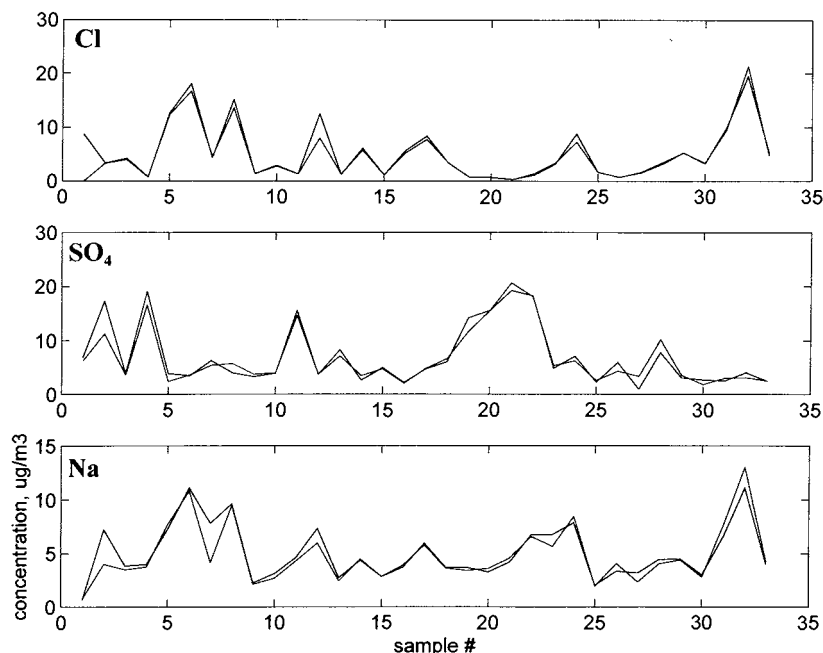


Fig. 7. Three examples showing an excellent agreement between the real and calculated time series concentrations ($\mu\text{g m}^{-3}$) for Cl^- , SO_4^{2-} and Na^+ .

0.2 with SO_4^{2-}). Under these circumstances, doubts may arise regarding the convenience (or not) of including such variables in the multivariate works. Thus, a second study omitting pH and conductivity values was carried out. The results indicated a slightly better sample group differentiation, denoting that pH and conductivity were not essential variables in our data set. Regarding the chemical background for this behaviour, it was supposed that:

1. since only anions and cations were considered, they can explain only a portion of the total conductivity letting, accordingly, another portion of unexplained conductivity (which might be attributed to e.g. other ionized substances as F^- , dissociated acids, carbon particles, organic matter, etc.).
2. the identified pollution sources (city, refinery, etc.) are quite close to our sampling site so the air masses appeared to be enhanced with NO_x and/or SO_x instead of their acidic forms (NO_3^- , SO_4^{2-}) therefore affecting the typical pH correlations. This point will be considered again latter on. Antilla et al. [11] presented

more reasons in order to explain similar problems in the pH performance.

Table 2 presents the loadings for the main principal components, after Varimax rotation and Fig. 2 presents the PC1-PC2-PC3 score subspace. Regarding Table 2 the following conclusions can be extracted:

1. The first factor can be closely related to a marine influence, as expected owing to the peninsular situation of A Coruña city. Samples # 32, 31, 5, 6 and 8 present the highest PC1-scores and wind directions coming from the W, S and WSW, i.e. those from the sea but also from the refinery and the industrial area. This fact is not so surprising as the 'pure sea-salt effect' could not be assessed. The reason is that the sampling site simultaneously monitor both sea- and industrial-originated aerosols and particles. In this respect, and although this factor reveals a clear sea-salt pattern, it is also reasonable to accept that samples combining both the marine and industrial sources will present the highest values for Cl^- and Na^+ . Some authors (e.g. Ohta and Okita [14]) have dis-

cussed methods to differentiate sea-salt chloride and/or sea-salt sulphate from other sources. Such studies are intended as univariate tools and they are inappropriate as multivariate ones. This is explained by how the correlation matrix is constructed. Obviously, the correlation between sulphate and excess sulphate, as it was called there [14], is perfect since we are defining variables which are linear combinations of the original variables and, thus, the data matrix become singular and the multivariate statistics (mostly PCA) are in danger. Therefore, instead of using this kind of univariate approaches, it was preferred to use the more comprehensive source apportionment technique described in the previous sections. Nevertheless, some preliminary studies were carried out using some equations given in [14] and no benefits were observed.

2. The second factor (ca. 22% of the initial variance) can be attributed to an industrial origin, whereas the fourth one can be grossly representative of the intensive road traffic and other urban inputs (NO_x , NO_3^-). These hypothesis became reinforced as the highest PC2-scores (samples # 21, 4, 20) have a clear origin in the NW to SW quadrant, i.e. from the industrial area. However, most samples with high NO_3^-

contents have wind directions blowing from the N, ENE and NE, i.e. from the urban area. Additionally, there was a strong association between NO_3^- and Pb ($r = 0.78$).

3. Rotated PC3 and PC5 are associated to K^+ and Ca^{2+} , respectively though they are not associated to the sea-salt effect (of course, a marine and crustal origin cannot be totally disregarded). Both K^+ and Ca^{2+} are quite uncorrelated to Cl^- and Na^+ , suggesting that they two may derive mainly from building and earthworking activities. Accordingly, K^+ and Ca^{2+} seem to be originated in the building works (dust, concrete, etc.). In Fig. 2, samples # 1, 24 and 27 present maximum values either for K^+ and Ca^{2+} and all of them are linked to winds blowing from the North (from such works).

Fig. 2 presents four main groups of samples, construction-derived material (samples 1, 24 and 27), a second group, placed at the right hand of the figure, showing medium-high PC2-scores, a third group, mostly at the left side, comprising samples with high levels in the marine factor (or marine plus industrial, samples # 31, 32, 26, 8) and a fourth group characterized by zero or negative score values for all the factors, thus describing those samples with the lower values for all the

Table 4

Average source profiles and Ion balance for the 4-model apportionment, $\mu\text{eq m}^{-3}$ (missing figures means that the contribution for this particular element is $<0.00010 \mu\text{eq m}^{-3}$)

Variable	Average profiles ($\mu\text{g m}^{-3}$)				Ion balance ($\mu\text{eq m}^{-3}$)				
	Urban	Industrial	Sea-salt	Building	Urban	Sea-salt	Industrial	Building	
Cl	0.0005	0.5637	0.0035	0.0624		0.0159		0.0018	
NO_3	0.3938	0.0089	0.0151	0.0238	0.0064		0.0002	0.0004	
SO_4	0.4886	0.0525	0.6112	0.2099	0.0101	0.0011	0.0127	0.0044	
Mg	0.0006	0.0161	0.0031	0.0004		0.0013			
Ca	0.0662	0.0122	0.0140	0.0648	0.0033	0.0006	0.0007	0.0032	
NH_4	0.0152	0.0016	0.2305	0.0152	0.0008		0.0128	0.0008	
Na	0.0328	0.3348	0.1124	0.3677	0.0014	0.0146	0.0049	0.0159	
K	0.0024	0.0102	0.0102	0.2557		0.0003	0.0003	0.0066	
					<i>Cations</i>				
					0.0055	0.0168	0.0187	0.0265	tot = 0.067
					<i>Anions</i>				
					0.0165	0.0170	0.0129	0.0066	tot = 0.053

variables. Interesting enough, almost all the samples in the fourth group were taken under rainy and/or drizzly conditions.

4.2. Cluster analysis

Although cluster analysis is a potentially useful technique for grouping samples, its application to atmospheric studies has not been broadly reported. One of the reasons might lie in the difficult interpretation associated to the dendrograms. Environmental variables may force unclear sample groups such that the dendrogram is difficult to interpret. In spite of this, it is considered that cluster analysis should be performed, at the very least, to confirm the sample score groups. Therefore, a cluster analysis was made using the autoscaled original data matrix, the squared euclidean distance as a measure of similarity and the complete linkage method as the clustering criterion. The dendrogram is depicted in Fig. 3.

It is not easy to find a single variable pattern dominating the sample grouping (e.g. increasing values of Cl^-), even using other similarity measures and clustering methods. Instead, the same general four groups discussed in the PC-score sample subspace get confirmed (where C means 'cluster') and, hence, the major pollution patterns identified using the PCA:

1. C1: comprises those samples with the highest levels of Cl^- , Na^+ and Mg^{2+} (marine related).
2. C2: comprises the samples showing the highest concentrations of SO_4^{2+} and NH_4^+ (industry-derived).
3. C3: groups all the remaining samples. Attention can be drawn onto an interesting subdivision, cluster C3B, which collects the samples with the lowest PC1-PC2-PC3 scores, and the lowest figures in almost all the original variables. Samples # 23, 26, 24, 1 and 27, present high values for K^+ and Ca^{2+} and 'normal' for the rest of the variables.

4.3. Source apportionment using positive matrix factorization

As in most multivariate techniques, there are

two initial steps in order to apply positive matrix factorization. First, to deal with the anomalous data and, second, to select the most adequate number of factors.

Regarding the first stage, an $(n \times p)$ -error matrix was defined (n = number of samples, p = number of variables) so that each value in the raw data matrix have its counterpart error estimate. Instead of using the same expression as Antilla et al. [11] to estimate the associated error, where the limit of detection was considered, it was preferred to estimate the error as in Eq. (4):

$$\sigma_{ij} = \sqrt{(\text{reproducibility})^2 + (0.05 x_{ij})^2} \quad (4)$$

since, we think, it would be better to consider the laboratory long-term precision errors (which comprise from cutting different pieces of the filter till analyzing them) which, hopefully, would take account for the sampling error (at least, partially). In that equation x_{ij} is every particular value in the raw data matrix, and method reproducibility (measured as within-laboratory long term SD) corresponds to each j th variable.

Additionally to this error matrix, the previous knowledge about the system (gained by the previous PCA) was used and the error estimated was increased (multiplying by 3) on these samples showing an outlier behaviour (i.e. samples 12 and 22). Table 3 resumes the error estimation for each variable and some cases specially considered. Such cases did not presented obvious anomalous figures and it was decided to increase their associated error after several trials where error estimation and residuals observation (after developing models) were carried out. This iterative approach is similar to the one selected by Garner et al. [15] when using the Generalized and Mardia's multivariate distances to deal with outlier values.

The second step is to select the most adequate number of factors (this expression will be maintained though they are not typical orthogonal nor orthonormal factors). Three different studies were conducted with 3, 4 and 5 factors, respectively in order to assess the best number of factors. It was found that the most understandable results arose when 4 factors were considered.

Fig. 4 depicts the explained variation for each variable by each factor. The values are normalized

so that the total explained variation for each variable is 1 (i.e. 100%). The first factor (the first barchart in Fig. 4) is mainly influenced by NO_3^- , Ca^{2+} and SO_4^{2-} , the second by Cl^- , Mg^{2+} and Na^+ , the third by SO_4^{2-} and NH_4^+ and the fourth by Ca^{2+} , Na^+ and K^+ . There is little doubt about the origin of the second and third source profiles, sea-salt (marine) and industry, respectively. The pollution source related to the first profile appears either as a consequence of the urban traffic or as a combination of the urban and industrial inputs. Of course, a sea-salt– SO_4^{2-} participation can not be totally disregarded. Due to the wind directions observed during the sampling days and the strong correlation between NO_3^- and Pb (see Section 4.1), it is thought that this factor is mainly related to the urban (traffic) pollution. The fourth source profile composed by K^+ , Ca^{2+} , Na^+ and, partially, SO_4^{2-} strongly suggests a building, roading and earthworking origin, dust, crustal erosion, concrete, etc. (remember that concrete and cement concrete are made of Ca^{2+} , Na^+ and aluminium-sulphates to a great extent).

All the variables exhibit a total explained variation > 0.80 , being the unique exception Mg^{2+} (ca. 0.72). This fact was consistently maintained for Mg^{2+} along the different studies and we have not found a satisfactory chemical reason. A similar behaviour was noted for K^+ by Antilla et al. [11] also without a detailed explanation.

Fig. 5 presents the influence of each factor along all the samples (this could be called ‘time series’). It is interesting to compare these pollution factor-profiles with the time series profiles for some variables (see Fig. 6). It can be verified that the concentration profiles for NO_3^- , Cl^- (Mg^{2+} and Na^+), SO_4^{2-} (and NH_4^+) and K^+ essentially agree with factors 1–4, respectively, being Ca^{2+} the unique variable without a definite corresponding factor profile. The lack of a corresponding factor profile for Ca^{2+} points towards a multi-source origin for Ca^{2+} , among them, sea-salt, building activities and crustal erosion.

One way to confirm that the essential pollution sources have been accounted for is to compare the ‘real’ and predicted concentrations for all the samples and for each variable. Fig. 7 shows just

two examples where an almost perfect agreement can be seen, the same behaviour was observed for the rest of the variables.

4.4. Ion balances

Thanks to the intrinsic mathematical behaviour of the positive matrix factorization algorithms, ion balances can be made in a straightforward manner. Ion balances can be used to assess if a distorted factorization was accepted and to gain insight about the chemical profiles of the pollution sources. As mentioned in the theoretical section, matrix **C** has the same units as the original values and matrix **Z** was normalized to get dimensionless figures. Additionally, the rows of **C** represent the chemical compositions of the pollution sources; moreover, each element of the rows of **C** (c_{kj} as stated above) represents the mean concentration of compound j , caused by the pollution source k . Therefore, the rows of **C** give the average composition (in original concentration units) of each source that it is reaching the sampling site and an ion balance can be performed to assess whether (on average) anions and cations become balanced. Most ion balances reported in literature are given in equivalent units, so, this was also used here.

Table 4 compiles both the average source profiles and their corresponding ion balance (translated to μeq units dividing by the equivalent weights). Two different behaviours are observed, the sea-salt and industrial-related factors are fairly well balanced whereas the other two suffer from a lack of cations and anions.

Several situations can take account of this little unbalance, namely:

1. As only the main water-soluble anions and cations were analyzed, there might be other ionic (or ionizable) substances that become not included in the balance. As it is almost impossible to consider every analyte in every study, this can be considered as a drawback of any apportionment method. Nevertheless, the unbalance is so little that it can be accepted that water-soluble ions constitute the main composition of the A Coruña particulate airborne

matter to a large extent, as it was assumed at the beginning of this work following Ali [1].

2. The sampler device was sited at the top of a hill two kilometres away from the core of the city and one kilometre away from the building and earthworking area. Such closeness to the pollution sources might imply that aerosol neutralization or stabilization might not be achieved before reaching the sampler and, accordingly, a lack of cations is observed for the NO_x , SO_x and automobile-based species and a lack of anions for the building-based pollutants.
3. Moreover, chemical reactions into the aerosol can not be discarded, for instance, the interaction between Cl^- and SO_2 and/or the interactions between NH_4^+ , SO_4^{2-} and Cl^- .

Table 4 also reveals that the global ion balance is rather well balanced. According to Antilla et al. [13] the ratio of the equivalent cation concentration to the sum of both anion and cation equivalent concentrations [$r = C_{\text{cat}} / (C_{\text{ani}} + C_{\text{cat}})$] should be close to 0.5 for a perfect balance. In this case, $r = 0.56$ thus pointing towards a little unbalance for anions.

5. Conclusions

An airborne particulate matter study was made in order to identify the main patterns influencing the aerosol quality during summer in A Coruña city. PCA and Cluster analyses were used as the first step to gain insight on the data and to simplify the chemical interpretation of the source apportionment and ion balances studies carried out by means of an apportionment technique called positive matrix factorization (PMF). All the PMF calculations and results are given in original units, which contribute to sound and reasonable

chemical conclusions. In this case, four main pollution patterns were identified, namely, marine, industrial, urban and building patterns (or factors). It is thought that they represent the geographical, social and industrial inputs to the local airborne particles and aerosols.

Acknowledgements

Thanks are given to the Galician Government (Xunta de Galicia) for its financial support (XUGA10303A92) and to the Meteorological Institute of A Coruña (Instituto Meteorológico de A Coruña).

References

- [1] A.Y. Ali-Mohamed, *Atm. Environ.* 25B (3) (1991) 397.
- [2] US-EPA, Protocol for applying and validating the CMB (chemical mass balance) Model, US Environmental Protection Agency, Research Triangle Park, NC, USA, May 1987.
- [3] P.K. Hopke, *Atm. Environ.* 22 (9) (1988) 1777.
- [4] G.D. Thurston, J.D. Spengler, *Atm. Environ.* 19 (1) (1985) 9.
- [5] R.M. Harrison, D.J.T. Smith, L. Luhana, *Environ. Sci. Technol.* 30 (1996) 825.
- [6] L. Poissant, *Atm. Environ.* 28 (12) (1994) 2129.
- [7] J.G. Watson, J.A. Cooper, J.J. Huntzicker, *Atm. Environ.* 18 (7) (1984) 1347.
- [8] J.G. Wang, P.K. Hopke, *Atm. Environ.* 23 (10) (1989) 2143.
- [9] S. Junnto, P. Paatero, *Environmetrics* 5 (1994) 127.
- [10] P. Paatero, U. Tapper, *Environmetrics* 5 (1994) 111.
- [11] P. Antilla, P. Paatero, U. Tapper, O. Järvinen, *Atm. Environ.* 29 (14) (1995) 1705.
- [12] L.J. Gleser, *Chemom. Intell. Lab. Syst.* 37 (1997) 15.
- [13] R. Carballal, R. Iglesias, M.E. López de Silanes, *Nova Acta Cient. Comp.* 1 (1990) 19.
- [14] S. Ohta, T. Okita, *Atm. Environ.* 24A (4) (1990) 815.
- [15] F.C. Garner, M.A. Stapanian, K.E. Fitzgerald, *J. Chemometrics* 5 (1991) 241.

Determination of mono- and sesquiterpenes in water samples by membrane inlet mass spectrometry and static headspace gas chromatography

Marja Ojala ^{a,b,*}, Raimo A. Ketola ^a, Timo Mansikka ^a, Tapio Kotiaho ^a,
Risto Kostianen ^c

^a VTT, Chemical Technology, P.O. BOX 1401, FIN-02044 VTT, Finland

^b University of Helsinki, Laboratory of Analytical Chemistry, P.O. Box 55, FIN-00014 University of Helsinki, Finland

^c University of Helsinki, Department of Pharmacy, Division of Pharmaceutical Chemistry, P.O. Box 56, FIN-00014 University of Helsinki, Finland

Received 4 June 1998; received in revised form 12 November 1998; accepted 16 November 1998

Abstract

A membrane inlet mass spectrometric (MIMS) method is presented and compared with a static headspace gas chromatographic method (HSGC) for the determination of terpenes in water. The MIMS method provides a very simple and fast analysis of terpenes in water, detection limits being relatively low, from $0.2 \mu\text{g l}^{-1}$ for monoterpenes to $2 \mu\text{g l}^{-1}$ for geraniol. The analysis of terpenes by the HSGC (equipped with flame ionization detector, FID) method is more time-consuming and the detection limits ($2 \mu\text{g l}^{-1}$ for monoterpenes to $100 \mu\text{g l}^{-1}$ for geraniol) are higher than with MIMS. However, the HSGC method has the advantage of determining individual mono- and sesquiterpene compounds, whereas MIMS provides only separation of different classes of terpenes. Both methods were applied to the analysis of mono- and sesquiterpenes in several condensation water samples of pulp and paper mills. © 1999 Elsevier Science B.V. All rights reserved.

Keywords: Membrane inlet mass spectrometry; Headspace gas chromatography; Terpenes; Water samples

1. Introduction

Mono- and sesquiterpenes are common constituents of volatile oils and several woods contain extractable terpenes, and they are found for ex-

ample in the condensation waters of pulp and paper mills [1,2]. Monoterpenes exist as hydrocarbons or as oxygenated compounds such as aldehydes, alcohols, ketones, esters or ethers. These may be acyclic, monocyclic, dicyclic or tricyclic in structure [3]. The solubility of mono- and dicyclic terpene hydrocarbons in water is low ($10\text{--}30 \text{ mg l}^{-1}$). However, monoterpenes containing the hydroxyl group have solubilities of $10\text{--}100\text{-fold}$

* Corresponding author. Tel.: +358-9-4565312; fax: +358-9-4567026.

E-mail address: Marja.Ojala@vtt.fi (M. Ojala)

compared to terpene hydrocarbons [4]. Due to their low solubility in water, terpene hydrocarbons have relatively high Henry's law constants [5,6] and therefore they partition predominantly into the atmosphere [7]. For this reason they have been analyzed more often in air [8–11] than in water.

Ekman et al. [12] have evaluated wood extractives in pulp and water samples by gas chromatography–mass spectrometry. Using gas chromatography, the turpentine extracted from wood has been studied and 15 different terpenes were found [13]. Kimball et al. [14] have identified 22 terpenoids from wood using GC combined with mass selective detection. Volatile sesquiterpenes and sesquiterpenoids in environmental and geological samples have been analyzed by a capillary gas chromatograph combined with a mass spectrometer after extraction and fractionation [15]. Furthermore, gas chromatography or gas chromatography-mass spectrometry has been used in the analysis of terpenes in waste water samples [1,16,17]. Static headspace gas chromatographic methods have been widely used in analysis of terpenes from essential oils, plant products and in aroma constituents [18–20]. Furthermore, headspace methods have been used in quantitation of volatile constituents, for example, terpenes in juices [21–23]. Mathieu et al. [24] have used dynamic headspace to analyze volatile organic compounds in red coffee berries and they found many mono- and sesquiterpene compounds. However, according to our study only one article reporting the measurements of terpenes from water by static headspace method was found in the literature [25]. The detection limits obtained for terpene hydrocarbons were $5 \mu\text{g l}^{-1}$, which are in good agreement with our results.

Although GC-methods are widely used, they are time-consuming, so that faster and more sensitive methods are needed. In addition, conventional GC-techniques are not well suited for on-line measurement, and therefore there is a need to develop rapid and sensitive on-line methods for the analysis of contaminated water samples. Membrane inlet mass spectrometry (MIMS) meets all these requirements [26,27]. The analysis with MIMS involves a flow of the sample over a

sheet polydimethylsiloxane membrane which extracts non-polar, medium polar and low molecular weight organic compounds from the matrix. After the extraction step the organics pervaporate through the membrane into the ion source of a mass spectrometer. The total analysis takes only a few minutes. The MIMS method has previously been applied to the analysis of volatile organic compounds (VOCs) in environmental water and air samples [28–34] as well as in the monitoring of chemical and biochemical processes [35–37]. Membrane inlet mass spectrometry has also been applied for continuous on-line waste water monitoring for VOCs [38,39]. This study compares the membrane inlet mass spectrometric (MIMS) method for the analysis of terpenes in water with the static headspace gas chromatographic (HSGC) method.

2. Experimental

2.1. Reagents and samples

The following reagents were obtained from Fluka: α -Pinene [80-56-8]; β -pinene [127-91-3]; limonene [138-86-3]; α -terpinene [99-86-5] Δ -3-carene [13466-78-9]; myrcene [123-35-3]; camphene [79-92-5]; longifolene [475-20-7]; α -cedrene [11028-42-5]; linalool [78-70-6]; and geraniol [106-24-1]. A stock solution (1 g l^{-1}) of each standard compound was prepared in methanol. The calibration standards ($0.1 \mu\text{g l}^{-1}$ – 1 mg l^{-1}) were prepared by dilution with deionized water (Millipore, Milli-Q Plus).

Authentic waste water samples from pulp and paper mills were used in comparison of the MIMS and HSGC methods. Many of the samples were unhomogenous due to their high terpene concentration and the low solubility of terpenes in water. Samples were diluted with deionized water before analysis as follows: Samples 10 and 11 were diluted by 1:250, sample 12 by 1:10 and sample 13 by 1:2 using deionized water for MIMS analysis. In addition, samples 10 and 12 were diluted by 1:10 and sample 11 by 1:50 for HSGC-analysis. All other samples were analyzed without dilution (Table 3).

Table 1
Standard terpene compounds and their electron impact mass spectra measured by MIMS

Compound	MW ^a	Ions m/z (RA) ^b
<i>Monoterpenes</i>		
α -pinene	136	93(100), 91(44), 92(37), 77(31), 79(25), 121(14), 105(13), 67(10), 53(10), 94(10), 136(6)
Camphene	136	93(100), 121(59), 79(48), 91(41), 67(32), 77(30), 107(30), 94(18), 53(16), 95(16), 136(11)
β -Pinene	136	93(100), 69(34), 91(32), 79(26), 77(26), 94(13), 121(13), 67(13), 92(12), 53(12), 136(6)
Myrcene	136	93(100), 69(76), 91(26), 79(20), 77(18), 53(15), 67(15), 92(11), 94(11), 53(15), 136(3)
Δ -3-carene	136	93(100), 91(53), 77(38), 79(35), 92(29), 80(22), 121(20), 105(16), 136(12) , 94(12)
α -terpinene	136	121(100), 93(91), 136(61) , 91(58), 77(36), 79(30), 119(29), 105(23), 107(12), 65(11)
Limonene	136	68(100), 67(74), 93(65), 79(36), 53(28), 91(27), 94(25), 92(24), 77(23), 121(22), 136(14)
<i>Monoterpene alcohols</i>		
Linalool	154	71(100), 55(84), 93(69), 69(50), 57(40), 56(40), 67(30), 80(27), 53(24), 121(19)
Geraniol	154	69(100), 93(24), 68(19), 67(18), 53(14), 91(13), 55(10), 79(10), 77(9), 123(9)
<i>Sesquiterpenes</i>		
Longifolene	204	161(100), 91(92), 105(76), 93(68), 107(67), 94(64), 79(63), 119(57), 133(54), 95(52), 204(26)
α -cedrene	204	119(100), 93(40), 105(33), 91(26), 161(18), 69(18), 204(16) , 77(15), 120(15), 121(14)

^a MW is molecular weight, molecular ions are bolded.

^b RA is relative abundance.

2.2. Mass spectrometric conditions

Samples were analyzed using a quadrupole

Table 2
Detection limits ($S/N = 3$) of selected terpenes by static HSGC and MIMS

Compound	Detection limit ($\mu\text{g l}^{-1}$)	
	HSGC	MIMS/SIM
<i>Monoterpenes</i>		
α -pinene	3	0.2
Camphene	3	0.5
β -pinene	3	0.2
Myrcene	2	0.2
Δ -3-carene	2	0.5
α -terpinene	2	0.5
Limonene	2	0.5
<i>Monoterpene alcohols</i>		
Linalool	30	0.5
Geraniol	100	2
<i>Sesquiterpenes</i>		
Longifolene	5	2
α -cedrene	5	0.5

mass spectrometer (Balzers QMG 421C, Balzers Aktiengesellschaft, Balzers, Liechtenstein) with a mass range 1–500 amu. This quadrupole instrument was equipped with an open cross-beam electron impact (70 eV) ion source. The data were collected either by scanning full mass spectrum (mass range m/z 50–210 amu), or by using a selected ion monitoring mode (SIM). The latter was used to determine detection limits. A sheet membrane inlet built at VTT Chemical Technology [40] was used. The membrane material was polydimethylsiloxane (Specialty Silicone Products, Ballston SPA, NY, USA) with a thickness of 110 μm and contact area of 28 mm^2 . During operation of the system, a water stream was continuously sucked through the membrane inlet via a peristaltic pump (Ismatec IPS4, Ismatec SA, Switzerland), with a typical flow rate of 10 ml min^{-1} , and with aliquots of sample solution (20–30 ml) injected into this stream. Using a heat exchanger, which was heated with a circulating water bath (Lauda M3, MGW, Germany), the water stream was heated to 70°C before the membrane inlet. Identification and quantitation of terpenes in water samples were done using a calculation pro-

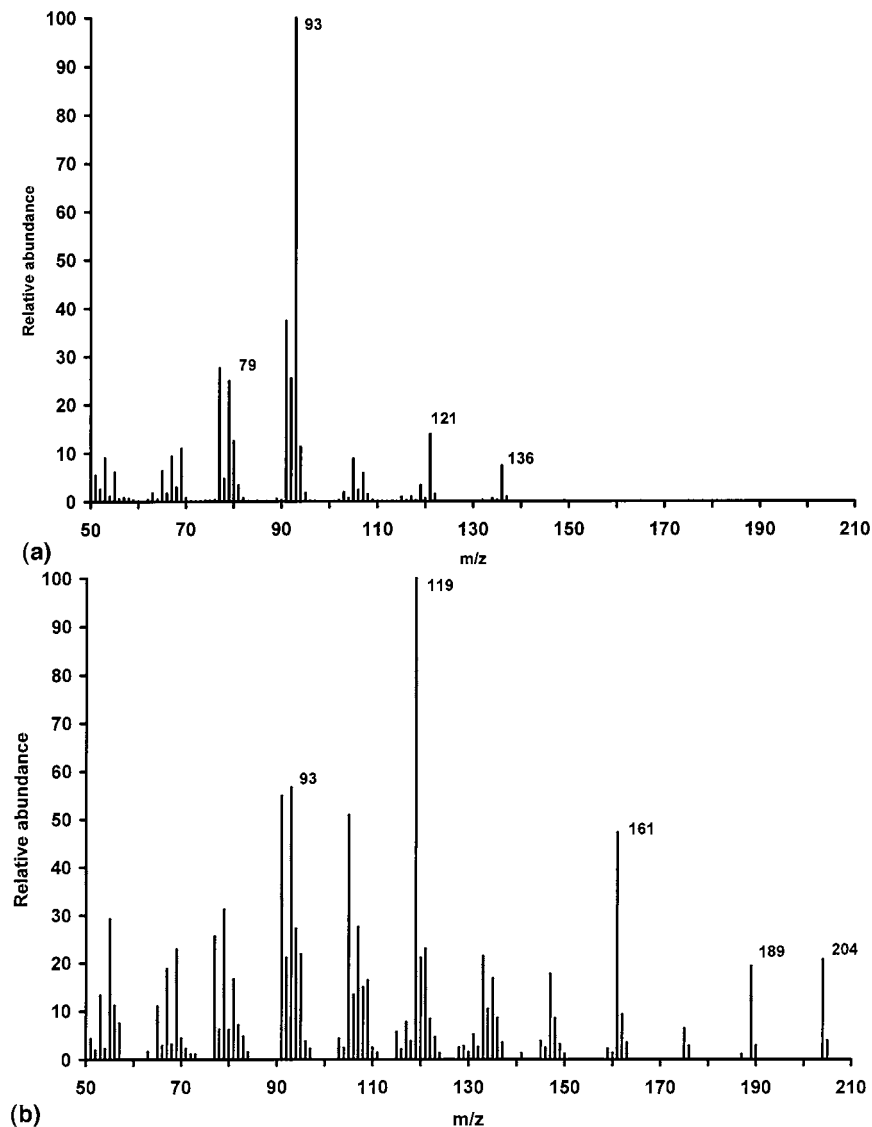


Fig. 1. (a) Electron impact mass spectrum of a mixture of α -pinene, β -pinene and Δ -3-carene (about $50 \mu\text{g l}^{-1}$ of each component). (b) Electron impact mass spectrum of a mixture of longifolene and α -cedrene (about $50 \mu\text{g l}^{-1}$ of each component). (c) Electron impact mass spectrum of a mixture of linalool and geraniol (about $100 \mu\text{g l}^{-1}$ of each component).

gram (Solver) designed at VTT Chemical Technology [41,42]. This calculation program uses a modified algorithm of the general deconvolution method, which assumes that the intensity of any mass-to-charge ratio (m/z) is a linear function of the concentration of the chemical compounds which contribute to that particular m/z .

2.3. Gas chromatographic conditions

The system used in this experiment was a gas chromatograph (HP 5890 Series II, Hewlett Packard, Palo Alto, CA, USA) equipped with two FIDs and a headspace sampler (HP 7694). Two columns were used, a SPB-1 ($30 \text{ m} \times 0.32 \text{ mm} \times$

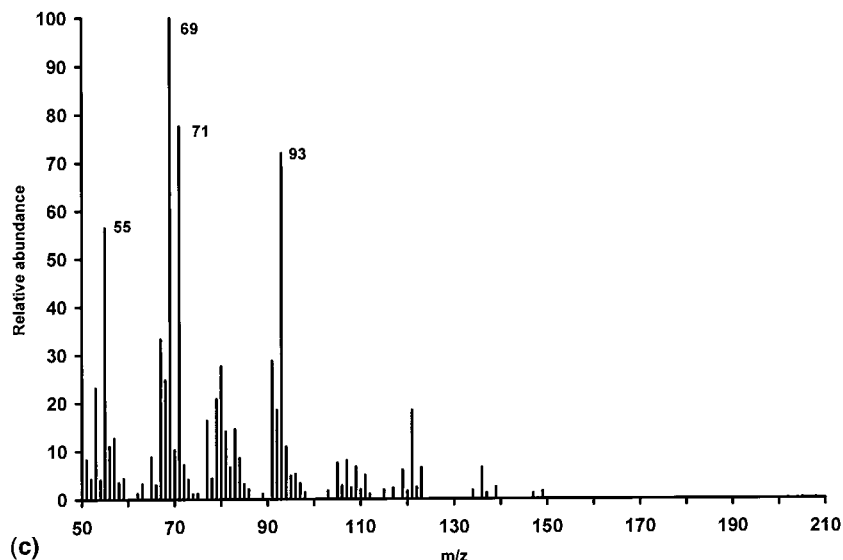


Fig. 1. (Continued)

1.0 μm , Supelco, Supelco Park, Bellefonte, PA 16823, USA) and a DB-1701 (30 m \times 0.32 mm \times 1.0 μm , J and W Scientific, Folsom CA, USA). The temperature program used was optimized for the separation of terpenes and it was 45°C, 5 min $\xrightarrow{10^\circ\text{C min}^{-1}}$ 210°C, 10 min. The temperatures of the injector and detectors were 220 and 250°C, respectively. In addition, the temperatures of sample vials and transferline between the headspace autosampler and the GC were 80 and 120°C, respectively.

3. Results and discussion

The analytical performance characteristics of the MIMS and HSGC methods were determined using the following standard compounds; monoterpenes: α - and β -pinene, limonene, α -terpinene, Δ -3-carene, myrcene and camphene, sesquiterpenes: longifolene and α -cedrene; and alcoholic derivatives of acyclic terpenes: linalool, and geraniol.

Electron impact (EI) mass spectra were measured for all these compounds using MIMS. Ten ions with the highest abundance and the molecular ions are presented in Table 1 and the mass spectra of the quantitation standard mixtures (a)

a monoterpene mixture consisting of α - and β -pinene and Δ -3-carene (about 50 $\mu\text{g l}^{-1}$ of each component); (b) a sesquiterpene mixture, longifolene and α -cedrene (about 50 $\mu\text{g l}^{-1}$ of each component), and (c) terpene alcohol mixture, linalool and geraniol (about 100 $\mu\text{g l}^{-1}$ of each component) are presented in Fig. 1. All the measured EI mass spectra (except linalool) agreed well with the EI mass spectra published in a reference mass spectral library [43]. The molecular ions m/z 136 for monoterpene hydrocarbons and m/z 204 for sesquiterpene hydrocarbons were recorded, but the molecular ion m/z 154 for linalool and geraniol was not observed. The EI spectra of monoterpenes were rather similar (Table 1), the base peak for nearly all monoterpenes was m/z 93 and the other fragment ions were nearly identical. EI spectra of sesquiterpenes, longifolene and cedrene, had many common fragment ions and the base peaks were m/z 161 and m/z 119, respectively. Due to the similarities in their mass spectra the identification of individual terpenes is very difficult without chromatographic separation. However, the mass spectra of mono- and sesquiterpenes are clearly different. Due to these differences the quantitation could be carried out by the MIMS method as monoterpene and sesquiterpene classes and it was performed using

Table 3

The terpene concentrations ($\mu\text{g l}^{-1}$) of analyzed authentic water samples using the HSGC and MIMS methods

Sample	Monoterpenes		Sesquiterpenes		Total	
	HSGC	MIMS	HSGC	MIMS	HSGC	MIMS
1	48	160	100	69	150	230
2	32	98	72	62	100	160
3	61	110	110	70	170	180
4	36	74	67	49	100	120
5	530	410	370	370	900	780
6	1500	1500	580	650	2100	2100
7	730	440	260	320	1000	760
8	1900	1800	540	750	2400	2600
9	860	610	330	450	1200	1100
10	23 000	37 000	37 000	5700	27 000	42 000
11	53 000	49 000	6100	4800	59 000	53 000
12	12 000	8500	2500	2000	15 000	11 000
13	2700	1100	670	470	3400	1600

the whole mass spectrum of a standard mixture (Fig. 1), in the calculations.

Detection limits with MIMS were measured using selected ion monitoring (SIM), and the base peak of each individual compound was used as the ion in measurement. The detection limits varied from 0.2 to $2 \mu\text{g l}^{-1}$ (Table 2). It is worth of notice that the detection limits measured by MIMS using the whole spectrum were about one order of magnitude higher compared to those measured by MIMS in a selected ion monitoring mode. The SIM results are reported here, because it is the typical method used for detection limit measurements in connection with MIMS and because the SIM method can be used to quantitate low levels of terpenes. Detection limits measured with HSGC were relatively low ($2\text{--}5 \mu\text{g l}^{-1}$), except for the more polar compounds linalool and geraniol, which had detection limits of 30 and $100 \mu\text{g l}^{-1}$, respectively (Table 2). The relatively high detection limit for linalool could be expected to be due to its low Henry's law coefficient, $0.002 \text{ kPa m}^3 \text{ mol}^{-1}$ [6]. The differences in detection limits can also be seen in the chromatogram presented in Fig. 2, which shows a gas chromatogram of a standard terpene mixture with about $20 \mu\text{g l}^{-1}$ of each terpene compound. On the basis of this chromatogram it is easy to see that the analysis time with the HSGC method is relatively long,

about 30 min. Whereas, with the MIMS method the analysis time was rather short, about five min, as in our earlier studies [31–34].

The repeatability and linear dynamic ranges of the MIMS method were tested using six compounds: α -pinene; α -terpinene; limonene; myrcene; longifolene; and geraniol. The measurements were done using at least four different concentrations (from 0.1 to $300 \mu\text{g l}^{-1}$) and triplicate analysis of every single concentration. Because of the poor solubility of terpenes in water, their linear dynamic ranges were measured only up to concentrations of about $300 \mu\text{g l}^{-1}$ with both the methods. The repeatability of the MIMS method was good [relative standard deviations (RSD) = 2.6–18%]. The repeatability of the HSGC technique was also good, the RSD being lower than 5% for every terpene compound (not determined for geraniol). The RSD values for the HSGC method were determined using four different concentrations of standard compounds and triplicate analysis of each. The linear dynamic ranges of the MIMS method were three orders of magnitude for all compounds, except for longifolene and geraniol, which had ranges of two orders of magnitude (correlation coefficients varied from 0.992 for geraniol to 1.000 for α -terpinene). The linear dynamic ranges by the HSGC method were only two decades and the correlation coefficients

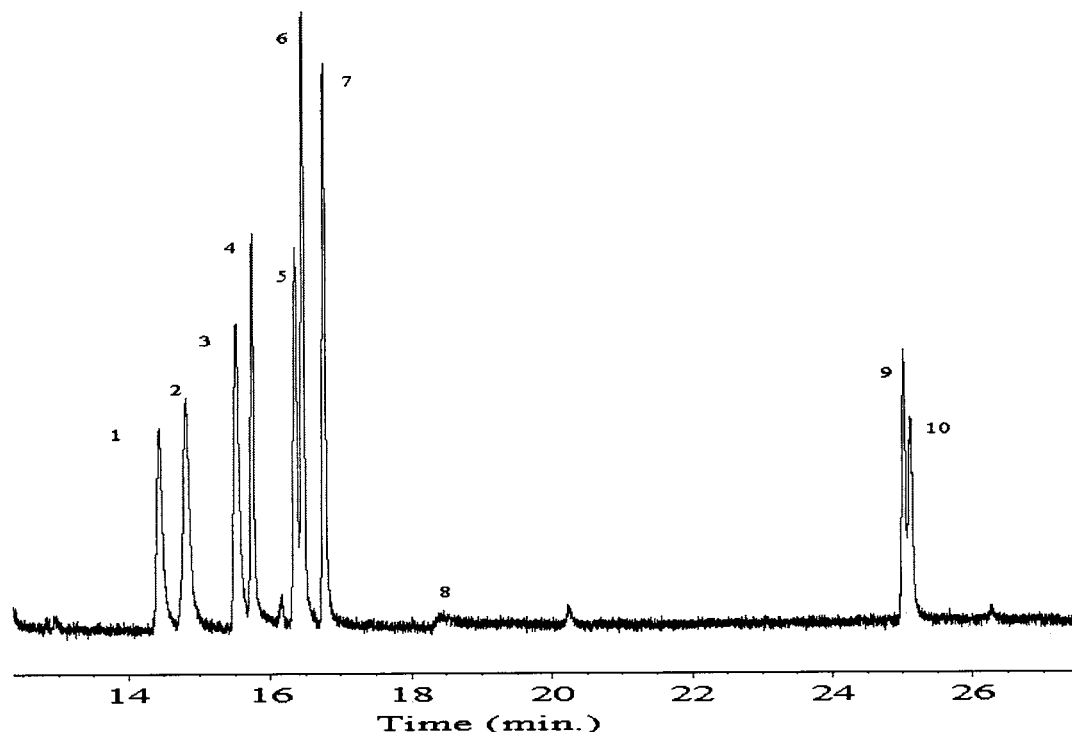


Fig. 2. A gas chromatogram of a standard terpene mixture (about $20 \mu\text{g l}^{-1}$ of each compound). Due to its high detection limit geraniol can not be seen in the chromatogram. It elutes between linalool and longifolene. Results are obtained using SPB-1 column. DB-1701 column could not separate longifolene and cedrene. 1. α -pinene, 2. camphene, 3. β -pinene, 4. myrcene, 5. Δ -3-carene, 6. α -terpinene, 7. limonene, 8. linalool, 9. longifolene, 10. α -cedrene.

varied from 0.995 for α -pinene to 1.000 for α -cedrene (measurement range 3–300 $\mu\text{g l}^{-1}$).

Authentic water samples were also analyzed for terpenes using the MIMS method and the results were compared with those obtained by the HSGC method. As an example of the measured results Fig. 3a shows the mass spectrum for the authentic water sample 13 (Table 3) and Fig. 3b shows the headspace gas chromatogram of the same sample. The same major ions as in the standard spectra 1a and 1b can be seen in this spectrum. Ion ratio between m/z 119 and 121 indicates that the concentration of monoterpenes is higher than that of sesquiterpenes as can also be seen in the gas chromatogram (Fig. 3b). According to the mass spectra and the gas chromatogram of the sample (Fig. 3), the concentration of linalool and geraniol was very low and they have not been quantitated. The gas chromatogram (Fig. 3b) shows good sep-

aration between terpene compounds and furthermore, several unknown peaks can be seen. Main compounds in the samples were α - and β -pinene and Δ -3-carene, in addition camphene, myrcene, limonene, longifolene and α -cedrene were found.

The quantitation of the mono- and sesquiterpene content in the authentic water samples by the MIMS method was performed using spectra 1a and 1b as standards for the Solver quantitation and identification program [41,42]. The mass spectra (Fig. 1c) for terpene alcohol mixture was not used since concentrations of these were very low as proved by the measured chromatogram and mass spectra.

The Solver program capability for quantitative analysis of terpenes in water samples was first thoroughly evaluated. All the eleven terpene compounds (Table 1) were used in testing. The first tests were made with solutions of only three

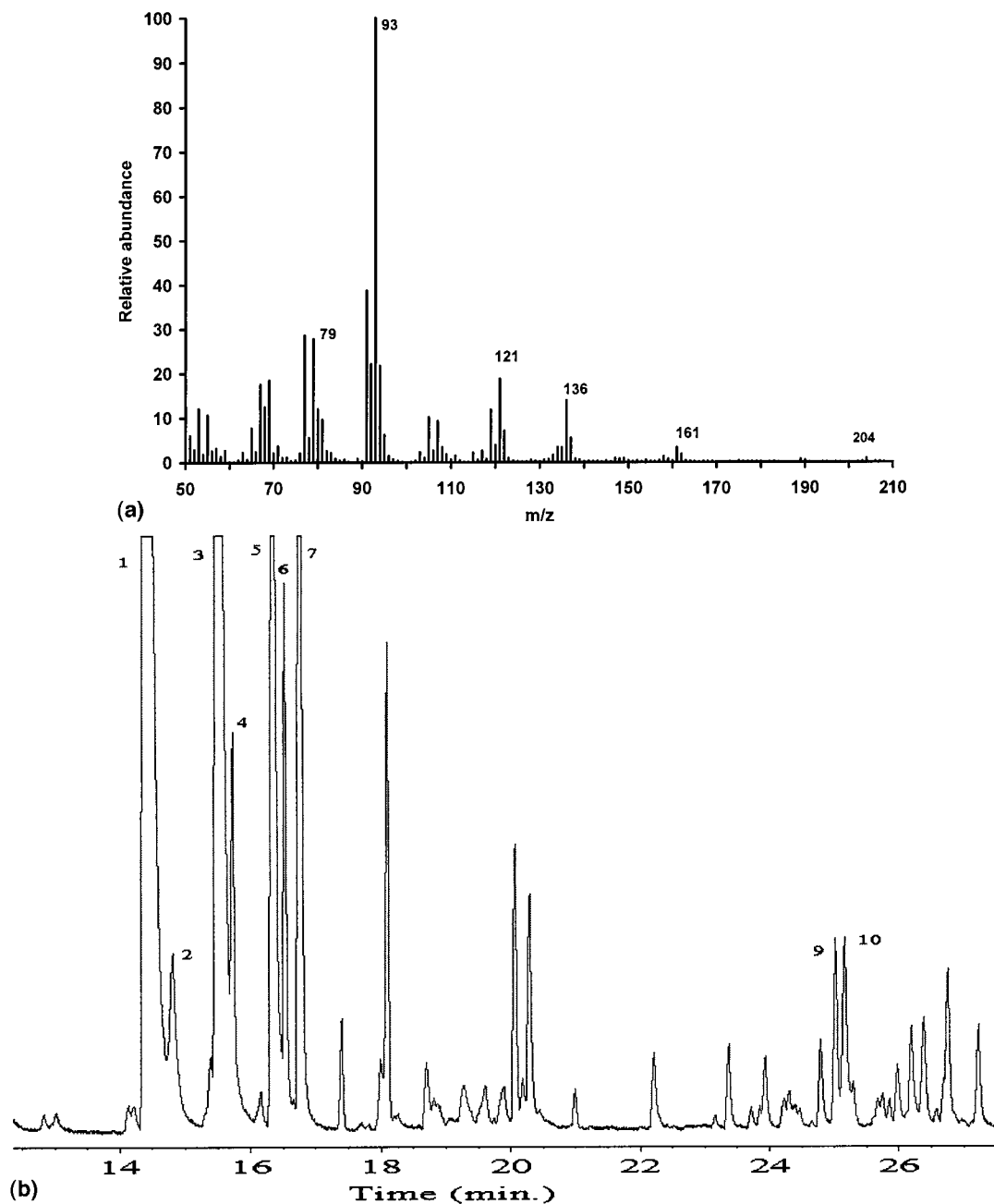


Fig. 3. (a) Electron impact mass spectrum of the authentic water sample 13 (Table 3, diluted by $\frac{1}{2}$ before analysis). (b) The gas chromatogram of the authentic water sample 13 (Table 3, diluted by $\frac{1}{2}$ before analysis). Results are obtained using SPB-1 column. DB-1701 column could not separate longifolene and cedrene.

monoterpenes i.e. α - and β -pinene and Δ -3-carene. Results of these measurements showed that the individual terpenes could be separated well from

three component mixtures at concentration range 20–100 $\mu\text{g l}^{-1}$. The relative standard deviations of the concentrations varied in the range 8–22%

Table 4
Results obtained in testing the quantitative capabilities of the Solver program

Compound	Concentration ($\mu\text{g l}^{-1}$)	Analyzed concentration ($\mu\text{g l}^{-1}$)			Mean	RSD (%)	Error (%)
<i>Monoterpenes</i> ^a	213	171	188	202	187	8.2	–12
	425	401	435	479	439	8.9	3.2
	850	806	949	963	906	9.6	6.6
<i>Sesquiterpenes</i> ^b	63.9	32.4	52.5	61.7	48.9	31	–24
	127	107	141	175	141	24	11
	256	206	290	330	275	23	7.5
<i>Terpene alcohols</i> ^c	75	59.7	73.0	81.9	71.5	16	–4.6
	150	137	156	165	153	9.1	1.8
	300	252	294	311	286	11	–4.4

^a α -pinene, camphene, β -pinene, myrcene, Δ -3-carene, α -terpinene and limonene.

^b Longifolene and cedrene.

^c Linalool and geraniol.

and the error of the concentration determination varied in the range 2–12%. However, when individual terpenes were quantitated from eleven component mixtures the result of the Solver program was poor, errors of the concentration determination varied in the range –16 to +100%. The reason for this is believed to be the fact that the terpene compounds used in testing have very similar EI mass spectra (Table 1). The next step was to test if different classes of terpenes can be reliably identified and quantitated by the Solver program. For these measurements mixtures of α - and β -pinene and Δ -3-carene were used as monoterpene hydrocarbon standards, mixtures of longifolene and cedrene were used as sesquiterpene hydrocarbon standards and mixtures of linalool and geraniol were used as terpene alcohol standards. The reference library, which the Solver program is utilizing in the calculations, contained only these three mixtures [42]. The results of these measurements are presented in Table 4. From Table 4 it can be noticed that the determination of monoterpene concentrations are repeatable and accurate and that the determination of terpene alcohols was rather good. Whereas, the determination of sesquiterpene concentrations was more inaccurate (RSD 20–30% and maximum relative error –24%). These results show that quantitation of different terpene classes with the Solver program works well and that the program can be utilized in the analysis of unknown samples. The

results presented in Table 3 for the authentic water samples are mean values of triplicate measurements, except for samples 1–4 and 10 only duplicate (RSD varied from 2 to 25%).

The total amount of terpenes in the authentic water samples (Table 3) were estimated by HSGC method using an external standard method (four different concentrations from 20 to 300 $\mu\text{g l}^{-1}$) and all the eleven individual compounds (Table 2) as standards. The amount of sesquiterpenes was calculated as the sum of longifolene, α -cedrene and the amount of unknown compounds eluted after limonene (number 7 in Fig. 3b). The concentration of these compounds were calculated by comparing their peak areas to the peak area of α -pinene. The HSGC results presented in Table 3 are means of duplicate determinations. The total amount of mono- and sesquiterpenes with both methods are in the same order. The differences between results with both methods varied from 0 to 60%, the average differences was 26%. The main reason for the differences between the results obtained by the different analytical methods is believed to be the high concentration of terpenes in the samples, which caused some inhomogeneity and the need to dilute samples before analysis. Furthermore, some non-terpeneic compounds could have been included in HSGC quantitation because the identification of unknown compounds was not possible using GC-FID.

In conclusion, quantitation by MIMS is fast (only a few minutes) and the results are reliable and respectable addition, MIMS is believed to be suitable for on-line terpene analysis, for example for on-line industrial waste water monitoring. The HSGC method is more time-consuming but better selectivity can be obtained due to good separation of the individual compounds.

References

- [1] D. Wilson, B. Hrutfiord, *Pulp Pap. Can.* 76 (1975) 91.
- [2] T.P. Churilova, G.D. Khamuev, *Gig. Sanit.* (1989) 78.
- [3] L.F. Fieser, M. Fieser, *Organic Chemistry*, 3rd ed., Maruzen, Tokyo, Japan, 1956, p. 935.
- [4] J.D. Weidenhamer, F.A. Macias, N.H. Fischer, G.B. Williamson, *J. Chem. Ecol.* 19 (1993) 1799.
- [5] J. Hine, P.K. Mookerjee, *J. Org. Chem.* 40 (1975) 292.
- [6] J. Li, E.M. Perdue, in: *Preprints of papers presented at the Two Hundredth and Ninth ACS National Meeting Anachem, CA*, 35 (1995) 134.
- [7] D. Mackay, W.Y. Shiu, *J. Phys. Chem. Ref. Data* 10 (1981) 1175.
- [8] T. Hoffmann, *Fresenius J. Anal. Chem.* 351 (1995) 41.
- [9] D.D. Riemer, P.J. Milne, C.T. Farmer, R.G. Zika, *Chemosphere* 28 (1994) 837.
- [10] K. Eriksson, J.O. Levin, M. Rhen, R. Lindahl, *Analyst* 119 (1994) 85.
- [11] F. Juettner, *J. Chromatogr.* 442 (1988) 157.
- [12] R. Ekman, B. Holmbom, *Nordic Pulp Paper Res. J.* 4 (1989) 16.
- [13] S.V. Kossuth, J.W. Munson, *Tappi* 64 (1981) 174.
- [14] B.A. Kimball, R.K. Craver, J.J. Johnston, D.L. Nolte, *J. High Resol. Chromatogr.* 18 (1995) 221.
- [15] V.O. Elias, B.R.T. Simoneit, J.N. Cardoso, *J. High Resol. Chromatogr.* 20 (1997) 305.
- [16] D.-K. Nguyen, A. Bruchet, P. Arpino, *J. High Resol. Chromatogr.* 17 (1994) 153.
- [17] L.V. Kosyokova, S.A. Konokova, *Gidroliz. Lesokhim. Prom-st.* (1978) 9.
- [18] T.L. Potter, *J. Essent. Oil. Res.* 7 (1995) 347.
- [19] G. Buchbauer, L. Jirovetz, M. Wasicky, A. Nikiforov, *Fresenius J. Anal. Chem.* 347 (1993) 465.
- [20] H. Vuorela, J. Pohjola, C. Krause, R. Hiltunen, *Flavour Fragrance J.* 4 (1989) 117.
- [21] M.G. Moshonas, P.E. Shaw, *J. Agric. Food Chem.* 45 (1997) 3968.
- [22] J.S. Paik, A.C. Venables, *J. Chromatogr.* 540 (1991) 456.
- [23] M.G. Moshonas, P.E. Shaw, *Food Sci. Technol.* 25 (1992) 236.
- [24] F. Mathieu, C. Malosse, A.-H. Cain, B. Frerot, *J. High Resol. Chromatogr.* 19 (1996) 298.
- [25] L.V. Kosyukova, Y.L. Belyaeva, *Zh. Anal. Khim.* 33 (1978) 794.
- [26] F.R. Lauritsen, T. Kotiaho, *Rev. Anal. Chem.* 15 (1996) 237.
- [27] T. Kotiaho, F.R. Lauritsen, T.K. Choudhury, R.G. Cooks, G.T. Tsao, *Anal. Chem.* 63 (1991) 875A.
- [28] R.G. Cooks, T. Kotiaho, in: J.J. Breen, M.J. Dellarco (Eds.), *ACS Symposium Series 508, Pollution Prevention in Industrial Processes: The role of Process Analytical Chemistry*, American Chemical Society, 1992, ISBN 0-8412-2478-1, pp. 126–154.
- [29] P.S.H. Wong, R.G. Cooks, M.E. Cisper, P.H. Hemberger, *Env. Sci. Technol.* 29 (1995) 215A.
- [30] T. Kotiaho, R.A. Ketola, M. Ojala, T. Mansikka, R. Kostiainen, *Am. Environ. Lab* 9 (1997) 19.
- [31] M. Ojala, R.A. Ketola, V. Virkki, H. Sorsa, T. Kotiaho, *Talanta* 44 (1997) 1253.
- [32] M. Ojala, R.A. Ketola, T. Mansikka, T. Kotiaho, R. Kostiainen, *J. High Resol. Chromatogr.* 20 (1997) 165.
- [33] R.A. Ketola, V.T. Virkki, M. Ojala, V. Komppa, T. Kotiaho, *Talanta* 44 (1997) 373.
- [34] V. Virkki, R. Ketola, M. Ojala, T. Kotiaho, V. Komppa, A. Grove, S. Facchetti, *Anal. Chem.* 67 (1995) 1421.
- [35] N. Srinivasan, R.C. Johnson, N. Kasthurikrishnan, P. Wong, R.G. Cooks, *Anal. Chim. Acta* 350 (1997) 257.
- [36] H. Degn, *J. Microbiol. Methods* 15 (1992) 185.
- [37] F.R. Lauritsen, D. Lloyd, in: C. Fenselau (Ed.) *ACS Symposium Series 541, Mass Spectrometry for Characterization of Microorganisms*, American Chemical Society, 1992, ISBN 0-8412-2478-1, pp. 126–154.
- [38] T. Kotiaho, R. Kostiainen, R.A. Ketola, et al., *Process Control Qual.* 11 (1998) 71.
- [39] M.A. LaPack, J.C. Tou, C.G. Enke, *Anal. Chem.* 63 (1991) 1631.
- [40] R.A. Ketola, M. Ojala, H. Sorsa, T. Kotiaho, R.K. Kostiainen, *Anal. Chim. Acta* 349 (1997) 359.
- [41] V. Virkki, R. Ketola, J. Juujärvi, E. Oja, H. Sorsa, M. Ojala, T. Kotiaho, Development of calculation program for the analysis of multicomponent spectra, in: *Presentation at XXIX Conference of the Finnish Physical Society, Jyväskylä, Finland, March 1995*.
- [42] R.A. Ketola, M. Ojala, V. Komppa, T. Kotiaho, J. Juujärvi, J. Heikkonen, *Rapid Commun. Mass Spectrom.* (submitted).
- [43] EPA/NIH Mass Spectral Data Base, U.S. Government Printing Office, Washington, 1978.

Performing procrustes discriminant analysis with HOLMES

Domingo González-Arjona ^{a,*}, G. López-Pérez ^a, A. Gustavo González ^b

^a Department of Physical Chemistry, University of Seville, 41012 Seville, Spain

^b Department of Analytical Chemistry, University of Seville, 41012 Seville, Spain

Received 10 September 1998; received in revised form 13 November 1998; accepted 16 November 1998

Abstract

Program HOLMES devised by target factor analysis has been updated for performing procrustes discriminant analysis (PDA). Computational details are outlined. The equivalence between PDA and partial least squares-discriminant analysis (PLS-DA) is established. Application of the PDA is illustrated by two case studies taken from literature. © 1999 Elsevier Science B.V. All rights reserved.

Keywords: Procrustes analysis; Target factor analysis; Discriminant analysis; Classification

1. Introduction

Target transformation or target factor analysis (TFA) is a technique of apportioning the measured value of a system to a series of independent causal processes [1] by means of an oblique factor rotation called procrustes rotation or procrustes transformation (PT) [2,3]. Accordingly, TFA and PT can be considered analogous. To unify the jargon the term PT will be used throughout the paper. PT is a powerful chemometric tool that easily allows a fit of the data to a model, taking the model variables as the number of proper independent underlying factors compatible with the data matrix. PT also allows one to individually test suspected arrays (target vectors) as possible real factors that are responsible for trends in

the data matrix. Thus, PT has been used in spectroscopy to identify pure spectra and quantify analytes [4–6] without the need for calibration. Moreover, PT has been adapted by statisticians to compare information from several measurement systems [7,8], such as, for example, sensory data and chemical data [9]. This adaptation is known as procrustes analysis or generalized procrustes analysis [10–14]

The application of PT for classification purposes is very scarce. The pioneer use of PT as a tool for pattern recognition was done by Weiner and Weiner [15] as Malinowski pointed out in his excellent textbook [16]. These authors examined the structure-activity relationships of 16 diphenylaminophenol drugs featured by 11 biological assays on mice. Several structural vectors based on the results of the uniqueness test were target tested. For example, the presence of a ring linked to the nitrogen atom in the drug was assumed to

* Corresponding author. Fax: +34-5-4557174.

E-mail address: dgonza@cica.es (D. González-Arjona)

be a factor and accordingly, a target column vector was built. Each entry in the vector was assigned a value of 0 or 1 dependent upon the presence or absence of a ring linkage in the drugs. By target testing, the separation of the drugs into two classes (drugs with and without ring linkage) was attained. This was a first insight on the so-called procrustes-discriminant analysis (PDA).

The aim of this paper is to present the new updated version of HOLMES [17,18] which incorporates PDA and to establish the equivalence between PDA and the technique of partial least squares-discriminant analysis (PLS-DA). For the sake of illustration, PDA is applied to two case studies and the results are compared with those obtained using class modeling linear discriminant analysis (CMLDA) [19] and artificial neural networks trained by back-propagation (BPNN) [20]

2. Equivalence between PDA and PLS-DA

PLS-DA may be considered as a PLS2 algorithm applied to classification problems [21–29]. The key feature of the PLS paradigm is to find latent variables in the descriptor space that have a maximum covariance with the predictor variables. Let us consider the data matrix \mathbf{X} (rxc) whose rows (r) are the objects or samples under study and whose columns (c) are the features or descriptors that best describe the samples. One common way to use PLS2 in classification problems is to introduce a class membership matrix \mathbf{Y} (rxk) whose rows (r) are the objects and whose columns (k) are the class coding for each object [30]. Thus, an element y_{ij} indicates the class membership of the object i for the class j . If the object belongs to the class, $y_{ij} = 1$ and otherwise $y_{ij} = 0$.

The emphasis on PLS2 is not only on regression but also on uncovering latent structure in both the \mathbf{X} and \mathbf{Y} spaces. This latent structure is made through a process of estimating the coefficients (\mathbf{p}) for the linear combinations of the \mathbf{X} variables. These so-called weight vectors \mathbf{p}_j are the eigenvectors of the matrix $(\mathbf{Y}'\mathbf{X})(\mathbf{Y}'\mathbf{X}) = \mathbf{X}'\mathbf{Y}\mathbf{Y}'\mathbf{X}$. This is generally carried out by using the NIPALS algorithm which gives the scores matrix \mathbf{T} (rxf) and the weight loadings matrix \mathbf{P} (cxf), f being the

number of significant factors so that $\mathbf{T} = \mathbf{X}\mathbf{P}$ [31]. The final PLS-DA model can be formulated as a regression equation

$$\mathbf{Y} = \mathbf{X}\mathbf{B} \quad (1)$$

where the estimated regression coefficients are given by [31]

$$\hat{\mathbf{B}}_{\text{PLS}} = \mathbf{P}(\mathbf{T}'\mathbf{T})^{-1}\mathbf{T}'\mathbf{Y} \quad (2)$$

and consequently, the \mathbf{Y} estimation according to the equation

$$\hat{\mathbf{Y}} = \mathbf{X}\hat{\mathbf{B}}_{\text{PLS}} = \mathbf{T}(\mathbf{T}'\mathbf{T})^{-1}\mathbf{T}'\mathbf{Y} \quad (3)$$

Let us consider now the procrustes transformation. To take into account the latent structure of both the \mathbf{X} and \mathbf{Y} matrices, assume that the scores and loading matrices \mathbf{T} and \mathbf{P} , respectively, are obtained after eigenanalysis of the covariance matrix $\mathbf{Z}'\mathbf{Z}$ (where $\mathbf{Z} = \mathbf{Y}'\mathbf{X}$). The suitable number of underlying factors, f , is selected by using the cross-validation technique [32]. The fundamental step in this technique is the oblique (procrustes) transformation of scores into the *true* target matrix \mathbf{Y} according to a transformation matrix \mathbf{W}

$$\mathbf{Y} = \mathbf{T}\mathbf{W} \quad (4)$$

This non-orthogonal transformation matrix may be easily estimated as follows:

$$\hat{\mathbf{W}} = (\mathbf{T}'\mathbf{T})^{-1}\mathbf{T}'\mathbf{Y} \quad (5)$$

and the estimated values of the target column vectors of \mathbf{Y} may be derived thereof by the procrustean transformation given in Eq. (4)

$$\hat{\mathbf{Y}} = \mathbf{T}\hat{\mathbf{W}} = \mathbf{T}(\mathbf{T}'\mathbf{T})^{-1}\mathbf{T}'\mathbf{Y} \quad (6)$$

But this is the same expression of Eq. (3) that leads to the inner equivalence between PLS-DA and PDA.

The matrix $\mathbf{G} = \mathbf{T}(\mathbf{T}'\mathbf{T})^{-1}\mathbf{T}'$ is called the projection matrix and exhibits some interesting features, like idempotency and symmetry, e.g.: $\mathbf{G}\mathbf{G} = \mathbf{G}$ and $\mathbf{G}' = \mathbf{G}$.

PDA may be considered equivalent to PLS-DA. The only discrepancies are that: (i) in PDA the eigenvectors are obtained from the covariance matrix $\mathbf{Z}'\mathbf{Z}$ by using the Jacobi or Householder techniques [33], and in PLS-DA the eigenvectors are sequentially obtained from the NIPALS al-

gorithm; and (ii) in PDA the selection of the optimum number of underlying factors may be carried out by using various methods (including cross-validation), and in PLS-DA the underlying factors are only selected by cross-validation.

3. Performing PDA for classification purposes

One excellent feature of PT is that it enables one to test target vectors (the columns of the \mathbf{Y} matrix) individually, that is

$$\hat{\mathbf{y}}_j = \mathbf{G}\mathbf{y}_j \quad (7)$$

These target vectors are column vectors whose rows are 0 or 1 depending on the class membership of the considered object (row). The elements of the predicted values $\hat{\mathbf{Y}}_j$ are rounded to the nearest integer 0 or 1. To assess the performance of the classification, the data are divided into the training or the calibration set ($\mathbf{X}_{\text{cal}}, \mathbf{Y}_{\text{cal}}$) and the prediction, validation or test set ($\mathbf{X}_{\text{test}}, \mathbf{Y}_{\text{test}}$). The optimal number of factors, f , is selected according to the cross-validation method, although it has been pointed out [21] that this choice may be done by minimization of the percent misclassification in the calibration set. Once the suitable number of factors is fixed, the projection matrix \mathbf{G} is obtained from the calibration set. The prediction of the \mathbf{Y} class membership matrices for both calibration and validation sets is as follows

$$\hat{\mathbf{Y}}_{\text{cal}} = \mathbf{G}\mathbf{Y}_{\text{cal}} \quad (8)$$

$$\hat{\mathbf{Y}}_{\text{test}} = \mathbf{G}\mathbf{Y}_{\text{test}}$$

The *recalling rate* (percent hits in the calibration set) and *prediction ability* (percent hits in the validation set) are evaluated after rounding of predicted class membership matrices to the nearest integer 0 or 1. PDA/PLS-DA can be applied to data matrices with $c > r$ like SIMCA, where the feature selection preliminary step is not needed.

4. Implementation and computational details

The new version of the HOLMES program

(HOLMES 98) presents the same implementation as in its early version [17,18]. Computational details are also the same with the exception of some alterations in three procedures: DATAIN, PREPROCESS and TFA. In the updated version, the user selects the procedure to be applied: TFA or PDA. The two different pathways are monitored in the different procedures by means of flags. The procedure DATAIN enables one to build in sequence the data file (ASCII file). The first input file is considered the calibration data set. In the procedure PREPROCESS, the \mathbf{Z} matrix is calculated and the covariance matrix \mathbf{Z}/\mathbf{Z} diagonalized. The proper number of latent variables, f , is evaluated from the procedure WOLD (cross-validation). Procedure REPX extracts both the scores matrix, \mathbf{T} (rxf), and the weight loadings matrix, \mathbf{P} (cxf). The calculation of the projection matrix \mathbf{G} and the prediction of the class memberships (calibration set) are performed by procedure TFA. The number of hits in each class is recorded. Then the user can use a second file as a validation set (which would be previously built with subroutine DATAIN). Then the procedure TFA applies the projection matrix \mathbf{G} (obtained from the calibration data) to predict the class membership of the validation set. Again, the number of hits in predicting the class membership is recorded. These data are needed to establish the sensitivity and specificity of the classification.

5. Features of HOLMES 98

HOLMES 98 allows the performance of factor analysis, TFA, iterative target testing and PDA. There are some commercialized programs that carry out PLS such as UNSCRAMBLER[®] [34], PARVUS [35] or the PLS-TOOLBOX for MATLAB [36]. These packages however, cannot perform directly PLS-DA. Instead, the user must be able to apply them in accord with theoretical or conceptual dictates on pattern recognition. Within the PDA/PLS-DA scope, HOLMES 98 could be more suitable for beginners in these topics because it directly accomplishes the discrimination analysis. Listing of HOLMES 98 are freely available from the authors upon request. The

HOLMES 98 program (QuickBasic source file, QuickBasic executable stand-alone file and some data samples) as well as a short user guide is also available via internet (contact by e-mail to dgonza@cica.es or agonzale@cica.es).

6. Worked examples

To show how HOLMES 98 achieves PDA/PLS-DA, two case studies have been taken from the literature.

The first one is a subset of a well-known reference data set: the Italian olive oils of Forina et al. [37–39], consisting of nine classes of olive oils according to the geographic origin: North Apulia, South Apulia, Calabria, Sicily, Inland Sardinia, Coastal Sardinia, East Liguria, West Liguria, and Umbria. The olive oils were featured by eight descriptors, the content of the following fatty acids: Palmitic, palmitoleic, stearic, oleic, linoleic, eicosanoic, linolenic and eicosenoic. Following [40–42], only the data corresponding to Calabria and Sicily were considered because they are the data that gave the most difficulties. Thus, the studied subset contains 92 samples and eight descriptors.

The second one is another reference data set dealing with 19 variables measured on 40 winged aphids (*aleate adelges*) caught in a light trap [43,44]. The 19 descriptors featuring the winged aphids are: body length, body width, fore-wing length, hind-wing length, spiracles number, antennal lengths (I to V modes), number of antennal spines, tarsus length, tibia length, femur length, rostrum length, ovipositor length, number of ovipositor spines, anal fold, and number of hind-wing hooks. For this set there are no predefined classes and unsupervised pattern recognition will be used to establish them.

For validation purposes, the studied data sets were randomly divided into a calibration set and a validation set, each containing about 50% of the cases of every class. Instead of considering as a key feature of the classification performance the recalling rate or the prediction ability, we will consider the sensitivity and specificity for every class against the universe. The sensitivity (SENS)

of a class corresponds to the rate of validation objects belonging to the class that are correctly classified. The specificity (SPEC) of a class corresponds to the rate of validation objects not belonging to the class that are correctly considered as belonging to a different class. This may be explained in terms of first and second kind risks associated with the prediction on the validation set. The first kind of error (α) corresponds to the probability of rejecting erroneously a member of the class as non a member (false negative). The second kind of error (β) corresponds to the probability of classifying erroneously non a member of the class as a member (false positive). For a given class (fractional scale): $\alpha = 1 - \text{SENS}$ and $\beta = 1 - \text{SPEC}$.

To compare the results obtained from PDA, another two very different in nature classification methods have been applied as indicated above: CMLDA [19] and BPNN [20]. For performing CMLDA, the CSS:STATISTICA package from StatSoft™ [45] and the SIGMAPLOT package for WINDOWS were applied [46]. To carry out BPNN, the program WinNN was used [47]. In the following paragraphs, the results obtained by applying PDA on the two data sets using HOLMES 98 are discussed and compared with those obtained using CMLDA and BPNN.

6.1. Olive oils data set

The projection of the objects onto the first two principal components (PC1 and PC2) (Fig. 1) gives an indication on the difficulty of discriminating the categories. According to [42] it may be considered that the Sicilian oils are surrounding the Calabrian ones. Once the calibration and validation sets together with the class membership coding were prepared, PDA, CMLDA and BPNN were applied.

When applying HOLMES 98, the number of underlying factors obtained by cross validation was three. The projection matrix, \mathbf{G} , calculated from the calibration set, was applied to the validation set to estimate its class membership.

CMLDA was applied to the same sets. The class radii obtained from the calibration test were 2.056 and 2.075 for Sicily and Calabria, respec-

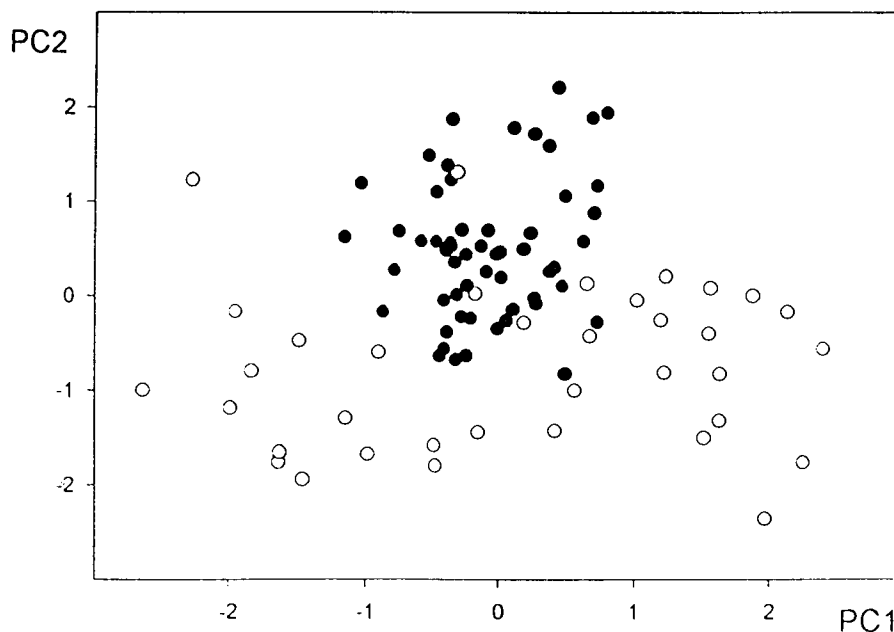


Fig. 1. Scores plot of Calabrian (●) and Sicilian (○) oils of the first two principal components.

tively. The F -test was applied at a confidence level of 95%.

Based on a preliminary study, BPNN was performed with the following architecture: eight input nodes plus bias, two output nodes (the two classes) and one hidden layer containing one node. Input values were normalized within -1 and 1 . Outputs were normalized within $0-1$. Initial weights were normalized between -0.1 and 0.1 . The target error was set to 0.15 . The sigmoidal function was chosen as the transfer function. The training rate was set at $\eta = 0.2$ and the momentum at $\mu = 0.5$. A maximum of 1000 epochs was selected for training.

The SENS and SPEC values of the two classes (Sicily and Calabria) for the validation set were calculated for every method and gathered in Table 1. These data will be analysed later, together with the results corresponding to the aphids data set, in the following paragraph.

6.2. Aphids data set

Considering that in the data set [44] no information about the class memberships of the stud-

ied aphids is given, some procedures for unsupervised learning pattern recognition were considered for establishing categories. The inspection of the scores plot for the first two PCs extracted from the whole data matrix by principal component analysis (PCA), suggests that the aphids (labelled from 1 to 40) seem to be assembled into four groups, as can be observed in Fig. 2. To assess this statement, optimization partitioning Cluster Analysis of samples was performed based on the k -medioid approach [48]. The optimal number of clusters was selected to give the maximum silhouette coefficient. In this

Table 1
Results for the olive oils data over the validation set

PRIVATE Method	Category	SENS (%)	SPEC (%)
PDA	Sicily	83.3	92.8
	Calabria	92.8	83.3
CMLDA	Sicily	83.3	85.7
	Calabria	85.7	83.3
BPNN	Sicily	94.4	96.4
	Calabria	96.4	94.4

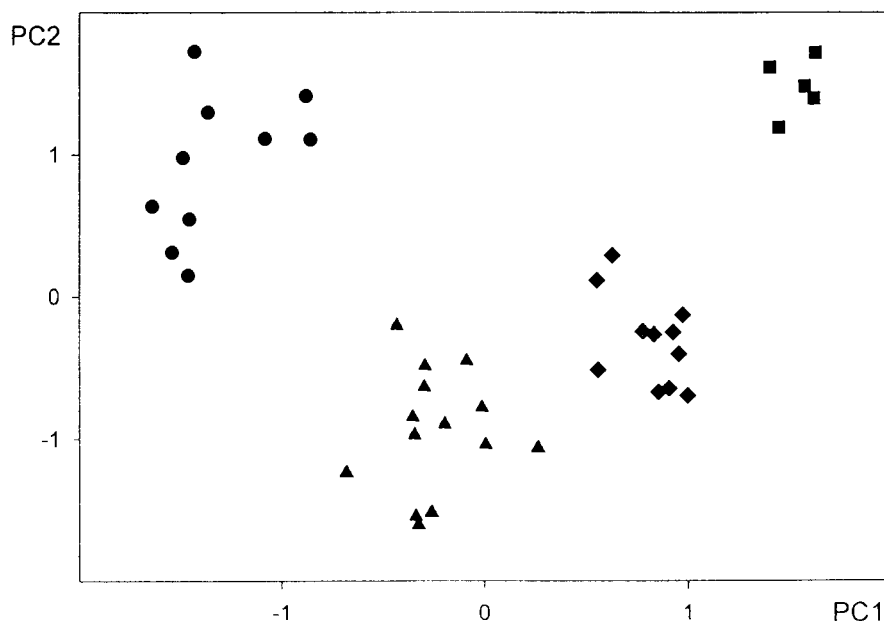


Fig. 2. Scores of the first and second principal components for the Aphids data set. C1 (●), C2 (■), C3 (▲) and C4 (◆).

case, four clusters appear. The four clusters were then assigned to classes C1, C2, C3 and C4 for the sake of supervised pattern recognition. The class membership of the aphids is indicated in Table 2. Once the class membership of the objects was established, the calibration and validation sets were built.

HOLMES 98 was applied to perform PDA. By using the cross-validation option of the program, the number of underlying factors was set to 5. Once the projection matrix \mathbf{G} was calculated, it was applied to the validation set to obtain the estimated class membership.

CMLDA was also applied to the same sets. The class radii obtained from the calibration test were

Table 2
Class membership of aphid data set

PRIVATE Class	Aphids (labels)
C1	1, 2, 3, 4, 5, 6, 7, 8, 9, 10
C2	11, 12, 13, 14, 15
C3	16, 17, 18, 19, 20, 21, 22, 23, 24, 25, 26, 28, 29, 30
C4	27, 31, 32, 33, 34, 35, 36, 37, 38, 39, 40

3.709, 3.910, 3.611, and 3.709 for C1, C2, C3 and C4 classes, respectively. The F -test was applied at a confidence level of 95%.

BPNN was performed with the following architecture: 19 input nodes plus bias, four output nodes (the four categories) and one hidden layer containing three nodes. The remaining parameters are the same as in the preceding case study.

Table 3
Results for the Aphids data over the validation set

PRIVATE Method	Category	SENS (%)	SPEC (%)
PDA	C1	100	100
	C2	100	100
	C3	100	92.9
	C4	85.7	100
CMLDA	C1	100	100
	C2	100	94.4
	C3	100	100
	C4	100	100
BPNN	C1	100	100
	C2	100	100
	C3	100	100
	C4	85.7	100

The SENS and SPEC of classes C1–C4 (validation set) were calculated for each method and are presented in Table 3.

As can be seen in Tables 1 and 3, PDA performs quite well in the two selected data sets, and the results produced by CMLDA and BPNN are in good agreement with those obtained when using HOLMES 98. However, it should be noted that specially from Table 1, BPNN gives better results than PDA or CMLDA. This fact could be explained by considering that neural networks based algorithms are intrinsically nonlinear and accordingly, classification problems due to nonlinear patterns will show much larger improvements when using neural networks. In the case of the olive data set, a linear separation between classes was not found (Fig. 1) and therefore, BPNN gives better results. A fairly linear separation is found, however, for the classes of the aphids data set (Fig. 2), and then all methods give comparable results [49].

7. Scope and limitations of PDA

PDA as was stated above is equivalent to PLS-DA. The only difference is the way in which the eigenvectors are obtained: simultaneously from the Jacobi or Householder methods (PDA) or sequentially from the NIPALS algorithm (PLS-DA). No matter what approach is used, the findings are the same. PDA have the normal advantages of PLS, being able to handle many and collinear X-variables, missing data in X and noisy X-variables [21]. By selecting the significant number of latent variables (underlying factors) by cross-validation, one gets a projection onto a hyperplane which constitutes the discriminant space. The coordinates in this plane are the X-scores which form predictors of the discriminant function, \hat{y} . An interesting feature of PDA derived thereof is that, like SIMCA [50,51], it can be applied to data sets with more variables than objects, $c > r$, without the need of a previous feature selection step as in CMLDA [19] or UNEQ [52]. As Varmuza pointed out in his superb textbook [53]: If the number of patterns is r and the dimension of the pattern space is d , then

the minimum requirement to be fulfilled to achieve a correct class separation is $r/d > 3$. In PDA, as explained above, the discrimination is performed not in the space of the c variables or features but in a principal factor modelled discriminant space whose dimension is given by the number of underlying factors, $d=f$. Thus, even for $c > r$, the requirement $r/d > 3$ is generally accomplished. Accordingly, PDA can be used when the number of X-variables in the data set is higher than the number of objects, like in spectral data or chromatographic profiles. It could be extremely useful to process the data produced by analytical techniques used for authentication purposes, such as Fourier transform infrared spectroscopy, gas chromatography/mass spectrometry or pyrolysis/mass spectrometry.

PDA, however, is a hard classification method [54]; that is, objects are classified into one of a number of defined classes, and consequently, outliers or multiclass membership cannot be considered. Nevertheless, since the X-scores in the discriminant space are linear combinations of the original scaled X-variables, they are approximately normally distributed, and hence can be the basis for the decision rules similarly to linear discriminant analysis (LDA). In addition, the X-residuals could be used to calculate the distance between new objects and the discriminant plane. This distance can provides an additional diagnostic in the detection outliers [21].

Theoretically PDA is prone to give some false positives because PDA deals with an implicit closed universe (because the Y variables have a constant sum) and consequently, it ignores the possibility of any strangers. The advantage of PDA is, however, that working on this closed universe, the method becomes more robust to class inhomogeneities [55].

Finally, like LDA, PDA works well in cases where the classes present inner similarities and are well separated from each other (minimization of the ratio of within classes sum of squares and between classes sum of squares). Thus, when dealing with data corresponding to non linear classes distributions, PDA is not a good choice; it should be more advisable to call on neural networks based algorithms for pattern recognition.

8. Conclusion

PDA is equivalent to PLS-DA and exhibits the same advantages and shortcomings. It may be easily applied by using the program HOLMES 98, which has been suitably adapted for this purpose. It has been set up in a flexible interactive way for easy use by beginners on the topics of pattern recognition.

References

- [1] P.K. Hopke, *Chem. Int. Lab. Sys.* 6 (1989) 7–19.
- [2] J.R. Hurley, R.B. Cattell, *Behav. Sci.* 7 (1962) 258–262.
- [3] R.A. Darton, *The Statistician* 29 (1980) 167–194.
- [4] M. Kubista, R. Sjöback, B. Albinsson, *Anal. Chem.* 65 (1993) 994–998.
- [5] I. Scarminio, M. Kubista, *Anal. Chem.* 65 (1993) 409–416.
- [6] A. Carlosena, J.M. Andrade, M. Kubista, D. Prada, *Anal. Chem.* 67 (1995) 2373–2378.
- [7] W.J. Krzanowski, F.H.C. Marriott, *Multivariate Analysis; Part I Distributions, Ordination and Inference*, Halsted Press, New York, 1994.
- [8] W.J. Krzanowski, *Principles of Multivariate Analysis, a User's Perspective*, Oxford University Press, 1988.
- [9] C. Demir, P. Hindmarch, R.G. Brereton, *Analyst* 121 (1996) 1443–1449.
- [10] G.J. Stucky, M.R. McDaniel, *J. Am. Soc. Brew. Chem.* 55 (1997) 65–72.
- [11] P. Hartwig, M.R. McDaniel, *J. Food Sci.* 60 (1995) 384–388.
- [12] J.R. Piggott, A. Paterson, J. Clyne, *Int. J. Food Sci. Technol.* 28 (1993) 629–637.
- [13] F.R. Jack, A. Paterson, J.R. Piggott, *Int. J. Food Sci. Technol.* 28 (1993) 293–302.
- [14] S.M. Rubico, M.R. McDaniel, *Chem. Senses* 17 (1992) 273–289.
- [15] M.L. Weiner, P.H. Weiner, *J. Med. Chem.* 16 (1973) 655.
- [16] E.R. Malinowski, *Factor Analysis in Chemistry*, Wiley, New York, 1991.
- [17] D. González-Arjona, J. A. Mejías, A. Gustavo González, *Anal. Chim. Acta* 295 (1994) 119–125; *idem ibidem* 297 (1994) 473.
- [18] D. González-Arjona, J.A. Mejías, A. Gustavo González, *HOLMES: target factor analysis program (QCMP135)*, *QCPE Bull.* 14 (1994) 63.
- [19] D. González-Arjona, A. Gustavo González, *Anal. Chim. Acta* 363 (1998) 89–95.
- [20] J. Zupan, J. Gasteiger, *Neural Networks for Chemists*, VCH, Weinheim, 1993, pp. 119–148.
- [21] M. Sjöström, S. Wold, B. Söderström, *PLS discriminant plots*, in: E.S. Geselma, L.N. Kanal (Eds.), *Pattern Recognition in Practice II*, Elsevier, Amsterdam, 1986, p. 486.
- [22] L. Stähle, S. Wold, *J. Chemometrics* 1 (1987) 185–196.
- [23] R. Vong, P. Geladi, S. Wold, K. Esbensen, *J. Chemometrics* 2 (1988) 281–296.
- [24] M. Carlin, T. Kavli, B. Lillekjendlie, *Chem. Int. Lab. Sys.* 23 (1994) 163–177.
- [25] M. Sjöström, S. Rannar, A. Wieslander, *Chem. Int. Lab. Sys.* 29 (1995) 295–305.
- [26] M.C. Ortiz, L.A. Sarabia, C. Symington, F. Santamaria, M. Iñiguez, *Analyst* 121 (1996) 1009–1013.
- [27] D.B. Dahlberg, S.M. Lee, S.J. Wenger, J.A. Vargo, *Appl. Spectrosc.* 51 (1997) 1118–1124.
- [28] J. Nouwen, F. Lindgren, B. Hansen, W. Karcher, H.J.M. Veerhar, J.L.M. Hermens, *Environ. Sci. Technol.* 31 (1997) 2313–2318.
- [29] D. Blanco-Gomis, P. Fernández-Rubio, M.D. Gutiérrez-Alvarez, J.J. Mangas-Alonso, *Analyst* 123 (1998) 125–129.
- [30] B.K. Alsberg, R. Goodacre, J.J. Rowland, D.B. Kell, *Anal. Chim. Acta* 348 (1997) 389–407.
- [31] A.J. Burnham, R. Viveros, J.F. Macgregor, *J. Chemometrics* 10 (1996) 31–45.
- [32] R.G. Brereton, *Multivariate Pattern Recognition in Chemometrics*, Elsevier, Amsterdam, 1992, pp. 222–226.
- [33] J.C. Sprott in association with Numerical Recipes Software, *Numerical Recipes, Routines and Examples in BASIC*, Cambridge University Press, 1991.
- [34] UNSCRAMBLER[®] 6.11, Camo ASA, Oslo, Norway.
- [35] M. Forina, S. Lanteri, C. Armanino, R. Leardi, G. Drava, *PARVUS*; an extendable package of programs for data explorative analysis; classification and regression analysis.
- [36] *PLS-TOOLBOX 2.0*, Eigenvector Research Inc. USA.
- [37] M. Forina, C. Armanino, *Ann. Chim.* 72 (1982) 179.
- [38] M. Forina, E. Tiscornia, *Ann. Chim.* 72 (1982) 143.
- [39] M. Forina, C. Armanino, S. Lanteri, E. Tiscornia, *Classification of olive oils from their fatty acid composition*, in: H. Martens, H. Russwurm (Eds.), *Food Research and Data analysis*, Applied Science Publishers, Barking, 1983.
- [40] M.P. Derde, L. Kauffmann, D.L. Massart, *J. Chemometrics* 3 (1989) 375.
- [41] M. Forina, C. Armanino, R. Leardi, G. Drava, *J. Chemometrics* 5 (1991) 435.
- [42] M.S. Sánchez, L.A. Sarabia, *Anal. Chim. Acta* 348 (1997) 533.
- [43] J.N.R. Jeffers, *Appl. Stat.* 16 (1967) 225.
- [44] R.G. Brereton, *Multivariate Pattern Recognition in Chemometrics*, Elsevier, Amsterdam, 1992, pp. 151–152.
- [45] *CSS:STATISTICA* package, StatSoft[™], Tulsa, OK, 1991.
- [46] *SIGMAPLOT 3.0* for WINDOWS, Jandel Scientific, Erkrath, Germany.
- [47] Y. Danon, *WinNN ver 0.97 Educational Program*, Arad, Israel, 1997.
- [48] L. Kaufman, P.J. Rousseeuw, *Finding groups in data: An introduction to cluster analysis*, Wiley, New York, 1990.
- [49] M.C. García-Parrilla, A. Gustavo González, F.J. Heredia, A.M. Troncoso, *J. Agric. Food Chem.* 45 (1997) 3487–3492.

- [50] S. Wold, *Patt. Recog.* 8 (1976) 127–139.
- [51] S. Wold, M. Sjöström, *ACS Symp. Ser.* 52 (1977) 243–282.
- [52] M.P. Derde, D.L. Massart, *Anal. Chim. Acta* 184 (1986) 33–51.
- [53] K. Varmuza, *Pattern Recognition in Chemistry*, Springer-Verlag, Berlin, 1980, p. 12.
- [54] C. Albano, W. Dunn III, U. Edlund, E. Johansson, B. Nordén, M. Sjöström, S. Wold, *Anal. Chim. Acta* 103 (1978) 429–443.
- [55] D.B. Dahlberg, S.M. Lee, S.J. Wenger, J.A. Vargo, D.C.S. Guyot, *Classification of Vegetable Oils using FTIR Spectra*. Communication presented in the VI International Conference of Chemometrics in Analytical Chemistry, Tarragona, Spain. 25–29 June 1996. Abstract Book page 142.

Analysis of 5-vinyl-1,3-oxazolidine-2-thione in complex matrices at ppb level

Nicolas Mabon *, Jean-Paul Wathelet, Michel Marlier

*Unité de Chimie Générale et Organique, Département d'Ingénierie des Biosystèmes,
Faculté Universitaire des Sciences Agronomiques, 2 Passage des Déportés, B-5030 Gembloux, Belgium*

Received 14 August 1998; received in revised form 23 November 1998; accepted 27 November 1998

Abstract

5-Vinyl-1,3-oxazolidine-2-thione (5-VOT) is a goitrogenic compound released by enzymatic degradation of progoitrin, the most important glucosinolate occurring in rapeseed meal. This paper describes an analytical method for determining the 5-VOT in complex matrices. The method proposed by Quinsac et al. [J. Assoc. Off. Anal. Chem., 75(3) (1992) 529] has been improved by modification of the extraction conditions and the purification steps. The extraction of 5-VOT is performed with hot acid buffer. The first purification step is achieved by solid-phase chromatography (C_{18}). The second purification step of 5-VOT is carried out by complexation with phenyl mercury acetate in cyclohexane and, afterwards, by decomplexation using an aqueous solution of sodium thiosulfate. These reactions move 5-VOT from an aqueous to an organic medium, and then back again to the aqueous phase. This procedure ensures a high purification efficiency. The precise quantification of 5-VOT is completed in 12 min by reverse-phase liquid chromatography (C_{18}), using an isocratic elution with an ultraviolet detector and with synthetic 4,4-dimethyl-1,3-oxazolidine-2-thione as internal standard. Using this modified method, 5-VOT can be determined in different matrices such as rapeseed meal, animal diets, muscle, several organs (thyroid, liver, kidney and lung) and biological fluids (plasma and milk). The quantification limit of 5-VOT in the sample is of 1 ppb ($1 \mu\text{g kg}^{-1}$), the recovery rate of 5-VOT is about 90% and the repeatability is over 97%. © 1999 Elsevier Science B.V. All rights reserved.

Keywords: 5-Vinyl-1,3-oxazolidine-2-thione; Analysis; Organs; Fluids

1. Introduction

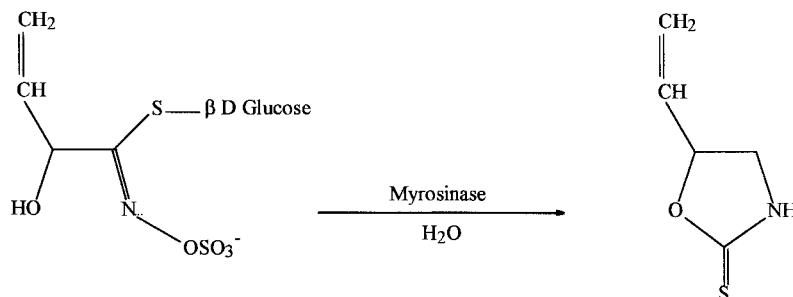
Rapeseed is an important source of protein for animal feed. Under the action of myrosinase, an

endogenous enzyme, or the action of the bacterial flora in animals, the glucosinolates can be degraded giving some by-products exhibiting antinutritional effects [1,2]. One of the most important of these effects is due to 5-vinyl-1,3-oxazolidine-2-thione (5-VOT), known as goitrin, the breakdown product of progoitrin (2-hydroxybut-3-enylglucosinolate) (Fig. 1). Its competition with thyroid

* Corresponding author. Tel.: +32-81-62-22-89; fax: +32-81-62-22-27.

E-mail address: mabon.n@fsagx.ac.be (N. Mabon)

a) Hydrolysis of 2-hydroxybut-3-enyl glucosinolate into 5-VOT



b) Synthetic internal standard, the 4,4-DMOT

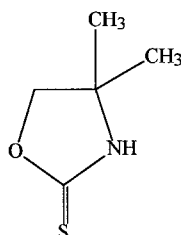


Fig. 1. (a) Hydrolysis of progoitrin into 5-VOT; (b) synthetic internal standard, 4,4-DMOT.

hormones causes strong metabolic disturbances [3], leading to the reduction of the zootechnic performances [4]. It is transferred to serum, milk, muscular tissues and to certain organs: liver, lung, kidney and, mainly, thyroid.

Experiments performed on ruminants showed that different levels of 5-VOT were found in biological fluids and tissues: from 3 to 8 $\mu\text{g kg}^{-1}$ in milk, 15–200 $\mu\text{g kg}^{-1}$ in plasma, 80–250 $\mu\text{g kg}^{-1}$ in urine [5], 70 $\mu\text{g kg}^{-1}$ in thyroid and less than 0.5 $\mu\text{g kg}^{-1}$ in liver or kidney [6].

Initially, 5-VOT found in plant extracts or milk was isolated by two-dimensional paper chromatography and then quantified by ultraviolet (UV) spectrometry [1,7]. Daxenbichler et al. [8] and van Etten et al. [9] used gas chromatography (GC), but the detection limits were insufficient for accurate analysis in such physiological environments. In 1978, McLeod et al. [10] introduced the

high pressure liquid chromatography (HPLC) technique in order to recover 5-VOT, prior to the analysis of the butylheptafluoro derivative by gas liquid chromatography (GLC) (electron capture detection mode). One year later, Josefsson and Akerström [11] and Bennis et al. [12] quantified 5-VOT by normal phase HPLC after liquid extraction. In 1982, 1984 and 1986, De Brabander and Verbeke [5,6,13] used a very selective extraction technique. It consists of a complexation with a mercuric compound, followed by GLC of the derivative formed by the pentafluorobenzoyl chloride. In 1992, Quinsac et al. [14] quantified the 5-VOT obtained by complexation with phenyl mercury acetate (PMA) using reverse-phase HPLC.

Some authors who performed 5-VOT analyses in physiological fluids [7,11,15] and tissues [6,15] observed a loss of 5-VOT during extraction.

Quinsac et al. [15] were convinced of the very fast degradation of 5-VOT during extraction at room temperature. The method proposed by these authors [15] has been modified in order to reduce the retention of 5-VOT in the biological matrices, to avoid the occurrence of emulsion during the extraction and to improve the purification procedure reducing the pollution of PMA. The method has been tested with samples of rapeseed meal, animal diets containing 40% of rapeseed meal, and with samples of liver, kidney, lung, muscle, thyroid, plasma and milk from an ewe fed with diets containing 40% of rapeseed meal.

2. Experimental

2.1. Apparatus

2.1.1. Liquid chromatograph

A model H.P. 1050 (Hewlett Packard, Atlanta, GA, USA) equipped with a pump (model 9852AX), automatic injector (model 79855A) with variable injection volume from 1 to 100 μl , spectrophotometric UV diode array detector (model G1306AX) and membrane mobile phase degasser. Software HPCHEM FOR HPLC (Rev. A.04.02.) (Hewlett Packard).

2.1.2. Analytical chromatographic column

Lichrospher C_{18} endcapped 5 μm , 125 \times 4 mm, and Lichrospher C_{18} endcapped 5 μm , 4 \times 4 mm precolumn with Manucart connectors (Merck, Darmstadt, Germany).

2.1.3. Solid-phase extraction system

Elution aspirating device 12 solid-phase extraction system (SPE) (Macherey Nagel, Düren, Germany), 13 \times 68 mm cartridges hand-packed with 2.5 g of C_{18} Chromabond-bonded silica, 40 μm , (Macherey Nagel).

2.1.4. Evaporator

Reacti Vap evaporator, catalogue number 18780 (Pierce Chemical, Rockford, USA).

2.1.5. Centrifuge

5000 t min^{-1} BB VV (Jouan, Saint-Nazaire, France), 16 \times 100 mm glass tubes with Teflon-coated screw caps (Sovirel).

2.2. Reagents

2.2.1. 5-VOT extraction

NaH_2PO_4 (UCB, Belgium) buffer, 100 mM, pH 2.5, methanol for chromatography (Alltech, Laarne, Belgium).

2.2.2. 5-VOT purification by SPE

Methanol and acetonitrile for chromatography (Alltech).

2.2.3. 5-VOT complexation–decomplexation

Na_2HPO_4 (UCB) buffer 50 mM, pH 9, 0.1 M sodium thiosulfate (UCB) solution in distilled water and saturated PMA (Sigma, St Louis, MI, USA) in cyclohexane (UCB), which is prepared as follows: heating 85 mg of PMA and 150 ml of cyclohexane in a 250 ml flask at reflux for 30 min; cooling; then passing the solution through a 0.45 μm Nylon filter (Gelman, Michigan, USA) and storing in darkness at room temperature.

2.2.4. HPLC analysis

Acetonitrile for chromatography (Alltech) in deionised water by a MilliQ system (Millipore Corporation, Bedford, USA) 10:90 (v/v).

2.2.5. Standard solutions

5-VOT (National Physical Laboratory, Teddington, UK) ($145.21 \text{ g mol}^{-1}$) at 100 mg l^{-1} in distilled water, 4,4-dimethyl-1,3-oxazolidine-2-thione (4,4-DMOT) (LCBA, Université d'Orléans, France) ($131.19 \text{ g mol}^{-1}$) at 100 mg l^{-1} in distilled water. The 4,4-DMOT solution is diluted to $250 \mu\text{g l}^{-1}$ ($1.906 \mu\text{mol l}^{-1}$). The ISTD, the 4,4-DMOT, has been synthesised by condensation of CS_2 on 2-amino-2-methyl-1-propanol in dioxane [16].

2.3. Sample preparation

Immediately after levy, the organs are frozen and stored at -18°C . Before analysis, the sam-

ples are thawed and blended in a baby-food mixer (10 s for a 40 g sample) in order to obtain a homogeneous paste.

2.4. 5-VOT extraction with acid buffer

The sample (3.0 g of liver, kidney, lung, muscle, thyroid or 3.0 ml of plasma or milk) is placed in a 16×100 mm glass tube with Teflon-coated screw caps. After preheating for 1 min in a 85°C water-bath, 4 ml of boiling phosphate buffer are added. Then, 500 μl of the aqueous solution of internal standard is added. The scattering of the blended matrices is achieved by vigorous manual shaking. The extract is kept in the water-bath for 10 min and stirred periodically with Vortex, then cooled and centrifuged at $1000 \times g$ for 10 min. The supernatant is transferred to a 15×100 mm test tube. The extraction is repeated twice but with 3 ml of phosphate buffer.

2.5. Purification with C_{18} -bonded silica

Before use, the SPE cartridges are solvated with 3 ml of methanol and 2 ml of acetonitrile, then washed with 20 ml of distilled water with special care in order to prevent any air from entering. The solution to be purified (about 10 ml) is placed in the cartridge reservoir and then percolated. The phase is rinsed with 2 ml of distilled water to eliminate most of the polluting substances and dried under aspiration for 1 min. The 5-VOT and 4,4-DMOT are finally eluted with 2 ml methanol/acetonitrile 50:50 (v/v) (Fig. 2).

The eluate is placed in a 10 ml conic flask and then evaporated to dryness with a rotating evaporator under vacuum (40°C). The 5-VOT and the 4,4-DMOT are recovered with 2×1 ml of phosphate buffer, pH 9, and transferred to a 16×100 mm glass tube with Teflon-coated screw caps. Selective extraction occurs by complexation and decomplexation

The aqueous phase is transferred to a tube and 1 ml of saturated PMA solution is added. After vigorous manual shaking for 1 min and centrifugation for 5 min at $1000 \times g$, the cyclohexanic phase is transferred to a second 16×100 mm glass tube with Teflon-coated screw caps. The

extraction is repeated. In this glass tube, 250 μl of aqueous sodium thiosulfate solution is added. After vigorous manual shaking (30 s) and centrifugation for 5 min at $1000 \times g$, the aqueous phase is ready for HPLC analysis. If the concentration of the 5-VOT in the sample is lower than $2.5 \mu\text{g kg}^{-1}$, it is necessary to concentrate the extract to 120 μl by evaporation under a gentle stream of nitrogen. By injecting 100 μl into the HPLC column, the quantification limit of $1 \mu\text{g kg}^{-1}$ is reached ($S/N=4$). A lower quantification limit can be achieved by increasing the sample weight (up to 5.0 g).

2.6. Chromatographic conditions

With a C_{18} chromatographic column and a 1 ml min^{-1} flow in isocratic mode, the analysis is performed in 12 min at 30°C . The compounds are detected at 240 nm.

3. Results and discussion

Neither the freeze-drying of samples nor the use of the Dangoumau grinder recommended by Quinsac et al. [14] are necessary. The blender, a baby-food mixer, is well adapted for fresh samples of mass below 50 g and facilitates obtaining a homogeneous paste. The blended samples are easy to manipulate and have an important contact surface with the buffer solution.

The homogenisation in the liquid medium used by Quinsac et al. [14] for liver and thyroid is not, therefore, required. The risks of emulsion with the extraction solution are furthermore avoided. The scattering of the matrices is easily achieved by manual shaking.

The authors who carried out the analysis of the physiological fluids [7,11,15] and tissues [6,15] observed a limitation and thought about a very fast degradation of the 5-VOT during extraction. By performing sample extraction at 95°C , Quinsac et al. [15] observed an improvement of extraction efficiency and showed that the 5-VOT is thermostable. They hypothesised the occurrence of an enzyme able to degrade the 5-VOT in biologic matrices such as liver. In fact, this problem cor-

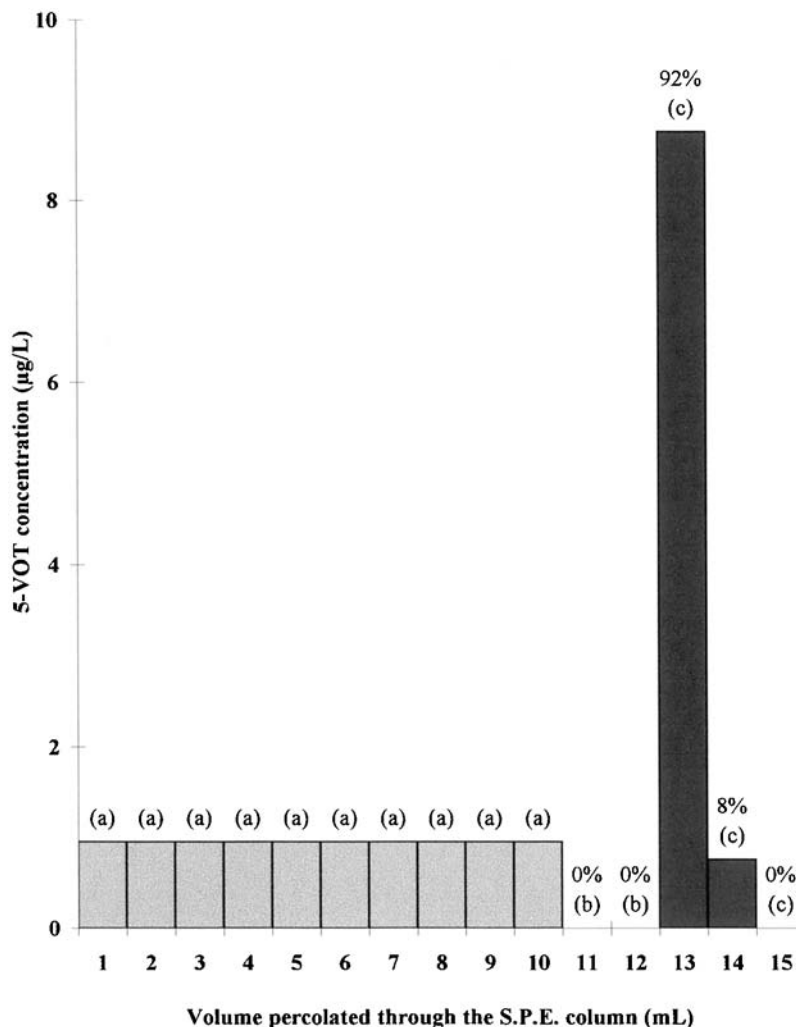


Fig. 2. Purification and concentration of 5-VOT aqueous solution ($1 \mu\text{g l}^{-1}$) on a SPE column (2.5 g of C_{18} -bonded silica, $40 \mu\text{m}$). (a) 5-VOT level in initial solution, (b) 5-VOT level in washing effluent (distilled water), (c) 5-VOT level in effluent, 50:50 methanol/acetonitrile. %, recovery of 5-VOT.

responds to the 5-VOT retention in complex matrices.

The tests performed with samples of liver have shown that, in order to avoid a stable emulsion that can hinder recovery of the organic phase, the pH of the extraction solution must be lower than 3. As the utilisation of an extraction cartridge of bonded silica C_{18} at the first step of purification imposes a pH equal to or higher than 2, we have retained the value of pH 2.5. Moreover, the acidity

of the extraction medium limits solubilisation of proteins and the raw extract remains clear. The recovery rate of the extraction process attains 95%.

The aqueous extract contains impurities which pollute the PMA during the extraction and greatly limit the extraction of 5-VOT. It is necessary to introduce a new purification step in the analytical procedure. So, the raw extract is purified by SPE. The 5-VOT and 4,4-DMOT are recovered in higher concentration (Fig. 3).

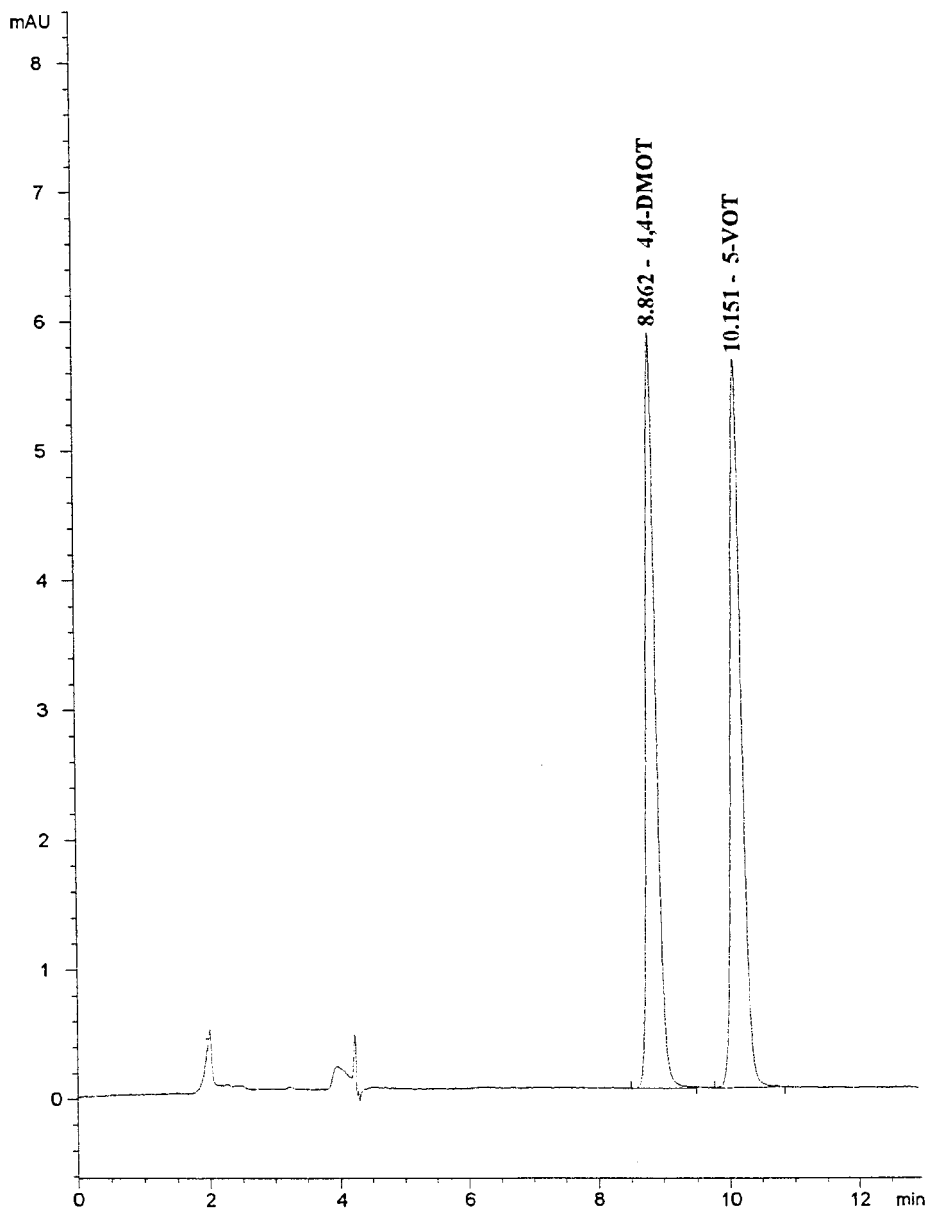


Fig. 3. Chromatogram of an aqueous standard solution of 4,4-DMOT and 5-VOT at $25 \mu\text{g l}^{-1}$, injection of $100 \mu\text{l}$. For HPLC conditions, see Section 2.

Some classic organic solvents (dichloromethane, diethyl ether) were used by several authors [4,7] for the 5-VOT extraction. They are currently out of date because of their poor selectivity. The second purification step of the 5-VOT is based on the selective complexation

with a mercuric compound. The aqueous phase is extracted by PMA in cyclohexanic medium. This agent, a particularly powerful complexant, has been previously used [5,6,13–15] to analyse biological samples. The PMA forms with the 5-VOT, at basic pH, a cyclohexane soluble complex.

The sodium thiosulfate has a strong capacity to form complexes with mercury and release the 5-VOT from PMA in the aqueous phase. This transfer between phases of very different polarities ensures the very high selectivity of the extraction. Using a small volume of thiosulfate solution, the 5-VOT is concentrated in the aqueous phase.

The 5-VOT analysis is achieved using HPLC with an UV detector. As the solution to be analysed contains only a few compounds to be separated (4,4-DMOT, 5-VOT and thiosulfate), a very fast analysis in the isocratic mode is feasible. With a C₁₈ column rather than a C₈ column [14] and a 1 ml min⁻¹ flow rate, the analysis is completed in 12 min. The retention times of 4,4-DMOT and 5-VOT are, respectively, 8.8 and 10.2 min.

The recovery rates are calculated with samples spiked with 10 µg kg⁻¹ 5-VOT. They reach 90% (Table 1). The PMA extraction leads to a high selectivity. The method is accurate: the repeatability calculated with samples of ewe muscle is improved to 97% and the reproducibility intra-laboratory is over 94%. The method shows a good linearity between 1 and 2000 µg kg⁻¹ with a correlation factor of 0.998. The low detection limit of this analysis (0.05 ng into the column) is

due to the strong absorption of 5-VOT in the UV ($\epsilon_{240} = 16\,000 \text{ l mol}^{-1} \text{ cm}^{-1}$) and the quantification limit in the sample has been decreased down to 1 µg kg⁻¹ (0.2 ng injected, S/N = 4). The efficiency of the extraction and the purification steps, and the use of an adapted internal standard allows us to obtain a rugged method.

The method described herein facilitates the analysis of various complex matrices: rapeseed meal, animal diets containing 40% of rapeseed meal and biologic samples such as liver, kidney, lung, muscle, thyroid, plasma and milk from an ewe fed with diets containing 40% of rapeseed meal (Table 1).

4. Conclusion

With this method, the 5-VOT stemming from the most important glucosinolate found in rapeseed, can be analysed at ppb (1 µg kg⁻¹) level. The marked improvement of 5-VOT extraction from organs and biologic fluids shows the importance of sample preparation and extraction conditions. Moreover, the analyses reveal the occurrence of 5-VOT in rapeseed meal, diets, plasma, milk and some target organs from an ewe fed with diets containing 40% of rapeseed meal.

This type of dosage, thanks to its high sensitivity, can also be used for experimentation on small animals. The simplicity of the material and the absence of derivation reagents make it accessible to all laboratories.

Table 1

5-VOT values obtained for various samples before and after addition of 1 ml of a 5-VOT solution at 30 µg l⁻¹ ($n = 3$)

Matrix	5-VOT level (µg kg ⁻¹)		Recovery rate (%)
	Before	After	
Vegetal			
Rapeseed meal	44.6	53.9	93
Diets (40% rapeseed meal)	25.3	34.4	91
Biologic tissues			
Liver	4.3	13.3	90
Kidney	4.6	13.8	92
Lung	5.2	14.5	93
Muscle	6.3	15.6	93
Thyroid	26.1	35.1	90
Biologic fluids			
Plasma	5.9	15.2	93
Milk	12.3	21.4	91

Acknowledgements

This work has been undertaken with the financial support of the 'Direction Générale Recherche et Développement du Ministère des Classes Moyennes et de l'Agriculture' and of the 'Direction Générale des Technologies, de la Recherche et de l'Energie du Ministère de la Région Wallone' of Belgium. The authors are grateful to Prof. P. Rollin (LCBA, Université d'Orléans, France) for supplying the 4,4-dimethyl-1,3-oxazolidine-2-thione.

References

- [1] E.B. Astwood, M.A. Greer, M.G. Ettlinger, *J. Biol. Chem.* 181 (1949) 121.
- [2] M.A. Greer, J.M. Deeney, *J. Clin. Invest.* 38 (1959) 1465.
- [3] G.R. Fenwick, R.K. Heaney, W.J. Mullin, *CRC Crit. Rev. Food Sci. Nutr.* 18 (1983) 123.
- [4] P.N. Maheshwari, D.W. Stanley, J.I. Gray, F.R. van de Voort, *J. Am. Oil Chem. Soc.* 56 (1979) 837.
- [5] H.F. De Brabander, R. Verbeke, *J. Chromatogr.* 252 (1982) 225.
- [6] H.F. De Brabander, R. Verbeke, *Proceedings of the 32nd European Meeting of Meat Research Workers*, Vol. 1, Gent, 1986, pp. 45–48.
- [7] M. Kreula, M. Kiesvaara, *Acta Chem. Scand.* 13 (1959) 1375.
- [8] M.E. Daxenbichler, G.F. Spencer, R. Kleiman, C.H. Van Etten, I.A. Wolff, *Anal. Biochem.* 38 (1970) 373.
- [9] C.H. Van Etten, M.E. Daxenbichler, N. Schroeder, L.H. Princen, T.W. Perry, *Can. J. Anim. Sci.* 57 (1977) 75.
- [10] H.A. McLeod, G. Benns, D. Lewis, J.F. Lawrence, *J. Chromatogr.* 157 (1978) 285.
- [11] E. Josefsson, L. Akerström, *J. Chromatogr.* 174 (1979) 465.
- [12] G. Benns, M.R. L'Abbé, J.F. Lawrence, *J. Agric. Food Chem.* 27 (1979) 426.
- [13] H.F. De Brabander, R. Verbeke, *Trends Anal. Chem.* 3 (1984) 162.
- [14] A. Quinsac, D. Ribailier, P. Rollin, M. Dreux, *J. Assoc. Off. Anal. Chem.* 75 (3) (1992) 529.
- [15] A. Quinsac, M. Dreux, D. Ribailier, *Proceedings of the Eighth International Rapeseed Conference*, Vol. 5, Saskatoon, Canada, 1992, pp. 1337–1342.
- [16] M. Skulski, D.L. Garmaise, A.F. Mac Kay, *Can. J. Chem.* 34 (1956) 81.

Comparison of two methods for the optimization of the analytical conditions for the determination of total sulfur

Teresa A.P. Rocha *, M. Teresa S.R. Gomes, Armando C. Duarte,
João A.B.P. Oliveira

Department of Chemistry, University of Aveiro, 3810 Aveiro, Portugal

Received 30 September 1998; received in revised form 30 November 1998; accepted 1 December 1998

Abstract

Response surface and simplex methods were used for optimizing the determination of total sulfur present in gaseous samples using a quartz crystal microbalance. The optimization methodology increased the analytical signal from three to five times. The simplex method showed the highest efficiency in the search for the maximum sensor response. However, the response surface allows ranking the variables according to their effects and highlights the existence of a plateau in the optimal region. © 1999 Elsevier Science B.V. All rights reserved.

Keywords: Simplex; Response surface; Optimization; Quartz crystal microbalance

1. Introduction

Sulfur compounds are widespread in the environment, and, mainly due to their notorious odor, may cause adverse effects in air quality mainly in the vicinity of landfills, pulp and paper mills, and sewage treatment plants. Due to increasing concern about the quality of the environment, there is a great need for methods easily applied to the monitoring of such compounds. Gas chromatography with flame photometric detection has been one of the methods used for determination of these compounds [1–4]. Abdallahi et al. [5] used a

Raney nickel wet chemical method for the determination of trace amounts of sulfur in naphthas, and Von Wandruszka et al. [6] used cathodic square wave stripping voltammetry for monitoring sulfur species.

In this work the analytical method proposed to detect and quantify sulfur compounds present in gaseous samples, is based on an oxidative combustion process, followed by detection of SO₂ with a piezoelectric quartz crystal [7]. In order to obtain high sensitivity to levels in the microgram range existing in some emissions, an optimization of the analytical conditions was performed with two different approaches: experimental design and simplex method.

* Corresponding author.

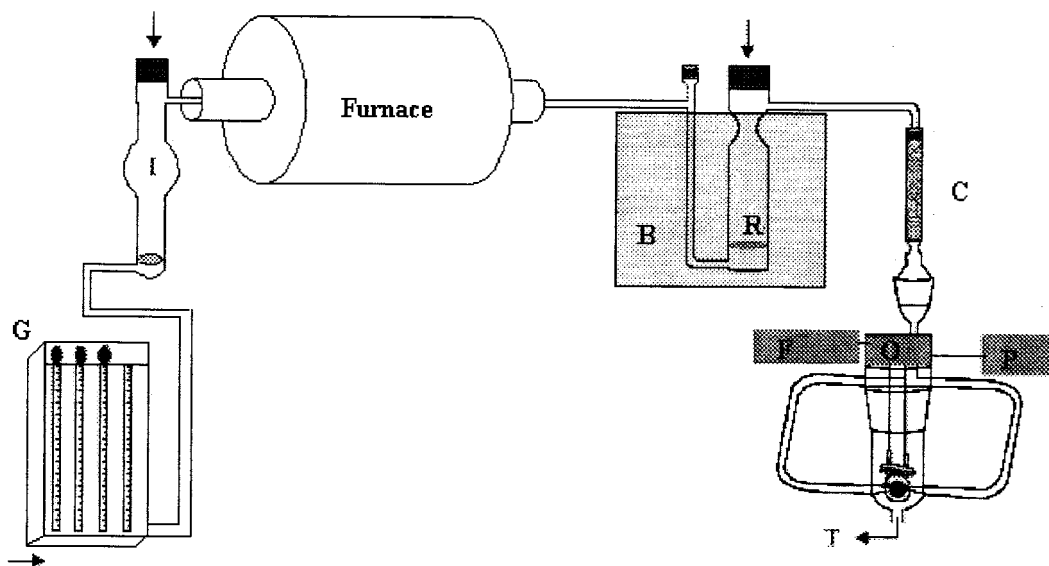


Fig. 1. Experimental apparatus: B, bath; C, column with desiccant (MgClO_4); G, gas proportioner; F, frequency meter; I, injection cell; O, oscillator; P, power supply; R, reaction cell.

2. Experimental

The experimental apparatus is shown in Fig. 1. A 100.00 cm^3 volume of working mercury solution was prepared from two stock solutions: HNO_3 0.1 mol dm^3 and HgNO_3 H_2O 0.01 mol dm^3 (in HNO_3 0.01 mol dm^3). An aliquot of 10.00 cm^3 was taken from the working mercury solution and introduced into the reaction cell. Due to the disproportionation of mercury, the $\text{Hg}(0)$ amalgamates onto the gold electrodes of the piezoelectric sensor, and a frequency decrease is observed. As soon as the frequency stabilized, $1.0 \times 10^{-6} \text{ dm}^3$ of ethanethiol ($43.35 \times 10^{-5} \text{ g}$ sulfur) was injected into the injection cell and was then carried by a mixture of nitrogen and oxygen (controlled with a gas proportioner) flowing into the quartz coil placed inside the furnace. After the oxidative combustion, the resulting SO_2 flows into the reaction cell and reacts with the $\text{Hg}(I)$ solution. The SO_2 promotes mercury disproportionation, more $\text{Hg}(0)$ is produced, and a new frequency decrease is observed, which is proportional to the mass of SO_2 generated and to the amount of sulfur compound injected. For safety reasons, there are two traps: one with sodium hypochloride and another

with potassium permanganate, for the sulfur compounds and $\text{Hg}(0)$, respectively.

Among the possible parameters that control the combustion process, the main ones are the oxygen and nitrogen flows, and furnace temperature. Temperature in the reaction cell, nitric acid and mercury(I) nitrate concentration are another three parameters that should be taken into account. The optimisation methodology based on response surface analysis of data obtained from experimental design was closely followed according to the software Unscrambler by Camo A/S [8]. The simplex method was performed according to the software designed and developed by Multisimplex [9].

3. Results and discussion

Since there are six design variables in the analytical process a full factorial design would require a total of 64 experiments. In order to save on the number of experiments without risking the optimization objective, a fractional factorial design 2^{6-2} (resolution IV) with two center samples was performed. The design variables T_{furnace} (temperature of furnace), OxygFlow (oxygen flow),

Table 1

Results obtained for the full set of experiments following experimental design procedures

Experiment number	HgVolume (cm ³)	AcidVolume (cm ³)	Tbath (°C)	Tfurnace (°C)	OxygFlow (cm ³ min ⁻¹)	TotalFlow (cm ³ min ⁻¹)	Dfreq (Hz)
1	0.10	1.0	20.0	700	10.0	25.0	2
2	1.0	1.0	20.0	700	20.0	25.0	1425
3	0.10	5.0	20.0	700	20.0	55.0	34
4	1.0	5.0	20.0	700	10.0	55.0	2
5	0.10	1.0	35.0	700	20.0	55.0	1359
6	1.0	1.0	35.0	700	10.0	55.0	10581
7	0.10	5.0	35.0	700	10.0	25.0	638
8	1.0	5.0	35.0	700	20.0	25.0	1400
9	0.10	1.0	20.0	1000	10.0	55.0	293
10	1.0	1.0	20.0	1000	20.0	55.0	872
11	0.10	5.0	20.0	1000	20.0	25.0	114
12	1.0	5.0	20.0	1000	10.0	25.0	3205
13	0.10	1.0	35.0	1000	20.0	25.0	1066
14	1.0	1.0	35.0	1000	10.0	25.0	473
15	0.10	5.0	35.0	1000	10.0	55.0	372
16	1.0	5.0	35.0	1000	20.0	55.0	12487
17	0.55	3.0	27.5	850	15.0	40.0	834
18	0.55	3.0	27.5	850	15.0	40.0	833
19	0.00	5.0	27.5	1000	15.0	40.0	0
20	1.10	5.0	27.5	1000	15.0	40.0	13449
21	0.55	5.0	18.3	1000	15.0	40.0	1299
22	0.55	5.0	36.7	1000	15.0	40.0	12741
23	0.55	5.0	27.5	1000	8.85	40.0	10576
24	0.55	5.0	27.5	1000	21.2	40.0	11759
25	0.55	5.0	27.5	1000	15.0	21.6	6065
26	0.55	5.0	27.5	1000	15.0	58.5	4981
27	0.55	5.0	27.5	1000	15.0	40.0	12089
28	0.55	5.0	27.5	1000	15.0	40.0	12110
29	0.55	5.0	27.5	1000	15.0	40.0	12050
30	0.55	5.0	27.5	1000	15.0	40.0	12035
31	0.55	5.0	27.5	1000	15.0	40.0	12008

AcidVolume (volume of nitric acid used in the preparation of the working mercury solution), HgVolume (volume of mercury(I) solution used in the preparation of the working mercury solution), Tbath (temperature of bath) and TotalFlow (sum of oxygen and nitrogen flows) defined an initial set of 18 experiments. Table 1 shows these results obtained for the 18 experiments. The analysis of effects [8] showed that all six design variables and respective second order interactions have a significant influence (P -value < 0.005) on the response variable (frequency decrease). Fig. 2 shows the normal probability plot of effects, where it can be observed that Tfurnace, OxygFlow and AcidVolume are likely to have similar main effects, but

not very significant. Only the variables HgVolume, Tbath and TotalFlow have significant main effects and/or interactions. Since those interactions are confounded, the design was extended in order to see which interactions are really significant. Some doubt may remain regarding the interaction effects AB and CE, which are confounded in this particular design. Since the effect of AcidVolume (variable B) is easier to predict (the more nitric acid added the higher the response), the OxygFlow (variable E) is kept for the new set of experiments. AcidVolume variable was fixed at 5.00 cm³ and Tfurnace at 1000°C (since the quartz coil temperature cannot be higher than 1050°C). The new design was obtained by deleting variables

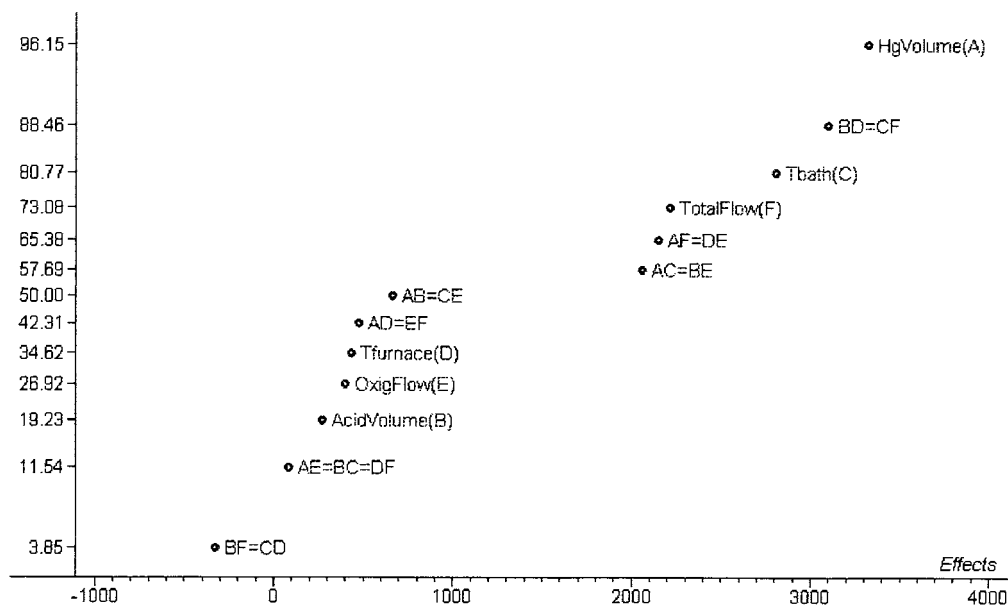


Fig. 2. Normal probability plot of the effects for the initial set of 18 experiments.

AcidVolume and Tfurnace, and extending the remaining part to a central composite design with new seven center samples. Table 1 also contains the results of these additional 13 experiments, and Fig. 3 shows the normal probability plot of the effects for the full set of 31 experiments. Assuming a full quadratic centered model, the response surface allows the estimation of the optimum for HgVolume of 0.88 cm^3 , T_{bath} of 32.9°C , OxygFlow of $12.3 \text{ cm}^3 \text{ min}^{-1}$ and TotalFlow of $46.2 \text{ cm}^3 \text{ min}^{-1}$. The predicted value for the response at the optimum value is $11\,070 \text{ Hz}$. Fig. 4 shows the response in terms of T_{bath} (new variable B) and HgVolume (new variable A) and it highlights the featureless aspect of the response surface without a well-defined peak in the optimum region. In fact, the region of the optimum is rather flat which complicates the search for optimum of the optimization procedure.

The simplex method was applied to the same variables, and the values of the initial simplex were generated from the ones reported by Suleiman and Guilbault [7]. Fig. 5 shows the evolution of the response (frequency decrease) and the variables along trials defined by the simplex method. The evolution of the variables confirms the exist-

tence of a response domain without important features: small increasing trend in response for a relatively large combination of variables. A very well stabilized response was reached at experiment 30, which includes four re-evaluations. The last two responses of the simplex evolution (experiments 29 and 30) were averaged, and optimum values were obtained for HgVolume of 0.54 cm^3 , T_{bath} of 34.3°C , OxygFlow of $20.2 \text{ cm}^3 \text{ min}^{-1}$, TotalFlow of $50.5 \text{ cm}^3 \text{ min}^{-1}$, AcidVolume of 3.64 cm^3 and Tfurnace of 992°C with a predicted response value of $16\,500 \text{ Hz}$.

The differences between the two optimal sets of conditions found by two different optimization procedures, can be attributed to the response domain which, besides showing a rather complex six-dimensional variable space, may also be a hypersurface without a well-defined maximum, and only with a plateau where different combinations of variables give similar values for the response.

Fig. 6 shows the results of experiments performed with another sensor for the conditions before and after optimization. Before optimization, the frequency decrease obtained for an injection of $1.00 \times 10^{-6} \text{ dm}^3$ of ethanethiol

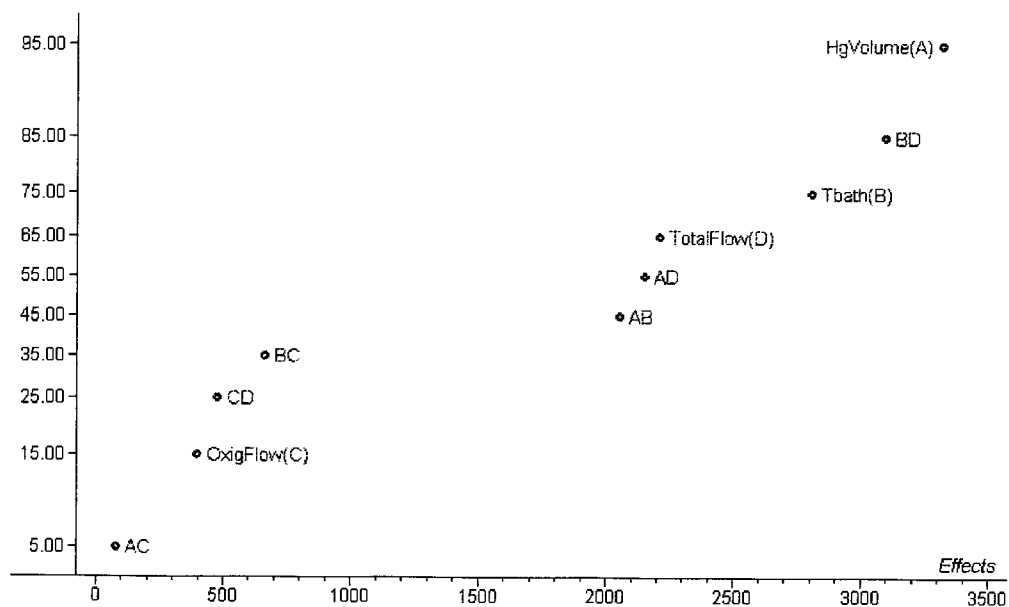


Fig. 3. Normal probability plot of the effects for the full set of 31 experiments.

-1.016e+03 1.327e+03 3.670e+03 6.014e+03 8.357e+03 1.070e+04

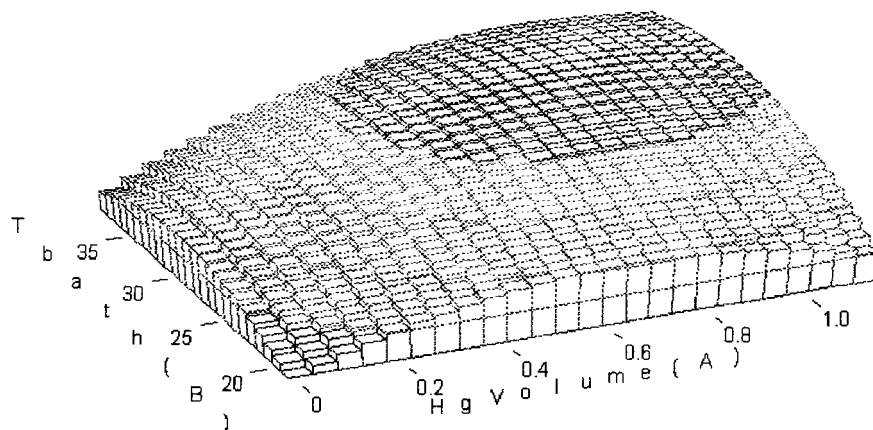


Fig. 4. Surface response in terms of Hg volume (new variable A) and bath temperature (new variable B).

(43.55×10^{-5} g of sulfur) was 3700 Hz for the following conditions [7]: HgVolume of 0.40 cm^3 , T_{bath} of 27.0°C , OxygFlow of 20.0 cm^3 and TotalFlow of $55.0 \text{ cm}^3 \text{ min}^{-1}$, AcidVolume of 2.5

$\text{cm}^3 \text{ min}^{-1}$ and T_{furnace} of 950°C . Frequency decrease for the same injection was 17 050 and 12 052 Hz for simplex optimization and experimental design optimization, respectively.

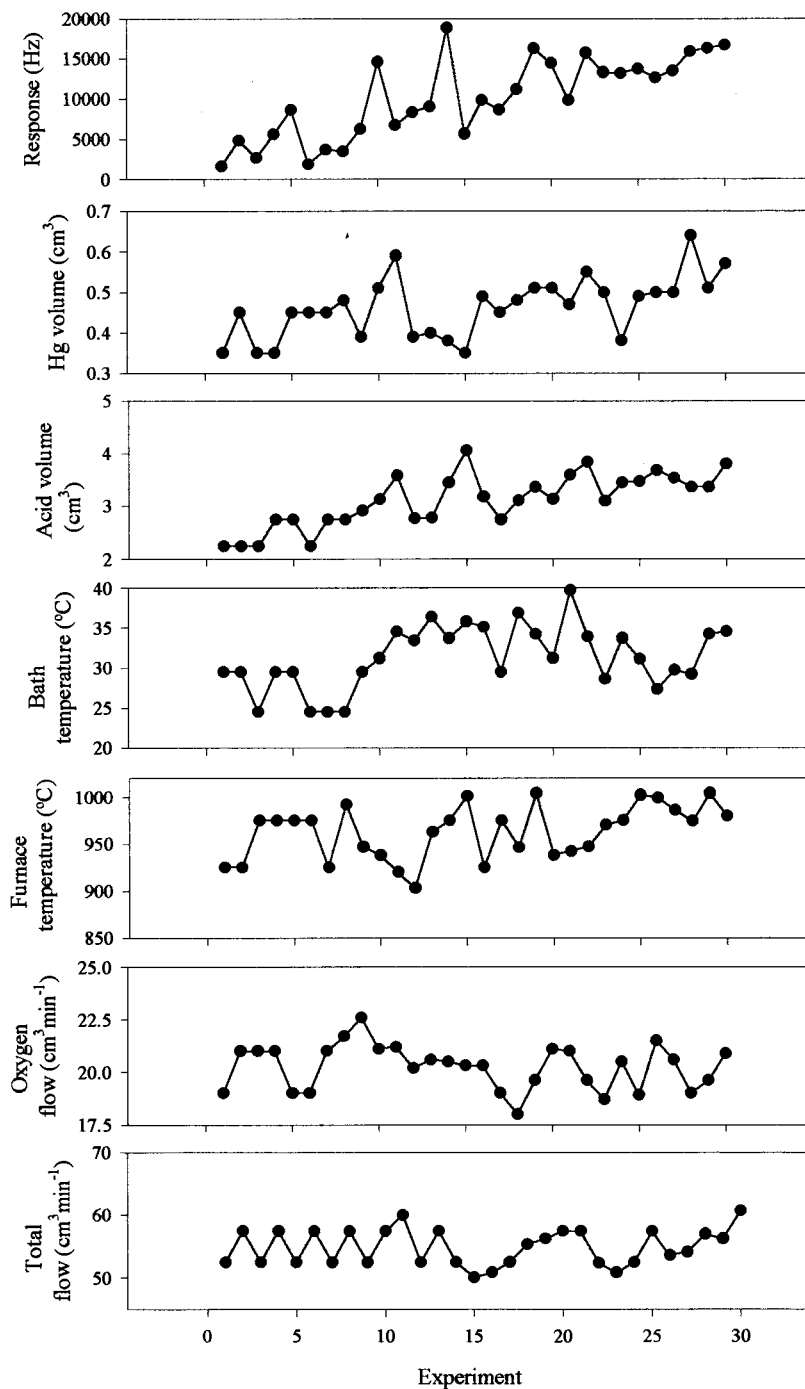


Fig. 5. Evolution of the response and variables with the trials defined by the simplex method.

After the optimization the analytical signal was increased from three to five times which allows

the monitoring of sulfur compounds at the microgram level.

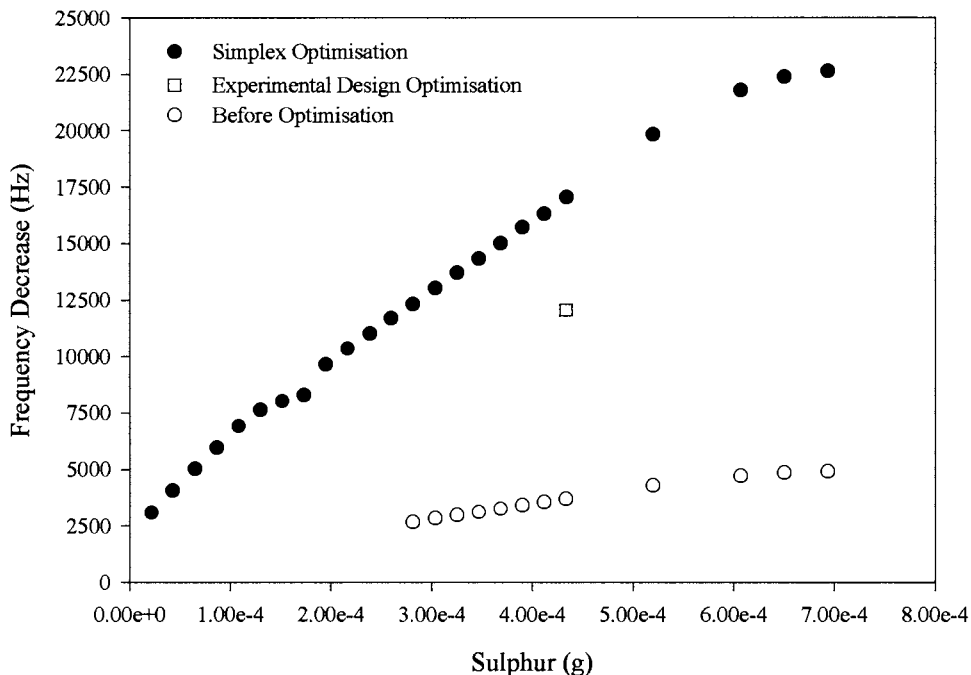


Fig. 6. Response of a QCM for conditions before and after both optimisation methods.

Acknowledgements

This work was partially financed through DGA funded project 'Desenvolvimento de Novos Sensores para a Monitorização de Nitrobenzeno e Compostos Sulfurosos' (Contract no. PEAM/NMA/656/95).

References

- [1] C. Persson, C. Leck, *Anal. Chem.* 66 (1994) 983.
- [2] J. Radford-Knoery, G.A. Cutter, *Anal. Chem.* 65 (1993) 976.
- [3] P.A. Steudler, W. Kijowski, *Anal. Chem.* 56 (1984) 1432.
- [4] R. Simo, J.O. Grimalt, J. Albaiges, *J. Chromatogr. A.* 665 (1993) 301.
- [5] M.M. Abdillahi, K. Alam, A. Bari, M. Siddiqui, M.A. Ali, *Analyst* 120 (1995) 1577.
- [6] R. Von Wandruszka, X. Yuan, M.J. Morra, *Talanta* 40 (1993) 37.
- [7] A. Suleiman, G.G. Guilbault, *Anal. Lett.* 17 (1984) 1927.
- [8] Camo A/S, 1996. *The Unscrambler. Computer-Aided Modelling A/S, Trondheim, Norway.*
- [9] MultiSimplex, 1997. Bergström and Öberg, Karlskrona, Sweden.

Flow injection dialysis for the determination of anions using ion chromatography[☆]

Kate Grudpan^{a,*}, Jaroon Jakmune^a, Ponlayuth Sooksamiti^b

^a Department of Chemistry, Faculty of Science, Chiang Mai University, Chiang Mai 50200, Thailand

^b Mineral Resources Region 3 (Chiang Mai), Chiang Mai 50200, Thailand

Received 8 December 1998; accepted 7 January 1999

Abstract

Flow injection dialysis (FID) coupling with ion chromatography (IC) is proposed for simultaneous determination of some anions (bromide, chloride, fluoride, nitrate, nitrite, phosphate and sulfate). A standard or sample containing the anions is injected into a donor stream of a mixture (0.022 M Na₂CO₃ and 0.028 M NaHCO₃) flowing into a dialysis cell. The bolus of the dialysate containing the anions, in the acceptor stream of water, flows to the IC injection valve where a portion of the bolus is injected into the IC and analysed under normal IC conditions, with a conductivity detector. FID provides on-line separation and dilution of the analytes from matrix especially from some species such as proteins, surfactant, particulates which may cause damage to the IC columns. Prolongation of life-time of the IC columns is an additional advantage to others which will be discussed. On-line dialysis–IC was also investigated. © 1999 Elsevier Science B.V. All rights reserved.

Keywords: Flow injection dialysis; On-line dialysis; Ion chromatography; Anion analysis

1. Introduction

Flow injection analysis (FIA) originated as a method for rapid assays [1,2] and later also served to introduce the sample into a detector. FIA could be used for and to enhance pretreatment steps [3]. FIA systems with on-line sample pretreatment are very beneficial [4–6]. These include,

for example, column [7,8], gas diffusion [9,10] and solvent extraction [11]. On-line dialysis could be incorporated with an FIA system to separate analytes from complicate matrices and provide dilution of analytes prior to the determination step [3,12] such as the determination of phosphate and chloride in blood serum [12] or chloride in milk samples [13]. Recently on-line dialysis has been applied to capillary electrophoresis [14].

FIA is now a tool to perform chemistry more efficiently. Various detection systems have been applied to FIA, although most are spectrophotometric, some use FIA for efficient sample introduction (such as AAS, ICP-AES, ICP-MS, ISE).

[☆] Presented at the Ninth International Conference on Flow Injection Analysis, Seattle, WA, USA, August 23–27, 1998.

* Corresponding author. Tel.: +66-53-943345; fax: +66-53-222268.

E-mail address: kate@chiangmai.ac.th (K. Grudpan)

FIA systems with detection techniques such as electrochemical [12,15], fluorometric [16], chemiluminescence and bioluminescence [17], radiometric [18] and even visual [19] have been reported. FIA has been applied to chromatography e.g. post-column derivative techniques such as a recent report on the determination of condensed phosphates [20].

In the present work, attempts have been made to couple flow injection dialysis (FID) with ion chromatography (IC), for sample cleaning or pre-treatment, for on-line separation and on-line dilution of some anions prior to their determination using an IC. An additional advantage of prolonging the life-time of the IC column would also be gained.

2. Experimental

2.1. Chemicals, solutions and samples

All chemicals were of analytical grade. Deionized water was used throughout. Inorganic anion stock solutions of 1000 mg l^{-1} were prepared from corresponding sodium salts except for phosphate and sulfate where potassium dihydrogen phosphate and potassium sulfate, respectively were used.

Standard solutions of each anion were prepared by appropriate dilution of the stock solutions. A mixed standard solution was obtained by mixing

the standard of each component with appropriate concentration.

The eluent for IC was prepared by mixing sodium hydrogen carbonate (0.44 M, 5 ml) with sodium carbonate (0.14 M, 20 ml) and diluting to a volume of 1 l. Stock solution of the former was prepared by dissolving 36.96 g NaHCO_3 (Merck) in water then making up to 1 l while for the latter by dissolving 14.84 g Na_2CO_3 (Merck) in 1 l. The eluent was degassed using an ultrasonic bath before use.

2.2. Dialysis cell

The dialysis cell used is depicted in Fig. 1. Two symmetric acrylic blocks, engraved for groove-path of solution, sandwich a sheet of dialysis membrane, commercially available as a wrapping foil (Somchai, Thailand).

2.3. Ion chromatograph

A Lachat Ion Chromatograph (Quik Chem 8000) was used including anion guard column (P/N 28085), anion separation column (Lachat EPA 300 A (P/N 28084)), suppressor column (Lachat P/N 28097), and conductivity detector (Lachat P/N A28982).

Recommended conditions (Quik Chem Method 10-510-00-1-A) were followed [21]. Lachat Omion IC software was also used. A sample ($200 \mu\text{l}$) was loaded and injected via a six-port injection valve (ICV1). With the eluent (a mixture of 0.0022 M NaHCO_3 and 0.0028 M Na_2CO_3), it passed through the guard and separation columns and entered a suppressor column, sitting in a 10-port valve (ICV2), then to the conductivity detector. The suppressor was automatically regenerated (by 0.25 M H_2SO_4 regenerant) via a switching valve (ICV2) while loading the sample at the injection valve (ICV1).

2.4. On-line dialysis-IC

The on-line dialysis-IC manifold is depicted in Fig. 2. A standard/sample is merged with a modifier stream passing through a mixing coil before entering into the dialysis unit. Dialysate

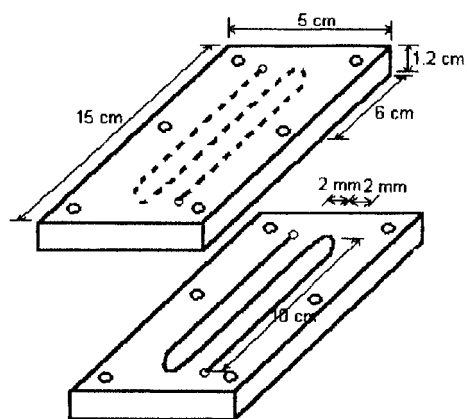


Fig. 1. Acrylic dialysis unit (membrane not shown).

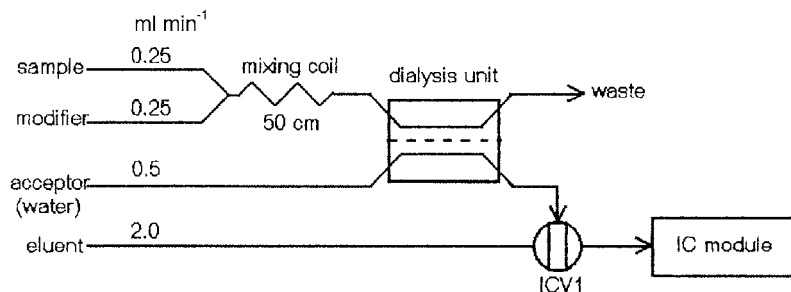


Fig. 2. Manifold for on-line dialysis–ion chromatography (see text).

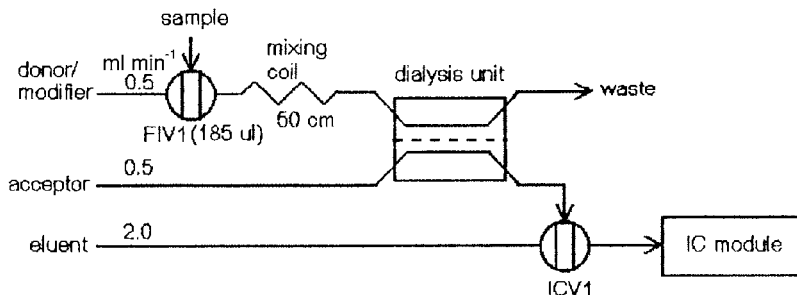


Fig. 3. Manifold for flow injection dialysis–ion chromatography (FID-IC) (see text).

permeates into the acceptor stream which then flows into an injection valve and is analysed by the IC (Fig. 2).

2.5. Flow injection dialysis (FID)–IC

Fig. 3 depicts the FID–IC manifold. FID is operated manually while the IC is manipulated via the Omnion software. Standard/sample (185 μ l) is injected via an injection valve (FIV1, FIALab-2000, Alitea) into a stream of donor/modifier, flowing through a mixing coil and the dialysis unit. The species of interest permeates to the acceptor stream. The dialysate bolus then flows to the IC injection valve (ICV1) where it is injected into the IC to be analysed. The two valves are operated under a timer control as indicated in Fig. 4. A standard/sample is injected into the FID by the valve, FIV1; 115 s after the injection at the valve, FIV1, the bolus of the dialysate containing the species of interest will reach the valve, ICV1 and at this moment the

valve, ICV1 is switched on; the dialysate flows into the sample loop, at this position for 70 s (200 μ l loop); then further automatically operated via the Omnion software, i.e. starting by switching the valve ICV1 into injection position and the valve, ICV2 to start the suppression process. Regenerating the suppressor takes place at the same time as sample loading. The IC data acquisition is made by the Omnion software and can be evaluated either by the software or manually.

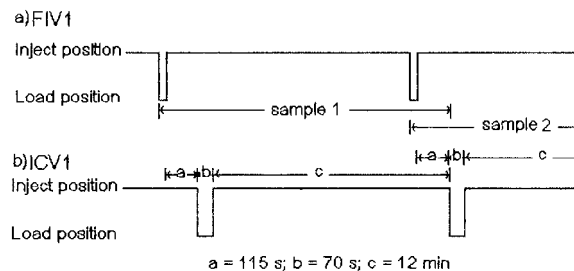


Fig. 4. Schematic diagram timer control for operation of valves in the FID–IC system.

Table 1
Effect of analyte concentration on % dialysis in on-line dialysis–IC (Fig. 2)

Analyte	% dialysis @ analyte concentration (mg l ⁻¹)						
	5	10	15	20	25	Mean	% RSD
<i>(a) Modifier: H₂O</i>							
F ⁻	3.4	3.9	4.1	4.1	3.3	3.8	10.2
Cl ⁻	7.8	6.3	5.6	5.3	4.3	5.9	22.3
NO ₂ ⁻	4.9	5.9	7.0	7.1	5.9	6.2	15.0
NO ₃ ⁻	4.0	5.4	6.3	6.5	5.4	5.5	17.9
PO ₄ ³⁻	1.1	1.8	1.8	1.8	1.4	1.6	20.4
SO ₄ ²⁻	3.0	1.7	1.4	1.2	1.0	1.7	48.3
<i>(b) Modifier: 0.01 M NaCl</i>							
F ⁻	11.0	8.5	9.9	8.9	8.5	9.4	11.6
Cl ⁻	10.1	10.3	11.1	10.5	10.8	10.6	3.8
NO ₂ ⁻	8.1	9.5	10.1	9.6	11.0	9.7	11.1
NO ₃ ⁻	9.2	10.1	10.6	10.1	11.2	10.2	7.4
PO ₄ ³⁻	3.1	3.8	4.0	3.3	4.0	3.6	10.8
SO ₄ ²⁻	4.3	3.3	3.0	2.6	2.8	3.2	21.6
<i>(c) Modifier: 20× eluent (0.044 M NaHCO₃+0.056 M Na₂CO₃)</i>							
F ⁻	7.6	–	8.5	–	9.1	8.4	8.9
Cl ⁻	13.5	–	11.9	–	12.4	12.6	6.5
NO ₂ ⁻	14.4	–	15.7	–	16.1	15.4	5.7
NO ₃ ⁻	12.8	–	14.4	–	14.9	14.0	7.8
PO ₄ ³⁻	5.2	–	5.8	–	5.8	5.6	6.4
SO ₄ ²⁻	8.1	–	6.6	–	6.4	7.0	13.3

2.6. Separation of species which possibly causes damage to IC columns

Using on-line dialysis–IC under optimum conditions, separation of species which may damage the IC column was investigated.

Surfactant sodium dodecyl sulfate (SDS, Fluka) (100 mg l⁻¹) was on-line dialysed. Fractions of the dialysate were collected and were analysed off-line using the standard methylene blue single extraction method [22]. The % dialysis was then estimated.

For proteins, fresh milk was tested, available from the local market and labelled as having 0.34% protein content. Fractions of the dialysate obtained from the on-line manifold were analysed, off-line by the biuret method [23]. Similarly albumin bovine (Sigma, St Louis, MO) (20 mg l⁻¹) was tried. The % dialysis in both cases was evaluated.

Particle slurry of silica gel (particle sizes < 10 µm) was present in the sample line (Fig. 2). Con-

tinuous monitoring was made for turbidity by setting the spectrophotometric detector at 520 nm.

3. Results and discussion

3.1. On-line dialysis–IC

Using the flow system described in Fig. 2, water was first used for both the modifier and acceptor streams. A mixture of seven anion standards resulted in a chromatogram with retention times the same as those directly (normal) injected into the IC: fluoride, chloride, nitrite, bromide, nitrate, phosphate and sulfate; 2.35, 3.25, 3.90, 5.27, 6.17, 8.58, and 10.43 min which agree with those reported previously [21]. Table 1 indicates the effect of analyte concentrations on % dialysis (defined as the percentage of the ratio of the concentration (mg l⁻¹) found to the analytical concentration). In general, % dialysis could not be well controlled when using water compared to 0.01 M NaCl and

Table 2
Effect of ionic strength, adjusted by sodium chloride of various concentrations, on % dialysis

Analyte ^a	% dialysis @ [NaCl] in modifier stream (M)								
	0 ^b	0.005	0.01	0.02	0.03	0.04	0.05	Mean	% RSD
F ⁻	6.6	7.4	7.6	7.8	7.0	8.1	7.8	7.5	6.9
Cl ⁻	8.3	12.1	11.6	10.2	9.0	8.9	8.4	9.8	15.8
NO ₂ ⁻	10.2	10.5	10.3	9.7	8.3	8.5	7.4	9.3	13.0
Br ⁻	10.6	11.6	11.8	11.9	10.1	12.1	11.6	11.4	6.5
NO ₃ ⁻	1.8	1.9	2.0	2.0	1.8	2.0	1.9	1.9	4.7
PO ₄ ³⁻	2.6	3.3	3.5	3.7	3.7	4.3	4.1	3.6	15.5
SO ₄ ²⁻	2.1	2.7	2.9	3.4	3.0	3.8	3.7	3.1	19.4

^a A mixture (concentration 50 mg l⁻¹ each of F⁻, Cl⁻, Br⁻, PO₄³⁻ and SO₄²⁻; 25 mg l⁻¹ each of NO₂⁻ and NO₃⁻).

^b Water.

the solution of the 20 times concentrations of the eluent mixture, (the highest % RSD in Table 1(a) compared to Table 1(b)Table 1(c) respectively).

This could be due to the effect of ionic strength on the dialysis mechanism. The mixture of 0.044 M NaHCO₃ and 0.056 M Na₂CO₃ having the

Table 3
Calibration graphs

Anion	Linear equation ($y = ax + b$)			r^2	Range (mg l ⁻¹)	Detection limit ^a (mg l ⁻¹)
	a	b	n			
<i>(a) Conventional IC</i>						
F ⁻	1.08×10^7	-5.39×10^5	5	0.999	0.05–5	0.12
Cl ⁻	7.29×10^6	-1.49×10^6	5	0.999	0.5–50	0.59
NO ₂ ⁻	1.51×10^7	-8.48×10^5	5	0.999	0.05–5	0.09
Br ⁻	2.24×10^6	-5.30×10^4	5	0.999	0.05–5	0.05
NO ₃ ⁻	1.38×10^7	-6.79×10^5	5	0.999	0.05–5	0.12
PO ₄ ³⁻	9.09×10^5	-1.42×10^4	5	0.999	0.05–5	0.08
SO ₄ ²⁻	5.20×10^6	-2.84×10^6	5	0.997	1–100	4.5
<i>(b) On-line dialysis-IC</i>						
F ⁻	9.79×10^4	-1.82×10^5	3	0.999	5–25	2.59
Cl ⁻	1.02×10^6	-1.27×10^6	3	0.999	5–25	2.77
NO ₂ ⁻	2.26×10^6	-2.56×10^6	3	0.999	5–25	2.19
Br ⁻	–	–	–	–	–	–
NO ₃ ⁻	4.17×10^5	-4.24×10^5	3	0.999	5–25	1.49
PO ₄ ³⁻	5.59×10^4	-3.45×10^4	3	0.999	5–25	0.97
SO ₄ ²⁻	6.74×10^5	-4.41×10^5	3	0.999	5–25	–
<i>(c) FID-IC</i>						
F ⁻	3.08×10^5	-1.32×10^5	5	0.999	1–50	1.00
Cl ⁻	2.87×10^5	-1.93×10^5	5	0.999	1–50	1.08
NO ₂ ⁻	6.44×10^5	-3.15×10^5	5	0.999	1–50	0.91
Br ⁻	1.19×10^5	-1.59×10^5	5	0.999	1–50	1.59
NO ₃ ⁻	1.41×10^5	-1.99×10^5	5	0.999	1–50	2.23
PO ₄ ³⁻	1.01×10^4	-1.02×10^4	5	0.999	1–50	0.37
SO ₄ ²⁻	6.64×10^4	3.46×10^4	5	0.999	1–50	0.91

^a 3 × standard deviation of the blank signals, estimated from the y-intercept [24].

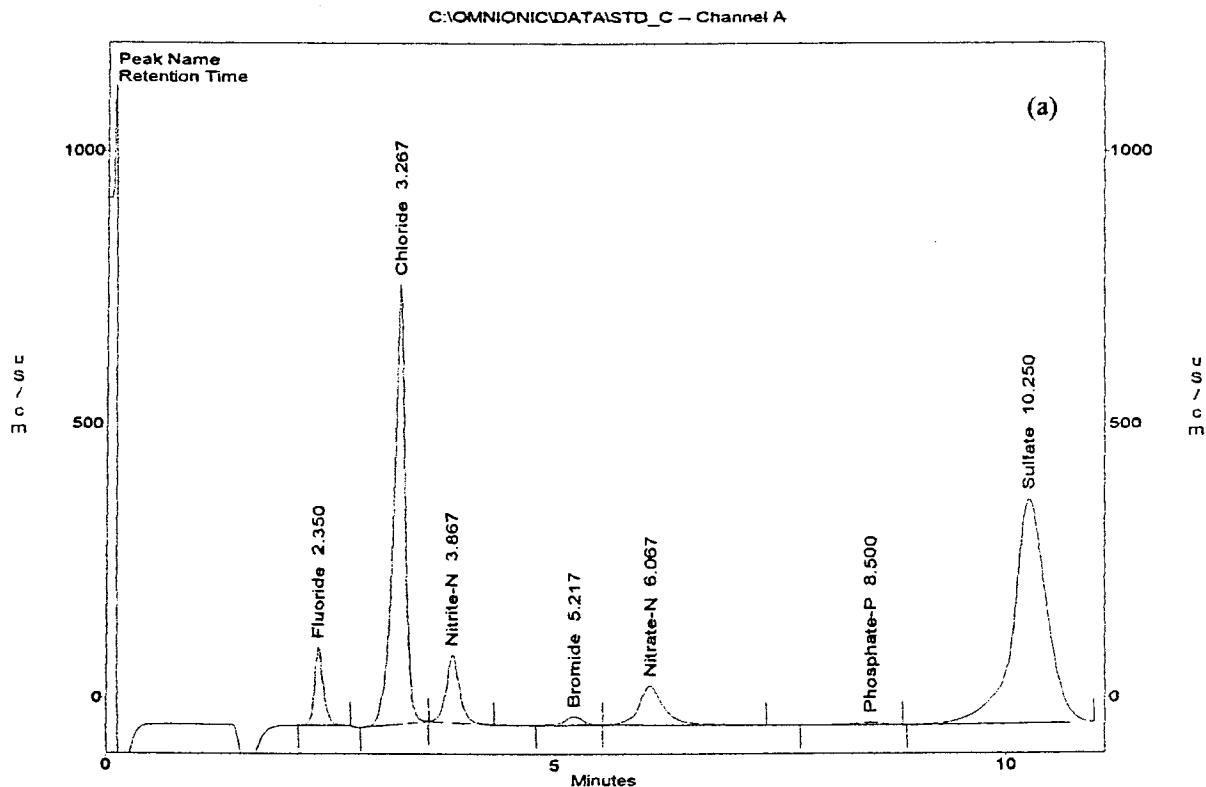


Fig. 5. Chromatograms of anions obtained by (a) conventional IC, (b) on-line dialysis-IC and (c) FID-IC.

highest ionic strength was found to be best, although ionic strength could be adjusted by using NaCl of various concentrations (Table 2) but chloride could not be analysed and the large chloride peak would also affect the neighboring peaks. Table 3 shows calibration graphs for the analytes when using the mixture of 0.044 M NaHCO₃ and 0.056 M Na₂CO₃.

3.2. Flow injection dialysis (FID)-IC

As found in the on-line dialysis-IC system, a mixture of 0.022 M NaHCO₃ and 0.028 M Na₂CO₃ (resulting from a stream of 0.044 M NaHCO₃ and 0.056 M Na₂CO₃ merging with equal flow rate of sample line becoming the donor of the dialysis unit) was satisfactory. This mixture was used as the donor stream (Fig. 3), although both sets of concentrations yielded the same sets of slopes of calibration graphs. Fig. 5 represents

chromatograms obtained by FID-IC together with those obtained by on-line dialysis-IC and those by conventional IC. Linear equations for calibration graphs of the anions are described in Table 3. FID-IC offers at least 10 times dilution which can be operated on-line with very good reproducibility (r^2 becoming unity). Analysis of the anions can be performed in a wider range of concentrations.

3.3. Separation of species which possibly causes damage to IC columns

Under optimum conditions for on-line dialysis-IC, with SDS (100 mg l⁻¹) chosen as a representative surfactant, only 0.8% dialysis was found; less than 0.5% dialysis of proteins was obtained from both the test species (fresh milk of 0.34% protein content and the albumin bovine (20 mg l⁻¹)). For the silica gel as test species for particu-

lates (sizes of $< 1 \mu\text{m}$), no signal different from the baseline was observed in the continuous turbidity monitoring.

It could also be concluded that under the conditions for the proposed FID–IC system, the anions of interest can be separated from the test surfactant, proteins and particulates which will not enter into the IC system. The life-time of IC columns which are usually expensive will be prolonged. This will be beneficial when analysing dirty samples such as natural water or waste water.

3.4. Analysis of real samples

Application of the proposed FID method was demonstrated by analysing natural water samples. Results (Table 4) obtained agree with those obtained by standard methods.

4. Conclusion

This work proposes flow injection dialysis for a simple on-line sample pretreatment for analysis of some anions (bromide, chloride, fluoride, nitrate, nitrite, phosphate and sulfate) by using ion chromatography (IC). FID offers simple on-line separation and on-line dilution of a sample for simultaneous analysis and determination. Under the proposed conditions, FID separates the anions of interest from the test proteins, surfactant and particulates leading preventing possible damage to the IC columns. The life-time of the column is then prolonged, especially when analysing dirty samples such as natural or waste water. Possible clogging effects on IC or on-line dialysis–IC procedures will be eliminated by applying FID. A wider range of concentrations can be obtained and with high reproducibility. Compared to on-line dialysis–IC, FID–IC needs a

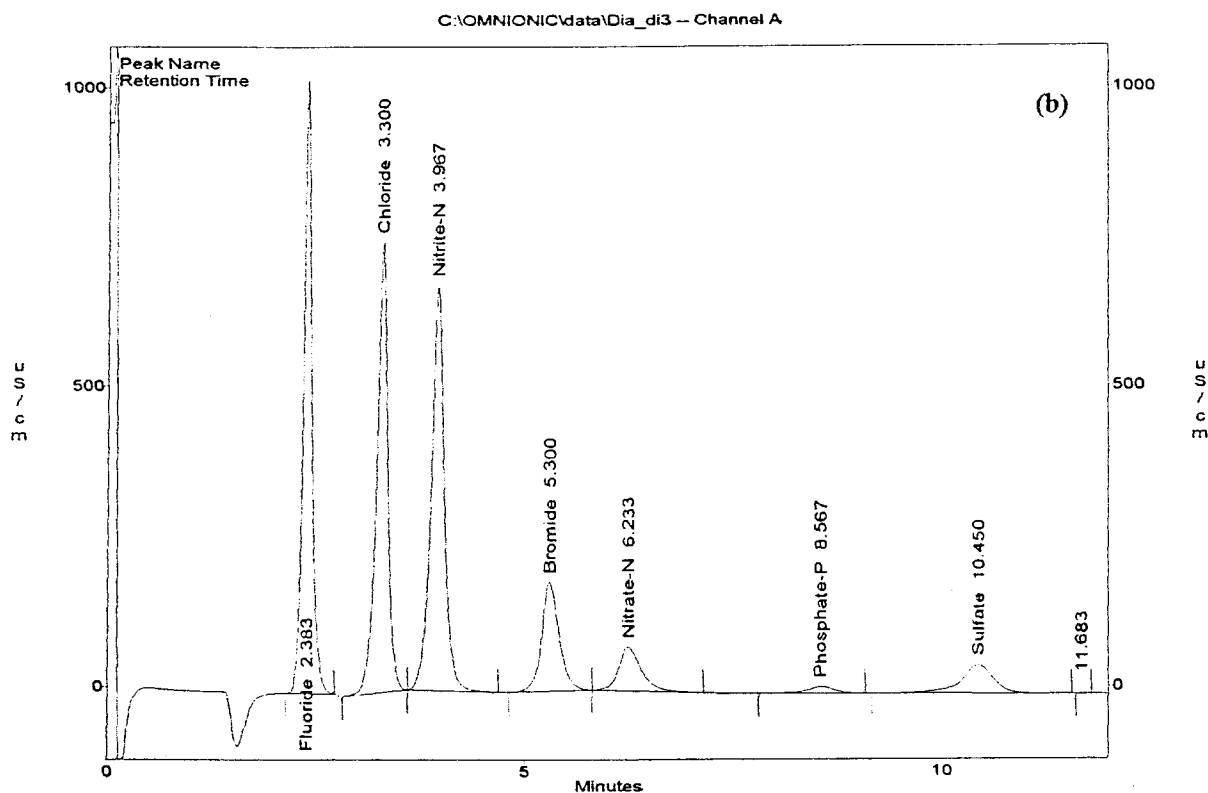


Fig. 5. (Continued)

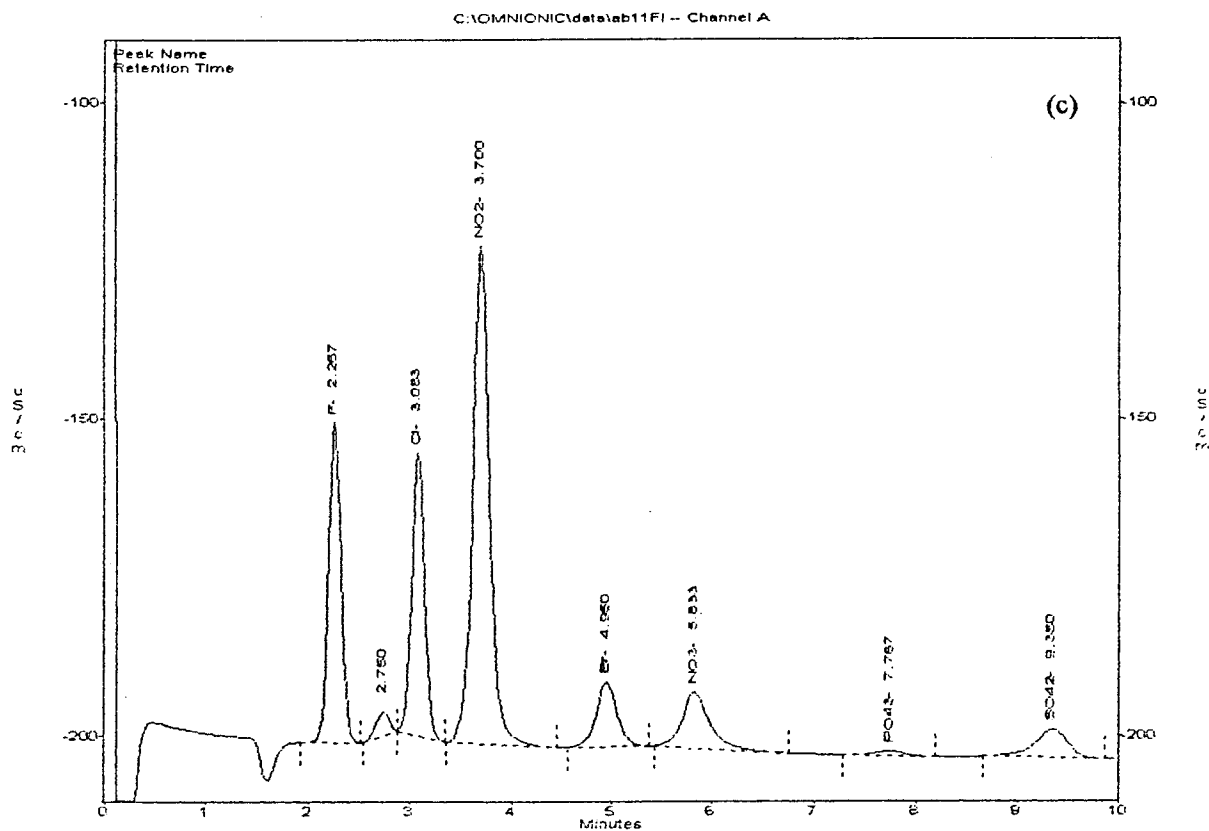


Fig. 5. (Continued)

Table 4
Analysis of natural water samples^a

Sample	Method	Concentration found (mg l ⁻¹) for						
		F ⁻	Cl ⁻	NO ₂ ⁻	Br ⁻	NO ₃ ⁻	PO ₄ ³⁻	SO ₄ ²⁻
1. Wanpen	FID-IC	12.0	15.3	ND	ND	0.4	ND	98
	REF	11.0	17.0	ND	-	ND	-	100
2. Saha	FID-IC	0.8	7.1	ND	ND	ND	ND	ND
	REF	0.8	7.6	ND	-	ND	-	ND
3. Maekeun	FID-IC	1.4	9.3	ND	ND	ND	ND	25.7
	REF	1.3	8.8	ND	-	0.1	-	20.5
4. Pipat	FID-IC	0.5	15.7	ND	ND	ND	ND	4.4
	REF	0.5	14.8	ND	-	0.1	-	3.0
5. MaeJam	FID-IC	1.9	7.3	0.7	ND	0.3	ND	944
	REF	-	-	-	-	-	-	1157
6. MaeLai	FID-IC	1.8	8.3	0.7	ND	0.4	ND	1005
	REF	-	-	-	-	-	-	1371

^a REF, reference methods [22]; ND, not detected; -, not determined.

much smaller sample volume (only μl order for FID–IC). The time for changing over from one sample to another in FID–IC is very short but would be more than 5 min for on-line dialysis–IC. For the former, total analysis time including separation and dilution is equal to the time for IC operation, but not for the latter which is much longer.

Investigations of FID–IC for the analysis of some cations and some other anions for samples with complicated matrices or high ionic strength such as waste water are now in progress.

Acknowledgements

The authors thank the National Research Council of Thailand (NRCT) and the Thailand Research Fund (TRF) for research grant support; Thai Unique, Bangkok, Thailand, for the loan of the ion chromatograph; and Dr R. Edwards and Professor G.D. Christian for useful discussions.

References

- [1] J. Ruzicka, E.H. Hansen, *Anal. Chim. Acta* 78 (1975) 145.
- [2] J. Ruzicka, E.H. Hansen, *Flow Injection Analysis*, 2nd edn, Wiley, New York, 1988.
- [3] G.D. Clark, D.A. Whitman, G.D. Christian, J. Ruzicka, *CRAC* 21 (1990) 357.
- [4] M. Valcarcel, M.D. Luque de Castro, *Flow Injection Analysis: Principles and Applications*, Ellis Horwood, Chichester, UK, 1981.
- [5] B. Karlberg, G.E. Pacey, *Flow Injection Analysis: A Practical Guide*, Elsevier, Amsterdam, 1989.
- [6] Z. Fang, *Flow Injection Separation and Preconcentration*, VCH, Weinheim, 1993.
- [7] H. Bergamin, B.F. Reis, A.O. Jacintho, E.A.G. Zagatto, *Anal. Chim. Acta* 117 (1980) 81.
- [8] P. Sooksamiti, H. Geckeis, K. Grudpan, *Analyst* 121 (1996) 1413.
- [9] H. Baadenhuijsen, H.E.H. Seuren-Jacobs, *Clin. Chem.* 25 (1979) 443.
- [10] K. Grudpan, C. Taylor, H. Sitter, C. Keller, *Fres. J. Anal. Chem.* 346 (1993) 882.
- [11] B. Karlberg, S. Thelander, *Anal. Chim. Acta* 98 (1978) 1.
- [12] E.H. Hansen, J. Ruzicka, *Anal. Chim. Acta* 87 (1976) 353.
- [13] C.F. Van Staden, *Anal. Lett.* 19 (1986) 1407.
- [14] P. Kuban, B. Karlberg, *Anal. Chem.* 69 (1997) 1169.
- [15] E.H. Hansen, J. Ruzicka, A.K. Ghose, *Anal. Chim. Acta* 100 (1978) 151.
- [16] K. Kina, K. Shirashi, N. Ishibashi, *Talanta* 25 (1978) 295.
- [17] S.W. Lewis, D. Price, P.J. Worsfold, *J. Bioluminesc. Chemiluminesc.* 8 (1993) 183.
- [18] K. Grudpan, D. Nacapricha, Y. Wattanakanjana, *Anal. Chim. Acta* 246 (1991) 325.
- [19] K. Grudpan, T. Thanasarn, *Anal. Proc.* 30 (1993) 10.
- [20] D.J. Halliwell, I.D. McKelvie, B.T. Hart, R.H. Dunhill, *Analyst* 121 (1996) 1089.
- [21] S. Karmarkar, Quik Chem Method 10-510-00-1-A, Determination of Inorganic Anions by Ion Chromatography, Lachat Instruments, 16 April 1997.
- [22] APHA, *Standard Methods for the Examination of Water and Wastewater*, 17th edn., American Public Health Association, Washington, DC, 1989.
- [23] S.J. Baum, W.R. Bowen, S.R. Poweter, *Laboratory Exercises in Organic and Biological Chemistry*, 2nd edn, Macmillan, New York, 1981, p. 176.
- [24] J.C. Miller, J.N. Miller, *Statistics for Analytical Chemistry*, Wiley, New York, 1984.

Book Review

***Multilingual Dictionary of Analytical Terms* by R.A. Chalmers, Blackwell, Oxford, 1994. ix + 275 pp. £42.50. ISBN 0-86542-859-X**

Earlier attempts to produce a multi-lingual dictionary of chemistry have not been particularly successful, and the reason lies in the need to understand completely the context before an individual word can be translated correctly. A big step forward was taken in the production of an EC sponsored multi-lingual dictionary of the North Sea oil industry, in which drawings were accompanied by short textual passages to give the correct meaning and the context in which words could be used.

This remarkable book, which deals only with the area of analytical chemistry, strives to achieve accuracy first by referring back to the two editions of the IUPAC 'Orange Book' a *Compendium of Analytical Nomenclature*, in which terms are defined, sometimes with additional commentary, so that context is always clear, and secondly, by giving a very full collection of terms—root words followed by phrases, such as *precision* followed by *precision of a weighing*. The reader will learn to think analytically in using this listing, because

internal standard is listed as such and not under *standard*. Further, *standard* itself is too general and is not listed, but instead we have collection of specific terms—standard deviation, standard solution, standard substance and so on.

The cross-referencing between the languages by way of a 2619×7 matrix of numbers seems at first a little unfriendly, but it does work, and anyway, could you think of a better way? Bed-time reading it is not, but a significant improvement over earlier attempts at a multilingual dictionary it most certainly is. Bob Chalmers, who has painstakingly assembled the endless pages of columns of words with corresponding columns of figures and managed not to get them all mixed up, must surely be congratulated on his work. The book is unique and will probably remain so—but buy your copy while it is available.

I. Marr
*Chemistry Department,
Aberdeen University,
Meston Walk,
Aberdeen,
AB24 3UE,
Scotland, UK*

Book Review

***Trends in Analytical Chemistry, Reference Edition, Volume 15, 1996.* Elsevier, Amsterdam, 1996, x + 677 + S190pp. ISSN 0167-2940.**

Once again I count myself lucky to be the recipient of a review copy of this volume. The reference editions are a mine of information about recent instrument developments, new techniques and applications. As usual the articles are written by experts in their fields who have been given the remit to make them easy to read, accessible and broad based. For subscribers to TrAC the reference edition comes ready bound at the end of the year as part of the annual fee, but it can be purchased separately (although this seems an unlikely scenario at US\$623.75!). This price represents a 12% increase on the previous year, but for this money you get an extra 338 pages; a good deal by any standards.

This volume contains the archival material from TrAC 1996 and is lifted directly from the journal. Now that the reference edition is getting so large it may be time to consider sorting the articles out into separate sections based on instrumentation, application area etc. I think that this

would be a useful idea for future issues. If this proved to be over complicated then I would suggest that putting all the 'trends', 'regional trends', 'internet column', 'computer corner' and 'quality assurance' articles together, would be a reasonable compromise.

The volume finishes with TrAC supplement number 3, which is the *Directory of Capillary Electrophoresis*. This 190 page section is a world-wide guide to leading scientists and manufacturers with an interest in CE. This supplement would make a useful place to begin a literature search on latest developments in CE instrumentation and in diverse application areas. In short, TrAC continues to deliver a high quality product which is a must for every analytical laboratory.

B.A. McGaw
*School of Applied Sciences,
The Robert Gordon University,
St. Andrews Street,
Aberdeen,
AB25 1HG,
Scotland, UK*

Book Review

***Current Practice of Liquid Chromatography–Mass Spectrometry* by W.M.A Niessen and R.D. Voyksner (editors), Elsevier, Amsterdam, 1998, ix + 438pp., US\$215.50. ISBN: 0-444-82938-5.**

The editors of this book have invited contributions from a number of distinguished LC-mass spectrometrists with interests in instrument development and in diverse applications. The book is a special issue of the *Journal of Chromatography A* (volume 794) and is divided into five sections, namely: pharmaceutical and biomedical applications of LC-products, electromigration techniques and, finally, fundamentals and instrumentation. All papers were subjected to peer review and the book has an author, but not a subject index.

As the editors state in the preface, 'LC-MS has a long history of promises and break-throughs', but this is timely contribution to the literature; coming at a time when LC-MS is, at last, fulfilling the expectations we had of the technique. The key to this has been the development of atmospheric pressure ionisation (APCI, ESI, SSI etc) and the interfacing of this to LC and to MS analysers. As a result of these developments LC-MS instru-

ments are robust, affordable and relatively easy to operate. The development of bench-top instruments has, in particular, signaled the beginning of a period of massive growth in application in biology, medicine and environmental science.

This book will be a great asset to the researcher and to those of us that teach about mass spectrometry. The editors have done a thorough job in the selection of papers, covering all aspects of LC-MS development and applications (including: LC-ICP/MS, LC-MS-MS, LC-ion trap-/reflectron TOF-MS and CE-MS). My final comments relate to the lack of a subject index (an oversight), to the price of this book (too high) and the quality of printing (at least four pages in the copy I have were smudged to the point where they are unreadable).

B.A. McGaw
*School of Applied Sciences,
The Robert Gordon University,
St. Andrews Street,
Aberdeen,
AB25 1HG,
Scotland, UK*

Book Review

An Introduction to Analytical Atomic Spectrometry
L. Ebdon, A. Fisher and S.J. Hill with E.H. Evans
(editor), Wiley, Chichester, 1998, x + 193 pp.,
£18.99. ISBN 0-471-97418-8 (paperback).

A well-presented, well-written, well-illustrated, concise, easy to understand, readable, textbook which encompasses both the older, e.g. flame atomic absorption spectrometry (FAAS) and electrothermal atomization, and the newer, e.g. plasma atomic emission spectrometry (PAES) and inductively coupled plasma mass spectrometry techniques. Chapter 1 presents a brief general overview of the basic analytical requirements of atomic spectrometry—here under instrumentation it would have been appropriate to have included the basics on monochromators and detectors rather than in the later chapter on PAES. Chapters 2–7 cover the theory, instrumentation, practice, sources of error and range of applications for all the currently used atomic emission and atomic absorption techniques.

There are several aids to self-study: heavy type is used to highlight keywords throughout the

text—this allows rapid assimilation of the important facts; short revision questions are used throughout individual chapters and, in an appendix, a further set of longer revision questions; in an appendix, an extensive, relevant bibliography which lists journals and general and specific texts which can be consulted for further information. A further appendix gives examples of laboratory practicals for all the major techniques. This appendix will represent best value for those who have or can get access to a well equipped laboratory.

This value-for-money text will be particularly relevant to students of analytical chemistry and others who wish to acquire knowledge of the techniques in this field through self-study.

R.R. Moody
School of Pharmacy,
The Robert Gordon University,
Schoolhill,
Aberdeen,
AB10 1FR,
Scotland, UK

Book Review

***Enzyme and Microbial Biosensors: Techniques and Protocols* by Ashok Mulchandani and Kim R. Rogers (editors) Humana Press, Totowa, NJ, 1998, xii + 264 pp., Us\$69.50, ISBN 0-896-03410-0.**
***Affinity Biosensors: Techniques and Protocols* by Ashok Mulchandani and Kim R. Rogers (editors), Humana Press, Totowa, NJ, 1998, xii = 249 pp., US\$69.50, ISBN 0-896-03539-5.**

As implied by the title, both these books are about techniques and protocols. The first chapter of each is an overview of sensor principles. The remaining chapters are all written in a prescribed format by practising scientists in the field. The first section is an introduction that describes the principles involved in the particular sensing approach that is described in that chapter and cites key references. The second section lists materials used in biosensor construction and evaluation and where they were obtained. Some of these sources are local to the authors and might not be the preferred source for scientists in other parts of the world. The third section is on methods. This includes reagent immobilization, sensor assembly and sensor calibration and evaluation. The information is presented in a manner so that the reader should be able to reproduce the procedure. The fourth section is entitled 'Notes' and includes a variety of comments on the experimental procedures. The content of this section varies from chapter to chapter. In some cases it contains very useful information about critical steps and possible failure modes. In other cases, it contains information about how the procedures may be extended to other analytes. The intent of the editors was to provide information that goes be-

yond what would be expected in the experimental section of a manuscript. In many cases, the Notes do this.

The chapter authors were chosen to provide complete coverage of the topic. In the case of enzyme and microbial sensors, this means several chapters on electrodes involving oxidase enzymes with different types of mediators as well as three chapters on potentiometric detection. In the case of affinity biosensors, this means chapters on immunosensors with a large number of different types of readouts from thermistors to various types of optical detection. The enzyme and microbial sensors can be used to sequentially analyze many samples or to monitor and change in concentration of analyte in a single solution. In contrast most of the affinity biosensors require regeneration after each measurement. Continuous affinity biosensors are included but are subject to serious kinetic limitations.

These books are appropriate for technicians who wish to make and apply a certain type of biosensor. They might be a convenience for researchers who wish to reproduce the work of others. However, these books do not provide comprehensive literature reviews or critical comparisons of different sensing approaches.

W.R. Seitz
Department of Chemistry,
University of New Hampshire,
Parsons Hall,
23 College Road,
Durham,
New Hampshire 03824-3598,
USA

Book Review

***Good Clinical Practice—standard operating procedures for clinical researchers* by J. Kolman, P. Meng and G. Scott (editors), Wiley, Chichester, 1998. xi + 177 pp., £29.95. ISBN 0-471-96936-2.**

The title of this text is rather misleading in that it gives the reader the impression that the material will be relevant to all fields of clinical research and the increasing range of healthcare professionals potentially involved in that research. On reading the first few pages of introduction, it however becomes obvious that the authors have focused on clinical trials, and have aimed for an audience of medical staff.

Standard operating procedures (SOPs) are defined as 'detailed, written instructions to achieve uniformity of the performance of a specific function'. While SOPs are widely used in drug industry sponsored clinical trials, this text aims to encourage their use in non-industry sponsored studies by producing a bank of SOPs. Clinical researchers are then encouraged to select and modify those for a particular study, thereby potentially increasing the quality of the study and data produced.

A brief introduction provides background material of clinical trial phases and trial design. Good clinical practice is covered in greater detail, describing the content of the chapters of the European Good Clinical Practice Guidelines, which can easily be confused with the structure of the present text. The remainder of the text is organised into 27 standard operating procedures, covering most aspects of clinical trials including: general study organisation, e.g. SOP 1 Study Organisation and Planning; pre-study, e.g. SOP 4 Local Management Requirements; during study, e.g. SOP 15 Obtaining Personal Written Informed Consent; end of study,

e.g. SOP 25 Trial Report. All SOPs are produced in a consistent format that outlines the background to each SOP, purpose of each SOP and procedure to be followed. In addition, many SOPs have detailed checklists. This presentation does, at first glance appear confusing and cumbersome, but generally provides the necessary detail. The majority of the SOPs are of high quality but some provide insufficient background information, e.g. estimation of patient numbers, SOP 7 relating to case report form review does not define a case report form. This is covered much later in SOP 19 dealing with case report form completion. In addition, no SOP covers development of the case report form.

SOP 5 deals with review and validation of the protocol. For those inexperienced in clinical trials, this may be one of the most important areas which could be more easily be presented in a series of SOPs covering the many sections contained within this SOP.

Following all 27 SOPs, there is a section summarising the FDA regulations concerning clinical trials. The relevance of this section is not entirely clear and indeed there is no mention of ABPI guidelines. While this text does encourage researchers to adopt the use of SOPs into their practice, thereby improving research, the general layout and the lack of detail provided relating to the development of the study protocol may reduce its general appeal.

D. Stewart,
School of Pharmacy,
The Robert Gordon University,
Schoolhill,
Aberdeen,
AB10 1FR,
Scotland, UK

Determination of methanol and ethanol by gas chromatography following air sampling onto florisil cartridges and their concentrations at urban sites in the three largest cities in Brazil

Pedro Afonso de Paula Pereira, Eliane Teixeira Sousa Santos,
Tatiana de Freitas Ferreira, Jailson B. de Andrade *

Instituto de Química, Universidade Federal da Bahia, Campus Universitário de Ondina, 40.170-290, Salvador, Bahia, Brazil

Received 23 February 1998; received in revised form 30 September 1998; accepted 5 October 1998

Abstract

A new sampling protocol was developed to determine methanol and ethanol in the gas phase, at low concentration levels, in urban atmospheres. The procedure involves collection of air samples (20.0–30.0 l) with three florisil cartridges connected in series, at a flow rate ranging from 1.0 to 2.0 l min⁻¹ and subsequent elution of the alcohols with water. Separation and quantification were done by gas chromatography (GC) coupled with a flame ionization detector, ‘SPI’ injector and column DB WAX (30 m × 0.53 mm × 1 μm). The minimum mass detected by the method, based on two times the average background mass on the blank cartridges, was 0.3 μg for both alcohols which, for a sampled volume of 30 l, resulted in detection limits of 7.6 and 5.3 ppbV for methanol and ethanol, respectively. The determined alcohol concentrations, in 42 different samples from the three largest cities in Brazil—São Paulo, Rio de Janeiro and Salvador—ranged from 72 ppbV to below the detection limit for methanol and from 355 to 12 ppbV for ethanol. © 1999 Elsevier Science B.V. All rights reserved.

Keywords: Atmospheric methanol; Atmospheric ethanol; Sampling

1. Introduction

In the last two decades, the use of oxygenated fuels, like methanol and ethanol, pure or mixed with gasoline, has been growing due to the benefits of improved air quality and also for

economic reasons. In Brazil, the number of light duty vehicles powered by pure hydrated ethanol is estimated at about 4 million [1–3], while the remaining vehicles actually utilize a mixture (22:78 v/v) of ethanol:gasoline. This results in an increase of alcohol emissions to the atmosphere in at least two ways: evaporation and as unburned fuel. Therefore, there is a need for the development of analytical procedures to determine these

* Corresponding author. Fax: +55-71-2375524.

E-mail address: jailsong@ufba.br (J.B. de Andrade)

compounds in the atmosphere, at low concentration levels, in order to permit an evaluation of possible impacts from their emissions on formation of chemical species in the atmosphere, such as ozone, aldehydes, carboxylic acids and other photochemical oxidants [4,5]. Unfortunately, there is very little information in the literature regarding analytical protocols for alcohol sampling at low concentration levels. Due to these low concentrations, the air volumes required to determine, in a quantitative way, the atmospheric levels of methanol and ethanol, are frequently in the range of several liters. Classical sample collection into glass impingers containing water is difficult and troublesome for handling during field campaigns, while the commonly used solid sorbents present very low breakthrough volumes for both compounds [6]. In fact, most of the analytical methods reported were developed for alcohol determination in vehicle exhaust [7–10] or alcoholic beverages [11–18]. In both cases the determinations involve high concentration levels.

The present work compares the use of water and three solid sorbents (silica, basic alumina and florasil) in terms of efficiency of collection for atmospheric methanol and ethanol, taking into account the breakthrough volumes for each. Florisil cartridges showed, among the collection media evaluated, the best mean results for methanol and ethanol sampling. Thus, this system was tested in real sites, by means of atmospheric determination of ethanol and methanol in urban places in Rio de Janeiro, São Paulo and Salvador. The first results of alcohol concentrations in these cities are reported here

2. Experimental

2.1. Material

The following were used: Tedlar and Teflon bags (80 l; BGI); Teflon chamber, transparent to sunlight, (3.5 m³); flowmeters; SEP-PAK (Millipore) solid sorbent cartridges: silica (80 µm × 690 mg × 30 mm × 9 mm i.d.), alumina (175 µm × 1850 mg × 27 mm × 9 mm i.d.) and florasil (125 µm × 900 mg × 24 mm × 9 mm i.d.); glass

impinger; Teflon and silicone tubes; ethanol, methanol and acetonitrile, analytical grade (Merck); water, distilled and further purified in an E-Pure (Altech) system; and 'zero' gases (nitrogen, air, helium).

2.2. Equipment

The following were used: gas chromatograph (Varian 3400), equipped with flame ionization detector and 'SPI' injector; DB WAX column (30

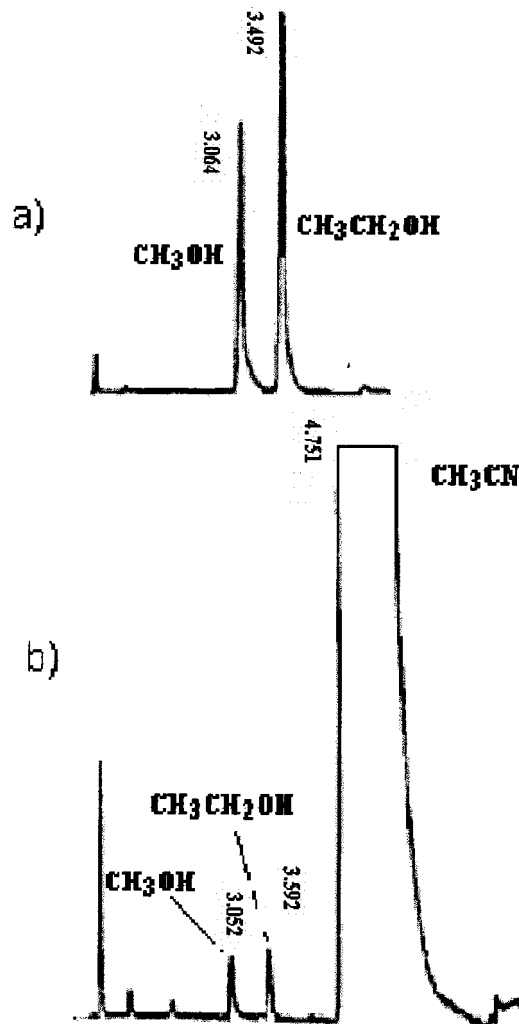


Fig. 1. Chromatograms for methanol and ethanol determinations from: (a) a standard dilution; and (b) a sample collected on florasil cartridge.

Table 1
Calibration curves for GC determination of methanol and ethanol [$H = aC + b$]^a

Alcohol	a (1 mg ⁻¹)	b	r^2
Methanol	2666	3.95	0.9992
Ethanol	1938	3.5	0.9998

^a a , slope (1 mg⁻¹); b , intercept; C , concentration (mg l⁻¹); H , peak height; r^2 = correlation coefficient.

m × 0.53 mm × 1 μm); Zero air supplier model 111 (Thermo Environmental); and vacuum pump.

Analysis were carried out according to the following conditions:

column oven: 45°C (1 min.) → 75°C (5°C min⁻¹) → 120°C (15°C min⁻¹) → 120°C (1 min)
injector: 150°C

FID detector: 200°C; sensib.: 10⁻¹² AFS;
atenn.: 2

carrier gas: helium (≈ 5 ml min⁻¹).

The GC analysis was completed in about 12 min. Typical chromatograms, for standard and sample, are shown in Fig. 1.

2.3. Procedure

Analytical curves for methanol and ethanol were done using external standards, ranging from 0 to 5.0 mg l⁻¹, prepared by dilution of a stock solution in purified water. Injections of 1.0 μl were made in the chromatographic system and the peak heights of methanol and ethanol determined. The analytical curves presented good linearity and correlation coefficients (r^2) in the order of 0.998, as shown in Table 1. The minimum mass detected by the method, based on two times the average background mass of alcohol on the blank cartridges, was 0.3 μg for both alcohols which, for a sampled volume of 30 l, resulted in detection

limits of 7.6 and 5.3 ppbV for methanol and ethanol, respectively.

All cartridges, prior sampling, were pre-conditioned by elution with water (5 ml) and acetonitrile (MeCN) (5 ml), followed by partial dryness passing helium or nitrogen throughout. Methanol (MeOH) and ethanol (EtOH) standard atmospheres were obtained by injection, with a microsyringe, into the bags, of known amounts (1 or 10 μl) of the respective alcohol using a 'zero' air flux as carrier gas (2.0–3.0 l min⁻¹), which, in turn, was used to fill the bag with specific air volumes (~ 70 l for small bags and 1000–2000 l for Teflon chamber). The exact concentration of methanol or ethanol, in each experiment, was determined taking into account the mass of alcohol put into the bag and the air volume used in dilution.

2.4. Breakthrough tests

For breakthrough tests, a known amount (6.8 μg) of MeOH or EtOH was collected on columns or impingers containing purified water, by means of a fixed volume (0.60 l) of standard atmosphere withdrawn from the Tedlar bag. Then, the columns or impingers were exposed to a 'zero' air flow, at 1 l min⁻¹, for variable periods, ranging from 0 to 75 min, one column or impinger for each time period. The air flow rate was controlled by a mass flowmeter, which was previously calibrated against a standard. After this time passing 'zero' air throughout, the column was eluted with 5 ml of water to a volumetric flask (10 ml) and the volume taken up. A 1.0-μl aliquot of this solution was injected and analyzed by GC. When using water as collection medium, an aliquot (1 μl) of the total volume (10 ml) was directly injected into the chromatograph immediately after each period passing 'zero' air. The scheme for alcohol sampling from the bag is shown in Fig. 2.

2.5. Samplings from bags, indoor, outdoor and urban atmospheric air

Samples were collected from Teflon bags (80 l) and Teflon chamber (3.5 m³), with concentrations ranging from 15 to 74 ppbV for methanol and

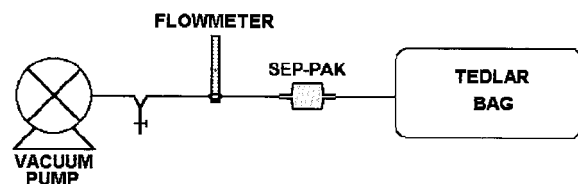


Fig. 2. Scheme for alcohol sampling from bag.

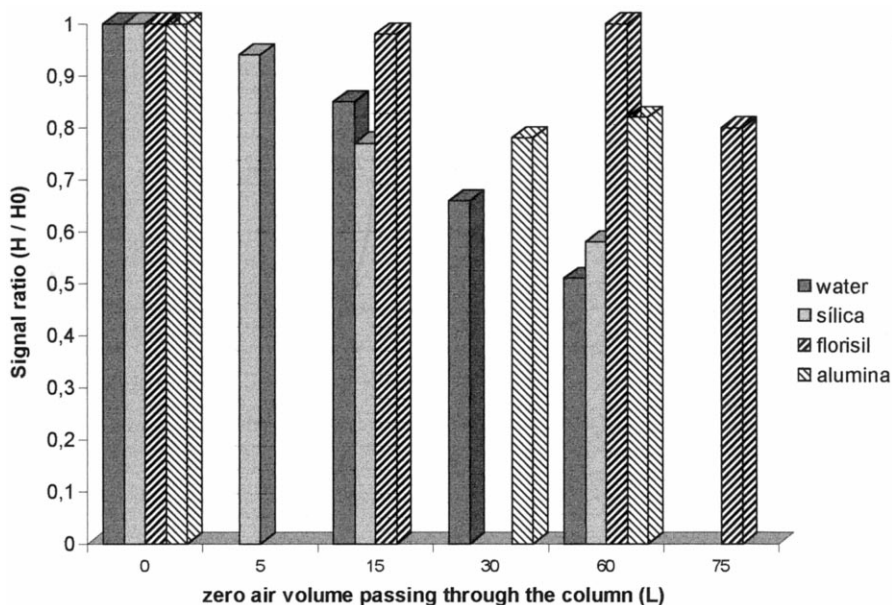


Fig. 3. Ethanol fraction still retained, as function of the sampling system and zero air volume through it.

from 10 to 51 ppbV for ethanol, from two sites inside the laboratory, outside the building of the Institute of Chemistry, and at urban sites in Salvador, Rio de Janeiro and São Paulo. The flow rates ranged from 1.0 to 2.0 l min⁻¹ and final volumes from 30.0 to 60.0 l for samples collected from bags, inside and outside the laboratory, while for urban atmospheric samples final volumes were 20.0 or 30.0 l. In all cases, three cartridges connected in series were used. The air flow rate was controlled in the same way as described above. The cartridges were then eluted with 3 ml of water to a volumetric flask. The volume of water used for elution was set at this time at 3 ml in order to exceed the hold-up volumes of cartridges (between 1.6 and 1.8 ml), and give a maximum sensitivity to detector responses. The efficiency of recovery for the compounds was checked by a second elution (3 ml) over 10% of each sample lot. A 1.0- μ l aliquot of the solution was injected and analyzed by GC. The interior of the laboratory and urban sites which were studied, are briefly described below.

2.5.1. Laboratory

The facilities of our research group, a set of three rooms with a total area of around 120 m², consist of an instrumental lab, a sample treatment lab and a third room for offices and computers.

2.5.2. Garibaldi Av. (Salvador)

This avenue, close to a car park of the university, has six traffic lanes (three in each direction) and near the sampling site is heavily occupied by commercial buildings and medical facilities. The sea is about 1 km away. Samples were collected \sim 1.0 m above the ground.

2.5.3. Muniz Barreto St. (Rio de Janeiro)

This is a secondary way that connects Praia de Botafogo and S. Clemente St. It has two traffic lanes in a single direction and near the sampling site has many residential and commercial buildings, as well as schools and clinical offices. The Botafogo beach—inside Guanabara's bay—is nearly 200 m away. Samples were collected \sim 1.0 m above the ground.

2.5.4. Rebouças Av. (São Paulo)

Located at Pinheiros, this avenue has six traffic lanes (three in each direction) and near the sampling site has residential, and commercial buildings and restaurants. The samples were taken from the 9th floor (≈ 30 m above ground level) of a residential flat.

3. Results and discussion

For a given compound, the breakthrough volume is defined as the volume of air or carrier gas, by unit mass of the sorbent, for which the compound retained into the sorbent cartridge begins to migrate away from it. This migration is a consequence of its partition equilibrium, between solid and gas phases, and is a function of sorbent and compound type, the compound concentration in the sample, the sampling temperature, the humidity of air, the air flow rate and flow velocity and the presence of other contaminants that can interfere with sampling. Volatile compounds, in general, have low breakthrough volumes [6,10].

The breakthrough tests with water, silica, basic alumina and florisil short columns were conducted in accordance with the experimental procedures previously described. The choice of the sorbents was based on their polarity, high activity grade and basic surface (basic alumina and florisil), which could enhance the interaction with alcohol molecules through the H atom in the OH group. The tests results are shown in Figs. 3 and 4, where a lack of data means that the experiment was not performed for that sampling media in that volume. For methanol (Fig. 4), neither of the three sorbents could retain its total mass for air volumes near to 15 l. At this volume, the relative mass of methanol that still remained in the florisil column (the sorbent showing the best results) was only 80% of the original. Silica and alumina presented lower performances than florisil. With 30 l of air passing through the column, mass still retained on these sorbents dropped drastically to a fraction equal to or below 20%. Water, on the other hand, still retained 52% of the original mass of methanol for an air volume of 60 l, while for florisil no methanol was detected at this volume. For ethanol (Fig. 3), florisil short columns showed

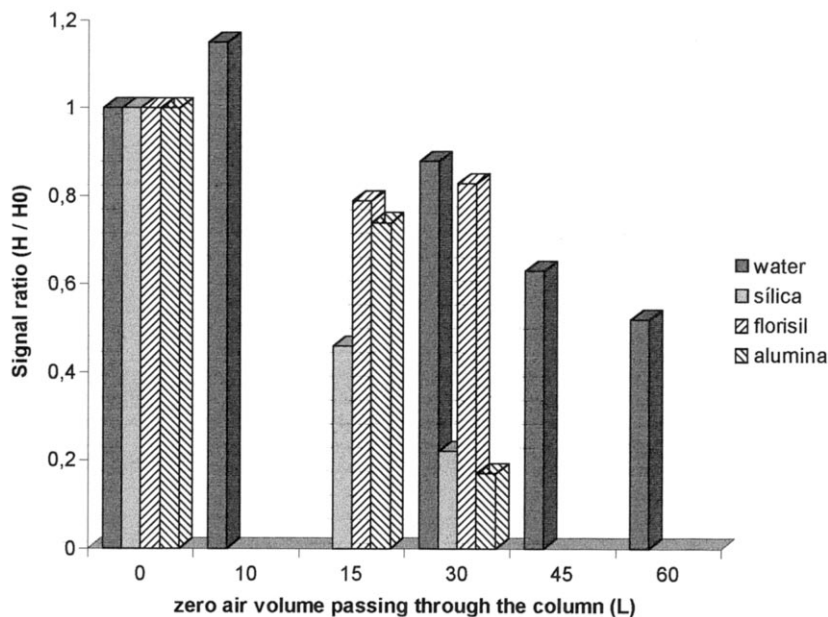


Fig. 4. Methanol fraction still retained, as function of the sampling system and zero air volume through it.

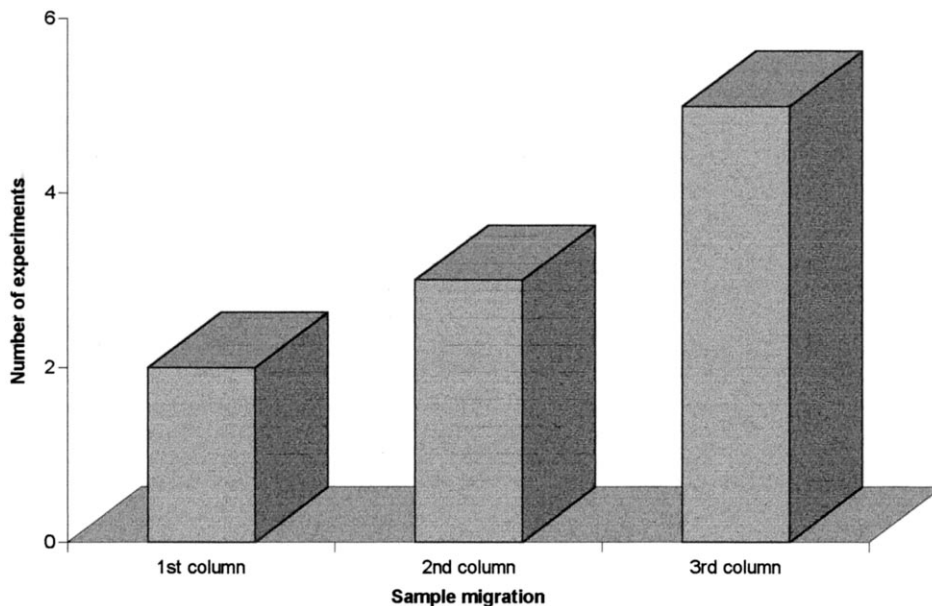


Fig. 5. Number of experiments as function of methanol migration through the columns (total experiments = 10).

the best results, being capable of retaining the totality of the alcohol for air volumes up to 60 l, and even 80% for 75 l. Florisil columns were then selected for the subsequent studies described below.

In order to evaluate the previously chosen sorbent, according to conditions closely related to real atmosphere samplings, the next test was to sample methanol or ethanol from larger air volumes (30–60 l) and concentrations near to the ones expected in the air, collected from Teflon bags (80 l) or Teflon chamber (3500 l), as described in Section 2. During these tests (ten), ethanol sampled was always observed in the first column or, at worst, in the second (one case), while for methanol, a significant number of experiments (five) showed migration up to the third column. These results are summarized in Figs. 5 and 6. Of the five experiments for which methanol migrated up to the third column, three were done with 60-l samplings at 1 l min^{-1} , one with 40 l at 1.4 l min^{-1} and the other with 30 l at 1.8 l min^{-1} . In this way, the breakthrough values for methanol in florisil cartridges seemed to be determined by the flow velocity, once higher air volumes correspond to lower flow rates and higher flow rates to

lower air volumes. Ethanol, on the other way, seems to be indifferent to the flow rate and flow velocity, at least at the range studied, which was chosen to give shorter sampling periods. In this way, to address a quantitative sampling for methanol, it was necessary to collect lower air volumes at lower flow rates, or to use more than three columns, although the last alternative would produce a high backpressure in the vacuum pump.

Finally, the florisil cartridges were used in real atmospheric samplings, as a mean to evaluate possible interference from other air contaminants, over retention of methanol and ethanol by the sorbent. Results for concentrations of methanol and ethanol, measured inside and outside the lab and at urban sites, are given in Table 2.

In all samples collected, the mass of methanol determined was predominantly at the third column, showing a strong migration. As consequence, results reported for this alcohol are only estimates of concentrations.

For ethanol, although migration had also occurred for 13% of the samples—probably due to competition for active sites with water and other organic compounds—the mass of this alcohol at

the third column, when present, was much lower than at first and second columns, showing a profile that makes it possible to predict that a fourth column should have ethanol at blank levels ($\approx 0.3 \mu\text{g}$). From the total of 53 samples, 52—or 98%—presented a quantitative retention for ethanol in the three cartridges, thus making florisil a good choice as a sorbent for its sampling in atmospheric air, especially if one takes it into account that common solid sorbents have very low breakthrough volumes for these compounds.

Breakthrough volumes at 20°C, reported for 11 sorbents used to collect organic compounds in atmospheric air [6,10,19] are in the range of 0.013–3.30 l g⁻¹ for ethanol and 0.006–0.950 l g⁻¹ for methanol. A unique exception was a carbon based sorbent, named Carbosieve SIII[®], with reported values of 7.50 and 55.0 l g⁻¹ at 20°C for methanol and ethanol, respectively [6]. Nevertheless, no information was available about water coadsorption interferences, a type of problem commonly associated with carbon based sorbents, as well as the efficiency of recovery of alcohols by elution with water. At present, our group have ordered this product and, as soon as we get it, these tests will be carried out.

4. Conclusions

Among the collection media evaluated, florisil showed, when sampling atmospheric methanol and ethanol, the best results besides presenting advantages including easy handling and field transportation. The breakthrough volumes presented, mainly for ethanol, are at least one order of magnitude higher than those for other common sorbents used for atmospheric air sampling. This is specially important if one considers the low atmospheric concentrations of methanol and ethanol.

The collection system chosen was then used for sampling indoor and outdoor sites at the Institute of Chemistry and urban sites in the three largest cities of Brazil: Rio de Janeiro, São Paulo and Salvador. At these urban sites, methanol and ethanol concentrations ranged, respectively, from 72 ppbV to below the detection limit, and from 355 to 12 ppbV. The largest mean concentration was detected for ethanol in Rio de Janeiro, namely 66.4 ppbV.

Samplings with florisil cartridges, followed by quantitation with GC-FID, were quantitative for ethanol in 52 of 53 collected samples. Meanwhile,

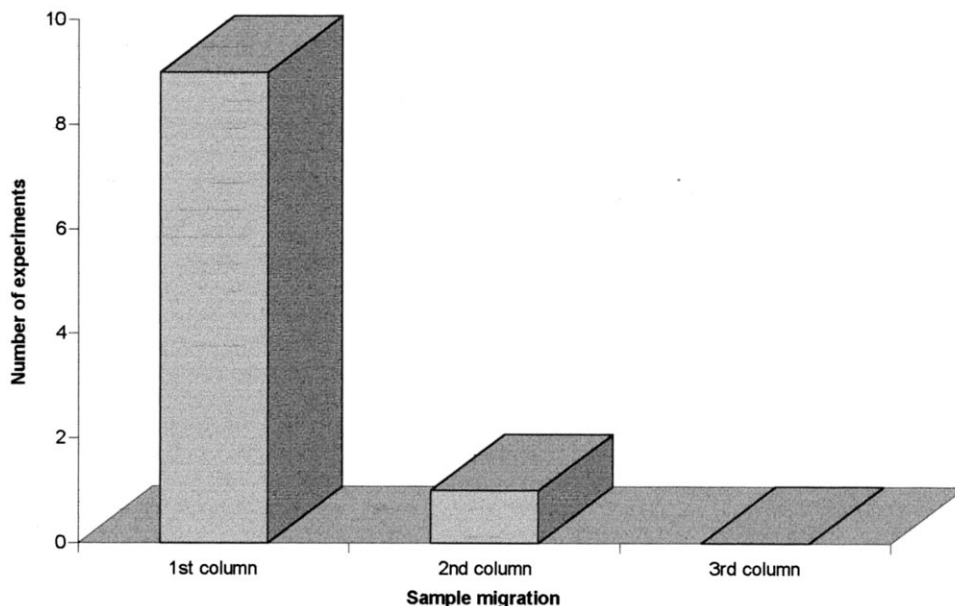


Fig. 6. Number of experiments as function of ethanol migration through the columns (total experiments = 10).

Table 2

Concentration of methanol and ethanol at the indoor, outdoor and urban sites

Locale	Number of collected samples	MeOH (ppbV)			EtOH (ppbV)		
		Maximum value	Minimum value	Mean value	Maximum value	Minimum value	Mean value
Inside the laboratory	06	99.2	8.9	41.3	768.6	10.6	271.2
Outside the laboratory	05	<7.6	<7.6	<7.6	35.5	<5.3	17.9
Garibaldi Av. (Salvador)	21	25.4	<7.6	9.8	354.6	21.3	65.4
Muniz Barreto St. (Rio)	12	25.4	<7.6	14.0	154.2	12.5	66.4
Rebouças Av. (SP)	09	72.5	<7.6	19.6	63.8	16.0	36.2

for methanol, the results are only an estimation of the real concentrations. For this alcohol, quantitative measurements should involve short volumes and lower flow rates to avoid its strong migration up to the third column.

Acknowledgements

The authors would like to thank Professor J.O.N. Reis for reviewing this paper as well as CAPES, CNPq and FINEP for financial support.

References

- [1] A.H. Miguel, *Environ. Sci. Technol.* 25 (4) (1991) 590.
- [2] A.H. Miguel, M.F. Andrade, J.B. de Andrade, Air pollution in large urban Brazilian centers, in: *Proceedings of the World Congress on Air Pollution in Developing Countries*, San Jose, Costa Rica, 21–26 October, 1996.
- [3] R.L. Tanner, A.H. Miguel, J.B. de Andrade, J.S. Gaffney, G.E. Streit, *Environ. Sci. Technol.* 22 (9) (1988) 1026.
- [4] S.M. Japar, T.J. Wallington, S.J. Rudy, T.Y. Chang, *Environ. Sci. Technol.* 25 (1991) 415.
- [5] D. Grosjean, *J. Braz. Chem. Soc.* 8 (4) (1997) 433.
- [6] Scientific Instrument Services, Selection and Use of Adsorbent Resins for Purge and Trap Thermal Desorption Applications, March, 1995 Application Note No 32.
- [7] F. Lipari, *J. Chromatogr.* 503 (1990) 51.
- [8] J.W. Butler, P.D. Maker, T.J. Korniski, L.P. Haack, F.E. McKelvy, A.D. Colvin, A System for On-Line Measurement of Multicomponent Emissions and Engine Operating Parameters, Society of Automotive Engineering, USA, 1985 Technical Paper Series No. 851657.
- [9] C.A. Gierczak, J.M. Andino, J.W. Butler, G.A. Heiser, G. Jesion, T.J. Korniski, FTIR: fundamentals and applications in the analysis of dilute vehicle exhaust, in: *Proceedings of the 1991 Society of Photo-Optical Instrumentation Engineers Symposium on Laser Spectroscopy*, 1991.
- [10] V.G. Berezkin, Y.S. Drugov, Gas Chromatography in Air Pollution Analysis. In: *Journal of Chromatography Library*, vol. 49, Elsevier, Germany, 1991, p. 46.
- [11] P.J. Worsfold, J. Ruzicka, E.H. Hansen, *Analyst* 106 (1981) 1309.
- [12] J. Mohns, W. Künnecke, *Anal. Chim. Acta* 305 (1995) 241.
- [13] F. Lázaro, M.D.L. de Castro, M. Valcárcel, *Anal. Chem.* 59 (1987) 1859.
- [14] M.J. Dennison, J.M. Hall, A.P.F. Turner, *Analyst* 121 (12) (1996) 1769.
- [15] W.R. LaCourse, D.C. Johnson, M.A. Rey, W. Slingsby, *Anal. Chem.* 63 (2) (1991) 134.
- [16] I.G. Casella, *Anal. Chim. Acta* 311 (1995) 37.
- [17] S.I. Montalvo, J.D. Ingle Jr., *Talanta* 40 (2) (1993) 167.
- [18] A. Pérez-Ponce, S. Garrigues, M. de la Guardia, *Analyst* 121 (7) (1996) 923.
- [19] A.R. Mastrogiacomio, E. Pierini, L. Sampaolo, *Chromatographia* 41 (9/10) (1995) 599.

Several modified piezoelectric quartz crystals for determination of omethoate

Fang Cheng, Wang Xianbao, Zhang Wuming, Zhou Xingyao *

Department of Chemistry, Wuhan University, Wuhan 430072, People's Republic of China

Received 26 January 1998; received in revised form 24 August 1998; accepted 18 November 1998

Abstract

Determination of omethoate by modified PQC (piezoelectric quartz crystal) sensor is described. Several modified films were studied and compared. Omethoate of 0.1–10 ppm can be determined directly and sensitively with PVC-dioctyl sebacate film modified PQC. The modified crystal has good reversibility and reproductivity. The lifetime is about 1 month. © 1999 Elsevier Science B.V. All rights reserved.

Keywords: PQC; PQC sensor; Organophosphorus compounds; Omethoate

1. Introduction

In the last few decades, much interest has been directed towards the analytical applications of the PQC (piezoelectric quartz crystal) sensor. King was the first who employed PQC in an analytical apparatus [1]. After Sauerbrey gave the relationship between the mass changes on the electrode surface of the piezoelectric crystal and the corresponding frequency shifts [2], much attention has been paid to the PQC sensor [3–5]. The utilization of the PQC as a sensor depended, almost entirely, on the advantage of high sensitivity in measuring very minute mass changes. The expanding application of the PQC sensor is also due to its simplicity and portability, its latent commercial benefits, and its ease of operation.

Organophosphorus compounds have become environmental pollutants because of their wide-ranging utilization as pesticides or insecticides. In addition, these compounds have also been developed for chemical warfare (CW). Therefore, the detection of organophosphorus compounds is of great practical importance and has received intensifying interest. A large number of papers have been published in this field [6–8]; the works of Guilbault and his co-workers are of great value [9–11].

Gas chromatography is a very suitable method for the detection of organophosphorus compounds [12], but it is difficult to make it portable. Despite the shortcoming in selectivity, PQC is an ideal method for in situ monitoring of the organophosphorus compounds. One way to increase the selectivity is to find a selective film coating on the surface of the electrode, which

* Corresponding author. Fax: +86-27-87882661.

E-mail address: xyzhou@whu.edu.cn (Z. Xingyao)

means to modify the PQC. In previous studies on selective films for detection of organophosphorus compounds, modified PQC has made considerable headway [13,14]. The modifying materials include not only transition metal complexes [15], organic compounds [16], but also enzymes and immunity agents [17]. Some authors [13] have pointed out that long-chain oxime complex could selectively respond to the organophosphorus compounds. This complex is a kind of imitated enzyme. Instruments have been built to carry out microgravimetric immunoassays, using microbial assays and gas phase immunosensor [18]. When used for the specific detection of the organophosphorus compounds, excellent results have been achieved [19].

Sometimes, however, the sensitivity is more important than the selectivity, either because the task is to determine the concentration of a known agent in the absence of interfering substance, or because the main interference could be discounted or avoided. Under these conditions, attention may be focused on how to improve the sensitivity.

In this paper, several common materials were selected to modify the PQC electrode for the sensitive detection of organophosphorus compounds. These materials were selected for the following reasons: (1) they were usually employed as absorbents or surface active agents; (2) if practical application is possible, the modified reagent must be economical and easily-preserved. In order to form the film, PVC (polyvinyl chloride) was used as film carrier due to its excellent film forming characteristics. Omethoate was utilized as a model compound in our investigation for a sensitive, reversible and reproducible PQC sensor for

organophosphorus compounds. There are two reasons to choose omethoate as a representative of organophosphorus compounds. First, omethoate is a type of insecticide that is applied commonly and extensively. Second, we purpose to detect organophosphorus compounds in gas phase; omethoate is volatile enough to obtain very minute concentration vapor without heating.

2. Experimental

2.1. Apparatus

A home-made TTL oscillator was employed. The piezoelectric crystals are 10 MHz AT-Cut quartz crystals with silver electrodes plated on both sides. The crystal diameter is about 1.0 cm and each silver electrode diameter is about 0.4 cm. All crystals were purchased from Wuhan Radio Component Factory (P. R. China). The frequency output from oscillator was recorded with a frequency counter (made in Taiwan, GFC-8010G).

The experiment set-up for the evaluation of PQC sensor is shown schematically in Fig. 1. Argon is selected as the carrier gas to avoid the interference of water vapor in air and other substances. A desiccator is used, which contains P_2O_5 as drying agent to absorb the water vapor in argon.

Omethoate was dissolved in acetone. A microsyringe was used to inject the acetone sample containing the omethoate insecticide into detector cell. We selected acetone as solvent not only because acetone changes into vapor readily, but also

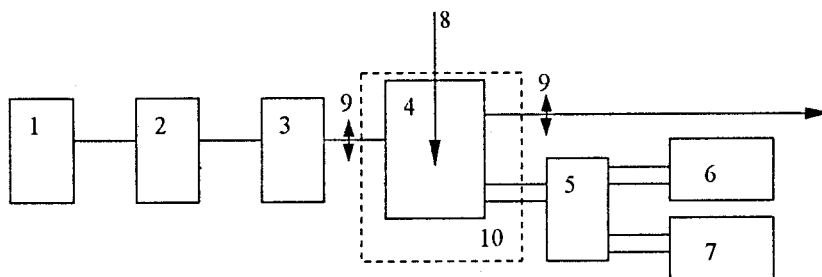


Fig. 1. Experimental apparatus: (1) argon pump; (2) desiccator (containing P_2O_5); (3) buffering bottle; (4) detector cell (100 ml); (5) oscillator; (6) frequency counter; (7) power supply; (8) microsyringe; (9) switch; (10) thermostat.

because acetone interference can be removed easily.

2.2. Reagents

o-Dimethyl benzene, dioctyl phthalate, dibutyl phthalate, dioctyl sebacate, butyl acetate, *o*-nitrotoluene, 4-methylpentanone, palmityl trimethyl ammonium bromide and omethoate (Hubei Provincial Agriculture Institution) were all analytical grade. They were used without further purification. All solvents used for preparation of coating solutions were of analytical reagent grade.

2.3. Crystal modification

PVC (0.10 g) was dissolved with cyclohexanone firstly, then diluted with acetone to 0.50% (m/v). Omethoate of 2.0% (v/v) was prepared with acetone and preserved at $\sim 0^{\circ}\text{C}$. All coating materials of 0.50% (m/v or v/v) were dissolved with acetone. The coating solutions were achieved when 1.0 μl acetone containing 0.50% coating material was added into 1.0 ml PVC solution. The modified crystals were prepared by dropping 1.0 or 2.0 μl coating solution onto the central of each electrode with a microsyringe separately. Then the crystals were placed in an oven at $60\text{--}80^{\circ}\text{C}$ for 3 h or in a desiccator overnight. After acetone was evaporated, a thin film was left on the crystal surface. The thickness of the modified film can be detected through the frequency shift.

2.4. Procedures

The measurement was conducted in argon. The volume of detection cell was 100 ml. Hence, when 5.0 μl acetone sample (2.0%) was injected into the cell and vaporized, 1.0 ppm omethoate vapor was obtained. After each measurement, pure argon was pumped in to purge the organophosphorus compounds and refresh the cell. At the same time, the crystal was regenerated, as verified from the digital changes in the frequency counter. Interferences were evaluated

using the same method. The temperature was maintained at $10 \pm 0.5^{\circ}\text{C}$.

3. Results and discussion

3.1. Calibration curves

Calibration curves corresponding to the different modified crystals are shown in Figs. 2 and 3. The calibration graphs are similar to those published previously [13]. In our study, a saturation effect was not observed as the crystal stopping oscillation. From these studies, PVC-dioctyl sebacate film was chosen as a model modified film.

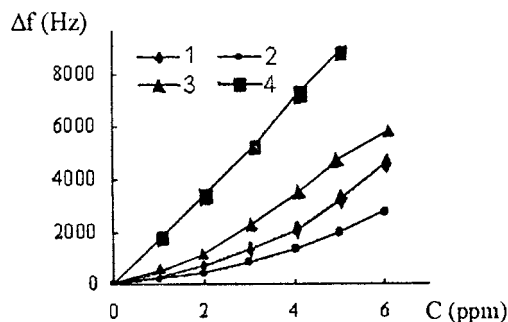


Fig. 2. Calibration curves for different modified films with omethoate. The modifying material is as follows: (1) *o*-dimethyl benzene; (2) dioctyl phthalate; (3) dibutyl phthalate; (4) dioctyl sebacate. All modified crystals were fresh.

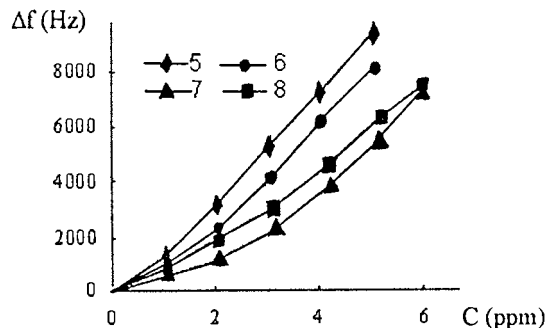


Fig. 3. Calibration curves for different modified films with omethoate. The modifying material is as follows: (1) *o*-dimethyl benzene; (2) dioctyl phthalate; (3) dibutyl phthalate; (4) dioctyl sebacate; (5) butyl acetate; (6) *o*-nitrotoluene; (7) 4-methylpentanone; (8) palmityl trimethyl ammonium bromide. All modified crystals were fresh.

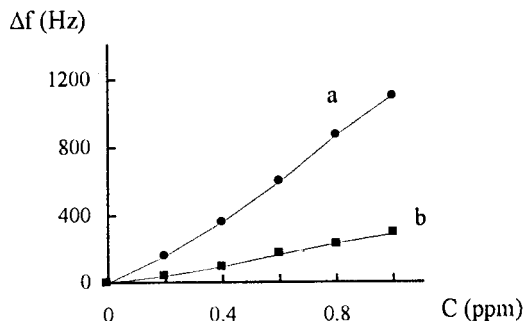


Fig. 4. Effect of the thickness of the PVC-dioctyl sebacate modified film. The coating solutions were: 2.0 μl (a) ($\Delta f = 11\,216$ Hz during modifying) or 1.0 μl (b) ($\Delta f = 6016$ Hz during modifying). The response is to omethoate. All modified crystals were fresh.

The exact mechanism of the interaction between vapor and film is complicated and not known exactly. From the sorption isotherm, a linear relationship can be obtained between the logarithm of concentration and the frequency shift. Furthermore, saturation phenomenon seems not to appear. Hence, the sorption belongs more to the Freundlich type than to the Langmuir type or Brunauer-Emmett-Teller (BET) type, which means that the sorption is not monolayer but multilayer. However, if the mass on the surface of the electrode is too large, whether this results from the sorption or the film itself, the crystal will cease to oscillate. Due to the interference of acetone, a concentration of 0–6 ppm of omethoate was determined in order to remove the frequency shift resulting from acetone readily.

3.2. Modified film

The film thickness is important for a good measurement. A thicker film can increase the sen-

sitivity as shown in Fig. 4. However, the crystal fails to oscillate if the modified film is too thick. For example, crystal no. 4 (#) (PVC-dioctyl sebacate film), 5 (#) (PVC-butyl acetate film), and 6 (#) (PVC-nitrotoluene film) stop oscillating after the sixth injection of the sample (about 6.0 ppm) due to the large frequency shifts of about 40 000 Hz during the modification, which can be seen from Table 1.

3.3. Response curve

The frequency varied with time after each injection. It takes some time for the frequency to stabilize, which can be seen in Figs. 5 and 6. The time required for stabilizing is determined by the following: (1) the speed that the sample changed into vapor, as determined by the volatility and the sample volume; (2) the interaction between the vapor and the film, which can be influenced not only by the sorption mechanism but also by the thickness of the modified

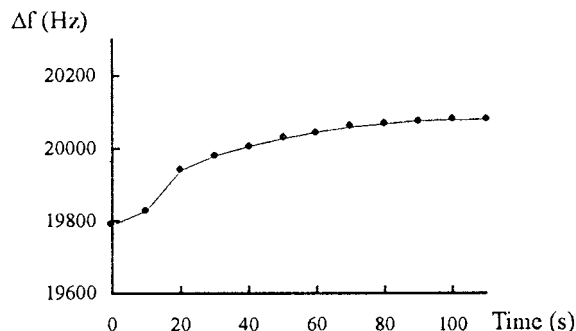


Fig. 5. PVC-dioctyl sebacate modified film responses to 0.20 ppm omethoate. The coating solution is 1.0 μl . The modified crystal was fresh.

Table 1
The frequency reading during the modifying (Hz)^a

No. of crystal (#)	1	2	3	4	5	6	7	8
Before modifying	2462	3155	3030	1766	1231	3300	1453	3505
After modifying	19 237	15 005	35 135	43 985	39 466	46 362	26 966	39 340
Δf	16 775	11 850	32 105	42 219	38 235	43 062	25 513	35 835

^a No. of the crystal is as the same as in Figs. 2 and 3.

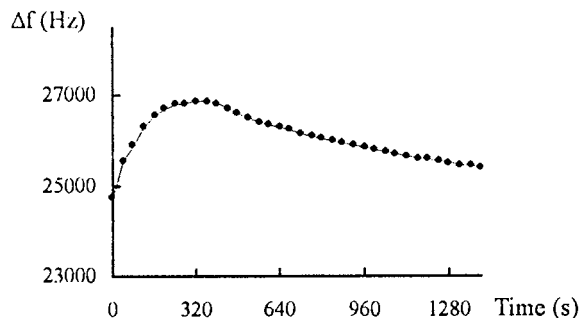


Fig. 6. PVC-dioctyl sebacate modified film responses to 5.0 ppm omethoate. The coating solution is 2.0 μl . The modified crystal was fresh.

film. So, the more readily the sample vaporizes, the faster the crystal arrives at a balance. For instance, it took only 5–10 s for an unchanging frequency to be achieved after 1.0 μl ether was injected into the detector cell, much less time than acetone which took 1–2 min. In addition, the greater the sample volume and the thicker the film, the longer time it took before a steady frequency reading could be obtained. Moreover, the sorption process can be different (Figs. 5 and 6).

In Fig. 6, a peak is observed. The possible reason is that vaporization causes a non-uniform distribution because the crystal was located too close to the injection position. The peak disappeared when the injection location was changed to a more distant point from the crystal or there was an agitator during the determination.

Sometimes, the frequency reading kept changing for a long time, as shown in Fig. 6. When this occurred, it was difficult to obtain a constant reading. In our experiment, if the changing reading is below 0.5% (frequency drift to frequency shift) per min, we think the sorption on the crystal has arrived at balance. That is to say, the standard deviations for frequency shift is below 0.5%.

3.4. Interference

Several organic vapors were expected as interferences in our study. These are summarized in Table 2. From the Table 2, a little interference was observed for all three kinds of materials, ether, acetone and ethyl alcohol (about 99%) for concentrations up to 100 times as that of omethoate. However, the water vapor disturbs the sample detection critically; hence each experiment was done in argon. In addition, Neither CO_2 nor N_2 has any interference.

Although ether has less interference and faster response, it is too volatile, which easily leads to changes of the sample concentration. Furthermore, the purchased omethoate sample is acetone solution. Therefore, we selected acetone as the solvent.

3.5. Measurement

The determination was carried out using PVC-dioctyl sebacate film as a model film. Fig. 7 shows the calibration curve. Each point is the

Table 2
Responses of the PVC-dioctyl sebacate modified film to acetone, ethyl alcohol and ether^{a,b}

No. of crystal	1	2	3	4	5	6	7	8
Acetone (500 ppm)	182	149	482	726	424	470	229	595
Ethyl alcohol (500 ppm)	805	289	562	157	531	115	113	159
Ether (500 ppm)	42	31	26	25	72	56	43	78

^a No. of the crystal is as the same as in Figs. 2 and 3.

^b The modified crystal was fresh.

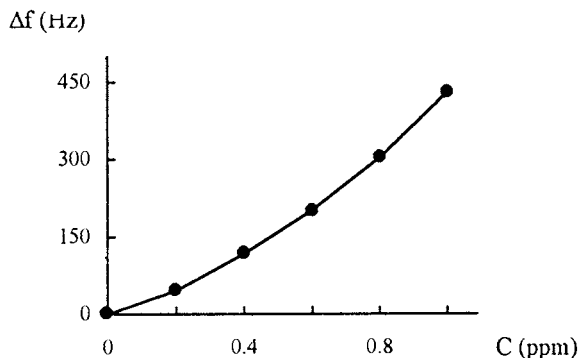


Fig. 7. Calibration curve of PVC-dioctyl sebacate modified crystal to methoate. The modified crystal was preserved for half a month with 2.0 μl coating solution.

mean value of two measurements obtained by deducting the interference of acetone of the same concentration. The determination employs the 'addition and recovery method'. The background in the detector cell is air (after desiccating). When the omethoate sample was added into the detector cell, a responding reading was obtained, which could be converted into concentration from the calibration curve. The determined concentration is compared with the added concentration. The results are shown in Table 3.

3.6. Lifetime

Satisfactory reversibility, reproductivity and lifetime are obtained, as seen in Tables 4, 5 and Fig. 8. A longer lifetime can be achieved if the crystal is washed with argon immediately after each detection and preserved in a desiccator. During washing the crystal regenerates, which can be monitored from the frequency shift. The

Table 3
The determination data of the addition and recovery method^a

Addition (ppm)	Δf (Hz)	Δf (removing acetone) (Hz)	Detection (ppm)	Recovery (%)
0.300	111	81	0.294	98.0
0.500	225	165	0.508	102

^a The modified crystal was preserved for half a month with 2.0 μl coating solution.

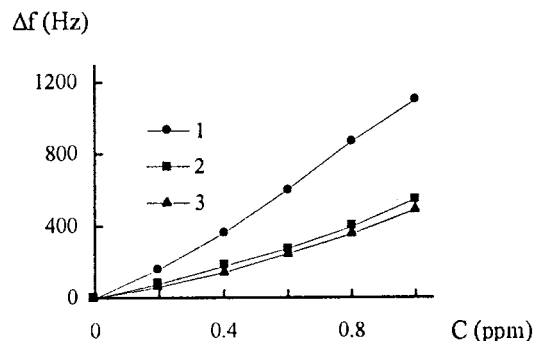


Fig. 8. The lifetime of the PVC-dioctyl sebacate modified crystal. (1) fresh; (2) after 3 days; (3) after half a month.

Table 4
The repeating experiment data of the PVC-dioctyl sebacate modified crystal in the determination of omethoate^a

Concentration (ppm)	0.2	0.4	0.6	0.8	1.0
Δf_1 (Hz)	63	142	250	362	501
Δf_2 (Hz)	63	148	249	370	511

^a The modified crystal has been preserved for half a month with 2.0 μl coating solution.

Table 5
The repeating experiment data of the PVC-dioctyl sebacate modified crystal in the determination of acetone^a

Concentration (ppm)	10	20	30	40	50
Δf_1 (Hz)	12	29	49	70	90
Δf_2 (Hz)	11	29	49	68	88

^a The modified crystal has been preserved for half a month with 2.0 μl coating solution.

sorption is reversible. The modified crystal has an excellent reproductivity for omethoate and acetone (Tables 4, 5 and Fig. 8). The crystal lifetime is about 1 month. However, the sensitivity decreases during preservation as indicated in Fig. 8. The dropping of the sensitivity was notable in the first few days. The crystal can be re-used after immersion in acetone overnight.

Acknowledgements

This work was supported by the Foundation of Chinese-France Cooperation Program on the Advance Research.

References

- [1] W.H. King Jr, *Res. Dev. Port* 1 20 (4) (1969) 28.
- [2] G.Z. Sauerbrey, *Z. Phys.* 155 (1959) 206.
- [3] J. Janata, A. Bezegh, *Anal. Chem.* 60 (1988) 64R.
- [4] H.T. James, L.G. Robin, *Anal. Chem.* 67 (1995) 3372.
- [5] B.L. Wu, H.W. Lei, C.S. Cha, *J. Electroanal. Chem.* 374 (1994) 97.
- [6] Y. Wang, Y. Sun, J. Huang et. al., *Wuhan University J. Nat. Sci.*, in press.
- [7] J. Ngeh-Ngwainbi, A.A. Suleiman, G.G. Guilbault, *Biosens. Bioelectron.* 5 (1990) 13.
- [8] L.V. Rajakovic, S. Strbac, *Anal. Chim. Acta* 315 (1995) 83.
- [9] Y. Tomita, G.G. Guilbault, *Anal. Chem.* 52 (1980) 1484.
- [10] G.G. Guilbault, J. Affolter, Y. Tomita, *Anal. Chem.* 53 (1981) 2057.
- [11] G.G. Guilbault, J. Kristoff, *Anal. Chem.* 57 (1985) 1754.
- [12] M. Agruilar, A. Farran, C. Serra, et al., *J. Chromatogr.* 778 (1997) 201.
- [13] Q. Dai, Q. Huang, Y. Deng, et al., *Chem. Sensor (in Chinese)* 16 (1996) 107.
- [14] J.M. John, *Analyst* 114 (1989) 1173.
- [15] J. Janata, M. Josowicz, D.M. Devancy, *Anal. Chem.* 66 (1994) 207R.
- [16] S. Milanko, S.A. Milinkovic, *Anal. Chim. Acta* 269 (1992) 289.
- [17] W. Wei, R.H. Wang, L.H. Lie, S.Z. Yao, *Instrum. Sci. Techol.* 25 (1997) 157.
- [18] M. Minunni, M. Mascini, G.G. Guilbault, B. Hock, *Anal. Lett.* 28 (5) (1995) 749.
- [19] A. Suleiman, G.G. Guilbault, *Anal. Lett.* 24 (1991) 1283.

Determination of the partition coefficient of triflupromazine between phosphatidylcholine vesicles and water by ^{19}F nuclear magnetic resonance spin-lattice relaxation time measurement

Keisuke Kitamura ^{a,*}, Masayoshi Yamamoto ^a, Shigehiko Takegami ^a,
Makiko Sugiura ^b

^a *Kyoto Pharmaceutical University, 5 Nakauchicho, Misasagi, Yamashina-ku, Kyoto 607-8414, Japan*

^b *Kobe Pharmaceutical University, 4-19-1 Motoyamakitamachi, Higashinada-ku, Kobe 658-8558, Japan*

Received 3 August 1998; received in revised form 20 November 1998; accepted 20 November 1998

Abstract

The ^{19}F nuclear magnetic resonance (NMR) spin-lattice relaxation time (T_1) of the trifluoromethyl signal of triflupromazine (TFZ) was measured in aqueous suspensions of phosphatidylcholine (lecithin) small unilamellar vesicles (SUV). The observed T_1 value depended on the concentration of SUV. Based on a simple two-site rapid exchange model, the partition coefficient (K_p) of TFZ between lecithin SUV and water was calculated from the relationship between the T_1 value and the lecithin concentration by using a nonlinear least-squares method. The obtained K_p value ($2.1 \pm 0.2 \times 10^5$) agreed well with that measured by a second-derivative spectrophotometric method. The ^{19}F NMR T_1 method will be useful for the determination of partition coefficients of drugs having fluorine atom(s), especially for the drugs which do not have absorption in the ultraviolet or visible region, or for those having absorption but do not show any changes according to their incorporation into the lecithin bilayers. The method does not require any separation procedure that may disturb the equilibrium conditions. © 1999 Elsevier Science B.V. All rights reserved.

Keywords: Partition coefficient; Triflupromazine; Spin-lattice relaxation time; ^{19}F nuclear magnetic resonance

1. Introduction

Partition coefficients of drugs between phospholipid bilayer vesicles and water have been

studied to investigate the drug interactions with biomembranes. Also, partition coefficients are important in the quantitative structure–activity relationships of drugs.

There are several kinds of important drugs containing fluorine atom(s) and, for these drugs, ^{19}F nuclear magnetic resonance (NMR) spec-

* Corresponding author. Fax: +81-075-595-4760.

E-mail address: kitamura@mb.kyoto-phu.ac.jp (K. Kitamura)

trometry is useful to obtain the information on their interactions with biological substances [1,2]. In this paper, we attempt to determine the partition coefficient of triflupromazine (TFZ) between phosphatidylcholine (lecithin) small unilamellar vesicles (SUV) and water by measuring the ^{19}F NMR spin-lattice relaxation time (T_1) of the trifluoromethyl signal of TFZ. As ^{19}F nuclei have a large magnetogyric ratio and 100% natural abundance, and are not contained in natural biological substances, it is comparably easy to measure the ^{19}F NMR T_1 values of drugs even in low concentrations (below millimolar) without interference by the background signals. The TFZ concentration employed in this study is 0.1 mM, which is sufficiently below the solubility of TFZ at the physiological pH of 7.4 [3]. The obtained value of the partition coefficient is confirmed by second-derivative spectrophotometric determination [4].

2. Theory

The molar partition coefficient (K_p) of TFZ between lecithin SUV and water is defined as [5]

$$K_p = \frac{(\text{mol of TFZ in lipid})/(\text{mol of lipid})}{(\text{mol of TFZ in water})/(\text{mol of water})}$$

This is equivalent to

$$K_p = \frac{D_p/[L]}{D_f/[W]} \quad (1)$$

where D_p and D_f represent moles of TFZ in the lecithin bilayer and water, respectively, and $[L]$ and $[W]$ are molar concentrations of lecithin and water, respectively. The motion of TFZ incorporated in the lecithin bilayer is restricted as compared with that of free TFZ in the water phase [6], so that the T_1 value of the trifluoromethyl signal of the partitioned TFZ will be different from that of the free TFZ. Then we express the T_1 value of the trifluoromethyl signal of TFZ in the water phase as T_{1f} and that in the lipid phase as T_{1p} . If the exchange rate of TFZ between water and lipid phases is fast enough at the time scale of ^{19}F NMR, the observed relaxation rate of the trifluoromethyl signal can be expressed as

$$\frac{1}{T_{1o}} = \frac{D_p}{D_f + D_p} \cdot \frac{1}{T_{1p}} + \frac{D_f}{D_f + D_p} \cdot \frac{1}{T_{1f}} \quad (2)$$

where T_{1o} denotes the observed T_1 value.

From Eqs. (1) and (2), K_p can be expressed as

$$K_p = \frac{T_{1o}T_{1p} - T_{1f}T_{1p}}{T_{1f}T_{1p} - T_{1o}T_{1f}} \cdot \frac{[W]}{[L]} \quad (3)$$

Finally, from Eq. (3), we get

$$T_{1o} = \frac{T_{1f}T_{1p}([L]K_p + [W])}{T_{1f}([L]K_p + T_{1p}[W])} \quad (4)$$

The values of K_p , T_{1p} and T_{1f} can be calculated from the experimental values of $[L]$, and T_{1o} by applying a nonlinear least-squares method (accompanying a Taylor expansion) [7] to Eq. (4).

3. Experimental

3.1. Chemicals, materials and apparatus

Triflupromazine hydrochloride was purchased from Sigma. The buffer used was 50 mM NaCl–10 mM 4-(2-hydroxyethyl)-1-piperazine-ethanesulfonic acid aqueous solution containing 10% deuterium oxide (HEPES buffer, pH 7.4). Egg-yolk lecithin purchased from Sigma was purified by column chromatography on alumina and silic acid, and the purity was monitored by thin-layer chromatography until it gave a single spot. The purified lecithin was stored as a 5% (w/v) chloroform stock solution at -30°C . Sonication for preparation of lecithin SUV was performed by an ultrasonicator (Kaijo-Denki TA-4280, maximum power 200 W). Size distribution of SUV was measured by a submicron particle size analyzer (Nicomp Model 370) with a 5-mW He–Ne laser light source. ^{19}F NMR experiments were performed at 470.36 MHz by using a Varian VXR-500 spectrometer locked onto the D_2O signal. The absorption spectra were measured by using a double-beam spectrophotometer (HITACHI U-3210). The spectrophotometer was connected to a personal computer (NEC PC-9801) through an RS-232C interface and the spectral data were stored in the PC.

3.2. Lecithin SUV preparation

An appropriate volume of the lecithin stock solution was evaporated and the residue was dried under vacuum for more than 4 h. The dried residue was suspended in the buffer using a vortex mixer. The suspension was then sonicated by the ultrasonicator operated at power level 3.5 (maximum level, 10) to produce SUV. Three minutes of sonication with a 3 min interval was repeated 10 times under a nitrogen stream in an ice-water bath. The sonicated suspension was centrifuged for 20 min at $2000 \times g$ (3500 rpm) to eliminate sediment from the sonication tip. The concentration of lecithin in the stock solution and the lecithin SUV suspensions was determined by phosphate analysis [4,8].

3.3. Size distribution measurement of SUV

The size distribution of the lecithin SUV was measured by the submicron particle size analyzer at an exciting wavelength of 632.8 nm after appropriate dilution of a SUV suspension with the buffer [9]. The results of size distribution measurement were further confirmed by gel chromatography using Sepharose CL-4B (Sigma). Every 4 ml of eluate was gathered and its lecithin concentration was determined by phosphate analysis [8].

3.4. Procedure for determining K_p , T_{1p} and T_{1f}

To each of several 2-ml volumetric flasks, 0.5 ml of a TFZ aqueous stock solution (0.4 mM) was added so that the final drug concentration in the sample solutions became 100 μM . A suitable aliquot of the lecithin SUV suspension was then added to each flask, and the buffer was further added to volume. Each flask was shaken for a short time, then ca. 1 ml of the sample solution was placed in a 5-mm NMR tube and after N_2 gas was passed, the tube was capped tightly. Measurement of T_1 was performed by an inversion recovery method [10] within 24 h after the samples were prepared. The pulse width used for a 180° pulse was 30.0 μs and a delay time introduced before repeating the pulse sequence was longer than five times each expected T_1 value. Eight-96 transients

were collected to improve the signal-to-noise ratio. The probe temperature was $21 \pm 2^\circ\text{C}$. With the obtained T_1 values, the nonlinear least-squares calculation of K_p , T_{1p} and T_{1f} were performed by a basic program.

3.5. UV absorption and second-derivative spectra

The UV sample solutions containing 100 μM of TFZ and various amounts of lecithin SUV were prepared in a similar manner to the NMR sample preparation. The reference solutions were those prepared without TFZ. An absorption spectrum of the sample solution was measured against the reference solution at $21 \pm 2^\circ\text{C}$ using 1-mm light-pass length cuvettes with a slit width of 2 nm and wavelength interval of 0.1 nm.

The second-derivative spectra were calculated in the same manner as previously reported [4].

4. Results and discussion

4.1. ^{19}F NMR T_1 study

From the results of volume-weighted size distribution measurements and with an assumption that the number of lecithin molecules forming each SUV is proportional to its surface area, it was found that 86.2% of the lecithin molecules in the SUV suspension are of the SUV with a mean diameter of 23 ± 4 nm, and the remaining 13.8% are of those with a mean diameter of 80 ± 14 nm. This was further supported by the result of gel chromatography, i.e. the lecithin contents in the fractions corresponding to the SUV with mean diameters of 23 and 80 nm were determined to be about 80 and 20%, respectively.

The ^{19}F NMR signal of the trifluoromethyl group of TFZ in this lecithin SUV (2 mM) suspension showed a slightly broadened (as compared with that measured in a buffer solution) single peak. Thus, the trifluoromethyl signals corresponding to the free TFZ and the TFZ bound to these SUV are sufficiently averaged to show a single peak. Therefore, the exchange rate of TFZ between the partitioned and free states in the sample suspensions can be considered to be fast enough at the time scale of ^{19}F NMR.

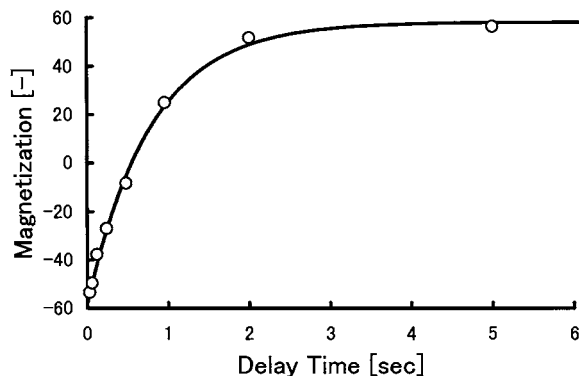


Fig. 1. Inversion-recovery profile of the ^{19}F NMR trifluoromethyl signal of TFZ in a 2 mM lecithin SUV suspension as a function of the delay time introduced between 180 and 90° pulses. Solid line shows the theoretical recovery curve calculated using the T_1 value and the equilibrium vertical magnetization obtained by a curve fitting to the experimental values (○).

Fig. 1 depicts one of the results of determining the T_1 value of the trifluoromethyl signal in the presence of the lecithin SUV. The solid line is a recovery curve calculated theoretically [10] using the values of equilibrium magnetization and T_1 that were obtained by a least-squares calculation with the values of magnetization measured at various delay times (plotted as open circles). Close fitness of the experimental values to the theoretical curve shows that the T_1 measurements were adequately performed and the assumption of rapid exchange was satisfied.

4.2. Calculation of K_p

Using the T_{1o} values measured in the presence of various amounts of lecithin SUV, the K_p , T_{1f} and T_{1p} values were calculated and are shown in Table 1. The T_{1f} value measured in a buffer

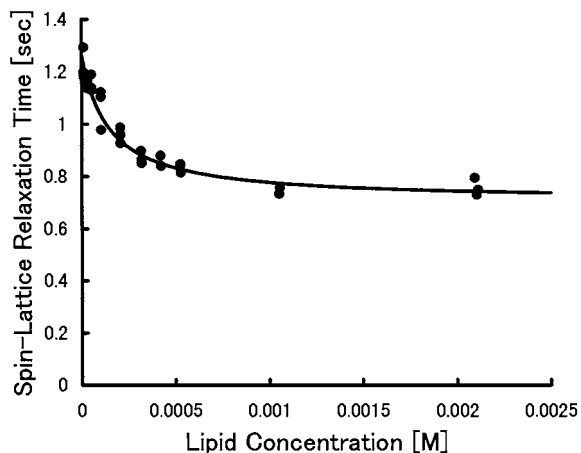


Fig. 2. The ^{19}F NMR trifluoromethyl spin-lattice relaxation time of TFZ in lecithin SUV suspensions as a function of lipid concentration. The filled circles show observed values and the solid line represents the theoretical curve calculated from Eq. (4) using the obtained K_p , T_{1f} and T_{1p} values.

solution is found to be 1.30 ± 0.06 s, which shows an appropriate agreement with the value in Table 1. The T_{1p} value is an average of several T_1 values corresponding to the TFZ molecules partitioned to some kinds of SUV of different diameters. As the T_{1p} value for each TFZ will depend on the size of SUV to which the TFZ is partitioned, the size distribution affects the obtained T_{1p} value. Therefore, it is required that the size distribution in the SUV dispersion is constant throughout the experiment.

The experimental T_{1o} values are plotted as a function of lecithin SUV concentration in Fig. 2. The plotted data show a good fitness with the theoretical curve calculated from Eq. (4) using the obtained K_p , T_{1f} and T_{1p} values.

Table 1
 K_p , T_{1f} and T_{1p} values of trifluoromazine

Method	K_p ($\times 10^{-5}$) ^a	T_{1f} (s)	T_{1p} (s)
T_1 measurement	2.13 ± 0.22	1.26 ± 0.03	0.71 ± 0.04
Second-derivative spectrophotometry	2.08 ± 0.18		

^a Mean \pm standard deviation ($n = 3$).

4.3. UV absorption and second-derivative spectra

To confirm the K_p value obtained by the ^{19}F NMR T_1 measurements, the K_p value was also determined by the second-derivative spectrophotometric method [4] using similar sample solutions as used in the ^{19}F NMR experiment.

The absorption and second-derivative spectra of TFZ in buffer solutions containing various amounts of lecithin SUV are depicted in Fig. 3(a) and (b), respectively. The absorption spectra in Fig. 3(a) show incomplete background compensation, whereas the second-derivative spectra in Fig. 3(b) show three derivative isosbestic points indicating entire elimination of the residual background effects. The derivative intensity change

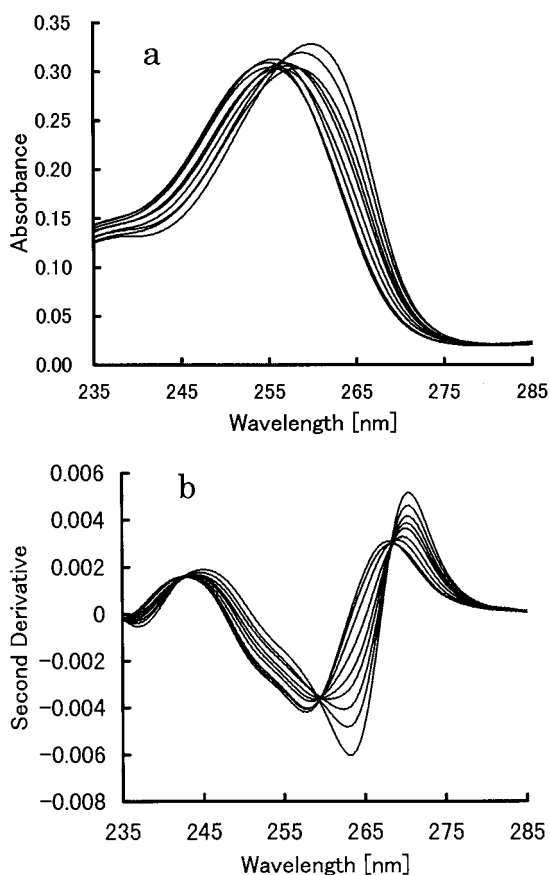


Fig. 3. Absorption (a) and second-derivative (b) spectra of TFZ in HEPES buffer solutions (pH 7.4) containing 0–1.0 mM SUV. Second-derivative spectra were calculated from absorption spectra of (a).

(ΔD) induced by the addition of lecithin SUV was measured at the λ (256 nm) and, from the relationship between the ΔD value and the lecithin concentration, the K_p value was calculated as previously reported [4], and is shown in Table 1. The K_p values obtained by the ^{19}F NMR and the second-derivative spectrophotometric methods show good agreement.

Consequently, the results of the present work indicate that for the drugs having fluorine atom(s), the ^{19}F NMR spin-lattice relaxation method is applicable to determine their K_p values without disturbing the equilibrium states of sample solutions by separation procedures. The method will be especially useful for the drugs which do not have absorption in the ultraviolet or visible regions, or for those having absorption but not showing any spectral changes according to their partition to lipid bilayers.

Acknowledgements

The authors are indebted to Dr N. Shimizu and H. Sasaki of Nippon Shinyaku for their courtesy of using a submicron particle analyzer, Nicomp 370.

References

- [1] P. Tang, B. Yan, Y. Xu, *Biophys. J.* 72 (1997) 1676.
- [2] P.N. Venkatasubramanian, Y.J. Shen, A.M. Wyrwicz, *Biochim. Biophys. Acta* 1245 (1995) 262.
- [3] K. Kitamura, M. Takenaka, S. Yoshida, M. Ito, Y. Nakamura, K. Hozumi, *Anal. Chim. Acta* 242 (1991) 131.
- [4] K. Kitamura, N. Imayoshi, T. Goto, H. Shiro, T. Mano, Y. Nakai, *Anal. Chim. Acta* 304 (1995) 101.
- [5] R. Welti, L.J. Mullikin, T. Yoshimura, G.M. Helmkamp Jr., *Biochemistry* 23 (1984) 6086.
- [6] Y. Kuroda, K. Kitamura, *J. Am. Chem. Soc.* 106 (1984) 1.
- [7] M. Sakoda, K. Hiromi, *J. Biochem.* 80 (1976) 547.
- [8] A.J. Christopher, T.R.F.W. Fennell, *Microchem. J.* 12 (1967) 593.
- [9] L.D. Mayer, M.J. Hope, P.R. Cullis, *Biochim. Biophys. Acta* 858 (1986) 161.
- [10] T.C. Farrar, E.D. Becker, *Pulse and Fourier Transform NMR*, Academic Press, New York, 1971, p. 20.

Inexpensive, in-situ monitoring of borohydride concentrations

Steven Amendola, Per Onnerud, Michael T. Kelly, Michael Binder *

Millennium Cell Co., 8 Cedar Brook Drive, Cranbury, NJ 08512, USA

Received 14 September 1998; received in revised form 23 November 1998; accepted 24 November 1998

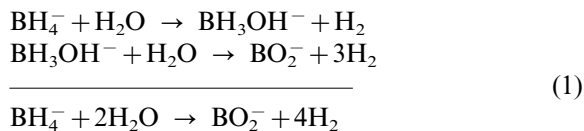
Abstract

Non-destructive, in-situ detection of 10^{-3} to 10^{-4} M borohydride ions in aqueous alkaline solutions containing borates can be easily and rapidly accomplished by simply measuring open circuit potentials of selected metals (relative to a suitable reference) immersed in these solutions. © 1999 Elsevier Science B.V. All rights reserved.

Keywords: Borohydride concentrations; Borates; Open circuit potentials

1. Introduction

Sodium borohydride, NaBH_4 , (tetrahydridoborate), is extensively used as an effective water-soluble reducing agent in chemical synthesis and electroless plating of metals. Aqueous borohydride solutions are generally kept strongly alkaline to prevent hydrolysis that occurs at lower pH. Borohydride hydrolysis involves a two step process to yield hydrogen gas.



In many applications, finding a simple, rapid, analytical method to monitor borohydride concentrations provides something of a challenge. Quantitative determination of borohydride anions, BH_4^- , in aqueous, alkaline solutions can be obtained by numerous methods including an iodate volumetric procedure [1]. Mirkin and Bard [2] used voltammetry to determine low borohydride concentrations in alkaline solutions. Their method, however, requires three electrodes and a potentiostat.

The present study was motivated by research into direct electrochemical synthesis (in aqueous, alkaline solutions) of borohydride from borate. This reaction is important for substantially reducing the cost of borohydride compounds and in the intriguing possibility of recharging our novel high-energy borohydride battery system [3]. We report a rapid, reliable, and non-destructive electrochemical method that can be used to determine relatively low $[\text{BH}_4^-]$ ranges in aqueous, alkaline

* Corresponding author. Tel.: +1-609-4099010; fax: +1-609-4091650.

E-mail address: steven@amendola.com (M. Binder)

solutions containing only borate and borohydride. This inexpensive, simple method requires only a reference electrode (such as a saturated calomel electrode, SCE), a small length of a specific metal wire, and a voltmeter. Any metal/alloy whose open circuit potential relative to a suitable reference is significantly different when immersed in 20% NaOH (no borohydride) or in 0.1 M NaBH₄-20% NaOH may be a candidate electrode for this method. We report data on three metals that are surprisingly good indicators of [BH₄⁻].

2. Experimental

We investigated open circuit (rest) potentials of platinum, rhodium, and cobalt wire immersed in various concentrations of NaBH₄ in 20% NaOH. All reported potentials were relative to a saturated calomel electrode (SCE) and performed at room temperature. In our experiments, we first measured rest potentials of these metals in 20% NaOH and then, using a burette, added increasing amounts of a freshly prepared NaBH₄-20% NaOH solution of known concentration that had been saturated with sodium metaborate, NaBO₂. Open circuit potentials for these metals were monitored as a function of added borohydride solution (similar to a potentiometric titration). Our solutions were saturated with sodium metaborate to simulate conditions where borohydride would be formed in low concentrations during electrochemical conversion of borate to borohydride (where excess borate would initially be present).

3. Results

3.1. Cobalt

Fig. 1 shows measured open circuit potentials of cobalt rhodium and platinum wire as a function of NaBH₄ concentration in 20% NaOH. Open circuit potentials for Co were relatively constant at approximately -0.95 V for [BH₄⁻] < 1 × 10⁻² M. At [BH₄⁻] = 6 × 10⁻³ M, the open circuit potential for Co changed in a step-function manner to approximately -1.3 V and remained

relatively constant with time at that potential even for higher [BH₄⁻].

3.2. Rhodium

Rh immersed in 20% NaOH, 40% NaOH, or for [BH₄⁻] < 2 × 10⁻³ M had a constant open circuit potential of approximately -0.2 V relative to SCE. For [BH₄⁻] = 2 × 10⁻³ M, Rh potentials changed abruptly to approximately -1.1 V and remained relatively constant with time at that potential even for higher [BH₄⁻]. In NaBH₄-40% NaOH solutions the step function change in Rh open circuit potential occurred at slightly higher concentrations, i.e. [BH₄⁻] = 2.6 × 10⁻³.

3.3. Platinum

The open circuit potential of Pt in 20% NaOH was approximately -0.15 V. As borohydride concentrations increased, Pt open circuit potentials gradually became more negative. At [BH₄⁻] = 3 × 10⁻⁴ M the Pt potential underwent a step-function change from approximately -0.28 V to approximately -0.8 V and remained relatively invariant with time at that level even for higher [BH₄⁻].

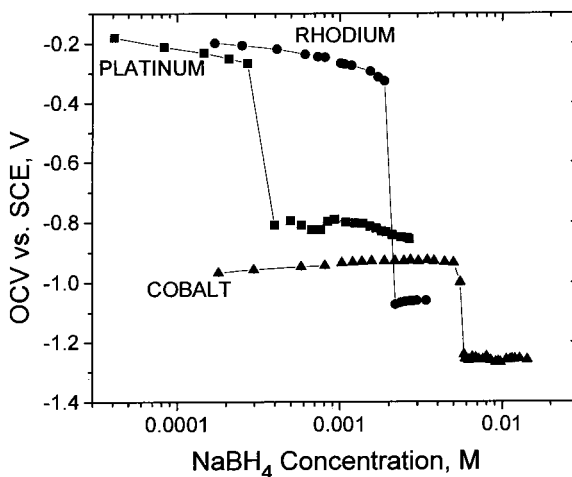
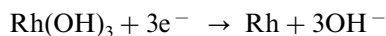


Fig. 1. Open circuit potentials of Co, Rh, and Pt wire (relative to a saturated calomel electrode) plotted as a function of borohydride concentration in 20% NaOH.

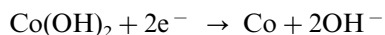
4. Discussion

We will first suggest a process to explain measured open circuit potentials for Rh and Co in 20% NaOH solution. The -0.2 -V open circuit potential observed for Rh could be due to reduction of rhodium hydroxide



whose potential relative to the standard hydrogen electrode (SHE) is 0.0 V which translates into -0.24 V versus SCE.

For Co, the redox potential for the reaction



is -0.73 V relative to SHE which translates into -0.97 V relative to SCE. Thus, our observed experimental open circuit potentials are in excellent agreement with expected thermodynamic values. Deviations from thermodynamic values (usually reported for $\text{pH} = 14$) may be due to slight differences in $[\text{OH}^-]$.

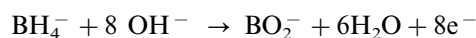
To explain step function changes in open circuit potentials of Co, Rh, and Pt as a function of borohydride concentration, we propose two distinct operating mechanisms. One mechanism pertains to Rh and Pt; the other pertains to Co. It is known that these transition metals are capable of catalyzing borohydride hydrolysis even in strongly alkaline solutions [4]. Catalytic activity towards borohydride hydrolysis follows the trend: $\text{Rh} > \text{Pt} > \text{Co}$.

For Rh and Pt (which are much stronger borohydride hydrolysis catalysts than Co) it is likely that hydrogen formed by borohydride hydrolysis is adsorbed on the metal surface. Adsorbed hydrogen may be responsible for the more negative open circuit potential observed on these metals at high borohydride concentrations. Once the metal surface is covered with adsorbed hydrogen, open circuit potentials abruptly change.

To substantiate our hypothesis that adsorbed hydrogen is responsible for the sharp change in potential, a glass H-cell was utilized in which the anode and cathode compartments were separated by an ion permeable membrane. Both anode and cathode compartments were filled with 20% NaOH. A Monel working electrode was immersed

in the cathode compartment and a stainless steel screen counter electrode was immersed in the anode compartment. An SCE reference electrode was placed in the cathode compartment. A PAR 273 potentiostat was used to apply -1.6 V (relative to the SCE) to the working electrode. This caused reduction of water on the cathode thus evolving copious amounts of hydrogen bubbles. Rh, Pt and Co wires were immersed in the cathode compartment and their open circuit potential monitored as a function of electrolysis time. As electrolysis proceeded (and hydrogen gas evolved), open circuit potentials of Rh and Pt became increasingly more negative and within a few minutes reached potentials similar to those observed when these metals were immersed in concentrated borohydride solutions. This observation indicated that the step-potential change of Rh and Pt at specific borohydride concentrations were not due to borohydride anions per se, but to its hydrolysis product, i.e. adsorbed hydrogen. This is because in our H-cell experiment, where no species other than hydrogen was formed in the cathode compartment, we nevertheless observed dramatic changes in open circuit potentials for Rh and Pt (similar to the step-function potential changes for Rh and Pt in borohydride solutions).

In these H-cell experiments, however, open circuit potentials of Co immersed in the cathode compartment remained at the same potential as in 20% NaOH even after prolonged electrolysis (and extensive hydrogen evolution). This indicated that for Co, hydrogen adsorption does not appear to be the dominant mechanism for the step-function potential change. For Co at high borohydride concentrations, open circuit potentials could be due to borohydride oxidation on bare metal



whose reduction potential [3] is -1.24 V versus SHE (-1.48 V relative to SCE). Abrupt changes in Co open circuit potential as a function of borohydride concentration may be due to competition between hydroxide removal from Co, and borohydride oxidation on bare cobalt.

We also measured open circuit potentials of these metals as a function of increasing sodium tetrafluoroborate, NaBF_4 -20% NaOH, (which

does not undergo hydrolysis). In this solution, open circuit potentials of these metals remained constant with fluoroborate concentration. This clearly indicated that observed changes in open circuit potential for these metals in borohydride solutions were specifically related to either hydrolysis or oxidation of borohydride anion.

5. Conclusions

We have demonstrated proof-of-principle of a rapid, sensitive method in which aqueous, alkaline solutions can be qualitatively evaluated for $[\text{BH}_4^-]$. The key point is that large changes in open circuit potentials of specific metals occur over relatively narrow $[\text{BH}_4^-]$ ranges. By simply inserting a selected metal (or combination of metals) directly into a solution, borohydride concentration ranges can be rapidly determined in-

situ, without solution sampling, by simply monitoring open circuit potentials.

Acknowledgements

We thank Martin M. Pollak and Jerome I. Feldman of GP Strategies Inc. for their continued interest, enthusiastic support, and constant encouragement.

References

- [1] D.A. Lyttle, E.H. Jensen, W.A. Struck, *Anal. Chem.* 24 (1952) 1843.
- [2] A.J. Mirkin, A.J. Bard, *Anal. Chem.* 63 (1991) 532.
- [3] S. Amendola, P. Onnerud, M. Kelly, P. Petillo, M. Binder, Abstract 39, Proceeding of the 194th Meeting of the Electrochemical Society, Boston, MA, November 1–6, Electrochemical Society, Pennington, NJ, 1998.
- [4] H.C. Brown, C.A. Brown, *J. Am. Chem. Soc.* 84 (1962) 1993.

Potentiometric determination of potassium cations using a nickel(II) hexacyanoferrate-modified electrode

Roger J. Mortimer ^{a,*}, Paulo J.S. Barbeira ^b, Ana F.B. Sene ^c,
Nelson R. Stradiotto ^c

^a Department of Chemistry, Loughborough University, Loughborough, Leicestershire LE11 3TU, UK

^b Departamento de Química-ICEx-UFMG, Belo Horizonte (MG), Brazil

^c Departamento de Química-FFCLRP-USP, 14040-901-Ribeirão, Preto (SP), Brazil

Received 25 May 1998; received in revised form 23 November 1998; accepted 27 November 1998

Abstract

Electroactive nickel(II) hexacyanoferrate (NiHCF) thin film modified electrodes are effective potentiometric sensors for the determination of potassium ions. The NiHCF films are deposited onto glassy carbon electrodes by repetitive potential cycling in $K_3Fe(CN)_6/NaNO_3/Ni(NO_3)_2$ solution. The modified electrodes exhibit a linear response to potassium ions in the concentration range 1×10^{-3} to 2.0 mol dm^{-3} , with a near-Nernstian slope (45–49 mV per decade) at 25°C. In the determination of potassium ion in syrups used for treatment of potassium deficiency, the NiHCF-modified electrode gave comparable results to those obtained using flame emission spectrophotometry. © 1999 Elsevier Science B.V. All rights reserved.

Keywords: Modified electrodes; Nickel(II) hexacyanoferrate; Potassium ion

1. Introduction

The chemical modification of electrodes using inorganic films is an attractive approach in the development of electrochemical sensors [1]. One electrode modification scheme that has seen much interest is the generation of films of transition metal hexacyanoferrates such as Prussian blue

and its analogues [2]. The principle of the application of such modified electrodes as amperometric sensors has been demonstrated for a range of analytes including NADH [3], ascorbic acid [4], thiosulfate [5], dopamine [6] and hydrogen peroxide [7]. The voltammetric determination of formal potentials of composite electrodes made of graphite, paraffin and metal hexacyanoferrates has been used in the quantitative analysis of a range of cations [8,9]. However, few papers [10,11] report the use of metal hexacyanoferrate-modified thin film electrodes as potentiometric ion sensors

* Corresponding author. Tel.: +44-1509-222583; fax: +44-1509-223925.

E-mail address: r.j.mortimer@lboro.ac.uk (R.J. Mortimer)

and none demonstrate any practical applications. We describe here a study of a new potassium ion potentiometric sensor based on a nickel(II) hexacyanoferrate (NiHCF)-modified glassy carbon electrode. The potassium ion is the most common intracellular cation and is essential for maintaining osmotic pressure and electrodynamic cellular properties in organisms [12]. The recommended daily intake of potassium is 3500 mg, however, under normal circumstances dietary deficiency does not occur [13]. The most important cause of potassium deficiency is excessive losses, usually through the alimentary tract or the kidneys. The potentiometric method described here was applied to the determination of potassium ion in syrup used in the treatment of body potassium deficiency. The results were compared to those obtained using flame emission spectroscopy, the official method for determination of calcium, potassium and sodium ions in electrolyte replenishers [14].

2. Experimental

2.1. Apparatus and chemicals

For the voltammetric experiments a FAC-200A potentiostat, FAC-201B ramp generator and a EG&G RE 0091 X-Y recorder were used. A conventional electrochemical cell was employed, with a 2 mm diameter glassy carbon disc working electrode, a 1 cm² platinum plate auxiliary electrode and a saturated calomel reference electrode (SCE). The glassy carbon electrode was polished to a mirror finish with alumina (0.05 μm), then rinsed thoroughly with water, cleaned in an ultrasonic bath with water and, finally, rinsed with water and ethanol before use. Dry nitrogen was passed through the solution to remove oxygen and maintained flowing over the solution during runs. The potentiometric measurements were carried out using a HP-34702A multimeter.

All chemicals were of analytical reagent grade and distilled/deionised water was used for preparing the solutions. KCl (Merck), NaNO₃ (Merck), K₃Fe(CN)₆ (Carlo Erba) and Ni(NO₃)₂ (Merck) were used without further purification.

2.2. Electrode modification

NiHCF films can be prepared by electrochemical oxidation of nickel electrodes in the presence of hexacyanoferrate(III) ions [15] or by voltammetric cycling of inert substrate electrodes in solutions containing nickel(II) and hexacyanoferrate(III) ions [16]. In this study we employed the latter technique, following the solution composition used by Zhou et al. [5]. Thus NiHCF films were prepared by repetitive potential cycling, from 0.0 to +0.8 V vs SCE, in an oxygen-free 1.0 mol dm⁻³ NaNO₃ solution containing 1 × 10⁻³ mol dm⁻³ Ni(NO₃)₂ and 1 × 10⁻³ mol dm⁻³ K₃Fe(CN)₆. Film thicknesses were estimated by the method earlier used for cupric hexacyanoferrate [17].

2.3. Analytical procedure

Before potentiometry, the NiHCF-modified electrode was conditioned at +0.7 V vs SCE for 10 min in 1.0 mol dm⁻³ KCl solution. Electrode potentials were recorded after 2 min of immersion of working and reference electrodes in the sample solution. After each measurement the electrode was reconditioned in 1.0 mol dm⁻³ KCl solution for 2 min.

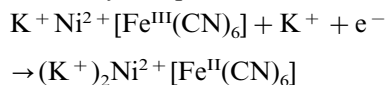
The commercial syrup samples, used in the treatment of potassium deficiency, were diluted with deionised water and introduced directly into the electrochemical cell. The flame emission spectroscopy measurements were carried out at 766.5 nm using a Shimadzu AA-680 spectrophotometer, equipped with an air/C₂H₂ burner. Potassium ion quantification was done using calibration (potentiometry) and standard addition (flame emission spectroscopy) methods.

3. Results and discussion

3.1. NiHCF film formation

Fig. 1 illustrates the steady current increase on repetitive potential cycling due to the accumulation of a NiHCF film on the glassy carbon electrode.

Transfer of NiHCF-modified electrodes to pure 1.0 mol dm^{-3} KCl supporting electrolyte revealed a single redox couple ($+0.36 \text{ V}$ vs SCE) represented by the process:



Cyclic voltammetric studies, with variation of scan rate, gave i_{pa} vs v ($r = 0.9998$), $i_{\text{pa}}/i_{\text{pc}} \approx 1$ and $|E_{\text{pc}} - E_{\text{pa}}| \approx 0$, indicative of rapid, reversible charge transfer to the surface-confined redox species. Successive potential scanning in pure supporting electrolyte showed that, after 100 cycles, there was a decrease of only 20% in the peak current, indicating good stability of the NiHCF-modified electrodes.

3.2. Potentiometric response to potassium ions

The potentiometric response of the NiHCF-modified electrodes to potassium ions was tested by measurements of the electrode potentials for a series of standard solutions of KCl (Fig. 2).

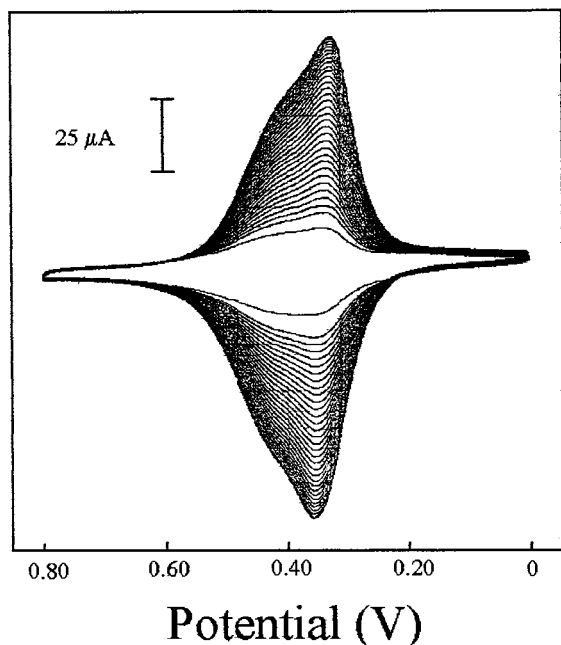


Fig. 1. Formation of the NiHCF-modified glassy carbon electrode in a 1.0 mol dm^{-3} NaNO_3 solution containing 1×10^{-3} mol dm^{-3} $\text{Ni}(\text{NO}_3)_2$ and 1×10^{-3} mol dm^{-3} $\text{K}_3\text{Fe}(\text{CN})_6$. Resulting film thickness = 38 nm.

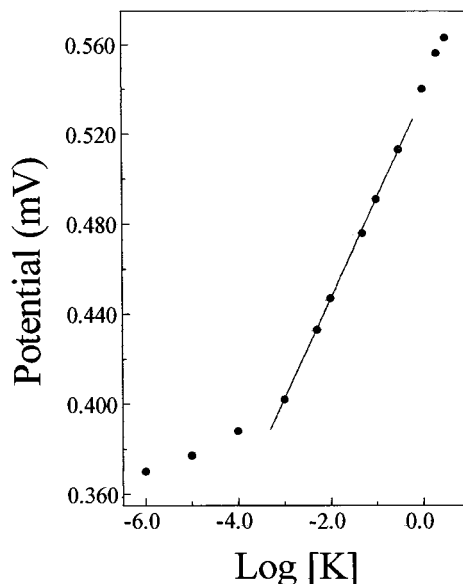


Fig. 2. Potentiometric response for potassium ion (as KCl solution) using a NiHCF-modified electrode. NiHCF film thickness = 38 nm.

The same curve was obtained for different NiHCF film thicknesses that had been prepared using different formation times (Table 1).

The best slope, detection and linear range were obtained with a NiHCF thickness of 38 nm (obtained after cycling at 100 mV s^{-1} for 10 min). The reproducibility of the electrode response was evaluated for a $1 \times 10^{-3} \text{ mol dm}^{-3}$ potassium ion solution, giving a relative S.D. of 2% ($n = 10$). The success of making reproducible potentiometric measurements with simple instrumentation is attributed to the use of thin films of NiHCF. Usually, voltammetric measurements are necessary to determine formal potentials of metal hexacyanoferrate systems [8,9], although a drawback of the potentiometric method described here is the high response times (Table 2). Square wave or differential pulse voltammetric measurements would allow fast measurements of formal potentials, with however, the penalty of the need for sophisticated instrumentation.

The selectivity of the modified electrode was tested by the mixed solution method, in which the potassium ion concentration was kept constant ($1 \times 10^{-3} \text{ mol dm}^{-3}$) and the interfering ion con-

Table 1

Effect of the NiHCF film thickness on the potentiometric response to potassium ion

Thickness (nm)	Linear range (mol dm ⁻³)	Detection limit (mol dm ⁻³)	Slope (mV mol dm ⁻³)
18	5 × 10 ⁻² –0.3	1 × 10 ⁻²	40–45
38	1 × 10 ⁻³ –2.0	3 × 10 ⁻⁴	45–49
49	5 × 10 ⁻³ –1.0	1 × 10 ⁻³	42–46

Table 2

Comparison of results obtained for potassium ion-selective electrodes based on metal hexacyanoferrate films

	NiHCF	CoHCF ^a	CuHCF ^b
Film thickness (nm)	38	35–40	30–40
Response time (s)	120	120	15
Linear range (mol dm ⁻³)	1 × 10 ⁻³ –2.0	3 × 10 ⁻⁵ –0.1	1 × 10 ⁻⁴ –1.0
Detection limit (mol dm ⁻³)	3 × 10 ⁻⁴	1 × 10 ⁻⁵	–
Slope (mV per decade)	45–49	48–54	42–50
Interfering [Li ⁺] (mol dm ⁻³)	1 × 10 ⁻²	1 × 10 ⁻¹	–
Interfering [Na ⁺] (mol dm ⁻³)	6 × 10 ⁻³	1 × 10 ⁻²	1 × 10 ⁻²
Interfering [NH ₄ ⁺] (mol dm ⁻³)	3 × 10 ⁻⁴	1 × 10 ⁻³	1 × 10 ⁻⁴

^a Ref. [10].^b Ref. [11].

centration was varied. A new NiHCF-modified electrode was prepared for each study and the concentration of the interfering ions were 1 × 10⁻², 6 × 10⁻³ and 3 × 10⁻⁴ mol dm⁻³ for Li⁺, Na⁺ and NH₄⁺, respectively (Table 2).

Thus in common with cobalt(II) hexacyanoferrate (CoHCF) and cupric hexacyanoferrate (CuHCF)-modified electrodes, the NiHCF-modified electrode had a selectivity sequence in the order NH₄⁺ > K⁺ > Na⁺ > Li⁺ (Table 2). This is in line with the ease of incorporation of these cations into the metal hexacyanoferrate lattices due the magnitude of the diameter of zeolitic channels in the NiHCF film relative to the effective hydrated diameter of the cations [17]. Compared to CoHCF and CuHCF-modified electrodes (Table 2), the NiHCF shows a lower sensitivity to potassium ion, but can be used at higher concentrations. The NiHCF-modified electrode has the further advantage that the NiHCF film is deposited in a single stage, whereas both the CoHCF and CuHCF films require initial electrodeposition of cobalt and copper respectively prior to generation of the metal hexacyanoferrate.

3.3. Determination of potassium ion in commercial syrups

The application of the NiHCF-modified electrode in the determination of potassium ion in two commercial syrups for the treatment of potassium deficiency was examined. Table 3 compares the results obtained using the potentiometric method with those using flame emission spectrophotometry. The value of *t* (Student's *t*-test) for both methods was 2.78 for 95% of confidence interval. Both methods showed good reproducibility, low standard deviations and good agreement

Table 3

Concentration of potassium ion (mg cm⁻³ of syrup) obtained by different analytical methods (five assays (*n* = 5))

Method	Syrup	
	A	B
Potentiometry	32.5 ± 0.7	4.9 ± 0.5
Flame emission spectrophotometry	29.9 ± 0.6	4.5 ± 0.4
Manufacturers' information	31.5	4.7

with the manufacturers' supplied data. However, the potentiometric method has the significant advantages of ease of operation and cost.

Acknowledgements

The authors are grateful for the financial support of CNPq, FAPESP, CAPES and the British Council.

References

- [1] J.A. Cox, R.K. Jaworski, P.J. Kulesza, *Electroanalysis* 3 (1991) 869.
- [2] K. Itaya, I. Uchida, V.D. Neff, *Acc. Chem. Res.* 19 (1986) 162.
- [3] B.F.Y. Yon Hin, C.R. Lowe, *Anal. Chem.* 59 (1987) 2111.
- [4] S. Dong, G. Che, *J. Electroanal. Chem.* 315 (1991) 191.
- [5] X. Zhou, S. Wang, Z. Wang, M. Jiang, *Fresenius J. Anal. Chem.* 345 (1993) 424.
- [6] D-M. Zhou, H-X. Ju, H-Y. Chen, *J. Electroanal. Chem.* 408 (1996) 219.
- [7] M.S. Lin, T.F. Tseng, W.C. Shih, *Analyst* 123 (1998) 159.
- [8] H. Düssel, A. Dostal, F. Scholz, *Fresenius J. Anal. Chem.* 355 (1996) 21.
- [9] M. Hermes, F. Scholz, *J. Solid State Electrochem.* 1 (1997) 215.
- [10] Z. Gao, X. Zhou, G. Wang, P. Li, Z. Zhao, *Anal. Chim. Acta* 244 (1991) 39.
- [11] D. Engel, E.W. Grabner, *Ber. Bunsenges. Phys. Chem.* 89 (1985) 982.
- [12] M. Sittig, D. Mota de Freitas, in S.P. Parker (ed.), *McGraw-Hill Encyclopedia of Science and Technology*, 8th ed., vol. 14, McGraw-Hill, New York, 1997, pp. 254–256.
- [13] Food and Nutrition board, Subcommittee on the tenth edition of the RDAs, R.J. Havel (Chairman). *Recommended Dietary Allowances*, 10th ed., National Academic Press, Washington, DC, 1989.
- [14] K. Helrich (ed.), *Official Methods of Analysis of the Association of Official Analytical Chemists*, 15th ed., 1990, pp. 503–504.
- [15] A.B. Bocarsly, S. Sinha, *J. Electroanal. Chem.* 137 (1982) 157.
- [16] J. Joseph, H. Gomathi, G.P. Rao, *Electrochim. Acta* 36 (1991) 1537.
- [17] L.M. Siperko, T. Kuwana, *J. Electrochem. Soc.* 130 (1983) 396.

The structural composition of humic compounds as indicator of organic carbon sources

N. Calace, M. Capolei, M. Lucchese, B.M. Petronio *

Department of Chemistry, University of Rome, 'La Sapienza', Piazzale A. Moro 5, 00185 Rome, Italy

Received 30 July 1998; received in revised form 26 November 1998; accepted 27 November 1998

Abstract

Various analytical techniques (^{13}C -NMR, FTIR, elemental analysis) have been used to study the structures of humic compounds present in the sediments of Martignano lake located 50 km from Roma city (Italy). The total amount of humic compounds present in the upper layer of sediments is practically constant; instead, considering humic (HA) and fulvic acids (FA) separately, it can be noticed that while HA increase remarkably from A_1 to A_3 , FA diminish, probably as a result of the continuous transformation of algal debris, present in large amount in A_1 , from compounds which are in an early stage of decomposition to more highly degraded organic matter. In deeper layers the percentage both of HA and FA is constant and slightly lower than that found in the upper layer, except for two sampling points. In these stations the amount of both HA and FA are very high and the carbohydrate peak areas of HA and FA increase along with the depth, reflecting the presence of a well localized source of organic carbon or different environmental conditions. © 1999 Elsevier Science B.V. All rights reserved.

Keywords: Lacustrine environment; Humic compounds structures; Sediments; Spectroscopic analysis

1. Introduction

Humic substances are ill-defined and heterogeneous mixtures of naturally-occurring molecules which are present in all soils, waters and sediments. They cannot be classified as any other chemical class of compounds and are traditionally defined according to their solubility: humic acids (HA) are insoluble at acidic pH values ($\text{pH} < 2$) and soluble at higher pH values, while fulvic acids (FA) are soluble in water at all pH values.

From an environmental point of view HA and FA are particularly interesting because in their molecular structures there are both polar and nonpolar substituents; therefore, they can interact both with water-soluble and -insoluble compounds [1,2].

Humic compounds are produced by abiotic chemical reactions, including condensations, polymerizations, oxidations and reductions, by which relatively low molecular weight compounds, such as degradation products of biopolymers (i.e. proteins and carbohydrates) and of lignin, are linked to one another [3].

* Corresponding author. Tel./fax: +39-6-499-13723.

E-mail address: petroniobm@axrma.uniroma1.it (B.M. Petronio)

The composition of the resulting humic compounds molecular structures vary depending on their source and location, partly as a result of different availability of low molecular-weight forms. FA are generally more aliphatic and less aromatic than HA and are richer in carboxylic, phenolic and ketonic groups. The abundance of phenolic moieties, in the structure of humic compounds, might be used as a biomarker of the terrestrial organic matter: phenolic acids liberated during the lignin degradation, that is unique to land plants, react with other fragments of degraded organic matter to form humic compounds.

The study and the characterization of humic compounds' structures provides therefore important information about the organic carbon source (aquatic or terrestrial) and the probable formation mechanisms.

In this work various analytical techniques (^{13}C -NMR, FTIR, elemental analysis) have been used to study the structures of humic compounds present in the sediments of Martignano lake (Italy). Martignano lake is a little volcanic lake located 50 km from Roma city (Italy), having an elliptic form and steep shores. The lake area is neither populated nor industrialized; consequently the environment is practically uncontaminated. Besides, a high production of algae, belonging to the *caracee* family, can be observed on the bottom of the lake, along the 10–15 m batimetric lines; *caracee* are present in all oligomesotrophos lakes and can be considered good indicators of the lacustrine atrophy and the environmental pollution.

2. Materials and methods

2.1. Materials

Sediment cores were collected in 12 points along the transept shown in Fig. 1. Samples were taken during different seasons and hydrological phases (six times in the year) along with the temperature values along the water column; furthermore, the oxygen content of the water in contact with sediments was determined. All sedi-

ment cores were subdivided into three sub-samples (0–10, 11–20 and 21–30 cm) and frozen at -30°C immediately after collection, except for samples A_0 and B_0 (cores of 10 cm collected on lake shores).

Spectra/Por Cellulose Ester membranes with a molecular weight cut off of 1000 Da were used; they are tubes with a diameter of 10 mm and a rate vol/length of 0.79 ml/cm.

Spectra/Por Cellulose Ester hydrophilic membrane discs with a molecular weight cut off of 500 Da (diameter 76 mm) were used.

2.2. Apparatus

A Philips mod. FTIR PU 9800 spectrophotometer working in diffuse reflectance conditions was employed. Results are given in Kubelka Munk units, a mathematical formula applied to diffuse reflectance spectra. For the analysis oven-dried samples (1.0 mg) were mixed with 100 mg of anhydrous potassium bromide.

An NMR Varian spectrometer mod. XL300 was employed. Samples were prepared in an NMR tube (5 mm) by dissolving 10 mg of lyophilized FA or HA in 1.0 ml of 0.5 N NaOD solution. Operating conditions were as follows: 75 MHz pulse 45° , acquisition time 0.1 s, delay 0.5 s. From 500 000 to 800 000 scans were accumulated.

Thermogravimetric analyses were carried out by a Perkin Elmer TGA thermogravimetric analyser in N_2 atmosphere, between 50 and 1200°C , using a scanning rate of $20^{\circ}\text{C min}^{-1}$, on 1.5 mg of sample.

Elemental analyses were performed by a Carlo Erba 240-B model CHN-analyzer.

An Amicon stirred ultrafiltration cell, model 8400, capacity 400 ml, equipped at the bottom with a 500 Da membrane disc (diameter 76 mm) was used for FA purification. The cell was connected to a reservoir (5 l) containing the diafiltrate solution (deionized water), which was nitrogen pressurized (4 atm). Varying the operational conditions, the cell can be used under nitrogen pressure (3.5 atm) without being interfaced with the reservoir. In this way, preconcentration conditions are settled.

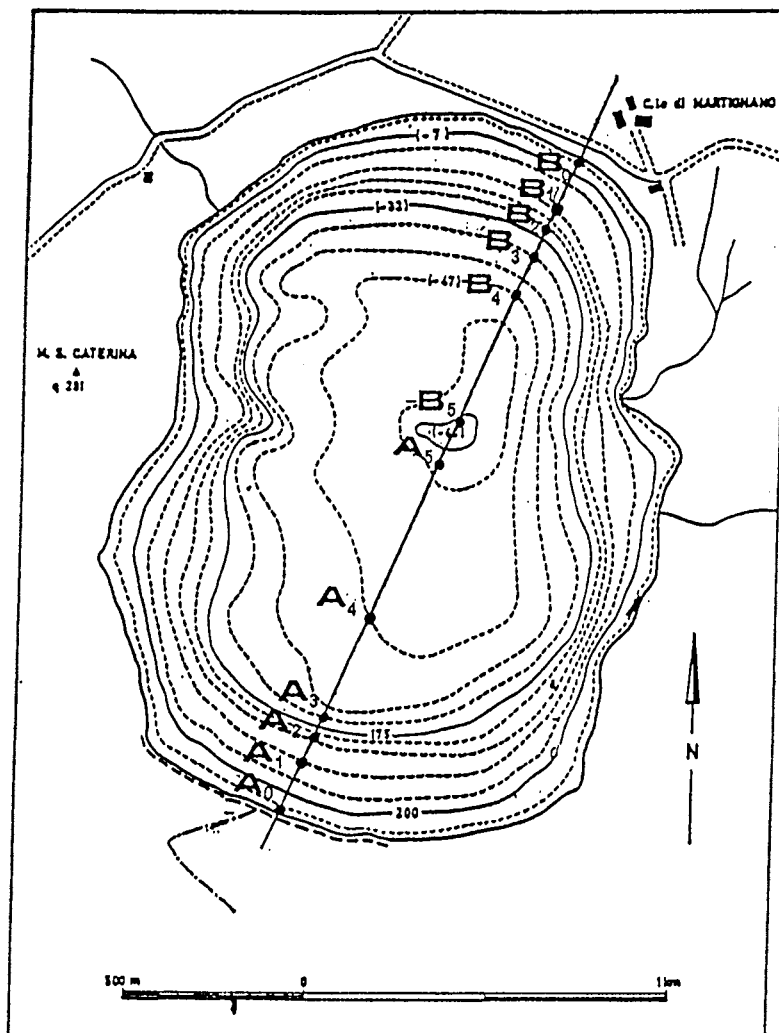


Fig. 1. Martignano lake: sampling point along the transept.

2.3. Recovery of HA and FA

Sediment samples were defrozen; HA and FA were then extracted with the King's procedure [4]. HA solutions were put in dialysis tubes (molecular size 1000 Da) and dialyzed against distilled water until chloride free. The solution was lyophilized.

The concentration and purification of FA from organic compounds with low molecular weight were carried out according to the procedure proposed by Thurman [5] for the recovery of humic

compounds from water. Briefly, acidic solutions containing FA extracted and separated from HA were passed through an Amberlite XAD-8 resin column (500 ml), then FA were recovered from resins by elution with 500 ml of 0.1 M NaOH. Basic eluates were neutralized and FA purified from inorganic salts by the ultrafiltration technique [6]. The ultrafiltration cell containing the FA solution was not connected to the reservoir. The solution was concentrated under nitrogen pressure up to 100 ml; the cell was then connected to the reservoir. Inorganic salts were removed

from the retentate with the pressurized diafiltrate solution (deionized water), crossing through the cell. At the end of the purification procedure (washings chloride free) the solution was lyophilized.

HA and FA were characterized by FTIR and ^{13}C -NMR spectroscopy, thermogravimetry and elemental analysis.

3. Results and discussion

Water temperature values show that, from spring to summer, a thermal stratification occurs along with the oxygen depletion taking place during late summer. In any other periods of the year oxygen reaches bottom sediments. In these conditions the organic matter decomposition is due both to aerobic processes, occurring at the sediment–water interface, and to anaerobic processes below.

Trends of percentage yields of HA and FA reported in Fig. 2 (July 1996) show that the total amount of humic compounds present in the upper layer of sediments is practically constant (Fig. 2, C); little difference between A_x and B_x samples may be due to higher amount of algae present in the A zone. Considering HA and FA separately (Fig. 2A, B), it can be noticed that while HA increase remarkably from A_1 to A_3 , FA diminish. Data of the B zone show a similar trend even though less evident. This behaviour is probably due to the continuous transformation of algal debris, present in large amounts in A_1 , from compounds which are in an early stage of decomposition to more highly degraded organic matter. The FAs' FTIR spectra (Fig. 3) support the interpretation: the A_1 spectrum is composed primarily of adsorptions which could be due to carbohydrate carbons (1050 cm^{-1}) whereas a decrease of this peak from A_1 to A_5 and an increase of the region of $1750\text{--}1500\text{ cm}^{-1}$ are observed. This suggest that FA of A_x are more highly degraded than those of A_1 . In fact, carbohydrates are the major constituents of algae and their content in humic compounds can be considered as a clue to the diagenesis state of sedimentary organic matter of algae origin; carbohydrate-rich HA indicate that

organic matter is in a very early stage of diagenesis [7]. No structural differences are shown by HAs' FTIR spectra of superficial samples, in which adsorptions due to CH bending of unsaturated structures ($1600\text{--}1450\text{ cm}^{-1}$), to OH deformation and CO stretching of alcohols and phenols ($1400\text{--}1100\text{ cm}^{-1}$), to CO adsorption and NH_2 deformation (amide I and II, $1650\text{--}1550\text{ cm}^{-1}$) are observed (Fig. 4, A). Besides, in ^{13}C -NMR spectra (Fig. 5, A) no prominent peaks due to methoxyl groups [8] (58 and 150 ppm) are present. The 0–50 ppm region, assigned to paraffinic carbons or carbons that are chemically bonded only to other carbons, is intense in all the spectra, indicating that paraffinic structures are major contributors. The major peak in this region is centred at 28 ppm, indicating aliphatic side chains. The aromatic carbon portion is small compared to terrestrial HA [9]. This reflects the lack of abundant aromatic precursors and the aquatic origin of the studied humic compounds [10–12]. Aromatic carbons present in humic structures probably derive from algae.

In deeper layers the percentage both of HA and FA is constant and slightly lower than that found in the upper layer, except for B_3 and B_4 sampling points. In these stations the amount of both HA and FA are very high (Fig. 2).

Elemental analysis percentage of HA obtained from all samples is reported in Table 1. Elemental composition is constant, except for HA obtained from deeper layers of B_3 and B_4 stations, where oxygen percentage, obtained as difference, is higher. A higher content of oxygen, even if less in comparison with B_3 and B_4 is also observed in the upper layer of the A_1 station, characterized by a high presence of algae.

FTIR and ^{13}C -NMR spectra referring to both HA and FA of different horizons are in agreement with elemental analysis data. In correspondence with B_3 and B_4 sampling points the carbohydrate peak areas of HA and FA increase along with the depth (Fig. 4A, B; Fig. 5), whereas carbohydrate content in HA and FA from deeper sediment samples shows generally less compositional differences when compared to that of near surface sediment samples.

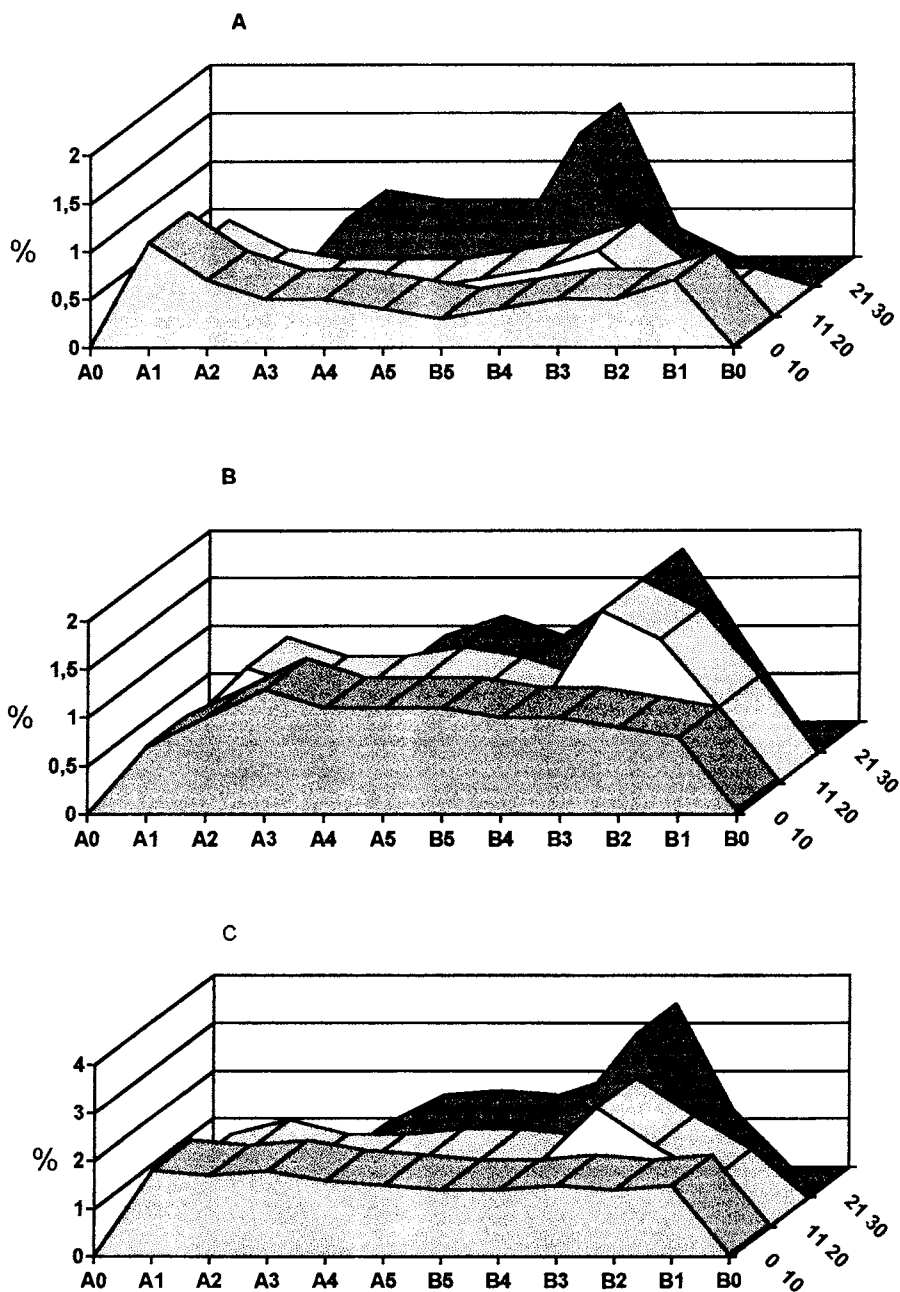


Fig. 2. Trends of percentage yields of fulvic acids (A), humic acids (B) and total humic compounds (C) in the three different layers of sediments.

Remarkable seasonal variations of the structural composition have not been observed both in HA and FA even though carbohydrate content in superficial FA of A₁ and B₁

is higher in summer, when the algae production is greater. Also FA concentration in this season is greater (0.70 and 0.27%, respectively).

In conclusion, regarding the general features of humic substances extracted by Martignano sediments, the ones extracted in the deeper layer of B₃ and B₄ stations show anomalous characteristics like the high amount of HA and FA in sediments, the higher oxygen percentage, the compositional differences (high carbohydrate content). These characteristics are also present by FA of A₁ and B₁ upper layer and are more evident in summer. It can be hypothesized that in correspondence with B₃ and B₄ stations it is a well localized source of organic carbon that concerns principally the deeper layers of lake sediments. Indeed, during some dives, a wooden structure has been found in this area. This structure consists of a set of

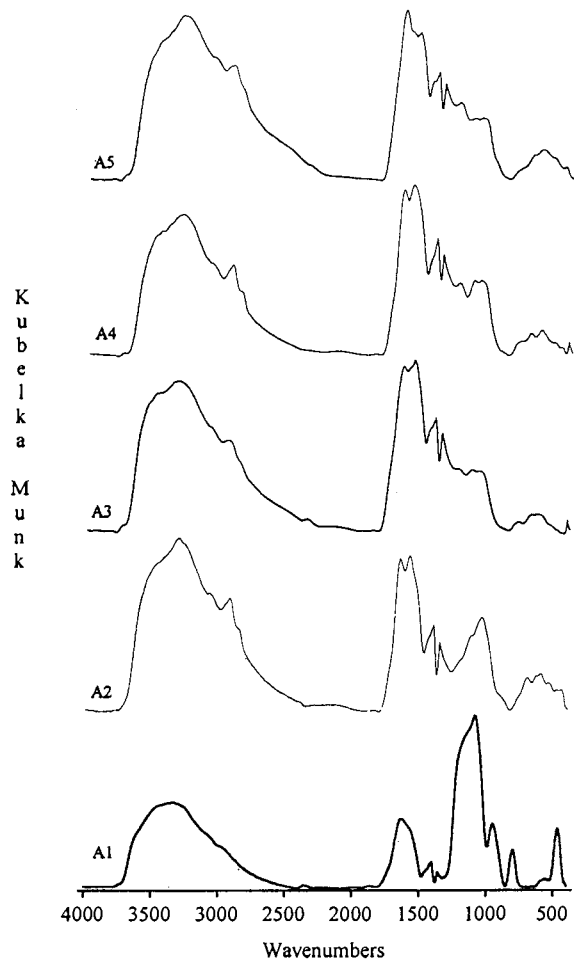


Fig. 3. FTIR spectra of superficial fulvic acids along the transept.

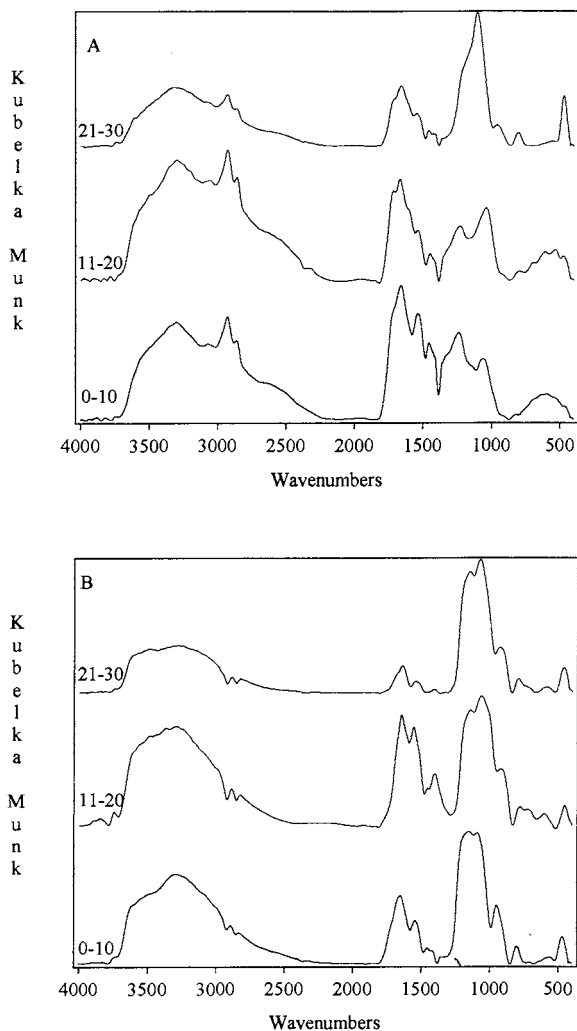


Fig. 4. FTIR spectra of humic acids in B₄ sampling point and of fulvic acids in B₃ sampling point.

branches, each one put on top of another one and of stakes without their barks; some of them are vertically thrust into the bottom of the lake, while others are horizontally placed. The set of branches is about 30 m long and 20 cm high and is placed on the edges of a highly sloping wall, which might have been the ancient shore.

Therefore, humic compounds characterized by different structural features are able to 'indicate' some anomalies in the environment that are being studied, such as the presence of carbon's punctual sources.

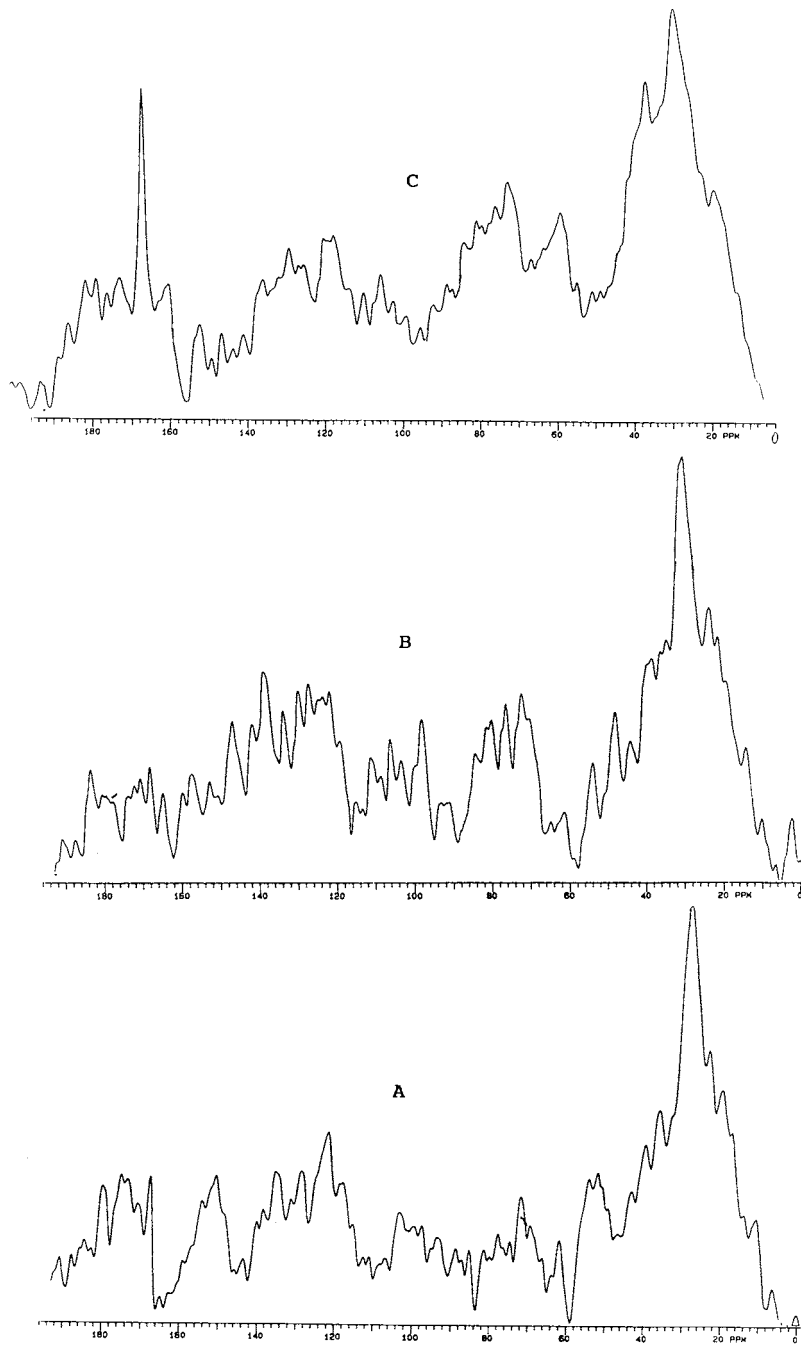


Fig. 5. ¹³C-NMR spectra of humic acids in B₃ sampling point; (A) 0–10 cm layer; (B) 11–20 cm layer; (C) 21–30 cm layer.

Table 1
Elemental analysis of humic acids

Samples		N (%)	C (%)	H (%)	O (%)
A ₀	0 10	4.4	47.3	4.4	43.9
A ₁	0 10	3.6	45.3	3.5	47.6
	11 20	5.3	51.5	5.5	37.7
A ₂	0 10	4.5	50.7	5.4	39.4
	11 20	4.9	51.5	5.4	38.2
A ₃	0 10	5.3	50.7	6.2	37.8
	11 20	4.5	51.5	6.0	38.0
	21 30	5.4	51.1	6.2	37.3
A ₄	0	4.5	46.6	5.3	43.6
	11 20	5.6	52.3	6.1	36.0
	21 30	5.5	51.6	6.3	36.6
A ₅	0 10	5.3	49.0	5.5	40.2
	11 20	5.9	53.5	6.6	34.0
	21 30	5.1	50.3	5.9	38.7
B ₅	0 10	5.5	51.7	5.8	37.0
	11 20	5.3	46.0	5.9	42.8
	21 30	4.9	47.1	6.1	41.9
B ₄	0 10	5.6	53.0	6.0	35.4
	11 20	5.1	48.6	6.0	40.3
	21 30	3.9	38.3	4.6	53.2
B ₃	0 10	4.9	48.4	5.6	41.1
	11 20	3.8	37.3	4.3	54.6
	21 30	3.2	32.9	3.8	60.0
B ₂	0 10	5.1	51.9	6.2	36.8
	11 20	5.4	53.1	6.2	35.3
	21 30	5.0	55.0	5.5	34.5
B ₁	0 10	5.8	54.7	5.9	33.6
	11 20	5.1	54.3	6.1	34.5
B ₀	0 10	4.5	48.9	5.3	41.3

References

- [1] J.F. McCarthy, J.M. Zachara, *Environ. Sci. Technol.* 23 (1989) 496.
- [2] P. LaFrance, O. Banton, P.G.C. Campbell, J.P. Villeneuve, *Wat. Sci. Tech.* 22 (1990) 15.
- [3] M.A. Rashid, *Geochemistry of Marine Humic Compounds*, Springer-Verlag, Heidelberg, 1985, p. 58.
- [4] M.A. Rashid, L.H. King, *Geochim. Cosmochim. Acta* 33 (1968) 147.
- [5] E.M. Thurman, R.L. Malcolm, *Environ. Sci. Technol.* 15 (1981) 463.
- [6] N. Calace, F. De Paolis, F. Minniti, B.M. Petronio, *Talanta* 47 (1998) 803.
- [7] P.G. Hatcher and W.H. Orem, *Organic Marine Geochemistry*, L. Sohn (ed), 1986, p. 142.
- [8] A.H. Gillam and M.A. Wilson, *Organic Marine Geochemistry*, L. Sohn (ed), 1986, p. 128.
- [9] W. Orem, P.G. Hatcher, *Int. J. Coal Geol.* 8 (1987) 33.
- [10] J.M. Dereppe, C. Moreaux, Y. Debyser, *Org. Geochem.* 2 (1980) 117.
- [11] H.M. Hurst and N. Burges, In: A.D. McLauren, G.H. Peterson (Eds.), *Soil Biochemistry*, Dekker, New York, 1967, cap II.
- [12] A. Nissenbaum, I.R. Kaplan, *Limnol. Oceanogr.* 17 (1972) 576.

Comparison of three derivatization reagents for the analysis of Se(IV) based on piaszelenol formation and gas chromatography-mass spectrometry

J.L. Gómez-Ariza ^{a,*}, J.A. Pozas ^b, I. Giráldez ^a, E. Morales ^a

^a *Departamento de Química y Ciencia de los Materiales, Escuela Politécnica Superior, Universidad de Huelva, La Rabida, Huelva, Spain*

^b *Departamento de Bioquímica, Bromatología y Toxicología, Facultad de Medicina, Universidad de Sevilla, Sevilla, Spain*

Received 15 October 1998; received in revised form 23 November 1998; accepted 27 November 1998

Abstract

A comparison between the performance of three derivatizing reagents (4-chloro-*o*-phenyldiamine, 4-nitro-*o*-phenyldiamine and 2,3-diaminonaphthalene) for the analysis of selenite in environmental samples using gas chromatography-mass spectrometry (GC-MS) has been evaluated. The effects of different parameters (pH, temperature and time of derivatization, type and volume of organic solvent and time and number of extractions) on the derivatization reaction and extraction of the derivatives have been evaluated. Derivatization using 2,3-diaminonaphthalene took a longer time compared to those obtained using the other reagents. The highest sensitivity was obtained using 4-chloro-*o*-phenyldiamine. No matrix interferences were observed in tap, river and seawater using the three reagents. © 1999 Elsevier Science B.V. All rights reserved.

Keywords: GC-MS; Selenium; Speciation; Piazselenol

1. Introduction

Selenium, being one of the biologically essential elements for man, is found in aquatic systems at concentrations ranging from less than 2 ng l⁻¹ to thousands of µg l⁻¹ [1]. The human nutritional requirement for selenium has been determined to be in the range 0.1–0.3 mg kg⁻¹. However, from

2 to 10 mg kg⁻¹, selenium produces chronic toxicity symptoms as liver carcinoma, cirrhosis, teeth, hair and nail losses, irritation of the eyes and paralysis [2].

A variety of analytical techniques for the determination of selenium has been developed [3–9]. Selenium species must be transformed to more volatile forms to be analysed by gas chromatography (GC). Both hydride generation [10] and alkylation [11] have been used for this purpose. The volatile compounds are usually trapped at low temperatures prior to the introduction into the

* Corresponding author. Tel.: +34-959-530246; fax: +34-959-350311.

E-mail address: ariza@uhu.es (J.L. Gómez-Ariza)

chromatographic device. Frequently, electron capture detection (ECD) has been used for selenium (Se(IV)) determination in natural matrices using *o*-phenylenediamines to form the corresponding volatile piaszelenol derivative. The highest sensitivity is obtained using 5-nitropiazselenol as a derivative to be determined by GC-ECD with an absolute detection limit of 1 pg [12]. However, ECD is not specific for selenium and spurious chromatographic peaks are usually observed close to the piaszelenol signal [13]. Therefore, other selenium-specific detectors have been proposed in selenium speciation such as microwave-induced plasma (MIP)-AES, flame photometric detector (FPD) and mass spectrometry (MS) [14]. The use of MS presents the added value of the possibility of combining it with isotope dilution (ID) [15]. Dissolved selenium species have been determined using MS after ID and formation of ions by thermal ionization. A precise determination at the parts per trillion level was achieved [16]. In that study, the mass spectrometric measurements were carried out with a high resolution (and costly) magnetic sector field instrument. Inorganic selenium species have been also determined using an ID-GC-ICP-MS system after piaszelenol formation, the accuracy was demonstrated and an absolute detection limit of about 3 pg was reached [17]. However, this approach is far from being a common technique for routine analysis available to environmental laboratories. Finally, quantitative determination of selenium in several environmental matrices was achieved by ID-GC-MS using a benchtop instrument and 4-nitro-*o*-phenylenediamine as reagent for the formation of the piaszelenol derivative [13].

Most of the analytical methods for the selenium determination based on the GC approach take advantage of the formation of piaszelenols and several reagents have been described in the literature [13,18]. Optimization of the different steps of the reaction is necessary and kinetic models may be derived from data resulting from these studies as demonstrated by Johansson et al. using 4,7-dibromo-5,6-benzopiazselenol synthesized by the same authors [19,20]. In their work, a great influence of both temperature and acid concentration as well as a little effect of the ligand concentration

on the rate of formation of piaszelenol was stated. Aggarwal et al. investigated the gas chromatographic behaviour of three derivatizing reagents for the determination of selenium in urine using ID-GC-MS and the performance of the reagents including memory effects and accuracy of isotope ratio measurements followed the order: 4-trifluoromethyl-*o*-phenylenediamine > 3,5-dibromo-*o*-phenylenediamine > 4-nitro-*o*-phenylenediamine [15].

The aim of this work is to establish an optimal derivatization reaction for Se(IV) determination by GC based on the use of three commercial *o*-phenylenediamines to form piaszelenols. The method has been performed for inorganic selenium species determination in natural waters from the southwest of Spain using GC-MS.

2. Experimental

2.1. Reagents, standards and apparatus

The analytical grade reagents and pesticide grade solvents (whose purity for organic compounds is checked by GC and HPLC) used in the experiments were obtained from Merck (Darmstadt, Germany) and Sigma (St. Louis, MO). Strong anionic exchange cartridges (SAX), 600 mg of sorbent, were obtained from Alltech (Deerfield, IL). Stock solutions of Se(IV) and selenate (Se(VI)) (1000 mg l⁻¹ of Se) were prepared from analytical-reagent grade selenium dioxide and anhydrous sodium selenate (Sigma), respectively. Intermediate solutions of 1 mg l⁻¹ of Se(IV) and Se(VI) were prepared by dissolving appropriate volumes of stock solutions and bringing the volume to 50 ml with water. Working solutions were prepared daily by appropriate dilutions of the intermediate solutions with water. Water used in the experiments was double-distilled and deionized (Milli-Q gradient, Millipore, Madrid, Spain). Plastic and glassware used for experiments were previously soaked in 0.08 mol l⁻¹ nitric acid for 24 h and rinsed carefully with double-distilled water.

Selenium species were determined by using an HP Model 5890 gas chromatograph, an HP

Table 1

Experimental conditions for piaszelenol formation, extraction and determination

PRIVATE	4-Chloro- <i>o</i> -phenyldiamine	4-Nitro- <i>o</i> -phenyldiamine	2,3-Diaminonaphthalene
Derivatization temperature (°C)	75	75	25
Derivatization time (min)	7	7	60
Extractant	2 × 3 ml of toluene	2 × 3 ml of toluene	2 × 3 ml of toluene
m^+/z of derivative	218	229	234
Retention time of derivative (min)	10.5	13.3	16.0
m^+/z internal standard	186	186	186
Retention time of internal standard (min)	9.8	9.8	9.8

Model 5970 mass detector and a fused silica capillary column, 25 m length, 0.20 mm i.d. and a film thickness of 0.33 μm HP-1 crosslinked methyl-silicone gum (Palo Alto, CA). Sample aliquots of 1 μl were manually injected using splitless injection mode (purge time = 0.5 min off). Helium was used as carrier gas at an inlet head pressure of 100 kPa. The interface temperature was operated at 260°C. Electron impact (EI) with an emission current of 0.4 mA and an electron energy of 70 eV were used to ionize the compounds eluting from the chromatographic column and the filament remained off until the solvent was eluted. A scan time of 1.0 s was used over a mass range of 40–500 m/z . Data were stored as total ion chromatogram (TIC) and quantification was performed by using single ion monitoring (SIM) mode.

2.2. Extraction of inorganic selenium species from water samples

Selenite was separated from selenate by solid phase extraction using a strong anion-exchange resin (SAX cartridge)[21]. The resin was conditioned by passing 10 ml of 3 M HCl followed by 10 ml of distilled water with a flow rate of 5 ml min^{-1} . The pH of the 500 ml water sample was adjusted to 7–8 using HCl or NaOH and then the sample was passed through the cartridge at a flow rate of 8 ml min^{-1} with the aid of a vacuum pump. Selenite and selenate were successively eluted with 25 ml of 1 M formic acid, which recovers Se(IV), and 25 ml of 3 M of hydrochloric acid for Se(VI), using a flow rate of 5 ml min^{-1} .

The hydrogen chloride extract containing Se(VI) was transferred to a Pyrex tube (50 ml) and selenate was quantitatively reduced to selenite by adding 10 ml of 5 M HCl and boiling for 30 min [22]. This digest was cooled to room temperature, the pH adjusted to 2 with NaOH and then derivatized.

2.3. Derivatization of Se(IV)

Five ml of either 0.1% (w/w) 4-chloro-*o*-phenyldiamine, 4-nitro-*o*-phenyldiamine or 2,3-diaminonaphthalene in 0.1 M HCl was added to the solution containing Se(IV) whose pH was previously adjusted to 2 with HCl. Both the derivatization temperature and the time to form the corresponding piaszelenol are depicted in Table 1. Once the derivatization was completed and after allowing the solution to cool to room temperature, the selenium derivative was extracted twice with 3 ml of toluene by shaking for 1 min. The organic phase was separated from the aqueous phase and reduced to just dryness under a N_2 stream. The residue was dissolved in 50 μl of hexane containing fluoro-di-nitrobenzene (FDNB) as internal standard (23 mg l^{-1}). Aliquots of 1 μl were analysed by GC-MS. The chromatographic analysis of the piaszelenols was performed using the following oven temperature program: 40°C for 1 min after injection, followed by a 60°C min^{-1} ramp to 125°C and maintaining this temperature for 1 min. Then a second heating ramp of 10°C min^{-1} up to 250°C and a final isotherm for 1 min. The injector block was heated to 240°C and the injection volume was fixed to 1 μl . Reten-

tion times and m^+/z used for quantitative analysis are presented in Table 1.

2.4. Calibration and performance parameters

Selenium concentrations were deduced from calibration curves derived from calibration solutions in seawater previously passed through SAX cartridge and using peak heights. The SAX cartridge is a styrene-divinylbenzene strong exchange resin containing 1.0 mEq of a quaternary amine and it is used in the acetate form. Standard addition procedures were performed to avoid possible matrix effects. The repeatability in a day was evaluated developing five analysis of an aqueous standard solution containing Se(IV). Other performance parameters of the proposed method such as reproducibility over a month, detection limits (evaluated as $3 \times \text{S.D.}$ of the mean blank + the value for the mean standard blank, for $n = 10$ standard blank runs), sensitivities (slope of the calibration curve) and correlation coefficients were also evaluated.

2.5. Statistical treatment

The data were analysed statistically for differences using factorial analysis of variance (ANOVA). Prior to analysis, all the data were tested for homogeneity of variance using the Bartlett and Levene tests. Parametric statistical test (Student's t -test) was applied to different hypothesis. An α -value of 0.05 was adopted as the critical level for all statistical tests giving a 95% confidence level (CSS: STATISTICA™).

2.6. Application to natural samples

The method was applied to the analysis of unfiltered and unacidified sea, river and tap water samples collected from the southwest of Spain with low suspended matter contents ($< 1 \text{ mg l}^{-1}$) and was validated for Se(IV) using the CRM CASS-3 (NRC, Canada) and 4-chloro-*o*-phenyldiamine as reagent for derivatization. The CRM consisted of a nearshore seawater with 0.5 mg l^{-1} of total dissolved organic matter,

acidified to pH 1.6 whose Se(IV) concentration is $0.020 \pm 0.005 \text{ } \mu\text{g l}^{-1}$.

3. Results and discussion

Conditions for the formation of three volatile and thermally stable piaszelenol derivatives based on the reaction of Se(IV) present in water with 4-chloro-*o*-phenyldiamine, 4-nitro-*o*-phenyldiamine and 2,3-diaminonaphthalene were studied. Physico-chemical parameters of the aqueous medium such as pH, temperature and time of derivatization, nature and volume of the organic solvent for piaszelenol extraction, number and time of extractions were optimized. For this purpose, $0.40 \text{ } \mu\text{g}$ of Se(IV) were derivatized and analysed by GC-MS using the derivatization procedure described under Section 2.

3.1. Formation of piaszelenol

Several pH values for the samples ranged from 0.4 and 4 were tested for the derivatization of $0.40 \text{ } \mu\text{g}$ of Se(IV) using 4-chloro-*o*-phenyldiamine, 4-nitro-*o*-phenyldiamine and 2,3-diaminonaphthalene, and the highest selenium derivatization yield was achieved for pH values between 1.5 and 2.5 (t -test, $P < 0.028$), which confirms previous studies carried out by other authors [13]. Consequently, the pH of the sample was adjusted to 2 for further experiments. Derivatization temperatures between 25 and 90°C were tested and the results are presented in Fig. 1. Significantly higher reaction yields were obtained for both the 5-chloro- and the 5-nitro-piazselenol using at least a temperature of 60°C (t -test, $P < 0.01$). However, optimum temperature for reaction of 2,3-diaminonaphthalene and Se(IV) was established at 25°C (t -test, $P < 0.001$). In Fig. 1, the results obtained from Se(IV) derivatization using different reaction times are presented. A reaction time of at least 3 min was necessary for the formation of 5-chloro- and the 5-nitro-piazselenol (t -test, $P < 0.001$) at 75°C and a longer period of time did not improve the reaction (ANOVA, $P > 0.719$). However, a reaction longer than 1 h was necessary to compensate the influence of the lower reaction temperature necessary for the derivatiza-

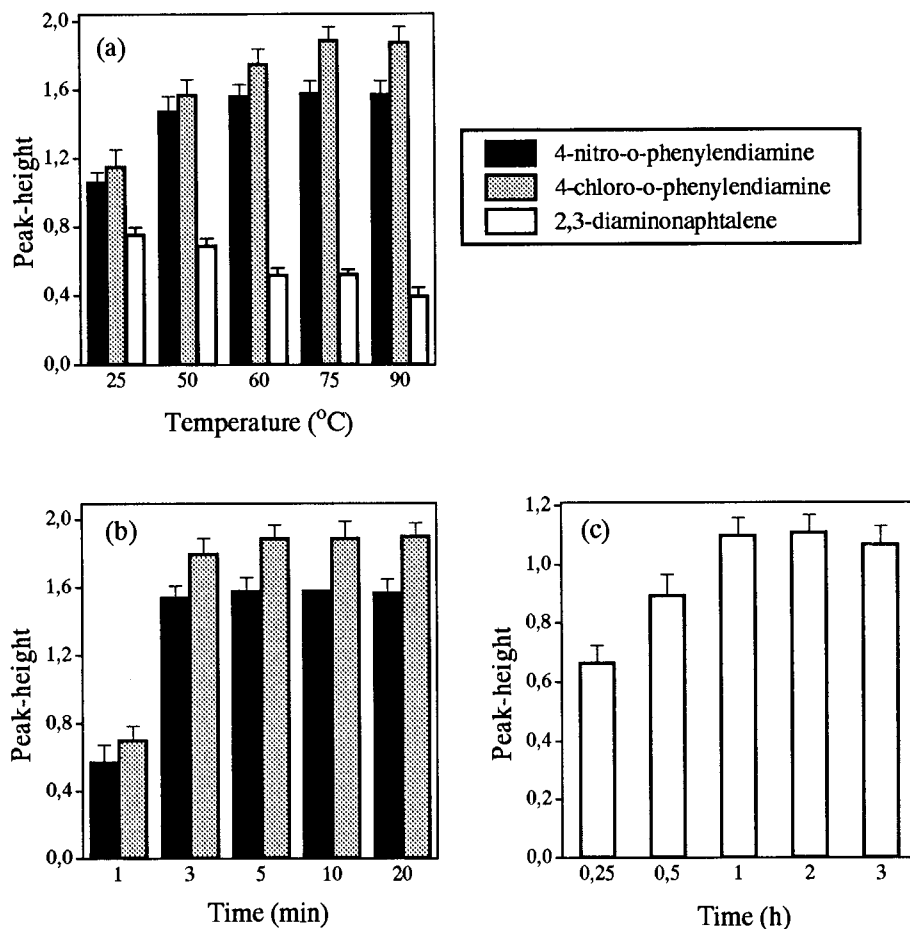


Fig. 1. (a) Effect of the temperature of reaction on the derivatization of 0.40 µg of Se(IV) for analysis by GC-MS; (b) effect of the time of reaction on the derivatization of 0.40 µg of Se(IV) using 4-chloro-*o*-phenyldiamine and 4-nitro-*o*-phenyldiamine for analysis by GC-MS; (c) effect of the time of reaction on the derivatization of 0.40 µg of Se(IV) using 2,3-diaminonaphthalene for analysis by GC-MS. Bars represent S.D.

tion with 2,3-diaminonaphthalene (*t*-test, $P < 0.003$).

3.2. Extraction of the piaszelenol

The piaszelenols have to be extracted into an organic solvent prior to the analysis by GC-MS. Several organic solvents were studied for the extraction of each piaszelenol using a single extraction into 1 ml of solvent. The results are presented in Fig. 2 and show that toluene is the best choice (*t*-test, $P < 0.001$). Therefore this solvent was used in further experiments. Different extraction times,

ranging from 1 to 10 min, were tested but no significant differences were found (ANOVA, $P > 0.37$). One minute was adequate to ensure a maximum extraction of the piaszelenols into toluene and was used in subsequent experiments. Up to three successive extractions were performed but no significant differences were found (ANOVA, $P > 0.14$) and two extractions were used in further experiments. Finally, volumes of solvent ranging from 1 to 10 ml were tested. There were no significant difference for the extraction yields obtained using different volumes of toluene (ANOVA, $P > 0.10$).

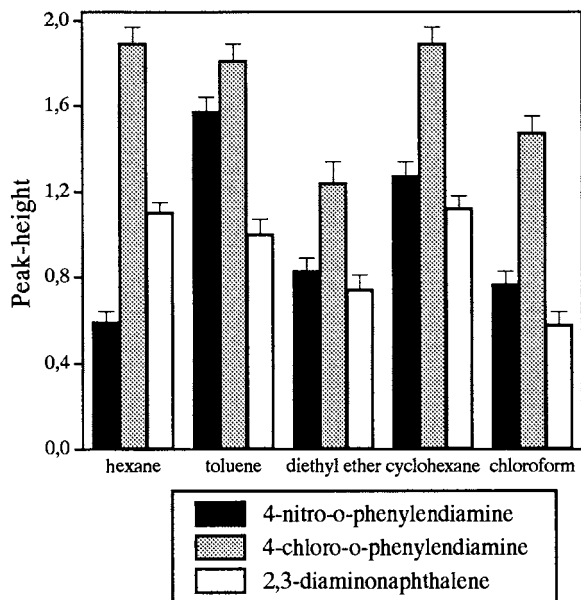


Fig. 2. Effect of the organic solvent used for the extraction of the piaszelenol derivative on the analysis of 0.40 μg of Se(IV) by GC-MS. Bars represent S.D.

3.3. Calibration and detection limits

The quantitative analysis of the selenium derivatives was carried out in the SIM mode for the following fragments: $m/z = 218$ (4-chloro-*o*-phenyldiamine), $m/z = 229$ (4-nitro-*o*-phenyldiamine), $m/z = 234$ (2,3-diaminonaphthalene) and $m/z = 186$ (internal standard). The dwell time of each mass was 100 ms. Five replicates of the samples were analysed using FDNB as internal standard. The quantification was carried out using peak height obtaining relative standard deviations lower than 5%, better than those obtained using peak area. The calibration curves were lin-

ear for selenium amounts from detection limit (1 ng) to less than 75 ng, with correlation coefficients greater than 0.99. The sensitivities (slope of the calibration curve) were 4.56 ± 0.03 , 3.70 ± 0.04 and $3.28 \pm 0.05 \mu\text{g}^{-1}$ for 4-chloro-*o*-phenyldiamine, 4-nitro-*o*-phenyldiamine and 2,3-diaminonaphthalene, respectively. The repeatability and the reproducibility of the derivatization method using aliquots of 75 ng of Se(IV) are presented in Table 2 and were lower than 10%.

3.4. Choice of the piaszelenol

According to the results obtained in the previous paragraphs and the data provided in the literature [13], the optimal conditions for the piaszelenol formation were obtained using pH values lower than 2.5. Moreover, longer derivatization times were necessary at lower derivatization temperatures. However, the relative sensitivities between the three piaszelenols change depending on the use of ECD or MS detector as can be observed by comparing our results using MS and data obtained by other authors using ECD [13]. Comparative sensitivities were obtained for both 5-nitro-piazselenol and 5,6-benzo-piazselenol using MS detector, which were 1.3 times lower than that for 5-chloro-piazselenol. This behaviour contrasts with those obtained using ECD which sensitivity for the 5-nitro-piazselenol has been reported as 7.5 and 28 times higher than that for 5-chloro-piazselenol and 5,6-benzo-piazselenol, respectively [13]. In addition, the derivatization using 2,3-diaminonaphthalene required a longer period of time than that using the other derivatization reagents.

Table 2
Analytical characteristics of the analysis of piaszelenols by GC-MS

PRIVATE	4-chloro- <i>o</i> -phenyldiamine	4-nitro- <i>o</i> -phenyldiamine	2,3-diaminonaphthalene
Detection limit (ng, as Se)	1	1	1
Sensitivity (μg^{-1} , as Se)	4.56 ± 0.03	3.70 ± 0.04	3.28 ± 0.04
Correlation coefficient	0.999	0.999	0.999
Repeatability (% R.S.D.) (75 ng)	4.9	5.0	5.3
Reproducibility (% R.S.D.) (75 ng)	7.1	8.2	8.3
Se(IV) in CASS-3 ($\mu\text{g l}^{-1}$)	0.017 ± 0.002	–	–

Table 3

Selenite and selenate concentration (average and S.D. for $n = 3$) in tap, river and seawater samples evaluated by GC-MS after piaszelenol formation

	Tap water, $\mu\text{g l}^{-1}$ (pH 7.1)		Seawater, $\mu\text{g l}^{-1}$ (pH 6.8)		River water, ng l^{-1} (pH 4.1)	
	External calibration	Standard addition	External calibration	Standard addition	External calibration	Standard addition
<i>Using 4-chloro-<i>o</i>-phenyldiamine as derivatizing reagent</i>						
Se(IV)	0.98 ± 0.09	0.95 ± 0.09	5.7 ± 0.4	6.0 ± 0.3	33 ± 3	35 ± 5
Se(VI)*	0.43 ± 0.03	0.43 ± 0.02	3.4 ± 0.2	3.6 ± 0.2	25 ± 2	29 ± 3
<i>Using 4-nitro-<i>o</i>-phenyldiamine as derivatizing reagent</i>						
Se(IV)	0.96 ± 0.08	1.09 ± 0.05	5.7 ± 0.5	5.8 ± 0.6	34 ± 2	37 ± 6
Se(VI) ^a	0.43 ± 0.03	0.45 ± 0.06	3.4 ± 0.3	3.6 ± 0.3	26 ± 2	28 ± 4
<i>Using 2,3-diaminonaphthalene as derivatizing reagent</i>						
Se(IV)	0.94 ± 0.07	1.0 ± 0.1	5.5 ± 0.3	5.5 ± 0.6	31 ± 3	32 ± 3
Se(VI) ^a	0.42 ± 0.03	0.42 ± 0.06	3.7 ± 0.3	3.7 ± 0.4	26 ± 2	25 ± 4

^a Indicative results.

3.5. Application to natural samples

A value of $0.017 \pm 0.002 \mu\text{g l}^{-1}$ of Se(IV) was found using 4-chloro-*o*-phenyldiamine as derivatizing reagent and GC-MS as the final analytical determination method for the CRM CASS-3 (in duplicate) in agreement with the certified value.

Selenium quantification in water samples collected from the southwest of Spain was carried out using both external calibration and standard addition methods. Samples were analysed in triplicate when external calibration was performed and three single additions of standards were carried out using the standard addition method. Results for the analysis of three types of water samples are presented in Table 3. No significant differences were found between the slopes of the calibration curve using both external calibration and standard addition methods (*t*-test, $P > 0.06$), which indicated the absence of matrix interferences. Moreover, no significant differences in selenium concentrations were found using the three derivatizing reagents (ANOVA, $P > 0.50$). However, the accuracy of the Se(VI) results are not guaranteed because no efforts were made to completely remove the organic matter from the sam-

ples. Transformations affecting the Se(VI) fraction are possible and known due to interferences from organic matter [23]. However, this was not the main purpose of this study.

4. Conclusion

The derivatization of Se(IV) to form piaszelenols using 4-chloro-*o*-phenyldiamine, 4-nitro-*o*-phenyldiamine and 2,3-diaminonaphthalene for selenium determination by GC-MS requires different reaction conditions. High temperature of reaction was necessary using 4-chloro-*o*-phenyldiamine. However, a shorter reaction time for 4-nitro-*o*-phenyldiamine was sufficient to obtain higher reaction yields. In addition, 4-chloro-*o*-phenyldiamine was judged more useful for the GC-MS determination of Se(IV) because of the higher sensitivity achieved using this derivative. The method can be applied to environmental waters from which Se(IV) and Se(VI) are quantitatively recovered and matrix interferences are not observed. However, it is possible to apply this method to other more complex matrices without requiring quantitative recovery if it is used in combination with the ID technique.

Acknowledgements

The authors wish to express their thanks to the DGICYT (Dirección General de Investigación Científica y Técnica) for Grant No PB95-0731.

References

- [1] J.E. Conde, M. Sanz-Alaejos, *Chem. Rev.* 97 (1997) 1979.
- [2] E.M. Bem, *Health Perspec.* 37 (1981) 183.
- [3] E.M. Donaldson, *Talanta* 24 (1977) 441.
- [4] I. Harrison, D. Littlejohn, G.S. Fell, *Analyst* 121 (1996) 1641.
- [5] V. Stibilj, M. Dermelj, A.R. Byrne, *Mikrochim. Acta* 123 (1996) 311.
- [6] H. Aydm, O. Oruc, *Fres. J. Anal. Chem.* 358 (1997) 859.
- [7] B. Lange, F. Scholz, *Fres. J. Anal. Chem.* 358 (1997) 736.
- [8] M.H. Hahn, K.A. Wolnik, F.L. Fricke, J.A. Caruso, *Anal. Chem.* 54 (1982) 1048.
- [9] P.M. Haygarth, A.P. Rowland, S. Stürup, K.C. Jones, *Analyst* 118 (1993) 1303.
- [10] M.H. Hahn, K.J. Mulligan, M.E. Jackson, J.A. Caruso, *Anal. Chim. Acta* 118 (1980) 115.
- [11] C.S. Evans, C.M. Johnson, *J. Chromatogr.* 21 (1967) 202.
- [12] C.F. Poole, N.J. Evans, D.G. Wibberley, *J. Chromatogr.* 136 (1977) 73.
- [13] S. Dilli, I. Sutikno, *J. Chromatogr.* 300 (1984) 265.
- [14] F. MacLeod, B.A. McGaw, C.A. Shand, *Talanta* 43 (1996) 1091.
- [15] S.K. Aggarwal, M. Kinter, D.A. Herold, *Anal. Biochem.* 202 (1992) 367.
- [16] D. Tanzer, K.G. Heumann, *Anal. Chem.* 63 (1991) 1984.
- [17] S.M. Gallus, K.G. Heumann, *J. Anal. Atom. Spectrom.* 11 (1996) 887.
- [18] A. Elaseer, G. Nickless, *J. Chromatogr. A* 664 (1994) 77.
- [19] K. Johansson, X. Luo, A. Olin, *Talanta* 42 (1995) 1979.
- [20] K. Johansson, Ö. Andersson, A. Olin, *Analyst* 120 (1995) 423.
- [21] J.L. Gómez-Ariza, J.A. Pozas, I. Giráldez, E. Morales, *The Analyst*, in press.
- [22] J. Pozas, *Especiación Analítica de Selenio Mediante el Acoplamiento GC-MS. Aplicación a Muestras Medioambientales*, PhD Thesis, Universidad de Huelva, 1996.
- [23] U. Örnemark, A. Olin, *Talanta* 41 (10) (1994) 67.

Optimization of performance and minimization of silicate interference in continuous flow phosphate analysis

J.-Z. Zhang^{a,b,*}, Charles J. Fischer^b, Peter B. Ortner^b

^a CIMAS, Rosenstiel School of Marine and Atmospheric Science, University of Miami, 4600 Rickenbacker Causeway, Miami FL 33149, USA

^b Ocean Chemistry Division, Atlantic Oceanographic and Meteorological Laboratory, National Oceanic and Atmospheric Administration, Miami, FL 33149, USA

Received 20 May 1998; received in revised form 9 November 1998; accepted 1 December 1998

Abstract

Specific reaction conditions for automated continuous flow analysis of phosphate are optimized in regard to minimizing coating and silicate interference, while maintaining high sensitivity. Use of Sb in the reagent increases sensitivity and yields absorbances with little temperature dependence. Coating can be minimized by using a final solution at a pH > 0.5. At final pH of 0.78 there is maximum interference from silicate in the sample. We recommend therefore as an optimal reaction condition with minimal silicate interference, the use of Sb, a final solution pH of 1.00, room temperature for the reaction and a $[H^+]/[Mo]$ ratio of 70. An equation is provided to correct silicate interference in high precision phosphate determination. © 1999 Elsevier Science B.V. All rights reserved.

Keywords: Phosphate determination; Silicate interference; Coating; Continuous flow analysis

1. Introduction

Phosphorus, together with nitrogen, is an essential nutrient supporting the plant growth in aquatic environments [1,2]. Due to the solubility limits of various phosphorus-containing minerals in earth's crust, phosphate concentrations are generally at low micromolar in the natural waters

[3,4]. In surface water, biological uptake through photosynthesis depletes phosphate concentration well below micromolar. Consequently, phosphorus becomes a nutrient that limits the primary productivity in many aquatic environments, especially in freshwater ecosystems [5–8]. To study the biogeochemical cycle of phosphorus, it is important to accurately measure the concentration of phosphate, which is the major form of phosphorus in natural waters. Quantitative analysis of phosphate in natural waters has relied on the formation of 12- molybdophosphoric acid and its

* Corresponding author. Tel.: +1-305-3614397; fax: +1-305-3614392.

E-mail address: zhang@aoml.noaa.gov (J.-Z. Zhang)

subsequent reduction to yield a blue-colored complex, the absorbance of which is readily measured by spectrometry [9–20]. Murphy and Riley's method [14] using Sb as a catalyst and ascorbic acid as a reductant has become the most widely used method for the analysis of phosphate in natural waters. Over the years numerous improvements on this method have been made. Among them the most important one has been that the ratio of $[H^+]/[Mo]$ in the final mixture must be kept at about 70 for rapid and stable color development [16–18]. However the coating and interference of this method have not been thoroughly investigated, especially the effects of pH and temperature on the coating and interference.

Coating is a well-known drawback of the molybdenum blue method for phosphate analysis. It results from the formation of a colloidal product that is readily adsorbed onto solid surfaces such as the cuvettes used in the absorbance measurement [19]. Additional rinses are often needed after each sample measurement. In automated continuous flow analysis the degree of coating is readily apparent in the shape of the sample peak on the recorder trace [15]. If there were no carryover due to coating the peak would be symmetrical and rectangular. Coating causes the distortion of this ideal peak to an asymmetric one with excessive tailing at the end. The tailing results from blue complex coating formed in the flowcell and tubing from a high concentration sample and re-dissolving in the subsequent wash solution and low concentration sample. The degree of coating is increased with increasing sample concentration and sample time. Consequently it takes a longer time, e.g. two to three sample-wash cycles, for the effect to disappear. The phenomenon is similar to the 'memory effect' in gas chromatography. Since an exact correction algorithm is not available it is desirable to minimize coating through optimization. A prolonged wash is often used to minimize coating effects but at the expense of sample throughput. In severe cases, it has been necessary to place a blank solution between samples [15]. The overall effect of coating is a decline in both precision and sample throughput.

An independent problem in phosphate analysis is competitive interference [11,21–24]. The method is subject to interference if arsenate and silicate are present in the sample since both can form similar blue complexes with molybdate [23,25–28]. Arsenate concentration is often much lower than phosphate in most natural waters (0.02 μM in open ocean [28]). However, in areas of arsenic pollution or hydrothermal activity arsenate concentrations can be comparable to phosphate concentrations [29,30]. In any case arsenate interference can be avoided by the addition of thiosulfate to reduce arsenate to arsenite which is non-reactive to molybdate reagent [31,32].

Unlike arsenate, silicate is often present in natural waters at concentrations that are one to three orders of magnitude higher than phosphate [33]. There is an abundance of silicon-containing minerals in the earth's crust and many are relatively soluble. It has been reported that at equilibrium dissolved silicate concentration is about 100 mM with quartz and about 2.3 mM with amorphous silica [34]. A high ratio of silicate to phosphate is often encountered in river, lake and ground water samples which contain low phosphate but a considerable amount of silicate resulting from the dissolution of ubiquitous amorphous silica minerals [35]. Interference from high silicate concentrations can overwhelm the phosphate signal. This artifact is evident when both phosphate and total dissolved phosphorus including dissolved organic phosphorus are measured in the same sample. The measured total dissolved phosphorus concentration can be lower than that of phosphate alone if the latter is not corrected for silicate interference. This anomaly results from the fact that the silicate interference is eliminated during the digestion procedure through which the dissolved organic phosphorus is oxidized to inorganic phosphate. Under the elevated temperature and pressure required for persulfate digestion silicate is polymerized in acidic solutions and becomes non-reactive to molybdate reagent when it undergoes subsequent phosphate analysis [36].

Murphy and Riley [14] noted an increase in absorbance of 0.002 due to 357 mM silicate in a blank solution. This is equivalent to 0.022 μM phosphate that was insignificant compared to 6.5

μM phosphate used in their interference study. Consequently, they concluded that no interference was caused by silicate at concentrations many times greater than its concentration in seawater. When Murphy and Riley's method was adapted to automatic continuous flow analysis, however, the interference increased to an equivalence of $0.06 \mu\text{M}$ phosphate in the presence of only $143 \mu\text{M}$ silicate [15]. Again this was considered a negligible error. Van Schouwenburg and Walinga [31] also reported no detectable interference from silicate concentration as high as 2.8 mM on the analysis of $48 \mu\text{M}$ phosphate samples. In contrast, Campbell and Thomas reported severe interference from silicate in an automated phosphate analysis in which interference equivalent to $1 \mu\text{M}$ phosphate resulted from a silicate concentration as low as $33 \mu\text{M}$ [36]. This severe interference was partially due to the high temperature (95°C) they used in the color forming reaction [36]. A linear correlation was found between silicate concentrations in the sample and resulting apparent phosphate concentrations. Instead of modifying the reaction conditions they made a significant correction to compensate for the interference [36]. A smaller degree of interference was reported in a later automated analysis with $<0.016 \mu\text{M}$ of apparent phosphate from 357 mM silicate when analyses were run at room temperature [32]. Ciavatta et al. [27] compared three manual methods of phosphate analysis and concluded the Murphy and Riley's method had the least interference from silicate.

With exception of Campbell and Thomas [36] and Ciavatta et al. [27] most earlier studies that concluded the silicate interference was negligible used a single silicate concentration and measured absorbance increase relative to a high phosphate concentration. Their phosphate concentrations were often much higher than those encountered in natural waters. As the sensitivity of phosphate analysis has been improved it is now possible to precisely quantify the silicate interference signals relative to the low phosphate concentrations typical of most surface water samples.

The various degrees of interference from silicate reported in the literature are not surprising given the very different experimental conditions used by

the different authors. The pHs used in past study varied widely, some studies used a pH as low as 0.2 [36–43]. Temperature also varied widely from 1 to 95°C [20,36]. The ratio of $[\text{H}^+]/[\text{Mo}]$ varied from 37 to 206. A systematic study is needed to quantify silicate interference with phosphate analysis as a function of reaction conditions, such as temperature and pH. Only with such a systematic study can an optimal reaction condition be defined for automated gas-segmented continuous flow phosphate analysis, providing both high sensitivity and minimal coating and silicate interference.

2. Experimental

The Alpkem Flow Solution auto-analyzer used for phosphate analysis consists of an auto-sampler, a peristaltic pump, a detector and a manifold containing mixing coils and a heater. The model 510 detector is a monochromator capable of measuring absorbance from 0.0005 to 2 Absorbance Units Full Scale (AUFS) at working wavelength ranged from 190 to 800 nm. The flow cell in the detector has a pathlength of 5.5 mm and a volume of $15 \mu\text{l}$. A flow diagram for phosphate analysis is shown in Fig. 1. Sample times and wash times were 90 and 30 s, respectively. Alpkem Softpac Plus software was used in the data processing.

The analytical method we used is essentially similar to the Murphy and Riley method [14]. Phosphate in the sample reacts with molybdate and potassium antimony tartrate in an acidic solution to form antimonymolybdophosphorus acid. The antimonymolybdophosphorus acid is then reduced by ascorbic acid to a molybdenum blue complex. The absorbance of the molybdenum blue complex is measured at 710 nm. For comparison the effect of Sb in the reagent, a few measurements were made using reagents without added Sb. Since the reaction product in the absence of Sb is molybdophosphorus acid that has a maximum absorbance at 840 nm [16], the measurements at 710 nm were corrected to 840 nm by absorbances measured on a Hewlett Packard 8453 spectrophotometer at both wavelength of 710 and 840 nm.

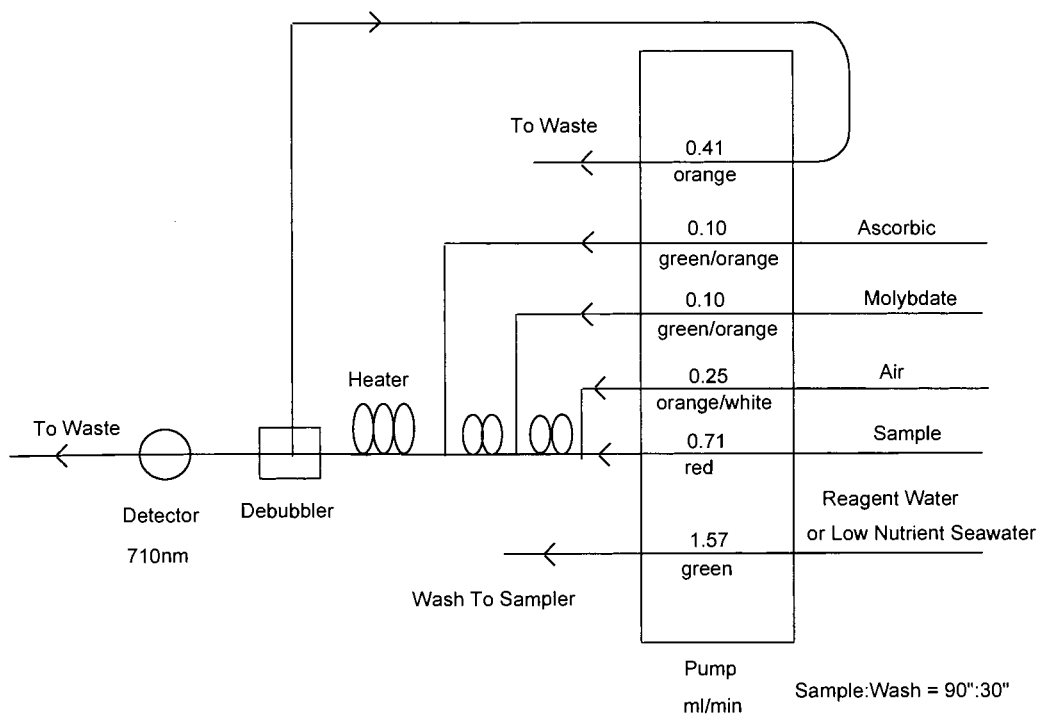


Fig. 1. Flow diagram and manifold configuration for automated gas segmented continuous flow phosphate analysis.

All reagents used were of analytical grade. Sodium dihydrogen phosphate was used to prepare the stock solution (2 mM) of phosphate standards. Sodium hexafluorosilicate was used to prepare silicate standards (2 mM). To ensure complete dissolution, a 0.3761 g of sodium hexafluorosilicate was stirred in ~800 ml of water for 24 h. The solution was then quantitatively transferred to a 1 l volumetric flask and diluted to the mark. Working standards of phosphate (50 nM–2 μ M) and silicate (20–100 μ M) were prepared daily by dilution. To avoid contamination from glassware silicate, plastic containers were used for handling standards, reagents and samples.

The effect of reaction temperature and final mixture pH upon the sensitivity, coating and interference from silicate were studied. The reaction temperature, final mixture pH were varied while the ratio of hydrogen ion to molybdenum ($[H^+]/[Mo]$) was held constant. Reaction temperature

was controlled to $\pm 0.1^\circ\text{C}$ and was varied from 25 to 70°C . pHs in final solutions ranged from 0.19 to 1.50. Precipitation of Sb precluded the study from final solution pH higher than 1.50. Concentrations of molybdate used (ranged from 0.45 to 9.6 mM) were calculated from a desired final pH such that ratios of $[H^+]/[Mo]$ remained at 70 ± 2 .

The extent of coating at various reaction conditions was estimated from carryover coefficients obtained using a high standard followed by two low standards (HLL scheme) as provided for within the Softpac Plus [44]. The apparent phosphate concentrations due to silicate interference were calculated from absorbances measured in the samples containing silicate alone using a calibration curve generated from phosphate standards. The concentrations of phosphate standards (0.05–1 μ M) used in each experiment were varied according to the magnitudes of silicate interference signals at given temperature and pH conditions.

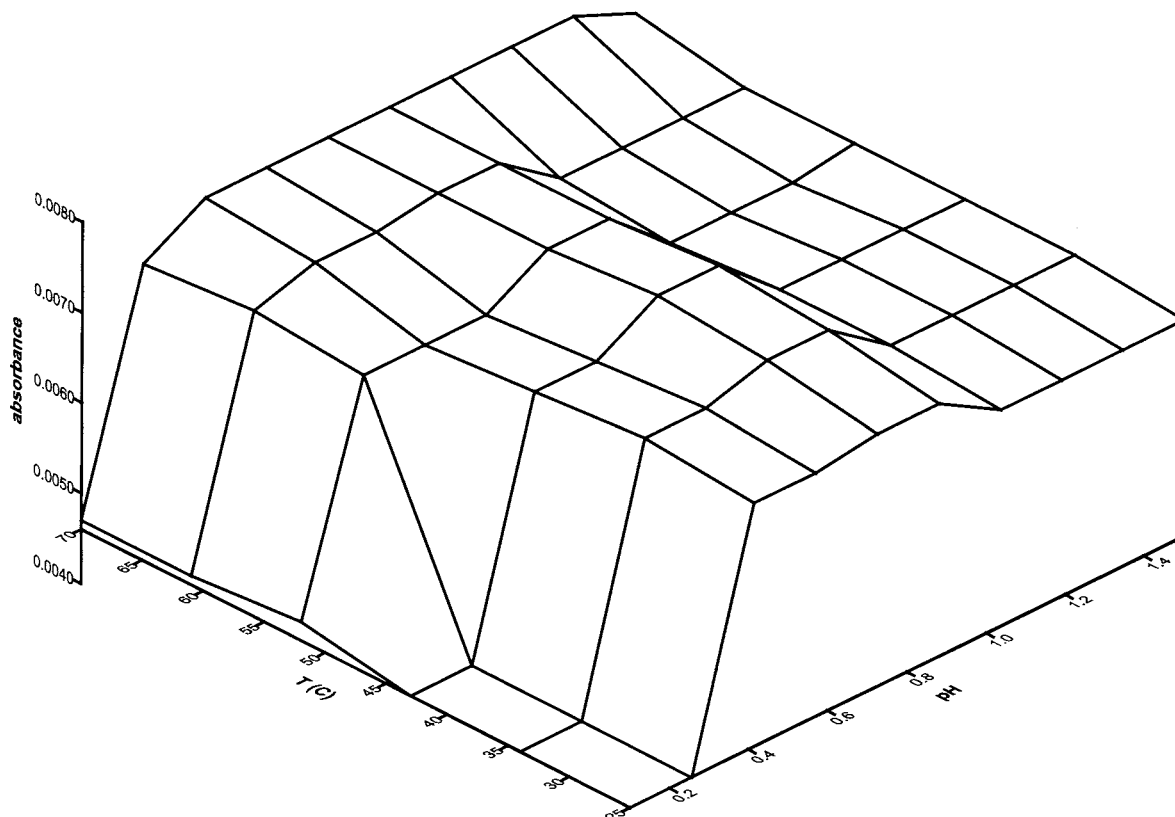


Fig. 2. Absorbances of 1 μM phosphate as a function of temperature and final solution pH at a $[\text{H}^+]/[\text{Mo}]$ ratio of about 70 with a 0.05 mM potassium antimony tartrate.

3. Results and discussion

3.1. Sensitivity

Since high sensitivity is essential given the low concentrations of phosphate typical of natural waters, the effect of reagent concentration, temperature and pH on overall method sensitivity was examined before considering the problems of coating and interference.

Effect of reaction temperature and pH of final solution on the absorbance was studied at a constant $[\text{H}^+]/[\text{Mo}]$ ratio of 70 in the presence of 0.05 mM of potassium antimony tartrate. Absorbances of phosphate normalized to 1 μM concentration as a functions of temperature and pH are shown in Fig. 2. At a given pH absorbances

are relatively constant over a temperature range of 25–70°C. This is likely due to the relatively fast reaction rate at a ratio of $[\text{H}^+]/[\text{Mo}]$ about 70 in the presence of Sb as potassium antimony tartrate. The time required for fully color development is only 2 min at room temperature [18]. The retention time in our automated analysis was about 7 min. This provided sufficient time for reaction completion even at room temperatures.

Method sensitivity was essentially constant within a pH range of 0.3–1.5 as shown in Fig. 2. This is in agreement with a previous study over a similar pH range of 0.36–1.06 at a $[\text{H}^+]/[\text{Mo}]$ ratio of 70 [18]. However, at a pH of 0.19 sensitivity was reduced about 40%. Since high concentrations of molybdate are required to maintain a constant ratio of $[\text{H}^+]/[\text{Mo}]$ at low pHs, polymer-

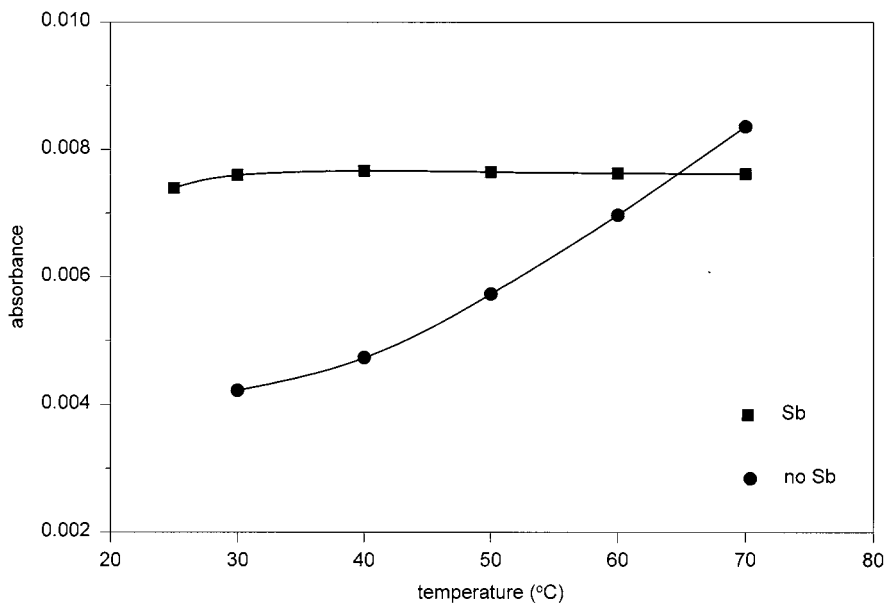


Fig. 3. The effect of Sb on absorbance as a function of temperature. Absorbances were measured from 1 μM phosphate at a final solution pH of 0.78 and a ratio of H^+/Mo of 70.

ization of molybdate at such high concentrations could hinder the molybdenum blue formation due to a lack of molybdenum dimmer [46].

In contrast, a positive temperature dependence was observed in a molybdate reagent with no added potassium antimony tartrate as shown in

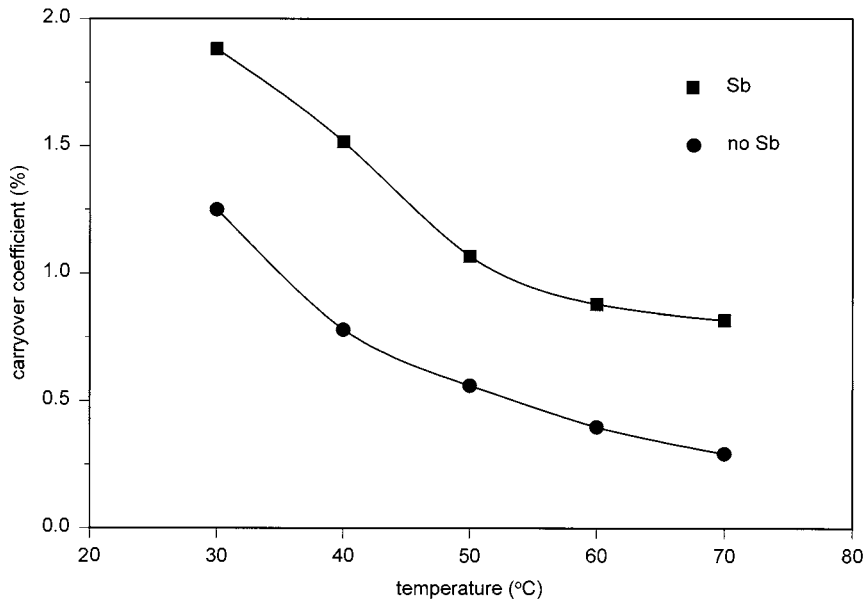


Fig. 4. The effect of Sb on the coating in automated phosphate analysis as a function of temperature at a $[\text{H}^+]/[\text{Mo}]$ ratio about 70 with 0.05 mM potassium antimony tartrate.

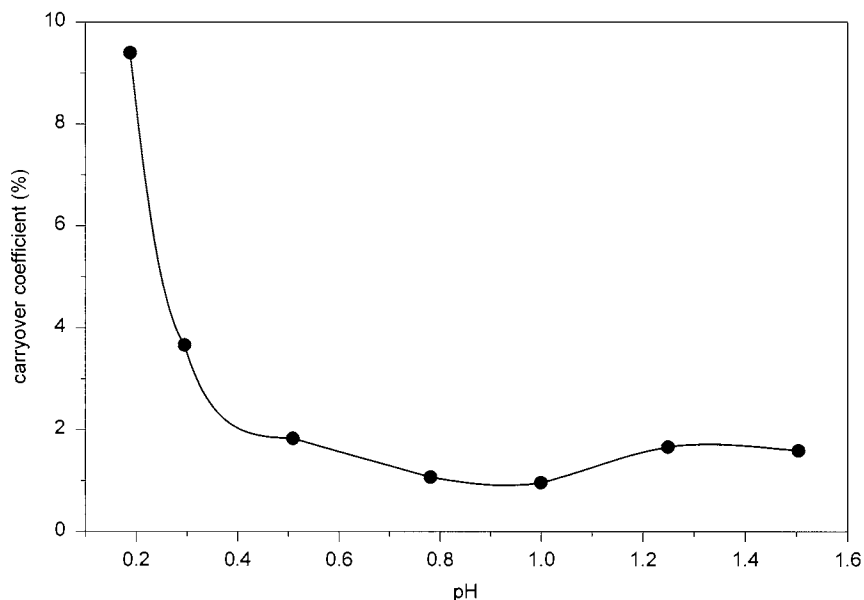


Fig. 5. Carryover coefficients as a function of final solution pH at a $[H^+]/[Mo]$ ratio about 70 with 0.05 mM of potassium antimony tartrate.

Fig. 3. At a temperature of 30°C absorbances of the same concentration of phosphate were about half of those measured in the presence of Sb due primarily to the slow reduction of molybdophos-

phorus acid. It has been reported that 24 h are needed to complete the reaction in the absence of Sb at room temperature [45]. The absorbances increase as temperature increases. At 70°C the

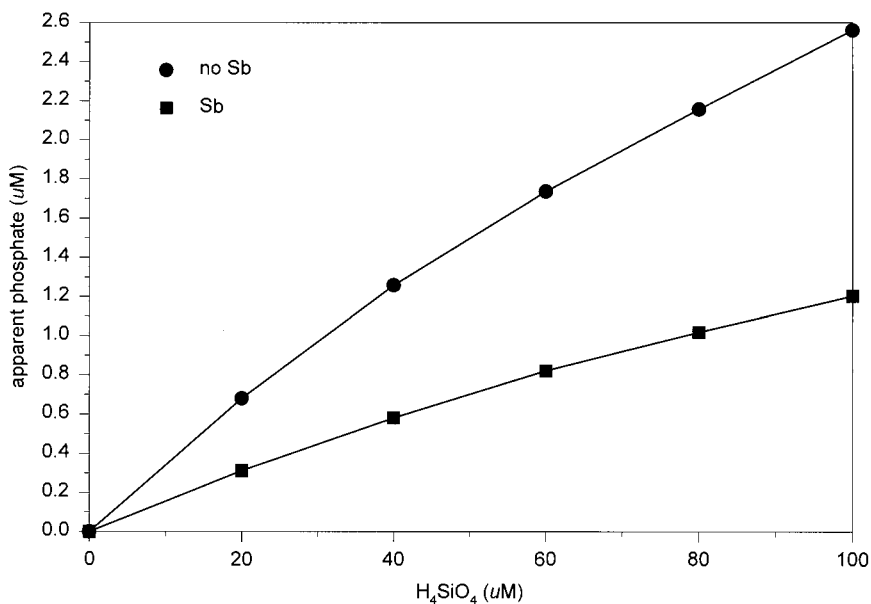


Fig. 6. The effect of Sb on apparent phosphate due to the silicate interference as a function of sample silicate concentration at 70°C, a final solution pH of 0.78 and a $[H^+]/[Mo]$ ratio of about 70.

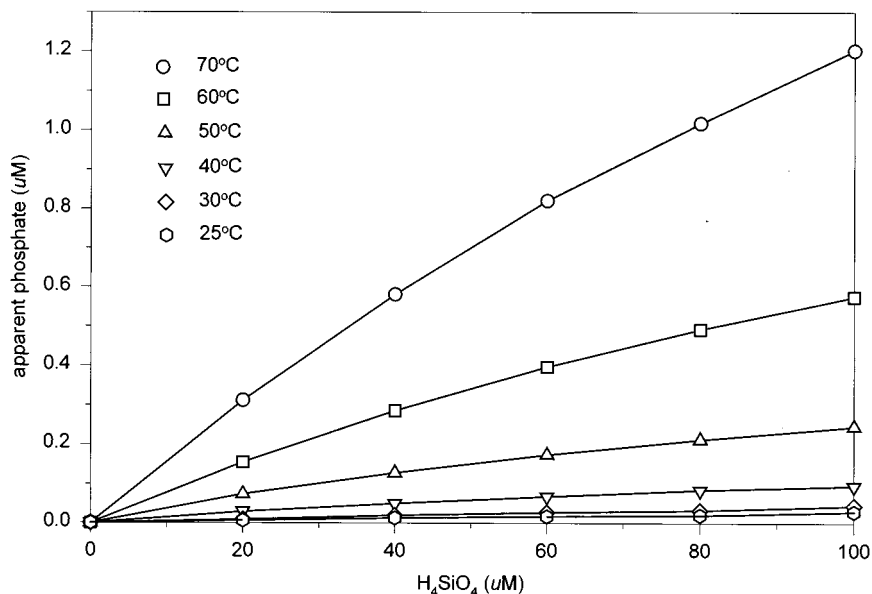


Fig. 7. Apparent phosphate due to silicate interference as a function of sample silicate concentration at various temperature with a final solution pH of 0.78 and a $[H^+]/[Mo]$ ratio of about 70.

absorbance measured from the reagent without Sb exceeds the value obtained with Sb.

Since the addition of Sb in the reagent increases sensitivity and reduces temperature dependence its use is clearly advantageous. We conclude that optimal conditions in respect to sensitivity are $pH > 0.3$ with the addition of Sb.

3.2. Coating

The effect of Sb on the coating as a function of temperature at a final solution pH of 0.78 is shown in Fig. 4. Carryover decreased with increasing temperature as one may expect since the solubility of colloidal molybdenum blue may increase with increasing temperature [46]. The carryover coefficients measured from a reagent mixture without Sb were slightly lower than those measured from a reagent containing Sb but the difference was not great.

Coating was almost constant over a pH range of 0.5 to 1.5 with carryover coefficients of 1–2% as shown in Fig. 5. They did, however, increase as pH decreased below 0.50. The carryover coefficient increased to about 9.5% at pH of 0.19.

Coating seemed to be related to the different characteristics of the molybdenum blue formed at different pH. The products formed at low pH seemed colloidal and tended to coat the flowcell and tubing. Over a wide range of pH (0.5–1.5) the products formed were sufficiently soluble and negligible coating effects were observed. At pH 0.78 and above carryover coefficients of about 1–2% are certainly acceptable since there were little differences from flow analysis of silicate and nitrite, which have essentially no coating effect. So an optimal condition for minimal coating is $pH > 0.5$.

3.3. Interference of silicate

Early studies found that absorbance due to silicate increases with time because the color development of silicomolybdenum blue is slower than that of phosphomolybdenum complex [19]. In manual analysis the time interval between reagent addition and absorbance measurement is difficult to keep constant from one sample to the next. A variable duration for color development will result in different degrees of silicate interfer-

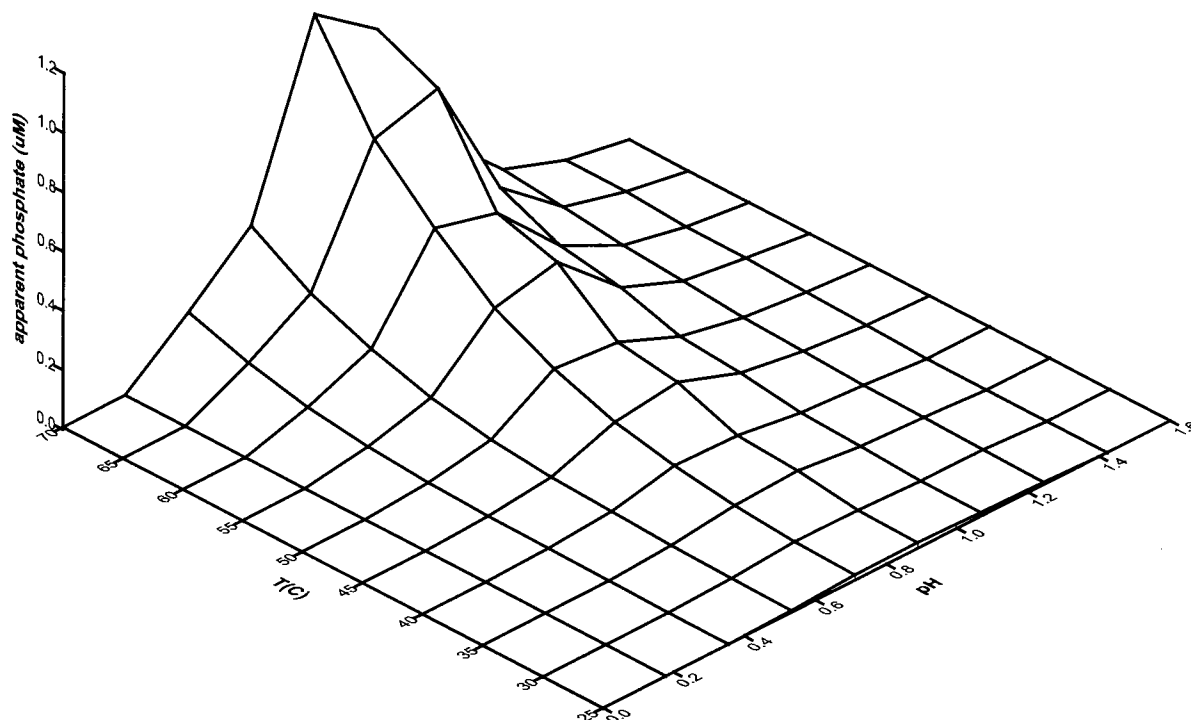


Fig. 8. Apparent phosphate due to the interference of 100 μM sample silicate as a function of temperature and final solution pH with a $[\text{H}^+]/[\text{Mo}]$ ratio of about 70.

ence. As a result it is, if not impossible, very difficult to correct for silicate interference in a manual method. One advantage of automated analyses over manual ones is precise timing and reagent mixing. The shorter interval between reagent addition and absorbance measurement in automated analysis also reduces the extent of interference given the slower formation of silico-molybdenum blue [19].

The potential interference of silicate on phosphate analysis is quantified by measuring absorbances in samples containing only silicate resulting from the phosphate analysis reactions. These absorbances can be translated to apparent phosphate concentrations using phosphate standards measured under the same conditions. Silicate concentrations in these samples ranged from 0 to 100 μM , concentrations commonly found in natural waters. We first tested the effect of Sb on potential silicate interference. The addition of Sb to the molybdate reagent not only increased sensi-

tivity as mentioned above but also reduced silicate interference to about 47% at 70°C as shown in Fig. 6. The relatively large interference from silicate reported by Campbell and Thomas at high temperature (95°C) was probably augmented by the absence of Sb in their reagent mixture [36]. Since addition of Sb to molybdate reagent has the advantages in sensitivity, color stability over a wide range of temperature and minimal effect on the coating as discussed above, Sb was used in all further experiments on silicate interference study.

Apparent phosphate increased as the silicate concentration increased in the samples. In contrast to a previous study [36], the response is non-linear, showing a pattern of exponential rise to maximum (see Fig. 7). The extent of apparent phosphate resulting from 100 μM in the sample as a function of temperature (ranged from 25 to 70°C) and pH (ranged from 0.19 to 1.50) is shown in Fig. 8. Temperature had a pronounced influence on apparent phosphate concentration. The

Table 1

Apparent phosphate concentrations (in μM) measured at various temperatures, pH of final mixture and silicate concentrations

Silicate (μm)	Temperature ($^{\circ}\text{C}$)					
	25	30	40	50	60	70
			pH = 0.19			
0		0.000		0.000		0.000
20		0.000		0.000		0.001
40		0.000		0.000		0.002
60		0.000		0.000		0.004
80		0.000		0.000		0.006
100		0.000		0.000		0.009
			pH = 0.30			
0		0.000	0.000	0.000	0.000	0.000
20		0.000	0.002	0.004	0.011	0.031
40		0.000	0.004	0.007	0.022	0.062
60		0.000	0.005	0.010	0.031	0.090
80		0.000	0.007	0.013	0.040	0.115
100		0.000	0.009	0.016	0.049	0.139
			pH = 0.51			
0	0.000	0.000	0.000	0.000	0.000	0.000
20	0.002	0.002	0.004	0.009	0.027	0.068
40	0.006	0.007	0.012	0.018	0.051	0.127
60	0.006	0.008	0.015	0.026	0.074	0.184
80	0.008	0.011	0.020	0.035	0.096	0.234
100	0.010	0.013	0.024	0.043	0.116	0.281
			pH = 0.78			
0	0.000	0.000	0.000	0.000	0.000	0.000
20	0.006	0.011	0.029	0.074	0.155	0.302
40	0.013	0.015	0.050	0.128	0.286	0.559
60	0.017	0.020	0.068	0.174	0.397	0.771
80	0.020	0.025	0.084	0.212	0.492	0.967
100	0.029	0.030	0.095	0.245	0.575	1.136
			pH = 1.00			
0		0.000	0.000	0.000	0.000	0.000
20		0.005	0.013	0.030	0.064	0.120
40		0.011	0.025	0.055	0.117	0.208
60		0.015	0.034	0.074	0.159	0.292
80		0.018	0.041	0.091	0.195	0.355
100		0.021	0.046	0.103	0.223	0.405
			pH = 1.25			
0	0.000	0.000	0.000	0.000	0.000	0.000
20	0.005	0.005	0.006	0.012	0.022	0.040
40	0.007	0.008	0.012	0.022	0.040	0.066
60	0.009	0.010	0.016	0.029	0.053	0.085
80	0.012	0.015	0.022	0.037	0.066	0.103
100	0.014	0.018	0.025	0.043	0.075	0.116
			pH = 1.50			
0				0.000	0.000	0.000
20				0.002	0.002	0.003
40				0.004	0.004	0.004
60				0.008	0.008	0.008
80				0.009	0.010	0.010
100				0.011	0.012	0.012

apparent phosphate concentration due to sample silicate increased with reaction temperature in all cases. A dramatic increase in silicate interference is found at temperatures higher than 40°C. Although low temperature (< 15°C) can cause an underestimate of phosphate concentration in samples with low phosphate content due to slow rate of the color formation [20], room temperature is sufficient to bring the reaction to completion under the automated conditions used here. Furthermore, reaction temperatures higher than 30°C should be avoided so that silicate interference will be minimal. This is important when analyzing water samples containing high ratios of silicate to phosphate (> 100).

Unlike the monotonic dependency on temperature or silicate concentration, apparent phosphate showed a maximum at pH 0.78 decreasing rapidly at higher or lower pHs (Fig. 8). Earlier workers suggested that the lower the pH the less the silicate interference. Based on this concept they recommended that the final solution pH should be lower than 1.0 [19]. Unfortunately there have been no systematic study on the formation kinetics of antimolybdsilicomolybdate acid. Further study is needed to elucidate the maximum silicate interference observed at pH of 0.78.

Apparent phosphate concentrations (in μM) measured by Murphy and Riley's method over a range of reaction conditions (pH = 0.19–1.5, $T = 25\text{--}70^\circ\text{C}$) and silicate concentrations (0–100 μM) are summarized in Table 1. A non-linear multi-parameter fitting of these experimental data yields the following equation:

$$[\text{PO}_4^{3-}]_a = (24594 \times 10^4 [\text{Si}] - 661951 [\text{Si}]^2) \left(\frac{1000}{T} \right)^{-23.6653} / 0.1587 e^{-(\text{pH}-0.78)^2 / 0.05037}$$

where $[\text{PO}_4^{3-}]_a$ is apparent phosphate concentration and $[\text{Si}]$ is silicate concentration in a sample, both in μM , T is the absolute temperature in K and pH is the value in the final solution. This equation has a correlation coefficient (r) of 0.992. It can be used to predict an apparent phosphate concentration due to the amount of silicate present in a sample given temperature and pH of the final solution used in the phosphate analysis.

In summary, lower sensitivity and pronounced coating effect have ruled out the feasibility using a final solution pH lower than 0.5. A pH of 0.78, as previously recommended, resulted in maximum interference from sample silicate at temperatures 40°C or higher. Precipitation of antimony from solutions of low acidity precludes reactions at a pH higher than 1.5. Room temperature for reaction is preferred for sufficient speed of reaction and minimal interference from sample silicate. Consequently, for our method of automated continuous flow phosphate analysis the optimal reaction condition for minimal silicate interference, maximum sensitivity and minimal coating would be a pH in final solution of 1.00, room temperature, a $[\text{H}^+]/[\text{Mo}]$ ratio of 70 and the addition of Sb. Under these optimal analytical conditions, a further improvement in the accuracy of phosphate determination can be achieved by applying the correction for the silicate interference given in the above equation.

Acknowledgements

The authors thank two anonymous reviewers for their constructive comments. This work was supported by the South Florida Ecosystem Restoration Prediction and Modeling Program, a part of NOAA's Coastal Ocean Program and OACES, a project of the NOAA's Climate and Global Change Program and USEPA (DW13936152-01-0).

References

- [1] S.V. Smith, *Limnol. Oceanogr.* 29 (1984) 1149.
- [2] P.G. Falkowski, *Nature* 387 (1997) 272.
- [3] R.E. Stauffer, *Geochim. Cosmochim. Acta* 46 (1982) 465.
- [4] P.N. Froelich, *Limnol. Oceanogr.* 33 (1988) 649.
- [5] S.V. Smith, M.J. Atkinson, *Nature* 307 (1984) 626.
- [6] J.H. Ryther, W.M. Dunstan, *Science* 171 (1971) 1008.
- [7] M.D. Krom, N. Kress, S. Brenner, L.I. Gordon, *Limnol. Oceanogr.* 36 (1991) 424.
- [8] D.W. Schindler, *Science* 195 (1977) 260.
- [9] J.E. Harwood, W.H.J. Hattingh, *Colorimetric methods of analysis of phosphorus at low concentrations in water*, in: E.J. Griffith, A.M. Beeton, J.M. Spencer, D.J. Michell (Eds.), *Environmental Phosphorus Handbook*, J. Wiley and Sons, New York, 1973, pp. 289–302.

- [10] D.F. Boltz, in: M. Hammann (Ed.), *Analytical Chemistry of Phosphorus Compounds*, Wiley, New York, 1972, pp. 9–65.
- [11] J.D. Burton, *Water Res.* 7 (1973) 291.
- [12] D.F. Boltz, C.H. Lueck, R.J. Jakubiec, in: D.F. Boltz, J.A. Howell (Eds.), *Colorimetric Determination of non-metals*, Chemical Analysis, Vol. 8, 2nd ed. Wiley, New York, 1978, pp. 337–369.
- [13] O. Broberg, K. Pettersson, *Hydrobiologia* 170 (1988) 45.
- [14] J. Murphy, J.P. Riley, *Anal. Chem. Acta* 27 (1962) 31.
- [15] K.M. Chan, J.P. Riley, *Deep-Sea Res.* 13 (1966) 467.
- [16] J.E. Going, S.J. Eisenreich, *Anal. Chim. Acta* 70 (1974) 95.
- [17] S.-C. Pai, C.-C. Yang, *Anal. Chim. Acta* 229 (1990) 115.
- [18] L. Drummond, W. Maher, *Anal. Chim. Acta* 302 (1995) 69.
- [19] F. Koroleff, Determination of phosphorus, in: K. Grasshoff, M. Ehrhardt, K. Kremling (Eds.), *Methods of seawater analysis*. Weinheim, Verlag Chemie, 1983, pp. 125–139.
- [20] A. Sjosten, S. Blomqvist, *Water Res.* 31 (1997) 1818.
- [21] A. Henriksen, *Analyst* 91 (1966) 290.
- [22] R.E. Stauffer, *Anal. Chem.* 55 (1983) 1205.
- [23] S. Blomqvist, K. Hjellstrom, A. Sjosten, *Intern. J. Environ. Anal. Chem.* 54 (1993) 31.
- [24] S. Blomqvist, S. Westin, *Anal. Chem. Acta* 358 (1998) 245.
- [25] C.Y. Shen, D.R. Dryoff, *Anal. Chem.* 34 (1962) 1367.
- [26] D.L. Johnson, *Environ. Sci. Technol.* 5 (1971) 411.
- [27] C. Ciavatta, L.V. Antisari, P. Sequi, *J. Environ. Qual.* 19 (1990) 761.
- [28] D.M. Karl, G. Tien, *Marine Chem.* 56 (1997) 77.
- [29] P.F. Reay, *J. Appl. Ecol.* 9 (1973) 557.
- [30] J. Shapiro, *Science* 171 (1971) 234.
- [31] J.C. Van Schouwenburg, I. Walinga, *Anal. Chim. Acta* 37 (1967) 269.
- [32] M.T. Downes, *Water Res.* 12 (1978) 743.
- [33] G. E. Hutchinson, *Treatise on Limnology*. Vol. 1. Wiley, New York, 1957.
- [34] P.M. Dove, J.D. Rimstidt, Silica–water interaction, in: P.J. Heaney, C.T. Prewitt, G.V. Gibbs (Eds.), *Silica: Physical behavior, geochemistry and materials applications*. Reviews in mineralogy Vol. 29. Mineralogical Society of America, 1994, pp. 259–308.
- [35] R.M. Garrels, C.L. Christ, *Solutions, Minerals and Equilibria*, Harper and Row, New York, 1965, pp. 450.
- [36] F.R. Campbell, R.L. Thomas, *Environ. Sci. Technol.* 4 (1970) 602.
- [37] H.P. Hansen, K. Grasshoff, Automated chemical analysis, in: K. Grasshoff, M. Ehrhardt, K. Kremling (Eds.), *Methods of seawater analysis*, Weinheim, Verlag Chemie, 1983, pp. 347–379.
- [38] S.A. Mostert, S. Afri, *J. Mar. Sci.* 1 (1983) 189.
- [39] Alpkem Corporation, Orthophosphate RFA methodology, Clackamas, Oregon, RFA Engineering Bulletin, 1990, A303–S200.
- [40] Alpkem Corporation, Methodology: Orthophosphate in seawater, Wilsonville, Oregon, 1994, DOC. 000629.
- [41] E.M.S. Woodward, Nutrient analysis techniques, Plymouth Marine Laboratory, Plymouth, UK, 1994.
- [42] Standard methods for the examination of water and wastewater. 1995. APHA, Washington, D.C. pp. 1193.
- [43] R.C. Antweiler, C.J. Patton, H.E. Taylor, Automated colorimetric methods for determination of nitrate plus nitrite, nitrite, ammonium and orthophosphate ions in natural water samples. US Geological Survey, 1996, Open-File Report pp. 93–638.
- [44] J.-Z. Zhang, *J. Automatic Chem.* 19 (1997) 205.
- [45] J. Murphy, J.P. Riley, *J. Mar. Biol. Assoc. UK* 37 (1958) 9.
- [46] S.R. Crouch, H.V. Malmstadt, *Anal. Chem.* 39 (1967) 1084.

Improvement of a monitoring tape for nitrogen dioxide in air

Kunio Nagashima ^{a,*}, Nobuo Nakano ^b

^a Faculty of Engineering, Kogakuin University, 2665-1, Nakanochō, Hachioji-shi, Tokyo, 192-0015, Japan

^b Riken Keiki Co., Ltd., 2-7-6, Azusawa, Itabashi-ku, Tokyo, 174-8744, Japan

Received 8 July 1998; received in revised form 9 November 1998; accepted 1 December 1998

Abstract

A porous cellulose tape containing a silica gel that was previously impregnated with a processing solution containing *p*-toluenesulfonic acid, sulfanilic acid, *N*-1-naphthyl ethylene diamine dihydrochloride, ethylene glycol and methanol has been developed to provide a highly sensitive detection of nitrogen dioxide in air. When the sample including nitrogen dioxide was passed through the tape, the color of tape changed to red, and the degree of color change could be recorded by measuring the intensity of reflecting light (555 nm). The calibration graph was linear up to ~0.10 ppm. The detection limit was 0.5 ppb for nitrogen dioxide with a sampling time of 8 min and a flow rate of 60 ml min⁻¹. No interferences were observed from ammonia (40 ppm), sulfur dioxide (51 ppm), carbon dioxide (21%), ozone (0.75 ppm), hydrogen sulfide (27 ppm) or nitrogen monoxide (99 ppm). © 1999 Elsevier Science B.V. All rights reserved.

Keywords: Nitrogen dioxide gas detection; Tape monitor; Sensitive tape for nitrogen dioxide gas; Saltzman's reagent

1. Introduction

The permitted level of nitrogen dioxide (NO₂) in atmospheric air in Japan is less than 40 ppb. There has been an increasing need for a NO₂ monitor that is inexpensive, small in size and sensitive to such low concentrations. Several gas sensors have been shown for the detection of NO₂, such as galvanic sensor using Ag⁺ conductor [1] and amperometric detection using sodium superionic conductor (NASICON) [2]. But these

gas sensors have a short lifetime due to the decrease in sensitivity because the surface of sensor is degraded by the exposure to sample gas. A liquid film/droplet of Saltzman absorbent was proposed for the detection of NO₂ [3]. Consequently, we chose a tape monitor [4] because of its high sensitivity and selectivity, easy maintenance, small size and low running cost. A monitoring tape [5] for Cl₂ has already been developed. The tape also can detect NO₂, but it has not been successful in detecting less than 1 ppm NO₂, even if the sampling time is extended to 10 min. In this experiment, we examined the tape using Saltzman's reagent [6] which has been recognized as an

* Corresponding author. Fax: +81-426-285647.

E-mail address: bt10450@ns.kogakuin.ac.jp (K. Nagashima)

excellent reagent for the colorimetric determination of NO_2 in air by the official method [7].

We had studied the tape [8,9] impregnated with the Saltzman's reagent in order to permit the determination of NO_2 concentrations less than 10 ppb in air. Glycerin was used as humectant in a previous report [8,9], but ethylene glycol was used instead of glycerin as a humectant in this report because the sensitivity of the tape for NO_2 increased two times and reaction rate increased three times.

2. Experimental

2.1. Reagents and samples

A processing solution was prepared as follows. In approximately 30 ml of water, 0.5 g of sulfanilic acid, 0.015 g of *N*-(1-naphthyl)ethylenediamine dihydrochloride, 0.088 g of *p*-toluenesulfonic acid and 20 ml of ethylene glycol were dissolved, then 45 ml of methanol was added to the solution, and the solution was diluted to 100 ml with water.

Standard NO_2 mixtures (0.01–0.5 ppm) were prepared by controlling the flow rate of streams of primary standard 8.9 ppm NO_2 (N_2 balance, Takachiho) and N_2 from a cylinder.

2.2. Monitoring tape

The porous cellulose tape (Whatman, 20 mm wide, 0.27 mm thick and 10 cm long) containing a silica gel was immersed in the processing solution for 5 min, evaporated to dryness under reduced pressure for 1 h and stored in a desiccator (silica gel). The reproducibility of the preparation of the monitoring tape was $\sim 4.1\%$ ($n = 8$).

2.3. Apparatus and procedure

The experimental apparatus was similar to that used previously [8,9]. The end of the tube (~ 1 cm in diameter) from the suction unit was attached tightly to a tape. The sample gas was sucked through the tape at a constant flow rate (60 ml min^{-1}) and sampling time (8 min). When the tape

was exposed to sample, Saltzman's reagent on the tape reacted with NO_2 to change its homogeneous color. The degree of color development was recorded by measuring the reflected light (555 nm). The section of the tape was renewed by moving the tape every 8 min. The response (reflection absorbance, A) is defined by

$$A = -\log V1/V0$$

where $V0$ and $V1$ are outputs of blank and of the sample, respectively. After the tape monitor was switched on, 30 min were required to measure the responses. All measurements were carried out at $25 \pm 2^\circ\text{C}$.

3. Results and discussion

3.1. Reflectance spectra and effect of concentration of Saltzman's reagent

After the tape was exposed to 0.1 ppm NO_2 for a sampling time of 8 min at a flow rate of 60 ml min^{-1} , the visible reflectance spectrum of exposed tape was obtained. The wavelength for the maximum absorbance of reflectance spectra was between 550 and 570 nm [8,9].

For the detection of NO_2 , the response for NO_2 was investigated with various concentrations of sulfanilic acid and *N*-1-naphthyl ethylenediamine dihydrochloride in the processing solution.

In this experiment, the pH of processing solution was adjusted to 2.5 with *p*-toluenesulfonic acid.

The response for NO_2 increased with increase in concentration of sulfanilic acid in processing solution and became constant above 0.5 wt.%.

The response was investigated with various concentrations of *N*-1-naphthyl ethylenediamine dihydrochloride in the range of 0.005–0.1 wt.% in the processing solution. Maximum response was obtained in the range 0.01–0.025 wt.% of *N*-1-naphthyl ethylenediamine dihydrochloride.

The processing solution used was prepared with 0.5 wt.% of sulfanilic acid and 0.015 wt.% of *N*-1-naphthyl ethylenediamine dihydrochloride.

3.2. Concentration of humectant

Effective humectant is essential to obtain a good response to NO_2 in this tape.

Ethylene glycol and glycerin as a humectant provide moistening of tape for the desired reaction of Saltzman's reagent.

The effect of humectant concentration of ethylene glycol and glycerin in the processing solution on the response is shown in Fig. 1. Maximum and almost constant responses were obtained at 15–24 v/v% of ethylene glycol and 25 vol.% of glycerin. The processing solution used was prepared so that the concentrations of ethylene glycol and glycerin were 20 and 25 v/v%, respectively.

3.3. Effects of flow-rate of sample gas on response

Table 1 shows the effect of sample gas flow-rate on responses using ethylene glycol and glycerin as humectant. The maximum responses were obtained at the flow-rates of 60 and 30 ml min^{-1} . The responses decreased with increasing sample gas flow-rate above 70 and 50 ml min^{-1} .

It can be considered that the reasons for decreasing response in high flow-rate were that the tape was dried by sample gas and the reaction of NO_2 with Saltzman's reagent did not proceed well.

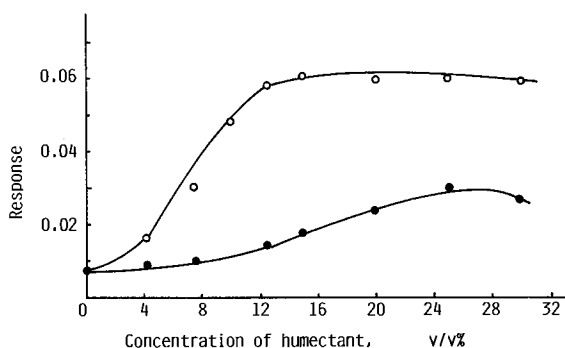


Fig. 1. Effect of humectant concentration in processing solution on response.

Table 1
Effect of sampling gas flow-rate on response^a

Gas flow-rate (ml min^{-1})	Response	
	Ethylene glycol	Glycerin
10	0.030	0.026
30	0.045	0.030
50	0.058	0.028
60	0.060	0.024
70	0.058	0.021
90	0.030	0.019
120	0.027	0.017

^a Concentration of NO_2 : 0.10 ppm.

3.4. Sampling time

The response for a fixed concentration of NO_2 (0.10 ppm) was plotted against various sampling times. The linear graphs between response and sampling time were obtained in the range 0–12 min (Fig. 2).

The reaction rate for ethylene glycol tape was double that of glycerin tape and sampling time, 8 min, was chosen for further experiment.

3.5. Calibration graph

Typical calibration graphs for NO_2 are shown in Fig. 3. The calibration graphs were linear up to ~ 0.10 ppm.

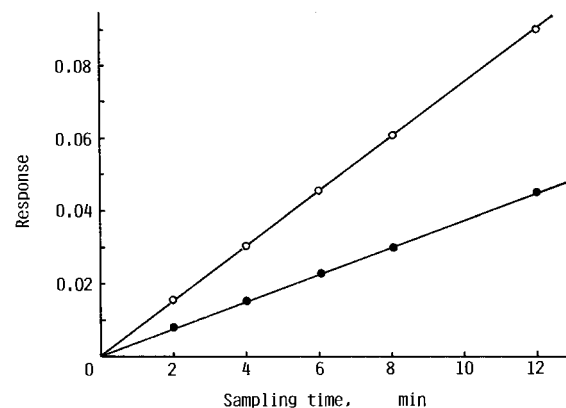


Fig. 2. Effect of sampling time.

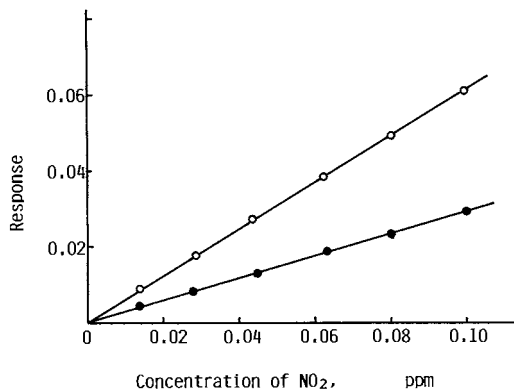


Fig. 3. Calibration graphs for NO₂.

The detection limits (signal to noise ratio = 3) by ethylene glycol tape and glycerin tape were 0.5 and 1.0 ppb, respectively.

3.6. Selectivity

The responses of the tape using ethylene glycol for ammonia (40 ppm v/v), sulfur dioxide (51 ppm), carbon dioxide (21%), ozone (0.75 ppm), hydrogen sulfide (27 ppm) and nitrogen monoxide (99 ppm) were less than 0.008.

4. Conclusion

The monitoring tape impregnated with Saltzman's reagent is very suitable for the determination of NO₂ 5–100 ppb. The detection limit was 0.5 ppb. This tape monitor method is simple, specific, capable of unattended operation and is recommended for field operation.

References

- [1] K. Nagashima, N. Nakano, Mater. Technol. 15 (1997) 146.
- [2] N. Miura, M. Iio, G.Y. Lu, N. Yamazoe, J. Electrochem. Soc. 143 (1996) 241.
- [3] A.A. Cardoso, P.K. Dasgupta, Anal. Chem. 67 (1995) 2562.
- [4] N. Nakano, K. Nagashima, J. Jpn Soc. Color Mater. 70 (1997) 124.
- [5] N. Nakano, A. Yamamoto, K. Nagashima, Talanta 43 (1996) 459.
- [6] J.L. Lambert, E.L. Trump, J.V. Paukstelis, Environ. Sci. Technol. 21 (1987) 497.
- [7] Japanese Industrial Standards (JIS) 1981, B7954.
- [8] N. Nakano, M. Inoue, K. Nagashima, Anal. Chim. Acta 321 (1996) 41.
- [9] N. Nakano, M. Inoue, K. Nagashima, Anal. Chim. Acta 334 (1996) 221.

An empirical relationship between distribution coefficients of phenols by polyurethane foams and their octanol–water distribution constants and pK_a values

S.G. Dmitrienko *, E.N. Myshak, L.N. Pyatkova

Analytical Chemistry Division, Department of Chemistry, Lomonosov Moscow State University, V-234 Vorob'evy Gory, 119899 Moscow, Russia

Received 15 July 1998; received in revised form 16 November 1998; accepted 1 December 1998

Abstract

Sorption of phenol, 3-cresol, 2-, 3-, 4-nitrophenols, 2,4-, 2,6-dinitrophenol, 2,4,6-trinitrophenol, and 1-naphthol by polyether- and polyester-type polyurethane foams (PUF) was investigated. The effects of sorption time, pH, phenol concentration and the structure of tested phenols and PUF were studied. The mechanism of sorption of tested compounds on foams is discussed. It is shown that the hydrophobicity ($\log P$, octanol–water distribution constant) and pK_a values of the compounds play an important role in the sorption process. A regression equation connecting distribution coefficient of phenols by PUF with their hydrophobicity parameter and pK_a values were derived. Good correlation between $\log D$ and values $\log P$ and pK_a was observed. © 1999 Elsevier Science B.V. All rights reserved.

Keywords: Phenols; Sorption; Polyurethane foam; Method of correlation ratio

1. Introduction

Polyurethane foams (PUF) are porous sorbents with hydrophobic polymeric matrices, which have various polar functional groups (urethane, amid, ester-, ether, urea-groups, etc.). Due to such a combination of properties, these sorbents are successfully used for effective sorption of both non-polar and polar molecules [1,2]. The part of a

solid phase in PUF is replaced with a gas, which exists in the polymer as numerous bubble-cells, forming the ordered system firm quasispherical membranes. Sorbed substance is dissolved in PUF membranes [2].

Considerable progress has been achieved in recent years in the use of PUF for effective sorption of organic compounds such as polychlorinated biphenyls [3–5], polycyclic aromatic hydrocarbons [6,7], different pesticides and insecticides [8–10], many organic dyes [11–15], ionogenic surfactants [16], aromatic acid [17,18] and phenols [17–21].

* Corresponding author. Tel.: +7-95-939-4675.

E-mail address: dmitrienko@analyte.chem.msu.ru (S.G. Dmitrienko)

Most of the studies dealing with sorption properties of PUF were aimed to practical problems of preconcentrating compounds from air and solutions; much less attention was focused on the peculiarities of sorption processes and sorption mechanisms. It was established that many organic compounds are extracted according to the neutral solvent extraction mechanism [17,18]. When a compound contains a group able to form hydrogen bonds, such as –OH, an additional factor appeared to be involved. Probably, this factor is hydrogen bonding between the polyurethane and the group of the organic compound [17–19,21]. In a dozen studies, the important role of nonspecific interactions in sorbing organic compounds by PUF was studied [13,15,19,21].

In this work the method of correlation ratios has been applied to reveal the correlation between the ability of a substance to be sorbed on PUF and its hydrophobicity and acid–base properties. A number of phenols with different values of correlated parameters—logarithm of the distribution constant in the octanol–water system (Hansch parameter, $\log P$) and acid dissociation constant (pK_a) was used as model compounds. To implement this, the sorption of phenols on polyether- and polyester-based PUF was studied.

2. Experimental

2.1. Reagents and materials

Except otherwise specified all the chemicals used were of analytical-reagent grade. Polyether (140, 5-30, and M-40 trade marks), polyester (2200 and 35-08 trade marks) foams and their copolymers (VP trade mark), produced by ‘Polimersintez’ (Vladimir, Russia) and ‘Radikal’ (Kiev, Ukraine) were used throughout (Table 1). Foam tablets of approximately 0.06 g were cut from a commercially available polymer sheet. To purify the tablets they were treated with a large quantity of 0.1 M HCl for 30 min, then washed with water up to pH 5–6 followed with acetone, and then dried in air and stored in brown-glass jars.

2.2. Apparatus

The absorbances of solutions were measured with a KFK-2 photoelectrocolorimeter; pH of solutions was monitored with a EV-74 potentiometer with H-selective glass electrodes.

2.3. Procedure

The sorption was carried out under batch conditions. The sample solution (25 ml) and the foam tablet (0.060 ± 0.002 g) were placed in a vessel with a ground stopper. Air bubbles were removed using a glass rod. The vessels were shaken with an automatic shaker for 30 min. Next, the tablets were removed, and the equilibrium concentrations of phenols were determined with a photometer by the absorption of the compounds or by azocoupling with 4-nitrophenyldiazonium tetrafluoroborate in alkaline solutions [22,23]. The sorption percentage (E , %) and the distribution coefficient (D) were calculated as follows:

$$E, \% = \frac{C_0 - C}{C_0} \cdot 100\% \quad (1)$$

$$D = \frac{E, \%}{(100 - E, \%)} \cdot \frac{V}{w} \quad (2)$$

where C_0 is the initial molar concentration of tested compound in solution before the sorption, C is the concentration in solution after the sorption, V is the volume of solution (l), and w is the mass of foam (kg). The reproducibility of the determined distribution coefficients is $RSD < 0.05$ ($n = 5-7$).

Sorption isotherms were obtained over a wide range of equilibrium concentrations (4×10^{-6} – 4×10^{-2} M) of the compounds at $20 \pm 1^\circ\text{C}$. The initial concentrations of phenols were varied from 2×10^{-5} up to 4.2×10^{-2} M, 4-nitrophenol from 4×10^{-5} up to 8×10^{-3} M, 2,4-dinitrophenol from 2×10^{-5} up to 5×10^{-3} M, 2,4,6-trinitrophenol from 4×10^{-5} up to 6×10^{-3} M, and 1-naphthol from 1.5×10^{-5} up to 2.8×10^{-3} M. The lower boundary of concentrations was determined by the sensitivity of photometric techniques used for the determination of the equilibrium concentrations of phenols; the upper boundary was limited by the solubility of phenols in water.

3. Results and discussion

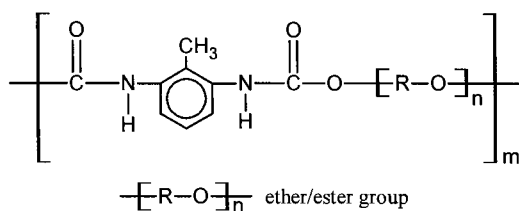
Phenols contain both a hydroxygroup and a hydrophobic aromatic nucleus; thus, they are convenient models for studying the regularities of the sorption of organic compounds by PUF. The structural variety of phenols makes it possible to systematically investigate the influence of acid–base properties of molecules and their hydrophobicity and the nature, the number, and the arrangement of the substitutes on the sorption of phenols by PUF of different types.

In this study, 1-naphthol, 2-, 3-, and 4-nitrophenols, 2,4- and 2,6-dinitrophenols, 2,4,6-trinitrophenol, and 3-cresol were selected as model compounds. For these phenols, the constant of acid dissociation (pK_a) changes from 0.7 up to

10.2 thus covering the whole range for this class of compounds. Moreover, phenols listed in Table 2 differ in their hydrophobicity, which is confirmed by the logarithms of their distribution constants in an octanol–water system.

Now, the distribution constants of compounds in an octanol–water system ($\log P$) are used as a standard parameter of hydrophobicity (Hansch parameter) [24]. Table 2 shows the values of $\log P$ for the non-ionized form ($\text{pH} \sim 0$) of phenols. Under experiment conditions (0.1 M HCl) all the tested phenols except for 2,4,6-trinitrophenol exist in the molecular form; thus, the values of $\log P$ at $\text{pH} \sim 0$ were used for calculations. Hansch parameter for 2,4,6-trinitrophenol was calculated from the formula $P_0 = P_{\text{app}} \cdot (1 + 10^{\text{pH} - \text{p}K_a})$, where P_0 and P_{app} are distribution coefficients in oc-

Table 1
Tested polyurethane foams



Polyurethane foam (trade mark)	Type	Ether/ester group
140	Polyethers	$[-(\text{CH}_2)_2-\text{O}-]_n$
5-30	Polyethers	$[-(\text{CH}_2)_2-\text{O}-(\text{CH}_2)_3-\text{O}-]_n$
M-40	Polyethers	$[-(\text{CH}_2)_3-\text{O}-]_n$
2200	Polyesters	$[-(\text{CH}_2)_m-\overset{\text{O}}{\parallel}{\text{C}}-\text{O}-]_n$
35-08	Polyesters	-
VP	Copolymer of polyesters (80%) and polyethers (20%)	-

Table 2
Sorption of phenols from 0.1 M HCl by 5-30 polyurethane foam^a

Compound	log <i>P</i> (octanol–water) [24]	p <i>K</i> _a in water [28]	<i>E</i> , %	log <i>D</i>
Phenol	1.48	10.00	31 ± 2	2.19 ± 0.05
	1.49			
3-Cresol	2.01	10.09	45 ± 2	2.53 ± 0.06
1-Naphthol	2.98	9.85	82 ± 5	3.27 ± 0.08
	2.31			
2-Nitrophenol	1.73	7.21	26 ± 3	2.18 ± 0.08
	1.79			
3-Nitrophenol	2.00	8.39	58 ± 2	2.77 ± 0.06
4-Nitrophenol	1.91	7.16	56 ± 2	2.75 ± 0.02
2,4-Dinitrophenol	1.51	4.11	54 ± 3	2.70 ± 0.03
2,6-Dinitrophenol	1.18	4.15	49 ± 3	2.62 ± 0.03
	1.25			
2,4,6-Trinitrophenol	2.03	0.71	88 ± 5	3.53 ± 0.09

^a Conditions: 20 ± 1°; 25-ml aliquot of 1 × 10⁻⁴ M aqueous solution of phenol, 0.06 g of the foam, sorption time 30 min, *n* = 5, *P* = 0.95.

tanol–water system for the non-ionized form of phenol and under given pH, respectively [25]. The calculated value of log *P* for 2,4,6-trinitrophenol in 0.1 M HCl is 1.56.

3.1. Sorption time

Preliminary experiments on the sorption of tested phenols from 0.1 M aqueous solution of HCl by 5-30 polyether foam showed that the sorption is fast, and the equilibrium is attained in less than 30 min (Fig. 1). The sorption efficiency among the tested phenols is significantly different as shown in Table 2. Similar results were obtained for other tested foams.

3.2. Effect of pH on the sorption

Phenols are weak organic acids. They exist in solution both as neutral and ionized forms. Therefore, pH plays an important role in their sorption. The effect of pH of the aqueous phase on the sorption of phenol, 3-cresol, 1-naphthol, 3- and 4-nitrophenols, 2,4-dinitrophenol, and 2,4,6-trinitrophenol by 5-30 polyether foam was investigated over a wide range of pH (pH 1–12). Fig. 2 shows that all the curves have almost the same sharpness. The maximum values of the sorption of phenols are reached at pH of the aqueous

solution of p*K*_a – 2 or below; with an increase pH of the aqueous solution up to p*K*_a + 2 or higher, the sorption of phenols decreases down to nothing. A correlation between a decrease in the sorption and p*K*_a of phenols was observed: the lower are p*K*_a values, the lower is pH at which the sorption starts to decrease. Thus, the most profound change in the extraction factor of phenols is observed at pHs equal to p*K*_a values. For phenols with similar p*K*_a values—phenol, 3-cresol, and 1-naphthol—pH ranges, at which sorption becomes higher are identical. This suggested effect gives evidence of the fact that phenols are sorbed in the molecular form. These results are in good agreement with the data reported by Chow et al. [17,18].

3.3. Effect of the type PUF on the sorption

The sorption of phenols and 1-naphthol from 0.1 M HCl by polyether (140, 5-30 and M-40), polyester (2200 and 35-08) foams and their copolymers (VP) was studied. Although sorption profiles have the same shape, the sorption in the case of polyester foams frequently differs from the case of polyether foams. As one can see from Table 3, the distribution coefficients on polyether foams are often higher than on polyester foams. The PUF on the basis of copolymers of ethers

and esters (VP) is in the middle. The sorption of phenols by polyether foams depends on the structure of the polymer unit: 5-30 foam containing both ethylene oxide and propylene oxide are more efficient than M-40 foam based on propylene oxide; 140 foam based on ethylene oxide are characterised by lower parameters of sorption of phenols. The latter fact seems to be connected with the competition of HCl in the sorption process. The results obtained may be accounted for by the formation of hydrogen bonds between phenol hydroxy group and oxygen atoms of ether groups of the polymer. Ether groups form hydrogen bonds more easily than ester groups. Trends similar to this have been reported by previous researches [17,18,21].

The comparison of the distribution coefficients (Fig. 2, Table 2) shows that the sorption of phenols is significantly affected by their acid–base properties and hydrophobicity. The highest values of distribution coefficients are achieved for the

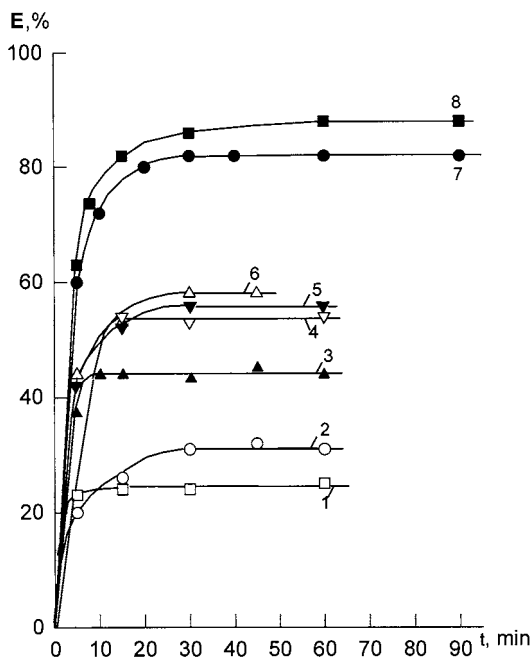


Fig. 1. Dependence of the sorption degree of 2-nitrophenol (1), phenol (2), 3-cresol (3), 2,4-dinitrophenol (4), 4-nitrophenol (5), 3-nitrophenol (6), 1-naphthol (7), 2,4,6-trinitrophenol (8) by 5-30 polyurethane foam on the phase contact time. $C_{Ph} = 1 \times 10^{-4}$ M, $C_{HCl} = 0.1$ M, $V = 25$ ml, $m_{PUF} \sim 0.06$ g.

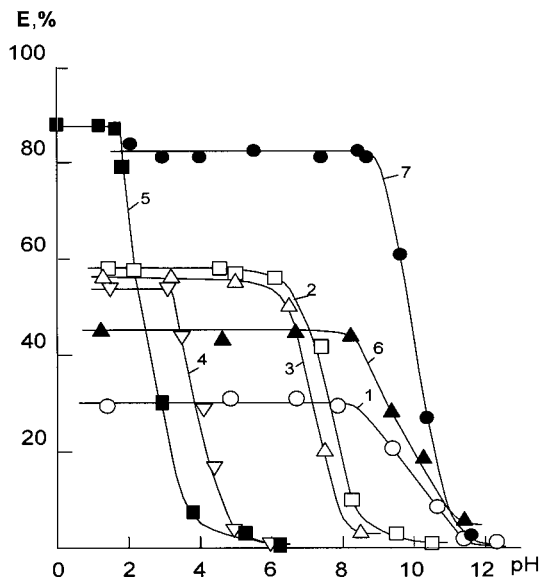


Fig. 2. Dependence of the sorption degree of phenol (1), 3-nitrophenol (2), 4-nitrophenol (3), 2,4-dinitrophenol (4), 2,4,6-trinitrophenol (5), 3-cresol (6) and 1-naphthol (7) by 5-30 polyurethane foam on pH. $C_{Ph} = 1 \times 10^{-4}$ M, $V = 25$ ml, $m_{PUF} \sim 0.06$ g.

strongest acid, 2,4,6-trinitrophenol, and for the most hydrophobous compound, 1-naphthol. Among the pairs of compounds with approximately identical pK_a values, the more hydrophobous one is sorbed better. 2,4,6-Trinitrophenol, being the strongest acid among nitrophenols ($pK_a = 0.71$), shows the best results. However, the values of distribution coefficients of 3-nitrophenol ($pK_a = 8.39$), 4-nitrophenol ($pK_a = 7.16$), 2,4-dinitrophenol ($pK_a = 4.11$), and 2,6-dinitrophenol ($pK_a = 4.15$) are similar, though the constants of acid dissociation of nitrophenols and dinitrophenols differ by as much as 3–4 order. 2-Nitrophenol, which can form intramolecular hydrogen bonds, is sorbed worse than 3- or 4-nitrophenol. These facts allowed one to suppose that the main types of sorbent–sorbate interactions are hydrophobic and those resulting in the formation of hydrogen bonds between a proton of phenol hydroxy group and electron–donor polar groups of PUF are like amido-, tertiary amino-, ether, ester etc. Table 3 shows that the differences in the sorption properties of

polyether and polyester foams become less appreciable as the hydrophobicity of phenols increases. This effect may be due to the hydrophobic interactions. It has been shown that PUF tested in this work do not differ in hydrophobicity [16].

3.4. Sorption isotherms

Sorption isotherms of phenol, 4-nitro-, 2,4-dinitro-, and 2,4,6-trinitrophenols and 1-naphthol on 5-30 PUF are shown in Fig. 3. Compounds selected as sorbates differ in size, hydrophobicity, and the ability to form hydrogen bonds.

The shape of sorption isotherms is similar. All the dependences have two increasing sections, differing by the slope (the value for the second section is lower), and plateaus. Apart from this the sorption isotherm of phenol has another increasing section with the slope greater than for two other sections. The arrangement of initial sections of sorption isotherms and their slopes (Fig. 3(b)) correlate with distribution coefficients in Table 2. In the case of 2,4,6-trinitrophenol, the initial section of sorption isotherm has a large slope as compared with 4-nitro- and 2,4-dinitrophenols, and especially phenol; also the point at which the isotherm reaches the plateau is shifted to lower initial concentrations.

An additional increase in the sorption after plateau is due to a change in the orientation of the sorbate molecules at the surface [26]. In the case of sorption of phenols, a change in the orientation of sorbate molecules after the first

plateau seems quite possible. In fact, the hydroxyl proton of a phenol molecule can interact simultaneously with several donor atoms of the chain of a polymeric sorbent, e.g. with several oxygen atoms of the polyester fragments of foam thus forming hydrogen or dipole–dipole bonds. A similar picture is observed when cyclic polyethers bind proton-donating molecules [27]. Such a ‘coordination number’ should be determined by the structure of the polymer and the type and the arrangement of corresponding polar groups. It is obvious that an increase in the concentration of phenol molecules in the sorbent phase would decrease the ‘coordination number’ and freed donor atoms of oxygen cause an additional increase in sorption. A decrease in the average number and/or in the interaction between the phenol and PUF chain must decrease the free energy of the sorption and the slope of the isotherms, as was observed in the studied case. The third increase on the sorption isotherm of phenol is apparently connected with formation of aggregate sorbate molecules in the solid phase. This mechanism is in good concordance with the repeatedly described ability of phenol to associate both in solutions and in the phase of different sorbents.

3.5. Model of sorption

The following equilibria are established in the process of sorption of phenols (HA) on PUF (based on the data received experimentally, anion A^- was not sorbed on PUF):

Table 3

Comparison of the distribution coefficients ($\log D$) of phenols sorbed from 0.1 M HCl by polyether and polyester foams^a

Compound	Polyurethane foam					
	140	5-30	M-40	VP	2200	35-08
Phenol	1.81	2.19	1.96	2.10	1.76	1.67
3-Cresol	2.25	2.53	2.38	2.42	2.32	2.25
1-Naphthol	3.14	3.27	3.10	3.13	3.16	3.14
4-Nitrophenol	2.26	2.75	2.56	2.29	2.13	2.26
2,4-Dinitrophenol	2.33	2.70	2.64	2.56	2.45	2.51
2,4,6-Trinitrophenol	3.05	3.53	3.16	2.76	2.66	2.60

^a Conditions: $20 \pm 1^\circ$; 25-ml aliquot of 1×10^{-4} M aqueous solution of phenol, 0.06 g of the foam, sorption time 30 min, $n = 5$, $P = 0.95$.

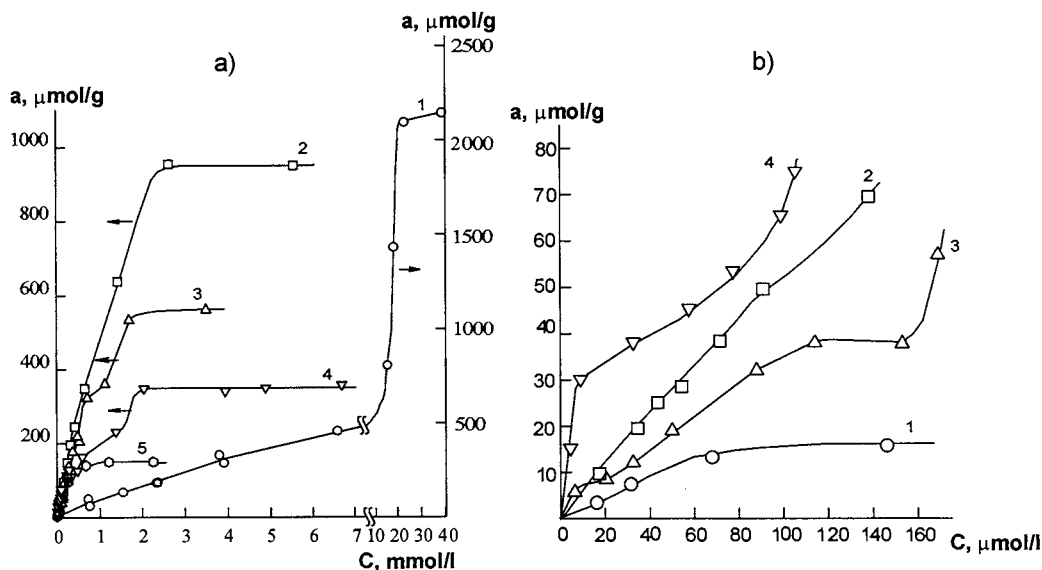
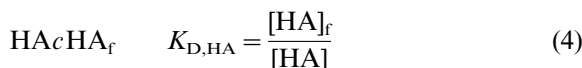
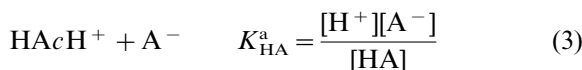


Fig. 3. Sorption isotherm of phenol (1), 4-nitrophenol (2), 2,4-dinitrophenol (3), 2,4,6-trinitrophenol (4) and 1-naphthol (5) by 5-30 polyurethane foam (a) and its initial sections (b). $C_{\text{HCl}} = 0.1 \text{ M}$, $V = 25 \text{ ml}$, $m_{\text{PUF}} \sim 0.06 \text{ g}$.



The distribution coefficient of phenols is equal to

$$D = \frac{[\text{HA}]_f}{[\text{HA}] + [\text{A}^-]} \quad (5)$$

From Eqs. (3) and (4) the following is obtained

$$D = \frac{[\text{H}^+] \cdot K_{\text{D,HA}}}{[\text{H}^+] + K_{\text{HA}}^a} \quad (6)$$

The Eq. (6) becomes simpler in the case of sorption of phenols from the solutions at $\text{pH} < \text{p}K_{\text{a}} - 2$:

$$D = K_{\text{D,HA}} \quad (7)$$

In order to guide and facilitate the search for improvements in gut permeability within this family of compounds, one hoped to identify a physicochemical marker which could readily be determined for a large series of compounds, and which might be used to predict the sorption behaviour of a given class of analogs. There is an extensive literature attempting such correlations

[29]. All the available methods for estimating the distribution coefficients involve empirical relationships with a certain property of the molecules [29]. These relationships are regression equations obtained from various data sets and are usually expressed in the log–log form. As the whole complex of physicochemical and structural parameters of molecules affects the retention characteristics, the correlation of retention indices and characteristics of the molecule may be described by the equation:

$$\log D = \sum_{i=1}^n a_i \log x_i + b_i$$

where x_i is the physicochemical and structural parameters of compounds; a_i, b are constants. As a rule, the parameter that has been employed in such studies is $\log P$, the octanol–water distribution constant, which is generally considered to be a measure of hydrophobicity. It is supposed that for a number of phenols with approximately similar values of acid–base dissociation constants, the difference in the sorption would be defined by the difference in their hydrophobicity. Really, in the number of phenol–3-cresol–1-naphthol ($\text{p}K_{\text{a}} \sim 10$) the distribution coefficients increase with the

increase of the molecule hydrophobicity. Moreover, the logarithm of the distribution coefficient and the parameter of the phenol hydrophobicity (Fig. 4) correlate linearly. The estimation of the obtained regression equations was made by the Fisher criterion. For all the investigated foams, the values of the coefficients of correlation are no less than 0.999 ($n = 3$), the correlation equations are given below:

PUF	The correlation equation	F_{exp}
5-30	$\log D = 1.243 + 0.640 \cdot \log P$	1.1×10^6
140	$\log D = 0.492 + 0.888 \cdot \log P$	1.4×10^4
M-40	$\log D = 0.846 + 0.757 \cdot \log P$	3466
VP	$\log D = 1.057 + 0.692 \cdot \log P$	443
2200	$\log D = 0.418 + 0.925 \cdot \log P$	358
35-08	$\log D = 0.244 + 0.975 \cdot \log P$	1030

$F_{\text{tabl}} = 99.00$ ($P = 0.99$)

In a similar way, it is possible to construct a series of substituted phenols with a gradual change in their ability to form hydrogen bonds (a decrease of pK_a): phenol-2,4-dinitrophenol-2,4,6-trinitrophenol. The major tendency is obvious: with an increase in the acidity of the proton of the OH-group, the distribution coefficients of phenols grow (Tables 2 and 3) although a linear correlation is not observed.

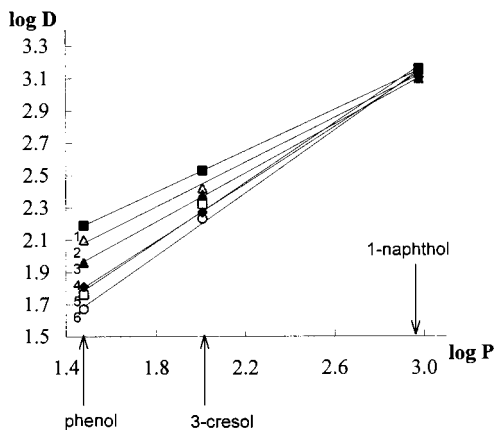


Fig. 4. Dependence of distribution coefficients of phenol, 3-cresol and 1-naphthol on the parameter of hydrophobicity by 5-30 (1) VP (2), M-40 (3), 140 (4), 2200 (5) and 35-08 (6) polyurethane foams. $C_{\text{Ph}} = 1 \times 10^{-4}$ M, $C_{\text{HCl}} = 0.1$ M, $V = 25$ ml, $m_{\text{PUF}} \sim 0.06$ g.

In this work, it is attempted to reveal the correlation dependence between the logarithm of the distribution coefficients with the values of pK_a and $\log P$ (the parameters of hydrophobicity). The values of $\log D$ of phenol, 3-cresol, 1-naphthol, 3-, 4-nitrophenols, 2,4-, 2,6-dinitrophenols and 2,4,6-trinitrophenol (Tables 2 and 3), found experimentally (sorption from 0.1 M HCl, the concentration of phenols was on the linear part of the sorption isotherms) were used throughout. The calculations were carried out using the unit of correlation regression analysis from Statistica for Windows, version 4.3 (StatSoft, 1993). The values of octanol–water distribution constants and pK_a of phenols were calculated by $\log P$ and pK_a software (©ACD, Toronto, Canada) or found in the databases included in these software packages. As a result, the two-parametrical correlation equations connecting the phenols $\log D$ values on different PUF with the values of pK_a and $\log P$ (Table 4) were produced. The derived equations describe the sorption of phenols with reliability that makes it possible to predict sorption behaviour of the compounds in this row. The coefficients of correlation of the derived equations are 0.968; 0.963; 0.996; 0.932; 0.939; 0.976 for PUF 5-30, 140, M-40, VP, 2200 and 35-08, respectively.

The compounds of phenol series with various substituents and several aromatic hydroxycompounds were chosen as a model to check the accuracy of the calculated equations. The values of the distribution coefficients of model compounds on polyether foams calculated from the equation and obtained experimentally are given in Table 5. The values of calculated distribution coefficients and obtained experimentally values for resorcinol, pyrocatechol, hydroquinone, 4-iodophenol, 3,4-dimethylphenol, 8-hydroxyquinoline, and 4-(2-pyridylazo)-resorcinol are in good concordance. A worse picture for experimental and calculated values for pyrogallol, 3-methyl-4-chlorophenol, nitrosonaphthol, and 1-(2-pyridylazo)-2-naphthol results from fact that the sorption of the above compounds involves not only hydrophobic interactions and hydrogen bond but also other interactions, which are not taken-considered the obtained two-parametrical equation.

Table 4

Calculate equations of dependence of distribution coefficient of phenols ($\log D$) on Hansch parameter ($\log P$) and constants of acid dissociation ($\text{p}K_{\text{a}}$)^a

Polyurethane foam	Correlation equilibrium	r	n	F_{exp}	F_{crit}	s_r
5-30	$\log D = 2.130 + 0.867 \cdot \log P - 0.131 \cdot \text{p}K_{\text{a}}$	0.968	8	37.71	5.79	0.124
140	$\log D = 1.423 + 1.010 \cdot \log P - 0.122 \cdot \text{p}K_{\text{a}}$	0.963	6	19.25	9.55	0.179
M-40	$\log D = 1.903 + 0.835 \cdot \log P - 0.121 \cdot \text{p}K_{\text{a}}$	0.996	6	166.73	9.55	0.055
VP	$\log D = 1.634 + 0.741 \cdot \log P - 0.070 \cdot \text{p}K_{\text{a}}$	0.932	6	9.95	9.55	0.171
2200	$\log D = 1.229 + 0.977 \cdot \log P - 0.093 \cdot \text{p}K_{\text{a}}$	0.939	6	11.17	9.55	0.212
35-08	$\log D = 1.124 + 1.029 \cdot \log P - 0.096 \cdot \text{p}K_{\text{a}}$	0.976	6	30.74	9.55	0.134

^a r , coefficient of correlation; n , number of points; F_{exp} , F_{crit} , experimental and critical values of Fisher's test, respectively ($P = 0.95$); s_r , relative standard derivation.

Table 5

Experimental and calculated values of distribution coefficients for phenols and aromatic hydroxy compounds on polyurethane foams^a

Compound	$\log P$	$\text{p}K_{\text{a}}$	$\log D$					
			PUF 5-30		PUF 140		PUF M-40	
			Exp.	Calc.	Exp.	Calc.	Exp.	Calc.
1-(2-Pyridylazo)-2-naphthol	2.74	11.00	3.8 ± 0.4	3.06	3.9 ± 0.4	2.85	3.9 ± 0.4	2.86
4-(2-Pyridylazo)-resorcinol	1.64	11.91	2.2 ± 0.1	1.99	1.6 ± 0.1	1.63	1.8 ± 0.1	1.83
8-Hydroxyquinoline	1.45	9.85	2.3 ± 0.2	2.10	2.2 ± 0.2	1.69	2.2 ± 0.2	1.92
	1.96			2.54		2.20		2.35
Resorcinol	0.88	9.30	1.9 ± 0.1	1.67	1.9 ± 0.1	1.18	1.8 ± 0.2	1.51
Pyrocatechol	1.01	9.5	2.0 ± 0.1	1.76	1.5 ± 0.1	1.28	1.7 ± 0.1	1.6
Hydroquinone	0.54	9.82	1.3 ± 0.1	1.31	0.87 ± 0.04	0.77	1.2 ± 0.1	1.17
	0.50	9.85		1.27		0.73		1.13
Pyrogallol	0.29	8.94	2.7 ± 0.2	1.21	2.7 ± 0.2	0.63	2.5 ± 0.1	1.06
4-Iodophenol	2.91	9.21	3.5 ± 0.4	3.45	3.4 ± 0.4	3.24	3.5 ± 0.4	3.22
3-Methyl-4-chloro-phenol	2.89	9.63	2.2 ± 0.2	3.37	2.5 ± 0.2	3.17	1.6 ± 0.1	3.15
3,4-Dimethyl-phenol	2.40	10.43	2.9 ± 0.4	2.84	2.7 ± 0.2	2.57	2.9 ± 0.2	2.64
1-Nitroso-2-naphthol	2.42	7.65	2.8 ± 0.2	3.23	2.7 ± 0.2	2.93	2.7 ± 0.2	3.00

^a Conditions: $20 \pm 1^\circ$; 25-ml aliquot of 1×10^{-4} M aqueous solution of phenol, 0.06 g of the foam, sorption time 30 min, $n = 5$, $P = 0.95$.

4. Conclusions

The obtained results demonstrate that tested phenols at $\text{pH} \leq \text{p}K_{\text{a}} - 2$ are sorbed in their molecular form. The sorption of different phenols by tested PUF increases in the row: phenol < 4-nitrophenol, 3-cresol < 2,4-dinitrophenol < 2,4,6-trinitrophenol < 1-naphthol. The data obtained allows one to suggest that two factors should be consider in studying the sorption of phenols.

Namely they are the hydrophobicity of phenols and their ability to form hydrogen bond.

It was shown, that in the series of phenols with similar values of $\text{p}K_{\text{a}}$, distribution coefficients depend linearly on the phenol hydrophobicity (Hansch parameter). In the series of phenols with approximately identical hydrophobicity, values of $\log D$ increase with a decrease in $\text{p}K_{\text{a}}$. The results of a linear combination of these two parameters with distribution coefficients of

phenols are regression equations presented in Table 4.

The mathematical model of the sorption showing the influence of the hydrophobicity and pK_a of sorbed compounds allowed the prediction of the sorption behaviour of the compounds, i.e. a priori the calculation of the distribution coefficients by PUF with different structures of the polymer unit.

Acknowledgements

This work was supported by the Russian fund of fundamental researches (grant No 96-03-33578à).

References

- [1] T. Braun, J.D. Navratil, A.B. Farag, *Polyurethane Foam Sorbents in Separation Science*, CRS Press, Boca Raton, FL, 1985.
- [2] T. Braun, *Fr. Z. Anal. Chem.* 333 (1989) 785.
- [3] H.D. Gesser, A. Chow, F.C. Davis, et al., *Anal. Lett.* 4 (1971) 883.
- [4] C.G. Simon, T.F. Bidleman, *Anal. Chem.* 51 (1979) 1110.
- [5] P.R. Musty, G. Nickless, *J. Chromatogr.* 100 (1974) 83.
- [6] J. Saxena, J. Kozuchowski, D.K. Basu, *Environ. Sci. Technol.* 11 (1977) 682.
- [7] D.K. Basu, J. Saxena, *Environ. Sci. Technol.* 12 (1978) 791.
- [8] A.B. Farag, A.M. El-Wakil, M.S. El-Shahawi, M. Mashaly, *Anal. Sci.* 5 (1989) 415.
- [9] M.S. El-Shahawi, S.M. Aldhaheri, *Anal. Chim. Acta* 320 (1996) 277.
- [10] M.S. El-Shahawi, A.M. Kiwan, S.M. Aldhaheri, M.H. Saleh, *Talanta* 42 (1995) 1471.
- [11] A. Chow, W. Branagh, J. Chance, *Talanta* 37 (1990) 407.
- [12] R. Werbowesky, A. Chow, *Talanta* 43 (1996) 263.
- [13] S.G. Dmitrienko, E.V. Loginova, E.N. Myshak, V.K. Runov, *Zh. Fiz. Khim.* 68 (1994) 1295 [*Russ. J. Phys. Chem. (Engl. Transl.)* 68 (1994) 1172].
- [14] S.G. Dmitrienko, E.V. Loginova, E.N. Myshak, V.K. Runov, *Zh. Fiz. Khim.* 71 (1997) 317 [*Russ. J. Phys. Chem. (Engl. Transl.)* 71 (1997) 258].
- [15] S.G. Dmitrienko, L.N. Pyatkova, N.V. Malinovskaya, V.K. Runov, *Zh. Fiz. Khim.* 71 (1997) 709 [*Russ. J. Phys. Chem. (Engl. Transl.)* 71 (1997) 623].
- [16] S.G. Dmitrienko, L.N. Pyatkova, E.N. Myshak, V.K. Runov, *Mendeleev Commun.* 4 (1996) 137.
- [17] L. Schumack, A. Chow, *Talanta* 34 (1987) 957.
- [18] P. Fong, A. Chow, *Talanta* 39 (1992) 497.
- [19] S.G. Dmitrienko, O.A. Kosyreva, O.I. Okina, I.V. Pletnev, *Zh. Fiz. Khim.* 66 (1992) 1421.
- [20] El-Shahawi, *Talanta* 41 (1994) 1481.
- [21] K. Rzeszutek, A. Chow, *Talanta* 46 (1998) 507.
- [22] S.G. Dmitrienko, E.N. Myshak, V.K. Runov, Yu.A. Zolotov, *Chem. Anal. (Warsaw)* 40 (1995) 291.
- [23] S.G. Dmitrienko, E.N. Myshak, A.V. Zhigulyev, V.K. Runov, Yu.A. Zolotov, *Anal. Lett.* 30 (1997) 2527.
- [24] C. Hansch, A.J. Leo, *Substituent Constants for Correlation Analysis in Chemistry and Biology*, Wiley, New York, 1979.
- [25] J. Sangster, *J. Phys. Chem. Data* 18 (1989) 1111.
- [26] G.D. Parfitt, C.H. Rochester (Eds.), *Adsorption From Solution at the Solid/Liquid Interface*, Academic Press, London, 1983.
- [27] Yu.A. Zolotov (Ed.), *Microcyclic compounds in the analytical chemistry*, Chemical Analysis Series, Vol. 143, Wiley, New York, 1997.
- [28] G.D. Kharlampovich, Yu.V. Churkin, *Phenoly (Phenols)*, Khimiya, Moskva, 1974 In Russian.
- [29] W.J. Lyman, W.F. Reehl, D.H. Rosenblatt (Eds.), *Handbook of chemical property estimation methods. Environmental Behavior of Organic Compounds*, American Chemical Society, Washington, DC, 1990.

A study on electrochemistry of histidine and its metabolites based on the diazo coupling reaction

Chen Guo Nan ^{a,*}, Wu Xiao Ping ^a, Duan Jian Ping ^b, Chen Hong Qing ^b

^a Department of Chemistry, Fuzhou University, Fuzhou, Fujian 350002, PR China

^b Analytical and Testing Center, Fuzhou University, Fuzhou, Fujian 350002, PR China

Received 23 July 1998; received in revised form 9 November 1998; accepted 1 December 1998

Abstract

The diazo coupling reaction of diazotized *p*-aminoacetophenone (DPAAP) with histidine and its metabolites form the basis of the differential pulse adsorption stripping voltammetry (DPASV) method for determination of histidine and its metabolites. The adsorption and electrochemical reaction mechanism of the coupling products were studied in detail by structure analysis, cyclic voltammetry, chronocoulometry, control potential electrolysis, electrocapillary curves, UV spectroscopy and the effect of temperature and surfactants. The adsorption of azo-histidine was found to obey Frumkin adsorption isotherm. The calculation results of the maximum surface excess ($\Gamma_m = 3.08 \times 10^{-11}$ mol cm²), diffusion coefficient ($D = 2.27 \times 10^{-6}$ cm² s⁻¹), adsorption coefficient ($\beta = 1.06 \times 10^7$) and interactive factor ($\gamma = 0.9900$) showed that the azo-histidine conjugation molecules adsorbed on the mercury electrode surface were attracted each other and the electrode process was adsorption controlled. © 1999 Elsevier Science B.V. All rights reserved.

Keywords: Histidine and its metabolites; Adsorption; Electrochemistry; Differential pulse stripping voltammetry

1. Introduction

Histidine (His) is one of the necessary basic amino acids in biological bases, constitutes the active center of many enzymes and function protein, and controls the transmission of metal elements in biological bases. His exists widely in muscular and nervous tissue, and constitutes the brain nervous peptide.

Metabolism of His is very important in physiology. In the metabolism process of His, histamine (Hst), imidazole acetic acid (Ima) and methyl imidazole acetic acid (Mic) are the main intermediates and products [1], and they are all biologically important compounds [2–4]. Some studies on the electrochemistry of His at the solid electrodes and mercury electrode in aprotic solvent have been reported [5,6]. As His is electrochemically inactive in water and is easily adsorbed on the surface of electrode to inactivate electrode, therefore, comparatively little attention has been paid to the electrochemical studies of His and its metabolites in water.

* Corresponding author. Fax: +86-591-3713866.

E-mail address: gn.chen@fzu.edu.cn (C. Guo Nan)

The coupling reaction between diazonium salts and proteins in alkaline solution has been widely studied. It was found that the stable coupling reaction only occurred with histidyl and tyrosyl residues of proteins [7]. In view of the fact that azo compounds usually possess adsorptivity and an electroactive group ($-N=N-$), so His and its metabolites can be derived to be electroactive compounds for further electrochemical determination. *p*-Amino-acetophenone (PAAP) was used as the diazo coupling reagent for His, Hst, Ima, Mic and Im in this paper. The electrochemical behavior and mechanism of the azo coupling compounds at a static mercury drop electrode was studied in detail, and a differential-pulse adsorptive stripping voltammetric method has been developed for determination of these compounds.

2. Experimental

2.1. Apparatus

A BAS-100 Electrochemical Analyzer (Bioanalytical Systems, Purdue, IN, USA) with a PAR (Princeton Applied Research) Model 303 static mercury drop electrode system was employed for all the electrochemical techniques. All potentials were measured against an Ag/AgCl (3 M KCl) reference electrode and the auxiliary electrode for all experiments was platinum electrode.

Controlled potential electrolysis was undertaken by using a stirred mercury pool (approximately 55 mm in diameter) working electrode. The auxiliary electrode consisted of platinum mesh immersed in a glass jacket containing 3 M KCl and separated from the test solution by a glass sinter. Electrode potentials were measured with respect to an Ag/AgCl (3 M KCl) reference electrode. A thermostatic cell was used to examine the effect of temperature.

A Perkin-Elmer Lambda 9 Spectrophotometer was used for UV measurement.

2.2. Chemicals

Histidine (GC grade, Shanghai Chemical), histamine (biological reagent, Shanghai Biological

Chemistry Institute), 1-methyl-4-imidazoleacetic acid (Sigma), imidazole-acetic acid (Sigma), and imidazole (AR, Guang Yao Chemical, Jiangsu, China) were used. Other reagents were of analytical grade or better and used without further purification. All water used was doubly distilled in a fused-silica apparatus.

2.3. Procedure

2.3.1. Preparation of diazotized *p*-amino-acetophenone (DPAAP)

A total of 10 ml 0.02 mol^{-1} PAAP and 5.0 ml 0.12 mol^{-1} HCl were added to a 50-ml beaker, and the mixture was cooled in ice-bath for 10 min. Then 5 ml 0.04 mol^{-1} NaNO_2 was added in drops under stirring, and kept in ice-bath for more than 10 min; 0.01 mol^{-1} DPAAP was then obtained.

2.3.2. Coupling of DPAAP with His

A 10- μl 0.01 mol^{-1} DPAAP solution was added to the Clark-Lubs buffer solution (pH 9.6) containing His in a 10-ml volumetric flask, and diluted with buffer solution to volume. The reaction was permitted to proceed for 30 min at room temperature. A blank assay was carried out in parallel with each determination.

The procedure for coupling of DPAAP with other metabolites of His is basically the same as that for His.

2.3.3. The procedure for differential-pulse adsorptive stripping voltammetry (DPASV)

A total of 10 ml derivative His or its metabolites solution was placed in a quartz voltammetric cell. The solution was purged with nitrogen for 5 min (subsequently, a 15 s de-oxygenation procedure was carried out between adsorptive stripping cycles). The derivative compound was then concentrated on SMDE at 0 V with stirring of nitrogen for 60 s. After standing for 5 s, a scan in negative direction was performed between 0 and -1.00 V . The whole experiment was performed at room temperature ($25 \pm 2^\circ\text{C}$, controlled by air conditioning).

3. Results and discussion

3.1. Selection of diazo coupling reagents and supporting electrolytes

Imidazole ring, which is present in His and its metabolites, is an electron-rich system and favorable for electrophilic substitution [8]. Diazonium salt itself is not a strong electrophile reagent, but the azo group is easy to conjugate with benzene ring to give a stable product, and the ortho or para electron attractive substituent on benzene ring can improve both reactivity and selectivity.

Diazotized sulphanilic acid (DSA) has been used to couple with His, and a DPASV method has been developed for determination of this coupling product [9]. Therefore, DSA was first selected as the coupling reagent. Unfortunately, except His the coupling products of Hst, Ima and Mic were found very unstable. In order to obtain a better result of the diazo coupling reaction, diazotized *p*-nitroaniline, *p*-sulphanilic acid, sulfonamide, *p*-amino-acetophenone, *p*-aminobenzoic acid and β -naphthylamine have been tried as the coupling reagents. It was found that high blank value was obtained with *p*-nitroaniline due to the reduction of the diazotized *p*-amino-acetophenone, and DPAAP is better than other compounds in sensitivity, stability and shape of stripping peak. DPAAP was selected as the coupling reagent in subsequent experiments.

3.2. Differential-pulse adsorptive stripping voltammetry behavior

DPAAP could be adsorbed at mercury electrode in Clark-Lubs (CL) buffer solution to give a stable reductive peaks at -0.12 , -0.37 , -0.54 and -0.89 V. However, except for the first peak,

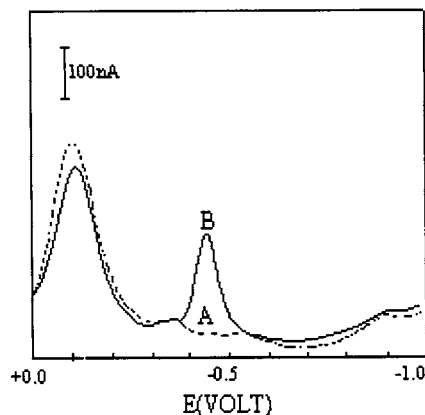


Fig. 1. Differential pulse adsorption stripping voltammogram for His coupling system. (A) DPAAP ($2.0 \times 10^{-5} \text{ mol}^{-1}$); (B) A + His ($1 \times 10^{-5} \text{ mol}^{-1}$). Coupling reaction time: 30 min; deposition time: 55 s; deposition potential: 0.0 V; pH: 9.6.

the other three peaks were very small, which did not even appear when the concentration was low; it was regarded that the first peak occurred due to a one-electron reduction of the diazonium salt [9], while it was possible that the other peaks responded to two-electron reduction of undissociated hydroxyazo-compound in alkaline solution, and which were pH dependence. When diazonium salt was coupled with His, a new reductive peak was appeared at about -455 mV, the peak was narrow and sharp, and peak potential and peak height were stable (Fig. 1). This peak could be ascribed to the reduction of coupling product at mercury electrode. The coupling products of other metabolites could be also reduced at mercury electrode, and their peak potentials are shown in Table 1. In general, N substituted imidazole derivatives are not regarded to occur coupling reaction [10]. However, it was found that Mic could be coupled with DPAAP in high concentration as the electron-repelling group $-\text{CH}_3$ was

Table 1
The peak potential of DPASV for His and its metabolites

	His ($1 \times 10^{-5} \text{ mol}^{-1}$)	Hst ($6 \times 10^{-6} \text{ mol}^{-1}$)	Im ($4 \times 10^{-5} \text{ mol}^{-1}$)	Mic ($1.4 \times 10^{-3} \text{ mol}^{-1}$)	Ima ($2.2 \times 10^{-5} \text{ mol}^{-1}$)
P_1 (mV)	-455	-500	-310	-340	-330
P_2 (mV)	-	-	-	-430	-440

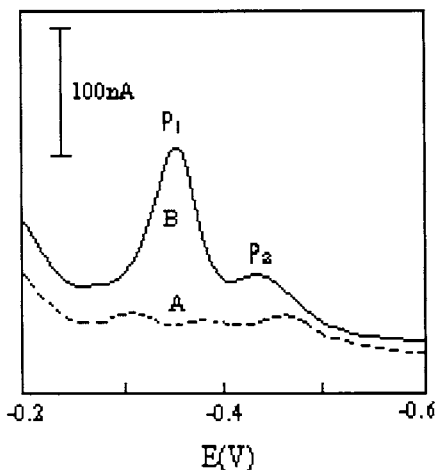


Fig. 2. Differential pulse adsorption stripping voltammogram for Mic coupling system (A) DPAAP ($1.6 \times 10^{-5} \text{ mol l}^{-1}$); (B) A + Mic ($1.4 \times 10^{-3} \text{ mol l}^{-1}$). Coupling reaction time: 20 min; deposition time: 35 s; deposition potential: 0.0 V; pH: 9.6.

substituted at N. This coupling product gave a reductive peak P_1 at -340 mV and another weaker peak P_2 at -430 mV (Fig. 2). P_2 could be inhibited by controlling the reaction conditions, P_1 was then used for quantitative determination. Ima was similar to Mic in giving two reduction peaks, and their mechanism for competitive reaction will be discussed later.

3.3. Optimum conditions for electroanalysis

In differential-pulse adsorption stripping voltammetry, the chemical reaction conditions and electrochemical parameters should be optimized to get the maximum adsorption of analyte at electrode, and then to obtain the maximum peak current. The coupling product of His and DPAAP was taken as an example for the selection of the optimum conditions.

3.3.1. Effect of DPAAP concentration

The effect of DPAAP concentration on the peak height has been determined, and the results show that the peak current reaches a maximum and constant value at $\sim 1.5\text{--}2.5 \times 10^{-5} \text{ mol l}^{-1}$ DPAAP and at higher concentration a decrease of the peak current is observed. This is due to the competitive adsorption on the electrode surface between the excess of DPAAP and coupling

product. In subsequent experiments $2.5 \times 10^{-5} \text{ mol l}^{-1}$ was used.

3.3.2. Effect of pH

The effect of pH for the coupling reaction on peak height has been examined, and the results show that the coupling reaction occurred mainly in the range of pH 8–11. The peak current was increased with pH when pH was between 8.0 and 9.4. In the range of pH 9.4–10.0, the coupling reaction was completed, and the peak current reached maximum and constant. After pH 10.0, diazo-cation was transferred to diazoic acid anion [11] with pH, and coupling reaction would occur by diazonium salt itself or between diazonium salt and diazo-phenol, so the coupling reaction rate of His would be decreased, and peak current would be decreased too. pH 9.5 was chosen as the optimum pH for subsequent experiments.

3.3.3. Effect of coupling time

The effect of coupling time on peak current was determined, and it was found that the azo-compound was formed completely in 25 min, and peak current was constant for 60 min, after that the peak current decreased gradually due to dissociation of coupling product. In subsequent experiments 30 min were selected.

3.3.4. Effect of deposition potential and deposition time

The effect of deposition potential on the peak current has been investigated, and the results showed that the highest peak current is obtained when the deposition potential is in the range of 0.0– -0.10 V . At more negative deposition potentials, the peak current is decreased, but the peak potential is unchangeable.

The effect of deposition time on the peak current has also been examined, and was found that when the deposition time is less than 40 s, the peak current is linear with the deposition time, while the peak current reaches a maximum and constant value when the deposition time is 50–65 s, which indicates that the surface of electrode is saturated by adsorption. In subsequent experiments, 0.0 V was chosen as the deposition potential and 55 s as the deposition time.

Table 2

The optimum conditions of DPASV for the coupling products of His and its metabolites^a

IMS	[DPAAP] × 10 ⁻⁵ M	pH	CRT (min)	DT (s)	DP (mV)	DL (M)	LR (M)	RSD (%)	PA	PP
His	2.5	9.5	30	55	0	1.4 × 10 ⁻⁷	8 × 10 ⁻⁷ -1.0 × 10 ⁻⁵	1.7	50	200
Hst	1.5	10.5	10	50	0	1.2 × 10 ⁻⁷	1 × 10 ⁻⁶ -1.2 × 10 ⁻⁵	2.4	50	200
Im	4.0	9.6	30	60	0	3.3 × 10 ⁻⁶	5 × 10 ⁻⁶ -2.0 × 10 ⁻⁴	1.9	50	200
Mic	1.5	9.6	20	35	0	5.0 × 10 ⁻⁵	1 × 10 ⁻⁴ -1.4 × 10 ⁻³	4.8	50	200
Ima	2.1	9.7	75	30	0	1.1 × 10 ⁻⁶	5 × 10 ⁻⁶ -6.0 × 10 ⁻⁵	3.5	50	200

^a CRT, coupling reaction time; DL, detection limit; DP, deposition potential; DT, deposition time; IMS, His and its metabolites; LR, linear range; PA, pulse amplitude; PP, pulse period.

3.3.5. The effect of temperature

The effect of temperature on the peak current of His coupling product has been tested. The results show that when $T < 10^{\circ}\text{C}$, the electrode reaction of coupling product was slow, and peak current (i_p) was small. The optimum temperature for the electrode reaction of coupling product was shown to be 15–40°C. At temperature higher than 40°C, the smaller peak currents obtained were caused by desorption of the coupling product. The effects of temperature on other metabolites were similar to that of His. In general, a room temperature of $25 \pm 2^{\circ}\text{C}$ controlled by air conditioning was used in subsequent experiments.

The optimum conditions for the coupling products of other metabolites and DPAAP were similar to that of His, and the results are shown in Table 2.

3.4. Linear response range, detection limit and precision

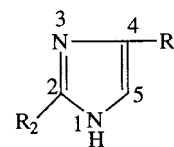
Under the above optimum conditions, the linear response range for the coupling products of His and metabolites were measured and the results are shown in Table 2. The detection limit was defined as three times the concentration corresponding to the standard deviation of the blank. The detection limit and precision for His and metabolites are also given in Table 2.

3.5. Interference

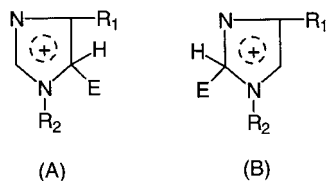
Of the 20 basic amino acids, glycine, alanine, valine, leucine, isoleucine, serine, threonine, methionine, glutamate, aspartic acid, asparagine, arginine, lysine, phenlalanine and proline were shown not to interfere at the 10-fold of His. It was found that tyrosine and tryptophan would react with DPAAP, and their coupling products would give a peak very close to that of His. Moreover, cysteine and cystine would adsorb at the electrode surface giving a peak partially overlapped and interfered with by the azo His peaks.

3.6. The coupling reaction mechanism

It was generally considered that a three-step-course was involved in the coupling reaction between diazonium salts and aromatics compounds: π -complex was first formed, π -complex was then rearranged to a carbonium ion (σ -complex) which would be transformed into a stable aromatic azo-compound after losing proton by attack of base. The structure of His and its metabolites are shown as follows:



By means of Huckel molecular orbital method, the charging density distribution of these compounds was obtained and are shown in Table 3, and the results indicate that the electron density on C_5 was higher than that on C_2 for all above compounds, therefore, C_5 was the prior position being attacked by electrophilic reagent. We infer that the electrophilic substitution influences the competition result and two possible σ -complexes in coupling reaction process can be described as follows:



where E represents diazo ion, R_1 represents the monosubstituted group on the imidazole ring, R_2 is $-\text{CH}_3$. According to the effect of monosubstituted group, the electrophilic reaction ability of His is stronger than Im. However, Mic is special as it has two substitution group, so its space resistance is higher, and a electron-repelling group $-\text{CH}_3$ is substituted at N, so its electrophilic reaction ability is lower than that of Im.

It is found that the coupling products of Mic and Ima have two reductive peaks at their cyclic voltammetry curve. We think this is due to the existence of the competition reaction as follows,

Table 3

The charging density distribution of His and its metabolites

Number of C	Charging density distribution			
	His	Hst	Mic	Ima
C_1	-0.1914	-0.1914	-0.1523	-0.1908
C_2	0.5726	0.5725	0.5502	0.5724
C_3	-0.9945	-0.9948	-1.0270	-0.9944
C_4	0.2415	0.2422	0.3024	0.2529
C_5	0.0461	0.0459	0.0331	0.0485
C_6	-	-	0.1485	-
C_7	-0.0486	-0.0595	-0.2393	-0.0158

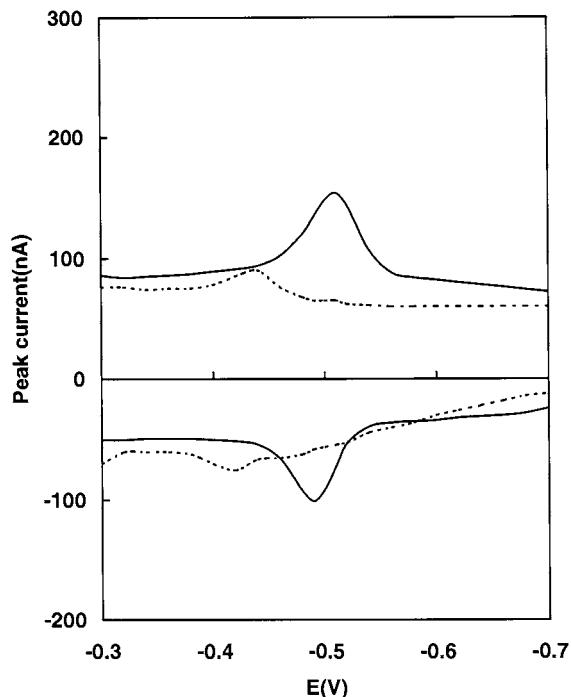
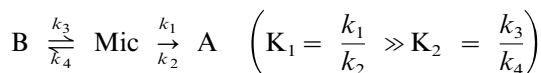


Fig. 3. Cyclic voltammogram of DPAAP-His at pH 9.6; (---), DPAAP; (—), $[\text{DPAAP-His}] = 2 \times 10^{-5} \text{ mol}^{-1}$.



where A represents C_5 coupling products and B represents C_2 coupling products. At the beginning of reaction, the formation of product A is dynamically controlled, so the main product is A, however, as the existence of competition reaction K_2 (although $K_2 \ll K_1$), so few product B would be occurred when reaction equilibrium is reached, therefore, the coupling products give two reductive peaks at mercury electrode.

To sum up, the ability order for His and its metabolites to react with diazonium salt is $\text{Hst} > \text{His} > \text{Ima} > \text{Im} > \text{Mic}$.

3.7. Adsorption characteristic of coupling products

3.7.1. Cyclic voltammetry

The cyclic voltammetry curve of DPAAP in Clark-Lubs buffer solution is shown in Fig. 3a, which gives a pair of symmetrical redox adsorptive peaks, and the corresponding redox potentials

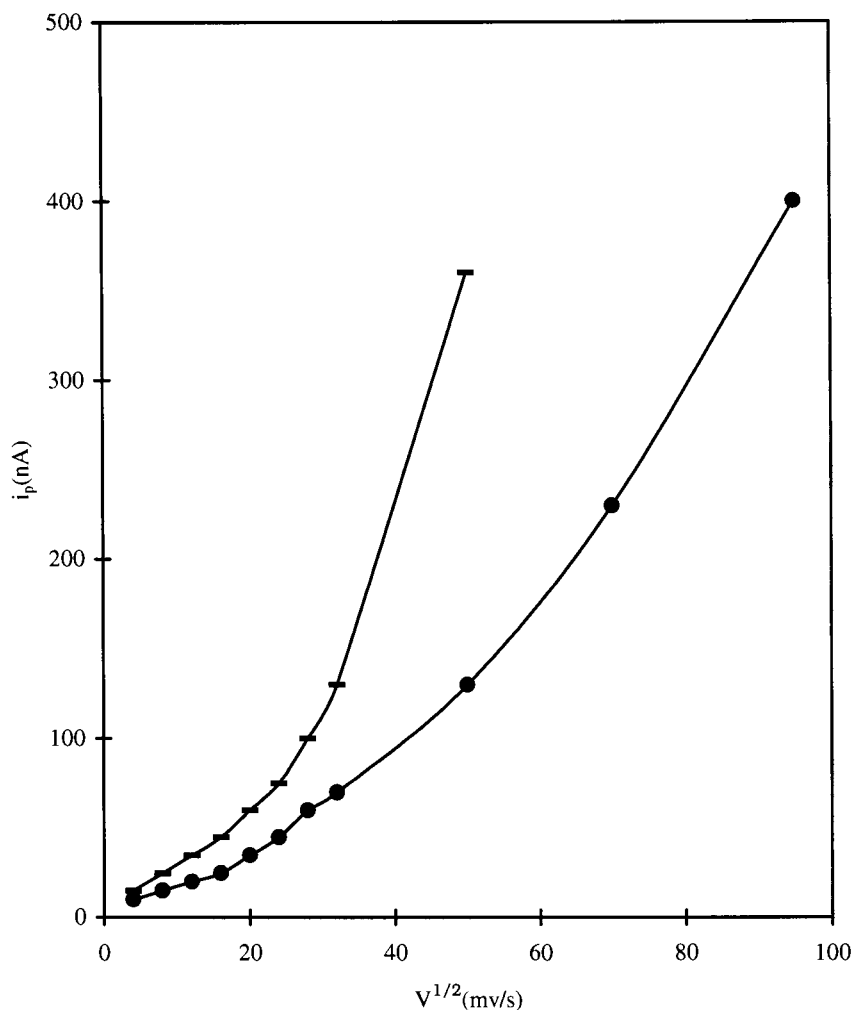


Fig. 4. The relationship between peak current and square root of scan rate for His system; $i_{pc} \sim V^{1/2}$; $-: i_{pa} \sim V^{1/2}$.

are $-418/410$ mV. The cyclic voltammetry curve for the coupling product of DPAAP and His is shown in Fig. 3b. From Fig. 3b it can be seen that the redox peak of coupling product is sharp and symmetrical, $E_{pa} = -498$ mV, $E_{pc} = -487$ mV, $i_{pa} \approx i_{pc}$, which indicates that the electrode process is reversible.

The cyclic voltammetry data of His coupling product under different scan rates are shown in Table 4. The plots of i_{pc} and i_{pa} against square root of scan rate ($V_s^{1/2}$) are made and shown in Fig. 4, which is turn up and departure from Randles Sevcik Equation [12]. When scan rate

(V_s) is between 100 and 1000 mV s^{-1} , the linear relationship can be obtained by making the plots of i_{pc} and i_{pa} against V_s (Table 4), and $i_{pa}/i_{pc} \approx 1$, which indicates that both reactant and product can be adsorbed on electrode to form the adsorbed film. When V_s is lower than 1000 mV s^{-1} , the differential of cathode and anode potential (ΔE_p) is not changed much, and $i_p/V_s^{1/2}$ is not V_s dependent, which illuminates that the electrode process is a fast and reversible electron transfer process. When V_s is higher than 1000 mV s^{-1} , as the electron transfer rate cannot catch up V_s , so ΔE_p is increased, and the electrode process is

Table 4
The CV data of His coupling product under different scan rates^a

	V_s (mV s ⁻¹)									
	10	50	100	200	350	500	800	1000	2500	5000
E_{pc} (mV)	-501	-503	-502	-503	-502	-504	-507	-510	-513	-516
E_{pa} (mV)	-488	-492	-495	-494	-493	-490	-491	-491	-482	-466
E_p (mV)	13	11	7	9	9	14	16	19	31	50
i_{pc} (nA)	7.9	17.8	27.7	36.3	50.2	63.4	74.5	82.2	143.2	232.1
i_{pa} (nA)	6.0	19.2	31.0	40.4	58.9	78.1	110.0	139.8	330.5	488.7
i_{pa}/i_{pc}	0.76	1.08	1.12	1.11	1.18	1.23	1.48	1.70	2.30	2.11

^a [His] = 2×10^{-5} mol⁻¹; [DPAAP] = 1×10^{-5} mol⁻¹; pH = 9.6.

Table 5
The CV data for coupling products of His and its metabolites

Products	E_{pa}/E_{pc} (mV)				
	His	Hst	Im	Mic	Ima
Main product	–498/–487	–540/–530	–405/–403	–425/–405	–430/–424
Competition product	–	–	–	–503/–498	–509/–499

changed into a semi-reversible process. When V_s is lower than 50 mV s^{-1} , $i_{pa}/i_{pc} < 1$, and E_p is shifted positively, the electrode reaction may have enough time to occur, so some intermediates are probably present in the process [13].

The cyclic voltammetry curve for the coupling products of other metabolites have been also investigated in detail, and their redox peak potentials are shown in Table 5.

3.7.2. Electrocapillary curve

The electrocapillary curve of His coupling system is shown in Fig. 5. It can be seen from Fig. 5 that DPAAP can be adsorbed on the surface of mercury electrode in the range of $0 \sim -1.2 \text{ V}$ (vs Ag/AgCl). When DPAAP is coupled with His, the electrocapillary curve is further lowered, and the surface tension (σ) near the zero charge point (ϕ_o) is decreased more obviously. A turning point in electrocapillary curve of coupling product can be observed at reductive potential about -0.40 V .

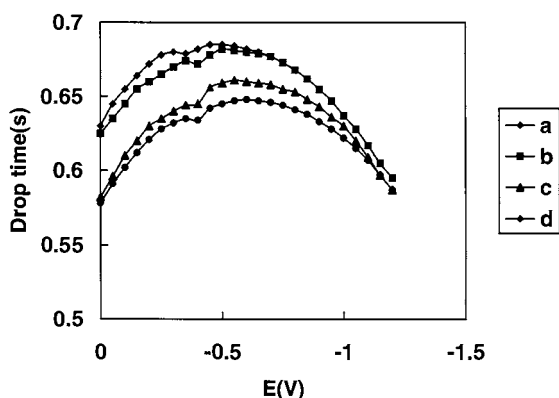


Fig. 5. The electrocapillary curves for His system. (a) $[\text{His}] = 0$; (b) $[\text{His}] = 2 \times 10^{-4} \text{ mol l}^{-1}$; (c) $[\text{His}] = 6 \times 10^{-4} \text{ mol l}^{-1}$; (d) $[\text{His}] = 8 \times 10^{-4} \text{ mol l}^{-1}$.

When the potential is more negative than -0.8 V the curve is recovered as the coupling product adsorbed on electrode is replaced by water molecule. The adsorbate on the surface of mercury electrode would be increased with the concentration of His, and the surface tension of mercury drop would be decreased.

The electrocapillary curves of other coupling products have been also investigated, and the results showed that all the coupling products of other metabolites and DPAAP can be adsorbed on the surface of mercury electrode to reduce its surface tension. All the electrocapillary curves of these coupling products give a small turning point around -0.4 V , which proves that the appearance of a sharp reductive peak between -0.3 and -0.5 V in differential pulse adsorption stripping voltammetry is due to the strong adsorptive reduction of coupling products on mercury electrode. As the drop time (t) of mercury is decreased with the increase of surface adsorbance, therefore, the order of adsorptivity for the coupling products of His and its metabolites can be found by comparing their drop time: $\text{Ima} > \text{His} > \text{Im} > \text{Hst} > \text{Mic}$.

3.7.3. Effects of surfactants

The effect of three surfactants, bromo-cetyltrimethylamine (CTMAB, cationic surfactant), Triton X-100 (non-ionic surfactant) and dodecyl sulfobenzoic acid sodium (SDS, anionic surfactant) on His, Hst and Im coupling system under the optimum conditions of DPASV has been investigated in detail, and the results showed that the addition of surfactants (CTMAB $2\text{--}5 \times 10^{-7} \text{ mol l}^{-1}$, Triton X-100 $2\text{--}5 \times 10^{-6} \text{ mol l}^{-1}$, SDS $5 \times 10^{-5}\text{--}1 \times 10^{-4} \text{ mol l}^{-1}$) will significantly reduce the peak current of coupling products, which

indicates that the surfactant is in the form of single molecule in dilute solution, and can interact with the electroactive substance adsorbed on the surface of mercury drop to bring about competitive adsorption to reduce the adsorptive peak current. In view of the inhibitive ability of these surfactants, we found that CTMAB > Triton X-100 > SDS, which indicates that the electroactive coupling product is in the form of anion, and the order of the inhibitive ability is His > Im > Hst, which corresponds to the order of adsorptive ability mentioned in electrocapillary effect.

3.7.4. Chronocoulometry

A $Q \sim t$ curve for coupling product of His and an $Q \sim t^{1/2}$ linear relationship for different concentration of His has been determined by using chronocoulometry. When concentration of reactant is zero, the slope of $Q \sim t^{1/2}$ is $B_0 = 0$, and intercept $I_0 \cong Q_{dl}$. When the concentration of His is lower, intercept I_j is increased quickly, which indicates that both reactant and product are strongly adsorbed on the electrode surface. When $[\text{His}] > 2 \times 10^{-4} \text{ mol l}^{-1}$, intercept I_j is not changed much, but slope B_j is increased, which shows that the adsorption of molecule has been in the saturate region of isotherm. While I_j is decreased the concentration of His is increased to $6 \times 10^{-4} \text{ mol l}^{-1}$, which is due to the competitive adsorption of solvent molecule and coupling product on electrode.

It is also found that ΔI_j , the differential between the intercept of coupling product I_j and the intercept of blank solution I_0 is proportional to the His concentration C_{His} , i.e. the charging coulomb of double layer Q_{dl} was basically unchanged under different C_{His} , therefore, when the concentration of DPAAP is adjusted to react with His completely (the concentration ratio was 1:2), an equation can be inferred for blank solution,

$$Q_0 = B_0 t^{1/2} + Q_{dl} + Q_{ads(0)} \cong B_0^{1/2} + Q_{dl} \quad (1)$$

and for coupling product,

$$Q_i = B_j t^{1/2} + Q_{dl} + Q_{ads(i)} \quad (2)$$

therefore,

$$\Delta I_j = I_j - I_0 = Q_{ads(i)} - Q_{ads(0)} \approx dQ_{ads(i)} \quad (3)$$

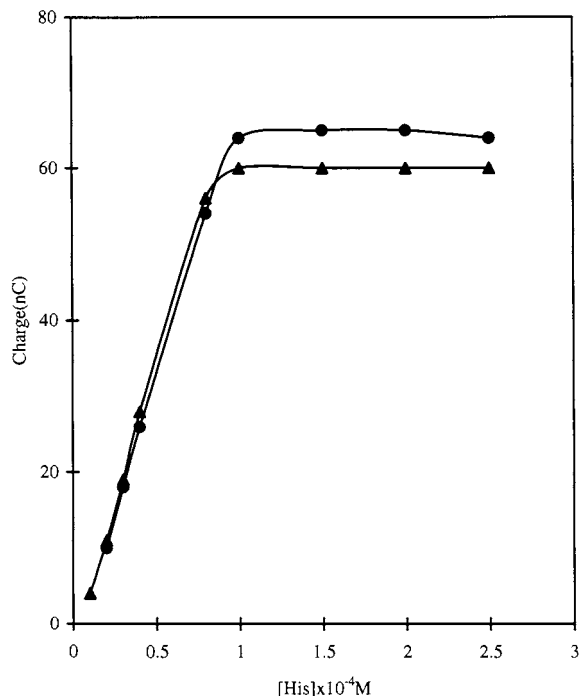


Fig. 6. The adsorption isothermal curves for His system; ●, reactant; ▲, product.

i.e.

$$\Delta I_j = Q_{ads(i)} = nFA\Gamma_i \quad (4)$$

The adsorption isotherm of His coupling product is shown in Fig. 6. It can be seen from Fig. 6 that electrode reactant and product have the same linear relationship for $Q_{ads} \sim C_{\text{His}}$ in the unsaturated adsorption region, while in the saturated region, which indicates that the reactant and product are basically equal adsorption. The type of adsorption on the surface of electrode is Frumkin adsorption [12], and molecules on the surface of electrode are intermolecular attractive. According to Eq. (4), the maximum adsorption under $[\text{His}] = 1 \times 10^{-4} \text{ mol l}^{-1}$ can be calculated as follows:

$$\Gamma_m = \frac{Q_{ads(max)}}{nAF} = 3.08 \times 10^{-11} \text{ mol cm}^2$$

($T = 16^\circ\text{C}$, $n = 2$), i.e. the area that each adsorbed coupling molecule occupies is 5.38 nm^2 , such large area for a molecule that we can infer

Table 6
The relationship between E_p and pH for coupling systems in DPASV

Coupling system	[IMS] (mol^{-1})	E_p (mV) ~ pH	Relative coefficient
azo-His	1×10^{-5}	$E_p = 74.7\text{--}55.6$ pH	0.9994
azo-Hst	1×10^{-5}	$E_p = 95.6\text{--}56.6$ pH	0.9972
azo-Im	4×10^{-5}	$E_p = 214.9\text{--}56.3$ pH	0.9739
azo-Ima	5×10^{-5}	$E_{p1} = 397.9\text{--}78.2$ pH	0.9607
azo-Mic	1×10^{-4}	$E_{p2} = 45.4\text{--}52.2$ pH	0.9848

the coupling molecule is adsorbed on the mercury electrode in the form of conjugate plane [14–17].

The diffusion coefficient D can be calculated by the slope of $Q \sim t^{1/2}$,

$$B = \frac{\Delta Q}{\Delta t^{1/2}} = \frac{2nFACD^{1/2}}{\sqrt{\pi}} \quad (5)$$

A diluted His solution (1×10^{-8} mol cm^3) was used under the optimum condition to get the slope $B = 0.0011$ $\mu\text{C ms}^{1/2}$, and then to obtain $D = 2.27 \times 10^{-6}$ $\text{cm}^2 \text{s}^{-1}$.

According to Frumkin adsorption isothermal equation,

$$\beta C = \theta / (1 - \theta) e^{(-2\gamma\theta)\gamma} \quad (6)$$

Where, $\theta = Q_{\text{balance}} / Q_{\text{saturated}}$, β is the adsorption coefficient, C is concentration of reactant (mol cm^3), and γ is interaction factor. A series value of C and θ can be calculated and substituted into Eq. (6) to obtain $\beta = 1.06 \times 10^7$, $\gamma = 0.9900$. Here β is quite large, which illuminates that the coupling product is strongly adsorbed on the surface of mercury electrode. Meanwhile, γ is positive, which further verifies that the coupling molecules adsorbed on the surface of electrode are intermolecular attractive.

3.8. Electrochemical reaction mechanism

In the investigation of acidic effect, it was found that the stripping peak potential was linearly shifted toward negative direction with pH, which indicated that H^+ transfer was involved in the electrode reaction. Table 6 gives the relationship between stripping peak potential of coupling product and pH of solution; the slopes are in the range of $-0.0556 - -0.0602$ (V pH^{-1}).

According to literature [18], for the reaction in which H^+ transfer is involved, a relationship exists as follows,

$$E_p(V) = E_p^0 - 0.059 \frac{m}{n} \text{pH} \quad (7)$$

From the slopes we can obtain that $m/n \approx 1$, i.e. the proton transfer number is equal to the electron transfer number.

In order to obtain the electron transfer number, a controlled potential electrolysis (CPE) was performed for the His coupling system at room temperature. The potential was controlled at -700 mV (vs SCE), UV absorption spectra and CV

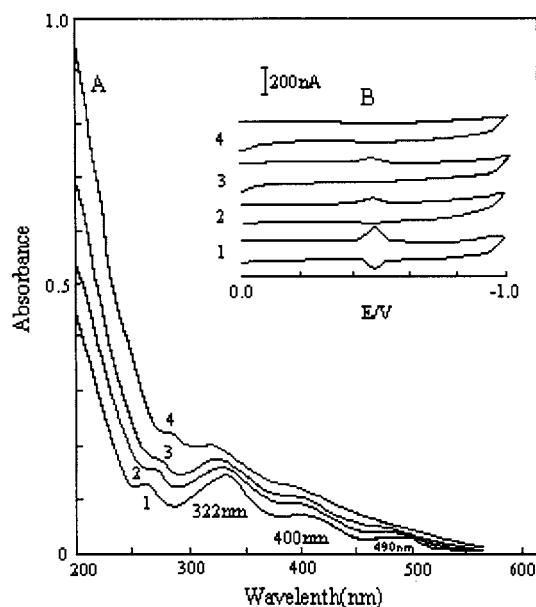
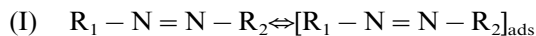


Fig. 7. The UV absorption spectra and cyclic voltammograms for His coupling system during the controlled potential electrolysis. Sampling time: (1) 0; (2) 1; (3) 2; (4) 3 h.

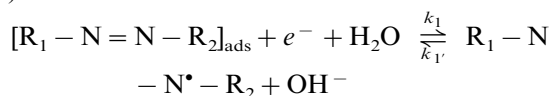
curves (Fig. 7) were measured to observe the situation of electrolysis. During the electrolysis, the color of solution changed gradually from yellow to uncolored, and there was no appearance of solid in solution or on the surface of electrode.

After completion of CPE, a net charge of 0.051369 coulomb was obtained (three replicates), according to Faraday law, $n = 2.1 \approx 2$ can be obtained. It has been known that $m/n = 1$, therefore, a reversible two-electron and two proton transfer is involved in the electrode reaction.

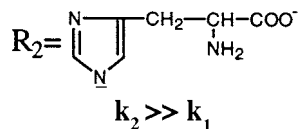
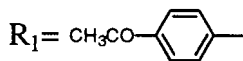
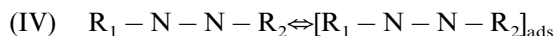
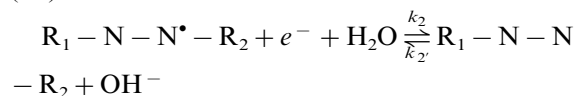
To sum up, the electrochemical reaction processes for His coupling system can be shown as follows,



(II)



(III)



$K_2 \gg k_1$

The electrochemical reaction processes for other metabolites are similar to that of His.

Acknowledgements

This project was financially supported by the National Nature Sciences Funding of China (29675003) and Nature Sciences Funding of Fujian Province, China.

References

- [1] C.Y. Zhang (Ed.), Biochemistry. In: Chinese Medical Encyclopaedia, vol. of, Shanghai Science and Technology Press, Shanghai, 1987, p. 20.
- [2] R. Draisci, S. Cavalli, L. Lucentini, A. Stacchini, Chromatographia 35 (1993) 9.
- [3] G.T. Liu, Shengwu Huaxue Yu Shengwu Wuli Jingzhang 15 (2) (1988) 182.
- [4] T. Gajda, B. Henry, J. Delpuech, J. Chem. Soc. Perkin Trans. 2 (1994) 157.
- [5] Y. Okazaki, T. Otsuki, Re. Polarog. 14 (1967) 3.
- [6] S. Sideny (Ed.), Instrumental Method of Organic Functional Group Analysis, Wiley, New York, 1972.
- [7] G. Candiano, G.M. Ghiggeri, G. Delfino, C. Queirolo, F. Ginevri, Anal. Chim. Acta 184 (1986) 323.
- [8] A.R. Katritzky, Handbook of Heterocyclic Chemistry, Pergamon, Oxford, 1985.
- [9] J.C. Moreira, A.G. Fogg, Analyst 116 (1991) 249.
- [10] A.R. Katritzky, C.W. Rees, Comprehensive Heterocyclic Chemistry, vol. 5, Pergamon, Oxford, 1984, p. 345 Part 4A.
- [11] Y.H. Wu, C. Li, X.M. Shen, Organic Chemistry, Chinese Science and Technology Press, Beijing, 1994, p. 182.
- [12] F. Anson, Electrochemistry and Electroanalytical Chemistry, Beijing University Press, Beijing, 1981 Translated by W.Z. Huang.
- [13] M.M. Baizer, H. Lund (Eds.), Organic Electrochemistry, Marcel Dekker, New York, 1983.
- [14] A.M. Bond, D.J. Tucker, Q. Zhang, D.E. Rivett, J. Electroanal. Chem. 261 (1989) 127.
- [15] A.M. Bond, D.J. Tucker, Q. Zhang, D.E. Rivett, J. Electroanal. Chem. 309 (1991) 173.
- [16] A.M. Bond, D.J. Tucker, Q. Zhang, D.E. Rivett, J. Electroanal. Chem. 315 (1991) 125.
- [17] A.M. Bond, D.J. Tucker, Q. Zhang, D.E. Rivett, J. Electroanal. Chem. 317 (1991) 203.
- [18] R.P. Gupta, Physical Methods in Heterocyclic Chemistry, Wiley, New York, 1984 Chapter 8.

Investigation on the relationship between analytical precision and concentration with iteratively reweighted least-squares linear regression method

Zhi Gao ^a, Xiwen He ^{a,*}, Guizhu Zhang ^a, Yuhuan Li ^b, Xiaoyu Wu ^b

^a *Department of Chemistry, Nankai University, Tianjin300071, People's Republic of China*

^b *Tianjin Geological Academy, Tianjin300181, People's Republic of China*

Received 8 September 1998; received in revised form 30 November 1998; accepted 1 December 1998

Abstract

It is very important to investigate the relationship between analytical precision and concentration for quality control and assessment of analytical results. A set of analytical data of trace elements in soil and water deposits (Chinese certified reference materials) was studied for the relationship between the analytical precision of collaboration trials (i.e. reproducibility) and the concentration of the analytes. Iteratively reweighted least-squares (IRLS) linear regression, a robust method, was employed in this study. The linear relationship between the standard deviation and concentration was successfully established. On comparison with the conventional least-squares (LS) method, the results of IRLS linear regression are superior to those of LS. © 1999 Elsevier Science B.V. All rights reserved.

Keywords: Standard deviation; Analytical precision; Collaborative trials; Iteratively reweighted least-squares; Linear regression

1. Introduction

In analytical determination, one usually expects that the results should be as precise as possible. However, such an expectation will not always be achieved. It is almost a fact that the analytical standard deviation increases with the concentration of the analyte. Investigation on the relationship between the analytical precision and the concentration is helpful for us to understand the sources and nature of the analytical error, which

would provide a reference for quality assurance. Establishing the relationship between the analytical precision and the concentration with a simple and reasonable model has been given more and more attention. Zitter and God [1] presented two models. One is the linear function that the analytical standard deviation increases with the concentration linearly. The other is the variance function that the square of the standard deviation (variance) is related to the concentration by a linear function of the square of the concentration. Thompson and Howarth [2] studied the relationship between the analytical precision and the concentration theoretically. They conclude that, as a

* Corresponding author. Fax: +86-22-23502458.

E-mail address: chenczl@sun.nankai.edu.cn (X. He)

first order of approximation, the standard deviation of analysis for the same analytical system is related with the concentration by a linear function. They also used the Monte Carlo simulation technique to testify the theory [3]. ISO standards [4] suggested three possible models which are linear functions (with and without intercept) and logarithm functions. Horwitz et al. [5] studied the analytical results of the main and trace amounts of constituents in foods and medicines in 50 laboratories, and established a general equation in the form of an exponent function for the relationship between the standard deviation and the concentration for the collaborative trails, regardless of the analyte, the matrix and the analytical method. Hughes and Hurley [6] also studied the relationship between the analytical precision and the concentration. Thompson [7] investigated a data set consisting of the analyses of about 700 geochemical materials for 25 elements, in respect of the relationship between the standard deviation of duplicated within-batch determination and the concentration of the analytes. He found that the simple linear model with a positive intercept is a good fit for nearly all of the analytes with the weighted regression; the variance model, which might be more satisfactory for theoretical explanation, is as good as the simple linear model, but its statistical treatment is much more complex; the logarithm model is the worst for the fitness of the data and also gives rise to some theoretical difficulties.

Linear function, with its simplicity in statistical treatment and reasonability in theoretical explanation, has been accepted for the relationship between the analytical standard deviation and the concentration. The best statistical method to estimate such a relationship is linear regression, from which the optimal estimates of the parameters are obtained. Two kinds of methods can be used in the regression, the conventional least-squares and the robust techniques. The conventional least-squares linear regression is based on the assumption of an independent and normal (Gaussian) error distribution with constant variance. Therefore, the outliers (caused by objective or subjective reasons) affect the final results of regression greatly, or even lead the results to be statistically

meaningless. The robust techniques can solve such problems [8]. Iteratively reweighted least-squares (IRLS) is a commonly used technique in robust statistics [9].

In this paper, IRLS linear regression was used to study the relationship between the analytical precision of collaborative trails of different laboratories (i.e. reproducibility) and the concentration of the trace or micro-amounts of elements in soil and water deposits. The results indicate that this relationship can be fitted as a linear function very well for each element. The simple functions are expected to be valuable in the quality assessment and quality control of the analytical data.

2. Theoretical

2.1. The relationship between the analytical precision and the concentration

The analytical precision is usually expressed as the standard deviation (σ_c). Many functions have been studied in order to fit the relationship between the standard deviation and the concentration (Table 1).

Since different models would result in different results for the same set of analytical data, it is very important to chose the appropriate model in the regression. An inappropriate model would cause big errors in the estimates of the parameters of the function, or even lead the fitted function to be out of practical significance. As can be seen

Table 1
Relationship between the standard deviation and the concentration of the analytes

Model	Function ^a	Reference
Linear	$\sigma_c = \sigma_0 + \theta c$	[1,2,4]
Linear	$\sigma_c = \theta c$	[4]
Exponent	$\sigma_c = 0.02c^{0.8495}$	[5]
Exponent	$\sigma_c = qc^{0.5}$	[6]
Exponent	$\sigma_c = qc^p$ ($p < 1$)	[4]
Logarithm	$\log \sigma_c = \log q + p \log c$	[4]
Variance	$\sigma_c^2 = \sigma_0^2 + \theta^2 c^2$	[1]

^a σ_c and σ_0 are the standard deviations at concentrations c and zero, respectively. θ, p, q are constants.

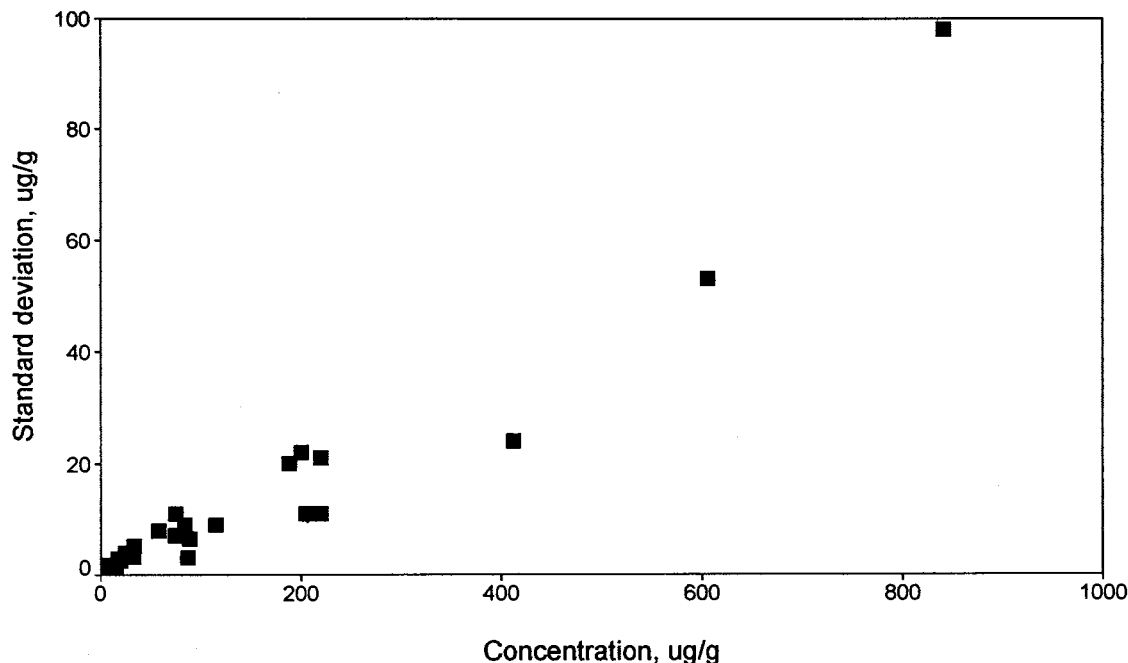


Fig. 1. Relationship between the standard deviation of the collaborative trials and the concentration of As in soil and water deposits.

from Table 1, the linear function is in the simplest form. Because of its simplicity in statistical treatment and reasonability in theory, the linear model with an intercept was employed for the estimation. The linear regression was computed with the IRLS technique. Conventional LS was also used as a comparison.

2.2. Robust linear regression IRLS technique [9]

In the practical analysis, the standard deviation s for a limited number of determinations is calculated as the optimal estimate of the standard deviation of the system σ for $n \rightarrow \infty$.

For an analyte in an analytical system, the linear relationship of standard deviation (s) and concentration (c) is in the following form:

$$s_c = \theta c + s_0 \quad (1)$$

where θ is the slope which represents the rate of the change of the standard deviation with the concentration, and s_0 is the standard deviation of the blank determinations.

For a set of data ($s_i, c_i, i=1, 2, \dots, n$), the traditional LS lacks robustness. It is easily influenced by the outliers. IRLS, on the contrary, is a robust method [9]. It gives weights (w_i) to the squares of the residuals (r_i) and minimizes $\sum r_i^2 w_i$. The parameters of the linear function are estimated by the following equation.

$$\mathbf{P} = (\mathbf{C}^t \mathbf{W} \mathbf{C})^{-1} \mathbf{C}^t \mathbf{W} \mathbf{S} \quad (2)$$

where \mathbf{P} is the matrix of the parameters, \mathbf{C} is the matrix of the concentrations, \mathbf{C}^t is the transposed matrix of \mathbf{C} , \mathbf{S} is the matrix of standard deviations and \mathbf{W} is the matrix of weights whose elements (W_i) are commonly given by the Tukey biweight function

$$w_i = [1 - (r_i/k r_s)^2]^2 \quad |r_i| < k r_s$$

$$w_i = 0 \quad |r_i| \geq k r_s \quad (3)$$

where, k is a constant which determines how harshly the residuals are treated. r_s is a measure of scale which is given by the median of the absolute values of the residuals

$$r_s = \text{median}\{|r_i|\} \quad (4)$$

The principle algorithm of IRLS is the process of iteration, so the initial weights are very important to the regression. We presented a robust method for the determination of the initial weights (called robust initial weights for simplicity) as follows:

1. fitted all of the original data with the conventional LS;
2. calculated the residuals, and the measure of scale r_s ;
3. rejected the data point(s) with absolute value(s) of the residual(s) greater than $2r_s$;
4. fitted the rest of the original data with the conventional LS;
5. calculated the residuals, the measure of the scale r_s and the weights for all of the original data.

After the initial weights were obtained, the IRLS linear regression was carried out by the routine procedure [9].

3. Experimental

Fifteen trace or micro-amounts of elements in 32 Chinese Certified Reference Materials (CRMs)

Table 2

Results of conventional LS linear regression on the relationship between the standard deviation and concentration

Elements	Results of the LS linear regression ^a				
	s_0 ($\mu\text{g g}^{-1}$)	$s_c(s_0)$ ($\mu\text{g g}^{-1}$)	θ	$s_c(\theta)$	β
Ag	-0.004	0.010	0.16	0.01	0.9769
As	-0.62	1.09	0.099	0.005	0.9635
Be	-0.32	0.13	0.25	0.01	0.9799
Bi	0.05	0.14	0.10	0.01	0.9169
Cd	0.069	0.018	0.048	0.003	0.9295
Co	0.72	0.10	0.087	0.004	0.9644
Cr	2.3	0.6	0.074	0.005	0.9411
Cu	1.69	0.38	0.043	0.001	0.9920
Li	-0.74	0.33	0.077	0.007	0.9042
Mo	0.26	0.10	0.091	0.004	0.9679
Ni	1.07	0.25	0.075	0.003	0.9791
P	21	5	0.040	0.007	0.7347
Pb	4.9	1.0	0.038	0.002	0.9717
Sb	-0.12	0.14	0.20	0.01	0.9892
Zn	-0.78	1.13	0.078	0.002	0.9942

^a $s_c(s_0)$ and $s_c(\theta)$ are the standard errors of s_0 and θ , respectively. β is the correlation coefficient.

of soil and water deposits were chosen in the study. Each CRM provides the concentration and standard deviation for each element. The standard deviation and the concentration varies with the CRMs for each element. The standard deviations represent the precision of collaborative trials. The CRMs studied are GBW07301-07312 and GBW07401-07411 (Institute of Physical and Chemical Exploration, and Institute of Rock and Mineral Resources Testing, Ministry of Geology and Mineral Resources) and GBW(E)070003-070011 (Tianjin Geological Academy, Ministry of Metallurgical Industry). These CRMs have almost the same matrix. The regressions were performed with MS-EXCEL 7.0 and SPSS 6.0 on a Great-Wall computer. The regressions continued until the relative change of the parameters of the last two iterations were less than 5%.

4. Results and discussion

4.1. Illustration of the relationship between the standard deviation and the concentration

The analytes Ag, As, Be, Bi, Cd, Co, Cr, Cu, Li, Mo, Ni, P, Pb, Sb and Zn were investigated.

Table 3

Changes of IRLS linear regression parameters with the number of iteration using robust and LS initial weights for the relationship between the standard deviation and the concentration of As

Parameters	Initial weight	Number of iterations					
		0	1	2	3	4	5
s_0 ($\mu\text{g g}^{-1}$)	LS	-0.62	0.64	0.74	0.80	0.82	0.83
	Robust	0.44	0.50	0.51	0.51		
θ	LS	0.099	0.092	0.090	0.089	0.088	0.088
	Robust	0.098	0.099	0.099	0.100		

As an example, the relationship between the standard deviation and the concentration for As is illustrated in Fig. 1. The other elements have a similar relationship. It is obvious to see that the standard deviation increases with the concentration in a general view. Such a relationship is in coincidence with that of within-batch precision with concentration [7].

4.2. Results of the conventional LS linear regression

The conventional LS linear regression was first used to estimate the function of the relationship between the standard deviation and the concentration (Table 2). As can be seen from the table, the linear function for each element reflects the general trend of the standard deviation changing with the concentration to some extent. The slopes are in the range of 0.03–0.25 with relative small standard errors. The correlation coefficients are greater than 0.9 for all elements except P, which indicates that the standard deviation strongly correlates with the concentration. However, the intercepts (s_0) are not satisfactory. The standard errors of the intercepts are relatively large, and 40% of the intercepts are negative, which have no practical meaning. Therefore, some limitations exist for the conventional LS as a technique for the linear regression of the relationship between the standard deviation and concentration. This is caused by outliers. The robust method should be used.

4.3. IRLS linear regression

4.3.1. Effect of the initial weights on the results of the IRLS linear regression

One of the important conditions in the IRLS linear regression is the initial weights. Phillips and Eyring [9] found that the weights obtained directly from the LS linear regression often result in divergence or incorrect convergence results. Taking As, for example, we investigated the effect of initial weights on the IRLS linear regression (Table 3). Two initial weights are considered. One is the robust initial weight, the other is the initial weight calculated from the residuals of LS linear regression (called LS initial weight for simplicity). As can be seen from Table 3, the robust initial weight gives a faster convergence rate.

4.3.2. Effect of the constant k in the Tukey biweight function on the regression results

The constant k in the Tukey biweight function determines the degree of harshness with which the residuals are treated in calculating the weights. It also determines the fraction of the original data being rejected ($w_i = 0$) in the regression. If k is too large, the linear regression would be greatly influenced by the outliers for $w_i \approx 1$. If k is too small, there would be too many points of data being rejected in the regression. Such results which would not represent the overall relationship of the original data. The effect of different values of k on the regression results of As was investigated as listed in Table 4. It is obvious to see that s_0

increases, θ and E decreases with k . The standard error of θ is relatively small and varies slightly with k . The standard error of s_0 increases with k , which indicates that the regression results lack robustness for large values of k . By balancing the robustness and the representativity, we choose $k = 6$ as the optimum value.

4.3.3. Results of the IRLS linear regression

The estimates of the IRLS linear regression on the relationship between the standard deviation of collaborative trials and the concentration are listed in Table 5. This shows that the standard errors of the slopes and the intercepts are small, which indicates that the relationship between the standard deviation and the concentration complies with a linear function very well. All the intercepts, except that of Sb, are greater than zero (the intercept of Sb is not significantly different from zero by the test of $t = |s_0/s_c(s_0)|$). Such intercepts(s_0) are good estimates of the practical standard deviations for the blank analyses. By comparing with the results of LS (Tables 2 and 5), we find that the slopes of both methods are similar for all elements except Be, Cd and Li; and the correlation coefficients of IRLS are better than those of LS for all elements except Li. The standard errors of the parameters by IRLS method are equal to or smaller than those of LS. So, we can conclude that the IRLS linear regression produces more

precise estimates than LS. We also find that the fraction of the original data being rejected is less than 20% for each element. Therefore, the linear functions are satisfactory estimates of the relationship between the standard deviation of collaborative trials and the concentration. When such equations are available, we can predict the standard deviations and make assessment on the analytical reproducibility of the analytes by the concentrations.

5. Conclusion

Taking Chinese CRMs of soil and water deposits as examples, the relationship between the analytical precision and concentration of 15 trace or micro-amounts of elements were investigated. The relationship can be fitted as a linear function very well. The regression should be treated with a robust method. Both LS and IRLS techniques were used in this study. By comparison, the results of IRLS are superior to those of conventional LS. Thompson [7] once concluded that the linear function with an intercept is a good estimate for the relationship between the standard deviation of within-batch analyses. We conclude from this study that the linear function with an intercept is also a good estimate for the relationship between the standard deviation of collaborative trials (reproduci-

Table 4

The effect of the constant k in the Tukey biweight function to the IRLS linear regression results for the relationship between the standard deviation and the concentration of As

k	Results of IRLS linear regression ^a					
	s_0 ($\mu\text{g g}^{-1}$)	$s_c(s_0)$ ($\mu\text{g g}^{-1}$)	θ	$s_c(\theta)$	β	E (%)
3	0.42	0.18	0.103	0.003	0.9937	28
6	0.50	0.27	0.100	0.003	0.9860	19
9	0.84	0.33	0.089	0.002	0.9906	9
12	0.77	0.40	0.087	0.003	0.9857	6
18	0.79	0.62	0.080	0.004	0.9640	3

^a E is the fraction (in percent) of the original data being rejected in the regression. The meanings of the rest of the parameters are the same as Table 2.

Table 5
Results of LS linear regression on the relationship between the standard deviation and concentration

Element	Results of the IRLS linear regression ^a				
	s_0 ($\mu\text{g g}^{-1}$)	$s_c(s_0)$ ($\mu\text{g g}^{-1}$)	θ	$s_c(\theta)$	β
Ag	0.002	0.002	0.153	0.003	0.9947
As	0.50	0.27	0.100	0.003	0.9853
Be	0.06	0.03	0.151	0.004	0.9884
Bi	0.03	0.01	0.117	0.003	0.9911
Cd	0.020	0.003	0.088	0.003	0.9893
Co	0.70	0.09	0.086	0.004	0.9720
Cr	1.9	0.4	0.079	0.003	0.9741
Cu	1.38	0.20	0.043	0.001	0.9966
Li	0.3	0.2	0.042	0.005	0.8465
Mo	0.11	0.02	0.109	0.001	0.9988
Ni	0.99	0.17	0.075	0.002	0.9899
P	21	4	0.038	0.006	0.7374
Pb	3.6	0.4	0.037	0.002	0.9787
Sb	−0.01	0.04	0.192	0.002	0.9986
Zn	0.7	0.5	0.079	0.001	0.9988

^a See Table 2.

bility) and the concentration. The functions vary with the analytes. Such functions would be very helpful in the quality control and the quality assessment in analytical determination.

Acknowledgements

This project was financially supported by the National Natural Science Foundation of China (No.29575200).

References

- [1] H. Zitter, C. God, *Fres. Z. Anal. Chem.* 255 (1971) 1.
- [2] M. Thompson, R.J. Howarth, *Analyst* 101 (1976) 690.
- [3] R.J. Howarth, M. Thompson, *Analyst* 101 (1976) 699.
- [4] International Standard, ISO 5725-2, 1994.
- [5] W. Horwitz, L.R. Kamps, K.W. Boyer, *J. Assoc. Off. Anal. Chem.* 63 (1980) 1344.
- [6] H. Hughes, P.W. Hurley, *Analyst* 112 (1987) 1445.
- [7] M. Thompson, *Analyst* 113 (1988) 1579.
- [8] Y.-L. Xie, J.-H. Wang, Y.-Z. Liang, R.-Q. Yu, *Chin. J. Anal. Chem.* 22 (1994) 294.
- [9] G.R. Phillips, E.M. Eyring, *Anal. Chem.* 55 (1983) 1134.

Complexation and fluorescence behavior of diazacrown ether carrying two anthryl pendants

Kanji Kubo ^{a,*}, Ryoichi Ishige ^b, Tadimitsu Sakurai ^b

^a Institute of Advanced Material Study, 86, Kyushu University, Kasuga-koen, Kasuga, Fukuoka, 816-8580, Japan

^b Department of Applied Chemistry, Faculty of Engineering, Kanagawa University, Kanagawa-ku, Yokohama, 221-0802, Japan

Received 28 July 1998; received in revised form 19 November 1998; accepted 2 December 1998

Abstract

Photoinduced electron transfer (PET) fluoroionophores (**1b**, **2b**) that consist of diazacrown and two 9-anthryl pendants show fluorescent enhancement with various guest salts. The diaza-12-crown-4 derivative (**2b**) exhibited Zn^{2+} selectivity and in the presence of this cation the host fluorescence intensity was increased by a factor of 182. The guest cation-induced fluorescence enhancement of **2b** was larger than the diaza-18-crown-6 derivative (**1b**). © 1999 Elsevier Science B.V. All rights reserved.

Keywords: Photoinduced electron transfer; Fluoroionophores; Fluorescence; Diazacrown ether; Anthryl pendants

1. Introduction

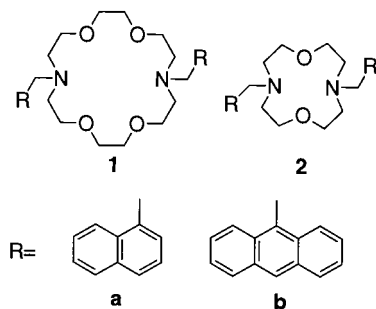
PET (photoinduced electron transfer) fluoroionophores, which give rise to a specific emission spectral change upon selective complexation with guest cations, have attracted considerable attention as spectrophotometric analytical reagents for the detection of particular guest cations [1–6]. Azacrown ethers have been important building blocks for constructing host molecules in supramolecular chemistry [7].

Of particular interest, it was found that the azacrown ethers act as electron donors in a typical

exciplex-forming system that involves an appropriate electron acceptor [8,9]. The addition of metal salts enhanced the fluorescence emission intensity of *N,N'*-bis(1-naphthylmethyl)-diazacrown ethers (**1a**, **2a**) by a factor of 43 for **2a**-Zn(-SCN)₂ [10] and 41 for **1a**-Ba(SCN)₂ [11]. However, the crown ether with naphthyl groups displayed fluorescence with a low quantum yield. As an effective PET fluoroionophore is designed, some important factors are that the PET fluoroionophores have low emission quantum yield by PET from amine donor to excited chromophore, high emission quantum yield in complexation with guest molecules and high binding constant. As an approach to the manipulation of PET fluoroionophore [10–16], we now report the fluorescence behavior of the diazacrown (**1b**, **2b**)

* Corresponding author. Fax: +81-92-5837810.

E-mail address: kubo-k@cm.kyushu-u.ac.jp (K. Kubo)



Scheme 1.

with two anthryl pendants in the presence of guest salts (Scheme 1).

2. Experimental

Elemental analyses were performed by Perkin Elmer PE2400 series II CHNS/O analyzer. Melting points were obtained with a Yanagimoto Micro Melting Point Apparatus and were uncorrected. NMR spectra were measured on a JEOL JNM-500 Model spectrometer in CDCl_3 ; the chemical shifts were expressed by a δ unit using tetramethylsilane as an internal standard. IR spectra were recorded on a Hitachi Model 270-30 infrared spectrophotometer. Fluorescence spectra were measured with a Hitachi Model F-4500 spectrofluorimeter.

2.1. Preparation of *N,N'*-bis(9-anthrylmethyl)-1,7-dioxa-4,10-diazacyclododecane (**2b**)

A tetrahydrofuran-toluene solution (5 + 5 ml) of 1,7-diaza-12-crown-4 (44 mg, 0.20 mmol), triethylamine (0.5 ml, 3.6 mmol), 9-chloromethylanthracene (227 mg, 1.00 mmol) was refluxed for 12 h. The mixture was then diluted with 1.0 M NH_3 (10 ml), extracted with ethyl acetate (50 ml). The solvent was evaporated and the residue was purified by column chromatography over silica gel (70–230 mesh, Merck) using hexane and ethyl acetate (1:1 *v/v*) as the eluent. The analytically pure sample (94 mg, 85%) showed the following physical and spectroscopic properties.

N,N'-Bis(9-anthrylmethyl)-1,7-dioxa-4,10-diazacyclododecane (**2b**): yellow crystals, 172–173°C, $^1\text{H-NMR}$ (CDCl_3) δ = 2.82 (8H, t, J = 5.0 Hz), 3.33 (8H, t, J = 5.0 Hz), 4.54 (4H, s), 7.44 (4H, ddd, J = 1.5, 6.7, 8.6 Hz), 7.48 (4H, ddd, J = 1.5, 6.7, 8.2 Hz), 7.96 (4H, d, J = 8.2 Hz), 8.37 (2H, s), 8.54 (4H, d, J = 8.6 Hz), $^{13}\text{C-NMR}$ δ = 53.06 (2C), 55.08 (4C), 69.03 (4C), 124.80 (4C), 125.41 (4C), 125.51 (4C), 127.44 (2C), 128.88 (4C), 130.48 (2C), 131.30 (4C), 131.40 (4C). IR (KBr) ν 723, 882, 1059, 1119, 1290, 1366, 1446, 1617, 2842 cm^{-1} . Found; C, 82.20; H, 6.92; N, 5.01%, calc. for $\text{C}_{38}\text{H}_{38}\text{N}_2\text{O}_2$: C, 82.28; H, 6.90; N, 5.05%.

2.2. Fluorescence spectral measurement of diazacrown (**1b**, **2b**) and its complexes

Fluorescence intensities of **1b**, **2b** (5.00×10^{-6} M, 1 M = 1 mol l^{-1}) and 9-methylanthracene (1.00×10^{-5} M) excited at 366 nm, were measured in methanol-chloroform (9:1 *v/v*) under nitrogen at room temperature, as shown in Fig. 1. The titrations were conducted by adding a crown ether solution (5.00×10^{-6} M for **1b** and **2b** in methanol-chloroform, 9:1 *v/v*) progressively containing excess metal salts, using a 0.25 ml syringe, to a cuvette containing 2.0 ml of the crown ether solution (5.00×10^{-6} M for **1b** and **2b** in methanol-chloroform, 9:1 *v/v*). The solutions were homogenized by ultrasonic waves for 3 min. The spectrum was recorded after each addition. The added equivalents of the cation were then plotted against the emission-intensity change at 413–421 nm (excited at 366 nm). The association constants (K) for guest cation complexes were determined at least in duplicate at $25 \pm 1^\circ\text{C}$ by the self-written non-linear curve-fitting computer program in the previous study [16,17].

3. Result and discussion

The anthracene-functionalized diazacrown ether (**2b**) was prepared by the *N*-alkylation of 1,7-diaza-12-crown-4 with 9-chloromethylanthracene in triethylamine-toluene-tetrahydrofuran solution. The structure and purity of **2b** were

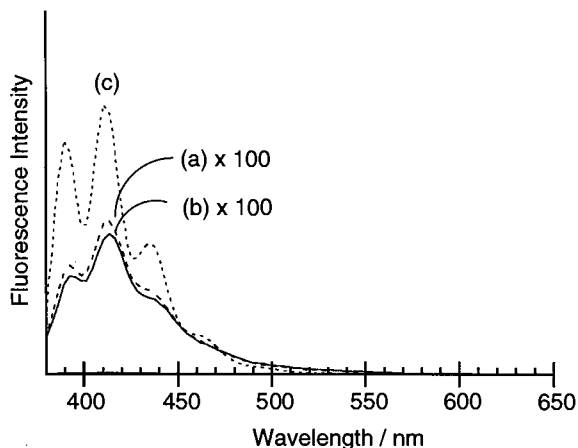


Fig. 1. Fluorescence spectra of (a) **1b** (5.00×10^{-6} M), (b) **2b** (5.00×10^{-6} M), and (c) 9-methylanthracene (1.00×10^{-5} M) in methanol-chloroform (9:1 *v/v*) at room temperature.

ascertained by NMR spectroscopy and elemental analysis.

Fluorescence spectral behavior of **1b** and **2b** (5.00×10^{-6} M) gave weak emission band at 414 nm. The emission-band intensities of **2b** were reduced to approximately one-196th that of standard substance (9-methylanthracene: 1.00×10^{-5} M, 9-MA). This indicates that the quenching of the excited-state anthracene chromophore by the

azacrown unit proceeds in a mechanism similar to that for the classical fluorescent-aliphatic amine system [18–21]. The quenching efficiency (I_{2b}/I_{9-MA} : 5.1×10^{-3}) of **2b** is similar to that (I_{1b}/I_{9-MA} : 5.6×10^{-3}) [14] of the diaza-18-crown-6 (**1b**). This means the PET from the nitrogen atoms in the crown to excited fluorescent moieties occurs efficiently.

Fig. 2 illustrates the relative fluorescence spectral behavior of guest cation complexes **2b** (5.00×10^{-6} M) in methanol-chloroform (9:1 *v/v*) at room temperature. A dramatic change in the emission intensity of **2b** (I_{2b}) was observed upon the addition of various amounts of guest cations (Li^+ , Na^+ , K^+ , Rb^+ , Cs^+ , Ca^{2+} , Ba^{2+} , Zn^{2+} , Mg^{2+} and NH_4^+). When the guest cations were added, the relative emission intensity ($I_{\text{complex}}/I_{2b}$), being used as a measure of the molecular recognition sensing, changed from 1 to 182 depending on the nature of guest cations such as size, valency, and electronic properties.

Fig. 3 illustrates the relative emission intensity of **2b** against the guest cations concentration. Clearly, the emission intensity increases with an increase in the guest cation concentration. Interestingly, the intensity ratio ($I_{\text{complex}}/I_{2b}$), (which was being used as a measure of the molecular

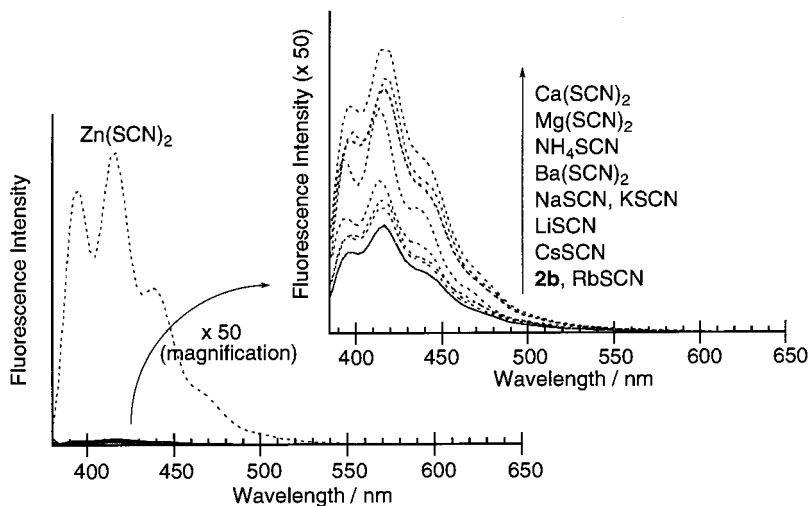


Fig. 2. Fluorescence spectra of **2b** (5.00×10^{-6} M) with and without various guest cations (2.5×10^{-4} M) in methanol-chloroform (9:1 *v/v*), as excited at 366 nm.

sensing), was different among bound guest cations and decreased in the following order: Zn^{2+} (182) > Ca^{2+} (4.2) > Mg^{2+} (3.7) > NH_4^+ (3.3) > Ba^{2+} (2.2) > Na^+ , K^+ (1.3) > Li^+ (1.2) > Cs^+ (1.1) > Rb^+ (1.0). The order of $I_{\text{complex}}/I_{2\text{b}}$ differs from that of $I_{\text{complex}}/I_{1\text{b}}$ (K^+ (24) > Zn^{2+} (13) > Rb^+ (11) > Na^+ (8.5) > Ca^{2+} (8.7) > NH_4^+ (7.0) > Ba^{2+} (5.0) > Mg^{2+} (3.2) > Cs^+ (2.7) > Li^+ (1.2)) [14]. The order depends upon the nature of ionophore properties [7]. Complexation of

2b with Zn^{2+} increased the fluorescence intensity of the host by a factor of 182. The Zn^{2+} -induced fluorescence enhancement is due to coordination from the two nitrogen atoms of the diazacrown to the zinc ion. The strength of this binding interaction modulates the PET from the amine to anthracene.

In Table 1 is illustrated the fluorescence intensity ratio ($I_{\text{complex}}/I_{\text{standard substance}}$) of guest cation complexes for the corresponding standard substance (9-MA, 1-MN: 1-methylnaphthalene), as a measure of the guest cation-induced fluorescence recovery and a parameter instead of emission quantum yield. The fluorescence recovery ($I_{1\text{b-Zn complex}}/I_{1\text{-MN}}$, $I_{2\text{b-Zn complex}}/I_{9\text{-MA}}$) of 12-crown-4 derivatives (**1b**, **2b**) for Zn^{2+} was larger than that ($I_{\text{complex}}/I_{\text{standard substance}}$) of the other complexes. Interestingly, the fluorescence recovery ($I_{2\text{b-Zn complex}}/I_{9\text{-MA}} = 0.93$) of **2b** for Zn^{2+} was larger than that ($I_{2\text{a-Zn complex}}/I_{1\text{-MN}} = 0.73$) of the corresponding naphthyl derivative (**2a**). The fluorescence intensity of **2b-Zn(SCN)₂** complex was similar to that of 9-methylanthracene. This means that the 12-crown-4 derivatives having two anthryl pendants (**2b**) have a high fluorescence switch-on ability as PET fluoroionophore.

Guest concentration dependence of the fluorescence intensity (Fig. 3) allowed us to determine the association constants (K) by the non-linear curve-fitting method [16,17] (Table 2). Although the K values of 12-crown-4 derivatives (**2**) for various guest cations were larger than those of the corresponding 18-crown-6 derivatives (**1**), the K values of the anthracene derivative (**2b**) for various guest cations were smaller than those of the naphthalene derivative (**2a**). This means the two large anthracene rings may block the incorporation of guest cations in host. The diazacrown derivatives (**1**, **2**) showed the following cation selectivity (**1a**: $\text{Li}^+ < \text{Ca}^{2+} < \text{Cs}^+ < \text{Na}^+ < \text{Zn}^{2+} < \text{Rb}^+ < \text{Ba}^{2+} < \text{NH}_4^+ < \text{K}^+ < \text{Mg}^{2+}$, **1b**: $\text{Ca}^{2+} < \text{Li}^+ < \text{Zn}^{2+} < \text{Ba}^{2+} < \text{NH}_4^+ < \text{Cs}^+ < \text{Rb}^+ < \text{Na}^+ < \text{Mg}^{2+} < \text{K}^+$, **2a**: $\text{NH}_4^+ < \text{Cs}^+ < \text{Rb}^+ < \text{K}^+ < \text{Na}^+ < \text{Mg}^{2+} < \text{Ba}^{2+} < \text{Li}^+ < \text{Ca}^{2+} < \text{Zn}^{2+}$, **2b**: $\text{Mg}^{2+} < \text{Ba}^{2+} < \text{NH}_4^+ < \text{Ca}^{2+} < \text{Zn}^{2+}$). Comparison of the selectivity order for **1** and **2** confirms that the size and electronic property of

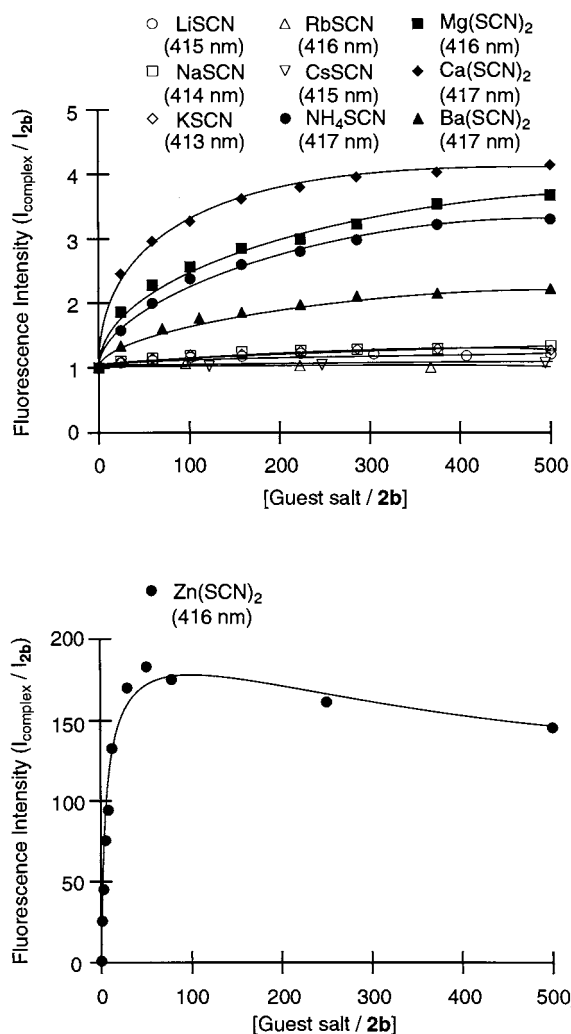


Fig. 3. Dependence of fluorescence intensities of **2b** (2.00×10^{-5} M) at 413–417 nm on the concentration of various guest cations (added as thiocyanate salts) in methanol–chloroform (9:1 v/v).

Table 1

The fluorescence intensity ratio ($I_{\text{complex}}/I_{\text{1 or 2}}$ and $I_{\text{complex}}/I_{\text{standard substance}}$) of the guest cation complexes of **1** and **2**^a

	1a		1b		2a		2b	
	MeOH		MeOH:CHCl ₃ (9:1 v/v)		MeOH		MeOH:CHCl ₃ (9:1 v/v)	
	$I_{\text{complex}}/I_{\text{1-MN}}$	$I_{\text{complex}}/I_{\text{1a}}$	$I_{\text{complex}}/I_{\text{9-MA}}$	$I_{\text{complex}}/I_{\text{1b}}$	$I_{\text{complex}}/I_{\text{1-MN}}$	$I_{\text{complex}}/I_{\text{2a}}$	$I_{\text{complex}}/I_{\text{9-MA}}$	$I_{\text{complex}}/I_{\text{2b}}$
Free	2.3×10^{-3}	–	5.6×10^{-3}	–	1.7×10^{-2}	–	5.1×10^{-3}	–
LiSCN	2.7×10^{-3}	1.2	6.7×10^{-3}	1.2	1.9×10^{-2}	1.1	6.1×10^{-3}	1.2
NaSCN	5.0×10^{-3}	2.2	4.8×10^{-2}	8.5	2.0×10^{-2}	1.2	6.6×10^{-3}	1.3
KSCN	6.4×10^{-3}	2.8	0.13	24	2.0×10^{-2}	1.2	6.6×10^{-3}	1.3
RbSCN	3.4×10^{-3}	1.5	6.2×10^{-2}	11	1.7×10^{-2}	1.0	5.1×10^{-3}	1.0
CsSCN	2.7×10^{-3}	1.2	1.5×10^{-2}	2.7	2.0×10^{-2}	1.2	5.5×10^{-3}	1.1
NH ₄ SCN	1.1×10^{-2}	4.9	3.9×10^{-2}	7.0	2.9×10^{-2}	1.7	1.7×10^{-2}	3.3
Zn(SCN) ₂	1.2×10^{-2}	5.4	7.3×10^{-2}	13	0.73	43	0.93	182
Mg(SCN) ₂	8.0×10^{-3}	3.5	1.8×10^{-2}	3.2	2.7×10^{-3}	1.6	1.9×10^{-2}	3.7
Ca(SCN) ₂	3.4×10^{-2}	15	4.9×10^{-2}	8.7	2.7×10^{-2}	1.6	2.1×10^{-2}	4.2
Ba(SCN) ₂	9.3×10^{-2}	41	2.8×10^{-2}	5.0	2.2×10^{-2}	1.3	1.1×10^{-2}	2.2

^a Standard substance: 1-MN, 1-methylnaphthalene; 9-MA, 9-methylantracene.

Table 2

Association constants ($\log K \text{ M}^{-1}$) of **1** and **2** for guest salts in methanol and methanol-chloroform (9:1 v/v)

	Log $K \text{ (M}^{-1}\text{)}$							
	1a		1b		2a		2b	
	CH ₃ OH	CH ₃ OH:CHCl ₃ (9:1 v/v)	CH ₃ OH	CH ₃ OH:CHCl ₃ (9:1 v/v)	CH ₃ OH	CH ₃ OH:CHCl ₃ (9:1 v/v)	CH ₃ OH	CH ₃ OH:CHCl ₃ (9:1 v/v)
LiSCN	1.43 ± 0.09	0.78 ± 0.08	4.12 ± 0.13	–	–	–	–	–
NaSCN	2.09 ± 0.03	2.70 ± 0.10	3.97 ± 0.03	–	–	–	–	–
KSCN	3.27 ± 0.08	3.29 ± 0.17	3.97 ± 0.08^a	–	–	–	–	–
RbSCN	2.48 ± 0.03	2.65 ± 0.05	3.71 ± 0.25	–	–	–	–	–
CsSCN	1.99 ± 0.16	2.11 ± 0.03	3.69 ± 0.09	–	–	–	–	–
NH ₄ SCN	3.17 ± 0.05	2.08 ± 0.04	3.67 ± 0.02	3.26 ± 0.05	3.67 ± 0.02	3.26 ± 0.05	3.26 ± 0.05	3.26 ± 0.05
Zn(SCN) ₂	2.10 ± 0.05	0.85 ± 0.15	5.28 ± 0.02	4.46 ± 0.09	5.28 ± 0.02	4.46 ± 0.09	4.46 ± 0.09	4.46 ± 0.09
Mg(SCN) ₂	3.51 ± 0.03	3.07 ± 0.08	4.01 ± 0.02	3.13 ± 0.09	4.01 ± 0.02	3.13 ± 0.09	3.13 ± 0.09	3.13 ± 0.09
Ca(SCN) ₂	1.79 ± 0.03	0.48 ± 0.18	4.33 ± 0.02	3.58 ± 0.04	4.33 ± 0.02	3.58 ± 0.04	3.58 ± 0.04	3.58 ± 0.04
Ba(SCN) ₂	2.85 ± 0.07	1.77 ± 0.06	4.05 ± 0.19	3.24 ± 0.05	4.05 ± 0.19	3.24 ± 0.05	3.24 ± 0.05	3.24 ± 0.05

^a The association constant ($\log K$) of **2a** for KSCN in CH₃OH:CHCl₃ (9:1 v/v) was 3.45 ± 0.03 .

ionophore attached with aromatic pendants. The pendants may control the selectivity of the host toward guest cations in a delicate manner.

In conclusion, the diazacrown (**2b**) exhibited Zn²⁺ selectivity and the emission intensity of this host was greatly enhanced in the presence of zinc salts, establishing that **2b** has a high fluorescence switch-on ability for complexation. The diaza-12-crown-4 having two anthryl pendants may be

utilized as a new PET fluorescent sensor for guest cations.

References

- [1] H.G. Löhr, F. Vögtle, Acc. Chem. Res. 18 (1985) 65.
- [2] R.A. Bissell, A.P. Silva, H.Q.N. Gunaratne, P.L.M. Lynch, G.E.M. Maguire, K.R.A.S. Sandanayake, Chem. Soc. Rev. 21 (1992) 187.

- [3] L. Fabrizzi, A. Poggi, *Chem. Soc. Rev.* 24 (1995) 197.
- [4] J.-M. Lehn (Ed.), *Supramolecular Chemistry*, VCH, Weinheim, 1995.
- [5] A.P. de Silva, H.Q.N. Gunaratne, T. Gunnlaugsson, C.P. McCoy, R.S. Maxwell, J.T. Rademacher, T.E. Rice, *Pure Appl. Chem.* 48 (1996) 1443.
- [6] T.D. James, K.R.A.S. Sandanayake, S. Shikai, *Supramol. Chem.* 6 (1995) 141.
- [7] J.S. Bradshaw, K.E. Krakowiak, R.M. Izatt (Eds.), *Aza-Crown Macrocycles*, Wiley, New York, 1995.
- [8] N. Kh. Petrov, A.I. Shushin, E.L. Frankevich, *Chem. Phys. Lett.* 82 (1981) 339.
- [9] N. Kh. Petrov, V.N. Borisenko, M.V. Alfimov, T. Fiebig, H. Staerk, *J. Phys. Chem.* 100 (1996) 6368.
- [10] K. Kubo, E. Yamamoto, T. Sakurai, *Heterocycles* 48 (1998) 2133.
- [11] K. Kubo, R. Ishige, N. Kato, E. Yamamoto, T. Sakurai, *Heterocycles* 45 (1997) 2365.
- [12] K. Kubo, N. Kato, T. Sakurai, *Bull. Chem. Soc. Jpn.* 70 (1997) 3041.
- [13] K. Kubo, E. Yamamoto, T. Sakurai, *Heterocycles* 45 (1997) 1457.
- [14] K. Kubo, R. Ishige, T. Sakurai, *Heterocycles* 48 (1998) 347.
- [15] K. Kubo, E. Yamamoto, T. Sakurai, *Heterocycles* 48 (1998) 1477.
- [16] K. Kubo, R. Ishige, J. Kubo, T. Sakurai, 1999. *Talanta* (accepted 18 June 1998).
- [17] K.A. Connors (Ed.), *Binding Constants*, Wiley, New York, 1987.
- [18] H. Leonhardt, A. Weller, *Ber. Bunsen-Ges. Phys. Chem.* 67 (1963) 791.
- [19] Davidson, R.S., Trethewey, K.R., *J. Chem. Soc. Chem. Commun.* 20 (1976) 827.
- [20] R. Foster (Ed.), *Photophysical Aspects of Exciplexes* Molecular Association, Academic Press, London, 1979.
- [21] X.-J. Luo, G.S. Beddard, G. Porter, *J. Chem. Soc. Faraday Trans. 1* 78 (1982) 3467.

Measurement of dioxygen by electrocatalytic reduction on microelectrodes modified with Nafion and methyl viologen

Wenliang Sun ^a, Jian Xue ^a, Junshui Chen ^a, Lanqun Mao ^a, Litong Jin ^{a,*},
K. Yamamoto ^b, Shuguang Tao ^b, Jiye Jin ^c

^a Department of Chemistry, East China Normal University, Shanghai, 200062, People's Republic of China

^b BAS Co., Ltd. No. 36-6, 1-Chome, Oshiage, Sumida-Ku, Tokyo, 131, Japan

^c Department of Chemistry, Faculty of Engineering, Gifu University, Yanagido1-1, Gifu, 501-11, Japan

Received 30 July 1998; received in revised form 1 December 1998; accepted 2 December 1998

Abstract

Nafion/methyl viologen (MV) has been chemically modified on a gold disk microelectrode (GDME). The electrochemistry of the Nafion/MV modified GDME is investigated by cyclic voltammetry (CV). Linear sweep voltammetry (LSV) and differential pulse amperometry (DPA) show that the Nafion/MV modified GDME exhibits very high electrocatalytic activity toward dioxygen reduction with good reproducibility and high sensitivity. The electrocatalytic peak current is found to be linear with the dioxygen concentration in the range of 3.44×10^{-7} to 2.59×10^{-4} mol l⁻¹ (at 25°C), with a correlation coefficient of 0.9978. The detection limit (signal/noise = 3) is calculated to be 0.19 μmol l⁻¹. The response time of the microsensor for dioxygen measurement is less than 15 s. For ten parallel measurements for 8.50 μmol l⁻¹ dioxygen, the relative standard deviation (RSD) is found to be 2.7%. The sensitivity of the microsensor is 0.17 nA μmol⁻¹ l⁻¹. This microsensor has been successfully employed to measure the concentration of dioxygen in real samples. The quantity of dioxygen, released from the three kinds of chloroplasts of plant leaves under different illumination, is monitored by the Nafion/MV modified gold microsensor. In order to survey the dioxygen concentration in vivo, a Nafion/MV modified carbon fiber microelectrode (CFME) is fabricated by a modification procedure similar to that of the Nafion/MV GDME. As a preliminary test, the dioxygen levels in the different areas of rat brain are determined by the Nafion/MV modified carbon fiber microsensors. The mechanism of the catalytic reaction is also addressed. © 1999 Elsevier Science B.V. All rights reserved.

Keywords: Chemically modified microelectrode; Methyl viologen; Nafion; Dioxygen; Catalytic reduction

1. Introduction

The electrocatalytic reduction of dioxygen has received continuous interest regarding its importance in many biological redox processes [1]. Var-

* Corresponding author. Fax: +86-21-62451876.

E-mail address: ltjin@ch.ecnu.edu.cn (L. Jin)

ious redox mediators for accelerating the irreversible reduction of dioxygen at conventional electrodes have been reported, including metal phthalocyanines [2–6], microparticles [7–10], metalloporphyrins [11–14], bipyridinium compounds [15,16] and conducting polymers [17]. These mediators, when chemically modified on electrode surfaces or dissolved in aqueous or organic solutions, exhibit effective electrocatalytic activity toward dioxygen reduction. Chemical modification has been the subject of more investigation [18–26].

A chemically modified microelectrode is favorable for dioxygen measurement *in vivo* if it has the following characteristics: (i) good selectivity; (ii) high sensitivity; (iii) fast response and long-term stability; and (iv) significant ability against fouling. Zimmerman and Wightman have reported the *in vivo* detection of dioxygen at a Nafion coated carbon fiber microelectrode using fast-scan cyclic voltammetry [27]. *In vivo* measurement of dioxygen also has been conducted at a lipid-treated carbon paste electrode by differential pulse amperometry [28]. On the other hand, the Nafion/methyl viologen (MV) chemically modified electrodes have been investigated extensively [21–26]. However, up to now determination of dioxygen *in vivo* using the Nafion/MV modified microelectrode has been little explored.

In this work, a microsensor for dioxygen determination is fabricated by chemically modifying Nafion and methyl viologen (MV) onto a gold disk microelectrode (GDME). Nafion, a cation-exchange polymer, can form a film on the electrode surface and thus improve the selectivity during implantation in real samples. Furthermore, Nafion film can entrap MV easily, which charges positively in aqueous solution [25,26]. The Nafion/MV modified microelectrode shows electrocatalytic activity toward dioxygen reduction with high sensitivity and good reproducibility. This microsensor has been successfully employed for the measurement of dioxygen, which is released from three kinds of chloroplasts of plant leaves under different illumination. In order to monitor the dioxygen levels *in vivo*, the Nafion/MV modified carbon fiber microelectrodes (CFMEs) have been prepared according to a sim-

ilar modification procedure. As a preliminary test, the dioxygen levels in the different areas of rat brain are monitored by the Nafion/MV modified carbon fiber microsensors using linear sweep voltammetry (LSV).

2. Experimental

2.1. Instrumentation

All *in vivo* and *in vitro* electrochemical experiments were performed on CHI-832 Electrochemical Analyzer (CHI, USA) or on Bio-sensing Unit (BAS, Japan). A conventional electrochemical cell was employed, which consisted of a Nafion/MV modified gold disk microelectrode (10 μm i.d., 4 mm o.d.; BAS) as the working electrode, a gold wire (200 μm) as the counter electrode and a KCl saturated Ag/AgCl microelectrode (self-made) as the reference electrode. All potentials were measured and reported versus the Ag/AgCl reference microelectrode. The whole electrochemical system was shielded in a home-made Faraday cage. A Model 501 Super-thermostat (Shanghai Experimental Instrumental Factory) was employed to control the temperature. To determine the dioxygen released from the chloroplasts of three plant leaves under illumination, a conventional Br-W lamp (24 V, 300 W, illuminating intensity > 50,000 lux) was used as the light source. The illuminating intensity was surveyed by the ST-III illuminator (Photoelectrical Instrument Factory of Peking Normal University, P.R. China). To monitor the dioxygen levels *in vivo*, the self-made Nafion/MV modified carbon fiber microelectrodes (CFMEs; 7 μm i.d., 30 μm o.d.) were employed as the working electrodes.

2.2. Chemicals and materials

Methyl viologen (> 98%) was purchased from Fluka. Nafion (5% w/w in ethanol solution) was obtained from Aldrich. Phosphate buffered saline (PBS) solution, containing 137.0 mmol l^{-1} NaCl, 2.7 mmol l^{-1} KCl, 8.0 mmol l^{-1} Na_2HPO_4 and 1.5 mmol l^{-1} KH_2PO_4 , was prepared and adjusted to pH 7.4. Tris-HCl buffer solution (pH

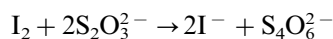
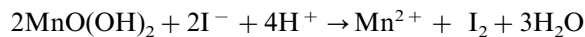
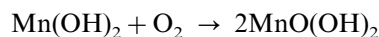
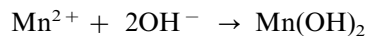
8.0) was used to extract the chloroplasts from the plant leaves. Other chemicals were of analytical grade and were used as received. All solutions were prepared in doubly distilled water. Unless otherwise mentioned, all experiments were performed in PBS solutions with the three-electrode system at $25.0 \pm 0.2^\circ\text{C}$. Prior to use, the buffer solutions were thoroughly deoxygenated for at least 15 min. The electrochemical experiments were carried out under nitrogen atmosphere.

2.3. Preparation of the Nafion/MV modified gold disk microelectrode

The bare gold disk microelectrode (GDME) was mechanically polished to a mirror-finish with 0.05- μm alumina, rinsed with deionized water, sonicated successively in acetone, 1:1 HNO_3 , 1.0 mol l^{-1} NaOH, and doubly distilled deionized water to remove any trapped alumina. The dried GDME was dipped into the 0.80% Nafion/methol solution for several seconds. Then the GDME was taken out and dried in air. A few minutes later, the same dip-coating process was repeated for a second time. After being coated twice with Nafion, the GDME was cycled in 0.010 mol l^{-1} MV solution in the potential range of 0.20 to -1.20 V for 10 min. Then the Nafion/MV modified GDME was taken out and cycled in the blank PBS solution between 0 and -0.70 V until a steady electrode response was obtained. Except for the measurement of dioxygen *in vivo*, the Nafion/MV modified GDMEs were used throughout the experiment. The Nafion/MV modified GDMEs were stable when stored in air (*vide infra*).

2.4. Calibration of the Nafion/MV modified microsensor

The calibration of the microsensors is mainly accomplished by the three-point method [27,28]. However this method is often limited by the temperature and atmospheric pressure. In this work, classic iodimetry [29], together with differential pulse amperometry (DPA), is used to calibrate the Nafion/MV modified microsensor. Classic iodimetry is based on the following reactions [29]:



Differential pulse amperometry (DPA), where a double pulse of fixed potential difference is applied at constant amplitude, has been used *in vivo* for the detection of dioxygen [28]. In order to define the position of dioxygen reduction at the Nafion/MV modified microsensor, linear sweep voltammetry (LSV) was conducted. The potentials used for the two cathodic pulses were chosen from the linear sweep voltammograms (see below). The parameters for the differential pulse amperometry are given in the following: the first pulse was applied from the resting potential (-0.10 V) to -0.20 V; and the second was adopted from -0.20 to -0.45 V.

The calibration of the microsensor was performed at $37.0 \pm 0.2^\circ\text{C}$ for the measurement of dioxygen *in vivo*, and in other tests the calibration was conducted at $25.0 \pm 0.2^\circ\text{C}$.

2.5. Extraction of the chloroplasts from the plant leaves

Three kinds of chloroplasts were extracted from the green leaves of the following plants: Chinese cabbage (A), morning glory (B) and Chinese parasol (C). All these plant leaves were collected in the campus. The extraction was conducted according to the procedure described in the literature [30]. Each kind of plant leaf (50 g, sheared into pieces of 2–3 cm^2) was added to the solution containing 0.35 mol l^{-1} NaCl (100 ml) and 0.10 mol l^{-1} Tris-HCl buffer (10 ml, pH 8.0). Then the mixture was ground for 30 s and filtered with a nylon net. The filtrate was centrifuged at 2000 rpm for 4 min. The precipitate was diluted by 0.35 mol l^{-1} NaCl (~ 40 ml), which was again centrifuged for 4 min at the same rate. Then the precipitate was diluted with 0.35 mol l^{-1} NaCl ($\sim 2-3$ ml). After its illumination under different light intensities for 10 s, the obtained suspension was suitable for the determination of dioxygen released from the chloroplasts. All these procedures were conducted

at under 4°C. Before its use, the suspension was shaded and stored in a refrigerator (0°C).

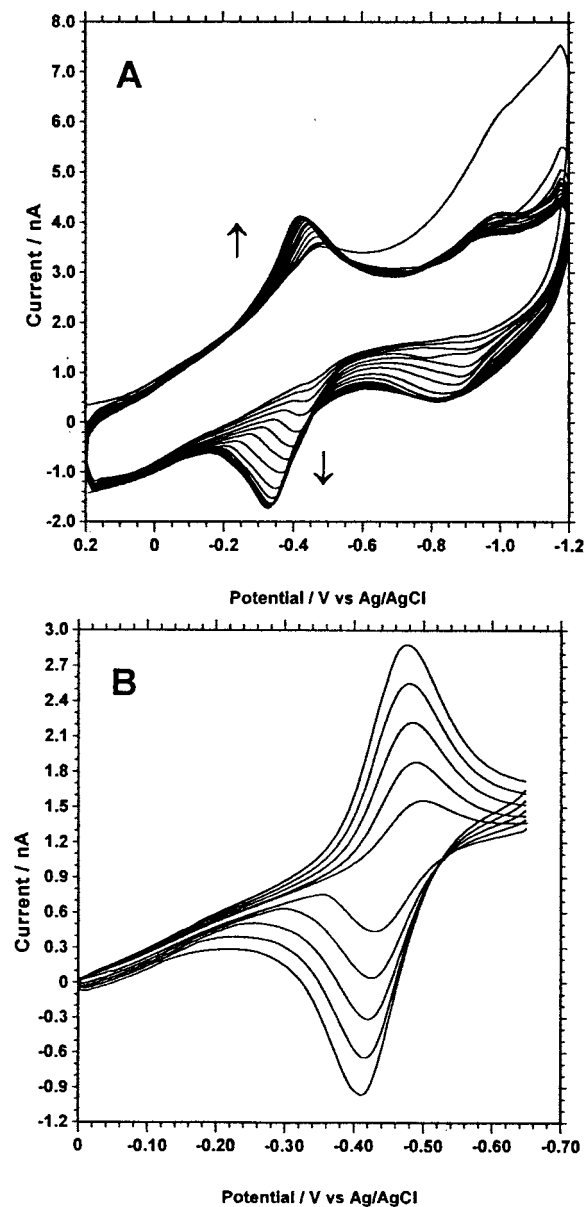


Fig. 1. Successive cyclic voltammograms of (A) the Nafion modified GDME in the PBS buffer solution (pH 7.4) containing 0.010 mol l^{-1} methyl viologen. Scan rate: 100 mV s^{-1} ; (B) the Nafion/MV modified GDME in the deoxygenated PBS buffer solution at different scan rates (from inner to outer): 20, 40, 60, 80 and 100 mV s^{-1} .

2.6. Fabrication of the Nafion/MV modified carbon fiber microelectrodes

The commercially available GDME (10 μm i.d., 4 mm o.d.) is unsuitable for usage *in vivo*. On the other hand, the bare gold wire microelectrode (10 μm in diameter) is too flexible to insert into rat brain. Carbon fiber microelectrodes (CFMEs) and carbon paste microelectrodes (CPMEs) have been demonstrated to be the alternative approaches to solve this problem [27,28,31,32]. CFMEs are extensively used, mainly because of their small diameter (5–50 μm), easily varied length (0–500 μm) and high sensitivity. Hence in this work the Nafion/MV modified CFMEs (7 μm i.d., 30 μm o.d., home-made) were employed to monitor the dioxygen levels *in vivo*. Before chemical modification, the CFMEs were washed successively with acetone, 1:1 HNO_3 , 1.0 mol l^{-1} NaOH, and doubly distilled water in an ultrasonic bath. All these CFMEs were electrochemically pre-activated by the following sequence: the electrode potential was first applied at 2.0 V for 30 s and -1.0 V for 10 s. Then a triangular wave (from 0.0 to 1.0 V) was performed at a scan rate of 100 mV s^{-1} until a stable current-voltage curve was obtained. After pre-activation, the CFMEs were chemically modified by Nafion and MV. The modification procedure was the same as that of the Nafion/MV modified GDME. The characterization and calibration of the modified CFMEs were also conducted using the same procedures.

2.7. *In vivo* techniques

The *in vivo* procedures were very similar to those described previously [27,28]. Adult Sprague–Dawley rats (male, 280–320 g) were anesthetized with urethane (ethyl carbamate, 1350 mg kg^{-1}) and positioned in a stereotaxic frame. Body temperature was maintained at 37°C with a heating pad. The skull was surgically exposed, and small holes were drilled for the electrode implantation. In order to measure the dioxygen levels in the different areas of the central nervous system (CNS) *in vivo*, several Nafion/MV modified carbon fiber microelectrodes were implanted into the rat brain. The Ag/AgCl reference

microelectrode was fixed in the region (AP 2.0, R 2.5, H 3.0, all dimensions of the coordinates are in millimeters according to the stereotaxic atlas of the rat brain [33]). The counter microelectrode (Ag wire, 200 μm) was placed between the skull and dura mater. All the electrodes were fixed to the skull with screws and dental acrylate. The rats were then allowed to recover from anesthesia. Post-operative analgesia was provided by the injection of buprenorphine (0.10 mg kg^{-1}), given immediately after the surgery. The welfare of the animals was assessed following recovery according to guidelines [34,35] and all procedures were specially licensed under the Animals (Scientific Procedures) Act 1986. The electrodes were connected to the Bio-sensing Unit, on which *in vivo* measurements of dioxygen were conducted by linear sweep voltammetry (LSV). All data were determined and reported as means \pm S.E.M. with n = number of the modified microelectrodes.

3. Results and discussion

3.1. Preparation and electrochemical behavior of the Nafion/MV modified GDME

Uniform coverage of modifiers at the microelectrode surface is a requisite factor for *in vivo* measurement. It has been reported [36] that dip-coating twice is suitable to coat a uniform Nafion film on the microelectrode surface. Therefore both the bare GDMEs and CFMEs are modified with Nafion film by dip-coating twice.

Fig. 1A shows the fixation of MV on the Nafion-coated GDME. The electrode potential is swept over the range where both MV^{2+} and MV^+ are reduced with one electron, respectively. It follows from the increases of the peak currents of MV^{2+} and MV^+ that the Nafion film incorporates MV^{2+} and MV^+ cations from the MV solution via ion-exchange with the Na^+ counter-ion of the fixed sulfonic acid groups. Both the peak potentials of the two redox couples ($\text{MV}^{2+}/\text{MV}^+$ and MV^+/MV^0) shift positively with the increase of the scan cycles (Fig. 1A). In addition, the ion-exchange selectivity of the Nafion film for MV^{2+} is apparently much higher than that for MV^+ .

The Nafion/MV modified GDME exhibits two pairs of well-defined redox peaks in a deoxygenated MV-free PBS solution. In order to simplify the question, the potential sweep range is restricted to the first pair of peaks (corresponding to the $\text{MV}^{2+}/\text{MV}^+$ redox couple). The second pair of redox peaks at more negative potentials (corresponding to the MV^+/MV^0 redox couple) is not studied further in this research. The typical cyclic voltammogram of the Nafion/MV modified GDME is shown in Fig. 1B, which is recorded in a deoxygenated PBS solution without any soluble MV present. A pair of redox peaks is obtained, with E_{pa} and E_{pc} of -0.42 and -0.48 V, respectively (E_{pa} and E_{pc} represents the anodic and cathodic peak potentials, respectively). The peak currents are found to be linear with the scan rates in the range of 20–100 mV s^{-1} , what is exactly as expected for a non-diffusion-controlled electrode process.

The total amount of MV^{2+} incorporated in the Nafion film can be quantitatively exchanged for Na^+ ions by the immersion of the Nafion/MV modified GDMEs into a saturated NaCl solution. In such a case, no redox waves can be detected on the modified GDMEs in the same potential window as that shown in Fig. 1B. The redox waves of the $\text{MV}^{2+}/\text{MV}^+$ couple reappear in the MV-free buffer after the modified GDMEs are scanned under the same conditions as described in Fig. 1A. The conversion of the MV^{2+} form to the Na^+ form and back again can be repeated many times (more than five) without an apparent loss of the exchange capacity of the Nafion film. Similar results have been reported by others [26]. Therefore it is a reasonable assumption that the MV^{2+} cations enter the Nafion film by exchange of Na^+ and form an efficient microsensor with a three-dimensional structure.

The concentration of the Nafion solution plays an essential role in the dip-coating procedure. To survey the relationship between the response of the Nafion/MV modified GDME and the Nafion concentration, several GDMEs of the same size are dip-coated twice with Nafion in different concentrations. The result is clearly shown in Fig. 2. The electrode response increases quickly with the

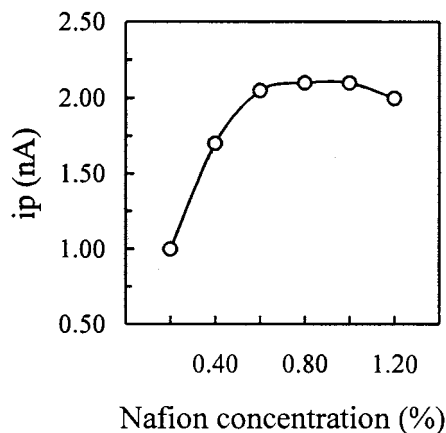


Fig. 2. The dependence of the Nafion/MV modified GDME response on the Nafion concentration. The Nafion/MV modified GDME is prepared by scanning the Nafion-coated GDME in the PBS solution containing 0.010 mol l^{-1} MV in the potential range of 0.20 to -1.20 V for 10 min. The data are collected on the modified GDME in air-saturated PBS solution. Scan rate: 100 mV s^{-1} .

increase of the Nafion concentration. When the range of the Nafion concentration varies from 0.60 to 1.00%, the peak currents of the modified GDMEs become almost constant. The response of the Nafion/MV modified GDME declines when the Nafion concentration is larger than 1.00%. Hence the 0.80% Nafion/methanol solution is selected for the modification of Nafion on the electrode surface.

The voltammetric peak currents, obtained immediately after the Nafion/MV modified GDME is transferred to the pure supporting electrolyte, are strongly dependent on both the time it scanned in the MV solution and the concentration of the MV solution. As mentioned above, several GDMEs coated twice with the 0.80% Nafion solution are tested in the 0.010 mol l^{-1} MV solution with different scan times. A typical result is given in Fig. 3. The dependence of the peak current on the scan time clearly shows that when the scan time $< 8 \text{ min}$ (~ 17 cycles), the electrode response increases quickly with the scan time. However the peak current remains almost constant when the scan time $\geq 10 \text{ min}$ (~ 22 cycles), indicating that the maximum amount of MV^{2+} has been fixed in the Nafion film. Therefore 10 min is chosen as the fixation time in this work.

The successive cyclic voltammograms of the Nafion/MV modified GDMEs in a deaerated PBS solution show that the peak currents decrease a little ($< 5\%$) in the first ten repetitious cycles and become steady after continuous potential scanning for 500 cycles. On the other hand, $91 \pm 4\%$ of the original electrode responses is obtained for the Nafion/MV modified GDMEs ($n = 3$) after those modified GDMEs have been placed in air for a month. However, the peak currents of the modified glassy carbon electrode prepared by the adsorption of MV [19] decrease much faster with repetitious sweeps. It is found that only 80% of the original electrode response remains after 50 successive scans. All these results suggest that MV^{2+} cations are more strongly immobilized by potential scanning at the Nafion-coated GDMEs.

3.2. Catalytic reduction of dioxygen at the Nafion/MV modified GDME

Dioxygen is readily able to permeate into the Nafion film and reach the electrode surface for reduction [27,37]. It has been reported [19,20,27,28,38] that dioxygen reduction is a two-electron process at the surfaces of most electrodes (e.g. gold or glassy carbon) and the predominate

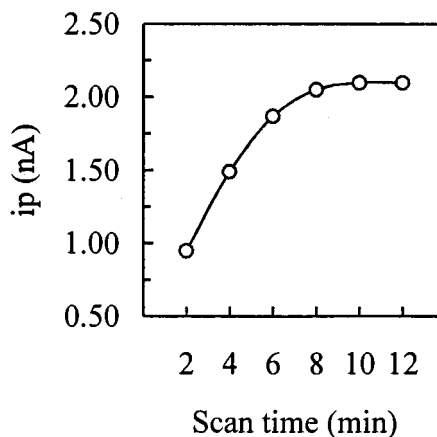


Fig. 3. The relationship between the cathodic peak current of the Nafion/MV modified microsensor and the scan time. The Nafion/MV modified GDME is fabricated by scanning the Nafion-coated GDME in the potential range of 0.20 to -1.20 V with different cycles (scan time). Other conditions are the same as in Fig. 2.

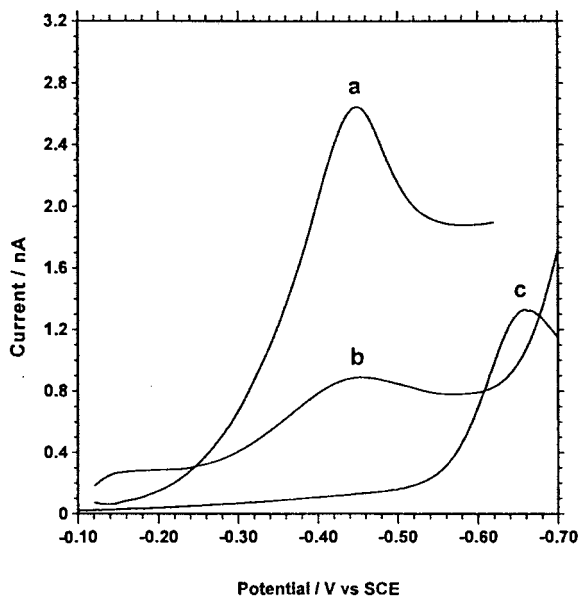
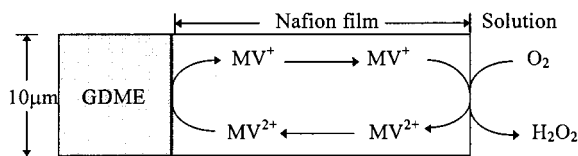


Fig. 4. Linear sweep voltammograms of the Nafion/MV modified GDME (a and b) and the bare GDME (c) in PBS solutions: (a, c) air-saturated; (b) nitrogen-saturated. Scan rate: 100 mV s^{-1} .



Scheme 1. The catalytic mechanism of dioxygen reduction on the Nafion/MV modified GDME.

product is hydrogen peroxide, which is not oxidized on these electrodes, leading to irreversible electrochemical behavior. The rate-limiting step for the reduction of dioxygen involves the initial one-electron transfer followed by protonation of the superoxide ion and further reduction [38].

The linear sweep voltammogram of dioxygen is consistent with its known electrochemical behavior (Fig. 4). Dioxygen is found to be irreversibly reduced at -0.66 V on the bare GDME (curve c, Fig. 4). However, dioxygen reduction is easier on the Nafion/MV modified GDME. The reduction peak is observed at -0.45 V , which is same as the cathodic peak potential of the Nafion/MV modified GDME itself (curves a and b, Fig. 4).

Thus a decrease in the overvoltage ($\sim 210 \text{ mV}$) and an increase in the reduction peak current (~ 2.5 times the size of that obtained on the bare GDME) are obtained on the Nafion/MV modified GDME. These results clearly demonstrate that the Nafion/MV modified GDME has an excellent catalytic activity for the dioxygen reduction. The $\text{MV}^{2+}/\text{MV}^+$ redox couple has a high electron self-exchange rate that facilitates the electron transfer between the electrode and dioxygen in PBS solution. The regeneration of MV^{2+} produced by the chemical reaction greatly enhances the peak current and anodically shifts the potential of dioxygen reduction. However, no changes are observed on the Nafion/MV modified GDMEs after hydrogen peroxide is added into the deoxygenated PBS buffer solution. On the other hand, the decomposition rate of hydrogen peroxide is very slow in the neutral or basic solutions. Therefore the corresponding procedure of the catalytic reaction can be expressed as follows:

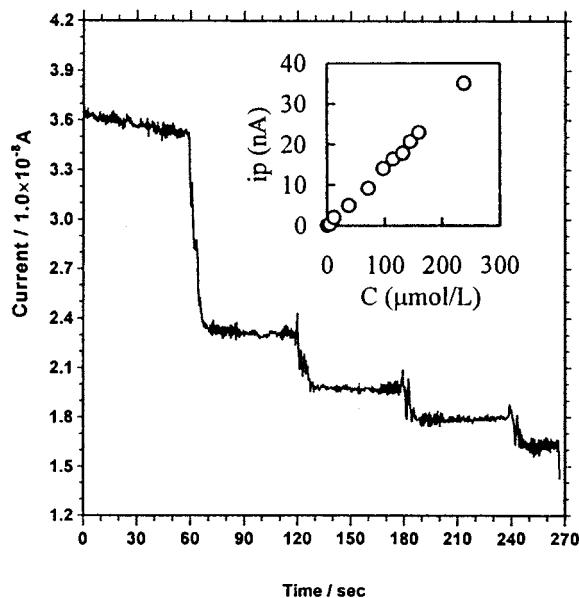
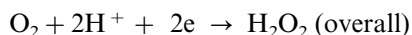
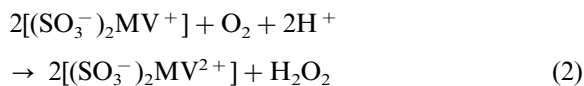
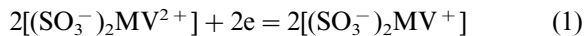


Fig. 5. Differential pulse amperometric response of dioxygen at the Nafion/MV modified GDME. The inset shows the relationship between the electrode response (the peak current) and the concentration of dioxygen.

Table 1
Determination of dioxygen by the Nafion/MV modified GDME^a

Order	1	2	3	4	5	6	7	8	9	10	Mean	RSD (%)
Current (nA)	1.45	1.40	1.48	1.41	1.49	1.46	1.51	1.45	1.39	1.45	1.45	2.7

^a Data are collected from the DPA response of the Nafion/MV modified GDME in the PBS solution (pH 7.4) containing 8.50 $\mu\text{mol l}^{-1}$ dioxygen.



The catalytic mechanism is shown in Scheme 1.

The potentials used for the two cathodic pulses of the differential pulse amperometry (DPA) are also chosen from the linear sweep voltammograms. The first pulse is set from the resting potential (-0.10 V) to -0.20 V, which corresponds to the root of the reduction wave for dioxygen. The second pulse is applied from -0.20 to -0.45 V, which is relevant to the peak of the reduction wave for dioxygen (Fig. 4).

3.3. Calibration of the Nafion/MV modified GDME

The electrode response for dioxygen measurement is standardized by classic iodimetry [29] together with differential pulse amperometry (DPA), as described in Section 2. A section of the resultant calibration curve is shown in Fig. 5. The electrode response is found to be linear with the dioxygen concentration over the range from 3.44×10^{-7} to 2.59×10^{-4} mol l^{-1} (at 25°C), with a correlation coefficient of 0.9978. The detection limit, defined as the analyte (dioxygen) concentration yielding a signal equal to three times the standard deviation of the background current, is calculated to be 0.19 ± 0.05 $\mu\text{mol l}^{-1}$ ($n = 4$). To meet the requirements, calibrations of the modified microelectrodes are conducted at different temperatures. The sensitivity of the microsensor is 0.17 ± 0.04 $\text{nA } \mu\text{mol}^{-1} \text{ l}^{-1}$ ($n = 5$).

3.4. Response time and life

The response time of the microsensor, defined as the required period when the steady response is obtained on the modified microsensors for dioxygen measurement, is less than 15 s. For ten parallel measurements of 8.50 $\mu\text{mol l}^{-1}$ dioxygen, the relative standard deviation (RSD) is found to be 2.7% (Table 1). No significant changes of the electrode responses are observed after the modified microelectrodes have been placed in air for 1 month, as mentioned above. On the other hand, the cyclic voltammograms of the Nafion/MV modified GDMEs show no obvious changes ($< 8\%$, $n = 3$) after the modified microsensors have been cycled continuously in the PBS solu-

Table 2

In vitro DPA response of the Nafion/MV modified GDMEs ($n = 3$) for a variety of potential interferents expressed as a percentage of the dioxygen (100.0 $\mu\text{mol l}^{-1}$) current in the PBS solution (pH 7.4)^a

Interferent	Dioxygen (%)
–	100 (17 ± 4 nA)
Ca^{2+}	< 0.01
Na^+	< 0.01
K^+	< 0.01
Cl^-	< 0.01
HCO_3^-	< 0.01
AA	2.87 ± 0.79
UA	0.48 ± 0.18
DA	0.54 ± 0.22
5-HT	1.03 ± 0.65
5-HIAA	1.58 ± 0.46
DOPAC	0.85 ± 0.23

^a The concentrations of Ca^{2+} , Na^+ , K^+ , Cl^- , HCO_3^- , ascorbic acid (AA) and uric acid (UA) are all 10.0 mmol l^{-1} . The concentrations of dopamine (DA), 5-hydroxytryptamine (5-HT), 5-hydroxyindole-3-acetic acid (5-HIAA) and 3,4-dihydroxyphenylacetic acid (DOPAC) are all 500.0 $\mu\text{mol l}^{-1}$.

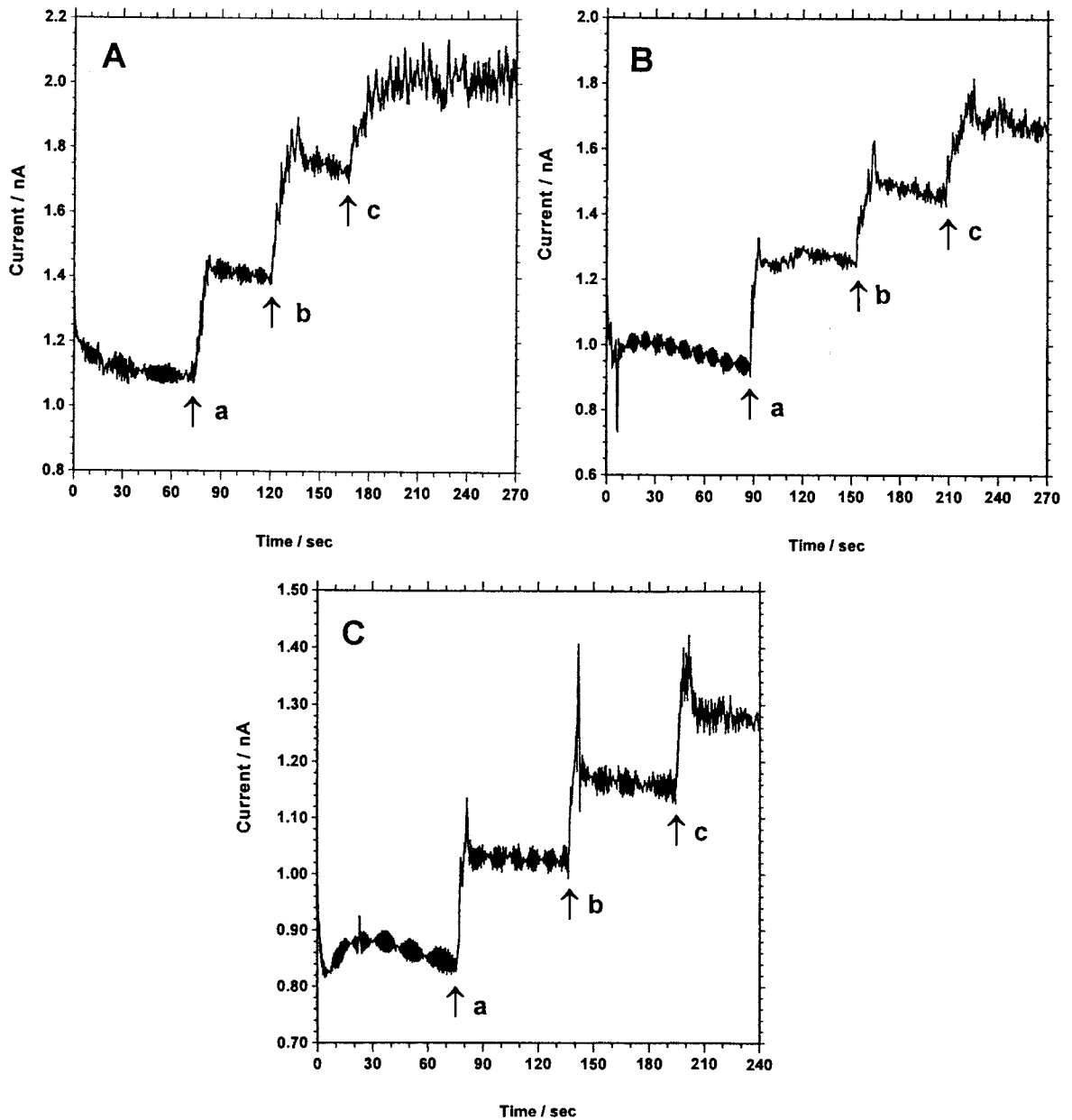


Fig. 6. DPA response of dioxygen released from the three kinds of chloroplasts of plant leaves (A: Chinese cabbage; B: morning glory; and C: Chinese parasol) under illumination (10 s) with different intensities: (a) 40 klux; (b) 34 klux and (c) 28 klux. The arrows indicate the start of illumination (10 s).

tions for 5 days. All these results suggest that the Nafion/MV modified microelectrodes can meet the requirements for dioxygen measurements *in vivo*.

3.5. Selectivity

The selectivity of the microsensor for dioxygen determination, relative to a variety of potential

interferents present in real samples, is also characterized in vitro. The interferents tested include the neurotransmitters (5-hydroxytryptamine, 5-HT and dopamine, DA), their metabolites (5-hydroxyindole-3-acetic acid, 5-HIAA and 3,4-dihydroxyphenylacetic acid, DOPAC) and other species such as Ca^{2+} , Na^+ , K^+ , Cl^- , HCO_3^- ; ascorbic acid (AA) and uric acid (UA). The results are summarized in Table 2. From Table 2, it is clear that the above substances have no appreciable effects on the responses of the microsensor for dioxygen detection. Therefore these in vitro results also suggest that the Nafion/MV modified microsensors should have interference-free signals for dioxygen determination in vivo.

Changes in solution pH may occur in physiological tests, and these could influence the catalytic reduction of dioxygen because of the involvement of proton in the catalytic reaction. To test for the dependence of the microsensor response on the solution pH, the buffer pH values are varied from 7.1 to 7.8. No obvious changes are observed in either the catalytic peak potentials and the peak currents of the reduction.

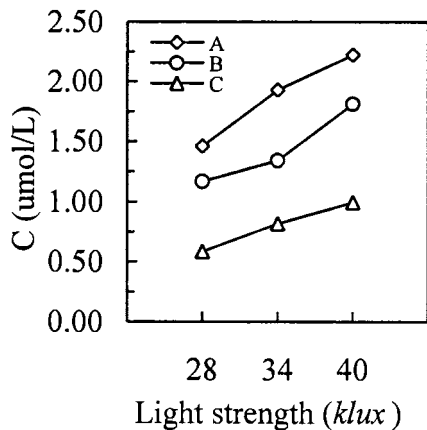


Fig. 7. The relationship between the dioxygen concentration released from the three kinds of chloroplasts of the plant leaves and the illumination intensity. (A: Chinese cabbage; B: morning glory; and C: Chinese parasol. Data are collected from Fig. 6).

3.6. Application

3.6.1. Measurement of dioxygen released from three kinds of chloroplasts

The Nafion/MV modified GDMEs are employed to determine the concentration of dioxygen, which is released from the three kinds of chloroplasts of the plant leaves under illumination (10 s) with different intensities. The extraction of the chloroplasts from the green leaves and the general procedures are conducted as described above. The results are shown in Figs. 6 and 7. For all three chloroplasts of these plant leaves, the amount of released dioxygen increases concomitantly with the increase of the light intensity (Fig. 7). On the other hand, the amount of dioxygen released from Chinese parasol (C) is less than that from morning glory (B). However, it is obvious that the chloroplast in the leaves of Chinese cabbage (A) releases the highest amount of dioxygen under the same conditions (Fig. 7). This microsensor therefore is applicable to evaluate the efficiency of dioxygen released from different plants.

3.6.2. Measurement of dioxygen in vivo

For in vivo measurement, the Nafion/MV modified CFMEs are fabricated and characterized in the PBS buffer at 37°C, as mentioned above. Similar electrochemistry and electrocatalytic activity toward dioxygen reduction are also observed on these Nafion/MV modified CFMEs. The Nafion/MV modified CFMEs are implanted in different areas of the rat brain. In vivo linear sweep voltammograms are obtained, while the cardiac rate is monitored with an oscillator and stored in a computer. It has been reported [39] that the dioxygen concentration in brain varies between 5.0 and 50.0 $\mu\text{mol l}^{-1}$. In this work, it is found that in the normal state of a rat, the concentrations of dioxygen in the dorsal hippocampus and the superior colliculus are 15.9 ± 3.3 and 36.9 ± 4.5 $\mu\text{mol l}^{-1}$, respectively ($n = 3$ animals). In the visual cortex (at the depth of H 500 and H 1500), the dioxygen levels are found to be 2.5 ± 0.6 and 53.1 ± 6.8 $\mu\text{mol l}^{-1}$, respectively ($n = 3$ animals). The concentration of dioxygen in the cerebral tissues maintains a dynamic balance due to the supply and consumption

of dioxygen. Dioxygen is supplied via blood flow in vessel and its consumption is related to the respiration and metabolism of the cells. Thus the dioxygen level obtained by in vivo measurement with the Nafion/MV modified CFMEs should vary in different regions. These results are very similar to those reported by the other workers [27,28].

4. Conclusion

A new type of chemically modified microsensor, including the Nafion/MV modified GDME and the Nafion/MV modified CFME, is prepared and studied for the determination of dioxygen. Several characteristics of the modified microsensors can be concluded. Firstly, the Nafion/MV modified microsensors exhibit efficient catalytic activity toward dioxygen reduction; secondly, these microsensors are very sensitive and reproducible to dioxygen determination; finally, it is shown by the in vitro signals that the determination of dioxygen is free of direct interference from several endogenous substances present in mammalian brain. All these results make it possible for in vivo and in vitro determination of dioxygen using the Nafion/MV modified microsensors. Preliminary experiments in vivo also suggest that these microsensors do have reliable response to dioxygen. Further work on in vivo characterization is currently under investigation in our laboratory and will be communicated after its completion.

Acknowledgements

This project was supported by the China Postdoctoral Science Foundation and Natural Scientific Foundation of Shanghai, P.R. China.

References

- [1] R.D. Jones, D.A. Summerville, F. Basolo, *Chem. Rev.* 79 (1979) 139.
- [2] J. Zagal, P. Bindra, E. Yeager, *J. Electrochem. Soc.* 127 (1980) 1506.
- [3] A. Elzing, A. Van Der Putten, W. Visscher, E. Barendrecht, *J. Electroanal. Chem.* 233 (1987) 99.
- [4] C. Hinnen, F. Coowar, M. Savy, *J. Electroanal. Chem.* 264 (1989) 67.
- [5] J. Ouyang, K. Shigehara, A. Yamada, F.C. Anson, *J. Electroanal. Chem.* 297 (1991) 489.
- [6] S. Zecevic, B.S. Glavaski, E. Yeager, A.B.P. Lever, P.C. Minor, *J. Electroanal. Chem.* 196 (1985) 339.
- [7] K.M. Kost, D.E. Bartak, B. Kazee, T. Kuwana, *Anal. Chem.* 62 (1990) 151.
- [8] D. Cukman, M. Vukovic, *J. Electroanal. Chem.* 279 (1990) 273.
- [9] D. Cukman, M. Vukovic, *J. Electroanal. Chem.* 279 (1990) 283.
- [10] S. Dong, Q. Qin, *J. Electroanal. Chem.* 314 (1991) 223.
- [11] A. Bettelheim, R.J.H. Chan, T. Kuwana, *J. Electroanal. Chem.* 10 (1980) 93.
- [12] R.R. Durand Jr., F.C. Anson, *J. Electroanal. Chem.* 134 (1982) 273.
- [13] D.O.R. Harth, U. Mor, A. Bettelheim, *J. Electroanal. Chem.* 266 (1989) 109.
- [14] T. Sawaguchi, T. Itabashi, T. Matsue, I. Uchida, *J. Electroanal. Chem.* 279 (1990) 219.
- [15] L. Pospisil, R. Fuoco, P. Papoff, *J. Electroanal. Chem.* 256 (1988) 83.
- [16] J.E. Nolan, J.A. Plambeck, *J. Electroanal. Chem.* 294 (1990) 1.
- [17] M. Fabrizio, G. Mengoli, M.M. Musiani, F. Paolucci, *J. Electroanal. Chem.* 300 (1991) 23.
- [18] Q. Chi, S. Dong, *J. Electroanal. Chem.* 369 (1994) 169.
- [19] L. Jin, P. Jin, J. Ye, Y. Fang, *Talanta* 39 (1992) 145.
- [20] W. Sun, J. Kong, J. Deng, *Anal. Lett.* 29 (1996) 2425.
- [21] T. Ohsaka, N. Oyama, K. Sato, H. Matsuda, *J. Electrochem. Soc.* 132 (1985) 1871.
- [22] A.M. Hogdes, O. Johansen, J.W. Loder, A.W.H. Mau, J. Rabani, W.H.F. Sasse, *J. Phys. Chem.* 95 (1991) 5966.
- [23] Z. Porat, Y.M. Tricot, I. Rubinstein, B. Zinger, *J. Electroanal. Chem.* 315 (1991) 217.
- [24] I. Rubinstein, *J. Electroanal. Chem.* 188 (1985) 227.
- [25] K. Shigehara, E. Tsuchida, F.C. Anson, *J. Electroanal. Chem.* 175 (1984) 291.
- [26] J. Weber, P. Janda, L. Kavan, A. Jegorov, *J. Electroanal. Chem.* 199 (1986) 81.
- [27] J.B. Zimmerman, R.M. Wightman, *Anal. Chem.* 63 (1991) 24.
- [28] J.P. Lowry, M.G. Bontelle, R.D. O'Neill, M. Fillenz, *Analyst* 121 (1996) 761.
- [29] Y. Fang, L. Jin, B. Xu, *Environmental Analysis and Monitoring*, East China Normal University Publishing House, 1987.
- [30] D. Li, J. Ye, *Zhi Wu Sheng Li Xue Tong Xun* 5 (1986) 56.
- [31] R. Kelly, R.M. Wightman, *Anal. Chim. Acta* 187 (1986) 79.
- [32] E.W. Kristensen, W.G. Kuhr, R.M. Wightman, *Anal. Chem.* 59 (1987) 1752.

- [33] L.J. Pellegrino, et al., *A Stereotaxic Atlas of the Rat Brain*, Plenum, New York, 1979.
- [34] D.B. Morton, P.H.M. Griffiths, *Vet. Rec.* 116 (1985) 431.
- [35] S. Wolfensohn, M. Lloyd, *Handbook of Laboratory Animal Management and Welfare*, Oxford University Press, Oxford, 1994.
- [36] H. Chen, H. Xu, Y. Xun, *Anal. Chem.* 66 (1994) 4538.
- [37] D. Lawson, L.D. Whitely, C.R. Martin, M.N. Szentirmai, J.I. Song, *J. Electroanal. Chem.* 135 (1988) 2247.
- [38] R.J. Taylor, A.A. Humffray, *J. Electroanal. Chem.* 64 (1975) 85.
- [39] Z.C. Feng, E.L. Roberts, T.J. Sick, M. Rosenthal, *Brain Res.* 445 (1988) 280.

The application of chemical modification in electrothermal vaporization-inductively coupled plasma atomic emission spectrometry

Bin Hu *, Zucheng Jiang, Tianyou Peng, Yongchao Qin

Department of Chemistry, Wuhan University, Wuhan, 430072, People's Republic of China

Received 3 August 1998; received in revised form 23 November 1998; accepted 2 December 1998

Abstract

In this paper, several fluoride chemical modifiers have been tested for electrothermal vaporization-inductively coupled plasma atomic emission spectrometry (ETV-ICP-AES) determination of different volatile elements, such as refractory element Ti, medium volatile element Ni and easy volatile element Pb. Reagents tested include polytetrafluoroethylene (PTFE), NH_4F , NaF and $\text{CuF}_2 \cdot 2\text{H}_2\text{O}$. The best overall results are obtained using 6% PTFE added to sample. Under the compromise operating conditions, the detection limits of analytes are in the range of 0.8–59 ng ml^{-1} and the calibration curves are linear for over three orders of magnitude. The direct determination of Ti, Ni and Pb in GBW 08505 tea leaves reference sample is shown as an example of PTFE chemical modification. © 1999 Elsevier Science B.V. All rights reserved.

Keywords: Fluoride; Chemical modification; Electrothermal vaporization-inductively coupled plasma atomic emission spectrometry

1. Introduction

Electrothermal vaporization (ETV) as a means of sample introduction for inductively coupled plasma atomic emission spectrometry (ICP-AES) has been paid great attention by many researchers since its first report in 1974 [1]. It can offer many advantages over conventional pneumatic nebulization method of sample introduction. These include: high transport efficiency, small amount of sample required, low absolute detection limit and

the ability to analyse both liquid and solid samples. Recent developments of this technique have been reviewed by Carey and Caruso [2], Hu et al. [3] and Moens et al. [4], the authors summarizing most of its crucial aspects.

However, this approach inherits the disadvantages of electrothermal atomization with respect to the formation of refractory carbides by elements in group IVB to VIB, which leads to a decrease and sometimes complete suppression of the analyte signals. Carbide formation also results in carry-over of analyte from one determination to the next, thus causing memory effects. Several methods can be used in order to solve the prob-

* Corresponding author. Fax: +86-27-87882661.
E-mail address: zcjiang@whu.edu.cn (B. Hu)

lem of refractory carbide formation. For example, the use of carbide coated tubes [5], utilization of metal material vaporizers [6,7], and chemical modification via the addition of either halocarbons [8–17], Cl_2 [18] in the plasma gases or matrix modifiers in the furnace [19,20]. Of these, chemical modification via the addition of chemical modifiers has been proven to be one of the most effective methods.

Chemical modifiers are compounds or mixtures of compounds, which are used to change the chemical or physical properties of the sample, matrix or the vaporizer/atomizer surface (or a combination of these) in such a way as to improve analysis. The concept of chemical modification is not new, it has been used for a number of years in both graphite furnace atomic absorption spectrometry (GFAAS) and in dc arc spectrometry and the approaches are easily transferable to ETV-ICP spectrometry. Kirkbright and Snook [8] used CCl_4 /argon atmosphere to enhance analyte volatilization of carbide forming elements. Substantial improvements in detection limits were reported for carbide forming elements such as B, Cr, Mo, W, and Zr. Barnes and Fodor [9] and Hulmston and Hutton [10] added trifluoromethane to the injector gas and improved the detection limits of refractory elements. Ren and Salin [11,12], utilizing Freon-12 as halogenation reagent, reported near 100% vaporization for the powdered samples studied, Al_2O_3 , SiO_2 , ZrO_2 and TaC. The same was true for WC if BaCl_2 was used as a second halogenation reagent. Also, they have tested Freon-assisted graphite furnace vaporization ICP-AES for analysis of solid samples (zeolite) that are difficult to digest or to vaporize in a conventional furnace [13]. Goltz et al. [16] investigated the determination of yttrium and rare-earth elements in ETV-ICP-MS with and without modifier. They showed that the addition of Freons in graphite furnace ETV-ICP-MS controls carbide formation and reduces memory effects in the high-sensitivity high-temperature determination of yttrium and rare-earth elements. More recently, Wanner et al. [17] examined the role of various modifiers in ETV-ICP-MS and found the best reactivity of NH_4F as modifier for B and of CHF_3 for La and U determination.

Matousek et al. [18] converted the refractory carbides into volatile chlorides and introduced analytes into an ICP with the use of Cl_2 as chemical modifier. Ng and Caruso [19] used 7% NH_4Cl as chemical modifier to determine refractory elements Cr, Ti, U, V and Zr. Nickel et al. [20] showed that total evaporation of impurity elements from SiC ceramic powder could be achieved by mixing the sample with BaO and CoF_2 .

The objective of our research is to investigate the chemical modification of fluoride chemical modifiers in ETV-ICP-AES for determination of different volatile elements, such as refractory element Ti, medium volatile element Ni and easy volatile element Pb, and to test the method for the determination of different volatile elements.

2. Experimental

2.1. Instrumentation

The inductively coupled plasma source system and the graphite furnace sample introduction device used in this study were identical with that reported previously [21]. A commercial 27 ± 3 -MHz Ar ICP source (Beijing Broadcast Instrument Factory, Beijing, China) with 2-kW plasma generator was interfaced to a WDG 500-1A type monochromator (Beijing Second Optics, Beijing, China). The output of the photomultiplier (R456, Hamamatsu, Japan) was amplified and registered on a strip chart recorder (L23-104, Sichuan Forth Meters, Sichuan, China).

A WF-1 type heating device with a matching graphite furnace (Beijing Second Optics, Beijing, China) was used as the electrothermal vaporization device. The instrument operating conditions and wavelength used are given in Table 1.

2.2. Design of ETV system

For electrothermal vaporization sample introduction, a commercially available WF-4 graphite furnace atomizer that is similar to an HGA 500 is modified for use. A pair of the conventional graphite tube adaptors and electric terminals with

Table 1
Operating conditions

Element and wavelength	Ti 334.95 nm; Ni 231.60 nm; Pb 220.35 nm
Incident power	1.0 kW
Observation height	12 mm (above working coil)
Carrier argon gas	0.6 l min ⁻¹
Coolant argon gas	15 l min ⁻¹
Auxiliary argon gas	0.8 l min ⁻¹
Heating cycle of ETV	Drying stage, ramp. 10 s , holds 20 s at 100°C Ashing stage, ramp. 10 s , holds 20 s at 400°C Vaporization stage, 4 s at 2340°C
Sample introduction	10- μ l Micropipette with disposable polyethylene tip

cooling water jackets are retained, but the original silica windows at the two ends of the graphite furnace are replaced with two PTFE cylinders, one of them connected to the injector tube of the plasma via a plastic tube (4 mm i.d. \times 0.5 m). The other was blocked to prohibit air from entering the graphite furnace, and there are sealed rings between the graphite furnace body and the PTFE cylinders. In Fig. 1, apertures 1 and 2 are used as inlets for the flow of the outer argon, and apertures 3 and 4 are carrier gas inlets. The graphite tube is enclosed in the original graphite tube adaptors filled with argon, which is introduced through apertures 1 and 2 to protect the tube

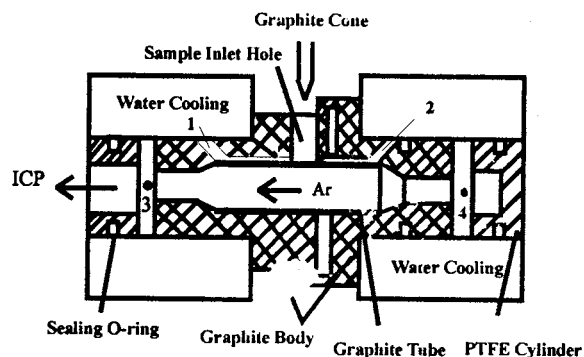


Fig. 1. The modified WF-4 commercial graphite furnace as an ETV assembly.

against oxidation during heating. Thus, after the sample is introduced into the graphite furnace, the injection hole is sealed with a graphite cone, and the vaporized analyte vapor is swept into the plasma by carrier gas, which enters through aperture 4.

2.3. Standard solutions and reagents

Stock titanium solution (1 g l⁻¹) was obtained by melting 0.1670 g of TiO₂ (Specpure grade, Shanghai Second Reagent Factory, Shanghai, China) with 10 g of K₂S₂O₇ (Analytical reagent grade, Shanghai Second Reagent Factory, Shanghai, China) in a platinum crucible, dissolving and transferring the melt with 5% H₂SO₄ solution into 100-ml calibrated flask.

The stock solution (1 g l⁻¹) of nickel was prepared from 99.99% pure metal of Ni and the acidity was adjusted with 0.1 mol l⁻¹ hydrochloric acid.

A lead stock solution (1 g l⁻¹) was prepared by dissolving an appropriate quantity of lead nitrate (Analytical grade reagent, Shanghai Second Reagent Factory, Shanghai, China) in 1% v/v nitric acid.

A 60% w/v PTFE slurry (viscosity 7–15 \times 10⁻³ Pa s) was purchased from Shanghai Institute of Organic Chemistry. NaF and NH₄F were analytical reagent grade and CuF₂·2H₂O was synthesized in our laboratory. Doubly distilled water was used throughout.

2.4. Sample preparation

The sample containing NH₄F was prepared by adding an appropriate quantity of NH₄F into a liquid sample and mixing.

The samples containing NaF, CuF₂·2H₂O and PTFE were prepared by adding an appropriate quantity of NaF, CuF₂·2H₂O and PTFE into liquid samples, respectively, and dispersing with ultrasonic processor for 15 min.

2.5. Procedure

After plasma stabilizing, 10 μ l prepared sample was pipetted into the graphite furnace with mi-

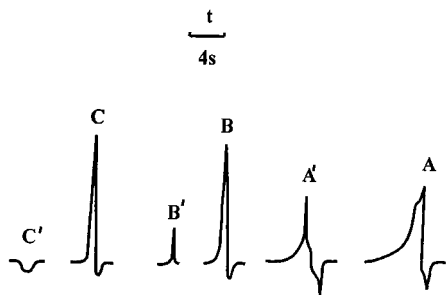


Fig. 2. Typical emission signal profiles for 10- μ l sample: A, B and C are 5.0 $\mu\text{g ml}^{-1}$ Ti, 1.0 $\mu\text{g ml}^{-1}$ Ni and 1.0 $\mu\text{g ml}^{-1}$ Pb, respectively; A', B' and C' are their residual signals of the empty firing, respectively.

crossyringe. The sample inlet hole was sealed with a graphite rod. After being dried and ashed, the analyte was vaporized and carried into the plasma under the selected conditions. A peak height measurement was used for calibration.

3. Results and discussion

3.1. Signal profiles of Ti, Ni and Pb without chemical modifier

In order to observe the vaporization behaviors of different volatile elements in ETV-ICP-AES, analyte emission temporal behavior was recorded. Typical results for 5 $\mu\text{g ml}^{-1}$ of Ti, 1 $\mu\text{g ml}^{-1}$ Ni and Pb are shown in Fig. 2. A weak and a broad signal profile with trailing was observed for Ti (Fig. 2A) and a severe memory effect was observed (Fig. 2A'), indicating slow and incomplete analyte volatilization. For Pb (Fig. 2C and C'), the signal observed is an intense and sharp peak and no memory effect was observed, indicating fast and complete analyte volatilization. A good signal profile was recorded for Ni (Fig. 2B), but the memory effect still existed (Fig. 2B'), indicating the vaporization behavior of Ni is between that of Pb and Ti.

During the drying/ashing cycle, an oxo-anion salt decomposes to form the corresponding oxide. A further increase in ETV temperature promotes either a reduction of the corresponding oxide to metal or carbide formation. Based on the thermo-

chemical properties of the oxides and carbides of the corresponding elements (Table 2), it can be concluded that without chemical modifier, Ti reacted with carbon to give refractory TiC during ETV heating cycle; this is verified in previous study[22]. For Pb, PbO was reduced into atom Pb by carbon, thus Pb was vaporized in the form of atom vapour. During graphite heating cycle, Ni was vaporized in the form of atom Ni through reduction reaction or decomposition of carbide.

3.2. Chemical modification of fluorides

The choice of appropriate materials to test as modifier was guided by the dc arc literature [23,24]. NaF, NH_4F , $\text{CuF}_2 \cdot 2\text{H}_2\text{O}$ and polytetrafluoroethylene (PTFE) were considered as suitable modifiers for the determination of Ti, Ni and Pb from multielement solution. For application of chemical modifiers, the concentration of the chemical modifiers had to be optimized. The concentration of the chemical modifier solution or slurry was varied between 0.1% and 10% w/v for NH_4F , NaF, $\text{CuF}_2 \cdot 2\text{H}_2\text{O}$ and PTFE. The effect of chemical modifier (NH_4F , NaF, $\text{CuF}_2 \cdot 2\text{H}_2\text{O}$ and PTFE) concentration (10- μ l injections) on the emission signal intensity of Ti, Ni and Pb was examined. Fig. 3 is the dependence of emission signal intensity of Ti, Ni and Pb on the PTFE concentration. It can be seen that the signal intensity of Ti and Ni was increased with the increase of concentration of PTFE and this enhancement effect levels off at a PTFE concentration of about 5%. However, PTFE showed no effect on the emission signal intensity of Pb in the concentration range used. Similar results can be obtained by examining NH_4F as chemical modifier, the only difference is the optimal chemical modifier concentration is 7% w/v for Ti and Ni. Both NaF and $\text{CuF}_2 \cdot 2\text{H}_2\text{O}$ as chemical modifier showed an adverse effect on the emission signal intensity of Pb in the concentration range used, whereas an obvious emission signal intensity increase for Ti and Ni can be observed with the increased modifier concentration of NaF and $\text{CuF}_2 \cdot 2\text{H}_2\text{O}$ up to a maximum of 5% w/v, followed by a decrease in signal intensity. Therefore, a concentration of 7% w/v solution of NH_4F , 5% w/v

Table 2
Melting and boiling point (°C) of Ti, Ni and Pb and their relative compounds

Element	M.P.	B.P.	Oxide	M.P.	B.P.	Carbide	M.P.	B.P.	Fluoride	M.P. ^a	B.P. ^a
Ni	1455	2730	NiO	1984	–	Ni ₂ C	–	–	NiF ₂	1000 ^{sub}	–
Pb	327	1740	PbO	886	–	Pb ₂ C	–	–	PbF ₂	885	1290
Ti	1660	3287	TiO ₂	1830	3000	TiC	3140	4820	TiF ₄	>400	284 ^{sub}

^a Sub means that this compound is sublimed at this temperature.

slurry of NaF and CuF₂·2H₂O, and 6% w/v slurry of PTFE was chosen for all further experiments.

After the optimal chemical modifier concentration had been found, the vaporization temperature was optimized. Fig. 4 shows the dependence of signal intensity for Ti, Ni and Pb on vaporization temperature by the use of PTFE as chemical modifier. There is an increase in signal intensity with increasing vaporization temperature up to 2340°C for Ti and Ni and 2240°C for Pb, whereas the signal intensity remains constant at higher temperatures. Therefore, 2340°C is chosen as vaporization temperature for determination of Ti, Ni and Pb from multielement solution.

Under the selected chemical modifier concentration and vaporization temperature, temporal signal profiles for Ti, Ni and Pb by use of various chemical modifiers are recorded. Typical results for Ti, Ni and Pb with NH₄F, NaF, CuF₂·2H₂O and PTFE modifiers compared with no chemical modifier are shown in Fig. 5. In general an enhancement of intensity of Ti was observed with four different fluoride modifiers, but this enhance-

ment was varied with fluoride modifier change. The greatest signal enhancement is achieved by the chemical modifier NH₄F and especially PTFE. These results allow the following sequence of investigated chemical modifiers to be arranged according to the increase of signal intensity of analyte and the decrease of the memory effects: PTFE > NH₄F > CuF₂·2H₂O > NaF. Similarly, an enhancement of signal intensity of Ni can be observed with four fluoride chemical modifiers and the ability of chemical modification can be concluded as follows: NH₄F > PTFE > CuF₂·2H₂O > NaF; whereas no enhancement was observed for Pb with PTFE and NH₄F chemical modifiers, but an obvious inhibition can be observed for Pb with NaF and CuF₂·2H₂O modifiers. The reasons for this are not clear right now; further examination should be carried out to investigate the effect mechanisms of the chemical modifier.

Based on above experimental results, some conclusions can be made: (a) the chemical modification of fluoride modifier is varied with the

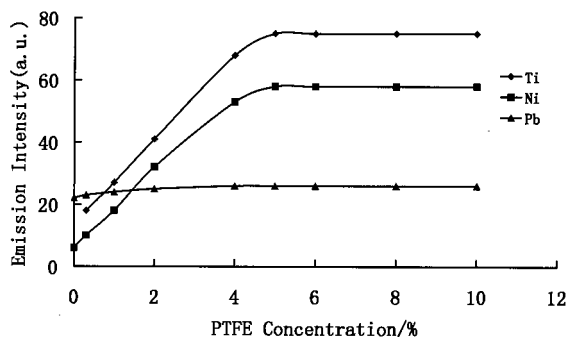


Fig. 3. The effect of PTFE concentration on signal intensity of 0.2 μg ml⁻¹ Ti, 0.2 μg ml⁻¹ Ni and 1.0 μg ml⁻¹ Pb with 10-μl sample.

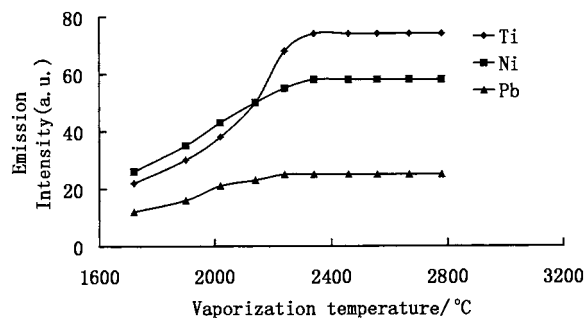


Fig. 4. The effect of vaporization temperatures on the signal intensity for 0.2 μg ml⁻¹ Ti (A), 0.2 μg ml⁻¹ Ni (B) and 1.0 μg ml⁻¹ Pb (C) with 6% w/v PTFE as chemical modifier.

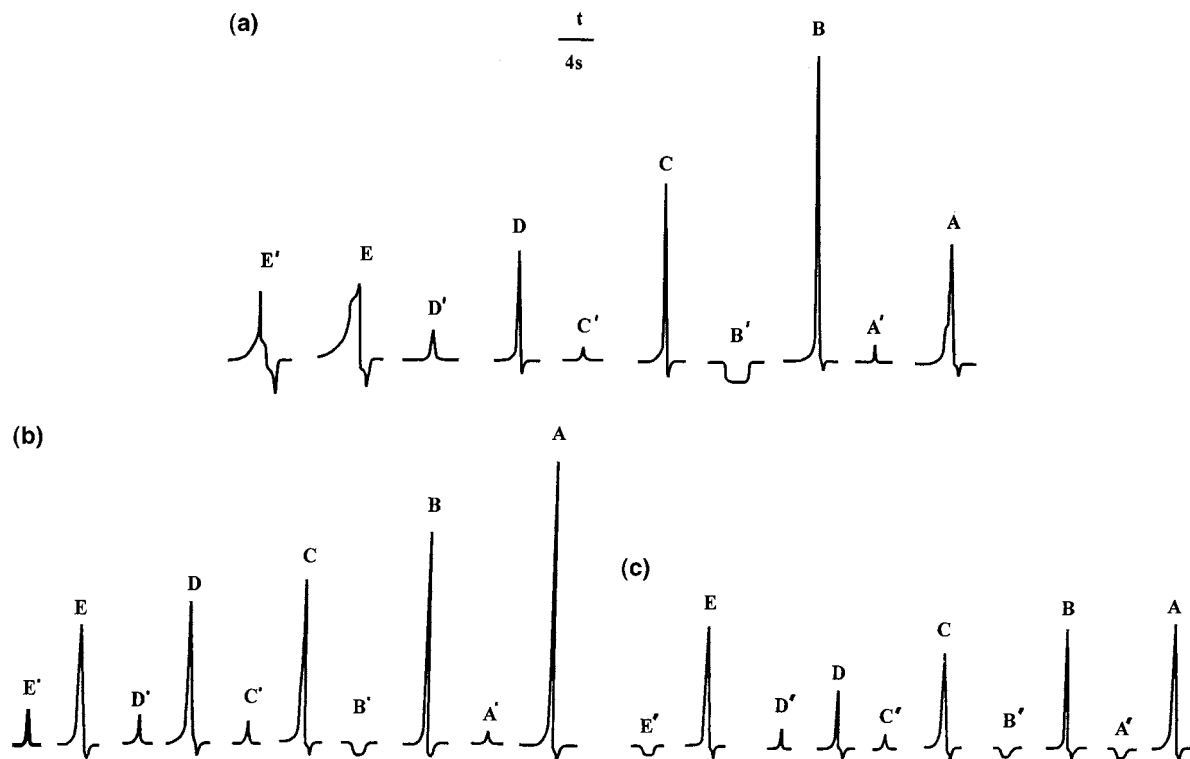


Fig. 5. Typical emission signal profiles of Ti (a), Ni (b) and Pb (c) with 10- μ l sample: (a) A: 1.0 $\mu\text{g ml}^{-1}$ Ti in 5% w/v $\text{CuF}_2 \cdot 2\text{H}_2\text{O}$; B: 0.2 $\mu\text{g ml}^{-1}$ Ti in 5% w/v PTFE; C: 0.4 $\mu\text{g ml}^{-1}$ Ti in 7% w/v NH_4F ; D: 1.0 $\mu\text{g ml}^{-1}$ Ti in 5% w/v NaF; E: 5.0 $\mu\text{g ml}^{-1}$ Ti without chemical modifier; A', B', C', D' and E' are their residual signals of the empty firing, respectively. (b) A: 0.2 $\mu\text{g ml}^{-1}$ Ni in 7% w/v NH_4F ; B: 0.2 $\mu\text{g ml}^{-1}$ Ni in 5% w/v PTFE; C: 1.0 $\mu\text{g ml}^{-1}$ Ni in 5% w/v $\text{CuF}_2 \cdot 2\text{H}_2\text{O}$; D: 1.0 $\mu\text{g ml}^{-1}$ Ni in 5% w/v NaF; E: 1.0 $\mu\text{g ml}^{-1}$ Ni without chemical modifier; A', B', C', D' and E' are their residual signals of the empty firing, respectively. (c) A: 1.0 $\mu\text{g ml}^{-1}$ Pb in 5% w/v PTFE; B: 1.0 $\mu\text{g ml}^{-1}$ Pb in 7% w/v NH_4F ; C: 1.0 $\mu\text{g ml}^{-1}$ Pb in 5% w/v $\text{CuF}_2 \cdot 2\text{H}_2\text{O}$; D: 1.0 $\mu\text{g ml}^{-1}$ Pb in 5% w/v NaF; E: without chemical modifier; A', B', C', D' and E' are their residual signals of the empty firing, respectively.

volatility of elements determined; (b) PTFE and NH_4F are the most suitable chemical modifiers for ETV-ICP-AES determination of refractory element (Ti) and medium volatile element (Ni). However, a problem emerged with NH_4F in that peak heights of a considerable intensity were observed even for a blank run for elements tested. These signals are due to impurities found in NH_4F utilized in these experiments. Clearly, measurements at concentration levels near or at the detection limit are not possible due to the low purity of the reagents utilized. As a result, PTFE is obviously the most useful chemical modifier of those tested.

3.3. Analytical characteristics

The ICP discharge parameters for Ti, Ni and Pb were established using a mixed standard slurry of Ti, Ni and Pb containing 6% PTFE, and the signal-to-background ratios were used to take the measurements. The compromise ICP discharge conditions for determination of above analytes are listed in Table 1.

Experiments were carried out to determine the best temperature and times for the various drying, ashing and vaporization steps. Optimum drying conditions were required to provide a smooth, even evaporation of the solvent with no splutter-

Table 3

Detection limits and relative standard deviations (RSD) obtained using ETV-ICP-AES with PTFE chemical modifier under compromise conditions

Element and wavelength	No chemical modifier			PTFE chemical modifier		
	Detection limit		RSD	Detection limit		RSD
	ng ml ⁻¹	ng	(%)	ng ml ⁻¹	ng	(%)
Ti 334.95 nm	280	2.8	–	0.8	0.008	1.9
Ni 231.60 nm	55	0.6	3.6	7.6	0.076	2.2
Pb 220.35 nm	59	0.6	3.0	59	0.59	2.8

ing; a drying temperature of 100°C was used. In order to optimize the ashing and vaporization temperatures, ashing and vaporization curves for Ti, Ni and Pb were constructed, and the compromise ETV operation conditions for the determination elements mentioned above were obtained (Table 1).

The calibration graphs for analytes, which were constructed from multielement solution of Ti, Ni and Pb with PTFE as a chemical modifier, were prepared by the recommended procedure. The relationships between emission intensity and analyte concentration were linear from 0.01 to 10, 0.3 to 100, and 1.0 to 1000 $\mu\text{g ml}^{-1}$ for Ti, Ni and Pb, respectively. Table 3 is the comparison of detection limits for analytes with and without PTFE as chemical modifier. These are 3 σ limits with the standard deviation of the blank determined by running nine blank runs. The most significant improvement in detection limit was observed for Ti. For easy volatile element Pb, there is little change in detection limit when the modifier is added. The relative standard deviation (RSD) of this method, obtained for nine replicate determinations at a concentration of 0.2 $\mu\text{g ml}^{-1}$ Ti, Ni and 1 $\mu\text{g ml}^{-1}$ Pb, were 1.9, 2.2 and 2.8%, respectively. This demonstrates that determination of Ti, Ni and Pb by ETV-ICP-AES with PTFE chemical modifier is possible.

3.4. The matrix effect

The effects of matrix elements on the determination of Ti, Ni and Pb by ETV-ICP-AES with PTFE as chemical modifier were investigated. The

tolerable amounts of matrix elements, which gave less than a 10% error for the determination of the above elements, were evaluated. Table 4 shows the tolerable amounts of matrix elements in this method. As can be seen, there is no obvious effect of the matrix elements on the determination of Ti, Ni and Pb by this method.

3.5. Sample analysis

The interest in adapting an electrothermal vaporization device for solid sample introduction into an ICP has recently increased significantly. Of all approaches for solid sampling ETV, slurry sample injection has demonstrated its potential as a promising method for direct solid analysis. Here, we reported a slurry sampling and ETV-ICP-AES method for direct determination of trace Ti, Ni and Pb in tea leaf sample.

A 1.0000-g sample of GBW 08505 tea leaves was weighed and carbonized in a quartz crucible at low temperature until no further smoke appeared and then charred at 450°C in a muffle furnace for 1 h. The ash was transferred quantitatively into a PTFE bottle and 0.1 ml of 60% (w/v) PTFE slurry, and 0.9 ml doubly distilled water was added. The suspension was homogenized with an ultrasonic processor for 30 min. The sample slurry (A), obtained by above method is used for determination of Pb. For determination of Ti and Ni, 0.2 ml of the above sample slurry (A) was taken and 0.38 ml of 60% (w/v) PTFE slurry added, then diluted to 4.0 ml. The suspension was dispersed with an ultrasonic processor for 30 min, after which the bottles were shaken

Table 4

The effect of matrix elements on the determination of Ti, Ni and Pb by ETV-ICP-AES with PTFE as chemical modifier

Element and wavelength	Concentration ($\mu\text{g ml}^{-1}$)	Tolerable amount of matrix elements (mg ml^{-1})									
		K	Na	Ca	Mg	Cu	Fe	Ni	Zn	Cd	
Ti 334.95 nm	0.2	5.0	5.0	5.0	5.0	5.0	5.0	5.0	2.0	5.0	
Ni 231.60 nm	0.2	5.0	5.0	5.0	3.0	5.0	5.0	–	3.0	1.0	
Pb 220.35 nm	1.0	5.0	5.0	5.0	5.0	5.0	5.0	5.0	5.0	1.0	

Table 5

Analytical results and recovery of Ti, Ni and Pb in GBW 08505 tea leaves sample by slurry sample injection ETV-ICP-AES with PTFE chemical modifier

Element and wavelength	Added amount	Found amount ^a	Recovery	Certified value
	μg	$\mu\text{g g}^{-1}$	%	$\mu\text{g g}^{-1}$
Ti 334.95 nm	0	35.2 ± 1.2	–	36
	30	64.1	96	
Ni 231.60 nm	0	8.10 ± 0.38	–	7.61 ± 0.48
	10	18.4	103	
Pb 220.35 nm	0	0.88 ± 0.10	–	1.06 ± 0.10
	1	1.85	97	

^a Average value obtained by three replicate determinations.

vigorously prior to sampling. The aqueous standard solutions containing 6% (w/v) PTFE chemical modifier, which were dispersed with ultrasonic processor for 15 min, were used for calibration. The analyte contents in sample were directly determined using external standards calibration method. The analytical results and the recovery of the method obtained by this method are given in Table 5. The agreement with the certified values was satisfactory.

4. Conclusions

From the results of the present study, it can be concluded that PTFE is the most useful chemical modifier of those tested and the chemical modification of fluoride varied with the volatility of elements tested. In the absence of chemical modifier, easy volatile element Pb can be volatilized from graphite furnace into ICP, while the addition of PTFE modifier has no adverse effects on the signal intensity of Pb. For evaporation of medium volatile element Ni and refractory

element Ti, the addition of PTFE modifier may be advantageously used. Compared with other kinds of halogenating reagents, which were used here or reported in the literature, PTFE slurry halogenating reagent presents certain advantages: (a) fluorine is sufficiently chemically active to combine with refractory materials; (b) PTFE has a suitable decomposition temperature, and allows a mild ashing temperature; (c) PTFE has a high fluorine content; (d) PTFE contains very low inorganic impurities, and the blank value is very low; and (e) PTFE slurry is easy to use. These characteristics may prove necessary for achieving complete vaporization and good analytical performance. The technique described permits determination of trace elements in solid sample without the need for labor intensive dissolution as required for conventional ICP-AES.

Acknowledgements

Financial support provided by the National Natural Science Foundation and the Education

Commission Foundation of China is gratefully acknowledged.

References

- [1] D.E. Nixon, V.A. Fassel, R. Kniseley, *Anal. Chem.* 46 (1974) 210.
- [2] J.M. Carey, J.A. Caruso, *Crit. Rev. Anal. Chem.* 23 (1992) 397.
- [3] B. Hu, Z. Jiang, Y. Zeng, *Henliang Fenxi* 9 (1993) 9.
- [4] L. Moens, P. Verrept, S. Boonen, F. Vankaecke, R. Dams, *Spectrochim. Acta* 50B (1995) 463.
- [5] K.C. Ng, J.A. Caruso, *Anal. Chim. Acta* 143 (1982) 209.
- [6] P. Barth, V. Krivan, *J. Anal. At. Spectrom.* 9 (1994) 773.
- [7] N. Shibata, N. Fudagawa, M. Kubota, *Anal. Chem.* 63 (1991) 636.
- [8] G.F. Kirkbright, R.D. Snook, *Anal. Chem.* 51 (1979) 1938.
- [9] R.M. Barnes, P. Fodor, *Spectrochim. Acta* 38B (1983) 1191.
- [10] P. Hulmston, R.C. Hutton, *Spectroscopy* (Eugene, OR) 6 (1991) 35.
- [11] J.M. Ren, E.D. Salin, *Spectrochim. Acta* 49B (1994) 555.
- [12] J.M. Ren, E.D. Salin, *Spectrochim. Acta* 49B (1994) 567.
- [13] J.-F. Alary, G. Hernandez, E.D. Salin, *Appl. Spectrosc.* 49 (1995) 1796.
- [14] G. Zaray, T. Kantor, G. Wolff, Z. Zadgorska, H. Nickel, *Mikrochim. Acta* 107 (1992) 345.
- [15] E.H. Bailey, A.J. Kemp, K.V. Ragnarsdottir, *J. Anal. At. Spectrom.* 8 (1993) 551.
- [16] D.M. Goltz, D.C. Goregoire, C.L. Chakrabarti, *Spectrochim. Acta* 50B (1995) 1365.
- [17] B. Wanner, P. Richner, B. Magyar, *Spectrochim. Acta* 51B (1996) 817.
- [18] J.P. Matousek, R.T. Satumba, R.A. Bootes, *Spectrochim. Acta* 44B (1989) 1009.
- [19] K.C. Ng, J.A. Caruso, *Analyst* 108 (1983) 476.
- [20] H. Nickel, Z. Zadgorska, G. Wolff, *Spectrochim. Acta* 48B (1993) 25.
- [21] M. Huang, L. Xu, Z. Jiang, Y. Zeng, *Gaodeng Xuexiao Huaxue Xuebao* 10 (1989) 709.
- [22] B. Hu, Z. Jiang, Y. Zeng, *Gaodeng Xuexiao Huaxue Xuebao* 14 (1993) 1165.
- [23] L.H. Ahrens, S.R. Taylor, *Spectrochemical Analysis*, Addison-Wesley, Reading, MA, 1961.
- [24] P.W.J.M. Boumans, *Theory of Spectrochemical Excitation*, Plenum, New York, 1966.

A potentiometric detector for hydrogen cyanide gas using silver dicyano complex

V. Kameswara Rao *, S. Suresh, A. Bhattacharya, N.B.S.N. Rao

Defence research and Development Establishment, Jhansi Road, Gwalior 474002, India

Received 15 June 1998; received in revised form 1 December 1998; accepted 3 December 1999

Abstract

A sensitive method capable of detecting Hydrogen cyanide gas in atmosphere at its TLV is being presented. This method makes use of two silver electrodes kept in two separate compartments which are in contact with a solution of constant concentration of Silver dicyano complex at a pH 11.5. One of the electrodes used as reference is concealed and the other used for sensing is exposed to the incoming air. In the absence of Hydrogen cyanide gas the potential difference between the two electrodes is zero, but when hydrogen cyanide gas is passed into the cell, the activity of Ag^+ ions nearer to the sensing electrode changes, there by generating a potential difference between the two electrodes. The plot between the potential vs. log of Concentration of Hydrogen cyanide gas is linear, in the concentration range 0.66–42.3 mg/m^3 with a slope nearer to 120mV and regression coefficient around 0.997. The standard deviation is 6% ($n = 4$). Minimum detectable limit is 0.66 mg/m^3 . Various concentrations of Silver dicyano complex used gave similar plots. © 1999 Elsevier Science B.V. All rights reserved.

Keywords: Electrochemical sensor; Potentiometric; Hydrogen cyanide

1. Introduction

Hydrogen cyanide gas is a well known toxic gas [1] which is generated during some organic reactions in laboratories and in electroplating processes where cyanide salts are used. Due to its toxicity persons working in such an atmosphere are liable to get affected so they should be provided with a reliable means of detecting hydrogen cyanide gas in the working environment. Normally Detector tubes are used for this purpose.

An electronic device capable of giving an alarm at the TLV of this gas is more useful. Several literature reports exist for determination of cyanide ion in solution. These are based on enzymatic [2,3], fiber-optic [4] potentiometric and amperometric methods which can be exploited for measurement of Hydrogen cyanide gas in atmosphere.

The enzymes are known for their ability to catalyze certain chemical reactions. The efficiency of catalysis is related to their activity, which in turn can be monitored with the help of an electrochemically regenerable redox species [3]. Some of the enzymes (Horseradish peroxidase, Tyrosinase) can be inhibited by cyanide ions reversibly. The

* Corresponding author. Fax: +91-751-341148.

E-mail address: drde@gwr1.dot.net.in (V. Kameswara Rao)

decrease in activity was related to the concentration of cyanide ions. Very low concentrations (ppb) of cyanide ions can be measured by this method. The enzymes are known to have a limited life time. Hence sensors based on them may not be useful for long term use.

Amperometric method of estimating cyanide in solution using silver [5,6] and gold [7,8] as anodes have been described. The principle is based on oxidation of silver or gold in the presence of cyanide ion to yield their respective complexes. Hydrogen cyanide gas in atmospheres can be found by passing it through a trap containing Sodium hydroxide solution and measuring the spontaneous anodic current at silver wire coupled to a platinum counter electrode [9]. Stetter et al. used KCl as electrolyte and gold as anode for testing their Hydrogen cyanide gas generator [10]. An amperometric method for determining Hydrogen cyanide in atmosphere using gold coated PTFE membrane and alkaline electrolyte was reported [11]. Bruckenstein described Pneumatometric method for determination of cyanide in solutions [12]. Coulometric determination of hydrogen cyanide in cigarette smoke was also reported [13]. An amperometric air-gap method for estimation of free cyanide in solution was described [14]. In this method a silver electrode was used as working electrode and calomel as reference electrode. The anodic current was found to be proportional to the concentration of cyanide in the samples.

In potentiometric method of sensing Hydrogen cyanide gas, the ion-selective electrodes and silver wire along with a solution of silver dicyano complex were used by air gap electrode method [15–17]. In this method silver wire or silver ion selective electrodes detects the changes in the Ag^+ ion activity in the electrolyte, when exposed to the Hydrogen cyanide gas [15]. Fligier et al. in their paper [16] described the response characteristics of the Silver and Silver ion selective electrodes prepared from Silver iodide and silver sulfide, towards determining hydrogen cyanide gas by an air-gap method and found that silver metal wire is best suited for measuring the Hydrogen cyanide. Even though this method is a very simple, it requires renewal of the electrolyte for each mea-

surement and thus not amenable for continuous monitoring. In this paper we present the details of a method for the continuous detection of hydrogen cyanide gas in atmosphere by using silver electrodes and an electrolyte containing Potassium silver dicyano complex, without the need to change the electrolyte. An electrochemical cell has been designed, in which a provision was made to keep the two silver electrodes separated by a distance of few millimeters and an electrolyte containing silver dicyano complex passes continuously over the electrodes with the help of a peristaltic pump. The changes in the activity of Ag^+ at the sensing electrode in the presence of Hydrogen cyanide gas results in a change in the development of potential difference between the electrodes, which is proportional to the log of concentration of Hydrogen cyanide gas.

2. Experimental

2.1. Chemicals

All reagents used were procured from E. Merck. Triple distilled water was used throughout this work. Stock solutions of cyanide were standardized by titration with silver nitrate solution using potentiometric method.

2.2. Generation of hydrogen cyanide gas

It was prepared by dynamic method by passing air through an impinger containing 30% Potassium cyanide solution in distilled water [18]. The concentration of Hydrogen cyanide generated was found by trapping it in a trap containing 0.1 M NaOH and analyzing subsequently with cyanide ion-selective electrode. Various gas concentrations were obtained by diluting this gas mixture with air.

2.3. Instrumentation

The ion-selective electrodes supplied along with model No. 901 ion-analyzer by Orion Research were used in analysis of cyanide solutions. A digital pH meter was used for measuring the

potential difference between the silver electrodes of the sensor.

2.4. Fabrication of sensor

The arrangement of the silver electrodes for sensing hydrogen cyanide gas is as shown in the Fig. 1. The sensor contains mainly an electrochemical Cell made of acrylic block of dimensions $3 \times 5 \times 3$ cm, in which the sensing and reference electrodes are located. The sensing electrode is in the form of a spiral while the reference electrode is made by folding silver wire several times. The diameter of silver wire used for both the electrodes is 0.3 mm. The volume of sensing chamber is 1.5 ml. The electrolyte was kept in a reservoir, which was passed in to the cell at a constant rate of 0.56 ml/min with the help of peristaltic pump. The electrolyte passes initially through a silver mesh of size 1000 squares per inch, so that any cyanide ions present in it during previous measurement, will get converted into silver dicyano complex. Then it passes into the sensing electrode chamber via the reference electrode, wherein it comes in contact with the incoming atmospheric air. As shown in the Fig. 1, the membrane pump creates a vacuum effect in the reservoir, which in turn is connected to the sensor chamber. Due to

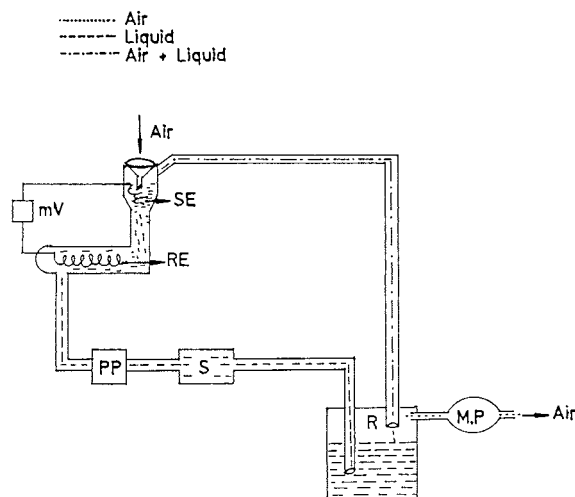


Fig. 1. Hydrogen cyanide sensor: SE, sensing electrode; RE, Reference electrode mV, milli voltmeter; PP, peristaltic pump; S, scrubber; R, reservoir, MP, membrane pump.

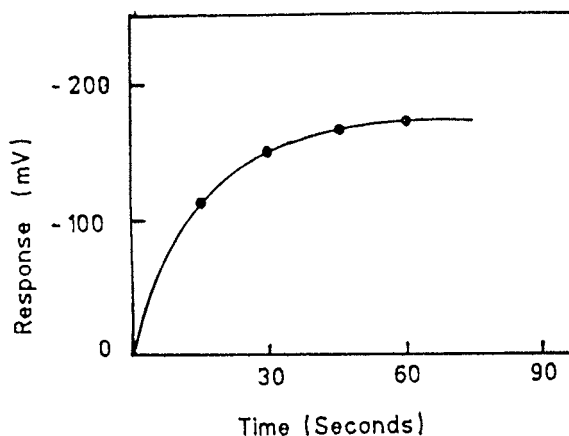


Fig. 2. Plot between response of the sensor vs. time for 6.66 mg/m^3 of HCN, concentration of Silver dicyano complex used is 0.03 mM.

this vacuum effect the air from atmosphere directly enters through the inlet situated above the sensing electrode at rate of 0.8 l/min. The air bubbles through the solution in sensor chamber. The electrolyte finally gets collected in the reservoir and the air goes out into the atmosphere.

3. Results and discussion

The plot between the response of the sensor with time is shown in Fig. 2. The response time for reaching 90% of the response value is around 35 s. The plots between response of the sensor and Hydrogen cyanide gas concentration, at various concentrations of silver dicyano complex in the electrolyte is shown in the Fig. 3. As described earlier, the electrochemical cell contains a pair of silver electrodes over which a silver dicyano complex solution is circulated with the help of a peristaltic pump. The silver electrodes responds to the concentration of the silver ions present in the solution. Since the electrodes are in contact with the same solution and that both the electrodes are made of same metal, the potential difference between them is zero. The potential at each electrode is given by [16,17]

$$E = E^0 + s \log[\text{Ag}^+] \quad (1)$$

where s is the nernstian slope. The silver ions present in the solution are due to the following equilibrium



and the potential at the electrode in terms of CN^- ion concentration is [VR1]

$$E = E^0 - 2s \log[\text{CN}^-] \quad (3)$$

When the solution surrounding the sensing electrode is effected by passing the hydrogen cyanide gas, the equilibrium as given in Eq. (2) is disturbed and concentration of the silver ions diminishes [15]. Hence a potential difference arises between the electrodes. Fig. 3 shows various plots between the potential difference between the electrodes and $\log(\text{HCN})$ at various concentrations of silver dicyano complex. The concentrations of silver dicyano complex used were 0.03, 0.3 and 3.0 mM. The regression coefficients for these plots at these concentrations of the complex are 0.996, 0.997 and 0.998 respectively and the slope values are 119.2, 120.2 and 124.6 mV/decade respectively. These slope values are very close to the expected double nernsteins slope, i.e. 118.16 mV/decade.

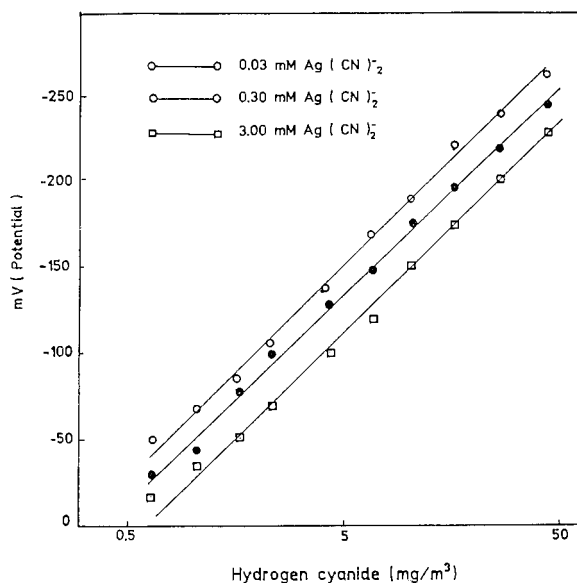


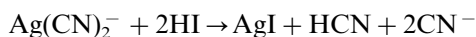
Fig. 3. Plot of response of sensor vs. concentration of hydrogen cyanide gas.

It may be noted from Fig. 3 that, the response for a given concentration of hydrogen cyanide gas is high when a low concentration of silver dicyano complex is used. This is because the changes brought in Silver ion concentration are high when low concentration (0.03 mM) of silver dicyano complex is used. When experiments were conducted at much lower concentrations of the complex, the reproducibility was found to be poor.

The plot between $\log(\text{HCN})$ and response of the sensor was found to be linear from 0.66 to 42.3 mg/m^3 . Experiments are limited to this concentration range since our interest is to develop a sensor for detecting at its TLV only. At higher concentrations (40 mg/m^3) the recovery time is high, like of the order of 10 min. The standard deviation in the measurement of 6.66 mg/m^3 by using 0.3 mM of the complex used is 6% for four assays. This is very nearer to the value of 5% reported for polyaniline based sensor [19].

The continuous monitoring of Hydrogen cyanide is possible because of the silver mesh scrubber used. The cyanide ions accumulated in the sensor chamber initially passes into the reservoir. Then it was passed through a silver mesh of size 1000 squares per inch folded and kept in a tube, so that all the free cyanide ions present in the solution get converted into dicyano complex. This electrolyte free from cyanide ions passes into the electrochemical cell. However the concentration of dicyano complex in the electrolyte does not vary much since the amount of cyanide ions collected during monitoring is very low and the volume of electrolyte taken in the reservoir is around 100 ml.

The potential interferences for this sensor are Hydrogensulfide and Hydroiodicacid due to the following reactions



The interference from these gases is not only because of the above reactions with silver dicyano complex but also because Silver sulfide and silver iodide precipitates will form a layer on the silver metal wire and change its function from a silver electrode to that of $\text{Ag}/\text{Ag}_2\text{S}$ and Ag/AgI elec-

trodes. These electrodes have different sensing characteristics for cyanide ions [16]. Once the sensor is exposed to these gases, it took a lot of time to recover. This device is not effected by 100 ppm Hydrochloric acid.

4. Conclusion

A method of detecting HCN gas in the atmosphere continuously by using a pair of silver electrodes and using a silver dicyano complex solution is presented. Unlike the air-gap cell method, the replenishment of the solution between measurements is not needed. It was made possible because of the silver scrubber used which will be able to convert the cyanide ions present in the solution into dicyano complex, there by keeping the solution free of cyanide ions before the next measurement is taken. The main interferences for this sensor are Hydrogen sulfide and Hydroiodic acid.

Acknowledgements

The authors are thankful to Dr R.V. Swamy Director D.R.D.E for his encouragement and giving permission to publish this work.

References

- [1] M. Sittig, *Hand Book of Toxic and Hazardous Chemicals and Carcinogens*, Noyes, London, 1985.
- [2] M.H. Smit, A.E.G. Cass, *Anal. Chem.* 62 (1990) 2429.
- [3] M.H. Smit, G.A. Rechnitz, *Anal. Chem.* 65 (1993) 380.
- [4] M.K. Freeman, L.G. Bachas, *Anal. Chim. Acta.* 241 (1990) 119.
- [5] B. Pihlar, L. Kosta, B. Hristovski, *Talanta* 26 (1979) 805.
- [6] G.W. Miller, L.F. Long, G.M. George, W.L. Skies, *Anal. Chem.* 36 (1964) 980.
- [7] D.B. Easty, W.J. Blaedal, L. Anderson, *Anal. Chem.* 43 (1971) 509.
- [8] J.A. McClosky, *Anal. Chem.* 33 (1961) 1842.
- [9] B. Baker, J.D. Johnson, *Anal. Chem.* 27 (1955) 1306.
- [10] Z. Tocksteinova, F. Opekar, *Talanta* 33 (1986) 688.
- [11] V. Kameswara Rao, S. Suresh, N.B.S.N. Rao, P. Rajaram, *Bull. Electrochem.* 13 (1997) 327.
- [12] F. Opekar, S. Bruckenstein, *Anal. Chim. Acta.* 169 (1985) 407.
- [13] C.H. Sloan, *Beitr. Tabakforschung. Int.* 10 (1980) 1064.
- [14] A. Nagy, G. Nagy, *Anal. Chim. Acta.* 283 (1993) 795.
- [15] J. Fligier, P. Czichon, Z. Gregorowie, *Anal. Chim. Acta.* 118 (1980) 145.
- [16] J. Fligier, M. Gtatzki, G. Nagy, E. Pungor, *Anal. Chim. Acta.* 134 (1982) 263.
- [17] R. Kalvoda (Ed.), *Electroanalytical Methods in Chemical and Environmental Analysis*, 1987, p. 101.
- [18] G.O. Nelson, *Gas Mixtures Preparation and Control*, Lewis, 1992, p. 200.
- [19] J. Langmaier, J. Janata, *Anal. Chem.* 64 (1992) 523.

Determination of total proteins: a study of reaction between quinones and proteins

D.A.M. Zaia^{a,*}, W.A. Verri Jr.^a, C.T.B.V. Zaia^b

^a Departamento de Química-CCE, Universidade Estadual de Londrina, 86051-990, Londrina, PR, Brazil

^b Departamento de Ciências Fisiológicas, Universidade Estadual de Londrina, 86051-990, Londrina, PR, Brazil

Received 18 August 1998; received in revised form 30 November 1998; accepted 3 December 1998

Abstract

A previous study was undertaken to test the reaction of several quinones (*p*-benzoquinone; 2,5-dichloro and 2,6-dichloro *p*-benzoquinone; tetrachloro-*p*-benzoquinone; tetrachloro-*o*-benzoquinone; 2,5-dichloro-3,6-dihydroxy-*p*-benzoquinone; benz[*a*]anthracene-7,12-dione) with bovine serum albumin (BSA). From this study, we have devised a spectrophotometric method for determination of total proteins. The quinone, tetrachloro-*p*-benzoquinone (*p*-chloranil), showed the best result. The product of reaction between proteins and *p*-chloranil absorbed at 360 nm and Beer's law was followed up to 200 $\mu\text{g ml}^{-1}$ of BSA. The product of reaction of BSA/*p*-chloranil was stable for 30 min, after that the absorbance increased 16% and kept stable for 24 h. The *p*-chloranil method showed a limit of detection (1.25 $\mu\text{g ml}^{-1}$) lower than the biuret method (52.0 $\mu\text{g ml}^{-1}$) or *p*-benzoquinone (PBQ) method (2.6–4.0 $\mu\text{g ml}^{-1}$). The method was applied to spectrophotometric determination of total proteins in blood plasma; the results were compared with the biuret method that is widely used in clinical analysis. © 1999 Elsevier Science B.V. All rights reserved.

Keywords: Spectrophotometric determination; Total proteins; Quinones; Proteins

1. Introduction

Determination of total proteins is important in clinical investigation, in food science, food technology, and in several research areas. For determination of total proteins five methods [1–5] are widely used, however as pointed out by Zaia et al. [6], those methods are not the final word in protein determination. In previous papers [7–10],

p-benzoquinone (PBQ) was used for spectrophotometric determination of total proteins in different media and it showed several advantages when compared with other methods; another quinone, *p*-chloranil, was also used for determination of specific proteins [11]. However, both methods require a heating step as long as 20 min, 100°C for PBQ method and 65°C for *p*-chloranil method. The *p*-chloranil method [11] was tested only for some purified proteins and the limit of detection was not so good as that of other methods. A spectrophotometric investigation was undertaken

* Corresponding author. Fax: +55-43-3284440.

E-mail address: zaiazaia@sercomtel.com.br (D.A.M. Zaia)

with several quinones (*p*-benzoquinone; 2,5-dichloro and 2,6-dichloro *p*-benzoquinone; tetrachloro-*p*-benzoquinone; tetrachloro-*o*-benzoquinone; 2,5-dichloro-3,6-dihydroxy-*p*-benzoquinone; benz[a]anthracene-7,12-dione) to eliminate the length and the high temperature of the heating step and to improve the limit of detection for determination of total proteins. The *p*-chloranil showed the best results among the other quinones. In this work, we describe a new spectrophotometric method using *p*-chloranil for determination of total proteins. With this method, a lower detection limit was reached, under lower heating time and temperature. The *p*-chloranil method was applied to determine total proteins in blood plasma of rats and the results were compared with those of the biuret method.

2. Experimental

2.1. Materials and reagents

Ultraviolet and visible spectrophotometry were carried out on spectrophotometers DMS-80 Varian and Shimadzu UV-1203. All reagents were of analytical reagent grade.

2.1.1. Bovine serum albumin (BSA)

A 6.0-g l⁻¹ BSA (Sigma) solution was prepared with distilled water and used as standard in all assays.

2.1.2. Tetrachloro-*p*-benzoquinone-(*p*-chloranil)

A 10-mM *p*-chloranil (Sigma) solution was prepared with DMSO and used in all assays.

2.2. Methods

2.2.1. Blood plasma

Blood plasma was obtained as described somewhere else [9].

2.2.2. Biuret method

The biuret method was used as described by Gornall et al. [1].

2.2.3. Standard curve

By dilution of the 6.0 g l⁻¹ of standard solution of BSA, a calibration curve was constructed using the following concentrations: 0.0, 30, 60, 90, and 120 µg ml⁻¹, 1 ml of ethanol was added to the tubes, and the volumes were adjusted to 1.8 ml with 0.1 M borate buffer pH 8.0. To each test tube, 200 µl of 10 mM *p*-chloranil was added; the tubes were shaken, incubated at 37°C for 5 min and cooled to room temperature. The absorbance at 360 nm was read against a suitable blank.

2.2.4. Assay with plasma

A 10-µl aliquot of blood plasma of rat was transferred to a test tube, 1 ml of ethanol was added, the volume was adjusted to 1.8 ml with 0.1 M borate buffer pH 8.0, and 200 µl of 10 mM *p*-chloranil was added; the tube was shaken and incubated at 37°C for 5 min. The tube was cooled to room temperature and the absorbance at 360 nm was read against the blank.

3. Results and discussion

An spectrophotometric investigation of the reaction between *p*-benzoquinone and BSA at 37°C in the pH range from 3.0 to 9.0 was carried out and the best specific absorbance was obtained with borate buffer pH 8.0. After that, using this buffer (borate pH 8.0), several quinones (Table 1) were reacted with BSA, and the product of reaction between *p*-chloranil and BSA showed the best specific absorbance. The reaction between *p*-chloranil and BSA performed in the pH range 7.5–9.0, confirmed that pH 8.0 with borate buffer was also optimal. Under these reaction conditions, and 10 min of heating at 37°C, the effect of *p*-chloranil concentration (from 0.20 to 4.00 mM) on the absorbance (360 nm) of the product of reaction of *p*-chloranil with BSA (75 µg ml⁻¹) was studied. The concentration of 1.0 mM of *p*-chloranil was chosen because its spectrum showed better shape than the other concentrations. We also tested the effect of the heating time from 2 to 40 min

at 37°C on the absorbance of the product of reaction *p*-chloranil (1.0 mM) with BSA (75 µg ml⁻¹), and the absorbance did not change after 5 min of heating. The band at 360 nm obeyed Beer's law up to 200 µg ml⁻¹ of BSA.

Time elapsed after heating was not critical for the measurement of proteins with *p*-chloranil, since the band of absorption at 360 nm of

the product of reaction was stable at the first 30 min. The absorbance increased 16% from 30 to 60 min and then the product of reaction was stable again up to 24 h. Therefore, the readings of the absorbances should be taken within the first 30 min after heating or 1 h after that.

The effect of selected potential interfering compounds on protein assay was studied. Potassium nitrate (30 mM), EDTA (100 mg l⁻¹), mixture of palmitic and oleic acids (100 mg l⁻¹), and sodium chloride (30 mM) did not interfere with *p*-chloranil method, but the assay showed to be susceptible to potassium nitrate (300 mM), ascorbic acid (100 mg l⁻¹), mixture of palmitic and oleic acid (1000 mg l⁻¹), triglycerides (10 mg l⁻¹), sodium chloride (300 mM), glucose (30 mM), and heparin (25 IU ml⁻¹).

In the straight line equation relating absorbance (*Y*) to BSA concentration (*X*), $Y = 8.00 \times 10^{-3}X + 4.80 \times 10^{-3}$ ($n = 8$, correlation coefficient, $r = 0.9923$, from 0 to 120 µg ml⁻¹ of BSA) for the *p*-chloranil method and $Y = 1.93 \times 10^{-4}X + 1.45 \times 10^{-2}$ ($n = 8$, correlation coefficient, $r = 0.9960$, from 0 to 3,000 µg ml⁻¹ of BSA) for the biuret method. The larger slope obtained for the *p*-chloranil method indicates its greater sensitivity. The detection limit with chloranil method (1.25 µg ml⁻¹) was about 40 times lower than that of the biuret method (52.0 µg ml⁻¹), about two to three times lower than PBQ method [8,9], and about two times larger than Lowry method [8].

The method using *p*-chloranil was applied to spectrophotometric determination of total proteins in blood plasma of rats and compared with the biuret method [1]. The results obtained were 65.3 ± 3.8 g l⁻¹ ($n = 6$) and 68.2 ± 1.3 g l⁻¹ ($n = 5$), respectively.

The data presented here show that the *p*-chloranil method can be used for routine analysis of total proteins.

Table 1

Maximum absorbance and specific absorbance following quinones and bovine serum albumin (BSA) reaction^a

Quinone (mM)	Maximum absorbance (nm)	Specific absorbance (cm ² µg ⁻¹ 10 ³)
<i>p</i> -Benzoquinone (1.00)	352	1.54
<i>p</i> -Benzoquinone (4.50)	353	2.42
2,5-Dichoro- <i>p</i> -benzoquinone (0.25)	355	0.90
2,5-Dichoro- <i>p</i> -benzoquinone (0.63)	363; 500	1.89; 0.23
2,5-Dichoro- <i>p</i> -benzoquinone (1.00)	356	1.47
2,5-Dichoro- <i>p</i> -benzoquinone (1.25)	370; 493	1.40; 0.25
2,6-Dichoro- <i>p</i> -benzoquinone (0.50)	359; 543	2.00; 0.17
2,6-Dichoro- <i>p</i> -benzoquinone (1.00)	359	1.74
2,6-Dichoro- <i>p</i> -benzoquinone (1.25)	363; 544	1.83; 0.32
Tetrachloro- <i>p</i> -benzoquinone (1.00)	360	3.10
Tetrachloro- <i>o</i> -benzoquinone (2.50)	340; 559	0.61; 0.11
Chloranilic acid (1.00) ^b	–	–
Chloranilic acid (5.00)	–	–
Benz[a]anthracene-7,12-dione (1.00)	425	0.74

^a The samples were heated at 37°C for 10 min, 0.1 M borate buffer pH 8.0 and 1.0 ml of ethanol in a total volume of 2.0 ml.

^b 2,5-Dichoro-3,6-dihydroxy-*p*-benzoquinone.

Acknowledgements

W.A.V. Jr. and C.T.B.V.Z. were recipients of

fellowships from CNPq/PIBIC and CNPq, respectively. This project was supported by CPG/UEL-330.734/95.

References

- [1] A.G. Gornall, C.J. Bardawill, M.M. David, *J. Biol. Chem.* 177 (1949) 751.
- [2] O.H. Lowry, N.J. Rosebrough, A.L. Farr, R.J. Randall, *J. Biol. Chem.* 193 (1951) 265.
- [3] M.M. Bradford, *Anal. Biochem.* 72 (1976) 248.
- [4] P.K. Smith, R.I. Krohn, G.T. Hermanson, A.K. Mallia, F.H. Gartner, M.D. Provenzano, E.K. Fujimoto, N.M. Goeke, B.J. Olson, D.C. Klenk, *Anal. Biochem.* 150 (1985) 76.
- [5] C.M. Stoscheck, General methods for handling proteins and enzymes: quantitation of protein, in: M.P. Deutscher (Ed.), *Methods in Enzymology: Guide to Protein Purification*, Academic Press, New York, 1990, p. 40.
- [6] D.A.M. Zaia, C.T.B.V. Zaia, J. Lichtig, *Química Nova* 21 (1998) 787.
- [7] W.J. Barreto, M. de Aquino, D.A.M. Zaia, *Anal. Letters* 23 (1990) 1279.
- [8] D.A.M. Zaia, S.R. Rockenbach, M.M. Obara, W.J. Barreto, S. Arizawa, R. Curi, J. Lichtig, *Anal. Letters* 25 (1992) 1225.
- [9] D.A.M. Zaia, M.M. Obara, S.R. Rockenbach, W.J. Barreto, L.C.J. Gaziri, C.T.B.V. Zaia, J. Lichtig, *Braz. J. Med. Biol. Res.* 25 (1992) 549.
- [10] D.A.M. Zaia, W.J. Barreto, N.J. Santos, A.S. Endo, *Anal. Chimica Acta* 277 (1993) 89.
- [11] S.A. Rahim, T.S. Al-Ghabsha, *Egypt. J. Chem.* 20 (1977) 627.

Fluorescence energy transfer between Acridine Orange and Safranin T and its application in the determination of DNA

Ying Cao, Xiwen He *, Zhi Gao, Lu Peng

Department of Chemistry, Nankai University, Tianjin 300071, People's Republic of China

Received 26 August 1998; received in revised form 30 November 1998; accepted 3 December 1998

Abstract

The fluorescence energy transfer (FET) between Acridine Orange and Safranin T, two intercalators of DNA, was studied in this paper. The FET efficiency between Acridine Orange and Safranin T is higher and the critical distance, R_0 , is longer in the intercalated state than in the free one. A new method for the determination of calf thymus DNA (ctDNA) was presented. The linear range of the calibration curve is $(0 \sim 1.1) \times 10^{-5} \text{ mol l}^{-1}$ in bases for ctDNA, and the limit of detection is $2.6 \times 10^{-7} \text{ mol l}^{-1}$. © 1999 Elsevier Science B.V. All rights reserved.

Keywords: Spectra probe; DNA; Fluorescence energy transfer; Acridine Orange; Safranin T

1. Introduction

Fluorescent reagents have been widely used as DNA probes, by which many methods have been developed for the determination of trace amount of DNA. Different probes react with the DNA in different ways. Among these methods, the fluorescence intensity of some probes is enhanced by DNA, such as ethidium bromide [1], 4',6-diamidino-2-phenylindole (DAPI) [2], Hoechst 33258 [3], etc., and the fluorescence of some other probes is quenched by DNA, such as (photochemical fluorescence probes) 9,10-anthraquinone-2-sulfonate [4] and Vitamin K₃ [5], etc. Fluorescence

energy transfer (FET) (or fluorescence resonance energy transfer), in which process the emission spectrum of the donor is absorbed by the acceptor [6], is a new method for the study of biological macromolecules [7,8]. It has been reported that DNA, a biopolymer featured by hydrophilic groups (the phosphate skeleton) and hydrophobic groups (the base pairs), can promote the electronic transfer by assembling the donor and the acceptor in the double helix of DNA [9]. In this paper, we studied the fluorescence energy transfer between two intercalators of DNA—Acridine Orange and Safranin T. The FET efficiency is enhanced by DNA, which was developed as a new probe of DNA. The influences of pH, ion strength and foreign substances on the FET were also investigated. A new method was subsequently pre-

* Corresponding author. Fax: +86-22-23502458.

E-mail address: chemczl@sun.nankai.edu.cn (X. He)

sented for the determination of trace amount of DNA, which is different from the above-mentioned methods with single fluorescence reagents as probes. The new method is featured by its high sensitivity and low detection limit.

2. Experimental

2.1. Apparatus

The fluorescence was measured with a Shimadzu RF-540 spectrofluorimeter (Kyoto, Japan). The electronic absorption spectra were measured with a Shimadzu UV-240 spectrophotometer (Kyoto, Japan). The pH values of the solutions were determined with a PHS-2 pH meter (Shanghai, People's Republic of China).

2.2. Reagents

A stock solution of DNA was prepared by dissolving calf thymus DNA (ctDNA) (Sino-American Biotechnology Engineering) into water and stored at 4°C. The concentration of DNA was determined by the absorbance at 260 nm ($\epsilon = 6600 \text{ l mol}^{-1} \text{ cm}^{-1}$, i.e. the concentrations of ctDNA are reported in bases) [10]. Stock solutions of Acridine Orange (AO) (microscope reagent; Fluka) and Safranin T (ST) (biological dye; Shanghai No.3 Chemical Reagent Plant) were prepared by dissolving the reagents into water. The working solutions were prepared by diluting the stock solutions with water. Tris-HCl was used as the buffer solution (pH 7.4). All the chemicals used were of biochemical or analytical reagent grade. The water used in the experiments was doubly deionized.

2.3. Procedure

Certain volumes of AO and ST working solutions were transferred to a 10-ml standard flask. Certain volumes of buffer solution were added and the solution mixed, and then certain volumes of ctDNA were added and mixed. After 10 min, the fluorescence spectrum and the fluorescence intensity were measured by spectrofluorimeter (ex-

citation wavelength, 491 nm; emission wavelength, 519 nm).

3. Results and discussion

3.1. Fluorescence energy transfer between AO and ST

Both AO and ST can intercalate into DNA [11,12]. The binding constants are $2.0 \times 10^6 \text{ l mol}^{-1}$ for AO and $6.1 \times 10^4 \text{ l mol}^{-1}$ for ST. The saturation numbers are 2.0 for AO and 6.7 for ST. As shown in Fig. 1, the emission spectrum of AO overlaps with the electronic absorption spectrum of ST either in the free or in the intercalated state. According to the Förster mechanism [6], fluorescence energy transfer can occur between AO (the donor) and ST (the acceptor).

3.2. Effect of ST on the fluorescence of AO

The fluorescence of AO can be quenched by ST in the absence of DNA. But, when a moderate amount of DNA was added to the AO-ST system, the quenching efficiency increased greatly (Fig. 2). The Stern-Volmer quenching constant changed from 0.94×10^6 to $1.75 \times 10^6 \text{ l mol}^{-1}$, respectively. For the AO-ST-DNA system, there are two possible reasons for the diminution of AO fluorescence upon the addition of ST. One is the FET between the intercalated AO and ST, and the other is the exclusion of the intercalated AO from the duplex DNA. However, we found that the electronic absorption spectrum of AO-DNA system almost did not change with the addition of ST in the experimental concentration range. This indicates that the intercalated AO is not exchanged from DNA by ST, although competitive intercalation may also occur. Therefore, the fluorescence quenching of the AO-DNA system is attributed to the FET between the intercalated AO and ST, instead of the exclusion of AO from the duplex DNA.

Due to the FET between AO and ST as already stated, the fluorescence of AO can be quenched by ST either with or without DNA. Besides, we found that DNA also quenches the fluorescence

of AO without ST. When the concentration of DNA is low, the quenching efficiency increases with the concentration of DNA. But when the concentration of DNA is higher, the quenching efficiency reaches a limit (Fig. 3). There is a poor

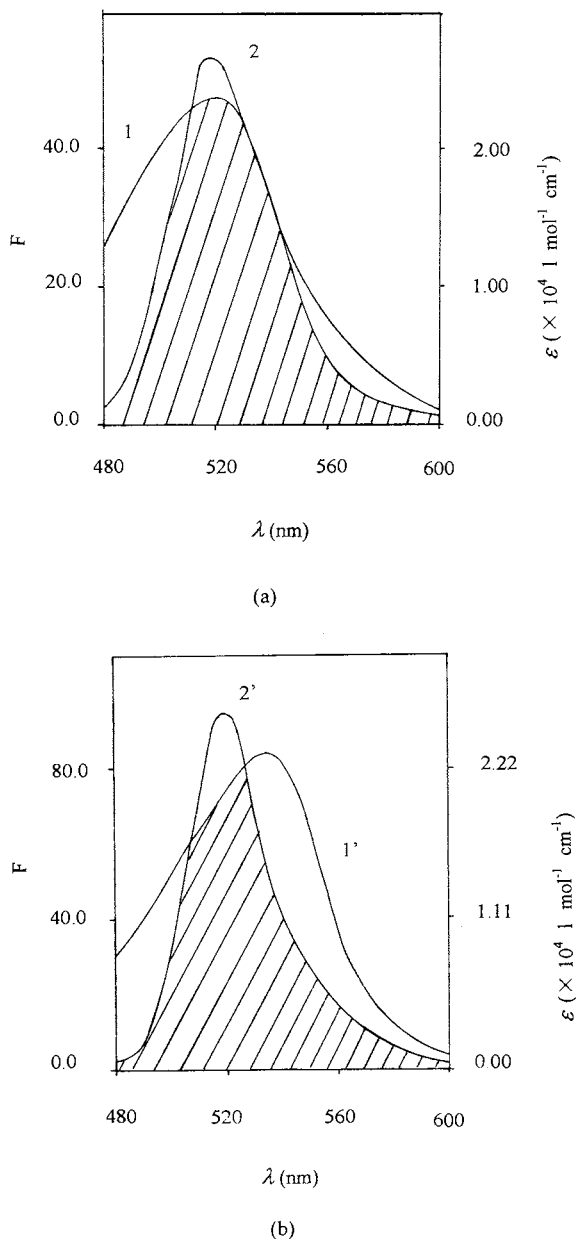


Fig. 1. Emission spectra of AO and the electronic absorption spectra of ST without (a) and with (b) DNA. (1,1') Electronic absorption spectra of AO, (2,2') emission spectra of ST.

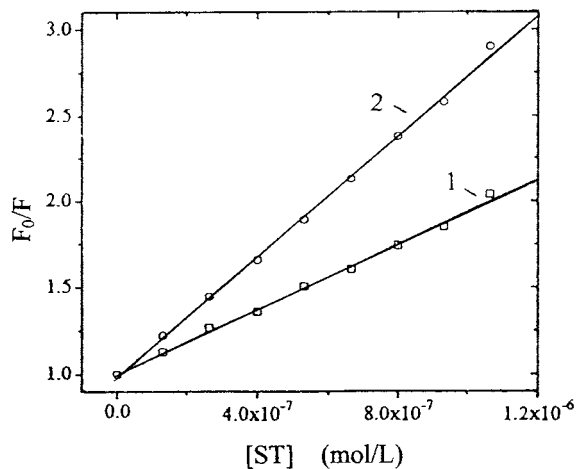


Fig. 2. Quenching effect of ST on the fluorescence of AO. (1) AO-ST system; (2) AO-ST-DNA system, $[DNA] = 1.64 \times 10^{-5} \text{ mol l}^{-1}$.

linear relationship between the concentration of DNA and the ratio of fluorescence intensities F_0/F (where F and F_0 are the fluorescence intensities of the systems with and without DNA, respectively), which is not convenient for AO itself as a DNA probe for quantitative determination of DNA, in spite of its strong fluorescence. By comparison, when ST coexists with AO, the calibration curve for the determination of DNA has a wide linear range (Fig. 3), which provides a good condition for the determination of trace amounts of DNA in solution.

3.3. Effect of DNA on the FET between AO and ST

The influence of DNA on the FET between AO and ST is complex, as shown in Fig. 4. The FET efficiency reaches a maximum at a moderate concentrations of DNA. The probable reasons are that when the concentration of DNA is low, only some of the AO and ST molecules intercalate into the DNA, and the others are still in their free states in which the fluorescence quenching is not effective; if the concentration of DNA is too high, the intercalated AO and ST will be kept apart at a much longer distance, which also decreases the FET efficiency.

According to the Förster mechanism [6], the critical distance (R_0) of FET between AO and ST can be calculated by the following equation:

$$R_0^6 = \frac{8.8 \times 10^{-25} K^2 \Phi_D J(\lambda)}{n^4} \quad (1)$$

where K is the orientation factor, $J(\lambda)$ is the spectral overlap intergral of the fluorescence spec-

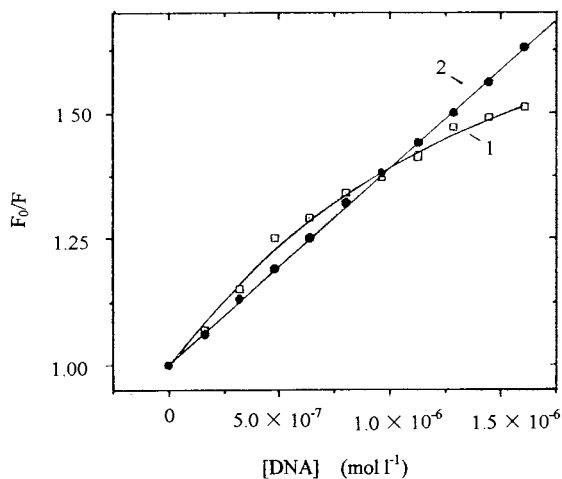


Fig. 3. Comparison of the fluorescence quenching curves of the AO-DNA and AO-ST-DNA systems. $[AO] = 0.5 \times 10^{-6} \text{ mol l}^{-1}$, $[ST] = 2.5 \times 10^{-6} \text{ mol l}^{-1}$. (1) AO-DNA, (2) AO-ST-DNA.

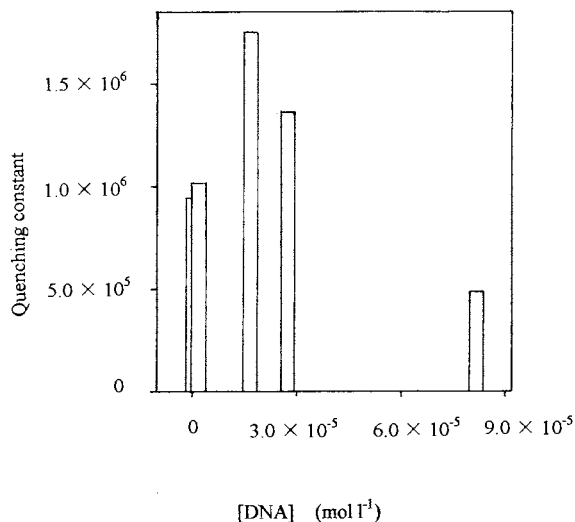


Fig. 4. Effect of DNA on the Stern-Volmer quenching constant of the AO-ST system. $[AO] = 3.67 \times 10^{-6} \text{ mol l}^{-1}$.

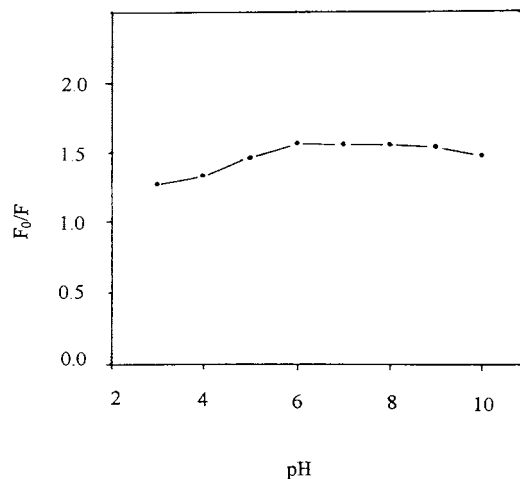


Fig. 5. Effect of pH on F_0/F of the AO-ST-DNA system. $[AO] = 0.5 \times 10^{-6} \text{ mol l}^{-1}$, $[ST] = 2.5 \times 10^{-6} \text{ mol l}^{-1}$, $[DNA] = 1.21 \times 10^{-6} \text{ mol l}^{-1}$.

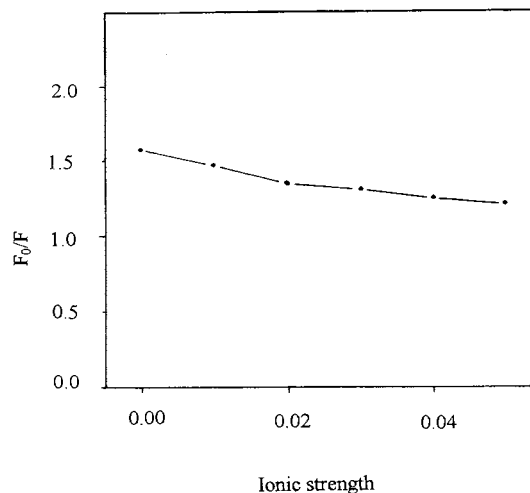


Fig. 6. Effect of ionic strength on F_0/F of the AO-ST-DNA system. $[AO] = 0.5 \times 10^{-6} \text{ mol l}^{-1}$, $[ST] = 2.5 \times 10^{-6} \text{ mol l}^{-1}$, $[DNA] = 1.21 \times 10^{-6} \text{ mol l}^{-1}$.

trum of AO and the electronic absorption spectrum of ST, n is the refractory index of the medium, and Φ_D is the fluorescence quantum yield for AO (intercalated into DNA or not) in the absence of ST. The fluorescence quantum yields were determined to be 0.67 for the intercalated AO and 0.22 for the free AO, by the method of comparison with Acridine Yellow [13]. The

overlap integrals for the systems with and without DNA were calculated to be 1.41×10^{-13} and $1.31 \times 10^{-13} \text{ l mol}^{-1} \text{ cm}^{-3}$, respectively. According to Eq. (1), the critical distances of the FET between AO and ST were calculated to be 5.17 and 4.19 nm for the systems with and without DNA. The net increase of R_0 is 0.98 nm, about the distance of three base pairs in the double-helix DNA.

3.4. Optimization of experimental conditions

All of the concentrations of AO, ST and DNA influence the FET efficiency of the system. If the concentration ratio of AO to ST is too low, the sensitivity for the detection of DNA by the AO–ST system will be decreased. On the contrary, the linear range will be narrow if the ratio is too high. From the balance between the sensitivity and the linear range, the optimum concentrations were chosen to be $0.5 \times 10^{-6} \text{ mol l}^{-1}$ for AO and $2.5 \times 10^{-6} \text{ mol l}^{-1}$ for ST.

The effect of pH on the FET between AO and ST was investigated as shown in Fig. 5. The value of F_0/F almost does not change in the range from

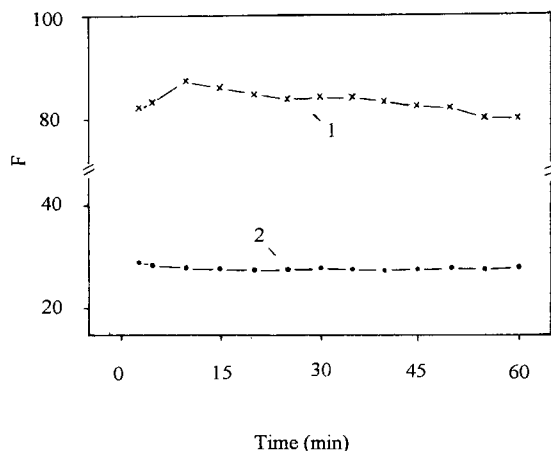


Fig. 7. Changes of the fluorescence intensities with time for the AO–ST and AO–ST–DNA systems. $[\text{AO}] = 0.5 \times 10^{-6} \text{ mol l}^{-1}$, $[\text{ST}] = 2.5 \times 10^{-6} \text{ mol l}^{-1}$, $[\text{DNA}] = 1.21 \times 10^{-6} \text{ mol l}^{-1}$. (1) AO–ST, (2) AO–ST–DNA.

Table 1
Tolerance of foreign substances^a

Foreign substances	Concentration (mol l ⁻¹)	Change of fluorescence intensity (%)
Bovine serum albumin	2.0×10^7	+7.7
Human serum albumin	5.0×10^6	+6.9
Adenine	4.0×10^5	-2.7
Guanine	0.9×10^5	-5.5
Cytosine	4.0×10^5	-3.1
Thymine	4.0×10^5	-3.1
Heparin	9.96×10^{2b}	-4.2
HPO ₄ ²⁻	3.0×10^3	+6.3
Ca(II) chloride	4.0×10^5	+9.7
Mg(II) chloride	2.0×10^5	+7.4
Al(III) sulfate	6.0×10^5	+2.5
Zn(II) chloride	1.0×10^5	+8.5
Fe(II) sulfate	1.0×10^5	+7.8
Fe(III) sulfate	6.0×10^5	2.4
Co(II) nitrate	0.8×10^5	+9.9
Ni(II) nitrate	0.2×10^5	+7.8
Cu(II) nitrate	2.0×10^5	+8.5
Mn(II) nitrate	1.2×10^5	+7.7
Pb(II) nitrate	0.8×10^5	+7.9
Cd(II) chloride	0.4×10^5	+7.6

^a $[\text{AO}] = 0.5 \times 10^{-6} \text{ mol l}^{-1}$, $[\text{ST}] = 2.5 \times 10^{-6} \text{ mol l}^{-1}$, $[\text{DNA}] = 4.86 \times 10^{-6} \text{ mol l}^{-1}$.

^b In mg ml⁻¹.

pH 6.0 to 8.0. So pH 7.4 was chosen as the optimal condition.

Ionic strength of the media has a great influence on the fluorescence quenching efficiency of the AO–ST–DNA system. The higher the ionic strength, the lower is the fluorescence quenching efficiency (Fig. 6). The reason is that high ionic strength weakens the intercalations of AO and ST into DNA. Therefore, a fixed amount of buffer solution was added into the system to keep a constant ionic strength.

After AO and ST are well mixed, the fluorescence is quenched rapidly. In the absence of DNA, the fluorescence intensity of the AO–ST system descends with the time if it is not protected from light. However, there is only little change for the AO–ST–DNA system (Fig. 7). The fluorescence intensity was measured 10 min after the reaction solutions were mixed.

Table 2

Analytical results of the synthetic samples ($n = 5$)^a

Number	Theoretical [DNA] (mol l ⁻¹)	Coexistent substances	Determined [DNA] (mol l ⁻¹)	Recovery (%)	RSD (%)
1 ^b	3.61×10^{-6}	A, T, C, G, HPO ₄ ²⁻	3.76×10^{-6}	98.9~110	4.5
2 ^c	3.61×10^{-6}	Ca(II), Mg(II), Al(III), BSA	3.49×10^{-6}	94.5~101	2.7

^a [AO] = 0.5×10^{-6} mol l⁻¹, [ST] = 2.5×10^{-6} mol l⁻¹.^b The concentrations of the foreign substances are [adenine] = 1.00×10^{-5} mol l⁻¹, [thymine] = 1.00×10^{-5} mol l⁻¹, [cytosine] = 1.00×10^{-5} mol l⁻¹, [guanine] = 0.40×10^{-5} mol l⁻¹ and [HPO₄²⁻] = 2.00×10^{-5} mol l⁻¹.^c The concentrations of the foreign substances are [Ca(II)] = 0.50×10^{-5} mol l⁻¹, [Mg(II)] = 0.50×10^{-5} mol l⁻¹, [Al(III)] = 0.50×10^{-6} mol l⁻¹ and [BSA] = 0.50×10^{-8} mol l⁻¹.

3.5. Tolerance of foreign substances

The interference of some foreign substances was tested at the optimal conditions. The results are listed in Table 1. As can be seen from the table, bovine serum albumin (BSA) and human serum albumin (HAS) severely interfere with the determination of DNA, and HPO₄²⁻ can be permitted to be as high as about 600 times of the concentration of DNA to be determined. Most metal ions, except Fe(III), increase the fluorescence intensity of the system. In other words, the quenching effect of ST–DNA on the fluorescence of AO is prevented by these metal ions, which may be caused by the competition of these metal ions with AO and ST in combining with DNA. BSA and HSA also prevent the quenching effect of ST–DNA on the fluorescence of AO. Actually, when BSA or HSA exist in the AO–ST–DNA system, they also combine with AO and ST, only part of the AO and ST intercalate into the DNA, and the quenching effect of BSA and HSA on the fluorescence of AO–ST is weaker than that of DNA. The interference of adenine, guanine, cytosine and thymine is positive. These bases are the constituents of DNA. We can deduce that the bases act in a similar way to DNA in quenching the fluorescence of the AO–ST system. We are giving here a simple explanation of the mechanisms of the interference. Further study will be needed for an explicit explanation.

3.6. Calibration curve

According to the cited conditions, the calibra-

tion curve for the determination of DNA was constructed. The linear range is $0 \sim 1.1 \times 10^{-5}$ mol l⁻¹ in bases for ctDNA. The regression equation is

$$F_0/F = 1.002 + 3.95 \times 10^5 c \quad (r = 0.9992) \quad (2)$$

where c is the concentration of ctDNA in mol l⁻¹. The limit of detection is 2.6×10^{-7} mol l⁻¹ for ctDNA ($n = 10$) by the 3σ method.

3.7. Analysis of synthetic samples

Synthetic samples were analyzed with the method presented (Table 2). The recoveries of the concentrations of ctDNA are satisfactory.

Acknowledgements

This project was supported by the National Natural Science Foundation of China.

References

- [1] W.O. Harriman, M. Wabl, *Anal. Biochem.* 228 (1995) 336.
- [2] P.D. Lipets, D.E. Brash, L.B. Joseph, H.D. Jewett, D.R. Lisle, L.E. Lantry, R.W. Hart, R.E. Stephens, *Anal. Biochem.* 121 (1982) 339.
- [3] B.C. Hyman, T.W. James, *Anal. Biochem.* 131 (1983) 205.
- [4] W.-Y. Li, X.-Q. Guo, J.-G. Xu, Q.-Z. Zhu, Y.-B. Zhao, *Anal. Chim. Acta* 340 (1997) 291.
- [5] W.-Y. Li, J.-G. Xu, X.-Q. Guo, Q.-Z. Zhu, Y.-B. Zhao, *Anal. Lett.* 30 (1997) 245.

- [6] G.-Z. Chen, X.-Z. Huang, Z.-Z. Zheng, J.-G. Xu, Z.-B. Wang, *Fluorimetry*, 2nd ed, Scientific Press, Beijing, 1990, p. 122 (in Chinese).
- [7] Z. Zhang, W.R. Seitz, K. O'Connell, *Anal. Chim. Acta* 236 (1990) 251.
- [8] A.-P. Wei, D.K. Blumenthal, J.N. Herron, *Anal. Chem.* 66 (1994) 1500.
- [9] P. Fromherz, B. Reiger, *J. Am. Chem. Soc.* 108 (1986) 5361.
- [10] J.K. Barton, J.M. Goldberg, C.V. Kumar, N.J. Turro, *J. Am. Chem. Soc.* 108 (1986) 2081.
- [11] F. Fredericq, C. Houssier, *Biopolymers* 9 (1970) 639.
- [12] Y. Cao, X.-W. He, *Spectrochim. Acta A* 54 (1998) 883.
- [13] C.A. Parker, W.T. Rees, *Analyst* 85 (1960) 587.

Calibration of the Hg chalcogenide glass membrane ion-selective electrode in seawater media

Roland De Marco *, James Shackleton

School of Applied Chemistry, Curtin University of Technology, GPO Box U 1987, Perth, WA 6845, Australia

Received 2 September 1998; received in revised form 7 December 1998; accepted 7 December 1998

Abstract

It is shown that a chalcogenide glass mercury^{II} ion-selective electrode (ISE) can be calibrated in chloride-free unbuffered and saline buffered standards, displaying near-Nernstian response over 19 orders of magnitude (i.e. 10^{-20} to 10^{-1} M Hg²⁺). Extended ageing of the ISE in seawater induced a memory effect, causing the electrode to respond in a sub-Nernstian fashion. Electrochemical impedance spectroscopy (EIS) demonstrated that the response of the Hg^{II} ISE is underpinned by a charge transfer process, and seawater matrix effects are due to electrode passivation. It is shown that standard addition ISE potentiometry may compensate for interferences caused by the seawater matrix. © 1999 Elsevier Science B.V. All rights reserved.

Keywords: Mercury; Ion-selective electrode; seawater media

1. Introduction

Mercury exists in the aquatic environment as a result of natural and man-made processes. Elevated levels of mercury, from any source, are of particular concern to environmental scientists. Mercury can be accumulated by marine organisms and passed down the food chain to humans. Mercury poisoning can have a devastating effect on a community, as evidenced by the Minnimata Bay incident in Japan, where a whole community was poisoned as a result of contaminated seafood [1].

Presently, there are numerous methods for the determination of mercury, although very few are able to detect mercury at the parts per million to parts per billion levels in seawater. Standard methods that are currently used to determine levels of total mercury in seawater include atomic absorption spectrometry, using a flame, cold vapour or graphite furnace, and atomic emission with an inductively coupled plasma. Electroanalytical methods (e.g. cathodic and/or anodic stripping voltammetry) can be used to determine concentrations of total and available mercury giving an indication of mercury speciation [2,3], while other techniques such as high performance liquid chromatography, X-ray fluorescence [4] and atomic fluorescence have been used to determine

* Corresponding author. Fax: +61-8-9266-2300.

E-mail address: r.demarco@info.curtin.edu.au (R. De Marco)

levels of total mercury [5]. Unfortunately, the non-electrochemical methods are costly, requiring extensive sample pretreatment, and clean room conditions for analysis.

Alternatively, it is possible to carry out electroanalyses of free Hg^{II} in natural waters using an ion-selective electrode (ISE), and this parameter is also useful in studies of inorganic and organic mercury speciation. By comparison with all of the standard instrumental methods of analysis, potentiometric detection with an ISE is inexpensive, simple, robust and portable, making it amenable to field analyses.

The literature on Hg^{II} ISEs is limited. Several research groups are developing solid-state [6–8] and neutral carrier-based polymer membrane [9] Hg^{II} sensors. Although it is reported that the detection limit of polymer membrane Hg^{II} ISEs may be reduced to 10^{-12} M through the use of internal metal buffer filling solutions [10], it is the authors' view that the best system for seawater analyses is the chalcogenide glass Hg^{II} ISE [6] because of its superior selectivity and chemical inertness. The Hg^{II} chalcogenide glass ISE [6] yields a detection limit of 10^{-7} M free Hg^{II} in unbuffered media, noting that such a high detection limit is probably attributable to electrode carry-over effects in the absence of buffering ligands like those found in seawater, and the chalcogenide glass Hg^{II} ISE is also completely free of ionic interferences. Regrettably, the elemental composition and response mechanism of the chalcogenide glass ISE membrane was not reported by Vlasov et al. [6]. It is possible to extend the working range of the Hg^{II} ISE to free Hg^{II} levels commensurate with those in seawater (i.e. $< 10^{-20}$ M) by using Hg^{II} buffered standards as demonstrated by Shatkin et al. [8], who calibrated their HgS Hg^{II} ISE down to 10^{-14} M Hg^{2+} .

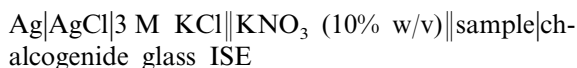
As there are no existing Hg^{II} ISE methods for the measurement of free Hg^{II} in seawater, an assessment of the behaviour of the Hg^{II} chalcogenide glass ISE in saline media was undertaken to ascertain if it is possible to use this system in the analysis of seawater. The potentiometric response of the chalcogenide glass Hg^{II} ISE has been studied in unbuffered chloride-free and buffered saline media. Standard addition Hg^{II} ISE

potentiometry has been trialled as a means of compensating for interferences caused by the seawater matrix. The unknown response mechanism of the Hg^{II} ISE has been studied using electrochemical impedance spectroscopy (EIS).

2. Experimental

2.1. Instrumentation

A Hg^{II} chalcogenide glass ISE was purchased from St Petersburg University's Institute of Chemical Sensors. The membrane was of unknown composition. The ISE was coupled with an ORION Research Incorporated model 90-02 double junction reference electrode. The IUPAC cell diagram of the system was:



The cell was connected to a EUTECH Cybernetics 200 pH meter. The instrument was directly connected to a laptop computer via its RS-232 serial output, where the signal was processed by EUTECH Cybernetics synapse[®]-lab computer program. At the 'plateau' in ISE response at a drift rate of 0.5 mV min^{-1} , the ISE potential was recorded.

2.2. Electrode pretreatment

Prior to use, the robust Hg^{II} chalcogenide glass ISE disc was polished using a tooth brush treated with STRUERS red lubricant and $3 \mu\text{m}$ diamond spray to remove the electrode's Hg-deficient modified surface layer, detected using EIS equivalent circuit modelling, restoring the reproducible response characteristics of a polished electrode. Following polishing, the electrode was buffed with soft tissue to a pearl-like finish. The electrode was then washed thoroughly with ultra-high-purity water.

2.3. Preparation of Hg^{II} buffers

Using the mintage2 software package (available at the Old Dominion University website <http://>

www.cce.odu.edu/cce/model/model.html), several known buffer systems were investigated. It was found that a chloride/bromide buffer system was able to produce the levels of free mercury found in environmental samples (namely 10^{-20} to 10^{-12} M). Standards were prepared in the pHg (i.e. $-\log[\text{Hg}^{2+}]$) range of 12–20 by adding mercury^{II} chloride, sodium chloride, sodium bromide and potassium nitrate to ultra-high-purity water, in the amounts specified by minteqa2 (refer to Table 1). The solutions were acidified to pH 2 through the addition of concentrated nitric acid, and each buffer was allowed to age for a period of approximately 24 h to ensure that chemical equilibrium had been established.

2.4. EIS studies

EIS studies of the Hg^{II} chalcogenide glass electrode were undertaken using an EG&G Princeton Applied Research Model 5120 potentiostat equipped with a lock-in amplifier. The EIS spectra were recorded using an overpotential of ± 10 mV, and a frequency range of 100 kHz to 1 mHz.

3. Results and discussion

3.1. Electrode response in buffered and unbuffered standards

In order to extend the working range of the Hg^{II} ISE to free Hg^{II} levels commensurate with those in seawater, it was necessary to employ Hg^{II} buffers for electrode calibration. It was found that a stable buffer system for free Hg^{II} over the pHg range 12–20 comprised mixtures of mercury chloride, sodium chloride and sodium bromide (potas-

sium nitrate was used as an ionic strength adjustor in some instances; see Table 1). In fact, the high level of buffer stability enabled the authors to use the same set of solutions for reproducible Hg^{II} ISE calibrations over the duration of the work (i.e. about 1 year). It can be seen in Fig. 1 that the lower limit of Nernstian response to free Hg^{II} in buffered standards (i.e. experimental slope is 28.6 mV per decade change in $[\text{Hg}^{2+}]$) is 10^{-18} M. The sub-Nernstian response between 10^{-20} and 10^{-18} M Hg²⁺ (refer to the dotted line in Fig. 1) is probably attributable to interferences by reagent impurities at these extremely low levels of free Hg^{II} (EIS data confirmed this hypothesis).

The collinearity of potentiometric response curves in unbuffered non-saline (Fig. 1, filled squares) and buffered saline Hg^{II} standards (Fig. 1, filled circles) demonstrates that the Hg^{II} ISE responds to free Hg^{II} over a wide dynamic range (i.e. 19 orders of magnitude). This behaviour resembles that of the glass pH electrode, and suggests that it may be possible to use the chalcogenide glass Hg^{II} ISE in a similar manner to a pH electrode (i.e. calibrate the Hg^{II} ISE in stable buffered solutions, and measure free Hg^{II} in well buffered media like seawater).

3.2. Response in UV-oxidised seawater

As the effect of natural organic ligands (i.e. humic and fulvic acids) on the Hg^{II} speciation of marine waters is unknown, a sample of Southern Ocean seawater was subjected to UV oxidation to decompose the uncharacterised organic ligands, leaving the well-known inorganic complexes of Hg^{II}. This enabled a reliable metal speciation calculation for free Hg^{II} in UV oxidised seawater using minteqa2 along with the seawater composition reported elsewhere in the literature [11].

The UV-oxidised seawater used in this study contained 75×10^{-12} M total Hg (as determined by inductively coupled plasma-mass spectrometry (ICP-MS)) and, when this level of total Hg is substituted into the seawater speciation model [11] entered into minteqa2, the pHg in seawater is estimated at 23.1. The actual response of the Hg^{II} ISE in filtered UV-oxidised Southern Ocean sea-

Table 1
Compositions (M) of chloride/bromide mercury^{II} buffers adjusted to pH 2

pHg	20.01	18.03	16.03	14.02	11.97
[HgCl ₂]	0.001	0.005	0.005	0.012	0.004
[NaCl]	0.446	0.486	0.526	0.22	0.02
[NaBr]	0.1	0.06	0.01	–	–
[KNO ₃]	–	–	–	0.302	0.518

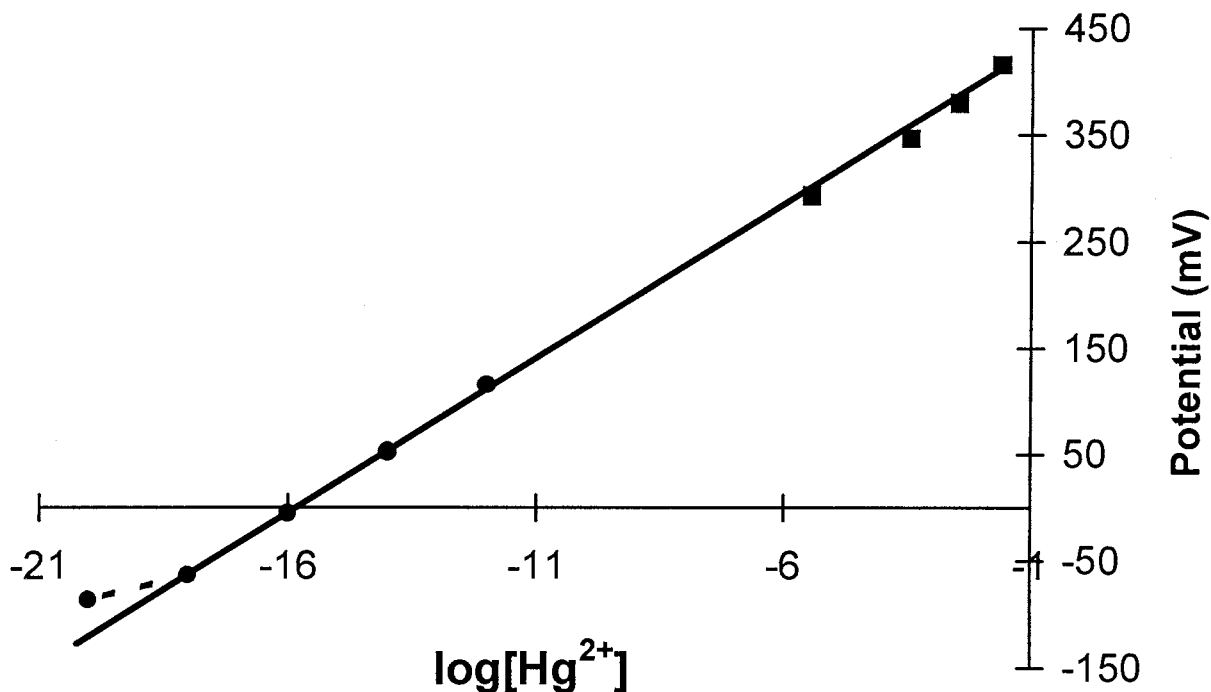


Fig. 1. Potentiometric response of the Hg^{II} chalcogenide glass ISE in (■) unbuffered Hg(NO₃)₂ standards and (●) chloride/bromide Hg^{II} buffers.

water yielded pHg 15.9. Note that electrode dissolution is partly responsible for the lower than expected pHg because ICP-MS analysis of seawater exposed to the Hg^{II} ISE for 5 min (i.e. analysis time) detected the release of 725×10^{-12} M Hg, and minteqa2 calculations demonstrated that this level of Hg contamination would have lowered the pHg value to 22.1. This finding demonstrates that electrode release of Hg is a minor contributor to the elevated Hg reading, and the extremely low Hg^{II} ISE pHg reading in seawater is due predominantly to a seawater matrix interference effect.

Ageing of the ISE in seawater over a 48-h period did not have a measurable effect on the electrode calibration characteristics in Hg^{II} buffers. Extended soaking of the Hg^{II} ISE in seawater for over 72 h led to the formation of a tenacious grey coating on the electrode surface (possibly a Cu and/or Fe selenide deposit). This coating was difficult to remove, requiring extended polishing on a rotary polisher. Note that the response of the poisoned electrode in Hg^{II}

buffers was sub-Nernstian (i.e. 20.4 mV per decade). This sub-Nernstian behaviour signifies that seawater's matrix is interfering with the Hg^{II} response of the chalcogenide glass ISE.

3.3. Standard addition potentiometry

As the large discrepancy between minteqa2 and ISE pHg values in seawater is attributable to a matrix interference, it was deemed appropriate to undertake a standard addition analysis of seawater. On two occasions, low spikes of Hg^{II} were employed (i.e. 0, 200, 600 and 3000 pM), and free Hg^{II} levels accompanying the spikes were calculated using minteqa2 (namely, pHg 23.1, 22.57, 22.18 and 21.52, respectively). Although there was significant scattering around the calibration curve ($E_{\text{Hg ISE}} = 565.31 + 23.2 \times \log[\text{Hg}^{2+}]$; $r^2 = 0.967$), the response was near-Nernstian (i.e. 23 mV per decade). It is important to note that ISE potentials in seawater spiked with mercury were extremely noisy due to electrode passivation by

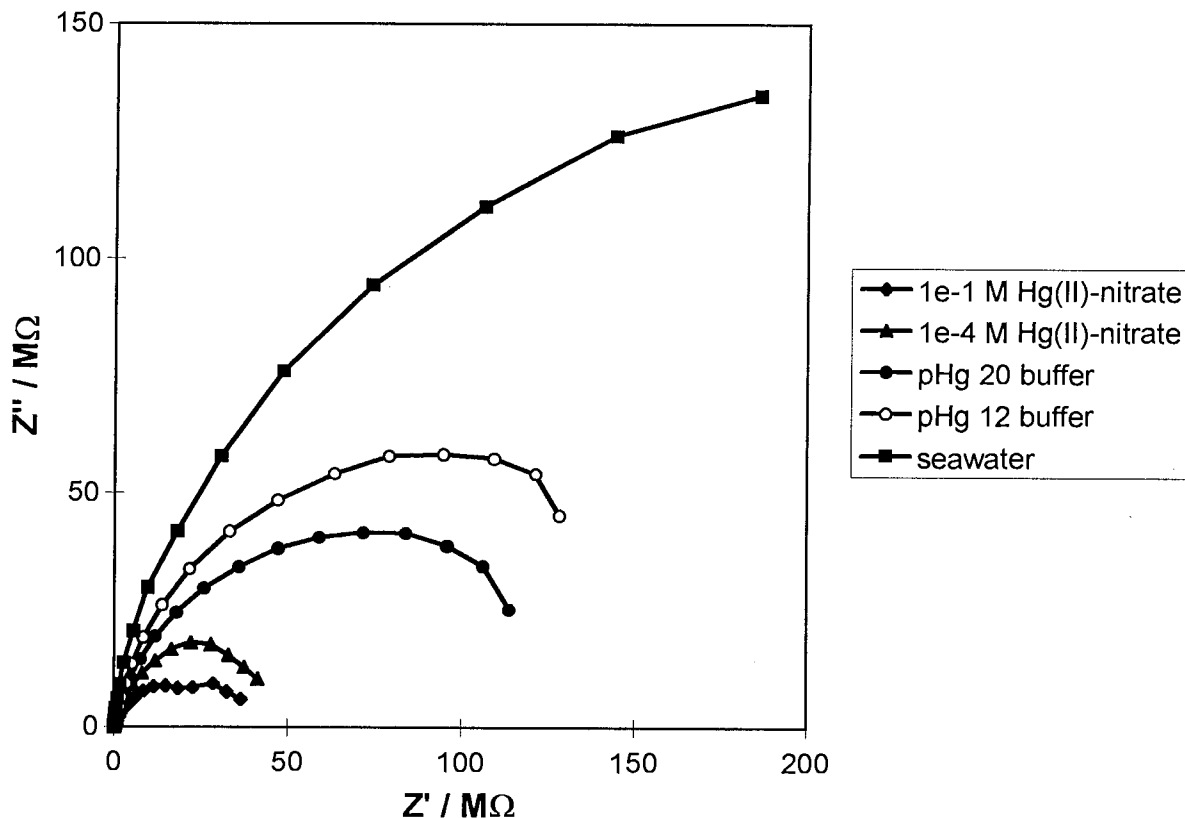


Fig. 2. EIS Nyquist plots for a Hg^{II} ISE in the following media: (\blacklozenge) 10^{-1} M $\text{Hg}(\text{NO}_3)_2$ in 0.6 M KNO_3 ; (\blacktriangle) 10^{-4} M $\text{Hg}(\text{NO}_3)_2$ in 0.6 M KNO_3 ; (\circ) saline Hg^{II} buffer containing 10^{-12} M Hg^{2+} ; (\bullet) saline Hg^{II} buffer containing 10^{-20} M Hg^{2+} ; (\blacksquare) UV-oxidised seawater.

seawater, yielding extremely low and spasmodic charge transfer rates as detectable by EIS. Despite these difficulties, the promising ISE standard addition results suggest that this approach may be able to compensate for interferences caused by the seawater matrix.

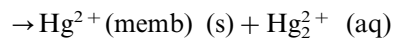
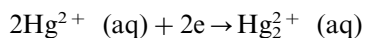
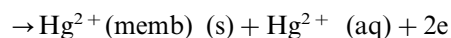
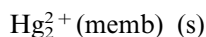
3.4. EIS studies

It has been found that the response of jalpaite Cu^{II} [12] and chalcogenide glass Fe^{II} [13,14] ISEs are underpinned by charge transfer processes occurring at the electrode/electrolyte interface, and these processes can be studied effectively using EIS. The Hg^{II} ISE is expected to display similar redox behaviour and, consequently, an EIS study of the Hg^{II} ISE was deemed appropriate.

Fig. 2 presents Nyquist plots for an EIS experiment involving exposure of the Hg^{II} ISE to unbuffered and buffered Hg^{II} standards along with UV-oxidised seawater. The low-frequency semi-circle (appearing at around 100 mHz) is indicative of a charge transfer process, probably involving the $\text{Hg}^{\text{II}}/\text{Hg}^{\text{I}}$ redox couple. Note that the charge transfer resistance (i.e. R_{CT}) is inversely proportional to the rate of charge transfer. It can be seen that the charge transfer resistance (i.e. R_{CT} given by the diameter of the low-frequency semi-circle) increases as the levels of free Hg^{II} in the standards diminish, with the exception of the buffer containing 10^{-20} M Hg^{2+} , demonstrating that the rate of the charge transfer reaction is suppressed at low concentrations of free Hg^{II} . The deviation in R_{CT} for the standard containing 10^{-20} M free

Hg^{II} is symbolic of an interference that facilitates the charge transfer process (possibly a copper and/or iron trace metal impurity interference that can be manifested only at very low levels of free Hg^{II}). Also noteworthy is the grossly dissimilar R_{CT} in the UV-oxidised seawater sample that is indicative of the seawater matrix interference. Clearly, the seawater matrix is severely impeding the charge transfer process occurring at the Hg^{II} ISE/solution interface, and is symbolic of electrode passivation.

Unfortunately, the composition of the Hg^{II} ISE membrane is unknown. Nevertheless, it is conceivable that the Hg^{II} chalcogenide glass membrane (assumed to be $\text{Hg}_2^{2+}(\text{memb})$ that is associated with an appropriate counterion) behaves in a similar manner to ISEs for Cu^{II} [12] and Fe^{III} [13,14] by displaying a selectivity towards an appropriate redox couple, namely $\text{Hg}^{\text{II}}/\text{Hg}^{\text{I}}$:



It is important to note that the only plausible solution redox chemistry for Hg^{2+} is reduction to Hg_2^{2+} , and the membrane must experience an accompanying oxidation process. Note that $\text{Hg}_2^{2+} (\text{aq})$ is normally susceptible to disproportionation, but avoids this fate at the electrode/electrolyte interface as it resides in Hg^{I} vacancies within the metal sublattice of the membrane, and the strong Coulombic forces experienced by Hg_2^{2+} in this chemical environment prevent it from disproportionating to Hg and Hg^{2+} . The suggestion of oxidation of $\text{Hg}_2^{2+}(\text{memb})$ yields a reaction stoichiometry that can be used in the derivation of a Nernst equation which correctly predicts divalent response to Hg^{2+} (i.e. 29 mV per decade):

$$E = E^\circ - \frac{2.303RT}{2F} \log\left(\frac{a\text{Hg}_2^{2+}}{a\text{Hg}^{2+}}\right) \quad (1)$$

Note that unit activities are assumed for mercury species within the glass membrane (i.e. $\text{Hg}_2^{2+}(\text{memb})$ and $\text{Hg}^{2+}(\text{memb})$), and if one also assumes that the background activity of Hg_2^{2+} is fixed through dissolution of the membrane (namely $\text{Hg}_2^{2+}(\text{memb})$), it is possible to simplify Eq. (1) to the following:

$$E = E_1^\circ + \frac{2.303RT}{2F} \log(a\text{Hg}^{2+}) \quad (2)$$

where

$$E_1^\circ = E^\circ - \frac{2.303RT}{2F} \log(a\text{Hg}_2^{2+}) \quad (3)$$

Most significantly, the mechanism and accompanying theory predicts correctly that the rate of the forward component of the reversible charge transfer process, and the net rate of charge transfer, will increase at elevated levels of Hg^{2+} .

4. Conclusions

The collinearity of calibration curves for the Hg^{II} ISE in chloride-free unbuffered and saline buffered standards demonstrates unambiguously that chloride does not interfere with the response of the Hg^{II} ISE.

EIS data have shown that the seawater matrix interference effect is due to passivation of the chalcogenide glass membrane. Standard addition potentiometry may compensate for the seawater matrix interference, albeit that electrode potentials in seawater are extremely noisy due to electrode passivation.

A preferred alternative for analysis would involve the use of Hg^{II} -spiked seawater standards and unspiked seawater samples that have been pretreated to remove the constituents that are passivating the electrode membrane. Work is in progress to determine the elemental composition of the Hg^{II} chalcogenide glass using ICP-MS, enabling the fabrication of Hg^{II} chalcogenide membranes that can be characterised using X-ray photoelectron spectroscopy to identify the passivation film.

Acknowledgements

The authors thank Dr Denis Mackey of the CSIRO Division of Marine Research for donating the Southern Ocean UV-oxidised seawater used in this study, and Dr John Watling of Curtin University for carrying out ICP-MS analyses of the UV-oxidised seawater. We also express our appreciation to Dr Andrey Legin of St Petersburg University for supplying the Hg^{II} chalcogenide glass ISE used in this study.

References

- [1] A. Jerne, in: E.D. Goldberg (Ed.), *The Sea*, vol. 5, Wiley Interscience, New York, 1974.
- [2] C. Belmont-Hebert, M.L. Tercier, J. Buffle, G.C. Fiaccabrino, N.F. de Rooij, M. Koudelka-Hep, *Anal. Chem.* 70 (1998) 2949.
- [3] L.A. Miller, K.W. Bruland, *Anal. Chim. Acta* 343 (1997) 161.
- [4] Q. Fernando, *Environ. Health Perspect.* 103 (suppl. 1) (1995) 13.
- [5] H. Morita, H. Tanaka, S. Shimomura, *Spectrochim. Acta* 50B (1995) 69.
- [6] Yu.G. Vlasov, E.A. Bychkov, A.V. Legin, *Talanta* 41 (1994) 1059.
- [7] M. Neshkova, E. Pancheva, *Anal. Chim. Acta* 300 (1995) 133.
- [8] J.A. Shatkin, H. Szenjwald Brown, S. Licht, *Anal. Chem.* 67 (1995) 1147.
- [9] X. Yang, D. Brynn Hibbert, P.W. Alexander, *Anal. Chim. Acta* 372 (1998) 387.
- [10] T. Sokalski, A. Ceresa, T. Zwickl, E. Pretsch, *J. Am. Chem. Soc.* 119 (1997) 11347.
- [11] A.E. Martell, R.J. Motekaitis, *Determination and Use of Stability Constants*, VCH, New York, 1988, pp. 145–157.
- [12] R. De Marco, R. Eriksen, A. Zirino, *Anal. Chem.* 70 (1998) 4683.
- [13] Y.G. Vlasov, E.A. Bychkov, *Ion-Selective Electrode Revs.* 9 (1987) 5.
- [14] R. De Marco, D.J. Mackey, *Mar. Chem.*, submitted.

Determination of organophosphorus pesticides in water by solid-phase microextraction

Pi-Guey Su, Shang-Da Huang *

Department of Chemistry, National Tsing Hua University, Hsinchu 300, Taiwan, ROC

Received 16 July 1998; received in revised form 1 December 1998; accepted 9 December 1998

Abstract

A solid-phase microextraction method coupled with a flame photometric detector was developed for the analysis of organophosphorus pesticides in water. Two kinds of fiber (100 μm polydimethyl siloxane (PDMS) and 85 μm polyacrylate (PA) fibers) were used and compared. Parameters that may affect the extraction, such as the duration of absorption and desorption, temperature of absorption, ionic strength, elutropic strength, and concentration of humic acid were investigated. Higher sensitivity and lower detection limits were achieved using a PA fiber than using a PDMS fiber. The detection limit is less than $0.3 \mu\text{g l}^{-1}$ for most of the analytes, except for mevinphos ($420 \mu\text{g l}^{-1}$). The precision is better than 9%. © 1999 Elsevier Science B.V. All rights reserved.

Keywords: Gas chromatography-flame photometric detector; Solid-phase microextraction; Organophosphorus pesticides; Polyacrylate; Polydimethyl siloxane; Water

1. Introduction

Sample pretreatment is generally required for the determination of trace organic pollutants in water. Pesticide samples are usually enriched by liquid–liquid [1,2] or solid-phase [3,4] extraction. Liquid–liquid extraction is time consuming and tedious, and often requires large quantities of toxic and environmentally unfriendly solvents. Solid-phase extraction requires less solvent but the presence of particulate matter in samples can cause plugging of the cartridges, breakthrough is sometimes experienced for highly concentrated

samples and a large volume of sample is generally required for trace analysis.

Solid-phase microextraction (SPME), a relatively new extraction technique, was introduced by Pawliszyn and co-workers [5–7]. The new trends in SPME were reviewed by Eisert and Pawliszyn [8]. The SPME technique integrates sampling, extraction, concentration, and sample introduction into a single step [9]. It is quick, highly sensitive and readily adapted to automation [7]. The applications of SPME studied by Pawliszyn and co-workers included volatile organic compounds such as substituted benzenes (benzene, toluene, ethylbenzene and the xylene isomers) and chlorinated hydrocarbons [7,10–13]; less volatile aromatic compounds such as polyaro-

* Corresponding author. Fax: +886-3-5736979.

E-mail address: sdhuang@chem.nthu.edu.tw (S.-D. Huang)

matic hydrocarbons (PAHs) [14], phenols and nitrophenols [15,16]; organochlorine pesticides [17]. A modification of this method for analysis from the headspace has been reported [18–20]. The SPME coupled with liquid chromatography has been developed for the analysis of PAHs [21], alkylphenol ethoxylate surfactants [22] or pesticides [23,24]. We reported on the applications of SPME on the analysis of priority pollutants listed in the USA Environmental Protection Agency (EPA) Method 609 (nitrobenzene, isophorone, 2,4-dinitrotoluene and 2,6-dinitrotoluene) [25], the haloethers [26] or the benzene derivatives [27] in water.

Organophosphorus pesticides are an important source of environmental contamination owing to their universal application in agriculture. Several studies have been reported on the analysis of organophosphorus pesticides in aqueous [28–37] or human body fluid samples [38] by using the SPME technique. Eisert et al. [28–30] determined a few pesticides in aqueous samples using SPME-gas chromatography-atomic emission detection (GC-AED), SPME-gas chromatography-nitrogen-phosphorus detection (GC-NPD) or SPME-gas chromatography-mass spectrometry (GC-MS). Boyd-Boland et al. [31] determined 60 pesticides in water using SPME-GC-MS. Sng et al. [32] determined two pesticides (malathion and parathion) in water by SPME-gas chromatography-flame ionization detection (GC-FID) using five kinds of fibers commercially available. Valor et al. [33] determined eight organophosphorus pesticides in water by SPME-GC-NPD. Pawliszyn and co-workers [34,35] determined a few organophosphorus pesticides in aqueous samples using SPME-GC-MS or SPME-GC-NPD. Mawhinney et al. [36] determined 46 nitrogen and phosphorus-containing pesticides of EPA Method 507 using SPME-GC-MS or SPME-GC-NPD. Lopez-Avila et al. [37] determined 49 organophosphorus pesticides in water by SPME-gas chromatography-thermionic selective detection (GC-TSD). Lee et al. [38] determined organophosphorus pesticides in human body fluids by the headspace-SPME-GC-NPD technique. Among these published works, flame photometric detection (FPD), which is the most

commonly used detector for organophosphorus pesticides analysis, was not used. FPD is very sensitive and selective for organophosphorus pesticide analysis. Use of a flame photometric detector will minimize interference from materials that do not contain phosphorus. It is thus of great interest to know whether SPME-GC-FPD is a useful technique for organophosphorus pesticides analysis. In the present work, we determined the organophosphorus pesticides (mevinphos, ethoprop, diazinon, disulfoton, fenthion), which were listed in the US EPA Method 622, using GC-FPD and a SPME fiber assembly. The effects of composition of the fibre coating, duration of absorption and desorption, temperature of absorption, ionic strength (Na_2SO_4), elutropic strength (methanol) and the concentrations of humic acid were investigated. Much higher sensitivity and lower detection limits were achieved using a polyacrylate (PA) fiber than those using polydimethyl siloxane (PDMS) fiber. The detection limits is less than $0.3 \mu\text{g l}^{-1}$ for most of the analytes, except for mevinphos ($420 \mu\text{g l}^{-1}$). The percentage relative standard deviation (%RSD) is better than 9%. This method was applied to an environmental sample (lake water) using an external calibration.

2. Experimental

2.1. Reagents and sample

Stock solutions of reagent grade (purity > 98%) mevinphos, ethoprop, diazinon, disulfoton, fenthion (Riedel-deHaen, Seelze Germany) were prepared in acetone (optima grade; Fisher, Fair Lawn, NJ, USA). Methanol (optima grade, Fisher), sodium sulphate (Osaca, Japan) and humic acid (technical grade, sodium salt; Aldrich, Milwaukee, WI, USA) were used to prepare the sample solution. Deionized water was prepared using a Milli-Q Millipore (Bedford, MA, USA) purification system. Lake water from the National Tsing Hua University served as the environmental sample.

2.2. Instruments and analysis

The SPME fiber assembly was purchased from Supelco. The microextraction fibres were coated with PDMS (100 μm) or PA (85 μm). SPME involves a few simple steps [9]. The fibre is withdrawn into the needle which is used to penetrate the septum of sample vial (4 ml). The fibre is then inserted into the sample solution by pushing the plunger. The fibre is completely immersed into the sample solution (3 ml). The sample solution in the vial is stirred with a magnetic stirring bar and controlled by a Digital/Magnetic Stirrer (Electrothermal HS 4000/5000). The speed of rotation of the stirring bar is 850 ± 10 rpm and the temperature of the sample solution is $25 \pm 2^\circ\text{C}$, unless otherwise specified. After sample absorption, the plunger is withdrawn to retract the fibre into the needle and the syringe needle is then removed from the vial. For desorption, the needle is inserted into the GC injection port and then the fibre is exposed again.

A gas chromatograph (Shimadzu GC-9-AM) with split/splitless injection system, flame photometric detector, and a capillary column (HP Ultra-2, 25 m \times 0.2 mm i.d., film thickness 0.33 μm) was used. The temperatures at the detector were 250°C for both PA and PDMS. The fibres were desorbed in the GC injector at 290°C for 5 min (PA) or 250°C for 7 min (PDMS). As the fibre began its desorption, the column temperature was kept at 50°C for 5 min (PA) or 7 min (PDMS), then increased at $40^\circ\text{C min}^{-1}$ to 180°C , held 1 min and then increased at 5°C min^{-1} to 220°C , and held 5 min. The carrier gas was nitrogen of purity 99.99%, further purified by passage through a gas purifier (Alltech) containing molecular sieve 5A and an oxygen-adsorbing gas purifier (OxiClear). The pressure of the carrier gas was 150 kPa and the flow-rate of make-up gas was 50 ml min^{-1} . The split flow-rate was 43 ml min^{-1} and the flow-rate for the septum purge was 1 ml min^{-1} . The fibres were injected in the splitless mode and the splitter was opened at the end of desorption period (delay time 5 min for PA fibre and 7 min for PDMS fibre). Peak areas of the FPD signals

were used to demonstrate the effect of parameters on the extraction. Peak area was most commonly used for the works of SPME (such as Refs. [25–33] and many others).

3. Results and discussion

3.1. Chromatogram of the SPME analysis

A chromatogram resulting from the SPME analysis of mixed standard of organophosphorus in water using PA fibre is shown in Fig. 1. Sharp peaks and good resolution were obtained. A similar chromatogram was obtained using the PDMS fibre.

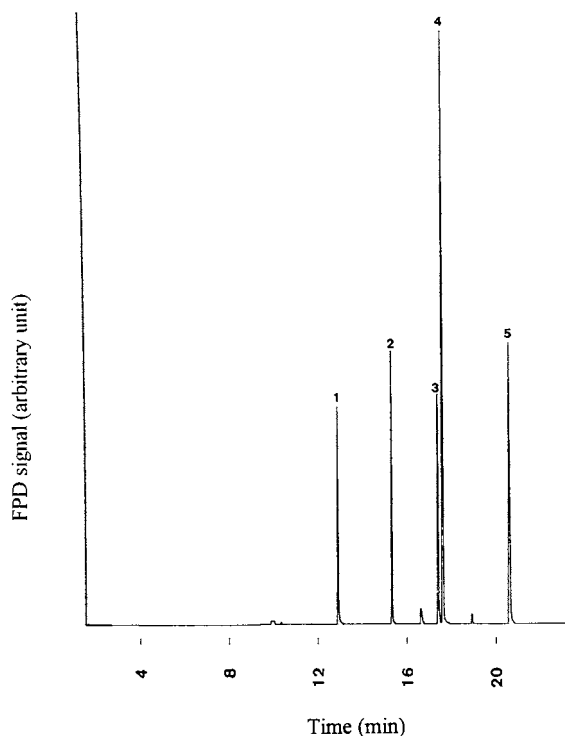


Fig. 1. Chromatogram of organophosphorus pesticides. Extracted with PA fibre from water for 30 min and desorbed in the GC injection port at 290°C for 5 min. 1, mevinphos (10 mg l^{-1}); 2, ethoprop ($125 \text{ } \mu\text{g l}^{-1}$); 3, diazinon ($12.5 \text{ } \mu\text{g l}^{-1}$); 4, disulfoton ($12.5 \text{ } \mu\text{g l}^{-1}$); 5, fenthion ($12.5 \text{ } \mu\text{g l}^{-1}$).

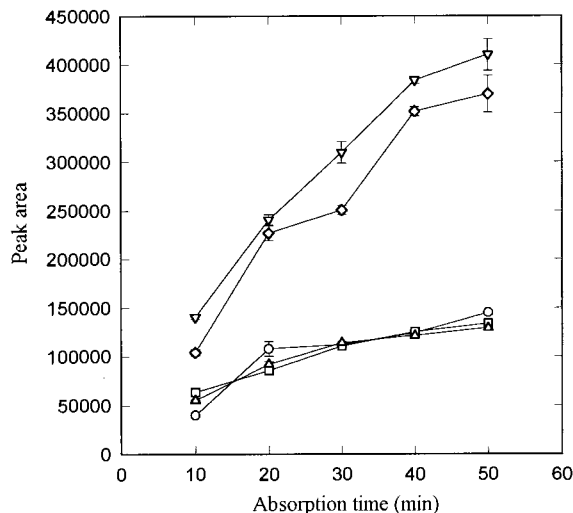


Fig. 2. Absorption–time profile for PA fibre. ○, mevinphos (10 mg l^{-1}); □, ethoprop ($125 \text{ } \mu\text{g l}^{-1}$); △, diazinon ($12.5 \text{ } \mu\text{g l}^{-1}$); ▽, disulfoton ($12.5 \text{ } \mu\text{g l}^{-1}$); ◇, fenthion ($12.5 \text{ } \mu\text{g l}^{-1}$). Desorption time, 5 min.

3.2. Absorption–time profile

The absorption–time profiles obtained using the PA or PDMS fibre are shown in Figs. 2 and 3. For PA fibre, the equilibration period re-

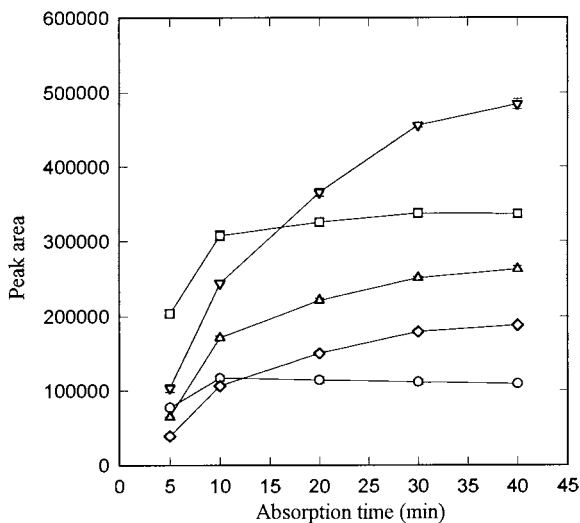


Fig. 3. Absorption–time profile for PDMS fibre. ○, mevinphos (20 mg l^{-1}); □, ethoprop ($250 \text{ } \mu\text{g l}^{-1}$); △, diazinon ($25 \text{ } \mu\text{g l}^{-1}$); ▽, disulfoton ($25 \text{ } \mu\text{g l}^{-1}$); ◇, fenthion ($25 \text{ } \mu\text{g l}^{-1}$). Desorption time, 5 min.

quired is longer than 50 min. For PDMS fibre, the equilibrium condition for the absorption of most analytes is almost reached after 30–40 min except for fenthion (longer than 40 min). Factors that influence the equilibration period were investigated by Pawliszyn and co-workers [7,10,13]. The equilibration rate is limited by: (1) the mass transfer rate of the analytes through a thin static aqueous layer at the fibre–solution interface; (2) the distribution constant of the analyte and (3) the thickness and kinds of the fibre coating. The longer period (50 min or more) for the partitioning of the analytes to reach equilibrium when the PA fibre was used, as compared with that using PDMS fibre, has two causes. First, the increased affinity of the polar analytes for the fibre with the more polar coating (PARL) requires larger amounts of the analytes to diffuse into the coating layer before equilibrium is reached. Second, the thickness of the static aqueous layer at the interface of the polar PA fibre and the aqueous phase may be larger than that at the surface of the non-polar PDMS fibre. Extraction periods of 30 min were chosen for both PA and PDMS fibres since it was approximately equivalent to the time required to run the GC chromatogram.

3.3. Desorption–time profile

The desorption–time profiles obtained using PA or PDMS fibre are shown in Figs. 4 and 5. A desorption period of 4–5 min was enough to desorb the analytes from the PA fibre (temperature of injection port, 290°C). A desorption period of 7 min was required from the PDMS fibre (temperature of injection port, 250°C). No carryover of any pesticide was observed.

3.4. Effect of temperature on extraction

The absorption–temperature profile obtained using a PDMS fibre is shown in Fig. 6. Optimum extraction efficiency was achieved in the range $25\text{--}35^\circ\text{C}$. The lower absorption of most of the analytes at 10°C was due to the decreased rate of diffusion of the analytes. The

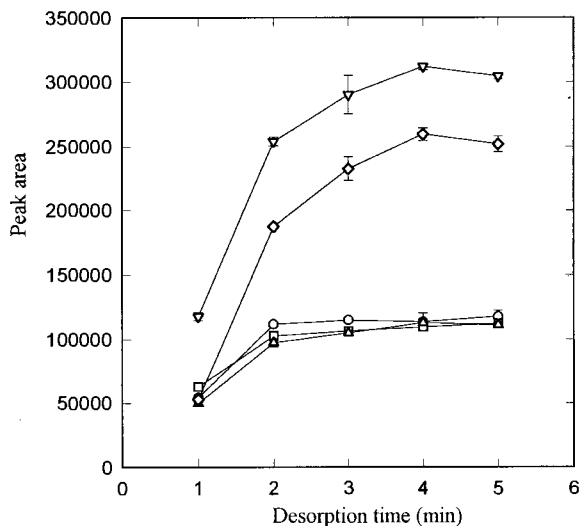


Fig. 4. Desorption–time profile for PA fibre. Absorption time, 30 min. Concentrations and symbols as in Fig. 2.

rate of diffusion of the analyte species through the static aqueous layer at the fibre–solution interface increases with increasing temperature, so that more analyte is absorbed at higher temperature if equilibrium has not been reached. The decreasing absorption with increasing temperature above 35°C is presumably due to a distribution constant which decreases with increasing

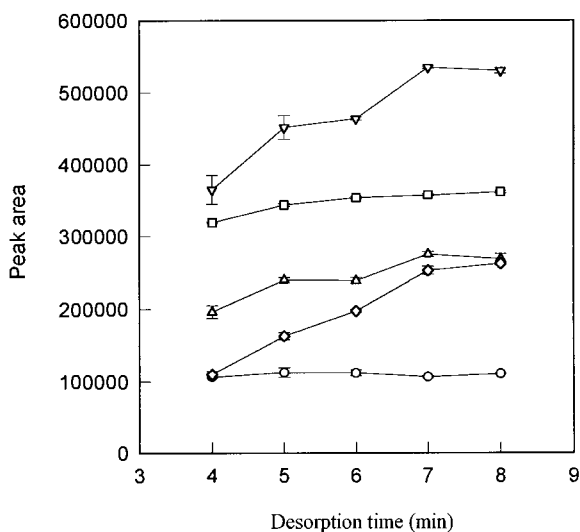


Fig. 5. Desorption–time profile for PDMS fibre. Absorption time, 30 min. Concentrations and symbols as in Fig. 3.

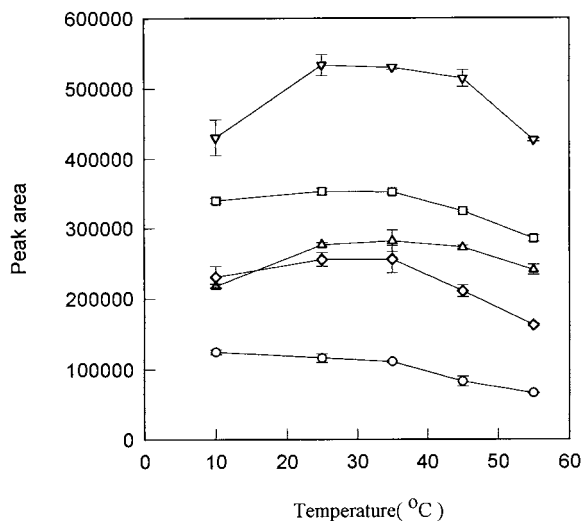


Fig. 6. Absorption–temperature profile for PDMS fibre. Absorption time, 30 min; desorption time, 7 min. Concentrations and symbols as in Fig. 3.

temperature. The absorption process is exothermic, thus lowering the temperature increases the distribution constant at equilibrium. In practical applications when the extraction is stopped before reaching the equilibrium, not only thermodynamic but also kinetic aspects be-

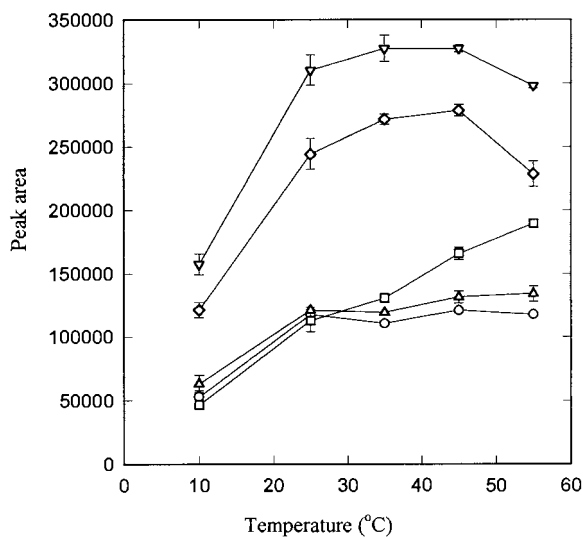


Fig. 7. Absorption–temperature profile for PA fibre. Absorption time, 30 min; desorption time, 5 min. Concentrations and symbols as in Fig. 2.

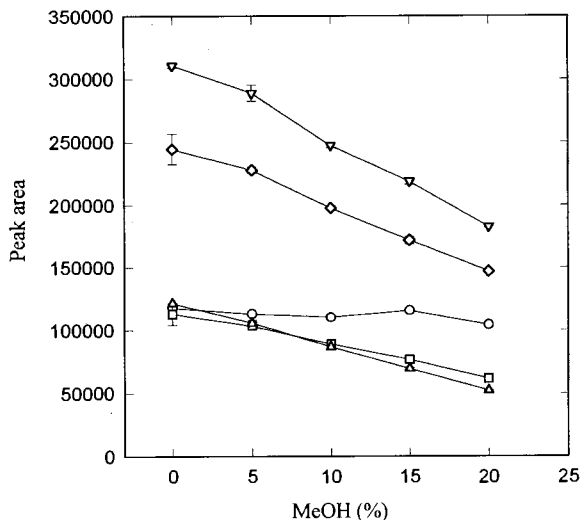


Fig. 8. Effect of methanol on absorption of organophosphorus pesticides by PA fibre. Absorption time, 30 min; desorption time, 5 min. Concentrations and symbols as in Fig. 2.

come important. The absorption–temperature profile obtained using PA fibre is shown in Fig. 7. The lower absorption of the analytes at 10°C was also observed. The amount of disulfoton and fenthion absorbed decreased as the extraction was performed at 55°C. An extraction temperature of 25°C was selected for further study using both fibers, because this temperature was most easily maintained, and the improvement in sensitivity at higher temperature is not very significant (except for extraction of ethoprop with PA fibre).

3.5. Effect of elutropic strength

The effect of elutropic strength of the sample on absorption was investigated by preparing a series of samples that contained methanol at concentrations from 0 to 20%. The absorption–elutropic strength profiles obtained using PA or PDMS fibre are shown in Figs. 8 and 9. As methanol concentration increases, less analyte was absorbed. An increased proportion of methanol in the aqueous solution decreases the polarity of the aqueous sample so that the distribution constant decreases [7]. This effect was also observed by other investigators [29,39].

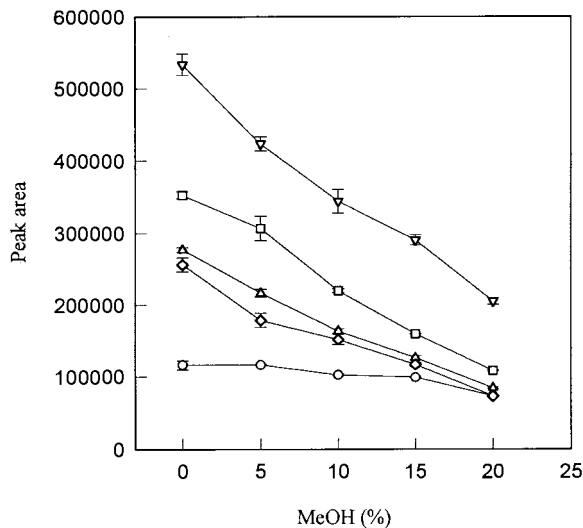


Fig. 9. Effect of methanol on absorption of organophosphorus pesticides by PDMS fibre. Absorption time, 30 min; desorption time, 7 min. Concentrations and symbols as in Fig. 3.

3.6. Effect of ionic strength

The effect of ionic strength on the absorption of analytes by a PA (Fig. 10) or a PDMS (Fig. 11) fibre was studied by preparing a series of samples that contained a Na_2SO_4 concentration range

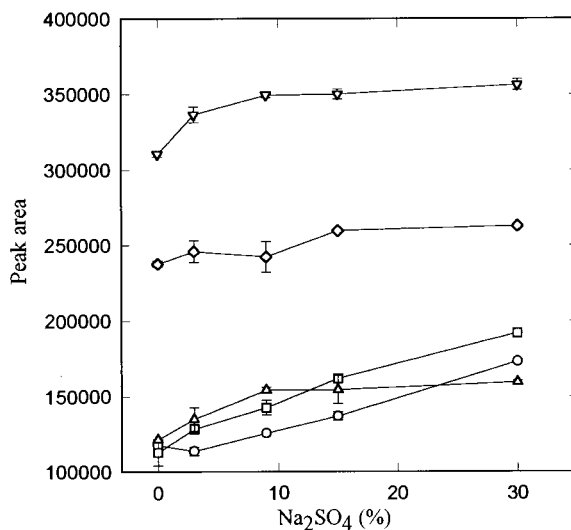


Fig. 10. Effect of ionic strength on absorption of organophosphorus pesticides by PA fibre. Absorption time, 30 min; desorption time, 5 min. Concentrations and symbols as in Fig. 2.

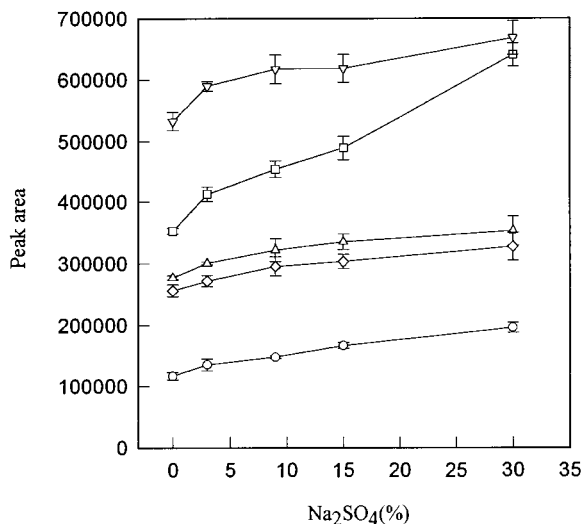


Fig. 11. Effect of ionic strength on absorption of organophosphorus pesticides by PDMS fibre. Absorption time, 30 min; desorption time, 7 min. Concentrations and symbols as in Fig. 3.

from 0 to 30%. The increase in absorption of the analytes, resulting from the 'salting-out effect', was observed using both fibres.

3.7. Effect of humic acid

The effect of humic acid on absorption of analytes by a PA (Fig. 12) or PDMS (Fig. 13) fibre was determined by preparing standards with a range of humic acid concentrations from 0 to 100 mg l⁻¹. At high concentrations of humic acid such as 100 mg l⁻¹, the response determined for fenthion shows a significant decrease > 20%. The absorption of the analytes was little affected by the humic acid when the concentration of humic acid is less than 10 mg l⁻¹.

3.8. Detection limits and precision

The detection limits and precision (RSDs) are shown in Table 1. Detection limits were calculated as three times the standard deviation of seven replicate runs. The detection limits for the analytes was lower by approximately two orders of magnitude using a PA fibre compared with that using a PDMS fibre except fenthion (0.12–0.10 µg

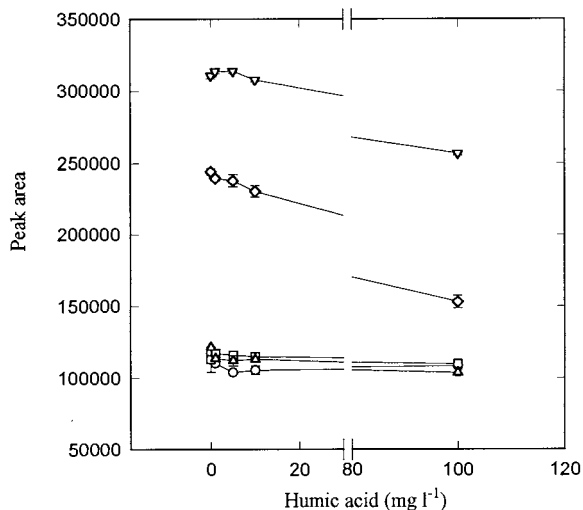


Fig. 12. Effect of humic acid on absorption of organophosphorus pesticides by PA fibre. Absorption time, 30 min; desorption time, 5 min. Concentrations and symbols as in Fig. 2.

l⁻¹). Precision of the method using either PA or PDMS fibres is better than 9%. Much lower LODs for the analysis of diazinon (0.025 µg l⁻¹) and disulfoton (0.013 µg l⁻¹) can be achieved using the SPME method (with both fibres) than that using EPA Method 622 (0.2 and 0.6 µg l⁻¹

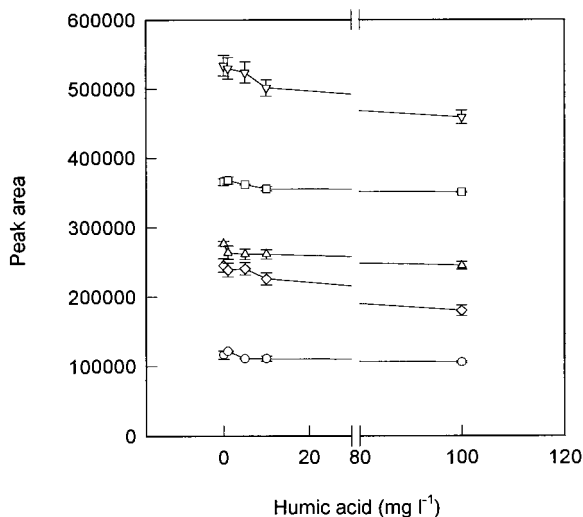


Fig. 13. Effect of humic acid on absorption of organophosphorus pesticides by PDMS fibre. Absorption time, 30 min; desorption time, 7 min. Concentrations and symbols as in Fig. 3.

Table 1

Comparison of detection limits^a (LOD) and relative standard deviations (RSDs) for the analysis of organophosphorus pesticides using PA or PDMS fibre

Compound	LOD ($\mu\text{g l}^{-1}$)		RSD (%) ^b	
	PA ^c	PDMS ^d	PA	PDMS
Mevinphos	420	860	9	8
Ethoprop	0.29	0.38	2	5
Diazinon	0.025	0.047	6	8
Disulfoton	0.013	0.030	3	6
Fenthion	0.10	0.12	8	6

^a Detection limits are calculated as three times the standard deviation of seven replicate runs.

^b Data obtained by extraction in seven replicate.

^c Concentrations of organophosphorus pesticides used for the run are 1 mg l^{-1} (mevinphos), $0.625 \mu\text{g l}^{-1}$ (ethoprop), $0.0625 \mu\text{g l}^{-1}$ (diazinon and disulfoton) and $0.25 \mu\text{g l}^{-1}$ (fenthion); absorption time, 30 min; desorption time, 5 min.

^d Concentrations of organophosphorus pesticides used for the run are 0.5 mg l^{-1} (mevinphos), $1.25 \mu\text{g l}^{-1}$ (ethoprop), $0.625 \mu\text{g l}^{-1}$ (diazinon and disulfoton) and $0.25 \mu\text{g l}^{-1}$ (fenthion); absorption time, 30 min; desorption time, 7 min.

for diazinon and disulfoton, respectively). The LODs for the analysis of fenthion and ethoprop are comparable for the SPME method and EPA

Method 622. Mevinphos showed a much higher LOD for the SPME method due to the low affinity of this polar analyte to the fibers. The SPME method provided comparable or better precision (RSDs 2–9%) compared with the EPA method 622 (RSDs 4–20%). SPME-GC is an equilibrium technique, but this procedure facilitates good sensitivity since the total amount of extracted material is transferred onto the GC column, which is different from that for liquid–liquid extraction (followed by determination with GC-FPD) used in EPA Method 622. Note that 1000 ml of sample solution is used for the EPA method, and as little as 3 ml of sample solution is used for the SPME method. The EPA method requires toxic solvent (methylene chloride and hexane) and the SPME method is a solvent-free technique. The procedures for the SPME method are much simpler than the EPA method.

In general, best selectivity and sensitivity (and lowest LODs) are achievable with SPME-GC-MS [29,31,35], but GC-FPD is much cheaper than GC-MS. SPME-GC-FPD is much more selective and sensitive (with lower LODs) for the analysis of organophosphorus pesticides than SPME-GC-

Table 2

Slopes and correlation coefficients of the calibration curve in deionized water (DIW) and lake water (LW)

Compounds	Matrix	PA ^a		PDMS ^b	
		Slope	Correlation coefficient	Slope	Correlation coefficient
Mevinphos ^c	DIW	12700	0.9991	5362	0.9995
	LW	12826	0.9984	5396	0.9989
Ethoprop ^d	DIW	849	0.9995	1431	0.9959
	LW	899	0.9998	1353	0.9957
Diazinon ^e	DIW	7566	0.9985	10873	0.9983
	LW	7662	0.9988	10725	0.9984
Disulfoton ^e	DIW	22414	0.9952	21555	0.9998
	LW	22773	0.9993	22624	0.9998
Fenthion ^e	DIW	17990	0.9982	10970	0.9965
	LW	18422	0.9992	10877	0.9982

^a PA fiber: absorption time, 30 min; desorption time, 5 min.

^b PDMS fiber: absorption time, 30 min; desorption time, 7 min.

^c Calibration curves with concentrations 2, 4, 10, 20, 40 mg l^{-1} for PA and PDMS.

^d Calibration curves with concentrations 12.5, 25, 50, 125 and 250 $\mu\text{g l}^{-1}$ for PA, and 12.5, 25, 50, 125, 250 and 500 $\mu\text{g l}^{-1}$ for PDMS.

^e Calibration curves with concentrations 1.25, 2.5, 5, 12.5 and 25 $\mu\text{g l}^{-1}$ for PA, and 1.25, 2.5, 5, 12.5, 25 and 50 $\mu\text{g l}^{-1}$ for PDMS.

FID [32,35] and SPME-GC-AED [28]. The selectivity and LODs are comparable for the methods of SPME-GC-NPD [30,33,35] and SPME-GC-FPD.

3.9. Environmental sample analysis

The results are shown in Table 2. Calibration curves of the analytes using either PA or PDMS fibres based on deionized water and lake water were compared. Correlation coefficients are better than $r = 0.9957$ for these organophosphorus pesticides. The slopes of the calibration curves were almost independent of the matrix of the sample solution (difference in slopes is less than 6%), which indicated that the SPME method can be used for the analysis of these organophosphorus pesticides in natural water using a simple calibration curve. We did not add salt to the samples and standards because the samples (lake water) did not contain a high concentration of salts. There is no interference from the matrix of the samples. The procedure is simpler if the addition of salt is not required. However, if the samples contain a high concentration of salt that can cause interference of the analysis, salt should be added. The addition of salt can also improve the sensitivities and LODs of the method.

SPME-GC-FPD is a simple, quick, solvent-free, sensitive and selective method for the analysis of organophosphorus pesticides in water.

Acknowledgements

We thank the National Science Council of Republic of China for support (grant no. NSC 87-2113-M007-042).

References

- [1] D. Barcelo, C. Porte, J. Cid, J. Albaiges, *Int. J. Environ. Anal. Chem.* 38 (1990) 199.
- [2] T.A. Bellar, W.L. Budde, *Anal. Chem.* 60 (1988) 2076.
- [3] C.H. Marvin, I.D. Brindle, C.D. Hall, M. Chiba, *J. Chromatogr.* 503 (1990) 167.
- [4] R. Carabias Martinez, E. Rodriguez Gonzalo, M.J. Amigo Moran, J. Hernandez Mendez, *J. Chromatogr.* 607 (1992) 37.
- [5] R.P. Belardi, J. Pawliszyn, *Water Pollut. Res. J. Can.* 24 (1989) 179.
- [6] C.L. Arthur, J. Pawliszyn, *Anal. Chem.* 62 (1990) 2145.
- [7] C.L. Arthur, L.M. Killam, K.D. Buchholz, J. Pawliszyn, J.R. Berg, *Anal. Chem.* 64 (1992) 1960.
- [8] R. Eisert, J. Pawliszyn, *Crit. Rev. Anal. Chem.* 27 (1997) 103.
- [9] Z. Zhang, M.J. Yang, J. Pawliszyn, *Anal. Chem.* 66 (1994) 884A.
- [10] D. Louch, S. Motlagh, J. Pawliszyn, *Anal. Chem.* 64 (1992) 1187.
- [11] C.L. Arthur, L.M. Killam, S. Motlagh, M. Lim, D.W. Potter, J. Pawliszyn, *J. Environ. Sci. Technol.* 26 (1992) 979.
- [12] M. Chai, C.L. Arthur, J. Pawliszyn, R.P. Belardi, K.F. Pratt, *Analyst* 188 (1993) 1501.
- [13] D.W. Potter, J. Pawliszyn, *J. Chromatogr.* 625 (1992) 247.
- [14] D.W. Potter, J. Pawliszyn, *Environ. Sci. Technol.* 28 (1994) 298.
- [15] K.D. Buchholz, J. Pawliszyn, *Environ. Sci. Technol.* 27 (1993) 2844.
- [16] K.D. Buchholz, J. Pawliszyn, *Anal. Chem.* 66 (1994) 160.
- [17] S. Magdic, J. Pawliszyn, *J. Chromatogr. A* 723 (1996) 111.
- [18] Z. Zhang, J. Pawliszyn, *J. High Resolut. Chromatogr.* 16 (1993) 689.
- [19] Z. Zhang, J. Pawliszyn, *Anal. Chem.* 65 (1993) 1843.
- [20] Z. Zhang, J. Pawliszyn, *Anal. Chem.* 67 (1995) 34.
- [21] J. Chen, J. Pawliszyn, *Anal. Chem.* 67 (1995) 2530.
- [22] A.A. Boyd-Boland, J. Pawliszyn, *Anal. Chem.* 68 (1996) 1521.
- [23] R. Eisert, J. Pawliszyn, *Anal. Chem.* 69 (1997) 3140.
- [24] K. Jinno, T. Muramatsu, Y. Saito, Y. Kiso, S. Magdic, J. Pawliszyn, *J. Chromatogr. A* 754 (1996) 137.
- [25] J.Y. Horng, S.D. Huang, *J. Chromatogr. A* 678 (1994) 313.
- [26] S.D. Huang, C.Y. Ting, C.L. Lin, *J. Chromatogr. A* 769 (1997) 239.
- [27] S.D. Huang, C.P. Cheng, Y.H. Sung, *Anal. Chim. Acta* 343 (1997) 101.
- [28] R. Eisert, K. Levsen, G. Wunsch, *J. Chromatogr. A* 683 (1994) 175.
- [29] R. Eisert, K. Levsen, *J. Am. Mass Spectrom.* 6 (1995) 1119.
- [30] R. Eisert, K. Levsen, *Fres. J. Anal. Chem.* 351 (1995) 555.
- [31] A. Boyd-Boland, S. Magdic, J. Pawliszyn, *Analyst* 121 (1996) 929.
- [32] M.T. Sng, F.K. Lee, H.A. Lakso, *J. Chromatogr. A* 759 (1997) 225.
- [33] I. Valor, J.C. Molto, D. Apraiz, G. Font, *J. Chromatogr. A* 767 (1997) 195.
- [34] T. Gorecki, R. Mindrup, J. Pawliszyn, *Analyst* 121 (1996) 1381.
- [35] S. Magdic, A. Boyd-Boland, K. Jinno, J.B. Pawliszyn, *J. Chromatogr. A* 736 (1996) 3259.

- [36] T.K. Choudhury, K.O. Gerhardt, T.P. Mawhinney, *Environ. Sci. Technol.* 30 (1996) 3259.
- [37] V. Lopez- Avila, R. Young, W.F. Beckert, J. High Resolut. *Chromatogr.* 20 (1997) 487.
- [38] X.P. Lee, T. Kumazawa, K. Sato, O. Suzuki, *Chromatogr* 42 (1996) 135.
- [39] L. Urruty, M. Montury, *J. Agric Food Chem.* 44 (1996) 3871.

A stopped-flow microdialysis sampling-flow injection system for automated multivessel high resolution drug dissolution testing

Qun Fang ^a, Shu-Sheng Liu ^b, Jin-Feng Wu ^b, Yu-Qing Sun ^a,
Zhao-Lun Fang ^{c,*}

^a *Shenyang Pharmaceutical University, 110015 Shenyang, China*

^b *Department of Communication Engineering, Northeastern University, 110006 Shenyang, China*

^c *Flow injection Analysis Research Center, Chemistry Department, Box 332, Northeastern University, 110006 Shenyang, China*

Received 15 July 1998; received in revised form 10 December 1998; accepted 10 December 1998

Abstract

A simple and robust flow injection on-line microdialysis system for multivessel drug dissolution testing is described. Microdialysis probes were used for sampling from the dissolution media. A stopped-flow dialysis mode with a 50-s stopped-flow period followed by 10-s injection at a perfusion rate of 2.8 ml min⁻¹ for each probe was used to achieve high resolution of dissolution events using relatively simple equipment and operation. The precisions obtained for simultaneous monitoring of dissolution profiles for six tablets were all better than 0.9% (RSD $n = 80$) and the overall sampling frequency of the system was 360 and 60 h⁻¹ for each test vessel. The dissolution profiles of isoniazid fast-release tablet from three sources were determined to demonstrate the performance of the system. © 1999 Elsevier Science B.V. All rights reserved.

Keywords: Flow injection; Microdialysis; Stopped-flow; Dissolution testing; Isoniazid

1. Introduction

The determination of the release rate of drugs through dissolution is essential for the development of testing new dosage forms and for quality control in pharmaceutical industries. Dissolution testing of pharmaceutical dosage forms is a laborious process that generates large number of sam-

ples, especially when the tests are performed with multivessels, as in most routine dissolution testing, or with high sampling frequencies. Various approaches have been proposed in the past to automate this testing procedure [1–3], and automated systems are commercially available.

In most approaches, on-line filtration techniques are used to separate the active ingredients and insoluble excipients of the preparation in the sample solution before the detection [4–8]. The main drawback of on-line filtration is the clogging

* Corresponding author. Tel.: +86-24-2389-3000, +86-24-2389-7659; fax: +86-24-238-90448.

of filters by insoluble constituents in the preparations, particularly when micropore filtration membranes, recommended for dissolution testing in most Pharmacopoeia [6,7,9], are used as filtering media [10], or when high sampling flow-rates are used.

The dialysis separation technique offers several advantages over filtration techniques. Active ingredients in drug formulations can be separated not only from insoluble excipient particles by dialysis, but also from soluble macromolecule components and additives present in dosage forms and dissolution media, which cannot be separated using conventional filtration techniques. Dialysis is driven by diffusion caused by the difference in analyte concentration on the two sides of the dialysis membrane and not by pressure difference, and therefore is less susceptible to clogging by insoluble excipients. A further advantage for dialysis operation is that it does not involve volume changes in sample solution, thus compensation of solution volume usually performed in systems using filtration is not required.

Macheras et al. [11] reported a flow injection serial dynamic dialysis system for dissolution testing in milk by drawing the sample solution out and pumping it through the dialyzer as practiced in conventional on-line dialysis systems, however this arrangement appears to be too complicated to be used in multivessel dissolution testing. The in situ sampling capability of microdialysis offers better potentials for multivessel sampling. Shah et al. [12] appeared to be the first to develop a microdialysis sampling technique for dissolution testing. Instead of pumping out the dissolution solution, microdialysis sampling is performed simply by immersing the microdialysis probe in the sample solution. With an appropriate perfusion medium, samples at extreme pH ranges can be buffered to a pH in the dialysate which is more compatible with column materials for on-line liquid chromatography (LC).

More recently, Shah et al. [13] reported an automated multivessel dissolution testing system using microdialysis sampling. Owing to the use of a non-stop continuous-flow dialysis mode in that system, low perfusion rates ($10\text{--}100\ \mu\text{l min}^{-1}$) were employed, giving rise to a low sampling frequency of $1\ \text{h}^{-1}$ for each of six dissolution

vessels in the study of dissolution profiles of controlled-release dosage forms. For fast release dosage forms, the dissolution profiles for only three tablets were measured simultaneously with a sampling interval of 6.5 min for each vessel.

In this work, a stopped-flow dialysis mode, which has been applied in conventional on-line dialysis but seldom in microdialysis systems, was used for microdialysis sampling in a six vessels drug dissolution system to shorten the sampling period, increase the analyte concentration, and improve the resolution of the dissolution process, particularly for multivessel monitoring of fast release dosage forms. Isoniazid tablets, in a rapid release dosage form, were used as test sample to demonstrate the performance of the system.

2. Experimental

2.1. Reagents and standard solutions

All chemicals were of analytical reagent grade and degassed demineralized water was used throughout.

Zinc chloride solution (50%, w/v) used for treatment of hollow dialysis fiber was prepared by dissolving 10 g zinc chloride in 10 ml water and made up to 20 ml with water.

The isoniazid standard solutions in the range of $25\text{--}125\ \text{mg l}^{-1}$ were prepared by dissolving 25, 50, 75, 100, 125 mg isoniazid standard (State Monitoring Center for Biological and Pharmaceutical Products, Beijing) in 100 ml water and made up to 1000 ml with water, respectively.

Isoniazid tablets were purchased on the market.

Water was used as carrier, i.e. perfusion solution, and dissolution medium.

2.2. Instrumentation

2.2.1. Microdialysis system

A loop-type microdialysis probe was used for sampling from the dissolution vessels. The dialyzer was produced using regenerated cellulose hollow dialysis fibers (280 mm i.d., 480 mm o.d., with a molecular weight cutoff of 1500 Da.; donated by Mr. Pinzao Yu of Hangzhou Water

Treatment Center of State Ocean Bureau). The construction of the microdialysis probe is shown in Fig. 1a.

The probe was produced by inserting 3 mm of both ends of a 10.6-cm length of hollow dialysis fiber into two 2-cm lengths of Micro-Line tubing (0.5 mm i.d., 1.6 mm o.d., Thermoplastics, Sterling, NY), and the connections were sealed with epoxy.

Prior to use, the fibers were treated with zinc chloride solution (50%, w/v) to enlarge the pores by first perfusing the probes with the zinc chloride solution, and then immersing the entire probe in the solution for 6 h, after which, the probes were washed with water, and immersed in water at 37°C for at least 10 h. The probes were stored in water before use.

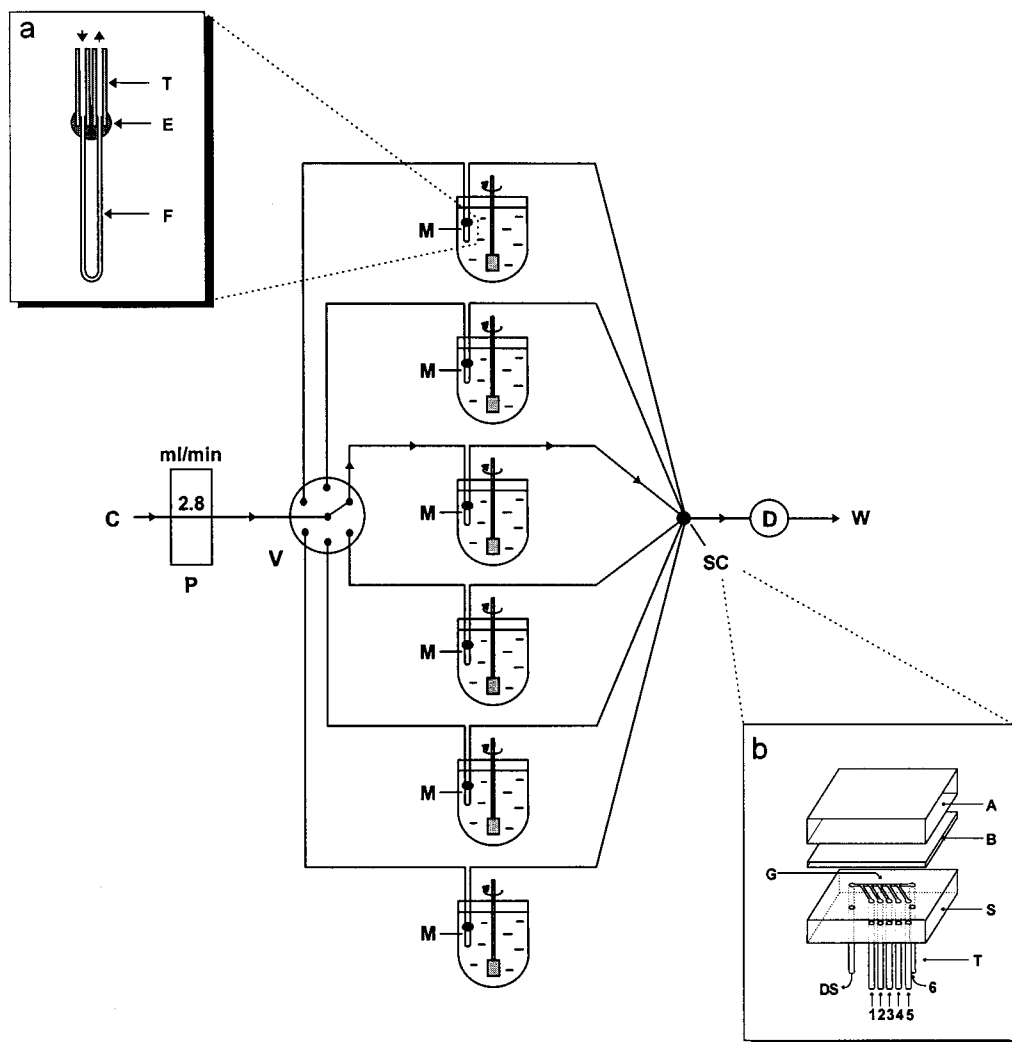


Fig. 1. Schematic diagram of the flow-injection on-line microdialysis system for multivessel dissolution test. C, carrier solution (perfusate); P, peristaltic pump; V, multiposition valve; SC, seven-way connector; D, detector, 254 nm; W, waste. (a) Schematic diagram of the microdialysis probe. E, epoxy glue; F, hollow dialysis fiber; T, connecting tubing. (b) Schematic diagram of the seven-way connector. A, upper plexiglas block; B, elastic PVC sheet; G, channels press-molded on the surface of lower PVC block, channel width, 0.8 mm, depth, 0.6 mm; S, lower PVC block; T, PTFE connection tubing, 0.5 mm i.d. and 1.3 mm o.d.; 1, 2, 3, 4, 5, 6, dialysates from six microdialysis probes, respectively; DS, detection system.

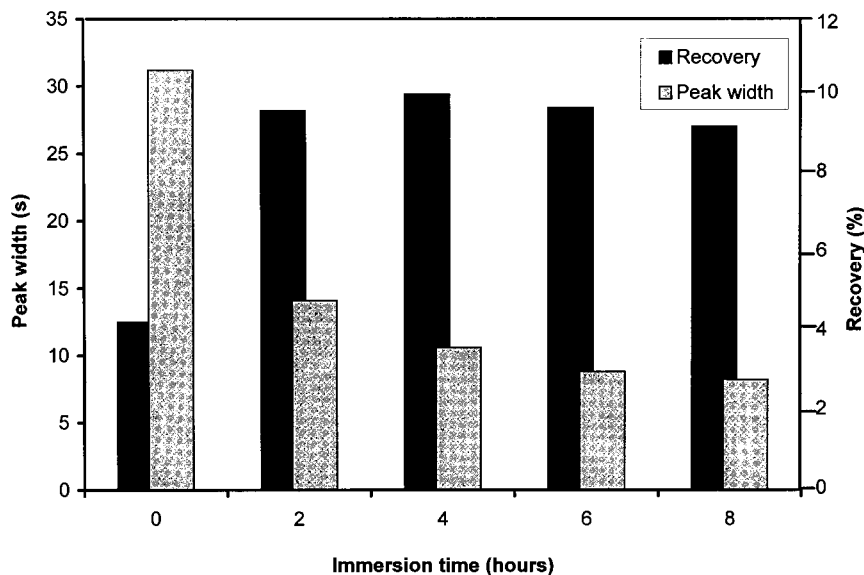


Fig. 2. Effect of immersion time of microdialysis fiber in 50% ZnCl_2 solution on peak width and dialysis recovery of microdialysis probes produced from the fibers. Effective dialysis fiber length: 10 cm, stopped-flow dialysis time: 50 s, carrier flow-rate: 2.8 ml min^{-1} ; sample solution, isoniazid standard (100 mg l^{-1}), 37°C .

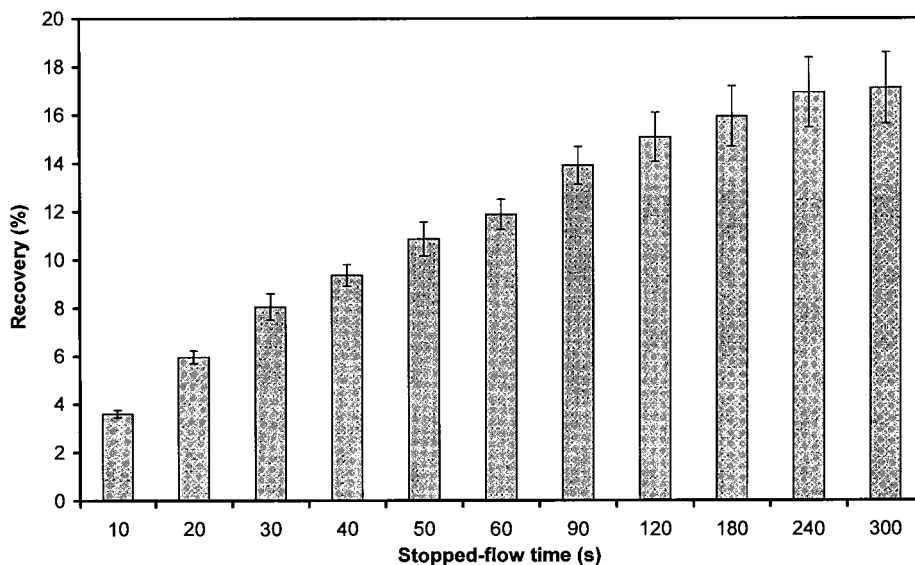


Fig. 3. Effect of stopped-flow time during microdialysis on dialysis recovery.

2.2.2. Sampling and detection system for dissolution testing with six vessels

A model LZ-1020 8-channel peristaltic pump (Zhaofa Instruments, Shenyang) and tygon pump tubings were used for delivery of dialysate and

carrier. A ten-position valve (Valco Instruments Co., Inc. Houston), in which only six positions were used in this work, and a home-made seven-channel connector were used for sequential sampling from six vessels. The sampling manifold is

shown schematically in Fig. 1. A drug dissolution system with six test vessels (Tianjin University, Radio Works, Tianjin) was used. The entire system was controlled by a computer program written in Visual Basic.

The seven-way connector (shown in Fig. 1b) was composed of two blocks. The lower block was made from hard polyvinylchloride (PVC), and furnished with six inlets for perfusates and an outlet for connection to the detector. 0.8 mm wide channels were press-molded on the surface of the lower block to a depth of 0.6 mm. The upper block was made from plexiglas. An elastic PVC sheet was sandwiched between the two blocks to seal the channels. The two blocks were held together by screws (not shown in Fig. 1b).

PTFE tubing of 0.5 mm i.d. and 1.1 mm o.d. was used for all connections. A knotted reactor (KR), made by tying interlaced knots in a 30-cm long PTFE tubing, was used to connect the outlet of the seven-way connector and the detector. The length of tubing connecting the probes and seven-way connector was 40 cm, which was the shortest applicable length with the equipment used.

A model DZ-254 liquid chromatograph UV detector (Scientific Instrument Works, Shanghai) was used at 254 nm wavelength with a 1-cm path length 10 μ l flow-cell. A model XTD-204 strip-chart recorder (Dahua Instruments, Shanghai) was used for readout.

2.3. Procedures

2.3.1. System optimization

Investigations were conducted at an early stage of this work using a single test vessel to facilitate optimization of the sampling system. In these experiments six microdialysis probes were placed in the same vessel containing only standard solutions. Other conditions were as described in Section 2.2.2.

The determination of isoniazid in the sample dialysate held in the dialysis probe following dialysis was conducted as follows: The multiposition valve was operated with a defined interval for each valve position. Six positions operated at 10 s intervals were used, unless mentioned otherwise. The carrier solution was pumped through the six

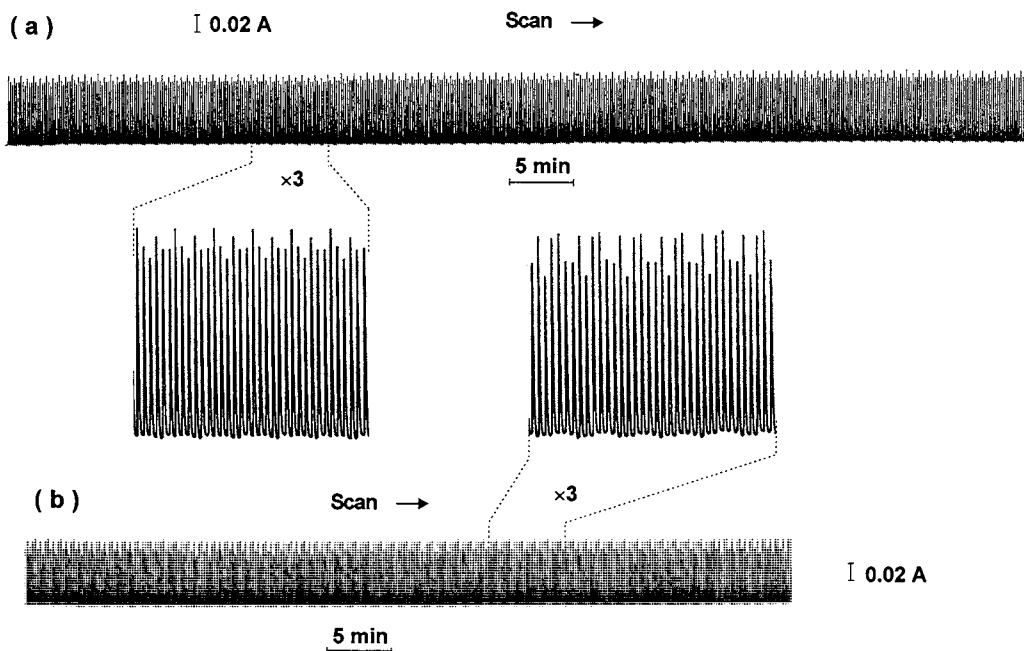


Fig. 4. Chart recordings obtained in reproducibility studies of the automated system for multivessel dissolution testing using isoniazid standard solution (100 mg l⁻¹) (a), and sample solution from origin B (ca. 100 mg l⁻¹) (b).

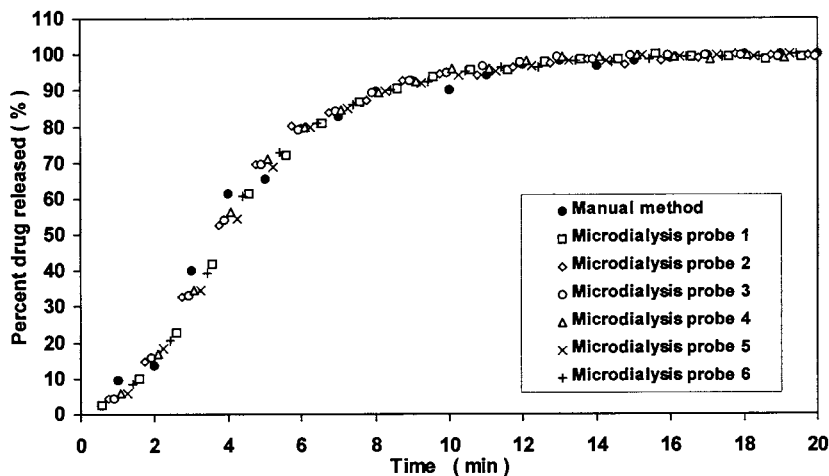


Fig. 5. Dissolution profiles of isoniazid tablets determined by the automated dissolution system using microdialysis sampling and compared to manual dissolution system. Conditions are as shown in Fig. 1.

microdialysis probes sequentially, and the dialysates in the six probes were transported via the seven-way connector into the detector flow-cell at 10 s intervals. Thus, for each probe, the stoppedflow time (i.e. dialysis sampling time) was 50 s, and the injection time was 10 s.

2.3.2. Dissolution testing

The experimental setup used is shown schematically in Fig. 1. The dissolution tests were performed mainly adopting conditions recommended for isoniazid tablets by Chinese Pharmacopoeia [9]. A total of 1000 ml of degassed water used as dissolution medium was filled into each testing vessel. A temperature of $37 \pm 0.5^\circ\text{C}$ was maintained in the system throughout the dissolution experiments with a circulated water bath. Baskets containing isoniazid tablets were rotated at 100 rpm at 3 cm distance from the bottom of the vessels. Six microdialysis probes were immersed in each of dissolution medium of the vessels. Microdialysis probes were fixed midway between the surface of the dissolving medium and the top of the basket, 1 cm away from the nearest wall of the test vessels. Water thermostated at 37°C was used as the carrier, which was initially pumped to the detector to achieve a stable baseline signal. Each basket containing an isoniazid tablet sample was lowered into its test

vessel at the beginning of the injection stage. Thus, the testings for the six samples were initiated successively at 10 s intervals. The dialysates held in the probes were injected and transported through the seven-way connector and the knotted reactor into the flow cell, and measured at 254 nm.

Calibration of the system using a standard series was performed at the beginning of each test, and recalibration using a 100 mg l^{-1} standard was performed after each test under the same conditions as for dissolution testing except that six probes were placed in a single vessel containing 1000 ml isoniazid standard.

2.3.3. Comparison of the microdialysis method with Chinese Pharmacopoeia method

The experiment was performed with six microdialysis probes in a single vessel using a single isoniazid tablet for the test, proceeding as described in Section 2.3.2. Simultaneously, a manual sampling from this vessel was also performed at a sampling frequency of 60 h^{-1} and each time withdrawing a sample volume of 2 ml. After filtering with $0.8 \mu\text{m}$ micropore membrane filter, the filtrates of the sample solutions were diluted 10-fold, and the absorbance measured at 254 nm. Results from the two sampling modes were compared.

3. Results and discussion

3.1. Considerations in the design of the FI on-line microdialysis system for dissolution testing with six vessels

The following were taken into consideration in designing a simple, rapid, reliable and automated system for multivessel dissolution testing:

In most reported microdialysis sampling systems, a continuous-flow mode was adopted to achieve continuous sampling from the dissolution

solutions; static perfusates were used only in non-flow dialysis systems. To our best knowledge, there has been only one reported application adopting the stopped-flow mode which was used for sampling from a small-volume bioreactor [14]. The stopped-flow mode was used in this case to reduce the effect of dialysis sampling on sample composition and not for improving the sampling frequency. In the continuous-flow mode, microdialyses were performed by perfusing the microdialysis probe with a defined solution at constant flow-rate to achieve non-interrupted continuous

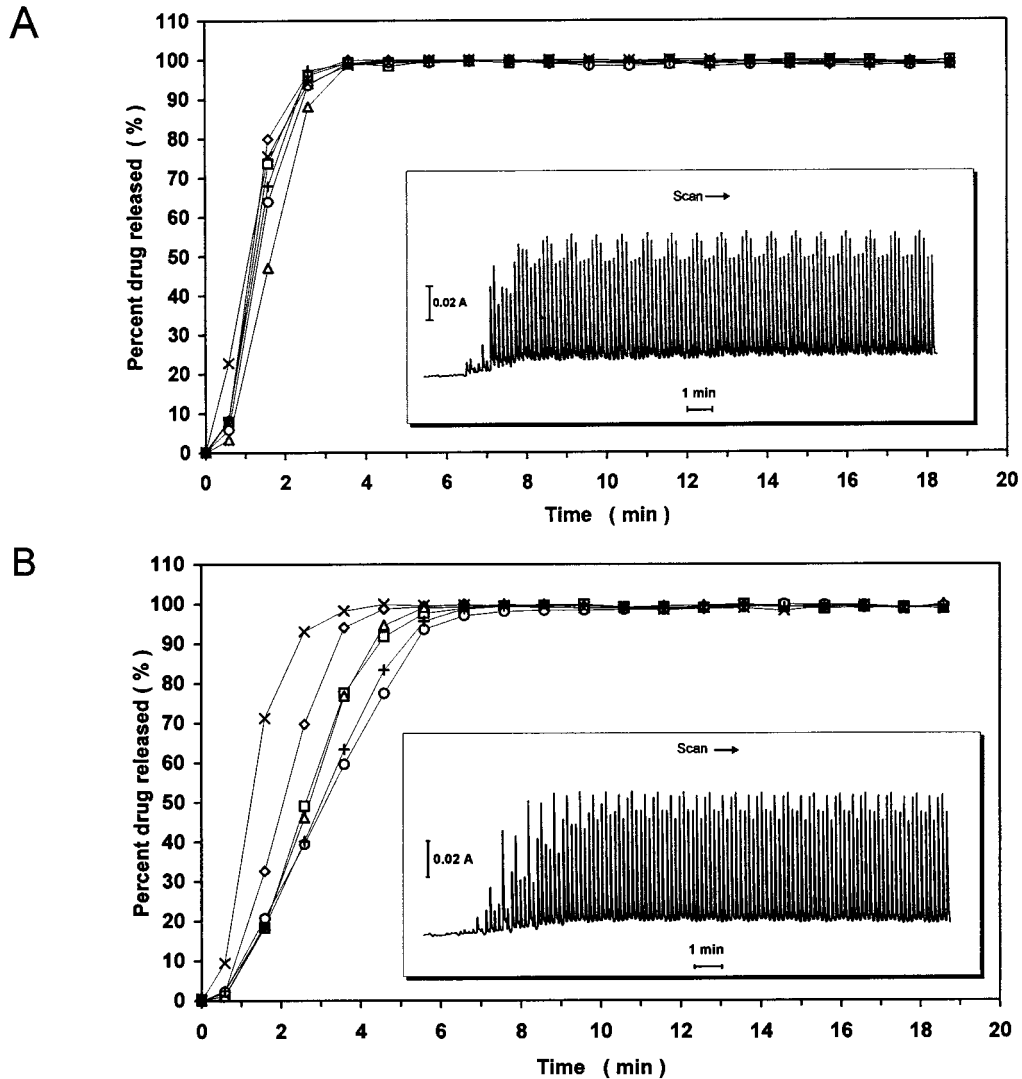


Fig. 6. A. B. C. Dissolution profiles and typical chart recordings (insert) obtained in dissolution test of six isoniazid tablets from origins A, B and C. Conditions are as shown in Fig. 1.

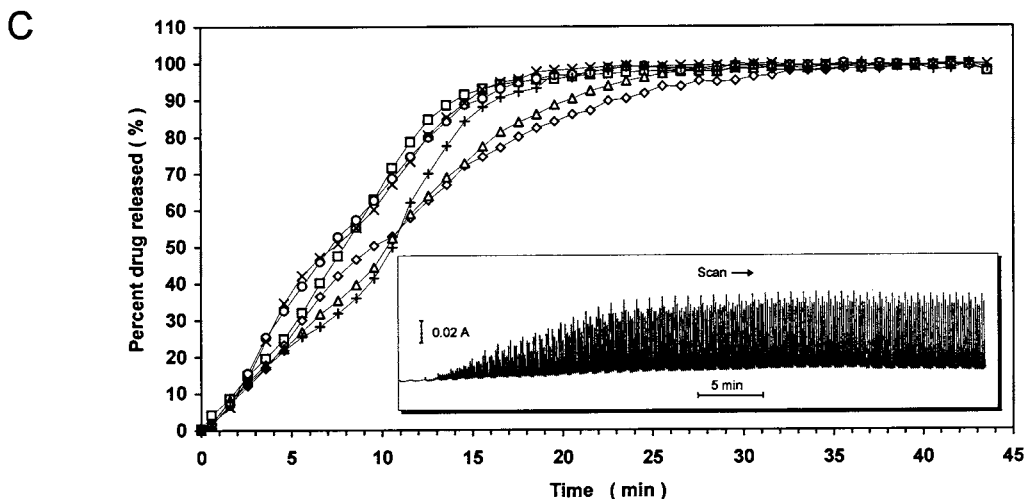


Fig. 6. (Continued)

operation. Extremely low perfusion rates ($1\text{--}50\ \mu\text{l min}^{-1}$) were usually used to achieve acceptable dialysis recoveries. The dialysates were transferred from the dialyzer into the sample loop of the valve also at this low flow-rate, resulting in low sampling frequencies. When applied to dissolution testing with multivessels, a multiposition valve would be required to achieve sampling from the vessels, which would increase the dead volume between the probe and sample loop, and further decrease the sampling frequency.

In this work, a stopped-flow dialysis mode, in which the sampling was performed under stopped-flow conditions for a defined period, and the dialysate transferred to the detection system by the perfusion flow, was adopted for sampling from multivessels. An advantage of the stopped-flow mode is that much higher perfusion rates ($>1\ \text{ml min}^{-1}$) can be used to decrease the dialysate transferring time and further increase sampling frequency without affecting the dialysis. A further advantage of this mode is that a common peristaltic pump could be used to deliver the perfusion solution, instead of the separate pumps working at low flow-rates usually used in the continuous-flow mode.

Instead of transferring the dialysate to the sample loop of an injection valve as in previously reported FI systems, in this work, the dialyzer

probe was made to function as a sample loop. The dialysates in the probes were transferred directly by the perfusion flow (carrier) into the flow-cell of the detector without an injection valve. With such a design, the manifold and operation were both simplified and the sampling frequency of the system was increased, which is most important for achieving high resolution of the dissolution process, particularly for multisample monitoring. However, when operated in such a mode, the baseline signal was not generated by the blank perfusate (carrier), since dialysis proceeded to some extent when the carrier was pumped through the dialysis probe. While monitoring the dissolution process, the baseline increased gradually following the release of the tablet owing to increase of analyte concentration in the dissolution medium. In actual measurements the analyte contribution to the baseline was about 10% that of the sample peak maximum. However, since the same effect occurred during the calibration this baseline drift compensated through calibration, and in the dissolution studies all evaluation of peak height were made referring to the baseline.

In this work, a multiposition valve and a seven-way connector were used to achieve six-vessel dissolution testing with stopped-flow microdialysis. An alternative would be to use two multiposi-

tion valves, but this complicates the system and makes the equipment more expensive. A shortcoming of the present system might be that when the carrier flows through one of the dialysis probes in the injection stage, the pressure generated could be transferred to the other probes operating in the stopped-flow stage and affect their dialysis process. However, no such effects were observed in this work, probably owing to the low flow-rates used.

3.2. Considerations on the expression of dissolution time

In this work in order to improve the monitoring resolution, a stopped-flow on-line dialysis approach is used for sampling from a drug dissolution medium in which the analyte concentration is under continuous change. Consequently, during each dialysis sampling stage not all the analyte in the dissolution medium experiences the same period of dialysis. As a continuous monitoring method, to which dissolution time does the analyte concentration in the final dialysate refer demands consideration.

Analyte concentration variations during drug dissolution processes are non-linear and occasionally described only by complicated concentration–time functions, however, within a short stopped-flow sampling period, t of less than a minute, the concentration variation with time can

be considered as almost linear, albeit with an intercept on the concentration axis. The concentration, C and dissolution time, T may be described by the equation:

$$C = kT + m \quad (T_0 \leq T \leq T_0 + t) \quad (1)$$

where k and m are constants, and T_0 the starting time of the stopped-flow period.

The recovery (% analyte dialyzed)–time relationship of a dialysis process is also non-linear, however, within the earlier stage of a dialysis, the recovery variation may be assumed to be directly proportional to the dialysis time. This assumption has been validated in this study (as shown in Fig. 3.). Thus the recovery, R of the dialysis at a stopped-flow time, t_s may be expressed by:

$$R = \frac{100C^d}{C} = 100at_s \quad (0 \leq t_s \leq t) \quad (2)$$

where C , and C^d are the analyte concentrations in the sample medium and dialysate respectively, and a is a constant determined by the dialysis system. Following a stopped-flow period of t_s , the analyte concentration of the dialysate, C_x^d may be expressed by the equation:

$$C_x^d = C_0^d + \int_{C_0}^{C_t} at_s dC \quad (3)$$

Combining Eqs. (1)–(3), the dissolution time, T_x corresponding to the analyte concentration in

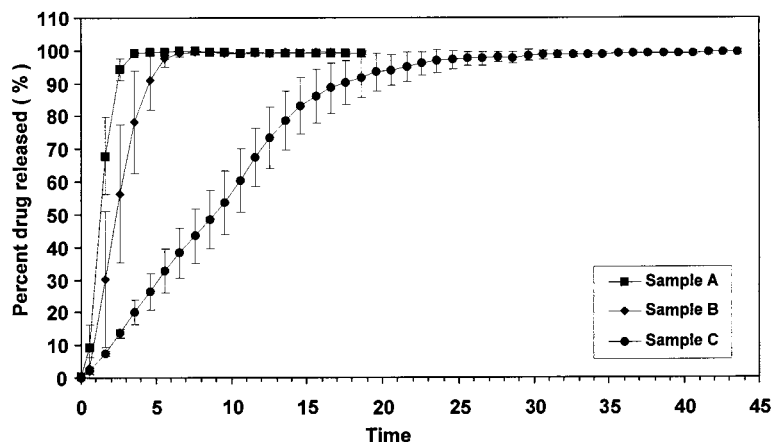


Fig. 7. Dissolution profiles of isoniazid tablets ($n=6$) from origin A, B and C. Conditions are as shown in Fig. 1.

the final dialysate, C_x^d is expressed by the equation:

$$T_x = T_0 + \int_{T_0}^{T_0 + t_s} \frac{t}{t} dT \quad (4)$$

Since

$$t_s = T_0 + t - T, \quad (5)$$

combining Eq. (4) and Eq. (5):

$$T_x = T_0 + \frac{t}{2} \quad (6)$$

Thus the dissolution time corresponds to the average of the starting and ending times of the stopped-flow period.

With a stopped-flow period of 50 s adopted in this study a correction of -25 s was applied to the injection time for the expression of the dissolution time.

3.3. Treatment of the dialysis fiber

The microdialysis probes were pretreated as described under Experimental in order to enlarge the pores of the dialysis membrane [15]. This was found necessary for decreasing the peak width, increasing the sampling frequency as well as for improving the dialysis recovery. The effect of immersion (pretreatment) time of the microdialysis fiber in $ZnCl_2$ solution on dialysis recovery and peak width obtained using probes produced from the fibers (10 cm effective length) were investigated using a 50 s stopped-flow dialysis period. The results are shown in Fig. 2. The recovery increased steeply within 3 h, but changed little thereafter. The peak width (measured at 1% peak height) decreased with increase in immersion time, up to 6 h. The molecular weight cutoff of the dialysis membrane was measured using aqueous solutions of polyethylene glycol with different molecular weights following known procedures [16]. An immersion time of 6 h was employed in this work to obtain sufficient porosity for achieving high sampling frequency, a molecular weight cutoff of 12 000 Da. was obtained with this pretreatment.

3.4. Optimization of the dialysis sampling system

The effect of perfusate (carrier) flow-rate within a range of 0.9 – 3.4 ml min^{-1} on the peak width was studied using 60-s stopped-flow periods. The results showed a decrease in peak width with increase in flow-rate. Higher flow-rates should be favored for increasing the sampling frequency, however, dialysate loss owing to ultrafiltration through the dialyzer membrane was induced at high perfusion-rates, and a moderate flow-rate of 2.8 ml min^{-1} was used in this study.

The effect of stopped-flow period in a range of 0–5 min on dialysis recovery was investigated employing six microdialysis probes. The result is shown in Fig. 3. The recovery increased steeply at short stopped-flow periods, but became much more gradual above 3 min. In this work, a 10-s injection time for each probe was employed to achieve high resolution of the dissolution process, thus the stopped-flow time for each probe in dissolution testing with six testing vessels was $10 \times (6 - 1) = 50$ s. The average dialysis recovery for six typical microdialysis probes under such conditions was $10.9 \pm 0.6\%$, $n = 6$. Under the same conditions, without stopped-flow, with a perfusion rate of 2.8 ml min^{-1} the dialysis recovery was only 0.3%, which was 3% that obtained in the stopped-flow mode.

3.5. Correction of Schlieren effect interferences

Under dissolution testing conditions, temperature differences between the perfusate within the dialysis probe (immersed in the dissolution medium thermostated at 37°C), and the perfusate in conduits outside the probe (exposed to ambient conditions) result in differences in refractive properties of the dialysate and carrier zones of the perfusate, giving rise to spurious peaks at the interface of the zones [17]. This Schlieren effect interference appeared even when the vessel for the perfusate was thermostated at 37°C during the monitoring process, apparently owing to cooling of the perfusate during transport through the pump tubing and transport conduits. When a blank solution was measured in this system, a spurious peak with a height of about 1/20 that of

a dialysate of a 100-mg l⁻¹ isoniazid standard solution, generated by Schlieren effect, was observed. A 30-cm long knotted reactor located downstream of the seven-way connector was found to decrease the blank signal as much as 50%, but could not be eliminated completely. However, owing to the small volume of dialysate injected (7 µl), the interfering peak maximum almost coincided with that of the dialysate, therefore a correction was made for the readout by simply subtracting the blank peak absorbance.

3.6. Performance of the system for dissolution testing with six vessels

Calibration graphs were linear in the range of 0–150 mg l⁻¹ for six typical microdialysis probes expressed by the following regression equations, with *r* values in the range 0.9992–0.9999:

$$A = 7.19 \times 10^{-4}C + 5.94 \times 10^{-4}$$

$$A = 7.27 \times 10^{-4}C + 1.10 \times 10^{-4}$$

$$A = 7.52 \times 10^{-4}C - 9.67 \times 10^{-4}$$

$$A = 8.20 \times 10^{-4}C - 5.98 \times 10^{-4}$$

$$A = 8.22 \times 10^{-4}C - 1.18 \times 10^{-4}$$

$$A = 8.42 \times 10^{-4}C + 3.27 \times 10^{-4}$$

A being the absorbance, and *C*, concentration of isoniazid.

The reproducibility of the system over 80- and 60-min periods was studied using constant concentration solutions composed of both an isoniazid standard solution (100 mg l⁻¹) and a sample solution (ca. 100 mg l⁻¹) prepared from a fully dissolved isoniazid tablet. The results are shown in Fig. 4. The peak height RSD for six microdialysis probes tested were generally better than 1% (0.87, 0.60, 0.61, 0.50, 0.78, 0.65% (*n* = 80) and 0.62, 0.40, 0.60, 0.43, 0.50, 0.71% (*n* = 60), respectively), which demonstrates the reliability and stability of the system for dissolution testing. The differences between the peak heights of individual probes were due to small variations in effective length of the dialysis fibers, this had no effect on the measurement, since each probe was calibrated separately. The overall sam-

pling frequency of the system was 360 h⁻¹, and for each test vessel 60 h⁻¹, which is high enough for simultaneous monitoring of dissolution process of fast-release drug preparations in multivessel dissolution testing.

Comparison of the microdialysis sampling method and Chinese Pharmacopoeia method [9] was made as described in Section 2. The results are shown in Fig. 5. The dissolution profiles of the microdialysis method agreed well with those obtained using the Chinese Pharmacopoeia standard method. The content of isoniazid in the sample tablet was also determined using the two methods. The results of the microdialysis method and pharmacopoeia method were 97.8 ± 0.5% (*n* = 5) and 98.2 ± 0.6% (*n* = 5) (expressed as the percentage of the specified content), respectively. No significant difference between the results was observed on subjecting to a statistic *t*-test (*α* = 0.05).

Dissolution tests for three isoniazid tablet samples from commercial sources A, B and C were performed using the described system with typical chart recordings and dissolution profiles shown in Fig. 6A, B and C. The average dissolution profiles of six samples from origins A, B and C shown in Fig. 7. demonstrate the strong capability of the present system in characterizing the kinetic features of the dissolution process of drug formulations.

Although the samples from origins A, B and C all satisfy the requirement of Chinese Pharmacopoeia, the kinetic features of their dissolution process vary significantly.

4. Conclusion

In this work, the stopped-flow microdialysis sampling mode was shown to be a simple, robust and automated system for multivessel dissolution testing capable of provide high resolution of the dissolution process. The system may provide a powerful tool for pharmaceutical research and quality control of drug formulations. The system demonstrates further potentials for applications to on-line process monitoring of other multisample systems.

References

- [1] A. Koupparis, P.I. Anagnostopoulou, *Anal. Chim. Acta* 204 (1988) 271.
- [2] Georgiou, G.N. Valsami, P.E. Macheras, M.A. Koupparis, *J. Pharm. Biomed. Anal.* 12 (1994) 635.
- [3] Solich, P.E. Macheras, M.A. Koupparis, *J. Pharm. Sci.* 84 (1995) 889.
- [4] D. Luque de Castro, M. Valcarcel, *J. Pharm. Biomed. Anal.* 8 (1990) 329.
- [5] E. Lamparter, C.H. Lunkenheimer, *J. Pharm. Biomed. Anal.* 10 (1992) 727.
- [6] United States Pharmacopoeial Convention, Inc., *The United States Pharmacopoeia XXIII*, 1995, p. 1791.
- [7] British Pharmacopoeia Commission, *British Pharmacopoeia*, 1993, p. A160.
- [8] C.A. Georgiou, G.N. Valsami, P.E. Macheras, M.A. Koupparis, *J. Pharm. Biomed. Anal.* 12 (1994) 635.
- [9] Chinese Pharmacopoeia Commission, *Chinese Pharmacopoeia*, 1995, p. 254.
- [10] Q. Fang, Y.-Q. Sun, *Yaowu Fenxi Zazhi* 15 (1995) 29.
- [11] P. Macheras, M. Koupparis, C. Tsaprounis, *Int. J. Pharm.* 33 (1986) 125.
- [12] K.P. Shah, M. Chang, C.M. Riley, *J. Pharm. Biomed. Anal.* 12 (1994) 1519.
- [13] K.P. Shah, M. Chang, C.M. Riley, *J. Pharm. Biomed. Anal.* 13 (1995) 1235.
- [14] N. Torto, G. Marko-Varga, L. Gorton, H. Stalbrand, F. Tjerneld, *J. Chromatogr. A* 725 (1996) 165.
- [15] L.C. Craig, W. Konigsberg, *J. Phys. Chem.* 65 (1961) 166.
- [16] Y.-X. Gao, L.-B. Ye, *Fundamentals of Membrane Separation Technique*, Science Press, Beijing, 1989, p. 166.
- [17] Z.-L. Fang, *Flow Injection Separation and Preconcentration*, VCH, Weinheim, 1993, p. 38.

Effect of tetrabutylammonium chloride as eluent modifier on the retention and enantioselectivity of D,L-dansyl amino acids using immobilized human serum albumin

Eric Peyrin *, Yves Claude Guillaume

Laboratoire de Chimie Analytique, Faculté de Médecine et Pharmacie, Place St Jacques, 25000 Besançon, France

Received 22 October 1998; received in revised form 10 December 1998; accepted 11 December 1998

Abstract

The influence of tetrabutylammonium (TBA) as a hydrophobic charged additive of the mobile phase was investigated in a chromatographic system involving D,L-dansyl amino acids as the test solute enantiomers and immobilized human serum albumin as the chiral stationary phase. By varying the column temperature, van't Hoff plots for solute retention and enantioselectivity were performed and thermodynamic parameters were calculated. An enthalpy–entropy compensation study revealed that the type of interaction between the analyte and stationary phase was independent of TBA concentration in the eluent. The counterion dependence on retention indicated that the coulombic interactions between dansyl amino acid and the site II binding cavity were of crucial importance in this association process. Also, the increasing variations of chiral discrimination with a TBA addition were attributed, by an analysis of the thermodynamic parameter trends, to a great facilitation of enantioselective H-bonding between solute and polar residues at the cavity rim. © 1999 Elsevier Science B.V. All rights reserved.

Keywords: Liquid chromatography; Tetrabutylammonium chloride; Immobilized human serum albumin; Chiral recognition

1. Introduction

The use of human serum albumin (HSA) immobilized on a high performance liquid chromatography (HPLC) support is useful for the separation of enantiomers. The characterization of the solute interaction mechanisms with the protein station-

ary phase is fundamental to obtain information on the selectivity processes. Several reports have examined the molecular mechanisms involved in the binding of chiral compounds on the HSA stationary phase. The effect of the solute structure on enantioselective separations was investigated using linear regression analysis and the construction of quantitative structure–enantioselective retention relationships by Wainer and coworkers [1,2]. The influence of subtle changes in the

* Corresponding author. Tel.: +33-3-81-665546; Fax: +33-3-81-665527.

protein's structure upon the selectivity properties has been examined by Tittelbach and Gilpin [3]. The binding of salicylic acid to HSA immobilized on agarose has been evaluated in Tris–HCl and phosphate buffers by Nakano et al. [4]. Hage and Loun [5,6] have investigated the thermodynamic and kinetic processes which occurred in the binding of warfarin enantiomers on a HSA column.

In earlier papers, Peyrin et al. studied the retention and the chiral recognition interactions which take place between test anionic solute enantiomers, i.e. D,L-dansyl amino acids, and immobilized HSA [7–11]. By the development of multiple physico-chemical models, it has been demonstrated that both hydrophobic [7,8], coulombic [9], H-bonding [10] and steric [11] forces are involved in the dansyl amino acid enantiomer binding to the HSA site II cavity. In order to gain more understanding on the relative contributions of these different interaction types, the aim of this paper was to assess the influence of mobile phase cationic additives such as tetrabutylammonium (TBA) on retention factor k' and enantioselectivity α of the test anionic compounds. This hydrophobic charged modifier was previously used by Schill et al. [12] to underscore the forces implied in the chiral selectivity of drugs on an alpha 1-acid glycoprotein (AGP) stationary phase. The k' and α values of dansyl amino acids were also determined over a range of TBA concentrations c and column temperatures T . From the temperature studies, van't Hoff plots were obtained and used to access thermodynamic parameters for dansyl amino acid transfer from the mobile to the stationary phases. Enthalpy–entropy compensation was examined to explore the retention mechanism at all mobile phase compositions. Finally, the retention factor and the selectivity variations with c were discussed to provide further knowledge of the mechanistic aspects of the solute binding.

2. Experimental section

2.1. Apparatus

The HPLC system consisted of a Merck Hitachi

pump L7100 (Merck, Nogent-sur-Marne, France), an Interchim Rheodyne injection valve model 7125 (Interchim, Montluçon, France) fitted with a 20 μ l sample loop and a Merck L 4500 diode array detector. An HSA protein chiral Shandon column (150 mm \times 4.6 mm) was used with controlled temperature in an Interchim Crococil oven TM N° 701. After each utilization, the column was stored at 4°C until further use. Throughout the study, the mobile phase flow rate was kept at 1 ml min⁻¹.

2.2. Solvents and samples

HPLC grade acetonitrile (Merck) was used without further purification. Sodium hydrogen phosphate and sodium dihydrogen phosphate were supplied by Prolabo (Paris, France). Water was obtained from an Elgastat option water purification system (Odil, Talant, France) fitted with a reverse osmosis cartridge. D,L-Dansyl norvaline and D,L-dansyltryptophan were obtained from Sigma Aldrich (Saint Quentin, France) and were made fresh daily at a concentration of 20 mg l⁻¹ in acetonitrile. Sodium nitrate was used as a dead time marker (Merck). The mobile phase consisted of a 0.01 M sodium phosphate buffer–acetonitrile (90–10 v/v) at pH 6.0 with TBA concentrations varying from 0 to 0.040 M. Twenty milliliters of each solute or a mixture of these was injected and the retention times were measured.

2.3. Temperature studies

Compound retention factors were determined over the temperature range 20–40°C. The chromatographic system was allowed to equilibrate at each temperature for at least 1 h prior to each experiment. To study this equilibration, the compound retention time of D-dansylnorvaline was measured after, 22, 23 and 24 h. The maximum relative difference of the retention time of this compound was always 0.8%, making the chromatographic system sufficiently equilibrated for use after 1 h. All the solutes were injected three times at each temperature and TBA concentration. Once the measurements were completed at

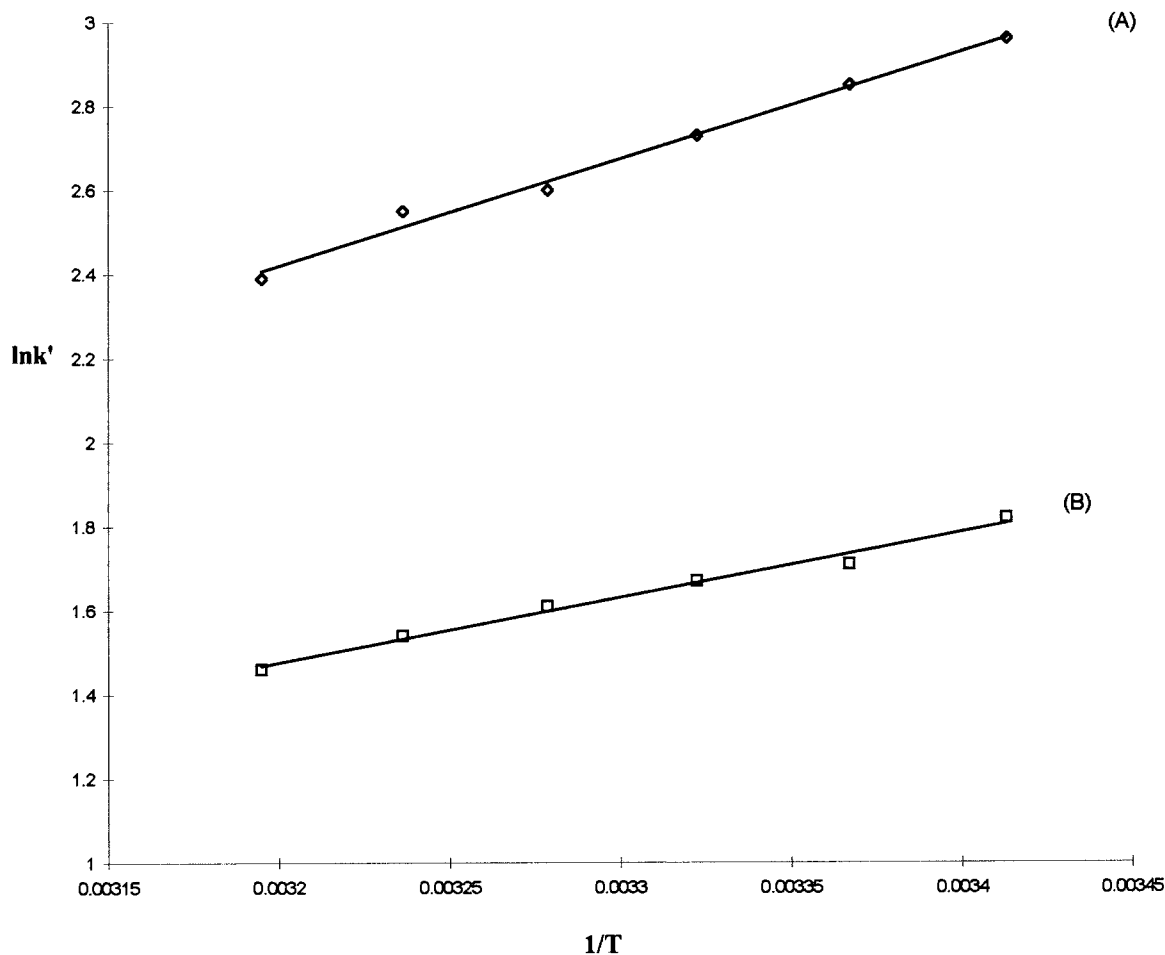


Fig. 1. Van't Hoff plots for k' values of D-dansyltryptophan (A) and D-dansylnorvaline (B) at a TBA concentration equal to 0.020 M.

the maximum temperature, the column was immediately cooled to ambient condition to minimize any denaturation of the immobilized HSA.

2.4. Thermodynamic relationships

Solute retention is usually expressed in terms of the retention factor k' which is proportional to the equilibrium constant K and can be written:

$$k' = \phi K \quad (1)$$

where ϕ is the phase ratio (volume of the stationary phase divided by the volume of the mobile

phase). Gibbs free energy ΔG° is related to the equilibrium constant by the equation:

$$\Delta G^\circ = -RT \ln K \quad (2)$$

where

$$\Delta G^\circ = \Delta H^\circ - T\Delta S^\circ \quad (3)$$

ΔH° (respectively ΔS°) is the enthalpy (respectively entropy) of transfer of the solute from the mobile to the stationary phase, T is the temperature and R the gas constant. Combining Eqs. (1) and (3), the capacity factor can be expressed by the equation:

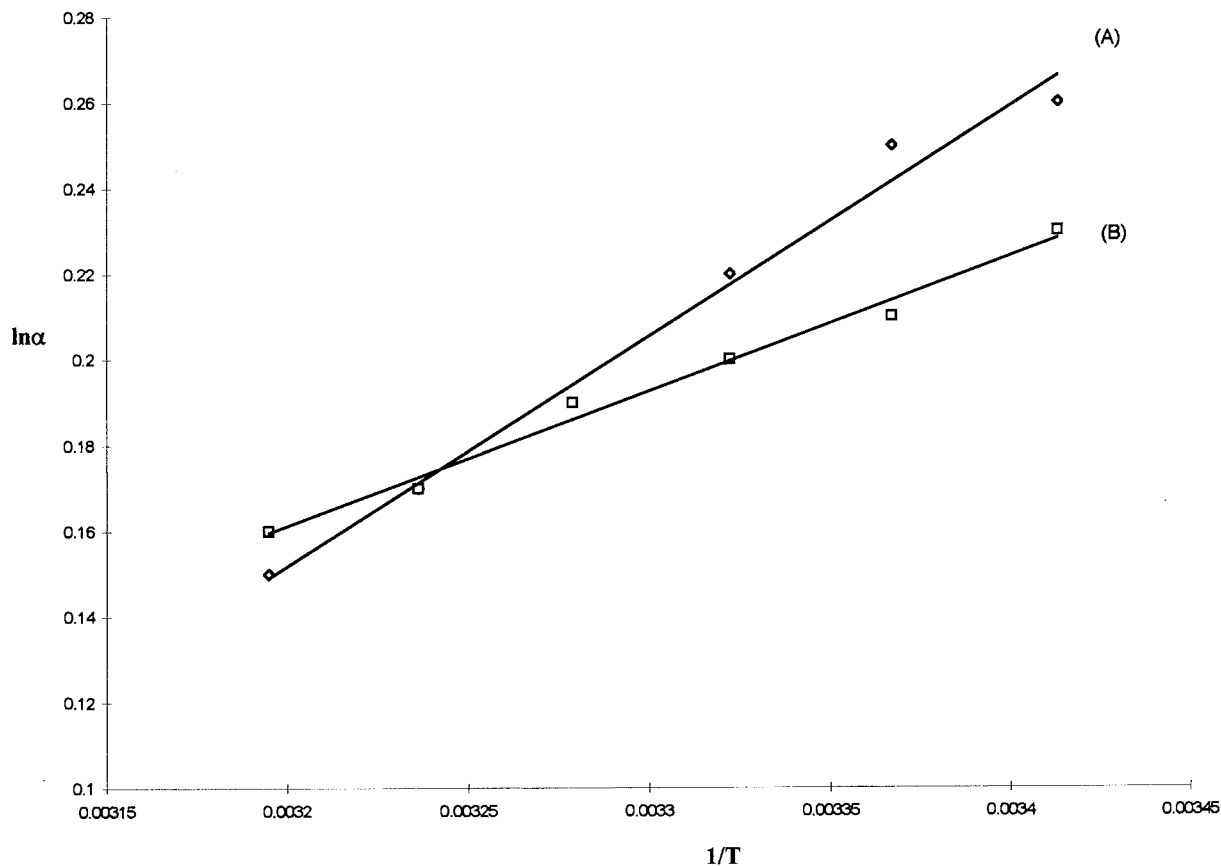


Fig. 2. Van't Hoff plots for α values of D,L-dansyltryptophan (A) and D,L-dansylnorvaline (B) at a TBA concentration equal to 0.020 M.

$$\ln k' = -\Delta H^\circ/RT + \Delta S^\circ/R + \ln \phi \quad (4)$$

Eq. (4) is a van't Hoff plot. From the slope and the intercept, ΔH° and $\Delta S^\circ/R + \ln \phi(\Delta S^{\circ*})$ can be respectively calculated.

Additionally, for a pair of D,L enantiomers, the separation factor α between the D and L enantiomers is given by the three following equations:

$$\alpha = k_D/k_L \quad (5)$$

and

$$\ln \alpha = -\Delta(\Delta H^\circ)/RT + \Delta(\Delta S^\circ)/R \quad (6)$$

with

$$\Delta(\Delta G^\circ) = \Delta(\Delta H^\circ) - T\Delta(\Delta S^\circ) \quad (7)$$

where k_D and k_L are the retention factors of D and L enantiomers and $\Delta(\Delta H^\circ)$ (respectively

$\Delta(\Delta S^\circ)$) is the dissolution enthalpy (respectively dissolution entropy) between the D and L enantiomers on the chromatogram. From a plot of $\ln \alpha$ versus $1/T$ (called a van't Hoff plot), Eq. (6) provides the calculation for $\Delta(\Delta H^\circ)$ and $\Delta(\Delta S^\circ)$ from the slope and intercept respectively.

3. Results and discussion

3.1. Van't Hoff plots for retention and selectivity

The van't Hoff plots for retention and enantioselectivity were all linear for the D,L-dansyl amino acids. The correlation coefficients for the linear fits were at least equal to 0.966. The relative typical standard deviations of the slope and the

Table 1

Thermodynamic parameters (TP) ΔH° (kJ mol⁻¹) and ΔS^{**} with standard deviations (in parentheses) at different TBA concentrations c for D- and L-dansyl amino acids

c (M)	TP	L-Dansylnorvaline	D-Dansylnorvaline	L-Dansyltryptophan	D-Dansyltryptophan
0	ΔH°	-7.2 (0.1)	-7.6 (0.1)	-15.5 (0.1)	-16.6 (0.1)
	ΔS^{**}	-0.4 (0.1)	-1.6 (0.1)	-0.7 (0.1)	-3.2 (0.1)
0.005	ΔH°	-8.1 (0.2)	-8.9 (0.1)	-16.6 (0.1)	-17.4 (0.1)
	ΔS^{**}	-0.8 (0.1)	-2.2 (0.1)	-0.9 (0.1)	-3.6 (0.1)
0.010	ΔH°	-9.2 (0.1)	-10.2 (0.2)	-16.8 (0.1)	-18.2 (0.1)
	ΔS^{**}	-1.1 (0.1)	-2.8 (0.2)	-1.1 (0.1)	-4.1 (0.1)
0.015	ΔH°	-10.6 (0.2)	-11.9 (0.1)	-17.4 (0.1)	-19.0 (0.1)
	ΔS^{**}	-1.2 (0.1)	-3.2 (0.1)	-1.2 (0.1)	-4.6 (0.1)
0.020	ΔH°	-12.0 (0.1)	-13.2 (0.1)	-19.3 (0.1)	-21.1 (0.1)
	ΔS^{**}	-1.5 (0.1)	-3.6 (0.1)	-1.3 (0.1)	-5.7 (0.1)
0.025	ΔH°	-13.1 (0.1)	-15.0 (0.1)	-21.3 (0.1)	-23.4 (0.1)
	ΔS^{**}	-1.8 (0.1)	-4.1 (0.1)	-2.3 (0.1)	-6.7 (0.1)
0.030	ΔH°	-15.2 (0.1)	-17.4 (0.1)	-23.5 (0.1)	-26.0 (0.1)
	ΔS^{**}	-2.2 (0.1)	-4.7 (0.1)	-2.9 (0.2)	-7.8 (0.1)
0.035	ΔH°	-17.5 (0.2)	-20.1 (0.1)	-23.6 (0.1)	-26.5 (0.1)
	ΔS^{**}	-2.4 (0.1)	-5.4 (0.1)	-3.1 (0.1)	-8.1 (0.1)
0.040	ΔH°	-18.5 (0.1)	-22.0 (0.1)	-23.8 (0.1)	-27.3 (0.2)
	ΔS^{**}	-2.7 (0.1)	-6.0 (0.1)	-3.3 (0.1)	-8.6 (0.1)

intercept were less than 0.008 and 0.03, respectively. Fig. 1 shows the van't Hoff plots for k' values of D-dansylnorvaline and D-dansyltryptophan at $c = 0.02$ M. The van't Hoff plots for α values of D,L-dansylnorvaline and D,L-dansyltryptophan at the same TBA concentration are presented in Fig. 2. These linear behaviors were thermodynamically what was expected when there was no change in retention and enantioselective

Table 2

Thermodynamic parameters $\Delta(\Delta H^\circ)$ (kJ mol⁻¹) and $\Delta(\Delta S^\circ)$ (J mol K⁻¹) with standard deviations (in parentheses) for dansyl amino acid enantiomers at different TBA concentrations c

c (M)	D,L-Dansylnorvaline		D,L-Dansyltryptophan	
	$\Delta(\Delta H^\circ)$	$\Delta(\Delta S^\circ)$	$\Delta(\Delta H^\circ)$	$\Delta(\Delta S^\circ)$
0	-0.5 (0.2)	-1.2 (0.1)	-1.0 (0.2)	-2.4 (0.3)
0.005	-0.7 (0.1)	-1.4 (0.1)	-1.3 (0.2)	-3.1 (0.2)
0.010	-0.9 (0.2)	-1.7 (0.2)	-1.5 (0.1)	-3.4 (0.2)
0.015	-1.1 (0.1)	-2.2 (0.2)	-1.6 (0.1)	-3.7 (0.1)
0.020	-1.2 (0.1)	-2.3 (0.1)	-1.8 (0.1)	-3.9 (0.1)
0.025	-1.7 (0.2)	-2.4 (0.1)	-2.1 (0.2)	-4.4 (0.2)
0.030	-2.1 (0.2)	-2.5 (0.2)	-2.4 (0.1)	-4.9 (0.2)
0.035	-2.5 (0.2)	-3.0 (0.1)	-3.0 (0.2)	-5.0 (0.1)
0.040	-3.3 (0.3)	-3.3 (0.2)	-3.6 (0.2)	-6.3 (0.1)

interactions over the temperature range studied [8,13]. Tables 1 and 2 contain a complete list of ΔH° , ΔS^{**} , $\Delta(\Delta H^\circ)$ and $\Delta(\Delta S^\circ)$ for dansylnorvaline and dansyltryptophan, respectively.

3.2. Enthalpy–entropy compensation study

An enthalpy–entropy compensation study was previously applied to chromatographic systems to evaluate the retention mechanisms [14,15]. Mathematically, enthalpy–entropy compensation can be expressed by the formula:

$$\Delta H^\circ = \beta \Delta S^\circ + \Delta G_\beta^\circ \quad (8)$$

where ΔG_β° is the Gibbs free energy of a physico-chemical interaction at a compensation temperature β . ΔH° and ΔS° are, respectively, the corresponding standard enthalpy and entropy. Rewriting Eq. (8) using Eq. (4) gives:

$$\ln k'_T = \ln k'_\beta - \frac{\Delta H^\circ}{R} \left(\frac{1}{T} - \frac{1}{\beta} \right) \quad (9)$$

where

$$\ln k'_\beta = - \frac{\Delta G_\beta^\circ}{R\beta} + \ln \phi \quad (10)$$

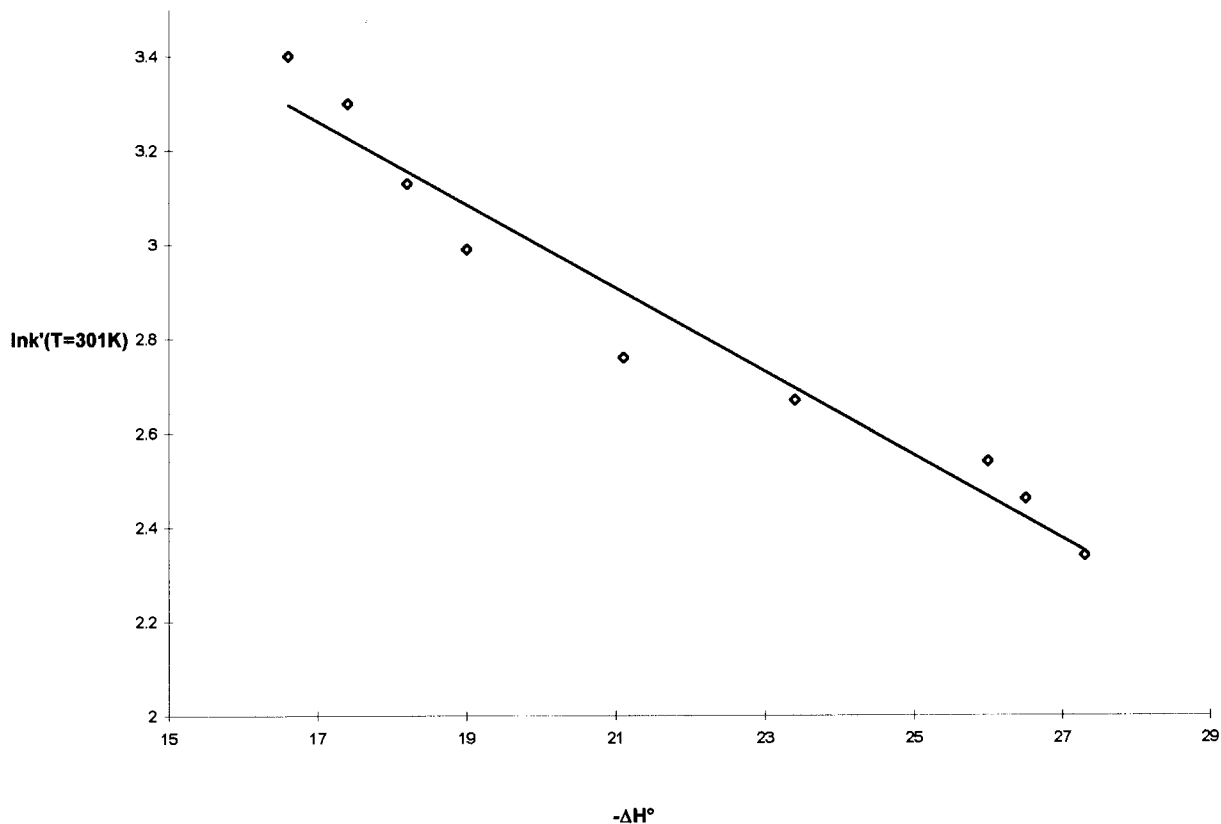


Fig. 3. Plots of $\ln k'_T$ ($T = 301$ K) against $-\Delta H^\circ$ (kJ mol $^{-1}$) for D-dansyltryptophan at different TBA concentrations.

Eq. (9) shows that, if a plot of $\ln k'_T$ against $-\Delta H^\circ$ is linear, then the solute is retained by an essentially identical interaction mechanism. A plot of $\ln k'_T$ ($T = 301$ K) calculated for dansyl amino acid enantiomers against $-\Delta H^\circ$ determined at the different values of the TBA concentration was drawn. The correlation coefficients for the linear fits were over 0.959. Fig. 3 shows $\ln k'_T$ values plotted as a function of $-\Delta H^\circ$ for D-dansyltryptophan. The degree of correlation can be considered to be adequate to verify enthalpy–entropy compensation [16], thus indicating that the interaction mechanism for solutes was independent of the TBA concentration in the mobile phase. Using Eq. (9), the β values were calculated from the slopes of the linear fits. For example, the compensation temperature for D-dansyltryptophan was equal to 246 K.

3.3. TBA dependence on retention

Dansyl amino acids exhibited the same variations in their retention factor values with a TBA concentration increase at each column temperature. Fig. 4 represents the change in $\ln k'$ vs c for D-dansyltryptophan at $T = 301$ K. The role of the counterion on charged analyte retention with immobilized protein has been examined in several papers. The solute affinity variations for the stationary phase with the addition of a charged additive are dependent on the relative contribution of the driving forces implied in the analyte transfer from the mobile to the stationary phases. Acetate counterion, when ion-paired to basic drugs, facilitated the approach of the solute to the AGP stationary phase, demonstrating that the hydrophobic effect played a greater role than electrostatic interactions in this retention process

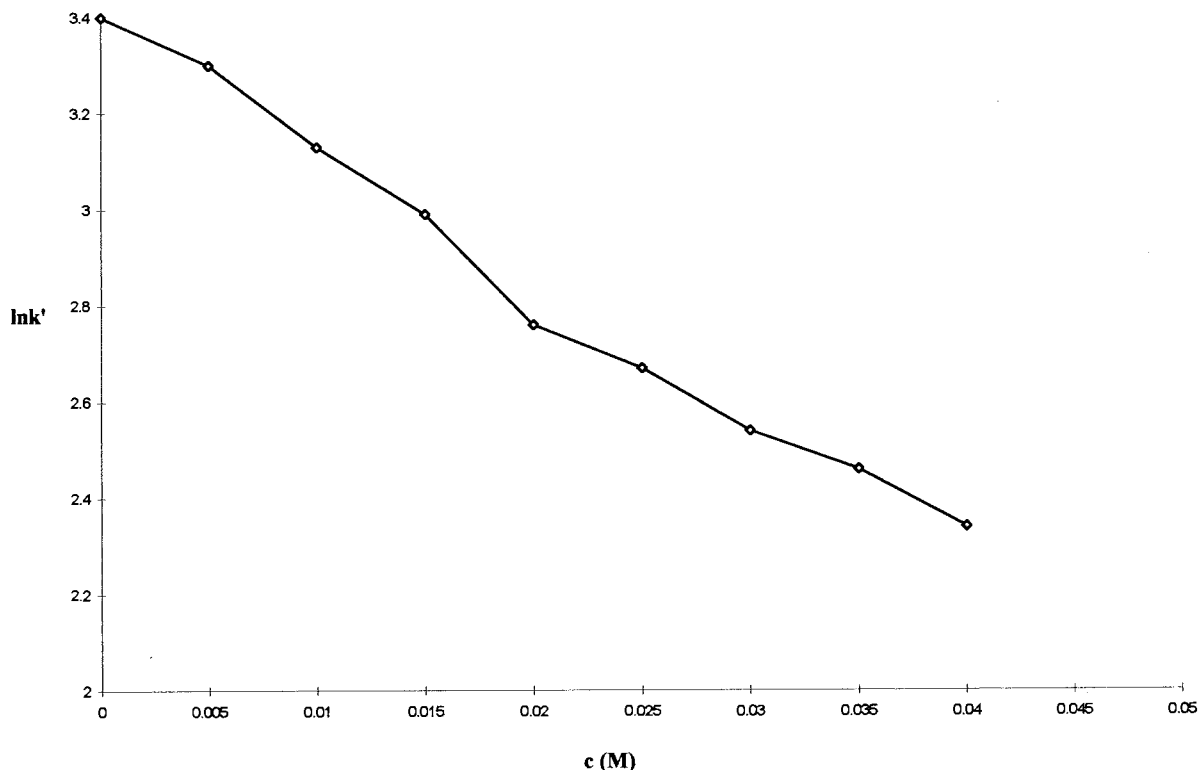


Fig. 4. Plots of $\ln k'$ vs TBA concentration c (M) for D-dansyltryptophan at $T = 301$ K.

[17]. On the other hand, the addition of octanoic acid in the mobile phase led to a retention decrease of alfuzosine on the same immobilized protein by a reduction in the coulombic interaction between the protonated amino groups of the solute and the negatively charged stationary phase [18]. It has been previously established that the retention process of dansyl amino acid on immobilized HSA is dependent on the long range forces which allow the approach of the solute to the opening of the site II binding cavity [9,13]. These interactions consist principally of a combination of both hydrophobic and coulombic effects [9,13]. The hydrophobic effect governs the association between the dansyl amino acid groups at large surface area such as dimethylaminonaphthyl and the apolar interior of the binding cavity [7,8,10,11]. The coulombic attraction is the result of the interaction between the carboxylate function (at pH 6.0) of the solute and the cationic residue of the site II cavity [9,13].

From Fig. 4, it is shown that the $\ln k'$ values of analyte decreased in the entire tetrabutylammonium chloride concentration range (0–0.04 M). In a previous study [19], a different retention behavior has been observed with sodium phosphate salt used as a nonhydrophobic ionic strength modifier. An initial decline in retention was observed in the sodium phosphate concentration range of 0–0.02 M followed by an increase in the 0.02–0.1 M range [19]. This result has been explained by the increased surface tension of the eluent and the concomitant increase in the hydrophobic interactions determined by the salting-out properties of the sodium phosphate salt [19,20]. The type of behavior shown in the case of the charged modifier tetrabutylammonium chloride (Fig. 4) could be rationalized in terms of TBA ion-pairing to the analyte and limiting the approach of the solute to the HSA site II. The ion-pair formation with the hydrophobic charged counterion acted through a coulombic interaction hindrance be-

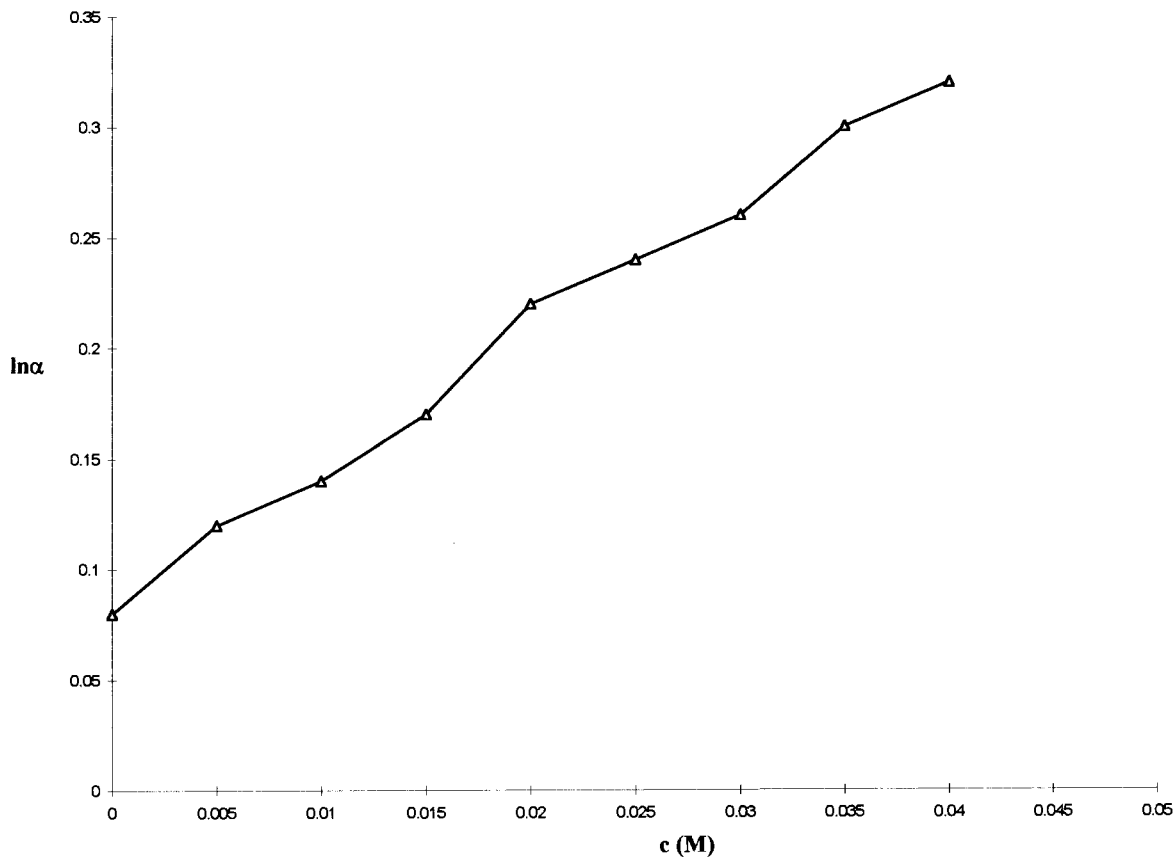


Fig. 5. Plots of $\ln \alpha$ vs TBA concentration c (M) for D,L-dansyltryptophan at $T = 301$ K.

tween the solute and the HSA stationary phase, rather than an enhancement of their hydrophobic attraction. This demonstrated the crucial role of the electrostatic binding mode in the solute site II

cavity association process. The thermodynamic parameter variations confirmed this observation. It is known that the association between two opposite charged species in an aqueous medium is characterized by both positive enthalpy and entropy changes [21]. As Table 1 shows, the ΔH° and ΔS° values became increasingly negative when c increased, corresponding to the limitation of the coulombic interaction between the solute and immobilized HSA due to the ion-pairing mechanism.

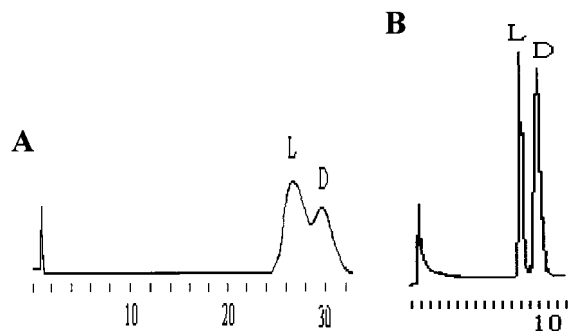


Fig. 6. Chromatograms of dansyltryptophan enantiomer mixture at 301 K (see the other conditions in the text).

3.4. TBA dependence on chiral discrimination

The logarithmic enantioselectivity variations of each enantiomer pair with c increasing were similar whatever the column temperature. Fig. 5 shows the plot of $\ln \alpha$ vs c for D,L-dansyltryp-

tophan at $T = 301$ K. The chiral recognition process of dansyl amino acid on the HSA stationary phase involves a mechanism based on short range forces between the solute and the rim of the binding cavity [9,11,13]. It has been verified that the solute inclusion process into the apolar interior of the pocket, depending on hydrophobic effects, limited the stereoselective interactions with residues at the opening of the cavity [9,13]. As can be seen in Fig. 5, enantioselectivity increased with an increase of TBA concentration. This observation can be explained in terms of a restricted process of the analyte inclusion. When dansyl amino acid was ion-paired with TBA, the large bulkiness of this ionic association provided significant steric hindrance to the solute insertion in the bottom of the binding cavity. Thus, solute binding became more dependent upon enantioselective interactions with residues at the cavity rim. $\Delta(\Delta H^\circ)$ and $\Delta(\Delta S^\circ)$ values decreased with c , corresponding to an enthalpically controlled chiral recognition increase. This was consistent with the favorable contribution of stereoselective H-bonding [13] between the polar solute groups and residues at the opening of the binding pocket.

An example illustrating this type of enantioselectivity behavior is shown in Fig. 6. For $T = 301$ K, in the chromatographic system used in the absence of TBA as mobile phase modifier, chiral discrimination for dansyltryptophan provided a minimum value equal to 1.08 associated with a large retention time and low resolution (Fig. 6(A)). Based on the trends noted in Figs. 4 and 5, it was possible to adjust the TBA concentration in order to obtain a greater enantiomeric separation with a reduced retention time. This was done by increasing the TBA concentration to 0.04 M. This provided an enantioselectivity equal to 1.35 with a good resolution (Fig. 6(B)).

4. Conclusion

In this paper, the role of the hydrophobic counterion TBA in controlling the retention and chiral discrimination interactions of dansyl amino acids on immobilized HSA was investigated. The reduction of solute affinity for the stationary phase

with a TBA concentration increase was described in terms of hindrance in the coulombic association between the carboxylate group of solute and cationic residue of the site II cavity of HSA. This indicated the preponderant role played by the electrostatic interaction in this ligand–receptor association process. The fact that chiral discrimination was enhanced in the TBA range was explained by an enhancement in stereoselective H-bonding between the solute and polar exterior of the binding pocket on the basis of thermodynamic parameter variations.

References

- [1] V. Andrisano, T.D. Booth, V. Cavrini, I.W. Wainer, *Chirality* 9 (1997) 178.
- [2] R. Kaliszan, T.A.G. Noctor, I.W. Wainer, *Mol. Pharmacol.* 42 (1992) 512.
- [3] V. Tittelbach, R.K. Gilpin, *Anal. Chem.* 67 (1995) 44.
- [4] N.I. Nakano, Y. Shimamori, S. Yamaguchi, *Chem. Pharm. Bull.* 33 (1985) 778.
- [5] B. Loun, D.S. Hage, *Anal. Chem.* 66 (1994) 3814.
- [6] B. Loun, D.S. Hage, *Anal. Chem.* 68 (1996) 1218.
- [7] E. Peyrin, Y.C. Guillaume, C. Guinchart, *Anal. Chem.* 69 (1997) 4979.
- [8] E. Peyrin, Y.C. Guillaume, N. Morin, C. Guinchart, *Anal. Chem.* 70 (1998) 2812.
- [9] E. Peyrin, Y.C. Guillaume, C. Guinchart, *Anal. Chem.* 70 (1998) 4235.
- [10] E. Peyrin, Y.C. Guillaume, N. Morin, C. Guinchart, *J. Chromatogr. A* 808 (1998) 113.
- [11] E. Peyrin, Y.C. Guillaume, C. Guinchart, *J. Chromatogr. Sci.* 36 (1998) 97.
- [12] G. Schill, I.W. Wainer, S.A. Barkan, *J. Chromatogr.* 365 (1986) 73.
- [13] E. Peyrin, Y.C. Guillaume, *Chromatographia* 48 (1998) 431.
- [14] M. Kucher, E. Kraus, V. Rejholec, V. Miller, *J. Chromatogr.* 449 (1988) 391.
- [15] Y.C. Guillaume, C. Guinchart, *J. Chromatogr. A* 727 (1996) 93.
- [16] L.A. Cole, J.G. Dorsey, *Anal. Chem.* 64 (1992) 1317.
- [17] J. Hermansson, A. Grahm, *J. Chromatogr. A* 694 (1995) 57.
- [18] A.M. Krstulovic, *J. Pharm. Biomed. Anal.* 6 (1988) 641.
- [19] E. Peyrin, Y.C. Guillaume, C. Guinchart, *Biophys. J.*, submitted for publication.
- [20] C. Horvath, W. Melander, I. Molnar, *J. Chromatogr.* 125 (1976) 129.
- [21] R. Lehmann, J. Seelig, *Biochim. Biophys. Acta* 1189 (1994) 89.

Combination of amperometric detector & UV detector for capillary electrophoresis

Xiaojing Huang, Tianyan You, Xiurong Yang, Erkang Wang *

Laboratory of Electroanalytical Chemistry and National Research Analytical Center of Electrochemistry and Spectroscopy, Changchun Institute of Applied Chemistry, Chinese Academy of Sciences, Changchun, Jilin, 130022, China

Received 1 July 1998; received in revised form 11 December 1998; accepted 14 December 1998

Abstract

A new electrochemical cell assembly with the combination of UV and amperometric detector (AD) based on their complementarity was described. A Nafion tubing junction was used to decouple the high voltage from the separation capillary in the rear of on-column UV detector. In this mode, the electroactive and inert compounds could be detected by UV and AD at the same time. Aromatic amines were determined with the UV and the end-column AD detection to evaluate the performances of the cell assembly. Such an improved electrochemical detector could match the capillary with different diameters. By simple adjustment of the screws, the positioning of the working electrode and the detection capillary was easily gained without microscope. It is also very easy to assemble and disassemble the working electrode when needed. © 1999 Elsevier Science B.V. All rights reserved.

Keywords: Combination; Amperometric detection; UV detection; Capillary electrophoresis

1. Introduction

After the introduction of high performance of capillary electrophoresis (HPCE) from last decade [1,2], it has been well developed and has become a powerful and indispensable separation technique.

As one of the most important factors to the separation and detection in HPCE, detectors have gained much attention. There are many most important requirements for the design of detectors suitable for capillary separation system, such as small volume detection cell, small contribution to

peak width, high sensitivity, large dynamic range, fast detector response, good resistance against temperature changes, reliable and convenient, ease of use, selective detection and non-selective detection [3]. There is no single detector available to provide all these properties. Several kinds of detectors have been coupled to the separation capillary as on-column, end-column and off-column. For on-column, peak tailing is minimized for there is no dead volume. However, the sensitivity is limited to optical detection modes by the small inner diameter and the short path length of the capillary, since the sensitivity is proportional to the path length. UV is one of the most popular methods of detection. It is easy to operate and

* Corresponding author. Fax: +86-431-568-9711.
E-mail address: ekwang@mail.jlu.edu.cn (E. Wang)

respond to a wide range of compounds. Moreover, certain species are easy to be determined by UV detection compared with others.

Wallingford and Ewing first reported amperometric detection coupled with CE in 1987 [4]. Amperometric detector shows more sensitive than UV detector. The amperometric detector is quite selective because only those electroactive compounds at a given potential can be detected. Thus, the analytes can be detected from the complex matrix, and its detection limit is very low. However, the separation current through the capillary is usually much higher than the faradaic current. To solve the problem, one way is to use small diameter capillary and another is to isolate electrochemical detector from the separation capillary by using a junction.

The combination of UV with amperometric detector in one run is interesting because of the complementary nature of the two techniques. The electroactive and inert components can be detected at the same time and the lower detection limit can be obtained. In this paper, considering the sensitivity of UV, a 75 μm diameter capillary was used. A Nafion tubing junction was used to isolate the amperometric detector from the separation capillary.

Since the placement of the capillary with respect to the electrode is critical for successful detection of sample, an equipment has been designed to adjust their relative position. In this study, a new electrochemical cell combined with the UV detection was described. The cell has many advantages such as easy to assemble and disassemble the working electrode, easy to position the working electrode and the outlet of the separation capillary by adjusting certain screws without the micropositioner, and the analytes can be determined by UV and AD detection at the same time.

2. Experimental

2.1. Materials

p-phenylenediamine (*p*-PDA) and phosphate buffer were from Beijing Chemical Plant. Aniline

sulfate (AS) and *p*-nitrophenylamine (NPA) were from Shanghai Reagent Factories. All chemicals were of analytical reagents.

All solutions were prepared with doubly distilled water. The background electrolyte for the separation and detection of aromatic amines was 10 mM phosphate buffer. For NPA the stock solution was prepared as 2 mM, the other two sample stock solutions were 10 mM. Samples were diluted to the desired concentrations with operating electrolytes prior to use. All solutions were filtered through 0.45- μm filters.

2.2. Apparatus

Polyimide-coated fused-silica capillary was used with an inner diameter of 75 μm , an outer diameter of 360 μm and a total length of 75 cm (41 cm from injection to UV detection). Capillary was filled with 0.1 M NaOH over night before use. The capillary was rinsed with H_2O , 0.1 M HCl, H_2O , 0.1 M NaOH, H_2O , running buffer respectively before each run. The high voltage was supplied by Spellman (High Voltage Electronics Corp. Modes CZE 1000 PN 30, Plainview, NY 11803).

The conventional three-electrode system was employed, a microelectrode made of 33 μm carbon fiber as a working electrode, an Ag/AgCl with saturated KCl as a reference electrode and a platinum wire as auxiliary electrode. An Esman Instrumentation Potentiostat 400 was used to control the potential for amperometric detection. Cyclic Voltammetry was performed with electrochemical analyzer (Model 832, CH Instruments, USA).

The UV absorbance detector was a Model CV⁴ obtained from ISCO and operated at 254 nm. Two-pen recorder was from Dahua Instrument Meter Factory (Shanghai, China). The samples were introduced into the capillary by hydrostatic pressure with utilizing gravity.

2.3. Equipment

The main part of the system for this two-dimensional detection was shown in Fig. 1. It is based on a CZE system, consisting of a fused-sil-

ica capillary, a high-voltage power supply, a UV detector, a Nafion junction, an amperometric detector, and platinum electrodes. The signals coming from the UV detector and amperometric detector were recorded simultaneously.

2.4. Electrochemical cell

An electrochemical detection cell was described previously [5]. Fig. 2 shows the diagram of the improving amperometric detection cell. For the reason of transparency, the two parts of the cell (block (a) and (b)) were made of plexi-glass. As seen in Fig. 2, the center of the each block was milled to be a half-global cavity, which acted as the buffer container. The cone-shaped section (b) was joined with the half-globe. At the end of the cone-shaped section, it became a cylinder (c). The Nafion junction was fixing in the conical section by the epoxy glue. By inserting a platinum into the column (a), the buffer container with the Nafion junction was grounded. The screws used to fix the configuration were through the columns (d) and (e). The auxiliary and reference electrodes were put in the column (f) which was joined with buffer container. The thin cylinder (g) acted as the channel of working electrode. The holes (h) were used to place screws in them. When the two parts of the configuration were put together, vertical and horizontal positioning was achieved by twisting the screws. In order to ensure the appropriate degree of tightness, a piece of silicon rubber was set between the two parts, and the springs were set at the end of the screws which were put through the columns (d) and (e). Fig. 2(c) gave the outline of the cell. One advantage of the design is to calibrate the capillary and electrode easily, conveniently and quickly, and it

is easy to handle the working electrode. The analytes can be detected by UV and AD detection simultaneously. The configuration as a whole can eliminates the outer disturbance in experiments. Moreover, it is suitable for different capillaries with different diameters.

2.5. Construction of the electrochemical cell

Firstly, the Nafion tubing joint assembly was made same as before [6]. A capillary cutter (ISCO, USA) was used to score the polyimide coating ca. 1 cm from the end of the capillary column. A 1-cm length of Nafion tubing was carefully threaded over the score mark. The two ends of the Nafion tubing were sealed to the capillary column with epoxy glue and then cured overnight. After it was cured, we applied gentle pressure to either end of the Nafion tubing to make the capillary fracture at the score. The end of the capillary (with Nafion tubing) was carefully inserted in (c) in block a and sealed to it using the epoxy glue and also cured overnight. The working electrode (WE) was inserted in a screw which has a hole that can match the outer diameter of the WE very well. Then the screw was placed to (g) in block (b). If the WE needs pretreated, the screw and the WE can be disassembled from block b easily as a whole by adjusting the screw. If the WE needs changed, it is very easy to change another one to the screw because all the electrodes have been made of the same outer diameter. The block (a) and (b) were put together with the screws through the holes of (d) and (e). The holes for fixing two blocks were made in oblate shape and the holes of one block perpendicular to that of the other, which makes the blocks move freely along their own directions (vertical and horizontal). When aligning the WE with the outlet of the capillary, the screws (d) and (e) were pushed gently until the WE was in close contact with the outlet of the capillary. The screw (h) was adjusted to move block (a) and (b) which makes sure the WE and the outlet of the capillary were at the same line (vertical and horizontal direction). The positioning can be successfully done after the vertical and horizontal positioning of the electrode is

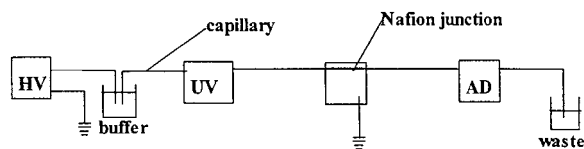


Fig. 1. Schematic diagram of the apparatus for two-dimensional detection for capillary electrophoresis.

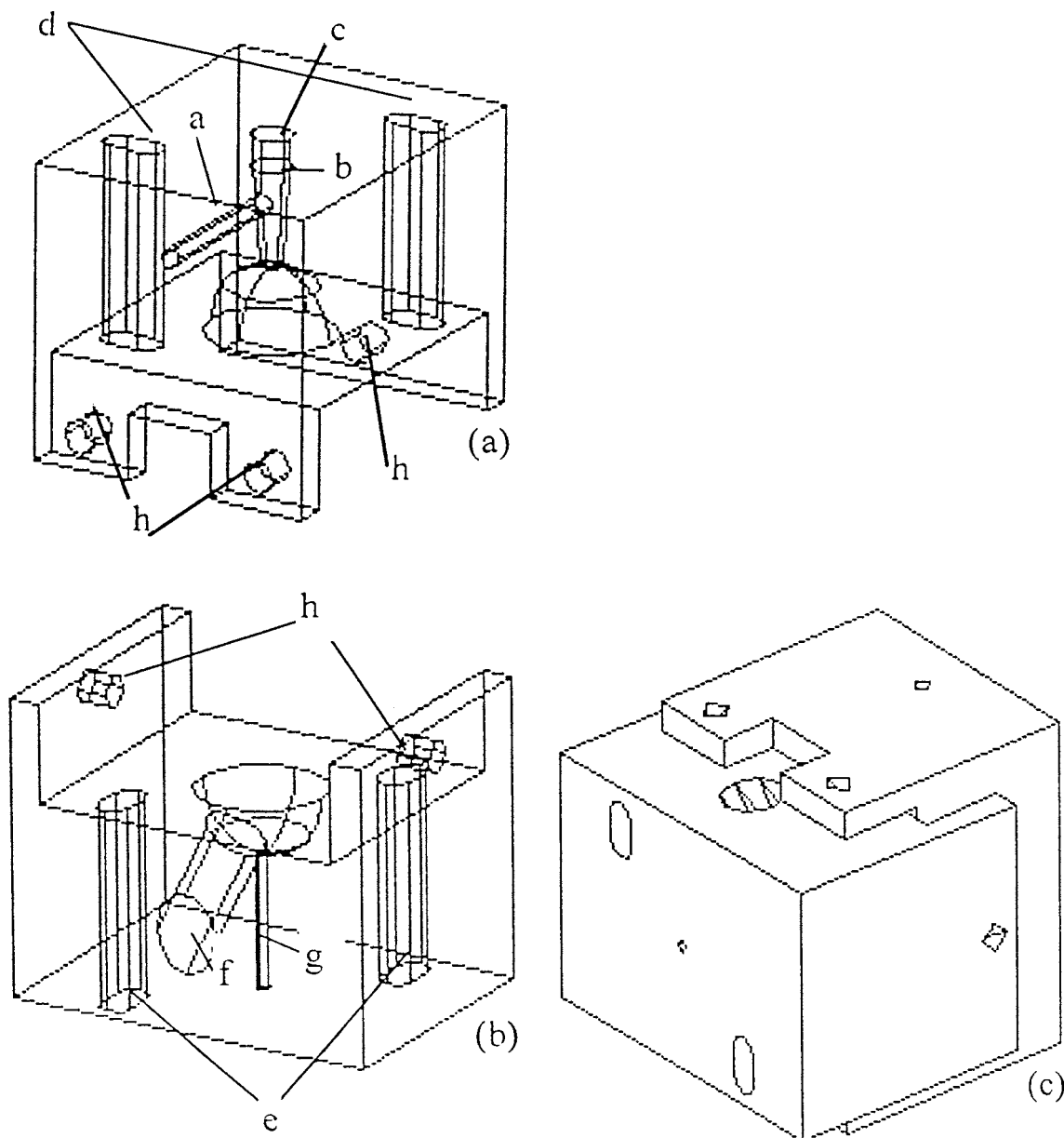


Fig. 2. Design of the amperometric detection device. (a) and (b): cell body; (c): the outline of the cell.

placed at the outlet of the capillary at the same line. Finally, every screw was tightened. A platinum wire was placed into (a) to ground the high voltage and the reference electrode and auxiliary were assembled to (f) with the same procedure as the WE. Then, the cell was filled with buffer and put into the Faraday cage.

3. Results and discussion

In order to evaluate the properties of this cell, we choose three kinds of aromatic amines as analytes: *p*-PDA, NPA, and AS. As we know, the electrochemical behavior of a molecule is determined by the nature of the electroactive func-

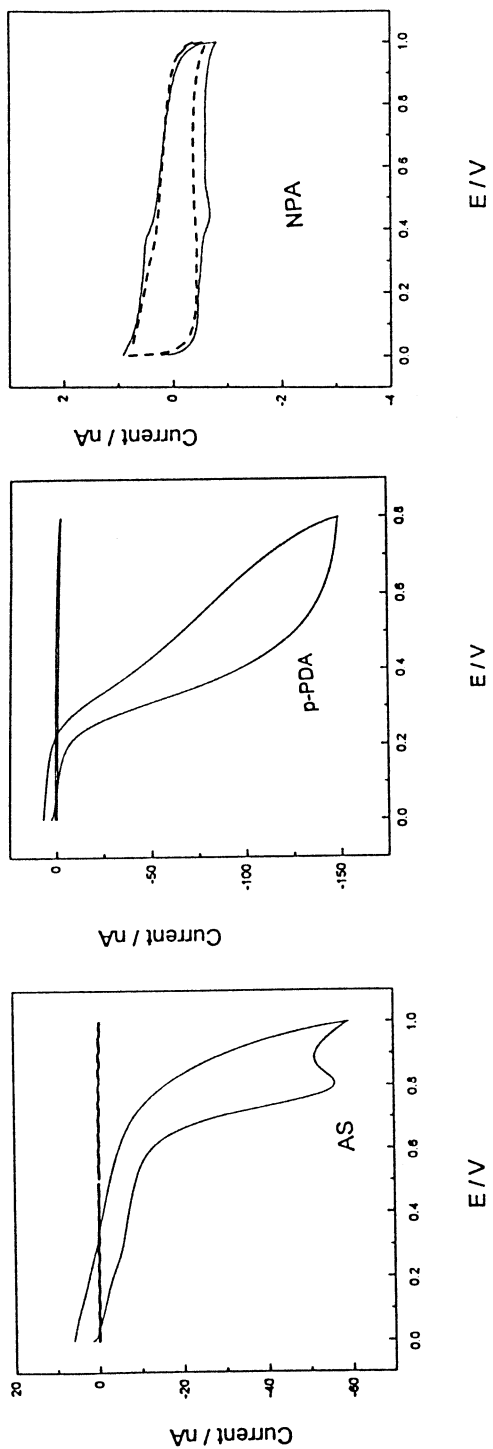


Fig. 3. Cyclic voltammograms of 5 mM AS, p-PDA and 1 mM NPA in 10 mM phosphate buffer, pH 4.75. The solid line is for samples, and the dash line is for buffer.

tional groups. Aromatic amines can be determined with the AD detection with high sensitivity. But, because of their different substitutional groups, each has different oxidation current and potential.

As shown in cyclic voltammograms (Fig. 3), AS and *p*-PDA are easily oxidized. They are suitable for amperometric detection. While for NPA, there is a pair of redox peaks at about 0.4 V with very small peak current, UV detection is better than electrochemical detection (AD) in this case. This idea would be shown later with the results of the capillary electrophoresis.

UV detector is used as on-column detection. A lot of species with functional groups are sensitive to UV detector, including bromine, iodine, and sulphur; two conjugated double bonds; a double bond vicinal to an atom having a single electron pair; a carbonyl group; an aromatic ring [3]. Although UV detector is more popular than amperometric detection, the amperometric detector has the advantages of good selectivity, high sensitivity and low detection limits over the UV detector.

Fig. 4 shows the electropherograms of 100 μM NPA, 50 μM AS and *p*-PDA separated by CE. Although these aromatic amines belong to the same family, they give the different properties. The UV sensitivity of NPA is higher than that of the amperometric detection, while the amperometric detection sensitivity of AS and *p*-PDA is much higher than that of the UV detector. The signals of AS and *p*-PDA are hardly identified from the noise in the electropherogram by the UV detection. Table 1 shows the result of the detection limit in the different detectors.

The satisfied results can be achieved by the combination of the UV detector and the amperometric detector simultaneously. Although the UV detector has the versatility for a large range of compounds, it is impossible to detect all these compounds at the same wavelength with the same high sensitivity. In this allied configuration, the use of special wavelength for UV and special potential for AD would save a lot of analytical time. From Fig. 4 we also learn that the peak symmetry of UV detector is better than that of AD detector. This is the advantage of the on-

column detector, because the band width was decreased in on-column detection, which improved the separation efficiency. Meanwhile, there is a decoupler (here is a Nafion tubing) to separate the high voltage applied to the separation capillary from the detection capillary, which leads to a certain degree of peak tailing compared with the UV detector. The other one is that some electroactive analytes have comparative low electron transfer. This can also lead to a certain degree of the trace tailing.

Since the HPCE was introduced, a great deal of work had been done to improve its separation efficiency. Many separation modes were devel-

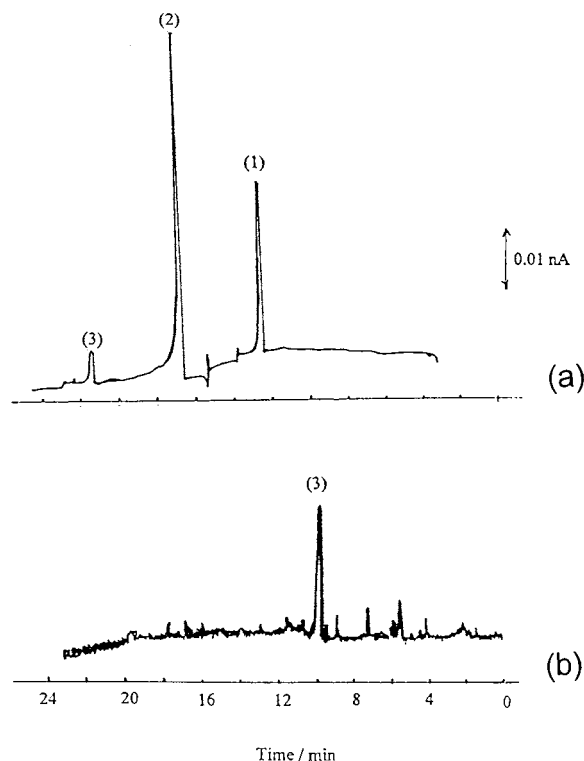


Fig. 4. Electrophoresis of 100 μM NPA and 50 μM *p*-PDA and AS in 10 mM phosphate buffer, pH 4.75. Polyimide-coated fused-silica capillary was used with an inner diameter of 75 μm , an outer diameter of 360 μm , and a total length of 75 cm (41 cm from injection to UV detection). Separation voltage: 15 kV. UV: 254 nm, sensitivity: 0.002. Electrochemical detection: 1.0 V. Sample injection: hydrostatic pressure by utilizing gravity (10 cm high), injection time: 10 s. (a) amperometric detection, (b) UV detection. (1) *p*-PDA, (2) AS, (3) NPA.

Table 1
The detection limit in different detectors^a

	NPA (pg)	AS (pg)	<i>p</i> -PDA (pg)
UV	16.4	67.6	25.8
AD	65.7	1.35	3.0

^a Sample in 10 mM phosphate buffer. Polyimide-coated fused-silica capillary was used with an inner diameter of 75 μm , an outer diameter of 360 μm , and a total length of 75 cm (41 cm from injection to UV detection). Separation voltage: 15 kV. UV: 254 nm, sensitivity: 0.002. Electrochemical detection: 1.0 V. Sample injection: hydrostatic pressure by utilizing gravity (10 cm high)

oped for different separation principles. But there are still some kinds of compounds not able to separate for the similar mass-charge ratio, or not able to baseline separate. In order to find out the best separation condition, much work should be done. The new construction may solve the problems in the certain extent for it has two kinds of the detection modes. For both UV and AD detection, the linearity ranges are relatively wide. If both compound A and B are in the same matrix having the response to UV detector, while the separation condition is difficult to fix, but only one (A or B) is electroactive. Then they can be detected by UV or AD respectively. The UV signal should be made out first, and the AD signal followed it. After the working curve was calculated for each analyte, the subtraction can be applied to get the quantity of the two compounds.

4. Conclusion

The united detection with both amperometric detector and UV detector was performed. The UV detection was on-column, while the amperometric detection was off-column. Such a combined method shows excellent versatility and selectivity. It is very easy to position the working electrode and the outlet of the capillary. And it is also easy to handle the working electrode when necessary. The electroactive and non-electroactive compounds could be detected by UV and AD modes at the same time. The aromatic amines had been successfully separated based on the united detection to evaluate the construction. Hopefully it could be used extensively in the future work.

References

- [1] J.W. Jorgenson, K.D. Lukacs, *Anal. Chem.* 53 (1981) 1298.
- [2] J.W. Jorgenson, K.D. Lukacs, *Science* 222 (1983) 226.
- [3] R. Kuhn, S. Hoffstetter-Kuhn, *Capillary Electrophoresis: Principles and Practice*, Springer, New York, 1993.
- [4] R.A. Wallingford, A.G. Ewing, *Anal. Chem.* 59 (1987) 1762.
- [5] Z. Liu, T. You, E. Wang, Abstracts for the fourth Asian Conference on Analytical Sciences, Fukuoba, Japan, May 21-23, 1997, p. 65.
- [6] T.J. O'Shea, R.D. Greenhagen, S.M. Lunte, C.E. Lunte, M.R. Smyth, D.M. Radzik, N. Watanabe, *J. Chromatogr.* 593 (1992) 305.

Computational program for evaluating and optimizing response–surface curves based on uniform shell designs

A. Gustavo González *, Domingo González-Arjona

Department of Analytical Chemistry, University of Seville, Seville 41012, Spain

Received 9 April 1998; received in revised form 30 October 1998; accepted 24 December 1998

Abstract

A program for optimizing uniform shell designs, called DOEHLOPT, is proposed. The scope and features of DOEHLOPT are discussed and compared with those of a general purpose program (GOSSET). DOEHLOPT was applied to a worked example for the sake of illustration. © 1999 Elsevier Science B.V. All rights reserved.

Keywords: Optimization methods; Uniform shell designs; Doehlert designs

1. Introduction

Many experiments in chemistry, chemical engineering, pharmacy,... belong to the extremum problem type: to determine the factor co-ordinates of the optimum response. A fruitful way to conduct experimental designs and optimization is according the response–surface methodology (RSM). In RSM, the experimental response y is taken as a function on several independent variables called factors (z_i) [1–4]. They occupy the called factor space and the plot of y on this space is the response surface. The region close to the extremum it is known as a ‘nearly stationary regions’ intrinsically non linear that can be suit-

ably described by using second order polynomials [5]

$$y = B_0 + \sum_{i=1}^f B_i z_i + \sum_{i=1}^f \sum_{j>i} B_{ij} z_i z_j + \sum_{i=1}^f B_{ii} z_i^2 + e \quad (1)$$

where f is the dimension of the factor space and e is the error associated to the y variable which is assumed to be normally distributed.

The number m of coefficients to be estimated in Eq. (1) is $m = (f + 1)(f + 2)/2$, and therefore, two-level factorial designs are insufficient to fit the model Eq. (1). In order to attain the optimum response, three-level factorial designs were developed by Box and Behnken [6]. However, these designs involve a very great number of runs $N = 3^f$ compared with the m coefficients to be determined. To alleviate this situation, central

* Corresponding author. Fax: +34-5-4557168.

E-mail address: agonzale@cica.es (A. Gustavo González)

composite designs (CCD) were issued. The introduction of extra runs (star points and centre of design) to augment two-level factorial designs was done to allow for an efficient way to estimate the coefficients of the model equation. The number of runs to be made in both orthogonal [7] or rotatable [8] CCD are $N = 2^f + 2f + 1$ (without replications), sensibly lower than three level factorial designs. For this reason, CCD are widely used in experimental optimization [9]. However, a more efficient design was devised by Doehlert in 1970 [10], who proposed uniform shell designs (USD) where the factor co-ordinates of experimental points are equally spaced distributed on centred circles, spheres or hyperspheres. These designs being more uniform than any other, show excellent interpolation features. In his paper [10], Doehlert applied an interesting technique to generate the USDs for f factors from a starting simplex containing $f + 1$ points. One of these points is the centre of design and the remainder f points lie on a sphere of radius unity from the centre of design. We will not consider here the way for building the USDs although his method was implemented as a procedure of our program. The total number of runs without replication needed for applying USD is $N = f^2 + f + 1$, even lesser than in CCD. Thus USD lead to the maximum efficiency (ratio between the number of coefficients to be evaluated, m , and the number of runs, N , in the design chose) [11]. For this reason, USD are highly applied in very different scientific frames [12–20].

The present paper deals with a computational procedure for optimizing USD. The program first constructs the USD for up $f = 10$ factors, evaluates the response surface curve from the $f^2 + f + 1$ experimental points and then performs the searching for the maximal response within the experimental working range; the optimization procedures involve eigenanalysis and derivative techniques.

2. Outline of the method

Within the realm of experimental design, two programs about optimization of mixture designs

[21] and CCD [9] have been devised by us. Some QuickBasic procedures applied in the present program have been already used in the former programs and they will be not discussed here. Accordingly, aside from the factor coding, which is somewhat different from CCD, the description on the curve fitting by multiple linear regression, the corresponding ANOVA and the way for finding the optimum response are literally the same as published in reference [9]. Therefore, these topics will be briefly referred for avoiding superfluous repetitions.

2.1. Coding the factors

Factor coding in USD is a key feature because the way in which these designs are built generates a data matrix dealing with coded units always [10,11]. In CCD, the number of levels for each factor is always the same. In USD however, is different for each factor. Remembering that the USD are generated in coded units, we need a rule for decoding these values into real levels. According to the different number of levels for each factor in USD, each factor is separately coded/decoded. Consider a given factor x ; whose maximum and minimum coded (generated) levels are x_i^{\max} and x_i^{\min} ($x_i^{\min} = -x_i^{\max}$). The real factor z_i have the extreme z_i^{\max} and z_i^{\min} . Any uncoded intermediate level z_i^* may be deduced from the coded intermediate level x_i^* according to the uncoding equation

$$z_i^* = z_i^{\max} - \frac{(x_i^{\max} - x_i^*) (z_i^{\max} - z_i^{\min})}{2x_i^{\max}} \quad (2)$$

In the coded units in which the USD are generated, Eq. (1) may be rewritten as

$$y = b_0 + \sum_{i=1}^f b_i x_i + \sum_{i=1, j>i}^f b_{ij} x_i x_j + \sum_{i=1}^f b_{ii} x_i^2 + e \quad (3)$$

In the remainder the symbols b will have significance in the coded factor space only.

As indicated above, when using these designs, the most complex factor should be modelled with the largest number of levels. For more than two factors, the number of levels for the first and the last factors is five and three, respectively, and the

number of levels for the remainder factors is seven always.

2.2. Performing the fit

Model Eq. (3) may be rewritten in matrix form as

$$\mathbf{y} = \mathbf{X}\mathbf{B} \quad (4)$$

where \mathbf{X} is the USD data matrix. In this matrix, each column represents the values of the factors in the following order: 1, $x_1, x_2, \dots, x_f, x_1^2, x_2^2, \dots, x_f^2, x_1x_2, x_1x_3, \dots, x_1x_f, x_2x_3, x_2x_4, \dots, x_2x_f, x_{f-1}x_f$. The design matrix \mathbf{D} is within X (columns x_1, x_2, \dots, x_f). There are $f^2 + 2f + 1$ rows. The least squares estimate for \mathbf{B} is

$$\mathbf{B} = (\mathbf{X}^T\mathbf{X})^{-1}\mathbf{X}^T\mathbf{y} \quad (5)$$

Multiple regression computations involving the variance/covariance matrix and ANOVA calculations are performed for testing the model adequacy. The variance of each regression coefficient b , $s^2(b)$, is easily obtained from the diagonal elements of the variance–covariance matrix. Once it is known, the coefficient is tested for significance according to the Student t -test: $t = b/s(b)$.

The coefficient is significant if t is higher than the critical tabulated value $t_{\text{crit}}(N-m, \alpha)$ for $N-m$ degrees of freedom and a given α significance level [9].

2.3. Finding the optimum

Once the form of the model Eq. (3) is known, the maximum for y occurs for the factor co-ordinates $(x_1^{\text{opt}}, x_2^{\text{opt}}, \dots, x_f^{\text{opt}})$ for which

$$\frac{\partial y}{\partial x_i} = 0 \quad \text{for } i = 1, 2, \dots, f \quad (6)$$

If the maximum exists, the column vector \mathbf{x}^{opt} is calculated as

$$\mathbf{x}^{\text{opt}} = \frac{-\mathbf{S}^{-1}\mathbf{s}}{2} \quad (7)$$

where \mathbf{s} is the column vector of the single order coefficients (b_1, b_2, \dots, b_f) and \mathbf{S} is an $f \times f$ matrix whose diagonal contains the second order coefficients b_{ii} and where any diagonal element ij equals

to the half value of the corresponding second order mixed coefficient, $b_{ij}/2$.

A canonical analysis can be carried out by eigenanalysis of matrix \mathbf{B} for a previous scrutiny of the singular point, which may be not a maximum, but a minimum or a saddle point [9].

3. Computational details

A program called DOEHLOPT that performs the outlined method, has been written in Quick-Basic 4.5 for IBM compatible PCs. For avoiding slow computations, 80486 or Pentium processors are recommended.

When using DOEHLOPT, the number of factors f (in the range 2–10), the number of replications at the centre of design n_0 , and the minimum and maximum working levels and units for the considered factors are typed from keyboard as data inputs. The program generates internally the USD coded matrix and then decodes it and displays the design matrix including the uncoded levels needed for the considered factors in order to perform the experimental runs. Once the runs have been performed, the experimental response corresponding to each run is entered from keyboard by the user and may be saved in an ASCII file for possible further use. The program then estimates: the coefficient of the model equation by multiple linear regression according Eq. (4), the optimum co-ordinates from Eq. (7) and the canonical analysis. The program produces the following outputs (monitor display or printer): (i) The ANOVA of the regression model, indicating sources of variation, degrees of freedom, sum of squares and variances. The experimental and critical tabulated values of Fisher F -test are also shown with the correlation coefficient for the fit; (ii) the estimated coefficients of the model equation and their standard deviations with indication of their significance according the Student t -test; (iii) the eigenvalues of matrix \mathbf{S} indicating if the stationary point is a maximum, minimum or saddle point; and (iv) the coded and uncoded co-ordinates of the singular point. The DOEHLOPT program is available from the authors upon request (including the source code).

4. Scope and features

As it was explained above, DOEHLPT has been implemented to evaluate and optimizing response–surface curves based on USD.

Allowing for that the user would be interested in a comparison of the performance of DOEHLPT with another well-known programs, we have selected the program GOSSET, developed by Hardin and Sloane [22] and perhaps the most compendious general-purpose program within the frame of experimental designs. It can be downloaded from ftp.research.att.com, login as anonymous. The remaining path is bin/dist/njas/gosset, and the files to be downloaded are readme, manual.ps (postscript file of the manual), codelib.a (library of precomputed designs) and codemart.cpio (GOSSET source code) [23]. Following section 9 of the manual, a private GOSSET copy may be installed only in a computer with unix/linux operating systems.

GOSSET consists of about 15 000 lines of C code, and at present only a UNIX version is available. It enables the construction of any response surface design, including the USD. However, as can be read in page 4 of the manual, 'GOSSET constructs only designs. We assume that you will use one of the standard statistical programs as... to analyse the data obtained by running the design'.

Concerning user facilities, DOEHLPT is a whole program implemented in a flexible interactive way towards the user, intended to the construction of USD and the optimization of the response data. GOSSET is a general purpose big program that only enables the user to build the design in accord with theoretical or conceptual dictates. For analysing the response data, another statistical program must be applied. For the sake of comparison some USD generated from GOSSET and analysed with standard statistical packages yield the same results that those produced by DOEHLPT.

Thus, within the USD frame only, DOEHLPT could therefore be more suitable for users which are not very familiarized on these topics and are only concerned in optimizing their experiments.

5. Worked example

In order to illustrate how DOEHLPT works, a case study taken from literature has been discussed.

Benzo et al. [24] studied the influence of three factors on the molybdenum determination by electrothermal atomic absorption spectroscopy, namely, acid concentration (x_1), ashing temperature (x_2) and atomization temperature (x_3). These factors were varied as follows: x_1 : 0–10% v/v in HCl, x_2 : 400–2200°C and x_3 : 2400–2800°C. The response measured (Y_{Mo}) is the absorbance at 313.3 nm. Before the application of our program and discuss the results, we will outline the procedure and results obtained by the authors in order to make comparisons. Benzo et al. applied the Doehlert procedure by performing 13 experiments as the average of two replications and eight runs (measured among experiments) at the centre of design that were averaged to a central point. Thus, the authors adjust the responses to a third degree polynomial plus interactions giving

$$Y_{Mo} = 0.274 - 0.020x_1 - 0.027x_2 + 0.161x_3 \\ - 0.013x_1^2 - 0.033x_2^2 - 0.071x_3^2 - 0.009x_1x_2 \\ + 0.002x_1x_3 - 0.003x_2x_3 + 0.064x_1^3 \\ - 0.027x_2^3 + 0.000x_3^3 - 0.001x_1x_2x_3$$

Then, by plotting the response surface at the 'optimal' atomization temperature, the authors attain an 'optimal experimental field' in the region 2–8% V/V HCl and a 400–1030°C ashing temperature.

Our aim is not to criticize the way used for the authors in order to attain optimal conditions from the Doehlert design, but some shortcomings derived therefrom should be considered.

First of all, most of the authors codify the maximum and minimum factor levels to 1 and -1 . In the worked example considered, the authors codify the limiting levels for the acid concentration in %V/V HCl (factor x_2) as follows: 0% is -1 and 10% is 1. However, beyond the first factor (x_1) the coded levels 1 and -1 are not considered in the Doehlert design. In fact, the range of the coded levels uniformly decreases

from ± 0.866 (three factors) to ± 0.745 (ten factors). Thus, limiting levels for factors other than x , will never be involved in experiments when the coding (high level = 1, low level = -1) is blindly applied to all factors.

On the other hand, the use of second order models like Eq. (3) ensures a good enough approach to attain optimal conditions and moreover, this enables us to perform an error analysis. Replications at the centre of design are the key feature for a full ANOVA of the regression. Finally, once the response surface is modelled, the derivative method for searching optimum conditions is very straightforward.

Now we will discuss the results obtained by applying DOEHLOPT to the data of Benzo et al. We have considered 12 runs ($f^2 + 2f$) (average of two measurements) plus eight replications at the centre of design. In order to use the authors' data for our purposes, the working range of factor levels is now: x_1 : 0–10% v/v in HCl, x_2 : 521–2079°C and x_3 : 2437–2763°C because the uncoded levels corresponding to the coded 1 and -1 ones are not used for x_2 and x_3 . Thus, the

uncoded data matrix including response is gathered in Table 1.

Considering that the number of coefficient to be estimated from Eq. (3) for three factors is 10 and we have 12 + 8 (replications at the centre of design) data, it is possible to perform the analysis of errors. From the variance-covariance matrix and the variance of residuals, the standard deviations associated to the coefficients are calculated and the ANOVA is carried out. The results are depicted in Table 2 and Table 3. The F -test between the variances for the lack of fit and for pure error (replications) leads to the value $F = 8.78$, higher than the tabulated critical value at significance level of 0.05, $F_{crit} = 3.97$, indicating a fair adjustment, which is also featured by a correlation coefficient of about 0.99. Better fit cannot be expected because the theoretical model should be rather a sigmoidal function on x_2 and x_3 , the absorbance mainly depending on the amount of element volatilized and atomised. The quadratic equation is used to approximate the experimental behaviour near to extremes. If the temperature range is chosen such that it does not contain the full sigmoid, the approximation is acceptable.

Table 1

Experimental data matrix for the Doehlert design in the optimization of molybdenum signal (from Ref. [24])^a

Acid concentration (x_1)	Ashing temperature (x_2)	Atomization temperature (x_3)	Response (Y_{Mo})
0	1300	2600	0.217
10	1300	2600	0.305
2.5	521	2600	0.285
7.5	2079	2600	0.200
2.5	1040	2437	0.098
7.5	1560	2763	0.341
7.5	521	2600	0.289
2.5	2079	2600	0.212
7.5	1040	2437	0.095
2.5	1560	2763	0.346
5	1819	2437	0.065
5	781	2763	0.370
5	1300	2600	0.266
5	1300	2600	0.286
5	1300	2600	0.282
5	1300	2600	0.271
5	1300	2600	0.269
5	1300	2600	0.287
5	1300	2600	0.261
5	1300	2600	0.272

^a All factor levels are uncoded.

Table 2
Error analysis and significance of the estimated coefficients

Coefficient	Value \pm SD ^a	Significance ^b
b_0	0.274 \pm 0.006	Yes
b_1	0.020 \pm 0.009	Yes
b_2	-0.043 \pm 0.009	Yes
b_3	0.163 \pm 0.009	Yes
b_4	-0.01 \pm 0.01	No
b_{22}	-0.03 \pm 0.01	Yes
b_{33}	-0.07 \pm 0.01	Yes
b_{12}	-0.009 \pm 0.02	No
b_{13}	0.002 \pm 0.02	No
b_{23}	-0.003 \pm 0.02	No

^a SD, standard deviation.

^b The significance is evaluated according to the Student *t*-test at a significance level of 0.05. If the coefficient is significant, then the result is Yes, otherwise, No.

Inasmuch as, according to Table 2, coefficients b_{11} , and second order interaction ones, b_{12} , b_{13} and b_{23} are non significant. Thus, b_{11} being not significant, it is not possible to find a singular point (maximum or minimum) in three dimensions. However, it is possible to obtain more insight proceeding in the following way: If we do not neglect the non significant coefficients, we find a maximum in the surface corresponding to the co-ordinates (1.156, -0.890, 1.183) in coded scale or (10.8%, 499°C, 2836°C) in uncoded scale. The x_1 co-ordinate is meaningless and therefore one may consider the values x_2 cat 500°C and x_3 cat 2800°C as nearly optimum levels. By taking these values in coded levels as fixed ones in our model equation we obtain a linear response of the molybdenum absorbance against the acid concentration:

Table 3
ANOVA of the regression model

Source	Degrees of freedom	Sum of squares	Variance
Regression	9	0.126309	0.014034
Residual	10	0.003084	0.000308
Replication	7	0.000648	0.000092
Lack of fit	3	0.002436	0.000812
Total	19	0.129393	0.006810

$$Y_{Mo} = 0.305 + 0.02x_1$$

the response being increased with the acid concentration. The extremes for x_1 are 1 and -1, and therefore the limiting values for the response at x_2 and x_3 fixed ranges within 0.325–0.285. Accordingly, as the authors [24] pointed out, it is advisable to use diluted acid solution to prevent pyrolytic graphite deterioration, and consequently levels of about 2% v/v (-0.6 in coded level) are appropriate. Thus, the optimum co-ordinates in uncoded levels are (2%, 500°C, 2800°C) in fair agreement with the obtained by Benzo et al. [24] (2%, 700°C, 2800°C). The only discrepancy being the value of the final ashing temperature: 500 versus 700°C. We have obtained our value by searching the optimum considering all terms of the model equations as significant and then disregarding the first factor. The authors selected the optimum for the ashing temperature midway of the optimum range chosen (400–1030), which is cat 700°C. Taking into account that the use of low ashing temperatures to preclude possible losses of molybdenum due to volatilization, it seems to be more suitable working at 500°C.

References

- [1] R.H. Myers, A.I. Khuri, W.H. Carter Jr., *Technometrics* 31 (1989) 137.
- [2] R. Mead, D.J. Pike, *Biometrics* 31 (1975) 803.
- [3] A.C. Atkinson, *Int. Stat. Rev.* 56 (1988) 99.
- [4] A.G. González, *Int. J. Pharm.* 97 (1993) 149.
- [5] N.A. Armstrong, K.C. James, *Pharmaceutical experimental design and interpretation*, Taylor and Francis, London, 1996, pp. 181–187.
- [6] G.E.P. Box, D.W. Behnken, *Technometrics* 2 (1960) 455.
- [7] G.E.P. Box, K.B. Wilson, *J. R. Stat. Soc. Ser. B* 13 (1951) 1.
- [8] G.E.P. Box, J.S. Hunter, *Ann. Math. Stat.* 28 (1957) 195.
- [9] A.G. González, D. González-Arjona, *Anal. Chim. Acta* 298 (1994) 65.
- [10] D.H. Doehlert, *Appl. Stat.* 19 (1970) 231.
- [11] Y. Hu, D.L. Massart, *J. Chromatogr.* 485 (1989) 311.
- [12] P. Gratteri, S. Furlanetto, E. La Porta, S. Pinzauti, *Farmaco* 51 (1996) 231.
- [13] Y. Berrah, P. Lanteri, R. Longaray, B. Kadri, B. Fabre, A. Accary, *Entropie* 32 (1996) 31.
- [14] T. Dagnac, J.M. Guillot, P. Le Cloirec, *J. Anal. Appl. Pyrolysis* 37 (1996) 33.

- [15] M.A. Carsol, I. Pouliquen, P. Giamarchi, G. Lesgards, M. Sergent, R. Phan Tan Luu, *Analisis* 24 (1996) 195.
- [16] M. De Meo, M. Laget, C. Di Giorgio, H. Guiraud, A. Botta, M. Castegnaro, G. Dumenil, *Mutat. Res.* 340 (1996) 51.
- [17] C.G. Hounsa, J.M. Aubry, H.C. Dubourguier, J.P. Hornez, *Appl. Microbiol. Biotechnol.* 45 (1996) 764.
- [18] L. Fernández Ruano, X. Tomas, *Afinidad* 52 (1995) 335.
- [19] M. Nechar, F.M. Molina, L. Cuadros, J.M. Bosque, *Anal. Chim. Acta* 316 (1995) 185.
- [20] A.M. García Campaña, L. Cuadros Rodríguez, A. Lupiáñez González, F. Alés Barrero, M. Román Ceba, *Anal. Chim. Acta* 348 (1997) 237.
- [21] D. González-Arjona, A.G. González, *Anal. Chim. Acta* 293 (1994) 205; *Idem*, *QCPE Bulletin*, 14 (1994) 43.
- [22] R.H. Hardin, N.J.A. Sloane, *J. Stat. Plan. Inference* 37 (1993) 339–369.
- [23] <http://www.research.att.com/~njas/gosset/index.html>
- [24] Z. Benzo, P. Araujo, A. Sierraalta, F. Ruetter, *Anal. Chim. Acta* 65 (1993) 1107.

Voltammetric determination of the phenolic antioxidants 3-tert-butyl-4-hydroxyanisole and tert-butylhydroquinone at a polypyrrole electrode modified with a nickel phthalocyanine complex

C. de la Fuente, J.A. Acuña, M.D. Vázquez, M.L. Tascón,
P. Sánchez Batanero *

Department of Analytical Chemistry, Faculty of Sciences, University of Valladolid, Valladolid, Spain

Received 28 May 1998; received in revised form 17 December 1998; accepted 24 December 1998

Abstract

The voltammetric behaviour of the antioxidants 3-tert-butyl-4-hydroxyanisole (BHA) and tert-butylhydroquinone (TBHQ), at a polymer electrode modified with nickel phthalocyanine as electron mediator, is described, and an electroanalytical method for the determination of these antioxidants based on their electrochemical oxidation on the modified electrode is proposed. Cyclic voltammograms showed well-defined oxidation peaks slightly shifted towards less positive potentials with respect to those obtained at the platinum disk electrode for both antioxidants. The peak currents measured at the modified electrode are considerably higher than those obtained at the unmodified electrode. A scan rate of 100 mV s^{-1} , a minimum methanol percentage of 0.5% and a 0.1-M Britton-Robinson medium were chosen as working conditions. The obtained results suggest that the BHA oxidation produces the TBHQ reduction product. This product is oxidised during the second cyclic scan, to generate the mentioned TBHQ as final product. These studies also reveal that sensitive response for both antioxidants can be obtained by using the differential pulse voltammetry (DPV) technique. Responses observed are dependent on the nature of the control solution (% methanol and pH) and the nature of voltammetric conditions (potential amplitude, ΔE , and scan rate, v_b). These factors have been modified in order to find the best analytical conditions. The mutual interferences between both antioxidants and the measurement reproducibility were tested. Using cyclic voltammetry (CV) and differential pulse voltammetry, BHA and TBHQ linear calibration graphs were obtained. The detection limits were 2.1 ppm for both when CV was used, and 18.7 ppm (BHA) and 1.23 ppm (TBHQ) for DPV. The developed methods were applied to the determination of BHA in spiked glaze biscuits and TBHQ in spiked mushroom cream. © 1999 Elsevier Science B.V. All rights reserved.

Keywords: Antioxidant; 3-tert-Butyl-4-hydroxyanisole; tert-Butylhydroquinone; Polypyrrole electrode; Nickel phthalocyanine complex

* Corresponding author.

1. Introduction

The use of antioxidants in the food and pharmaceutical industries is particularly important to prevent the decomposition of organic compounds present in prepared products.

Biological and toxicological aspects, detection, estimation and evaluation of antioxidants used as food additives have been described by Hudson [1]. Among the most common additives used as antioxidants we considered the phenolic compounds. They are currently added to food products in order to prevent oxidative degradation of fats and oils. Two of the most commonly employed are tert-butylhydroxyanisole (BHA) and tert-butylhydroquinone (TBHQ). BHA resists heat well, so it is effective in bakery and confectionery products subjected to cooking. As for their toxicity, there is large discrepancy among investigators, some classifying it as carcinogenic and others as not carcinogenic. Typical products where these antioxidants appear are cookies, sweets, raisins, fruit pastries, margarine, prepared food, etc. The authorised maximum quantities in oils are 200 mg kg^{-1} and in margarine 100 mg kg^{-1} . TBHQ is less used. In oils the allowed maximum quantity is 200 mg kg^{-1} .

Methods for the determination of phenolic antioxidants including BHA and TBHQ have been reviewed [2]. Undoubtedly HPLC is the most widely used method, for example, for the simultaneous determination of phenolic antioxidants in food, and cosmetic and pharmaceutical products [3]. Also BHA (with others antioxidants) has been determined in oil and butter [4–8]. This kind of food is also analysed using spectrophotometric and fluorimetric methods, [9–11]. Other kinds of products, where TBHQ and BHA have been determined, are plastics [12–14], peanut [15], fat [16] and drugs [17]. Electrochemical methods are relatively scarce in this area. Differential pulse voltammetry at stationary [18] and rotating [19] electrodes, as well as preconcentration at a carbon paste electrode [20], has been reported. A carbon paste electrode modified with nickel phthalocyanine has been used in [21] for the determination of a phenolic antioxidant in diethylether. Finally, flow-injec-

tion methods based on antioxidant oxidation at a glassy carbon electrode have been described [22].

The areas of analytical application of chemically modified electrodes are those where immobilised electron-transfer mediators are the most used to catalyse slow electrode reactions [23–26]. Metal phthalocyanines are one of the most employed inorganic modifiers, having been reviewed by Cox et al. [27], and by Zagal [28]. Baldwin's group [29–32] has demonstrated the suitability of metal phthalocyanines for analytical purposes.

Voltammetry has been used for the determination of numerous electroactive vitamins, antioxidants, preservatives, metals and organics in foods and drinks. With advanced pulse voltammetric techniques such analytes can be determined down to the submicromolar level. While reducible components are determined polarographically at the mercury electrode, oxidizable components are commonly measured at carbon or platinum surfaces. Recent advances in the areas of modified micro and ultramicroelectrodes, sensors arrays, and advanced voltammetric waveforms should greatly enhance the power of voltammetry in the food industry. For example, it is important to emphasise that the electroanalytical methods are very useful for the determination of organic compounds, due to their sensitivity, selectivity and accuracy, as well as to the important information on the electrochemical mechanisms which sometimes are comparable to those taking place in metabolic processes in living organisms. In this sense, we can mention the reviews of Bersier and Bersier [33,34], and Kalvoda [35].

The aim of this work is to investigate cyclic voltammetry and pulse differential voltammetry behaviour of BHA and TBHQ at a polypyrrole electrode modified with tetrasulfonated nickel phthalocyanine complex in order to develop a method for the determination of these antioxidants based on their electrochemical oxidation. The methods have been applied to the determination of the mentioned antioxidants in different food samples, in which these antioxidants may be present.

2. Experimental

2.1. Reagents

Sodium nickel (II) phthalocyanine tetrasulfonate (NiPcTs, Aldrich); sodium *p*-toluenesulfonate (TsNa, Fluka); pyrrole (Merck); tert-butylhydroxyanisole (BHA) and tert-butylhydroquinone (TBHQ) (Sigma); boric acid (Merck); acetic acid (Merck); orthophosphoric acid (Panreac); sodium hydroxide (Panreac); methanol (Merck); aluminum oxide (Metrohm 6.2802.000); and sodium dichromate (Panreac) were used. All reagents were of analytical grade. Ultrapure water was obtained from the Barnstead System.

2.2. Instrumentation

Potentiostat AUTOLAB PSTAT 10 ECO-CHEMIE (Holland) using the GPES software; ultrasonic bath P-Selecta (Spain); mechanical stirrer vibromatic 384 P-Selecta (Spain); rotary vacuum evaporator Büchi (Italy); and thermostatic bath P-Selecta (Spain), were used.

2.3. Electrodes

Ag/AgCl/KCl_(sat), reference electrode; Pt wire (home made), as auxiliary electrode; and Pt disk electrode, 0.076 cm² (Metrohm) as working electrode, were used.

3. Procedure

3.1. Electrogeneration of modified polypyrrole electrodes

The polypyrrole coated electrode was prepared on disk platinum surface (diameter = 3 mm) by the electrochemical polymerisation of pyrrole monomers from a 0.1-mol l⁻¹ pyrrole solution. The polymerisation was performed at 0.8 V for 60 s versus Ag/AgCl/KCl_(sat), at the Pt electrode. The generation solution was deoxygenated by bubbling N₂ gas. Pyrrole was dissolved in aqueous solution containing NiPcTs (1·10⁻⁴ mol l⁻¹), or TsNa (4·10⁻⁴ mol l⁻¹). Polypyrrole electrodes

prepared by this procedure have been described elsewhere [36].

3.2. Treatment of commercial food samples

A procedure similar to that proposed by King et al. [37] was followed for the determination of BHA in glaze biscuits and for the TBHQ determination in mushroom cream. Samples were powdered in an agate mortar. Then, three portions of 0.50 g of these samples, to which a controlled volume of BHA or TBHQ standard solutions in methanol were added, were placed in a 20-ml centrifuge tube. In all cases, extraction was carried out with three 5-ml portions of a 50% MeOH/water solution. The tube was mechanically shaken for 15 min, and after centrifugation at 7000 rpm for 20 min, all the extracts were combined in a 100-ml vessel of the rotary vacuum evaporator, and concentrated up to a final volume of ~1 ml. This extract was transferred into a 25-ml volumetric flask, and then diluted to the mark with Britton-Robinson buffer solution. This solution was transferred to the electrochemical cell, where BHA or TBHQ were voltammetrically determined by using the standard additions method. Similar procedure was done on a blank sample, to which neither BHA nor TBHQ had been added.

To modify the pH, maintaining the other parameters constant, a Britton-Robinson solution was employed. Therefore, to vary the pH, a 2-mol l⁻¹ NaOH solution was added to the Britton-Robinson solution in sufficient amount to reach the necessary pH values.

All the experiments were carried out at constant temperature (20 ± 1°C), maintaining the electrocells thermostated.

4. Results and discussion

4.1. Catalytic effect

In order to ascertain if BHA and TBHQ are electrocatalytically oxidised at the Pt/PPy/NiPcTs electrode, voltammograms of both were obtained in a Britton-Robinson 0.1-M solution of pH 1.1

(control solution), at different working electrodes: Pt, Pt/PPy/Ts and Pt/PPy/NiPcTs, where Ts is *p*-toluenesulphonate, a counterion with no electrocatalytic properties. These voltammograms are displayed in Fig. 1 for BHA, and Fig. 2 for TBHQ. As can be seen and as expected, the peak potentials shifted toward less positive values and antioxidant peak intensities are substantially increased when working with a Pt/PPy/NiPcTs electrode, showing that electrocatalytic effects are produced.

The cyclic voltammograms obtained, when using a Pt/PPy/NiPcTs electrode in pure (blank) electrolyte, show a high background current, similar to that observed in other investigations [36], where explanations were given. But this large background current observed does not interfere with the electrochemical measurements. No signal of Ni(II) oxidation is produced because NiPcTs is an example of a redox inactive transition metal phthalocyanine [38].

4.2. Optimisation of voltammetric parameters

4.2.1. Influence of pH and methanol/water ratio on voltammetric peak height and peak potential

Both the effect of pH and the methanol percentage on the electrochemical responses of BHA and TBHQ were examined using cyclic voltammetry at a potential scan rate of 100 mV s⁻¹. Voltammograms were obtained at the modified polymer electrode with NiPcTs. Fig. 3a,b shows the influence of pH on E_p for 1·10⁻³ M BHA in a 2% methanol/0.1-M Britton-Robinson buffer medium and for 6·10⁻⁴ M TBHQ in a 0.45% methanol/0.1-M Britton-Robinson buffer medium, respectively. The peak potential for both antioxidants decreased linearly ($y = 0.73 - 0.052x$, $r^2 = 0.984$ for BHA and $y = 0.43 - 0.056x$, $r^2 = 0.996$ for TBHQ) with increasing pH. The peak currents describe similar curves for BHA and TBHQ (Fig. 4a,b): first it increases to pH 4.5, but then, for higher pH values, the peak intensity decreases considerably. This behaviour is similar to that observed for phenolic antioxidants at other modified polymer electrodes [36].

Taking into account these results, a 0.1-M Britton-Robinson solution (pH 1.1) was chosen for

further studies. This is not the optimal pH value, but we can obtain good sensitivity and, more important, the experiments are very simple.

The effect of methanol percentage on the peak current of 1·10⁻³ M BHA and 8·10⁻⁴ M TBHQ in 0.1-M Britton-Robinson solution was examined over the range 0–28% (v/v). A linear decrease of I_p values was observed as the methanol percentage increased. Consequently, a smaller methanol percentage (~0.4%) was chosen as working medium for subsequent experiments.

4.2.2. Influence of scan rate in cyclic voltammetry

Cyclic voltammograms of 6.0·10⁻⁴-mol l⁻¹ BHA (0.12% methanol) solutions were recorded at different scan rates between 5 and 600 mV s⁻¹. With the experimental data, we have deduced that as the scan rate was increased the peak current increased, as well as the background current and the peak potential. A clear shift of E_p was produced as expected for irreversible electrochemical reactions. I_p versus $v^{1/2}$ and the I_p versus v showed some linear relationships, with a slope change at 150 mV s⁻¹. In addition, the ratio $I_p/C_{v^{1/2}}$ increases with the logarithm of the potential scan rate. This behaviour suggests that the oxidation process is controlled by diffusion as well as by adsorption mechanism [39].

On the other hand, cyclic voltammograms of a 1.2·10⁻³-mol l⁻¹ TBHQ solution, were recorded at different scan rates between 5 and 1000 mV s⁻¹; in this case, by analysing the results, an increase of E_p is observed when the scan rate increases. I_p showed a linear relationship versus $v^{1/2}$ and versus v up to 125 mV s⁻¹, but the linearity is lost at faster scan rates. In addition, the ratio $I_p/C_{v^{1/2}}$ increases with the logarithm of the potential scan rate until 500 mV s⁻¹. The conclusions are similar to the case of BHA.

With these results, a scan rate of 100 mV s⁻¹ was chosen for all further studies.

4.2.3. Influence of potential amplitude, ΔE , and scan rate, v , in potential and height antioxidant peaks, using differential pulse voltammetry

4.2.3.1. Influence of potential amplitude, ΔE . A study of the influence of potential amplitude of

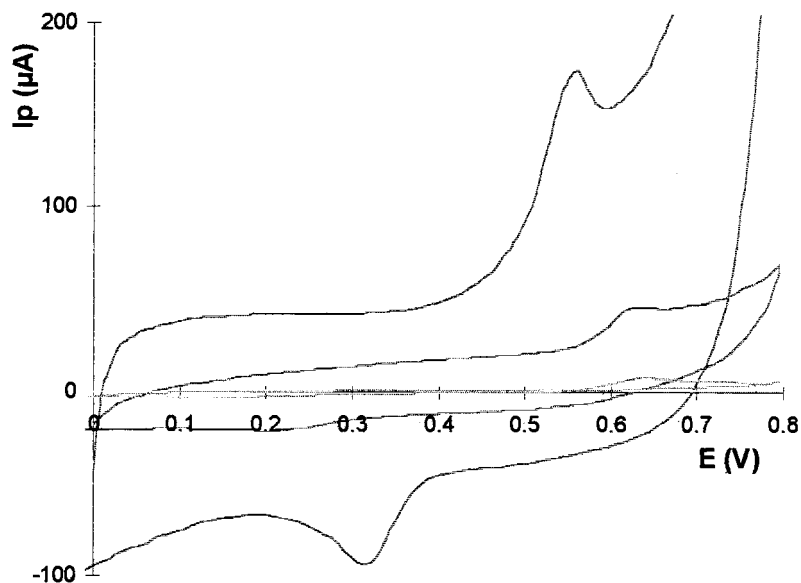


Fig. 1. Cyclic voltammograms obtained in a Britton-Robinson 0.1 mol l^{-1} -solution (pH 1.1; 1.4% methanol; $v = 100 \text{ mV s}^{-1}$ with $4.0 \cdot 10^{-4} \text{ mol l}^{-1}$ BHA at different working electrodes): (a) WE Pt: $E_p = 0.634 \text{ V}$, $I_p = 1.00 \mu\text{A}$; (b) WE Pt/PPy/Ts: $E_p = 0.624 \text{ V}$, $I_p = 10.45 \mu\text{A}$; (c) WE Pt/PPy/NiPcTs: $E_p = 0.549 \text{ V}$, $I_p = 51.50 \mu\text{A}$.

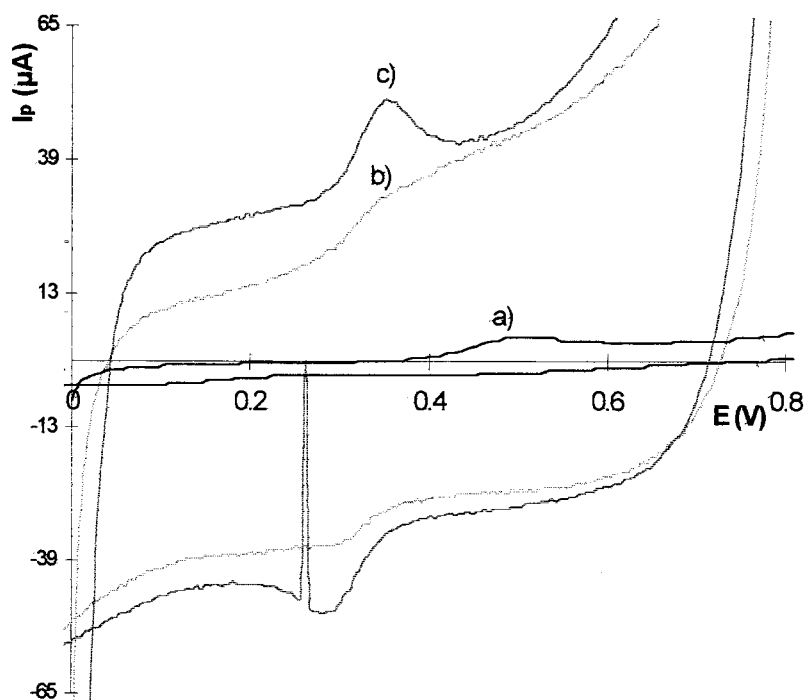


Fig. 2. Cyclic voltammograms obtained in a Britton-Robinson 0.1 mol l^{-1} solution (pH 1.1; 0.5% methanol; $v = 100 \text{ mV s}^{-1}$ with $4.0 \cdot 10^{-4} \text{ mol l}^{-1}$ TBHQ at different working electrodes): (a) WE Pt: $E_p = 0.485 \text{ V}$, $I_p = 2.4 \mu\text{A}$; (b) WE Pt/PPy/Ts: $E_p = 0.378 \text{ V}$, $I_p = 4.1 \mu\text{A}$; (c) WE Pt/PPy/NiPcTs: $E_p = 0.352 \text{ V}$, $I_p = 11.8 \mu\text{A}$.

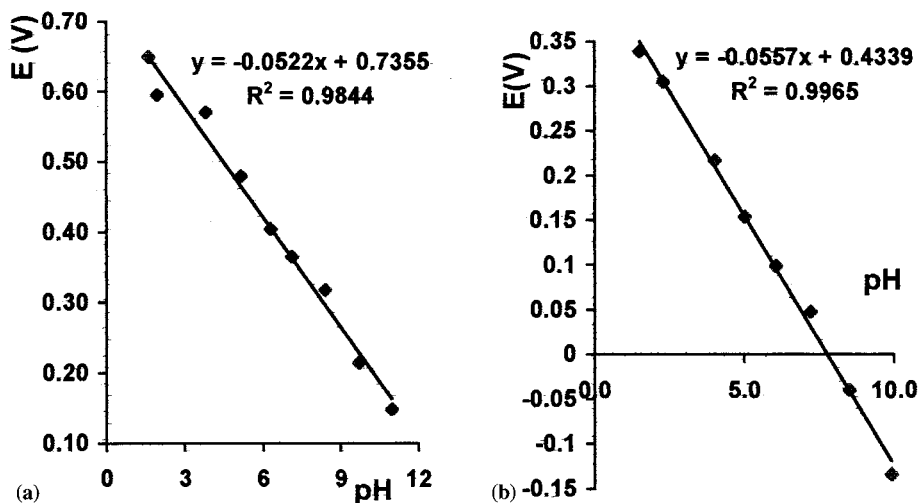


Fig. 3. Effect of pH on BHA peak potential (a) and on TBHQ peak potential (b) for cyclic voltammetry at a nickel (II) phthalocyanine tetrasulfonate modified polypyrrole electrode (Pt/PPy/NiPcTs) using working conditions described in the text.

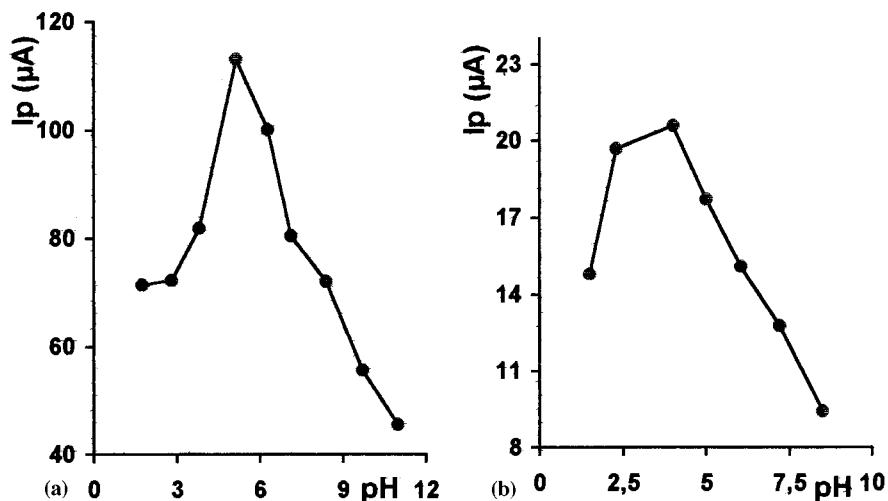


Fig. 4. Effect of pH on BHA peak intensity (a) and on TBHQ peak intensity (b) for cyclic voltammetry at a nickel (II) phthalocyanine tetrasulfonate modified polypyrrole electrode (Pt/PPy/NiPcTs) using working conditions described in the text.

the peak height of antioxidants was carried out by using differential pulse voltammetry (modifying this parameter and at a fixed scan rate of 25 mV s^{-1}). The BHA concentration was $4 \cdot 10^{-4} \text{ M}$ and the TBHQ concentration was $4 \cdot 10^{-5} \text{ M}$. Fig. 5 shows all the plots of experimental results. Taking into account these figures, the best results are obtained in the potential amplitude interval of 90–130 mV. But the background intensity is increased with the potential amplitude, therefore a

value of 90 mV for both antioxidants was chosen for subsequent studies.

4.2.3.2. Influence of scan rate, v_b . In this study we have modified the scan rate used in the experiments, maintaining all other parameters fixed. The BHA concentration was $4 \cdot 10^{-4} \text{ M}$ and that of TBHQ was $4 \cdot 10^{-5} \text{ M}$. In all cases the potential peak does not undergo important variations whereas the background intensity is increased

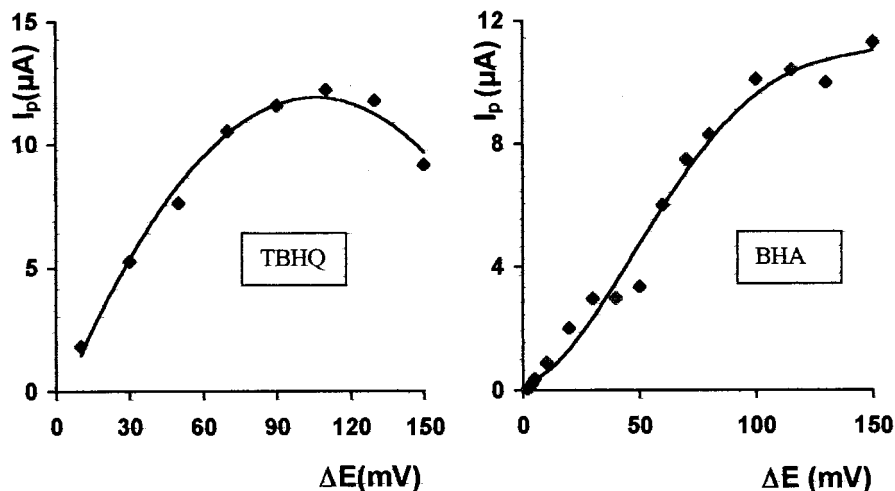


Fig. 5. Effect of potential amplitude on antioxidant peak current and potential peak obtained with differential pulse voltammetry (DPV) at a nickel (II) phthalocyanine tetrasulfonated modified polypyrrole electrode (Pt/PPy/NiPcTs).

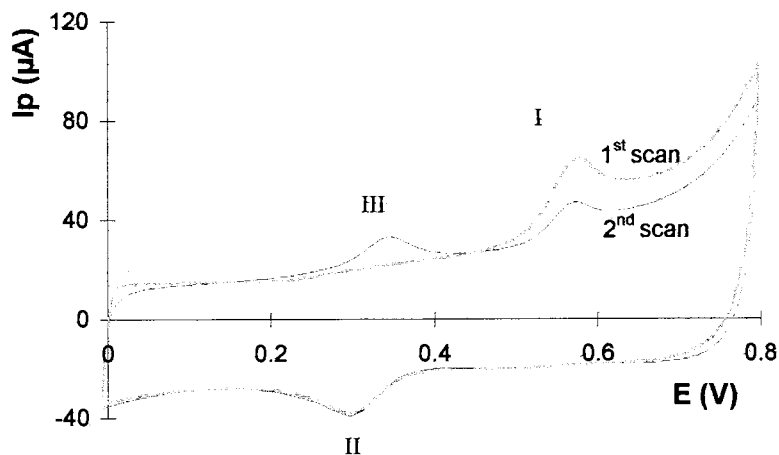


Fig. 6. First and second successive cyclic voltammograms of a BHA solution.

when the scan rate is increased. With these results, and in order to obtain good sensibilities, scan rates of 40 mV s^{-1} for BHA and 25 mV s^{-1} for TBHQ were chosen for subsequent studies, since the relation between peak and background intensities is high.

4.2.4. Successive cyclic voltammograms

Cyclic voltammograms corresponding to two consecutive scans of $6 \cdot 10^{-4} \text{ M}$ BHA, on the same modified working electrode, are plotted in Fig. 6. The first scan shows an oxidation peak (peak I) at 0.571 V and a reduction peak (peak II) at 0.302 V;

at the second scan, we can also see a new oxidation peak (peak III) at 0.341 V. Peaks II and III do not appear when the potential scan finishes at a smaller potential than the BHA oxidation. So, these two peaks could be due to reduction and subsequent oxidation of a product generated during the BHA oxidation. The consulted bibliography [40] indicates that formation of phenoxonium ions is involved in the oxido-reduction of phenolic compounds. Therefore, the BHA oxidation could involve *t*-butylquinone (TBO) formation, which is the product obtained when TBHQ is oxidised. To confirm this hypothesis, cyclic voltammogram of

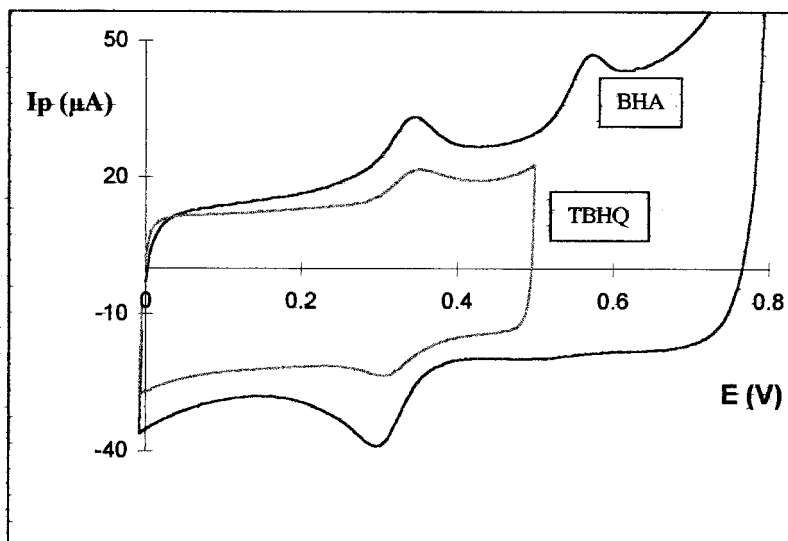


Fig. 7. Second successive cyclic voltammograms of a BHA solution and cyclic voltammograms of a TBHQ solution obtained using the same working conditions.

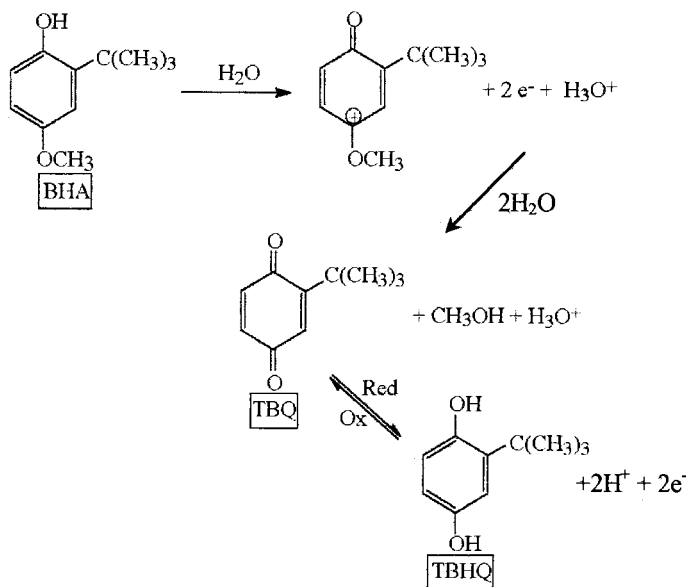


Fig. 8. BHA oxidation reaction proposed.

a TBHQ solution, obtained at the same working-conditions, was compared with the second BHA scan cyclic voltammogram, as can be seen in Fig. 7. As expected, peaks II and III are present in both voltammograms, confirming the reactions plotted in Fig. 8.

If the same working electrode remains in the solution some minutes, when new voltammograms are registered, the described behaviour is repeated, registering only one oxidation peak (peak I) in the first cycle. But the peak I height increases slightly in successive experiments, possi-

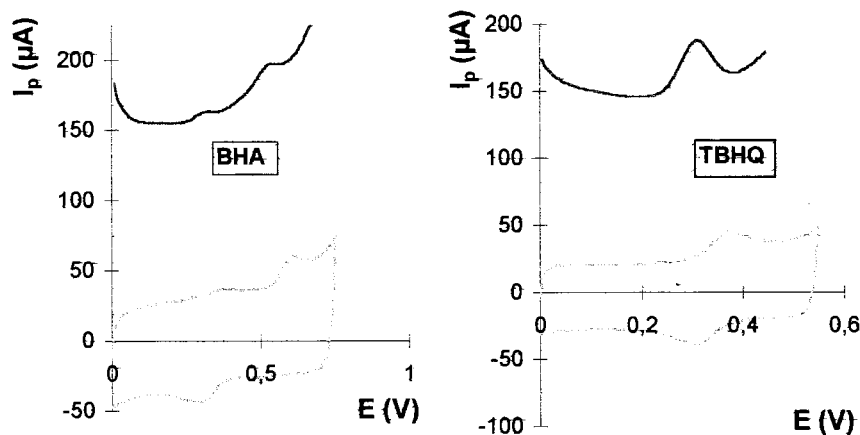


Fig. 9. Comparative curves obtained by using cyclic voltammetry and pulse differential voltammetry. (a) $2 \cdot 10^{-4}$ -M BHA solution: CV ($v_b = 100 \text{ mV s}^{-1}$); DPV ($\Delta E = 90 \text{ mV}$; $v_b = 25 \text{ mV s}^{-1}$), (pH 1.2; % methanol = 0.4); (b) $2 \cdot 10^{-5}$ M TBHQ solution: CV ($v_b = 100 \text{ mV s}^{-1}$); DPV ($v_b = 25 \text{ mV s}^{-1}$; $\Delta E = 90 \text{ mV}$), (pH 1.2; % methanol = 0.4).

bly due to small adsorption. For a $8 \cdot 10^{-4}$ -M TBHQ solution, the mean intensity for 12 measurements carried out with one electrode was $25 \pm 1 \mu\text{A}$.

4.2.5. Reproducibility with cyclic voltammetry and with differential pulse voltammetry techniques

In order to check the reproducibility in the preparation of the modified polypyrrole electrodes, several Pt/PPy/NiPcTs electrodes (11 for the TBHQ and 15 for the BHA experiments) were obtained under the same experimental conditions (60 s at 0.80 V). BHA and TBHQ cyclic voltammograms were recorded after immersing the electrodes for 2 min into the analyte solutions. These analytical solutions contain a $6.0 \cdot 10^{-4}$ -M BHA and a $8.0 \cdot 10^{-4}$ -M TBHQ solution with a methanol percentage of 0.4%. BHA peak current mean values of $27.8 \pm 0.4 \mu\text{A}$ ($n = 15$; RSD = 3.1%) and $41.1 \pm 0.7 \mu\text{A}$ ($n = 11$; RSD = 3.2%) for TBHQ were obtained. These results indicate a good reproducibility when cyclic voltammetry was used.

On the other hand, two BHA and TBHQ differential pulse voltammograms have been recorded: the first, immediately after the electrode was immersed into the analyte solution and the second after immersing the electrodes for 3 min in the analyte solution. The peak current mean values obtained for both antioxidants were the following: for BHA ($4 \cdot 10^{-4}$ M) peak current mean values of

12.7 ± 0.5 and $11.4 \pm 0.7 \mu\text{A}$ were obtained for time 0 min and time 3 min, respectively; for TBHQ ($2.0 \cdot 10^{-4}$ M), $35 \pm 1 \mu\text{A}$ ($t = 0$) and $35 \pm 2 \mu\text{A}$ ($t = 3$). The peak potentials are the same in all cases.

The results obtained with both voltammetry techniques are fairly good if we consider that good reproducibility with this type of electrodes is not easy to achieve since, during the electropolymerisation procedure, dimers, trimers, tetramers, etc., are formed. These forms consume polymerisation charge and they are very difficult to control and quantify.

In addition, the curves I - E obtained for the two antioxidants by using cyclic voltammetry and by using differential pulse voltammetry are shown in Fig. 9; the experimental conditions are described in the caption of this figure.

4.2.6. Interferences.

Mutual interferences between BHA and TBHQ were checked by cyclic voltammetry at the NiPcTs modified electrode. Two well separated oxidation peaks were obtained for mixtures of BHA with TBHQ. However, in order to check for the degree of interference of each tested compound, the following study has been done. First, voltammograms of solutions containing $1 \cdot 10^{-4}$ M BHA and different concentrations of TBHQ were registered. Then, the TBHQ concentration was fixed

Table 1

Lineal relationships and detection limits obtained for BHA and TBHQ using cyclic voltammetry

	Range·10 ⁴ (mol l ⁻¹)	r ²	Slope·10 ⁻⁵ (μA Lmol ⁻¹)	Intercept (μA)	% RSD
BHA	2–20	0.994	40.5 ± 1.2	-0.65 ± 1.38	4.6
	1–3	0.996	5.99 ± 0.15	-2.83 ± 0.32	2.6
	Detection limit 1.19·10 ⁻⁵ mol l ⁻¹ = 2.1 ppm Determination limit = 3.97·10 ⁻⁵ M				
TBHQ	2–18	0.994	2.80 ± 0.01	-0.12 ± 0.09	4.8
	0.4–2.6	0.998	0.68 ± 0.01	2.20 ± 0.26	2.3
	Detection limit 2.31·10 ⁻⁵ mol l ⁻¹ = 2.1 ppm Determination limit = 4.36·10 ⁻⁵ M				

varying the BHA concentration each time. Relative errors below 10% were obtained for a 1/20 BHA/TBHQ ratio or higher, but for lower ratios the relative error was increased, because high TBHQ content gave rise to a very high TBHQ peak whose descending part overlapped the BHA peak yielding a flattened peak with decrease of its height. On the other hand, the presence of BHA affected the TBHQ signal for a TBHQ/BHA ratio of 1/22 (a relative error of 9.9% was obtained for that ratio). Smaller ratios have higher error percentages, probably due to the poor BHA solubility in the working medium.

4.2.7. Influence of antioxidant concentrations on their voltammetric signals

Using cyclic voltammetry under the optimised conditions, e.g. pH 1.1, $v = 100 \text{ mV s}^{-1}$ and 0.4% methanol, linear relationships between peak intensity and concentration, in the range from $2.0 \cdot 10^{-4}$ to $20 \cdot 10^{-4} \text{ M}$ and from $1.0 \cdot 10^{-4}$ to $3.0 \cdot 10^{-4} \text{ M}$ for BHA, and from $2.0 \cdot 10^{-4}$ to $18 \cdot 10^{-4} \text{ M}$ and from $4.0 \cdot 10^{-5}$ to $2.6 \cdot 10^{-4} \text{ M}$ for TBHQ, were obtained. The detection limits can be calculated according to the Miller and Miller criteria [41]. In this case, a detection limit of $1.2 \cdot 10^{-5} \text{ M}$ (2.1 mg l^{-1}) for BHA and $2.3 \cdot 10^{-5} \text{ M}$ (2.1 mg l^{-1}) for TBHQ were reached. These results are shown in Table 1. On the other hand, using differential pulse voltammetry under optimised conditions, linear relationships between peak intensity and concentration, summarised in Table 2, were obtained. Analytical characteristics of the method are included in this table. The conclusion is that

BHA shows a smaller detection limit when cyclic voltammetry was used; we have not found a clear reason to explain why DPV is worse than VC. For TBHQ the results obtained with differential pulse voltammetry are better than those obtained using the cyclic voltammetry technique.

4.2.8. Application of the analytical methods to antioxidant determination in commercial food samples

Recovery studies of BHA in commercial glazed biscuits, containing this compound as antioxidant, and of TBHQ in commercial mushroom cream, containing propylgallate (PG) as antioxidant but not tert-butylhydroquinone, were carried out by applying the procedure described in the experiment. Thus, in both cases, the described procedure was applied to 0.5-g sample of food. To determine the concentration of antioxidants the standard additions method was used. Results obtained using cyclic voltammetry for three glaze biscuit samples gave a mean recovery of $93 \pm 1\%$. For three mushroom cream samples a mean recovery of $99 \pm 5\%$ was obtained.

To verify the accuracy of the differential pulse method, recovery studies of TBHQ were carried out on mushroom cream samples, after adding controlled aliquot of antioxidant standard solutions ($10 \mu\text{l}$ of 0.05 M TBHQ). Thus the described procedure was applied to 0.5-g blank sample. No differential pulse voltammetric signal was registered for this blank sample. The mean recovery for three samples is $97 \pm 3\%$ for a significance level of 0.05.

Table 2

Lineal relationships and detection limits obtained for BHA and TBHQ using differential pulse voltammetry (DPV)

	Range·10 ⁵ (mol l ⁻¹)	r ²	Slope·10 ⁻⁵ (μA Lmol ⁻¹)	Intercept (μA)	% RSD
BHA (ΔE = 90 mV; v _b = 25 mV s ⁻¹)	20–100	0.991	55 ± 3	2.5 ± 0.2	5.35
	Detection limit 1.04·10 ⁻⁴ mol l ⁻¹ = 18.7 ppm Determination limit = 3.4·10 ⁻⁴ M				
TBHQ (ΔE = 90 mV; v _b = 25 mV s ⁻¹)	12–22	0.996	0.96 ± 0.03	0.2 ± 0.5	0.96
	2–14	0.997	1.73 ± 0.04	0.9 ± 0.4	2.89
	Detection limit 7.4·10 ⁻⁶ mol l ⁻¹ = 1.23 ppm Determination limit = 2.5·10 ⁻⁵ M				

These results were for a significance level of 0.95, showing the validity of the proposed method for the determination of BHA and TBHQ in samples of this kind, using CV and DPV technique.

5. Conclusions

Electrochemical polymerisation at controlled potential is an appropriate method to prepare nickel (II) phthalocyanine tetrasulfonated modified polypyrrole electrodes. This system exerts an important electrocatalytic effect on the anodic oxidation of tert-butylhydroquinone and tert-butylhydroquinone, by comparing these voltammograms with those obtained by using a bare Pt electrode. So, working with the modified polypyrrole electrode, Pt/PPy/NiPcTs, some E_p values less positive than those of the bare Pt electrode were obtained, as well as higher I_p values. The optimal values were pH 1.1, methanol percentage of 0.5% and scan rate of 100 mV s⁻¹. A mutual interference study has been carried out, showing that, approximately, for two antioxidants, a 1/20 analyte-antioxidant/interferent-antioxidant ratio does not cause high % errors. Detection limits of ppm range were found for both phenolic antioxidants. The application of the proposed method to determine BHA in glaze biscuits and TBHQ in mushroom cream, using the standard addition method, gives a recovery of 93 ± 1% (BHA) and of 99 ± 5% (TBHQ), indicating that this electro-analytical method is suitable

for BHA and TBHQ determination in this type of sample.

The Pt/PPy/NiPcTs modified electrode also showed an analytical response when the DPV technique was used, so the mentioned electrode can be used for the sensitive determination of phenolic antioxidant. Studies described in this paper have demonstrated that the coated electrode shows a good reproducibility. The developed method has been successfully used in TBHQ detection in commercial samples of mushroom cream. On the other hand, this electrode seems to be suitable as indicator electrode in flowing systems when electrochemical detection of antioxidants must be carried out.

Acknowledgements

The authors thank the Ministerio de Educación y Ciencia of Spain for the financial support granted to carry out this work (Project DGICYT PB 92-0259).

References

- [1] B.J.F. Hudson, Food Antioxidants, Elsevier, London, 1990.
- [2] K. Robards, S. Dilli, Analysis 112 (1987) 933.
- [3] J. Irache, F.A. Vega, I. Ezpeleta, Pharm. Acta Helv. 67 (1992) 152 Chem. Abstr. 117:97416k (1992).
- [4] Y. Kitada, Y. Ueda, M. Yamamoto, K. Shinomiya, H. Nakazawa, J. Liq. Chromotogr. 8 (1985) 47.

- [5] C. Takao, *Hokkaidoritsu Eisei Kenkyushoho* 39 (1989) 19.
- [6] M. Garbarino, *Boll. Chim. Ig. Parte Sci.* 41 (1990) 325.
- [7] A. Muñoz de la Peña, F. Salinas, T. Galeano, A. Guiberteau, *Anal. Chim. Acta* 234 (1990) 263.
- [8] J.Y. Maslowaska, M. Bielawski, *Prezm. Che.* 68 (1989) 551 *Chem. Abstr.* 112:137663.
- [9] U.V. Prasad, T.E. Divakar, K. Hariprasar, D.S. Sastry, *Food Chem.* 25 (1987) 159.
- [10] M.C. Gutiérrez, A. Gómez-Hens, D. Pérez-Bendito, Z. Fresenius, *Anal. Chem.* 334 (1989) 344.
- [11] C.S. Sastry, S.G. Rao, *J. Food Sci. Technol.* 29 (1992) 101.
- [12] N. Yagoubi, A.E. Baillet, F. Pellerin, D. Bayloq, *J. Chromatogr.* 522 (1990) 131.
- [13] P.J. Arpino, D. Dilettato, K. Nguyen, A. Bruchet, *J. High Resolut. Chromatogr.* 13 (1990) 5.
- [14] H. Egsgaard, E. Larsen, W.P. Pedersen, L. Carlsen, *Trends Anal. Chem.* 11 (1992) 164.
- [15] I. Vomberg, *Acta Chim. Hung.* 127 (1990) 553.
- [16] A. Guiberteau, T. Galeano, F. Salinas, *Analysis* 19 (1991) 262.
- [17] R. Boussendaji, M. Porthault, A. Berthod, *J. Pharm. Biomed. Anal.* 11 (1993) 71.
- [18] S.C. Rifkin, D.H. Evans, *Anal. Chem.* 48 (1976) 2174.
- [19] C.H. Brieskorn, K. Mahlmeister, *Z. Lebensm. Unters. Forsch.* 171 (1980) 348.
- [20] D. Wang, B.H. Freiha, *Anal. Chim. Acta* 154 (1983) 87.
- [21] M.A. Ruiz, P. Yáñez-Sedeño, J.M. Pingarrón, *Electroanalysis* 6 (1994) 475.
- [22] P. Yáñez-Sedeño, J.M. Pingarrón, L.M. Polo, *Anal. Chim. Acta* 252 (1991) 153.
- [23] R.W. Murray, A.G. Ewing, A.A. Durst, *Anal. Chem.* 59 (1987) 379A.
- [24] S. Dong, Y. Wang, *Electroanalysis* 1 (1989) 99.
- [25] E. Wang, H. Ji, W. Hou, *Electroanalysis* 3 (1991) 1.
- [26] R.P. Baldwin, K.N. Thomsen, *Talanta* 38 (1991) 1.
- [27] J.A. Cox, R.K. Jaworski, P.J. Kulesza, *Electroanalysis* 3 (1991) 869.
- [28] J.H. Zagal, *Coord. Chem. Rev.* 119 (1992) 89.
- [29] A.M. Tolbert, R.P. Baldwin, *Electroanalysis* 1 (1989) 389.
- [30] A.M. Tolbert, R.P. Baldwin, L.M. Santos, *Anal. Lett.* 22 (1989) 683.
- [31] L.M. Santos, R.P. Baldwin, *Anal. Chim. Acta.* 206 (1988) 85.
- [32] L.M. Santos, R.P. Baldwin, *Anal. Chem.* 59 (1987) 1766.
- [33] P.M. Bersier, J. Bersier, *Analytical voltammetry in pharmacy*, in: G. Svehla (Ed.), *Wilson and Wilson's Comprehensive Analytical Chemistry*, vol. XXVII, 1992, p. 159.
- [34] P.M. Bersier, J. Bersier, *Analytical voltammetry in environmental science II. Organic and organometallic species*, in: G. Svehla (Ed.), *Wilson and Wilson's Comprehensive Analytical Chemistry*, vol. XXVII, 1992, p. 381.
- [35] R. Kalvoda, in: R. Kalvoda (Ed.), *Electroanalytical Methods in Chemical and Environmental Analysis*, Plenum, New York, 1987.
- [36] C. de la Fuente, J.A. Acuña, M.D. Vazquez, M.L. Tascón, M.I. Gómez, P. Sánchez Batanero, *Talanta* 44 (1997) 685.
- [37] W.P. King, K.T. Joshep, *J. Assoc. Off. Anal. Chem.* 63 (1980) 137.
- [38] C.C. Leznoff, A.B.P. Lever, *Phthalocyanines*, vol. 1, VCH, New York, 1993, p. 27.
- [39] A.M. Bond, *Modern Polarographic Methods in Analytical Chemistry*, Marcel Dekker, New York, 1980.
- [40] M. Baizer, H. Lund (Eds.), *Organic Electrochemistry*, Marcel Dekker, New York, 1983 Chapter 16.
- [41] J.C. Miller, J.N. Miller, *Statistic for Analytical Chemistry*, Ellis Horwood, New York, 1984.

Simultaneous determination of caffeine and non-steroidal anti-inflammatory drugs in pharmaceutical formulations and blood plasma by reversed-phase HPLC from linear gradient elution

M.J. Martín, F. Pablos*, A.G. González

Department of Analytical Chemistry, University of Seville, 41012 Seville, Spain

Received 15 May 1998; received in revised form 18 December 1998; accepted 24 December 1998

Abstract

A reversed-phase HPLC procedure based on methanol–water gradient elution for determining caffeine and non-steroidal anti-inflammatory drugs with UV absorbance detection is proposed. Chromatographic operational conditions were selected by considering the peak resolution and the retention times of the first and last eluted compounds. The method was suitably validated and successfully applied to the determination of: caffeine, indoprofen, ketoprofen, naproxen, fenbufen and ibuprofen in blood plasma samples and several analgesic/antiphlogistic pharmaceutical formulations © 1999 Published by Elsevier Science B.V. All rights reserved.

Keywords: High performance liquid chromatography; Non-steroidal anti-inflammatories; Blood plasma; Pharmaceutical preparations

1. Introduction

Within the pharmacologic group of non-steroidal anti-inflammatory drugs, arylpropionic derivatives (APDs) are very suitable drugs for preparing analgesic, antiphlogistic and antipyretic formulations because of their good tolerance. APDs actions are due to the inhibition of the cyclooxygenase enzyme, which in turn, prevents

the synthesis of certain prostaglandines [1,2]. Besides these actions, APDs act as middling central nervous system (CNS) depressors. Thus, for preventing this soft CNS depression, central stimulants (i.e. caffeine) are added sometimes to dosage forms.

Today, analytical techniques based on reversed-phase high performance liquid chromatography (RP-HPLC) have become the procedures of choice for determining drugs either in pharmaceutical formulations or biological fluids [3]. Although several RP-HPLC methods have been proposed to assay APDs, they generally deal with a single compound or a few ones [4]. In other

* Corresponding author. Tel.: +34-95-4557173; fax: +34-95-4557168.

E-mail address: fpablos@cica.es (F. Pablos)

cases, some special features about column temperature [5], or detection other than based on absorbance [6,7] are needed.

The aim of this paper is to present an RP-HPLC assay method for determining caffeine and some typical APDs such as indoprofen, ketoprofen, naproxen, fenbufen and ibuprofen in human blood plasma and pharmaceutical dosage forms. An ODS based column, photometric detection at 254 nm and a methanol–water mobile phase have been used.

2. Experimental

2.1. Reagents

Methanol and acetonitrile (Romil, Cambridge, UK) were of HPLC grade. Milli-Q (Millipore, Milford, MA, USA) treated water (with resistivity less than 18 M Ω cm) was used throughout. Other chemicals used in this study were of analytical reagent grade (Merck, Darmstadt, Germany). Arylpropionic acids: indoprofen, naproxen (SIGMA, Steinheim, Germany), fenbufen, ketoprofen and ibuprofen (ICN, Costa Mesa, CA, USA) and caffeine (Merck, Darmstadt, Germany) were used as received. Table 1 shows the generic INN (International nonproprietary name), proprietary names and Chemical Abstracts Service (CAS) registry numbers for each APD studied [8].

2.2. Apparatus

The HPLC system consisted of an assembly of two 510 Waters (Milford, MA, USA) pumps

monitored by a Waters AGC-680 automated gradient controller, a Rheodyne 7120 injection valve with a 20 μ l sample loop, a Waters 440 tunable absorbance detector operated at 254 nm and a Hewlett Packard (Palo Alto, CA, USA) HP3395 integrator.

A 150 \times 4 mm Spherisorb ODS2 5 μ m column (Teknokroma, Barcelona, Spain) was used for the separation.

2.3. Procedure

A two solvent gradient elution was performed, solvent A being an aqueous formic acid/formate buffer (0.1 M) of pH 3, and solvent B methanol. The starting mobile phase was 90% A, 10% B, and the linear gradient was run over 10 min to proportion of 45% A, 55% B, then continued to a final proportion of 100% B at 30 min. The flow rate was 1.5 ml min⁻¹.

2.4. Samples

Seven pharmaceutical dosage forms (belonging to the Spanish catalogue of pharmaceutical preparations) marketed in Spanish chemists' were analysed for APDs and/or caffeine according to the proposed method. In all cases the dosage forms were capsules or tablets. For the assay preparation, the content of about 20 tablets or capsules was powdered in a mortar. A weighted portion of the powder equivalent to the suitable amount of drug (according to the label claimed) was transferred into a 50ml-volumetric flask. The drug was fully dissolved with methanol and then diluted with this solvent to the mark. After mixing, a portion of the solution was filtered through a disposable 0.45 μ m filter unit into a vial and injected.

Drug-free human blood plasma samples were provided by the Military Hospital of Seville. Plasma samples were prepared by spiking concentrated methanol solutions of the studied analytes to attain the suitable concentrations in plasma and methanol (up to a total added volume of 400 μ l) to 200 μ l of plasma into a vial. The vial was then vortex-mixed gently for a few seconds and plasma proteins were precipitated. A portion of

Table 1
Identification features of the studied APDs

INN ^a	Proprietary names	CAS registry number
Indoprofen	Flosint, Isindone	31842-01-0
Ketoprofen	Alreumun, Ketalgin	22071-15-4
Naproxen	Naprosyn, Nycopren	22204-53-1
Fenbufen	Cinopal, Bufemid	36330-85-5
Ibuprofen	Amersol, Brufen	15687-27-1

^a International nonproprietary name.

Table 2
Gradient program

Time (min)	% Aqueous buffer	% Cosolvent
0	90	10
10	45	55
30	0	100

the content was transferred to a syringe and filtered through a disposable 0.45 μm filter unit into another vial and injected.

3. Method development

3.1. Experimental design and gradient scouting

To select properly the mobile phase composition for the separation of the APDs studied and caffeine, we applied gradient scouting runs [9]. A two-level factorial design was applied to get started. The factors to be varied were: the pH of the aqueous buffer (3 or 5), the nature of cosolvent (methanol or acetonitrile) and the flow rate (1 or 1.5 ml min^{-1}). The criteria to select a given combination of levels was the peak resolution and the omega peak (analysis time). Linear gradients were performed according to the program shown in Table 2, devised from a previous knowledge of the polarity of the compounds according to the octanol–water partition constants and data on ionization constants and solubility parameters [10–12].

Gradient runs were carried out on a standard methanolic solution of the considered analytes (caffeine 40 mg l^{-1} , indoprofen 20 mg l^{-1} , ketoprofen 10 mg l^{-1} , naproxen 40 mg l^{-1} , fenbufen 20 mg l^{-1} and ibuprofen 80 mg l^{-1}) with photometric detection at 254 nm. After the eight runs (2^3 experiments) the combination that leads to the best response (higher resolution and shorter analysis time) corresponds to the use of an aqueous buffer of pH 3, methanol as cosolvent and a flow rate of 1.5 ml min^{-1} .

The next decision to be made from the scouting runs is whether to go on with an isocratic or a gradient run. For this purpose, the so-called retention range (Δt), which is the difference between

the retention time of the last and first eluted analyte, can be calculated. Then, the obtained value is divided by the gradient time (t_g). If the ratio is less than 0.25, the use of an isocratic run is recommended, otherwise, a gradient run should be used [9]. In our case, $\Delta t = 18.8$ (ibuprofen) – 6.8 (caffeine) = 12, and $t_g = 30$, which led to a ratio of $0.4 > 0.25$ and consequently, a gradient method is the way to achieve the separation. Accordingly, the selected operational conditions were: methanol–aqueous buffer (pH 3) as mobile phase with a linear gradient elution according to the program indicated in Table 2, at a flow rate of 1.5 ml min^{-1} and photometric detection at 254 nm. A chromatogram obtained under these conditions is depicted in Fig. 1.

3.2. Peak identification

APDs were identified by retention times by matching their values with those of standard solutions. At the selected operational conditions, the retention times (in min) rounded up to the last significant figure for the studied APDs are indicated in the following: 6.8 (caffeine), 13.6 (indoprofen), 14.3 (ketoprofen), 15.0 (naproxen), 15.5 fenbufen) and 18.8 (ibuprofen).

4. Method validation

Method validation establishes that the method performance characteristics are suitable for the intended use. Validation entails evaluation of various parameters of the method such as selectivity, accuracy, precision, linearity (concentration–detector response relationship), sensitivity, detection and quantitation limit and recovery from the matrix [13].

4.1. Selectivity

For chromatographic methods, specificity is the ability of the method to accurately measure the analyte response in presence of all potential sample components. The selectivity criterion for an assay method is that analyte peaks will have

baseline chromatographic with suitable resolution from all the other sample components (analytes and no analytes). In our case, the peaks show resolutions ≥ 1.5 except the couple naproxen and fenbufen that is 1.1.

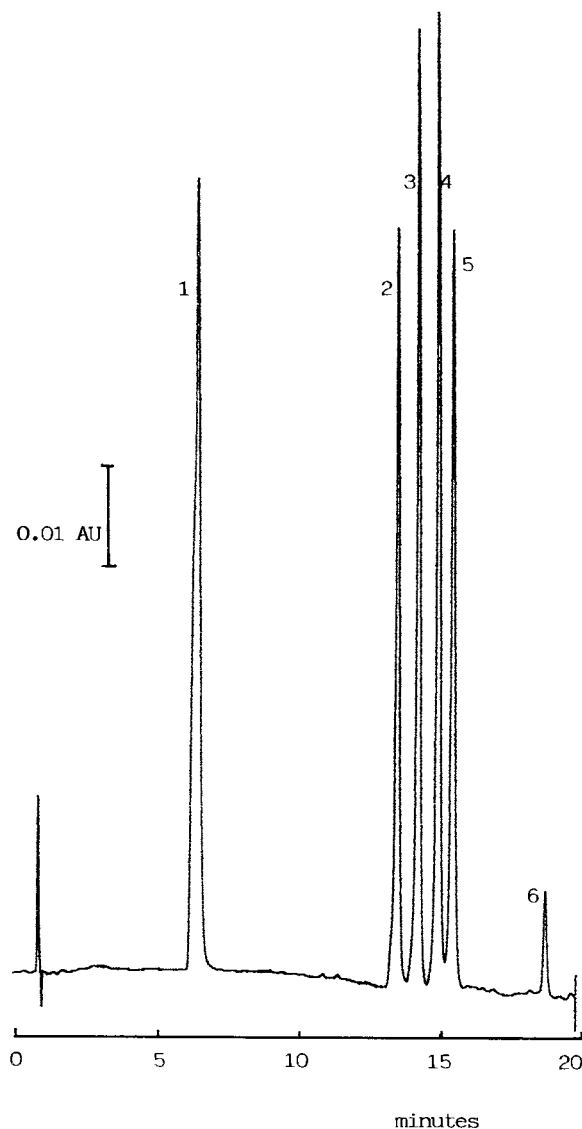


Fig. 1. Chromatogram of a standard solution. (1) caffeine (40 mg l^{-1}), (2) indoprofen (20 mg l^{-1}), (3) ketoprofen (10 mg l^{-1}), (4) naproxen (40 mg l^{-1}), (5) fenbufen (20 mg l^{-1}), (6) ibuprofen (80 mg l^{-1}). Chromatographic conditions are given in Section 2.

Table 3
Linearity results for caffeine and APDs

APD	Range (mg l^{-1})	Equation ^a	S_R^b
Caffeine	10–35	$y = (172.7 \pm 1.7)x$	98
Indoprofen	25–50	$y = (148.5 \pm 1.3)x$	122
Ketoprofen	5–35	$y = (304.9 \pm 1.6)x$	96
Naproxen	30–55	$y = (204.2 \pm 0.8)x$	88
Fenbufen	25–55	$y = (204.0 \pm 1.0)x$	106
Ibuprofen	60–120	$y = (11.8 \pm 0.1)x$	17

^a y , peak height; x , concentration (mg l^{-1}).

^b Standard deviation of regression.

4.2. Linearity

The linearity of the analytical response, here the peak height using absorbance detection at 254 nm, was studied for each APD. Table 3 shows the equation of the regression line concentration–analytical response, the standard deviation of the regression line and the optimum linear range (mg l^{-1}) for each compound.

After a previous study, the intercept of the calibration line was non-significant. Accordingly, using a zero intercept, excellent linearity was obtained in all cases with correlation coefficients higher than 0.999. Optimum linearity ranges were evaluated according to the EURACHEM procedure [14] by plotting the ratio (analytical response/concentration) versus the logarithm of the concentration. These linear ranges should not be considered as absolute ones but rather as the concentration intervals for achieving optimal measurements. Thus quantitation limits evaluated as explained below may fall outside these optimum ranges.

4.3. Limit of detection and quantitation

The detection limit (LOD) of a method is the lowest analyte concentration that produces a response detectable above the noise level of the system, typically taken as three times the noise level. The quantitation limit (LOQ) is the lowest level of analyte that can be accurately measured, and it is often evaluated as ten times the noise level. Both detection and quantitation limits need

Table 4
Detection and quantitation limits (mg l^{-1}) for caffeine and APDs

Compound	LOD ^a	LOQ ^b
Caffeine	1.7	5.7
Indoprofen	2.5	8.2
Ketoprofen	0.9	3.1
Naproxen	1.3	4.3
Fenbufen	1.6	5.2
Ibuprofen	4.3	14.2

^a LOD, limit of detection.

^b LOQ, limit of quantitation.

to be determined only for impurity methods. In our case, the proposed method is for assay of caffeine and APDs in pharmaceutical formulations, and consequently the detection and quantitation limits are not required [15]. However, we have evaluated both quantities according to the procedure of Miller and Miller [16] calculated as three and ten times, respectively, the ratio between the standard deviation of regression and the slope of the calibration line. From these values (Table 3) the detection and quantitation limits have been evaluated as depicted in Table 4. LOQ data generally fall outside the optimum linear ranges for every analyte. However, as was men-

tioned above these ranges should be regarded as limiting optimum values instead of absolute ones. Thus, analytes at concentrations higher than the LOQ can be determined without risks from the calibration graph.

The LOQ data, with respect to the potential applications of this method are very suitable because the analysis of formulation dosage forms can be conducted to ensure analyte concentrations higher than LOQ values. Besides, plasma concentration–time curves for the studied analytes exhibit maxima higher than their corresponding LOQs [17–19].

4.4. Accuracy and recovery

The accuracy of the method was evaluated from recovery assays. In our case instead of preparing placebos, the recovery study was made on the formulation samples. Thus, known amounts of caffeine and each APD were spiked into their corresponding formulation (except for indoprofen, which is not used as active ingredient in the Spanish catalogue of pharmaceutical formulations), and the recovery was calculated according to Cuadros et al. [20]. For assay methods, spiked matrices were prepared in triplicate at three levels. In our case, the average recovery was

Table 5
Method accuracy from recovery assays for the studied analytes^a

Compound	Spiked amount (mg l^{-1})	Found amount (mg l^{-1})	Averaged recovery (%)
Caffeine	15	13.8	97.1
	20	20.2	
	25	24.6	
Ketoprofen	15	14.7	98.2
	20	19.5	
	25	24.8	
Naproxen	30	29.4	99.4
	40	40.3	
	50	49.7	
Fenbufen	30	29.8	101.2
	40	40.7	
	50	51.2	
Ibuprofen	30	29.2	99.7
	40	40.5	
	50	50.3	

^a Except for indoprofen.

Table 6
Content of caffeine and APDs expressed as % with respect to the label claim

Brand	Drug	Drug (mg) dosage unit ⁻¹ %		
		Claimed	Found	
1	Naproxen	550	545.6	99.2
2	Naproxen	250	249.5	99.8
3	Fenbufen	300	304.8	101.6
4	Ibuprofen	200	200.6	100.3
	Caffeine	50	50.4	100.8
5	Ibuprofen	200	198.2	99.1
6	Ketoprofen	50	46.2	92.5
7	Ketoprofen	50	46.0	92.1

calculated as the mean value obtained by spiking the analyte studied at three levels within the working range (concentrations higher than LOQ). Each solution was injected in triplicate. By applying the Student *t*-test to the average recoveries [21], the null hypothesis (the recovery is close to unity and the method is accurate) was accepted at a 5% significance level. Data corresponding to these recovery assays for the studied analytes are presented in Table 5.

4.5. Precision

To test the precision of the method, triplicate determinations of each analyte in each selected

formulation were carried out on different days. The precision expressed as % relative standard deviation (RSD) always remained < 1% for all the studied components in the different dosage forms.

5. Determination of caffeine and APDs in pharmaceutical formulations and blood plasma samples

The method was applied to seven different pharmaceutical formulations (capsules or tablets) for determining the content of caffeine and APDs. In the Spanish catalogue of pharmaceutical formulations, indoprofen is not used as active ingredient, and consequently it was not assayed. The results are expressed in Table 6 as the drug percentage with respect to the label claim. As can be observed, the values ranged within 92–102%, very acceptable values according to the AOAC guidelines [22]. Caffeine and APDs were also determined in spiked plasma samples following the procedure indicated in Section 2.4. Plasma samples were spiked at two levels within the working linear range of the studied analytes and the recoveries were calculated from the data found by the proposed procedure. The averaged results are presented in Table 7. They also fulfil the AOAC requirements and accordingly were considered suitable for analytical purposes.

Table 7
Recovery assays for the spiked blood plasma samples

Compound	Spiked amount (mg l ⁻¹)	Found amount (mg l ⁻¹)	Averaged recovery (%)
Caffeine	17.0	18.1	102.8
	34.0	33.7	
Ketoprofen	11.6	14.7	98.2
	23.2	24.8	
Naproxen	26.4	25.2	97.5
	52.8	52.6	
Indoprofen	22.0	21.2	100.4
	44.0	46.0	
Fenbufen	25.2	24.4	99.2
	50.4	51.2	
Ibuprofen	54.0	56.0	100.6
	108.0	105.2	

6. Conclusion

Several APDs together with caffeine have been analysed in pharmaceutical formulations and spiked blood plasma samples using the proposed RP-HPLC method. This procedure is straightforward, simple and feasible enabling the simultaneous determination of the analytes indoprofen, ketoprofen, naproxen, fenbufen, ibuprofen and caffeine with a methanol–water gradient elution, ODS column and photometric detection at 254 nm.

References

- [1] J.E. Dinchuk, B.D. Car, R.J. Focht, et al., *Nature* 378 (1995) 406.
- [2] J.J. Li, M.B. Norton, E.J. Reinhard, et al., *J. Med. Chem.* 39 (1996) 1846.
- [3] M.K. Ghosh, *HPLC methods on drug analysis*, Springer-Verlag, Heidelberg, 1992.
- [4] T. Hirai, S. Matsumoto, I. Kishi, *J. Chromatogr. B* 692 (1997) 375.
- [5] H.J. Battista, G. Wehinger, R. Henn, *J. Chromatogr.* 345 (1985) 77.
- [6] A.K. Singh, Y. Jang, U. Mishra, K. Granley, *J. Chromatogr.* 568 (1991) 351.
- [7] A.G. Kazemifard, D.E. Moore, *J. Chromatogr.* 533 (1990) 125.
- [8] *The Merck Index*, 12th ed., Merck, Whitehouse Station, NJ, 1996.
- [9] J.W. Dolan, *LC-GC Int* 9 (1996) 130.
- [10] A. Fini, M. Laus, I. Orienti, V. Zecchi, *J. Pharm. Sci.* 75 (1986) 23.
- [11] A.F.M. Barton, *Handbook of Solubility Parameters and other Cohesion Parameters*, 2nd ed., Boca Raton, CRC Press, 1991.
- [12] A.G. González, M.A. Herrador, *Anal. Chim. Acta* 356 (1997) 253.
- [13] A.C. Mehta, *Analyst* 122 (1997) 83R.
- [14] L. Huber, *LC-GC Int.* 11 (1998) 96.
- [15] J.M. Green, *Anal. Chem.* 68 (1996) 305A.
- [16] J.C. Miller, J.N. Miller, *Statistics for Analytical Chemistry*, Horwood, Chichester, 1988.
- [17] A. Avgerinos, A.J. Hutt, *J. Chromatogr. B* 380 (1986) 468.
- [18] D.G. Kaiser, R.S. Martin, *J. Pharm. Sci.* 67 (1978) 514.
- [19] G.E.M. Janssen, J.F. Venema, *Int. Med. Res.* 13 (1985) 68.
- [20] L. Cuadros, A.M. García Campaña, F. Alés, C. Jiménez, M. Román Ceba, *J. AOAC Int* 78 (1995) 471.
- [21] M.J. Martín, F. Pablos, M.A. Bello, A.G. González, *Fresenius J. Anal. Chem.* 357 (1997) 357.
- [22] AOAC, Peer verified method program, Manual on policies and procedures, Arlington, VA, USA, November 1993.

Normal-phase high-performance liquid chromatographic determination of spiramycin in eggs and chicken

Naoto Furusawa *

Faculty of Human Life Science, Osaka City University, Sumiyoshi-ku, Osaka 558-8585, Japan

Received 22 October 1998; received in revised form 23 December 1998; accepted 4 January 1999

Abstract

A precise method is presented for determination of residual spiramycin (SP) in chicken eggs and tissues by high-performance liquid chromatography (HPLC). The sample preparation was performed by homogenizing with a mixture of acetonitrile and n-hexane (5:4, v/v) to minimize the fat amount followed by ultra-filtration using a MolCutII®. The extracts containing SP were free from interfering compounds when examined by the normal-phase HPLC using a LiChrosorb® NH₂ column and a mobile phase of acetonitrile–water (85:15, v/v) with a photo-diode array detector. The average recoveries from spiked SP (0.1, 0.5 and 1.0 ppm) were in excess of 89.0% with coefficients of variation between 1.4 and 2.4%. The limit of detection was 0.1 ppm. © 1999 Elsevier Science B.V. All rights reserved.

Keywords: Spiramycin; High-performance liquid chromatography; Ultra-filtration unit

1. Introduction

Spiramycin (SP) is widely used in veterinary medicine to treat diseases or as feed additives to promote growth. The use of this compound can result in the appearance of residues in livestock products. The residues can result from incorrect use of the drug and lack of withdrawal times and pharmacokinetic data, and may have toxic effects on consumers. Therefore, the EU has set the maximal residue limits (MRLs) [1] for SP in live-

stock products. The MRL in animal muscles is 0.2 ppm. No MRL for SP in eggs has been fixed up to now. In order to monitor drug residues in livestock products, a simple and precise analytical method for the determination would be indispensable.

Numerous methods have been reported for SP residue in livestock products using high-performance liquid chromatography (HPLC) [2–10]. However, most of these methods are complicated and time-consuming, and do not permit monitoring of a large number of samples. In particular, a method for determination of SP in eggs is lacking. Since eggs contain many proteins and lipids have

* Tel.: +81-6-605-2864; fax: +81-6-605-2914.

E-mail address: furusawa@life.osaka-cu.ac.jp (N. Furusawa)

high emulsion power, it is difficult to extract/clean-up the residual drugs. Because they are highly nutritious as shown above, cheap, and readily available, eggs are a very important food. Most consumers believe that eggs are nutritionally 'perfect food'.

Previous reports [11–19] of pharmacokinetic/residual studies of veterinary drugs in eggs support the view that the risk of SP residue in the egg is great. A biological half-life of SP (2.4 days) after the withdrawal, which indicates the rate of decrease of SP in the egg, was greater than those of other drugs, such as oxytetracycline (1.1 days), chlortetracycline (1.6 days), tylosin (1.3 days) and some sulphonamides (0.9–1.23 days), and suggests that the SP residue continues over a long period.

The aim of this study was to develop a simple and precise method for determination of SP in eggs. This paper describes the procedure for determination of this antibiotic in eggs and chicken muscle by HPLC with a photo-diode array detector.

2. Experimental

2.1. Materials and reagents

SP standard was obtained from Sigma (St. Louis, MO). Other chemicals were obtained from Wako (Osaka, Japan): distilled water, acetonitrile and methanol were of HPLC grade; acetic acid was of analytical chemical grade; anhydrous sodium sulfate was of pesticide residue grade.

Standard solutions of SP were prepared by accurately weighing 10 mg, dissolving it in 100 ml of distilled water and diluting to the desired volume with distilled water. These solutions kept at 4°C for up to 1 month.

2.2. Apparatus

Instruments used in sample preparation were as follows: a Model PH-91 SMT[®] auto-homogenizer (Mitsui Denki-Seiki, Tokyo, Japan); a

Model H-103N centrifuge (Kokusan-Enshinki, Tokyo, Japan); a Model Eyela N-1M vacuum rotary evaporator; MolCutII[®] (Model no. UFP1 LCC 24, fractionating molecular weight, 5000) ultra-filtration unit (Nippon Millipore, Kogyo, Tokyo, Japan).

The standard and extracted compound were introduced into a Jasco HPLC (Model PU-980 pump and DG-980-50 degasser) (Jasco, Tokyo, Japan) equipped with an SPD-M10A_{VP} Diode Array detector (Shimadzu, Kyoto, Japan) interfaced with a Fujitsu FMV-5133D7 personal computer (Fujitsu, Tokyo, Japan). The separation was performed on a LiChrosorb[®] NH₂ (7 µm) column (250 × 4 mm i.d.) (Merck, Darmstadt, Germany) with a guard column (4 × 4 mm i.d.) (Merck) using a mixture of acetonitrile–water (85:15, v/v) as the mobile phase at a flow-rate of 1.0 ml/min at ambient temperature.

2.3. Egg and muscle samples

Besides commercial eggs and chicken tissues (sample a), eggs and muscles from laying hens that were kept in individual cages and given a SP-free basal layer diet continuously were also used as blank samples (sample b). In order to validate the present method for routine monitoring, eggs with residual SP and muscles from laying hens that were fed a diet containing 400 ppm SP for 7 days were also used as sample c.

2.4. Procedure

Two grams of sample accurately weighed was mixed sufficiently with 10 g of anhydrous sodium sulfate and homogenized at high speed for 2 min with 30 ml of acetonitrile (saturated with n-hexane) and 25 ml of n-hexane. After centrifugation at 3500 rpm for 5 min, the supernatant was poured into a separating funnel through a funnel. The acetonitrile layer was evaporated to dryness and the residue was dissolved in 1 ml 20% (v/v) methanol solution (in water). The solution was ultra-filtered through MolCutII. A 20-µl volume of the ultra-filtrate was injected into the HPLC system.

2.5. Recovery test

The recovery of SP was determined from blank samples (samples a, b) spiked at 0.1, 0.5 and 1.0 ppm. In this test, fortified samples were allowed to stand at 4°C for 12 h after the addition followed by mixing.

3. Results and discussion

3.1. Extraction and clean-up

An advantage of the proposed extraction (homogenizing with acetonitrile–hexane) is that the fat extraction is minimised. With the egg samples, the extract did not form an emulsion that would hinder the recovery of SP. After centrifugation, it was completely recovered in the acetonitrile layer without giving residue losses in the hexane layer. Also, 2 g of the sample was mixed with 10 g of anhydrous sodium sulfate to remove the moisture in the sample, so that the treatment resulted in a satisfactory extraction and good operability [20] preventing sample adhesion to the homogenizer-edge.

The extract obtained was further purified to remove interfering materials. As a simple clean-up technique to replace the conventional liquid–liquid partition [2,4,5,7,10], the use of commercial pre-packed (C_{18} or Diol) cartridges for the purification of residual drugs in foods of animal origin has been used [8,9,21–24]. To simplify the procedure further, the present study used a MolCutII as the ultra-filtration unit. This process was able to deproteinize the extracted solution easily only with syringe-pressure. A considerable saving of time was achieved.

3.2. HPLC operating conditions

SP was dissolved in 20% (v/v) methanol solution and its absorption spectra was measured using a photo-diode array detector. Maximum absorption for SP was 231 nm. The monitoring wavelength was adjusted to 231 nm and the flow-rate was 1.0 ml/min.

As for the HPLC analysis of SP the reverse-phase system used the C_{18} column as a mainstream [8–10]. The present study examined the separation of target compound obtained with two C_{18} columns (LiChrospher® 100 RP-18 and TSKgel ODS-80T_M) and a LiChrosorb NH_2 normal-phase column with a mixture of acetonitrile–water as the mobile phase. With the two C_{18} columns, SP was detected as a ‘broad peak’. It was difficult to separate SP and the interference originating in the sample and to prevent the broad peak. The best chromatogram with a sharp peak of SP and clear retention time was obtained with the normal-phase LiChrosorb NH_2 column and acetonitrile–water (85:15, v/v) as the mobile phase. The retention time of SP was 1.6 min.

Fig. 1 shows typical HPLC traces of blank and SP in the eggs. The resulting extract was free from interference. There is no difference between chro-

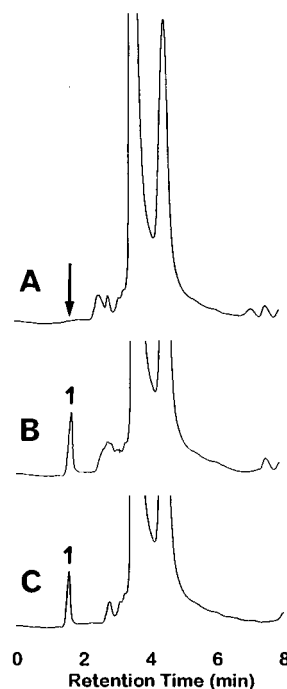


Fig. 1. HPLC chromatograms (photo-diode array set at 231 nm). For other HPLC operating conditions see text. A, blank egg sample; B, spiked (0.5 ppm) egg sample; C, egg laid by the hen fed a diet containing 400 ppm of SP for 7 days (sample c, see text). Peaks: 1, SP (retention time, 1.6 min). Arrow indicates the retention time 1.6 min.

Table 1
Recoveries^a of spiramycin (SP) from eggs and chicken muscle

Spiked (ppm)	<i>n</i>	Eggs	Muscle
0.1	10	89.5 (2.1)	89.0 (2.4)
0.5	10	91.8 (1.4)	92.8 (1.4)
1.0	10	96.0 (2.0)	96.0 (2.4)

^a Data are average recoveries (%) from samples a (*n* = 5) and b (*n* = 5) (see text). Values in parentheses are coefficients of variation (%).

matograms obtained from the sample a and b. Fig. 1C demonstrates that the present method is valid for practical usage. Similar results were obtained from the muscle samples.

3.3. Calibration and recovery

The calibration graph was linear over range 2–40 ng for SP. The correlation coefficient, 0.9997, was highly significant ($P < 0.01$). The detection limit of SP was 2 ng. The precision of the procedure was obtained from the relative standard deviation of areas calculated for five replicate injections of 10 ng of SP. The value was below 1.0%.

Table 1 summaries the average recoveries of the target compound from eggs and chicken muscles at three different spiking levels (0.1, 0.5 and 1.0 ppm). Overall, satisfactory results were obtained. The average recoveries were greater than 89.0% and their coefficients of deviation (C.V.) were within 2.4% (*n* = 10). In a practical analysis, the limit of detection (signal-to-noise ratio > 5) in eggs and chicken tissues was 0.1 ppm for SP. The value was below the MRL (0.2 ppm in muscle) [1]. The total time required for the analysis of one sample was around 30 min. The high recovery and low C.V. together with the economical analysis time prove that this method has good precision and may be accurate.

4. Conclusions

Characteristics of the procedure developed and described here are as follows: (1) simple; (2)

higher efficiency of clean-up; (3) shorter analysis time; (4) highly precise. Therefore, this method can be considered as reliable for the routine monitoring of residual SP in chicken products.

Acknowledgements

Support of this study by a grant from the Ministry of Education of Japan (in 1998) is gratefully acknowledged.

References

- [1] Commission of the European Communities, The rules governing medical products in the European Community, Vol. VI, Commission of the European Communities, 1991.
- [2] W.A. Moats, *J. Agric. Food Chem.* 43 (1995) 931.
- [3] E.J. Mulders, D. van de Lagemaat, *J. Pharm. Biomed. Anal.* 7 (1987) 1829.
- [4] C.R. White, W.A. Moats, *J. Assoc. Off. Anal. Chem. Int.* 76 (1993) 549.
- [5] M.H. Tomas, *J. Chromatogr.* 72 (1989) 564.
- [6] S.M. Croubels, K.E. Vanoosthuyze, C.H. van Peteghem, *J. Chromatogr. B* 690 (1997) 173.
- [7] T. Nagata, M. Saeki, *J. Assoc. Off. Anal. Chem.* 69 (1986) 644.
- [8] B. Delepine, D. Hurtaud, P. Sanders, *Analyst* 119 (1994) 2717.
- [9] B. Delepine, D. Hurtaud-Pessel, P. Sanders, *J. Assoc. Off. Anal. Chem. Int.* 79 (1996) 397.
- [10] P. Leroy, D. Decolin, A. Nicolas, P. Archimbault, *Analyst* 119 (1994) 2743.
- [11] M. Yoshida, D. Kubota, S. Yonezawa, H. Nakamura, R. Yamaoka, H. Yoshimura, *Jpn. Poult. Sci.* 10 (1973) 254.
- [12] M. Yoshida, D. Kubota, S. Yonezawa, H. Nakamura, R. Yamaoka, H. Yoshimura, *Jpn. Poult. Sci.* 10 (1973) 261.
- [13] M. Yoshida, D. Kubota, S. Yonezawa, H. Nakamura, R. Yamaoka, H. Yoshimura, *Jpn. Poult. Sci.* 10 (1973) 29.
- [14] M. Yoshida, D. Kubota, S. Yonezawa, H. Nakamura, H. Azechi, N. Terakado, *Jpn. Poult. Sci.* 8 (1971) 103.
- [15] B. Rouaut, J.P. Moretain, *Br. Poult. Sci.* 31 (1990) 661.
- [16] M.F. Geertsma, J.F. Nouws, J.L. Grandel, M.M.L. Aerts, T.B. Vree, C.A. Kan, *Vet. Q.* 9 (1987) 67.
- [17] N. Furusawa, T. Mukai, *Jpn. Poult. Sci.* 32 (1995) 34.
- [18] N. Furusawa, T. Mukai, M. Yoshida, *Jpn. Poult. Sci.* 31 (1994) 168.
- [19] N. Furusawa, Y. Tsuzukida, H. Yamaguchi, *Br. Poult. Sci.* 39 (1998) 241.
- [20] M. Murayama, S. Uchiyama, Y. Saito, *J. Food Hyg. Soc. Jpn.* 32 (1991) 155.
- [21] M.C. Rouan, *J. Chromatogr.* 340 (1985) 361.

- [22] S.A. Barker, C.C. Walker, *J. Chromatogr.* 624 (1992) 195.
- [23] K. Fujita, K. Ito, E. Araki, K. Tanno, M. Murayama, Y. Saito, *J. Food Hyg. Soc. Jpn.* 38 (1997) 12.
- [24] H. Oka, Y. Ikai, J. Hayakawa, K. Masuda, K. Harada, M. Suzuki, V. Martz, J.D. MacNeil, *J. Agric. Food Chem.* 41 (1993) 410.

Short communication

Determination of traces of Ni, Co and Fe in $\text{Li}_2\text{CO}_3/\text{K}_2\text{CO}_3$ melts by flame atomic absorption spectrometry

Silvera Scaccia *

Dipartimento Energia. Divisione Tecnologie Energetiche Avanzate. Sezione R&S Conversione Elettrochimica dell'Energia, ENEA, C.R.E Casaccia, Via Anguillarese 301, I-00060, Rome, Italy

Received 13 May 1998; received in revised form 6 November 1998; accepted 1 December 1998

Abstract

A flame atomic absorption spectrometry (AAS) method is described for the determination of trace levels of Ni, Co, and Fe in 62 mole percent (mol.%) Li_2CO_3 and 38 (mol.%) K_2CO_3 melts after dissolution of the sample in dilute nitric acid. A pneumatic nebulizer with a glass impact bead is used to sample introduction. The effect of the high salt loading of the solution on the analytical signals is minimized by optimization of acetylene flow-rate and height of observation above the burner head. Under the optimum conditions, the results of the analysis of synthetic sample solutions by aqueous standards calibration graphs well agree with those obtained by the method of standard additions. Recoveries ranged from 99 to 101% and the relative standard deviation is around 1%. Detection limits for Ni, Co and Fe in Li/K carbonate salts are similar to that in aqueous solutions, i.e. 0.5×10^{-6} g analyte/g ($\text{Li}_{0.62}, \text{K}_{0.38}$) $_2\text{CO}_3$. Furthermore, a background absorption is easily compensated by D_2 background correction, which does not affect the sensitivity. The proposed method is applied to the determination of cobalt in real melt samples. © 1999 Elsevier Science B.V. All rights reserved.

Keywords: Flame atomic absorption spectrometry; $\text{Li}_2\text{CO}_3/\text{K}_2\text{CO}_3$ melts; Molten carbonate fuel cells; Transition metals

1. Introduction

The determination of Ni, Co and Fe in $\text{Li}_2\text{CO}_3/\text{K}_2\text{CO}_3$ melts is of great interest in the technology of molten carbonate fuel cells (MCFCs), because the cathode materials, such as NiO, LiCoO_2 and

LiFeO_2 may dissolve in the electrolyte during operation shortening the lifetime of the cell [1]. Although it is felt that solubility data are needed for these materials, the experimental details on solubility measurements are often lacking. Among the spectroscopic techniques, flame atomic absorption spectrometry (F-AAS) makes it attractive to be used for trace metal's assay in alkali salts owing to the high precision and accuracy, selectivity and sensitivity, easy to use and speed,

* Corresponding author. Tel.: +39-6-30483815; fax: +39-6-30486357.

E-mail address: silvera@casaccia.enea.it (S. Scaccia)

and relative freedom from interferences of the matrix [2,3]. Infact, one difficulty often encountered with spectroscopy techniques is the blockage of nebulizer and/or solid deposition at the burner head when using high salt loading solutions. However, the nebulizers commonly used in F-AAS [4–6] allow greater tolerance to high salt loading of the analyte solution as compared to the nebulization systems of other spectroscopic techniques, such as inductively coupled plasma atomic emission spectrometry (ICP-AES) [7], inductively coupled plasma mass spectrometry (ICP-MS) [8] and microwave induced plasma atomic emission spectrometry (MIP-AES) [9], for which, owing to orifice clogging problems that occur during sample introduction into the plasma, labourious and time-consuming analyte/matrix separation methods are required.

In the present paper a simple and reliable analytical method for the determination of trace levels of Ni, Co and Fe in 62 mol.% Li_2CO_3 and 38 mol.% K_2CO_3 melts by F-AAS is described. The interference effects produced by the high levels of lithium and potassium on the absorbance signal of the analytes are markedly reduced by optimization of some operating parameters, such as the acetylene flow-rate and the height of observation above the burner head. Under the optimized AAS conditions the detection limits, sensitivities, accuracy and precision are evaluated for each analyte in Li/K carbonate melt. The proposed method can be applied to the solubility measurements of nickel, iron and cobalt based cathode materials in Li/K carbonate melts.

2. Experimental

2.1. Instrumentation

The Varian Techtron Spectr-AA 10 atomic absorption spectrometer with a deuterium lamp background corrector was used. Varian Techtron hollow cathode lamps of Ni, Co, and Fe were used as sources. A pneumatic nebulizer with a glass impact bead was used. The most sensitive analytical wavelengths were chosen for analytes

and were: 232.0 nm (Ni), 240.8 nm (Co) and 248.3 nm (Fe). Slit width was 0.2 nm. Integration time was 4 s. Observation height was varied between 6

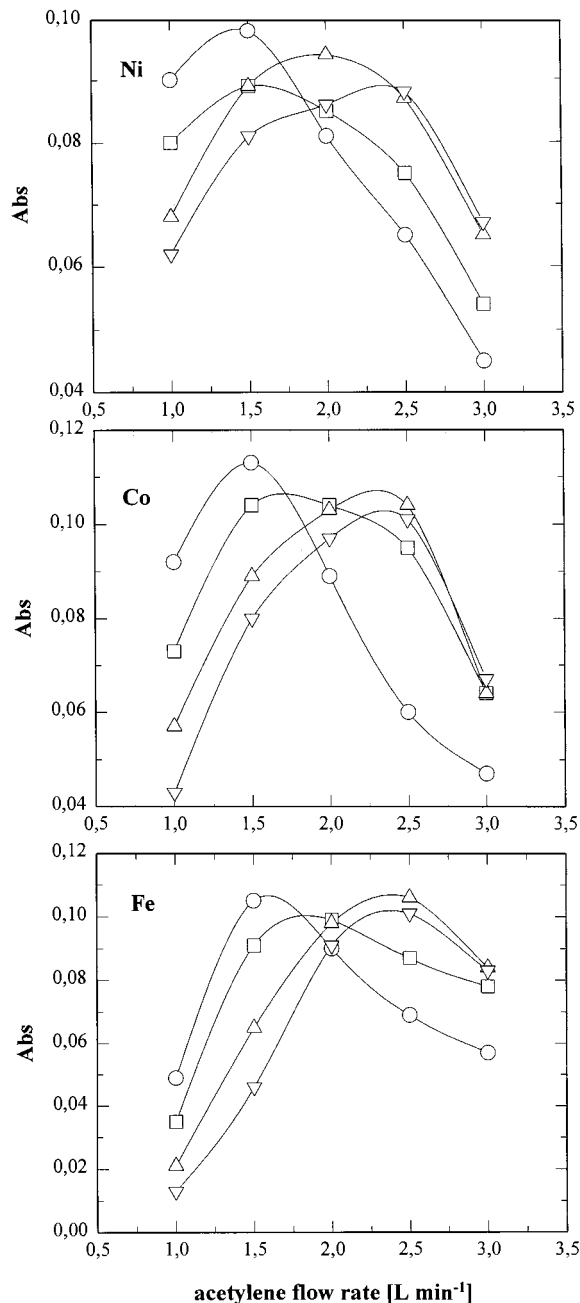


Fig. 1. The effect of acetylene flow rate on absorption signals of 1 mg l⁻¹ Ni, Co, and Fe aqueous solutions at different observation heights: 6 mm (○), 8 mm (□), 10 mm (△), and 12 mm (▽).

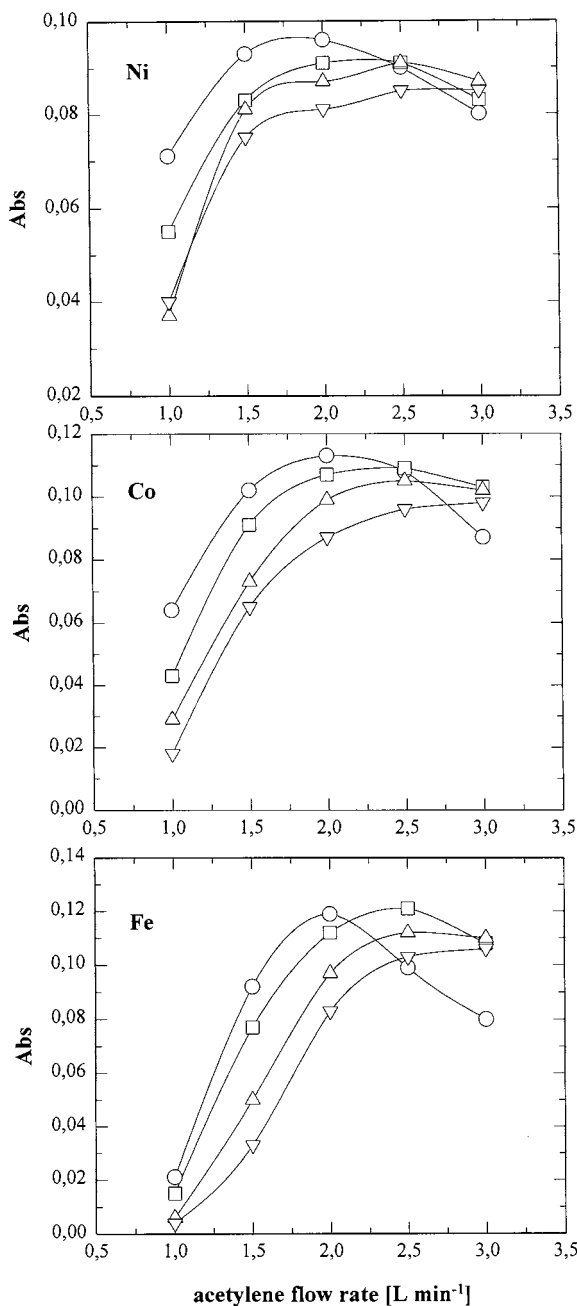


Fig. 2. The effect of acetylene flow rate on absorption signals of 1 mg l^{-1} Ni, Co, and Fe in 0.25 M Li and 0.16 M K solutions at different observation heights: 6 mm (\circ), 8 mm (\square), 10 mm (\triangle), and 12 mm (∇).

and 12 mm . A slot burner for air-acetylene flame was used. Acetylene flow-rate was varied between

1.0 and 3.0 l min^{-1} ; air flow was kept constant at 16 l min^{-1} .

2.2. Reagents and standard solutions

All acids were of analytical-reagent grade. De-ionized water ($18 \text{ M}\Omega \text{ cm}^{-1}$) produced by a Milli-Q water purification system (Millipore Corporation) was used throughout. Aqueous standard solutions from 0.5 to 2 mg l^{-1} were daily prepared by using 1000 mg l^{-1} atomic absorption stock solutions (Aldrich Chemical Company). Appropriate amounts of Li_2CO_3 and K_2CO_3 (Suprapur, Merck, dried at 250°C for 4 h) were dissolved in water to make 0.25 M Li and 0.16 M K solutions and used to prepare the blank solution and the standards at the same concentration as aqueous standards for the standard additions method. All solutions contained 0.5 M HNO_3 . The impurities in the carbonate salts were all under the limit of detection of this method.

2.3. Decomposition of melts

About 1.0 g of carbonate melt ($62 \text{ mol.}\%$ Li_2CO_3 and $38 \text{ mol.}\%$ K_2CO_3) was transferred to 50-ml covered beaker and dissolved in 3 ml of concentrated nitric acid by gentle heating and magnetic stirring on a hot plate. After cooling, the solution was transferred to 50-ml clean volumetric flask and made up to volume with deionized water. The sample solution was directly analyzed for the content of cobalt in five replicate runs.

2.4. Procedure

The two sets of standard solutions were introduced alternatively in the nebulizer for different values of acetylene flow rate at a given observation height, being the other parameters kept constant. To avoid salt deposition at the burner head, deionized water was aspirated until the red zone of the flame seen when aspirating Li/K containing solutions completely disappeared. The matrix effect M (%) was defined as the percentage difference in the signals between the Li/K containing and the aqueous standard solutions.

3. Results and discussion

3.1. Optimization of acetylene flow and height of observation

The variation of absorption signals of 1 mg l⁻¹ Ni, Co and Fe aqueous solutions with acetylene flow-rate and height of observation is depicted in Fig. 1. The effect of acetylene flow-rate seems to be more significant as compared to the effect of observation height. The maximum absorbance signal for the analytes is achieved with acetylene flow-rates around 1.5 l min⁻¹ and observation height of 6–8 mm. As it can be seen from Fig. 2, the absorbance signals of 1 mg l⁻¹ of Ni, Co and Fe solutions in presence of approximately 1700 mg l⁻¹ Li and 6000 mg l⁻¹ K increase with increasing the acetylene flow rate up to 2.0 l min⁻¹ and then level off at any observation height, suggesting that the same physical-chemical features control the atom concentration in the flame (Table 1). The suppression of analyte signal in fuel lean flame may be attributable to the inclusion of analyte in a solvated particle of high salt concentrations, which may take longer to volatilize than analyte particles alone. The favourable effect of lithium and potassium in fuel rich flame is rather due to the fast release of analyte atoms during atomization step by lithium carbide formation [10], than to shift the analyte ionization equi-

librium towards the free atoms in presence of easily ionizable alkali elements. The extent of analyte suppression/enhancement caused by a single concomitant element at a time has been evaluated. The concomitant lithium has a greater positive effect on each analyte in fuel rich flame than potassium. Fig. 3 shows that matrix effects change from depressing to enhancement ones passing across $M(\%) = 0$, where the matrix effect can be considerably reduced. The optimum acetylene flow-rate and observation height for all analytes are as follow: 2.0 l min⁻¹ and 12 mm for Ni; 2.0 l min⁻¹ and 10 mm for Co; 2.5 l min⁻¹ and 8 mm for Fe.

A non-specific absorbance signal of the matrix is observed at the wavelengths of each of analytes. No significant difference in absorption with gas composition and height of observation is found, indicating a light scattering effect by particles in the flame with samples having a high salt content. The background level is easily corrected by using deuterium background correction, which does not affect the sensitivity.

3.2. Calibration, limits of detection, accuracy and precision

Direct calibration with aqueous standards and the method of standard additions are used for all the analytes. The slopes of the two curves are

Table 1
Recovery and precision of Ni, Co and Fe in synthetic samples^a

Element	Concentration added, mg l ⁻¹	Concentration found, mg l ⁻¹		RSD (%) ^b	Recovery(%)
		Direct calibration	Standard addition method		
Ni	0.4	0.40	0.40	1.2	101
	0.8	0.81	0.81	0.9	101
	1.0	0.99	0.99	0.8	99
Co	0.4	0.40	0.40	1.0	101
	0.8	0.81	0.80	0.8	101
	1.0	0.99	0.99	0.9	99
Fe	0.4	0.40	0.40	1.5	101
	0.8	0.80	0.80	1.0	100
	1.0	1.00	0.99	0.8	100

^a Optimum acetylene flow rates and observation heights: 2.0 l min⁻¹ and 12 mm for Ni, 2.0 l min⁻¹ and 10 mm for Co, 2.5 l min⁻¹ and 8 mm for Fe.

^b Relative standard deviations of five replicate measurements.

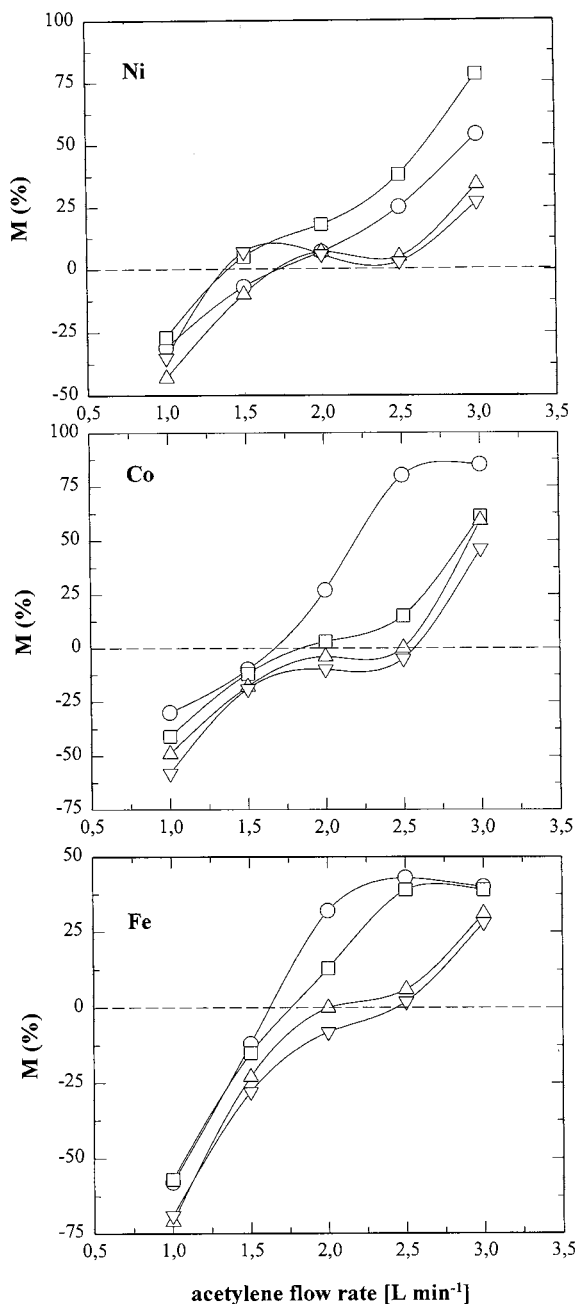


Fig. 3. Matrix effect (M%) of 0.25 M Li and 0.16 M K on absorption signals of 1 mg l^{-1} Ni, Co, and Fe as a function of acetylene flow-rate at different observation heights: 6 mm (○), 8 mm (□), 10 mm (△), and 12 mm (▽).

compared by means of the *t*-test [11] and any statistically significant difference was found, indi-

cating that the matrix interference in the measurements of any metals is overcome. Calibration curves are linear over two orders of magnitude from detection limits to 2 mg l^{-1} with correlation coefficient better than 0.999 under the proper AAS operating conditions. The detection limits, based on three times the standard deviation of ten measurements of the blank solution to the slope of the calibration graphs, are similar to those in aqueous solutions, i.e. 0.01 mg l^{-1} for all the analytes and are converted in solid detection limits, i.e. $0.5 \cdot 10^{-6} \text{ g analyte/g (Li}_{0.62}\text{, K}_{0.38})_2\text{CO}_3$ by multiplying each calculated by a factor of 50 (considering that all constituents in the melt are diluted 50-fold according to the decomposition of the sample). The reliability of the proposed method is assessed by analysing a series of synthetic samples because certified values of Ni, Co and Fe in Li_2CO_3 and K_2CO_3 are not available. The synthetic samples are prepared by adding known amounts of elements to Li/K carbonate solutions so that the final matrix in analysis is simulated. The percentage recoveries ranged from

Table 2
Determination of cobalt in real melt samples^a

Time (h)	g Co/g ($\text{Li}_{0.62}\text{, K}_{0.38}$) ₂ CO_3 ^b	RSD (%) ^c	$X_{\text{Co}} \cdot 10^6$ $= n_{\text{Co}} /$ $n_{(\text{Li}_{0.62}\text{, K}_{0.38})_2\text{CO}_3}$ ^d
0	<D.L.	–	<D.L.
24	2.7×10^{-6}	20	4.5
48	3.3×10^{-6}	20	5.5
72	4.3×10^{-6}	9.3	7.2
96	5.2×10^{-6}	9.6	8.7
148	6.7×10^{-6}	7.5	11.2
192	6.6×10^{-6}	7.6	11.0
216	6.3×10^{-6}	8.6	10.5

^a Acetylene flow rate of 2.0 l min^{-1} and observation height of 10 mm.

^b Solid concentration values obtained by multiplying each solution concentration by a factor of 50.

^c Relative standard deviation of five replicate measurements.

^d $X_{\text{Co}} \cdot 10^6 = n_{\text{Co}} / n_{(\text{Li}_{0.62}\text{, K}_{0.38})_2\text{CO}_3} =$ mole fraction of cobalt in the melt obtained by multiplying the solid concentration by the factor 1.67, i.e. 98.3 molecular weight of $(\text{Li}_{0.62}\text{, K}_{0.38})_2\text{CO}_3 / 58.9$ atomic weight of Co; n_{Co} = number of moles of cobalt and $n_{(\text{Li}_{0.62}\text{, K}_{0.38})_2\text{CO}_3}$ = number of moles of lithium and potassium carbonates in the sample.

99 to 101% and are in good agreement with those obtained using the method of standard additions. The precision, expressed as relative standard deviation, is better than 1% ($n=5$) for all the analytes.

3.3. Analysis of melts

The results of the analysis of cobalt in melt samples withdrawn at different times [12] are given in Table 2, together with the RSDs. The gathered results are also given in mole fraction for an easier comparison with literature data. The amount of cobalt increases with the increasing of the time up to 148 h, after that the value of cobalt does not vary for more than 5% suggesting that this value can be taken as the solubility value of cobalt in the Li/K carbonate melt. The complete decomposition of the melt sample requires a rather long time period because the amount of lithium carbonate in the melt is near the limit of solubility in water [13]. Care has to be taken in the decomposition of melt to ensure complete dissolution of any precipitate that arises from the Li_2CO_3 if a dilution factor less than 33 is used.

The proposed method allows the determination of trace levels of Co, Fe and Ni in 62/38 mol/o $\text{Li}_2\text{CO}_3/\text{K}_2\text{CO}_3$ melts using aqueous standard for calibration without the need of matrix matching or using the method of standard additions. The time required for the melt decomposition, prepa-

ration of solutions and analysis is about 4 h for any metal. Moreover, the method offers the advantage of time saving using a low cost AA spectrometer.

References

- [1] L. Plomp, E.F. Sitters, J.B.J. Veldhuis, R.C. Makkus, S.B. van der Molen, Performance and dissolution-precipitation behavior of Molten Carbonate Fuel Cells, Proceedings of the Third International Symposium on Molten Carbonate Fuel Cell Technology, The Electrochemical Society, Pennington, NJ, 1993.
- [2] Z.A. Grosser, C.A. Scheider, *At. Spectrosc.* 17 (1996) 209–210.
- [3] E. Ivanova, I. Havezov, *Talanta* 42 (1995) 1259–1263.
- [4] R. Lobinski, Z. Marzenko, in: S.G. Weber (Ed.), *Comprehensive Analytical Chemistry*, vol. XXX, Elsevier, Amsterdam, 1997, p. 48.
- [5] L. Kekedy-Nagy, *Talanta* 44 (1997) 1919–1922.
- [6] T.S. Conner, J. Yang, J.A. Koropchak, *Spectrochim. Acta, Part B* 52B (1997) 1087.
- [7] J.D. Doyon, T. Gilbert, G. Davies, L. Paetsch, *J. Electrochem. Soc.* 134 (1987) 3035.
- [8] J.A. Olivares, R.S. Houk, *Anal. Chem.* 58 (1986) 20–25.
- [9] D. Ye, H. Zhang, Q. Jin, *Talanta* 43 (1996) 535–544.
- [10] B. Welz, *Atomic Absorption Spectrometry*, 2nd, completely revised edition, VCH, Weinheim, 1985, p. 169.
- [11] J.C. Miller, J.N. Miller, *Statistics for Analytical Chemistry*, 2nd edition, Horwood, Chichester, UK, 1988.
- [12] L. Giorgi, M. Carewska, M. Patriarca, S. Scaccia, E. Simonetti, A. Di Bartolomeo, *J. Power Sources* 49 (1994) 227.
- [13] R.C. Weast, S.M. Selby, C.D. Hodgman, *CRC Handbook of Chemistry and Physics*, 53rd edition, 1972–1973.

Short communication

Solution equilibria between ethylenediamine-*N,N'*-di-3-propionate and some transition metal(II) ions

Jelena Disic, Srecko Trifunovic, Slobodan Grujic, Predrag Djurdjevic *

Faculty of Science, Institute of Chemistry, P.O. Box 60, 34000 Kragujevac, Yugoslavia

Received 15 September 1998; received in revised form 24 November 1998; accepted 8 December 1998

Abstract

Solution equilibria between the ligand ethylenediamine-*N,N'*-di-3-propionate (eddp^{2-}) and copper(II), nickel(II) or cobalt(II) ions were studied by glass electrode pH-metric and spectrophotometric measurements in 0.1 M NaCl ionic medium at 298.0 ± 0.2 K. In the concentration limits $1.0 \leq [\text{metal(II)}] \leq 5.0$, $1.0 \leq [\text{eddp}] \leq 10.0$ and $2.5 \leq -\log [\text{H}^+] \leq 10.0$ mM, the formation of the following complexes with their overall stability constants, $\log(\beta \pm \sigma)$, was proved by the non-linear least-squares data treatment: Cu(eddp), 14.23 ± 0.04 ; Cu(Heddp), 16.17 ± 0.08 ; Cu(OH)eddp, 3.08 ± 0.06 ; Ni(eddp), 8.89 ± 0.02 ; Ni(OH)eddp, -2.15 ± 0.06 ; Co(eddp), 7.16 ± 0.03 ; Co(OH)eddp, -0.83 ± 0.04 ; Co(OH)₂eddp, -10.54 ± 0.05 . The mechanism of the formation and structure of the complexes, as well as their possible analytical use, were discussed. © 1999 Elsevier Science B.V. All rights reserved.

Keywords: Solution equilibria; Complexes; Ethylenediamine-*N,N'*-di-3-propionate

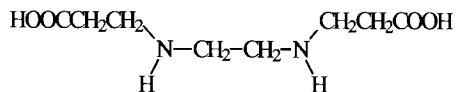
1. Introduction

A unique place among chelating ligands is taken by complexonates containing carboxylic acid residues. Chelates of ethylenediaminetetraacetate (edta)-type ligands have been studied for

over half of a century, owing to their importance in chemistry, medicine, agriculture, etc. [1–4]. In analytical chemistry, chelating agents of edta-type are of particular interest since most metal ions could be relatively easily determined in various samples, by a fast and simple procedure employing the complexation reaction. Of particular practical and theoretical interest among dicarboxylic complexones is ethylenediamine-*N,N'*-di-3-propionic acid (H_2L , H_2eddp ; eddp^{2-} = ethylenediamine-*N,N'*-di-3-propionate) containing two frag-

* Corresponding author. Fax: +381-34335-040.

E-mail address: preki@knez.uis.kg.ac.yu (P. Djurdjevic)



Scheme 1.

ments of natural β -alanine amino acid (Scheme 1). The lower charge of eddp^{2-} should be an advantage over edta^{4-} since there is complete charge neutralization for eddp complexes of divalent metal ions. In addition, the elongated side chain of eddp can encircle the metal(II) ion more favorably by forming a six-membered ring of enhanced stability.

The metal(II) complexes with the eddp ligand were comparatively little studied. While with the related ligand, ethylenediamine-*N,N'*-diacetic acid (edda) there are a number of recent studies concerning the structure and synthesis of the complexes with Zn(II) [5,6], Co(II) and Co(III) [7,8], Fe(III) [9], Cr(III) [10] and Pt(II) [11] ions, so far only a few metal–eddp complexes have been synthesized and characterized. These include copper(II)–eddp [12], nickel(II)–eddp [13], and vanadyl(IV)–eddp [14] complexes. In order to evaluate the analytical potential of eddp, it is necessary to determine the stability of complexes with many metal ions. The stability constants of eddp chelates with transition metal ions have been determined by Martell et al. [15]. It seems that after Martell et al.'s work, no other data on metal(II)–eddp solution equilibria have been reported. Hence, in view of recent findings related to the structure of eddp complexes with Co(III) [16], Cu(II) [12] and Ni(II) [13] ions, Martell et al.'s values for metal(II) stability constants need to be reinvestigated in terms of the precision of the calculated stability constants, as well as the speciation scheme in the metal(II)–eddp systems.

In the present work, we report the study with copper(II), nickel(II) and cobalt(II) ions. In continuation with our previous studies of edta-type metal(II) and metal(III) complexes [17–20], we paid particular attention to the formation of mixed ternary complexes (hydroxy and protonated) which, so far, have not been characterized in metal(II)–eddp systems.

2. Experimental

2.1. Reagents and analysis

All chemicals used were of analytical purity grade, products of Merck (Darmstadt, F.R.G.). The $\text{H}_2\text{eddp} \times 2 \text{HCl}$ was prepared according to the procedure described by Martell and Chaberek [21]. The final product was recrystallized from hot water. Elemental analysis gave: C, 35.0%; H, 6.81%; N, 10.50% (calculated for $\text{C}_8\text{H}_{16}\text{N}_2\text{O}_4$: C, 34.67%; H, 6.54%; N, 10.10%). The chloride content was determined potentiometrically by the titration with standard solution of AgNO_3 , using a Gran plot, and gravimetrically by precipitation as AgCl . Both methods gave the same result (25.3%), within the relative error of 0.2%. The stock solutions of the ligand, metal(II) chlorides, HCl, NaOH and NaCl, were prepared and analyzed as described previously [19].

2.2. Instruments and procedure

2.2.1. Potentiometric measurements

A Tacussel Isis 20|000 pH meter equipped with a Tacussel TC-100 combined electrode was used for pH measurements. The apparatus and the procedure for calibration of the electrode system in terms of hydrogen ion concentration, were described in detail earlier [17,18]. During the calibration of the glass electrode, the ionic product of water was calculated and found to be $\text{p}K_w = 13.54 \pm 0.02$. All measurements were made in 0.1 M NaCl ionic medium at $298.0 \pm 0.2 \text{ K}$, as a series of potentiometric titrations. The standard NaOH (0.165 M) was used as a titration agent. A Metrohm (Donau, Switzerland) Dosimat model 665 was used for delivering the base. Purified argon was bubbled through the titrated solution, which, in addition, was magnetically stirred.

The total concentrations of metal ions were 1.0, 3.0 and 5.0 mM with ligand to metal concentration ratios 1.2:1, 1.5:1 and 2:1. Within these concentration ranges, no effect of ionic medium on the stability constants should be expected. The main contribution to the ionic medium stems from the chloride ion, whose concentration, during the titration, changes very little (less than 3%)

and thus, activity coefficients of charged species may be assumed to remain constant. The free hydrogen ion concentration, $[H^+]$, was decreased by adding CO_2 -free NaOH solution to an acidified mixture of metal(II) ion and ligand. For each system, five to 10 different titrations with 80–120 pH readings were carried out within the limits $2.5 \leq -\log [H^+] \leq 8.5$ –10 (depending on the metal–eddp system).

2.2.2. Spectrophotometric measurements

The UV–visible spectra were recorded on a Varian SuperScan 3 spectrophotometer in a 350–800 nm wavelength range. The quartz cells of 1 cm pathlength were used; the reference cell being filled with corresponding metal-free solution. The spectra of pure metal(II) chlorides, in 0.1 M HCl solution were recorded separately and used for the correcting the corresponding metal–eddp spectra. For each metal(II)–eddp system, 20 solutions were prepared with total metal concentrations 3.0 or 5.0 mM and ligand to metal concentration ratios 1:1 or 2:1. The pH of the solutions was adjusted with the addition of standard NaOH or HCl solution; thus, the pH was varied within the limits $3.0 \leq -\log [H^+] \leq 8.0$ –8.5 (depending on the metal–eddp system). Care was taken to avoid the influence of atmospheric oxygen on cobalt(II) + eddp solutions by preparing the solutions in inert (argon) atmosphere and storing, before measurements, in volumetric flasks equipped with Teflon corks. Additional protection was made with ‘parafilm’ folio.

2.3. Preparation of binary and hydroxy complexes

A solution of metal(II) chloride (5 mM) was added to an aqueous solution of H_2eddp (5.2 mM) with heating to 40°C and stirring. After cooling to room temperature, the pH of the mixture was adjusted, by gradual addition of 20 wt% NaOH, to 9.0 for copper(II) and nickel(II) + eddp, and to 8.0 for cobalt(II) + eddp solution. The obtained solutions were heated to 40°C for 5 min and left to cool again to room temperature. At this temperature, the solutions were allowed to stand, in a vacuum desiccator,

for several days. Solutions were then passed through an ion-exchange column (Dowex 1X8) to give one dominant band and some small residual material, which was completely eluted with 0.1 M NaCl. The dominant band was eluted with water, the solution was evaporated to small volume and crystallized after 1 day in a desiccator containing methanol. The results of elemental microanalysis are in agreement with the formula $M^{II}(eddp) \times H_2O$ ($M^{II} = Cu, Ni$ or Co). The eluant obtained with 0.1 M NaCl was desalted using a G-10 Sephadex column. From the obtained solutions, it was not possible to isolate any pure substance due to precipitation of metal(II) hydroxides during the crystallization.

2.4. Data treatment

The concentration stability constants $\beta = [M_p H_q L_r] / [M]^p [H]^q [L]^r$ were calculated with the aid of the SUPERQUAD [22] and SQUAD [23] programs. Negative values of q denote hydroxy complexes. The SUPERQUAD was used for evaluation of potentiometric data while SQUAD was applied to spectrophotometric data. The quality of fit of the potentiometric data was judged by the statistical parameters U , χ^2 , s and σ . The parameter U is defined as $U = \Sigma(pH_{calc} - pH_{obs})^2$, χ^2 (Pearson’s test) is a measure of the normality of the distribution of the residuals, $pH_{calc} - pH_{obs}$, s is a standard deviation in residuals and σ is standard deviation in calculated stability constants. The fit was considered as acceptable when χ^2 was less than 12.6 (at 95% confidence level with six degrees of freedom), s less than 2.0 (with standard deviation in pH measurements of 0.001 pH units and that in volume readings 0.001 ml) and σ less than 0.15 logarithmic units.

In SQUAD calculations, the statistical parameters S and SD were used to assess the quality of fit of the spectral data. The SD is a standard deviation in residuals ($A_{calc} - A_{obs}$), while $S = \Sigma(A_{calc} - A_{obs})^2$ where A denotes absorbance. The fit was adequate if both SD and S were simultaneously less than 1×10^{-2} .

Table 1

Stability constants, $\beta_{p,q,r}$ of the complexes formed in metal(II)–eddp systems in 0.1 mol l⁻¹ NaCl ionic medium at 298 K. The constants refer to the equilibrium: $pM^{2+} + qH^+ + reddp^{2-} \rightleftharpoons M_pH_q(eddp)_r$

Complex	log ($\beta_{p,q,r} \pm \sigma$)	
	Potentiometry	Spectrophotometry
H(eddp) ⁻	9.38 ± 0.01	–
H ₂ (eddp) ⁰	15.86 ± 0.01	–
H ₃ (eddp) ⁺	19.14 ± 0.02	–
H ₄ (eddp) ²⁺	22.06 ± 0.03	–
Cu(Heddp) ⁺	16.17 ± 0.08	16.09 ± 0.005
Cu(eddp) ⁰	14.23 ± 0.04	14.22 ± 0.01
Cu(OH)eddp ⁻	3.08 ± 0.06	3.10 ± 0.02
Ni(eddp) ⁰	8.89 ± 0.02	8.90 ± 0.01
Ni(OH)eddp ⁻	-2.15 ± 0.06	–
Co(eddp) ⁰	7.16 ± 0.03	7.14 ± 0.002
Co(OH)eddp ⁻	-0.83 ± 0.04	-1.12 ± 0.06
Co(OH) ₂ eddp ²⁻	-10.54 ± 0.05	–
Co ₂ (OH) ₂	–	0.73 ± 0.09
eddp ²⁻	–	–

3. Results and discussion

3.1. Protonation constants of the eddp²⁻ ion

The protonation constants of the eddp²⁻ ion were determined potentiometrically under the same medium and temperature conditions as for complexation measurements. In total, five titrations were carried out within the concentration limits $1.0 \leq [\text{eddp}]_{\text{tot}} \leq 5.0$ mM, $2.0 \leq -\log [H^+] \leq 10.0$. About 350 titration points were included in calculation. The results of least-squares data treatments with the aid of SUPERQUAD and MAGEC [24] programs are given in Table 1.

3.2. Potentiometric measurements

The treatment of the potentiometric complexation data was initiated by making Bjerrum plots of $Z = f(-\log [\text{eddp}])$, where Z is an average ligand number defined as:

$$Z = \frac{[\text{eddp}]_{\text{tot}} - \frac{[H]_{\text{tot}} - [H^+] + [OH^-]}{Z_H}}{[M]_{\text{tot}}}$$

where M denotes Cu, Ni or Co, Z_H is an average proton number of eddp²⁻ while index tot denotes total stoichiometric concentration of the species. The maximal values of the average ligand number were 1 for Cu(II) + eddp and Ni(II) + eddp, and 1.5 for Co(II) + eddp system. The formation curves show a steep increase at $Z \sim 0.3$ – 0.6 for all the systems studied. Change of the total metal ion concentration has no effect on the formation curve, thus indicating the formation of mononuclear complexes only. From the maximal average ligand number values attained, it may be concluded that no stepwise complex formation takes place, i.e. no formation of bis or higher binary complexes is significant. The formation curves obtained for the Co(II) + eddp system indicate intensive hydrolysis in the system at pH values higher than ~ 6.0 .

The results of SUPERQUAD data treatment are given in Table 1. The ‘best’ model of the Cu(II) + eddp system involves the (1, 1, 1), (1, 0, 1), (1, -1, 1) complexes. The statistical parameters $\chi^2 = 13.4$ and $s = 2.1$ indicate acceptable fit. However, scatter or residuals at pH > 8.0 showed a systematic trend. Therefore, the stability constants of the (1, 0, 1) and (1, 1, 1) complexes were fixed, and calculation was repeated only with points in the pH interval 8.0–10.0. The complexes (1, -1, 1) and (1, -2, 1) were accepted ($\chi^2 = 12.0$ and $s = 1.3$) with the stability constant of the (1, -2, 1) complex, $\log \beta_{1,-2,1} = -8.33 \pm 0.06$. In a final calculation cycle, all points from pH 2.5 to 10.0 were included with the stability constants of (1, 1, 1) and (1, 0, 1) complexes fixed, while these of (1, -1, 1) and (1, -2, 1) were allowed to float. The diol, (1, -2, 1) was rejected with a set of statistics ($\chi^2 = 12.9$, $s = 1.1$) indicating good fit of the data. Since the concentration of the diol is less than 0.2% at pH values between 9.0 and 10.0, it could be excluded from the speciation scheme. From the distribution diagram (Fig. 1(a)), one can see that hydrolytic complex (1, -1, 1) is only a minor species in the system at pH < 8.0 (its concentration was less than 0.1%). Upon increasing the pH, its concentration increases up to 6% at pH 10.0. Nonetheless, this species is not shown in the Fig. 1(a) since it reaches the appreciable concentration in the pH region which is not ana-

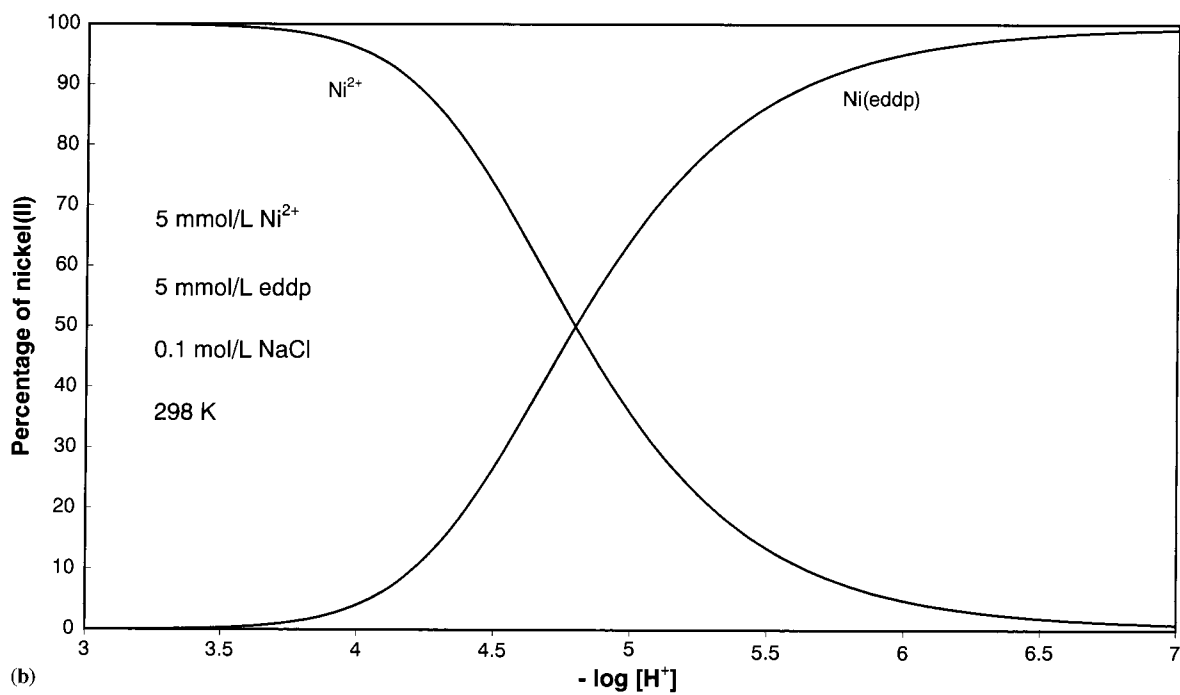
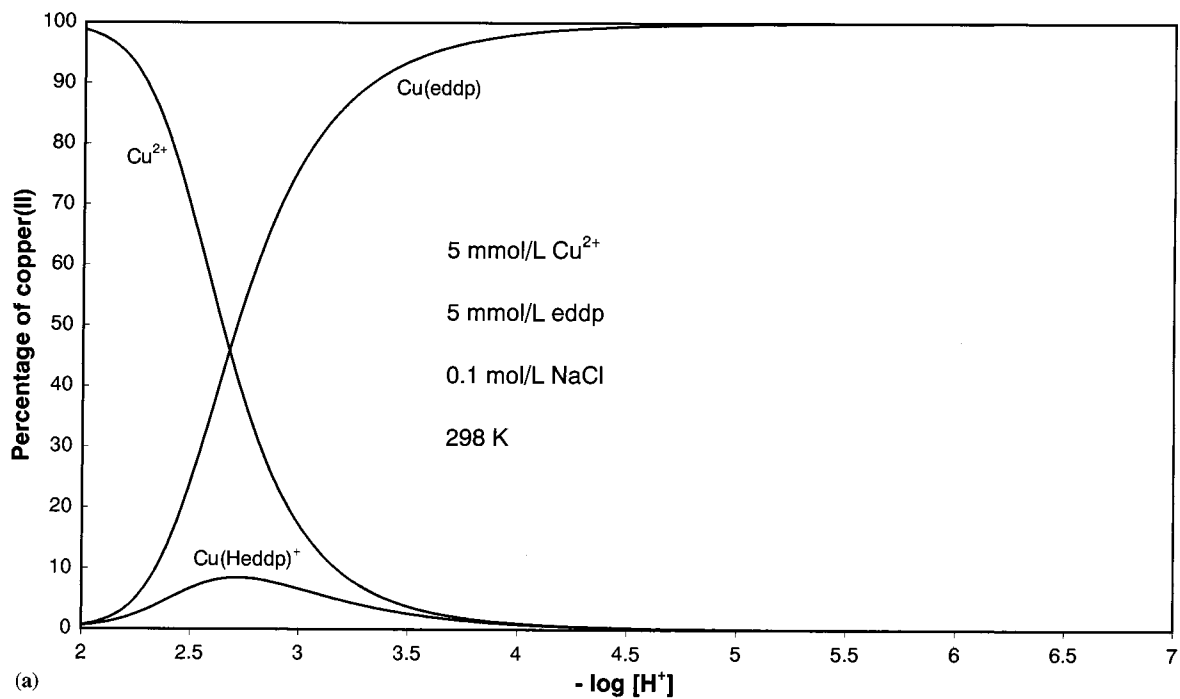


Fig. 1. Distribution diagram for (a) Cu(II) + eddp, (b) Ni(II) + eddp and (c) Co(II) + eddp systems.

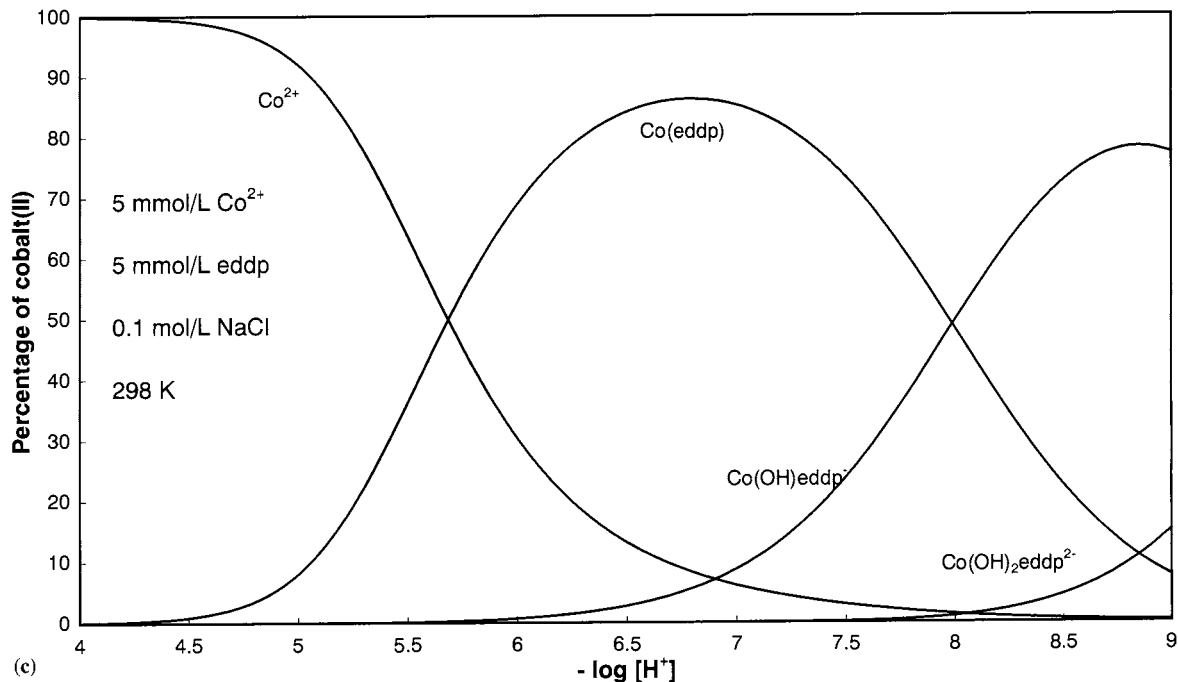


Fig. 1. (Continued)

lytically interesting. The protonated complex is formed in significant amounts in the pH interval between 2.0 and 3.5. Since the formation of the simple binary complex $\text{Cu}(\text{eddp})$ starts in the same pH region, both complexes are formed by the parallel mechanism. As is widely accepted, the mechanism of the formation involves the bonding of N from the diamine ring to $\text{Cu}(\text{II})$, followed by the bonding of the N' donor and carboxylates with release of four protons. In the case of the formation of the protonated complex, in competition for an oxygen donor, the proton wins, so that probably, the carboxyl group is not coordinated to copper, although in our previous work [19], we found that the 3-propionic carboxyl group (from ethylenediamine- N,N' -diacetato-di-3-propionic acid) could be coordinated to copper through the hydroxyl group.

In the nickel(II) + eddp system, formation of the binary complex $\text{Ni}(\text{eddp})$ dominates in the entire pH region studied, with the concentration of the hydroxy species, $\text{Ni}(\text{OH})\text{eddp}$, being less than 1% at $\text{pH} \sim 9.0$ (Fig. 1(b)). The calculated

statistical parameters ($\chi^2 = 12.3$, $s = 1.1$) indicate good fit of the data. A somewhat different situation is seen in the cobalt(II) + eddp system. Poor fit was obtained when all points from the pH range 3.0–8.5 were included in the calculation. Only the binary complex $\text{Co}(\text{eddp})$ was accepted with too bad a set of statistics. The stability constant of this complex was therefore calculated from the points lying in the pH interval 3.0–5.0 and fixed in all subsequent calculation cycles. The pH region was then broadened, to $\text{pH} \sim 7.5$ and calculations were repeated. The hydroxy complex was accepted with a greatly improved set of statistics. Both constants were then fixed and calculations were made in the pH interval 7.5–8.5. The complexes (1, 0, 1) and (1, -1, 1) gave acceptable fit ($\chi^2 = 13.6$, $s = 2.0$); however, inclusion of the diol (1, -2, 1) somewhat improved the set of statistics ($\chi^2 = 12.6$, $s = 1.8$). In addition, better scatter of residuals was obtained in the pH region between 7.0 and 8.5. From these reasons, the diol was accepted in the speciation scheme. No formation of protonated complex was observed, but

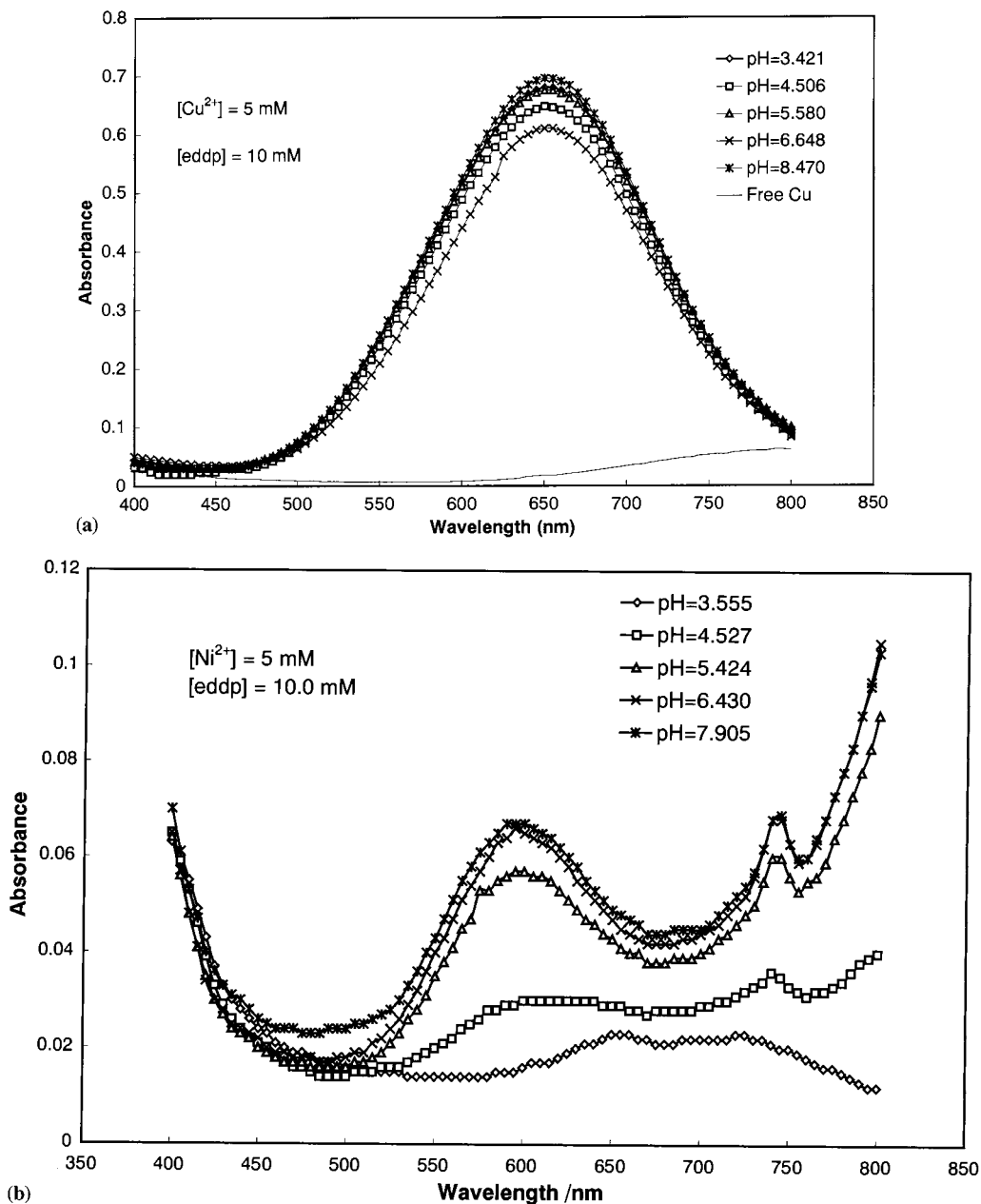


Fig. 2. UV-visible spectra of (a) Cu(II) + eddp, (b) Ni(II) + eddp and (c) Co(II) + eddp systems.

both hydroxy complexes, Co(OH)eddp^- and $\text{Co(OH)}_2\text{eddp}^{2-}$, are formed in significant concentration at $\text{pH} > 7.0$ (Fig. 1(c)). From the distribution diagram, it may be assumed that these complexes are formed by the hydrolysis of the binary complex, Co(eddp) .

3.3. Spectrophotometric measurements

The spectra of the Cu(II) + eddp, Ni(II) + eddp and Co(II) + eddp systems are shown in Fig. 2(a)–(c), respectively. In the Cu(II) + eddp system, the spectra, within pH limits from 3 to 8,

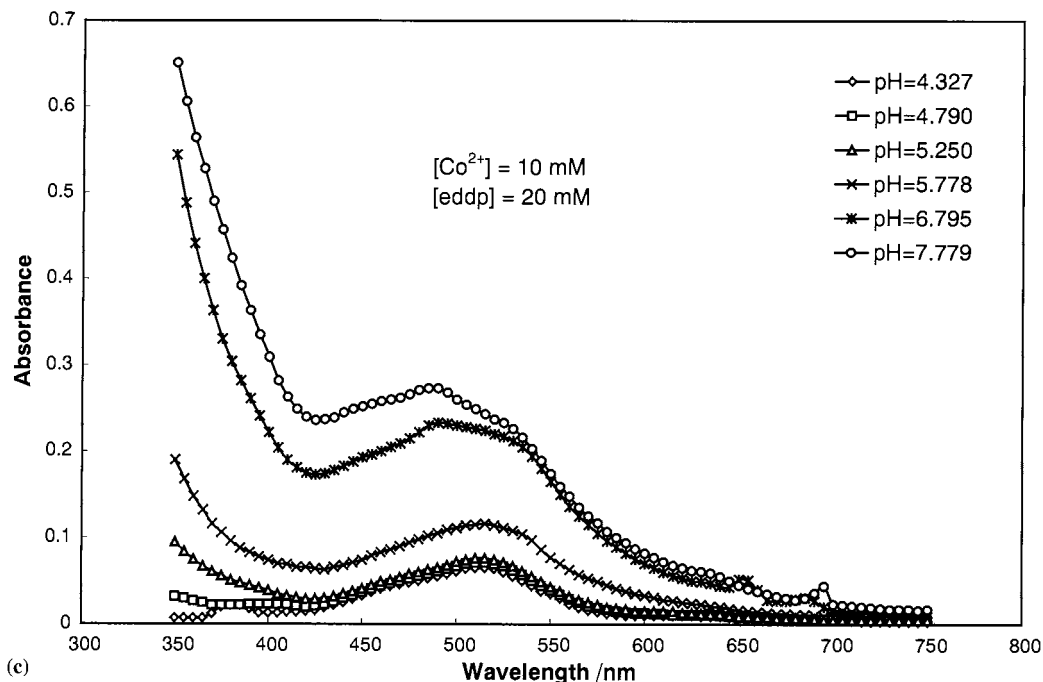


Fig. 2. (Continued)

show an irregular trend upon increasing the pH, thus indicating the formation of several species. The blue shift of the copper band centered at 800–640 nm is due to the formation of a very stable complex. In the Ni(II) + eddp and Co(II) + eddp systems, the spectra are pH dependent, in terms of the position of the absorption maxima as well as the shape of the absorption bands. In the Ni(II) + eddp system, upon increasing the pH from 3 to 8, a band centered at 660 nm shifts toward the blue region for approximately 40 nm and, at the same time, its intensity increases approximately fourfold. In the cobalt(II) + eddp system, the band centered at 515 nm shifts to 490 nm upon increasing the pH from 3 to 7. At pH values higher than 6.5, a new maximum centered at 540 nm appears, indicating intensive hydrolysis at higher pH values.

The results of SQUAD calculations are summarized in Table 1. The copper(II) + eddp system can be modeled with a satisfactorily good set of statistics ($SD = 2 \times 10^{-3}$, $S = 1 \times 10^{-3}$) with

three complexes: the protonated one, $\text{Cu}(\text{Heddp})^+$, the binary one, $\text{Cu}(\text{eddp})$, and the hydroxy complex $\text{Cu}(\text{OH})\text{eddp}^-$. The spectrophotometrically determined formation constants agree very well with these obtained by potentiometry. In the case of the nickel(II) + eddp system, various combinations of complexes did not give acceptable fit. In conjunction with the binary complex, $\text{Ni}(\text{eddp})$, all other complexes were rejected or caused the procedure to diverge. Thus, spectra of Ni(II) + eddp solutions could be interpreted in terms of the formation of only the $\text{Ni}(\text{eddp})$ complex. Its formation constant is in excellent agreement with the potentiometric one. Fitting the cobalt(II) + eddp spectra proved to be a difficult task. Various combinations of complexes were tried. The potentiometrically determined model did not give acceptable fit. Therefore, along with mononuclear complexes, some polynuclears were tested too. The satisfactorily good fit ($SD = 3 \times 10^{-3}$, $S = 2 \times 10^{-3}$) was obtained with the model involving $\text{Co}(\text{eddp})$, $\text{Co}(\text{OH})\text{eddp}^-$ and $\text{Co}_2(\text{OH})_2\text{eddp}$ complexes.

Table 2
Spectral characteristics of the metal(II)–eddp complexes

Complex	λ_{\max} (nm)	ϵ_{\max} (calc)	ϵ_{\max} (obs)
Cu(eddp)	650	110	130
Ni(eddp)	595	9.2	8.6
	745	10.2	9.6
Co(eddp)	515	14	12

The complex $\text{Co}(\text{OH})_2\text{eddp}$ was not accepted in the model. Both the diol and the dimer are formed at pH values higher than 6, probably by the attachment of eddp^{2-} to the corresponding hydrolytic species. The obtained results are in agreement with chromatographic data. Comparison of calculated absorption maxima and those obtained experimentally for binary complexes show excellent agreement (Table 2). At the same time, elution of residual material with 0.1 M NaCl indicates formation of -1 charged species in all systems. This is in agreement with the formation of the hydroxy complexes, although in very small concentration.

In Table 3, the stability constants of eddp complexes are compared with those of other edda- and edta-type ligands. Complexes with edda possess considerably higher stability constants owing to the formation of in-plane five-membered rings. The stability constants with eddp are close to these with the edtp ligand. This is in agreement

with the observation that the two 3-propionate groups, in edtp complexes in the axial position, are only loosely bound to the metal [25]. Thus, the hydrolytic tendencies of the eddp complexes may be explained taking into account their structure, where four donors are in-plane, forming one five-membered and two six-membered rings, with two unequivalent water molecules in the axial position. In the case of the $\text{Cu}(\text{eddp})$ complex, one water molecule is closer to the metal while the other is at such a distance that it is difficult to speak, whether it belongs to the structure of the complex or not. More tightly bound water is responsible for the hydrolysis of the complex. The hydrolysis of the $\text{Cu}(\text{eddp})$ complex occurs at pH values higher than 8 and proceeds very moderately before precipitation, at $\text{pH} \sim 11$. The small extent of the hydrolysis of the $\text{Cu}(\text{eddp})$ complex may be a consequence of a relatively long distance between the water molecule and copper ion so that the electronic cloud around copper influences the water molecule relatively little. The hydrolysis of $\text{Ni}(\text{eddp})$ is very sluggish and slight. Its extent, before precipitation occurs, is very small. The $\text{Co}(\text{eddp})$ complex is very prone to hydrolysis. The hydrolysis begins at pH values around 7 and steeply increases upon increasing the pH. It seems that coordinated water molecules are in a close position to the 3-propionate carbonyl groups, thus forming a spatial arrangement which facilitates the hydrolysis.

Table 3
Stability constants of ML complexes of metal(II) ions with edda- and edta-type chelating ligands^a

Complex	$\log \beta$					
	ida ^b	idp ^c	edda ^d	eddp ^e	edta ^f	edtp ^g
CuL	10.63	9.36	16.2	14.23 (15.1)	18.3	14.85
NiL	8.19	6.14	13.5	8.89 (9.3)	18.4	10.38
CoL	6.97	4.92	11.2	7.16 (7.3)	16.1	8.68

^a ida, iminodiacetate; idp, iminodipropionate; edda, ethylenediaminediacetate; eddp, ethylenediamine-di-3-propionate; edta, ethylenediaminetetraacetate; edtp, ethylenediaminetetra-propionate. Literature values for eddp complexes [15] are given in parentheses.

^b Ref. [27], 20°C, $\mu = 0.1$ M.

^c Ref. [27], 20°C, $\mu = 0.1$ M.

^d Ref. [28], 30°C, $\mu = 0.1$ M.

^e This work, 25°C, $\mu = 0.1$ M; Ref. [15], 30°C, $\mu = 0.1$.

^f Ref. [29], 20°C, $\mu = 0.1$ M.

^g Ref. [30], 25°C, $\mu = 0.1$ M.

As seen from the distribution diagrams (Fig. 1(a)–(c)), the maximum formation of the complexes is achieved at different pH values. The Cu(eddp) complex reaches the maximum concentration at pH 4.0, Ni(eddp) at pH 6.0 and Co(eddp) at pH 7.0. At pH 4.0, the eddp complex with cobalt(II) does not form while that with nickel(II) forms in negligible concentration. It means that copper could be determined in the presence of Ni or Co by the titration with eddp in a buffered solution at pH 4.0. That these ions could be simultaneously determined indicates large spacing between formation curves and different position of the absorption maxima of their eddp complexes. Convenient analytical methods could be spectrophotometry, polarography or ion-selective potentiometry, as in the case of other edda- and edta-related ligands [26].

References

- [1] F.L. Garvan, Metal chelates of ethylenediaminetetraacetate acid and related substances, in: F.P. Dwyer, D.P. Mellor (Eds.), *Chelating Agents and Metal Chelates*, Academic Press, New York, 1964.
- [2] G. Anderegg, *Complexones*, in: G. Wilkinson (Ed.), *Comprehensive Coordination Chemistry*, vol. 2, Pergamon Press, Oxford, 1987.
- [3] R.A. Bulman, *Structure Bonding* (Berlin) 67 (1987) 91.
- [4] B.E. Douglas, D.J. Radanovic, *Coord. Chem. Rev.* 128 (1993) 139.
- [5] Y. Fujibayashi, H. Saji, K.H. Suzuki, K. Torizuka, A. Yokoyama, I. Yomoda, *Eur. J. Nucl. Med.* 11 (1986) 488.
- [6] Y. Fujibayashi, H. Adachi, K. Horiuchi, R. Hosotani, K. Inoue, K. Kawai, S. Miyata, T. Okuno, H. Saji, K. Torizuka, Y. Unuma, A. Yokoyama, *Int. J. Nucl. Med. Biol.* 12 (1986) 447.
- [7] T. Taura, *Polyhedron* 11 (1992) 1463.
- [8] I. Bernal, J. Cetrullo, J. Myrczek, J.W. Cai, W.T. Jordan, *J. Chem. Soc. Dalton Trans.*, (1993) 1771.
- [9] Y. Nishida, S. Ito, *Polyhedron* 14 (1995) 2301.
- [10] N. Sakagami, M. Nakahamada, K. Ino, A. Hioki, S. Kaizaki, *Inorg. Chem.* 35 (1996) 683.
- [11] R.E. Shepherd, S.S. Zhang, R. Kortés, F.T. Lin, C. Maricondi, *Inorg. Chem. Acta* 244 (1996) 15.
- [12] Z. Matovic, G. Pelosi, S. Ianelli, G. Ponticelli, D.D. Radanovic, D.J. Radanovic, *Inorg. Chem. Acta* 268 (1998) 221.
- [13] D.J. Radanovic, V. Matovic, Z. Matovic, L.P. Battaglia, G. Pelizzi, G. Ponticelli, *Inorg. Chem. Acta* 237 (1995) 151.
- [14] E. Alberico, G. Micera, D. Sanna, A. Desi, *Polyhedron* 13 (1994) 1763.
- [15] R.C. Courtney, S. Chaberek, A.E. Martell, *J. Am. Chem. Soc.* 75 (1953) 4814.
- [16] N. Sakagami, T. Yasui, H. Kawaguchi, T. Ama, S. Kaizaki, *Bull. Chem. Soc. Jpn.* 67 (1994) 680.
- [17] P. Djurdjevic, D.J. Radanovic, M. Cvijovic, D.S. Veselinovic, *Talanta* 38 (1991) 455.
- [18] P. Djurdjevic, D.J. Radanovic, J. Jovanovic, D.S. Veselinovic, *Transition Met. Chem.* 17 (1992) 84.
- [19] P. Djurdjevic, D.J. Radanovic, M. Cvijovic, M. Dimitrijevic, D.S. Veselinovic, *Polyhedron* 11 (1992) 197.
- [20] B. Prelesnik, D.D. Radanovic, Z. Tomic, P. Djurdjevic, D.J. Radanovic, D.S. Veselinovic, *Polyhedron* 15 (1996) 376.
- [21] A.E. Martell, S. Chaberek, *J. Am. Chem. Soc.* 72 (1950) 5357.
- [22] P. Gans, A. Sabatini, A. Vacca, *J. Chem. Soc. Dalton Trans.*, (1985) 1195.
- [23] ,Squad: Stability quotients from absorbance data, D.J. Leggett (Ed.), *Computational Methods for the Determination of Formation Constants*, Plenum Press, New York, 1985, pp. 159–220.
- [24] P.M. May, D.R. Williams, Magec: a program for the definite calibration of the glass electrode, in: R.E. Leggett (Ed.), *Computational Methods for the Determination of Formation Constants*, Plenum Press, New York, 1985, pp. 37–71.
- [25] N.M. Dyatlova, K. Ya. Temkina, K.I. Popov, *Kompleksny i Kompleksonati Metallov* (Complexones and Metal Complexonates), Khimiya, Moskva, 1988.
- [26] R. Prshibil, *Analiticheskie Primeneniya Etilendiamintetraakusnoi Kisloty i Rodstvenyh Soedinenii* (Analytical Applications of Ethylenediaminetetraacetic Acid and Related Compounds), Mir, Moskva, 1975.
- [27] A. E. Martell, R.M. Smith, *Critical Stability Constants*, vols. 1 and 5, Plenum Press, London, 1974, 1982.
- [28] S. Chaberek, A.E. Martell, *J. Am. Chem. Soc.* 74 (1952) 5052.
- [29] G. Anderegg, *Critical Survey of Stability Constants of EDTA Complexes*, Pergamon Press, Oxford, 1977.
- [30] L.H.J. Lajunen, P. Kokkonen, H. Knutti, J. Jokisaari, *Acta Chem. Scand.* 431 (1989) 2.

Trace determination of zinc in standard alloys, environmental and pharmaceutical samples by fourth derivative spectrophotometry using 1-2-(thiazolylazo)-2-naphthol as reagent and ammonium tetrphenylborate supported on naphthalene as adsorbent

Anju Bhalotra, Bal Krishan Puri *

Chemistry Department, Indian Institute of Technology, Hauz Khas, New Delhi, 110 016, India

Received 10 August 1998; received in revised form 11 December 1998; accepted 28 December 1998

Abstract

A highly sensitive, selective, economical and rapid method for the trace determination of zinc using fourth derivative spectrophotometry has been proposed with 1-2-(thiazolylazo)-2-naphthol (TAN) as an analytical reagent and ammonium tetrphenylborate (ATPB)-naphthalene as an adsorbent. Zn-TAN is quantitatively retained on ATPB naphthalene in the pH range 6.5–9.5. The calibration plot is linear in the concentration range 0.02–1.4 $\mu\text{g ml}^{-1}$ Zn of DMF solution. The sensitivity of the method as determined from the slope of the calibration plot is 2.640 ($d^4A/d\lambda^4$)/($\mu\text{g ml}^{-1}$). Nine replicate determinations of 5.0 μg of zinc in 5 ml of DMF give a mean signal height of 2.660 (peak to peak height between $\lambda_1 = 597$ nm and $\lambda_2 = 585$ nm) with a relative standard deviation of 1.1%. The various conditions have been optimized and the developed method has been used for the determination of zinc in standard alloys, environmental and pharmaceutical samples. © 1999 Elsevier Science B.V. All rights reserved.

Keywords: Zinc; 1-2(Thiazolylazo)-2-naphthol; Ammonium tetrphenylborate-naphthalene; Fourth derivative spectrophotometry; Standard alloys; Environmental and pharmaceutical samples

1. Introduction

For the growth of both plant and animal life, the presence of small quantities of zinc is essential [1]. Zinc exerts beneficial effects on cardiocircula-

tory function and prevention of black foot disease [2]. It is used in the protection of steel against corrosion, dry batteries, photoengraving and lithography[1]. Therefore, sensitive, selective and rapid methods for the determination of zinc are in great demand. Atomic absorption spectrometry (AAS) [3], graphite furnace atomic absorption spectroscopy (GFAAS) [4], neutron activation analysis (NAA) [5], inductively coupled plasma-

* Corresponding author. Fax: +91-11-686-2037.

E-mail address: bkpuri@chemistry.iitd.ernet.in, balkpuri@hotmail.com (B.K. Puri)

atomic emission spectroscopy (ICP–AES) [6], inductively coupled plasma–mass spectrometry (ICP–MS) [7], direct current plasma atomic emission spectrometry (DC–PAES) [8], X-ray fluorescence [9] are widely applied to the determination of zinc at trace level. However, zinc can alternatively be determined by spectrophotometric method. Furthermore, the use of derivative spectrophotometry offers a useful means of enhancing the selectivity of the method due to narrow peaks. The sensitivity is also enhanced due to high signal as compared to zero order [10]. Various recent spectrophotometric reagents reported in the literature for the determination of zinc are summarized in Table 1. Most of these reagents are less sensitive and the preconcentration factor is also limited as compared with the present method.

Preconcentration technique allows the improvement of detection limit as well as the selectivity of the method. Preconcentration may be achieved by evaporation, osmosis, solvent extraction, coprecipitation, ion exchange (column and batch mode), modified solid supports, electro chemical deposition and on line concentration. Some of the above mentioned methods are non-selective, tedious and requires rigorous control of experimental conditions. Moreover, the preconcentration factor achieved is not much favoured [11].

In the present work, ammonium tetraphenylborate (ATPB) supported on naphthalene has been used as an adsorbent for preconcentration of zinc–1-2-thiazolylazo-2-naphthol (TAN) complex from its aqueous solution since zinc forms an ion associated ternary complex (zinc–TAN–TPB) when aqueous solution of Zn–TAN is passed over the adsorbent. Various parameters viz. pH, flow rate, aqueous volume, reagent concentration, choice of solvent and interference of large number of metal ions and anions are optimized to determine zinc content in various alloys, environmental and pharmaceutical samples.

2. Experimental

2.1. Apparatus and reagents

A Hitachi-330 spectrophotometer with 1.0 cm

quartz cells was used for normal and derivative spectrophotometric measurements. An Elico pH analyzer model LI-612 with combined glass-calomel electrode was used for pH measurements. All atomic absorption measurements were made with atomic absorption spectrometer model 4129 supplied by Electronic Corporation of India Ltd. Funnel tipped glass tube (60 mm × 6 mm id) was used as a column for the preconcentration purposes. The column was plugged with polypropylene fibre and then filled with the adsorbent to a height of 1.0–1.2 cm after pressing lightly with a flat glass rod. All glasswares were kept overnight in a mixture of nitric and sulphuric acid (1 + 1) and washed with doubly distilled water before use.

A 1000 $\mu\text{g ml}^{-1}$ zinc solution was prepared by dissolving 4.3970 g of $\text{ZnSO}_4 \cdot 7\text{H}_2\text{O}$ in 1000 ml of distilled water and standardized [12]. A 2.0 $\mu\text{g ml}^{-1}$ working solution of zinc was prepared by diluting the stock solution. TAN was procured from Sigma Co. (St. Louis, USA) and was used without further purification. A 0.01% solution of TAN was prepared in methanol and stored in an amber coloured bottle. Buffer solutions of pH 3–7 and 7–11 were prepared by mixing appropri-

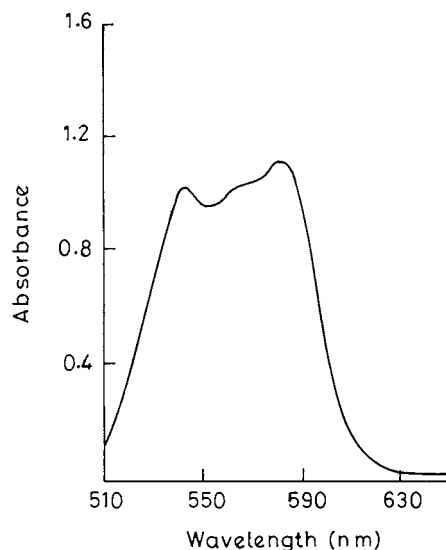


Fig. 1. Zero order spectrum of Zn(II)–TAN–ATPB–naphthalene complex. Zn(II): 5.0 μg ; pH = 8, TAN: 2 ml of 0.01% solution; Buffer 2 ml, Flow rate: 2 ml min^{-1} , Solvent: 5 ml of DMF, Reference: Reagent blank.

Table 1

Comparison of the present method for the determination of zinc with some of the recent spectrophotometric methods reported in the literature

S. No.	Reagent	Remarks	Reference
1	1-(2-Pyridylazo)-2-naphthol	$\epsilon = 5.15 \times 10^4 \text{ l mol}^{-1} \text{ cm}^{-1}$. Medium—sodium dodecylsulphate/ <i>n</i> -butanol/ <i>n</i> -heptane/water microemulsion medium limited aqueous phase volume. Concentration range: 0–3.4 μg of zinc/10 ml.	[14]
2	<i>O</i> -Hydroxybenzenediazo-aminoazo benzene	$\epsilon = 1.50 \times 10^5 \text{ l mol}^{-1} \text{ cm}^{-1}$ presence of emulsifier <i>n</i> -octyl polyethylene glycol phenylether, limited aqueous phase volume. Concentration range: 0–13 μg of zinc/25 ml.	[15]
3	Xylenol orange	$\epsilon = 1.4 \times 10^4 \text{ l mol}^{-1} \text{ cm}^{-1}$, a few metal ions interfered. Concentration range: 0–5 μg of zinc/ml.	[16]
4	$\alpha,\beta,\gamma,\delta$ -Tetrakis (3,4-hydroxy phenyl) porphine	$\epsilon = 8.1 \times 10^4 \text{ l mol}^{-1} \text{ cm}^{-1}$, limited aqueous phase, some metal ions interfered. Concentration range: 0–0.24 μg of zinc/ml.	[17]
5.	Bathophenanthroline	$\epsilon = 7.3 \times 10^4 \text{ l mol}^{-1} \text{ cm}^{-1}$ limited aqueous phase.	[18]
6.	1,3-Bis(4-phenylazophenyl) triazine	$\epsilon = 1.63 \times 10^5 \text{ l mol}^{-1} \text{ cm}^{-1}$, in the presence of triton X-100, limited aqueous phase volume. Concentration range: 0–8 μg of zinc/25 ml.	[19]
7.	1-(2-Imidazolylazo)-2-naphthol-4-sulfonic acid	$\epsilon = 4.01 \times 10^4 \text{ l mol}^{-1} \text{ cm}^{-1}$, in the presence of Triton X-100, limited aqueous phase volume. Concentration range: 0–20 μg of zinc/25 ml.	[20]
8	Eriochrome azurol 6B, quinoline	$\epsilon = 1.1 \times 10^5 \text{ l mol}^{-1} \text{ cm}^{-1}$, in the presence of cetyltrimethyl ammonium bromide, limited aqueous phase volume. Concentration range: 0–16 μg of zinc/25 ml.	[21]
9	Dithizon	$\epsilon = 8.5 \times 10^4 \text{ l mol}^{-1} \text{ cm}^{-1}$, a few metal ions interfered, limited aqueous phase volume. Concentration range: 0–6 μg of zinc/12.75 ml.	[22]
10	4- <i>p</i> -Nitrobenzoyl 2,4-dihydro-5-methyl-1-phenylpyrazol-3,one	$\epsilon = 1.09 \times 10^4 \text{ l mol}^{-1} \text{ cm}^{-1}$, preconcentration factor limited	[23]
11	1-(<i>p</i> -Azophenyl)-3-(2-thiazolyl)-triazene	$\epsilon = 9.6 \times 10^4 \text{ l mol}^{-1} \text{ cm}^{-1}$, in the presence of non-ionic surfactant triton X100, limited aqueous phase volume. Concentration range: 0–24 μg of zinc/25 ml.	[24]
12	Antipyrinyldiazo amino 2,4-dinitrobenzene	$\epsilon = 1.75 \times 10^5 \text{ l mol}^{-1} \text{ cm}^{-1}$, in the presence of triton X-100, limited aqueous phase volume, metal ions interfere. Concentration range: 0–12 μg of zinc/25 ml.	[25]
13	Salicylfluorne	$\epsilon = 7.7 \times 10^4 \text{ l mol}^{-1} \text{ cm}^{-1}$, in the presence of cetyltrimethylammonium bromide, limited aqueous phase volume. Concentration range: 1–8 μg of zinc/25 ml. Detection limit 0.04 $\mu\text{g ml}^{-1}$.	[26]
14	1-2-Thiazolylazo-2-naphthol (Present method)	$\epsilon = 7.2 \times 10^4 \text{ l mol}^{-1} \text{ cm}^{-1}$. Sensitivity, 2.64 ($d^4A/d\lambda^4$)/ $\mu\text{g ml}^{-1}$ Concentration range: 0.02–1.4 μg of zinc/ml of DMF. Preconcentration factor-100, a few metal ion interfered that too were easily masked with common masking agents. Selectivity further enhanced by pre-concentration and derivative spectrophotometry. Detection limit 9.5 ng ml^{-1} .	

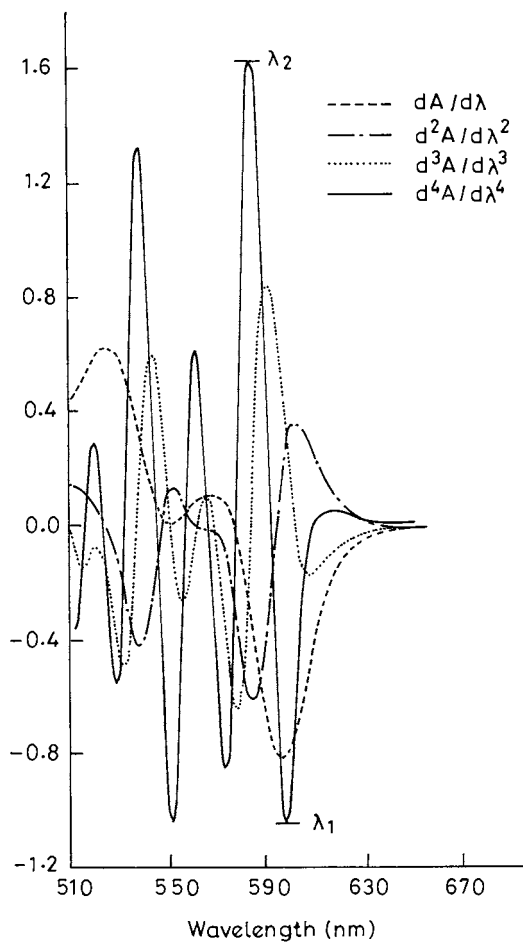


Fig. 2. First, second, third and fourth order spectrum of Zn(II)-TAN-ATPB-naphthalene complex. Conditions same as in Fig. 1.

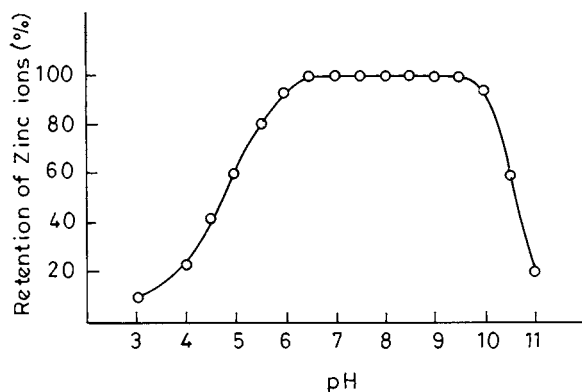


Fig. 3. Effect of pH. Conditions same as in Fig. 1.

ate ratios of 0.5 M solution each of acetic acid–sodium acetate and 0.5 M ammonium acetate–ammonia respectively. All other reagents used were of analytical grade. Double distilled water was used throughout the present work.

2.2. Preparation of ATPB–naphthalene adsorbent

A solution of naphthalene was prepared by dissolving 20 g naphthalene in 35 ml of acetone on a magnetic hot plate stirrer at 40°C. This naphthalene solution was added in a fast stream with continuous stirring into a beaker containing 1500 ml of doubly distilled water which was conditioned to pH \approx 9.5 by adding 25 ml of 1 M ammonium acetate and 75 ml of 1 M ammonia solution. Then, to this solution, 500 ml of an aqueous solution containing 1.7 g of sodium tetrphenylborate was added. The naphthalene coprecipitated with NH_4^+ and TPB^- was stirred for about 2 h on a magnetic stirrer. The supernatant solution was decanted off and the remaining solid mass was washed twice with doubly distilled water. The adsorbent in the form of a slurry was stored in a bottle for subsequent use.

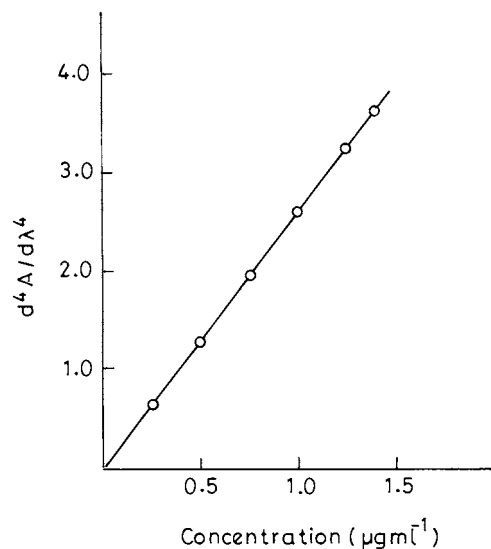


Fig. 4. Calibration plot for Zn(II) by fourth derivative spectrophotometry from peak to peak measurements between λ_1 (597 nm) and λ_2 (585 nm). pH = 8, TAN: 2 ml of 0.01% solution; Buffer 2 ml, Flow rate: 2 ml min $^{-1}$, Solvent: 5 ml of DMF, Reference: Reagent blank.

Table 2
Effect of diverse ions on the estimation of 5.0 µg of zinc

Salt of the anion/metal ion added	Tolerance limit/µg
Sodium fluoride	2000
Sodium nitrate	3000
Potassium iodide	10,000
Potassium chloride	8000
Sodium potassium tartrate	1000
Potassium thiocyanate	10,000
Thiourea	10,000
Ammonium phosphate	2000
Dimethylglyoxime	5000
Sodium citrate	5000
Sodium thiosulphate	2000
Ascorbic acid	1000
Sodium sulphate	500
Au(III)	200
Pt(IV)	200
Pd(II)	80
Ir(III)	250
Ru(III)	280
Mg(II)	300
Ba(II)	400
Sn(IV)	80
Zr(IV)	500
Co(II)	100 ^a
Rh(III)	170
Ni(II)	100 ^a
Cu(II)	100 ^b
Fe(III)	80 ^c
Cr(VI)	400
Al(III)	150
Mo(VI)	50
Bi(III)	60
Th(IV)	70
As(III)	65
Sb(III)	80
Ca(II)	450
Ge(IV)	400

^a After masking with 5 ml of 0.1% of dimethylglyoxime.

^b pH was maintained at 9.5 and masking was done with 5 ml of 0.1% of thiourea.

^c After masking with 2 ml of 0.1% of NaF.

2.3. General procedure

An aliquot of a solution containing 0.1–7.0 µg of zinc was taken in a beaker containing 15 ml of doubly distilled water. To this solution, 2 ml of ammonia–ammonium acetate buffer (pH ≈ 8) and 2 ml of 0.01% TAN solution were added. The

column loaded with the adsorbent was conditioned to pH ≈ 8 by passing 5 ml of a buffer solution and then sample solution was passed through it at a flow rate of 2 ml min⁻¹. The packing in the column was aspirated strongly for a few minutes to eliminate excess of water attached to the adsorbent. The metal complex along with the adsorbent was dissolved out of the column with 5 ml of DMF. The normal and the derivative spectra were recorded against the reagent blank.

3. Results and discussion

3.1. Spectral characteristics

Derivative spectrophotometry is an analytical technique of great utility for extracting both qualitative and quantitative information from spectral curves composed of unsolved bands. The zero-order spectrum (Fig. 1) and derivative spectra (Fig. 2) of zinc were recorded against the reagent blank. The peak height of the derivative spectra depends on various parameters such as scan speed, slit width, response time and the wavelength interval over which the spectra are recorded ($\Delta\lambda$). In the present study, a scan speed of 60 nm min⁻¹; slit width 2 nm; response time 1.0 s and $\Delta\lambda = 10$ nm were selected from the preliminary study. The sensitivity in case of zero order, 1.1 A/µg ml⁻¹; first order, 0.93 (dA/dλ)/µg ml⁻¹; second order, 0.96 (d²A/dλ²)/µg ml⁻¹; third order, 1.50 (d³A/dλ³)/µg ml⁻¹ and fourth order, 2.64 (d⁴A/dλ⁴)/µg ml⁻¹. The sensitivity in the fourth order is considerably improved (≈ 2.75 times more than the second order) because peaks become much sharper in the fourth order as compared to the lower orders and thus resulting in much more increase in the magnitude of the signal (Fig. 2). It is seen that derivative leads to sharper zero order bands and gives higher signals in the resulting spectra thus reducing the spectral interferences. Since sensitivity and resolution in case of fourth order derivative are much higher as compared to normal mode and other lower derivative hence further studies were carried out using fourth derivative spectrophotometry. The peak to peak

height between λ_1 (597 nm) and λ_2 (585 nm) was measured as the analytical signal.

3.2. Reaction conditions

The reaction conditions were established using 5 μg of zinc. The retention of zinc–TAN complex was maximal and constant on ATPB naphthalene adsorbent in the pH range 6.5–9.5 (Fig. 3). It was noted that 0.5–9.0 ml of a buffer of pH \approx 8 did not effect the peak to peak height and 2 ml was recommended in the present work. The flow rate was varied from 0.5–10 ml min^{-1} . The retention of zinc complex was not affected when the flow rate did not exceed 8 ml min^{-1} and flow rate of 2 ml min^{-1} has been used for safe side. However, in case of large volume of the aqueous phase, a flow rate of 8 ml min^{-1} may be used. It was observed that zinc retention was maximal and constant when the volume of the aqueous phase did not exceed 500 ml. Thus, a 100-fold preconcentration is achieved. It was noted that peak to peak distance is maximal and constant when 0.5–7.0 ml

0.01% TAN solution was used and 2 ml of 0.01% of TAN was recommended in present study. If the other possible interfering ions are present along with zinc, 5 ml of TAN solution may be used. Various solvents were tried for dissolving zinc complex along with naphthalene. In the present work, DMF was preferred because of high solubility and stability of the metal complex in it. It was found that 2–3 ml of DMF was sufficient to dissolve the complex along with naphthalene, thus further increasing the sensitivity of the method.

3.3. Retention characteristic of ATPB naphthalene

Preliminary studies indicated that the retention capacity of adsorbent is considerably improved with the use of tetraphenylborate. It may be acting as a counter ion in the formation of neutral complexes. Tetraphenylborate forms a weakly bonded ion pair with NH_4^+ in aqueous solution and coprecipitate with microcrystalline naphthalene as follows:

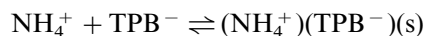


Table 3
Determination of zinc in standard alloys

Sample	Certified composition (%)	Concentration of zinc (%)	
		Certified Value	Observed value ^a
NKK No.920 (Al Alloy)	Si, 0.78; Fe, 0.72; Cu, 0.71; Mg, 0.46; Cr, 0.27; Ni, 0.29; Ti, 0.15; Sn, 0.20; Pb, 0.10; V, 0.15; Bi, 0.06; Ga, 0.05; Co, 0.10; Sb, 0.10; Ca, 0.03	0.80	0.794 \pm 0.017
NKK No.1021 (Al–Si–Cu–Zn alloy)	Si, 5.56; Fe, 0.99; Cu, 2.72; Sn, 0.10; Mg, 0.29; Cr, 0.03; Ni, 0.14; Ti, 0.04; Pb, 0.18; V, 0.007; Zr, 0.01; Bi, 0.01; Sb, 0.01, Ca, 0.004	1.76	1.745 \pm 0.029

^a Average of five determinations \pm S.D.

Table 4
Analysis of Zinc in Environmental Samples

Sample	Amount of zinc found by present method ($\mu\text{g g}^{-1}$) ^a	Amount of zinc found by AAS method ($\mu\text{g g}^{-1}$) ^a
Flyash near Indraprastra power station, New Delhi, India	126.2 \pm 3.2	126.5 \pm 3.25
Soil Near Wazirpur Industrial Area, New Delhi, India	24.71 \pm 0.4	24.80 \pm 0.5

^a Average of five determinations \pm S.D.

Table 5
Analysis of zinc in pharmaceutical sample

Sample	Certified composition	Certified value of zinc (mg)	Value by present method of zinc (mg) ^a
Fefol-Z (Smithkline Beecham Pharmaceutical, Bangalore, India)	Iron sulphate I.P. ^b = 150 mg; Zinc sulphate monohydrate = 61.8 mg (22.5 mg of elemental zinc); Folic Acid 0.5 mg	22.5	22.1 ± 0.39
Zincovit (Apex Laboratories Pvt. Ltd., Sidco Pharmaceutical Complex, Alathur, India)	Vitamin A I.P. 5000 I.U.; Vitamin D ₃ I.P.4000 I.U.; Vitamin E I.P.151 I.U.; Thiamine Mononitrate I.P.10 mg; Riboflavin I.P. 10 mg; Pyridoxine hydrochloride 2.0 mg; Cyanocobalamin 7.5 mcg; Niacinamide 50 mg; Calcium Pantothenate 10 mg; Ascorbic Acid 75 mg; Magnesium oxide 30 mg; Manganese sulphate 2.8 mg; Copper sulphate 2.0 mg; Zinc sulphate 100.0 mg; Selenium dioxide 70 mg.	100.0 (reported as zinc sulphate)	99.7 ± 1.2 (reported as zinc sulphate)

^a Average of five determinations ± S.D.

^b I.P. Indian Pharmacopoeia.

$\text{NH}_4^+ - \text{TPB}^-$ ion pair produced from TPB and ammonium acetate in aqueous solution when supported on naphthalene was unstable and partly desorbed from the surface of naphthalene in the column on passing the buffer solution. Thus, the $\text{NH}_4^+ - \text{TPB}^-$ ion pair was prepared in acetate buffer pH ≈ 9.5 . The adsorbent shows excellent adsorption characteristic towards retention of metal ions. In the present work TPB^- is selected as the counter ion because of its high purity and moderate price.

3.4. Calibration, sensitivity and detection limit

On the basis of the above developed optimum conditions, a calibration graph was constructed according to the general procedure (Fig. 4). It was linear over the concentration range 0.02–1.4 μg of zinc per ml of DMF solution. Nine replicate determination of 5 μg of zinc in 5 ml of DMF solution gave mean intensity (peak to peak height between λ_1 and λ_2) 2.660 with relative standard deviation of 1.1%. The sensitivity of the method was $[2.640(d^4A/d\lambda^4)/(\mu\text{g ml}^{-1})]$ from the slope of the calibration plot. The detection limit of the method was 9.5 ng ml^{-1} [13].

3.5. Effect of diverse ions

The effect of various salts of anions and cations on the adsorption and subsequently on the derivative spectrophotometric determination of 5 μg of zinc were studied. The tolerance limit (error < 3%) is given in Table 2. Among the salts examined, most did not interfere when present 400 times in excess. Among the metal ions studied, most did not interfere when present 15 times in excess. However, Cu(II), Fe(III), Co(II) and Ni(II) could be tolerated to higher levels by masking, Cu(II) with thiourea–sodium thiosulphate, Fe(III) with sodium fluoride or ascorbic acid and Co(II) and Ni(II) with dimethylglyoxime respectively.

4. Analytical applications

The accuracy and applicability of the proposed method was evaluated by its application on vari-

ous standard alloys, environmental and pharmaceutical samples.

4.1. Application to the analysis of standard alloys

A 0.1 g sample of each standard alloy was dissolved in 50–60 ml of 6 M HCl by heating on hot plate, then 3–5 ml of 30% hydrogen peroxide was added to it. The excess of the peroxide was decomposed by heating the solution on a hot plate. The solution was cooled, filtered if needed and diluted to 1000 ml with distilled water in a calibrated standard flask. Then, 10 ml of this solution was taken and made up to 250 ml in a volumetric flask. Then, 50–100 ml of the sample solution of standard alloys was taken and analyzed by the general procedure. The results are given in Table 3.

4.2. Application to the analysis of environmental samples

Solid environmental samples were oven dried at 200°C for 2 h. A 1.0–5.0 g of each of the sample was decomposed with 50–60 ml of 6 M HCl, then 3–5 ml of 30% hydrogen peroxide was added to it. The mixture was heated on a hot plate almost to dryness. The residue was dissolved in 10 ml of 1 M HCl filtered if needed, and the solution was made up to 1000 ml with doubly distilled water in a calibrated standard flask. The 50–100 ml of each solution was taken individually and analyzed by the general procedure after masking Fe(III) with NaF. The results are given in Table 4.

4.3. Application to the analysis of pharmaceutical samples

The tablet/capsule (one of each) was dissolved in 10 ml of 70% perchloric acid. The solution was evaporated to dryness, digested with 5 ml of 0.1 M HCl, then filtered if needed. The solution was made up to 1000 ml with doubly distilled water in a calibrated flask. Then 1.0 ml of this solution was taken and made up to 250 ml in a calibrated flask. A 50–75 ml of this solution was taken and analyzed by the general procedure after masking iron with NaF. The results are given in Table 5.

Acknowledgements

Sincere thanks of the authors are due to CSIR (India) for the award of a senior research fellowship to one of them (AB).

References

- [1] S.W.K. Morgan, Zinc and its Alloys and Compounds, Ellis Horwood, Chichester, UK, 1985, pp. 170–171.
- [2] C.J. Horng, S.R. Lin, Talanta 45 (1997) 75.
- [3] K.A. Mohamed, E. Kourashy, A. Ghany, E. Hagrassy, Anal. Methods. Instrum. 2 (1995) 190.
- [4] T. Tanaka, Y. Aoki, M. Sasaki, Nara-Ken Eisei Kenkyusho Nenpo 9 (1995) 133.
- [5] B.S. Shanbhag, Z.R. Turel, J. Radioanal. Nucl. Chem. 197 (1995) 417.
- [6] P. Wilharlitz, S. Dreew, R. Krismer, O. Bobleter, Mikrochim. Acta 125 (1997) 45.
- [7] T. Saito, K. Saito, Tohoku J. Exp. Med. 178 (1996) 11.
- [8] P.K. Prakash, M. Sai, M.R. Rao, S. Bapu, Int. Sugar J. 97 (1995) 268.
- [9] X. Yin, G. Hao, Fenxi Shiyanshi 15 (1996) 80.
- [10] N.K. Agnihotri, V.K. Singh, H.B. Singh, Talanta 45 (1997) 331.
- [11] K. Robards, P. Worsfold, Analyst 116 (1991) 549.
- [12] A.I. Vogel, Textbook of Quantitative Inorganic Analysis, Longman, London, 1989, p. 329.
- [13] J.N. Miller, Analyst 116 (1991) 3.
- [14] X. Zhu, R. Guo, Fenxi Huaxue 20 (1992) 452.
- [15] W. Yang, W. Chen, H. Chunggin, W. Wei, Talanta 39 (1992) 187.
- [16] C. Xu, Diandu Yu Huanbao 11 (1991) 31.
- [17] J. Yan, C. Wu, H. Liu, B. Wu, Fenxi Huaxue 20 (1992) 1057.
- [18] B. Mikula, Pr. Nauk. Uniw. Slask. Katowicach 1119 (1990) 32.
- [19] Y. Zhu, W. Jiang, C. Deng, G. Jin, Fenxi Huaxue 20 (1992) 1309.
- [20] F. Pan, S. Zhang, Huaxue Shiji 15 (1993) 119.
- [21] Z. Li, D. Cheng, A. Chen, Yejin Fenxi 13 (1993) 28.
- [22] X. Huang, J. Lihua, Huaxue Fence 28 (1992) 290.
- [23] A. Kumar, Indian J. Chem. Sect. A 35A (1996) 246.
- [24] Y. Zhu, G. Wu, W. Jiang, G. Jin, Fenxi Shiyanshi 14 (1995) 22.
- [25] B. Xu, Z. Lu, Fenxi Kexue Xuebao 10 (1994) 55.
- [26] S. Zou, G. Aodeng, Y. Sai, H. Liu, Neimenggu Daxue Xuebao, Ziran Kexueban 26 (1995) 567.

Spectrophotometric study on the supramolecular interactions of Nile blue sulphate with nucleic acids

Cheng Zhi Huang*, Yuan Fang Li, Dao Jian Zhang, Xiao Ping Ao

Institute of Environmental Chemistry, Southwest Normal University, Chongqing, 400715, People's Republic of China

Received 6 August 1998; received in revised form 14 December 1998; accepted 29 December 1998

Abstract

The supramolecular interaction of Nile blue sulphate (NBS) with nucleic acids was studied by investigating the characteristics of the interaction absorption spectra on the basis of the drug binding process in organic system in which small amount of drug interacting with large amount of biological macromolecules involves, and an accordingly binding model for organic dyes with large amount of macromolecules was established. At pH 7.40 and ionic strength 0.004, the *H*-aggregation of NBS occurs with increasing NBS concentration. The NBS aggregates can be bound to both calf thymus DNA and fish sperm DNA by the ratio of each nucleotide residue with a molecule of NBS if the concentration of DNAs is more than 15-fold excessive. The corresponding binding constant for the interaction of NBS with DNAs is about 10^3 order, with which thermodynamic parameters for the interactions, such as the change of free energy, enthalpy and entropy at 25°C, were calculated. It was found that the binding of NBS with thermally denatured DNA is similar to that with native yeast RNA, which indicates *H*-aggregation of NBS can be encouraged by single stranded nucleic acids. © 1999 Elsevier Science B.V. All rights reserved.

Keywords: Nucleic acids; Nile blue sulphate; Absorption spectrum

1. Introduction

The study of the supramolecular recognition of organic dyes with biological macromolecules has become an increasingly interested research field for the recent decades, especially in the field to study the interactions of functional organic dyes

with biological macromolecules in order to investigate the micro-structure of biological macromolecules and to simulate the biophysical process [1,2]. The studies on the supramolecular interacting systems, because of the formation of the complex species of the interacting subunit by virtue of the intermolecular linkage, resulting in organized structures and functions which none of the interacting subunits should have, can be studied by investigating the binding characteristics of organic dyes [3]. Depending on the molecular symmetry

* Corresponding author. Tel.: +86-23-6825-3822; fax: +86-23-6886-6796.

E-mail address: chengzhi@swnu.edu.cn (C.Z. Huang)

and the environmental conditions, the interactions of organic dyes with nucleic acids generally involve in three mechanisms: the intercalation of the organic dyes into the base pairs of the double stranded structure of nucleic acids [4]; the groove binding in which the organic dyes locate in the major or minor groove of DNA [4]; and the long range assembly of the organic dyes on the molecular surfaces of nucleic acids [5,6]. Based on those bindings, analytical methods of biological macromolecules have been established [7–13].

In the drug binding process in a practical organism system, a common observed case is the interaction of small amount of drug with large amount of biological macromolecules [14]. On this account, we try to establish interaction models of organic dyes with nucleic acids on the basis of drug binding in the presence of large amounts of biological macromolecules in the present paper. It was found that each molecule of NBS is bound to one nucleotide residue of DNA and the reaction is not affected significantly by ionic strength if the concentration of nucleic acids is 15-fold larger than that of NBS. Binding constant is about 10^3 order, which indicates that the interaction is weak and new supramolecular complexes are formed [15].

2. Experimental

2.1. Reagents

The stock solutions of DNAs and RNA were prepared by dissolving commercially purchased calf thymus DNA (ctDNA, Beitai Biochemical Co., Chinese Academy of Sciences, Beijing, China), fish sperm DNA and yeast RNA (fsDNA and yRNA, Shanghai Institute of Biochemistry, Chinese Academy of Sciences, Shanghai, China) in doubly distilled water. For DNAs, 24 h or more were needed at 4°C, with gentle shaking occasionally. The concentrations of nucleic acids were determined according to the absorbances at 260 nm after establishing that the absorbance ratio A_{260}/A_{280} was in the range 1.80–1.90 for DNAs and 1.90–2.00 for yRNA. The molarities of nucleic acids were calculated by using $\epsilon_{\text{DNA}} =$

$6600 \text{ M}^{-1} \text{ cm}^{-1}$ and $\epsilon_{\text{RNA}} = 7800 \text{ M}^{-1} \text{ cm}^{-1}$, respectively [16]. 0.003 M and 7.5×10^{-5} M working solution of nucleic acids, including ctDNA, fsDNA and yRNA, were used according to necessity.

The stock solution of Nile blue sulphate (NBS) was prepared by dissolving the crystallized product (The Third Chemical Reagent Plant of Shanghai, Shanghai, China) in water. Its working solution was 2.0×10^{-4} M.

Tris–HCl buffer solution (pH 7.40) buffer was used to control the acidity, while 0.1 and 1.0 M of NaCl solution was used to adjust the ionic strength of the aqueous solutions.

All other reagents were of analytical-reagent grade without further purification. Doubly distilled water was used throughout.

2.2. Apparatus

All absorption determination was made by using a Hitachi U-3400 Spectrophotometer (Tokyo, Japan). A pH S-10A digital pH meter (Xiaoshan Scientific Instruments Plant, Zhejiang, China) was used to measure the pH values of the solutions, and an MVS-1 vortex mixer (Beide Scientific Instrumental Ltd., Beijing, China) was used to blend the solutions in the volumetric flasks.

2.3. Method

Into a 10-ml volumetric flask were added appropriate working solution of nucleic acids and 1.0 ml of buffer solution, vortexed and then added NBS solution. The mixture at last was diluted to 10.00 ml by using doubly distilled water and mixed thoroughly. All absorption measurements were obtained against the blank treated in the same way without nucleic acids.

3. Results and discussion

3.1. Absorption characteristics

Fig. 1 shows the absorption characteristics of NBS and those for the interactions of NBS with ctDNA. At pH 7.40, NBS has its maximum ab-

sorption in the region from 640.2 to 637.6 nm. By increasing its concentration, NBS has its a maximum absorption band characterized a few nanometer's hypsochromic shift, with the appearance of an increasingly apparent absorption band at 603.4 nm. It was found that the ratio of $A_{\max}/A_{603.4}$ decreases with increasing NBS concentration (Table 1), which indicates some aggregation of NBS occur with increasing NBS concentration and the band located at 603.4 nm should be ascribed to *H*-aggregation species of NBS [17]. The change of A_{\max}/A_H can come to 0.338 with increasing NBS concentration from 0.4×10^{-5} to 2.0×10^{-5} M. In addition, the aggregation mechanism of NBS in the aqueous medium at pH 7.40 can be supported by the absorption in the region of 640.2–637.6 nm which

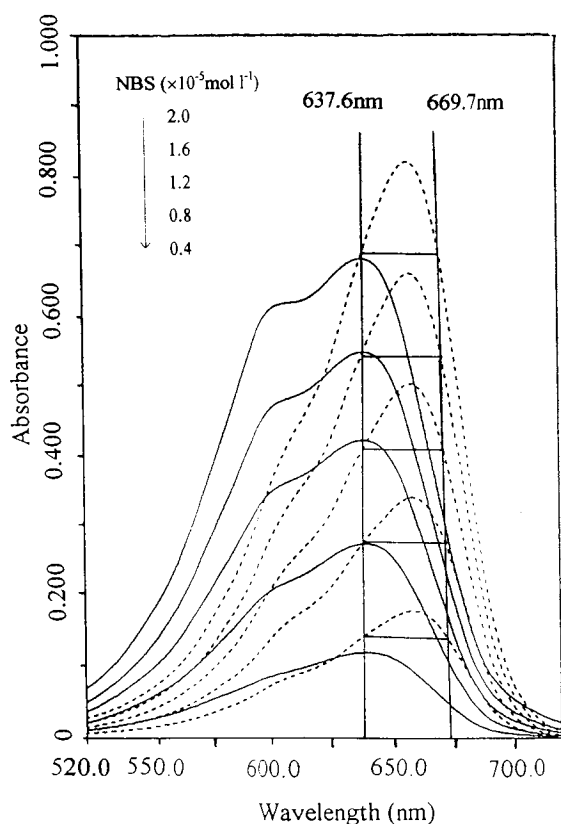


Fig. 1. Absorption spectra of NBS and NBS-ctDNA mixtures. ctDNA concentration constant at 3.0×10^{-4} mol l $^{-1}$; pH, 7.40; Ionic strength, 0.004. Solid line: NBS; dashed line: NBS-ctDNA.

does not follow Beer's law if the concentration of NBS is higher than 1.2×10^{-5} M.

In contrast to the *H*-aggregation mechanism of NBS, a new absorption band at 657.8 nm appears without any shift of the absorption band with increasing NBS concentration if the concentration of ctDNA or fsDNA is 15-fold more than that of NBS in the interacting system. One important phenomenon is that the new band at 657.8 nm shows significant hyperchromic effect compared to the band in the region from 640.2 to 637.6 nm, and no significant shoulder peak can be observed at the corresponding *H*-aggregation band of NBS. These absorption spectra indicate that the interaction of NBS with ctDNA or fsDNA results in new complex. It is worth noting that the absorption band should be ascribed to the absorption of the new complex because nucleic acids have no absorption band in the region under consideration, and their concentrations, 15-fold more than that of NBS, keep the concentration of free NBS very small, and to be neglected. Fig. 1 shows the newly formed complexes have larger absorptivity than that of NBS at their maximum absorption wavelength. It was found that the absorbance ratio at their maximum wavelength, $A_{\text{DNA-NBS}}/A_{\text{NBS}}$, decreases with increasing NBS concentration until 1.2×10^{-5} M (Table 1), and then keeps constant. This phenomenon possibly indicates that the aggregation of NBS occurs with increasing NBS concentration.

From Fig. 1, it is obvious that the absorption increases with increasing NBS concentration in the presence of 3.0×10^{-4} M ctDNA, and two equal absorption points can be obtained at 637.6 and 669.7 nm for each absorption spectrum of different concentration of NBS. The two equal absorption points, which can be obtained arbitrarily to some degree, should be carefully determined by measuring the absorbances at different concentration levels of NBS. In the same way, we can obtain the equal absorption points at 637.6 and 670.8 nm for the interaction of NBS with fsDNA. However, we can not find the equal absorption points for the interactions of NBS with native yRNA, which is similar to the interaction of NBS with thermally denatured ctDNA (Fig. 2). So we can conclude that the interaction of NBS with

Table 1

Aggregation of NBS supported by A_{\max}/A_H and $A_{\text{DNA-NBS}}^{\max}/A_{\text{NBS}}^{\max}$ ratio in aqueous medium^a

	Concentration of NBS ($\times 10^{-5}$ M)				
	0.4	0.8	1.2	1.6	2.0
<i>NBS</i>					
λ_{\max}	640.2	639.2	638.7	637.9	637.4
A_{\max}/A_H	1.443	1.279	1.200	1.158	1.105
<i>DNA-NBS</i>					
$A_{\text{DNA-NBS}}^{\max}/A_{\text{NBS}}^{\max}$	1.343	1.248	1.186	1.201	1.206

^a A_H was determined at 603.4 nm, where the absorption peak of *H*-aggregation band located. pH: 7.40; ionic strength: 0.004; Concentration of DNAs: 3.0×10^{-4} M. The change of A_{\max}/A_H with was 0.338 with increasing NBS concentration from 0.4×10^{-5} to 2.0×10^{-5} M.

nucleic acids can be used to explore the helix structure of nucleic acids.

3.2. Binding number of the interaction determined by dual wavelength

Since nucleic acids have no absorption band in the region under consideration, and the concentrations of DNA are more than 15-fold excessive, so the absorption band shown in Fig. 1 should be ascribed to the absorption of the new complex. Therefore, the absorbance at any wavelength for NBS–DNA interacting system can be expressed as:

$$A = A_{\text{NBS}} + A_{\text{NBS-DNA}} = \varepsilon[\text{NBS}] + \varepsilon'[\text{NBS-DNA}] \quad (1)$$

where ε and $[\text{NBS}]$ are the molar absorptivity and the concentration of free NBS at equilibrium, while ε' and $[\text{NBS-DNA}]$ are the molar absorptivity and the concentration of bound NBS at equilibrium, respectively. So, the absorbance difference at 637.6 and 669.7 nm, ΔA , can be described by:

$$\begin{aligned} \Delta A &= A_{637.6} - A_{669.7} \\ &= (\varepsilon'_{637.6} - \varepsilon'_{669.7})[\text{NBS-DNA}] \\ &\quad + (\varepsilon_{637.6} - \varepsilon_{669.7})[\text{NBS}] \end{aligned} \quad (2)$$

Since the equal absorption of the complex at 637.6 and 669.7 nm, namely, $\varepsilon'_{637.6} = \varepsilon'_{669.7}$, Eq. (2) can be expressed as:

$$\Delta A = (\varepsilon_{637.6} - \varepsilon_{669.7})[\text{NBS}] \quad (3)$$

namely, ΔA is in proportion to the free concentration of NBS at equilibrium. So, by determining the absorbance difference at 637.6 and 669.7 nm we can calculate the value of $[\text{NBS}]$, the free concentration of NBS in NBS–ctDNA interacting system; and by determining the absorbance difference at 637.6 and 670.8 nm we can calculate the value of $[\text{NBS}]$ in NBS–fsDNA interacting system.

Define the average binding number of NBS with each nucleotide residue of DNA, n , as:

$$n = \frac{c_{\text{NBS}} - [\text{NBS}]}{c_{\text{DNA}}} \quad (4)$$

where c_{NBS} and c_{DNA} are the total concentration of NBS and nucleic acids, respectively. Rearrange Eq. (4), we have,

$$\frac{c_{\text{NBS}}}{c_{\text{DNA}}} = n + \frac{[\text{NBS}]}{c_{\text{DNA}}} \quad (5)$$

so $c_{\text{NBS}}/c_{\text{DNA}}$ has linear relationship with $[\text{NBS}]/c_{\text{DNA}}$ by the intercept of n , the binding number of NBS with each nucleotide residue. Table 2 lists the binding number for the interactions of NBS with ctDNA and fsDNA with the dual wavelength method, from which we can conclude that each NBS molecule binds with one nucleotide residue of double-stranded DNA. So it is possible in the newly formed complex of DNA that NBS exists in monomer state, not in aggregate state.

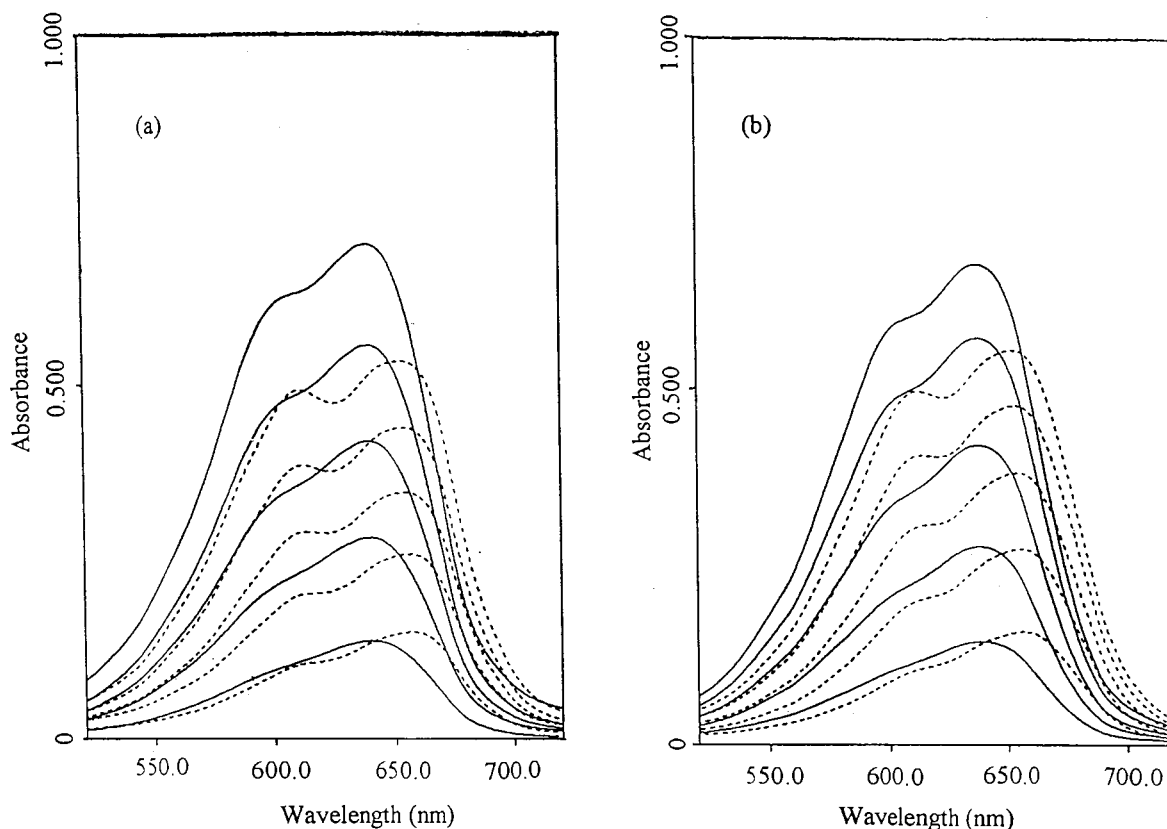


Fig. 2. Absorption spectra of the interactions of NBS with single-stranded nucleic acids. (a) NBS with thermally denatured ctDNA; (b) NBS with native yRNA. Concentrations of nucleic acids constant at $3.0 \times 10^{-4} \text{ mol l}^{-1}$; pH, 7.40; Ionic strength, 0.004. Solid line: NBS; dashed line: NBS with nucleic acids. Concentration of NBS in order of increasing at their maximum absorption wavelength ($\times 10^{-5} \text{ mol l}^{-1}$): 0.4; 0.8; 1.2; 1.6; 2.0.

3.3. Binding constant of the interaction determined by average molar absorptivity

According to the results of Table 2, each NBS molecule binds one nucleotide residue of DNA, so we can establish following equilibrium:



then the apparent binding constant, K_{app} , can be expressed as:

$$K_{\text{app}} = \frac{[\text{NBS-DNA}]}{[\text{DNA}][\text{NBS}]} \quad (6)$$

where $[\text{DNA}]$ is the equilibrium concentration of DNA. When the concentration of DNA is large enough, 15-fold excessive, for instance to keep $[\text{DNA}] = c_{\text{DNA}}$, we can express K_{app} as:

$$K_{\text{app}} = \frac{[\text{NBS-DNA}]}{c_{\text{DNA}}[\text{NBS}]} \quad (7)$$

Define average absorptivity, ε_{app} , as the ratio of the total absorbance of the solution with the total concentration of NBS, c_{NBS} , namely:

$$A = \varepsilon_{\text{app}} c_{\text{NBS}} = \varepsilon_{\text{app}} [\text{NBS-DNA}] + \varepsilon_{\text{app}} [\text{NBS}] \quad (8)$$

where the thickness of sample cell was considered as 1 cm. Since

$$A = \varepsilon [\text{NBS}] + \varepsilon' [\text{NBS-DNA}] \quad (9)$$

so Eq. (8) can be expressed as:

$$\frac{[\text{NBS-DNA}]}{[\text{NBS}]} = \frac{\varepsilon - \varepsilon_{\text{app}}}{\varepsilon_{\text{app}} - \varepsilon'} \quad (10)$$

Substitute Eq. (10) to Eq. (7), yielding

Table 2

The binding number of NBS with DNAs determined by dual wavelength method^a

Nucleic acids	Concentration of nucleic acids ($\times 10^{-6}$ mol l^{-1})	Linear regression equation	Linear correlation coefficient (r)
ctDNA	3.0	$y = 1.31 + 1.03x$	0.9998
	6.0	$y = 1.26 + 1.15x$	0.9997
fsDNA	3.0	$y = 1.08 + 1.08x$	0.9902
	6.0	$y = 1.16 + 1.10x$	0.9984

^a [NBS] was determined by using $\Delta A = -0.0066 + 17616.4$ [NBS] ($r = 0.9985$) which was obtained by the absorbance difference at 637.6 and 669.7 nm for a series of concentration of NBS. pH: 7.40; ionic strength: 0.004.

$$K_{app} = \frac{\varepsilon - \varepsilon_{app}}{c_{DNA}(\varepsilon_{app} - \varepsilon')} \quad (11)$$

Rearrange Eq. (11), we can obtain:

$$(\varepsilon - \varepsilon_{app}) = \frac{\varepsilon_{app} - \varepsilon'}{K_{app}c_{DNA}} + (\varepsilon - \varepsilon') \quad (12)$$

Namely, by plotting $(\varepsilon - \varepsilon_{app})$ against $(\varepsilon_{app} - \varepsilon')/c_{DNA}$, which can yield a slope of K_{app}^{-1} , we can calculate the binding constant. Table 3 lists the values of the binding of NBS with ctDNA and fsDNA, respectively, which were calculated according to Eq. (12) with the absorption data obtained at wavelength 637.6 nm.

3.4. Binding equilibrium as studied by absorbance change

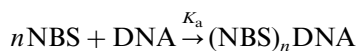
When NBS coexists with DNA, suppose NBS can interact only to one kind of separated binding site of DNA, then,

$$\Delta A = (1 - x)A_0 + xA_b \quad (13)$$

where x is the molar ratio of bound NBS with DNA to free NBS, A_0 is the absorbance at the wavelength considered without addition of DNA, and A_b is the absorbance of the NBS–DNA complex at the wavelength considered. By rearranging Eq. (13), we have,

$$\frac{[NBS]'}{c_{NBS}} = \frac{\Delta A - A_0}{A_b - A_0} \quad (14)$$

where [NBS]' is the total concentration of bound NBS with DNA. If DNA has an n separately independent binding site for NBS, then the interaction of NBS with DNA can be expressed as:



where n is the number of NBS bound to each nucleotide of DNA, and $(\text{NBS})_n\text{DNA}$ stands for the NBS–DNA complex. So we can get the binding constant of the interaction, K_a ,

$$K_a = \frac{[n(\text{NBS})_n\text{DNA}]}{[\text{NBS}][n\text{DNA}]} = \frac{[NBS]'}{[NBS][n\text{DNA}]} \quad (15)$$

According to material equilibrium principle, we have

$$[NBS] = c_{NBS} - [NBS]' \quad (16)$$

and

$$[DNA] = \frac{nc_{DNA} - [NBS]'}{n} \quad (17)$$

Substitute Eq. (15) with Eq. (16) and Eq. (17), yielding:

$$\frac{c_{NBS}}{[NBS]'} = \frac{1}{K_a(nc_{DNA} - [NBS]')} + 1 \quad (18)$$

Combine Eq. (14) with Eq. (18), yielding

$$\frac{A_0 - \Delta A}{A_0 - A_b} c_{NBS} = nc_{DNA} - \frac{A - \Delta A}{\Delta A - A_b} \frac{1}{K_a} \quad (19)$$

So by using the slope and the intercept of the chart of $(A_0 - \Delta A)c_{NBS}/(A_0 - A_b)$ against $(A_0 - \Delta A)/(\Delta A - A_b)$, we can obtain the binding number, n , and the binding constant, K_a . Table 4 lists the binding number and constant for the interactions of NBS with ctDNA and fsDNA, respectively. It can be seen that the results of Table 4 are identical with those of Tables 2 and 3.

Generally, the binding of organic dyes with biological macromolecules is depicted by using

Table 3
Binding constant of NBS with DNAs determined by average molar absorptivity^a

Nucleic acids	Linear regression equation	Linear correlation coefficient (<i>r</i>)	Binding constant (mol ⁻¹ l)
ctDNA	$y = 0.00006 + 0.00031x$	0.9999	3225.8
fsDNA	$y = 0.000015 + 0.00030x$	0.9999	3333.3

^a All data were obtained at wavelength 637.6 nm at 25°C. pH: 7.40; ionic strength: 0.004; Concentrations of DNAs: 3.0×10^{-4} mol l⁻¹.

Scatchard plot [17]. It is obvious that the binding study according to Eq. (19) is different from Scatchard analysis. At first, the data treatment according Eq. (19) is very simple, it does not involve complicate calculation. In addition, Scatchard analysis treats the reaction as a true combination of the ligand with specific sites on the macromolecules, but the reality is not often the case [17].

3.5. Effects of the state of nucleic acids on the equilibrium

Because of the negative backbone of nucleic acids which originates from the phosphate ion, the stranded structure of nucleic acids is very sensitive to the change of ionic strength. Generally, the controller of ionic strength of the solution, Na⁺, for instance, acts as a counter ion to reduce the unwinding tendency due to electrostatic repulsion between the negatively charged phosphate groups on adjacent nucleotides, and lead stability of the double stranded structure of the DNAs if the ionic strength is higher than 0.01 [3–5]. In this report, however, the concentration of nucleic acids is too excessive, the sensitive effect of ionic strength seems disappear if the ionic strength in the solution is lower than 0.02. Table 4 lists the binding number and binding constant of NBS with ctDNA and fsDNA, from which it can be seen that if the ionic strength is higher than 0.02, the binding number and binding constant decrease.

One important phenomenon is the similarity between the binding of NBS with single-stranded DNA and that with native RNA. Fig. 2 shows the binding of NBS with thermally denatured ctDNA and with native RNA, respectively. It can be seen

that the interactions of NBS with thermally denatured DNA and native RNA, namely, single-stranded nucleic acids, produces two absorption bands around 610 and 655 nm, showing hypochromic effect and bathochromic shift compared with the characteristic absorption bands of NBS itself. The band located at 610 nm, corresponding the *H*-aggregation band of NBS itself, scarcely shows wavelength shift with increasing the concentration of NBS; the band around 655 nm, however, having larger absorptivity than that of the *H*-aggregation band. The absorbance ratio for the two bands, A_{\max}/A_H , decreases with increasing NBS concentration from 0.4×10^{-5} to 2.0×10^{-5} M, with the A_{\max}/A_H change from 0.365 to 0.414 for thermally denatured ctDNA–NBS binding and yRNA–NBS binding, respectively (Table 5). The A_{\max}/A_H ratio change, which greatly depends on increasing NBS concentration indicates that the interactions of NBS with single stranded nucleic acids result in aggregation species of NBS complex [3]. As Table 5 can be seen that the change of absorbance ratio is obviously larger than that of NBS itself in Table 1, that possibly indicates the aggregation of NBS in the presence of single stranded nucleic acids occur. In other words, *H*-aggregation of NBS can be encouraged by single stranded nucleic acids.

3.6. Thermodynamic parameters of the interactions of NBS with DNAs

In the binding system of supramolecular interactions, Gibbs free energy change, ΔG_{cpl}^0 , is a very important parameters, which reflects the binding degree and the stability of the newly formed supramolecular complex. ΔG_{cpl}^0 can be calculated according following equation [18]:

Table 4
Binding number and constant of NBS with nucleic acids determined by the change of absorbance^a

Nucleic acids	Ionic strength	Linear regression equation	Linear correlation coefficient (<i>r</i>)	Binding number	Binding constant (mol ⁻¹ l)
ctDNA	0.004	$y = 0.00029 + 0.00031x$	0.9967	0.97	3225.8
fsDNA	0.004	$y = 0.00031 + 0.00029x$	0.9991	1.02	3448.3
ctDNA	0.010	$y = 0.00030 + 0.00030x$	0.9971	1.00	3333.3
ctDNA	0.020	$y = 0.00028 + 0.00031x$	0.9981	0.93	3225.8
ctDNA	0.030	$y = 0.00025 + 0.00035x$	0.9979	0.83	2857.1
ctDNA	0.040	$y = 0.00020 + 0.00042x$	0.9991	0.67	2380.1

^a All data were obtained at 25°C at the wavelength 657.8 nm. pH: 7.40; Concentrations of DNAs 3.0×10^{-4} mol l⁻¹.

$$\Delta G_{\text{cpl}}^0 = -RT \ln K \quad (20)$$

where the R is molar gas constant with the value $8.31 \text{ J K}^{-1} \text{ mol}^{-1}$, T the absolute temperature, K the binding constant. The calculated ΔG_{cpl}^0 is related to the change of Helmholtz free energy, ΔH_{cpl}^0 , and entropy change, ΔS_{cpl}^0 , of the supramolecular interactions [18]:

$$\Delta G_{\text{cpl}}^0 = \Delta H_{\text{cpl}}^0 - T\Delta S_{\text{cpl}}^0 \quad (21)$$

Since the study was constructed at constant temperature and pressure, ΔH_{cpl}^0 approximates to zero. So we can calculate the values of ΔS_{cpl}^0 for the interactions of NBS with DNAs. Table 6 lists the thermodynamic parameters for the supramolecular interactions of NBS with DNAs. From Table 6 it can be seen that the interaction is a spontaneous process characterized entropy increase.

4. Conclusion

At near physiological acidity and ionic strength 0.004, the H -aggregation of NBS resulting from increasing NBS concentration was characterized, and the aggregation band locates at 603.4 nm. It was found that the H -aggregation of NBS was

encouraged by single stranded nucleic acids. Considering the drug binding process in organic system in which small amount of drug interacting with large amount of biological macromolecules involves, an binding model for organic dyes with large amount of macromolecules was established, by which the interaction of NBS with double stranded nucleic acids were investigated. It was found that the interaction of NBS with double stranded nucleic acids occurs by the ratio of each nucleotide residue of DNAs binding one NBS molecule with the binding constant at 10^{-3} order. Calculation of the thermodynamic parameters of the interaction, including Gibbs free energy change, ΔG_{cpl}^0 , Helmholtz free energy, ΔH_{cpl}^0 , and entropy change, ΔS_{cpl}^0 , shows supramolecular complexes formed, in which NBS exists in monomer.

Acknowledgements

This research gets the supports of the National Natural Science Foundation of China (NSFC No.: 29875019) and the Municipal Science Foundation of Chongqing for Young and Middle Scientists(No.: 97-4729).

Table 5
Aggregation of NBS in the presence of single-stranded nucleic acids^a

Concentration of NBS ($\times 10^{-5}$ M)	0.4	0.8	1.2	1.6	2.0	
ctDNA–NBS ^b	λ_{\max} (nm)	657.6	656.8	654.6	654.1	652.3
	A_{\max}/A_H	1.448	1.287	1.194	1.135	1.085
yRNA–NBS ^c	λ_{\max} (nm)	657.3	657.4	654.2	654.1	652.3
	A_{\max}/A_H	1.536	1.376	1.258	1.180	1.117

^a pH: 7.40; ionic strength: 0.004; Concentration of nucleic acids: 3.0×10^{-4} M. The change of A_{\max}/A_H was 0.365 and 0.414 for thermally denatured ctDNA–NBS binding and native yRNA–NBS binding, respectively, with increasing NBS concentration from 0.4×10^{-5} to 2.0×10^{-5} M.

^b Thermally denatured ctDNA.

^c Native yRNA.

Table 6
Thermodynamic parameters of the interactions of ST with nucleic acids^a

Thermodynamic parameters	ΔG_{cpl}^0 (kJ mol ⁻¹)	ΔH_{cpl}^0 (kJ mol ⁻¹)	ΔS_{cpl}^0 (kJ mol ⁻¹ ·K)
ctDNA	-20.006	0	26.806
fsDNA	-20.172	0	28.655

^a $T = 298$ K; pH: 7.40; ionic strength: 0.004.

References

- [1] Y.J. Wei, S.Y. Tong, K.A. Li, Acta Chim. Sinica 53 (1995) 83.
- [2] C.Z. Huang, Y.F. Li, N. Li, K.A. Li, S.Y. Tong, Bull. Chem. Soc. Jpn. 71 (1998) 1791.
- [3] C.Z. Huang, Y.F. Li, X.D. Liu, Chemistry (Chin. Chem. Soc. Taipei) 25 (1998) 25.
- [4] R.F. Pasternack, E.J. Gibbs, J.J. Villafranca, Biochemistry 22 (1983) 2405.
- [5] C.Z. Huang, K.A. Li, S.Y. Tong, Bull. Chem. Soc. Jpn. 70 (1997) 1843.
- [6] C.Z. Huang, K.A. Li, S.Y. Tong, Chem. J. Chin. Univ. 18 (1997) 525.
- [7] C.Z. Huang, K.A. Li, S.Y. Tong, Anal. Chem. 68 (1996) 2259.
- [8] C.Z. Huang, K.A. Li, S.Y. Tong, Anal. Chem. 69 (1997) 514.
- [9] C.Z. Huang, K.A. Li, S.Y. Tong, Anal. Chem. Acta 345 (1997) 235.
- [10] C.Z. Huang, Y.F. Li, H.Q. Luo, X.H. Huang, Anal. Lett. 31 (1998) 1149.
- [11] J. Rao, W.R. Otto, Anal. Biochem. 207 (1992) 186.
- [12] J.T. Petty, M.E. Johnson, P.M. Goodwin, J.C. Martin, J.H. Jett, R.A. Keller, Anal. Chem. 67 (1995) 1775.
- [13] B.B. Haab, R.A. Mathies, Anal. Chem. 67 (1995) 3253.
- [14] S.E. Osborne, A.D. Ellington, Chem. Rev. 97 (1997) 349.
- [15] K.L. Yin, R.J. Xue, Y.Z. Xue, Chem. Prog. 9 (1997) 337.
- [16] Z.Y. Chen, J. Liu, D. Luo, Biochemistry Experiment, China University Press of Science and Technology, Hefei, China, 1994, p. 111.
- [17] O. Ohno, Y. Kaizu, H. Kobayashi, J. Chem. Phys. 99 (1993) 4128.
- [18] Y.J. wei, K.A. Li, S.Y. Tong, Talanta 43 (1996) 1.

Asynchronous merging zones system: spectrophotometric determination of Fe(II) and Fe(III) in pharmaceutical products

André Fernando Oliveira, Joaquim A. Nóbrega, Orlando Fatibello-Filho *

Departamento de Química, Grupo de Química Analítica, Centro de Ciências Exatas e de Tecnologia, Universidade Federal de São Carlos, Caixa Postal 676, CEP 13.560-970, São Carlos, SP, Brazil

Received 2 September 1998; received in revised form 15 December 1998; accepted 29 December 1998

Abstract

An asynchronous merging zones was proposed with simultaneous introduction of the sample and of the modifier reagent, ascorbic acid in the studied case, for sequential determination of Fe(II) and Fe(III) in pharmaceutical products. The sample and reagent attained a merging point at different times owing to the use of a delay reactor in the reagent channel. By inserting a large sample and controlling the dispersion in the flow system, Fe(II) and Fe(III) were sequentially measured in the front and in the rear of the sample zone, respectively. The results obtained for Fe redox speciation in pharmaceutical products are in agreement at a 95% confidence level with those obtained with a manual spectrophotometric procedure. The analytical frequency with the proposed flow analysis system was 54 samples h^{-1} , i.e. 108 determinations h^{-1} . © 1999 Elsevier Science B.V. All rights reserved.

Keywords: Sequential determination; Asynchronous merging zones; Redox iron speciation

1. Introduction

To increase the versatility of the flow analysis systems several strategies have been proposed for simultaneous or sequential determinations. These systems were based on diverse schemes, such as the use of various sample loops, flow splitting, combination of various detectors and multielementar detection [1].

The serial insertion of sample loops separated by a large coil (1400-cm) was proposed by Fernandez et al. [2] and the parallel insertion of a sample loop with different residence times was evaluated by Kozuka et al. [3]. In both cases the analytes had distinct reaction rates.

Cosano et al. [4] proposed an asymmetric merging zones system with parallel injection of the sample and Nessler's reagent. When the injector is in the sampling state, a large volume of sample is inserted in a loop composed by three stages, i.e. a first sample region, an enzymatic column containing urease and a second sample region positioned

* Corresponding author. Fax: +55-16-2608350.

E-mail address: bello@dq.ufscar.br (O. Fatibello-Filho)

in this sequence. One fraction of the sample aspirated flowed through the enzymatic column twice; the other fraction of the sample did not flow through the column. With this strategy it was possible to determine ammonia and urea in the front and in the rear of the sample zone, respectively. This is a creative strategy, but it is not a general one and obviously different analytes require distinct enzymatic columns. The asymmetric merging zones is an extension of the merging zone concept proposed by Bergamin's group in the end of the 1970s [5–7].

Alonso et al. [8] proposed a sandwich technique for multicomponent determination. In this paper, a reducing reagent (ascorbic acid) was introduced in series and it mixed partially with a large sample zone. In spite of the ingenious flow diagram, the potential disadvantages are the use of a single line system and the possibility of carryover between the reducing reagent presented in the rear of the sample zone and the front of the next injected sample.

Yamane and Goto [9] also determined Fe total and Fe(II) with 1,10-phenanthroline. In this case, a merging zones system was designed to insert in a parallel and synchronous way a large sample loop and an acid ascorbic loop. In the merging zone, occurred a partial mixing between the front of the sample zone and the reagent. The system must be designed to avoid the penetration of the reducing solution in the rear part of the sample zone, in which only Fe(II) should react forming the ferroin complex.

The zone penetration approach was also exploited by the Center for Process Analytical Chemistry group for multicomponent analysis. These authors demonstrated the chemical possibilities coming from the production and interpretation of complex chemical gradients in flow systems [10].

More recently Fe(II) and Fe(III) were sequentially determined by inserting a confluent reagent point in the sample loop [11]. The best characteristic of this flow system is the possibility to create different regions in the sample zone by confluent introduction of the reagent.

In this work it is proposed an asynchronous merging zones system in which a large sample

volume and a smaller reagent volume, called as modifier reagent, since it acts chemically to modify part of the sample zone, are simultaneously introduced, but they attain a merging point at different times owing to the use of a delay reactor in the reagent channel. By inserting a large sample volume and by proper control of the dispersion in the flow system, two analytes can be sequentially determined in the front and in the rear of the sample zone.

The synchronous system proposed by Yamane and Goto [9] and the asynchronous system here proposed are similar but they differ in the carry-over effect that can occur in the sample zone. As depicted on Fig. 1 the introduction of the modifier reagent in the front of the sample zone can imply in the dispersion of the modifier reagent zone inside the rear of the sample zone (intra-sample

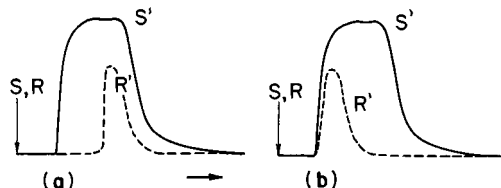


Fig. 1. The letters S and R represent the introduction point (sample and reagent). The letters S' and R' represent the sample zone profile and the reagent zone profile, respectively. (a) Asynchronous merging zones system: reagent zone is formed in the rear of the sample zone (system proposed here), (b) Synchronous merging zones system: reagent zone is formed in the front of the sample zone.

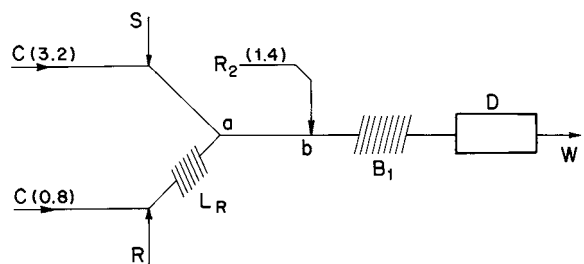


Fig. 2. Flow diagram of the asynchronous merging zones system. The capital letters C, S, R, and R₂ represent the carrier (water), sample loop (400 cm, 2000 µl), ascorbic acid loop (10 cm, 50 µl), and 1,10-phenanthroline solution, respectively. L_R, B₁, and D are a 75 cm delay reactor, a 100 cm tubular reactor, and a spectrophotometric detector ($\lambda = 520$ nm), respectively. Confluence points are represented as a and b. Numbers in parentheses are the flow rates in ml min⁻¹. W-waste.

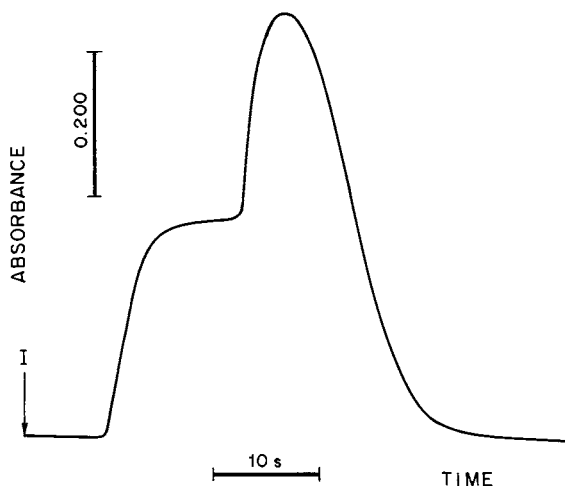


Fig. 3. Transient signal showing two well-resolved signals in the same sample zone, the first one a plateau corresponding to Fe(II) and the second one a peak corresponding to (Fe(II) + Fe(III)).

carryover), which is undesirable. On the other hand, when the modifier reagent is inserted in the rear of the sample zone as proposed, it disperses in the carrier and its carryover in the next injected sample can be easily avoided. The present proposal can be readily implemented for the determination of two analytes in two distinct points of the sample zone taking full advantage of the dispersion characteristics and of the chemistry involved. The feasibility of this proposal was showed using a model system for determination of total Fe and Fe(II) in pharmaceutical products.

2. Experimental

2.1. Apparatus

An eight channel Ismatec (Zurich, Switzerland) model 7618-40 peristaltic pump supplied with Tygon pump tubing was used for propulsion of fluids. The manifold was constructed with polyethylene tubing (0.8 mm i.d.). Absorbance was measured at 520 nm with a Micronal (São Paulo, Brazil) model B342II spectrophotometer using a Hellma flow-through cell (optical path 1.0 cm) and connected to a Cole Parmer (Niles, IL,

USA) model Chicago II three channel strip-chart recorder. Samples and/or reference solutions injection were performed using a temporized proportional Micronal (São Paulo, Brazil) model B352 commutator. Reference solutions containing Fe(II) and Fe(III) were prepared using a Schott Geräte model T80/20 and a Braud Brinkmann model Digital Buret II burettes.

2.2. Reagents and solutions

All reagents used were of analytical-reagent grade and all solutions were prepared with water from a Millipore (Bedford, MA, USA) Milli-Q system (model UV Plus Ultra-low Organics water).

Reference solutions containing Fe(II) and Fe(III) were made by diluting stock solutions (200 mg l^{-1}). The Fe(II) stock solution were prepared from $\text{Fe}(\text{NH}_4)_2(\text{SO}_4)_2 \cdot 6\text{H}_2\text{O}$ (Mohr's salt) and the Fe(III) stock solution was prepared with this same salt and adding $0.02 \text{ mol l}^{-1} \text{ KMnO}_4$ solution, until a persistent pink colour was obtained, before diluting to 1000 ml with 0.014 mol l^{-1} nitric acid.

The chromogenic reagent was prepared dissolving 0.500 g of 1,10-phenantroline in 50 ml of 2.0 mol l^{-1} acetate buffer (pH 5.5) and diluting to 500 ml with deionized water. The modifier reagent ($1\% \text{ w/v}$ ascorbic acid solution) was daily prepared by dissolving ascorbic acid (Merck) in water.

The manual thiocyanate procedure for the determination of Fe(III) used was identical to that recommended by Marczenko [12].

Pharmaceutical products samples (Combiron, Ferrous sulfate solution) were prepared by dilution of commercial liquid samples in 0.014 mol l^{-1} nitric acid solution.

2.3. Analytical procedure

The diagram of the flow analysis system used is shown in Fig. 2. Samples containing Fe(II) and Fe(III) and the modifier reagent (ascorbic acid) were introduced simultaneously by a proportional comutator in each carrier. The reagent zone flowed through a delay coil and merged with the rear of the sample zone in the point *a*, reducing

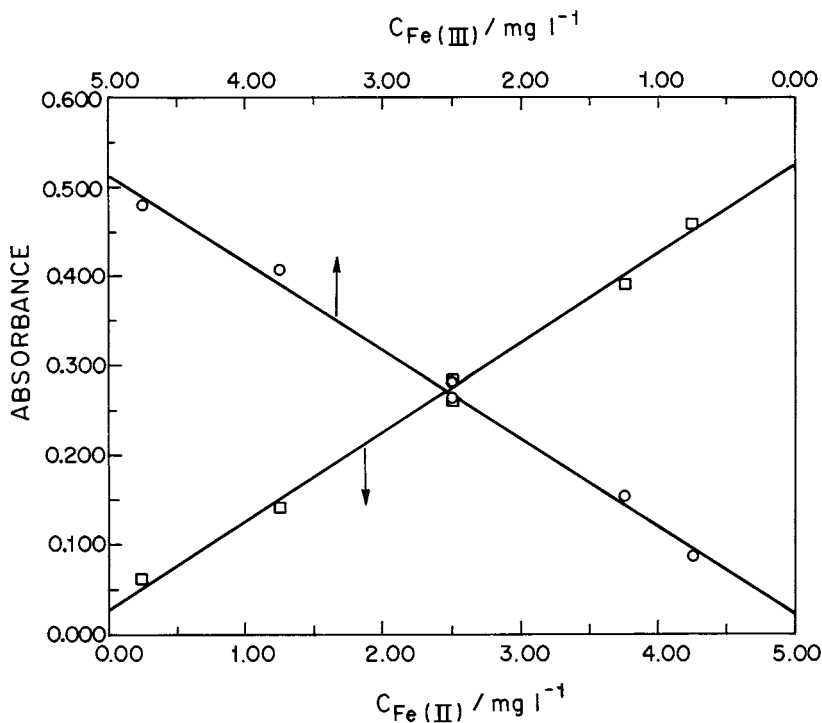


Fig. 4. Experimental demonstration of the additivity condition: analytical curves for Fe(II) □ and Fe(III) ○.

Fe(III) to Fe(II) in this zone. At point *b*, the 1,10-phenanthroline solution is inserted by confluence in the sample zone. The reducing and colorimetric reactions developed in the B_1 coil and the absorbance of the formed ferroin was measured at 520 nm.

3. Results and discussion

A flow analysis system with asynchronous merging zones was projected to attain two main objectives: the sensitivity for Fe(II) in the front and in the rear of the sample zone should be the same, and the sensitivity reached for Fe(III) in the rear of the sample zone should be equivalent to that obtained for Fe(II). These conditions were called as additive principle and the adoption of it implied in a simplification of the analytical procedure, since the analytical curve obtained for one of the analytes can be used for the determination of both and the difference between the absorbance

signal related to Fe total (the rear of the sample zone) and the absorbance signal related to Fe(II) (the front of the sample zone) is directly proportional to the concentration of Fe(III).

In the Fig. 3 is shown a transient signal generated by inserting 2000 μl of reference solution containing 2.5 mg l^{-1} Fe(II) plus 2.5 mg l^{-1} Fe(III) and 50 μl of ascorbic acid (1% w/v) employing the flow diagram depicted on Fig. 2. It can be seen a clear separation between the first plateau signal formed by the ferroin complex formed from Fe(II) and the second peak generated by the ferroin complex formed from total Fe, since the rear of the sample zone was modified by action of the modifier agent.

The effect of each carrier flow rate, i.e. the sample and the reagent carrier, on the formation of the sample zone is pronounced. The system was adjusted to guarantee the asynchronous character and the volume of each loop was chosen to control the carryover between sample and reagent in the sample zone. The best condition to form two

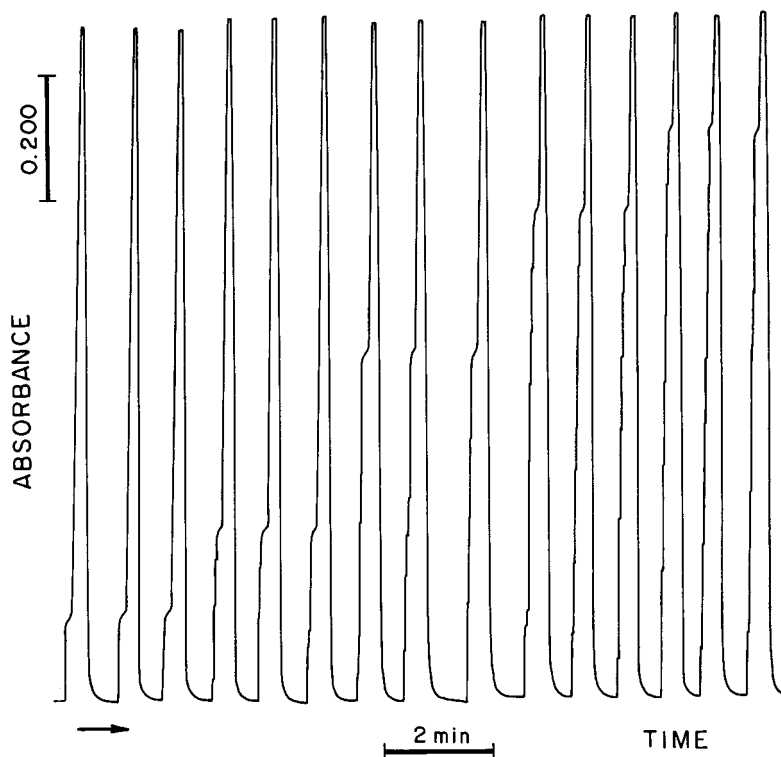


Fig. 5. Triplicate transient signals for reference solutions containing each one 5.0 mg l^{-1} (Fe(II)+Fe(III)) generated by combination of different concentrations of Fe(II) and Fe(III).

well-resolved signals in the same sample zone was attained using flow rates of 3.2 and 0.8 ml min^{-1} for sample and reagent, respectively (Fig. 3).

To reach conditions compatible with the additive principle, it is suitable to use a sample volume which led to two distinct regions of signal maxima and this was attained using a sample loop larger than $1000 \mu\text{l}$. Unless when mentioned, a $2000 \mu\text{l}$ sample loop was used in all experiments. The establishment of two distinct regions of signal maxima is not essential when using a very reproducible equipment for propulsion of solutions and a digital system for data acquisition.

The effect of the volume of ascorbic acid inserted in the system was evaluated and it was observed that with volumes smaller than $250 \mu\text{l}$ there is no carryover between the rear of the sample zone containing the modifier reagent and the front of the next injected sample.

Other aspect relevant is to establish suitable experimental conditions to reach the additive condition. When the delay coil (L_R) varied from 55 to 75 cm , the additive condition was obeyed and the analytical curves for Fe(II) and for Fe(III) presented the same sensitivity. In the Fig. 4 are showed analytical curves prepared from solutions containing 5.0 mg l^{-1} of total Fe, but with different concentrations of Fe(II) and Fe(III) in each. The transient signals are showed in the Fig. 5. The relative standard deviation for total Fe concentration determined by summation of the Fe(II) and Fe(III) was 0.74% ($n = 15$).

The repeatabilities obtained for eleven consecutive injections of a reference solution containing 2.5 mg l^{-1} Fe(II) and 2.5 mg l^{-1} Fe(III) was 1.81 and 1.30% , respectively ($n = 11$). The mean concentrations of Fe(II) and Fe(III) did not differ at a 95% confidence level.

Table 1

Determination of Fe(II) and Fe(III) using the proposed asynchronous merging zones system and a manual procedure^a

Sample	Proposed procedure (g l ⁻¹)		Comparative procedure (g l ⁻¹)	
	Fe(II)	Fe(III)	Fe(II)	Fe(III)
A	7.34 ± 0.03	1.79 ± 0.08	7.25 ± 0.06	1.83 ± 0.07
B	6.92 ± 0.03	2.07 ± 0.07	6.98 ± 0.04	2.14 ± 0.07
C	7.12 ± 0.05	2.52 ± 0.08	7.16 ± 0.05	2.68 ± 0.08

^a Mean values and S.D. (*n* = 3)

To evaluate the effect of the Fe(II) and Fe(III) concentration ratio an experiment was carried out maintaining constant the Fe(II) concentration in 0.25 mg l⁻¹ and varying the Fe(III) concentrations from 1.0 to 7.5 mg l⁻¹. When the Fe(III) concentration was 5.0 mg l⁻¹, i.e. 20-fold higher than Fe(II) concentration, the intra-sample carry-over was 10%.

The analytical frequency attained with the proposed flow analysis system was 54 samples h⁻¹, i.e. 108 determinations h⁻¹. The flow analysis method was applied to the determination of Fe(II) and Fe(III) in pharmaceutical products used as a supplement of iron and supposed to contain only Fe(II) since this is the form of Fe easily absorbed in our body. The results are showed in Table 1 and it can be seen that all samples contained an appreciable amount of Fe(III) probably formed by oxidation after starting using the product or after expiration of the shelf lifetime, since some samples were collected from old flasks. There is no difference at a 95% confidence level between the results obtained with the proposed method and those obtained with a manual spectrophotometric procedure.

The asynchronous system is feasible and it could be adopted for others sequential determinations since the chemistry involved is properly adjusted. Its application to redox speciation, as demonstrated for Fe(II) and Fe(III) determination, and blank corrections is straightforward. The analytical frequency attained with this system was better than that reached with the reagent introduction in the sample loop [11], without

causing adverse effects on sample and reagent dispersion.

Acknowledgements

Financial support from FAPESP, PADCT/CNPq, and also the scholarship granted by CNPq to AFO is gratefully acknowledged. O.F.F. and J.A.N. are grateful to CNPq by researchships.

References

- [1] V. Kuban, Crit. Rev. Anal. Chem. 23 (1992) 15.
- [2] A. Fernandez, M.D. Luque de Castro, M. Valcárcel, Analyst 113 (1987) 803.
- [3] S. Kozuka, K. Saito, K. Oguma, R. Kuroda, Analyst 115 (1990) 431.
- [4] J.S. Cosano, J.L. Calle, J.L. Pinillos, P. Linares, M.D. Luque de Castro, M. Valcarcel, Anal. Chim. Acta 221 (1989) 173.
- [5] H. Bergamin Filho, E.A.G. Zagatto, F.J. Krug, B.F. Reis, Anal. Chim. Acta 101 (1978) 17.
- [6] E.A.G. Zagatto, F.J. Krug, H. Bergamin Filho, S.S. Jorgensen, B.F. Reis, Anal. Chim. Acta 104 (1979) 279.
- [7] B.F. Reis, H. Bergamin Filho, E.A.G. Zagatto, F.J. Krug, Anal. Chim. Acta 107 (1979) 309.
- [8] J. Alonso, J. Bartroli, M. Del Valle, R. Barber, Anal. Chim. Acta 219 (1989) 345.
- [9] T. Yamane, E. Goto, Anal. Sci. 5 (1989) 221.
- [10] D.A. Whitman, M.B. Seasholtz, G.D. Christian, J. Ruzicka, B.R. Kowalski, Anal. Chem. 63 (1991) 775.
- [11] A.F. Oliveira, O. Fatibello-Filho, M.C.T. Diniz, J.A. Nóbrega, Anal. Chim. Acta 366 (1998) 281.
- [12] Z. Marczenko, Separation and Spectrophotometric Determination of Elements, 2nd edn, Ellis-Horwood, Chichester, 1986, p. 667.

Studies on 1:12 phosphomolybdic heteropoly anion film modified carbon paste electrode

Lu Guanghan *, Wu Xiaogang, Lan Yanhua, Yao Shenlai

Department of Chemistry, Central China Normal University, 430079 Wuhan, People's Republic of China

Received 15 April 1998; received in revised form 30 December 1998; accepted 5 January 1999

Abstract

A 1:12 phosphomolybdic anion film modified carbon paste electrode (PMo_{12} electrode) is prepared by electrochemical deposition and its application is studied by cyclic voltammetry. The film modified electrode can adsorb PMo_{12} selectively and thus be used for the determination of trace phosphorus. In a solution containing $2 \mu\text{g ml}^{-1}$ phosphorus, the relative standard deviation is 4.69% ($n = 4$), the peak height also varies linearly with the concentration of phosphorus over the range $0.4\text{--}25 \mu\text{g ml}^{-1}$, and the detection limit is $0.04 \mu\text{g ml}^{-1}$. The method is convenient and rapid. It has been used for the determination of inorganic phosphorus in phytic acid directly with satisfactory results. © 1999 Elsevier Science B.V. All rights reserved.

Keywords: Chemically modified electrode; Phosphomolybdic acid; Phosphorus; Phytic acid

1. Introduction

In recent years, more and more attention has been introduced to the electrochemical study of isopoly and heteropoly oxometalates [1–10]. Up to now, modifications with isopoly and heteropoly acids has been restricted to glassy carbon electrode chiefly and carbon paste electrode is rarely discussed. In this report, a 1:12 phosphomolybdic anion (PMo_{12}) electrode is prepared by cycling the potential at 100 mV s^{-1} between 0.6 and 0.1 V in $0.5 \text{ mol l}^{-1} \text{ H}_2\text{SO}_4$ containing $10 \mu\text{g ml}^{-1}$ phosphorus, $3 \times 10^{-3} \text{ mol l}^{-1}$ paramolybdate and 16%

(V/V) acetone. The electrode is applied to the determination of inorganic phosphorus in phytic acid without any pretreatment. The procedure is easy and convenient to operate, and the results are in accordance with those obtained by the comparison method. The detection limit is $0.04 \mu\text{g ml}^{-1}$ and most anions and cations do not interfere. The method is also very promising because it supplies a voltammetric determination for the elements which are difficult to determine by voltammetry.

2. Experimental

2.1. Apparatus

Electrochemical experiments were performed on

* Corresponding author. Fax: +86-27-87876070.
E-mail address: lugh@163.net (L. Guanghan)

an XJP-821B neopolarography (Jiansu Electro-analysis Instrumental Factory, China) equipped with a Model 3033 X-Y recorder (Sichuan, China). A three electrode system was used. The reference electrode was a saturated calomel electrode (SCE), the counter electrode was a platinum sheet and the working electrode was a PMo_{12} electrode. The electrolytic cell was a 50 ml beaker. A U-2000 double beam spectrophotometry (Japan) was used for method comparison.

2.2. Reagents

Unless otherwise specified, all solutions were prepared from analytical-reagent chemicals and triply distilled water.

A 1 mg ml^{-1} stock phosphorus solution was prepared from KH_2PO_4 which had been dried at $105 \sim 110^\circ\text{C}$ for 2 h. Standard solutions were obtained by diluting the stock solution with water.

Mixed solution was prepared by adding 139 ml concentrated sulfuric acid into 300 ml water, dissolving 18.5 g $(\text{NH}_4)_6\text{Mo}_7\text{O}_{24}\cdot 4\text{H}_2\text{O}$ after cool, and then diluting to 1000 ml with water.

Electrode modification solution was composed of $10 \text{ } \mu\text{g ml}^{-1}$ phosphorus, $3 \times 10^{-3} \text{ mol l}^{-1}$ paramolybdate, 0.5 mol l^{-1} sulfuric acid and 16% (V/V) acetone. It should be allowed to stand for about 5 min before use.

2.3. Preparation of PMo_{12} electrode

Carbon paste that contained 5 g graphite powder (spectroscopically pure) and 2 ml paraffin oil (chemically pure) was put into a glass tube (4.0 mm i.d) and a copper rod was inserted through the opposite end to establish electrical contact. The carbon paste surface was smoothed on transparent paper until the surface had a shiny appearance. Thus, a carbon paste electrode was obtained and used as the working electrode. After seven scans between 0.6 and 0.1 V at a scan rate of 100 mV s^{-1} in the modification solution, the working electrode was taken out and washed with water to remove excess PMo_{12} . Thus, the PMo_{12} electrode was prepared (Fig. 1).

2.4. Procedure

To the standard or sample solution ($0.4\text{--}25 \text{ } \mu\text{g ml}^{-1}$ phosphorus), added 10.00 ml mixed solution and 8.0 ml acetone. Diluted to 50 ml and mixed thoroughly. The solution was allowed to stand for 5 min. The measurements were carried out after an open circuit adsorption for about 30 s while the solution was gently stirred. After a rest period of 15 s, the cyclic voltammogram was recorded between 0.6 and 0.1 V at a scan rate of 100 mV s^{-1} (Fig. 2). After each determination, the PMo_{12} electrode needed rinsing with water. $i_{p,c1}$ ($E_{p,c1} = 0.33 \text{ V vs SCE}$) was used for quantitative analysis.

3. Results and discussion

3.1. Process of electrode modification

A comparison of modified gold, glassy carbon and carbon paste electrodes showed that the sensitivity of modified carbon paste electrode was the highest. Therefore, carbon paste electrode was selected as the matrix.

The acidity of the modification solution had a considerable effect on the formation of PMo_{12} . In the experiments, 0.5 mol l^{-1} sulfuric acid was

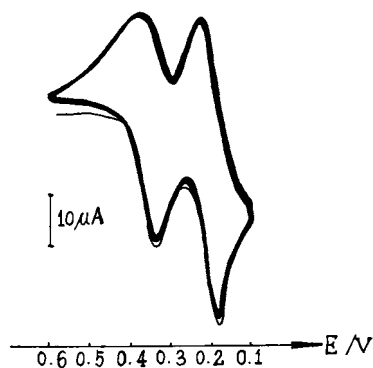


Fig. 1. Repetitive cyclic voltammograms of the process of electrode modification. $10 \text{ } \mu\text{g ml}^{-1}$ phosphorus + $3 \times 10^{-3} \text{ mol l}^{-1}$ paramolybdate + 0.5 mol l^{-1} sulfuric acid + 16% (V/V) acetone.

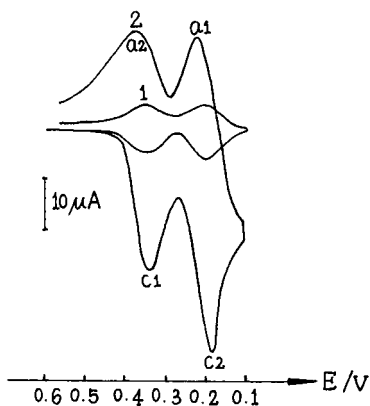


Fig. 2. Cyclic voltammograms of 1:12 phosphomolybdic anion (PMo_{12}) electrode in solutions to be analysed. (1) 3×10^{-3} mol l^{-1} paramolybdate + 0.5 mol l^{-1} sulfuric acid + 16% (V/V) acetone. (2) $10 \mu\text{g ml}^{-1}$ phosphorus + 3×10^{-3} mol l^{-1} paramolybdate + 0.5 mol l^{-1} sulfuric acid + 16% (V/V) acetone.

chosen because PMo_{12} could be completely formed and well-defined peaks could be obtained at this acidity.

Acetone can be used as a spiked and stabilized reagent in analysis [11]. The electrodes were immersed (carbon paste electrode as working electrode) into the newly prepared modification solution and the time $\sim i_{\text{p,c1}}$ experiments were carried out. For a modification solution without acetone, the peak height increased with the accretion of time up to 5 min, above which it started to decline (Fig. 3). With the addition of 16% (V/V) acetone, the peak height increased considerably and became stable after 5 min (Fig. 4).

When cycling between 0.6 and 0.1 V, two pairs of well-defined oxidation–reduction waves were obtained (Fig. 1). After seven scans, the peak height became stable and thus the PMo_{12} electrode was prepared. Both the sensitivity and reproducibility of the PMo_{12} electrode were good.

3.2. Characterization of PMo_{12} electrode

PMo_{12} could be selectively adsorbed at the PMo_{12} electrode under open circuit. In order to obtain a stable peak height, the solution to be analysed was required to stand for 5 min because

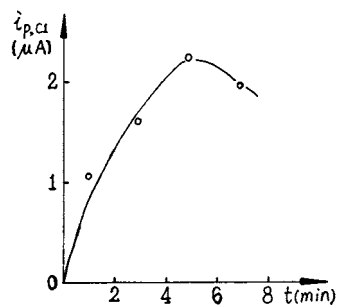


Fig. 3. Dependence of the $i_{\text{p,c1}}$ peak height of phosphorus on the time in a modification solution without acetone. $10 \mu\text{g ml}^{-1}$ phosphorus + 3×10^{-3} mol l^{-1} paramolybdate + 0.5 mol l^{-1} sulfuric acid.

of the complete reaction between PO_4^{3-} and $\text{Mo}_7\text{O}_{24}^{6-}$. Considering the solubility of $\text{H}_3\text{PMo}_{12}\text{O}_{40}$, $\text{K}_3\text{PMo}_{12}\text{O}_{40}$ and the nearly reversible character of the two pairs of oxidation–reduction peaks showed by Fig. 2, the electrode only needed rinsing with water before the next determination. The same PMo_{12} electrode was used to determine the solutions containing 10, 1 $\mu\text{g ml}^{-1}$ phosphorus alternately, and the relative standard deviations both were less than 5% ($n=4$). This result suggested that PMo_{12} adsorbed on the PMo_{12} electrode was not the formation of new film but the result of selective adsorption.

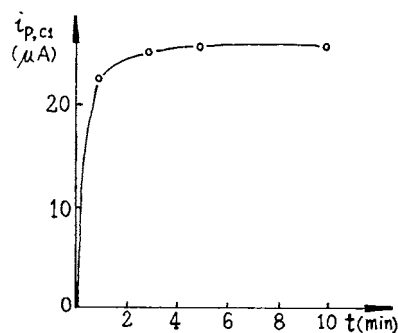


Fig. 4. Dependence of the $i_{\text{p,c1}}$ peak height of phosphorus on the time in a modification solution containing 16% (V/V) acetone. $10 \mu\text{g ml}^{-1}$ phosphorus + 3×10^{-3} mol l^{-1} paramolybdate + 0.5 mol l^{-1} sulfuric acid + 16% (V/V) acetone.

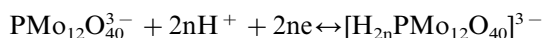
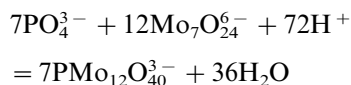
Table 1
Determination of inorganic phosphorus in the samples

Samples	This method (%)	Spectrophotometric method (%)	Recovery (%)
Phytic acid 1	10.09 ± 0.47 ^a	10.39 ± 0.14	102.9
Phytic acid 2	4.82 ± 0.15	4.98 ± 0.19	96.1
Phytic acid 3	2.18 ± 0.03	2.74 ± 0.04	89.2

^a Values are expressed as mean ± S.D. ($n = 3$).

The effect of scan rate on the peak current was examined over the range 20–200 mV s⁻¹ in a solution containing 10 µg ml⁻¹ phosphorus. It showed that the peak height increased linearly with the square root of scan rate, as expected for a diffusion-controlled process. Considering the sensitivity and reagent blank, the scan rate was chosen to be 100 mV s⁻¹.

In a solution containing 10 µg ml⁻¹ phosphorus, ΔE_p of the two pairs both were nearly 30 mV. According to the equation ΔE_p = 59 mV n⁻¹, 25°C [12], $n_1 = 2$, $n_2 = 2$. Thus, the possible stoichiometry is:



When cycling between 0.6 and 0.1 V, n is equal to 1 and 2.

3.3. Principle of quantitative

All the four peaks had linear relationships between the peak currents and the phosphorus concentration over the range 0.4–25 µg ml⁻¹. The linear regression equations and the correlation coefficients were as follows:

$$i_{p,c1} \sim C_p, \quad y = 5.11 + 2.13x, \quad r = 0.9990;$$

$$i_{p,c2} \sim C_p, \quad y = 4.84 + 1.39x, \quad r = 0.9948;$$

$$i_{p,a1} \sim C_p, \quad y = 4.25 + 3.00x, \quad r = 0.9991;$$

$$i_{p,a2} \sim C_p, \quad y = 3.41 + 1.18x, \quad r = 0.9978.$$

From these, it can be seen that $i_{p,c1}$ and $i_{p,a1}$ are better. In these experiments, $i_{p,c1}$ was chosen for its good ability to resist interference.

3.4. Interferences

The tolerance for various foreign ions was studied for the determination of 2 µg ml⁻¹ phosphorus. The results showed that at least 500-fold Na⁺, K⁺, SO₄²⁻, NO₃⁻, 100-fold Cu²⁺, Cd²⁺, SiO₄²⁻, BO₃⁻, 50-fold AsO₄³⁻, TeO₄³⁻, 5-fold Pb²⁺ had little effect on the determination.

3.5. Sample analysis

In this practical analysis, the method was applied to the determination of inorganic phosphorus in three different phytic acid samples. The results are summarized in Table 1. The samples used for method comparison should be introduced into a column filled with 717 basic anion-exchanger, inorganic phosphorus was eluted with 0.2 mol l⁻¹ NaCl and then applied to a spectrophotometric method [13], respectively (Table 1). In order to evaluate the validity of the proposed method, recovery studies were carried out on samples to which known amounts of phosphorus had been added (Table 1).

References

- [1] A.G. Fogg, N.K. Bsebsu, *Analyst* 106 (1981) 369.
- [2] E. Papaconstantinou, M.Z. Hoffman, *Inorg. Chem.* 21 (1982) 2087.
- [3] K. Unoura, N. Tanaka, *Inorg. Chem.* 22 (1983) 2963.
- [4] B. Keita, L. Nadjjo, *J. Electroanal. Chem.* 191 (1985) 441.
- [5] B. Keita, L. Nadjjo, *J. Electroanal. Chem.* 227 (1987) 265.
- [6] J.E. Toth, F.C. Anson, *J. Electroanal. Chem.* 256 (1988) 361.
- [7] L. Chen, S. Li, F. Zhao, H. Zhou, *Fenxi Huaxue* 20 (1992) 945.

- [8] B. Wang, S. Dong, *Electrochim. Acta* 37 (1992) 1859.
- [9] S. Dong, X. Xi, M. Tian, *J. Electroanal. Chem.* 385 (1995) 227.
- [10] C. Rong, F.C. Anson, *Inorg. Chim. Acta.* 242 (1996) 11.
- [11] G. Lu, C. Zhu, Y. Wang, S. Yao, *Anal. Lett.* 22 (1989) 2531.
- [12] G. Pu, Z. Yuan, S. Wu, *Electroanalytical Chemistry*, China University of Science and Technology Press, China, 1993, p. 178.
- [13] M.A. Franson, *Standard Methods for the Examination of Water and Waste Water*, 14th edition, American Public Health Association, Washington, 1976, pp. 481–482.

End-column amperometric detection of melatonin by high performance capillary electrophoresis

Tianyan You, Zhiming Liu, Xiurong Yang, Erkang Wang *

Laboratory of Electroanalytical Chemistry and National Analytical Research Center of Electrochemistry and Spectroscopy, Changchun Institute of Applied Chemistry, Chinese Academy of Sciences, Changchun 130022, China

Received 21 July 1998; received in revised form 4 January 1999; accepted 5 January 1999

Abstract

A rapid and sensitive method is described for the detection of melatonin in rat pineal gland and melatonin tablets. Capillary electrophoresis (CE) with electrochemical detection (EC) was used. This method had high sensitivity and good reproducibility. The detection limit of melatonin was as low as 1.3×10^{-9} mol/l (0.30 fg). There was a linear range of concentration from 3.9×10^{-7} to 3.25×10^{-5} mol/l with a correlation coefficient of 0.999. The linear equation was $Y = 8.27 + 0.0042X$ with a slope of 0.0042 pA/nM. The relative standard deviations of the peak current response and the migration time for 16 continuous injections of 6.5 μ M melatonin were 4.5 and 0.48%, respectively. The proposed method was applied to detect melatonin in the rat pineal gland and the melatonin tablets. Good results were obtained compared with previous reports. © 1999 Elsevier Science B.V. All rights reserved.

Keywords: End-column; Amperometric detection; Melatonin; Capillary electrophoresis

1. Introduction

Melatonin, a hormone of pineal gland, plays a very important role in many mammalian physiological functions. Increasing attention has been focused on it because of its important influence on mammalian life. Melatonin may delay the aging process perhaps owing to its ability to scavenge free radicals [1,2]. The temporal changes of melatonin level can lead to reproductive malfunctions [3–5], neurological and psychiatric disorders [6,7], and can also affect some genomic actions [8]. So,

in recent years, there has been an increased interest in developing accurate analytical methods valid for the quantitation of melatonin including amino acid method [9], gas-liquid chromatography with electron-capture detection [10], gas chromatography-mass spectrometry (GC-MS) [11], high performance liquid chromatography with radioimmunoassay (RIA) [12], fluorometric [13] and amperometric detection [14–16]. However, these methods have some limitations on sensitivity, selectivity or versatility.

High performance capillary electrophoresis (HPCE) has become a very important technique in separation and detection areas because of its minimal sample volume requirement, short analy-

* Corresponding author. Fax: +86-431-5689711.

E-mail address: ekwang@mail.jlu.edu.cn (E. Wang)

sis time and high separation efficiency. Moreover, HPCE coupled with electrochemical detection (EC) can also provide high sensitivity and selectivity. The detection of melatonin by HPCE-EC has advantages over other methods mentioned above such as rapid speed, high sensitivity and good selectivity. Moreover, this method was very reproducible.

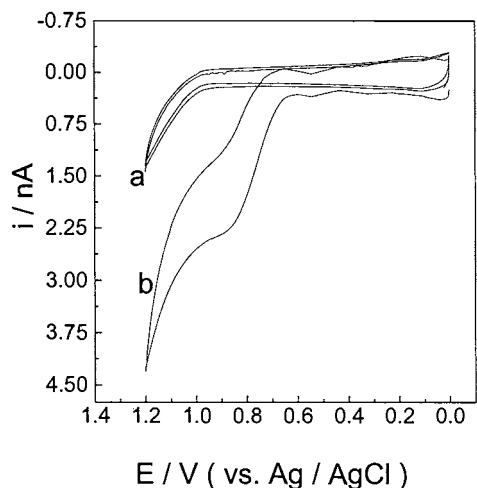


Fig. 1. Cyclic voltammograms of MES buffer (10 mM, pH 5.44) (a) without and (b) with 0.25 mM melatonin at the CFE. Scan rate: 50 mV/s.

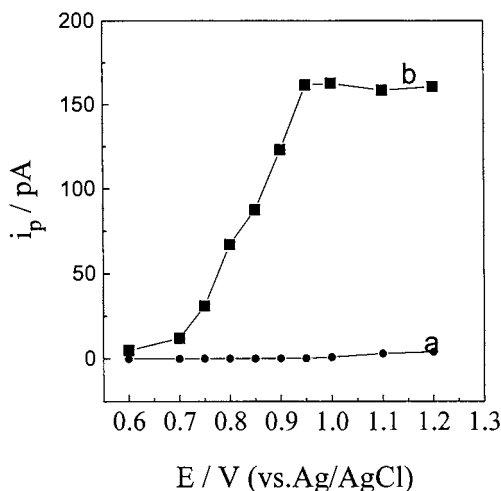


Fig. 2. Hydrodynamic voltammograms of MES buffer (10 mM, pH 5.44) (a) without and (b) with 32.5 μM melatonin at the CFE. Separation capillary, 25 μm i.d., 40 cm long. Operating voltage, 15 kV. Sample injection, 2 s at 15 kV.

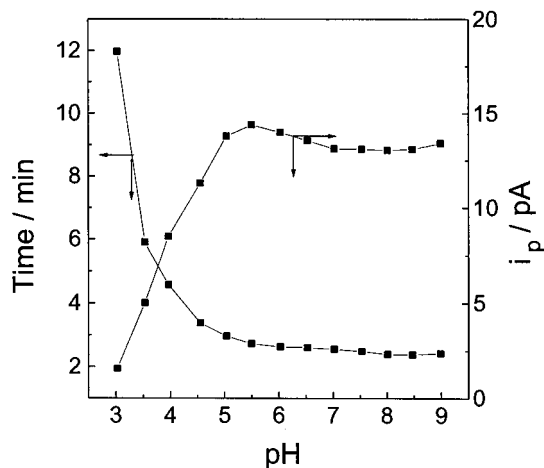


Fig. 3. The effect of 10 mM MES running buffer pH on the (a) peak current and (b) migration time of 32.5 μM melatonin at the CFE. Separation capillary, 25 μm i.d., 40 cm long. Operating voltage, 15 kV. Sample injection, 2 s at 15 kV. Detection potential, +1.0 V vs. Ag/AgCl.

In this work, a 33- μm carbon fiber microdisk electrode (CFE) was used for end-column amperometric detection of melatonin. It is a rapid and sensitive method for the determination of melatonin. The detection limit of melatonin was as low as 1.3×10^{-9} mol/l (0.30 fg). There was a linear range of concentration from 3.9×10^{-7} to 3.25×10^{-5} mol/l with a correlation coefficient of 0.999. The linear equation was $Y = 8.27 + 0.0042X$ with slope of 0.0042 pA/nM. The relative standard deviations of the peak current response and the migration time for 16 continuous injections of 6.5 μM melatonin were 4.5 and 0.48%, respectively. This method was used to detect melatonin in rat pineal gland and melatonin tablets.

2. Materials and methods

2.1. Reagents

Melatonin was obtained from Aldrich (Milwaukee, WI) and 2-(*N*-morpholinol)-ethanesulfonic acid (MES) ($\text{p}K_a$ 6.15) was purchased from Sigma. Melatonin tablets were made by Zhejiang Huangyan Pharmaceuticals. All chemicals were

analytical reagent grade and used as received. A stock solution of melatonin (1.3 mM) was made in doubly distilled water and stored at -70°C . Working solutions were freshly prepared daily to the required concentration with doubly distilled water (passed through a $0.45\text{-}\mu\text{m}$ membrane filter).

2.2. Apparatus

Electrophoresis in the capillary was driven by a high-voltage power supply (Spellman CZE 1000R, Plainview, NY). A 40-cm length of $25\text{-}\mu\text{m}$ i.d., $320\text{-}\mu\text{m}$ o.d. uncoated fused-silica capillary was used (Yongnian Optical Fiber Factory, Hebei, China). The capillary was flushed with 0.1 mol/l sodium hydroxide solution overnight before use.

The construction of the complete CE system with electrochemical detection was built in the laboratory [18]. End-column detection was employed using a wall-jet configuration. Detection was performed in the amperometric mode using a three-electrode system, with a carbon fiber microdisk ($33\text{ }\mu\text{m}$ diameter) working electrode, a Ag/AgCl (saturated KCl) reference electrode and a platinum auxiliary electrode. Potential control and current output was provided by a PAR Model 400 amperometric detector (USA). Data collection from the electropherogram was provided by a Philips computer configured as a Gilson 715 HPLC system controller software.

Cyclic voltammetry was carried out with a Model 832 computerized voltammetric analyzer (CH Instruments, TN) in a three-electrode system cell which was similar to the detection cell system.

Sample introduction was accomplished by an electromigration system and the volume injected was calculated in the continuously filling mode by recording the time required for the sample to reach the detector.

2.3. Sample preparation

Samples for the determination of melatonin were obtained from male albino rats of weight ca. 200 g. The animals were killed at 07:00 h under a very dim red light and the pineal were removed. The pineals were stored at -70°C until use. Before analysis, the pineals were dissolved in 0.1 M perchloric acid and then thoroughly disrupted. After that, the tissue homogenate was immediately centrifuged at $2500\text{ rev. min}^{-1}$ for 20 min at 0°C . The clear supernatant was rapidly frozen in poly(propylene) tubes at -70°C .

The melatonin tablets were crushed to fine powder and dissolved in doubly distilled water. The

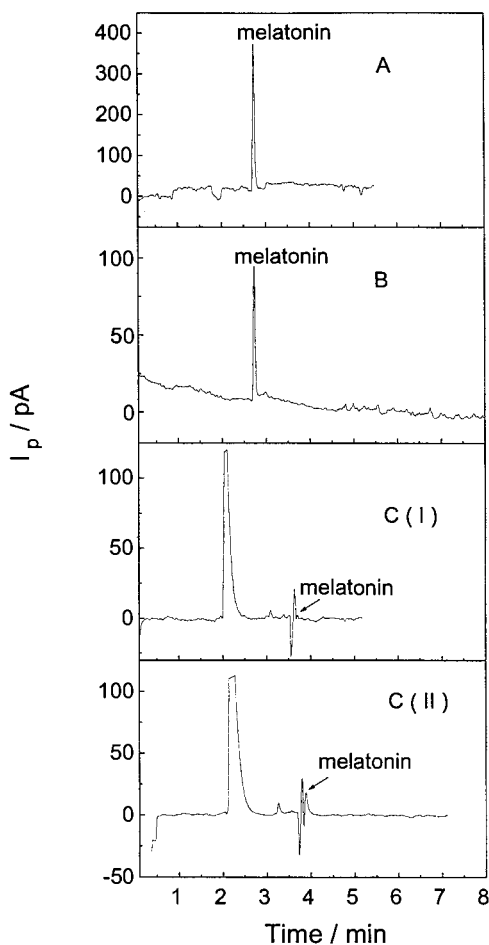


Fig. 4. Electropherograms of (A) $130\text{ }\mu\text{M}$ standard melatonin, (B) melatonin tablets, (C) rat pineal gland (I) without spiked melatonin and (II) with spiked $10\text{ }\mu\text{M}$ melatonin. Other conditions (A) and (B): MES buffer (10 mM , $\text{pH } 5.44$); (C) MES buffer, (0.1 M , $\text{pH } 5.44$). Separation capillary, $25\text{ }\mu\text{m}$ i.d., 40 cm long. Operating voltage, 15 kV . Sample injection, 2 s at 15 kV . Detection potential, $+1.0\text{ V}$ vs. Ag/AgCl.

solution was filtered through a membrane filter (0.45 μm). This stock sample was further diluted with the electrophoretic medium before injection.

3. Result and discussion

3.1. Cyclic voltammetry

The cyclic voltammogram of melatonin at the CFE is shown in Fig. 1. It can be seen that melatonin can be easily oxidized with peak potential at 0.85 V.

3.2. End-column CE-EC system using a carbon fiber microdisk electrode

Compared to the normal-sized electrode, a microelectrode has many advantages, including rapid mass transport towards the electrode, very rapid relaxation, very small ohmic drop values, and in flow systems a high signal-to-noise ratio owing to edge effect [17]. A 33- μm CFE was employed in our work.

Fig. 2 shows the hydrodynamic voltammograms (HDVs) of the CFE with and without melatonin in the buffer electrolyte over the applied potential range between 0.6 and 1.2 V (vs. Ag/AgCl). From the HDVs, it can be seen that the response of the melatonin increases with increasing positive potential until reaching a plateau at 0.95 V. As a compromise of high sensitivity and low background current, a potential of 1.0 V vs. Ag/AgCl was chosen for melatonin detection.

The effect of pH of MES running buffer on peak current and migration time with CE-EC of melatonin at the CFE was investigated over a range of pH from 3.06 to 9.00 (Fig. 3). When pH changed from low to high, the peak current increased and migration time decreased. After pH 5.50, the tendency of both peak current and migration time was towards the plateau. Considering both the sensitivity and migration time of melatonin, a pH value 5.44 was chosen for CE-EC.

The electropherogram of melatonin is shown in Fig. 4A. The different concentrations of melatonin were measured and the response versus concentration for melatonin is linear from $3.9 \times$

10^{-7} to 3.25×10^{-5} mol/l. The linear equation was $Y = 8.27 + 0.0042X$ with a correlation coefficient of 0.999 ($n = 6$). The detection limit was found to be 1.3×10^{-9} mol/l (S/N = 3). Based on an injection volume of 1.0 nl, this corresponds to 0.30 fg. The slope of the curve obtained was 0.0042 pA/nM.

In order to observe the reproducibility of this method, the response of melatonin at the CFE in the CE-EC system was studied by making 16 replicate injections of 6.5 μM melatonin. To guarantee reproducibility, the capillary was rinsed with doubly distilled water (1 min), 0.1 M sodium hydroxide (1 min), doubly distilled water (1 min) and running buffer (5 min) before each run. The relative standard deviations of current response and migration time were 4.5 and 0.48%, respectively.

3.3. Application

In order to examine the application of the method, the level of melatonin was measured in melatonin tablets. The electropherogram for melatonin tablet is shown in Fig. 4B. The content of melatonin in each piece of melatonin tablet was found to be 18.2 μg by the internal standard addition method.

Fig. 4C (I) and (II) are the electropherograms of the rat pineal gland sample without and with spiked melatonin. The level of melatonin in rat pineal gland was very low. But as the amperometric detection in capillary electrophoresis has high sensitivity and selectivity, it can be applied to detect melatonin in the rat pineal gland. The concentration of melatonin in the rat pineal gland was 19.3 ± 4.5 pg/pineal which is similar to a previous report [15].

3.4. Life of the electrode

When the standard melatonin sample and melatonin tablets sample were analysed, in order to obtain good reproducibility, only the capillary was washed before each run as mentioned above and the electrode was not treated. When detecting the rat pineal gland, some species from the sample was adsorbed onto the surface of the electrode, so

the electrode was required to be reactivated. The electrode can be refreshed by means of cyclic potential scanning for 3 min between -0.5 and 1.5 V vs. Ag/AgCl at a scan rate of 100 mV/s without dislocating from CE-EC cell body. The electrode can be used continuously for about 6 months.

4. Conclusion

The present study demonstrates that an end-column CE-EC system with a CFE can be used to detect melatonin. This method has high sensitivity and good reproducibility. The detection limit of melatonin was as low as 1.3×10^{-9} mol/l (0.30 fg). A linear range of concentration was from 3.9×10^{-7} to 3.25×10^{-5} mol/l with a correlation coefficient of 0.999. The linear equation was $Y = 8.27 + 0.0042X$ with a slope of 0.0042 pA/nM. The relative standard deviations of the peak current response and the migration time for 16 continuous injections of 6.5 μ M melatonin were 4.5 and 0.48%, respectively. It can be applied to practical samples such as melatonin tablets and rat pineal gland.

Acknowledgements

This work was supported by the National Nat-

ural Science Foundation of China.

References

- [1] G.P. Trentini, A.R. Genazzani, M. Criscuolo, *Neuroendocrinology* 56 (1992) 364.
- [2] W. Pierpaoli, W. Regelson, *Proc. Natl. Acad. Sci. USA* 91 (1994) 787.
- [3] D.P. Cardinali, *Endocr. Rev.* 2 (1981) 327.
- [4] J.P. Preslock, *Endocr. Rev.* 5 (1984) 282.
- [5] S. Binkley, *The Pineal: Endocrine and Nonendocrine Function*, Prentice-Hall, Englewood Cliffs, NJ, 1988.
- [6] B. Claustrat, J. Brun, G. Chazot, *Nucl. Med. Biol.* 17 (1990) 625.
- [7] R.J. Reiter, *Endocr. Rev.* 12 (1991) 151.
- [8] A. Menendez-Pelaez, R.J. Reiter, *J. Pineal Res.* 15 (1993) 59.
- [9] M. Wilkinson, G.A. Iacohicei, D.V. Meyers, *Anal. Biochem.* 70 (1976) 479.
- [10] D.H. Degen, J.R. Doamaral, J.D. Barchas, *Anal. Biochem.* 45 (1972) 634.
- [11] F. Cattabeni, S.H. Koslow, E. Costa, *Science* 178 (1972) 166.
- [12] M.D. Rollay, G.D. Niswender, *Endocrinology* 98 (1976) 482.
- [13] A.A. Vitale, C.C. Furrari, H. Aldana, J.M. Affanni, *J. Chromatogr. B.* 681 (1996) 381.
- [14] A. Takaharu, S. Atsuko, A. Kazuhiro, S. Hiroyoshi, M. Yusuke, *J. Chromatogr.* 530 (1990) 47.
- [15] T. Raynaud, P. Révet, *J. Chromatogr.* 564 (1991) 103.
- [16] R. Vieira, J. Míguez, M. Lima, M. Aldigunde, *Anal. Biochem.* 205 (1992) 300.
- [17] W. Hou, H. Ji, E. Wang, *Anal. Chim. Acta* 230 (1990) 207.
- [18] Z. Liu, T. You, E. Wang, *J. Anal. Chem.* 6 (1998) 786 In Chinese.

Determination of arsenic in sea water by sorbent extraction with hydride generation atomic absorption spectrometry

S. Karthikeyan, T. Prasada Rao *, C.S.P. Iyer

*Centre for Marine Analytical Reference and Standards (C-MARS), Regional Research Laboratory (CSIR),
Trivandrum 695 019, India*

Received 25 August 1998; received in revised form 2 November 1998; accepted 5 January 1999

Abstract

A rapid and sensitive sorbent extraction hydride generation-flow injection analysis atomic absorption spectrometric (HG-FIAS-AAS) method is described for the determination of As(III) and As(V) based upon online preconcentration on a microcolumn packed with activated alumina. In the present procedure these arsenicals are complexed with quinolin-8-ol-5-sulphonic acid from neutral solutions in the flow injection system and adsorbed on the column. The preconcentrated species are eluted with 10% HCl, mixed with 0.5% sodium borohydride and carried to the HG-FIAS cell with a carrier gas flow rate of 75 ml min⁻¹. The retention efficiency is found to be better than 98% with sensitivity enhancement of 12 and 10 for As(III) and As(V), respectively, for a 20 s preconcentration period. The respective detection limits are 0.05 and 2 ng ml⁻¹ for As(III) and As(V). The throughput of the samples is found to be 60 h⁻¹, with a loading time of 20 s. The method has been applied to sea water samples. © 1999 Elsevier Science B.V. All rights reserved.

Keywords: Arsenic; Sea water; Atomic absorption spectrometry

1. Introduction

The detection of arsenic species can be greatly increased through the use of hydride generation (HG) [1–8], HG-total reflection X-ray fluorescence [9] and HG-graphite furnace atomic absorption spectrometry (AAS) [10] have been used for the determination of arsenic in biological materi-

als and food respectively. Magnuson et al. [11] have recently developed an ion-chromatographic separation for arsenic species with a HG system and inductively coupled plasma-mass spectrometric (ICP-MS) detection. Palladium and iridium are used as modifiers during determination of arsenic by electrothermal vaporisation-ICP-MS following in-situ trapping of hydrides [12]. Mester and Foder [13] have measured different arsenic species by using HG-atomic fluorescence spectrometry.

* Corresponding author. Fax: +91-471-490186/491712.
E-mail address: rao@csrrlrd.ren.nic.in (T. Prasada Rao)

Table 1
Flow injection analysis (FIA) procedures for As(III)/As(V)

SI. no.	Species	Detection method	Sample	Sample frequency (samples h ⁻¹)	Detection limit	Linear range	FIA	References
(1)	(2)	(3)	(4)	(5)	(6)	(7)	(8)	(9)
1.	As(III)	AAS	–	–	8 µg l ⁻¹	40 ng–0.5 µg ml ⁻¹	Hydride generation	[22]
2.	As(III)	ICPAES	–	–	5.2 µg ml ⁻¹	–	”	[23]
3.	As(III)	GFAAS	–	–	–	–	”	[24]
4.	As(III)	UV-Vis	–	30	–	–	”	[25]
5.	As(III)	AAS	–	–	3.9 µg l ⁻¹	–	”	[26]
6.	As(III)	AAS	–	–	–	–	”	[27]
7.	As(III) and As(V)	AAS	–	10	0.25 µg ml ⁻¹	Upto 30 µg ml ⁻¹	”	[28]
8.	As(III) and As(V)	AAS	–	–	0.4 µg l ⁻¹	Upto 100 µg ml ⁻¹	”	[29]
9.	As(III)	ICPAES	–	–	50 µg l ⁻¹	Upto 100 µg ml ⁻¹	”	[30]
10.	As(III)	UV-Vis	Soil	15	–	–	”	[31]
11.	As(III)	PSA	–	–	–	–	–	[32]
12.	As(III)	AAS	–	33	0.003 µg l ⁻¹	–	Coprecipitation on La(OH) ₃ or Hf(OH) ₄	[33]
13.	As(III) and As(V)	AAS	–	180	0.111 µg l ⁻¹	–	Hydride generation	[34]
14.	As, Sb, Bi, Se	AAS	–	–	–	–	”	[35]
15.	As, Hg, Se, Sb, Sn and Bi	GFAAS	–	–	–	–	”	[36]
16.	As, Sb, Bi, Hg, Se and Te	AFS	–	–	0.02–0.2	Upto 300 µg l ⁻¹	”	[37]
17.	As, Sb, Se	ICPAES	–	–	1 µg l ⁻¹	–	Hydride generation	[38]
18.	As and Se	AAS	Environment	–	10–20 pg ml ⁻¹	–	Cold trap collection	[39]
19.	As and Se	AAS	CRMs of water liver, citrus	–	10–20 pg ml ⁻¹	–	”	[40]
20.	As, Se, Mo, S and Cr	ICPAES	–	–	13 µg l ⁻¹	–	Anion exchange	[41]
21.	As	ICPMS	Estuarine water	–	–	92 pg	–	[42]
22.	As(III) and As(V)	AAS	CRMs for sediment, lobster, and sea plants and seawater	60	0.05, 2 µg l ⁻¹	0–2, 2–100 µg l ⁻¹	Sorbent extraction	Present method

The growing interest in the use of flow-injection analysis (FIA), in conjunction with atomic spectrophotometric techniques was highlighted in several reviews [14–20] and in a recent book [21]. Various FIA procedures described for arsenic since 1990 have been summarised in Table 1. Of these FIA procedures described for arsenic, only one procedure utilizes anion exchange preconcentration prior to determination by ICP-AES [41]. Siska et al. [39,40] have described AAS procedures in combination with cold trap collection. Recently, sorbent extraction FIA-AAS procedures for the determination of Mo [43], Cu, Cd and Pb [44], Fe, Co, Ni, Mn and Zn [45] were described and in speciative determination of chromium [46]. In the present study, a sorbent extraction based on sorption of As(III)/As(V) in presence of quinoline-8-ol onto activated alumina and subsequent HG-FIAS-AAS determination is described. This method is useful for the determination of total arsenic in sea water samples.

2. Experimental

2.1. Apparatus

A Perkin Elmer Model 3100 AAS was used. The instrumental parameters are given in Table 2. A standard HG system was used with a carrier gas flow rate of 75 ml min⁻¹.

A Perkin Elmer FIAS-200 flow injection system connected to the HG cell was used for on-line sorbent extraction of As(III) or As(V). The automatic operation of the injector valve and

two multichannel peristaltic pumps were programmed using the spectrometer software. Tygon pump tubes were used to propel sample and reagent solutions. A conically shaped micro-column of 50 µl capacity (Perkin Elmer, Uberlingen, Germany) packed with 20 mg of activated alumina (40–60 µM size) was used.

Time resolved absorbance signals of the As(III) or As(V) were displayed on the computer monitor and were printed with peak-height and integrated absorbance values.

2.2. Reagents

All reagents were of analytical reagent grade purity. Ultrapure water (18.2 MΩ) was used. Quinoline-8-ol-5-sulphonic acid (Aldrich, USA) (0.02%) was prepared in 0.2 M ammonium acetate (E merck) (pH 7.0 ± 1.0) 10% HCl (E merck, Suprapure) and 0.5% sodium borohydride (Aldrich, USA) were used for elution and for hydride generation, respectively.

Standard solutions of As(III) or As(V) were prepared by standardising the solutions obtained by dissolving sodium arsenite (E Merck) or sodium arsenate (E Merck) by standard titrimetric procedures. Quality assurance was carried out by analysing standard reference materials viz, MESS (Marine sediment reference material supplied by NRC, Canada), TORT (Biological reference material supplied by NRC, Canada), BCR 279 (Seaplant-Sealautice supplied by IAEA), and IAEA 140 (Seaplant supplied by International atomic energy agency).

2.3. Procedure

The FI manifold (0.3 mm i.d. type) for online preconcentration and elution is shown in Fig. 1. Samples and quinoline-8-ol-5-sulphonic acid solutions were pumped simultaneously and mixed online. The preconcentration time was usually 20 s. The duration and function of each sequence are given in Table 3. Linear calibration graphs were obtained over the concentration ranges of 0–2 and 0–100 ppb for As(III) and As(V), respectively, using aqueous standard solutions.

Table 2
Instrumental parameters

Parameter	As(III) or As(V)
Hollow cathode lamp current (mA)	18
Wavelength (nm)	193.7
Slit width (mm)	0.7
Measurement mode	AA
Carrier gas flow rate (ml min ⁻¹)	75
Cell temperature (°C)	900

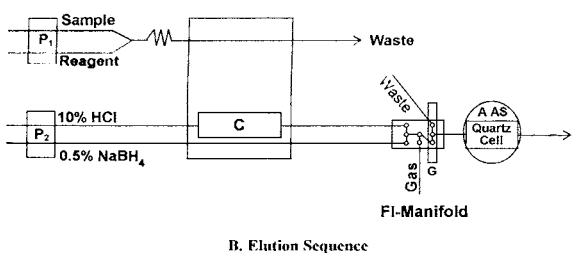
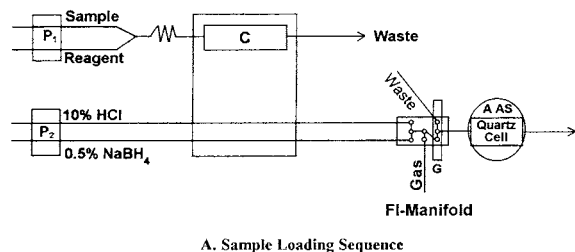


Fig. 1. Hydride generation-flow injection analysis (HG-FIAS) manifold for online preconcentration P_1 , P_2 , peristaltic pumps; C, microcolumn packed with activated alumina; G, gas-liquid separator; AAS, atomic absorption spectrometer; (A) sample loading sequence; (B) elution sequence.

2.4. Analysis of standard reference materials

2.4.1. MESS (marine sediment, NRC Canada)

To 0.2 g MESS, add 10 ml of 48% HF, 5 ml of 70% HNO_3 and 1 ml of 70% HClO_4 and digest in a Mega 240 Milestone microwave digester (digestion programme 5 min, 250 W; 1 min, 0 W; 5 min, 400 W; 10 min, 500 W; 2 min, 600 W). After digestion, HF was evaporated off, 40 ml of water added and pH was adjusted to 7 ± 1 by using HCl

or NaOH and made up to 50 ml. These solutions were subjected to HG-FIAS-AAS determination by following the procedure described above.

2.4.2. TORT (Lobster Pancreas, NRC, Canada) BCR 279 (sea plant), IAEA 140 (sea plant)

To 0.2 g of sample, 5 ml of 70% HNO_3 and 1 ml of 70% HClO_4 were added and then digested in the microwave digestion. Subsequently the procedure described above was followed.

2.4.3. Sea water

Sea water samples were collected at various locations in Arabian sea (5 km from the shore) and filtered through a 0.45μ membrane filter. These samples were oxidised by digesting in a microwave digestion with 5 ml of 70% HNO_3 and 2 ml of 30% H_2O_2 to convert various forms of arsenic to As(V). They were then subjected to sorbent extraction and hydride generation AAS by following the procedure described above for the determination of arsenic.

3. Results and discussion

Preliminary studies indicated that As(III) or As(V) were sorbed on C_{18} bonded silica gel in the presence of quinoline-8-ol-5-sulphonic acid or diethyl ammonium dithiocarbamate. Both As(III) and As(V) are sorbed in the presence of quinoline-8-ol-5-sulphonic acid, onto activated alumina column and can be eluted easily with 10% HCl. The detailed evaluation and optimisation of various analytical parameters during sorbent extraction HG-FIAS-AAS determination are given below. (A summary of which is given in Table 4.)

Table 3

Sequence of operations for on-line flow injection (FI) sorbent extraction preconcentration for the determination of As(III) and As(V) by hydride generation-flow injection analysis atomic absorption spectrometric (HG-FIAS-AAS)

Sequence	Stage of operation	Time (s)	Pump 1	Pump 2	Valve position	Pumped medium	
			(ml min ⁻¹)			Pump1	Pump2
1.	Prefill	20	6.0, 2.5	4.0	Elute	Sample, HO_x	HCl
2.	Load	20	6.0, 2.5	Off	Load	Sample, HO_x	–
3.	Elution	20	Off	4.0	Elute	Off	HCl
	Total	60					

Table 4
Optimal ranges and optimal concentrations of various parameters

Parameters	Optimal range		Optimal concentrations	
	Arsenic (III)	Arsenic (V)	Arsenic (III)	Arsenic (V)
Quinoline-8-ol-5-sulphonic acid (% w/v)	0.01–0.05	0.01–0.05	0.02	0.02
Ammonium acetate concentration (M)	0.05–0.2	0.05–0.2	0.2	0.2
pH	6–8	5–9	7.0	7.0
Acidity of the HCl eluent (% w/v)	10–15	10–15	10	10
Sodium borohydride concentration (% w/v)	0.2–0.5	0.5–1.0	0.5	0.5
Carrier gas flow rate (ml min ⁻¹)	50–100	50–100	75	75

3.1. Optimisation of analytical parameters for the determination of As(III) and As(V)

3.1.1. Effect of sample pH

The quinoline-8-ol complex of As(III) or As(V) was effectively sorbed on activated alumina in the pH range 6–8 and 5–8, respectively, and there was no significant influence on the retention efficiency in this pH range (Fig. 2). However, there is a decrease in retention efficiency at higher and lower pH values. Hence the sample was adjusted 7.0 ± 1.0 with dilute HCl or NaOH before analysis.

3.1.2. Effect of quinolin-8-ol-5-sulphonic acid(HO_x) concentration

Variation of HO_x concentration from 0.01 to 0.05% did not effect the retention efficiency of As(III) or As(V) on activated alumina. Therefore, a concentration of 0.02% of HO_x was used for subsequent studies.

3.1.3. Effect of ammonium acetate concentration

Variation of ammonium acetate buffer concentration from 0.05–0.2 M did not effect the retention efficiency of As(III) or As(V) on activated alumina. A concentration of 0.2 M of ammonium acetate was used as buffer in subsequent studies.

3.1.4. Effect of acidity of the eluent

As(III) or As(V) complex of HO_x on activated alumina was stripped quantitatively in the range 10–15% (w/v) HCl. Hence, 10% (w/v) HCl was used to strip the As(III) or As(V) sorbed on activated alumina in the presence of HO_x.

3.1.5. Effect of sodium borohydride concentration

The sodium borohydride concentration was varied from 0.1 to 1.0% (w/v) (in steps of 0.1) during the formation of AsH₃ from As(III) or As(V). The absorbance reaches maximum when sodium borohydride concentration is 0.2–0.5 or 0.5–1.0% for As(III) and As(V), respectively.

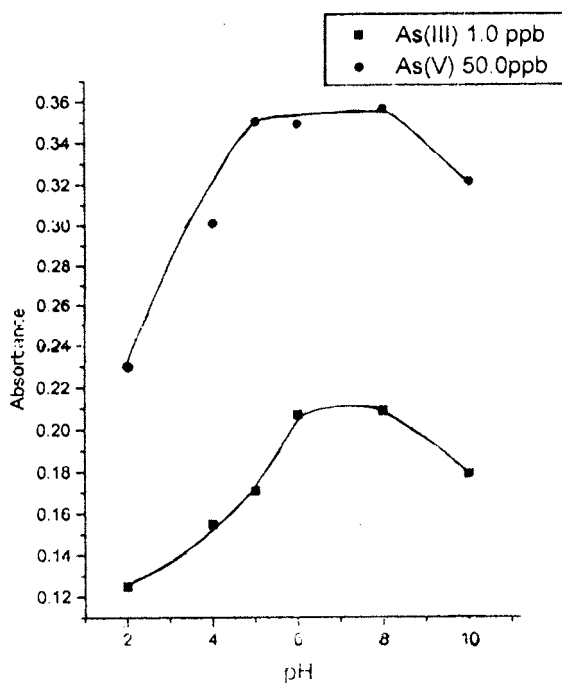


Fig. 2. Effect of pH on the analytical signal of $1.0 \mu\text{g l}^{-1}$ of As(III) and $50 \mu\text{g l}^{-1}$ of As(V) (after subtracting blank) eluted with 10% HCl and reduced with 0.5% NaBH₄ after preconcentration on activated alumina in the presence of quinoline-8-ol-5-sulphonic acid as sorbing agent.

Hence, 0.5%(w/v) sodium borohydride was used in subsequent studies.

3.1.6. Effect of carrier gas flow rate

The carrier gas flow rate was varied from 10 to 100 ml min⁻¹ during the determination of As(III) or As(V) after sorbent preconcentration. The optimum carrier gas flow rate was found to be 50–100 ml min⁻¹ for both As(III) and As(V), and hence 75 ml min⁻¹ was chosen in subsequent studies.

3.2. FI flow condition optimisation

High sample loading flow rates are needed for efficient preconcentration as well as high sample throughput. In general, FI sample flow rates are limited by the back pressure produced by the column and/or the sorption efficiency, which decreases with increasing flow rate. No degradation in sorption efficiency was observed upto a loading flow rate of 7.0 ml min⁻¹ for As(III) and As(V), which is the highest flow rate that can be handled with reproducibility by the peristaltic pump and the type of column used in this work. The reagent flow rate adds to the total loading flow rate and hence calls for a proportional reduction of the sample flow rate. For good mixing of sample and reagent solutions the reagent flow should not be too low. A flow rate of 2.5 ml min⁻¹ was used in all subsequent experiments. The elution flow rate of 4.0 ml min⁻¹ was selected which provides optimum sensitivity and elution peaks with minimum tailing.

3.3. Performance of online sorbent extraction preconcentration system

Characteristic data for the performance of the online preconcentration system is summarised in Table 5. The efficiency of sorption was investigated by analysing the previously collected column eluent of a standard solution of As(III) or As(V) using the same preconcentration technique. From the results obtained by this repeated preconcentration, retention efficiencies of 99 and 98% were calculated for As(III) and As(V), respectively. The sorption/elution is highly reproducible

Table 5

Performance data for online preconcentration by activated alumina

Parameters	Arsenic (III)	Arsenic (V)
Working range (ng ml ⁻¹)	0–2	2–100
Sensitivity enhancement ^a	12	10
Precision (% R.S.D.)	3.6	5.0
Sample consumption (ml)	2.5	2.5
Sample frequency (number h ⁻¹)	60	60
Limit of detection (ng ml ⁻¹)	0.05	2.0

^a Compared to normal hydride generation-flow injection analysis atomic absorption spectrometric (HG-FIA-AAS) determination.

giving an overall precision of 3.6 and 5.0% for As(III) and As(V), respectively (Table 5.). A linear relation was observed between preconcentration time and absorbance from 5 to 40 s of preconcentration time only. With a preconcentration time of 20 s, 12- and 10-fold enhancement in sensitivity (compared to normal HG-FIA-AAS method) was obtained for As(III) and As(V), respectively, allowing a sample frequency of 60 h⁻¹. Higher sensitivities could be obtained by modifying the method using longer preconcentration periods upto 40 s at the expense of reduced sample throughput.

3.4. Interference studies

The interference due to the coexisting ions on the determination of 0.1 or 10 µg l⁻¹ of As(III) or As(V) was studied. NaCl (5%), KCl (0.1%), MgCl₂ (0.25%), CaCl₂ (0.1%), KI (0.2%), Cu, Cd, Pb, Zn, Fe, Mn, Hg, Se, Sb (all 1 µg ml⁻¹), NO₃⁻ (500 µg ml⁻¹), PO₄³⁻ (500 µg ml⁻¹) and MoO₄²⁻ (10 µg ml⁻¹) do not interfere in the sorbent extraction-HG-FIAS determination of As(III) or As(V). Twenty-fold amounts of As(V) do not interfere in the determination of 0.1 µg l⁻¹ of As(III). On the other hand, As(III) interferes at all concentrations during the determination of As(V).

Table 6
Analysis of reference materials

Sample	Amount of total arsenic found ^a ($\mu\text{g g}^{-1}$)	Certified value for total arsenic ($\mu\text{g g}^{-1}$)
MESS	12.4 ± 1.0	10.6 ± 1.2
TORT	22.4 ± 1.3	24.6 ± 2.2
BCR279	3.20 ± 0.12	3.09 ± 0.20
IAEA140	46.4 ± 4.0	44.3 ± 4.0

^a Average of three determinations.

3.5. Analysis of standard reference materials (SRM)

SRMs MESS, TORT, BCR 279 and IAEA 140 were analysed by the developed sorbent extraction-HG-FIAS-AAS procedure for the determination of total arsenic as As(V) and compared with the certified values (Table 6). The results agree well with the certified values indicating that the present procedure can be reliably used for the analysis of total arsenic in sediments and marine biota.

3.6. Analysis of sea water samples

The sea water samples collected from various locations of Arabian sea were analysed by the proposed sorbent extraction-HG-FIA-AAS procedure for total arsenic as described in Section 2. The data obtained are shown in Table 7.

4. Conclusions

The sorbent extraction preconcentration of As(III) or As(V) in the presence of quinoline-8-ol-

Table 7
Analysis of sea water sample

Location of sample in Arabian sea	Total arsenic found ^a ($\mu\text{g l}^{-1}$)
Sangumukham	4.4 ± 0.7
Kayamkulam	3.9 ± 0.7
Alleppey	4.8 ± 0.6

^a Average of three determinations.

5-sulphonic acid results in 12- or 10-fold enhancement in sensitivity compared to normal HG-FIA-AAS method. The determination of As(III) is highly selective as several other anions and cations at >1000-fold level and 20-fold amounts of As(V) do not interfere. On the other hand As(V) is determined only after reduction to As(III) (which is little slow) and then generation of AsH₃ vapour. So As(III) determination is more sensitive and interferes at all concentrations in As(V) determination. Further, the proposed method was successfully used for the determination of ultra trace amounts of total As in sea water samples.

References

- [1] M.L. Magnuson, J.T. Creed, C.A. Brockoff, *J. Anal. At. Spectrom* 11 (1996) 893.
- [2] C.J. Hwang, S.J. Jiang, *Anal. Chim. Acta* 289 (1994) 205.
- [3] X-C Le, W.R. Cullen, K.J. Reimer, *Talanta* 41 (1994) 495.
- [4] W.C. Story, J.A. Caruso, D.T. Heitkemper, L. Perkins, *J. Chromatogr. Sci.* 30 (1992) 427.
- [5] R. Roehl, M.M. Alforque, J. Riviello, Paper presented at the 1992 Winter Conference on Plasma Spectrochemistry, January 6–11, 1992.
- [6] S. Branch, W.T. Corns, L. Ebdon, S. Hill, P. O'Neil, *J. Anal. At. Spectrom* 6 (1991) 155.
- [7] X. Wang, M. Viczian, A. Lasztity, R.M. Barnes, *J. Anal. At. Spectrom.* 3 (1988) 821.
- [8] M. Thompson, J.N. Walsh, *A Handbook of Inductively Coupled Plasma Spectrometry*, Blackie, Glasgow, 1983.
- [9] J. Messerschmidt, A.V. Bohlen, F. Alt, R. Klochenkamper, *J. Anal. At. Spectrom* 12 (1997) 1251.
- [10] P.N. Fedorob, G.N. Ryabchuck, A.V. Zverev, *Spectrochim. Acta* 52B (1997) 1517.
- [11] M.L. Magnuson, J.T. Creed, C.A. Brockoff, *J. Anal. At. Spectrom.* 12 (1997) 689.
- [12] H.Th. Uggerud, W. Lund, *J. Anal. At. Spectrom* 12 (1997) 1169.
- [13] Z. Mester, P. Fodor, *Spectrochim. Acta* 52B (1997) 1763.
- [14] J.F. Tyson, S.R. Bysouth, K. Grazeszczyk, E. Debrah, *Anal. Chim. Acta* 261 (1990) 75.
- [15] J.F. Tyson, *Anal. Chim. Acta* 234 (1990) 3.
- [16] Z. Fang, L. Sun, S. Xu, *Anal. Chim. Acta* 261 (1992) 557.
- [17] M. Valcarcel, M.D. Luque Decastro, *Microchem. J.* 45 (1992) 189.
- [18] M. Trojanowicz, Olbrych-Sleszynska, *Chem. Anal.* 37 (1992) 111.
- [19] Yu.A. Zolotov, L.K. Shpigun, *Microchem. J.* 45 (1992) 225.
- [20] Z.L. Fang, S.K. Xu, *Fenxi Shiyanshi* 12 (1993) 1997.

- [21] M. Trojanowicz, *Flow Injection Analysis, Instrumentation and Applications*, World Scientific, Singapore, 1996.
- [22] G.D. Marshall, J.F. Van Sladen, *J. Anal. At. Spectrom.* 5 (1990) 675.
- [23] H. Chen, Z. Jiang, L. Kang, Y. Zen, *Fenxi Ceshi Tangbao* 9 (1990) 9.
- [24] Y. An, S.N. Willie, R.E. Sturgeon, *Spectrochim. Acta* 47B (1992) 1403.
- [25] G.Q. Liu, C.X. Wang, B. Xie, W.H. Wu, *Fenxi Huaxue* 20 (1992) 810.
- [26] J.F. Tyson, S.G. Offley, N.J. Seare, H.A.B. Kibble, C. Fellows, *J. Anal. At. Spectrom.* 7 (1992) 315.
- [27] P.D. Wentzell, N.G. Sundin, C. Hogeboom, *Analyst* 119 (1994) 1403.
- [28] B. Welz, Y. He, M. Sperling, *Talanta* 40 (1993) 1917.
- [29] D. Schaumloeffel, B. Neidhart, *Fresenius J. Anal. Chem.* 354 (1996) 866.
- [30] B. Jamoussi, M. Zafzouf, B. Benhassin, *Fresenius J. Anal. Chem.* 356 (1996) 331.
- [31] G.Q. Liu, C.X. Wang, F.X. Cao, *Fenxi Huaxue* 24 (1996) 1429.
- [32] J.H. Aldstadt, A.F. Martin, *Analyst* 121 (1996) 1387.
- [33] S. Nielsen, J.J. Sloth, E.H. Hansen, *Talanta* 43 (1996) 867.
- [34] S. Nielsen, E.H. Hansen, *Anal. Chim. Acta* 343 (1997) 5.
- [35] G.D. Marshall, J.F. van Staden, *J. Anal. At. Spectrom.* 5 (1990) 681.
- [36] Y.P. Ma, *Fenxi Shiyanshi* 12 (1993) 87.
- [37] T. Guo, M. Liu, W. Schrader, *J. Anal. At. Spectrom.* 7 (1992) 667.
- [38] H.N. Wang, Y. Chen, J. Wang, *Anal. Proc.* 31 (1994) 357.
- [39] P. Siska, J. Borszeki, E. Gegus, *Magy. Kem. Foly.* 63 (1996) 248.
- [40] R. Siska, J. Borszeki, E. Gegus, *J. Appl. Spectrosc.* 40 (1995) 117.
- [41] E. Liu, W.J. Chen, C.Y. Zhao, *Fenxi Huaxue* 21 (1993) 328.
- [42] J.T. Creed, M.L. Magnuson, C.A. Brockoff, I. Chamberlain, M. Sivaganesan, *J. Anal. At. Spectrom.* 11 (1996) 505.
- [43] C.S.P. Iyer, T. Prasada Rao, S. Karthikeyan, A.D. Damodaran, *At. Spectrosc.* 15 (1994) 234.
- [44] S. Karthikeyan, B. Vijayalekshmy, S. Chandramouleeswaran, T. Prasada Rao, C.S.P. Iyer, *Anal. Lett.* 30 (1997) 1037.
- [45] K.A. Tony, S. Karthikeyan, B. Vijayalekshmy, T. Prasada Rao, C.S.P. Iyer, *Analyst* (in press).
- [46] T. Prasada Rao, S. Karthikeyan, B. Vijayalekshmy, C.S.P. Iyer, *Anal. Chim. Acta* 369 (1998) 69.

Spectrophotometric study of the reaction of iodine and bromine with two new macrocycle diamides and di-ortho methoxybenzoyl thiourea in chloroform solution

Hashem Sharghi *, Ahmad R. Massah, Mohamad Abedi

Department of Chemistry, Shiraz University, Shiraz, 71454, Iran

Received 6 May 1998; received in revised form 30 December 1998; accepted 6 January 1999

Abstract

The complex formation reactions of iodine and bromine with two new macrocycle diamides (**1** and **2**) and di-ortho methoxybenzoyl thiourea (DOMBT) (**3**) have been studied spectrophotometrically at various temperatures in chloroform solution. In all cases the resulting 1:2 (macrocycle to halogen) or (DOMBT to halogen) molecular complexes were formulated as (macrocycle...X⁺)X₃⁻ or (DOMBT... X⁺)X₃⁻. The formation constants of the resulting molecular complexes were evaluated from computer fitting of the absorbance-mole ratio data. For iodine complexes we found that the values of K_f vary in the order of **1** \approx **2** > **3**. In the case of bromine complexes the values of K_f are larger ($> 10^8$) and vary in the order of **1** > **2** > **3**. The enthalpy and entropy of complexation reactions of iodine with **1**, **2** and **3** were determined from the temperature dependence of the formation constants. In all cases it was found that the complexation reactions are enthalpy stabilized, but entropy destabilized. © 1999 Elsevier Science B.V. All rights reserved.

Keywords: Spectrophotometry; Complexation; Macrocylic diamide; Hallogen

1. Introduction

The macrocyclic polyethers, a class of compound firstly synthesized by Pederson [1] were shown to bind cations much more powerfully than mono functional and linear poly functional ethers of similar basicity [2–5]. Studies on neutral molecule–macrocycles interactions have been far fewer in number than those on cation–macrocycle

interactions. The motivation to study neutral molecule–macrocycle interactions is understandable because the function of neutral molecules is as important as that of charged molecules in many chemical and biochemical processes. In addition there is increasing interest in molecular complexes of macrocyclic compounds by their possible application in different areas such as separation process, catalytic chemical reactions, conversion of chemical reactions to optical or electronic signals and to separate certain neutral molecules from environmental systems [6–9].

* Corresponding author. Tel: +98-71-276013; fax: +98-71-20027.

Much work has been done on the interaction of iodine and bromine with different donor compounds. In some of these reactions stable charge transfer complexes were isolated as solids where halogen is converted to polyhalogen unites, such as X_3^- and X_5^- [9–14].

In the present work thermodynamic and kinetic studies of the complexation of iodine with 1,15-diaza-3,4; 12,13-dibenzo-5,8,11-trioxacyclohexadecane-16-thiocarbonyl-2,15-dione (**1**) and 1,18-diaza-3,4; 15,16-dibenzo-5,8,11,14-tetraoxacyclonadecane-19-thiocarbonyl-2,18-dione (**2**) which we synthesized in our laboratory [15], were carried out spectrophotometrically in chloroform solution. In addition, we report the result of a spectrophotometric investigation of complex formation of bromine with these new dilactam macrocycles, in chloroform solution. Respective results are compared with a linear compound, di-ortho methoxybenzoyl thiourea (**3**), of similar basicity.

2. Experimental

2.1. Chemicals

Reagents grade iodine, bromine and chloroform were obtained from Merck and used without further purification. The macrocycles (**1**, **2**) and di-ortho methoxy benzoyl thiourea (**3**) were prepared and purified according to [15].

2.2. Apparatus

IR spectra were recorded on a Nicolet Impact 400D FTIR spectrophotometer. All UV–Vis spectra were recorded on a Philips PUB 8750 spectrophotometer and the absorbance measurements were made with a Philips PU 8675 spectrophotometer at various temperature ($\pm 0.5^\circ\text{C}$). Conductance measurements were carried out with a metrohm 660 conductivity meter.

2.3. Mole ratio data

The stoichiometry of 1:2 complexes between donors (**1**, **2**, **3**) and iodine or bromine were

determined by absorbance measurements at λ 510 nm for iodine and 272 nm for bromine in which varying concentration of donors were added to fixed concentration of iodine (3.8×10^{-4} mol dm^{-3}) or bromine (3×10^{-3} mol dm^{-3}) in chloroform at 25°C . The plot of absorbance vs. macrocycle/ I_2 or Br_2 mole ratios indicated the formation of 1:2 (donor to iodine or bromine) complexes (Figs. 2 and 4).

2.4. Formation constants

For the evaluation of the formation constants of the resulting molecular complexes, k_f , from the absorbance–mole ratio data, a non-linear least-squares curve fitting program KINFIT was used [16]. The program is based on the iterative adjustment of calculated values of absorbance to the observed values by using either the Wentworth matrix technique [17,18] or the Powell procedure [19]. Adjustable parameters are k_f and ε , where ε is the molar absorption coefficient of iodine.

The observed absorbance of an iodine solution in chloroform at its λ_{max} is given by:

$$A_{\text{obs}} = \varepsilon b [\text{I}_2] \quad (1)$$

The mass balance equations can be written as:

$$C_{\text{I}} = [\text{I}_2] + 2[(\text{donor} \dots \text{I}^+) \text{I}_3^-] \quad (2)$$

$$C_{\text{donor}} = [\text{donor}] + [(\text{donor} \dots \text{I}^+) \text{I}_3^-] \quad (3)$$

The formation constant of complex is equal to:

$$K_f = \frac{[(\text{donor} \dots \text{I}^+) \text{I}_3^-]}{[\text{donor}][\text{I}_2]^2} \quad (4)$$

Substitution of Eq. (2) and Eq. (3) into Eq. (4) and rearrangement yields:

$$K_f[\text{I}_2]^3 + K_f(2C_{\text{donor}} - C_{\text{I}})[\text{I}_2]^2 + [\text{I}_2] - C_{\text{I}} = 0 \quad (5)$$

The free iodine concentration, $[\text{I}_2]$, were calculated from Eq. (5) by means of a Newton–Raphson procedure. Once the value of $[\text{I}_2]$ had been obtained, the concentration of all other involved species were calculated from the corresponding mass balance equations by using the estimated value of K_f at the current iteration step of the program. Refinement of the parameters is continued until the sum-of-squares of the residuals be-

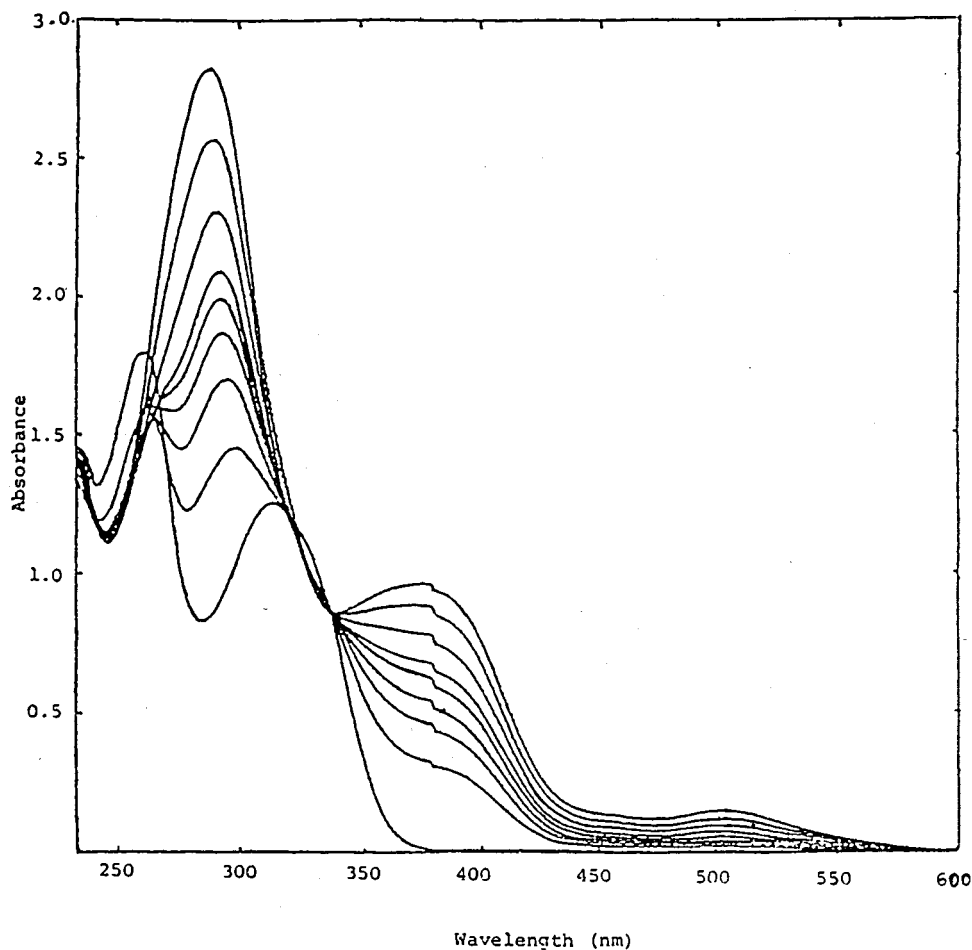


Fig. 1. Absorption spectra of 1.2×10^{-4} mol dm $^{-3}$ macrocycle **2** in chloroform in the presence of various concentration of I $_2$. The I $_2$: macrocycle mol ratios from the bottom to the top spectrum are: 0.0, 0.2, 0.4, 0.6, 0.8, 1.0, 1.2, 1.4, 1.6:1.

tween calculated and observed values of absorbance for all experimental points is minimized. The output of program KINFIT comprises the refined parameters, the sum-of-squares and the standard deviations of data.

2.5. Thermodynamic data

In order to understanding the thermodynamics of the complexation reactions of iodine with the used macrocycles and DOMBT, it is useful to consider the enthalpic and entropic contributions of these reactions. The enthalpy and entropy of the complexation reactions were determined by

measuring the formation constants as a function of temperature [20]. The formation constants of all molecular complexes in chloroform at various temperatures, obtained by computer fitting of the corresponding absorbance–mole ratio data and are listed in Table 2. The fair agreement between the observed and calculated absorbances is a further support of the occurrence of a 1:2 complexation between used donors and I $_2$ in chloroform solution. For obtaining the thermodynamic parameters, plots of $\log K_f$ vs. $1/T$ are considered for the all studied cases. The enthalpies and entropies of complexation were determined in the usual manner from the slopes and intercepts of

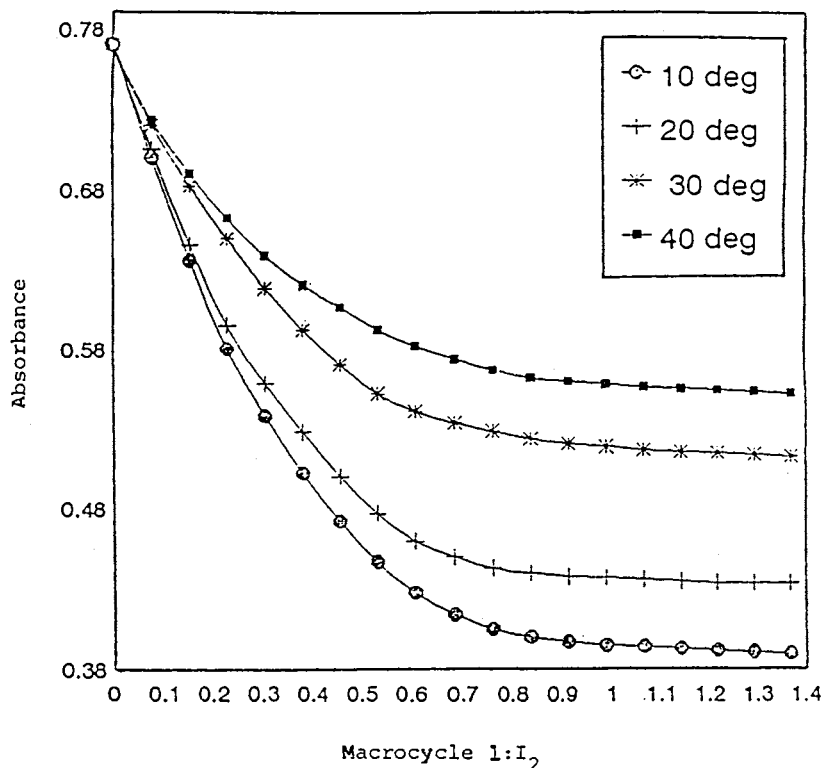


Fig. 2. Plots of absorbance vs. macrocycle 1: I₂ mole ratio in chloroform solution at 510 nm and various temperature.

plots respectively. The results are also included in Table 2.

2.6. Kinetic data

In order to investigate the kinetics of triiodide formation, the absorbance at 364 nm was monitored as a function of time in a chloroform solution containing the reactants in I₂:macrocycle mole ratio about 18:1 (analytical concentration of I₂ = 5.0 × 10⁻⁴ mol dm⁻³) at 25°C. The absorbance changes were found to be in accord with first order kinetics. The rate constants were calculated by the Guggenheim method using the relationship:

$$\ln(A_{\infty} - A_t) = -k(t_{\infty} - t_0) + \ln(A_{\infty} - A_0) \quad (6)$$

The rate values obtained from the slope of the corresponding plots of $\ln(A_{\infty} - A_t)$ vs. $(t_{\infty} - t_0)$. As is seen in Table 2, the rate constants vary in the order of $1 \approx 2 > 3$.

3. Results and discussion

3.1. Part A: complexation with iodine

The electronic absorption spectra of macrocycle **2** in the presence of increasing amounts of iodine in chloroform solution at 25°C is shown in Fig. 1. The corresponding spectra for macrocycle **1** and DOMBT (**3**) are very similar to those of macrocycle **2** and thus are not included. Addition of donors to iodine results in two new absorption bands at 292 and 364 nm. The existence of these bands are presumably due to the formation of iodine–macrocycle complex (or iodine–DOMBT complex). These bands are well known to be characteristic for the formation of triiodide ion, I₃⁻, in the complex formation process between iodine and different electron pair donating ligands [14,21,22].

For understanding of the stoichiometry of reactions the mole ratio method was used. The plot of

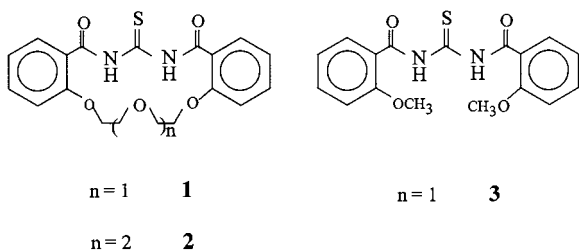
Table 1

Conductivity of macrocycle donors, DOMBT and their complexes with iodine and bromine in chloroform solution at 25°C

Donors	Conc. mM ^a	$k \times 10^5, \Omega^{-1} \text{ cm}^{-1}$		
		Before X ₂ addition	After Br ₂ addition	After I ₂ addition
1	1.24	0.218	0.872	0.667
2	1.07	0.202	0.720	0.621
3	1.16	0.224	0.488	0.432

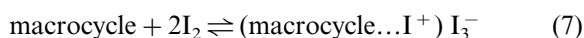
^a [I₂] = 2.85 mM, [Br₂] = 2.88 mM.

absorbance vs. macrocycle/I₂ mole ratio indicated the formation of a 1:2 (macrocycle to iodine) and (DOMBT to iodine) complexes in chloroform solution. (Fig. 2) Moreover, the existence of an isosbestic point in the spectra (see Fig. 1) supports the occurrence of a simple complexation equilibrium in solution. It is interesting to note that, the curvature of absorbance–mole ratio plots decrease in the order of **1** ≈ **2** > **3** which reflects a decrease in the stability of the resulting iodine complexes in this sequence.

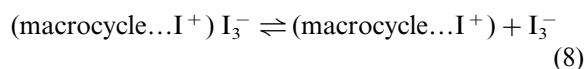


For supporting of the formation of triiodide ion the conductivity of solution was measured before and after addition of iodine to macrocycle solution. The increasing of the conductivity of solution (Table 1) indicates the formation of I₃⁻ in the solution.

Based on the observed spectral behavior and conductivity measurements, the formation of triiodide ion can be reasonable assumed to occur in two steps: The first step involves the formation of a molecular complex in the form of (macrocycle...I⁺) I₃⁻ in which the I₃⁻ ion exists as a contact ion paired anion, i.e.



The formation of such molecular complexes have been reported previously [21–23]. In the second step, which is actually the rate determining step for the formation of triiodide ion, the resulting molecular complex is further decomposed to release free I₃⁻ ion into chloroform solution, as:



As the data in Table 2 indicate, the stability of both macrocycle complexes with iodine are similar and, especially, for DOMBT complexes are several times of magnitude smaller than macrocyclic donors with iodine. This results exhibit, the effect of macrocyclic cavity on the stability of the resulting complexes. In other word the cavity can surrounded the I⁺ ion and keep it, but the flexibility of DOMBT is larger and cannot completely keep the I⁺ ion, therefore, the stability of complex is decreased.

As can be seen in Table 2, the iodine complexes with macrocycles **1**, **2** and DOMBT are enthalpy stabilized but entropy destabilized. It should be noted that similar behavior was previously observed for the macrocyclic complexes with iodine in different solvents [12–14]. The data indicate that, the entropy of reaction of iodine with macrocyclic donors are more negative than DOMBT. The degree of flexibility is maybe responsible for this effect. Because of the larger flexibility of DOMBT than macrocyclic donors, the I⁺ ion can change the conformation of DOMBT partially and thus the change of entropy is less negative. The reported thermodynamic data

Table 2

Rate constants and thermodynamic data for the formation of molecular complexes between iodine and macrocycles **1**, **2** and DOMBT in chloroform solution

Donors	k (min ⁻¹)	log K_f					ΔH (kJ mol ⁻¹)	ΔS (J mol ⁻¹ ° ⁻¹)
		10°C	20°C	25°C	30°C	40°C		
1	0.83	6.17	6.07	5.89	5.79	5.60	-35.29	-14.22
2	0.79	6.15	6.06	5.82	5.73	5.57	-40.9	-24.66
3	0.025	4.29	4.15	4.03	3.93	3.75	-30.6	-6.34
18-C-6 ^a	—	—	—	0.69	—	—	-13.7	-32.6

^a Data taken from [12].

for the 18-crown-6 system are included for comparison.

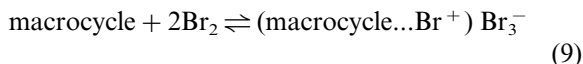
3.2. Part B: complexation with bromine

The complexation of macrocycle **1** AND **2** and DOMBT (**3**) with bromine were studied in chloroform solution at 25°C. The electronic absorption spectra of bromine in the presence of increasing amount of macrocycle **1** is shown in Fig. 3. The corresponding spectra for macrocycle **2** and DOMBT **3** are very similar to those with **1** and thus are not included. The observed blue shift of bromine visible bond and increasing the intensity of bromine UV-band with increasing of macrocycle concentration can be attributed to the formation of charge transfer complex. Bromine in the presence of tetrabutylammonium bromide in chloroform solution has shown such absorption behavior. It should be noted that 272 nm band is well known to be characteristic for the formation of tribromide ion, Br₃⁻, in the process of complex formation between bromine and different electron donors [24,25].

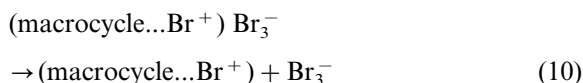
The mole ratio method was used for evaluation of stoichiometry of the resulting molecular complexes, which absorbance versus mole ratio plots of the resulting molecular complexes are exhibited in Fig. 4. From the figures, the mole ratio of 0.5 indicates 1:2 stoichiometry of the complexes obviously. Moreover, the existence of a well defined isosbestic point in the spectra of bromine upon titration with the macrocycle

(Fig. 3) further supports the occurrence of a simple complexation equilibrium in solution.

The formation of tribromide ion is supported by conductivity measurement of fixed donors concentration prior and former the addition of bromine to the solutions (see Table 1). The conductivity enhancement can be attributed to the releasing of Br₃⁻ from contact ion pair to free or solvent separated ion pair. Based on spectral behavior and conductivity measurements the formation of tribromide ion can be reasonably assumed to occur in two steps: the first step involves the formation of a molecular complex as (macrocycle...Br⁺) Br₃⁻ in which the Br₃⁻ ion exists as a contact ion paired anion, i.e.



In the second step, the resulting molecular complex is further decomposed and finally forms the free tribromide ion, as:



for the evaluation of the formation constants of the resulting molecular complexes, the absorbance–mole ratio data were obtained at 367 nm at 25°C and by using a non-linear least-squares curve fitting program KINFIT [14,16], the values of K_f were calculated. For both of macrocyclic donors complexes with bromine the $K_f \gg 10^8$. It should be noted that this method generally becomes unreliable for very strong complexes with $K_f > 10^8$.

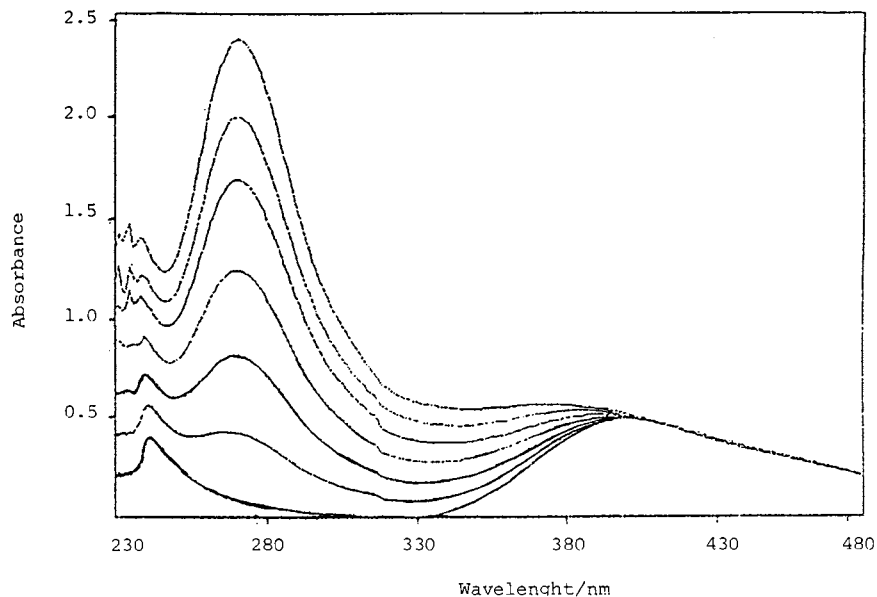


Fig. 3. Absorption spectra of 3×10^{-3} mol dm $^{-3}$ bromine in chloroform in the presence of various concentration of macrocycle **1**. The macrocycle: Br $_2$ mol ratios from the bottom to the top spectrum are 0.0, 0.18, 0.36, 0.54, 0.72, 0.9 and 1.02: 1

The FTIR spectra of both macrocycles show the C=O vibrational frequency shifted to higher frequency in the complexes than free donors, (1729 \rightarrow 1750 cm $^{-1}$ for **1**, 1729 \rightarrow 1736 cm $^{-1}$ for **2**) and the intensity of all bands show a considerable increasing in the complexes. This effects have been observed previously for some other charge-transfer complexes [23]. Two proba-

ble factors are responsible for these increasing shifts. The first effect is more contribution of non-bonding electrons of nitrogen in resonance with C=S, which increases the electron density of sulfur, and its ability to donation of electron to σ^* orbital of bromine. The second effect may be attributed to the more symmetrical shape of the macrocycle molecule after complexation with bromine.

The conductivity, spectrophotometric and IR data indicate that the cavity of macrocycle **1** is fitter than **2** for Br $^+$ ion. Probably higher flexibility of **2** and its larger size, can not keep Br $^+$ ion completely. On the other hand the corresponding results for the linear DOMBT–bromine complex show that the stability of this complex is very smaller than macrocyclic donors with bromine and it is attributed to the effect of macrocycles cavity and more donor sites of these compounds on the stability of the resulting complexes. Therefore, the cavity can surround the Br $^+$ ion and keep it, whereas the flexibility of DOMBT is larger so can't keep Br $^+$ ion completely, consequently the stability of complex is decreased considerably.

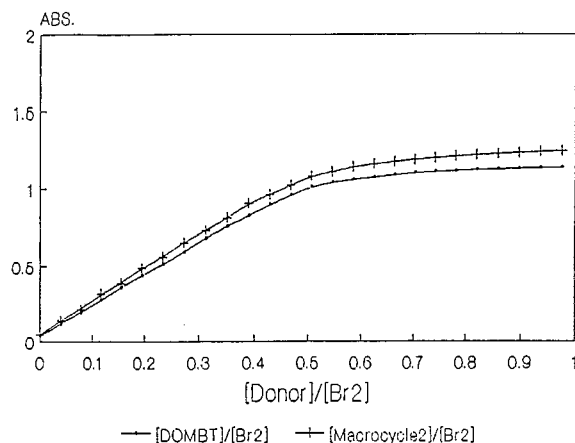


Fig. 4. Plots of absorbance vs. macrocycle **2**: Br $_2$ and DOMBT: Br $_2$ in chloroform solution at 272 nm and 25°C.

Acknowledgements

We are thankful to Shiraz University Research Council for their financial support.

References

- [1] C.J. Pedersen, *J. Am. Chem. Soc.* 89 (1967) 7017.
- [2] E. Shchori, J. Jagur-Grodzinski, Z. Luz, M. Shporer, *J. Am. Chem. Soc.* 93 (1971) 7133.
- [3] R.M. Izatt, J.J. Bradshaw, K. Pawalk, R.L. Bruning, *Chem. Rev.* 91 (1991) 1721.
- [4] M.R. Gangali, H. Eshghi, H. Sharghi, M. Shamsipur, *J. Electroanal. Chem.* 405 (1996) 177.
- [5] H. Sharghi, H. Eshghi, *Tetrahedron* 51 (1995) 913.
- [6] L.J. Andrew, R.M. Keefer, *Molecular Complexes in Organic Chemistry*, Holden-Day, New York, 1964.
- [7] R.V. Ball, G.M. Eckert, F. Gutmann, D.K.Y. Wong, *Anal. Chem.* 66 (1994) 1198.
- [8] W. Hirsch, G. Greenman, R. Pizer, *Can. J. Chem.* 71 (1993) 2171.
- [9] R.M. Izatt, J.J. Bradshaw, K. Pawalk, R.L. Bruning, B.J. Tarbet, *Chem. Rev.* 92 (1992) 1261.
- [10] S.R. Salman, S.M. Al-Marsumi, *Spectrochim. Acta Part A.* 49 (1993) 435.
- [11] A. Semnani, M. Shamsipur, *Spectrochim. Acta Part A.* 49 (1993) 411.
- [12] H.P. Hopkins, D.V. Jahagirdar, F. Windlar, *J. Phys. Chem.* 82 (1978) 1254.
- [13] M. Abedi, MS. Thesis, Shiraz University, Shiraz, IRAN.
- [14] A. Semnani, M. Shamsipur, *J. Chem. Soc. Dalton Trans.* (1996) 2215.
- [15] H. Sharghi, A.R. Massah, H. Eshghi, Kh. Niknam, *J. Org. Chem.* 63 (1998) 1455.
- [16] V.A. Nicely, J.L. Dye, *J. Chem. Educ.* 48 (1971) 443.
- [17] W.E. Wentworth, *J. Chem. Educ.* 42 (1962) 96.
- [18] W.E. Wentworth, *J. Chem. Educ.* 42 (1962) 162.
- [19] M.J.D. Powell, *Comput. J.* 7 (1964) 155.
- [20] M. Hassani, M. Shamsipur, *J. Inclusion Phenomen.* 16 (1993) 123.
- [21] M. Mizuno, J. Tanaka, I. Harada, *J. Phys. Chem.* 85 (1981) 1789.
- [22] L.J. Andrew, E.S. Prochaska, A. Loewenschuss, *Inorg. Chem.* 19 (1980) 463.
- [23] Y.A. Serguchev, T.I. Petrenko, *Teor. Eksp. Khim.* 13 (1977) 705.
- [24] H.D. Spivey, T. Shedlovsky, *J. Phys. Chem.* 71 (1967) 2165.
- [25] E. Shchori, J.J. Grodzinski, *J. Am. Chem. Soc.* 94 (1972) 7957.

Multiwavelength spectrophotometric determination of acid dissociation constants

Part IV. Water-insoluble pyridine derivatives

K.Y. Tam ^{a,*}, M. Hadley ^b, W. Patterson ^b

^a *Sirius Analytical Instruments Ltd., Riverside, Forest Row Business Park, Forest Row, East Sussex, RH18 5DW, UK*

^b *SmithKline Beecham Pharmaceuticals, Old Powder Mills, Near Leigh, Tonbridge, Kent TN11 9AN, UK*

Received 3 November 1998; received in revised form 29 December 1998; accepted 6 January 1999

Abstract

A multiwavelength spectrophotometric (WApH) titration method for determination of acid dissociation constants (pK_a values) of ionizable compounds developed previously was applied in the case of pyridine derivatives of pharmaceutical interest. Specifically, UV absorption spectra of the drug solution are acquired in the course of a pH-metric titration using an optical device based on a fibre optics dip probe, a light source and a diode array detector. Target factor analysis was applied to deduce the pK_a values from the spectral data recorded at different pH. Using this technique, the pK_a values of six pyridine derivatives were determined successfully. It was demonstrated that the WApH technique in this case outperforms conventional pH-metric methods with respect to the measurement of pK_a values of the sparingly water soluble samples reported in this study. © 1999 Elsevier Science B.V. All rights reserved.

Keywords: Acid dissociation constants; Spectrophotometric titration; Target factor analysis; Pyridine

1. Introduction

Acid dissociation constants (pK_a values) are important parameters to denote the extent of ionization of molecules in solution at different pH values. In the context of pharmaceutical drug discovery and development, the aqueous solubility of compounds may not be high enough for precise

pK_a determination using conventional pH-metric titration. If the sample is sufficiently soluble in a water-miscible organic solvent, it is possible to determine pH-metrically the apparent pK_a (p_sK_a) in co-solvent mixtures [1]. Aqueous pK_a values can be determined by extrapolation of the p_sK_a values, using the Yasuda–Shedlovsky method, to zero organic solvent content (a plot of $p_sK_a + \log[H_2O]$ vs. $A/\epsilon + B$, where $[H_2O]$, ϵ , A and B represent, respectively, the molar concentration of water, the dielectric constant of the co-solvent mixture, the slope and the intercept of the plot)

* Corresponding author. Tel.: +44-1324-820-720; fax: +44-1324-820-725.

E-mail address: sirius@cix.compulink.co.uk (K.Y. Tam)

[2]. We have recently reported the use of eight popular organic solvents for this purpose [3]. However, it may even be difficult to apply this technique for water-insoluble samples that are only sparingly soluble in the co-solvent mixtures.

Spectrophotometric pK_a determination is an alternative method provided the compound is water soluble to the extent of 10^{-6} M and it contains chromophore(s) in proximity to the ionization centre(s). Traditionally, spectral data at a single analytical wavelength is acquired from the sample in a series of solutions with known pH values. If the molar absorptivities of the reacting species are known, the pK_a value(s) can be computed by fitting the experimental data to established formulae [1]. Computer programs used for calculating the acid dissociation constants from multiwavelength spectrophotometric data have been reported [4,5, and the refs. therein]. Most of these methods involve a least-squares procedure whereby the differences between the theoretical and experimental absorbance values are minimized by means of the Gauss–Newton–Marquardt algorithm [5]. To this end, the unknown pK_a values and/or the molar absorptivity of individual reacting species are treated as adjustable parameters. Chemometric approaches based on factor analysis have been applied to determine acid dissociation constants from spectroscopic titrations [6,7]. In these reported procedures, the molar absorptivities are usually not required for analysis. However, explicit equations for the equilibrium expression are necessary to rotate the eigenvector(s) to give the correct concentration profiles. It may be difficult to generalize these explicit equations for multistep ionization systems. For instance, [6] called for the Henderson–Hasselbalch equation as the parametrized model while [7] needed to solve each element of the transformation matrix algebraically which is obviously tedious for real-life ionizable drug substances with larger number of unknown pK_a s than those studied in the paper.

In our previous work [8], we developed a multi-wavelength spectrophotometric (WApH) titration approach to interrogate drug compounds with one or two pK_a values. Specifically, we used a fibre optics dip probe, a UV light source and a

photodiode array (PDA) detector in conjunction with a commercially available titrator (Sirius PCA101) to capture the absorption spectra of the sample in the course of a pH-metric titration. Target factor analysis (TFA) was applied with success to deduce the pK_a values of drug substances and resolve the absorption spectra of the reacting species, without prior knowledge of their optical properties. In another study [9], we have shown that the TFA method outperforms the established first derivative technique in terms of obtaining pK_a results. Moreover, the WApH technique has been utilized to examine several multiprotic ionization drugs which involved four unknown pK_a s [10]. In particular, some of these pK_a values were within mid pH range which were difficult to determine because of insufficient spectra data acquired in the un-buffered region of the titration curve. With the aid of the WApH technique in coupled with an optically transparent buffer, all the unknown pK_a values have been successfully determined and were in excellent agreement with the pH-metric results. In contrast to the related approaches using factor analysis method [6,7], we generated the target matrices (i.e. the theoretical concentration profiles) using the Cramer's rule method [8] which is relatively easy to extend to multiprotic ionization systems [10].

In this work, we have examined six pharmaceutical intermediates (pyridine derivatives) with structures given in Fig. 1. We deliberately selected samples that were: I) soluble in water, acetonitrile–water or methanol–water mixtures (SKF-75250, SB-209471 and SB-221789) and II) sparingly soluble in water and other co-solvent mixtures (SB-221787, SB-209247 and SB-234013) to exemplify the use of the WApH technique in measuring the pK_a values. It is envisaged that the pK_a s of these substituted pyridine compounds are less than 2 which implies precise potentiometric determination would be difficult [1]. Moreover, the solubilities of type II compounds in water and other co-solvent mixtures are so low such that pH-metric titration is hard to obtain reliable results. In the framework of spectrophotometric titration, the pK_a values are derived from the spectral changes recorded at the extreme region of pH (< 2) whereby the pH data may be problem-

atic. Here, we employed an established four-parameter equation to calibrate the pH electrode [2,3,11] so giving more reliable measurements as compared with the conventional electrode calibration protocols using two or three buffer solutions [12]. The goal of this study is to apply the WApH technique in conjunction with a robust electrode calibration procedure to determine the pK_a values which are virtually impossible to measure by means of conventional pH-metric titration. In the following discussion, a brief account on the TFA and WApH methods is presented. It was demonstrated that, when available, the pK_a values ob-

tained from pH-metric co-solvent titrations agree with those deduced by the WApH technique.

2. Calculations

With WApH titrations, the data obtained consist of a series of spectra acquired at different pH values. According to Beer's law, the absorbance matrix, **A**, can be expressed as follows:

$$\mathbf{A} = \mathbf{CE} \quad (1)$$

where **C** and **E** represent, respectively, the concentration–pH profile of the ionization system and the molar absorptivity matrix with the inclusion of the optical path length. The unknown pK_a values are derived from the **A** matrix using the mathematical treatment as shown below.

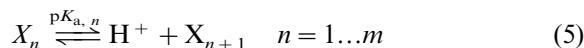
Principal component analysis [13–15] is first applied to **A** to calculate an abstract solution for **C** and **E**, namely, \mathbf{C}_{abs} and \mathbf{E}_{abs} , which contain only the primary eigenvalues (λ_r) and eigenvectors (\mathbf{Q}_r). The residual standard deviation [14], IND function [13,14], eigenvalue ratio [16] and reduced eigenvalue ratio [17,18] are utilized to identify the number of principal components (independent light absorbing species) present in the chemical system. In the TFA treatment, the abstract solution can be rotated to the one with relevant physical significant \mathbf{C}_p and \mathbf{E}_p by a transformation matrix **T** [14,19,20] as given below:

$$\mathbf{T} = \lambda_r^{-1} \mathbf{C}_{\text{abs}}^T \mathbf{C}_t \quad (2)$$

$$\mathbf{A} \approx \mathbf{C}_{\text{abs}} \mathbf{T} \mathbf{T}^{-1} \mathbf{E}_{\text{abs}} \quad (3)$$

$$\mathbf{A} \approx \mathbf{C}_p \mathbf{E}_p \quad (4)$$

where the superscripts -1 and **T** denote, respectively, inverse and transpose operations. The test matrix \mathbf{C}_t in Eq. (2) contains the concentration–pH profiles of the m -step ionization system which are generated theoretically by solving the following mass balance equations [8].



$$Y = \sum_{n=1}^{m+1} C(n) \quad (6)$$

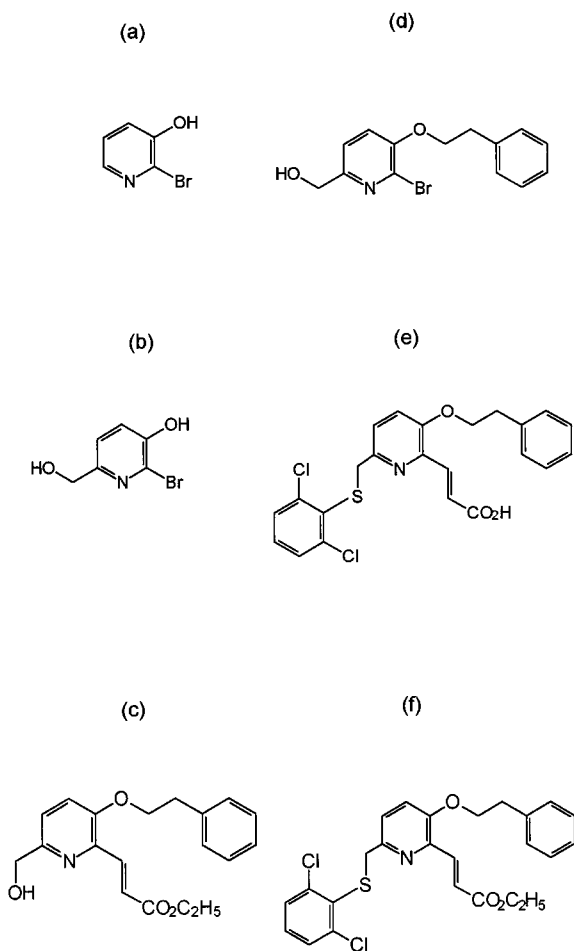


Fig. 1. Structural formula of (a) SKF-75250, (b) SB-209471, (c) SB-221789, (d) SB-221787, (e) SB-209247 and (f) SB-234013.

where $pK_{a,n}$ and X_n represent, respectively, the acid dissociation constant and the individual reacting species (with charge being excluded for clarity) while Y and $C(n)$ symbolize the initial concentration and concentration of X_n , respectively. In this study, the concentration pH value ($p_cH(= -\log[H^+])$) is related to the operational pH reading by a multiparametric equation as given below [2,3,11]:

$$pH = \alpha + Sp_cH + j_H[H^+] + j_{OH} + \frac{K_w}{[H^+]} \quad (7)$$

The intercept parameter α corresponds to the negative logarithm of the activity coefficient of H^+ at working temperature and ionic strength. The S term denotes the ratio between the actual slope and the Nernst slope. The j_H term corrects pH readings for the non-linear pH response due to liquid junction and asymmetry potentials in moderately acidic solution (pH 1.2–2.5), while the j_{OH} term corrects for any high-pH (pH > 11) non-linear effects. These parameters are determined by a weighted non-linear least squares procedure [11]. The ionization constants of water (K_w) as a function of temperature and ionic strength, were taken from Sweeton et al. [21].

The SPOIL function as derived by Malinowski [14,20] is utilized to determine whether a test matrix is acceptable or not. In general, a test matrix in which the SPOIL function is minimized to a value not greater than 3.0 is considered as the solution for the target transformation procedure [8–10,14,19,20,22]. For a particular **A** matrix, the SPOIL function depends only on **C_t** which in turn is a function of the sought pK_a values (see Eqs. (5) and (6)). The TFA computation optimizes the pK_a values for a global minimum of the SPOIL function. The SIMPLEX method [23] can be used for this purpose.

3. Experimental

3.1. Reagents and apparatus

Pharmaceutical intermediates SKF-75250, SB-209471, SB-221789 (hydrochloride salt), SB-221787, SB-209247 and SB-234013 (hydrochloride

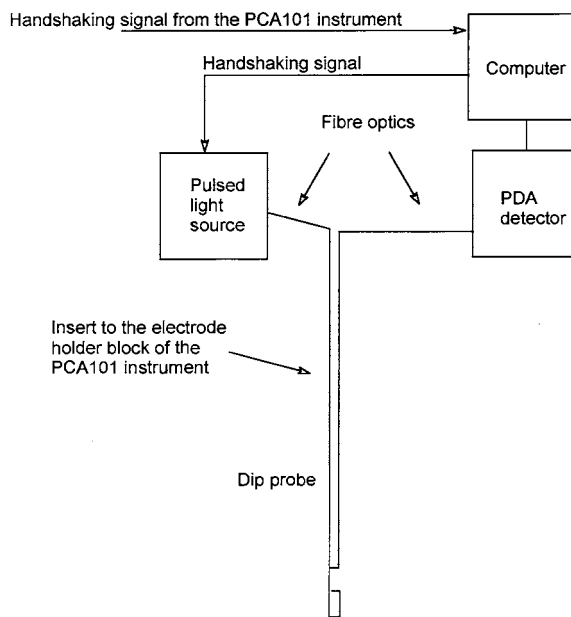


Fig. 2. Schematic for the experimental setup utilized in the WApH titration.

salt) were provided by SmithKline Beecham Pharmaceuticals (Tonbridge, Kent, UK). Acetonitrile (far UV grade) was supplied by Romil (Cambridge, UK). Methanol and potassium chloride (all AR grade) were obtained from Fisher (Loughborough, UK). Solutions were prepared in deionized water of resistivity $> 10^{14} \Omega \text{ cm}$. The preparation and standardization of HCl and KOH solutions have been described elsewhere [11]. Potassium chloride was added to standardize the ionic strength of water and solvent–water mixtures. All titrations were performed by using a PCA101 or a GLp K_a automatic titrator (Sirius, Forest Row, UK) [2]. The pH electrode was supplied by Orion (Ross™ type, Beverly, USA) and was calibrated titrimetrically in the pH range of 1.6–12.2 in the relevant solvent media before use [2,11]. The processing of the pH-metric data, calculations of p_sK_a values via a non-linear least square procedure and Yasuda–Shedlovsky extrapolation treatments were carried out using $pK_a\text{LOGP}^{\text{TM}}$ software (v5.01, Sirius).

For the WApH titration, a schematic diagram of the experimental setup is given in Fig. 2. The optical system consists of a pulsed deuterium

lamp (Cathodeon, Cambridge, UK) and a 256-element photodiode array (PDA) detector (Carl Zeiss, Herts., UK). This combination offers a spectral range of 200–735 nm with blaze wavelength at 220 nm. A bifurcated fibre optics dip probe (Custom Sensor & Technology, MO, USA) with optical path length of 1-cm was connected to the deuterium lamp and the PDA detector. Synchronization of the titrator, pulsed deuterium lamp and spectrum acquisition by the PDA detector was accomplished using a terminate-and-stay-resident system [24]. The program for TFA treatment on the WApH data was coded in a Turbo C environment [8–10].

3.2. UV/pH titrations

All titrations were performed in solutions of 0.15 M KCl under argon atmosphere at $25 \pm 0.5^\circ\text{C}$ using standardized 0.5 M HCl or 0.5 M KOH titrants. In the present study, sample concentrations of 1.6×10^{-3} – 4.7×10^{-3} M and 5.5×10^{-6} – 4.4×10^{-5} M were employed, respectively, for pH-metric and WApH titrations. In general, sample solutions of 10–20 ml volumes were pre-acidified to a relatively low pH value (ca. 1.4) and then titrated alkalimetrically to an appropriate high pH value (4.0–8.0). The pH change per titrant addition was limited to ca. 0.1 pH units. pH data were acquired when the drift was less than 0.01 pH units min^{-1} . For each co-solvent experiment, a weighed amount of sample was dissolved in 8–40 wt.% of acetonitrile or methanol before titration. For the WApH titration, a stock solution was prepared either by dissolving ca. 1.0 mg of sample in 1.0 ml 80 wt.% methanol or 50.0 ml acidified water. 50- μl or 1.0-ml aliquots of the stock solutions were then transferred into a sample vial containing 10–20 ml 0.15 M KCl solution to produce the required sample concentration. Spectral data were recorded in the region of 200–450 nm after each pH adjustment.

4. Results and discussion

Six pharmaceutical intermediates of pyridine derivative were interrogated in this study. In the

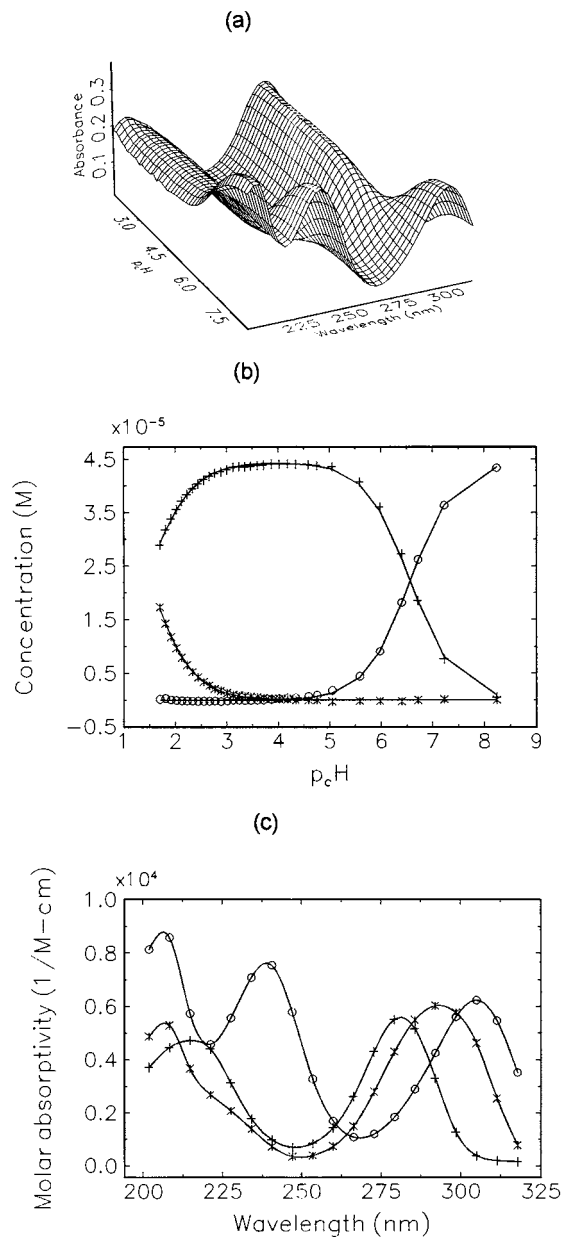


Fig. 3. (a) Absorption spectra of SKF-75250, (b) Distribution of species for SKF-75250 as a function of $p_c\text{H}$ with the symbols (* fully protonated species, + mono-protonated species, o fully deprotonated species) represent the C_p matrix and solid lines denote the C_t matrix. (c) Molar absorptivity coefficients of SKF-75250. The symbols (see (b)) represent the elements in matrix E_p . Solid lines are generated using the cubic spline interpolation method.

Table 1

pK_a values of SKF-75250, SB-209471, SB-221789, SB-221787, SB-209247 and SB-234013 as determined using the WApH and the pH-metric techniques at 25°C and an ionic strength of 0.15 M

Type			WApH ^a	pH-metric		
				Aqueous ^a	Acetonitrile–water ^b	Methanol–water ^b
I	SKF-75250	$pK_{a,1}$	1.48 ± 0.07	1.79 ± 0.02	1.43 ± 0.32	— ^c
		$pK_{a,2}$	6.59 ± 0.07	6.56 ± 0.01	6.54 ± 0.02	6.33 ± 0.39
	SB-209471	$pK_{a,1}$	1.21 ± 0.05	—	—	—
		$pK_{a,2}$	6.52 ± 0.04	6.51 ± 0.01	6.56 ± 0.05	6.61 ± 0.06
SB-221789	$pK_{a,1}$	2.74 ± 0.03	—	2.51 ± 0.07	2.65 ± 0.19	
II	SB-221787	$pK_{a,1}$	1.55 ± 0.03	—	—	—
	SB-209247	$pK_{a,1}$	1.64 ± 0.04	—	—	—
		$pK_{a,2}$	3.14 ± 0.08	—	—	—
	SB-234013	$pK_{a,1}$	1.47 ± 0.02	—	—	—

^a Uncertainties equal to the standard deviation of the pK_a values from three experiments.

^b Values obtained using the Yasuda–Shedlovsky extrapolation method [2,3] (uncertainty represents the estimated standard deviation).

^c Not available.

subsequent discussion, we classified the compounds into two types:

Type I: Compounds soluble in water, acetonitrile–water or methanol–water mixtures, e.g. SKF-75250, SB-209471 and SB-221789

Type II: Compounds sparingly soluble in water and co-solvent mixtures, e.g. SB-221787, SB-209247 and SB-234013

4.1. Type I compounds

SKF-75250 and SB-209471 were water soluble up to mM concentrations while SB-221789 was soluble in acetonitrile–water and methanol–water mixtures at similar concentrations. This permitted a direct comparison of the pK_a values determined using the WApH technique with pH-metric results. TFA was applied to absorption spectra of these three compounds and in all cases the correct number of light-absorbing species was identified. Fig. 3 shows the absorption spectra, the distribution of species and the resolved molar absorptivity coefficients of SKF-75250. The unknown pK_a values were successfully determined with the SPOIL function of each component less than 3.0. Table 1 lists the pK_a values of SKF-75250, SB-209471 and SB-221789 obtained by the WApH and the pH-metric techniques. It can be seen that the agree-

ment between the WApH and the pH-metric results is generally good. However, when using pH-metric measurements, accurate determination of the low pK_a values of the 2-bromo-pyridine derivatives such SKF-75250 as SB-209471 was difficult due to the potentiometric data at the extreme region of pH (< 2) being relatively noisy compared with the data obtained from the mid-range of pH. It has previously been established that a sample concentration > 15 mM (or 400 times the buffer capacity of water) should be utilized for measuring pK_a values in the extreme pH region [25]. However, this concentration level was difficult to obtain for the type I compounds. The WApH technique was able to determine the pK_a values of the pyridine derivatives in this extreme region of pH.

4.2. Type II compounds

The solubilities of the type II samples in water, acetonitrile–water and methanol–water mixtures were so low that reliable pH-metric determination was difficult. TFA treatment revealed the correct number of principal components in these chemical systems. Fig. 4 shows the absorption spectra, the distribution of species and the resolved molar absorptivity coefficients of SB-234013. Again, the

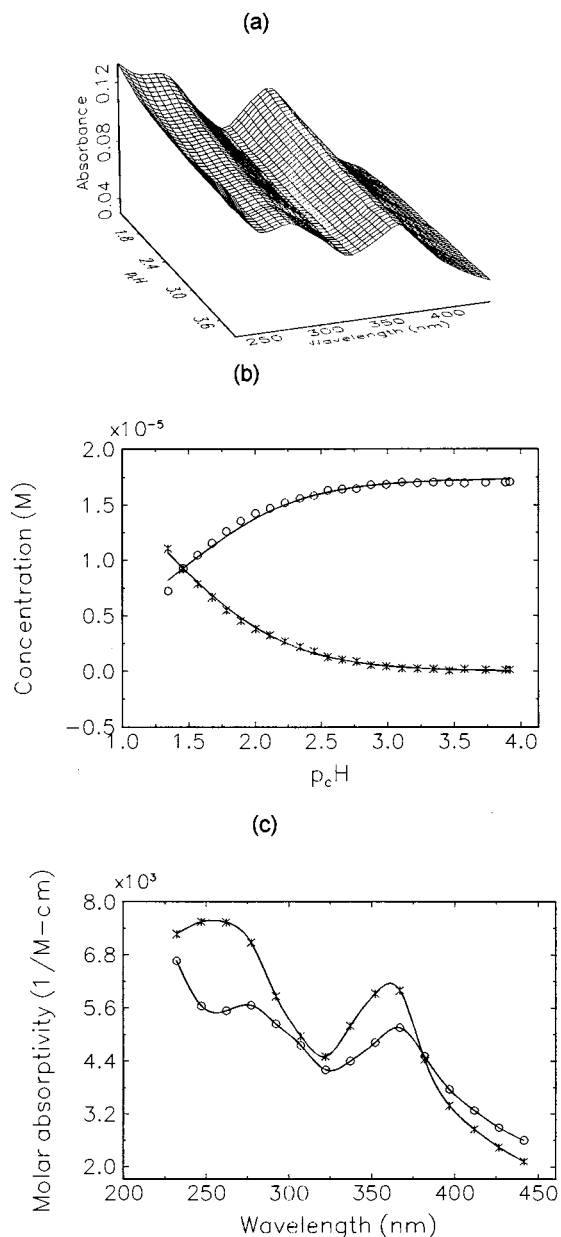


Fig. 4. (a) Absorption spectra of SB-234013, (b) Distribution of species for SB-234013 as a function of p_cH with the symbols (* fully protonated species, O fully deprotonated species) represent the C_p matrix and solid lines denote the C_t matrix. (c) Molar absorptivity coefficients of SB-234013. The symbols (see (b)) represent the elements in matrix E_p . Solid lines are generated using the cubic spline interpolation method.

SPOIL function was found to be less than 3.0 for each component. Table 1 gives the pK_a values of type II compounds derived using the WApH method. By considering the pK_a values of type I and II compounds, it can be seen that the pK_a value of the pyridine group varies with the nature of the substituents in the 2-position which may be summarized as below:

1. Bromo-substituent: $1.2 < pK_a < 1.8$ (SKF-75250, SB-209471, SB-221787)
2. Phenylthio- and propenoic ester-substituent: $1.4 < pK_a < 1.7$ (SB-209247, SB-234013)
3. Propenoic ester-substituent: $2.5 < pK_a < 2.8$ (SB-221789)

The WApH results derived from the analysis of the compounds examined are generally in line with expected values. The presence of the bromo group at the 2-position would be expected to exert a strong negative inductive effect on the pyridine nitrogen, reducing its basicity markedly in comparison to 3-hydroxypyridine (pK_a value ca. 4.8, [26]). Replacement of the bromo group with other less electronegative substituents eg. propenoic ester or acid groups has the effect of reducing the negative inductive effect and reducing basicity to a lesser extent in comparison to the bromo substituent.

5. Concluding remarks

A multiwavelength spectrophotometric titration (WApH) method was developed for the determination of pK_a values of ionizable compounds. The WApH technique was applied with success to determine the pK_a values of several water-insoluble pyridine derivatives of pharmaceutical interest. Typically, a 10–20 ml sample of concentration in the region of 10^{-6} M is sufficient for measurement. It was demonstrated that for water-insoluble samples with low pK_a values, the WApH technique in this case outperforms conventional pH-metric methods. It was also demonstrated that the pK_a value of the pyridine group present in the series of compounds examined depends very much on the nature of the substituents in the 2-position.

Acknowledgements

We thank Mr. J.E.A. Comer (Sirius) for various helpful comments.

References

- [1] A. Albert, E.P. Serjeant, *The Determination of Ionization Constants*, 3rd edn, Chapman and Hall, London, 1984.
- [2] A. Avdeef, J.E.A. Comer, S.J. Thomson, *Anal. Chem.* 65 (1993) 42.
- [3] A. Avdeef, K.J. Box, J.E.A. Comer, M. Gilges, M. Hadley, C. Hibbert, W. Patterson, K.Y. Tam, *J. Pharm. Biomed. Anal.*, in press.
- [4] H. Gampp, M. Maeder, C.J. Meyer, A.D. Zuberbühler, *Talanta* 32 (1985) 257.
- [5] P. Gans, A. Sabatini, A. Vacca, *Talanta* 43 (1996) 1739.
- [6] R.J. Pell, B. R. Kowalski, *J. Chemom.* 5 (1991) 375.
- [7] M. Kubista, R. Sjöback, B. Albinsson, *Anal. Chem.* 65 (1993) 994.
- [8] R.I. Allen, K.J. Box, J.E.A. Comer, C. Peake, K.Y. Tam, *J. Pharm. Biomed. Anal.* 17 (1998) 699.
- [9] K.Y. Tam, K. Takács-Novák, *Pharm. Res.*, in press.
- [10] R.C. Mitchell, C.J. Salter, K.Y. Tam, *J. Pharm. Biomed. Anal.*, in press.
- [11] A. Avdeef, J.J. Bucher, *Anal. Chem.* 50 (1978) 2137.
- [12] H. Galster, *pH Measurement*, VCH, Weinheim, 1991, p. 57.
- [13] E.R. Malinowski, *Anal. Chem.* 49 (1977) 612.
- [14] E.R. Malinowski, *Factor Analysis in Chemistry*, Wiley, New York, 1991.
- [15] P.J. Gemperline, *J. Chemom.* 3 (1989) 549.
- [16] H.B. Woodruff, P.C. Tway, L.J.C. Love, *Anal. Chem.* 53 (1981) 81.
- [17] P.J. Gemperline, J.C. Hamilton, *Factor analysis of spectro-chromatographic data*, in: H.L.C. Meuzelaar (Ed.), *Computer-Enhanced Analytical Spectroscopy*, vol. 2, Plenum, New York, 1990, pp. 27–48.
- [18] E.R. Malinowski, *J. Chemom.* 1 (1987) 33.
- [19] M. D'Amboise, B. Lagarde, *Comput. Chem.* 13 (1989) 39.
- [20] M. McCue, E.R. Malinowski, *Appl. Spectrosc.* 37 (1983) 463.
- [21] F.H. Sweeton, R.E. Mesmer, C.F. Baes, *J. Solution Chem.* 3 (1974) 191.
- [22] K.Y. Tam, F.T. Chau, *Chemom. Intell. Lab. Syst.* 25 (1994) 25.
- [23] J.A. Nelder, R. Mead, *Comput. J.* 7 (1965) 308.
- [24] K.Y. Tam, F.T. Chau, *Comput. Chem.* 19 (1995) 389.
- [25] J.E.A. Comer, A. Avdeef, K.J. Box, *Am. Lab. April* (1995) 36C.
- [26] S.B. Asensio, E. Lopez-Cantarero, J. Llor, *Can. J. Chem.* 70 (1992) 1635.

New approach for screening polycyclic aromatic hydrocarbons in water samples

Erik D. Hagestuen, Andres D. Campiglia *

Department of Chemistry, North Dakota State University, Fargo, ND 58105 5516, USA

Received 30 October 1998; received in revised form 12 January 1999; accepted 13 January 1999

Abstract

For the first time, solid-phase extraction (SPE) has been combined to room-temperature phosphorimetry (RTP) to determine the 16 polycyclic aromatic hydrocarbons related as major pollutants by the US Environmental Protection Agency (EPA). These include naphthalene, anthracene, acenaphthylene, acenaphthene, fluorene, fluoranthene, benzo(a)anthracene, benzo(k)fluoranthene, benzo(b)fluoranthene, benzo(a)pyrene, indeno(1,2,3-cd)pyrene, pyrene, chrysene, phenanthrene, benzo(g,h,i)perylene and dibenzo(a,h)anthracene. The pre-concentration factor obtained by SPE, combined with the sensitivity of RTP, resulted in calibration curves with linear dynamic ranges at the parts-per-billion level (ng ml^{-1}). The limits of detection were estimated at the parts-per-trillion level (pg ml^{-1}). Several pollutants usually encountered in water samples were tested for interference. These included polychlorinated biphenyls, pesticides, and volatile organic compounds. As a result of the appropriate combination of excitation wavelength (330 nm) and phosphorescence enhancers (0.1 M TINO_3 and 0.05 M sodium dodecyl sulfate, SDS), no interference was observed. The results demonstrate the potential of SPE-RTP for screening polycyclic aromatic hydrocarbons (PAHs) in environmental waters. © 1999 Elsevier Science B.V. All rights reserved.

Keywords: Solid-phase extraction; Room-temperature phosphorimetry; PAHs

1. Introduction

There is a critical demand to have rapid and simple screening techniques for polycyclic aromatic hydrocarbons (PAHs) in environmental samples. The development of screening techniques leads to shorter turnaround analysis time and

reduced costs for environmental monitoring and remediation.

A typical assay for the analysis of PAHs includes an extraction procedure followed by a chromatographic determination scheme. Gas chromatography-mass spectrometry (GC-MS) [1–4] and high-performance liquid chromatography (HPLC) [5–9] are major tools for the analysis of PAHs in water samples. Because of their lipophilic character, PAHs attach chemically to organic carbon in stream-bottom sediments. The partitioning process into sediment results in very

* Corresponding author. Tel.: +1-701-231-8702; fax: +1-701-231-8831.

E-mail address: campiglia@prairie.nodak.edu (A.D. Campiglia)

low concentrations in water samples below the limits of detection of the chromatographic method. Therefore, a concentration step is usually performed prior to chromatographic analysis.

Recently, the US Environmental Protection Agency (EPA) adopted solid-phase extraction (SPE) as the pre-concentration technique for PAHs in water and biological samples [10]. PAHs are separated from the sample onto a non-polar solid matrix by reversed phase mechanisms. The adsorbent phases are packaged in two basic formats: cartridges or membranes. For water analysis, membranes are preferred over cartridges, since the larger cross-sectional area and the shorter depth of extraction disks result in high flow rates and short analyses times [10].

The composition of SPE membranes consists of alkyl bonded silica particles enmeshed in an inert support. Unfortunately, free silanol (Si–OH) groups are also present on the silica which result in non-reversed phase interactions. The strong adsorption of PAHs on the silica surface results in low analyte recoveries. It is common to observe recoveries as low as 40%. Thermally assisted desorption, sonication of the adsorbent material, and microwave-assisted elution are often employed to improve analyte recoveries [11,12]. Although thermal desorption improves extraction efficiencies to acceptable recoveries for analytical use, this approach increases analysis time and provides ample opportunity for introduction of laboratory contaminants, loss of target compounds, and worker exposure. Time and labor to perform these and other necessary tasks are important since they affect analytical costs and delays in obtaining results.

In this study, a new approach for screening PAHs in water samples is presented. The new analytical tool combines SPE with solid-surface (SS) room-temperature phosphorimetry (RTP) [13,14]. Since the analysis of PAHs is performed on the adsorbing material, the drawbacks associated with SPE procedures are eliminated. The lack of interference from pollutants commonly encountered in water samples demonstrates the selectivity necessary for the determination of total PAHs. The pre-concentration factor obtained by SPE, combined with the sensitivity of RTP to-

wards PAHs, results in limits of detection at the ppt (pg ml^{-1}) level of concentration. The studies demonstrate that SPE-RTP provides a simple, rapid, and inexpensive experimental procedure for routine screening of PAHs in water samples.

2. Experimental

2.1. Chemicals

All chemicals were analytical-reagent grade and were used without further purification. Nanopure water was employed throughout. Octyl (C_8) and C_{18} membranes were obtained from Ansys Diagnostics. Their composition consists of bonded silica particles enmeshed in a glass fiber support. The average size and mean pore size of the silica particles were 30 μm and 7 nm, respectively. The mean thickness and diameter of the membranes were 1000 μm and 47 mm, respectively. Naphthalene, phenanthrene, pyrene, chrysene, 1,12-benzperylene [benzo(g,h,i)perylene], dibenz(a,h)anthracene [1,2:5,6-dibenzoanthracene], anthracene, acenaphthylene, acenaphthene, fluorene, fluoranthene, 1,12-benzanthracene [benzo(a)anthracene], 11,12-benzfluoranthene [benzo(k)fluoranthene], 3,4-benzfluoranthene [benzo(b)fluoranthene], benzo(a)pyrene, thallium(I) nitrate, lead(II) acetate, and sodium dodecyl sulfate (SDS) were purchased from Aldrich at their highest purity available. Indeno(1,2,3-cd)-pyrene, 2-chloro-4-ethylamino-6-isopropylamino-s-triazine [atrazine], 3,5-dibromo-4-hydroxybenzotrile [bromoxynil], 3-(3,4-dichlorophenyl)-1,1-dimethylurea [diuron], 2-chloro-*N*-[2-ethyl-6-methylphenyl]-*N*-[2-methoxy-1-methylethyl]acetamide [metolachlor], *N*-[5-(1,1-dimethylethyl)-1,3,4-thiadiazol-2-yl]-*N,N'*-dimethylurea [tebuthiuron], a,a,a-trifluoro-2,6-dinitro-*N,N*-dipropyl-*p*-toluidine [trifluralin], 2,3-dihydro-2,2-dimethyl-benzofuran-7-yl methylcarbamate [carbofuran], bis(2-ethylhexyl)phthalate, 1,1-bis(4-chlorophenyl)-2,2,2-trichloroethane (*p,p'*-DDT), and 2,2-bis(4-chlorophenyl)-1,1-dichloroethylene (*p,p'*-DDE) were purchased from Chem Service at their highest purity available.

Methanol was acquired from EM Science at 99.8% purity.

Note: Use extreme caution when handling thallium and lead salts, PAHs, and organochlorine compounds that are known to be extremely toxic.

2.2. Background reduction treatment

SPEC disks from several lots were tested for RTP measurements. The disks were solvent extracted with *n*-hexane for 8 h, cut into 1 × 2 cm tabs, and introduced into quartz tubes for UV irradiation (8 h). No significant difference was observed in the background emission of tabs from the same lot or within tabs from different lots. Similar behavior was observed in the analyte signal of compounds adsorbed on tabs from the same lot or tabs from different lots. The relative standard deviations reported for RTP measurements account for the effect of possible variations existing among silica grain size, binder coverage and coverage by octadecyl chains. The irradiated membranes were stored in a desiccator to be used as solid substrates.

2.3. Standard solutions and synthetic mixture preparation

Stock solutions of PAHs were prepared in methanol. Working solutions were obtained by appropriate dilution in methanol. Thallium nitrate, lead acetate, and sodium dodecyl sulfate (SDS) solutions were prepared in methanol/water 50:50 v/v.

Interference studies were carried out with a synthetic mixture of PAHs prepared in methanol. The concentration of each PAH in the mixture was 10 ppm. Standard solutions of atrazine, bromoxynil, diuron, metolachlor, tebuthiuron, trifluralin, carbofuran, bis(2-ethylhexyl)phthalate, *p,p'*-DDE and *p,p'*-DDT were prepared in methanol. Their potential interference was evaluated individually (at the 100 ppm concentration level) or in a mixture containing each pesticide at the 10 ppm level.

2.4. Sample procedure

2.4.1. Phosphorescence measurements

All solutions were spotted on solid substrates with 10- μ l micropipettes (Oxford Labware). Five μ l of surfactant and heavy-atom solutions were successively spotted on the solid substrate and dried in an oven for 15 min at 110°C. The substrates were placed into a desiccator (containing CaSO₄ chips) to be used for RTP measurements. A volume of 5 μ l of PAH solution was used in all the studies. The same volume was used for all the interference studies. After spotting the analyte solution (or interferent solution) on the solid substrate, the samples were placed into a desiccator until measurement time.

2.4.2. SPE-RTP measurements

SPE was performed by the usual procedure [10]. The extraction membrane was conditioned with 10 ml of methanol prior to sample application. Vacuum suction was adjusted to allow 1 l of sample to pass through the membrane in approximately 45 min. For a 38 mm active diameter disk, this flow rate is equivalent to a linear velocity of 0.03 cm s⁻¹, which is significantly slower than the maximum linear velocity (0.18 cm s⁻¹) recommended by EPA [15]. By working at 0.03 cm s⁻¹, a high retention efficiency of organic pollutants was assured.

Following water extraction, the SPE disk was cut in six pieces to fit in the spectrofluorimeter sample holder. After adding 5 μ l of 0.1 M TiNO₃ to each substrate, the samples were dried in an oven for 15 min at 110°C. The samples were then placed into a desiccator until measurement time.

2.5. Instrumentation

The collection of phosphorescence spectra, signal intensities and lifetime measurements were performed with a Fluorolog-3 spectrofluorimeter (ISA, JobinYvon-Spex, model FL3-11). A pulsed-lamp phosphorimeter attachment (Spex 1934) provided signal-gating circuitry so that a selected window of sample emission (gate time), after excitation (delay time), was allowed to reach the detector. The pulsed source consisted of a UV-vis

Xenon lamp with adjustable pulse rate between 0.05 and 33 flashes s^{-1} . The full-width, half maximum (FWHM) of each pulse was 3 μs . Two single-grating (1200 grooves mm^{-1}) spectrometers were used for wavelength selection. The excitation and emission blaze wavelengths were 250 and 500 nm, respectively. The detector was a photomultiplier tube (Hamamatsu, model R928) operating at room temperature in a photon-counting mode. Appropriate software (dM 3000, Spex Industries) was used for automated scanning and data acquisition.

The UV irradiation treatment for background reduction of solid substrates was carried out in a Rayonet photochemical reactor (Southern N.E. Ultraviolet Middletown) using eight lamps with maximum wavelength of emission (λ_{em}) at 254 nm, four with λ_{em} at 300 nm, and another four with λ_{em} at 350 nm.

3. Results and discussion

3.1. Comparison of C_8 and C_{18} membranes

Recently, the feasibility of detecting phosphorescence emission from PAHs adsorbed on octadecyl (C_{18}) extraction membranes was demonstrated. The RTP signals of pyrene, phenanthrene, 1,2:3,4-dibenzanthracene, 1,2:5,6-dibenzanthracene, benzo[g,h,i]perylene and chrysene were enhanced by co-spotting 0.1 M $TiNO_3$ and 0.05 M SDS on SPE disks. The limits of detection were estimated at the nanogram (ng) to sub-ng level [16].

As a tentative means of improving the limits of detection of PAHs, the phosphorescence enhancing efficiencies of C_8 and C_{18} extraction membranes were compared. RTP studies performed by Ciolino and Dorsey [17,18] on bonded silica substrates showed an inverse correlation between the phosphorescence emission of phenanthrene and the length of the alkyl group bonded to the silica surface. Since octyl membranes are suitable materials for the extraction of PAHs from contaminated waters, their use could lead to an improvement in the limits of detection.

The studies were carried out with three model compounds: phenanthrene, fluoranthene and benzo[a]pyrene. The extraction membranes were treated for background reduction [16,19]. A combination of solvent extraction (*n*-hexane) and UV irradiation results in a 50% reduction of the background signal. In addition to background reduction, the treatment causes a $2 \times$ improvement in the standard deviation of the blank, which contributes to lower limits of detection.

Table 1 shows the phosphorescence intensities of the model compounds adsorbed on C_8 and C_{18} membranes. 0.1M $TiNO_3$ and 0.05M SDS were used as phosphorescence enhancers [16]. Although the background emission (I_B) of C_{18} membranes was higher than the one observed from C_8 membranes, the net analyte signals (I_A) were higher on C_{18} membranes. Apparently, the octadecyl alkyl chains provide higher analyte rigidity than the octyl groups suggesting that the entrapment of analyte molecules within the alkyl chains plays an important role in the phosphorescence enhance-

Table 1
Phosphorescence emission^a of polycyclic aromatic hydrocarbons (PAHs)^b on octyl (C_8) and octadecyl (C_{18}) extraction membranes^c

Analyte	$\lambda_{exc}/\lambda_{em}$	$I_{A+B} \pm S_{A+B}^d$	$I_B \pm S_B^e$	$I_A \pm S_A^f$	$I_{A+B} \pm S_{A+B}^d$	$I_B \pm S_B^e$	$I_A \pm S_A^f$
Phenanthrene	292/500	810 \pm 28.3	113 \pm 13.0	697 \pm 31.1	561 \pm 35.4	84.4 \pm 4.15	477 \pm 35.6
Fluoranthene	374/542	260 \pm 14.4	92.1 \pm 6.65	158 \pm 15.9	135 \pm 13.3	49.6 \pm 1.04	85.4 \pm 13.3
Benzo[a]pyrene	400/685	37.2 \pm 3.67	21.5 \pm 0.90	15.7 \pm 3.78	22.4 \pm .07	17.2 \pm 1.96	5.20 \pm 2.85

^a Phosphorescence intensities in thousands of counts per second (cps).

^b A 5 μl spot of 10 ppm analyte was applied to the solid-phase extraction (SPE) surface.

^c Five microliter volumes of 0.05 M SDS and 0.1 M $TiNO_3$ were employed as phosphorescence enhancers.

^d I_{A+B} , analyte signal. Each value is the average of three samples. S_{A+B} , standard deviation of the analyte signal.

^e I_B , blank intensity. Each value is the average of three samples. S_B , standard deviation of the blank signal.

^f I_A , net analyte signal. $(I_{A+B} - I_B) = I_A$. S_A , standard deviation of the net analyte signal.

Table 2

Heavy atom effect^a on the phosphorescence emission^b of polycyclic aromatic hydrocarbons (PAHs)^c adsorbed on octadecyl membranes

Analyte	$\lambda_{\text{exc}}/\lambda_{\text{em}}$	Tl(I)			Pb(II)		
		$I_{A+B} \pm S_{A+B}^d$	$I_B \pm S_B^e$	$I_A \pm S_A^f$	$I_{A+B} \pm S_{A+B}^d$	$I_B \pm S_B^e$	$I_A \pm S_A^f$
Naphthalene	294/505	269 ± 31.2	128 ± 1.70	141 ± 31.3	96.1 ± 3.32	76.6 ± 8.52	19.5 ± 9.14
Anthracene	255/675	22.1 ± 2.61	17.5 ± 1.17	4.60 ± 2.86	10.8 ± 1.57	10.2 ± 0.73	^g
Phenanthrene	292/500	810 ± 28.3	113 ± 13.0	697 ± 31.1	356 ± 36.1	65.5 ± 4.94	291 ± 36.4
Fluoranthene	374/542	260 ± 14.4	92.1 ± 6.65	158 ± 15.9	127 ± 16.3	59.7 ± 5.20	67.3 ± 17.1
Benzo[a]pyrene	400/685	37.2 ± 3.67	21.5 ± .90	15.7 ± 3.78	16.3 ± 0.85	9.10 ± 0.20	7.20 ± 0.87

^a Five microliter volumes of 0.05 M SDS, 0.5 M Pb(OAc)₂, 0.1 M TlNO₃ were employed as phosphorescence enhancers.

^b Phosphorescence intensities in thousands of counts per second (cps).

^c A 5 µl spot of 10 ppm analyte was applied to the C₁₈ membrane surface.

^d I_{A+B} , analyte signal. Each value is the average of three samples. S_{A+B} , Standard deviation of the analyte signal.

^e I_B , blank intensity. Each value is the average of three samples. S_B , standard deviation of the blank signal.

^f I_A , net analyte signal. $(I_{A+B} - I_B) = I_A$. S_A , standard deviation of the net analyte signal.

^g No analyte signal detected.

ment of PAHs. It is important to mention that the results are not contradictory to those previously reported by Ciolino and Dorsey [17,18]. The membranes tested in the studies contain glass fiber as a binder, which was not present on the bonded silica phases previously investigated [17,18].

3.2. Heavy-atom salts and SDS

The phosphorescence characteristics of PAHs have been investigated under a wide variety of experimental conditions [20–43]. In general, filter paper has been the substrate of choice, and Tl(I) and Pb(II) appear to be the most effective phosphorescence enhancers. Considering that the heavy-atom effect is also related to the nature of the solid substrate [13,14], the enhancing efficiency of Tl(I) and Pb(II) on C₁₈ membranes was evaluated. Benzo[a]pyrene, fluoranthene, chrysene, phenanthrene, and pyrene were employed as model compounds. The heavy-atom and surfactant concentrations were selected based on previous RTP studies [17,41,42]. Table 2 shows the obtained results. For all the studied compounds, the highest phosphorescence enhancements were observed in the presence of 0.1 M TlNO₃.

Since the mass of heavy-atom and surfactant on the solid substrate play an important role in the enhancement of phosphorescence emission [44],

the optimization of TlNO₃ and SDS concentrations was performed. The maximum analyte signals were observed with 0.1 M TlNO₃ and 0.05 M solutions. Heavy-atom and surfactant concentrations above these values reduced the analyte signal. These concentrations, therefore, were used for all further studies.

3.3. Nitrogen purging studies

Previous studies on octadecyl membranes showed a certain degree of oxygen quenching. The presence of oxygen was minimized by purging the sample compartment of the spectrofluorimeter with nitrogen gas. The maximum phosphorescence intensities were observed after 9 min of nitrogen purging [16].

As a tentative means of increasing sample throughput without compromising the limits of detection of SPE-RTP, two new substrate holders for extraction membranes were designed (see Fig. 1). The outer dimensions of both sample holders were 1.2 cm × 1.2 cm × 7.8 cm, approximately the width and depth of a standard cuvette designed to fit most commercial spectrofluorimeters. Both configurations were machined to collect phosphorescence emission at a right angle from the excitation beam. The main difference between the two designs is the nitrogen flow path. While the sub-

strate holder in Fig. 1A delivers the nitrogen flow to the front surface of the solid substrate, the one in Fig. 1B directs the passage of nitrogen through the sample from the backside of the solid substrate. In both cases, nitrogen is fed to the substrate holders via an orifice in the base of the sample chamber. When the substrate holders are positioned for phosphorescence measurements, the alignment between the orifice located in the base of the sample chamber and the one in the substrate holder provides continuous path to the nitrogen flow.

The performances of both designs were compared to purging nitrogen into the entire sample compartment of the spectrofluorimeter. This is a

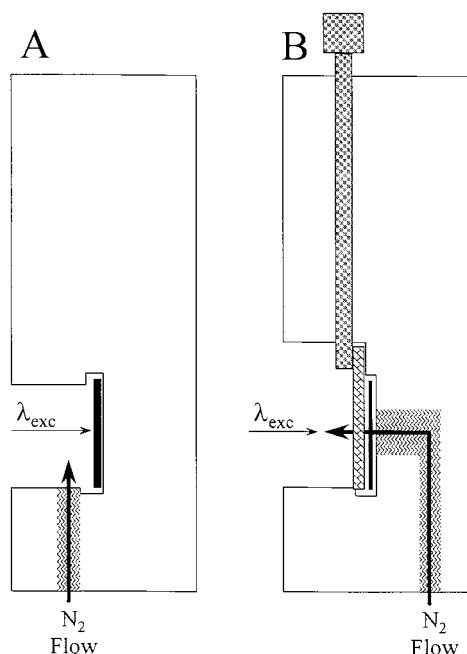


Fig. 1. Solid-phase extraction (SPE) disk holder configurations delivering nitrogen upon the face (A) and the backside (B) of the SPE disk. In configuration 1B, the sample is held in place by a copper plate with a hole drilled through the middle. The hole position in the copper plate is optimized for the incident beam and the passing nitrogen. The restraining pin is designed to hold the top of the copper plate in place with the bottom firmly wedged into a machined ridge. Figure key is as follows: ▨, nitrogen flow (hole in aluminum); ■, SPE disk; □, copper plate (low luminescent paint covering); ■, restraining pin (designed to hold copper plate in place at high nitrogen flow velocities).

common procedure in SS-RTP analysis. Since commercial sample compartments are designed for measurements in pre-deoxygenated liquid solutions, the nitrogen flow in RTP measurements is not directed towards the solid substrate. Phenanthrene was used as a model compound. 0.1 M TiNO₃ and 0.05 M SDS were employed as phosphorescence enhancers. Fig. 2 shows the obtained results. Phosphorescence intensities were measured in 2 min increments from 0 to 20 min. A flow meter was used to keep a constant purging rate. Each point plotted in the graphs is the result of three analyte and blank signal measurements. As expected, directing the nitrogen flow towards the solid substrate enhanced phosphorescence emission. Moreover, the highest enhancing efficiency was observed by forcing the nitrogen flow through the SPE membrane (configuration 1B). This design is also the most efficient approach to reach maximum intensity in the shortest period of nitrogen purging time. Taking these features into consideration, all further studies with the sample holder shown in Fig. 1B.

3.4. Analytical figures of merit (AFOM)

The AFOM of the 16 PAHs included in the EPA's priority list [15] were estimated on octadecyl extraction membranes. According to the literature survey, the RTP characteristics of acenaphthylene, benzo(b)fluoranthene, benzo(k)fluoranthene, and indeno(1,2,3-cd)pyrene were investigated for the first time. Fig. 3 shows their excitation and emission spectra.

All phosphorescence measurements were performed after 5 min of nitrogen purging. Assuming a similar behavior for all PAHs to the one observed for phenanthrene (see Fig. 2), 5 min of nitrogen purging would provide approximately 80% of maximum phosphorescence emission. All samples were prepared by spotting 5 μl of surfactant, heavy-atom and analyte solutions on SPE membranes. Table 3 shows the obtained results. The correlation coefficients of the calibration curves were close to unity, indicating a linear relationship between analyte concentration and phosphorescence intensity. Depending on the limits of detection, the linear dynamic ranges varied

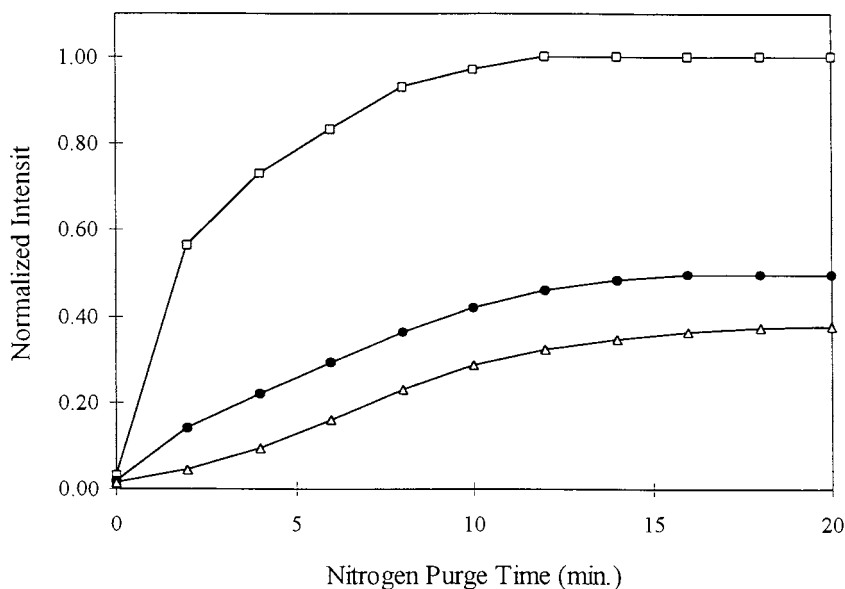


Fig. 2. Phosphorescence intensity of phenanthrene as a function of nitrogen purging time: (—△—) purging into the sample compartment; (—●—) front sample delivery; (—□—) backside nitrogen delivery.

from 1 to 3 orders of magnitude. In all cases, the upper linear concentrations were lower than 100 ng. The phosphorescence lifetimes included short and long-lived components. Their values were calculated by the stripping method [45]. The least-squares analysis of the long-decay components yield correlation coefficients higher than 0.999.

The ALOD varied from picograms (pg) to ng levels. Although these values are comparable to those estimated on paper substrates [20–42], the limits of detection on octadecyl membranes can be improved by taking advantage of the high-pre-concentration factors of SPE. Fig. 4 shows the phosphorescence spectra of a 10 ppb (ng ml⁻¹) phenanthrene solution on octadecyl membranes. The samples were prepared either by SPE (A) or by conventional SS-RTP (B). In both cases, the heavy-atom and surfactant solutions were added to the substrate after analyte deposition on the membrane.

When compared to the conventional sampling procedure, SPE increases the amount of phenanthrene on the solid substrate by approximately 6 L. By processing 1 L of water through the extraction membrane, it was possible to deposit 10 ng of

phenanthrene on the solid substrate. This is approximately 100 × the mass estimated as the ALOD for phenanthrene (see Table 3). On the other hand, the SS-RTP procedure—which typically employs 5 μl of sample volume—deposited on the solid substrate 5 × 10⁻¹⁴ g of phenanthrene, which is well below its ALOD. As a consequence, the spectral characteristics of the compound were not distinguishable. It is important to mention that spotting larger volumes of sample with a syringe is inappropriate because solutions migrate to the edges of the substrate causing analyte losses [13,14]. Therefore, the determination of phenanthrene by conventional SS-RTP is not possible at the ppb level.

A calibration curve for phenanthrene ($y = 165939x + 43220$; $R^2 = 0.9981$) was obtained by SPE-RTP. Each point plotted in the calibration graph was the average of six phosphorescence measurements. For each concentration, 1 L of standard solution was processed through the SPE membrane. The heavy-atom and surfactant solutions were spotted on the substrate after sample deposition. The linear dynamic range of the calibration curve was extended from 0.5 to 10 ppb.

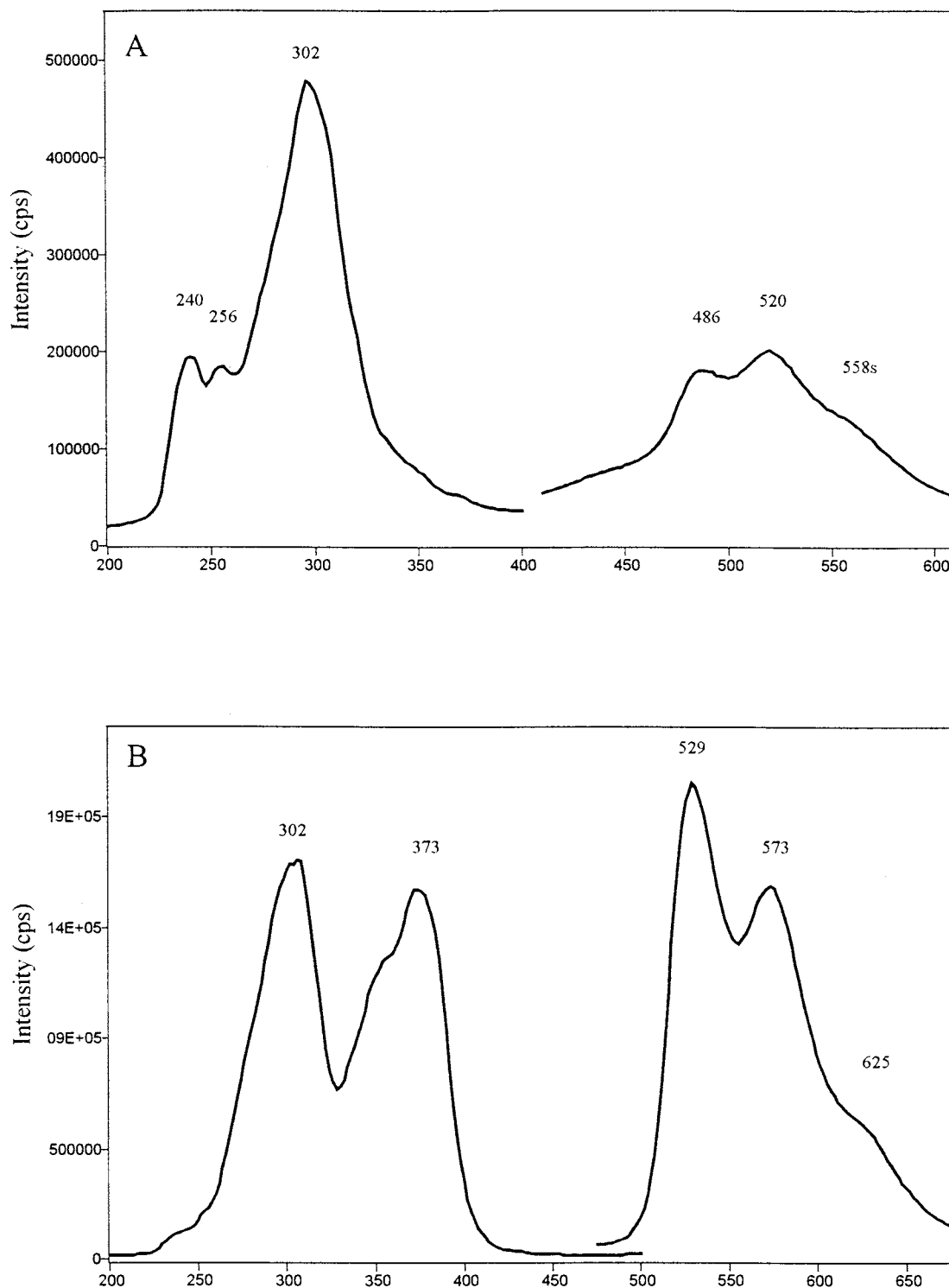


Fig. 3. Excitation and emission spectra of (A) acenaphthylene, (B) benzo(b)fluoranthene, (C) benzo(k)fluoranthene, and (D) indeno(1,2,3-cd)pyrene. A total of $100 \mu\text{g ml}^{-1}$ standard solutions were used for A and D. A total of $20 \mu\text{g ml}^{-1}$ concentrations were used for B and C. The excitation (λ_{exc}) and emission (λ_{em}) wavelengths used to obtain the spectra were the following: (A) 240/520 nm; (B) 373/529 nm; (C) 410/567 nm; (D) 434/656 nm. Spectra are not corrected for instrumental response.

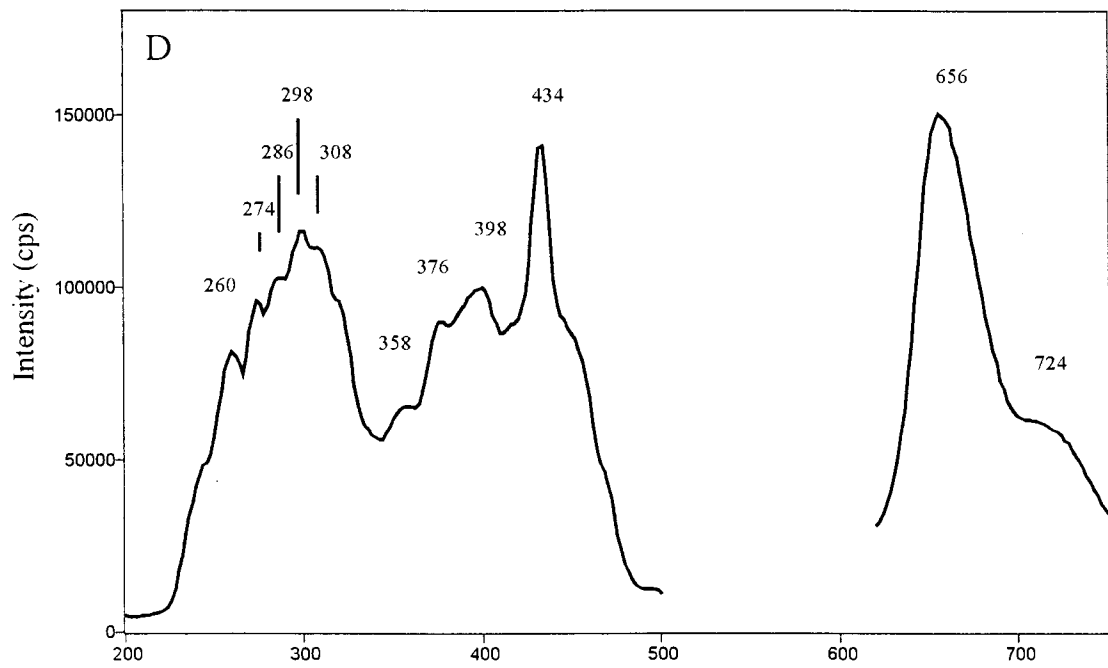
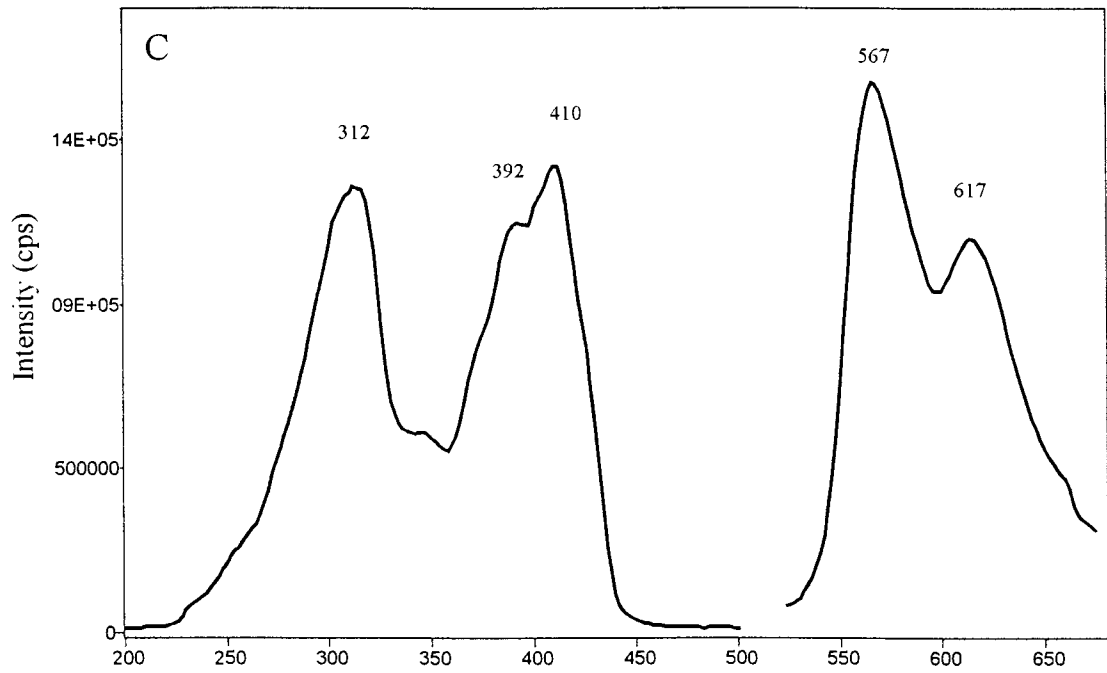


Fig. 3. (Continued)

Since there was interest in estimating the limit of detection, no attempts were made to establish the upper linear concentration of the calibration curve. The relative standard deviation of six measurements—resulting from one SPE disk—was approximately 5%. The limit of detection ($LOD = 3s_B/m$) [46] was estimated as 2 pg ml^{-1} .

3.5. Interference studies

The composition of water samples is complex and diverse. It depends on the surrounding industry and various run-off sources such as agriculture, sewer, rain water and oil spills. Recently, the US Geological Survey published a comprehensive

Table 3

Analytical figures of merit for the 16 EPA PAH priority pollutants obtained on octadecyl extraction membranes^a

Compound	Excitation (nm) ^b	Emission (nm) ^b	LDR (ng) ^c	R^d	ALOD (ng) ^e	Short Tau (ms) ^f	Long Tau (ms) ^f
Naphthalene	240, 256, 282, <u>294</u>	472, <u>505</u> , 541	1.6–44	0.9991	1.6	1.20 ± 0.05	3.99 ± 0.12
Anthracene	255*, <u>285</u> , 350, 368, 385	<u>675</u> , 730s	8.3–44	0.9984	8.3	0.37 ± 0.06	1.45 ± 0.09
Phenanthrene	270, <u>292</u> , 302	468, <u>500</u> , 534s	0.1–44	0.9991	0.1	1.26 ± 0.08	3.90 ± 0.24
Acenaphthylene	240*, 256, <u>297</u>	486, <u>520</u> , 558s	10.7–88	0.9990	10.7	0.82 ± 0.06	4.22 ± 0.26
Acenaphthene	238*, 254, <u>306</u>	482, <u>514</u> , 554	0.4–44	1.0000	0.4	0.74 ± 0.02	3.55 ± 0.04
Fluorene	236s, 282, <u>304</u>	427s, <u>449</u> , 481s	0.2–22	0.9992	0.2	0.97 ± 0.02	3.16 ± 0.04
Fluoranthene	256, 270, <u>296</u> , 358, 374*	<u>542</u> , 584	0.2–44	0.9996	0.2	0.96 ± 0.01	3.66 ± 0.10
Benzo(a)anthracene	<u>298</u> , 354*, 372	<u>598</u> , 654	0.2–44	1.0000	0.2	0.85 ± 0.03	3.70 ± 0.04
Pyrene	254, 280, 328s, <u>344</u>	<u>590</u> , 645	0.1–44	1.0000	0.1	1.09 ± 0.02	3.26 ± 0.18
Chrysene	<u>278</u> , 316 330s, 370	510, <u>544</u> , 590s	0.07–44	0.9991	0.07	1.32 ± 0.04	3.31 ± 0.01
Benzo(k)fluoranthene	312, 346, 392, <u>410</u>	<u>567</u> , 617, 661	0.03–44	0.9999	0.03	1.23 ± 0.03	3.51 ± 0.07
Benzo(b)fluoranthene	248, <u>306</u> , 360s, 373*	<u>529</u> , 573, 625	0.08–44	0.9994	0.08	1.69 ± 0.09	4.19 ± 0.05
Benzo(a)pyrene	262, 286, <u>300</u> , 312, 382s, 400*	685	0.4–22	0.9991	0.4	0.40 ± 0.02	1.42 ± 0.08
Indeno(1,2,3-cd)pyrene	260, 274, 298, 358, 376, 398, <u>434</u>	<u>656</u> , 724	0.4–22	0.9998	0.4	0.48 ± 0.02	1.37 ± 0.14
Benzo(ghi)perylene	304, 374, <u>392</u>	<u>618</u> , 674	0.03–33	0.9990	0.03	1.04 ± 0.01	3.42 ± 0.03
Dibenz(a,h)anthracene	<u>304</u> , 342, 360s	<u>554</u> , 600, 654	0.02–44	0.9981	0.02	1.49 ± 0.06	4.17 ± 0.01

^a Octadecyl membranes previously spotted with $5 \mu\text{l}$ of 0.1 M TiNO_3 and $5 \mu\text{l}$ of 0.05 M SDS .

^b Maximum excitation and emission wavelengths. The peak with maximum intensity is underlined. Symbol (*) represents the maximum excitation ratio of analyte to blank. Figures of merit were therefore established at this wavelength (S, shoulder).

^c Linear dynamic range (LDR) is estimated from the limit of detection to the upper linear calibration.

^d R , correlation coefficient of the calibration curve.

^e ALOD, absolute limit of detection. Calculated on a basis of the equation $LOD = 3s_B/m$, where s_B is the standard deviation of the blank and m is the slope based upon four concentrations within the linear dynamic range.

^f Short and long lifetime components based upon stripping method from J.N. Demas, Excited State Lifetime Measurements, Academic Press, New York, 1983.

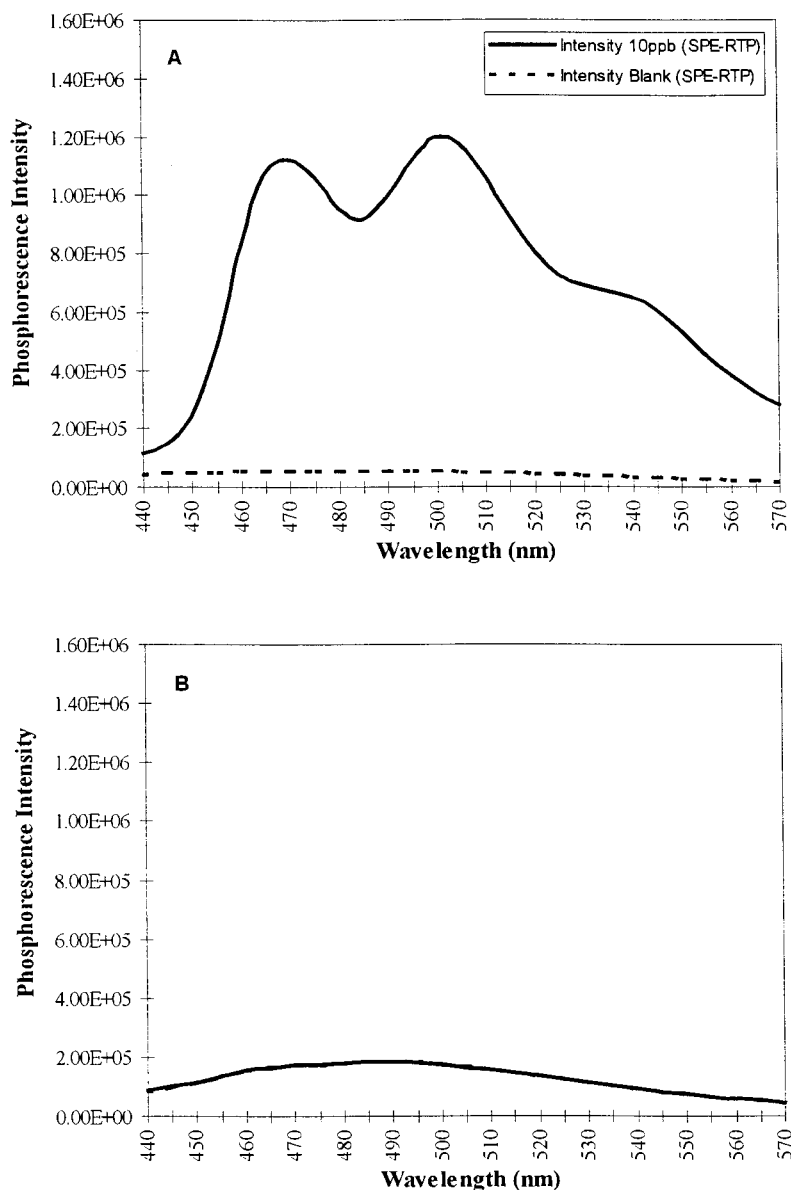


Fig. 4. Phosphorescence emission of a 10 ng l^{-1} phenanthrene solution deposited on octadecyl extraction membranes. The samples were prepared by processing 1 l of sample through the SPE membrane (A) and by the conventional solid-surface room-temperature phosphorimetry (SS-RTP) procedure using $5 \mu\text{l}$ of sample (B).

survey assessing the water-quality conditions of more than 50 of the Nation's largest river basins and aquifers [47]. In the specific case of the Red River of the North Basin (MN, ND and SD), the major organic pollutants present in the aquatic ecosystem are PAHs, pesticides, polychlorinated

biphenyls (PCBs) and volatile organic compounds (derivatives of benzene such as mono-, di- and tri-methylbenzenes).

The potential interference of concomitants were evaluated taking into consideration two simple criteria: (i) their potential retention by the SPE

matrix; (ii) their ability to show phosphorescence emission. These criteria ruled out the inorganic species not retained by the SPE membrane—such as mercury and nitrate—and the pollutants with no aromaticity in their molecular structure. Table 4 shows the remaining list of compounds tested for interference under the experimental conditions optimized for PAHs. Benzene was included in the list as a representative compound of benzene derivatives.

Each compound was tested individually by the conventional RTP sampling procedure, i.e. by spotting the standard solution on the solid substrate with a microliter syringe. The same procedure was used for the deposition of heavy-atom and surfactant solutions on the solid substrate. The phosphorescence intensities of 100 ppm solutions were measured at two excitation wavelengths: 280 and 330 nm. These wavelengths were selected based on the excitation characteristics of PAHs (see Table 3). Due to their broad excitation spectra, sample excitation at 280 or 330 nm promotes the phosphorescence emission of the 16 PAHs. No phosphorescence emissions were observed from the potential interferents when the substrates were excited at 330 nm. Their phosphorescence signals were exactly the same as those

observed from the blanks. Similar results were obtained with a synthetic mixture containing all the interferents at the 10 ppm level.

To check for interfering effects that could alter the spectral features of the PAHs mixture, the interferents were mixed with the 16 PAHs prior to their deposition on the solid substrate. The concentration of each PAH in the final mixture was 10 ppm. The phosphorescence characteristics of the PAHs mixture in the presence of interferents were compared with those from a mixture containing the 16 PAHs at the same level of concentration. For a confidence interval (CI) of 95% ($P = 0.05$) and four determinations ($N = 4$) [46], no statistical difference was observed in the intensity of the phosphorescence signal and the spectral features of the PAHs mixture.

4. Conclusions

The studies demonstrate the feasibility of combining SPE and RTP for the analysis of PAHs in water samples. The high pre-concentration factors obtained by SPE, associated with the sensitivity of RTP, result in limits of detection at the pg ml^{-1} level. Taking into consideration that PAH concentrations range from pg ml^{-1} in pure ground water supplies to $\mu\text{g ml}^{-1}$ in heavily contaminated sewage [48], it can be stated that SPE-RTP has the sensitivity required for screening PAHs in water samples. It is important to mention that PAHs at lower concentrations than ppt levels could be detected by processing larger volumes of sample through the SPE membrane.

The selective retention of PAHs by SPE, combined with the forbidden nature of the phosphorescence electronic transition, reduces the number of potential interferents in the analysis of water samples. Several organic pollutants commonly encountered in aquatic ecosystems did not show phosphorescence emission at the excitation wavelength (330 nm) selected for the determination of PAHs. In the analysis of complex mixtures with several phosphorescent concomitants, the selectivity towards PAHs can be enhanced by selective-external heavy-atom perturbation (SEHAP), time-resolved phosphorimetry (TRP) and synchronous excitation techniques [13]. [14]

Table 4
List of organic pollutants^a tested for interferences

Pesticides

Alachlor, Atrazine, Bromoxynil, Cyanazine, Diuron,
Metolachlor, Simazine, Tebuthiuron, Trifluralin

Insecticides

Carbofuran, Diazanone

PCBs

4-Chlorobiphenyl, 4,4-Dichlorobiphenyl,
3,4-Dichlorobiphenyl, 3,3-Dichlorobiphenyl,
3,3,5,5-Tetrachlorobiphenyl,
3,3,4,4,5-Pentachlorobiphenyl,
3,3,4,4,5,5-Hexachlorobiphenyl, Arochlor 1016, Arochlor
1242, Arochlor 1221

Volatile organics

Benzene, bis(2-Ethylhexyl)phthalate

Organochlorine compounds

p,p'-DDE, *p,p'*-DDT, *o,p'*-DDT

^a The commercial names are listed for some of the pollutants. See Section 2.1 for the IUPAC nomenclature.

The experimental procedure of SPE-RTP is relatively simple. Since the PAHs are detected on the extraction membrane, the drawbacks associated to elution steps in SPE procedures are eliminated. In addition, the use of organic solvents is avoided, which reduces analysis costs and avoids disposal of toxic solvents. After performing SPE, the RTP procedure takes approximately 20 min. Since several SPE membranes can be dried simultaneously, which takes 15 min per batch, the sample throughput is appropriate for routine analysis of a large number of samples. The new substrate holder optimizes oxygen removal and provides reasonable phosphorescence intensities with 2 min of nitrogen purging.

Shorter analyses times can be obtained by reducing the length of the drying step. This parameter is under optimization in our laboratory. However, it is important to mention that the drying step should not be considered a disadvantage when the technique is compared to chromatographic analysis. The efficient elution of PAHs from the octadecyl membrane prior to chromatographic analysis depends on prior removal of water sorbed to the silica surface. This can be accomplished by using an eluent that is miscible with water, such as ethyl acetate/toluene (50:50 v/v). Toluene is added to ethyl acetate to increase the solubility of PAHs and to enhance their elution from the solid phase. If a more hydrophobic solvent is required to remove highly non-polar compounds, such as hexane or methylene chloride, the sorbent must be carefully dried and free of water [49].

Acknowledgements

A.D. Campiglia gratefully acknowledges the ND EPSCoR Program and the NDSU Grant-in-Aid Program for financial support. Erik D. Hagestuen is grateful to the ND EPSCoR Doctoral Dissertation Fellowship Program for his award.

References

- [1] G. Gmeiner, G. Stehlik, H. Tausch, *J. Chromatogr. A* 767 (1997) 163.
- [2] B. Janoszka, K. Tyrpien, D. Bodzek, *J. Planar Chromatogr.* 9 (1996) 450.
- [3] R. Hartmann, *Int. J. Environ. Anal. Chem.* 62 (1996) 161.
- [4] L. Rivera, M.J.C. Curto, P. Pais, M.T. Galceran, L. Puignou, *J. Chromatogr. A* 731 (1996) 85.
- [5] G. Kiss, A. Gelencser, Z. Krivacsy, J. Hlavay, *J. Chromatogr. A* 774 (1997) 349.
- [6] T. Renner, D. Baumgarten, K.K. Unger, *Chromatographia* 45 (1997) 199.
- [7] B. Bodzek, B. Janoszka, C. Dobosz, L. Warzecha, M. Bodzek, *J. Chromatogr. A* 774 (1997) 177.
- [8] R. Ferrer, J. Guiteras, L. Beltran, *Anal. Lett.* 29 (1996) 2201.
- [9] E. Manoli, C. Samara, *Chromatographia* 43 (1996) 135.
- [10] R.E. Majors, *LC-GC May* (1998) S8.
- [11] Z. Zhang, M.J. Yang, J. Pawliszyn, *Anal. Chem.* 66 (1994) 844A.
- [12] O. Fiehn, M. Jekel, *Anal. Chem.* 68 (1996) 3083.
- [13] T. Vo-Dinh, *Room Temperature Phosphorescence for Chemical Analysis*, Wiley, New York, 1984.
- [14] R.J. Hurtubise, *Phosphorimetry: Theory, Instrumentation and Applications*, VCH, New York, 1990.
- [15] J.W. Eichelberger, T.D. Behymer, W.L. Budde, *Determination of Organic Compounds in Drinking Water by Liquid-Solid Extraction and Capillary Column Gas Chromatography Mass Spectrometry*, EPA Method 525, Environmental Monitoring Systems Laboratory, US Environmental Protection Agency, 1988.
- [16] E.D. Hagestuen, A.D. Campiglia, *Appl. Spectrosc.* 52 (1998) 1096.
- [17] L.A. Ciolino, J.G. Dorsey, *Anal. Chem.* 66 (1994) 3223.
- [18] L.A. Ciolino, J.G. Dorsey, *J. Chromatogr. A* 678 (1994) 201.
- [19] A.F. Arruda, A.D. Campiglia, *Determination of trace levels of polychlorinated biphenyls on reversed phase octadecyl bonded silica membranes*, *Anal. Chim. Acta* 386 (1999) 271.
- [20] T. Vo-Dinh, E. Lue Yen, J.D. Winefordner, *Talanta* 24 (1977) 146.
- [21] T. Vo-Dinh, G.L. Walden, J.D. Winefordner, *Anal. Chem.* 49 (1977) 1126.
- [22] T. Vo-Dinh, R.B. Gammage, *Anal. Chem.* 50 (1978) 2054.
- [23] E. Lue-Yen Bower, J.D. Winefordner, *Anal. Chim. Acta* 102 (1978) 1.
- [24] E. Lue-Yen Bower, J.D. Winefordner, *Appl. Spectrosc.* 33 (1979) 9.
- [25] G.D. Boutillier, J.D. Winefordner, *Anal. Chem.* 51 (1979) 1391.
- [26] T. Vo-Dinh, J.R. Hooyman, *Anal. Chem.* 51 (1979) 1915.
- [27] T. Vo-Dinh, R.B. Gammage, *Anal. Chim. Acta* 107 (1979) 261.

- [28] S.Y. Su, J.D. Winefordner, *Can. J. Spectrosc.* 28 (1983) 21.
- [29] T. Vo-Dinh, T.J. Bruewer, G.C. Colovos, T.J. Wagner, R.H. Jungers, *Environ. Sci. Technol.* 18 (1984) 477.
- [30] T. Vo-Dinh, *Environ. Sci. Technol.* 19 (1985) 997.
- [31] G.R. Ramos, M.C. Garcia Alvarez-Coque, A.M. O'Reilly, I.M. Khasawneh, J.D. Winefordner, *Anal. Chem.* 60 (1988) 416.
- [32] M.A. Mignardi, J.J. Laserna, J.D. Winefordner, *Microchem. J.* 38 (1988) 313.
- [33] L.M. Perry, A.D. Campiglia, J.D. Winefordner, *Anal. Chim. Acta* 225 (1989) 415.
- [34] A.D. Campiglia, L.M. Perry, J.D. Winefordner, *Appl. Spectrosc.* 43 (1989) 1341.
- [35] L.M. Perry, A.D. Campiglia, J.D. Winefordner, *Anal. Chem.* 61 (1989) 2328.
- [36] A.D. Campiglia, A. Berthod, J.D. Winefordner, *Anal. Chim. Acta* 231 (1990) 289.
- [37] A.D. Campiglia, L.M. Perry, J.D. Winefordner, *Appl. Spectrosc.* 44 (1990) 729.
- [38] A.D. Campiglia, A. Berthod, J.D. Winefordner, *J. Chromatogr.* 508 (1990) 37.
- [39] L. Bruzzone, R. Badía, *Anal. Lett.* 23 (1990) 1113.
- [40] A.D. Campiglia, T. Vo-Dinh, *Talanta* 43 (1996) 1805.
- [41] A.D. Campiglia, D.M. Hueber, T. Vo-Dinh, *Polyc. Arom. Comp.* 8 (1996) 117.
- [42] A.D. Campiglia, D.M. Hueber, T. Vo-Dinh, *Appl. Spectrosc.* 50 (1996) 252.
- [43] J. Chen, R.J. Hurtubise, *Talanta* 45 (1998) 1081.
- [44] R.Q. Aucelio, A.D. Campiglia, *Anal. Chim. Acta* 309 (1995) 345.
- [45] J.N. Demas, *Excited State Lifetime Measurements*, Academic Press, New York, 1983.
- [46] J.C. Miller, J.N. Miller, *Statistics for Analytical Chemistry*, Wiley, New York, 1984.
- [47] US Department of the Interior, *Water Quality in the Red River of the North Basin, Minnesota, North Dakota, and South Dakota*, US Geological Survey Circular 1169, 1992–1995.
- [48] T. Vo-Dinh, *Chemical Analysis of Polycyclic Aromatic Compounds*, Wiley, New York, 1990.
- [49] E.M. Thurman, M.S. Mills, in: J.D. Winefordner (Ed.), *Solid-Phase Extraction: Principles and Practice*, Wiley, New York, 1998.

The use of 1-[pyridyl-(2)-azo]-naphthol-(2) in the presence of TX-100 and *N,N'*-diphenylbenzamidine for the spectrophotometric determination of copper in real samples

Manisha Thakur, Manas Kanti Deb *

School of Studies in Chemistry, Pt. Ravishankar Shukla University, Raipur-492 010, M.P., India

Received 18 June 1998; received in revised form 25 October 1998; accepted 14 January 1999

Abstract

A simple and sensitive field detection and spectrophotometric method for determination of copper described herewith is based on the formation of a red coloured species of copper(II) with 1-[pyridyl-(2)-azo]-naphthol-(2) (PAN), TX-100 and *N,N'*-diphenylbenzamidine (DPBA) at pH range 7.8–9.4. The red coloured Cu(II)-PAN-(TX-100)-DPBA complex in chloroform shows maximum absorbance at 520 nm with molar absorptivity value of $1.14 \times 10^5 \text{ l mol}^{-1} \text{ cm}^{-1}$. The detection limit of the method is 2 ng ml^{-1} organic phase. The system obeys Beer's law up to $0.6 \mu\text{g Cu(II) ml}^{-1}$ in organic solution. Most of the common metal ions generally found associated with copper do not interfere. The repeatability of the method was checked by finding relative standard deviation (RSD) ($n = 10$) value for solutions each containing $0.2 \mu\text{g ml}^{-1}$ of Cu(II) and the RSD value of the method was found to be 1.5%. The validity of the method has been satisfactorily examined for the determination of copper in soil and airborne dust particulate samples. © 1999 Elsevier Science B.V. All rights reserved.

Keywords: Spectrophotometry; Copper determination; 1-[Pyridyl-(2)-azo]-naphthol-(2) (PAN); Soil and airborne dust particulates; Field detection

1. Introduction

Copper is both micro-nutrient as well as toxic element for living beings, depending up on the concentration level [1]. Inhalation of dusts, fumes and mists of Cu-salts results in congestion of

nasal mucous membranes, ulceration with perforation of the nasal septum on occasion and sometimes, pharyngeal congestion [2]. It is also a gastrointestinal tract irritant [3].

Many techniques i.e. AAS [4], ICP-AES [5,6], voltammetry [7], spectrophotometry [8] have been reported for the determination of copper. AAS and ICP-AES are most selective and sensitive techniques used for the determination of copper. These techniques, however, are quite expensive

* Corresponding author. Tel.: +91-0771-528367; fax: +91-0771-545984.

E-mail address: manish@lakshya.kalptaru.com (M.K. Deb)

and require costly maintenance and skilled hands for operation. Voltammetry is the most sensitive technique but suffers from matrix interference [9,10]. Various organic and inorganic reagents viz. Phenols [11,12], amines [13–15], carbazones [16–19], carbamates [20,21], oximate [22], thioamides [23,24], carbonohydrazide [25] and azo [26–29] compounds have been proposed for the spectrophotometric determination of copper at trace levels. These methods, however, are not entirely suitable due to the involvement of one or more of the following reasons: the tedium involved in the methods, critical pH ranges, poor sensitivity and the problem of matrix interference. Some other reagents like alizarin *s*-methyl violet-poly(vinyl alcohol) system [30], 4-(2,3-dihydro-1,4-phthalazinedione-5-triazeno)-azobenzene [31], 5-Br-PADAP [32], diphenylcarbazide [33] have also been reported for the spectrophotometric determination of copper.

The present paper deals with a simple and sensitive method for the field identification and spectrophotometric determination of copper in soil and airborne dust particulates using 1-[pyridyl-(2)-azo]-naphthol-(2) (PAN) in presence of TX-100 and *N,N'*-diphenylbenzamidine.

2. Experimental

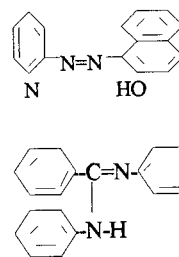
2.1. Apparatus

A Carl-Zeiss Jena spectrophotometer fitted with EK-5 unit and matched quartz cells of 1 cm path length was used for all absorbance measurements. A Systronic digital pH-meter type 335 was employed for the measurement of pH value of solutions.

2.2. Reagents

All chemicals used were of analytical reagent grade, BDH/E. Merck/Glaxo or SD fine Chem. The standard Cu(II) solution was prepared by digestion of a weighed amount of copper metal (99.9%) in 5 ml concentrated nitric acid. The excess of nitric acid was removed by heating the

dried mass with concentrated hydrochloric acid. The solution was heated up to dryness. The dried mass was dissolved in 1 ml of 10 mol l⁻¹ hydrochloric acid and diluted to 100 ml with distilled water. The working standard solutions were prepared by suitably diluting with distilled water. *N,N'*-Diphenylbenzamidine (DPBA), as shown by its structural formula below, was synthesized according to the procedure in the literature [34] and its 7.3 × 10⁻³ mol l⁻¹ (or 0.2%, w/v) solution in chloroform was employed for extraction. A 4.01 × 10⁻³ mol l⁻¹ (or 0.1%, w/v) 1-[pyridyl-(2)-azo]-naphthol-(2) (PAN), as shown by its structural formula below, solution was prepared in chloroform for colour development and 1.54 × 10⁻³ mol l⁻¹ (or 0.1%, w/v) of Triton X-100 was prepared in distilled water. NaOH-H₃BO₃ buffer solution [35] (≈ pH 8.5) was used for adjusting the pH of aqueous solution.



2.3. Procedure

An aliquot of the standard solution containing up to 6.0 μg Cu(II) was taken in a 125 ml separatory funnel. To the above solution, mix 0.7 ml of TX-100 and 1 ml of PAN solution. Adjust pH of the aqueous solution at 8.5 ± 0.2 with buffer solution in a total volume of 10 ml. Shake the above solution vigorously for 2 min with 2 × 2 ml of DPBA solution in chloroform. Wash the aqueous phase with 1 ml fresh chloroform. Combine the extracts and dry over anhydrous sodium sulphate (≈ 2 g). Make up the total organic phase to the mark with chloroform in 10 ml volumetric flask. Measure the absorbance of the complex against reagent blank at λ_{max} 520 nm.

2.4. Field detection of copper

Take 0.1–1.0 g of test samples viz. crushed soil (200 mesh) and airborne solids in a micro test tube. Add to this 0.5–2.0 ml of hot (30–60°C) 0.1 mol l⁻¹ nitric acid. Shake the tube gently and leach out the samples. Put 2–3 drops of the leachate in another micro test tube using capillary tube or dropper. Add 0.2–0.5 ml of buffer, into it, adjust pH around 8.5 and add 2–3 drops each of PAN, DPBA and aqueous TX-100. The presence of copper in test samples is indicated by generation of intense red colouration in the organic phase which persisted for several minutes.

2.5. Determination of copper in soil and airborne dust particulates

This method has been applied to the determination of Cu(II) in soil and airborne dust particulate samples. The samples were collected from different representative places of Raipur city, M.P., India viz. from residential, commercial, industrial and heavy traffic areas. Weighed amount of dust samples were taken, digested with nitric acid and excess of hydrochloric acid (1:3). The samples were neutralised with ammonium hydroxide (1:8) and its excess was removed by boiling. The solutions were filtered and the filtrates diluted to a

known volume (10 ml). Aliquots of this solution were analysed for Cu(II).

3. Results and discussion

While establishing the optimum concentration ranges for various analytical parameters for determination of 2.0 µg Cu(II) 10 ml⁻¹ organic phase (for which, $A_{\max} = 0.360$) all parameters, except the one whose optimal range was being determined, were employed within the obtained optimum ranges

3.1. Absorption spectra

The absorption spectra of Cu(II)-PAN-(TX-100)-DPBA complex shows maximum absorption around 520 nm against reagent blank in chloroform at an extraction pH of 8.5. Fig. 1 exhibits the family curves at different concentration of Cu(II) and different pH values.

3.2. Effect of pH

The effect of pH on the extraction of Cu(II)-PAN-(TX-100)-DPBA complex was seen in an optimum pH range of 7.8–9.4 of aqueous solution, Fig. 2. Therefore, a pH 8.5 was kept con-

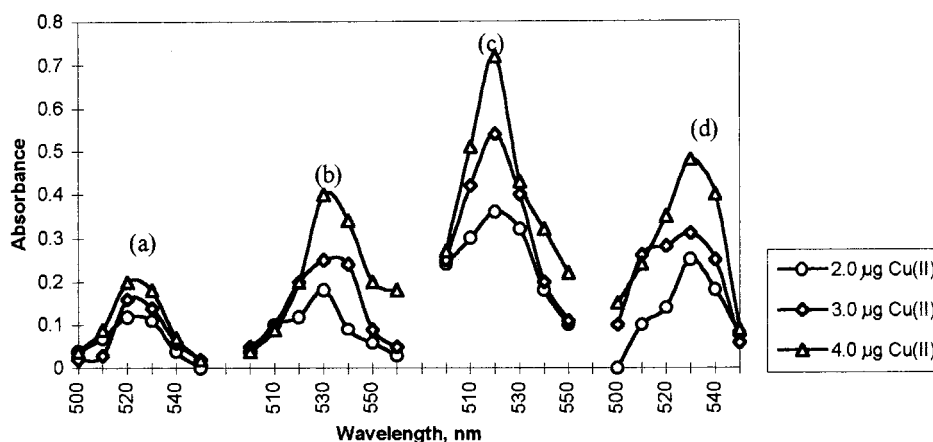


Fig. 1. Absorption spectra of Cu(II)-PAN-(TX-100)-DPBA complex in chloroform against their respective reagent blanks at different pH of extraction of the complex with 3 different concentrations of the analyte; a, pH 5.0; b, pH 7.0; c, pH 8.5; d, pH 10.5; $C_{\text{PAN}} = 4.0 \times 10^{-4}$ M, $C_{\text{TX-100}} = 1.1 \times 10^{-4}$ M, $C_{\text{DPBA}} = 1.5 \times 10^{-3}$ M.

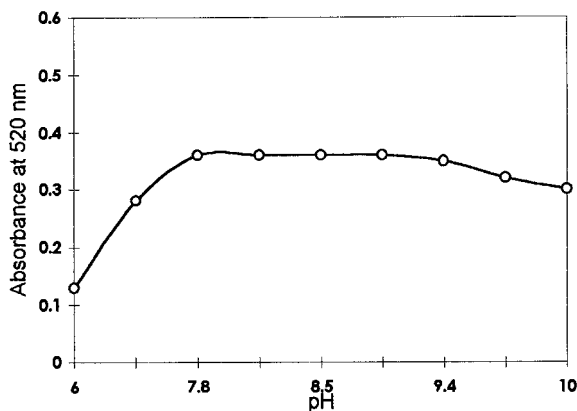


Fig. 2. Effect of pH on the extraction and absorbance of the Cu(II)-PAN-(TX-100)-DPBA complex in chloroform; $C_{\text{TX-100}} = 1.1 \times 10^{-4}$ M, $C_{\text{PAN}} = 4.0 \times 10^{-4}$ M, $C_{\text{DPBA}} = 1.5 \times 10^{-3}$ M.

stant throughout the experiment by using NaOH- H_3BO_3 buffer.

3.3. Solvent effect

The effect of various organic solvents on the formation and extraction of Cu(II)-PAN-(TX-100)-DPBA complex was studied. The values of molar absorptivity at the wavelength of maximum absorption of the complex in different solvents are as follows: toluene (ϵ , 4.8×10^4 ; λ_{max} , 520), benzene (ϵ , 2.2×10^4 ; λ_{max} , 520), n-butyl alcohol (ϵ , 3.8×10^4 ; λ_{max} , 525), xylene (ϵ , 5.4×10^4 ; λ_{max} , 525), and chloroform (ϵ , 1.14×10^5 l mol $^{-1}$ cm $^{-1}$; λ_{max} , 520 nm). Complete extraction and maximum absorbance of the complex is observed with chloroform as compared to the other solvents. Due to its superiority, chloroform was therefore chosen as solvent for extraction of Cu(II) complex.

3.4. Effect of reagents

The results obtained indicated that at least $(1.2\text{--}2.0) \times 10^{-3}$ mol l $^{-1}$ DPBA in chloroform was adequate for complete extraction of the complex of Cu(II). Therefore, a 1.5×10^{-3} mol l $^{-1}$ DPBA was employed throughout the experiment. It was observed that a concentration range of

$(3.5\text{--}6.0) \times 10^{-4}$ mol l $^{-1}$ PAN solution was adequate for maximum colour development of Cu(II)-PAN-(TX-100)-DPBA complex. The concentration of PAN beyond the upper limit caused enhanced blank absorbance. Therefore, 4.0×10^{-4} mol l $^{-1}$ PAN was employed. The studies on the effect of concentration of TX-100 indicated that a concentration range of $(0.73\text{--}1.54) \times 10^{-4}$ mol l $^{-1}$ TX-100 solution was sufficient for maximum colour development of Cu(II)-PAN-(TX-100)-DPBA complex. Therefore, 1.1×10^{-4} mol l $^{-1}$ TX-100 solution was kept constant throughout the experiment.

3.5. Beer's law, molar absorptivity, precision and detection limit

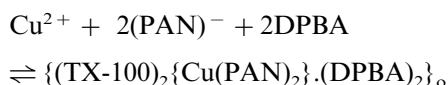
The system obeyed Beer's law up to 0.6 μg Cu(II) ml $^{-1}$ with an excellent linearity in terms of correlation coefficient value [36] of 0.997. The molar absorptivity of the Cu(II)-PAN-(TX-100)-DPBA complex, calculated in terms of Cu(II), is 1.14×10^5 l mol $^{-1}$ cm $^{-1}$ at λ_{max} 520 nm. The precision of the method in terms of relative standard deviation ($n = 10$) for the determination of 2.0 μg Cu(II) is 1.5%. In this method the detection limit, defined as for photometry, the concentration of analyte causing more absorbance than twice the standard deviation of ten replicate measurements of blank absorbance at 95% probability [37], of copper is 2 ng ml $^{-1}$ in the organic phase. The lowest concentration of copper that can be detected in real samples is 2.6 ng Cu g $^{-1}$.

3.6. Composition of the Cu(II)-PAN/(TX-100)/DPBA complex

The complex of the copper complex was determined by the curve fitting method [38]. The molar ratio of metal to PAN, TX-100 and DPBA was determined by logarithmic value of distribution ratio of metal [$\log\{A_{\text{eq}}/(A_{\text{max}} - A_{\text{eq}})\}$] (where, A_{max} = maximum absorbance of the complex at λ_{max} under optimum reagent concentrations at a level of 2.0 μg Cu(II) per 10 ml organic phase and A_{eq} /absorbance of Cu(II) complex at equilibrium concentration, obtained by equilibration with different known concentrations of reagents viz.

PAN/TX-100/DPBA) versus logarithmic values of varied known concentrations of PAN/ TX-100/ DPBA in chloroform.

The inclination of the curves for PAN, TX-100 and DPBA were found to be very closed to integer 2 in all cases. Thus, a 1:2:2 molar ratio complex of Cu: PAN: TX-100: DPBA in chloroform was predicted. Fig. 3 indicates sets of curves for the metal-ligand ratio pertaining to three different concentrations of the analyte viz. 2.0, 3.0, and 4.0 μg . It is quite evident that virtually all curves are superimposed in all different concentrations of the analyte in the determination of molar composition of all individual ligands. This shows that the composition of the complex, Cu(II)-PAN-(TX-100)-DPBA, does not change on variation of the concentration of Cu(II). The probable overall reaction mechanism can be represented as:



subscript 'o' here describes the organic phase or chloroform.

3.7. Effect of diverse ions

The effect of various diverse ions on the de-

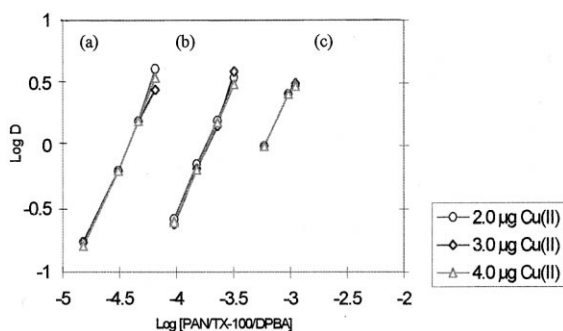


Fig. 3. Plot of curve fitting data for the determination of stoichiometry of the Cu(II)-PAN-(TX-100)-DPBA complex in chloroform at three different concentrations of the analyte viz. 2.0, 3.0, and 4.0 μg . a, PAN ($C_{\text{TX-100}} = 1.1 \times 10^{-4}$ M, $C_{\text{DPBA}} = 1.5 \times 10^{-3}$ M); b, TX-100 ($C_{\text{PAN}} = 4.0 \times 10^{-4}$ M, $C_{\text{DPBA}} = 1.5 \times 10^{-3}$ M); c, DPBA ($C_{\text{PAN}} = 4.0 \times 10^{-4}$ M, $C_{\text{TX-100}} = 1.1 \times 10^{-4}$ M).

Table 1

Tolerance limit of diverse ions in the determination of 2.0 μg Cu(II)/10 ml at pH 8.5 ± 0.2

Ions added	Tolerance limit ^a mg 10 ml ⁻¹ or- ganic phase
Cd(II)	0.04
Zn(II)	0.1
SCN ⁻	0.3
Tartarate	0.4
Fe(III), NO ₃ ⁻	0.5
Cl ⁻ , SO ₄ ²⁻ , EDTA	0.8
Cr(III), Pb(II), Bi(III)	1.0
Br ⁻	1.6
Co(II), Ag(I), Sn(IV), PO ₄ ³⁻	2.0
Fe(II)	2.5
Ni(II)	3.0
V(V), Mn(VII)	4.0
Mo(VI)	5.0
Cr(VI)	8.0
Ca(II), Mg(II)	9.0

^a Ions were considered to interfere when they caused a change in the absorbance of the Cu(II)-PAN-(TX-100)-DPBA complex ($A = 0.360$) by $\geq \pm 2\%$

termination of 2.0 μg of Cu(II) was studied as per the proposed procedure. Only Zn(II) and Cd(II) were found to interfere in the determination of Cu(II). The field test as well as the determination procedure for Cu(II) is completely free from interfering ions under the optimum conditions of the method. The real sample analysis is completely free from matrix interference because, in the present method, at least 20 and 50-fold concentrations of Cd(II) and Zn(II) respectively, are tolerated in the determination of 2.0 μg of Cu(II). Usually, all soils and airborne dust particulates are reported to have contained Cu(II), Cd(II) and Zn(II) in a proportion of $\approx 120:5:80$ ppm, respectively [39]. This concentration ratio of Zn(II) and Cd(II) with Cu(II) is too far less than that tolerated by the present method. However, these interferences could be removed by prior extraction with 3 ml chloroform solution of dithizone (0.1%, w/v) at pH 3.0 ± 0.2 [40]. The tolerance limits of various diverse ions are summarized in Table 1.

4. Application of the present work and its validation

The method has been satisfactorily applied for the determination of Cu(II) in airborne dust particulate and field detection of soil. The actual content of Cu(II) in real samples were determined with the help of the calibration curve [37]. The results obtained for Cu(II) content of these samples were also verified by AAS method. The AAS determination were carried out on the same solution used for the photometric determination. The Cu(II) concentration in various soil and airborne solid samples have been incorporated in Table 2. The comparison of the results indicates good correlation between the recommended procedure and AAS method.

Various standard and certified reference materials including different kind of steel, some alloy and rock samples have been tested for the determination of Cu using the proposed method for the purpose of test of validation of the present method. A weighed amount of standard samples (0.1–0.5 g) were digested with acid treatment as according to the standard method[41]. The acidic samples were then neutralised with the addition of ammonium hydroxide (1:3). Excess ammonia was removed by boiling the solution. The volume of the samples were then made up to the mark with distilled water in a 50 ml volumetric flask. Different aliquots of the samples were then taken for analyses. For samples with high concentration of Cu, five observations were made, whereas ten observations were carried out for those samples

Table 2
Determination of copper in soil and airborne dust particulate samples^a

Samples	Cu(II) found by		Relative standard deviation of the present method, $n = 5$ (%)
	PRESENT METHOD PPM	AAS METHOD (PPM)	
<i>Soil samples</i>			
S-1	9.26	9.97	1.6
S-2	6.78	6.81	1.7
S-3	4.33	4.30	1.7
S-4	6.74	6.77	1.8
S-5	6.88	6.90	1.8
S-6	7.29	7.26	1.7
S-7	9.89	9.81	1.9
S-8	6.67	6.63	1.8
S-9	4.78	4.81	1.7
S-10	5.77	5.78	1.8
<i>Dust fall samples</i>			
Df-1	0.130	0.132	2.7
Df-2	0.070	0.091	2.6
Df-3	0.104	0.105	2.6
Df-4	0.104	0.106	2.5
Df-5	0.075	0.081	2.6
Df-6	0.083	0.086	2.4
Df-7	0.035	0.038	2.4
Df-8	0.030	0.033	2.6
Df-9	0.225	0.237	2.5
Df-10	0.100	0.109	2.5

^a S-1, ..., S-10 and Df-1, ..., Df-10 are soil and dust fall samples, respectively, collected from different representative locations of Raipur, M.P., India.

^b GBC Flame, AAS model 932.

^c Wavelength, 324.7 nm; slit width, 0.5 nm.

Table 3

The validation of the present method based on analysis of standard reference samples for the spectrophotometric determination of copper^a

Samples (%)	Actual content of copper (%)	Content of other major matrix (%)	Cu found by present method, $N = 10$ ($x \pm SD$) (%)
<i>Carbon steel</i>			
BCS No. 218/2	0.23	Mn-0.64, Cr-0.10, Mo-0.027	0.21 ± 0.03
152/2	0.16	Mn-0.91, Cr-0.085, Mo-0.035, Sn-0.025	0.15 ± 0.04
<i>Alloy steel</i>			
BCS No. 233	5.09	Co-23.4, Ni-11.22, Sn-7.95, Mn-0.235	5.03 ± 0.12
266	3.33	Co-23.4, Ni-13.3, Al-7.95	3.30 ± 0.10
<i>Mild steel</i>			
BCS No. 275	0.205	W-0.20, Cr-0.165, Mo-0.095, Ni-0.080	0.21 ± 0.04
<i>Low alloy steel</i>			
BCS No. 253	0.495	Ni-2.92, Mo-0.94, Cr-0.34, V-0.220	0.47 ± 0.03
251	0.090	Ni-5.15, Mo-0.185, Mn-0.165, Co-0.07	0.09 ± 0.04
<i>Aluminium base alloy</i>			
BCS No. 216/1	4.42	Mn-0.73, Fe-0.40, Zn-0.11, Ti-0.10	4.18 ± 0.61
262	0.026	Mg-10.57, Fe-0.19, Mn-0.06	0.03 ± 0.01
<i>Copper base alloy^b</i>			
BCS No. 207	86.84	Sn-9.8, Zn-2.53, Pb-0.41	87.7 ± 1.3
179	58.8	Zn-33.9, Sn-1.75, Al-1.62, Mn-1.03, Ni-1.01, Fe-0.91	58.6 ± 1.7
<i>Rock samples^c</i>			
USGS W-2	106.2	Cr-91.51, Zn-79.6, Pb-37.66, Cd-3.10, Sb-0.85	110.2 ± 7.8
BIR-1	124.7	Cr-372.5, Zn-69.6, Pb-33.11, Cd-3.17, Sb-0.50	129.3 ± 9.9

^a BCS, British Chemical Standards, Bureau of Analysed Samples Ltd., Middlesborough, England; USGS, US Geological Survey, Mafic Rock Reference Samples, Washington, USA.

^b $N = 5$.

^c Concentrations are expressed in ppm for Cu including other metals.

with low content of Cu for each and individual standard sample. Prior extraction with dithizone in chloroform was carried out in samples with comparatively high concentration of zinc to avoid interference [40]. A high degree of correlation was observed between the results obtained by our method and the actual Cu content. The analytical data are incorporated in Table 3.

5. Conclusion

A simple and sensitive field test and extraction-spectrophotometric method for the determination

of Cu(II) at trace level in soil and airborne dust particulates has been described. The extraction in chloroform of red coloured Cu(II)-PAN-(TX-100)-DPBA complex makes the method very sensitive and selective as well. As little as 2 ng Cu(II)/ ml in organic solution could be detected by this method. A comparison of characteristic features of some spectrophotometric methods reported earlier for the determination of copper made in Table 4 reveals the suitability of the present work in the terms of molar absorptivity, matrix interference, linear dynamic range, etc. The present method overcomes all the drawbacks of classical PAN method and other reported photometric methods [11–33].

Table 4
Comparison of characteristic features of various spectrophotometric methods for the determination of copper(II)^a

Reagents	λ_{\max} (nm)	Molar absorptivity, ϵ (l $\text{mol}^{-1} \text{cm}^{-1}) \times 10^5$	Linear dynamic range, $\mu\text{g ml}^{-1}$	Remarks	References
2,6-Dichlorophenolindophenol	562	-	5-300	V(IV), Cd(II) interfere	[11]
2-(5-Bromo-2-pyridylazo) -5-diethyl-aminophenol	545	0.87	0–0.5(BL)	Co(II), Ni(II), Fe(III), Zn(II) interfere	[12]
5-(5-Chloropyridylazo-2,4)diamine	540	0.51	1.0 (DL)	Ni(II), Co(II), Fe(III) interfere	[13]
N,N'-bis(pyridylmethylene)- ethylenedi- amine	740	0.06	1–10 (BL)	Poor sensitivity, Ti(IV), Fe(III), Co(II), CN-, EDTA interfere	[14]
1-(2-Chlorophenyl) -3-hydroxy-3-methylazen	415	0.01	3.2–25.4	Very poor sensitivity	[15]
p-Anisaldehydethiosemi-carbazone	402	0.06	0.1–1.0	Poor sensitivity, Fe, Pt, Pd, Os interfere	[16]
2,4-Dihydroxyacetophenone-thiosemicar- bazone	360	0.14	1.0–10	λ_{\max} at near-UV, Fe ³⁺ , Cr ³⁺ interfere	[17]
Diphenylcarbazone	540	0.63	0.05–1.4	less sensitive	[18]
Biacetyl-2-pyridylhydrazon-ethylo-semicar- bazone	520	0.56	–	Fe, Co, Ni interfere	[19]
Dithiocarbamate	434	0.13	0.0544 \pm 0.0017 (DL)	Poor sensitivity, Fe, Ni, Co interfere, crit- ical pH	[20]
Diethyldithiocarbamate	445	–	0.5–9 (BL)	Ag(I), Hg(I), Bi(III) interfere, critical pH	[21]
Phenanthrene-9,10-quine- monoximate	470	0.63	9.6 (DL)	Fe(II), Co(II), Ni(II), Pb(II), Os(VIII) in- terfere	[22]
N-((-Pyridyl)-2-thioquinaldiamide	520	0.05	3–12	Poor sensitivity	[23]
3-Thiobenzoyl-1-p-tolylthio- carbamide	420	0.10	0.5–4.5	Poor sensitivity, EDTA, Ni, Co interfere	[24]
1,5-bis(di-2-pyridylmethylene)- thiocar- bonohydrazide	420	0.42	0.1–1.3	Co(II), Ni(II), Fe(III), Hg(I), Hg(II) inter- fere	[25]
Antipyrinylazo/pentane-2,4- dione	535	0.13	0.2–15	Poor sensitivity, Zn interfere	[26]
1-(2-Pyridylazo)-2-naphthol	595	–	0.5–3.6	Many metals interfere	[27]
1-(2-Pyridylazo)-2-naphthol	555	0.52	0.08–4.0	Fe, Co, Cd, Hg, Ni, Mn, Zn interfere, less sensitive	[28]
Pyridylazo dye	532	0.47	–	less sensitive	[29]
1-(2-Pyridylazo)-2-naphthol-(2) /TX-100/N-phenyl-N'-(4-methylphenyl) -benzamidine	520	1.14	0.05–5.0	highly sensitive and selective, only Zn and Cd interfere but could be removed	Present method

^a DL, Detection limit, BL, Beer's law.

Acknowledgements

The authors are thankful to the Madhya Pradesh Council of Science and Technology, MAPCOST, Bhopal for the grant-in-aid under the project code Env. Sci. 56/95.

References

- [1] B.K. Sharma, Environmental Chemistry, Goel Publishing House, Meerut, India, 1997.
- [2] W.M. Raymond, R.L. Donahue, Soils in our Environment, 7th ed., Prentice-Hall of India, New Delhi, 1997.
- [3] T.Z. Judith, T. Peter, T. Thomas, Immunotoxicology of Environment Occupational Metals, School of Medicine, New York, 1998.
- [4] N. Goyal, P.J. Purohit, A.G. Page, M.D. Shastry, Talanta 39 (1992) 775.
- [5] E.H. Van Veen, M.T.C. de Loss-Vollebergt, A.P. Wassink, H. Kalter, Anal. Chem. 64 (1992) 1643.
- [6] K. Lobinski, W. Van Borm, J.A.C. Broekaert, P. Tschopel, G. Tolg, Fresenius, J. Anal. Chem. 342 (1992) 563.
- [7] L. Brown, S.J. Hacwell, M.M. Rhead, P.O. Neill, K.C.C. Bancroft, Analyst 108 (1983) 1511.
- [8] A.F. Allen, P.K.N. Bartlett, G. Ingrom, Analyst 109 (1984) 1075.
- [9] F. Queirolo, P. Valenta, Fresenius J. Anal. Chem. 328 (1987) 93.
- [10] R.N. Khandekar, R.M. Tripathi, R. Raghunath, V.C. Mishra, Indian J. Environ. Health 30 (1988) 98.
- [11] M.I. Prodormidis, C.D. Stalikas, P. Th. Veltsistas, M.I. Karayannis, Talanta 41 (1994) 1645.
- [12] D. Xia, Q. Lin, Fenxi Huaxue 13 (1985) 65.
- [13] G. Zhang, Y. Hu, G. Xu, G. Liu, Fenxi Huaxue 13 (1985) 124.
- [14] J.A. Munoz Leyva, P. Salazar Palma, Microchem. J. 31 (1985) 332.
- [15] D.N. Purohit, M.P. Tyagi, S. Shivpuri, Acta Cien. Indi. Chem. 10 (1984) 134.
- [16] K.N. Thimmaiah, H. Sanke Gowda, S.M. Ahmed, Indian J. Chem., A 22 (1983) 690.
- [17] K.H. Reddy, K.G. Reddy, K.M.M.S. Prakash, D.V. Reddy, Indian J. Chem., A 23 (1984) 535.
- [18] J. Song, Y. Zhang, B. Yin, Fenxi Shiyanshi 7 (1988) 27.
- [19] V.D. Pillay, V.M. Shinde, Indian J. Chem, Sect. A 34 (1995) 401.
- [20] Li. Shine, Li. Shenquan, A. Chen, Talanta 40 (1993) 1085.
- [21] Alvarez-Coque Garcia, M.C. Martinez Vaya, R.M. Villanueva Camanas, Mongay-fernandes, Qui. Anal. 5 (1986) 329.
- [22] A. Wasey, B.K. Puri, M. Katyal, M. Satake, Int. J. Environ. Anal. Chem. 24 (1986) 169.
- [23] A.K. Chakrabarti, Indian J. Chem. A. 25 (1986) 886.
- [24] D.M. Ambhore, A.P. Joshi, J. Indian Chem. Soc. 68 (1991) 175.
- [25] A.M. Garcia Rodriga, F.Z.A. Garcia de Torres, J. M. Cano Pavon, C. Bosh Ojeda, Talanta 40 (1993) 1861.
- [26] T. Inshizaki, H. Wada, G. Nakagawa, Anal. Chim. Acta 212 (1988) 253.
- [27] A. Gallardo Malgarejo, A. Gallardo Cespedes, J.M. Cano Pavon, Analyst 114 (1989) 109.
- [28] N.K. Agnihotri, K. Singh, H.B. Singh, Talanta 45 (1997) 331.
- [29] O.M. Baudino, B.A. Gill, P.M. Molinsde, An. Quim. Ser. B 86 (1992) 613.
- [30] M. Yuhuman, Lu. Ming, Y. Yongshen, Z. Xiaoyan, L. Tianyan, Huaxue Fence 33 (1997) 162.
- [31] M. Huimin, H. Yuexian, L. Shugian, Fenxi Shiyanshi 16 (1997) 5.
- [32] Z. Zhigian, L. Jianyan, Huaxue Fence 33 (1997) 74.
- [33] S. Dengming, W. Feng, Y. Dawen, Fenxi Huaxue 24 (1996) 1673.
- [34] R.L. Shriner, F.W. Newmann, Chem. Rev. 35 (1944) 151.
- [35] J.A. Dean, Lange's Handbook of Chemistry, 13th ed, Mc-Graw Hill, International Editions Chemistry, New York, 1987.
- [36] P. Moore, J. Cobby, Introductory Statistics for Environmentalists, Prentice Hall, Oxford, 1998.
- [37] G.D. Christian, Analytical Chemistry, Wiley, New York, 1986.
- [38] L.G. Sillen, Acta Chem. Scand. 10 (1956) 185.
- [39] S.S. Dara, A Text book of Environmental Chemistry and Pollution Control, S. Chand, New Delhi, 1997.
- [40] E.B. Sandell, Colorimetric Determination of Traces of Metals, 3rd ed, Interscience Publishers, New York, 1965.
- [41] W. Gallay, Environmental Pollutants: Selected Analytical Methods, Butterworths, London, 1975.

Different valency chlorine species analysis by non-suppressed ion-chromatography with double cell quartz crystal detector

Po Chen¹, Wan-Zhi Wei, Shou-Zhuo Yao*

New Materials Research Institute, Hunan University, Changsha 410082, People's Republic of China

Received 18 August 1998; received in revised form 13 January 1999; accepted 14 January 1999

Abstract

A non-suppressed ion-chromatographic assay combined with a novel double cell quartz crystal (DCQC) detector is developed for analysis of different valency chlorine species including chlorite, chloride, chlorate, hypochlorite. The retention characteristics of the anions are discussed. The chromatographic system involves the use of a Shimadzu Shim-pack IC-A1 anion analysis column with 0.5 mM potassium acid phthalate (KHP), pH 6.7, as a mobile phase. The DCQC detector has a low temperature coefficient and a high conductance sensitivity independent of the background from 7.2 to 2500 μ S. The analysis of sample is completed without the use of an ion suppression device. © 1999 Elsevier Science B.V. All rights reserved.

Keywords: Double cell quartz crystal; Chromatography; Chlorine dioxide

1. Introduction

Chlorine is an active element. There are many different valency species in nature including chloride, hypochlorite, chlorite and perchlorate. Each of the chlorine species has definite effects on human, animal and plant, chloride has an important biological effect on bio-body, hypochlorite is usually used as a disinfectant. Perchlorate and chlorate from industrial waste are recognized as

reactive chemical hazards. Because of the requirements of the environment control and water quality control, the analysis of the different valency chlorine species is very important.

There have been many analytical methods for the chlorine species, such as high-performance liquid chromatography (HPLC), ion-chromatography (IC), photolytic spectroscopy, flow injection analysis (FIA), electrical chemical assay etc.[1–8]. Most IC methods used suppressed conductivity technology to detect the species. The methods are complex and difficult to operate.

Bulk acoustic wave (BAW) sensor exhibits sensitive response to the change of the solution conductivity. In this laboratory, series piezoelectric

* Corresponding author. Fax: +86-731-8824505.

E-mail address: szyao@hunu.edu.cn (S.-Z. Yao)

¹ Working in Hunan Health and Anti-Epidemic Station, Changsha 410005, People's Republic of China now.

quartz crystal (SPQC) detector and electrode-separated piezoelectric crystal (ESPC) detector based on the BAW sensor have been developed and applied in HPLC and non-suppressed IC [9–13]. The high sensitivity, low cost and conceptual simplicity of the detectors are their advantages versus conventional conductivity detector. In this paper, a novel double cell quartz crystal (DCQC) detector is proposed for use in non-suppressed IC. It has many advantages such as a low temperature coefficient and a high conductance sensitivity, independent of the background conductance. Different chlorine species have been determined simultaneously using this new technique. The retention characteristics of the chlorine species have been discussed.

2. Experimental section

2.1. Reagents and chemicals

Sodium chlorite (80% pure, Aldrich), sodium chlorate (analytical-reagent grade), sodium chloride (analytical-reagent grade), sodium hypochlorite (available chlorine 10–13%, ACS-grade chemicals, Fisher Scientific, Pittsburgh, PA) and perchloric acid were used to prepare standard

solutions. Water was purified using a Milli-Q system ($> 80 \text{ M}\Omega$, Waters Chromatography Division, Millipore Corporation, Milford, USA). All other chemicals were of analytical reagent grade and were used as received without further purification. The mobile phase and sample solutions were filtered through a $0.45 \mu\text{m}$ filter membrane (Millipore, USA).

2.2. Apparatus

IC analyses were performed using a Waters 246 liquid chromatograph coupled to a Waters U6K manual injector, a 590 solvent deliver pump and a Baseline 810 chromatographic workstation. Separations were performed on a Shim-pack IC-A1 ($10 \text{ cm} \times 4.6 \text{ mm ID}$) anion analysis stainless steel column packed with an anion exchange resin of a polymethacrylate support with a particle size of $10 \mu\text{m}$ incorporating a quaternary ammonium base as a functional group (Shimadzu, Japan).

2.3. DCQC detector

The detection of the analytical column elutes was completed by a novel DCQC detector. Schematic diagram of the detector is shown in Fig. 1.

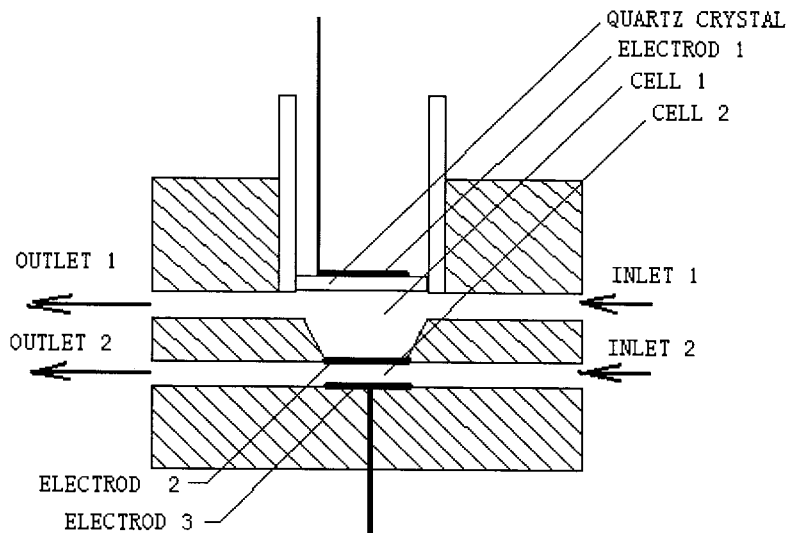


Fig. 1. Diagram of the double cell quartz crystal (DCQC) detector.

Table 1
The retention characteristics of chlorine species^a

Mobile	Retention time of ions (min)				
	ClO ₂ ⁻	ClO ⁻	Cl ⁻	ClO ₃ ⁻	ClO ₄ ⁻
Method 300.1 [14]	3.63	–	4.67	9.28	–
KHP (pH 6.7)	2.12	2.43	3.52	7.42	24.92
Phenol (pH 6.5)	2.51	2.57	3.84	9.27	34.25
NaOH	1.02	1.02	1.34	2.78	3.27
Benzoic acid (pH 6.2)	3.41	3.52	4.01	10.97	29.42
Sodium benzoate (pH 6.7)	2.27	2.31	3.42	5.74	15.42

^a Flow rate is 1.2 ml min⁻¹. Injection volume is 40 µl.

The piezoelectric quartz crystal was mounted on the top of a Teflon column with one side facing liquid. The electrode on this side was removed, therefore the two opposite electrodes inducing an alternating electrical field across the crystal were separated by two flow-through conductivity cells, cell 1 and cell 2. Cell 1 was the adjustment cell and one side of the crystal contacts with liquid in this cell. Cell 2 was the sample cell and mobile from the chromatographic column flows through the cell. The cell constant of cell 1 can be adjusted by changing the position of the PTFE column with the crystal and the cell constant of cell 2 is 0.85 cm. The piezoelectric quartz crystal used was 9 MHz and AT-Cut. A frequency-to-voltage converter (made in this laboratory [9]) was used to transform the frequency signal of the DCQC detector to a Baseline 810 chromatographic workstation, which was used to record chromatograms in real-time and to integrate peak areas.

2.4. Chromatographic conditions

Chromatographic runs consisted of isocratic elution. The flow-rate of mobile phase, 0.5 mM potassium acid phthalate (KHP) (pH 6.7), was 1.2 ml min⁻¹. All solutions were filtered through a type HA 0.45 µm membrane filter (Millipore, Bedford, MA) and degassed by vacuum. Temperature can affect the response stability of the DCQC detector. Hence, the detector temperature must be maintained constant. In the experiments, to keep the thermal equilibrium, the flow cell of

the DCQC detector was maintained at 40°C and the temperature of the analysis column was maintained at 40°C too. No detector drift due to thermal effects was observed.

The eluent was pumped into the chromatographic system. The sample solution was introduced after the baseline was stabilized (f_0 and v_0), and the voltage signals (v_1) was recorded versus time by Baseline 810. The concentrations of the tested ions were calculated from the obtained frequency shift versus time chromatogram by comparison with the standard.

2.5. Standard solutions preparation

The pH of standard solutions must be maintained at over 8.0 to avoid hydrolysis of the chlorine species. And the standard solutions were prepared daily

3. Results and discussion

3.1. Mobile selection

Several common ion chromatography mobile phase, including potassium hydrogen phthalate, sodium hydroxide, sodium benzoate, benzoic acid and phenol, were investigated. Table 1 shows the retention characteristics of the chlorine species under the same concentration (0.5 mM) of the different mobiles. Otherwise, USEPA has reported a method of determination of inorganic anions in drinking water by IC. The method uses

chemically-suppressed IC to analyze the common anions (Part A) and the inorganic disinfection by-products (Part B)[14]. The retention time of chlorine species of the method is also listed in Table 1.

From the results, separation of chlorite and hypochlorite is found to be the most difficult among the five chlorine species. The retention ability of chlorite and hypochlorite is poor on the column. Phenol is a good mobile for poor retention anion separation in general, but chlorite and hypochlorite can not be separated using phenol as a mobile phase, though they are well-known as poor retention anions on the column. KHP is an optimum mobile phase for the chlorine species separation among the mobile phases studied. Each chlorine species ion can be separated completely by using this mobile phase.

Because of the possibility of interference of common ions, several ions were tested for their possible interference with 0.5 mM KHP (pH 6.7) as the mobile phase. The retention time is as follow: F^- 1.72 min, NO_3^- 4.73 min, Br^- 5.21 min, NO_2^- 6.21 min, CO_3^- 11.27 min. Hence, chlorine species ions can be separated completely even in presence of these commonly wet interference ions.

3.2. pH of mobile effect on separation

pH of the mobile affected dramatically the retention characteristics of the anions of chlorine species. When pH of the mobiles increased, the retention time of the ions decreased obviously. Fig. 2 shows the relationship of retention time of the anions with pH of the mobile. When $pH > 7.0$, chlorite and hypochlorite can not be separated completely. From Table 1, it can be seen that strong base mobile can elute the anions chlorine species quickly. So, if pH of the mobile is larger than 7.0, the hydroxy ion in the mobile has a major effect for the anions elution. When $pH < 7.0$, the concentration of phthalate ion in the KHP mobile increases with increasing pH of the mobile. So the elution ability of the mobile increases and the retention time of the chlorine species ions decreases with increasing pH.

3.3. Working condition of the DCQC

For the DCQC detector, the ΔF versus ΔG relationship ($\Delta F/\Delta G$) is linear when all other parameters are kept unchanged. And it was found that the response sensitivity of the DCQC is independent of the background conductivity of solution in cell 2 (G_2) when conductivity of solution in cell 1 (G_1) is ca. 500 μS . Cell constants can affect the detector performance. In this work, the cell constants were optimized $k_1 = 1.0$ cm, $k_2 = 0.85$ cm.

For conventional conductivity detector, its detection sensitivity depends on the background conductivity. So, the advantage of the DCQC detector over the conventional conductimetric detector is its independence on the background conductivity and its response stability. Table 2 shows comparison results of detection sensitivity of these two detectors at different background conductivity. It is obvious that the response of the DCQC is more stable than the conventional conductimetric detector.

For the SPQC detector, the response sensitivity is good when the mobile conductivity is on a range of 150–1200 μS [10]. When the mobile conductivity is over 3000 μS , the detector does

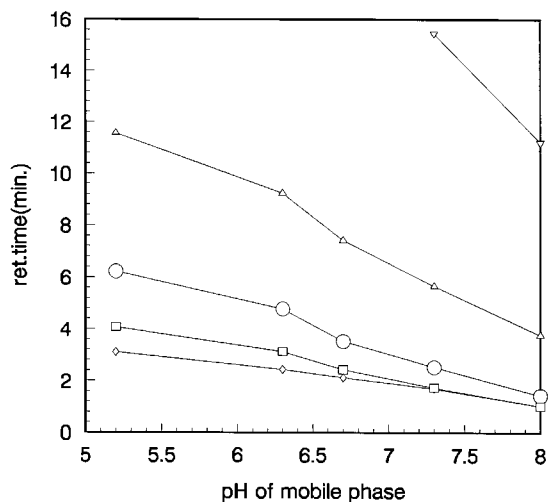


Fig. 2. Relationship of retention time of anions with pH of the mobile. \diamond , ClO_2^- ; \square , ClO^- ; \circ , Cl^- ; \triangle , ClO_3^- ; ∇ , ClO_4^- .

Table 2

Sensitivity comparison of conventional conductivity detector and double cell quartz crystal (DCQC) detector at different background^a

Background (μS)	Response of detector ($\mu\text{V s}^{-1}$)	
	DCQC	Conventional
127	6.42×10^6	5.21×10^6
254	6.33×10^6	5.14×10^6
783	6.24×10^6	4.11×10^6
1543	5.94×10^6	1.13×10^6
2674	5.78×10^6	0.21×10^6

^a 20 ppm Cl^- , 5 μl injection.

not work satisfactorily. In the DCQC detector, because there are two solution cells between the crystal and electrode, the total conductivity between them can be adjusted through a changing solution conductivity in these two cells to meet the requirement of the crystal oscillation. In this way, the working region of the DCQC detector is much wider than that of the SPQC detector reported earlier [10]. It extends to 7.2–2500 μS . Because the crystal does not contact with the mobile directly, the crystal oscillation stability is not affected by the liquid flowing in the sample cell. Therefore, the DCQC oscillation is very stable.

Using DCQC to detect the anions of chlorine species, the calibration graphs for chlorite, hypochlorite, chloride and chlorate were linear over ranges 0.1–20, 0.1–15, 0.2–25 and 0.5–20 $\mu\text{g ml}^{-1}$, respectively. The correlation coefficients of the calibration graphs were >0.9995 . The detection limits (signal-to-noise ratio = 3, noise 1 Hz) were 0.02 $\mu\text{g ml}^{-1}$ for chlorite, 0.02 $\mu\text{g ml}^{-1}$ for hypochlorite, 0.05 $\mu\text{g ml}^{-1}$ for chloride and 0.08 $\mu\text{g ml}^{-1}$ for chlorate.

3.4. Application

The chlorine species was detected in chlorine disinfecting drinking water and chlorine dioxide for daily use. The results are shown in Tables 3 and 4.

The results shown in Table 3 are that of water at different points in water output tube network

Table 3

Determination results of drinking water samples

Sample	Results of determination ($\mu\text{g ml}^{-1}$)			
	Chlorite	Hypochlorite	Chloride	Chlorate
Water 1	<0.01	0.45	24	0.33
Water 2	<0.01	0.78	54	0.52
Water 3	<0.01	2.12	121	1.47
Water 4	<0.01	3.71	132	1.87
Water 5	<0.01	2.54	142	2.01
Water 6	<0.01	2.92	151	1.91

of a drinking water factory. In this factory, the major disinfecting technology is adding liquid chlorine to water. Water 1 and 2 were samples obtained from points in water factor. Water 3 was obtained from point which is located between the factory and the users. Water 4, 5 and 6 were obtained from user's homes. From the results, the concentration of chlorine species in water increases with water transportation. In Chinese national standard for drinking water, the free chlorine margin is a disinfecting index and chloride is a sanitation index. It is thought that the concentration of hypochlorite may be used as a disinfecting index for liquid chlorine disinfecting water factory.

From Table 4, it can be seen that the quality of chlorine dioxide disinfectant for daily use from different manufactures is not stable. Maybe the different quality of the manufacturing sources caused this problem. Sample # 5 was a counter-

Table 4

Results of determination of chlorine dioxide disinfectant for daily use

Sample	Concentration (% w/v)			
	Chlorite	Hypochlorite	Chloride	Chlorate
1 #	1.50	0.002	0.23	0.12
2 #	2.01	0.010	0.46	0.11
3 #	1.66	0.007	0.33	0.27
4 #	3.12	0.003	0.52	0.74
5 #	0.02	4.56	2.30	0.12
6 #	1.10	0.072	1.01	0.52

Table 5
Determination results comparison of different analysis methods

Ions	Determination results of (mg ml ⁻¹)	
	IC-DCQC	Potentiometric
Chlorite	0.02	0.04
Hypochlorite	4.56	4.00
Chloride	2.30	2.35
Chlorate	0.12	0.13

feit chlorine dioxide disinfectant obtained from a market. Because ionic chlorine in stability chlorine dioxide disinfectant is mainly chlorite, the content of chlorite can reflected the false or true chlorine dioxide disinfectant. Sample # 5 contained mainly hypochlorite, no chlorite. So, # 5 disinfectant is a counterfeit chlorine dioxide disinfectant.

For investigating the difference of determination results between the proposed method and the conventional method for chlorine species analysis, the IC-DCQC method and direct potentiometric method [2] were used to analyze a disinfectant simultaneously. The results are shown in Table 5. From Table 5, the results for chlorite and hypochlorite are different. When determining two ions by potentiometric method, they can interfere with each other. So, results of these two methods have differences.

4. Conclusions

The non-suppressed IC-DCQC method described here has a high resolving power, a high sensitivity and a high anti-interference ability for

chlorine species analysis. The method is simple, rapid and accurate. The possibility of application of the DCQC detector in single column IC has been demonstrated. In this method, the use of the ion suppression device is not necessary. The method can be used to monitor the quality of drinking water and chlorine disinfectant.

Acknowledgements

This work was supported by the Natural Science Foundation of China.

References

- [1] Mark Johnson, et al., *Analyst* 121 (1996) 1075–1078.
- [2] Luke C. Adam, et al., *Anal. Chem.* 67 (1995) 535–540.
- [3] Mark K. Bettler, et al., *J. AOAC Int.* 78 (1995) 878–883.
- [4] A.M. Dietrich, et al., *Anal. Chem.* 64 (1992) 496–504.
- [5] E.M. Aieta, et al., *J. Am. Water Works Assoc.* 76 (1984) 64–70.
- [6] K Suzuki, et al., *Anal. Chem.* 50 (1978) 1596–1597.
- [7] G. Gordon, et al., *J. Am. Water Works Assoc.* 9 (1993) 89–97.
- [8] A.I. Vogel, *Quantitative Inorganic Analysis*, 3rd edition, Wiley, New York, 1969.
- [9] P. Chen, L. Nie, S. Yao, X. Fan, *Instrum. Sci. Technol.* 23 (1995) 137–145.
- [10] P. Chen, L.H. Nie, S.Z. Yao, *J. Chromatogr. Sci.* 33 (1995) 268.
- [11] P. Chen, L.H. Nie, S.Z. Yao, *J. Chromatogr. B* 637 (1995) 153.
- [12] B. Yu, P. Chen, L. Nie, S. Yao, *Anal. Lett.* 29 (1) (1996) 43–57.
- [13] K. Chen, P. Chen, L. Nie, S. Yao, *J. Chromatogr. A* 753 (1996) 171–176.
- [14] Daniel P. Hautman, David J. Murch, *Method 300.1 Revision 1.0, Parts A and B*, USEPA, Office of Water, 1997.

Influence of the guests, the type and degree of substitution on inclusion complex formation of substituted β -cyclodextrins

Ágnes Buvári-Barcza, Lajos Barcza *

Institute of Inorganic and Analytical Chemistry, L. Eötvös University, P.O. Box 32, 1518 Budapest 112, Hungary

Received 6 July 1998; received in revised form 6 November 1998; accepted 15 January 1999

Abstract

The stability of inclusion complexes (i.e. the measure of molecular recognition between a guest and β -cyclodextrin, CD) is highly influenced by the fit of the guest into the cavity of the host and by secondary bonds among the functional groups getting in close connection. The guests themselves influence these interactions by their sizes, shapes and functional groups. On the other hand, both the size of the cavity and the reactivity of β -CDs are altered when the hydroxy groups are substituted. As best models, the interactions among hydroxypropylated CDs of different average degree (and pattern) of substitution (DS) and phenolphthalein (as a model for 'large' guests) or *p*-nitrophenol/*p*-nitrophenolate (*p*-NP/*p*-NPate) couple (as for 'small' ones) have been studied. The formation constants of phenolphthalein–hydroxypropyl- β -CD (HP-CD) complexes are continuously decreasing, while those of *p*-NP and *p*-NPate ones show a maximum with increasing DS. Similarly, the pattern of substitution has a significant effect on the quality of the interaction, too. The change of the DS on O(6) position alters the type of the interactions most, and a series of different findings prove that this change is the basis in the chiral selectivity of different CD derivatives, too. The ratio of the average DS on primary and secondary hydroxy rims [$R_{DS} = DS(6)/DS(2,3)$] is recommended as the simplest possibility for characterizing the substitution pattern. © 1999 Elsevier Science B.V. All rights reserved.

Keywords: Cyclodextrins; Substitution pattern; Molecular recognition; Analytical separation

1. Introduction

Cyclodextrins (CDs) are cyclic oligosaccharides produced in enzymatic hydrolysis of starch. The α -, β - and γ -CDs contain six, seven or eight

glucose units, respectively. They are molecules with a shape of truncated cone, having hydrophobic cavity (Fig. 1). The diameter of the cavities are estimated as 4.7, 6.8 and 10 Å, while their volumes are of 176, 346 and 510 Å³, respectively [1]. Many hydroxy groups are situated on the outer part of the ring which make the CDs both hydrophilic and soluble in water. It is well known that CDs can form inclusion complexes and the

* Corresponding author. Tel.: +36-1-209-0555; fax: +36-1-209-0602.

E-mail address: barcza@ludens.elte.hu (L. Barcza)

properties of the encapsulated molecules are modified by this complex formation, e.g. water solubilities and chemical stabilities are increased, etc. [1–4]. CDs have a wide range of practical application in pharmaceutical, cosmetic, food, chemical and several other industries [2,3] and are often used in separation techniques of analytical chemistry. Not only structurally dissimilar compounds but also isomers can be separated, and CDs are thought to be the best chiral selector

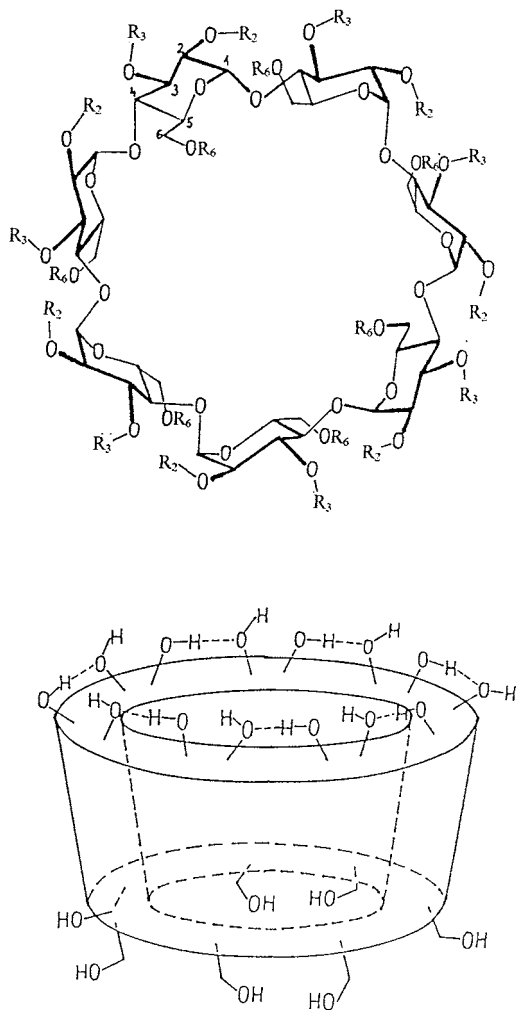


Fig. 1. Sketchy representation of β -cyclodextrin (CD). (On the top: its atom-to-bond formula, where R_2 , R_3 and R_6 represents the substituents on O(2,3 or 6) position. At the bottom: its shaped truncated cone representation with the intramolecular 'flip-flop' H-bondings [31].)

[3–6]. The theoretical background of chiral discrimination is based on the general theory of intermolecular forces [7,8], surveyed recently from the point of view of CD inclusion complexes, too [9]. The opinions vary about the effect of substitutions on the enantiomer discrimination: using molecular dynamics calculations, the enantiodiscriminating domain of permethyl- β -CD was found to be inside the macrocyclic cavity [10], while others found no distinctive effect by NMR (and other) methods, when all of the hydroxyls were alkylated in α - or β -CDs [11].

The number of guests investigated is growing every day and it is nearly inestimable, while 1562 monomeric CD derivatives and several polymeric, etc. CDs are surveyed by a recent compilation [12]. The substituted CDs are characterized by the average degree of substitution (DS), which means generally the average number of substituents per one CD (or sometimes that of the substituents per one glucose unit) [2,3].

Among the most interesting CD derivatives, 2-hydroxypropyl- β -CD (HP-CD) [13] could be emphasized and used as the best example.

HP-CDs are produced by a condensation of β -CD with propylene oxide in alkaline solution. The hydroxypropylation of O(2) secondary hydroxyls (and much less that of O(3)) is favoured by relatively low alkali hydroxide concentration while high alkali hydroxide content (≥ 10 M) promotes the formation of O(6) derivatives [13–15], still the products are always substituted randomly concerning the distribution among the different glucose units. The DS values depend on the ratio of reactants, reaction time and temperature. It follows that the composition of HP-CD samples shows high variability which is reflected in the chemical and physical properties, too.

It can be well understood, that the solubilizing power of (amorphous) HP-CD was investigated above all because of its practical importance, and the 'aqueous solubility enhancement' was found to depend extremely on the kind of guests [13]. The effect of the substitution pattern both on the solubility and inclusion complex forming ability had been recognized before long [14], and that of the DS in the next step [15]. The chiral selectivity in analytical separations, which is in close correla-

tion with both the molecular recognition and the stability of inclusion complexes, is effected by the change in DS of HP-CD as demonstrated experimentally [16,17]. It seems that this fact is not realized up to now by most of the authors working on this field, since the DS value is hardly mentioned in most of the papers as if the HP-CD were a discrete compound.

It seems a rather general phenomenon among the substituted β -CD derivatives that their stereospecificity is influenced by both their substitution pattern and DS (with the exception of homogeneously and totally substituted 'per' ones). The apparent contradiction mentioned earlier [10,11] may originate from the fact, that using molecular dynamics calculations [10,18,19], permethylated (i.e. trimethyl-) β -CD was used as the model of the host (where the proton donor abilities of β -CD are ceased and its proton acceptability is also diminished), and most of the guest molecules selected for modelling were of poor proton donating capacity. (Nevertheless, the enantiodifferentiating forces can be estimated as significant as 10% of the binding forces [18].)

The dependence of chiral selectivity of heptakis(2,3-di-OMe)- β -CD derivatives has been investigated as the function of the size of the substituent on O(6) position from the point of view of gas chromatography (GC) (i.e. at higher temperature up to 250°C) [20]. Starting with (6-F)-6-deoxy derivative, the 6-O-methyl, *-i*-pentyl, *-n*-propyldimethylsilyl, *-t*-butyldimethylsilyl and *-tris(i-propyl)silyl* derivatives were studied. The chiral selectivity was detected to vary significantly with the size of the substituent: the best effect was found for nearly all types of guests investigated in the case of *-t*-butyldimethylsilyl substitution [20].

It is not surprising, that synthesizing mono(6-O-X)-, mono[(6-N-X)-6-deoxy]-, mono[(6-Se-X)-6-deoxy]-, etc. derivatives of β -CD, the stability of the complexes (using mainly L-tryptophan as model guest) change significantly, e.g. the derivatives containing Se(6) instead of O(6) form less stable complexes [21]. The high effects of DS and substitution pattern of HP-CD on chiral separation of four basic drugs (using the capillary electrophoretic method) are also discussed [22].

Concerning the stabilities of HP-CD inclusion complexes, a large series of stability constants, determined parallel for α -CD, β -CD and HP-CD (of DS = 6) were recently published [23,24]. The values for 68 aliphatic compounds with β -CD and HP-CD are very close to each other. All of the stability constants of the ketones studied are higher for HP-CD than for β -CD, except the single aromatic one, the acetophenone [24]. It can be seen that depending on the kind of the guest, the HP-substitution can either increase or decrease the stability of the complexes. All of these findings point to the rather close connection between the stability of the inclusion complex formed and the size of the guest, i.e. to the primary importance of the fit of the guest into the CD cavity.

Since the aim was to study the phenomena mentioned, appropriate model guests had to be chosen. Phenolphthalein (PP) and the *p*-nitrophenol/*p*-nitrophenolate (*p*-NP/*p*-NPate) couple seemed ideal ones because aromatic compounds are typical guests for complexation and on the other hand, the changes in absorbances make easy to follow the complex formation. PP was thought for modelling the 'large' guests, as only a part of its rather rigid molecule is included during the complex formation [25], and the *p*-NP/*p*-NPate couple [26] served as the model of 'small' molecules, for they can penetrate the CD cavity rather easily and the fitting is not too tight.

The earlier results are supplemented in this paper with those obtained with some new, differently substituted HP-CDs, together with the more detailed information about the hosts got by high performance liquid chromatography-mass spectrometry (HPLC-MS). Comparing the trends in the stability constants for different hosts and guests, some more general conclusions are drawn.

2. Experimental

Most of the HP-CD samples were from Cyclo-lab (Hungary), except two ones, purchased from Aldrich. These last samples were labelled equally (as 'HP- β -CD') but the Cat. Nos. were different (which meant (A) DS = 4.2 and (B) DS = 6.3,

respectively). All other materials were of analytical grade and were used without further purification.

The guests (G) investigated (PP, *p*-NP and *p*-NPate) form 1:1 inclusion complexes with the host (H = HP-CD), where the stability constants are by definition:

$$K = [H - G]/([H] \times [G]) \quad (1)$$

The stability constants of PP inclusion complexes have been determined by spectrophotometry, using Spectromom 195D instrument, measuring the equilibrium concentration of free PP in solutions of pH 10.5 (in presence of 0.02 M sodium carbonate) at $\lambda = 550$ nm since the complexed form is colourless [25]. Knowing [PP] (= [G]) and the total concentrations:

$$c_G = [G] + K \times [G] \times [H] \quad (2)$$

$$c_H = [H] + K \times [G] \times [H] \quad (3)$$

the stability constants can be calculated easily.

Using the same spectrophotometer, the interaction of *p*-NP and *p*-NPate with HP-CD has been investigated by means of the shift in the concentrations of the conjugate acid and base forms, which is caused by the different stabilities of the corresponding complexes [26]. The measurements were carried out at three different wavelengths ($\lambda = 300, 317$ and 402 nm) and at three different pH values (pH 6.4, 6.8 and 7.2; adjusted by phosphate buffers which are the most indifferent for CDs). Since the molar absorptivities of *p*-NP and *p*-NPate can be separately measured in acidic and alkaline solutions, respectively, the equation characterizing the measured absorbance can be set up. Combining this equation with those of mass balances (which are similar to Eqs. (2) and (3)), the stability constants can be evaluated using an iterative computer program.

In every experiment, the temperature was kept constant as $25 \pm 1^\circ\text{C}$.

The HP-CD samples were analysed by Spectrophysics HPLC gradient system, VG Quattro MS/MS equipped with electrospray interface (Ficous Instrument, Altricham) with C8 column and an eluent of 50:950:1 acetonitrile/water/formic acid has been used.

3. Results

The soft ionization mass spectrometry gives the common [27] heterogeneous (multicomponent) picture for every sample, but connected with reversed phase HPLC, very interesting differences can be found. Figs. 2 and 3 represent the results of samples (A) and (B) (DS = 4.2 and 6.3, respectively) in a very illustrative way: the mass spectra of the different fractions obtained by HPLC are shown, and the \sim DS value of the main species in the given fraction is noted on the ordinate instead of ionic mass ranges. (The mean of ionic masses, characteristic for the fractions, can be easily recalculated knowing the molecular mass of β -CD and HP substituent.) The two measurements were done under the same conditions exactly, so it is demonstrated that sample (A) consists of more similarly substituted species, it is relatively consistent, while sample (B) is more complex, proved also by the higher and different retention times.

The HP-CD samples from Cyclolab could be grouped principally in two categories: (i) where first of all the secondary [O(2) and less probably O(3)] hydroxy groups are substituted; and (ii) where the substitution on the primary hydroxy rim [O(6)] predominates.

The substitution pattern can be characterized by R_{DS} values, by the ratio of DSs on primary and secondary hydroxy rims:

$$R_{DS} = [R_{DS(6)/DS(2,3)}] = DS(6)/[DS(2) + DS(3)] \\ = DS(6)/DS(2,3) \quad (4)$$

Accordingly, the case (i) can be characterized by $R_{DS} \ll 1$, and (ii) by $R_{DS} > 1$. A third, intermediate case is also possible, when (iii) $R_{DS} \sim 1$.

The stability constants of PP–HP-CD inclusion complexes are represented on Fig. 4 as a function of DS. The symbols indicating the values measured with HP-CD samples of $R_{DS} \ll 1$ could be connected by a straight line and show a continuous decreasing trend. The PP complexes with samples of other substitution pattern always have lower stabilities, but the decrease of constants as a function of DS can be followed also in these cases. Fig. 4 contains the data measured with 2,6-dimethyl and 2,3,6-trimethyl β -CD, too, and their relative locations are very informative.

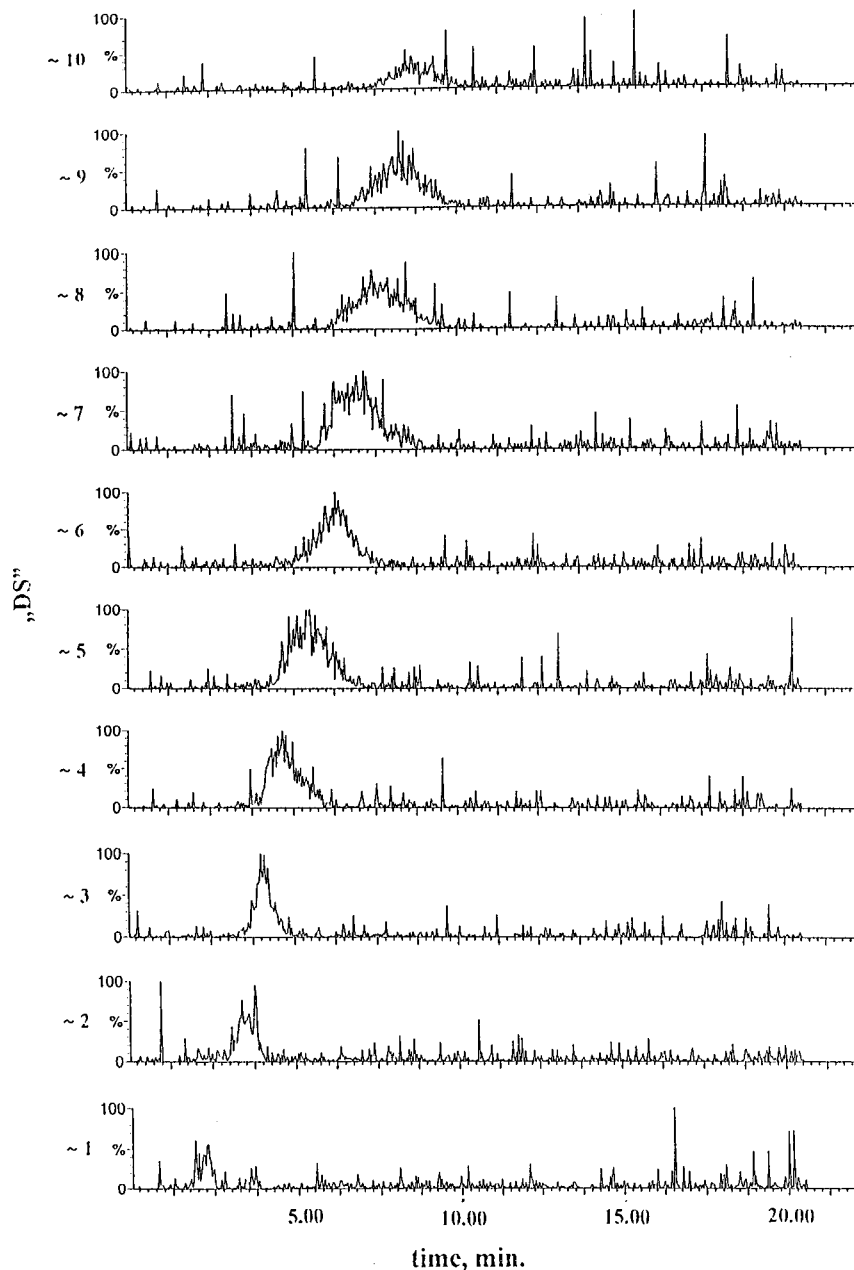


Fig. 2. The high performance liquid chromatography-mass spectrometry (HPLC-MS) chromatogram of sample (A) (see text). (The ionic masses are substituted by ~ 'degree of substitution' ('DS') values and sensitivity data are omitted for clarity.)

The stability constants of HP-CD-*p*-NP/*p*-NPate complexes are summarized in Table 1 (together with their standard deviation) and grouped into three categories reflecting the substitution

pattern of HP-CD. Samples 2–7 with $R_{DS} \ll 1$ form one of the groups (b in Table 1), the next group (c) collects the samples (8–11) with $R_{DS} \sim 1$, while samples 12–13 (d) are those having $R_{DS} > 1$.

In general, the stability constants of inclusion complexes formed between HP-CD and *p*-NPate or *p*-NP increase with increasing DS of HP-CD at the beginning then passing a maximum at DS =

6–8 they decrease at higher DS values.

The change in substitution pattern of HP-CD decrease all the formation constants measured as it is demonstrated especially with the case of three

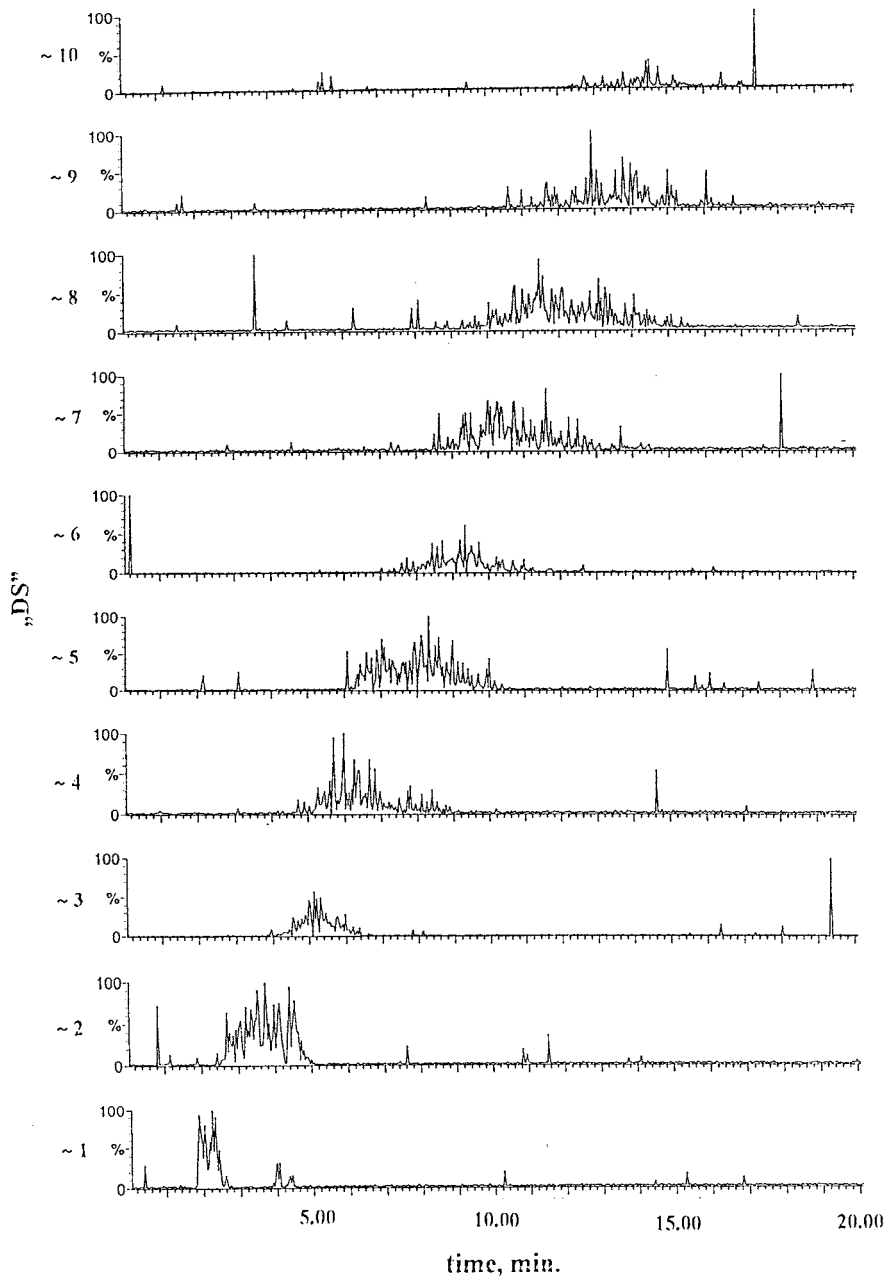


Fig. 3. The high performance liquid chromatography-mass spectrometry (HPLC-MS) chromatogram of sample (B). (Notes as at Fig. 2.)

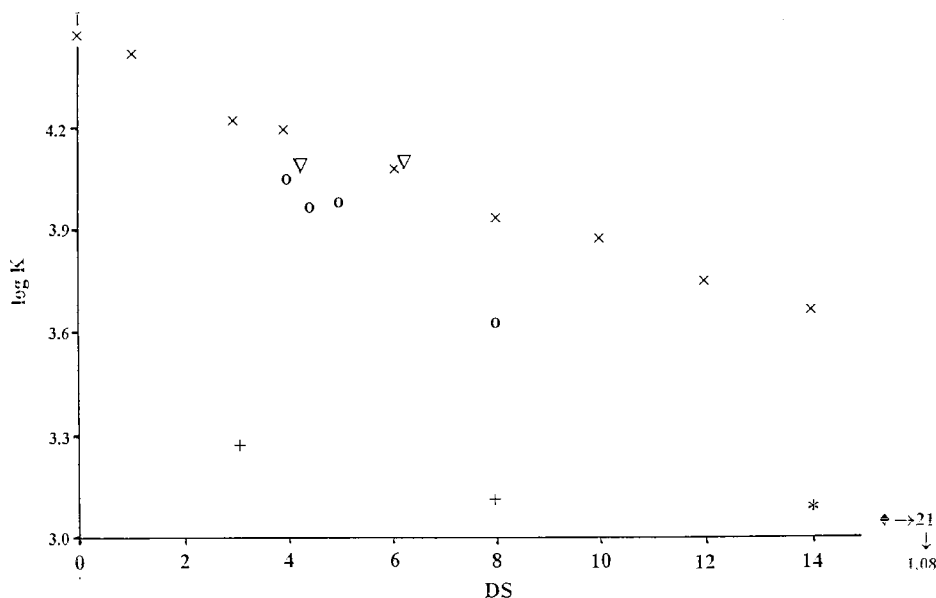


Fig. 4. log K values of phenolphthalein–2-hydroxypropyl- β -cyclodextrins (PP–HP-CD) inclusion complexes as a function of degree of substitution (DS) values. [x, indicates samples of $R_{DS} \ll 1$; o, represents those of $R_{DS} \sim 1$; +, represents those of $R_{DS} > 1$; while ∇ , represents samples (A) and (B) (see text). *, stands for O(2,6)-dimethyl and \blacklozenge , for trimethyl β -CD derivatives.]

HP-CD samples having identical DS values (DS = 8) but different substitution pattern (see Fig. 4 and Table 1). However, this change is not identical for the inclusion complexes of different guests: its trend can be characterized qualitatively as $PP > p\text{-NPate} \gg p\text{-NP}$. Even the very typical and important difference between the values of $K_{p\text{-NPate-CD}}$ and $K_{p\text{-NP-CD}}$ disappears and their quotient (Q in Table 1) nears to 1 when the value of R_{DS} is increasing.

4. Discussion

The cavity of CD is extended by HP substitution, which can mean either (i) the protection of the included guest or (ii) the sterical hindrance of the inclusion. (The possibility of the formation of new H-bonds (iii) can be added as a third factor—when the guest possesses any H-donor or H-acceptor abilities—because these new H-bondings also influence the stability of the inclusion complex.) It must be mentioned that the consequence of these opposite interactions was experi-

enced rather early, therefore, only HP-CD samples of DS < 8 were recommended for practical use [13].

The larger and less flexible guests, like PP are more sensitive against the sterical hindrance (ii) and no stability maximum exists [28] with (PP HP-CD) inclusion complexes as a function of DS. As it is shown by the stability constants in the case of PP, the three-site interaction [25] is disturbed first of all by the substitution of the primary hydroxy rim (6-O-HP). The change (decrease) of the stability constants can be well correlated with the change of the induced circular dichroism spectra of the given inclusion complex [29], proving the common origin of these phenomena.

The inclusion of $p\text{-NP}$ and its deprotonated form, $p\text{-NPate}$ is both promoted by the hydroxypropylation of β -CD at the beginning, where the protecting (i) and the H-bonding (iii) effects exceed the sterical hindrance (ii). At higher DS, the sterical hindrance becomes more and more predominant: the increase of constants stop first then a decreasing trend appears. Very interestingly the change of the substitution pattern, first of all the

relative increase of the substitution on O(6) position alters the type of the interaction between HP-CD and *p*-NPate anions, as the resonance charge delocalization of the latter one (which was the first motive for the unusual stability of β -CD-*p*-NPate complex [26]) seems to lose its priority. The explanation can be similar as for the case of PP complex [30], where even the signs of maxima in circular dichroism spectra may

change: the *p*-NPate (and possibly also the *p*-NP) molecule is left by the increasing substitution of the primary rim in an inclined position a bit further out of the cavity (but bound by H-bonds with HP hydroxy groups).

The dependence of chiral selectivity of heptakis(2,3-(di-OMe)- β -CD derivatives on the size of the substituents on O(6) position [20] points again to the high probability of the role of O(6) substituent.

It is very interesting that entirely different effects can be determined by the capillary electrophoretic method during the enantioseparation of four basic drugs varying the DS and substitution pattern of HP-CD [22]: decrease, increase or maximum can be equally found in the effectiveness of the separations. It seems very likely that the R_{DS} (the substitution pattern) and the special interactions with the guest are of crucial importance in these cases, too.

Table 1

Stability constants of *p*-nitrophenol (*p*-NP) and *p*-nitrophenolate (*p*-NPate) inclusion complexes with 2-hydroxypropyl- β -cyclodextrins (HP-CDs)

No.	DS	$K_{p\text{-NP-HP-CD}} \pm 3\sigma$	$K_{p\text{-NPate-HP-CD}} \pm 3\sigma$	Q^a
1 ^b	0.0	$(1.30 \pm 0.15) \times 10^2$	$(4.10 \pm 0.40) \times 10^2$	3.15
2 ^b	2.9	$(4.40 \pm 1.60) \times 10^2$	$(8.50 \pm 2.30) \times 10^2$	1.93
3 ^b	6.0	$(5.40 \pm 0.66) \times 10^2$	$(1.22 \pm 0.08) \times 10^3$	2.26
4 ^b	8.0	$(4.93 \pm 0.40) \times 10^2$	$(1.26 \pm 0.12) \times 10^3$	2.55
5 ^b	10.0	$(4.32 \pm 0.39) \times 10^2$	$(1.22 \pm 0.10) \times 10^3$	2.82
6 ^b	12.0	$(4.06 \pm 0.12) \times 10^2$	$(1.06 \pm 0.33) \times 10^3$	2.62
7 ^b	14.0	$(2.54 \pm 0.11) \times 10^2$	$(6.80 \pm 0.15) \times 10^2$	2.68
8 ^c	4.0	$(2.46 \pm 0.26) \times 10^2$	$(5.25 \pm 0.44) \times 10^2$	2.13
9 ^c	4.4	$(3.25 \pm 0.22) \times 10^2$	$(8.13 \pm 0.27) \times 10^2$	2.50
10 ^c	5.0	$(2.72 \pm 0.20) \times 10^2$	$(5.50 \pm 0.30) \times 10^2$	2.02
11 ^c	8.0	$(3.89 \pm 0.47) \times 10^2$	$(5.74 \pm 0.67) \times 10^2$	1.48
12 ^d	3.1	$(3.10 \pm 0.50) \times 10^2$	$(3.10 \pm 0.35) \times 10^2$	1.00
13 ^d	8.0	$(2.50 \pm 0.07) \times 10^2$	$(2.85 \pm 0.03) \times 10^2$	1.14

^a The $K_{p\text{-NPate-HP-CD}}/K_{p\text{-NP-HP-CD}}$ ratio.

^b $R_{DS} \ll 1$ (see text).

^c $R_{DS} \sim 1$.

^d $R_{DS} > 1$.

5. Conclusion

The molecular recognition, i.e. both the stability constant of inclusion complex formed and the possibility of any analytical separation are determined equally by the properties of the interacting guest and the CD. Since the variety of guests is nearly infinite and the interactions are extremely delicate, the selection of some good models (like PP for ‘large’ and *p*-NP for ‘small’ guests, etc.) can be recommended for comparing the effect of different CDs.

The characterization of partially or heterogeneously substituted CDs is even more complicated, since none of them can be regarded chemically uniform compound. As it was demonstrated, both the DS and substitution pattern (can) alter the results and neither separations nor stability constant determinations can be reproduced without the exact qualification of the CD derivative used.

For characterizing the substitution pattern, the ratio of DSs on primary and secondary hydroxy rims [$R_{DS} = DS(6)/DS(2,3)$] is the simplest but most appropriate value.

Acknowledgements

Financial support of this work from the Hungarian Research Foundation (OTKA 019493) is gratefully acknowledged. We thank Cyclolab (Hungary) for the selected CD samples, Dr T. Karancsi and M. Tarnai for helping in HPLC-MS investigations.

References

- [1] J. Szejtli, *Cyclodextrins and Their Inclusion Complexes*, Akadémiai Kiadó, Budapest, 1982, p. 34.
- [2] J. Szejtli, *Cyclodextrin Technology*, Kluwer, Dordrecht, 1988.
- [3] D. Duchene (Ed.), *New Trends in Cyclodextrins and Derivatives*, Edition de Santé, Paris, 1991.
- [4] J. Szejtli and T. Osa (Eds.), *Cyclodextrins*, In: J.-M. Lehn, J.L. Atwood, J.E.D. Davies, F. Vögtle (Eds.), *Comprehensive Supramolecular Chemistry*, Vol. 3, Pergamon, Oxford, 1996.
- [5] S. Li, W.G. Purdy, *Chem. Rev.* 92 (1992) 1457.
- [6] H. Nishi, S. Terabe, *J. Chromatogr. A* 675 (1994) 245.
- [7] P.L. Huyskens, W.A.P. Luck, T. Zeegers-Huyskens (Eds.), *Intermolecular Forces*, Springer, Berlin, 1991.
- [8] H. Dodziuk, *Modern Conformational Analysis*, VCH, New York, 1995.
- [9] K. Kano, *J. Phys. Org. Chem.* 10 (1997) 286.
- [10] K.B. Lipkowitz, R. Coner, M.A. Peterson, A. Morreale, J. Shackelford, *J. Org. Chem.* 63 (1998) 732.
- [11] A. Gafni, Y. Cohen, R. Katakay, S. Palmer, D. Parker, *J. Chem. Soc. Perkin Trans. 2* (1998) 19.
- [12] L. Jicsinszky, E. Fenyvesi, H. Hashimoto, A. Ueno, *Cyclodextrin Derivatives*, Pergamon, Oxford, 1996, pp. 57–188.
- [13] L. Szente, C.E. Strattan, *Hydroxypropyl β -Cyclodextrins, Preparation and Physicochemical Properties*, Edition de Santé, Paris, 1991, pp. 57–98.
- [14] C.T. Rao, B. Lindberg, J. Lindberg, J. Pitha, *J. Org. Chem.* 56 (1991) 1327.
- [15] C.T. Rao, J. Pitha, B. Lindberg, J. Lindberg, *Carbohydr. Res.* 223 (1992) 99.
- [16] B.W. Müller, U. Brauns, *J. Pharm. Sci.* 75 (1986) 571.
- [17] I.E. Valko, H.A.H. Billiet, J. Frank, K.C.A.M. Luyben, *J. Chromatogr. A* 678 (1994) 139.
- [18] K.B. Lipkowitz, G. Pearl, B. Coner, M.A. Peterson, *J. Am. Chem. Soc.* 119 (1997) 600.
- [19] K.B. Lipkowitz, R. Coner, M.A. Peterson, *J. Am. Chem. Soc.* 119 (1997) 11269.
- [20] A. Shitangkoon, G. Vigh, *J. Chromatogr. A* 738 (1996) 31.
- [21] Y. Liu, B.H. Han, B. Li, Y.M. Zhang, P. Zhao, Y.T. Chen, T. Wada, Y. Inoue, *J. Org. Chem.* 63 (1998) 1444.
- [22] X.Y. Fu, C.R. Sun, J.D. Lu, Y.Z. Chen, *Chem. J. Chin. Univ.* 18 (1997) 1957.
- [23] O.S. Tee, T.A. Gadosy, J.B. Giorgi, *Can. J. Chem.* 74 (1996) 736.
- [24] O.S. Tee, A.A. Fedortchenko, P.G. Loncke, T.A. Gadosy, *J. Chem. Soc. Perkin Trans. 2* (1996) 1243.
- [25] Á. Buvári, L. Barcza, M. Kajtár, *J. Chem. Soc. Perkin Trans. 2* (1988) 1687.
- [26] Á. Buvári, L. Barcza, *J. Chem. Soc. Perkin Trans. 2* (1988) 543.
- [27] J. Pitha, J. Milecki, H. Fales, L. Pannell, K. Uekama, *Int. J. Pharm.* 29 (1986) 73.
- [28] Á. Buvári-Barcza, L. Barcza, *Anal. Quim. Int. Ed.* 94 (1998) 98.
- [29] Á. Buvári-Barcza, J. Kajtár, L. Szente, L. Barcza, *J. Chem. Soc. Perkin Trans. 2* (1996) 489.
- [30] Á. Buvári-Barcza, J. Kajtár, L. Barcza, *J. Incl. Phenom.* 24 (1996) 211.
- [31] C. Betzel, W. Saenger, B.E. Hingerty, G.M. Brown, *J. Am. Chem. Soc.* 106 (1984) 7545.

Simultaneous spectrophotometric determinations of cobalt, nickel and copper using partial least squares based on singular value decomposition

T. Khayamian, Ali A. Ensafi *, B. Hemmateenejad

College of Chemistry, Isfahan University of Technology, Isfahan, Iran

Received 21 September 1998; received in revised form 19 January 1999; accepted 20 January 1999

Abstract

The partial least squares modeling based on singular value decomposition was applied for the simultaneous spectrophotometric determination of Co(II), Ni(II) and Cu(II) as their ammonium 2-amino-1-cyclohexan-1-dithiocarbamate complexes. The latent variable calculation in this partial least squares modeling is not an iterative technique. The detection limits for Co(II), Ni(II) and Cu(II) were 0.072, 0.021 and 0.063 $\mu\text{g/ml}$, respectively. The application of the method was confirmed by analysis of these metals in sample alloys. © 1999 Elsevier Science B.V. All rights reserved.

Keywords: Partial least squares; Simultaneous; Singular value decomposition; Co–Ni–Cu; Spectrophotometry

1. Introduction

The combination of cobalt, nickel and copper are used in different alloys [1]. The analysis of these metals by univariate calibration methods, at first requires using one of the separation techniques. Wada et al. [2] determined Co(II), Ni(II) and Cu(II) by derivatizing the metals with 2-(4-methyl-2-quinolylazo)-5-diethyl-aminophenol and using reversed-phase high performance liquid chromatography. In this paper, partial least squares (PLS), as a multivariate calibration

method [3–5], was applied to the simultaneous spectrophotometric determination of these metals with no need for previous separation. The spectrophotometric determination of the metals was done by preparing the complexes of the cations with ammonium 2-amino-1-cyclohexan-1-dithiocarbamate (AACD). This reagent was synthesized by Takeshima et al. [6] in 1979 and forms a complex with most transition metal cations. Co(II), Ni(II) and Cu(II) are the cations that form a stable complex with AACD, with the formulae $\text{Co}(\text{AACD})_3$, $\text{Ni}(\text{AACD})_2$ and $\text{Cu}(\text{AACD})_2$. The peak absorbance of these complexes in the visible region is at 445, 535 and 470 nm, respectively [7–9]. The PLS was applied for modeling the absorbance spectra of Co–AACD, Ni–AACD

* Corresponding author. Tel.: +98-31-891-2351; fax: +98-31-891-2350.

E-mail address: ensafi@cc.iut.ac.ir (A.A. Ensafi)

and Cu–AACD in solutions containing these three cations.

PLS is a factor analysis that was originally suggested by Wold and coworkers [10,11], and consequently different algorithms for PLS modeling were developed [12–16]. Lorber et al. [17], in 1987, suggested an alternative method for PLS modeling. It is different from any modeling that used an iteration technique to find the latent or factor variables for PLS modeling. In the following, a brief summary of the PLS algorithm is shown [17].

In the classical least squares (CLS) method, the concentration of all components in the calibration samples must be known. This is called the total calibration model. When the concentrations of all constituents are not known, it is named partial calibration. Consider a sample with k constituents. If the responses of this sample are measured in J sensors, the response vector \mathbf{r}_{un} , can be written in matrix notation as:

$$\mathbf{r}'_{\text{un}} = \mathbf{c}'_{\text{un}}\mathbf{S} + \mathbf{e}' \quad (1)$$

where \mathbf{r}_{un} is the $J \times 1$ response vector, \mathbf{c}_{un} is the $k \times 1$ vector analyte concentrations in the sample, \mathbf{S} is the $k \times J$ matrix of sensitivities and \mathbf{e}' is the $J \times 1$ error vector.

For predicting analyte concentrations in an unknown sample, it is necessary to determine the matrix of sensitivities \mathbf{S} and it is determined in the calibration step.

$$\mathbf{R} = \mathbf{C}\mathbf{S} + \mathbf{E} \quad (2)$$

If I samples are used, \mathbf{R} is an $I \times J$ response matrix and $\mathbf{C} = I \times K$ concentration matrix. Solving the calibration equation for \mathbf{C} gives:

$$\mathbf{C} = \mathbf{R}\mathbf{S}^+ \quad (3)$$

The superscript $+$ denotes the pseudo inverse matrix. Multiplying both sides by \mathbf{R}^+ results in

$$\mathbf{R}^+\mathbf{C} = \mathbf{R}^+\mathbf{R}\mathbf{S}^+ = \mathbf{S}^+ \quad (4)$$

Thus, $\mathbf{S}^+ = \mathbf{R}^+\mathbf{C}$

Solving Eq. (1) for concentration gives

$$\mathbf{c}_{\text{un}} = \mathbf{r}'_{\text{un}}\mathbf{S}^+ \quad (5)$$

Substituting Eq. (4) into Eq. (5) gives:

$$\mathbf{c}_{\text{un}} = \mathbf{r}'\mathbf{R}^+\mathbf{C} \quad (6)$$

For one component, Eq. (6) can be written as:

$$c'_{\text{un}} = \mathbf{r}'_{\text{un}}\mathbf{R}^+\mathbf{c} \quad (7)$$

where \mathbf{c} is the concentration vector from calibration for the desired analyte only, and \mathbf{c}_{un} is the estimated concentration of this analyte in the unknown sample. By singular value decomposition \mathbf{R}^+ can be determined:

$$\mathbf{R} = \mathbf{U}\cdot\mathbf{S}\cdot\mathbf{V}' \quad (8)$$

$$\mathbf{R}^+ = \mathbf{V}\mathbf{S}^{-1}\mathbf{U}' \quad (9)$$

This is the case where the full mathematical rank of \mathbf{R} is included in the estimation of \mathbf{R}^+ . One objective of PLS is to approximate \mathbf{R} by the minimum number of the components required to predict the concentration of the analyte. This algorithm uses a PLS approach to obtain an estimate of \mathbf{R}^+ which is not simply the inverse or pseudo inverse of \mathbf{R} , and the estimation of each PLS component is not an iterative procedure. A good estimate of \mathbf{R}^+ means to find the required number of latent variables for building the model.

In this paper, the PLS-1 algorithm based on an estimate of \mathbf{R}^+ was written in MATLAB and was used to determine the concentration of Co(II), Ni(II) and Cu(II) in artificial mixtures and real samples. According to our knowledge, this is the first report of the application of the written algorithm for simultaneous determination of metals with satisfactory results.

2. Experimental

2.1. Reagents and chemicals

All chemicals were analytical grade. Doubly distilled water was used for preparation of the solutions.

Stock standard solutions (1000 $\mu\text{g/ml}$) of cations were prepared by dissolving 1.235, 1.239 and 0.982 g of $\text{Co}(\text{NO}_3)_2\cdot 6\text{H}_2\text{O}$, $\text{Ni}(\text{NO}_3)_2\cdot 6\text{H}_2\text{O}$ and $\text{CuSO}_4\cdot 6\text{H}_2\text{O}$ compounds, respectively, in 250 ml volumetric flask and diluted to the mark with distilled water.

AACD reagent was synthesized by the procedure explained by Takeshima et al. [6]. AACD solution (1.7×10^{-2} M) was prepared by dissolving 0.3130 g of the reagent in 100 ml acetone.

2.2. Apparatus

A Perkin-Elmer double beam spectrophotometer (Model 551) equipped with 10.0-mm quartz cells was used for fixed-wavelength measurements. For recording the absorbance spectrum, a double-beam spectrophotometer (Shimadzu, Model UV-240) equipped with 10.0-mm quartz cells was used.

The PLS algorithm was written in MATLAB (Math Works, version 4) for running on a personal computer (Windows 95 operating system).

2.3. Procedure

2.3.1. One component calibration

In order to find the linear dynamic range of concentration of each cation, one component calibration was performed for each element. Different volumes of 10 $\mu\text{g/ml}$ solution of cobalt(II) were added to 5.0 ml AACD solution in 10.0 ml volumetric flask and diluted to the mark with distilled water. After 8 min, the absorbance was recorded at the 445 nm vs. the blank solution of AACD containing no analyte. The same procedure was followed for Ni(II) and Cu(II). The absorbance of Ni(II) and Cu(II) solutions were recorded at 535 and 470 nm, respectively.

2.3.2. Ternary standard solutions

Two sets of standard solutions were prepared. The calibration set contains 20 standard solutions and the prediction set contains 15 standards. The concentrations of each cation in solution were in the linear dynamic range of the cation. For the preparation of each solution, different volumes of three cations solutions (10 $\mu\text{g/ml}$) were added to 5.0 ml AACD solution in a 10-ml volumetric flask. After 8 min, the absorption spectra of the mixtures were recorded vs. the blank solution of the reagent between 420 and 620 nm.

2.3.3. Data processing and model building

The absorbance data of each standard solution were collected in 4-nm intervals (51 data points for each solution) using the absorbance spectra. At first, the variables were mean centered (zero mean) and variance-scaled (unit variance). The latent variables or factors for each element were determined by the cross-validation technique. The prediction error was calculated for each element for the prediction set, which are samples not participating in the construction of the model. This error was expressed as prediction residuals error sum of squares (PRESS). PRESS was calculated for the first latent variable, which built the PLS modeling in the calibration step. After that, another latent variable was added for the model building and the PRESS was calculated again. These calculations were repeated for one to 10 latent variables, which were used in the PLS modeling. The numbers of latent variables that give the minimum PRESS for each element were selected for the PLS modeling. This procedure was repeated for each element and the number of latent variable were determined. The PLS-1 modeling for each element had different number of latent variables.

2.3.4. Analysis of alloy samples

Take an alloy sample (0.1–0.2 g) in a beaker, add 15 ml of aqua regia, heat the beaker until the contents become syrup, then heat up to dryness. Add 20 ml of distilled water to the residua and mix. Then filter off the insoluble material using filter paper (Whatman No. 1), and wash the filter three times with water. The filtrate was collected in a 100-ml volumetric flask and diluted with water. Then, 1.0 ml of the solution was diluted to 100 ml with water in a volumetric flask. The Ni(II), Cu(II), and Co(II) contents were determined by the recommended procedure.

2.3.5. Detection limit determination

Several different approaches have been reported for the determination of the detection limit in multivariate calibration procedures [18–20]. Some authors are still applying the univariate definition of this parameter to evaluate it in a multivariate procedure [21,22].

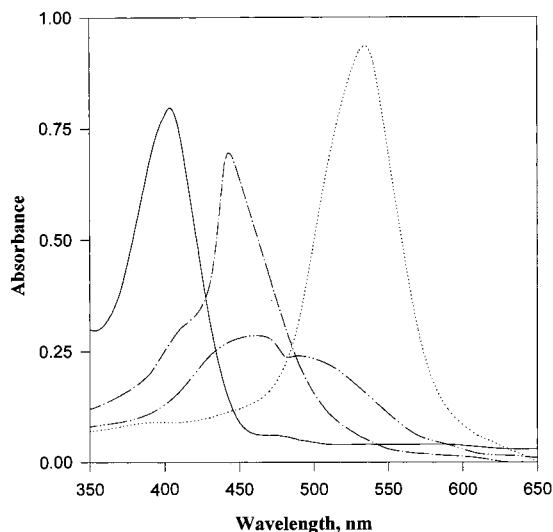


Fig. 1. Absorption spectra of AACD (—) vs. solvent blank and their Co^{2+} (---), Ni^{2+} (.....) and Cu^{2+} (-·-·-) complexes vs. reagent blank; Conditions: solvent, acetone–water mixture (1:1); AACD, 8.5×10^{-3} M; Co^{2+} , 0.80 $\mu\text{g/ml}$; Ni^{2+} , 1.00 $\mu\text{g/ml}$; Cu^{2+} , 1.00 $\mu\text{g/ml}$.

In this paper, the detection limit has been calculated from the univariate definition as described by Garcia et al. [21] and Ketterer et al. [22]. The absorbance for three blank solutions was obtained from 420 to 620 nm (51 points). From the PLS modeling for each element, the predicted concentrations were calculated. The standard deviation of predicted concentrations for each cation was calculated (S_b). Then, three times the S_b for each element was taken as the detection limit.

3. Result and discussion

The absorbance spectra of AACD, Co–AACD, Ni–AACD and Cu–AACD are shown in Fig. 1. Co–AACD and Cu–AACD spectra have been considerably overlapped with each other, and the Ni–AACD spectrum has also overlapped to some extent with the other spectra. Thus, multivariate calibration was used to resolve the spectrum of each pure components in the mixtures.

An optimum condition for spectrophotometric determinations of Co(II), Ni(II) and Cu(II) complexes with AACD was obtained. These com-

Table 1
Calibration set composition

Solution number	Cobalt(II) ($\mu\text{g/ml}$)	Nickel(II) ($\mu\text{g/ml}$)	Copper(II) ($\mu\text{g/ml}$)
1	1.7000	2.1000	0.0250
2	0.5000	0.2000	0.7500
3	2.3000	0.0100	0.0500
4	2.0000	1.0000	1.4000
5	0.3000	1.4000	0.9000
6	0.8000	1.9000	0.0700
7	2.5000	0.8000	0.6000
8	0.4000	0.6000	0.3000
9	0.3000	0.0060	1.3000
10	1.2000	1.7000	0.0800
11	3.0000	0.5000	1.0000
12	2.9000	2.1000	0.0800
13	2.0000	3.0000	0.7500
14	0.9000	2.7000	0.3000
15	1.7000	0.0400	1.1000
16	0.3300	1.8000	0.2500
17	2.2000	0.0700	0.8000
18	1.7500	2.7000	0.4000
19	1.3000	0.5000	0.7000
20	1.7000	2.2000	0.4000

Table 2
Prediction set composition and their predicted value

Solution number	Co ²⁺ (μg/ml)			Ni ²⁺ (μg/ml)			Cu ²⁺ (μg/ml)		
	Actual value	Predicted value	RE (%)	Actual value	Predicted value	RE (%)	Actual value	Predicted value	RE (%)
1	1.70	1.73	1.76	0.04	0.03	−9.05	1.10	1.04	−5.42
2	0.33	0.33	6.06	1.80	1.82	1.31	0.25	0.28	13.2
3	2.20	2.23	1.70	0.07	0.06	4.40	0.80	0.86	8.33
4	1.75	1.80	3.03	2.70	2.68	−0.74	0.40	0.45	14.07
5	1.30	1.43	10.03	0.50	0.50	1.61	0.70	0.70	0.90
6	1.70	1.79	0.38	2.20	2.22	0.95	0.40	0.40	1.81
7	2.00	2.18	9.14	0.40	0.42	6.08	1.00	0.95	−4.64
8	2.50	2.72	8.87	2.30	2.45	6.88	0.35	0.37	7.07
9	2.90	2.71	−6.25	0.50	0.47	−4.65	0.08	0.08	0.13
10	2.40	2.51	4.79	3.20	3.56	11.3	0.80	0.84	5.03
11	1.40	1.43	2.37	3.10	3.34	8.00	1.70	0.66	−4.90
12	2.10	2.02	−3.62	0.08	0.07	−9.00	0.30	0.29	1.36
13	2.75	2.82	2.78	1.20	1.17	2.06	0.90	0.95	6.23
14	1.50	1.44	−3.70	1.30	1.25	−3.69	0.25	0.23	−6.66
15	1.00	1.05	0.94	3.00	3.05	1.85	1.60	1.57	1.50

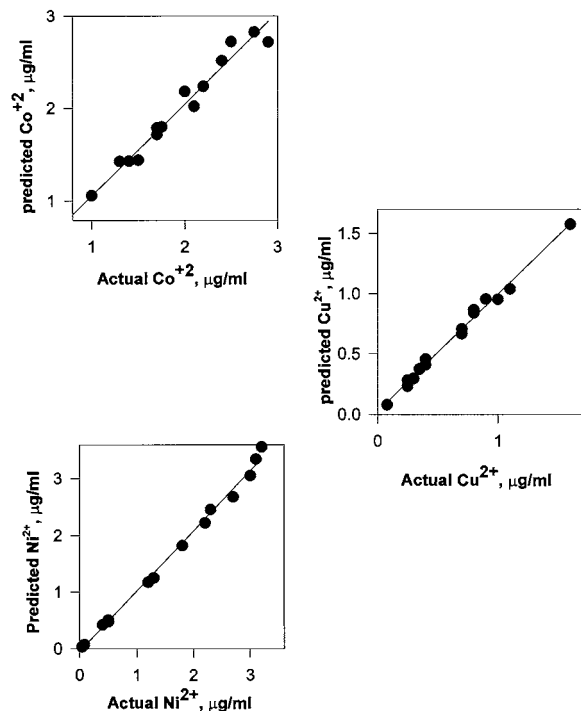


Fig. 2. Plots of predicted concentration vs. actual concentration for three cations in the prediction set.

plexes are stable in the pH range 3.0–9.5 [7]. Thus, this study was performed in the solutions without addition of any buffer solution. This condition was: a mixture of water–acetone (1:1) as solvent, and a concentration of 8.5×10^{-3} M (greater than 100 times of the most concentrated cation solution) of AACD in all experiments (no need for using of buffer solution). All of the complexes were stable after 8 min.

3.1. Experimental design for calibration and prediction standards

The concentrations of each component in stan-

Table 3
Statistical parameters

Cations	Number of factors	PRESS	RMSE	R^2	REP
Co ²⁺	5	0.117	0.109	0.978	0.169
Ni ²⁺	4	0.132	0.039	0.995	0.026
Cu ²⁺	9	0.038	0.115	0.991	0.202

dards were in their linear dynamic ranges of 0.005–3.5 µg/ml for Ni(II), 0.10–3.00 µg/ml for Co(II) and 0.025–1.50 µg/ml for Cu(II). Standard samples were prepared so that the concentrations of the constituents to be determined cover the entire dynamic ranges for each element. Two sets of standard solutions, a training set and a prediction set (randomly selected), were prepared. In both cases, the correlation between concentrations of the elements were avoided because collinear components in the training set data tend to cause over-fitting in the PLS models. The compositions of calibration and prediction standards are summarized in Tables 1 and 2, respectively (the spectral region between 420 and 620 nm with 51 absorbance data points was selected for analysis).

3.2. Selection of optimal number of factors

PRESS values are minimum in the number of factors of 4, 5 and 9 for cobalt, nickel and copper, respectively. Therefore, these numbers of latent variables were selected as the optimum number of factors for PLS models building. The predicted concentrations and their relative errors for each element in prediction standard solutions are shown in Table 2. The results show that the accuracy of the method that is less than 10% (except for a few samples). In Fig. 2, plots of these predicted concentrations vs. actual concentrations are shown for Co(II), Ni(II) and Cu(II) with the correlation coefficients for each plot being 0.989, 0.998 and 0.996, respectively, indicating the good performance of the PLS model based on singular value decomposition.

3.3. Statistical parameters for the optimized model

Three parameters were selected to evaluate the prediction ability of the model. The root mean

Table 4
Artificial mixture analysis ($n = 5$)

Sample ^a	Cobalt found ($\mu\text{g/ml}$)	Recovery (%)	Nickel found ($\mu\text{g/ml}$)	Recovery (%)	Copper found ($\mu\text{g/ml}$)	Recovery (%)
Co ²⁺ (1.5), Ni ²⁺ (2.0), Cu ²⁺ (0.80)	1.46 (± 0.05)	97.3	2.05 (± 0.05)	102.5	0.78 (± 0.04)	97.5
Co ²⁺ (0.50), Ni ²⁺ (1.20), Cu ²⁺ (0.15), Mn ²⁺ (1.50), Fe ²⁺ (1.00), Cd ²⁺ (0.80)	0.47 (± 0.03)	94.0	1.13 (± 0.04)	94.2	0.16 (± 0.03)	107.2
Co ²⁺ (2.20), Ni ²⁺ (0.45), Cu ²⁺ (1.00), Fe ³⁺ (1.50), Zn ²⁺ (2.20), Al ³⁺ (2.50)	2.33 (± 0.06)	105.9	0.43 (± 0.02)	95.6	1.09 (± 0.05)	109.0
Co ²⁺ (1.00), Ni ²⁺ (1.00), Cu ²⁺ (0.50), Fe ²⁺ (2.70), Sn ²⁺ (0.50), Cd ²⁺ (1.50)	0.94 (± 0.03)	94.0	1.07 (± 0.04)	107.0	0.46 (± 0.04)	92.0
Co ²⁺ (2.80), Ni ²⁺ (0.08), Cu ²⁺ (0.30), Mn ²⁺ (2.00), Fe ³⁺ (1.00), Al ³⁺ (1.80)	3.02 (± 0.06)	107.8	0.085 (± 0.01)	106.25	0.32 (± 0.03)	106.7

^a The number in parentheses indicates the concentration of element taken for analysis in $\mu\text{g/ml}$.

Table 5
Some industrial alloys analysis ($n = 5$)

Alloys	Composition ^a	Cobalt (%) ^b		Nickel (%) ^b		Copper (%) ^b	
		<i>a</i>	<i>b</i>	<i>a</i>	<i>b</i>	<i>a</i>	<i>b</i>
Permute	Cu(49), Ni(21), Co(30)	31.1 (± 1.0)	30.0 (± 1.02)	20.05 (± 0.4)	21.00 (± 0.5)	50.1 (± 1.2)	49.3 (± 1.1)
CuNiCo(No. 1)	Cu(50), Ni(21), Co(20)	28.4 (± 0.9)	29.8 (± 1.0)	21.7 (± 0.5)	20.9 (± 0.5)	51.4 (± 1.3)	50.2 (± 1.4)
CuNiCo(No. 2)	Cu(35), Ni(41), Co(24)	25.3 (± 0.8)	24.2 (± 0.7)	39.8 (± 0.9)	41.1 (± 1.1)	35.2 (± 0.9)	35.5 (± 1.0)
Lemaiguand	Cu(39), Ni(7), Co(8), Zn(7) Sn(9), Fe(30)	8.5 (± 0.3)	7.9 (± 0.4)	7.6 (± 0.4)	7.05 (± 0.4)	38.1 (± 1.0)	39.4 (± 1.1)
Alloy sample No. 1	Cu(7.0), Ni(19.0), Co(5.3), Zn(7.7), Cr(6), Fe(55)	5.6 (± 0.3)	4.5 (± 0.3)	18.7 (± 0.7)	19.5 (± 0.9)	7.4 (± 0.5)	6.5 (± 0.4)
Alloy sample No. 2	Co(4.7), Ni(12.7), Zn(50), Sn(4.6), Cr(18), Mo(10)	4.6 (± 0.3)	5.2 (± 0.2)	12.4 (± 0.5)	13.0 (± 0.6)	0.12 (± 0.06)	Not found

^a The numbers in parentheses are percent composition of each element in the alloys: *a*, for the proposed method; *b*, atomic absorption spectrometry.

^b The numbers in parentheses are standard deviations.

squares error (RMSE), i.e. the standard deviation of residuals, determines the average error in the analysis of each cation. Another parameter was relative error of prediction (REP), which shows the predictive ability of the model and is calculated as:

$$\text{REP} = \left(\frac{\sum_{i=1}^n (\hat{c}_i - c_i)^2}{\bar{c}} \right)^{1/2} \times 100 \quad (10)$$

where \hat{c}_i is the predicted concentration and \bar{c} is the average concentration of prediction set.

The square of correlation coefficient (R^2), which indicates the fitting of data in a straight line, was calculated as:

$$R^2 = \frac{\sum_{i=1}^n (\hat{c}_i - c_i)^2}{\sum_{i=1}^n (c_i - \bar{c}_i)^2} \quad (11)$$

The values of REP, RMSE, R^2 , number of factors and PRESS in the optimum number of factors that calculated for Co(II), Ni(II) and Cu(II) concentrations in prediction set are summarized in Table 3. The detection limits (DL) that calculated from the discussed procedure are 0.072, 0.021 and 0.063 $\mu\text{g/ml}$ for cobalt, nickel and copper ions, respectively. From these data, it can be concluded that predictive ability of the model is better for nickel because of the low overlapping character of its spectrum with the spectrum of ACCD. The DL for nickel is lower than cobalt and copper because of low overlapping its spectrum with the reagent spectrum.

3.4. Applications of model for analyzing ternary mixtures in artificial mixtures and real alloy samples

The predictive ability of the model was evaluated for the simultaneous determination of Co(II), Ni(II) and Cu(II) in synthetic solutions alloy samples. The results are summarized in Tables 4 and 5.

The complexes of manganese(II), cadmium(II), iron(III) and iron(II) with AACD have spectra overlapping with the spectra of Co–AACD, Ni–AACD and Cu–AACD and, therefore, they can cause spectral interference [8]. However, the results in Tables 4 and 5 show that the PLS model

is able to predict the concentrations of each element in the presence of those interferences.

4. Conclusion

A PLS algorithm based on singular value decomposition (SVD) [17] was written. Simultaneous determination of Co(II), Ni(II) and Cu(II) as their AACD complexes in combination with the PLS modeling was established, with good prediction ability in the artificial samples. The PLS modeling was able to deal with interferences from some metal–AACD complexes. The results confirm that the model can be used for the determination of cobalt, nickel and copper in real sample analysis.

References

- [1] W. Betteridge, Cobalt and Its Alloys, Ellis Horwood Limited, Chichester, UK, 1982.
- [2] H. Niwa, T. Yasui, T. Ishizuki, A. Yuchi, H. Yamada, H. Wada, Talanta 45 (1997) 349.
- [3] E.V. Thomas, Anal. Chem. 66 (1994) 795A.
- [4] K.R. Beebe, R.B. Kowalski, Anal. Chem. 59 (1987) 1007A.
- [5] E.R. Malinowski, D.G. Howery, Factor Analysis in Chemistry, Wiley, New York, 1980.
- [6] T. Takeshima, A. Yano, N. Fukada, Y. Hirose, M. Muraoka, J. Chem. Res. 4 (1979) 140.
- [7] A.A. Ensafi, M.Sc. Thesis, Shiraz University, Shiraz, Iran, 1988.
- [8] A. Safavi, A.A. Ensafi, M. Massoumi, Talanta 38 (1991) 229.
- [9] A.A. Ensafi, T. Khayamian, B. Hemmateenejad, Anal. Lett. (in press).
- [10] K.G. Joreskog, H. Wold, System Under Indirect Observations, North Holland, Amsterdam, 1982.
- [11] R.W. Gerlach, B.R. Kowalski, H. Wold, Anal. Chim. Acta 112 (1979) 417.
- [12] I.E. Frank, J. Feikema, N. Constantine, B.R. Kowalski, J. Chem. Inf. Comput. Sci. 24 (1984) 20.
- [13] D.M. Haaland, E.V. Thomas, Anal. Chem. 60 (1988) 1193.
- [14] P. Geladi, B.R. Kowalski, Anal. Chim. Acta 185 (1986) 1.
- [15] F. Despagne, D. Masart, C.E. Noord, Anal. Chem. 69 (1997) 3391.
- [16] C.H. Spiegelman, M.G. Mcshane, M.G. Goetz, M. Motamedi, Q. Liyue, G.L. Cote, Anal. Chem. 70 (1998) 35.
- [17] A. Lorber, L. Wangen, B.R. Kowalski, J. Chemometr. 1 (1987) 19.
- [18] A. Lorber, Anal. Chem. 58 (1986) 1167.

- [19] G. Bauer, W. Wegscheid, H.M. Ortner, *Fres. J. Anal. Chem.* 340 (1991) 135.
- [20] K.S. Booksh, B.R. Kowalski, *Anal. Chem.* 66 (1994) 782A.
- [21] M. Toribio, G.F. Garcia, A. Izquierdo-Ridorsa, R. Tauler, G. Rauret, *Anal. Chim. Acta* 310 (1995) 297.
- [22] M.E. Ketterer, J.J. Reschl, M.J. Peters, *Anal. Chem.* 61 (1989) 2031.

Fast determination of calcium, magnesium and zinc in honey using continuous flow flame atomic absorption spectrometry

I. López-García, P. Viñas, C. Blanco, M. Hernández-Córdoba *

Department of Analytical Chemistry, Faculty of Chemistry, University of Murcia, 30071 Murcia, Spain

Received 22 October 1998; received in revised form 21 January 1999; accepted 21 January 1999

Abstract

A procedure is described for the rapid determination of calcium, magnesium and zinc in honey with no previous mineralization stage. The samples are dissolved in a solution containing dilute hydrochloric acid and a lanthanum salt, and then directly introduced into the flame atomic absorption spectrometer by means of a simple continuous-flow manifold. The computer-controlled system performs an automatic on-line dilution of the solutions, in this way decreasing matrix effects due to the organic matter content and allowing analytical signals within the linear response range to be obtained. Calibration is carried out against aqueous standards. Reproducibilities for calcium and magnesium measurements in the honey samples are close to $\pm 3\%$. The detection limit for zinc is $0.2 \mu\text{g g}^{-1}$, the reproducibility obtained for a honey sample containing $1.7 \mu\text{g g}^{-1}$ zinc being $\pm 5.2\%$. The results agree with those obtained by means of a lengthy mineralization-based procedure, the main advantages of the non-conventional methodology reported being automation, saving of time and a decrease in the contamination risk. © 1999 Elsevier Science B.V. All rights reserved.

Keywords: Flame atomic absorption spectroscopy; Calcium; Magnesium; Zinc; Honey

1. Introduction

Flame atomic absorption spectrometry (FAAS), due to its relatively low cost and excellent analytical performances, is probably the most widely used technique for analyzing a variety of metals in foods. The conventional way to carry out such determinations involves a mineralization

stage to obtain finally a solution suitable for introduction in the spectrometer. Such a stage is recommended even for liquid or water-soluble foodstuffs, the destruction of the organic matter preventing both spectral interferences and the accumulation of residues in the burner head and spray chamber. The conventional practice of FAAS can also pose a drawback since the linear response range of the atomic absorption spectrometer is narrow. For this reason, once solutions have been obtained, they must often be

* Corresponding author. Tel.: +349-68-307-100; fax: +349-68-364-148.

diluted to varying degrees, depending on the sensitivity of each particular analyte. These are easy-to-perform stages, but affect the time taken for the determination to be carried out.

Honey is used worldwide as a basic foodstuff, either by direct ingestion or as a sweetener in a variety of foodstuffs. The mean content of mineral substances in honey has been calculated to be 0.17%, although this can vary within a wide range [1]. Some of the components of this mineral fraction can be determined by FAAS either after a mineralization stage [2] or simply by dissolving the samples in water containing a small amount of acid and then directly introducing the solutions in the spectrometer [3]. In the latter case, some of the afore-mentioned difficulties appear due to the high organic matter content of the samples. In addition, calibration against aqueous standards is hindered by the different physicochemical properties of the solutions that are being aspirated into the spectrometer. The drawbacks can be greatly alleviated if the solutions are not continuously aspirated, but introduced in the spectrometer by means of a flow injection (FI) manifold [4].

Recent advances in continuous flow techniques also offer other approaches that simplify the handling of samples which are problematic when measured by direct aspiration. This communication reports the results obtained when a new methodology to introduce the solutions in FAAS [5] was applied to the determination of three elements of nutritional interest in honey, namely calcium, magnesium and zinc. The non-conven-

tional way of operation applied here minimizes the problems caused by the organic matter contained in the solution since it is continuous and automatically diluted on-line, thus reducing the amount of organic compounds which are supplied to the nebulizer. In addition, the system avoids the need of manually diluting the solutions to obtain signals within the linear response range, because the task is carried out automatically. The system, which can be useful for other similar analytical situations, does not depend on special requirements and can easily be adapted to the needs of every laboratory.

2. Experimental

2.1. Apparatus

The manifold used is shown in Fig. 1. All the connecting lines were of 0.8 mm i.d. poly(tetrafluoroethylene), the distance between the T-piece and the nebulizer entry being maintained as short as physically possible (about 15 mm). All the measurements were obtained with an ATI Unicam Model 919 Solaar atomic absorption spectrometer. The analogical output of the instrument was connected to a personal computer via a PCLab 818 PG card. Home-made software permitted both the direct plotting in the computer screen of the absorbance–time relationship and the absorbance–time data pairs to be saved in ASCII format, which facilitated their later handling by using ordinary software for data treatment. The pump was a peristaltic Gilson Minipuls 3 provided with an interface allowing the turning speed to be varied by applying an external voltage between 0 V (pump stopped) and 5 V (pump turning at the maximum speed of 47.9 rpm). The pump speed could therefore be varied by the computer equipped with the afore-mentioned card. A 1.42 mm nominal i.d. pump tube was used. When the pump was equipped with this tube and operated at its maximum turning speed, the flow rate delivered was equal to the nebulizer uptake rate.

Air acetylene flames were used exclusively. Measurements were performed at 422.7, 285.2 and

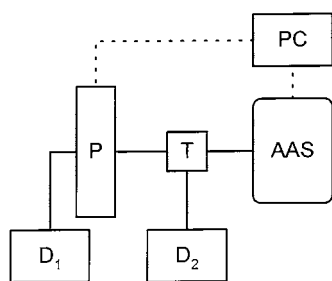


Fig. 1. Manifold used: P, variable-speed peristaltic pump; PC, computer; T, piece to connect pump channel to compensation channel; D₁ and D₂, vessels containing the sample solution and the diluent solution, respectively.

213.9 nm using ordinary hollow cathode lamps operated at 6, 4 and 10 mA for calcium, magnesium and zinc, respectively. It was experimentally verified that background correction was unnecessary, which is probably due to the peculiar way in which the continuous flow manifold operates and to the high dilution degree of the solutions entering to the nebulizer.

2.2. Reagents

Aqueous calcium, magnesium and zinc solutions ($1000 \mu\text{g ml}^{-1}$) were obtained from Panreac (Spain) and used after appropriate dilutions. All other chemicals were obtained from Merck. All solutions were prepared using ultrapure water obtained from a Milli-Q System of Millipore. No calcium, magnesium or zinc could be detected by FAAS in this water.

2.3. Operation of the manifold: procedures

The manifold shown in Fig. 1 operates in such a way that a constant flow is supplied to the nebulizer through a T-piece. If a standard solution of the analyte is pumped using an increasing flow rate starting from zero up to the nebulizer uptake rate while pure water, or an appropriate diluent solution, is aspirated through the compensation channel, a calibration graph can be obtained automatically [5]. If a sample solution is pumped using a decreasing flow rate while diluent is aspirated through the T-piece, the sample solution is diluted on-line, which is useful to obtain analytical signals from solutions that are too concentrated to be aspirated directly. For high analyte concentrations, a curve is found for the absorbance–time relationship at the beginning of the experiment and only when the pumped solution is sufficiently diluted is a straight line obtained. The concentration of the unknown solution is calculated from the absolute value of the slope, S_x , of this linear portion and from the slope, S_0 , of a calibration line, using the equation $C_x = C_0 \cdot S_x / S_0$, where C_x and C_0 indicate the concentration of analyte in the sample solution and in the standard solution, respectively. A detailed description of this manifold, its different analytical

possibilities as well as its limitations is given elsewhere [5,6].

Commercial honey samples were purchased in a supermarket. Portions of the samples were accurately weighed (typical amounts were in the 1–5 g range) and diluent solution (2% v/v concentrated hydrochloric acid and 0.6% m/v $\text{La}(\text{NO}_3)_3 \cdot 6\text{H}_2\text{O}$) was added to obtain 50 ml of solution. This was repeatedly shaken for homogenization and then placed in the vessel of the pump. Diluent solution was placed in the compensation channel. By means of a simple keystroke on the computer keyboard, the pump started and the turning speed was immediately decreased linearly with time to zero. The variation in the turning speed was carried out by decreasing the voltage applied at the pump at a rate of 100 mV s^{-1} and, consequently, the time invested in the measurement was 50 s. To decrease the supply of organic matter to the nebulizer and, at the same time, to enlarge the time during which the system is working within the linear response range, most of the experiments were carried out by starting the pump at 80% of its maximum turning speed [6].

For comparison purposes, the samples were analyzed in the following way. Fractions of 1g were weighed in platinum crucibles, 0.1 ml of concentrated nitric acid was added and the crucibles irradiated with an infrared lamp during 1 h. Next, the crucibles were placed in a furnace, the temperature being raised to 500°C and maintained during 8 h. The white ashes thus obtained were dissolved using 1 ml of concentrated nitric acid, the solution being finally diluted up to 10 ml. Calcium, magnesium and zinc were determined in this solution after appropriate dilutions by using FAAS in the conventional aspiration mode.

3. Results and discussion

The most convenient way to operate the manifold, shown in Fig. 1, is to use the compensation channel to introduce the sample solution, the diluent being propelled by the peristaltic pump because this makes it possible to maintain a high sampling frequency. However, it was thought that

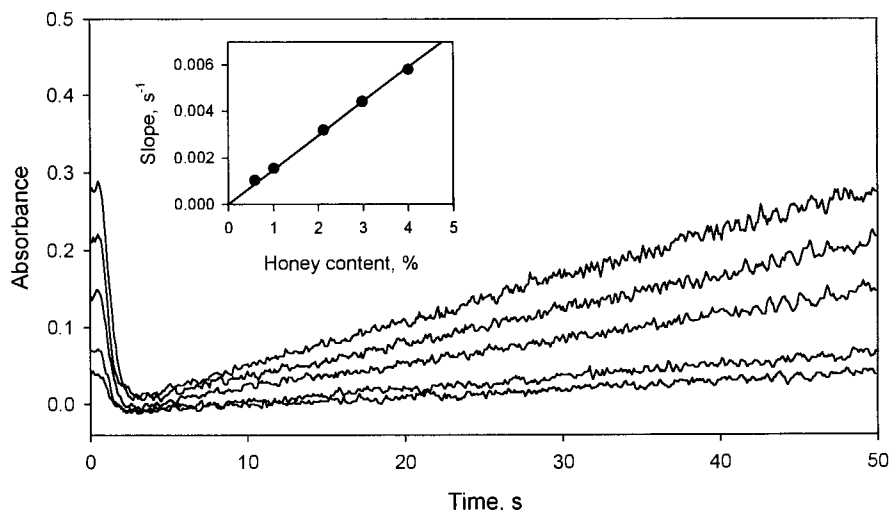


Fig. 2. Absorbance–time profiles of calcium obtained when solutions containing different proportions of a same honey sample were aspirated through the compensation channel, the pump delivering diluent solution at a decreasing rate.

the variation of the physicochemical properties of the solutions with the proportion of honey might affect the nebulizer uptake rate, thus rendering the direct calibration against aqueous standards unsuitable. To verify this, several solutions containing different proportions of the same honey sample were prepared and introduced in the spectrometer through the compensation channel, while the pump propelled water and decreased its turning speed from the maximum (which produced a flow rate equal to the nebulizer uptake rate) to zero. As can be seen in Fig. 2, where the absorbance–time profiles for calcium thus obtained are shown, when low or moderate proportions of honey were used, there was a linear relationship between the slopes of the absorbance–time profiles and the concentration in honey of the solution being aspirated. On the contrary, when solutions containing high proportions of honey (up to 10%) were assayed, the variation in the suction through the compensation channel led to an appreciable decrease of the analytical signal. Such an effect disappeared when the sample solution was not aspirated through the compensation channel, but propelled by the pump (Fig. 3). Consequently, to render the direct calibration with aqueous standards feasible even with solutions containing high proportions of honey,

the rest of the experiments were carried out by operating the system in this way. It is important to note that concentrations higher than 10% m/v are unsuitable due to slight variations in the flow rate delivered by the pump. In addition, there is in such a case a serious risk of clogging the system and abundant carbonaceous residues are deposited in the burner head.

The well-known interference of phosphate on calcium determination was suppressed by adding

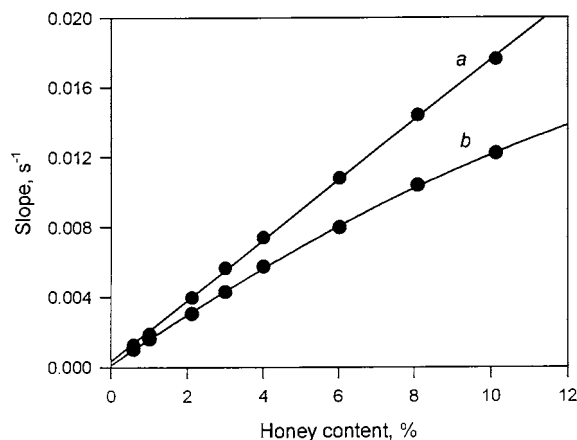


Fig. 3. Slopes of absorbance–time profiles of calcium. The sample solution was propelled by the pump (line a) or introduced through the compensation channel (line b).

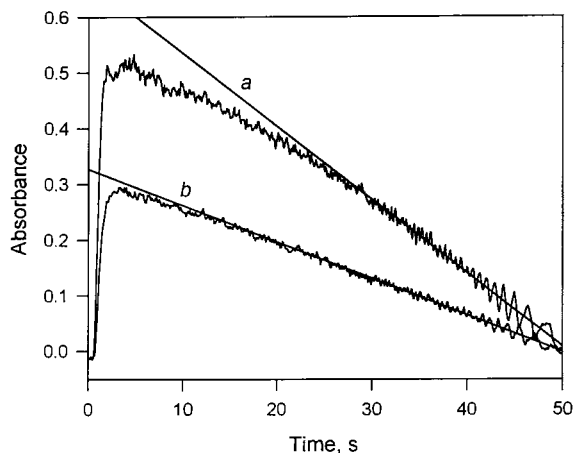


Fig. 4. Absorbance–time profiles of calcium obtained using the recommended conditions. Graphs a and b correspond to solutions prepared from samples 3 and 2, respectively.

lanthanum salts. A number of experiments were carried out by incorporating the suppressor in both the sample and diluent solutions and by adding it only to the latter solution. In neither case did the slopes of the absorbance–time tracings show significant statistical differences (95% confidence level) with the slopes of calibration graphs obtained from aqueous standards in the same experimental conditions. Consequently, for simplicity purposes, the lanthanum salt was incorporated only to the diluent solution. Fig. 4 shows some absorbance–time profiles from solutions containing honey obtained in the conditions recommended. It should be noted that these profiles

were not submitted to a smoothing procedure and are shown here exactly as they were seen on the computer screen.

The repeatability obtained from 15 consecutive measurements obtained from the same sample solution was $\pm 3.7\%$. The results obtained for the calcium content of four commercial honey samples are shown in Table 1 together with those found by the conventional and lengthy procedure based on the previous ashing of the samples. The application of a common statistical test (*t*-test) did not reveal significant differences (95% confidence level) between the two sets of results [7].

No particular problems were found when the approach was applied to the determination of magnesium. To check the absence of a matrix effect and to confirm that the simplest calibration against aqueous standards was valid, standard addition graphs were obtained from solutions prepared from four available commercial honey samples. The mean value of the slopes ($0.016 \pm 0.002 \text{ s}^{-1} \mu\text{g}^{-1}\text{ml}$, two solutions of each sample; each graph being constructed with four points, and three measurements being obtained at each point) did not reveal significant statistical differences with the slopes ($0.017 \pm 0.002 \text{ s}^{-1} \mu\text{g}^{-1}\text{ml}$) of calibration graphs obtained from aqueous standards. The repeatability for 15 measurements of the same sample solution was $\pm 2.5\%$. The final results obtained are given in Table 1, where the results obtained using a mineralization-based procedure are also shown for comparison purposes.

Table 1

Results obtained for the determination of calcium, magnesium and zinc in honey samples

Sample	Calcium ($\mu\text{g g}^{-1}$)		Magnesium ($\mu\text{g g}^{-1}$)		Zinc ($\mu\text{g g}^{-1}$)	
	Obtained ^a	Reference ^b	Obtained	Reference	Obtained	Reference
1	47 ± 2	46 ± 3	5.8 ± 0.3	6 ± 0.8	1.2 ± 0.1	1.5 ± 0.1
2	65 ± 1	67 ± 3	16 ± 1	15 ± 1	2.3 ± 0.1	2.1 ± 0.1
3	132 ± 1	131 ± 2	173 ± 8	175 ± 6	1.7 ± 0.1	1.5 ± 0.1
4	92 ± 1	94 ± 4	25 ± 1	24 ± 2	1.3 ± 0.1	1.6 ± 0.2

^a Mean value \pm confidence interval for 15 measurements obtained from five solutions prepared from each sample.

^b Mineralization-based procedure.

No significant differences at the 95% confidence level were found between the two sets of results (since the data were not normally distributed, the Mann–Whitney test was used in this case) [7].

The zinc content in honey is low, which required one to prepare solutions containing high proportions of the foodstuff. As stated, the absence of a matrix effect was verified by comparing the slopes of standard additions graphs with the slopes of calibration graphs obtained from aqueous standards in the same experimental conditions. The determination limit for solutions containing the maximum proportion of honey recommended (10% m/v) was calculated to be $0.2 \mu\text{g g}^{-1}$. The repeatability obtained from 15 consecutive measurements of the same solution prepared from a sample containing $1.7 \mu\text{g g}^{-1}$ zinc was $\pm 5.2\%$. Table 1 shows the results obtained. As occurred in the cases of calcium and magnesium, no statistical (*t*-test) significant differences were found with the results obtained by the conventional method based on a previous ashing.

Acknowledgements

The authors are grateful to the Spanish DGI-CYT (Project PB96-1100) and to Fundación Séneca (CARM, Spain, Project PB/7/FS/97) for financial support.

References

- [1] J.W. White, in: E. Crane (Ed.), *A Comprehensive Survey of Honey*, Heinemann, London, 1979 Chapter 5.
- [2] J.L. Rodríguez-Otero, P. Paseiro, J. Simal, L. Terradillos, A. Cepeda, *J. Apic. Res.* 31 (1992) 65.
- [3] E. Sauri Duch, J.C. Hernández Chávez, *Rev. Esp. Cienc. Tecnol. Aliment.* 34 (1994) 450.
- [4] F. Salinas, V. Montero de Espinosa, E. Osorio, M. Lozano, *Rev. Esp. Cienc. Tecnol. Aliment.* 34 (1994) 441.
- [5] I. López-García, P. Viñas, M. Hernández-Córdoba, *J. Anal. Atom. Spectrom.* 9 (1994) 553.
- [6] I. López-García, P. Viñas, N. Campillo, M. Hernández-Córdoba, *Fres. J. Anal. Chem.* 355 (1996) 57.
- [7] J.C. Miller, J.N. Miller, *Statistics for analytical chemistry*, 3rd ed., Ellis Horwood, Chichester, 1993.

Separation and transport of lithium of 10^{-5} M in the presence of sodium chloride higher than 0.1 M by 2,3,7,8,12,13,17,18-octabromo-5,10,15,20-tetrakis(4-sulfonatophenyl)porphyrin

Haiping Sun, Masaaki Tabata *

Department of Chemistry, Faculty of Science and Engineering, Saga University, 1 Honjo-machi, Saga 840-8502, Japan

Received 2 December 1998; received in revised form 22 January 1999; accepted 25 January 1999

Abstract

A water-soluble porphyrin (2,3,7,8,12,13,17,18-octabromo-5,10,15,20-tetrakis(4-sulfonatophenyl)porphyrin ($H_2(obtpps)^{4-}$, H_2P^{4-}) synthesized in our laboratory was applied to a solvent extraction method and a liquid membrane transport of lithium as low as 10^{-5} M ($M = \text{mol dm}^{-3}$) in the presence of sodium chloride higher than 0.1 M. The lithium porphyrin with five negative charges was extracted successfully into chloroform with tetrabutylammonium ion (But_4N^+) at pH 12.7. The extraction constant for the reaction of $[\text{LiP}^{5-}]_a + 5[\text{But}_4\text{N}]_a^+ \rightleftharpoons [(\text{But}_4\text{N})_5\text{LiP}]_o$ was found to be $(1.9 \pm 0.3) \times 10^{18} \text{ M}^{-5}$, where the subscripts a and o denote chemical species in aqueous and organic phases, respectively. Lithium was transported to an aqueous phase at pH 7 through a chloroform liquid membrane containing $[(\text{But}_4\text{N})_5\text{HP}]$. The extraction and transport mechanism was discussed on the basis of extraction constants, chemical species and transportation rate. Lithium in sea water or serum sample was separated and its concentration was determined spectrophotometrically by the present method without any interference from sodium chloride. The interference from transition and heavy metal ions was masked by Mg-EDTA. A calibration curve was linear over a range of 2×10^{-6} to 2×10^{-5} M at a precision of 1.51% (RSD). © 1999 Elsevier Science B.V. All rights reserved.

Keywords: Lithium; Separation; Transport; Porphyrin

1. Introduction

Lithium is an important element for lithium battery and clinical treatment of manic depres-

sion. Thus, rapid and accurate methods for the determination of lithium and its separation and collection of lithium in recycling are receiving great attention [1–3]. Because of the high concentrations of Na^+ in sea water and blood, very high Li^+/Na^+ selectivity is required for the separation and determination of Li^+ at concentrations less than 10^{-4} M (700 ppb) in a large excess of Na^+ .

* Corresponding author. Tel.: +81-952-28-8560; fax: +81-952-28-8548.

E-mail address: tabatam@cc.saga-u.ac.jp (M. Tabata)

Crown ethers have often been selected as ligands to form complexes with lithium ion, because the oxygen atom is 'a hard base' and preferably binds to the lithium ion, which is a hard acid [4,5]. Bartsch and coworkers synthesized a series of novel crown-4 compounds in which the crown ether ring size systematically varied from 13 to 16 atoms [6,7]. The Li^+ extracting ability decreased as the crown ring size was varied: 14-crown-4 > 13-crown-4 \geq 15-crown-5 > > 16-crown-4. This order was rationalized in terms of the size-fit concept [8]. The methylene-substituted 14-crown-4 compounds exhibited very high Li^+ selectivity with $\text{Li}^+/\text{Na}^+ = 44.9$ [7]. Sholl and Southerland synthesized azaphenol cryptand and extracted Li^+ from aqueous solutions into chloroform with very high selectivity of $\text{Li}^+/\text{Na}^+ = 400$ [9]. Much higher selectivity, however, is required for separation and determination methods of lithium in sea water or human blood which contains Na^+ of 0.5 or 0.15 M, respectively.

Recently, we synthesized a water-soluble porphyrin, octabromoporphyrin, 2,3,7,8,12,13,17,18-octabromo-5,10,15,20-tetrakis(4-sulfonatophenyl) porphyrin ($\text{H}_2(\text{obtpps})^{4-}$, H_2P^{4-} ; Fig. 1) and demonstrated a reaction of the porphyrin with lithium ion in aqueous solution [10]. The synthesized porphyrin is highly electron deficient, resulting in a decrease in the basicity of porphyrin due to the presence of eight bromine atoms that directly attach to the β -pyrrole positions [10–13]. We also reported a spectrophotometric method

for the determination of lithium in aqueous solution [14]. However, the overlap of absorption spectra of the lithium porphyrin, $[\text{LiP}]^{5-}$, on that of free porphyrin, HP^{5-} , resulted in a small change in absorption spectra caused by the binding of lithium to the free-base porphyrin. After that work, we found that $[\text{LiP}]^{5-}$ could be extracted into chloroform with tetrabutylammonium ion (But_4N^+) [15].

We report here the methods of separation, transport and determination of lithium as low as 10^{-5} M in the presence of Na^+ greater than 0.1 M. The selectivity of Li^+/Na^+ is higher than 10^4 . The present method was also applied to the separation and determination of Li^+ in sea water and in blood serum.

2. Experimental

2.1. Reagents

A water-soluble octabromoporphyrin ($\text{H}_2(\text{obtpps})^{4-}$) was synthesized by bromination and sulfonation of tetraphenylporphyrin as reported previously [10]. Other reagents were of analytical-reagent grade and were used without further purification.

2.2. Apparatus

Absorption spectra were recorded on Shimadzu UV-2100 and JASCO Ubest spectrophotometers. Concentration of lithium was determined by a Hitachi Z-6100 Polarized Zeeman Atomic Absorption Spectrophotometer. The pH values were determined with a Radiometer Ion 85 Analyzer with a combined electrode (GK2401C). A 1.000×10^{-2} M nitric acid solution containing 0.09 M sodium nitrate was employed as a standard hydrogen ion concentration ($-\log[\text{H}^+] = 2.000$). From the pH meter reading of sample solutions containing various hydrogen ion concentrations, the pH meter and electrode system was calibrated in terms of $-\log[\text{H}^+]$ at an ionic strength of 0.1 M NaCl.

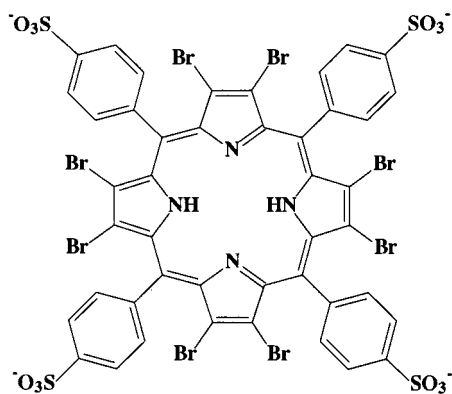


Fig. 1. 2,3,7,8,12,13,17,18-Octabromo-5,10,15,20-tetrakis(4-sulfonatophenyl)-porphyrin ($\text{H}_2(\text{obtpps})^{4-}$, H_2P^{4-}).

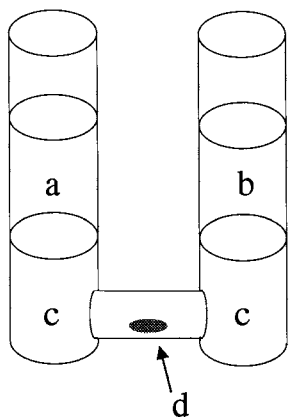


Fig. 2. Apparatus for measuring lithium ion transport across a chloroform membrane consisting of aqueous source phase (a), aqueous receiving phase (b), chloroform membrane (c) and magnetic stirring bar (d).

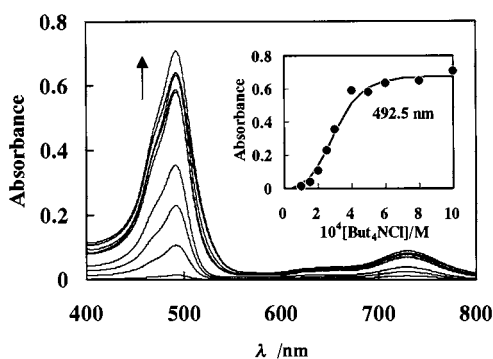


Fig. 3. Change in the absorbance of $[\text{LiP}]^{5-}$ extracted into organic phase with increasing of But_4NCl in the presence of $4.34 \times 10^{-6} \text{ M H}_2(\text{obtpps})^{4-}$ and $1.0 \times 10^{-5} \text{ M Li}^+$ at pH 12.7.

2.3. Procedure of solvent extraction

Into a 50 ml sample tube with a screw cap were added 10 ml of chloroform and 10 ml of aqueous solution containing Li^+ (1×10^{-2} or $1 \times 10^{-5} \text{ M}$), tetrabutylammonium chloride (But_4NCl) (4×10^{-5} to $1 \times 10^{-3} \text{ M}$), NaCl (0.1 M) and buffers (0.01 M) of 2-[4-(2-hydroxyethyl)-1-piperazinyl]propanesulfonic acid (HEPES) for pH 6–7.5, sodium borate for pH 10, or NaOH (0.01–0.1 M). The two phases were mixed vigorously by a shaker for 5 min and followed by centrifugation for 5 min to separate the two phases completely.

The absorption spectra of the organic and aqueous phases were measured. The absorption maxima of H_2P^{4-} , HP^{5-} and LiP^{5-} in the chloroform phase were observed at 474.5, 502 and 492.5 nm, respectively, in the presence of tetrabutylammonium chloride. All experiments were carried out at $25 \pm 1^\circ\text{C}$ and at an ionic strength of 0.1 ($\text{Na}(\text{Cl}^-, \text{OH}^-)$).

2.4. Procedure of lithium transport

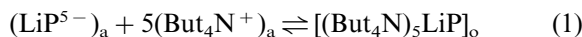
A U-type glass tube, shown in Fig. 2, was used for measurement of the transport of lithium ion. It consisted of a 10-ml chloroform liquid membrane (c) facing both a 10-ml source phase (a) and a 10-ml receiving phase (b). The source phase contains lithium (10^{-2} to 10^{-5} M), 0.1 M NaOH and $10^{-3} \text{ M But}_4\text{NCl}$, and the receiving phase contains 0.01 M HEPES buffer (pH 7.0) and $10^{-3} \text{ M But}_4\text{NCl}$. First, a 10 ml of chloroform containing $8 \times 10^{-6} \text{ M}$ of porphyrin was placed at the bottom of the tube, then aqueous solutions for source and receiving phases were poured into the both sides. Only the chloroform phase was stirred mechanically at 200 rpm min^{-1} by a Teflon-coated magnetic stirring bar (b) located at the bottom of the tube. The transport of lithium ion was initiated by addition of the aqueous solutions. Lithium concentration was determined by a flame spectrophotometer.

3. Results and discussion

3.1. Extraction of lithium(I) by $\text{H}_2(\text{obtpps})^{4-}$ with But_4NCl

Since a preliminary experiment on extraction of lithium porphyrin has been reported in the proceedings of Asianalysis, 1997 [15], we will give here some essential data which are not described in the proceedings and required for the determination of lithium by solvent extraction and lithium transport. The octaboromoporphyrin exists mainly as HP^{5-} at pH higher than 10 [14] and reacts with lithium ion to form a stable lithium complex, $[\text{LiP}]^{5-}$. The lithium(I) porphyrin complex was easily extracted into chloroform in the

presence of tetrabutylammonium chloride. Fig. 3 shows the change in absorbance of organic phase in different concentrations of But_4NCl in aqueous phase. With increasing the concentration of But_4NCl , the absorbance of chloroform phase increased at 492.5 nm at pH 12.7 and at $[\text{Li}^+] = 1.0 \times 10^{-5}$ M. Lithium(I) of 10^{-5} M was completely extracted into chloroform at the concentrations of But_4NCl higher than 6.0×10^{-4} M. The extraction constant can be expressed as:



with

$$K_{\text{ex(LiP)}} = [(\text{But}_4\text{N})_5\text{LiP}]_{\text{o}} / [\text{LiP}^{5-}]_{\text{a}} [\text{But}_4\text{N}^+]_{\text{a}}^5 \quad (2)$$

The extraction constant of $[(\text{But}_4\text{N})_5\text{LiP}]$ was determined from the change in absorbance of the chloroform phase at different concentrations of tetrabutylammonium chloride (Fig. 3) by taking into account of the distribution constant of But_4NOH into chloroform: $\log K_{\text{ex}(\text{But}_4\text{NOH})} = \log([\text{But}_4\text{NOH}]_{\text{o}} / [\text{But}_4\text{N}^+]_{\text{a}} [\text{OH}^-]_{\text{a}}) = -0.83$ [16]. The values of $K_{\text{ex(LiP)}}$ was found to be $(1.9 \pm 0.3) \times 10^{18} \text{ M}^{-5}$. The extraction constants of the porphyrin species (HP^{5-} and H_2P^{4-}) unbound to Li^+ were also determined from the change in absorbance by the same method as LiP^{5-} in the presence of But_4NCl at pH 7.5 and 12.7, respectively. The extraction constants are

$$\begin{aligned} K_{\text{ex(HP)}} &= (\text{But}_4\text{N})_5\text{HP}]_{\text{o}} / [\text{HP}^{5-}]_{\text{a}} [\text{But}_4\text{N}^+]_{\text{a}}^5 \\ &= (4.7 \pm 0.4) \times 10^{16} \text{ M}^{-5}, \end{aligned}$$

$$\begin{aligned} K_{\text{ex(H}_2\text{P)}} &= [(\text{But}_4\text{N})_4\text{H}_2\text{P}]_{\text{o}} / [\text{H}_2\text{P}^{4-}]_{\text{a}} [\text{But}_4\text{N}^+]_{\text{a}}^4 \\ &= (9.5 \pm 1.5) \times 10^{13} \text{ M}^{-4}. \end{aligned}$$

Since the ionic radius of lithium(I) (73 pm) is comparable to that of zinc(II) (74 pm) [17], lithium ion can incorporate well into porphyrin core, which leads to stabilized lithium(I) porphyrin. The HP^{5-} was less extracted into chloroform than LiP^{5-} due to the solvation of water to iminate anion (HP^{5-}) that is formed by the dissociation of a proton bound to the pyrrole nitrogen of $\text{H}_2(\text{obtpps})^{4-}$ [14]. Consequently, the organic phase gave mainly the absorption spectrum of the extracted $[\text{LiP}]^{5-}$ and the absorption spectra of non-reacted HP^{5-} was negligible in the presence of tetrabutylammonium. That

prevented from an overlap of absorbance of HP^{5-} ($\lambda_{\text{max}} = 502 \text{ nm}$) on that of $[\text{LiP}]^{5-}$ at 492.5 nm and led to selective detection of $[\text{LiP}]^{5-}$.

3.2. Determination of lithium by solvent extraction method

These results were applied to the determination of Li^+ in sea water and human blood serum. Lithium(I) ($(2-20) \times 10^{-6} \text{ M}$) was extracted into a 10 ml of chloroform at $5 \times 10^{-6} \text{ M H}_2(\text{obtpps})^{4-}$ and 0.1 M NaOH by the method described in Section 2.3. The absorbance was measured at 492.5 nm and the concentration of Li^+ was determined from a calibration curve. The calibration curve was a linear in a range of 1×10^{-6} to 2×10^{-5} which afforded to determine lithium after a dilution of 100 times a therapeutic sample, of which the concentration is $(0.5-1.5) \times 10^{-3} \text{ M}$ [18]. A sample containing $1 \times 10^{-5} \text{ M}$ lithium ion was determined with a precision of 1.51% (RSD).

3.2.1. Effect of foreign ions

Since porphyrins form stable complexes with transition and heavy metal ions like copper(II), zinc(II) and lead(II) [19], these metal ions were masked by addition of a solution of ethylenediamine-*N,N,N',N'*-tetraacetatomagnesium(II), $[\text{Mg}(\text{edta})]^{2-}$, ($5 \times 10^{-3} \text{ M}$)¹ [20]. Table 1 summarizes the effect of foreign metal ions and anions for the determination of lithium ion ($1 \times 10^{-5} \text{ M}$) by the present method. Metal ions usually encountered in natural water samples were masked by $[\text{Mg}(\text{edta})]^{2-}$; and Na^+ and K^+ greater than 0.1 M did not interfere with the determination of Li^+ , as well as chloride.

3.2.2. Determination of Li^+ in sea water and human serum

3.2.2.1. *Sea water.* Sea water contains a large amount of Na^+ and Cl^- , but these ions did not

¹ $[\text{Na}(\text{edta})]^{3-}$ cannot be used to mask heavy metals like Zn^{2+} and Cu^{2+} due to the formation of $[\text{Li}(\text{edta})]^{3-}$ in alkaline solution. Thus, $[\text{Mg}(\text{edta})]^{2-}$ was used to mask Zn^{2+} and Cu^{2+} ($\log K_{\text{Zn}(\text{edta})}(16.44) > \log K_{\text{Mg}(\text{edta})}(8.83) > \log K_{\text{Li}(\text{edta})}(2.85) > \log \log K_{\text{Na}(\text{edta})}(1.64)$).

Table 1

The effect of foreign ions on the determination of Li^+ by the present method

Ions	Concentration (M)	Recovery (%)	Ions	Concentration (M)	Recovery (%)
Al^{3+}	1.0×10^{-5}	99.5	Cu^{2+}	1.0×10^{-5}	96.4
Fe^{3+}	1.0×10^{-5}	99.2	Pb^{2+}	1.0×10^{-5}	94.1
Cd^{2+}	1.0×10^{-5}	100.9	Mn^{2+}	1.0×10^{-5}	96.2
Zn^{2+}	1.0×10^{-5}	91.4	Cl^-	1.0×10^{-1}	97.2
Co^{2+}	1.0×10^{-5}	93.3	Br^-	1.0×10^{-5}	95.2
Ca^{2+}	1.0×10^{-5}	101.3	F^-	1.0×10^{-5}	96.2
Mg^{2+}	1.0×10^{-5}	100.1	SCN^-	1.0×10^{-5}	96.1
K^+	1.0×10^{-1}	97.2	CO_3^{2-}	1.0×10^{-5}	99.3
Na^+	1.0×10^{-1}	97.9	SO_4^{2-}	1.0×10^{-5}	99.5
			PO_4^{3-}	1.0×10^{-5}	102.5

interfere with the determination of Li^+ by the present method. Since Mg^{2+} and Ca^{2+} exist in sea water at much higher concentration than that of heavy metal ions, an equivalent amount of $[\text{Na}_2(\text{edta})]^{2-}$ to Mg^{2+} and Ca^{2+} was added into sample solutions to form $[\text{Mg}(\text{edta})]^{2-}$ and $[\text{Ca}(\text{edta})]^{2-}$, which mask heavy metal ions such as Zn^{2+} and Cu^{2+} . The concentration of Li^+ in a sea water was determined from a calibration curve and was found to be $(2.40 \pm 0.01) \times 10^{-5}$ M. The concentration was confirmed by a flame photometry and found to be $(2.42 \pm 0.04) \times 10^{-5}$ M.

3.2.2.2. Human blood serum. Protein reacted with the porphyrin and reduced absorbance. Thus, protein in serum was removed by the method described previously [14]. After protein was removed, the serum solution was diluted 100–500 times and analyzed by the present method. Since serum contains a few millimoles of Cu^{2+} and Zn^{2+} , $[\text{Na}_2(\text{edta})]^{2-}$ (1.00×10^{-4} M) was added to mask them in the serum. A recovery of lithium ion in the serum sample is shown in Fig. 4. The lithium concentration was recovered sufficiently after removing protein. However, if protein was not removed, the recovery decreased greatly (Fig. 4).

3.3. Transport of lithium

The presented solvent extraction study suggests that Li^+ is transported from an alkaline aqueous solution containing Li^+ to another acidic aqueous solution through a chloroform liquid membrane.

The lithium transport was monitored by determination of the concentration of Li^+ in both aqueous phases by a flame photometry at different pH values and concentrations of lithium and But_4NCl , and in various transportation times. Transport of lithium was negligible in the absence of the porphyrin.

3.3.1. Effect of pH in source and receiving phases

The transport of lithium ion is driven by a proton gradient between source and receiving phases. A plot of the concentration of transported lithium against pH is shown in Fig. 5. The concentration of Li^+ in the receiving phase, $[\text{Li}^+]_r$, increases rapidly at pH greater than 10. The results are in agreement with the protonation constant of $\text{H}_2\text{obtypps}^{4-}$ ($\text{p}K_a = 10.0$) [14]. A proton

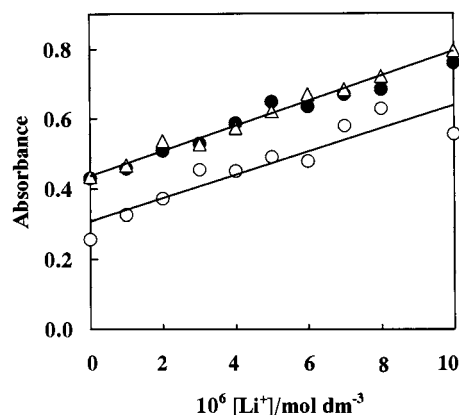


Fig. 4. Recovery of lithium by the addition of accurate amount of lithium to serum before (○) and after (●) removing protein, and to pure water (△).

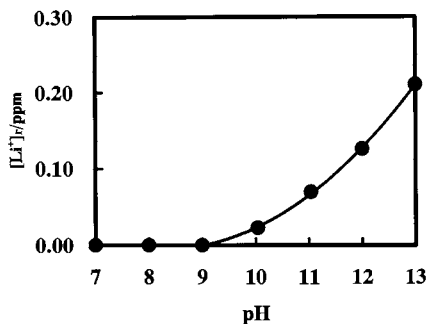


Fig. 5. Concentration of Li^+ transported into the receiving phase at different pH values.

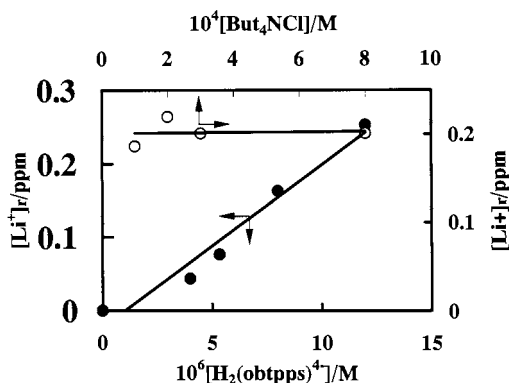


Fig. 6. Concentration of Li^+ transported into the receiving phase at different concentrations of $\text{H}_2(\text{obtpps})^{4-}$ (●) and But_4NCl (○) in the source phase.

removal of the porphyrin is an important step for the reaction of Li^+ with $\text{H}_2(\text{obtpps})^{4-}$. Therefore, the source phase must be alkaline for taking place of lithium transport. In the receiving phase, Li^+ was released from the lithium porphyrin complex, $[(\text{But}_4\text{N})_5\text{LiP}]_{\text{m}}$, in the chloroform membrane at an acidic condition and moved to the receiving phase. However, the acidic conditions lower than pH 6 caused a leak of the porphyrin unbound to Li^+ into the receiving phase from the membrane. This can be explained by the protonation of H_2P^{4-} to form H_3P^{3-} ($\text{p}K_{\text{a}1} = 4.83$ [14]) at pH lower than 5.0. The protonated porphyrin (H_3P^{3-}) is very hydrophilic so that H_3P^{3-} cannot be extracted into chloroform by formation of an ion-pair complex with But_4N^+ . Based on these results, the pH values were adjusted to 12.7 (0.1

M NaOH) for the source phase and 7.0 for the receiving phases, respectively.

3.3.2. Effect of the concentrations of porphyrin, But_4NCl and Li^+ on the lithium transfer

Since Li^+ is transported to the receiving phase by the formation of $[(\text{But}_4\text{N})_5\text{LiP}]$, the enhanced lithium transfer is expected. The results are given in Fig. 6. Lithium ion in the receiving phase increased with the concentrations of the porphyrin and Li^+ was transported to the receiving phase at a constant ratio in the presence of But_4NCl higher than 10^{-3} M in the source phase. In the receiving phase, a lack of But_4NCl caused a leak of the porphyrin to the receiving phase from the liquid membrane, and higher concentration of But_4NCl than 10^{-2} M decreased the lithium transfer a little, due to back extraction of lithium from the receiving phase to the liquid membrane. Usually, 1×10^{-3} M But_4NCl in both source and receiving phases is suitable for lithium transportation.

The amount of lithium ion transported into the receiving phase increased with lithium ion in the source phase, but became constant over a concentration of 10^{-2} M lithium, where the transport of Li^+ is controlled by the dissociation rate of $[(\text{But}_4\text{N})_5\text{LiP}]$ by a proton, as described in the following kinetics study.

3.3.3. Kinetics of Li^+ transport

The diffusion of chemical species in a liquid membrane is usually assumed to be a rate-determining step for ion transportation, while, in our experiment, the liquid membrane phase was stirred continuously so that the transport of lithium is not affected by diffusion rate of $[(\text{But}_4\text{N})_5\text{LiP}]$ in the membrane. Therefore, the transport rate of lithium was controlled by both kinetic processes of the extraction of Li^+ into the liquid membrane and the dissociation of $[(\text{But}_4\text{N})_5\text{LiP}]$ at the interface of water and chloroform. Fig. 7 shows a downhill transport of Li^+ at different transportation times. In the first 30 min, the lithium concentration in the source phase decreased sharply, but lithium transport into the receiving phase was not observed. This means fast formation of $[\text{LiP}]^{5-}$ and extraction of

[(But₄N)₅LiP] into the chloroform membrane. The concentration of Li⁺ extrapolated to *t*=0 is comparable to the concentration of the porphyrin. The dissociation rate of [(But₄N)₅LiP] in the re-

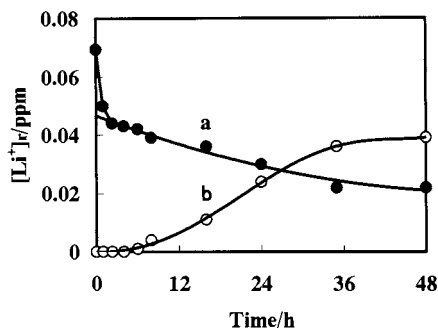
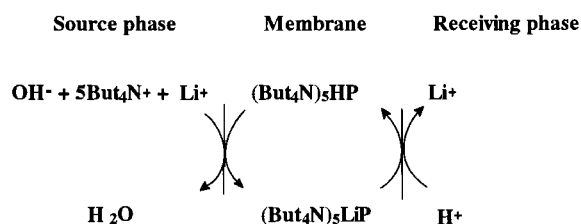


Fig. 7. Transport of 10^{-5} M Li⁺ from source phase (a) at pH 12.7 to the receiving phase (b) at different transportation times and at 8.0×10^{-6} M H₂(obtpps)⁴⁻ in the chloroform membrane.



Scheme 1. Reaction scheme of the lithium ion transport across a chloroform liquid membrane containing of H₂(obtpps)⁴⁻ in the presence of tetrabutylammonium chloride (But₄NCl).

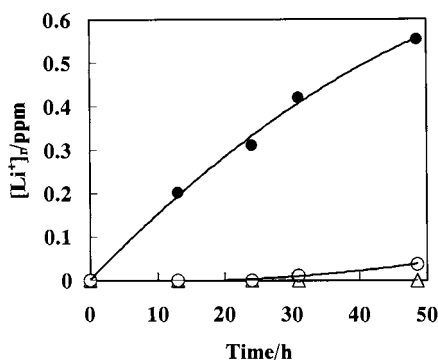


Fig. 8. Competitive transport of Li⁺ (●), Na⁺ (△) and K⁺ (○) across a chloroform liquid membrane at 10^{-2} M Li⁺, 0.1 M Na⁺ and 0.1 M K⁺ as their initial concentrations in the source phase.

ceiving phase is apparently slower than the uptake of lithium. Thus the lithium transfer rate is controlled by the dissociation reaction of the lithium complex. The reaction mechanism of the lithium transfer is given in Scheme 1.

3.3.4. Competitive transport of Li⁺, Na⁺ and K⁺

As described in the solvent extraction of lithium, the synthesized octabromoporphyrin reacts selectively with Li⁺ in a large excess of Na⁺ or K⁺. In order to know the selectivity of Li⁺/Na⁺ and Li⁺/K⁺ in the lithium transport, we carried out an experiment for lithium transfer in the presence of 0.1 M Na⁺ or K⁺. Sodium ion did not transfer at all, even after 48 h, but potassium ion did a little after 48 h reaction time (Fig. 8). Any change in absorption spectra was not observed for the chloroform membrane equilibrated with an aqueous solution containing of K⁺. Potassium ion may be transported with a weak ion-pair complex such as [K⁺][(But₄N)₄(LiP)⁻], where K⁺ interacts with [LiP⁵⁻] as a positive counter ion like But₄N⁺. Potassium ion shows some hydrophobicity that makes it possible for K⁺ to transfer into the receiving phase along with the lithium porphyrin through a chloroform membrane. Sodium ion has high hydration energy that prevents Na⁺ from transporting across the chloroform membrane with the lithium porphyrin. The competitive transport of Li⁺, Na⁺ and K⁺ is shown in Fig. 8.

4. Conclusions

The octabromo groups of the synthesized water-soluble porphyrin (Fig. 1) lower the basicity of the porphyrin ring and enhance the proton dissociation of the pyrrole protons, making it easy for Li⁺ to bind to the porphyrin. Due to an inflexibility of ring size of the porphyrin, Na⁺ cannot bind to the porphyrin. Thus, Li⁺ less than 10^{-5} M was selectively extracted into chloroform and transported in the presence of Na⁺ greater than 0.1 M. The present method was applied to the separation and determination of Li⁺ in sea water

and serum, and to Li^+ transport through a liquid membrane. The method is simple, selective and sensitive. The sensitivity for the determination of Li^+ increased 30 times by the solvent extraction method compared with the direct determination of Li^+ in aqueous solution due to a decreased overlap of absorption spectra of $[\text{HP}]^{5-}$ on that of $[\text{LiP}]^{5-}$ in chloroform phase. This method will be extended to an ion-selective electrode monitoring lithium of a lower concentration in blood and environmental discharges, and to collection of lithium from sea water and for recycling in industry.

Acknowledgements

We are grateful for the Grant-in Aid for Scientific Research (No 08454238) from the Ministry of Education, Science and Culture of Japan.

References

- [1] R.O. Bach, *Lithium—Current Application in Science, Medicine and Technology*, Wiley, New York, 1985.
- [2] A.-M. Sapse, P. von, R. Schleyer, *Lithium Chemistry*, John Wiley & Sons, New York, 1995.
- [3] J.c. Nardi, M. Yoshio, A. Kozawa, *Progress in Batteries & Battery Materials*, ITE, vol. 16, JEC Press, Japan, 1997.
- [4] R.G. Pearson, *Hard and Soft Acids and Bases*, Dowden Hutchinson and Ross, Stroudsburg, PA, 1973.
- [5] R.M. Izatt, K. Pawlak, J.S. Bradshaw, R.L. Bruening, *Chem. Rev.* 91 (1991) 1721 and references cited therein.
- [6] B.P. Czech, D.A. Babb, B. Son, R.A. Bartsch, *J. Org. Chem.* 49 (1984) 4805.
- [7] R.A. Bartsch, M. -J. Goo, G.D. Christian, X. Wen, B.P. Czech, E. Chapoteau, A. Kumar, *Anal. Chim. Acta* 272 (1993) 285.
- [8] S. Kitazawa, K. Kimura, H. Yano, T. Shono, *J. Am. Chem. Soc.* 106 (1984) 6978.
- [9] A.F. Sholl, I.O. Southerland, *J. Chem. Soc. Chem. Commun.* (1992) 1716.
- [10] M. Tabata, J. Nishimoto, A. Ogata, T. Kusano, N. Nahar, *Bull. Chem. Soc. Jpn.* 69 (1996) 673.
- [11] F. D'Souza, Y.-Y. Hsieh, G.R. Deviprasad, *J. Electroanal. Chem.* 426 (1997) 17.
- [12] F. D'Souza, R.G. Deviprasad, Y.-Y. Hsieh, *J. Electroanal. Chem.* 411 (1996) 167.
- [13] R.A. Richards, K. Hammons, M. Joe, G.M. Miskelly, *Inorg. Chem.* 35 (1996) 1940.
- [14] M. Tabata, J. Nishimoto, T. Kusano, *Talanta* 46 (1998) 703.
- [15] S. Haiping, J. Nishimoto, M. Tabata, *Anal. Sci.* 13 (1997) 119.
- [16] E.V. Dehmolow, S.S. Pehmlow, *Phase Transfer Catalysis*, Cerlay Chemie, Weinheim, 1980.
- [17] R.D. Shannon, *Acta Crystallogr.* A32 (1976) 751.
- [18] A. Amidsen, *DMB Dan, Med. Bull.* 22 (1975) 277.
- [19] M. Tabata, M. Tanaka, *Trends Anal. Chem.* 10 (1991) 128.
- [20] A.E. Martell, R.M. Smith, *Critical Stability Constants*, vol. 1, Plenum Press, New York, 1974.

Electrochemical studies and square wave adsorptive stripping voltammetry of the antidepressant fluoxetine

A.M.S. Roque da Silva ^a, J.C. Lima ^a, M.T. Oliva Teles ^b,
A.M. Oliveira Brett ^{c,*}

^a *CEQUP/Departamento de Química-Física, Faculdade de Farmácia, Universidade do Porto, R. Anibal Cunha, 164, 4050 Porto, Portugal*

^b *Departamento de Eng. Química, Instituto Superior de Engenharia do Porto, R. S. Tomé, 4000 Porto, Portugal*

^c *Departamento de Química, Faculdade de Ciências e Tecnologia, Universidade de Coimbra, 3049 Coimbra, Portugal*

Received 29 September 1997; received in revised form 20 January 1999; accepted 26 January 1999

Abstract

The electrochemical reduction of the antidepressant drug fluoxetine was investigated by cyclic, linear sweep, differential pulse and square wave voltammetry using a hanging mercury drop electrode in alkaline buffer solution in water and in a water/acetonitrile mixed solvent. Cyclic voltammograms in aqueous solution showed very strong adsorption of fluoxetine on the electrode with formation of a compact film. The effect of addition of different percentages of acetonitrile on the voltammetric response was evaluated. It is shown that acetonitrile protects the electrode surface, thus preventing the adsorption of fluoxetine as a compact film, although reduction occurs at more negative potentials. Adsorption was used to accumulate the drug onto the electrode surface. The adsorbed species were measured voltammetrically by reduction at -1.3 V in an aqueous 0.05 M Ringer buffer, pH 12, 20% acetonitrile v/v. Linear calibration graphs were obtained in the range 0.52–5.2 M. The quantification of fluoxetine in pharmacological formulations existing in the market was performed using adsorptive square wave cathodic stripping voltammetry, and compared with data from UV spectrophotometry. The method is simple and not time-consuming. A comparative high performance liquid chromatography assay with UV detection was performed. Recovery data for both methods are reported. © 1999 Elsevier Science B.V. All rights reserved.

Keywords: Fluoxetine; Electrochemistry; Antidepressant; Pharmaceutical formulations

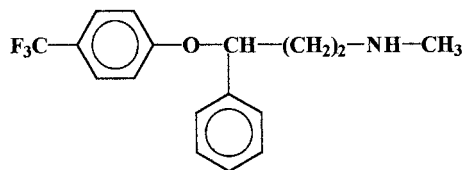
1. Introduction

The continuous demand for anti-depressive drugs with minimal side effects, mainly cardiovascular accidents or anticholinergic activity, gave rise to the development of the anti-depressant

* Corresponding author. Tel.: +351-39-835-295; fax: +351-39-935-295.

E-mail address: brett@cygnus.ci.uc.pt (A.M. Oliveira Brett)

drug fluoxetine, *N*-methyl-8-14-(trifluoromethyl) phenoxybenzenepropanamine.



It works by inhibiting the uptake of serotonin by the neurons in the brain, enhances serotonin neurotransmission and has the longest half-life of all the selective serotonin reuptake inhibitors (SSRIs). It has been used for the treatment of major depression, obsessive–compulsive disorder, borderline personality and panic disorders, nervous anorexia and bulimia, autism, obesity, alcoholism, geriatrics, and deintoxication by cocaine [1–5]. Fluoxetine is clinically administered orally in the form of chlorhydrates and is the most widely prescribed antidepressant in the USA. The precise mechanism of action is not clear but it has less sedative, anticholinergic and cardiovascular effects than the tricyclic antidepressant drugs. Fluoxetine is metabolized to norfluoxetine which is also active. It is highly protein-bound and readily crosses the blood–brain barrier and the placenta, consequently also appearing distributed into breast milk. Carcinogenic studies provided evidence that fluoxetine is neither a complete carcinogen nor a tumor promoter [6].

The control of fluoxetine and norfluoxetine has been accomplished in blood serum using gas chromatography [7–12] and, to a larger extent, by high pressure liquid chromatography (HPLC) with fluorescence or UV detection [13–24].

This paper is concerned with the study of the adsorptive voltammetric behaviour of fluoxetine using a hanging mercury drop electrode (HMDE) in different buffer solutions. In the literature, no references were found concerning the use of electroanalytical techniques for the determination of this substance or studies of the electron transfer mechanisms of fluoxetine. Based on the results obtained, a square wave adsorptive voltammetric quantification method was developed. This procedure was applied to the determination of fluoxetine in commercial preparations existing in the market and the results were compared with those

obtained by the same determination using HPLC with UV detection.

2. Experimental

Fluoxetine chlorhydrate was kindly supplied by the laboratory El Lilly Pharmaceuticals (Indianapolis, IN, USA). All the chemicals used were of reagent grade quality and they were employed without further purification. The most conclusive experiments were performed in 0.05 M Ringer buffer ($\text{HPO}_4^{2-}/\text{PO}_4^{3-}$) in the range pH 9–12, and were prepared using purified water from a Millipore Milli-Q system.

The working electrode was a Metrohm multi-mode HMDE, the counter electrode a carbon rod and the reference electrode was AgCl/Ag/3 M KCl, used in a one-compartment cell of a 663 VA stand Metrohm. Voltammograms were recorded using a Autolab PSTAT 10 potentiostat/galvanostat running with model GPES version 3 software, from Eco-Chemie, Netherlands. The potential range studied was from -0.8 to -1.8 V vs. Ag/AgCl, cyclic voltammetry scan rates varying from 20 to 800 mV s^{-1} . Differential pulse voltammetry conditions were: pulse amplitude, 40 mV; pulse width, 70 ms; scan rate, 6 mV s^{-1} ; and square wave voltammetry conditions were: pulse amplitude, 40 mV; frequency, 50 Hz; potential step, 6 mV.

The HPLC system used was a Sykan model A 1210 liquid chromatograph, equipped with a model 3200 UV/Vis detector and connected to a computing integrator model PRIME version 2.2.6 chromatography data station. For chromatographic separation, a Technopak 10 C_{18} column (250×4 mm, 5 μM particle size) was employed. The separation was carried out at room temperature using, as the mobile phase, 40% acetonitrile:60% 0.05 M potassium dihydrogenphosphate (pH 4.7) filtered through a 0.45 μm filter and degassed with a helium sparge. A Hamilton 50 μl syringe was used for sample injection.

The pharmaceutical samples were prepared by mixing and the content of 10 capsules followed by weighing exactly around one-tenth of it. To this powder aliquot was added 80 ml of water in a 100

ml dilution flask. This was placed during 15 min in an ultrasonic bath, before completing the volume up to 100 ml with water. This procedure was repeated 10 times.

Adsorptive voltammetry measurements were carried out in the square wave voltammetry mode (SWV) under the following optimized conditions: accumulation potential, -0.8 V and accumulation time, 5 s, with stirring at 500 rpm. An equilibrium time of 5 s was allowed to elapse between the end of the stirring and the start of the potential scan from -1.0 to -1.8 V. The adsorptive cycle was repeated three times using a new mercury drop each time, the result being expressed as the average of the four measurements. Quantification of fluoxetine was performed by means of the standard addition method.

To calculate the recovery, another aliquot of the powder sample was weighed and a known number of milligrams of fluoxetine clorhydrate were added; the quantification procedure already described was carried out.

3. Results and discussion

The electrochemical reduction process of fluoxetine at the HMDE leads to very strong adsorption on the electrode surface, as seen from the cyclic voltammograms in Fig. 1, at pH 12. The shape of the cyclic voltammograms suggests that, in the conditions used, they correspond to a

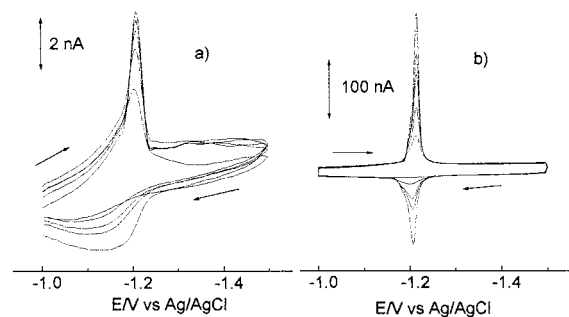


Fig. 1. Cyclic voltammograms of fluoxetine at scan rates of: (a) 90 mV s^{-1} ; (b) 600 mV s^{-1} . Concentrations: 6.36, 7.93, 9.50, 11.1 and $12.6 \text{ } \mu\text{M}$ in 0.05 M Ringer buffer, pH 12, $t_{\text{dep}} = 5 \text{ s}$ at $E_{\text{dep}} = -0.8 \text{ V}$.

quasi-reversible system for adsorbed species, since there is only a very little separation of 10 mV between anodic and cathodic peaks. The curve is almost symmetric round E_p , the width at half-height, $W_{1/2}$, decreases slightly as the concentration increases, and the peak current is proportional to the scan rate, ν , for both the anodic and the cathodic peaks. Also the peak potential does not vary with scan rate, ν , and the oxidation peak only appears for very high scan rates (Fig. 1b). However, the adsorption peak height for the reduction does not vary linearly with concentration, suggesting blocking by formation of a compact film on the electrode surface [29–32].

The strong adsorption process taking place on the electrode surface corresponding to the accumulation of fluoxetine was confirmed by repetitive cyclic voltammograms recorded after dipping the HMDE in a stirred solution of the drug for a period of 5 s at -0.8 V. The short accumulation time gives substantial enhancement of the cathodic peak (first scan) compared with those of non-accumulated species (subsequent scans), thus indicating a rapid desorption of fluoxetine from the electrode surface.

The study of peak potential, E_p , versus pH, in Britton Robinson buffer, showed that the reduction signal for fluoxetine appears only for pH values higher than 8.5. This is because reduction only occurs at very negative potentials, as is predicted for this type of compound [24,25]. Consequently, the reduction peak can only be expected to be observed when very high pH value supporting electrolytes are used because in those experimental conditions, the negative potential range for HMDE is increased up to -2.0 V vs. Ag/AgCl, and the reduction peak can be recorded. Fluoxetine molecules are potentially basic on account of the unshared electron pair of the oxygen atom and at these pH values it is the unprotonated form that is reacting (Fig. 2). The peak potential was only shifted slightly to more positive values as the pH was increased, the slope corresponds to 6.1 mV per unit of pH. Thus the reduction of fluoxetine is pH independent.

The reduction reaction mechanism of fluoxetine is quite general for aromatic compounds [25–28]

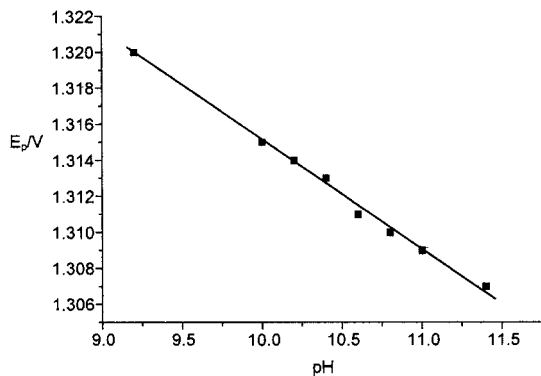


Fig. 2. Plot of E_p vs. pH for a 6.36 M fluoxetine solution in 0.05 M Ringer buffer solutions. The line corresponds to a slope of 6.1 mV per unit of pH.

and is considered to require the formation of a radical anion formed by electron transfer into an antibonding orbital of the arene linked to the oxygen. The peak current increased until pH 10.5 and then became constant until pH 12.5. Since the best definition of peaks was observed for pH 12 in Ringer buffer, this supporting electrolyte was chosen for subsequent experiments.

The strong adsorption process of fluoxetine on the electrode surface depended on the accumulation time and was investigated further. Without accumulation, when the concentration was lowered to 1 μM , a negligible current was observed. However, a well-defined peak was observed if a 60 s accumulation period preceded the potential scan. For micromolar concentrations, besides the adsorption peak, a diffusion peak, due to the reduction of diffusing molecules, appears for a long deposition time. Fig. 3 shows the diffusion peak as a shoulder before the adsorption peak in the negative potential scan [29]. A deposition potential of -0.8 V was chosen and accumulation times varying from 5 to 80 s were evaluated, after which CVs were recorded. For concentrations less than 1 M, 20 s deposition time led to the maximum current. However, at higher concentrations, the shape and peak height, in reduction as in oxidation, shows the same behaviour as described elsewhere [29–32] for the case of strong adsorption with formation of a compact film on the electrode surface. The peak potential was

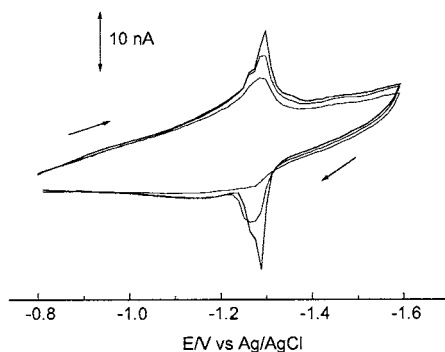


Fig. 3. Cyclic voltammograms of fluoxetine at 600 mV s^{-1} . Concentrations: 1.46, 2.04 and $2.62 \mu\text{M}$ in 0.05 M Ringer buffer, pH 12, $t_{\text{dep}} = 60 \text{ s}$ at $E_{\text{dep}} = -0.8 \text{ V}$.

shifted to more negative values and $W_{1/2}$ decreased as the concentration or the accumulation time was increased.

Quantitative determinations of fluoxetine were very irreproducible due to the very strong adsorption causing decrease of peak height in successive scans. When a buffer supporting electrolyte in an acetonitrile/water mixed solvent was used, the reproducibility of the peaks and the resolution of the peaks improved although the peak potentials were shifted ~ 200 mV to more negative values. Comparison between Fig. 4a and Fig. 4b shows the effect of using 20% acetonitrile/80% water as solvent.

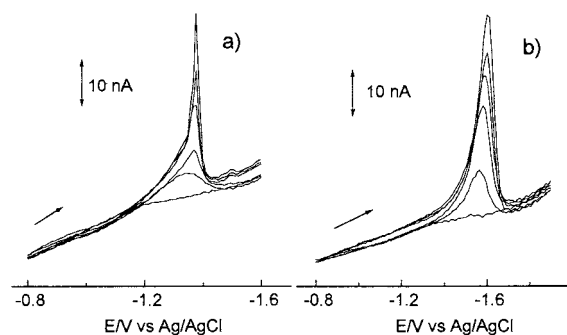


Fig. 4. Adsorptive linear sweep voltammetry of fluoxetine, (a) 0.05 M Ringer buffer, pH 12; (b) 0.05 M Ringer buffer, pH 12, 20% acetonitrile v/v. Scan rate, 800 mV s^{-1} ; concentrations: 0.92, 1.85, 2.76, 3.68 and $4.59 \mu\text{M}$, $t_{\text{dep}} = 20 \text{ s}$ at $E_{\text{dep}} = -0.8 \text{ V}$.

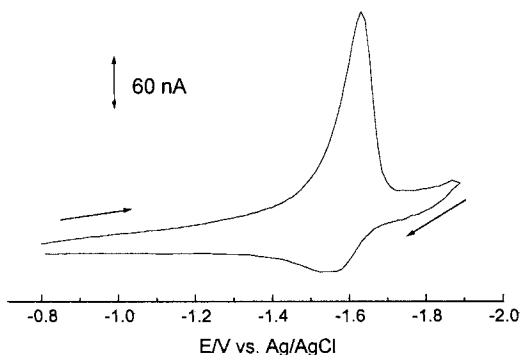


Fig. 5. Cyclic voltammogram of 12.5 μM fluoxetine in 0.05 M Ringer buffer, pH 12, 20% acetonitrile v/v. Scan rate, 800 mV s^{-1} ; $t_{\text{dep}} = 20$ s at $E_{\text{dep}} = -0.8$ V.

According to Ref. [33], the differential capacity of the electric double layer is a very sensitive function of the adsorption of organic molecules at the mercury electrode surface. At high positive and negative surface charges, the adsorption–desorption peaks on the C vs. ϕ curves, are very much lower or vanish entirely in the case of solution in organic solvents in comparison with aqueous solutions. The influence of the mixture of aqueous with organic electrolyte in the height and position of the peaks on the C vs. ϕ curves is caused by the salting-out of the organic substance [34], giving rise to a shift of the cathodic peak in the negative direction and an increase of the peak height. This is in good agreement with our experiments where the shift of the peak potentials ~ 200 mV to more negative potentials was observed.

The influence of different percentages of acetonitrile in the solvent was evaluated and it was found that 0.05 M Ringer buffer, 20% acetonitrile v/v, led to the best improvement of peak definition and height (Fig. 5). The cyclic voltammogram after accumulation of fluoxetine at -0.8 V shows that acetonitrile protects the electrode surface by preventing irreversible adsorption of fluoxetine.

In the presence of acetonitrile, the symmetry of the differential pulse voltammetric peak also improves and, since the resolution is better, it is possible to determine lower concentrations of fluoxetine down to 3.2×10^{-7} M. In these condi-

tions, the non-linear relationship between peak current, i_p , and $v^{1/2}$ shows again that the reduction process is not only diffusion controlled, but there is an important adsorption component.

In the presence of acetonitrile, different potential scan modes, i.e. linear sweep voltammetry (LSV), differential pulse voltammetry (DPV) and square wave voltammetry (SWV), were applied to the stripping analysis of the adsorbed fluoxetine (Fig. 6). It was found that the use of pulse techniques improves the sensitivity, as expected. The largest slope value in the plot of peak current vs. concentration, 14.3 nA M^{-1} , was obtained using SWV while values of 6.18 and 0.93 nA M^{-1} were achieved using LSV and DPV respectively. Therefore, square wave voltammetry was chosen for further work since this technique is less time consuming and shows the best peak resolution.

For electroanalytical purposes, the optimised conditions for square wave adsorptive stripping voltammetry found were accumulation of fluoxetine on the electrode surface during a total of 10 s at a potential of -0.8 V, 5 s with stirring at 500 rpm, followed by 5 s without stirring, supporting electrolyte 0.05 M Ringer buffer, 20% of acetonitrile v/v, frequency 50 Hz, pulse amplitude 40 mV, potential step 6 mV, and scan from -1.0 to -1.6 V.

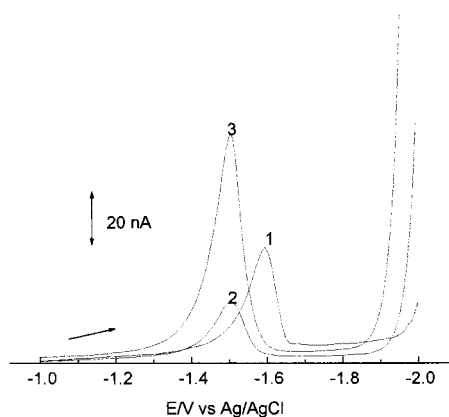


Fig. 6. Adsorptive stripping voltammograms of a 5.19 μM fluoxetine solution in 0.05 M Ringer buffer, pH 12, 20% acetonitrile v/v, $t_{\text{dep}} = 5$ s at $E_{\text{dep}} = -0.8$ V: (1) linear sweep voltammetry, scan rate 800 mV s^{-1} , (2) differential pulse voltammetry, scan rate 6 mV s^{-1} , (3) square wave voltammetry, frequency 50 Hz and potential step 6 mV.

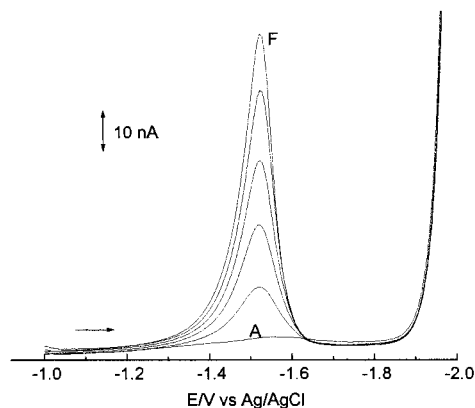


Fig. 7. Square wave adsorptive stripping voltammograms obtained after increasing the fluoxetine concentration in 1.05 μM steps from 0 (A) to 5.19 μM (F), $t_{\text{dep}} = 5$ s at $E_{\text{dep}} = -0.8$ V.

In these conditions, a value of 3.9×10^{-8} M was determined for the detection limit (defined as three times the noise). The dependence of peak current on fluoxetine concentration was found to be linear over a range from 0.52 to 5.2 μM . Fig. 7 shows square wave voltammograms obtained after successive standard additions of fluoxetine chlorhydrate, each addition corresponding to a 1.05 μM increase in concentration. A least-square treatment of the data in Fig. 7 yields a slope of 14.3 nA M^{-1} and an intercept of 0.42 nA, with a correlation coefficient of 0.9998. Precision was calculated by 10 successive measurements of a 5.19 μM fluoxetine solution (accumulation for 5 s at -0.8 V) with a relative standard deviation of 2.8%.

The fluoxetine content of commercially available capsules, prepared as described in Section 2,

was determined directly using adsorptive linear sweep square wave voltammetry method, using the standard addition method. The results obtained by the electroanalytical method were in good agreement with those obtained by HPLC with UV detection using the same samples (Table 1).

4. Conclusions

The reduction of fluoxetine is pH independent and occurs at very high potentials, which means that it can be studied only at pH values higher than 8.5. The use of buffer electrolyte in a mixed acetonitrile/water solvent proved very convenient for preventing strong adsorption of the analyte on the electrode surface and enabling better reproducibility and sensitivity. Adsorptive linear sweep square wave voltammetry permitted accurate quantification of fluoxetine in commonly used pharmaceutical drugs in the micromolar range after a very simple and rapid sample treatment. Good precision was obtained (relative standard deviation = 2.8%; $n = 10$). This electroanalytical method can be used for determination of therapeutic doses of fluoxetine in biological fluids if coupled with high performance liquid chromatography (HPLC) with electrochemical detection.

Acknowledgements

El Lilly Pharmaceuticals (Indianapolis, IN USA) very kindly supplied the fluoxetine chlorhydrate used in this work. This work was supported by a grant PRAXIS/P/QUI/10109/1998 (Portugal).

Table 1
Electrochemical quantification of fluoxetine in pharmacological formulations^a

Sample	SWV			HPLC		
	mg/cap	RSD (%)	Recovery (%)	mg/cap	RSD (%)	Recovery (%)
A	20.0	3	100	23.0	6	112
B	19.6	0.3	101	19.0	4	116
C	20.0	3	98	20.0	7	120
D	20.0	3	102	20.0	2	100

^a All formulations refer to 20 mg of fluoxetine per capsule. RSD (%), relative standard deviation.

References

- [1] A. Wood, *Int. Clin. Psychopharmacol.* 8 (1993) 295.
- [2] G.A. Bray, *Ann. Intern. Med.* 1197 (1993) 707.
- [3] J.R. Cornelius, I.M. Salloum, M.D. Cornelius, J.M. Perel, M.E. Thase, J.G. Ehler, J.J. Mann, *Psychopharmacol. Bull.* 29 (1993) 195.
- [4] M.G. Harris, P. Bentley, *Drugs Aging* 6 (1995) 64.
- [5] S.L. Walsh, K.L. Preston, J.T. Sullivan, R. Fromme, G.E. Bigelow, *J. Clin. Psychopharmacol.* 14 (1994) 396.
- [6] R.A. Bendele, E.R. Adams, W.P. Hoffman, C.L. Gries, D.M. Morton, *Cancer Res.* 52 (1992) 6931.
- [7] J.F. Nash, R.J. Bopp, R.H. Carmichael, K.Z. Farid, L. Lamberger, *Clin. Chem.* 28 (1982) 2100.
- [8] V. Dixit, H. Nguyen, V.M. Dixit, *J. Chromatogr.* 563 (1991) 379.
- [9] R.J. Lantz, K.Z. Farid, J. Koons, J.B. Tenbarger, R.J. Bopp, *J. Chromatogr.* 614 (1993) 175.
- [10] G.A. Torok-Both, G.B. Baker, R.T. Coutts, K.F. McKenna, L.J. Aspeslet, *J. Chromatogr.* 579 (1992) 99.
- [11] T.P. Rohring, R.W. Prouty, *J. Anal. Toxicol.* 13 (1989) 305.
- [12] R.T. Sane, A.B. Jani, J.K. Ghade, A.J. Vaidya, S.S. Kotwal, *Indian Drugs* 29 (1992) 237.
- [13] M.A. Raggi, R. Mandrioli, G. Casamenti, F. Bugamelli, V. Volterra, *J. Pharm. Biomed. Anal.* 18 (1998) 193.
- [14] A. El Jazigi, D.A. Rainer, *Ther. Drug Monit.* 15 (1993) 305.
- [15] S.H.J. Wong, S.S. Dellafera, R. Fernandes, *J. Chromatogr.* 499 (1990) 601.
- [16] P. Thomare, K. Wans, V. Van-der-Meersh-Mougeout, B. Diquet, *J. Chromatogr.* 583 (1992) 217.
- [17] A.L. Peyton, R. Carpenter, R. Kowski, *Pharm. Res.* 8 (1991) 1528.
- [18] P.R. Puopolo, J.G. Flood, *Clin. Chem.* 37 (1991) 1304.
- [19] R.F. Suckow, M.F. Zhang, T.B. Cooper, *Clin. Chem.* 38 (1992) 1756.
- [20] A. El-Maani, I. Combourieu, M. Bonini, E.E. Creppy, *Clin. Chem.* 39 (1993) 1749.
- [21] J.H. Nichols, J.R. Charlson, G.H. Lawson, *Clin. Chem.* 40 (1994) 1312.
- [22] B.D. Potts, C.J. and C. Bethea, *Drug Dev. Ind. Pharm.* 18 (1992) 257.
- [23] S. Raghuver, A.B. Avadhanulu, A.R.R. Poentulu, *Indian Drugs* 30 (1993) 83.
- [24] C.K. Mann, K.K. Barnes, *Electrochemical Reactions in Nonaqueous Systems*, Marcel Dekker, New York, 1970.
- [25] A. Zeig, A.H. Maurer, B.G. Roberts, *J. Org. Chem.* 32 (1967) 1322.
- [26] J.K. Brown, D.R. Burnham, N.A.J. Rogers, *J. Chem. Soc. (B)* (1969) 1149.
- [27] A.J. Birch, *Quart. Rev.* 4 (1950) 69.
- [28] A.J. Birch, H. Smith, *Quart. Rev.* 12 (1958) 17.
- [29] E. Laviron, *Collect. Czech. Chem. Commun.* 36 (1971) 363.
- [30] H. Angerstein-Kozłowska, J. Klinger, B.E. Conway, *J. Electroanal. Chem.* 75 (1977) 61.
- [31] H. Angerstein-Kozłowska, B.E. Conway, *J. Electroanal. Chem.* 95 (1979) 1.
- [32] E. Laviron, in: A. Bard (Ed.), *Electroanalytical Chemistry*, Marcel Dekker, New York, 1982, pp. 12–54.
- [33] B.B. Damaskin, O.A. Petrii, V.V. Batrakov, *Adsorption of Organic Compounds on Electrodes*, Plenum Press, New York, 1971.
- [34] Grigorev, N.B., Damaskin, B.B., *Advances in the Electrochemistry of Organic Compounds*, Izd. Nauka, Moscow, 1968, p. 66.

Determination of arsenic compounds in reference materials by HPLC-(UV)-HG-AFS

Zdenka Šlejkovec^{a,b,*}, Johannes T. van Elteren^a, Anthony R. Byrne^b

^a *Interfaculty Reactor Institute, Delft University of Technology, Mekelweg 15, 2629 JB Delft, Netherlands*

^b *Jožef Stefan Institute, Jamova 39, 1000 Ljubljana, Slovenia*

Received 27 November 1998; received in revised form 25 January 1999; accepted 26 January 1999

Abstract

Arsenic compounds were determined in six reference materials of biological origin. None of them has yet been certified for arsenic compounds but some are in the process of certification; for most of these reference materials indicative literature values are available. Eight commonly used arsenic standards were used for quantification using a recently developed hyphenated speciation system comprising high performance liquid chromatography (HPLC) and atomic fluorescence spectrometry (AFS), interfaced via a UV-photoreactor and a hydride generation (HG) unit. Absolute detection limits were ca. 0.2 and 0.4 ng As for separation on anion and cation exchange columns, respectively. Our results agree well with indicative literature values which were generated by different authors using various separation and detection methods. The HPLC-(UV)-HG-AFS system validated in this way is suitable for quantification of eight arsenic compounds. Moreover, the system is capable of separation of at least six more compounds in the mentioned reference materials, of which two could be attributed to arsenosugars (OH and phosphodiester form) but due to the lack of standards, quantification was not possible. For accurate and extensive speciation analysis the availability of certified reference materials and standards for arsenic compounds should be promoted. © 1999 Elsevier Science B.V. All rights reserved.

Keywords: Arsenic; Speciation; Reference materials

1. Introduction

The arsenic compounds found in environmental samples are arsenite (As(III)), arsenate (As(V)), monomethylarsonic acid (MMAA), dimethylarsinic acid (DMAA), arsenobetaine (AsB), ar-

senocholine ion (AsC), tetramethylarsonium ion (TETRA) and trimethylarsine oxide (TMAO). Next to these compounds more than ten arsenosugars have been found in various species of marine algae; most of them are dimethylarsinoyl-ribosides [1,2].

The reliability of speciation data depends on the accuracy of the speciation procedure. A common way to verify analytical procedures is to analyse certified reference materials (CRMs). Un-

* Corresponding author. Tel.: +31-15-2782709; fax: +31-15-2783906.

E-mail address: slejkovec@iri.tudelft.nl (Z. Šlejkovec)

fortunately, in speciation analysis only few suitable CRMs are available. As an intermediate solution, reference materials certified for total element concentrations may be used if speciation results have been reported, especially when a consensus of agreement has been reached.

For arsenic speciation, NBS SRM Oyster tissue 1566a (*Crassostrea gigas*) [3–5] and NBS SRM toxic metals in freeze-dried Urine 2670 [6–9] from the National Institute of Standards and Technology (NIST, USA), NIES No. 6 (Mussel tissue, *Mytilus edulis*) [3,4] from the National Institute

for Environmental Studies (NIES, Japan), DORM-1 (Dogfish muscle) [3,4,10–17], TORT-1 (Lobster hepatopancreas) [4,15] and DOLT-1 (Dogfish liver) [3,11,15] from the National Research Council of Canada (NRCC) are being used for this purpose.

In 1990 NIES started a program on the preparation and certification of environmental and biological CRMs for elemental speciation. After the preparation of NIES CRM No. 11 and 12 (both for tin) and NIES CRM No. 13 (for mercury) [18,19], two CRMs are in preparation for speciation of arsenic. NIES CRM No. 14 (Brown algae) is in the process of certification for As(V) and NIES CRM No. 15 (Scallop) for AsB [19,20].

In this work a recently developed [21,22] high performance liquid chromatography (HPLC)-(UV)-HG-AFS system with anion and cation exchange chromatography has been applied to determine arsenic compounds in six reference materials (certified for total As or candidates for As compounds) from NIST (NBS SRM 1566 a), NRCC (DOLT 1, DORM 1, TORT 1) and NIES (No. 14, No. 15).

2. Experimental

2.1. Reagents and standards

All chemicals were of analytical reagent grade. As_2O_3 and As_2O_5 were purchased from Merck (Darmstadt, Germany) and MMAA, DMAA, AsB-bromide, TMAO, AsC and TETRA-iodide were gifts from Prof. K.J. Irgolic (Karl-Franzens University Graz, Austria). Stock solutions of the arsenic compounds containing about 1000 mg l^{-1} arsenic were prepared in water and kept at 4°C . The exact concentration of arsenic in the stock solutions was determined by instrumental neutron activation analysis (INAA). Working solutions with arsenic concentrations of $10\text{--}100 \text{ ng ml}^{-1}$ were prepared fresh daily. Millipore (Milford, MA, USA) Milli-Q Plus water ($18.2 \text{ M}\Omega \text{ cm}$) was used for all solution preparations. Next to the commonly available arsenic compounds mentioned above, NBS SRM Oyster tissue 1566a was used as a comparative sample with two known arsenosugars [4,5].

Table 1

Experimental conditions for arsenic speciation with the HPLC-(UV)-HG-AFS system

HPLC

Anion exchange:

Column Hamilton PRP-X100, $250 \times 4.1 \text{ mm}$
Mobile phase KH_2PO_4 solution, 15 mmol l^{-1} , pH 6.1 (NH_4OH)

Cation exchange:

Column Alltech Adsorbosphere SCX 5U, $250 \times 4.6 \text{ mm}$

Mobile phase Pyridine, 2.5 mmol l^{-1} , pH 2.65 (citric acid)

Flow rate 1 ml min^{-1}

Injection volume $100 \mu\text{l}$

On-line UV-reactor (optional)

Ultraviolet lamp 8 W (Camag), 254 nm

Digestion coil FEP Teflon tubing (3.1 m , 0.5 mm i.d.)

$\text{K}_2\text{S}_2\text{O}_8$ 2% (m/v) in 2% (m/v) NaOH, (anion exchange) or 4% (m/v) in 4% (m/v) NaOH, (cation exchange)

Flow rate 1.35 ml min^{-1}

Hydride generation

HCl 4.4 mol l^{-1} , 3.0 ml min^{-1}

NaBH_4 1.5% (m/v) in 0.1% (m/v) NaOH, 3 ml min^{-1}

Argon (gas-liquid separator) 340 ml min^{-1}

Nitrogen (drying) 1 l min^{-1}

AFS

Detector Excalibur (PS Analytical, Kent, UK)

Lamp Arsenic, 189.04, 193.76 and 197.26 nm (Photron Pty. Ltd., Superlamp 803S)

Primary current 27.5 mA

Boost current 35 mA

Table 2
Arsenic speciation data for some reference materials.

Material	HPLC separation	Detection	Compounds reported ($\mu\text{g g}^{-1}$ dry weight)	Ref.
DORM 1	RP, gel permeation	ICP/MS	AsB (15.6), DMAA (0.60), TETRA (0.46), U ^a (0.41)	[11]
	Anion, cation exchange	ICP/MS	AsB (14.1), TETRA (0.34), TMAO (0.02), AsC (0.02), U ^a (0.41)	[15]
	Anion exchange	AAS	AsB (13.8), DMAA (0.39), TETRA (0.36), AsC (0.04), As(V) (0.21), MMAA (1.33), U ^a (0.31)	[17]
	Anion, cation exchange	ICP/MS	AsB (15.6), TETRA (0.38), AsC (0.04), U ^a (0.33)	[16]
	Anion exchange	UV-HG-ICP/OES	AsB (16.2), DMAA (0.66)	[13]
	Anion exchange	UV-HG-QFAAS	AsB (15.9), DMAA (0.83), U ^a (0.57)	[10]
	Anion exchange Ion exchange	ICP/AES INAA	AsB (16.5) AsB (15.9), DMAA (0.61)	[14] [12]
DOLT 1	RP, gel permeation	ICP/MS	AsB (5.69), DMAA (0.78), U ^a (0.80)	[11]
	Anion, cation exchange	ICP/MS	AsB (4.16), DMAA (1.64), TETRA (0.01), TMAO (0.04), AsC (0.02), As(V) (0.09), U ^a (0.54)	[15]
TORT 1	Anion, cation exchange	ICP/MS	AsB (16.0), DMAA (1.64), TETRA (0.05), TMAO (0.13), AsC (0.04), As(V) (0.09), U ^a (0.73), U ^{2a} (0.04)	[15]
	Anion, cation exchange	ICP/MS	AsB (16.1), DMAA (1.01), sugar 1 ^b (0.71), sugar 2 ^c (0.18)	[4]
NBS 1566a	Anion, cation exchange	ICP/MS	AsB (1.24), DMAA (1.69), As(V) (0.07), MMAA (0.04), TMAO (0.01), AsC (0.02), U ^a (1.3), U ^{2a} (0.01)	[15]
	Anion, cation exchange	ICP/MS	AsB (1.24), DMAA (0.86), sugar 1 ^b (1.13), sugar 2 ^c (1.22)	[4]
NIES No. 14	RP	ICP/MS	As(V) (nq ^d), sugar (sulphite form, nq ^d), sugar (sulphate form, nq ^d)	[19]
	RP	ICP/MS	As(V) (nq ^d), sugar 1 ^a (nq ^d), sugar 2 ^b (nq ^d), sugar (sulphite form, nq ^d), sugar (sulphate form, nq ^d)	[20]
NIES No. 15	RP	ICP/MS	AsB (nq ^d)	[19]
	RP	ICP/MS	AsB (nq ^d), 2 other compounds (nq ^d)	[20]

^a Unidentified compound.

^b Dimethylarsinyl-riboside, OH form.

^c Dimethylarsinyl-riboside, phosphodiester form.

^d Not quantified.

2.2. Extraction of As compounds from the sample

For preparation of the extract, 10 ml of a water–methanol mixture (1:1 for NIES candidate reference materials No. 14 and 15; 1:10 for other materials) was added to the sample (0.2–0.5 g). Although a water–methanol mixture of 1:10 is the preferred extractant for organoarsenic compounds, materials with high inorganic arsenic

content show poor extraction behaviour [23]. Yoshinaga [20] reported satisfactory extraction of arsenic compounds from NIES candidate reference materials No. 14 and 15 using a water–methanol mixture of 1:1. After sonication (60 min) and centrifugation (3000 rpm, 10 min), the extract was decanted. The procedure was repeated with the residual pellet and the two extracts were combined and dried using a rotary evaporator.

The dry residue was taken up in water (10 ml), filtered (0.45 μm) and kept frozen (-20°C) until analysis. For each reference material, three extracts were prepared. Extracts were analysed within one week of preparation to prevent changes in species [24]. For determination of the moisture content samples were weighed in a glass vial and dried (85°C) to constant weight (ca. 4 h).

2.3. Analysis

2.3.1. Total arsenic in solid materials

Total arsenic was determined by radiochemical

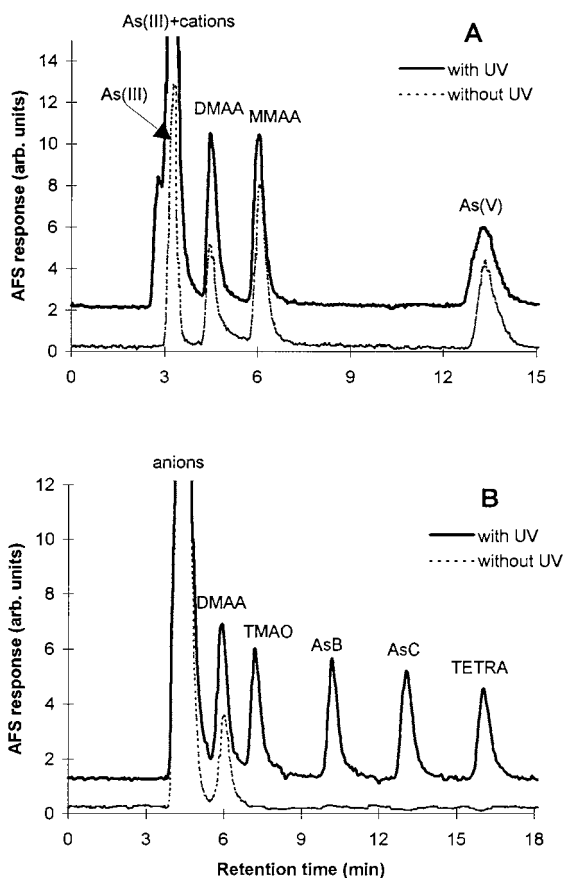


Fig. 1. Anion (A) and cation (B) exchange separation of a mixture of As(III), As(V), MMAA, DMAA, TMAO, AsB, AsC and TETRA (100 ng g^{-1} As each); for experimental details see Table 1.

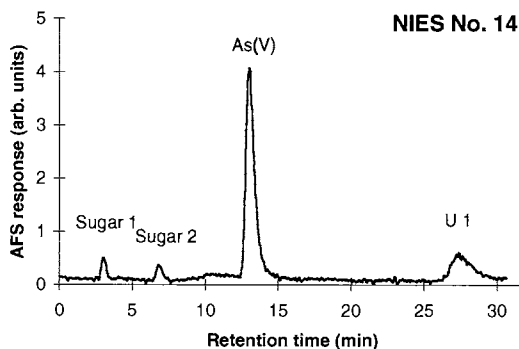
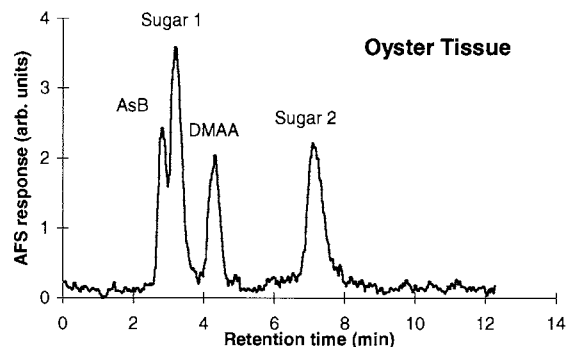


Fig. 2. Anion exchange separation of arsenic compounds in extracts of NBS SRM Oyster Tissue 1566a and NIES No. 14; sugar 1 is dimethylarsinyl-ribose, OH form and sugar 2 is dimethylarsinyl-ribose, phosphodiester form. For experimental details see Table 1 (with UV-decomposition).

neutron activation analysis (RNAA), employing mineralisation of the sample with a mixture of HNO_3 and H_2SO_4 followed by addition of H_2O_2 to complete the destruction of organic material, boiling, addition of KI, extraction of AsI_3 into toluene and measurement of the ^{76}As activity at 559 keV [25].

2.3.2. Total arsenic in extracts

Total arsenic in extracts was determined by HG-AFS (flow-injection mode) [26] after mineralisation of the sample similarly to the method described above. The arsenic in the acid digest was measured by the method of standard additions.

2.3.3. Separation and determination of arsenic compounds in extracts

A description of the HPLC-(UV)-HG-AFS system used can be found elsewhere [21,22]. A summary of experimental details is given in Table 1. Of the eight commonly used arsenic standard compounds only the anionic ones (As(III), As(V), MMAA and DMAA) form volatile hydrides, while the cationic ones are not (AsB, AsC and

TETRA) or only slightly (TMAO) susceptible to hydride generation and have to undergo UV-decomposition to be detectable. The method of standard additions was used for identification and quantification, i.e. anionic arsenic standards (for anion exchange chromatography) or cationic arsenic standards (for cation exchange chromatography) were added to aliquots of the extracts. Retention times of arsenic compounds could be (slightly) shifted as a result of matrix composition and of column ageing. For each of the three extracts, triplicate separation and quantification runs were made

3. Results and discussion

For the reference materials under study literature data have been reported for arsenic speciation (Table 2). The main speciation method used is ion exchange chromatography interfaced with ICP-MS. Arsenic compounds identified and quantified in the reference materials mentioned comprise AsB, DMAA, TETRA, AsC, TMAO, As(V), MMAA and two arsenosugars (dimethylarsinyl-riboside, OH and phosphodiester form); some unidentifiable compounds were found as well.

In arsenic speciation research generally up to eight commonly available standard arsenic compounds can be determined, whereas a few authors were able to quantify some arsenosugars as well. Since we have no access to these arsenosugars, with our HPLC-(UV)-HG-AFS system we quantified the eight arsenic standards. By combining anion exchange chromatography (without UV-decomposition) and cation exchange chromatography (with UV-decomposition) we are able to separate and detect the eight arsenic standards (Fig. 1A and B).

Additionally, two more arsenic compounds can be identified in the chromatogram by comparison with an extract of NBS oyster tissue (Fig. 2) in which two arsenosugars have been characterised previously (dimethylarsinyl-riboside, OH and phosphodiester form) [4,5]. Since these arsenosugars behave as anions under the conditions applied and do not form hydrides, they can only be

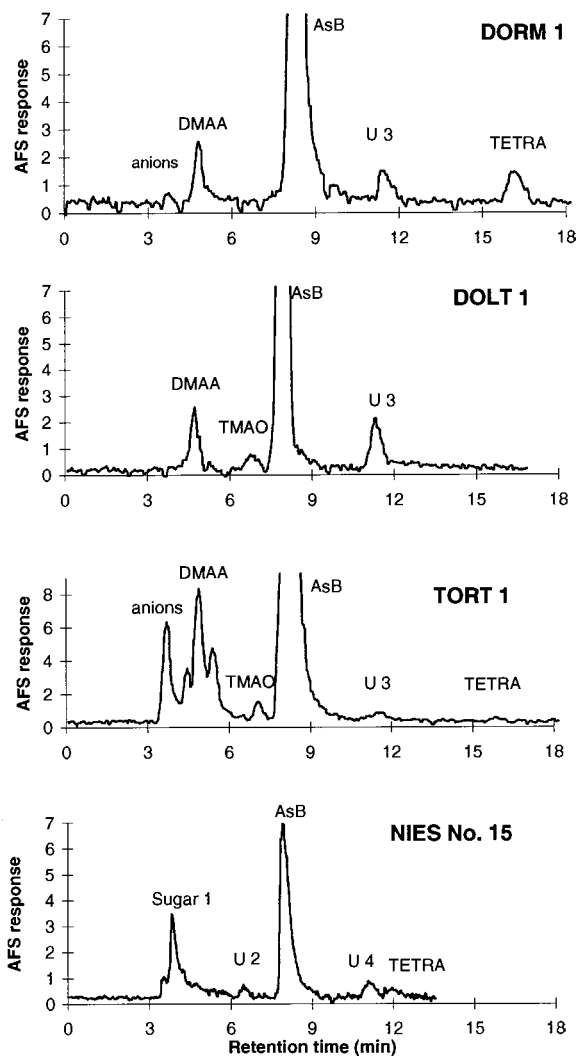


Fig. 3. Cation exchange separation of arsenic compounds in extracts of DORM 1, DOLT 1, TORT 1 and NIES No. 15; for experimental details see Table 1 (with UV-decomposition).

Table 3

Arsenic compounds detected in the reference materials and their positions in the anion or cation exchange chromatograms; the asterisk indicates that the compound is detectable with HG-AFS.

Arsenic compound	Capacity factor k'	Response (without UV)	Response (with UV)
<i>Anion exchange column</i>			
AsB, AsC, TMAO, TETRA, U? ^a	0		*
As(III)	0.08	*	*
Sugar 1 ^b	0.11		*
DMAA	0.50	*	*
MMAA	0.83	*	*
Sugar 2 ^c	1.50		*
As(V)	3.45	*	*
U 1 (Brown algae)	9.00		*
<i>Cation exchange column</i>			
As(V), As(III), MMAA, DMAA, U? ^d	0		*
DMAA	0.33		*
TMAO	0.94		*
U 2 (Scallop)	1.05		*
AsB	1.22		*
U 3 (DORM, DOLT, TORT)	2.28		*
AsC	2.42		*
U 4 (Scallop)	2.85		*
TETRA	3.50		*

^a Unknown cationic compounds which might elute in the void volume.

^b Dimethylarsinyl-riboside, OH form.

^c Dimethylarsinyl-riboside, phosphodiester form.

^d Unknown anionic compounds which might elute in the void volume.

separated and detected using anion exchange chromatography with UV-decomposition. Quantification of these arsenosugars, and also of unknown compounds, without authentic standards is not possible as the detector response depends on the degree of decomposition in the UV-reactor; different compounds show different decomposition behaviour [27]. This implies that for speciation of arsenic in the reference materials in this study the contribution of the two arsenosugars and unknown compounds can only be roughly estimated by evaluation of the peak area relative to the total area under the chromatogram.

The ion exchange chromatograms of the other reference materials are given in Figs. 2 and 3; in Table 3 the peak positions and detectability of all arsenic compounds found are summarised. Table 4 shows our data for the arsenic compounds quantified and other arsenic compounds detected. From Table 4 it can be seen that the extractability of arsenic is 57% (Oyster tissue) to 95% (DORM

1). Of the arsenic extracted 30% (Oyster tissue) to 100% (TORT 1) can be assigned to particular compounds, depending on the arsenic species present in the reference materials; the remainder of the extractable arsenic can be attributed to arsenosugars and unknown compounds. A visualisation of the comparison of our results (Table 4) with indicative literature data (Table 2) for five arsenic compounds in DOLT1, DORM1, TORT1 and NBS 1566a is given in Fig. 4. A regression line with a slope of 1 is an indication of a perfect correlation; an overall regression line with a slope of 0.90 ± 0.02 and an intercept of 0.16 ± 0.19 was found ($R^2 = 0.988$). Regarding the variation in the literature data (shown as a spread in vertical data) the slope found suggests a good correlation, especially taking into account that at least one of the AsB outliers in the plot (indicated with an arrow) was questioned in a recent publication [16]. It is obvious that the HPLC-(UV)-HG-AFS system used in this investigation generates data

similar to that of other hyphenated speciation systems with different set-ups.

4. Conclusions

The performance of the HPLC-UV-HG-AFS system with anion and cation exchange column was suitable for the identification and quantification of eight arsenic compounds available as standards. Data generated with this system were comparable with the ones obtained with the more expensive HPLC- ICP/MS set-ups.

Due to a lack of (commercially) available arsenic standards only partial speciation of arsenic in reference materials was possible, although the system was capable of separation of at least six more compounds. The major findings of this study were in agreement with work done by other workers on the same materials.

The preparation of certified reference materials for arsenic compounds should be given the highest priority to verify the accuracy of the speciation procedures presently in use or under development in many laboratories.

Acknowledgements

The authors would like to thank Dr M. Horvat for stimulating this research, Dr J. Yoshinaga for donating the NIES candidate reference materials, Dr M. Rossbach for donating the NBS SRM 1566a, J. Smrke for total arsenic analyses with RNAA and Professor J.J.M. de Goeij for constructive discussions. The Ministry of Science and Technology of the Republic of Slovenia is acknowledged for the financial support of the projects J1-7268-0106-96 and J1-8907-0106-97.

Table 4

Concentrations (in $\mu\text{g g}^{-1}$ dry weight) of total arsenic, extractable arsenic and arsenic compounds and estimations (in % of total area under chromatogram) of arsenosugars and unknown compounds in reference materials. Three parallel extracts of each reference material were prepared and each was analysed in triplicate

Found	DOLT 1	DORM 1	TORT 1	NBS 1566a	NIES No. 14	NIES No. 15
Total As, $\mu\text{g g}^{-1}$	10.1 ± 1.4^a	17.7 ± 2.1^a	24.6 ± 2.2^a	13.4 ± 1.9^a	74.1 ± 6.9^b	3.29 ± 0.19^b
Extractable As, $\mu\text{g g}^{-1}$	6.3 ± 0.5	16.7 ± 1.9	19.6 ± 1.7	7.6 ± 0.4	50.7 ± 4.1	2.84 ± 0.23
Quantified As compounds, $\mu\text{g g}^{-1}$						
As(III)	<0.02	<0.02	<0.02	<0.03	<0.01	<0.02
DMAA	0.69 ± 0.03	0.64 ± 0.03	1.20 ± 0.05	1.05 ± 0.04	<0.01	<0.02
MMAA	Traces	Traces	Traces	<0.03	<0.01	<0.02
As(V)	0.05 ± 0.02	<0.02	0.39 ± 0.03	<0.04	26.9 ± 1.7	<0.02
TMAO	0.11 ± 0.02	Traces	0.17 ± 0.06	<0.06	<0.02	<0.04
AsB	4.63 ± 0.32	16.5 ± 0.6	19.5 ± 1.5	1.26 ± 0.09	<0.02	2.59 ± 0.34
AsC	<0.04	<0.04	<0.04	<0.06	<0.02	<0.04
TETRA	<0.04	0.49 ± 0.04	Traces	<0.06	<0.02	Traces
Other As compounds detected, % of total area under chromatogram						
sugar 1 ^c	–	–	–	25%	3%	< 10%
sugar 2 ^d	–	–	Traces	30%	3%	–
U 1	–	–	–	–	30%	–
U 2	–	–	–	–	–	Traces
U 3	7%	2%	0.5%	–	–	–
U 4	–	–	–	–	–	Traces

^a Certified value.

^b Determined by RNAA.

^c Dimethylarsinyl-riboside, OH form.

^d Dimethylarsinyl-riboside, phosphodiester form.

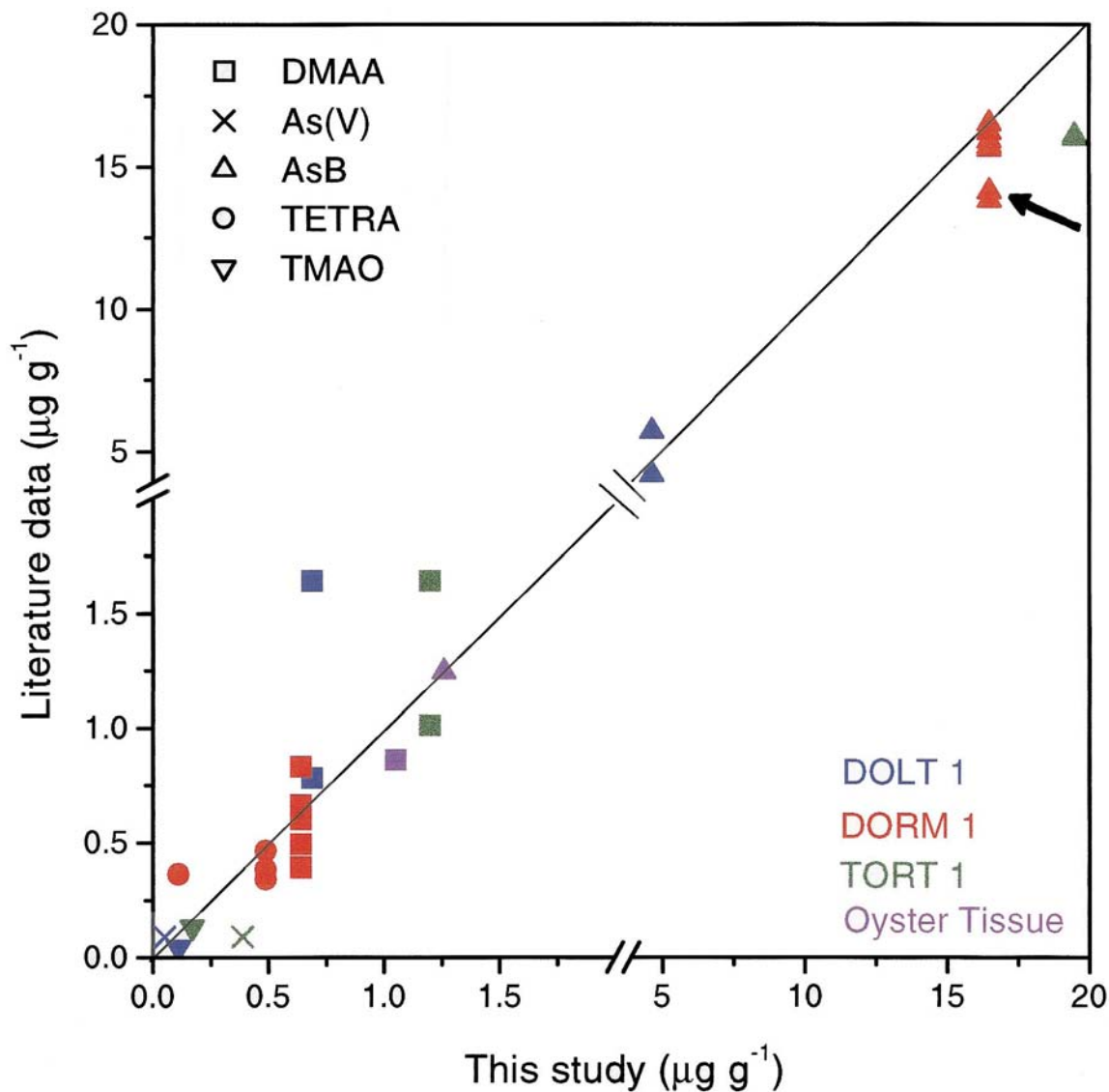


Fig. 4. Comparison of data from this study with data reported in literature; a regression line for a perfect correlation (slope = 1) has been drawn. Colours refer to the standard reference materials and symbols to arsenic compounds.

References

- [1] K. Francesconi, J.S. Edmonds, *Adv. Inorg. Chem.* 44 (1997) 147.
- [2] D.J.H. Phillips, *Aquatic Toxicol.* 16 (1990) 151.
- [3] Y. Shibata, M. Morita, *Appl. Organomet. Chem.* 6 (1992) 343.
- [4] E.H. Larsen, *Fresenius J. Anal. Chem.* 352 (1995) 582.
- [5] X.C. Le, W.R. Cullen, K.J. Reimer, *Environ. Sci. Technol.* 28 (1994) 1598.
- [6] M. Ma, X.C. Le, *Clin. Chem.* 44 (1998) 539.
- [7] X.C. Le, M. Ma, *Anal. Chem.* 70 (1998) 1926.
- [8] J.L. Gomez-Ariza, D. Sanchez-Rodas, R. Beltran, W. Corns, P. Stockwel, *Appl. Organomet. Chem.* 12 (1998) 439.
- [9] R. Ritsema, L. Dukan, T.R. i Navarro, W. van Leeuwen, N. Oliveira, P. Wolfs, E. Leuret, *Appl. Organomet. Chem.* 12 (1998) 591.
- [10] R. Rubio, J. Alberti, A. Padro, G. Rauret, *TRAC* 14 (1995) 274.

- [11] Y. Shibata, M. Morita, *Anal. Chem.* 61 (1989) 2116.
- [12] A.R. Byrne, Z. Šlejkovec, T. Stijve, L. Fay, W. Goessler, J. Gailer, K.J. Irgolic, *Appl. Organomet. Chem.* 9 (1995) 305.
- [13] J. Alberti, R. Rubio, G. Rauret, *Fresenius J. Anal. Chem.* 351 (1995) 415.
- [14] N. Ybáñez, D. Velez, W. Tejedor, R. Montoro, *J. Anal. Atom. Spectrom.* 10 (1995) 459.
- [15] E.H. Larsen, G. Pritzl, S.H. Hansen, *J. Anal. Atom. Spectrom.* 8 (1993) 1075.
- [16] W. Goessler, D. Kuehnelt, C. Schlagenhafen, Z. Šlejkovec, K.J. Irgolic, *J. Anal. At. Spectrom.* 13 (1998) 183.
- [17] G. Momplaisir, T. Lei, W.D. Marshall, *Anal. Chem.* 66 (1994) 3533.
- [18] J. Yoshinaga, M. Morita, K. Okamoto, *Fresenius J. Anal. Chem.* 357 (1997) 279.
- [19] K. Okamoto, J. Yoshinaga, M. Morita, *Mikrochim. Acta* 123 (1996) 15.
- [20] J. Yoshinaga, Y. Shibata, T. Horiguchi, M. Morita, *Accred. Qual. Assur.* 2 (1997) 154.
- [21] Z. Šlejkovec, J.T. van Elteren, A.R. Byrne, *Anal. Chim. Acta* 358 (1998) 51.
- [22] Z. Šlejkovec, J.T. van Elteren, A.R. Byrne, J.J.M. de Goeij, *Anal. Chim. Acta* 380 (1998) 63.
- [23] Z. Šlejkovec, A.R. Byrne, T. Stijve, W. Goessler, K.J. Irgolic, *Appl. Organomet. Chem.* 11 (1997) 673.
- [24] M.A. Palacios, M. Gómez, C. Cámara, M.A. López, *Anal. Chim. Acta.* 340 (1997) 209.
- [25] A.R. Byrne, A. Vakselj, *Croatica Chem. Acta* 46 (1974) 225.
- [26] J.T. van Elteren, Z. Šlejkovec and H.A. Das, *Spectrochim. Acta B* 54 (1999) 311.
- [27] Z. Šlejkovec, J.T. van Elteren, A.R. Byrne, *Acta Chim. Slov.* 44 (1997) 225.

pH-Metric determination of acid values in oilseeds without titration

I. Kuselman *, Ya.I. Tur'yan, T. Burenko, I. Goldfeld, B. Anisimov

The National Physical Laboratory of Israel, Danziger 'A' Bldg., The Hebrew University, Givat-Ram, Jerusalem 91904, Israel

Received 30 November 1998; received in revised form 25 January 1999; accepted 26 January 1999

Abstract

A new pH-metric method for determination of acid values in oilseeds without titration has been developed in the range 0.6–10 and more mg KOH/g. The method is based on a rapid (1–2 min) selective and complete extraction of free fatty acids from an oilseed test portion into a special reagent A, separation of the solution from the solid oilseed material by centrifugation or filtration, transfer of an aliquot of the solution into a pH-metric cell with reagent B for measurement of conditional pH'_1 of the formed mixture, addition of standard acid (HCl or H_2SO_4) and pH'_2 measurement. The reagents are non-toxic, and the method is rapid. Its metrological parameters for Soybean, Canola and Sunflower oilseeds are satisfactory for practical purposes. © 1999 Elsevier Science B.V. All rights reserved.

Keywords: Acid value; Oilseeds; pH-metry; Metrological parameters

1. Introduction

Acid value (AV) is an important index of oilseed quality. AV is expressed by KOH (mg) necessary for titration of the free fatty acids (FFA) contained in 1 g oil in oilseeds. The standard method for AV determination [1,2] is based on the extraction of oil from oilseeds by hexane using Soxhlet during 4 h or more, and then acid–base titration of the FFA in the non-aqueous system. An alternative pH-metric method without titration for AV determination in oilseeds has been developed [3]. It was based on the use of a special

reagent for rapid extraction of FFA. The reagent consisted of triethanolamine (TEA) dissolved in the mixture of diethyl ether + ethanol + water. A review of such methods was published by us in [4] (see also Ref. [5]). The extraction of FFA in Ref. [3] was carried out directly from the oilseed in the pH-metric cell. However, in this way, other acids (for example, probably from proteins) were extracted simultaneously. To obtain results of AV determination close to those from the standard titration, the pH measurements were done after a limited time of the extraction. That is why the method could not assure reproducible results. Later, we proposed extraction of the FFA and possible other acids in reagent A consisting of TEA dissolved in isopropanol + heptane + water

* Corresponding author. Tel.: +972-2-6536-534; fax: +972-2-6520-797.

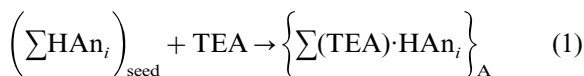
E-mail address: kuselman@netvision.net.il (I. Kuselman)

solvent [6]. From this mixture, FFA were displaced into heptane phase by sulfuric acid addition [7,8]. An aliquot of the heptane phase was then introduced into the pH-metric cell in another reagent, B, for pH-metric AV determination. Reagent B consisted of TEA in isopropanol + water solvent. The drawbacks of this technique are caused by incomplete FFA re-extraction into the heptane phase (included, partly, isopropanol and water traces) and sulfuric acid penetration in this phase instead of FFA. Such substitution can be one reason for problems with accuracy of the AV determination. In the present work, these drawbacks were overcome, and a new pH-metric method for the acid value determination in oilseeds without titration with satisfactory metrological characteristics is described.

2. Principles

To decrease the probability of extraction of other acids besides FFA, the polarity of the solvent in reagent A [6] and the TEA concentration in it were minimized with maintaining the reagent homogeneity [9]. Thus, the new reagent A consists of 0.06 M TEA in the solvent 55.7% isopropanol + 42.9% heptane + 1.4% water (throughout, percent is volumetric if not otherwise indicated).

Reagent A ensures rapid (1–2 min), complete and selective extraction of FFA from an oilseed according to the following scheme:

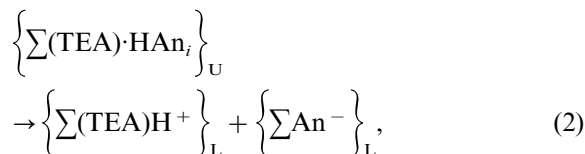


where HAn_i is i -th free fatty acid; $\{\sum (\text{TEA}) \cdot \text{HAn}_i\}_{\text{A}}$ is the corresponding TEA salt in reagent A, partly or completely dissociated. Therefore, the use of reagent A proposed here eliminates the necessity of FFA separation from other acids by their re-extraction to the heptane phase as it was proposed earlier [6–8].

For pH-metric determination of AV, we used reagent B: 0.2 M TEA + 0.01 M KNO_3 in the solvent 50% isopropanol + 50% water. This reagent was developed by us [10] for pH-metric determination of AV in vegetable oils. This technique was adopted by AOAC International as a

peer-verified one [11]. At the contact of reagent B with an aliquot of reagent A, the TEA salts $\{\sum (\text{TEA}) \cdot \text{HAn}_i\}$ are transferred from reagent A to reagent B, and pH-metric determination of their sum, i.e. AV, in isopropanol–water phase, becomes possible. Because reagent B contains a high concentration of water and has increased polarity, extraction of the other acids besides FFA at its contact with the oilseed material must be avoided. Therefore, the oilseed material is removed from reagent A by centrifugation or filtration before the aliquot of reagent A is added to reagent B.

At mixing of reagent A aliquot with reagent B, their composition and volumes are changed and two phases are formed: instead of reagent B, the lower isopropanol + water phase is formed (defined by index ‘L’), and instead of reagent A, the upper heptane phase (defined by index ‘U’). If the transfer of the TEA salts from phase U into phase L is complete:



the concentration of TEA salts in phase L $\{\sum (\text{TEA})\text{H}^+\}_{\text{L}}$ is equivalent to the FFA concentration N_a . In buffer mixture TEA + $(\text{TEA})\text{H}^+$ in phase L at TEA high excess, in comparison to the sum of FFA, the following dependence takes place [10,11]:

$$\text{pH}' = A - \lg N_a \quad (3)$$

where pH' is conditional pH because pH-measurements are carried out with an aqueous reference electrode and glass working electrode calibrated by usual aqueous buffer solutions; A is a constant for the specific pH-sensor, TEA concentration and ionic strength regulated by KNO_3 addition.

Using the method of standard additions (for example, H_2SO_4 addition), the calculation of the AV in the oilseed sample is carried out on the basis of Eq. (4):

$$\begin{aligned} \text{AV} &= (\text{AV})_{\text{al}} \times V/V_{\text{al}} \quad \text{and} \\ (\text{AV})_{\text{al}} &= (56.1 \times 100 \times N_{\text{st}} \times V_{\text{st}}) \\ & \quad / [G \times P \times (10^{\Delta \text{pH}} - 1)] \end{aligned} \quad (4)$$

Table 1
Mass of test portion of oilseeds

Expected AV (mg KOH/g)	Mass (g)
0.6–2	5–10
2–5	2–5
5–10	1–2
>10	<1

where $(AV)_{al}$ is the acid value corresponding to the aliquot of reagent A used for pH measurements (mg KOH /g); V is the total volume of reagent A contacted with the oilseed test portion (30 ml); V_{al} is the volume of the aliquot of reagent A (mL); 56.11 is the molecular weight of KOH; N_{st} is the concentration of H_2SO_4 solution used for the standard acid addition (0.1 N); V_{st} is the volume of the standard acid addition (mL), which is considerably less than volume of phase L (~ 60 mL); G is the mass of the oilseed test portion (g); P is the oil content in the oilseed (%); $G \times P/100$ is the analyzed oil mass (g); $\Delta pH = pH'_1 - pH'_2$, where pH'_1 is the pH' of reagent B after addition of the aliquot of reagent A with the extracted FFA salts, and pH'_2 is the pH' after the following addition of the standard acid.

3. Experimental

3.1. Apparatus

Coffee grinder (SEB, France), Drying oven (Tuttenauer, Israel), pH-Meter (Metrohm 744) (resolution, ± 0.01 pH) with glass working elec-

trode 6.0133.100 and reference Ag/AgCl electrode (Shwitzerland). Gas chromatograph with flame-ionization detector HP 5880A (USA) and fused-silica capillary column FFAP CB, $L = 25$ m, $d = 0.32$ mm, $d_f = 0.30$ μ m from Crompack (Holland). Disposable test-tube for centrifugation, graduated capacity 50 ml from Medical Products (Israel). Mechanical hand pipetters up to 5 ml from Gilson (France). Analytical balance with uncertainty ± 0.0002 g (Sartorius 2400, Germany). Centrifuge from MSE (USA). Mixer Reax 2000 from Heidolph (Germany).

3.2. Reagents

TEA was supplied by Fluka (Switzerland). *n*-Heptane, *n*-hexane, diethyl ether, ethanol, isopropanol and potassium hydroxide were from Frutaron (Israel). Sulfuric acid was from Palacid (Israel); Oleic acid was from Merck (Germany). Boron trifluoride methanol complex and buffers at pH 7.00 and 9.22 were from BDH (UK). Potassium chloride and nitrate were from Baker (NY). The oilseeds (Sunflower, Soybean and Canola) were purchased from local suppliers. Heptadecanoic acid, methyl ester, Oil reference standards AOCS No.1, 3 and for Low Erucic Rapeseed Oil were from Sigma (USA).

3.3. Procedures

3.3.1. Reagent A preparation

TEA (7.46 g) was dissolved in 500 ml of the mixture 97.5% isopropanol and 2.5% water. This solution was then mixed with 375 ml of *n*-heptane.

Table 2
Influence of the time of FFA extraction on the results of pH-metric AV determination

Time of extraction (min)	Soybean		Canola	
	Mass (g)	AV (mg KOH/g)	Mass (g)	AV (mg KOH/g)
1	2.4919	1.7	2.6176	4.7
2	2.5064	2.1	2.5168	4.5
3	2.5665	1.9	2.5908	4.4
5	2.5722	2.0	3.1100	4.8
10	–	–	2.8494	4.7

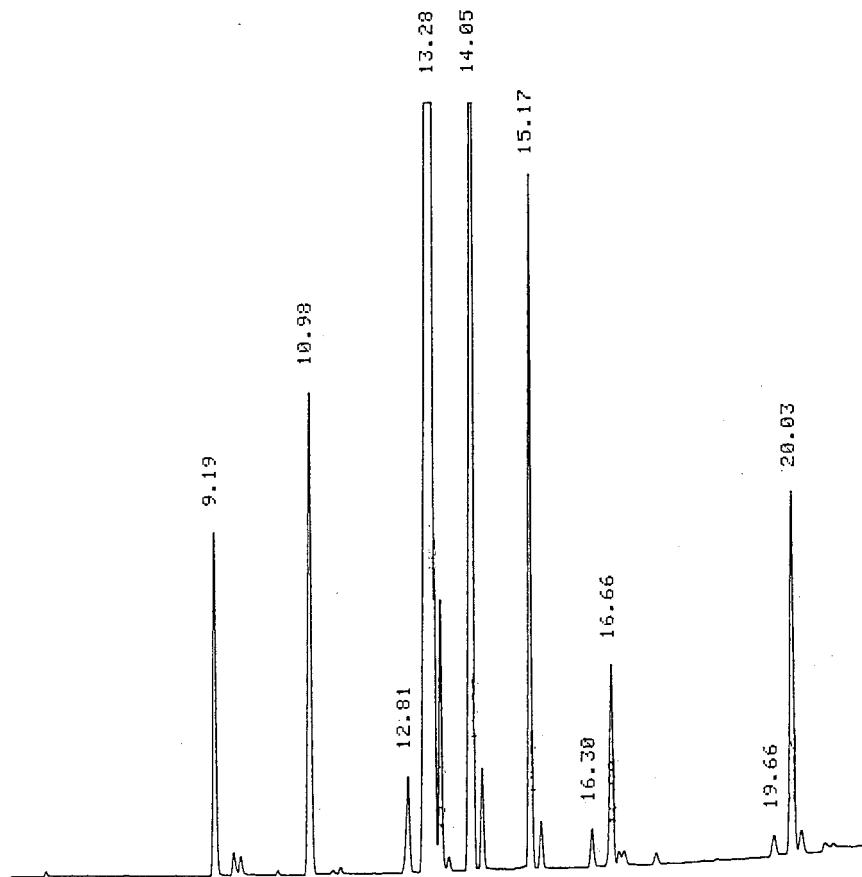


Fig. 1. Gas chromatogram of free fatty acids extracted from the canola sample. The numbers in the chromatogram are the retention time (min): in accordance with the time, there are peaks of palmitic, heptadecanoic (internal standard), stearic, oleic, linoleic, linolenic, arachidic, *cis*-eicosenoic, behenic and erucic acids.

3.3.2. Reagent B preparation

KNO_3 (1.0 g) and TEA (29.8 g) were dissolved in the 1 l solvent 50% water + 50% isopropanol. A small amount of aqueous 0.1 M KOH was added to the indicated solution to reach $\text{pH}'_0 = 11.30 \pm 0.05$ for neutralization of CO_2 traces.

3.3.3. System suitability test

The pH measurement system suitability was tested by the control of the dependence of conditional pH' versus logarithm of concentration of the standard (sulfuric) acid added into reagent B. With that aim in view, 100, 100, 200, 400 and 800 μl of 0.1 N H_2SO_4 were introduced subsequently in 50 ml of reagent B in the pH-metric cell and the

corresponding pH'_1 , pH'_2 , pH'_3 , pH'_4 and pH'_5 were measured. The test was successful if the differences $\text{pH}'_1 - \text{pH}'_2$, $\text{pH}'_2 - \text{pH}'_3$, $\text{pH}'_3 - \text{pH}'_4$ and $\text{pH}'_4 - \text{pH}'_5$ are 0.30 ± 0.02 in analogy with Eq. (3).

3.3.4. Sample preparation

Dry oilseeds were ground in the coffee grinder until homogeneous meal state. Oilseed sample should be not less than 15–20 g (for two, three or more test portions). Recommended masses of a test portion for oilseeds with minimal oil content $P = 20\%$ are shown in Table 1 (a greater mass corresponds to a lesser expected AV). If $P > 20\%$, the recommended mass of the test portion in Table 1 is decreased $P/20$ times.

3.3.5. Standard procedures

The oil contents in the oilseed samples were determined by the standard extraction technique [2], and the AV values were obtained by the standard titration technique [1]. These AV values were assumed to be correct ('true') ones.

3.3.6. Chromatographic procedures

For comparison the FFA extracted by reagent A according to the new method and by hexane according to the standard gas chromatographic technique [2], after FFA derivatization to methyl esters with $\text{BF}_3/\text{CH}_3\text{OH}$ [12] was used. The chromatograms were recorded at an oven temperature from 170°C (hold 5 min) to 250°C with a gradient of 5°C/min (hold 30 min); carrier gas helium at a flow rate of 0.8 ml/min; injector

temperature was 280°C, detector temperature was 300°C.

3.3.7. Determination of the distribution coefficient

To study the equilibrium distribution of TEA and its salts $\text{TEA}\cdot\text{HAN}_i$, the salt of TEA and oleic acid $\text{TEA}\cdot\text{HOI}$ was used.

The distribution coefficient K_i is the ratio of the equilibrium concentrations of TEA and $\text{TEA}\cdot\text{HOI}$ (mol/l), in the upper heptane phase C_i^U and the lower isopropanol–water phase C_i^L , correspondingly:

$$K_i = C_i^U / C_i^L \quad (5)$$

where i is TEA or $\text{TEA}\cdot\text{HOI}$.

For the determination of K_i values, concentrations of TEA and $\text{TEA}\cdot\text{HOI}$ were determined in

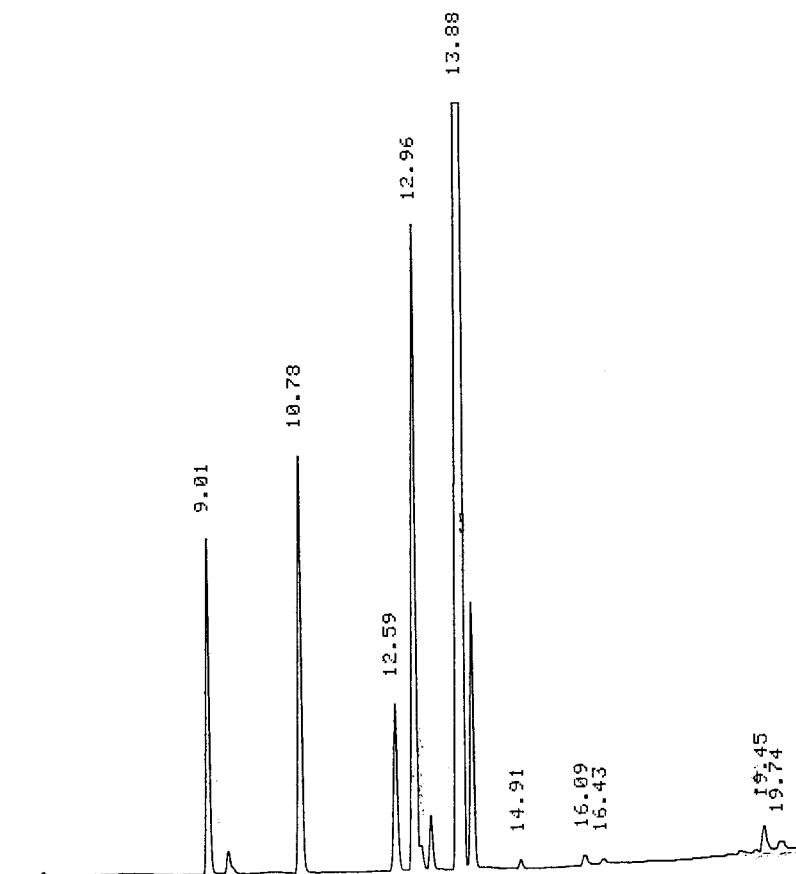


Fig. 2. Gas chromatogram of free fatty acids extracted from the sunflower sample. The acids are the same as in Fig. 1.

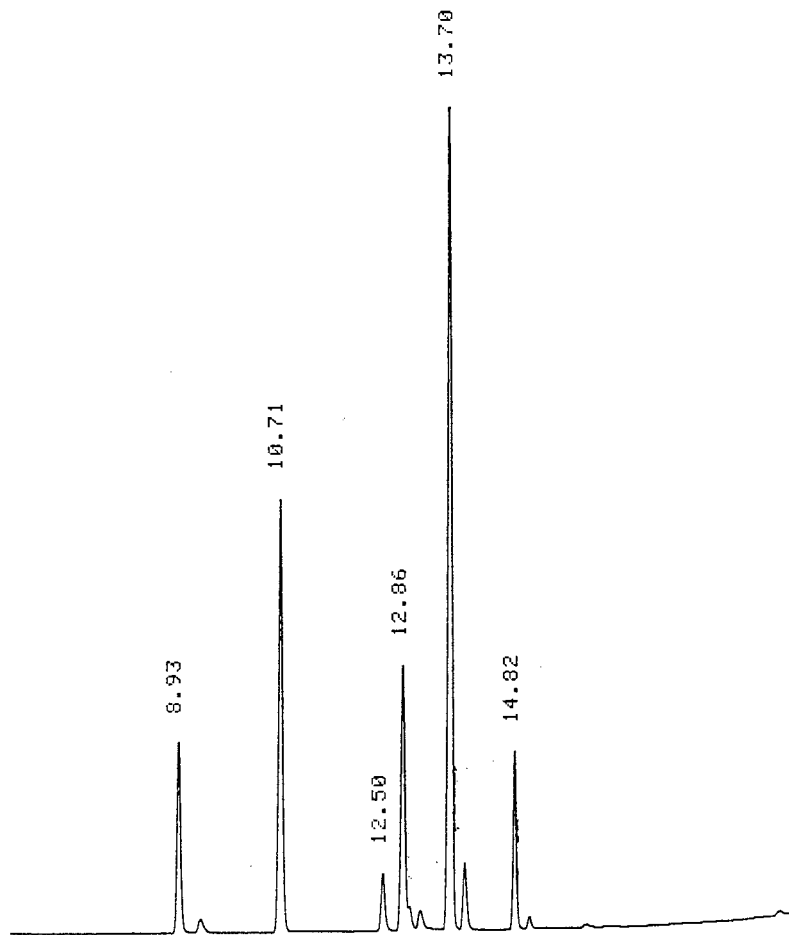


Fig. 3. Gas chromatogram of free fatty acids extracted from the soybean sample. The acids are the same as in Fig. 1.

the upper and lower phases of the mixture of 50 ml reagent B, $(20 - X)$ ml reagent A and X ml of the following solution: 0.26 M TEA + ~ 0.20 M HOI dissolved in the solvent 55.7% isopropanol + 42.9% heptane + 1.4% water. The X values were 0.5, 1.0 and 2.5 ml.

The TEA·HOI equilibrium concentrations (after intensive shaking for 1–3 min) were determined by titration of $(\text{TEA})\text{H}^+$ against KOH by analogy with the standard [1]. The equilibrium concentrations of free TEA were found by titration against H_2SO_4 solution with the methyl-orange indicator.

The equilibrium composition and volumes of the phases were calculated from the data obtained by Vorob'eva and Karapet'yants [9].

3.3.8. pH-Metric procedure

Thirty milliliters of reagent A are added to a disposable test-tube with an oilseed test portion. The test-tube is closed and shaken intensively with the mixer or by hand for 1–2 min. After that, the test-tube is centrifuged during 1 or 2 min for the phase separation (filtration can be used for this purpose also). An aliquot of the upper liquid phase (5–20 ml) is removed from the test-tube using a mechanical pipetter into the pH-metric cell. Approximately 50 ml of reagent B are added into the cell and a stirrer is turned on to provide a good mixing of the components and to assure extraction of salts of free fatty acids with triethanolamine from the aliquot into the phase of reagent B.

Table 3

Composition of free fatty acids extracted from oilseeds by reagent A (new method) and by hexane (standard procedure)^a

Free fatty acids	Canola oilseeds		Sunflower oilseeds		Soybean	
	New method (%)	Standard method (%)	New method (%)	Standard method (%)	New method (%)	Standard method (%)
Palmitic	4.2	4.4	6.7	7.1	11.9	13.1
Stearic	1.6	1.4	4.0	4.0	4.0	3.7
Oleic	57.2	56.4	17.2	16.2	19.6	13.8
Linoleic	19.2	20.9	70.7	71.7	54.5	58.2
Linolenic	9.2	10.2	0.1	n.d.	10.0	11.2
Arachidic	0.5	0.6	0.2	0.2	n.d.	n.d.
<i>cis</i> -Eicosenoic	2.5	2.2	0.3	n.d.	n.d.	n.d.
Behenic	0.3	n.d.	0.7	0.5	n.d.	n.d.
Erucic	5.4	4.0	0.1	0.3	n.d.	n.d.

^a % is the peak area of the acid in percent of total peak area on the chromatogram; n.d. is not detected.

The electrodes are introduced into the cell with reagent B and the aliquot, and after 1–2 min stable pH'_1 is read. Then a certain volume (0.2 ml or other) of the standard 0.1 N H_2SO_4 aqueous solution is added through stirring during 1 min and stable pH'_2 is read. The optimal standard acid addition should assure $\Delta\text{pH} = \text{pH}'_1 - \text{pH}'_2 \approx 0.25 - 0.35$ [13].

The calculation of the AV in the oilseed sample is carried out according to Eq. (4). Corresponding uncertainty of the AV was considered by us earlier [13].

3.3.9. Fortification procedure

A fortified sample is prepared from an i -th test portion (G_i , g) of the previously analyzed oilseed sample (initial sample). The 0.1 M oleic acid in heptane is added to this test portion in test-tube before introduction of reagent A. The volume of the oleic acid solution (V_{oa} , ml) should be calculated assuming that the AV_f in the fortified sample is n times greater than AV_i in the initial sample (i.e. $\text{AV}_f = n\text{AV}_i$):

$$V_{\text{oa}} = 2 \times 10 \times G_i \times P \times \text{AV}_i / [C_{\text{oa}} \times M_{\text{oa}} \times (199 - n \times \text{AV}_i)]$$

$$= 0.708 \times G_i \times P \times \text{AV}_i / (199 - n \times \text{AV}_i) \quad (6)$$

where M_{oa} and C_{oa} are the molecular weight (g) and concentration (0.1 M) of oleic acid, 199 is the

ratio between molecular weights of potassium hydroxide and oleic acid multiplied by 1000.

The first sample of Canola oilseed fortified in this way is intended to have AV 1.5 times ($n = 1.5$) higher than in the initial purchased oilseed, the second fortified sample, AV 2.0 times ($n = 2$) higher than in the initial oilseed. For Soybean and Sunflower oilseed, the fortification procedure should assure a three ($n = 3$) and six ($n = 6$) times increase of initial AV: first and second fortified samples, correspondingly. The n values for Canola oilseeds are less because of large AV of the purchased sample.

Table 4

Coefficient of the distribution of TEA·HOI between upper (heptane) and lower (water+isopropanol) phases and the part of the salt (%) remaining in the upper phase^a

C_s^o (M)	C_s^U (M)	C_s^L (M)	K_s	% of salt
5.90×10^{-3}	2.25×10^{-4}	1.86×10^{-3}	0.12	1.4
1.20×10^{-2}	4.68×10^{-4}	3.71×10^{-3}	0.13	1.5
1.20×10^{-2}	4.95×10^{-4}	3.74×10^{-3}	0.13	1.6
2.90×10^{-2}	1.21×10^{-3}	9.11×10^{-3}	0.13	1.6

^a C_s^o is the TEA·HOI concentration in the mixture of reagent A and solution of TEA and HOI; C_s^U is the equilibrium concentration of the TEA·HOI in the upper phase; C_s^L is the equilibrium concentration of the TEA·HOI in the lower phase.

Table 5
Recovery values for fortified oilseed samples^a

Oilseed	Sample number	AV _i (mg KOH/g)	G _i (g)	V _{oa} (ml)	AV _f (mg KOH/g)	Recovery (%)
Canola	1	4.75	2.1998	0.333	7.07	101
	2	4.75	2.0826	0.641	9.22	94
Soybean	1	1.01	3.4655	0.179	3.25	108
	2	1.01	1.5294	0.326	9.37	99
Sunflower	1	1.04	4.4526	0.822	3.12	103
	2	1.04	4.5208	3.548	9.38	96

^a AV_i is the AV of the initial oilseed sample; G_i is the mass of the oilseed test portions; V_{oa} is the volume of the oleic acid solution (0.1 M) added to the test portion; AV_f is the AV of the fortified sample.

4. Results and discussion

4.1. Extraction of free fatty acids and interphase distribution

To study the influence of the time of FFA extraction from an oilseed in the new method on the result of the AV determination, the experiment was performed with samples of Soybean and Canola (Table 2). AV of the samples determined by the standard technique [1,2] are for Soybean, 1.8 mg KOH/g, and for Canola, 4.7 mg KOH/g. As can be seen from Table 2, after 1–2 min extraction, the results of the AV determination by the new method do not differ from the results obtained by the standard ones. So, the concentrations of extracted acids in the two methods are equivalent. Further contact of the oilseeds with reagent A after 1–2 min does not influence the results of the extraction. Identity of extracted acids is confirmed by comparison of the chromatograms of FFA extracted in reagent A and in hexane (after the Soxhlet extraction during 4 h [2]). Visually they are the same. Therefore, chromatograms are shown in Figs. 1–3 only for reagent A. Detailed analysis of ratios between FFA concentrations ('profiles' of the chromatograms) is described in Table 3. The 'profiles' are close. Thus, chromatographic data confirm also selectivity and completeness of the FFA extraction from oilseeds by reagent A.

After introduction of an aliquot of reagent A (20 ml) in reagent B (50 ml), the equilibrium is achieved during 1 and 2 min between the two phases: upper heptane and lower isopropanol–

water ones. The composition of these phases is calculated by us using the data by Vorob'eva and Karapet'yants [9]: the upper phase consists of 89.7% heptane + 9.7% isopropanol + 0.6% water, and the lower one is 1.8% heptane + 50.8% isopropanol + 47.4% water. The volume of the upper phase is 7.5 ml and the lower phase is 62.5 ml.

The distribution coefficients for TEA, $K_{\text{TEA}} = 0.015$ (see Section 3.3.7) and for TEA·HOI, $K_s = 0.13$ were determined by us using TEA and TEA·HOI equilibrium concentrations (mol/l) shown in Table 4. The correlation $K_s > K_{\text{TEA}}$ is caused by the effect of the affinity of TEA·HOI to the low-polar reagent A due to HOI. The distribution coefficient of TEA·HOI allows one to make the conclusion about the practically complete extraction of the FFA from the upper (heptane) phase to the lower (isopropanol–water) phase in which pH measurements are performed.

Unlike the heptane phase differing from initial reagent A, the composition of the isopropanol–

Table 6
Comparison of the results of acid value determination by the standard and the new methods^a

Oilseeds	AV _{new}	S _{new}	AV _{st}	S _{st}	F	t
Canola	4.75	0.10	4.68	0.12	1.44	1.59
Soybean	0.98	0.04	1.01	0.05	1.56	1.65
Sunflower	1.04	0.05	1.01	0.06	1.44	1.36

^a AV_{new} and AV_{st} are the average results obtained by the new and the standard methods; S_{new} and S_{st} are the standard deviations characterizing repeatability of the results obtained by the new and the standard methods; F is the Fisher's ratio, t is the Student's ratio.

water phase and of initial reagent B are close. Therefore, properties of reagent B for the AV pH-metric determination [10,11] are maintained: the pH' versus $\lg N_a$ dependence (Eq. (3)) is linear with the slope equal to one.

4.2. Metrological parameters

Since for the new method accuracy demonstration is most important, recovery values averaged for 20 oilseed test portions are shown in Table 5 as an index of accuracy. These values are more and also less than 100%. To be sure that the deviations from 100% are acceptable (accuracy is satisfactory), an additional experiment was performed.

The experiment consisted of $n_{st} = 10$ replicate AV determinations by the standard method during a day, and of $n_{new} = 20$ determinations by the new method, four replicates per day during a week (5 days). Table 6 shows the average results obtained by the standard AV_{st} and new AV_{new} methods; standard deviations of the replicates, S_{st} and S_{new} with $f_{st} = n_{st} - 1 = 9$ and $f_{new} = n_{new} - 5 = 15$ numbers of degrees of freedom, correspondingly; Fisher's ratio $F = S_{st}^2/S_{new}^2$; and Student's ratio $t = |AV_{st} - AV_{new}|/(S_{st}^2/n_{st} + S_{new}^2/n_{new})^{0.5}$.

The critical value for Fisher's ratio is 2.60 at the 0.95 level of confidence and the numbers of degrees of freedom, 9 and 15. For Student's ratio, the critical value is 2.06 at the 0.95 level of confidence and $f_{st} + f_{new} = 24$ degrees of freedom. From the comparison of the F -data with the critical value, it follows that the difference between repeatability of results obtained by the standard and the new method is insignificant (all F -values are less than the critical one). The accuracy for these techniques is approximately the same because deviations of AV_{new} from AV_{st} are insignificant in comparison with standard deviations characterizing repeatability: all t values are less than the critical value (2.06). So, recovery

deviations from 100% should also be accepted as admissible.

4.3. Advantages of the method

1. Time for one determination is no more than 9–10 min. while the standard AV determination needs 4 h or more.
2. Reagents are not toxic.
3. Low cost instruments are used.
4. Facility for automation is obvious.

Acknowledgements

The authors express their gratitude to Prof. E. Schoenberger for helpful discussion.

References

- [1] Oilseeds—Determination of Acidity of Oils, Standards of International Organization for Standardization, Switzerland, 1988, ISO 729: 1988-11-01.
- [2] Oilseeds—Determination of Hexane Extract (or Light Petroleum Extract), Colled 'Oil Content', Standards of International Organization for Standardization, Switzerland, 1988, ISO 659: 1988-02-15.
- [3] T.M. Lapshina, Ya.I. Tur'yan, S.I. Danilchuk, J. Anal. Chem. USSR 46 (1991) 833.
- [4] O.Yu. Berezin, Ya.I. Tur'yan, I. Kuselman, A. Shenhar, Talanta 42 (1995) 507.
- [5] Ya.I. Tur'yan, E. Stochkova, O.Yu. Berezin, I. Kuselman, A. Shenhar, Talanta 47 (1998) 53.
- [6] O.Yu. Berezin, Ya.I. Tur'yan, I. Kuselman, A. Shenhar, J. Am. Oil. Chem. Soc. 73 (1996) 1707.
- [7] V.P. Dole, H. Meinertz, J. Biol. Chem. 235 (1960) 2595.
- [8] W.E. May, D.J. Hume, J. Am. Oil. Chem. Soc. 70 (1993) 229.
- [9] A.I. Vorob'eva, M.Kh. Karapet'yants, Russ. J. Phys. Chem. 41 (1967) 1061.
- [10] Ya.I. Tur'yan, O.Yu. Berezin, I. Kuselman, A. Shenhar, J. Am. Oil. Chem. Soc. 73 (1996) 295.
- [11] I. Kuselman, Ya.I. Tur'yan, O.Yu. Berezin, L. Kogan, A. Shenhar, J. AOAC Int. 81 (1998) 873.
- [12] K.-S. Liu, J. Am. Oil. Chem. Soc. 71 (1994) 1179.
- [13] I. Kuselman, A. Shenhar, Accred. Qual. Assur. 2 (1997) 180.

Flow injection potentiometry for enzymatic assay of cholesterol with a tungsten electrode sensor

Manihar Situmorang, Peter W. Alexander, D. Brynn Hibbert *

Department of Analytical Chemistry, University of New South Wales, Sydney, NSW 2052, Australia

Received 4 November 1998; accepted 27 January 1999

Abstract

Flow injection potentiometry (FIP) for the enzymatic determination of cholesterol is reported. The assay utilises a combination of three enzymes: cholesterol esterase (CE), cholesterol oxidase (COD) and peroxidase (POD). The method is developed by the use of a tungsten wire electrode as a sensor vs. Ag/AgCl in conjunction with a redox mediator ferrocyanide. CE converts esterified cholesterol to free cholesterol, which is then oxidised by COD with hydrogen peroxide as product. Ferrocyanide is converted to ferricyanide by hydrogen peroxide, catalysed by POD, and the tungsten electrode responds to the ratio of ferricyanide to ferrocyanide. Flow injection potentiometry gave well-defined peaks for cholesterol samples with a fast response (30 s). Linear calibration was obtained from 0.05 to 3.0 mM cholesterol, with a slope of 60.2 mV/decade change in cholesterol concentration, and detection limit 0.01 mM cholesterol ($S/N = 3$). Repeatability was 3% (CV). Interferences from commonly found species were shown to be negligible. The sensor cell is simple to construct, and it was free from surface contamination problems over long periods of use. The application of the sensor for the determination of serum cholesterol was demonstrated. © 1999 Elsevier Science B.V. All rights reserved.

Keywords: Cholesterol; Flow injection potentiometry; Tungsten electrode; Enzymatic analysis

1. Introduction

The determination of serum cholesterol is important in clinical diagnosis, because atypical total cholesterol in serum is an indicator of abnormality in lipid metabolism, of arteriosclerosis and hypertension. Epidemiological and clinical studies have demonstrated a strong positive correlation between the total cholesterol in human blood serum and the incident of coronary heart

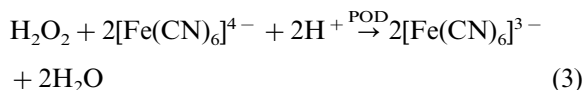
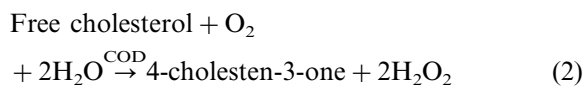
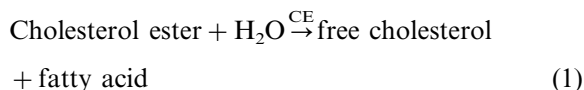
diseases [1]. As awareness of the importance of cholesterol levels has increased, numerous screening programs have been set up to identify individual concentrations of cholesterol in human serum [2]. Various analytical methods have been used for cholesterol assays including colourimetric [3] spectrometric [4–13] and electrochemical methods [14–34]. For human blood cholesterol assays, enzymatic procedures are mainly employed, due to their rapid, selective, sensitive nature and the great accuracy obtained in the measurements.

* Corresponding author.

Electrochemical detection systems for cholesterol assay are frequently based on the monitoring of the consumption of oxygen [14–17] or the rate of production of hydrogen peroxide [18–22] by an enzymatic reaction. Amperometric methods [23–26] commonly operate at a high potential (0.6–0.7 V vs. Ag/AgCl), and at such potentials, many other species are oxidised. To minimise the effect of interferences, techniques have been developed using the redox mediator ferrocyanide ($[\text{Fe}(\text{CN})_6]^{4-}$) [27–30] to reduce hydrogen peroxide, making the product ferricyanide ($[\text{Fe}(\text{CN})_6]^{3-}$) which can be detected at low potentials. However, this measuring system was affected by air oxidation of ferrocyanide that takes place as a competitive reaction during the enzymatic oxidation.

Potentiometric detection is a very attractive method because of the inherent wide detection range. However, the few works have that been reported for cholesterol, use ion selective electrodes (ISEs) [31,32]. This might be due to the difficulty of measuring the redox potential of the enzymatic reaction of cholesterol. An indirect method, by the use of ferrocyanide to couple the hydrogen peroxide produced on enzymatic oxidation of cholesterol in flow injection system has been reported [33], and immobilisation of enzyme [34] in a reactor has also been shown to be applicable for FIA.

The proposed system is based upon previous research [33,34] and upon a successful glucose assay [35]. The enzymatic determination of cholesterol by this system is based on a sequence of three enzyme reactions:



The hydrolysis of cholesterol ester is catalysed by the enzyme cholesterol esterase (CE) to produce free cholesterol and fatty acid. Subsequently,

the free cholesterol is oxidised by presence of cholesterol oxidase (COD) to produce 4-cholesten-3-one and hydrogen peroxide. Reduction of hydrogen peroxide by ferrocyanide, in the presence of peroxidase (POD), yields the ferricyanide. The reaction product from cholesterol or its ester is converted stoichiometrically to ferricyanide. The redox potential developed in this manner can be related to the change of the concentration of $[\text{Fe}(\text{CN})_6]^{3-}/[\text{Fe}(\text{CN})_6]^{4-}$ by the Nernst equation.

Assume that cholesterol ester is converted stoichiometrically to cholesterol, and the total cholesterol is in turn converted to hydrogen peroxide, which then reacts with ferrocyanide. Let the initial concentrations of cholesterol ester, free cholesterol and ferrocyanide be $[\text{CH E}]_0$, $[\text{CH}]_0$, and $[\text{FeII}]_0$ respectively. Then if $[\text{P}]$ and $[\text{FeIII}]$ are the concentrations of peroxide and ferricyanide generated during the reaction, and ferrocyanide is in excess:

$$[\text{FeIII}] = 2 \times [\text{P}] = [\text{CH}]_0 + [\text{CH E}]_0 \quad (4)$$

and the concentration of ferrocyanide after reaction $[\text{FeII}]$ becomes

$$[\text{FeII}] = [\text{FeII}]_0 - [\text{FeIII}] \quad (5)$$

Applying the Nernst equation to the redox active species:

$$E = \text{const} + \frac{RT}{F} \ln \left(\frac{[\text{FeIII}]}{[\text{FeII}]} \right) \quad (6)$$

$$E = \text{const} + \frac{RT}{F} \ln \left(\frac{[\text{CH}]_0 + [\text{CH E}]_0}{[\text{FeII}]_0 - ([\text{CH}]_0 + [\text{CH E}]_0)} \right) \quad (7)$$

Eq. (7) predicts linear Nernstian behaviour while $[\text{FeII}]_0 \gg [\text{FeIII}]$. $[\text{FeII}]_0 = 5$ mM, and Nernstian behaviour would be expected up to a cholesterol concentration of about 1 mM. The redox potential is monitored with a tungsten electrode vs. Ag/AgCl. In flow injection mode, the baseline is established by the ratio of ferrocyanide to ferricyanide and this is independent of the enzyme reaction, ensuring a return to a constant baseline after each injection.

The purpose of this paper is to describe a simple method for constructing a flow injection

potentiometric (FIP) method for enzymatic determination of cholesterol, using a tungsten wire electrode as a sensor vs. Ag/AgCl, in conjunction with the redox mediator ferrocyanide. The resulting sensor exhibits a good performance with a sensitive and rapid response to cholesterol, wide linear range, good precision, and is free from normal interferences.

2. Experimental

2.1. Chemicals and reagents

All chemicals used were laboratory reagent grade. COD (E.C.1.1.3.6) from pseudomonash 33 units/mg, POD (E.C.1.11.1.7.2) from horse radish 179 units/mg, cholesterol, accutrol chemistry control normal/abnormal, lipid control normal/elevated, control serum type IA normal/type IIA abnormal, and Triton X-100 were all obtained from sigma Chem. Co. USA. CE (E.C. 1.1.13) from porcine pancreas 18.1 units/mg was from ICN Biochemical Co. Reagents $K_4Fe(CN)_6$, $K_3Fe(CN)_6$, K_2HPO_4 , KH_2PO_4 , and KCl were purchased from Ajax Chem. Australia. 4-cholesten-3-one was supplied from Aldrich, Australia. Hydrogen peroxide (27.5%) was obtained from the Pacific Manufacturing Co. Sydney, Australia. Human blood samples were donated by the University of Health Service, the University of New South Wales Australia. Sera were centrifuged at 5000 rpm for 15 min to separate the serum from blood plasma. The control solutions

and human blood sera were diluted 1:8 (v/v) with phosphate buffer containing 1% isopropanol and 1% Triton X-100, and were then heated to 40°C for a few minutes to make the cholesterol soluble in aqueous solution.

Cholesterol is insoluble in water, and so samples were first dissolved in a small volume of isopropanol containing a surfactant. The stock solution of 10.0 mM cholesterol was prepared by dissolving 0.19335 g cholesterol in a 50 ml volumetric flask containing a mixture of 5 ml isopropanol and 5 ml Triton X-100. The mixture was swirled and heated gently at 40°C. After the cholesterol had dissolved, the solution was diluted to the mark with redistilled water. The stock solution throws a hazy precipitate if refrigerated overnight, but gently heating at 40°C will redissolve the cholesterol. Standard solutions in the range 0.1–5 mM cholesterol were prepared by diluting the cholesterol stock solution with 10 mM phosphate buffer, pH 7.0.

2.2. Instrumentation

A schematic diagram of the FIP system is shown in Fig. 1. The flow rate was regulated with a peristaltic pump (Dessaga STA, type 131900, Heidelberg, West Germany). The electrodes assembled with a tungsten wire electrode versus Ag/AgCl reference electrodes separated by saturated KCl bridge in agar gel, placed in a modified flow through cell [36]. Potentiometric measurements were made with a Keithley 177-Microvolt Digital Multi Meter (Keithley Instrument, USA) connecting with MacLab/8 Analog Digital Instrument, Sydney, Australia, for data acquisition.

2.3. Procedures

The two channels of the FIP system were flowed continuously at a constant flow rate of 1.15 ml/min at 30°C. The cholesterol assay was carried out by incubation of cholesterol ester with 0.5 unit/ml CE for 5 min, followed by oxidation with 0.8 unit/ml COD for 10 min in the reaction tube. An 50 μ l of aliquot was then injected in to the flow channel containing 5 mM ferrocyanide in phosphate buffer which then merged with the 0.75

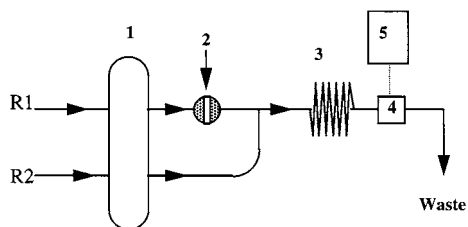


Fig. 1. FIP manifold for the potentiometric determination of cholesterol: (1) peristaltic pump, (2) injection port, (3) mixing coils, (4) flow cell, (5) voltmeter and micro computer. Carrier solutions of 5 mM $K_4Fe(CN)_6$ (R1), and 0.75 unit/ml peroxidase (R2) were dissolved in 10 mM phosphate buffer, pH 7.0.

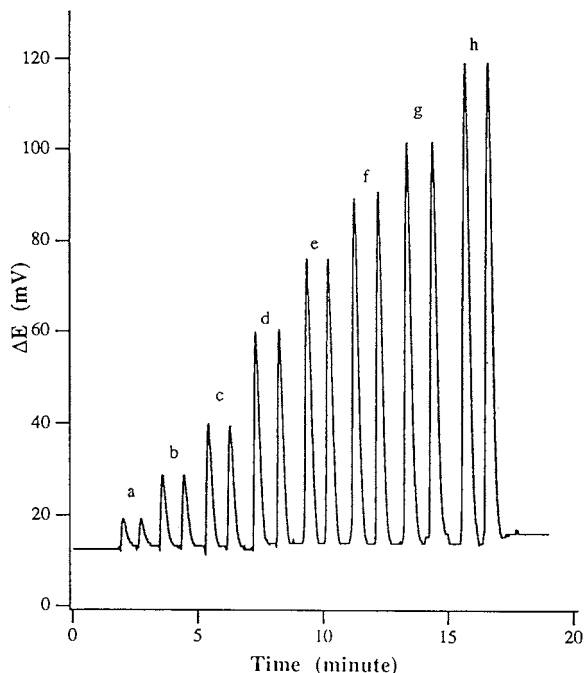


Fig. 2. Typical FIP peaks corresponding to successive duplicate injections of 50 μ l of cholesterol solution into the carrier stream (10 mM phosphate buffer, pH 7.0, containing of 5.0 mM ferrocyanide and 0.75 unit/ml POD). (a) 0.05 mM, (b) 0.08 mM, (c) 0.1 mM, (d) 0.3 mM, and (e) 0.5 mM, (f) 0.8 mM, (g) 1.0 mM, (h) 1.5 mM cholesterol. Cholesterol was diluted in 1% v/v Triton X-100 and isopropanol, incubated with 0.8 units/ml COD for 15 min, flow rate 1.15 ml/min, at 30°C.

unit/ml POD. The potential change caused by the reaction was recorded with a voltmeter and the data was stored in a microcomputer. Calibration was carried out by duplicate injections of the incubated 0.01–3 mM cholesterol standard solutions into the carrier stream, followed by the analysis of the diluted control solutions and human blood samples.

3. Results and discussion

A typical signal output for the determination of cholesterol is presented in Fig. 2. The peak height increased linearly in proportion to the log concentration of cholesterol injected. The signal decay to base line was fast at 30 s, and samples were

injected at 1-min intervals. As the concentration of cholesterol injected increases, the concentration of ferricyanide in the carrier stream also increases, causing the observed signal.

Electrode responses to hydrogen peroxide and standard ferricyanide solution were also measured to provide convincing evidence that the response signal results from the oxidation of cholesterol. Injection of 50 μ l of 1 mM hydrogen peroxide or ferricyanide buffered solutions, in the absence of cholesterol and in the presence of peroxidase, gave the same response peak to those observed with the injection of an equivalent amount of cholesterol. No change in potential was observed when 50 μ l of 1 mM cholestenone was injected into the carrier stream. These results support the hypothesis that the source of the potentiometric signal is the catalysed oxidation of ferrocyanide by the hydrogen peroxide released from the enzymatic oxidation of cholesterol.

The selectivity of the measurement for cholesterol was demonstrated by the following experiment. Various concentrations (1–10%) of the bacterium *E. coli* were added to 1 mM cholesterol standard solution containing a rich broth growth medium. Aliquots of the mixture were incubated for 15 min, then injected into the carrier stream. The peak height for cholesterol decreased linearly in proportion to the increasing concentration of *E. coli* in solution (Fig. 3). *E. coli* consumes the oxygen in solution and so its presence leads to a decrease in the enzymatic reaction.

3.1. Optimisation of the FIP system

Experimental parameters affecting the determination of cholesterol were optimised. The procedure was optimised in two stages, namely the incubation reaction of the substrate with two enzymes in the reaction vessel, then the peroxidase reaction in the carrier stream. The optimum conditions of the FIP system are summarised in Table 1.

The pH is known to be a critical parameter of enzymatic activity and stability in aqueous media. The effect of pH on the overall reaction for enzymatic oxidation of 1 mM cholesterol was studied. The dependence of the enzymatic reac-

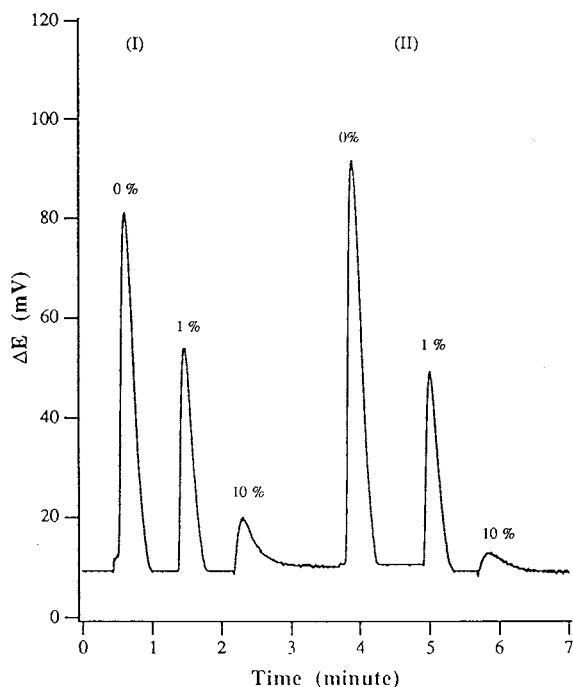


Fig. 3. Typical FIP output following injection of 50 μ l lots of 1.0 mM cholesterol standard solution containing 0–10% of bacterial culture (*E. coli*), incubated with the enzymes: for (I) 10 min, and (II) 15 min. The solutions contain rich nutrient broth to support the bacteria. Other FIP conditions are the same as for Fig. 2.

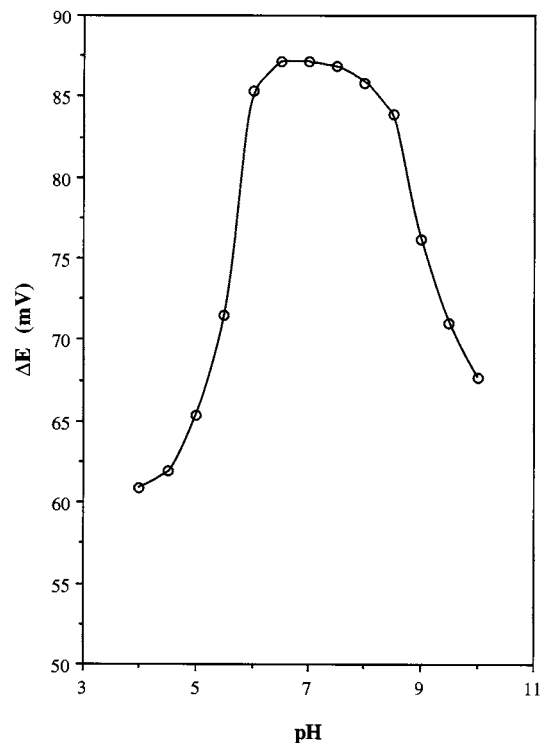


Fig. 4. pH dependence of FIP signal. 50 μ l aliquots of 1 mM cholesterol standard solution were injected into various buffer solutions. Other FIP conditions are the same as for Fig. 2.

Table 1
Optimum conditions for the enzymatic FIP determination of cholesterol

Parameter being optimised	Optimum conditions
Redox mediator	5.0 mM $K_4Fe(CN)_6$
Phosphate buffer (NaH_2PO_4 / Na_2HPO_4)	pH 7.0, 10.0 mM + 10.0 mM KCl
Enzymes	0.5 unit/ml CE, 0.8 unit/ml COD and 0.75 unit/ml POD
Flow rate	1.15 ml/min
Mixing coil (delay time)	30 cm
Injection volume	50 μ l
Temperature	30°C
Diameter of tungsten wire electrode	0.5 mm

tion rate to the pH of the phosphate buffer was examined in the range of pH 4.0–10.0 (Fig. 4). The most sensitive response accompanied by a good baseline was observed using phosphate buffer, pH 7.0.

Different procedures were applied for the preparation of cholesterol standard solutions. Non ionic surfactant Triton X-100 and isopropanol were found to be effective lipid solubilising agents for cholesterol solution. Triton X-100 is used to ensure the cholesterol and COD remains in the solution, while isopropanol acts as an emulsifier [25]. However, the ratio of the surfactant to the cholesterol is essentially determined by a compromise between solubilising the cholesterol and controlling the interference of the enzyme activity caused by the surfactant (Fig. 5). The peak height increased as the concentration of Triton X-100 increased, reaching an optimum response at 1% Triton X-100 after which inhibition of the reaction dominates.

The effect of isopropanol on the sensitivity of the measurement was also studied. The peak height decreased as the concentration of isopropanol in the solution increased. The slope of the electrode response curve decreased as the concentration of isopropanol increased. That a less sensitive response was obtained at higher concentrations of isopropanol is possibly a result of decrease in ionisation of the electrolyte due to reduction in relative permittivity of the solution. A concentration of 1% of each additive was chosen to be used in the experiment.

Incubation in a reaction tube was chosen to save the consumption of enzyme per assay. To obtain information on the effect of COD on the reaction rate, the development of potential with incubation time of 1 mM cholesterol at various concentrations of COD was measured. The con-

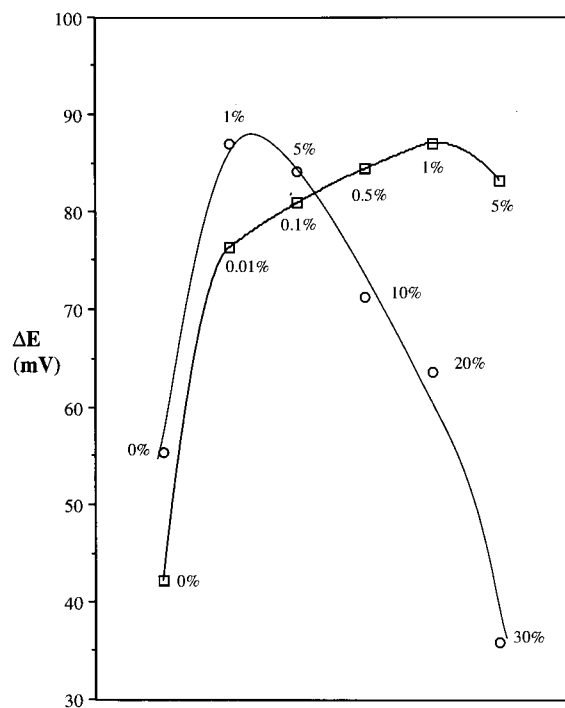


Fig. 5. The effect of isopropanol and Triton X-100 on the sensitivity of measurement of 1 mM cholesterol diluted with 10 mM phosphate buffer containing (○) various concentrations of isopropanol at a constant concentration of 1% Triton X-100, and (□) various concentrations of Triton X-100 at a constant concentration of 1% isopropanol. Other FIP conditions are the same as for Fig. 2.

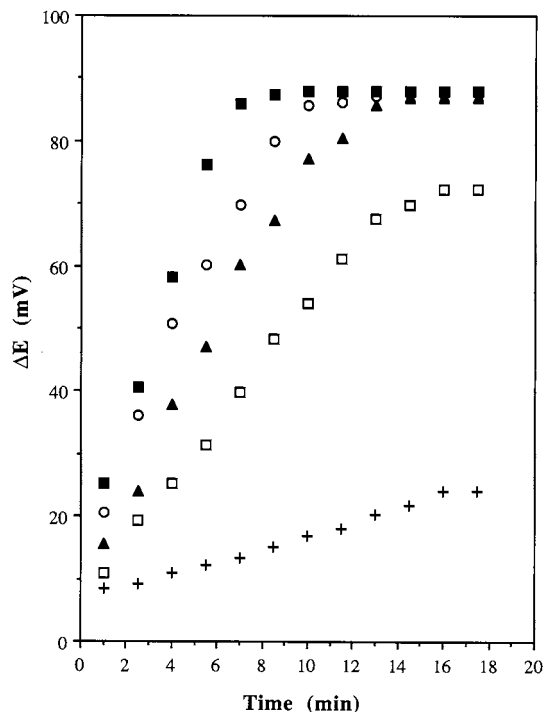


Fig. 6. The time development of the peak height for the oxidation of 1 mM cholesterol as a function of the concentration of COD (+) 0.1, (□) 0.4, (▲) 0.6, (○) 0.8, and (■) 1.0 unit/ml. Other FIP conditions are the same as for Fig. 2.

centration of hydrogen peroxide produced from the reaction was dependent on the enzyme concentration from 0.1–0.8 units/ml COD (Fig. 6). The incubated reaction was complete in 15 min using 0.8 unit/ml COD and 10 min using 1 unit/ml COD. The response peak did not increase further for a longer incubation time. The concentration of 0.8 unit/ml COD appeared to be adequate for the experiments, and 15 min was found to be satisfactory for complete oxidation of free cholesterol to produce hydrogen peroxide.

The enzyme CE is used to hydrolyse cholesterol ester into free cholesterol and fatty acid. Using a constant concentration of 0.8 unit/ml COD, the effect of CE on the sensitivity of the electrode was studied with normal lipid control solutions. Peak heights for the optimisation of the concentration of CE are presented in Fig. 7. A concentration of 0.5 unit/ml CE was found adequate for the hydrolysis of the ester, and the reaction was com-

pleted in about 5 min. No further increase in sensitivity was observed when using higher concentrations of CE. It is seen that the limiting potential in the absence of CE (Fig. 7) establishes the amount of free cholesterol and the potential when CE was added gives the esterified cholesterol.

3.2. Calibration

Calibration curves for free cholesterol standard solutions were constructed under optimum FIP system conditions. Typical signals resulting from duplicate injections of cholesterol standard solutions are presented in Fig. 2, and a plot of the peak heights (ΔE) against log concentration of cholesterol (Fig. 8) shows a linear range from 0.05

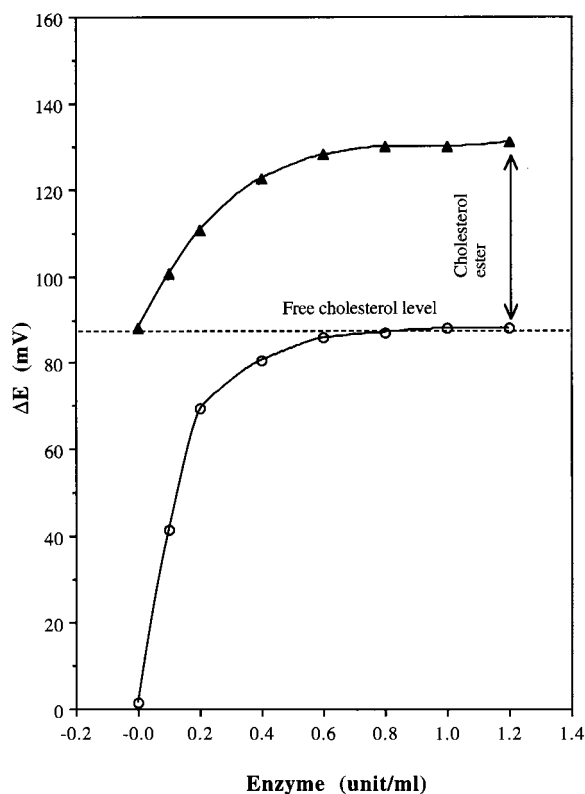


Fig. 7. The response of the tungsten electrode to a lipid normal control solution incubated with 0.8 unit/ml COD with different amounts of CE (▲) and to different amounts of COD in the absence of CE (○). Other FIP conditions are the same as for Fig. 2.

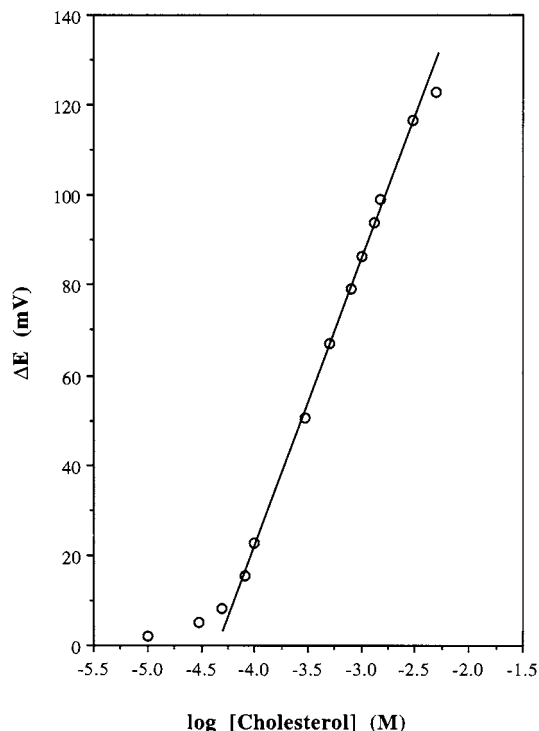


Fig. 8. Calibration graph for the FIP of cholesterol. FIP conditions are the same as for Fig. 2.

to 3 mM cholesterol, with a calibration slope of 60.2 mV/decade concentration change. The detection limit for the injection of a 50 μ l volume is 0.01 mM cholesterol ($S/N = 3$).

3.3. Evaluation of the method

To assess the precision and recovery of the FIP method, eight replicate injections of various concentrations of cholesterol standard solutions were made, followed by lipid control solutions and serum control solutions, and the results are presented in Table 2. The coefficient of variation (CV) was less than 3% for all solutions which is recommended for methods used in a clinical laboratory [37]. The same solution was analysed repeatedly on different days and maintained good precision.

The accuracy of the method was demonstrated by comparing the measured concentration with assigned values of cholesterol in lipid control and

Table 2

Repeatability of electrode response for eight replicate injection of standard and control cholesterol solutions under optimum conditions in the FIP system

Cholesterol standard and control	ΔE (mV) ^a	SD $n = 8$ (mV)	CV (%)
0.1 mM	29.3	0.7	2.6
0.5 mM	61.5	1.4	2.3
1.0 mM	87.1	1.7	1.9
Lipid control normal ^b	87.6	1.1	1.2
Lipid control elevated ^b	104.3	1.7	1.6
Control serum I A normal ^b	68.6	1.1	1.7
Control serum I A Elevated ^b	91.7	1.7	1.8

^a Mean of eight replicate injections of the substrate.

^b Samples are diluted 1:8 with phosphate buffer (10 mM, pH 7.0), containing 1% (v/v) Triton X-100 and isopropanol.

serum control solutions. The concentrations of cholesterol in the control solutions analysed by

this present method were mostly within the range of the assigned values (Table 3). The results obtained with the FIP method for sample of human serum also agree well with those obtained by the conventional auto-analyser method used in hospital.

The use of an unmodified tungsten electrode that responds to a well-behaved redox couple in FIA mode has the great advantage of long term stability. Throughout this study (2 years) a number of tungsten wires were used repeatedly with occasional cleaning. No loss of activity or change in the appearance of the electrodes was seen.

This present method has been applied for the determination of cholesterol in human blood serum. Ten patient's sera were analysed independently by two methods: the present FIP method and the standard auto-analyser method used in hospital which is a similar enzyme method in which the peroxide produced is reacted to produce a coloured product [38]. The concentration of cholesterol in human blood samples was deter-

Table 3

Analysis of cholesterol in control solutions and human blood serum samples by two methods, the standard auto-analyser method and the present FIP method

Sample	Cholesterol			
	Assigned value (mM) ^a		FIP method (mM) ^b	
	Free	Total	Free	Total
Accutrol Chem. Control Normal	–	3.68	3.90 ± 0.12	4.00 ± 0.11
Accutrol Chem. Control Abnormal	–	3.00	2.65 ± 0.10	3.03 ± 0.11
Lipid Control Normal	5.31	6.42	5.88 ± 0.15	6.32 ± 0.14
Lipid control Elevated	9.65	9.78	8.57 ± 0.17	9.88 ± 0.18
Serum Control type I A Normal	–	3.50	3.40 ± 0.10	3.62 ± 0.11
Serum Control type II A Elevated	–	6.90	6.50 ± 0.16	7.00 ± 0.15
Human blood serum 1	–	5.20	4.94 ± 0.14	5.38 ± 0.13
Human blood serum 2	–	5.50	4.37 ± 0.11	4.37 ± 0.12
Human blood serum 3	–	4.70	3.75 ± 0.11	4.70 ± 0.11
Human blood serum 4	–	4.60	3.58 ± 0.12	4.50 ± 0.11
Human blood serum 5	–	4.10	2.08 ± 0.10	3.90 ± 0.10
Human blood serum 6	–	5.60	4.98 ± 0.11	6.37 ± 0.12
Human blood serum 7	–	5.50	4.60 ± 0.13	5.67 ± 0.12
Human blood serum 8	–	5.10	4.83 ± 0.13	5.40 ± 0.15
Human blood serum 9	–	5.10	4.51 ± 0.13	5.10 ± 0.14
Human blood serum 10	–	5.00	4.40 ± 0.15	5.30 ± 0.14

^a Obtained from supplier or from hospital with auto-analyser method

^b Mean from three measurements ± 95% confidence limit.

Table 4

The effect of interfering agents on the sensitivity of measurements of a 1 mM cholesterol standard.

Interfering agents (constituents) ^a	Concentration (mM)	ΔE (mV) ^b	Change in response (mV)
Cholesterol standard	1.0	87.1	–
Ascorbic acid	5.0	67.5	–19.6
Uric acid	5.0	80.2	–5.6
Palmitic acid	10.0	105.4	18.3
Tripalmitin	10.0	92.4	5.3
	5.0	87.4	0.3
Phosphatidyl colin	10.0	102.6	15.5
Sodium azide	5.0	85.3	–2.8

^a Constituents were added into 1 mM cholesterol standard solution.

^b Mean of duplicate injection of the substrate.

mined independently on the day of collection, and the mean values of cholesterol measurements are summarised in Table 4. A plot of the results obtained by FIP against those from the auto-analyser method, gave a correlation coefficient of 0.972 (Fig. 9). This result reveals a close agreement between the present method and the standard clinical method, and confirms that the FIP method meets the rigid demands expected for cholesterol analysis in a clinical laboratory. The present method gives values that are on average 0.13 mM greater than the conventional method, but by a paired *t*-test the difference was only significant at the 59% level ($t = 0.588$).

3.4. Interference studies

Several concentrations of possible interfering agents that might be present in a blood sample were added to a cholesterol standard. These included reducing agents, proteins, organic acids, cations and anions. Other compounds of a lipid nature that may accompany the cholesterol in the solution, such as fatty acids, triglycerides, and phospholipids, were also tested. The sensitivity of measurements in the presence of (1–10 mM) interfering agents was evaluated for 1 mM cholesterol (Table 4). High concentrations of 5 mM ascorbic acid and uric acid gave negative errors in the measurement, but the presence of normal concentrations of 1 mM of those interfering agents did not disturb the measurement. A high concentration of 10 mM of the lipids palmitic

acid, tripalmitin and phosphatidyl colin gave positive errors in measurements, but lower than 5 mM of these compounds, which is above the average for human blood serum, is free from interference. The presence of 5 mM sodium azide,

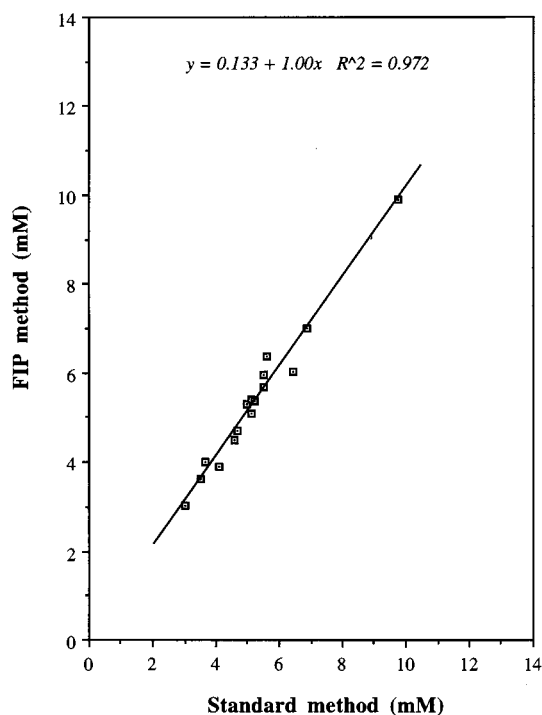


Fig. 9. Correlation plot for cholesterol values of human serum as determined by the present FIP method and by the conventional auto-analyser method used in a hospital. The best fit line is drawn.

which is usually used as a preservative for serum samples, reduces the sensitivity of the sensor, however, this value is above the average of azide in the samples. Other interfering agents such as proteins, uric acid and bilirubin, that have interfered in the enzymatic determination of cholesterol by other methods [11,20] had negligible effects on this FIP method. These results lead to the conclusion that the use of ferrocyanide redox mediator in this FIP system is very selective for cholesterol. The analytical method can be used for the determination of cholesterol in the presence of interfering agents in normal concentrations found in serum. Therefore, the sample can be analysed without pretreatment, except dilution with 1% of Triton X-100 and isopropanol.

4. Conclusions

This potentiometric method with the use of ferrocyanide as mediator in a FIP system has several advantages in selectivity, sensitivity, rapidity, wide linear calibration range and freedom from interference. The FIP technique described in the experiment has been shown to be a reliable analysis tool for applications in clinical chemistry. The tungsten wire electrode has several advantages when used as a sensor electrode. It has a fast response to the analyte and because of its low electrical resistance which is suitable for potentiometric flow injection systems, can be used for routine assays over prolonged periods of time without suffering from interferences, surface deterioration or electrode poisoning. Moreover, it is possible to construct miniature electrodes from tungsten wire that is commonly available and of low cost in comparison with conventional ion selective electrodes. The FIP method developed has therefore been shown to function acceptably with low cost instrumentation that is easily fabricated in a well-equipped laboratory.

References

- [1] H.K. Naito, *Clin. Chem.* 34 (1988) 444–449.
- [2] R.I. Levy, *Clin. Chem.* 27 (1981) 653–662.
- [3] J.S. Moshides, *Clin. Chem.* 34 (1988) 1799–1804.
- [4] P.W. Wentz, R.E. Cross, J. Savory, *Clin. Chem.* 22 (1976) 188–192.
- [5] W. Richmond, *Clin. Chem.* 19 (1973) 1350–1356.
- [6] R. Deeg, J. Ziegenhorn, *Clin. Chem.* 29 (1983) 1798–1802.
- [7] J.M. Fernandez-Romero, M.D. Luque de Castro, M. Valcarcel, *Clin. Chim. Acta* 167 (1987) 97–104.
- [8] N.L. Malavolti, D. Pilosof, T.A. Nieman, *Anal. Chim. Acta* 170 (1985) 199–207.
- [9] A. Taniguchi, Y. Hayashi, H. Yuki, *Anal. Chim. Acta* 188 (1986) 95–100.
- [10] A. Nabi, A. Rashid, M. Yaqoob, *Anal. Lett.* 29 (1996) 2281–2288.
- [11] T. Nakaminami, S. Kuwabata, H. Yoneyama, *Anal. Chem.* 69 (1997) 2367–2372.
- [12] A. Krug, R. Gobel, R. Kellner, *Anal. Chim. Acta* 287 (1994) 59–64.
- [13] M.J. Valencia-Gonzalez, M.E. Diaz-Garcia, *Anal. Chem.* 66 (1994) 2726–2731.
- [14] A. Kumar, G.D. Christian, *Clin. Chim. Acta* 74 (1977) 101–108.
- [15] A. Noma, K. Nakayama, *Clin. Chem.* 22 (1976) 336–340.
- [16] I. Satoh, I. Karube, S. Suzuki, *Biotech. Bioeng.* 19 (1977) 1095–1099.
- [17] G.F. Hall, A.P.F. Turner, *Anal. Lett.* 24 (1991) 1375–1388.
- [18] H.S. Huang, S.S. Kuan, G.G. Guilbault, *Clin. Chem.* 23 (1977) 671–676.
- [19] C. Bertrand, P.R. Coulet, D.C. Gautheron, *Anal. Lett.* 12 (1979) 1477–1488.
- [20] W. Trettnak, I. Lioni, M. Mascini, *Electroanalysis* 5 (1993) 753–763.
- [21] T. Yao, M. Satomura, T. Nakahara, *Anal. Chim. Acta* 296 (1994) 271–276.
- [22] T. Yao, M. Satomura, T. Nakahara, *Electroanalysis* 7 (1995) 143–146.
- [23] M. Masoom, A. Townshend, *Anal. Chim. Acta* 174 (1985) 293–297.
- [24] I. Karube, K. Hara, H. Matsuoka, S. Suzuki, *Anal. Chim. Acta* 139 (1982) 127–132.
- [25] G.J. Moody, G.S. Sanghera, J.D.R. Thomas, *Analyst* 113 (1988) 1419–1422.
- [26] J. Motonaka, L.R. Faulkner, *Anal. Chem.* 65 (1993) 3258–3261.
- [27] T. Yao, M. Sato, Y. Kobayashi, T. Wasa, *Anal. Biochem.* 149 (1985) 387–391.
- [28] T. Yao, T. Wasa, *Anal. Chim. Acta* 207 (1988) 319–323.
- [29] Y. Hahn, C.L. Olson, *Anal. Chem.* 51 (1979) 444–449.
- [30] U. Wellenbrg, M. Kuhn, F. Scheller, V. Deppmeyer, M. Janchen, *Bioelectrochem. Bioeng.* 11 (1983) 307–310.
- [31] D.S. Papastathopoulos, G.A. Rechnitz, *Anal. Chem.* 47 (1975) 1792–1796.

- [32] I. W. Siddiqi, *Clin. Chem.* 28 (1982) 1962–1967.
- [33] S. Thahir, M. Situmorang, P.W. Alexander, Proceedings of the 13th Australian Symposium on Analytical Chemistry, Darwin, 1995, pp. AO12-1–AO12-2.
- [34] S. Silalahi, M. Situmorang, I. Nurwahyuni, Proceedings of the 14th Australian Symposium on Analytical Chemistry, Adelaide, 1997, pp. 376–378.
- [35] M. Situmorang, P.W. Alexander, Proceedings of the 10th Australian Symposium on Analytical Chemistry, Tasmania, 1991, p. 116.
- [36] P.W. Alexander, P.R. Haddad, M. Trojanowicz, *Anal. Chim. Acta* 171 (1985) 151–163.
- [37] H.K. Naito, *Special Rep. Clin. Chem.* 34 (1988) 193–201.
- [38] P. Trinder, *Ann. Clin. Biochem.* 18 (1981) 64–70.

Chemical accumulation and voltammetric determination of traces of nickel(II) at glassy carbon electrodes modified with dimethyl glyoxime containing polymer coatings

Chen Bing ^a, Roshan Deen ^a, Goh Ngho Khang ^a, Chia Lian Sai ^a,
Lars Kryger ^{b,*}

^a *Division of Chemistry, School of Science, National Institute of Education, Nanyang Technological University, 469 Bukit Timah Road, Singapore 259756*

^b *Department of Chemistry, Aarhus University, Langelandsgade 140, DK-8000, Aarhus C, Denmark*

Received 17 November 1998; received in revised form 1 February 1999; accepted 2 February 1999

Abstract

The objective of the present study was to develop a solid mercury free electrode for the voltammetric determination of traces of nickel(II) in solution. For this purpose chemically modified electrodes (CME's) were constructed from glassy carbon coated with dimethylglyoxime-containing polymers. CME's based on a composite matrix, which contained polyvinyl chloride, polyaniline, and dimethylglyoxime were shown to possess the ability to accumulate traces of nickel(II) from ammonia buffered aquatic solutions by a purely chemical attachment. Moreover the nickel(II) contents of such solutions could be determined using voltammetric quantitation of the nickel(II) dimethylglyoximate deposits on the CME surfaces and the standard addition technique. The CME surfaces could subsequently be regenerated by acid treatment. The limit of detection for Ni(II) following a 240 s chemical deposition was estimated as $18 \mu\text{g Ni l}^{-1}$, and the CME results for traces of Ni(II) in fresh water compared well with the results obtained by atomic absorption spectroscopy. Moreover the CME's retained their sensitivity for more than two days, i.e. significantly longer than the 3 h, during which analogous carbon paste electrodes completely lost their affinity to nickel(II). © 1999 Elsevier Science B.V. All rights reserved.

Keywords: Nickel(II); Trace; Polymer coating; Dimethyl glyoxime; Mercury free electrode

1. Introduction

While traces of nickel(II) can be found in many environments, elevated concentrations in the aquatic environment may arise from mining e.g. of nickel sulphides or nickel laterites. It is gener-

* Corresponding author. Fax: +45-86-196199.
E-mail address: kryr@kemi.aau.dk (L. Kryger)

ally accepted that nickel(II) concentrations below the $100 \mu\text{g Ni l}^{-1}$ level in natural waters are harmless to aquatic organisms and irrigated plants [1]. However, since higher concentrations, e.g. in fresh waters, present a potential hazard to the human organism, the development of reliable, yet affordable, analytical approaches for the determination of Ni(II) in concentrations down to the $100 \mu\text{g Ni l}^{-1}$ level seems worthwhile.

While spectroscopic methods have previously been preferred in environmental analysis, electrochemical methods, voltammetric as well as potentiometric, have now reached a state where they constitute a reliable and low-cost alternative for determination of e.g. sulphides in the coastal environment [2,3] and traces of heavy metals in decomposed industrial waste [4] and sea water [5]. Conventional stripping methods, which are based on electrolytic deposition and subsequent redissolution of metallic species at mercury electrodes are among the most sensitive electrochemical methods. Because of their inherent pre-concentration step these techniques are extremely useful for the determination of e.g. Pb(II), Cd(II), Cu(II), and Tl(I) which may be reduced to form dilute amalgams and subsequently be reoxidized via almost ideal electrode processes, i.e. processes which are transport controlled at low overpotentials. The electrode processes for Ni(II) at mercury electrodes are however far from ideal, in particular because nickel is only sparingly soluble in mercury. Thus stripping methods for Ni at such electrodes are not sufficiently sensitive for environmental investigations. A number of studies have therefore been focused on the development of alternative electrochemical methods for Ni(II). These methods are based on accumulation/stripping at chemically modified electrodes (CME's). CME's have chemically selective groups (modifiers) attached to their surfaces [6], and many are based on carbon or graphite such that the use of mercury is avoided, and such that applications of the electrode, from an environmental point of view, is more acceptable. In CME procedures the analyte is first accumulated on the electrode via a 'chemical deposition', i.e. a non electrochemical interaction with the modifier such as covalent linkage, complexation, or ion ex-

change, and subsequently quantitated by a voltammetric approach [7–20]. Depending on the selectivity of the modifier-analyte interaction this approach may introduce an additional dimension of selectivity in the pre-concentration step. As regards the determination of Ni(II), CME's based on dimethyl glyoxime (DMG) have previously been constructed and used for the determination of trace concentrations of Ni(II) [11]. These CME's, which were based on carbon paste matrices, were shown to be both sensitive and selective devices for the determination of traces of Ni(II). However, on continued use, their affinity to Ni(II), and hence the sensitivity, was lost after 3 h, such that a fresh CME-surface had to be generated. This problem, which was attributed to leakage of DMG and Ni(DMG)₂ from the soft carbon paste matrix, could however, be reduced by operation of the carbon paste CME in a closed (and relatively complex) flow system, in which no significant loss of sensitivity was observed after more than 4 h of continuous operation [21]. In view of these results, and with future routine CME applications in mind, it was decided to develop and investigate analogous CME's, operated without the complications of a flow system, but using solid polymer matrices, which, mechanically, are more robust than carbon paste.

The present communication reports on the results obtained using CME's, which were constructed from glassy carbon coated with DMG-containing polymer matrices. The experiments included a search for a polymer matrix which adhered well to the glassy carbon surface and which was sufficiently conductive for voltammetric quantification. In this context DMG solutions were mixed with polyvinyl chloride (PVC) solutions, with solutions of the more conductive polyaniline (PA) [22], and with mixtures of the PVC and PA solutions. Droplets of the resulting solutions were subsequently placed on the glassy carbon electrode surface and allowed to evaporate such that polymer coated CME's were obtained.

The performance of the CME's were subsequently studied in the following fashion: Initially tests were made to study whether Ni(II) could be deposited on the CME's by a purely chemical attachment, and whether such deposits could be

quantitated by voltammetric means. As shown below Ni(II) could indeed be determined in this fashion. Therefore, in order to optimize the sensitivity to Ni(II), a search was subsequently made to identify the most suitable CME matrix and voltage excitation wave form. Moreover a suitable acid regeneration scheme for the CME surfaces was established. In all cases the CME was studied by a procedure [11], which included: (a) open loop exposure of the electrode surface to metal solutions or blanks for a well defined period of time, (b) transfer of the CME to a separate medium, (c) connection of the CME to the working electrode terminal of a voltammetric analyzer, (d) recording of the current versus potential curve for the CME, and (e) open loop exposure of the electrode surface to an acidic solution for a well defined period of time. The CME-procedure was subsequently characterized by establishing relationships for Ni-response versus Ni(II) concentration and for Ni-response versus chemical deposition time. Furthermore the limit of detection was estimated. As regards interference the metallic species, which is most likely to interfere with the CME determination of Ni in ammonia buffers (pH 8–10), is Co(II) [11]. Like Ni(II), Co(II) forms a stable and sparingly soluble complex with DMG. Moreover this complex is known to be reducible near the reduction potential of the Ni(DMG)₂-complex. Consequently, in order to investigate this possibility the effects on the Ni-response of Co(II) additions was also studied. Finally the practical utility of the CME's was studied by investigation of: (a) their long term stability; and (b) their performance in a practical analytical situation (CME-analysis of fresh water samples and comparison of the CME-results with those found by an independent analytical method, atomic absorption spectroscopy (AAS)).

2. Experimental

2.1. Instrumentation

Voltammetric measurements were carried out using a computerized potentiostat/galvanostat

(Model 273A, EG and G, Princeton Applied Research with Model 270/250 Research Electrochemistry Software 4.00). The three electrode assembly included a 50 ml glass cell equipped with a rotating disk electrode assembly (Model 616, EG and G, Princeton Applied Research), a rotating glassy carbon working electrode (area 0.13 cm²), a saturated Ag–AgCl reference electrode, and a Pt wire counter electrode. Atomic absorption measurements were carried out using an AA-680 Atomic Absorption/Flame Emission Spectrophotometer (Shimadzu) equipped with a Ni-hollow cathode lamp (Koto Bunkogen Co. Ltd., Japan) filled with Ne-gas. The flame was produced by combustion of a mixture of acetylene (2.0 l min⁻¹) and air (8.0 l min⁻¹), and the AAS measurements were based on the absorption at 232.0 nm, a slit width of 0.2 nm and a maximum lamp current of 20 mA.

2.2. Reagents, solutions and equipment

Polyvinyl chloride (PVC) (Aldrich), dimethyl glyoxime (DMG) (Baker), and tetrahydrofuran (THF) (Merck) were used as received. Polyaniline (PA) was prepared according to MacDiarmid and co-workers [23]. Ultra filtered de-ionized water (Model D 4755, Barnstead, USA), 60% HNO₃ (Aristar, BDH), 30% NH₄OH (Analytical Grade, Baker), KNO₃ (Analytical Grade, Merck), and 1000 mg l⁻¹ standard solutions of Ni(II) and Co(II) (spectrosol, BDH) were used throughout the study. Dilute standards of Ni(II) and Co(II) were prepared daily by dilution of the 1000 mg l⁻¹ solutions with doubly distilled water. The medium used for voltage scanning was an ammonia buffer prepared by addition of 0.2 M HNO₃ to the 30% NH₄OH until pH 8.5. Metal solutions for chemical depositions were prepared by addition the appropriate dilute metal standards to a blank medium, which was identical to the medium used for voltage scanning. Standard additions and dilution's were carried out using micropipettes. Regeneration of CME surfaces was carried out by exposure to 1 M HNO₃. Before use flasks and containers were soaked in 6 M HNO₃ for at least 24 h, then rinsed with de-ion-

ized water and equilibrated with portions of the sample for analysis.

2.3. Fresh water samples

The artificially contaminated fresh water samples were obtained by mixing tap water from the Singapore fresh water supply with Ni(II) solutions. While the samples for analysis by atomic absorption were analyzed directly, the samples for analysis by the electrochemical method were prepared by mixing 4 ml of the water sample with 6 ml of ammonia buffer.

2.4. Preparation of polymer solutions, chemically modified electrodes, and unmodified (plain) electrodes

The preparation of polymer solutions is summarized in Table 1. Three types of CME's were constructed using the polymer solutions no. 3, 4, and 5 (Table 1), respectively. All CME's were prepared by placing 5 μ l of the appropriate polymer solution on the surface of the glassy carbon electrode, and allowing the solvent to evaporate at room temperature. Unmodified (plain) electrodes were prepared in the same fashion omitting the DMG component.

Table 1
Preparation of polymer solutions

No.	Solution	Components ^a	Preparation
1	PVC-THF	PVC: 150 mg THF: 3 ml	b
2	PA-THF	THF: 3 ml PA: 50 mg	c
3	PVC-THF saturated with DMG	PVC-THF: 100 μ l DMG: 150 mg THF 5 ml	c
4	PA-THF saturated with DMG	PA-THF: 100 μ l DMG: 150 mg	c
5	PVC-PA-THF saturated with DMG	PVC-THF: 100 μ l PA-THF: 200 μ l DMG: 150 mg	c

^a THF, tetrahydrofurane; PA, polyaniline; PVC, polyvinyl chloride, DMG, dimethylglyoxime.

^b Components mixed and sonicated in an ultrasonic bath until complete dissolution. Solution stored in a vial.

^c Components mixed and sonicated in an ultrasonic bath for 10 min. Solution left to settle overnight. Precipitates removed by filtration. Filtrate stored in a vial.

2.5. Analytical procedure

The analytical procedure included the following steps.

1. Forty millilitres of ammonia buffer were placed in the electrochemical cell and purged with nitrogen gas for 5 min.
2. The CME was conditioned in the ammonia buffer and using five cyclic linear sweeps (range: +0.2 to -1.3 V, scan rate 50 mV s⁻¹) and two cyclic square wave scans (range: +0.2 to -1.22 V, frequency: 60 Hz, pulse height: 50 mV, scan increment: 2 mV). Further conditioning was carried out with the CME disconnected from the potentiostat, using a 10 s CME exposure to ammonia buffer containing 100 (M Ni(II) followed by a 30 s exposure to 1 M HNO₃ and a 30 s rinse in distilled water. This conditioning cycle was repeated five times.
3. Metallic species were chemically deposited on the conditioned CME surface. This step was carried out with the CME disconnected from the potentiostat and using a fixed time exposure of the CME to the non-deaerated, stirred (magnetic bar, 500 rpm) metal solution.
4. Metallic species attached to the CME (step 3) were quantitated voltammetrically under quiet

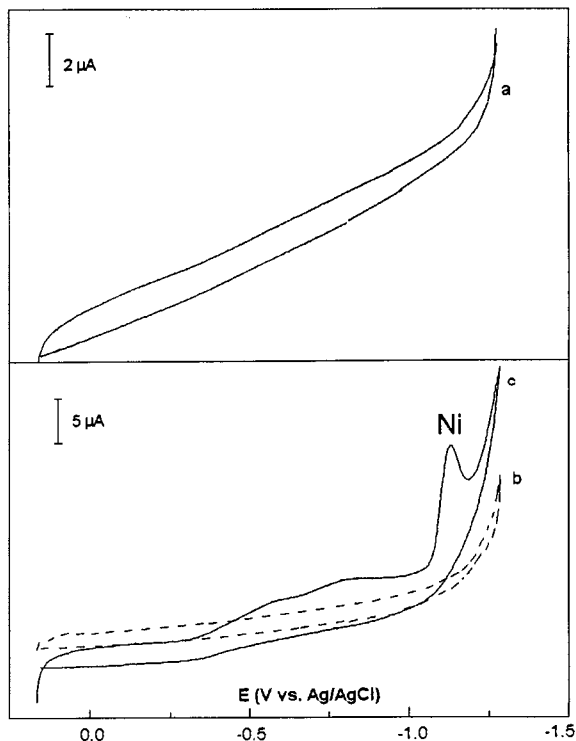


Fig. 1. Cyclic linear scan voltammograms (50 mV s^{-1} , ammonia buffer) obtained after 120 s (open loop) electrode exposures. (a) Electrode film: PVC/PA. Exposure to ammonia buffer spiked with $174 \mu\text{M Ni(II)}$. (b) Electrode film: PVC/PA/DMG. Exposure to ammonia buffer. (c) Electrode film: PVC/PA/DMG. Exposure to ammonia buffer spiked with $174 \mu\text{M Ni(II)}$.

conditions using a cathodic square wave voltammetric scan ($+0.2$ to -1.22V , frequency: 60 Hz , pulse height: 50 mV , scan increment: 2 mV) followed a potential step to $+0.2\text{V}$.

5. The CME surface was regenerated by disconnecting the CME from the potentiostat and by subsequent exposure of its surface to a 1 M HNO_3 solution which was stirred (500 rpm) with magnetic bar.
6. The analytical response (S) was obtained as the difference between the reduction peak current for the Ni(DMG)_2 -deposit and the baseline current, which was obtained at the peak potential after CME surface regeneration (step 5).

2.6. Atomic absorption measurements

The atomic absorption measurements were based on calibration against a standard curve. This curve was prepared from absorbance measurements on standard solutions, which contained $20, 25, 100, 150,$ and $200 \mu\text{g Ni l}^{-1}$.

3. Results and discussion

3.1. Choice of polymer matrix

The PVC-DMG film obtained using polymer solution 3 (Table 1) adhered well to the glassy carbon surface. However even after extended ($> 10 \text{ min}$) exposures to mM concentrations of Ni(II) no analytical signals for Ni(II) could be obtained using this type of CME. Moreover, low voltammetric background currents indicated that the conductivity of the film was too low for the voltammetric quantitation. By contrast the PA-DMG film (solution 4), gave clear voltammetric responses for nickel(II). This film, however, did not adhere well to glassy carbon. Therefore a compromise between the two types of film, a PVC-PA-DMG film (prepared from solution 5) and the corresponding unmodified PVC-PA film, was subsequently studied. As regards the unmodified electrode its PVC-PA film was clearly conductive and chemically inert with respect to Ni(II) . This aspect was demonstrated by the significant cell currents, and the featureless linear scan cyclic voltammogram, which were obtained with the electrode following a 2 min exposure to an ammonia buffer which contained 174 (M Ni(II)) (Fig. 1a). In addition to good electrical conductivity the composite PVC-PA-DMG CME exhibited an obvious reactivity with respect to Ni(II) . These properties are demonstrated in Fig. 1b and c. Shown are the featureless voltammogram obtained after a 2 min exposure of the CME to a blank ammonia buffer (Fig. 1b) and the well developed voltammetric response (from -1100 to -1200 mV) which was subsequently observed after spiking the ammonia buffer with $174 \mu\text{M Ni(II)}$ (Fig. 1c).

While this latter response increased with Ni(II) addition (cf. Section 3.4) the two responses (in the range from -500 mV to -800 mV) which were also developed after Ni(II) uptake did not. Consequently these two responses were attributed to changes in the electrode surface properties and hence its capacitance, introduced by the Ni(DMG)₂ deposit. As a consequence of these observations CME's based on the PVC-PA-DMG film (which in the dry state had a slight yellowish colour) were used for the remaining part of the study. Moreover only the response from -1100 mV to -1200 mV was used for quantitation of Ni(II).

3.2. Choice of voltage excitation waveform

Fig. 2 shows the cyclic square wave voltammograms obtained following a 240 s CME exposure to the ammonia buffer before and after spiking with $3.4 \mu\text{M}$ Ni(II). As shown the square wave excitation waveform afforded a viable approach to quantitation of the Ni(DMG)₂ deposit. Subsequent experiments revealed that the sensitivity (defined as the ratio between the analytical

response and Ni(II) concentration) for equal deposition times could be improved by a factor of ≈ 2 by utilizing square wave rather than linear scan voltammetry. Moreover, since the square wave scan was more rapidly accomplished, square wave voltammetry was chosen as the excitation waveform for the remaining part of the study.

3.3. Regeneration of the chemically modified electrode surface

Experiments showed that deposits of Ni(DMG)₂ on the CME could be dissolved by exposure to 1 M HNO_3 . The time required for complete removal of Ni deposits were typically longer than the 5 s, which were sufficient for CME's based on DMG containing carbon paste [11]. This observation was attributed to slower transport of HNO_3 and the Ni(DMG)₂ complex within the polymer matrix. However, experiments also showed that if the CME was exposed for 2 min to 1 M HNO_3 (stirred with a magnetic stirrer bar, 500 rpm) all evidence of previous exposure to Ni(II) was removed such that subsequent voltage scanning resulted in featureless voltammograms like Fig. 1b. As a consequence of this observation a regeneration time of 2 min was chosen for the remaining part of the study.

3.4. Characterization of the chemically modified electrodes

The surface to surface reproducibility for the CME's was studied by observing the variation in Ni(II)-responses obtained using ten different CME's under identical conditions (240 s chemical depositions from $3.0 \mu\text{M}$ Ni(II)). While the variation obtained in this case was rather large (relative standard deviation: 16%, the variation for a single electrode surface was considerably smaller: More specifically, once a single CME had been conditioned its surface could be used for at least 10 cycles of Ni(II)-accumulation (240 s from $3.0 \mu\text{M}$ Ni(II)), voltage scanning, and acid regeneration with no systematic drift in its chemical affinity to the analyte and a relative standard deviation ($n = 10$) of only 4%. Experiments carried with such conditioned CME's showed that the analytical

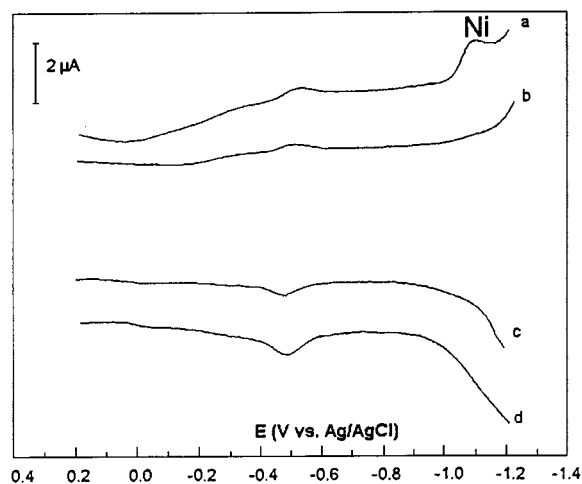


Fig. 2. Cyclic square wave voltammograms (frequency: 60 Hz, pulse height: 50 mV, scan increment: 2 mV) obtained after 240 s (open loop) exposures of the PVC/PA/DMG-CME to the blank ammonia buffer and the ammonia buffer spiked with $174 \mu\text{M}$ Ni(II). (a) cathodic scan, spiked buffer. (b) cathodic scan, blank buffer. (c) anodic scan, blank buffer. (d) anodic scan, spiked buffer.

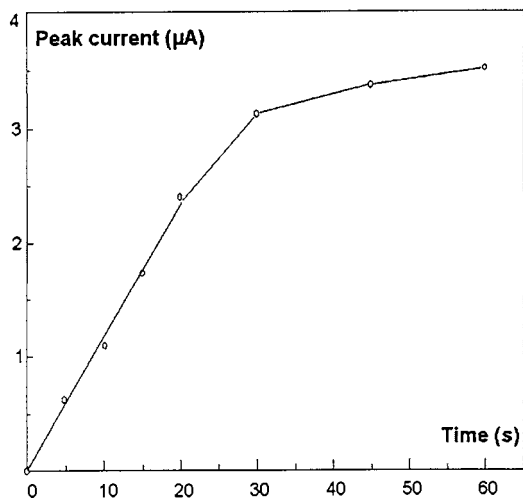


Fig. 3. Plot of voltammetric peak current against chemical deposition time. Deposition solution: ammonia buffer spiked with 17.4 μM Ni(II).

Ni-response, and hence the sensitivity of the analytical procedure, increased with the chemical deposition time. Experiments also revealed that the increase in sensitivity was larger for shorter exposures of the CME, an effect, which was attributed

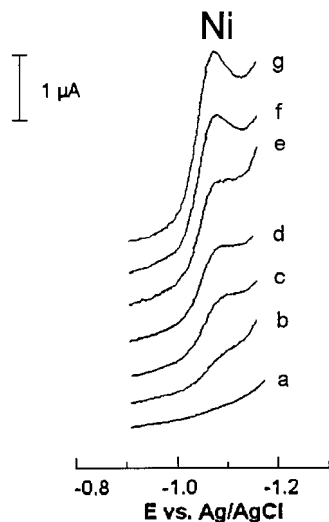


Fig. 4. Cathodic square wave voltammograms obtained after 240 s exposures of an acid regenerated CME surface to ammonia buffer spiked with increasing concentrations of Ni(II). Ni(II) concentration: (a) 0.00 μM , (b) 0.34 μM , (c) 0.68 μM , (d) 1.02 μM , (e) 1.36 μM , (f) 2.04 μM , (g) 3.00 μM .

to gradual saturation of the CME-surface for longer deposition periods. This aspect is illustrated in Fig. 3, which shows the plot of the voltammetric peak current against chemical deposition time for ammonia buffer spiked with 174 (M Ni(II). For a constant chemical deposition time the analytical Ni-signal increased with increasing concentrations of Ni(II). This increase is shown in Fig. 4 which was obtained after 240 s exposures of the CME surface to the blank ammonia buffer and to the buffer spiked with Ni(II) in concentrations ranging from 0.34 to 3.00 μM . For the six standard additions shown in Fig. 4 the analytical response, S (μA), (cf. step 6 of the analytical procedure outlined in the experimental section) was a linear function of the Ni(II)-concentration, C (μM), (regression line: $S = 0.237 + 0.837C$; correlation coefficient: 0.986). Further standard addition resulted in gradually decreasing sensitivity (i.e. negative deviation from linear behaviour). As above, this effect was attributed to saturation of the available CME-binding sites. However, since the linear range was sufficiently wide for quantitative determination of Ni(II) by the standard addition method, this approach was used for the remaining part of the study.

Repetitive experiments in which 240 s chemical deposition was carried out from ammonia buffers spiked with 0.34 μM Ni(II) resulted in weak, yet clearly discernible, Ni-responses analogous to Fig. 4 b. Consequently, for a 240 s deposition from ammonia medium, the limit of detection for Ni(II) (signal/noise > 3) was of the order of 0.3 μM or about 18 $\mu\text{g Ni l}^{-1}$. Thus, since Ni(II) concentrations in aquatic medium below the 100 $\mu\text{g Ni l}^{-1}$ level are considered harmless to aquatic organisms and irrigated plants, it was concluded that the CME technique was useful for detection of Ni(II) in a range of concentrations which are of interest in an environmental context.

As shown in Fig. 5 the Co(II)-addition experiments revealed, that the CME could indeed accumulate Co(II). However the reduction of the Co(DMG)₂-complex took place at a potential, which was about 180 mV more positive than that for the reduction of the Ni(II)-deposit. Moreover, for a chemical deposition of 240 s the addition of 24 μM Co(II) did not influence the signal from 3.4 μM Ni(II).

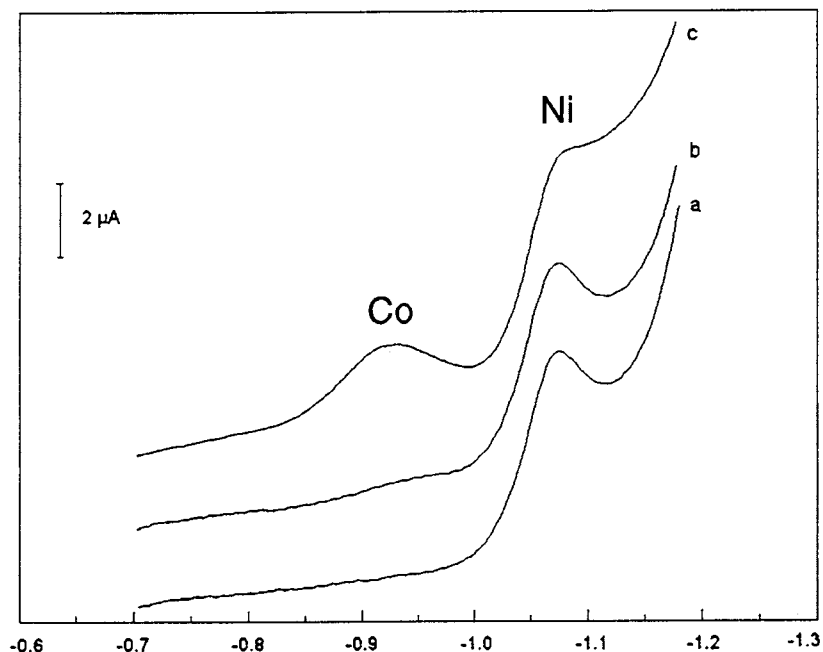


Fig. 5. Effect of Co(II) additions on the CME-response for Ni. Chemical deposition for 240 s from 3.40 μM Ni(II) in ammonia buffer. Co(II) concentration added: (a) 0.00 μM , (b) 22.1 μM , (c) 124.0 μM .

3.5. Long term CME-stability

Once a CME-surface had been conditioned it could be used for extended periods of time. In fact, if the CME was stored in distilled water overnight, the decrease in sensitivity to Ni(II) observed over a 2 day period was less than 10%. Thus, when operated under analogous conditions and without the complications of a closed flow system, the polymer based CME was stable for much longer than the 3 h during which the carbon paste CME lost its activity [11].

3.6. Water analysis

The CME-analysis revealed that the fresh water samples were such that their Ni(II) concentrations could not be detected following a 240 s chemical deposition. In other words, their Ni(II) concentrations were lower than the 18 $\mu\text{g Ni l}^{-1}$ limit of detection and well below the above mentioned 100 $\mu\text{g Ni l}^{-1}$ safety level. In view of these observations the performance of the CME was studied

after introducing an artificial contamination of the fresh water. This contamination was introduced in such a way that results for Ni(II) could be obtained using both the CME technique and AAS. The CME and the AAS results for eight separate analyses of the Ni(II)-contaminated fresh water are given in Table 2. As shown the results obtained by the polymer coated CME were almost indistinguishable from those obtained by AAS.

Table 2

Mean value^a and 95% confidence limits of CME^b and AAS^c results for Ni(II) in contaminated fresh water

CME results:	$45.1 \pm 0.5 \mu\text{g Ni l}^{-1}$
AAS results:	$45.0 \pm 1.2 \mu\text{g Ni l}^{-1}$

^a Number of experiments: $n = 8$.

^b CME results obtained using a 240 s chemical deposition and standard addition.

^c AAS results obtained using calibration. Calibration line obtained by linear regression of absorbance measurements (A) on Ni(II)-standards (C $\mu\text{g Ni l}^{-1}$): $A = -0.00056 + 0.0070 \cdot C$; Correlation coefficient: 0.9997.

4. Conclusions

In view of these results it was concluded that the polymer coated CME, like the analogous graphite paste CME's, could be used for the determination of traces of Ni(II). It was also concluded the CME procedure was sufficiently sensitive to be used for concentration levels, which are of interest in an environmental context. In addition, it was observed that the CME results for Ni(II) in fresh water compared favourably with results obtained by the well established AAS technique. Finally the long term stability of the polymer based CME was better than that observed for the analogous carbon paste CME. This stability suggests, that conductive polymer–ligand based CME's should be further studied for their suitability in practical applications.

Acknowledgements

This work was supported by the National Institute of Education Research Fund, Grant no. RP 24/92 LK. Chen Bing acknowledges a scholarship granted by the National Institute of Education. The authors wish to thank Arne Lindahl for technical assistance.

References

- [1] R.E. Train, *Quality Criteria for Water*, Castle House Publications Ltd, 1979, pp. 105–106.
- [2] L. Kryger, S.K. Lee, *Biogeochem.* 35 (1996) 367.
- [3] L. Kryger, S.K. Lee, *Environ. Int.* 21 (1995) 85.
- [4] J.K. Christensen, L. Kryger, N. Pind, *Anal. Chim. Acta* 141 (1982) 131.
- [5] B. Chen, L. Kryger, *Bull. Singapore Nat. Inst. Chem.* 23 (1995) 91.
- [6] R.W. Murray, What chemically modified electrodes are and why they are interesting, in: A.J. Bard (Ed.), *Electroanalytical Chemistry*, Marcel Dekker, New York, 1984, vol. 13, pp. 191–368.
- [7] *Sensor Electrodes*, L. Kryger, L. (Ed.), *Talanta Special Issue*, Pergamon Press, Oxford, January 1991.
- [8] J.F. Price, R.P. Baldwin, *Anal. Chem.* 52 (1980) 1940.
- [9] G.T. Cheek, R.F. Nelson, *Anal. Lett.* 11 (1978) 393.
- [10] J.A. Cox, M. Majda, *Anal. Chem.* 52 (1980) 861.
- [11] R.P. Baldwin, J.K. Christensen, L. Kryger, *Anal. Chem.* 58 (1986) 1790.
- [12] S.V. Prabhu, R.P. Baldwin, L. Kryger, *Electroanalysis* 1 (1989) 13.
- [13] L.D. Kong, L. Kryger, J.K. Christensen, K.N. Thomsen, *Talanta* 38 (1991) 101.
- [14] J.A. Cox, P.J. Kulesza, *Anal. Chim. Acta* 154 (1983) 71.
- [15] J. Wang, B. Greene, C. Morgan, *Anal. Chim. Acta* 158 (1984) 15.
- [16] P. Hernández, E. Alda, L. Hernández, *Fresenius Z. Anal. Chem.* 327 (1987) 676.
- [17] J. Wang, T. Martinez, *Anal. Chim. Acta* 207 (1988) 95.
- [18] C.G. Murray, R.J. Nowak, D.R. Rolison, *J. Electroanal. Chem.* 164 (1984) 205.
- [19] B. Chen, L. Kryger, *Talanta* 43 (1996) 153.
- [20] L.M. Wier, A.R. Guadalupe, H.D. Abruña, *Anal. Chem.* 57 (1985) 2009.
- [21] K.N. Thomsen, L. Kryger, R.P. Baldwin, *Anal. Chem.* 60 (1988) 151.
- [22] M.E.R. Dam, K.N. Thomsen, P.G. Pickup, K.H. Schröder, *Electroanalysis* 7 (1995) 57.
- [23] A.G. MacDiarmid, J.C. Chiang, A.F. Richter, A.J. Epstein, *Synth. Met.* 18 (1987) 285.

Potentiometric detection of ascorbate using a graphite carbon electrode

ZuLiang Chen ^{a,*}, Jimmy C. Yu ^b

^a Department of Plant Sciences, The University of Western Australia, Nedlands, WA 6907, Australia

^b Department of Chemistry, The Chinese University of Hong Kong, Shatin, NT, Hong Kong, People's Republic of China

Received 28 September 1998; received in revised form 3 February 1999; accepted 4 February 1999

Abstract

A graphite carbon electrode was used for the potentiometric detection of ascorbate. The electrode exhibits a linear response with a slope of -42 ± 1.0 mV decade⁻¹ in concentrations ranging from 5×10^{-4} to 5.0×10^{-2} M in 0.1 M NaOH solution with a detection limit of 5.0×10^{-6} M. The response mechanism of this electrode was investigated by potentiometry, voltammetry, and scanning electron microscopy (SEM), and it suggests that the electrode potential change resulted from the ion-exchange adsorption and subsequent oxidation of ascorbate on the electrode surface at pH 12–13. The electrode exhibits high sensitivity, selectivity and reproducibility. © 1999 Elsevier Science Ireland Ltd. All rights reserved.

Keywords: Ascorbate; Graphite carbon electrode; Potentiometric detection

1. Introduction

The detection of l-ascorbic acid in biological samples has long been essential in bioanalysis. Electroanalytical methods such as voltammetry and amperometry have been widely used in the detection of ascorbic acid due to its electroactive substance [1,2]. Much attention has been focused on the development of various chemically modified electrodes, where immobilized reagent on the surface of the electrode. Consequently, chemically modified electrodes were constructed and used for the determination of ascorbic acid in

which the overpotential for the ascorbic acid oxidation was reduced by electrocatalytic oxidation due to the coating of the reagent at the electrode surface. Such recently reported reagents include ferrocen derivatives [3], polypyrrole–dodecyl sulphate [4], poly(glycine) [5], and poly(indole-3-acetic acid) [6], which have been used in voltammetric detection of ascorbic acid. Amperometric sensors based on chemically modified electrodes are frequently used for the determination of ascorbic acid [7–9]. Despite the sensitivity and selectivity of chemically modified electrodes, response is subject to electrode fouling by oxidation products[10], and hence the electrodes require regeneration to obtain reproducible response.

* Corresponding author. Fax: +61-08-93801108.

E-mail address: zchen@agric.uwa.edu.au (Z. Chen)

Potentiometric detection should be possible for continuous monitoring use due to its stability and reproducibility. However, the use of a potentiometric sensor for the detection of ascorbic acid has received little attention, particularly the use of a carbon-based electrode [1,2]. A sensor using ferrocene modified on a platinum wire was developed to detect ascorbic acid with a response slope of -50 mV decade $^{-1}$ [11]. Further, a carbon microfiber electrode with a base coat of an electrodeposited cobalt chelate of a cobalt tetramethylpyridopyrroazine derivative has been reported. This electrode had a linear response to ascorbic acid in the concentration range from 1×10^{-6} to 1×10^{-2} M with a super-Nernstian slope of -62 mV decade $^{-1}$ [10]. More recently, a carbon electrode based on the mixture of spectroscopic graphite powder and di-iso-octylphthalate has been constructed, and the electrode responded to ascorbic acid with slope -95 mV decade $^{-1}$ [12].

In a previous paper, a spectroscopic graphite electrode was used as a sensor for the potentiometric detection of Fe^{3+} with high sensitivity and good selectivity in 0.1 M H_2SO_4 solution. The mechanism of this electrode involves the process of adsorption and reduction of Fe^{3+} at the electrode surface [13]. We report here on the use of a graphite carbon electrode for the potentiometric detection of ascorbate because of its ruggedness, sensitivity, simplicity and low cost [1]. This study involved (1) cyclic voltammetry, potentiometry and SEM to elucidate the electrochemical behaviours of ascorbate at a graphite carbon electrode, and (2) the effect of pH and interference of other anions on the electrode response.

2. Experimental

2.1. Reagents and solution

All reagents were of analytical grade. Standard ascorbic solutions were prepared in Milli-water. The others chemicals were obtained from Merck, BDH, May and Baker and Ajax. All correspond-

ing solutions were prepared in 0.1 M NaOH solution.

2.2. Graphite electrode

A spectroscopic graphite rod (5×40 mm, Aldrich, Sydney, Australia) and Ag–AgCl electrode (model 90-01 Orion single-junction reference electrode with saturated potassium chloride) were used as the indicator and reference electrodes, respectively. The graphite electrode was sealed into the polyethylene tube and connected with a shielded wire. Prior to experiments, the electrode was polished manually on a cloth with an aqueous slurry of $3 \mu\text{m}$ alumina (Buehler, Lake Bluff, USA). The electrochemical cell used for potential measurements was:

Graphite electrode | Ascorbate, 0.1 M NaOH solution || 0.1 M KCl, AgCl(s) | Ag

2.3. EMF measurements

All EMF measurements were carried out using a home-made digital mV meter in combination with a PC computer via interface for data recording. The ascorbic acid concentrations in this study ranged from 1.0×10^{-6} – 5.0×10^{-2} M. The interference effect of organic acid and anions on the potential response of the electrode to ascorbic acid was studied in 0.1 M NaOH solution with 5×10^{-4} M ascorbic acid by mixed method [14]. Each solution was stirred continuously and its potential was measured at a steady state at 25°C .

2.4. Cyclic voltammetry

Voltametric measurements were performed using a BAS-100 B (Bioanalytical System, West Lafayette, IN, USA) electrochemical analyzer with a three-electrode cell using graphite carbon as a working electrode, Ag–AgCl as a reference electrode and platinum wire as an auxiliary electrode. The carbon graphite electrode was polished prior to each CV measurement. During each measurement nitrogen gas was passed over the solution.

2.5. Scanning electron microscopy (SEM) measurement

The surface of the electrode was examined using a JEOL 6300 field emission scanning electron microscope (FESEM). Composition of the electrode surface was determined using energy dispersive X-ray spectroscopy (EDS) at 8 kV and Phi-Rho-Z ($\phi(\rho z)$) quantitative analysis technique.

3. Results and discussion

3.1. Voltammetry

Cyclic voltammetry was used in an attempt to elucidate ascorbate behaviour at the electrode surface. Fig. 1 shows cyclic voltammograms recorded with a graphite carbon electrode in a 0.1 M NaOH solution against a AgCl–Ag reference

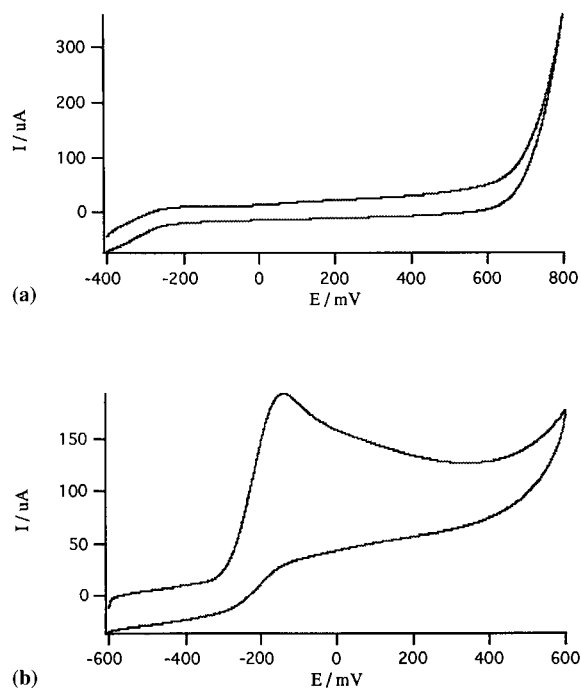


Fig. 1. Cyclic voltammograms of the electrode in a 0.1 M NaOH solution against AgCl–Ag reference electrode at a scan rate of 100 mV s^{-1} . (a) 0.1 M NaOH solution, (b) 0.001 M ascorbate acid in 0.1 M NaOH solution.

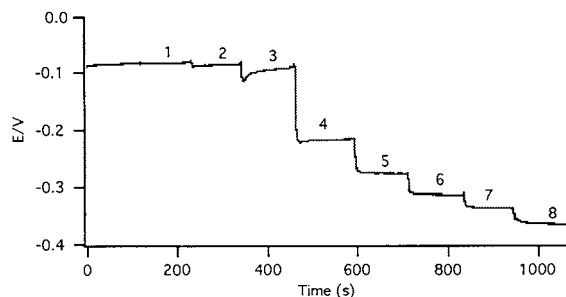


Fig. 2. A typical electrode response to ascorbate obtained at the graphite carbon electrode by steady-state measurement. (1) 5×10^{-6} , (2) 2.5×10^{-5} , (3) 5×10^{-5} , (4) 2.5×10^{-4} , (5) 5.0×10^{-4} , (6) 2.5×10^{-3} , (7) 5.0×10^{-3} , and (8) 5.0×10^{-2} M. Electrolyte solution, 0.1 M NaOH.

electrode at a scan rate of 100 mV s^{-1} . Fig. 1(a) was obtained from the blank solution. No oxidation peaks were observed in the cyclic voltammogram. In contrast, as shown in Fig. 1(b), an oxidation peak appeared at approximately -160 mV in the presence of 1 mM ascorbate in the 0.1 M NaOH solution. A similar behaviour was observed with the use of a glassy carbon electrode for the voltametric detection of ascorbate, where ascorbate appeared to adsorb onto the electrode surface and irreversible oxidation at glassy carbon electrode surface [15]. Thus, a preliminary adsorption equilibrium, and subsequently the irreversible oxidation of ascorbate on the electrode surface was possible.

3.2. Potentiometry

A typical dynamic potentiometric response of the electrode to ascorbate in 0.1 M NaOH solution is shown in Fig. 2. The response of the electrode is fast, reaching a steady-state in a relatively short time ($< 45 \text{ s}$) for ascorbate in the concentration range of 1×10^{-4} to 1×10^{-2} M. However, the electrode has a relatively long equilibrium time ($> 45 \text{ s}$) for concentrations of ascorbate below 1×10^{-4} M. It was observed that the electrode potential returned to the original potential when the electrode was placed in 0.1 M NaOH solution (without ascorbate), which indicated that the adsorption of ascorbate on the electrode surface was reversible.

Table 1

Response characteristics of ascorbate acid on the graphite carbon electrode in 0.1 M NaOH solution

Parameters	
Linear range (M)	5.0×10^{-4} to 5.0×10^{-2}
Slope(mV/log C)	-42 ± 1.5
Response time (s)	<60
pH range	12–13
Detection limits (M)	5.0×10^{-6}

The response characteristics of the electrode were evaluated by the recommendation of IUPAC[16]. The data from Fig. 2 were plotted and the correlation between potential against the ascorbate concentration determined. The electrode has a linear response to ascorbate with a slope of -42 ± 1.0 mV decade⁻¹ in the concentration range from 5×10^{-4} to 5×10^{-2} M (R^2 , 0.999). A detection limit with signal to noise ratio (S/N) equal to 3 was estimated to be 5×10^{-6} M. The response characteristics are listed in Table 1.

Interference from a variety of anions was studied by the mixed solution method [14], where the solution contained a fixed concentration of ascorbate (5×10^{-4} M) in 0.1 M NaOH and various concentrations of interfering ions. The selectivity coefficients are listed in Table 2. Clearly, the selectivity coefficient levels for the interferences tested were in the order of 10^{-4} or lower. This demonstrates that interference does not hinder the determination of ascorbate and the graphite electrode exhibits high selectivity in 0.1 M NaOH solution.

Table 2

Selectivity coefficients using the mixed method for the graphite carbon electrode in 0.10 M NaOH

Interfering anion	$\log K_{ij}^{\text{pot}}$	Interfering anion	$\log K_{ij}^{\text{pot}}$
Cl ⁻	1.2×10^{-4}	Benzoate	3.7×10^{-4}
SO ₄ ⁼	3.4×10^{-4}	l-Histidine	5.4×10^{-4}
HPO ₄ ²⁻	4.5×10^{-4}	Citrate	4.9×10^{-4}
SO ₃ ⁼	2.12×10^{-4}	Tartrate	5.0×10^{-4}
	2.7×10^{-4}	Oxalate	3.8×10^{-4}

While the electrode shows high sensitivity and selectivity towards ascorbate in alkaline solution, the drift of the potential is of concern for continuous monitoring. Hence, the study of EMF stability of the electrode was also carried out. The average potential reading obtained from ten measurements for the 5×10^{-4} M ascorbate was -185 ± 2.5 mV with a 1.4 RSD%, showing the electrode has a good reproducibility. The drift rate was 0.5 mV h⁻¹ after the electrode was equilibrated with 5×10^{-4} M ascorbate solution and the noise level was about 0.1 mV.

The influence of the electrolyte pH on the electrode response was tested in the 0.1 M NaOH solution containing 5×10^{-4} M ascorbate. The electrode response decreased as pH dropped from 13–11. Such an effect may result from the graphite electrode suffering from H⁺ interference because the surface oxidation of graphite electrode creates an ion-exchange layer, which confers some degree of the selective response [17]. Consequently, the adsorption of ascorbate on the electrode surface by ion-exchange decreased as the electrolyte pH decreased. The specificity of ion-exchange on the electrode surface may also explain why the graphite carbon electrode responds to ascorbate with high selectivity and then is oxidized by the dissolved oxygen in 0.1 M NaOH solution.

3.3. Scanning electron microscopy (SEM)

In spite of the fact that the nature of this mechanism is not fully understood, we suggest that the observed electrode response to ascorbate in 0.1 M NaOH solution may be attributed to the ion-exchange occurring between the electrode surface and ascorbate [18]. The results show that the electrode surface contains pores of varying size which may affect ion-exchange adsorption of ascorbate onto the electrode surface and electrolyte diffusion (i.e. electrolyte concentration in the pores differs from that outside the pores). Ion-exchange on the electrode surface and then oxidation of ascorbate seems probable at the porous electrode surface [17]. SEM quantitative analysis showed that the surface of the electrode, which was thoroughly washed with distilled water

after being used, contained hydrogen and oxygen elements which may facilitate adsorption of ascorbate.

4. Conclusion

The spectroscopic graphite carbon electrode described here is useful as a low cost sensor for the potentiometric detection of ascorbate in alkali electrolyte. It offers high sensitivity, selectivity and stability with lost cost. The data obtained from cyclic voltammetry, potentiometry and scanning electron microscopy, suggest that the electrode response to ascorbic acid may result from the adsorption of ascorbate on the electrode surface by ion-exchange and then oxidation at high pH solution. Such an electrode is suitable for the direct potentiometric detection of ascorbate, as well as being used as a means of end-point detection of ascorbate redox titrations.

Acknowledgements

The authors thank the reviewers for their valuable suggestions on the manuscript.

References

- [1] K. Kalcher, M.J. Kauffmann, J. Wang, I. Svancara, K. Vytras, C. Neuhold, Z. Yang, *Electroanalysis* 7 (1995) 5.
- [2] K. Kalcher, *Electroanalysis* 2 (1990) 419.
- [3] M. H. Pournaghizar, R. Ojani, *Talanta* 42 (1995) 1839.
- [4] Z.Q. Gao, B. Chen, M.X. Zi, *J. Electroanal. Chem.* 365 (1994) 197.
- [5] A.M. Yu, H.L. Zhang, H.Y. Chen, *Electroanalysis* 9 (1997) 788.
- [6] A.M. Yu, D.M. Sun, H.Y. Chen, *Anal. Lett.* 30 (1997) 1643.
- [7] I.G. Casella, M.R. Guascito, *Electroanalysis* 9 (1997) 1381.
- [8] L.E. Leon, *Talanta* 43 (1996) 1275.
- [9] H.M. Li, R.L. Ge, E.K. Wang, *Anal. Chim. Acta* 292 (1994) 107.
- [10] H. Lerner, J. Giner, J.S. Soeldner, C.K. Colton, *J. Electrochem. Soc.* 126 (1979) 43.
- [11] M. Petersson, *Anal. Chim. Acta* 147 (1983) 359.
- [12] X. Hu, Z. Leng, *Anal. Lett.* 28 (1995) 2263.
- [13] Z. Chen, X. Yang, X. Lu, *Electroanalysis* 10 (1998) 567.
- [14] K. Srinivasan, G.A. Rechnitz, *Anal. Chem.* 41 (1969) 1203.
- [15] E.M. Strochkova, Y.I. Turyan, I. Kuselman, A. Shenhar, *Talanta* 44 (1998) 1923.
- [16] IUPAC Analytical Chemistry Division, Commission on Analytical Nomenclature. Recommendations for nomenclature of ion selective electrodes. *Pure Appl. Chem.* 48 (1976) 127.
- [17] D. Midgley, D.E. Mulcahy, *Ion-Sel. Electrode Rev.* 5 (1983) 165.
- [18] H.V. Malmstadt, D.A. Vassallo, *Anal. Chem.* 31 (1959) 862.

The use of polymers coupled with metallised electrodes to allow H₂O₂ detection in the presence of electrochemical interferences

D.J. Daly, C.K. O'Sullivan, G.G. Guilbault *

Laboratory of Sensor Development, Department of Chemistry, University College Cork, Cork, Ireland

Received 1 July 1998; received in revised form 21 December 1998; accepted 12 February 1999

Abstract

One of the most important parameters to be considered when developing a biosensor based on the use of oxidase enzymes is the selective determination of H₂O₂ in the presence of easily oxidisable interferents. In this work one approach was taken to overcome this problem—the use of metallised carbon electrodes in conjunction with polymers. Polymers, both conducting and nonconducting, have recently become very interesting materials for the suppression of interferences. They are easy to grow on any electrode surface and the extensive range of polymers available provides a huge scope for the large variety of sensors that exist today. They can be grown in organic or aqueous media. In this work, three polymers (polypyrrole, polyaniline and 1,3-diaminobenzene) were examined for their interferent—preventing potential on several types of electrodes. Previous work carried out at the Laboratory of Sensor Development has shown the co-deposition of ruthenium and rhodium on carbon to provide an electrode surface which is highly catalytic and selective towards H₂O₂ [1]. The co-deposition of Ru, Rh and Pt, as well as Pt on Ru–Rh electrodes was investigated and all these transducers were coupled with the use of the polymers for enhanced elimination of interferences with highly promising results obtained. The best system was seen to be a Ru–Rh metallised electrode polymerised with poly(1,3-diaminobenzene). At an applied potential of +100 mV the response to H₂O₂ was ≈200 times greater than the response of any of the potential interferences. © 1999 Elsevier Science B.V. All rights reserved.

Keywords: H₂O₂ detection; Metallisation; Biosensors; Electropolymerisation

1. Introduction

A biosensor may be defined as a sensor that utilises a biological sensing component and a

transducer that changes this response into an analytically useful signal. One of the greatest problems encountered in the development of biosensors based on H₂O₂ detection is the effect of electrochemical interferents. Two approaches can be taken—to lower the applied potential required for the detection of H₂O₂ by the use of mediators or metallised surfaces and the use of

* Corresponding author. Tel.: +353-21-902403; fax: +353-21-903103.

E-mail address: stch8059@ucc.ie (G.G. Guilbault)

polymers or membranes to allow selective detection of H_2O_2 based on ‘sieving’ properties of charge and size.

Various types of polymers have already been exploited for constructing electrochemical sensors, especially the glucose biosensor [2–24]. Polymers have many advantages over traditional membranes. Their growth and thickness can be easily controlled, and their physical and chemical properties can be changed by the incorporation of various counter ions. They also have many uses in chromatography [25–29]. The pore size of polymers can also be of use in the blocking of interferents from the electrode.

The main polymers used for the above applications and others are poly(pyrrole) [30–35], poly(aniline) [36–40] and poly(thiophene) [41–45]. Of these three polymers, poly(pyrrole) is regarded as the most useful. Since it is electropolymerised in aqueous media at a neutral pH, there is a large range of counterions that can be incorporated. Poly(aniline) suffers from the fact that it must be produced in acidic media, and thiophene is only soluble in organic solvents. Substituted pyrroles have also been used [46–50]. The polymers mentioned are also electroactive, i.e. they are capable of being oxidised or reduced themselves.

Nonconducting polymer films, such as poly(1,2-diaminobenzene) have also been used [51–54]. They impart a film of uniform thickness, unlike conducting polymer films. This occurs because, when the polymer forms on the electrode surface, it forms an insulating layer beyond which no more electropolymerisation can take place [53,55]. Conducting polymers, such as poly(pyrrole), on the other hand, form a conducting layer on the electrode surface which can then be polymerised further. Thus, there are a lot more variables affecting polymer film thickness and reproducibility for conducting polymer films. Since nonconducting polymers are not electroactive or conducting, they are mainly used for blocking interferents and for the immobilisation of biocomponents [51,52,55,56].

There are several methods of depositing polymers on surfaces. *Solvent casting* has been used extensively for application of films to elec-

trodes. The method consists of applying a polymer solution to the electrode surface. The film is formed by evaporation of the polymer solution. *Spin coating* produces a film of uniform thickness on an electrode surface. The polymer solution is dropped onto an electrode surface which is rotating at an extremely high speed. The film is then air-dried. This procedure is mainly used in the electronics industry [57]. It is also possible to *physically adsorb* a polymer film onto an electrode surface, but the method suffers from the inability to control the film thickness. This technique often precedes electropolymerisation.

Electropolymerisation is the preferred method of polymer film formation [15,58–62]. Faraday’s law governs this method [63]. Current density determines the rate at which polymer film formation occurs and the total amount of charge transferred influences the amount of polymer generated. There are several techniques available for polymer film formation via electropolymerisation-potential cycling, fixed potential, pulsed potential and galvanostatic methods are all viable and have been used [56]. Polymerisation at a fixed potential is the method by which the polymer films were produced in this report.

2. Experimental

All solutions were prepared using doubly distilled water. L-cysteine ($\text{C}_3\text{H}_7\text{NO}_2\text{S}\cdot\text{HCl}\cdot\text{H}_2\text{O}$), uric acid ($\text{C}_5\text{H}_4\text{N}_4\text{O}_3$), potassium chloroplatinate (K_2PtCl_6), 1,3-diaminobenzene ($\text{C}_6\text{H}_8\text{N}_2$), aniline ($\text{C}_6\text{H}_7\text{N}$), ruthenium and rhodium atomic absorption standard solutions were obtained from Sigma (Poole, England). Potassium hydroxide pellets (KOH), dipotassium hydrogen phosphate (K_2HPO_4), L-ascorbic acid ($\text{C}_6\text{H}_8\text{O}_6$), and sodium chloride (NaCl) were purchased from Merck (Poole, England). Disodium hydrogen phosphate (Na_2HPO_4), and potassium chloride (KCl) were obtained from Analar (Poole, England). Pyrrole ($\text{C}_4\text{H}_5\text{N}$) was supplied from Fluka Chemika (Gillingham, England).

3. Procedure

The polymer films were produced on metallised electrodes by a fixed potential method applied by an Amperometric Biosensor Detector, Model 3001, (Universal Sensors Inc., New Orleans, USA) Metallisation and all cyclic voltammograms were performed using the Autolab Electrochemical Analyser, which was controlled by the software package GPES 4.4 (Utrecht, Holland). Metallisation and electropolymerisation were both performed using a three-electrode system. The reference electrode was an Ag–AgCl electrode and the counter electrode was a Pt wire. The working electrodes used were glassy carbon (diameter, 3×10^{-3} m, working area, 5.58×10^{-5} m²) and platinum disc (diameter, 1.5×10^{-3} m, working area, 1.45×10^{-5} m²) electrodes. Before use, the glassy carbon electrodes were hand polished with 0.05 μ m alumina slurry for ca. 5 min and then sonicated in doubly distilled water for 3 min. All solutions were deoxygenated by bubbling with nitrogen for 10 min. A nitrogen atmosphere was maintained throughout the metallisation. Platinised glassy carbon electrodes (working area, 1.36×10^{-4} m²) were prepared by cycling the potential in a 1 mg ml⁻¹ solution of potassium chloroplatinate in phosphate buffer at pH 7.4 from -0.75 to $+0.25$ V versus Ag–AgCl for 30 scans at 0.05 V s⁻¹.

For Ru–Rh–Pt metallised electrodes (working area, 9.12×10^{-5} m²), the concentration of each metal was 333.3 μ g ml⁻¹, so that the total metal concentration was 1 mg ml⁻¹. Similarly, for the Ru–Rh metallised electrodes (working area, 9.80×10^{-5} m²), the concentration of each of the metals was 500 μ g ml⁻¹. For the Ru–Rh–Pt and Ru–Rh solutions, the pH was adjusted to 2.5 by addition of concentrated KOH solution. For all metallisations the glassy carbon electrode was activated before use. Activation of the glassy carbon electrodes improves electrochemical response, reversibility, sensitivity and dynamic range. This appears to be a result of the formation of a graphite oxide film which appears when the electrode is subjected to high positive potentials in neutral media [64]. The metallisation was accomplished by scanning from -0.625 to 1.0 V versus

Ag–AgCl for the Ru–Rh–Pt and Ru–Rh electrodes. This potential range had previously been determined to be the optimum range for metallisation of Ru–Rh and Ru–Rh–Pt in this laboratory [1]. After metallisation, the electrodes were stored at room temperature with plastic caps protecting the surfaces.

4. Results/discussion

4.1. Metallisation

Typical cyclic voltammograms of some metallised surfaces on glassy carbon electrodes are shown in Figs. 1–4. The first cyclic voltammogram (Fig. 1) is that of codeposited Ru–Rh on glassy carbon. On the cathodic wave, two peaks are visible: at -0.08 and -0.45 V. One peak is seen on the anodic wave at -0.25 V. The peaks visible at -0.45 and -0.25 V are characteristic for adsorption/desorption of the H₂ molecule [65]. The second cyclic voltammogram is that of Ru–Rh–Pt on glassy carbon. It is almost exactly the same as the cyclic voltammogram for Ru–Rh on glassy carbon (Fig. 2). Due to the similarity of both cyclic voltammograms, it is reasonable to assume that there is very little platinum deposited on the Ru–Rh–Pt electrode. The third cyclic voltammogram (Fig. 3) is Pt deposited on the Ru–Rh electrode, the Ru–Rh electrode having been previously metallised onto a glassy carbon electrode. This looks totally different from the previous two cyclic voltammograms. Two peaks are visible on the anodic wave and one on the cathodic wave. The peak on the cathodic wave is at -0.16 V and the anodic peaks are at -0.02 and -0.2 V. Again the peak at -0.2 V is due to H₂ adsorption/desorption, where the peak at the more negative potential may have been suppressed. The presence of the other peaks may indicate that the metal is depositing onto the glassy carbon electrode.

The cyclic voltammogram depicted in Fig. 4 is that of Pt metallised on a glassy carbon electrode. There are four peaks visible: at -0.2 and -0.02 V on the forward sweep and at -0.21 and -0.55 V on the negative sweep. These are due

again to H₂ adsorption/desorption and to the oxidation of Pt (0) to Pt (II) to Pt (IV) and the reduction back to Pt (0). The peaks are very well defined compared to Fig. 3, that of Pt on Ru–Rh, possibly demonstrating the better surface of the glassy carbon electrode compared to that of the Ru–Rh electrode.

4.2. Polymerisation

The electrodes to be examined were tested initially at +650 mV (the applied potential required

for electrocatalysis of H₂O₂ using non-membrane electrodes) without a polymer on the surface for comparison purposes with H₂O₂, together with the major interferents in blood serum; L-ascorbic acid, acetaminophen (paracetamol), L-cysteine and uric acid, as these are among the major interferents in blood serum. All amperometry was carried out at room temperature in a quiescent solution. The electrodes were also tested at +100 mV, as this applied potential was shown in our laboratory to be the most useful for a maximum H₂O₂: interferent ratio. The results are shown in

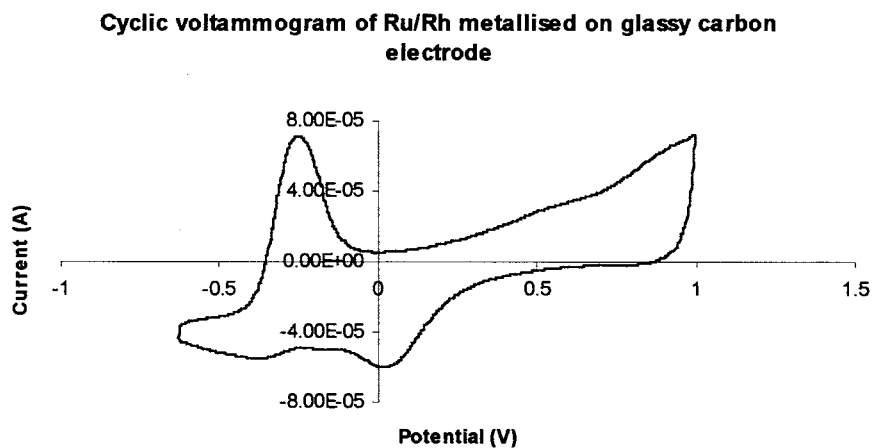


Fig. 1. Cyclic voltammogram of Ru–Rh metallised onto glassy carbon electrode. Reference Ag–AgCl, counter Pt wire, working glassy carbon.

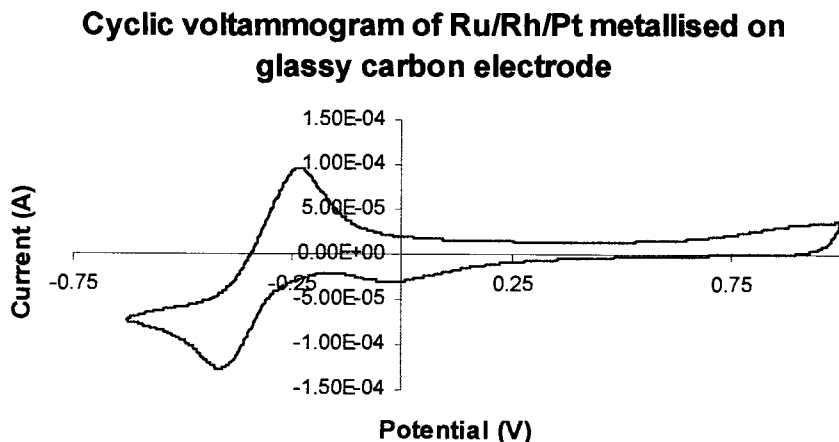


Fig. 2. Cyclic voltammogram of Ru–Rh–Pt metallised onto glassy carbon electrode Reference Ag–AgCl, counter Pt wire, working glassy carbon.

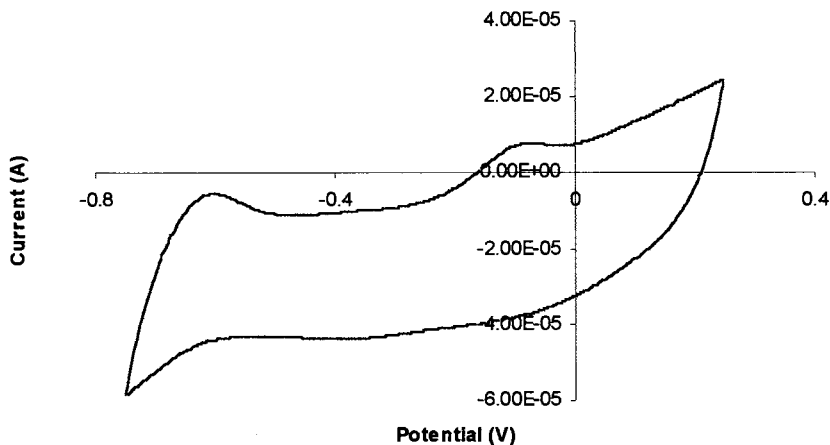


Fig. 3. Cyclic voltammogram of Pt metallised onto Ru–Rh electrode. Reference Ag–AgCl, counter Pt wire, working glassy carbon.

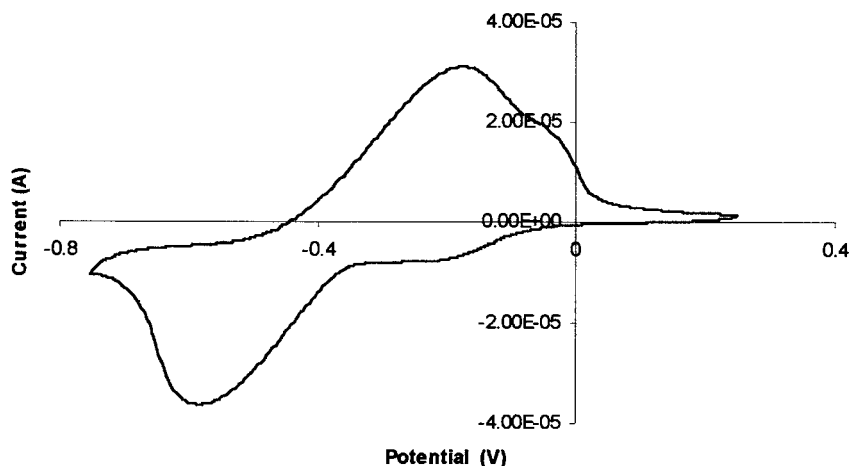


Fig. 4. Cyclic voltammogram of Pt metallised onto glassy carbon electrode Reference Ag–AgCl, counter Pt wire, working glassy carbon.

Figs. 5 and 6. For the electrodes tested at +100 mV (Fig. 5), the results are not very good. The response to hydrogen peroxide for the first four electrodes is smaller than the interferences listed above and thus, if the electrodes were used in an assay, the interferent response would be too large for any useful measurement to be made. The largest interferent by far in the case of the glassy carbon and platinum disc electrodes is acetaminophen. For the Pt on glassy carbon and the Pt on Ru–Rh electrodes, the responses to all substances are tiny. The last two electrodes (Ru–

Rh and Ru–Rh–Pt) show a H_2O_2 response that is larger than the interferences. However, in the case of these electrodes, the interferent response is still too large for a good measurement.

For the same electrodes tested at +650 mV (Fig. 6) the responses were not good either. The H_2O_2 response is larger for all the electrodes, except glassy carbon, but the interferent response is also very large, with acetaminophen, L-ascorbic acid and uric acid all giving large responses. Obviously, these electrodes are of little use due to the large interferences, so the surfaces of the elec-

trodes were modified by polymers to see if the interferences could be reduced.

The first polymer to be investigated was poly(pyrrole). Pyrrole was electropolymerised on a glassy carbon electrode at +0.75 V versus Ag–AgCl until 0.32 mC of charge had passed. This amount of charge was assumed to yield a film of 0.1 μm thickness, according to the equation described by Diaz et al [66]. The electrode was tested amperometrically at +0.65 V versus Ag–AgCl with the same solutions as used for the unpolymerised electrodes, i.e. H_2O_2 , L-ascorbic acid, acetaminophen, L-cysteine and uric acid. However, the results obtained from this electrode were irreproducible.

The polymerisation was repeated on the glassy carbon, Pt disc, Ru–Rh, Ru–Rh–Pt, Pt on Ru–Rh and Pt on glassy carbon electrodes. Since 0.32 mC of charge seemed to be too little for efficient polymerisation, the pyrrole was polymerised until 3.2 mC of charge was passed. This took ca. 40 min to complete. The platinum disc electrode was electropolymerised with pyrrole until 0.8 mC of charge had passed, as the surface area of this electrode was smaller than the other electrodes. The results are shown graphically in Fig. 7 (100 mV) and Fig. 8 (650 mV). The results for the +100 mV electrodes are generally better than those obtained with the unpolymerised electrodes. Primarily, the hydrogen peroxide response is

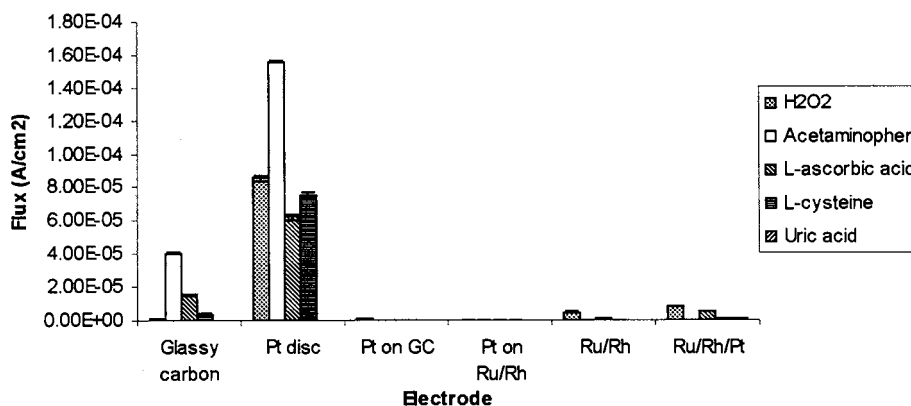


Fig. 5. Plot of flux (A cm^{-2}) versus electrode type for unpolymerised electrodes. Potential = 100 mV.

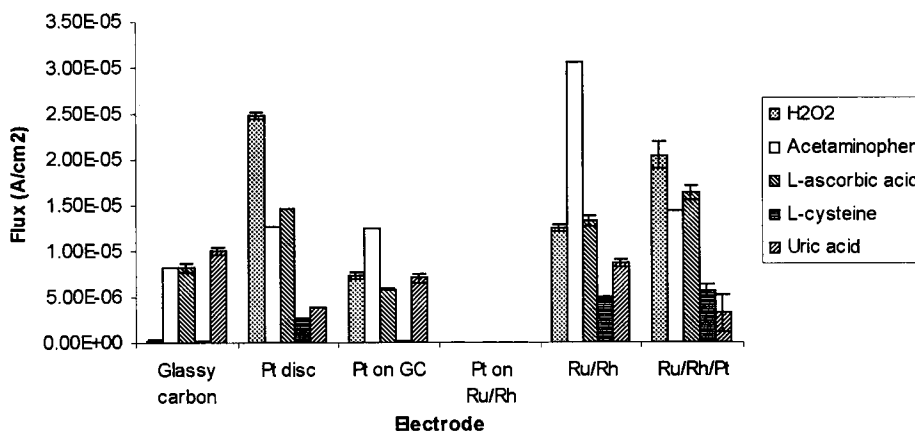


Fig. 6. Plot of flux (A cm^{-2}) versus electrode type for unpolymerised electrodes. Potential = 650 mV.

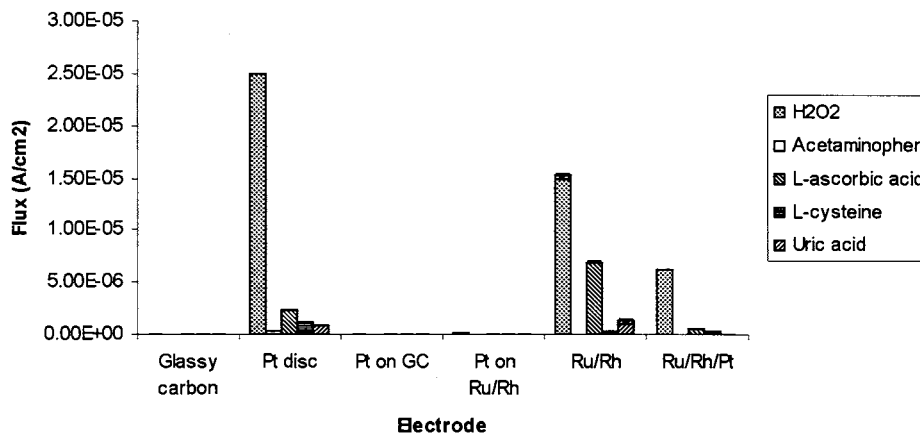


Fig. 7. Plot of flux (A cm^{-2}) versus electrode type for electrodes polymerised with poly(pyrrole), potential = 100 mV.

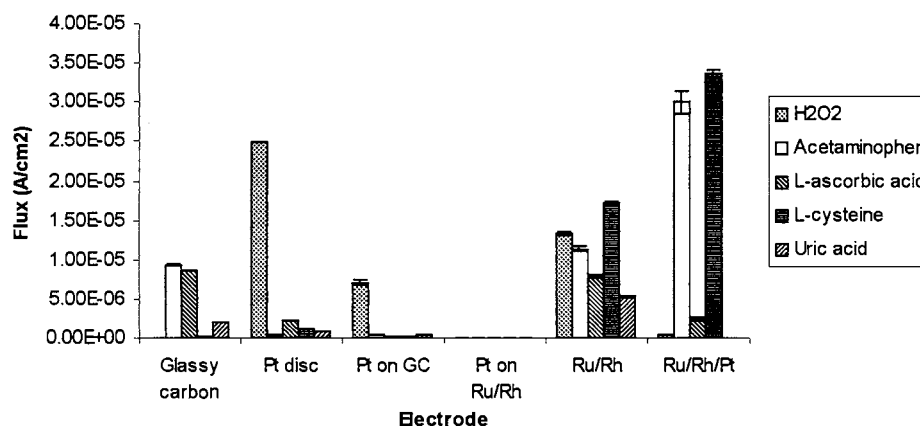


Fig. 8. Plot of flux (A cm^{-2}) versus electrode type for electrodes polymerised with poly(pyrrole), potential = 650 mV.

larger in almost all cases. The only large interferent is L-ascorbic acid, and that is only for the Ru–Rh metallised electrode. The only problem is that three electrodes, the glassy carbon, Pt on glassy carbon and Pt on Ru–Rh, gave extremely small responses for all substances. For those electrodes examined at the higher potential, the results were worse, with the interferent response very high compared to that obtained for hydrogen peroxide.

After these electrodes were tested, attention was turned to other polymers. Poly(aniline) was chosen and prepared in 1.2 M HCl, as described in the method of Trojanowicz et al. [6]. No change was noticed on the surface of the Pt disc electrode

after polymerisation with aniline. However, the surface of the Ru–Rh–Pt electrode became a shiny purple and the surface of the Pt on Ru–Rh turned a dark green. Electrodes were tested with H₂O₂, L-cysteine, L-ascorbic acid, acetaminophen and uric acid, as before. The results are presented graphically in Figs. 9 and 10. However, after testing, the previously shiny purple surface of the Ru–Rh–Pt electrode lost its lustre and the surface of the Pt on Ru–Rh electrode became dark yellow-green. This change in colour of the polymer was probably due to the oxidation or reduction of the polymer as it was exposed to the atmosphere.

The results for the poly(aniline)-covered electrodes were not as good. The electrodes examined

at 100 mV had major problems with interferences from L-ascorbic acid, with the H_2O_2 response being dwarfed in comparison. The response for cysteine is also quite large. However, the responses due to uric acid and acetaminophen are very small. For the electrodes tested at 650 mV, it was much worse. The responses for H_2O_2 were improved, but the interferent response increased as well, including those for uric acid and acetaminophen. The electrodes covered with poly(aniline) and used at +650 mV would thus be unusable.

Finally, a nonconducting polymer, poly(1,3-diaminobenzene), was investigated. The polymerisation was continued until the current decreased to a minimum, which took about 45 min. This hap-

pened because when the polymer film grew, the polymer formed a nonconducting surface, on which no more polymerisation would take place. The films obtained from this type of polymer would be expected to be more uniform than those obtained with the conducting polymers. The electrodes were tested with the usual substances and at 100 and 650 mV, except for glassy carbon, which was tested at 100 and 750 mV.

The results obtained from these electrodes were extremely encouraging. As can be seen in Figs. 11 and 12, for the electrodes examined at 100 mV, there are almost no responses from the interferents. The only interferents that can be seen are those of cysteine and uric acid, and in both cases, the hydrogen peroxide response is far larger than

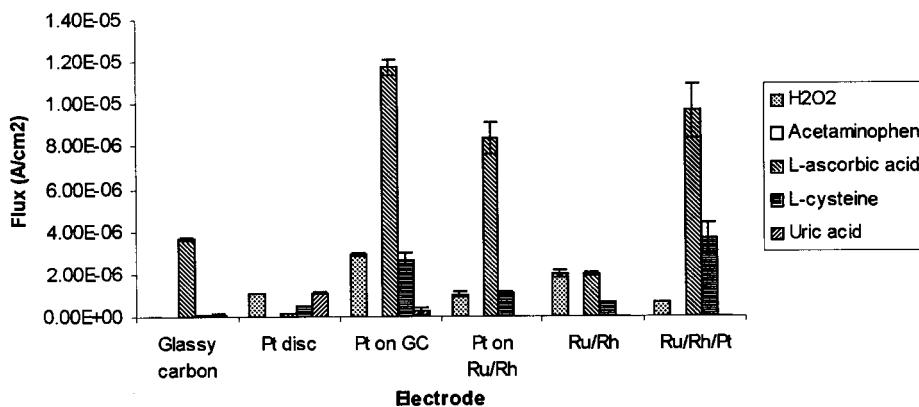


Fig. 9. Plot of flux (A cm^{-2}) versus electrode type for electrodes polymerised with poly(aniline), potential = 100 mV.

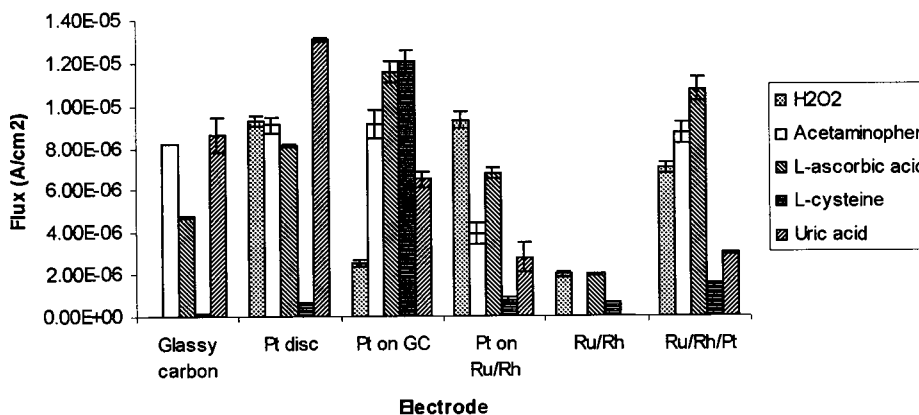


Fig. 10. Plot of flux (A cm^{-2}) versus electrode type for electrodes polymerised with poly(aniline), potential = 650 mV.

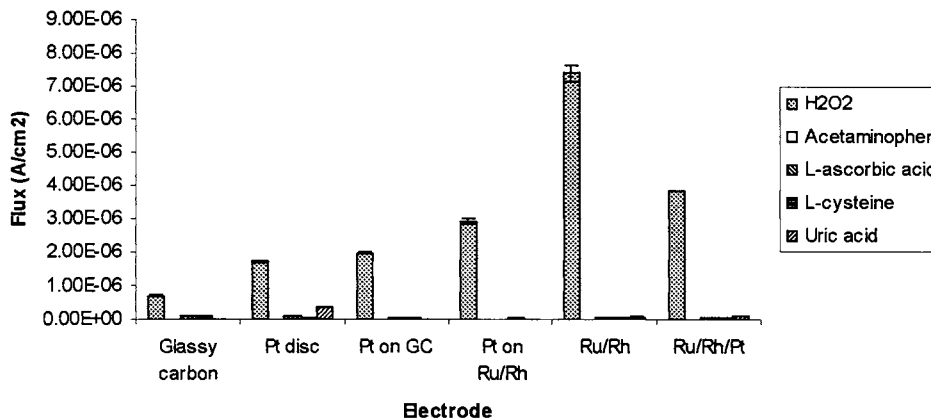


Fig. 11. Plot of flux (A cm^{-2}) versus electrode type for electrodes polymerised with poly(1,3-diaminobenzene), potential = 100 mV.

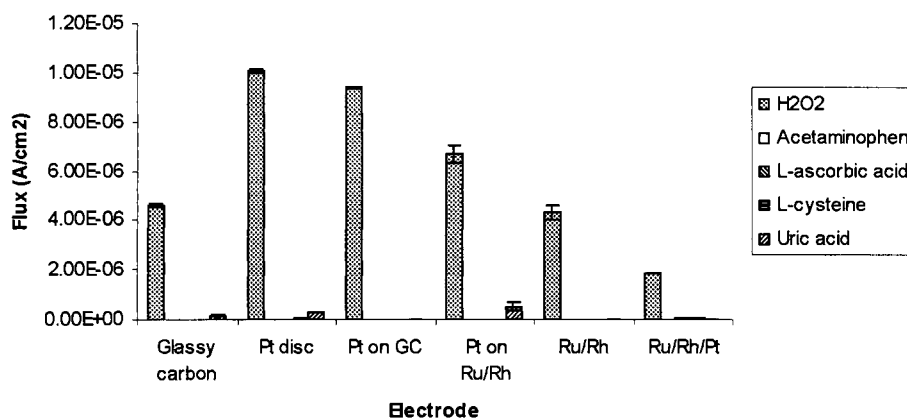


Fig. 12. Plot of flux (A cm^{-2}) versus electrode type for electrodes polymerised with poly(1,3-diaminobenzene), potential = 100 mV.

both of them. The results for the electrodes investigated at 650 mV is also very good. The uric acid response is larger than for the electrodes tested at 100 mV, but the interferences are still far smaller than the H_2O_2 . The hydrogen peroxide response is slightly larger for those electrodes investigated at 650 mV, so this potential is probably the preferential one to use. The largest H_2O_2 response was obtained from the Ru–Rh electrodes at 100 mV and the Pt on Ru–Rh for 650 mV.

The flux, which is the current per unit area, was also calculated. The responses of the electrodes thus far are independent of area, whereas the flux takes the differing working areas of the electrodes into account. The theoretical areas of the elec-

trodes were determined by a visual measurement and the working areas were determined by chronocoulometry (Table 1)

Table 1
Theoretical and working areas of electrodes

Electrode	Working area (m^2)	Theoretical area (m^2)
Glassy carbon	6.95×10^{-5}	2.83×10^{-5}
Platinum disc	1.45×10^{-5}	1.77×10^{-6}
Pt on GC	6.95×10^{-5}	2.83×10^{-5}
Pt on Ru–Rh	1.36×10^{-4}	2.83×10^{-5}
Ru–Rh	9.80×10^{-5}	2.83×10^{-5}
Ru–Rh–Pt	9.12×10^{-5}	2.83×10^{-5}

Table 2

Ratio of flux ($A\text{ cm}^{-2}$) to polymerised (with poly(pyrrole)) and unpolymerised electrodes at: (a) 650 mV; (b) 100 mV

Substance	Glassy carbon	Pt disc	Pt on GC	Pt on Ru–Rh	Ru–Rh	Ru–Rh–Pt
<i>(a)</i>						
H ₂ O ₂	2.36E-02	2.92E-01	7.23E-02	2.83E+01	3.19E+00	7.35E-01
Acetaminophen	0.00E+00	2.17E-03			0.00E+00	
L-ascorbic acid	9.23E-05	3.78E-02			7.90E+00	9.65E-02
L-cysteine	4.00E-04	1.50E-02	2.50E-02	5.09E+00	3.42E+00	5.13E-01
Uric acid	2.50E-02		0.00E+00	0.00E+00		0.00E+00
<i>(b)</i>						
H ₂ O ₂	4.15E-02	1.00E+00	9.61E-01	4.87E+00	1.06E+00	2.45E-02
Acetaminophen	1.13E+00	2.68E-02	3.69E-02	4.55E+00	3.72E-01	2.07E+00
L-ascorbic acid	1.04E+00	1.60E-01	2.62E-02	2.11E+00	5.97E-01	1.50E-01
L-cysteine	5.86E-01	4.40E-01	5.69E-01	1.72E+00	3.56E+00	5.93E+00
Uric acid	2.02E-01	2.13E-01	6.07E-02	4.63E+00	6.16E-01	0.00E+00

Table 3

Ratio of flux ($A\text{ cm}^{-2}$) to polymerised (with poly(aniline)) and unpolymerised electrodes at: (a) 650 mV; and (b) 100 mV

Substance	Glassy carbon	Pt disc	Pt on GC	Pt on Ru–Rh	Ru–Rh	Ru–Rh–Pt
<i>(a)</i>						
H ₂ O ₂	0.00E+00	1.29E-02	4.26E+00	1.41E+02	4.16E-01	8.08E-02
Acetaminophen	0.00E+00	0.00E+00		0.00E+00		
L-ascorbic acid	2.32E-01	2.22E-03		2.27E+00	1.80E+00	
L-cysteine	1.60E-02	6.42E-03	2.34E+01	1.93E+02	5.89E+00	5.48E+00
Uric acid	1.00E+00		3.20E+00	0.00E+00		0.00E+00
<i>(b)</i>						
H ₂ O ₂	5.18E-02	3.75E-01	3.41 E-01	5.73E+02	1.58E-01	3.45E-01
Acetaminophen	9.97E-01	7.21 E-01	7.28E-01	6.61 E+02	0.00E+00	6.02E-01
L-ascorbic acid	5.79E-01	5.57E-01	1.99E+00	7.75E+02	1.50E-01	6.56E-01
L-cysteine	5.55E-01	2.41 E-01	5.23E+01	2.63E+02	1.40E-01	2.65E-01
Uric acid	8.64E-01	3.37E+00	9.28E-01	3.99E+02	0.00E+00	9.48E-01

The theoretical areas of the Pt on glassy carbon, Pt on Ru–Rh, Ru–Rh–Pt and the Ru–Rh electrodes are the same as that of the ‘bare’ glassy carbon electrode because the metallisations were accomplished on the glassy carbon electrode. The only electrode to have a different theoretical surface area was the platinum disc electrode, as the diameter of the glassy carbon electrode was twice that of the Pt disc electrode. The working area of the electrodes was larger than the theoretical area mainly because the surfaces of the electrodes were not perfectly smooth, even after polishing. Small imperfections on the surface, too minute to be detected by the naked eye, exist on all of the electrodes, and these give rise to a larger surface area.

The higher the flux, the better the response. According to the data for the poly(pyrrole) at both potentials, the best response is obtained from the platinum disc electrode (Table 2). Despite the small area of this electrode, the response obtained from it was consistently high, so when the area was taken into account, it meant that the electrode performed very well.

For the poly(aniline) covered electrodes, the Pt disc and Pt on Ru–Rh gave the best results at 650 mV, while the Pt on GC electrode performed best at 100 mV, followed by the Ru–Rh, Pt on Ru–Rh and Pt disc electrodes (Table 3). The electrodes covered with the nonconducting polymer poly(1,3-diaminobenzene) gave the best results for the Pt disc and Pt on Ru–Rh electrodes again

Table 4

Ratio of flux ($A\text{ cm}^{-2}$) to polymerised (with poly(1,3-diaminobenzene)) and unpolymerised electrodes at: (a) 650 mV; and (b) 100 mV

Substance	Glassy carbon	Pt disc	Pt on GC	Pt on Ru–Rh	Ru–Rh	Ru–Rh–Pt
<i>(a)</i>						
H ₂ O ₂	8.91 E-01	2.01 E-02	2.91 E+00	4.03E+02	1.55E+00	4.56E-01
Acetaminophen	0.00E+00	0.00E+00		0.00E+00		
L-ascorbic acid	5.82E-03	1.44E-03		3.50E-02	6.94E-03	
L-cysteine	3.24E-02	9.17E-04	3.38E-01	5.35E+00	3.30E-01	5.74E-02
Uric acid	0.00E+00		0.00E+00	0.00E+00		1.18E-01
<i>(b)</i>						
H ₂ O ₂	1.65E+01	4.06E-01	1.28E+00	4.09E+02	3.45E-01	9.14E-02
Acetaminophen	0.00E+00	1.64E-03	0.00E+00	0.00E+00	0.00E+00	0.00E+00
L-ascorbic acid	0.00E+00	2.36E-03	0.00E+00	2.27E+00	0.00E+00	3.48E-03
L-cysteine	1.23E-01	2.14E-02	7.50E-02	1.01E+01	2.13E-03	1.24E-02
Uric acid	1.15E-02	6.91E-02	0.00E+00	7.68E+01	0.00E+00	0.00E+00

at 650 mV, while the Ru–Rh electrodes were far better than the others at 100 mV, although the rest gave good results (Table 4).

5. Conclusion

In conclusion, the data presented here shows that if the correct potential and polymer is chosen well, a very good improvement can be obtained from electrochemical assays. Metallisation of electrodes, coupled with the technique of electropolymerisation can provide enhanced results by lowering the response due to interference while still keeping the response of interest, hydrogen peroxide, relatively high. The technique is also well suited to miniaturisation, as both metallisation and electropolymerisation can be done on screen-printed electrodes or those made by photolithographic methods.

References

- [1] P.J. O'Connell, C.K. O' Sullivan, G.G. Guilbault, *Anal. Chim. Acta* 373 (1998) 261.
- [2] M. Umana, J. Waller, *Anal. Chem.* 58 (1986) 2979.
- [3] C. Iwakura, Y. Kajiya, H. Yoneyama, *J. Chem. Soc. Chem. Commun.* 15 (1988) 1019.
- [4] N.C. Foulds, C.R. Lowe, *J. Chem. Soc. Faraday Trans.* 82 (1986) 1259.
- [5] M. Trojanowicz, W. Matuszewski, M. Podsiadia, *Biosens. Bioelectron.* 5 (1990) 157.
- [6] D.T. Hoa, T.N. Suresh Kumar, N.S. Puneekar, R.S. Srinivasa, R. Lal, A.R. Contractor, *Anal. Chem.* 64 (1992) 2645.
- [7] M. Trojanowicz, O. Geschke, T. Krawczynski vel Krawczyk, K. Cammann, *Sens. Actuators B* 28 (1995) 191.
- [8] P.J.H.J. van Os, A. Bult, C.G.J. Koopal, W.P. van Bennekom, *Anal. Chim. Acta* 335 (1996) 209.
- [9] N.C. Foulds, C.R. Lowe, *Anal. Chem.* 60 (1988) 2473.
- [10] D. Belanger, J. Nadreau, G. Fortier, *J. Electroanal. Chem.* 274 (1989) 143.
- [11] M.-C. Shin, H.-S. Kim, *Biosens. Bioelectron.* 11 (1996) 161.
- [12] M.-C. Shin, H.-S. Kim, *Biosens. Bioelectron.* 11 (1996) 171.
- [13] C. Malitesta, F. Palmisano, L. Tori, P.G. Zambouin, *Anal. Chem.* 62 (1990) 2735.
- [14] W. Schuhmann, R. Lammert, B. Uhe, H.-L. Schmidt, *Sens. Actuators B* 1 (1990) 537.
- [15] P.N. Bartlett, Z. Ali, V. Eastwick-Field, *J. Chem. Soc. Faraday Trans.* 88 (1992) 2677.
- [16] M. Shaolin, X. Huaiguo, Q. Bidong, *J. Electroanal. Chem.* 304 (1991) 7.
- [17] H. Shinohara, T. Chiba, M. Aizawa, *Sens. Actuators* 13 (1988) 79.
- [18] S.E. Wolowacz, B.F.Y. Yon-Hin, C.R. Lowe, *Anal. Chem.* 64 (1992) 1541.
- [19] B.F.Y. Yon-Hin, C.R. Lowe, *J. Electroanal. Chem, Interfacial Electrochem.* 374 (1994) 167.
- [20] K. Yokahama, S. Lee, E. Tamaya, et al., *Anal. Chim. Acta* 263 (1992) 101.
- [21] G. Fortier, D. Belanger, L. Casavant, C. Wilson, M.F. Lawrence, *Anal. Lett.* 25 (1992) 1835.
- [22] S. Mu, H. Xue, *Sens. Actuators B* 31 (1996) 155.

- [23] M.C. Shin, H.C. Yoon, H.S. Kim, *Anal. Sci.* 12 (1996) 597.
- [24] L.V. Lukachova, A.A. Karyakin, E.E. Karyakina, L. Gorton, *Sens. Actuators B* 44 (1997) 356.
- [25] G.G. Wallace, K.E. Wallace, T.W. Lewis, A.J. Hodgson, M.J. Spencer, *J. Liq. Chromatogr.* 13 (1990) 3091.
- [26] S.D. Alexander, *Sep. Purif. Methods.* 17 (1988) 67.
- [27] C. Grob-Rhode, H.G. Kicinski, A.J. Kettrup, *Chromatographia* 26 (1988) 209.
- [28] D. Kolla, J. Kohler, G. Schomberg, *Chromatographia* 23 (1987) 465.
- [29] N. Tanaka, K. Hashizume, M. Araki, *J. Chromatogr.* 400 (1987) 33.
- [30] A. Michalska, A. Ivanska, A. Lewenstam, *Anal. Chem.* 69 (1997) 4060.
- [31] Z. Cai, C.R. Martin, *J. Electroanal. Chem.* 300 (1991) 35.
- [32] O.A. Sadik, M.J. John, G.G. Wallace, D. Barnett, C. Clarke, D.G. Laing, *Analyst* 119 (1994) 1997.
- [33] X. Zhang, B. Ogorevc, G. Tavcar, I.G. Svegl, *Analyst* 121 (1996) 1817.
- [34] Y.J. Shi, Y.F. Lang, J.Q. Kan, S.L. Mu, Y.F. Li, *Biosens. Bioelectron.* 12 (1997) 655.
- [35] P.N. Bartlett, J.N. Cooper, *J. Electroanal. Chem.* 362 (1993) 1.
- [36] Y. Yang, S. Mu, *J. Electroanal. Chem.* 432 (1997) 71.
- [37] H. Wang, S. Mu, *J. Electroanal. Chem.* 436 (1997) 43.
- [38] T.A. Sergeeva, N.V. Lavrik, S.A. Piletsky, A.E. Rachkov, A.V. El'skaya, *Sens. Actuators B* 34 (1996) 283.
- [39] D.M. Zhou, J.J. Xu, H.Y. Chen, H.Q. Fang, *Electroanalysis* 9 (1997) 1185.
- [40] A.L. Kukla, Y.M. Shishov, S.A. Piletsky, *Sens. Actuators B* 37 (1996) 135.
- [41] P. Audebert, L. Guyard, M. Nguyen Dinh An, P. Hapiot, M. Chahma, C. Combélas, A. Thiebault, *J. Electroanal. Chem.* 407 (1996) 169.
- [42] K. Imanishi, M. Satoh, Y. Yasuda, R. Tsushima, S. Aoki, *J. Electroanal. Chem.* 260 (1989) 469.
- [43] R.G. Sandberg, L.J. Van Houten, J.L. Schwartz, R.P. Bigliano, S.M. Dallas, J.C. Silvja, M.A. Cabelli, V. Narayanswamy, *Biosensor design and applications*, American Chemical Society, Washington DC (1992) 224.
- [44] G. Tourillon, F. Garnier, *J. Electroanal. Chem.* 161 (1984) 51.
- [45] R.J. Waltman, J. Bargon, A.F. Diaz, *J. Phys. Chem.* 87 (1983) 1459.
- [46] T.A. Skotheim, M.V. Rosenthal, A. Melo, M.I. Florik, *J. Electroanal. Chem.* 185 (1985) 97.
- [47] H.E. Ge, S.A. Ashraf, K.J. Gilmore, C.O. Too, G.G. Wallace, *J. Electroanal. Chem.* 340 (1992) 41.
- [48] S. Asavapiriyant, G.K. Chandler, G.A. Gunawardena, D. Pletcher, *J. Electroanal. Chem.* 177 (1984) 245.
- [49] T. Inagaki, M. Hunter, X.Q. Yang, T.A. Skotheim, Y. Okamoto, *J. Chem. Soc. Chem. Commun.* 2 (1988) 126.
- [50] Z. Deng, D.C. Stone, M. Thompson, *Analyst* 122 (1997) 1129.
- [51] M.B. Madaras, R.P. Buck, *Anal. Chem.* 68 (1996) 3832.
- [52] S.V. Sasso, R.J. Pierce, R. Walla, A.M. Yacynych, *Anal. Chem.* 62 (1990) 1111.
- [53] Q.S. Li, S.L. Zhang, J.T. Yu, *Anal. Lett.* 28 (1995) 2161.
- [54] P. Manowitz, P.W. Stoeker, and A.M. Yacynych, *Biosens. Bioelectron.* 10 (1995) 359.
- [55] R.J. Geise, J.M. Adams, N.J. Barone, A.M. Yacynych, *Biosens. Bioelectron.* 6 (1991) 171.
- [56] S.A. Emr, A.M. Yacynych, *Electroanalysis* 7 (1995) 913.
- [57] R.W. Murray, *Electroanalytical Chemistry*, vol. 13, in: A.J. Bard (Ed.), Marcel Dekker, New York, 1984, pp. 462–507.
- [58] P.N. Bartlett, R.G. Whitaker, *J. Electroanal. Chem.* 224 (1987) 27.
- [59] R.J. Waltman, J. Bargon, A.F. Diaz, *J. Phys. Chem.* 87 (1983) 1459.
- [60] P.N. Bartlett, D.J. Caruna, *Analyst* 119 (1994) 175.
- [61] H. Yamato, M. Ohwa, W. Wernet, *J. Electroanal. Chem.* 397 (1995) 163.
- [62] M.D. Imisides, R. John, P.J. Riley, G.G. Wallace, *Electroanalysis* 3 (1991) 879.
- [63] B.L. Funt, *Encyclopaedia of Polymer Science and Engineering*, vol. 5, in: H.F. Mark, N.M. Bikales, C.G. Overberger, G. Menges, J.I. Kroschwitz (Eds.), John Wiley, New York, 1986, pp. 587–601.
- [64] E. Sakslund, J. Wang, O. Hammerich, *J. Electroanal. Chem.* 371 (1994) 71.
- [65] N. Georgolios, D. Jannakoudakis, P. Karabinas, *J. Electroanal. Chem.* 264 (1989) 235.
- [66] A.F. Diaz and J.I. Castille, *Chem. Ser.* 17 (1981) 1.

Synchronous-derivative phosphorimetric determination of 1- and 2-naphthol in irrigation water by employing β -cyclodextrin

Miguel Hernández López ^{*,1}, Manuel Algarra González,
Ma Isabel López Molina

Department of Analytical Chemistry, Faculty of Sciences, University of Málaga, Campus de Teatinos s/n, 29071 Malaga, Spain

Received 5 August 1998; received in revised form 10 February 1999; accepted 12 February 1999

Abstract

A room-temperature phosphorimetric (RTP) study of the inclusion process between 1- and 2-naphthol, β -cyclodextrin (β -CD) and 3-bromo-1-propanol as heavy atom perturber has been performed. Experimental conditions were optimized for the formation of trimolecular complexes with lifetimes of 10.82 and 9.41 ms for 1- and 2-naphthol, respectively. A synchronous-derivative room-temperature phosphorimetric method has been proposed to the analysis of both naphthols in synthetic mixtures and irrigation water in the ratio 1:10 to 10:1; the limit of detection is 0.02 $\mu\text{g ml}^{-1}$ and the relative standard deviation (RSD) is about 6%. © 1999 Elsevier Science B.V. All rights reserved.

Keywords: Phosphorimetry; Cyclodextrins; 1-Naphthol and 2-naphthol; Synchronous-derivative technique; Irrigation water

1. Introduction

Since the first study about room temperature phosphorimetry (RTP) in fluid solution [1], several approaches have been used to produce emission phosphorescence from the metastable triplet state in this medium, such as sensitized-RTP [2] or by the use of micelles [3,4], cyclodextrins (CD) [5–7] or their mixtures [8], vesicles [9,10], microe-

mulsions [11,12] and water-soluble copolymers [13]. CDs are the organized media which have been commonly used as hosts to originate inclusion complexes with a great variety of guest molecules; their analytical applications have been reviewed [14–16]. On the other hand, 1- and 2-naphthol have been determined in their mixtures by different techniques such as FIA with photometric detection [17], high-performance liquid chromatography (HPLC) [18], normal [19] and synchronous-derivative fluorimetry [20,21]. No references there are in the literature to the phosphorimetric quantitative analysis of mixtures of both naphthols, only qualitative data have

* Corresponding author. Tel./fax: + 34-95-2131-886.

E-mail address: sulphur@uma.es (M. Hernández López)

¹ Presented at the Xth International Symposium on Molecular Recognition and Inclusion, 20–25 June, 1998, Warsaw, Poland.

been found [22]. Synchronous technique has been proposed as a means of increasing the selectivity of phosphorimetry [23] due to its associated band-narrowing effect and together with derivative spectroscopy is a useful tool to discriminate mixtures of analytes with severe overlapped spectra. This approach, employed earlier in spectrofluorimetry [24,25] and in spectrophotometry [26] offers acceptable levels of precision and accuracy. In the present study the luminescence characteristics of the inclusion compounds of 1- and 2-naphthol in β -cyclodextrin (β -CD) aqueous solution have been investigated with the object of characterizing the inclusion process involved and proposing a phosphorimetric method for the determination of these compounds in their mixtures and in irrigation water. The proposed method shows good sensitivity and a higher selectivity due to the phosphorescence spectroscopy [7] coupled to synchronous-derivative technique together with the restrictive cavity of β -CD.

2. Experimental

2.1. Apparatus

All the fluorimetric and phosphorimetric measurements were carried out on a Perkin-Elmer (Norwalk, CT) LS-5 luminescence spectrophotometer equipped with a xenon discharge lamp (9.9 W) pulsed at line frequency (10 μ s half-width, 50 Hz), Monk-Gillieson f/3 monochromators and 1 \times 1 cm quartz cell which was capped with a teflon stopper. The spectrometer was connected to a Perkin-Elmer model 3600 data station provided with a PECLS II application software. Phosphorescence lifetimes were measured with an Obey-Decay application program on the mentioned software and the data were obtained automatically. When scanning phosphorescence spectra the delay time (t_d) and the gate time (t_g) were set at 1 and 11 ms and the excitation and the emission slits were set at 5 and 20 nm, respectively. The system responds to spectral derivatives and the structure calculates the first and second derivative of a spectrum. The cell holder and samples were controlled thermostatically by a thermostatic bath

Frigitem, Selecta (Barcelona, Spain) at $20 \pm 0.5^\circ\text{C}$.

2.2. Reagents

1- and 2-Naphthol were purchased from Sigma (St Louis, MO) and Merck, (Darmstadt, Germany) respectively and used without further purification. 2000 $\mu\text{g ml}^{-1}$, stock solutions were prepared in 1-propanol and working solutions were obtained by dilution with this solvent. Anhydrous β -CD (Sigma) was used as received. Cyclodextrin solutions (0.01 M) were prepared in deionized water. A buffer solution (pH 4.8) was prepared from 1 M sodium acetate and acetic acid. Purified water (Milli Q/Milli-Q2 system, Millipore, Bedford, MA) was used. Unless otherwise stated, the reagents used were of analytical reagent grade.

2.3. Procedures

2.3.1. Study of inclusion phenomena

To aliquots of naphthols in acetone, gently evaporated, were added increasing volumes of 1×10^{-2} M β -CD solution and deionized water up to a final volume of 10 ml. These samples were sonicated during 10 min and their fluorescence spectra were recorded.

2.3.2. Phosphorimetric determination of 1- and 2-naphthol

Aliquots containing 0.5–100 μg of 1- and 2-naphthol in 1-propanol were transferred into a 10 ml calibrated flask. Add 1-propanol up to a final volume of 50 μl , 1.5 ml of pH 4.8 acetic–acetate buffer solution, 100 μl of 3-bromo-1-propanol and dilute to the mark with 0.01 M aqueous β -CD. The samples were stirred by hand for 3 min, left for 20 min and the second derivative synchronous spectra were recorded between 280 and 380 nm against a reagent blank with the following instrumental parameters: $\Delta\lambda = 180$ nm, a scanning speed of 240 nm min^{-1} , a response time of 2 s and an integer factor of 20. The second derivative analytical values were measured as the vertical difference in the d^2I_p scale from the corre-

sponding isodifferential point to the break with the second derivative curves (329.1 nm for 2-naphthol and 342.9 nm for 1-naphthol). The concentration of 1- and 2-naphthol in the binary mixtures is determined from the corresponding calibration graph previously run under similar conditions to those of the mixture.

2.3.3. Determination of 1- and 2-naphthol in irrigation water

To aliquots of samples, without filtration, 50 μl of 1-propanol, 1.5 ml of pH 4.8 buffer solution, 100 μl of 3-bromo-1-propanol and 94.7 mg of solid β -CD (final concentration 8.35×10^{-3} M) were transferred into a 10 ml calibrated flask. The samples were sonicated for 3 min, left for 20 min and their phosphorescence was measured as previously described.

3. Results and discussion

3.1. Spectral characteristics

Both naphthols form inclusion compounds with β -CD with stoichiometry 1:1 calculated by continuous variations method. The association constants of both naphthols were calculated from fluorescence data, by using the changes produced on the fluorescence spectra, for the expression described previously [27] and the values obtained were 644 ± 50 and 718 ± 40 M^{-1} for 1- and 2-naphthol, respectively. The phosphorescence excitation and emission spectra of both species in a β -CD medium, at pH 4.8 are shown in Fig. 1. The excitation spectra show maxima at 255, 265 and 300 nm for 1-naphthol and 240, 255 and 330 nm for 2-naphthol. The emission spectra present

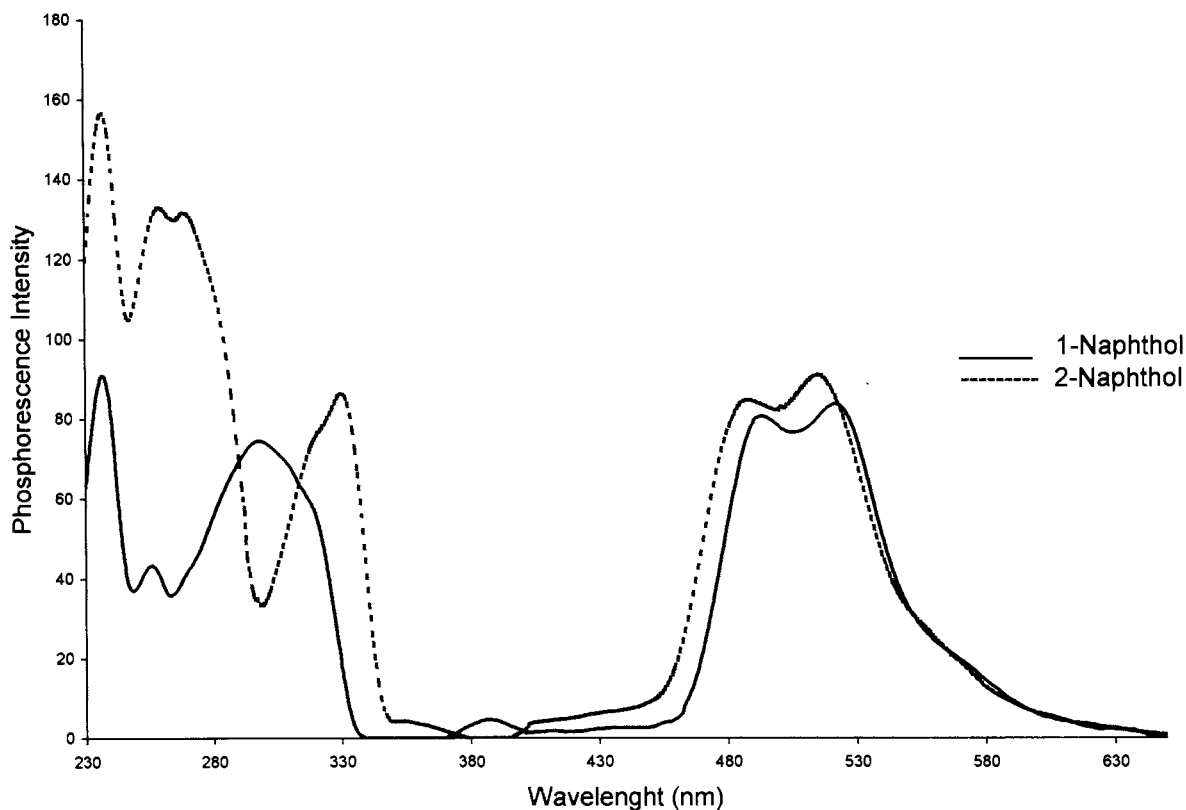


Fig. 1. Excitation and emission spectra of 1- and 2-naphthol. [1-naphthol] = $1 \mu\text{g ml}^{-1}$ and [2-naphthol] = $3 \mu\text{g ml}^{-1}$, [β -cyclodextrin (CD)] = 8.3×10^{-3} M, pH 4.80, [3-Br-1-propanol] = 0.11 M, scanning speed 240 nm min^{-1} , response 2 s.

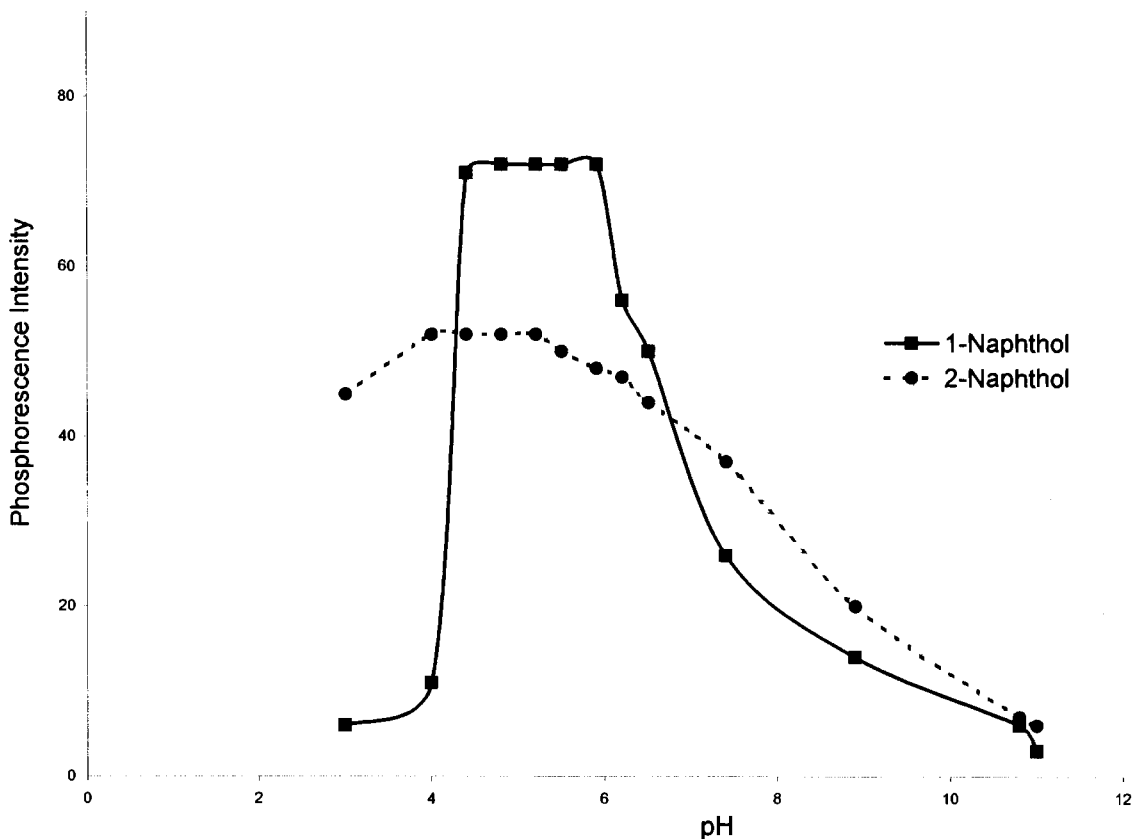


Fig. 2. Effect of pH on the phosphorescence intensity of 1-naphthol (1) and 2-naphthol. [Naphthol] = $1 \mu\text{g ml}^{-1}$, [β -cyclodextrin (CD)] = 8.3×10^{-3} M, [3-Br-1-propanol] = 0.11 M, $t_d = 1$ ms, $t_g = 11$ ms.

broad bands with maxima at 490 and 520 nm for 1-naphthol and 486 and 518 nm for 2-naphthol.

3.2. Effect of varying reaction conditions

3.2.1. Effect of pH

Fig. 2 shows the dependence of phosphorescence of both naphthols with pH; the curves present maximum and constant intensity in the range 4–6 U of pH. Acetic–acetate buffer was used to adjust at pH 4.8.

3.2.2. Effect of solvent

To avoid the elimination of solvent by heating samples and then to have to sonicate, a study to choose an adequate solvent was done. Acetone, methanol, and ethanol totally quench the phos-

phorescence emission, this fact was not observed with 1-propanol. The influence of concentration of 1-propanol is shown in Fig. 3. From these kinetic curves it can be observed that the equilibrium is attained slower as the concentration of alcohol increases, with the values of the slope of the kinetic curve 0.128 s^{-1} in the absence of alcohol and decreasing to 0.101 s^{-1} for 6.6×10^{-2} M in 1-propanol for 1-naphthol and 0.028 s^{-1} for 2-naphthol (curve 7). The molecules compete between the apolar cavity of β -CD and its affinity or solubility in 1-propanol. Similar behaviour was observed for 2-naphthol. A compromise concentration between rapidity and facilities to prepare samples of both naphthols in 1-propanol was decided (6.6×10^{-2} M, i.e. 50 μl in a final volume of 10 ml).

3.2.3. Influence of heavy atom

Several aliphatic alkane halides, halogenated alcohols and mineral salts were investigated as heavy atoms perturbers. Generally, no RTP of the naphthols was observed from mineral salts (KBr, TiNO₃,...), but with some aliphatic alkane halides (1,2-dibromoethane, 1,3-dibromopropane...) and with some halogenated alcohols, RTP emission was obtained in turbid solutions, less in samples prepared with halogenated alcohols, due to the immiscibility of the heavy atom. Maximum emission was obtained by employing 3-bromo-1-propanol (Table 1). Its concentration affects the kinetic of the formation of the trimolecular complex β -CD-heavy atom-analyte and the intensity of the phosphorescence signal in the

equilibrium. At lowest concentrations of heavy atom ($< 5.5 \times 10^{-2}$ M) the coupling S–T is poor and the subsequent population of the triplet state is slow, and at highest concentrations ($> 8.3 \times 10^{-2}$ M) the equilibrium is attained at 15 min for 1-naphthol and 20 min for 2-naphthol. This last time is fixed to obtain the measurements and 100 μ l of 3-bromo-1-propanol in 10 ml of sample (11.1×10^{-2} M) is added. The data show that phosphorescence emission is observed, generally, with heavy atoms non-ionics, aliphatic alkanes containing bromine (not chlorine) and the rest of the upper alkane to methyl group. The heavy atom may act as a wedge which gives more strength to the inclusion compound to adjust the molecule of naphthol to the cavity and to favour

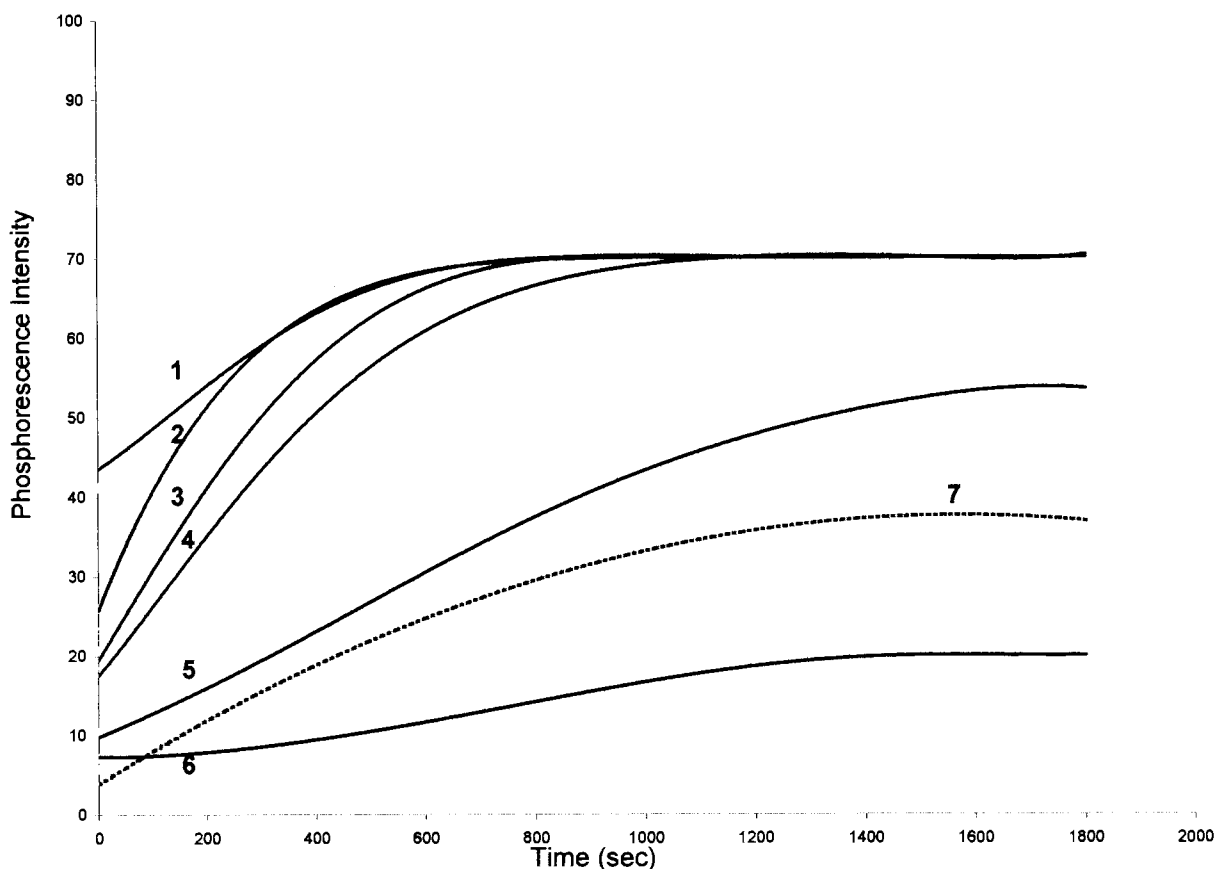


Fig. 3. Dependence of the phosphorescence emission of 1- and 2-Naphthol aqueous solution of β -cyclodextrin (CD) (8.3×10^{-3} M) as a function of the concentration of 1-propanol; for 1-naphthol: (1) 0; (2) 0.013 M; (3) 0.066 M; (4) 0.13 M; (5) 0.26 M; (6) 0.52 M; for 2-naphthol: (7) 0.066 M; [naphthol] = $1 \mu\text{g ml}^{-1}$, pH 4.80.

Table 1
Phosphorescence intensity (I_p) and lifetime (τ) of 1- and 2-naphthol with different heavy atoms^a

Heavy atom	1-Naphthol		2-Naphthol	
	τ (ms)	I_p	τ (ms)	I_p
1,2-Dibromoethane	1.32	12	1.09	15
1,3-Dibromopropane	4.07	38	3.79	–
Dibromomethane	–	–	0.79	7
2-Bromoethanol	–	–	–	–
3-Bromo-1-propanol	10.81	85	9.41	20
1,3-Dichloro-2-propanol	–	–	–	–
Bromoform	–	–	–	–
Chloroform	–	–	–	–
AgNO ₃	–	–	4.88	17

^a Other heavy atoms assayed were: Pb(NO₃)₂, Hg(NO₃)₂, HgI₂, KBr, KI, TiNO₃, and 2-bromoethylammonium bromide. All of them were in 0.1 M concentration. [Naphthol] = 1 $\mu\text{g ml}^{-1}$.

the increase of the coupling S–T due to a great proximity of the heavy atom and originating a trimolecular complex (Fig. 4). The heavy atom can probably orient itself into the cavity with the –OH hydrophilic terminal directed to aqueous bulk and can interact by hydrogen bonding with the –OH group of naphthol fixing the molecule, while the hydrophobic terminal is directed into the cavity adjusting as a wedge and increasing its immobility and decreasing the vibronic effects. The –OH group in location 1 (1-naphthol) is more protected than the group in location 2 (2-naphthol) in relation to the aqueous environment. In this case this group can interact more easily with water molecules and for this reason its ac-

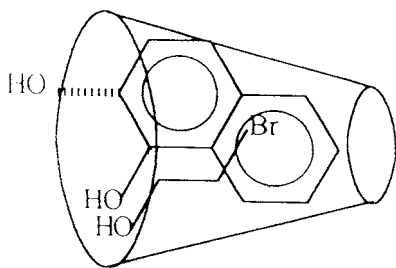


Fig. 4. Schematic representation of the phosphorescent trimolecular complex β -cyclodextrin (CD): naphthol: 3-Br-1-propanol in aqueous solution. (—, 1-naphthol; ···, 2-naphthol).

commodation in the cavity is more slow and the coupling S–T is more disfavoured (phosphorescence emission is less intense). Table 1 present the lifetimes (τ) of naphthols obtained with different heavy atoms. The lifetimes were calculated by employing the Obey-Decay application program with delay times between 0.03 and 7 ms, doing ten measurements with correlation coefficients between 0.993 and 0.999 considering a monoexponential decay (with 3-bromo-1-propanol, τ for 1-naphthol is 10.82 ms implying a longer time in the excited state than 2-naphthol, τ is 9.41 ms). A delay time of 1 ms and a gate time of 11 ms were chosen for giving the best signal to noise ratio (SNR).

3.2.4. Influence of β -CD concentration, temperature and order of addition

The phosphorescence intensity increases as the β -CD concentration does (Fig. 5), and the time to attain the equilibrium is shorter in all the experiments if β -CD concentration was maintained at 8.85×10^{-3} M. It is not necessary to eliminate the oxygen in the β -CD solution. The addition of sodium sulphite does not ameliorate the kinetic of the phosphorescence process. The equilibrium is attained at 5 min for 1-naphthol and 20 min for 2-naphthol; this time is chosen for this work. Sonication of the samples has no influence. Raising the temperature from 15 to 45° decreases the relative phosphorescence intensity of 1-naphthol from 100 to 5%. The work reported here was carried out at $20 \pm 0.5^\circ$. Under these conditions, the phosphorescence intensity remains stable for at least 2 days. The order of the addition is important and the sequence sample, buffer, heavy atom and CD is recommended.

3.2.5. Selection of instrumental parameters

The phosphorescence spectra of both naphthols present broad bands whose overlapping does not allow the discrimination of the individual components in mixtures. However, the band narrowing effect and the associated spectral profile simplification provided by synchronous scanning phosphorimetry, together with the derivative approach, permit the quantitative and simultaneous determination of both naphthols in mix-

tures. Optimum $\Delta\lambda$ value ($\lambda_{em} - \lambda_{ex}$) was determined by recording various synchronous phosphorescence spectra at different values near the singlet–triplet splitting of two naphthols with the criterion of the largest, narrowest signal and maximal difference in the synchronous peaks. Fig. 6 shows the synchronous spectra of 1- and 2-naphthol registered at various $\Delta\lambda$, $v_{scan} = 240 \text{ nm min}^{-1}$ and response time of 2 s. It can be observed that there is a difference of 26 nm between the wavelength maxima when $\Delta\lambda$ is increased from 130 to 190 nm, the difference being only 7 nm for 2-naphthol. As a compromise situation between maximum spectral intensity, half bandwidth at half maximum intensity and separation between wavelength maxima of both naphthols, a $\Delta\lambda$ of 180 nm have been chosen. At this $\Delta\lambda$ (the separation between maxima is 15 nm) the over-

lapped synchronous spectral bands impede the quantitative discrimination of both species. But the synchronous derivative approach adds a great power of discrimination. The main instrumental parameters affecting the shape of the derivative spectra are: the derivative order, wavelength scan speed and the response time. In the case of LS-5 spectrofluorimeter the number of data points has to be optimized; high numbers give better SNR in both first and second derivatives, thus 81 data points, corresponding to an integer factor of 20, were chosen for the experimental work. The synchronous-second derivative phosphorescence spectra of both naphthols are shown in the Fig. 7 which appear at isodifferential points at 329.1 and 342.9 nm. These points are of analytical interest because the contribution to the derivative amplitude from one component is zero in the isodiffer-

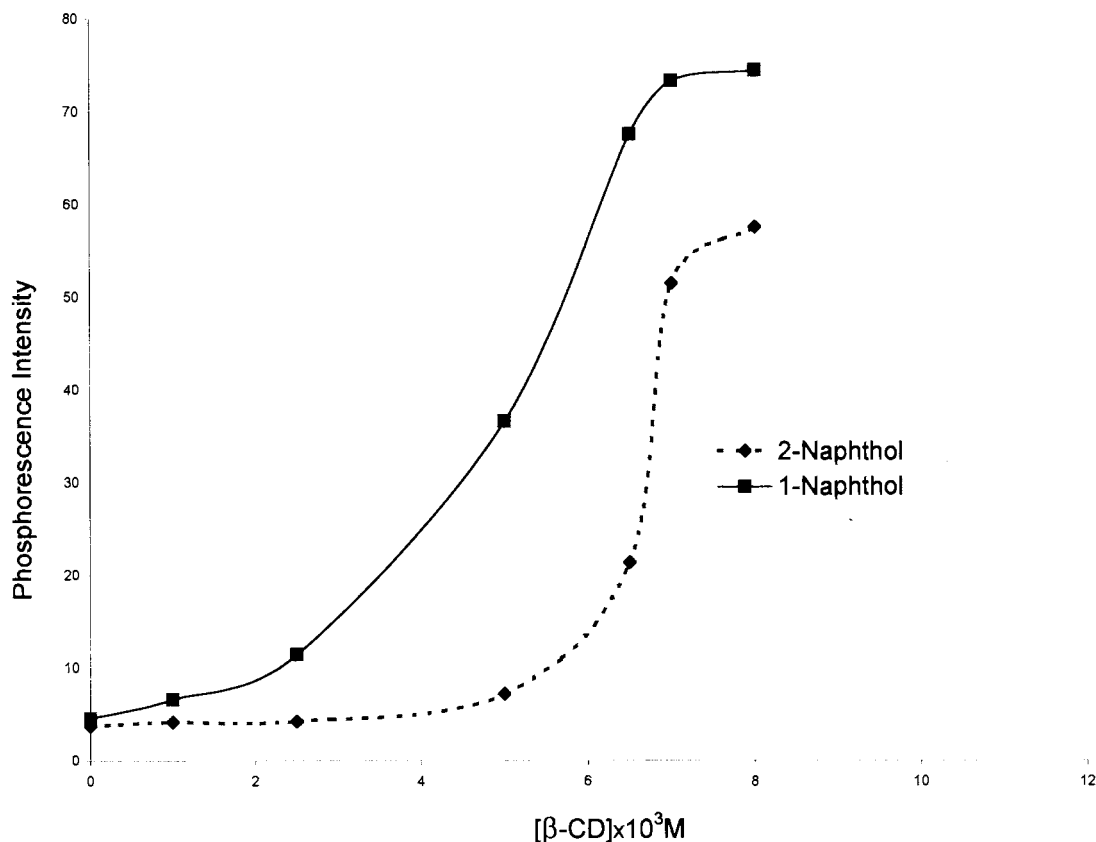


Fig. 5. Influence of the concentration of β -cyclodextrin (CD) on the phosphorescence emission of 1- and 2-naphthol; [naphthol] = $1 \mu\text{g ml}^{-1}$, [3-Br-1-propanol] = 0.11 M.

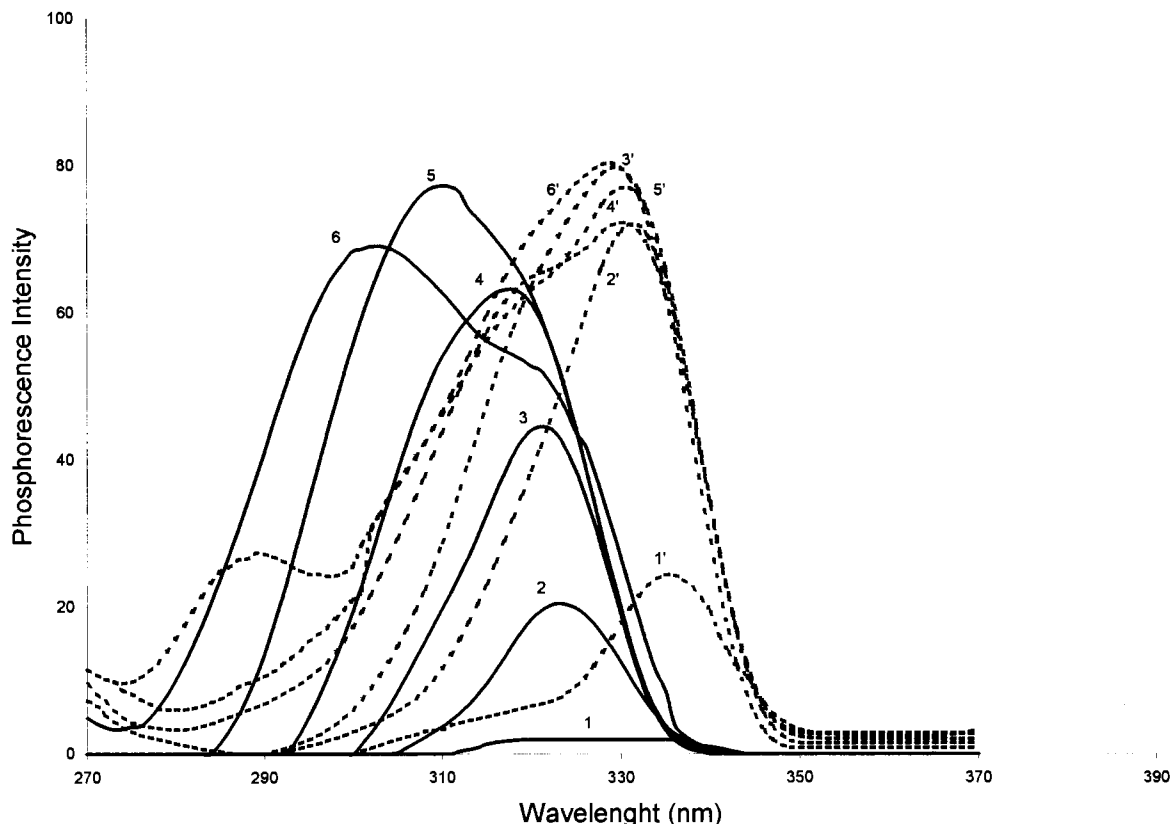


Fig. 6. Synchronous phosphorescence spectra of 1-naphthol (a) and 2-naphthol (b) at different $\Delta\lambda$, ($\lambda_{em} - \lambda_{ex}$): (1, 1'), 130 nm; (2, 2'), 150 nm; (3, 3'), 160 nm; (4, 4'), 170 nm; (5, 5'), 180 nm; (6, 6'), 190 nm; scanning speed, 240 nm min⁻¹, response 2 s.

ential scale; consequently, in a mixture, measurements from these points are independent of the concentration of this compound.

3.2.6. Quantitative analysis and main analytical figures of merit

It is assumed that Beer's law is obeyed in the concentration range studied and that the derivative of a spectral band is the sum of the derivatives of its individual bands. The intensity of phosphorescence is given by the following expression:

$$I_p = 2.3\Phi_p I_0 \epsilon bc \quad (1)$$

where I_p is the phosphorescence intensity, Φ_p is the phosphorescence quantum yield, I_0 is incident source intensity, ϵ is molar absorptivity, b is path-

length, and c is the concentration in mol l⁻¹ (this expression is valid if the product ϵbc is < 0.01). The calibration graphs, in normal phosphorimetry, were linear over the range 0.3–10 $\mu\text{g ml}^{-1}$ for both naphthols and fitted by the least-squares treatment are expressed by:

$$I_p = 207 [\text{1-naphthol}] \quad r = 0.999$$

$$I_p = 90.4 [\text{2-naphthol}] \quad r = 0.998$$

where I_p is the phosphorescence intensity, r the correlation coefficient and the [Naphthol] is in $\mu\text{g ml}^{-1}$. Other analytical parameters are given in Table 2.

The second derivative of (1) is:

$$d^2 I_p / d\lambda^2 = 2.3\Phi_p I_0 bc \, d^2 \epsilon / d\lambda^2 \text{ or } k\Phi_p c \, d^2 \epsilon / d\lambda^2$$

For one mixture of two components:

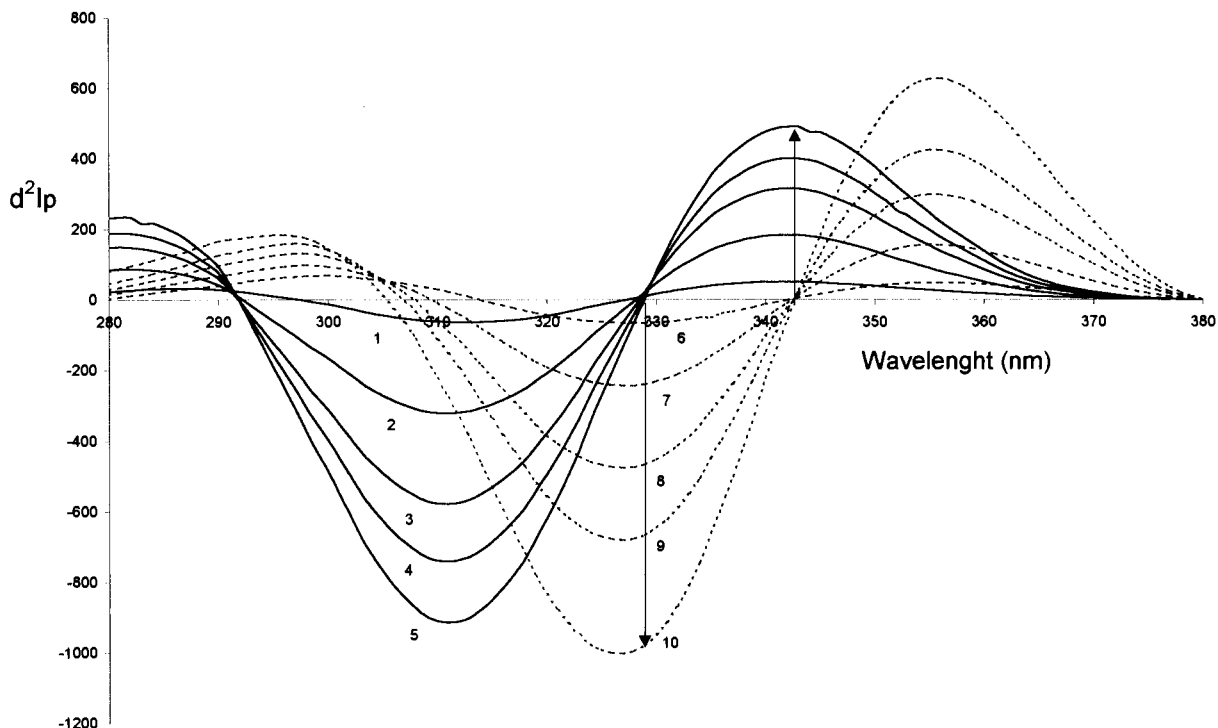


Fig. 7. Synchronous second-derivative phosphorescence spectra of 1-naphthol (1–5) and 2-naphthol (6–10). [Naphthol] = 1, 3, 5, 7 and 10 $\mu\text{g ml}^{-1}$; pH 4.80, $\Delta\lambda = 180 \text{ nm}$; scanning speed 240 nm min^{-1} , response 2 s.

at $\lambda_{1 \text{ iso}}$

$$d^2I_p/d\lambda_1^2 = k\Phi_{p1}c d^2\varepsilon/d\lambda_1^2 + k\Phi_{p2}c d^2\varepsilon/d\lambda_1^2$$

at $\lambda_{2 \text{ iso}}$

$$d^2I_p/d\lambda_2^2 = k\Phi_{p1}c d^2\varepsilon/d\lambda_2^2 + k\Phi_{p2}c d^2\varepsilon/d\lambda_2^2$$

When $d^2\varepsilon/d\lambda_1^2 = 0$ or a constant value, the contribution of component 1 to the over-all amplitude is zero, and for this reason component 2

may be measured free of interference by component 1. The same applies to component 2 when $d^2\varepsilon/d\lambda_2^2 = 0$. Relationships between $d^2I_p/d\lambda^2$ and the concentration of naphthols obtained from these isodifferential points are:

$$d^2I_p/d\lambda^2 = -102.0 [2\text{-naphthol}] + 34.2,$$

$$r = 0.999,$$

$$\text{at } \lambda_{\text{iso}} = 329.1 \text{ nm (at this } \lambda, I_p \text{ is 15)}$$

Table 2
Analytical parameters

Method	Species	λ_{ex} (nm)	λ_{em} (nm)	λ_{iso} (nm)	LDR ^a ($\mu\text{g ml}^{-1}$)	C_L ($k=3$) ($\mu\text{g ml}^{-1}$)	C_Q ($k=10$) ($\mu\text{g ml}^{-1}$)	R.S.D. ^b (%)
Normal	1-Naphthol	300	520	–	0.10–7	0.03	0.10	3.7
Normal	2-Naphthol	334	518	–	0.17–10	0.05	0.17	5.3
2nd derivative	1-Naphthol	–	–	342.9	0.07–7	0.02	0.07	6.5
2nd derivative	2-Naphthol	–	–	329.1	0.07–10	0.02	0.07	5.7

^a Linear dynamic range.

^b Relative standard deviation (R.S.D.), at $1 \mu\text{g ml}^{-1}$ level.

Table 3

Phosphorimetric analysis of 1- and 2-naphthol in synthetic binary mixtures and irrigation water

Ratio I/II (w/w)	Amount (I) ($\mu\text{g ml}^{-1}$)		Error (%)	Amount (II) ($\mu\text{g ml}^{-1}$)		Error (%)
	Taken	Found ^a		Taken	Found ^a	
1:1	5.0	5.20	4.0	5.0	4.99	-0.2
1:1	1.0	1.10	10.0	1.0	1.05	5.0
1:5	1.0	1.12	12.0	5.0	5.10	2.0
1:5	0.1	0.11	10.0	0.5	0.48	-4.0
1:7	1.0	1.10	10.0	7.0	6.77	-3.2
1:10	0.1	0.11	10.0	1.0	1.04	4.0
1:10	1.0	1.08	8.0	10.0	9.30	-7.0
3:5	3.0	2.95	-1.7	5.0	5.00	0.0
3:7	3.0	2.92	-2.6	7.0	6.77	-3.2
5:1	0.5	0.49	-2.6	0.1	0.11	10.0
7:1	7.0	7.15	0.7	1.0	1.07	7.0
10:1	1.0	1.10	10.0	0.1	0.11	10.0
Sample 1	1.0	1.05	5.0	1.0	1.08	8.0
Sample 2	5.0	5.12	2.4	5.0	5.25	5.0
Sample 3	0.5	0.52	4.0	5.0	4.80	-4.0
Sample 4	5.0	4.91	-1.8	0.5	0.55	10
Sample 5	1.0	1.07	7.0	10	9.20	-8.0

^a Mean of three separate determinations.

$$d^2I_p/d\lambda^2 = 58.2 [1\text{-naphthol}] + 8, \quad r = 0.999,$$

$$\text{at } \lambda_{\text{iso}} = 342.9 \text{ nm (at this } \lambda, I_p \text{ is 4),}$$

(where the concentration of naphthols is expressed in $\mu\text{g ml}^{-1}$).

From the results obtained in the determination of synthetic binary mixtures of both naphthols (Table 3), it can be deduced that the reported method gives good results even at high ratios with acceptable levels of precision and accuracy.

4. Applications

The synchronous-derivative phosphorimetric procedure was applied to the determination of 1- and 2-naphthol in irrigation water samples taken in the Axarquía (area of east Malaga province) spiked with both naphthols. Table 3 summarizes the results; it can be concluded that acceptable accuracy and precision was obtained in the analysis of 1- and 2-naphthol in irrigation water.

5. Conclusions

It has been shown that 1- and 2-naphthol form inclusion compounds in β -CD aqueous solution

with formation constants of 644 ± 50 and $718 \pm 40 \text{ M}^{-1}$, respectively. By employing 3-bromo-1-propanol, as heavy atom perturber, an intense phosphorescence emission in β -CD aqueous solution is observed, with a maximum at 520 and 518 nm for 1- and 2-naphthol, being a strong overlapping of emission bands. Lifetimes were calculated from decay curves (10.82 and 9.41 ms, respectively). The variables affecting the formation of both complexes of inclusion have been studied. The kinetic of inclusion process for 2-naphthol is slower than 1-naphthol due to the different position of the group -OH in the molecule which is more protected in 1-naphthol. Mixtures of both species in the ratio 1:10 to 10:1 were simultaneously determined in irrigation water from a single scan by employing the synchronous-derivative technique with a relative standard deviation (R.S.D.) between 5 and 10% and limits of detection of 0.02–0.05 $\mu\text{g ml}^{-1}$.

Acknowledgements

The authors acknowledge the Consejería de Educación y Ciencia de la Junta de Andalucía (Group FQM 0148) for financial this work.

References

- [1] C.A. Parker, C.G. Hatchard, *J.Phys. Chem.* 30 (1962) 276.
- [2] J.J. Donkerbroek, C. Gooijer, N.H. Velthorst, R.W. Frei, *Anal. Chem.* 54 (1982) 891.
- [3] S. Scypinski, L.J. Cline Love, *Anal. Chem.* 56 (1984) 331.
- [4] M.E. Díaz Garcia, A. Sanz Medel, *Anal. Chem.* 58 (1986) 1436.
- [5] S. Scypinski, L.J. Cline Love, *Anal. Chem.* 56 (1984) 331.
- [6] Y.S. Wei, W.J. Jin, R.H. Zhu, G.W. Xing, C.S. Liu, S.S. Zhang, B.L. Zhou, *Spectrochim. Acta Part A* 52 (1996) 683.
- [7] M. Algarra Gonzalez, M. Hernandez Lopez, *Analyst* 123 (1998) 2217.
- [8] X. Du, Y. Zhan, Y. Jiang, X. Huang, G. Chen, *Talanta* 44 (1997) 511.
- [9] M.R. Fernandez de la Campa, Y.M. Liu, M.E. Diaz Garcia, A. Sanz Medel, *Anal. Chim. Acta* 238 (1990) 297.
- [10] S.L. Neal, M.M. Villegas, *Anal. Chem.* 67 (1995) 2659.
- [11] W.J. Jiu, Y.S. Wei, W.S. Duan, C.S. Liu, *Anal. Chim. Acta* 287 (1994) 95.
- [12] G.R. Ramos, I.M. Khasawneh, M.L. Garcia-Alvarez Coque, J.D. Winefordner, *Talanta* 35 (1988) 41.
- [13] I. Soutar, L. Swanson, *Analyst* 116 (1991) 671.
- [14] S. Li, W.C. Purdy, *Chem. Rev.* 92 (1992) 1457.
- [15] K.A. Connors, *Chem. Rev.* 97 (1997) 1325.
- [16] L. Szente, J. Szejtli, *Analyst* 123 (1998) 735.
- [17] M.C. Quintero, M. Silva, D. Perez-Bendito, *Talanta* 36 (1989) 717.
- [18] A. Vincze, M.L. Huszar, *J. Liquid Chromatogr.* 12 (1989) 2887.
- [19] D.M. Hércules, L.B. Rogers, *Anal. Chem.* 30 (1958) 96.
- [20] Y.Q. Li, X. Z. Huang, J.G. Xu, G.Z. Chen, *Talanta* 41 (1994) 695.
- [21] A.M. Afonso Perera, J.H. Ayala Diaz, A. Gonzalez Armas, V. Gonzalez Diaz, *Anal. Lett.* 26 (1993) 2251.
- [22] R.A. Dalterio, R.J. Hurtubise, *Anal.Chem.* 56 (1984) 819.
- [23] T. Vo-Dinh, R.B. Gammage, *Anal. Chem.* 50 (1978) 2054.
- [24] F. Garcia Sanchez, M Hernandez Lopez, J.C. Marquez Gomez, *Spectrochim. Acta* 43A (1987) 101.
- [25] F. Garcia Sanchez, J.C. Marquez Gomez, M. Hernandez Lopez, *Analyst* 112 (1987) 649.
- [26] F. Garcia Sanchez, M. Hernandez Lopez, J.C. Marquez Gomez, *Anal. Chim. Acta* 197 (1987) 275.
- [27] M.M. Hoshino, S. Imamura, K. Ikehara, Y. Hama, *J. Phys. Chem.* 85 (1981) 1820.

Solid-phase UV spectroscopic multisensor for the simultaneous determination of caffeine, dimenhydrinate and acetaminophen by using partial least squares multicalibration

M.J. Ayora Cañada ^a, M.I. Pascual Reguera ^a, A. Molina Díaz ^{a,*},
L.F. Capitán-Vallvey ^b

^a *Department of Physical and Analytical Chemistry, Faculty of Experimental Sciences, University of Jaén, Paraje Las Lagunillas, s/n, E-23071 Jaén, Spain*

^b *Department of Analytical Chemistry, Faculty of Sciences, University of Granada, E-18071 Granada, Spain*

Received 8 December 1998; received in revised form 9 February 1999; accepted 12 February 1999

Abstract

A straightforward flow-through multisensor was developed for the fast simultaneous determination of caffeine (CF), dimenhydrinate (DMH) and acetaminophen (AAP) based on the integration of their retention and UV detection. A diode array spectrophotometer was used to monitor the inherent UV full-spectra in the range 245–310 nm of the analytes retained on C₁₈ bonded phase beads packed in a flow cell, without requiring additional reagents or derivatization processes. The extensively overlapped spectra of the analytes retained on the solid support could be resolved by partial least squares (PLS) regression. After collecting the response of the multisensor, its active microzone was regenerated by using methanol as the eluting agent, leaving it ready for the next determination. The proposed multisensor has been satisfactorily applied for the analysis of synthetic and real samples with different nominal contents of these active principles. © 1999 Elsevier Science B.V. All rights reserved.

Keywords: Solid-phase spectroscopy; PLS multicalibration; Flow-through sensor; Pharmaceuticals

1. Introduction

There are few flow-through spectrophotometric sensing systems based on the use of a sorbent

material where the analyte is temporarily retained while monitoring of its native absorption is performed [1]. One of the most promising aspects of this type of sensor is the possibility of performing multi-component analysis using photometric diode-array detectors to monitor simultaneously the absorbance at various wavelengths or record the entire spectra in a fraction of a second. The joint use of this principle, and chemometric ap-

* Corresponding author. Tel.: +34-953-212-147; fax: +34-953-212-141.

E-mail address: amolina@ujaen.es (A.M. Díaz)

proaches allows the development of multi-parameter sensors. Despite their outstanding advantages there are only few examples of this type of systems. Thus, mixtures of amines could be determined on the basis of their intrinsic absorbance by injecting a large sample volume into a methanol–water carrier in order to drive the plug to a flow cell packed with C_{18} bonded silica beads for temporary retention [2]. A careful selection of the wavelengths at which the individual spectra are most markedly different from one another, must be done in order to allow mixture resolution by solving the 9-equations system obtained from measurements made at nine wavelengths.

In recent years, multivariate calibration methods have an increasing importance in multicomponent analysis, especially those using the partial least squares (PLS) method with decomposition into latent variables. PLS is a factor-based method, which exhibit many of the full-spectrum advantages of the classical least squares (CLS) method without suffering many of the disadvantages of this more classical statistical tool. The basic concept of PLS regression was originally developed by Wold [3]. The use of PLS method for chemical applications was pioneered by Wold et al. [4] and nowadays PLS is a well-established technique [5]. This method had been successfully used in various instances: in fluorimetry [6], in ultraviolet-visible [7] and near-infrared [8] spectrometry and in kinetic analysis [9]. To date no flow-through spectrophotometric sensors that use a full-spectra calibration method to resolve complex mixtures have been described, since research in this area has been dominated by the search for more selective sensors. However, through the use of sensing devices and chemometrics, more intelligent instrumentation can be developed which permits those contributions to the total signal, arising from primary and interfering species, to be decoupled, allowing thus accurate determination of individual components in mixtures.

The purpose of this study was to develop a straightforward flow-through spectrophotometric multisensor for the simultaneous determination of dimenhydrinate (DMH), caffeine (CF), and

acetaminophen (AAP). DMH (diphenhydramine salt of 8-chlorotheophylline) is an antihistaminic compound, widely used in pharmaceuticals formulations as antinauseant to avoid travel sickness. The principal side effects of DMH are somnolence, decrease in the capacity of concentration and incoordination, therefore it is frequently combined with CF (1,3,7-trimethylxanthine) in pharmaceuticals preparations. Acetaminophen (*N*-acetyl-*p*-aminophenol), on the other hand, is used as an analgesic and antipyretic drug, appearing associated with CF and DMH in many commercial formulations.

This paper deals, for the first time, with the use of sorbent retention for the optosensing of target species, exploiting not only their spectral features with the aid of a multicalibration chemometric approach but also their different kinetic behavior in the retention–elution process onto the solid support by selecting the spectra at two adequate time values which provides the most different behavior. In addition, the solid support, placed in the flow cell enhances the signal compared with the same system in homogeneous solution, so also increasing the sensitivity.

2. Experimental

2.1. Reagents

Stock standard solutions of $1000 \mu\text{g ml}^{-1}$ of CF (Merck), DMH (Guinama, Valencia, Spain) and AAP (Fluka), were prepared by dissolution in doubly distilled water under sonication. Working solutions were prepared daily by appropriate dilution with doubly distilled water. All chemicals such as perchloric, nitric, hydrochloric and orthophosphoric acids (Panreac) were of analytical-reagent grade. HPLC grade methanol (Panreac) was used as eluent. C_{18} bonded silica (Waters) with average particles sizes of 55–105 μm was used as solid support, ion exchange resins Sephadex SP C-25 and QAE A-25 (Fluka) were also tested. All solutions were prepared in doubly distilled water.

2.2. Apparatus and software

A Milton Roy Spectronic 3000 diode-array spectrophotometer was used for spectra recording, using the Milton Roy software RapidScan 2.01 for all data acquisition. The GRAMS/32 (from GALACTIC) software package, with the PLSplus/IQ application software [10] running in a 486 PC was used for the statistical treatment of the data and the application of the PLS method. The equipment was also used to import to its own format the absorbance spectra of samples and standards.

A flow-through cell Hellma Model 138-QS with 1 mm optical path length (50 μl inner volume) was packed with the support by introducing it in a methanol suspension with the aid of a syringe. A four channel peristaltic pump (Gilson Minipuls 3) was used to generate the flowing streams. Two six-way rotary injection valves Rheodyne 5041 (one of which acted as a selecting valve) and

PTFE tubing of 0.8 mm i.d. were used. An ultrasonic bath (Ultrason, Selecta) and a Crison Model 2002 pH-meter, fitted with a glass saturated calomel electrode assembly and a temperature probe were also used.

2.3. Treatment of samples

Tablets were dissolved in doubly distilled water by shaking them in an ultrasonic bath for 15 min. Solutions were filtered through a 0.45 μm Millipore filter and diluted conveniently with doubly distilled water.

2.4. Flow diagram and general procedure

A schematic diagram of the flow system is shown in Fig. 1. The sample (600 μl) containing between 0.5 and 5.0 $\mu\text{g ml}^{-1}$ of CF, from 1.0 to 6.0 $\mu\text{g ml}^{-1}$ of DMH and from 5 to 40 $\mu\text{g ml}^{-1}$ of AAP, was inserted into the carrier

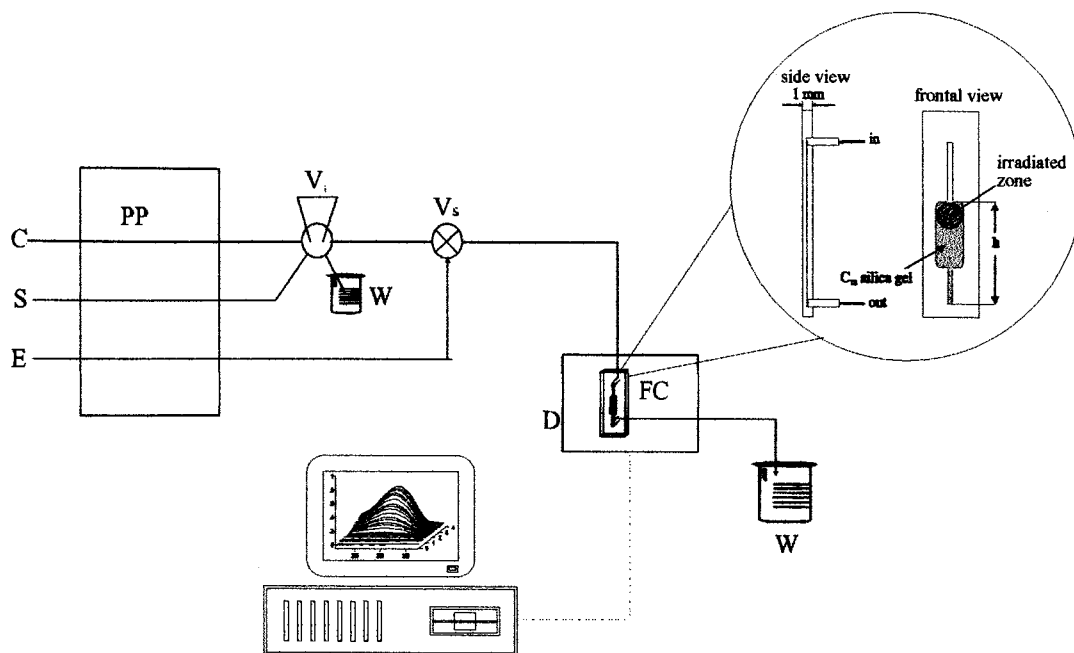


Fig. 1. Flow system diagram. C, carrier solution (0.7% HClO_4 , flowing at 2.1 ml min^{-1}); S, sample; E, eluent (methanol); W, waste; V_i , injection valve; V_s , selecting valve; D, diode-array detector; FC, flow-cell (0.1 cm optical path length) packed with C_{18} . Inset, expanded diagram of the flow cell indicating as h the level of solid support in it.

Table 1
Calibration matrix^a

Sample	Caffeine	Dimenhydrinate	Acetaminophen
1	1.0	2.0	–
2	–	2.0	20
3	1.0	–	20
4	3.0	6.0	20
5	0.5	1.0	40
6	5.0	4.0	40
7	0.5	1.0	5
8	2.0	6.0	10
9	0.5	2.0	5
10	3.0	1.0	10
11	1.0	4.0	5
12	2.0	6.0	40
13	3.0	2.0	10
14	1.0	6.0	20
15	0.5	6.0	5
16	2.0	4.0	10
17	5.0	1.0	30
18	2.0	4.0	10
19	5.0	2.0	30
20	2.0	–	–
21	–	6.0	–
22	–	–	20
23	5.0	–	–
24	–	2.0	–
25	–	–	40
26	3.0	2.0	–

^a Concentrations are expressed as $\mu\text{g ml}^{-1}$.

stream (HClO_4 0.7%) at a flow rate of 1.2 ml min^{-1} . The analytes were retained on the solid support when passing through the flow cell while spectra were being recorded between 245 and 310 nm (using data resolution of 0.35 nm) at 8 s intervals during all the retention process (4 min). Selecting valve was then switched to the eluent stream (methanol), which removed the analytes from the support. For calibration, 26 synthetic mixtures of CF, DMH and AAP were employed (according to Table 1). The concentration ranges were selected within the previously established linear calibration range for each compound. All the levels and ratios of these active principles in the most common commercialized pharmaceuticals are included in these range values.

3. Results and discussion

CF, AAP and DMH are highly absorbing substances in the UV region. CF and DMH (8-chlorotheophylline) show highly overlapping absorption maxima at 275 and 280 nm, respectively, therefore, conventional spectrophotometry cannot be applied satisfactorily to the determination of the mixture. The overlapping between the spectrum of AAP and the other two analytes is lower in conditions near to isoabsorption. But CF and DMH are minor constituents in most commercial pharmaceutical preparations in which binary or ternary mixtures of these analytes are found, so the overlapping among their spectra becomes rather intense making the resolution of the mixture quite difficult as can be seen in Fig. 2. No changes in the positions of absorption maxima were observed when the species were retained on the sorbent. The use of a solid support on which the analytes show a different kinetic behavior of retention–elution together with the powerful capability of the PLS method to discriminate complex mixtures allowed the simultaneous determination of CF, DMH and AAP. The temporal evolution of the spectra of the three analytes is shown in Fig. 3.

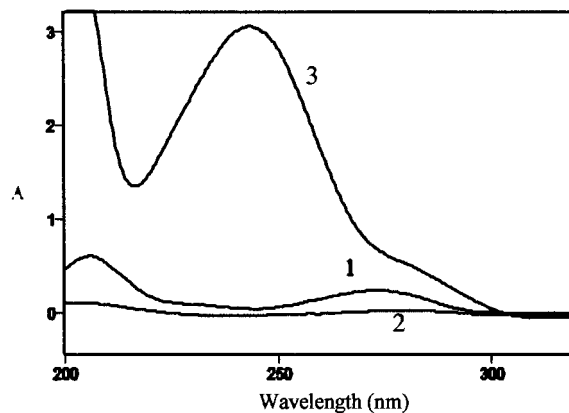


Fig. 2. UV spectra of (1) $5 \mu\text{g ml}^{-1}$ of caffeine (CF), (2) $1.5 \mu\text{g ml}^{-1}$ of dimenhydrinate (DMH), and (3) $50 \mu\text{g ml}^{-1}$ of acetaminophen (AAP). Concentrations are in the same ratio as in the nominal content of 'Saldeva forte' sample (1 cm optical path length).

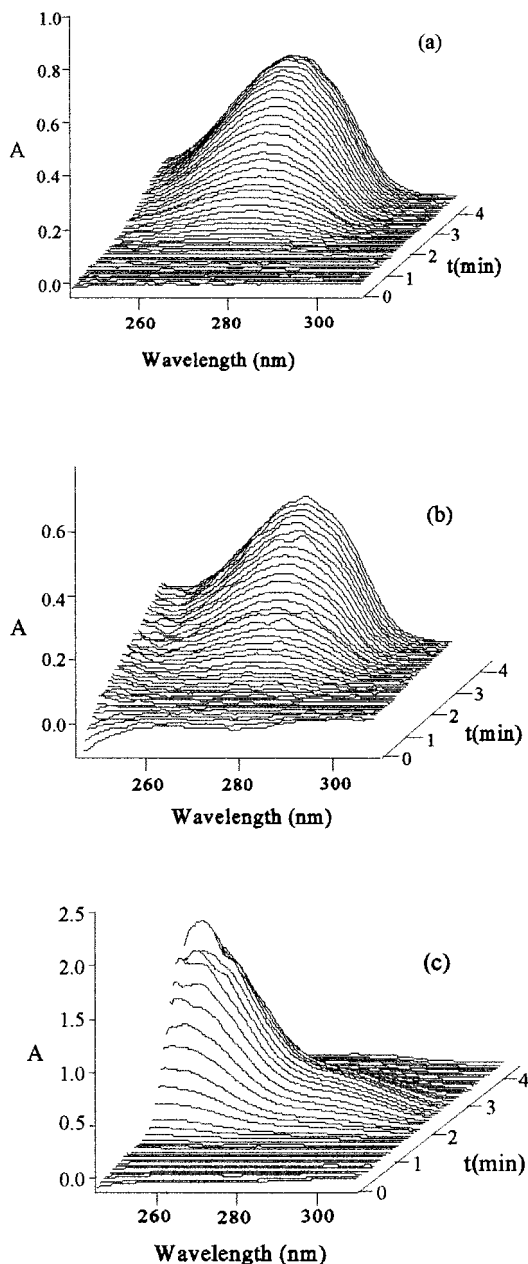


Fig. 3. Temporal evolution of the absorption spectra of (a) $3 \mu\text{g ml}^{-1}$ of caffeine (CF), (b) $6 \mu\text{g ml}^{-1}$ of dimenhydrinate (DMH) and (c) $20 \mu\text{g ml}^{-1}$ of acetaminophen (AAP), measured on C_{18} . Injection of $600 \mu\text{l}$ volumes were performed at $t = 1 \text{ min}$. Elution step was carried out after $t = 4 \text{ min}$ in all cases.

3.1. Optimization of procedure

Optimization studies were carried out for each individual constituent and compromise values of the experimental variables were selected. The variables influencing the system can be divided into three groups: those related to the retention-detection unit, chemical variables and flow system variables.

3.1.1. Variables of the integrated retention-detection unit

Different supports were tested under the same experimental conditions. Cation exchange resin Sephadex SP C-25 was found to fail to retain the analytes; also anionic exchange resin Sephadex QAE A-25 retained only DMH and AAP at alkaline pH values. A non-polar sorbent, octadecylsilane (C_{18}), was selected for further studies due of its large interaction capability with all the three analytes. Decreasing particle size of the support increased the compactness of the solid and resulted in an increasing of the absorption of the baseline; moreover, this fact causes a decrease on permeability of the support and hence problems due to the appearing pressure increase. So the greatest particle size commercially available ($55\text{--}105 \mu\text{m}$) was selected providing an acceptable absorbance background. The level of the sorbent in the flow cell was a key variable: for too high support level a large amount of the analytes is retained just on top of the cell, where the incoming flow just contacts the solid support, falling outside of the detection area (above the light beam). On the other hand, with lower levels the light beam pass through the solution. The optimum height of packing level was found to be 17 mm .

3.1.2. Chemical variables

The effect of pH on the sorption of the three analytes was examined. The retention of CF was found to be independent of pH from 1.0 to 8.0 whereas signal of AAP decreased at $\text{pH} > 7.0$ (see Fig. 4). Because of the extent of the AAP ionization, a decrease in the analytical signal of about 40% was observed at $\text{pH} 11.0$. As can also be seen in Fig. 4, the strongest dependence on pH was

that of the DMH retention, where beyond pH 7.0 the analyte is not sorbed on the C_{18} silica gel. Since DMH exhibits a low absorbance relative to the other two compounds, pH 1.0 was selected to further experiments. Below this pH value a decrease in all the three analytes signals was observed. Different acids (hydrochloric, perchloric, orthophosphoric and nitric) were tested. Perchloric acid was found to give a slightly larger signal (about 10%), so a 0.1 M perchloric acid solution was chosen for further experiments. Under this working conditions AAP was weakly retained so it was eluted from the solid support by the carrier solution itself whereas CF and DMH were strongly retained. In this way, a large enhancement is achieved in sensitivity with regard to conventional spectrophotometry in solution for CF (60 times more) and DMH (50 times more) due to their preconcentration in the solid support. On the other hand the response for PCT in the working conditions do not suffer any enhancement so, by means of the solid support, we obtain a selective increase in sensitivity which allows to keep the absorbance values within the appropriate range to be measured by the detector.

In order to regenerate the sensor, a study of potential different solvents as eluting agents was carried out. Acetonitrile, ethanol, methanol and acetone were tested as eluting agents in water–or-

ganic solvent mixtures ranged between 10 and 100%. The use of methanol resulted in the fastest elution, the speed of which increased by increasing its content in the solvent, therefore, pure methanol was selected in order to achieve a complete and fast (1 min) regeneration of the sensor. The pH of the samples was not critical (signals were found to be constant in the pH range of 1.0–12.0 for CF and AAP and 1.0–9.0 for DMH) because of the partial dispersion of the sample plug (600 μ l) in the carrier stream. Therefore, it was not necessary to buffer the samples before injecting them into the flow system eliminating any sample pre-treatment.

3.1.3. FIA variables

The effects of the sample volume and the flow rate were studied. Decreased flow rates resulted, as expected, in increased residence times and increased peak heights, indicating that the adsorption of the analytes was not instantaneous. A flow-rate of 1.2 ml min⁻¹ was selected. Increasing sample volumes yielded increasing analytical signals and residence times, as a result of the larger amount of analyte retained. This fact makes it possible to select the most appropriate volume of sample taking into consideration the concentration of the samples that are going to be analyzed. A volume of 600 μ l was chosen. The length of the transport system between the injection valve and the flow cell was kept as short as possible because of the absence of a derivatization reaction.

3.2. PLS treatment of spectrophotometric data

UV absorbance data from a calibration set of 26 standard samples (see Table 1) were taken between 245 and 310 nm (at data intervals of 0.35 nm) during the retention–elution process. In order to select the optimum time for PLS resolution, six matrices at different measurement times were optimized. Hence, the absorption spectra of 26 standard samples, at six different time values, were used to optimize six calibration matrices (designated in Table 2 as matrices 1, 2, 3, 4, 5, 6). The upper and lower limits of the studied concentrations used for the calibration matrices were established within the linear range for each indi-

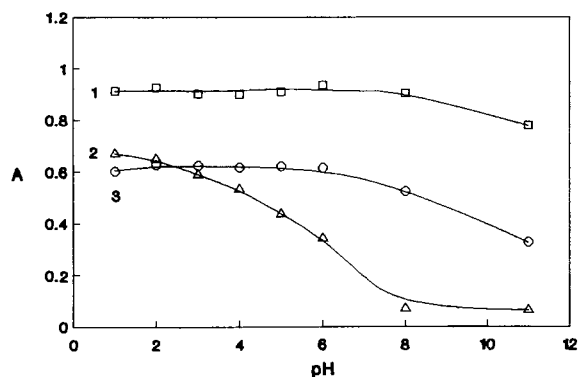


Fig. 4. Effect of the pH on the carrier solution on sensor response (0.1 cm optical path length). Signals at $t = 2.33$ min after injecting the sample. (1) Caffeine (CF) (3 μ g ml⁻¹, $\lambda_{\max} = 275$ nm), (2) dimenhidrate (DMH) (5 μ g ml⁻¹, $\lambda_{\max} = 280$), and (3) acetaminophen (AAP) (40 μ g ml⁻¹, $\lambda_{\max} = 250$).

Table 2
Statistical parameters

Time (min)	Matrix	Caffeine					Dimenhydrinate					Acetaminophen				
		No. Fact	R^2	RMSD	REP	AIC	No. Fact	R^2	RMSD	REP	AIC	No. Fact	R^2	RMSD	REP	AIC
1.75	1	5	0.7283	0.8781	47.6	3.240	4	0.5113	1.5400	57.2	30.46	1	0.8932	4.509	30.1	80.31
1.92	2	4	0.9360	0.3788	25.7	-42.57	4	0.9650	0.4205	15.2	-37.92	9	0.9916	1.506	10.5	39.31
2.08	3	7	0.9472	0.3765	21.6	-36.93	6	0.9244	0.5773	23.3	-16.56	8	0.9707	2.274	17.4	58.71
2.33	4	5	0.9777	0.1975	12.7	-74.35	7	0.9530	0.4471	20.2	-27.86	4	0.9453	2.892	21.6	63.21
2.50	5	7	0.9964	0.1007	5.98	-105.7	7	0.9962	0.1403	5.51	-87.71	4	0.6200	9.101	60.7	122.8
2.75	6	6	0.9709	0.2812	16.1	-53.99	6	0.8687	0.8247	30.0	1.871	2	0.4331	10.687	71.2	127.2

vidual component and in order to include the maximum and minimum levels and ratios for these three active principles in the most common commercially available pharmaceuticals. The model was mean centered and PLS calibration carried out using PLS-1.

To select the number of factors, in order to model the system without overfitting the concentration data, a cross-validation method, leaving out one sample at a time, was used [11]. Cross-validation consists of systematically removing one of the observations in turn and using the remaining observations for construction of latent factors and their regression. The predicted concentrations were compared with the known concentrations of the compounds in each sample and the prediction error sum of squares (PRESS) was calculated. This parameter is a measurement of how well a particular model fits the concentration data. The PRESS was calculated in the same manner each time adding a new factor to the model. The maximum number of factor used was selected at 14 (half of the number of standards plus 1). To select the optimum number of factors, the criterion of Haaland and Thomas was taken into account [12]. According to this, rather than the selection of the model which yields a minimum in PRESS that usually leads to some overfitting, the model to be selected is the one with a minimum number of factors that provides a PRESS value not significantly greater than the minimum one. Haaland and Thomas empirically determined that an *F*-ratio probability of 0.75 was a good choice. So the number of factors for the first PRESS value showing an *F*-ratio probability below 0.75 was selected as the optimum for each matrix at each different time value. The statistical results obtained for all the matrices are summarized in Table 2. The values of the root mean square difference (RMSD) (1), the relative error of prediction (REP), which is the square root of the mean square of the error in the prediction for each component, expressed as a percentage of the mean of the true concentrations (2), the determination coefficient (D) (3) and the Akaike information criterion (AIC) (4) are included in order to give an indication both of the average error in the analysis and the quality of fit of all data to a

straight line, for each component. The most suitable model is the one which gives the lowest value of both the AIC and RMSD, thus matrix 2 (1.92 min after injection) must be used for AAP calibration and matrix 5 (2.5 min after injection) must be used in the case of CF and DMH.

$$\text{RMSD} = \left[\frac{1}{n} \sum_{i=1}^n (\hat{c}_i - c_i)^2 \right]^{0.5} \quad (1)$$

$$\text{REP} (\%) = \frac{100}{\bar{c}} \left[\frac{1}{n} \sum_{i=1}^n (\hat{c}_i - c_i)^2 \right]^{0.5} \quad (2)$$

$$D = \frac{\sum_{i=1}^n (\hat{c}_i - \bar{c}_i)^2}{\sum_{i=1}^n (c_i - \bar{c}_i)^2} \quad (3)$$

$$\text{AIC} = n \ln \frac{\text{RSC}}{n} + 2m \quad (4)$$

where *n* is the total number of samples in the set, \hat{c}_i is the true concentration of the analyte in the sample *i*, c_i represents the estimated concentration of the analyte in the sample *i*, \bar{c} is the mean of the true concentrations in the set, *m* is the number of parameters (factors) and RSC is sum of squared residual.

It can be observed that the best simultaneous D and REP values are obtained from matrix 2 for AAP whereas CF and DMH can be predicted with REP values about 5% and a good linear correlation coefficient by using matrix 5. So the best results for AAP are obtained when it begins to be eluted from the solid support, meanwhile the best results for the other analytes are found when AAP is rather completely desorbed. It was not possible to quantify the three analytes by using only one of the matrices with acceptable REP values for all of them, therefore, it is necessary to use two different calibration matrices. It must be emphasized that it does not mean that two different experiments had to be done but spectra at two time values recorded with only one injection of the sample had to be selected in order to build the two matrices.

In Table 2 the optimum number of factors for each component and matrix is shown. For the matrices that are going to be used in prediction of real samples, seven latent variables were used in

Table 3
Validation set^a

Sample	Caffeine			Dimenhydrinate			Acetaminophen		
	C_{added}	C_{found}	Rec $\pm \sigma$ (%)	C_{added}	C_{found}	Rec $\pm \sigma$ (%)	C_{added}	C_{found}	Rec $\pm \sigma$ (%)
1	1.50	1.53	102 \pm 3	1.00	1.03	103 \pm 2	15.0	15.4	103 \pm 13
2	2.00	2.01	100 \pm 2	2.50	2.40	96 \pm 7	20.0	18.1	91 \pm 2
3	1.50	1.44	96 \pm 5	1.50	1.56	103 \pm 1	30.0	36.0	120 \pm 3
4	4.00	3.92	98 \pm 2	3.00	3.41	113 \pm 1	15.0	14.1	94 \pm 12
5	1.00	1.14	114 \pm 2	2.00	1.89	94 \pm 2	40.0	42.0	105 \pm 2
6	2.00	1.90	95 \pm 2	–	–0.07	–	–	–0.34	–
7	–	–0.03	–	–	–0.06	–	30.0	30.3	101 \pm 2
8	–	–0.06	–	3.00	2.54	85 \pm 1	15.0	15.4	102 \pm 7
9	2.50	2.37	95 \pm 4	1.50	1.58	105 \pm 1	20.0	21.1	111 \pm 7
10	4.00	3.80	95 \pm 2	0.50	0.52	103 \pm 3	30.0	31.7	106 \pm 2
11	1.50	1.60	94 \pm 6	2.50	2.66	106 \pm 3	30.0	27.3	91 \pm 4
12	0.75	0.71	94 \pm 3	4.00	3.85	96 \pm 2	15.0	15.7	105 \pm 3
13	3.00	3.09	103 \pm 3	1.00	0.95	95 \pm 4	30.0	32.2	107 \pm 3
14	0.50	0.53	106 \pm 5	5.00	4.83	97 \pm 3	25.0	24.3	97 \pm 3
15	1.00	0.97	97 \pm 2	1.00	1.05	105 \pm 4	40.0	36.5	91 \pm 3
16	2.00	1.90	95 \pm 3	2.00	2.03	102 \pm 3	–	0.33	–
17	3.50	3.17	91 \pm 5	2.50	2.73	109 \pm 3	25.0	26.3	105 \pm 2
18	0.75	0.77	103 \pm 1	1.00	1.09	109 \pm 5	15.0	16.5	110 \pm 6
19	0.50	0.44	88 \pm 4	3.00	3.17	106 \pm 3	40.0	42.5	106 \pm 2
20	3.00	3.14	105 \pm 4	1.50	1.48	99 \pm 3	25.0	28.0	112 \pm 6

^a C_{added} , concentration added expressed as $\mu\text{g ml}^{-1}$; C_{found} , concentration found. Values are mean of three independent determinations expressed as $\mu\text{g ml}^{-1}$. Rec $\pm \sigma$ (%), mean percentage of recovery \pm S.D.

modeling both CF and DMH while nine of them were used in modeling AAP. If the three components system were linear, only three latent variables would be required. However, the retention onto a solid support can cause the appearance of nonlinear effects, as well as differences both in the intensity of light scattered by the solid support and in compactness. As reported by other authors [13–15], linear calibration techniques like PCR and PLS can give good approximations to non linearity by incorporating extra factors in the calibration model.

3.2.1. Validation set

In order to test the performance of the proposed method, it was applied to the determination of artificial mixtures containing various concentrations of the three compounds. A set of 20 synthetic mixtures was predicted by using the selected matrices (matrix 2 for AAP and matrix 5 for CF and DMH). Results are summarized in Table 3. As can be seen, the amounts added and

found were consistent and the relative standard deviations low. Higher errors of prediction are found for AAP probably due to the lower reproducibility of data taken in its elution step. The results are excellent considering not only the spectral overlapping but also the 10-fold difference between the concentrations of AAP and the other two analytes.

3.3. Applications

The proposed sensing system has been used in the simultaneous determination of the three analytes in commercially available pharmaceutical formulations with different proportions of these active principles (most of them are binary mixtures, a ternary mixture and an individual component sample were included). The results obtained and the percentage of recovery with respect to the contents reported by the manufacturers are shown in Table 4. All the constituents were predicted with acceptable errors. The highest errors were

Table 4
Analytical applications^a

Pharmaceutical	Caffeine		Dimenhydrinate		Acetaminophen	
	C_{found}	Rec $\pm \sigma$ (%)	C_{found}	Rec $\pm \sigma$ (%)	C_{found}	Rec $\pm \sigma$ (%)
'Cinfamar Infantil'	–	–	26.2	105 \pm 6	–	–
'Cinfamar Cafeína'	54.2	108 \pm 7	51.7	103 \pm 8	–	–
'Biodramina C'	53.3	107 \pm 8	54.3	109 \pm 3	–	–
'Salvarina'	43.1	86 \pm 2	11.6	77 \pm 4	–	–
'Saldeva Forte'	45.9	92 \pm 2	13.4	89 \pm 3	518	105 \pm 8
'Analgilasa'	26.5	89 \pm 5	–	–	556	111 \pm 5

^a Nominal contents of pharmaceuticals (per component): 'Cinfamar Infantil' (dimenhydrinate 25 mg); 'Cinfamar Cafeína' (dimenhydrinate 50 mg, caffeine 50 mg); 'Biodramina C' (dimenhydrinate 50 mg, caffeine 50 mg, pyridoxine HCl 15 mg); 'Salvarina' (ibuprofen 200 mg, caffeine 50 mg, dimenhydrinate 15 mg); 'Saldeva forte' (acetaminophen 500 mg, caffeine 50 mg, dimenhydrinate 15 mg); 'Analgilasa' (acetaminophen 500 mg, caffeine 50 mg, codeine phosphate 10 mg). Results are mean of three independent determinations. C_{found} , concentration found in mg per component. Rec $\pm \sigma$ (%), mean of percentage of recovery \pm S.D.

about 10% (tolerance level established in the USP Pharmacopeia for this type of drug [16]). Although the relative prediction errors are higher than those obtained with the validation set, this is a good prediction if we take into account the absence, in the calibration standards, of a compensation involving the presence of excipients and active principles which are present in some of the formulations. Hence, the high error of prediction for DMH in 'Salvarina' can be attributed perhaps to the great amount of ibuprofen, in fact, due to this reason the determination would not have been possible in the absence of the solid support, as ibuprofen is much more weakly retained than CF and DMH. Additionally, the method provides accurate and precise results in a wide range of concentrations which varies from 15 mg/U of DMH to 500 mg/U of AAP.

4. Conclusions

The integrated PLS spectrophotometric multi-sensor developed for the simultaneous determination of CF, DMH and AAP offers interesting features such as simplicity, sensitivity, low cost and flexibility. The solid support placed in the flow cell acts both on increasing the sensitivity (in a selective way depending on the analyte) and selectivity of the detection. Thus, the discrimination is made by the features of the detector, the

chemometric PLS approach used for data treatment and the capability of the solid support to reveal different retention–elution kinetic behaviors of the analytes. This is the first spectrophotometric sensing device combining this feature. Moreover the proposed procedure is very fast, requiring only the dissolution of the samples in water and filtration before injecting them into the flow system.

Acknowledgements

The authors acknowledge the financial support of the Ministerio de Educación y Cultura (Dirección General de Enseñanza Superior e Investigación Científica), project PB97-0849.

References

- [1] K. Yoshimura, Anal. Chem. 59 (1987) 2922.
- [2] B. Fernández Band, F. Lázaro, M.D Luque de Castro, M. Valcárcel, Anal. Chim. Acta 229 (1990) 177.
- [3] H. Wold, in: F. David (Ed.), Research Papers in Statistics, Wiley, New York, 1966, p. 411.
- [4] H. Wold, in: H. Joreskog, H. Wold (Eds.), Systems Under Indirect Observation, vol. 2, North-Holland, Amsterdam, 1982, p. 1.
- [5] H. Martens, T. Naes, Multivariate Calibration, Wiley, Chichester, 1989.
- [6] M. Del Olmo, C. Díez, A. Molina, I. De Orbe, J.L. Vilchez, Anal. Chim. Acta 335 (1996) 23.

- [7] I. Durán Meras, A. Muñoz de la Peña, A. Espinosa Mansilla, F. Salinas, *Analyst* 118 (1993) 807.
- [8] F.J. Rambla, S. Garrigues, M. De la Guardia, *Anal. Chim. Acta* 344 (1997) 41.
- [9] J. Havel, J. Jiménez, R.D. Bautista, J.J. Arias León, *Analyst* 118 (1993) 1355.
- [10] Grams/32 Software Package, PLSplus/IQ Add-on Application Software, Galactic Industries, Salem, NH.
- [11] M. Stone, *J. R. Stat. Soc. B* 36 (1974) 111.
- [12] D.M. Haaland, E.V. Thomas, *Anal. Chem.* 60 (1988) 1193.
- [13] M.K. Phelan, C.H. Barlow, J.J. Kelly, T.M. Jinguji, J.B. Callis, *Anal. Chem.* 61 (1989) 1419.
- [14] W.P. Carey, L.E. Wagen, J.T. Dyke, *Anal. Chem.* 61 (1989) 1667.
- [15] P.J. Gemperline, J.R. Long, V.G. Gregoriu, *Anal. Chem.* 63 (1991) 2313.
- [16] United States Pharmacopeia XXIII revision, 1990 USP Convention, Rockville, MD, 1990.

Voltammetric determination of traces of Cr(VI) in the flow system in the presence of bipyridyne

Mieczysław Korolczuk *, Małgorzata Grabarczyk

Faculty of Chemistry, Maria Curie-Skłodowska University, 20-031 Lublin, Poland

Received 8 February 1999; accepted 12 February 1999

Abstract

The voltammetric method of Cr(VI) determinations in the flow system, based on the combination of selective accumulation of the product of Cr(VI) reduction on HMDE and a very sensitive method of chromium determination in the presence of bipyridine [Z. Gao K.S. Siow, *Electroanalysis* 8 (1996) 602] is proposed. The calibration graphs were linear from 3×10^{-9} to 3×10^{-8} and from 5×10^{-10} to 5×10^{-9} mol l⁻¹ for accumulation times 120 and 600 s, respectively. The relative standard deviation (R.S.D.) was 6.5% ($n = 5$) for Cr(VI) concentration 1×10^{-8} mol l⁻¹ and the accumulation time 120 s. The influence of foreign ions commonly present in water samples is presented. Validation of the method was made by comparison of the results of analyses of tap water by another electrochemical method and by recovery test for river and mineral water. © 1999 Elsevier Science B.V. All rights reserved.

Keywords: Chromium speciation; Voltammetry; Water; Flow system

1. Introduction

The hexavalent chromium is about 100–1000 times more toxic than the trivalent [1], so the methods for differentiation between these two states are important in water analysis. A number of voltammetric procedures for chromium determination with low detection limit have been recently developed [2–10], but only some of them can be used for Cr(VI) determination in the presence of Cr(III) [5–10]. Only the procedure pro-

posed by Turyan et al. [10] seems to be highly selective and sensitive; however, it requires the regeneration of the working electrode before each measurement. In other procedures [5–9] the determinations of Cr(VI) can be carried out only to 10–100-fold excess of Cr(III).

This paper presents the application of a voltammetric method of total chromium determination [2] for determination of Cr(VI) in the presence of a large excess of Cr(III) ions. The method is based on selective accumulation of the product of Cr(VI) reduction in the form of Cr(OH)₃ onto HMDE, its complexation with bipyridine and then reduction of the complex in the presence of nitrite.

* Corresponding author. Fax: +48-81-533-3348.

E-mail address: mkorolcz@hermes.umcs.lublin.pl (M. Korolczuk)

2. Experimental

2.1. Apparatus

Measurements were made with the use of an EA 9 electrochemical analyzer and a static mercury drop electrode both made by MTM Poland. The schematic diagram of the flow cell used is presented in Fig. 1. The volume of the cell was about 0.5 ml. A HMDE with a surface area of 1.4 mm² was used. All potentials reported are referred to an Ag/AgCl electrode. The solutions were delivered to the cell from a constant headspace reservoir elevated 0.5 m above the cell. The flow-rates of each solution were about 18 ml min⁻¹.

2.2. Reagents

A stock standard solution of Cr(VI) (0.01 mol l⁻¹) was prepared by dissolving K₂CrO₄ in water. A standard solution of Cr(III) (0.01 mol l⁻¹) was prepared by dissolving CrCl₃·6 H₂O in 0.5 mol l⁻¹ HCl. A 0.01 mol l⁻¹ stock solution of 2,2-bipyridine was prepared by dissolving the reagent in absolute ethanol. A 0.2 mol l⁻¹ CH₃COONa/CH₃COOH buffer (pH 4.5) was prepared from reagent grade CH₃COOH and NaOH. Triply distilled water was used throughout.

2.3. Procedure

Each measurement consisted of three steps:

- selective accumulation of the product of Cr(VI) reduction in the form of Cr(OH)₃ onto the HMDE;
- washing of the cell; and
- complexation of the product of Cr(VI) reduction by bipyridine and then reduction of the complex.

The standard measuring procedure was as follows: the flow of 0.002 mol l⁻¹ acetate buffer of pH 4.5 containing 2 × 10⁻³ mol l⁻¹ Al(III) and 3 × 10⁻⁸ mol l⁻¹ K₂CrO₄ was directed into the electrochemical cell and the accumulation of the product of Cr(VI) reduction onto the mercury drop was carried out within 120 s at -0.25 V. Then the potential was changed to -0.6 V and the cell was washed with the 0.001 mol l⁻¹ acetate

buffer within 120 s. Next the complexing solution 0.1 mol l⁻¹ NaNO₂ + 0.1 mol l⁻¹ NH₄Cl + 5 × 10⁻⁶ mol l⁻¹ EDTA + 5 × 10⁻⁶ mol l⁻¹ bipyridine + NH₄OH (pH 9.3) was directed into the cell within 30 s. Then the potential was changed to -1.0 V and after an equilibration time of 15 s the differential pulse voltammogram was recorded, while the potential was scanned to -1.45 V. The scan rate of 50 mV s⁻¹ and the pulse height 50 mV were chosen. During the accumulation and the washing steps the solutions were stirred. The oxygen from the complexing solution was removed by passing pure nitrogen through the solution in the reservoir all the time as the measurements were performed. After each measurement the flow of the 0.001 mol l⁻¹ acetate buffer was started for at least 60 s before the next measurement. The blank voltammogram was obtained according to the above procedure, though using triply distilled water as a sample.

2.4. Sample preparation

Transfer 80 ml of river or mineral water or 50 ml of tap water into a 100 ml volumetric flask and add 1.6 ml 0.125 mol l⁻¹ NH₄Al(SO₄)₂. Then add 1 ml acetate buffer and make to mark with triply distilled water.

3. Results and discussion

The procedure of Cr(VI) determination presented in this paper is based on the combination

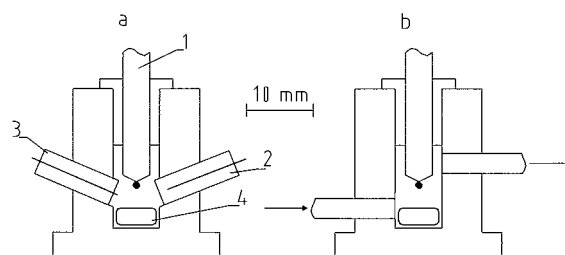


Fig. 1. A schematic diagram of the flow cell used for Cr(VI) determination. (A) and (b) front and side view, respectively. 1, HMDE; 2, Ag/AgCl electrode; 3, Pt electrode; 4, magnetic stirring bar.

of selective accumulation of the product of Cr(VI) reduction in the form of Cr(OH)₃ on HMDE and a voltammetric method of total chromium determination in the presence of bipyridine [2]. The voltammetric procedure described in paper [2] with a very low detection limit 20 pmol l⁻¹ has not been used to distinguish between chromium species. Because the chromium species show different toxicity it was decided to adapt this method to selective determination of Cr(VI) in the presence of excess of Cr(III). For minimisation of interferences from Cr(III) and other ions the measurements were performed in a flow system. In this system the substances present in the sample which can potentially interfere are removed from the electrochemical cell before the detection step.

3.1. Cyclic voltammetry

To explain the mechanism of the catalytic process the cyclic voltammetric experiments were performed following the accumulation within 60 s at potential -1.0 V from quiescent solutions. Ammonium buffer concentration in these experiments was 0.003 mol l⁻¹, because at higher concentrations the catalytic peak of chromium is overlapped by a peak of bipyridine reduction. In this buffer, bipyridine is reduced, with the peak at potential -1.34 V forming on the voltammogram (Fig. 2a). On the cyclic voltammogram from a solution containing bipyridine and Cr(VI) ions (Fig. 2b) a new cathodic peak appears at potential -1.44 V and an anodic one at -1.38 V. The appearance of these new peaks can be explained in the following way. During the accumulation period at -1.0 V, Cr(VI) ions are reduced to Cr(III) and in the presence of bipyridine the Cr(III)-bipyridine (Cr(III)-By) complex is formed. As shown in the paper [2], this complex is adsorbed on the electrode. Then during the negative direction scan the complex is reduced to Cr(II)-By and a corresponding peak at -1.44 V is observed on the voltammogram. When the direction of the polarisation scan is changed the Cr(II)-By complex is oxidised to Cr(III)-By and an anodic peak is formed. Such explanation of the reduction-oxidation process is confirmed by the voltammogram presented in Fig. 2c. In this case after the cathodic

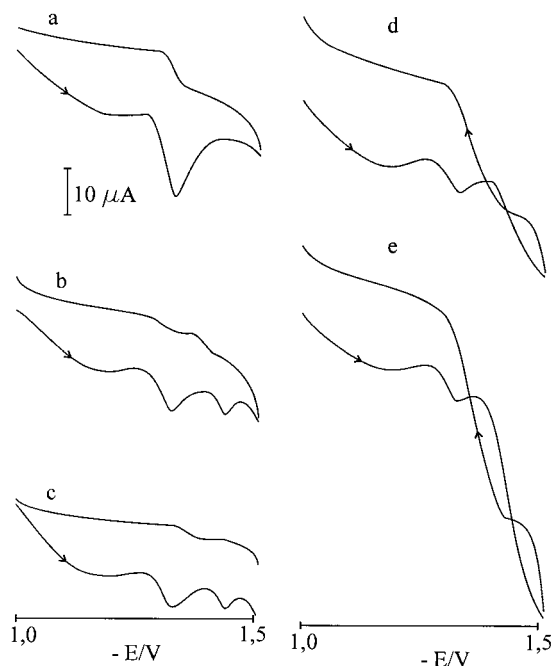
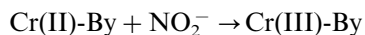
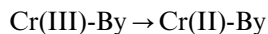


Fig. 2. Cyclic voltammograms following accumulation within 60 s at potential -1.0 V from quiescent solutions: (a) 0.003 mol l⁻¹ NH₄Cl + NH₄OH (pH 9.2) + 1 × 10⁻⁵ mol l⁻¹ bipyridine; (b) as (a) + 1 × 10⁻⁶ mol l⁻¹ K₂CrO₄; (c) as (b) but the potential was stopped for 30 s at -1.53 V after the cathodic scan; (d) as (b) + 5 × 10⁻⁴ mol l⁻¹ NaNO₂; (e) as (b) + 1 × 10⁻³ mol l⁻¹ NaNO₂. Scan rate 200 mV s⁻¹.

scan the potential was stopped for 30 s and then the anodic part of the voltammogram was recorded. The absence of the anodic peak can be explained by diffusion of Cr(II)-By complex into the bulk of the solution (the reduction product of Cr(III)-By complex as shown in [2] is not adsorbed at the mercury electrode). The concentration of Cr(II)-By on the electrode is limited by diffusion of Cr(VI) ions to the electrode. Because the concentration of Cr(VI) in the solution is low, the anodic peak is not observed on the voltammogram. The absence of the anodic peak on the voltammogram also confirms that Cr(III)-By is not reduced to metallic chromium, because in such a case the anodic peak should increase as a result of the accumulation process. The addition of nitrites to the solution containing Cr(VI) and bipyridine causes the increase of the current in the potential range corresponding to Cr(III)-By re-

duction (Fig. 2d, e). This increase of current can be explained by the following cyclic reactions:



It must be stated that in the absence of chromium the nitrites are not reduced on the electrode at this potential range. Probably, in the catalytic process complexes containing not only bipyridine but also ammonia ligands react with nitrites, because the concentration of ammonia influences the current of the chromium peak.

3.2. Effect of composition and pH of the supporting electrolyte

For selective accumulation of the product of Cr(VI) reduction in the form of Cr(OH)₃ onto the mercury film electrode Vidal et al. [11] proposed the acetate/acetic acid buffer as the supporting electrolyte and the accumulation potential -0.3 V versus SCE. The preliminary experiments show that the acetate buffer of pH 4.5 and the accumulation potential -0.25 V are suitable for selective accumulation of the product of Cr(VI) reduction onto the HMDE. At these conditions only the Cr(III) ions generated on the electrode are accumulated on its surface, while the Cr(III) ions present in the solution are accumulated with very low efficiency. It may be explained by different adsorption properties of Cr(III) compounds formed from the ions generated on the electrode and those present in the solution. Different reactivity of these two forms of Cr(III) are known [5]. To confirm such hypothesis, experiments were carried out according to the proposed procedure but with an additional washing step after the accumulation period. In this washing step the acetate buffer containing 1×10^{-8} mol l⁻¹ of Cr(III) was used. The concentration of Cr(III) in this solution was equal to Cr(VI) concentration used in the accumulation step. It was observed that the peak of chromium decreased three times and nearly disappeared after the introduction of the washing periods of 20 and 40 min, respectively. During such a long washing time the form of accumulated Cr(III) changes, desorption of

accumulated Cr(III) proceeds and as a consequence the peak of chromium decreases. It was found that under chosen conditions of accumulation, the Cr(III) ions do not give any response up to the concentration of 1×10^{-6} mol l⁻¹. At higher concentrations Cr(III) ions interfere as shown in Fig. 3b. The interference can be minimized by the addition of NH₄Al(SO₄)₂ to the sample solution (Fig. 3a) so the determinations of Cr(VI) can be carried out even at Cr(III) concentrations exceeding 1×10^{-6} mol l⁻¹ although small interference should be taken into account. Al(III) was added to the concentration of 2×10^{-3} mol l⁻¹ although it did not influence the Cr(VI) response up to the concentration 1×10^{-2} mol l⁻¹. The change of acetate buffer from 0.001 to 0.004 mol l⁻¹ as well as the pH of the solution in the range from 3 to 5 does not influence the current of the peak corresponding to Cr(VI). For further measurements the pH 4.5 was chosen because at higher pH the coprecipitation of hydroxide was observed.

3.3. Effect of the accumulation potential

The effect of the accumulation potential was studied for both oxidation states of chromium Cr(VI) and Cr(III) at concentrations 3×10^{-8} and 3×10^{-4} mol l⁻¹, respectively. The accumu-

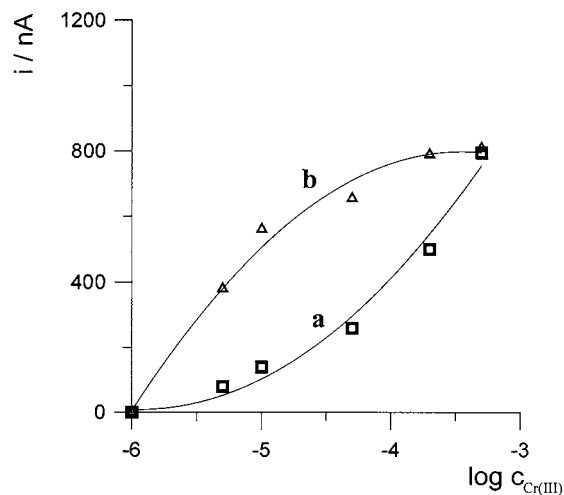


Fig. 3. Comparison of Cr(III) interference in the presence (a) and absence (b) of Al(III). Accumulation time 120 s.

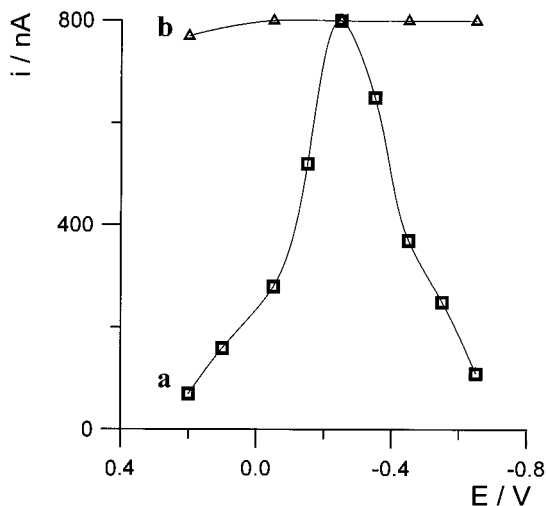


Fig. 4. Effect of the accumulation potential on the Cr(VI) (a) and Cr(III) (b) peak. Accumulation time 120 s. Concentrations of Cr(VI) and Cr(III) were 3×10^{-8} and 3×10^{-4} mol l⁻¹, respectively.

lation potential was changed from +0.2 to -0.65 V. The results are presented in Fig. 4. On the basis of the result obtained in further measurements the potential -0.25 V was chosen.

3.4. Effect of the accumulation time

The current of the peak increases linearly with the accumulation time to 180 and 600 s for Cr(VI) concentrations 3×10^{-8} and 3×10^{-9} mol l⁻¹, respectively.

3.5. Effect of the complexation time

The equilibration time of 15 s is sufficient for complexation of the accumulated product of Cr(VI) reduction by bipyridine.

3.6. Calibration graph

The calibration graph for accumulation time of 120 s was linear from 3×10^{-9} to 3×10^{-8} mol l⁻¹ and obeyed equation $y = 30.4x + 17$, where y and x are peak current (nA) and

Cr(VI) concentration (nmol l⁻¹), respectively. The linear correlation coefficient $r = 0.997$. The relative standard deviations (R.S.D.) from the five determinations were 9.2 and 6.5% for Cr(VI) concentrations 3×10^{-9} and 1×10^{-8} mol l⁻¹, respectively. The calibration graph for accumulation time of 600 s was linear from 5×10^{-10} to 5×10^{-9} mol l⁻¹ and obeyed equation $y = 167x + 4$ ($r = 0.999$). Fig. 5 shows the differential pulse voltammograms for the blank and for spiked distilled water samples. Fig. 4a shows that even when Cr(VI) ions were not added to the sample solution the peak on the voltammogram was observed. Gao et al. [2] also reported the presence of the peak for blank solution in the course of chromium determination in the presence of bipyridine, and concluded that the detection limit of the method is limited by the impurities of chromium in the supporting electrolyte. The experiments carried out at different concentrations of the ammonia buffer indicate that the peak in the blank corresponds to bipyridine reduction. The peak is not influenced by the buffer concentration while the peak of chromium increases as the buffer concentration increases from 3×10^{-3} to 0.1 mol l⁻¹. In the course of analyses of samples containing Cr(VI) performed at the buffer concentration of 3×10^{-3} mol l⁻¹ two peaks were observed on the voltammogram. The first one at potential -1.3 V, which increases linearly as the concentration of bipyridine increases and is not influenced by Cr(VI) concentration, corresponds to bipyridine reduction. The second one at potential -1.34 V is linearly dependent on the chromium concentration. The above results show that the lower peak in the blank can be obtained only if the concentration of bipyridine is lower. However, the decrease in the bipyridine concentration also causes the decrease of the chromium peak, so the bipyridine concentration of 5×10^{-6} mol l⁻¹ was used as proposed in the original paper for total chromium determination [2].

The limit of detection estimated from (3σ) for low concentrations of Cr(VI) was about 1×10^{-9} and 2×10^{-10} mol l⁻¹ for accumulation times 120 and 600 s, respectively.

3.7. Effect of foreign ions

The influence of foreign ions on the determination of Cr(VI) was studied using fixed concentration of Cr(VI), 1.5×10^{-8} mol l⁻¹ and the accumulation time 120 s. The addition of Cr(III) up to the concentration 1×10^{-6} mol l⁻¹ does not influence the current of the peak corresponding to Cr(VI). Further results showed that at least 10³-fold amounts of Zn²⁺, Pb²⁺, Fe³⁺, Ni²⁺, Mn²⁺, MnO₄⁻, Cd²⁺; 10²-fold amounts of Cu²⁺, Co²⁺, VO₃⁻, MoO₄⁻ do not interfere. The addition of MgSO₄ or CaCl₂ at concentration 0.01 mol l⁻¹ also does not influence the current of the peak. The influence of surface active substances was studied using Triton X-100. It was found that the addition of Triton X-100 at the concentration 0.2 mg l⁻¹ causes about 22% decrease of the peak.

3.8. Analytical applications

The procedure proposed was applied to Cr(VI) determination in tap water from Chełm (industrial

area). The result obtained was 8.6 nmol l⁻¹ and R.S.D. 5.7% ($n = 3$), while the analyses performed by another voltammetric procedure [5] give the result 8.9 nmol l⁻¹ and R.S.D. 4.5% ($n = 3$). Analyses of tap water samples spiked additionally with Cr(III) to the concentration 1×10^{-6} mol l⁻¹ performed by the proposed method give the same result, while the DTPA method in such conditions give the result about three times higher. Recovery studies with Cr(VI) and/or Cr(III) spiked river and mineral water samples yielded recoveries ranging from 93 to 113% as shown in Table 1. Agreement between the results obtained by the proposed procedure with that obtained by DTPA method for tap water and acceptable recoveries for river and mineral water shows that the proposed procedure can be used for determination of Cr(VI) in natural water samples. The results show that the proposed procedure allows for Cr(VI) determinations in the presence of higher excess of Cr(III) than the commonly used DTPA procedure [5]. The detection limit of the proposed procedure is about five times higher than that of the DTPA method.

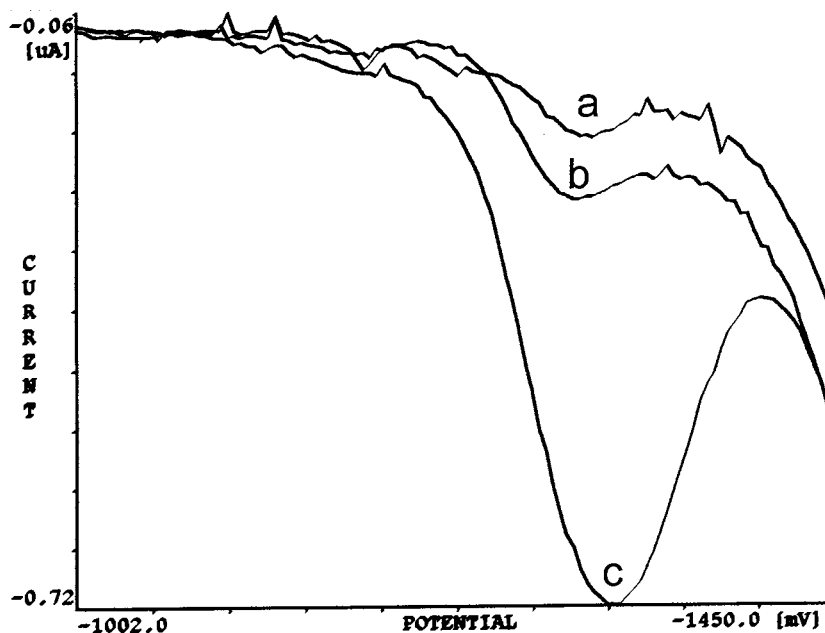


Fig. 5. The differential pulse voltammograms obtained after accumulation for 600 s from water samples: (a) triply distilled water; (b) as (a) + 5×10^{-10} mol l⁻¹ Cr(VI); (c) as (a) + 3×10^{-9} mol l⁻¹.

Table 1
Recovery tests for the Bystrzyca river and mineral water samples

Sample	Cr(VI) added (nmol l ⁻¹)	Cr(III) added (nmol l ⁻¹)	Cr(VI) found (nmol l ⁻¹)	Recovery of Cr(VI) (%)	R.S.D. (n = 3) (%)
Bystrzyca river water	3	–	3.2	106	7.4
	–	1000	<1	–	–
	3	1000	3.4	113	10.2
	10	–	9.5	95	5.2
	10	1000	10.6	106	5.5
Mineral water 'Żywiec Zdrój'	3	–	2.8	93	8.3
	10	–	11	110	6.1

Acknowledgements

This work was supported by KBN (Poland) grant (project 3 T09A 038 15).

References

- [1] R.M. Cespón-Romero, M.C. Yebra-Biurrun, M.P. Bermejo-Barrera, *Anal. Chim. Acta* 327 (1996) 37.
- [2] Z. Gao, K.S. Siow, *Electroanalysis* 8 (1996) 602.
- [3] J. Wang, J. Lu, *Analyst* 117 (1992) 1913.
- [4] A.M. Dobney, G.M. Greenway, *Analyst* 119 (1994) 293.
- [5] M. Boussemart, C.M.G. van den Berg, M. Ghaddaf, *Anal. Chim. Acta* 262 (1992) 103.
- [6] C. Elleouet, F. Quentel, Ch. Madec, *Anal. Chim. Acta* 257 (1992) 301.
- [7] M.A. Ghandour, S.A. El-Shatoury, A.M.M. Aly, S.M. Ahmed, *Anal. Lett.* 29 (1996) 1431.
- [8] E.M. Souza, A.L. Wagener, P. Farias, *Croat. Chem. Acta* 70 (1997) 259.
- [9] D.V. Vukomanovic, G.V. van Loon, K. Nakatsu, D.E. Zoutman, *Microchem. J.* 57 (1997) 86.
- [10] I. Turyan, D. Mandler, *Anal. Chem.* 69 (1997) 894.
- [11] J.C. Vidal, J.M. Sanz, J.R. Castillo, *Fresenius J. Anal. Chem.* 344 (1992) 234.

In-situ external reflection FTIR spectroelectrochemical and XPS investigations of cobalt-cyanometallates as inorganic polymeric materials on a platinum electrode

Ai Li Bo ^a, Xiang Qin Lin ^{b,*}

^a *Laboratory of Electroanalytical Chemistry, Changchun Institute of Applied Chemistry of Chinese Academy of Sciences, Changchun 130022, China*

^b *Department of Chemistry, University of Science and Technology of China, Hefei 230026, China*

Received 8 July 1998; received in revised form 18 December 1998; accepted 29 December 1998

Abstract

Cobalt-cyanometallate films electrochemically deposited on a platinum electrode were studied by cyclic voltammetry (CV), in-situ FTIR spectroelectrochemistry (FTIRs) and potential resolved XPS measurements. The experimental results reveal that the CoHCF film on Pt electrode exists in two forms. The major form of the inner layer of the film is $(M^+)_2Co(II)Fe(II)(CN)_6$ where M^+ denotes a cationic counter ion, in which both the Fe^{2+} and Co^{2+} centers can be oxidized to Fe^{3+} and Co^{3+} in the potential range of 0–1.0 V vs. Ag/AgCl in NaCl solution. The major form of the outer layer is $Co(II)_2Fe(II)(CN)_6$, in which electrochemical reactions in this potential range are limited by kinetic sluggishness. The FTIR and XPS spectra indicated that the Co centers change from high-spin state to low-spin state accompanying the Co^{2+}/Co^{3+} oxidation reaction. In addition, the cations' effect on electrochemical reactions of CoHCF is also discussed. © 1999 Elsevier Science B.V. All rights reserved.

Keywords: Cobalt-cyanometallates; Cyclic voltammetry; FTIR; XPS; Platinum electrode

1. Introduction

A variety of chemically modified electrodes (CME) have been studied for deliberation of controlling the reactivity of the electrode/electrolyte interface. One of these has made significant progress is for the polymer film coated electrodes

[1–8]. During the past decade, the mixed valence heavy-metal hexacyanometallates, as one kind of inorganic conducting polymers, have been paid much attention due to their potential application in electrocatalysis, electrochromism and electroanalytical applications etc. Among this kind of inorganic polymeric material, Prussian Blue (PB) is the first compound that raised electrochemists' interest. The PB analogues, such as CoHCF (cobalt-hexacyanoferrite), PdHCF, TiHCF etc.

* Corresponding author. Fax: +86-551-3631760.
E-mail address: xqlin@ustc.edu.cn (X. Qin Lin)

[9–11], have also been electrochemically synthesized. Studies that have been carried out indicate that the electrochemical properties of CoHCF are very similar to that of PB, and this compound has many attractive applications in chemistry and physics [12]. However, the studies showed very different behavior on glassy carbon electrode (GCE) [9], compared with that on wax-impregnated graphite electrode (WIGE) [12]. For example, on the GCE, CoHCF has only a set of redox peaks at about 0.39 V which were assigned to the $\text{Fe}^{2+}/\text{Fe}^{3+}$ reaction [9], while on the CoHCF film coated WIGE, two-step reactions were involved: one was ascribed to the electrochemical reaction of $\text{Co}^{2+}/\text{Co}^{3+}$ at 0.38 V and the other to $\text{Fe}^{2+}/\text{Fe}^{3+}$ transition at 0.82 V [12].

It is possible that not only deposition conditions and counter cations but also the electrode materials can play important roles on the structure and properties of the prepared CoHCF CMEs. CV (cyclic voltammetry) data alone is obviously not enough for characterization of CoHCF modified electrodes with other substrates. In-situ FTIRs (FTIR spectroelectrochemistry) and ex-situ potential resolved XPS method can be used along with the CV technique for this investigation.

2. Experimental

$\text{Co}(\text{NO}_3)_2$ and NaCl (Beijing Chemical Factory, Beijing), $\text{K}_3\text{Fe}(\text{CN})_6$ and $\text{K}_4\text{Fe}(\text{CN})_6 \cdot 3\text{H}_2\text{O}$ (Shanghai Reagent Cooperation, Shanghai) and other chemicals were of certified analytical grade and employed as received. All solutions were prepared with double distilled water.

Electrochemical measurements were performed using a CH Instrument Model 630 Electrochemical Analyzer. In-situ FTIR measurements were conducted using a Nicolet 520 FTIR Spectrometer with a DTGS detector. The external reflectance system was constructed from a variable angle specular reflectance attachment (Spectra Tech.). All spectra were displayed in units of $\Delta R/R$ [13]. The FTIR spectroelectrochemical thin layer cell is a self-constructed three-electrode cell with a CaF_2 window against the flat surface of the

Pt disk working electrode (9.6 mm in diameter). The liquid path length of the IR cell is about 1 μm depending on the treatment of the electrode surface. A KCl saturated Ag/AgCl electrode was used as the reference electrode.

Prior to each film deposition, the Pt working electrode was polished to a mirror-like surface using alumina paste of 1.0, 0.3, and 0.05 μm successively, followed by dipping the electrode into alcohol, acetone, and 0.05 M HCl successively for 5 min. Then it was cleaned ultrasonically in water to remove any adherent particles.

CoHCF film was prepared by cycling the platinum electrode between 0 and 1.0 V at 1000 mV/s for 5–10 min in the solution containing 1 mM $\text{Co}(\text{NO}_3)_2$ + 1 mM $\text{K}_3\text{Fe}(\text{CN})_6$ + 1 M NaNO_3 . After the deposition, the electrode was rinsed thoroughly with water, and made ready for further experiments.

XPS (X-ray photoelectron spectroscopy) was performed using an ESCALAB-MK II instrument (VG, UK) with a monochromatic Al $K\alpha$ X-ray source under 6.5×10^{-5} Pa pressure. The binding energies were referenced to graphitic C_{1s} ($E_b = 284.6$ eV). Element ratios were calculated from the high-resolution XPS spectra. The platinum plate substrate used for XPS detection was pre-treated by quenching. CoHCF films were electrochemically deposited on this plate according to the procedure described above.

3. Results and discussion

3.1. In-situ growth and cyclic voltammetry of the CoHCF film on Pt electrode

Fig. 1 shows the cyclic voltammograms of the Pt electrode cycling from 0.0 to 1.0 V in 1 mM $\text{K}_3\text{Fe}(\text{CN})_6$ + 1 mM $\text{Co}(\text{NO}_3)_2$ + 1 M NaNO_3 solution for 25 cycles.

At the beginning of the cycling, the redox peaks of the $\text{K}_4[\text{Fe}(\text{CN})_6]/\text{K}_3[\text{Fe}(\text{CN})_6]$ process appeared at $E_m(1) = 0.25$ V. With increasing cyclic times, two sets of redox peaks at E_m s of about 0.5 and 0.94 V, respectively, emerged and became higher and higher accompanied by a decrease of the $E_m(1)$ peaks, which indicates the formation of polymerized CoHCF film on the Pt electrode.

The CV response of the prepared CoHCF|Pt electrode placed in 1 M NaCl was similar to the final CV curve shown in Fig. 1. Two sets of quite symmetric peaks at $E_m(2) = 0.44$ V and $E_m(3) = 0.91$ V can be observed. Comparing the results for the CoHCF|GC electrode [9], the $E_m(2)$ can be assigned to the $\text{Fe}^{2+}/\text{Fe}^{3+}$ transition in the structure of $\text{Na}_2\text{CoFe}(\text{CN})_6$. According to the structure of CoHCF and comparing the redox potential of free and weakly complexed species of $\text{Co}^{2+}/\text{Co}^{3+}$, the anodic peak of $E_m(3)$ at 0.91 V should be due to the $\text{Co}^{2+}/\text{Co}^{3+}$ transition.

Analysis shows that both the anodic and cathodic peak current of $E_m(2)$ is proportional to the scan rate up to 200 mV/s. This nature of typical surface waves is consistent to the formation of surface-bonded thin films on this electrode.

The surface coverage of the CoHCF film on the Pt electrode can be calculated by using the following equation [14]

$$i_p = n^2 F^2 A \Gamma v / 4RT$$

where v is the scan rate, A is the surface area of the electrode, Γ is the surface coverage of the redox moieties, and n , F , R , and T have their usual significance. Accordingly, the surface charge

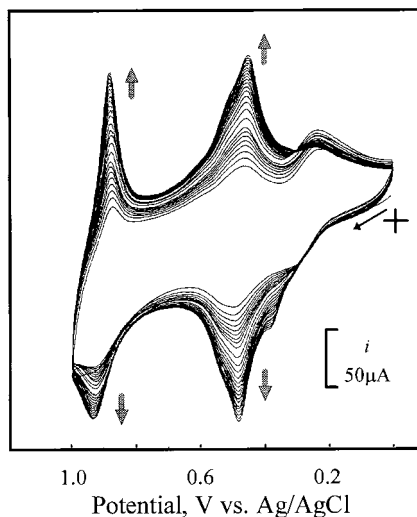


Fig. 1. Accumulation of CoHCF film on Pt electrode by cyclic voltammetry in 1 mM $\text{K}_3\text{Fe}(\text{CN})_6$ + 1 mM $\text{Co}(\text{NO}_3)_2$ + 1 M NaNO_3 solution at 100 mV/s.

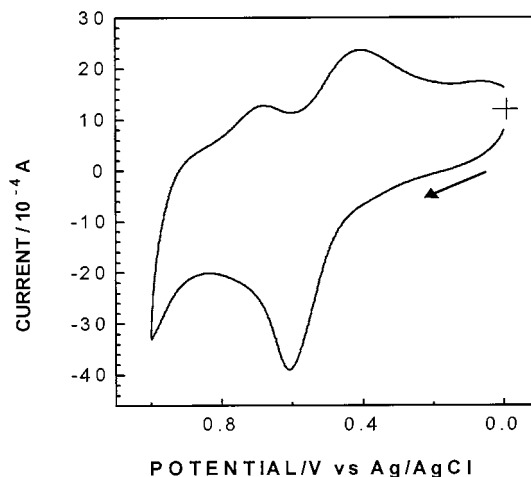


Fig. 2. Cyclic voltammogram of CoHCF|Pt electrode in 1.0 M KCl solution at a scan rate of 100 mV/s.

estimated from these experiments corresponds to ca. 10^{-5} C cm^{-2} , and this works out at a Γ -value of ca. 10^{-10} mol cm^{-2} .

In the literature, the approximate upper limit for the monolayer coverage is reported as 2×10^{-9} mol cm^{-2} [15]. The much lower Γ -value in our case indicates that only part of the surface layer is electrochemically active.

The CoHCF microstructures, such as Prussian Blue, are zeolitic and may act as molecular sieves. So, it can be expected that the electrochemistry of the CoHCF film is affected by the type of electrolyte cations. Fig. 2 shows the CV of this prepared CoHCF|Pt electrode in 1 M KCl solution. Only one anodic peak appeared at 0.61 V, and the corresponding cathodic peak appeared at 0.40 V. This corresponds to the $\text{Fe}^{2+}/\text{Fe}^{3+}$ transition at $E_m(2) = 0.50$ V, and the 210 mV peak separation indicates the irreversibility of this redox process. The oxidation potential for the $\text{Co}^{2+}/\text{Co}^{3+}$ transition shifts positively so that only a sloped anodic baseline can be seen at potentials higher than 0.91 V; a small cathodic peak at 0.70 V may correspond to the re-reduction reaction of the $E_m(3)$ step.

The CV behavior of the CoHCF|Pt is more reversible in NaCl solution than in KCl solution. The CoHCF film can even be destroyed at potentials more positive than 1.0 V in KCl solution.

The size of the CoHCF lattice should be reduced or expanded upon oxidation or reduction due to doping or di-doping process, similar to the case in PB oxidation [18]. The smaller the size of the cation, the smaller will be the distortion of the lattice. This CoHCF|Pt electrode preference for Na^+ may reflect the lower flexibility of the coated CoHCF film.

3.2. In-situ FTIR spectroelectrochemistry

In order to study the surface structure and reaction mechanism of the CoHCF|Pt electrode, in-situ FTIRs investigation was carried out. Fig. 3 shows the potential resolved FTIR spectra of CoHCF|Pt from 0.3 to 0.7 V in 1 M NaCl. The spectra were normalized by the reference spectrum acquired at 0 V. An upward band appeared at 2084 cm^{-1} and became stronger and stronger with the potential shifting positively. This band corresponds to the disappearance of

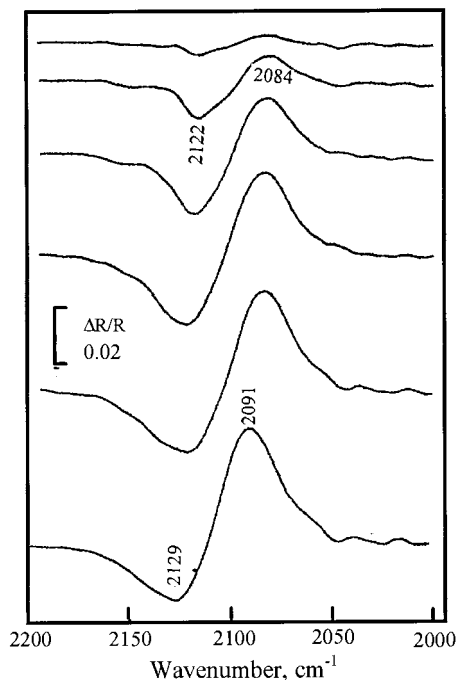


Fig. 3. In-situ FTIR spectra of CoHCF|Pt in 1 M NaCl. Reference potential: 0 V. Sample potential (from top to bottom): 0.3, 0.4, 0.5, 0.6, 0.7, 0.8 V vs Ag/AgCl. Signal averaging: 100 scans.

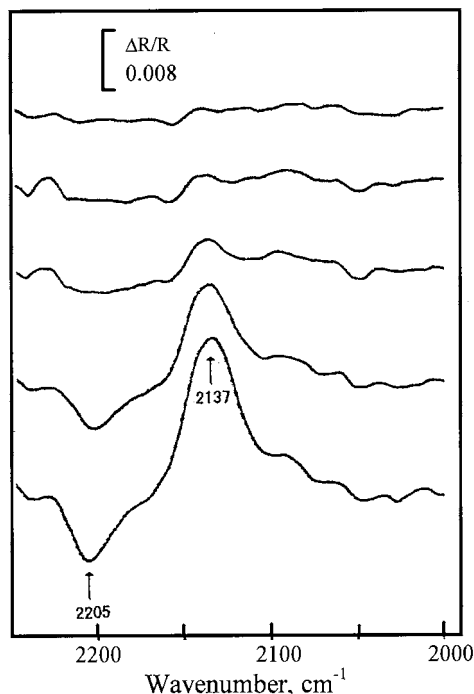


Fig. 4. In-situ FTIR spectra of CoHCF|Pt in 1 M NaCl. Reference potential: 0.7 V. Sample potential (from top to bottom): 0.75, 0.80, 0.85, 0.90, 1.0 V vs Ag/AgCl. Signal averaging: 50 scans.

$\text{Na}_2\text{Co(II)Fe(II)(CN)}_6$ during the oxidation and can be ascribed to the vibrational mode of bridge-bonded $-\text{C}\equiv\text{N}-$ in Co(II)-CN-Fe(II) structure [4]. At the same time, a downward band appeared at 2122 cm^{-1} , corresponding to the vibrational mode of bridge-bonded $-\text{C}\equiv\text{N}-$ in the Co(II)-CN-Fe(III) structure. These two bands indicate that the transition from Fe^{2+} to Fe^{3+} occurred.

It is also shown in Fig. 3, with the potential increasing from 0.3 to 0.7 V, both these upward and downward bands have about 7 cm^{-1} blue-shift. This shift may be caused by the Stark effect.

In-situ IR spectra of the electrochemical reaction at $E_m(3)$ in NaCl solution are shown in Fig. 4. As seen in this figure, an upward band at 2137 cm^{-1} and a downward band at 2205 cm^{-1} appeared when the electrode potential shifted from 0.70 to 1.0 V. Considering the $\nu(\text{CN})$ at 2080 cm^{-1} for Fe(II)-CN-Fe(III) and 2167 cm^{-1} for $\text{Fe(III)-CN-Fe(III)}$ in PB|Pt electrode [17], about

45 cm^{-1} blue shifts resulted for the Co(II/III)–CN–Fe(III) structure. This suggests that the Co(III) and Co(II) centers attract electrons from the coordinated $\text{N}\equiv\text{C}$ more strongly than the Fe(III) and Fe(II) do.

The interactions between transition metal–CN bond can be described in terms of s-bonding and p-bonding mechanisms [20]. Co^{3+} tends to be in a low-spin state with the highest outer electron distribution $\uparrow\downarrow\uparrow\downarrow\uparrow\downarrow$ [21]. The two empty d orbitals are ready to accept electrons from CN^- forming a strong σ bonding between Co^{3+} and C–N. However, the Fe^{3+} in PB should be in a high spin state with the highest outer electron distribution $\uparrow\uparrow\uparrow\uparrow\uparrow\uparrow$ with no empty d orbital, and making the σ bond of Fe^{3+} – CN^- weaker. This is probably the main reason why the vibration frequency of C)N is so high in Co–NC–Fe. This is also inconsistent with the report [19] that the higher the ionization energy of transition metal connected to CN, the higher the $\nu(\text{CN})$. The third ionization energy is 3232 KJ/mol for Co^{3+} , and 2957.4 KJ/mol for Fe^{3+} [22].

In-situ FTIR spectra of CoHCF|Pt in 1 M KCl are shown in Fig. 5; an upward band at 2109 cm^{-1} and a downward band at 2142 cm^{-1} appeared during the first oxidation step. These two bands can be assigned to the vibration modes of bridge-bonded CN group in Co(II)–CN–Fe(II) and Co(II)–CN–Fe(III), respectively. In comparison with the spectra in NaCl, about 14 cm^{-1} blue shifts result in KCl electrolyte.

The square opening or hole in the face of the cube lattice is smaller than the cube center [9]. So that, even if the doping cation should partially take off its hydrated shell before penetrating into the lattice, the hydrated shell may be reformed after entering. In this way, only small enthalpy and entropy changes are needed for the doping and di-doping processes. The small radius of naked Na^+ ion makes it easy to penetrate into the lattice; however the larger radius of hydrated Na^+ makes the lattice expand which reduces the bond strength of CN and its vibration frequency.

3.3. XPS analysis of the CoHCF|Pt electrode

Although the electrochemical behavior of CoHCF has been well studied, no XPS data were reported in the previous literature. We employed XPS as a surface technique to investigate the film structure of the CoHCF|Pt electrode in 1 M NaCl solution at different potentials. Analyses of XPS spectra are shown in Table 1.

As seen in this table, the expected signals of Co, Fe, Na and N from CoHCF film were observed in the XPS spectra, which demonstrate that the CoHCF film had been deposited on the Pt surface. It was noted that when the potential changed from 0 to 0.75 V, $\Delta\text{BE}(2\text{p}_{3/2} - 2\text{p}_{1/2})$ was reduced by a small amount and the binding energy of $\text{Co}2\text{p}_{3/2}$ increased to 782.6 eV. From the XPS spectra, it was found that the band width of $\text{Co}2\text{p}_{3/2}$ was also reduced. However, these changes in binding energy are not statistically significant since the uncertainty of the XPS measurements is ± 0.2 eV.

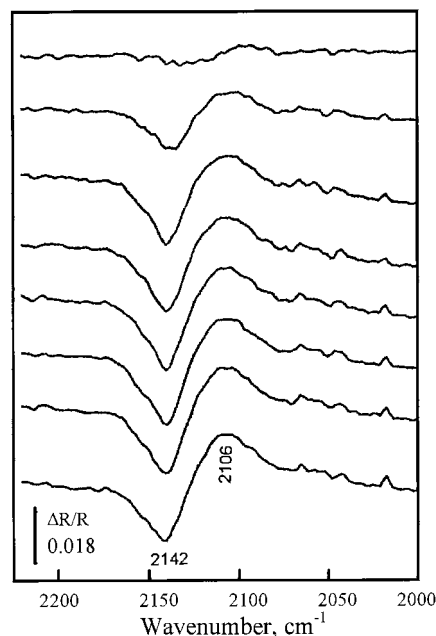


Fig. 5. In-situ FTIR spectra of CoHCF|Pt in 1 M KCl. Reference potential: 0 V. Sample potential (from top to bottom): 0.45, 0.5, 0.55, 0.6, 0.65, 0.7, 0.8, 0.9 V vs Ag/AgCl. Signal averaging: 50 scans.

Table 1
XPS data for CoHCF modified electrode in 1 M NaCl

Sample	Binding energy (± 0.2 eV)						
	Co2p _{3/2}	$\Delta BE(2p_{3/2} - 2p_{1/2})$	Fe2p _{3/2}	Na _{1s}	N _{1s}	Co:Fe	N:Na
K ₃ Fe(CN) ₆ powder	–	–	709.6	–	–	–	–
Co(NO ₃) ₂ powder	782.0						
CoHCF Pt at 0 V	782.0	15.4	708.5	1071.6	397.8	1.87:1	2.2:1
CoHCF Pt at 0.75 V	782.6	15.2	708.4	1071.5	398.1	1.55:1	24:1
CoHCF Pt at 1.1 V	782.4	15.0	708.3	1071.5	397.8	1.77:1	20:1

With the potential shifting from 0.75 to 1.1 V, both the binding energy and $\Delta BE(2p_{3/2} - 2p_{1/2})$ of the Co decreased and the band width increased, indicating a transition of Co²⁺ to Co³⁺. However, this is not in agreement with the case reported in the literature that the Co center is non-electroactive in the potential range from 0 to 1 V [16].

Interestingly, there are no XPS bands corresponding to Fe³⁺ centers even at 1.1 V indicating that the outer layer of the CoHCF is electrochemically inactive during the oxidation. According to the study of PB [17], the porous and relative random layer of Co(II)₂Fe(II)(CN)₆ may be formed and become the major composition of the outer layer. This outer shell could not be oxidized or the electrochemical oxidation reaction is kinetically very slow, possibly because the Co²⁺ cations in the lattice are not free from diffusion.

From the Co:Fe ratio of about 1.9 at 0 V and 1.8 at 1.1 V, the composition of the CoHCF film can be estimated. Because the Co:Fe ratio for Na₂Co(II)Fe(II)(CN)₆ is one and for Co(II)₂Fe(II)(CN)₆ is two, it can be simply estimated according to the XPS data that the Co(II)₂Fe(II)(CN)₆ lattice should be the major composition (90% at 0 V) in the outer layer of the CoHCF film. This should be the reason why the formal surface coverage value, Γ , calculated above is about 20 times less than the expected value of a monolayer coverage.

The N:Na ratio of 2.2 at 0 V is much lower than the expected value of six for the composition of 90% Co₂Fe(CN)₆ + 10% Na₂Co(II)Fe(II)(CN)₆. However, a NO₃⁻ band at 407.3 eV was observed in the XPS spectra at 0 V, indicating

that a certain amount of NO₃⁻ was codeposited in the CoHCF film, which should bring up the same amount of Na⁺ ions. The amount of Na⁺ was drastically reduced at potentials of 0.75 and 1.1 V, which strongly supports the mechanism that the Na⁺ ions diffuse out of the film for charge balancing upon oxidation. The N:Na ratio of 24 at 0.75 V and 20 at 1.1 V, much larger than six, apparently shows over balancing of the charge. It may imply that the anion codeposition is important for CoHCF film construction.

4. Conclusion

In comparison with the results obtained for GCE [9] and WIGE [12], the electrode substrate in contact with the electrochemically deposited CoHCF film plays an important role in the film structure and electrochemical property. The structure of CoHCF film on platinum electrode is composed of two major structures, Na₂CoFe(CN)₆ and Co₂Fe(CN)₆. The Na₂CoFe(CN)₆ structure is formed in the inner layer of the film and is electroactive for both the Fe and Co centers in NaCl solution which is similar to the case for WIGE [12]. However, our investigation shows that the $E_m = 0.44$ V step is attributed to the Fe²⁺/Fe³⁺ and the $E_m = 0.91$ V to the Co²⁺/Co³⁺ reaction based on the in-situ FTIRs detection. The major (ca. 90%) Co₂Fe(CN)₆ structure is formed in the outer layer of the film and its electrochemical activity is sluggish, which is well demonstrated by the ex-situ potential resolved XPS detection. A significant

amount of codeposited NO_3^- anions exist in the CoHCF film, which may play important an role for the charge balancing process of the film upon redox reactions.

Acknowledgements

The authors gratefully acknowledge financial support from the National Natural Science Foundation of China, and the Open Laboratory of Electroanalytical Chemistry, Chinese Academy of Science.

References

- [1] U.C. Pham, P.C. Lacaze, F. Genoud, L.H. Dao, M. Nguyen, *J. Electrochem. Soc.* 140 (1993) 912.
- [2] V.A. Christensen, A. Hamnett, *Electrochim. Acta* 36 (1991) 1063.
- [3] X.Q. Lin, H.Q. Zhang, *Electrochim. Acta* 41 (1996) 2019.
- [4] S.N. Hoier, D.S. Ginley, S.M. Park, *J. Electrochem. Soc.* 135 (1988) 9.
- [5] M.S. Wrighton, *Science* 231 (1996) 32.
- [6] N. Oyama, F.C. Anson, *J. Electroanal. Chem.* 127 (1980) 247.
- [7] F.C. Anson, T. Ohsaka, T.M. Sayeant, *J. Am. Chem. Soc.* 105 (1983) 4883.
- [8] A.R. Guadalupe, H.D. Abruna, *Anal. Chem.* 57 (1985) 1471.
- [9] M. Jiang, X. Zhou, Z. Zhao, *Ber. Bunsen Ger. Phys. Chem.* 95 (1991) 720.
- [10] M. Jiang, Z. Zhao, *J. Electroanal. Chem.* 292 (1990) 281.
- [11] M. Jiang, X. Zhou, Z. Zhao, *J. Electroanal. Chem.* 292 (1990) 289.
- [12] J. Joseph, H. Gomathi, G.P. Gao, *J. Electroanal. Chem.* 304 (1991) 263.
- [13] K. Ashley, S. Pons, *Chem. Rev.* 86 (1988) 673.
- [14] R.W. Murray, in: A.J. Bard (Ed.), *Electroanalytical Chemistry*, Ch. 3, vol. 13, Marcel Dekker, New York, 1984.
- [15] D.M. Kolb, in: H. Gerischer, C.W. Tobias (Eds.), *Advances in Electrochemistry and Electrochemical Engineering*, Ch. II, vol. 11, Wiley, New York, 1978.
- [16] H.Q. Zhang, X.Q. Lin, *Talanta* 44 (1997) 2069.
- [17] P.A. Christensen, A. Hamnett, S.J. Higgins, *J. Chem. Soc. Dalton Trans.* 2233 (1990).
- [18] A. Dostal, G. Kauschka, S.J. Reddy, F. Scholz, *J. Electroanal. Chem.* 406 (1996) 155.
- [19] G.B. Bonino, G. Fabbri, *Atti accad. nazl. Lincei Class sci. fits. mat. enat.* 25 (1958) 410.
- [20] Xizhang Cao et al. (Eds.), *Inorganic Chemistry*, Ch. 11 and 12, Advanced Education Press, Beijing.
- [21] Y. Yin, *Advanced Chemical Handbook*, Ch. 5, Shandong Science and Technology Press, Jinan.

Determination of cadmium in sewage sludge by differential pulse anodic stripping voltammetry

Richard A. Pacer *, Cynthia K. Scott Ellis, Ruzhan Peng

Department of Chemistry, Indiana University Purdue University Fort Wayne, Fort Wayne, IN 46805-1499, USA

Received 24 August 1998; received in revised form 20 January 1999; accepted 28 January 1999

Abstract

A procedure was developed for the determination of cadmium in sewage sludge by differential pulse anodic stripping voltammetry. A sodium peroxide fusion carried out in zirconium crucibles was found to give satisfactory results, based on analysis of standard reference materials. Samples collected from the municipal sludge lagoon in Fort Wayne, Indiana were found to have cadmium abundances ranging from 120 to 250 ppm, with most samples falling in the 120 to 170 ppm range. Interference from zinc is easily eliminated by carrying out the deposition step at -0.95 V vs. Ag/AgCl. Lead-to-cadmium ratios as high as 50:1 (ppm basis) have no effect on the height of the cadmium peak. © 1999 Published by Elsevier Science B.V. All rights reserved.

1. Introduction

The impetus for this work, begun as an undergraduate research project, stemmed from two articles appearing in the Fort Wayne, Indiana newspapers. The January 15, 1995 edition of the Journal Gazette [1] described an operation carried out by the U.S. Army in which germ-sized particles of zinc cadmium sulfide were dropped from the air over Fort Wayne as a part of a top-secret program studying biological warfare. The second article appeared in the January 16, 1997 edition of The News Sentinel [2] in which it was stated that the cadmium levels of bio-solids in the sludge at the Lake Avenue sludge lagoons exceeded the

limits set by the Indiana Department of Environmental Management.

Sewage sludges contain some valuable resources, such as nitrogen, phosphorus, and organic matter. Hence their use in both home gardening and in agricultural applications is widespread [3]. From a practical standpoint, the ability to safely use municipal sewage sludge for home gardening and other applications depends, at least in part, on its lack of toxic chemicals, such as cadmium. There is evidence that soil treated with sewage sludge has resulted in cadmium being taken up from the soil by food crops. Elevated Cd concentrations (3–7- or 8-fold enhancement when compared to normal crops) have been found in lettuce, cabbage, spinach, carrots, potatoes, wheat, corn, and soybeans grown in soils containing greater than 1 mg/kg of cadmium [4–10].

* Corresponding author. fax: +1-219-481-6070.
E-mail address: pacer@ipfw.edu (R.A. Pacer)

(Peas, beans, and tomatoes, on the other hand, tend not to accumulate cadmium [6]).

Is there a 'typical' or narrow range of cadmium abundance in sewage sludge? Evidently not, given the results of Jing and Logan [5], who examined the trace element content of 17 different sludges, and found a 30-fold variation in the total cadmium content of the sludges. The values fell into three distinct groups: the Chicago sludge (227 ppm Cd); the Ashtabula, Elyria, Bellefontaine, and Fremont sludges (34–140 ppm Cd); and the remaining sludges (8–25 ppm Cd).

In what chemical form does cadmium exist in sewage sludge? Theoretical considerations and indirect methods suggest that sludge Cd probably exists as a combination of organically complexed metal, adsorbed forms, and coprecipitates with Fe, Al, and Ca solid phases [5]. As a result, plant uptake of Cd is strongly dependent on pH (inverse correlation between plant uptake and soil pH), temperature, chloride salinity, organic matter, and calcium concentration [8].

Turning next to the analysis of the sewage sludge samples for cadmium, differential pulse anodic stripping voltammetry (DPASV) is ideal for determining heavy metals, such as zinc, cadmium, lead, and copper, routinely capable of achieving detection limits down to the parts per billion level. However, interelement interferences are possible in DPASV. Thus it was necessary to ensure that the specific DPASV procedure adopted was free of interelement interferences as well as free of matrix effects in general. This latter concern is normally taken care of by a standard addition procedure.

A major concern in any analytical procedure is finding an optimum sample dissolution technique. Wet ashing, dry ashing, and extraction techniques [3,11–14] have been used for sewage sludge samples. Regulations in some countries often specify an aqua regia treatment [13]. A total sample digestion using oxidative acids followed by hydrofluoric acid treatment is too time-consuming and regarded as unnecessary in providing a reliable estimate of important trace metal concentrations [13]. Ackers et al. [14] report that metals which are most readily released from the sample matrix (Cu, Cd and Zn) give analytical results

with the greatest precision; and therefore for these metals, the choice of digestion technique from among a wide range used by participants in a study appeared not to matter.

While Jenniss et al. [4] report that losses of cadmium and lead greater than 10% can occur when muffle furnace ignition is used on sludge samples, Ritter [15] found no such problem with using a dry-ashing method of preparing sewage sludge for AAS analysis of cadmium, lead, and other elements.

Among the dissolution techniques for sewage sludge samples reported in the literature were a CaCl_2 extraction procedure, described by Delschen and Werner [16]; a wet ashing procedure given by Murphy [17]; and a sodium peroxide fusion procedure as given by Kaye, Strebin, and Nevissi [18]. Of the three, the sodium peroxide fusion procedure was found to be most promising. A comparison by us of the wet ashing and fusion procedures found the latter to give better precision and to be much less time-consuming. Consequently, it was decided to adopt the fusion procedure, to modify it so as to ensure complete oxidation of our actual samples, and to test it by analyzing several NBS (now NIST) standard reference materials for cadmium. The fusion/DPASV procedure was used to analyze several actual municipal sewage sludge samples.

The results for these samples are given.

2. Experimental

2.1. Apparatus

An EG & G Princeton Applied Research Model 174 A Polarographic Analyzer with a Model RE0074 X–Y recorder and an EG & G PARC Model 303 SMDE (static mercury drop electrode) were used for all of the DPASV scans.

All pH measurements were made with an Orion Research Model 701A/digital Ionalyzer, using a combination electrode.

A Thermolyne Type 1500 furnace was used for the initial fusion work.

2.2. Reagents

Sodium peroxide, >93% ACS reagent, was obtained from Aldrich Chemical Co., Inc.

Hydrochloric acid used was Baker 'Intra-analyzed' grade for trace metal analysis.

The zirconium crucibles used were new, purchased from B-J Scientific Products, Inc.

The 0.50 M acetic acid/0.50 M sodium acetate buffer was made from Baker 'Intra-analyzed' $\text{CH}_3\text{CO}_2\text{H}$ and ACS reagent grade $\text{CH}_3\text{CO}_2\text{Na}$. All other materials were of ACS reagent grade quality.

2.3. Procedure

Samples of sewage sludge were collected from the sludge lagoon located at 5510 Lake Avenue in Fort Wayne, IN. Six samples were taken altogether. The area where the sludge was located had piles of sludge arranged in an almost horseshoe-like formation. The sludge samples were collected approximately three feet from each other around the edge of the sludge piles. The samples were labeled A, B, C, D, E, and F, respectively. The order in which the samples were collected was from left to right (while facing into the mouth of the U-shape of the horseshoe-like formation).

Sludge samples C and D were used to evaluate the wet ashing and Na_2O_2 fusion methods. This preliminary work indicated that the fusion method gave greater precision and required considerably less time than the wet ashing procedure. For the fusion procedure, 0.25 g samples of sludge were mixed with 2.5 g of Na_2O_2 in a nickel crucible and allowed to heat for 30 min in a furnace which had been heated to 500°C . After the crucibles cooled to room temperature, 6 M HCl was used to extract the melt. However, in some cases, a rather dark product resulted, indicating that oxidation of the sample may have been incomplete. A revised fusion procedure was developed, as follows:

2.3.1. Fusion procedure

1. Weigh three zirconium crucibles (crucibles were newly purchased for this work).

2. Subdivide Sludge Sample A by a mixing/coning and quartering technique (sample is ground in a mortar and pestle, mixed, piled into a cone, after which the cone is quartered and alternate quarters are discarded; the process is repeated with the quarters retained until a suitable-sized lab sample remains).
3. Weigh three ≈ 0.2 g samples (to ± 0.0001 g) into Zr crucibles.
4. Add ≈ 2.0 g Na_2O_2 to each and mix thoroughly.
5. Heat over a Bunsen burner for 10 min after the mixture melts, with swirling, using the full heat of the burner during this 10-min period.
6. After allowing the crucible to cool, a 2nd fusion is carried out, this time using 1.0 g Na_2O_2 and 5 min of full burner heating after melting occurs.
7. To each crucible, ≈ 18 ml of 6 M Baker 'Intra-Analyzed' HCl was added, dropwise, followed by quantitative transfer to a 250 ml beaker.
8. Next, the pH of each solution was adjusted to 4.00 ± 0.02 by the addition of solid sodium acetate.
9. Each solution was then treated with 20.00 ml of 0.50 M $\text{CH}_3\text{CO}_2\text{H}$ /0.50 M $\text{CH}_3\text{CO}_2\text{Na}$ buffer, followed by volumetric dilution to 100.0 ml.
10. Blank solutions were prepared following this same procedure.

Sewage Sludge Samples B, E, and F were treated in exactly the same way. The triplicate samples of each were designated by letter and number, such as B-1, B-2 and B-3.

Each solution was then run by DPASV, using a standard addition procedure. The following parameters and conditions were used:

2.3.2. DPASV parameters

Initial $E_{\text{APPLIED}} = -0.95$ V vs. Ag/AgCl; rate, 10 mV/s; direction, +; range, 1.5 V; operating mode, differential pulse; modulation amplitude, 25 mV(PP); clock, 0.5 s; low pass filter, OFF; mode, HDME; drop size, small; purge (N_2) time, 4 min; sensitivity, 2 μA full-scale (adjusted as needed to give peaks of reasonable height); sample size, 10.00 ml; spikes: three additions of 1.00

ml each of 5.00 ppm Cd^{2+} (1.00 ppm Cd^{2+} when spiking the blank).

In order to evaluate the method for possible bias, two NBS (now NIST) standard reference materials were analyzed by the above method: NBS Standard Reference Material 1648, Urban Particulate Matter; and NBS Standard Reference Material 1645, River Sediment.

Because SRM 1648 has a much higher abundance of lead than the sewage sludge samples we analyzed, a separate study was conducted to see if high abundances of lead would have any effect on the DPASV peak for cadmium. We looked at solutions in which the $\text{Pb}^{2+}/\text{Cd}^{2+}$ ppm ratio varied from 0 to 100 and observed the effect (if any) on the current due to the Cd^{2+} peak.

3. Results and discussion

In developing the fusion procedure, it was noted that the melt had a rather dark brown color, even after heating the Zr crucible with the Na_2O_2 /sewage sludge mixture for 10 min at the full heat of a

Bunsen burner. Consequently, the second fusion step was added (1.0 g Na_2O_2 additional, plus 5 min of full heat). After cooling, the solidified material had a pale yellow color.

After the dropwise addition of 6 M HCl, dilution, and transfer to a volumetric flask, the solution was observed to be yellow in color, with a white, flocculent solid settled out on the bottom (presumably silica).

The initial pH of the HCl solution of the melt was ≈ 0.5 . As $\text{NaC}_2\text{H}_3\text{O}_2$ was added, the solution took on an orange color when the pH rose above ≈ 3 (probably a hydroxy species of Fe(III)). No further change in appearance was noted as the pH was brought to 4.00 ± 0.02 . (Blank solutions were all colorless when their pH was similarly adjusted to 4.00).

If an initial E_{APPLIED} (vs. Ag/AgCl) of -1.20 V is used for the deposition (pre-concentration) step in the DPASV procedure, four distinct peaks may be observed, as noted in Fig. 1, which shows the results for Sample B-2. The peaks, from left to right, are assigned (vs. Ag/AgCl) to:

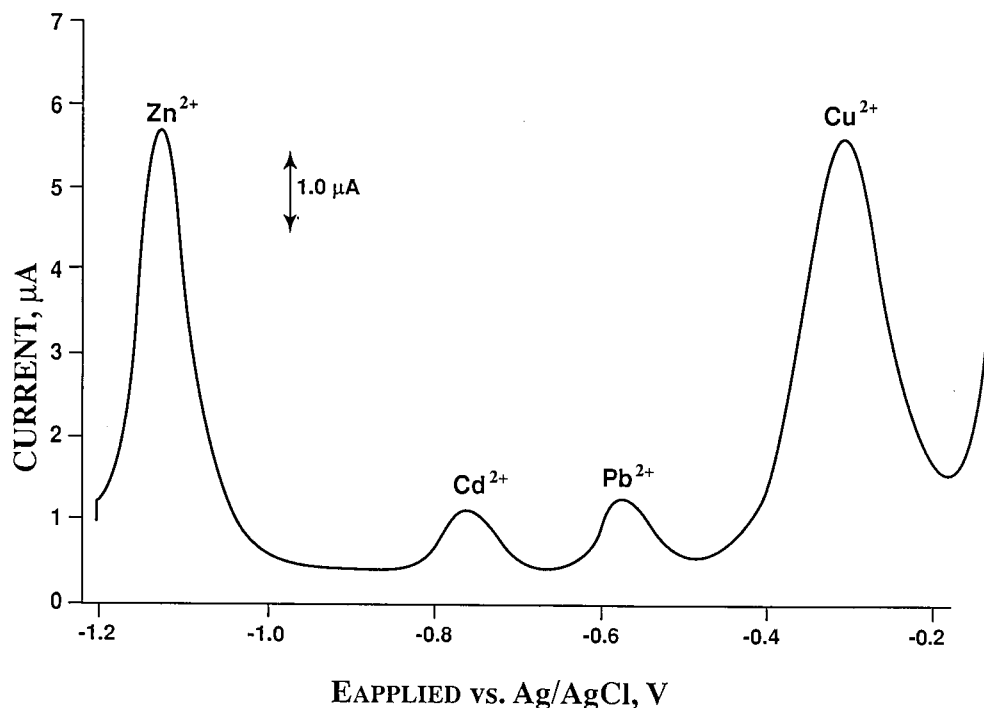


Fig. 1. Analysis of sewage sludge sample B-2 by DPASV initial $E_{\text{APPLIED}} = -1.20$ V vs. Ag/AgCl.

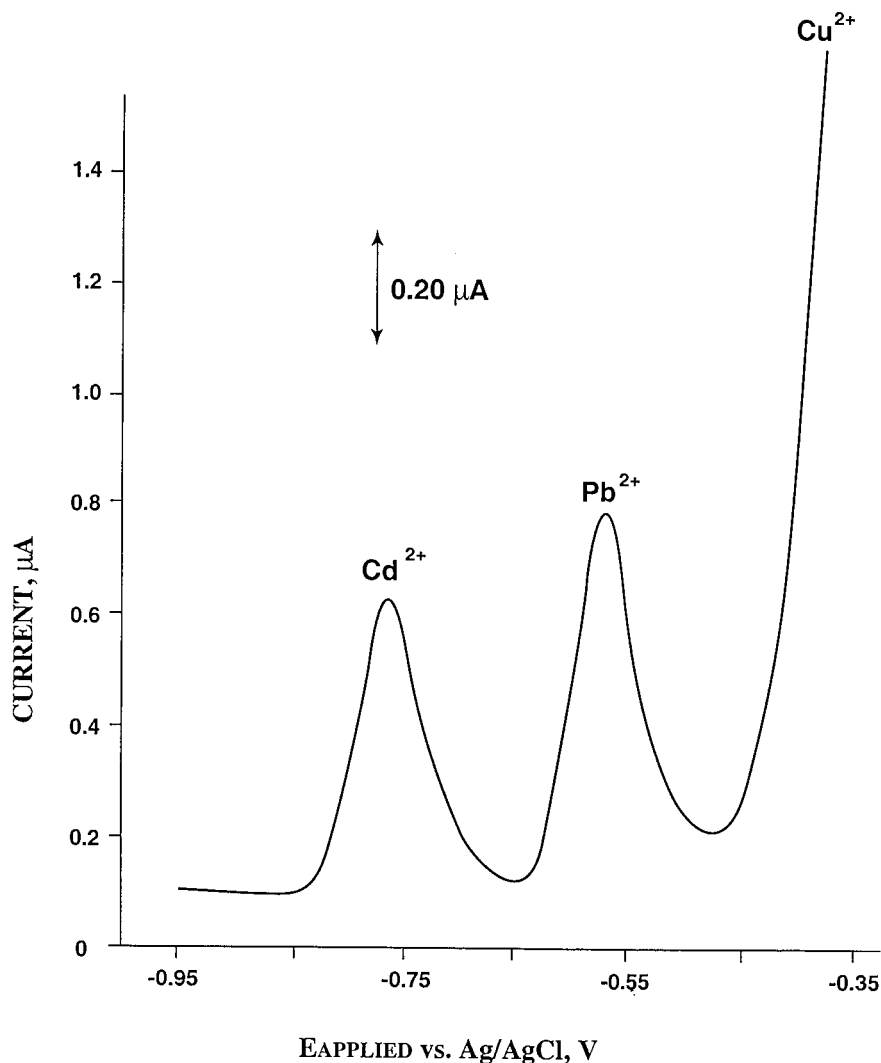


Fig. 2. Analysis of sewage sludge sample B-2 by DPASV initial $E_{\text{APPLIED}} = -0.95$ V vs. Ag/AgCl.

Zn^{2+}	-1.13 V
Cd^{2+}	-0.765 V
Pb^{2+}	-0.575 V
Cu^{2+}	-0.310 V

While the Zn^{2+} and Cd^{2+} peaks are well separated, the much greater current due to the Zn^{2+} peak limits the current sensitivity setting which may be used; a more sensitive setting would be

desirable to enhance the Cd^{2+} peak and minimize uncertainties in measuring peak height. By using an initial E_{APPLIED} of -0.95 V (vs. Ag/AgCl) for the deposition step, the Zn^{2+} peak is eliminated. This is shown in Fig. 2, which is a DPASV run at -0.95 V for the same solution (B-2), but at a 5-fold greater sensitivity setting (2 μA full-scale vs. 10 μA full-scale for Fig. 1). Note in Fig. 2 that the Cd^{2+} and Pb^{2+} peaks are well-resolved, and somewhat similar in height. This was typical of all the sludge samples analyzed. Fig. 3 shows the

results of the standard addition procedure, in which Solution B-2 is spiked with three successive 500 μL portions of 5.00 ppm Cd^{2+} solution. Before plotting current vs. $\mu\text{g Cd}^{2+}$ added, for the standard addition procedure, all current values were corrected for dilution and for the Cd^{2+} abundance in the blank. A typical calibration curve is shown in Fig. 4.

Table 1 illustrates the nature of the calculations carried out, using Sewage Sludge Sample A-1 as typical. A linear least squares plot of current in

μA (corrected for dilution) vs. $\mu\text{g Cd}^{2+}$ added to the sample yielded an intercept of $0.572_{54} \mu\text{A}$ and a slope of $0.177_{00} \mu\text{A}/\mu\text{g Cd}$, with an RVAL of 0.99964.

Thus,

$$y = mx + b$$

$$0 = (0.17700)x + 0.57254$$

$$X = -3.23_5 \mu\text{g Cd}$$

and

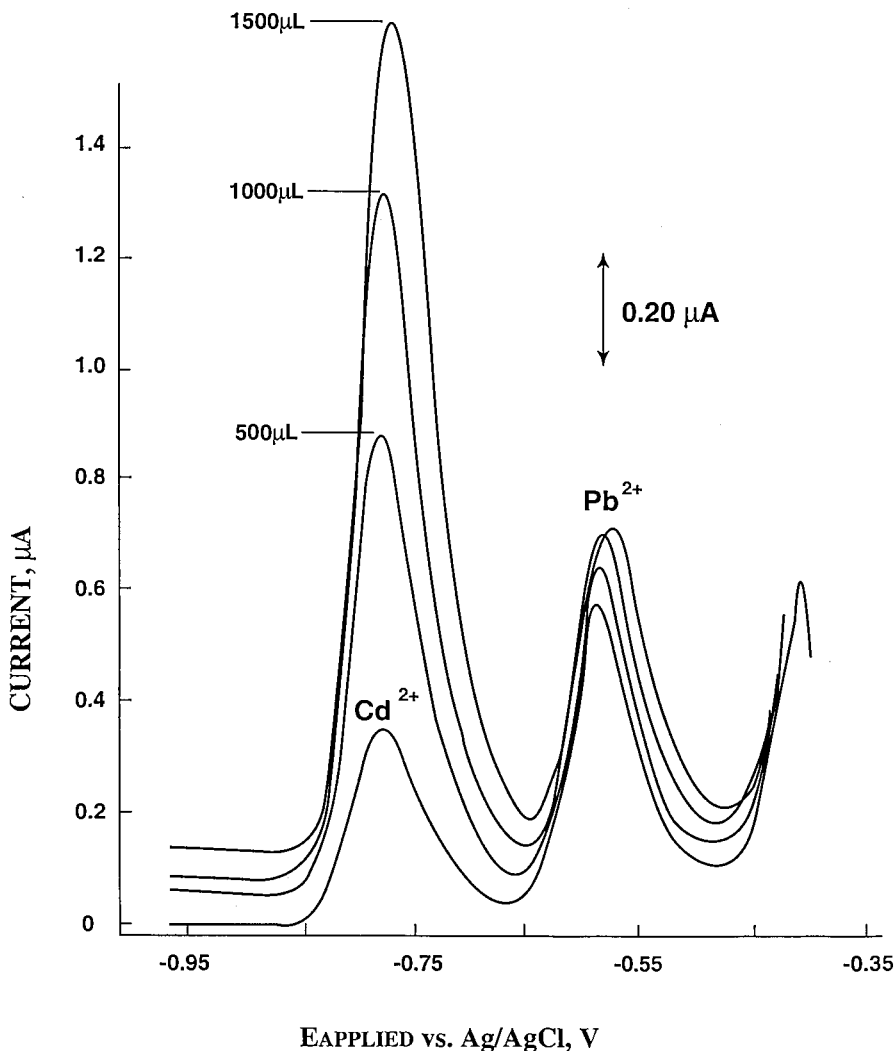


Fig. 3. Standard addition spiking of sewage sludge sample B-2 with 500 μL portions of 5.00 ppm Cd^{2+} .

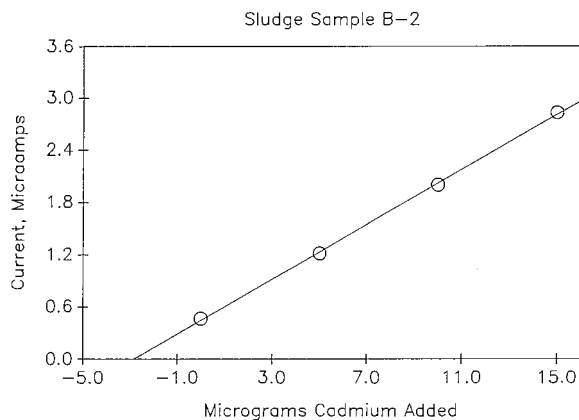


Fig. 4. Calibration curve for sewage sludge sample B-2.

$$\frac{3.235 \mu\text{g Cd}}{9.969 \text{ ml}} \times \frac{100.0 \text{ ml}}{\text{sample}} - \frac{0.155 \mu\text{g Cd}}{\text{sample}} (\text{blank value})$$

$$\frac{0.1981 \text{ g (mass of sample A1-1)}}{0.1981 \text{ g (mass of sample A1-1)}}$$

$$= 163 \mu\text{g Cd/g sample A-1}$$

$$= 163 \text{ ppm Cd in Sewage Sludge Sample A-1}$$

The results obtained for the four sewage sludge samples, each analyzed in triplicate, are given in Table 2, which includes mean and standard deviation data as well. The results show cadmium abundance values ranging from 120 to 250 ppm, with most values falling in the 120–170 ppm range. In order to evaluate any possible bias in the method, two NBS (NIST) standard reference materials were analyzed in triplicate. The results and standard deviations are given in Table 3. The data show no conclusive evidence of bias, giving results which are 23% low (SRM 1648) in one case and 35% high (SRM 1645) in the other. Rather, they suggest that the results are associated with a fairly large relative uncertainty. Thus,

Table 2
Results for sewage sludge samples analyzed

Sample	Cd ²⁺ (ppm)	Sample	Cd ²⁺ (ppm)
A-1	163	E-1	301
A-2	199	E-2	230
A-3	151	E-3	210
A (ave)	171	E (ave)	247
s _A	25	s _E	48
B-1	118	F-1	139
B-2	133	F-2	115
B-3	122	F-3	138
B (ave)	124	F (ave)	131
s _B	8	s _F	14

the results given for the sewage sludge samples may well have uncertainties of the order of 30%. If a standard reference material sewage sludge had been available for analysis, it would be possible to make a more definite statement about the results.

Another point of concern was the possibility that the Pb²⁺ peak might interfere with the peak for Cd²⁺, in the case of SRM 1648. The certified values for SRM 1648 are:

Cadmium	75 ± 7 μg/g
Copper	609 ± 27 μg/g
Lead	0.655 ± 0.008% (or 6550 ± 80 μg/g)

Thus there is 87 times as much lead as cadmium (ppm basis) in SRM 1648. Does this high ratio of Pb to Cd have any effect on the size of the Cd peak? (Again, no such concern existed with regard

Table 1
Summary of DPASV results for sewage sludge sample A-1

5.00 ppm Cd ²⁺ added to sample (ml)	Cd added to sample (μg)	Peak height (div.)	Full-scale (fs = 100 div.) (μA)	Gross current (μA)	Current corrected for dilution (μA)
0.00	0.00	29.6	2	0.592	0.592
1.00	5.00	65.8	2	1.316	1.4476
2.00	10.00	38.4	5	1.920	2.304
3.00	15.00	50.1	5	2.505	3.2565

Table 3
Results for standard reference materials

SRM	Reported value (ppm Cd ²⁺)	This work (ppm Cd ²⁺)
1648, urban particulate matter	75 ± 7	58.1 ± 6.9
1645, river sediment	10.2 ± 1.5	13.8 ± 4.7

to the sewage sludge samples themselves, where abundances of Cd and Pb are comparable, based on peak height; and there is no evidence whatsoever of mutual peak interference). To test this possibility solutions were prepared in which the Pb²⁺/Cd²⁺ ppm ratio ranged from 0 to 100 and the current due to Cd²⁺ was measured. The results are given in Table 4. It may be seen that for Pb²⁺/Cd²⁺ ratios ranging from zero to 50 (ppm/ppm basis), increasing ratios have no effect on the height of the Cd²⁺ peak. There may be a peak suppression effect at higher ratios, but this would need to be investigated further.

If one looks at Fig. 5, which gives the Pb²⁺ and Cd²⁺ voltammograms for Pb²⁺/Cd²⁺ ratios (ppm/ppm) of 0, 1 and 50, it is obvious that there is an increasing overlap of the peaks as the Pb²⁺/Cd²⁺ ratio increases. However, if one uses the baseline to the left of the Cd²⁺ peak as the reference baseline, this overlap has no effect on the height of the Cd²⁺ peak and its calculated current. For example, Table 4 shows that the current for a 1.00 ppm Cd²⁺ solution, in which Pb²⁺/Cd²⁺ ratios vary from 0 to 50, remains essentially constant at 1.70 ± 0.06 µA.

Table 4
Investigation of possible lead interference on cadmium measurement

Cd ²⁺ concentration (ppm)	Pb ²⁺ /Cd ²⁺ ratio (ppm/ppm)	Cd ²⁺ current (µA)	Cd ²⁺ current (µA) per ppm Cd ²⁺
1.00	0.00	1.675	1.675
1.00	1.00	1.78	1.78
1.00	5.00	1.64	1.64
1.00	10.00	1.67	1.67
1.00	50.00	1.755	1.755
0.50	100.00	0.685	1.37

4. Conclusion

Sewage sludge samples obtained from the municipal sludge lagoon in Fort Wayne, IN were found to contain 171, 124, 247, and 131 ppm Cd, for an average of 168 ppm Cd. A sodium peroxide fusion in zirconium crucibles, followed by leaching with HCl and pH adjustment to 4.00, gave solutions which were then analyzed by differential pulse anodic stripping voltammetry. By carrying out the deposition step at −0.95 V vs. Ag/AgCl, interference from zinc was easily eliminated. Lead was not a problem, inasmuch as lead-to-cadmium ratios as high as 50:1 (ppm) have no effect on the current due to Cd; and the actual sludge samples had much lower Pb:Cd ratios. Analysis of standard reference materials indicated the procedure used was satisfactory.

The average value of 168 ppm Cd falls within the range reported for sewage sludges by Jing and Logan [5]; that is, it is less than the 227 ppm Cd reported for the Chicago sludge, but greater than the upper end of the range of 34–140 ppm Cd reported for the Ashtabula–Elyria–Bellefontaine–Fremont sludges. It is, in fact, very similar to the 170 ppm value reported back in 1975 as typical of the sewage sludge used by Braude et al. [19] in their work on the uptake of Cd by soybeans grown on sludge-amended soil.

There is no evidence, based on this work, that the abundance of Cd in Fort Wayne municipal sewage sludge was enhanced by the zinc cadmium sulfide dropped on Fort Wayne. In view of the elevated Cd concentrations in selected crops grown on sewage sludge treated soil (lettuce, cabbage, spinach, carrots, potatoes, wheat, corn, and soybeans), which could be as great as an 8-fold

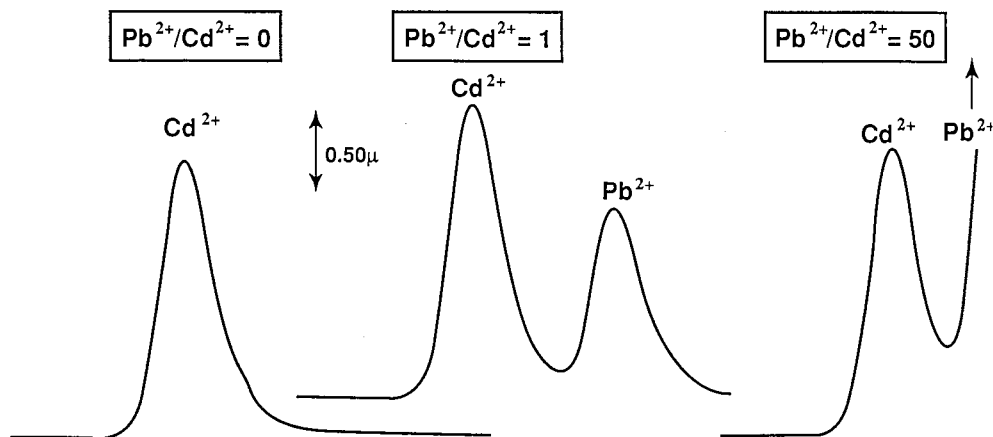


Fig. 5. Effect of the $\text{Pb}^{2+}/\text{Cd}^{2+}$ ratio on the current for the Cd^{2+} peak.

enhancement when compared to normal crops, it is recommended that Fort Wayne municipal sewage sludge not be used when growing such crops.

Acknowledgements

We wish to thank Stacey J. Petrovas, agronomist for the City of Fort Wayne Utilities, for his part in the sewage sludge acquisition.

References

- [1] D. Noell, L. Stedman, *The Journal Gazette*, Fort Wayne, Indiana, January 15, 1995, 1A.
- [2] A. Jarosh, *The News Sentinel*, Fort Wayne, Indiana, January 16, 1997, 1A, 9A.
- [3] S.B. Sterrett, R.L. Chaney, C.H. Gifford, H.W. Mielke, *Environ. Geochem. Health* 18 (1996) 135–142.
- [4] S.W. Jenniss, S.A. Katz, T. Mount, *Am. Lab.* 12 (1980) 18, 20, 22–23.
- [5] J. Jing, T.J. Logan, *J. Environ. Qual.* 21 (1992) 73–81.
- [6] J.C. Sherlock, *Proceedings of the 4th Int. Cadmium Conference*, Munich, 1983, pp. 107–109.
- [7] M.J. Dudas, S. Pawluk, *Can. J. Soil Sci.* 55 (1975) 239–243.
- [8] A.P. Jackson, B.J. Alloway, *Plant Soil* 132 (1991) 179–186.
- [9] L. Linnman, A. Andersson, K.O. Nilsson, B. Lind, T. Kjellström, L. Friberg, *Arch. Environ. Health* 27 (1973) 45–47.
- [10] C.S. Reddy, C.R. Dorn, *Environ. Res.* 38 (1985) 377–388.
- [11] A. Meyer, U. De la Chevallier-Haaf, G. Henze, *Fresenius Z. Anal. Chem.* 328 (1987) 565–568.
- [12] J.F.N. Maaskant, A.H. Boekholt, P.J. Jenks, *Fresenius J. Anal. Chem.* 360 (1998) 406–409.
- [13] B. Griepink, H. Muntau, E. Colinet, *Fresenius Z. Anal. Chem.* 318 (1984) 490–494.
- [14] C.J. Ackers, M.J. Gardner, J.E. Ravenscroft, *Fresenius J. Anal. Chem.* 354 (1996) 596–601.
- [15] C.J. Ritter, *Am. Lab.* 14 (1982) 72–73.
- [16] T. Delschen, W. Werner, *Landwirtschaft. Forsch.* 42 (1989) 29–39.
- [17] T.J. Murphy, in: R. Mavrodineau (Ed.), *Procedures used at the National Bureau of Standards to Determine Selected Trace Elements in Biological and Botanical Materials*, National Bureau of Standards, 1977, pp. 6–7.
- [18] J.H. Kaye, R.S. Strebin, A.E. Nevissi, *J. Radioanal. Chem.* 180 (1994) 197–200.
- [19] G.L. Braude, A.M. Nash, W.J. Wolf, R.L. Carr, R.L. Chaney, *J. Food Sci.* 45 (1980) 1187–1189, 1199.

Synthesis, complexation, and fluorescence behavior of armed crown ethers carrying naphthyl group

Kanji Kubo ^{a,*}, Seiji Sakaguchi ^b, Tadamitsu Sakurai ^b

^a Institute of Advanced Material Study, 86, Kyushu University, Kasuga-koen, Kasuga, Fukuoka, 816-8580 Japan

^b Department of Applied Chemistry, Faculty of Engineering, Kanagawa University, Kanagawa-ku, Yokohama, 221-8686 Japan

Received 16 November 1998; received in revised form 21 January 1999; accepted 28 January 1999

Abstract

Armed crown ethers (**1–4**) bonding through an amine, amide, ether, or ester linkage to naphthyl group were found to display unique photophysical properties in the presence of guest salts. Complexation of PET fluoroionophores (**1a** and **1b**) with Zn^{2+} increased the fluorescence intensities of the host by a factor of 2.4 and 2.7, respectively. ¹H and ¹³C NMR analyses of this complexation behavior of **1a** revealed that Zn^{2+} strongly coordinates with the armed crown nitrogen to cause a dramatic decrease in an intramolecular charge-transfer character. The armed crowns (**2** and **3**), bonding through an ether or ester linkage to a naphthalene, gave fluorescence quenching with guest thiocyanates. While the amide derivative (**4**) exhibited high Ba^{2+} fluorescence selectivity and in the presence of this cation the host fluorescence intensity was by a factor of 3.69. © 1999 Elsevier Science B.V. All rights reserved.

Keywords: Photoinduced electron transfer; Fluoroionophore; Fluorescence behavior; Armed crown ethers

1. Introduction

Photo-responsive supramolecular systems are of great significance particularly for their potential application to nanoscale devices for cation sensor and switch [1]. Recently, there are extensive investigations toward the characterization of fluoroionophores including podands, crown ethers, calixarenes, cyclophanes, and cyclodextrins derivatives with fluorophore [2–4]. Moreover, de Silva et al. created a photoinduced

electron transfer (PET) fluoroionophores, an azacrown ether having an anthryl group [5–7]. In our previous papers, we reported that the diazacrown ethers carrying two fluorophores have a higher fluorescence switch-on ability for guest cation complexation than the monoazacrown derivatives [8–17]. Thus, it is interesting to investigate the complex formation with guest cations using fluorescence spectroscopy. While, armed crown ethers such as lariat ethers and double armed crowns are a class of cation-host molecules, which are characterized by parent macrocyclic ring and ligating arms [18,19]. Since their cation-binding properties are essentially determined by coordination characters of macrocycle and donor arms,

* Corresponding author. Tel.: +81-92-5837807; fax: +81-92-5837810.

E-mail address: kubo-k@cm.kyushu-u.ac.jp (K. Kubo)

wide variations of basic structures may lead to the design of new and specific host molecules for a given guest cation [20,21]. By combining armed crown ether and fluorophore, a fluoroionophore having a novel property could be produced. Here, we describe the synthesis and fluorescence behavior of the armed crown ether containing naphthyl pendants.

2. Experimental

Elemental analyses were performed by Perkin Elmer PE2400 series II CHNS/O analyzer. Melting points were obtained with a Yanagimoto Micro Melting Point Apparatus and were uncorrected. NMR spectra were measured on a JEOL JNM-500 Model spectrometer in CDCl_3 and $\text{DMSO}-d_6$; the chemical shifts were expressed by an δ unit using tetramethylsilane as an internal standard. IR spectra were recorded on a Hitachi Model 270-30 infrared spectrophotometer. Fluorescence spectra were measured with a Hitachi Model F-4500 spectrofluorimeter. Mass spectra were measured with a JEOL 01SG-2 spectrometer.

2.1. Preparation of compounds **1a**, **1b**, **2**, **3**, and **4**

Compound **1a** was prepared according to literature procedure [13].

2.1.1. Synthesis of 2-[*N,N*-bis(1-naphthylmethyl)-aminomethyl]-1,4,7,10,13-pentaoxacyclopentadecane (**1b**)

A toluene solution (10 cm^3) of 2-(aminomethyl)-15-crown-5 (0.116 g, 0.5 mmol), triethylamine (1.0 cm^3 , 7.2 mmol), 1-chloromethylnaphthalene (0.588 g, 3.3 mmol) was refluxed for 6 h. The mixture was then diluted with 1 M NH_3 (30 cm^3), extracted with ethyl acetate (50 cm^3). The solvent was evaporated and the residue was purified by column chromatography over silica gel (70–230 mesh, Merck) using hexane and ethyl acetate (1:1 *v/v*) as the eluent.

1b (colorless oil); ^1H NMR: $\delta = 2.62$ – 2.70 (2H, m), 3.04 – 3.21 (4H, m), 3.43 (2H, t, $J = 4.6$ Hz),

3.48 – 3.63 (13H, m), 3.99 (2H, d, $J = 12.8$ Hz), 4.10 (2H, d, $J = 12.8$ Hz), 7.19 (2H, ddd, $J = 8.2$, 7.0 , 1.5 Hz), 7.36 (2H, dd, $J = 8.1$, 7.0 Hz), 7.39 (2H, ddd, $J = 8.2$, 8.1 , 1.5 Hz), 7.44 (2H, d, $J = 7.0$ Hz), 7.72 (2H, d, $J = 8.2$ Hz), 7.78 (2H, d, $J = 8.2$ Hz), and 7.99 (2H, d, $J = 8.2$ Hz); ^{13}C NMR: $\delta = 55.5$, 59.2 , 69.4 , 70.1 , 70.4 , 70.5 , 70.55 , 70.6 , 70.8 , 70.9 , 72.5 , 77.9 (2C), 125.0 (2C), 125.3 (2C), 125.48 (2C), 125.50 (2C), 128.1 (2C), 128.2 (2C), 128.3 (2C), 132.5 (2C), 133.8 (2C), and 135.0 (2C). IR (NaCl) ν 777, 840, 948, 1116, 1254, 1290, 1350, 1449, 1596, 1941, 2848, and 3040 cm^{-1} . HR (FAB) MS: m/z 530.2908. Calcd for $\text{C}_{33}\text{H}_{40}\text{NO}_5$: 530.2906.

2.1.2. Synthesis of 2-[(1-naphthylmethoxy-methyl)]-1,4,7,10,13-pentaoxacyclopentadecane (**2**)

A toluene solution (10 cm^3) of 2-hydroxymethyl-15-crown-5 (0.116 g, 0.5 mmol) and NaH (0.096 g, 4.0 mmol) were refluxed for 1 h. To the mixture 1-chloromethylnaphthalene (0.588 g, 3.3 mmol) was added and refluxed for 5 h. The mixture was then diluted with 1 M HCl (30 cm^3), extracted with ethyl acetate (50 cm^3). The solvent was evaporated and the residue was purified by column chromatography over silica gel (70–230 mesh, Merck) using ethyl acetate as the eluent.

2 (colorless oil); ^1H NMR: $\delta = 3.55$ – 3.82 (21H, m), 4.98 (2H, s), 7.42 (1H, dd, $J = 8.2$, 8.2 Hz), 7.45 – 7.53 (3H, m), 7.79 (1H, d, $J = 8.2$ Hz), 7.85 (1H, d, $J = 8.2$ Hz), and 8.12 (1H, d, $J = 8.6$ Hz); ^{13}C NMR: $\delta = 70.2$, 70.41 , 70.44 , 70.47 , 70.52 , 70.53 , 70.7 , 70.8 , 71.0 , 71.4 , 72.0 , 78.7 , 124.2 , 125.2 , 125.7 , 126.1 (2C), 126.4 , 128.5 , 128.6 , 131.8 , and 133.8 . IR (NaCl) ν 776, 1124, 1288, 1346, 1448, 1598, 1724, and 2860 cm^{-1} . EA: Calcd for $\text{C}_{22}\text{H}_{30}\text{O}_6$: C; 67.67, H; 7.74. Found: C; 67.50, H; 7.55.

2.1.3. Synthesis of 1,4,7,10,13-pentaoxacyclopentadec-2-ylmethyl 1-naphthalene carboxylate (**3**)

A toluene–tetrahydrofuran solution (15 + 15 cm^3) of 2-hydroxymethyl-15-crown-5 (0.049 g, 0.2 mmol) and NaH (0.015 g, 0.6 mmol) were refluxed for 1 h. To the mixture 1-naphthoyle chloride (0.265 g, 1.0 mmol) was added and

refluxed for 5 h. The mixture was then diluted with 1 M HCl (30 cm³), extracted with ethyl acetate (50 cm³). The solvent was evaporated and the residue was purified by column chromatography over silica gel (70–230 mesh, Merck) using ethyl acetate as the eluent.

3 (colorless oil); ¹H NMR: δ = 3.63–3.93 (18H, m), 4.04 (1H, qui, *J* = 5.3 Hz), 4.43 (1H, dd, *J* = 11.6, 5.3 Hz), 4.57 (1H, dd, *J* = 11.6, 5.3 Hz), 7.49 (1H, ddd, *J* = 8.2, 7.0, 1.2 Hz), 7.53 (1H, ddd, *J* = 8.2, 7.0, 1.2 Hz), 7.60 (1H, ddd, *J* = 8.5, 7.0, 1.2 Hz), 7.87 (1H, d, *J* = 8.2 Hz), 8.01 (1H, d, *J* = 8.2 Hz), 8.19 (1H, dd, *J* = 7.3, 1.2 Hz), and 8.92 (1H, d, *J* = 8.5 Hz); ¹³C NMR: δ = 65.0, 70.49, 70.53, 70.58, 70.67, 70.68, 70.9, 71.0, 71.2, 71.3, 77.7, 124.5, 125.9, 126.2, 127.2, 127.7, 128.5, 130.9, 131.4, 133.4, 133.9, and 167.4. IR (NaCl) ν 776, 1124, 1194, 1242, 1340, 1450, 1506, 1592, 1706, 2864 cm⁻¹. EA: Calcd for C₂₂H₂₈O₇: C; 65.33, H; 6.98. Found: C; 65.42, H; 6.85.

2.1.4. Synthesis of synthesis of 1,4,7,10,13-pentaoxacyclopentadec-2-ylmethyl 1-naphthalene carboxamide (**4**)

A toluene solution (10 cm³) of 2-(aminomethyl)-15-crown-5 (0.240 g, 1.0 mmol), triethylamine (1.0 cm³, 7.2 mmol), 1-naphthoyl chloride (0.380 g, 2.0 mmol) was refluxed for 12 h. The mixture was then diluted with 1 M HCl (20 cm³), extracted with ethyl acetate (50 cm³). The solvent was evaporated and the residue was purified by column chromatography over silica gel (70–230 mesh, Merck) using ethyl acetate as the eluent.

4 (colorless oil); ¹H NMR: δ = 3.52–3.91 (21H, m), 6.68 (1H, t, *J* = 5.1 Hz), 7.44 (1H, dd, *J* = 8.2, 7.3 Hz), 7.50 (1H, ddd, *J* = 8.9, 7.1, 1.5 Hz), 7.53 (1H, ddd, *J* = 8.3, 7.1, 1.5 Hz), 7.61 (1H, dd, *J* = 7.3, 1.5 Hz), 7.85 (1H, dd, *J* = 8.9, 1.5 Hz), 7.89 (1H, d, *J* = 8.2 Hz), and 8.34 (1H, dd, *J* = 8.3, 1.5 Hz); ¹³C NMR: δ = 41.6, 69.8, 70.41, 70.44, 70.57, 70.73, 70.91, 70.93, 71.2, 72.4, 77.6, 124.7, 125.0, 125.6, 126.3, 127.0, 128.2, 130.2, 130.4, 133.7, 134.8, and 169.6. IR (NaCl) ν 780, 930, 1113, 1245, 1293, 1353, 1512, 1626, 2146, 2860, 3046, and 3298 cm⁻¹. HR(FAB) MS: *m/z* 404.2079. Calcd for C₂₂H₃₀NO₆: 404.2073.

2.2. Fluorescence spectral measurement of armed crown ethers (**1–4**) and its complexes

Fluorescence intensities of the fluoroionophores (**1**: 2.00 × 10⁻⁵ M, **2–4**: 4.00 × 10⁻⁵ M, 1 M = 1 mol dm⁻³) and 1-methylnaphthalene (4.00 × 10⁻⁵ M) excited at 278–288 nm measured in methanol under nitrogen at room temperature. The titrations were conducted by adding a crown ether solution (**1**: 2.00 × 10⁻⁵ M, **2–4**: 4.00 × 10⁻⁵ M in methanol) progressively containing excess guest salts, using a 0.25 cm³ syringe, to a cuvette containing 2.0 cm³ of the crown ether solution (**1**: 2.00 × 10⁻⁵ M, **2–4**: 4.00 × 10⁻⁵ M in methanol). The solutions were homogenized by ultrasonic waves for 3 min. The spectrum was recorded after each addition. The added equivalents of the cation were then plotted against the emission-intensity change. The association constants (*K*) for guest cation complexes were determined at least in duplicate at 25 ± 1°C by the self-written nonlinear curve-fitting computer program in the previous studies [10,15,22].

3. Results and discussion

The naphthalene-functionalized armed crown ethers (**1–4**) were prepared by *N*-alkylation, etherification, esterification, amidation of the corresponding armed crown ethers with 1-chloromethylnaphthalene or 1-naphthoyl chloride (Scheme 1).

3.1. Fluorescence spectral studies

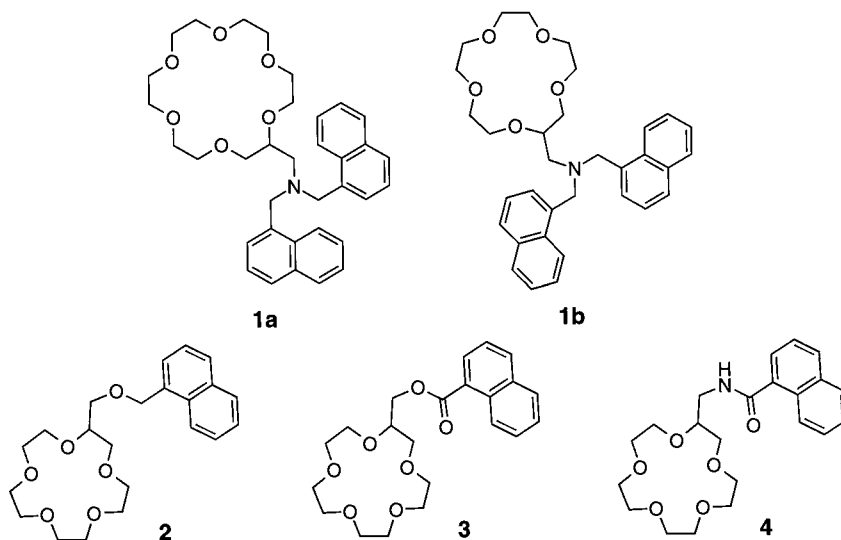
Fig. 1 is illustrated the fluorescence spectral behavior of **1–4** and 1-methylnaphthalene in methanol at room temperature. Fluoroionophore (**1**), when excited at 281 nm, gave a broad emission band with a maximum at 460 nm in addition to the normal naphthalene fluorescence at 334 nm. The formation of intramolecular exciplex and excimer should be responsible for the appearance of the emission band at 460 nm. The emission-band intensities at 334 nm of **1a** and **1b** (2.00 × 10⁻⁵ M) was reduced to approximately one-270th and one-330th that of 1-methylnaphthalene (1-

MN, 4.00×10^{-5} M), which was accompanied by the exciplex fluorescence. This indicates that the quenching of the excited-state naphthalene chromophore by the amino unit proceeds in a mechanism similar to that for the classical naphthalene-aliphatic amine system [23–25].

The formation of the intramolecular exciplex is very likely to be responsible for the observed emission quenching. In fact, the quenching efficiency (I_{1a}/I_{1-MN} : 3.7×10^{-3} , I_{1b}/I_{1-MN} : $3.0 \times$

10^{-3}) is similar to that (I/I_{1-MN} : 2.3×10^{-3}) of *N,N'*-bis(1-naphthylmethyl)-1,4,10,13-tetraoxa-7,16-diazacyclooctadecane [9]. This result suggested that the quenching of the excited-state naphthalene chromophore proceed PET occurring from the nitrogen atoms in the sidearm unit.

For the armed crown bonding through ether linkage **2** (4.00×10^{-5} M), when excited at 278 nm, the emission-band intensity at 332 nm was reduced to approximately one half that of 1-



Scheme 1. Naphthalene—functionalized armed crown ethers (1–4).

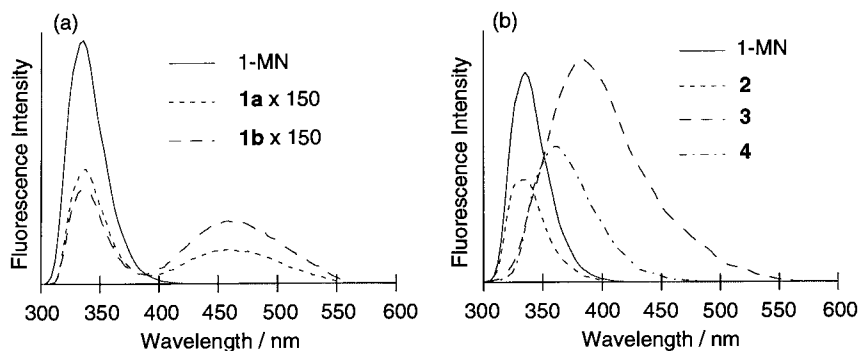


Fig. 1. Fluorescence spectrum of: (a) **1** (2.00×10^{-5} M) and 1-methylnaphthalene (4.00×10^{-5} M) in methanol as excited at 281 nm; (b) **2–4** (4.00×10^{-5} M) and 1-methylnaphthalene (4.00×10^{-5} M) in methanol (excitation wavelength: **2**, 278 nm; **3**, 288 nm; **4**, 279 nm).

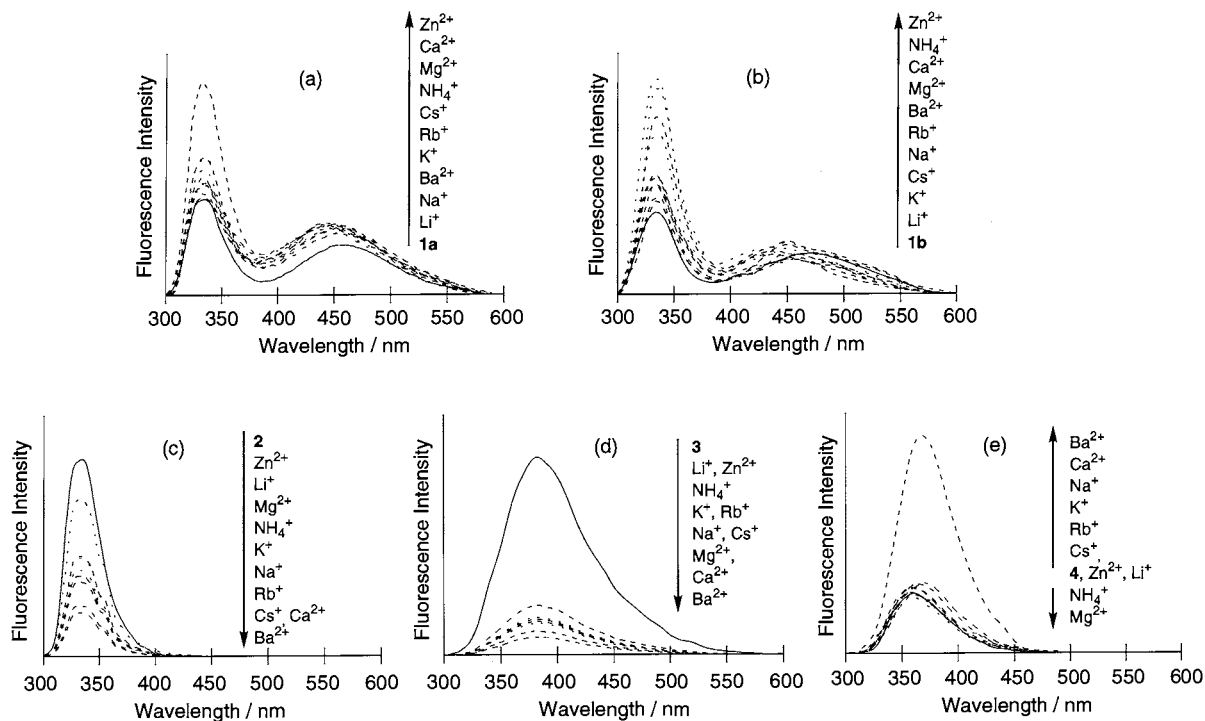


Fig. 2. Fluorescence spectral changes of armed crown ethers (**1a**, **1b**, **4**, 2.00×10^{-5} M; **2**, **3**, 4.00×10^{-5} M) with and without various guest salts (1.00×10^{-3} M for **1a**, **1b**, **4**, 8.00×10^{-2} M for **2**, **3**) in methanol.

methylnaphthalene (4.00×10^{-5} M). The quenching is due to PET occurring from the oxygen atoms of sidearm and crown ether to the excited state naphthalene. The armed crown (**3** and **4**) bonding through ester and amide linkage, when excited at 288 for **3** and 279 nm for **4**, gave a emission band at 372 and 360 nm.

A dramatic change in the emission intensity of **1–4** was observed upon the addition of various amounts of guest cations (Li^+ , Na^+ , K^+ , Rb^+ , Cs^+ , NH_4^+ , Zn^{2+} , Mg^{2+} , Ca^{2+} , and Ba^{2+}) as shown in Fig. 2. Fig. 3 illustrates the relative emission intensity of **1–4** (I_{1-4}) against the guest cation concentration.

When the guest cations were added (50 molar equivalent), the relative emission intensity ratio (I_{complex}/I_1), being used as a measure of the molecular recognition sensing, changed from 2.4 to 1.2 for **1a** and from 2.7 to 1.2 for **1b** depending on the nature of guest cations. The intensity ratio

(I_{complex}/I_1) was different among bound metal ions and decreased in the following order: (**1a**: Zn^{2+} (2.4) > Ca^{2+} , Mg^{2+} (1.6) > NH_4^+ , Cs^+ (1.4) > Rb^+ , K^+ (1.3) > Ba^{2+} , Na^+ , Li^+ (1.2), **1b**: Zn^{2+} (2.7) > NH_4^+ (2.6) > Ca^{2+} (2.2) > Mg^{2+} (2.0) > Ba^{2+} (1.5) > Na^+ , Rb^+ (1.4) > Cs^+ (1.3) > Li^+ , K^+ (1.2)).

In Table 1 is illustrated the fluorescence intensity ratio ($I_{\text{complex}}/I_{1\text{-MN}}$) of guest cation complexes for 1-methylnaphthalene (1-MN), as a measure of the guest cation-induced fluorescence recovery and a parameter instead of emission quantum yield.

This fluorescence recovery means that the complexation for guest cations inhibit the PET occurring from the nitrogen atoms in the sidearm to the naphthalene. Zinc ion binding can then cause high fluorescence recovery. This recovery is due to coordination from the nitrogen atoms of the armed crown to the zinc ion. The strength of this

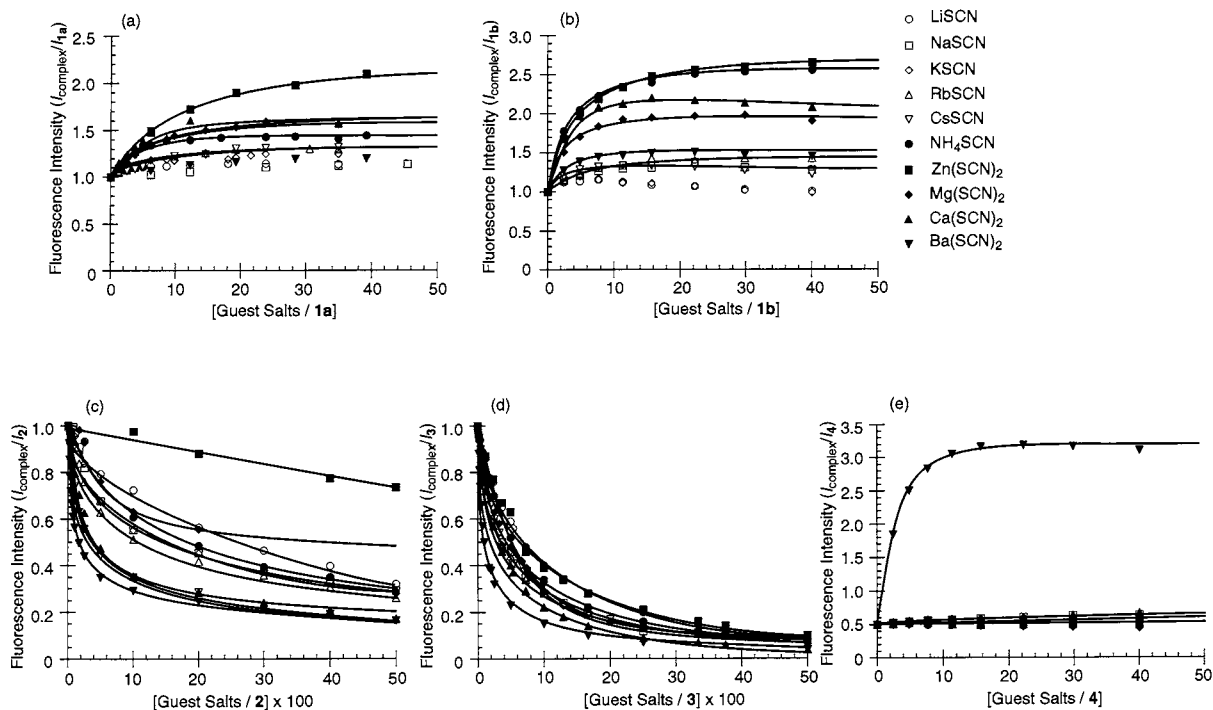


Fig. 3. Dependence of fluorescence intensities of: (a) **1a** (2.00×10^{-5} M) at 334 nm; (b) **1b** (2.00×10^{-5} M) at 334 nm; (c) **2** (4.00×10^{-5} M) at 332 nm; (d) **3** (4.00×10^{-5} M) at 372 nm; (e) **4** (4.00×10^{-5} M) at 360 nm on the concentration of various guest salts in methanol.

binding interaction modulates the PET from the amine to naphthalene. However, the recovery ($I_{1a-Zn\ complex}/I_{1-MN} = 8.9 \times 10^{-3}$, $I_{1b-Zn\ complex}/I_{1-MN} = 8.4 \times 10^{-3}$) of the armed crown (**1**) for Zn^{2+} is lower than that of the N,N',N'',N''' -tetrakis(1-naphthylmethyl)-cyclam ($I_{Zn\ complex}/I_{1-MN} = 0.11$) [12] and N,N' -bis(1-naphthylmethyl)-diaz-12-crown-4 ($I_{Zn\ complex}/I_{1-MN} = 0.73$) [14]. While, the emission intensity of **2** and **3** decreases with an increase in the guest cation concentration. Furthermore, it is noteworthy that the **2** and **3**-guest thiocyanate complex exhibited a decrease in its emission intensity relative to that of **2** and **3**, itself. This suggests that the observed quenching is due to the presence of thiocyanate ion. A similar quenching by the thiocyanate anion was explained based on the photoinduced electron transfer from this anion to the naphthalene chromophore [26,27]. On the other hand, the amide derivative (**4**) exhibited high Ba^{2+} fluorescence

selectivity and in the presence of this cation the host fluorescence intensity was by a factor of 3.69.

Table 1

Fluorescence intensity ratio ($I_{complex}/I_1$ and $I_{complex}/I_{1-MN}$) of guest cation complexes of **1a** and **1b** for 1-methylnaphthalene (1-MN)

	I_{1a}/I_{1-MN}	$I_{complex}/I_{1a}$	I_{1b}/I_{1-MN}	$I_{complex}/I_{1b}$
Free	3.7×10^{-3}	–	3.1×10^{-3}	–
LiSCN	4.4×10^{-3}	1.2	3.7×10^{-3}	1.2
NaSCN	4.4×10^{-3}	1.2	4.3×10^{-3}	1.4
KSCN	4.8×10^{-3}	1.3	3.7×10^{-3}	1.2
RbSCN	4.8×10^{-3}	1.3	4.3×10^{-3}	1.4
CsSCN	5.2×10^{-3}	1.4	4.0×10^{-3}	1.3
NH_4SCN	5.2×10^{-3}	1.4	8.1×10^{-3}	2.6
$Zn(SCN)_2$	8.9×10^{-3}	2.4	8.4×10^{-3}	2.7
$Mg(SCN)_2$	5.9×10^{-3}	1.6	6.2×10^{-3}	2.0
$Ca(SCN)_2$	5.9×10^{-3}	1.6	6.8×10^{-3}	2.2
$Ba(SCN)_2$	4.4×10^{-3}	1.2	4.7×10^{-3}	1.5

Table 2
Association constants (K/M^{-1}) of **1–4** for various metal salts in methanol

	1a	1b	2	3	4
LiSCN	–	–	8.1 ± 0.9	35.8 ± 0.6	–
NaSCN	–	–	21.0 ± 1.8	75.0 ± 4.5	1920 ± 150
KSCN	–	–	21.9 ± 2.0	66.0 ± 0.6	17900 ± 5500
RbSCN	8500 ± 690	3070 ± 380	23.0 ± 2.0	66.2 ± 0.7	4200 ± 830
CsSCN	990 ± 580	5890 ± 630	118 ± 2.0	54.0 ± 2.2	–
NH ₄ SCN	19000 ± 6400	10900 ± 900	13.9 ± 1.9	41.8 ± 0.8	–
Zn(SCN) ₂	3600 ± 400	37000 ± 1500	1.0 ± 0.2	34.7 ± 0.8	–
Mg(SCN) ₂	6500 ± 800	47300 ± 5600	38.2 ± 10.5	44.5 ± 1.7	–
Ca(SCN) ₂	10100 ± 2500	28100 ± 3000	41.8 ± 4.2	87.3 ± 2.3	–
Ba(SCN) ₂	–	29000 ± 3000	68.2 ± 9.0	144 ± 5	18400 ± 4500

3.2. Association constants

Guest cation concentration dependence of the emission intensity (Fig. 3) allowed us to determine the association constants (K) by the non-linear curve-fitting method (Table 2) [10,15,22].

The armed crowns (**1**) showed the following cation selectivity (K): (**1a**: $\text{Cs}^+ < \text{Zn}^{2+} < \text{Mg}^{2+} < \text{Rb}^+ < \text{Ca}^{2+} < \text{NH}_4^+$, **1b**: $\text{Rb}^+ < \text{Cs}^+ < \text{NH}_4^+ < \text{Ca}^{2+} < \text{Ba}^{2+} < \text{Zn}^{2+} < \text{Mg}^{2+}$). This selectivity order for **1a** is distinct from that for *N,N'*-bis(1-naphthylmethyl)-1,4,10,13-tetraoxa-7,16-diazacyclooctadecane (K : Li^+ (27) < Ca^{2+} (61) < Cs^+ (97) < Na^+ (123) < Zn^{2+} (126) < Rb^+ (305) < Ba^{2+} (710) < NH_4^+ (1490) < K^+ (1850) < Mg^{2+} (3240)) [9], *N*-(1-naphthylmethyl)-1,4,7,10,13-pentaoxa-16-azacyclooctadecane (K : Zn^{2+} (1330) < Li^+ (2400) < Na^+ (3890) < Cs^+ (6260) < Ca^{2+} (7100) < NH_4^+ (15800) < Mg^{2+} (29600) < Ba^{2+} (51300) < Rb^+ (51400) < K^+ (98200)) [15] and *N,N'*-bis(1-naphthylmethyl)-1,4,10-trioxa-7,13-diazacyclopentadecane (K : K^+ (246) < Zn^{2+} (597) < Ca^{2+} (794) < Ba^{2+} (1067) < NH_4^+ (2210) < Mg^{2+} (4620)) [17]. The association constants of **1** for various guest cations are larger than those of the corresponding crown, suggesting that the complexation based on cooperative actions of crown and amino sidearm. The association constants of **2** and **3** were smaller than those of **1**. This means that the ether or ester sidearm does not participate in the complexation but hinder the complexation with guest cations.

While the amide derivative (**4**), has a greatly fluorescence enhancement in the presence of Ba^{2+} , exhibited Ba^{2+} selectivity. Comparison of the selectivity order for **1–4** confirms that the cation ligating side-arm property may control the selec-

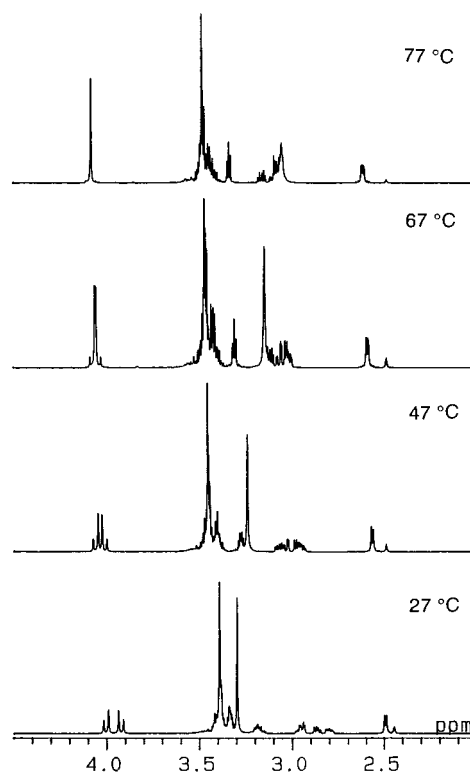


Fig. 4. Temperature-dependent ^1H NMR spectra of **1a** in $\text{DMSO-}d_6$ at 27, 47, 67, and 77°C.

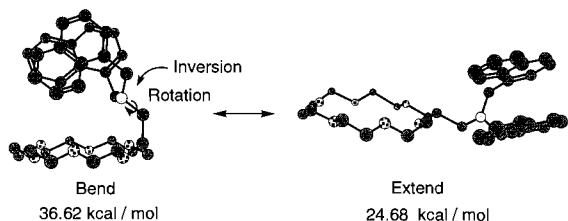


Fig. 5. Structure of **1a** generated by MM2 calculation.

tivity of the host toward guest cations in a delicate manner. In spite of the small association constant for **1** and **4** in methanol, the emission

intensity of this host was greatly enhanced in the presence of metal salts, establishing that **1** and **4** have a high fluorescence switch-on ability for complexation with various guest cations.

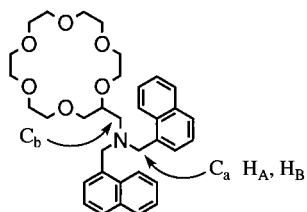
3.3. NMR studies

At room temperature the ^1H NMR spectrum of **1a** in $\text{DMSO-}d_6$ exhibits the usual *AB* splitting pattern of the methylene protons (naphthylmethyl group) as shown in Fig. 4. This means that inter-conversional (rotational or inversional) barrier ex-

Table 3

Changes of ^1H and ^{13}C NMR chemical shifts (δ) and induced shifts ($\delta_{\text{complex}} - \delta_{\text{1a}}$) of **1a** (1.0×10^{-2} M) with various metal salts (1.0×10^{-2} M) in $\text{CD}_3\text{CN-CDCl}_3$ (1:1 *v/v*)

	Naphthylmethyl group -CH ₂ -			
	H _A	H _B	C _a	C _b
1a	3.96	4.13	59.58	54.50
LiSCN	3.93	4.21	59.79	53.35
NaSCN	(−0.03)	(+0.08)	(+0.21)	(−1.19)
KSCN	3.93	4.20	59.83	53.61
RbSCN	(−0.03)	(+0.07)	(+0.25)	(−0.91)
CsSCN	3.89	4.22	59.82	52.78
NH ₄ SCN	(−0.07)	(+0.09)	(+0.24)	(−1.76)
Ba(SCN) ₂	3.95	4.18	59.74	53.43
Ca(SCN) ₂	(−0.01)	(+0.05)	(+0.16)	(−1.11)
Mg(SCN) ₂	3.98	4.14	59.69	53.77
Zn(SCN) ₂	(+0.02)	(+0.01)	(+0.11)	(−0.77)
	3.93	4.20	59.78	53.06
	(−0.03)	(+0.07)	(+0.20)	(−1.48)
	3.89	4.30	59.79	52.41
	(−0.07)	(+0.17)	(+0.21)	(−2.13)
	3.86	4.33	59.67	52.35
	(−0.10)	(+0.20)	(+0.09)	(−2.19)
	3.97	4.24	59.86	54.23
	(+0.01)	(+0.11)	(+0.28)	(−0.31)
	4.45, 8.82	4.95, 5.74	59.41, 57.97	56.69



ist between extended and bended conformations as illustrated in Fig. 5. The MM2 calculations [28] were applied to the bend and extend conformations. The geometries were optimized so as to give minimum energy. Thus, we are led to the bend conformation (36.62 kcal mol⁻¹) being sterically less stable than extend conformation (24.68 kcal mol⁻¹). To determine the barriers of the armed crown (**1a**), the temperature-dependent ¹H NMR measurement employed.

The rate of interconversion at the coalescence temperature was calculated from the expression $k_{\text{coalescence}} = \pi(\Delta\nu^2 = 6J^2)/(2^{1/2})$ where $\Delta\nu$ is the difference in chemical shift between the centers of the coupling constant. Substituting this value into the rate equation gives the expression $\Delta G^\ddagger = RT \ln(6.62 \times 10^{12}/k_{\text{coalescence}})$ [29]. From these measurements, the coalescence temperature (T_c) is 77°C and the free energy of activation for the interconversion was determined as 16.5 kcal mol⁻¹.

Further detailed information on the cation binding behavior for **1a** was obtained by ¹H and ¹³C NMR spectroscopy. The chemical (δ) and induced ($\Delta\delta$) shifts of the selected proton and carbon signals of the host (**1a**) with and without guest cations are summarized in Table 3.

Interestingly, Zn²⁺ produced even more remarkable chemical-shift change and peak splitting for the methylene proton and carbon signal of naphthylmethyl group. The induced shift was clearly demonstrating that the nitrogen atom in the armed crown (**1a**) has a propensity to strongly coordinate with Zn²⁺. As already mentioned, the binding of guest cations to the armed crown (**1a**) caused an emission-intensity enhancement. The change is considered to result from the guest cation-dependent coordinated structure and the strength of coordination between nitrogen atoms and guest cations.

4. Conclusion

In conclusion, the PET armed-crown ethers (**1a**, **1b**) recognized guest cations and the fluores-

cence enhanced in the presence of these cations. The guest cation-induced emission-intensity enhancement originates from the affinity of the nitrogen atom in the armed crown ether for cations. The fluorescence of armed-crown ether (**2**, **3**) bonding through an ester or ether linkage to naphthalene were quenched with various guest thiocyanates. The fluorescence intensities quenching of the host itself occurs by photoinduced electron transfer from this counter anion to the naphthalene. These armed crown ether having naphthyl pendants may be utilized as a new fluorescent sensor for guest salts.

References

- [1] J.-M. Lehn (Ed.), *Supramolecular Chemistry*, VCH Verlagsgesellschaft mbH, Weinheim, 1995.
- [2] H.G. Löhr, F. Vögtle, *Acc. Chem. Res.* 18 (1985) 65.
- [3] L. Fabbrizzi, A. Poggi, *Chem. Soc. Rev.* 24 (1995) 197.
- [4] E. Kimura, T. Koike, *Chem. Soc. Rev.* 27 (1998) 179.
- [5] A.P. de Silva, S.A. de Silva, *J. Chem. Soc., Chem. Commun.* 23 (1986) 1709.
- [6] A.P. de Silva, H.Q.N. Gunaratne, T. Gunnlaugsson, C.P. McCoy, R.S. Maxwell, J.T. Rademacher, T.E. Rice, *Pure & Appl. Chem.* 48 (1996) 1443.
- [7] A.P. de Silva, H.Q.N. Gunaratne, T. Gunnlaugsson, A.J.M. Huxley, C.P. McCoy, J.T. Rademacher, T.E. Rice, *Chem. Rev.* 97 (1997) 1515.
- [8] K. Kubo, E. Yamamoto, T. Sakurai, *Heterocycles* 45 (1997) 1457.
- [9] K. Kubo, R. Ishige, N. Kato, E. Yamamoto, T. Sakurai, *Heterocycles* 45 (1997) 2365.
- [10] K. Kubo, N. Kato, T. Sakurai, *Bull. Chem. Soc. Jpn.* 70 (1997) 3041.
- [11] K. Kubo, R. Ishige, T. Sakurai, *Heterocycles* 48 (1998) 347.
- [12] K. Kubo, E. Yamamoto, T. Sakurai, *Heterocycles* 48 (1998) 1477.
- [13] K. Kubo, S. Sakaguchi, T. Sakurai, *Rep. Inst. Adv. Mat. Study, Kyushu Univ.* 12 (1998) 11.
- [14] K. Kubo, E. Yamamoto, T. Sakurai, *Heterocycles* 48 (1998) 2133.
- [15] K. Kubo, R. Ishige, J. Kubo, T. Sakurai, *Talanta* 48 (1999) 181.
- [16] K. Kubo, R. Ishige, T. Sakurai, *Talanta*. (In press).
- [17] K. Kubo, E. Yamamoto, T. Sakurai, *Rep. Inst. Adv. Mat. Study, Kyushu Univ.* 12 (1998) 137.
- [18] J.S. Bradshaw, K.E. Krakowiak, R.M. Izatt (Eds.), *Aza-Crown Macrocycles*, Wiley, New York, 1995.

- [19] G.W. Gokel, O.F. Schall (Eds.), *Comprehensive Supramolecular Chemistry*, vol. 1, Pergamon Press, Oxford, 1996.
- [20] H. Tsukube, *Coord. Chem. Rev.* 48 (1996) 1.
- [21] H. Tsukube, S. Shinoda, Y. Mizutani, M. Okano, K. Takagi, K. Hori, *Tetrahedron* 53 (1997) 3487.
- [22] K.A. Connors (Ed.), *Binding Constants*, John Wiley and Sons, New York, 1987.
- [23] H. Leonhardt, A. Weller, *Ber. Bunsen-Ges. Phys. Chem.* 67 (1963) 791.
- [24] R.S. Davidson, K.R. Trethewey, *J. Chem. Soc., Chem. Commun.* 20 (1976) 827.
- [25] R. Foster (Ed.), *Photophysical Aspects of Exciplexes Molecular Association*, Academic Press, London, 1979.
- [26] S. Iwata, K. Tanaka, *J. Chem. Soc., Chem. Commun.* 15 (1995) 1491.
- [27] S. Iwata, H. Matsuoka, K. Tanaka, *J. Chem. Soc., Perkin Trans. 1.* 16 (1997) 1357.
- [28] Computer calculations were performed with the CS Chem3D pro (ver. 3.5.1) program from Cambridge Soft Corporation.
- [29] R.J. Kurland, M.B. Rubin, W.B. Wise, *J. Chem. Phys.* 40 (1964) 2426.

Determination of gaseous acidic compounds by measuring fluorescence after their reaction with tetra-substituted amino aluminum phthalocyanine

Dong-Hui Li, Qiu-Ying Chen, Qing-Zhi Zhu, Fang Li, Hong Zheng,
Shi-Yao Yang, Jin-Gou Xu *

*The Research Laboratory of SEDC of Analytical Science for Material and Life Chemistry, Department of Chemistry,
Xiamen University, Xiamen 361005, China*

Received 2 July 1998; received in revised form 1 December 1998; accepted 4 February 1999

Abstract

Based on the fluorescence enhancement of a red-region fluorescent dye, tetrasubstituted amino aluminum phthalocyanine (TAAIPc), in strongly acidic medium, a new method was developed for the detection of four strong acids (HCl, HBr, HNO₃ and H₂SO₄). Under optimal conditions the linear ranges of the calibration curves were 0.04–0.67 mol/l (HCl), 0.04–0.67 mol/l (HBr), 0.04–0.80 mol/l (HNO₃) and 0.02–0.80 mol/l (H₂SO₄), respectively. The detection limits were 0.007 mol/l for HCl, 0.006 mol/l for HBr, 0.005 mol/l for HNO₃ and 0.007 mol/l H₂SO₄. This method has been applied to the analyses of four artificial samples with satisfactory results. © 1999 Published by Elsevier Science B.V. All rights reserved.

Keywords: pH; Strong acid; Phthalocyanine; Near-infrared; Detection

1. Introduction

The determination of pH or acidity of a solution has been very important throughout all phases of chemistry and biochemistry. Many new methods have been developed and a variety of reagents have been applied for the determination of pH in recent years [1–4]. Although a wide range of pH can be determined by various methods, the measurement of pH at extreme values is

still a problem [5]. Efforts have been made for the purpose of resolving such a difficulty lately [6–8]. Methods based on the absorption spectroscopy or fluorescence spectroscopy principles have been investigated for the determination of strong acid such as the detection of hydrogen chloride gas [9,10]. A new trend in this area is the application of dyes with absorption or fluorescence bands in red or near-infrared region, for example, the cyanine [11] and phthalocyanine [12] compounds.

Phthalocyanine and its derivatives are widely used in many areas such as photodynamic treatment of tumor (PDT) [13], the investigation of

* Corresponding author. Fax: +86-592-218-8054.
E-mail address: jgxu@xmu.edu.cn (J.-G. Xu)

solar energy transfer [14], and fluorimetric immunoassay (FLIA) [15] because of their chemical, optical and thermal stability and high fluorescence quantum yield. Recently, two phthalocyanine dyes have been employed in the detection of acids based on their absorbance variation in near-red spectral region caused after exposure to hydrogen chloride or acetic acid atmosphere [12].

A novel method for the determination of strong acids by using tetra-amino aluminum phthalocyanine as the probe is described in this article. The fluorescence of the probe was obviously enhanced when strong acids were added and the relative fluorescence intensity of the probe increased in logarithmic form with the increase of the concentration of strong acid. To our knowledge, similar investigations have not been reported previously.

2. Experimental

2.1. Apparatus

A Hitachi Model 650-10S fluorescence spectrophotometer equipped with a xenon lamp, dual monochromators, a 1×1 cm quartz cell and a functional recorder was employed. The slit-width for both of the excitation and emission was set at 5 nm.

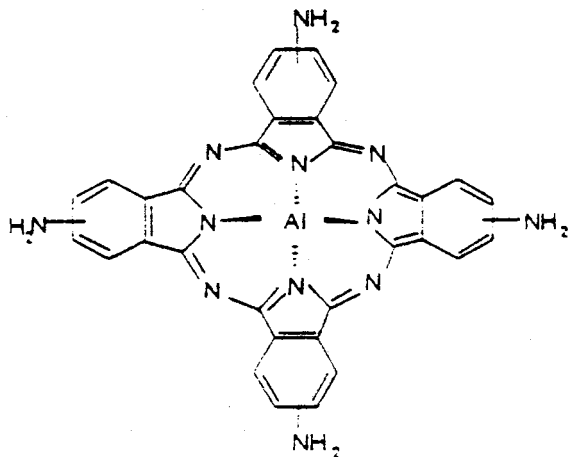


Fig. 1. Molecular structure of TAAIPc.

2.2. Reagents

The fluorescent probe, 4, 4', 4'', 4'''-tetra amino aluminum phthalocyanine (named in short as TAAIPc in the following) was synthesized and purified according to the method reported formerly [10]. Stock solution of TAAIPc (1.0×10^{-3} mol/l) was prepared by dissolving solid TAAIPc in redistilled dimethyl formamide. Stock solutions of four kinds of strong acids were prepared by diluting the concentrated acids with double-deionized water, followed by titration using standard NaOH solution which had been titrated by potassium biphthalate, affirming that the concentrations of HCl, HBr, HNO₃, and H₂SO₄ are 2.0, 2.0, 2.0, and 1.0 mol/l, respectively.

All of the chemicals were of analytical grade and were used directly without further purification. Double-deionized water was used throughout.

2.3. Method

To a 10-ml volumetric flask a certain volume (e.g. 0.2 ml) of 1.0×10^{-4} mol/l TAAIPc solution was added, followed by adding the strong acid to be tested, and the mixture was diluted to 10.0 ml with double-deionized water. Then the relative fluorescence intensity of the solution was measured at the excitation wavelength of 370 nm and the emission wavelength of 678 nm.

3. Results and discussion

3.1. Structure and spectral characteristic of TAAIPc

The structure of TAAIPc is given in Fig. 1. The ring of phthalocyanine is substituted with four amino groups. The addition of peripheral groups greatly increases the solubility of the phthalocyanine moiety because the symmetry of phthalocyanine ring is reduced and thus the aggregation decreases [16]. So, the stock solution of TAAIPc could be prepared at a concentration of 1.0×10^{-3} mol/l. With the addition of HCl, the absorption spectrum of TAAIPc changed obviously (Fig. 2),

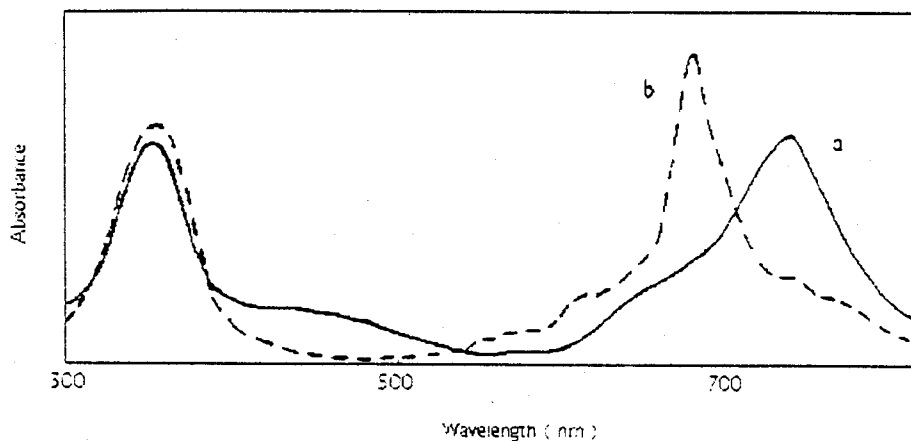


Fig. 2. Absorption spectra of TAAIPc in (a) water and (b) 0.40 mol/l HCl. [TAAIPc] = 6.0×10^{-6} mol/l.

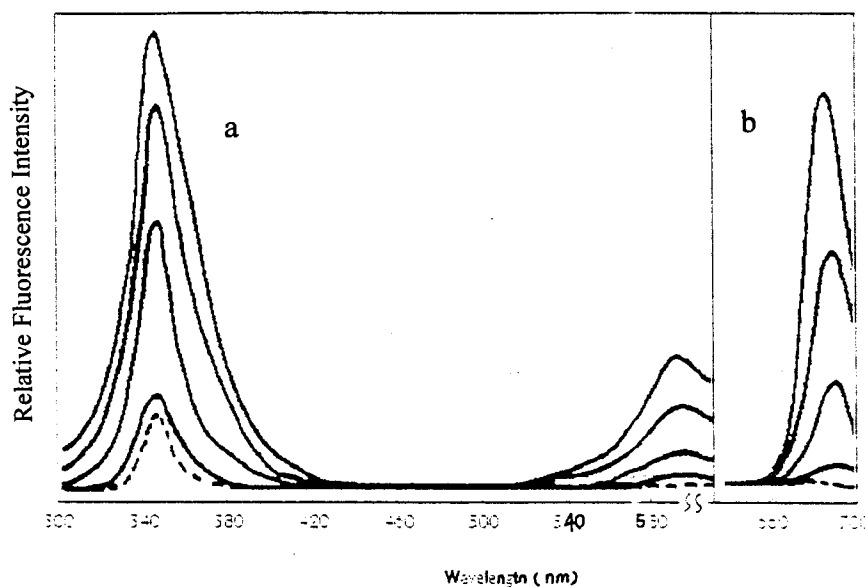


Fig. 3. Excitation and emission spectra. Excitation spectra (a) Emission spectra (b) dotted curves: obtained in water medium. Solid curves: obtained in hydrochloric acid (0.2 mol/l) medium.

the absorption peak at long-wavelength region (Q band) was blue-shifted for about 60 nm. It could be seen that a broaden peak between 350 and 500 nm existed in the absorption spectrum of TAAIPc, which was a result of the intramolecular charge transfer induced by the amino groups, but disappeared when HCl was added. These phenomena which agreed with those reported in literatures [16,17] can be explained by the proto-

nation of amino groups on the phthalocyanine ring when they were in strong acidic environment.

The excitation and emission spectra of TAAIPc in water and strong acidic media were given in Fig. 3. The spectra show that TAAIPc is almost non-fluorescent in neutral medium, but fluorescent in strongly acidic medium.

This reveals that TAAIPc is sensitive to the high acidity of environment. The phenomenon agrees

with the previous report that electron withdrawing groups are benefit to the fluorescence of phthalocyanine, but electron donating groups are opposite [18]. When a strong acid was added to the aqueous solution of TAAIPc, the amino groups changed to $-\text{NH}_3^+$, an electron withdrawing group, thus the fluorescence of TAAIPc was enhanced. It was found in the experiments that the fluorescence emission peak of TAAIPc was at 678 nm in strongly acidic medium and two excitation peaks occurred, one at short-wavelength region (Soret band), another at long-wavelength region (Q band). It is clear from Fig. 3 that the excitation at Soret band is more sensitive than that at Q band. Therefore, the excitation at short-wavelength region was chosen. It should be pointed out that in order to avoid the interference of secondary scattered light, the excitation wavelength was chosen not at the peak position but at 370 nm.

It should be noted that the small peak appearing at short-wavelength region (340 nm) in the condition without the addition of acid is caused by the scattering light.

3.2. Relationship between the concentration of strong acid and the fluorescence of TAAIPc

The relative fluorescence intensity of TAAIPc

increases in logarithmic form with increasing the concentration of hydrochloric acid (Fig. 4). When making a logarithmic conversion of the concentration, a straight line is obtained (Fig. 5).

3.3. Effects of different strong acids on the fluorescence of TAAIPc

The changes of the fluorescence intensity of TAAIPc with the concentration of different kinds of strong acids are shown in Fig. 4. It can be seen from Fig. 4 that the curves of HCl, HBr and HNO_3 are almost overlapping with a somewhat deviation of H_2SO_4 , which may be explained by its dibasic character and its incomplete second dissociation. The results imply that TAAIPc may be used as a new fluorescent probe for the acidity determination of strongly acidic medium containing monobasic strong acids usually encountered.

3.4. Effect of TAAIPc concentration on the linear range of calibration curves

The experimental results about the effect of TAAIPc concentration on the linear range of working curves are shown in Table 1. It can be seen from the table that when the concentration of TAAIPc is 6.0×10^{-6} mol/l, a working curve

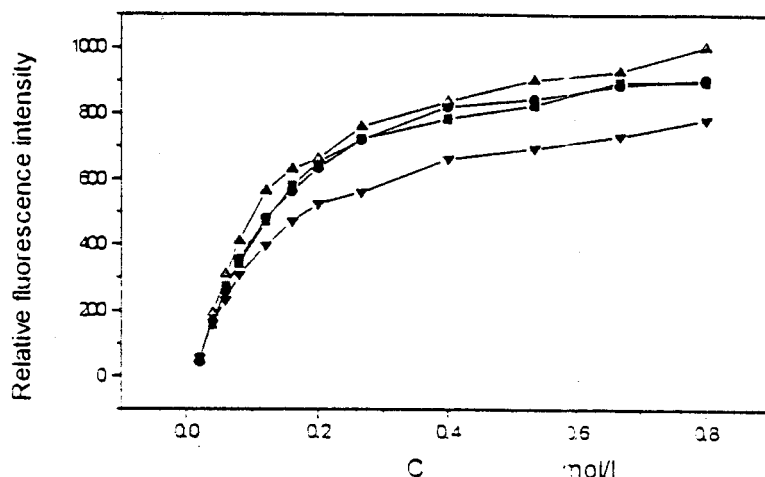


Fig. 4. Effects of concentration of different acids on the relative fluorescence: ■ HCl; ● HBr; ▲ HNO_3 ; ▼ H_2SO_4 ; The excitation and emission wavelengths for constructing these curves were 370 and 678 nm, respectively.

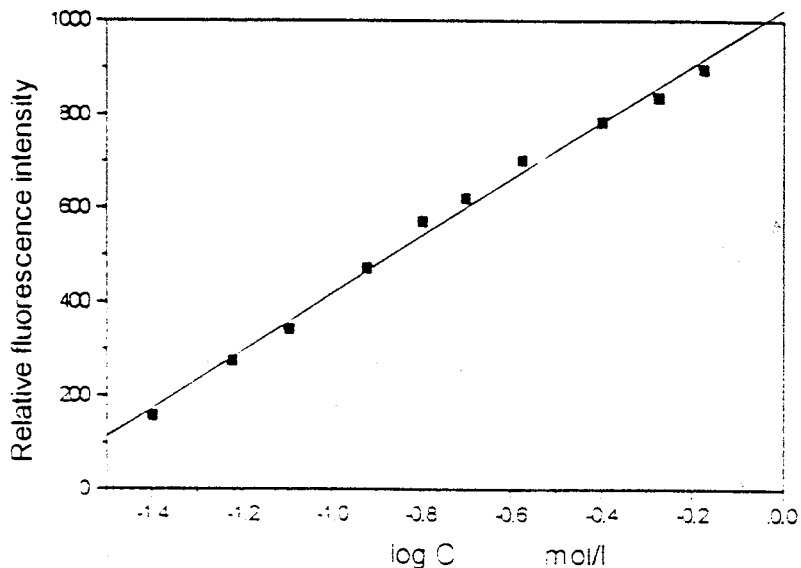


Fig. 5. The calibration curve of HCl.

with the largest dynamic range is obtained. So, in our experiments, the concentration of TAAIPc was fixed at 6.0×10^{-6} mol/l when constructing the standard curves of acids.

3.5. Interference of weak acids

Four kinds of weak acids (acetic acid, ethanedioic acid, citric acid and phosphoric acid) used as the interfering components were investigated. It was found that even 100 times of acetic acid (molecular ratio of acetic acid to strong acid determined) did not disturb the determination. But the tolerance of ethanedioic acid and citric acid was only one-fold, the interference of phosphoric acid was even more serious. This may be due to their larger first dissociation constants.

3.6. Calibration curves and the determination of artificial samples

The calibration curves for HCl, HBr, HNO_3 and H_2SO_4 are given in Table 2. To simulate the circumstances usually encountered in practice, four kinds of gases, such as HCl, HBr, NO_2 and SO_3 , were prepared and dissolved in double-deionized water, and then determined by this method. The results are listed in Table 3.

The results indicate that this method is accurate and reproducible, and it has the potential in applying to the detection of waste gases let out from industries. We also think it is possible for TAAIPc to be used as chemical sensor, this work is under consideration.

4. Conclusions

Tetrasubstituted aminophthalocyanine(-TAAIPc) was investigated as a new red-region fluorescent probe for the detection of strong acids. It was found that the relative fluorescence intensity of TAAIPc was proportional to the logarithm

Table 1
Effect of TAAIPc concentration on the linear range of calibration curve

Concentration of TAAIPc	Linear range (mol/l) ($\times 10^{-6}$ mol/l)
2.0	0.04–0.533
4.0	0.04–0.533
6.0	0.04–0.667
8.0	0.04–0.533
10.0	0.04–0.40

Table 2
Characteristic parameters of calibration curves

Strong acids	Linear range (mol/l)	Linear regression equation	Limit of detection	<i>r</i>
HCl	0.04–0.67	$F = 1052 + 633 \log C$	0.0069	0.9978
HBr	0.04–0.67	$F = 1062 + 640 \log C$	0.0065	0.9968
HNO ₃	0.04–0.80	$F = 1073 + 604 \log C$	0.0052	0.9940
H ₂ SO ₄	0.02–0.80	$F = 833 + 472 \log C$	0.0074	0.9978

Table 3
Determination results of artificial samples

Samples	Mean concentration found (mol/l, <i>n</i> = 6)	Recoveries (% , <i>n</i> = 6)	RSD (%)	Taken values of acids ^a (mol/l)
HCl	0.0951	102.2–107.2	3.8	0.098
HBr	0.180	100.6–104.5	3.3	0.187
HNO ₃	0.158	101.6–107.4	1.6	0.151
H ₂ SO ₄	0.116	103.3–106.6	3.8	0.124

^a Obtained by NaOH titration.

mic value of the concentration of strong acid. Four kinds of strongly acidic gases were prepared and detected by this method with satisfactory results.

Acknowledgements

This work is supported by the National Natural Science Foundation of China (NNSFC, No. 29775021), all the authors wish to make a grateful acknowledgment.

References

- [1] H. Hismato, M. Tsububu, T. Enomoto, et al., *Anal. Chem.* 68 (1996) 3871.
- [2] A. Talaie, *Polymer* 38 (1997) 1145.
- [3] K.I. Mullen, D.X. Wang, L.G. Cane, K.T. Carron, *Anal. Chem.* 64 (1992) 930.
- [4] Y. Cros, N. Jafferezicrenault, J.M. Chvelon, *J. Electrochem. Soc.* 139 (1992) 507.
- [5] C.N. Konodari, C.G. Nanos, M.I. Karayannis, *Analyst* 118 (1993) 711.
- [6] E.W. Baumann, *Talanta* 42 (1995) 457.
- [7] L.R. Allain, K. Sorasaene, Z.L. Xue, *Anal. Chem.* 69 (1997) 3076.
- [8] G.J. Mohr, O.S. Wolfbeis, *Anal. Chim. Acta* 292 (1994) 41.
- [9] N. Nakano, A. Yamamoto, Y. Kobayashi, Nagashina, *Analyst* 118 (1993) 1539.
- [10] N. Nakano, H. Yake, K. Nagashima, M. Kamaga, *Bunseki Kagaku* 44 (1995) 151.
- [11] Jyh-Myng, G. Patonay, *Anal. Chem.* 63 (1991) 2934.
- [12] L.E. Norena-Franco, F. Kvasnik, *Analyst* 121 (1996) 1115.
- [13] I. Rosenthal, *Photochem. Photobiol.* 53 (1991) 859.
- [14] K. Kuninobu, *Coordination Chem. Rev.* 32 (1980) 67.
- [15] R.F. Devlin, W.B. Dandliker, M.L. Hsu, U.S. patent application 856176, 1992.
- [16] J.B. Liu, F.Q. Zhao, Y. Zhao, et al., *Acta Physico-Chim. Sinica* 12 (1996) 491.
- [17] X.F. Zhang, H.J. Xu, *Chem. J. Chin. Univ.* 15 (1994) 917.
- [18] C. Ye, *Chin. J. Appl. Chem.* 8 (1991) 14.

DNA-modified electrodes; part 4: optimization of covalent immobilization of DNA on self-assembled monolayers

Yuan-Di Zhao ^a, Dai-Wen Pang ^{a,*}, Shen Hu ^a, Zong-Li Wang ^a,
Jie-Ke Cheng ^a, Hong-Ping Dai ^b

^a Department of Chemistry, Wuhan University, Wuhan 430072, PR China

^b State Key Laboratory for Physical Chemistry of Solid Surfaces, Institute of Physical Chemistry, Department of Chemistry, Xiamen University, Xiamen 361005, PR China

Received 5 October 1998; received in revised form 2 February 1999; accepted 4 February 1999

Abstract

The covalent immobilization of DNA onto self-assembled monolayer (SAM) modified gold electrodes (SAM/Au) was studied by X-ray photoelectron spectrometry and electrochemical method so as to optimize its covalent immobilization on SAMs. Three types of SAMs with hydroxyl, amino, and carboxyl terminal groups, respectively, were examined. Results obtained by both X-ray photoelectron spectrometry and cyclic voltammetry show that the largest covalent immobilization amount of dsDNA could be gained on hydroxyl-terminated SAM/Au. The ratio of amount of dsDNA immobilized on hydroxyl-terminated SAMs to that on carboxyl-terminated SAMs and to that on amino-terminated SAMs is (3–3.5): (1–1.5): 1. The dsDNA immobilized covalently on hydroxyl-terminated SAMs accounts for 82.8–87.6% of its total surface amount (including small amount of dsDNA adsorbed). So the hydroxyl-terminated SAM is a good substrate for the covalent immobilization of dsDNA on gold surfaces. © 1999 Elsevier Science B.V. All rights reserved.

Keywords: DNA-modified electrodes; Covalent immobilization; Self-assembled monolayers; Modified gold electrodes

DNA-modified electrodes are crucially important for developing electrochemical DNA biosensors [1,2] and studying the interactions of DNA with other molecules [3–6], which are highlighted recently. Some different methods for immobilizing DNA onto electrode surfaces have been appear-

ing. Controlled-potential adsorption method was adopted by Wang [7] to anchor DNA to carbon paste electrodes. Herne et al. [8] synthesized DNA fragments modified with a mercapto group by the use of a DNA synthesizer and then immobilized DNA onto gold electrode surfaces through self-assembly of the mercapto-modified DNA. They found that hybridization of surface-bound HS-ss-DNA depends on surface coverage, which is af-

* Corresponding author. Fax: +86-27-87882661.

E-mail address: dwpang@whu.edu.cn (D.-W. Pang)

fect by the concentration of buffer solutions. More precise control over surface coverage was achieved by creating mixed monolayers of HS-ss-DNA and a spacer thiol to largely remove non-specifically adsorbed DNA. A simple method for preparing DNA-modified gold and glass carbon electrodes by adsorption–drying of DNA solution was developed by our research group [9]. The above methods are of their features, but also of shortages. In general, the preparation of DNA-modified electrodes by adsorption is simple and only small amounts of DNA samples are required. The modified electrodes obtained are suitable for the study of the interactions between DNA and other molecules [6], but they cannot be used for DNA biosensors. In view of keeping fully biological activities of DNA, including its function of hybridization and bio-affinity, the most perfect method for DNA immobilization on electrodes should be covalent coupling method, by which DNA strands are anchored with either of its terminals and dangled from the surfaces. However, it is inconvenient to use the method for preparing DNA-modified electrodes by self-assembly of mercapto-modified DNA because the yields of synthesis of mercapto-containing DNA is quite low. Thus the method is tedious, time-consuming and costly. So, it is of significance to explore new methods for preparing DNA-modified electrodes and screen them by characterizing the electrodes.

Reported here is the covalent immobilization of double-stranded DNA (dsDNA) onto gold surfaces through layer-by-layer self-assembly. That is, self-assembled monolayers (SAMs) of thiols formed first on gold surfaces, and then the condensation reaction between 5'-phosphate end or 3'-hydroxy end of DNA and the terminal group of SAMs resulted in the immobilization of DNA on the surfaces. It is predictable that the difference in the terminal groups of SAMs would lead to different amounts of DNA covalently immobilized on SAMs. The influence of different terminal groups of SAMs on the covalent immobilization of DNA on gold was investigated by X-ray photoelectron spectrometry (XPS) and cyclic voltammetry (CV). The results will be helpful for the study of the covalent attachment of DNA to electrodes.

1. Experimental section

1.1. Reagents

Calf thymus DNA, obtained from Sino-American Biotechnical Company, was purified as described elsewhere [2] to reach a high purity (OD_{260}/OD_{280} was larger than 1.8, where OD represents the optical density). Three ethylene-containing thiols, 2-mercaptoethanol (GIBCO), 2-mercaptoethamine (Sigma), and 3-mercapto-propionic acid (Fluca) were used as received. Tris(2,2'-bipyridyl)cobalt(III) perchlorate [$Co(bpy)_3(ClO_4)_3$] was prepared from cobalt(II) chloride, hydrogen peroxide, perchloric acid, and 2,2'-bipyridyl (bpy) [10]. Other chemicals were of analytical reagent grade. Water used was doubly distilled and sterilized.

1.2. Immobilization of double-stranded DNA on self-assembled monolayers on gold electrodes

A gold electrode (1.25 cm²) was heated in boiling concentrated HNO₃ for 5 min followed by rinsing with water and then sonicating in water for 3 min. The electrode was voltammetrically cycled and characterized in 1 M H₂SO₄ until a stable cyclic voltammogram was obtained. The freshly-pretreated electrode was rinsed with water and then immersed in a 40 μM thiol solution for 6 h. Then the electrode was washed thoroughly with water. Thus a SAM-modified gold electrode (SAM/Au) was obtained. The SAM/Au was reacted with 1 mg ml⁻¹ dsDNA in the presence of 1 mg ml⁻¹ 1-ethyl-3-(3-dimethylaminopropyl) carbodiimide hydrochloride (EDAC) in a 40 mM 2-[N-morpholino]ethanesulfonic acid (MES) buffer (pH 6.5) for 24 h, and then washed with MES buffer. Thus a SAM/Au modified with dsDNA was obtained. It is denoted as dsDNA-SAM/Au throughout.

A SAM/Au electrode for control experiments was prepared as mentioned above for the dsDNA-SAM/Au except no EDAC in MES buffer.

1.3. CV measurements

A three-electrode cell was used in the measurements, with a bare gold electrode or SAM/Au or

dsDNA-SAM/Au as the working electrode, a saturated calomel reference electrode (SCE) immersed in the electrolyte through a Luggin capillary situated at the working electrode and a platinum wire counter electrode. Voltammograms were recorded using MCEC-II Electrochemistry and Electroanalysis System (Xiamen University). Experiments were conducted at 25°C. All reported potentials are against the SCE.

1.4. XPS experiments

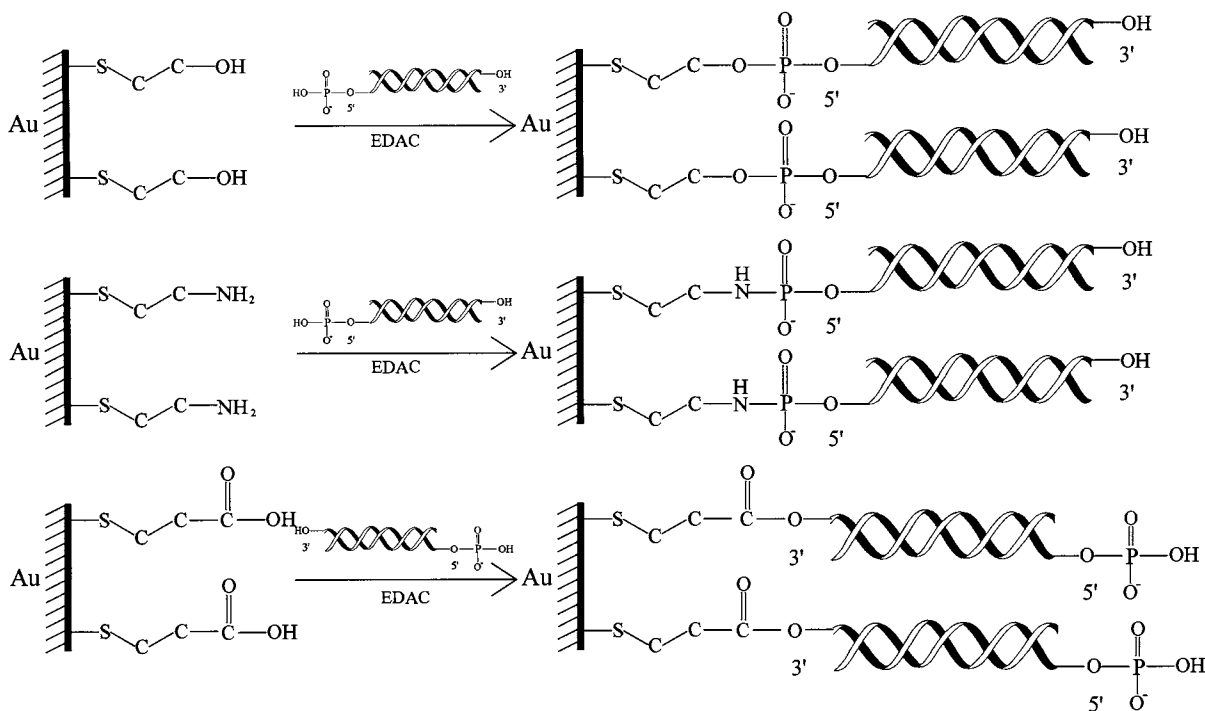
The dsDNA-SAM/Au and SAM/Au for control experiments were dried after washed with water, and transferred into a chamber for XPS immediately. The XPS spectra were recorded on a VG ESCA-LAB MKII spectrometer using Mg radiation. The data were acquired and processed by XPS-AES sampling/processing program (Version 5.0, Tsinghua University). The radiation gun was operated at 10 kV and 20 mA; and the

electron multiplier voltage was set at 2.9 kV; 20 scans were used. The PE mode was set for the analyzer.

2. Results and discussion

2.1. Electrochemical characterization of dsDNA-SAM/Au prepared from SAMs with different terminal groups

To optimize the covalent immobilization of dsDNA on SAMs, three ethylene-containing thiols, 2-mercaptoethanol, 2-mercaptoethamine, and 3-mercaptopropionic acid, whose terminal groups are respectively hydroxyl, amino and carboxyl, were used to prepare different SAMs with different terminal groups. Hydroxyl and amino groups can react with 5'-phosphate end of DNA, and carboxyl group with 3'-hydroxy end of DNA.



Scheme 1. Illustrative presentation of the covalent immobilization of dsDNA on SAMs with different terminal groups.

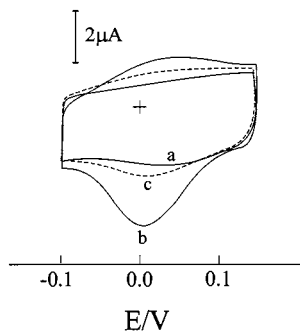


Fig. 1. Cyclic voltammograms of $10 \mu\text{M Co}(\text{bpy})_3^{3+}$ in 5 mM Tris (pH 7.1) containing 5 mM NaCl at a (a) hydroxyl-terminated SAM/Au, (b) hydroxyl-terminated SAM/Au treated with EDAC and dsDNA, and (c) control experiment electrode. Scan rate: 100 mV s^{-1} .

The covalent immobilization of dsDNA on SAM/Au surfaces is illustrated in Scheme 1. The dsDNA was covalently immobilized onto SAM/Au via phosphate ester, phosphoramidate and carboxylate ester linkages, respectively.

$\text{Co}(\text{bpy})_3^{3+}$ was used to characterize dsDNA-SAM/Au due to its strong interaction with dsDNA at low ionic strength [1,11]. Fig. 1a is the CV curve of $10 \mu\text{M Co}(\text{bpy})_3^{3+}$ at a hydroxyl-terminated SAM/Au, a pair of redox peaks appearing at a formal potential (E°) value of 82 mV . Fig. 1b shows the CV curve of $10 \mu\text{M Co}(\text{bpy})_3^{3+}$ obtained at a hydroxyl-terminated SAM/Au treated with EDAC and dsDNA. It can be seen that the cathodic peak current increased notably, and the E° shifted from 82 mV negatively to 20 mV , indicating that dsDNA has been immobilized on the SAM/Au. The increased current and negative shift in E° resulted from the electrostatic interaction of dsDNA immobilized on the SAM/Au with $\text{Co}(\text{bpy})_3^{3+}$ [6]. Fig. 1c obtained at the control experiment electrode in the same solution shows that the cathodic peak current slightly increased compared with that in Fig. 1a and the E° shifted to 27 mV , which resulted from a small amount of dsDNA adsorbed because there is only dsDNA adsorbed possibly on the SAM/Au surface for control experiments.

From the above results, it can be concluded that dsDNA is able to be covalently immobilized on hydroxyl-terminated SAM/Au surfaces under

the activation of EDAC to obtain dsDNA-SAM/Au, at the same time, only a small amount of dsDNA is adsorbed onto the surfaces. The surface concentration (Γ) of $\text{Co}(\text{bpy})_3^{3+}$ preconcentrated on the SAM/Au surface can be calculated from the integrated charge of its CV peaks before and after modification of the SAM/Au with dsDNA. The surface concentration of $\text{Co}(\text{bpy})_3^{3+}$ estimated from Fig. 1b is $(1.55 \pm 0.15) \times 10^{-11} \text{ mol cm}^2$, and Γ at the control experiment electrode is $(2.66 \pm 0.28) \times 10^{-12} \text{ mol cm}^{-2}$. Because the surface concentration of $\text{Co}(\text{bpy})_3^{3+}$ preconcentrated at a SAM/Au depends directly on the amount of dsDNA immobilized on the surface, the relative amounts of dsDNA immobilized at different SAM/Au electrodes can be evaluated from the surface concentration of $\text{Co}(\text{bpy})_3^{3+}$. In the case of Fig. 1b, the dsDNA on the electrode surface was dominantly immobilized through covalent bonds besides a small amount of adsorbed dsDNA. Assuming that in this case the adsorbance of dsDNA is close to that on the control experiment electrode, on which only adsorbed dsDNA exists, then the covalently immobilized dsDNA are estimated to account for 82.8% of total amount of dsDNA on the hydroxyl-terminated SAM/Au.

Accordingly, the covalent immobilization of dsDNA on amino-terminated and carboxyl-terminated SAM/Au surfaces was examined. Table 1 presents the results obtained on these SAMs. Amino groups can be protonized, the negatively-charged DNA should be easy to adsorb on the amino-terminated SAM/Au surface, and the condensation reaction would be hard to take place. So the amount of covalently immobilized dsDNA will be small. As was indeed observed, only 23.1% of the total amount of dsDNA on amino-terminated SAM/Au was immobilized through covalent bonds. On carboxyl-terminated SAM/Au surfaces, although the covalently immobilized dsDNA reached up to 92.2% of the total amount of dsDNA, in fact, the total amount itself is small. So the amount of covalently immobilized dsDNA is only as large as 1/3 of that on the hydroxyl-terminated SAM/Au surfaces. The reason for this is that the negatively-charged SAM/Au surface resulting from the disassociation of carboxyl group

will electrostatically repel negatively-charged dsDNA, so that dsDNA is difficult to approach carboxyl-terminated SAM/Au surface and react with the carboxylate group, even hard to adsorb on the surface.

2.2. XPS characterization of dsDNA-SAM/Au prepared from SAMs with different terminal groups

Phosphorus element, P, is the best evidence for the existence of DNA, so it can be used as an indicator for the immobilization of DNA on SAM/Au. Fig. 2 shows the XPS spectra of P obtained under different conditions. Fig. 2(1) is the P2p spectra of a hydroxyl-terminated SAM/Au (curve a) after treated with EDAC and dsDNA, and a hydroxyl-terminated SAM/Au for control experiments (curve b). It is clear that there is plenty of P on the dsDNA-SAM/Au surface, but there is little P in the case of the slight adsorption of DNA on the SAM/Au surface. From the peak intensities obtained under these conditions, the amount of P, corresponding to the amount of dsDNA on surfaces, can be calculated. As shown in Table 1, 87.6% of dsDNA was covalently immobilized on the hydroxyl-terminated SAM/Au, which is quite close to that obtained by CV.

The P2p spectra of an amino-terminated and a carboxyl-terminated SAM modified covalently

with dsDNA are presented in Fig. 2(2a) and Fig. 2(3a), respectively. Curve b in Figs. 2(2) and 2(3) is for the SAMs for control experiments. Similarly, the relative amounts of the dsDNA covalently immobilized on the dsDNA-SAM/Au surfaces can be estimated. The results are listed in Table 1.

As shown in Table 1, the relative amount of the dsDNA covalently immobilized on the hydroxyl-terminated SAM/Au is the largest of all the three SAMs, accounting for 82.8–87.6% of the total amount of dsDNA on the surface. And the amino-terminated SAM is poor for covalent immobilization of dsDNA. The amount ratio of the covalently immobilized dsDNA on the three dsDNA-SAM/Au surfaces is (3–3.5):1:(1–1.5). In the meantime, the amount ratio of adsorbed dsDNA is (5–5.6):30:1, which is consistent with the order of electric positivity of the SAM surfaces. Covalent immobilization of dsDNA is the prerequisite for DNA-modified electrodes to be used as electrochemical DNA biosensors. It is being expected that DNA is covalently immobilized on electrode surfaces as much as possible, while DNA is adsorbed in an amount as small as possible. To sum up, the hydroxyl-terminated SAM is a good substrate for the covalent immobilization of dsDNA on gold surfaces.

Comparing the data in Table 1, it can be seen that the results obtained by CV are quite consis-

Table 1
Comparison of covalent immobilization of dsDNA on the SAMs with different terminal groups^{a,b,c}

		HOCH ₂ CH ₂ S/Au	H ₂ NCH ₂ CH ₂ S/Au	HOOCCH ₂ CH ₂ S/Au
A ₁ : A ₂	CV	5.8:1	1.3:1	12.8:1
	XPS	8.1:1	1.4:1	15:1
(A _c /A ₁) × 100%	CV	82.8%	23.1%	92.2%
	XPS	87.6%	28.8%	93.1%
A _c :A _c :A _c	CV	3.5	1	1.5
	XPS	3	1	1
A ₂ :A ₂ :A ₂	CV	5.6	29.5	1
	XPS	5	30	1

^a A₁, data obtained from CV or XPS corresponding to the total amount of dsDNA on a dsDNA-SAM/Au.

^b A₂, data obtained from CV or XPS corresponding to the amount of adsorbed dsDNA on a SAM/Au for control experiments.

^c A_c = A₁ – A₂, corresponding to the amount of covalently immobilized dsDNA.

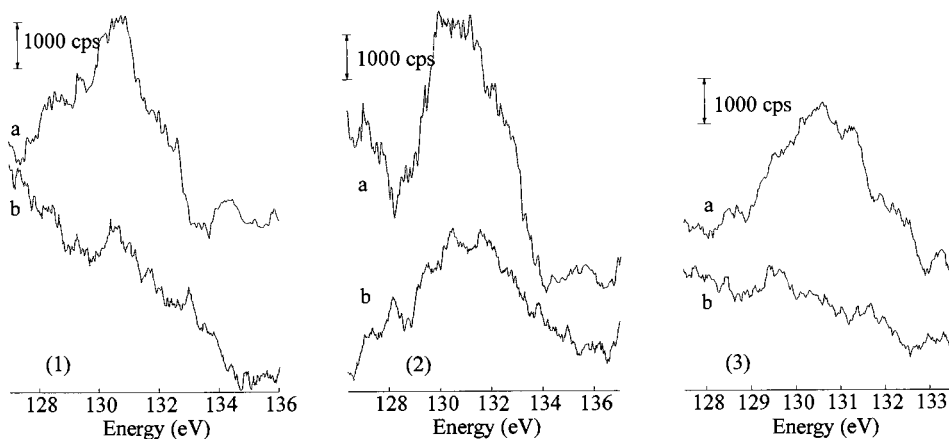


Fig. 2. P2p XPS spectra of a hydroxyl-terminated SAM/Au (1), amino-terminated SAM/Au (2), and carboxyl-terminated SAM/Au (3). Curve a: dsDNA-SAM/Au; curve b: control experiment electrode.

tent with those by XPS. This provides a possibility to use simple CV method to evaluate the amount of dsDNA immobilized on SAM/Au surfaces, which was determined by XPS technique in the past. This will facilitate the study of DNA-modified electrodes.

Acknowledgements

This work was supported by the National Natural Science Foundation of China (Grant Nos. 39370213; 39770220; 29773034), Ministry of Education, the Natural Science Foundation of Hubei Province (China) (Grant No. 96J037) and the State Key Laboratory for Physical Chemistry of Solid Surfaces (Xiamen University). The authors also wish to thank Professor Zhong-Hua Lin, Professor Zhong-Qun Tian, Professor Bing-Wei Mao, Professor Shui-Jiu Wang and Cai-Hui Shi for their kind help.

References

- [1] K.M. Millan, A.J. Spurmanis, S.R. Mikkelsen, *Electroanalysis* 4 (1992) 929.
- [2] D.W. Pang, Y.P. Qi, Z.L. Wang, J.K. Cheng, J.W. Wang, in: E.B. Feng, (Ed.) *Proceedings First China Postdoctoral Academic Congress*, vol. II, National Defense Industry Press, Beijing, 1993, p. 1654.
- [3] D.W. Pang, Y.P. Qi, Q.S. Du, Z.L. Wang, J.K. Cheng, M. Zhang, *Kexue Tongbao* 39 (1994) 1605.
- [4] Y.D. Zhao, D.W. Pang, Z.L. Wang, J.K. Cheng, Y.P. Qi, *J. Electroanal. Chem.* 431 (1997) 203.
- [5] Y.D. Zhao, D.W. Pang, Z.L. Wang, J.K. Cheng, Z.F. Luo, C.J. Feng, H.Y. Shen, X.C. Zhang, *Acta Chim. Sinica* 56 (1998) 178.
- [6] D.W. Pang, H.D. Abruna, *Anal. Chem.* 70 (1998) 3162.
- [7] J. Wang, M. Chicharro, G. Rivas, X. Cai, N. Dontha, P.A.M. Farias, H. Shirashi, *Anal. Chem.* 68 (1996) 2251.
- [8] T.M. Herne, M.J. Tarlov, *J. Am. Chem. Soc.* 119 (1997) 8916.
- [9] D.W. Pang, M. Zhang, Z.L. Wang, Y.P. Qi, J.K. Cheng, Z.Y. Liu, *J. Electroanal. Chem.* 403 (1996) 183.
- [10] F.H. Burstall, R.S. Nyholm, *J. Chem. Soc.* (1952) 3570.
- [11] M.T. Carter, M. Rodriguez, A.J. Bard, *J. Am. Chem. Soc.* 111 (1989) 8901.

Transport of organic dyes through ether-type polyurethane membrane

Kathy Rzeszutek, Art Chow *

Department of Chemistry, University of Manitoba, Winnipeg, MB, Canada R3T 2N2

Received 27 October 1998; received in revised form 2 February 1999; accepted 4 February 1999

Abstract

Transport of various anthraquinone, acidic and basic dyes in aqueous solution through ether-type polyurethane membrane has been studied to better define the factors affecting the removal of organic compounds by the polyurethane membrane and to complement the previously proposed sorption mechanism. The effects of pH, salts, dye geometry and size, initial dye concentration, thickness of the membrane, and solution temperature on the rate of transport were investigated. Transport was found to be dependent upon the pH conditions of the starting and the receiving solutions. An increased rate of transport was observed with increased solution temperature and with the use of a thinner polyurethane membrane. The differences in the rates of transport can be attributed to the relative solubility of the organic dyes in the membrane and in solution, and to the strength and extent of intermolecular interactions with the polymer. Dye concentration, geometry and size, and the presence of salts in solution had no significant effect on the rate of transport. All of the studied dyes were found to exist as neutral species in the membrane. © 1999 Elsevier Science B.V. All rights reserved.

Keywords: Organic dyes; Ether-type polyurethane membrane; Non-porous membrane transport

1. Introduction

Due to more rigorous government regulations for the disposal of waste effluents and the increased environmental awareness of the public, the manufacturers and industrial consumers of organic compounds have been forced to strictly monitor their wastewater for the presence of organic chemicals. As a result, more focus has been placed on the development of advanced waste

purification techniques for the removal of organic compounds from industrial effluents. Currently, the most extensively employed purification procedure is adsorption of organic pollutants on activated carbon [1]. Unfortunately, this process alone is neither very efficient nor economical [1]. Because adsorption takes place from an aqueous solution, the organic species which are polar and soluble in water are not efficiently removed by the relatively non-polar carbon; water-insoluble non-polar compounds tend to form colloidal dispersions from which migration and adsorption on the carbon surface are also not very effective [1].

* Corresponding author. Fax: +1-204-4747608.

E-mail address: achow@cc.umanitoba.ca (A. Chow)

Current industrial wastewater purification operations are a combination of physical, chemical and/or biological degradation procedures which are applied prior to exposure of the effluent to carbon. However, this entire process is quite expensive and time-consuming because of the many steps involved [1].

In the last few years, applications of membrane separations to organic pollution control have been extensively researched [2–14]. Membrane separation is a relatively new type of separation process which is predicted, ultimately, to replace a majority of the conventional separation systems. At present, there is little interest in using biological membranes for this purpose. On the other hand, the possibility of separations with various synthetic polymeric membranes is highly appealing because no conventional single step purification treatment offers the same potential and versatility as those of synthetic membranes. In membrane processes, the separation is achieved via a membrane which acts as a barrier between two homogeneous phases and as a sorbing medium. The separation is governed by both the chemical and the physical nature of the membrane material and it occurs because of differences in shape, size, chemical properties, or charge of the species to be separated [2–14]. Transport through the membrane can be achieved when a driving force such as a pressure or concentration difference, for example, is applied or created during adsorption. Membrane technology is already being used to some extent in many industrial areas such as food and beverage, metallurgy, pulp and paper, textile, pharmaceutical, automotive, dairy, biotechnological and chemical industries. The membrane processes have become particularly important in water treatment for industrial and domestic water where membrane technology can be applied in cleaning operations [2–14]. For instance, in textile plants membranes are used to treat dye house effluents to remove the dyestuff and allow the reuse of auxiliary chemicals for dyeing, or to concentrate the dyestuffs and auxiliaries and produce purified water [15].

One of the more important categories of membranes comprises the non-porous polymeric membranes which are most widely adopted in current

industrial membrane separations [2–15]. Polyurethane membrane is an example of a non-porous synthetic membrane. Ether-type polyurethane membrane is manufactured through a copolymerisation condensation reaction of polyols with polyisocyanates [16]. These two components aggregate into two distinct regions during the reaction which results in the formation of hard and soft domains. The hard domain is very rigid in structure due to the presence of aromatic rings; the soft domain, comprising the polyol segments, is more fluid and amorphous. Extensive intermolecular hydrogen bonding takes place between the individual crystalline segments and the soft segments. As a result, the ether-type polyurethane membrane is resistant to extreme pH and temperature conditions which makes it an attractive candidate for industrial membrane separation applications.

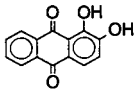
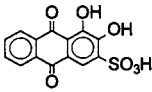
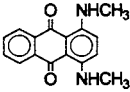
Our earlier work on the mechanism of extraction of phenols and benzoic acids by the polyurethane membrane shows that this polymer is capable of sorbing organic compounds from solution [17,18]. Carbon adsorption of organic dyes from waste effluents is relatively ineffective for the reasons previously mentioned, and consequently effluents containing organic dyes are very difficult to treat in environmental systems [1]. We chose to investigate the transport of organic dyes for the purpose of better defining the factors affecting sorption of organic compounds by the polyurethane membrane in general, and to explore the possibility of practical industrial applications. This comprehensive study should help to promote the use of the polyurethane membrane for separations in various segments of industry.

2. Experimental

2.1. Instrumental analysis and reagents

UV-visible spectra and absorbance readings were taken using a Hewlett-Packard Model 8452A diode-array spectrophotometer. Solution pH was measured with an Orion Expandable Ion Analyser EA940. Water was obtained from a Barnstead Nanopure II™ purification system fed with water

Table 1
Anthraquinone organic dyes

Name	Structure	C. I. Number
Alizarin		58000
Alizarin Red S		58005
Disperse Blue 14		61500

purified by reverse osmosis. Polyether-type polyurethane membranes PT6100S and PT6310S 0.025 and 0.051 mm thick, respectively were supplied by Deerfield Urethane Inc., South Deerfield, MA. The organic dyes were obtained from BASF Co., Ludwigshafen, Germany and from a biological stain kit, Chem-Supply Model No. BS-100, provided by Chem Service, Inc., West Chester, PA. The molecular structures and the Colour Index (C.I.) numbers of the dyes used for this study are listed in Tables 1–3. The purity of these dyes was checked by TLC using a 50:10:15 ratio of *n*-butanol:ethanol:water mobile phase composition. Because the compounds appeared to be in their pure form, they were used without further purification. All other chemicals were of a reagent grade.

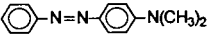
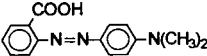
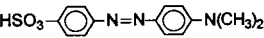
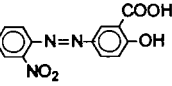
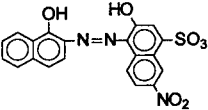
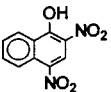
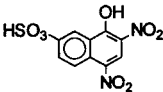
2.2. Experimental apparatus and procedure

Enough of each dye was weighed out to give a final solution concentration of about 1.9×10^{-5} M in 1.0 M HCl or in 1.0 M NaOH unless otherwise specified. The choice of this concentration was dictated by the solubility limit of the least soluble dye in 1.0 M HCl. Parameters such as salt, acid, or base concentrations were adjusted accordingly.

The dye classification shown Tables 1–3 was adopted from textile science and is based not only on the type of substituents on the dye molecule but also on the application conditions used in textile operations utilizing those particular dyes [19].

The apparatus used for membrane testing consisted of two separate glass ‘cells’ (a starting and a receiving cell) having capacities of 260 ml. The flanges of both cells were covered lightly with Dow Corning high vacuum silicone grease in order to obtain a better seal of the two cells. All cells had short sidearms which allowed access for solutions and sampling. Ether-type polyurethane membrane 0.025 mm thick (unless otherwise specified) was cut into squares and placed between the flanges of the two cells which were then clamped together. The membrane was not subjected to any cleaning prior to use and we assumed that it does not swell in aqueous solution due to its hydrophobic nature. The surface area of the membrane exposed to solutions was 23.8 ± 0.2 cm². The starting cell contained 250 ml of aqueous dye solution; the receiving cell contained 250 ml of 1.0 M HCl solution without the dye (unless otherwise specified). Teflon stirrers were placed inside each cell to keep the solutions stirred throughout the experiment. Sep-

Table 2
Acidic organic dyes

Name	Structure	C. I. Number
Solvent Yellow 2		11020
Methyl Red		13020
Methyl Orange		13025
Alizarin Yellow GG		14025
Eriochrome Black T		14645
Martius Yellow		10315
Naphthol Yellow S		10316

arate magnetic stirrers were used for each cell. After the sample and the receiving solutions were transferred into the cells, the sidearm openings of the cells were closed with glass stoppers and Parafilm™ to eliminate evaporation and pH variations. The entire apparatus was then wrapped in aluminum foil for the duration of the experiment to prevent any possible decomposition of the dye due to light. Each experiment was repeated at least twice to establish reproducibility.

The UV-visible spectra (190–820 nm) of the original solutions were taken prior to the experiment (A_I) and compared with the absorbances of

the starting and receiving solutions taken after a known period of time (A_{FS} , A_{FR}). % dye in starting cell and % dye in receiving cell are the concentrations of dye in the starting and the receiving solutions, respectively at a known time. The concentration of dye in the membrane at a specific time, reported as % dye in membrane, can be calculated.

$$\% \text{ Dye in starting cell} = A_{FS}/A_I \times 100\% \quad (1)$$

$$\% \text{ Dye in receiving cell} = A_{FR}/A_I \times 100\% \quad (2)$$

$$\% \text{ Dye in membrane} = 100\% - (\% \text{ dye in starting cell} + \% \text{ dye in receiving cell}) \quad (3)$$

Table 3

Basic organic dyes

Name	Structure	C. I. Number
Victoria Blue R		44040
Wool Green S		44090

3. Results and discussion

3.1. Effect of the solution pH on the transport of organic dyes through polyurethane membrane

Our previous work on the mechanism of extraction of phenols [17] and benzoic acids [18] by the polyurethane membrane shows that two conditions must be met in order for extraction to occur. First, the organic compound must be transferred from solution onto the membrane surface. Second, more of this compound will be removed from solution after the initial sorption only if the species sorbed on the membrane surface can migrate deeper into the polymer. An increase in the degree of sorption is observed until the capacity of the membrane has been reached. Through the study of the extraction of phenols and benzoic acids, we have found that the polyurethane membrane can only hold un-

charged organic species. Based on what we know about the mechanism of extraction of phenols and benzoic acids, we hypothesized that it should be possible to increase the amount of the organic compound removed from the starting solution if the sorbed compound could be transported through the membrane into a receiving solution. To test this hypothesis, we investigated the transport of a series of organic dyes (Tables 1–3) which are representatives of dyes frequently used in the textile industry [19,20].

The solution conditions for these dyes were chosen such that majority of the dye molecules would exist as charged or as neutral species. Both 1.0 M HCl and 1.0 M NaOH solutions were used for the extraction and transport of the anthraquinone dyes Alizarin and Alizarin Red S, all of the acidic dyes, and the basic dye Wool Green S. Anthraquinone Disperse Blue 14 is insoluble in

Table 4

Qualitative analysis of transport of anthraquinone, acidic and basic organic dyes^a

Dye	Dye in starting solution	Dye in receiving solution	Dye in membrane
<i>Anthraquinone</i>			
Alizarin	1.0 M HCl: yellow	Yellow	Yellow
	1.0 M NaOH: violet	None	None
Alizarin Red S	1.0 M HCl: light yellow	Light yellow	Light yellow
	1.0 M NaOH: purple	None	None
Disperse Blue 14	1.0 M HCl: pink	Pink	Blue
<i>Acidic</i>			
Solvent Yellow 2	1.0 M HCl: red	Red	Red
	1.0 M NaOH: yellow	None	None
Methyl Red	1.0 M HCl: red/pink	Red/pink	Red/pink
	1.0 M NaOH: yellow	None	None
Methyl Orange	1.0 M HCl: red	None	None
	1.0 M NaOH: yellow	None	None
Alizarin Yellow GG	1.0 M HCl: orange	Orange	Orange
	1.0 M NaOH: yellow	None	None
Eriochrome Black T	1.0 M HCl: burgundy	Burgundy	Burgundy
	1.0 M NaOH: yellow	None	None
Martius Yellow	1.0 M HCl: light yellow	Yellow	Yellow
	1.0 M NaOH: orange	None	None
Naphthol Yellow S	1.0 M HCl: light yellow	Light yellow	Light yellow
<i>Basic</i>			
Victoria Blue R	1.0 M NaOH dark yellow	None	None
	1.0 M HCl: yellow	None	None
Wool Green S	Water: blue	Blue	Blue
	1.0 M HCl: green	None	None
	1.0 M NaOH: blue	None	None

^a Conditions: $25.0 \pm 2.0^\circ\text{C}$, 250-ml aliquot of $\approx 1.9 \times 10^{-5}$ M aqueous dye solution in the starting cell, 250-ml aliquot of solvent in the receiving cell, 0.025 mm thick ether-type membrane, active surface area of 23.8 ± 0.2 cm².

basic solution, and therefore it was tested only in 1.0 M HCl. The basic dye, Victoria Blue R, is also insoluble in basic solution but it dissolves in water (pH \approx 5.0) and in 1.0 M HCl. Table 4 shows the qualitative results for the extraction and transport of the selected dyes from the corresponding starting solutions. The receiving solution for each dye had a similar acidity or basicity to the starting solution in which the dye was dissolved. The color of each dye in the starting solution, the receiving solution, and the membrane corresponds to the type of species present (i.e. charged vs. uncharged). The anthraquinone and the acidic dyes (with the exception of Methyl Orange) were found to extract and transport out of acidic solution but not from basic solution. The acidic Methyl Orange and the basic dye Wool Green S showed no extraction or trans-

port from either solution used. Basic Victoria Blue R was extracted and transported out of water but not out of acidic solution.

In 1.0 M HCl, the anthraquinone dyes that have acidic substituents are neutral, e.g. Alizarin and Alizarin Red S. During extraction and transport of these dyes from acidic solution, the membrane had the same color as the starting dye solutions. In 1.0 M NaOH, Alizarin and Alizarin Red S are negatively charged; no extraction or transport was observed from basic solutions of these dyes. Organic dyes such as disperse blue 14 having basic substituents are positively charged in 1.0 M HCl. During the transport of Disperse Blue 14, the starting and receiving solutions contained charged species (pink), but the membrane was blue in color. The blue color of Disperse Blue 14 is observed when

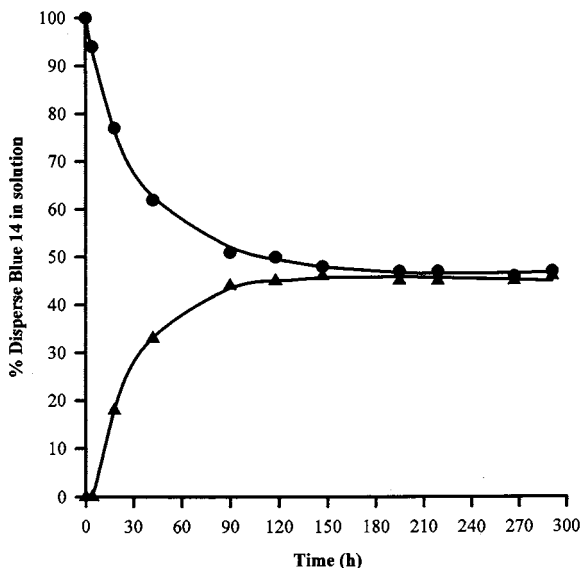


Fig. 1. Transport of Disperse Blue 14 through 0.025 mm thick ether-type polyurethane membrane. Conditions: $25.0 \pm 2.0^\circ\text{C}$, 250-ml aliquot of $\approx 1.9 \times 10^{-5}$ M aqueous dye solution in 1.0 M HCl in the starting cell, 250-ml aliquot of 1.0 M HCl in the receiving cell, 0.025 mm thick ether-type membrane, active surface area of 23.8 ± 0.2 cm². Decrease in dye concentration in the starting cell, ●; increase in dye concentration in the receiving cell, ▲.

the dye molecules are uncharged (e.g. when the dye is dissolved in a non-polar solvent such as hexane). The data collected on transport of the anthraquinone dyes suggests that only a neutral form of these dyes is retained by the membrane. Clear visual evidence for this conclusion is the transport of Disperse Blue 14 during which we observe a color change when the dye is being transferred from solution into the polymer and vice versa.

Similar conclusions were reached from extraction and transport of acid dyes. In 1.0 M HCl, a majority of acidic dye species will be neutral. Similarly to the anthraquinone dyes, the acidic dyes were extracted and transported from and into acidic solution but not from basic solution. Methyl Orange, however, was an exception. The lack of extraction of this dye can be accounted for by the high probability that the dye never actually exists as an extractable uncharged species i.e. the closest instance in which it resembles an uncharged species is when it forms a zwitterion. The

net charge on the zwitterion is zero, but the individual ends of this species are either positively or negatively charged. Consequently, no initial transfer onto the membrane surface can occur, and hence no transport into the receiving cell was observed.

Similar reasoning can be used to account for the unextractability of basic Wool Green S. Like Methyl Orange, the probability of Wool Green S being uncharged is unlikely due to the presence of the basic substituents and the sulfonic acid group on the dye molecule. Under acidic conditions, the sulfonic acid group on the dye will be neutral, but amino groups (other than the ion-paired substituent which is not considered to be truly charged because the positive charge is closely associated with the negative ions) may be protonated. The opposite will be true in basic solution. Since no neutral species is formed, there is no extraction and therefore no transport. Basic Victoria Blue R, has only basic substituents in addition to the ion-paired quaternary ammonium group. The majority of Victoria Blue R molecules are neutral in water (again, the ion-paired group is not considered to be charged), and therefore this dye is extracted and transported out of water. No extraction or transport occurred out of 1.0 M HCl due to the presence of positively charged species.

These results further support the hypothesis that the presence of a neutral species of an organic compound is a deciding factor which determines whether the initial transfer of an organic compound from solution onto the membrane surface will take place. After successful initial sorption, the transport through the membrane into a receiving solution will occur only if the receiving solution conditions are favorable for desorption of the organic species from the membrane. For example, the anthraquinone dyes are transported into acidic receiving solutions but not into water in which they are only sparingly soluble. In conclusion, the transport of organic dyes from one solution into another using the polyurethane membrane as the transporting medium is contingent upon both the initial sorption of the dye from solution onto the polymer surface and the chemical properties of the receiving solution.

3.2. Effect of dye geometry, size, and chemical properties on transport through polyurethane membrane

As pointed out in Section 3.1, the first step in the overall transport process (Fig. 3) is the sorption of the dye onto the membrane surface. It is hypothesized that the efficiency with which the dye in solution is initially transferred onto the polymer surface will be dependent on the relative solubilities of the dye in the solvent and in the membrane which will take into account all the different possible specific and non-specific interactions [21]. After the initial sorption has taken place, the ability of the sorbed species to separate the individual segments of the polymer and migrate deeper into the bulk is largely driven by the strength and the extent of the intermolecular interactions that can take place between the species and the constituent groups on the hard and soft segments of the polymer [17,18]. Because all of the dyes used in this study are relatively non-polar with substituents capable of intermolecular interactions and aromatic rings which are also found in the matrix of the membrane, they should be soluble in this polymer. For the remainder of this discussion we will only be concerned with the neutral form of the dyes since

it is the only species that is retained by the membrane. Using this information on extraction and transport within the polymer matrix, we anticipated that the rate of transport of the dye from the starting into the receiving solution through the polymer will be affected by the morphology and the chemical characteristics of the dye molecule. To test this hypothesis, the dyes were dissolved in the solvent from which extraction and transport were previously observed (Table 4) to give a concentration of 1.9×10^{-5} M. Ether-type 0.025 mm thick polyurethane membrane was used in all instances. The results reported in Table 5 show the time at which no further change was measured in the receiving and the starting cells, the percentage dye detected in each of the cells at that time, and the percentage dye calculated to be in the membrane. Unlike all other dyes that were tested, Eriochrome Black T and Naphthol Yellow S show significantly lower concentrations in the receiving cell than in the starting cell at the reported times. This suggests that the transport of the two dyes must be very slow, and therefore the change in concentration at the time of measurement may be too small to detect. We found that some dyes, for example Alizarin, Disperse Blue 14 and Solvent Yellow 2, are not well retained by the membrane but quite efficiently

Table 5
Effect of dye morphology and chemical properties on the rate of transport^a

Dye	Time (h)	% Dye in starting cell	% Dye in receiving cell	% Dye in membrane
<i>Anthraquinone</i>				
Alizarin	163	48 ± 3	42 ± 4	10 ± 3
Alizarin Red S	929	50 ± 3	45 ± 3	5 ± 3
Disperse Blue 14	147	47 ± 1	46 ± 1	7 ± 1
<i>Acidic</i>				
Solvent Yellow 2	235	54 ± 1	45 ± 1	1 ± 1
Methyl Red	183	18 ± 2	15 ± 2	65 ± 1
Alizarin Yellow GG	240	14 ± 3	5 ± 2	81 ± 2
Eriochrome Black T	216	39 ± 3	15 ± 4	46 ± 3
Martius Yellow	43	29 ± 3	29 ± 3	42 ± 3
Naphthol Yellow S	408	90 ± 1	8 ± 3	2 ± 1
<i>Basic</i>				
Victoria Blue R	733	30 ± 1	26 ± 1	40 ± 1

^a Conditions: $25.0 \pm 2.0^\circ\text{C}$, 250-ml aliquot of $\approx 1.9 \times 10^{-5}$ M aqueous dye solution in the starting cell in a solvent from which transport occurs (Table 4), 250-ml aliquot of solvent (identical to that in the starting cell) in the receiving cell, 0.025 mm thick ether-type membrane, active surface area of 23.8 ± 0.2 cm².

transported. Other dyes such as Methyl Red, Alizarin Yellow GG, Eriochrome Black T, Martius Yellow, and Victoria Blue R are very well retained and transported through the polyurethane membrane. Two of the studied dyes, Alizarin Red S and Naphthol Yellow S, are very poorly extracted and transported by this polymer.

Dyes which show very inefficient extraction and transport (Alizarin Red S and Naphthol Yellow S) are small, compact and both contain a single sulfonic acid substituent (Tables 1 and 2). Because of the small size of these dyes, the effect of individual substituents on the chemical characteristics of the entire molecule is more significant than it would be for a larger dye. Thus, in the case of Alizarin Red S and Naphthol Yellow S, the presence of the sulfonic acid group imparts more polarity to both compounds. The relatively polar character of these dyes hinders efficient initial sorption onto the membrane surface and results in the very slow transport into the receiving cell. The dyes which were effectively retained and transported by the membrane are generally non-polar in nature (Tables 2 and 3). For example Eriochrome Black T, in spite of the presence of the sulfonic acid group, remains quite non-polar because of a greater number of non-polar aromatic rings. Unlike Alizarin Red S and Naphthol Yellow S, this dye is sorbed and transported quite efficiently. Martius Yellow which has chemical structure identical to that of Naphthol Yellow S (Table 2) but lacks the sulfonic acid group is highly retained by the membrane and very quickly transported which again indicates that it is the resultant polarity of the dye molecule (and therefore the solubility) and not the polarity of the individual substituents that plays an important role in the transport process. Dyes which showed high extraction and efficient transport are quite diverse in geometry and size. Examples are large non-linear dyes such as Eriochrome Black T and Victoria Blue R, smaller linear Methyl Red and Alizarin Yellow GG, and even smaller Martius Yellow (Tables 2 and 3). We can therefore conclude that the morphology and size of the dye alone are not important factors controlling the transport process. The percent concentration of the linear dyes, Methyl Red and Alizarin Yellow GG, in the membrane is significantly higher than that of, for

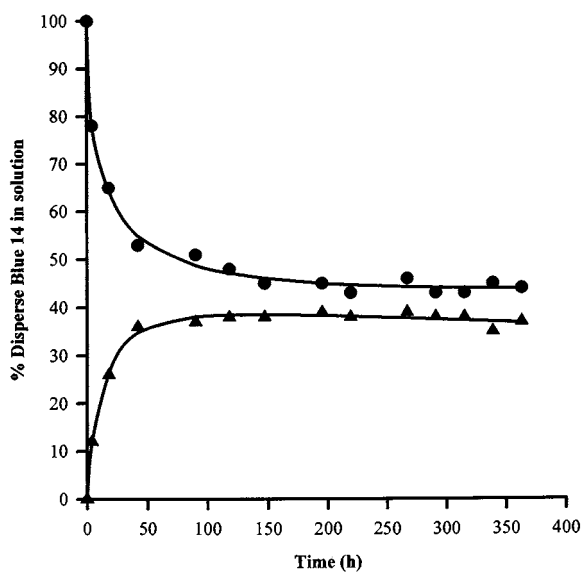


Fig. 2. Transport of Disperse Blue 14 through 0.051 mm thick ether-type polyurethane membrane. Conditions: $25.0 \pm 2.0^\circ\text{C}$, 250-ml aliquot of $\approx 1.9 \times 10^{-5}$ M aqueous dye solution in 1.0 M HCl in the starting cell, 250-ml aliquot of 1.0 M HCl in the receiving cell, 0.051 mm thick ether-type membrane, active surface area of 23.8 ± 0.2 cm². Decrease in dye concentration in the starting cell, ●; increase in dye concentration in the receiving cell, ▲.

example, Eriochrome Black T or Martius Yellow. This can be accounted for by the presence of carboxylic acid groups on both Methyl Red and Alizarin Yellow GG which are also found in the polymer matrix. The presence of the carboxylic acid groups increases the probability for more hydrogen bonding interactions between the dye and the polymer, and increases the solubility of the dye in the polymer matrix. These results support the hypothesis on the importance of intermolecular

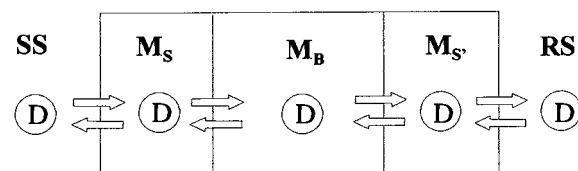


Fig. 3. Pictorial representation of transport of an organic dye through a polyurethane membrane. SS is the starting solution, D is the neutral dye species, M_S is the membrane surface on the starting solution side, M_B is the membrane bulk, $M_{S'}$ is the membrane surface on the receiving solution side, RS is the receiving solution.

interactions. Dyes such as Alizarin, Disperse Blue 14 and Solvent Yellow 2 (Tables 1 and 2) were not well retained by the membrane, but they were transported quite efficiently. These dyes are capable of forming hydrogen bonds and are relatively non-polar. The low concentration of these dyes in the membrane, in spite of the effective transport, must be a result of their relative solubility in the solvent and in the polymer. The strength of hydrogen bonding of the dyes with the solvent must be slightly higher than with the polymer, and therefore we observed preferential partitioning of these dyes into the aqueous phase.

In conclusion, the rate of transport is not controlled by the geometry or size of the dye molecule but rather by the relative solubility of the dye in the polymer and in the solvent, and by the relative strength and extent of the intermolecular interactions with the polymer and the solvent. These findings are in agreement with the conclusions reached from our earlier study of the mechanism of extraction of phenols and benzoic acids by the polyurethane membrane [17,18].

3.3. Dependence of the rate of transport on thickness of the polyurethane membrane

The relationship between the thickness of the polyurethane membrane and the rate of transport of the dye molecules through this polymer is exemplified by the transport of Disperse Blue 14. This dye having a concentration of 1.9×10^{-5} M in 1.0 M HCl was transported into 1.0 M HCl using 0.025 and 0.051 mm thick ether-type polyurethane membranes. Figs. 1 and 2 show the time taken to achieve an equilibrium between the starting cell, the receiving cell and the membrane when the 0.025 and 0.051 mm thick membranes were used respectively. Equilibrium was achieved within about 195 h with the 0.025 mm thick membrane and within 219 h with the 0.051 mm thick membrane. At the observed equilibrium, the 0.025 mm thick membrane contained $6 \pm 2\%$ of the starting concentration of the dye, and the 0.051 mm thick membrane contained $19 \pm 1\%$ of the initial

Table 6

Effect of the initial concentration of Disperse Blue 14 on the rate of transport^a

	Initial concentration of Disperse Blue 14	
	1.9×10^{-6} M	1.9×10^{-5} M
Equilibrium time (h)	146	146
% Dye in starting cell	27 ± 4	48 ± 1
% Dye in receiving cell	27 ± 4	45 ± 1
% Dye in membrane	46 ± 4	7 ± 1

^a Conditions: $25.0 \pm 2.0^\circ\text{C}$, 250-ml aliquot of aqueous dye solution of appropriate concentration in the starting cell in 1.0 M HCl, 250-ml aliquot of 1.0 M HCl in the receiving cell, 0.025 mm thick ether-type membrane, active surface area of 23.8 ± 0.2 cm².

dye solution concentration. The masses corresponding to the active surface (23.8 ± 0.2 cm²) of 0.025 mm and 0.051 mm thick membranes prior to exposure to the dye were ≈ 0.120 and 0.235 g, respectively.

An attempt was made to determine the overall diffusion coefficient for the transport process. At a steady state, the diffusion coefficient can be evaluated by using a so called 'time-lag' method [22,23]. Initially, in the non-stationary state the amount of dye diffusing through the membrane is mathematically represented by

Table 7

Effect of the initial concentration of Solvent Yellow 2 on the rate of transport^a

	Initial concentration of Solvent Yellow 2	
	1.9×10^{-6} M	1.9×10^{-5} M
Equilibrium time (h)	235	235
% Dye in starting cell	55 ± 1	52 ± 1
% Dye in receiving cell	43 ± 1	47 ± 1
% Dye in membrane	2 ± 1	1 ± 1

^a Conditions: $25.0 \pm 2.0^\circ\text{C}$, 250-ml aliquot of aqueous dye solution of appropriate concentration in the starting cell in 1.0 M HCl, 250-ml aliquot of 1.0 M HCl in the receiving cell, 0.025 mm thick ether-type membrane, active surface area of 23.8 ± 0.2 cm².

Table 8
Successive removal of Disperse Blue 14 from aqueous solution^a

	Dye concentration in starting cell at equilibrium (M)	Dye concentration in receiving cell at equilibrium (M)	Dye concentration in membrane at equilibrium (M)
Initial conditions ^b	1.9×10^{-5}	0	0
Initial transport	8.9×10^{-6}	8.7×10^{-6}	1.4×10^{-6}
First successive transport	4.3×10^{-6}	3.9×10^{-6}	1.6×10^{-6}
Second successive transport	2.1×10^{-6}	2.3×10^{-6}	1.5×10^{-6}

^a Conditions: $25.0 \pm 2.0^\circ\text{C}$, 250-ml aliquot of aqueous dye solution in the starting cell in 1.0 M HCl, 250-ml aliquot of 1.0 M HCl in the receiving cell, 0.025 mm thick ether-type membrane, active surface area of $23.8 \pm 0.2 \text{ cm}^2$.

^b Note: initial conditions represent the initial concentration in the starting cell before any extraction or transport has occurred; the time required to reach equilibrium was $\approx 147 \text{ h}$ for the initial and successive transports.

$$Q = F\Delta x C_A \left[\frac{D_t}{\Delta x^2} - \frac{1}{6} - \frac{2}{\pi^2} \sum \frac{(-1)^n}{n^2} \exp \left(\frac{-D_n^2 n^2}{x^2} \right) \right] \quad (4)$$

As time increases and the equilibrium is approached, the above equation can be simplified to

$$Q = \frac{DC_A F}{\Delta x} \left[t - \frac{\Delta x^2}{6D} \right] \quad (5)$$

If the thickness of the membrane, Δx , and the time, Δt , taken to reach the steady state ('time-lag') are known, the diffusion coefficient can be calculated using [22,23]

$$D = \frac{\Delta x^2}{6\Delta t} \quad (6)$$

The transport of disperse blue 14 through the 0.025 mm thick membrane required about 195 h for the dye in the membrane to reach a steady state (i.e. when no further change in dye concentration was observed in the starting and receiving solutions and in the membrane). The approximate diffusion coefficient calculated using Eq. (6) is $5.34 \times 10^{-7} \text{ mm}^2 \text{ h}^{-1}$. The transport of Disperse Blue 14 through the 0.051 mm thick membrane required about 219 h to reach a steady state. The approximate value of the diffusion coefficient is $1.98 \times 10^{-6} \text{ mm}^2 \text{ h}^{-1}$.

As expected, the overall equilibrium for the transport of Disperse Blue 14 was achieved more quickly when the thinner membrane was used.

This can be accounted for by the shorter path that the dye had to diffuse through in order to reach the receiving cell solution. The more quickly the dye appears on the receiving cell side of the membrane, the more rapidly it can be desorbed into the receiving solution. The concentration of the dye in the membrane increases until the steady state is reached where no further sorption or transport are observed. The amount of dye in the thinner membrane was calculated to be approximately one third of that in the thicker polymer. The thicker membrane can retain a higher amount of the dye because it has more of the polymer material by weight that is available for interactions with the dye molecules. The calculated diffusion coefficients for the transport are broad approximations of the true values. The mathematical representation of the entire diffusion is beyond the scope of this paper and will be addressed in a later publication.

3.4. Dependence of the rate of transport on the initial dye solution concentration

Disperse Blue 14 and Solvent Yellow 2 were used to study the effect of the initial concentration of the dye on the rate of transport through the polyurethane membrane. The choice of the initial dye concentrations in the sample cells was dictated by the solubility of the dyes in 1.0 M HCl and the detection limit of the UV-visible spectrophotometer. The starting concentrations used

for both Solvent Yellow 2 and Disperse Blue 14 were 1.9×10^{-6} and 1.9×10^{-5} M. Table 6 and Table 7 show the time taken to achieve equilibrium at the two concentrations for both dyes, and the corresponding percentage of each dye in the starting and the receiving cells and in the membrane. Regardless of the starting concentration used, equilibrium was achieved within ≈ 146 h for Disperse Blue 14 and 235 h for Solvent Yellow 2. When 1.9×10^{-6} M Disperse Blue 14 was extracted, a higher percentage of the dye was retained by the membrane and lower final concentrations were detected in the starting and the receiving solutions than in the extraction of 1.9×10^{-5} M solution of this dye. This was not observed for the transport of the corresponding solutions of Solvent Yellow 2.

In the case of Disperse Blue 14, although the membrane contained a higher proportion of the dye, the calculated molar concentration of the dye in the membrane was approximately the same as the molar concentration for the extraction of the more concentrated solution of Disperse Blue 14. This suggests that the membrane can remove the dye from solution until its capacity for the dye is reached. In the case of Solvent Yellow 2, the capacity of the membrane has probably been reached at 2% even at the 1.9×10^{-6} M dye concentration. Therefore, a change in the percentage of this dye in the membrane was not observable as with the Disperse Blue 14.

To determine whether the polyurethane membrane already containing a dye could be used to

transport more dye if a fresh receiving solution was provided, we investigated a stepwise removal of Disperse Blue 14. The starting concentration of Disperse Blue 14 was 1.9×10^{-5} M. After equilibrium was achieved between the two cells and the membrane, the molar dye concentrations in both cells and in the membrane were calculated. Next, the receiving cell solution containing the dye was discarded and replaced with new 1.0 M HCl solution. The cells were again allowed to come to equilibrium, and the concentrations were calculated. This process was repeated until an instrumental detection limit for the dye was reached.

The calculated molar concentrations of Disperse Blue 14 in the starting and receiving cells at equilibrium for each successive extraction are shown in Table 8. The concentration of Disperse Blue 14 in the membrane gradually increased during the initial extraction/transport until equilibrium. This membrane dye concentration remained constant for all of the subsequent successive extraction/transport experiments regardless of the time at which the measurements were taken and the solution dye concentration being transported. Furthermore, because the time needed to achieve equilibrium for all of the successive extractions was approximately the same as for the initial extraction/transport, we can conclude that the transporting properties of the membrane have not been affected by the presence of the dye in the matrix. These results prove that the membrane will extract the dye until its capacity for the dye is reached (i.e. the solubility limit for the dye in the membrane is

Table 9
Effect of salt on the rate of transport of Disperse Blue 14 and Solvent Yellow 2^a

	Equilibrium time (h)	% Dye in starting cell	% Dye in receiving cell	% Dye in membrane
Disperse Blue 14				
No salt added	147	48 ± 1	46 ± 1	8 ± 1
0.5 M LiCl	195	48 ± 2	40 ± 2	10 ± 2
Solvent Yellow 2				
No salt added	234	52 ± 1	46 ± 1	2 ± 1
0.5 M LiCl	234	58 ± 2	41 ± 2	1 ± 2

^a Conditions: $25.0 \pm 2.0^\circ\text{C}$, 250-ml aliquot of $\approx 1.9 \times 10^{-5}$ M aqueous dye solution in the starting cell in 1.0 M HCl with salt concentration appropriately adjusted, 250-ml aliquot of 1.0 M HCl in the receiving cell, 0.025 mm thick ether-type membrane, active surface area of 23.8 ± 0.2 cm².

Table 10
Effect of temperature on the rate of transport of Disperse Blue 14^a

Temperature (°C)	% Dye in starting cell at 24 h	% Dye in receiving cell at 24 h	% Dye in membrane at 24 h
4	88 ± 1	6 ± 1	6 ± 1
23	69 ± 1	24 ± 1	7 ± 1
37	58 ± 1	36 ± 1	6 ± 1
66	45 ± 1	43 ± 1	7 ± 1

^a Conditions: temperature, ± 2.0°C, 250-ml aliquot of $\approx 1.9 \times 10^{-5}$ M aqueous dye solution in the starting cell in 1.0 M HCl, 250-ml aliquot of 1.0 M HCl in the receiving cell, 0.025 mm thick ether-type membrane, active surface area of 23.8 ± 0.2 cm².

reached). In order for this membrane to continue removing the remaining dye in the starting solution, a flow of dye through the membrane into the receiving solution must occur.

3.5. Effect of salt on the rate of transport through polyurethane membrane

Disperse Blue 14 and Solvent Yellow 2 were chosen as examples to illustrate the effect of salt on the rate of transport. The extraction efficiency and the time taken to achieve equilibrium for transport of both dyes (1.9×10^{-5} M) from 1.0 M HCl solutions containing 0.5 M LiCl were compared with the results for solutions without the salt. 0.5 M and 1.0 M aqueous solutions of NaCl, KCl, RbCl, CaCl₂, and Al₂(SO₄)₃ in 1.0 M HCl and in water were also tested to determine whether any transport of the cations and/or anions was occurring. The percentages of the dyes in the starting and the receiving cells and in the membrane at equilibrium for the sample solutions with and without salt are presented in Table 9. None of the cations and anions were transported through the membrane from any of the starting salt solutions as confirmed by analysis using atomic absorption spectroscopy. The extraction efficiency of Disperse Blue 14 and Solvent Yellow 2 from starting solutions containing the salt and the rates of transport into the receiving cells are almost identical (within experimental error) to the corresponding solutions of these dyes without the salt. Furthermore, the presence of salt does not change the saturation amount of each of the dyes that can be retained by the polyurethane membrane.

As discussed in Section 3.1, the majority of Disperse Blue 14 species in 1.0 M HCl are posi-

tively charged. These positively charged species are, however, at equilibrium with a small percentage of uncharged molecules of Disperse Blue 14. The opposite is true for the solution of Solvent Yellow 2 in 1.0 M HCl in which the predominant species is the uncharged dye molecule. When salt is added to solutions containing charged organic species, ion pair formation can take place [24–26] and the overall solution becomes more polar. Because of the increased solution polarity in the presence of salts, we would expect a ‘salting out’ effect where the non-polar uncharged species becomes more insoluble in the solvent, and therefore partitions more efficiently into the non-polar membrane which results in a more rapid extraction and transport of both dyes. Because no significant changes in extraction and transport rates have been observed, we concluded that addition of salt does not cause a sufficiently high change in the relative solubility of the dye species in solution and the membrane. These findings are in agreement with the conclusions reached for the earlier investigation of the extraction of phenols and benzoic acids by the polyurethane membrane [17,18].

3.6. Dependence of the rate of transport on solution temperature

1.9×10^{-5} M solutions of Disperse Blue 14 in 1.0 M HCl were transported into a 1.0 M HCl solution using 0.025 mm polyurethane membrane at 4, 23, 37, and 66°C. The percentages of the dye in the starting and the receiving cells and in the membrane at 24 h for each of the temperatures are shown in Table 10. The percentage of the dye retained by the membrane is approximately the

same at all four temperatures. However, the rate of removal of the dye from the starting cell and the rate of transport into the receiving cell were found to increase with increased temperature.

The above results do not correlate with the temperature data that we collected for extraction of phenols and benzoic acids by the ether-type polyurethane membrane [17,18]. For the extraction of phenols and benzoic acids, we found that as the temperature was increased, the extraction decreased because of the exothermic nature of the extraction process. In this study, however, in addition to extraction we have transport into a receiving solution. Unlike the simple extraction, the transport is probably controlled not only by thermodynamic factors but also by the concentration gradient created during the process. The fact that the membrane retains approximately the same amount of dye at all of the temperatures suggests that the solubility of the dye in the polymer remains relatively the same. The increased rates of removal and transport of the dye at higher temperatures suggest that the physical properties of the membrane matrix must be different at those temperatures. The most likely explanation is that due to the higher energy in the membrane segments at the increased temperature, some of the intermolecular interactions among the individual segments within the polymer may be weakened or broken; this results in the matrix being more fluid in nature and, consequently, more accessible to the dye species in solution. Therefore, at higher temperatures (e.g. 66°C), the dye species sorbed on the surface can migrate more freely through the bulk of the polymer and into the receiving solution which is evidenced by the significantly shorter time in which equilibrium is achieved (e.g. within 146 h at 23°C vs. 24 h at 66°C).

4. Conclusion

The rate at which various organic dyes will transport through the ether-type polyurethane membrane is dependent on the solution pH, the overall polarity and capability of the dye molecule to engage in hydrogen bonding interactions with the polymer, the relative solubility of the dye

species in the polymer and in the solvent, and the temperature at which the transport is occurring. The ether-type polyurethane membrane can retain only neutral species of the organic dyes.

In order to obtain an initial transport through the bulk of the membrane, the pH of the starting solvent must be favorable for the formation of a neutral species which is the only species soluble in the membrane. Furthermore, a flow of the species in the membrane into the receiving solution will be observed only if a driving force resulting from the differences in dye concentration in the starting and receiving solutions and the membrane (or a concentration gradient) is present. The rate of transport is dependent on chemical factors such as the efficiency with which the dye can partition into the membrane surface and then migrate through the membrane bulk, and on the physical experimental conditions such as the temperature. For example, species with comparable solubility in the polymer and in solution is transported from the starting cell into the receiving cell quite efficiently. On the other hand, if the solubility of the species is relatively higher in one of the media, the transport may be hindered due preferential partitioning. The partitioning of the dye between the solution and membrane phases and the rate of migration through the bulk of the polymer can be significantly altered by changing the temperature. The rate of transport of the dyes through the polyurethane membrane increased when higher temperatures were used. The increase in the transport rate at increased temperatures can be accounted for by change in the physical properties of the membrane matrix which becomes more fluid, and therefore more exposed and accessible to the dye species in solution.

Overall, the results from this study provide a deeper insight into the mechanism of extraction and transport process of organic compounds by the polyurethane membrane and show that this membrane has considerable potential in commercial applications for removal of organic compounds from aqueous solutions.

Acknowledgements

The authors would like to acknowledge the

financial support of the University of Manitoba and the Natural Sciences and Engineering Research Council of Canada.

References

- [1] A. Reife, H.S. Freeman, *Environmental Chemistry of Dyes and Pigments*, Wiley-Interscience, New York, 1996, pp. 3–32.
- [2] R. Singh, *CHEMTECH* 28 (4) (1998) 33.
- [3] R. Singh, *CHEMTECH* 26 (6) (1996) 46.
- [4] K. Scott, R. Hughes, *Industrial Membrane Separation Technology*, Chapman and Hall, London, 1996.
- [5] M. Mulder, *Basic Principles of Membrane Technology* 2nd ed., Kluwer Academic Publishers, Dordrecht/Boston/London, 1996.
- [6] J.A. Howell, A. Noworyta, *Towards Hybrid Membrane and Biotechnology Solutions for Polish Environmental Problems*, Wrocław Technical University Press, Wrocław, 1995.
- [7] K. Scott, *Handbook of Industrial Membranes*, 1st ed., Elsevier Advanced Technology, 1995.
- [8] R.D. Noble, S.A. Stern, *Membrane Separation Technology: Principles and Applications*, Elsevier Science, Amsterdam, 1995.
- [9] T. Matsuura, *Synthetic Membranes and Membrane Separation Processes*, CRC Press, Boca Raton, 1993.
- [10] P. Aptel, Membrane pressure driven processes in water treatment, in: J.G. Crespo, K.W. Broddeker (Eds.), *Membrane Processes in Separation and Purification*, NATO ASI Series, Series E: Applied Sciences, Kluwer Academic Publishers, 272 (1993) 263.
- [11] M. Mulder, The use of membrane separation processes in environmental problems, in: J.G. Crespo, K.W. Broddeker, *Membrane Processes in Separation and Purification*, NATO ASI Series, Series E: Applied Sciences, Kluwer Academic Publishers, 272 (1993) 233.
- [12] W.S. Winston Ho, K.K. Sirkar, *Membrane Handbook*, Van Nostrand Reinhold, New York, 1992.
- [13] J.A. Howell, *The membrane alternative: energy implications for industry*, Report number 21, Elsevier, London and New York, 1990, pp. 2–8.
- [14] L. Cecille, J.-C. Toussaint, *Future industrial prospects of membrane processes*, Elsevier, London and New York, 1989, pp. 3–7, 44, 55.
- [15] L. Cecille, J.-C. Toussaint, *Future Industrial Prospects of Membrane Processes*, Elsevier, London and New York, 1989, pp. 190–195.
- [16] G. Woods, *The ICI Polyurethanes Book*, ICI Polyurethanes and John Wiley & Sons Publication, Toronto, 1987, pp. 27–54.
- [17] K. Rzeszutek, A. Chow, *Talanta* 46 (1998) 507.
- [18] K. Rzeszutek, A. Chow, *Talanta* 47 (1998) 697.
- [19] D.M. Nunn, *The Dyeing of Synthetic-Polymer and Acetate Fibres*, Dyers Company Publications Trust, Bradford, West Yorkshire, 1979, pp. 2–53.
- [20] E.P.G. Gohl, L.D. Vilensky, *Textile Science: an Explanation of Fibre Properties*, 2nd ed., Longman Cheshire Pty Ltd., Melbourne, 1983, pp. 120–164.
- [21] C.L. Bird, W.S. Boston, *The Theory of Coloration of Textiles*, The Dyers Company Publications Trust, Bradford, West Yorkshire, England, 1975, pp. 294–298.
- [22] I.D. Rattee, M.M. Breuer, *The Physical Chemistry of Dye Adsorption*, Academic Press, London and New York, 1974, pp. 72–77.
- [23] J. Crank, *The Mathematics of Diffusion*, Clarendon Press, Oxford, 1975, pp. 44–68.
- [24] L. Shumack, A. Chow, *Talanta* 34 (1987) 957.
- [25] P. Fong, A. Chow, *Talanta* 39 (1992) 497.
- [26] R. Werbowesky, A. Chow, *Talanta* 43 (1996) 263.

Solid-phase extraction with liquid chromatography and ultraviolet detection for the assay of antidepressant drugs in human plasma

A. Bakkali, E. Corta, J.I. Ciria, L.A. Berrueta, B. Gallo *, F. Vicente

Department of Analytical Chemistry, Faculty of Sciences, University of the Basque Country, P.O. Box 644, 48080 Bilbao, Spain

Received 21 December 1998; received in revised form 10 February 1999; accepted 10 February 1999

Abstract

A solid-phase extraction (SPE) method for sample clean-up followed by a reversed-phase high-performance liquid chromatography (HPLC) procedure for the assay of five antidepressant drugs (trazodone, doxepin, desipramine, maprotiline and imipramine) is reported. The drugs were recovered from plasma buffered at a suitable pH using C18 Bond-Elut cartridges and mixtures of methanol–aqueous buffer as washing and elution solvents. The recoveries of the drugs using other sorbent materials (C8, C2, cyclohexyl, cyanopropyl and phenyl Bond Elut and copolymer HLB waters cartridges) were also examined. The selectivity of SPE was examined by using spiked plasma samples and the CH cartridge gave rise to the cleanest extracts. Cyclohexyl cartridges were conditioned successively with 2 ml of methanol and 1 ml of acetic acid–sodium acetate buffer (0.1 M, pH 4.0). Plasma sample was buffered at pH 4.0 and then applied to the sorbent. The washing step was performed subsequently with 1.5 ml of acetate buffer (0.1 M, pH 4.0), 100 μ l of acetonitrile and 1 ml of methanol–acetate buffer (30:70, v/v). Finally, the analytes were eluted with 0.5 ml of methanol–acetate buffer (70:30, v/v). The extract was evaporated to dryness, reconstituted in mobile phase, and chromatographed on a reversed-phase C18 column with ultraviolet detection at 215 nm. The recoveries of trazodone, doxepin, desipramine, maprotiline and imipramine from spiked plasma samples using the CH cartridge were 58.2, 84.3, 83.3, 83.3 and 82.2%, respectively. The within-day and between-day repeatabilities were lower than 6% and 9%, respectively. The linearity of calibrations for the five antidepressants was between 0.005 and 2 μ g/ml. The limits of detection were 1 ng/ml for trazodone, doxepin and desipramine and 2 ng/ml for maprotiline and imipramine. © 1999 Published by Elsevier Science B.V. All rights reserved.

Keywords: Antidepressant drugs; Plasma; Solid-phase extraction

1. Introduction

The treatment of depressive disorders is usually accomplished by the use of different compounds known as antidepressants and these drugs are frequently encountered in emergency toxicology

* Corresponding author. Tel.: +34-94-6012000; fax: +34-94-4648500.

E-mail address: qapgaheb@lg.ehu.es (B. Gallo)

screening, drug-abuse testing and forensic medical examinations [1]. Many studies have indicated that the clinical effects of this group of compounds are concentration dependent, at least in endogenously depressed patients [2,3]. Monitoring of plasma levels of some antidepressants may be clinically useful in certain situations, providing valuable information for a more rational use of these drugs in clinical practice.

Although several analytical methods are available for the determination of antidepressants in biological fluids, including gas–liquid chromatography [4–6], the most advantageous technique, in terms of both versatility and reliability, has proven to be the high-performance liquid chromatography (HPLC) [7–10].

A classical standard procedure for the extraction of antidepressants from biological samples is based on liquid–liquid extraction after alkalization [11,12]. In some methods, an aqueous acidic solution is used for back-extraction of antidepressants from the organic phase [7,10,13–18]. Such an approach is often tedious and time-consuming. An interesting alternative consists in the isolation of the analytes by solid-phase extraction (SPE) using disposable extraction cartridges (DECs) [19–23].

SPE is a consolidated preparation technique for biological samples. It is widely used for removing interfering components and for trace enrichment of analytes prior to chromatography. The advantages of SPE include minimal waste solvent generation, the ability to handle a wide range of sample volumes, ease of use, potentially excellent selectivity due to a wide range of available sorbents, and, to a greater extent than liquid–liquid and supercritical fluid extraction, the ability to extract and retain polar and ionic analytes.

This paper deals with the optimization of all the experimental variables that affect the recoveries obtained in the SPE of five widely used antidepressants, not only physicochemical variables such as the nature of the solid and liquid phases used and the sample pH, but also other hydrodynamic variables such as the flow-rate at which liquid phases are passed through the adsorbent or the volume of air used to forced the liquids through the solid.

2. Experimental

2.1. Reagents and chemicals

Imipramine hydrochloride, desipramine hydrochloride, maprotiline hydrochloride, doxepin hydrochloride, trazodone hydrochloride and the internal standard *p*-hydroxybenzoic acid *n*-butyl ester (butyl paraben) were from Sigma (Madrid, Spain). Methanol and acetonitrile (Romil Chemicals Ltd, Heidelberg, Germany) were of HPLC grade. The water used in all experiments was purified on a Milli-Q system from Millipore (Bedford, MA, USA). Sodium acetate, acetic acid, phosphoric acid, sodium hydrogen and dihydrogen phosphates, boric acid, sodium borate, sodium carbonate, sodium hydrogen carbonate, sodium hydroxide, concentrated ammonia (25%) and triethylamine were of analytical quality from Merck (Darmstadt, Germany). Aqueous buffers were prepared in order to buffer the aqueous standard and spiked plasma samples. The buffers (1 M and 0.1 M) were $\text{H}_3\text{PO}_4\text{--NaH}_2\text{PO}_4$ (pH 2.0), HAc--NaAc (pH 4.0–5.0), $\text{NaH}_2\text{PO}_4\text{--Na}_2\text{HPO}_4$ (pH 6.0–8.0), $\text{H}_3\text{BO}_3\text{--NaH}_2\text{BO}_3$ (pH 9.0–10.0), $\text{NaHCO}_3\text{--Na}_2\text{CO}_3$ (pH 11.0–12.0) and NaOH (pH 13.8). Stock standard solutions of antidepressant drugs were prepared in methanol at a concentration of 1 mg/ml and were stored at 4°C in the dark.

The SPE cartridges used were Bond-Elut (Varian, Barcelona, Spain) octadecyl (C18), octyl (C8), ethyl (C2), cyclohexyl (CH), cyanopropyl (CN) and phenyl (PH) silica bonded phases (100 mg) and Waters (Barcelona, Spain) copolymer Hydrophilic–Lipophilic Balance (HLB) sorbent (30 mg).

2.2. Instrumentation

The extraction was performed with an ASPEC XL equipment from Gilson (Villiers le Bel, France). The extracts were evaporated to dryness using a Zymark (Barcelona, Spain) Turbo Vap LV evaporator. No recovery or selectivity problems were observed when the same cartridge was used twice for plasma samples and up to 15 times with aqueous standard samples.

HPLC was used for the determination of the recoveries of the drugs eluted from the cartridges. The chromatographic system consisted on a Pharmacia LKB (Barcelona, Spain) 2248 pump, a Hewlett-Packard (Barcelona, Spain) 1100 automatic sample injector with a sample loop of 100 μ l and a Waters (Barcelona, Spain) 484 UV-visible detector. A reversed-phase Waters (Barcelona, Spain) Nova-Pack C18 column (15 cm \times 3.9 mm I.D., 4 μ m particle size) and a Waters Nova-Pack C18 guard-column (20 \times 3.9 mm I.D., 4 μ m particle size) were used. The effluent was monitored at 215 nm. The mobile phase was acetonitrile–0.02 M triethylamine (pH 5.5 with 0.75 M H_3PO_4) (35:65, v/v) delivered at a flow-rate of 1 ml/min. Organic modifier content and pH of the mobile phase were optimized for the proper separation of the analytes using the mentioned column. Triethylamine was used in order to avoid tailing peaks. The system was operated at room temperature.

3. Optimization of the extraction procedure

3.1. SPE studies in aqueous standard samples

Buffered aqueous standard samples at a concentration level of 0.5 μ g/ml were prepared daily by dilution from stock solutions using the appropriate 0.1 M aqueous buffer. The extraction was performed by the ASPEC system in a sequential mode as follows. The SPE cartridge was activated with 2 ml of methanol and washed with 1 ml of 0.1 M aqueous buffer. Then, 1 ml of buffered aqueous sample was added and the compounds of interest were eluted with 1 ml of a convenient elution liquid.

For the study of the effect on recoveries of sample pH, pure methanol was selected as a starting elution solvent. On the other hand, when recoveries were evaluated as a function of the composition of the elution solvent, methanol–1.0 M aqueous buffer mixtures were used.

3.2. SPE studies in spiked plasma samples

Blood samples were collected using sodium citrate as anticoagulant, centrifuged and plasma was

separated and stored at -20°C . Blank plasma samples were spiked with 0.5 μ g of imipramine, desipramine, maprotiline, doxepin and trazodone per ml and buffered with the appropriate 1.0 M buffer (3: 1, v/v). The SPE procedure was similar to the case of the aqueous standard samples, but after loading with 1 ml of the spiked plasma sample the cartridge was washed subsequently with 1.5 ml of aqueous acetate buffer, 100 μ l of acetonitrile and 1 ml of the convenient washing solvent prior to elution with 1 ml of the adequate elution solvent. The compositions of the washing and elution solvents used were those obtained as optima in the studies in aqueous standard samples.

The extracts from all studies were evaporated to dryness under a nitrogen stream at 45°C and reconstituted with 200 μ l of mobile phase containing 5 μ g/ml of internal standard, and 20 μ l of this solution was injected into the chromatographic system.

Recoveries were calculated against the initial amount of analytes spiked on the sample (aqueous or blank plasma), using linear calibration curves based on standard solutions of analytes and internal standard.

4. Results and discussion

When recoveries of the five test compounds from aqueous standard samples buffered at different pH values within the range 2–14 were examined by using the C18 cartridges, the most apolar, and pure methanol as elution solvent, large variations in recoveries and reproducibilities were observed with small pH changes.

In order to assure that no losses of analytes would occur in the loading of sample on the SPE cartridge, the sample was collected and analyzed after being passed through the sorbent and no chromatographic peaks corresponding to the antidepressant analytes were found. In conclusion, retention of the compounds is complete in the loading step, but 1 ml of pure methanol is not able to completely elute the analytes in some circumstances. A greater volume of methanol or a change in the nature of the elution liquid used was required.

Table 1
Recoveries (% R.S.D. of $n = 4$ determinations) of the analytes from aqueous standard samples using C18 cartridges as a function of the sample pH

	pH 4.0			pH 7.0			pH 11.0		
	MeOH	1% NH ₃ ^a	MeOH–buffer (9:1) ^b	MeOH	1% NH ₃ ^a	MeOH–buffer (9:1) ^b	MeOH	1% NH ₃ ^a	MeOH–buffer (9:1) ^b
Trazodone	86 ± 4	89 ± 1	94 ± 2	90 ± 5	83 ± 1	80 ± 1	97 ± 10	95 ± 5	93 ± 2
Doxepin	1.9 ± 0.1	82 ± 3	95 ± 1	78 ± 7	81 ± 1	74 ± 2	42 ± 8	70 ± 4	91 ± 2
Desipramine	2.1 ± 0.2	85 ± 2	87 ± 1	45 ± 9	75 ± 1	66 ± 1	77 ± 9	83 ± 4	89 ± 1
Maprotiline	3.7 ± 0.8	78 ± 4	94 ± 1	28 ± 7	78 ± 2	71 ± 1	80 ± 6	86 ± 3	88 ± 1
Imipramine	2.3 ± 0.2	71 ± 3	86 ± 1	64 ± 9	62 ± 1	77 ± 1	33 ± 5	62 ± 4	90 ± 2

^a MeOH–concentrated NH₃ (99:1, v/v).

^b Buffer is aqueous acetate buffer (pH 4.0, 1.0 M).

The antidepressants studied are basic in character, thus pK_a values for trazodone, doxepin, imipramine, desipramine and maprotiline are 6.7, 8.0, 9.4, 10.2 and 10.5, respectively. Retention of basic drugs onto modified silica is not only due to hydrophobic interactions between analyte and apolar groups of silica modified surface, but also to cation-exchange processes with charged residual silanols when the medium pH is acid enough to maintain the drug in its charged form [24–26]. In order to obtain good recoveries of analytes, all retention mechanisms must be suppressed during the elution step. This is probably the biggest source of difficulty in developing good SPE methods.

In general, organic solvents alone are inefficient in eluting the adsorbed antidepressants from the extraction cartridges [27]. Narasimhashari [28] used a relatively large volume (10 ml) of a mixture of hexane–isopropyl alcohol (9:1) to elute antidepressants from Sep-Pak C18 cartridge. The efficiency of elution can be increased by adding a competing cation such as ammonium or triethylamine to the organic elution solvent to block the charged silanol groups of the extraction cartridge [29] or by making the organic solvent acidic enough to maintain the silanol groups uncharged [30,31].

Table 1 collects the recoveries of the five antidepressants assayed at different sample pH values using different elution solvents and the C18 cartridges. Complete recoveries of the five antidepressants were found when the sample pH was 4

or 11 and methanol–aqueous acetate buffer (pH 4.0) (9:1, v/v) was used for elution. The good performance of the addition of the acetate buffer to methanol is due to the lower degree of ionization of silanol groups and the competing effect of the high concentration of sodium cation in the elution medium.

In order to select an appropriate washing solvent, the elution of the antidepressant compounds was examined for C18 cartridge as a function of the composition of the elution liquid by using mixtures of methanol and 1.0 M acetic acid–sodium acetate buffer at pH 4.0. The recoveries reached are shown in Table 2. The elution profiles obtained by plotting the recovery versus the methanol percentage of the elution solvent gives information about the best composition of the washing solvent (the one with the highest methanol percentage without eluting the drug) and the best elution solvent (the lowest methanol percentage that gives complete recovery of the drug). Fig. 1 shows the elution profiles found for the tested compounds when C18 cartridges were employed. The correct selection of the washing and elution solvents will provide the cleanest samples in the SPE process and therefore the best selectivity in the analytical method. Thus, the optimum conditions found in the aqueous standard samples study, using the apolar cartridge C18, for the five drugs were 1 ml of methanol–acetate buffer (30:70, v/v) as the washing solvent and 1 ml of methanol–acetate buffer (70:30, v/v) as the elution solvent, fixing the pH of the samples at 4.0.

Table 2

Recoveries (% R.S.D. of $n = 4$ determinations) of the analytes from aqueous standard samples at pH 4.0 using C18 cartridges as a function of the composition of the elution mixture (1 ml of methanol: 1.0 M aqueous acetate buffer, pH 4.0)

MeOH (%)	C18				
	Trazodone	Doxepin	Desipramine	Maprotiline	Imipramine
90	94.0 ± 0.2	91.9 ± 0.4	89.5 ± 0.4	91.6 ± 0.8	88 ± 1
80	96.9 ± 0.5	96.9 ± 0.6	93.9 ± 0.4	95.0 ± 0.4	92.3 ± 0.4
70	92.8 ± 0.3	94.1 ± 0.3	91.9 ± 0.4	94.2 ± 0.3	91.0 ± 0.4
60	85.1 ± 0.2	84.2 ± 0.3	64.1 ± 0.7	61.9 ± 0.8	48 ± 1
50	57.4 ± 0.7	31 ± 1	33 ± 2	32 ± 3	21 ± 3
40	18.4 ± 4	11 ± 1	3 ± 9	6 ± 7	9 ± 1
30	<0.2	<0.2	<0.2	<0.4	<0.4

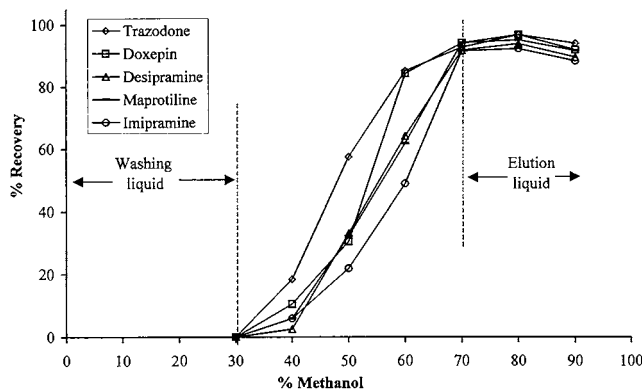


Fig. 1. Plot of the recoveries of the antidepressants from aqueous standard samples at pH 4.0 using C18 cartridges versus the composition of the elution mixture (1 ml of methanol–aqueous buffer).

Once the complete recoveries of the tested analytes on C18 were checked, the SPE from aqueous standard samples was studied with other sorbent materials using the optimum conditions for C18 (sample pH 4; washing solvent 1 ml of methanol–1.0 M acetate buffer (30:70, v/v); elution solvent 1 ml of methanol–1.0 M acetate buffer, 70:30, v/v). Good recoveries (90%) were obtained with all the sorbent materials tested (C8, C2, cyclohexyl, phenyl, cyanopropyl and HLB), except for C2 cartridges, for which poor recoveries for trazodone were found, and cyanopropyl cartridges, for which low recoveries were attained for all compounds assayed (Fig. 2).

In order to select the most appropriate sorbent material, the selectivity provided by each one was assayed using blank plasma samples spiked with 0.5 µg of imipramine, desipramine, trazodone, doxepin and maprotiline per ml. All the assayed cartridges (C18, C8, C2, CH, PH and HLB) gave rise to chromatograms with several interfering peaks from plasma endogenous components, the number of which increased the higher the hydrophobic nature of the sorbent. The cleanest chromatograms were obtained using DEC's packed with hexyl silica (CH) bonded phase. To improve even more the cleanness of the extracts, two additional washing steps were introduced prior to the application of methanol–buffer washing solvent. Once the plasma sample was applied, the cartridge was washed with 1.5 ml of aqueous acetate

buffer and then with 100 µl of acetonitrile. The volume of acetonitrile used in this washing step was limited to 100 µl since a significant decrease in the analyte recoveries (especially for trazodone) was observed when increasing the volume. Table 3 shows the recoveries obtained for the antidepressants using the three washing steps and different sorbent materials. The CH cartridges provided the best recovery and selectivity.

Other experimental variables related to the hydrodynamic performance of the ASPEC equipment were also tested using spiked plasma samples and the CH bonded phase. The main

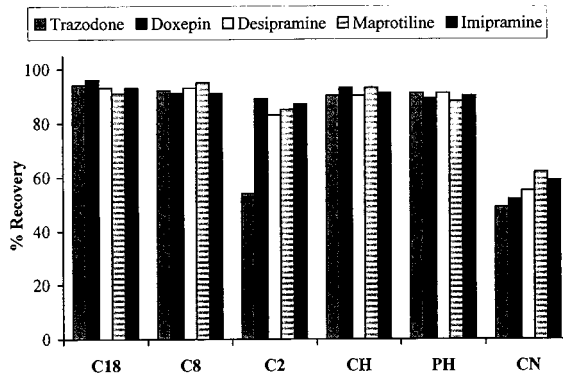


Fig. 2. Recoveries of the antidepressants from aqueous standard samples at pH 4.0 using different types of cartridges. Washing and elution solvents were 1 ml of methanol–1.0 M acetate buffer (30:70, v/v) and 1 ml of methanol–1.0 M acetate buffer (70:30, v/v), respectively.

Table 3

Recoveries (% R.S.D. of $n=4$ determinations) of the analytes from spiked plasma samples as a function of the sorbent material, using the SPE conditions optimized in aqueous standard samples

	C18	C8	C2	CH	PH	HLB
Trazodone	41 ± 2	54 ± 1	8 ± 1	53 ± 2	53 ± 2	12 ± 1
Doxepin	92 ± 2	91 ± 3	34 ± 4	84 ± 3	83 ± 2	33 ± 4
Desipramine	80 ± 3	77 ± 3	34 ± 3	81 ± 2	70 ± 3	45 ± 3
Maprotiline	77 ± 1	78 ± 4	47 ± 4	80 ± 2	72 ± 3	49 ± 1
Imipramine	74 ± 3	77 ± 3	38 ± 3	80 ± 3	74 ± 3	51 ± 2

three variables are the air volume passed through the cartridge after the sample loading and after the washing steps (inadequate drying of SPE column can cause losses in recovery), the volume of elution solvent used and the flow-rate at which the sample and elution solvent are passed through the cartridge. No significant decreases in recoveries were observed in the case of the air volume passed after the sample loading and the washing steps (volumes between 0 and 10 ml were tested). Antidepressant drugs are highly protein-bound in plasma, thus their recovery by SPE can be variable and low due to incomplete liberation of the drugs bound to proteins. The simplest approach to minimize the effect of protein binding is to pass the sample through the sorbent at a low rate [32]. Finally, losses in recoveries were found when volumes of elution solvent lower than 0.5 ml (Fig. 3A) and flow-rate of the elution process higher than 1.0 ml/min (Fig. 3B) were used.

Thus, the optimum conditions finally proposed for the SPE of the tested compounds in plasma samples were (total cycle 18.1 min.):

- Cartridge conditioning (flow-rate 6.0 ml/min; air volume 1 ml): the cartridge (CH) was first conditioned with 2.0 ml of methanol and then with 1.0 ml of acetate buffer (pH 4.0, 0.1 M).
- Loading with sample (flow-rate 1 ml/min; air volume 1.5 ml): 1 ml of sample buffered with acetate buffer (pH 4.0, 1 M) was dispensed on the cartridge.
- Washing (flow-rate 3.0 ml/min; air volume 2 ml): the cartridge was subsequently washed with 1.5 ml of acetate buffer (pH 4.0, 0.1 M), 100 μ l of acetonitrile and 1 ml of methanol–acetate buffer (pH 4.0, 1.0 M) (30:70, v/v).

- Elution (flow-rate 1 ml/min; air volume 2 ml): 0.5 ml of methanol–acetate buffer (pH 4.0, 1.0 M) (70:30, v/v) was applied to the cartridge.

Typical chromatograms of a blank plasma extract and an extract of blank plasma spiked with the five antidepressant are given in Fig. 4. The extract of drug free plasma shows the absence of endogenous peaks from the plasma matrix at the retention times corresponding to analytes.

Plasma samples spiked with different concentration levels of the drugs were analyzed using the

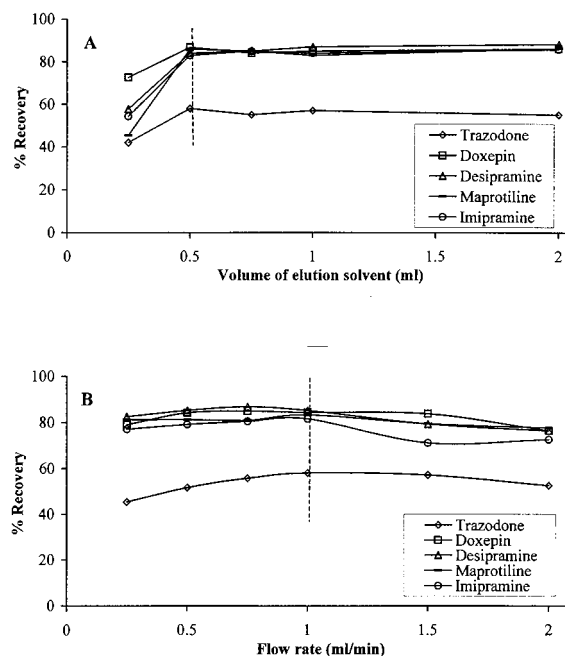


Fig. 3. Effects on recoveries of the volume of elution solvent passed through the SPE column (A) and the flow-rate of the elution step (B).

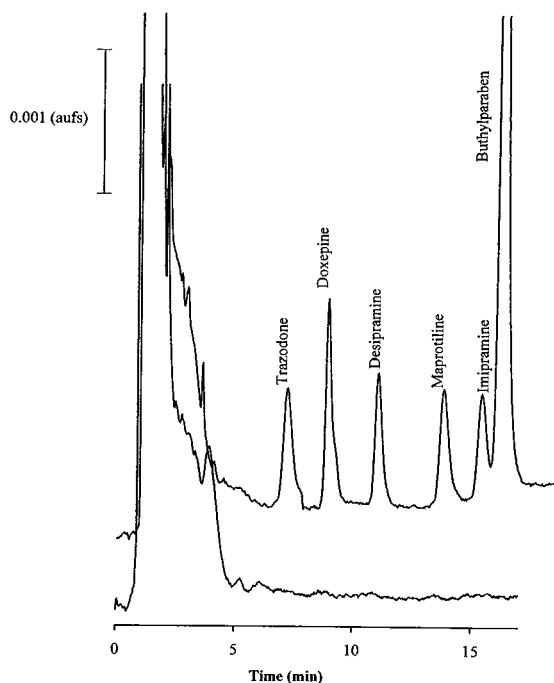


Fig. 4. Typical chromatograms obtained by coupling the semi-automated SPE sample preparation to HPLC: (A) blank plasma and (B) plasma sample spiked with 0.2 µg each of trazodone, doxepin, desipramine, maprotiline and imipramine per ml, respectively.

optimum SPE conditions. The peak area ratios (analyte/internal standard) showed a linear relationship with the concentration over the range 0.005–2.0 µg/ml for the five antidepressants. The equations obtained were:

$$\text{Trazodone: } y = (0.00238 \pm 0.00005)x + (0.02 \pm 0.03) \quad (r^2 = 0.9991)$$

$$\text{Doxepin: } y = (0.00314 \pm 0.00003)x + (0.03 \pm 0.02) \quad (r^2 = 0.9991)$$

$$\text{Desipramine: } y = (0.00202 \pm 0.00002)x + (0.01 \pm 0.02) \quad (r^2 = 0.9991)$$

$$\text{Maprotiline: } y = (0.00225 \pm 0.00003)x + (0.02 \pm 0.02) \quad (r^2 = 0.9990)$$

$$\text{Imipramine: } y = (0.00209 \pm 0.00002)x + (0.01 \pm 0.02) \quad (r^2 = 0.9991)$$

where y is the peak–area ratio and x the drug concentration in plasma samples (µg/ml).

Using the optimum SPE conditions, the absolute recoveries of the analytes at three different concentration levels (0.01, 0.1 and 1 µg/ml) were examined. The mean absolute recoveries for trazodone, doxepin, desipramine, maprotiline and imipramine were 58 ± 2 , 84 ± 3 , 83 ± 3 , 83 ± 3 and $82 \pm 2\%$, respectively. The precision of the bioanalytical method, expressed by the coefficient of variation (CV), was estimated by measuring the within-day and between-day repeatabilities at three different concentration levels, 0.01, 0.1 and 1.0 µg/ml (Table 4). Intra-day repeatabilities were less than 6% and inter-day repeatabilities less than 9% in all cases.

The limits of detection, calculated as the spiked analyte concentration that produces a chromatographic peak whose height is three times the baseline noise of chromatograms of blank plasma samples, were 0.001 µg/ml for trazodone, doxepin and desipramine and 0.002 µg/ml for maprotiline and imipramine.

Finally, the method was applied to plasma samples from healthy subjects following the intake of an oral dose of 25 mg of imipramine hydrochloride (Fig. 5A), 75 mg of doxepin hydrochloride (Fig. 5B), 75 mg of maprotiline hydrochloride (Fig. 5C) or 100 mg of trazodone hydrochloride (Fig. 5D), respectively.

5. Conclusion

When analysing drugs from biological fluids using SPE, the selection of the convenient extraction conditions (sample pH, composition of the washing and elution solvents, and nature of the sorbent material) provides the cleanest samples for the later chromatographic analysis and is an important factor in the selectivity of the entire analytical method. Losses in recoveries and/or poor repeatabilities in the SPE processes owing to the presence of mixed interactions on the silica based sorbent surface can be avoided by adding appropriate modifiers to the solvents employed in the extraction.

Table 4
 Within-day ($n = 4$) and between-day ($n = 3$) repeatabilities of the SPE–HPLC determination method

Amount added ($\mu\text{g/ml}$)	Trazodone		Doxepin		Desipramine		Maprotiline		Imipramine	
	Amount found ($\mu\text{g/ml}$)	CV (%)	Amount found ($\mu\text{g/ml}$)	CV (%)	Amount found ($\mu\text{g/ml}$)	CV (%)	Amount found ($\mu\text{g/ml}$)	CV (%)	Amount found ($\mu\text{g/ml}$)	CV (%)
<i>Intra-day re-peatability</i> ($n = 4$)										
0.01	0.0056 ± 0.0003	5.5	0.0086 ± 0.0004	4.6	0.0082 ± 0.0004	4.2	0.0083 ± 0.0004	5.2	0.0085 ± 0.0004	5.0
0.1	0.056 ± 0.002	3.9	0.083 ± 0.003	3.9	0.085 ± 0.002	2.1	0.083 ± 0.003	3.0	0.083 ± 0.002	2.7
1	0.59 ± 0.02	2.9	0.83 ± 0.03	3.4	0.82 ± 0.02	2.6	0.83 ± 0.02	1.8	0.82 ± 0.02	2.5
<i>Inter-day re-peatability</i> ($n = 3$)										
0.01	0.0059 ± 0.0005	8.6	0.0081 ± 0.0005	6.1	0.0089 ± 0.0009	6.6	0.0087 ± 0.0007	8.2	0.0081 ± 0.0006	7.7
0.1	0.061 ± 0.004	6.9	0.089 ± 0.005	5.9	0.081 ± 0.006	7.2	0.080 ± 0.004	4.4	0.080 ± 0.004	5.6
1	0.55 ± 0.04	7.7	0.83 ± 0.04	5.1	0.83 ± 0.03	3.8	0.85 ± 0.04	4.6	0.86 ± 0.05	5.8

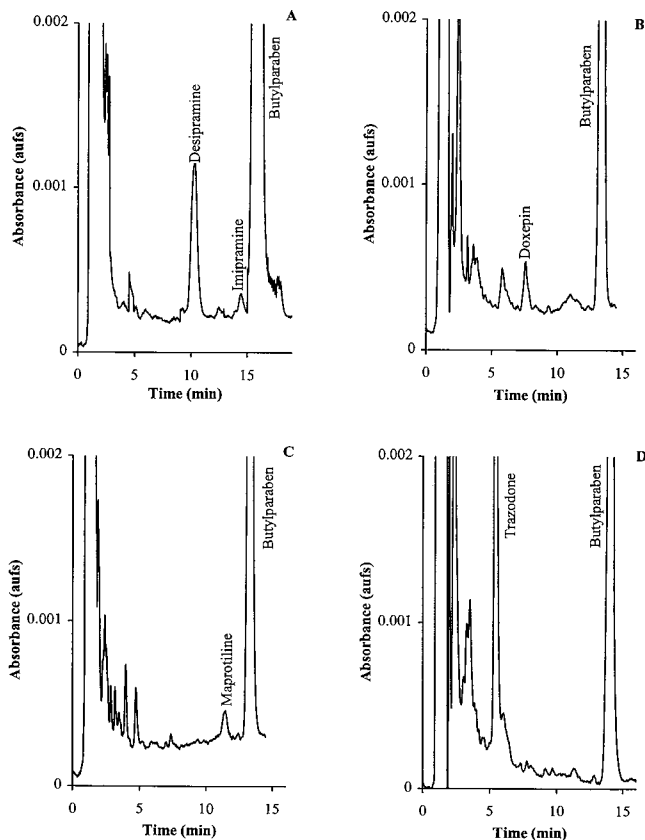


Fig. 5. Chromatograms corresponding to plasma samples from four healthy volunteers following the intake of an oral dose of: (A) 25 mg of imipramine hydrochloride (blood collected after 4 h of intake); (B) 75 mg of doxepin hydrochloride (blood collected after 2.5 h of intake); (C) 75 mg of maprotiline hydrochloride (blood collected after 8 h of intake); (D) 100 mg of trazodone hydrochloride (blood collected after 2 h of intake).

Acknowledgements

These studies were supported by the Basque Government (project PI95/002) and the University of the Basque Country (UPV, project EA003/94).

References

- [1] J.R. Roberts, J.A. Tafuri, in: L.M. Haddad, J.F. Winchester (Eds.), *Clinical Management of Poisoning and Drug Overdose*, W.B. Saunders, Philadelphia, PA, 1990, p. 402.
- [2] L.F. Gram, P. Kragh-Sorensen, C.B. Kristensen, M. Moller, O.L. Peredsen, P. Thayssen, in: P.J. Clayton, J.E. Barrett (Eds.), *Treatment of Depression: Old Controversies and Approches*, Raven Press, New York, 1983, p. 85.
- [3] M. Asberg, in: E. Usdin, M. Åsberg, L. Bertilsson, F. Sjöqvist (Eds.), *Frontiers in Biochemical and Pharmacological Research in Depression*, Raven Press, New York, 1984, p. 399.
- [4] S. Ulrich, J. Martens, *J. Chromatogr. B* 696 (1997) 217.
- [5] P. Lillsunde, T. Korte, *J. Anal. Toxicol.* 15 (1991) 71.
- [6] M.L. Rao, U. Staberock, P. Baumann, C. Hiemke, *Clin. Chem.* 40 (6) (1994) 929.
- [7] P.M. Kabra, *Clin. Chim. Acta* 111 (1981) 123.
- [8] B.K. Kudelin, L.V. Gavrilina, Y.L. Kaminsku, *J. Chromatogr.* 636 (1993) 243.
- [9] A. Poklis, L.E. Edinboro, J.S. Lee, C.R. Crooks, *Clin. Toxicol.* 35 (1) (1997) 77.
- [10] J.A. Politou, K. Tsarpalis, A. Koutselinis, *J. Liq. Chromatogr.* 17 (18) (1994) 3969.
- [11] A. Tracqui, P. Kintz, P. Mangin, *J. Forensic Sci.* 40 (2) (1995) 254.
- [12] E. Tanaka, M. Terada, T. Nakamura, S. Misawa, C. Wakasugi, *J. Chromatogr. B* 692 (1997) 405.

- [13] J.P. Foglia, D. Sorisio, J.M. Perel, *J. Chromatogr. B* 572 (1991) 247.
- [14] R.N. Gupta, *J. Chromatogr. B* 576 (1992) 183.
- [15] K.K. Nielsen, K. Brøsen, *J. Chromatogr. B* 612 (1993) 87.
- [16] A.G. Chen, Y.K. Wing, H. Chiu, S. Lee, C.N. Chen, K. Chan, *J. Chromatogr. B* 693 (1) (1997) 153.
- [17] K. Keiko, J. Narumi, I. Tohru, *J. Anal. Toxicol.* 21 (3) (1997) 185.
- [18] G. Aymard, P. Livi, Y. Thu, B. Diquet, *J. Chromatogr. B* 700 (1997) 183.
- [19] T.R. Krishnan, I.J. Ibrahim, *J. Pharm. Biomed. Anal.* 12 (1994) 287.
- [20] R.E. Major, *LC-GC Int.* 13 (1995) 542.
- [21] T.W. Hermann, *Chem. Anal.* 42 (1997) 1.
- [22] S. Hartter, B. Hermes, C. Hiemke, *J. Liq. Chromatogr.* 18 (17) (1995) 3495.
- [23] H. Lindeman, S.J.F. Hoekstra-Oussoren, *J. Chromatogr. B* 689 (1997) 221.
- [24] B. Law, S. Weir, N.A. Ward, *J. Pharm. Biomed. Anal.* 10 (1992) 167.
- [25] R.J. Ruane, I.D. Wilson, G.P. Tomkinson, in: E. Reid (Ed.), *Bioanalysis of Drugs and Metabolites, Especially Anti-Inflammatory and Cardiovascular*, vol. 18, Plenum Press, New York, 1997, p. 221.
- [26] G.M. Roberts, C.S. Henn, *Biomed. Chromatogr.* 1 (1986) 49.
- [27] V. Makro, L. Šoltes, K. Rodová, *J. Chromatogr. Sci.* 28 (1990) 403.
- [28] N. Narasimhashari, *J. Chromatogr.* 225 (1981) 189.
- [29] M. Mazhar, S. Binder, *J. Chromatogr.* 497 (1989) 201.
- [30] R.N. Gupta, M. Steiner, *J. Liq. Chromatogr.* 13 (1990) 3785.
- [31] G. Musch, D.L. Massart, *J. Chromatogr.* 432 (1988) 209.
- [32] W. Lin, P.D. Frade, *Ther. Drug Monit.* 9 (1987) 448.

Extraction equilibria of various metal picrates with 19-crown-6 between benzene and water. Effect of the extra methylene group on extraction ability and selectivity

Shoichi Katsuta ^{a,*}, Masaomi Kanazawa ^a, Yasuyuki Takeda ^a, Mikio Ouchi ^b

^a Department of Chemistry, Faculty of Science, Chiba University, Yayoi-cho, Inage-ku, Chiba 263-8522, Japan

^b Department of Applied Chemistry, Faculty of Engineering, Himeji Institute of Technology, 2167 Shosha, Himeji, Hyogo 671-2201, Japan

Received 28 September 1998; received in revised form 8 February 1999; accepted 11 February 1999

Abstract

The overall extraction equilibrium constants (K_{ex}) of picrates of Li^+ , Na^+ , K^+ , Rb^+ , Cs^+ , Ag^+ , Tl^+ , and Sr^{2+} with 19-crown-6 (19C6) were determined between benzene and water at 25°C. The K_{ex} values were analyzed into the constituent equilibrium constants, i.e. the extraction constant of picric acid, the distribution constant of the crown ether, the formation constant of the metal ion–crown ether complex in water, and the ion-pair extraction constant of the complex cation with the picrate anion. The effects of an extra methylene group of 19C6 on the extraction ability and selectivity are discussed in detail by comparing the constituent equilibrium constants of 19C6 with those of 18-crown-6 (18C6). The K_{ex} value of 19C6 for each metal ion is lower than that of 18C6, which is mostly attributed to the higher lipophilicity of 19C6. The extraction ability of 19C6 for the univalent metal ions decreases in the order $\text{Tl}^+ > \text{K}^+ > \text{Rb}^+ > \text{Ag}^+ > \text{Cs}^+ > \text{Na}^+ \gg \text{Li}^+$, which is the same as that observed for 18C6. The difference in $\log K_{\text{ex}}$ between the univalent metals is generally smaller for 19C6 than for 18C6. The extraction selectivity of 19C6 is governed by the selectivity in the ion-pair extraction, whereas that of 18C6 depends on both the selectivities in the ion-pair extraction and in the complexation in water. © 1999 Elsevier Science B.V. All rights reserved.

Keywords: Solvent extraction; Constituent equilibria; Metal picrates; 19-Crown-6; Effect of extra methylene group

1. Introduction

The complexing ability and the selectivity of crown ethers for ions are considered to be governed by various factors such as size and shape of

cavity, type and number of donor atoms, and ring conformation [1]. 19-Crown-6 (19C6) has an extra methylene group than 18-crown-6 (18C6). By using CPK models [2], the cavity radius of 19C6 is evaluated to be 1.35 Å, which is almost the same as that of 18C6 (1.30 Å). These two crown ethers have the same number of donor oxygen atoms. However, the CPK models reveal that the less symmetrical arrangement of the oxygen atoms

* Corresponding authors. Fax: +81-43-290-2781.

E-mail addresses: katsuta@scichem.c.chiba-u.ac.jp (S. Katsuta), takeda@scichem.c.chiba-u.ac.jp (Y. Takeda)

induced by the extra methylene group leads to an unfavorable conformation for complexation compared with symmetrical 18C6. Ouchi et al. [2] synthesized *x*-crown-6 ethers (*x* = 19, 20, 22) and examined their extraction ability for Na⁺, K⁺, Rb⁺, and Cs⁺ into dichloromethane. They reported that the introduction of extra methylene groups into the 18C6 ring decreases the extraction ability. Recently, formation constants of 19C6 complexes with various uni- and bivalent metal ions were determined in water by conductometry; for the metal ions which are larger in size than Na⁺, the formation constants of the 19C6 complexes are smaller than those of the 18C6 ones, but the contrary holds for the cations smaller than Na⁺ [3]. One should note that the extraction-ability and -selectivity do not always reflect the complexation-ability and -selectivity in water, because the overall extraction equilibrium consists of several equilibria, e.g. the distribution of the crown ether, the formation of the metal ion–crown ether complex in water, and the ion-pair extraction of the complex cation with the counter anion. In order to understand the effect of the extra methylene group on the extraction-ability and -selectivity of 19C6 from the standpoint of equilibrium, it is necessary to evaluate the overall extraction equilibrium on the basis of the constituent equilibria.

In this study, the overall extraction equilibrium constants of various univalent metal picrates and strontium(II) picrate with 19C6 in a benzene–water system were determined, and analyzed into four constituent equilibria. Each of the equilibrium constants was compared with that of 18C6, and the effect of the extra methylene group was discussed quantitatively.

2. Experimental

2.1. Materials

The preparation of 19C6 was just the same as that described in the previous paper [2]. Benzene, picric acid, LiOH·H₂O, NaOH, KOH, RbOH, CsOH, AgNO₃, and TlNO₃ were of analytical grade; Sr(NO₃)₂ was a suprapur-grade reagent

from Merck. Benzene was washed three times with deionized water. The concentrations of the metal hydroxides and picric acid in stock solutions were determined by acid–base titrations. The water used was distilled and further purified with a Milli-Q system (Millipore).

2.2. Extraction of metals

10 ml of benzene and an equal volume of an aqueous solution containing 19C6 (2.3×10^{-4} – 2.0×10^{-2} M; 1 M is 1 mol dm⁻³), picric acid (1.0×10^{-4} – 1.6×10^{-2} M), and metal hydroxide or nitrate (2.3×10^{-3} – 1.0×10^{-1} M) were placed in a stoppered glass tube (30 ml), shaken in a thermostated water bath at $25 \pm 0.2^\circ\text{C}$ for 2 h, and centrifuged. The shaking period was confirmed to be sufficient to attain equilibrium. The pH of the aqueous phases measured by a glass electrode was 11.5–12.5 and 2.2–3.2 for the metal hydroxide and nitrate systems, respectively. A 5 ml portion of the benzene phase was pipetted into a beaker and evaporated to dryness. The residue containing an alkali metal was dissolved in a 5 ml 1.0×10^{-2} M NaOH aqueous solution; the residue containing Ag, Tl, or Sr was dissolved in a 1.0×10^{-2} M nitric acid aqueous solution. The concentrations of alkali metals were obtained through spectrophotometric determination of picrate ($\lambda_{\text{max}} = 356$ nm, $\epsilon = 1.45 \times 10^4$ cm⁻¹ M⁻¹). The concentrations of Ag, Tl, and Sr were determined with a polarized zeeman atomic absorption spectrophotometer (Hitachi Z-6100) at 328.1, 276.8, and 460.7 nm, respectively. It was found that there was no or a slight extraction in the absence of 19C6. Extractions of Ca²⁺ and Ba²⁺ were also conducted in a similar manner; however, the concentrations of the metals extracted are too low to determine by atomic absorption spectrophotometry.

2.3. Distribution of 19C6

12 ml of benzene and an equal volume of an aqueous solution of 19C6 (1.8×10^{-4} – 3.8×10^{-3} M) in a stoppered glass tube (No. 0) were shaken for 2 h at $25 \pm 0.2^\circ\text{C}$, and centrifuged. A 10 ml portion of the benzene phase was transferred into

a beaker and evaporated to dryness. After the residue was dissolved in 10 ml water, a 9 ml portion of the aqueous solution was transferred into another tube (No. 1) where 9 ml of dichloromethane (DCM) and 9 ml of an aqueous solution saturated with potassium picrate were placed, and the tube was shaken; by this operation, 19C6 was extracted as a 19C6–potassium picrate 1:1:1 complex into DCM. A 16 ml portion of the aqueous phase of the tube No. 1 was further shaken with 8 ml of DCM in a tube (No. 2) to complete the extraction of 19C6. In order to complete the complexation of 19C6 with potassium picrate in DCM, 8 and 7 ml of the DCM phases of the tubes No. 1 and No. 2 were shaken with equal volumes of the saturated potassium picrate solution in tubes No. 3 and No. 4, respectively. 7 and 6 ml of the aqueous phases of the tubes No. 3 and 4 were shaken again with equal volumes of DCM in tubes No. 5 and 6, respectively. Four milliliters of the DCM phases in the tubes No. 3–6 are transferred into beakers and evaporated to dryness. The residues were dissolved in 4 ml of a 0.01 M NaOH aqueous solution, and the concentrations of picrate were determined spectrophotometrically. From the sum of the picrate concentrations, the 19C6 concentration of the benzene phase in the tube No. 0 was calculated. The distribution constant determined was $(3.91 \pm 0.10) \times 10^{-1}$ as the average of 11 measurements.

3. Results and Discussion

3.1. Analysis of extraction equilibria

The overall extraction equilibrium constant of a metal cation (M^{m+}) with a crown ether (L) and picric acid (HA) is defined as

$$K_{\text{ex}} = \frac{[\text{MLA}_m]_{\text{o}}[\text{H}^+]^m}{[\text{M}^{m+}][\text{L}]_{\text{o}}[\text{HA}]_{\text{o}}^m} \quad (1)$$

where the subscript ‘o’ and the lack of a subscript denote the species in the organic and aqueous phases, respectively. The overall extraction constant can be expressed using the distribution constant of the crown ether ($K_{\text{D,L}} = [\text{L}]_{\text{o}}[\text{L}]^{-1}$), the

extraction constant of picric acid ($K_{\text{ex,HA}} = [\text{HA}]_{\text{o}}[\text{H}^+]^{-1}[\text{A}^-]^{-1}$), the formation constant of a metal ion–crown ether complex in water ($K_{\text{ML}} = [\text{ML}^{m+}][\text{M}^{m+}]^{-1}[\text{L}]^{-1}$), and the ion-pair extraction constant of the complex cation with the picrate anion ($K_{\text{ex,ip}} = [\text{MLA}_m]_{\text{o}}[\text{ML}^{m+}]^{-1}[\text{A}^-]^{-m}$):

$$K_{\text{ex}} = K_{\text{ML}}K_{\text{ex,ip}}^{-1}K_{\text{D,L}}^{-1}K_{\text{ex,HA}}^{-m} \quad (2)$$

The distribution ratio of the metal is considered to be expressed as

$$D = \frac{[\text{MLA}_m]_{\text{o}}}{[\text{M}^{m+}] + [\text{ML}^{m+}] + [\text{MLA}_m]} \quad (3)$$

Assuming that $[\text{M}^{m+}] \gg [\text{ML}^{m+}] + [\text{MLA}_m]$, Eq. (3) can be transformed into

$$D = \frac{[\text{MLA}_m]_{\text{o}}}{[\text{M}^{m+}]} = K_{\text{ex}}K_{\text{ex,HA}}^m[\text{L}]_{\text{o}}[\text{A}^-]^m \quad (4)$$

In this case, the concentrations, $[\text{M}^{m+}]$, $[\text{L}]_{\text{o}}$ and $[\text{A}^-]$, are calculated as follows:

$$[\text{M}^{m+}] = [\text{M}]_{\text{t}} - [\text{MLA}_m]_{\text{o}} \quad (5)$$

$$[\text{L}]_{\text{o}} = \frac{[\text{L}]_{\text{t}} - [\text{MLA}_m]_{\text{o}}}{1 + K_{\text{D,L}}^{-1}} \quad (6)$$

$$[\text{A}^-] = \frac{[\text{HA}]_{\text{t}} - m[\text{HLA}_m]_{\text{o}}}{1 + (K_{\text{HA}} + K_{\text{ex,HA}})[\text{H}^+]} \quad (7)$$

where the subscript ‘t’ denotes the total concentration and $K_{\text{HA}} = [\text{HA}][\text{H}^+]^{-1}[\text{A}^-]^{-1}$. The values of $K_{\text{ex,HA}}$ and K_{HA} at 25°C are 247 [4] and 1.9₅ [5], respectively. Plots of $\log(D/[\text{A}^-]^m)$ vs. $\log[\text{L}]_{\text{o}}$ are shown in Fig. 1. Each plot gives a straight line with a slope of unity, proving the validity of Eq. (4). It was also confirmed that a plot of $\log(D/[\text{L}]_{\text{o}})$ vs. $\log[\text{A}^-]$ for Sr^{2+} gives a straight line with a slope of two, as expected from Eq. (4).

The K_{ex} values were determined from Eq. (1) by using the $[\text{L}]_{\text{o}}$, $[\text{M}^{m+}]$ and $[\text{HA}]_{\text{o}}$ values calculated from the following equations in which the formation of ML^{m+} in the aqueous phase is considered:

$$[\text{L}]_{\text{o}} = \frac{[\text{L}]_{\text{t}} - [\text{MLA}_m]_{\text{o}}}{1 + K_{\text{D,L}}^{-1} + K_{\text{ML}}K_{\text{D,L}}^{-1}[\text{M}^{m+}]} \quad (8)$$

$$[\text{M}^{m+}] = \frac{[\text{M}]_{\text{t}} - [\text{MLA}_m]_{\text{o}}}{1 + K_{\text{ML}}K_{\text{D,L}}^{-1}[\text{L}]_{\text{o}}} \quad (9)$$

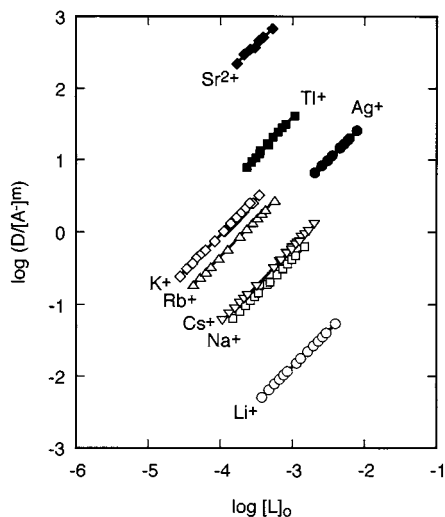


Fig. 1. Plots of $\log(D/[A^-]^m)$ vs. $\log [L]_o$ for solvent extraction of uni- ($m = 1$) and bivalent ($m = 2$) metal picrates with 19C6.

$$[HA]_o = \frac{[HA]_t - m[MLA_m]_o}{1 + ([H^+]^{-1} + K_{HA})K_{ex,HA}^{-1}} \quad (10)$$

The K_{ex} and $K_{ex,ip}$ obtained are summarized in Table 1, together with the K_{ML} values used for calculations [3]. For comparison, the equilibrium constants for 18C6 [3,4,6,8–10] are also listed in

Table 1, where the K_{ex} values were recalculated by using Eqs. (8)–(10) and $K_{D,L} = 5.32 \times 10^{-2}$ [7].

The extraction constants of Ag^+ and Tl^+ with the picrate anion ($K_{ex,MA} = [MA]_o[M^+]^{-1}[A^-]^{-1}$) were reported previously: $\log K_{ex,MA} = -2.65$ [11] and -3.07 [12] for Ag^+ and Tl^+ , respectively. Using these values, the formation constants of the MLA complexes in the benzene phase ($K_{MLA,o} = [MLA]_o/[MA]_o^{-1}[L]_o^{-1}$) were obtained by the equation $K_{MLA,o} = K_{ex}/K_{ex,MA}$: $\log K_{MLA,o} = 3.56, 5.11, 4.78,$ and 7.06 for $AgA-19C6, TlA-19C6, AgA-18C6,$ and $TlA-18C6,$ respectively. The MA forms a less stable complex with 19C6 in benzene than with 18C6. For both 19C6 and 18C6, the $K_{MLA,o}$ of Tl^+ is always greater than the corresponding one of Ag^+ , which agrees with the size-fit concept. The selectivity of 19C6 for TlA over for AgA is lower than that of 18C6. It was reported that the extra methylene group of 19C6 generally decreases the complex stability and the selectivity for M^+ in water [3]. The same is true for the MA in benzene.

3.2. Extraction ability of 19C6

From Table 1, the difference in $\log K_{ex}$ between 19C6 and 18C6, $\log\{K_{ex}(19C6)/K_{ex}(18C6)\}$, is al-

Table 1

Summary of the equilibrium constants in the extraction of metal picrates with 19C6 and 18C6 between benzene and water at 25°C

Metal ion	r_M (Å) ^a	$\log K_{ex}$			$\log K_{ML}$			$\log K_{ex,ip}$ ^b		
		19C6	18C6 ^c	(19C6–18C6) ^d	19C6 ^e	18C6	(19C6–18C6) ^d	19C6	18C6	(19C6–18C6) ^d
Li ⁺	0.76	-1.26 ± 0.00	-0.37	(-0.89)	0.76	0.0 ^f	(0.8)	-0.04	0.8	(-0.8)
Na ⁺	1.02	0.24 ± 0.00	1.07	(-0.83)	0.93	0.73 ^e	(0.20)	1.29	1.46	(-0.17)
K ⁺	1.38	1.56 ± 0.01	3.62	(-2.06)	1.27	2.03 ^{g,h}	(-0.76)	2.27	2.71	(-0.44)
Rb ⁺	1.52	1.27 ± 0.01	3.11	(-1.84)	1.33	1.56 ^h	(-0.23)	1.92	2.67	(-0.75)
Cs ⁺	1.67	0.38 ± 0.02	2.01	(-1.63)	0.71	0.99 ^h	(-0.28)	1.65	2.14	(-0.49)
Ag ⁺	1.15	0.91 ± 0.00	2.13	(-1.22)	0.93	1.50 ^h	(-0.57)	1.96	1.75	(0.21)
Tl ⁺	1.50	2.04 ± 0.02	3.99	(-1.95)	1.08	2.27 ^h	(-1.19)	2.94	2.84	(0.10)
Sr ²⁺	1.18	3.35 ± 0.02	4.93	(-1.58)	1.83	2.72 ^h	(-0.89)	5.90	5.72	(0.18)

^a Ref. [13].

^b Calculated from $\log K_{ex,ip} = \log K_{ex} - \log K_{ML} + \log K_{D,L} + m \log K_{ex,HA}$; $m = 1$ for univalent metal ions and $m = 2$ for Sr^{2+} .

^c Refs. [4,6] (see text).

^d $\log\{K(19C6)/K(18C6)\}$.

^e Ref. [3].

^f Ref. [8].

^g Ref. [9].

^h Ref. [10].

ways negative, proving that the introduction of an extra methylene group in the 18C6 ring decreases the extraction constant. The absolute value of $\log\{K_{\text{ex}}(19\text{C6})/K_{\text{ex}}(18\text{C6})\}$ decreases in the order $\text{K}^+ > \text{Tl}^+ > \text{Rb}^+ > \text{Cs}^+ \approx \text{Sr}^{2+} > \text{Ag}^+ > \text{Li}^+ \approx \text{Na}^+$. From the ionic radii of the metals (r_{M}) [13], it can be seen that the decrease in $\log K_{\text{ex}}$ from 18C6 to 19C6 caused by the extra methylene group is relatively large for the size-fitting and -misfitting larger cations, whereas is small for the size-misfitting smaller cations.

According to Eq. (2), the difference in $\log K_{\text{ex}}$ between two crown ethers, L_1 and L_2 , for a given metal ion can be explained in terms of the differences in $\log K_{\text{ML}}$, $\log K_{\text{ex,ip}}$, and $\log K_{\text{D,L}}$:

$$\log \frac{K_{\text{ex}}(L_1)}{K_{\text{ex}}(L_2)} = \log \frac{K_{\text{ML}}(L_1)}{K_{\text{ML}}(L_2)} + \log \frac{K_{\text{ex,ip}}(L_1)}{K_{\text{ex,ip}}(L_2)} - \log \frac{K_{\text{D,L}}(L_1)}{K_{\text{D,L}}(L_2)} \quad (11)$$

The $\log\{K_{\text{ML}}(19\text{C6})/K_{\text{ML}}(18\text{C6})\}$ is negative for all the metal ions except Li^+ and Na^+ ; the lower complexation ability of 19C6 for the metal ions of larger sizes than Na^+ is ascribed to the less favorable orientation of the donor oxygen atoms to the ions owing to the unsymmetrical structure of 19C6 [3]. The $\log\{K_{\text{ex,ip}}(19\text{C6})/K_{\text{ex,ip}}(18\text{C6})\}$ is negative for the alkali metal ions, but positive for Ag^+ , Tl^+ , and Sr^{2+} . The $\log\{K_{\text{D,L}}(19\text{C6})/K_{\text{D,L}}(18\text{C6})\}$ is positive (0.86) because of the lipophilicity of the extra methylene group. For Li^+ and Na^+ , contributions of $\log\{K_{\text{ML}}(19\text{C6})/K_{\text{ML}}(18\text{C6})\}$ and $\log\{K_{\text{ex,ip}}(19\text{C6})/K_{\text{ex,ip}}(18\text{C6})\}$ cancel each other, resulting in $\log\{K_{\text{ex}}(19\text{C6})/K_{\text{ex}}(18\text{C6})\} \approx \log\{K_{\text{D,L}}(19\text{C6})/K_{\text{D,L}}(18\text{C6})\}$ (Eq. (11) and Table 1). For K^+ , Rb^+ , and Cs^+ , the two terms concerning K_{ML} and $K_{\text{ex,ip}}$ in Eq. (11) are both negative, leading to the smaller $\log\{K_{\text{ex}}(19\text{C6})/K_{\text{ex}}(18\text{C6})\}$ values of K^+ , Rb^+ , and Cs^+ than those of Li^+ and Na^+ because the term $\log\{K_{\text{D,L}}(19\text{C6})/K_{\text{D,L}}(18\text{C6})\}$ in Eq. (11) is constant. In the case of Ag^+ , Tl^+ , and Sr^{2+} , the negative contributions of $\log\{K_{\text{ML}}(19\text{C6})/K_{\text{ML}}(18\text{C6})\}$ and $\log\{K_{\text{D,L}}(19\text{C6})/K_{\text{D,L}}(18\text{C6})\}$ surpass the positive one of $\log\{K_{\text{ex,ip}}(19\text{C6})/K_{\text{ex,ip}}(18\text{C6})\}$, resulting in the large negative $\log\{K_{\text{ex}}(19\text{C6})/K_{\text{ex}}(18\text{C6})\}$ value. The lower ex-

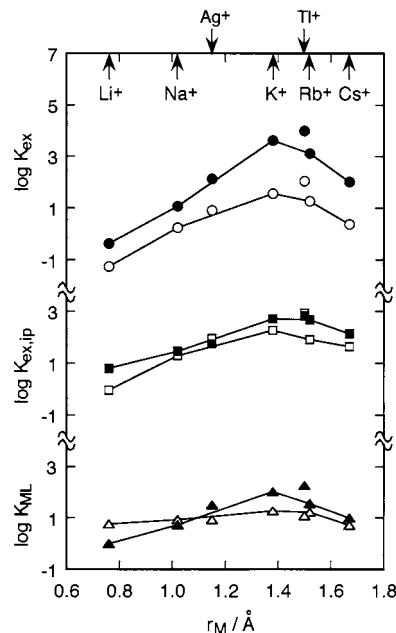


Fig. 2. Plots of $\log K_{\text{ex}}$, $\log K_{\text{ex,ip}}$, and $\log K_{\text{ML}}$ vs. ionic radii of univalent metals. \circ \bullet : K_{ex} ; \square \blacksquare : $K_{\text{ex,ip}}$; \triangle \blacktriangle : K_{ML} . The open symbols denote 19C6, and the filled ones 18C6. The solid lines join the values for the alkali metals.

traction constant of 19C6 is mostly attributed to the higher lipophilicity of 19C6 compared with 18C6.

The $K_{\text{ex,ip}}$ is expressed as a product of two elementary equilibria, i.e. the ion-pair formation constant in water and the distribution constant of the ion-pair. These elementary equilibrium constants are necessary for a detailed discussion of the ion-pair extraction equilibrium. The underlying constants have been determined for the 18C6–alkali metal picrate systems [7], but not for the 19C6 systems; thus no further discussion of $K_{\text{ex,ip}}$ can be given at this stage.

3.3. Extraction selectivity of 19C6

In Fig. 2, the equilibrium constants of 19C6 and 18C6 for the univalent metals are plotted against the ionic radii of the metals. The K_{ex} value of 19C6 decreases in the order $\text{Tl}^+ > \text{K}^+ > \text{Rb}^+ > \text{Ag}^+ > \text{Cs}^+ > \text{Na}^+ \gg \text{Li}^+$, which is the same as that observed for 18C6. The K_{ex} order for

the alkali metals is in agreement with the size-fit concept, i.e. the metal which is more closely fitted into the cavity is more extractable. The K_{ML} and $K_{ex,ip}$ of 19C6 for the univalent metals decrease in the order $Rb^+ \approx K^+ > Tl^+ > Ag^+ = Na^+ > Li^+ \approx Cs^+$ and $Tl^+ > K^+ > Ag^+ \approx Rb^+ > Cs^+ > Na^+ \gg Li^+$, respectively; the sequence of K_{ex} is almost consistent with that of $K_{ex,ip}$, but considerably different from that of K_{ML} . Whereas the K_{ML} and $K_{ex,ip}$ of 18C6 decrease in the order $Tl^+ > K^+ > Rb^+ \approx Ag^+ > Cs^+ > Na^+ > Li^+$ and $Tl^+ > K^+ \approx Rb^+ > Cs^+ > Ag^+ > Na^+ > Li^+$, respectively; the sequence of K_{ex} is almost the same as both the sequences of K_{ML} and $K_{ex,ip}$.

According to Eq. (2), the difference in $\log K_{ex}$ between two metals, M_1 and M_2 , is determined by the differences in $\log K_{ML}$ and in $\log K_{ex,ip}$:

$$\log \frac{K_{ex}(M_1)}{K_{ex}(M_2)} = \log \frac{K_{ML}(M_1)}{K_{ML}(M_2)} + \log \frac{K_{ex,ip}(M_1)}{K_{ex,ip}(M_2)} \quad (12)$$

The values of $\log\{K_{ex}(M_1)/K_{ex}(M_2)\}$, $\log\{K_{ML}(M_1)/K_{ML}(M_2)\}$, and $\log\{K_{ex,ip}(M_1)/$

$K_{ex,ip}(M_2)\}$ for all the couples of univalent metals are shown in Table 2. In most cases, the $\log\{K_{ex}(M_1)/K_{ex}(M_2)\}$ value for 19C6 largely depends on the $\log\{K_{ex,ip}(M_1)/K_{ex,ip}(M_2)\}$ one, while that for 18C6 is determined by both the $\log\{K_{ML}(M_1)/K_{ML}(M_2)\}$ and $\log\{K_{ex,ip}(M_1)/K_{ex,ip}(M_2)\}$ ones (Eq. (12) and Table 2). This means that the extraction selectivity of 19C6 is governed by the selectivity in the ion-pair extraction rather than that in the complexation in water, whereas the extraction selectivity of 18C6 depends on both the selectivities in the complexation and in the ion-pair extraction.

The absolute value of $\log\{K_{ex}(M_1)/K_{ex}(M_2)\}$ is always smaller for 19C6 than for 18C6 except for the cases of Na/Li, Tl/K, and Ag/Cs. The overall extraction selectivity of 19C6 is generally lower than that of 18C6. The absolute value of $\log\{K_{ML}(M_1)/K_{ML}(M_2)\}$ is also always smaller for 19C6 than for 18C6 except for the cases of Cs/Rb and Ag/Rb, indicating that the complexation selectivity of 19C6 is lower. In some cases, the

Table 2
Differences in $\log K_{ex}$, $\log K_{ML}$, and $\log K_{ex,ip}$ between univalent metals

M_1/M_2	19C6			18C6		
	$\log \frac{K_{ex}(M_1)}{K_{ex}(M_2)}$	$\log \frac{K_{ML}(M_1)}{K_{ML}(M_2)}$	$\log \frac{K_{ex,ip}(M_1)}{K_{ex,ip}(M_2)}$	$\log \frac{K_{ex}(M_1)}{K_{ex}(M_2)}$	$\log \frac{K_{ML}(M_1)}{K_{ML}(M_2)}$	$\log \frac{K_{ex,ip}(M_1)}{K_{ex,ip}(M_2)}$
Na/Li	1.50	0.17	1.33	1.44	0.7	0.7
K/Li	2.82	0.51	2.31	3.99	2.0	1.9
Rb/Li	2.53	0.57	1.96	3.48	1.6	1.9
Cs/Li	1.64	-0.05	1.69	2.38	1.0	1.3
Ag/Li	2.17	0.17	2.00	2.50	1.5	1.0
Tl/Li	3.30	0.32	2.98	4.36	2.3	2.0
K/Na	1.32	0.34	0.98	2.55	1.30	1.25
Rb/Na	1.03	0.40	0.63	2.04	0.83	1.21
Cs/Na	0.14	-0.22	0.36	0.94	0.26	0.68
Ag/Na	0.67	0.00	0.67	1.06	0.77	0.29
Tl/Na	1.80	0.15	1.65	2.92	1.54	1.38
Rb/K	-0.29	0.06	-0.35	-0.51	-0.47	-0.04
Cs/K	-1.18	-0.56	-0.62	-1.61	-1.04	-0.57
Ag/K	-0.65	-0.34	-0.31	-1.49	-0.53	-0.96
Tl/K	0.48	-0.19	0.67	0.37	0.24	0.13
Cs/Rb	-0.89	-0.62	-0.27	-1.10	-0.57	-0.53
Ag/Rb	-0.36	-0.40	0.04	-0.98	-0.06	-0.92
Tl/Rb	0.77	-0.25	1.02	0.88	0.71	0.17
Ag/Cs	0.53	0.22	0.31	0.12	0.51	-0.39
Tl/Cs	1.66	0.37	1.29	1.98	1.28	0.70
Tl/Ag	1.13	0.15	0.98	1.86	0.77	1.09

absolute value of $\log\{K_{\text{ex,ip}}(\text{M}_1)/K_{\text{ex,ip}}(\text{M}_2)\}$ is greater for 19C6 than for 18C6; in other cases, the contrary holds. However, the variation in $\log\{K_{\text{ex,ip}}(\text{M}_1)/K_{\text{ex,ip}}(\text{M}_2)\}$ between 19C6 and 18C6 is often smaller than that in $\log\{K_{\text{ML}}(\text{M}_1)/K_{\text{ML}}(\text{M}_2)\}$. In most cases, the lower extraction selectivity of 19C6 is attributed to the lower complexation selectivity in water compared with 18C6. It is interesting that, for Tl/K and Ag/Cs, the extraction selectivity of 19C6 is higher than that of 18C6; the extra methylene group causes the gain in the ion-pair extraction selectivity over the loss in the complexation selectivity.

References

- [1] B.G. Cox, H. Schneider, *Coordination and Transport Properties of Macrocyclic Compounds in Solution*, Elsevier, Amsterdam, 1992.
- [2] M. Ouchi, Y. Inoue, T. Kanzaki, T. Hakushi, *J. Org. Chem.* 49 (1984) 1408.
- [3] Y. Takeda, Y. Mochizuki, M. Tanaka, Y. Kudo, S. Katsuta, *J. Incl. Phenom.* 33 (1999) 217.
- [4] Y. Takeda, H. Kato, *Bull. Chem. Soc. Jpn.* 52 (1979) 1027.
- [5] G. Kortün, W. Vogel, K. Andrussov (Eds.), *Dissociation Constants of Organic Acids in Aqueous Solution*, Butterworths, London, 1961.
- [6] Y. Takeda, H. Goto, *Bull. Chem. Soc. Jpn.* 52 (1979) 1920.
- [7] Y. Takeda, A. Kawarabayashi, K. Endo, T. Yahata, Y. Kudo, S. Katsuta, *Anal. Sci.* 14 (1998) 215.
- [8] Y. Kudo, Y. Takeda, H. Matsuda, *J. Electroanal. Chem.* 396 (1995) 333.
- [9] Y. Takeda, O. Arima, *Bull. Chem. Soc. Jpn.* 58 (1985) 3403.
- [10] R.M. Izatt, R.E. Terry, B.L. Haymore, L.D. Hansen, N.K. Dalley, G.A. Avondet, J.J. Christensen, *J. Am. Chem. Soc.* 98 (1976) 7620.
- [11] Y. Takeda, F. Takahashi, *Bull. Chem. Soc. Jpn.* 53 (1980) 1167.
- [12] Y. Takeda, M. Nemoto, S. Fujiwara, *Bull. Chem. Soc. Jpn.* 55 (1982) 3438.
- [13] R.D. Shannon, C.T. Prewitt, *Acta Cryst.* A32 (1976) 751.

Determination of bromhexine in cough–cold syrups by absorption spectrophotometry and multivariate calibration using partial least-squares and hybrid linear analyses. Application of a novel method of wavelength selection

Héctor C. Goicoechea ^{a,b}, Alejandro C. Olivieri ^{b,*}

^a Departamento de Química, Facultad de Bioquímica y Ciencias Biológicas, Universidad Nacional del Litoral, Paraje El Pozo, Santa Fe 3000, Argentina

^b Departamento de Química Analítica, Facultad de Ciencias Bioquímicas y Farmacéuticas, Universidad Nacional de Rosario, Suipacha 531, Rosario 2000, Argentina

Received 28 September 1998; received in revised form 8 February 1999; accepted 11 February 1999

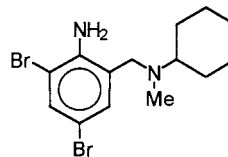
Abstract

The mucolytic bromhexine [*N*-(2-amino-3,5-dibromobenzyl)-*N*-methylcyclohexylamine] has been determined in cough suppressant syrups by multivariate spectrophotometric calibration, together with partial least-squares (PLS-1) and hybrid linear analysis (HLA). Notwithstanding the spectral overlapping between bromhexine and syrup excipients, as well as the intrinsic variability of the latter in unknown samples, the recoveries are excellent. A novel method of wavelength selection was also applied, based on the concept of net analyte signal regression, as adapted to the HLA methodology. This method allows one to improve the performance of both PLS-1 and HLA in samples containing nonmodeled interferences. © 1999 Elsevier Science B.V. All rights reserved.

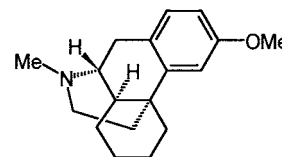
1. Introduction

Bromhexine [*N*-(2-amino-3,5-dibromobenzyl)-*N*-methylcyclohexylamine] is a mucolytic agent used in the treatment of respiratory disorders associated with viscid or excessive mucus. Its has been shown to enhance the penetration of erythromycin into bronchial secretions and to im-

prove the symptoms and ventilatory function in elderly patients being treated for acute exacerbations of chronic bronchopulmonary disease [1].



Bromhexine



Dextromethorphan

* Corresponding author. Fax: +54-41-372704.

E-mail address: aolivier@fbioyf.unr.edu.ar (A.C. Olivieri)

Bromhexine has been determined spectrophotometrically after derivatization with different reagents [2–4]. Recently, first-derivative electronic absorption spectroscopy was used for the determination of both bromhexine and the codeine-related central cough suppressant dextromethorphan [5] (*d*-3-methoxy-*N*-methylnorphinan) in pharmaceutical tablets [6]. Other methods, such as high performance liquid chromatography (HPLC) [7–9], preparative thin layer chromatography [10] and gas–liquid chromatography [11] have been applied for the simultaneous determination of bromhexine and other drugs in pharmaceutical preparations. An interesting indirect determination of bromhexine by atomic absorption spectrometry was also reported [12].

Multivariate calibration methods [13–15] applied to both absorptive and emissive spectral data as well as to electrochemical signals are being increasingly used for the analysis of complex pharmaceutical mixtures [16–22]. They have the advantage of using full spectral information, and allow for a rapid determination of mixture components; often with no need of prior separation or sample pre-treatment. For routine pharmaceutical quality control programs, they are more rapid and of lower cost when compared to HPLC. We have recently reported the resolution of binary mixtures of antiepileptics [23] and antihistaminics [24] as well as a ternary mixture of antibiotics [25] in pharmaceutical preparations by partial least squares (PLS) regression using the PLS-1 formalism. The latter is one of the simplest multivariate methods, and can be performed with easily accessible statistical software.

An additional advantage of robust multivariate methods, such as PLS and the recently introduced variant of hybrid linear analysis (HLA) [26], is that calibration can be performed by ignoring the concentrations of all other components except the analyte of interest. This makes these methods especially appealing for the determination of the active components in syrups, whose excipients may show absorption spectra which are severely overlapped with those from the analytes. Furthermore, syrups belong to a class of samples composed of a variable complex matrix and a small

number of analytes of interest (in our case only bromhexine). Thus, several multivariate methods have been applied to the determination of the active principles in syrups [27–29].

In the present report we discuss the possibility of determining bromhexine in syrups by applying electronic absorption measurements together with robust multivariate calibration analyses (PLS-1 and HLA). It should be noticed that in these cases, where the unknown samples may contain components not modeled by the method during calibration, variable selection criteria becomes critical. We have thus applied a novel method for wavelength selection which minimizes the effect of nonmodeled potential interferences [30], based on the concept of net analyte signal (NAS). The prediction abilities of PLS-1 and HLA are similar, although the latter is simpler to implement, uses less factors, and can be easily adapted to the formalism of wavelength selection.

2. Experimental

2.1. Apparatus

Electronic absorption measurements were carried out on a Beckman DU-640 spectrophotometer, using 1.00 cm quartz cells. All spectra were saved in ASCII format, and transferred to a PC Pentium 166 microcomputer for subsequent manipulation. PLS-1 and HLA were applied with in-house programs written in Quick Basic according to refs. [13] and [26] respectively. Wavelength selection was achieved by applying a moving window/NAS calculation strategy, similar to that described for ordinary least-squares analysis [31], but adapted to the HLA methodology [30].

2.2. Reagents

All experiments were performed with analytical-reagent grade chemicals. Stock solutions of bromhexine hydrochloride (1.0×10^{-3} mol l⁻¹) and dextromethorphan (4.0×10^{-3} mol l⁻¹) were prepared by dissolving the compounds in methanolic HCl 0.1 mol l⁻¹. Solutions of the excipients present in a commercial bromhexine

syrup, i.e. ethanol, glycerol, sorbitol, tartaric acid, sodium benzoate, carboxymethylcellulose, orange essence and amarant were also prepared in methanolic HCl 0.1 mol l^{-1} .

The analyzed samples were from Lafedar Laboratories (Paraná, Argentina), and were prepared by diluting 10.00 ml of syrup with methanolic HCl 0.1 mol l^{-1} in a 100.00 ml volumetric flask, and then sonicating for 5 min.

2.3. Calibration set

In the presently studied syrup samples, the analyte of interest is embedded in a complex mixture of a large number of components. A training set of 12 samples (in this case mixtures of the studied component with three different levels of a blank syrup sample) were prepared for calibration, with the concentrations of bromhexine lying in the known linear absorbance–concentration range. The syrup blank was added to these samples in such a manner that three solutions contained 50%, six contained 100% and the other three contained 150% of a syrup blank provided by the manufacturing laboratory (see Table 1).

Table 1

Composition of the calibration set for applying both PLS-1 and HLA analyses

Calibration sample	Syrup blank added (%) ^a	Bromhexine added ($\text{mol l}^{-1} \times 10^4$)
1	50	1.55
2	50	2.06
3	50	2.58
4	100	1.55
5	100	2.06
6	100	2.58
7	100	1.55
8	100	2.06
9	100	2.58
10	150	1.55
11	150	2.06
12	150	2.58

^a The % is relative to a usual commercial syrup blank taken as 100%.

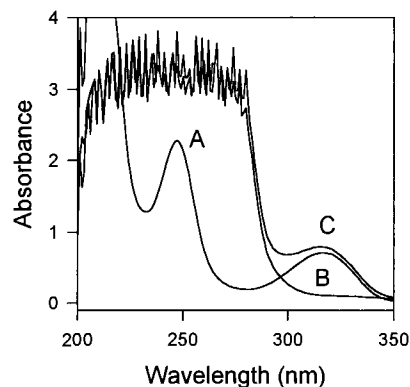


Fig. 1. Electronic absorption spectra of: (A) bromhexine $1.94 \times 10^{-4} \text{ mol l}^{-1}$ in methanolic HCl 0.1 mol l^{-1} , (B) excipients present in a typical syrup, and (C) a commercial syrup sample. Samples (B) and (C) were diluted (1:10) with methanolic HCl 0.1 mol l^{-1} .

2.4. Validation set

A validation set was built with different levels of bromhexine between 0 and $2.66 \times 10^{-4} \text{ mol l}^{-1}$, also containing a variable syrup blank. Additional test samples were prepared containing potential interferences, such as: (a) dextromethorphan, which was absent in the calibration set, and (b) excipients whose absorption signals lie near the bromhexine maximum at 316 nm (i.e. sodium benzoate and orange essence, see Fig. 1), but added in higher amounts than those modeled during calibration.

2.5. Spectrum of pure bromhexine

HLA requires the knowledge of a very accurate spectrum of the pure analyte of interest. In order to obtain such a spectrum for bromhexine, four solutions were prepared, with concentrations in the linear range. The absorbance data (in the range 285–348 nm, digitized every 1.0 nm, 64 points per spectrum) were subjected to least-squares analysis at each wavelength in order to obtain the pure spectrum at unit concentration.

3. Theory

In the PLS method, the $m \times n$ data matrix \mathbf{A} (m is the number of calibration samples; n is the number of wavelengths) is decomposed into:

$$\mathbf{A} = \mathbf{T}_a \mathbf{B}_a \quad (1)$$

where \mathbf{B}_a and \mathbf{T}_a are the $h \times n$ loading and $m \times h$ scores matrix respectively, and h is the number of PLS factors. The $m \times l$ (l is the number of components) calibration mixture matrix \mathbf{C} is similarly decomposed:

$$\mathbf{C} = \mathbf{T}_c \mathbf{B}_c \quad (2)$$

where \mathbf{T}_c ($m \times h$) and \mathbf{B}_c ($h \times l$) are the concentration loading and scores matrixes respectively. During calibration, the following equation holds:

$$\mathbf{T}_c = \mathbf{T}_a \mathbf{V} \quad (3)$$

where \mathbf{V} is an $h \times h$ matrix which establishes the internal relation between \mathbf{T}_c and \mathbf{T}_a . During prediction, the component score is obtained from the unknown spectrum \mathbf{a} as $\mathbf{t} = \mathbf{B}_a \mathbf{a}$, and the unknown concentration from $c_i(\text{pred}) = \mathbf{t}^t \mathbf{V} \mathbf{b}_{ci}$, where \mathbf{b}_{ci} is the appropriate $h \times 1$ vector associated with the component of interest. Notice that individual components are independently modeled by PLS-1, using an optimum h value for each of them. This method offers the additional advantage of ignoring the concentrations of all other components except i during calibration, provided the former are present and can be adequately modeled.

In the HLA method, on the other hand, a blank data matrix $\mathbf{S} = [\mathbf{A} - \mathbf{c}_i(\text{cal})\mathbf{s}_i^t]$ is created, where the $n \times 1$ \mathbf{s}_i vector contains the pure spectrum of analyte i at unit concentration and the $m \times 1$ $\mathbf{c}_i(\text{cal})$ vector the calibration concentrations of analyte i . Then the first h eigenvectors of \mathbf{S} are used to define a column space \mathbf{X} , from which the concentration of i in an unknown sample is obtained as:

$$c_i(\text{pred}) = \mathbf{b}^t \mathbf{a} \quad (4)$$

where \mathbf{a} is the spectrum of the unknown sample, $\mathbf{b} = \mathbf{s}_{\text{net},i} / \mathbf{s}_i^t \mathbf{s}_{\text{net},i}^t$ and $\mathbf{s}_{\text{net},i} = (\mathbf{I} - \mathbf{X}\mathbf{X}^t)\mathbf{s}_i$ (\mathbf{I} is an $n \times n$ unitary matrix). It may be noticed that $\mathbf{s}_{\text{net},i}$ is the so-called NAS spectrum of pure i .

Wavelength selection is achieved in HLA by calculating an error indicator (EI) as a function of a moving window, starting from the NAS regression plot (NASRP) for each sample. The latter is a plot of the elements of the vector \mathbf{a}_{net} vs. those of \mathbf{s}_{net} (see below). The expression for EI used in the present context is [31]:

$$\text{EI} = \frac{\left[s^2 \left(1 + \frac{N^2 s^2}{4 \|\mathbf{a}_{\text{net}}\|^2} \right) \right]^{1/2}}{\|\mathbf{a}_{\text{net}}\|} \quad (5)$$

where $\|\mathbf{a}_{\text{net}}\|$ is the norm of the net analyte spectrum $\mathbf{a}_{\text{net}} = \mathbf{a}(\mathbf{I} - \mathbf{X}\mathbf{X}^t)$ (\mathbf{a} is the spectrum for the unknown sample, \mathbf{X} is the column space spanned by the first h eigenvectors of \mathbf{S} in HLA and the norm is understood as the square root of the sum of the squared elements of the vector), s is the standard deviation of the best fitted straight line to the NASRP plot (in a given spectral region) and N is the number of points in the latter plot [30].

4. Results and discussion

Fig. 1 shows the electronic absorption spectra of bromhexine and a commercial syrup blank. As can be seen, the region 200–280 nm is uninformative. The analysis of the spectra suggests that a convenient working region is 285–348 nm (Fig. 1), although certain degree of spectral overlapping between bromhexine and the excipients still persists. A usual method for resolving mixtures, which can be applied to the present case, is partial least squares analysis (PLS). An alternative to analyzing mixtures when spectral overlapping occurs involves the use of hybrid linear analysis (HLA, see above) [26].

Electronic absorption spectra for the samples shown in Table 1 were recorded in the range 285–348 nm and subjected to both PLS-1 and HLA analyses. For the selection of the optimum number of factors, the cross validation method proposed by Haaland and Thomas was used in both cases [13]. Hence, two factors were used for prediction using HLA and three factors using PLS-1 (Table 2). This latter table also gives the values of the optimal regions used in calibration,

Table 2

Optimum number of factors and statistical parameters for calibration when applying HLA and PLS-1 in the full spectral range 285–348 nm

Statistical parameters ^a	HLA	PLS-1
Factors	2	3
REP%	0.94	0.73
R ²	0.998	0.999

$${}^a R^2 = 1 - \frac{\sum_1^m (c_{\text{act}} - c_{\text{pred}})^2}{\sum_1^m (c_{\text{act}} - \bar{c})^2}, \bar{c} \text{ is the average component concentration in the } m \text{ calibration mixtures; REP(\%) = } \frac{100}{\bar{c}} \left[\frac{1}{m} \sum_1^m (c_{\text{act}} - c_{\text{pred}})^2 \right]^{1/2}.$$

square of the correlation coefficient (R^2) and relative error of prediction (REP), which give an indication of the quality of fit of all the data. Table 3 collects the prediction results for the validation set. As can be seen, both PLS-1 and HLA yield excellent recoveries, although the latter method requires less factors due to the introduction of the information corresponding to the pure spectrum of the analyte of interest in the model.

Wavelength selection is a critical step for increasing the predictive ability of multivariate analyses, and should ideally eliminate both uninformative and/or highly correlated data. A num-

ber of selection methods have been proposed in the literature [32–35]. The presence of nonmodeled chemical components is a major problem common to all multivariate methods. In factor-based methods, it can be alleviated by expanding the calibration set to include samples containing potential interferences. This has been implemented in a previous study of syrups by including in the calibration some commercial samples for which the content of the analyte of interest was determined by HPLC [27]. This is possible since a knowledge of the concentrations of the interferences (or, in extreme cases, their chemical identities) is not needed in the case of robust techniques such as PLS or HLA in order to achieve successful calibration and prediction. However, no method is completely free from interferences which may be present in unknown samples, and were not adequately modeled during calibration.

In order to study the effect of nonmodeled interferences, two types of test samples were designed (see Section 2). In one case, dextromethorphan was added to a syrup sample. In the other one, the concentrations of the excipients whose spectra are overlapped with that of bromhexine in the working range 285–348 nm were increased to a proportion not present in the calibration set

Table 3

Composition of the validation set and results obtained by applying PLS-1 and HLA analyses

Validation sample	Syrup blank (%) ^a	Bromhexine (mol l ⁻¹ × 10 ⁴)		
		Actual	Found (HLA)	Found (PLS-1)
1	75	1.96	1.97	1.98
2	125	2.16	2.18	2.19
3	100	0.00	0.00	0.00
4	100	0.82	0.87	0.84
5	100	1.02	1.08	1.04
6	100	1.33	1.39	1.36
7	100	1.84	1.94	1.93
8	100	2.35	2.42	2.43
9	100	1.94	2.00	1.98
10	100	2.14	2.19	2.18
11	100	2.24	2.26	2.25
REP (%) ^b			3.3	2.7

^a The % is relative to a usual commercial syrup blank taken as 100%.

^b This value of REP (%) corresponds to the validation set and may be different to that for the calibration (see Table 2).

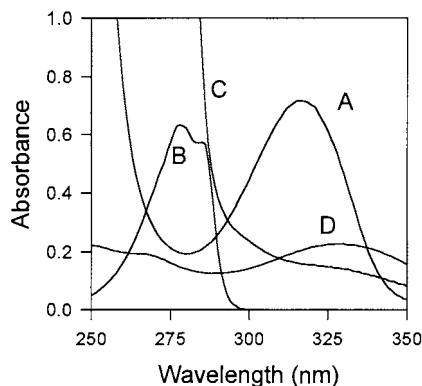


Fig. 2. Electronic absorption spectra of: (A) bromhexine $1.94 \times 10^{-4} \text{ mol l}^{-1}$, (B) dextromethorphan $4.00 \times 10^{-4} \text{ mol l}^{-1}$, (C) sodium benzoate 4 g l^{-1} (200% of the content in a commercial syrup blank) and (D) methanolic orange essence at a concentration which is twice that in a normal syrup (see Fig. 1). Solutions A, B and C are in methanolic HCl 0.1 mol l^{-1} .

(Fig. 2). To each of these samples a strategy based on HLA/NAS calculations was applied in order to identify the potential presence of an interference and to alleviate its effects [30]. As an example, the NASRP for sample 12 (Table 4) in the full spectral region 285–348 nm is shown in Fig. 3A. As can be seen, linearity is not fulfilled, strongly indicating the presence of nonmodeled interfer-

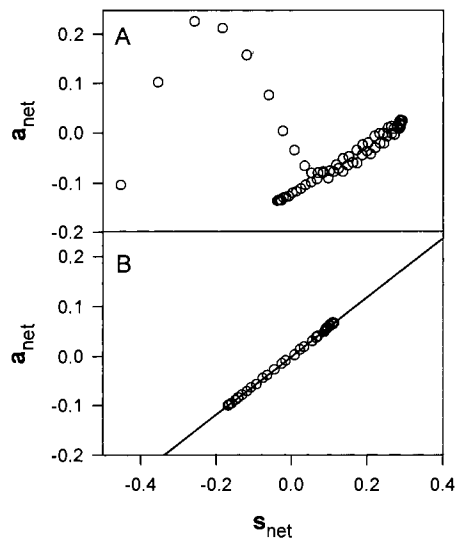


Fig. 3. (A) NASRP for sample 12 using the calibration wavelength range 285–348 nm. (B) NASRP in the range 315–344 nm, as predicted from the analysis of the EI parameter (Table 4). The solid line is the best linear fit to the calculated points.

ences. A search for the minimum value of EI as a function of all possible wavelength ranges indicates that the corresponding NASRP in the restricted region 315–344 nm (Fig. 3B) is seemingly linear (see also the values of EI in Table 4). It

Table 4

Results obtained by applying PLS-1 and HLA analyses to samples with nonmodeled interferences, before and after wavelength selection

Sample	Interference	Wavelength range (nm)	EI	Bromhexine ($\text{mol l}^{-1} \times 10^4$)		
				Actual	Found ^a (HLA)	Found ^a (PLS-1)
12	Dextromethorphan $8.0 \times 10^{-4} \text{ mol l}^{-1}$	285–348	0.5	2.66	2.17(2)	2.13(3) ^b
		315–344	0.005	2.66	2.68(1)	2.68(2)
13	Sodium benzoate 4 g l^{-1} ; 200% of the amount in the syrup blank	285–348	0.06	2.66	2.95(2)	2.94(3) ^b
		312–344	0.011	2.66	2.75(1)	2.78(2)
14	Orange essence, 200% of the amount in the syrup blank	285–348	0.21	2.04	2.39(2)	2.44(3) ^b
		285–315	0.02	2.04	2.51(1)	2.53(2)

^a The number of factors used for prediction are given in parenthesis.

^b Considered as an outlier by PLS-1, on the basis of the calculation on the spectral F ratio, i.e. $F(\mathbf{a}) = m \sum_{k=1}^n (e_{a,k})^2 / \sum_{i=1}^m \sum_{k=1}^n (e_{i,k})^2$, where $e_{a,k}$ are the spectral residues of the unknown sample \mathbf{a} , and $e_{i,k}$ are the corresponding residues of the m calibration samples.

may be noticed that the latter spectral range avoids the contribution from dextromethorphan (Fig. 2). Table 4 shows the predictions from HLA and PLS-1 for all test samples containing potential interferences, before and after wavelength selection by the above procedure. Both for samples 12 and 13, the use of NASRP allows to select the regions where the interferences do not show significant absorptions. The case of sample 14, however, deserves a comment. In the region selected by the NASRP criterion, the predicted bromhexine concentration is overestimated, although linearity is satisfactorily fulfilled (Table 4). Interestingly, PLS-1 considers samples 12–14 as outliers when the full spectral region 285–348 nm is used, but does not detect anomalies in the regions of minimum EI. The latter results can be ascribed to the fact that the spectrum of the interference present in sample 14 (orange essence) is approximately collinear with that of bromhexine in the region 285–315 nm (Fig. 2). Thus PLS-1 does not recognize the sample as an outlier, and HLA chooses the region where the interference is present. As a consequence, both methods overestimate the concentration of bromhexine in this particular sample (Table 4). It should be noticed that orange essence is present in sample 14 in a large excess as compared to the usual composition of the commercial syrup blank. This sample was included in order to test the limits of the present wavelength selection procedure. Nevertheless, the results shown in Table 3 indicate that changes by $\pm 25\%$ in the concentrations of excipients do not significantly alter the quality of multivariate predictions. Although it would be interesting to compare the present wavelength selection technique with other reported methods, no direct comparison is possible since the latter only use the calibration data, whereas the present one focuses also on the spectrum of a particular sample.

5. Conclusions

Cough suppressant syrups were studied as regards the content of bromhexine [*N*-(2-amino-3,5-dibromobenzyl)-*N*-methylcyclohexylamine] with

the aid of spectrophotometric measurements, together with the multivariate methods of partial least-squares (PLS-1) and hybrid linear analysis (HLA). Although the spectra of bromhexine and the syrup excipients are overlapped, and the concentration of the syrup blank was varied by $\pm 25\%$, the recoveries are excellent. In order to improve the performance of both PLS-1 and HLA in samples containing nonmodeled interferences, a novel method of wavelength selection was applied, based on the concept of net analyte signal regression, adapted to the HLA methodology.

Acknowledgements

Financial support from CONICET (Consejo Nacional de Investigaciones Científicas y Técnicas), the University of Rosario and Fundación Antorchas is gratefully acknowledged. H.C. Goicoechea thanks FOMEC (Programa para el Mejoramiento de la Calidad de la Enseñanza Universitaria) for a fellowship.

References

- [1] W. Martindale, The Extra Pharmacopeia, 30th. Edition, The Pharmaceutical Press, London, 1993.
- [2] M.I. Santoro, M.M. Dos Santos, J.F. Magalhaes, J. Assoc. Off. Anal. Chem. 67 (1984) 532.
- [3] S.S. Zarapker, R.V. Rele, V.J. Doshi, Indian Drugs 26 (1988) 38.
- [4] B. Gala, A. Gomez Hens, D. Perez Bendito, Anal. Lett. 26 (1993) 2607.
- [5] J.L. Benn, R. Peck, Drug Saf. 7 (1992) 190.
- [6] V. Tantishaiyakul, J. Pharm. Biomed. Anal. 17 (1998) 237.
- [7] N. Badwe, A. Garg, D. Eapem, P.D. Sethi, East. Pharm. 38 (1995) 179.
- [8] O. Lau, C. Mok, J. Chromatogr. A 693 (1995) 45.
- [9] J. Rauha, H. Salomies, M. Aalto, J. Pharm. Biomed. Anal. 15 (1996) 287.
- [10] P. Parimoo, P. Umapathi, J. Samuel, East. Pharm. 36 (1993) 125.
- [11] E.V. Rao, R.G. Rao, S. Raghuvveer, P. Khadgapathi, Analyst 112 (1987) 871.
- [12] C. Nerin, A. Garnica, J. Cacho, Anal. Chem. 58 (1986) 2617.
- [13] D.M. Haaland, E.V. Thomas, Anal. Chem. 60 (1988) 1193.

- [14] H. Martens, T. Naes, *Multivariate Calibration*, Wiley, Chichester, 1989.
- [15] K.R. Beebe, B.R. Kowalski, *Anal. Chem.* 59 (1989) 1007A.
- [16] A. Guiberteau Cabanillas, T. Galeano Díaz, A. Espinosa-Mansilla, F. Salinas Lopez, *Talanta* 41 (1994) 1821.
- [17] A. Espinosa-Mansilla, A. Muñoz de la Peña, F. Salinas, M. Martínez Galera, *Anal. Chim. Acta* 276 (1993) 141.
- [18] M. Sánchez Peña, A. Muñoz de la Peña, F. Salinas, M.C. Mahedero, J.J. Aaron, *Analyst* 119 (1994) 1177.
- [19] A. Espinosa-Mansilla, F. Salinas, A. Zamoro, *Analyst* 119 (1994) 1183.
- [20] A. Guiberteau Cabanillas, T. Galeano Díaz, A. Espinosa-Mansilla, P.L. López de Alba, F. Salinas López, *Anal. Chim. Acta* 302 (1995) 9.
- [21] A. Bozdogan, A.M. Acar, G.K. Kunt, *Talanta* 39 (1992) 977.
- [22] Durán Merás, A. Muñoz de la Peña, M.I. Rodríguez Cáceres, F. Salinas López, *Talanta* 45 (1998) 899.
- [23] H.C. Goicoechea, A.C. Olivieri, *Talanta* 47 (1998) 103.
- [24] H.C. Goicoechea, A.C. Olivieri, *J. Pharm. Biomed. Anal.*, in press.
- [25] H.C. Goicoechea, A.C. Olivieri, *J. Pharm. Biomed. Anal.*, in press.
- [26] A.J. Berger, T. Koo, I. Itzkan, M.S. Feld, *Anal. Chem.* 70 (1998) 623.
- [27] M. Blanco, J. Coello, M. Elaamrani, H. Iturriaga, S. MasPOCH, *J. Pharm. Biomed. Anal.* 15 (1996) 329.
- [28] M. Blanco, J. Coello, H. Iturriaga, S. MasPOCH, C. de la Pezuela, *Anal. Chim. Acta* 333 (1996) 147.
- [29] M. Blanco, J. Coello, H. Iturriaga, S. MasPOCH, S. Alaoui-Ismaili, *Fresenius J. Anal. Chem.* 357 (1997) 967.
- [30] H.C. Goicoechea, A.C. Olivieri, *Analyst*, in press.
- [31] J. Ferré, F.X. Rius, *Anal. Chem.* 70 (1998) 1999–2007.
- [32] S.D. Osborne, R.B. Jordan, R. Künnemeyer, *Analyst* 122 (1997) 1531.
- [33] F. Lindgren, P. Geladi, S. Rännar, S. Wold, *J. Chemom.* 8 (1994) 349.
- [34] A.G. Frenich, D. Jouan-Rimbaud, D.L. Massart, S. Kutatharmmakul, M. Martínez Galera, J.L. Martínez Vidal, *Analyst* 120 (1995) 2787.
- [35] I.E. Frank, *Chemom. Intell. Lab. Syst.* 1 (1987) 233.

Modelling the matrix interference of iron in the multivariate determination of copper by stripping voltammetry

Instrument standardization

Ana Herrero *, M. Cruz Ortiz

Dpto Química, Fac. de Ciencias, Universidad de Burgos, Pza. Misuel Banuelos s/n, 09001 Burgos, Spain

Received 23 November 1998; received in revised form 15 February 1999; accepted 16 February 1999

Abstract

Two different standardization procedures have been applied in order to minimize the experimental effort necessary to determine copper in presence of iron by differential pulse anodic stripping voltammetry. The significant matrix interference caused by iron in the voltammetric determination of copper has been successfully solved by using partial least squares (PLS) regression. The use of this multivariate regression implies a large number of training set samples, so a standardization method was required. In fact, the standardization methods used have reduced the calibration samples needed in future determinations by up to 75%. Moreover, PLS regression allowed both metals to be determined simultaneously by using an adequate experimental design, without any limitation to their respective concentrations and without the need to know the level of interference. © 1999 Elsevier Science B.V. All rights reserved.

Keywords: Instrument standardization; Matrix interference; Multivariate analysis; Stripping voltammetry

1. Introduction

Multivariate regression methods [1–3] such as principal components (PC) or partial least squares (PLS) regressions, have been demonstrated to be very useful tools for modelling analytical signals by using all the information they contain. How-

ever, in multianalyte determinations, a large number of samples is usually necessary to build each regression model, and this must be recalculated again if a new instrument is used, or the experimental response changes because of time, drift, etc. To reduce the experimental effort that is necessary in new calibration models, several standardization methods have been proposed [4–13]; these methods are based on suitably relating two different instrumental situations by means of a reduced number of calibration samples (standardization subset) measured on both situations.

* Corresponding author. Tel.: +34-94-725-8800; fax: +34-94-725-8831.

E-mail address: aherrero@ubu.es (A. Herrero)

Some of these approaches consist of correcting the signals measured for example on a secondary instrument to the format that would have been obtained if they had been measured on the primary or master instrument, and then the regression model built for this instrument can be used with the transformed signals. Those developed by Shenk et al [5] and by Wang et al [6–9] belong to these kinds of methods. Other methods are based on the correction of the primary model in such a way that it can be used for measurement data from the secondary instrument [13].

Most of the standardization applications come from the field of NIR spectroscopy, but many of the strategies and methods described can also be applied to calibration transfer problems in other analytical fields such as electrochemistry. Since the multivariate techniques have been successfully applied to some electrochemical problems where interferences such as complex relations between sensors or overlapping signals exist [14–16], the possibility of standardizing an electrochemical instrument to obtain a significant reduction in the calibration sets seems to be suitable when these interferences are present [17–19].

A common kind of interference which generates overlapping responses in stripping voltammetry [20] can be due to solution-phase electroactive species present in the sample, as is the case of iron in the determination of copper because the voltammetric peaks of these two metals are close together in most supporting electrolytes. Several univariate procedures that have been used to overcome this interference include separation of iron by extraction with diethyl ether [21], medium exchange procedures [22], selective complexation of either metal [23,24], subtractive approaches [25], etc. But most of these procedures cannot be effective or suitable in some cases.

In this article, the use of PLS regression in the stripping voltammetric determination of copper in presence of high concentration of iron is shown as an alternative procedure to avoid any prior separation procedure by modelling the

concentration of both metals: copper (considered as analyte of interest) and iron (interferent which causes the matrix effect). This is a particular electrochemical interference where copper is anodically stripped from the electrode after a deposition period while iron gives a direct voltammetric response due to its level of concentration in the solution which overlaps the stripping voltammetric response of copper.

Next, in order to minimize the experimental effort required by the multivariate procedure (a large number of calibration samples are usually needed), two different standardization procedures, the piecewise direct standardization (PDS) method developed by Wang et al. and another method proposed by Forina et al., have been applied. The successful reduction of the calibration samples (by up to 75%) is described.

2. Theory

2.1. Piecewise direct standardization method

The PDS [6] method consists of relating the predictor variables from two different instruments, A and B, through a transformation matrix, F (dimensions $p \times p$, p being the number of measured variables). It is based on taking a small subset (standardization subset) of the full calibration set (X_{As} and X_{Bs} being the voltammograms obtained on instruments A and B, respectively, for the standardization subset) and then, relating each variable, $x_{A,i}$, from instrument A to the variables in a small window, Z_i , at instrument B by means of a local multivariate regression.

$$X_{As} = X_{Bs}F \quad (1)$$

$$Z_i = [x_{B,i-j}, x_{B,i-j+1}, \dots, x_{B,i+k-1}, x_{B,i+k}] \quad (2)$$

$$x_{A,i} = Z_i b_i \quad (3)$$

Each regression vector, b_i , can be calculated by PCR or PLS to subsequently be arranged along the main diagonal of the transformation matrix (the rest of the elements being zero).

Then, F matrix is used to transform any measured sample on instrument B to the A format in such a way that the regression model built with the full

calibration set measured on instrument A can be used for calculating the concentration of these new samples.

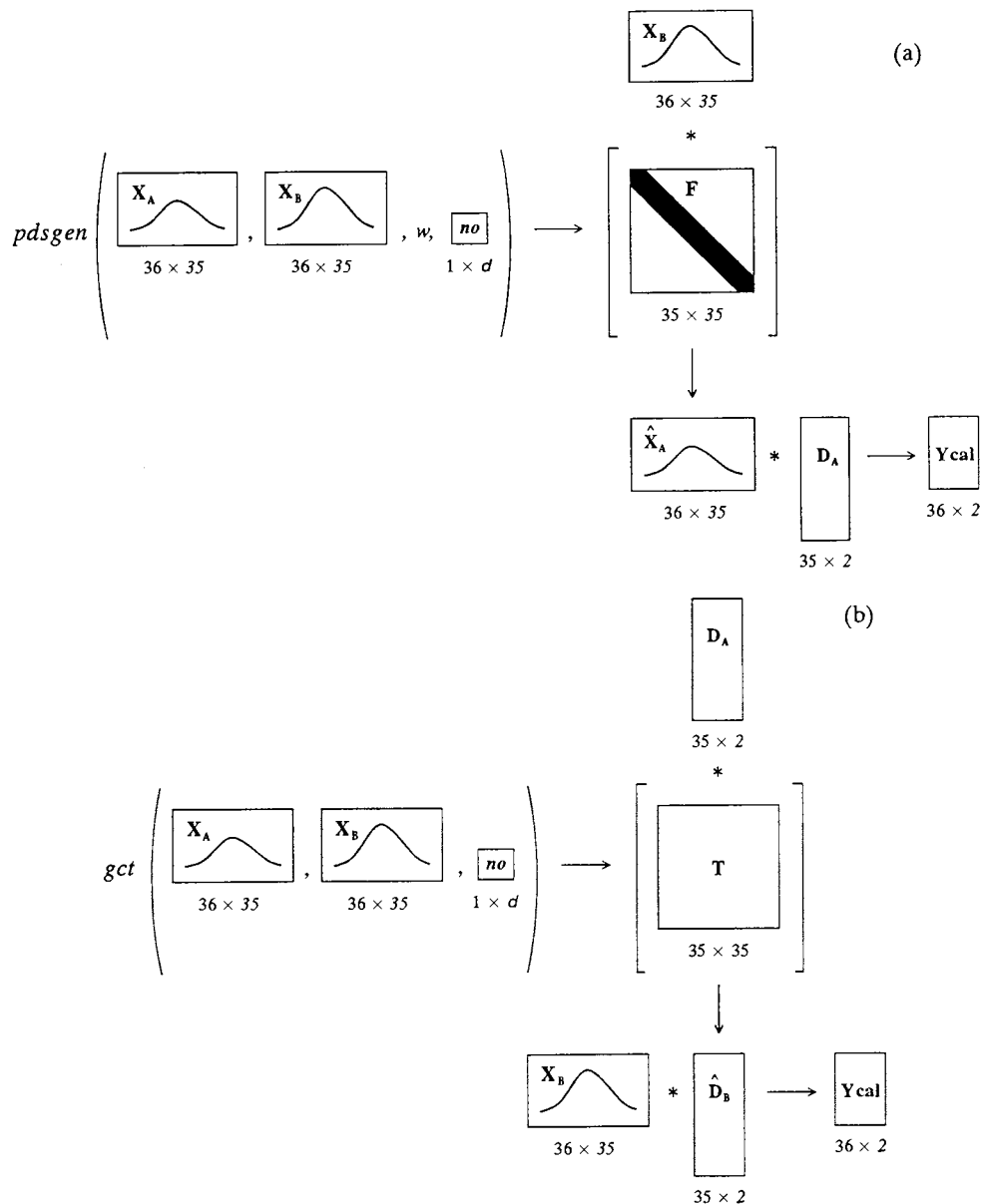


Fig. 1. Schematic representation of PDS (a) and GCT (b) standardization procedures. X_A and X_B are the voltammograms of both data sets, F and T are the respective transformation matrix, D_i is the PLS regression vector matrix for instrument i and Y_{cal} is the calculated concentration matrix for samples measured on instrument B. For PDS method w is the window size, no is the standardization index sample vector and \hat{X}_A is the corrected voltammograms matrix for instrument B; for GCT method \hat{D}_B is the regression vector matrix estimated.

$$\hat{x}_A = x_B F \quad (4)$$

The whole standardization method is shown in Fig. 1a.

2.2. Global calibration transfer method

The approach proposed by Forina et al [13], named in this paper as global calibration transfer method, GCT, uses the PLS regression twice. Firstly, to relate the original training set measured on instrument A, X_A , and the standardization subsets of instruments A and B to the response:

$$y = X_A b_A \quad (5)$$

$$y_s = X_{As} b_A \quad (6)$$

$$y_s = X_{Bs} b_B \quad (7)$$

where y and y_s are the calibration set and standardization subset responses, and b_A and b_B are the regression vectors for the models of instruments A and B, respectively.

Next, PLS is used to relate the standardization subsets of both instruments through the coefficient transformation matrix, T :

$$X_{As} = X_{Bs} T \quad (8)$$

So Eq. (6) can be written:

$$y_s = X_{As} b_A = X_{Bs} T b_A \quad (9)$$

and by comparing Eq. (7) with Eq. (9), an estimation of the regression vector for instrument B is achieved:

$$\hat{b}_B = T b_A \quad (10)$$

Then, the estimated regression vectors can be used to determine the concentration of samples measured on this instrument, such is indicated in Fig. 1b where the whole procedure is illustrated.

3. Experimental

3.1. Apparatus

The experiments were performed by using

DPASV on two separate instruments. Instrument A: μ AUTOLAB system from Eco Chemie in conjunction with a Metrohm 663 VA stand, equipped with a Metrohm multimode electrode (MME) used in the hanging mercury drop electrode (HMDE) mode (nominal area 0.40 mm²), and connected to the Interface to Mercury Electrodes IME 663. The three electrode system was completed by means of an Ag/AgCl/KCl (3 M) reference electrode and a glassy carbon auxiliary electrode. Instrument B: Metrohm 646 VA processor with a 647 VA stand in conjunction with a MME used in the HMDE mode (nominal area 0.40 mm²) together with an Ag/AgCl/KCl (3 M) reference electrode and a platinum auxiliary electrode.

3.2. Reagents

Analytical reagent grade chemicals were obtained from Merck, Darmstadt (Germany). All the solutions were prepared with deionised water from a Barnstead NANO Pure II system. All voltammetric measurements were carried out in a citrate-citric acid supporting electrolyte/buffer (pH 4.7) medium. Nitrogen (99.997%) was used to remove dissolved oxygen.

3.3. Procedure

Each solution was placed in the voltammetric cell and purged with nitrogen for 10 min. Once the solution had been deoxygenated a deposition potential of -1.3 V was applied to the working electrode for 60 s. At the end of this deposition time the stirrer was switched off and, after 30 s had elapsed, an anodic potential scan was initiated from -0.154 to 0.050 V with scan rate 10 mV/s (interval time 0.6 s). For the instrument A, pulse amplitude 49.95 mV and stirring rate 1500 rev/min were used, while for instrument B the available parameters were 50.00 mV and 1290 rev/min, respectively. After each addition, the solution was stirred and deoxygenated for 15 s before applying the voltammetric procedure again.

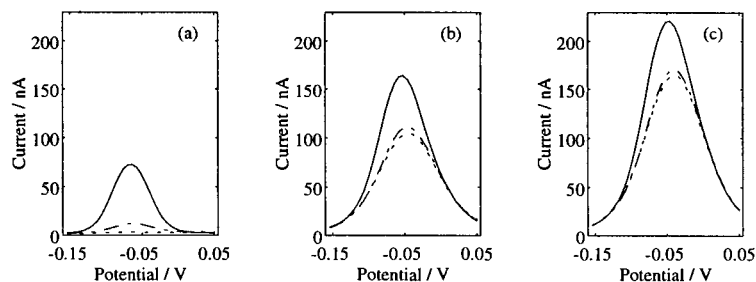


Fig. 2. Voltammograms recorded for copper and iron with deposition time: 60 s (solid line) and 0 s (dash-dot and dotted line). Iron concentration: (a) 0 M; (b) 6.06×10^{-5} M; (c) 9.97×10^{-5} M. Copper concentration: 0 M (dotted line); 4×10^{-7} M (dash-dot and solid line).

4. Results and discussion

4.1. Univariate approaches

The individual or simultaneous voltammetric determination of copper and iron in most of the electrolytes is complicated by the close electrode potentials at which their peaks appear. In most cases this results in the overlapping of their responses and, hence, in an analytical error. That is why the voltammetric determination of copper in the presence of iron usually involves experimental methods [21–24] to remove or avoid this interference.

Another approach to overcome this matrix interference is the procedure proposed by Bonelli et al [25] who use a subtractive approach that corrects for the current contribution from iron. These authors consider that, since the peak current from iron is independent of deposition time (because iron does not form an amalgam in the mercury electrode), a zero deposition time voltammogram can be recorded and subtracted from a normal stripping voltammogram for samples and standards alike. In this way, the iron contribution to the signal recorded has been compensated, and these are the net signals used in the standard additions method subsequently applied. This procedure presents the advantage of eliminating the contribution of iron to the signal independently of its concentration. But the contribution of copper is not taken into account. The usefulness of this univariate procedure has been analysed in this work for copper concentrations high enough to produce a small voltam-

metric response at zero deposition time for different levels of Fe(III). Relative errors from -25% to -40% have been found.

As can be seen in Fig. 2, the voltammograms recorded at zero deposition time for those samples which only contain iron (dotted lines) do not coincide in any case with those recorded for samples with the same iron concentration when a certain quantity of copper is present (dash-dot lines). So, if the latter voltammogram (dash-dot lines) is considered as the iron contribution, as the Bonelli procedure proposes, and then subtracted from the stripping signal (solid lines) to eliminate the interference, it is clear that a part of the subtracted signal is related to the copper. This leads to the high relative errors found.

Possibly, this univariate approach could be suitable for lower concentrations of copper, at which no direct response is obtained for this analyte. But, if the concentration of copper is such that copper has a small contribution to the voltammogram recorded at zero deposition time, the subtraction approach leads to significant analytical errors which are a priori unknown (when no iron is present, relative errors of about -25% have been found). Since, in practice, the voltammogram corresponding to the iron contribution alone is not available, the error associated with the determination cannot be estimated.

4.2. Multivariate analysis

An alternative to this univariate procedure is the use of multivariate methods such as the partial least

squares (PLS) regression, which allows one to model the interference of iron in the determination of copper and, with the same experimental effort, to simultaneously determine the concentration of the interferent, without any limitation to their respective concentrations and without the need to previously know the level of the interference. This approach is based on modelling the interference that each metal, copper and iron, causes on the voltammetric determination of the other. And, once the multivariate model is built, it can be used for the instrumental standardization procedure which gives a significant reduction in the experimental effort required in later calibrations.

With this aim, 36 solutions of copper-iron were prepared with concentrations varying from 0 to 1.01×10^{-6} M for copper and from 0 to 1.01×10^4 M for iron in such a way that six equally spaced levels of concentration were obtained for each metal in the training set. Another set of four solutions ($t1$ to $t4$) was prepared as test set, the copper and iron concentrations (in μM) being 0.31 and 20.54 for $t1$, 0.50 and 80.05 for $t2$, 0.80 and 50.03 for $t3$, and 0.98 and 88.36 for $t4$. The

voltammograms of the sample solutions were recorded following the above experimental procedure on both instruments A and B (Fig. 3). Evident differences exist between both calibration set voltammograms, the most significant being that the peak current is lower and the peak potential is more negative on instrument A. But, on both instruments the copper peak occurs always at the same potential whereas the iron peak is shifted to more positive potentials according to the increase of the iron concentration, so the peak potential of the overlapping peak obtained depends largely on the iron concentration.

Two PLS models have been built on the basis of the data from instrument A, independently for the analyte of interest and the interferent. The explained and full crossvalidated variances corresponding to both models were 99.39 and 99.35% for copper and 99.98 and 99.95% for iron with five and seven latent variables respectively (which were chosen taking into account the highest cross-validated variance criterium). These high and close variance values point out the stability and prediction ability of the models built. Moreover, both standard error of prediction (SEP) and stan-

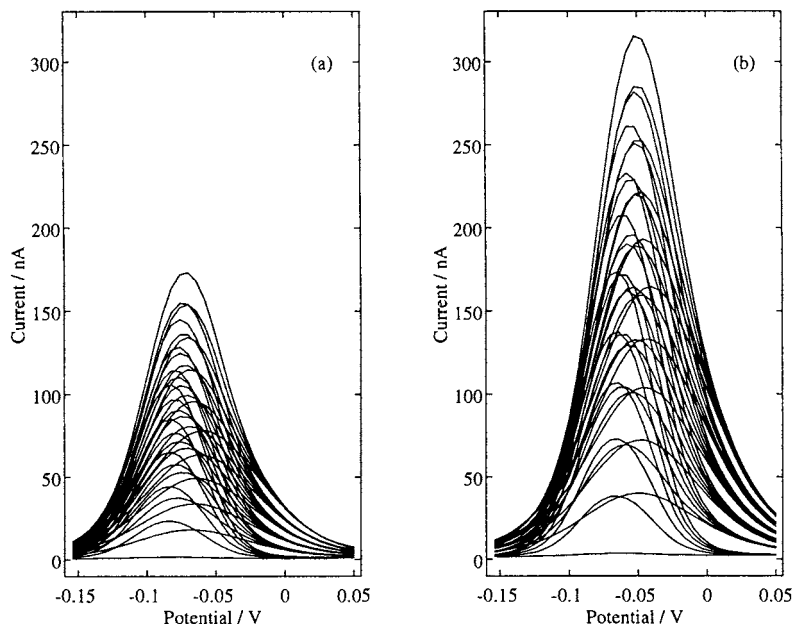


Fig. 3. Training set voltammograms recorded on instruments A (a) and B (b).

Table 1

SEP and SET values corresponding to the PLS models and to the standardization procedures carried out with the standardization parameters named in the text for each metal

Metal	Conc. range (μM)	PLS models ^a				Standardization procedures ^b			
		Instrument A		Instrument B		PDS		GCT	
		SEP	SET	SEP	SET	SEP	SET	SEP	SET
Copper	0.00–1.01	0.0224	0.0107	0.0379	0.0155	0.0095	0.0339	0.0302	0.0195
Iron	0.00–101.03	0.2236	0.1815	0.4178	0.4919	1.0831	1.7727	1.04	0.7716

^a Errors calculated from the raw data measured on instruments A and B, respectively (PLS regression).

^b Errors calculated from the data measured on instrument B (standardization methods).

dard error for the training set (calculated in the same way as SEP but for the training set samples, named SET) corresponding to these PLS models are shown in columns 3 and 4 of Table 1. The regression vectors have been computed by means of the Marengo-Todeschini algorithm [26] implemented in PARVUS [27].

Fig. 4 shows the scores obtained for the first three latent variables of the PLS model for copper, which were very similar to those corresponding to the iron PLS model. It shows that the PLS regression has been able to model the iron matrix interference, by including latent variables related to this metal that subtract its contribution to the signal in spite of the shifting observed in the peak potential. The scores' structure in the plane of the first two latent variables (Fig. 4a) approximately reproduces the experimental design used, but the inclusion of more latent variables is needed to model a certain curvature that scores show, as can be seen in Fig. 4b, probably due to the shift observed on signals when iron concentration changes.

Similar PLS models have been obtained from the raw data recorded on instrument B for the same sample solutions. Table 1 shows the SEP and SET values corresponding to them, whereas Table 2 shows the relative errors related to each sample, columns 3 and 7, to compare the standardization procedures results.

4.3. Multivariate instrumental standardization

Two different standardization methods have been used: the piecewise direct standardization

(PDS) method developed by Wang et al. [6] and the global calibration transfer (GCT) proposed by Forina et al. [13]. Instrument A has been considered the primary instrument whereas instrument B was the secondary instrument in both standardization procedures.

To search for a suitable standardization set, several subsets have been chosen from the calibration set based on the following criteria: (1) reasonable number of calibration samples (fewer samples); (2) easy to achieve, even by addition of standards; (3) following a more or less orthogonal design; and (4) sufficiently covering the experimental domain. Fig. 5 shows the standardization subsets used in the analysis. In this case, no method based on the leverage values has been used because previous experiences pointed out that, generally, a standardization subset leads to different results for each analyte, although for all of them the same voltammograms are used [28].

When PDS method was performed, to calculate the transformation matrix the *m*-function *pdsgen*, implemented in the PLS Toolbox by Wise [29], was used (Fig. 1a). Both the standardization subset (*no*) and window size (*w*) have been changed in order to obtain the best results; the subsets used are shown in Fig. 5 and the window sizes were 3, 5, 7, ..., 33 and 35 (17 in all).

Once the standardization procedure was carried out, to evaluate the usefulness of the method, both SEP and SET were calculated. The former standard error is related to the test set samples and evaluates the real prediction ability of the method. While the second, which is calculated from all the training set

samples, is related both to the standardization subset samples and to the rest of the samples (which had not been used to build the PLS model of the primary instrument either), so this error also evaluates to some extent the prediction ability of the standardization procedure. Those samples that do not belong to the standardization subset are real test samples. Because of this, SET has been analysed together with SEP in this paper.

Differences exist between the SEP for both metals. Standardization subsets 2, 5 and 8 give the lowest SEP values for copper with small window sizes, whereas it is subset 11 which gives the best results for iron. An additional analysis of both standard errors by means of the multiple range tests of Tukey and Newman-Keuls for a significance level $\alpha = 0.05$ (considering the standardization subsets as replicates when the window sizes are analysed and vice versa) points out that the homogeneous group with the best SEP contains the standardization parameters $no = 5$ and $w = 7$ for copper and $no = 11$ and $w = 9$ for iron. The SEP and SET obtained in the standardization procedures carried out with these parameters are shown in Table 1, where they can be compared with those corresponding to the PLS models directly built with the voltammograms recorded on instrument B for the same sample sets.

The standardization procedure has transformed the voltammograms measured on instrument B in such a way that SEP value has been reduced for copper. The very characteristics of sample *t3* and other samples with similar concentrations to it, see Table 2, seem to be included in the primary

PLS model, so the corresponding results are better. But, instead, the contrary effect has been caused on the SET values, which can be explained by the corresponding relative errors in Table 2. This could be due to the fact that, since PDS is a local procedure, its results can be excessively dependent on any standardization subset sample. Similar results have been obtained for iron, but in this case, both errors are higher than those corresponding to the PLS models built for instrument B. This standardization method seems not to be able to transfer the different potential shifting that the iron peak undergoes depending on its concentration.

With regard to the number of calibration samples measured on instrument B implied in the procedure, as a different standardization subset is used for each metal, a total of 14 samples are needed, versus the 36 samples that constituted a complete recalibration. In this way, this standardization procedure leads to a reduction in the experimental effort of about 61%.

On the other hand, the GCT method (Fig. 1b) was performed with home-made Matlab [30] sub-routines taking into account the same standardization subsets as in the preceding procedure. In this case, subsets 2, 4, 5, 6 and 7 give the lowest SEP values for both copper and iron, subsets 5 and 6 being related also to the lowest SET values. Table 1, shows SEP and SET corresponding to $no = 5$, which has been chosen as the best standardization subset for both metals because it implies a slightly lower number of samples, only eight.

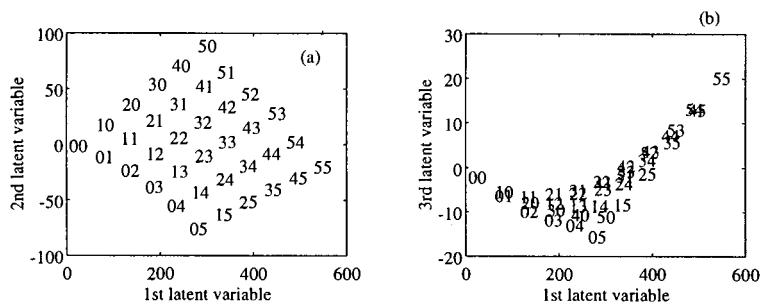


Fig. 4. Scores corresponding to the first three latent variables of the PLS model for copper. (a) First–second latent variables; (b) first–third latent variables. The numbers indicate the level of copper and iron, respectively.

Table 2

Relative errors for measured samples on instrument B, with the whole training set (PLS models) and with the standardization procedures, PDS and GCT methods, respectively

Run ^a	Copper			Iron				
	Concentration (μM)	Relative error (%)			Concentration (μM)	Relative error (%)		
		PLS	PDS	GCT		PLS	PDS	GCT
00	0.0000	–	–	–	0.0000	–	–	–
10	0.2074	–0.01	–2.95	2.24	0.0000	–	–	–
20	0.4121	–0.19	–2.34	0.76	0.0000	–	–	–
30	0.6141	0.05	–2.80	0.49	0.0000	–	–	–
40	0.8135	–2.49	–4.26	–1.72	0.0000	–	–	–
50	1.0103	0.18	–0.09	1.28	0.0000	–	–	–
01	0.0000	–	–	–	20.7417	5.02	3.18	5.47
11	0.2061	3.98	–2.47	3.33	20.6053	–5.76	–3.26	–5.50
21	0.4094	1.13	2.86	2.81	20.4706	0.47	1.56	–0.63
31	0.6101	0.84	3.43	2.74	20.3377	–2.92	–2.07	–6.16
41	0.8083	2.78	8.61	5.49	20.2065	–3.25	–3.45	–9.18
51	1.0038	3.05	11.48	6.43	20.0769	–1.65	–5.14	–8.86
02	0.0000	–	–	–	41.2105	0.06	1.89	1.52
12	0.2047	1.45	–2.69	–1.36	40.9412	0.29	2.39	1.40
22	0.4068	–6.37	–3.94	–6.22	40.6753	0.55	1.73	0.79
32	0.6062	–5.42	0.09	–3.88	40.4129	1.38	2.32	–0.20
42	0.8031	–5.75	–0.28	–4.33	40.1538	0.04	1.20	–1.43
52	0.9975	0.25	10.02	3.07	39.8981	–0.59	–3.52	–3.59
03	0.0000	–	–	–	61.4118	–0.67	–1.13	0.02
13	0.2034	3.82	0.75	1.27	61.0130	0.08	–0.04	0.35
23	0.4041	–0.64	3.05	–0.66	60.6194	1.54	1.25	1.23
33	0.6023	0.83	5.29	1.87	60.2308	0.08	0.32	–0.60
43	0.7980	0.85	6.35	1.94	59.8471	0.70	1.56	0.18
53	0.9911	1.11	6.93	2.01	59.4684	–0.05	1.54	–0.13
04	0.0000	–	–	–	81.3506	–1.05	–3.28	–1.16
14	0.2021	–0.43	–3.93	–3.27	80.8258	–0.62	–2.60	–0.97
24	0.4015	–0.76	–0.96	–1.75	80.3077	–1.40	–2.87	–1.82
34	0.5985	–2.15	–1.32	–2.64	79.7962	0.26	–0.07	–0.16
44	0.7929	–2.04	–2.05	–2.83	79.2911	0.19	1.99	0.49
54	0.9849	–1.90	–2.79	–2.89	78.7925	–0.19	3.67	0.58
05	0.0000	–	–	–	101.0320	0.73	–4.63	–0.05
15	0.2008	–2.81	3.78	–1.77	100.3840	0.05	–4.54	–1.12
25	0.3990	0.35	3.22	0.62	99.7452	–0.01	–2.98	–1.08
35	0.5947	0.81	2.79	0.68	99.1139	0.40	–1.10	0.01
45	0.7879	2.11	2.60	1.64	98.4906	0.21	0.21	–0.07
55	0.9788	2.09	–0.45	1.53	97.8750	–0.21	2.38	–0.02
<i>t1</i>	0.3081	–2.35	–2.27	–1.67	20.5377	1.12	3.09	1.00
<i>t2</i>	0.5003	–1.75	0.61	–1.39	80.0511	–0.42	–1.99	–1.42
<i>t3</i>	0.8005	–9.33	–1.73	–7.37	50.0319	–0.15	–2.63	–2.32
<i>t4</i>	0.9818	0.61	1.08	0.98	88.3636	–0.82	–0.16	–1.46

^a The run indicates the level of copper (first number) and iron (second number).

The SEP and SET values obtained for copper with this standardization procedure, Table 1, are comparable to those obtained by the PLS model

built with the measurements carried out on instrument B for the same sample set, i.e. with and without standardization procedure. Instead, SEP

and SET related to the standardization procedure are a little higher than those of the PLS model for iron (the SET value for GCT is lower than that for PDS method); anyway, for the interferences the relative errors associated with both methods are really low (average of the absolute value of the relative error for the test set is 0.63% with the PLS model and 1.55% with the GCT standardization procedure). GCT method allows one to find a single standardization subset that simultaneously satisfies the conditions for the instrumental standardization transfer for both metals with acceptable predictions. This procedure seems to obviate the over-fitting problem, giving results very similar to those corresponding to the complete recalibration PLS models.

This indicates that it is possible to determine copper in presence of iron, and also to know the concentration of interferent, with only eight standardization samples, an experimental effort significantly lower than a complete recalibration (36 samples), by means of the GCT standardization procedure. The reduction in the experimental effort is, in this case, up to 78%.

Both standardization methods have been applied again to a different calibration set measured on instrument B and similar results were obtained, proving the standardization procedures carried out, i.e. it is also possible to standardize an electrochemical instrument over time.

5. Conclusions

The multivariate techniques used have obviated the serious matrix interference caused by iron in the voltammetric determination of copper in the concentration range analysed. The PLS regression allows the simultaneous determination of copper and iron by stripping voltammetry, without needing to know the level of the interference.

On the other hand, the two standardization procedures carried out, PDS and GCT, lead to a reduction in the experimental effort in future determinations up to 61 and 78% respectively, with relative errors comparable to those corresponding to a complete recalibration.

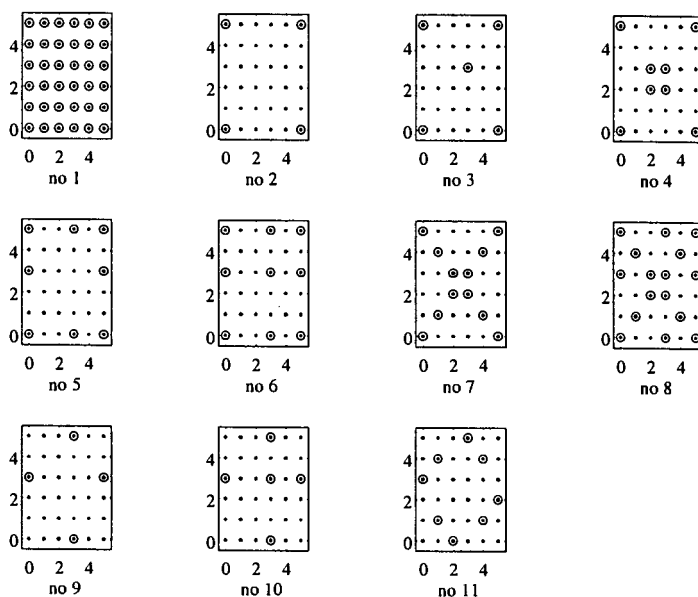


Fig. 5. Standardization subsets (samples signalled with a circle). Ordinates show the level of copper, the abscissae the level of iron.

Acknowledgements

This work has been partially supported by Ministerio de Educación y Cultura under project PB97-0596 and by Junta de Castilla y León under project BU16/98.

References

- [1] K.R. Beebe, B.R. Kowalski, *Anal. Chem.* 59 (1987) 1007A.
- [2] H. Martens, T. Næs, *Multivariate Calibration*, 2nd ed., Wiley, New York, 1992.
- [3] B.R. Kowalski, M.B. Seasholtz, *J. Chemometr.* 5 (1991) 129.
- [4] O.K. De Noord, *Chemometr. Intell. Lab. Syst.* 25 (1994) 85.
- [5] J.S. Shenk, M.O. Westerhaus, *Crop Sci.* 31 (1991) 1694.
- [6] Y. Wang, D.J. Veltkamp, B.R. Kowalski, *Anal. Chem.* 63 (1991) 2750.
- [7] Y. Wang, M.J. Lysaght, B.R. Kowalski, *Anal. Chem.* 64 (1992) 562.
- [8] Y. Wang, B.R. Kowalski, *Anal. Chem.* 65 (1993) 1174.
- [9] Z. Wang, T. Dean, B.R. Kowalski, *Anal. Chem.* 67 (1995) 2379.
- [10] E. Bouveresse, D.L. Massart, P. Dardenne, *Anal. Chem.* 67 (1995) 1381.
- [11] E. Bouveresse, C. Hartmann, D.L. Massart, I.R. Last, K.A. Prebble, *Anal. Chem.* 68 (1996) 982.
- [12] B. Walczak, E. Bouveresse, D.L. Massart, *Chemometr. Intell. Lab. Syst.* 36 (1997) 41.
- [13] M. Forina, G. Drava, C. Armanino, R. Boggia, S. Lanteri, R. Leardi, P. Corti, P. Conti, R. Giangiaco, C. Galiena, R. Bigoni, I. Quartari, C. Serra, D. Ferri, O. Leoni, L. Lazzeri, *Chemometr. Intell. Lab. Syst.* 27 (1995) 189.
- [14] A. Henrion, R. Henrion, G. Henrion, F. Scholz, *Electroanalysis* 2 (1990) 309.
- [15] A. Herrero, M.C. Ortiz, J. Arcos, J. Lopez-Palacios, L.A. Sarabia, *Anal. Chim. Acta* 2 (1994) 277.
- [16] M.C. Ortiz, M.J. Arcos, L.A. Sarabia, *Chemometr. Intell. Lab. Syst.* 34 (1996) 245.
- [17] A. Herrero, M.C. Ortiz, *Anal. Chim. Acta* 348 (1997) 51.
- [18] A. Herrero, M.C. Ortiz, *Electroanalysis* 10 (1998) 717.
- [19] A. Herrero, M.C. Ortiz, *Talanta* 46 (1998) 129.
- [20] J. Wang, *Stripping Analysis. Principles, Instrumentation and Applications*, VCH Publishers, Deerfield Beach, FL, 1985.
- [21] V. Meenakumari, *Analyst* 120 (1995) 2849.
- [22] S. Gottesfeld, M. Ariel, *J. Electroanal. Chem.* 9 (1965) 112.
- [23] M.I. Ismail, S.H. Etaiw, *J. Electroanal. Chem.* 108 (1980) 229.
- [24] M.E. Vázquez Díaz, J.C. Jiménez Sánchez, M. Callejón Mochon, A. Guiraúm Pérez, *Analyst* 119 (1994) 1571.
- [25] J.E. Bonelli, H.E. Taylor, R.K. Skogerboe, *Anal. Chim. Acta* 118 (1980) 243.
- [26] E. Marengo, R. Todeschini, *Chemometr. Intell. Lab. Syst.* 12 (1991) 117.
- [27] M. Forina, R. Leardi, C. Armanino, S. Lanteri, *PARVUS: An Extendable Package of Programs for Data Exploration, Classification and Correlation*, Release 1.2 (provisionally available from the authors).
- [28] A. Herrero, 1996. *Análisis Multivariante y Transferencia de Calibrado en Voltamperometría*, PhD Thesis, University of Burgos, Spain.
- [29] B.M. Wise, *PLS Toolbox for Use with MATLAB*, Version 1.3 (available from the author).
- [30] Matlab, *The MathWorks, Matlab*, Natick, MA, 1992.

Near infrared thermal lens spectrometry for the real-time monitoring of supercritical fluid extraction

J. Amador-Hernández, J.M. Fernández-Romero, M.D. Luque de Castro *

Department of Analytical Chemistry, Faculty of Sciences, University of Córdoba, E-14004-Córdoba, Spain

Received 2 December 1998; received in revised form 9 February 1999; accepted 16 February 1999

Abstract

A commercially available supercritical fluid extractor provided with carbon dioxide was coupled to a dual-beam thermal lens spectrometer with a pumpprobe coaxial configuration, pumped by a pulsed Nd-YAG laser operating at the fundamental wavelength of 1064 nm. As a preliminary step, several compounds were studied in batch regime using carbon tetrachloride as solvent, in order to observe the influence of overtones and combinations involving distinct chemical bonds on thermal lens spectrometry (TLS). Several factors related with supercritical fluid extraction (SFE) under hydrodynamic conditions were studied in order to establish their influence both in the extraction yield and thermal lens signal magnitude obtained. The advantages and limitations of the hyphenated SFE-TLS technique proposed are discussed, and the possibility of on-line detection in SFE with a pulse thermal lens spectrometer was demonstrated. © 1999 Elsevier Science B.V. All rights reserved.

Keywords: Near-infrared; Thermal lens spectrometry; Pulsed laser; Supercritical fluid extraction

1. Introduction

During the last years, the development of different molecular absorption techniques in the near infrared radiation region (NIR) has been undertaken with interesting results, owing to the fact that the low absorptivities of absorption bands are compatible with concentrated samples, besides the use of long path lengths that enables spectra to be measured by transmission through intact materials. Both aspects allow rapid and low-cost

analysis because sample preparation is either avoided or minimized. On the other hand, the low absorptivity of water makes the region suitable for the analysis of samples containing a high proportion of water such as food and natural products, likewise beverages. Thus, spectroscopic techniques such as NIR spectrophotometry, NIR reflectance, NIR transmittance, NIR transreflectance and NIR diffuse reflectance have been successfully applied for the determination of various food constituents in the food and beverage industry [1], for the non-invasive in vivo monitoring of metabolites in humans [2], and quality control of solid pharmaceutical formulations [3], among others.

* Corresponding author. Tel.: +34-957-218-614; fax: +34-957-218-606.

E-mail address: qallucam@uco.es (M.D. Luque de Castro)

However, NIR spectroscopy has been regarded as a strongly sample matrix dependent technique and the use of NIR techniques for quantitative purposes involves preliminary exhaustive calibration steps, many of which require chemometric methods for the treatment of data such as partial least squares regression, enclosed in the multivariate calibration techniques. Undoubtedly, the effort involved in those calibrations is not justified unless large number of similar samples have to be analysed [4,5].

On the other hand, supercritical fluid extraction (SFE) has emerged as an advantageous alternative for solid sample treatment in comparison with conventional organic solvent extraction. The principal aspects to be considered are: (a) the availability of non-toxic supercritical fluid solvents, i.e. carbon dioxide and water; (b) the attractive physico-chemical properties of the fluid in the supercritical region, namely high solvent strength, high diffusivity and no surface tension, which enable its easy penetration through the solid material for the quantitative extraction of the analyte; and (c) the reduction of the extraction time [6]. The growing interest for its adoption in the automation of the analytical process has led to the development of the on-line coupling of the supercritical fluid extractor to several molecular spectroscopic detectors [7,8]. Between the detection techniques considered of higher interest in the last few years, thermal lens spectrometry (TLS) has been shown to be a high sensitive technique in the UV and visible region. Therefore, the present authors proposed by the first time the coupling of a thermal lens spectrometer, pumped by a pulsed dye laser emitting in the visible region, with a commercially available supercritical fluid extractor [9]. Providing an environment with reduced potential for its oxidation and low extraction temperatures, the SFE of trans- β -carotene (an important but unstable natural product) and on-line detection by pulsed laser TLS was carried out satisfactorily. For a sample concentration of $80 \mu\text{g g}^{-1}$, an extraction yield of 23% expressed as mean recovery percentage was obtained, with a relative standard deviation (R.S.D.) of 12%. The limit of detection was estimated as 5×10^{-6} absorbance units.

As can be deduced, only a sensitive spectroscopic technique such as TLS would be applied satisfactorily for the on-line monitoring of an extraction process with small quantities of the compound of interest involved, similar to the monitoring of an efficient SFE process of a compound that absorbs weakly. Considering the increasing incorporation of SFE in industrial processes, i.e. to the decaffeination of coffee and tea and to extraction of hops and spices [10–12], it results in, with great interest, the development of an SFE-near infrared TLS hyphenated technique. As a consequence, the characteristics of both analytical techniques described above could be improved at the same time. In first term, complex solid samples can be analysed without interferences of the matrix and reduced sample treatment. Secondly, the near infrared source allows a wide variety of analytes to be analysed by TLS (not just those which absorb visible or ultraviolet radiation owing to the presence of chromogenic groups), such as the improvement in the limit of detection owing to the high energy of the excitation lasers.

In relation to the photothermal techniques, some authors have reported the application of continuous wave (CW) and pulsed lasers operating in the NIR and IR regions as excitation sources in the construction of dual-beam thermal lens spectrometers [13,14]. Thus, the ultrasensitive determination of dichlorodifluoromethane by photothermal deflection spectrometry (PDS) using an analyzer etalon as detector [15] or the sensitive determination of isotopic purity of several solvents by TLS in the infrared region [16,17], are examples of the significant improvements in the analytical approaches developed in the last years such as the enhancement of detection limits performed. However, many of the laser excitation sources were constructed in the laboratory, which rose up the price of the equipment employed and reduced the possibilities of its application in routine analyses.

In this work, the coupling of a supercritical fluid extractor with a thermal lens spectrometer pumped by a commercially available pulsed laser operating in the NIR region, and provided with a high pressure flow cell interface, is proposed for

the first time for the continuous, real-time monitoring of SFE processes. As a preliminary step, the TLS signal magnitude of several compounds was studied in batch using carbon tetrachloride as solvent. Then, the study of the influence of the principal variables affecting the extraction process was carried out far from the critical point. The TLS-SFE system suggested would be of interest in the real-time monitoring of industrial SFE and the monitoring of reactions in or with supercritical fluids, particularly when low absorptivity solutes would be involved.

2. Experimental

2.1. Apparatus

The experimental arrangement of the dual beam thermal lens spectrometer used in this work is shown in Fig. 1. The excitation radiation was provided by a pulsed Nd:YAG laser, with a max-

imum 650 mJ pulse energy and 6–9 ns pulse duration at the fundamental wavelength of 1064 nm (Spectron Laser Systems, UK, Model SL454G), which was focused in the flow cell with a 135 mm focal length plano-convex lens (25 mm in diameter), while the probe beam was provided by a 632.8 nm He–Ne laser (Melles Griot, Irvine, CA, Model 05 LPL 903070), focused by other plano-convex lens of the same characteristics at the confocal distance with the beam waist occurring after the sample cell. Other details have been described elsewhere [18]. The signal was acquired by a real-time digital oscilloscope (Tektronix, Beaverton, OR) at a sampling rate of 200 s^{-1} and the data were sent to a PENTIUM microcomputer via an RS232C serial interface for their storage and treatment using a homemade QBA-SIC program.

A supercritical fluid extractor (Hewlett Packard, Palo Alto, CA, Model 7680A) with carbon dioxide as the supercritical solvent was used without fluid modifier. It was furnished with a 7 ml

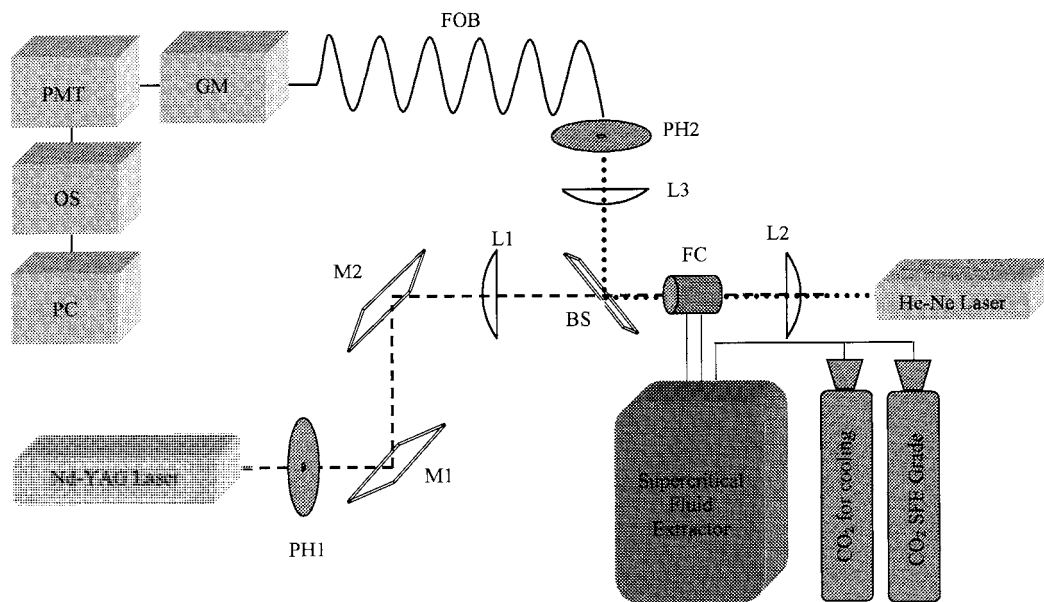


Fig. 1. Scheme of the layout: M1 and M2, beam steering mirrors; L1 and L2, 135 mm focal length planoconvex lenses; L3, 25 mm focal-length plano-convex lens; BS, beamsplitter; FC, flow cell; PH1 and PH2, pinhole masks; FOB, fiber optic bundle; GM, grating monochromator; PMT, photomultiplier tube; OS, oscilloscope, PC personal computer. Excitation and probe beams provided by a pulsed Nd:YAG laser and by a He–Ne laser, respectively. The supercritical fluid extractor was provided with carbon dioxide cylinders for extraction and cooling operations.

sample container and hypersyl ODS (octadecyl chains bonded to silica balls, 30–40 µm diameter) analyte trap packing, and coupled to a 486 PC provided with the proper software for the equipment control. The direct coupling of the supercritical fluid system to the thermal lens spectrometer was made through a high-pressure flow cell interface designed in the laboratory, with 50 mm of optical pathlength and 350 µl inner volume. The flow cell allowed routine working pressures at least up to 180 bar without leaking.

A spectrophotometer (Hitachi, Tokyo, Model U2000) equipped with a standard quartz batch cell of 10 mm optical pathlength was employed for conventional absorbance measurements at 275 nm. Finally, a rotary vacuum evaporator (Tokyo Rikakikai, Tokyo) was also used.

2.2. Reagents

All chemicals were of analytical-reagent grade. Lauric acid, myristic acid, palmitic acid, stearic acid, 3-pentadecyl-phenol (3PDP), polyoxyethylene octylphenol, polyoxyethylen-laurylether and diatomaceous earth (acid-washed, not further calcined) were obtained from Sigma (St. Louis, MO); phenol, *p*-cresol, *m*-cresol, benzoic acid, *n*-hexane, carbon tetrachloride and diethyl ether were purchased from Merck (Darmstadt, Germany); methyl laurate, methyl myristate, methyl stearate were obtained from PolyScience (Evanston, IL). Finally, carbon dioxide (SFC/SFE grade and 99.995 minimum purity for cooling operations) obtained from Carbueros Metálicos (Barcelona, Spain) was also used.

A stock solution containing 1000 mg l⁻¹ of 3PDP in *n*-hexane and stock solutions of lauric acid, myristic acid, palmitic acid, stearic acid, methyl laurate, methyl myristate, methyl stearate, 3PDP, phenol, *p*-cresol, *m*-cresol, benzoic acid, polyoxyethylene octylphenol, and polyoxyethylen-laurylether with a 1% (w/v) concentration in carbon tetrachloride were prepared and stored at 0–4°C. All stock solutions were filtered and degassed in an ultrasonic bath for 10 min before batch measurements. For the extraction study, the solid samples were prepared daily.

2.3. Procedures

2.3.1. Solid sample preparation

An adequate portion of diatomaceous earth in a 250 ml flask was spiked with 3PDP to give a final concentration of ca. 6% (w/w); then, 100 ml of diethyl ether was added and the mixture stirred for 15 min. Finally, the organic solvent was evaporated under vacuum at 25°C and the solid sample thus obtained was homogenized in a mortar.

In order to establish the actual concentration of the analyte in the diatomaceous earth before each study, 0.1 g of the solid material and 5 ml of *n*-hexane were shaken vigorously for 2 min and centrifuged (3500 rpm, 10 min). Then, 1 ml of the supernatant portion was transferred to a 25 ml volumetric flask and diluted to volume with *n*-hexane. The analyte concentration was spectrophotometrically determined in triplicate.

2.3.2. SFE-TLS experiences

The solid sample (0.3 g) with 3PDP was placed in the sample container; after static and dynamic successive periods of extraction (20 and 15 min, respectively) under the proposed conditions (Table 3), the analyte deposited in the trap was removed with 1.8 ml of *n*-hexane. The extraction process of 3PDP was monitored through the thermal lens signal magnitude obtained in real-time, while the extraction efficiency was determined by TLS and/or spectrophotometric measurements. Each experience was done in triplicate.

2.3.3. Spectrophotometric determination of 3PDP

Appropriate volumes of the stock solution of 3PDP in *n*-hexane to give final concentrations of 20–200 mg l⁻¹ were introduced into 5 ml volumetric flasks and diluted to volume with *n*-hexane. The absorbance of each sample was measured at 275 nm and the corresponding calibration equation was calculated.

2.3.4. Data collection and processing

The unprocessed signal was recorded as the variation of the probe beam intensity produced by absorption of the pump pulses, while the analytical TLS signal was calculated as ($\Delta I/I$), where ΔI is the difference of intensities at the probe beam

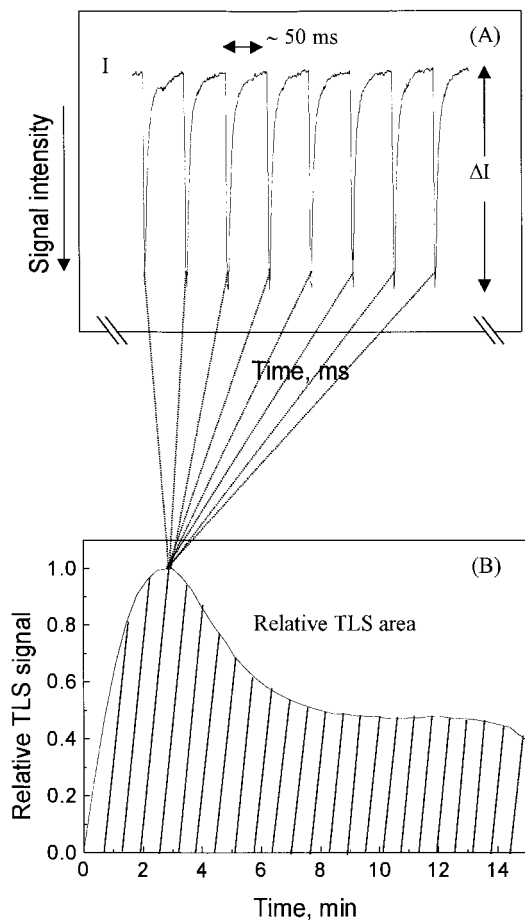


Fig. 2. Thermal lens detection in the supercritical fluid extraction process. (A) perturbation of the probe beam by a pump pulse used (unprocessed signal); I , baseline; ΔI , intensity change produced. (B) Diagram of the extraction kinetics; the relative TLS area was obtained as a result of the integration of the relative thermal lens spectrometry (TLS) signals.

center when measured before (initial baseline intensity) and immediately after the incidence of a pump pulse, and I is the initial baseline intensity (Fig. 2A). Thus, once the real-time unprocessed signals were stored along the extraction process, the thermal lens signal magnitudes were calculated, smoothed by the Savitzky–Golay algorithm [19] and integrated by means of the trapezoidal rule method, in order to estimate the corresponding TLS signal area (TLS area, Fig. 2B). It worth noting that the analytical TLS signal data ob-

tained along each working session were divided by the maximum absolute value obtained in that session; in this way, all reported $(\Delta I/I)$ values were normalized between 0 and 1. Owing to the nature of the TLS-SFE approach proposed, the development of a suitable software for acquisition, storage and treatment of data was mandatory. Major details of the QBASIC language program used have been described elsewhere [9].

3. Results and discussion

According to the theoretical models describing the thermal lens phenomenon, the sensitivity enhancement factor is proportional to the power of the laser excitation source; therefore, the use of high powered pulsed lasers such as Nd-YAG lasers operating at the fundamental wavelength of 1064 nm could be used for the improvement of the limits of detection in the near infrared region. Thus, the coupling of a supercritical fluid extractor with a near infrared thermal lens spectrometer for the real-time monitoring of the extraction process, could be considered as a new and interesting alternative for the automation of the analysis of solid samples, since the proper adjustment of the laser output energy could increase considerably the quantification range from concentrated to diluted samples with a wide variety of matrices coming from the food and pharmaceutical industries, environmental field, etc.

However, at high laser energies optical saturation of the analytes begins to occur, where non-linear intensity dependent signal magnitudes result from multiphoton absorption or optical transition saturation. Both of these effects depend on the rate at which excited species relax relative to the rate at which stimulated emission takes place in a given photothermal technique (PDS or TLS), producing distinct signal intensity behaviors. As the intensity of the pump laser exceeds the saturation intensity, the temperature profile in the sample begins to resemble a top-hat profile and the curvature of the temperature profile decreases while the maximum gradient increases. Since the PDS signal is proportional to the temperature gradient and the TLS signal is propor-

tional to the curvature of the temperature profile, the PDS signal has been observed to be greater than the TLS signal under saturation conditions [20–22].

According to these considerations, the improvement in the limit of detection using a high power excitation source (e.g. a Nd:YAG laser operating at 1064 nm), is limited by optical saturation phenomena related with the structure of the analyte, such as the experimental conditions employed.

3.1. Preliminary NIR-TLS study

3.1.1. Background signal

Although several authors have reported the use of TLS as a detection technique in the NIR and IR regions, a study of the thermal lens response of the solvents used (CCl₄ and CO₂ in supercritical phase) was necessary as a starting point in this work, using the dual-beam thermal lens spectrometer proposed. Undoubtedly, a high background absorption is undesirable in this type of experiments, principally at low concentration levels.

In general terms, the absorption bands observed in the near infrared region are a consequence of the overtones and combinations of the molecule's vibrational modes, principally those involving hydrogen. Consequently, the absorptivity coefficients of carbon tetrachloride and carbon dioxide in NIR would be expected to be negligible. However, the absorption of pump pulses with energies higher than 30 mJ produced a quick perturbation of the probe beam followed by a slower decay curve in both solvents, as a result of photothermal phenomena. On the other hand, carbon dioxide in the supercritical state showed a major distortion of the baseline signal intensity than carbon tetrachloride. In this case, the strong dependence of the physicochemical properties of the fluid from the thermodynamic state of the system in the supercritical region (namely the temperature coefficient of the refractive index and thermal conductivity), plays a major role. In addition, absorption from the cell windows material or atmosphere could be occurring. In this case, a laser energy output of 30 mJ was used, in order to obtain negligible background signals.

3.1.2. NIR-TLS detection of organic compounds

At this point, the comparison of the TLS signal magnitude of several organic compounds in the near infrared region (1064 nm) was carried out in batch conditions, for the subsequent selection of the substance used as analyte in the real-time monitoring of the SFE process.

Theoretically, most NIR spectra can be explained by assignment of the bands to overtones and combinations of fundamental vibrations involving hydrogenic stretching modes, which principal absorption bands observed around 1064 nm are described in Table 1 [1]. Even when the amine group shows a band around 1060 nm, it was not considered in this study owing to its high polarity and therefore low solubility in CO₂ under supercritical conditions. In practice, the efficient SFE of polar compounds with CO₂ is carried out with the aid of a cosolvent or modifier, in order to increase the polarity of the extractant phase. However, the presence of a modifier is not recommended in this case owing to the great difference of the refractive index between CO₂ and cosolvent in different phases, which produces a large dispersion of the probe laser beam thus hindering monitoring of the TLS signal.

In this work, four groups of organic compounds (fatty acids, fatty acidic esters, phenolic derivatives and compounds such as benzoic acid and some surfactants) were considered for the study of their TLS signal at 1064 nm according to their chemical structure, using the batch cell and 1% (w/v) stock solutions in carbon tetrachloride.

Table 1
Assignment of some observed absorption bands around 1064 nm

Wavelength (nm)	Chemical bond	Structure
1053	2 × C–H (stretching vibration) + 2 × C–H (deformation vibration) + (CH ₂) <i>n</i>	RCH ₂ R'
1060	N–H (stretching vibration, second overtone)	RNH ₂
1080	2 × C–H (stretching vibration) + 2 × C–C (stretching vibration)	Benzene

Table 2
Sensitivity comparison of some organic compounds by thermal lens spectrometry (TLS) at 1064 nm

Group	Organic compound	Condensated formula	Relative TLS signal magnitude
Fatty acids	Lauric acid	$C_{12}H_{24}O_2$	0.53
	Myristic acid	$C_{14}H_{28}O_2$	0.82
	Palmitic acid	$C_{16}H_{32}O_2$	0.88
	Stearic acid	$C_{18}H_{36}O_2$	0.93
Fatty acidic esters	Methyl laurate	$C_{13}H_{27}O_2$	0.45
	Methyl myristate	$C_{15}H_{31}O_2$	0.49
	Methyl stearate	$C_{19}H_{39}O_2$	0.53
Phenolic derivatives	Phenol	C_6H_6O	0.61
	<i>p</i> -cresol	C_7H_8O	0.50
	<i>m</i> -cresol	C_7H_8O	0.66
	3-Pendadecyl-phenol	$C_{21}H_{36}O$	1.00
Others	Benzoic acid	$C_6H_6O_2$	0.46
	Polyoxyethylene octylphenol	–	0.59
	Polyoxyethylen-laurilether	$C_{58}H_{118}O_{24}$	0.98

The results obtained are showed in Table 2. As can be observed, the maximum relative TLS signal magnitude was provided by 3PDP; according to the chemical bond assignments detailed in Table 1, the absorption involved in the thermal lens phenomenon was mainly due both to the presence of C–H bonds in the large saturated hydrocarbon chain (CH_2 units), with the theoretical maximum absorption band at 1053 nm, and to the presence of C–H and C–C bonds in the aromatic part of the structure with the maximum absorption band located at 1080 nm. On the other hand, an increase of the relative TLS signal magnitude was observed when an increased number of CH_2 units in the hydrocarbon chain of both fatty acids and fatty acid esters, as could be expected. In contrast, slower TLS signal magnitudes were noticed in the methyl esters than in the corresponding fatty acids, probably owing to the chemical bonds associated with the carbonyl group, physical impediments and resonant effects of the chemical structures.

Nevertheless, some considerations about saturation phenomena should be taking into account at this point since a high energy excitation source was used throughout. Theoretically, for different molecular structures there are different saturation intensities and/or multiphoton absorption phenomena. A non-linear behavior between the pho-

tothermal signal and the excitation laser pulse energy is greatly influenced by the rates at which excited-states species can couple or relax into background or heath-bath rovibrational states relative to the rate of optical excitation, and the density of these rovibrational states at the excited state energy [23]. If the density of states is high and coupling into these states is rapid, neither saturation nor multiphoton absorption will occur. Since a high density of rovibrational states occurs in large polyatomic molecules and medium-sized polyatomics with heavy atoms, a linear relationship between the thermal signal and output laser energy and high saturation intensity are expected. In contrast, the low density of rovibrational states in small to medium sized molecules induced the presence of saturation or multiphoton absorption; therefore, small species with high absorption coefficients are more likely to exhibit non-linear absorption behavior [22]. Also, in gas-phase conditions, the increasing pressure increases the saturation intensity, as a result of the greater rate of collisional deactivation [20]. For these reasons, when a high energy excitation source is used in a photothermal technique, the examination of the absorption characteristics of the absorbing compound is required.

In this case, the study described above was carried out as a preliminary step for the subse-

quent selection of the analyte in the real-time monitoring of the SFE process. Therefore, the linear dependence of the corresponding TLS signal upon the excitation energy was not studied for all compounds, since more in deep studies was out of the scope of this work. Owing to the relative TLS signal magnitude observed for 3PDP and a linear relationship between the photothermal signal and pulse energy, it was used through the SFE study.

3.2. SFE

Although several compounds such as ammonia, nitrous oxide, water, pentane, etc., have been used as supercritical solvents, they are not ideally suited for routine analysis owing to their unfavorable physicochemical properties, reactivity, solvating power, non-existent or high cost commercial instrumentation [6]. In contrast, carbon dioxide is a useful solvent in SFE, since they possess feasible critical parameters, non-toxicity and moderate cost. For this reason, it was used in this study.

Since they are closely related with the efficiency of the extraction process, the optimization of the static and dynamic extraction time was carried out under the experimental conditions described in Table 3. The chamber, nozzle and trap temperature was maintained at the default values suggested by the SFE equipment manufacturers (40, 45 and 40°C, respectively).

Table 3
Optimum operating parameters for the extraction process

Parameter	Selected conditions
Sample size (g)	0.3
Equilibration time (min)	20
Extraction time (min)	15
Flow rate (ml min ⁻¹)	0.5
Density (g ml ⁻¹)	0.8
Chamber temperature (°C)	60
Nozzle temperature (°C)	55
Trap packing	ODS
Trap temperature (°C)	40
Rinse solvent	<i>n</i> -Hexane
Rinse volume (ml)	1.8

First, the influence of the CO₂-analyte equilibration time over the extraction efficiency was studied; accordingly, three distinct periods of 0, 10 and 20 min of static extraction were used prior to identical dynamic extraction processes. The highest total product yield was obtained with a static extraction time of 20 min, which was selected as optimum. The diffusion of the analyte through the porous structure of the matrix enhanced with the sample-extractant contact time.

Secondly, the optimization of the dynamic extraction time was carried out varying it from 5 to 30 min. The major quantity of the extracted compound was obtained at the first 15 min (74.7% recovery). This period was selected for subsequent experiments, in order to avoid unnecessary consumption of carbon dioxide SFE/SFC grade.

3.3. SFE-TLS hyphenated system

A typical kinetic curve of the extraction process obtained with the SFE-TLS hyphenated approach is shown in Fig. 2B. The displacement of extracted 3PDP through the sample container and stainless steel transport tubing was slow as a consequence of both the flow rate employed (0.5 ml min⁻¹) and physical dimensions of the experimental approach. For this reason, small quantities of the phenolic derivative were detected during the first 2 min of dynamic extraction approximately; after that, the highest amount of analyte in the effluent appeared at different times, depending of the operating parameters utilized for the extraction process. As can be observed in Fig. 2B, the knowledge of the kinetics of the SFE under given experimental conditions is possible by real-time monitoring of the process with a detection technique such as TLS. In practice, the selection of the proper dynamic extraction period can be made with a single experience without unnecessary consumption of the solvent. Besides, the influence of the operating parameters over the extraction process can be studied in more detail, even if the major goal of the suggested approach is the improvement in automation of solid material analysis.

The study of the influence of thermodynamic and physicochemical properties of the supercriti-

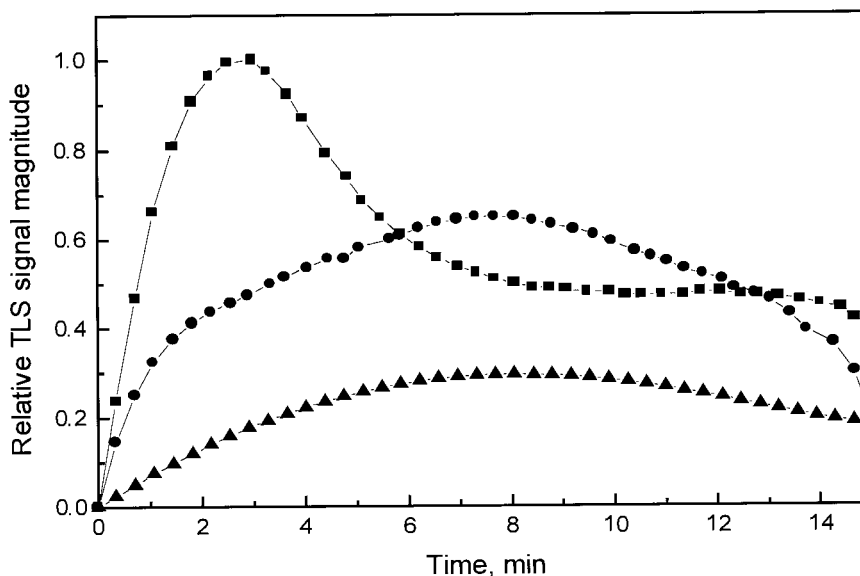


Fig. 3. Influence of density in the kinetics of the supercritical fluid extraction process, under the working conditions described in Table 3: (■), 0.8 g ml⁻¹; (●) 0.7 g ml⁻¹; (▲), 0.6 g ml⁻¹. The trap temperature was maintained constant at 40°C.

cal fluid on both the efficiency of the extraction process and the TLS signal magnitude was carried out simultaneously. Likewise in a previous work [9], the relative TLS signals obtained during a dynamic extraction process were integrated and the corresponding area (arbitrarily denominated relative TLS area) was compared with the concentration of the analyte spectrophotometrically determined at the end of the extraction step.

The study of the *influence of density* on the extraction process was carried out from 0.6 to 0.80 g ml⁻¹ at a constant chamber temperature of 40°C, with the corresponding changes in pressure values from 97 to 164 bar. The kinetic curves obtained are shown in Fig. 3. According to these, the maximum quantity of 3PDP in the effluent was detected at a shorter time at the highest pressure and density conditions studied. This fact is a consequence of the considerable increase of solvent strength as a result of the favorable solvation energy relationship between the solute and the solvent. Under these conditions, the suitable physicochemical properties of the supercritical fluid enabled the beginning of removal of the phenolic derivative from the inert matrix during the static extraction period; therefore, the greatest

amount of the compound was monitored through the detection cell during the first 5 min of the process. In contrast, the decrease in the density–pressure conditions reduced considerably the solubility of 3PDP. In addition, a larger time was necessary to reach the maximum of the kinetic extraction process. As reported in a previous work [9], an approximately proportional relationship between the relative TLS area and the total quantity of the phenolic compound extracted was observed. The recovery results expressed as percentage are shown in Fig. 4. The optimum pressure and density conditions selected were 164 bar and 0.80 g ml⁻¹, respectively.

The study of the *influence of temperature* over the efficiency of the extraction process was developed from 40 to 60°C maintaining a constant pressure of 164 bar, with the corresponding change in the density of the solvent from 0.55 to 0.80 g ml⁻¹. The recovery results of the phenolic compound, expressed as percentage, are shown in Fig. 4. As can be observed, a complete extraction of the analyte was obtained at 60°C, owing to the increase of the analyte solubility in the supercritical solvent. On the other hand, the kinetic curves obtained as a result of the monitoring of the

corresponding extraction processes are presented in Fig. 5. As in the density–pressure study described above, a relationship between the relative TLS signal magnitude and the concentration of the organic compound was observed.

Theoretical aspects of the relationship between some physicochemical properties of the supercritical fluids and the thermodynamic conditions of the system, besides their influence in the TLS enhancement factor, could be of interest at this point for the improvement of the proposed SFE-TLS hyphenated approach.

In a one-component system, compressibility and constant-pressure heat capacity becomes infinite at the critical point. As a result, physicochemical properties such as thermal conductivity and the temperature coefficient of the refractive index shows strong divergences in the critical region. Thus, according to the results obtained by Harris and Leach [24,25], a 150-fold sensitivity improve-

ment relative to measurements in carbon tetrachloride was obtained using carbon dioxide as supercritical fluid near the critical conditions, in the visible region. However, the presence of critical opalescence, which refers to light scattered from refractive index fluctuations due to the critical density fluctuations driven by compressibility, can appear under these conditions. In contrast, the solubility of the analyte as a function of the thermodynamic state of the system is the most important aspect in the optimization of a SFE process, and, generally, the suitable experimental conditions are far from the critical parameters, where the thermophysical properties of the solvent are not the best for TLS sensitivity improvement. Fortunately, the enhancement factors obtained in supercritical fluids could be similar to those obtained in liquids even at pressure and temperature conditions far from the critical region.

4. Conclusions

The viability of the real-time monitoring of a dynamic SFE process by means of a thermal lens spectrometer pumped by a pulsed laser emitting in the near infrared region has been demonstrated throughout. The use of a commercially available Nd-YAG laser operating at the fundamental wavelength of 1064 nm enables the detection of a large number of organic compounds, since RCH_2R' , RNH_2 and benzene derivatives have absorption bands around this wavelength. Unfortunately, a limited selectivity is obtained. In order to diminish this problem, the application of tunable lasers could be considered.

On the other hand, although during the optimization of certain parameters in the SFE process the TLS signal magnitude variations resulted from both the change of the concentration of the analyte and physicochemical properties of the supercritical solvent, a near to linear relationship between the concentration of the compound of interest and the analytical signal can be suggested in a wide range if the study is developed far from the critical point. However, once the extraction process is optimized, a satisfactory estimation of the concentration of the analyte can be obtained.

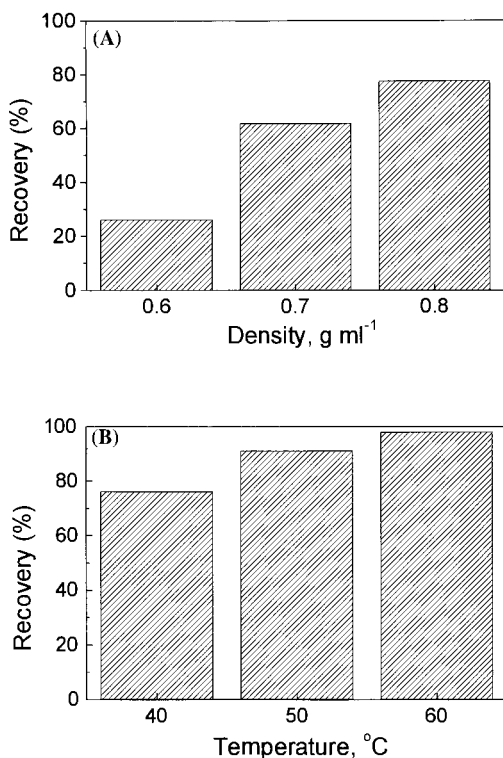


Fig. 4. Recovery percentage results as a function of (A) density and (B) temperature conditions, in the supercritical fluid extraction (SFE) process.

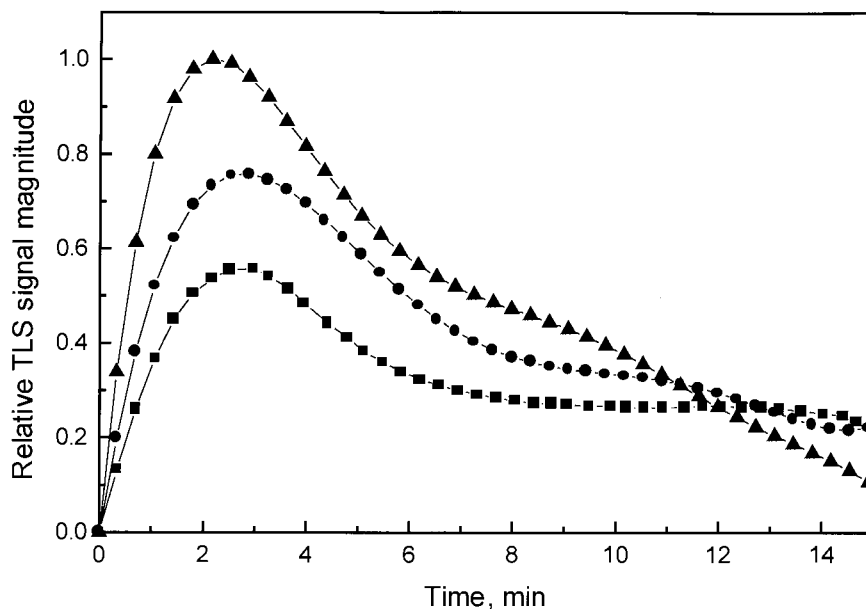


Fig. 5. Influence of temperature in the kinetics of the supercritical fluid extraction process, under the working conditions described in Table 3: (■), 40°C; (●) 50°C; (▲), 60°C. Pressure was maintained constant at 164 bar.

Acknowledgements

The Dirección General de Investigación Científica y Técnica (DGICYT) of Spain is thanked for financial support (project No. PB95/1265); J.A.H. expresses her gratitude to Consejo Nacional de Ciencia y Tecnología (CONACyT), México, for a grant.

References

- [1] B.G. Osborne, T. Fearn, P.H. Hindle, *Practical NIR Spectroscopy with Applications in Food and Beverage Analysis*, Longman Scientific and Technical, Singapore, 1993.
- [2] D.J. Anderson, et al., *Anal. Chem.* 69 (1997) 165R.
- [3] E. Dreassi, G. Ceramelli, P. Corti, M. Massacesi, P.L. Peruccio, *Analyst* 120 (1995) 2361.
- [4] M. Blanco, J. Coello, H. Iturriaga, S. Maspoch, C. de la Pezuela, *Anal. Chim. Acta* 333 (1996) 147.
- [5] K.H. Norris, P.C. Williams, *Cereal Chem.* 61 (1984) 158.
- [6] M.D. Luque de Castro, M. Varcárcel, M.T. Tena, *Analytical Supercritical Fluid Extraction*, Springer, Berlin, 1994.
- [7] J.K. Rice, R.A. Dunbar, F.V. Bright, *Appl. Spectrosc.* 48 (1994) 1030.
- [8] M.T. Tena, M.D. Luque de Castro, M. Varcárcel, *Anal. Chem.* 68 (1996) 2386.
- [9] J. Amador-Hernández, J.M. Fernández-Romero, G. Ramis-Ramos, M.D. Luque de Castro, *Anal. Chim. Acta* (1998) in press.
- [10] K. Zosel, *Process for the decaffeination of coffee*, U.S. Patent 4, 247, 580 (1981).
- [11] R. Vollbrecht, *Chem. Ind.* 19 (1982) 397.
- [12] P. Hubert, O.G. Vitzthum, *Agnew. Chem. Int. Ed. Eng.* 17 (1978) 710.
- [13] T. Higashi, T. Imasaka, N. Ishibashi, *Anal. Chem.* 56 (1984) 2010.
- [14] S. Kawasaki, T. Imasaka, N. Ishibashi, *Anal. Chem.* 59 (1987) 523.
- [15] S.E. Bialkowski, Z. Fang He, *Anal. Chem.* 60 (1988) 2674.
- [16] C.D. Tran, V.I. Grishko, *Appl. Spectrosc.* 48 (1994) 96.
- [17] C.D. Tran, V.I. Grishko, *Anal. Biochem.* 218 (1994) 197.
- [18] J. Amador-Hernández, J.M. Fernández-Romero, G. Ramis-Ramos, M.D. Luque de Castro, *Appl. Spectrosc.* 52 (1998) 1465.
- [19] A. Savitzky, M.J.E. Golay, *Anal. Chem.* 36 (1967) 1627.
- [20] G.R. Long, S.E. Bialkowski, *Anal. Chem.* 56 (1984) 2806.
- [21] G.R. Long, S.E. Bialkowski, *Anal. Chem.* 57 (1985) 1079.
- [22] S.E. Bialkowski, G.R. Long, *Anal. Chem.* 59 (1987) 873.
- [23] J.I. Steinfeld, *Molecules and Radiation*, 2nd edition, MIT Press, Cambridge, MA, 1985.
- [24] R.A. Leach, J.M. Harris, *Anal. Chem.* 56 (1984) 1481.
- [25] R.A. Leach, J.M. Harris, *Anal. Chem.* 56 (1984) 2801.

Properties of a high capacity iminodiacetate–agarose adsorbent and its application in a flow system with on-line buffering of acidified samples for accumulation of metal ions in natural waters

Payman Hashemi¹, Barbro Noresson, Åke Olin*

Department of Analytical Chemistry, Uppsala University, P.O. Box 531, S-751 21 Uppsala, Sweden

Received 4 September 1998; received in revised form 19 February 1999; accepted 22 February 1999

Abstract

Adsorption properties of a fast iminodiacetate–agarose adsorbent, IDA–Novarose, with a capacity of 120–140 $\mu\text{mol/ml}$ were studied for preconcentration of eight transition elements. A FIA–ICP–AES system was used in the study. It was shown that 0.3 ml of the adsorbent, packed in a column, can quantitatively accumulate Cr^{3+} , Mn^{2+} , Fe^{3+} , Co^{2+} , Ni^{2+} , Cu^{2+} , Zn^{2+} and Cd^{2+} from standard solutions in the pH range between 4 and 8 at high loading flow rates (10–80 ml/min). The rate of adsorption was studied in batch experiments and found to be fast and equal for the divalent metal ions but relatively slow for accumulation of Cr^{3+} and Fe^{3+} . On-line buffering of acidified samples improved the accumulation of metal ions from synthetic samples spiked with humic acid. Quantitative uptakes were observed for most of the studied metals. The accumulation of Cr^{3+} was found to be quite sensitive to the ionic strength and some loss of inert complexes of Fe^{3+} was also observed. The method was applied to the analysis of certified riverine water (SLRS-3), a tap water and a lake water. With few exceptions the results obtained by ICP–AES after preconcentration agreed well with the certified concentrations and results found by ICP–MS. © 1999 Elsevier Science B.V. All rights reserved.

Keywords: Iminodiacetate adsorbent; Preconcentration; ICP–AES; Natural waters

1. Introduction

Iminodiacetic acid (IDA) chelating adsorbents have been widely used for the preconcentration of heavy metal ions from water samples prior to their determination by different instrumental techniques. Flame atomic absorption spectrometry (FAAS) [1–3], graphite furnace atomic absorption spectrometry (GFAAS) [4], inductively cou-

* Corresponding author; Tel.: +46-18-471-3689; fax: +46-18-471-3692.

E-mail address: ake.olin@kemi.uu.se (Å. Olin)

¹ Present address: Department of Chemistry, Lorestan University, Khoramabad, Iran.

pled plasma–atomic emission spectrometry (ICP–AES) [5–9] and—mass spectrometry (ICP–MS) [10–13] have been employed in conjunction with these sorbents. IDA containing sorbents based on hydrophobic organic polymers, however, show considerable volume changes in different media and/or low adsorption rates [1,2]. These properties complicate their use in on-line preconcentration systems. Introduction of more hydrophilic phases that increase mass transfer rates and decrease the time required for loading and regeneration of the adsorbent column are hence of interest.

An adsorbent containing iminodiacetate groups bonded to a highly crosslinked agarose support, IDA–Novarose, was studied in two previous works [14,15]. Equilibrium and kinetic properties of the adsorbent were investigated together with the effects on adsorption of the total metal binding capacity (0–45 $\mu\text{mol/ml}$) of the material. These studies showed that IDA–Novarose was about 50 times faster than Chelex-100 (50–100 mesh) in accumulation of Ni^{2+} , Cu^{2+} and Cd^{2+} from standard solutions in the batch mode [14]. The ions were quantitatively captured at flow rates up to 100 ml/min in the column mode. The volume of the packed sorbent was constant and independent of pH, ionic strength and flow rate.

The adsorption of eight frequently occurring transition elements from standard solutions and samples of natural waters onto IDA–Novarose has been studied in the present investigation. A sorbent preparation with a higher capacity than previously used (140 $\mu\text{mol/ml}$) was utilised in order to enhance recovery of more weakly sorbed ions, such as manganese, and diminish chemical interference from the matrix. A method, in which the necessary pH adjustment and buffering of an acid preserved water sample is performed on-line just before the sample enters the sorbent column, will also be presented.

2. Experimental

2.1. Chemicals

The IDA–Novarose chelating adsorbents with

a particle size of 30–60 μm were obtained from Inovata AB (Stockholm, Sweden). Adsorbents with metal binding capacities of 120–140 and, occasionally, 45 $\mu\text{mol/ml}$ were used and will be referred to as IDA140 and IDA45, respectively.

Test solutions were made by appropriate dilution of a stock solution containing eight transition elements. The stock solution was prepared from AAS standards (Reference material AB, Sweden) and the concentrations of Cr^{3+} , Mn^{2+} , Fe^{3+} , Co^{2+} , Ni^{2+} , Cu^{2+} , Zn^{2+} and Cd^{2+} were 25, 10, 50, 25, 75, 25, 25 and 25 mg/l, respectively (the concentrations roughly reflect the relative sensitivity in the ICP–AES determination of the elements). Humic acid, as sodium salt, was obtained from Aldrich and a 100 mg/l stock solution was prepared according to Liu and Ingle Jr. [16].

The other chemicals used were of analytical grade (Merck) and all solutions were made up with Milli-Q filtered deionised water. Stock solutions of ammonium acetate and acetic acid were used for buffering, usually at a total buffer concentration of 0.01 or 0.09 M for initially strongly acidified water samples. Buffers were purified by passage through an IDA140 column in order to diminish blanks.

2.2. Samples

The samples were a communal drinking water from Uppsala, one lake water from its neighbourhood and a riverine water reference material, SLRS-3, from Institute for National Measurement Standards, Canada. The first two samples were acidified by 0.5 ml of suprapure HNO_3 /100 ml and passed through a 0.45 μm Millipore filter. Sub-samples were sent to the accredited laboratory Svensk Grundämnesanalys AB (SGAB), Luleå, Sweden and analysed by ICP–MS.

2.3. Apparatus and analysis

Metal ion concentrations were determined by ICP–AES (Spectroflame, Spectro, Kleve, Germany) or GFAAS (Perkin–Elmer 5000) using the platform technique and deuterium or tungsten

background correction. The instrumental settings of the manufacturers were followed.

The pH measurements were made with a Radiometer PHM 84 (Radiometer, Copenhagen, Denmark) equipped with a combined glass electrode.

The components of the flow injection equipment were the same as reported previously [14]. Glass columns of 6.5 mm i.d. and variable length (Om-nifit) held the adsorbent.

2.4. The FIA–ICP–AES system

The previously presented FIA-system [14] was modified to include the new on-line buffering procedure and is shown in Fig. 1. Pump-B, a piston pump, was connected to the sample flow with a three port connection. It was utilised for on-line pH adjustment of the acidified sample by adding ammonium acetate, usually at a flow rate of 4 ml/min, to the sample stream just in front of the column. This system will be called the on-line buffering of acidified samples (OBAS) system. When the ordinary system was applied for pre-buffered samples, the flow of Pump-B was set to zero.

The piston pump A contained an acetic acid–ammonium acetate buffer solution used for dis-

placing major cations from the column by NH_4^+ , for injection of 2 M HCl as eluent from the 1 ml loop and reconditioning of the column after elution. The flow rate was 2 ml/min. When the ICP was not engaged, the peristaltic pump of the ICP instrument continuously introduced acetate buffer into the plasma at a flow rate of 2 ml/min through V-4.

The sample and buffer, respectively, enter the column from V-2 and go to waste via V-3 during the enrichment, Fig. 1a, and washing cycles. After the washing step, the settings of the valves are changed so that the eluent can enter the column at the bottom. The analytes are carried to V-4 for off-line collection or directed to the ICP–AES instrument, Fig. 1b.

In the recovery measurements, the eluate was collected off-line and analysed by ICP–AES against matched standards.

In the on-line mode, the ICP background signals were found to be somewhat affected when the acid elution plug passed by. Measurement of the blank variation from preconcentrated volumes of buffered and neat MQ between 0 and 300 ml resulted in the following estimates of the detection limits (element, DL(3σ)/ng): Mn, 0.5; Fe, 50; Co,

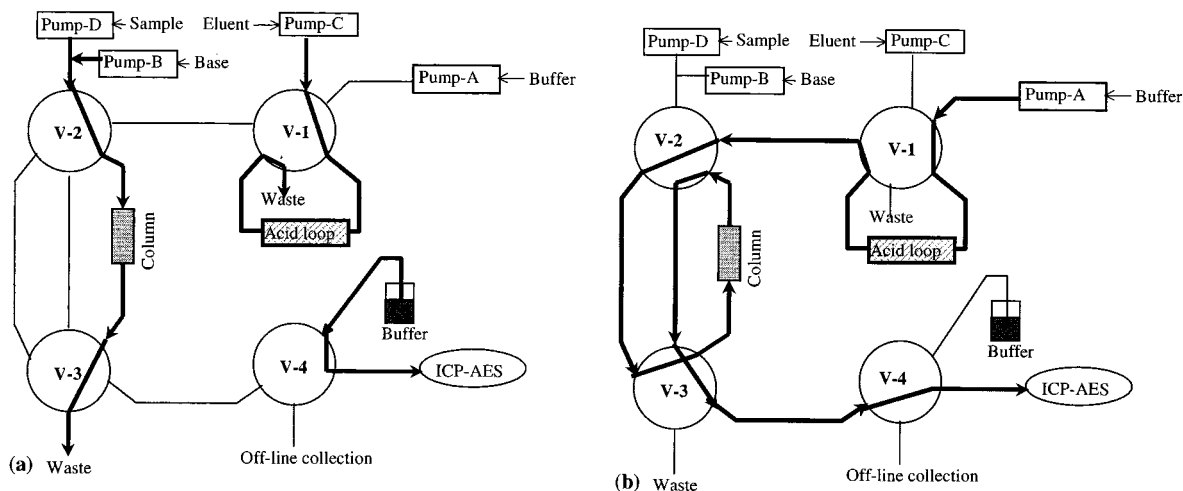


Fig. 1. The FIA–ICP–AES system with four pumps, four seven-port valves, a 1 ml eluent loop and the IDA–Novarose column. Pump-B was only used in the on-line buffering system (OBAS). Its flow rate was set to zero in the ordinary system. (a) The thick lines show the flows during the sampling step and the filling of the eluent loop. (b) The flow during elution is shown.

3.5; Ni, 10; Cu, 10; Zn, 2.5; Cd, 3. The analytical calibration curve, i.e. peak area vs. ng of analyte, was established from measurements of a MQ blank and a standard solution. The same volume and reagent additions were used in the calibration as for the sample. The sensitivity of the analytical curve (counts/ng) was independent of preconcentration volume. A slight increase in the blank with volume for Fe^{3+} (0.3 ng/ml) and for Zn^{2+} (0.03 ng/ml) indicated that some contamination occurred from the equipment and reagents despite treatment of the buffer by passage through IDA140 before use. No blanks were detected for the other elements.

2.5. Adsorption rates and equilibrium concentrations

The measurement of adsorption rates and equilibrium concentrations were performed in the batch mode as described earlier [14]. The start solution was prepared by diluting the metal stock solution 1:100 and at the same time the solution was buffered to the desired pH. To a 200 ml portion of this solution, 0.5 ml of IDA140 was added at the start of the experiment.

2.6. Accumulation and recovery experiments

The uptake of the metal ions in the batch mode as a function of pH was studied by a titration technique. The start solution consisted of 200 ml of the metal stock solution diluted 1:100 and adjusted to pH 2. A 1 ml portion of IDA140 was added and the mixture stirred by a suspended magnetic bar [14]. The pH of the sample was increased in a stepwise manner by addition of 1 M NH_4Ac or NaOH. A 5 ml portion of the solution was sampled through a filter not earlier than 0.5 h after a pH adjustment had been made and analysed by ICP–AES against matched standards. The ionic strength changed from 0.01 to 0.05 M during the experiment.

The metal ion uptake in the column mode was studied with test solutions prepared by diluting the metal stock solution 1:1250 and adjusting the pH to the desired value by 1 M NH_4Ac or NaOH. A 60 ml sample was enriched at a flow rate of 40

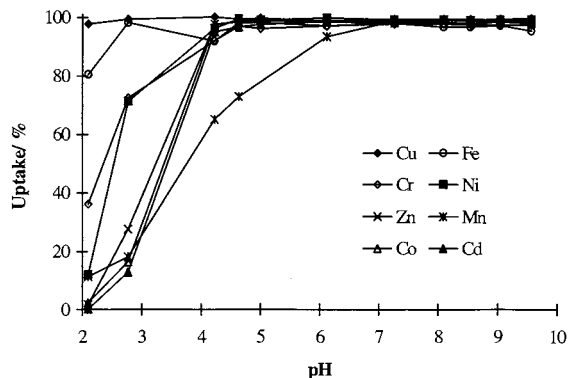


Fig. 2. Batch mode adsorption of metal ions on IDA140 as a function of pH. The uptakes were calculated from the equilibrium concentrations in the aqueous phase. Test solution: 200 ml of stock solution diluted 1:100. Adsorbent: 0.5 ml of IDA140.

ml/min in each experiment. The uptake was found from an analysis of the column eluate by ICP–AES and/or the effluent by GFAAS.

3. Results and discussion

3.1. pH dependence of the adsorption

The adsorption of the metal ions was studied over the pH range from 2 to 9 in batch experiments with a stepwise increase of pH from the lower limit. Fe^{3+} and Cr^{3+} are extensively hydrolysed over most of the investigated pH interval and a number of the other ions form hydroxo complexes in the upper part of the region [21]. The percentage of the test ions taken up by the adsorbent as a function of pH is shown in Fig. 2. All the metal ions, except Mn^{2+} , were quantitatively adsorbed from 200 ml of the test solution onto 0.5 ml of IDA140 when the pH was raised to a value slightly above 4. To confirm the results obtained by the stepwise pH increase, the experiment was repeated with two samples adjusted directly to pH 4.7 and 7.0, respectively, before addition of the sorbent. The solutions were sampled 0.5 and 2 h after addition of the sorbent. The results were equal for the two sampling occasions and in good agreement with the stepwise experiment. No desorption of the metal ions was ob-

served due to formation of hydroxo complexes at high pH.

Recoveries from column enrichments were determined in the same pH range as used in the batch experiment. Column effluents were also collected and analysed by GFAAS. For Mn^{2+} , Co^{2+} , Ni^{2+} , Zn^{2+} and Cd^{2+} the recovery, calculated from analysis of the column eluate, was $103 \pm 2\%$ and independent of pH between pH 4 and 8. It then decreased somewhat up to pH 9, the highest pH investigated. The pattern was similar for Cu^{2+} but the decrease started already at pH 6. The recovery of Fe^{3+} was about 70% in the whole pH region and the recovery of Cr^{3+} increased with pH but did not exceed 60%. Determination of the concentrations of Cr^{3+} , Fe^{3+} and Cu^{2+} in the effluent, on the other hand, indicated that only a few per cent of the ions passed the column unadsorbed in the pH region 3–8.5.

The interpretation of recovery experiments at high pH is made difficult by the hydrolysis and even precipitation of metal ions. For the present set of ions, equilibrium calculations indicate precipitation of Fe(III) above pH 4 and of Cr(III) and Cu(II) at the highest pH values used. Insertion of a 5 μm titanium in-line filter before the column substantially lowered the recoveries above pH 6 and strongly suggests formation of solids. Part of the uptake by the column of these metals may therefore be a filtering effect. However, the incomplete recovery obtained for Fe^{3+} and Cu^{2+} is at variance with the batch experiments and a study was performed to find out the reason for the discrepancy.

The efficiency of the elution was tested first as a possible explanation for the analyte loss. Use of different eluents, higher acid concentrations and volumes, up to 3 ml of 2 M HCl, and even a stop flow elution technique, resulted in no improvement in the recoveries. Elution profiles were also studied in on-line experiments, which showed that 1 ml of acid suffices for elution and no significant difference was observed between the profiles from samples collected at different pH. It can thus be concluded that the losses of the analytes occurred before the enrichment column.

Hirata et al. [5,6] used an on-line buffering system to avoid precipitation in high pH samples.

In this way, the pH is adjusted under the dynamic conditions of the flow system with less risk of precipitation or adsorption onto the walls. This method was tested here by on-line mixing of the sample (pH 2) with a 4 ml/min flow of 1 M NH_4Ac solution. The resulting pH varied with the sample flow rate and changed from 5.5 to 6.3, when the sample flow rate decreased from 60 to 10 ml/min. With the exception of Cr^{3+} , quantitative recoveries were obtained for the metal ions at all flow rates. The low affinity of the adsorbent for Cr^{3+} makes the recovery very sensitive to the matrix composition. The recovery decreased from 91 to 4% when the buffer concentration increased from 0.07 (at 60 ml/min) to 0.3 M (at 12 ml/min).

With on-line pH adjustment we can imagine that a metal ion is captured by the adsorbent before the hydrolysis reactions have proceeded to yield precipitates or hydroxo complexes prone to adsorption on container or tubing walls. On the other hand, the average metal ion spends a considerable time on the adsorbent at high pH during the enrichment. The initially formed adsorbent–metal bond may therefore be subsequently broken by hydrolysis and the metal desorbed as hydroxo species. The on-line experiments as well as the accumulation experiments in batch show that such reactions do not lead to a release of the metal ion from the adsorbent.

The experiment with on-line buffering shows that the low recoveries of some elements in the previous experiments were not due to inefficiency of the adsorbent, but rather to the experimental technique used. None of the methods normally utilised is entirely satisfactory for a determination of the pH dependence of the metal ion accumulation by an adsorbent column. The results obtained with pH adjusted samples may be affected by hydrolysis and precipitation leading to losses by adsorption and filtering effects in the equipment used. The method of on-line buffering, even though more reliable as demonstrated here, can lead to errors for metals whose adsorption is weak and sensitive to the ionic strength. Preservation of solutions by complexing agents or different buffering systems [17] is also unreliable due to incorporation of kinetic effects and equilibrium displacements. Hernandez-Torres et al. [18] used

column effluent concentrations for the calculation of retention in their pH studies rather than recovery. In the high pH region, this may be the only way to find out if there are any loss of metal ions to the effluent. However, as the concentrations of the dissolved ions entering the enrichment column at a high pH are not exactly known, measurements of effluent concentrations can lead to erroneous conclusions on the suitability of an adsorbent for analytical purposes. On the other hand, when the purpose is to study the efficiency of an adsorbent in removal of dissolved metal ions, this method will give the most reliable results. Suppose, for instance, that there is a 5% loss of copper at pH 8 on an adsorbent and that 30% of the copper has already been precipitated or adsorbed before it reaches the column. Only 70% of the total amount of copper will thus reach the column and from that amount 5% will be lost. A measurement on the eluate will give the erroneous result of a 33.5% loss, whereas a measurement on the effluent will result in a 3.5% loss by the column, which is only slightly different from the true value. At a low pH, measurements on eluates and effluents would be equally reliable.

Fig. 3 depicts the adsorption performance of an IDA140 column as a function of pH. The uptakes were obtained from column recoveries at low pH with no hydrolysis and from effluent concentra-

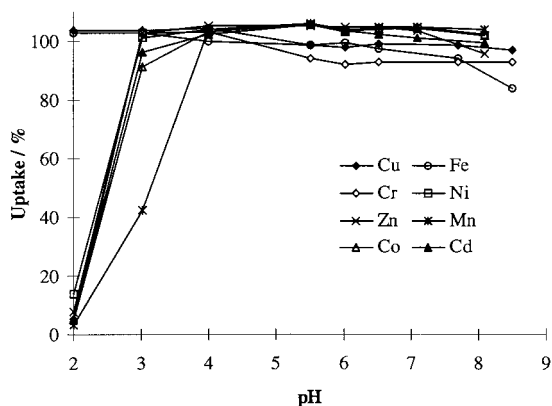


Fig. 3. Column mode adsorption of metal ions on IDA140 as a function of pH. The uptakes were calculated either from eluate or effluent concentrations. Test solution: 60 ml of stock solution diluted 1:1250. Column: 6.5 mm i.d. \times 9 mm. Flow rate: 40 ml/min. Enrichment volume: 60 ml.

tions at high pH. It can be seen from the results that the IDA–Novarose column efficiently accumulates all the studied metal ions in the pH range of 4–8. Since the pH of natural waters is situated within this range, it can be concluded that if the adsorption had been unaffected by the presence of humic and other substances, buffering or pH adjustment of the samples would be unnecessary. Greater pH dependence has been reported for other adsorbents with the same [5,6,12,19] or different [18,20] functional groups.

3.2. Adsorption rates and equilibrium concentrations

Conditional first order rate constants for the adsorption of the metal ions on IDA140 in 0.01 M acetate buffer, pH 5.5, were calculated from the kinetic experiments described in the experimental part. The adsorption rates were quite similar for Mn^{2+} , Co^{2+} , Ni^{2+} , Cu^{2+} , Zn^{2+} and Cd^{2+} , while the rate of adsorption was considerably slower for Cr^{3+} and Fe^{3+} than for the other ions. The trivalent ions are extensively hydrolysed at pH 5.5 and the test solution is supersaturated with respect to FeOOH(s) [21]. The results indicate that mass transfer is rate limiting for the simple ions, whereas for the hydrolysed ions a chemical step determines the adsorption rate.

The equilibrium concentrations, which were close to the detection limits of the ICP–AES instrument for all the metal ions except Mn^{2+} , are presented in Table 1. This table also contains data from measurements in the presence of 0.01 M Ca^{2+} , which was used to represent major cations in fresh water samples. Ca^{2+} affected both the equilibrium concentrations and the adsorption rates. The equilibrium concentrations increased, particularly for manganese and chromium, Table 1. The adsorption rates decreased, but the distinction between the two groups of metal ions was preserved.

The equilibrium data have been used to estimate the sample volume, V_R , which can be enriched on a 0.3 ml column of IDA140 [15]. These volumes are entered in Table 1. They would be sufficient for a determination by ICP–AES of the test ions at the concentrations present in natural

Table 1

Equilibrium concentrations and predicted retention volumes of eight transition elements on IDA140 in the presence and absence of Ca^{2+} ^a

$[\text{Ca}^{2+}]/\text{M}$	Cr	Mn	Fe	Co	Ni	Cu	Zn	Cd
<i>Equilibrium concentrations (%)^b</i>								
0	1.6	9.0	2.0	<0.1	<0.1	<0.1	1.0	1.2
0.01	19.6	87.7	7.0	3.1	<0.1	<0.1	1.5	3.5
<i>Predicted retention volumes (l)</i>								
0	7.3	1.2	5.7	>100	>100	>100	11.4	9.6
0.01	0.5	<0.02	1.6	3.7	>100	>100	7.9	3.3

^a Test solution: 200 ml of stock solution diluted 1:100 and adjusted to pH 5.5. Adsorbent: 0.5 ml of IDA140. The retention volumes were calculated for a 0.3 ml column.

^b Relative to the initial concentration.

waters, which requires enrichment of 50–100 ml of sample. In order to test the equilibrium model, a 60 ml portion of test solution, adjusted to pH 5.5, was enriched on a 0.3 ml column at flow rates between 10 and 80 ml/min. Cr^{3+} and Fe^{3+} were excluded in this study due to their extensive hydrolysis at pH 5.5. The recoveries of Mn^{2+} , Co^{2+} , Ni^{2+} , Cu^{2+} , Zn^{2+} and Cd^{2+} were quantitative in the absence of Ca^{2+} in accordance with the predicted retention volumes. In 0.01 M Ca^{2+} , the recovery of Mn^{2+} was no longer quantitative and the highest result, 50%, was obtained at a flow rate of 10 ml/min. Loss of Mn^{2+} is predicted, since V_R is estimated to about 20 ml in this medium. Contrary to expectation, loss of Ni^{2+} was observed in the presence of Ca^{2+} . The recovery dropped from 97 to 80% when the flow rate increased from 10 to 80 ml/min. The recovery of the other four ions was quantitative also in the presence of Ca^{2+} .

3.3. Some observations with the OBAS system

When a water sample is enriched on a chelating column, only free metal ions or ions bound in labile complexes can be taken up. Inert complexes will pass the column unless captured by simple ion exchange. Hence, quantitative recoveries will be possible only if the metal ions are released in some way. For this purpose digestion techniques are used to decompose organic complexing agents, but they are generally time consuming and require addition of chemicals to the samples with accompanying problems with the blank.

A loss of copper amounting to about 30% was found when tap water samples were enriched by the ordinary enrichment system on IDA45. On the other hand, almost complete recovery of copper was obtained if the tap water sample was acidified to $\text{pH} < 2$ and enriched by the on-line buffering (OBAS) system. Increased recoveries of complexed metal ions by the OBAS system were also found by measurements on test solutions to which humic acid had been added. Table 2 indicates a significant increase in the result for Ni^{2+} and Cu^{2+} , whereas the accumulation of the weaker complex formers Co^{2+} , Zn^{2+} and Cd^{2+} is little affected. The loss of Mn is caused by the diminished distribution ratio in the presence of major cations (see Table 1), in this case NH_4^+ . The improved recovery with the OBAS system

Table 2

Comparison of the recoveries of seven metal ions obtained by the ordinary and OBAS enrichment systems in the presence of 8 mg/l of humic acid^a

System	Recovery (%)						
	Cu	Ni	Cd	Zn	Mn	Fe	Co
Ordinary	21	56	88	91	100	10	93
OBAS	79	100	97	101	79	(161) ^b	100

^a Sample: Metal stock solution diluted 1:1250 and pH adjusted to 7 for the ordinary and 1.6 for the OBAS system. Sample flow rate: 40 ml/min. Sample volume: 60 ml. Column: 0.3 ml of IDA140.

^b Not corrected for contamination of the humic acid by iron.

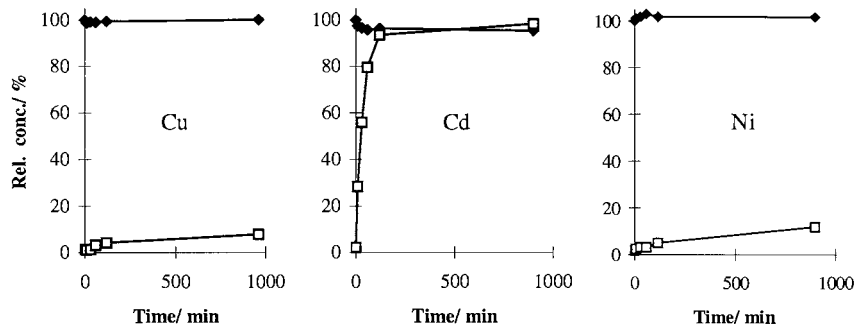


Fig. 4. Concentrations in the aqueous phase during adsorption and stripping of Cu^{2+} , Cd^{2+} and Ni^{2+} in the presence of $5\ \mu\text{M}$ EDTA as a function of time. Filled symbols: Adsorption, the concentrations are expressed relative to the initial values. Open symbols: Stripping, the concentrations are expressed relative to the expected values for complete release. Experimental conditions: 200 ml of solution, 0.5 ml of IDA140, pH 5.

can be understood if humate and other complexes, ML, are essentially dissociated at a low pH. When the acidified sample is buffered on-line at a high flow rate, the residence time after the pH adjustment is so short, that the complexes do not have sufficient time to reform before the solid phase extraction of the free metal ions. The mean time spent by the sample between the pH adjustment and the column is about 0.1 s at a flow rate of 40 ml/min. The half time for the re-formation of the dissociated complex, M–L, should then be longer than 3 s, as otherwise more than 2% of M–L would be reformed.

An ion captured on the column is in contact with the percolating solution between 0 and 150 s for a sample volume of 100 ml and a flow rate of 40 ml/min. When the thermodynamic stability of the adsorbent–metal ion complex, M–R, is substantially greater than the stability of M–L, there is little risk of elution of adsorbed M by L passing through the column. On the other hand, any adsorbed M would be more or less completely eluted when M–R is a weaker complex than M–L. In this case, the kinetics of the exchange reaction $\text{M–R} + \text{L} = \text{M–L} + \text{R}$ will be decisive for the recovery obtained. These points can be illustrated by the behaviour of the system IDA140(R)–EDTA(L)– Ni^{2+} , Cu^{2+} , Cd^{2+} , (M). Very little or no adsorption was observed when IDA140 was added to a solution containing the metal ions and $5\ \mu\text{M}$ EDTA in a batch experiment, Fig. 4. Hence, M–L is a stronger complex

than M–R. In the next set of batch experiments, $5\ \mu\text{M}$ EDTA was added after the metal ions had first been allowed to adsorb on the IDA140 beads. The metal ions were stripped from the adsorbent at very different rates as shown in the same figure. Cd^{2+} was quickly eluted, whereas Cu^{2+} and Ni^{2+} were eluted very slowly.

As a consequence of the thermodynamic stabilities of the EDTA complexes, no recovery of the metal ions was obtained in the presence of $5\ \mu\text{M}$ EDTA with the ordinary system. In the OBAS system, with a pH adjustment from 1.5 to 5, the recovery was a few per cent for Cu^{2+} and Cd^{2+} , whereas the recovery for Ni^{2+} was 85%. From kinetic data [22] the conditional half-time for the formation of NiEDTA can be estimated to 5–10 s, while the half-times for Cu^{2+} and Cd^{2+} are several orders of magnitude shorter. The NiEDTA complex is decomposed at pH 1.5 and the time is too short to re-establish the complex at pH 5 before the sample reaches the column, which captures Ni^{2+} . The slow exchange reaction on the column prevents Ni^{2+} from elution during the sampling time. CuEDTA and CdEDTA on the other hand have time to reform before the sample reaches the column and are therefore not taken up.

These simple experiments demonstrate the intricacies of dynamic preconcentration on a column and points towards advantages of on-line pH adjustment of samples preserved by acid.

3.4. Analysis of natural waters

The detection limits of the FIA–ICP–AES system reported in the experimental part necessitate preconcentration from substantial sample volumes in order to obtain reliable results for low-level analytes. This is exemplified for a lake water in Table 3. The concentrations have been evaluated from calibration curves established at the particular sample volume used. For copper and zinc stable results are obtained already at a sample volume of 50 ml, whereas the low cadmium concentration requires accumulation from about 200 ml of sample. The somewhat varying result for zinc is connected with contamination problems made evident from the calibration curves obtained for different enrichment volumes.

Washing of the column by a buffer before elution was important for replacement of Ca^{2+} and other matrix ions as they interfere with the ICP–AES determination [15]. The extent of such interferences was studied by a comparison of the slopes and intercepts of calibration curves of the analytes in the presence of different concentrations of Ca^{2+} . For all metals the sensitivity decreased and the intercept increased with the Ca^{2+} concentration. The NH_4^+ ion was used to displace Ca^{2+} by a washing step inserted between the accumulation and elution steps. It is reported that a 1 M acetate buffer is required for efficient removal of the matrix ions from Chelex-100 [23]. Displacement experiments indicated that both the ammonium concentra-

tion and pH are important factors. At pH 9, it was not possible to wash out Ca^{2+} with a 16 ml portion of 1 M NH_4^+ . On the other hand, the same volume of a 0.25 M acetate buffer, pH 4.7, sufficiently decreased the amount of calcium to allow interference-free determinations. All test elements were retained after this treatment except chromium that was largely lost.

The water samples (preserved by acid) were analysed by the OBAS system and the ordinary system after adjustment of pH to 4.7 with ammonium acetate. The flow rate was 40 ml/min. No attempt was made to determine Cr(III) which is unretained by IDA140 at the high NH_4^+ concentration present after the pH adjustment. The results for the ordinary and OBAS methods in Table 4 were calculated from triplicate determinations on sample volumes of 125 and 250 ml for Fe, Ni, Cu and Zn, and from triplicate determinations on 250 ml for Co and Cd. For Mn a sample volume of 20 ml was used since the breakthrough volume is about 50 ml. With few exceptions the results from the ordinary and OBAS determinations agree well with one another.

The measured concentrations of Fe and Co fall outside the 95% confidence limits of the SLRS-3 reference sample. In the case of Fe this definitely indicates the presence of iron species, which pass the adsorbent without being retained. The substantial improvement observed with the rapid pH adjustment in the OBAS system suggests that pH dependent equilibria are involved. The discrepancy for Co is not surprising considering the large correction from the overlap of a Fe line. The correction amounts to about 0.1 ng/ml.

The values entered for the determinations made by SGAB are the mean and range obtained for two submitted subsamples, one from each bottle used to hold the test sample. Again the agreement between the sets of data is good and shows the capability of IDA–Novarose to sequester very low metal ion concentrations at a high flow rate from natural waters. A notable exception is Cu. For this metal, the total concentration measured directly by ICP–MS on the lake water sample is significantly larger than the

Table 3
The variation of the analytical results with the enriched volume^a

Volume (ml)	Concentration (ng/ml)		
	Cu	Zn	Cd
20	1.47 ± 0.04	3.42 ± 0.03	0.064 ± 0.018
50	1.49 ± 0.07	3.24 ± 0.08	0.047 ± 0.009
125	1.45 ± 0.02	3.19 ± 0.01	0.023 ± 0.005
250	1.48 ± 0.01	3.27 ± 0.02	0.025 ± 0.008

^a Mean values ± S.D. from triplicate measurements of a lake water sample.

Table 4

Mean values and uncertainty estimates, as detailed in the text, within parentheses for three natural waters analysed by the ordinary and OBAS systems

Sample/method	Concentrations ng/ml						
	Mn	Fe	Co	Ni	Cu	Zn	Cd
<i>SLRS-3</i>							
Ordinary ^a	3.99 ± 0.05	52 ± 3	–	0.79 ± 0.01	1.38 ± 0.08	1.16 ± 0.10	0.014 ± 0.004
OBAS ^a	3.86 ± 0.05	77 ± 2	0.042 ± 0.004	0.79 ± 0.01	1.42 ± 0.03	1.10 ± 0.04	0.015 ± 0.004
Certified ^b	3.9 ± 0.3	100 ± 2	0.027 ± 0.003	0.83 ± 0.08	1.35 ± 0.07	1.04 ± 0.09	0.013 ± 0.002
<i>Tap water</i>							
Ordinary ^a	17.2 ± 0.2	6.0 ± 0.3	0.054 ± 0.003	0.75 ± 0.02	4.89 ± 0.20	63.0 ± 1.6	0.11 ± 0.01
OBAS ^a	15.8 ± 0.2	5.7 ± 0.1	0.050 ± 0.003	0.71 ± 0.01	4.68 ± 0.02	57.7 ± 0.4	0.10 ± 0.01
SGAB ^c	18.1 ± 0.9	6.4 ± 1.0	0.053 ± 0.009	0.62 ± 0.03	4.37 ± 0.11	54.5 ± 0.7	0.0975 ± 0.000
<i>Lake water</i>							
Ordinary ^a	47.4 ± 0.3	95.5 ± 2.4	0.034 ± 0.013	1.39 ± 0.06	1.14 ± 0.01	3.52 ± 0.03	0.030 ± 0.004
OBAS ^a	49.6 ± 0.7	87.4 ± 2.7	0.048 ± 0.008	1.41 ± 0.03	1.46 ± 0.02	3.23 ± 0.04	0.025 ± 0.008
SGAB ^c	49.3 ± 1.9	97.3 ± 4.1	0.042 ± 0.010	1.38 ± 0.24	1.86 ± 0.43	3.70 ± 0.39	0.026 ± 0.009

^a Estimated ± S.D.

^b 95% confidence limits (±).

^c Range. Analysis by ICP–MS.

concentration obtained by the ordinary system, while the result from the OBAS system lies in between. The observation that the result for Cu from the OBAS system is significantly larger than from the ordinary system has been made repeatedly on specimens of natural waters and indicates that Cu is the element most strongly complexed by humic substances.

4. Conclusions

The improved detection by the ICP–MS instrumentation has made preconcentration procedures less important for many sample types, which needed them previously. Adsorbents should, however, still be useful in the ICP–MS or ICP–AES laboratory for matrix modification and improvement of detection limits by preconcentration. The IDA–Novarose adsorbent is well suited for these purposes. Quantitative recovery is obtained over a broad pH range and the rapid kinetics and open structure allow high flow rates, up to 80 ml/min. The moderate strength of iminodiacetate com-

plexes also affords an estimate of the relative availability of the metal ions by a determination of the total amount of metal and the amount adsorbed by IDA–Novarose.

References

- [1] J.P. Riley, D. Taylor, *Anal. Chim. Acta* 40 (1968) 479.
- [2] Z. Fang, J. Ruzicka, E.H. Hansen, *Anal. Chim. Acta* 164 (1984) 23.
- [3] S. Hirata, K. Honda, T. Kumamaru, *Anal. Chim. Acta* 221 (1989) 65.
- [4] F. Baffi, A.M. Cardinale, R. Bruzzone, *Anal. Chim. Acta* 270 (1992) 79.
- [5] S. Hirata, Y. Umezaki, M. Ikeda, *Anal. Chem.* 58 (1986) 2602.
- [6] S. Hirata, K. Honda, T. Kumamaru, *Anal. Chim. Acta* 221 (1989) 65.
- [7] K. Vermeiren, C. Vandecasteele, R. Dams, *Analyst* 115 (1990) 17.
- [8] V. Dupont, Y. Auger, C. Jeandel, M. Wartel, *Anal. Chem.* 63 (1991) 520.
- [9] S. Caroli, A. Alimonti, F. Petrucci, Zs. Horvath, *Anal. Chim. Acta* 248 (1991) 241.
- [10] L. Ebdon, A. Fisher, H. Handley, P. Jones, *J. Anal. At. Spectrom.* 8 (1993) 979.

- [11] S.F. Durrant, A. Krushevskaya, D. Amarasiriwardena, M.D. Argentine, S. Romon-Guesnier, R.M. Barnes, *J. Anal. At. Spectrom.* 9 (1994) 199.
- [12] M.J. Bloxham, S.J. Hill, P.J. Worsfold, *J. Anal. At. Spectrom.* 9 (1994) 935.
- [13] S.M. Nelms, G.M. Greenway, D. Koller, *J. Anal. At. Spectrom.* 11 (1996) 907.
- [14] P. Hashemi, Å. Olin, *Talanta* 44 (1997) 1037.
- [15] B. Noresson, P. Hashemi, Å. Olin, *Talanta* 46 (1998) 1051.
- [16] Y. Liu, J.D. Ingle Jr., *Anal. Chem.* 61 (1989) 525.
- [17] B. Mohammad, A.M. Ure, D. Littlejohn, *Microchim. Acta* 113 (1994) 325.
- [18] O. Hernandez-Torres, J.J. Arias-Leon, *Int. J. Environ. Anal. Chem.* 54 (1993) 15.
- [19] M. Satake, K. Ishida, B.K. Puri, S. Usami, *Anal. Chem.* 58 (1986) 2502.
- [20] B. Pasullean, C.M. Davidson, D. Littlejohn, *J. Anal. At. Spectrom.* 10 (1995) 241.
- [21] C.F. Baes Jr., R.E. Mesmer, *The Hydrolysis of Cations*, Wiley, New York, 1976.
- [22] N. Tanaka, Y. Sakuma, *Bull. Soc. Chem. Jpn.* 32 (1959) 578.
- [23] H.M. Kingston, I.L. Barnes, T.J. Brady, T.C. Rains, M.A. Champs, *Anal. Chem.* 50 (1978) 2064.

Chelating 2-mercaptobenzothiazole loaded resin. Application to the separation of inorganic and alkylmercury species for their atomic absorption spectrometry determination in natural waters

J. Chwastowska *, A. Rogowska, E. Sterlińska, J. Dudek

Institute of Nuclear Chemistry and Technology, Department of Analytical Chemistry, ul. Dorodna 16, 03-195 Warsaw, Poland

Received 16 December 1998; received in revised form 17 February 1999; accepted 22 February 1999

Abstract

A new 2-mercaptobenzothiazole loaded Bio-Beads SM-7 resin has been prepared and its analytical properties were established. The sorbent was applied to the separation and preconcentration of inorganic and alkylmercury from natural waters. Optimum conditions of separation as pH, flow rate on column, volume of samples and desorbing agent were established. The cold vapour atomic absorption method determination of both forms of mercury after their successive reduction by tin(II) was used. The low limit of determination for this method was established as 10 ng l^{-1} for 1.0 l water sample. Accuracy and precision of the method was estimated by using test water standards and samples of natural water spiked with known amounts of mercury species. © 1999 Elsevier Science B.V. All rights reserved.

Keywords: 2-mercaptobenzothiazole sorbent; Inorganic; Alkylmercury; CVAAS

1. Introduction

Mercury belongs to the toxic, dangerous for human health elements, whose concentration in the environment should be kept under permanent control.

The toxicity of mercury depends to a high degree on its chemical form. The inorganic compounds of mercury(II) and its methyl derivatives are particularly dangerous because of their neuro- and embriotoxicity. It results from the literature data [1,2] that methylmercury is of great interest owing to its toxicity and its prevalence in the environment.

The admissible concentrations of individual forms of mercury in natural waters are usually below the determination limit of most of commonly used analytical techniques. Therefore,

* Corresponding author. Tel.: +48-22-8112737; fax: +48-22-8111532.

E-mail address: jchwasto@orange.ichtj.waw.pl (J. Chwastowska)

many applied procedures are based on separation and preconcentration followed by determination.

Solid-phase extraction, using chelating sorbents obtained by immobilization of a suitable organic agent on a resin bed, is the most effective method of trace preconcentration. The typical sorbents used for mercury separation contain organic agents with sulphhydryl groups that form stable complexes with mercury, e.g. ditzone [3,4], thio-carbamates [3,5–7], thionalide [8]. Terada et al. [9] used 2-mercaptobenzothiazole (MBT) loaded silica gel for preconcentration of copper and Pu et al. [10] investigated the sorption of silver by MBT fixed on modified silica gel. Also the sorption of mercury, cadmium, lead and zinc by MBT immobilized on the specially treated natural clay was studied [11]. The results obtained showed that MBT-sorbent may be an effective for mercury(II).

In the present work sorbent obtained by MBT immobilization on a macroporous acrylic ester polymer bed (Bio-Beads SM-7) was studied and applied for inorganic and alkylmercury preconcentration followed by sequential determination of both of these forms of mercury from the same sample by CV AAS after their successive reduction by tin(II).

2. Experimental

2.1. Apparatus

A Thermo Jarrel Ash Smith-Hieftie 4000 atomic absorption spectrometer, equipped with TJA 440 atomic vapour accessory, deuterium arc background correction and Visimax II mercury hollow-cathode lamp (Thermo Jarrell Ash).

A Mettler-Toledo Delta 340, pH-meter.

A SWAN γ -ray spectrometer (Institute for Nuclear Studies, Świerk) with an Ortec HPGe detector (resolution 1.8 for $E_{\gamma} = 1332$ keV, relative efficiency 40%) was used for activity measurements.

IR measurements were carried out using a Perkin–Elmer Model 577 spectrometer

Glass columns 4 mm in internal diameter were used in column experiments.

2.2. Reagents and solutions

All water used purified by Water Purification System—Milipore.

Nitric and hydrochloric acids purified by sub-boiling distillation were used.

Bio-Beads SM-7 resin (acrylic ester polymer), 20–50 mesh, Bio-Rad.

2-Mercaptobenzothiazole (MBT), analytical grade, Fluka.

Chelating resin-MBT loaded Bio-Beads SM-7 (MBT-BB) was prepared as follows: 3 g Bio-Beads SM-7 resin 20–50 mesh, previously washed with ethanol, were shaken with 25 ml 0.1 M MBT solution in acetone for 10 min. The resin was then filtrated off under reduced pressure and allowed to dry in the air for about 2 h. It should be stored in darkness at 4°C.

A radiotracer ^{197}Hg ($T = 65$ H, $E_{\beta} = 77$ keV) was obtained by irradiation of HgCl_2 solution in a nuclear reactor.

Stock inorganic mercury solution, 1 mg ml $^{-1}$, was prepared by dissolution of 0.1 g Hg, analytical grade, POCH, in concentrated nitric acid and diluted to 100 ml with water.

Stock methyl- and ethylmercury solutions in the concentration of 1 mg ml $^{-1}$ were prepared by dissolution of 0.0659 g CH_3HgCl (Johnson–Matthey) in 6 ml of 96% $\text{C}_2\text{H}_5\text{OH}$ and of 0.0660 g of $\text{C}_2\text{H}_5\text{HgCl}$ (Johnson–Matthey) in 10 ml acetone, then dilute to 50 ml with water.

Working solutions of all forms of mercury were prepared before use, by dilutions of the stocks solutions with water.

Tin chloride 10% solution, was prepared daily by dissolution of 5.95 g $\text{SnCl}_2 \cdot 2\text{H}_2\text{O}$, analytical grade, POCH, in 4 ml concentrated hydrochloric acid and diluted to 50 ml with water.

Potassium hydroxide, analytical grade, POCH, 30% solution in water.

Cadmium chloride, 1% solution, was prepared by dissolution of 1.25 g $\text{CdCl}_2 \cdot 2.5\text{H}_2\text{O}$ in 100 ml of water, analytical grade, POCH.

Thiourea, 5% solution, was prepared by dissolution of 5 g thiourea, analytical grade, Fluka, in 100 ml 0.005 mol l $^{-1}$ hydrochloric acid.

Test water solution was of the following composition (mg l^{-1}): Na^+ , 15; K^+ , 4; Mg^{2+} , 20; Ca^{2+} , 55; Cl^- , 124; SO_4^{2-} , 80; Zn^{2+} , 0.2; Fe^{3+} , 0.2, Cd^{2+} , 0.01 and Pb^{2+} , Ni^{2+} , Co^{2+} , Cu^{2+} , 0.05.

Glassware were cleaned by soaking in 20% nitric acid (48 h) and then rinsed with water.

2.3. Examination of MBT–BB properties

The amount of MBT loaded on the resin was determined spectrophotometrically at 322 nm after removal from the sorbent with ethanol.

The stability of the sorbent was determined by measuring the amount of MBT on the sorbent after definite time intervals after its preparation.

IR spectra of sorbent MBT–BB and of MBT and resin BB were measured in the range 800–3500 cm^{-1} . The samples were ground, mixed with KBr and pelletized.

The retention capacity was determined for mercury(II) by the batch method.

2.4. Conditions for sorption experiments

2.4.1. Batch experiments

Sorption of Hg^{2+} was examined over a pH range 0–6. The proper acidity was adjusted by addition of diluted hydrochloric acid or sodium hydroxide solution. 20 ml of solution of a suitable acidity countering the radiotracer ^{197}Hg ($\approx 1 \mu\text{g}$) was shaken with 0.2 g of MBT–BB for 30 min. It was then filtered off and the sorbent was washed twice with 2-ml portion of solutions of the same acidity. The washings were combined with the filtrate. The sorption of element was calculated from the difference of the activity of the primary solution and filtrate by measurement of the ^{197}Hg 77 keV photopeak.

2.4.2. Column experiments

A glass column was filled with 0.2 g of the sorbent ($70 \times 4 \text{ mm}$) and conditioned with a solution of suitable acidity. A sample adjusted to suitable acidity was passed through the column at the rate of $0.7\text{--}1 \text{ ml min}^{-1}$. The column was washed with 5 ml of water acidified to the same

acidity and the washing was added to the effluent. Mercury retained on the column was eluted with 10 ml 5% thiourea and the inorganic mercury was determined in the same way as in the batch experiments. Since the labelled alkylmercury compounds were not available the sorption efficiency of CH_3Hg^+ and $\text{C}_2\text{H}_5\text{Hg}^+$ was estimated by the CV AAS method.

2.5. Conditions for CV AAS determination

2.5.1. Modified procedure for cold vapour generation

Tin(II), used for successive reduction of inorganic and alkylmercury, shows a strong adsorption on the walls of the reaction vessel. When the commercial accessory for cold vapour generation (e.g. TJA 400 atomic vapour accessory) is used, tin adsorbed in the vessel during the analysis of the first sample reduces prematurely mercury in the succeeding samples and causes its losses. Therefore, the original procedure of sequential reduction of various forms of mercury, proposed by Magos [12], required a modification [8].

The applied procedure was as follows:

7 ml of 30% solution of potassium hydroxide was put into the reaction vessel, closed and purged with argon for 20 s. Next 2 ml of tin chloride solution was introduced into the vessel and 5 ml of the sample was injected using a syringe pipette. The inorganic mercury was reduced for 1.5 min. and then the mercury vapour was transported with the stream of argon to the vapour cuvette of the spectrometer and measured. The reduction procedure was repeated without opening the reaction vessel, but this time, after purging the vessel with argon, only 1 ml of 1% cadmium chloride solution was added. Mercury bound as alkyl compounds was replaced by cadmium and reduced to the metallic form by tin(II) present in an excess. After 1.5 min the evolved vapours were transported again to the spectrometer and measured as the alkylmercury.

All results were based on the peak height absorbance.

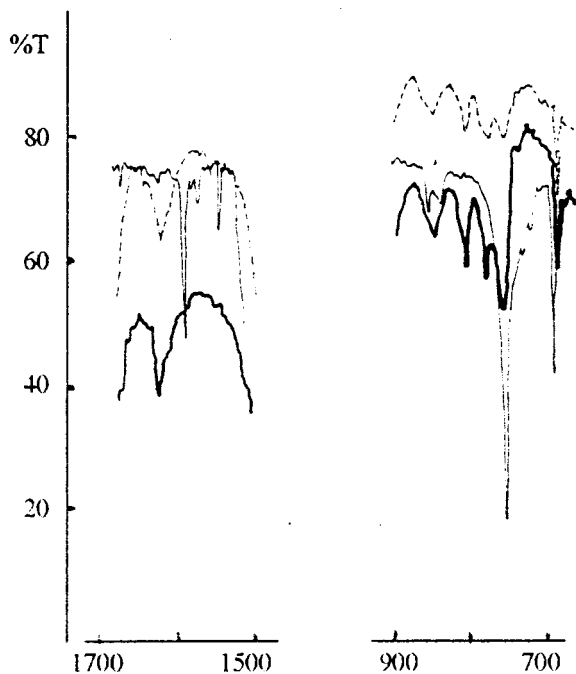


Fig. 1. IR spectra of (thin solid lines) MBT, (dashed lines) Bio-Beads SM-7 resin, and (thick solid lines) MBT-BB.

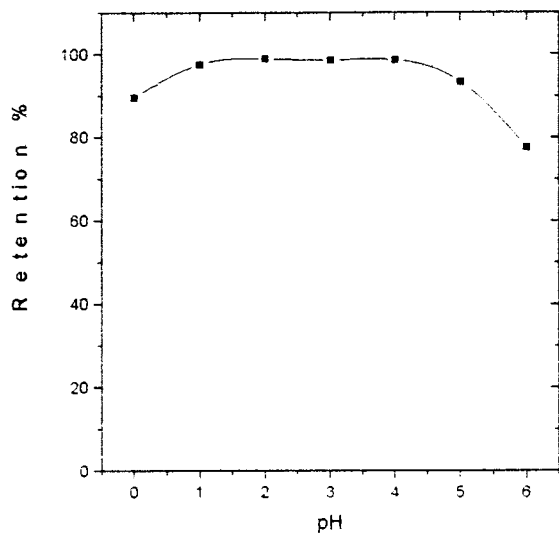


Fig. 2. Dependence on the efficiency of mercury sorption on pH solution.

Table 1

Recovery of inorganic and alkylmercury compounds in test water

	Sample I		Sample II
	Hg ²⁺	CH ₃ Hg ⁺	C ₂ H ₅ Hg ⁺
Added (ng l ⁻¹)	50	50	50
Found ^a (ng l ⁻¹)	49.5	49.0	49.0
Recovery (%)	99.0	98.0	98.0
S _r (%)	7.0	8.0	8.0

^a Mean of four determinations.

Table 2

Determination of mercury in natural waters

Sample	<i>n</i>	Hg ²⁺ (ng l ⁻¹)	S _r (%)
River water	9	35.7	8.2
Ground water	4	<10	

2.5.2. Instrumental settings for AAS measurements

Wavelength	253.7 nm
Band pass width	1.0 nm
Signal pulse lamp current	3.0 mA
Background pulse lamp current	6.0 mA
Integration time	8.0 s
Purge gas—argon	6.0 l min ⁻¹

2.6. Analytical procedure

0.2 g of MBT-BB was placed in the glass column (70 × 4 mm), which was previously washed with 15 ml of 5% thiourea solution, 10 ml of water and 10 ml of 0.01 mol l⁻¹ hydrochloric acid. The sample of water to be analyzed (1.0 l) was filtered using 0.45 μm cellulose filter, acidified with hydrochloric acid to pH = 3, passed through the column with flow rate 5 ml min⁻¹ and then

the column was rinsed with 5 ml of water. All the mercury was desorbed using 10 ml of 5% thiourea solution in 0.05 mol l⁻¹ hydrochloric acid with flow rate 1 ml min⁻¹. 5 ml of the eluate was used for the successive determination of inorganic and organic mercury by cold vapour AAS according to the modified procedure described above.

3. Results and discussion

3.1. Characteristics of the sorbent

The amount of MBT loaded on Bio-Beads SM-7 varied in the range 42.5–43.5 mg g⁻¹ and is stable for at least 6 weeks, if it is stored in darkness at 4°C.

The IR spectra of MBT–BB, MBT and resin are shown in Fig. 1. It can be seen that the bands in the range 1645–1615 cm⁻¹ characteristic for the C=N group, clearly visible in the spectrum of MBT, disappear in the spectrum of MBT–BB. On the other hand the bands in the range 800–600 cm⁻¹, characteristic for the C–S group, are present in the spectrum of the sorbent. The concentration of MBT in the sorbent is lower than that in the spectrum of MBT alone but the presence of C–S bands in the spectrum of sorbent may to prove that disappearance of C=N bands is caused by the fact, that MBT molecules are attached to the support (Bio-Beads SM-7) through the electrons of C=N groups.

The average retention capacity of MBT–BB for mercury(II) from solution of pH = 3 is equal 55 mg mercury(II) for 1 g of sorbent This gives a mole ratio of MBT to the mercury (in sorbent) 1:1 and suggests that the sorption process is accompanied by the reduction of mercury(II). The reduction of cuprous during the sorption of Cu(II) on the MBT loaded silica gel was suggested by Terada et al. [9].

3.2. Retention of mercury compounds

The investigation of Hg retention on the MBT–BB sorbent by batch method (shaking time 10 min) as function of pH (Fig. 2) shows that the efficiency of sorption is constant and equal to 98% in the range of pH values from 1 to 4. In the column process the obtained results were very similar, however, then the sorption efficiency was higher, about 100%. The value of pH = 3 was considered as optimal. In these conditions mercury in the form of methyl and ethyl compounds was also adsorbed quantitatively with similar efficiency.

At the optimal acidity it was found that a flow rate up to 5 ml min⁻¹ and a sample volume up to 1.0 l do not deteriorate the efficiency of mercury sorption.

3.3. Analytical applications

The accuracy of the method was checked on the basis of the artificially prepared test water samples containing main components present in

Table 3
Recovery of inorganic mercury in spiked natural waters

Sample	Added		n	Found ^a (ng l ⁻¹)	Recovery (%)	S _r
	Form	Amount (ng l ⁻¹)				
River water	Hg _{inorg}	50	4	49	98.0	9.3
River water	¹⁹⁷ Hg _{inorg}	100	2	97	97.0	
Ground water	Hg _{inorg}	50	4	51	102.0	9.0
Ground water	¹⁹⁷ Hg _{inorg}	100	2	99	99.0	

^a Results after subtraction of amount determined in water.

natural waters and known concentrations of inorganic, methyl and ethylmercury. The results are shown in Table 1. The accuracy of the method was found to be correct and the precision may be considered as satisfactory ($S_r = 7.0; 8.0$) for this level of concentration.

The lower limit of determination for elaborated method was estimated as 10 ng l^{-1} for water sample volume equal to 1 l.

Examples of the determination of mercury in river and ground water are presented in Table 2. They are limited to the determination of inorganic mercury only, since we were not able to find the natural samples containing detectable amounts of alkylmercury.

The recovery of inorganic mercury in natural waters was determined after spiking the samples of natural waters with known amounts of mercury. The test was carried out in two ways: using the proposed analytical method and using the radiotracer ^{197}Hg (Table 3). The determined recovery is comparable to that presented in Table 1.

Acknowledgements

The authors thank Professor L. Pszonicki for discussions.

References

- [1] E.A. Mackey, D.A. Becker, *Analyst* 123 (1998) 779.
- [2] Y. Madrid, C. Cabrera, T. Perez-Coroma, C. Camara, *Anal. Chem.* 67 (1995) 750.
- [3] M.F. Garcia, R.P. Garcia, N.B. Garcia, A. Sanz-Medel, *Talanta* 41 (1994) 1833.
- [4] T. Braun, A.B. Farag, *Anal. Chim. Acta* 75 (1974) 133.
- [5] K. Kinagawa, Y. Takizawa, I. Kifune, *Anal. Chim. Acta* 115 (1980) 103.
- [6] H. Emteborg, D.C. Baxter, W. French, *Analyst* 118 (1993) 1007.
- [7] P. Lansen, C. Mauleman, M. Leemarkers, W. Baeyens, *Anal. Chim. Acta* 234 (1990) 417.
- [8] J. Chwastowska, W. Skwara, E. Sterlińska, J. Dudek, L. Pszonicki, *Chem. Anal.(Warsaw)* 43 (1998) 995.
- [9] K. Terada, K. Matsumoto, H. Kimura, *Anal. Chim. Acta* 153 (1983) 237.
- [10] Q. Pu, Q. Sun, Z. Hu, Z. Su, *Analyst* 123 (1998) 239.
- [11] N.L. Filho, Y. Gushikem, W.L. Polito, *Anal. Chim. Acta* 306 (1995) 167.
- [12] L. Magos, *Analyst* 96 (1971) 847.

Spectrophotometric determination of the dissociation constants of methyl yellow in mixed protic solvents

Jing Fan *, Xuejing Shen, Jianji Wang

Department of Chemistry, Henan Normal University, Xinxiang, Henan 453002, People's Republic of China

Received 5 August 1998; received in revised form 17 February 1999; accepted 25 February 1999

Abstract

The concentration dissociation constants (pK_a) of methyl yellow, MY (H^+In) in mixed aqueous solvents of methanol, ethanol, iso-propanol, tert-butanol have been accurately determined from spectrophotometric measurements at 25°C and a constant ionic strength of 0.1 mol l⁻¹. It has been shown that in these solvents, the pK_a values decrease with increasing composition of the organic co-solvent. A linear relationship between pK_a and the mole fraction (x_2) of the co-solvent was observed in a limited range of the compositions for each of the solvent systems. The results have been discussed in the light of transfer thermodynamic properties of the species existing in the dissociation equilibrium, solvent basicity and solute–solvent interactions. Furthermore, it was also observed that with the change of the solvents, the absorption spectra of MY shifted apparently and the color transition changed accordingly. The solvent effect on the spectra has been attributed to the isomerization equilibria of MY. A simple application of MY was also shown to the sodium acetate-hydrochloric acid titrations in the mixed solvents. © 1999 Elsevier Science B.V. All rights reserved.

Keywords: Spectrophotometry; Dissociation constant; Methyl yellow; Mixed protic solvents

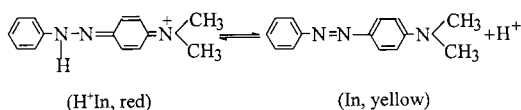
1. Introduction

Recently, mixed solvents have been widely used in analytical chemistry with the extension of research fields and the development of non-aqueous analytical technique and methods. These solvents are advantageous to the titrations of the acids and

bases which are too weak or insoluble in water [1–3]. So it is important to select suitable indicators and to plan optimum analytical procedures for these titration systems. The aim of the recent work was therefore to determine the pK_a values of a set of acid–base indicators in mixed solvents. These data would enhance the applicability of the indicators in nonaqueous titrations.

Methyl yellow (MY) is one of the most used acid–base indicators. Its acid–base equilibrium in solution may be represented by

* Corresponding author. Fax: +86-373-3383145.
E-mail address: wjjly@public.zz.ha.cn (J. Fan)



The dissociation constants for MY in water, methanol and ethanol are well known [4–6]. However, pK_a values of this indicator in mixed solvents have been reported only in aqueous solutions of methanol (40, 60, 80 vol.%) [7], ethanol (40, 60, 80 vol.%) [7], acetone (40, 60, 80 vol.%) [7], dioxane (20, 40, 60 vol.%) [8] and *N,N*-dimethyl formamide (10–80 vol.%) [9]. As a part of the systematic studies on *para*-(dimethylamino)azobenzene indicators in mixed solvents [10], the acid dissociation constants for MY in water–methanol, –ethanol, –isopropanol and –tert-butanol mixed solvents are represented here at 25°C and an ionic strength of $I = 0.1 \text{ mol l}^{-1}$ KCl. The effect of solvent on the visible absorption spectra and color transition range of MY has been investigated. A simple application of MY has also been given to the sodium acetate–hydrochloric acid titration in the mixed solvents. The co-solvents (methanol, ethanol, iso-propanol and tert-butanol) were chosen in order to examine the effect of alkyl chain size in co-solvent molecules on the dissociation constants.

2. Experimental

2.1. Reagents and stock solutions

MY (A.R., Hopkin and Williams, UK) was used after drying for several hours under vacuum. Methanol (MeOH), Ethanol (EtOH), isopropanol (i-PrOH) and tert-butanol (t-BuOH) (A.R., all from Beijing Chemical Factory) were dried over 4A type molecular sieves before use. Hydrochloric acid, potassium chloride, sodium hydroxide and anhydrous sodium acetate (A.R., all from Shanghai Chemical Reagent Co.) were used without further purification.

The stock solution of sodium hydroxide (0.1 mol l^{-1}) was made in water and standardized by potassium acid phthalate. Then, this solution was

used to standardize the stock solution of hydrochloric acid (0.1 mol l^{-1}). Stock solutions of MY were made in pure organic solvents investigated because of the very low solubility of this indicator in water. Test solutions were prepared by dilution of the respective stock solutions. The ionic strength in all solutions was maintained to be 0.1 mol l^{-1} by using potassium chloride as background. Deionized and redistilled water was used throughout the experiment.

2.2. Apparatus

Absorbance measurements were made on a shanghai spectrophotometer (Model 721) equipped with cells of path length 1.0 cm. The measurements of H^+ concentration was conducted in cell (A)

glass electrode | 0.1 mol l^{-1} (KCl + HCl),
SH, $\text{H}^+ \text{In} | \text{AgCl} - \text{Ag}$ (A)

where SH denotes solvent. A shanghai pH glass electrode (Model 231) and a thermal electrolytic $\text{AgCl} - \text{Ag}$ reference electrode without liquid junction [11] were used. The cell potentials were recorded by means of a shanghai ion-analyzer (model PXSJ-216). The absorbance and potential measurements were thermostatically controlled at $25 \pm 0.05^\circ\text{C}$ by circulating water from a modified Shanghai thermostat (model 501).

2.3. Procedure

Solutions for absorbance and potential measurements were prepared by weight. Into a 50-ml volumetric flask, transfer 5.00 ml of the stock solution of sodium hydroxide and 1.00 ml of the stock solution of MY, add 0.3728 g potassium chloride, the necessary amount of pure alcohol and water to the mark in order to obtain a $0.0100 \text{ mol l}^{-1}$ sodium hydroxide in the required mixed solvent. A $0.0100 \text{ mol l}^{-1}$ hydrochloric acid in the same mixed solvent can be similarly obtained. Both solutions should have the same proportion of alcohol and the same ionic strength. Twenty five ml of this hydrochloric acid solution was added to cell (A) and titrated with

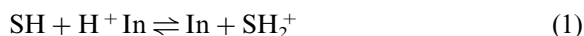
small additions of the sodium hydroxide solution until an equivalent point. After each titration, the volume of the titrant (V) and the corresponding potential (E) of the cell were recorded.

In 25-ml flasks 0.50 ml of the MY stock solution, the necessary amount of potassium chloride, pure alcohol, small volumes of nitric acid at different concentrations and redistilled water were added to the mark to obtain a series of solutions of MY at different pH values. Each of these solutions was used to the potential measurements and the absorbance measurements against a solvent blank. The solution containing only the acid form of the indicator was used to choose the working wavelength.

3. Results and discussion

3.1. Determination of the dissociation constants

Dissociation equilibrium of the MY in mixed solvents can be described as follows



where SH_2^+ denotes solvated proton, $\text{H}^+ \text{In}$ and In refer to the acid and basic forms of MY, respec-

tively. The concentration dissociation constant ($\text{p}K_a$) for the indicator can be calculated [10] from

$$\text{p}K_a = \text{p}[\text{SH}_2^+] + \log[(A - A_2)/(A_1 - A)] \quad (2)$$

where A_1 and A_2 are the absorbances of the acid and the basic forms of MY, respectively. A is the absorbance of the equilibrium mixtures of acid and base forms at a particular pH. A , A_1 and A_2 are determined spectrophotometrically. Concentration of the solvated proton in the mixed solvent, $[\text{SH}_2^+]$, can be known potentiometrically as stated below.

The potential of cell (A) is given [12] by

$$E = E_a^{0'} - k \log[\text{SH}_2^+] \quad (3)$$

where $E_a^{0'}$ is the specific constant of the cell and k the experimental slope of the glass electrode. Based on the acid–base titration data mentioned in Section 2, they can be obtained for a particular mixed solvent by means of the linear relationship between E and $\log[\text{SH}_2^+]$. Then, the potential data of a series of solutions of MY can be used to calculate $[\text{SH}_2^+]$ in each mixed solvent by using Eq. (3).

As an example, the observed absorbances of MY, potentials of cell (A) at different pHs, the calculated $\text{p}[\text{SH}_2^+]$ and $\text{p}K_a$ values in 30 wt.%

Table 1

The observed absorbance of methyl yellow (MY), potentials of the cell at different pHs, the calculated values of $\text{p}[\text{SH}_2^+]$ and $\text{p}K_a$ in 30 wt.% ethanol–water mixture (25°C, $I = 0.1$)^a

No.	A^b	E (mV)	$\text{p}[\text{SH}_2^+]$	$\log \frac{A - A_2}{A_1 - A}$	$\text{p}K_a$
1	0.255	191.9	3.104	−0.603	2.50
2	0.299	198.5	2.997	−0.495	2.50
3	0.348	204.2	2.904	−0.389	2.52
4	0.408	211.7	2.782	−0.272	2.51
5	0.462	218.1	2.678	−0.174	2.50
6	0.506	222.2	2.611	−0.098	2.51
7	0.574	229.5	2.493	0.018	2.51
8	0.635	235.2	2.401	0.122	2.52
9	0.676	240.5	2.314	0.193	2.51
10	0.724	247.2	2.206	0.281	2.49
Mean					2.51 ± 0.01

^a $A_1 = 1.077$, $A_2 = 0.050$, $E_a^{0'} = 383.0 \pm 0.2$, $K = -61.57 \pm 0.009$.

^b $\lambda_{\text{max}} = 519$ nm.

Table 2

pK_a values of methyl yellow (MY) in aqueous solutions of alcohols (25°, $I = 0.1$)

Alcohol (wt.%)	pK_a			
	MeOH–H ₂ O	EtOH–H ₂ O	i-PrOH–H ₂ O	t-BuOH–H ₂ O
0	3.23 ^a	3.21 ^a	3.26 ^a	3.24 ^a
15	– ^b	– ^b	2.87 ± 80.03	2.71 ± 70.02
20	– ^b	2.94 ± 0.02	–	2.35 ± 0.02
25	– ^b	–	2.38 ± 0.01	–
30	2.84 ± 0.02	2.51 ± 0.01	–	1.88 ± 0.01
35	–	–	1.99 ± 0.01	–
40	2.64 ± 0.02	2.12 ± 0.02	1.89 ± 0.01	1.66 ± 0.01
50	2.45 ± 0.01	1.89 ± 0.01	1.65 ± 0.02	1.50 ± 0.01
60	2.27 ± 0.03	1.77 ± 0.02	1.51 ± 0.02	–
70	2.13 ± 0.02	1.63 ± 0.02	–	–
80	2.05 ± 0.03	–	–	–

^a The extrapolated values from Eq. (4).

^b The pK_a values can not be accurately determined because of the very low solubility of MY in these mixed solvents.

ethanol–water mixed solvent have been listed in Table 1. The pK_a values of MY in the mixed solvents are given in Table 2. The pK_a value in pure water reported here is an extrapolated value which was calculated according to the linear relationship between pK_a and the mole fraction of the co-solvent (x_2) in water-rich region (Eq. (4)). An average value of 3.24 ± 0.02 was obtained which is in excellent agreement with the value of 3.25 reported in the literature [9]. Katoh [7] determined pK_a values of MY in 40, 60, 80 vol.% alcohol (methanol, ethanol)–water solvents at $24 \pm 0.5^\circ\text{C}$ and an unstated ionic strength. After correction for the concentration scale of alcohol in mixed solvents, it is found that agreement of the pK_a values in these solvents with those reported by Katoh is quite reasonable considering the difference in temperature. No pK_a data in other mixed solvents has been reported in literature.

3.2. Solvent effect on the dissociation equilibrium

As can be seen from Table 2, the pK_a values of MY decrease with the addition of alcohol. This is similar to the results of MY and methyl orange in aqueous *N,N'*-dimethylformamide solutions [9]. It was found that the variation of pK_a for MY is largely dependent on both the mole fraction (x_2) and the nature of the co-solvent in the mixed

solvents. As shown in Fig. 1, there is a linear relation between pK_a and x_2 in a limited range of co-solvent compositions for each of the solvent systems. Using a least-squares regression procedure, pK_a values in the linear ranges (30–70 wt.%

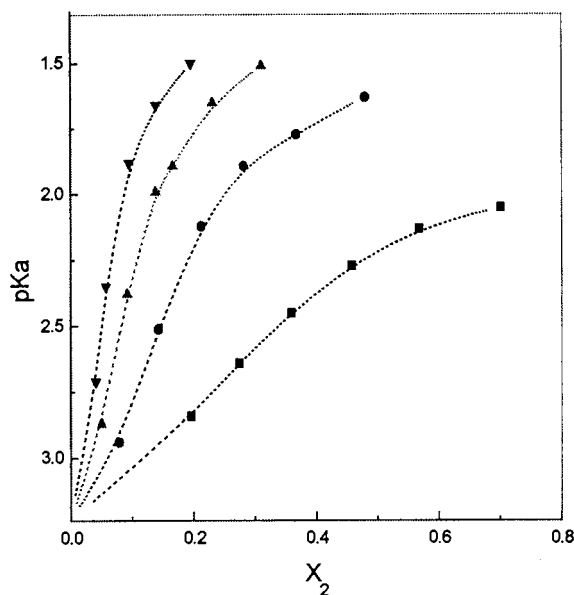


Fig. 1. Variation of the concentration dissociation constants (pK_a) as a function of mole fraction (x_2) of alcohol in the mixed solvents: (■), MeOH; (●), EtOH; (▲), i-PrOH; (▼), t-BuOH.

MeOH–H₂O, 20–50 wt.% EtOH–H₂O, 15–40 wt.% i-PrOH–H₂O, 15–30 wt.% t-BuOH–H₂O) were respectively analyzed to give the following equations:

$$\begin{aligned} \text{p}K_{\text{a}}(\text{s}) &= 3.23 - 1.98x_2 & R &= 0.996 \\ \text{p}K_{\text{a}}(\text{s}) &= 3.21 - 4.85x_2 & R &= 0.997 \\ \text{p}K_{\text{a}}(\text{s}) &= 3.26 - 9.16x_2 & R &= 0.996 \\ \text{p}K_{\text{a}}(\text{s}) &= 3.24 - 14.39x_2 & R &= 0.996 \end{aligned} \quad (4)$$

where $\text{p}K_{\text{a}}(\text{s})$ is the $\text{p}K_{\text{a}}$ value in mixed solvent, R is the linear correlation coefficient. Obviously, the intercept of the linear equation is the $\text{p}K_{\text{a}}$ value in pure water $\text{p}K_{\text{a}}(\text{w})$, and the slope reflects the extent of co-solvent effect on the $\text{p}K_{\text{a}}$ values in the water-rich regions. It is apparent that the $\text{p}K_{\text{a}}$ values decrease with increasing composition of the co-solvent in the order:

t-BuOH > i-PrOH > EtOH > MeOH

MeOH, EtOH, i-PrOH and t-BuOH are mono-hydric alcohols. The number of –OH groups in these molecules is identical. Their difference is only in the size of alkyl groups. So, it is expected that there is a correlation between the slope of the above equations and the size of alkyl groups. In fact, MeOH, EtOH, i-PrOH and t-BuOH can be regarded as the derivatives of H₂O in which one hydrogen atom is, respectively, replaced by CH₃, CH₃CH₂, CH₃CHCH₃ and C(CH₃)₃ groups. According to the group additivity assumption suggested by Hakin et al. [13,14], CH₃ is equivalent to 1.5 CH₂, and CH equivalent to 0.5 CH₂. In addition, it is assumed that C is equivalent to a CH₃ [15]. Thus, the number of CH₂ groups in the alkyl chains of these alcohol molecules will increase successively from 1.5 (MeOH), 2.5 (EtOH), 3.5 (i-PrOH) to 6 (t-BuOH). The dependence of the slopes on the number of CH₂ groups is shown in Fig. 2. It can be seen that the slope decreases linearly with an increasing number of CH₂ groups. This means that at a particular x_2 , K_{a} will increase with increasing number of CH₂ group in the co-solvents. The alkyl groups of the co-solvent are helpful for the dissociation of MY.

It is known that the standard free energy change for the dissociation process of MY in water is given by

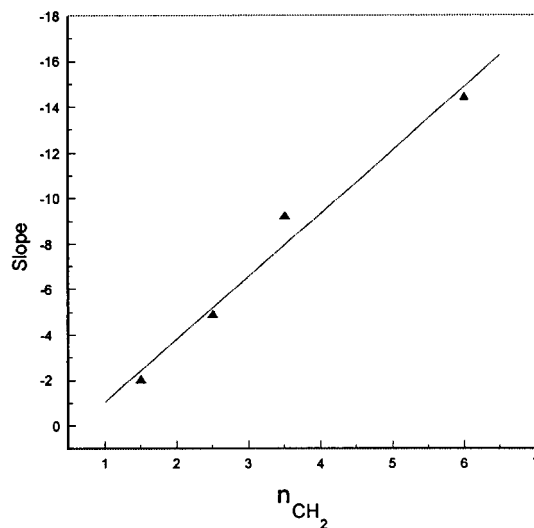


Fig. 2. Variation of the slope of Eq. (4) as a function of number of CH₂ in alkyl groups of alcohol molecules.

$$\Delta G_{(\text{w})}^0 = 2.303RT\text{p}K_{\text{T}}(\text{w}) \quad (5)$$

Similarly, the standard free energy change for the dissociation process in the mixed solvent is given by

$$\Delta G_{(\text{s})}^0 = 2.303RT\text{p}K_{\text{T}}(\text{s}) \quad (6)$$

Therefore, the solvent effect on the dissociation equilibria of MY can be represented by

$$\Delta G_{\text{T}}^0 = 2.303RT[\text{p}K_{\text{T}}(\text{s}) - \text{p}K_{\text{T}}(\text{w})] \quad (7)$$

where $\text{p}K_{\text{T}}(\text{s})$ and $\text{p}K_{\text{T}}(\text{w})$ are the thermodynamic dissociation constant in the mixed solvent and in water, respectively. ΔG_{T}^0 is the standard Gibbs energy of transfer of the dissociation reaction from water to the mixed solvents. As shown in Eq. (1), the dissociation of MY is an isoelectric reaction. The thermodynamic dissociation constant can be represented by

$$\text{p}K_{\text{T}} = \text{p}K_{\text{a}} - \log(\gamma_{\text{H}^+} \gamma_{\text{In}} / \gamma_{\text{H}^+ \text{In}}) \quad (8)$$

where γ is the activity coefficient, which is a function of the charge Z of the species, the permittivity D , the absolute temperature T and the ionic strength I [16]:

$$\begin{aligned} -\log \gamma &= [1.825 \times 10^6 Z^2 (DT)^{-3/2} I^{1/2}] \\ &/[1 + 251.45 (DT)^{-1/2} I^{1/2}] \end{aligned} \quad (9)$$

It is evident that γ value for H^+ is equal to that for H^+ In at the same T , D and I . And γ is usually assumed to be 1 for neutral molecule In. Therefore, the difference between pK_T and pK_a for MY is negligible. $pK_a(s)$ and $pK_a(w)$ determined in this work can be directly used to calculate ΔG_t^0 by Eq. (7) without serious error. Values of ΔG_t^0 thus obtained are given in Table 3.

On the other hand, ΔG_t^0 can be represented by the standard Gibbs energies of transfer of the species existing in dissociation equilibrium from water to mixed solvents

$$\Delta G_t^0 = \Delta G_t^0(H^+) + \Delta G_t^0(In) - \Delta G_t^0(H^+ In) \quad (10)$$

where $\Delta G_t^0(H^+)$, $\Delta G_t^0(In)$ and $\Delta G_t^0(H^+ In)$ refer to the standard Gibbs energies of H^+ , In and $H^+ In$ from water to mixed solvents.

It has been stressed [17] that $\Delta G_t^0(H^+)$ reflects the basicity of the mixed solvent relative to water. Lahiri et al. [17–19] determined the Gibbs energies of transfer of H^+ from water to water + alcohol (MeOH, EtOH, *i*-PrOH, *t*-BuOH) mixtures. The interpolated values in the appropriate solvents are included in Table 3. Values of $[\Delta G_t^0(In) - \Delta G_t^0(H^+ In)]$ calculated from ΔG_t^0 and $\Delta G_t^0(H^+)$ at particular proportions of the co-solvents are also included in Table 3.

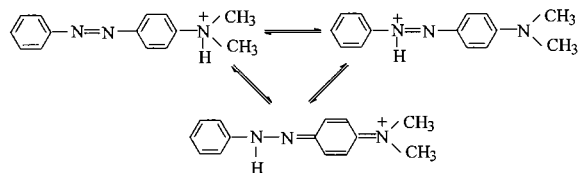
The data in Table 3 shows that in all the mixed solvents studied, $\Delta G_t^0(H^+)$ values are all negative and become increasingly negative with increasing composition of the organic co-solvents. This indicates that the binary mixtures are more basic than water. The basicity of the mixed solvents varies in the order: *t*-BuOH > *i*-PrOH > EtOH > MeOH. This is consistent with the order experimentally observed. Thus, the more basic characteristic of the mixed solvents compared to water is one of the important factors for the observed increase of K_a in the alcohol–water mixtures.

It is noted from Table 3 that values of $[\Delta G_t^0(In) - \Delta G_t^0(H^+ In)]$ are increasingly negative with addition of the co-solvent for a given alcohol–water solvent system. They are also increasingly negative in the order: *t*-BuOH > *i*-PrOH > EtOH > MeOH, at a particular composition for different solvent systems. This is related to the hydrophobic interaction between MY molecule and the alkyl group of alcohols. As shown in the

Section 1, the main difference between H^+ In and In is that there is a positive charge on the dimethylaniline moiety in H^+ In. According to the suggestion of Brandts et al. [20], hydrophobic interaction is only possible with the uncharged part of the indicator molecules. Therefore, the hydrophobic interaction of the alkyl group of alcohols with In should be greater than that with H^+ In. Accordingly, values of $\Delta G_t^0(In)$ should be more negative compared to those of $\Delta G_t^0(H^+ In)$. From the above discussion, it can be concluded that the overall behavior of the dissociation process of MY can be dictated by the specific solute–solvent interactions besides the relative solvent-basicities.

3.3. Effect of solvent on the visible absorption spectra of MY

A red shift of λ_{max} for the acid form of MY (H^+ In) was observed with addition of the alcohol in water. For instance, the λ_{max} in water is 508 [21], whereas in 30 and 80 wt.% MeOH– H_2O solvents, it is 515 and 524 nm, respectively. This may be due to the shift of position of the tautomeric equilibrium of H^+ In shown as follows



It has been proved that the equilibrium is sensitive to the polarity of the solvent [22]. On the other hand, the color transition range of MY is also changed because of shift of the dissociation equilibrium in the mixed solvents. For example, pH range of color change in water [21] is 2.9 (red)–4.0 (yellow), while it changes to be 2.1 (red)–3.3 (yellow) in 50 wt.% MeOH– H_2O , 1.7 (red)–2.9 (yellow) in 50 wt.% EtOH– H_2O , 1.3 (red)–2.4 (yellow) in 50 wt.% *i*-PrOH– H_2O and 1.3 (red)–2.3 (yellow) in 50 wt.% *t*-BuOH– H_2O . This is interesting from a practical point of view. The indicator can be used to indicate the end points of the acid–base titrations, which are not

Table 3

Values of ΔG_t^0 , $\Delta G_t^0(\text{H}^+)$ ^a and $[\Delta G_t^0(\text{In}) - \Delta G_t^0(\text{H}^+\text{In})]$ from water to aqueous alcohol mixed solvents at 25°C (in kJ·mol⁻¹)

Alcohol (wt.%)	MeOH–H ₂ O			EtOH–H ₂ O			i-PrOH–H ₂ O			t-BuOH–H ₂ O		
	ΔG_t^0	$\Delta G_t^0(\text{H}^+)$	Δ^b	ΔG_t^0	$\Delta G_t^0(\text{H}^+)$	Δ^b	ΔG_t^0	$\Delta G_t^0(\text{H}^+)$	Δ^b	ΔG_t^0	$\Delta G_t^0(\text{H}^+)$	Δ^b
15	–	–	–	–	–	–	–2.1	–2.0	–0.1	–3.0	–2.5	–0.5
20	–	–	–	–1.7	–2.2	0.5	–	–	–	–5.0	–3.2	–1.8
25	–	–	–	–	–	–	–4.9	–3.6	–1.3	–	–	–
30	–2.2	–2.0	–0.2	–4.2	–3.1	–1.1	–	–	–	–7.7	–4.0	–3.7
35	–	–	–	–	–	–	–7.1	–4.3	–2.8	–	–	–
40	–3.4	–2.8	–0.6	–6.3	–4.1	–2.2	–7.6	–4.9	–2.7	–9.0	–3.7	–5.3
50	–4.5	–3.6	–0.9	–7.6	–5.1	–2.5	–9.0	–5.4	–3.6	–9.9	–2.8	–7.1
60	–5.5	–4.6	–0.9	–8.3	–5.6	–2.7	–9.8	–5.6	–4.2	–	–	–
70	–6.3	–5.4	–0.9	–9.1	–5.6	–3.5	–	–	–	–	–	–
80	–6.7	–5.5	–1.2	–	–	–	–	–	–	–	–	–

^a $\Delta G_t^0(\text{H}^+)$ values have been taken from Refs. [17–19] by interpolation.^b $\Delta = \Delta G_t^0(\text{In}) - \Delta G_t^0(\text{H}^+\text{In})$.

possible in water, by choosing appropriate co-solvent and changing the co-solvent content of the mixed solvents.

As an example, The application of MY to the titration of sodium acetate by hydrochloric acid is described here. Two series of titrations were conducted in cell (A). One is the titration of 1.0 mol l^{-1} sodium acetate by 1.0 mol l^{-1} hydrochloric acid in water. The other is that of 1.0 mol l^{-1} sodium acetate by 1.0 mol l^{-1} hydrochloric acid in 50 wt.% EtOH–H₂O solvent. The titration end points were indicated by MY indicator and potentiometric technique simultaneously. The results are shown in Fig. 3. It has been observed that pH value is 3.71 at the titration end point indicated by MY in water. This dose not coincide with the pH value (2.15) for the end point of potentiometric titration in water. So MY fails to indicate the end point for sodium acetate–hydrochloric acid titrations in water. However, the situation is quite different for the

titration in the mixed solvent. The pH value is 2.59 at the titration end point indicated by MY, which is in excellent agreement with the pH value (2.46) for the potentiometric titration end point in the mixed solvent. In addition, the color change of the indicator in the mixed solvent is very sharp in the vicinity of the equivalent point. Obviously, MY can be used as an indicator for the sodium acetate–hydrochloric acid titration in 50 wt.% EtOH–H₂O solvent.

References

- [1] M. Georgiva, G. Velinov, O. Budevsky, *Anal. Chim. Acta* 90 (1977) 83.
- [2] M. Georgiva, G. Velinov, O. Budevsky, *Anal. Chim. Acta* 101 (1978) 139.
- [3] M. Georgiva, G. Velinov, O. Budevsky, *Anal. Chim. Acta* 110 (1979) 183.
- [4] I.M. Kolthoff, *J. Phys. Chem.* 35 (1931) 2732.
- [5] I.M. Kolthoff, L.S. Guss, *J. Am. Chem. Soc.* 60 (1938) 2516.
- [6] L.S. Guss, I.M. Kolthoff, *J. Am. Chem. Soc.* 62 (1940) 249.
- [7] K. Katoh, *Jpn. Analyst* 13 (1964) 514.
- [8] K. Katoh, *Jpn. Analyst* 17 (1968) 1055.
- [9] A.G. Gonzalez, M.A. Herrador, A.G. Asuero, *Anal. Chim. Acta* 246 (1991) 429.
- [10] J. Fan, X. Shen, J. Wang, *Anal. Chim. Acta* 364 (1998) 275.
- [11] G.J. Ives, G.J. Janz, *Reference Electrodes, Theory and Practice*, Academic Press, New York, 1961, p. 209.
- [12] J. Tencheva, G. Velinov, O. Budevsky, *J. Electroanal. Chem.* 68 (1976) 65.
- [13] A.W. Hakin, M.M. Duke, L.L. Groft, J.L. Marty, M.L. Rushfeldt, *Can. J. Chem.* 73 (1995) 725.
- [14] A.W. Hakin, M.M. Duke, J.L. Marty, K.E. Preuss, *J. Chem. Soc. Faraday Trans.* 90 (1994) 2027.
- [15] K. Zhuo, J. Wang, W. Liu, J. Lu, *Proceedings of the First Symposium of Henan Province for Young Scientist*, Chinese Science and Technology Press, Beijing, 1995, p. 107.
- [16] M. Galus, S. Glab, K. Grekulak, A. Hulanicki, *Talanta* 26 (1979) 109.
- [17] D. Sengupta, A. Pal, S.C. Lahiri, *J. Chem. Soc. Dalton Trans.* (1983) 2685.
- [18] A.K. Bhattscharyya, D. Sengupta, S.C. Lahiri, *Z. Phys. Chem. (Leipzig)* 265 (1984) 372.
- [19] S.K. Chakravorty, D. Sengupta, S.C. Lahiri, *Z. Phys. Chem. (Leipzig)* 267 (1986) 969.
- [20] P.M. Brandts, W.J. Gesema, C.L. De Ligny, *J. Chromatogr.* 438 (1988) 181.
- [21] S. Zhang, F. Tang, T. Zhang, *Modern Handbook of Chemical Reagents*, Vol. 2, (Chinese version), Chemical Industry Press, Beijing, 1987, p. 15.
- [22] L. Skulski, W. Walcuwek, A. Szurowska, *Bull. Acad. Pol. Sci. Chim.* 20 (1972) 463.

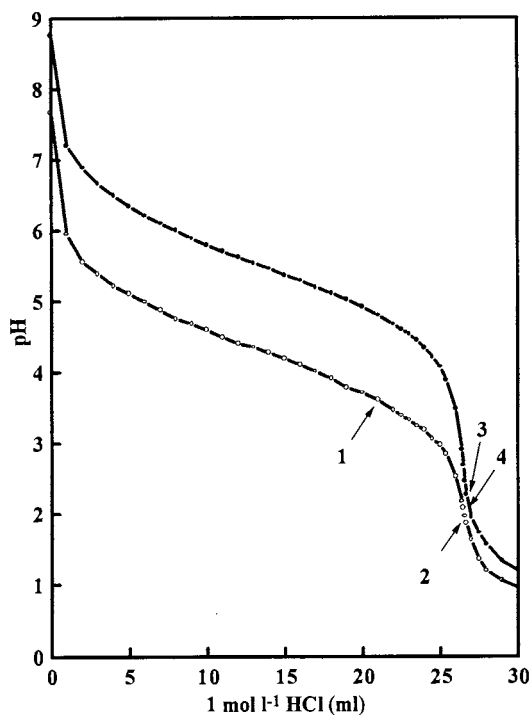


Fig. 3. pH titration curves of sodium acetate with hydrochloric acid. --○-- in water; --●-- in 50 wt.% ethanol–water mixed solvent. 1 and 3, end points indicated by methyl yellow (MY); 2 and 4, end points of the potentiometric titrations.

A practical and accurate method for the determination of ^{234}Th simultaneously with ^{210}Po and ^{210}Pb in seawater

Guebuem Kim ^{a,*}, Najid Hussain ^a, Thomas M. Church ^a, Han-Soeb Yang ^b

^a College of Marine Studies, University of Delaware, Newark, DE 19716, USA

^b College of Marine Sciences and Technology, Bukyong National University, Namgu, Pusan 608-737, South Korea

Received 6 October 1998; received in revised form 11 February 1999; accepted 25 February 1999

Abstract

A practical technique has been developed for the determinations of ^{234}Th simultaneously with ^{210}Po and ^{210}Pb in seawater samples, which greatly simplifies the on-board chemical procedures and enables an accurate correction of ^{234}Th ingrowth. A unique feature of this technique lies in the exact determination of co-precipitated ^{238}U following $\text{Fe}(\text{OH})_3$ precipitation which leads to an exact correction of ingrown ^{234}Th between $\text{Fe}(\text{OH})_3$ precipitation and U/Th separation. Such a correction eliminates several cumbersome on-board chemistry steps (such as Po plating, Fe^{2+} oxidation, and 9 N HCl anion exchange) required in regular procedures to eliminate the ^{234}Th ingrowth. The total time required for on-board sample treatment (spike equilibration, $\text{Fe}(\text{OH})_3$ co-precipitation and filtration) could be less than 10 h which significantly increases the sample processing efficiency and data throughput. © 1999 Elsevier Science B.V. All rights reserved.

Keywords: Seawater; Chemical purification; ^{234}Th

1. Introduction

The relatively short-lived, naturally occurring, radionuclides of the ^{238}U decay series (^{234}Th , ^{210}Po , and ^{210}Pb) have provided important information on the fate of trace elements in the ocean [1–4]. More recently they have been utilized as

tracers of carbon export in the ocean which plays an important role in global atmospheric CO_2 variation [5–9].

For in-situ ^{234}Th determination in seawater, quick separation of ^{234}Th from ^{238}U is required to prevent significant ingrowth corrections being applied during sample storage. To do so, HCl anion exchange has been most commonly done on board ship [5,7,10]. McKee et al. [11] used a column containing 5–10 g of manganese-impregnated acrylic fiber to selectively adsorb Th after spike equilibration and acidification (pH 2). Bues-

* Corresponding author. Present address: Department of Oceanography, Florida State University, Tallahassee, FL 32306, USA. Tel.: +1-850-644-9032; fax: +1-850-644-2581.

E-mail address: gkim@ocean.fsu.edu (G. Kim)

seler et al. [12] developed a nondestructive gamma technique which involves filtration of about 1000 l seawater through a manganese fiber column and subsequent direct gamma counting.

However, for simultaneous analyses of ^{210}Po , ^{210}Pb and ^{234}Th in the same sample, ^{210}Po needs to be plated prior to U–Th separation since ^{210}Po is to be analyzed but strongly adsorbed to 9 N HCl anion exchange resin, which is generally used for the U–Th separation. After Po plating, other oxidation steps also need to be carried out using strong acids before U–Th separation [8]. This poses significant hazards at sea and also limits the number of samples which can be processed over the duration of the cruise since the procedure is time intensive.

Although simultaneous measurement of ^{210}Po , ^{210}Pb , and ^{234}Th in the open ocean is not easy, their use is equally important in understanding marine processes and the biogeochemistry of the surface ocean [5,6,8,13]. A simple, labor and time efficient on-board technique has been developed to analyze these isotopes in a single seawater sample. The ease of this technique allows processing dozens of samples a day, without compromising the accuracy of the ^{234}Th , ^{210}Po , and ^{210}Pb determinations. In practice, we have used this method during many cruises off Bermuda for the analyses of hundreds of samples.

2. Experimental

2.1. Sampling and on-board procedures

The 20 l seawater samples were obtained from the Sargasso Sea using a rosette sampler. For filtered samples, water was passed through 0.45 μm cartridge filters using a small pump (JABSCO). The filtration was completed on-board within an hour of sampling in order to minimize particle sinking, decomposition, and adsorption on the walls of sampling bottles.

Soon after collection (or filtration in case of filtered samples), samples were acidified with about 50 ml of concentrated HNO_3 ($< \text{pH } 1$) and transferred into 40 l plastic buckets. The samples were then spiked using 16 dpm of ^{230}Th standard,

0.5 dpm of ^{209}Po , 25 mg of Pb^{2+} carrier and 70 mg of Fe^{3+} carrier. After stirring and bubbling with N_2 gas for 10–30 min for equilibration of the spike and carriers, samples were allowed to stand for an additional 3 h to ensure complete equilibration. Na_2CrO_4 was then added to precipitate PbCrO_4 after adjusting the pH to 4 using NH_4OH . The Th, Po, and remaining Pb were co-precipitated with $\text{Fe}(\text{OH})_3$ at pH 8.

After allowing the precipitate to settle for 4–5 h, the supernatant was siphoned off and the residual mixture filtered through Whatman 54 quantitative grade paper. The precipitate was dissolved in 0.5 N HCl and subsequently spiked with ^{236}U . This procedure allowed the exact content of ^{238}U in the precipitate to be determined enabling the exact ^{234}Th ingrowth correction to be applied later. The entire procedure was completed within 10 h of the sample collection. The sample solution was then brought back to the laboratory for further analyses. A simplified flowchart of the analytical procedures is shown in Fig. 1. The choice of ^{236}U spike was to avoid any interference of beta emission from the spike or its daughters (e.g. ^{232}U) in beta counting of ^{234}Th .

2.2. Chemical purification and source preparation in a laboratory

In the laboratory, the solution was transferred to a Teflon beaker. After adding 0.5 g of ascorbic acid, the solution was heated to 90°C and Po was spontaneously plated onto a silver disc [14–16].

The remaining solution was evaporated and the oxidised residue dissolved in 1 ml of 9 N HCl. After repeating the step twice, the residue was taken in 5 ml of 9 N HCl and loaded on a preconditioned 9 N HCl anion exchange column (AG 1-X8 resin, 100–200 mesh). The U and Po were retained on the column while Th and Pb were brought down in the effluent. The column was eluted with hot H_2O ($70\text{--}85^\circ\text{C}$) to obtain a U fraction. Further U purification using an 8 N HNO_3 anion exchange column (AG 1-X8 resin, 100–200 mesh) followed (Fig. 1).

The effluent, containing Th and Pb, was dried and the residue dissolved in 8 N HNO_3 . This step was repeated twice. The solution was then loaded

on a preconditioned 8 N HNO₃ anion exchange column. The effluent from this column contained Pb (free from Po) and was stored for more than 6 months for ²¹⁰Po ingrowth from ²¹⁰Pb. The chemical yield of Pb was determined by measuring the stable Pb recovery on a flame atomic absorption spectrometer. The exact date for 8 N HNO₃ column exchange was recorded in order to calculate ²¹⁰Pb activity precisely from ingrown ²¹⁰Po since Po is removed completely by use of the 9 N HCl and 8 N HNO₃ columns. Th was eluted from the column with 9 N HCl. The eluent was dried and 1 ml of concentrated HNO₃ was added to oxidize the residue. After the concentrated HNO₃

solution was completely dried, 1 ml of 0.01 N HNO₃ was added and the solution was transferred to an electrodeposition cell.

The plating method of Puphal and Olsen [17] was used with a mixed oxalate–chloride electrolyte and stainless steel planchet as cathode. This method has advantages over several others in its low material costs and short deposition time (35 min). Other available techniques use a chloride electrolyte with a silver disc as cathode for 2 h [18], a chloride electrolyte with a platinum planchet for 20 min [5,19] or a sulfate electrolyte with a stainless steel disc for 2 h [12]. Briefly, in the evaporated beaker, 2 ml of saturated ammo-

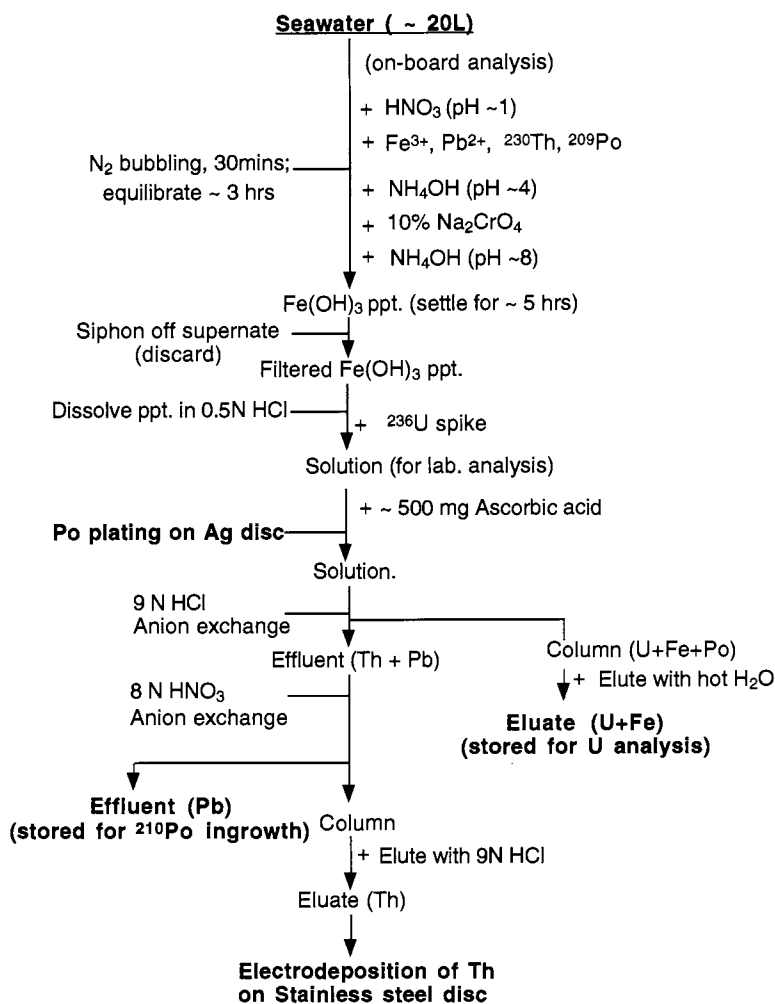


Fig. 1. Schematic illustration of the analytical procedure.

nium oxalate and 2 ml of 10% NH_4Cl solution are added and transferred to an electrodeposition cell to wash the beaker completely. The solution is electrodeposited by adjusting the initial current to 0.9 A at a constant voltage of 10 V. After 35 min, the current drops below 0.5 A, a few drops of 50% NH_4OH solution are added before turning off the current. The planchet is rinsed with distilled water and singed briefly with a burner. The same electrodeposition procedures are applied to the U fraction (Fig. 1).

2.3. Alpha spectrometry and beta counting

The activity ratios of ^{209}Po and ^{210}Po are measured using a silicon surface barrier detector coupled to a multichannel analyzer. The ^{234}Th sources are beta counted via ingrown $^{234\text{m}}\text{Pa}$. Low energy beta particles and alpha particles are eliminated by a gold mylar absorber covering the source (6.8 mg cm^{-2}). The decay curve for ^{234}Th is followed over a period of about 2 months to ensure the purity of the source [20]. Chemical yield of Th is determined via alpha counting the ^{230}Th spike.

A proper intercalibration between alpha and beta detectors is desirable as ^{234}Th is beta counted and ^{230}Th is alpha counted on the same source. The detector efficiency of the alpha counter is calibrated using a ^{230}Th or ^{238}Pu standard and that of beta counter using a $^{234}\text{Th}/^{238}\text{U}$ standard source [5,12,21]. This method leads to possible uncertainties in alpha and beta inter-calibration as it uses different standard sources. A source of pure U is prepared and ^{234}Th is allowed to grow into equilibrium with ^{238}U on the planchet. It is not necessary to know exactly the emerging dpm of ^{238}U or ^{234}Th in the source as the same source was counted in both beta and alpha detection systems to determine the alpha to beta ratio. Similar ratio in the sample (from $^{230}\text{Th}/^{234}\text{Th}$) is then compared with this standard ratio to calculate the exact activity of ^{234}Th in the sample [8,19].

When ^{238}U to ^{236}U activity ratios are determined using an alpha counter, the small corrections (less than 5%) for the interference of natural ^{235}U energy in the range of ^{236}U energy peaks

(centroids at 4.33, 4.44, 4.49 MeV) are made based on natural ^{238}U to ^{235}U ratios (activity ratio: 21.7) in seawater.

3. Results

3.1. Calculations

The activity of ^{210}Po is calculated based on the background corrected peak-area ratios of $^{210}\text{Po}/^{209}\text{Po}$ multiplied by the activity of the added ^{209}Po spike. Mean field blank activity is then subtracted from such calculated ^{210}Po activity. Activity of ^{210}Pb , via ^{210}Po , is also calculated by assaying the ingrown ^{210}Po over the period of ingrowth between the first and second ^{210}Po separations. Appropriate ingrowth and decay corrections are then applied using Eq. (1) to obtain the ^{210}Pb activity (A_{Pb}):

$$A_{\text{Pb}} = A_{\text{Po}} \cdot \frac{\lambda_{\text{Po}} - \lambda_{\text{Pb}}}{\lambda_{\text{Po}} \cdot (e^{-\lambda_{\text{Pb}}t} - e^{-\lambda_{\text{Po}}t})} \quad (1)$$

where A_{Po} is measured ingrown ^{210}Po activity, λ_{Po} and λ_{Pb} are the decay constants of ^{210}Po and ^{210}Pb , respectively, and t is the time elapsed between the last Po/Pb separation (8 N HNO_3 column exchange) by the anion exchange column and the Po plating time. In addition, a further decay correction is made for the time lapse between Po plating and counting.

Owing to a relatively shorter half-life ($t_{1/2} = 24$ days), ingrowth and decay corrections for ^{234}Th become very important. Once a sample for ^{234}Th is collected (time t_1), generally its deficient in-situ activity starts changing due to ingrowth from abundant ^{238}U in the sample before U–Th separation (between the time of acidification and spike/carrier equilibration). For the case of seawater, the amount of ^{238}U in the sample over this period is given by the U-salinity relationship [22]. The $\text{Fe}(\text{OH})_3$ precipitation (t_2) produces yet another disequilibrium between ^{238}U and ^{234}Th by scavenging preferentially ^{234}Th in the precipitate. Uranium scavenging is significantly reduced if the sample is not bubbled with N_2 prior to precipitation, whereas Th scavenging remains unaffected [18,23]. Thus, following precipitation (t_2) until

U–Th separation (t_3), growth of ^{234}Th will occur from the ^{238}U content in the precipitate which can no longer be obtained based on U-salinity relationship in the seawater. To counter this problem, we add ^{236}U spike to the $\text{Fe}(\text{OH})_3$ precipitate and calculate exactly the amount of ^{238}U within the precipitate that enables an exact ingrowth correction for ^{234}Th . Once the U–Th separation is complete (9 N HCl column, Fig. 1), ^{234}Th decays with its own half-life over the period of further purification, plating of the source, and counting. The activity of ^{234}Th at the time of sample collection from the activity at the time of U–Th separation is thus given by Eq. (2):

$$A_{\text{Th}}^0 = \left[\frac{C_{\text{Th}-234}}{C_{\text{Th}-230} \cdot DE_{\beta/\alpha} \cdot V} - U_2(1 - e^{-\lambda(t_3 - t_2)}) \right] \cdot e^{-\lambda(t_3 - t_1)} - U_1(e^{\lambda(t_2 - t_1)} - 1) \quad (2)$$

where A_{Th}^0 is the ^{234}Th activity in the sample at the time of sample collection, $C_{\text{Th}-234}$ is the ^{234}Th count rate at U/Th separation time based on ^{234}Th decay curve analysis as discussed later, $C_{\text{Th}-230}$ is the ^{230}Th count rate, and $DE_{\beta/\alpha}$ (typically ~ 2) is the ratio of detector efficiency determined using a $^{234}\text{Th}/^{238}\text{U}$ equilibrated source, V is the sample volume, λ is the decay constant of ^{234}Th , U_1 is the ^{238}U activity in seawater sample which is calculated from salinity, U_2 is the measured ^{238}U activity in the $\text{Fe}(\text{OH})_3$ precipitate (following addition of ^{236}U spike) and t_1 , t_2 , t_3 are the time of sample collection, $\text{Fe}(\text{OH})_3$ recovery and the U–Th separation, respectively.

Instead of using a single count rate of ^{234}Th for calculation, Hussain and Krishnaswami [20] suggested use of the slope of its decay line which also ensures the purity of the source. For this, the prepared ^{234}Th source is counted repeatedly at regular time intervals following plating and a regression line is drawn between gross count rate and an appropriate ^{234}Th decay factor ($e^{-\lambda t}$, $t = 0$ at t_3). An excellent fit suggests no contamination of the source by other relatively longer or shorter half-life beta emitting nuclides. Besides, use of the slope cancels out the detector background and any relatively long half-life beta emitting nuclides.

Backgrounds of each sample based on intercepts of regressions (Fig. 2) ranged between 0.2

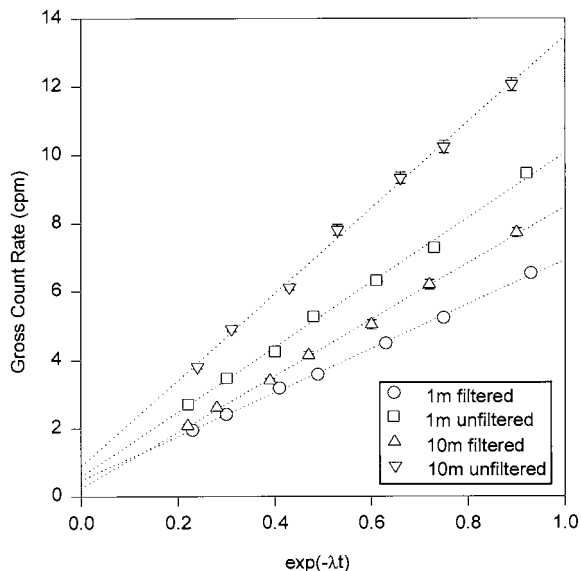


Fig. 2. Decay curves obtained from the beta counting of ^{234}Th sources of filtered and unfiltered samples. Uncertainties in activities smaller than the symbols are not shown by the error bars. Excellent fit to the data shows high purity of the sources. The ‘ t ’ is the time lapse between U/Th separation and mid-time of counting. Thus, the slope is the activity of ^{234}Th at the time of U/Th separation.

and 1 cpm (counts per minute) whereas the signal from the sample was between 8 and 15 cpm at the first count. Standard deviation of the slope was used to indicate 1σ uncertainties due to counting statistics. Also, field and reagent blanks were run separately as controls on our ^{234}Th analyses. The activities from reagent blanks were less than the 1σ uncertainties on the sample signals.

3.2. Calibration experiment

Results of ^{234}Th analyses for standard samples measured using this technique and calibrations are shown in Table 1. The agreement between the standard ^{238}U (in equilibrium with ^{234}Th) activity and recovered ^{234}Th shows the accuracy of calibrations for detector efficiency and a ^{230}Th spike. A few archived samples have also been analyzed as further checks. The ratios between expected and measured ^{234}Th are 0.99 ± 0.02 (expected ^{234}Th activities are based on in-situ ^{238}U concentrations). Results confirm the applicability of our

Table 1
Accuracy and precision of ^{234}Th measurements.

PRIVATE Standard	Expected ^{234}Th activity (dpm l^{-1})	Measured ^{234}Th activity (dpm l^{-1})	Activity ratio (measured/expected)
Seawater (20 l) ^a	2.50 ± 0.02	2.54 ± 0.06	1.02
Seawater (20 l) ^b	2.41 ± 0.02	2.34 ± 0.06	0.97
Seawater (20 l) ^b	2.41 ± 0.02	2.38 ± 0.06	0.99
^{238}U Standard ^c	41.15 ± 0.05	41.54 ± 0.72	0.99
			Mean: 0.99 ± 0.02

^a Archived seawater samples were collected at 500m water depths on 4 October, 1996 from the BATS site off Bermuda. The samples were filtered and acidified soon after collection. The ^{234}Th was measured on 12 February, 1997 (about 94% equilibration time of ^{234}Th is allowed). The expected activities were calculated based on in-situ dissolved ^{234}Th activity at 500m (in a duplicate sample) and ^{238}U activity calculated from salinity in the sample [^{238}U (dpm l^{-1}) = 0.06807 ± 0.00057 Sal (‰), Chen et al. [22]].

^b Archived unfiltered seawater samples were taken from 1000 m on 14 February, 1997 (generally, in situ ^{234}Th is in equilibrium with ^{238}U at this depth). The ^{234}Th was measured on 18 April, 1997. The expected activity of ^{234}Th is the same as ^{238}U activity in the sample.

^c The ^{238}U standard certified by National Institute of Standards and Technology, which is in equilibrium with ^{234}Th and was also used for determining the detector efficiency ratio of alpha and beta counters used in this study.

technique to obtain accurate ^{234}Th concentrations of seawater samples.

As a further check on the technique, duplicate samples were analyzed using two different approaches. In one sample, U–Th separation was done on board immediately after collection (preventing the ingrowth of ^{234}Th) and the other was spiked with ^{236}U and processed as stated above. The delay between sample collection and U–Th separation in this case ranged between 4 days and a week. Fig. 3 shows an excellent agreement between both methods within experimental uncertainties. A few duplicate samples were collected with a time lag (up to 2 days) between them, and that may be responsible for the scatter in Fig. 3 due to diurnal variation of ^{234}Th activity in the ocean surface. An overall agreement for both methods (a mean activity ratio of 1.01 ± 0.04) shows the accuracy of the ^{234}Th ingrowth correction using the ^{236}U spiking method.

4. Discussions

Since this technique applies a precise ingrowth correction for ^{234}Th in seawater, it is appropriate to discuss the scavenging characteristics of U from seawater with $\text{Fe}(\text{OH})_3$ precipitate. Harada and Tsunogai [18] reported that about 10% of U

in seawater co-precipitates with calcium carbonate and ferric hydroxides after acidification (< pH 1) and vigorous stirring. This U co-precipitation efficiency can be increased to as much as 50% when a sample is oxidized with a mixture of nitric, perchloric, and hydrochloric acids [23]. During our Bermuda experiments, it was found that the

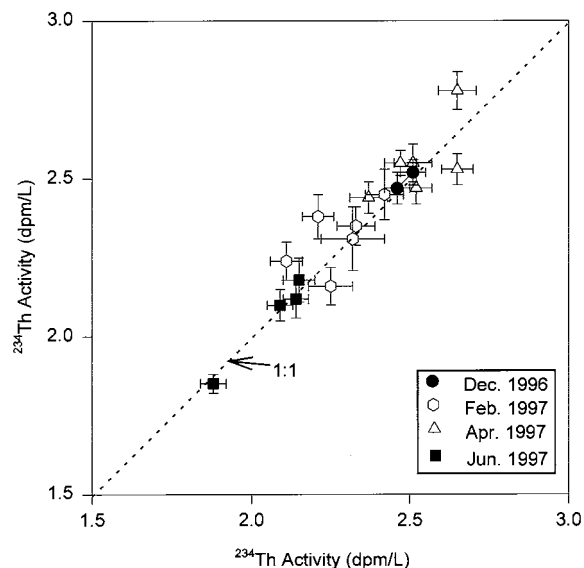


Fig. 3. The plot of ^{234}Th activities measured via on board U/Th separation (x axis) vs via the ^{236}U spiking method (y axis).

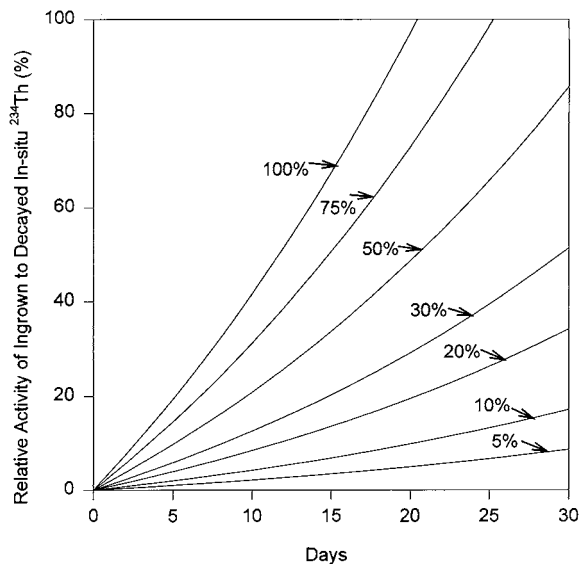


Fig. 4. Variation of the contribution of ingrown ^{234}Th with time for various ^{238}U precipitation recoveries (5–100%). The percentage of ingrown ^{234}Th to in-situ ^{234}Th , which decays away with time, is shown. The x-axis is the time elapsed between $\text{Fe}(\text{OH})_3$ precipitation and U–Th separation.

^{238}U precipitation efficiency through $\text{Fe}(\text{OH})_3$ coprecipitation and siphoning of supernatant remains variable ($17 \pm 7\%$ compared to $60 \pm 14\%$ for ^{234}Th over all procedures for 44 samples). The U precipitation efficiency increases with increasing bubbling rate and the total time of bubbling.

Therefore, most previous calculations of gross ingrowth correction (i.e. an equation by Huh and Prahl [24]), from sample collection to U–Th separation, based on in-situ ^{238}U activity of the seawater (actually measured or estimated from salinity) could over-correct ^{234}Th ingrowth. The magnitude of over-correction will depend on the time lapse between $\text{Fe}(\text{OH})_3$ precipitation and Th/U separation as well as the extent of U co-precipitation with $\text{Fe}(\text{OH})_3$. Such over-correction should be larger where simultaneous analyses of ^{234}Th and ^{210}Po are made. Modeled contribution of the ingrown ^{234}Th from in-situ ^{238}U , relative to the decay of in-situ ^{234}Th in a sample, for various extent of ^{238}U co-precipitation, is shown in Fig. 4. One can easily see the extent of over-correction if proper U co-precipitation efficiencies are not taken into account.

Accounting for the actual recovery of ^{238}U in the precipitate via ^{236}U spiking method not only improves the precision of ^{234}Th determinations, but also renders complete processing of a sample on-board unessential, thereby increasing the data throughput. The technique's applicability can easily extend up to at least one half-life of ^{234}Th (24 days), once ^{210}Po is separated from ^{210}Pb .

This technique of simultaneous determination of ^{234}Th , ^{210}Pb and ^{210}Po via spiking the $\text{Fe}(\text{OH})_3$ precipitate with ^{236}U , provides a better methodology for determining accurate concentrations in seawater samples during cruises with limited duration, laboratory space, and personnel. This could be of particular advantage when higher throughput is required without compromising the sensitivity and accuracy of results.

Acknowledgements

This research was supported by a grant from the Ocean Science Division of NSF (OCE-9522004) awarded to TMC and NH. The study was greatly assisted by Drs Maureen Conte, Laurent Alleman, and the crew members aboard the R/V Weatherbird. Drs M.M. Sarin and Bill Burnett provided many useful comments on the manuscript.

References

- [1] M.P. Bacon, D.W. Spencer, P.G. Brewer, *Earth Planet Sci. Lett.* 32 (1976) 277.
- [2] Y. Nozaki, J. Thomson, K.K. Turekian, *Earth Planet Sci. Lett.* 32 (1976) 304.
- [3] M. Minagawa, S. Tsunogai, *Earth Planet Sci. Lett.* 47 (1980) 5.
- [4] J.K. Cochran, M.P. Bacon, S. Krishnaswami, K.K. Turekian, *Earth Planet. Sci. Lett.* 65 (1983) 433.
- [5] K.H. Coale, K.W. Bruland, *Limnol. Oceanol.* 30 (1985) 22.
- [6] K.H. Coale, K.W. Bruland, *Limnol. Oceanol.* 32 (1987) 189.
- [7] J.W. Murray, J.N. Downs, S. Strom, C.-L. Wei, H.W. Jannasch, *Deep-Sea Res.* 36 (1989) 1471.
- [8] M.M. Sarin, S. Krishnaswami, R. Ramesh, B.L.K. Somayajulu, *Continental Shelf Res.* 14 (1994) 251.

- [9] K.O. Buesseler, J.A. Andrews, M.C. Hartman, R. Belastock, F. Chai, *Deep-Sea Res.* 42 (1995) 777.
- [10] C.-L. Wei, J.W. Murray, *Deep-Sea Res.* 38 (1991) 855.
- [11] B.A. McKee, D.J. DeMaster, C.A. Nittrouer, *Earth Planet Sci. Lett.* 68 (1984) 431.
- [12] K.O. Buesseler, J.K. Cochran, M.P. Bacon, H.D. Livingston, S.A. Casso, D. Hirschberg, M.C. Hartman, A.P. Fleer, *Deep-Sea Res.* 39 (1992) 1103.
- [13] D. Kadko, *J. Geophys. Res.* 98 (1993) 857.
- [14] W.W. Flynn, *Anal. Chim. Acta.* 43 (1968) 221.
- [15] H. Narita, K. Harada, W.C. Burnett, S. Tsunogai, W.J. McCabe, *Talanta* 36 (1989) 925.
- [16] T.M. Church, N. Hussain, T.G. Ferdelman, S.W. Fowler, *Talanta* 41 (1994) 243.
- [17] K.W. Puphal, D.R. Olsen, *Anal. Chem.* 44 (1972) 284.
- [18] K. Harada, S. Tsunogai, *J. Oceanogr. Soc. Jpn.* 41 (1985) 98.
- [19] M.M. Sarin, R. Bhushan, R. Rengarajan, D.N. Yadav, *Ind. J. Marine Sci.* 21 (1992) 121.
- [20] N. Hussain, S. Krishnaswami, *Geochim. Cosmochim. Acta* 44 (1980) 1287.
- [21] C.-L. Wei, C.-C. Hung, *J. Oceanogr.* 48 (1992) 427.
- [22] J.H. Chen, R.L. Edwards, G.L. Wasserburg, *Earth Planet Sci. Lett.* 80 (1986) 241.
- [23] A.E. Lally, Chemical procedures, in: M. Ivanovich, R.S. Harmon (Eds.), *Uranium Series Disequilibrium: Application to Environmental Problems*, Oxford University Press, New York, 1982, pp. 79–106.
- [24] C.-A. Huh, F.G. Prahl, *Limnol. Oceanogr.* 40 (1995) 528.

A potentiometric and spectrophotometric study on acid–base equilibria in ethanol-aqueous solution of acetazolamide and related compounds

Eduardo E. Chufán, Fernando D. Suvire, Ricardo D. Enriz,
José C. Pedregosa *

*Area de Química General e Inorgánica 'Dr. Gabino Puelles', Facultad de Química, Bioquímica y Farmacia,
Universidad Nacional de San Luis (PIP-CONICET 4929/86), Chacabuco y Pedernera, 5700 San Luis, Argentina*

Received 10 November 1998; received in revised form 16 February 1999; accepted 25 February 1999

Abstract

Acid–base equilibria in ethanol-aqueous solution of 5-acetamido-1,3,4-thiadiazole-2-sulfonamide (acetazolamide, H₂acm), 5-tertbutyloxycarbonylamido-1,3,4-thiadiazole-2-sulfonamide (B-H₂ats), 5-amino-1,3,4-thiadiazole-2-sulfonamide (Hats) and 5-amino-1,3,4-thiadiazole-2-thiol (Hatm) at 25°C, 0.15 mol dm⁻³ ionic strength (NaNO₃), have been investigated by potentiometry and UV spectrophotometry. The ionization constants were calculated with SUPERQUAD program from potentiometric measurements and by a method according to Edsall et al. using the mole fractions determined by complementary tri-stimulus colorimetry (CTS). The constants obtained by potentiometry were: B-H₂ats, $pK_{a_1} = 7.33(3)$ and $pK_{a_2} = 9.27(1)$; Hats, $pK_{a_1} = 2.51(3)$ and $pK_{a_2} = 8.49(1)$; Hatm, $pK_{a_1} = 1.92(1)$ and $pK_{a_2} = 6.81(1)$; whereas the constants determined by spectrophotometry were: H₂acm, $pK_{a_1} = 7.78(1)$ and $pK_{a_2} = 9.57(2)$; B-H₂ats, $pK_{a_1} = 7.71(2)$ and $pK_{a_2} = 9.61(2)$; Hats, $pK_{a_1} = 2.19(3)$ and $pK_{a_2} = 8.61(2)$; Hatm, $pK_{a_2} = 6.90(2)$. Theoretical calculations using MO semiempirical and ab-initio RHF/6-31G* computations for the compounds were also performed. It was possible to clarify the preferred deprotonation mechanism of acetazolamide and B-H₂ats in which the first deprotonation takes place at the carbonamido group. © 1999 Elsevier Science B.V. All rights reserved.

Keywords: Acidity constant; 1,3,4-Thiadiazole-sulfonamides; Potentiometry; Spectrophotometry; Deprotonation mechanism; Molecular orbitals calculations

1. Introduction

Carbonic anhydrase, a Zn(II) metalloenzyme, is an extremely efficient catalyst of the reversible

hydration of carbon dioxide. Heterocycles sulfonamides constitute an important group of carbonic anhydrase inhibitors. The inhibition of this enzyme by sulfonamides drugs finds clinical application in the treatment of glaucoma, epilepsy and others disorders. On the other hand, these compounds have played an important role in the

* Corresponding author. Fax: +54-2652-430224.

E-mail address: jpedreg@unsl.edu.ar (J. Pedregosa)

physico-chemical and enzymatic studies on carbonic anhydrase.

Acetazolamide (5-acetamido-1,3,4-thiadiazole-2-sulfonamide) has shown to be one of the most potent inhibitors [1] and has been used clinically from 1954 [2]. In order to obtain new sulfonamides with major potency, two acetazolamide derivatives have been synthesized, 5-tertbutyloxy-carbonylamino-1,3,4-thiadiazole-2-sulfonamide (B-H₂ats) [3] and 5-amino-1,3,4-thiadiazole-2-sulfonamide (Hats) [4]. Their anticonvulsant properties were measured in mice and the results showed that they are three times more potent than acetazolamide [5].

A knowledge of the interactions of sulfonamides with carbonic anhydrase is of immense pharmacological and therapeutic interest. On the basis of X-ray crystallographic studies of carbonic anhydrase–acetazolamide complex at 1.9–2.0 Å resolution it is accepted that the inhibitor acts as monodentate [6] and pseudo-bidentate ligand [7] in the hydrophobic pocket of the active site.

In an attempt to contribute new data, studies on the coordination behaviour of these new potent sulfonamides have been initiated. In a previous paper, the crystal structure of a copper complex [Cu(B-ats)(NH₃)₂]₂ has been reported [3] where *B-ats* ligand acts as a doubly deprotonated specie. Recently, Borja et al. reported the crystal structure of [Zn(ats)₂(NH₃)₂]·H₂O [8] where *ats* ligand acts as a monodeprotonated specie. Furthermore, ternary complexes have been synthesized and characterized with the Hats ligand and triamines (as diethylenetriamine and dipropylenetriamine) which mimic the active site of the enzyme [9].

As part of the studies the coordination properties of the 1,3,4-thiadiazole ring has been analyzed which has three potential donor atoms. Thus, the 5-amino-1,3,4-thiadiazole-2-thiol ligand (Hatm) was chosen which is an analogue of Hats without the sulfonamido moiety. Recently, two copper complexes were synthesized with the following stoichiometries: [Cu(atm)₂(H₂O)] and [Cu(Hatm)-(HIm)₂(SO₄)], where Hatm is present in its monodeprotonated form in the first complex and as neutral specie in the last one [10].

In this work the potentiometric and spectrophotometric study of acetazolamide, B-H₂ats, Hats and Hatm ligands, have been carried out in order to determine the species present at different pH values. The measurements were taken from ethanol-water solution because of the synthesis are carried out in ethanol or ethanol-water medium due to the poor solubility of these molecules in water. To better understand the above experimental results we conducted a computer-assisted molecular orbital study using AM1 and ab-initio RHF/6-31G* calculations on the compounds reported here. The obtained data are important for understanding the deprotonation mechanism of acetazolamide and B-H₂ats which is matter of discussion in the literature [2,11,12].

As the deprotonation of these sulfonamides is directly associated to metal complexes formation, the analytical data obtained in this work are useful for designing new methods of synthesis and characterization of metal complexes. On the other hand, the results presented here can be of interest for researchers dealing with acid–base equilibria of these pharmaceutically important products.

2. Experimental

2.1. Reagents

Acetazolamide was provided by Sigma, St. Louis, MO. B-H₂ats was prepared and purified by the technique described in Ref. [3]. Hats was prepared by acidic hydrolysis of acetazolamide and recrystallized from methanol:water (1:1) [13]. Hatm was provided by Aldrich. Sodium nitrate (Merck p.a.) was used to keep the ionic strength constant at 0.15 mol dm⁻³. Standard HNO₃ solutions were prepared from concentrated HNO₃ (Merck p.a.) and standardized with THAM buffer (Merck p.a.). 0.1 M carbonate-free NaOH solutions were prepared from NaOH ampoules and diluted in appropriated ethanol-water amounts to obtain a final 50 vol.% ratio. The NaOH solutions were standardized with HNO₃ 0.1 M. Ethanol (Merck p.a., ACS, ISO) dried over molecular sieves (4 Å) and tested by CG-EM analysis (Finnigan-MatGCQ-Plus) was used to prepare the

mixture 50 vol.% ethanol-water. Doubly freshly distilled water of high purity tested by conductivity was used throughout.

2.2. Potentiometric study

2.2.1. Potentiometric measurements

The potentiometric titrations were carried out in an automatic system controlled by an Apple II microcomputer. The system consisted of: (1) a Radiometer PHM 84 Research pH-meter using an Ingold-combined electrode, (2) a Crison 2002 microburette, (3) a Crison thermostated cell, and (4) a Julabo Paratherm U8 electronic thermostat coupled with a Julabo Tauchkübler Immersion Cooler FT200 cryostat. All the e.m.f. measurements (with 0.1 mV resolution) were carried out in ethanol-aqueous solution at 25.0°C and $I = 0.15 \text{ mol dm}^{-3} \text{ NaNO}_3$. The glass electrode was calibrated as a hydrogen concentration probe by titration of well-known amounts of HNO_3 with 0.1 M carbonate-free NaOH solution and determination of the equivalent point by the Gran's method [14,15]. The pK_w value was in agreement with the literature [16].

2.2.2. Calculation of ionization constants from potentiometric data

The computer program SUPERQUAD [17] was used to calculate the protonation constants and to corroborate the equilibrium model. The titration curves for each system were treated either as a single set or as separated entities without significant variations in the values of the constants. In all cases, σ (S.D. of the protonation constants) was less than 3.00 and χ^2 (goodness-of-fit) less than 12.60, condition for the 95% confidence level.

2.3. Spectrophotometric study

2.3.1. Spectrophotometric measurements

Absorption spectra of ethanol-aqueous solutions were measured in the ultraviolet region with a Shimadzu UV-160 A recording spectrophotometer with a CPS-240A cell positioner using quartz cells (light-path = 10 mm); the temperature was maintained at $25 \pm 0.1^\circ\text{C}$ during the measure-

ments. In order to make reliable spectrophotometric determinations of the ionization constants, 5–10 spectra (such as those presented in Fig. 1 for acetazolamide; those corresponding for B-H₂ats are similar) were collected at pH values in the range ± 2 pH units around the pK_a value to be determined, titrating the solutions with carbonate-free NaOH. The pH measurements (with 0.002 pH units resolution) were carried out with a ORION EA 940 ionanalyzer equipped with a combination pH electrode which was calibrated with standard solutions (pH 4.00; 7.00; 10.00). The concentrations of the investigated compounds solutions were chosen on the basis of their absorptivities estimated from previous measurements.

2.3.2. Calculation of ionization constants from spectrophotometric data

Since the Qr plot (Fig. 2), obtained from the change in absorbance caused by dissociation of the carbonamido and sulfonamido groups (for acetazolamide and B-H₂ats) or of the ammonium and sulfonamido groups (for Hats), showed two straight lines, the ionization constants could be calculated by complementary tri-stimulus colorimetry (CTS) [18]. Then, the mole fractions (q_{NH}) of the species present at different pH values were calculated for the regions a–b and b–c from this plot. The M_{NH} value defined by Edsall et al. [19] is given in Eq. (1):

$$M_{\text{NH}} = \frac{[\text{H}^+] \cdot q_{\text{NH}}}{(1 - q_{\text{NH}})} \quad (1)$$

which can be rewritten as [20]:

$$k_{a_1} \cdot [\text{H}^+]^2 - k_{a_1} \cdot k_{a_2} \cdot M_{\text{NH}} - M_{\text{NH}} \cdot [\text{H}^+]^2 = 0 \quad (2)$$

The dissociation constants k_{a_1} and k_{a_2} of acetazolamide, B-H₂ats and Hats were calculated from Eq. (2) for two different proton concentrations. For Hatm, as no change in the absorption spectra is observed on ionization of the protonated amino group, the first dissociation constant could not be obtained by spectrophotometry. The second dissociation constant was determined by CTS method from the straight line of its Qr plot.

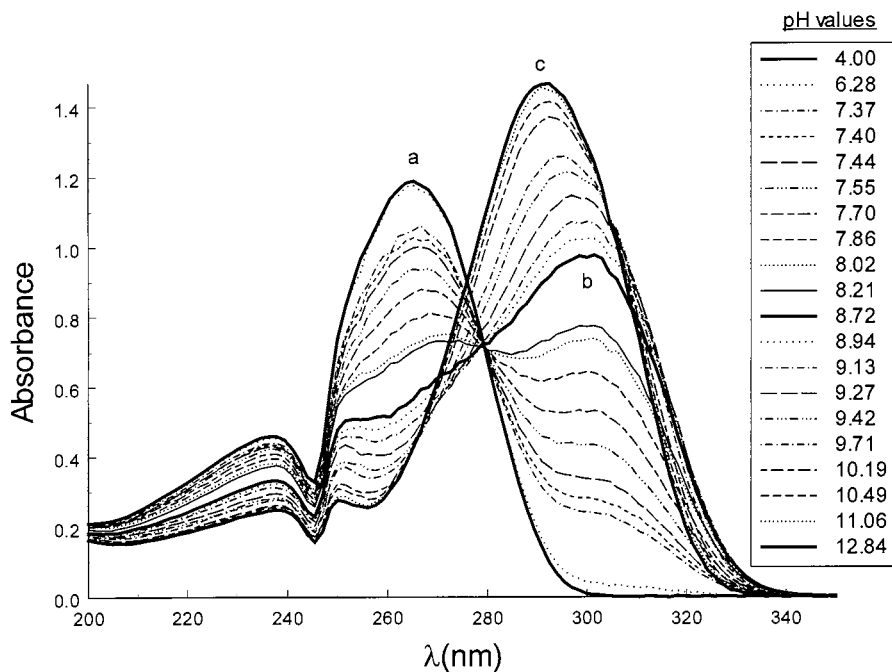


Fig. 1. Absorption spectra of acetazolamide at different pH values.

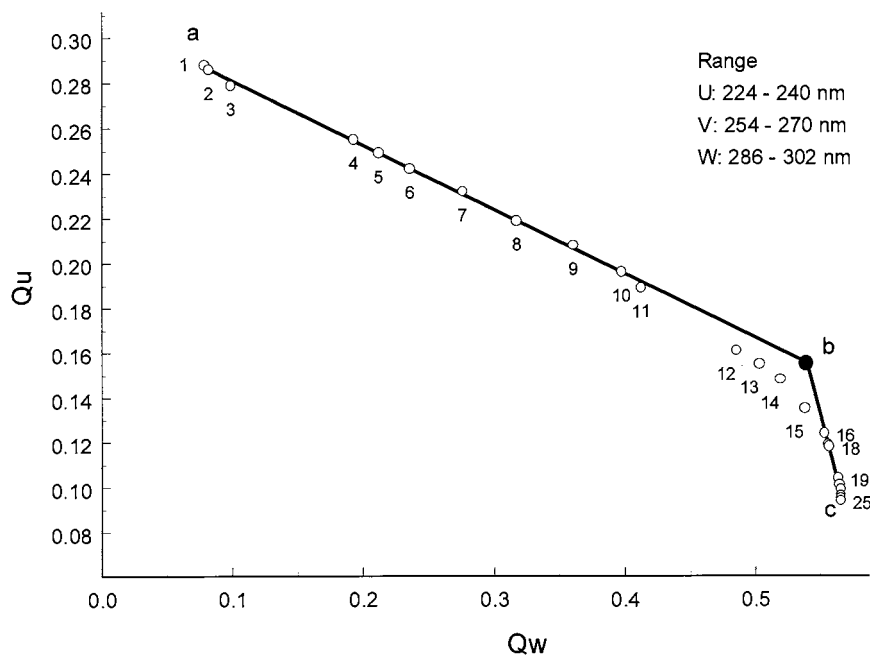


Fig. 2. Qu–Qw plot for acetazolamide: (a) fully protonated form; (b) singly deprotonated form; (c) doubly deprotonated form. Point, pH value: 1, 3.10; 2, 4.00; 3, 6.28; 4, 7.37; 5, 7.40; 6, 7.44; 7, 7.55; 8, 7.70; 9, 7.86; 10, 8.02; 11, 8.21; 12, 8.72; 13, 8.94; 14, 9.13; 15, 9.27; 16, 9.42; 17, 9.64; 18, 9.71; 19, 10.19; 20, 10.35; 21, 10.49; 22, 11.06; 23, 11.54; 24, 12.30; 25, 12.84.

Table 1

pK_a values of acetazolamide, 5-tertbutyloxycarbonylamido-1,3,4-thiadiazole-2-sulfonamide (B-H₂ats), 5-amino-1,3,4-thiadiazole-2-sulfonamide (Hats) and 5-amino-1,3,4-thiadiazole-2-thiol (Hatm) determined in 50 vol.% ethanol-water solution

Ligand	Potentiometry		Spectrophotometry	
	pK_{a_1}	pK_{a_2}	pK_{a_1}	pK_{a_2}
Acetazolamide	7.52 (1) ^a	9.41 (1) ^a	7.78 (1)	9.57 (2)
B-H ₂ ats	7.33 (3)	9.27 (1)	7.71 (2)	9.61 (2)
Hats	2.51 (3)	8.49 (1)	2.19 (3)	8.61 (2)
Hatm	1.92 (1)	6.81 (1)	–	6.90 (2)

^a ref. [11]. Values in parenthesis are S.D. in the last significant figure.

2.4. Molecular orbital calculations

Quantum chemical calculations were carried out by the Gaussian 94 suite of programs [21]. Geometry optimizations were carried out for all the compounds treated here at the semiempirical AM1, SM2 and ab-initio RHF/6-31G* levels of theory. Semiempirical calculations were performed from SPARTAN program [22]. The use of these methods was previously reported with excellent results [23–25]. All the structural parameters of the investigated compounds were fully optimized in order to obtain reliable molecular structures.

3. Results and discussion

The ionization constants for the compounds under study, determined by potentiometry and spectrophotometry, are summarized in Table 1. The values obtained by both techniques are in good agreement. However, the pK_a values for a particular compound determined by spectrophotometry are systematically higher than those obtained by potentiometry, probably due to the different electrode calibration procedures recommended for each one of these methods [17,20].

For Hats, pK_{a_1} refers to dissociation of the proton from the ammonium group, $-\text{NH}_3^+$, and pK_{a_2} to the proton from the sulfonamido one. The

pK_{a_2} value of this compound has been previously reported by Young et al. [26], determined by the ‘Spectrotitrimeter’ method in aqueous solution and the value obtained was 7.68. The determination carried out in the mixed ethanol-water solvent shows that Hats is less acidic in this medium, as it is usually observed [11,27]. The IR spectrum of crystals obtained from strongly acidic solutions in comparison with the corresponding to Hats crystallized at neutral pH shows an additional strong band at 1400 cm^{-1} assigned to the δ_{ammonium} mode [28]; this fact confirms the protonation at the amino group.

The great separation between the two pK_a values of Hats indicates the preference of the neutral form over the zwitterion one (see Scheme 1). The tautomeric constant of a related molecule, 4-amino-benzenosulfonamide, $K_t = 10^{4.07}$, is a clear reference of it [29]. Theoretical calculations are an additional support for these data. Both semiempirical AM1 and ab-initio RHF/6-31G* calculations indicate that the neutral form of Hats is the highly preferred form for the acid–base dissociation in this protonated molecule (see Table 2).

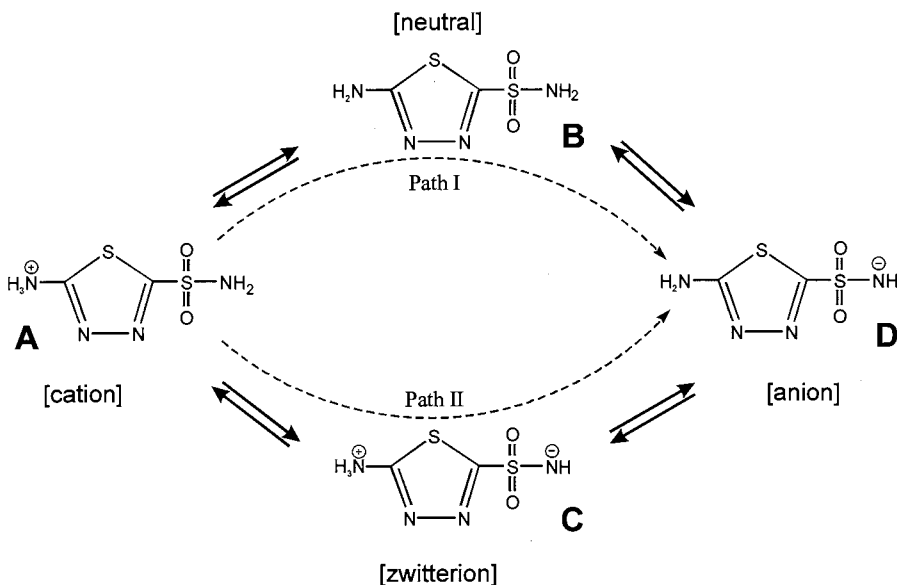
The acid–base behaviour of Hatm is similar to that just described for Hats, being the thiol group more acidic than the sulfonamido one (see Table 1). On the other hand, Hatm is more acidic than aliphatic mercaptanes due to the delocalization of the negative charge by the thiadiazole ring on anion formation [30].

The pK_{a_2} value determined for Hatm explains the presence of the ligand in different forms in $[\text{Cu}(\text{atm})_2(\text{H}_2\text{O})]$ and $[\text{Cu}(\text{Hatm})(\text{HIm})_2(\text{SO}_4)]$. In the synthesis of the last complex, imidazole (HIm) (a very weak base) was used and then a portion of ligand is present in the reaction medium as a neutral form (*Hatm*) whereas for the first complex, a stronger base (ammonia) was used being the ligand completely deprotonated (atm^{1-}).

Acetazolamide and B-H₂ats have two titrable protons which can be attributed to the carbonamido and the sulfonamido groups. The proximity between the pK_{a_1} and pK_{a_2} values suggests both deprotonations occur simultaneously, establishing the equilibria showed in Scheme 2. However, three spectral patterns (a, b, c) with maxima at 265, 301 and 292 nm for acetazolamide and at

265, 302 and 293 nm for B-H₂ats, respectively, are observed in the UV spectra of acetazolamide and B-H₂ats at different pH values. All the curves between the spectral patterns a and b intersect a

point, named isobestic point, indicating that only one ionization equilibrium occurs in the pH range from acidic medium to pH 8.7–8.8, for both sulfonamides [31]. This observation evidences the



Scheme 1. Scheme of ionization equilibrium of 5-amino-1,3,4-thiadiazole-2-sulfonamide (Hats).

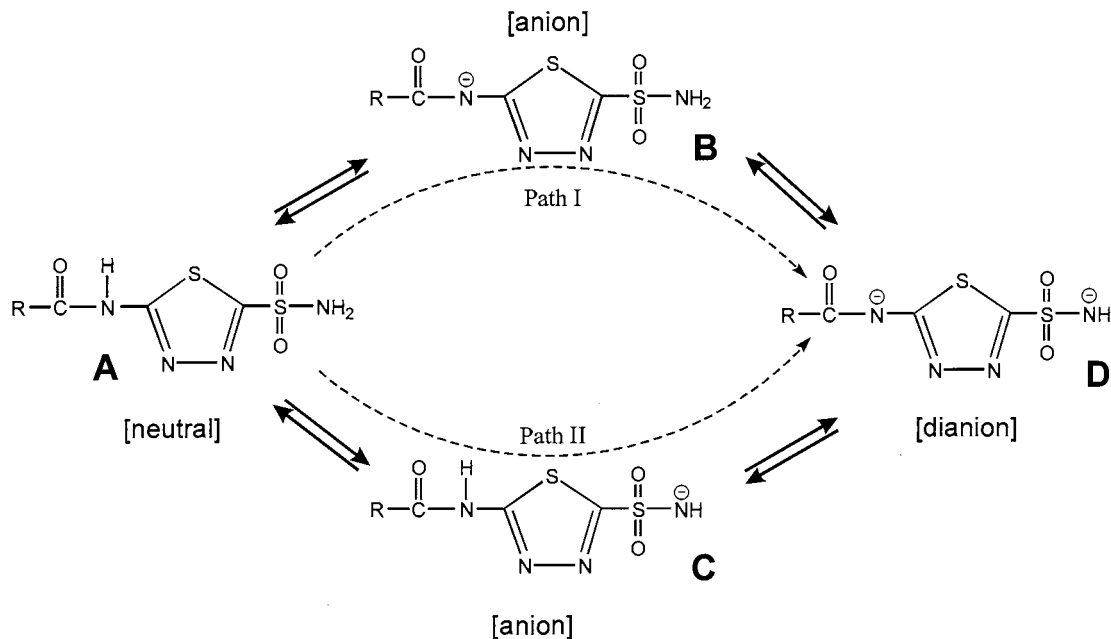
Table 2

Energy gap between the stationary points (B and C) using semiempirical AM1, solvation and ab-initio calculations

	Ab-initio		Semiempirical			
	6-31G*		AM1	SM2 (C-T)		
	Energy ^a	Energy gap ^b	Heat of Formation ^b	Energy gap ^b	Heat of Formation ^b	Energy gap ^b
<i>Acetazolamide</i>						
Form B	-1391.72467	0.00	-103.19	0.00	-194.02	0.00
Form C	-1391.70458	12.61	-76.28	26.91	-187.36	6.66
<i>B-H₂ats</i>						
Form B	-1583.70255	0.00	-154.61	0.00	-245.04	0.00
Form C	-1583.68529	10.83	-125.69	28.91	-238.43	6.61
<i>Hats</i>						
Form B	-1240.47552	0.00	-15.62	0.00	-80.35	0.00
Form C	-1240.34083	84.52	54.95	70.57	-56.75	23.59
<i>Hatm</i>						
Form B	-1035.80018	0.00	59.92	0.00	20.30	0.00
Form C	-1035.72273	48.60	94.22	34.29	33.59	13.29

^a Values in Hartrees.

^b Values in kcal mol⁻¹.



Scheme 2. Scheme of ionization equilibrium of acetazolamide (R = methyl) and 5-tertbutyloxycarbonylamido-1,3,4-thiadiazole-2-sulfonamide (B-H₂ats) (R = tert-butylxy).

preferred formation of one specie over its tautomer.

A question that readily comes out is which is the group undergoing deprotonation first. The acidity constants of acetazolamide have been determined by different methods several times [11,32–35] but there is no agreement about which proton is more acidic. If a comparison is made between acetazolamide and related molecules which just present a protonable group (sulfonamido), it should be assumed that the first deprotonation of acetazolamide and B-H₂ats takes place on the sulfonamido moiety [2,11]. However, the presence of the 1,3,4-thiadiazole ring linked to the carbonamido group markedly enhances its acidity via π delocalization.

In an attempt to provide information about the stereoelectronic aspects that may aid in the understanding of the reaction mechanism of B-H₂ats and acetazolamide, the change of potential energy with the variation of carbonamido hydrogen bond distance ($r_{C_{N-H}}$) and sulfonamido hydrogen bond distance ($r_{S_{N-H}}$) has been then compared (Fig. 3). The potential energy surface indicates

two possible reaction paths for the deprotonation process from A (neutral form) to D (dianionic form). These theoretical results are in complete agreement with the working hypothesis of Scheme 2. In order to evaluate in detail both reaction paths I and II, a one-dimensional (1D) plot which is shown in Fig. 4 has been performed. The 1D cross-section is neither along $r_{C_{N-H}}$ nor along $r_{S_{N-H}}$, but along a combination of these two internal coordinates. Such combinations of internal coordinates are called reaction coordinates if the energy along such lines represent the shallowest ascent. Two distinct reaction paths are seen on Scheme 2, one corresponding to I and the other to the II route. The energy values and the energy gap between the stationary points (B and C) are listed in Table 2. AM1 calculations predict an energy gap between B and C of about 27 kcal mol⁻¹ for acetazolamide whereas ab-initio RHF/6-31G* computations indicate that this difference is about 13 kcal mol⁻¹. It should be noted that both AM1 and ab-initio calculations were performed for an isolated molecule in vacuo and some change in these results due to solvent effect was expected. In

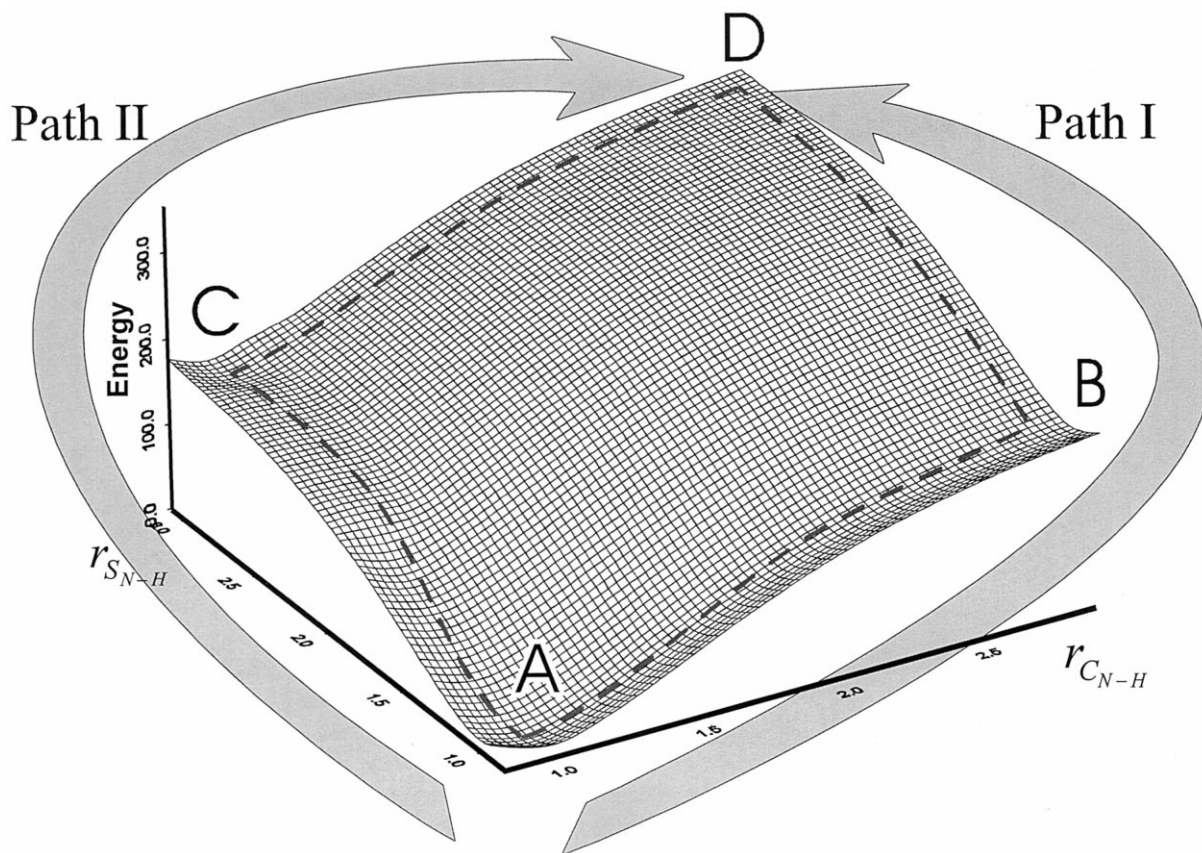


Fig. 3. Three dimensional potential energy surface of deprotonation obtained from AM1 calculations. The probable reaction paths are also indicated.

view of these observations, the next stage in our analysis was to compare these results with AM1 calculations including the effects of solvation. These calculations were performed using the SM2 method developed by Cramer and Truhlar [22] and are shown in Table 2. The energy gap predicted by SM2 calculations was lower in comparison with those obtained by calculations in gas-phase at both level of theory. Elsewhere the energy gap obtained between B and C was large enough to suggest that the tautomeric equilibrium between the above forms is somewhat restricted. Thus, theoretical calculations indicate that the reaction path I is thermodynamically preferred.

On the other hand, it is worth mentioning that the hypsochromic shift observed in the UV spec-

tra maxima for the proposed dissociation of the sulfonamido moiety (301–292 nm for acetazolamide and 302–293 nm for B-H₂ats) is in agreement with the shift observed for the same dissociation in Hats (281–270 nm).

On the basis of the experimental and theoretical results it was concluded that the acid–base dissociation of acetazolamide and B-H₂ats follows one preferred reaction path in which the first deprotonation takes place at the carbonamido group.

It was possible to prepare and characterize by single crystal X-ray diffraction (XRD) some acetazolamide complexes where the ligand acts monodeprotonated at the carbonamido group in according with the conclusions [36,37].

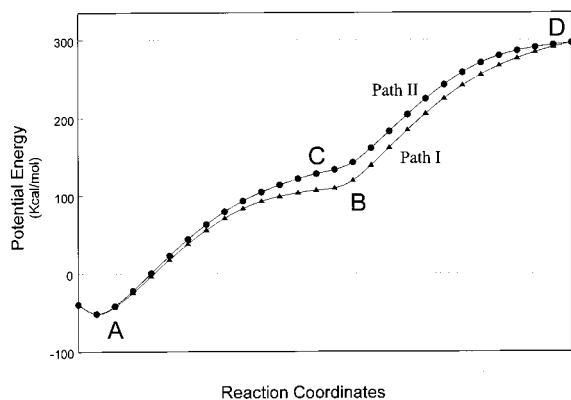


Fig. 4. Potential energy profiles along the reaction coordinates (variation of carbonamido hydrogen bond distance, $r_{\text{C-N-H}}$, and sulfonamido hydrogen bond distance, $r_{\text{S-N-H}}$).

Acknowledgements

This work was supported by 'Consejo Nacional de Investigaciones Científicas y Técnicas de la República Argentina' and 'CyT-Universidad Nacional de San Luis'. The authors are also indebted to Drs Rosa Ortiz and Mónica Ruiz for their comments and assistance with the potentiometric study.

References

- [1] J.L. Evelhoch, D.F. Bocian, J.L. Sudmeier, *Biochemistry* 20 (1981) 4951.
- [2] C.T. Supuran, in: I. Puscas (Ed.), *Carbonic Anhydrase and Modulation of Physiologic and Pathologic Processes in the Organism*, Helicon, Timisoara, Romania, 1994, pp. 29–113.
- [3] J.C. Pedregosa, J. Casanova, G. Alzuet, J. Borrás, S. García-Granda, M.R. Díaz, A. Gutierrez-Rodriguez, *Inorg. Chim. Acta* 232 (1995) 117.
- [4] J.C. Pedregosa, G. Alzuet, J. Borrás, S. Fustero, S. García-Granda, M.R. Díaz, *Acta Cryst. C* 49 (1993) 630.
- [5] E.E. Chufán, J.C. Pedregosa, O.N. Baldini, L.B. Blanch and II Farmaco, submitted, April (1999).
- [6] J. Vidgren, A. Liljas, N.P.C. Walker, *Int. J. Biol. Macromol.* 12 (1990) 342.
- [7] S. Chakravarty, K.K. Kannan, *J. Mol. Biol.* 243 (1994) 298.
- [8] P. Borja, G. Alzuet, J. Casanova, J. Server-Carrió, J. Borrás, M. Martínez-Ripoll, C.T. Supuran, *Main Group Met. Chem.* 21 (1998) 279.
- [9] E.E. Chufán, J.C. Pedregosa, G. Alzuet, J. Borrás and C.T. Supuran, *ICCC XXXII*, 1997.
- [10] E.E. Chufán, J.C. Pedregosa, J. Borrás, *Vib. Spectrosc.* 15 (1997) 191.
- [11] S. Ferrer, J. Borrás, E. Garcia-España, *J. Inorg. Biochem.* 39 (1990) 297.
- [12] G. Alzuet, L. Casella, A. Perotti and J. Borrás, *J. Chem. Soc., Dalton Trans.* (1994) 2347.
- [13] C. Supuran, A.T. Balaban, M.D. Gheorghiu, A. Schike-tanz, A. Dinculescu, I. Puscas, *Rev. Roum. Chim.* 35 (1990) 399.
- [14] G. Gran, *Analyst (London)* 77 (1952) 661.
- [15] F.J. Rossotti, H. Rossotti, *J. Chem. Educ.* 42 (1965) 375.
- [16] B. Trémillon, *La Chimie des Solvants Non-Aqueux*, Presses Universitaires de France, France, 1971.
- [17] P. Gans, A. Sabatini and A. Vacca, *J. Chem. Soc., Dalton Trans.* (1985) 1195.
- [18] H. Flaschka, *Talanta* 7 (1960) 90.
- [19] J.T. Edsall, R.B. Martin, B.R. Hollingworth, *Proc. Natl. Acad. Sci. USA* 44 (1958) 505.
- [20] T. Ishimitsu, S. Hirose, H. Sakurai, *Talanta* 24 (1977) 555.
- [21] M.J. Frisch, G.W. Trucks, H.B. Schlegel, P.M.W. Gill, B.G. Johnson, M.A. Robb, J.R. Cheeseman, T.A. Keith, G.A. Petersson, J.A. Montgomery, K. Raghavachari, M.A. Al-Laham, V.G. Zakrzewski, J.V. Ortiz J.B. Foresman, J. Cioslowski, B.B. Stefanov, A. Nanayakkara, M. Challacombe, C.Y. Peug, P.Y. Ayala, W. Chen, M.W. Wong, J.L. Andres, E.S. Replogle, R. Gomperts, R.L. Martin, D.J. Fox, J.S. Binkley, D.J. Defrees, J. Baker, J.P. Stewart, M. Head-Gordon, C. Gonzalez, and J.A. People, *Gaussian 94 (Revision D.1)*, Gaussian, Pittsburgh, PA, 1995.
- [22] SPARTAN version 4.0, Wavefunction, Inc., 18401 Von Karman Ave., # 370, Irvine, CA 92715, USA.
- [23] R.D. Enriz, E.A. Jauregui, F. Tomas-Vert, *J. Mol. Struct. (THEOCHEM)* 306 (1994) 115.
- [24] F.D. Suvire, R.D. Enriz, E.A. Jauregui, *Acta Farm. Bonaerense* 14 (4) (1995) 237.
- [25] A.M. Rodriguez, H.A. Baldoni, F.D. Suvire, R. Nieto Vázquez, G. Zamarbide, R.D. Enriz, O. Farkas, A. Perczel, M.A. McAllister, L.L. Torday, J.G. Papp, I.G. Csizmadia, *J. Mol. Struct. (THEOCHEM)* 455 (1998) 275.
- [26] R.W. Young, K.H. Wood, J.A. Eichler, J.R. Vaughan Jr., G.W. Anderson, *J. Am. Chem. Soc.* 78 (1956) 4649.
- [27] D.B. Rorabacher, W.J. MacKellar, F.R. Shu, Sister M. Bonavita, *Anal. Chem.* 43 (1971) 561.
- [28] K. Nakamoto, *Infrared and Raman Spectra of Inorganic and Coordination Compounds*, 5th edition, Wiley, New York, 1997.
- [29] H. Sakurai, T. Ishimitsu, *Talanta* 27 (1980) 293.
- [30] M.C. Aragoni, M. Arca, G. Crisponi, F. Cristiani, F. Isaia, V.M. Nurchi, *Talanta* 43 (1996) 1357.
- [31] E.J. King, *The International Encyclopedia of Physical Chemistry and Chemical Physics*, Topic 15, vol. 4, 1st edition, Pergamon Press, Oxford, 1965, p. 97.

- [32] T.H. Maren, *Physiol. Rev.* 47 (1967) 595.
- [33] M. Mathew, G.J. Palenik, *J. Chem. Soc., Perkin II* (1976) 532.
- [34] *The Index Merck*, 9th edition, Merck, NI Rahway, USA, 1976.
- [35] F. Malecki, R. Starosciak, *Pharmazie* 38 (1983) 174.
- [36] S. Ferrer, J. Borrás, C. Miratvilles, A. Fuertes, *Inorg. Chem.* 28 (1989) 160.
- [37] S. Ferrer, J.G. Haasnoot, R.A.G. de Graaf, J. Reedijk, J. Borrás, *Inorg. Chim. Acta* 192 (1992) 129.

Analysis of trace metals in water by in-situ sample pre-concentration combined with wavelength dispersive X-ray fluorescence spectroscopy and inductively coupled plasma-optical emission spectroscopy

Mark E. McComb *, Hyman D. Gesser

Department of Chemistry, University of Manitoba, Manitoba, WB R3T 2N2, Canada

Received 30 November 1998; received in revised form 24 February 1999; accepted 25 February 1999

Abstract

In this paper an earlier work on the use of poly(acrylamidoxime) cloth for use as a passive monitor for trace metals in water by characterizing the sorption of several metals onto the cloth using a continuous flow chamber is extended. The monitor consists of amidoxime chelating groups covalently bound to the surface of a textile encased in a common 35 mm slide holder. Placement of this device in the water to be sampled resulted in the uptake of heavy metals by the chelating groups. After removal of the monitor from water, the metals were analyzed using wavelength dispersive X-ray fluorescence spectroscopy (WDXRF) as well as by acid extraction followed by inductively coupled plasma-optical emission spectroscopy (ICP-OES). Correlation between the two methods of analysis varied with maximum correlation of 0.99897 observed for Pb and a minimum correlation of 0.16512 for Mg. The order of the distribution coefficients for the seven metals tested was: $Pb \geq Cu > Zn > Cd > Mn > Fe > Mg$, in agreement with the order of the stability constants for the amidoxime/hydroxamic acid group for the chelation of the same metals at a pH of 5, with the exception of Fe. Field testing of the monitors was also carried out and a comparison made between active sampling of river water and sampling with the monitors. Results indicated that semiquantitative analysis of trace metals in water may be performed using the passive monitors. © 1999 Elsevier Science B.V. All rights reserved.

Keywords: WDXRF; Trace metals; ICP-OES

1. Introduction

The monitoring of trace metals in the environment has been a subject of great concern over the

last decade and will continue to be so as there is an ever increasing amount of metals that are to be found in the environment. The sources of heavy metals in the environment, and more specifically in water systems, has been attributed primarily to man made sources, such as waste discharge and stack emissions from industrial sources and coal power production. The amounts released are stag-

* Corresponding author. Tel.: +1-204-474-6561; fax: +1-204-474-7608.

E-mail address: mccomb@cc.umanitoba.ca (M.E. McComb)

gering, with values in the millions of tonnes per year for a single metal [1]. This results in the subsequent contamination of fresh water resources and an ever increasing accumulation of these toxins in the human food chain [2]. Research over the last 20 years indicates that consumption of heavy metals, for example Pb, may be detrimental to a person's health at levels lower than those which were once thought to be safe [2,3]. Thus, there exists the need for the continuous monitoring of both fresh water supplies and essentially all water sources, including the oceans, in order to better understand the sources, transport and amounts of these toxic heavy metals [4–6].

The most common method of water analysis today involves the collection of an aqueous grab sample from the location of interest followed by direct instrumental analysis at a dedicated central laboratory [7–9]. A number of extra steps may be taken with regards to the initial sample, before the actual analysis is carried out, dependent on the information which is wanted. These include bulk filtration to remove humic material and other particulate matter which may interfere with analysis [10], addition of a preservative to ensure that there is no sample loss on the container walls during storage [11,12], and sample preconcentration which is carried out in order to improve the detection limits and analytical working range of the analysis [13,14]. The net result of this is a sampling protocol for a single sample which is not only time consuming and costly, but which must be carried out by a skilled technician both at the location of sampling as well as in the laboratory. For multiple samples from a single location the time involved in sampling and the initial preparation steps can run into several hours or even days. The cost of this on a per sample basis can be excessive. This type of approach is hardly applicable if profile monitoring, pollutant source identification or transport modelling are to be done, in which a large number of samples must be gathered over an extended period of time.

A solution to this is the method of passive sampling which involves the measurement of the concentration of an analyte as a weighted function of the time of analysis. In this way, the

concentration of the analyte is integrated over the time of sampling. The principal advantage of this over the more traditional method of grab sampling is that only one device is necessary at a sampling location for the entire time of sampling. In the case of a grab sample, the number of samples collected over the same period of time may be large in order to gain the same time averaged information.

Passive monitors for trace metals in water are not common with work predominantly directed towards *in vitro* experiments with very little actual field studies being done. There are several different approaches to *in situ* aqueous sample collection or measurement of trace heavy metals as a function of the time of analysis. These range considerably and include the following: collection of an aqueous grab sample at preset time intervals via mechanical devices in what can be considered a semi continuous mode [15–17], *in situ* collection and speciation via dialysis, again in a semi continuous mode [18–20], *in situ* measurement via electrochemical means as is the case with ion selective electrodes [21], and sample sorption/preconcentration on a suitable sorbent [22–28].

Recently, the use of a woven cloth containing the amidoxime chelating group was introduced for use as a means to extract trace metals from water [29,30]. The amidoxime chelating group was specifically chosen for a number of reasons. Foremost was its ability to chelate a large number of different heavy metals without taking up alkali and alkaline earth metals [31]. Another factor was the great amount of work that has been done in the past with regards to using the amidoxime group for the preconcentration and analysis of trace metals in water [32–38]. Additionally, work performed by Lin on the use of poly(acrylonitrile) fibres containing the amidoxime group for the extraction of Au from water [39,40], and by others for the preconcentration of U from seawater [41–48] demonstrated the ease of preparing poly(-acrylamidoxime) chelating fibres from the poly(-acrylonitrile) (Orlon) precursor.

The passive monitor consists of amidoxime chelating groups covalently bound to a poly(acrylonitrile) textile encased it in a common commercial 35 mm slide holder made of plastic. The idea

for this approach came from previous work in this laboratory with regards to passive monitors for organic compounds in air and water [49,50]. Placement of this device in the water to be sampled results in the uptake of heavy metals by the chelating groups. After removal of the monitor from water, the metals may then be analyzed. Previously, several physical properties of the poly(acrylamidoxime) cloth were characterized and measured several parameters which affect the sorption of metals onto the cloth. Analysis was performed using energy dispersive X-ray fluorescence spectroscopy (EDXRF) and wavelength dispersive X-ray fluorescence spectroscopy (WDXRF). In this paper an earlier work is extended by characterizing the sorption of several metals on the cloth monitors using a continuous flow chamber (in-vitro experiments). Field testing of the monitors was also carried out and a comparison made between active sampling of river water and sampling with the monitors. Analysis was performed by WDXRF via the thin sample technique directly on the monitors. Quantitative analysis was performed by removing the metals from the cloth by acid extraction followed by inductively coupled plasma-optical emission spectroscopy (ICP-OES). WDXRF spectroscopy was chosen as it provides for relatively sensitive, simultaneous multi-elemental analysis, while avoiding costly and time consuming acid extraction. ICP-OES was used as a comparative method and to quantify the WDXRF results.

2. Experimental

2.1. Reagents

Reagents used in the conversion of the nitrile groups on poly(acrylonitrile) cloth to amidoxime chelating groups, $\text{NH}_2\text{OH}\cdot\text{HCl}$, NH_4OH , NaOH , and ethanol (95%) were reagent grade (Fisher) while methanol (100%) used was electronic grade (Fisher). Metals used in the in vitro tests and in standard solutions were prepared from the nitrate salts and were reagent grade (Fisher). Solutions used in ICP-OES analysis were prepared in environmental grade HNO_3 (Anachemia). Water used

for the in vitro tests in the flow chambers was derived from reverse osmosis feedstock (ro). Water used in the standards for ICP-OES, and in the conversion process, was further purified by passage through a four stage Barnsted Nano-Pure II purification system (nanopure). The film used in the preparation of samples for WDXRF spectroscopy was $6.3\ \mu\text{m}$ X-ray polypropylene film supplied by Chemplex Industries, NY, USA. The poly(acrylonitrile) cloth used in the monitors was obtained from Test Fabrics and used as received [51].

2.2. Apparatus

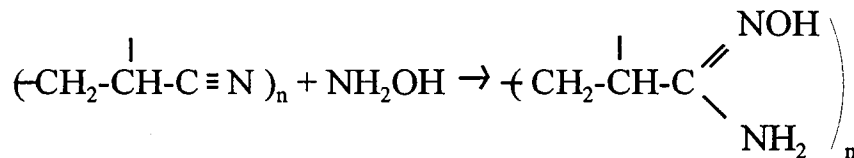
For the in vitro experiments, a constant flow chamber was set up in which the monitors could be placed. This consisted of a 200 l polyethylene barrel connected to a glass flow chamber (height $\sim 30\ \text{cm}$, diameter $\sim 10.6\ \text{cm}$) via glass and silicon rubber tubing. A small immersible mechanical pump provided solution flow through the flow chamber. A diagram of the flow chamber and a sample holder has been previously described [29].

2.3. WDXRF spectroscopy

WDXRF spectroscopy was performed on an American Research Laboratories spectrometer. Analysis of the monitors was carried out on the cloth samples after removal from their plastic frames. The cloth pieces were placed on a cardboard backing followed by encasement in $6.3\ \mu\text{m}$ polypropylene film. This small packaged sample was then placed in the supplied sample holders. Spectral acquisition was carried out by recording spectra for three 30 s intervals for each element examined with the exception of Zn, for which the acquisition time was only two seconds. Representative blanks were recorded for all analysis.

2.4. ICP-OES

Analysis of metals taken up by the cloth samples by ICP-OES was performed using a Varian Liberty 200 ICP-OES. Standards were prepared in 1% HNO_3 by serial dilution of stock $1000\ \text{mg}\ \text{l}^{-1}$ solutions of the respective metal salts. Metals



Scheme 1. Reaction of a poly(acrylonitrile) monomer unit with hydroxylamine to produce poly(acrylamidoxime).

taken up by the cloth were analyzed after extraction with 1% HNO_3 . A total of three extractions per sample were performed, the extracts combined, and made up to 25 ml. The degree of extraction was calculated previously to be better than 95% [29].

2.5. Preparation of the passive monitors

The preparation of the passive monitors began with the conversion of the nitrile groups on the surface of the poly(acrylonitrile) cloth to amidoxime chelating groups via the reaction in methanolic hydroxylamine as described by Lin [52]. The reaction is depicted in Scheme 1.

Conversion was carried out via a batch process by exposing pieces of cloth to a methanolic solution of hydroxylamine. After conversion the cloth was washed with water (ro) and allowed to dry in air before use. A complete description of the preparation process is given elsewhere [30]. The properties of the cloth used in the monitors are summarized in Table 1. Small pieces of the amidoxime containing cloth were cut into 2×2 cm squares for use in the *in vitro* experiments. As well, 3.5×4 cm pieces were cut and placed into standard 35 mm slide holders to produce the passive monitors.

3. Results and discussion

3.1. *In vitro* experiments

Characterization of the sorption of different metals onto the cloth from solution was performed using the flow chamber. A total of seven metals were used: Pb(II), Cu(II), Mn(II), Mg(II), Cd(II), Zn(II), and Fe(III). The flow rate was fixed at $\sim 4.7 \text{ l min}^{-1}$, with a linear velocity of

$\sim 52 \text{ cm min}^{-1}$. The initial concentrations of metals in solution were fixed at $0.300 \mu\text{mol l}^{-1}$ in $\sim 150 \text{ l}$. The cloth samples ($2 \times 2 \text{ cm}$) were placed in the flow chamber for times ranging from 17 h to 60 days. After exposure, they were removed from the chamber and dried in air prior to analysis by WDXRF and ICP-OES.

3.2. Comparison of methods

In general the sample preparation for the WDXRF analysis was less time consuming and easier to perform than the ICP-OES work. As the WDXRF method was nondestructive the samples could be re-analyzed with ease. Because of the design of the monitor, the cloth samples could literally be stored indefinitely prior to analysis. The one limitation to this method is that quantitation is not readily performed. Either thin sample standards may be prepared or, as in this case, select samples can be quantified via a second method such as ICP-OES and the results correlated to the first.

In comparison with ICP-OES great care was taken to ensure that sample contamination did not occur during the acid extraction and subse-

Table 1
Properties of poly(acrylamidoxime) cloth used in the passive monitors

Property	
Degree of conversion	$45 \pm 2\%$
Texture	Flexible and soft
Mass	0.043 g cm^{-2}
Area of cloth in monitor	8.05 cm^2 (one side)
Mass of cloth exposed	0.346 g
Amount of amidoxime group	206 mmol cm^{-2}
Capacity for Pb, 7 days	2.17 mmol g^{-1}
Capacity for Cu, 7 days	1.12 mmol g^{-1}

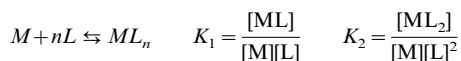
Table 2
Sorption of metals onto poly(acrylamidoxime) cloth^a

Metal	Correlation	Sampling rate ^b		K_d^d	Formation constants ^c	
		$\mu\text{mol g}^{-1} \text{ day}^{-1}$	$\text{ml g}^{-1} \text{ day}^{-1}$		K_1	K_2
Pb	0.99897	0.35	940	35 000	6.7	10.7
Cu	0.98953	0.29	710	34 000	7.9	–
Cd	0.76375	0.065	240	4000	4.5	7.8
Fe	0.43513	0.0070	50	350	11.42	21.10
Mn	0.99153	0.033	140	880	4.0	6.9
Zn	0.9850	0.10	430	5400	5.4	9.6
Mg	0.16512	0.0089	80	140	2.4 ^e	–

^a Correlation between wavelength dispersive X-ray fluorescence spectroscopy (WDXRF) and inductively coupled plasma-optical emission spectroscopy (ICP-OES) measurements, rates of metal uptake and distribution coefficients (K_d) for the sorption of metals from dilute solution. Initial metal concentration in solution = $0.300 \mu\text{mol l}^{-1}$.

^b Average rate over 60 days of exposure per g cloth.

^c Formation constants acetohydroxamic acid [54] ($\log K_{eq}$) derived from the following equation:



^d K_d measured at 60 days of exposure. $K_d = \frac{(\mu \text{ mol metal}) (\text{g cloth})^{-1}}{(\mu \text{ mol metal}) (\text{ml solution})^{-1}}$

^e The value for Ca was used as the value for Mg was not available [55].

quent analysis. The actual time required to wash all laboratory glassware and perform the extractions was long while at the same time demanding constant attention. Once the metals were extracted from the cloth they were immediately analyzed by ICP-OES in order to eliminate possible loss during storage. However, quantitation was straight forward and estimated to be linear over four orders of magnitude with linear calibration coefficients better than 0.99995.

The correlation between the WDXRF and the ICP-OES results are given in Table 2. It is noted that the WDXRF and the ICP-OES results did not correlate as well as expected for all the metals analyzed. For Pb, Mn, Cu and Zn the correlation between the two methods was better than 95% which indicates excellent agreement with the two methods. The remaining metals analyzed did not correlate as well. The poor degree of correlation for Fe (0.43513) and Mg (0.16512) was suspected to be due to the low amount of each metal present on the cloth, in the low ppm range according the ICP-OES analysis. The metals which did correlate well were found in relatively high concentrations

on the cloth. Overall the best correlation between the two methods was for Pb with a correlation of 0.99897 between the two methods.

3.3. Kinetics of metal uptake

The results showing the amount of metal taken up by the cloth with respect to the time of exposure to the solution within the flow chamber are given in Fig. 1. It was observed that the results varied considerably for each of the metals tested in the in vitro experiment. The general shapes of the curves in Fig. 1 (Pb, Cu, Cd, Zn and Mn) indicate that the rate of uptake of the metals was initially quite rapid, after which, the rate was observed to decrease slightly. The profile observed was similar to the general shape of results reported by others with respect to the rates of metal uptake by chelating polymers such as resins [41–44] and fibres [47,48]. Pb, Cu, Zn and Cd, all showed an increase in the amount taken up over the entire time of exposure. Initially, the amount of Mn taken up increased with the time of exposure after which the amount levelled off. Fe was

taken up by the cloth only marginally over the duration of exposure.

The rate of metal uptake was calculated using an average rate for the duration of exposure. The values are given in Table 2, values slightly lower than those observed for the sorption of $\text{UO}_2(\text{VI})$ of $200 \mu\text{g g}^{-1} \text{day}^{-1}$ ($0.84 \mu\text{mol g}^{-1} \text{day}^{-1}$) from seawater onto amidoxime containing fibres [53]. A material balance on the amount of metals in solution indicated that the concentration of the metals in the barrel decreased by less than 10% over the duration of the experiment and thus for the sake of simplicity was considered constant. The smaller rates observed may be because a smaller net surface area of fibre was exposed on the cloth as some of the fibre surface is covered with other fibres due to the woven nature of the cloth. In addition, the cloth had only approximately 45% of the nitrile groups converted to the amidoxime group.

The amounts of metal sorbed are also represented in the form of the equilibrium distribution coefficient K_d [37,54]. The K_d values for each of the metals tested are presented in Table 2.

$$K_d = \frac{(\mu\text{mol metal}) (\text{g cloth})}{(\mu\text{mol metal}) (\text{ml solution})}$$

This provides a measure of the degree of sample preconcentration from solution and at the same time normalizes the results with respect to each other. The order observed: $\text{Pb} > \text{Cu} > \text{Zn} > \text{Cd} > \text{Mn} > \text{Fe} > \text{Mg}$ is in agreement with the order of the stability constants for the amidoxime/hydroxamic acid group for the chelation of the same metals at a pH of 5, with the exception of Fe [55–58]. This indicates that chelation is selective for metals which form stable complexes with the amidoxime group under these conditions. Thus in

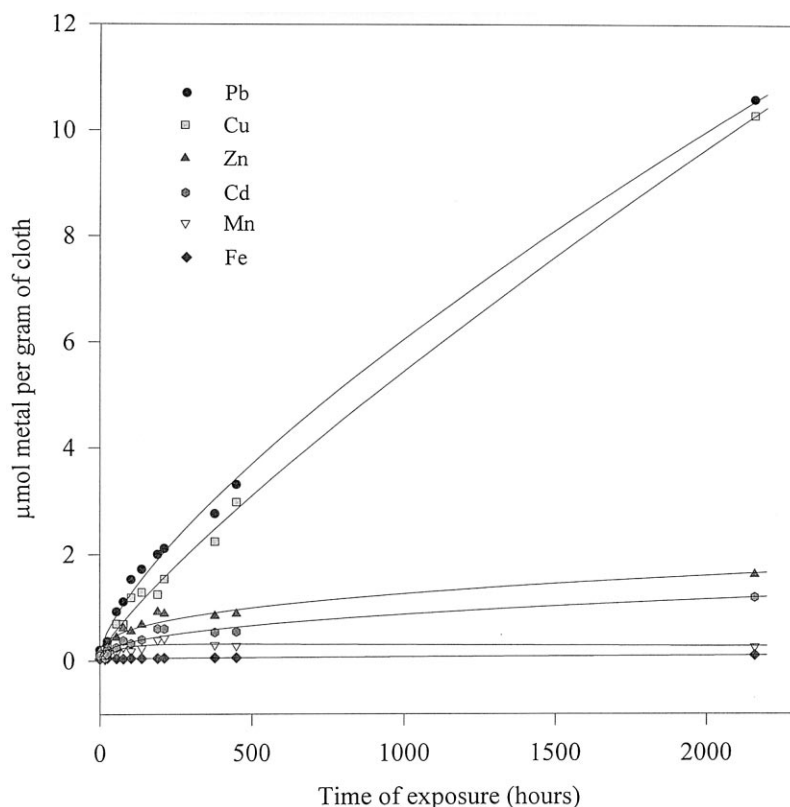


Fig. 1. Kinetics of metal sorption onto poly(acrylamidoxime) chelating cloth. Initial concentrations of each metal in the flow chamber were $0.300 \mu\text{mol l}^{-1}$.

order to monitor other metals, which are not preferred by the amidoxime group, one would have to select a different chelating group. The discrepancy for Fe is not known. It is suspected that Fe may form such a strong complex with the amidoxime group that it may not penetrate into the cloth fibres to any extent and thus after a surface equilibrium is established there would be no net further uptake of Fe. This correlates with our earlier results with respect to the amount of Cu sorbed on cloth with low degrees of conversion to amidoxime chelating groups [30]. The absolute values of K_d for Cu and Pb represent a degree of sample pre-concentration per gram of cloth of $\sim 35\,000$. This indicates that the level of metal which can be detected with this method can be extremely small. An estimate of the concentration that may be detected for Pb and Cu per g of cloth is <0.010 ppb in water, values that rival ICP-MS.

Given a fixed sampling rate of metals by the cloth, presumably diffusion limited [29], the amount of metal taken up by the cloth will be representative of its concentration in solution, the time of exposure and the calculated rate of uptake from solution under similar conditions, or at equilibrium, its K_d value. In this case, equilibrium has yet to be established for the metals tested. Thus, the amount of metal taken up by the cloth may be related to the original concentration of metal in solution by the following equation:

$$A_m = C_m \times R_m \times t$$

A_m is the amount of metal taken up on the cloth, $\mu\text{mol (g cloth)}^{-1}$; C_m is the original concentration of metal in solution, $\mu\text{mol ml}^{-1}$; R_m is the rate of uptake of the metal, $\text{ml (g cloth)}^{-1} \text{ day}^{-1}$; t is the time of exposure to solution, day.

3.4. Field tests

In order to demonstrate the use of these monitors for the quantitative analysis of trace metals in water a series of field tests were conducted with the assistance of personnel from Manitoba

Table 3

Concentrations of metals found in the Red River floodway for the month of June, 1995^a

Metal	Concentration (mg l^{-1})	$\mu\text{mol ml}^{-1}$
Pb	0.0020	9.6×10^{-6}
Cu	<0.01	150×10^{-6}
Cd	<0.001	8.9×10^{-6}
Fe	2.41	43×10^{-3}
Mn	0.29	5.0×10^{-3}
Zn	0.02	0.3×10^{-3}
Mg	35.5	1400×10^{-3}

^a Sampling conditions: 500 ml grab sample, filtered 0.45 μm , 2.5% in HNO_3 as preservative. Turbidity = 120 NTU, conductance = 735 W^{-1} .

Environment. Monitors were deployed in the Red River Floodway at Selkirk, Manitoba, near sampling locations used by Manitoba Environment to collect monthly water samples, as part of the routine analysis of the water near Winnipeg, Manitoba. A total of three monitors were exposed to water in the river and subsequently analyzed. The monitors were deployed ~ 0.5 km upstream of the site of grab sampling, for a period of 7 days. The concentration of metals in the Red River at the time of sampling are given in Table 3. Water conditions at the time of sampling were as follows: fast flow $\sim 0.5\text{--}1$ m s^{-1} , with a high degree of turbidity. After exposure the monitors were placed in polyethylene bags for ~ 2 h while they were transported to the laboratory. The results in Table 4 show the amount of metal taken up per g cloth for the three monitors. After exposure Mg, Mn, Fe and Zn were found in the largest amounts on the cloth. This was not unexpected as these metals were found in relatively large concentrations in the water tested. The other metals analyzed for were present on the cloth in slightly lower amounts.

An attempt was made to quantify and provide a degree of correlation with respect to the amounts of metals observed on the monitors and the amounts of metals analyzed from the grab samples. The initial concentration of metals in the river based on the passive monitor results were calculated using the rates of uptake measured in

the in vitro experiments. The results in Fig. 2 show the comparison between the results of the grab sample and the values derived from the passive monitors. The calculated values for Pb and Mn were in agreement with the grab sample results. The results for the remainder of the metals were all approximately one order of magnitude less in concentration in comparison with the measured values. The degree of correlation between the two sets of results are given in Table 4. The correlation between the measurements indicated good agreement between the measured amounts and the calculated amounts.

Several factors may contribute to the differences between the measured and calculated results. The velocity of the river water, the presence of other metals in the river as well as the amount of humic material all may contribute to the amount of metals sorbed. The comparison also is influenced by the limitation in the measurement of Cu and Cd in the Red River at the time of sampling as they were not measured quantitatively and are presented as being less than a minimum value. In spite of this, the results did correlate well and although the calculated values were not exact, they were systematically lower than the measured values. This is similar to field measurements of Zhang and Davidson's passive sampler [28]. They observed calculated values for Zn to be lower than values

obtained from grab samples and attributed the results to a difference between labile metals in solution and those bound by organic matter. The reproducibility in the field measurements was of the order of 14–89% for the three samplers. The precision in replicate measurements was less than results obtained in-situ [29,30]. Possible explanations for this are that the metals in the river water were all present in relatively low concentrations and that the samplers were influenced by turbulent flow and the presence of humic material. A longer exposure time, and more careful placement of the monitors may improve the reproducibility in these measurements.

These results demonstrate that qualitative analysis and semi-quantitative analysis (within an order of magnitude) is possible with these monitors and that quantitative analysis is feasible. In order to more accurately quantify the results all that is necessary is to know the concentration of a single metal on the cloth and to measure the remaining metals relative to the first. In addition, if used for a monitoring process, it would not be necessary to measure an absolute concentration of metals in the water to be tested. Instead, it is only necessary to measure a difference between subsequent sets of monitors over the duration of sampling and correlate one set with an active grab sample for quantitative analysis.

Table 4
Results for the monitors deployed in the Red River at Selkirk, Manitoba^a

Metal	Amount of metal: $\mu\text{mol (g cloth)}^{-1}$			Mean \pm S.D.
	# G8	# G2	# G5	
Pb	11×10^{-3}	89×10^{-3}	46×10^{-3}	$48 \pm 39 \times 10^{-3}$
Cu	21×10^{-3}	3.7×10^{-3}	15×10^{-3}	$13 \pm 8.8 \times 10^{-3}$
Cd	0.79×10^{-3}	0.75×10^{-3}	0.93×10^{-3}	$0.82 \pm 0.095 \times 10^{-3}$
Fe	170×10^{-3}	770×10^{-3}	670×10^{-3}	$540 \pm 320 \times 10^{-3}$
Mn	630×10^{-3}	2800×10^{-3}	1800×10^{-3}	$1700 \pm 1100 \times 10^{-3}$
Zn	62×10^{-3}	81×10^{-3}	65×10^{-3}	$69 \pm 10 \times 10^{-3}$
Mg	18.8	37.4	34.1	30 ± 9.9
Correlation	0.99973	0.99964	0.99927	0.99955 ± 00024

^a Amount of metal sorbed for three monitors for 7 days exposure and their correlation with the measured concentration in the Red River obtained from the grab sample.

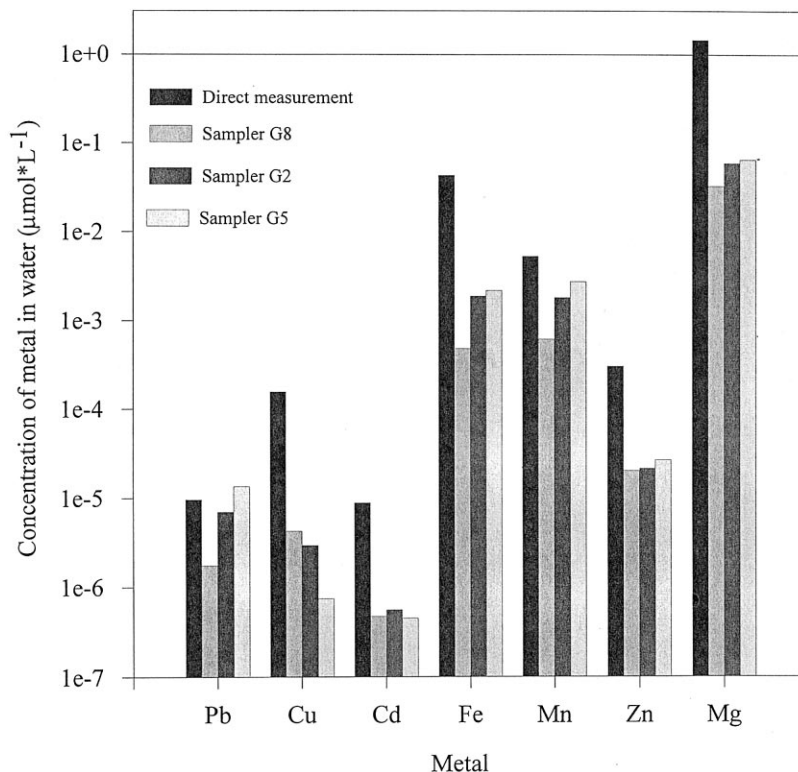


Fig. 2. Field testing of three monitors deployed in the Red River at Selkirk, Manitoba. Comparison between the concentration measured from a grab sample and amounts calculated using the passive monitors.

4. Conclusions

A number of conclusions can be made with respect to the preparation and use of poly(acrylamidoxime) cloth as a passive monitor for trace metals in water. The *in vitro* experiments demonstrated the feasibility of the passive *in situ* sorption of trace metals by the cloth followed by either WDXRF or ICP-OES analysis. Sensitivity in the $\mu\text{g l}^{-1}$ and sub $\mu\text{g l}^{-1}$ range was observed. Non-destructive analysis by WDXRF greatly simplified the measurement of sub $\mu\text{g l}^{-1}$ levels of metals and avoided time consuming and costly acid extraction. The physical nature of the monitor suggests an indefinite storage time both before and after deployment. The actual size of the monitors proved to be ideal for WDXRF analysis as well as for acid extraction followed by ICP-OES analysis. The choice of amidoxime as a ligand was acceptable and proved to be selective to several

metals of interest. The kinetics of metal sorption and distribution coefficients were similar to those of resins and fibres from previous work. The *in vitro* experiments demonstrated the sensitivity of this method with K_d values in the 10^5 range for Cu and Pb.

The field test demonstrated the feasibility of using the monitors for the semi-quantitative analysis of trace metals in water. Concentrations of metals in the environment were observed on the monitors at levels lower than those typically measured thus indicating the sensitivity of the method and the ability of the cloth to concentrate the trace metals into the working range of WDXRF and ICP-OES.

There are several significant benefits to the development of a passive monitor for trace metals in water. A passive monitor will allow the reduction in the cost per sample analyzed for many types of environmental monitoring and sampling, and al-

low for the direct application for the analysis of many aspects of environmental pollutants. The low cost would allow for an increase in the amount of monitoring that could be done at any given location. For example, fresh water supplies could be monitored continuously for trace metals thus ensuring their quality. Continuous monitoring of predetermined sites would allow for pollutant source identification over long term exposure and allow for the enforcement of pollution control guidelines. This could be applied in the cases of acid mine tailings, waste effluent and discharge from industry, as well as other sources. Other beneficial applications include the study of transport phenomena of metals in water. Metal concentration profiles in a lake or river could be studied over both short and long time frames by using a large number of monitors at a relatively low cost. As well, the study of water pollution could be carried out to the same degree with the aim to reduce human exposure to these pollutants.

Acknowledgements

The author thanks AECL Pinawa for the use of the WDXRF instrument and Manitoba Environment for their assistance. Gratitude is expressed towards W. Blonski for his assistance with the ICP-OES work. We thank H. Perreault for support and the University of Manitoba for a Fellowship awarded to M.E. McComb.

References

- [1] J.O. Nriagu, J.M. Pacyna, *Nature* 333 (1988) 134.
- [2] D.D. Chiras, *Environmental Science*, 3rd edition, Benjamin Cummings, California, 1991.
- [3] WHO report, 1995.
- [4] L.H. Keith, W.A. Telliard, *Environ. Sci. Technol.* 13 (1979) 416.
- [5] Ph. Quevauviller, E.A. Maier, *Int. J. Environ. Anal. Chem.* 57 (1994) 255.
- [6] K.J.M. Kramer, *Int. J. Environ. Anal. Chem.* 57 (1994) 179.
- [7] W. Slavin, *At. Spectr.* 1 (1980) 66.
- [8] D.F.S. Natusch, P.K. Hopke, *Analytical Aspects of Environmental Chemistry*, vol. 64, Wiley, New York, 1983.
- [9] I.L. Marr, M.S. Cresser, *Environmental Chemical Analysis*, International Textbook Company, New York, 1983.
- [10] E. Michnowsky, L.M. Churchland, P.A. Thomson, P.H. Whitfield, *Water Res. Bull.* 18 (1982) 129.
- [11] R. Masee, F.J.M. Maessen, *Anal. Chim. Acta.* 127 (1981) 181.
- [12] D.P.H. Laxen, R.M. Harrison, *Anal. Chem.* 53 (1981) 345.
- [13] Z.B. Alifasi, C.M. Wai, *Preconcentration Techniques for Trace Elements*, CRC Press, Boca Raton, FL, 1992.
- [14] C. Kantipuly, S. Katragadda, A. Chow, H.D. Gesser, *Talanta* 37 (1990) 491.
- [15] H.F. Padden, U.S. Patent No. 05319986, 1994.
- [16] R.L. Nichols, U.S. Patent No. 05293931, 1994.
- [17] R.K. Harris, U.S. Patent No. 05353870, 1994.
- [18] P. Beneš, E. Steinnes, *Water Res.* 8 (1974) 947.
- [19] P. Beneš, *Water Res.* 14 (1980) 511.
- [20] S.C. Apte, M.J. Gardner, D.T.E. Hunt, *Environ. Tech. Lett.* 10 (1989) 201.
- [21] S.K. Srivastava, V.K. Gupta, S. Jain, *Analyst* 120 (1995) 495.
- [22] K. Srikameswaran, H.D. Gesser, M.J. Venkateswaran, *Environ. Sci. Health A15* (1980) 323.
- [23] K. Srikameswaran, H.D. Gesser, *J. Environ. Sci. Health A13* (1978) 415.
- [24] C.H. Lochmüller, J.W. Galbraith, R.L. Walter, *Anal. Chem.* 46 (1974) 440.
- [25] T. Saito, *Talanta* 41 (1994) 811.
- [26] K. Srikameswaran, H.D. Gesser, *J. Environ. Sci. Health A19* (1984) 83.
- [27] E.O. Skogley, U.S. Patent No. 05355736, 1994.
- [28] H. Zhang, W. Davidson, *Anal. Chem.* 67 (1995) 3391.
- [29] M.E. McComb, H.D. Gesser, *Anal. Chim. Acta* 341 (1997) 229.
- [30] M.E. McComb, H.D. Gesser, *J. Appl. Polym. Sci.* 65 (1997) 1175.
- [31] Technical Sheet, Duolite CS-346, Diamond Shamrock.
- [32] T.W. Kyffin, Ph.D. Thesis, University of Salford, 1976.
- [33] M.B. Colella, S. Siggia, R.M. Barnes, *Anal. Chem.* 52 (1980) 967.
- [34] Technical Sheet, Duolite ES-346, Dia-Prosium, 1977.
- [35] É.M. Kats, E.K. Vul'fson, N.G. Zhukova, S.B.Z. Makarova, *Prikl. Him.* 64 (1991) 1263.
- [36] M.B. Colella, S. Siggia, R.M. Barnes, *Anal. Chem.* 52 (1980) 2347.
- [37] T. Hirotsu, S. Katoh, K. Sugasaka, M. Senō, T. Itagaki, *Sep. Sci. Tech.* 21 (1986) 1101.
- [38] N. Kabay, H. Egawa, *Tr. J. Chem.* 17 (1993) 62.
- [39] W. Lin, Y. Lu, H. Zeng, *React. Polym.* 17 (1992) 255.
- [40] W. Lin, Y. Lu, H. Zeng, *J. Appl. Polym. Sci.* 49 (1993) 1635.
- [41] T. Hirotsu, S. Katoh, K. Sugasaka, M. Senō, T. Itagaki, *J. Appl. Polym. Sci.* 36 (1988) 1741.
- [42] N. Kabay, H. Egawa, *Sep. Sci. Tech.* 28 (1993) 1985.
- [43] K. Sugasaka, S. Katoh, N. Takai, H. Takahashi, Y. Umezawa, *Sep. Sci. Tech.* 16 (1981) 971.

- [44] T. Hirotsu, S. Katoh, K. Sugasaka, N. Takai, M. Senō, T. Itagaki, *Ind. Eng. Chem. Res.* 26 (1987) 1970.
- [45] Y. Kobuke, T. Aoki, H. Tanaka, I. Tabushi, T. Kamaishi, I. Hagiwara, *Ind. Eng. Chem. Res.* 29 (1990) 1662.
- [46] N. Kabay, A. Katakai, T. Sugo, H. Egawa, *J. Appl. Polym. Sci.* 49 (1993) 599.
- [47] S. Katoh, K. Sugasaka, K. Sakane, N. Takai, H. Takahashi, Y. Umezawa, K. Itagaki, *Bull. Soc. Sea Water Sci. Jpn.* 9 (1982) 1155.
- [48] S. Katoh, K. Sugasaka, K. Sakane, N. Takai, H. Takahashi, Y. Umezawa, K. Itagaki, *Bull. Soc. Sea Water Sci. Jpn.* 9 (1982) 1449.
- [49] E. Giller, H.D. Gesser, *Environ. Int.* 21 (1995) 839.
- [50] E. Giller, M.Sc. Thesis, University of Manitoba, 1994.
- [51] Technical Catalog, Test Fabrics, Middlesex, NJ, 1992.
- [52] W. Lin, Y. Lu, H. Zeng, *J. Appl. Polym. Sci.* 47 (1993) 45.
- [53] H.J. Fischer, K.H. Lieser, *Fresenius, J. Anal. Chem.* 346 (1993) 934.
- [54] G.H. Luttrell Jr., C. More, C.T. Kenner, *Anal. Chem.* 43 (1971) 1370.
- [55] R.M. Smith, A.E. Martel, *Critical Stability Constants*, vol. 2, Amines, Plenum Press, New York, 1982.
- [56] F. Vernon, *Pure Appl. Chem.* 54 (1982) 2151.
- [57] T. Hirotsu, S. Katoh, K. Sugasaka, *Sep. Sci. Tech.* 21 (1986) 1101.
- [58] F. Vernon, H. Eccles, *Anal. Chim. Acta.* 82 (1976) 369.

Spectrofluorimetric determination of cisatracurium and mivacurium in spiked human serum and pharmaceuticals

Rut Fernández, Miguel Angel Bello *, Manuel Callejón, Juan Carlos Jiménez, Alfonso Guiraúm

Department of Analytical Chemistry, Faculty of Chemistry, 41012-Seville, Spain

Received 12 October 1998; received in revised form 9 February 1999; accepted 26 February 1999

Abstract

Spectrofluorimetric methods to determine cisatracurium and mivacurium are proposed and applied to the determination of both substances in human serum and to the determination of mivacurium in pharmaceuticals. The fluorimetric methods allow the determination of 5–500 ng ml⁻¹ of mivacurium in aqueous solutions and 5–500 ng ml⁻¹ of cisatracurium in water–acetonitrile solutions, both containing acetic acid–sodium acetate buffer (pH 5.5) with $\lambda_{\text{exc}} = 230$ nm and $\lambda_{\text{em}} = 324$ nm. © 1999 Elsevier Science B.V. All rights reserved.

Keywords: Cisatracurium determination; Fluorescence; Mivacurium determination; Serum

1. Introduction

Cisatracurium besylate {(1*R*,1'*R*,2*R*,2'*R*)-2,2-[1,5-pentanediy]bis-[oxy(3-oxo-3,1-propanediy)]}-bis[1 - [(3,4 - dimethoxyphenyl) - methyl] - 1,2,3,4 - tetrahydro - 6,7 - dimethoxy - 2 - methylisoquinolinium] dibenzene sulfonate} (Fig. 1) and mivacurium {(*E*)-(1*R*,1'*R*)-2'-[4-octenedioyl-bis(oxytrimethylene)]bis[1,2,3,4-tetrahydro-6,7-dimethoxy-2-methyl-1-(3,4,5-trimethoxybenzyl)-isoquinolinium] dichloride} (Fig. 2) are non-depolarizing

neuromuscular blocking agents. Mivacurium consists of a mixture of three stereoisomers. Cisatracurium is one of ten stereoisomers (*R-cis*, *R'-cis*) that comprise atracurium which represents approximately 15% of the atracurium mixture and is approximately 3-fold more potent than the mixture that constitutes the parent drug [1].

Several reports describe high-performance liquid chromatography (HPLC) methods for the analysis of plasma concentrations of cisatracurium alone using either ultraviolet [2] or mass spectrometry detection [3]; ion chromatography with fluorescence detection [4] also has been used. For mivacurium, HPLC methods with ultraviolet [5] and fluorescence detection [6–9] have been described.

* Corresponding author. Tel.: +34-954557172; fax: +34-954557168.

E-mail address: mabello@cica.es (M.A. Bello)

This work constitutes the first stage of a research schedule focused on the proposal of new analytical procedures for the determination of cisatracurium and mivacurium as alternatives to the HPLC methods. This paper describes the spectrofluorimetric determination of cisatracurium and mivacurium in serum and also has been applied to the determination in pharmaceuticals.

2. Experimental

2.1. Reagents

Cisatracurium besylate and mivacurium were kindly provided by Glaxo-Wellcome (Greenford, Middlesex, UK). Acetic acid, sodium acetate, picric acid, acetonitrile, sulfuric acid and isopropanol were of analytical-reagent grade and purchased from Merck (Darmstadt, Germany); dichloromethane of HPLC grade was obtained from Romil (Cambridge, UK). High-purity water was obtained from a Millipore (Milford, MA, USA) Milli-Q Plus system. Stock standard mivacurium and cisatracurium solutions of $100 \mu\text{g ml}^{-1}$ and working standard solution of $1 \mu\text{g ml}^{-1}$ were prepared by dissolving the corresponding substance in high-purity water; both solutions were stable for several months at room temperature. Serum pooled samples were obtained from healthy volunteers. To adjust the pH of the solutions, an acetic acid–sodium acetate 0.1 M pH 5.5 buffer was used. Picric acid solution was prepared by dilution 1:50 (v/v) from aqueous saturated picric acid solution.

2.2. Apparatus

Fluorescence intensity was measured on a Perkin-Elmer (Norwalk, CT, USA) LS-5 luminescence spectrometer equipped with a xenon lamp and an Acer Model 1030 computer working with the FLUORPACK software from Sciware (Mallorca, Spain). All measurements were performed in a standard 10-mm pathlength quartz cell, thermostatted at $25.0 \pm 0.5^\circ\text{C}$, with 5 nm bandwidths for the emission and excitation monochromators. A Philips (Eindhoven, Netherlands) Model PU-8720 UV/VIS spectrophotometer was used for the absorbance measurements. The pH was measured on a Crison (Barcelona, Spain) MicropH 2002 pH-meter. Centrifugation of serum samples was carried out with a Sigma (Osterode, Germany) Laborzentrifugen 4-10. For agitation in the serum extraction procedure, a Selecta (Barcelona, Spain) Vibromatic 384 shaker was used.

2.3. Spectrofluorimetric determination of cisatracurium

Into 25-ml calibrated flasks were pipetted suitable aliquots of working solution of cisatracurium containing 125–12 500 ng of cisatracurium; 5 ml of 0.1 M acetic acid–sodium acetate buffer (pH 5.5) and 5 ml of acetonitrile were added and diluted to the mark with water. The solutions were thermostatted at $25 \pm 0.1^\circ\text{C}$ and the fluorescence measured at 324 nm using an excitation wavelength of 230 nm against a blank solution. The concentration of cisatracurium in the sample was determined from a calibration graph prepared

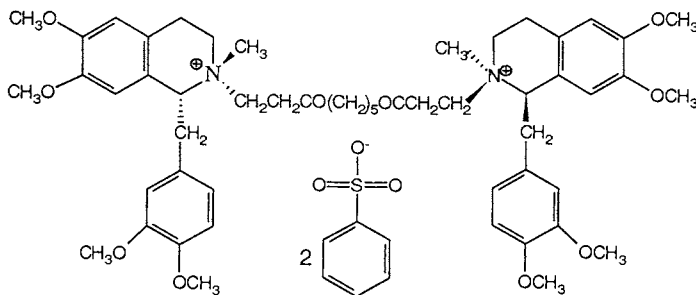


Fig. 1. Chemical formula of cisatracurium besylate.

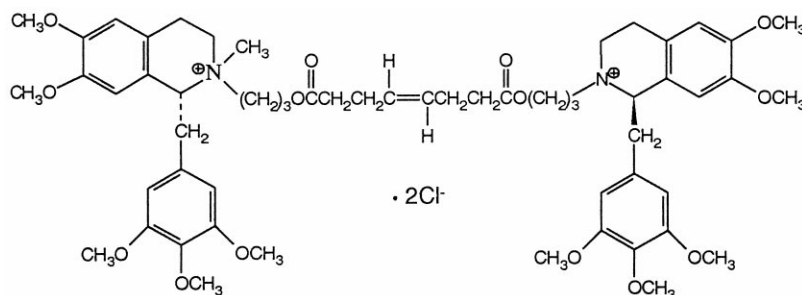


Fig. 2. Chemical formula of mivacurium dichloride.

under identical conditions. The prepared solutions remain stable for at least 24 h.

2.4. Spectrofluorimetric determination of mivacurium

Into 25-ml calibrated flasks were pipetted suitable aliquots of working solution of mivacurium containing 125–12 500 ng of mivacurium; 5 ml of 0.1 M acetic acid–sodium acetate buffer (pH 5.5) was added and diluted to the mark with water. Solutions were thermostatted at $25 \pm 0.1^\circ\text{C}$ and the fluorescence was measured at 324 nm using an excitation wavelength of 230 nm against a blank solution. The concentration of mivacurium in the sample was determined from a calibration graph prepared under identical conditions. The prepared solutions remain stable for at least 24 h.

2.5. Samples

The proposed procedure for the determination of mivacurium was applied to the direct determination in one Spanish commercialized pharmaceutical formulation (Mivacron[®] injection blisters). The method was also applied to the determination of mivacurium and cisatracurium in spiked human pooled sera which were kindly provided from hospitals in the city.

2.5.1. Serum preparation

Serum (0.5 ml) spiked with a suitable quantity of cisatracurium or mivacurium was poured into a 15-ml centrifuge tube with a thread lock and then 0.25 ml of picric acid solution, three drops of

sulfuric acid 1:2 (v/v), 0.4 ml of isopropanol and 2.1 ml of dichloromethane were added. The tube was vigorously shaken in a mechanical shaker for 10 min and then centrifuged ($6000 \times g$) for 5 min. The organic layer was transferred to a reservoir for collecting subsequent organic phases. The aqueous phase was treated with 1 ml of dichloromethane, agitated for 10 min by the mechanical shaker and centrifuged for 5 min. The last organic extract was also transferred to the reservoir and all the combined organic extracts were then evaporated to dryness under a nitrogen stream. The tube was removed immediately after drying and the solution reconstituted with 5 ml of acetic acid–sodium acetate buffer. The sample was then treated and measured according to the spectrofluorimetric determination procedures described in Sections 2.3 and 2.4. A blank was prepared under the same conditions but without cisatracurium or mivacurium spiking. Samples prepared from sera must be filtered ($0.45 \mu\text{m}$) prior to fluorescence intensity measurements.

3. Results and discussion

3.1. Study of the emission features of the cisatracurium and mivacurium solutions

Fig. 3(A) shows the excitation spectra for aqueous solutions of cisatracurium and mivacurium, in which a maximum at 230 nm can be clearly observed for both substances. Fig. 3(B) shows the emission spectra for aqueous cisatracurium and mivacurium using $\lambda_{\text{exc}} = 230 \text{ nm}$; a

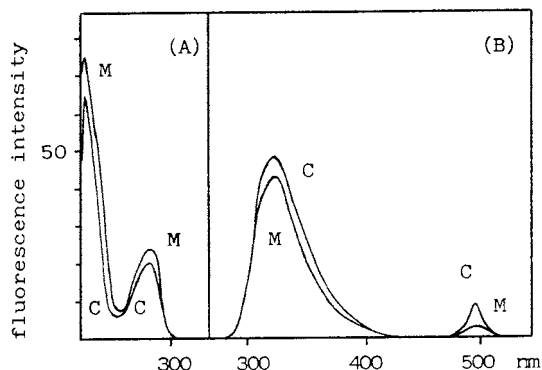


Fig. 3. Excitation spectra (A) and emission spectra with $\lambda_{\text{exc}} = 230$ nm (B) for aqueous solutions of cisatracurium (C) and mivacurium (M).

maximum at 324 nm can be observed for both substances. This is in agreement with the similar molecular structures of cisatracurium and mivacurium.

The influence of pH on the fluorescence intensity of cisatracurium and mivacurium solutions can be observed in Fig. 4. Using as excitation wavelength 230 nm, the fluorescence intensity measured at 324 nm exhibit a maximum within a

pH range of 3.5–6 for cisatracurium and 4.4–10.7 for mivacurium. Thus, an acetic acid–sodium acetate buffer solution of pH 5.5 was chosen for the spectrofluorimetric determination of cisatracurium and mivacurium.

The effect of the concentration of the buffer solution was studied. Fluorescence intensity remains stable for total buffer concentrations lower than 4×10^{-2} M and 2×10^{-2} M for cisatracurium and mivacurium, respectively; higher buffer concentrations lead to fluorescence decay. Accordingly, a 5-ml aliquot of 0.1 M buffer solution for 25 ml of total volume was selected as a suitable volume for the recommended procedure.

With the aim to study the influence of the ionic strength, aqueous solutions of cisatracurium and mivacurium containing buffer at various concentrations of KCl were prepared. The results obtained show that no significant changes occur in the fluorescence intensity of cisatracurium and mivacurium for concentrations between 0 and 1 M KCl.

The effect of the presence of organic miscible solvents was tested for methanol, ethanol and acetonitrile. For cisatracurium, an important increase in the fluorescence intensity was noticeable

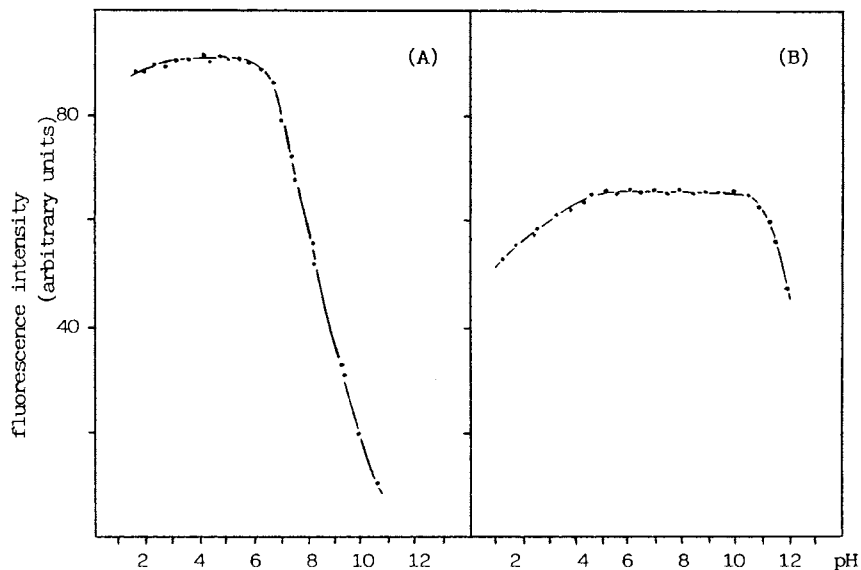


Fig. 4. Influence of pH on the fluorescence intensity for cisatracurium (A) and mivacurium (B) solutions ($\lambda_{\text{exc}} = 230$ nm; $\lambda_{\text{em}} = 324$ nm).

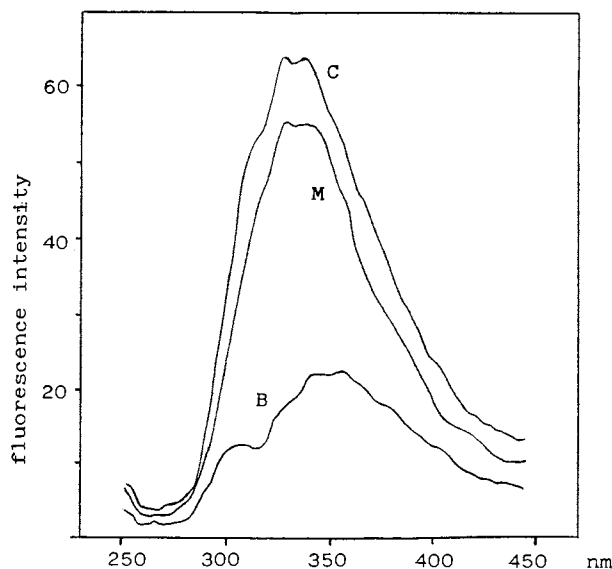


Fig. 5. Emission spectra ($\lambda_{\text{exc}} = 230$ nm) for blank serum (B) and for sera spiked with cisatracurium (C) and mivacurium (M).

when water-miscible organic solvents were added. The best results were found for acetonitrile, yielding an increase of 100% in the fluorescence intensity for an addition of 20% (v/v) of this solvent. Poor increases in the fluorescence intensity were found for mivacurium even at higher organic solvent concentrations.

The influence of the temperature on the fluorescence intensity shows a nearly linear (negative) relationship between temperature and fluorescence intensity for cisatracurium and mivacurium. When the temperature is decreased the fluorescence is enhanced, as expected. Hence samples were thermostatted at $25 \pm 0.5^\circ\text{C}$ in the proposed procedure.

3.2. Selectivity: effect of interfering substances

A study of some potential interferences in the spectrofluorimetric determination of mivacurium and cisatracurium was performed by selecting the excipients often used in pharmaceutical formulations or as possible co-active substance.

Samples containing a fixed amount of cisatracurium or mivacurium (100 ng ml^{-1}) and variable concentrations of potential interfering compounds were measured. Lactose, sucrose,

glucose, fructose and succinylcholine did not cause interference at weight ratios (interfering substance/active substance) $\leq 10\,000$, and ≤ 5000 for succinylcholine/mivacurium. Metamizole causes interference for ratios ≥ 15 for cisatracurium and ≥ 1 for mivacurium. Ratios ≤ 20 for bupivacaine/mivacurium and ≤ 1 for bupivacaine/cisatracurium did not cause interference.

3.3. Linearity of the response

A series of standard solutions (five replicates) of cisatracurium and mivacurium were prepared by following the procedures described in Section 2. The calibration graphs of fluorescence intensity (y) versus cisatracurium or mivacurium concentration (x) were found to be linear over the range $5.0\text{--}500.0 \text{ ng ml}^{-1}$ for cisatracurium (Eq. (1)) and mivacurium (Eq. (2)):

$$y = (-0.1 \pm 0.3) + (0.429 \pm 0.002)x$$

$$(n = 10, r = 0.9997) \quad (1)$$

$$y = (0.0 \pm 0.2) + (0.426 \pm 0.001)x$$

$$(n = 10, r = 0.9998) \quad (2)$$

The application of Student's *t*-test shows that the intercepts are non-significant and accordingly the straight lines pass through the origin.

3.4. Precision

Eleven replicates carried out on different days within a month of 100 ng ml⁻¹ target solutions of cisatracurium and mivacurium were made by using the proposed procedures. The results were 99.8 ± 0.3 and 100.1 ± 0.2, respectively, which leads to a R.S.D. between-day precision of 0.3% and 0.2%, respectively.

3.5. Detection and quantitation limit

According to the Analytical Methods Committee [11], the detection limit (LOD) is the concentration of cisatracurium or mivacurium corresponding to a signal equal to the blank mean (y_B) plus three times the standard deviation of the blank (s_B). Eleven blank measurements gave an average signal blank $y_B = 0.2$ and a standard deviation $s_B = 0.1$ for the cisatracurium blank and $y_B = 0.1$ and $s_B = 0.1$ for the mivacurium blank. Thus, the analytical signal corresponding to LOD is $y_B + 3s_B$. This value is transformed in LOD through the equations of the calibration lines, giving 1.39 ng ml⁻¹ for cisatracurium and 0.93 ng ml⁻¹ for mivacurium.

From the calibration straight lines it is also possible to estimate the quantitation limits as the concentration corresponding to the ratio between three times the S.D. of the intercept and the slope of the calibration line [12].

This leads to a quantitation limit of 2.1 ng ml⁻¹ for cisatracurium and 1.4 ng ml⁻¹ for mivacurium.

3.6. Validation of the spectrofluorimetric determinations of cisatracurium and mivacurium

3.6.1. Analysis of pharmaceutical samples

Five injection blisters of Mivacrom® (Glaxo-Wellcome) with a mivacurium label content of 2 mg ml⁻¹ were directly analyzed with the proposed method from external calibration obtaining a result of 1.9 ± 0.2 mg ml⁻¹ of mivacurium. The application of an independent method (direct spectrophotometric determination at 280.7 nm) shows a result of 2.0 ± 0.2 mg ml⁻¹; as can be observed, there is good agreement between both methods.

3.6.2. Analysis of spiked sera

Serum samples were spiked with cisatracurium or mivacurium to obtain concentrations in serum of 5 and 10 µg ml⁻¹ and treated according to the above described preparation and spectrofluorimetric determination procedures; the final solutions measured contained 100 and 200 ng ml⁻¹ of the active substance, respectively.

Fig. 5 shows the emission spectra with $\lambda_{exc} = 230$ nm for the samples obtained from blank serum (B) and from sera spiked with cisatracurium (C) and mivacurium (M).

Poor recoveries were found for mivacurium, ranging from 65 to 70%, values very similar to those obtained by other authors [6]. In order to avoid matrix effects that affect the results, the standard additions method [10] was used for mi-

Table 1
Results for the analyzed samples of spiked sera

Substance	Spiked concentration (µg ml ⁻¹)	HPLC method (µg ml ⁻¹) ^{a,b}	Proposed method (µg ml ⁻¹) ^b
Cisatracurium	5.0	4.9 ± 0.2	4.8 ± 0.3
	10.0	10.2 ± 0.1	10.2 ± 0.3
Mivacurium	5.0	5.0 ± 0.1	4.9 ± 0.2
	10.0	10.0 ± 0.2	10.2 ± 0.1

^a For details of the method see text.

^b Average of five determinations ± S.D.

vacurium. For cisatracurium it is possible to apply external calibration. The samples were also analyzed by HPLC methods using UV detection at 280 nm for cisatracurium [2] and at 210 nm for mivacurium [5]. The results obtained are collected in Table 1.

As can be seen, good agreement was found between the HPLC and the proposed methods (statistically proved according to the paired *t*-test [12]) with respect to the spiked concentration (the application of Student's *t*-test indicates that the method is accurate (null hypothesis accepted) [12]).

4. Conclusions

The results obtained show that the proposed method may be useful to determine cisatracurium or mivacurium in spiked human serum at the levels obtained after the administration of normal clinical doses, and it would be a method of choice for monitoring these substances in patients. The method for mivacurium has also been applied to the determination of the active constituent in a commercial pharmaceutical preparation.

Acknowledgements

The authors gratefully acknowledge Glaxo-Wellcome for supplying cisatracurium and mivacurium.

References

- [1] A. Bryson, D. Faulds, *Drugs* 53 (5) (1997) 848.
- [2] H. Zhang, P. Wang, M.G. Bartlett, J.T. Stewart, *J. Pharm. Biomed. Anal.* 16 (7) (1998) 1241.
- [3] G.J. Dear, J.C. Harrelson, A.E. Jones, T.E. Johnson, S. Pleasance, *Rapid Commun. Mass Spectrom.* 9 (14) (1995) 1457.
- [4] B.J. Bryant, C.D. James, D.R. Cook, J.C. Harrelson, *J. Liq. Chromatogr.* 20 (13) (1997) 2041.
- [5] R. DeAngelis, P. Loebis, R. Maehr, J. Savarese, R.M. Welch, *J. Chromatogr.* 525 (1990) 389.
- [6] A. Brown, C. James, R. Welch, J. Harrelson, *J. Chromatogr. Biomed. Appl.* 578 (1992) 302.
- [7] W. Biederbick, G. Aydinouglou, C. Diefenbach, M. Theisohn, *J. Chromatogr. Biomed. Appl.* 685 (1996) 315.
- [8] M. Weindlmayr-Goettel, G. Weberhofer, H. Gilly, H.G. Kress, *J. Chromatogr. Biomed. Appl.* 685 (1996) 123.
- [9] S.I. Lugo, N.D. Eddington, *J. Pharm. Biomed. Anal.* 14 (6) (1996) 675.
- [10] L. Cuadros, A.M. García, M. García Campaña, F. Alés, C. Jiménez, M. Román Ceba, *J. AOAC Int.* 78 (1995) 471.
- [11] Analytical Methods Committee, *Analyst* 112 (1987) 199.
- [12] J.C. Miller, J.N. Miller, *Statistics for Analytical Chemistry*, 3rd ed., Ellis Horwood-Prentice Hall, Chichester, 1993.

Parafac decomposition of three-way kinetic-spectrophotometric spectral matrices corresponding to mixtures of heavy metal ions

Joaquim C.G. Esteves da Silva *, César J.S. Oliveira

LAQUIPAI, Chemistry Department, Faculdade de Ciências, R. Campo Alegre 687, P4150 Porto, Portugal

Received 23 June 1998; received in revised form 14 December 1998; accepted 1 March 1999

Abstract

Binary and ternary mixtures of some of the following heavy metal ions Zn(II), Ni(II), Pb(II), Co(II) and Cd(II) were analyzed by a ligand substitution kinetic method. Three-way data matrices were generated by acquisition of UV–Vis spectra (332–580 nm) as a function of the time of a substitution reaction observed between the complex of the heavy metal ions with the non selective metallochromic indicator 4-(2-pyridylazo) resorcinol (PAR) and EDTA, and of different relative concentration of the metal ions (1–6 mM). The PARAFAC trilinear model, without restrictions, was used in the data analysis. A full decomposition of the data matrices was obtained (spectra, concentration and time profiles). It was shown that ligand substitution kinetic methods coupled to three-way chemometric analytical methods can be used for the development of robust sensors for the analysis of binary [Zn(II) + Ni(II), Pb(II) + Cd(II), Zn(II) + Pb(II)] or ternary [Zn(II) + Pb(II) + Co(II)] mixtures of metal ions in the micromolar concentration range. © 1999 Elsevier Science B.V. All rights reserved.

Keywords: Kinetic-spectrophotometric data; Mixtures of heavy metal ions; PARAFAC

1. Introduction

The simultaneous determination of metal ions at trace amounts in complex samples usually requires relatively expensive analysis, involving atomic absorption or emission spectrophotometric equipment. Kinetic methods of analysis constitutes a much simpler alternative to the analysis of

mixtures of metal ions [1–13]. Indeed, with a standard UV–Vis spectrophotometer, analytical methodologies can be developed based on metal ion complex formation reactions and, for example, on the different rates of ligand substitution reactions.

If a UV–Vis spectrophotometer equipped with a diode array detector is used in the acquisition of spectra as function of the time of a reaction, each sample generates a two-way data matrix (spectra versus time), i.e. a second-order analytical device is obtained [7–13]. Kinetic methods based on this

* Corresponding author. Tel.: + 351-2-6082869; fax: + 351-2-6082959.

E-mail address: jcsilva@fc.up.pt (J.C.G. Esteves da Silva)

type of instruments have one great advantage over traditional kinetic-spectrophotometric methods which is the unnecessary to formulate a kinetic model. Indeed, multivariate calibration techniques allow the development of empirical calibration models to predict the concentrations of analytes in unknown samples. Chemometric calibration techniques of principal components regression, partial least squares and artificial neural networks [14,15] have been used to model kinetic-spectrophotometric data [7–13]. However, these calibration techniques take advantage of only a fraction of all the information available in the data generated by the second-order instrument, i.e. the possibility of analyte quantification in the presence of unknown interferences and complex backgrounds is not possible.

A three-way data matrix is created when a set of two-way data matrices having different relative proportions of the metal ions under analysis are put together. From the simultaneous analysis of these three-way data matrices robust analytical methods for the simultaneous quantitative analysis of metal ions can be developed based on the so-called ‘second-order advantage’, i.e. robust estimation of the analytes concentration in mixtures that contains unknown interferences [16–18]. The second order advantage achieved from the analysis of three-way data is an application of the ‘unique decomposition property’ which was first investigated in the field of psychometrics [19–22]. The unique decomposition of kinetic-spectrophotometric matrices should allow the calculation without any a priori information of the three basic properties of the constituents of the mixture under analysis (spectra, concentrations time profiles), which are related to the respective kinetic properties.

The analysis of three-way data matrices in analytical chemistry studies began with a liquid chromatography work [23] and the number of applications is increasing [24–39]. Nevertheless, the number of studies using experimental data is still very limited. One method that is being used to check if a three-way chemical structure is candidate to a unique decomposition is PARAFAC (parallel factor analysis) [22] because of two facts: (1) from a theoretical point

of view this method allows a unique decomposition; and (2) this method has a basic trilinear model which is compatible with analytical data structures involving spectrophotometric measurements.

This paper presents a method for the experimental generation of three-way kinetic-spectrophotometric matrices that can be uniquely decomposed by PARAFAC. Data matrices correspond to binary and ternary mixtures of the following heavy metal ions: Zn(II); Ni(II); Pb(II); Co(II); Cd(II). Three-way matrices were generated by the acquisition of spectra of standards, with different relative concentration of the metal ions, during the ligand substitution reaction that is observed when EDTA is added to mixtures of the metal ions and the non-selective metallochromic indicator 4-(2-pyridylazo) resorcinol (PAR).

The objective of this work was to evaluate the performance of the PARAFAC model in the decomposition of three-way kinetic-spectrophotometric data matrices. The results obtained in this work may constitute the basis for the development of analytical methodologies for the detection of heavy metal ions in the micromolar concentration range, that take advantages of the second-order advantage.

2. Theory

A three-way data structure corresponding to a kinetic-spectrophotometric experiment can be expressed by the following equation:

$$a_{ijk} = \sum_{s=1}^{nf} t_{is} w_{js} c_{ks} + e_{ijk}$$

$$i = 1, \dots, nt \quad j = 1, \dots, nw \quad k = 1, \dots, ns \quad (1)$$

where a_{ijk} are the elements of the experimental matrix of absorbances **A**, w_{js} are the elements of the matrix **S** containing the spectra (each one with nw wavelengths) of the spectroscopically active species (ns species), t_{is} are the elements of the matrix **T** containing the time profiles (each one with nt time points) of the ns species, c_{ks} are the elements of the matrix **C** which contain

the relative concentration of the ns species, nf is the number of factors of the model, e_{ijk} are the elements of the matrix of the spectroscopic error.

Eq. (1) also represents the basic three-way PARAFAC model [22]. After selecting nf , the three basic unknown matrices **T**, **S** and **C** are calculated by an iterative alternating least squares method without any restrictions, taking as a first approximation for the three matrices a random generated set; several independent runs are performed to check for a unique decomposition. The number of factors of the model is the intrinsic dimensionality of the data matrix and correspond to the observed no correlated spectral variations. If the absorbance readings are always directly proportional to the concentration of the ns species, i.e. the Lambert–Beer law is obeyed in the concentration, wavelength and time ranges used in the experiments, the generated three-way data structure is trilinear. Under this condition, nf is equal to ns . The number of spectroscopically active species in the kinetic-spectroscopic experiments is equal to the number of metal ions plus one corresponding to the metallochromic indicator.

The quality of the fit of experimental data to the tested model is assessed by the value of the loss function after convergence is achieved, which is defined by:

$$\sum_{i=1}^{nt} \sum_{j=1}^{nw} \sum_{k=1}^{ns} e_{ijk}^2 = \sum_{i=1}^{nt} \sum_{j=1}^{nw} \sum_{k=1}^{ns} (a_{ijk} - a'_{ijk})^2 \quad (2)$$

where a'_{ijk} are the predicted elements of the experimental matrix. In this work, a quite low value for this function (1.0×10^{-8}) was always used as criteria to stop the alternating least squares process.

The elements of the concentration matrix are of particular importance in this work because of the heavy metal ion quantification objective and were subjected to a quality of prediction analysis. This test consisted in the plot of the predicted versus real concentrations and calculation of the following regression parameters: intercept and corresponding confidence interval at 95%; correlation coefficient.

3. Experimental

3.1. Reagents

All reagents were of analytical grade and used without purification. About 1.0 mM aqueous solutions of the metal ions were prepared by weighting the following salts: $\text{CoCl}_2 \cdot 6\text{H}_2\text{O}$; $\text{Zn}(\text{NO}_3)_2 \cdot 4\text{H}_2\text{O}$; $\text{Cd}(\text{NO}_3)_2 \cdot 4\text{H}_2\text{O}$; $\text{Pb}(\text{NO}_3)_2$; $\text{NiCl}_2 \cdot 6\text{H}_2\text{O}$. Borax buffer (pH 9.50) was prepared by mixing 4.77 g of borax, 75 ml of 0.10 M NaOH and the necessary volume of 0.10 M KNO_3 until a total volume of 500 ml. PAR [4-(2-pyridylazo) resorcinol] solution (1.0 mM) was prepared in the borax buffer. Standard 0.100 M EDTA solution was prepared from a concentrated solution (Titrisol Merck).

Solutions to be analyzed were prepared by mixing the metal ions to the final concentration in the micromolar range, PAR (20–40 μM) and borax buffer. The design of metal ion solutions followed a full factorial experimental design with four levels for binary mixtures and three levels for ternary mixtures. EDTA solution to be used in the analysis (1.00–6.00 mM) were prepared by diluting the concentrated 0.100 M solution with borax buffer.

3.2. Instruments

A Hewlett-Packard 8452A diode-array spectrophotometer controlled by a Hewlett-Packard computer and equipped with a 1-cm pathlength quartz cell with a cell stirring module (Hewlett-Packard 89054A and 89055A) was used for UV–Vis spectra acquisition. Spectra were acquired between 332 and 580 nm (2 nm resolution), with 0.2 s integration time and 0.5 s cycle time during a 30-s time window (one experiment generated 60 spectra). These integration and cycle times allow the acquisition of relatively low noise spectra at a relatively fast rate.

3.3. Experimental procedures

The mixture of metal ions, PAR and borax buffer (3.00 ml) was placed in the quartz cell together with a magnetic bar (Hewlett-Packard 9301-1161) to promote mixing. Spectra acquisi-

tion began with the injection of the diluted EDTA solution (30 μl). The mixtures of heavy metals analyzed in this work, as well as the total concentration of the three constituents involved in the ligand substitution reactions, i.e. metal ion, PAR and EDTA, are shown in Table 1.

3.4. Data analysis

Spectra were translated to ASCII format using homemade software developed in Turbo Pascal (Borland, USA). Each spectrum was composed of 125 points and, to reduce the dimension of the three-way data matrices, each experiment was composed of the first 49 spectra (the last 11 spectra were not considered) because no marked spectral variation was observed in the last spectra. The program TRILIN, obtained from P.M. Kroonenberg (Department of Education, Leiden University), was used for the PARAFAC decomposition.

4. Results and discussion

4.1. Preliminary analysis of spectral data

Fig. 1 shows typical two-way data matrices

corresponding to single and mixtures of heavy metal ions. A preliminary analysis of this figure shows a common feature, i.e. a decrease of intensity of a band located at about 500 nm and the increase of the intensity of the band at 414 nm. The decreasing band correspond to the complex formed between PAR and the metal ions and the decreasing trend is due to the substitution reaction of PAR by EDTA, resulting in a spectroscopically inactive species in the visible wavelength range. The band that appears at 414 nm is due to the uncomplexed PAR which free concentration increases with time. In the case of the mixtures (Fig. 1d–f) no marked differences are detected when compared with the single heavy metal ion spectral data (Fig. 1a–c) revealing similar spectral properties. Indeed, the maximum of the band of the complexes observed between PAR and the heavy metal ions fall in a narrow wavelength range of 16 nm. The maximum of the bands of the complexes are (the width at 50% high is about 80 nm): PAR + Zn(II), 490 nm plus a shoulder at 520 nm; PAR + Ni(II), 495 nm plus a shoulder at 526 nm; PAR + Pb(II), 516 nm; PAR + Co(II), 500 nm; PAR + Cd(II), 490 nm plus a shoulder at 522 nm. The broad band characteristic of the

Table 1
Experimental concentrations used to generate three-way data matrices from the mixtures of heavy metal ions

Mixture	Metal ion	Concentration ^a		
		Metal ion	PAR	EDTA
<i>Binary mixtures</i>				
Zn(II)+Ni(II)	Zn(II)	0.0; 1.0; 2.0; 4.0	20.0	13.3
	Ni(II)	0.0; 1.0; 2.0; 4.0		
Pb(II)+Cd(II)	Pb(II)	0.0; 1.0; 3.0; 6.0	20.0	13.3
	Cd(II)	0.0; 1.0; 2.0; 3.0		
Zn(II)+Pb(II)	Zn(II)	0.0; 1.0; 2.0; 3.0	20.0	13.3
	Pb(II)	0.0; 1.0; 3.0; 6.0		
<i>Ternary mixture</i>				
Zn(II)+Pb(II)+Co(II)	Zn(II)	1.0; 3.0; 6.0	40.0	60.0
	Pb(II)	1.0; 3.0; 6.0		
	Co(II)	1.0; 2.0; 3.0		

^a The concentrations of the metal ions and PAR are expressed in μM and the concentrations of EDTA are expressed in mM .

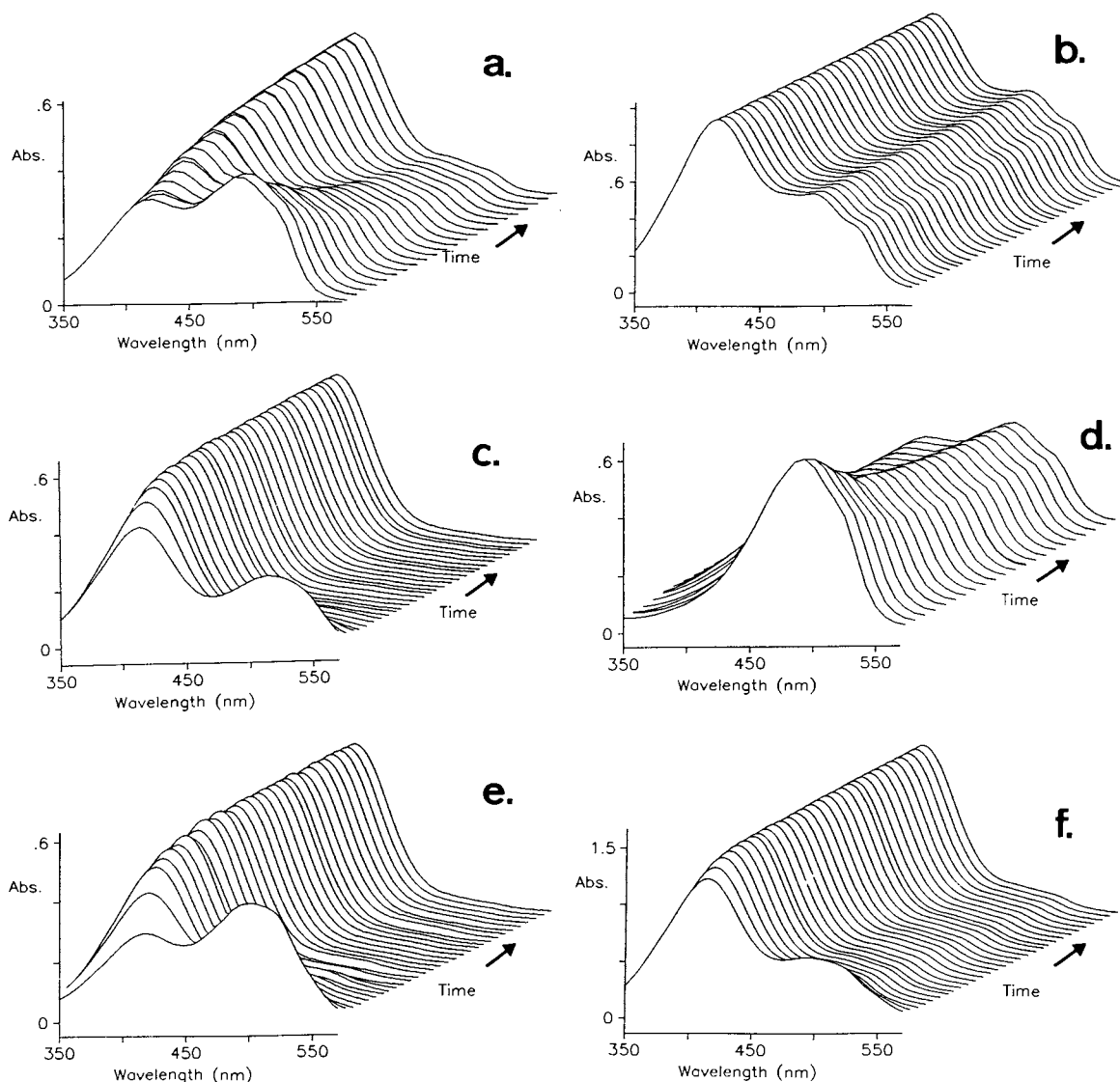


Fig. 1. Three-way spectral data matrices corresponding to the following metal ions or mixtures: (a) Zn(II) (4.0 μM); (b) Ni(II) (6.0 μM); (c) Pb(II) (6.0 μM); (d) Zn(II)+Ni(II) (4.0 μM both ions); (e) Pb(II)+Cd(II) (6.0 and 3.0 μM , respectively); (f) Zn(II)+Pb(II)+Co(II) (6.0, 3.0 and 1.0 μM , respectively).

spectra of the PAR complexes is also responsible for the relatively high spectral overlap.

The direct analysis of the decreasing band at 520 nm for the data sets corresponding to single ions (Fig. 2) allowed to obtain a relative sorting of the ligand substitution reaction rates (decreasing order): Pb(II) > Cd(II) > Zn(II) > Ni(II) \approx Co(II).

4.2. Single ion three-way data matrices

PARAFAC decomposition of three-way spectral matrices corresponding to single ions was performed using two factors to check for the trilinearity of the single ion data structures. Fig. 3 shows a typical decomposition result [Ni(II) experiments] and Table 2 presents some linear re-

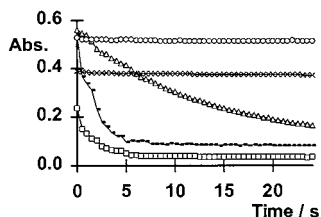


Fig. 2. Absorbance decreasing curves of the spectral band corresponding to the complex formed between the metal ions and PAR with time: (Δ) Zn(II); (\circ) Ni(II); (\square) Pb(II); (\times) Co(II); (—) Cd(II).

gression parameters observed between the predicted and experimental concentrations.

The analysis of the calculated spectra of the two factors (Fig. 3a) shows that one (the first) has only positive values and the other (the second) has a negative and a positive section. The first one corresponds to the constant spectra (no variation is observed with time) and is constituted by the PAR band at about 414 nm and by the band of the fraction of the unreacted complex, if at the end of the monitoring time (about 30 s) the metal ion complex is not fully exchanged by EDTA. The negative part of the other calculated spectrum corresponds to the band of the complex formed

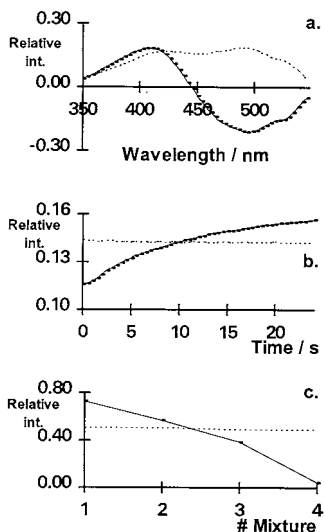


Fig. 3. Typical decomposition results for one metal ion spectral data set [Ni(II)]: (a) spectra; (b) time profiles; (c) estimated concentration (arbitrary units) of the components in the mixtures.

between the metal ion and PAR which concentration decreases with time. The positive section of this spectrum is due to the increasing band of the free PAR. These two sections of the second spectra are a consequence of the opposite but correlated spectral variations of the two chemical species involved: when the concentration of the metal ion PAR complex decreases the concentration of free PAR increases.

The calculated time profiles have a similar shape, but with different intensity, to that shown in Fig. 3b. The profile corresponding to the constant spectra is, as expected, a horizontal line, showing no time dependence. The other profile is a curve, with an increasing or decreasing trend, corresponding to the observed spectral variation as the substitution reaction is occurring. From the point of view of the metal ion PAR complex a time profile with a decreasing trend is expected because the concentration of the complex is decreasing. On the contrary, and from the point of view of the free PAR, an opposite trend is expected for the free PAR. Because the time variation of the metal ion PAR complex and free PAR are negatively correlated, one profile can be obtained from the other.

For quantitative analysis the most important information is the concentrations of the heavy metal ions that constitute the mixture. In order to assess the estimated values (arbitrary units), plots representing the estimated values as function of the experimental concentration (molar concentration) were obtained. The correlation coefficients and confidence intervals about the intercept are calculated to check for linearity and are shown in Table 2. As shown in Table 2 relatively high correlation coefficients and confidence intervals including the zero support the existence of linearity. However, these statistical parameters were obtained when the zero concentration was not included in the calculations; if this value was included, deviations from linearity were observed.

4.3. Mixtures of metal ions

PARAFAC decomposition of three-way spectral matrices corresponding to mixtures of ions was performed using a number of factors equal to

Table 2

Typical linear regression parameters observed between the predicted (arbitrary units) and experimental (μM) concentrations of heavy metal ions

Mixture	Metal ion	R^a	Intercept	Confidence interval (95%)
<i>Single ions^b</i>				
Zn(II)	Zn(II)	0.9932	-1.0×10^{-7}	$[-4.2 \times 10^{-6}; 4.0 \times 10^{-6}]$
Ni(II)	Ni(II)	0.9747	-2.6×10^{-7}	$[-1.7 \times 10^{-5}; 1.2 \times 10^{-5}]$
Pb(II)	Pb(II)	0.9955	-8.2×10^{-7}	$[-6.4 \times 10^{-6}; 4.8 \times 10^{-6}]$
Co(II)	Co(II)	0.9927	3.6×10^{-6}	$[8.4 \times 10^{-7}; 6.3 \times 10^{-6}]$
Cd(II)	Cd(II)	0.9989	-2.2×10^{-7}	$[-1.6 \times 10^{-6}; 1.2 \times 10^{-6}]$
<i>Binary mixtures</i>				
Zn(II)+Ni(II)	Zn(II)	0.9794	-2.7×10^{-7}	$[-5.8 \times 10^{-7}; 4.2 \times 10^{-8}]$
	Ni(II)	0.9981	3.7×10^{-6}	$[3.6 \times 10^{-6}; 3.8 \times 10^{-6}]$
Pb(II)+Cd(II)	Pb(II)	0.9527	8.3×10^{-7}	$[7.3 \times 10^{-8}; 1.6 \times 10^{-6}]$
	Cd(II)	0.7252	-1.0×10^{-6}	$[-2.6 \times 10^{-6}; 5.7 \times 10^{-7}]$
Zn(II)+Pb(II)	Zn(II)	0.9820	-3.3×10^{-8}	$[-2.6 \times 10^{-7}; 1.9 \times 10^{-7}]$
	Pb(II)	0.9545	1.2×10^{-7}	$[-5.1 \times 10^{-5}; 7.1 \times 10^{-7}]$
<i>Ternary mixture</i>				
Zn(II)+Pb(II)+Co(II)	Zn(II)	0.9970	1.2×10^{-7}	$[-3.4 \times 10^{-7}; 9.7 \times 10^{-8}]$
	Pb(II)	0.9603	4.6×10^{-7}	$[-3.2 \times 10^{-7}; 1.2 \times 10^{-6}]$
	Co(II)	0.9959	8.0×10^{-6}	$[7.6 \times 10^{-6}; 8.5 \times 10^{-6}]$

^a Correlation coefficient.

^b Single ion sets constituted by three two-way data matrices correspond to subsets of binary mixtures where the other ion has zero concentration.

the number of metal ions present plus one, to account for the existence of the constant PAR spectra and other constant spectral sections. Several binary and ternary mixtures of the five metal ions were tested but only some were uniquely decomposed with success by PARAFAC (shown in Table 2). It was observed that the most important factor to take into consideration in the design of mixtures candidate to a unique decomposition is the time profile. The greater the differences are in the kinetic properties of the ligand substitution reaction for the metal ions constituents of the mixtures the better the decomposition is achieved.

Fig. 4 [binary mixture of Zn(II) + Pb(II)] and Fig. 5 [ternary mixture of Zn(II) + Pb(II) + Co(II)] show typical decomposition results and Table 2 presents some linear regression parameters observed between the calculated (arbitrary units) and experimental concentrations.

The calculated spectra of the PAR complexes (Fig. 4a and Fig. 5a) have a similar shape to

that obtained in the single ions study. The calculated spectra of the PAR complexes exactly matches those observed experimentally. The analysis of Fig. 4a and Fig. 5a also shows that besides the high overlap of the bands, i.e. a relatively low resolution in the wavelength order, the PARAFAC decomposition was able to reconstruct the individual spectral bands without restrictions.

The calculated time profiles (Fig. 4b and Fig. 5b) for the individual constituents of the mixtures followed the expected trend presented above.

The calculated concentrations, shown as examples in Fig. 4c and Fig. 5c, are good estimation of the experimental values, i.e. they are directly proportional, with a prediction quality similar to that obtained for the single ions (Table 2). Worst correlation was obtained for the estimation of Cd(II) in the binary mixture of Pb(II) + Cd(II) which is due to the somewhat similar time profiles of these two cations.

5. Limitations of the unique decomposition process

The general rule to obtain a unique decomposition of the kinetic-spectrophotometric data matrices corresponding to binary or ternary mixtures of the five heavy metal ions analyzed in this work is that the metal ions in the mixture must have different spectra and time profiles. For example, because the species PAR + Zn(II) and PAR + Cd(II) have similar spectra (maximum of the band at 490 nm plus a shoulder at about 520 nm) these two ions do not generate kinetic-spectrophotometric data matrices candidates to a unique decomposition. The same is observed for mixtures of Co(II) and Ni(II), because they have similar time profiles (Fig. 2).

Nevertheless, in the case of mixtures containing ions with similar spectral or kinetic properties the modification of the experimental system, for example the pH or the metallochromic indicator, can give origin to more selective information. Alternatively, other decomposition processes with specific design restrictions could be used [40,41].

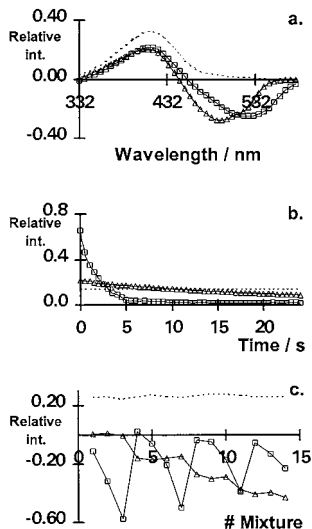


Fig. 4. Typical decomposition results for the mixtures of two metal ions [Zn(II) + Pb(II)]: (a) spectra; (b) time profiles; (c) estimated concentration (arbitrary units) of the components in the mixtures. The symbols correspond to the following metal ions: (Δ) Zn(II); (\square) Pb(II).

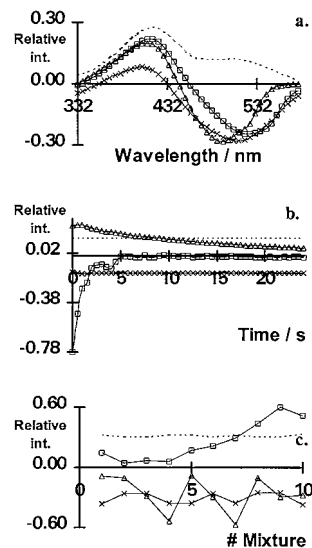


Fig. 5. Typical decomposition results for the mixtures of three metal ions [Zn(II) + Pb(II) + Co(II)]: (a) spectra; (b) time profiles; (c) estimated concentration (arbitrary units) of the components in the mixtures. The symbols correspond to the following metal ions: (Δ) Zn(II); (\square) Pb(II); (\times) Co(II).

6. Conclusion

It was shown that simple kinetic-spectrophotometric experimental procedures are able to generate trilinear data structures from mixtures of heavy metal ions candidates to a unique decomposition process. As consequence, there is the potential for the development of analytical methodologies for the simultaneous and robust quantitative analysis of heavy metal mixtures at the micromolar concentration range.

The PARAFAC model successfully interpreted analytical chemistry data presented in this work. This result supports the usefulness of PARAFAC based chemometric techniques to solve some complex analytical chemistry problems.

Acknowledgements

A PBIC/QUI/C/2177/95 project grant is acknowledged to F.C.T. (Lisbon). A PhD grant (BD/9187/96) to C.J.S. Oliveira is acknowledged to PRAXIS XXI (Lisbon).

References

- [1] M. Tanaka, S. Funashi, K. Shirai, *Anal. Chim. Acta* 39 (1967) 437.
- [2] G.M. Ridder, D.W. Margerum, *Anal. Chem.* 49 (1977) 2090.
- [3] L. Ballesteros, D. Péres-Bendito, *Analyst* 108 (1983) 443.
- [4] D. Péres-Bendito, *Analyst* 109 (1984) 891.
- [5] E. Mentasti, V. Dlask, J.S. Coe, *Analyst* 110 (1985) 1451.
- [6] O. Abollino, E. Mentasti, C. Sarzanini, V. Porta, L.J. Kirschenbaum, *Analyst* 116 (1991) 1167.
- [7] J. Havel, F. Jiménez, R.D. Bautista, J.J.A. León, *Analyst* 118 (1993) 1355.
- [8] M. Blanco, J. Coelho, H. Iturriaga, S. Maspoch, J. Riba, E. Rovira, *Talanta* 40 (1993) 261.
- [9] M. Blanco, J. Coelho, H. Iturriaga, S. Maspoch, J. Riba, *Anal. Chem.* 66 (1994) 2905.
- [10] M. Blanco, J. Coelho, H. Iturriaga, S. Maspoch, M. Redon, *Appl. Spectrosc.* 48 (1994) 37.
- [11] M. Blanco, J. Coelho, H. Iturriaga, S. Maspoch, M. Redon, *Anal. Chim. Acta* 303 (1995) 309.
- [12] M. Blanco, J. Coelho, H. Iturriaga, S. Maspoch, M. Redon, *Anal. Chim.* 67 (1995) 4477.
- [13] T.F. Cullen, S.R. Crouch, *Mikrochim. Acta* 126 (1997) 1.
- [14] E.R. Malinowski, *Factor Analysis in Chemistry*, 2nd ed., Wiley, New York, 1992.
- [15] J. Zupan, J. Gasteigner, *Neural Networks for Chemistry*, VCH, Weinheim, 1993.
- [16] K.S. Booksh, B.R. Kowalski, *Anal. Chem.* 66 (1994) 782A.
- [17] Z. Lin, K.S. Booksh, L.W. Burgess, B.R. Kowalski, *Anal. Chem.* 66 (1994) 2552.
- [18] K.S. Booksh, Z. Lin, Z. Wang, B.R. Kowalski, *Anal. Chem.* 66 (1994) 2561.
- [19] J.K. Carrol, J.J. Chang, *Psychometrika* 35 (1970) 283.
- [20] J.B. Kruskal Jr., *Multilinear models*, in: H.C. Law, C.W. Snider Jr., J.A. Hattie, R.P. McDonald (Eds.), *Research Methods for Multimode Data Analysis*, Praeger, New York, 1984, pp. 36–62.
- [21] J.B. Kruskal, Rank, Decomposition and uniqueness for 3-way and N-way arrays, in: R. Coppi, S. Bolasco (Eds.), *Multway Data Analysis*, Elsevier, Amsterdam, 1989, pp. 7–18.
- [22] R.A. Harshman, M.E. Lundy Jr., The PARAFAC model for three-way factor analysis and multidimensional scaling, in: H.C. Law, C.W. Snider Jr., J.A. Hattie, R.P. McDonald (Eds.), *Research Methods for Multimode Data Analysis*, Praeger, New York, 1984, pp. 122–215.
- [23] C.J. Appellof, E.R. Davidson, *Anal. Chem.* 53 (1981) 2053.
- [24] M.D. Russel, M. Gouterman, *Spectrochim. Acta* 44A (1988) 857.
- [25] M.D. Russel, M. Gouterman, *Spectrochim. Acta* 44A (1988) 863.
- [26] M.D. Russel, M. Gouterman, J.A. van Zee, *Spectrochim. Acta* 44A (1988) 873.
- [27] D.S. Burdick, X.M. Tu, L.B. McGown, D.W. Millican, *J. Chemometr.* 4 (1990) 15.
- [28] E. Sanchez, B.R. Kowalski, *J. Chemometr.* 4 (1990) 29.
- [29] A.K. Smilde, D.A. Doornbos, *J. Chemometr.* 5 (1991) 345.
- [30] A.K. Smilde, *Chemometr. Intell. Lab. Syst.* 15 (1992) 143.
- [31] Y. Zeng, P.K. Hopke, *J. Chemometr.* 6 (1992) 65.
- [32] S. Leurgans, R.T. Ross, *Statist. Sci.* 7 (1992) 289.
- [33] J.M. Henshaw, L.W. Burgess, K.S. Booksh, B.R. Kowalski, *Anal. Chem.* 66 (1994) 3328.
- [34] R. Tauler, A.K. Smilde, J.M. Henshaw, L.W. Burgess, B.R. Kowalski, *Anal. Chem.* 66 (1994) 3337.
- [35] A.K. Smilde, R. Tauler, J.M. Henshaw, L.W. Burgess, B.R. Kowalski, *Anal. Chem.* 66 (1994) 3345.
- [36] M. Gui, S.C. Rutan, A. Agbodjan, *Anal. Chem.* 67 (1995) 3293.
- [37] I.E. Bechmann, *Talanta* 44 (1997) 585.
- [38] P. Hindmarch, K. Kavianpour, R.G. Brereton, *Analyst* 122 (1997) 871.
- [39] J.C.G. Esteves da Silva, S.A.G. Novais, *Analyst* 123 (1998) 2067.
- [40] R. Tauler, A. Smilde, B. Kowalski, *J. Chemometr.* 9 (1995) 31.
- [41] R. Bro, *Chemometr. Intell. Lab. Sys* 38 (1997) 149.

Determination of Cu(II) and Zn(II) using silica gel loaded with 1-(2-thiasolylazo)-2-naphthol

O. Zaporozhets *, N. Petruniok, O. Bessarabova, V. Sukhan

Taras Shevchenko Kyiv University, 64 Volodymirska Street, Kyiv 252033, Ukraine

Received 26 October 1998; received in revised form 26 February 1999; accepted 1 March 1999

Abstract

The silica gel with 1-(2-thiasolylazo)-2-naphthol adsorbed was obtained. The adsorption of Cu(II) and Zn(II) from an aqueous solution onto loaded silica gel was studied. The capabilities of 1-(2-thiasolylazo)-2-naphthol immobilized for Cu(II) and Zn(II) preconcentration, visual and diffusion reflectance spectroscopic detection was evaluated. The detection limits were 10 and 15 $\mu\text{g l}^{-1}$, respectively. Visual test scales for metal ions determination in the range 0.65–13 μg per sample were worked out. The developed methods were applied to Cu(II) and Zn(II) determination in natural and tap water. The obtained results agreed well with the reported value. © 1999 Elsevier Science B.V. All rights reserved.

Keywords: 1-(2-Thiasolylazo)-2-naphthol; Loaded silica gel; Cu(II) determination; Zn(II) determination

1. Introduction

Attention has recently been focused on the development of sorption-spectroscopic and visual test methods by using sorbents modified with analytical reagents [1]. A sorption separation of the trace elements prior to analysis serves the dual purpose of increasing their concentrations to levels at which they can be reliably determined and of removing them from the natural water matrix [2]. The using of specific chromophorous reagents as a modifying agent allows for the increase in

selectivity and sensitivity of determination. The sorbents can be modified via ion-exchange, impregnation, adsorption or covalent grafting of analytical reagents [3]. The previous studies [4–7] have shown wide use of chelating sorbents for Cu(II) and Zn(II) determination in different types of water. The resins loaded with organic reagent, 1-(2-thiasolylazo)-2-naphthol (TAN) and 1-(2-thiasolylazo)-2-naphthol-3,6-disulfonic acid (TAN-3,6-S), are known to be one of the effective preconcentration substrates [8,9]. However, they show a lack of stability in high ionic strength media [10]. Simultaneously, the reagents immobilization on the silica supports offers some distinct advantages over immobilization on the organic polymer supports: short time for equilibration, excellent swelling resistance in different solvents,

* Corresponding author. Tel.: +380-44-2210211; fax: +380-44-2244188.

E-mail address: smyk@akcecc.kiev.ua (O. Zaporozhets)

ease of surface modification with analytical reagent by adsorption. The preparation of modified silicas with a reagent adsorbed is rather simple, and their chemical–analytical properties do not yield to those of the sorbent with covalent grafted reagent [11]. Such solid-phase reagents are promising for analytical practice. As far as we know, no silica with TAN adsorbed has been proposed for heavy metal ion determination.

In the present work, we have studied the adsorption of TAN from organic solvents onto a silica surface, and established the TAN immobilized usefulness in the sorption–spectroscopic and visual test determination of copper and zinc.

2. Experimental

2.1. Reagents

Water and hexane were purified according to [12] and by flowing over metallic sodium, respectively. TAN was synthesized and purified according to [13]. All other chemicals were of analytical reagent grade. Stock Zn(II) and Cu(II) solutions were prepared by nitrates dissolving in 1 mmol l⁻¹ nitric acid and standardized by complexometry. Sodium chloride (4.0 mol l⁻¹), fluoride, hydroxide (0.1 mol l⁻¹) and thiosulphate (0.5 mol l⁻¹), potassium iodide (1.0 mol l⁻¹) and saturated hydrazine sulphate aqueous solutions were prepared by dissolving appropriate substances. The standard solutions of metal salts were acidified with nitric acid and further diluted as required. The aqueous solutions of TAN-3,6-S, 4-(2-pyridylazo)-naphthol (PAN), hexane and acetone solutions of TAN were obtained by dissolving appropriate substances. Silica gel Silpearl UV 250 (SG) for chromatography (Chemapol, Prague, Czech Republic) was digested in hydrochloric acid, washed with purified water and dried at 80°C for 8 h, and then at 200°C for 12 h. Nonporous highly dispersed silica Silics (Kalush, Ukraine, specific surface area $S = 300 \text{ m}^2\text{g}^{-1}$) was dried in vacuum at 68°C for 10 h to remove water adsorbed on the sorbent surface [14].

2.2. Apparatus

The absorbance spectra of solutions and reflectance spectra of sorbents were registered with a UV/Vis spectrophotometer Specord M-40 (Carl Zeiss Jena, Germany). The IR spectra of sorbents were registered with an automatic IR photometer UR-20 (Carl Zeiss Jena, Germany), samples being prepared as thin films between KBr windows. Atomic absorption measurements were recorded on an atomic absorption spectrometer model Saturn (Severodonetsk, Ukraine) equipped with a standard burner for use with an air–propane–butane flame. Standard hollow-cathode lamps were used as a line source for all elements.

A potentiometer model EV-74 with glass electrode (Gomel, Belarus) was used for pH measurements.

The ultrasound destruction of Cu(II) complexes with organic substances of natural water were realized by using USDN-A (Sumy, Ukraine).

2.3. Procedures

The batch technique was used for the research of TAN, Cu(II) and Zn(II) adsorption onto unloaded silicas and metal ions adsorption onto silica gel modified with TAN (TAN-SG). The reagent desorption from TAN-SG surface into aqueous solutions at a different pH was studied by this technique also.

2.3.1. Adsorption of TAN from hexane solution

Silicas (0.01 g) was stirred with 5 ml of 0.05–1.0 mmol l⁻¹ TAN hexane solution for 1–60 min. The TAN residue in the hexane solution after a sorbent separation was controlled spectrophotometrically by an absorbance at 480 nm. The amount of reagent adsorbed was calculated as: $a = (C_0 - [C]) * V / 1000 * m$, where C_0 , $[C]$, mol l⁻¹ were initial and equilibrium TAN concentrations in solution, respectively; V (ml) was volume of solution; and m , g was sorbent mass.

2.3.2. Desorption of TAN from TAN-SG surface into aqueous solution at different pH

The aqueous solution (5–100 ml) at the desired pH (2–8) was stirred for 1–60 min with weighed

amount (0.01–0.1 g) of sorbents containing a known amount of TAN (a , $\mu\text{mol g}^{-1}$: 1.0, 2.5, 25 or 50). The portion (4.5 ml) of solution after sorbent separation was mixed with 0.5 ml of acetone. The amount of TAN removed from surface into solution was determined spectrophotometrically by the own absorbance in aqueous–acetone (9:1) mixture at 450 nm. The equation of calibration graph was $A_{450} = 0.091 \cdot C$ ($\mu\text{mol l}^{-1}$).

2.3.3. The preparation of silics loaded with TAN for IR spectroscopy measurement

The silics (0.1 g) were stirred with 10 ml of hexane solutions containing 1.0, 25 or 250 $\mu\text{mol l}^{-1}$ of TAN for 15 min. Then sorbents were separated and dried in a vacuum at room temperature for 1 h. The amount of reagent adsorbed was a , $\mu\text{mol g}^{-1}$: 0.3, 7.5 and 69.

2.3.4. Adsorption of Zn(II) and Cu(II) onto SG and TAN-SG

Zinc containing an aqueous solution (30 ml) at pH 6.0 was stirred with 0.05 g of SG and TAN-SG with different reagent amounts on the surface (a , $\mu\text{mol g}^{-1}$: 1.0, 2.5, 25 or 50). Copper adsorption was realized from the 0.5 mol l^{-1} NaCl aqueous solution with pH 3.5. Zn(II) and Cu(II) residue in the solution was controlled spectrophotometrically with PAN [5] and TAN-3,6-S [9], respectively. The amount of metal ions adsorbed onto the silicas surface was determined as before. Sorbents with metal ions adsorbed were separated and dried at 60°C for 1 h.

2.3.5. Ultrasound destruction of Cu(II) complexes with organic substances in natural water samples

The sample of natural water (10 ml) was acidified to pH 1.0 (0.1 mol l^{-1} HNO_3) and exposed to ultrasound at 44 kHz, at an intensity of ≤ 10 Watts cm^{-2} for 3 min [15].

3. Results and discussion

3.1. TAN adsorption onto SG

The adsorption of TAN onto SG from chloro-

form, toluene, hexane and their mixtures was studied. It was found that the best TAN adsorption was observed when hexane was used. That is why modification of SG with TAN has been carried out from a hexane solution.

The kinetics experiments shown that the equilibrium of TAN adsorption from a hexane solution onto SG surface was reached in 5 min ($m = 0.01$ –0.1 g, $V = 5$ –10 ml). TAN adsorption as a function of reagent concentration in solution was studied. The results obtained testify that SG capacity in relation to TAN ($a_{\text{max}} = 69 \mu\text{mol l}^{-1}$) was limited by reagent solubility in hexane. The isotherm of TAN adsorption is represented in Fig. 1 (curve 1). Its initial part shows that the reagent adsorbed completely ($a > 0$ at $[C] = 0$) from dilute solutions ($C \leq 5.3 \mu\text{mol l}^{-1}$). This fact is known to indicate strong adsorbate connection with a sorbent [16]. That may be a result of interaction between TAN functional groups and OH-groups of SG surface [17]. The maximum value of TAN full adsorption is $2 \mu\text{mol g}^{-1}$. The further reagent adsorption ($a > 2 \mu\text{mol g}^{-1}$) may take place onto new surface (SG with TAN adsorbed) and caused intermolecular interaction. Low affinity of TAN molecules for new surface may explain S-shape of

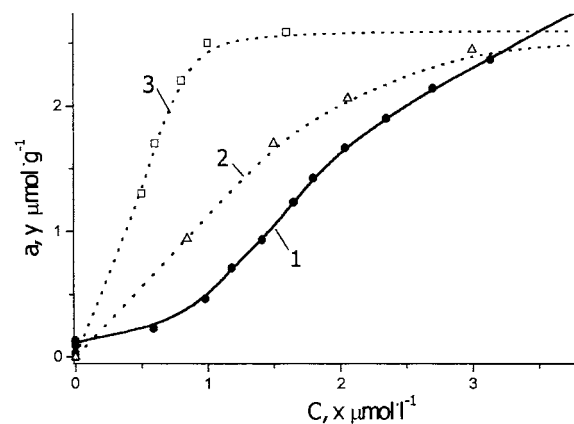


Fig. 1. Isotherms of TAN adsorption onto SG (1) and Zn(II) (2), Cu(II) (3) onto TAN-SG.; a_{TAN} , mmol g^{-1} : 25(2), 2.5(3); pH 6.0(2), 3.5(3); x : 20(1), 1(2,3); y : 20(1), 10(2), 1(3); $C_{\text{NaCl}} = 0.5 \text{ mol l}^{-1}$ (3); $m = 0.01$ g; $V = 5$ ml; $T = 293.0 \pm 0.5$.

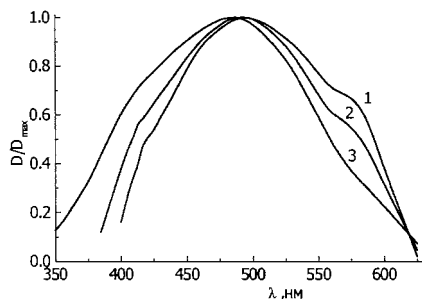


Fig. 2. Standardized diffusion reflectance spectra of TAN-SG. a , $\mu\text{mol}\cdot\text{g}^{-1}$: 0.5(1), 1(2), 5(3).

isotherm second part at $C > 5.3 \mu\text{mol}\cdot\text{l}^{-1}$ [17]. The diffusion-reflectance spectra of TAN-SG with different reagent content on the surface were compared for this supposition examining. Fig. 2 shows that the polarizing effect of SG on TAN molecule is decreased with the increasing of reagent content on the surface. The diffusion-reflectance spectra of TAN-SG with $a > 5.0 \mu\text{mol}\cdot\text{g}^{-1}$ is similar to absorbance spectra of TAN solution in polar solvent. This fact confirms TAN second layer formation as a result of intermolecular interaction.

The nature of TAN binding with the SG surface has also been investigated using IR-spectroscopy [18]. The IR spectra of silics modified with TAN are shown in Fig. 3. They indicate that the absorbance band at 3749 cm^{-1} belonging to valence vibration of singular surface OH-groups [18] becomes less intensive as TAN surface content increases. Simultaneously, the absorbance band at $3200\text{--}3600 \text{ cm}^{-1}$ corresponding to valence vibration of hydrogen bonded silanol groups becomes more intensive. This may be the result of hydrogen bonds forming between N or S atoms of reagent molecules and surface OH-groups at TAN fixation.

To establish the possibility of new solid-phase reagent application to analytical practice, reagent desorption from TAN-SG surface as a function of pH of solution was studied. The data obtained show that TAN desorption at pH 3.5–7.0 (sorbent mass $\geq 0.01 \text{ g}$, aqueous solution volume $\leq 100 \text{ ml}$, time of phases contact $\leq 60 \text{ min}$) was not more than 15, 10, 2 and 1% for reagent surface 1.0, 2.5, 25 and $50 \mu\text{mol}\cdot\text{g}^{-1}$, respectively. It is known [9] that the sorbents with maximum capacity in relation to a reagent are useless in determining metal ions because of the strong inter-

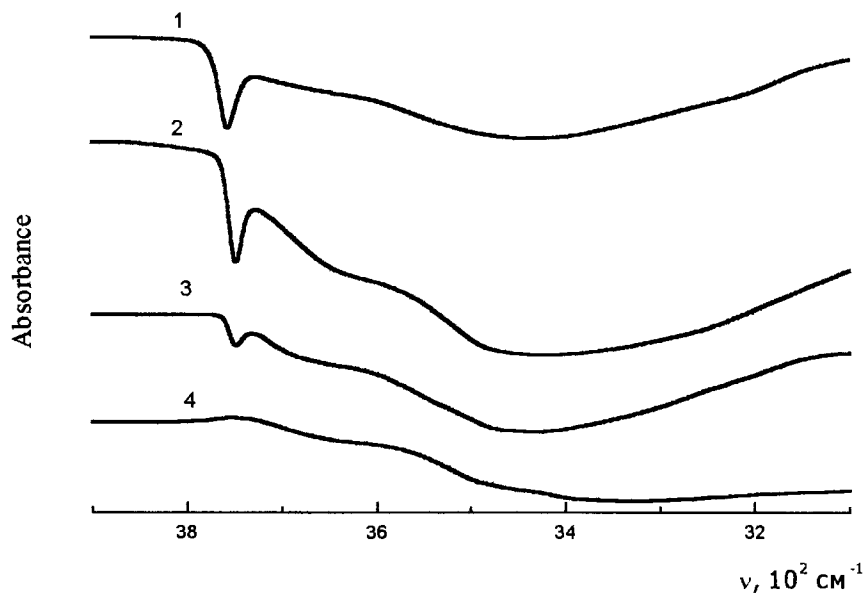


Fig. 3. IR spectra of silica modified with TAN containing on the surface, $\text{mmol}\cdot\text{g}^{-1}$: 0(1), 1(2), 5(3), 70(4).

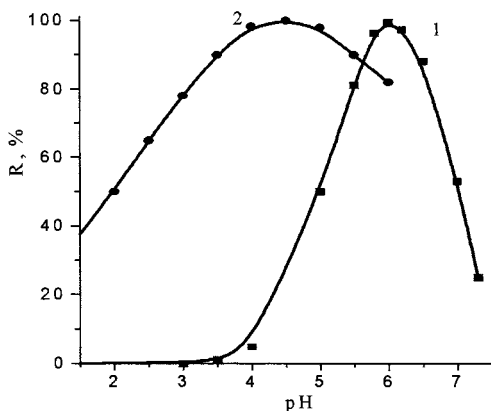


Fig. 4. Adsorption of Zn(II) (1) and Cu(II) (2) onto TAN-SG as function of pH. Initial concentration of metal ions 1 mmol l^{-1} ; a_{TAN} , mmol g^{-1} : 25(1), 2.5(2); $m = 0.01 \text{ g}$; $V = 5 \text{ ml}$.

molecular attraction between molecules of a modifying agent, making complexing centers inactive. Therefore, the silicas with TAN surface content $2.5\text{--}25 \text{ } \mu\text{mol g}^{-1}$ were used for the study of Cu(II) and Zn(II) adsorption.

3.2. Zn(II) adsorption onto TAN-SG

The pH dependence of Zn(II) adsorption by TAN-SG from an aqueous solution ($m \leq 0.05 \text{ g}$, $V \leq 30 \text{ ml}$, $a = 25 \text{ } \mu\text{mol g}^{-1}$) is represented in Fig. 4 (curve 1). The Zn(II) recovery seems to be complete at pH 5.5–6.8. Zinc ions are not adsorbed onto unloaded silica gel under these conditions [19]. The dependence of Zn(II) adsorption as a function of TAN surface content was studied. The data obtained indicates that the maximum recovery was reached at $a \geq 25 \text{ } \mu\text{mol g}^{-1}$. Therefore, TAN-SG with $a = 25 \text{ } \mu\text{mol g}^{-1}$ was used to further investigate Zn(II) adsorption.

Kinetic experiments shown that the Zn(II) adsorption equilibrium was reached in 10 min. The sorbent mass and solution volume dependencies of Zn(II) adsorption onto TAN-SG were studied. The maximum concentration factor was found to be 600 ml g^{-1} at volume of solution 30 ml and mass of sorbent 0.05 g.

The isotherm of Zn(II) adsorption onto TAN-SG is shown in Fig. 1 (curve 2). Its shape (L-type)

may testify about chemical interaction between Zn(II) and TAN immobilized. The chelating capacity of TAN-SG was $25 \text{ } \mu\text{mol g}^{-1}$ Zn(II) for $25 \text{ } \mu\text{mol g}^{-1}$ reagent. It was assumed that the complex with the ratio Zn:TAN = 1:1 has been formed on the surface of TAN-SG. Spectra shown in Fig. 5 confirmed such surface complex formation.

3.3. Cu(II) adsorption onto SG and TAN-SG

The pH dependence of Cu(II) adsorption onto TAN-SG from an aqueous solution was studied. For escaping difficulties, with insoluble hydroxide of Cu(II) conformation at $\text{pH} > 3$, the adsorption from the NaCl aqueous solution was investigated [21]. It was found experimentally, that optimum concentration of sodium chloride was more than 0.5 mol l^{-1} . The pH-dependence is represented in Fig. 4 (curve 2). The optimum pH range of Cu(II) adsorption was 3.3–4.6. For comparison, an attempt to adsorb Cu(II) onto unloaded SG was carried out, but there was no effect under such conditions.

The Cu(II) adsorption as a function of TAN content on the SG surface was studied. It was found that Cu(II), in contrast to Zn(II), Co(II) and Fe(III), was quality recovered by sorbent which contained $\leq 2.5 \text{ } \mu\text{mol g}^{-1}$ TAN ($m = 0.01\text{--}0.1 \text{ g}$, $V = 5\text{--}100 \text{ ml}$). This is why the

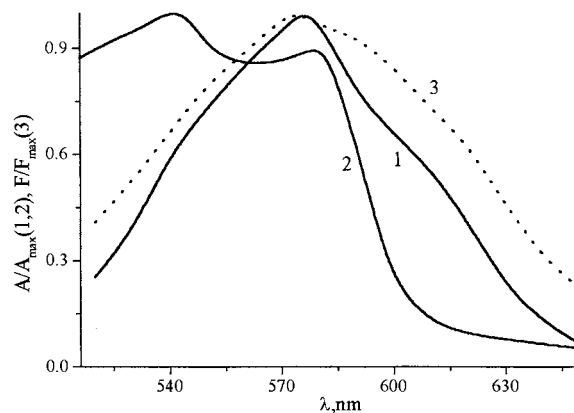


Fig. 5. Standardized absorbance spectra of ZnTAN aqueous-acetone solution (1); $\text{Zn}(\text{TAN})_2$ benzene solution [20] (2); and diffusion reflectance spectra of TAN-SG with Zn(II) adsorbed (3).

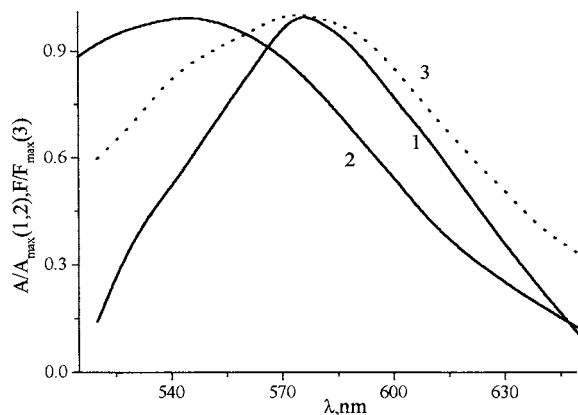


Fig. 6. Standardized absorbance spectra of CuTAN aqueous-acetone solution (1); Cu(TAN)₂ benzene solution [20] (2); and diffusion reflectance spectra of TAN-SG with Cu(II) adsorbed (3).

modified sorbent with $a = 2.5 \mu\text{mol}\cdot\text{g}^{-1}$ was used for Cu(II) adsorption.

Kinetics experiments show that the time taken for maximum Cu(II) recovery was 15 min. The sorbent mass and solution volume dependencies of Cu(II) adsorption onto TAN-SG were studied. It was found that the maximum concentration factor of Cu(II) was $1000 \text{ ml}\cdot\text{g}^{-1}$ at volume of solution 100 ml and mass of sorbent 0.1 g.

The isotherm of Cu(II) adsorption onto TAN-SG is shown in Fig. 1 (curve 3). It may be referred to L-type. The chelating capacity of TAN-SG was $2.6 \text{ mmol}\cdot\text{g}^{-1}$ Cu(II) for $2.5 \text{ mmol}\cdot\text{g}^{-1}$ TAN. Therefore, the formation of complex with the ratio immobilized reagent: Cu(II) = 1:1 on the TAN-SG surface may be supposed. The comparison of absorbance spectra of CuTAN and Cu(TAN)₂ solutions with a diffusion reflectance spectrum of TAN-SG with Cu(II) adsorbed (Fig. 6) confirmed this fact.

3.4. The interference of foreign ions

The maximum adsorption of metal ions can be reached during complex with the ratio metal ion:immobilized reagent = 1:1 formed on a surface [22]. It is known [8], that among natural water components, only Co(II), Cu(II), Zn(II), Fe(III), Hg(II) and Ag(I) form such complexes with TAN in aqueous-acetone solution. There-

fore, their influence on zinc and copper determination was studied. It was shown that Hg(II) and Ag(I) do not interact with TAN immobilized at pH 3.0–7.0. Fe(III) ($\leq 10 \text{ mg}\cdot\text{l}^{-1}$) in the presence of $0.01 \text{ mol}\cdot\text{l}^{-1}$ NaF and cobalt ($\leq 0.5 \mu\text{g}\cdot\text{l}^{-1}$) do not interfere with Zn(II) and Cu(II) determination. Zinc at concentration $\leq 0.1 \text{ mg}\cdot\text{l}^{-1}$ does not influence $\geq 10 \mu\text{g}\cdot\text{l}^{-1}$ Cu(II) determination by using TAN-SG with chelating capacity $2.5 \mu\text{mol}\cdot\text{g}^{-1}$. Copper at concentration $\leq 1 \text{ mg}\cdot\text{l}^{-1}$ in the presence of $0.01 \text{ mol}\cdot\text{l}^{-1}$ Na₂S₂O₃ does not interfere with Zn(II) determination.

3.5. Application of modified SG to zinc and copper ions determination

The possibility of TAN-SG application to Cu(II) and Zn(II) ions determination in water has been studied.

3.5.1. Zn(II) determination in water by using TAN-SG

The diffusion reflectance spectroscopic (DRS) method for Zn(II) determination was developed. The calibration graph was linear in the range 0.5–25 μg per sample. The calibration equation was: $R_{570} = 0.01 + 0.07 \cdot C$ (μg per sample), $r = 0.99$. The detection limit was $15 \mu\text{g}\cdot\text{l}^{-1}$ (for 30 ml of sample solution). Therefore, TAN-SG can be conveniently used to detect zinc ions in natural water at values as low as 0.15 MAC [23].

The colour scale for zinc visual test determination was prepared by stirring 10 ml of Zn(II) solution containing 0, 0.65, 1.95, 3.25, 6.50, 9.80 and 13.00 μg at pH 6.0 with 0.05 g of TAN-SG ($a = 25 \mu\text{mol}\cdot\text{g}^{-1}$) for 10 min. The sorbents were separated. The sorbent colour changed from orange to violet with Zn(II) concentration increasing. The scale stored without air access has been stable for more than 4 months. The characteristics of developed and known visual test (VT) methods for Zn(II) determination are compared in Table 1. The data indicate that the test proposed is more sensitive.

Zn(II) is known to form unstable complexes with organic substances of natural water [24]. Therefore, it is possible to determine the Zn(II) concentration in water without mineralization.

The sample of water ($V = 10$ ml) containing ≥ 1 μg of Zn(II) at pH 6.0 was mixed with 0.1 ml of 1.0 mol l^{-1} NaF and 0.1 ml of 1.0 mol l^{-1} $\text{Na}_2\text{S}_2\text{O}_3$ and stirred mechanically with 0.05 g of TAN-SG ($a = 25 \mu\text{mol g}^{-1}$) for 10 min. Sorbent was separated and its colour was compared with the standard scale. The dried sorbent was examined using diffusion reflectance spectroscopy.

3.5.2. The Cu(II) determination in water by using TAN-SG

The DRS method of Cu(II) determination was developed. The calibration graph was linear in the range 1.0–10.4 μg per sample. The calibration equation was: $R_{560} = 0.004 + 0.03 \cdot C$ (μg per sample), $r = 0.98$. The detection limit was $10 \mu\text{g l}^{-1}$ (for 100 ml of sample solution and sorbent mass 0.1 g). Therefore, TAN immobilized may be applied to Cu(II) determination in natural water at a content as low as 0.05 MAC level [23].

The colour scale for Cu(II) visual test determination in the range 0.65–13 μg per sample was developed. It was prepared by stirring 10 ml solution containing 0, 0.65, 1.3, 2.6, 5.2, 6.4 and 13 μg of Cu(II) and 0.5 mol l^{-1} NaCl at pH 3.5 with 0.1 g TAN-SG ($a = 2.5 \mu\text{mol g}^{-1}$) for 15 min. The sorbents were separated. The colour of sorbents changed from light-pink to violet with Cu(II) concentration increasing. The scale stored without air access has been stable for more than 4 months. The comparison of developed and known

VT methods for Cu(II) determination represented in the Table 1 shows higher sensitivity of test proposed.

Copper forms the stable complexes with organic substances of natural water [24], so it becomes inactive in reaction with TAN immobilized. Therefore, the natural water was analyzed after the ultrasound mineralization.

The sample ($V = 10$ ml) of mineralized water was neutralized with 1 mol l^{-1} NaOH up to pH 3.5, mixed with 1.25 ml of 4 mol l^{-1} NaCl, 1 ml of 0.1 mol l^{-1} NaF and stirred mechanically with 0.1 g of TAN-SG ($a = 2.5 \mu\text{mol g}^{-1}$) for 10 min. The sorbent was separated and its color was compared with standard scale. Dried sorbent was examined by using diffusion reflectance spectroscopy.

The results of the zinc and copper determination in natural and tap water by using developed and flame atomic absorption spectroscopic (FAAS) [23] methods are represented in Table 2. The data obtained show that the method proposed gives reproducible and reliable results. The comparison of results of copper determination in tap and river water indicate the necessity for prior mineralization in both cases.

The developed DRS and VT methods on the base of silica with TAN adsorbed are simple and rapid in procedure and appear to offer a faster and more effective route to natural water analysis.

Table 1

Comparative description of visual test methods of Cu(II) and Zn(II) determination^a

Ion	Sorbent	Detection limit (mg l^{-1})	Detection range (mg per sample)	Reference
Cu(II)	TM-cellulose	0.05	0.05–2*	[25]
	DETC-polymer fiber	0.05	0.5–10	[26]
	PAN-Silochrome	0.1	0.5–5.0	[27]
	Copper Test Aquaquant	0.05	0.05–0.5*	[28]
	TAN-SG	0.010	0.65–13	Proposed
Zn(II)	Dz-textile with ion exchanger	0.1	1.0–5.0	[26]
	PAN-Silochrome	0.03	5.0–50	[27]
	Zinc test aquaquant	0.1	0.1–5.0*	[28]
	TAN-SG	0.015	0.65–13	Proposed

* mg l^{-1} .

^a TM-4,4'-Bis-(dimethylamino)-thiobenzophenone, DETC, Diethylthiocarbazon; PAN-1-(2-Pyridylazo)-2-naphthol, Dz, Diphenylthiocarbazon.

Table 2

Results of Cu(II) and Zn(II) determination using the VT, DRS and FAAS methods ($n = 3$, $P = 0.95$)

Ion	Sample	Concentration (mg l ⁻¹)			
		Added	Founded		
			VT	DRS	AAS
Cu(II)	Standard solution	0.55	0.52 ± 0.3	0.55 ± 0.2	0.55 ± 0.05
	Tap water	0.64	0.4 ± 0.1	0.45 ± 0.2	0.61 ± 0.06
	River water	—	<0.07	<0.1	0.06 ± 0.01
	River water*	—	0.13 ± 0.07	0.10 ± 0.3	0.06 ± 0.01
Zn(II)	Standard solution	0.2	0.20 ± 0.07	0.20 ± 0.02	0.22 ± 0.02
	Tap water	0.2	0.98 ± 0.15	1.00 ± 0.05	1.10 ± 0.07
	River water	—	0.13 ± 0.03	0.12 ± 0.03	0.09 ± 0.01

* After ultrasound destruction.

Acknowledgements

This work was partly supported by the International Soros Science Education Program through grants N SPU073063; N APU073033.

References

- [1] R.E. Clement, G.A. Eiceman, C.J. Koester, *Anal. Chem. Applic. Rev.* 67 (1995) 221R.
- [2] H. Watanabe, *Anal. Chem.* 53 (1981) 738.
- [3] O.A. Zaporozhets, O.M. Gawer, V.V. Sukhan, *Russian Chem. Rev.* 66 (1997) 637.
- [4] H. Watanabe, K. Goto, Sh. Taguchi, J.W. McLaren, S.S. Berman, D.S. Russell, *Anal. Chem.* 53 (1981) 738.
- [5] G. Giraudi, C. Pari, E. Mentasti, *Ann. Chim. (Italian)* 74 (1984) 307.
- [6] Chi-Chung Wan, S. Chiang, A. Corsini, *Anal. Chem.* 57 (1985) 719.
- [7] S. Przeszlakowski, R. Kocjan, *Analyst* 110 (1985) 1077.
- [8] G.D. Brykina, N.S. Stepanova, A.V. Stefanova, L.S. Krysinina, T.A. Belyavskaya, *Zh. Anal. Khim.* 38 (1983) 33.
- [9] G.D. Brykina, T.V. Martchak, L.S. Krysinina, T.A. Belyavskaya, *Zh. Anal. Khim.* 54 (1980) 2294.
- [10] P. Battistoni, S. Bompadre, G. Fava, G. Gobbi, *Talanta* 30 (1983) 15.
- [11] M.A. Marshall, H.A. Mottola, *Anal. Chem.* 57 (1985) 729.
- [12] *Methods of Analysis of Pure Chemical Reagents*, Chemistry, Moscow, 1984 (in Russian).
- [13] B. Skytle, *Jensen Acta Chem. Scand.* 14 (1960) 927.
- [14] R. Iler, *The Chemistry of Silica*, Wiley-Interscience, New York, 1979.
- [15] F.A. Chmilenko, A.N. Baklanov, V.T. Chuiko, *Khim. Tekhnol. Vody.* 12 (1990) 1039.
- [16] S.G. Perry, R. Amos, P.I. Brewer, *Practical Liquid Chromatography*, Plenum Press, New York, 1974.
- [17] N.H. Gilles, T.N. MacEwan, S.H. Nakhwa, D. Smith, *J. Chem. Soc.* (1960) 3973.
- [18] A.V. Kiseliyov, V.I. Lygin, *The infra red spectra of surface compounds*, Nauka, Moscow, 1972 (in Russian).
- [19] N.N. Vlasova, N.K. Davidenko, V.I. Bogomaz, A.A. Chuiko, *Colloids Surf. A: Physicochem. Eng. Aspects* 104 (1995) 53.
- [20] O. Navratil, *Collect. Czech. Chem. Com.* 29 (1964) 2490.
- [21] G.D. Brykina, N.S. Stepanova, T.A. Belyavskaya, *Zh. Anal. Khim.* 37 (1982) 208.
- [22] G.D. Brykina, T.V. Martchak, L.S. Krysinina, T.A. Belyavskaya, *Zh. Anal. Khim.* 38 (1983) 1463.
- [23] G.S. Fomin, *Water, Inspection of Chemical, Bacteriological and Radiation Safety according to International Standards*, Encyclopedical Handbook, Protector, Moscow, 1995 (in Russian).
- [24] I. Yu. Andreeva, N.V. Komarova, S.V. Drogobuzhskaya, Yu. E. Kazakevich, *Zh. Anal. Khim.* 51 (1996) 777.
- [25] R.P. Pantaler, L.A. Egorova, L.I. Avramenko, A.B. Blank, *Zh. Anal. Khim.* 51 (1996) 997.
- [26] O.P. Shvoeva, V.P. Dedkova, A.G. Gitlits, S.B. Savvin, *Zh. Anal. Khim.* 52 (1997) 89.
- [27] S.A. Morozko, V.M. Ivanov, *Zh. Anal. Khim.* 50 (1995) 629.
- [28] *Chemicals reagents*, Merck, KGaA, Darmstadt, 1999/2000.

Low-level mercury determination with thiamine by fluorescence optosensing

A. Segura-Carretero ^a, J.M. Costa-Fernández ^b, R. Pereiro ^b, A. Sanz-Medel ^{b,*}

^a Department of Analytical Chemistry, University of Granada, 18071 Granada, Spain

^b Department of Physical and Analytical Chemistry, University of Oviedo, Julián Clavería, 8, 33006 Oviedo, Spain

Received 9 November 1998; received in revised form 25 February 1999; accepted 1 March 1999

Abstract

A sensitive fluorescence optosensing method for the determination of Hg(II) in water samples is described. The method, using a flow injection technique, is based on the immobilization on a non-ionic-exchanger solid support (packed in a flow cell placed in a conventional fluorimeter) of the thiochrome formed by the oxidation of thiamine with Hg(II) in a continuous flow carrier at pH 8.1. Experimental parameters such as the solid support, the carrier pH, the thiamine concentration and the flow-rate were investigated to select the optimum operating conditions. The proposed optosensor showed a relative standard deviation of $\pm 3.0\%$ for ten replicates analysis of 100 ng ml^{-1} of mercury(II). A detection limit of 3 ng ml^{-1} for mercury(II) was achieved for 4-ml sample injections. A detailed study of interferences (possible elements present in natural waters) demonstrated that this optosensing method is virtually specific for this metal, because it allows the determination of mercury in the presence of relatively large amounts of other heavy metals and compounds present in natural waters, such as Mg(II) or Ca(II). The method was successfully applied to the determination of Hg(II) in spiked samples of mineral, tap and sea water. © 1999 Elsevier Science B.V. All rights reserved.

Keywords: Fluorescence; Mercury; Optosensing

1. Introduction

The determination of trace amounts of heavy metal ions is of growing interest in several fields including environmental analysis, process control, biology, medicine, etc., and there is now a partic-

ular need for simple and fast field analytical tests.

In contrast to well-established laboratory methods, such as atomic absorption or emission spectrometry, mass spectrometry or voltammetry, (bio)chemical sensors have attracted a great deal of interest in the last decade because of their great potential for in the field, in situ, continuous and remote, if required, applications [1]. Fluorimetric optical sensors are particularly suited for low-level monitoring of heavy metals because of the intrinsic sensitivity of this detection technique. The so-called 'sensing phase' consists of a reagent dye

* Corresponding author. Tel.: +34-98-510-34-74; fax: +34-98-510-31-25.

E-mail address: asm@sauron.quimica.uniovi.es (A. Sanz-Medel)

immobilized in organic or inorganic solid matrices. Photoluminescence of this sensitive layer occurs when the analyte reacts with the dye on the solid surface (solid surface luminescence) [2].

The combination of flow-injection analysis (FIA) techniques with optically active surfaces, having an immobilised indicator in a flow-through cell, has been called 'optosensing flow-injection analysis' [3], and has proved to offer important advantages in the optical sensors field [4]. Particularly, optosensing with luminescence detectors is especially suited to combine with flow measurements because of their high sensitivity and selectivity, good precision, simplicity and low cost. Moreover, flow injection methods allow direct monitoring of analyte concentrations without any sample pre-treatment, or, conversely, the conventional on-line sample pretreatment needed is carried out in an easy and fast way.

Mercury (Hg) is a very toxic element which is of great environmental concern because it is widespread in the lithosphere and water [5,6]. Few publications on optical sensors for heavy metal ions seem to be available [7] while optical sensors for mercury are usually based on immobilized absorptiometric dyes (reflectance changes of 4-phenylazo-3-aminorhodamine (PAAR) [8] or absorbance changes of certain porphyrins [9–11] or of neutral ionophors such as dithiocarbamates [12] have been described). Also, the change of the fluorescence of an amphiphilic immobilized ox-acarboxyanine dye [13] has been used as an optical transducer for mercury. Unfortunately, these sensors suffer from lack of selectivity to Hg(II) over other toxic heavy metals such as Ag(I), Cd(II) and Pb(II).

Moreover, biosensors have demonstrated their potential for the detection of toxic heavy metals. The inhibition effect of mercury on immobilized horseradish peroxidase [14] and urease [15] was employed to develop optical tests for Hg(II) and a novel microbial biosensor has been described using a genetically modified firefly luciferase. It enables the determination of Hg(II) with good selectivity over Cd(II) and exhibits a sensitivity in the picomolar concentration range [16]. A general disadvantage of the biosensing approach, however, is their limited robustness in terms of operational stability compared to chemical sensors.

Very few conventional batch solution methods for fluorimetric Hg(II) determination have been described. They are based on the quenching effect of Hg(II) on the fluorescence of rhodamine B [17], on the catalytic effects of Hg(II) on the autoxidation of 2,2'-dipyridylketone hydrazone [18] or on the oxidation of thiamine to thiochrome which is highly fluorescent [19]. This last method is highly sensitive and selective to Hg(II) but requires a reaction time of about 1 h before measurements [17].

In the present paper, a fluorescence optosensor for Hg(II) low levels determination is described. It is based on the reaction of thiamine with Hg(II) to form the highly fluorescent thiochrome in a flow system, while the formed thiochrome is immobilized on-line onto a solid support and its fluorescence measured. The analytical performance of the proposed optosensor for mercury analysis is evaluated and its application to trace analysis of Hg in mineral, tap and sea waters is discussed.

2. Experimental

2.1. Materials and solutions

The selected reagent, thiamine, was provided by Sigma-Aldrich (Steinheim, Germany) and used as received. A stock solution of Hg(II) ($1000 \mu\text{g ml}^{-1}$) in HNO_3 0.5 M was obtained from Merck (Darmstadt, Germany). Working Hg(II) standards were prepared daily by appropriate dilution of the stock solution.

The buffer carrier solution consisted typically of 0.05 M di-sodium tetraborate decahydrate (Merck)–HCl with a pH of 8.1.

Different types of solid supports were used to immobilize the fluorophore, including Amberlite XAD-2 and Amberlite XAD-4 (cross-linked copolymers of styrene and divinylbenzene), Amberlite XAD-7 (a cross-linked polymer of methyl methacrylate), Kieselgel Davisil Typ 646 and Kieselgel Merck Typ 10181 (non-ionic exchangers), Dowex 50WX8-200 (a strongly cationic anion-exchange resin) and the strongly basic anion-exchange resin Dowex 1X2-200. All these

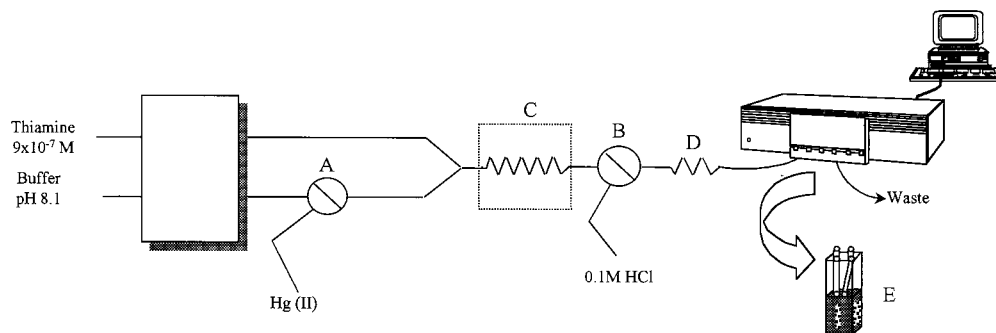


Fig. 1. Schematic flow diagram of the system employed. A and B, valves; C, thermostatted water bath; D, cooling coil; E, fluorescence flow cell.

solid supports were purchased from Aldrich Chemical Co. (Gillingham, Dorset, UK). The possible solid support impurities were removed by washing (first with ethanol, then with 2 M hydrochloric acid and finally with de-ionized water).

Analytical reagent-grade chemicals were employed for the preparation of all the solutions. Freshly prepared ultrapure de-ionized water (Milli-Q 3 RO/Milli-Q2 system, Millipore, UK) was used in all experiments. Special care was taken in the preparation and handling of solutions and containers to minimize any possible risk of Hg(II) contamination. Calibrated flasks were left overnight in 10% (v/v) HNO₃ (analytical reagent grade) and rinsed with ultra-pure Milli-Q water, to eliminate contamination, before use.

2.2. Instrumentation

Fig. 1 illustrates the optosensing FIA manifold used. A four-channel Gilson Minipuls-2 peristaltic pump was used to generate the flowing streams. Omnifit 1106 rotary valves were used for sample introduction (valve A in Fig. 1) and for elution of the retained compound (valve B). Omnifit 2401 mixing T-piece, PTFE tubing (0.8 mm i.d.) and fittings were used to connect the flow-through cell, the rotary valves and the carrier solution reservoirs.

A conventional Hellma flow-cell (Model 176.52) of 25 μ l volume was used. At the bottom of the flow cell, a small piece of nylon net was placed to prevent particle displacement by the

carrier (see Fig. 2). The solid support was loaded with the aid of a syringe and the other end of the flow cell was kept free [20]. The cell was then connected to the flow system and 10 min allowed for the particles to settle. In order to ensure that the compound first retained by the packing solid material was in the light path, the resin level was maintained 1 mm lower than that of the cell window. The resin packed in this way could be used for at least 4 weeks with satisfactory fluorescence readings.

A Shimadzu Model RF-5000 spectrofluorimeter coupled to a data station (Shimadzu, Model DR-15) was employed for all the fluorescence emission measurements. Instrument excitation and emission slits were set at 5 nm and 2.5 nm, respectively.

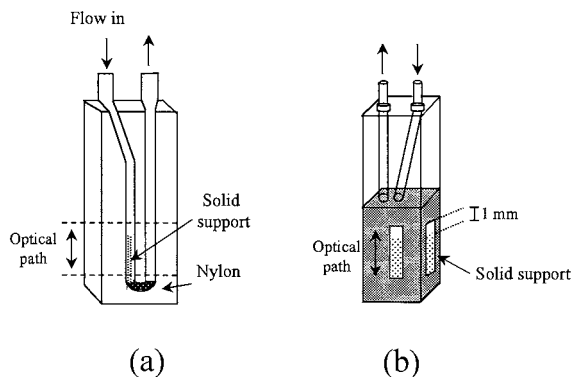


Fig. 2. Schematic diagram of the fluorescence flow cell employed. A: section view; B: front view.

The pH measurements were made by using a WTW pHmeter Model 139 (Wiss. Tech. Werk-states, Weilheim) and a Radiometer GK-2401-C combination glass–saturated calomel electrode.

2.3. General procedure

In the flow-injection system, a Hellma flow-through cell with the solid support was placed in the conventional sample compartment of the detector (see Fig. 1). Sample or standard solutions were injected via valve A (sampling volume 4 ml) into the carrier stream at a flow rate of 1.2 ml min⁻¹. This stream was mixed with the thiamine solution in a T-piece and passed through the reaction coil C (1 ml volume) which was immersed in a thermostatted water bath to increase the kinetics of the thiamine oxidation. A cooling coil of 0.5 ml (D) was used to decrease the flow temperature to the room temperature. Finally, the thiochrome formed went through the flow cell (E) where it was retained on the packed resin. The high fluorescence emitted by the thiochrome, retained on the solid support, was measured at the spectral maxima of 380 nm for excitation and 430 nm for emission.

Once the fluorescence measurement was taken, 2 ml of 0.1 M HCl was injected via valve B (to strip the thiochrome retained on the solid phase), before proceeding with the next sample injection. Typical flow-injection fluorescence signals versus time were taken and measured.

3. Results and discussion

3.1. Selection of solid support

The solid support for flow-injection solid surface fluorescence optosensing should be ideally translucent, so that reflected or absorbed light entering or leaving the probe would be negligible. In our case, the fluorescence intensity of the thiochrome was influenced by the nature of the solid support onto which this fluorophore was adsorbed. The interactions between the solid support and the thiochrome, that resulted in observation of fluorescence, were studied for different

Table 1
Selection of solid support (Hg(II) concentration of 100 ng ml⁻¹)

Resin type (particle size 0.160-0.080 mm)	Relative fluorescence net signal
Amberlite XAD-2	48
Amberlite XAD-4	100
Amberlite XAD-7	26
Kieselgel Davisil Typ 646	1
Kieselgel Merck Typ 10181	1
Dowex 50WX8-200	5
Dowex 1X2-200	2

commercial polymeric resins. Table 1 shows the fluorescence intensities observed for thiochrome immobilized onto seven different solid supports.

The immobilization of thiochrome onto solids such as Amberlite XAD-2, Amberlite XAD-4, Amberlite XAD-7, Kieselgel Davisil Typ 646 and Kieselgel Merck Typ 10181 (all non-ionic exchangers) should be through hydrophobic interactions. Using ionic resins (Dowex 1X2-200 or Dowex 50WX8-200) the main interaction with the adsorbed thiochrome molecules should be mainly via electrostatic interactions between the charged groups of the compound and the ionic moieties of the resins. As can be seen from Table 1, the highest fluorescence net intensities for a given amount of Hg(II) introduced in the FIA system (Fig. 1) were obtained when using Amberlite XAD-4.

Different particle sizes of the packed resins were also assayed by using several sieves to select particles sizes. Three ranges were assayed: 0.160–0.080 mm, 0.080–0.063 mm and 0.037–0.063 mm. The best results were achieved when using particles with diameters between 0.080–0.160 mm. Thus this particle size range was selected for further packing of the cell in analytical measurements.

3.2. pH and thiamine concentration

The pH of the carrier influences the kinetics of the oxidation reaction Hg(II) + thiamine and, therefore, the observed fluorescence signal. The observed effect of variations in the pH of the

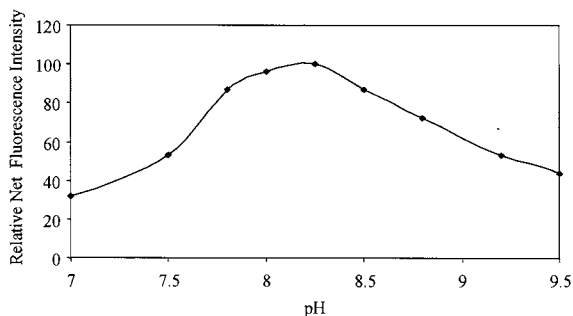


Fig. 3. Effect of pH on the fluorimetric signal of Hg. Hg(II) concentration of 100 ng ml^{-1} . λ_{ex} and λ_{em} of 380 and 430 nm, respectively. Slits: 5 nm for excitation and 3 nm for emission.

carrier (pH range 5.5–10.5) on the analytical signal is shown in Fig. 3. As can be seen, the highest analytical signal was obtained in the interval from pH 7.8 to 8.5 and so a pH of 8.1 was selected for subsequent studies.

The observed effect of thiamine concentration in solution has been plotted in Fig. 4. For concentrations of thiamine above $1.5 \times 10^{-6} \text{ M}$ a sharp decrease of the fluorescence was observed, probably due to ‘inner filter’ effects on the solid surface. Thus, a final thiamine concentration of $9 \times 10^{-7} \text{ M}$ was selected for subsequent work.

3.3. Conditions of the flow-system

The influence of the carrier flow-rate was also investigated over the range $0.6\text{--}2.5 \text{ ml min}^{-1}$. Fig. 5 shows the observed effects of flow rate, both on the relative net fluorescence intensity

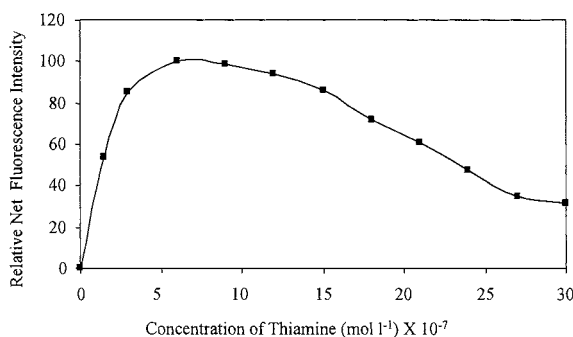


Fig. 4. Effect of thiamine concentration on the fluorimetric signal. Experimental conditions as in Fig. 3.

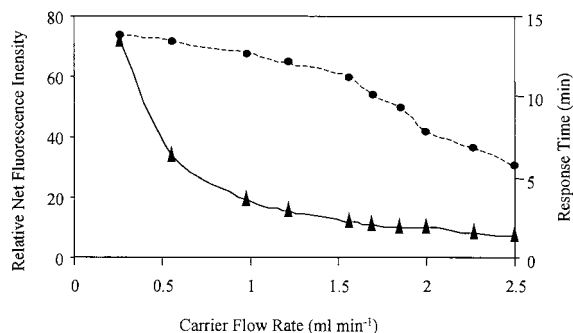


Fig. 5. Effect of flow rate on the fluorimetric signal (●) and the response time (▲). Experimental conditions as in Fig. 3.

and on the time elapsed between sample injection and measurement. From such results, a compromise flow-rate of 1.2 ml min^{-1} was selected for further experiments.

Different reaction coil lengths (from 0.75 to 2 ml volumes) were studied at the selected flow rate. It was observed that the fluorescence signal gives a maximum for a coil length of 1 ml when this is placed into a water bath at 80°C . The temperature of the water bath used to heat the reaction coil was also investigated and before reaching 80°C the observed fluorescence signals increased with temperature up to a plateau was reached. Temperatures higher than 80°C did not show any further increase of signals.

Finally, elution of the formed thiochrome, adsorbed on the solid support, was studied by using HCl, at different concentrations, as stripping agent. Regeneration of the reagent phase can be accomplished by passing 2 ml of 0.1 M HCl which washed out the immobilized thiochrome rapidly and completely from the resin ion-exchanger.

3.4. Interferences

Following the described procedure, the effect of foreign elements (typical in natural waters) over the response of the optosensor for mercury was studied. The potential interferences were added to a standard mercury solution containing 100 ng ml^{-1} of the analyte and their effect on the Hg(II) fluorescence signal was investigated.

The influence of adding increasing amounts of NaCl (a major component in sea water) on the Hg signal was investigated first and the results showed that Na:Hg ratios up to 15 000 (maximum level tested) did not affect the Hg signal. For calcium and magnesium, tolerance ratios 'interference:Hg(II)' of 1000 were observed.

The most serious effect was due to Fe^{3+} and Cu^{2+} , which quenched the luminescence of the thiochrome very efficiently at ratios higher than 10:1. Fortunately, interference from such cations can be easily overcome by removing Fe^{3+} and Cu^{2+} in an 'in-line' mini-column (e.g. packed with the 8-hydroxyquinoline derivative Kelex 100 immobilised on Amberlite XAD-7) as described previously [21].

Other metals (Cd^{2+} , Pb^{2+} , Mn^{2+} , Co^{2+}) which could be present in natural waters at low levels did not interfere the proposed determination of mercury even at 100:1 ratios.

3.5. Analytical performance characteristics

Fig. 6 shows the observed effect of sample volume injected on the analytical signal. As can be seen, the higher the sample volume the higher the relative net signal intensity. However, considering that higher volumes give also rise to higher response times, a compromise sample volume of 4 ml was chosen. With the proposed method, it is possible to analyse 12 samples per hour, when using 4 ml sample injection volumes.

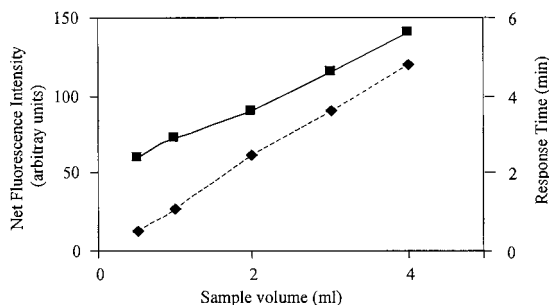


Fig. 6. Effect of sample volume on the analytical signal (◆) and the response time (■). Experimental conditions as in Fig. 3.

Analytical performance characteristics of the proposed method were evaluated under selected optimum conditions. Calibration graphs were prepared from the results of triplicate 4 ml injections of Hg standard solutions of increasing concentration and proved to be linear from 10 to 150 ng ml^{-1} of Hg(II). The detection limit, calculated as the concentration of mercury which produced an analytical signal three times the standard deviation of the blank signal, was 3 ng ml^{-1} of Hg and the precision of the proposed flow-through fluorimetric optosensor, evaluated as the R.S.D. of ten replicates of a sample containing 100 ng ml^{-1} of Hg(II), was $\pm 3.0\%$.

3.6. Analysis of real samples

The usefulness of the proposed method was evaluated for the determination of mercury(II) in mineral, tap and sea water samples by following the general procedure described in Section 2.

Mineral and tap waters (in which Hg(II) concentration was not detectable with the proposed method) were spiked with Hg(II) at different concentration levels and analyzed with the proposed optosensor. No other previous pretreatment was required for these water samples. The results obtained are collected in Table 2 and show good agreement between the expected and found values.

Sea water samples from Gijón bay (Asturias) were filtered and analyzed without any other previous treatment of the samples. As no fluorimetric Hg signals were obtained from such waters, they were spiked in the laboratory with Hg(II) at two different concentration levels and then analyzed with the proposed FIA–optosensing system. Results showed poor recoveries: 68% for an addition of 150 ng ml^{-1} of Hg(II) and 62% for an addition of 90 ng ml^{-1} of Hg(II). At the same time, a darkening of the solid support was observed after passing the sea water sample. Therefore, the spiked sea water samples were first filtered (by passing them through an Omnifit column, 50 mm long and 3 mm inner diameter, packed with the anionic-exchange resin Dowex 1X2-200, at a flow rate of 0.4 ml min^{-1}) in order to remove oils and other organic impurities present in such sea wa-

Table 2
Recovery study of spiked Hg(II) in mineral, tap and sea waters

Sample	Hg(II) spiked (ng ml ⁻¹)	Hg(II) recovered (ng ml ⁻¹)	Recovery (%)
Mineral water 1	60	64.5 ± 2.5	107.5
Mineral water 2	100	101.0 ± 3.0	101.0
Mineral water 3	130	127.8 ± 1.6	98.3
Tap water 1	45	46.3 ± 1.6	102.9
Tap water 2	60	58.4 ± 2.6	97.3
Tap water 3	80	78.0 ± 2.7	97.5
Sea water 1	50	54.5 ± 2.9	109.0
Sea water 2	90	90.8 ± 3.6	100.9
Sea water 3	120	114.6 ± 3.5	95.5

ters. These impurities adsorbed on the Amberlite XAD-4 resin would be responsible for the interferences observed on the Hg(II) determination (by decreasing the desired adsorption of the formed thiocrome). The resin-filtered sea water samples were then analyzed, with clearly improved recoveries (around 80%). In order to improve further such Hg recoveries, sea water samples were then diluted 1 + 1 with de-ionized water. Such diluted samples analyzed with the proposed optosensor provided excellent Hg(II) recoveries as demonstrated by the results given in Table 2.

Acknowledgements

Financial support from European Union (DG XII Science, Research and Development) through the project ref. MAS3-CT97-0143 (MEMOSEA) is gratefully acknowledged.

References

- [1] W.R. Seitz, in: O.S. Wolfbeis (Ed.), *Fiber Optic Chemical Sensors and Biosensors*, vol. II, CRC Press, Boca Raton, FL, 1991, p. 1.
- [2] R.J. Hurtubise, *Solid Surface Luminescence Analysis: Theory, Instrumentation, Applications*, Marcel Dekker, New York, 1991.
- [3] M. Valcárcel, M.D. Luque de Castro, *Flow-through (Bio)Chemical Sensors*, Elsevier, Amsterdam, 1994.
- [4] A. Sanz-Medel, *Anal. Chim. Acta* 283 (1993) 367.
- [5] E. Merian, *Metals and Their Compounds in the Environment*, VCH, Weinheim, 1991.
- [6] R.P. Mason, J.R. Reinfelder, F.M.M. Morel, *Water Air Soil Pollut.* 80 (1995) 915.
- [7] I. Oehme, O.S. Wolfbeis, *Mikrochim. Acta* 126 (1997) 177.
- [8] S.B. Savvin, L.M. Trutneva, O.P. Shvoeva, K.A. Efendiev, *J. Anal. Chem. Engl. Tr.* 46 (1991) 709.
- [9] A. Morales-Bahnik, R. Czolk, J. Reichert, H.J. Ache, *Sens. Actuat. B* 13 (1993) 424.
- [10] M. Plaschke, R. Czolk, H.J. Ache, *Anal. Chim. Acta* 304 (1995) 107.
- [11] R. Czolk, J. Reichert, H.J. Ache, *Sens. Actuat. B* 7 (1992) 540.
- [12] M. Lerchi, E. Reiter, W. Simon, E. Pretsch, D.A. Chowdhury, S. Kamata, *Anal. Chem.* 6 (1994) 1713.
- [13] I. Murkovic, O.S. Wolfbeis, *Sens. Actuat. B* 38–39 (1997) 246.
- [14] T.N. Shekhovtsova, S.V. Chernetskaya, *Anal. Lett.* 27 (1994) 2883.
- [15] C. Preininger, O.S. Wolfbeis, *Biosens. Bioelectron.* 11 (1996) 981.
- [16] M. Virta, J. Lampinen, M. Karp, *Anal. Chem.* 67 (1995) 667.
- [17] G. Oshima, K. Nagasawa, *Chem. Pharm. Bull.* 18 (1970) 687.
- [18] F. Grases, F. García Sánchez, M. Valcárcel, *Anal. Chim. Acta* 119 (1980) 359.
- [19] J. Holzbecher, D.E. Ryan, *Anal. Chim. Acta* 64 (1973) 333.
- [20] R. Pereiro García, Y.M. Liu, M.E. Díaz García, A. Sanz-Medel, *Anal. Chem.* 63 (1991) 1759.
- [21] R. Pereiro, M.E. Díaz García, A. Sanz-Medel, *Analyst* 115 (1990) 575.

Speciation of selenium (IV) in natural waters by solid phase spectrophotometry

M.C. Valencia, E. Arana Nicolas, L.F. Capitán-Vallvey *

Department of Analytical Chemistry, Faculty of Sciences, University of Granada, 18071 Granada, Spain

Received 27 November 1998; received in revised form 2 March 1999; accepted 3 March 1999

Abstract

A method for the speciation of selenium (IV) based on solid-phase spectrophotometry (SPS), has been developed. In acidic conditions selenium (IV) oxidizes potassium iodide and the I_3^- forms an ionic association with Rhodamine B (RB) which is fixed on a dextran type lipophilic gel. The gel phase absorbances at 590 and 800 nm are measured directly, and allows for the determination of selenium (IV) in the range of 0.7–18.0 $\mu\text{g l}^{-1}$, with a relative standard deviation (RSD) of 2.8%. The method has been applied to the determination of Se(IV) in natural waters. © 1999 Elsevier Science B.V. All rights reserved.

Keywords: Solid-phase spectrophotometry; Selenium (IV) speciation; Natural waters

1. Introduction

The speciation of the oxidation states of selenium, namely selenium (IV) and selenium (VI), is necessary for elucidation of its distribution, mobilization and toxicity in environmental waters, specially taking into account the small difference between its essential and toxic levels and the wide distribution of this non-metallic element.

The usual techniques used in these studies included absorption spectrometry using both hydride generation in a quartz furnace and electrothermal atomization [1], differential pulse

cathodic stripping voltammetry [2], high-performance liquid chromatography (HPLC) with on-line detection by inductively coupled mass spectrometry or flame atomic absorption spectrometry [3] and capillary electrophoresis [4]. The lack of enough sensitivity and selectivity of some of the methods used requires a preconcentration step, such as coprecipitation [5], adsorption on XAD-resin [6] or iron (III)-loaded Chelex-100 resin [7], functional resin [8,9], activated carbon [10,11], thiol cotton [12] and extraction [13], among others.

In this paper an attempt is made to try to solve the problem using solid phase spectrometry (SPS), a group of hybrid analytical techniques that combine two operational aspects of the analytical process, the sorption or fixation of the analyte or a derivative product on a solid phase from a

* Correspondence author. Tel./fax: +34-58-248436.

E-mail address: lcapitan@goliat.ugr.es (L.F. Capitán-Vallvey)

solution, and the subsequent measurements of any appropriate optical property (UV-Vis spectrophotometry [14], spectrofluorimetry [15], spectrophosphorimetry [16] and photoacoustic photometry [17]) directly in the solid phase.

The fixation of the analyte in the solid phase prior to the measurement of the analytical signal, provides a series of advantages, with a noticeable increase in the sensitivity as consequence of the preconcentration process and, many times, a high selectivity as a consequence of the selective fixation of the analytes in the appropriate solid support, derived from its differences in charge or polarity [18]. The right selection of solid support taking into account the chemical properties of the analyte or its derivative and the optical properties of the whole is the key factor in SPS methods.

The solid phases used in SPS are mostly organic solid particles of diverse granulometry and composition, specially adsorbents or ion exchangers. Among the first, silica gel or modified silica (i.e. C-18 silica gel) and polydextran gels (Sephadex) and as exchangers, cationic or anionic exchangers coming from styrene or polydextran type. As can be seen these solids are of hydrophilic nature, except C-18 silica. In this paper the use of an organic lipophilic solid support to retain the derivative that originates the analytical signal is explored.

The selenium (IV) oxidation of iodide to triiodide and back formation of an ionic association with Rhodamine B (RB) that is fixed in a lipophilic dextran type gel give us a way to speciate selenium (IV) at $\mu\text{g l}^{-1}$ level. The proposed method has been satisfactorily applied to the determination of selenium in water samples.

2. Experimental

2.1. Apparatus and software

A Perkin Elmer model Lambda 2 spectrophotometer interfaced to an IBM SX-486 micro-computer for the spectral acquisition and subsequent manipulation of experimental data. Furthermore, an Agitator 2000 rotating bottles

agitator (Tecnotrans, Barcelona, Spain), a desk centrifuge (URA Technic 2610, Barcelona, Spain) and a Crison Model 501 pH-meter (Crison Instruments, Barcelona, Spain) were used with a combined glass-saturated calomel electrode. The absorbance measurements were carried out in two matching glass cells (Hellma, type 100, Müllheim, Germany) with a 1 mm path length. For the treatment of the spectral data the following programmes were used: PECSS software v.4.2, Perkin Elmer, Ueberlingen, Germany, 1992 and the Data Leader Software Package, Beckman, Fullerton, CA, 1987.

2.2. Reagents

Stock solutions of (1000 mg l^{-1}) selenium (IV), (Titrisol Merck) as SeO_2 in nitric acid 0.5 M. The working solutions were obtained by dilution with HNO_3 solution until a 6.3% of HNO_3 was obtained. Other reagents included: RB, $1.29 \times 10^{-3} \text{ M}$ aqueous solution (Carlo Erba), this solution stored in dark bottle remains stable for 1 week; potassium iodide 1 M and hydrochloric acid (HCl) 4 M (both Aldrich).

The lipophilic Sephadex LH-20 gel (mesh 25–100 μm) (Sigma, St. Louis, MO) in its original dry state without pretreatment was used as solid support.

All reagents were of analytical-reagent grade unless stated otherwise. Reverse osmosis quality water was used throughout and all experiments were carried out at room temperature.

2.3. Absorbance measurements

The absorbance (really attenuation) of the ionic pair sorbed in the gel was measured in a 1 mm cell at 590 nm (corresponding to the absorption maximum of the derivative) and 800 nm (the latter is in the 700–850 nm range, where only the gel 'absorbs' light), and compared with a 1 mm cell packed with gel equilibrated with blank solution. The net absorbance was calculated by difference as in a previous report [19].

2.4. Procedures

(A) For 100 ml final volume, an appropriate volume of sample containing 5.0–120.0 $\mu\text{g l}^{-1}$ (0.5–12.0 μg) of selenium (IV) was transferred into a 100 ml flask and then 4 ml of 4 mol l^{-1} HCl and 4 ml of 1 mol l^{-1} KI were placed levelling off to the mark with water. After standing for 15 min in the dark, the solution was transferred to a 1 l polyethylene bottle, adding 0.8 ml of 2.67×10^{-4} mol l^{-1} Rodamine B solution and 60 mg of Lipophilic Sephadex LH-20 (25–100 mesh) gel.

The mixture was stirred mechanically for 5 min and the coloured gel was collected by filtration under suction and, using a little pipette, packed into a 1 mm cell together with a small volume of the filtrate. The cell was centrifuged at 2500 rpm for 30 s. A blank solution containing all the reagents except selenium was prepared and treated in the same way as the sample. The absorbance difference between sample and blank, measured as described under ‘absorbance measurements’, provides an estimation of the net absorbance.

(B) For 500 ml final volume, an appropriate volume of sample containing 1.1–26.0 $\mu\text{g l}^{-1}$ (0.5–13.0 μg) of selenium (IV) was transferred into a 500 ml flask, using amounts of reagents increased by a factor of 5 and a constant amount of gel. The stirring time was 20 min, following the same steps as indicated above.

(C) For 1000 ml final volume, an appropriate volume of sample containing 0.7–18.0 $\mu\text{g l}^{-1}$ (0.7–18 μg) of selenium (IV) was transferred into a 1000 ml flask, using amounts of reagents increased by a factor of 10 and the same amount of gel. The equilibration time was 35 min, operating as indicated below.

The calibration graphs were constructed in the same way, using selenium solution of known concentration.

2.5. Treatment of samples

The natural water was preserved with concentrated HNO_3 (0.25 ml/1000 ml), filtered through a 0.45 μm membrane filter (Millipore) and collected

in a polyethylene container carefully cleaned with nitric acid. The samples were stored at 4°C until analysis. The analyses were performed with the least possible delay. The usual general precautions were taken to avoid contamination [20].

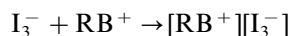
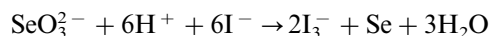
2.6. Distribution measurements

Rodamine B, HCl solution, KI and 60 mg of Sephadex LH-20 gel were added to a 500 ml aqueous solution containing 0.126 μmol of Se(IV). After 30 min of equilibration, the gel was separated by filtration under suction. The ionic pair concentration in the coloured gel was determined as described in the 500 ml procedure. Subsequently the aqueous phase was treated in the same way with a further batch of gel and the ionic pair remaining in the aqueous phase was measured as before. The distribution ratio, D (μmol of ionic pair sorbed per gram of resin/ μmol of ionic pair per ml of solution), was calculated in the usual way from the initial and equilibrium concentrations in the solution. An average value of D of $(2.00 \pm 0.26) \times 10^5 \text{ ml g}^{-1}$ was obtained from four replicate experiments.

3. Results and discussion

3.1. The fixation of rhodamine and its ionic pair

Selenium (IV) oxidizes iodide in a weak acid medium to iodine, which in aqueous solution is as a triiodide complex. In the presence of the cationic xanthene dye RB a less soluble violet ionic pair is formed, according to the equations:



It was found that the ionic pair is not fixed on ion-exchangers as QAE or DEAE Sephadex anion exchangers, as well as in the cation exchangers (SP) or hydrophilic adsorbents as G-25 Sephadex. On the contrary, the ionic pair was strongly fixed in lipophilic Sephadex (hydroxypropyl beaded dextran) as indicated by its distribution ratio of $(2.00 \pm 0.26) \times 10^5 \text{ ml g}^{-1}$, giving

a red colour with an absorption maximum at 590 nm, compared with 580 nm observed in solution. RB at pH 3 and when selenium is not present, was less strongly fixed in the lipophilic Sephadex showing an absorption maximum at 564 nm (552 nm in aqueous solution [21]) (Fig. 1).

3.2. Optimization of variables

3.2.1. HCl concentration

From hydrochloric acid, phosphoric acid and sulphuric acid, the first gave the highest absorbance and stability. Optimum HCl concentration for the formation and fixation of the species falls in the range 0.12–0.18 M. At concentrations higher than 0.18 M and lower than 0.12 M the absorbance decreases significantly. The working HCl concentration selected for the formation and fixation of the ion-association in the gel phase is 0.16 mol l⁻¹. The optimum HCl concentration is the same for all sample volumes studied. It should be pointed out that the optimum acidity in the gel phase is lower than in homogeneous solution (0.32 M) [21].

An increase in the ionic strength decreases the absorbance, an effect that may be attributed to the competition of the other ions in the ion-pair formation.

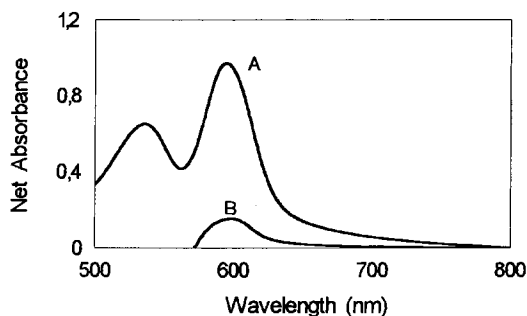


Fig. 1. Net absorption spectra of ion-association (blank as reference). (A) Gel spectrum [Se(IV)] = 26 $\mu\text{g l}^{-1}$; [KI] = 0.04 M; [RB] = 2.13×10^{-6} M; [HCl] = 0.16 M; lipophilic Sephadex = 60 mg; stirring time = 20 min; sample volume = 500 ml. (B) Solution spectrum [Se(IV)] = 100 $\mu\text{g l}^{-1}$; [KI] = 0.08 M; [RB] = 8×10^{-5} M; [HCl] = 0.32 M.

3.2.2. Rodamine B and iodide concentrations

Absorbance increases together with Rodamine B concentration and the optimum values are obtained for concentrations of RB between 1.86×10^{-6} and 2.4×10^{-6} mol l⁻¹ (for 500 ml sample) decreasing immediately after. Consequently, a 14 [RB]/[Se] ratio was chosen for 500 ml. However, for 100 and 1000 ml, 1 and 8 ml of RB solution 2.67×10^{-4} M were recommended, respectively, using the same molar ratio. Working with the optimum Rodamine B concentration, a maximum absorbance value in the range 0.035–0.05 M was observed for potassium iodide concentration. In the standard procedures 4.0×10^{-2} M was selected as optimum.

3.2.3. Other experimental conditions

For the optimum development of the ion-association, 15 min was necessary before equilibration with the gel. The optimum stirring time depended on the sample volume. Stirring times of 5, 20 and 35 min were necessary for 100, 500 and 1000 ml, respectively. The fixed species is stable for at least 1 day after equilibration. As the centrifugation of the gel into the measurement cell increases the signal and decreases its fluctuation a centrifugation time of 0.5 min at 2500 rev min⁻¹ (25 g) was used here. The use of a large amount of resin lowered the absorbance as usual [19], consequently only the amount required to fill the cell and to facilitate handling was used for all the measurements (60 mg). The order of addition used here was: selenium + HCl + KI + RB + solid phase.

3.3. Analytical data

The analytical parameters are summarized in Table 1. The reproducibility was established for the proposed method by measuring the selenium concentration for 100, 500 and 1000 ml sample solutions with a Se(IV) concentration of 50, 16 and 6 ng ml⁻¹, respectively. For ten determinations, the relative standard deviation (RSD) was 2.0, 2.3 and 2.8%, respectively. It was possible verifying that one of the main contributions to the RSD comes from the variability of the packing of the gel. Because of this, reproducibility is im-

Table 1
Analytical parameters

Parameter	Volume of sample system		
	100 ml	500 ml	1000 ml
Intercept	−0.012	−0.010	−0.012
Slope	0.008	0.037	0.052
LDR ($\mu\text{g ml}^{-1}$)	5.0–120.0	1.1–26.0	0.7–18.0
Correlation coefficient	0.9986	0.9991	0.9996
Detection limit ($K = 3$) ($\mu\text{g ml}^{-1}$)	4.1	1.1	0.7
Determination limit ($K = 10$) ($\mu\text{g ml}^{-1}$)	13.7	3.6	2.5
RSD (%) ($n = 10$)	2.0	2.3	2.8

proved if the cells packed with the gel phase are centrifuged before spectrophotometric measurements are taken. With centrifugation for 0.5 min at 2500 rpm before the absorbance measurements were carried out, the RSD decreased and the absorbance values increased about a 10%.

The sensitivity, expressed as molar absorptivity, of the proposed methods, is compared with that of spectrophotometric procedures cited in the literature (Table 2). It is shown that the increase in sensitivity obtained with the proposed method is substantial, especially in relation to the solution methods using the same reagent.

Table 2
Comparison of sensitivities for spectrophotometric selenium methods^a

Reagent	Molar absorptivity ($\times 10^4$ $1 \text{ mol}^{-1} \text{ cm}^{-1}$)	Reference
SnCl ₂	0.17	[22]
DAB	1.02	[23]
J-acid	1.48	[24,25]
Dithizone	7.0	[26]
Rhodamine B-I [−]	19.7	[21]
Thiocyanate-BR	64.0	[27]
Procedure 100 ml	612	This paper
Procedure 500 ml	2868	This paper
Procedure 1000 ml	4001	This paper

^a J-acid, 6-amino-1-naphthol-3-sulphonic acid; DAB, 3,3'-diaminebenzidine; BR, butylrhodamine.

Table 3
Effect of foreign ions in the determination of $12 \mu\text{g l}^{-1}$ of selenium (IV)

Foreign ion or species	Tolerance level ($\mu\text{g l}^{-1}$)
Cl [−] , K(I), Na(I), Be(II), Mn(II)	>5000
NO ₃ [−] , SO ₄ ^{2−}	5000
SiO ₃ ^{2−}	3000
Ca(II), Mg(II), Co(II), CDTA	2000
Cr(III)	800
PO ₄ ^{3−} , Zn(II), W(VI)	250
Pb(II)	150
F [−] , Mo(VI), EDTA	100
Te(IV)	80
Hg(II)	25
Cd(II), Ascorbic acid	12
Bi(III)	5
S ^{2−} , Cu(II), Fe(III)	<1

The increase in sensitivity with the sample volume taken for analysis can be calculated by measuring the absorbance of gel equilibrated with different volumes of solutions containing the same concentration of Se(IV) and a proportional amount of the other reagents. In practice, the increase in the absorbance with the sample volume can also be predicted from the slope of the calibration graphs. The sensitivity ratios (S) for the samples analyzed here are: $S_{1000/500} = 1.4$; $S_{1000/100} = 6.5$ and $S_{500/100} = 4.6$.

The S.D. of the background absorbance measured for the blank, which is necessary for the estimation of the IUPAC detection limit ($K = 3$), was taken as the average of ten determinations and noted as RSD units. Values calculated for the 100, 500 and 1000 ml samples were ± 0.011 , ± 0.013 and ± 0.016 , respectively (Table 1).

3.4. Effect of foreign ions

A study of interference effects was carried out for cations and anions, in amounts ranging up to $5000 \mu\text{g l}^{-1}$, with $6 \mu\text{g}$ of selenium. Ions were considered as not interfering if they produced an error less than $\pm 5\%$ in the determination of the analyte. The tolerance limits for the ions studied are shown in Table 3. The interference level is lower than the solution method [21] for the ions assayed. The most serious interferences are caused

Table 4
Recovery study for Se(IV) in natural waters

Mineral water ^a	Se(IV) in sample ($\mu\text{g l}^{-1}$)	Se(IV) added ($\mu\text{g l}^{-1}$)	Total Se(IV) found ($\mu\text{g l}^{-1}$)	Average recovery (%)
Ortigosa del Monte	0.00	3.00	3.03	101.0
	0.00	4.50	4.40	97.8
Lanjaron	0.00	3.00	2.96	98.6
	0.00	5.50	5.62	102.2
Fuente Liviana	0.00	3.00	2.94	98.0
	0.00	6.00	5.86	97.7
Solan de Cabras	3.25	3.00	6.33	102.7
	3.25	6.00	9.40	102.5
	3.25	9.00	12.15	98.9

^a Sample volume 500 ml levelled off to 1000 ml. Standard addition calibration graph method. The data represent the average from three determinations.

by ions which may oxidize I^- to I_3^- under the experimental conditions, such as Cu(II), Fe(III); ions which may reduce Se(IV) or I_3^- such as S^{2-} or ascorbic acid and, finally, ions which may form anionic complexes able to form ion-associates with RB, such as Bi or Cd.

3.5. Applications

The proposed method has been applied to the determination of selenium in mineral waters by the standard additions method. Due to the presence of interfering ions in waters, a previous treatment to eliminate those ions using a cationic exchanger was developed (1 g for 2 l of water; Sephadex CM C25; exchange capacity 5.3 meq g^{-1}). Water and ion exchanger were equilibrated for 20 min, then the gel was separated by filtration and the selenium content determined in the water, as described in the standard procedure. The method used was the general procedure for the 1000 ml sample system and the selenium contents in three natural water samples (Ortigosa del Monte (Segovia), Lanjarón (Granada) and Fuente Liviana (Cuenca), all from Spain), selected because its different mineralization level, were lower than the determination limit of the method. The selenium content in other natural water (Solan de Cabras, also from Spain) was $3.25 \mu\text{g l}^{-1}$. To check the accuracy of the proposed method in selenium analysis in water, a recovery

study was carried out in the waters mentioned above. To do so, different amounts of Se(IV) were added to water samples, obtaining a recovery acceptable in the standard conditions established. Table 4 shows the results obtained for all water samples.

Acknowledgements

This study was found by the General Subdirectorate for Training and Knowledge-sharing of the Spanish Ministry of Education and Culture (Project No. PB96-1404).

References

- [1] D.A. Martens, D.L. Suarez, Environ. Sci. Technol. 31 (1997) 133.
- [2] F. Seby, M. Potin-Gautier, A. Castebon, M. Astruc, Analisis 23 (1995) 510.
- [3] G. Alsing Pedersen, E.H. Larsen, Fresenius J. Anal. Chem. 358 (1997) 591.
- [4] D. Schlegel, J. Mattusch, R. Wennrich, Fresenius J. Anal. Chem. 354 (1996) 535.
- [5] Th.A. Kouimtzi, M.C. Sofoniou, I.N. Papadoyannis, Anal. Chim. Acta 123 (1981) 315.
- [6] Y. Sugimura, Y. Suzuki, J. Oceanog. Soc. Jpn. 33 (1997) 23.
- [7] T. Ferri, P. Sangiorgio, Anal. Chim. Acta 321 (1996) 185.
- [8] M. Nakayama, M. Chikuma, H. Tanaka, Talanta 30 (1983) 455.

- [9] M. Nakayama, T. Tanaka, M. Tanaka, M. Chikuma, K. Itoh, H. Sakurai, H. Tanaka, T. Nakagawa, *Talanta* 34 (1987) 435.
- [10] H.J. Robberecht, R.E. Van Grieken, *Anal. Chem.* 52 (1980) 449.
- [11] M.I. Castilla, J.V. Llopis, *Agrochimica* 39 (1995) 233.
- [12] Mu-Quing Yu, Gui-Quin Liu, Qinhan Jin, *Talanta* 30 (1983) 265.
- [13] M. Ejaz, M.A. Qureshi, *Talanta* 34 (1987) 337.
- [14] M.L. Fernández de Córdova, A. Ruíz Medina, A. Molina Diaz, *Fresenius J. Anal. Chem.* 357 (1997) 44.
- [15] H. Waki, S. Noda, M. Yamashita, *Reactive Polymers* 7 (1988) 227.
- [16] T. Vo-Dinh (Ed.), *Room Temperature Phosphorimetry for Chemical Analysis*, Wiley, New York, 1984.
- [17] S. Yamada, K. Yoshimura, *Talanta* 39 (1992) 1013.
- [18] L.F. Capitan-Vallvey, R. Avidad, M.D. Fernandez Ramos, *Recent Res. Dev. Pur. Appl. Anal. Chem.* 1 (1998) 149.
- [19] P. Ortega Barrales, A. Molina Diaz, M.I. Pascual Reguera, L.F. Capitan-Vallvey, *Anal. Chim. Acta* 353 (1997) 115.
- [20] American Public Health Association. American Water Works Association and Water Pollution Control Federation. *Standard Methods for the Examination of Water and Wastewater*, 15th edition. A.P.H.A., Washington D.C., 1981.
- [21] Liu-Shaopu, Zhou-Guangming and Huang Zhigui, *Talanta* 37 (1990) 749.
- [22] N. Léontovich, *Chim. Anal. (Paris)* 41 (1959) 56.
- [23] G.R. Desai, J. Paul, *Mikrochim. J.* 22 (1977) 176.
- [24] K.N. Ramachandran, R. Kaveeshwar, V.K. Gupta, *Talanta* 40 (1993) 781.
- [25] R. Manish, K.N. Ramachandran, V.K. Gupta, *Talanta* 41 (1994) 1623.
- [26] B. Kasterka, J. Dobrowolski, *Chim. Anal.(Warsaw)* 15 (1970) 303.
- [27] X. Li, H. Hu, *Fenxi Huaxue* 17 (1989) 1119.

A sensitive colorimetric method for the micro determination of iodine in marine water

Omi Agrawal, G. Sunita, V.K. Gupta *

School of Studies in Chemistry, Pt. Ravishankar Shukla University, Raipur 492010 M.P., India

Received 16 September 1998; received in revised form 26 February 1999; accepted 6 March 1999

Abstract

More than 70% of the earth surface is covered by water bodies. Marine pollution is associated with the discharge of oils, petroleum products, sewage agricultural wastes, pesticides, heavy metals, waste substances and dumping of radioactive waters in sea. This in turn results in hazards to human health, hindrance to aquatic organisms and impairment of quality for use of sea water. Sea water is reported to contain iodine but the concentration varies according to the location and depth. Here a simple and sensitive method is described for the determination of iodine using leucocrystal violet as a reagent in different samples of sea water. The method is based on the oxidation of iodine to iodate with bromine water and the liberation of free iodine from the iodate by addition of potassium iodide in acidic medium. This iodine selectively oxidises leucocrystal violet to form the crystal violet dye. Beer's law is obeyed over the concentration range of 0.04–0.36 ppm of iodine at λ_{\max} 592 nm. The dye was further extracted in chloroform. The extracting system obeys Beer's law in the range of 0.008–0.08 ppm at λ_{\max} 588 nm. © 1999 Elsevier Science B.V. All rights reserved.

Keywords: Colorimetric method; Iodine; Marine water

1. Introduction

Iodine is an essential element in nutrition. Iodine and its compounds are used in analytical chemistry, medicine, photography and in the making of dye stuff and numerous organic compounds. It is liberated from its salts by the action of oxidising agent and purified by sublimation. Formally obtained from the ash of seaweed, it is now obtained chiefly from the mother liquors

remaining in the preparation of chille saltpetre or from natural occurring brines in the US [1].

For the prevention of endemic goitre iodides are added to the table salt, but chronic intoxication including irritation and nervousness have been seen from the ingestion of excessive amount of iodides. The ingestion of iodine may cause occurrence of fatal poisoning due to nitrogen retention and anuria. Inhalation of iodine vapour acts as an irritant causing a rapidly developing pulmonary oedema [2,3]. Its industrial exposure shows lacrymation and burning sensation in the eyes, blepharitis, rhinitis, catarrhal, stomatitis and chronic pharyngitis. The threshold concentration

* Corresponding author. Fax: +91-771-428-824.

for iodide is 0.1 ppm or 1 mg m^{-3} in air as adopted by the American Conference of Governmental Industrial Hygienists [1,4,5].

Due to its importance, various instrumental methods such as high-performance liquid chromatography (HPLC) [6], gas chromatography (GC) [7], GC/mass spectrometry (MS) [8], neutron activation analysis [9], voltametry [10], Plasma MS [11] etc. have been reported for the determination of iodine in various environmental and biological samples. A number of spectrophotometric methods are reported in the literature [12–19]. Some of the methods lack sensitivity and are based on catalytic reactions [12] in which Hg (II) seriously interferes even in traces [13].

Other methods using different reagent, i.e. neutral red [14], $\text{Ce}(\text{SO}_4)_2$ [15] etc. are also reported for the spectrophotometric determination of iodine but these methods suffer from drawbacks such as instability of colour, insufficient, sensitivity, absorbance variation of the blank, interferences from foreign ions etc.

In the present communication, a simple, sensitive and non catalytic method is proposed for the determination of iodine in different samples. Iodine is oxidised to iodate with saturated bromine water. In acidic medium the iodate is treated with potassium iodide to liberate free iodine. This iodine selectively oxidises leucocrystal violet to form crystal violet dye which shows maximum absorbance at 592 nm. The dye was further extracted in chloroform. The clear organic layer was separated and transferred quantitatively into a graduated tube and was made up to 10 ml. The absorbance of this extraction system was measured at 588 nm against the reagent blank. Beer's law was obeyed in the concentration range of 0.04–0.36 ppm in aqueous system and 0.008–0.08 ppm in extraction system.

2. Experimental

2.1. Apparatus

All spectral measurements were made with systronics UV-VIS 108 spectrophotometer. Systronics pH meter model 331 was used for pH measurement.

2.2. Reagents

2.2.1. Iodine stock solution

Stock solution of iodine of 1 mg ml^{-1} was prepared in 30% ethanol. The working standard solution was prepared by the appropriate dilution of stock with water.

2.2.2. Bromine water

A saturated solution of bromine water was prepared daily.

2.2.3. Formic acid

Aqueous solution (50%) was used.

2.2.4. Potassium Iodide

Aqueous solution (0.1%) was used.

2.2.5. Leucocrystal violet (Sigma, St. Louis, MO)

To a 1 l volumetric flask 200 ml of water, 3 ml of 85% phosphoric acid and 250 mg of leucocrystal violet, i.e. 4,4',4''-methylidynetris (*N,N'*-dimethylaniline) ($\text{CH}[\text{C}_6\text{H}_4\text{N}(\text{CH}_3)_2]_3$) were added and shaken gently until the dye gets dissolved. The content of the flask was then diluted to 1 l with water.

2.2.6. Sodium hydroxide

Aqueous solution (0.5 M) was used.

2.3. Procedure

To an aliquot containing 1–9 mg of iodine, 0.5 ml of bromine water was added and shaken for 2 min. The excess of bromine was removed by the dropwise addition of formic acid. To this 1 ml of potassium iodide and 1 ml of leucocrystal violet were added. The pH of the solution was adjusted between 4.5 and 5.5 with the use of sodium hydroxide. The contents were diluted to 25 ml with water and kept for about 25 min for complete colour development. The absorbance was measured at 592 nm against the reagent blank.

The aliquot containing 0.8–8 mg in 100 ml of deionised water was taken. The dye was developed from the above procedure. The dye was further extracted in chloroform. The clear organic layer was separated and transferred quantitatively

into a graduated tube and was made up to 10 ml. The absorbance of this extraction system was measured at 588 nm, against the reagent blank.

3. Results and discussion

3.1. Spectral characteristics

The absorption spectrum of the dye formed shows maximum absorbance at 592 nm. The reagent blank showed negligible absorbance at this wavelength.

3.2. Adherence to Beer's law, molar absorptivity and Sandell's Sensitivity

Beer's law was obeyed over the concentration range of 1–9 μg (0.04–0.36 ppm) of iodine in a final solution of 25 ml in aqueous system. The molar absorptivity and sandell's sensitivity were found to be $2.82 \times 10^5 \text{ l mol}^{-1} \text{ cm}^{-1}$ and $0.00045 \mu\text{g cm}^{-2}$ for iodine in aqueous phase. In extraction system Beer's law obeys over the

range of 0.8–8.0 μg in 100 ml solution (0.0008–0.08 ppm). The molar absorptivity and Sandell's sensitivity were found to be $1.01 \times 10^6 \text{ l mol}^{-1} \text{ cm}^{-1}$ and $0.00012 \mu\text{g cm}^{-2}$, respectively.

3.3. Effect of reagent concentration

It was found that 0.5 ml bromine water, 1 ml of potassium iodide and 1 ml of leucocrystal violet were sufficient for complete colour reaction. For the removal of excess of bromine two to three drops of formic acid was sufficient. It was found that on increasing the amount of formic acid the sensitivity decreased (Fig. 1).

3.4. Effect of time and temperature

It was observed that 2 min were sufficient for the oxidation of iodine. Free iodine was liberated immediately in acedic medium. Full colour development required 25 min. It was found that 35–45°C was the most suitable temperature for the colour reaction. The temperature was obtained by keeping the solution in a thermostat maintained at 45°C. At lower and higher tem-

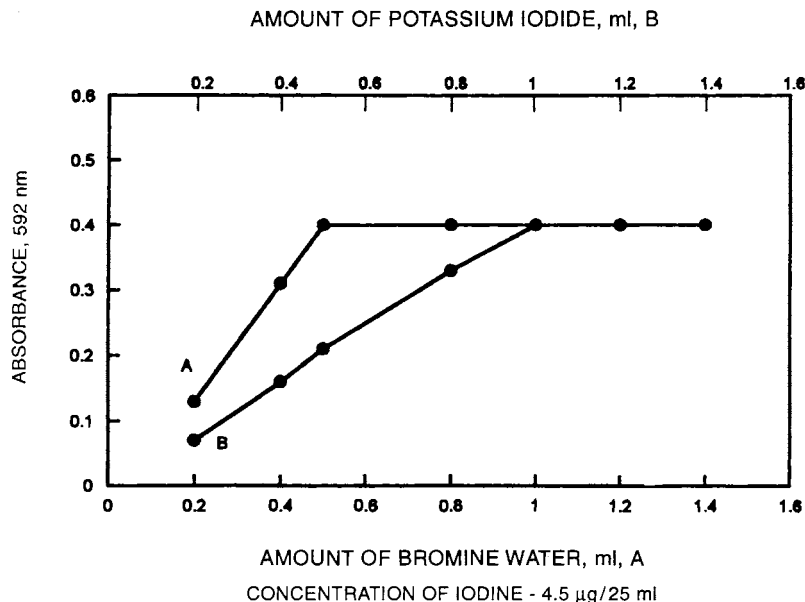


Fig. 1. Effect of amount of bromine water and potassium iodide on colour reaction.

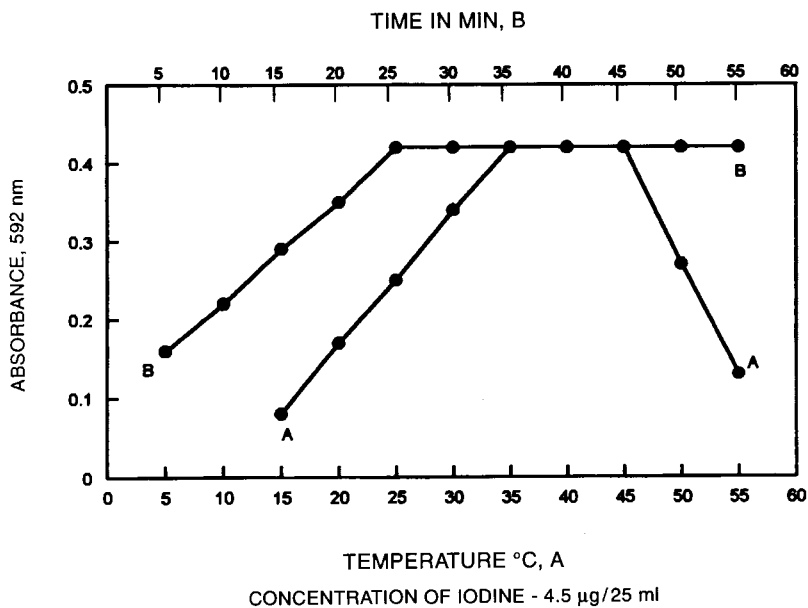


Fig. 2. Effect of temperature and time on colour reaction.

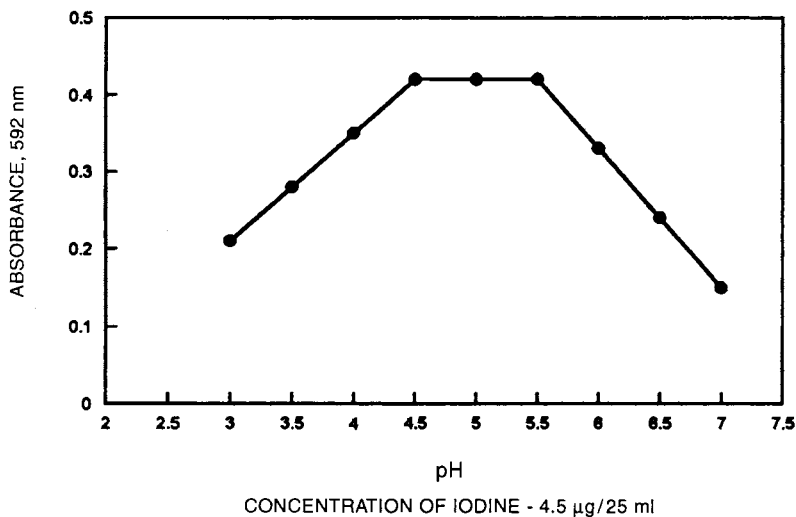


Fig. 3. Effect of pH on colour reaction.

perature the colour intensity gradually decreased (Fig. 2).

3.5. Effect of pH

Under optimum conditions pH of 4.5–5.5 was found to be the best for the formation of crystal violet from leucocrystal violet. Above the pH 5.5

stability and the sensitivity of the colour was severely affected (Fig. 3).

3.6. Stability of colour

The crystal violet dye formed was stable for several days under optimum conditions.

Table 1
Effect of foreign species^a

Foreign species	Tolerance limit ^b (µg/25 ml)
SO ₄ ²⁻ , PO ₄ ³⁻	62 500
NO ₃ ⁻	50 000
HCO ₃ ⁻ , phenol	37 500
Cd ²⁺ , Sr ²⁺ , Ba ²⁺ , Ca ²⁺ , Fe ³⁺	31 250
Zn ²⁺ , Al ³⁺	25 000
Co ²⁺ , Cu ²⁺	21 250
Pb ²⁺ , Sn ⁴⁺	20 000
Br ⁻ , Cl ⁻	6250
Hg ²⁺ , Mn ²⁺	625

^a Concentration of iodine 4.5 µg/25 ml, 0.18 ppm.

^b The amount causing 2% error in absorbance values.

3.7. Reproducibility

The reproducibility of the method was assessed by carrying out seven replicate analysis of the final solution containing 4.5 µg per 25 ml of iodine. The standard deviation (S.D.) and relative standard deviation (R.S.D.) were found to be ± 0.006 and 1.50%, respectively.

Table 2
Determination of iodine in marine water

Sample ^b	Amount of iodine initially found ^a (µg)	Amount of iodine added (µg)	Total iodine found ^a (µg)	% Recovery
Sample 1	2.18	2	4.13	97.50
	2.19	4	6.15	99.00
	2.18	6	8.10	98.66
Sample 2	3.40	2	5.37	98.50
	3.39	3	6.35	98.66
	3.41	4	7.39	99.50
Sample 3	4.10	4	8.07	99.25
	4.12	4	8.07	98.75
	4.12	4	8.02	97.50
Sample 4	2.25	2	4.23	99.00
	2.25	4	6.15	97.50
	2.25	6	8.17	98.66
Sample 5	1.87	2	3.84	98.50
	1.90	4	5.82	98.00
	1.92	6	7.79	97.83

^a Mean of three replicate analysis.

^b Aliquot of the sample solution = 5 ml after treatment described in the Section 4.

3.8. Effect of foreign species

The validity of the method was assessed by investigating the effect of common foreign species in the analysis of iodine. The tolerance limit values of different foreign species in a solution containing 4.5 µg per 25 ml of iodine are given in Table 1. The anions Cl⁻, Br⁻, SO₄²⁻, PO₄³⁻, NO₃⁻ did not interfere under the optimum conditions.

4. Application

Sea water is reported to contain iodine but the concentration varies according to the location and depth [4]. The method was applied for the determination of iodine in marine water. Different samples of marine water was collected in 1 l glass bottles and filtered. For the analysis of the water sample dry combustion was carried out in which water sample was heated in a suitable evaporation vessel. The dry residue was used for the further separation process. Selective adsorption isolates certain substances in water which are difficult to concentrate. Then the water was again filtered in order to remove any solid matter present [20].

Then aliquots of the sample was analysed. The results are given in the Table 2.

5. Conclusion

The proposed method is simple and sensitive. The method is highly selective as most of the common ions do not interfere. The method is fairly reproducible and can be compared favourably with the standard methods reported by Kolthoff et al. [16,17] using cerium salt having a sensitivity of 0.05 μg and Velculescu et al. [18] having a sensitivity of 5 μg using silver nitrate. H. Weisz proposed a sensitivity of 0.3 μg using starch solution [19]. The method should be applicable for the determination of iodine in different environmental samples.

Acknowledgements

The authors are thankful to Pt. Ravishankar Shukla University, Raipur for providing laboratory facilities. One of them (O.A.) is thankful to Pt. R.S.U., Raipur for providing financial assistance and (G.S.) is thankful to CSIR, New Delhi for Senior Research Fellowship.

References

- [1] F.A. Patty, *Industrial Hygiene and Toxicology*, vol. 2, 2nd edition, Interscience, New York, 1962, p. 854.
- [2] R. Finkelstein, M. Jacobi, *Ann. Intern. Med.* 10 (1937) 1283.
- [3] A.B. Luckhardt, F.C. Koch, W.F. Schroeder, A.H. Weiland, *J. Pharmacol. Exp. Ther.* 15 (1920) 1.
- [4] N.I. Sax, *Dangerous Properties of Industrial Materials*, 6th edition, Van Nostrand Reinhold, New York, 1984, p. 1616.
- [5] M. Crawford, *Air Pollution Control Theory*, Tata McGraw Hill, New Delhi, 1980, p. 10.
- [6] S. Ohshiro, N. Hokama, N. Habaro, *Byoin Yakugaku* 23 (1997) 202, (JP) C.A., 127 (6) (1997) 86189 u.
- [7] Z. Fu, Q. Ge, M. Yu, Y. Wang, *Fenxi Huaxue* 24 (1996) 198 (ch), C.A., 124 (13) (1996) 169704 x.
- [8] S.H. Sang, O.S. Yunsuk, K.J. Hwan, R.J. Keun, *J. Chromatogr. A* 732 (1996) 327.
- [9] M. Dermelj, A.R. Byrne, *J. Radioanal. Nucl. Chem.* 216 (1997) 13.
- [10] Q. Wu, R. Wu, K. Liu, J. Lihua, *Huaxue Fence* 31 (1995) 82 (ch), C.A., 123 (8) (1995) 92606 m.
- [11] E.H. Larsen, M.B. Ludurigen, *J. Anal. Al. Spectrom.* 12 (1997) 435.
- [12] Z. Guo, S. Zhang, *Fenxi Shiyanshi* 14 (1995) 31 (ch) C.A., 124 (22) (1996) 305774 z.
- [13] M. Pesaventa, *Anal. Chim. Acta* 153 (1983) 249.
- [14] H. Yamada, M. Sugahara, H. Kosaka, A. Katayama, K. Takahashi, K. Yonebayashi, *Soi. Sci. Plant. Nutr.* 42 (1996) 367.
- [15] Y. Chen, *Zhongguo Tiaoweipin* 4 (1995) 29 (ch), C.A., 123 (17) (1995) 226190 g.
- [16] I.M. Kolthoff, E.B. Sandell, *J. Am. Chem. Soc.* 56 (1934) 1426.
- [17] I.M. Kolthoff, E.B. Sandell, *Microchim. Acta* 1 (1937) 9.
- [18] A.J. Velculescu, J. Cornea, *Z. Anal. Chem.* 94 (1933) 255.
- [19] H. Weisz, *Microchim. Acta* (1956) 1225.
- [20] W. Fresenius, K.E. Quenlin, W. Schneider (Eds.), *Water Analysis*, Springer-Verlag, New York, 1988, pp. 71, 264.

Determination of trace rare earth elements by X-ray fluorescence spectrometry after preconcentration on a new chelating resin loaded with thorin

Irma E. De Vito *, Adriana N. Masi, Roberto A. Olsina

*Department of Analytical Chemistry 'Dr Carlos B. Marone', Faculty of Chemistry, Biochemistry and Pharmacy,
National University of San Luis, San Luis, Argentina*

Received 25 September 1998; received in revised form 25 February 1999; accepted 6 March 1999

Abstract

A very stable chelating resin was prepared by adsorption of (*o*-[3,6-disulfo-2-hidroxy-1-naphthylazo]-benzenearsonic acid) (thorin) on a macroporous resin Amberlite XAD-7. The optimal conditions for preparing it were obtained through the study of the adsorption properties of the resin and the thermodynamic quantities of the adsorption processes. Likewise, the behavior of the loaded resin with the rare earth elements (REE) were studied (pH of retention, sorption kinetics, etc). The conditions to prepare a thin film with this system were also evaluated. The loaded resin was successfully used for the separation and preconcentration of Sm(III), Eu(III) and Gd(III) prior to their determination by X-ray fluorescence (XRF) spectrometry. The preconcentration factor obtained was 500 and the concentrations at low detection limit were 13.8, 17 and 15.7 $\mu\text{g l}^{-1}$ for Sm, Eu and Gd, respectively. © 1999 Elsevier Science B.V. All rights reserved.

Keywords: Rare earth elements; X-ray fluorescence spectrometry; Thorin

1. Introduction

Great efforts and investigations have been made for obtaining chelating resins with selective chelating groups covalently attached to different supports [1–6]. These resins can be synthesized by direct polymerization and copolymerization of monomers containing the groups of interest by

chemical modification of the polymer. But, the application of these resins in the field of analytical chemistry seems to be limited by the complexity of their synthesis.

During the last years, the development of new functional resins which have chelating properties, prepared by simple immobilization of complexing organic reagents, by ion exchange and/or adsorption onto conventional anion exchange resins or non ionic adsorbents, has acquired great importance [7–10]. These modified resins can react with

* Corresponding author. Fax: + 54-2652-43-0224.

E-mail address: devito@unsl.edu.ar (I.E. De Vito)

a variety of metal ions by complex formation and can be used to preconcentrate trace of them preparing a selective resin.

The determination of lanthanides in geological samples is one of the most difficult and complicated analytical task, especially at trace levels, because of the similarity of their chemical behavior. The knowledge of the fundamental laws governing the distribution and redistribution of elements during metamorphic process, etc, enables geochemists to predict the probability of the occurrence of economically interesting minerals in a particular geological environment. The rare earth elements (REE), due to their similarity, serve as a particularly suitable group of indicator elements. The determination of REE in other materials is also of interest. The presence of trace quantities of REE in high purity metals, semiconductors and glasses have an important influence on the electrical, magnetic, mechanical, nuclear and optical properties [11].

The present work is devoted to the preparation and characterization of a new chelating resin prepared by sorption of (*o*-[3,6-disulfo-2-hidroxy-1-naphthylazo]-benzenearsonic acid) (thorin) on a macroporous resin Amberlite XAD-7 and evaluation of the analytical properties of it. This loaded resin reacts with some REE for which its preconcentration capability has been studied. Another advantage of using this loaded resin is the possibility of preparing thin films with them, which implies that absorption-enhancement effects are negligible because neither primary nor analyte X-rays line are significantly absorbed in such a thin layer.

Thorine is a reagent that has been used for absorptiometric determination of REE [12], but its use in chelating resins or as a precocentrating agent has not been reported. Although thorine reacts with the REE, in this work only Sm, Eu and Gd were chosen for their study since they represent the transition between light (Sm) and heavy (Gd) REE. Eu shows a behavior that takes aside from general trend that characterize the rest of the REE. This is known as Eu anomaly and can be positive or negative depending if the concentration relation is smaller or higher than 1.

2. Experimental

2.1. Reagents and apparatus

The resin Amberlite XAD-7 (Rohm and Haas) has a specific surface area of $450 \text{ m}^2 \text{ g}^{-1}$, pore diameter 8 nm and bead size 20–50 mesh.

REE standard solutions were prepared by dissolving their oxides in HCl 0.1 mol l^{-1} and diluting with water.

A $5 \times 10^{-3} \text{ mol l}^{-1}$ solution of thorine was prepared by dissolving the reagent in water. Diluted solutions were prepared by adding water to the concentrated solutions

Membrane filter papers were Millipore of $0.45 \mu\text{m}$ pore size.

All other chemicals were of analytical grade and doubly distilled water was used throughout.

A Philips PW1400 X-ray fluorescence (XRF) spectrometer was used for Sm, Eu and Gd L_{α} line measurement. The parameters were appropriately selected.

A Gilford response UV-visible spectrometer was used with glass cells of 10 mm path length.

The ICP-AES measurements were performed with a sequential inductively coupled plasma spectrometer (Baird ICP 2070).

The pH of the solutions were measured by an Orion 701-A pH meter with Ag/AgCl electrode.

The filtrations were performed in a special filtration apparatus with a vacuum pump.

2.2. Preparation of the resin

The XAD-7 resin was ground with an acetone–water mixture in a ceramic mortar and sieved with a mesh sifter to obtain 100–200 mesh grains. Then the resin was soaked with methanol– 4 mol l^{-1} HCl (1:1) solution overnight and washed with water [3].

2.3. Effect of pH on the sorption

Amberlite XAD-7 was shaken during 1 h with solutions of $5 \times 10^{-4} \text{ mol l}^{-1}$ thorine. The pH was adjusted with NaOH or HCl (0.01 mol l^{-1}), the resin was filtered and equilibria concentrations of thorine were determined spectrometrically at 491 nm at pH 9.

2.4. Effect of shaking time on the sorption

The resin was shaken with $3.5 \times 10^{-4} \text{ mol l}^{-1}$ solutions of thorine during different periods of time at pH 3.5 and the filtered liquids were measured spectrometrically.

2.5. Effect of temperature and concentration of reagent on the sorption

The resin was shaken for 60 min at pH 3.5 with thorine solution in a concentration range of 0.5×10^{-5} to $5 \times 10^{-5} \text{ mol l}^{-1}$. The filtered liquids were determined spectrometrically. The procedures were realized at different temperatures.

2.6. Preparation of the loaded resin

Under the optimized adsorption conditions, the organic reagent was loaded on the grinded resin (Amberlite XAD-7). Resin (1 g) was shaken overnight with a 200 ml of $5 \times 10^{-3} \text{ mol l}^{-1}$ solution of thorine containing 2% v/v Triton X-100 at room temperature.

2.7. Effect of pH on the retention of Sm, Eu and Gd

Portions (10 ml) of solutions containing Sm 10 mg l^{-1} were adjusted to different pH values with sodium hydroxide or hydrochloric acid. They were mechanically shaken with 10 mg portions of the loaded resin for 2 h. The resins were then filtered on Millipore membrane using a vacuum pump. The papers were covered with Mylar and the L_{α} lines of the analyte were measured in the XRF spectrometer. The same procedure was carried out with solutions containing Eu and Gd.

2.8. Preparation of the thin film

Different amounts (5, 10, 15, 20, 25, 30 mg) of the loaded resin containing the preconcentrated elements were used to prepared the films and they were then measured by XRF, in order to determine the critical thickness of the film.

2.9. Determination of Sm, Eu and Gd in synthetic and reference samples

2.9.1. Sample treatment

The procedure for dissolving the reference sample G-2 from the United States Geochemical Standards (USGS) was the following: 1 g of sample was weighed and put into a teflon vessel. The sample was moistened with drops of water and 2 ml of HNO_3 (c). Then, 2 ml of HClO_4 (c) and 20 ml of HF (c) in portions of 3 ml each were added, looking the result of the dispersion in each step. The sample was heated in a sand bath up to dryness. In a case that some of the residue was resistant to the attack, the addition of HClO_4 and HF was repeated. At last, the residue was taken with HCl (c), in such a way that the final concentration was 2 mol l^{-1} . The solution was diluted up to 50 ml.

The separation of the matrix elements was carried out by ion exchange and the procedure used was that of Crock et al. [13]: the ion exchange apparatus consisted of a $30 \times 1 \text{ cm}$ glass column, packed with a 20 cm long bed of 200–400 mesh Dowex 2×8 cation exchange resin. This resin was washed with HNO_3 8 mol l^{-1} in order to eliminate iron, up to the washed liquid analyzed by ICP revealed no signal of Fe.

The resin was first activated with 50 ml of 1 mol l^{-1} HCl and then 25 ml of 2 mol l^{-1} HCl. Sample solution (50 ml) dissolved in 1 mol l^{-1} hydrochloric acid was loaded. The elution was realized with 50 ml of 2 mol l^{-1} HCl, followed by 50 ml 2 mol l^{-1} HNO_3 with a flow rate of 1 ml min^{-1} , discarding both eluates. Then the resin was eluted with 75 ml of 7.5 mol l^{-1} HNO_3 . The eluates were collected and combined, evaporated to dryness and carried to a final volume of 10 ml for subsequent REE determination.

The synthetic sample was prepared with the same composition of the reference samples GS-N of USGS.

A series of appropriate standards solutions of Sm, Eu and Gd were preconcentrated on the loaded resin by the described method and measured by XRF spectrometry. The measuring parameters were $66.23 2\theta$ for Sm L_{α} , $67.57 2\theta$ for Eu L_{α} and $61.10 2\theta$ for Gd L_{α} ; Rh tube, 50 kV 50

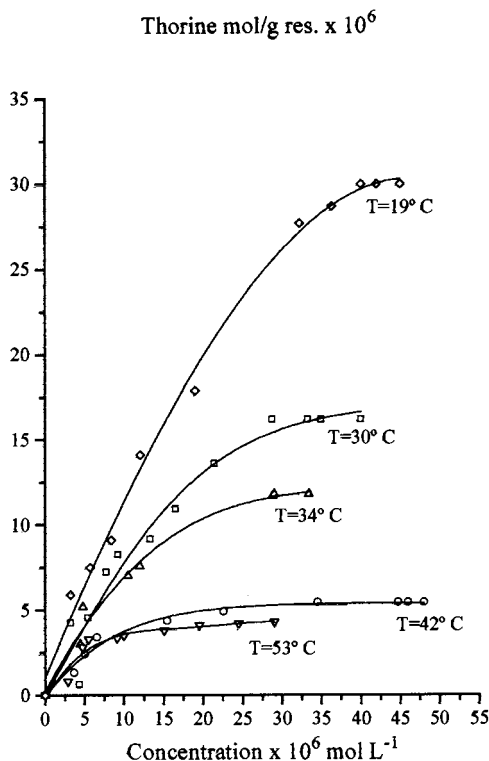


Fig. 1. Adsorption isotherms for thorin on amberlite XAD-7.

mA, LiF (200) crystal; 75–25 window width, counting time for peak and background 100 s; gas proportional-scintillation counter in tandem.

3. Results and discussion

Through the realized sorption studies it was established that the sorption of the reagent thorine on the surface of the poliacylate type resin Amberlite XAD-7 is a physic sorption due

to, probably, π – π dispersion forces between the aromatic rings of the reagent and no saturated bonds of the resin. This sorption behavior was confirmed through the adsorption isotherms (Fig. 1), in which it can be seen that the quantity of reagent increases as the solution concentration increases up to the saturation value, but decreases with increasing temperature. The same conclusion was obtained with the adsorption constants calculated for each temperature through the Langmuir isotherms (in Table 1). This behavior is typical for the adsorption process and the linearity of Langmuir isotherms shows that the reagent is adsorbed in a complete monolayer, on the opposite the isotherms were not linear.

The variation of the adsorption constants with temperature and Vant'Hoff equation enables the calculation of the thermodynamic parameters for the sorption process like enthalpy changes, entropy changes and standard free energy. Table 1. The low values of enthalpy changes can also confirm that the sorption is realized through physical forces because the chemisorption requires more energy to be produced. The negative entropy change values are in accordance with the 'order' produced when the molecules are adsorbed onto the surface of the resin.

Another important data obtained by these isotherms was the maximal loading capacity of the reagent on the resin. The average loading capacity calculated for this resin was $39.20 \times 10^{-5} \text{ mol g}^{-1}$. This gave the idea of a possible preconcentration factor, considering that the quantity of reagent loaded is proportional to the quelate formed.

Respect to the sorption mechanism on this type of resin, Lee et al. [14] have claimed that it occurs

Table 1

Thermodynamic variables of the adsorption process of thorine on Amberlite XAD-7 at different temperatures

T (°C)	ΔH^0 (Kcal mol ⁻¹)	ΔS^0 (Kcal (K mol) ⁻¹)	ΔG^0 (Kcal mol ⁻¹)	K_{Ads} (L mol ⁻¹)
19	-0.16744	0.01589	-4.80732	3982.7
30	-0.16744	0.01560	-4.89424	3398.4
34	-0.16744	0.01436	-4.57596	1812.5
42	-0.16744	0.01332	-4.36324	1066.9
53	-0.16744	0.01325	-4.48694	1020.0

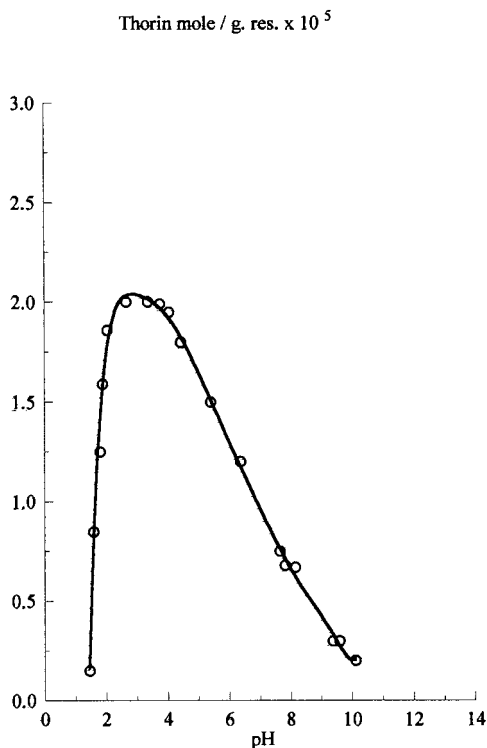


Fig. 2. Adsorption of thorin on Amberlite XAD-7 as function of pH.

between electrically neutral molecules and at higher or lower pH values the molecules are electrically charged, so the sorption becomes smaller or negligible. The results are in accordance with this theory since the experiences showed that the maximal pH of sorption is between pH 2 and 4, in which the reagent molecule remain without electric charge, Fig. 2.

The studies of sorption show that sorption equilibria is reached in 1 h, but for practical purposes it is convenient to leave the macroporous resins in contact with the reagent solution for a longer period of time.

3.1. Preconcentration and determination of Sm, Eu and Gd

In Fig. 3. it can be seen that the retention of trace amounts of Sm, Eu and Gd as a function of pH are evaluated by the batch method. These REE were optimally retained from solutions of

pH 9.5, 11 and 10, respectively, and after 120 min of shaking with the loaded resin they were totally retained.

Working with these optimal experimental parameters the enrichment factor obtained was 500, considering 10 ml of initial volume of sample, a final volume in the thin film of 20 mm³ and practically 100% of retention determined spectrometrically by the arsenazo method [12] in the filtrate. This factor can be enhanced working with an initial volume of 50 or 100 ml (it is unpractical to work with bigger volume). The concentrations at the lower detection limit were 13.8, 17 and 15.7 $\mu\text{g l}^{-1}$ for Sm, Eu and Gd, respectively.

The method was applied with good results to synthetic samples containing Sm, Eu and Gd in the same quantities as the references samples AGV-1 and GS-N of the USGS. In the same way, but with a previous dissolution treatment the certified rocks G-2 were analyzed. During the determination it was found that in samples containing different REE there were some spectral interferences between the analytes lines and the other REE present in the sample, so they ought to be corrected.

3.2. Correction of spectral interferences

The spectral interferences between the measured elements (analytes) and the other REE present in the analyzed certified samples by the developed methodology, were corrected using a factor obtained relating the intensity of the interference line in the 2θ angle corresponding to the analyte line and the intensity of a line of the interference element that can be measured on the specimen and without any type of interferences.

This relation was obtained measuring the intensities in samples containing only the element of interest by dissolution of its oxide. For each specimen, the intensity of the interferent line can be calculated from the measured intensity, free from interferences, of the second line of the interferent element.

The elements analyzed in this work Sm(III), Eu(III) and Gd(III) are spectrally interfered by the other REE which are present in granitic rocks like that analyzed by the authors.

The total intensity measured in a sample at the 2θ angle corresponding to an element i which is spectrally interfered by other j is [15]:

$$(I^x)_{i,T} = (I^x)_i + (I^y)_j \quad (1)$$

where $(I^x)_{i,T}$, total intensity (T) of the line x of element i measured at the position 2θ which is interfered by element j ; $(I^x)_i$, intensity of line x of element i without interference (at position 2θ); $(I^y)_j$, intensity of the line y of interfering element j at position 2θ of the analyte line.

If it is possible to measure the intensity of a line of element j free from interferences, then the intensity $(I^y)_j$ of this element can be written as a function of this line:

$$(I^y)_j = (k^{z,y})_{ji}(I^z)_j$$

$(k^{z,y})_{ji}$, fraction of the intensity of line y of interfering element j at position 2θ of the line x of analyte i , with respect to the intensity $(I^z)_j$ of line z of the interfering element j measured free from interferences. This factor involves atomic properties and instrumental parameters.

Knowing $(k^{z,y})$, it is factible to calculate the line intensity of the analyte free from interferences $(I^x)_i$, measuring the analyte intensity interfered $(I^x)_{i,T}$, and a line of the interferent element $(I^z)_j$, free from interferences [15].

In this case, the interference of Ce $L_{\gamma 1}$ on Gd $L_{\alpha 1}$, when Gd(III) is measured in a sample which also contains Ce(III) is:

$$(I^{L_{\alpha 1}})_{Gd,T} = (I^{L_{\alpha 1}})_{Gd} + (k^{L_{\alpha 1},L_{\gamma 1}})_{Ce,Gd}(I^{L_{\alpha 1}})_{Ce}$$

$$(I^{L_{\gamma 1}})_{Ce} = (k^{L_{\alpha 1},L_{\gamma 1}})_{Ce,Gd}(I^{L_{\alpha 1}})_{Ce} \quad (2)$$

the intensity of Gd(III) free from interferences will be:

$$(I^{L_{\alpha 1}})_{Gd} = (I^{L_{\alpha 1}})_{Gd,T} - (I^{L_{\gamma 1}})_{Ce} \quad (3)$$

If Eq. (2) is replaced in Eq. (3):

$$(I^{L_{\alpha 1}})_{Gd} = (I^{L_{\alpha 1}})_{Gd,T} - (k^{L_{\alpha 1},L_{\gamma 1}})_{Ce,Gd}(I^{L_{\alpha 1}})_{Ce}$$

Using the same methodology employed in the preparation of standards of the different elements determined in this work, the standards of Ce (III)

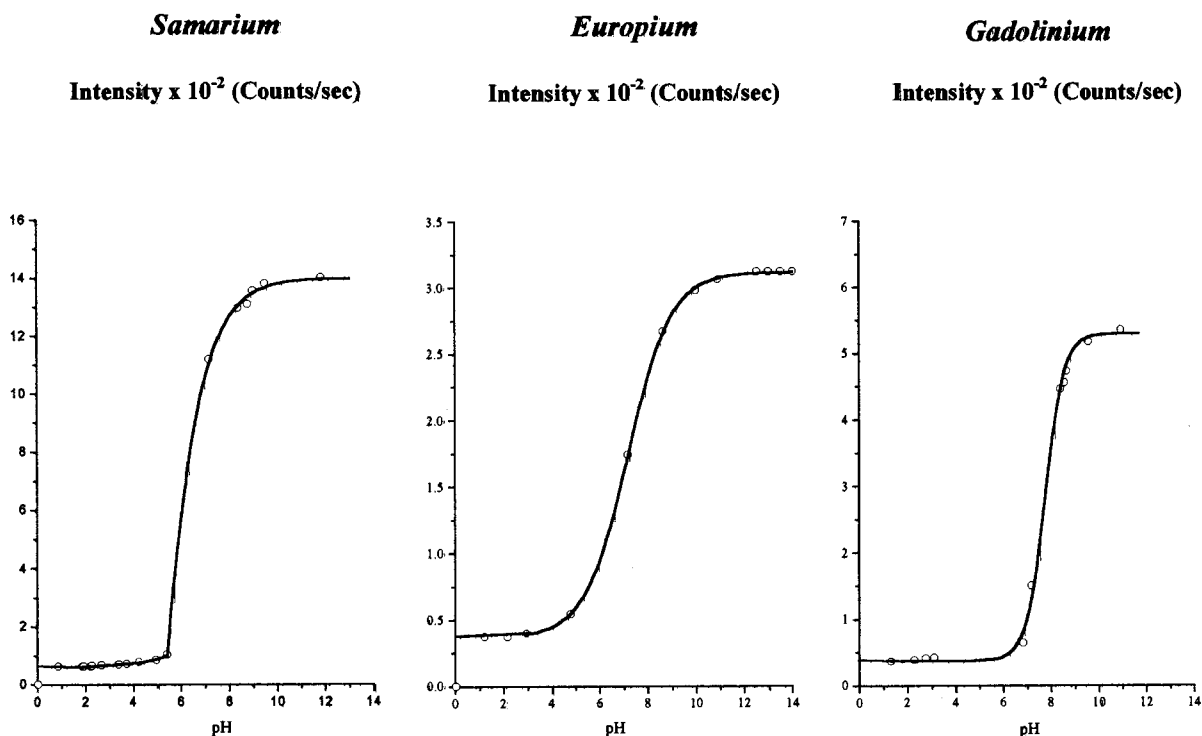


Fig. 3. Retention of Sm(III), Eu(III) and Gd(III) on Thorin-XAD-7 as function of pH.

Table 2
Determination of Sm, Eu and Gd in different samples

Sample	Contents (mg l ⁻¹)			Quantity found (mg l ⁻¹)			Error (%)			Correction factors		
	Sm	Eu	Gd	Sm	Eu	Gd	Sm	Eu	Gd	Sm	Eu	Gd
G-2 Certif by USGS	5	1.5	7.3	4.7	1.3	7.5	6.0	13.3	2.6	0.362	0.488	0.264
GS-N (synthetic)	7.7	1.7	5.2	7.57	1.6	5.8	1.7	5.8	11.5	–	–	–
AGV-1 (synthetic)	5.9	1.7	5.5	5.8	1.53	5.1	1.7	10	7.3	–	–	–

were prepared. A line of Ce spectrally pure (Ce L_{α1} 2θ 79.01) and the analyte line Gd L_{α1} 2θ 61.10 were measured by XRF on these standards. In this way the correction factor ($k^{z,y}$)_{ij}, could be obtained, which represents the relation between the intensities of the lines *z* and *y* of the interferent element Ce(III).

$$k = (I^{L_{\gamma 1}})_{\text{Ce}} / (I^{L_{\alpha 1}})_{\text{Ce}}$$

$$= 408\,76 \text{ counts s}^{-1} / 1547\,96 \text{ counts s}^{-1}$$

$$= 0.264$$

In the same manner were calculated the correction factor for Sm(III) measuring the line Sm L_{α1} 2θ 66.23 which is interfered by Ce(III) and Eu L_{α1} 2θ 63.57 interfered by Pr(III). In this last case the pure line measured was Pr L_{β1} 2θ 68.24. All correction factors are shown in Table 2.

4. Conclusions

The method proposed in this work results very useful for a precise determination and pre-concentration of trace REE by XRF spectrometry. The preparation of the loaded resin is simple, quick and has the advantage that the resin can be presented to X-ray spectrometer as a thin film, which eliminates the interelemental effects in the sample. In addition, high enrichment factors and low detection limits are obtained.

Acknowledgements

The authors wish to thank Dr Jose Gasquez for his worthy and interested contribution to this work. This work was supported by CINICET and the national University of San Luis.

References

- [1] K. Terada, Anal. Sci. 7 (1991) 187–198.
- [2] A. Masi, R. Olsina, Anal. Quim. 89 (3) (1993) 341–345.
- [3] K. Isshiki, E. Nakayama, Anal. Chem. 59 (1987) 291–295.
- [4] R. Kocjan, S. Przeszlakowski, Talanta 39 (1) (1992) 63–68.
- [5] P. Burba, P.G. Willmer, Fres. Z. Anal. Chem. 329 (1987) 539–545.
- [6] A. Hase, T. Kawabata, K. Terada, Anal. Sci. 6 (1990) 747–751.
- [7] R. Pathak, G.N. Rao, Talanta 44 (1997) 1447–1453.
- [8] V.K. Jain, S.S. Sait, P. Shrivastav, Y.K. Agrawal, Talanta 45 (1997) 397–404.
- [9] Chang H. Lee, Moo Y. Suh, Kih S. Joe, Tae Y. Eom, Won Lee, Anal. Chim. Acta 351 (1997) 57–63.
- [10] M. Torre, M.L. Marina, Crit. Rev. Anal. Chem 24 (5/6) (1994) 327–361.
- [11] C.J. Kantipuly, A.D. Westland, Talanta 35 (1) (1988) 1–13.
- [12] Z. Marczenko, Spectrophotometric Determination of Elements, Springer-Verlag, Berlin, 1983.
- [13] J.G. Crock, F.E. Lichte, G.O. Riddle, C.L. Beech, Talanta 33 (7) (1987) 601–606.
- [14] D.W. Lee, Ch.H. Eum, I.H. Lee, S.J. Jeon, Anal. Sci. 4 (1988) 505.
- [15] J.A. Gasquez, E. Perino, E. Marchevsky, R. Olsina, A. Riveros, X-Ray Spectrom. 26 (1997) 272–274.

Anomalies in the spectrophotometric and extractive behaviour of zirconium and hafnium Evidence of a synergistic effect

Patricio Peralta-Zamora ^{a,*}, José W. Martins ^b

^a *Universidade Federal do Paraná, Departamento de Química, CP 19081, CEP 81531-990, Curitiba-PR, Brazil*

^b *Universidade Estadual de Campinas, Instituto de Química, Campinas-SP, Brazil*

Received 23 November 1998; received in revised form 24 February 1999; accepted 6 March 1999

Abstract

In this work, some observations that confirm non-specific interactions between zirconium and hafnium are presented. This phenomenon, which induces significant differences between the spectrophotometric and extractive behaviour of the isolated elements related to their mixtures, indicates the existence of an important synergistic effect on the depolymerisation reactions involved in the aqueous chemistry of the elements. All experimental evidences suggest that the presence of zirconium can minimise the polymerisation of hafnium, favouring its reaction with the studied complexing agent. © 1999 Elsevier Science B.V. All rights reserved.

Keywords: Zirconium; Hafnium; Polymerisation

1. Introduction

The determination of zirconium–hafnium mixtures is one of the most classical problems in analytical chemistry, mainly due to the exceptional similarity between the chemical properties of these elements. Usually, the analytical problems associated with the inter-element interferences can be overcome only by the application of modern instrumental analytical techniques [1–3].

An interesting revision on this subject has been presented by Serbinovich et al. [3].

Generally, the application of spectrophotometric methods based on the formation of coloured chelates of the metallic ions is not possible due to the low selectivity of the chromogenic agents. With the aim of finding analytical alternatives, many scientists have developed differential colorimetric methodologies based on the specific behaviour of zirconium or hafnium under different acidic conditions or in the presence of specific masking agents. Among these, it is worth mentioning the methodologies based on the masking effect of hydrogen peroxide on the reaction of zirconium with xylenol orange (proposed by

* Corresponding author.

E-mail address: zamora@quimica.ufpr.br (P. Peralta-Zamora)

Cheng [4–6]), the significant reduction of the absorption signal of the hafnium–arsenazo III complex in acidic media (proposed by Elinson and Mirzoyan [7]), the absorption differences between zirconium and hafnium complexes with xylenol orange with different acidities (proposed by Chalis [8]) and the absorption differences between zirconium and hafnium sulphate complexes in the 205–220 nm region (proposed by Yagodin et al. [9]). At least in theory, all of above mentioned methodologies work adequately; unfortunately, the behaviour of the isolated elements is very different to that observed for their mixtures, due to several unspecified interactions between zirconium and hafnium.

In this work, evidences are provided to confirm the significant interaction that exists between zirconium and hafnium. Evidences that also could indicate a synergistic effect on the depolymerisation reactions of these elements.

2. Experimental

2.1. Instrumental

Spectrophotometric measurements were carried out in a Hitachi U-2000 spectrophotometer, using 1 cm quartz cells. Standard solution volumes were taken with a Metrohm microburette, using 0.5000 ml taps.

2.2. Chemicals and solutions

The zirconium standard solution was prepared by direct dissolution of $ZrOCl_2 \cdot 8H_2O$ (99.5%, Riedel-de Haen) in 2 mol l^{-1} HCl.

The hafnium standard solution was prepared from hafnium oxide (HfO_2 , Specpure, Johnson, Mathey). The oxide was dissolved in a $HF-H_2SO_4$ (1:1 v/v) mixture and heating several times almost to dryness with successive additions of concentrated H_2SO_4 . To eliminate the sulphate ions, hafnium hydroxide was precipitated with an aqueous solution of NH_3 and redissolved in HCl (final concentration of HCl, about 2 mol l^{-1}).

Both solutions were standardised by a gravimetric procedure using mandelic acid [10].

2.3. Analytical procedures

All of the analytical procedures were carried out according to the methodologies described in the literature, that is, colorimetric determination by xylenol orange according to Cheng [4–6], UV-Vis determination of the sulphate complexes according to Yagodin et al. [9], and single-phase extraction according to Silva and Martins [11].

3. Result and discussions

3.1. Experimental observations

The methodology proposed by Yagodin's et al. [9] is based on the fact that the absorbance of the hafnium sulphate complex at 205 nm is negligible compared to the signal related to the zirconium sulphate complex. Even though this observation is true for the isolated ions, accurate determination of zirconium in a mixture of hafnium and zirconium is not possible, because hafnium modifies the linear relationship between the observed absorbance and the concentration of zirconium, therefore, interfering in the proposed additivity of the absorbance signals. A schematic representation of this phenomenon is presented in Fig. 1. It is evident in this representation that the presence of one element interferes in the normal spectrophotometric behaviour of its congener. A very similar anomaly in the additivity of the absorbance signals was observed when the Cheng's methodology was applied (Fig. 2). Both observed effects on the absorbance signals are highly significant when compared with the typical observed standard deviation (S.D.) of spectrophotometric measurements (about 0.005 absorbance units).

Certainly, the more remarkable results are represented by the observations carried out on the study of the effect of a prior thermal treatment on hafnium complexation with xylenol orange (Table 1). When the standard solutions were previously evaporated to almost dryness, followed by resuspension in 0.5 mol l^{-1} $HClO_4$ and finally added to the xylenol orange solution, hafnium did not react with xylenol orange while zirconium alone reacted in an apparently normal way. Further-

more, when the two ions elements were subjected to the same treatment as a mixture, the absorbance signal was significantly increased, indi-

cating that the presence of zirconium promotes hafnium complexation, even when the experimental conditions are unfavourable.

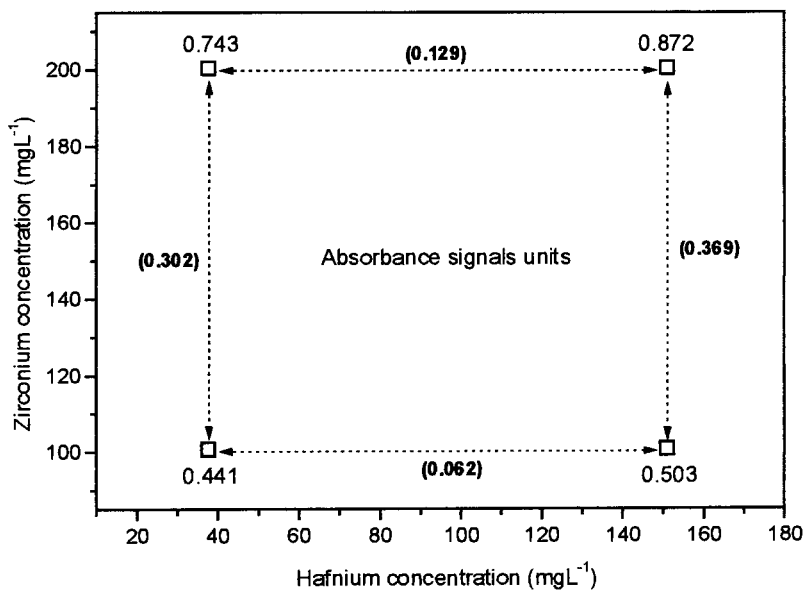


Fig. 1. Anomalies in the observed absorbance signals units of zirconium and hafnium sulphate complexes at 205 nm (determination according Yagodin et al. [9]). * Absorbance differences are represented in brackets.

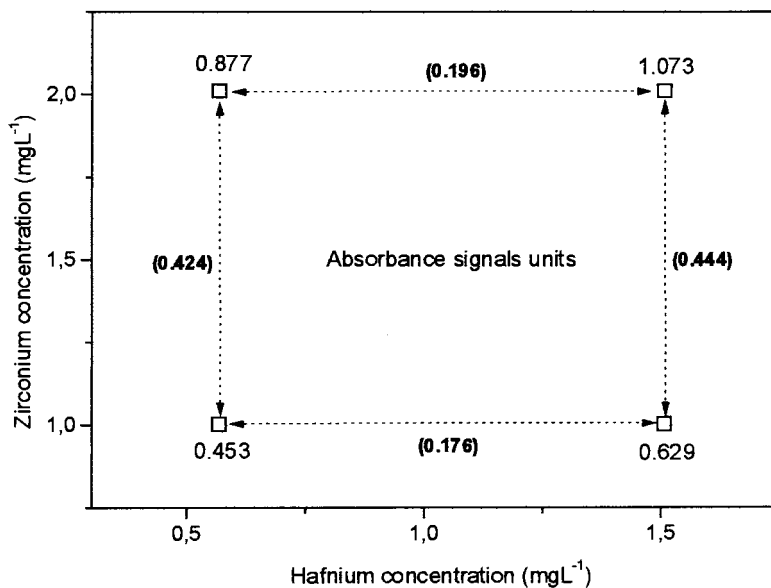


Fig. 2. Anomalies in the observed absorbance signals units of zirconium and hafnium xylenol orange complexes at 550 nm (determination according Cheng [4–6]). * Absorbance differences are represented in brackets.

Table 1
Effect of the thermal treatment on the complexation of zirconium and hafnium with xylenol orange^a

Conc. Zr (mg l ⁻¹)	Conc. Hf (mg l ⁻¹)	Absorbance Zr	Absorbance Hf	Absorbance mixture
1.0	–	0.330	–	–
1.5	–	0.620	–	–
2.5	–	1.190	–	–
–	0.82	–	wdc ^b	–
–	1.24	–	wdc	–
–	2.06	–	wdc	–
1.0	2.06	–	–	0.645
1.5	1.24	–	–	0.809
2.5	0.82	–	–	1.290

^a λ , 545 nm; media, 0.5 mol l⁻¹ HClO₄; optical path length, 1.0 cm.

^b wdc, without development of colour.

Table 2
Liquid–liquid single-phase extraction of zirconium and hafnium^a

Element	Conc. HCl (mol l ⁻¹)	Extraction Zr (%)	Extraction Hf (%)
Hafnium	0.69	–	0.0
Hafnium	1.03	–	0.0
Zirconium	0.69	46.0	–
Zirconium	1.03	48.5	–
Hafnium–zirconium	0.69	47.5	33.4
Hafnium–zirconium	1.03	50.6	35.7

^a Zr, 1230 μ g; Hf, 545 μ g; HTTA, 1.7×10^{-2} mol l⁻¹ (in single-phase); system:water:ethanol:methylisobutylketone (2:7.5:5 v/v); volume of system, 14.5 ml.

A very similar observation was obtained in studies related to liquid–liquid single-phase extraction of zirconium–hafnium mixtures using water:ethanol:methylisobutylketone solution containing thenoyltrifluoroacetone. In the absence of zirconium, hafnium was not extracted from a 0.69–1.03 mol l⁻¹ aqueous HCl solution. However, under the same conditions, hafnium was partially extracted (33.4–35.7%) from mixtures of the two elements. Again, the presence of zirconium induced the complexation reaction of hafnium (Table 2).

3.2. Proposed interpretations

Zirconium and hafnium are chemical species that show a high tendency to polymerise in aqueous solutions through reactions that depend on exper-

imental conditions such as pH, concentration of the elements, nature and concentration of mineral acids present, age of the solutions, temperature, among others [1]. Consequently, the chemistry of these species are closely connected to their capability to form polymeric species such as $[Zr_x(OH)_y]^{4x-y}$ and $[Hf_x(OH)_y]^{4x-y}$, which can modify the reactivity of the elements to the complexing agent. Recently, small-angle X-ray scattering measurements demonstrated an equilibrium condition between octameric $(Zr_8(OH)_{20}-(H_2O)_{24}Cl_{12})$ and tetrameric $([Zr_4(OH)_8(H_2O)_{16}Cl_6]^{2+})$, species of zirconium at 0.05 mol l⁻¹ in highly acidic solutions [12]. Other studies also indicated that the primary particles are formed at pH of 1.2 [13]. By increasing the pH or the temperature, these primary particles form large aggregates while retaining the primary particle structure.

Taking into account the experimental observations reported above, it would be very natural to assume that hafnium presents a higher tendency to polymerise in aqueous solutions, forming polymeric species that hinder its complexation with could therefore minimise the occurrence of these polymerisation reactions, favouring the subsequent reaction with the complexing agent.

At the moment, studies are in progress to further elucidate the possible mechanism of this 'synergistic effect'.

Acknowledgements

The authors thank Professor Carol Collins for critically reading the manuscript.

References

- [1] A.K. Mukherji, Analytical Chemistry of Zirconium and Hafnium, Pergamon Press, Oxford, 1970.
- [2] A. Brookes, A. Townshend, Analyst 95 (1970) 529.
- [3] U.V. Serbinovich, V.P. Antonovich, N.A.J. Pshetkovskaya, Anal. Chem. USSR 41 (1986) 867.
- [4] K.L. Cheng, Talanta 2 (1959) 266.
- [5] K.L. Cheng, Talanta 3 (1959) 81.
- [6] K.L. Cheng, Anal. Chim. Acta 28 (1963) 41.
- [7] S.V. Elinson, N.A. Mirzoyan, Zavod. Lab. 27 (1961) 798.
- [8] H.J.G. Challis, Analyst 94 (1969) 94.
- [9] G.A. Yagodin, A.M. Chekmarev, L.M. Vladimirova, Russ. J. Inorg. Chem. 11 (1966) 167.
- [10] R.S. Barbieri, J.C. Rocha, V.R. Terra, A. Marques Neto, Eclét. Quim. 14 (1989) 101.
- [11] J.F. Silva, J.W. Martins, Talanta 39 (1992) 1307.
- [12] A. Singhal, L.M. Toth, J.S. Lin, K. Affholter, J. Am. Chem. Soc. 118 (1996) 11529.
- [13] A. Singhal, L.M. Toth, G. Beaucauge, J.S. Lin, J.J. Peterson, Colloid Interface Sci. 194 (1997) 470.

Erratum

Erratum to “Further development of catalase, tyrosinase and glucose oxidase based organic phase enzyme electrode response as a function of organic solvent properties”[☆]
[Talanta 46 (1998) 595–606]

L. Campanella *, G. Favero, M.P. Sammartino, M. Tomassetti

Department of Chemistry, University ‘La Sapienza’, p.le A. Moro, 5, 00185 Rome, Italy

The publisher regrets the following error in this article: page 598: in reaction a), “hydroquinone” should read “o-quinone”. This was as a result of an error printed in an earlier publication which the publisher also regrets: Talanta, 41 (1994), 1015–1023: page 1017: in reaction at line 17, “hydroquinone” should read “o-quinone”.

[☆] PII of original article: PII S0039-9140(97)00311-1

* Corresponding author. Tel.: +39 6 49913744; +39 6 490375; e-mail: campanellal@axrma.uniroma1.it

Erratum

Erratum to “Determination of stability constants of complexes of $M_iK_jH_kL$ type in concentrated solutions of mixed salts”[☆]
[48 (1999) 1191]

Dariusz Janecki ^a, Katarzyna Doktor ^a, Tadeusz Michałowski ^{b,*}

^a Faculty of Chemistry, Jagiellonian University, ul. R. Ingardena 3, 30-060 Cracow, Poland

^b Department of Analytical Chemistry, Faculty of Engineering and Chemical Technology, Technical University of Cracow, ul. Warszawska 24, 31-155 Cracow, Poland

Received 17 July 1998; received in revised form 27 October 1998; accepted 30 October 1998

The publisher regrets the following errors which refer to the formulae (6b), (8) and equation for z_1 . The correct form of these are found below:

$$x_0 = b_0 + b_1 \cdot [M] + b_2 \cdot [K] + b_3 \cdot [M]^2 + b_4 \cdot [K]^2 + b_5 \cdot [M] \cdot [K] \quad (6b)$$

$$[M] \gg \sum_i [M_i K_j H_k L], \quad [K] \gg \sum_j [M_i K_j H_k L] \quad (8)$$

$$z_1 = (C_1 V_{MB} - C_2 V_{KB}^*) / V_f$$

[☆] PII of original article: S0039-9140(98)00345-2

* Corresponding author. Tel.: +48-12-33-03-00; fax: +48-12-33-33-74

Book review

Selectivity and Optimisation in Capillary Electrophoresis, Edited by Z. El Rassi and R.W. Giese, Elsevier, Amsterdam, 1998. ISBN 0-444-82915-6, US\$244.00

This book, reprinted from the Journal of Chromatography, brings together articles on the general theme of selectivity in both free zone capillary electrophoresis and micellar electrokinetic chromatography. It contains some 15 review articles and 21 original papers organised into six different sections. It will be of most use to researchers active in developing applications of the technique of capillary electrophoresis dealing as it does with fundamental theory and strategies for obtaining selectivity.

The first section is general and includes reviews on the effects of organic solvents and also on the selectivity achieved by micelles, chiral selectors and non-aqueous solvents. The subsequent collection of original papers covers many applications ranging from the separation of drugs such as sulphonamides and impurities in penicillins to carbohydrates, peptides and ribonucleotides. The second part is devoted to micellar electrokinetic chromatography. There is a very comprehensive review of the fundamental properties of micelles and also a review of polymers and polymer surfactants which offer alternatives to conventional surfactants used in MEKC. There are original papers on amine, fatty acid and dye separations. The most extensive section of the text is the third part dealing with chiral separations. This includes a very wide ranging overview of the principles of chiral separation using buffer additives and a comprehensive collection of drug applications. Other reviews in this section deal

with parameters controlling separation when using inclusion compounds, charged selectors and mixed cyclodextrins. There are, in addition, three review articles on enantiomeric separation using macrocyclic antibiotics, polysaccharides and proteins, respectively. The original papers in this section range from thermodynamics of selectivity to the separation of small chiral peptides. The two subsequent sections deal with the use of cyclodextrins for micellar electrokinetic chromatography and with various other methods of obtaining selectivity including ion pairing and achiral separations using cyclodextrins. The book concludes with a review of selectivity strategies for the separation of metal species. Overall this book shows great insight on the part of the editors. They recognise, as is stated in the Foreword, that no separation can take place in the absence of selectivity. They have also identified and provided coverage of the various selectivity techniques and strategies which have been used to exploit the acknowledged high theoretical plate number which is the hallmark of CZE and MEKC. The text represents a good balance between review articles dealing with more or less broad themes and reports of original specific research. Such a collection of reviews and papers must necessarily become dated particularly when dealing with a rapidly advancing field such as capillary electrophoresis. Nevertheless this appraisal of the state of the art was timely and the only obvious current omission is the absence of any reference to capillary electrochromatography. This mode of capillary electrophoresis is perhaps one where the selectivity aspects will be most versatile although its development currently lags behind that of other modes.

R.B. Taylor

Book review

Mass Spectra and GC Data of Steroids—Androgens and Estrogens, Edited by H.L.J. Makin, D.J.H. Trafford, J. Nolan, Wiley-VCH, Weinheim, 1998. ISBN 3-527-29644-1; £299.00

This collection of steroid mass spectral data belongs to the SpecBook series and aims to support researchers 'who are not satisfied with purely electronic products'. It contains approximately 2500 mass spectra of androgens and estrogens and their derivatives (trimethyl ethers, *O*-methyloximes and acetates).

All the steroids have had their retention index and EI(+) mass spectra newly measured. The source of each of the steroids analysed is given in the index under Spectrum Number Index. The steroid mass spectra are presented in order of increasing molecular weight and each entry includes the structure, systematic and trivial names, the molecular formula, molecular weight, CAS number and retention index. In addition the publishers have allocated a spectrum number to each entry for cross-reference. Due to the enormous number of steroids reported, 616

pages are required to accommodate all the entries.

The final section of the compilation contains a separate index for Molecular Formula, Spectrum Number, Retention Index, CAS Registry Number and Dictionary of Steroids Number. With the range of indexes presented, the process by which the identity of an unknown steroid is made, becomes easier.

The very last page of the book is an advertisement for an electronic form of this collection of mass spectral data. One wonders how researchers in this area, whose instrumentation will undoubtedly have dedicated microprocessors to handle the data being produced, could ever not be satisfied with a 'purely electronic product' such as being offered. Surely this would be more effective.

Although the price of the book is formidable, there is no doubt it would be invaluable for those researchers in this area who do not have open access to mass spectral libraries and instrumentation.

A.S. Low

Book review

Understanding Mass Spectra: A Basic Approach, Edited by R.M. Smith and K.L. Busch, Wiley, Chichester, 1999. ISBN 0-471-29704-6; £38.95

This book concentrates on the interpretation of mass spectra and is aimed at upper level undergraduates, beginning postgraduates and practitioners in the field. It is highly commendable because of three features: many worked examples, many problems with solutions provided, and something rarely seen but extremely useful, strategies to use for MS interpretation. The book was written by a practising forensic chemist (RMS), and many of the examples are mass spectra of illicit narcotic substances and their metabolites. The other author (KLB) provides technical expertise in terms of instrumentation. The book was originally written to counter the plethora of books currently being published on new MS techniques, to give a basic grounding in MS interpretation to those with little or no previous experience. The authors' reason is that these new techniques have not altered the basic fragmentations observed in mass spectra, and that EI is still the most often used ionisation technique.

The book is divided into nine chapters, the last of which is solutions to the problems. Chapter one covers the instrumentation and compares EI with other ionisation techniques. Ionisation reactions are mentioned followed by brief coverage of mass analysers (magnetic sector, quadrupole, TOF, FT-ICR) after which hyphenated techniques are discussed (MS-MS, GC-MS). All parts of the MS systems are covered including the electron multiplier. A very important section covers data systems, and the power of the use of library searches.

The authors stress here the importance of visual inspection of spectra selected by the library search, and also give some criteria for 'good spectra'.

Chapter 2 goes into detail about isotopic abundance and how this affects the shape of the isotope clusters observed. There are simple explanations and examples of how to calculate peak intensities, using binomial expansions, or using a neat trick involving Pascal's triangle. The best and most important section in the whole book follows, and this alone makes this book worth buying, and this is 'A reasoned approach to MS interpretation'. This set of rules should be at the forefront of every practitioner's mind when interpreting mass spectra.

Chapter 3 covers ionisation, fragmentation and electron accounting. This details the basics of even and odd electron species and the site of initial ionisation. There is a foray into frontier orbital theory here to explain these phenomena. The final part of this chapter talks about energetic considerations in fragmentations.

Chapters 4–6 use specific examples to explain different types of fragmentation processes. Chapter 4 covers neutral losses and ion series, and the mass spectra of aromatic compounds. In chapter 5 alpha cleavage comes to the fore, and several examples are given, benzylic cleavage and cleavage next to aliphatic N or O. The last part of this chapter talks about secondary elimination from alpha cleavage ions. Rearrangements are the main focus of chapter 6, with the McLafferty and retro Diels–Alder being the most important.

Chapter 7 shows the reader how to write MS fragmentation mechanisms and good use is made of curly arrows. Again there is a very useful set of

guidelines as to how to set about drawing a fragmentation mechanism. This chapter also gives some very specific and useful examples. The final chapter of text before the solutions to problems gives examples of structure determinations of complex compounds. Many of these are drawn from the first author's own field, and we see drugs such as MDA (an ecstasy analogue) and metabolites of cocaine, which should certainly rouse students' interests.

On the whole this book comes highly recommended, mainly because of the large number of worked examples and solved problems. The unique feature which really makes it worth buying for anyone who wants to know more about mass spectral interpretations is the short sections on strategy and guidelines for mass spectral interpretation.

M. Jaspers

Book review

Signal Processing Using Optics, Edited by B.G. Boone, OUP, Oxford, 1998. ISBN 0-19-508424-1; £57.50

This book covers the basics of optical signal processing and is directed towards practising engineers/scientists and final year students or first year postgraduates. As an Electronics Engineer specialising in Digital Signal Processing and with no prior knowledge of Optical Signal Processing I found this subject fascinating and very much enjoyed reviewing this text. Chapter 1 presents analytically the fundamentals of two-dimensional linear systems. The extensive use of diagrams throughout this chapter is of a great benefit in the comprehension of the processes described. Chapter 2 addresses the stochastic processes and non-linear systems that are found in real optical processing devices.

The most commonly used mathematical transforms in optical processing (Frensel, Hilbert, Radon, Mellin and Wavelet) are covered in detail in Chapter 3. Chapter 4 describes the fundamental properties of light and how it interacts with rectilinear glass structures. This chapter concludes with summary of simple lenses and lens combinations.

In Chapter 5 diffraction, interference and coherence are introduced, again supplemented by clear diagrams of their effects. The important properties of lens systems is covered in Chapter 6 and also the analogies between time-domain signal processing and optics. I found this chapter particularly enlightening as I could clearly relate to the time-domain analogies. Chapter 7

details the principles of operation of light sources and detectors including Light Emitting Diodes, Laser diodes, diode arrays and Charged Coupled Device detectors. The characteristics of these devices that are required for optical signal processing are summarised.

Chapter 8 describes Spatial Light Modulators (SLMs) and their use as transducers and for implementing amplification, arithmetic and Boolean operations. The implementation of spectrum analysis and correlation are described in detail in Chapter 9. Different types of optical signal processing architectures are categorised with specific examples of each analysed in depth. Image spatial filtering techniques and its variants are described in Chapter 10. Improvements in the basic matched filter are considered which make it less susceptible to distortions of the input image. The specific application of optical signal processing to radar signal processing and pattern recognition are covered in Chapters 11 and 12. In particular the ambiguity function, synthetic aperture radar processing, optical feature extraction, matrix vector multiplication and neural networks.

Each Chapter concludes with problem exercises with hints and solutions to selected exercises presented in Appendix D. Appendix B contains the bibliography which lists the most well-known and recent textbooks on Optical Signal Processing and Fourier Optics. Very useful comments are made on the contents of these texts. Appendix C contains a summary of modelling and simulation methodology for synthesising and analysing Optical Processing Systems.

There are software listings (MATLAB) which were invaluable in demonstrating the various techniques described in the preceding Chapters. I have enjoyed reading this book and would recom-

mend it to anyone who would like to gain an understanding of Optical Signal Processing.

S. Elder

Book review

Protein NMR Techniques, Edited by David G. Reid, Humana, Totowa, 1997. ISBN 0-896-03309-9; US\$79.50

The field of protein NMR spectroscopy is moving too fast and has become too complex and multidisciplinary for any single text to provide comprehensive coverage of the state-of-the art. This is particularly true of books which purport to deal with techniques at the expense of theory. Another disadvantage of 'methods' books is that they often fall between two stools—they are too detailed for the non-specialist but pedestrian by the standards of those practising the art. However, this new book on NMR—'Protein NMR Techniques', edited by David Reid—should still manage to find a place on library shelves.

'Protein NMR Techniques' is a multiauthor text dealing with all aspects of the eponymous topic, from protein expression to calculation of structures. Like other works in the series 'Methods in Molecular Biology' this 60th volume benefits from a well-thought out overall structure, a high standard of editing and a good quality of printing and figure reproduction. A well-illustrated Introduction directs readers to appropriate later chapters where they can benefit from the efforts of acknowledged specialists who bring their experience and expertise to bear in a clear and instructive manner. Membrane proteins,

protein-metal interactions and protein-ligand interactions are covered as well as mainstream three-dimensional structure determination. The study of protein dynamics, flexibility and folding is a sad omission. The book is reasonably up-to-date but unfortunately went to press too early to catch the exciting developments from the groups of Wuthrich, Bax and others which set the protein NMR community buzzing in 1998.

As its title suggests, the text places a strong emphasis on practical and technical aspects of protein NMR. In this respect it occupies a fairly narrow niche, somewhere between Cavanagh et al.'s very rigorous treatment of the subject in their tome, 'Protein NMR Spectroscopy. Principles and Practice' (Academic Press, 1996) and Roberts' methods-based compilation, 'NMR of Macromolecules' (Oxford University Press, 1993). This niche is shared with Evans' monograph, 'Biomolecular NMR Spectroscopy' (Oxford University Press, 1995). Evans' book is stronger on theory and enzymology and is more coherent by virtue of its single authorship. However Reid's book is definitely worth a look. Its scope is broad, and it could be a reasonable investment as a reference book in the library—or even in the labs of NMR spectroscopists who feel they are becoming overly specialised within the field.

P. Barlow

SIAMate—a compact and modular sequential injection analysis controller

Nils Kullberg^{a,b,*}, Michael Vilén^{a,b}, Pernilla Sund^{a,b}, Markus Talaslahti^{a,b},
Rolf Sara^{a,b}

^a Centre for Biotechnology, Åbo Akademi University, PO Box 123, 20521 Åbo, Finland

^b University of Turku, Turku, Finland

Abstract

A number of sequential injection analysis (SIA) measurement methods have been developed during the last years. Almost all have been used in laboratory conditions with good results, but very few have been implemented as on-line methods, applied to non-stop measurements, producing immediate results for process control. The transfer of an SIA system from laboratory to an industrial facility [J. Ruzicka, *Anal. Chim. Acta* 261 (1992) 3] requires a whole new range of details to be taken into account. Some SIA platform related topics will be discussed. There are numerous ways of building an SIA system that meets the needs of the industry. One alternative, *SIAMate*, is presented. © 1999 Published by Elsevier Science B.V. All rights reserved.

Keywords: SIAMate; Sequential injection analysis controller; Industry; On-line analysis

1. Introduction

The objective of the Biosense project at Turku Centre for Biotechnology has been to develop on-line analysis methods for mammalian cell culturing systems [1]. The analyses included ammonia, glucose and the end product (often a monoclonal antibody) [2]. Sequential injection analysis (SIA) was chosen as the basic technology, and direct ion selective sensors were abandoned due to their long-term instability.

It soon became clear that there were no available SIA systems that would fulfill the specifica-

tions for an industrial analyzer. Therefore the project has developed an SIA controller software suitable for on-line process analysis [3]. The resulting software, *AnalySIA*, has been presented at several conferences and will not be covered in the present paper.

Once the project had suitable SIA software, the work with the hardware started. The first four analyzers were built using off-the-shelf parts, and some problems were encountered: (1) all devices used their own, proprietary communications scheme; (2) the controlling computer always had to be enhanced with lots of different i/o ports; and (3) the long analog pathways from the detectors to the A/D card in the computer caused trouble in terms of interference tolerance. To be

* Corresponding author. Tel.: +358-40-501-2535.

E-mail address: nils.kullberg@btk.utu.fi (N. Kullberg)

able to transfer the developed methods to the industry the project had to continue by designing a new SIA platform.

This paper is focused on the SIA hardware platform, the *SIA controller*. Other important issues when transferring methods to the industry are on-line sampling, analyzer interface to a process control system, maintenance of the analyzer as well as ensuring stable calibration.

A laboratory SIA analyzer brought to the industry to serve as an on-line analyzer is not the optimal solution. Some of the topics involved are:

- the physical size and shape of the analyzer
- the communication between the analyzer and the controlling computer
- the need for manual tuning of the detector(s) used
- the need for on-site service of the analyzer

The Biosense group focused on the above details as well as on other topics involved with bringing SIA into the industry when designing *SIAMate*. The end result was a traditional SIA controller with certain new features implemented. Some of the new features are presented below.

2. A rugged and compact design

SIA does not require the hardware to be large and cumbersome. A typical SIA system consists of a pump, a multiport valve, a detector and few bottles. One additional benefit of SIA (especially compared to FIA) is that one single manifold often can be used to perform several different analyses [4]. This gives the method designer a good starting point for the conversion of a laboratory tested measurement method into an industrial on-line application.

The commonly used 19-inch instrumentation rack is a natural choice for an industrially oriented SIA analyzer, as the rack is both compact, easy to enhance with a plastic cover for desktop usage, and easy to mount in a 19-inch wall-mount or sealed housing (Fig. 1).

The use of a 19-inch rack as the basis for an SIA analyzer further enhances the simplicity and reliability of the SIA system, due to almost no loose wires in the analyzer. All electric power,

measured readings and control signals are transferred via the back-plane bus of the rack. The detector being one of the devices in the rack gives very short analog wire paths, which will be discussed later in this paper.

In the case of *SIAMate*, the 19-inch rack is capable of housing seven devices, *modules*, of which one is the combined computer interface and power supply unit. This leaves the method developer with six slots for SIA modules like pumps, valves, detectors, mixing chambers and so forth.

3. Interference tolerant communication

The communications protocol between the controlling computer and the SIA hardware has to cope with a lot more interference in an industrial location than in a laboratory. This does not only apply to the controlling of pumps and valves, but even more to the measurement sampling and transfer of the sampled results to the computer.

Almost all laboratory detectors supply their measured signal as an analog output, that is connected to an analog-to-digital (A/D) board inside or outside the computer. This leads to unnecessary long analog paths that not only collect noise from the environment, but often cause modulations of the surrounding electromagnetic fields on the signal. This is even more apparent in an industrial environment where there often are high-power electrical machines close to the analyzer.



Fig. 1. SIAMate rack with plastic cover.

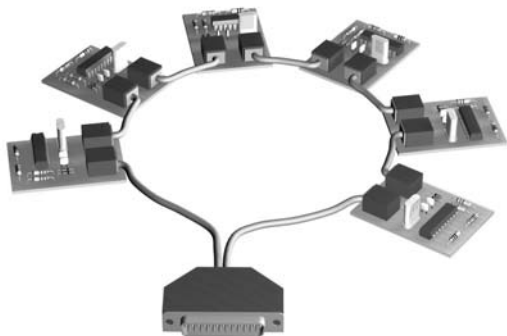


Fig. 2. BrokenRing.

Traditionally RS485 has been used as the means of communication between the various devices, due to its low impedance and symmetric nature. This communications protocol has two major drawbacks, however, namely the lack of an RS485 port on a standard PC computer and the need for a very precise bit-rate on the bus itself. Small, integrated microcontrollers in the devices often use most of their computing power just to satisfy the needs of RS485, whereas a synchronous transmission would release most of the power of these microcontrollers to the device itself.

As a part of the Biosense/Modcon project at the Turku Centre for Biotechnology a new communications protocol has been introduced. The new protocol is called *BrokenRing*TM, and is especially designed to be suitable and efficient for SIA control.

BrokenRing utilizes three wires; ground, data and clock. No exact bit-rate is required either from the PC or from the microcontrollers. The clock signal propagates from one device to another as soon as the device is capable of recognizing the incoming clock pulse. Hence the name BrokenRing (Fig. 2).

The parallel port of a PC can be used directly as a BrokenRing interface, and no extra hardware is required. The impedance of a parallel port is low enough to ensure error-free transmission even in electrically noisy environments.

Any one PC parallel port can control two BrokenRings, consisting of up to 14 devices per ring. All SIamate devices are equipped with a small microcontroller, a PIC16F84, which implements both the BrokenRing interface and most of the device application software (pump control, valve control, sampling, etc.).

The approximate transfer rate of BrokenRing depends on both the number of devices on the ring and on the latency times of each device. The transfer rate can be estimated as:

$$\text{BitRate (kb s}^{-1}\text{)} = 1/(\# \text{ devices} * 0.025 \text{ ms})$$

For a four device ring this gives $\sim 40 \text{ kb s}^{-1}$, which means ~ 525 19-bit packets per second. Each packet can contain any data, i.e. commands, device status, sampled data, etc. The BrokenRing speed also sets an upper limit on the sampling frequency of any detector used. A detector producing 16-bit data would be limited to ~ 250 samples per second, which is acceptable for many detectors, but too little for detectors like spectrophotometers.

The benefit of having digital transfer of measurements to the controlling computer is the gained interference tolerance, which cannot be achieved any other way.

A definition for a bitstream transfer mode for BrokenRing is part of the current research. The bitstream mode would enable detectors to use a higher bandwidth for data transfer to the controlling computer, thereby making measurements like time lapse spectrograms possible.

4. Self-tuning detector units

An analyzer working stand-alone in an industrial facility has to survive with at least two forms of long term drift: (1) reagent decay; and (2) slow, cyclic variations in the ambient temperature. Both require a built-in ability to retune the detector units at given intervals, or at given fluctuations in the environment.

There are two ways of implementing self-tuning detectors units: (1) built-in algorithms for retuning; and (2) open-ended control capabilities that can be used from the controlling computer. The

SIAMate concept implements the latter one, thereby making the detector's self-tune algorithm a part of the overall measurement method.

The advantages of this arrangement are that it is possible to reduce the amount of electronics and software needed in the detector itself, as well as enabling the measurement method developer (usually a chemist) to adjust, end even redesign, the self-tuning algorithm according to needs.

4.1. LedSpecII self-tuning

The basic detector of an SIAMate analyzer is at the moment an LED-based photometric detector, *LedSpecII*. Being a device on the BrokenRing it can be controlled directly from the computer and retuned by the measurement method itself. The LedSpecII is equipped with an internal A/D converter, which leads to very short analog paths and very good measurement signal quality.

In the text below '*light liquid*' is a liquid with low absorbance at the wavelength being measured, and '*dark liquid*' is a liquid absorbing as much as the calibration needs at the given wavelength. The light liquid is usually plain carrier solution and the dark liquid should produce the signal of the highest concentration of standard solution. The basic tuning algorithm is as follows:

1. Introduce light liquid into the detector.
2. Adjust the detector offset to a maximum readout.
3. Introduce dark liquid into the detector.
4. Adjust the detector gain to a minimum readout.

The algorithm involves liquid transfers, which the pump normally handles. If the detector would have been designed to contain a retuning procedure like the one above, this would imply that the detector ought to be able to give commands to the pump to get the necessary liquid transfers done. This would induce further unnecessary complexity into the system, and a simpler solution is to let the measurement method control the tuning of the detector. The controlling computer, equipped with the retuning algorithm, uses exactly the same mechanisms for the retuning as is used for normal analysis.

5. A higher degree of modularity

Certain parts of an analyzer have well-defined, but limited lifespans. Both the pump syringe and the valve inner parts have to be replaced at given intervals, but even electronics may malfunction, albeit at longer intervals.

Process technicians, who seldom know the exact behavior or theory of an instrument, usually maintain industrial analyzers. They have to replace malfunctioning parts like syringes, but they also have to be able to replace whole modules if needed.

To achieve this, the devices of the analyzer have to be very modular and easy to replace. In the case of SIAMate the modules are fitted with four screws on the front panel. A module can be removed and replaced by opening these four screws only (Fig. 3).

The complete removal of the rack is very seldom needed, but easily done as the rack itself is fitted to its mountings by four screws in the front panel.

6. Precise measurement timing

One of the first industrial analyses produced with the SIAMate controller was Cr(IV) in chromium conversion baths. The amount of chromium in such baths is comparatively high, $\sim 3 \text{ g l}^{-1}$, which is too high to be measured photometrically without diluting the sample.

The dilution is done in two 1:5 steps. The SIA method takes about 3 min per sample, which makes the method relatively time consuming (Fig. 4).

The time consuming dilution is more sensitive to variations in diffusion, dispersion and changes in the viscosities of the liquids used, than a straightforward, simple analysis method.

Not surprising we got variations in the measurement results [5]. The variations were, however, greater than 5%, which led us to recheck the function of the syringe pump as well as the valve. Neither of them showed any variations of this magnitude. The main reason proved to be variations in the total execution time of the method.

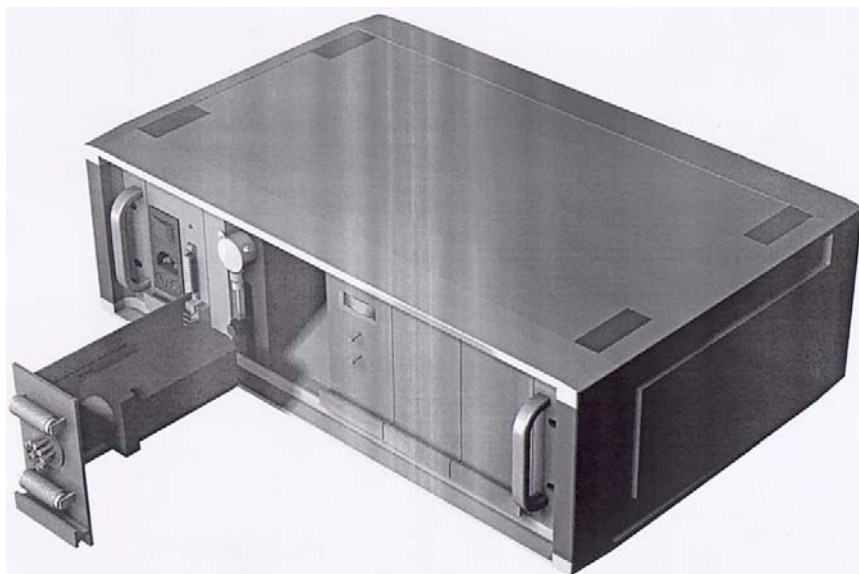


Fig. 3. SIamate valve removed.

The variation in the execution time was caused by the controlling PC running Microsoft Windows. It is almost impossible to get the PC to run the measurement method at a precise pace, due to

network traffic, mouse movements and other software requiring attention.

6.1. Command buffering

To get the method running at the same pace for each measurement, the AnalySIA BrokenRing driver program was redesigned so that it buffers the commands generated by the measurement method. Once a device has executed its command, the driver will immediately send the next command to a device. This is done at a very low level, compared to Windows and any application programs, and therefore gives a more predictable latency time.

The result is that the devices (mostly the pump and the valve) control the execution speed of the method, which gives a very steady pace, regardless of the PC's workload. The only thing required of the PC and the overlaying measurement method is that they produce commands fast enough so that the BrokenRing driver always has a new command ready when the last one is finished.

With this modification implemented, the overall reproducibility of the measurement method was reduced to less than 1%.

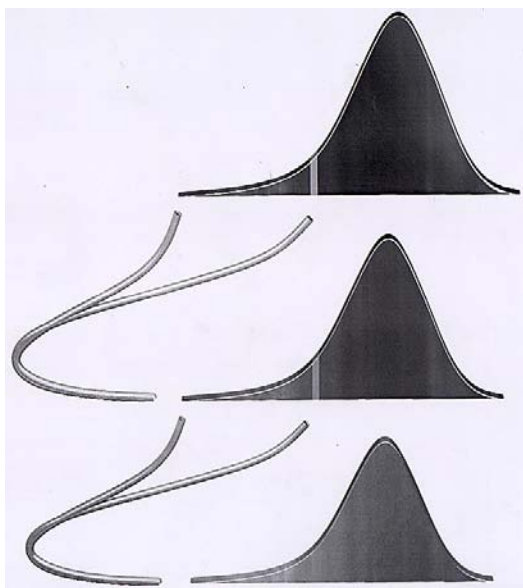


Fig. 4. On-line two-step dilution.

7. Methods produced

At the present time two methods have been produced using the SIAMate controller.

7.1. Mg^{2+} in high Ni^{2+} matrix

- 0–600 ppm of Mg^{2+}
- 15 000 ppm of Ni^{2+}
- Eriochrome Blue Black B (EBBB) color indicator
- 635 nm LED
- On-line sampling from two process lines

7.2. Cr(VI) in chromium conversion baths

- 0–3 g l^{-1} of Cr(VI)
- On-line dilution of sample
- Small amounts of Fe, Ti, Zn, Al and F in the matrix
- 558 nm LED
- Harsh industrial environment

7.3. Solutions

All reagents were of analytical grade. The bromothymol blue (BTB) solution used for testing of the gain was 1×10^{-5} M. The BTB stock solution was prepared by dissolving 0.0650 g BTB (Sigma B8630) into 100 ml of 0.01 M Borax solution. A volume of 1 ml of the stock solution was then diluted to 100 ml with 0.01 M Borax solution and used as sample when the effect of the gain settings was studied. The carrier solution was 0.01 M Borax (Sigma S9640) solution.

For Mg^{2+} analysis the following solutions were used: The carrier was 1.5 M NH_3-NH_4Cl buffer solution, pH ~ 10.5 , the 7% Triethylenetetramine (Trien) solution was prepared by diluting 70 ml Trien solution (Sigma T 7262) to 1000 ml with the buffer solution used as carrier. The metal indicator reagent solution Eriochrome Blue Black B (EBBB) was prepared by dissolving 0.2085 g EBBB (Sigma E 2252) in 50 ml ethanol and diluted to 250 ml with the NH_3-NH_4Cl buffer solution. The high- and low-standards were prepared by dissolving

67.182 g $NiSO_4 \cdot 6H_2O$ (Sigma N 4882) and 6.084 g $MgSO_4 \cdot 7H_2O$ (Sigma M5921), for the high-standard, to 1000 ml with deaerated distilled water. Wash solution was prepared by diluting 800 ml ethanol to 1 l with 1.5 M NH_3-NH_4Cl buffer solution.

For Cr(VI) analysis the following solutions were used: the buffer was 0.04 M H_2SO_4 and the 0.1% diphenylcarbazide solution was prepared by dissolving 50 mg of diphenylcarbazide (Aldrich 25,922-5) into 10 ml of acetone and by diluting it to 50 ml with water. The 0.5 M KF solution for masking iron was prepared by dissolving 1.45 g of KF (Sigma P2569) in 0.04 M H_2SO_4 and diluting the solution to 50 ml with the same acid solution. The 10 g l^{-1} Cr(VI) stock solution was prepared by dissolving 2.829 g of $K_2Cr_2O_7$ (Sigma P6535) into 0.04 M H_2SO_4 solution and diluting the solution to 100 ml with the acid solution. The Cr(VI) standard solution was prepared by diluting 30 ml of the stock solution to 100 ml with 0.04 M H_2SO_4 .

7.4. Mg^{2+} analysis

The high nickel concentration 15 g l^{-1} in the sample matrix strongly disturbs the analysis of magnesium in the range 0–600 mg l^{-1} . The nickel is masked with Trien at pH > 10 . EBBB forms a red complex with magnesium. The formed Ni-Trien complex has an absorbance maximum at 560 nm. The Mg-EBBB complex formed has an absorbance maximum at 580 nm, which is fairly close to the Ni-Trien absorbance maximum. Due to the close maxima the wavelength 635 nm is chosen and the signal for the unreacted EBBB solution is used as the analytical signal (Fig. 5). This causes the calibration curve to become a falling one (Fig. 6).

7.5. Mg^{2+} manifold

A 2500 μl syringe was used. All tubings were of PTFE with an inner diameter of 0.76 mm. The holding coil length was 2.00 m and the reaction coil length 1.00 m. A 635 nm LED was chosen.

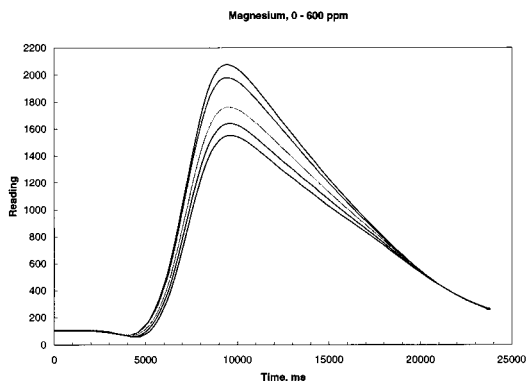


Fig. 5. SIA peaks of a Mg^{2+} calibration run.

7.6. Cr(VI) analysis

To test the performance of the detector in real determinations a method of analysis for Cr(VI) in chromate conversion baths was developed for the *SIAMate* using the *LedSpecII* detector. Chromate conversion baths are used in metal industry mainly to improve corrosion resistance of the metal and to improve the adhesion of paint or plastic coatings to the metal surface. During the process the Cr(VI) is consumed and concentrated Cr(VI) solution is added to maintain the bath composition at a proper level. The method of analysis was developed with eventual on-line measurements in mind and no manual pretreatment of the bath sample was made. The Cr(VI) concentration in the bath is quite high, between 1.8 and 2.2 $g\ l^{-1}$, making it necessary to dilute the sample

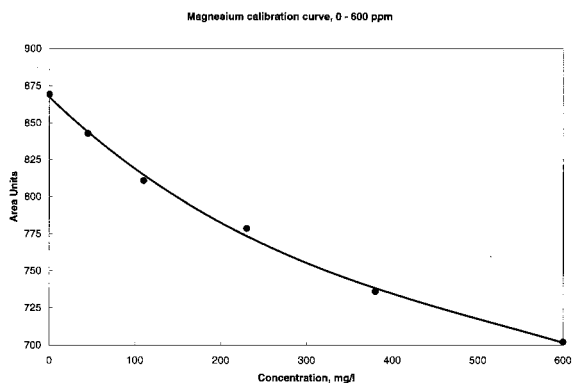


Fig. 6. Mg^{2+} calibration curve.

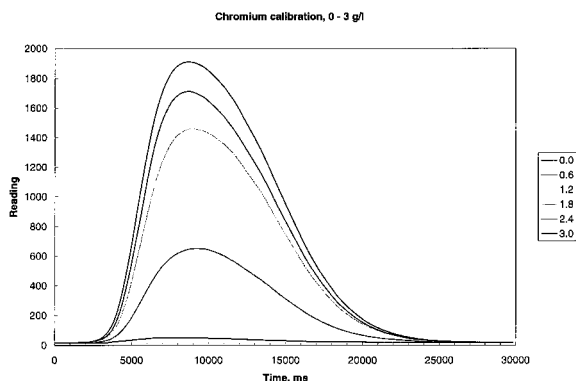


Fig. 7. SIA peaks of a Cr(VI) calibration run.

before the photometric determination with diphenylcarbazide. The solubility of diphenylcarbazide in water is quite limited and in practice it sets the limit for the highest measurable concentration of Cr(VI) with this method.

Due to this, a method with on-line dilution of the sample was developed based on the principle described by van Staden et al. [5]. In this technique the dispersion of the sample with the carrier solution is utilised by pumping most of the sample peak into a waste line and then taking a small part of the tail of the peak as a sample. A two-stage dilution was found to give the best results when diluting the sample to approximately 5% of the original concentration.

The calibration curve for the determination was constructed using only one standard solution that was diluted on-line to different calibration concentrations. The dilutions were done by first aspirating standard and then buffer, keeping the sum of the volumes constant. The on-line diluted calibration concentrations were matched against known manually prepared standards. This matching has to be done only once for each manifold.

With this technique only one port position of the multi-position valve is needed for calibration. The peaks for the calibration runs are given in Fig. 7. Each curve is the median value of three identical consecutive runs. The calibration points are determined using the delta method described above and the calibration curve is given in Fig. 8. As can be seen the curve is slightly bent, as is often the case when LEDs are used as light sources.

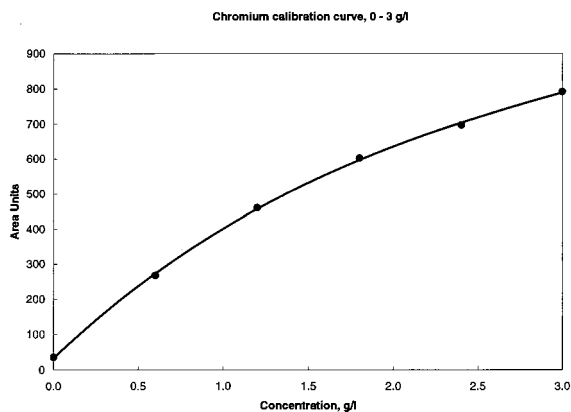


Fig. 8. Cr(VI) calibration curve.

When a third order polynomial is fitted to the calibration points, a nearly perfect fit is obtained ($r^2 = 0.999972$). The value can be regarded as quite satisfactory when considering that a two-stage dilution is performed in the determination. The curvature of the calibration curve is caused by a mismatch of the emission and absorption spectra. The relative standard deviation for repeated determinations of a bath sample was 0.9%.

7.7. Cr(VI) manifold

A 2500 μl syringe was used. All tubings were of PTFE with an inner diameter of 0.76 mm. The holding coil length was 2.00 m and the reaction coil length 1.00 m. A 558 nm LED was chosen. The manifold was the same as in the magnesium method.

Both measurement methods are in constant use, either producing results directly to the process control system or used as fast verifications of the process liquids.

8. Conclusions

An analyzer based on SIA technology can be designed rugged enough to suit the needs of the industry. Several topics related to the physical appearance of the analyzer have not been ad-

ressed in the present paper, like the placement of the reagent bottles, proper on-line sampling and possible filtering of the samples, but the basis for a rugged and sturdy SIA analyzer has been developed.

The communication between the various SIA devices and the PC needs further standardization at several levels. A totally digital communication is mandatory, but also the higher-level command protocols would need to be defined by approved, SIA suitable standards. Uniform communications protocols would ensure further enrichment of the set of available devices, as well as maintain interchangeability among different brands and manufacturers.

LED based photometers can be competitive both in terms of performance and pricing. A computer controlled LED photometer meets the requirements of industrial applications, not only because of its stability but also because of the very short, and well shielded analog paths, that give an impressive signal to noise ratio.

The effects of variations in method execution time, especially in conjunction with on-line dilution of the sample, needs further investigation. Diffusion plays an important role, but the magnitude of the variations in the results is surprisingly high.

The analyzer presented in this paper works both reliably and accurately. It is an example of how an industrial SIA analyzer can be built, and clearly shows that SIA as a methodology is very competitive in on-line analysis.

References

- [1] U. Spohn, J. van der Pol, R. Eberhardt, B. Joks, C. Wandrey, *Anal. Chim. Acta* 292, 281.
- [2] J. van der Pol, C. de Gooijer, M. Biselli, C. Wandrey, J. Tramper, *Tibtech* 14 (1996) 471.
- [3] G.D. Marshall, J.F. van Staden, *Process Control Qual.* 3 (1992) 251.
- [4] J. Ruzicka, G.D. Marshall, *Anal. Chim. Acta* 237 (1990) 329.
- [5] J.F. van Staden, R.E. Taljaard, *Fresenius J. Anal. Chem.* 357 (1997) 577.

Automated nucleic acid isolation and purification from soil extracts using renewable affinity microcolumns in a sequential injection system

Darrell P. Chandler ^{a,*}, Beatrice L. Schuck ^a, Fred J. Brockman ^a,
Cynthia J. Bruckner-Lea ^b

^a Environmental Microbiology Group, Battelle Pacific Northwest National Laboratory, 902 Battelle Blvd., P.O. Box 999, Mail Stop P7-50, Richland, WA 99352, USA

^b Chemical Sensors and Microanalytical Systems, Battelle Pacific Northwest National Laboratory, 902 Battelle Blvd., Richland, WA 99352, USA

Received 26 January 1999; accepted 4 February 1999

Abstract

We have combined affinity purification concepts with novel renewable-surface microcolumns in a sequential injection system for the automated and rapid isolation and purification of nucleic acids directly from crude soil extracts. *Geobacter chapellii* DNA was spiked at femtomolar concentrations into clean solutions or crude soil extracts containing picomolar concentrations of competitive DNA, humic acids and other soluble soil constituents. The 16S rDNA targets (indigenous and spiked) were purified and eluted in less than 20 min in a form suitable for direct polymerase chain reaction (PCR) amplification and detection. The extraction efficiency of the automated system was equivalent to a 4-h batch reaction using identical reagents. The estimated efficiency of isolation and purification was maximally 30% under the conditions employed here, with levels comparable to those obtained with soils/sediments processed by standard techniques, and a detection limit of 1.7 attamoles (10^6 copies) *Geobacter* target in a soil extract containing a competitive background of 10^9 genomes. This manuscript represents the first report of automated nucleic acid purification from an environmental sample using sequential injection fluidic systems and renewable microcolumn technology, and provides an excellent platform from which to optimize and accelerate the development of an integrated microbial/nucleic acid detector. © 1999 Published by Elsevier Science B.V. All rights reserved.

Keywords: Sequential injection; Flow injection analysis; Renewable columns; Affinity; DNA; Soil; Sample preparation

1. Introduction

The need to rapidly detect specific microorganisms or gene sequences is both varied and extensive, encompassing basic biochemical, genetic and ecological research; numerous applications in clin-

* Corresponding author. Tel.: +1-509-3768644; fax: +1-509-3761321.

E-mail address: dp.chandler@pnl.gov (D.P. Chandler)

ical diagnostics and genetic identification of disease; drug discovery; genomics and gene expression analysis; law enforcement and forensics; pathogen detection in food, air, water, soil, agricultural products or physiological fluids; and wastewater, bioprocess and in situ bioremediation monitoring. Advanced nucleic acid technologies for the detection and analysis of microorganisms combine PCR amplification and/or labeling of DNA with detection of nucleic acid hybridization on oligonucleotide arrays. Array technology is currently being used to develop novel DNA sequencing strategies, study oligonucleotide hybridization interactions, identify genetic polymorphisms and profile microbial communities [1–7]. However, routine deployment of microarray (and other) gene detection methods in many diagnostic or environmental applications is limited by (i) the time and labor required for manual sample handling, nucleic acid purification and associated volume reduction, (ii) inefficient purification/concentration of nucleic acids at low target concentrations, especially in environmental samples, and (iii) the co-purification of inhibitory compounds that interfere with subsequent molecular manipulations (e.g. PCR; [8]). Idealized microbial- or gene-detection systems, then, require an integrated sample processing capability which provides nucleic acid isolation, purification, and concentration functions for delivery to downstream PCR or other gene-based detectors, with the ability to process diverse sample matrices, solution chemistries and target concentrations in a spectrum of genetic and chemical backgrounds.

A multitude of nucleic acid isolation and purification techniques now exist for processing samples recovered from any source, most of which are based upon standard protocols originally developed for routine microbial cultures or clinical specimens [9,10]. These methods have been further adapted to detect and analyze nucleic acids in numerous environmental systems [11–17]. Most protocols are predicated upon significant target densities, high overall biomass ($\geq 10^7$ – 10^8 cells), preconcentration of aqueous samples by filtration, and dilution of nucleic acid extracts to overcome PCR inhibition. However, standard molecular biology protocols are inefficient for recovering

target nucleic acids from low biomass ($\leq 10^6$ cells) environmental samples [12,18,19], considerations that are especially relevant for the timely detection of human, animal and plant pathogens in a variety of sample matrices [20–26].

In order to overcome the limitations of current sample preparation technology and the difficulties associated with the automation and field-deployment of benchtop nucleic acid manipulations (e.g. centrifugations, precipitations, organic extractions), we have combined affinity purification concepts with novel renewable-surface microcolumns in a sequential injection system for the automated and rapid isolation and purification of nucleic acids. Renewable microcolumns provide a simple method for automatically removing and replacing column matrices [27–29], and sequential injection systems provide the necessary fluidics platform for handling microliter to milliliter sample volumes typically required for the isolation, separation and detection of nucleic acids in environmental samples. In this report, we demonstrate the utility of sequential injection technology and renewable microcolumns for mixed-phase nucleic acid analyses. We also present proof-of-concept data for nucleic acid purification from soil, representing one of the most difficult chemical and genetic backgrounds from which to recover and purify nucleic acids for subsequent detection and analysis.

2. Materials and methods

2.1. Control DNA

All extraction and purification experiments were conducted using a specific target DNA in clean salt solutions of spiked into crude soil extracts. Target DNA for all experiments was obtained from *Geobacter chapellii*, an anaerobic, iron-reducing organism not readily isolated from surface soils and incapable of growing as a contaminant within the flow system (e.g. as a biofilm). Cultures of *G. chapellii* were grown anaerobically in 100 ml serum bottles containing an 80% N₂, 20% CO₂ gas headspace and (per liter): 5 mg tryptone, 3 mg yeast extract, 1 mg glucose, 420 mg KH₂PO₄, 220 mg K₂HPO₄, 200

mg NH₄Cl, 380 mg KCl, 360 mg NaCl, 40 mg CaCl₂·2H₂O, 100 mg MgSO₄·7H₂O, 1.8 g NaHCO₃, 500 mg Na₂CO₃, 8.0 g fumarate, 10 ml mineral elixer (per liter: 2.14 g nitriloacetic acid, 100 mg MnCl₂·4H₂O, 300 mg FeSO₄·7H₂O, 170 mg CoCl₂·6H₂O, 200 mg ZnSO₄·7H₂O, 30 mg CuCl₂·2H₂O, 5 mg AlK(SO₄)₂·12H₂O, 5 mg H₃BO₃, 90 mg Na₂MoO₄, 110 mg NiSO₄·6H₂O, 20 mg Na₂WO₄·2H₂O), 25 ml 2 M lactate, 1 ml 1 mM Na₂SeO₃. After sterilization, 150 µl vitamin mix (per liter: 2 mg biotin, 2 mg folic acid, 10 mg pyridoxine-HCl, 5 mg riboflavin, 5 mg thiamine, 5 mg nicotinic acid, 5 mg pantothenic acid, 0.1 mg cyanocobalamin, 5 mg *p*-aminobenzoic acid, 5 mg thioctic acid) was added anaerobically to each serum bottle. Bottles were inoculated with 1 ml log-phase culture and grown in the dark at ambient temperature for 2 weeks prior to DNA isolation.

Geobacter cells were collected by centrifugation and genomic DNA isolated by a standard CTAB (hexadecyltrimethylammonium bromide) procedure [9]. Genomic DNA was sheared to 4–10 Kbp in size by ballistic disintegration for 1 min at 5000 oscillations s⁻¹ in an eight-place bead beater (BioSpec Products, Bartlesville, OK). DNA size fractions of 0.4–1.5 Kbp and 0.3–0.6 Kbp were obtained by sonication with a Heat Systems Ultrasonics model W-375 sonicator. After shearing, DNA concentrations were determined by fluorometry [30] and sizes determined by gel electrophoresis on 1.2% agarose (SeaKem GTG, FMC, Rockland, ME) gels in 1 × TAE running buffer, both containing ethidium bromide. All DNA targets were added at 1 or 100 ng to 200 µl soil extract in 0.3 M NaCl, representing 1 × 10⁶ or 1 × 10⁸ genomic targets (genome size of 1 fg cell⁻¹) or 3 × 10⁹–3 × 10¹¹ PCR targets, in a competitive DNA background of 6 × 10⁸ genomes (see below).

2.2. DNA extraction from soil

Nucleic acid extracts were prepared from a garden soil by aliquoting 12 × 0.5 g soil into 2.0-ml screw-cap microfuge tubes containing 1.5 g 0.1-mm glass beads and 1 ml extraction buffer (0.2 M NaPO₄, 0.1 M EDTA, 2% SDS, pH 8.0).

Slurries were frozen at –80°C for 1 h, thawed at 65°C for 30 min and cells lysed by ballistic disintegration at 5000 oscillations s⁻¹ for 2 min. Glass beads, sediment and cell debris were removed by centrifugation at 14 600 × *g* for 10 min at 18°C, and the supernatants pooled. Crude extracts were dialyzed against several changes of sterile water, passed through a 0.2-µm syringe-filter and the salt concentration adjusted to 0.3 M NaCl. While unnecessary for affinity capture in the flow system or in batch solution (not shown), the Na⁺ concentration of the soil extract was adjusted to 0.3 M to provide solution conditions comparable to those normally encountered in solution hybridization studies, standard membrane hybridizations and sequence-specific purification systems based on oligo-dT or biotinylated oligonucleotides and streptavidin-coated paramagnetic particles.

Due to spectroscopic interference by humic acids and other soil constituents, total DNA in the soil extract was quantified by ethidium bromide staining after gel electrophoresis. Assuming that 100% of the in situ biomass represents prokaryotic microorganisms, 5 fg DNA cell⁻¹, and equivalent EtBr incorporation between the crude extract relative to a sheared *E. coli* control DNA standard, the estimated nucleic acid concentration in 200 µl soil extract used for all automated captures was ~3 µg, or 6 × 10⁸ cell equivalents of genomic DNA. To illustrate the utility of and rationale for an affinity purification approach for soil extracts, pure DNA or soil DNA spiked with *G. chapellii* was also purified with Qiagen genomic DNA resin (Chatsworth, CA) that relies upon non-specific binding of nucleic acids to silica in a chaotropic salt, or a biotinylated primer/streptavidin-coated magnetic bead strategy (Promega, Madison, WI) that relies upon specific oligonucleotide-target DNA interactions to purify target sequences.

2.3. Sequential injection system

The nucleic acid purification system is based upon sequential injection technology [31], including a precision stepper motor syringe pump, holding coil and simple microvalves operated under computer control. Adapting the sequential injection

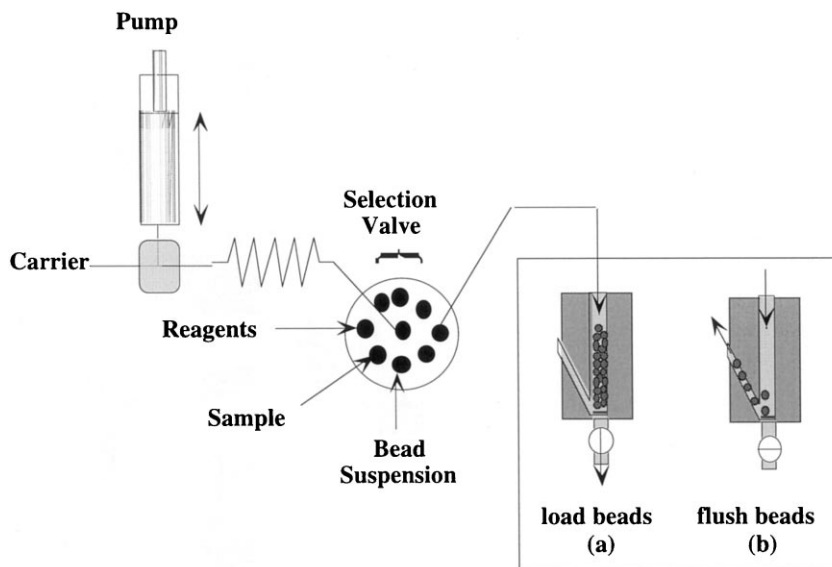


Fig. 1. Schematic representation of automated nucleic acid extraction and purification system including the renewable column concept (inset).

tion system for mixed-phase affinity capture of nucleic acids relies on the manipulation of suspended microparticles and the temporary immobilization of those solids in a suitable flow cell, otherwise known as flow injection of renewable surfaces (FIRS). FIRS was developed by Ruzicka and co-workers [27,29], and has since been used for applications ranging from the investigation of antigen-antibody interactions [27,29] to the solid-phase extraction of radionuclides [28]. For nucleic acid separations, we miniaturized and modified a renewable column [28] that incorporates frit restriction for trapping beads and microvalves for controlling the delivery and removal of beads from the column. This renewable microcolumn (Fig. 1) is a very simple and rugged device with no moving parts within the microcolumn itself.

A variety of bead materials, bead sizes and solution conditions were initially tested to evaluate the hydraulic properties of the system and various beads prior to on-line nucleic acid captures. Spherical beads composed of glass, polystyrene, acrylamide and sepharose, ranging in size from 10 to 150 μm in diameter were manipulated in water, $2 \times$ and $0.5 \times$ SSC ($20 \times$ SSC = 3.0 M NaCl, 0.3 M NaCitrate, pH 7.0), 0.3 M

NaCl or phosphate extraction buffer (see above) and evaluated for their ability to form reproducible microcolumns that are easily delivered, perfused and flushed from the fluidic system and renewable column.

Automated nucleic acid extractions were performed with an Alitea sequential injection system, FiaLab software (Seattle, WA) and a laptop computer. For a typical analysis, samples and reagents are aspirated through a ten-port selection valve (Valco, Cheminert) into a holding coil. The valve position is then switched and the sample, wash solutions and elution reagents delivered in sequence to the column. After sample clean-up and nucleic acid elution, the microbeads are flushed from the system, tubing is automatically cleaned with bleach and detergent to prevent DNA carry-over, and a new microbead column is emplaced in the flow cell in preparation for the next sample. Experiments were conducted in which the nucleic acid extract passed once and ten times through the microcolumn. A syringe pump (Cavro) was used for single pass experiments, and an Eldex reciprocating pump was added for recirculating the sample through the column. An overall schematic of the fluidic system is shown in Fig. 1, with a typical analytical protocol outlined in Table 1.

Table 1

Summary of the automated DNA sample processing procedure used for extraction of *G. chapellii* DNA spiked into clean solutions and crude soil extracts^a

Procedural step	Solution composition	Solution volume (μl)	Flowrate (μl/s)
Add column	15 mg/ml Tepnel 1392r beads in 0.3 M NaCl	To produce 7-μl packed bed volume	3
Inject sample	1 ng or 100 ng <i>G. chapellii</i> DNA in 0.3 M NaCl (or soil extract) (DNA concentration is 8.3×10^{-13} M or 8.3×10^{-15} M)	200	0.9
Rinse column	0.3 M NaCl	80	3
Wash column	$0.5 \times$ SSC (0.075 M NaCl, 0.0075 M NaCitrate)	1700	3
Elute DNA	Water	100	0.3

^a Tepnel microbeads derivatized with universal 16S rRNA oligonucleotide 1392r were used for the purification. The flowrates for sample injection and DNA elution are average flowrates produced by alternating flow at 3 μl/s and stopped flow.

2.4. Nucleic acid isolation and purification with renewable affinity microcolumns

The affinity matrix used throughout this study for on-line affinity purification of DNA was obtained from Tepnel Life Sciences (Cheshire, England) and included universal 16S rDNA oligonucleotide 1392r with a dT₈ linker (lower case) covalently attached to 60-μm microbeads (bead- 5' tttttttACGGGCGGTGTGTRC). The binding capacity was estimated to be 2 pmol mg⁻¹ (or cm²) beads (1.27×10^{12} capture probes mg⁻¹) based upon a competitive hot/cold assay using complementary oligonucleotides (Tepnel). Underivatized beads were also obtained to test for non-specific binding of nucleic acids. Before experimenting with Tepnel reagents in the mesofluidic system, we performed batch capture experiments which varied in hybridization time (30 min or 4 h), wash stringency ($0.5 \times$ or $0.05 \times$ SSC) and elution temperature (room temperature or 100°C), using both underivatized and 1392r-derivatized microbeads.

For each nucleic acid size and quantity, automated capture experiments were performed with 200 μl blank extract (no DNA), purified *G. chapellii* genomic DNA in 0.3 M NaCl, and at least two replicate captures of *G. chapellii* genomic DNA in 200 μl soil extract. The sample processing times for the primary separation events are shown in Table 2. The nucleic acid capture

program was initiated by delivering the affinity matrix from a stirred slurry (15 mg ml⁻¹ in 0.3 M NaCl) to the renewable column, resulting in a 7-μl bed volume (1.6 mm I.D. \times 3.5 mm column height) containing approximately 3.7 mg bead material, 3.5 cm² surface area and 4.4×10^{12} capture probes.

Nucleic acid extracts (200 μl) were heat denatured at 100°C for 10 min, quick-chilled on ice and perfused over the microcolumn at 0.9 μl s⁻¹ for a total contact time of approximately 3 min. The unbound flow-through was collected for subsequent analysis. Beads were washed by perfusing 80 μl 0.3 M NaCl to remove nucleic acid extract, bound nucleic acids were washed in 1.7 ml $0.5 \times$ SSC (3 μl s⁻¹), and hybridized target was eluted with 100 μl water at room temperature with a 5.5-min contact time. The total sample processing time from injection to elution was 18 min. The experimental conditions were identical for the ten pass sample recirculation experiments, except the extract and hybridization solutions were recirculated ten times over the column at a flow rate of 3 μl s⁻¹, resulting in a sample contact time of approximately 11 min instead of 3 min, and a total hybridization time of 19 min (Table 2). Eluted nucleic acids were lyophilized to dryness and resuspended in 20 μl water prior to PCR detection. Between captures, the flow system was washed extensively with a sequence of 0.16% Roccal microbial disinfectant, 10% bleach, and water.

Table 2

DNA extraction summary and comparison of processing times from DNA sample introduction to DNA elution^a

	One pass automated	Ten pass automated	Batch manual
Sample contact time (flowrate, $\mu\text{l/s}$)	3 min 6 s (0.9)	11 min 7 s (3)	240 min
Total hybridization time, min ^b	3.5	19	240
Rinse, min (flowrate, $\mu\text{l/s}$)	9 (3)	9 (3)	10 ^c
Elution, min	5.5	5.5	10 ^c
Total processing time, min	18	33.5	260

^a Processing times are summarized for one pass of DNA through the renewable column, ten passes (recirculation) of the DNA sample, and a manual batch reaction. In all cases the sample volume was 200 μl , and the elution volume was 100 μl . Processing times in the automated system were not optimized for speed, and therefore do not necessarily reflect a lower limit on processing speed within the system and for other sample matrices.

^b Total hybridization time is the sample contact time plus the time elapsed during column washing with the hybridization solution (0.3 M NaCl).

^c Approximately 20 min are required to manually wash/collect microbeads and elute DNA in batch, using a standard $3 \times 0.5\text{-ml}$ bead rinse protocol.

2.5. PCR amplification and capture efficiency

Geobacter 16S rDNA and total eubacterial 16S rDNA were detected and enumerated with a dilution-to-extinction PCR-based approach [32] to estimate capture efficiency and, for captures in soil extracts, to provide a functional assay for DNA purity that cannot be obtained by scintillation counting of radiolabeled DNA. Estimates of capture efficiency were calculated by (PCR detection limit) \times (dilution factor) \times (conversion factor to account for entire eluant). For example, with a 64 copy detection limit, 5^3 dilution to the last positive PCR signal, and a 2- μl DNA input into the fivefold dilution series (10% of the total recovered DNA), 8×10^4 copies of DNA were recovered. At 1-ng input DNA (1×10^6 copies of target, assuming one 16S rDNA copy per genome), the capture efficiency is therefore $(8 \times 10^4 / 1 \times 10^6) \times 100$, or 8%. Capture efficiencies calculated in this manner are conservative estimates and underestimate the actual capture efficiency. That is, the true extinction point of the PCR lies between the last positive signal and the next dilution in the fivefold series. Further, the positive control used to calibrate the enumeration was non-fragmented, highly purified DNA rather than sheared DNA isolated from a soil extract (which may amplify with lower efficiency than the standard). These variables bias the calculation of capture efficiency downward, such that the actual capture efficiency

calculated in the example above is $\geq 8\%$ but $\leq 40\%$.

Purified DNA was serially diluted in a fivefold series immediately prior to PCR. PCR primers were synthesized by Keystone Labs (Camarillo, CA): Gbc.1300f (5' CGGTCTCAGTTCGGATTG) and Gbc.1400r (5' GGACCAATCGACTCCCGT) (this study); S- δ 401F-20 (5' caucacaucuAASCCTGACGCAGCRACGCC) and S- δ 683aR-20 (5' cuacuacuacuacuaTCTACGGATTCACTCCTACAC) (modified from [33]); universal eubacterial primers fD1 (5' ccgaattcgtcgacaacAGAGTTTGATCCTGGCTCAG) and rP2 (5' ccgggatccaagcttACGGCTACCTTGTTACGACTT) [34]. Lower case letters designate cloning tails. For both sets of *Geobacter*-specific primers, PCR reactions were carried out in 25 μl total volume, utilizing a Perkin-Elmer (Foster City, CA) 9600 thermal cycler and 0.2-ml thin-walled reaction tubes. Final reaction conditions were 2 μl purified DNA (or dilutions thereof), 10 mM Tris pH 8.3, 50 mM KCl, 2.5 mM MgCl_2 , 200 μM each dNTP, 0.2 μM each primer, and 0.625 U Taq polymerase (Perkin Elmer) which had been pretreated with TaqStartTM antibody at $0.5 \times$ the recommended concentration (Sigma, St. Louis, MO). Assembled reactions were heated to 80°C for 5 min (hot start) and amplifications were conducted by performing five cycles at 94°C for 40 s, 60°C for 10 s, 72°C for 75 s followed by 40 cycles at 94°C for 12

s, 65°C for 10 s, 72°C for 80 s with a 2-s extension per cycle. A final 20 min, 72°C extension was performed before chilling reactions to 4°C. Control reactions included no template, solution blank and system washes (pre- and post-capture), affinity-purified nucleic acids (i.e. system eluant) spiked with 250 fg *G. chapellii* genomic DNA, and a dilution series of *G. chapellii* genomic DNA. PCR conditions for universal eubacterial primers fD1/rP2 were essentially identical, except we utilized 1.5 mM MgCl₂ and a thermal profile consisting of five cycles at 94°C for 40 s, 55°C for 10 s, 72°C for 75 s, 30 cycles at 94°C for 12 s, 65°C for 10s, 72°C for 80 s with a 2-s extension per cycle, and a 20 min, 72°C final extension.

Positive controls (with known concentrations of target) were used to determine the PCR detection limit for each experiment and calibrate the PCR enumeration. Spiked controls (eluant amended with 250 fg target DNA) were used to visualize and estimate the extent of PCR inhibition due to co-purified soil constituents. The entire contents of each PCR were analyzed on 1% NuSieve, 1% Seakem GTG agarose (FMC Bioproducts, Rockland, ME) gels in 1 × TAE running buffer, both containing ethidium bromide, and gel images captured with a BioRad (Hercules, CA) Gel-Doc station and Molecular Analyst software.

3. Results

The rationale for using sequence-specific affinity purification reagents for automated purification of nucleic acids from crude environmental samples is illustrated by the PCR results in Fig. 2. While DNA purification resins that rely upon electrostatic or ion exchange principles (e.g. Qiagen resin) can capture very dilute DNA in pure solution (50 fg μl^{-1} shown here), they also bind humic acids, metals, inorganics and other soil constituents which are co-eluted from the matrix and destroy the PCR. Consequently, even 100 ng of specific target (10^8 copies) in the crude soil background could not be detected after Qiagen purification (lanes 29–31) whereas 10 pg (10^4 copies) were easily detected using pre-purified DNA template (lanes 26–28). We have observed

similar purification difficulties with non-specific resins sold by other vendors, so the results presented here are not unique to the Qiagen product. On the other hand, sequence-specific affinity purification generated DNA free of enzymatic inhibitors (lanes 16–17) with an absolute detection sensitivity equaling that of the non-specific resin in pure solution (e.g. 10^4 copies, lanes 11–12). These simple results illustrate the practical limitations of non-specific resins in an environmental context and underscore the need for using (and developing) affinity reagents for automated DNA extraction and purification from soils and other difficult sample matrices.

It was important to differentiate between specific and non-specific binding of nucleic acids to the affinity support matrix, and ensure that the experimental conditions used within the fluidic system were suitable for DNA extraction and elution. Batch capture experiments indicated that target DNA binding to the Tepnel reagent included both specific and non-specific interactions. The difference between non-specific interaction with the solid support and sequence-specific selection by the tethered oligonucleotide was apparent after washing the microbeads with solutions of varying ionic strength. There was a 25–125 × decrease in target DNA recovery from underivatized beads when they were washed at high stringency ($0.05 \times \text{SSC}$) compared to washes at low stringency ($0.5 \times \text{SSC}$), whereas the 1392r beads retained an equivalent amount of target DNA under both wash conditions (not shown). A 100°C elution temperature did not appreciably increase the amount of target DNA recovered from either matrix (underivatized or 1392r) relative to the recovery of DNA eluted at room temperature. These results suggest that non-specific interactions between the underlying support matrix and nucleic acids contribute to the initial binding event, but that target molecules are specifically bound by the tethered oligonucleotide on the 1392r microbeads.

The addition of bovine serum albumin to the hybridization solution blocked the non-specific binding of DNA to the underivatized matrix but also decreased binding to the 1392r reagent, suggesting that non-specific interactions between the

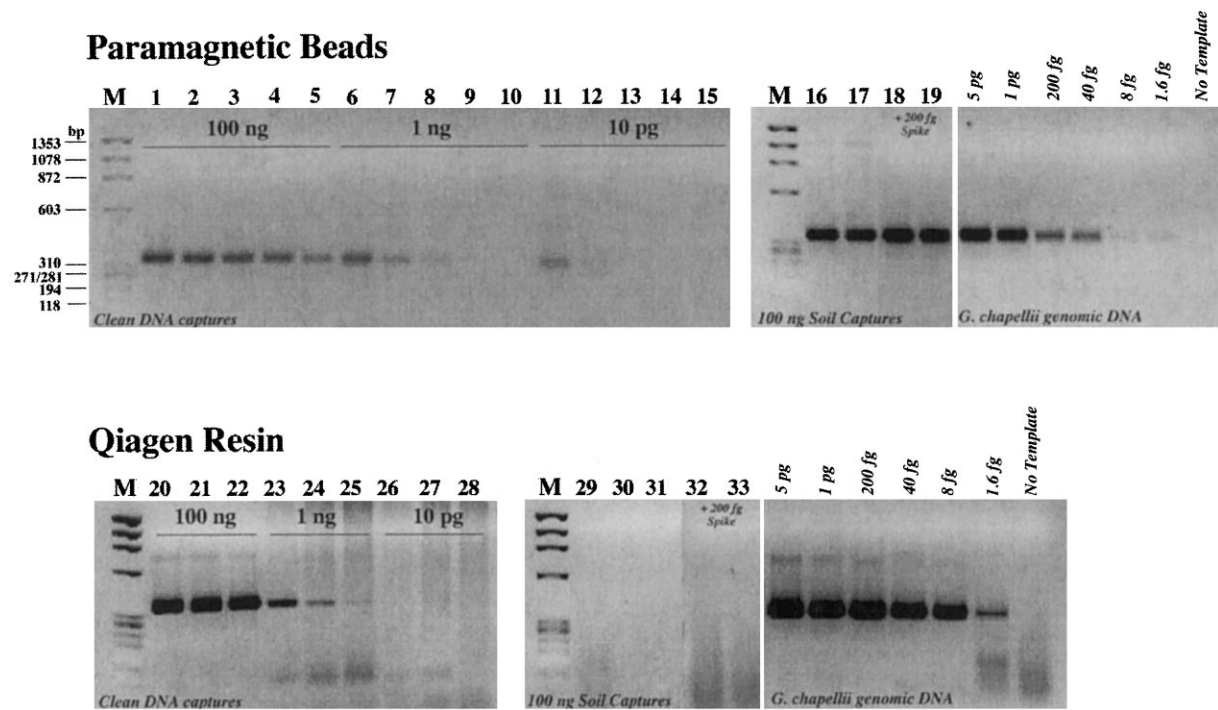


Fig. 2. Comparison of affinity purification approach to non-specific binding resin in a soil extract. *G. chapellii* 4–10 Kb sheared genomic DNA was reconstituted in a 200- μ l 0.3 M NaCl at the indicated quantities and processed according to the manufacturer's instructions (Promega, Qiagen). Purified eluant from the paramagnetic beads was lyophilised to dryness and reconstituted in 20 μ l water prior to PCR. Purified eluant (\sim 1 ml) from the Qiagen resin was ethanol precipitated before reconstituting in 20 μ l for dilution-to-extinction PCR detection. Lane assignments are: M, ϕ X174 \times HaeIII molecular weight marker, with fragment sizes indicated in the margin; 1–5, 100 ng genomic DNA capture and elution, with lane 1 is 1:5¹ dilution of template prior to PCR; 2, 1:5² dilution prior to PCR; 3, 1:5³; 4, 1:5⁴; 5, 1:5⁵; 6–10 are the same as 1–5, except a dilution series from 1 ng genomic DNA capture and dilution; 11–15 are the same as 1–5, except from 10 pg DNA capture and dilution; 16, undiluted eluant from 100 ng *G. chapellii* genomic DNA capture in the presence of 200 μ l competitive soil background; 17, same as 16, except diluted 1:5 prior to PCR; 18 and 19 are the same as 16 and 17, except spiked with an additional 200 fg control DNA prior to PCR; 20–22 are the same as 1–3 except purified with Qiagen resin; 23–25 are the same as 6–8; 26–28 are the same as 16–17, except with an additional fivefold dilution (lane 31); 32 and 33 are the same as 29 and 30, except spiked with an additional 200 fg control DNA prior to PCR. *G. chapellii* control DNA and standard curve are indicated in both panels.

microbead and organic compounds within the sample matrix may decrease DNA capture efficiency. Based upon these results from batch reactions, automated capture experiments with 1392r microbeads utilized 0.3 M NaCl hybridization buffer, no BSA blocking, 0.5 \times SSC washes and elution at room temperature.

Relative to batch capture protocols, the automated capture was faster (18 versus 260 min total processing time; Table 2) and resulted in an extraction efficiency that was equivalent to or better than that obtained in solution. The best batch capture efficiency was only 2% using 100 ng of

4–10 Kb DNA and a hybridization time of 240 min, and \leq 0.4% for a 30-min hybridization. Automated capture of the same DNA size fraction and concentration resulted in an extraction efficiency of 6.25%, with a single pass through the column and a hybridization time of 3.5 min (i.e. time elapsed during sample delivery and column wash with hybridization solution).

DNA capture with one pass over the renewable affinity column varied appreciably as a function of target size and absolute target concentration (Table 3). At 1 ng of input genomic DNA (\sim 1.7 attamoles target), capture efficiency declined with

Table 3

Capture efficiency of *G. chapellii* 16S rDNA with the Tepnel 1392r reagent and one pass through the renewable affinity column^a

	Genomic DNA				No spike
	4–10 Kbp sheared	1 Kbp sheared	0.5 Kbp sheared	300-bp PCR product	
<i>1 ng</i>					
Clean, %	8	1.6	0.3	0.00001	0
(Background, %)					
Soil, %	0.3	0.3	0.3	0.00001	0
(Background, %)					(0.04)
<i>100 ng</i>					
Clean, %	6	31	6	0.0004	0
(Background, %)					
Soil, %	0.3	0.3	0.002	0.000003	0
(Background, %)	(0.1)	(0.1)	(1)	(0.2)	(0.3)

^a Each value is the average of at least two capture experiments. 1 ng of *G. chapellii* genomic DNA = 10^6 cell equivalents (1 fg cell⁻¹) or 10^6 copies of target assuming 1 copy cell⁻¹. 1 ng of the 300-bp PCR product = 3×10^9 copies of target. The estimated DNA content of the soil extract background was $\sim 3 \mu\text{g}$ per capture, or $\sim 3 \times 10^9$ competitive DNA targets assuming 5 fg cell⁻¹ and one 16S rDNA target fg⁻¹ (or Mb⁻¹). Values in parentheses indicate capture efficiency of total 16S rDNA target based on PCR enumerations with universal 16S rDNA primers fd1/rP2.

the smaller DNA fragment sizes; for 100 ng genomic DNA inputs, capture efficiencies were relatively constant and represented the highest observed capture efficiencies (6–30%). PCR analysis of the sample flow-through, column eluent and spent microbeads (Fig. 3) showed that the majority of DNA applied to the column could be detected in the flow-through fraction, indicating that significant amounts of DNA were not adsorbed by the fluidics system (tubing, valves) and detectable target DNA was not retained on the microbeads after elution. Automated capture of 1 Kbp sheared DNA after ten passes (~ 19 min hybridization time) over the microcolumn showed no improvement relative to single-pass experiments, suggesting that the capture efficiency was not limited by column contact time alone. Further, the maximal amount of target DNA recovered from 1 ng genomic DNA captures was ~ 80 pg ($\sim 8 \times 10^4$ copies), whereas the amount of target DNA recovered from the 100 ng genomic captures was 6–30 ng (6×10^6 – 3×10^7 copies). Therefore, the limited capture of 1 ng target at all size ranges was not due to surface saturation of available binding sites, suggesting that kinetic and/or thermodynamic effects limited nucleic acid capture at the lower target concentrations.

The capture efficiency for competitive eubacterial 16S rDNA from unspiked soil extract was 0.3%, similar to the capture efficiency of *Geobacter* genomic DNA targets that were also spiked into the soil background (Table 3). At both 1 ng and 100 ng 4–10 Kbp and 1 Kbp DNA inputs into the soil background, the capture of *G. chapellii* 16S rDNA specific capture and total eubacterial 16S rDNA capture was constant and of similar magnitude (0.3% capture efficiency), even though 100 ng of *G. chapellii* target constituted $\sim 3\%$ of the total 16S rDNA and 1 ng represented only 0.03% of total 16S rDNA target. These results indicate that the spiked DNA (up to 10^8 additional targets) did not appreciably change the availability or binding efficiency of *Geobacter* targets relative to total, eubacterial, competitive 16S rDNA targets, and that humic acids did not bias the affinity binding for or against the added *Geobacter* DNA relative to indigenous 16S rDNA. In addition, these results indicate that the competitive DNA background did not bias the affinity capture system for or against low-copy genomic DNA targets (*Geobacter* 16S rDNA) in solution. However, the binding of competitive 16S rDNA sequences to the 1392r microbeads or non-specific binding of humic acids precluded more

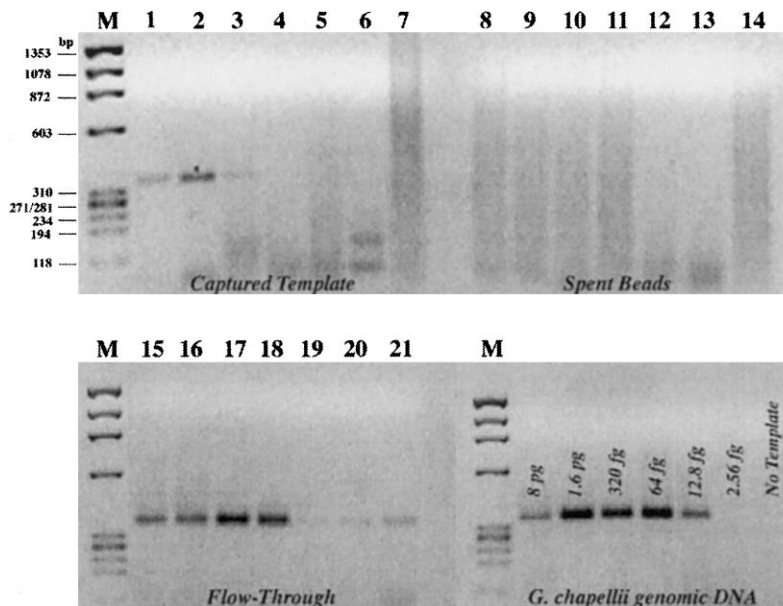


Fig. 3. Partitioning of target DNA within the automated purification system. The single-pass capture protocol was implemented on 1 ng 4–10 Kb sheared genomic DNA. The flow-through fraction was ethanol precipitated and reconstituted in 20 μ l water prior to dilution-to-extinction PCR. After elution of bound target in water, spent microbeads were heated in boiling water for 5 min and the supernatant concentrated by ethanol precipitation. Fivefold serial dilutions of eluted and concentrated target were analysed by PCR with primers S- δ 401F-20 and S- δ 683aR-20. Lane assignments are: M, ϕ X174 \times HaeIII molecular weight marker, with fragment sizes indicated in the margin; 1–7 are serial fivefold dilutions of purified eluant, where lane 1 is 1:5¹ dilution of 1392r-captured and eluted template prior to PCR; 2, 1:5² dilution prior to PCR; 3, 1:5³; 4, 1:5⁴; 5, 1:5⁵; 6, 1:5⁶; 7, 1:5⁷; lanes 8–14 are the same as 1–7, except from spent microbeads; lanes 15–21 are the same as 1–7, except from the unbound flow-through fraction. *G. chapellii* control DNA and standard curve is indicated in the figure.

efficient binding of *Geobacter* target DNA, since purified *Geobacter* DNA was captured with up to 30% efficiency (at 100 ng) whereas *Geobacter* targets spiked into a soil background (at 100 ng) were only captured with 0.3% efficiency.

Importantly, nucleic acid eluant purified from the crude soil extracts was not inhibitory to the PCR (Fig. 4), in contrast to results obtained with non-specific resins (Fig. 2), validating the mixed-phase affinity purification approach for purifying nucleic acids from soil (and similar environmental) extracts. Some level of PCR inhibition was occasionally observed in concentrated (20 μ l) eluants from soil extracts (not shown). However, eluted nucleic acids were always concentrated fivefold prior to PCR (e.g. 100 μ l eluant lyophilized and reconstituted in 20 μ l water), and PCR inhibition was always relieved by the first fivefold dilution, indicating that the original eluant (100 μ l volume) was suitable for direct PCR analysis.

4. Discussion

As reflected in the literature [11–17], current methods of nucleic acid extraction from environmental samples fail to meet many of the practical criteria for technology deployment outside of the research laboratory and are ill-suited for automation. Non-specific purification resins employed for routine molecular biology applications also fail to remove many environmental contaminants that interfere with subsequent analyses (Fig. 2). The affinity purification principle, however, provides the most straightforward, simple and robust purification method currently available for environmental samples. In this paper, we have shown that the affinity purification principle can be automated, miniaturized and applied with reasonable purification and recovery efficiency (6–30%) to one of the most challenging sample preparation

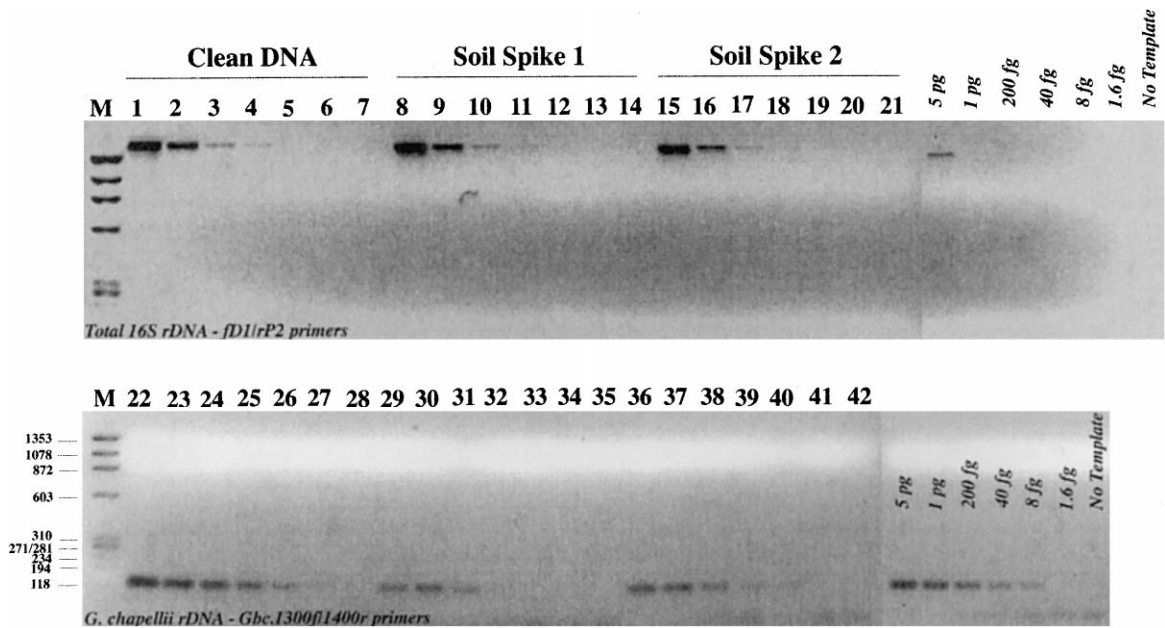


Fig. 4. Automated isolation and purification of *G. chapellii* from a competitive soil extract. A total of 100 ng 4–10 Kb sheared genomic DNA was added to 200 μ l soil extract containing $\sim 3 \mu$ g competitive genomic DNA background and processed with the automated purification system. Total eubacterial 16S rDNA captured by the Tepnel-1392r renewable microcolumn was estimated by dilution-to-extinction PCR with universal eubacterial primers fD1 and rP2. *G. chapellii*-specific isolation and purification was detected/quantified with primers Gbc.1300f/1400r. Lane assignments are: M, \emptyset X174 \times HaeIII molecular weight marker, with fragment sizes indicated in the margin; 1–7 are serial fivefold dilutions of eluant from purified DNA captured and eluted in clean buffer solutions, where lane 1 is 1:5¹ dilution of 1392r-captured and eluted template prior to PCR; 2, 1:5² dilution prior to PCR; 3, 1:5³; 4, 1:5⁴; 5, 1:5⁵; 6, 1:5⁶; 7, 1:5⁷; lanes 8–14 are the same as 1–7, except from *G. chapellii* genomic DNA added to a crude soil extract prior to automated purification; lanes 15–21 are the same as 8–14, except from a replicate soil purification; lanes 22–28 are the same as 1–7 except detecting *G. chapellii*-specific rDNA; lanes 29–35 are the same as 8–14, and lanes 36–42 are the same as 15–21. *G. chapellii* control DNA and standard curve is indicated in the figure.

matrices (soil) for subsequent gene-based detection/analysis.

For real-time, on-line environmental applications, a nucleic acid purification and detection system must meet a number of (competing) criteria that are not limiting in a laboratory environment. For example, devices should be field portable (or miniaturized), reliable, and have a rapid response time (i.e. 1–2 h). The system should require little (if any) hands-on time for maintenance, repair and sample manipulation, use minimal solution volumes and few (if any) consumables, and avoid the use of noxious or hazardous chemicals. The system and reagents should be capable of handling nucleic acid extracts from soils, sediments, sludge, industrial process streams, undefined aqueous media, swabs and

other notoriously ‘filthy’ sample matrices. Typical environmental samples also represent grams of solid or tens of milliliters of liquid that must be concentrated to microliter volumes for subsequent nucleic acid or gene-based detection (i.e. PCR, MALDI-MS, oligonucleotide arrays). Advanced, microfabricated ‘lab-on-a-chip’ devices are restricted to pl-nl manipulations and run the risk of clogging by even the smallest colloid or suspended particle, and are therefore inappropriate sample acquisition/preparation platforms for many environmental applications.

These requirements were the primary conceptual drivers for the fluidics system and renewable column as illustrated in Fig. 1. Sequential injection systems and renewable surface techniques provide the up-front capacity, volume reduction,

and sample purification capabilities necessary to utilize microfabricated detection devices for biomolecular analysis in an environmental context. The affinity purification approach described here utilizes harmless salts and buffer solutions for complete sample preparation, avoiding the hazards associated with standard purification protocols and greatly simplifying engineering requirements and system architecture. The simplicity of sequential injection systems also allows us to physically separate ‘dirty’ reagents or processes from downstream, ‘clean’ reagents and processes, a design feature that has resulted in more than 1 year of experimentation without a single instance of DNA cross-contamination between samples. Most important, however, is the concept of an automated, renewable affinity microcolumn, which eliminates the need for routine operator intervention, disposables and consumables, and is therefore a significant departure from other instruments or techniques that utilize microparticles (affinity or non-specific binding) for nucleic acid separations. This fundamental departure from standard practices and traditional commercial applications provides the opportunity to develop free-standing, field-deployable, continuous monitoring capabilities in a range of environmental applications, including the detection of pathogenic microorganisms in food, air, water, soil, agricultural products or physiological fluids, and microbial community profiling in wastewater treatment processes, reactor bioprocessing, and in situ bioremediation monitoring.

The affinity microbead format for nucleic acid isolation is a significantly different biophysics problem than solution-based hybridizations, with a number of added complexities and variables affecting hybridization kinetics and overall efficiency. In addition to buffer composition, pH, ionic strength, temperature, nucleic acid concentration (relative and absolute), and target size, mixed-phase hybridizations are affected by surface derivatization and charge density, probe spacing, loading density, probe length, and competing solution-phase reannealing reactions, to name a few. These variables have been investigated primarily within the context of oligonucleotide arrays [3–5,35–38], in which a short

oligonucleotide probe is tethered to a planar solid support and used to ‘capture’ oligonucleotides or short PCR products from solution. We are primarily interested in the purification of large nucleic acid fragments (i.e. > 1.5 Kb, usually 4–10 Kb) from environmental samples, a specific hybridization objective that has not been explicitly addressed or optimized for affinity microbead purification resins. We therefore initiated our studies with a reagent of defined surface coverage under low-stringency solution hybridization and wash conditions that do not require more elaborate engineering requirements for a fieldable device. Under these conditions, the primary hypotheses were that target size and concentration would affect nucleic acid capture efficiency, with small or numerous targets captured with greater efficiency than large or rare targets [35,39].

Automated capture results with pre-purified genomic DNA showed that low-copy (10^6) targets were isolated with a lower frequency than abundant (10^8) targets, but that the recovery efficiency was dependent upon target size (Table 3). At 1 ng of spiked genomic DNA, the increase in capture efficiency with increasing target size was counter to our hypothesis but in agreement with predictions and experimental data for (non-specific) protein and polymer adsorption on surfaces at a low surface coverage [40], suggesting some level of binding ‘cooperativity’ or networking on the microbead surface. At 100 ng of genomic DNA target, capture efficiencies were uniform and independent of target size, or at least within the fivefold uncertainty imposed by the dilution-to-extinction PCR detection method. Significant amounts of target DNA were not retained within the fluidics system during the capture protocol (Fig. 3), and elution temperature [41] did not increase the recovery of bound DNA from the microbeads. These results are in contrast to theoretical [35] and experimental [38] data generated in the context of oligonucleotide arrays. What, then, are the experimental and physical parameters limiting purification efficiency of our automated system?

The 8% maximum capture efficiency (8×10^4 copies) at 1 ng of genomic target DNA was not due to surface saturation or inaccessibility of

probe binding sites; in absolute terms, the binding capacity of the microcolumn was at least 10^7 targets as indicated by the 30% capture efficiency at 100 ng of DNA (Table 2). The probe density of a 7- μ l microcolumn is approximately 4.4×10^{12} molecules, or 10^4 – 10^6 excess over the spiked DNA targets and 10^3 excess over competitive 16S rDNA targets in solution. The diffusion constant for 2.6 Kbp DNA is 3.8×10^{-8} cm² s⁻¹ [35], resulting in 130 ms for a DNA diffusion distance of 1 μ m. Even for the largest DNA fragments (10 Kb), the diffusion constant (1.69×10^{-8} cm² s⁻¹ [35]) results in a 300-ms diffusion time over the same interval. We therefore do not expect mass transport of DNA from solution to the microbead surface to be limiting as nucleic acids traverse the tortuous path of the microcolumn. This hypothesis is also supported by the ten-pass (19 min) and batch (240 min) hybridization experiments, which did not improve the DNA capture efficiency relative to the one-pass experiment (3.5 min) regardless of DNA concentration (10^6 or 10^8 copies of target).

Reannealing of target DNA in solution could be a limiting factor for effective nucleic acid capture at a surface. However, our target DNA was present in low concentration (femtomolar) and cooled on ice prior to delivery to the column, and capture efficiency in solution increased with increasing time, so we expect that solution-phase reannealing was not significant during the time course of our experiments (min). DNA hybridization requires a nucleation event followed by strand zipping to form a double helix. It is known that the rate limiting step for solution-phase hybridization is the primary nucleation event [42]. For mixed-phase hybridizations, however, the initial binding event may be driven by non-specific interactions between the target DNA and microbead surface and/or random base pairing with the tethered oligonucleotide. Once the target nucleic acid is on the microbead surface, it can rapidly interact and hybridize with the tethered probe via two-dimensional diffusion and hybridization [35]. Our data with 1 ng target DNA is consistent with simple Langmuir adsorption followed by two-dimensional diffusion:

$$C_s = K_e C \quad (1)$$

where C_s is the surface concentration of DNA, C is the solution concentration of DNA and K_e is the apparent equilibrium constant. With 1 ng of 0.5 Kb sheared DNA, we measured an extraction efficiency of 0.3%, which corresponds to a binding constant (K_e) of 8.5×10^{-4} cm, within the range measured for the adsorption of oligonucleotides onto glass substrates (3.3×10^{-6} cm [43] to 1.71×10^{-3} cm [36]). If the extraction efficiency is governed by simple Langmuir adsorption at low target concentrations, then the most straightforward method for increasing the capture efficiency in our system is to increase the column size (or surface area).

Clearly, the renewable microcolumn is a very complex biophysical system, but the operation of the sequential injection extraction system is simple and straightforward. Using a simple (and possibly sub-optimal) extraction protocol, indigenous soil 16S rDNA ($\sim 3 \times 10^9$ competitive targets) was captured with ~ 0.1 – 1% efficiency (Fig. 4, Table 3), in general agreement with all experiments in which pre-purified *G. chapellii* targets were spiked into the soil background, and in agreement with the recovery/purification efficiency of indigenous nucleic acids from soil matrices by standard benchtop methods [13,44,45]. These results also demonstrate an ability to isolate and purify target DNA in a single step, without carry-over of PCR inhibitors. The stoichiometry of *G. chapellii* capture relative to total 16S rDNA capture was maintained at both target concentrations (0.3% capture efficiency), indicating that a complex genetic background ($\sim 10^3$ different species [46,47]) and solution-phase reannealing does not bias the mixed-phase affinity capture principle for or against low-copy targets in solution. Therefore, the automated, mixed-phase affinity purification method is well-suited for quantitative nucleic acid purification from, and analyses of, environmental samples.

To the best of our knowledge, this report represents the first proof-of-principle demonstration for automated nucleic acid purification from an environmental sample, with a 1-attomole (10^6 copy) capture, elution, and detection limit in a

competitive background of $\sim 10^9$ genomes. It also represents the first use of sequential injection technology and renewable-surface micro-columns to study nucleic acid interactions at a surface. The estimated efficiency of isolation and purification of femtomolar target concentrations was maximally 30% for purified *Geobacter* 16S rDNA, and 1% for spiked targets in a soil background containing 10^9 competitive targets. Our data for low target concentrations in soil backgrounds highlights the complexity of the mixed-phase affinity purification method and some of the limitations of non-specific DNA binding reagents for automated nucleic acid purification from environmental and/or low-biomass samples. It is clear that significant, fundamental research is still required to determine the optimal bead size, bead surface chemistry, probe spacing, target size, solution conditions, packed bed volumes and hydraulic parameters for each class of sample processing applications. Advanced technologies and/or reagents will also be required to overcome diffusion-controlled, mixed-phase hybridization kinetics and increase the isolation/purification efficiency of nucleic acids from low-biomass environments. Nevertheless, the system and approach presented herein provides an excellent platform from which to examine each of these variables, and should accelerate integrated microbial/nucleic acid detector development specifically for environmental samples and on-line applications.

Acknowledgements

We thank Sam-Seung H. Lee and Ronald Mick for excellent technical assistance, and Dr Jarja Ruzicka for insightful discussions. The continued support of Dr Barbara Seiders is greatly appreciated. This research was supported in part by a grant from the US Department of Energy (DOE) Laboratory Technology Research program. Pacific Northwest National Laboratory is operated for the US DOE by Battelle Memorial Institute under contract DE-AC06-76RLO 1830.

References

- [1] Z.G. Guo, A. Guilfoyle, A.J. Thiel, R. Wang, L.M. Smith, *Nucleic Acids Res.* 22 (1994) 5456.
- [2] G. Yershov, V. Barsky, A. Belgovskiy, E. Kirillov, E. Kreindlin, I. Ivanov, et al., *Proc. Natl. Acad. Sci. USA* 93 (1996) 4913.
- [3] E.M. Southern, S.C. Case-Green, J.K. Elder, M. Johnson, K.U. Mir, L. Wang, J.C. Williams, *Nucleic Acids Res.* 22 (1994) 1368.
- [4] A.C. Pease, D. Solas, E.J. Sullivan, M.T. Cronin, C.P. Holmes, S.P.A. Fodor, *Proc. Natl. Acad. Sci. USA* 91 (1994) 5022.
- [5] U. Maskos, E.M. Southern, *Nucleic Acids Res.* 21 (1993) 4663.
- [6] J.C. Williams, S.C. Case-Green, K.U. Mir, E.M. Southern, *Nucleic Acids Res.* 22 (1994) 1365.
- [7] D.Y. Guschin, B.K. Mobarry, D. Proudnikov, D.A. Stahl, B.E. Rittmann, A.D. Mirzabekov, *Appl. Environ. Microbiol.* 63 (1997) 2397.
- [8] C.C. Tebbe, W. Vahjen, *Appl. Environ. Microbiol.* 59 (1993) 2657.
- [9] F.M. Ausubel, R. Brent, R.E. Kingston, D.D. Moore, J.G. Seidman, J.A. Smith, K. Struhl, *Current Protocols in Molecular Biology*, Wiley, New York, 1995.
- [10] J. Sambrook, E.F. Fritsch, T. Maniatis, *Molecular Cloning: A Laboratory Manual*, 2nd ed, Cold Spring Harbor Laboratory Press, New York, 1989.
- [11] C.S. Jacobsen, O.F. Rasmussen, *Appl. Environ. Microbiol.* 58 (1992) 2458.
- [12] A. Ogram, W. Sun, F.J. Brockman, J.K. Fredrickson, *Appl. Environ. Microbiol.* 61 (1995) 763.
- [13] R.J. Steffan, J. Goksoyr, A.K. Bej, R.M. Atlas, *Appl. Environ. Microbiol.* 54 (1988) 2908.
- [14] T. Volossiouk, E.J. Robb, R.N. Nazar, *Appl. Environ. Microbiol.* 61 (1995) 3972.
- [15] S. Ekendahl, J. Arlinger, F. Ståhl, K. Pedersen, *Microbiology* 140 (1994) 1575.
- [16] T.A. Hovanec, E.F. DeLong, *Appl. Environ. Microbiol.* 62 (1996) 2888.
- [17] R.T. Noble, J.A. Fuhrman, *Appl. Environ. Microbiol.* 63 (1997) 77.
- [18] D.P. Chandler, F.J. Brockman, J.K. Fredrickson, *Mol. Ecol.* 6 (1997) 475.
- [19] D.P. Chandler, C.A. Wagon, H. Bolton Jr., *Appl. Environ. Microbiol.* 64 (1998) 669.
- [20] Y.-L. Tsai, B. Tran, L.R. Sangermano, C.J. Palmer, *Appl. Environ. Microbiol.* 60 (1994) 2400.
- [21] Y.-L. Tsai, M.D. Sobsey, L.R. Sangermano, C.J. Palmer, *Appl. Environ. Microbiol.* 59 (1993) 3488.
- [22] C. Laroche, E.B. Drouet, P. Brousset, C. Pain, A. Boibieux, F. Biron, J. Icart, G.A. Denoyel, A. Niveleau, *J. Med. Virol.* 46 (1995) 66.
- [23] G.N. Frerichs, in: W. Ahne, E. Kurstak (Eds.), *Viruses of Lower Vertebrates*, Springer, Heidelberg, 1989, pp. 317–332.

- [24] E.M. Deacon, G. Pallesen, G. Niedobitek, J. Crocker, L. Brooks, A.B. Rickinson, L.S. Young, *J. Exp. Med.* 177 (1993) 339.
- [25] P.P. Chiou, B.S. Drolet, J.C. Leong, *J. Aquat. Anim. Health* 7 (1995) 9.
- [26] R.L. Atmar, F.H. Neill, J.L. Romalde, F. LeGuyader, C.M. Woodley, T.G. Metcalf, M.K. Estes, *Appl. Environ. Microbiol.* 61 (1995) 3014.
- [27] O. Egorov, J. Ruzicka, *Analyst* 119 (1995) 1925.
- [28] O. Egorov, M.J. O'Hara, J.W. Grate, J. Ruzicka, *Anal. Chem.* 70 (1998) 977–984.
- [29] J. Ruzicka, *Analyst* 119 (1994) 1925.
- [30] C. Labarca, K. Paigen, *Anal. Biochem.* 102 (1980) 344.
- [31] J. Ruzicka, E.H. Hansen, *Flow Injection Analysis*, 2nd ed, Wiley, New York, 1988.
- [32] D.P. Chandler, *J. Ind. Microbiol.* 21 (1998) 128–140.
- [33] N.K. Fry, J.K. Fredrickson, S. Fishbain, M. Wagner, D.A. Stahl, *Appl. Environ. Microbiol.* 63 (1997) 1498.
- [34] W.G. Weisburg, S.M. Barns, D.A. Pelletier, D.J. Lane, *J. Bacteriol.* 173 (1991) 697.
- [35] V. Chan, D.J. Graves, S.E. McKenzie, *Biophys. J.* 69 (1995) 2243.
- [36] V. Chan, D.J. Graves, P. Fortina, S.E. McKenzie, *Langmuir* 13 (1997) 320.
- [37] M.S. Shchepinov, S.C. Case-Green, E.M. Southern, *Nucleic Acids Res.* 25 (1997) 1155.
- [38] W.G. Beattie, L. Meng, S.L. Turner, R.S. Varma, D.D. Dao, K.L. Beattie, *Mol. Biotechnol.* 4 (1995) 213.
- [39] T.R. Gingeras, D.Y. Kwoh, G.R. Davis, *Nucleic Acids Res.* 15 (1987) 5373.
- [40] A. Silberberg, in: J.D. Andrade (Ed.), *Surface and Interfacial Aspects of Biomedical Polymers*, Plenum, New York, 1985, pp. 321–337.
- [41] U. Maskos, E.M. Southern, *Nucleic Acids Res.* 20 (1992) 1679.
- [42] P. Tijssen, in: P.C. van der Vliet (Ed.), *Laboratory Techniques in Biochemistry and Molecular Biology*, Elsevier, New York, 1993.
- [43] J.B. Lamture, K.L. Beattie, B.E. Burke, M.D. Eggers, D.J. Ehrlich, R. Fowler, M.A. Hollis, B.B. Kosicki, R.K. Reich, S.R. Smith, et al., *Nucleic Acids Res.* 22 (1994) 2121.
- [44] S.Y. Lee, J. Bollinger, D. Bezdicek, A. Ogram, *Appl. Environ. Microbiol.* 62 (1996) 3787.
- [45] D.P. Chandler, F.J. Brockman, *Appl. Biochem. Biotechnol.* 57/58 (1996) 971.
- [46] V. Torsvik, R. Sørheim, J. Goksoyr, *J. Ind. Microbiol.* 17 (1996) 170.
- [47] V. Torsvik, J. Goksoyr, F. Lise Daae, *Appl. Environ. Microbiol.* 56 (1990) 782.

Does the chromatomembrane cell improve the quality of environmental analysis?

Jürgen Simon ^{a,*}, Leonid N. Moskvina ^b

^a Free University of Berlin, Institute for Inorganic and Analytical Chemistry, Fabeckstrasse 34-36, D-14195 Berlin, Germany

^b St. Petersburg State University, Department of Chemistry, 198904 St. Petersburg, Russian Federation

Received 26 October 1998; accepted 20 November 1998

Abstract

With the intention of combining partition chromatography and membrane techniques, we succeeded in developing the chromatomembrane cell which has proved to be reliable as an extraction and preconcentration manifold in flow injection analysis. With this technique, two immiscible phases can be induced to flow independently through a block of biporous (macro and micro) PTFE in order to promote analyte exchange. Consequently, the application of chromatomembrane cells in environmental analysis resolves all problems of sample pretreatment simply and effectively whenever a preconcentration step by gas/liquid or liquid/liquid solvent extraction is included. The link-up with analyzers (AAS, UV–Vis photometry, GC, IC, HPLC, voltammetry, ion selective electrodes, etc.) makes possible computer aided automatization for environmental monitoring. © 1999 Elsevier Science B.V. All rights reserved.

Keywords: Chromatomembrane cell; Environmental analysis; Flow-injection analysis

1. Introduction

It is a vast subject to report on modern instrumentation used today for accurate analytical information. Despite the great variety of methods being applied in our laboratories, careful sample preparation affects all of them. It is only now that we have at our disposal modern flow-techniques which allow pretreatment procedures to integrate into automated process analysis. In particular, the separation of the analyte by means of liquid/liq-

uid or gas/liquid extraction is a basic technique, but its implementation in flow systems hardly meets the requirements of computer controlled processes. The text book of Fang [1] reports comprehensively on some results for special applications in this field but, as remarkable as these results may be, none work so universally as to be compared with the activities of the former analyst using his shaking funnel. But as time passes, tools improve.

Mention must be made of the novel extraction technique in flow injection analysis using for instance replaceable organic wetting films on Teflon tubing developed by Luo et al. [2]. In the past few

* Corresponding author. Fax: +49-30-8382424.

E-mail address: behrens@chemie.fu-berlin.de (J. Simon)

years the ‘jet ring cell’ introduced by Ruzicka’s group [3] gained importance. This method uses microbeads as renewable surfaces for analyte adsorption with the aim of monitoring by optical measurements. Moskvina and coworkers [4,5] presented a new concept for the implementation of extraction procedures in flow systems combining partition chromatography with membrane techniques. The chromatomembrane cell can be applied without the special preconditions mentioned above whenever analyte transfer by liquid/liquid or gas/liquid extraction is required for automated sample pretreatment.

Authorities responsible for environment protection have established many regulations by which environmental samples have to be analyzed. In order to replace historical batch operations for extraction we demonstrate the possibilities for on-line applications of chromatomembrane cells in automated pretreatment procedures with several examples. Moreover, the mode of processing allows trace analytes to preconcentrate within the chromatomembrane cell so that the accuracy of monitoring increases remarkably.

We provide here an overview of the findings of published work on the chromatomembrane cell, with a brief description of its principles, construction and operation, and a summary of the benefits of the cell observed in the studies.

2. The chromatomembrane cell

The chromatomembrane cell consists of a rectangular block of hydrophobic PTFE with two types of pores, namely micropores and macropores. Polar liquids fill the macropores whereas the micropores remain available only for gases or non-polar liquids. The capillary pressure of polar liquids prevents their penetration into micropores. Some precautions make possible an independent flux of two immiscible phases. Two opposite sides of the block are covered with microporous membranes. Only the non-polar liquid is allowed to flow in this direction. Two sides are open for the flux of the polar liquid whereas any flux in the third possible direction is excluded by sealing the pores completely on the matching sides (Fig. 1).

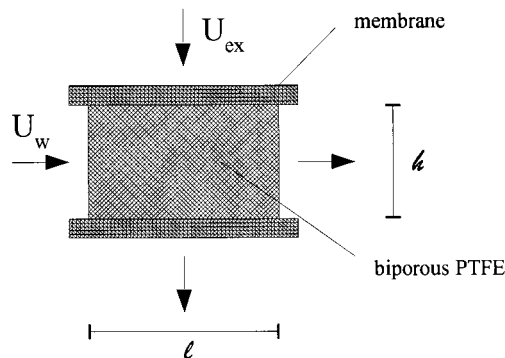


Fig. 1. The chromatomembrane cell. Macropores filled with polar liquid, micropores filled with non-polar liquid or gas.

The margin of pressures—which can be used for the supply of polar and non-polar phases—is set by the capillary pressure of the polar liquid within the micropores.

The enclosure of the chromatomembrane body is constructed from non-corroding metals, pressing the microporous membrane onto biporous PTFE. An undisturbed flow of the non-polar phase is ensured whereas the membrane works perfectly as a water barrier. (Fig. 2). Moreover all the materials made from PTFE are easily exchangeable which makes the device renewable whenever necessary. The stopped flow mode is one of the principles of applying the chro-

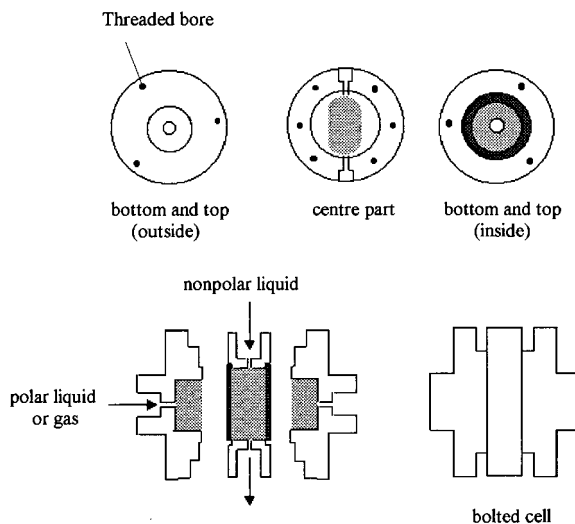


Fig. 2. The chromatomembrane cell enclosed in the case.

matomembrane cell to extraction procedures: the polar liquid flows with rate U_w while the flux of the non-polar phase is stopped. Normal partition chromatography takes place with a rate of component-zone shift:

$$U_i = \frac{U_w}{1 + K(V_{\text{ex}}/V_w)}$$

where K is the partition coefficient and V_{ex} , V_w are the volumes of the contacting phases. Just before breakthrough takes place the polar liquid is stopped. By starting the flux of the non-polar phase the analyte becomes rewashed from the cell. Preconcentration followed by complete extraction has resulted. Computer-controlled processing is made possible when using multifunctional valves.

A complete extraction will be realized by a continuous flow mode as well (both phases are flowing) under the condition that:

$$\frac{U_i}{l} < \frac{U_{\text{ex}}}{h}$$

Neglecting this condition completely (i.e. $U_w \gg U_{\text{ex}}$) leads to the situation that both phases contain the analyte. In the limiting case its concentrations meet the partition law $c_{\text{ex}}/c_w = K$, i.e. the inlet concentration of the aqueous phase equals that of the outlet and a maximum value of c_{ex} will be obtained. Such practice is applicable in the case of major partition constants, and an alternative to the head space analysis is obtained for instance.

So we can conclude that the benefits from the application of chromatomembrane cells for extraction procedures in FIA are based on the

- small volumes of the contacting phases (100–200 μl);
- fast adjustment of the distribution equilibrium because the distance to the phase boundary is always short;
- no problems with phase separation;
- continuous extraction or preconcentration procedure according to your choice;
- completely automated sample pretreatment on request.

We investigated several applications of the chromatomembrane cell in the field of environmental analysis:

1. liquid/liquid extraction on-line to UV/Vis spectrometry:
 - Methylene-Blue Index (MBAS)-anionic surfactants [6]
 - Phenol-Index by using 4-aminoantipyrin (4-AAP)
2. Liquid/liquid extraction on-line to HPLC:
 - determination of organic pollutants
3. gas/liquid extraction on-line to IC:
 - determination of acid compounds in atmospheric air [7]
4. gas/liquid extraction on-line to ion-selective electrodes:
 - determination of ammonia in atmospheric air [8]
5. liquid/gas extraction on-line to GC:
 - determination of volatile organic compounds (VOCs) in waste waters (headspace analysis) [9].

3. Automation and accuracy

Commercial equipment (i.e. pumps, multifunctional valves, etc.) combined with chromatomembrane cells result in productively working units which are programmable and suitable in every respect for on-line coupling with modern analytical instrumentation. As the chromatomembrane cell has characteristics of chromatographic columns, all preconcentration procedures allow the phase transition of the analyte to be complete if required. The extracted volume V_{ex} has to be transported with the flux of the extracting solvent to the detector. The recovery of the analyte depends on the size of the sample loop, i.e. whether the volume of the sample loop exceeds V_{ex} or not. The accuracy is found to be better than manual procedures.

The economic application of analytical instrumentation requires sophisticated concepts of automation. Sampling and sample pretreatment are more time-consuming than the detection step. Therefore one can position such independent units to operate somewhere in the field for sampling. Later in the laboratory this unit will supply the sample pretreated to the detector.

So we can conclude that the application of chromatomembrane cells improves the quality of environmental analysis whenever sample preparation requires preconcentration and extraction procedures.

The reason is that

1. the sample size decreases whereas the reproducibility remains constant or improves;
2. the waste production decreases;
3. automatization enhances reproducibility in combination with computer aided on-line processing.

As a result we observe an increased sample throughput performance and manual processing faults do not occur. And last but not least, the workload of expensive analytical equipment improves.

Analytical procedures including the application of chromatomembrane cells are compatible with Analytical Assurance Programs so that the required accuracy is available. The manufacturer of analytical instrumentation, however, can provide a modular concept for customer's specific problem solving.

Our experience with this new method gained in the wide field of environmental monitoring is with the optimization of the technical standard of the chromatomembrane cell, so that the improve-

ments made in the past few years (Fig. 2) now warrant its application in routine analysis.

Acknowledgements

The authors thank the Deutsche Forschungsgemeinschaft (DFG) and the Russian Foundation for Fundamental Researches (RFFI) for the support of this work.

References

- [1] Z. Fang, *Flow Injection Separations and Preconcentrations*, VCH, Weinheim, 1993.
- [2] Y. Luo, R.A. Othman, J. Ruzicka, G.D. Christian, *Analyst* 121 (1996) 601.
- [3] J. Ruzicka, C.H. Pollema, K.M. Scudder, *Anal. Chem.* 65 (1993) 3566.
- [4] L.N. Moskvina, J. Simon, *Talanta* 41 (1994) 1765.
- [5] L.N. Moskvina, *J. Chromatogr. A.* 669 (1994) 81.
- [6] L.N. Moskvina, J. Simon, P. Löffler, N.V. Michailova, D.N. Nicolaevna, *Talanta* 43 (1996) 819.
- [7] H. Erxleben, L.N. Moskvina, T.G. Nikitina, J. Simon, *Fresenius J. Anal. Chem.* 361 (1998) 324.
- [8] P. Löffler, J. Simon, A. Katruzov, L.N. Moskvina, *Fresenius J. Anal. Chem.* 352 (1995) 613.
- [9] L.N. Moskvina, O.V. Rodinkov, *J. Chromatogr. A.* 725 (1996) 351.

Design of two channel flow cells for simultaneous determination of copper and iron[☆]

Tadao Sakai^{a,*}, Yoshihito Maeda^a, Nobuo Ura^b

^a Department of Applied Chemistry, Aichi Institute of Technology, 1247 Yachigusa, Yakusa-cho, Toyota 470-0392, Japan

^b Soma Optics, Hinode-cho, Nishitama, Tokyo 190-0181, Japan

Received 23 August 1998; accepted 19 October 1998

Abstract

Two compact double and serial flow cells were designed for simultaneous determination of trace copper and iron ions. 2-(5-Bromo-2-pyridylazo)-5-(*N*-propyl-*N*-sulfopropylamino)aniline(5-Br-PSAA) was used as a chromogenic reagent. 5-Br-PSAA reacted with Cu(II) and Fe(II) to form red chelate compounds and did not react with Cu(I) and Fe(III). Based on these characteristics, a three-lines flow system using two channel flow cells was assembled for the simultaneous determination of trace amounts of copper and iron and applied to the assay of ground water. © 1999 Elsevier Science B.V. All rights reserved.

Keywords: 5-Br-PSSA; Double and serial flow cells; Copper and iron

1. Introduction

Pyridylazo compounds such as 2-[2-(3,5-dibromopyridyl)-azo]-5-dimethylaminobenzoic acid [1], 2-[2-(3,5-dibromopyridylazo)-5-diethylaminobenzoic acid [2] and 2-(2-thiazolylazo)-5-diethylaminobenzoic acid derivatives [3], have been synthesized as new and highly sensitive chromogenic reagents for the determination of several metal ions. These reagents reacted with iron, copper,

nickel and cobalt and the chelate compounds formed had a molar absorptivity of $10^5 \text{ l mol}^{-1} \text{ cm}^{-1}$. These are suitable for the analysis of trace heavy metals. However, the reagents were designed for the use of solvent extraction.

In order to eliminate the solvent extraction process, water-soluble reagents such as 2-nitroso-5-(*N*-ethyl-*N*-sulfopropylamino)phenol [4], 2-(2-thiazolylazo)-4-methyl-5-(sulfopropylamino)benzoic acid [5] and 2-(5-bromo-2-pyridylazo)-5-(*N*-propyl-*N*-sulfopropylamino)aniline(5-Br-PSAA) [6] have been synthesized without losing characteristics of high sensitivity and wide optimal pH range. These water-soluble reagents were applied to the determination of trace amounts of metals by a flow injection (FI) system [5,7–9]. These

[☆] Presented at 8th International Conference on Flow Injection Analysis (ICFIA '98), held in Seattle, WA, USA, 23–27 August, 1998.

* Corresponding author. Fax: +81-565-48-0076.

E-mail address: tadsakai@ac.aitech.ac.jp (T. Sakai)

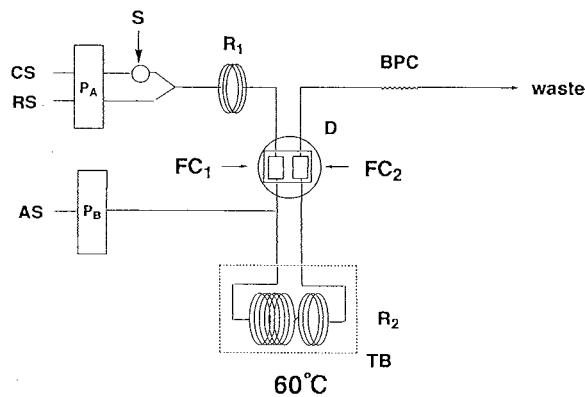


Fig. 1. Schematic flow diagram for simultaneous determination of copper and iron. CS, carrier solution (0.01 mol l^{-1} HCl containing $1 \times 10^{-4} \text{ mol l}^{-1}$ NaIO_4); RS, reagent solution ($1 \times 10^{-4} \text{ mol l}^{-1}$ 5-Br-PSAA buffered at pH 4.5); AS, $2 \times 10^{-2} \text{ mol l}^{-1}$ sodium ascorbate; P_A , double-plunger pump (0.45 ml min^{-1}); P_B , (0.2 ml min^{-1}); S, sample injection valve ($200 \mu\text{l}$); R_1 , reaction coil ($0.5 \text{ mm i.d.} \times 0.2 \text{ m}$); R_2 , reaction coil ($0.5 \text{ mm i.d.} \times 9 \text{ m}$); TB, reaction system, 60°C ; FC, flow cells; D, double beam spectrophotometer; BPC, back pressure coil ($0.25 \text{ i.d.} \times 2 \text{ m}$).

methods have a disadvantage which it is difficult to determine several elements simultaneously with a single detection system. For simultaneous detection, Faizullah and Townshend proposed the FI method to analyse Fe(II) and total iron using a

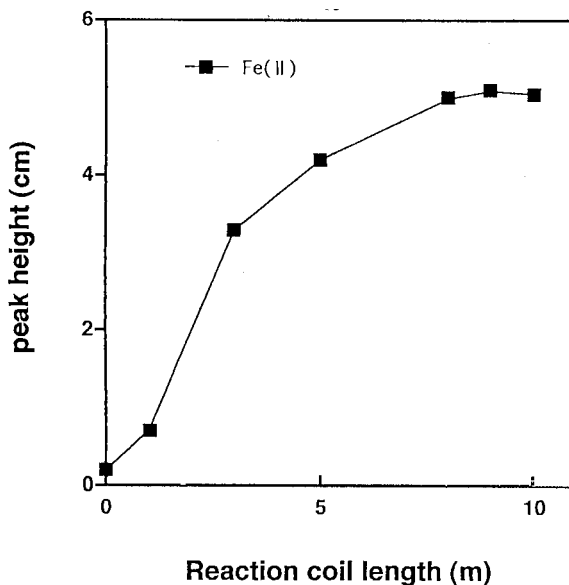


Fig. 3. Effect of reaction coil length (R_2). Sample, 10 ppb Fe(II) ; RS, $1 \times 10^{-4} \text{ mol l}^{-1}$ 5-Br-PSAA buffered at pH 4.5; AS, $2 \times 10^{-2} \text{ mol l}^{-1}$ sodium ascorbate; AU, 0.05 AU .

Jones reductor mini-column [10]. Kuroda et al. also reported the analysis of Fe(III) and total iron utilizing the formation of the complex between Tiron and Fe(III) by irradiation with ultraviolet

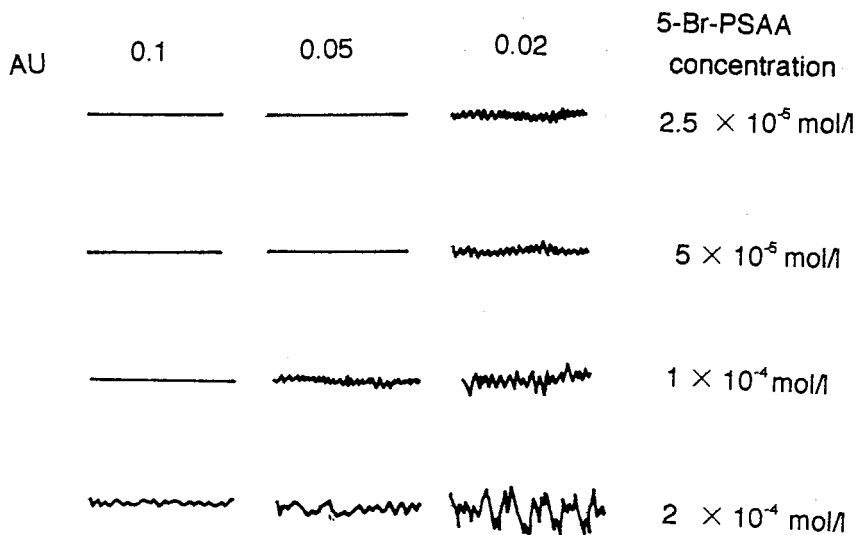


Fig. 2. Influence on base line caused by absorbance unit (AU) in the detector and 5-Br-PSAA concentration.

radiation [11]. The system consists of a single detector with two flow cells or of that with single flow cell circulating the sample without and with UV irradiation twice. On the other hand, the sample injection at two inlet points was proposed for the determination of Fe(III) and Ti(IV) [12] and doublet peaks in a single-line system were used for the Ni(II) and Fe(II) [13]. In addition, two flow cells in a double beam spectrophotometer and a twin-compartment flow-through cell were proposed for the analysis of two elements [14,15]. However, the detailed configurations were not shown in the text.

This paper describes the function of a double and serial flow cell designed newly and the simultaneous determination system of trace amounts of Cu(II) and Fe(II) in ground water using 5-Br-PSAA.

2. Experimental

2.1. Apparatus

A Hitachi U-2000 spectrophotometer with 10-mm quartz cells was used for measuring absorption spectra. A Hitachi-Horiba F-7II pH meter

with a combined glass electrode was used to measure pH.

2.2. Reagents

All reagents used were of analytical-reagent grade and distilled water was used throughout.

2.2.1. 5-Br-PSAA ($1 \times 10^{-4} \text{ mol l}^{-1}$) solution

A total of 0.048 g of 2-(5-bromo-2-pyridylazo)-5-(*N*-propyl-*N*-sulfo-propylamino)aniline sodium (Dojindo, Kumamoto) was dissolved in 100 ml of distilled water to prepare $1 \times 10^{-3} \text{ mol l}^{-1}$. The stock solution was diluted with buffer solution (pH 4.5) 10-fold for use.

2.2.2. Standard Cu(II) and Fe(II) solutions, 1000 ppm

A total of 0.100 g of copper metal (99.99%) was dissolved in dilute nitric acid (1 + 1) and diluted with distilled water to 100 ml.

A Fe(II) solution was prepared by dissolving 0.4317 g of ammonium Fe(II) sulphate in 100 ml of 0.1 mol l^{-1} sulphuric acid.

Working solutions were prepared by appropriate dilution with 0.1 mol l^{-1} HCl as required.

2.2.3. Buffer solutions

Acetate buffer solution was prepared by dissolving 34 g of sodium acetate trihydrate in 500 ml of water and adjusting the pH to 4.5 by dropwise addition of 5 mol l^{-1} acetic acid.

2.2.4. Sodium ascorbate solution, $2 \times 10^{-2} \text{ mol l}^{-1}$

A total of 0.99 g of sodium ascorbate was dissolved in 250 ml of buffer solution.

2.2.5. Sodium metaperiodate solution

A $1 \times 10^{-4} \text{ mol l}^{-1}$ sodium metaperiodate solution was prepared by dissolving 0.023 g of sodium metaperiodate in 0.01 mol l^{-1} HCl.

Super purified HCl (Tama pure-AA-100, Tama Chemicals, Tokyo) and super pure water were used for dilution and carrier stream for the trace metal detection.

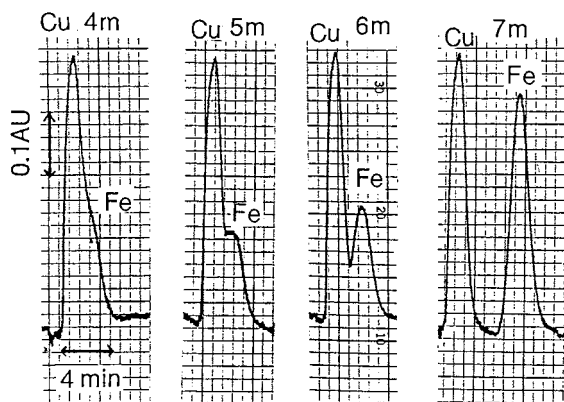


Fig. 4. Separation profiles caused by various R_2 lengths in a serial flow cell. Cu(II), 100 ppb; Fe(II), 100 ppb.

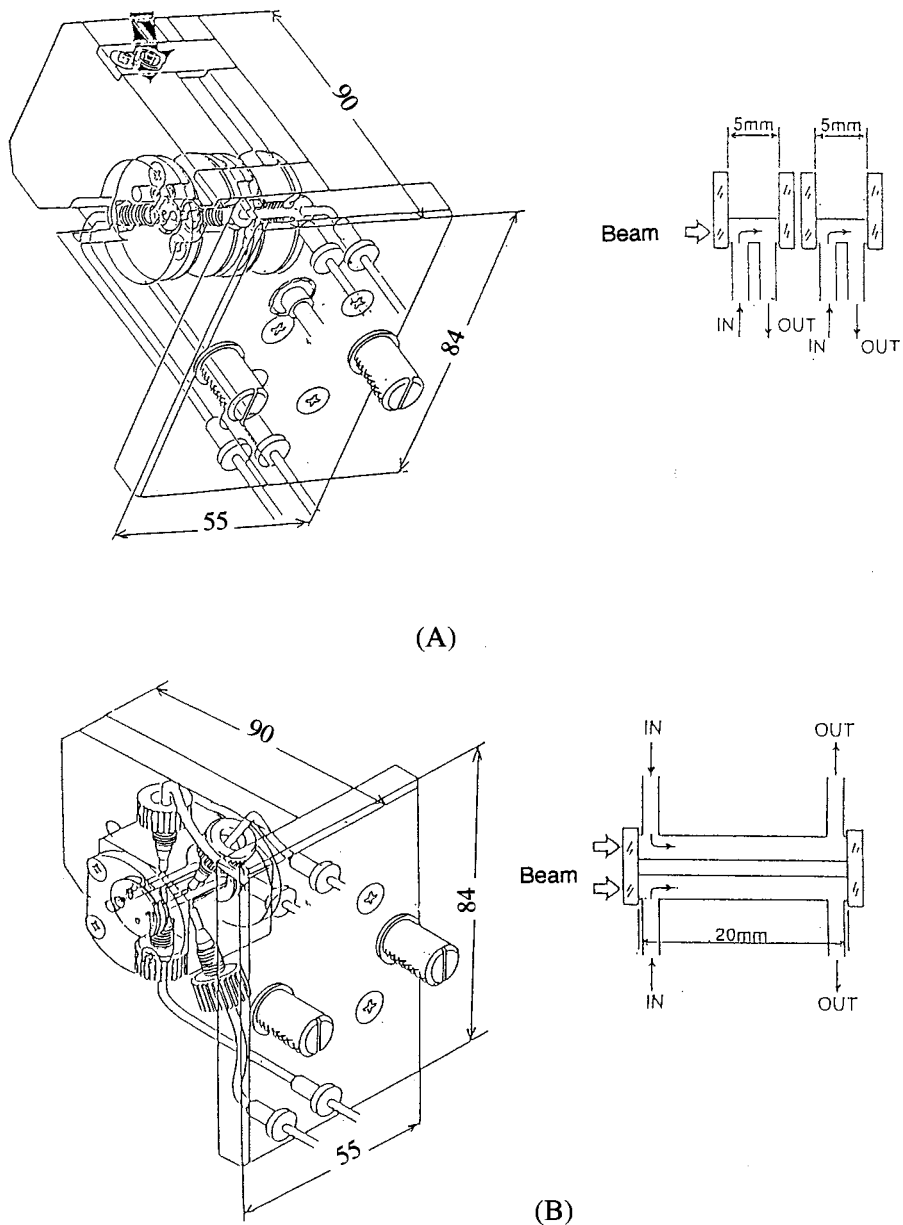


Fig. 5. Configuration of serial (A) and double (B) flow cells. (A) $55 \times 84 \times 90$ mm; path length, 5 mm; cell volume, 4 μl . (B) Path length, 20 mm; cell volume, 30 μl .

2.3. FI procedure with 5-Br-PSAA

The manifold of the FI system is shown in Fig. 1. Two double plunger micro-pump (Sanuki Kogyo DM2U-1026, Tokyo) were used to pump the solutions. The 0.01 mol l^{-1} HCl containing $1 \times$

$10^{-4} \text{ mol l}^{-1}$ sodium metaperiodate and $1 \times 10^{-4} \text{ mol l}^{-1}$ 5-Br-PSAA buffered at pH 4.5 are delivered at the flow rate of 0.45 ml min^{-1} . The samples (200 μl), containing up to 100 ppb of Cu(II) and Fe(II), are injected into the carrier stream by means of a six-way injection valve to

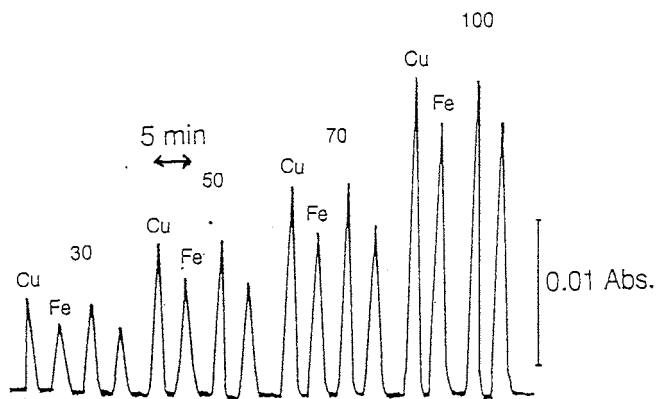


Fig. 6. Peak signals for the determination of copper and iron using serial flow cell. Sample, 30, 50, 70, and 100 ppb; sample volume, 200 μ l; AU, 0.1 AU.

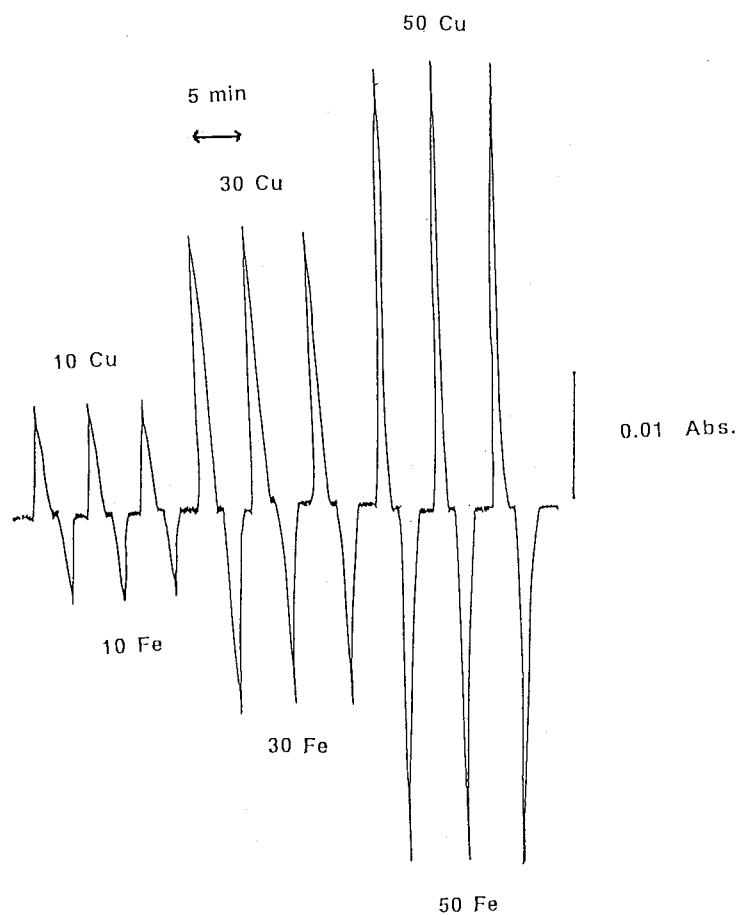


Fig. 7. Flow signals for the determination of copper and iron using double flow cell with 20 mm path length. Sample, 10, 30, and 50 ppb; sample volume, 200 μ l; AU, 0.1 AU.

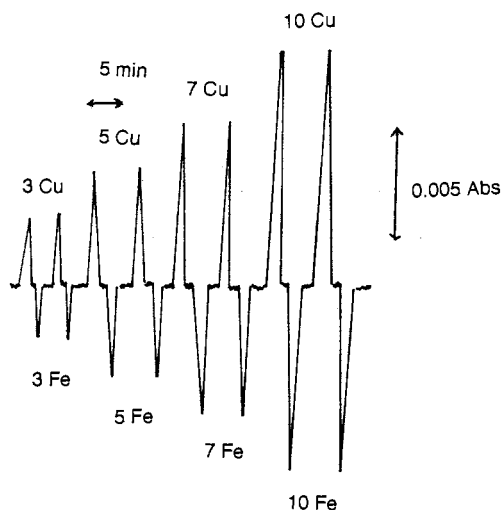


Fig. 8. Calibration graphs of trace amounts of Cu(II) and Fe(II) with 20 mm path length double flow cell and 0.05 AU. Sample, 3, 5, 7, and 10 ppb.

Table 1
Recoveries of Cu(II) and Fe(II) in synthetic mixtures

Added (ppm)		Found (ppm) ^a			
Cu	Fe	Cu	Rec. ^b (%)	Fe	Rec. ^b (%)
0.05	0.10	0.052	104	0.101	101
0.05	0.20	0.051	102	0.210	105
0.10	0.10	0.101	101	0.103	103
0.10	0.20	0.100	100	0.200	100
0.15	0.10	0.150	100	0.100	100
0.15	0.20	0.154	103	0.198	99
0.20	0.10	0.20	100	0.101	101
0.20	0.20	0.20	100	0.198	99

^a Average of three determinations.

^b Rec, recovery (%).

which a volume control loop is attached. A double beam spectrophotometric detector (Soma Optics, S-3250, Tokyo), fitted with the flow cell designed newly is used. The Cu(II) chelates are rapidly formed in the 20-cm reaction coil (R_1) and its absorbance is measured at the first flow cell (FC_1) at 558 nm. The stream passed through the cell is mixed with 2×10^{-2} mol l^{-1} sodium ascorbate delivered at 0.4 ml min^{-1} . The chelate formation with Fe(II) reduced is accelerated in the reaction system (reaction coil 0.5 mm i.d. \times 9 m (R_2), Soma Optics, S-3850) which has tempera-

tures kept at 60°C. The absorbance of the coloured product is monitored in the second flow cell (FC_2) at the same wavelength mentioned above. The peak signal is recorded using a Toa Electronics FBR 251A recorder. The PTFE tubing is 0.5 mm i.d. except for the back-pressure coil which is 0.25 mm i.d. (2 m long).

3. Results and discussion

3.1. Absorption spectra and effect of pH

5-Br-PSAA reacted with Cu(II) and Fe(II) to form coloured complexes, but did not react with Cu(I) and Fe(III). The absorption maximum of the Cu(II) complex was at 578 nm and that of the Fe(II) complex, at 558 and 714 nm.

The effects of pH on the Cu(II) and Fe(II) chelate formation were investigated. Maximum and constant absorbances were obtained in the pH ranges 4.0–5.8 for the Cu(II)-5-Br-PSAA complex, 4.3–7.0 for that of Fe(II). To determine both Cu(II) and Fe(II), pH 4.5 was chosen.

3.2. Measuring wavelength in the FI system

For the simultaneous determination of Cu(II) and Fe(II), the measuring wavelengths were investigated. The molar absorptivity of the 5-Br-PSAA-Cu(II) complex at 578 nm was large and that of the Fe(II) complex at 558 nm was larger than that at 578 nm. However, as there is a large and wide shoulder which has sufficient sensitivity between 550 and 560 nm in the absorption spectra of the Cu(II) complex, 558 nm was chosen in the manifold.

3.3. Effect of reagent concentration

The effect of 5-Br-PSAA concentration on the colour development was investigated in the range 8×10^{-5} – 1.5×10^{-4} mol l^{-1} for 10 ppb of Cu(II) and Fe(II). The peak heights were maximum and constant over 1×10^{-4} mol l^{-1} 5-Br-PSAA. However, since the reagent blank is coloured, the higher concentration of the reagent was not preferable in the flow injection analysis (FIA). To enhance the sensitivity, the relationship

between the gain (absorbance unit, AU) in the detector and the concentration of 5-Br-PSAA was investigated. Fig. 2 shows the influence on noise level caused by different AU and various 5-Br-PSAA concentrations. When the concentration of 5-Br-PSAA was less than $5 \times 10^{-5} \text{ mol l}^{-1}$, even with AU 0.02, the base line was very smooth. When the 5-Br-PSAA concentration was $1 \times 10^{-4} \text{ mol l}^{-1}$, the slight irregularity in the base line was found at AU 0.05. However, it did not give a large influence on the reproducible and sharp peak heights. When AU 0.02 in the detector was used, the large disorder of the base line was observed at both 1 and $2 \times 10^{-4} \text{ mol l}^{-1}$ 5-Br-PSAA. Therefore, the AU 0.05 and $1 \times 10^{-4} \text{ mol l}^{-1}$ 5-Br-PSAA were used to determine Cu(II) and Fe(II) less than 10 ppb, while Cu(II) and Fe(II) in the concentration range 10–50 ppb were detectable even using AU 0.1.

3.4. Effect of reducing agent concentration

When 5-Br-PSAA is used as a chromogenic reagent, both Cu(I) and Fe(III) do not form a coloured chelate. To detect only Fe(II), the reducing agent has to be added before the solution passes through the second flow cell. The effect of sodium ascorbate concentration was studied for reducing Fe(III). The concentration was varied from 5×10^{-3} to $2.5 \times 10^{-2} \text{ mol l}^{-1}$. Maximum and reproducible peak height was obtained over $2 \times 10^{-2} \text{ mol l}^{-1}$ for 10 ppb. In this work, $2 \times 10^{-2} \text{ mol l}^{-1}$ sodium ascorbate was used.

3.5. Effect of reaction coils, R_1 and R_2

The effects of the reaction coils R_1 and R_2 (Fig. 1) were examined. The R_1 length was varied from 10 to 100 cm. The maximum peak was obtained at a length of 20 cm. The effect of the R_2 length was also investigated in the range 1–9 m (Fig. 3). The longer the coil length, the higher the peak height. However, when the length was short (< 7 m), the separation of the first peak for Cu(II) and of the second peak for Fe(II) was not satisfactory and the formation of the Fe chelate was not complete. And also, the separation profiles with various R_2 lengths in the serial flow cell are shown in Fig. 4. Over 7 m length, the good separation on the Cu(II) and Fe(II) signals was observed. A 9 m coil length was used in consideration of separation and sensitivity. To accelerate the formation of Fe(II)-5-Br-PSAA, the temperature in the reaction system was kept at 60°C.

3.6. Design of two channel flow cells

Fig. 5 shows the configuration of serial (A) and double (B) flow cells designed newly. The path length of the serial flow cell is 5 mm and the volume of the cell is 4 μl . The size of the cell holder is $55 \times 84 \times 90$ mm and it is compact. The peak signals for Cu(II) and Fe(II) with the serial flow cell in the range 30–100 ppb are shown in Fig. 6. The sample throughput was 12 h^{-1} . The double flow cells which have 10 and 20 mm path

Table 2
Simultaneous determination of copper and iron in ground waters

Sample no.	Contents ^a (ppb)					
	FIA method		ICP-AES		AAS	
	Cu	Fe	Cu	Fe	Cu	Fe
1	39.4 ± 0.23	3 ppb <	38.7	ND	–	–
2	2.7 ± 0.1	15.2 ± 0.17	2.99	–	–	–
3	48.0 ± 0.04	ND			48.0	ND
4	10.0 ± 0.05	ND			11.0	ND
5	10.0 ± 0.08	ND			10.0	<0.01
6	28.2 ± 0.17	3 ppb <			28.0	1.0

^a Mean values \pm S.D. of three determinations.

lengths were also designed. The volume in the 10 mm path length cell was 8 μl and that of the 20 mm length cell (B in Fig. 5), 30 μl . The flow signals with 20 mm length cell is shown in Fig. 7.

To detect Cu(II) and Fe(II) below 10 ppb, the flow cell with 20 mm path length is useful.

3.7. Calibration graphs

The calibration graphs for both Cu(II) and Fe(II) were made using 5-Br-PSAA and double flow cells with 10 and 20 mm path lengths. The calibration graphs were linear for 10–80 ppb. Each calibration graph is as follows; for Cu(II), $y = 0.101x$, Fe(II), $y = 0.079x$ with 10 mm path length; Cu(II), $y = 0.201x$, Fe(II), $y = 0.160x$ with 20 mm path length in the double flow cell; Cu(II), $y = 0.5x$, Fe(II), $y = 0.4x$ with the serial flow cell. As a matter of course, when the cell with 20 mm path length was used, the slope of the calibration graph was 2-fold compared with that of 10 mm path length. The relative standard deviation (R.S.D.) ($n = 5$) with 10 mm path length was 0.8% for 30 ppb Cu(II), 0.9% for 30 ppb Fe(II). The R.S.D. with 20 mm path length was 0.6% for 30 ppb Cu(II), 0.99% for Fe(II). When the 20 mm path length cell and AU 0.05 in the detector were used, Cu(II) and Fe(II) in the range 3–10 ppb could be detected quantitatively and R.S.D. for 10 ppb Cu(II) was 0.5%, for 10 ppb Fe(II), 0.6%. The determination limit was 1 ppb for both ions. The detection less than 5 ppb Fe(II) using AU 0.1 was impossible. Fig. 8 shows the flow signals in the range 3–10 ppb metal ions using 0.05 AU. The sampling rate was 12 h^{-1} .

3.8. Recoveries of Cu(II) and Fe(II) in synthetic mixtures

Known amounts of Cu(II) and Fe(II) were determined to assess the proposed method. The recoveries are shown in Table 1. The satisfactory results were obtained, respectively.

3.9. Application

Copper and iron in the ground water were

determined by the proposed FI manifold using 5-Br-PSAA and the double flow cell with 20 mm path length. The sample was heated for 2 h at 80°C after adding HCl (super pure, Tama Chemicals, Tokyo) and was diluted with super purified water to give a final concentration of 0.01 mol l^{-1} . The results are shown in Table 2. Although the detection of copper was easy, the determination less than 3 ppb iron was uncertain because the check by other methods was impossible.

4. Conclusion

A serial and double flow cells with different path lengths were newly designed for the simultaneous determination of copper and iron. 5-Br-PSAA was preferable for the chelate formation with Cu(II) and Fe(II). A three-channel system using double flow cell with 20 mm path length was available for trace amounts (ppb level) of copper and iron.

References

- [1] T. Katami, T. Hayakawa, M. Furukawa, S. Shibata, *Anal. Chim. Acta* 188 (1986) 289.
- [2] T. Katami, T. Hayakawa, M. Furukawa, S. Shibata, T. Hara, *Anal. Sci.* 2 (1986) 169.
- [3] M. Furukawa, S. Shibata, *Bunseki Kagaku* 39 (1990) 589.
- [4] M. Saito, D. Horiguchi, K. Kina, *Bunseki Kagaku* 30 (1981) 635.
- [5] H. Wada, T. Ishizuki, G. Nakagawa, *Mikrochim. Acta* 235 (1983) III.
- [6] D. Horiguchi, M. Saito, T. Imamura, K. Kina, *Anal. Chim. Acta* 151 (1983) 457.
- [7] N. Ohno, T. Sakai, *Analyst* 112 (1987) 1127.
- [8] T. Sakai, N. Ohno, *Anal. Chim. Acta* 214 (1988) 217.
- [9] N. Ohno, T. Sakai, M. Nakabayashi, H. Sasaki, *Bunseki Kagaku* 39 (1990) 399.
- [10] A.T. Faizullach, A. Townshend, *Anal. Chim. Acta* 167 (1985) 225.
- [11] R. Kuroda, T. Nara, K. Oguma, *Analyst* 113 (1988) 1557.
- [12] S. Kozuka, K. Saito, K. Oguma, R. Kuroda, *Analyst* 115 (1990) 431.
- [13] D.A. Whiteman, G.D. Christian, J. Ruzicka, *Anal. Chim. Acta* 214 (1988) 197.
- [14] A. Fernandez, M.D.L. de Castro, M. Valcarcel, *Anal. Chem.* 56 (1984) 1146.
- [15] H. Muller, V. Muller, E.H. Hansen, *Anal. Chim. Acta* 230 (1990) 113.

On-line extraction-spectrophotometric determination of neostigmine in pharmaceuticals using double membrane phase separator and monovalent dyestuff

Tadao Sakai *, Xiaoqin Liu ¹, Yoshihito Maeda

Department of Applied Chemistry, Aichi Institute of Technology, Yachigusa, Yakusa-cho, Toyota 470-0392, Japan

Received 23 August 1998; accepted 19 October 1998

Abstract

A simple, sensitive and rapid spectrophotometric method for the determination of neostigmine by flow injection analysis (FIA) coupled with an ion associate extraction has been developed. The three-line manifold was assembled. Neostigmine (200 μ l) was injected into a distilled water stream and the pH was adjusted to 10 with a borate–phosphate buffer solution. Then, the stream was mixed with the ion-pairing tetrabromophenolphthalein ethylester (TBPEH)-1,2-dichloroethane solution. After phase separation with a double membrane phase separator, absorbance was measured at 610 nm. A linear calibration graph was obtained between 1×10^{-7} mol l⁻¹ and 5×10^{-7} mol l⁻¹ of neostigmine. Up to 48 samples h⁻¹ could be processed with a relative standard deviation (R.S.D.) of 0.5% ($n = 5$) for 4×10^{-7} mol l⁻¹ neostigmine. The proposed system was applied to the simple, reproducible and rapid determination of neostigmine in commercial pharmaceuticals. © 1999 Elsevier Science B.V. All rights reserved.

Keywords: Neostigmine determination; Blue ion associate with tetrabromophenolphthalein ethylester; Flow injection extraction

1. Introduction

Bromophenol Blue (BPB) [1–3], Bromocresol Green (BCG) [4] and Orange(II) [5] have been used as ion-association reagents for the extraction-spectrophotometric determination of quaternary ammonium salts and Sakai has reported [6]

that BPB reacted with a quaternary ammonium ion to form a yellow 1:1 or a blue 1:2 associate in the acidic or alkaline media. However, the molar absorptivities of associates mentioned above were small and the sensitivity was poor for trace analysis. Tetrabromophenolphthalein ethylester potassium (TBPEK), which has a molar absorptivity of 10^5 l mol⁻¹ cm⁻¹, was proposed for the sensitive spectrophotometric determination of trace amounts (10^{-6} mol l⁻¹ level) of berberine [7]. Moreover, it was found that TBPEH obtained below pH 3 dissolved in 1,2-dichloroethane (DCE) and TBPEH–DCE solution was preferable

* Corresponding author. Fax: +81-565-48-0076.

E-mail address: tadsakai@ac.aitech.ac.jp (T. Sakai)

¹ On leave: Nanjing University of Chemical Technology, Chemical Engineering Research Center, No.5 New Model Road, Nanjing Jiangsu 210009, People's Republic of China.

to the flow injection (FI) spectrophotometric determination of berberine and benzethonium [8] coupled with solvent extraction. For efficient segments, extraction and phase separation, lots of papers were published [9–17] and also the review related to extraction flow injection analysis (FIA) was reported by Kuban [18]. In a previous paper [8], a phase separator with a sloped groove and a porous PTFE membrane (0.8 μm) proposed by Motomizu et al. [14] was used. However, the durability of a single membrane was not sufficient for long runs.

This paper describes a durable extraction FI system using a double membrane phase separator for sensitive and rapid determination of neostigmine in pharmaceuticals. There are few spectrophotometries for the neostigmine determination [18,19]. Neostigmine shows a pharmacological action for anticholinesterase. Its methylsulfate and bromide are combined in the injection ampoule and eye-drops. Although titrimetry is proposed as an official method [20], the procedure is tedious and the sensitivity is poor (mg ml^{-1} level).

2. Experimental

2.1. Apparatus

A Hitachi Model U-3000 double-beam spectrophotometer was used with 10 mm light-path cells for absorbance measurements. A Horiba M-GL pH meter with a glass electrode was used. Extraction was carried out with an Iwaki Model KM shaker.

2.2. Reagents

All reagents were of analytical-reagent grade and were used without further purification.

2.2.1. Stock standard neostigmine solution

Prepared by dissolving 0.0606 g of neostigmine bromide (Wako, Osaka) in 100 ml of distilled water to make a 2×10^{-3} mol l^{-1} . Working solutions were prepared by appropriate dilution.

2.2.2. Tetrabromophenolphthalein ethylester (TBPEH) solution

A 5×10^{-4} mol l^{-1} TBPEH–DCE solution was prepared according to Ref. [8]. TBPEH is not available commercially.

2.2.3. Buffer solution, pH 7–10.5

Prepared by mixing equal volumes of 0.3 mol l^{-1} potassium dihydrogen phosphate and 0.1 mol l^{-1} sodium borate. The pH was adjusted with 1 mol l^{-1} sulfuric acid or sodium hydroxide.

2.2.4. Procedure for the FI method

A schematic diagram of the extraction-FI system used is shown in Fig. 1. The absorbance was measured at 610 nm using a Soma Optics (Tokyo) Model S-3250 double-beam spectrophotometer with a 10 mm light-path flow cell (8 μl). Signals were recorded with a Shimadzu (Kyoto) R-11 recorder. Double-plunger micro-pumps (Sanuki Kogyo, Tokyo, DMZU-1026) was used to deliver the carrier, buffer and reagent solutions. The carrier and buffer solution (pH 10) were delivered at the flow rate of 0.85 ml min^{-1} and the flow rate of 5×10^{-5} mol l^{-1} TBPEH–DCE solution was 0.55 ml min^{-1} . The samples (200 μl) were injected into the carrier stream by a 6-way injection valve.

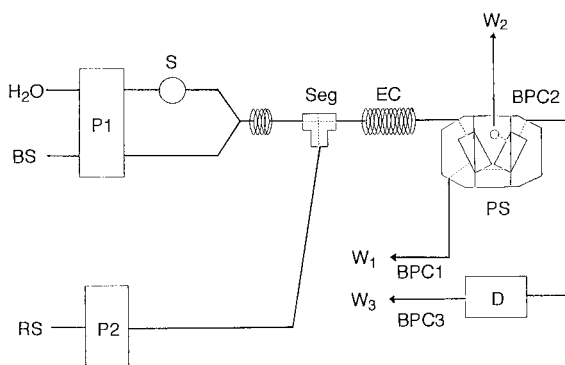


Fig. 1. Schematic diagram of the extraction-flow injection (FI) system for neostigmine determination. BS, buffer (pH 10); RS, 5×10^{-5} mol l^{-1} tetrabromophenolphthalein ethylester (TBPEH)–1,2-dichloroethane (DCE) solution; P1, P2, pumps (BS, H_2O 0.85 ml min^{-1} , RS 0.55 ml min^{-1}); S, sample injection (200 μl); Seg, segmentor; EC, extraction coil (0.5 mm i.d., $\times 3$ m); PS, phase separator; D, spectrophotometer (610 nm); BPC, back pressure coil (0.25 mm i.d., BPC1 1 m, BPC2 6 m, BPC3 1.5 m).

The phase separator with double membranes made of porous poly(tetrafluoroethylene) (PTFE, pore size 0.8 μm), reported in the previous papers [21,22], was used for separation of organic phase. Flow lines were of PTFE tubing (0.5 mm i.d.) and the back pressure coil were of 0.25 mm i.d. PTFE tubing.

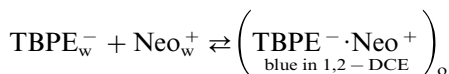
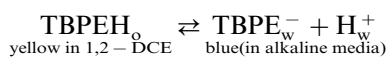
3. Results and discussion

3.1. Batchwise study

3.1.1. Absorption spectra

In a previous paper [7], TBPEK solution was used as an extracting reagent for the sensitive determination of berberine, however, TBPEH–DCE solution was used as an extracting reagent and solvent.

The yellow TBPEH in 1,2-DCE is back-extracted into the alkaline solution ($\text{pH} > 7$) and the blue TBPE anion is liberated in the aqueous phase. And then, TBPE anion reacts with neostigmine (Neo^+) to form a blue ion associate as follows;



where the subscripts o and w refer organic and aqueous phases. The $\text{TBPE}^- \cdot \text{Neo}^+$ associate was successfully extracted into 1,2-DCE with about 100% extraction percentage. The absorption maximum was at 610 nm and absorbance of the reagent blank was about 0.030. The molar absorptivity for the neostigmine associate was $75\,000\ \text{l mol}^{-1}\ \text{cm}^{-1}$.

3.1.2. Effect of pH on extraction

The effect of pH on the extraction of neostigmine associates was examined in the pH range 7.3–10.8 with $5 \times 10^{-4}\ \text{mol l}^{-1}$ TBPEH–DCE solution. The results are shown in Fig. 2. The optimum pH range was 9.8–10.8. At $\text{pH} > 11$, the absorbance of the associates slightly decreased because TBPE anion was gradually hydrolyzed in the higher alkaline media.

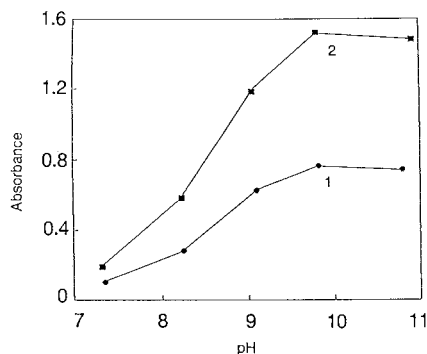


Fig. 2. Effect of pH on the extraction of $\text{TBPE}^- \cdot \text{Neo}^+$ associates by the batchwise method. Neostigmine, (1) $2 \times 10^{-6}\ \text{mol l}^{-1}$; (2) $4 \times 10^{-6}\ \text{mol l}^{-1}$; tetrabromophenolphthalein ethylester (TBPEH), $5 \times 10^{-4}\ \text{mol l}^{-1}$; wavelength, 610 nm.

3.2. FI study

3.2.1. Flow system

On the basis of the experimental conditions obtained by the batchwise method, the three-channels FI system was assembled (Fig. 1) and examined for rapid and sensitive determination of neostigmine. The pH was varied from 7 to 10.8. Over pH 10.8, the base line became noisy. The reproducible peaks were obtained at pH 10. The TBPEH concentration was varied from 5×10^{-5} to $5 \times 10^{-4}\ \text{mol l}^{-1}$ for $4 \times 10^{-7}\ \text{mol l}^{-1}$ neostigmine. The higher the concentration of TBPEH, the higher was the signal peak for the neostigmine associate. However, when $5 \times 10^{-5}\ \text{mol l}^{-1}$ TBPEH was delivered, a stable base line and reproducible signal were obtained.

3.2.2. Effect of back-pressure coil length

The function of phase separator is important for liquid–liquid extraction in FIA. Several phase separating systems were proposed using a PTFE porous membrane which is permeable to an organic phase, but impermeable to an aqueous phase [10–17]. Although the separation efficiency by the separators mentioned above was sufficient, the durability of the membrane was not satisfactory. The life-time of two 1.0 μm pore size PTFE membranes with polyethylene backing was about 2 h [11]. A double-membrane phase separator was

designed [21] to prevent that moisture passes through the membrane and reaches to the flow cell. In the previous paper [22], the phase separator mentioned above was improved to facilitate the tube connection and the efficiency for the (MIBK + toluene = 1 + 1) extraction system was investigated. The recovery of the organic phase depended on the back-pressure coil lengths (BPC1, BPC2, BPC3 in Fig. 1). In this study, the function for a heavy gravity solvent was also studied. The volumes of aqueous and organic phases which are conducted to W1 (waste 1), W2 and W3 were compared by varying the back-pressure coil length. When the volume of organic phase conducted to W3 was maximum, the condition was best. Consequently, BPC1 1 m, BPC2 6 m and BPC3 1.5 m were chosen in the system. The recovery of organic phase in W3 was 87%. The durability of the separation system was improved compared with a single membrane system [23] and the continuous about 5 h run was possible without replacement of membranes. To examine the efficiency of extraction, the length of the extraction coil was varied from 1 to 4 m. A 3 m length gave the maximum peak height.

3.2.3. Effect of flow rate of aqueous phase to organic phase

The flow rate of organic solvent was maintained at 0.55 ml min^{-1} and the flow rates of the carrier and buffer stream were varied from 0.53 to 0.97 ml min^{-1} . As two streams were delivered by the same micro-plunger pump, the flow rate was identical. The results obtained are shown in Fig. 3. The peak height increased with an increase in the ratio of the aqueous phase to the organic phase ($V_{\text{aq}}/V_{\text{org}}$). The increase shows the concentration effect by solvent extraction. In order to achieve a high and constant extraction, the flow rate of aqueous phase should be 0.85 ml min^{-1} and the rate of organic phase, 0.55 ml min^{-1} .

3.2.4. Effect of sample volume

In general, it is well-known that the peak height increases with increasing sample injection volume. The volume of sample injected was varied by changing the length of the sample loop in the injection valve. The peak height remarkably in-

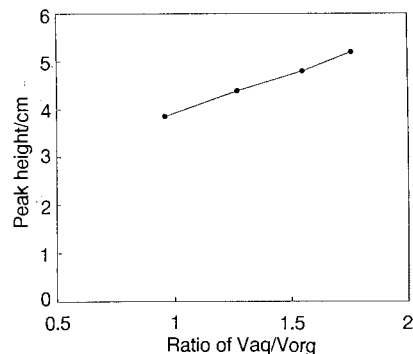


Fig. 3. Effect of ratio of V_{aq} and V_{org} by the flow injection (FI) method. Neostigmine, $4 \times 10^{-7} \text{ mol l}^{-1}$; extraction coil, 3m; sample volume, 200 μl ; V_{org} , 0.55 ml min^{-1} ; pH 10.

creased in the range of 50–200 μl and it slightly increased over 200 μl . However, when 400 μl of sample was injected, a double peak shape was obtained. It is assumed that parts of ion associates were adsorbed on the surface of the membrane and double extraction occurred. A total of 200 μl was injected in this work.

3.2.5. Calibration graph

By using the flow system shown in Fig. 1, the calibration graph was constructed and the profile

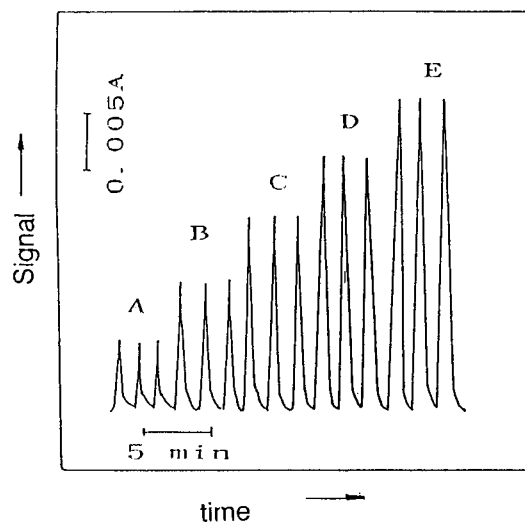


Fig. 4. Flow signals for neostigmine determination. (A) $1 \times 10^{-7} \text{ mol l}^{-1}$; (B) $2 \times 10^{-7} \text{ mol l}^{-1}$; (C) $3 \times 10^{-7} \text{ mol l}^{-1}$; (D) $4 \times 10^{-7} \text{ mol l}^{-1}$; (E) $5 \times 10^{-7} \text{ mol l}^{-1}$.

Table 1
Determination of neostigmine in pharmaceuticals

Sample	Nominal	Found ^a	Recovery
Eye-drops	0.005%	0.00506 ± 0.000007%	101.2%
Injection ampoule	0.5 mg ml ⁻¹	0.492 ± 0.0023 mg ml ⁻¹	98.4%
Diluted powder	5 mg g ⁻¹	4.94 ± 0.051 mg g ⁻¹	98.6%

^a S.D. for three determination.

of flow signals is shown in Fig. 4. The calibration graph was linear over the range 1×10^{-7} mol l⁻¹ (0.03 µg ml⁻¹)– $\times 10^{-7}$ mol l⁻¹ (0.152 µg ml⁻¹) of neostigmine when 200 µl of the standard solution was injected. The relative standard deviation (R.S.D.) ($n = 5$) was 0.5% for 4×10^{-7} mol l⁻¹ neostigmine and the detection limit (S/N = 3) was 1.8×10^{-8} mol l⁻¹. Sampling frequency was 48 h⁻¹.

3.2.6. Determination of neostigmine in commercial pharmaceuticals

Aliquot amounts of commercial eye-drops, injection ampoule or debited powder were dissolved in 100 ml of distilled water. After filtration or dilution, sample solutions were determined by the recommended FI method. The results are shown in Table 1. The recoveries against the nominal values were within 98.4–101.2%.

4. Conclusion

Neostigmine reacts with TBPE anion which is back-extracted from TBPEH–1,2-DCE solution to form the blue ion associate. The ion associate system was introduced into the FI method. The

three-channels FI system with liquid–liquid extraction and the double membrane phase separator was developed for the sensitive, reproducible and rapid determination of neostigmine in pharmaceutical formulations.

References

- [1] E. Auerbach, *Ind. Eng. Chem. Anal. Ed.* 15 (1943) 492.
- [2] Y. Kaneda, M. Iwada, *Eisei Kagaku* 22 (1976) 370.
- [3] K. Arai, M. Kimura, F. Kusu, K. Takamura, *Bunseki Kagaku* 45 (1996) 783.
- [4] H.M.N.H. Irving, J.J. Markham, *Anal. Chim. Acta* 39 (1967) 7.
- [5] G.V. Scott, *Anal. Chem.* 40 (1968) 768.
- [6] T. Sakai, *Analyst* 108 (1983) 608.
- [7] T. Sakai, *Bunseki Kagaku* 24 (1975) 135.
- [8] T. Sakai, *Analyst* 116 (1991) 187.
- [9] B. Karlberg, S. Thelander, *Anal. Chim. Acta* 98 (1978) 1.
- [10] J. Kawase, *Anal. Chem.* 52 (1980) 2124.
- [11] L. Nord, B. Karlberg, *Anal. Chim. Acta* 118 (1980) 285.
- [12] T. Imasaka, T. Harada, N. Ishibashi, *Anal. Chim. Acta* 129 (1981) 195.
- [13] K. Backstrom, L.-G. Danielsson, L. Nord, *Anal. Chim. Acta* 169 (1985) 43.
- [14] S. Motomizu, M. Oshima, *Analyst* 112 (1987) 295.
- [15] S. Motomizu, K. Korechika, *Anal. Chim. Acta* 220 (1989) 275.
- [16] V. Kuban, L.-G. Danielson, F. Ingman, *Talanta* 37 (1990) 1169.
- [17] T. Miyaji, K. Hibi, T. Sakai, *Bunseki Kagaku* 39 (1991) 73.
- [18] V. Kuban, *Crit. Rev. Anal. Chem.* 22 (1991) 477.
- [19] J.M. Calatayud, *Flow Injection Analysis of Pharmaceuticals-Automation in the Laboratory*, Talor and Francis, London, 1996.
- [20] *The Japanese Pharmacopoeia*, XII, Hirokawa, Tokyo, 1991, p. C-2160.
- [21] T. Sakai, Y.S. Chung, N. Ohno, S. Motomizu, *Anal. Chim. Acta* 276 (1993) 127.
- [22] T. Sakai, H. Harada, X.-Q. Liu, N. Ura, K. Takeyoshi, K. Sugimoto, *Talanta* 45 (1998) 543.
- [23] T. Sakai, *Analyst* 117 (1992) 211.

Simultaneous potentiometric determination of $\text{ClO}_3^- - \text{ClO}_2^-$ and $\text{ClO}_3^- - \text{HClO}$ by flow injection analysis using Fe(III)–Fe(II) potential buffer

Hiroki Ohura ^a, Toshihiko Imato ^{b,*}, Sumio Yamasaki ^a

^a Department of Industrial Chemistry, Faculty of Engineering, Kyushu Sangyo University, Matsugadai, Higashi-ku, Fukuoka 813-8503, Japan

^b Department of Chemical Systems and Engineering, Graduate School of Engineering, Kyushu University, Hakozaki, Higashi-ku, Fukuoka 812-8581, Japan

Received 24 August 1998; received in revised form 2 December 1998; accepted 3 December 1998

Abstract

A rapid potentiometric flow injection technique for the simultaneous determination of oxychlorine species such as $\text{ClO}_3^- - \text{ClO}_2^-$ and $\text{ClO}_3^- - \text{HClO}$ has been developed, using both a redox electrode detector and a Fe(III)–Fe(II) potential buffer solution containing chloride. The analytical method is based on the detection of a large transient potential change of the redox electrode due to chlorine generated via the reaction of the oxychlorine species with chloride in the potential buffer solution. The sensitivities to HClO and ClO_2^- obtained by the transient potential change were enhanced 700–800-fold over that using an equilibrium potential. The detection limit of the present method for HClO and ClO_2^- is as low as 5×10^{-8} M with use of a 5×10^{-4} M Fe(III)– 1×10^{-3} M Fe(II) buffer containing 0.3 M KCl and 0.5 M H_2SO_4 . On the other hand, sensitivity to ClO_3^- was low when a potential buffer solution containing 0.5 M H_2SO_4 was used, but could be increased largely by increasing the acidity of the potential buffer. The detection limit for ClO_3^- was 2×10^{-6} M with the use of a 5×10^{-4} M Fe(III)– 1×10^{-3} M Fe(II) buffer containing 0.3 M KCl and 9 M H_2SO_4 . By utilizing the difference in reactivity of oxychlorine species with chloride in the potential buffer, a simultaneous determination method for a mixed solution of $\text{ClO}_3^- - \text{ClO}_2^-$ or $\text{ClO}_3^- - \text{HClO}$ was designed to detect, in a timely manner, a transient potential change with the use of two streams of potential buffers which contain different concentrations of sulfuric acid. Analytical concentration ranges of oxychlorine species were $2 \times 10^{-5} - 2 \times 10^{-4}$ M for ClO_3^- , and $1 \times 10^{-6} - 1 \times 10^{-5}$ M for HClO and ClO_2^- . The reproducibility of the present method was in the range 1.5–2.3%. The reaction mechanism for the transient potential change used in the present method is also discussed, based on the results of batchwise experiments. The simultaneous determination method was applied to the determination of oxychlorine species in a tap water sample, and was found to provide an analytical result for HClO, which was in good agreement with that obtained by the *o*-tolidine method and to provide a good recovery for ClO_3^- added to the sample. © 1999 Elsevier Science B.V. All rights reserved.

Keywords: Flow-injection; Oxychlorine species; Fe(III)–Fe(II) potential buffer; Potentiometric detection

* Corresponding author. Fax: +81-92-642-4134.

E-mail address: imato@cstf.kyushu-u.ac.jp (T. Imato)

1. Introduction

Although chlorine has been widely used for the disinfection of drinking water, the toxicity of trihalomethanes which are derived from reactions of organic compounds in raw water with chlorine, has been noted and as a result, considerable interest in the use of alternative disinfectants has recently developed. Chlorine dioxide is extensively used for as an alternative to chlorine, in the disinfection of water, because of its advantages over chlorine with respect to negligible reaction with ammonia to form chloramines and with organic compounds to form chlorinated organic compounds [1]. However, ClO_3^- is known to be generated by the reaction of chlorine dioxide with organic compounds during water treatment, and the reaction of chlorine dioxide with the resulting ClO_3^- is known to induce a disproportionation to form oxychlorines such as HClO and ClO_2^- [2]. Since the oxychlorines are considered to be hazardous to general health, a level of residual oxychlorines in the drinking water is important for health safety, and it requires routine monitoring. The EPA requires that the maximum contaminant limit of oxychlorine species be less than 1.0 mg l^{-1} for drinking water because of possible adverse health effects by oxychlorine species [3]. Iodometry has been adopted as one of the standard methods to determine oxychlorine species [4]. This method is capable of determining the total oxychlorine species in drinking water. One drawback to the method is that other oxidizing species which coexist in the sample can interfere with the determination.

A sensitive and accurate analytical method for oxychlorinated species such as HClO , ClO_2^- , ClO_3^- and ClO_2 in water is required in water treatment process. Furthermore, since HClO and ClO_2^- are unstable and are easily decomposed by air oxidation, a rapid analytical method which can be operated in a substantially closed system, is desirable. Flow injection analysis (FIA) [5] has been recognized to be a versatile and valuable tool which is capable of rapid, automatic sample analysis and is suitable for analyzing unstable substances such as HClO and

ClO_2^- . Gordon et al. [6–9] reported an analytical method for oxychlorine species, ClO_2^- , ClO_3^- and ClO_2 by using the FIA technique. Their method is based on the spectrophotometric detection of iodine generated by the reaction of oxychlorine species with iodide in acidic media. This method is designed to enhance the selectivity among oxychlorines by utilizing different reaction kinetics depending on the acid concentration in the reaction media and by combining a gas-diffusion unit in the flow system. Numerous reports have appeared concerning the determination of residual chlorine, total oxychlorine HClO , ClO^- and Cl_2 [10–13] using this method. However, only a few reports on the simultaneous potentiometric determination of a mixture of oxychlorine species, i.e., HClO , ClO_2^- and ClO_3^- have been published.

In earlier papers, a novel application of the potentiometric FIA method has been proposed for the rapid and accurate determination for redox compounds such as bromate, glucose and hydrazine [15,16] with use of potential buffer solutions such as $\text{Fe(III)}-\text{Fe(II)}$, $\text{Fe(CN)}_6^{3-}-\text{Fe(CN)}_6^{4-}$ and $\text{Ce(IV)}-\text{Ce(III)}$ and the use of a redox electrode detector. The method is based on the detection of the potential change of the redox electrode which is caused by the composition change in the potential buffer as the result of a reaction of the redox sample with the potential buffer. It has recently been found that the addition of chloride or bromide to the $\text{Fe(III)}-\text{Fe(II)}$ potential buffer enhances the sensitivity to some oxidative species such as residual chlorine [14] and hydrogen peroxide [17]. For example, highly sensitive determination of residual chlorine in tap water has been achieved by the detection of a large transient potential change which is temporarily increased as the result of the generation of intermediate chlorine during the reaction of the sample with chloride added to the potential buffer.

In this paper, the application of this method [14] is described to the simultaneous determination of trace amounts of oxychlorines such as HClO , ClO_2^- and ClO_3^- , as a method for monitoring water. The factors which effect the reactivity of the oxychlorines with the potential

buffer were examined in a batchwise system. Based on the batchwise examination of the simultaneous determination of mixed oxychlorines, an FIA system was designed which consists of two detectors, two streams of an Fe(III)–Fe(II) potential buffer containing different concentrations of sulfuric acid and two reaction coils which serve to control the reaction time.

2. Experimental

2.1. Reagents and preparation of solutions

A stock solution of HClO was prepared by filtering a commercially available sodium hypochlorite solution (10% available chlorine; Taisei Yakuhin, Japan) through a membrane filter (0.45 μm pore size) and diluting the filtrate with deionized water appropriately, as described previously [14]. A stock solution of 0.1 M NaClO₂ was prepared by dissolving 9.044 g NaClO₂·3H₂O into 1 dm³ of deionized water, after purifying commercially available sodium chlorite (Katayama, Japan) by recrystallization from water [18]. A stock solution of NaClO₃ was prepared by dissolving analytical grade sodium chlorate (Katayama, Japan) with deionized water. Both stock solutions of 0.1 M Fe(III) and 0.1 M Fe(II) in 0.1 M H₂SO₄ were prepared from ammonium iron(III) sulfate and ammonium iron(II) sulfate (Katayama, Japan), respectively, according to procedures described previously [14]. An Fe(III)–Fe(II) potential buffer solution was prepared by mixing the Fe(III) and Fe(II) stock solutions appropriately and by adding sulfuric acid. This potential buffer solution is hereafter referred to as buffer-A. Another Fe(III)–Fe(II) potential buffer solution, abbreviated as buffer-B, was prepared by the same procedure as used for buffer-A except for the further addition of potassium chloride.

A cation-exchange resin column in the Fe(II) form was prepared by packing cation-exchange resin (Amberlite IR-118, 20–50 mesh) into a polyacrylic resin tube (6 cm-long, 7 mm i.d.) and then eluting it with a 1×10^{-4} M Fe(II) solution.

2.2. Procedure for the determination of single component of oxychlorine species in flow system

A schematic diagram of a two-channel flow system is shown in Fig. 1(A). The apparatus consisted of a peristaltic pump (P), a sample injection valve (S), a flow-through redox electrode detector (D) which has a gold-plated electrode and a silver/silver chloride reference electrode, a potentiometer and a recorder, as described previously [15]. PTFE tubing of 0.5 mm i.d. was used for the manifold. The potential buffer solution and water were pumped at a flow rate of 0.7 ml min⁻¹ as the reagent stream (RS) and as a carrier stream (CS), respectively. A sample solution (140

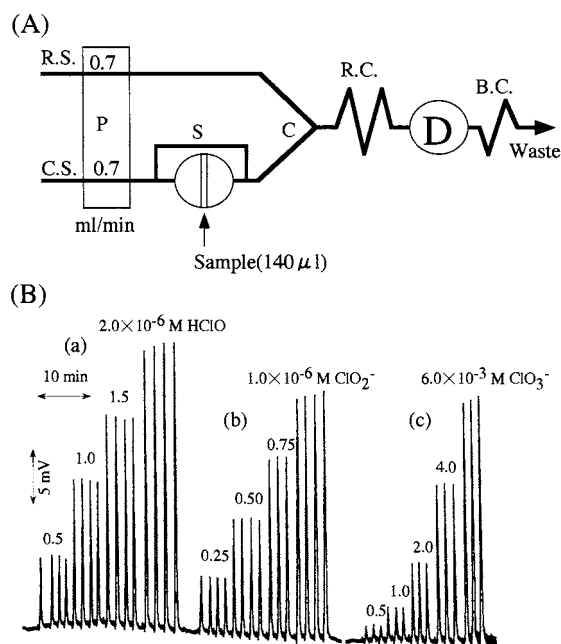


Fig. 1. Schematic diagram of a two-channel flow injection analysis (FIA) system for oxychlorine species (A) and calibration peaks for oxychlorine species (B). RS, reagent stream (5×10^{-3} M Fe(III)– 1×10^{-2} M Fe(II), 0.3 M KCl and 0.5 M H₂SO₄); CS, carrier stream (H₂O); RC, reaction coil (70 cm \times 0.5 mm i.d.); BC, back-pressure coil (5 m \times 0.5 mm i.d.); S, sample injector (140 μl); D, flow-through type redox electrode detector; C, confluence point; temperature of the RS and CS was controlled at $25 \pm 0.5^\circ\text{C}$. Oxychlorine species: (a) HClO; (b) ClO₂⁻; (c) ClO₃⁻.

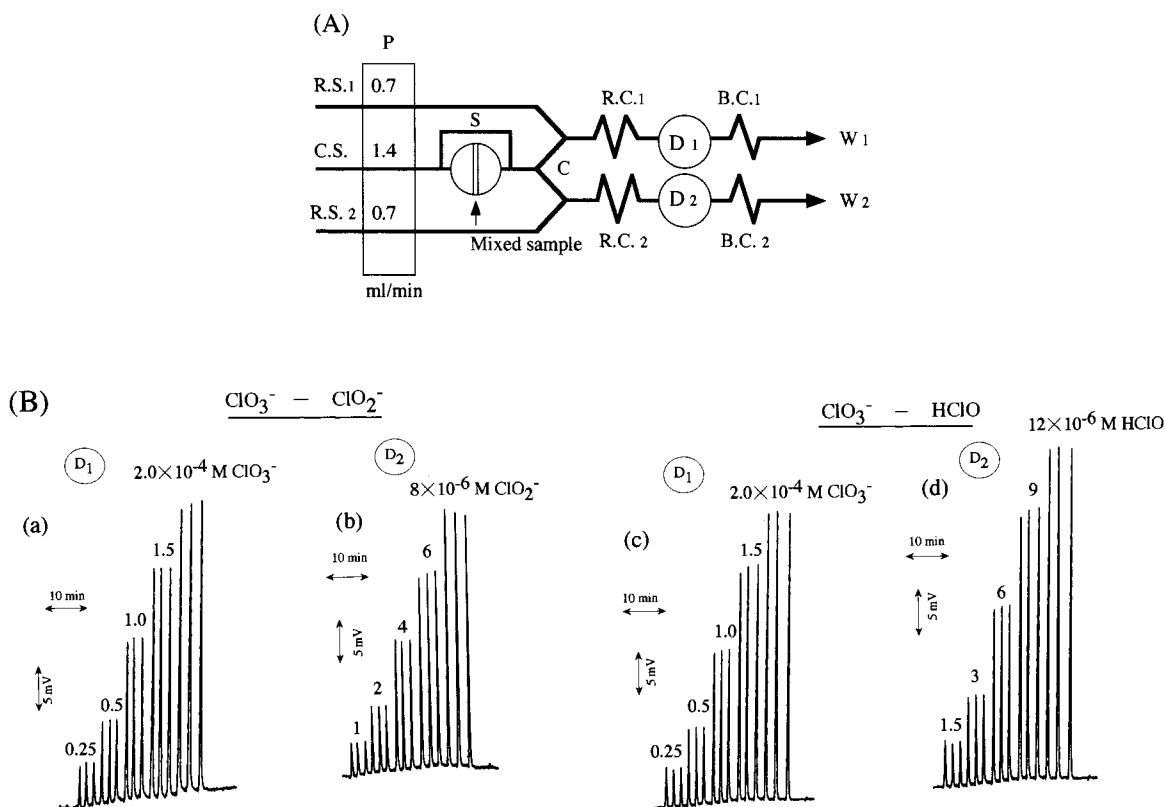


Fig. 2. (A) Schematic diagram of a three-channel flow injection analysis (FIA) system for the simultaneous determination of ClO_3^- – HClO or ClO_3^- – ClO_2^- (for the case of $[\text{ClO}_3^-] > [\text{ClO}_2^-]$ and $[\text{ClO}_3^-] > [\text{HClO}]$). RS₁, reagent stream 1 (5×10^{-3} M Fe(III)– 1×10^{-2} M Fe(II), 0.3 M KCl and 9 M H_2SO_4); RS₂, reagent stream 2 (5×10^{-3} M Fe(III)– 1×10^{-2} M Fe(II), 0.3 M KCl and 0.3 M H_2SO_4); RC₁, reaction coil 1 (200 cm \times 0.5 mm i.d.); RC₂, reaction coil 2 (60 cm \times 0.5 mm i.d.); D₁ and D₂, the same detectors as in Fig. 1. The other experimental conditions are the same as that in Fig. 1(A). (B) Calibration peaks ((a), (b)) for ClO_3^- and ClO_2^- obtained with detectors D₁ and D₂, respectively. Concentrations of ClO_3^- and ClO_2^- in the mixed sample are indicated in the figure. Calibration peaks ((c), (d)) for ClO_3^- and HClO obtained with detectors D₁ and D₂, respectively. Concentrations of ClO_3^- and HClO in the mixed sample are indicated in the figure.

μl) containing a single component of oxychlorine (HClO , ClO_2^- or ClO_3^-) was injected into the carrier stream, and merged with the reagent stream at the confluence point (C). The mixed stream was led to the redox electrode detector, after passing through the reaction coil (RC). A back-pressure coil (BC) was connected to an outlet of the detector to suppress the generation of bubble in the RC and the detector. The potential change of the detector was measured with the potentiometer and the signal therefrom was recorded on the recorder.

2.3. Procedure for the simultaneous determination of ClO_3^- – ClO_2^- and ClO_3^- – HClO in flow system

In the case of the mixed sample solution containing ClO_3^- – ClO_2^- or ClO_3^- – HClO under the concentration condition $[\text{ClO}_3^-] > [\text{ClO}_2^-]$ or $[\text{ClO}_3^-] > [\text{HClO}]$, a three-channel flow system shown in Fig. 2(A) was used. The mixed sample solution was injected into the CS. The carrier stream was divided into two streams at the point (C) and the divided streams were merged with two

different potential buffer streams. The potential buffer (RS₁) contains potassium chloride and sulfuric acid at very high concentration. The potential buffer (RS₂) contains potassium chloride and sulfuric acid at low concentration. A half portion of the sample zone was led to the detector (D₁) after mixing with RS₁ and passing the reaction coil (RC₁). The other half was directed to the detector (D₂) after mixing with RS₂ and passing the reaction coil (RC₂). ClO₂⁻ or HClO in the mixed sample was selectively detected with detector D₂ even in the presence of ClO₃⁻ in the sample. Only ClO₃⁻ was detected with detector D₁ by setting length of RC₁ longer than that of RC₂, even when ClO₂⁻ or HClO was present in the sample solution under the concentration conditions mentioned above.

In the case of a mixed sample solution containing ClO₃⁻–ClO₂⁻ or ClO₃⁻–HClO under the concentration condition [ClO₃⁻] ≅ [ClO₂⁻] or [ClO₃⁻] ≅ [HClO], a four-channel flow system shown in Fig. 3(A) was used. A sample solution was injected into the CS. The carrier stream was divided into two streams at point (C). A half portion of sample zone was merged with a stream of RS₃, 1 × 10⁻⁴ M Fe(II) solution containing 0.01 M H₂SO₄, and was passed through an Fe(II) form cation-exchange resin column (EC). ClO₂⁻ and HClO in the sample containing ClO₃⁻ were reduced to chloride by reaction with Fe(II) in the RS₃ stream and with Fe(II) on the ion-exchange resin. ClO₃⁻ in the mixed sample did not react with Fe(II) in the RS₃ stream or the Fe(II) on the ion-exchange resin. Thus, the unreacted ClO₃⁻ in the sample zone was reacted with the potential buffer (RS₁) containing chloride and sulfuric acid at very high concentration and was led to the detector D₁. Therefore, the signals from the detector D₁ are attributed only to ClO₃⁻ even in the presence of ClO₂⁻ or HClO in the sample solution. Another half portion of the sample zone was merged with the stream of RS₂. The RS₂ stream is a solution of buffer-A, the Fe(III)–Fe(II) potential buffer containing sulfuric acid. ClO₂⁻ or HClO in the mixed sample solution reacted with Fe(II) in the reagent solution of RS₂, while chlorate did not react with Fe(II) in the reagent solution of RS₂ containing sulfuric acid at low

concentration during the short period required for passage through RC₂. Thus, ClO₂⁻ or HClO could be detected with detector D₂ even in the presence of ClO₃⁻. About 3 and 0.25 min were required from the time of sample injection to the appearance of the maximum peak with the detectors D₁ and D₂, respectively. The stream of RS₃ was used as the reagent solution to regenerate the exchange column in the Fe(II) form.

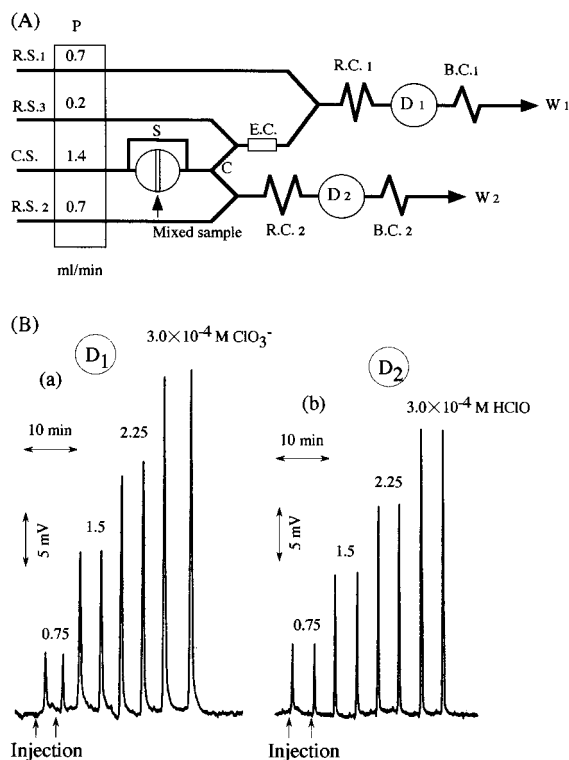


Fig. 3. (A) Schematic diagram of a four-channel flow injection analysis (FIA) system for the simultaneous determination of ClO₃⁻ and HClO (for the case of [ClO₃⁻] ≅ [HClO]). RS₁, reagent stream 1 (5 × 10⁻³ M Fe(III)–1 × 10⁻² M Fe(II), 0.3 M KCl and 9 M H₂SO₄); RS₂, reagent stream 2 (1 × 10⁻³ M Fe(III)–2 × 10⁻³ M Fe(II), 0.3 M H₂SO₄); RS₃, reagent stream 3 (1 × 10⁻⁴ M Fe(II), 1 × 10⁻² M H₂SO₄); RC₁, reaction coil 1 (200 cm × 0.5 mm i.d.); RC₂, reaction coil 2 (250 cm × 0.5 mm i.d.); EC, cation-exchange resin column in Fe(II) form. The other experimental conditions are the same as that in Fig. 2(A). (B) Calibration peaks ((a), (b)) for ClO₃⁻ and HClO obtained with detectors D₁ and D₂, respectively. Concentrations of ClO₃⁻ and HClO in the mixed sample are indicated in the figure.

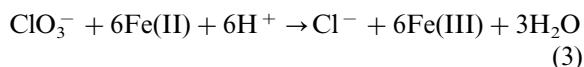
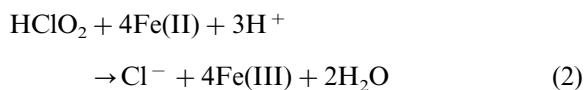
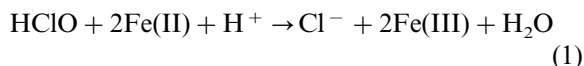
2.4. Procedure of measurement of potential change using a batch system

The relationship between the potential change of the redox electrode caused by the reaction of oxychlorine species with the potential buffer and the reaction time was examined by using the same batch-beaker system as described previously [14]. A sample solution of oxychlorine (100 μ l) was added quickly to the potential buffer solution (10 ml) in which the redox electrode and the reference electrode were immersed. The potential change of the redox electrode was measured with a potentiometer as a function of time and recorded on recorder.

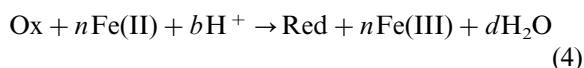
3. Results and discussion

3.1. Response potential of redox electrode caused by the reaction of oxychlorine with Fe(III)–Fe(II) potential buffer

The overall reactions of oxychlorines such as HClO, HClO₂ and ClO₃⁻, with Fe(II) in the potential buffer containing sulfuric acid can be expressed by Eqs. (1)–(3) [19].



Eqs. (1)–(3) can be generally rewritten by Eq. (4) when oxychlorines and their reduced species, Cl⁻, are abbreviated by Ox and Red, respectively.



where, n , b and d are stoichiometric coefficients.

The potential of the redox electrode, E_1 , in the Fe(III)–Fe(II) potential buffer containing Fe(III) and Fe(II) at the concentration of [Fe(III)]_o and [Fe(II)]_o, respectively, can be expressed by

$$E_1 = E^0 + 0.059 \log\left(\frac{[\text{Fe(III)}]_o}{[\text{Fe(II)}]_o}\right) \quad (\text{V at } 25^\circ\text{C}) \quad (5)$$

where E^0 is the formal redox potential.

Oxychlorine at the concentration of [Ox]_o is added to the Fe(III)–Fe(II) potential buffer and if the reaction is then completed, according to Eq. (4), the change of potential of the redox electrode, ΔE , i.e. the potential difference between before and after an addition of oxychlorines can be obtained using Eq. (5) and expressed by

$$\Delta E = 0.059 \log\left\{\frac{1 + n[\text{Ox}]_o/[\text{Fe(III)}]_o}{1 - n[\text{Ox}]_o/[\text{Fe(II)}]_o}\right\} \quad (\text{V}) \quad (6)$$

The relationship between ΔE and [Ox]_o depends on both the ratio of [Fe(III)]_o/[Fe(II)]_o and the value of n , as expected from Eq. (6). Indeed by numerical calculation of Eq. (6), a linear relationship exists between ΔE and [Ox]_o where ΔE is within ca. 35 mV, when the ratio of [Fe(III)]_o/[Fe(II)]_o is 0.5. The sensitivities, defined as the slope of the linear portion are calculated to be 15.0, 30.0 and 45.0 mV mM⁻¹ for $n = 2, 4$ and 6 , respectively from Eq. (6). These values for the sensitivities correspond to the theoretical sensitivity to HClO, ClO₂⁻ and ClO₃⁻, respectively. These values are also given in column (B) of Table 1.

Based on the batchwise procedure described in the experimental section, the potential changes of the redox electrode were examined by adding oxychlorine solutions to buffer-A and the buffer-B. Curves (A)-(a), -(b) and -(c) in Fig. 4 show the time-courses of the potential change when 100 μ l of 1×10^{-2} M HClO, ClO₂⁻ and ClO₃⁻, respectively, were added to 10 ml of the buffer-A, which consists of 5×10^{-3} M Fe(III)– 1×10^{-2} M Fe(II) and 0.5 M H₂SO₄. As can be seen from curves (A)-(a) and -(b), the potential increases quickly within 10 s and then decreases with time after passing through a maximum, and finally reaching constant values after 20 s or longer when HClO and ClO₂⁻ were added to buffer-A. The potential difference between the initial potential and the equilibrium potential after 20 s were 1.8 and 3.3 mV for curve (A)-(a) and -(b), respectively. The values of these potential differences are

Table 1
Sensitivities to oxychlorine species

Oxychlorine species	Sensitivity (mV/mM) ^a		Enhancement factor
	(A) Observed in FIA system ^b	(B) Calculated ^c	(A)/(B)
HClO	1.2×10^4	15 ($n = 2$)	800
ClO_2^-	2.1×10^4	30 ($n = 4$)	700
ClO_3^-	3.4	45 ($n = 6$)	0.08
ClO_3^-	4.3×10^{2d}	45 ($n = 6$)	9.8

^a Sensitivities defined as slope of the potential change versus sample concentration curves.

^b Slope of calibration curves observed at flow injection analysis (FIA) system shown in Fig. 1.

^c Sensitivity calculated from Eq. (6); n indicates the number of moles of Fe^{2+} reacted with 1 mole of Ox (Eq. (4)).

^d Slope of calibration curve observed in the FIA system with buffer-B containing 9.0 M H_2SO_4 and a reaction coil (RC) of 200 cm in length.

in agreement with that of the potential change calculated from Eq. (6). This indicates that the assumption of completion of the reactions (1) and (2) is valid and Eq. (6) holds for HClO and HClO_2 . On the other hand, no significant potential change of the redox electrode for ClO_3^- was observed, as can be seen from curve (A)-(c) in Fig. 4, although the highest sensitivity to ClO_3^- is expected among oxychlorines, judging from the calculated value based on Eqs. (3) and (6). This indicates that the rate of the reaction of ClO_3^- with Fe(II) is much slower than that of HClO and HClO_2 under the present conditions.

If the reaction of oxychlorine with Fe(II) proceeds in accordance with Eq. (4), a monotonous potential increase from the initial potential E_1 of Eq. (5) to the equilibrium potential $E_1 + \Delta E$ is expected, though the time required to reach the equilibrium potential may depend on the reaction rate of Eq. (4). However, mountain-shaped potential changes (curves (A)-(a) and -(b)) were in fact obtained when HClO and ClO_2^- were added to the buffer-A, as shown in Fig. 4. This suggests that the reaction of HClO or HClO_2 with Fe(II) is not a simple reaction such as is expressed by Eqs. (1) and (2), but may include several elementary reactions, generating an intermediate substance with higher redox potential. For an explanation of the mountain-shaped curves (A)-(a) and -(b), the following reactions can be considered as feasible elementary reactions.

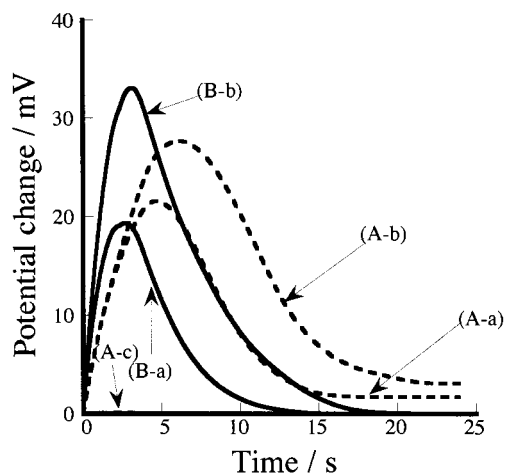
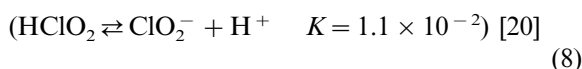
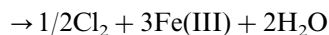
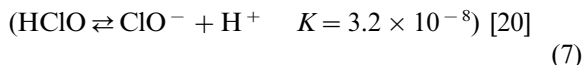
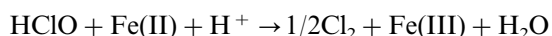
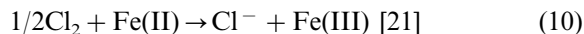
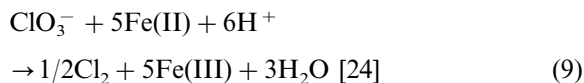


Fig. 4. Potential changes of the redox electrode caused by reaction of oxychlorine samples with buffer-A or -B in a batch system. (A) Broken lines represent potential changes obtained by the addition of 100 μl of 1.0×10^{-2} M oxychlorine to 10 ml of the buffer-A (5×10^{-3} M Fe(III)– 1×10^{-2} M Fe(II) and 0.5 M H_2SO_4). (A)-(a) HClO; (A)-(b) ClO_2^- ; (A)-(c) ClO_3^- . (B) Solid lines represent potential changes obtained by the addition of 100 μl of 1.0×10^{-4} M oxychlorine to 10 ml of buffer-B (5×10^{-3} M Fe(III)– 1×10^{-2} M Fe(II), 0.3 M KCl and 0.5 M H_2SO_4). (B)-(a) HClO; (B)-(b) ClO_2^- .



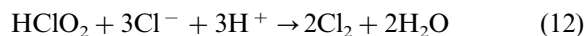
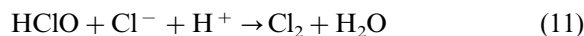
That is, the potential raising observed just after the addition of HClO and ClO_2^- may be due to reactions (7) and (8) to generate the intermediate chlorine, Cl_2 , which has a higher redox potential of Cl_2/Cl^- couple than the redox potential of $\text{Fe(III)}/\text{Fe(II)}$ couple [20]. As a result, the potential descending may be due to a decrease in chlorine concentration as the result of the reaction of chlorine with Fe(II), according to Eq. (10). As is also shown in the curves (A)-(a) and -(b) in Fig. 4, the magnitude of the observed potential changes for ClO_2^- was slightly larger than that for HClO. This is probably due to the larger reactivity of HClO_2 with Fe(II) than HClO. The sum of the elementary reactions (7) and (10) or (8) and (10) are identical to overall reactions (1) or (2), respectively. A lack of response to ClO_3^- suggests that the rate of reaction (9) may be very slow in dilute acidic media such as 0.5 M H_2SO_4 . As is subsequently described, an increase in sulfuric acid in the potential buffer results in a mountain-shaped potential change for ClO_3^- , the same as for ClO_2^- and HClO. It is probable that reactions (9) and (10) would occur as the elementary reaction of reaction (3).

3.2. Effect of the addition of potassium chloride to the potential buffer on potential change

Curves (B)-(a) and -(b) in Fig. 4 show the potential changes of the redox electrode obtained by the addition of 100 μl of 1×10^{-4} M HClO and ClO_2^- , respectively, to 10 ml of the buffer-B which consists of 5×10^{-3} M Fe(III)– 1×10^{-2} M Fe(II), 0.5 M H_2SO_4 and 0.3 M KCl. As can be seen from the curves (B)-(a) and -(b), mountain-shaped potential changes similar to those with the buffer-A were obtained, even though the concentrations of HClO and ClO_2^- added to the buffer-B are lower by two order of magnitude than those added to buffer-A. It is noteworthy that the magnitude of the transient potential change was much larger than that obtained with the buffer-A. The

potential changes at the maximum normalized by the concentration of oxychlorine added to the buffer were 2.2×10^4 mV mM^{-1} for HClO and 3.8×10^4 mV mM^{-1} for ClO_2^- when buffer-B was used, while they were 2.4×10^2 mV mM^{-1} for HClO and 2.8×10^2 mV mM^{-1} for ClO_2^- when the buffer-A was used. The peak maxima appeared at around 2–5 s which was shorter than those observed for buffer-A, and the potential after 20 s was nearly identical to the initial value.

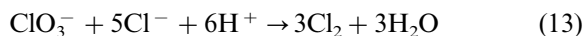
Since the difference in composition between the buffer-A and -B is the absence or presence of chloride in the buffer, the larger transient potential change for ClO_2^- and HClO obtained with buffer-B may be related to the presence of chloride. The following reactions are known [19], and are thought to provide a possible explanation of the large transient potential change.



When the concentration of potassium chloride in buffer-B was varied from 0.1 to 1.0 M, the transient potential change increased with increasing concentration of potassium chloride up to 0.3 M and became nearly constant at concentrations of 0.5 M and higher. Since chloride exists in a much higher concentration than Fe(II) in buffer-B, HClO and ClO_2^- must react with chloride preferentially. Therefore, the raising transient potential changes are due to chlorine generated by reactions (11) and (12) rather than by reactions (7) and (8). The rate of the generation of chlorine by reaction (12) is estimated to be faster than that by reaction (11) based on the fact that the potential change of the curve (B)-(b) is larger than that of the curve (B)-(a), providing the descending of the potential after a maximum occurs via the same path as reaction (10). The potential changes for ClO_2^- and HClO became larger when the potential buffer consisting of a lower concentration of the Fe(III)–Fe(II) couple containing 0.5 M H_2SO_4 and 0.3 M KCl was used. For example, the potential changes for HClO and ClO_2^- were about 6-fold higher when a 5×10^{-5} M Fe(III)– 1×10^{-4} M Fe(II) buffer solution was used, compared with the potential change obtained with the

5×10^{-3} M Fe(III)– 1×10^{-2} M Fe(II) buffer solution. This suggests that reaction (10) occurs simultaneously with the reactions (11) or (12) and that the rate of reduction of chlorine by Fe(II) (reaction (10)) determines the magnitude of the potential changes. In the case where buffer-B was used, the sum of the elementary reactions (11) and (10) or (12) and (10) are identical to the overall reaction (1) or (2), respectively. That is, the presence of chloride in buffer-B may act as a homogeneous catalyst for the successive reactions involving chlorine as the intermediate. Since the transient potential changes for HClO and ClO_2^- are much larger when buffer-B was used, a more sensitive analysis for HClO and ClO_2^- could be expected by using buffer-B, provided the maximum potential change which appears transiently can be detected in a timely manner.

On the other hand, by the addition of 100 μl of 1×10^{-3} M ClO_3^- to 10 ml of buffer-B consisting of 5×10^{-3} M Fe(III)– 1×10^{-2} M Fe(II), 0.3 M KCl and 4.5 M H_2SO_4 , no potential change similar to that of curve (A)–(c) was observed. However, a mountain-shaped potential change was observed when a concentration of ClO_3^- higher than 10^{-3} M was added to buffer-B. This potential change may be due to the simultaneous elementary reactions (13) and (10), i.e. cases similar to that of HClO and ClO_2^- .



The rate of reaction (13) is thought to be relatively slower than that of reactions (11) and (12), based on the fact that the concentration of ClO_3^- used to observe the mountain-shaped potential change was higher than that of HClO and ClO_2^- . As describe below, reaction (13) was accelerated by increasing the concentration of sulfuric acid in buffer-B.

3.3. Effect of concentration of sulfuric acid in the potential buffer on the potential change for chlorate

The concentrations of sulfuric acid as well as chloride in the potential buffer would be expected to affect the magnitude of the potential change, judging from the fact that a proton is included in

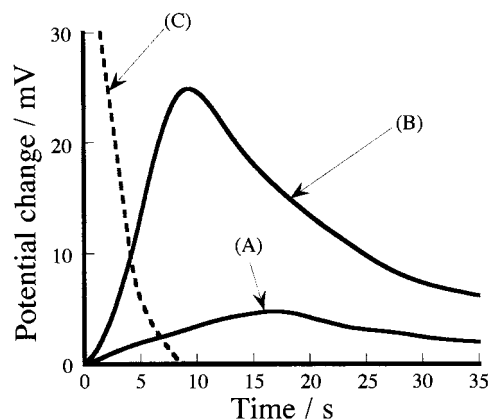


Fig. 5. Potential changes of the redox electrode caused by the reaction of oxychlorine samples with the buffer-A or -B containing 4.5M H_2SO_4 in the batch system. (A) The potential change obtained by the addition of 100 μl of 2×10^{-3} M ClO_3^- to 10 ml of the buffer-A (5×10^{-3} M Fe(III)– 1×10^{-2} M Fe(II) and 4.5 M H_2SO_4). (B) The potential change obtained by the addition of 100 μl of 2×10^{-3} M ClO_3^- to 10 ml of buffer-B (5×10^{-3} M Fe(III)– 1×10^{-2} M Fe(II), 0.3 M KCl and 4.5 M H_2SO_4). (C) The potential changes obtained by the addition of 100 μl of 1×10^{-4} M ClO_2^- or HClO to 10 ml of buffer-B (5×10^{-3} M Fe(III)– 1×10^{-2} M Fe(II), 0.3 M KCl and 4.5 M H_2SO_4).

left hand side of reactions (11), (12) and (13). Chlorine is known to be generated according to reaction (13) when ClO_3^- is added to a chloride solution containing sulfuric acid at a high concentration [22,23]. Therefore, the effect of sulfuric acid concentration in buffer-A and -B on the potential change for chlorate was examined. Indeed, when 100 μl of 2×10^{-3} M ClO_3^- was added to 10 ml of the buffer-B containing 4.5 M H_2SO_4 , a mountain-shaped potential change of 26 mV with a maximum at around 10 s was observed, as shown in Fig. 5(B), and a constant potential after passing through the maximum was 60 s or longer. This indicates that reaction (13) was accelerated by the presence of high concentrations of sulfuric acid. Curve (A) in Fig. 5 shows the time-course of the potential change when 100 μl of 2×10^{-3} M ClO_3^- was added to 10 ml of the buffer-A, which consists of 5×10^{-3} M Fe(III)– 1×10^{-2} M Fe(II) and 4.5 M H_2SO_4 . A mountain-shaped potential response was also obtained, but the potential change at the maximum was about one-fifth that of the curve (B) in Fig. 5.

The maximum appeared at around 18 s for buffer-A, which was longer than the time for the maximum observed for the curve (B) in Fig. 5. These results indicate that the presence of chloride and high concentrations of sulfuric acid in the potential buffer enhanced the transient potential change for ClO_3^- . The potential change normalized by the concentration of ClO_3^- was ca. 200 times larger, when concentration of sulfuric acid in the buffer-B was 4.5 M, as compared with the potential change observed for the buffer-B which contained 0.5 M H_2SO_4 .

The potential changes of the redox electrode for HClO and ClO_2^- were also examined by using the above buffer-B containing 4.5 M H_2SO_4 . The potential change is shown in the curve (C) in Fig. 5, when 100 μl of 2×10^{-4} M HClO or ClO_2^- was added to 10 ml of the buffer-B. The potential changes for both oxychlorines were very large and so fast that the peak maxima were not observed by the present batch system. Only the potential descending was observed and the response potential returned to the initial potential within 10 s, which is prior to the peak appearance for ClO_3^- . These results indicate that the increase in the concentration of sulfuric acid in buffer-B accelerates, not only the generation rate of chlorine by reaction (11) and (12), but also the reduction rate of chlorine by reaction (10).

From the above results based on batchwise experiments, the simultaneous determination of ClO_3^- – HClO and ClO_3^- – ClO_2^- in a mixture is attainable, provided the transient potential changes are detected in a timely manner by controlling the concentrations of sulfuric acid in the potential buffer solution. For example, HClO and ClO_2^- at a concentration of 10^{-6} M could be detectable even in the presence of ClO_3^- at concentrations below 10^{-4} M in the mixed sample if buffer-B containing 0.5 M sulfuric acid is used and if the reaction time is controlled to be in the vicinity of 5 s. On the other hand, ClO_3^- at the concentration level of 10^{-5} M may be detectable even in the presence of HClO and ClO_2^- concentrations below 10^{-5} M in the mixed sample if buffer-B containing 4.5 M H_2SO_4 is used and if the reaction time is controlled to be in the vicinity of 20 s, since the reaction of HClO or ClO_2^- with

the buffer-B would already have been completed within 20 s, as expected from Fig. 5. Therefore, no interference from HClO and ClO_2^- may occur for the detection of ClO_3^- .

3.4. Determination of single species of oxychlorine by the two-channel FIA system

Since a flow injection technique has the advantage of controlling the timing of detection, this technique would be expected to be suitable for detecting the transient potential change described in previous sections. The flow system shown in Fig. 1(A) was designed to detect the transient potential change that appeared at about 5–10 s after mixing of the sample with the potential buffer in the batch system. The residence time of the sample zone in the RC was set at about 6 s by controlling the length of the RC and the flow rates of the water and the buffer streams as indicated in Fig. 1(A). The detection peak signals for HClO , ClO_2^- and ClO_3^- , respectively, are shown in Fig. 1(B)-(a), -(b) and -(c) where a 5×10^{-3} M Fe(III) – 1×10^{-2} M Fe(II) buffer solution containing 0.3 M KCl and 0.5 M H_2SO_4 was used. Good reproducible signals for three repeated injection of the same sample were obtained. The peak heights for three oxychlorine species were nearly linear with concentrations in the indicated ranges. The sensitivities, i.e. the slopes of the calibration peaks versus concentration (mV mM^{-1}) obtained from Fig. 1(B) are given in column (A) of Table 1. The theoretical sensitivities which were calculated from Eq. (6), assuming completion of reactions (1), (2) and (3) are also given in column (B) of Table 1. The sensitivity enhancement factors, defined as the ratio of the observed sensitivity to the theoretical, were 700–800 for HClO and ClO_2^- . The minimum concentrations of HClO and ClO_2^- which could be detected, were as low as 5×10^{-8} M using buffer-B which consisted of 5×10^{-4} M Fe(III) – 1×10^{-3} M Fe(II) and contained 0.3 M KCl and 0.5 M H_2SO_4 . With respect to ClO_3^- , the sensitivity obtained from the slope of the calibration peaks versus concentration in Fig. 1(B)-(c) was 3.4 mV mM^{-1} less than 1/10 of the theoretical. However, ClO_3^- at a concentration level of

10^{-5} M was detected with use of buffer-B containing 9 M H_2SO_4 , and a RC which was 200 cm in length in order to provide a reaction time of around 20 s. In this case, the sensitivity to chlorate was 4.3×10^2 mV mM^{-1} , approximately 100-fold enhancement over the sensitivity obtained for buffer-B containing 0.5 M H_2SO_4 , as shown in bottom line of Table 1. The relative standard deviation (R.S.D.) was 1.1% ($n = 5$) for measurement of a 5×10^{-5} M ClO_3^- sample. The fluctuation and the drift of the baseline potential with use of buffer-B containing 9 M H_2SO_4 were 0.8 mV and ca. 2.5 mV h^{-1} , respectively. The detection limit (signal/noise, $S/N = 3$) of ClO_3^- was 2×10^{-6} M, when buffer-B consisted of 5×10^{-5} M Fe(III)– 1×10^{-4} M Fe(II) containing 0.3 M KCl and 9M H_2SO_4 was used.

3.5. Simultaneous determination of ClO_3^- –HClO or ClO_3^- – ClO_2^- in mixture

As described in the previous sections, the magnitude and time when the peak maximum was appeared for the transient potential changes of the redox electrode were different for the various oxychlorine species. This is due to difference in the reactivity of oxychlorines with the potential buffer depending on the composition of the buffer. The reactivity of ClO_3^- with buffer-B containing sulfuric acid at low concentration was low, but was enhanced by increasing the sulfuric acid concentration. On the other hand, the reactivities of ClO_2^- and HClO with buffer-B were high even when the buffer contained sulfuric acid at a low concentration. Therefore, the simultaneous determination of a mixture of ClO_3^- –HClO or ClO_3^- – ClO_2^- can be expected if two buffer-Bs containing sulfuric acid at different concentrations are used for the reagent solutions in the flow system.

For the case of a mixed sample solution containing ClO_3^- – ClO_2^- and ClO_3^- –HClO under the condition of $[\text{ClO}_3^-] > [\text{ClO}_2^-]$ or $[\text{ClO}_3^-] > [\text{HClO}]$, the simultaneous determination of the mixed solution was examined by the flow system shown in Fig. 2(A). As described in Section 2, ClO_3^- would be expected to be detected by the detector D_1 even in the presence of HClO or ClO_2^- in the mixed sample solution and HClO

and ClO_2^- would be expected to be detected by the detector D_2 if kinetic discrimination can be successfully performed. Fig. 2(B)-(a) and -(b) show the calibration peaks for ClO_3^- obtained using detector D_1 and for ClO_2^- obtained using detector D_2 , respectively, where the mixed sample solutions contained ClO_3^- and ClO_2^- at different concentration but the same molar ratio $[\text{ClO}_3^-]/[\text{ClO}_2^-] = 25$ were injected three times for one sample solution. Peak heights for ClO_3^- and ClO_2^- were nearly proportional to the concentration for the concentration ranges indicated in Fig. 2(B)-(a) and -(b), respectively. The R.S.D. for peak heights obtained by six repeated injections were 1.5% for 2.0×10^{-4} M ClO_3^- and 2.3% for 8×10^{-6} M ClO_2^- . When 8×10^{-6} M ClO_2^- without ClO_3^- was injected, no peak was observed with detector D_1 and a peak with the same height as the sample which contained 2.0×10^{-4} M ClO_3^- and 8×10^{-6} M ClO_2^- was observed with detector D_2 . In addition when 2.0×10^{-4} M ClO_3^- solution without ClO_2^- was injected, no peak was observed with the detector D_2 and a peak with the same height as the sample containing 8×10^{-6} M ClO_2^- and 2×10^{-4} M ClO_3^- was observed with detector D_1 . These results indicate that interference from ClO_2^- to detector D_1 and that from ClO_3^- to detector D_2 are negligibly small. Fig. 2(B)-(c) and -(d) show the calibration peaks for ClO_3^- obtained with detector D_1 and for HClO obtained with detector D_2 , respectively, when a mixed sample containing ClO_3^- and HClO was injected three times for one sample. In this case, the concentrations of ClO_3^- and HClO in the mixed sample solution were different but the molar ratio $[\text{ClO}_3^-]/[\text{HClO}]$ was 16.7. The R.S.D. for peak heights obtained by six repeated injections were 1.8% for 2.0×10^{-4} M ClO_3^- and 2.1% for 12×10^{-6} M HClO. When a 12×10^{-6} M HClO solution without ClO_3^- was injected, no response peak for HClO was observed with detector D_1 , and a peak with the same height as the sample which contained 2×10^{-4} M ClO_3^- and 12×10^{-6} M HClO was observed with detector D_2 . In the flow system shown in Fig. 2(A), interference from HClO was negligibly small for the determination of ClO_3^- with detector D_1 if HClO or ClO_2^- exists in the mixed solution at a concen-

tration less than 1/20 that of the ClO_3^- concentration. However, when the concentration of ClO_2^- or HClO in the mixed solution was the same as that of ClO_3^- (2×10^{-4} M), ca. 70% of positive relative error was observed.

For the simultaneous determination of the mixed sample solution containing ClO_3^- or HClO at the same concentration as ClO_2^- , the flow system which combined the cation-exchange resin column in the Fe(II) form shown in Fig. 3(A) was designed in order to eliminate interference by ClO_2^- or HClO. HClO or ClO_2^- in the mixed sample is reduced to chloride by the column, whereas ClO_3^- in the mixed sample passes through the column without reduction and reacts with the components of the potential buffer RS_1 in the reaction coil RC_1 . As a result, ClO_3^- is detected by detector D_1 and HClO or ClO_2^- is detected by detector D_2 . Fig. 3(B)-(a) and -(b) show the calibration peaks for ClO_3^- obtained with detector D_1 and for HClO obtained with detector D_2 , respectively, where the mixed sample contains ClO_3^- and HClO at the same concentration. Buffer-A in which no chloride was contained, was used as RS_2 , in order to determine HClO at moderately high concentration as ClO_3^- . As can be seen from Fig. 3(B), a good linear relationship exists between the peak height and concentration for both ClO_3^- and HClO. The baseline potential was good for both detectors D_1 and D_2 , and the reproducibility of the response peak was good. Calibration peaks for the mixed solution of ClO_3^- and ClO_2^- were also obtained with nearly the same sensitivity and reproducibility as that obtained for the mixed solution of ClO_3^- and HClO. When the 3×10^{-4} M HClO solution without ClO_3^- was injected, no peak was observed with detector D_1 and a peak with the same height as the sample containing ClO_3^- and HClO at 3×10^{-4} M was observed with detector D_2 . This indicates that interference from HClO was completely eliminated by the cation-exchange resin column, as expected. However, in the case of the mixed sample containing oxychlorine under conditions of $[\text{HClO}] > [\text{ClO}_3^-]$ or $[\text{ClO}_2^-] > [\text{ClO}_3^-]$, an accurate determination of ClO_3^- was not possible with detector D_1 in the present flow system. A positive error was observed for detector

D_1 due to the interference from ClO_2^- and HClO. This is probably due to the fact that the reduction of ClO_2^- and HClO on the cation-exchange column in the Fe(II) form was incomplete.

3.6. Application to oxychlorine species in city water

Simultaneous determination method using the three-channel flow system shown in Fig. 2 was applied to determine the oxychlorine species in tap water, which was collected at four taps in the university. At first, the existence of oxychlorine species in the tap water was examined by an iodometry method in batchwise test, according to the procedure reported by Gordon et al. [8]. Detectable amount of ClO_2^- and ClO_3^- was not present in the all samples, though the presence of HClO in the sample water was confirmed. The applicability of the present method to the real sample was then evaluated by using the tap water samples, to which 1×10^{-4} M ClO_3^- was added. As described in Section 3.5, HClO and ClO_3^- detected with detectors D_2 and D_1 , respectively. The analytical results of HClO in the tap water samples were calculated by using the peak heights obtained with detector D_2 and the calibration, which was shown in Fig. 2(B)-(d), and listed in Table 2. As can be seen from Table 2, all analytical values obtained the present method were in good agreement with those obtained by a conventional spectrophotometric method with use of *o*-tolidine[4]. On the other hand, recovery of peak heights for 1×10^{-4} M ClO_3^- added to the tap water sample, which were simultaneously observed with detector D_1 , were within 95–105% compared with the standard calibration peak, which was shown in Fig. 2(B)-(c).

Table 2
Analytical results of HClO in tap water

Sample	Concentration of HClO (M)	
	Present method	<i>o</i> -Tolidine method
A	5.0×10^{-6}	4.2×10^{-6}
B	7.8×10^{-6}	8.3×10^{-6}
C	8.2×10^{-6}	9.0×10^{-6}
D	6.0×10^{-6}	6.9×10^{-6}

As described in a previous paper [14], the case of the two-channel flow system shown in Fig. 1, the existence of ionic species (Ca^{2+} , Mg^{2+} , etc.), which are usually present in tap water up to 10^3 -fold of HClO , was tolerable for the determination of 5×10^{-6} M HClO (0.35 mg l^{-1} as residual chlorine), when the variation in peak height within 3% was regarded as tolerated. The presence of monochloramine interfered with the determination of HClO since the sensitivity of the present method to the monochloramine was one-fifth of that to HClO . Various heavy metal ions (Cr^{3+} , Ni^{2+} , Zn^{2+} , Cd^{2+} , Cu^{2+} , Co^{2+}) did not interfere when their concentration were less than 20 times the HClO concentration.

4. Conclusion

A simultaneous determination method for $\text{ClO}_3^- - \text{ClO}_2^-$ and $\text{ClO}_3^- - \text{HClO}$ is demonstrated by use of the $\text{Fe(III)} - \text{Fe(II)}$ potential buffer solution containing chloride and the redox electrode detector. Based on the difference in reactivity of oxychlorine with the potential buffer, the simultaneous determination of $\text{ClO}_3^- - \text{HClO}$, or $\text{ClO}_3^- - \text{ClO}_2^-$ was achieved by designing the flow system combined the cation-exchange column in the Fe(II) form. The present method is suitable for analyses of samples containing ClO_2^- or HClO at the same concentration as ClO_3^- . The limitation of the present method is subject to interference from ClO_2^- and HClO in the determination of ClO_3^- , where a mixed sample contains ClO_2^- or HClO at a higher concentration than ClO_3^- . A more effective reduction column than the cation-exchange column in the Fe(II) form could possibly expand the applicability of the present method.

References

- [1] W.J. Masschelen, Chloride Dioxide, Ann Arbor Science, Ann Arbor, MI, 1979, p. 154.
- [2] G. Gordon, S. Tachiyashiki, Environ. Sci. Technol. 25 (1991) 468.
- [3] S.U.S. Regli, Environmental Protection Agency Status Report on Development of Regulations for Disinfectants and Disinfection By-Products, Washington, D.C., June 1991.
- [4] American Public Health Association, Standard Method for the Examination of Water and Wastewater, 14th edition, APHA, Washington, DC, 1975, pp. 304–349.
- [5] J. Ruzicka, E.H. Hansen, Anal. Chim. Acta 78 (1975) 145.
- [6] K.G. Miller, G.E. Pacey, G. Gordon, Anal. Chem. 57 (1985) 734.
- [7] D.A. Hollowell, G.E. Pacey, G. Gordon, Anal. Chem. 57 (1985) 2851.
- [8] G. Gordon, K. Yoshino, D.G. Themelis, D.W. Wood, G.E. Pacey, Anal. Chim. Acta 224 (1989) 383.
- [9] D.G. Themelis, D.W. Wood, G. Gordon, Anal. Chim. Acta 225 (1989) 437.
- [10] T. Aoki, M. Munemori, Anal. Chem. 55 (1983) 209.
- [11] J.R. Gord, G. Gordon, G.E. Pacey, Anal. Chem. 60 (1988) 2.
- [12] A.N. Tsaousis, C.O. Huber, Anal. Chim. Acta 178 (1985) 319.
- [13] M. Trojanowicz, W. Matuszewski, A. Hulanicki, Anal. Chim. Acta 136 (1982) 85.
- [14] N. Ishibashi, T. Imato, H. Ohura, S. Yamasaki, Anal. Chim. Acta 214 (1988) 349.
- [15] H. Ohura, T. Imato, S. Yamasaki, N. Ishibashi, J. Flow Injection Anal. 8 (1991) 2.
- [16] H. Ohura, T. Imato, S. Yamasaki, Bunseki Kagaku 45 (1996) 689.
- [17] H. Ohura, T. Imato, S. Yamasaki, N. Ishibashi, Talanta 43 (1996) 943.
- [18] The Chemical Society of Japan, New Experimental Chemistry Course 8, Maruzen, Tokyo, Japan 1977, p. 469 (in Japanese).
- [19] Gmelin-Institut, Gmelins Handbuch der Anorganischen Chemie, 8, auflage, Chlor, Teil B-Lieferung 2, Verlag Chemie, Weinheim, 1969.
- [20] W.M. Latinen, Oxidation Potentials, 2nd edition, Prentice-Hall, Englewood Cliffs, NJ, 1952.
- [21] H. Taube, H. Dodgen, J. Am. Chem. Soc. 71 (1949) 3330.
- [22] C.C. Hong, F. Lenzi, W.H. Rapson, Can. J. Chem. Eng. 45 (1967) 349.
- [23] S. Yamasaki, H. Ohura, I. Nakamori, Nippon Kagaku Kaishi (1975) 1315.
- [24] A.M. Azzam, I.A.W. Shimi, Z. Phys. Chem. 33 (1962) 190.

Simultaneous flow injection determination of calcium and fluoride in natural and borehole water with conventional ion-selective electrodes in series[☆]

J.F. van Staden *, R.I. Stefan

Department of Chemistry, University of Pretoria, Pretoria 0002, South Africa

Received 26 October 1998; accepted 4 January 1999

Abstract

An on-line automated system for the simultaneous flow injection determination of calcium and fluoride in natural and borehole water with conventional calcium-selective and fluoride-selective membrane electrodes as sensors in series is described. Samples (30 μ l) are injected into a TISAB II (pH = 5.50) carrier solution as an ionic strength adjustment buffer. The sample-buffer zone formed is first channeled to a fluoride-selective membrane electrode and then via the calcium-selective membrane electrode to the reference electrodes. The system is suitable for the simultaneous on-site monitoring of calcium (linear range 10^{-5} – 10^{-2} mol l⁻¹ detection limit 1.94×10^{-6} mol l⁻¹ recovery 99.22%, RSD < 0.5%) and fluoride (linear range 10^{-5} – 10^{-2} mol l⁻¹ detection limit 4.83×10^{-6} mol l⁻¹ recovery 98.63%, RSD = 0.3%) at a sampling rate of 60 samples h⁻¹. © 1999 Elsevier Science B.V. All rights reserved.

Keywords: Simultaneous detection; Calcium-selective membrane electrode; Fluoride-selective membrane electrode; Flow injection analysis

1. Introduction

Since its conception in 1974–1975 flow injection analysis (FIA) has developed into a well established analytical technique [1–3]. According to the numerous publications to date, spectrophotometric determination still seems to be the most

popular choice in FIA systems, but there has been an increase in the use of electrochemical detection in flowing streams. Various types of automatic or semi-automatic electrochemical sensors have been employed in continuous-flow measurements [1,2,4]. However, in most of the methods reported, the emphasis was placed on the determination of a single species in a sample. A survey of literature indicated a lack of procedures describing the simultaneous determination of more than one species in the same sample [5,6]. Although ICP or chromatographic methods offer the possibility for simultaneous determinations, the expen-

[☆] Presented at ICFA'98, August 23–27, 1998, Seattle, WA, USA.

* Corresponding author. Tel.: +27-12-4202515; fax: +27-12-3625297.

E-mail address: koos.vanstaden@chem.up.ac.za (J.F. van Staden)

sive instrumentation (ICP) or laborious and time consuming (chromatography) procedures make these systems not very suitable for small routine laboratories and on-site field analysers. The use of ion-selective electrodes (ISE) in FIA on the other hand seems very attractive because of a number of advances [6], such as simple low cost instrumentation, little or no pretreatment of the sample [7], no interference from sample colour and turbidity [8,9], reliability, compatibility, capability, etc. [10]. Růžicka et al. [11] used a cascade electrode arrangement to determine sodium and potassium simultaneously in blood serum and Mascini and Palleschi [12] glucose and urea in serum samples. Virtanen [13] developed a method for the simultaneous determination of potassium, sodium, calcium and chloride in serum by placing four cascade ion-selective electrodes sequentially in an FIA system with the reference electrode downstream. The same idea of electrodes in series was implemented by Hansen et al. [14] for the simultaneous determination of pH and calcium in serum. Van Staden [15] exploited the concept of flow-through tubular arrangements for the simultaneous determination of chloride and pH in a single sample. It has been recognised that one of the fundamental requirements for the successful performance of ion-selective electrode arrays in flow injection analysis is high selectivity coefficients with respect to the primary ions [16–18]. One of the advances associated with ion-selective electrode arrays in FIA is an enhanced selectivity [17,18] for the primary ion over interferents due to the hydrodynamic conditions of the sample plug at the detector, where the response is under kinetic rather than equilibrium control. These simultaneous detection systems are necessary in clinical analysis (e.g. for the determination of Na^+ , K^+ and Ca^{2+} in blood) [17,18] as well as in environmental analysis [19]. The miniaturization of these sensor arrays also made possible the simultaneous in vivo assay of inorganic cations and pH [20,21].

In South Africa, water is a very scarce commodity, and in some rural areas, where the people depend on borehole water, water quality should be controlled very carefully. There is therefore a need for a robust low-cost field analyser for the

on-site simultaneous monitoring of calcium and fluoride in natural and borehole water. Our laboratory was approached by the water authorities to adapt and combine the two single conventional automated segmented systems currently in use for the determination of calcium and fluoride with conventional electrodes into one robust low-cost ISE-FIA on-site field analyser capable of simultaneous determination of both components on a single sample. This present paper therefore describes a simultaneous detection system for calcium and fluoride ions in natural and borehole water, using a conventional calcium-selective membrane electrode in series with a conventional fluoride-selective membrane electrode in a flow injection system.

2. Experimental

2.1. Reagents and solutions

All reagents were prepared from analytical reagent grade chemicals unless specified otherwise. Deionised water from a Modulab system (Continental Water Systems, San Antonio, TX) was used for dilution. The solutions were prepared as follows:

TISAB II was used as carrier stream; 57 ml glacial acetic acid and 74 g reagent grade potassium chloride were carefully dissolved in 500 ml distilled water in a 1-l beaker. The pH was adjusted to 5.50 by adding 5 mol l^{-1} KOH solution. The solution was quantitatively diluted to mark in a 1-l volumetric flask with distilled water.

Standard working calibration solutions containing both calcium and fluoride ions were prepared by serial dilutions from standard 0.10 mol l^{-1} CaCl_2 and NaF stock solutions.

2.2. Apparatus

Two ion-selective membrane electrodes: calcium-selective membrane electrode (Orion Research) Model 93-20 and fluoride-selective membrane electrode (Orion Research) Model 94-09 were used for all measurements in combination with two double junction reference electrodes

(Orion Research) Model 90-02. The potentials were measured at room temperature using two Orion Research (Model 901) microprocessor Ionalyzers.

2.3. Flow injection system

The electrodes were incorporated into the conduits of a flow injection system with basic design similar to that previously described [15,22]. A Carle microvolume two-position sampling valve (Carle No. 2014) containing two identical sample loops was used. Each loop has a volume of 30 μl . A Cenco peristaltic pump operating at 10 rev. min^{-1} supplied the carrier streams to the manifold system. Tygon tubing (0.51 mm i.d.) was used to construct the manifold; coils were wound round suitable lengths of glass tubing (15 mm o.d.). The carrier solution containing the sample is first channeled to a fluoride-selective membrane electrode and then via the calcium-selective membrane electrode to the reference electrodes. A 60-s cycle sampling time was used, giving the system a capacity of about 60 samples h^{-1} .

Data acquisition and device control were achieved using a PC30-B interface board (Eagle Electric, Cape Town, South Africa). The FlowTEK [23] software package (obtainable from MINTEK) for computer-aided flow analysis was used throughout for device control and data acquisition.

3. Results and discussion

The main purpose of this investigation was to combine the two single automated segmented systems using two conventional calcium and fluoride electrodes currently in use by the water authorities into a single robust low-cost FIA-ISE on-site field analyser for the simultaneous determination of both components on a single sample as requested. As a result the incorporation and performance of the electrodes in array in an FIA system was investigated.

The response characteristics and selectivity coefficients of both the fluoride- and calcium-selective electrodes incorporated in series into the

conduits of the flow injection system were evaluated under optimum running conditions. Preliminary experiments indicated that the position of the fluoride- and calcium-selective electrodes in the series of arrays in the flow injection system is important and this was investigated. It was found that the best results were obtained when the fluoride-selective membrane electrode was placed before the calcium-selective membrane electrode in the series. The analytical applicability of the proposed system was further evaluated on natural and borehole water.

3.1. Electrodes response

The electrode characteristics of both electrodes incorporated into the FIA system are summarised in Table 1. The equations for the calibration graphs are:

$$H = H^\circ - 0.06 \text{ pCa}$$

and

$$H = H^\circ - 0.25 \text{ pF}$$

where H are the relative peak heights; $\text{pCa} = -\log[c_{\text{Ca}^{2+}}]$ and $\text{pF} = -\log[c_{\text{F}^-}]$; with correlation coefficients of 0.9670 and 0.9787, respectively. It is clear from the results in Table 1 that with the linear response ranges between 10^{-5} and 10^{-2}

Table 1
Response characteristics of the ion-selective membrane electrodes incorporated into the conduits of the flow injection analysis system^a

Parameter	Response	
	Ca ²⁺ -selective membrane electrode	F ⁻ -selective membrane electrode
Slope of calibration graph	0.060 \pm 0.002	0.250 \pm 0.002
Intercept, H°	0.932 \pm 0.020	1.323 \pm 0.070
Linear range	10 ⁻⁵ –10 ⁻² mol l ⁻¹ (approximately 0.4–400 mg l ⁻¹)	10 ⁻⁵ –10 ⁻² mol l ⁻¹ (approximately 0.19–190 mg l ⁻¹)
Detection limit	1.94 \times 10 ⁻⁶ mol l ⁻¹ (about 0.078 mg l ⁻¹)	4.83 \times 10 ⁻⁶ mol l ⁻¹ (about 0.092 mg l ⁻¹)

^a All measurements are the average of 10 determinations.

Table 2

Selectivity coefficients of the calcium- and fluoride-selective membrane electrodes incorporated into the FIA system^a

Electrode	Interfering species						
	Na ⁺	Mg ²⁺	Ca ²⁺	F ⁻	Cl ⁻	Br ⁻	CO ₃ ²⁻
Ca ²⁺ -selective	1.2 × 10 ⁻³	6.0 × 10 ⁻³	–	<<10 ⁻⁴	–	–	–
F ⁻ -selective	–	–	<<10 ⁻⁵	–	1.4 × 10 ⁻⁵	4.0 × 10 ⁻⁵	1.0 × 10 ⁻⁵

^a All measurements are the average of seven determinations.

mol l⁻¹ (approximately 0.4–400 mg l⁻¹ Ca²⁺) and 10⁻⁵–10⁻² mol l⁻¹ (approximately 0.19–190 mg l⁻¹ F⁻), the very low detection limits of 1.94 × 10⁻⁶ mol l⁻¹ (about 0.078 mg l⁻¹ Ca²⁺) and 4.83 × 10⁻⁶ mol l⁻¹ (about 0.092 mg l⁻¹ F⁻), the very high precision obtained and stability of the ISE-FIA system with time for both electrodes, the proposed on-line ISE-FIA system seems to be ideally suitable as a reliable and effective low-cost robust field analyser.

3.2. Selectivity of the electrodes

One of the main requirements for electrodes in series is that for ideal conditions no mutual interferences should occur and that the electrodes should have high selectivity coefficients with respect to the primary ions [16–18]. The effect of some possible mutual interferences on the response of both electrodes as well as possible interferences from other anions and cations were studied with the proposed ISE-FIA system. The selectivity coefficients presented in Table 2 shows that sodium, magnesium and fluoride do not interfere in the response of the calcium-selective membrane electrode even when the ratio between the calcium and interfering ions (mol l⁻¹) was 1:100 (1:10² for fluoride) and that the response of the fluoride-selective membrane electrode was not affected by the presence of Br⁻, Cl⁻ and CO₃²⁻ ions even when the ratio between the concentration of fluoride and interfering ions (mol l⁻¹) was 1:1000 (1:10³ for calcium). This fact demonstrates the specificity of the two electrodes for the primary ions and that the electrodes could be used in series.

3.3. Analytical applications

The response characteristics as well as the selectivity of both ion-selective membrane electrodes incorporated in series into the conduits of the FIA system ensure a reliable simultaneous detection of calcium and fluoride ions in natural and borehole water without any sample preparation. The accuracy of the proposed ISE-FIA system was tested by comparing the results of a number of natural and borehole water samples with those obtained by a standard automated segmented method. Results compare favourably as can be seen from Table 3. The RSD (%) for water samples having different concentrations of calcium and fluoride was less than 0.5 and 0.3% for calcium and fluoride respectively on 10 tests of each sample. Analyses were also performed in a random order to test carry-over effects. Carry-over from one sample to another is negligible at a sample throughput of 60 samples h⁻¹. The average recoveries of calcium and fluoride in natural and borehole water samples are 99.22 and 98.63%, respectively.

4. Conclusion

The proposed ISE-FIA system using a conventional calcium-selective membrane electrode and a conventional fluoride-selective membrane electrode as detectors in series is suitable for the simultaneous on-line monitoring of calcium and fluoride at a rate of approximately 60 actual water samples h⁻¹. The very high selectivity coefficients obtained for both ion-selective electrodes with respect to their primary ions coupled with their

Table 3

Performance and reproducibility of the proposed ISE-FIA system for the simultaneous determination of calcium and fluoride ions in natural and borehole water^a

Sample	Automated segmented method [Ca ²⁺] (mg)	Proposed ISE-FIA system [Ca ²⁺] (mg)	RSD (%)	Automated segmented method [F ⁻] (mg)	Proposed ISE-FIA system [F ⁻] (mg)	RSD (%)
1	8.4	8.0	0.2	0.123	0.112	0.3
2	60.1	59.6	0.1	0.133	0.130	0.2
3	61.9	55.2	0.1	0.338	0.315	0.2
4	51.5	49.2	0.3	0.311	0.294	0.1
5	5.0	6.1	0.5	0.136	0.136	0.1

^a Mean result of 10 tests in each case, with relative standard deviation for the proposed ISE-FIA system.

response characteristics contributed to the successful performance of both sensors in series in the FIA system. As a low-cost, low maintenance (especially with the low cost calcium- and fluoride-selective electrodes as detectors) reliable analyser, the system satisfies the requirements given to us by the water authorities and can be particularly attractive for on-site water laboratories where natural and borehole water streams could be monitored continuously.

References

- [1] M. Valcárcel, M.D.L. de Castro, *Flow-injection Analysis. Principles and Applications*, Ellis Horwood, Chichester, UK, 1987.
- [2] J. Růžička, E.H. Hansen, *Flow Injection Analysis*, 2nd edn, Wiley, New York, 1988.
- [3] J.L. Burguera, *Flow Injection Atomic Spectroscopy*, Marcel Dekker, New York, 1989.
- [4] K. Štulík, V. Pacáková, *Electroanalytical Measurements in Flowing Liquids*, Ellis Horwood, Chichester, UK, 1987.
- [5] M.D. Luque de Castro, M. Valcárcel, *Analyst* 109 (1984) 413.
- [6] A. Izquierdo, M.D. Luque de Castro, *Electroanalysis* 7 (1995) 505.
- [7] M.E. Meyerhoff, P.M. Kovach, *J. Chem. Educ.* 60 (1983) 766.
- [8] M.E. Meyerhoff, Y.M. Fraticelli, *Anal. Lett.* 14 (1981) 415.
- [9] E. Pungor, Z. Feher, G. Nagy, K. Toth, G. Horvai, M. Gratzl, *Anal. Chim. Acta* 109 (1979) 1.
- [10] J.F. van Staden, *Anal. Chim. Acta* 179 (1986) 407.
- [11] J. Růžička, E.H. Hansen, E.A. Zagatto, *Anal. Chim. Acta* 88 (1977) 1.
- [12] M. Mascini, G. Palleschi, *Anal. Chim. Acta* 145 (1983) 213.
- [13] R. Virtanen, in: E. Pungor (Ed.), *Ion-selective Electrodes 3. Proceedings of the Third Symposium, Matrafüred, Hungary, October 1980; Analytical Symposium Series, Volume 8*, Elsevier, Amsterdam, 1981, p. 375.
- [14] E.H. Hansen, J. Růžička, A.K. Ghose, *Anal. Chim. Acta* 100 (1980) 151.
- [15] J.F. van Staden, *Analyst* 111 (1986) 1231.
- [16] Y.G. Vlasov, *Ann. Chim.* 87 (1997) 261.
- [17] D. Diamond, R.J. Forster, *Anal. Chim. Acta* 276 (1993) 75.
- [18] R.J. Forster, F. Regan, D. Diamond, *Anal. Chem.* 63 (1991) 876.
- [19] Y.G. Vlasov, A.V. Legin, A.M. Rudnitskaya, A. Damico, C. Dinatale, *J. Anal. Chem.* 52 (1997) 1087.
- [20] L. Ratton, T. Kunt, T. Mcavoy, T. Fuja, R. Cavicchi, S. Semancik, *Sensors Actuators B* 41 (1997) 105.
- [21] V.V. Cosofret, M. Erdösy, A.J. Timothy, R.P. Buck, R. Bruce Ash, M.R. Neuman, *Anal. Chem.* 67 (1995) 1647.
- [22] J.F. van Staden, *Analyst* 112 (1987) 595.
- [23] G.D. Marshall, J.F. van Staden, *Anal. Instrum.* 20 (1992) 79.

Flow injection spectrophotometric or conductometric determination of ascorbic acid in a vitamin C tablet using permanganate or ammonia[☆]

Kate Grudpan *, Kiattisak Kamfoo, Jaron Jakmunee

Department of Chemistry, Faculty of Science, Chiang Mai University, Chiang Mai 50200, Thailand

Received 8 December 1998; accepted 7 January 1999

Abstract

Two simple flow injection (FI) procedures for the determination of ascorbic acid content in a vitamin C tablet are proposed: spectrophotometric involving injection into a stream of acidic potassium permanganate solution and monitoring its color change due to the redox reaction; FI conductometry based on the neutralization of ascorbic acid injected into a flowing ammonia solution yielding a change in conductivity. The procedures have been applied to the analysis of locally commercial vitamin C tablet samples. A through-put of at least 90 injections h^{-1} can be achieved. The relative standard deviation was found to be 2.5% (for a 50 mg vitamin C tablet; $n = 7$) for both. Results obtained by either procedure agree with a standard titrimetric method. © 1999 Elsevier Science B.V. All rights reserved.

Keywords: Ascorbic acid; Vitamin C; Flow injection; Spectrophotometry; Conductometry; Permanganate; Ammonia

1. Introduction

Ascorbic acid is considered to be an essential vitamin with a recommended daily intake, although from various sources, including vitamin C tablets. There have been a number of methods proposed for the determination of ascorbic acid in various matrices and at different levels [1–4]. Various flow injection (FI) procedures have also

been reported, such as redox titration with cerium(IV) [5], amperometry (iodometry) [6], enzymetry [7] and chemiluminescence [8]. Some FI procedures make use of the reducing property of ascorbic acid to produce a color change which can be spectrophotometrically monitored, for example, photochemical reduction of methylene blue [9], reduction of Fe(III) to Fe(II) for complex formation with 1,10-phenanthroline [10]; reduction of a Co(III) complex [11] or vanadotungstophosphoric acid [12]. This paper describes two FI procedures with spectrophotometric and conductometric detection using permanganate or ammonia reagents, respectively which are simple, versatile, economic and rapid.

[☆] Presented at the Ninth International Conference on Flow Injection Analysis, Seattle, WA, August 23–27, 1998.

* Corresponding author. Tel.: +66-53-943345; fax: +66-53-222268.

E-mail address: kate@chiangmai.ac.th (K. Grudpan)

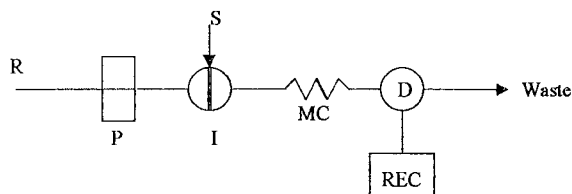


Fig. 1. Manifold for FI determination of ascorbic acid. R, reagent; P, pump; S, standard/sample; I, injection valve; MC, mixing coil; D, flow-through cell and detector; REC, recorder (see text).

2. Experimental

2.1. Reagents

Deionized water was used for the preparation of all reagents.

A stock standard aqueous ascorbic acid solution (10 g l^{-1}) was prepared from L (+) ascorbic acid (Merck). Other standard ascorbic acid solutions were obtained by appropriate dilutions of the stock solution. Potassium permanganate stock solution ($2 \times 10^{-4} \text{ M}$) was prepared by dissolving KMnO_4 (BDH) 0.030 g in sulfuric acid (Carlo Erba) (0.1 M) and making up a volume of 1 l. The stock was further diluted for other concentrations.

Ammonia solutions were prepared from conc. ammonia (BDH) (0.91 g ml^{-1}).

2.2. Manifold for FI spectrophotometry

A single line manifold (Fig. 1) was assembled using a peristaltic pump (FIA Lab, Alitea, or Eyela, Japan), an injection valve (Alitea) or a home-made two-loop injection valve with a suction system using an aquarium pump as described previously [13], a mixing coil and a detector. The detector was a Spectronic 21 (Bausch & Lomb) or laboratory-made digital read-out LED colorimeter, with a flow-through cell (Hellma, 1 cm Suprasil 1 window or home-made, modified from that previously reported [14]). Signals were recorded by either a chart recorder (OmniScribe, Houston Instruments) or direct digital reading for light transmission of the laboratory made colorimeter (with maximum value holding). All the tubing was of PTFE (1 mm i.d.), apart from

Table 1

Conditions for the determination of ascorbic acid in a vitamin C tablet by spectrophotometric FI

Concentration of permanganate (R)	$2 \times 10^{-4} \text{ M}$
Concentration of sulfuric acid (R)	0.1 M
Flow rate	4 ml min^{-1}
Sample injection volume	80 μl
Mixing coil length (MC)	100 cm, 1 mm i.d.
Wavelength	525 nm
Recorder sensitivity	10 mV f.s.d.
Chart speed	0.5 cm min^{-1}

pump tube which was silicone rubber. Connections were made with flexible sleeves.

Standard/sample solutions of ascorbic acid were injected into a stream of aqueous permanganate in sulfuric acid solution (R in Fig. 1). A bolus of fading permanganate color resulting from the redox reaction in the mixing coil (MC) flowing into the detector to be continuously monitored (at 525 nm) for a decrease in absorbance or increase in transmittance. Optimum conditions are listed in Table 1.

Optimization was achieved by injections of 40–200 ppm ascorbic acid standards with certain parameters of the manifold adjusted over the following ranges: permanganate (0.9×10^{-4} – $6.3 \times 10^{-4} \text{ M}$); flow rate (2 – 7 ml min^{-1}); mixing coil length (10–200 cm) and wavelength (310, 506, 525 and 545 nm).

2.3. Manifold for FI conductometry

The manifold used was similar to that for FI spectrophotometry, except using a digital read-out conductivity detector, a modified one from the earlier design [15]), with a flow-cell (using stainless steel to replace the copper contact described in Ref. [15]). Signals were recorded by a chart recorder or by direct reading from the digital meter of the detector.

Under the conditions in Table 2, into a flowing stream of ammonia solution (R in Fig. 1), a standard/sample (ascorbic acid) was injected. Neutralization of the acid with the base took place along the mixing coil. An increase in conductivity due to the reaction product was observed (D in Fig. 1).

Table 2

Conditions for the determination of ascorbic acid in a vitamin C tablet by FI conductometry

Concentration of ammonia (R)	5×10^{-3} M
Sample injection volume	80 μ l
Mixing coil length (MC)	50 cm, 1 mm i.d.
Flow rate	5 ml min ⁻¹
Recorder sensitivity	1 V f.s.d.
Chart speed	0.5 cm min ⁻¹

Optimization was investigated by injection of a series of ascorbic acid standards (0.02–0.10% w/v) under a set of parameters: ammonia (2×10^{-3} – 7×10^{-3} M); flow rate (1–5 ml min⁻¹).

2.4. Analysis of samples

Various vitamin C tablet samples, commercially available locally, were analyzed for ascorbic acid content by both procedures. Twenty tablets were weighed and an average weight of a tablet was calculated before being ground into fine powder. A portion of the powder, equivalent to the average weight of a tablet was dissolved in water and filtered before making a volume of 100 or 250 ml. Appropriate dilution may be required. Replicate injections were made. The samples were also analyzed in duplicate by a standard titrimetric method [1] for referee purposes.

Table 3

Analysis of ascorbic acid content in vitamin C tablets by FI and by standard titrimetry [1]

Sample	Labeled amount (mg/tablet)	Found					
		Titrimetry ^a		FI spectrophotometric ^b		FI conductometric ^b	
		mg/tablet	% label	mg/tablet	% label	mg/tablet	% label
1. Sweetcec	50	50.0 ± 0.0	100	50.5 ± 0.6	101	50.5 ± 0.8	101
2. The United Drug ^c	50	47.5 ± 0.0	95	40.6 ± 0.0	81	45.9 ± 0.4	92
3. Chinta Trading ^c	100	72.9 ± 0.0	73	76.6 ± 0.0	77	89.9 ± 1.9	90
4. Takeda-100	100	97.8 ± 1.2	98	99.8 ± 2.2	100	94.2 ± 2.1	94
5. Hicee-500	500	492.5 ± 0.0	99	516.1 ± 0.0	103	462.6 ± 2.4	93
6. Nopparat-500	500	498.1 ± 4.2	100	494.2 ± 0.0	99	488.3 ± 2.3	98
7. Silom-500	500	524.9 ± 0.0	105	533.5 ± 5.5	107	535.8 ± 2.1	107

^a Duplicate titrations.

^b Triplicate injections.

^c Intensely colored solution obtained.

3. Results and discussion

3.1. Analytical characteristics

Calibration graphs were found to be linear at least up to 200 ppm ($y = 0.006x + 7.00$; $r = 0.99$) and 8000 ppm ($y = 0.002x - 4.29$; $r = 0.99$) for the FI spectrophotometric and conductometric procedures, respectively with relative standard deviation for analysis of a 50 mg vitamin C tablet being 2.5% ($n = 7$) for both.

At least 90 injections h⁻¹ can be performed by both methods. No significant change in the response was obtained from other ingredients in nominal amounts (reducing sugars (sucrose (30 mg) and lactose (30 mg)), and stearate salts (10 mg as calcium- or magnesium-salt) in a tablet).

3.2. Analysis of samples

Analysis of locally commercially available vitamin C tablets are summarized in Table 3. Although the results obtained from both procedures agree with the titrimetric analysis, a tendency was observed for the spectrophotometric values to be lower than the conductometric ones, for a sample resulting in an intensely colored solution, which would cause a negative bias.

Comparative linear regression of all titrimetric (x) versus FI (y) values from Table 3 shows the spectrophotometric procedure to exhibit a regression line slope closer to unity, a lower intercept and a higher correlation coefficient (spectrophotometric: $y = 1.02x - 1.69$, $r^2 = 0.999$; conductometric: $y = 0.97x + 4.44$, $r^2 = 0.996$).

4. Conclusion

The very simple and rapid FI procedures described in this paper can be an alternative to the more complex and expensive methods for assay of ascorbic acid content in vitamin C tablets. For the proposed FI spectrophotometric procedure, potassium permanganate solution which is economic but unstable for a batch procedures, can be used; thus giving an additional advantage to the other advantages, usually obtained by FI, similar to that of unstable murexide reagent for calcium determination [16].

The FI conductometric method is very versatile and useful especially for an intensely colored sample.

Acknowledgements

Thailand Research Fund (TRF) is gratefully

acknowledged for support of this research. We thank Supachai Chaisawad for design and construction of detectors and Professor G.D. Christian for useful discussion.

References

- [1] US Pharmacopoeia, 23rd edn, 1995.
- [2] British Pharmacopoeia, 1993.
- [3] K. Helrich, AOAC Official Methods of Analysis, 15th edn, AOAC, Virginia, 1990.
- [4] Y.-S. Fung, S.-F. Luk, *Analyst* 110 (1985) 201.
- [5] S.M. Sultan, *Talanta* 4 (1994) 125.
- [6] M.A. Abdalla, H.H. Al-Swaiden, *Analyst* 114 (1989) 583.
- [7] G.M. Greenway, P. Ongomo, *Analyst* 115 (1990) 1297.
- [8] A.A. Alwarthan, *Analyst* 118 (1993) 639.
- [9] L.E. Leon, J. Catapano, *Anal. Lett.* 26 (1993) 1741.
- [10] S.M. Sultan, A.M. Abdennabi, F.E.O. Suliman, *Talanta* 41 (1994) 125.
- [11] M.I. Albero, M.S. Garcia, C. Sanchez-Pedreno, J. Rodriguez, *Analyst* 117 (1992) 1635.
- [12] D. Thorburns, N. Chimpalee, D. Chimpalee, *Anal. Chim. Acta* 243 (1991) 187.
- [13] K. Grudpan, C. Taylor, H. Sitter, C. Keller, *Fres. Z. Anal. Chem.* 346 (1993) 882.
- [14] K. Grudpan, D. Nacapricha, Y. Wattanakanjana, *Anal. Chim. Acta* 246 (1991) 325.
- [15] K. Grudpan, P. Sritharathikhun, J. Jakmunee, *Anal. Chim. Acta* 363 (1998) 199.
- [16] K. Grudpan, J. Jakmunee, Y. Vaneesorn, S. Watanesk, U.A. Maung, P. Sooksamiti, *Talanta* 46 (1998) 1245.

Selective flow injection analysis of ultra-trace amounts of Cr(VI), preconcentration of it by solvent extraction, and determination by electrothermal atomic absorption spectrometry (ETAAS)[☆]

Steffen Chen Nielsen ^a, Stefan Stürup ^b, Henrik Spliid ^c, Elo Harald Hansen ^{a,*}

^a Department of Chemistry, Technical University of Denmark, Building 207, DK-2800 Lyngby, Denmark

^b Risø National Laboratory, Plant Biology and Biogeochemistry Department, Building 124, Postbox 49, DK-4000 Roskilde, Denmark

^c Department of Mathematical Modeling, Building 321, Technical University of Denmark, Building 207, DK-2800 Lyngby, Denmark

Received 29 October 1998; accepted 11 December 1998

Abstract

A rapid, robust, sensitive and selective time-based flow injection (FI) on-line solvent extraction system interfaced with electrothermal atomic absorption spectrometry (ETAAS) is described for analyzing ultra-trace amounts of Cr(VI). The sample is initially mixed on-line with isobutyl methyl ketone (IBMK). The Cr(VI) is complexed by reaction with ammonium pyrrolidine dithiocarbamate (APDC), and the non-charged Cr(VI)–PDC chelate formed is extracted into IBMK in a knotted reactor made from PTFE tubing. The organic extractant is separated from the aqueous phase by a gravity phase separator with a small conical cavity and delivered into a collector tube, from which 55 μl organic concentrate is subsequently introduced via an air flow into the graphite tube of the ETAAS instrument. The operations of the FI-system and the ETAAS detector are synchronously coupled. A significant advantage of the approach is that matrix constituents, such as high salt contents, effectively are eliminated. The extraction procedure was optimized by a simplex approach. A central composite design was subsequently employed to verify the estimated operational optimum. An 18-fold enhancement in sensitivity of Cr(VI) was achieved after preconcentration for 99 s at a sample flow rate of 5.5 ml min^{-1} , as compared to direct introduction of 55 μl of sample, yielding a detection limit (3σ) of 3.3 ng l^{-1} . The sampling frequency was 24.2 samples h^{-1} . The proposed method was successfully evaluated by analyzing a NIST Cr(VI)-reference material, synthetic seawater and waste waters, and waste water samples from an incineration plant and a desulphurization plant, respectively. © 1999 Elsevier Science B.V. All rights reserved.

[☆] Presented at the Ninth International Conference on Flow Injection Analysis (ICFIA '98) held in Seattle, WA, USA, 23–27 August 1998.

* Corresponding author. Fax: +45-4588-3136.

E-mail address: ehh@kemi.dtu.dk (E.H. Hansen)

Keywords: On-line preconcentration of Cr(VI); Extraction of Cr(VI)–PDC complex; FI-ETAAS; Assay of inorganic Cr(VI)

1. Introduction

Due to environmental restrictions and authoritative limitations, water-quality monitoring in process effluents has attained high national and international priority, especially in respect to the so-called heavy metals. Furthermore, as several of the individual metals may be present in various oxidation states and/or in different chemical forms, the toxicity of which may vary widely, chemical speciation has attained increased interest. For the very same reasons, the focus of current analytical chemistry is shifting from determination of total concentrations towards development of selective assays of individual chemical species. Considering the number of analyses at hand, it is in this context of particular interest to devise automated procedures. Chromium is one of the most toxic elements, existing in solution as Cr(III) and Cr(VI), where the latter oxidation state is much more toxic than the trivalent chromium, which, in fact, plays a significant role in the body [1]. Therefore, and in continuation of the current research activities of this group, the present paper is centered on the selective determination of Cr(VI).

For determination of extremely low levels of Cr, electrothermal atomic absorption spectrometry (ETAAS) appears to be one of the most attractive detection options. However, a preliminary separation/preconcentration step is often required prior to the analysis of the sample in order to isolate the analyte from interfering matrix constituents and to bring its concentration into the dynamic measuring range of the instrument. Thus, for determination of samples of low content, such as those found in drinking water and seawater where typical concentrations are in the 0.1–0.5 $\mu\text{g l}^{-1}$ range [2], it is necessary to incorporate a preconcentration step in the analytical procedure. To develop reliable and robust systems for this purpose, the flow injection (FI) technique with its inherent technical advantages and manip-

ulatory versatility presents itself as an obvious avenue of choice.

So far, FI on-line preconcentration procedures have been based predominantly on incorporation of column reactors packed with different ion-exchange resins [3], or, following formation of suitable complexes, with non-polar materials such as silanised C_{18} [4], or on (co)-precipitation/adsorption procedures where the precipitate formed initially is entrapped in a knotted reactor and subsequently is eluted with a suitable eluent [5]. However, preconcentration procedures utilizing solvent extraction have not been exploited to any appreciable extent despite the inherent and obvious advantages, and to the authors' best knowledge this does, indeed, hold true for the assay of chromium. This is so much more surprising as much effort have been invested into developing suitable batch-wise solvent extraction procedures, where the one using the well-known APDC-IBMK extraction is especially noteworthy [6,7]. Actually, liquid–liquid extraction is one of the most frequently used separation techniques in the analytical laboratory. Despite its indisputable effectiveness in the removal of interfering matrix constituents, and potentials for facilitating the preconcentration of the analyte, its popularity has been somewhat restricted when used under batch conditions. This is partly due to the laboriousness of operation, and partly to risks of contamination from utensils and the laboratory environment which may induce complications in trace analysis. A further drawback of batch extractions is the often annoying odor and the toxicity of the organic solvent vapors released into the laboratory atmosphere. Such undesirable consequences may be avoided completely by using the enclosed FI liquid–liquid extraction systems, and may be considered as another merit which adds to the general advantages of FI on-line separation/preconcentration methods. An additional advantage of FI liquid–liquid extraction is that, in contrast to most other FI separation techniques, much higher phase transfer factors can be achieved. FI liquid–

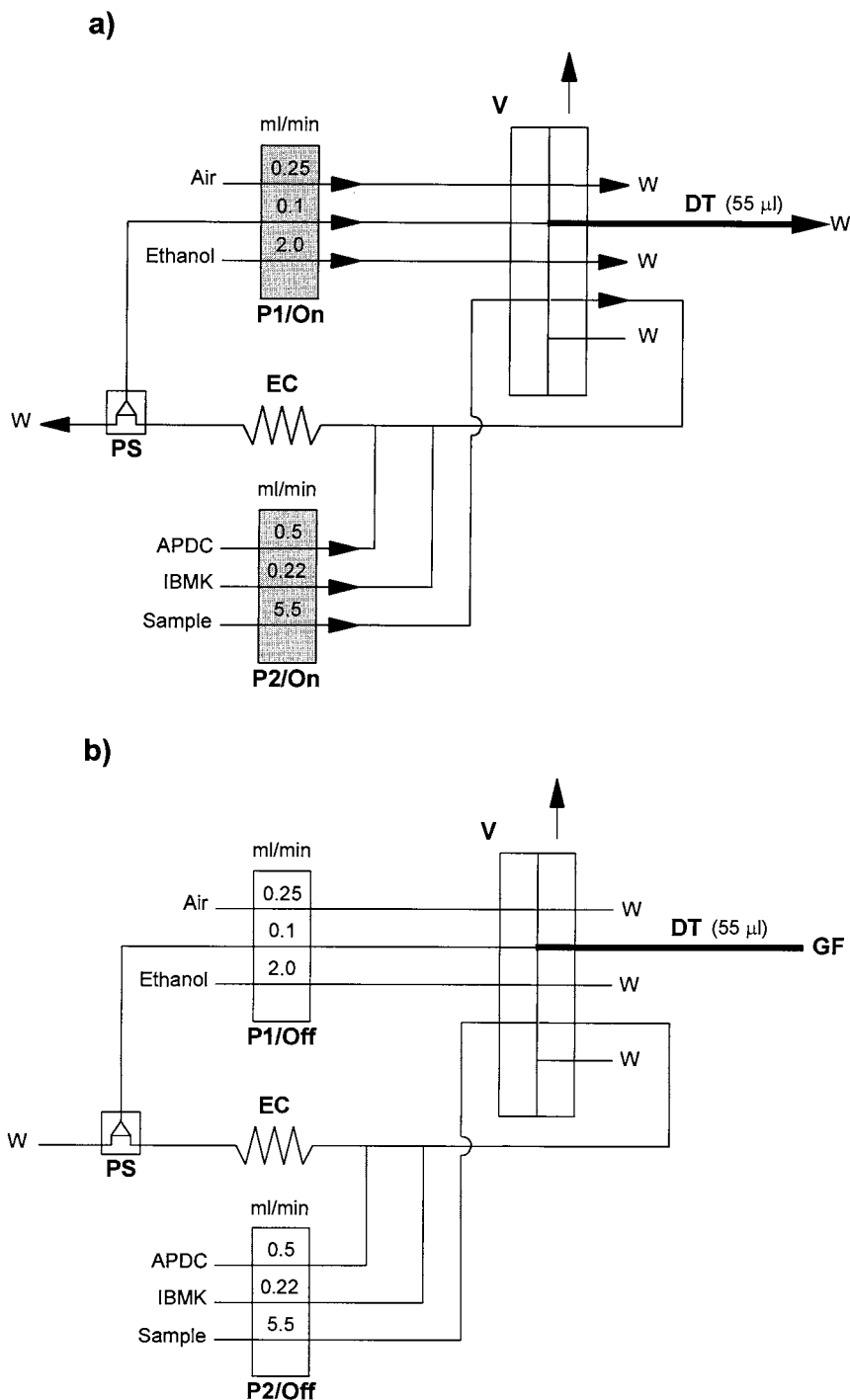
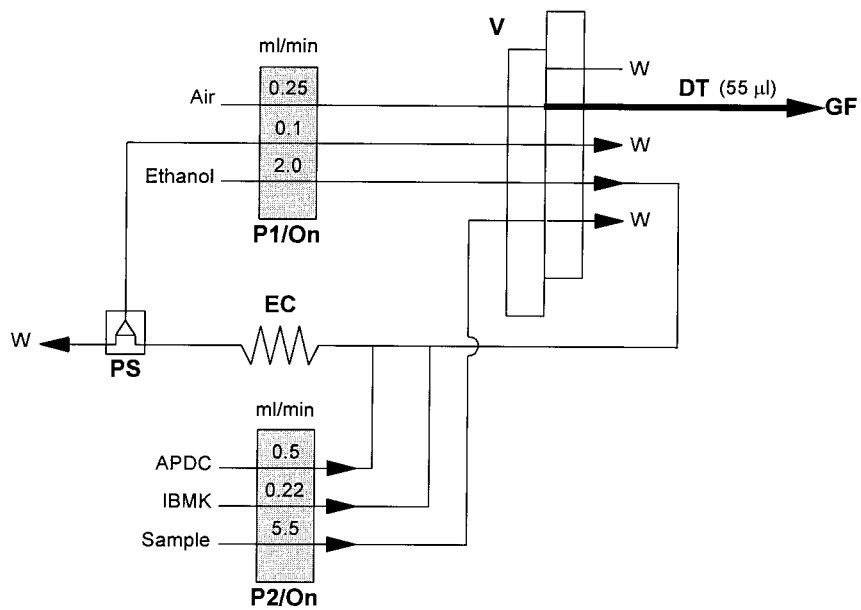


Fig. 1. Schematic diagram of the FI-manifold for sample extraction/preconcentration and the operational sequences involved. The purpose and duration of each sequence of a–d are given in Table 1 and described in detail in Section 2.3. The pumping rates of the peristaltic pumps, P1 and P2, are those ultimately adopted. APDC, ammonium pyrrolidine dithiocarbamate; IBMK, isobutyl methyl ketone; WS, washing solution; W, waste; EC, extraction coil (knotted, $L_{EC} = 350$ cm); PS, phase separator; DT, delivery tube; V, valve. (a) On-line extraction and preconcentration; (b) Intermittent stop for positioning of the tip of the delivery tube (DT) into the graphite furnace, and sample exchange; (c) Introduction of concentrate via air, and wash of pertinent conduits; (d) Conditioning of the FI-system and elimination of carry-over.

c)



d)

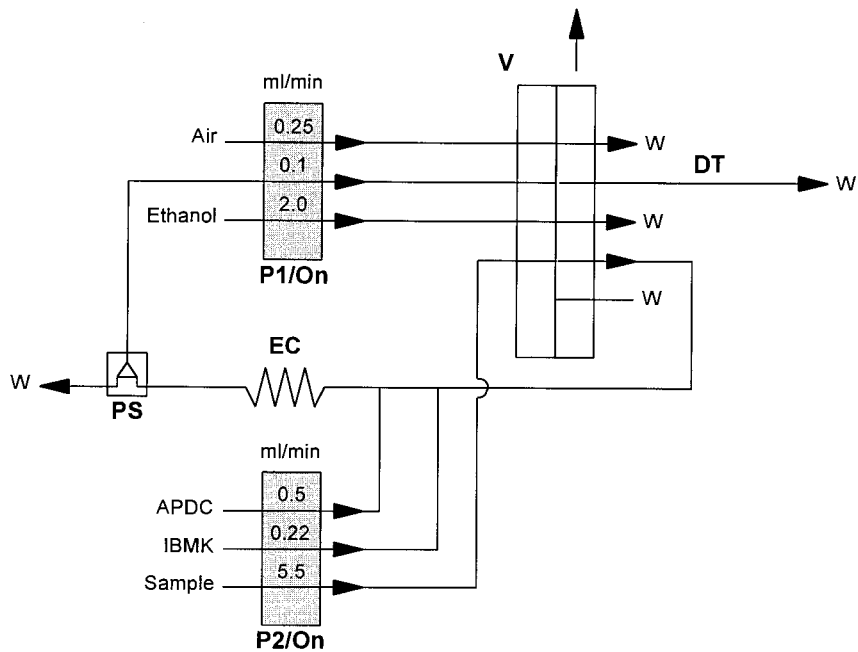


Fig. 1. (Continued)

liquid extraction systems are readily automated [8]. However, the phase separators available until recently, such as the sandwich-type gravitational phase separator or the sandwich-type membrane phase separator, are not considered sufficiently effective and robust, and that goes especially for the types incorporating a membrane.

Recently, Tao and Fang proposed an ingenious design for a liquid–liquid phase separator [9], the concept of which eliminates the use of a membrane. Thus, when incorporated into a FI-system, the application of liquid–liquid extraction does promise to constitute an attractive unit operational procedure provided, of course, that it would, via conscientious fabrication, facilitate a reliable long-term operational lifetime

In this work, an attempt was made to develop a practical and robust time-based FI procedure for the selective determination of ultra-trace amounts of Cr(VI) incorporating on-line preconcentration and extraction of the analyte followed by detection by ETAAS. Considering the provisions outlined above, special emphasis was placed on the design of the liquid–liquid separator, the dimensions of which were studied in great detail and experimentally verified via the construction of an array of individual separation units. Furthermore, an important part of this work was to exploit the potential of response surface models (RSM) to reach optimal operational conditions for the FI-procedure employed in a systematic manner.

2. Experimental

2.1. Apparatus

A Perkin-Elmer Model 2100 atomic absorption spectrometer was used in combination with a Perkin-Elmer Model FIAS-200 flow injection system (equipped with two individually controlled peristaltic pumps and a 5-port FI-valve). A chromium hollow cathode lamp (S. & J. Juniper, Harlow, Essex, UK) was used at a wavelength of 357.9 nm with a spectral bandpass of 0.7 nm, and was operated at 10 mA. The output signals were processed with a time constant of 0.5 s in the peak area mode and recordings from the graphics

screen were printed out by an Epson Model FX-850 printer. The sample manipulations of the FI-procedure were controlled automatically by a five-port valve (V) and via the activation of two peristaltic pumps (P1 and P2) (Fig. 1). The actuation times of the injector valve and the operation of the two pumps were programmed and controlled by a separate computer. A schematic diagram of the phase separator (PS), which is composed of two blocks, is depicted in Fig. 2. The

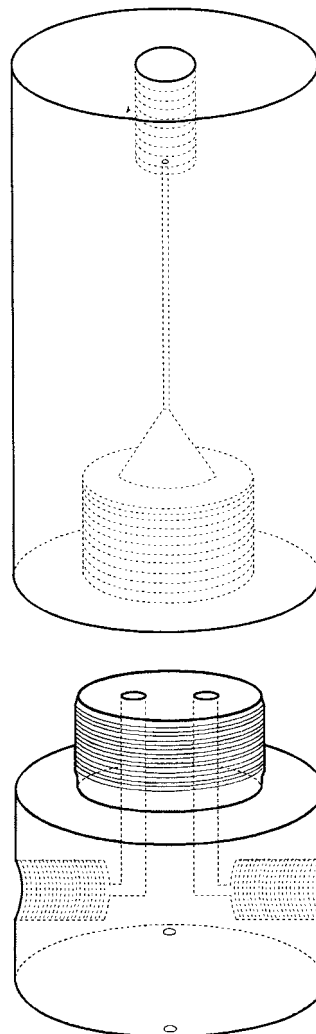


Fig. 2. Illustration of the phase-separator, consisting of a lower part, machined from stainless steel, and an upper block fabricated from PTFE. For operational details, see text.

upper block, which is produced from poly-tetrafluoroethylene (PTFE), is shaped to contain a conical cavity and furnished with a single outlet for the separated phase (i.e. the organic concentrate), while the lower block is fabricated from stainless steel provided with an inlet and outlet for the combined reaction mixture and the waste flow, respectively. When assembled, the dead volume of the conical cavity has a well-defined volume. The organic concentrate is drawn out of the top of the conical cavity by means of a PTFE pump tube (i.d./o.d.) = (0.5/1.3 mm) which offers a very controllable and reproducible flow-rate; the remainder of the aqueous/organic flow leaves as waste. A PTFE pump tube (i.d./o.d.) = (0.5/1.3 mm) was also used to introduce IBMK rather than a displacement bottle which would have made the system more complicated. In general, PTFE tubing used as pump tube works extremely well when the flow rate is less than 0.5 ml min^{-1} . In fact, by proper adjustment of the peristaltic pump a PTFE pump tube can readily be used to provide a constant flow-rate for 100–200 h!

The concentrate was introduced into the ETAAS instrument via the valve of the FI-system and a 50-cm PTFE delivery tube (DT) of i.d. 0.25 mm which was mounted at the end with a quartz capillary of volume of $7.5 \mu\text{l}$ ($L = 6.5 \text{ cm}$; i.d. = 0.40 mm). With the total tubing volume corresponding to $22.5 \mu\text{l}$ and considering the dead volume of the valve conduit, the total volume of the collected concentrate amounted to $55 \mu\text{l}$ (Fig. 1). The quartz capillary was inserted into the graphite tube of the ETAAS instrument manually by means of a specially made sampler-arm that is easily adjusted to the optimal position three-dimensionally [5]. Thus, the introduction of the concentrate onto the platform in the graphite tube is at least as reproducible as when using an auto-sampler arm.

The extraction coils (EC) (knotted; made by tying interlaced knots of approximately 5 mm diameter loops) and all the other connections and conduits in the FI-manifold (Fig. 1) consisted of (i.d./o.d.) = (0.50/1.70 mm) PTFE-tubing.

Ismaprene pump tubes were employed to propel the sample, reagent and air, respectively, while the washing solution (ethanol) was introduced by

means of a silicone pump tube. The FI-manifold, tubings and components were arranged and affixed by LEGO®-blocks (LEGO, Denmark).

2.2. Reagents and standard solutions

All reagents were of analytical grade, and distilled water was used throughout. Ammonium pyrrolidine dithiocarbamate (APDC) (Fluka) (0.05% (w/v)) was prepared from a 0.5% (w/v) solution of APDC. Standard solutions of Cr(VI) for calibration were made by three-stage dilution of a 1000 mg l^{-1} stock solution made by dissolving 3.3735 g of potassium chromate, K_2CrO_4 , in 1000 ml of deionized water. The IBMK used was a Merck product of analytical grade. Industrial 96% (v/v) ethanol was used as wash solution.

The FI extraction procedure was evaluated by analyzing a NIST Cr(VI)-reference material (certified Cr(VI) content of $1000 \pm 4 \text{ mg l}^{-1}$); spiked synthetic seawater and waste water samples; and waste water samples from an incineration plant (IPS) and from a desulphurization plant (DPS), respectively.

The synthetic seawater sample, corresponding to coastal seawater, was made by dissolving 33.8 g NaCl, 10.92 g $\text{MgSO}_4 \cdot 7\text{H}_2\text{O}$ and 0.22 g NaHCO_3 , respectively, making the solution up to 2000 ml in distilled water, and adjusting the acidity to 0.012 M by hydrochloric acid.

The waste water samples (obtained from a Danish electricity power plant) were initially preserved with 5% (v/v) Suprapure nitric acid, filtered through $0.45\text{-}\mu\text{m}$ acid-resistant Millipore filters, and finally the pH was adjusted to 1.9 by addition of Suprapure NH_4OH .

Further, to verify the capacity of the FI-procedure, two synthetic waste water samples (SWW1 and SWW2) were made and analysed. These were prepared according to information supplied by an end-user as to the presence of main macro constituents in natural waste water samples, that is, SWW1 and SWW2, were spiked with $0.100 \mu\text{g l}^{-1}$ Cr(VI) in a matrix composed of $\text{CaCl}_2 \cdot 2\text{H}_2\text{O}$, NaCl, $\text{Mg}(\text{SO}_4)_2 \cdot 6\text{H}_2\text{O}$ and Fe(III), where the composition of the two samples were as follows: SWW1: 20 g l^{-1} Ca, 50 g l^{-1} Cl^- , 0.23 g l^{-1} Mg, 0.3 g l^{-1} S, and $60 \mu\text{g l}^{-1}$ Fe(III); and

Table 1

Sequences of operations for the on-line FI extraction-preconcentration procedure

Sequence	Figure	Valve position	Time (s)	Operation of performance
1	1a	Fill	99	Extraction/preconcentration
2	1b	Fill	5	Positioning of DT in graphite furnace and sample exchange
3	1c	Inject	15	Introduction of concentrate to ETAAS and wash of pertinent conduits
4	1d	Fill	30	Conditioning of FI-system

SWW2: 3 g l⁻¹ Ca, 10 g l⁻¹ Cl⁻, 1 g l⁻¹ Mg, 1.32 g l⁻¹ S, and 20 µg l⁻¹ Fe(III)). Finally, the acidity in both samples was adjusted to 0.012 M by hydrochloric acid.

All glassware was soaked for at least 24 h in 1 M nitric acid, and finally rinsed in distilled water before use.

2.3. Operational procedure

The FI-manifold for the extraction/preconcentration and the attached cycle of operation sequences are shown in Fig. 1 and Table 1. The FI-procedure runs through a cycle of four sequences, that is, preconcentration, introduction of the concentrate into the graphite furnace (ETAAS) by means of air, washing of the knotted reactor (KR) and the phase separator, and finally conditioning of the FI-system to prepare it for the following sample run. A complete cycle of the FI-procedure lasts 149 s. The operations of the FI-system and the ETAAS detector are synchronously coupled.

In sequence 1 (Fig. 1a)—wherein the extraction/preconcentration takes place—both pumps are activated for 99 s with the valve (V) in the fill-mode position. The aspirated sample is initially mixed on-line with isobutyl methyl ketone (IBMK). The Cr(VI) is complexed by reaction with ammonium pyrrolidine dithiocarbamate (APDC) added downstream, and the Cr(VI)–PDC chelate formed is extracted into IBMK in the knotted reactor made from PTFE tubing. The organic extractant is separated from the aqueous phase by the gravity phase separator (PS) (Fig. 1) and forwarded via the PTFE pump tube into the delivery tube (DT) which, as mentioned above, has a volume of 55 µl.

In sequence 2 (Fig. 1b) the valve is retained in the fill-mode position, both pumps are stopped for 5 s and the tip of the delivery tube, which is furnished with a quartz capillary, is inserted into the graphite furnace of the ETAAS instrument by means of the manually operated rocker-arm. During this sequence the sample is exchanged so that the new sample solution is used to wash out the previous one, thereby preparing the system for the next sample run.

In sequence 3 (Fig. 1c) the valve is automatically switched into the inject-mode position and both pumps are activated for 15 s. Thus, the organic concentrate contained within the delivery tube (DT) is guided into the graphite tube by an air flow, and at the same time the ETAAS program is initiated. Simultaneously the sample conduit is rinsed by ethanol to avoid any carry-over between samples.

Finally, in sequence 4 (Fig. 1d), which lasts 30 s, both pumps are still activated while the valve is switched back to the fill-mode position. Thus, the FI-system is conditioned to prepare for the following sample run. If the sample is not interchanged (in step 2), sequence 4 can be omitted.

The FI-system and the ETAAS instrument are coupled and operated completely synchronously. Thus, as soon as the delivery of the concentrate to the ETAAS by means of air has been completed (sequence 3), the pre-programmed ETAAS firing sequence is initiated (Table 2), while the FI-system is finishing sequence 4 before it is restarted.

3. Results and discussion

When developing an FI on-line preconcentration procedure to handle more complex sample

matrices such as seawater and waste water, it is important, as detailed previously [5], that the approach adopted allows several ancillary manipulatory operations of the sample to be included before introducing the concentrate to the detector. Thus, when utilizing a column or a knotted reactor to retain the analyte, suitable operations must include wash of the surface of the retained analyte in the preconcentration unit in order to remove possible interfering matrix component, quantitative dissolution of the retained analyte in the smallest possible eluent volume, and reliable transport of the concentrate to the detector at a minimum dispersion, for instance via mono-segmentation by air of the entrapped eluent zone of concentrate, and finally thorough cleansing of the pertinent conduits in the FI-system in order to avoid carry-over between individual samples. When arranging an intelligent interfacing of the continuously operating FI-system with the discontinuously operating ETAAS detector, it is especially important to apply the feature of mono-segmentation in order to satisfy the volumetric requirements of the graphite tube (platform).

However, by exploiting the features of liquid–liquid extraction the necessary manipulatory operations can be reduced to a minimum partly because the analyte is automatically separated from possible interfering matrix components and partly because a homogeneous concentrate is collected in a holding coil from which it can be reproducibly metered and introduced directly to the detector. Thus, in order to place it optimally onto the platform of the graphite tube, it is merely necessary to guide the concentrate generated to

the detector in a smooth way, that is, by limiting the dispersion of the concentrate on its way to the detector. This is readily effected by forwarding the sample extract by means of air as illustrated in Fig. 1.

3.1. Design of the FI on-line solvent extraction system

It is well-known that that Cr(VI) and APDC in acid milieu form the complex Cr(VI)–PDC. This feature was exploited previously via preconcentration by effective adsorption of the complex on the inner wall of PTFE tubing followed by elution in a discrete zone of eluent [5]. However, since the complex formed is uncharged, it is readily soluble in a non-polar solvent, such as IBMK. Therefore, to achieve maximum sensitivity in the present instance, the sample was initially mixed on-line with IBMK and subsequently with APDC. To eliminate any carry-over in the pertinent conduits, ethanol was used as wash solution instead of water. Further, any precipitate generated in the extraction coil would effectively be dissolved by ethanol. Thereby an accessible conditioning of the system was ensured which is especially important when more complicated sample matrices are to be analyzed.

Compared with the system presented by Tao and Fang [9], the design of the present FI-system was improved considerably in several aspects. Firstly, the dimensions of the phase separator, that is, the i.d. of the conduits in both the lower and upper blocks and the internal cavity serving as the separation entity, were thoroughly investigated and optimized, and secondly the entrap-

Table 2

Graphite furnace temperature program for the determination of Cr(VI) in the organic concentrate of IBMK using a pyrolytic coated tube furnished with platform

Step	Temperature (°C)	Ramp (s)	Hold (s)	Argon flow-rate (ml min ⁻¹)
1	60	5	25	300
2	90	5	10	300
3	140	10	10	300
4	1400	5	20	300
5	2300	0	5	0
6	2800	1	3	300

ment and introduction of the concentrate to the graphite furnace was reorganized. Thus, the volume of the concentrate to be introduced into the detector was readily fixed by exploiting the valve position and subsequently guiding the concentrate to the detector by air after rotating the valve (Fig. 1). Hence, this approach greatly improves the accuracy of determination and lowers the RSD.

3.2. Optimization of the phase separator, PS

Before the optimization of the FI-procedure itself, the dimensions of the phase separator (PS) were studied in detail. To achieve a high preconcentration factor, the ratio between the sample plus APDC flow-rates and the flow-rate of IBMK, $(Q_S + Q_{APDC})/Q_{IBMK}$, must be relatively high at a suitable flow-rate of the reagent APDC, that is, $Q_{APDC} = 0.5 \text{ ml min}^{-1}$. Based on previous investigations performed by Tao and Fang [9], the performance was improved at a fixed IBMK flow-rate of $Q_{IBMK} = 0.22 \text{ ml min}^{-1}$, and a fixed aspiration-rate of organic phase (concentrate) of $Q_{\text{Conc.}} = 0.10 \text{ ml min}^{-1}$ from the top of the phase separator module, i.e. about half of the inflow rate of the organic phase. Thereby, a small fraction of the organic phase was forced to leave the separator as waste. This sacrifice eliminated the chance of entraining small aqueous droplets into the separated organic phase, and with its simple construction the phase separator allowed the organic–aqueous reaction mixture to be separated effectively and automatically within the conical space of the unit without the need for a membrane.

After having fixed the individual pumping rates, the goal was to obtain the highest sample flow-rate which would result in a constant aspiration-rate of the pure organic phase from the top of the phase separation module. To measure the efficiency of the phase separators to be tested, a hydrochloric acid solution of 0.01 M was used as sample. Without going through all the combinations of interest tested (dimensions and shape of the upper and lower part of the phase separator and the conduits within the individual components), it turned out that the optimal dimensions ultimately adopted allowed us to obtain a ratio of

$(Q_S + Q_{APDC})/Q_{IBMK} = (6.0 + 0.5)/0.22 = 29.55$ without entraining anything but organic concentrate—except, of course, the amount of water that can be dissolved in IBMK at room temperature (the solubility of IBMK in water is 2.04% (w/w) at 20°C). Further, when introducing IBMK at a flow-rate of 0.22 ml min^{-1} it was not possible to achieve a flow-rate of pure organic phase (concentrate) higher than $0.100\text{--}0.105 \text{ ml min}^{-1}$. If higher flow-rates of the sample are needed, then the flow-rate of the organic concentrate must be lowered relatively. But this will further lower the sample frequency (see Section 3.5). However, with increasing sample flow-rate it also becomes increasingly difficult to maintain a constant efficiency of separation (constant ratio between the streams) in long-term operation. Therefore, and because robustness of operation against small fluctuations in sample delivery was given the highest priority, a sample flow rate of 5.5 ml min^{-1} was selected for the following optimization procedure.

3.3. Optimization of sample acidity, $[H^+]_S$, and the APDC concentration, $[APDC]$

An important part of this work was to exploit the potentials of response surface models (RSM) to reach optimal conditions for the FI-procedure in a systematic way. Unfortunately, usually publications within FI are based on the so-called OVAT approach, that is, One Variable At a Time optimization. This method often suffers from finding optimum without appropriate knowledge about the system concerned or where a large number of experiments are run. There are several effective models such as steepest ascent, Box-Wilson, simplex, second-order models, which would be able to find optimum or near optimum conditions within a relatively small number of experiments. Of course, in order to limit the number of experimental factors, a screening of the experimental factors would be valuable, i.e. by performing a simple factorial screening experiment. In this work the extraction procedure was optimized by using a regular simplex optimization. Thus, when k variables are being studied, then the number of trials in the design is $n = k +$

1. The n observations are taken at the vertices of a regular simplex, which for $k = 2$ is a triangle and for $k = 3$ a tetrahedron. The advantage of this iterative procedure relative to a factorial design is that fewer trials are required. Thus, the simplex is a type of a ‘automatic’ steepest ascent procedure to finding the optimum (or minimum) [10]. The mathematical optimization algorithm is as follows:

Let the design contain the points P_1, \dots, P_{k+1} , in the k -dimensional simplex with $(k + 1)$ points, where each point defines one set of the design variables, i.e. one set of experimental conditions. When using the procedure, the design point with lowest signal, P_j , say, is replaced by a new point P_j^* . This point is determined by mirroring P_j in the average experimental conditions of the remaining points. Mathematically this can be expressed in vectors as (for a detailed description, see Ref. [11]):

Define:

$$F = \sum_{i=1}^{k+1} P_i - P_j$$

then

$$P_j^* = \frac{2}{k} \times F - P_j$$

Essentially, there are only two critical parameters in the extraction process, that is, the sample acidity $[H^+]_s$ and the APDC concentration [APDC]. This, of course, makes it easy to visualize the regular simplex procedure. The results obtained thereby are shown in Fig. 3 and Table 3.

As it is seen, the simplex procedure was performed smoothly, and the optimum conditions were found to be near the center of the points 10, 13 and 14, that is, $[H^+]_s = 0.012$ M and [APDC] = 0.065% (w/v) (Table 3).

Subsequently, to verify the expected optimum conditions a two-parameter central composite design (CCD) including five center points was performed around the estimated optimum (experimental conditions shown by the black circles in Fig. 3). Thereby each parameter was tested at five different (concentration) levels. Thus, with nine different design points, which gives 13 degrees of freedom, the CCD-design enables a second-order model to be estimated completely, that is:

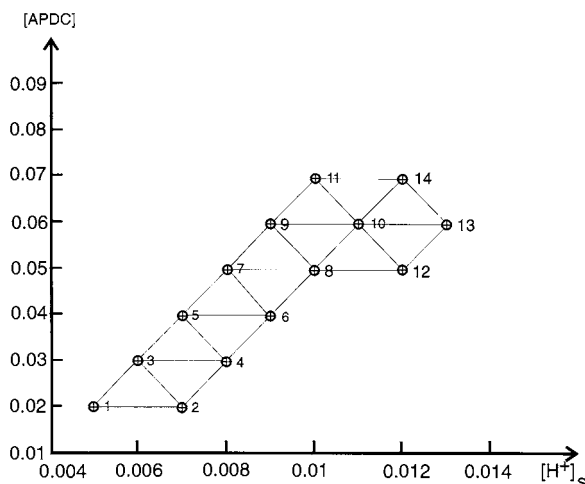


Fig. 3. Experimental sequence with a regular simplex procedure for optimizing the sample acidity $[H^+]_s$ and the APDC concentration [APDC] using a $0.40 \mu\text{g l}^{-1}$ Cr(VI) standard. $L_{EC} = 250$ cm and $T_E = 99$ s. Operational conditions are otherwise as given in Fig. 1.

$$y = \beta_0 + \sum_{i=1}^k \beta_i x_i + \sum_{i < j} \beta_{ij} x_i x_j + \sum_{i=1}^k \beta_{ii} x_i^2 + \varepsilon \quad (1)$$

where X_1 = sample acidity and X_2 = concentration

Table 3

Results obtained by the experimental sequence with a regular simplex procedure for optimizing sample acidity $[H^+]_s$ and APDC concentration [APDC] (Fig. 3) using a $0.40 \mu\text{g l}^{-1}$ Cr(VI) standard^a

Experiment number	Relative response (%)
1	43.9
2	43.3
3	53.8
4	58.7
5	62.0
6	74.4
7	78.0
8	90.8
9	87.2
10	100.0
11	78.4
12	87.5
13	97.7
14	99.0

^a The results are based on the average of three replicates of each set of the experimental conditions. L_{EC} , 250 cm and T_E , 99 s. Operational conditions are otherwise as given in Fig. 1.

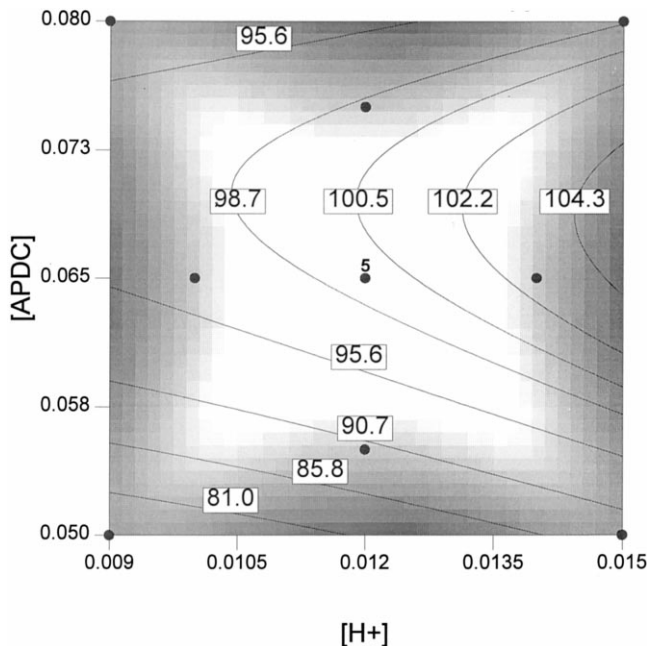


Fig. 4. Central composite design (CCD) for verifying the optimized parameters for the sample acidity $[H^+]_s$ and the APDC concentration $[APDC]$ using a $0.40 \mu\text{g l}^{-1}$ Cr(VI) standard. $L_{EC} = 250$ cm and $T_E = 99$ s. Operational conditions are otherwise as given in Fig. 1.

of APDC. The remaining degrees of freedom are assigned to higher order effects and a so-called residual (error) (ε), which cannot be explained by the model.

The results achieved by the two-parameter CCD are shown by response gradients (expressed in percentage) in Fig. 4. These results confirmed that the estimated optimum found by the simplex procedure described above is reasonable. However, it is seen that a slightly higher signal could perhaps be obtained by moving from the estimated optimum to the right (Fig. 3) according to the response gradients which are derived on the basis of the statistical model described below. Yet, as indicated by the more intense color, the relative standard deviation thereby increased. Therefore, the signal achieved for $[H^+]_s = 0.012$ M and $[APDC] = 0.065\%$ (w/v) was a suitable compromise.

The response gradients shown in Fig. 3 are described by an expression of Eq. (1). From the statistical analysis of variance (ANOVA) given in Table 4, the following conclusions can be made: The 'Lack of Fit' variation is not significant when

tested against the 'Pure Error' variation. Subsequently the 'Residual' variation is found by pooling the sums of squares for 'Pure Error' and 'Lack of Fit', and the model is tested against this 'Residual' variation. It is seen that the model is strongly significant (Table 4).

The final equation in terms of natural factors expressed as relative response is:

$$y = -177.6 + 1790.84 [H^+]_s + 7471.71 [APDC] + 80\,032.21 [H^+]_s^2 - 50\,798.71 [APDC]^2 - 34\,444.44 [H^+]_s [APDC] \quad (2)$$

In fact, as the factors $[H^+]_s^2$ and the interaction $[H^+]_s [APDC]$ are not significant, the model (Eq. (1)) could be reduced to:

$$y = \beta_0 + (\beta_1 x_1 + \beta_2 x_2) + \beta_{22} x_{22}^2 + \varepsilon \quad (3)$$

which depicted graphically would show a cylindrical response surface which is increasing slightly, linearly, in the direction of $[H^+]_s$.

If it is important to reach the 'real' optimum conditions, e.g. for economical reasons or statisti-

Table 4
ANOVA for response surface quadratic model of the CCD experiment

Source	Sum of squares	df	Mean square	F-value	Probability > F-value	
Model	632.03	5	126.41	22.70	0.0003 (strongly significant)	
Residual	38.98	7	5.57			
Lack of fit	29.67	3	9.89	4.25	0.0980 (not significant)	
Pure error	9.31	4	2.33			
Cor total	671.01	12				
Factor	Coefficient estimate (coded)	df	Standard error	<i>t</i> for H_0 coeff = 0	Probability > <i>t</i>	VIF
Intercept	99.58	1	0.87			
A-[H ⁺]	4.42	1	1.07	4.14	0.0044	1.00
B-[APDC]	6.82	1	1.07	6.39	0.0004	1.00
A^2	0.72	1	2.76	0.26	0.8019	3.51
B^2	-11.43	1	2.76	-4.14	0.0044	3.51
AB	-1.55	1	1.18	-1.31	0.2304	1.00

cal reasons, rather than finding reasonably good conditions (as in the present case), the described simplex procedure should be modified at the moment where the increase of signal is becoming small compared to the experimental uncertainty. Thus, the regular simplex procedure should be changed into a variable simplex procedure where the above described mirroring is modified to use smaller steps while keeping the design regular or almost regular.

In the present case this was not considered necessary as the steps in the regular simplex procedure were already relatively small and, in fact, the RSDs achieved were typically around 0–2%. And more important, when using an RSM the process improvement should be regarded as a continuing, iterative process, and any optimum found in any given experiment should perhaps not be considered as important as what one clearly gains in process improvement and what one learns about the process in general [10] (p. 242).

3.4. Optimization of the length of the extraction coil, L_{EC}

In the FI-procedure IBMK is mixed with the sample at a pumping rate which is 25 times smaller than the sample pumping rate. Subsequently, when the combined reaction medium enters the knotted extraction coil, the organic phase becomes effectively dispersed within the aqueous phase in such

small droplets that the combined solution for the naked eye actually appears to look completely homogeneous. This is most advantageous because that means that the interface between the two phases, despite the low organic-to-aqueous phase ratio, is very large, thereby facilitating effective phase-transfer of the complex. By optimizing the length of the knotted extraction coil, i.e. the extraction time, the results shown in Fig. 5 were obtained.

It is seen that the results did not increase further beyond a length of 350 cm, which corresponds to a residence time of 7 s. Therefore, to avoid unnecessary back-pressure and deteriorated flow stability a coil length of 350 cm was selected.

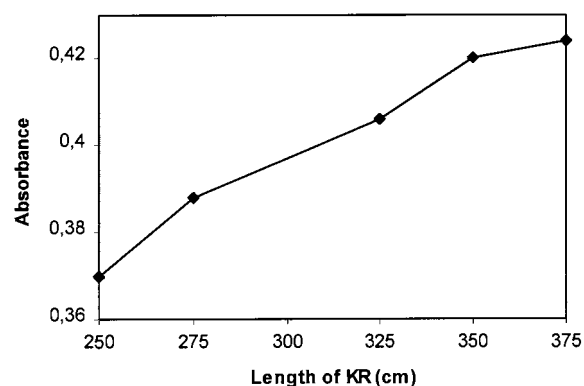


Fig. 5. Effect of the length of the extraction coil (EC, knotted) as determined for a $0.40 \mu\text{g l}^{-1}$ Cr(VI) standard. $T_E = 99$ s. Operational conditions are otherwise as given in Fig. 1.

3.5. Variation of the preconcentration time, $t_{Preconc.}$

The signal increased gradually until a preconcentration period of 90–95 s, which can be explained by the volume of the conduit in which the concentrate has to move from the phase separator to the end of the delivery tube (Fig. 1). This volume was estimated to be 90 μl ($V_{Concentrate} = 55 \mu\text{l}$). Thus, since $Q_{conc.} = 100 \mu\text{l min}^{-1}$, it takes 54 s to guide the concentrate from the phase separator to the end of the delivery tube. Further, during the first ca. 40 s there is a concentration gradient in the concentrate aspirated from the PS, which is easily observed by judging the composition of drops coming out of the delivery tube (Fig. 1). These consist of IBMK (concentrate) and ethanol (which was used to clean the system in step 3). Consequently, it takes about 40 s before the concentrate aspirated from the phase separation module has become completely uniform (equilibrium state), that is, there was no concentration gradient in the concentrate after 40 s. Therefore, to ensure a very robust system a preconcentration period of 99 s was chosen. Of course, a shorter preconcentration time could be used, but by aspirating a completely uniform concentrate from the PS it was possible partly to exploit the systems capacity completely and partly to ensure more robust conditions and thereby low RSD values.

3.6. Variation of the sample flow-rate, Q_s

By varying the sample flow-rate the separation efficiency of the PS was not influenced.

Thus, the integrated absorbance increased linearly vs. sample flow-rate, at least until a flow-rate of 5.5 ml min^{-1} . This does not necessarily mean that the solvent extraction is quantitative. In this context it should be considered that although the degree of extraction should be higher at lower sample flow-rates because of longer extraction time, this would, on the other hand, entail relative dilution of the concentrate generated since the amount of IBMK was kept constant.

Table 5

Characteristics of performance for the FI-ETAAS on-line extraction/preconcentration system

Sample flow rate (ml min^{-1})	5.5
Calibration range ($\mu\text{g l}^{-1}$)	0.005–0.6
Regression equation in calibration range (eight standards, $n = 3$, $C_{Cr(VI)}$ in $\mu\text{g l}^{-1}$)	$1.067 C_{Cr(VI)} + 0.006$ (Corr. = 0.9992)
Sample volume per assay (ml) (Loading time, $t_{preconcentration} = 99 \text{ s}$)	$9.2 + 4.6$
Sample frequency (f) (samples h^{-1})	24.2
RSD (%) ($n = 11$, $0.2 \mu\text{g l}^{-1}$)	0.83
Limit of detection (3σ) (ng l^{-1})	3.3
Enrichment factor (EF)	18.4
Concentration efficiency (CE = $\text{EF}/60$)	7.4

4. Performance of the system

4.1. Calibration runs of synthetic samples

Table 5 shows the operational characteristics which were obtained for the selective determination of Cr(VI) using the FI-ETAAS system developed. In this context it is particularly interesting to note the very high sensitivity and the extremely low detection limit obtained. The capacity of the system can also be illustrated by a typical signal output. Thus, in Fig. 6 is depicted a readout for a $0.40 \mu\text{g l}^{-1}$ sample, and as it is seen the RSD is merely 1.2% for these three replicates.

4.2. Investigation of interferences

If the FI-ETAAS procedure is to have any practical utility, e.g. for assays of natural water and seawater, it is essential that it can tolerate the presence of pertinent ions, and at the concentration levels at which they might occur in the sample concerned. Hence, the effects of representative potential interfering species were tested, that is, Cu^{2+} , Cd^{2+} , Zn^{2+} , Pb^{2+} , Ni^{2+} , Co^{2+} and Fe^{3+} .

Besides, the system was evaluated with the presence of CaCl_2 , NaCl and MgSO_4 , respectively, as

these are the main constituents of the waste water samples tested (see Section 5). The effect of these ionic constituents on the determination of Cr(VI) is summarized in Table 6A,B.

In the last column of Table 6A the tolerated interferent/analyte ratio is shown, that is, at this level the interferent does not impair the assay noticeably, i.e. less than 5%. In preparation for testing the waste water samples it is especially noteworthy that the procedure is not influenced by the very high salt concentrations (see Section 5). Only in the case of very high concentrations of chloride is there a moderate decrease in the sensitivity (see Table 6B).

5. Evaluation of the FI-ETAAS procedure

Solvent extraction should intuitively be able effectively to separate the analyte from interfering matrices. Therefore it was of great interest to test complicated sample matrices, that is, synthetic seawater, waste water samples originating from an incineration plant (IPS) (total chromium content of $0.24 \mu\text{g l}^{-1}$), and from a desulphurization plant (SPS) (total chromium content of $0.53 \mu\text{g l}^{-1}$), respectively. Further, to verify the high capacity of the FI-procedure calibrations of two corresponding synthetic waste water samples were tested; SWW1 and SWW2,

PERKIN-ELMER

M 2100

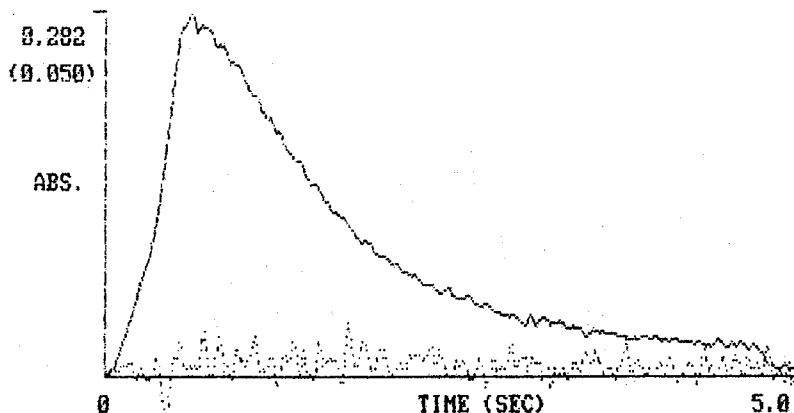
98/05/25

PAGE 1

Element Run - FURNACE
 Element File: CR-LIQ98
 Element: Cr - PEAK AREA
 Repl. 0 of 3

Printer: OFF
 BG Corr: ON
 Units :
 Ch.Mass:

0.445



READY

Peak Area (A-s)
 AA-BG: 0.444
 BG : 0.008

Peak Height (A)
 AA-BG: 0.282
 BG : 0.007

Statistics

Mean: 0.445
 SD: 0.006
 RSD(%): 1.2

Energy: 65 Wavelength: 357.8 Slit: 0.7 L Lamp: 1 Current: 10 mA
 HGA/AS : Off STEP of 6 TEMP.: °C TIME: s AS LOC:

PERKIN-ELMER

M 2100

98/05/26

PAGE 1

Fig. 6. Typical peak readout for a $0.40 \mu\text{g l}^{-1}$ Cr(VI) standard as obtained by using the FI-ETAAS system depicted in Fig. 1. Operational conditions are as given herein.

Table 6

(A) Investigation of the tolerance of potentially interfering ions. (B). Investigation of the tolerance of the main species present in the matrices of the waste water samples tested (see Section 5)^a

Interferent	Concentration ^b	Recovery (%)	Interferent/analyte ratio ^c
(A)			
Cu(II)	100	98.1	333
	200	65.5	
Cd(II)	100	101.1	333
	200	72.8	
	1000	52.6	
Zn(II)	100	103.0	1333
	400	99.4	
	1000	91.9	
Pb(II)	100	99.8	667
	200	95.1	
	1000	67.4	
Ni(II)	200	104.4	667
	400	67.6	
	1000	39.9	
Co(II)	200	97.2	667
	1000	57.6	
Fe(III)	80	98.3	267
	100	92.7	
	200	70.0	
	500	50.9	
(B)			
Ca ²⁺ /Cl ⁻	3/5.3	102.1	
Ca ²⁺ /Cl ⁻	20/35.4	89.3	
Na ⁺ /Cl ⁻	6.5/10	101.3	
Na ⁺ /Cl ⁻	32.4/50	74.2	
Mg ²⁺ /SO ₄ ²⁻	1/3.9	123.7	

^a The concentration of Cr(VI) was in all cases 0.3 $\mu\text{g l}^{-1}$. The effect is expressed as the recovery for the levels added.

^b Concentration in (A) is in $\mu\text{g l}^{-1}$ and in (B) in g l^{-1} .

^c The tolerated interferent/analyte ratio is shown, that is, at this level the interferent does not impair the assay at any noticeable degree.

respectively (see Section 2.2). Finally, in addition to these calibrations a determination of Cr(VI) in a NIST reference material (certified Cr(VI) content of $1000 \pm 4 \text{ mg l}^{-1}$) was performed.

The actual results achieved from the determination of Cr(VI) in the NIST reference material and a synthetic seawater sample are shown in Table 7. Both of the calibrations, which were made by standard addition, are most satisfactory. The sensitivity of both the NIST reference material and the synthetic seawater sample was similar to that obtained with the deionized Cr(VI)-standard solutions (Table 5), that is

1.067 [Abs s ($\mu\text{g l}^{-1}$)⁻¹]. Therefore, the matrix of the synthetic seawater does not in any manner influence the extraction/separation mechanism. Admittedly, the results of both samples were ca. 4.8% higher than the stipulated spiked concentrations of $0.10 \mu\text{l l}^{-1}$. But as the precision in both cases was very high a plausible explanation of this difference might be a bias due to the three-stage dilution of the stock solution of the two materials.

The results of the determination of Cr(VI) in the samples originating from an incineration plant (IPS) and from a desulphurization plant (DPS), respectively, revealed that the procedure

is completely unaffected in spite of the very high salt contents (Table 8). The waste water samples do not contain any Cr(VI), that is, the chromium content of the samples appears to be Cr(III). The sensitivities were 10–15% higher compared to when using deionized Cr(VI)-standard solutions.

The results achieved by the calibrations of the corresponding synthetic waste water samples tested, SWW1 and SWW2, respectively, are shown in Table 9. When comparing the sensitivities obtained for these two samples with those for the real waste water samples (IPS and DPS) they do not seem to correspond completely. This might be explained by unidentified components in the real samples and/or that the concentrations of the individual matrix components, as supplied by the provider of the samples, are not correct. In both calibrations of the synthetic waste water samples the sensitivity achieved was somewhat lower compared to the sensitivity of the real samples. This indicates that the content of one or more components probably appears at lower concentrations than informed. Surprisingly, the sensitivity of the SWW1 calibration was somewhat higher than that obtained for SWW2. This pattern should have been opposite considering the influence of a high concentration of chloride (see Section 4.2). On the other hand, the calibration of IPS also resulted in a slightly higher sensitivity than the calibration of DPS. However, when using the approach of standard addition for determining the concentration of the individual samples, these small changes in the sensitivities do not play any role at all.

It can be concluded that, contrary to what was previously reported [5], in which reference the

adsorption-preconcentration process was described as being dependent on the ionic strength of the reaction media, the IBMK-extraction procedure appears, for all practical purposes, to be virtually independent of the ionic strength of the sample. Therefore, and since, irrespective of the matrix, there is no blank value recorded, standard addition could for screening purposes be replaced by use of normal external calibration.

6. Conclusion

A key to the success of the FI-system developed is the design of the phase separation module, which, compared to the unit suggested by Tao and Fang [9], in this work was markedly improved through a detailed investigation of the dimensions of the component. The unique feature of the phase separator is that, despite its simple construction, the organic–aqueous reaction mixture is separated automatically within the conical space of the phase separator without the need for the incorporation of a membrane.

The FI-system is very robust and simple in performance. It fulfills all the requirements to handle complex sample matrices like seawater and waste water without deteriorating the sensitivity. Thus, it is noteworthy that the procedure is not influenced by the very high salt concentrations which makes the developed FI-procedure very promising in industrial respect. In particular, the results of the determination of Cr(VI) in two samples originating from an incineration plant and from a desulphurization plant are interesting.

Table 7

Determination of Cr(VI) in a NIST-Cr(VI) reference material and a synthetic seawater sample, respectively, using the proposed FI-ETAAS procedure

	Cr(VI) ^a	Cr(VI) ^b
Regression equation ($n = 4$, $C_{\text{Cr(VI)}}$ in $\mu\text{g l}^{-1}$) ^c	$1.078C_{\text{Cr(VI)}} + 0.113$ (Corr. = 0.9995)	$1.108C_{\text{Cr(VI)}} + 0.116$ (Corr. = 0.9992)
Concentration found ($\mu\text{g l}^{-1}$)	0.1047 ± 0.0019	0.1047 ± 0.0017

^a Certified Cr(VI) NIST-sample (certified content of $1000 \pm 0.004 \text{ mg l}^{-1}$), diluted until a concentration of $0.10 \mu\text{g l}^{-1}$ by a three-stage dilution, as determined by four-level standard addition by adding 0, 0.1, 0.2 and $0.3 \mu\text{g l}^{-1}$ Cr(VI) to the sample.

^b Synthetic seawater sample, spiked with Cr(VI) to a concentration of $0.10 \mu\text{g l}^{-1}$, as determined by standard addition by adding 0, 0.1, 0.2 and $0.3 \mu\text{g l}^{-1}$ Cr(VI) to the sample.

^c The regression equations of the multiple standard addition calibrations were determined within a confidence interval of 95%.

Table 8
Determination of Cr(VI) in waste water samples using the proposed FI-ETAAS procedure

	IPS ^a	DPS ^b
Regression equation ($n = 5$, $C_{\text{Cr(VI)}}$ in $\mu\text{g l}^{-1}$) ^c	$1.22C_{\text{Cr(VI)}} + 0.0004$ (Corr. = 0.9997)	$1.17C_{\text{Cr(VI)}} - 0.0008$ (Corr. = 0.9993)
Concentration found ($\mu\text{g l}^{-1}$)	0.002 ± 0.000	0.003 ± 0.000

^a Waste water from a incineration plant as determined by standard addition by adding 0, 0.1, 0.2, 0.3 and 0.4 $\mu\text{g l}^{-1}$ Cr(VI) to the sample.

^b Waste water from a desulphurization plant as determined by standard addition by adding 0, 0.1, 0.2, 0.3 and 0.4 $\mu\text{g l}^{-1}$ Cr(VI) to the sample.

^c The regression equations of the multiple standard addition calibrations were determined within a confidence interval of 95%.

Table 9
Determination of Cr(VI) in the corresponding simulated synthetic waste water samples (see also Table 8).

	SWW1 ^a	SWW2 ^b
Regression equation ($n = 5$, $C_{\text{Cr(VI)}}$ in $\mu\text{g l}^{-1}$) ^c	$1.095C_{\text{Cr(VI)}} + 0.101$ (Corr. = 0.9992)	$0.87C_{\text{Cr(VI)}} + 0.088$ (Corr. = 0.9991)
Concentration found ($\mu\text{g l}^{-1}$)	0.0998 ± 0.0017	0.1011 ± 0.0015

^a Synthetic incineration waste water sample, produced according to the information provided by the supplier, and spiked with Cr(VI) to a concentration of 0.10 $\mu\text{g l}^{-1}$, as determined by standard addition by adding 0, 0.1, 0.2 and 0.3 $\mu\text{g l}^{-1}$ Cr(VI) to the sample.

^b Synthetic desulphurization waste water sample, produced according to the information provided by the supplier, and spiked with Cr(VI) to a concentration of 0.10 $\mu\text{g l}^{-1}$, as determined by standard addition by adding 0, 0.1, 0.2 and 0.3 $\mu\text{g l}^{-1}$ Cr(VI) to the sample.

^c The regression equations of the multiple standard addition calibrations were determined within a confidence interval of 95%.

These samples are very severe, because they contain a high background of salts (from the neutralization procedure used), and therefore they are generally not accessible to analyze directly by AAS. However, by using the proposed procedure, the salt matrix was conveniently eliminated, which—in addition to the preconcentration feature—makes this approach very attractive for practical assays.

At present, the only ‘missing link’ in the combined FI-ETAAS system is the need for improving the software so that the sampler arm could be controlled fully automatically. The use of the manual sampler arm was simply dictated by the fact that the auto-sampler arm of the detector and the FI-system cannot operate in parallel. Therefore, it was necessary to control the FI-system and the graphite furnace system individually by the use of two independent computers.

The system developed could obviously be employed directly for industrial purposes. However, to achieve a long-term stable FI-system that can work eventually without supervision, the peristaltic

pumps should be exchanged by syringe pumps. This is simply because pump tubes are aging and therefore need to be adjusted regularly. With syringe pumps the system should be able to operate completely without any adjustment. Thus, the FI-system described herein could perform exactly the same processes via the use of three syringe pumps.

Finally, concerning the ‘chemical robustness’ of the procedure, that is, its selectivity as demonstrated for its tolerance of potential interfering species/agents, it was found that at high concentrations of certain cations, the recovery was well below 100% (see Section 5). This is due to the fact that APDC actually forms complexes with many metal ions, and therefore at high levels of interfering cations there is a competition between these foreign ions and the analyte for the APDC present. However, this feature can also be turned around and made into an advantage; that is, if one were to apply a multi-detection device one could use the present FI-extraction system in conjunction with a multi-detection device such as an

ICP-MS or a spectrophotometer and thereby determine several metal species simultaneously. Using an ICP-MS would, of course, require ultrasonic nebulization and membrane desolvation in order to remove IMBK before the sample reaches the plasma.

Acknowledgements

The authors wish to extend their appreciation to The Brothers Hartmann's Foundation (Denmark) and to The COWI-Foundation (Denmark) for financial support, and to the mechanical workshop of this department for conscientious machining of the many individual phase separators made and tested. Thanks are also due to Edith Thomsen of the Southern Jutland Electricity Power Plant for providing the industrial waste water samples analysed.

References

- [1] B. Mennen, <http://www.chromium.edu/intro.htm>.
- [2] H.J. Bowen, *Environmental Chemistry of the Elements*, Academic Press, London, 1979.
- [3] S. Olsen, L.C.R. Pessenda, J. Ruzicka, E.H. Hansen, *Analyst* 108 (1983) 905.
- [4] J. Ruzicka, A. Arndal, *Anal. Chim. Acta* 216 (1989) 243.
- [5] S. Nielsen, E.H. Hansen, *Anal. Chim. Acta* 366 (1998) 163–176.
- [6] K.S. Subramanian, J.C. Méranger, *Analyst* 105 (1980) 620.
- [7] K.S. Subramanian, *Anal. Chem.* 60 (1988) 11.
- [8] Z.L. Fang, *Flow Injection Separation and Preconcentration*, VCH, Weinheim, 1993, p. 1993.
- [9] G.H. Tao, Z.L. Fang, *Spectrochim. Acta Part B* 50 (1995) 1747.
- [10] R.H. Meyer, D.C. Montgomery, *Response Surface Methodologies; Process and Product Optimization Using Designed Experiments*, Wiley, New York, 1995.
- [11] H. Spliid, *Simple Methods for Optimizing Response Surfaces*, Polyteknisk Boghandel, Denmark, 1978 in Danish.

Chromium speciation using an automated liquid handling system with inductively coupled plasma — mass spectrometric detection

Mary Kate Donais, Rob Henry *, Tom Rettberg

VG Elemental, 27 Forge Parkway, Franklin, MA 02038, USA

Received 3 November 1998; received in revised form 10 February 1999; accepted 22 February 1999

Abstract

The speciation of inorganic chromium in environmental samples is required for accurate assessment of pollution levels. Of the two chromium oxidation states, Cr (VI) is a known carcinogen, while Cr (III) is an essential element. Total chromium measurement cannot be used to determine actual environmental impact due to the considerable difference in toxicity of the two elemental forms. An automated liquid handling system, the PrepLab™, can be used with an inductively coupled plasma-mass spectrometer (ICP-MS) to quantify Cr (III) and Cr (VI) in liquid samples. An autosampler is used to introduce discrete sample volumes into a solid-phase chelation resin column. The Cr (III) and Cr (VI) species are separated and are introduced on-line into the VG PlasmaQuad 3 ICP-MS for detection. The chromatographic data are collected in time resolved analysis mode with the capability of simultaneous multiple-isotopic detection. © 1999 Elsevier Science B.V. All rights reserved.

Keywords: Automated liquid handling system; Chromium speciation; Mass spectrometry

1. Introduction

Chromium is a naturally occurring element found in rocks, animals, plants, soil, and in volcanic dust and gases. Humans are exposed when eating food, drinking water, and inhaling air that may contain chromium. The average daily intake from air, water, and food is estimated to be 0.01–0.03 µg, 2 µg/l, and 60 µg, respectively.

Dermal exposure to chromium may occur during the use of products that contain chromium such as wood treated with copper dichromate or leather tanned with chromic sulfate. Occupational exposure to chromium occurs from chromate production, stainless-steel production, chrome plating, and the tanning industries. Occupational exposure can be two orders of magnitude higher than exposure in the general population. People who live in the vicinity of chromium waste disposal sites or chromium manufacturing and processing plants have a greater probability of elevated chromium exposure than the general population.

* Corresponding author. Tel.: +1-303-939-9012; fax: +1-303-939-9017.

E-mail address: rhenry1812@aol.com (R. Henry)

Chromium occurs in the environment in two major valence states, trivalent chromium {Cr (III)} and hexavalent chromium {Cr (VI)}. Cr (III) compounds are sparingly soluble in water, while Cr (VI) compounds are readily soluble which may result in enhanced levels of Cr (VI) in water sources. Cr (VI) is more toxic than Cr (III) and is a known carcinogen. The reference dose (RfD)¹ for Cr (VI) is 0.005 mg/kg per day and the RfD for Cr (III) is 1 mg/kg per day. The US Environmental Protection Agency (EPA) estimates that consumption of these doses or less over a lifetime is unlikely to result in the occurrence of chronic non-cancer effects. Cr (III) is also an essential element in humans, with a daily recommended intake of 50–200 µg/day for an adult; it is essential to normal glucose, protein, and fat metabolism. The body is capable of detoxifying some Cr (VI) to Cr (III) which leads to increased levels of Cr (III) in the body. Laboratory tests can detect chromium in the blood, urine, and hair of exposed individuals, however it is difficult to separate Cr (VI) from Cr (III); therefore analysis is usually limited to total chromium.

1.1. Chromium speciation

Due to the widely different toxicity of the two forms of chromium, total chromium measurement cannot be used to determine actual environmental impact. The speciation of chromium in environmental samples is therefore necessary to accurately assess pollution levels. EPA Method 7196A was developed for the determination of Cr (VI) in EP/TCLP extracts and ground waters [1]. The method requires the addition of diphenylcarbazide and sulfuric acid to the water sample followed by measurement of the solution absorbance

¹ The RfD is not a direct estimator of risk but rather a reference point to gauge the potential effects. Exceeding the RfD does not imply that an adverse health effect would necessarily occur. As the amount and frequency of exposures exceeding the RfD increase, the probability of adverse health effects also increases. The RfD for Cr (VI) is 0.005 mg/kg per day of body weight based on no effects noted in rats exposed to chromium in the drinking water. The RfD for Cr (III) is 1 mg/kg per day based on no effects observed in rats exposed to Cr (III) in the diet.

at 540 nm. A method using ion chromatography (IC) to separate Cr (VI) from Cr (III) prior to complexation with 1,5-diphenylcarbohydrazide and absorbance measurement has also been reported by the EPA [2]. This IC method utilizes an additional ICP-MS measurement to compensate for the reduction of Cr (VI) to Cr (III) during sample collection. Without the use of the ICP-MS data, the Cr (VI) measurements would be erroneous.

Chromium speciation methods utilizing chromatographic column separations followed by spectrometric detection also have been reported. Cox and coworkers used an activated alumina micro-column in an FIA manifold to separate and pre-concentrate Cr (VI) from Cr (III) followed by inductively coupled plasma atomic emission spectrometric detection [3]. A method using a chelating ion-exchange column to separate and pre-concentrate Cr (III) from Cr (VI) followed by flame atomic absorption spectrometric detection has been reported by Milosavljevic and coworkers [4].

Recent definitive studies of the interconversion of Cr (III) to Cr (VI) and Cr (VI) to Cr (III) during sample preparation call to question the accuracy of results generated using previously reported analytical procedures [5,6]. Speciated isotope dilution mass spectrometry (SIDMS)² can be used to study and correct for these interconversion reactions during sample analysis [7].

² Speciated Isotope Dilution Mass Spectrometry (SIDMS). Isotope Dilution Mass Spectrometry is a highly accurate technique that has been used for the determination of metals in a range of matrices. The methodology relies on addition of an internal spike of the same element, of known but different isotopic composition to that of the sample for calibration. Also any loss of metal during sample preparation is compensated for, since the only measurement made is for isotopic ratios. SIDMS takes the method one stage further by addition of species-specific isotopically-enriched spikes, one spike for each metal specie to be measured. Therefore when the isotope ratios are determined using ICP-MS after chromatographic separation it is possible to calculate the original concentration of each species in the original sample. Obviously great care should be taken to avoid loss of speciation during sample preparation and analysis in order that the isotopic ratios can be determined accurately and precisely.

1.2. Chromium detection

Many spectrophotometric techniques are available for the detection of chromium, e.g. UV-VIS Spectrophotometers, atomic absorption spectrometers (AAS), and inductively coupled plasma spectrometers (ICP) all of which have different detection limit capabilities. Inductively coupled plasma–mass spectrometry (ICP-MS) has the advantage of achieving very low ng/l detection limits for chromium, which are needed for the analysis of environmental samples. ICP-MS is also relatively easily interfaced to many liquid chromatographic techniques [8] to allow automated, on-line separation and detection of the chromium species at ng/l concentrations in solution. Lastly, ICP-MS provides multiple-mass isotopic data for the separated species.

In this work an automated method was developed for the separation and determination of Cr (VI) and Cr (III) using low-pressure chromatographic separation of the species coupled with on-line ICP-MS detection. The method was developed to demonstrate analytical capability before implementation of a SIDMS procedure for chromium speciation in environmental samples.

2. Experimental section

2.1. Reagents and materials

All solutions were prepared using 18 M Ω deionized water. The following chemicals were used for preparation of sample loading solutions and eluting solutions: ammonium acetate (A.C.S. grade, Fisher Scientific, Pittsburgh, PA, USA), ammonium sulfate (A.C.S. grade, Fisher Scientific, Pittsburgh, PA, USA), ammonium nitrate (A.C.A. grade, GFS Chemicals, Columbus, OH, USA), ammonium hydroxide (cleanroom grade, Ashland Chemicals, Columbus, OH, USA), and nitric acid (redistilled, GFS Chemicals, Columbus, OH, USA). Individual certified stock solutions containing 1000 ppm Cr (III) and Cr (VI) (High Purity Standards, Charleston, South Carolina, USA) were used to prepare test solutions of the two chromium species.

2.2. Ion chromatography

Chromatographic separations of the chromium species were achieved using the PrepLab™; a metal-free, automated, liquid handling system (VG Elemental, Winsford, UK) (Fig. 1). The output of the PrepLab was connected directly by a short length of polyethylene tubing to the sample introduction system of the ICP-MS. Two, solid-phase chelation resins were evaluated: Chelex 100 (50–100 mesh, Bio-Rad Laboratories, Hercules, CA, USA) and Prosep-Chelating I (particle size 75–125 μ m, Bioprocessing Limited, Consett, Co Durham, UK). The chelation resins were hand-packed into 3 mm \times 25 mm glass columns with standard $\frac{1}{4}$ "-28 tube fittings and PTFE frits (Om-nifit, Cambridge, UK). An Oakton pH Tester 3 (Cole-Parmer, Vernon Hills, IL, USA) was used to measure the pH of the mobile phases and solutions.

2.3. Inductively coupled plasma–mass spectrometry

A PlasmaQuad 3™ ICP-MS instrument (VG Elemental, Winsford, UK) fitted with an AutoRange Plus™ simultaneous detector and 64 000 channel Multi-channel Analyzer was used for chromium detection. The ICP-MS sample introduction system consisted of a concentric nebulizer (Glass Expansion, Victoria, Australia) and a low-volume impact-bead quartz spray chamber. A low volume, sample introduction system with rapid

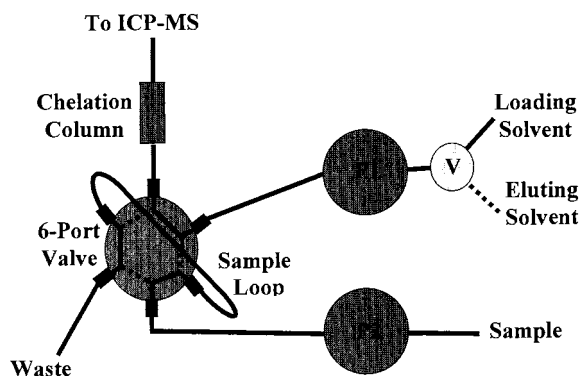


Fig. 1. PrepLab™ automated liquid handling system.

Table 1
ICP-MS instrument parameters

Gas flows	
Cool (l/min)	13.0
Auxiliary (l/min)	0.90
Nebulizer (l/min)	0.80
Plasma power (W)	1310
Sample flow rate (ml/min)	1.0

washout characteristics was preferred in order to minimize chromatographic peak broadening. The instrument software (PQVision™) was configured to control the complete analytical system including separation, detection and reporting using time resolved analysis (TRA) data acquisition. ICP-MS instrument parameters used for the chromium speciation experiments are provided in Table 1.

2.4. Implementation of PrepLab™ for separation of Cr (III) and Cr (VI)

A three-step PrepLab™ procedure was developed for the separation of Cr (III) and Cr (VI) using a solid-phase chelation resin column. A 0.5 ml sample loop is filled with sample while the loading solution flows through the column to the ICP-MS. The six-port valve is then switched so that the sample flows through the column. During this step, the chelation resin must have specificity in the solvent or buffer for one Cr species but not the other, such that one species remains bound to the resin while the other flows through to the ICP-MS. Switching of the mobile phase to an eluting solution then removes the species bound to the resin so that it flows to the ICP-MS for detection. This procedure also allows pre-concentration of the bound species during the loading step.

3. Results

3.1. Evaluation of Chelex 100 resin

Chelex 100 is a styrene-divinylbenzene co-polymer with iminodiacetic acid functional groups.

Metals are reversibly bound to the functional groups depending on the solvent in contact with the co-polymer. Chelex 100 has been used routinely to remove metal contamination from various solvents and to pre-concentrate metals for analysis [9,10]. The resin functions as a chelating resin from pH 4 to 12 and as an anion exchanger below pH 4.

MilliQ water, 0.05 M ammonium hydroxide, and 10 mM ammonium sulfate adjusted to pH 9 with ammonium hydroxide were evaluated as loading solutions for the separation of Cr (III) and Cr (VI). The eluting solution for all tests was 2 M nitric acid.

Since ICP-MS cannot differentiate between Cr (III) and Cr (VI) the binding specificity of the resin for each species was evaluated independently. Individual solutions containing 50 ppb Cr (III) and 50 ppb Cr (VI) in deionized water were prepared. Neither species exhibited specificity for the Chelex 100 resin with any of the three loading solutions.

A solution of 0.4% nitric acid was also tried as the loading solution since, at low pH, the resin behaves as an anion exchanger. A slight increase in the Cr signal followed by a leveling off was observed during the first 100 s after the Cr (VI) was introduced to the column. A wash of 2 M nitric acid did not produce any additional signal. The Cr (VI) appeared to initially bind to the resin and then slowly elute from the column with time. A much stronger binding between a Cr species and the resin is required for this separation to be effective.

3.2. Evaluation of Prosep-Chelating I

Prosep-Chelating I contains the same iminodiacetic acid functional group as Chelex 100 but the stationary phase support is porous glass rather than a co-polymer. Prosep-Chelation I functions as a chelating resin in the pH range from 1 to 9 and has been used to pre-concentrate metals for analysis (S. Nelms, 1997, personal communication). A 50 mM ammonium nitrate solution adjusted to pH 9 with ammonium hydroxide was evaluated as a loading solution. In this study 1 M nitric acid was used as the eluting solution.

Individual solutions of 50 ppb Cr (III) and 50 ppb Cr (VI) in water were analyzed first to evaluate the binding specificity of the resin. During sample loading with the 50 mM ammonium nitrate solution, Cr (VI) was not bound and flowed through the column to the ICP-MS detector. On the other hand, Cr (III) remained bound to the resin during sample loading with the 50 mM ammonium nitrate solution. When the eluent was switched to 1 M nitric acid, the bound Cr (III) eluted from the column. A solution containing both Cr (III) and Cr (VI) was analyzed next in order to test the separation capabilities of the resin (Fig. 2). Prosep-Chelating I demonstrated the required specificity for the separation of the two Cr species, which were separated in less than 5 min.

In order to further test the resin, individual solutions of Cr (III) and Cr (VI) in water were analyzed using the same analytical conditions. Fig. 3 illustrates that while Cr (III) resulted in only one peak at the Cr (III) retention time, Cr (VI) analysis resulted in peaks with retention times of both Cr (III) and Cr (VI). The small amount of Cr (III) detected during the analysis of the Cr (VI) solution could be caused by either Cr (III) contamination in the Cr (VI) solution or inter-conversion of Cr (VI) to Cr (III) during the analysis.

4. Discussion

To investigate whether the small amount of Cr (III) detected during analysis of the Cr (VI) solution was caused by contamination in the certified solution, further information on the production of the solution was obtained from the manufacturer. The manufacturer does not perform a Cr (VI)-specific test on the solution to obtain the certified concentration, but instead assumes that the solution contains only Cr (VI) because it is prepared from 99.998% pure solid potassium dichromate in water. Upon testing the pH of the standard solution it was determined to be acidic ($< \text{pH } 3.5$). At pH less than 6.5, the predominant Cr (VI) species is the strong oxidizer hydrogen chromate. Under these acidic conditions, Cr (VI) can be converted to Cr (III) [2] and thus create Cr (III) contamination in the certified Cr (VI) solution. On the other hand, the basic conditions (pH 9.0) used during steps 1 and 2 of the IC-ICP-MS method described in this paper would discourage the conversion of Cr (VI) to Cr (III). Further studies using SIDMS at each step of the analysis procedure are planned in order to determine definitively the source of the Cr (III) contamination. Analysis of the Cr (VI) standard using a method such as EPA Method 7196A would not provide a definitive answer to the question of the source of the Cr (III) contamination as noted earlier.

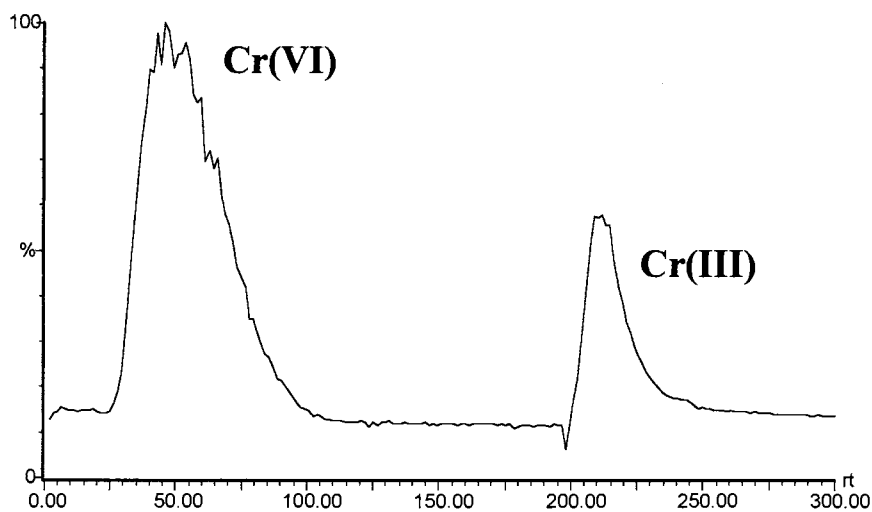


Fig. 2. Chromatography of a mixture of Cr (III) from Cr (VI) using Prosep-Chelating I.

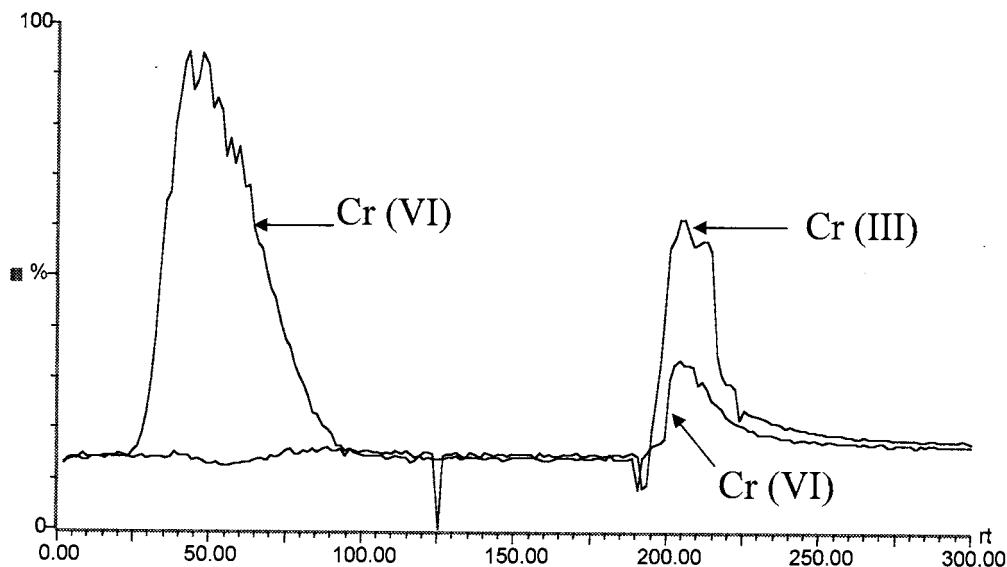


Fig. 3. Chromatography of individual Cr (III) and Cr (VI) runs using Prosep-Chelating I.

5. Summary

Cr (III) and Cr (VI) can be successfully separated using Prosep-Chelating I. On-line ICP-MS detection is sensitive enough to meet US EPA criteria. Further studies are necessary, however, to complete the evaluation of this method for the analyses of real environmental samples. Additional studies of interconversion of Cr (III) and Cr (VI) must be performed using SIDMS as well as investigation of possible interferences due to matrix ions such as Fe, Ca, K, and Na, which are present in water samples. Evaluation of sample storage containers and preservatives is also needed so that the chromium speciation in the sample remains unchanged from sampling site to analysis. Lastly, an evaluation of column design is planned to study peak shape and peak broadening.

References

- [1] USEPA Method 7196A. Chromium, Hexavalent (Colorimetric). July 1992.
- [2] E.J. Arar, S.E. Long, T.D. Martin, S. Gold, *Environ. Sci. Technol.* 26 (10) (1992) 1944–1950.
- [3] A.G. Cox, I.G. Cook, C.W. McLeod, *Analyst* 110 (1985) 331–333.
- [4] E.B. Milosavljevic, L. Lolujic, J.H. Nelson, J.L. Hendrix, *Mikrochim. Acta* III (1985) 353–360.
- [5] H.M.S. Kingston, D.W. Huo, Y.S. Lu, S. Chalk, *Spectro. Chim. Acta B* 53 (2) (1998) 299–309.
- [6] H.M. Kingston, *Environ. Sci. Technol.* 32 (21) (1998) 3418–3423.
- [7] Kingston H.M., US Patent No. 5414259.
- [8] M.K. Donais, *Spectroscopy* 13 (9) (1998) 30–35.
- [9] H.M. Kingston, R.R. Greenberg, *Anal. Chem.* 55 (1983) 1160.
- [10] R.R. Greenberg, H.M. Kingston, *J. Radioanal. Chem.* 71 (1982) 147.

Chemiluminescence method for the assay of perphenazine in drug formulation using permanganate in sulphuric acid with flow injection technique and a chemometrical optimization approach

Salah M. Sultan *, Abdullah M.S. Abdennabi, Ala'ddin M. Almuaibed

Chemistry Department, King Fahd University of Petroleum and Minerals, KFUPM Box No. 2026, Dhahran 31261, Saudi Arabia

Received 5 November 1998; received in revised form 21 December 1998; accepted 30 December 1998

Abstract

An accurate selective flow injection chemiluminescence (CL) method for the assay of perphenazine was explored. In the method 394 ppm permanganate solution was used as a chemiluminogenic reagent in 0.289 mol dm⁻³ sulphuric acid media. A photomultiplier tube was used as a detector at a total flow rate of 4.94 ml/min. Perphenazine was determined by a linear calibration plot of the following equation in the range 50–350 ppm: $mV = -4.488 + 0.1162C$, with a correlation coefficient of 0.9989 for five measurements and a relative standard deviation less than 2.33. A sampling frequency not less than 110 samples h⁻¹ was established. Three factors namely, the flow rate, sulphuric acid and permanganate concentrations were found to have an influence on the amount of chemiluminescence intensity produced. Therefore, their interaction effects were thoroughly investigated by employing the 2³ factorial design chemometrical approach and the results obtained revealed a higher interaction between sulphuric acid and permanganate and a less significant interaction for both reagents with the flow rate. The interaction of variables observed necessitated the conduct of the super modified simplex optimization procedure which has resulted in offering the proper optimum conditions as stated above and led to the quantitative assay of perphenazine. An interference study indicated that the method was suitable for application in pharmaceutical preparations. © 1999 Elsevier Science B.V. All rights reserved.

Keywords: Perphenazine; Permanganate; Factorial design; Simplex optimization; Chemiluminescence

1. Introduction

Perphenazine is chemically known as 4-[3-(2-chloro-1 OH-phenothiazine-10-yl) propyl]-1-piperazineethanol which belongs to the phenothiazines family of drugs. It is used as an

* Corresponding author. Tel.: +966-3-860-2532; fax: +966-3-860-5534.

E-mail address: smsultan@kfupm.edu.sa (S.M. Sultan)

antihistamine, antiemetic, and for the treatment of Parkinson's disease. Recently [1], perphenazine has been determined by FIA-spectrophotometry using dichromate as an oxidant but with poor sensitivity, reproducibility, and very limited linear dynamic range. In the method described [1], the system and chemical variables were optimized superficially using a univariate procedure. The metavanadate FI method [2] for the determination of perphenazine is also another proof that perphenazine oxidation product is less sensitive and irreproducible than the other phenothiazine derivatives. The official method for the assay of prephenazine, described in both the British Pharmacopoeia (BP) [3] and the United States Pharmacopoeia (USP) [4], is a titrimetric method in which the drug is dissolved in acetic acid and titrated versus perchloric acid using crystal violet indicator. CL coupled with flow injection technique [5,6] has been the most successful approach to monitor CL reactions because of the nature of such reactions which are known to be rapid, taking only a few seconds. CL reactions have also proven to be more sensitive than any spectrophotometric technique. Therefore, the present work is considered to be a better alternative with respect to sensitivity, selectivity and speed. This paper describes a FI-CL method for the determination of perphenazine by its oxidation with permanganate in sulphuric acid media using a photomultiplier tube for detection. The interaction of chemical as well as system variables were investigated employing the factorial design [7] chemometrical approach. Optimum conditions of the variables were established using the super modified simplex computer programme [8–10].

2. Experimental

2.1. Reagents

2.1.1. Perphenazine

Perphenazine stock solution (1000 ppm) was prepared by dissolving 0.1 g of the pure analytical reagent grade compound (supplied by

Rhone-Poulenc, batch No. D11) in 100 ml 0.001 M sulphuric acid.

2.1.2. Potassium permanganate

Stock solution (2000 ppm) was prepared by dissolving exactly 1.0 g of potassium permanganate (BDH AnalaR, Merck, UK) in 500 ml 0.04 M sulphuric acid. This solution is usually used after standardisation against potassium oxalate.

2.1.3. Sulphuric acid

Stock sulphuric acid solution (3 mol dm⁻³) was prepared by diluting Analar grade concentrated acid (97.80%, specific gravity 1.84 kg/l, Fisons, UK).

Working solutions were prepared from the stocks by appropriate dilutions in the appropriate sulphuric acid concentration. Distilled deionised water has been used for all preparations.

2.2. Apparatus

Fig. 1 shows the double-line manifold FI system, which was used for all measurements. The system consists of a peristaltic pump (Gilson, Minipuls, France) which delivers both the acid carrier and the permanganate oxidant streams to a PTFE T-piece, which allows the two streams to mix. The resulting stream is then passed into a coiled glass flow cell of 330 μ l volume and 1.5 mm i.d., which is backed by a polished stainless

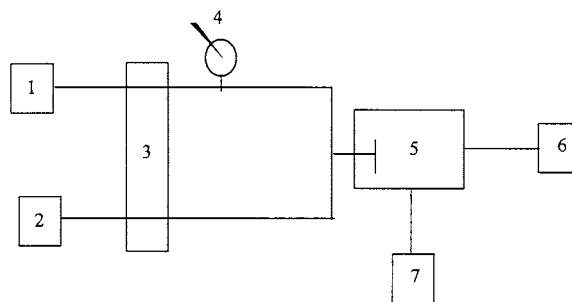


Fig. 1. Two line manifold composed of 1, 0.289 M H₂SO₄ carrier solution; 2, 394 ppm potassium permanganate; 3, peristaltic pump; 4, injector valve of 25 μ l loop size; 5, PMT; 6, XY recorder; and 7, product waste.

steel surface and faced by a photomultiplier tube detector (PMT) of the type B2F/RFI (Thorn EMI, UK). The PMT is operated at -1000 V provided by a stable high voltage power supply unit Model M312 (Wallis Hivolt, UK). The carrier was pumped through a poly (vinyl chloride) (PVC) pump tubing of 0.5 mm i.d. A Rheodyne sample injector (Cotati, CA) Model 5020 four-way PTFE rotary valve with a 25 μ l injection loop was used. A chart recorder of the type BD 4004 (Kipp and Zonen, Holland) was used for tracing at the sensitivity of 10 mV.

2.3. Computer programmes

The software package 'Chemometrical Optimization by Simplex' (COPS; Elsevier Scientific, Amsterdam) was employed for the chemometrical optimization procedure. Both Sigma plot (Jandel Scientific) and Chem Win were used for the statistical analyses as well for obtaining plots and diagrams.

2.4. Procedure

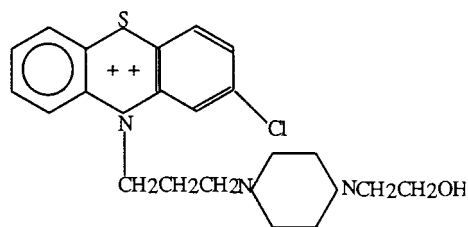
A 25 μ l drug sample was injected into 0.289 mol dm^{-3} sulphuric acid flowing at a speed of 2.47 ml/min. The permanganate solution (394 ppm) which was prepared in 0.289 mol dm^{-3} sulphuric acid was propelled at a speed of 2.47 ml/min as a carrier stream. The carrier acid solution together with the injected drug zone were then mixed with permanganate solution at the PTFE T-piece. FI tracings were recorded at a speed of 4 mm/s once the product reached the PMT.

3. Results and discussion

3.1. The chemical system

The perphenazine–permanganate redox reaction in sulphuric acid media was explored and found to give a prominent chemiluminescence (CL) emission. The nature and mechanism of the CL emission is thought to be of a direct chemiluminescent reaction type referred to earlier by

Calokerinos et al. [11]. Many oxidation reactions with permanganate were found to be occurring with the generation of CL emission when conducted with various organic compounds [11–16]. In the presence of formaldehyde and/or polyphosphate, permanganate was found to give more CL emission for the oxidation of organic species [14–16]. However, the CL emission obtained with perphenazine was high enough and does not require further treatment by adding such compounds. The oxidation of the perphenazine with permanganate was believed to be producing the dication diradical species, illustrated in the diagram below, which is responsible for the CL radiation of the permanganate. Other phenothiazines such as chlorpromazine hydrochloride, promethazine theoclate and trimeprazine tartrate were tested for CL by permanganate but gave no emission



The production of the dication diradical species in the case of oxidation of perphenazine with dichromate [1] and metavanadate [2] has been reported but with no mention of CL emission phenomenon. During this work cerium(IV) was used but no CL emission was produced. Preliminary studies revealed that this emission requires a thorough investigation to establish the best conditions to generate higher reproducibility and analytically acceptable intensity. With a flow injection technique, the reaction coil was made short enough (25 cm long) to minimise CL emission losses before reaching the photomultiplier tube detector. The flow rate was considered together with other chemical factors affecting but responsible for the CL such as sulphuric acid and permanganate concentrations. The three factors were rigorously investigated by studying their interaction effects, if any, and then subjected to an optimisation procedure to decide on the optimum conditions for quantitative assay of the drug.

Table 1

Full treatment combinations in both their original and coded values along with the responses obtained

Experiment no.	Flow rate (ml/min)	Sulphuric acid (M)	Permanganate (ppm)	Response (mm)
1	2.0	0.10	300	76
2	2.47	0.147	323	96
3	2.12	0.289	324	86
4	2.59	0.336	300	84
5	2.12	0.147	394	84
6	2.70	0.144	396	84
7	2.28	0.213	361	100
8	2.50	0.300	400	100
1	-1	-1	-1	76
2	+1	-1	-1	96
3	-1	+1	-1	86
4	+1	+1	-1	84
5	-1	-1	+1	84
6	+1	-1	+1	84
7	-1	+1	+1	100
8	+1	+1	+1	100

3.2. Interactions of variables

Prior to making a decision on what optimisation procedure should be followed to determine the conditions under which the assay method is quantitative and applicable, the interaction effect between the variables was investigated using the factorial design approach. An experiment was designed employing the simplest and most popular class of factorial design in which all the factors have only two levels denoted by a 2^f class where f is the number of variables [7]. The full treatment combinations in both their original concentrations and coded values, along with the responses obtained are depicted in Table 1. Eight runs were needed to perform the experiment with the lower level assigned the value -1 and the higher level assigned $+1$. The lower level between 2.00 and 2.15 ml/min was considered for the flow rate, 0.10–0.20 mol dm⁻³ for the sulphuric acid concentration and 300–350 ppm for the permanganate concentration. The higher level was considered between 2.16 and 2.3 ml/min for the flow rate, 0.21–0.32 mol dm⁻³ for the sulphuric acid concentration and 351–400 ppm for the permanganate concentration. The interaction effects between the factors were calculated and found to be $+8.5$ between sulphuric acid and permanganate, -5.5 between the flow rate and sulphuric acid and -4.5 between the flow rate and permanganate. It was clear that the interaction involving the flow rate was always not additive and that the interaction between sulphuric acid and permanganate is significant. Three-dimensional plots for each of the three possible interactions are presented in Figs. 2–4. The figures clearly indicated

ganate, -5.5 between the flow rate and sulphuric acid and -4.5 between the flow rate and permanganate. It was clear that the interaction involving the flow rate was always not additive and that the interaction between sulphuric acid and permanganate is significant. Three-dimensional plots for each of the three possible interactions are presented in Figs. 2–4. The figures clearly indicated

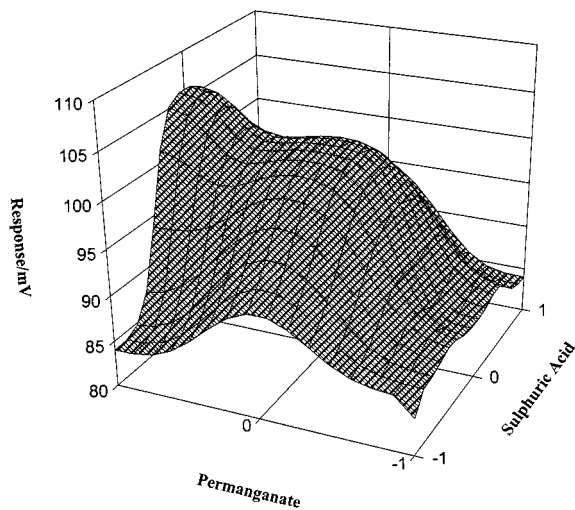


Fig. 2. Surface plot of the response in mV versus sulphuric acid and permanganate levels.

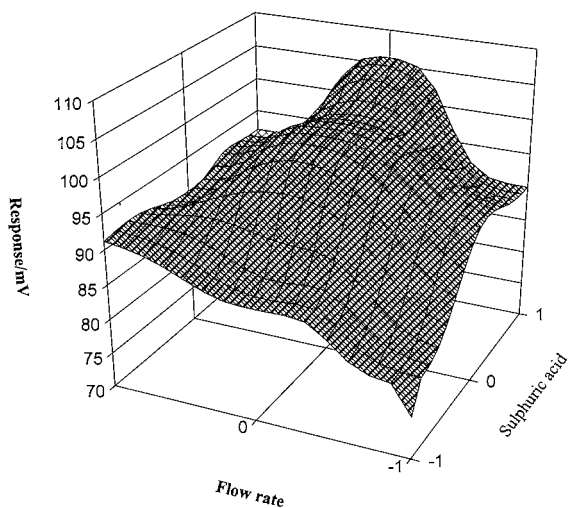


Fig. 3. Surface plot of the response in mV versus flow rate and sulphuric acid levels.

agreement with the mathematical findings. Fig. 2 shows that both sulphuric acid and permanganate have positive effects on the CL emission intensity while Figs. 3 and 4 indicate that the flow rate has a low effect on the CL emission intensity which could be attributed to the shorter reaction coil fixed earlier. This finding reveals that our flow injection system was properly set for the experiment and that the chemistry involved is posing more effect on CL emission. This is quite sensible due to the well known fact that the reduction potential for the permanganate increases by increasing the acidity of the solution.

3.3. Optimisation

The above successful treatment reveals a clear interaction between sulphuric acid and permanganate and also shows that both have a positive impact on the CL emission intensity. It was therefore decided necessary perform the simplex optimization procedure [8–10] since the iterative univariate method of optimization would not be the right choice and is not expected to give the representative best optimum conditions. The super modified simplex programme was carried out and the necessary parameters for the lower and upper boundaries of variables and the start and

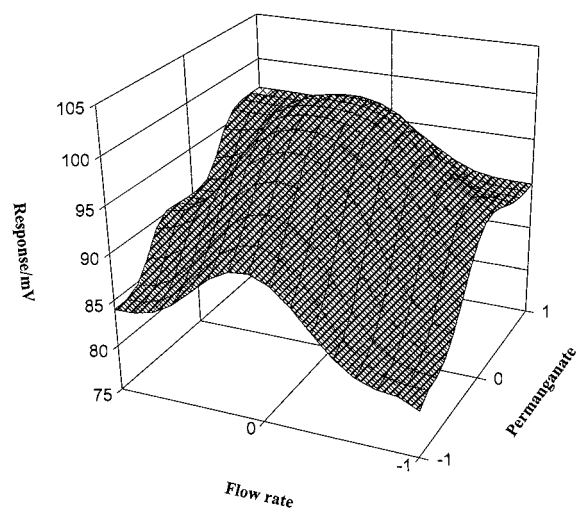


Fig. 4. Surface plot of the response in mV versus flow rate and permanganate levels.

size of steps were fed to the computer as listed in Table 2. The first experiment was designed on the basis of preliminary investigations and the previous interaction study. The initial simplex was designed by injecting 300 ppm permanganate with the flow rate fixed at 2.00 ml/min, 0.10 mol dm⁻³ sulphuric acid. The response factor for the CL emission intensity was chosen to measure the sys-

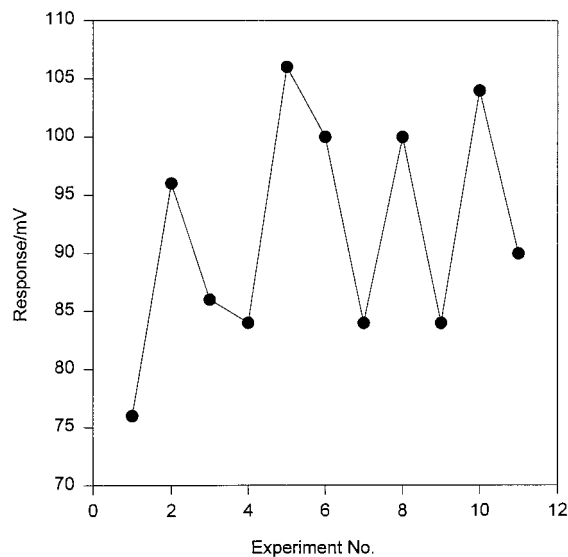


Fig. 5. Response function progress of the simplex.

Table 2
The simplex computer programme parameters

Parameter	Flow rate (ml/min)	Sulphuric acid (M)	Permanganate (ppm)
Lower	2.0	0.05	20
Upper	4	0.75	400
Start value	2	0.10	300
Step	0.5	0.20	10

tem performance and the optimum conditions for the variables chosen at the maximum response value. The progress of the simplex is shown on Fig. 5 which indicates a gradual improvement in the response function generated by having three reflection points at runs 4, 6 and 8. Only 11 runs were found to be sufficient to judge the optimum variable conditions and to halt the optimisation procedure. Finally, the best conditions obtained for maximum reproducible responses were 2.47 ml/min flow rate, 0.289 mol dm⁻³ sulphuric acid 394 ppm permanganate.

3.4. Analytical appraisal and application

A series of standard solutions of perphenazine was analysed under the optimum conditions of 2.47 ml/min flow rate, 0.289 mol dm⁻³ sulphuric acid and 394 ppm permanganate. Each run was repeated five times to calculate reproducibility and precision. The calibration plot was found to be linear over a perphenazine concentration range of 50–350 ppm with 0.9989 correlation coefficient for five measurements, 2.33 relative standard deviation (RSD) for five injections and a sampling frequency not less than 110 samples h⁻¹. The calibration equation obtained under this condition was as follows:

$$mV = -4.488 + 0.1162C$$

where C was in ppm and response was in millivolts (mV).

The method was applied to the determination of perphenazine in synthetic samples containing ingredients similar to those usually added as excipients in any pharmaceutical preparations such as starch, glucose, sucrose and maltose. The synthetic samples were prepared by dissolving the

perphenazine together with starch, glucose, maltose with concentrations as much as twice the concentration of the drug. In addition to that equimolar concentrations of chlorpromazine hydrochloride, promethazine theoclate and trimeprazine tartrate were added. It is worth mentioning here that proprietary drugs containing phenothiazines are controlled and not accessible. From the results obtained as listed in Table 3 and from the t -test values calculated when compared with the results obtained by the standard FIA-metavanadate [2] method, no interference was present from such ingredients, even if added as much as ten times the concentration of the perphenazine, indicating high accuracy and suitability for quality assurance in drug formulations.

4. Conclusion

The present method is highly specific and selective especially since other phenothiazine deriva-

Table 3
Results of statistical analysis of synthetic samples containing perphenazine obtained by the CL method compared with those obtained by the FIA-metavanadate method [2]

Species added	% Recovery \pm S.D. ^a		t -test ^b
	CL method	FIA-metavanadate method	
Starch	100.1 \pm 0.7	99.7 \pm 0.8	1.4
Glucose	99.3 \pm 0.5	99.0 \pm 0.8	1.7
Lactose	99.2 \pm 0.9	99.2 \pm 0.6	0.2
Maltose	99.6 \pm 1.0	100.4 \pm 0.8	2.0

^a Standard deviation calculated from five determinations, 300 ppm perphenazine.

^b Student t -test calculated, theoretical value = 2.228 (P = 0.05).

tives showed no CL emission under the same conditions. This method is superior when compared to the FIA-metavanadate method with respect to the stability of the oxidised product and precision of the response. The method is better than the BP and USP official procedure with respect to speed and sample throughput. The chemometrics involved, although not new, validate the method and are considered novel.

Acknowledgements

Thanks are due to KFUPM for help in allowing the main author to present this paper at the International Conference on Flow Injection Conference (ICFIA 98), Seattle, WA.

References

- [1] S.M. Sultan, A.M. Abdennabi, *Microchem. J.* 48 (1993) 343.
- [2] S.M. Sultan, *Analyst* 116 (1991) 177.
- [3] *British Pharmacopoeia*, 5th edn, HMSO, London, 1988, pp. 982–983.
- [4] *United States Pharmacopoeia*, 20th revision, 15th edn, Mark Printing, Easton, PA, 1980, pp. 601.
- [5] A. Townshend, *Analyst* 115 (1990) 495.
- [6] A.R. Bowie, M.G. Sanders, P.J. Worsfold, *J. Biolumin. Chemilumin.* 11 (1996) 61.
- [7] E.D. Morgan, *Chemometrics: Experimental Design*, Wiley, Chichester, 1991.
- [8] J.A. Nelder, R. Mead, *Comput. J.* 7 (1965) 308.
- [9] S.L. Morgan, S.N. Deming, *Anal. Chem.* 46 (1974) 1170.
- [10] W. Spendley, G.R. Hext, F.R. Himsforth, *Technometrics* (1962) 441.
- [11] A.C. Calokerinos, N.T. Deftereos, W.R.G. Baeyens, *J. Pharm. Biomed. Anal.* 13 (1995) 1063.
- [12] X.R. Zhang, W.R.G. Baeyens, G. Van Der Weken, A.C. Calokerinos, K. Imai, *Anal. Chim. Acta* 303 (1995) 137.
- [13] A.A. Al-Warthan, A. Townshend, *Anal. Chim. Acta* 185 (1986) 329.
- [14] N.T. Deftereos, A.C. Calokerinos, C.E. Efstathiou, *Analyst* 118 (1993) 627.
- [15] A.R.J. Andrew, A. Townshend, *Anal. Chim. Acta* 227 (1989) 65.
- [16] N.W. Barnett, D.G. Rolfe, T.A. Bowser, *Anal. Chim. Acta* 282 (1993) 551.

Determination of iron(II) and total iron in environmental water samples by flow injection analysis with column preconcentration of chelating resin functionalized with *N*-hydroxyethylethylenediamine ligands and chemiluminescence detection

Shizuko Hirata ^{a,*}, Hiroki Yoshihara ^b, Masato Aihara ^b

^a Chugoku National Industrial Institute, 2-2-2 Hiro-suehiro Kure, Hiroshima 737-0197, Japan

^b Kinki University, 1 Takaya-Umenobe, Higashi-Hiroshima, 739-2116, Japan

Received 26 October 1998; received in revised form 28 January 1999; accepted 1 February 1999

Abstract

A flow injection analysis (FIA) technique for the determination of Fe(II) and total-Fe in environmental water samples has been developed with a high sensitivity. The resin used for preconcentration of iron was the macroporous resin, Amberlite XAD-4 functionalized by *N*-hydroxyethylethylenediamine (HEED) groups. The technique employed was FIA by combination of on-line chelate resin preconcentration and chemiluminescence detection (CL), using brilliant sulfoflavine and hydrogen peroxide reagent solutions. The interference by coexisting Fe(III) could be eliminated by addition of 1×10^{-6} mol of deferroxamine B solution. The detection limits of Fe(II) and total-Fe were 0.80 and 0.36 nmol l⁻¹ for 5.6-ml seawater samples with a concentration of 2 nmol l⁻¹. The relative standard deviations for both samples were less than $\pm 4\%$. A typical analysis for Fe(II) can be performed in 7.5 min. The technique was ascertained by comparing the analytical value of total-Fe with the certified value of Fe in the reference standard seawater CASS-3. © 1999 Elsevier Science B.V. All rights reserved.

Keywords: Flow injection analysis; Amberlite XAD-4-HEED column; Fe(II); Environmental water samples

1. Introduction

Research related to fixation of carbon dioxide has been carried out widely to decrease the rate of global warming. As one countermeasure, the fixa-

tion of carbon dioxide by primary production of phytoplankton in oceans may possibly lower the concentration of carbon dioxide in air. The hypothesis that Fe limits primary production in the ocean [1–5] and acid rain problems [6] stimulate the iron research [7–11]. As a result, iron determination methods have been developed with high sensitivities. A number of chelating resins contain-

* Corresponding author. Fax: +81-823-72-1998.

E-mail address: hirata@cniri.go.jp (S. Hirata)

ing various functional groups (using ethylene diaminetetraacetic acid [12], iminodiacetic acid [13–15], *N*-phenylhydroxamic acid [16] and 8-quinolinole [17,18]) have been reported. Recently, with combination of on-line chelate resin preconcentration and spectrophotometric detection [19–21], or chemiluminescence (CL) detection [22–24], a number of analytical methods for iron with high sensitivities have been developed and have proved that it is very useful for determine iron in seawater. The methods mainly used resins with immobilized 8-hydroxyquinoline (8-HQ) as an on-line preconcentration column. These methods are summarized in Table 1.

In our previous study [25], we developed a flow system to determine cobalt in seawater, which had the advantage of a low detection limit. In the present work, the macroporous resin, Amberlite XAD-4 has been functionalized with *N*-hydroxyethylethylenediamine (HEED) groups [26], which has hydroxyl and amine functional groups as binding sites for metal ions and used for the preconcentration of iron. The resin has been characterized and sorption behavior of iron on the resin studied. The determination of iron(II) was measured by the method of Erlod et al. [23], which uses brilliant sulfoflavin (BSF) and hydrogen peroxide reagents, where there was interference from coexisting iron(III). The interference by coexisting iron(III) could be eliminated by addition of deferoxamine B solution, one of the siderophores known to be iron chelators and the determination of iron(II) in environmental water samples could be measured successfully.

2. Experimental

2.1. Apparatus

The chelating resin preconcentration and CL systems are shown in Fig. 1. The concentration column was a Teflon tube (4-mm i.d., 45-mm length) packed with XAD-4-HEED resin, which was sealed with two pieces of Teflon mesh (170 mesh). All the stages were switched with three-way solenoid valves which were controlled by a programmable valve controller (Tosoh, VC-8020). It employed a double-plunger pump which has 7.0-mm plungers (Sanuki Industries, DMX 2000-T) for the carrier solution, two peristaltic pumps for reagent solutions (Iwaki Industries, PST-100), a peristaltic pump for sampling (Masterflex, PA-71A), a CL detector (Japan Spectroscopic, 825-CL) and an analog recorder (Nippon Denshi Kagaku Industry, U-228). All flow lines were 1-mm i.d. Teflon tubing except for the peristaltic pump tubing (Tygon) and a flow line from the column to the CL detector (0.8-mm i.d. Teflon tubing). The length of line from the final T-piece to the flow cell was 11 cm and the volume of flow cell was 125 μ l which consisted of 0.8-mm Teflon tubing with a circular shape. Low density polyethylene containers (LDPE, Nalgene) for sample preservation were washed with hot 1 M hydrochloric acid for 3 h and hot pure water for 3 h, successively, after the usual washing with 5% Extran MA 01 (Merck).

Table 1
Recent advanced iron determination in seawater^a

Species	Reagent	Preconcentration	Detection	DL (ng ml ⁻¹)	Reference
Fe(II)	Ferrozine	C ₁₈ Sep-Pak	SP	0.6	King et al. [20]
Fe(II)	Ferrozine	C ₁₈ Sep-Pak	HPLC/SP	0.1	Yi et al. [19]
Fe(II)	BSF-H ₂ O ₂	TSK-8HQ	CL	4.4	Erlod et al. [23]
Fe(III)	PSAP	Silica-8HQ	SP	10	Kuma et al. [21]
Fe(III)	Luminol-H ₂ O ₂	MAF-8HQ	CL	0.05	Obata et al. [24]
Fe(II) + Fe(III)	DPD-H ₂ O ₂	Vinyl polymer -8HQ	SP	0.025	Measures et al. [22]

^a DL, detection limit; CL, chemiluminescence; SP, spectrometry; BSF, Brilliant sulfoflavine; PSAP, 2-nitroso-5-(*N*-propyl-*N*-sulfo-propylamino)phenol; DPD, *N,N*-dimethyl-*p*-phenylenediamine.

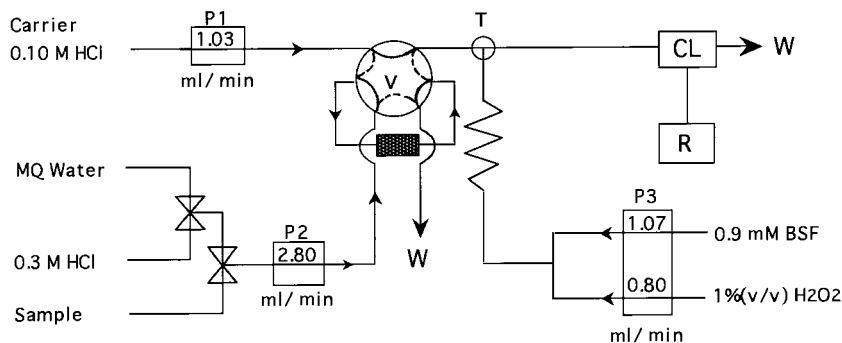


Fig. 1. Schematic diagram of manifold for the on-line column pre-concentrating CL system. P₁, Double syringe plunger pump; P₂, peristaltic pump; T, three-way joint; V, 6-way valve; column, Amberlite XAD-4-HEED (6 mm i.d., 45 mm); CL, chemiluminescence detector (volume of flow cell: 125 μ l); R, recorder; W, waste.

2.2. Reagents

Brilliant sulfoflavin (BSF, Tokyokasei), hydrochloric acid (Cica-Merck, for toxic metal analysis), hydrogen peroxide (Wako Pure Chemical Industries, for atomic absorption spectrometry), ammonia water (Cica-Merck, for toxic metal analysis) hydroxylamine hydrochloride (Wako Pure Chemical Industries, for atomic absorption spectrometry) and deferrioxamine B (Sigma) were used without further purification. All solutions were made up with Millipore Milli-Q (MQ) water.

The carrier solution (eluent) was 0.075 M hydrochloric acid; 0.9 mM BSF was dissolved in the phosphate buffer (pH 8.3) [23]. Hydrogen peroxide solution was 1.0% (v/v) and 3 M acetate buffer solution (pH 4.4) was prepared by acetic acid (Merck, Suprapur) and ammonia water (Merck, Suprapur). The final concentration of deferrioxamine B solution was 1×10^{-6} M.

2.2.1. Iron standards

Stock solutions (10 mM) of iron(II) and iron(III) were prepared from ferrous ammonium sulfate (Katayama Chemical Industries, special grade) and ferric chloride (Katayama Chemical Industries, special grade) by dissolving in 0.12 M hydrochloric acid, respectively. Working standards were prepared by diluting the stock solutions with MQ water. A 10^{-6} M iron(II) and iron(III) solution was made freshly every 3 weeks.

The concentrations of iron(II) and iron(III) with 10^{-4} M were certified by comparison with the commercial iron standard for atomic absorption spectrometry (Katayama Chemical). Artificial seawater was prepared by Lyman and Fleming [27] and purified by a MAF-8HQ (8-quinolinol-immobilized fluoride containing metal alkoxide glass) [24] column and an ODS-C₁₈ column before use. Standard solutions of 10 mM of Mn, Cu, Co, Ni, Zn, Pb, Cd, Cr(III) and Al were made from special grade reagents.

2.3. Preparation of XAD-4-HEED resin

Amberlite XAD-4 was functionalized after Dev and Rao [26]. XAD-4 beads (10 g) were first acylated by refluxing with acetic acid (20 ml) and anhydrous aluminium trichloride (1 g) in petroleum ether at 70°C for 30 h. The product was filtered off and washed with 50 ml of hexane. The intermediate product was then stirred into 500 ml of water containing 8.5 g of potassium permanganate and 10 g of sodium hydroxide at 40°C for 1 h. The product was filtered off, washed with water and treated with hydrochloric acid (1 + 1). The subsequent carboxylic acid was then refluxed with 50 ml of thionyl chloride at 60°C for 0.5 h. The intermediate resin was refluxed with HEED (2.0 ml) and sodium ethoxide (11.3 mM) in toluene at 100°C for 8 h. A light yellow resin was obtained.

2.4. Analytical procedure

The FIA system was operated as follows. With the injection valve in the load position, a sample was drawn and iron(II) was collected on the XAD-4-HEED column. The sample was typically pumped through the column for 2 min at a flow rate of 2.8 ml/min. The solenoid valve was switched and Milli-Q water was pumped through the column for 1 min at a flow rate of 2.8 ml min⁻¹. The injection valve was then switched to the elute position and 0.075 M HCl flowed through the column, eluting the iron. The injection valve remained in the elute position for 2 min. The HCl carrier stream containing the iron merged the mixture of both the BSF reagent and the H₂O₂ reagent solutions before entering the flow cell. The solenoid valve was switched, 0.3 M HCl washed through the column for 1 min, and after the solenoid valve was switched, MQ water was washed through the column for 1.5 min. The injection valve was then returned to the load position. Total analytical time was 7.5 min. The analytical procedure is shown in Fig. 2. Determination of total Fe was similar to the iron(II) method after the addition of buffer solution and

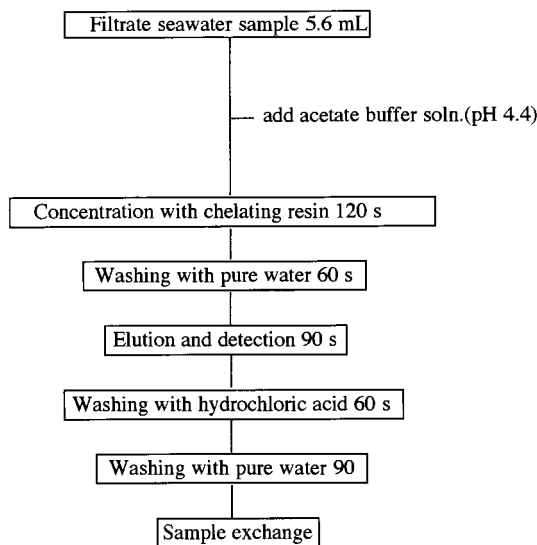


Fig. 2. A flow chart of the analytical procedure for the determination of iron(II) in a seawater sample by on-line chelate pre-concentration with CL detection.

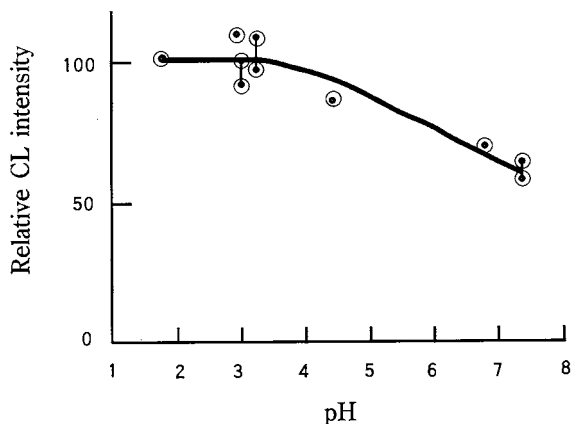


Fig. 3. Effect of reaction pH on the CL signals generated by a 10 nmol l⁻¹ Fe(II) addition.

hydroxylamine hydrochloride solution to a sample solution and being left for 30 min.

3. Results and discussion

The object of this work was to produce a method that could provide a precise determination of iron at the nanomolar level. Our efforts were focused on optimizing the chemistry and preconcentration for the shortest possible analysis times.

3.1. Evaluation of reaction chemistry parameter

The BSF-H₂O₂ CL method was optimized for FIA by Erlod et al. [23]. We also re-evaluated the chemical parameters using the XAD-4-HEED column. Although the optimal reaction pH with the concentration column was found to be between 2.5 and 3.5 (Fig. 3), in disagreement with the results of Erlod et al. [23], the noise and background signal of the system also increases with lowering pH value. We used pH 3.3.

The effect of H₂O₂ concentration on sensitivity was also determined. By using a 10 nM iron(II) standard solution, the effect of H₂O₂ concentration was investigated in the range from 0.5 to 1% (v/v) H₂O₂ concentrations. The results show that the sensitivity of the technique as measured by the slope of the standard curve continually increased

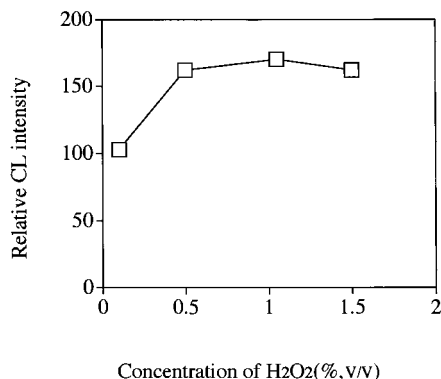


Fig. 4. Effect of H₂O₂ concentration on the signal generated by a 10 nmol l⁻¹ Fe(II) addition to MQ water containing a buffer solution (pH 4.4).

up to a H₂O₂ concentration of 1.0% (v/v) in the reagent stream; beyond this concentration there is no appreciable increase (Fig. 4). The concentration of H₂O₂ was adjusted to 1.0% (v/v).

The effect of BSF concentration at the optimum peroxide concentration (above) is shown in Fig. 5. Sensitivity peaks at a BSF concentration of 0.9 mM. We have adopted the plateau concentration of 0.9 mM.

3.2. Optimization of preconcentration column parameters

3.2.1. Sample pH

XAD-4-HEED resin was found to remove iron

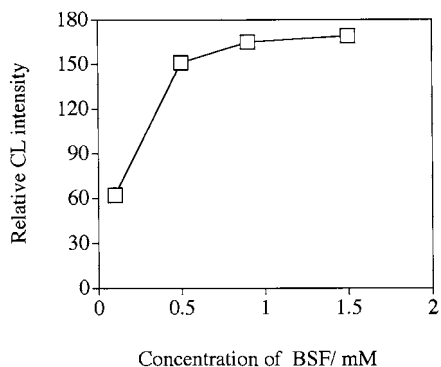


Fig. 5. Effect of BSF concentration on the signal generated by a 10 nmol l⁻¹ Fe(II) addition to MQ water containing a buffer solution (pH 4.4).

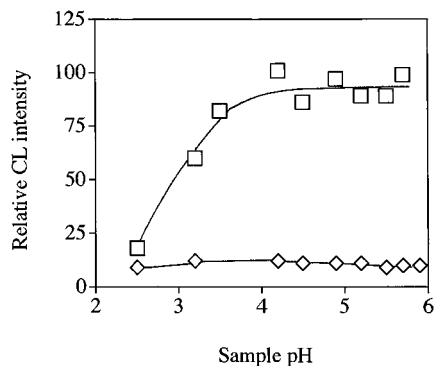


Fig. 6. Effect of sample pH on the CL signals generated by a 10 nmol l⁻¹ Fe(II) addition. (□) Fe(II), 10 nmol l⁻¹ in MQ water (pH 4.4); (◇) blank.

quantitatively from water samples in the pH range 4–6 (Fig. 6). We adopted pH 4.4 and then adjusted this with a 3 M ammonium acetate buffer solution to a target pH of 4.4 prior to iron absorption on the XAD-4-HEED column. The recoveries of iron(II) by the column were examined using a standard solution with 50 nM iron(II) both in MQ and in seawater. The solutions passed through the column were collected and iron(II) concentrations in the solutions were measured by the column preconcentration CL method. Since the iron(II) concentrations in them could not be detected, the recoveries of iron(II) were believed to be 100%.

3.2.2. Amounts of buffer solution

The amount of 3 M acetate buffer solution (pH 4.4) was examined in the range 0.1–1.0 ml added to a 100-ml sample solution; 0.1–0.2 ml addition of the buffer solution exhibited the highest signals, but the CL signals decreased with time. Since the CL signals of iron(II) in a sample solution with 0.4 ml of buffer solution added to a 100-ml sample were stable for 50 min (Fig. 7), 0.4 ml of buffer solution was added to a 100-ml sample.

3.3. Interferences of foreign ions

The column dimensions and exchange capacity is very important on the tolerance of interferences with the on-line preconcentration system. The ef-

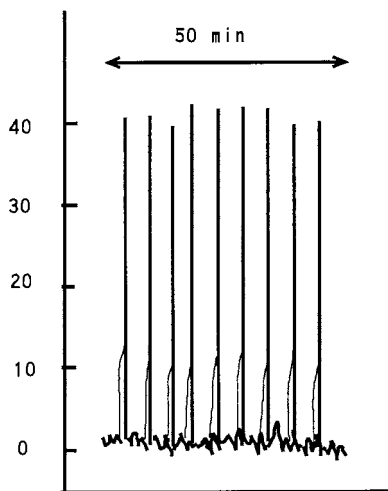


Fig. 7. Stability of CL signals generated by a 5 nmol l^{-1} Fe(II) MQ solution.

fect of foreign metal ions on the recovery of iron(II) was examined at pH 4.4 in the range 1–100 times higher than iron(II) concentrations; Mn^{2+} , Co^{2+} , Ni^{2+} , Pb^{2+} , Cd^{2+} , and Cr^{3+} had little effect, but Cu^{2+} and Fe^{3+} ions enhanced the CL signals as shown in Table 2. Since the concentration of Cu^{2+} in seawater is similar to iron, Cu^{2+} coexisting in seawater has not effect. However, since an equivalent amount of coexisting iron(III) enhanced 18% of the CL signal of iron(II), iron(III) must be separated from iron(II).

A masking solution for iron(III) in solution was investigated. Most terrestrial microorganisms

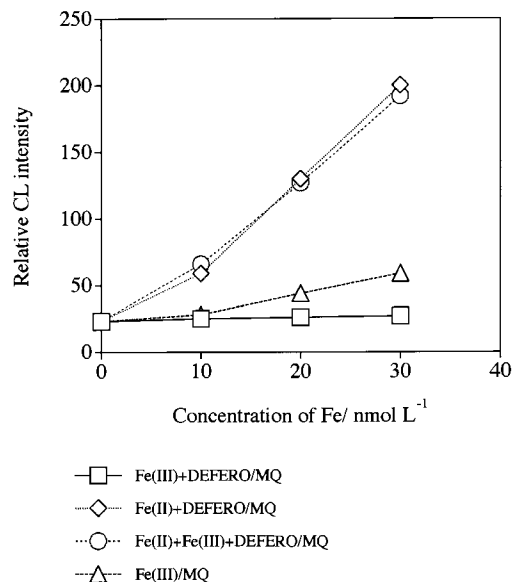


Fig. 8. Calibration curves of Fe(II) and effect of addition of deferrioxamine solution on the CL signals of Fe(III). □, Fe(III) + 10^{-6} M deferrioxamine solution; ◇, Fe(II) + 10^{-6} M deferrioxamine solution; ○, Fe(II) + Fe(III) + 10^{-6} M deferrioxamine solution; △, Fe(III) in MQ water.

acquire Fe through a siderophore-mediated uptake system [28,29]. Ferrioxamine B has a very high Fe^{3+} affinity constant ($\log K = 30.60 \sim 30.97$) [30]. By addition of 10^{-6} M deferrioxamine B, 10^{-7} M of iron(III) was chelated with deferrioxamine B completely (Fig. 8). So with an addition of deferrioxamine B solution, iron(II) could be determined separately from iron(III).

Table 2

Relative signals of the solutions containing 10 nmol l^{-1} iron(II) plus an additional trace metal at the concentration shown to the signal of 10 nmol l^{-1} iron(II) on XAD4-HEED

Amount of added metal (nmol l^{-1})	Signal for [metal+iron(II)]/signal for iron(II)									
	Mn^{2+}	Cu^{2+}	Ni^{2+}	Co^{2+}	Zn^{2+}	Pb^{2+}	Cd^{2+}	Cr^{3+}	Fe^{3+}	Al^{3+}
10	0.96	0.97	0.96	0.94	0.96	0.96	1.02	0.94	1.18	1.03
100	0.93	1.16	1.00	0.90	0.99	0.98	1.08	1.01	>2.00	1.07
1000	0.70	2.34	1.13	1.27	0.94	1.00	1.05	1.07	–	1.13

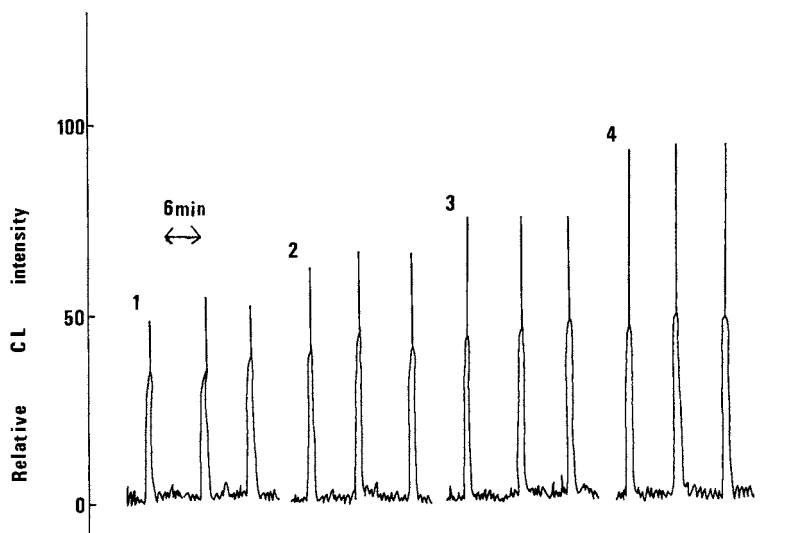


Fig. 9. Typical CL signals of total iron in artificial seawater samples containing a hydroxylamine hydrochloric acid solution.

3.4. Detection limit and precision

Although XAD-4-HEED resin could chelate iron(II) efficiently from a MQ water sample, the recovery of iron(II) from an artificial seawater sample was relatively low. Therefore the loading time for seawater samples was lengthened to 4 min against 2 min for MQ water samples. The detection limits of the method for the relative standard deviations for three replicate measurements using a concentration of 2 nmol l^{-1} iron(II) were 0.30 nmol l^{-1} iron(II) in a MQ water samples and 0.80 nmol l^{-1} iron(II) in seawater samples (Fig. 9). The precision of both samples was less than $\pm 4.0\%$. The calibration curves were linear in the concentration range of $0.8\text{--}200 \text{ nmol l}^{-1}$ iron(II).

3.5. Determination of total iron

3.5.1. Addition of reducing agent solution for iron(III) reduction

Total dissolved iron concentrations can be determined by reducing iron(III) to iron(II) prior to analysis. A hydroxylamine hydrochloride solution is suitable due to its rapid and efficient reducing power [10,31]. Therefore, addition of 0.2 mM amounts of hydroxylamine hydrochloride solution

were examined by using an artificial seawater sample with a concentration of 20 nmol l^{-1} iron(III). Since the CL signals did not change greatly by additions of 0.2 mM hydroxylamine hydrochloride solution in the range $0.1\text{--}0.5 \text{ ml}$ to a 50-ml sample, 0.3 ml of reducing solution was added to a 50-ml sample.

3.5.2. Standing time for reduction of iron(III)

Effect of standing time for reduction of iron(III) after addition of 0.3 ml of hydroxylamine hydrochloride solution was examined. Since the CL signals increased with time and was constant after 1 h, a standing time of 1 h was used.

Table 3

Comparison of dissolved iron values determined by this method and certified value for the trace metal standard seawater solution*

Reference material	Iron concentration (nmol l^{-1})	
	Certified	This method
CASS-3	22.56 ± 3.04	23.25 ± 0.25

* National Research Council of Canada, Marine Analytical Chemistry Standard Program.

Table 4

Iron(II), total-iron and iron(III) concentrations in rain water, tap water, river water and coastal seawater samples

Sample	Iron(II) (nM)	Total-iron (nM)	Iron(III) (nM)	Iron(II)/Total-iron (%)
Rain water	7.7 ± 1.3 (n = 3)	17.6 ± 0.7 (n = 3)	9.9 ± 1.3	43.8
Tap water	18.0 ± 1.0 (n = 2)	25.0 ± 1.0 (n = 3)	5.0 ± 1.0	72.0
River water	39.0 ± 3.0 (n = 3)	90.5 ± 0.5 (n = 2)	51.5 ± 3.0	43.1
Coastal seawater	53.3 ± 4.7 (n = 3)	67.7 ± 2.3 (n = 3)	14.4 ± 4.7	78.6

3.5.3. Accuracy

Accuracy of the method was ascertained by analyzing iron in the standard reference seawater obtained from National Research Council of Canada. The analytical result is shown in Table 3 and good agreement was found between our analytical value and the certified value for CASS-3 (Coastal Atlantic Surface Seawater).

3.6. Application to environmental samples

The method was applied to the determination of iron(II) and total-iron in the rain water, tap water, river water and coastal seawater samples. The calibrations for rain, tap and river water samples were made by MQ water and the calibrations for coastal seawater samples were made by artificial seawater. The analytical results are shown in Table 4. The concentrations of iron in the environmental samples were in the range 7.7 ~ 53.3 nM for iron(II) and in the range 17.6 ~ 90.5 nM for total iron, respectively. The ratios of iron(II) to total-iron were in the range 43.1 ~ 78.6%. Iron(II) and total-iron in the environmental samples could be determined successfully by the method.

4. Conclusions

Combination of on-line column preconcentration and CL detection demonstrates that the technique can be applied to iron(II) and total Fe determinations in environmental samples such as acid rain. Chelation of iron(III) with deferrioxam-

ine B solution has a possibility for determination of iron(II) in various environmental samples and the speciation of iron(II) and iron(III). The system is easy to construct and inexpensive. Furthermore since the running cost of the CL method is very cheap in contrast to an inductively coupled plasma-mass spectrometry instrument, it is very useful and convenient for analysis of environmental samples.

References

- [1] J.H. Martin, S.E. Fitzwater, *Nature* 331 (1988) 341.
- [2] J.H. Martin, R.M. Gordon, *Deep-Sea Res.* 35 (1988) 177.
- [3] J.H. Martin, R.M. Gordon, S.E. Fitzwater, *Deep-Sea Res.* 36 (1989) 649.
- [4] J.H. Martin, R.M. Gordon, S.E. Fitzwater, *Nature* 345 (1990) 156.
- [5] J.H. Martin, R.M. Gordon, S.E. Fitzwater, *Limnol. Oceanogr.* 36 (1991) 1793.
- [6] G. Zhuang, Z. Yi, R.A. Duce, P.R. Brown, *Nature* 355 (1992) 537.
- [7] M.L. Wells, N.G. Zorkin, A.G. Lewis, *J. Mar. Res.* 41 (1983) 731.
- [8] H.W. Rich, F.M.M. Morel, *Limnol. Oceanogr.* 35 (1990) 652.
- [9] D.W. O'Sullivan, A.K. Hanson, W.L. Miller, D.R. Kester, *Limnol. Oceanogr.* 36 (1991) 1727.
- [10] K.S. Jhonson, K.H. Coale, V.A. Elrod, N.W. Tindale, *Mar. Chem.* 46 (1994) 319.
- [11] G. Zhuang, Z. Yi, G.T. Wallace, *Mar. Chem.* 50 (1995) 41.
- [12] E.M. Moyers, J.S. Fritz, *Anal. Chem.* 49 (1977) 418.
- [13] M. Morhol, K.L. Cheng, *Talanta* 21 (1974) 751.
- [14] S. Tomoshige, M. Hirai, H. Ueshima, *Anal. Chim. Acta* 115 (1980) 285.
- [15] P. Figura, B. McDuffie, *Anal. Chem.* 49 (1977) 1950.
- [16] R. Mendez, V.N.S. Pillai, *Analyst* 115 (1990) 213.

- [17] S.N. Willie, R.E. Sturgeon, S.S. Berman, *Anal. Chim. Acta* 149 (1983) 59.
- [18] W.M. Landing, C. Haraldson, N. Paxeus, *Anal. Chem.* 58 (1986) 3031.
- [19] Z. Yi, G. Zhuang, P.R. Brown, R.A. Duce, *Anal. Chem.* 64 (1992) 2826.
- [20] D.W. King, J. Lin, D.R. Kester, *Anal. Chim. Acta* 247 (1991) 125.
- [21] K. Kuma, S. Nakabayashi, Y. Suzuki, I. Kudo, K. Matsunaga, *Mar. Chem.* 37 (1992) 15.
- [22] C.I. Measures, J. Yuan, J.A. Resing, *Mar. Chem.* 50 (1995) 2573.
- [23] V.A. Elrod, K.S. Johnson, K.H. Coale, *Anal. Chem.* 63 (1991) 893.
- [24] H. Obata, H. Karatani, E. Nakayama, *Anal. Chem.* 65 (1993) 1524.
- [25] S. Hirata, Y. Hashimoto, M. Aihara, G.V. Mallika, *Fresenius J. Anal. Chem.* 355 (1996) 676.
- [26] K. Dev, G.N. Rao, *Analyst* 120 (1995) 2509.
- [27] J. Lyman, R.H. Fleming, *J. Mar. Res.* 3 (1940) 134.
- [28] R.T. Reid, A. Butler, *Limnol. Oceanogr.* 36 (1991) 1781.
- [29] K. Murakami, S. Ohta, H. Fuse, O. Takimura, K. Kamimura, Y. Yamaoka, *Microbios* 84 (1995) 231.
- [30] G. Winkelmann, *Handbook of Microbial Iron Chelates*, CRC Press, Boca Raton, FL, 1991, p. 189.
- [31] K. Isshiki, Y. Sohrin, H. Karatani, E. Nakayama, *Anal. Chim. Acta* 224 (1989) 55.

Optimization for detection of flunarizine by high performance liquid chromatography/electrospray/mass spectrometry

Ming-Ren S. Fuh *, Chi-Jen Hsieh, Yu-Lun Tai

P.O. Box 86-72, Department of Chemistry, Soochow University, Taipei, Taiwan, ROC

Received 21 October 1998; accepted 10 November 1998

Abstract

This paper describes a newly developed high performance liquid chromatography/electrospray/mass spectrometry (HPLC/ES/MS) method for the determination of flunarizine (FZ) in artificial cerebrospinal fluid. The optimization for the detection of FZ in biological fluid by LC/ES/MS was investigated. The effects of solvent composition, the addition of modifier and flow rate on the detection of FZ by ES/MS were examined. The detection limit of this method (~ 0.8 nM) proved to be much better than previously reported methods. Satisfactory accuracy (98.2–106.0%) of this newly developed method was obtained. The application of this method was demonstrated by analyzing FZ in rat microdialysis samples. © 1999 Elsevier Science B.V. All rights reserved.

Keywords: High performance liquid chromatography/electrospray/mass spectrometry; Flunarizine; Artificial cerebrospinal fluid

1. Introduction

Flunarizine (FZ) [*trans*-1-cinnamyl-4-(4,4-difluorobenzhydryl) piperazine dihydrochloride], is one of the piperazine derivatives with antihistamine properties and calcium channel blocking activity. FZ is now widely used in the treatment of cerebral and peripheral vascular insufficiency [1,2]. A recent clinical study reported that FZ induced Parkinsonism in patients during chronic administration. Therefore, the development of a

sensitive analytical method is an important task that will help researchers investigate the pharmacokinetics of FZ and understand the cause of its side-effect.

Most of the previous studies focused on the concentrations of FZ in the plasma and few reports monitored the concentrations of FZ in the brain. A number of gas chromatography (GC) and high performance liquid chromatography (HPLC) methods for the determination of FZ were also reported [3–5]. The reported GC methods provided good sensitivity but they required a multiple-step extraction procedure prior to GC analysis. Some of the previous reported HPLC methods also required complex sample prepara-

* Corresponding author. Tel.: +886-2-28819471, ext. 6821; fax: +886-2-28811053.

E-mail address: msfuh@mail.scu.edu.tw (M.-R.S. Fuh)

tion to extract FZ from plasma; furthermore, some of them utilized a complex mobile phase at elevated temperature. Our laboratory has developed an HPLC with UV detection method to study the pharmacokinetics of FZ in the whole brain of Sprague–Dawley rat [6]. Although this method required little sample preparation, its relatively high detection limit (20 nM) makes it unsuitable for in situ microdialysis application.

HPLC/electrospray/mass spectrometry (HPLC/ES/MS) has emerged as an effective and useful analytical technique for many applications [7–13]. In this paper, we will discuss the optimization for the detection of FZ in biological fluid by LC/ES/MS and propose the possibility of adapting an LC/UV method for LC/ES/MS application.

2. Experiment

2.1. Reagents

HPLC grade acetonitrile (Mallinckrodt Baker, Paris, KY, USA) and water (HPLC grade, Labscan, Dublin, Ireland) were used throughout the experiment. Flunarizine dihydrochloride and sodium hydroxide were purchased from Sigma (St. Louis, MO, USA). Ammonia solution, sodium chloride, magnesium chloride, potassium chloride, calcium chloride, ascorbic acid and glucose were purchased from Nacalai Tesque (Kyoto, Japan).

2.2. Instrumentation

An HP-5989B mass spectrometer equipped with an HP-59987A electrospray interface (Hewlett Packard, Palo Alto, CA, USA) was used. Heated nitrogen gas (350°C, 12.5 l/min) evaporated solvent from the spray chamber. Compressed nitrogen (80 psi) was used for nebulization. The cylinder electrode in the spray chamber was set at –4000 V. The end plate and capillary entrance voltage were set at –3500 and –6000 V. The voltage of skimmer 1, lens 1, skimmer 2, lens 2 and lens 3 were set at 31.0, –1.0, 10.2, 12.4 and –86 V, respectively. Mass spectra collected in scan mode were obtained by scanning from 10 to

500 m/z in 0.5 s. Over the measured mass range, nine scans were averaged with a step size of 0.1. HP Chemstation analysis package (G1034C, version C.03.00) was utilized to determine the molecular mass.

An HP1050 four solvent gradient pump (Hewlett-Packard, Palo Alto, CA, USA) was used for LC and flow injection analysis. A syringe pump (model 22, Harvard Apparatus, Natick, MA, USA) was employed for flow infusion experiments. A Merck LiChroCART RP-18e (125 × 3 mm, 5 μm; Merck KGaA, Germany) with an on-line filter was used for chromatographic separation throughout the analysis.

2.3. Standard solution

Standard solutions (0.001 M) of FZ were prepared in acetonitrile/water (80/20, v/v) or artificial cerebrospinal fluid (ACSF). The stock solution was further diluted to yield the appropriate working solutions. All solutions were stored at 4°C in the dark. ACSF is composed of 0.13 M sodium chloride, 0.98 mM magnesium chloride, 2.65 mM potassium chloride, 1.2 mM calcium chloride, 0.25 mM ascorbic acid, and 10 mM glucose. The mixture was adjusted to pH 7.2–7.4 with 0.1 M sodium hydroxide.

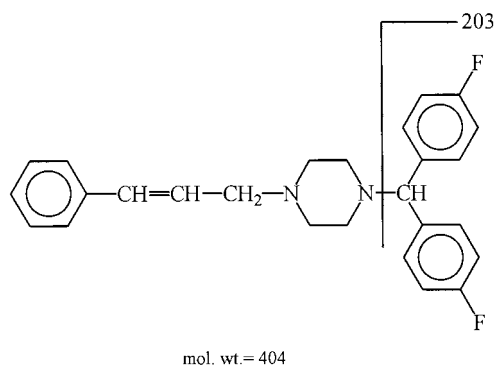


Fig. 1. Molecular structure of FZ.

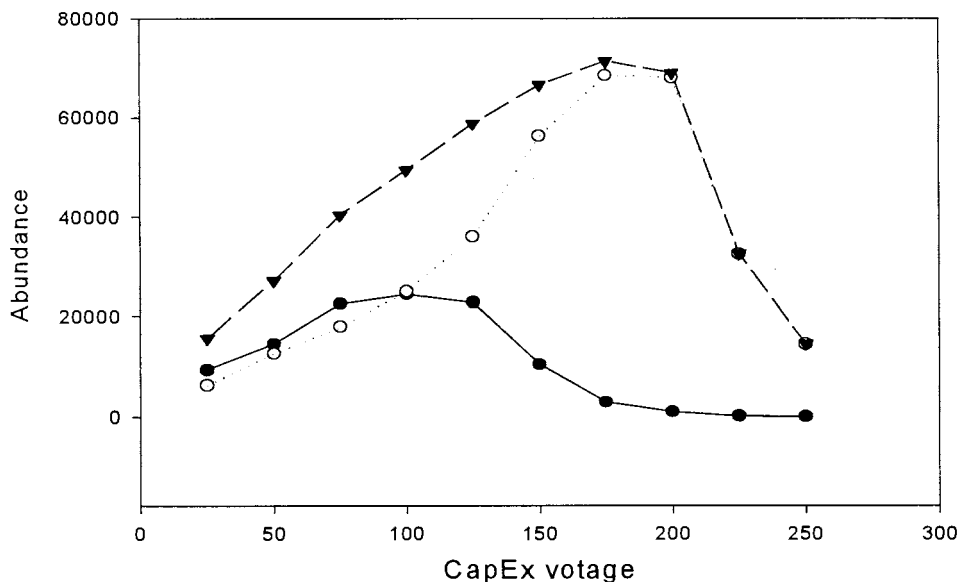


Fig. 2. Relative effect on abundance of $[M + H]^+$ ($m/z = 405$) and fragmented ($m/z = 203$) ions as capillary exit voltage (CapEX). ●, $m/z = 405$; ○ $m/z = 203$; ▼, $m/z = 405$ and 203 .

3. Results and discussion

An LC/UV method utilizing a C_{18} column and isocratic elution has been developed for the analysis of FZ in the brain of Sprague–Dawley rat [6]. A mixture of acetonitrile and water (80/20, v/v) with 0.14% of ammonium hydroxide was used as mobile phase. We attempted to adapt this LC method for LC/ES/MS application. Several parameters associated with LC separation and ES/MS detection were examined to develop a sensitive and accurate LC/ES/MS method to determine FZ in microdialysate for pharmacokinetic study.

ES/MS is a soft ionization technique, however, molecular fragmentation can be obtained through in-source collision-induced-dissociation (CID). For FZ, two major ions ($m/z = M + 1$ and 203) were detected in positive mode detection. The structures of FZ and proposed fragmented ion are shown in Fig. 1. The effect of CID voltage on the fragmentation of FZ was examined and the results are summarized in Fig. 2. When CID voltage increased from 25 to 100 V, the abundance of both ions ($m/z = 405$ and 203) increased. However, the abundance of $[M + H]^+$ ion decreased

while the abundance of fragmented ion ($m/z = 203$) increased as the CID voltage increased from 100 to 175 V. When CID voltage was higher than 175 V, a small amount of $[M + H]^+$ ion was detected and the abundance of fragmented ion ($m/z = 203$) decreased significantly as the CID voltage increased. In this study, CID voltage was set at 175 V and the selective ion monitoring ($m/z = 203$) was used for quantitative analysis to maximize sensitivity.

We examined the effects of solvent composition on the detection of FZ and LC separation. The effect of solvent composition on ES/MS detection of FZ was also examined. In addition to acetonitrile/water mixture, we tested the effectiveness of methanol/water mixture as a mobile phase. Although there is a small enhancement of the sensitivity of ES/MS detection when methanol/water mixture is used as solvent, the decline in efficiency of LC separation makes it unsuitable for our application.

From our previous study, we found adding ammonium hydroxide in mobile phase necessary to enhance LC separation of FZ in biological fluid sample. We investigated the effect of ammonium hydroxide on determination of FZ by ES/

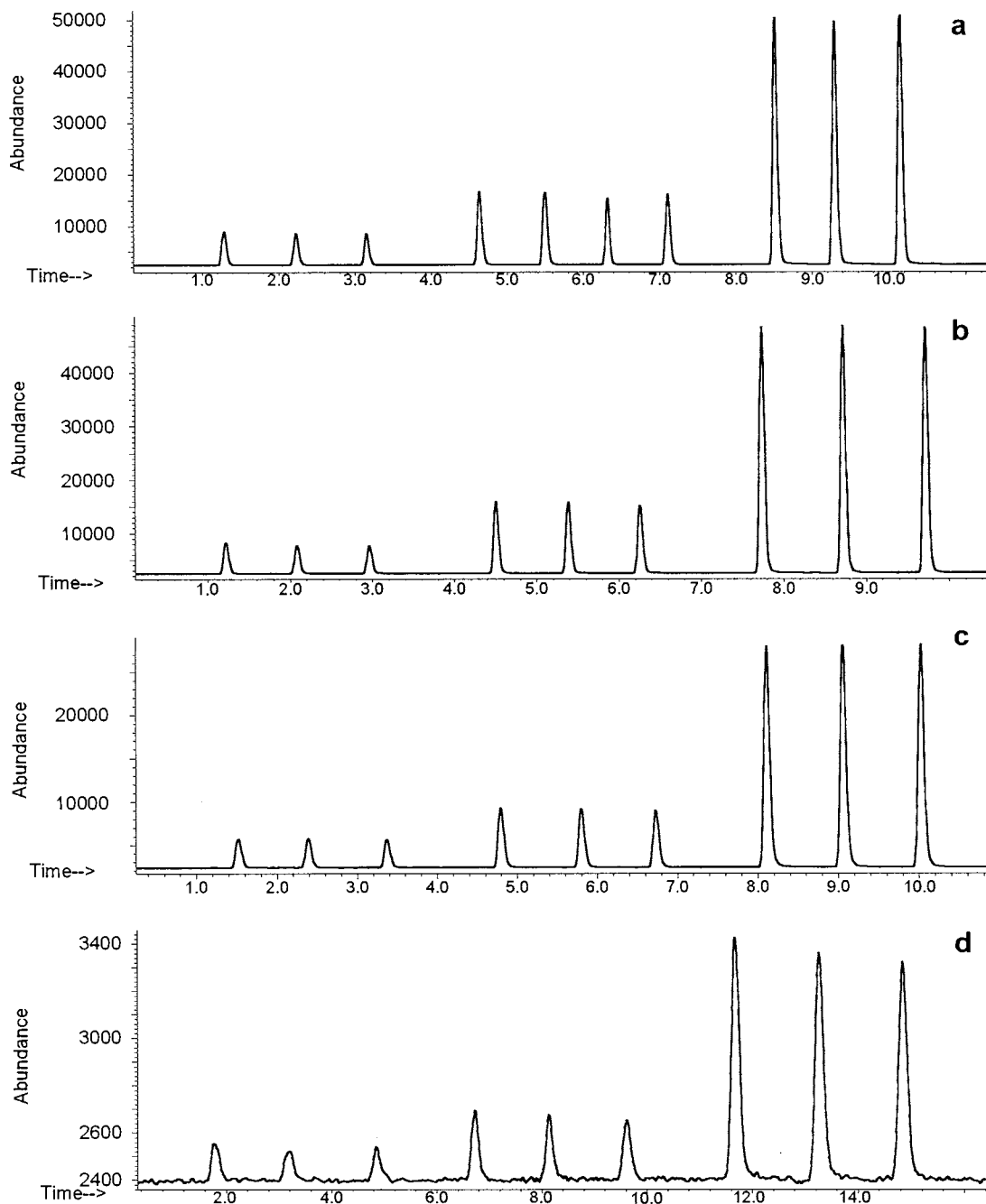


Fig. 3. ES/MS response at different split ratio. (a) No split, (b) 64%, (c) 28%, (d) 20%.

MS. The results show that there is $\sim 15\%$ decrease in ES/MS response when 0.14% of ammonium hydroxide was added in acetonitrile/water

mixture. This might be attributed to the decrease of the protonation of FZ in solution. Although the addition of ammonium hydroxide would re-

duce ES/MS sensitivity, it is needed for LC separation [6]. Hence, we have chosen acetonitrile/water (80/20, v/v) with 0.14% ammonia hydroxide as mobile phase for LC separation.

Another important parameter affecting the sensitivity of ES/MS is the flow rate of sample introduction [14]. For LC/ES/MS, the dimension of the LC column used for separation will determine the flow rate of sample introduction. However, post-column splitting could also be utilized to reduce the amount of LC elute being introduced into ES/MS. The effluent flow for most electro-spray interfaces is restricted to between 0.5 and 0.1 ml/min. A flow injection set-up was used for this study and a splitting-T was placed between sample injector and ES/MS to control the sample flow. The results of this study are shown in Fig. 3. The flow rate of pump was set at 0.5 ml/min and the splitting ratio was controlled by adjusting tube length connected to waste. No change in sensitivity was observed when the splitting ratio was set at 64% (0.32 ml/min of effluent was introduced into ES/MS) when compared to no splitting. However, significant decreases in sensitivity of ES/MS were detected as the splitting ratio decreased. We decided to use a 3.0-mm I.D. column whose flow rate was set at 0.5 ml/min with a splitting ratio at 64%. Although the reduction of effluent introduced into ES/MS would not affect the sensitivity, it would lessen the possible contamination from biological samples.

The linearity of this method was examined by analyzing various standards (from 0.05 to 5 μM). The correlation over the range examined was 0.99.

Table 1
Accuracy study of LC/ES/MS sample

Sample, μM	Measured ^a , μM	Recovery, %
0.05	0.053 \pm 0.001	106.0
0.05	0.051 \pm 0.001	102.0
0.50	0.491 \pm 0.002	98.2
0.50	0.497 \pm 0.005	99.4
1.00	1.050 \pm 0.016	105.0
1.00	1.025 \pm 0.020	102.5
5.00	4.985 \pm 0.036	99.7
5.00	5.013 \pm 0.026	100.3

^a Mean \pm S.D. deviation represents three measurements.

The detection limit of this method based on three times S/N is 0.8 nM, which proved to be much better than that of LC/UV assay. Table 1 shows the analytical results of LC/ES/MS method for some synthetic samples. Satisfactory recoveries ranging from 106.0 to 98.2% were determined. The application of this newly developed LC/ES/MS method was demonstrated by analyzing FZ in microdialysis samples. Typical LC/ES/MS results of FZ in ACSF and microdialysate of rat brain after FZ administration are shown in Fig. 4. FZ was eluted at approximately 6.05 min. FZ was detected at total ion chromatogram and extracted ion ($m/z = 203$) chromatogram but was not measured at $[\text{M} + \text{H}]^+$ ($m/z = 405$) channel. This is because that fragmented ion ($m/z = 203$) is the principal ion when CapEX was set at 175 V as shown in Fig. 2.

In summary, an LC/ES/MS method was developed for the determination of FZ in rat brain and microdialysate. Several parameters affecting the sensitivity of ES/MS detection and resolution of LC separation were examined and optimized. The effect of CID voltage on FZ fragmentation and ion abundance was evaluated. Some modification of LC/UV method was made to enhance the sensitivity of ES/MS. Post-column split was utilized to minimize the possible contamination from biological samples. The addition of a modifier, ammonium hydroxide, in mobile phase decreases the sensitivity of ES/MS; however, the modifier is needed to maintain the resolution of LC separation. The sensitivity of this newly developed method is much better than previously published ones. Currently, we are applying LC/ES/MS method to the study of the pharmacokinetics of FZ in rat brain.

Acknowledgements

We wish to express our thanks to the National Science Council of Taiwan for its financial support and to Dr Wynn Pan of National Yung-Ming University for his many valuable suggestions.

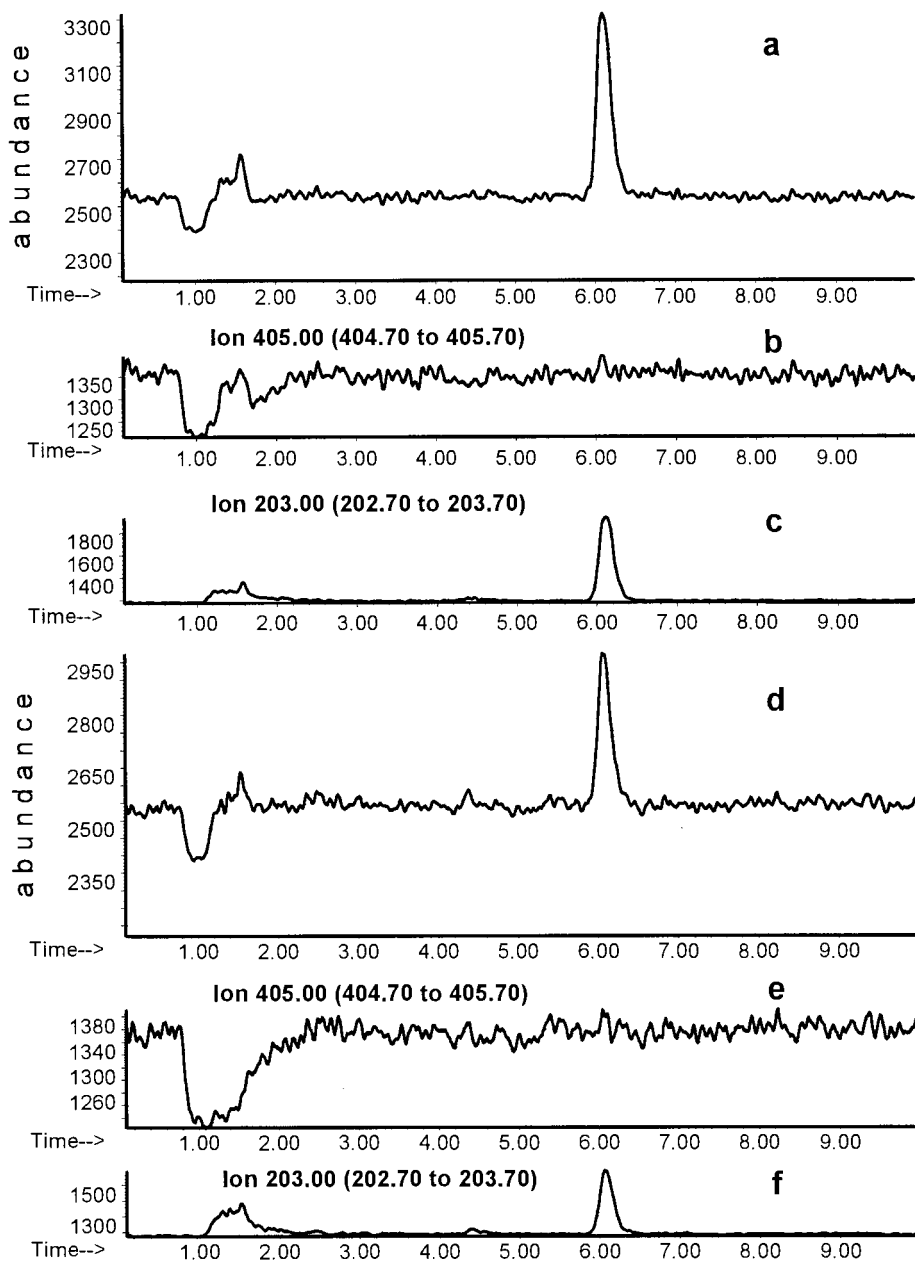


Fig. 4. LC/ES/MS reconstructed total ion and extracted ion chromatograms. (a) Total ion chromatogram (TIC) of FZ standard in ACSF. (b,c) Extracted ion chromatograms (EIC) of FZ in ACSF. (d) TIC of a microdialysis sample after FZ administration. (e,f) EIC of a microdialysis sample after FZ administration.

References

- [1] B.N. Singh, *Br. J. Clin. Pharmacol.* 21 (1986) 109S–212S.
- [2] P.A. Todd, P. Benfield, *Drug* 38 (1989) 481–499.
- [3] I.M. Kapetanovic, W.D. Yonekawa, H.J. Kupferberg, *J. Chromatogr.* 383 (1986) 223–228.
- [4] A. Yamaji, K. Kataoka, M. Oishi, N. Kanamori, T. Tagawa, T. Mimaki, *J. Chromatogr.* 421 (1987) 372–376.

- [5] F. Albani, R. Riva, G. Casucci, M. Contin, A. Baruzzi, J. Chromatogr. 374 (1986) 196–199.
- [6] M.S. Fuh, Y.F. Chan, W.H. Pan, I.P. Hunang, J. Liq. Chromatogr. Rel. Technol. (in press).
- [7] J. Keever, R.D. Voyksner, K.L. Tyczkowska, J. Chromatogr. A 794 (1998) 57.
- [8] P. Pais, E. Moyano, L. Puignou, M.T. Galceran, J. Chromatogr. A 775 (1997) 125.
- [9] W.M.A. Nissen, J.V.D. Greff, Liquid Chromatography Mass Spectrometry, Principle and Application. In: Chromatographic Science, vol. 58, Marcel Dekker, New York, 1992.
- [10] R.D. Voyksner, Environ. Sci. Technol. 28 (1994) 118A.
- [11] A. Di Corcia, C. Crescenzi, R. Samperi, L. Scappaticcio, Anal. Chem. 69 (1997) 2819.
- [12] H. Owabuchi, E. Kitazawa, N. Kobayashi, H. Watanabe, M. Kanai, K. Nakamura, Biol. Mass Spectrom. 23 (1994) 540.
- [13] X. He, M.W. Bernart, L. Lian, L. Lin, J. Chromatogr. A 796 (1998) 327.
- [14] G. Hopfgartner, K. Bean, J. Henion, R. Henry, J. Chromatogr. 647 (1993) 51.

Flow-injection spectrophotometry of manganese by catalysis of the periodate oxidation of 2,2'-azinobis(3-ethylbenzothiazoline-6-sulfonic acid)

Shigenori Nakano ^{a,*}, Kana Tanaka ^a, Rumiko Oki ^a, Takuji Kawashima ^b

^a Chemical Institute, Faculty of Education, Tottori University, Koyama-cho, Tottori 680-0945, Japan

^b Laboratory of Analytical Chemistry, Department of Chemistry, University of Tsukuba, Tsukuba 305-8571, Japan

Received 23 September 1998; received in revised form 4 November 1998; accepted 6 November 1998

Abstract

A sensitive flow-injection spectrophotometric procedure is proposed for the determination of manganese(II), based on its catalytic effect on the oxidation of 2,2'-azinobis(3-ethylbenzothiazoline-6-sulfonic acid) (ABTS) with periodate. By monitoring the change in absorbance of the oxidation product of ABTS at 415 nm, manganese(II) in the range 0.05–1.0 ng ml⁻¹ can be determined with a sampling frequency of 30 h⁻¹. A relative standard deviation (R.S.D.) ($n = 10$) is 1.6% at the 0.5 ng ml⁻¹ level. The proposed method suffers from few interferences and has been successfully applied to the determination of manganese in river, lake and seashore water samples. © 1999 Elsevier Science B.V. All rights reserved.

Keywords: Manganese determination; Catalytic method; Flow injection analysis; 2,2'-Azinobis(3-ethylbenzothiazoline-6-sulfonic acid); Periodate

1. Introduction

Kinetic–catalytic methods have been recognized as useful approaches to trace analysis. Extremely small concentrations of transition metal ions have been determined by utilizing their catalytic action in various indicator reactions, which are commonly monitored by such techniques as

spectrophotometry, fluorimetry, potentiometry, chemiluminescence and thermometric methods [1]. Furthermore, the use of flow-injection analysis (FIA) makes kinetic–catalytic methods more attractive because of easy handling of the mixing reagent and the time measurement [2].

Numerous oxidation processes of organic compounds with a suitable oxidant were employed for the catalytic determination of manganese(II) with batchwise procedures [3–11]. The oxidizing agents used in such reactions are periodate and dissolved oxygen as well as hydrogen peroxide. Several manganese(II)-catalyzed reactions have been

* Corresponding author. Fax: +81-857-31-5109.

E-mail address: nakano@fed.tottori-u.ac.jp (S. Nakano)

¹ Presented at the Ninth International Conference on Flow Injection Analysis, 23–27 August, 1998, Seattle, Washington, USA.

adapted to FIA for the manganese determination [12–21]. The catalytic effect on the oxidation of protocatechuic acid with hydrogen peroxide allowed the determination of up to 40 ng ml^{-1} manganese(II); it required the separation process to remove the interfering ions [12]. The periodate oxidations of *N,N*-diethylaniline [14,15] and Malachite Green [16,17] were adopted for the flow-injection determination of manganese(II) at nanogram levels after preconcentration and/or separation steps. Sensitive flow-injection methods were also developed for the catalytic determination of manganese(II) using the oxidative couplings of 3-methyl-2-benzothiazolinone hydrazone with *N,N*-dimethylaniline [18] and *N,N*-dimethyl-*p*-phenylenediamine with *m*-phenylenediamine [19] in the presence of hydrogen peroxide; the catalytic action of manganese(II) was improved by the addition of activators to the reaction systems. Although, these methods have high sensitivity, their applications were limited because of matrix effects.

2,2'-Azinobis(3-ethylbenzothiazoline-6-sulfonic acid) (ABTS) have been used as a chromogenic reagent for the spectrophotometric determination of hydrogen peroxide coupled with enzymatic reaction [22–25]. Mahuzier et al. [26] reported a colorimetric method for the determination of periodate using the oxidation of ABTS. However, there are no works on the application of this reaction in catalytic methods of analysis. This paper describes a flow-injection photometric method for the determination of manganese(II) at sub-ng ml^{-1} levels, based on its catalytic effect on the new indicator reaction between ABTS and periodate. The proposed method which is one of the methods having the highest level of the sensitivity has been applied satisfactorily to the determination of manganese in natural water without the need for any preconcentration step.

2. Experimental

2.1. Reagents

All solutions were prepared from analytical-reagent grade with deionized water purified with a Millipore Milli-Q system.

A standard manganese(II) solution (1.0 mg ml^{-1}) was obtained from Wako Junyaku, Japan. The working standard solutions were prepared daily by diluting the standard solution with $10^{-2} \text{ mol l}^{-1}$ HCl.

ABTS obtained from Wako Junyaku, Japan was used as received. A $2.0 \times 10^{-3} \text{ mol l}^{-1}$ ABTS solution was prepared in $5 \times 10^{-3} \text{ mol l}^{-1}$ sulfuric acid. A $2.0 \times 10^{-3} \text{ mol l}^{-1}$ potassium periodate solution was prepared. Stock solutions of 3-morpholinopropanesulfonic acid (MOPS, 0.5 mol l^{-1}), malonic acid (1.0 mol l^{-1}) and ammonia (2.0 mol l^{-1}) solutions were also prepared.

A working mixed solution of MOPS (0.1 mol l^{-1}), malonic acid ($8.0 \times 10^{-2} \text{ mol l}^{-1}$) and ammonia (0.4 mol l^{-1}) was prepared by mixing the stock solutions; the pH of the solution was adjusted to the desired value with 1 mol l^{-1} HCl.

2.2. Apparatus

A schematic diagram of the flow-injection system is given in Fig. 1. All tubing was made of Teflon, having a 0.5 mm i.d. Two double-plunger micropumps (Sanuki Kogyo, DMX-2400T) were used to propel the carrier and reagent solutions. A six-way injection valve (Sanuki Kogyo SVM-6M2) with a loop was used for injecting the standard manganese(II) and sample solutions. A circulating thermostated bath (Toyo LH-1000C)

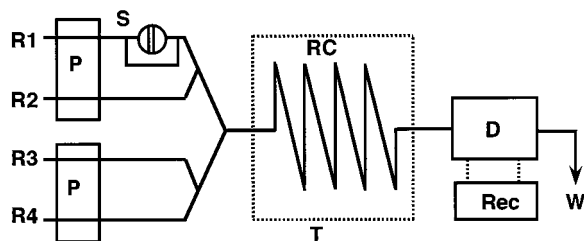


Fig. 1. Flow-injection system for the determination of manganese(II). R1, carrier ($10^{-2} \text{ mol l}^{-1}$ HCl); R2, KIO_4 ($2.0 \times 10^{-3} \text{ mol l}^{-1}$); R3, 2,2'-azinobis(3-ethylbenzothiazoline-6-sulfonic acid) (ABTS) ($2.0 \times 10^{-3} \text{ mol l}^{-1}$); R4, 3-morpholinopropanesulfonic acid (MOPS) (0.1 mol l^{-1})/malonic acid ($8.0 \times 10^{-2} \text{ mol l}^{-1}$)/ammonia (0.4 mol l^{-1}); P, micropump (1.0 ml min^{-1}); S, sample injector ($132 \mu\text{l}$); T, thermostated bath (30°C); RC, reaction coil (6 m); D, detector (415 nm); Rec, recorder; W, waste (pH 6.6–6.7).

was used for keeping a constant reaction temperature. A spectrophotometer (Nihon Bunko UVDIC -320) with a 10-mm micro flow-cell (20 μ l) and a recorder (Nippon Denshi Kagaku V1250) were used for detecting and recording the change in the absorbance.

A Hitachi 200-10 double-beam spectrophotometer with 10-mm cells was used for measurements of absorption spectra. A Toa Model HM-5S pH meter was used for pH measurements. A Hitachi Model 170-70 atomic absorption spectrometer (AAS) was used to evaluate the present method.

2.3. Procedure

Carrier (R1, 10^{-2} mol l^{-1} HCl) and reagent solutions in reservoirs R2 (potassium periodate), R3 (ABTS) and R4 (MOPS, malonic acid and ammonia) were pumped into the analytical line at a flow rate of 1.0 ml min^{-1} (Fig. 1). An aliquot of the sample solution (132 μ l) was introduced into the carrier solution by a loop-valve injector (S). The carrier stream was then mixed with the reagent solutions and passed through the reaction coil (RC, 6 m) immersed in a thermostatic bath at $30.0 \pm 0.1^\circ C$. The oxidation of ABTS with periodate took place in the coil, RC. The absorbance was continuously measured at 415 nm.

3. Results and discussion

ABTS is oxidized with periodate to form the radical cation ($ABTS^{\bullet+}$), which slowly disproportionates giving ABTS and the azodication [26,27]. The radical cation has absorption maximum at 415 nm together with a lesser maxima at 395, 640 and 725 nm. Throughout this work, the change in the absorbance at 415 nm was monitored. The catalytic action of manganese(II) in redox reactions with periodate involves the generation of manganese(III) and/or manganese(IV) [3,6]; the formation of $ABTS^{\bullet+}$ is catalytically accelerated by minute amounts of manganese as a result of the regeneration of manganese(III) and/or manganese(IV).

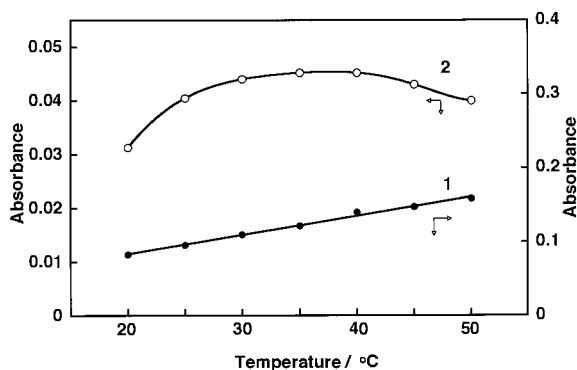


Fig. 2. Effect of reaction temperature on the uncatalyzed (1) and catalyzed (2) reactions. Conditions as in Fig. 1 except for temperature. $C_{Mn(II)}$, 0.5 ng ml^{-1} .

3.1. Effect of flow-injection and chemical variables

To optimize the conditions for the determination of manganese(II), variables were examined by using the flow system as shown in Fig. 1. The peak height for the catalyzed reaction depends on the reaction time, i.e. on the flow rate and the length of reaction coil. The lower flow rate and longer reaction coil gave higher and broader peaks. The heights of baseline for the uncatalyzed reaction also increased with lengthening the reaction time. The flow rate of solutions and reaction coil length were selected as 1.0 ml min^{-1} and 6 m, respectively, taking into account the sampling frequency and the baseline stability. The peak height and peak width increased with increasing sample volume; a 132- μ l sample solution was injected into the flow-line. Figure 2 shows the effect of reaction temperature on the uncatalyzed and catalyzed reactions. Although the heights of baseline for the uncatalyzed reaction increased with increasing temperature, the peak heights for the catalyzed reaction was almost constant in the range 30–40°C. It seemed that the deprotonation of $ABTS^{\bullet+}$ proceeded at higher temperatures. By considering the height of baseline, the reaction temperature was kept at 30°C.

The catalytic activity of manganese(II) in the indicator reaction occurred at a neutral medium. The suitability of several buffers was examined at a constant concentration of ammonia as an

alkaline. The buffers tested were as follows: bis (2-hydroxyethyl)iminotris(hydroxymethyl) methane (bis-tris), *N*-(2-acetamid)iminodiacetic acid (ADA), piperazine-*N,N'*-bis(2-ethanesulfonic acid (PIPES), *N*-(2-acetamid)-2-aminoethanesulfonic acid (ACES), 2-hydroxy-3-morpholinopropane-sulfonic acid (MOPSO) and MOPS. An increase in the concentrations of bis-tris, ADA and PIPES rapidly decreased the peak heights for the catalyzed reaction. On the other hand, the peak heights gradually decreased with increasing in the concentration of ACES, MOPSO and MOPS. Of these, MOPS was chosen as a buffer because of its lesser effect on the manganese(II)-catalyzed reaction; the MOPS concentration was fixed at 0.1 mol l^{-1} for the procedure. Effect of ammonia concentration was examined in the range $0.15\text{--}0.5 \text{ mol l}^{-1}$. The peak heights were almost constant at the concentrations above 0.3 mol l^{-1} ; a 0.4 mol l^{-1} ammonia solution was used. Figure 3 shows the effect of pH on the uncatalyzed and catalyzed reactions over the range 5.5–8.8 in the presence of MOPS and ammonia. A maximum peak height was obtained in the pH range 6.6–6.7, decreasing on both sides of this range. The pH of the reaction mixture in the reaction coil was adjusted in this range.

The effects of ABTS and periodate concentrations were examined. An increase in the ABTS concentration caused an increase in the rate of the uncatalyzed and catalyzed reactions. The concentration of ABTS was selected at $2.0 \times 10^{-3} \text{ mol}$

l^{-1} taking into account the baseline stability. With the increase in the periodate concentration, the rate of both reactions also increased. The peak height, however, reached its maximum at the concentration above $1.0 \times 10^{-3} \text{ mol l}^{-1}$. A $2.0 \times 10^{-3} \text{ mol l}^{-1}$ periodate solution was used.

3.2. Calibration graphs

The calibration graphs for the determination of manganese(II) were run under the optimal conditions as described in Fig. 1. Linear plots were obtained for the manganese(II) concentration range $0.05\text{--}1.0 \text{ ng ml}^{-1}$. The detection limit for a signal to noise ratio of 2 was 0.02 ng ml^{-1} . The relative standard deviations (R.S.D.) for ten determinations of 0.5 and 1.0 ng ml^{-1} of manganese(II) were 1.6 and 1.2%, respectively. The sampling frequency was about 30 h^{-1} .

3.3. Effect of diverse ions

From preliminary experiments, a positive interference from iron(III) was observed and its interference should be eliminated with the determination of manganese(II). Some complexing agents such as citric acid, diphosphate and malonic acid were examined as masking agents for iron(III). Among them, malonic acid at the concentrations above $4.0 \times 10^{-2} \text{ mol l}^{-1}$ effectively suppressed the interference of 100 ng ml^{-1} iron(III); at the same time, the presence of the agent slightly increased the peak height for the catalyzed reaction. The concentration of malonic acid was fixed at $8.0 \times 10^{-2} \text{ mol l}^{-1}$ for the procedure.

Table 1 summarizes the tolerance limits of other diverse ions on the determination of 0.5 ng ml^{-1} manganese(II) in the presence of malonic acid; an error of 5% are considered to be tolerable. Most of the ions examined did not interfere with the manganese(II) determination in concentrations up to at least 100-fold excesses. Negative interferences from As(III) and Ce(III, IV) at the 50 ng ml^{-1} level were observed; cobalt(II) at the amount of 10 ng ml^{-1} gave positive interference. The levels of these ions normally presented in the natural water samples were tolerable in the present method.

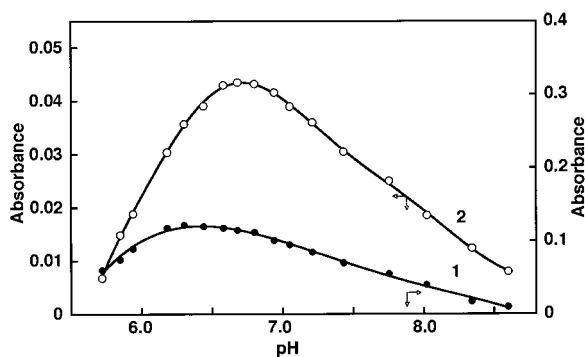


Fig. 3. Effect of pH on the uncatalyzed (1) and catalyzed (2) reactions. Conditions as in Fig. 1 except for pH. $C_{\text{Mn(II)}}$, 0.5 ng ml^{-1} .

Table 1

Tolerance limits for diverse ions in the determination of 0.5 ng ml⁻¹ manganese(II)

Tolerance limit (ng ml ⁻¹)	Ion added
10 000	As(V), Ba(II), Ca(II), K(I), Mg(II), Na(I), Sr(II), W(IV), BO ₃ ³⁻ , Br ⁻ , F ⁻ , NO ₃ ⁻ , PO ₄ ³⁻ , P ₂ O ₇ ⁴⁻ , SO ₄ ²⁻ , Oxalate, Tartrate
1000	Mo(VI), NO ₂ ⁻ , Citrate
100	Cu(II), Cr(VI), Fe(III), Hg(II), Ni(II), Se(IV), Sn(II), Sn(IV), Ti(IV), V(V)
50	Al(III), Cd(II), Cr(III), Pb(II), Zn(II)
10	As(III), Ce(III), Ce(IV)
1	Co(II)

3.4. Applications

The proposed flow-injection method was applied to the determination of manganese in river, lake and seashore water samples. These samples were filtered through a 0.45- μ m Millipore filter immediately after collection and then concentrated HCl was added to the filtrates (approximately pH 1). Both calibration curve and standard addition methods were carried out after appropriate dilution. These values were in good agreement with each other (Table 2). The same samples were also analyzed with graphite furnace atomic absorption spectrometry (GFAAS) [28]. As can be seen in Table 2, the values obtained by the present method are consistent with those by GFAAS.

4. Conclusion

The proposed catalytic flow-injection procedure is simple, rapid and convenient for the determination of manganese at sub-ng ml⁻¹ levels. There is no need for preliminary separation and concentration of manganese. The results obtained by the present method illustrate that the precision and accuracy are satisfactory.

Table 2

Determination of manganese in river, lake and seashore waters

Sample ^a	Dilution	Manganese in sample ^b (ng ml ⁻¹)		
		Proposed method		GFAAS
		(I) ^c	(II) ^d	
<i>River water</i>				
Kyu-fukuro-gawa	1/200	94 ± 1	95 ± 2	95 ± 4
Sendai-gawa	1/20	4.5 ± 0.1	4.3 ± 0.1	4.2 ± 0.3
Tenjin-gawa	1/50	9.5 ± 0.1	9.4 ± 0.1	9.3 ± 0.4
<i>Lake water</i>				
Tanega-ike	1/500	126 ± 4	128 ± 2	133 ± 12
Koyama-ike	1/100	66 ± 2	66 ± 1	68 ± 4
Togo-ike	1/200	94 ± 3	92 ± 2	89 ± 4
<i>Seashore water</i>				
Uradome	1/10	1.9 ± 0.1	1.8 ± 0.1	1.7 ± 0.2
Karo	1/10	1.0 ± 0.1	1.1 ± 0.1	1.1 ± 0.2
Natudo-mari	1/10	3.2 ± 0.1	3.1 ± 0.1	3.0 ± 0.3
Hawai	1/20	9.2 ± 0.1	9.5 ± 0.1	9.4 ± 0.4

^a Collected in Tottori Prefecture, Japan.

^b Corrected for addition ($n = 3$).

^c Calibration curve method.

^d Standard addition method.

References

- [1] D. Perez-Bendito, M. Silva, Kinetic Methods in Analytical Chemistry, Ellis Horwood, Chichester, 1988.
- [2] T. Kawashima, S. Nakano, Anal. Chim. Acta 261 (1992) 167.
- [3] A.A. Alexiev, K.L. Mutaftchiev, Mikrochim. Acta I (1982) 441.
- [4] A. Moreno, M. Silva, D. Perez-Bendito, M. Valcarcel, Talanta 30 (1983) 107.
- [5] S. Nakano, A. Ohta, T. Kawashima, Mikrochim. Acta II (1985) 273.
- [6] M.A. Ratina, G.A. Zolotova, I.F. Dolmanova, Zh. Anal. Khim. 42 (1987) 1502.
- [7] F. Salinas, J.J.B. Nevado, P. Valiente, Talanta 34 (1987) 321.
- [8] M.I. Karayanmis, P.G. Veltsistas, Analyst 115 (1990) 741.
- [9] L. Jianli, W. Budong, Z. Fenyan, Analyst 118 (1993) 1213.
- [10] R. Liu, A. Zhang, D. Liu, S. Wang, Analyst 120 (1995) 1195.

- [11] K. Watanabe, S. Takahashi, M. Itagaki, *Bunseki Kagaku* 45 (1996) 987.
- [12] T. Yamane, *Anal. Sci.* 2 (1986) 191.
- [13] S. Maspoch, M. Blanco, V. Cerda, *Analyst* 111 (1986) 69.
- [14] I.Y. Kolotyrkina, L.K. Shpigun, Y.A. Zolotov, *Zh. Anal. Khim.* 43 (1988) 284.
- [15] I.Y. Kolotyrkina, L.K. Shpigun, Y.A. Zolotov, G.I. Tsylin, *Analyst* 116 (1991) 707.
- [16] S. Kawakubo, T. Fukasawa, M. Iwatsuki, T. Fukasawa, *J. Flow Injection Anal.* 5 (1988) 14.
- [17] C. Zhang, S. Kawakubo, T. Fukasawa, *Anal. Chim. Acta* 217 (1989) 23.
- [18] Y. Miyata, T. Hirano, S. Nakano, T. Kawashima, *Anal. Sci.* 7 (1991) 97.
- [19] S. Nakano, M. Nozawa, M. Yanagawa, T. Kawashima, *Anal. Chim. Acta* 261 (1992) 183.
- [20] J.A. Resing, M.J. Mottl, *Anal. Chem.* 64 (1992) 2682.
- [21] Q. Lin, A. Guiraum, R. Escobar, F.F. de la Rosa, *Anal. Chim. Acta* 283 (1993) 379.
- [22] N. Hasegawa, E. Sugawara, T. Kashiwagi, *Bunseki Kagaku* 30 (1981) 470.
- [23] B. Olsson, *Mikrochim. Acta II* (1985) 211.
- [24] N. Majkic-Singh, L. Bogavac, V. Kalimanovska, Z. Jelic, S. Spasic, *Clin. Chim. Acta* 162 (1987) 29.
- [25] S. Ignjatovic, N. Majkic-Singh, *Anal. Chim. Acta* 285 (1994) 369.
- [26] G. Mahuzier, B.S. Kirkacharian, C. Harfouche-Obeika, *Anal. Chim. Acta* 76 (1975) 79.
- [27] R.E. Childs, W.G. Bardsley, *Biochem. J.* 145 (1975) 93.
- [28] M. Tominaga, Y. Umezaki, *Nippon Kagaku Kaishi* (1981) 7.

Catalytic flow injection determination of vanadium by oxidation of *N*-(3-sulfopropyl)-3,3',5,5'-tetramethylbenzidine using bromate[☆]

Tsuyoshi Shiobara^a, Norio Teshima^{a,1}, Makoto Kurihara^a,
Shigenori Nakano^b, Takuji Kawashima^{a,*}

^a *Laboratory of Analytical Chemistry, Department of Chemistry, University of Tsukuba, Tsukuba 305-8571, Japan*

^b *Chemical Institute, Faculty of Education, Tottori University, Koyama-cho, Tottori 680-0945, Japan*

Received 21 October 1998; accepted 23 November 1998

Abstract

A catalytic flow-injection (FI) method was developed for the determination of 10^{-9} mol l⁻¹ levels of vanadium(IV, V). The method is based on the catalytic effect of vanadium(V) on oxidation of *N*-(3-sulfopropyl)-3,3',5,5'-tetramethylbenzidine (TMBZ-PS) using bromate as oxidant to form a yellow dye ($\lambda_{\text{max}} = 460$ nm). The use of 5-sulfosalicylic acid (SSA) as an activator enhanced the sensitivity of the method. The calibration graphs with a working range 0.05–8.0 ng ml⁻¹ were obtained for vanadium(V). Vanadium(IV) was also determined, being oxidized by bromate. The detection limit (signal/noise, S/N = 3) was 0.01 ng ml⁻¹ (ca. 2×10^{-10} mol l⁻¹) vanadium. The relative standard deviations (R.S.D.) for 15 determinations of 0.5 ng ml⁻¹ vanadium, and for ten determinations of 0.1 and 1.0 ng ml⁻¹ vanadium were 0.41, 2.6 and 0.25%, respectively, with a sampling rate of 15 samples h⁻¹. The proposed method was successfully applied to the determination of vanadium in natural waters. © 1999 Elsevier Science B.V. All rights reserved.

Keywords: Catalytic flow-injection method; Vanadium determination; *N*-(3-sulfopropyl)-3,3',5,5'-tetramethylbenzidine

1. Introduction

It has been known that the determination of vanadium provides significant information regarding its biological effects [1,2] and/or the extent of air pollution [3,4]. Highly sensitive and selective methods are still required for the determination of sub-nanogram or less levels of vanadium in water samples [5].

[☆] Presented at The Ninth International Conference on Flow Injection Analysis (ICFIA 98), Seattle, Washington, USA, 23–27 August, 1998.

* Corresponding author. Tel.: +81-298-53-6521; fax: +81-298-53-6503.

E-mail address: kawashima@staff.chem.tsukuba.ac.jp (T. Kawashima)

¹ Present address: Department of Applied Chemistry, Aichi Institute of Technology, Toyota 470-0392, Japan.

Spectrophotometry is the most common technique used for vanadium determination [5]; especially, kinetic–catalytic spectrophotometric methods of analysis based on catalytic reactions are available techniques used for the determination of trace amounts of vanadium without pre-concentration [6]. In the last decade, many batchwise methods for the catalytic determination of vanadium have been reported, based on its catalytic effect on various coloration reactions of organic compounds in the presence of bromate or persulfate [7–13]. Batch methods are, however, sometimes complicated because care is needed in the mixing of reagents at regular time intervals to obtain accurate results. Such disadvantages in the batch procedure can be overcome by using flow-injection analysis (FIA), since FIA technique can strictly control the rate of catalyzed reaction, and the mixing of the solutions of reagents and sample with rapid sample throughput [14,15]. Vanadium in sub-nanogram levels can be determined by FI spectrophotometric methods utilizing the bromate oxidation of Bindschedler's green leuco base [16], *o*-phenylenediamine [17] and galloycyanine [18]. Already proposed are various indicator reactions for the catalytic determination of vanadium such as oxidative coupling of 4-aminoantipyrine (AA) with *N,N*-dimethylaniline (DMA) [19,20], *N*-phenyl-*p*-phenylenediamine with DMA [21], *p*-hydrazinobenzenesulphonic acid with *m*-phenylenediamine [22] in the presence of bromate or chlorate. In these studies, the use of tartrate [21,22], 5-sulfosalicylic acid (SSA) [20] and 1,2-dihydroxybenzene-3,5-disulfonate (Tiron) [19] as activators permits an improvement in their selectivity and sensitivity. The method for vanadium determination utilizing AA–DMA–KBrO₃ system as an indicator reaction can be successfully applied to the fractional determination of vanadium(IV) and vanadium(V) in natural waters by combining the solvent extraction technique [23–25].

This paper describes a highly sensitive FIA method for the determination of vanadium(IV, V) based on its catalytic effect on the bromate oxidation of *N*-(3-sulfopropyl)-3,3',5,5'-tetramethylbenzidine (TMBZ·PS) which is a new indicator reaction for the catalytic determination of vana-

dium. In this reaction system, SSA acted as an effective activator for the catalysis of vanadium. The interference from nitrite was effectively eliminated by adding amidosulfuric acid. The proposed method can determine vanadium in the range 0.05–8.0 ng ml⁻¹ and be successfully applied to the determination of vanadium in tap, pond and river waters.

2. Experimental

2.1. Reagents

All reagents used were of analytical-reagent grade and used without further purification. Water used to prepare the solutions was obtained from a Milli-Q PLUS water purification system (Millipore).

A commercial atomic absorption standard solution (Wako, Osaka, Japan) containing 1000 µg ml⁻¹ of vanadium(V) (ammonium metavanadate in 0.5 mol l⁻¹ sulfuric acid) was used. A stock solution of vanadium(IV) (5.0×10^{-2} mol l⁻¹, 2555 µg ml⁻¹) was prepared by dissolving vanadyl sulfate *n*-hydrate (Kanto) in 5×10^{-3} mol l⁻¹ sulfuric acid. The concentration of vanadium(IV) was determined by a standard potassium permanganate titration. Each working solution was prepared by serial dilution of the standard solutions with 5×10^{-3} mol l⁻¹ sulfuric acid. A 2×10^{-3} mol l⁻¹ TMBZ·PS stock solution was prepared by dissolving 0.38 g of *N*-(3-sulfopropyl)-3,3',5,5'-tetramethylbenzidine sodium salt (Dojindo) in 500 ml of water. A 0.25 mol l⁻¹ potassium bromate stock solution was prepared by dissolving 20.88 g of potassium bromate (Wako) in 500 ml of water. A 0.15 mol l⁻¹ SSA stock solution was prepared by dissolving 19.07 g of 5-sulfosalicylic acid dihydrate in ca. 100 ml of water; the pH of the solution was adjusted to pH about 2.8 with 0.5 mol l⁻¹ trisodium citrate dihydrate and diluted to 500 ml with water.

2.2. Apparatus

The FI system used for the determination of vanadium(IV, V) is schematically shown in Fig. 1.

All flow lines were made from Teflon tubing (0.5 mm i.d.). Carrier and reagent solutions were propelled by two double plunger micropumps (Sanuki Kogyo, DMX-2000). Sample solutions were injected into the carrier stream by a six-way injection valve (Sanuki Kogyo, SVM-6M2). Two thermostated baths (Taitec DX-10) were used to maintain the reaction temperature and to stabilize the baseline. The absorbance of the reaction product was measured at 460 nm with a spectrophotometer (Soma Kagaku S-3250) fitted with a flow-through cell (8 μ l volume, 10 mm path length) and recorded with a recorder (Yokogawa Model 3722). A pH meter (Shibata PH-810) was used for pH measurements.

2.3. Procedure

As shown in Fig. 1, a 5×10^{-3} mol l $^{-1}$ sulfuric acid as a carrier solution (R₁), a 0.15 mol l $^{-1}$ SSA in buffer solution (0.5 mol l $^{-1}$ trisodium citrate, pH 2.8) (R₂), a 2×10^{-3} mol l $^{-1}$ TMBZ·PS solution (R₃) and a 0.25 mol l $^{-1}$ potassium bromate solution (R₄) were pumped at a flow rate of 0.3 ml min $^{-1}$, respectively. A sample solution of 287 μ l was injected into the carrier stream, and then merged with a solution containing SSA,

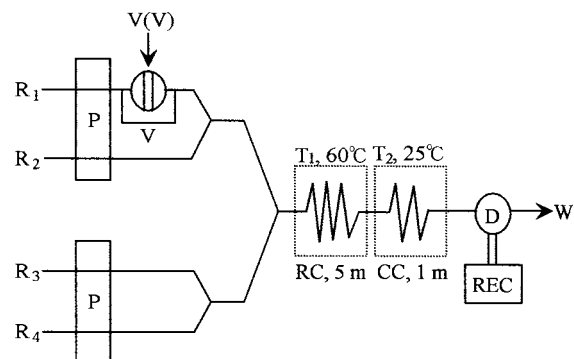
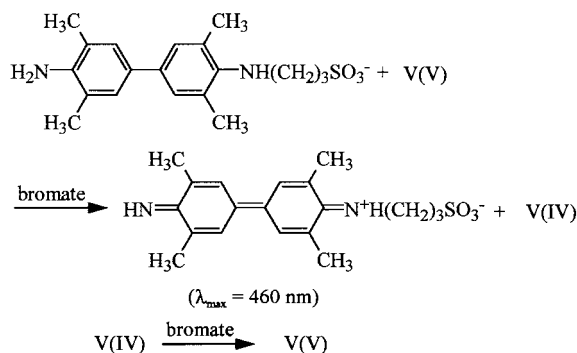


Fig. 1. Flow system for the catalytic determination of vanadium. R₁, carrier solution (H₂SO₄, 5×10^{-3} mol l $^{-1}$); R₂, 5-sulfosalicylic acid (SSA) (0.15 mol l $^{-1}$) + citrate buffer (pH 2.8); R₃, *N*-(3-sulfopropyl)-3,3',5,5'-tetramethylbenzidine (TMBZ·PS) (2×10^{-3} mol l $^{-1}$); R₄, KBrO₃ (0.25 mol l $^{-1}$); P, pump (0.6 ml min $^{-1}$); V, six-way valve (287 μ l); RC, reaction coil (5 m); CC, cooling coil (1 m); T₁ and T₂, thermostated baths (60 and 25°C); D, spectrophotometer (460 nm); Rec, recorder; W, waste (pH 2.8).

TMBZ·PS and bromate. The color development proceeded in the reaction coil of 5 m length at $60 \pm 0.1^\circ\text{C}$ and then the colored solution was passed through the cooling coil of 1 m length at 25°C and then the flow-through cell. The absorbance change of the dye formed was monitored continuously at 460 nm and recorded on a recorder.

3. Results and discussion

In the presence of bromate, TMBZ·PS is oxidized to produce a yellow dye, which has an absorption maximum at 460 nm. The rate of color-forming reaction is catalytically accelerated by vanadium(V). Vanadium(IV) reduced during this reaction is oxidized again by bromate to vanadium(V); the coloration is catalyzed by trace amounts of vanadium as a result of the regeneration of vanadium(V) in the presence of bromate. Therefore, vanadium(IV) can also be determined, being oxidized by bromate. These reactions are exemplified below:



The vanadium(V)-catalyzed reaction is activated in the presence of SSA.

3.1. Effect of reaction variables

The flow manifold and chemical variables affecting the catalyzed and uncatalyzed reactions were examined to obtain the optimum conditions for the determination of vanadium(V).

The effect of the flow rate was examined in the range 0.2–0.8 ml min $^{-1}$. The decrease in the flow rate increased the peak height for both the catalyzed and uncatalyzed reactions, but made the baseline unstable because of high baseline ab-

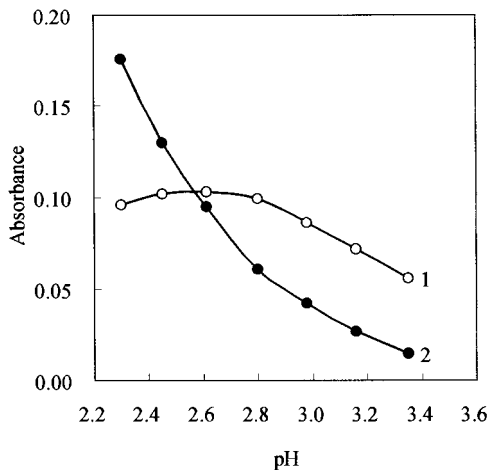


Fig. 2. The effect of pH on the peak height and baseline. (1) 1.0 ng ml⁻¹ vanadium(V); (2) baseline. $C_{SSA} = 0.1 \text{ mol l}^{-1}$, $C_{KBrO_3} = 0.15 \text{ mol l}^{-1}$. Other conditions as in Fig. 1.

sorbance. A flow rate of 0.3 ml min^{-1} was adopted by considering stable baseline and reasonable sensitivity. The length of reaction coil of RC was varied in the range 2.5–10 m. The peak height increased with increasing coil length; a 5 m of reaction coil length was chosen taking into account of sample frequency. The injection volume more than 287 μl showed almost constant peak height; a 287 μl sample solution was injected into the carrier stream.

The effect of reaction temperature was examined over the range 30–80°C. The peak height increased with an increase in temperature. However, an increase in temperature also increased the baseline. The reaction was carried out at 60°C for the sake of high sensitivity and reproducibility.

Fig. 2 shows the effect of pH on the peak height. The peak height was almost constant in the pH range 2.3–2.8, decreasing gradually on both sides of this pH range. Thus, the reaction was carried out in the pH range 2.4–2.7. The effect of bromate concentration was examined over the range 0–0.3 mol l⁻¹. Fig. 3 shows that the baseline linearly depends on the bromate concentration. A 0.25 mol l⁻¹ potassium bromate concentration was chosen to obtain the attainable sensitivity. The effect of TMBZ·PS concentration on the reaction rate is shown in Fig. 4. As can be seen, the peak height increases with increasing

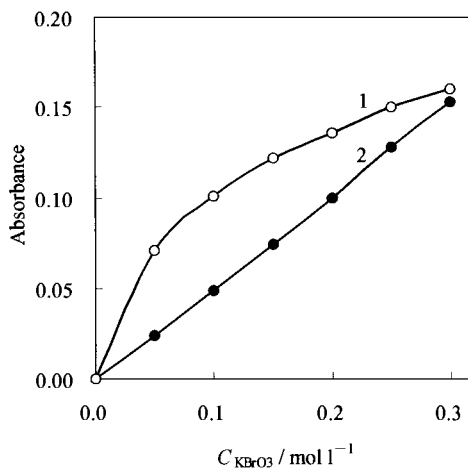


Fig. 3. The effect of bromate concentration on the peak height and baseline. (1) 1.0 ng ml⁻¹ vanadium(V); (2) baseline. $C_{SSA} = 0.1 \text{ mol l}^{-1}$. Other conditions as in Fig. 1.

TMBZ·PS concentration up to $4.0 \times 10^{-3} \text{ mol l}^{-1}$. A $2.0 \times 10^{-3} \text{ mol l}^{-1}$ TMBZ·PS concentration was adopted taking into account the solubility of the oxidation product.

The possibility for further increase in the sensitivity of catalytic method is the application of a suitable activator. The various activators examined were tartrate, citrate [13], SSA, salicylic acid, Tiron, gallic acid [17], catechol, *trans*-1,2-di-

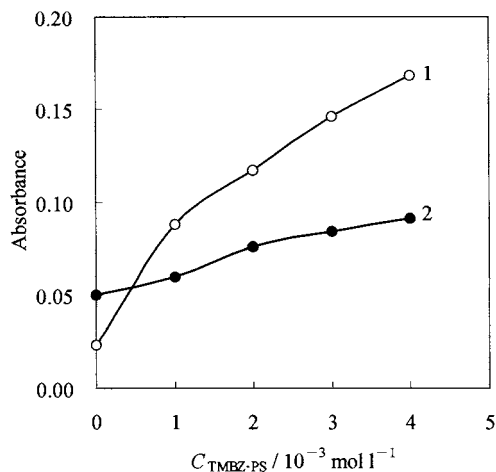


Fig. 4. The effect of *N*-(3-sulfopropyl)-3,3',5,5'-tetramethylbenzidine (TMBZ·PS) concentration on the peak height and baseline. (1) 1.0 ng ml⁻¹ vanadium(V); (2) baseline. $C_{SSA} = 0.1 \text{ mol l}^{-1}$. Other conditions as in Fig. 1.

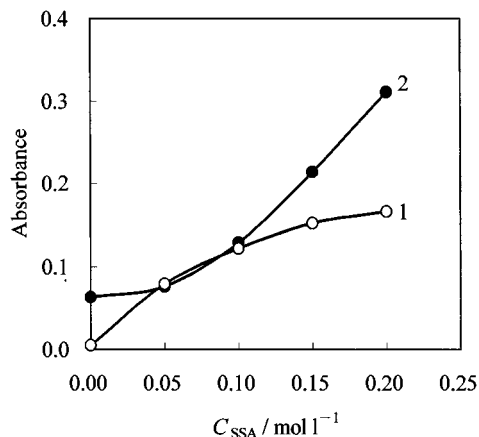


Fig. 5. The effect of 5-sulfosalicylic acid (SSA) concentration on the peak height and baseline. (1) 1.0 ng ml^{-1} vanadium(V); (2) baseline. Other conditions as in Fig. 1.

aminocyclohexane-*N,N,N',N'*-tetraacetic acid and 1,10-phenanthroline. Among them, SSA was found to have the greatest activating effect on this reaction. The effect of SSA on the coloration is shown in Fig. 5. The peak height for vanadium(V) increased with increasing the concentration of SSA up to 0.20 mol l^{-1} and then remained almost constant in the range $0.15\text{--}0.2 \text{ mol l}^{-1}$. Thus, an SSA concentration was selected as 0.15 mol l^{-1} for the procedure.

3.2. Calibration graphs

The calibration graphs for vanadium(V) in the range $0.05\text{--}8.0 \text{ ng ml}^{-1}$ were prepared under the optimum conditions. Although the calibration graph showed slightly upward curvature in the range $0.05\text{--}1.0 \text{ ng ml}^{-1}$, the reproducibility of the method was satisfactory; the relative standard deviation (R.S.D.) for 15 determinations of 0.5 ng ml^{-1} vanadium was 0.41% and for ten determinations of 0.01 and 1.0 ng ml^{-1} vanadium were 2.6 and 0.25%, respectively. The calibration graphs for vanadium(IV) were almost identical to those for vanadium(V) in the same concentration range within experimental error. The detection limit (signal/noise, $S/N = 3$) was 0.01 ng ml^{-1} vanadium and the sampling rate was $15 \text{ samples h}^{-1}$.

3.3. Interferences

The effect of foreign ions on the determination of 0.5 ng ml^{-1} vanadium(V) was investigated. A $\pm 5\%$ error was considered to be tolerable. The results are summarized in Table 1. Copper(II) and chromium(III) did not interfere with the determination of vanadium(V) at concentration up to 5000 ng ml^{-1} . Iodide and nitrite showed serious positive interferences on the color development. The positive interference from nitrite is attributable to its catalysis on this reaction. However, the interference of nitrite was effectively eliminated by adding $1 \times 10^{-1} \text{ mol l}^{-1}$ amidosulfuric acid as is seen in Table 1.

3.4. Applications to natural waters and standard reference material

The proposed method was applied to the determination of vanadium in tap, pond and river water samples. For tap water, the sample was collected after discharging tap water for about 30 min and boiled for 5 min to remove chlorine. Pond water sample was filtered through a Mil-

Table 1
Effect of foreign ions on the determination of 0.5 ng ml^{-1} of vanadium(V)

Tolerance limit ^a (ng ml^{-1})	Ion and compound added
50 000	K(I), Na(I), NH_4^+ , BO_3^- , Cl^- , ClO_3^- , ClO_4^- , IO_3^- , NO_3^- , PO_4^{3-} , SO_4^{2-} , acetate, amidosulfuric acid, citrate, tartrate
25 000	Pb(II), CO_3^{2-} , NO_2^- ^b
10 000	Ag(I), Ca(II), Cd(II), Co(II), Mn(II), Se(IV), Zn(II), F^- , SiO_3^{2-}
5000	Cu(II), Mg(II), Cr(III)
2500	As(III), Be(II), Li(I), Ni(II), Br^- , oxalate
1000	Ba(II), Ce(III), Mo(VI), Sr(II)
500	Al(III)
250	Fe(III), Rb(I)
100	Sb(III), W(VI)
50	Cr(VI), Sn(II)
25	I^-
5	NO_2^-

^a A $\pm 5\%$ error of the peak height for 0.5 ng ml^{-1} vanadium(V) was considered to be tolerable.

^b In the presence of $1 \times 10^{-3} \text{ mol l}^{-1}$ amidosulfuric acid.

Table 2
Determination of vanadium in natural waters

Sample	Dilution	V(V) added (ng ml ⁻¹)	V found (ng ml ⁻¹)	V in sample (ng ml ⁻¹)	Recovery (%)
Tap water ^a	1:12.5	0	0.179	2.24	–
		0.1	0.284	2.30	105
		0.2	0.380	2.25	102
		0.3	0.482	2.28	102
		0.4	0.585	2.31	102
				Average: 2.28 ± 0.03	
Pond water ^a	1:25	0	0.163	4.08	–
		0.1	0.262	4.05	99
		0.2	0.367	4.18	102
		0.3	0.469	4.23	102
		0.4	0.565	4.13	101
				Average: 4.13 ± 0.07	
SRM 1640 ^b	1:100	0	0.138	13.8	–
		0.1	0.237	13.7	99
		0.2	0.331	13.1	97
		0.3	0.429	12.9	97
		0.4	0.538	13.8	100
				Average: 13.5 ± 0.4	

^a Collected at University of Tsukuba.

^b Standard reference material (SRM) 1640 (Trace Element in Natural Water) issued by National Institute of Standard and Technology (NIST). The certified value of vanadium is 13.01 ± 0.37 ng ml⁻¹.

lipore membrane filter with a pore size of 0.45 µm. These two sample solutions were acidified by adding concentrated hydrochloric acid to pH about 1. In addition, the standard reference material (SRM) 1640 (Trace Elements in Natural Water) issued by National Institute of Standard and Technology (NIST) was employed without pre-treatment. These samples were injected into the flow line after appropriate dilution. All analytical results were obtained by the calibration method. To examine the recovery of vanadium, known amounts of vanadium(V) were added to the sample. The results are summarized in Table 2. The recovery of added vanadium(V) was found to be quantitative and the reproducibility was satisfactory. The results of the SRM 1640 were in good agreement with the certified value.

4. Conclusions

A new catalytic FI photometric method is pro-

posed for the determination of sub-nanogram levels of vanadium(IV, V). The method is based on the catalytic effect of vanadium(V) on the oxidation of TMBZ·PS in the presence of potassium bromate. The sensitivity was enhanced by adding SSA as an effective activator, being determined as low as 0.01 ng ml⁻¹ vanadium. The serious interference from nitrite can be effectively eliminated with amidosulfuric acid. The method is successfully applied to the analysis of vanadium in natural water samples without preconcentration and separation.

Acknowledgements

The authors gratefully acknowledge the financial support of this study by Grants-in-Aid for Scientific Research No. 09640715 from the Ministry of Education, Science, Sports and Culture.

References

- [1] D.C. Crans, M.S. Gottlieb, J. Tawara, R.L. Bunch, L.A. Theisen, *Anal. Biochem.* 188 (1990) 53.
- [2] B. Petel, G.E. Henderson, S.J. Haswell, R. Grzeskowiak, *Analyst* 115 (1990) 1063.
- [3] G.R. Cass, G.J. McRae, *Environ. Sci. Technol.* 17 (1983) 129.
- [4] G.J. Keeler, P.J. Samson, *Environ. Sci. Technol.* 23 (1989) 1358.
- [5] M.J.C. Taylor, J.F. van Staden, *Analyst* 119 (1994) 1263.
- [6] T. Kawashima, S. Nakano, M. Tabata, M. Tanaka, *Trends Anal. Chem.* 16 (1997) 132.
- [7] M.L. Lunar, S. Rubio, D. Perez-Bendito, *Anal. Chim. Acta* 237 (1990) 207.
- [8] A.C. Zotou, C.G. Papadopoulos, *Analyst* 115 (1990) 323.
- [9] M.L. Camacho, M.T. Rodriguez, M.C. Mochon, A.G. Perez, *Anal. Chim. Acta* 244 (1991) 89.
- [10] L. Darbha, J. Arunachalam, *Talanta* 40 (1993) 135.
- [11] A.A. Ensafi, A. Kazemzadeh, *Anal. Chim. Acta* 298 (1994) 27.
- [12] S. Kawakubo, B. Liang, M. Iwatsuki, T. Fukasawa, *Analyst* 119 (1994) 1391.
- [13] A.A. Mohamed, M. Iwatsuki, T. Fukasawa, M.F. El-Shahat, *Analyst* 120 (1995) 2281.
- [14] J. Ruzicka, E.H. Hansen, *Flow Injection Analysis*, 2nd edition, Wiley, New York, 1988.
- [15] T. Kawashima, S. Nakano, *Anal. Chim. Acta* 261 (1992) 167.
- [16] M. Sugiyama, T. Hori, *Anal. Chim. Acta* 261 (1992) 189.
- [17] S. Kawakubo, K. Kajihara, M. Iwatsuki, *Anal. Sci.* 12 (1996) 237.
- [18] A.A. Ensafi, A. Kazemzadeh, *Microchem. J.* 53 (1996) 139.
- [19] S. Nakano, M. Tago, T. Kawashima, *Anal. Sci.* 5 (1989) 69.
- [20] S. Nakano, C. Yamada, M. Sakai, T. Kawashima, *Anal. Sci.* 2 (1986) 61.
- [21] S. Nakano, H. Kasahara, M. Tanaka, T. Kawashima, *Chem. Lett.* 1981 (1981) 597.
- [22] T. Kawashima, S. Karasumaru, M. Hashimoto, S. Nakano, *Nippon Kagaku Kaishi* 1981 (1981) 175.
- [23] S. Nakano, S. Kinoshita, M. Ikuta, T. Kawashima, *Anal. Sci.* 6 (1990) 435.
- [24] S. Ueno, M. Ishizaki, *Nippon Kagaku Kaishi* 1979 (1979) 217.
- [25] M. Ishizaki, S. Ueno, *Talanta* 26 (1979) 523.

Catalytic determination of cobalt at sub-nanogram levels using the oxidative coupling of 3-methyl-2-benzothiazolinone hydrazone with *N*-ethyl-*N*-(2-hydroxy-3-sulfopropyl)-3,5-dimethoxyaniline by manual and flow-injection methods[☆]

Tetsuya Fujimoto^a, Norio Teshima^{a,1}, Makoto Kurihara^a,
Shigenori Nakano^b, Takuji Kawashima^{a,*}

^a *Laboratory of Analytical Chemistry, Department of Chemistry, University of Tsukuba, Tsukuba 305-8571, Japan*

^b *Chemical Institute, Faculty of Education, Tottori University, Koyama-cho, Tottori 680-0945, Japan*

Received 21 October 1998; accepted 12 November 1998

Abstract

A catalytic photometric method was developed for the determination of sub-nanogram levels of cobalt. The method is based on the catalytic effect of cobalt(II) on the oxidative coupling of 3-methyl-2-benzothiazolinone hydrazone with *N*-ethyl-*N*-(2-hydroxy-3-sulfopropyl)-3,5-dimethoxyaniline (DAOS) to form a colored dye ($\lambda_{\text{max}} = 525 \text{ nm}$) in the presence of hydrogen peroxide. In this reaction system, 1,2-dihydroxybenzene-3,5-disulfonate (Tiron) acted as an effective activator for the catalysis of cobalt(II). Variation of reaction time between 5 and 10 min allows the determination range to be extended from 0.01 to 1.0 ng ml⁻¹. The reaction system can also be successfully adapted to flow-injection analysis (FIA). The dynamic range of the proposed flow-injection method was 0.01–1.0 ng ml⁻¹ and detection limit (signal/noise, S/N = 3) was 5 pg ml⁻¹ at a sampling rate of 30 h⁻¹. Manual and flow-injection methods were applied to the direct determination of cobalt in pepperbush as a standard material. © 1999 Elsevier Science B.V. All rights reserved.

Keywords: Catalytic manual and flow-injection method; Photometry; Cobalt determination; Tiron as an activator

* Corresponding author. Tel.: +81-298-53-6521; fax: +81-298-53-6503.

E-mail address: kawasima@staff.chem.tsukuba.ac.jp (T. Kawashima)

¹ Present address: Department of Applied Chemistry, Aichi Institute of Technology, Toyota 470-0392, Japan.

[☆] Presented at The Ninth International Conference on Flow Injection Analysis (ICFIA 98), Seattle, Washington, USA, 23–27 August, 1998.

1. Introduction

Catalytic determinations of transition metal ions are the most widely used for the kinetic-based methods. In the past decade, various such methods have been developed by several authors [1–3]. By using a catalyzed reaction, ultratrace amounts of a catalyst can be determined through an increase in the reaction rate since the catalyst may take part in the number of cycles of the reaction. The best approach to enhance the rate of a catalyzed reaction is to use the appropriate activators.

The highly sensitive methods for determining cobalt at sub-ng ml⁻¹ levels have been increasingly required for the environmental, geochemical and ecological investigations. Many kinetic–catalytic methods have been reported by utilizing the oxidation processes of organic compounds such as 1,2-dihydroxybenzene-3,5-disulfonate (Tiron) [4,5], protocatechuic acid [6,7], Direct Blue 6B [8], Pyrogallol Red [9], *N*-phenyl-*p*-phenylenediamine [10], Amido Black 10B [12], *N,N'*-diethyl-*p*-phenylenediamine [11], 3,4-dihydroxybenzoic acid [13], Stilbazo and Pyrocatechol Violet [14].

Catalytic–photometric methods have also been reported for determining nanogram levels of copper(II) [15,16], chromium(III) [17], manganese(II) [18,19], cobalt(II) [20] and iron(II,III) [21] using an oxidative coupling of 3-methyl-2-benzothiazolinone hydrazone (MBTH) with *N,N*-dimethylaniline (DMA) in the presence of an oxidant. A suitable coupler including modified Trinder's reagents [22,23] instead of DMA was investigated, and it was found that *N*-ethyl-*N*-(2-hydroxy-3-sulfopropyl)-3,5-dimethoxyaniline (DAOS) was an effective coupler for MBTH in the presence of hydrogen peroxide and cobalt(II). Moreover, the catalytic activity of cobalt(II) was effectively enhanced by adding Tiron as an activator as previously reported [10,19]. This paper describes the highly sensitive manual and flow-injection photometric methods for the catalytic determination of cobalt(II) based on this reaction. Cobalt(II) in the range 0.01–1.0 ng ml⁻¹ can be determined by the manual and flow-injection methods. The meth-

ods permit the determination of sub-nanogram levels of cobalt and can be successfully applied to the determination of cobalt in peppercorn (National Institute for Environmental Studies (NIES) certified reference material No.1).

2. Experimental

2.1. Apparatus

A Hitachi U-1000 spectrophotometer was used for the absorbance measurements with 10-mm glass cells. A Horiba F8-AT pH meter and a Taiyo C-630 thermostated bath were also used.

The flow-injection system consisted of two double-plunger type pumps (Sanuki Kogyo, DM2M-1026), a six-way injection valve (Sanuki Kogyo, SVM-6M2), a Soma Kogaku S-3250 spectrophotometer equipped with a flow-through cell (8- μ l volume, 10-mm path length), a Chino EB 22005 recorder and two circulating thermostated baths (Taiyo, C-630). The flow lines were made from Teflon tubing (0.5 mm i.d.) and three-way connectors. The configuration of flow-injection manifold used is shown in Fig. 1 with optimum conditions.

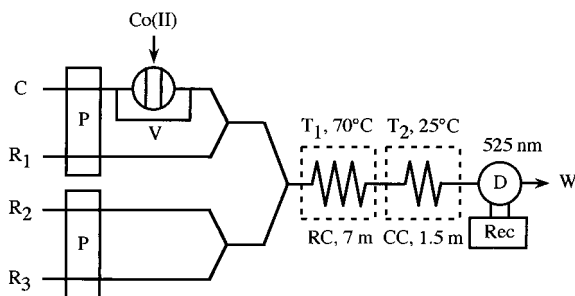


Fig. 1. Flow system for the catalytic determination of cobalt. C, carrier solution (HCl, 1.0×10^{-2} mol l⁻¹); R₁, Tiron (0.1 mol l⁻¹) + H₂O₂ (0.8 mol l⁻¹); R₂, *N*-ethyl-*N*-(2-hydroxy-3-sulfopropyl)-3,5-dimethoxyaniline (DAOS) (6.0×10^{-3} mol l⁻¹); R₃, 3-methyl-2-benzothiazolinone hydrazone (MBTH) (2.0×10^{-3} mol l⁻¹) + 2-amino-2-methyl-1,3-propanediol (AMP) (0.2 mol l⁻¹, pH 10.2); P, pump (0.5 ml min⁻¹); V, six-way valve (130 μ l); RC, reaction coil (7 m); CC, cooling coil (1.5 m); T₁ and T₂, thermostated baths (70 and 25°C); D, detector (525 nm); Rec, recorder; W, waste (pH 9.1).

2.2. Reagents

All reagents used were of analytical-reagent grade. The water purified with a Millipore Milli-Q PLUS system was used to prepare the solutions.

A 10 ng ml⁻¹ cobalt(II) stock solution was prepared by diluting a cobalt(II) standard solution (1000 µg ml⁻¹) for atomic absorption spectrometry (Kanto) in 0.05 mol l⁻¹ sulfuric acid. Working standard solutions were prepared by appropriate dilution before use. A 1.25 × 10⁻² mol l⁻¹ MBTH stock solution was prepared by dissolving 0.146 g of 3-methyl-2-benzothiazolone hydrazone hydrochloride (Tokyo Kasei) in 50 ml of water. A stock solution of 1.25 × 10⁻² mol l⁻¹ DAOS was prepared by dissolving 0.213 g of *N*-ethyl-*N*-(2-hydroxy-3-sulfopropyl)-3,5-dimethoxyaniline sodium salt (Dojindo) in 50 ml of water. Stock solutions of 2.0 mol l⁻¹ hydrogen peroxide and 0.1 mol l⁻¹ Tiron were prepared from the commercial reagents.

Other modified Trinder's reagents such as *N*-ethyl-*N*-(2-hydroxy-3-sulfopropyl)-3-methoxyaniline sodium salt dihydrate (ADOS), *N*-ethyl-*N*-(2-hydroxy-3-sulfopropyl)-3,5-dimethylaniline sodium salt monohydrate (MAOS), *N*-ethyl-*N*-(2-hydroxy-3-sulfopropyl)-3-methoxyaniline sodium salt dihydrate (TOOS), *N*-ethyl-*N*-(2-hydroxy-3-sulfopropyl)aniline sodium salt monohydrate (ALOS), *N*-(3-sulfopropyl)aniline sodium salt monohydrate (HALPS) were obtained from Dojindo Laboratories. A stock solution of 0.01 mol l⁻¹ DMA was prepared by dissolving *N,N*-dimethylaniline (Wako Junyaku) in 0.1 mol l⁻¹ hydrochloric acid.

Buffer solutions of 0.5 mol l⁻¹ tris(hydroxymethyl)aminomethane (tris), and 0.1 mol l⁻¹ 2-amino-2-methyl-1,3-propanediol (AMP) were also prepared in water. More diluted solutions were prepared from these stock solutions.

2.3. Manual procedure

To 20–25 ml of a sample solution containing less than 50 ng of cobalt(II) in a beaker, 4 ml of MBTH, 4 ml of DAOS, 5 ml of tris buffer, 4 ml of Tiron solutions are added. The pH of the mixed solution is adjusted to 8.1–8.2 by adding

hydrochloric acid and/or sodium hydroxide solution using a pH meter. The solution is transferred to a 50-ml volumetric flask. The solution is kept at 30.0 ± 0.1°C in a thermostated bath to attain thermal equilibrium for about 5 min. To initiate the reaction, 5 ml of hydrogen peroxide (30°C) is added. The solution is diluted to the mark with water. Exactly 5 and/or 10 min after the initiation of the reaction, a portion of the reaction mixture is pipetted into a 10-mm glass cell, the absorbance at 525 nm is measured against a water reference.

2.4. Flow-injection procedure

As shown in Fig. 1, the carrier solution of 1.0 × 10⁻² mol l⁻¹ hydrochloric acid (C), a mixed solution of 0.8 mol l⁻¹ hydrogen peroxide and 0.1 mol l⁻¹ Tiron (R₁), 6.0 × 10⁻³ mol l⁻¹ DAOS (R₂), a solution of 2.0 × 10⁻³ mol l⁻¹ MBTH containing 0.2 mol l⁻¹ AMP buffer (R₃) are pumped at a flow rate of 0.5 ml min⁻¹. A 130 µl sample solution is injected into the carrier stream. The color development proceeds in the reaction coil of 7 m length at 70°C, and then the colored solution is passed through the cooling coil of 1.5 m length at 25°C and the flow-through cell. The absorbance of the dye produced is monitored continuously at 525 nm.

3. Results and discussion

3.1. Preliminary studies

Tamaoku et al. [22,23] have synthesized the modified Trinder's reagents including DAOS, ADOS, MAOS, TOOS, ALOS and HALPS in order to determine hydrogen peroxide by using the coloration of the reagents with 4-aminoantipyrine. In the presence of hydrogen peroxide, MBTH also reacts with these Trinder's reagents to produce indamine dyes; cobalt(II) catalyzes these dye-forming reactions. The reactions involve the oxidation of cobalt(II) to cobalt(III); each color formation is accelerated by trace amounts of cobalt as a result of the regeneration of cobalt(III) by hydrogen peroxide.

Table 1
Characteristics of color formations of MBTH with various couplers^a

Coupler	λ_{\max} (nm)	pH	Initial rate ($\times 10^{-2}$ Δ abs min^{-1})
DAOS	525	9.1	2.8
ADOS	568	9.0	2.7
MAOS	570	8.6	2.1
TOOS	590	8.0	1.4
ALOS	601	7.9	0.37
DMA	588	8.0	0.21
HALPS	579	8.0	0.16

^a C_{coupler} , 1.0×10^{-2} mol l^{-1} ; C_{MBTH} , 1.0×10^{-2} mol l^{-1} ; $C_{\text{H}_2\text{O}_2}$, 3.0×10^{-2} mol l^{-1} ; $C_{\text{Co(II)}}$, 5.0 ng ml^{-1} ; temperature, 30°C; reaction time, 30 min. Abbreviations for couplers as in the text.

Preliminary investigations aimed at finding an appropriate coupler for MBTH. The oxidative coupling of these Trinder's reagents and DMA with MBTH in the presence of hydrogen peroxide and cobalt(II) were followed by monitoring the absorbances at optimum pH values. Table 1 shows the characteristics of these color formations. Relative large initial rates were observed in the cases of DAOS and ADOS. Among them, DAOS is the most sensitive reagent for this method; thus, DAOS was chosen as a coupler and the changes of absorbance were measured at 525 nm of the reaction product.

3.2. Optimization of the manual mode

In order to find the optimum conditions, the effects of pH, temperature and the concentrations of all the reagents on the reaction rate were studied at a cobalt(II) concentration of 1.0 ng ml^{-1} by using the fixed-time technique.

The effect of pH on the color development for the uncatalyzed and catalyzed reactions was examined for two reaction times of 5 and 10 min at 30°C. The maximal color development was obtained for the catalyzed reaction at pH 8.1–8.2 as shown in Fig. 2. The reaction proceeded faster with an increase in temperature, but a constant absorbance was obtained at temperatures above 35°C. The reaction temperature was fixed at 30°C for the sake of reproducibility.

The use of a suitable activator in catalytic methods permits an improvement in their sensitivity [1]. The effect of the concentrations of various complexing agents such as Tiron (3×10^{-3} – 5×10^{-2} mol l^{-1}), sulfosalicylic acid (6×10^{-5} – 1×10^{-2} mol l^{-1}), 2,2'-bipyridine (1×10^{-5} – 1×10^{-2} mol l^{-1}) and 1,10-phenanthroline (1×10^{-7} – 3×10^{-6} mol l^{-1}) was examined in relation to their use as possible activators. The catalytic activity of cobalt was suppressed in the presence of sulfosalicylic acid, 2,2'-bipyridine and 1,10-phenanthroline. On the other hand, Tiron effectively accelerated the cobalt(II)-catalyzed reaction. Fig. 3 shows the effect of Tiron concentration on the color development. As can be seen, the dependence of the reaction rate on activator concentration showed a maximum. Such a maximum is a characteristic feature for the types of activated reactions when the activator is concerned with the formation of ternary complexes of the activator-metal-substrate [1]; 2×10^{-2} mol l^{-1} Tiron was used for the procedure.

The color development was examined by changing concentration of MBTH at a constant concentration of DAOS. An increase in MBTH concentration increased in the absorbance for the catalyzed reaction. However, the formation of precipitate was observed in the reaction medium and the reproducibility became poorer at MBTH concentrations above 2.0×10^{-3} mol l^{-1} . Thus, a

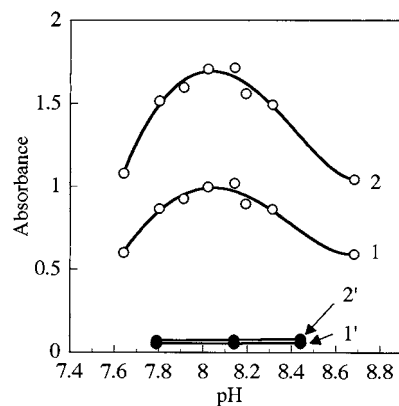


Fig. 2. Effect of pH on the color development. (1) and (2), 1.0 ng ml^{-1} cobalt(II); (1') and (2'), reagent blank. Reaction time: (1) and (1'), 5 min; (2) and (2'), 10 min. Other conditions as in the text.

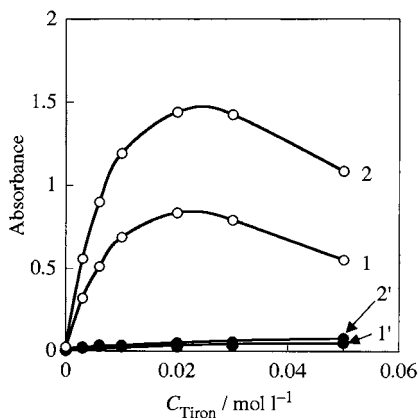


Fig. 3. Effect of Tiron concentration on the color development. (1) and (2), 1.0 ng ml^{-1} cobalt(II); (1') and (2'), reagent blank. Reaction time: (1) and (1'), 5 min; (2) and (2'), 10 min. Other conditions as in the text.

MBTH concentration of $1.0 \times 10^{-3} \text{ mol l}^{-1}$ was used for the procedure. Fig. 4 shows the effect of DAOS concentration on the color development for the reaction times of 5 and 10 min. A maximum absorbance was obtained at a DAOS concentration of $3.0 \times 10^{-3} \text{ mol l}^{-1}$; thus, this concentration was recommended. The effect of hydrogen peroxide concentration was examined over the range 3.0×10^{-2} – 0.6 mol l^{-1} . A maximum and constant absorbance for the catalyzed

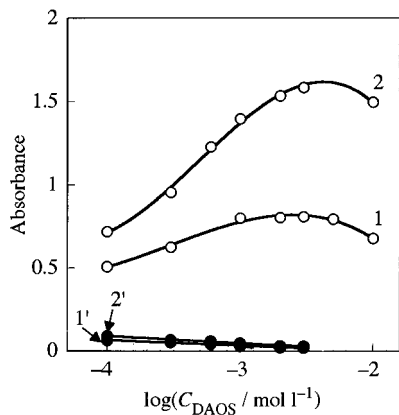


Fig. 4. Effect of *N*-ethyl-*N*-(2-hydroxy-3-sulfopropyl)-3,5-dimethoxyaniline (DAOS) concentration on the color development. (1) and (2), 1.0 ng ml^{-1} cobalt(II); (1') and (2'), reagent blank. Reaction time: (1) and (1'), 5 min; (2) and (2'), 10 min. Other conditions as in the text.

reaction was obtained in the concentration range 0.2 – 0.3 mol l^{-1} . A 0.2 mol l^{-1} hydrogen peroxide concentration was selected.

3.3. Calibration graphs for the manual method

Under the optimum conditions, two calibration graphs for the determination of cobalt(II) were prepared by the fixed-time method at 5 and 10 min. For a reaction time of 5 min, the calibration graph was linear over the range 0.1 – 1.0 ng ml^{-1} of cobalt(II). The apparent molar absorption coefficient was $5.0 \times 10^7 \text{ l mol}^{-1} \text{ cm}^{-1}$ with Sandell sensitivity of 1.2 pg cm^{-2} . At 10 min, it was linear in the range 0.01 – 0.1 ng ml^{-1} ; the apparent molar absorption coefficient and Sandell sensitivity were $1.1 \times 10^8 \text{ l mol}^{-1} \text{ cm}^{-1}$ and 0.55 pg cm^{-2} , respectively. The relative standard deviations (R.S.D.) ($n = 6$) for 0.6 and 0.06 ng ml^{-1} of cobalt(II) were 1.2 and 2.0%, respectively.

3.4. Interference studies for the manual method

The effect of diverse ions on the determination of 0.5 ng ml^{-1} of cobalt(II) at 5 min was examined. The tolerance ratio of each foreign ion was taken as the largest amounts yielding an error below $\pm 5\%$. No interference was observed from Ca(II), Na(I), NH_4^+ , K(I), BO_3^{3-} , Cl^- , CH_3COO^- , CO_3^{2-} , NO_3^- , PO_4^{3-} and citrate even at levels 10^4 times of the cobalt(II) concentration. Al(III), Mg(II) and Ti(IV) up to a 10^3 -fold excess and Cr(VI), Cd(II), Cu(II), Fe(III), Mn(II), Pb(II), Sn(II) and Zn(II) up to a 10^2 -fold excess did not interfere with the determination of cobalt(II). Positive interferences were observed from Ni(II) and V(V) up to 10^2 -fold excess; however, these ions up to 10-fold excess did not interfere.

3.5. Optimization of the flow system

On the basis of the conditions of the manual mode described above, the present reaction system was adapted to the flow-injection technique. By using the flow system as shown in Fig. 1, the variables were optimized by injecting a 1.0 ng ml^{-1} cobalt(II) solution.

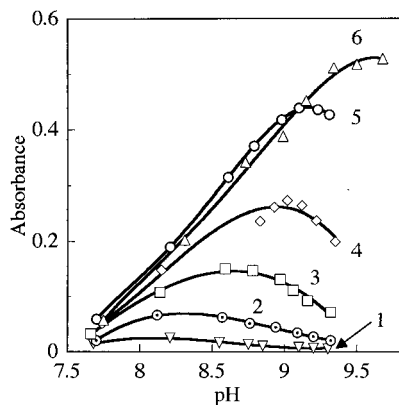


Fig. 5. Effects of pH and reaction temperature on the peak height. Curves (1)–(6) correspond to reaction temperature of 30, 40, 50, 60, 70 and 80°C, respectively. $C_{\text{Co(II)}}$, 1.0 ng ml⁻¹. Other conditions as in Fig. 1.

The effect of pH on the peak height was examined over the range 7.6–9.5 by adding AMP, hydrochloric acid and sodium hydroxide solutions at different reaction temperatures. The pH of the waste solution which was passed through the cooling coil of 1.5 m length at 25°C was measured. A maximum pH of the solution on the color development was shifted to higher pH values with increasing the reaction temperature. At higher temperatures, this shift might be attributable to the pH change of the solution in the RC of 7 m length to lower pH than that of the waste solution. In the case of a reaction temperature of 30°C, the maximal color development was obtained at pH around 8.1–8.2; this optimum pH range was the same as that obtained by the manual method as described in Section 3.2. The rate of cobalt(II)-catalyzed reaction increased with increasing in temperature and/or pH value (Fig. 5). However, the reproducibility became poorer at temperatures above 80°C; the reaction temperature and pH was therefore fixed at 70°C and 9.1, respectively. In order to carry out the cobalt(II)-catalyzed reaction at this pH, the mixed solution of MBTH and AMP in the reservoir R₃ was adjusted to pH 10.2. The length of the reaction coil was varied from 2 to 9 m. The peak heights increased with increasing the coil length. However, the wider peak width was observed at longer reaction coil length. A 7 m of reaction coil was

chosen taking into account of sampling frequency.

As described above, Tiron acted as an activator for the catalysis of cobalt(II). The peak height increased with increasing in the Tiron concentration up to 0.1 mol l⁻¹, and remained almost constant up to 0.2 mol l⁻¹. It began to decrease at concentrations above 0.2 mol l⁻¹. Therefore, 0.1 mol l⁻¹ Tiron concentration was selected. The peak height ratio between the presence of Tiron and its absence was about 180.

The effects of MBTH, DAOS and hydrogen peroxide concentrations on the catalyzed reaction were examined by varying their concentrations. The peak heights increased with increasing the MBTH concentration. However, MBTH at concentrations above 2.0×10^{-3} mol l⁻¹ was not sufficiently soluble in the reaction medium at pH 10.2. Therefore, a 2.0×10^{-3} mol l⁻¹ MBTH was selected as the recommended procedure. The peak heights were independent of the DAOS concentration; a 6.0×10^{-2} mol l⁻¹ DAOS concentration was chosen. The hydrogen peroxide concentration was varied from 0 to 2.0 mol l⁻¹. The peak heights increased up to hydrogen peroxide concentration of 0.6 mol l⁻¹, above which they became relatively independent of the hydrogen peroxide concentration. A hydrogen peroxide concentration of 0.8 mol l⁻¹ was therefore selected for the procedure.

3.6. Calibration graphs for the flow-injection method

By changing the sensitivity of the detector, two calibration curves in the concentration ranges 0.01–0.1 and 0.1–1.0 ng ml⁻¹ were prepared under the optimum conditions stated in the procedure. The linear range was obtained over the range 0.01–0.3 ng ml⁻¹. Although the peak heights deviated from a straight line at cobalt(II) concentration above 0.3 ng ml⁻¹, the dynamic range of the proposed method was obtained in the range 0.01–0.1 ng ml⁻¹ cobalt(II). The limit of detection for the proposed method is 5 pg ml⁻¹ (signal/noise, S/N = 3). The reproducibility was satisfactory with the R.S.D. of 1.6 and 0.64% for six determinations of 0.05 and 0.5 ng ml⁻¹ cobalt(II), respectively, with sampling rate of 30 h⁻¹.

Table 2
Determination of cobalt in pepperbush^a

Cobalt found ^b ($\mu\text{g g}^{-1}$)		Certified value ($\mu\text{g g}^{-1}$)
Manual method	FIA method	
22 \pm 1	22 \pm 1	23 \pm 3

^a The digested solution was diluted 100 (for manual method) or 1000 (for FIA method) times before measurement.

^b Average value for three determinations.

3.7. Interference studies for the flow-injection method

The interference of foreign ions in the present flow system was studied with the determination of 0.1 ng ml⁻¹ cobalt(II). The criterion for interference was a relative error of $\pm 5\%$. Up to 10⁵-fold excess for most foreign ions and a 10³-fold excess of Al(III), As(III), Cd(II), Fe(III), Mg(II), Mo(VI), Pb(II), Se(IV), Ti(IV), V(V), W(VI) and Zn(II) did not interfere. The excess of Cr(VI), Cu(II), Mn(II) up to 10²-fold caused no interference. Nickel(II) showed positive interference when present 10²-fold excess; 10-fold amounts of nickel(II) did not interfere in the same manner as the results of the manual method.

3.8. Application

In order to assess the utility of the proposed manual and flow-injection methods, they were applied to the determination of cobalt in pepperbush (NIES certified reference material No.1). A pressure decomposition in a Teflon bomb for the wet digestion of the sample (170.4 mg) was carried out by the procedure as described previously [24]. The decomposed sample was dissolved in 100 ml of 0.01 mol l⁻¹ hydrochloric acid. Analytical results were obtained by the calibration and standard addition methods after appropriate dilution. For the manual and flow-injection analysis (FIA) procedures, the results of cobalt obtained by the calibration method were a little higher than the certified value probably because of large amounts of co-existing matrices in the sample. However, the results obtained by the standard addition

method were in good agreement with the certified value (Table 2).

4. Conclusions

The oxidative coupling of MBTH with DAOS in the presence of hydrogen peroxide and Tiron is a sensitive catalytic reaction system for the determination of cobalt. The sensitivity of the manual and flow-injection photometric methods proposed here is superior and/or nearly equal to that of others [4–14]. The reproducibility of the methods was satisfactory with the R.S.D. below 2%. A 10²-fold excess of most foreign ions did not interfere with the determination. Cobalt in pepperbush can be easily determined by the proposed methods.

Acknowledgements

We gratefully acknowledge the financial support of this study by Grants-in-Aid for Scientific Research Nos. 09640715 and 0264 (N.T.) from the Ministry of Education, Science, Sports and Culture.

References

- [1] T. Kawashima, S. Nakano, *Anal. Chim. Acta* 261 (1992) 167.
- [2] D. Perez-Bendito, S. Rubio, *Trends Anal. Chem.* 12 (1993) 9.
- [3] T. Kawashima, S. Nakano, M. Tabata, M. Tanaka, *Trends Anal. Chem.* 16 (1997) 132.
- [4] K. Isshiki, E. Nakayama, *Talanta* 34 (1987) 277.
- [5] M.A.Z. Arruda, E.A.G. Zagatto, A.O. Jacintho, S.M.B. Brienza, *J. Braz. Chem. Soc.* 2 (1991) 47.
- [6] T. Yamane, K. Watanabe, H.A. Mottola, *Anal. Chim. Acta* 207 (1988) 331.
- [7] T. Kitamura, T. Yamane, *Bunseki Kagaku* 37 (1988) 360.
- [8] Z. Gregorowicz, D. Matysek-Majewska, T. Suwinska, *Mikrochim. Acta (Wien)* 1 (1985) 237.
- [9] M. Llobat-Estelles, A. Sevillano-Cabeza, J. Medina-Es-criche, *Analyst* 111 (1986) 193.
- [10] T. Kawashima, T. Minami, M. Ata, M. Kamada, S. Nakano, *J. Flow Injection Anal.* 2 (1985) 40.
- [11] A. Malahoff, I. Ya. Kolotyorkina, L.K. Shipigun, *Analyst* 121 (1996) 1037.

- [12] K. Watanabe, A. Tsutsumi, N. Koura, *Bunseki Kagaku* 38 (1989) 691.
- [13] M.T. Oms, R. Forteza, V. Cerda, *Anal. Chim. Acta* 258 (1992) 177.
- [14] T. Deguchi, A. Higashi, I. Sanemasa, *Bull. Chem. Soc. Jpn.* 59 (1986) 295.
- [15] S. Nakano, H. Ihara, M. Tanaka, T. Kawashima, *Mikrochim. Acta (Wien) I* (1985) 455.
- [16] K. Satoh, N. Iwamura, N. Teshima, S. Nakano, T. Kawashima, *J. Flow Injection Anal.* 10 (1993) 245.
- [17] S. Nakano, S. Hinokuma, T. Kawashima, *Chem. Lett.* 1983 (1983) 357.
- [18] S. Nakano, A. Ohta, T. Kawashima, *Mikrochim. Acta (Wien) II* (1985) 273.
- [19] Y. Miyata, T. Hirano, S. Nakano, T. Kawashima, *Anal. Sci.* 7 (1991) 97.
- [20] Zhu-Yue Yu, N. Teshima, S. Nakano, T. Kawashima, *Talanta* 43 (1996) 1519.
- [21] T. Tomiyasu, N. Teshima, S. Nakano, T. Kawashima, *Talanta* 47 (1998) 1093.
- [22] K. Tamaoku, Y. Murao, K. Akiura, Y. Ohkura, *Anal. Chim. Acta* 136 (1982) 121.
- [23] K. Tamaoku, K. Ueno, K. Akiura, Y. Ohkura, *Chem. Pharm. Bull.* 30 (1982) 2492.
- [24] K. Okamoto, K. Fuwa, *Anal. Chem.* 56 (1984) 1758.

Spectrophotometric determination of Cu(II) with sequential injection analysis[☆]

J.F. van Staden *, A. Botha

Department of Chemistry, University of Pretoria, Pretoria 0002, South Africa

Received 30 November 1998; received in revised form 2 February 1999; accepted 2 February 1999

Abstract

A sequential injection system, based on the reaction of Cu(II) with diethyldithiocarbamate (DDTC), was developed for the determination of Cu(II) in plant food and water samples. The extraction procedure, generally used to extract the Cu(II)–DDTC complex for subsequent analysis was eliminated in this procedure. The complex was detected spectrophotometrically in aqueous solutions at 460 nm. The physical and chemical parameters depicting the system were studied to obtain optimum conditions for sample analysis. The system developed is fully computerized and able to monitor Cu(II) in samples at seven samples per hour with a relative standard deviation of < 4.50%. The calibration curve is linear from 0.5–5.0 mg/l with a detection limit of 0.2 mg/l. Interferences were reduced by introducing multiple flow reversals, to increase mixing between the reagent and sample zones, and subsequently enhance working of the masking agents (EDTA/citrate). © 1999 Elsevier Science B.V. All rights reserved.

Keywords: Copper(II); Diethyldithiocarbamate; Sequential injection analysis; Multiple flow reversals; Plant food samples; Water samples

1. Introduction

The steady increase in pollution necessitates the analysis and monitoring of toxic species that could become a serious potential hazard if not controlled. Copper fulfils various roles in the agricultural field. Control thereof in terms of nutri-

tion of plants and its possible contamination of water, is necessary. Metal dithiocarbamates are widely used for analytical purposes due to their characteristic colours [1]. Diethyldithiocarbamate (DDTC) is often used as reagent for the selective determination of Cu(II) since the Cu(II)–DDTC stability constant is the highest, next to silver, compared with the stability constants of the other DDTC–metal complexes [2]. DDTC coordinates with Cu(II) through the two sulfur atoms to form a four-membered ring complex which can be spectrophotometrically detected.

An extensive study has already been conducted on the analysis of copper using its reaction with

[☆] Presented at the Ninth International Conference on Flow Injection Analysis (ICFIA'98) held in Seattle, WA, USA, August 23–27, 1998.

* Corresponding author. Fax: +27-12-362-5297.

E-mail address: koos.vanstaden@chem.up.ac.za (J.F. van Staden)

DDTC and the subsequent extraction of the complex formed into an organic medium [2–10]. Extraction of the Cu(II)–DDTC complex is preferred since it is slightly soluble in water and dissolves more readily in organic solvents [11]. A disadvantage of solvent-extraction is the use of toxic organic solvents that also have carcinogenic properties. A lot of emphasis is placed on conducting environmentally friendly analysis and eliminating the use of harmful substances. Spectrophotometric analysis of the Cu(II)–DDTC complex, without solvent-extraction, has also successfully been conducted by measurement of the coloured complex in aqueous medium [12–16]. The system developed in this study was based on the spectrophotometric measurement of the Cu(II)–DDTC complex in an aqueous medium.

The development of systems to conduct routine analysis is subjected to stringent requirements. Effective cost control plays a very important role in the efficient management of routine control laboratories and on-line process analysers. Low-cost instrumentation, minimum sample and reagent consumption therefore become important. Detectors like AAS and ICP, although very fast are expensive when compared to UV/Vis spectrophotometers, whereas the reagent consumption in flow injection analysis is relatively high compared to sequential injection analysis (SIA). An additional advantage of SIA is the relative ease of implementation as an on-line analyser. SIA is based on the sequential aspiration of microlitres of reagent and sample, as zones, into a holding

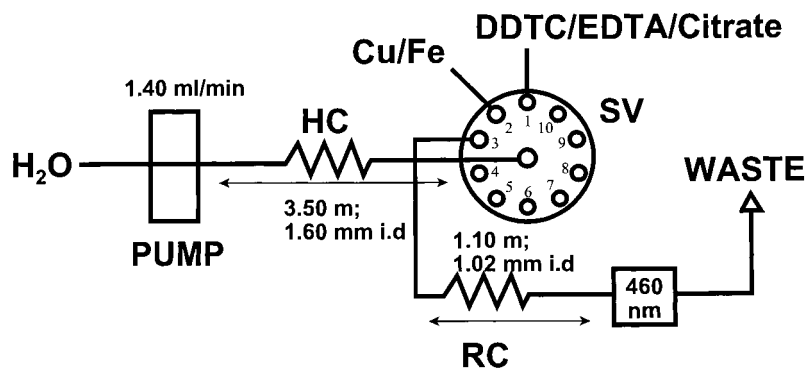


Fig. 1. A schematic diagram of the sequential injection analyser used for the determination of Cu(II) with DDTC. HC, holding coil; RC, reaction coil; SV, selection valve.

Table 1
Device sequence for one cycle of the sequential injection system

Time (s)	Pump	Valve	Description
0	Off	DDTC/EDTA/citrate	Pump off, select DDTC/EDTA/citrate stream (valve position 1)
5.0	Reverse		Draw up DDTC/EDTA/citrate solution
15.7	Off		Pump stop
16.7		Cu/Fe	Select Cu/Fe stream (valve position 2)
17.7	Reverse		Draw up Cu/Fe solution
49.8	Off		Pump stop
50.8		Detector	Select detector line (valve position 3)
51.8	Forward, reverse		Twenty-nine flow reversals of 4 s each
167.8	Forward		Pump stack of zones to detector
519.0	Off	Home	Pump off, return valve to starting position (valve position 1)

Table 2
Influence of different techniques to reduce interference from Fe(II)

	% Interference
Stopped-flow period (s)	
0	31.8
120	27.9
240	10.4
Flow reversals (#)	
1	52.0
10	32.2
20	28.6
30	13.6
Length of flow reversal (s)	
0	65.2
4	59.2
10	43.9
20	12.6

coil. After aspiration the flow is reversed and the well-defined zones are then propelled via a reaction coil to the spectrophotometer. The reagent and sample zones mutually penetrate one another to form a product zone which can then be detected.

The purpose of this work was to study the possibility of applying DDTC as reagent for the

spectrophotometric determination of Cu(II) with a SIA system. A sensitive and selective method was developed for the determination of Cu(II) in natural waters and plant food.

2. Experimental

2.1. Reagents and solutions

All reagents were prepared from analytical-reagent grade chemicals unless specified otherwise. All aqueous solutions were prepared using de-ionised water from a Modulab system (Continental Water Systems, San Antonio, TX). The de-ionised water used to prepare the aqueous solutions were degassed, by heating to boiling point and cooling before the solutions were made up.

2.1.1. Standard Cu(II) solution, 1000 mg/l

Pure copper metal coarse chips were used in the preparation of the Cu(II) stock solution. The copper metal was cleaned to remove any oxides and dissolved by heating 1.0 g of the copper metal in 10 ml 55% HNO₃ and ca. 10 ml of water. The subsequent solution was cooled and then diluted to 1000 ml with water.

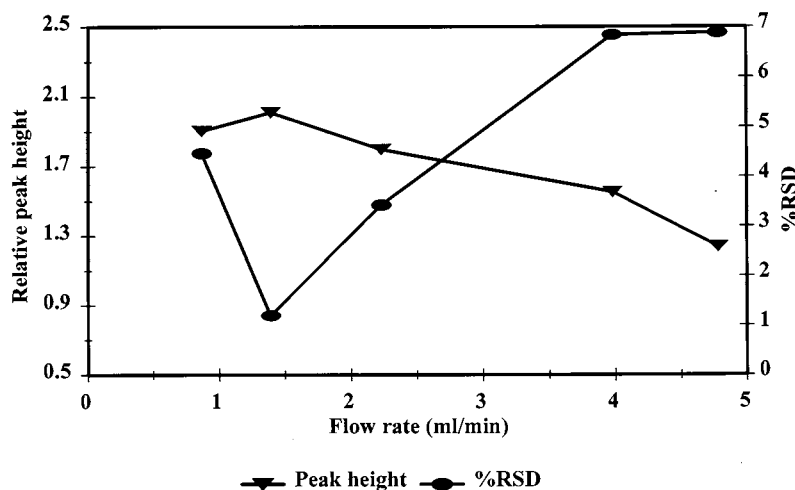


Fig. 2. Influence of flow rate on sensitivity and precision.

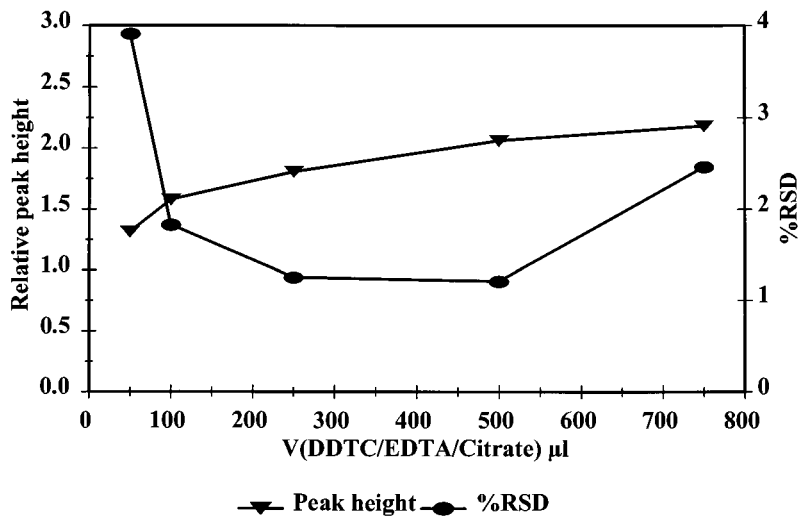


Fig. 3. Influence of reagent (DDTC/EDTA/citrate) volume on sensitivity and precision.

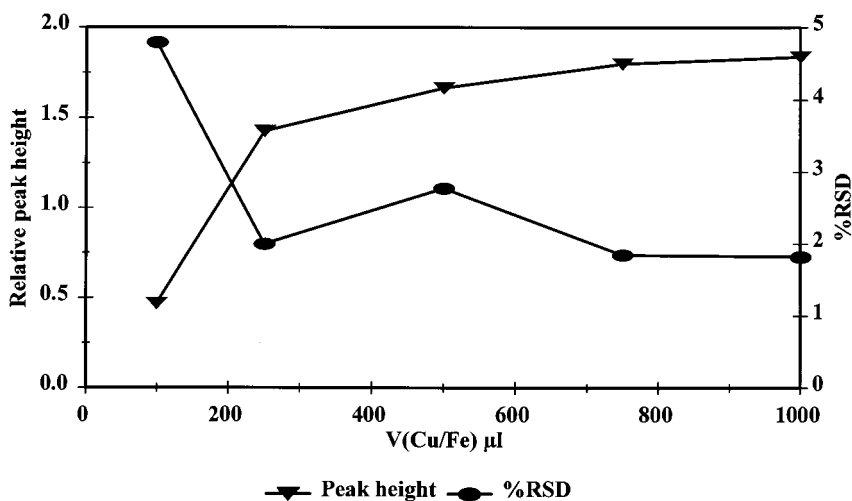


Fig. 4. Influence of sample (Cu/Fe) volume on sensitivity and precision.

2.1.2. Standard Fe(II) solution, 100 mg/l

$\text{Fe}(\text{NH}_4)_2(\text{SO}_4)_2 \cdot 6\text{H}_2\text{O}$ (0.0702 g) was dissolved in ca. 20 ml of water with 1.1 ml of 18.4 mol/l H_2SO_4 (98%). The final solution was diluted to 100 ml with water.

2.1.3. Cu(II)/Fe(II) working solution

A solution containing 3 mg/l Cu(II) and 15 mg/l Fe(II) was prepared in order to study the effect of Fe(II) as the largest interferent on the

Cu(II)–DDTC reaction [16] in the presence of the analyte. These solutions were made by appropriate dilutions of the 1000 mg/l Cu(II) and 100 mg/l Fe(II) standard solutions respectively.

2.1.4. DDTC/EDTA/citrate reagent solution

Sodium diethyldithiocarbamate (DDTC; 0.1% (m/v)) was dissolved in 50 ml water by heating the solution to 60°C. After the DDTC solution was cooled, 1.2 g ethylene-diamine-tetra-acetic acid

disodium salt (EDTA) together with 1.5 g triammonium citrate was dissolved in 25 ml water and added to the DDTC solution; 9.5 ml of a 2 mol/l NH_4Cl solution was then added to the DDTC/EDTA/citrate solution and the pH adjusted to 8.3 by adding an appropriate volume of 2 mol/l NH_3 . The final solution was made up to 100 ml with water.

2.2. Apparatus

The sequential injection system depicted in Fig. 1 was constructed from the following components: a Gilson Minipuls peristaltic pump (Model M312, Gilson, Villiers-le-Bel, France); a 10-port electrically actuated selection valve (Model ECSD10P; Valco Instruments, Houston, TX); and a UNICAM 8625 UV–visible spectrophotometer equipped with a 10-mm Hellma-type (Hellma, Mülheim/Baden, Germany) flow-through cell (volume 80 μl) for absorbance measurements.

Data acquisition and device control was achieved using a PC30-B interface board (Eagle Electric, Cape Town, South Africa) and an assembled distribution board (Mintek, Randburg, South Africa). The FlowTEK [17] software package (Mintek) for computer-aided flow anal-

ysis was used throughout for device control and data acquisition.

The wavelength of maximum absorption was identified by scanning the Cu(II)–DDTC complex solution over the 300–700 nm range with a Spectronic Genesys 5 spectrophotometer (Milton Roy). The optimum wavelength was chosen as 460 nm which corresponds to the wavelength used by previous authors conducting the same determination [13,16].

pH measurements of the DDTC/EDTA/citrate solution were conducted with an Orion pH meter (Model 420A; Orion Research) and an Orion pH Triode™ electrode.

2.3. Sample preparation

Cu(II) was determined in plant food (water soluble samples) and water samples. A predetermined mass was weighed, dissolved and finally diluted to 100 ml. The water samples were spiked with a known concentration of Cu(II).

2.4. Procedure

The device sequence for the determination of Cu(II) by sequential injection analysis is given in Table 1.

Table 3
Influence of sodium–DDTC concentration on peak height, precision and interference

% [Na–DDTC] (m/v)	Relative peak height (Cu)	Relative peak height (Cu/Fe)	% RSD (Cu/Fe)	% Interference
0.05	1.75	1.41	1.47	–19.22
0.10	1.74	1.57	2.86	–9.86
0.20	1.83	1.83	3.52	0.02
0.30	1.88	2.06	4.49	9.47
0.40	1.85	2.16	3.08	17.07

Table 4
Influence of pH of DDTC/EDTA/citrate solution on peak height, precision and interference

pH	Relative peak height (Cu/Fe)	% RSD (Cu/Fe)	% Interference
6.30	1.47	1.89	–10.52
7.30	1.67	3.42	0.95
8.30	1.54	1.34	–2.84
9.20	1.50	1.84	–6.11

Table 5
Influence of EDTA concentration on peak height, precision and interference

% [EDTA] (m/v)	Relative peak height (Cu/Fe)	% RSD (Cu/Fe)	% Interference
0.30	1.49	1.61	−9.14
0.60	1.52	1.36	−6.24
1.20	1.50	1.18	−4.35

3. Results and discussion

3.1. Optimization of the sequential injection system

It is well-known that changing the physical parameters of an SIA system influenced the sensitivity and precision of measurements [18–20]. These parameters also have a direct influence on the sensitivity and precision obtained when studying a chemical reaction. It was shown that the following chemical parameters affect the Cu(II)–DDTC reaction [16]: DDTC concentration, pH, EDTA and citrate concentration. Optimization of physical and chemical parameters was thus necessary to develop a system with optimum sensitivity and precision.

3.1.1. Physical parameters

3.1.1.1. Comparison of different techniques to reduce Fe(II) interference. According to previous studies it seems that Fe(II) interfered significantly, even from the smallest interfering ion:Cu(II) ratio when Cu(II) was determined with DDTC [16]. It was therefore decided to optimize the Cu(II)–DDTC complexation reaction in the presence of Fe(II) as interferent. Optimising the chemical parameters to a point where interference from Fe(II) was a minimum possibly also reduced other interferences. Three physical techniques that could contribute to reducing interference were studied. The results are tabulated in Table 2. The techniques were: stopped-flow period, flow reversals and length of the flow reversals. Although the interference for the zero stopped-flow period ('no stopped flow') should be equivalent to the interference for no flow reversals, since both just mean

simple sample aspiration and delivery to the detector, the repeated results obtained showed a % interference of 31.8% for 'no stopped-flow' and 65.2% for 'no flow reversal' respectively (Table 2).

The stopped-flow period was implemented for a fixed time directly after the flow was reversed. The length of the stopped-flow period was evaluated. A decrease in Fe(II) interference was observed for the longer periods, due to more time allowed for the masking agents to react with the interferent. A disadvantage of the stopped-flow period was, however, a decrease in sample frequency due to longer analysis times.

Flow reversals were obtained by propelling the flow forward and backwards in the flow conduit. By repeating this action more than once, zone penetration was enhanced and a mixing effect was obtained which allowed more effective mixing of the sample and reagent zones. This action contributed to a larger reaction between the masking and interfering components. The results showed that a decrease in Fe(II) interference was obtained with a larger number of flow reversals. Although sensitivity decreased due to increased dispersion of the zones for the larger number of flow reversals, viable analysis times and adequate sensitivity were achieved.

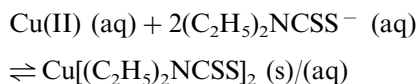
The length of a fixed number of flow reversals was changed by changing the time it takes for each reversal (counting one forward and backward motion as one reversal) to be completed. Increasing the length of the flow reversals effectively reduced interference although dispersion of the zones increased dramatically and sensitivity decreased as a result.

Thirty flow reversals were chosen as optimum to reduce interference effectively and still gave adequate sensitivity and analysis times.

Table 6
Influence of tri-ammonium citrate concentration on peak height, precision and interference

% [Citrate] (m/v)	Relative peak height (Cu)	Relative peak height (Cu/Fe)	% RSD (Cu/Fe)	% Interference
1.50	1.54	1.52	2.25	–1.05
3.00	1.60	1.71	2.01	7.11
6.00	1.72	1.86	1.10	7.98
10.00	1.82	1.99	1.45	9.05

3.1.1.2. *Flow rate.* The effect of flow rate on peak height is shown in Fig. 2. A flow rate of 1.4 ml/min, which gave the best sensitivity and precision compared to other flow rates, was chosen as optimum. A decrease in peak height was observed for the higher flow rates. This was attributed to a low Cu(II)–DDTC reaction rate. The formation of the Cu(II)–DDTC complex can be illustrated by the following equilibrium reaction ($(\text{C}_2\text{H}_5)_2\text{NCSS}^- = \text{DDTC}$):



At low flow rates, adequate time was available for the equilibrium to be attained. An adequate amount of Cu(II)–DDTC complex was therefore formed for spectrophotometric detection. With increased flow rates the formed product zone was propelled faster to the detector. The time available for complex formation was therefore shortened, thus less Cu(II)–DDTC complex was formed and a decrease in sensitivity was observed. Although higher flow rates resulted in higher sampling frequencies, it was characterised by a loss of sensitivity and decreased precision (Fig. 2).

3.1.1.3. *Reagent and sample volume.* The reagent volume was studied by aspirating increasing reagent volumes (50–750 μl) into the system, while keeping the sample volume constant. In Fig. 3 an increase in sensitivity with increasing reagent volume was initially observed. No further increase for the largest reagent volumes was noticed. An optimum of 250 rather than 500 μl was chosen although the sensitivity for 500 μl was higher. The reason for this was that by using a large reagent volume (e.g. 500 μl) an excess of DDTC reagent would be added to the system,

and subsequently a larger sample volume would be necessary to react with all the reagent to deliver a plateau (no further increase in sensitivity with increasing sample volume) in an increasing sample volume graph. For these systems longer analysis times would be required for flushing the system resulting in lower sampling frequencies.

With smaller reagent volumes (e.g. 250 μl), smaller sample volumes would be necessary to deliver a plateau in an increasing sample volume graph. An advantage of SIA is the reduction in reagent and sample consumption. By choosing a smaller reagent volume as optimum (250 μl) a decrease in sensitivity would be inevitable, but the analysis time could be kept as short as possible and reagent and sample consumption would be reduced.

Fig. 4 illustrates the change in peak height with changing sample volume (100–1000 μl), whilst the reagent volume is kept constant. The increase in peak height was attributed to the larger quantity of analyte available to react with the excess of reagent. A plateau is reached when the sample

Table 7
Comparison of results obtained by the proposed SIA system and flame-AAS

Sample	AAS (mg/l)	SIA (mg/l)	% RSD (SIA)
A	1.30	1.27	3.98
B	1.68	1.82	1.78
C	2.87	2.66	1.72
D	3.29	3.16	4.54
E	4.18	4.28	2.29
Plant food: A	4.88	4.47	2.76
Plant food: B	2.69	2.47	2.02

Table 8

Interference from foreign ion species studied for a 3.0 mg/l Cu²⁺ solution^a

Tolerance ratio of foreign species (<i>x</i>)	Foreign species
600	Mg ²⁺
300	SO ₄ ²⁻ , Mn ²⁺
200	NO ₃ ⁻
150	Ca ²⁺
40	Cl ⁻
20	Zn ²⁺ , K ⁺
10	CO ₃ ²⁻
5	Fe ²⁺ , Fe ³⁺

^a The ratio of foreign ion (mg/l) to Cu(II) is indicated as *x*:1.

reacts with most of the reagent in the reagent volume. Optimum sensitivity and precision were obtained for 750 µl of sample.

3.1.2. Chemical parameters

3.1.2.1. Sodium diethyldithiocarbamate (Na-DDTC) concentration. Increasing the % Na-DDTC concentration (m/v) resulted in increased peak heights (Table 3) for the Cu(II)/Fe(II) working solution. Although it was expected that the response would stay constant for higher reagent concentrations due to all the sample being used up by the reagent, the results obtained proved the contrary. The relatively constant peak height obtained for the reaction between Cu(II) and DDTC (in the absence of Fe(II)) suggested that all the Cu(II) had reacted and that by increasing the DDTC concentration no significant increase in complex formation was achieved. An increase in peak height was, however, observed for DDTC and the Cu(II)/Fe(II) sample. This increase was attributed to Fe(II) which was added as interferent to the Cu(II) sample. In this instance Fe(II) was also available to react with the DDTC after an optimum of Cu(II) had reacted. In addition to the detected Cu(II)–DDTC complex, the Fe(II)–DDTC complex might also contribute to the peak height.

It is also evident from Table 3 that the % interference changes from a large negative to a large positive value with increasing Na-DDTC concentrations. This is due to the possibility that

Fe(II) might have formed different complexes at various Na-DDTC concentrations. Increased Na-DDTC concentrations could affect the coordination of DDTC towards Fe(II) to form different complexes with differing absorption characteristics.

Choosing an optimum was based on a compromise regarding sensitivity and % interference and gaining with respect to precision. The 0.1% Na-DDTC concentration was chosen as optimum. The 0.2% concentration gave better sensitivity with less interference, but the precision was not that satisfactory. The interference experienced for the 0.1% concentration can be reduced by optimization of the masking agent concentrations.

3.1.2.2. pH of the DDTC/EDTA/citrate solution.

The most important feature of the dithiocarbamate ion is its protonation in acidic solutions and the subsequent decomposition into carbon disulphide and the protonated amine [1]. Preliminary experiments therefore showed that complex formation between Cu(II) and DDTC did not occur at a pH below 6, but that complex formation took place above a pH of 6. Due to possible interference from Fe(II) on the spectrophotometric determination of Cu(II), the pH range between 6 and 10 was studied to see whether pH might influence the overall sensitivity as well as interference from Fe(II).

Table 4 shows that a change in pH had a minor effect on the sensitivity of the measurements. The pH did however influence the complexation reaction. Since interference was minimised between a pH of 7.3 and 8.3, it can be concluded that the masking agents performed best in the mentioned range. Precision obtained at pH 8.3 was better than at pH 7.3 and was thus chosen as the optimum working condition. This compares well to the optimum pH used in previous studies [13,16].

3.1.2.3. Masking agents concentration.

The selectivity of the complexation reaction between Cu(II) and DDTC is enhanced considerably by using EDTA in combination with citrate as masking agent [1,2,7,13,16]. Increasing the EDTA concen-

tration did not affect the sensitivity and had a minor influence on precision (Table 5). As was expected the % interference decreased with higher EDTA concentrations. A 1.2% (m/v) EDTA concentration was chosen for masking interferences.

Table 6 shows an increase in sensitivity with increasing citrate concentration, both in the presence and absence of Fe(II). This observation is due to the fact that the citrate might react with either Fe(II) or Cu(II) to form complexes that absorb at the wavelength of interest to contribute to the Cu(II)–DDTC absorption signal. This also explained the increase in % interference with increasing citrate concentration. Least interference was experienced at 1.5% (m/v) citrate and this concentration was therefore chosen as optimum.

4. Method evaluation

The proposed SIA system was critically evaluated with regard to accuracy, precision, detection limit, linear range, sample interaction, sampling frequency and interferences.

4.1. Linearity, accuracy, precision and detection limit

The response of the proposed SIA system for the spectrophotometric determination of Cu(II) was evaluated under optimum conditions. The calibration curve was linear from 0.5 to 5.0 mg/l (response = $0.4984[\text{Cu(II)}] + 0.1367$; $r = 0.998$, $n = 5$). The calculated detection limit was 0.2 mg/l Cu(II).

The accuracy was evaluated by analysing two plant food samples and five tap water samples. The results, shown in Table 7, are in good agreement with the results obtained by flame-AAS. The precision determined for the analysed samples ($n = 5$) is also shown in Table 7. In all cases the RSD was $< 4.50\%$.

A sampling frequency of seven samples per hour was obtained. The lengthy analysis time (519 s) was ascribed to the time necessary to perform the flow reversals and time needed to rinse the system to minimise possible carry-over between analysis. The sample interaction between samples was smaller than 1%, which is negligible.

4.2. Interferences

Wang and coworkers [16] showed that some ions interfered in the spectrophotometric determination of Cu(II) with DDTC. The interferences of these ions with the proposed SIA system were studied and the results are highlighted in Table 8. It is clear from Table 8 that the level of tolerance is up to at least a 5:1 (foreign ion to Cu(II) ion) ratio for Fe^{2+} , an interference that has been dealt with in detail. The interference from the carbonate ion is mainly due to a change in pH that was eliminated by selecting the optimum pH working conditions as described.

5. Conclusion

The proposed system proved to be successful in analysing Cu(II) in plant food and water samples. Analysis was done without the necessity of introducing an extraction step thus complying with the need for conducting environmentally safe analysis. The lengthy analysis time that contributes to the low sample frequency was due to the flow reversals necessary to reduce interference and to flush the system. The flow reversals successfully reduced interference. The system is fully computerized and can be incorporated on-line if required. The calibration curve is linear from 0.5 to 5.0 mg/l with a detection limit of 0.2 mg/l. The system processes seven samples per hour with a relative standard deviation of $< 4.50\%$.

References

- [1] A. Hulanicki, Talanta 14 (1967) 1371.
- [2] J. Szpunar-Lobinska, M. Trojanowicz, Anal. Sci. 6 (3) (1990) 415.
- [3] T. Blanco, N. Maniasso, M. Fernanda-Gine, A.O. Jacintho, Analyst 123 (2) (1998) 191.
- [4] X.N. Ge, P.F. Jiang, W.S. Bo, Fenxi Huaxue 22 (8) (1994) 863.
- [5] Z. Yan, X. Jiang, Y. Yi, Y. Hu, Yaowu Fenxi Zazhi 13 (4) (1993) 275.
- [6] A.R. Fernandez-Alba, J.L. Martinez-Vidal, P. Aguilera, F. Freniche, A. Aguera, Anal. Lett. 25 (8) (1992) 1581.
- [7] M. Kan, H. Sakamoto, T. Nasu, M. Taga, Anal. Sci. 7 (6) (1991) 913.

- [8] H. Satoh, Y. Kikuchi, T. Suzuki, K. Sawada, *Bunseki Kagaku* 40 (10) (1991) 167.
- [9] K. Fujiwara, *Anal. Chim. Acta* 212 (1-2) (1988) 245.
- [10] B. Zuo, G. Chen, J. Han, *Huaxue Xuebao* 42 (1) (1984) 93.
- [11] B.J. Mueller, R.J. Lovett, *Anal. Chem.* 59 (1987) 1405.
- [12] M.P. San-Andres, M.L. Marina, S. Vera, *Analyst* 120 (2) (1995) 255.
- [13] P. Wang, D.L. Jia, Y. Wang, *Fenxi Huaxue* 23 (1) (1995) 36.
- [14] T. Kiriya, *Bunseki Kagaku* 42 (4) (1993) 223.
- [15] M.C. Garcia-Alvarez-Coque, M.C. Martinez-Vaya, G. Ramis-Ramos, R.M. Villanueva-Camanas, C. Mongay-Fernandez, *Quim. Anal.* 5 (3) (1986) 329.
- [16] P. Wang, S.J. Shi, D. Zhou, *Microchem. J.* 52 (1995) 146.
- [17] G.D. Marshall, J.F. van Staden, *Anal. Instrum.* 20 (1992) 79.
- [18] J.F. van Staden, A. Botha, *S.-Afr. Tydskr. Chem.* 51 (2) (1998) 100.
- [19] G.D. Marshall, J.F. van Staden, *Proc. Cont. Qual.* 3 (1992) 251.
- [20] T. Gübeli, G.D. Christian, J. Růžicka, *Anal. Chem.* 63 (1991) 2407.

Author Index

Volume 49 (1999)

- Aaron, J.-J., 107
Abdennabi, A.M.S., 1051
Abedi, M., 531
Acar, O., 135
Acuña, J.A., 441
Agrawal, O., 923
Aihara, M., 1059
Alexander, P.W., 639
Algarra González, M., 679
Almuaibed, A.M., 1051
Amador-Hernández, J., 813
Amendola, S., 267
Andrade, J.M., 165
Anisimov, B., 629
Antonov, L., 99
Ao, X.P., 495
Arana Nicolas, E., 915
Arias, J.J., 143
- Bakkali, A., 773
Barbeira, P.J.S., 271
Barcza, L., 577
Barefoot, R.R., 1
Bello, M.A., 881
Berrueta, L.A., 773
Bessarabova, O., 899
Bhagat, A.N., 41
Bhalotra, A., 485
Bhattacharya, A., 367
Binder, M., 267
Bing, C., 651
Biswas, J., 41
Blanco, C., 597
Blasco Gómez, F., 155
Bosch Reig, F., 155
Botha, A., 1099
Brockman, F.J., 969
Bruckner-Lea, C.J., 969
Burenko, T., 629
Buvári-Barcza, Á., 577
Byrne, A.R., 619
- Calace, N., 277
Callejón, M., 881
Campiglia, A.D., 547
Campíns Falcó, P., 155
Cañada, M.J.A., 691
Cao, Y., 377
Capewell, S.G., 25
Capitán-Vallvey, L.F., 691, 915
Capolei, M., 277
Chakravarty, S., 41
Chandler, D.P., 969
Cheng, F., 253
Cheng, J.-K., 751
Chen, J., 345
Chen, P., 571
Chen, Q.-Y., 745
Chen, Z.L., 661
Chow, A., 757
Chufán, E.E., 859
Chul Lee, S., 69
Church, T.M., 851
Chwastowska, J., 837
Ciria, J.I., 773
Coly, A., 107
Corta, E., 773
Costa-Fernández, J.M., 907
Cruz Ortiz, M., 801
- Dai, H.-P., 751
Daly, D.J., 667
Da, S.-L., 47
Díaz, A.M., 691
de Andrade, J.B., 245
Deb, M.K., 561
Deen, R., 651
de Freitas Ferreira, T., 245
de la Fuente, C., 441
De Marco, R., 385
de Paula Pereira, P.A., 245
De Vito, I.E., 929
Disic, J., 473
Djurdjevic, P., 473
- Dmitrienko, S.G., 309
Donais, M.K., 1045
Duarte, A.C., 207
Dudek, J., 837
- Ekmekçi, G., 83, 91
Enriz, R.D., 859
Ensafi, A.A., 587
Esteves da Silva, J.C.G., 889
- Fang, Q., 403
Fang, Z.-L., 125, 403
Fan, J., 843
Farghaly, O.A., 31
Fatibello-Filho, O., 505
Feng, Y.-Q., 47
Fernández, R., 881
Fernández-Romero, J.M., 813
Fischer, C.J., 293
Fuh, M.-R.S., 1069
Furusawa, N., 461
- Gallo, B., 773
Gao, Z., 331, 377
Gergov, G., 99
Gesser, H.D., 869
Ghandour, M.A., 31
Ghosh, D., 41
Giráldez, I., 285
Goldfeld, I., 629
Gomes, M.T.S.R., 207
Gómez-Ariza, J.L., 285
González, A.G., 189, 453
González-Arjona, D., 189, 433
Grabarczyk, M., 703
Grudpan, K., 215, 1023
Grujic, S., 473
Guanghan, L., 511
Guilbault, G.G., 667
Guillaume, Y.C., 415
Guiraúm, A., 881
Guo Nan, C., 319

- Gupta, K.K., 41
 Gupta, V.K., 923
 Gustavo González, A., 433

 Hadley, M., 539
 Hae Lee, J., 69
 Hagestuen, E.D., 547
 Hansen, E.H., 1027
 Hashemi, P., 825
 Hefter, G.T., 25
 Hemmateenejad, B., 587
 Henry, R., 1045
 Hernández-Córdoba, M., 597
 Hernández López, M., 679
 Hernández, O., 143
 Herrero, A., 801
 He, X., 331, 377
 Hibbert, D.B., 639
 Hirata, S., 1059
 Hong Qing, C., 319
 Hsieh, C.-J., 1069
 Huang, C.Z., 495
 Huang, S.-D., 393
 Huang, X., 425
 Hu, B., 357
 Huichun, Z., 77
 Hu, S., 751
 Hussain, N., 851
 Hu, Y.-L., 47
 Hwan Cho, M., 69
 Hyun Pang, J., 69

 Imato, T., 1003
 Isabel López Molina, M., 679
 Ishige, R., 339
 Iyer, C.S.P., 523

 Jakmunee, J., 215, 1023
 Jiang, Z., 357
 Jian Ping, D., 319
 Jiménez, A.I., 143
 Jiménez, F., 143
 Jiménez, J.C., 881
 Jin, J., 345
 Jin, L., 345

 Kameswara Rao, V., 367
 Kamfoo, K., 1023
 Kanazawa, M., 785
 Karthikeyan, S., 523
 Katsuta, S., 785
 Kawashima, T., 1077, 1083
 Kelly, M.T., 267
 Ketola, R.A., 179
 Khang, G.N., 651
 Khayamian, T., 587
 Kim, G., 851

 Kim, J.S., 69
 Kitamura, K., 261
 Kılıç, Z., 135
 Korolczuk, M., 703
 Kostiainen, R., 179
 Kotiaho, T., 179
 Kryger, L., 651
 Kubista, M., 99
 Kubo, K., 339, 735
 Kullberg, N., 961
 Kurihara, M., 1083
 Kuselman, I., 629

 Li Bo, A., 717
 Li, D.-H., 745
 Li, F., 745
 Lima, J.C., 611
 Linpei, J., 77
 Liu, S.-S., 125, 403
 Liu, X., 997
 Liu, Z., 517
 Li, Y., 331
 Li, Y.F., 495
 López-García, I., 597
 López-Mahía, P., 165
 López-Pérez, G., 189
 Lucchese, M., 277
 Lu, J.Y., 15
 Luque de Castro, M.D., 813
 Lu, T.-H., 59

 Mabon, N., 199
 Maeda, Y., 989, 997
 Ma, H.-B., 125
 Mansikka, T., 179
 Mao, L., 345
 Marlier, M., 199
 Martins, J.W., 937
 Martín, E., 143
 Martín, M.J., 453
 Masi, A.N., 929
 Massah, A.R., 531
 May, P.M., 25
 McComb, M.E., 869
 Morales, E., 285
 Mortimer, R.J., 271
 Moskvina, L.N., 985
 Myshak, E.N., 309

 Nagashima, K., 305
 Nakano, N., 305
 Nakano, S., 1077, 1083
 Nielsen, S.C., 1027
 Nóbrega, J.A., 505
 Noresson, B., 825
 Nygren, J., 99

 Ohki, A., 69
 Ohura, H., 1003
 Ojala, M., 179
 Oki, R., 1077
 Olin, Å., 825
 Oliva Teles, M.T., 611
 Oliveira, A.F., 505
 Oliveira Brett, A.M., 611
 Oliveira, C.J.S., 889
 Oliveira, J.A.B.P., 207
 Olsina, R.A., 929
 Onnerud, P., 267
 Ortner, P.B., 293
 O'Sullivan, C.K., 667
 Ouchi, M., 785

 Pablos, F., 453
 Pang, D.-W., 751
 Patterson, W., 539
 Pedregosa, J.C., 859
 Peng, L., 377
 Peng, T., 357
 Peralta-Zamora, P., 937
 Pereiro, R., 907
 Petronio, B.M., 277
 Petrov, V., 99
 Petruniok, N., 899
 Peyrin, E., 415
 Pozas, J.A., 285
 Prada, D., 165
 Prasada Rao, T., 523
 Prendes, P., 165
 Puri, B.K., 485
 Pyatkova, L.N., 309

 Qin Lin, X., 717
 Qin, Y., 357

 Ranganathan, S., 41
 Rao, N.B.S.N., 367
 Reguera, M.I.P., 691
 Rettberg, T., 1045
 Rocha, T.A.P., 207
 Rogowska, A., 837
 Roque da Silva, A.M.S., 611
 Rzeszutek, K., 757

 Sai, C.L., 651
 Sakaguchi, S., 735
 Sakai, T., 989, 997
 Sakurai, T., 339, 735
 Samatha, K., 53
 Sánchez Batanero, P., 441
 Sanz-Medel, A., 907
 Sara, R., 961
 Scaccia, S., 467
 Schroeder, W.H., 15
 Schuck, B.L., 969

- Segura-Carretero, A., 907
Sene, A.F.B., 271
Shackleton, J., 385
Sharghi, H., 531
Shenlai, Y., 511
Shen, X., 843
Shiobara, T., 1083
Simon, J., 985
Situmorang, M., 639
Šlejkovec, Z., 619
Somer, G., 83, 91
Sooksamiti, P., 215
Sousa Santos, E.T., 245
Spliid, H., 1027
Sreedhar, N.Y., 53
Stefan, R.I., 1017
Sterlišnska, E., 837
Stradiotto, N.R., 271
Stürup, S., 1027
Sugiura, M., 261
Sukhan, V., 899
Sultan, S.M., 1051
Sund, P., 961
Sun, H., 603
Sunita, G., 923
Sun, I.W., 59
Sun, W., 345
Sun, Y.-Q., 403
Su, P.-G., 393
Suresh, S., 367
Suvire, F.D., 859

Tabata, M., 603
Tai, Y.-L., 1069

Takeda, Y., 785
Takegami, S., 261
Talaslahti, M., 961
Tamaddon, A., 119
Tam, K.Y., 539
Tanaka, K., 1077
Tao, S., 345
Tascón, M.L., 441
Teshima, N., 1083
Thakur, M., 561
Tieli, Z., 77
Trifunovic, S., 473
Türker, A.R., 135
Tur'yan, Y.I., 629

Ura, N., 989

Valencia, M.C., 915
van Elteren, J.T., 619
Van Loon, J.C., 1
van Staden, J.F., 1017, 1099
Vázquez, M.D., 441
Verri, W.A., Jr., 373
Vicente, F., 773
Vilén, M., 961
Viñas, P., 597

Wang, E., 425, 517
Wang, J., 843
Wang, Z.-L., 751
Wathelet, J.-P., 199
Wei, W.-Z., 571
Wu, J.-F., 125, 403
Wuming, Z., 253

Wu, X., 331

Xianbao, W., 253
Xiaogang, W., 511
Xiao Ping, W., 319
Xingyao, Z., 253
Xue, J., 345
Xu, J.-G., 745

Yamamoto, K., 345
Yamamoto, M., 261
Yamasaki, S., 1003
Yamini, Y., 119
Yang, H.-S., 851
Yang, H.-Y., 59
Yang, S.-Y., 745
Yang, X., 425, 517
Yanhua, L., 511
Yao, S.-Z., 571
Yoshihara, H., 1059
You, T., 425, 517
Yu, J.C., 661

Zaia, C.T.B.V., 373
Zaia, D.A.M., 373
Zaporozhets, O., 899
Zhang, D.J., 495
Zhang, G., 331
Zhang, J.-Z., 293
Zhang, Q.-H., 47
Zhao, Y.-D., 751
Zheng, H., 745
Zhu, Q.-Z., 745

Subject Index

Volume 49 (1999)

- Absorption spectrum 495
Acid dissociation constants 539
Acidity constant 859
Acid value 629
Acridine Orange 377
Adsorption 319
Affinity 969
Aggregation 99
Airborne particles 165
Alkylmercury 837
Amberlite XAD-4-HEED column 1059
Ambient air 15
Ammonia 1023
Ammonium tetraphenylborate-naphthalene 485
Amperometric detection 425, 517
Analysis 199
Analytical precision 331
Analytical separation 577
Anion analysis 215
anodic slime 83, 91
Anthryl pendants 339
Antidepressant 611
Antidepressant drugs 773
Antioxidant 441
Armed crown ethers 735
Arsenazo(III) 155
Arsenic 523, 619
Artificial cerebrospinal fluid 1069
Ascorbate 661
Ascorbic acid 1023
Assay of inorganic Cr(VI) 1027
Asynchronous merging zones 505
Atmospheric ethanol 245
Atmospheric methanol 245
Atomic absorption spectrometry 125, 523
Automated liquid handling system 1045
2,2'-Azinobis(3-ethylbenzothiazoline-6-sulfonic acid) 1077
- Biosensors 667
Bismuth 135
Blood plasma 453
- Blue ion associate with tetrabromophenolphthalein ethylester 997
Body fluids 77
Borates 267
Borohydride concentrations 267
5-Br-PADAP 47
5-Br-PSSA 989
- Calcium 155, 597
Calcium-selective membrane electrode 1017
Canrenone 143
Capillary electrophoresis 425, 517
Carbodic carbon 41
Catalytic flow-injection method 1083
Catalytic method 1077
Catalytic reduction 345
Cesium chloride 25
Chemically modified electrode 511
Chemically modified microelectrode 345
Chemical modification 357
Chemical modifiers 135
Chemical purification 851
Chemiluminescence 1051
Chemometrics 99
Chiral recognition 415
Chlorine dioxide 571
Cholesterol 639
Chromatography 571
Chromatomebrane cell 985
Chromium speciation 703, 1045
Cisatracurium determination 881
Classification 189
Coating 293
Cobalt-cyanometallates 717
Collaborative trials 331
Colorimetric method 923
Combination 425
Complexation 531
Complexes 473
Conductometry 1023
Co-Ni-Cu 587
Constituent equilibria 785

- Continuous flow analysis 293
Copper and iron 989
Copper determination 561
Copper(I) 119
Copper(II) 1099
Covalent immobilization 751
19-Crown-6 785
Cu(II) determination 899
CVAAS 837
Cyclic voltammetry 31, 717
Cyclodextrins 577, 679
- Deltamethrin 53
Denuder 15
Deprotonation mechanism 859
Detection 745
Diazacrown ether 339
Diethyldithiocarbamate 1099
Differential pulse stripping voltammetry 319
Dimethyl glyoxime 651
Dioxygen 345
Discriminant analysis 189
Dissociation constant 843
Dissolution testing 403
DNA 377, 969
DNA-modified electrodes 751
Doehlert designs 433
Double and serial flow cells 989
Double cell quartz crystal 571
- Effect of extra methylene group 785
Electrochemical sensor 367
Electrochemistry 319, 611
Electropolymerisation 667
Electrothermal vaporization-inductively coupled plasma atomic emission spectrometry 357
End-column 517
Environmental analysis 985
Environmental and pharmaceutical samples 485
Environmental water samples 1059
Enzymatic analysis 639
ETAAS–Zeeman background correction 135
Ether-type polyurethane membrane 757
Ethylenediamine-*N,N'*-di-3-propionate 473
Extraction of Cr(VI)–PDC complex 1027
- Factorial design 1051
Fe(II) 1059
Fe(III)–Fe(II) potential buffer 1003
Field detection 561
FI-ETAAS 1027
Flame atomic absorption spectrometry 467
Flame atomic absorption spectroscopy 597
Flow injection 125, 403, 1023
Flow-injection 1003
Flow injection analysis 969, 1017, 1059
Flow-injection analysis 985
- Flow injection analysis 1077
Flow injection dialysis 215
Flow injection extraction 997
Flow injection potentiometry 639
Flow system 703
Flow-through sensor 691
Fluids 199
Flunarizine 1069
Fluorescence 339, 881, 907
Fluorescence behavior 735
Fluorescence energy transfer 377
Fluoride 357
Fluoride-selective membrane electrode 1017
Fluoroionophore 735
Fluoroionophores 339
Fluoxetine 611
¹⁹F nuclear magnetic resonance 261
Fosfomycin 47
Fourth derivative spectrophotometry 485
FTIR 717
- Gas chromatography-flame photometric detector 393
GC-MS 285
Gold 1
Graphite carbon electrode 661
- Hafnium 937
Hallogen 531
Headspace gas chromatography 179
High-performance liquid chromatography 461
High performance liquid chromatography 453
High performance liquid chromatography/electrospray/mass spectrometry 1069
Histidine and its metabolites 319
H₂O₂ detection 667
Honey 597
H-point standard addition 155
Humic compounds structures 277
Hydrogen cyanide 367
- ICP–AES 825
ICP-OES 869
Iminodiacetate adsorbent 825
Immobilized human serum albumin 415
Indirect spectrophotometry 47
Indium 135
Inductively coupled plasma mass spectrometry 1
Industry 961
Inorganic 837
Instrumental methods 1
Instrument standardization 801
Iodine 923
Ion chromatography 215
Ionic dyes 99
Ion-pairing 25
Ion-selective electrode 385
Ion-selective membrane electrodes 83, 91
Irrigation water 679

- Isoniazid 403
Iteratively reweighted least-squares 331
- Kinetics 143
Kinetic-spectrophotometric data 889
- Lacustrine environment 277
Lead 135
 $\text{Li}_2\text{CO}_3/\text{K}_2\text{CO}_3$ melts 467
Linear regression 331
Linear sweep and differential pulse stripping voltammetry 31
Liquid chromatography 415
Liquid membrane 69
Lithium 603
Loaded silica gel 899
Lomefloxacin 77
- Macrocyclic diamide 531
Magnesium 155, 597
Manganese determination 1077
Marine water 923
Mass spectrometry 1045
Matrix interference 801
Melatonin 517
Membrane inlet mass spectrometry 179
2-mercaptobenzothiazole sorbent 837
Mercury 385, 907
Mercury. 125
Mercury film electrode 59
Mercury free electrode 651
Metallisation 667
Metal picrates 785
Method of correlation ratio 309
Methyl viologen 345
Methyl yellow 843
Metrological parameters 629
Micellar effect 107
Microdialysis 403
Mivacurium determination 881
Mixed protic solvents 843
Mixtures of heavy metal ions 889
Modified electrodes 271
Modified gold electrodes 751
Molecular orbitals calculations 859
Molecular recognition 577
Molten carbonate fuel cells 467
Multiple flow reversals 1099
Multivariate analysis 801
- Nafion 59, 345
1-Naphthol and 2-naphthol 679
Natural waters 825, 915
Near-infrared 745, 813
Neocuproine 119
Neostigmine determination 997
Nickel(II) 651
Nickel(II) hexacyanoferrate 271
- Nickel phthalocyanine complex 441
Nile blue sulphate 495
Nitrogen dioxide gas detection 305
Non-porous membrane transport 757
Non-steroidal anti-inflammatories 453
N-(3-sulfopropyl)-3,3',5,5'-tetramethylbenzidine 1083
Nucleic acids 495
- Octadecylsilica membrane disks 119
Oilseeds 629
Omethoate 253
On-line analysis 961
On-line dialysis 215
On-line preconcentration of Cr(VI) 1027
Open circuit potentials 267
Optimization 207
Optimization methods 433
Optosensing 907
Organic dyes 757
Organophosphorus compounds 253
Organophosphorus pesticides 393
Organs 199
Oxychlorine species 1003
- PAHs 547
PARAFAC 889
Partial least squares 587
Partial least-squares regression 155
Particulate-phase mercury 15
Partition coefficient 261
Periodate 1077
Permanganate 1023, 1051
Perphenazine 1051
pH 745
Pharmaceutical formulations 611
Pharmaceutical preparations 453
Pharmaceuticals 691
Phenols 309
pH-metry 629
Phosphate determination 293
Phosphomolybdic acid 511
Phosphorimetry 679
Phosphorus 511
Photochemical fluorimetry 77
Photochemically-induced fluorescence 107
Photoinduced electron transfer 339, 735
Phthalocyanine 745
Phytic acid 511
Piazselenol 285
Plant food samples 1099
Plasma 773
Platinum electrode 717
Platinum group elements 1
PLS 143
PLS multicalibration 691
Podand 69
Polarography 53
Polyacrylate 393

- Polydimethyl siloxane 393
Polymer coating 651
Polymerisation 937
Polypyrrole electrode 441
Polyurethane foam 309
Porphyrin 603
Potassium ion 271
Potentiometric 367
Potentiometric detection 661, 1003
Potentiometry 859
PQC 253
PQC sensor 253
Precipitation 41
Preconcentration 825
Procrustes analysis 189
Proteins 373
Pulsed laser 813
Pyridine 539
1-[Pyridyl-(2)-azo]-naphthol-(2) (PAN) 561
- Quartz crystal microbalance 207
Quinones 373
- Rare earth elements 929
Redox iron speciation 505
Reference materials 619
Renewable columns 969
Response surface 207
Rice. 53
River water analysis 107
Room-temperature phosphorimetry 547
- Safranine T 377
Saltzman's reagent 305
Sample preparation 969
Sampling 245
Seawater 851
Sea water 135, 523
seawater media 385
Sediments 277
Selective complexation 69
selenium 83, 91, 285
Selenium (IV) speciation 915
Self-assembled monolayers 751
Sensitive tape for nitrogen dioxide gas 305
Separation 603
Sequential determination 505
Sequential injection 125, 969
Sequential injection analysis 1099
Sequential injection analysis controller 961
Serum 881
SIamate 961
Silicate interference 293
Simplex 207
Simplex optimization 1051
Simultaneous 587
Simultaneous detection 1017
Simultaneous determination 155
Singular value decomposition 587
Sodium ion 25
Soil 969
Soil and airborne dust particulates 561
Solid-phase extraction 547, 773
Solid-phase microextraction 393
Solid-phase spectrophotometry 915
Solid-phase spectroscopy 691
solid state membrane 91
Solution equilibria 473
Solvent extraction 69, 785
Sorption 309
Source apportionment 165
SPE 119
Speciation 285, 619
Spectra probe 377
Spectrophotometric determination 373
Spectrophotometric titration 539
Spectrophotometry 531, 561, 587, 843, 859, 1023
Spectroscopic analysis 277
Spin-lattice relaxation time 261
Spiramycin 461
Spironolactone 143
Square-wave voltammetry 59
Standard addition method 83
Standard alloys 485
Standard deviation 331
Steel 41
Stopped-flow 403
Storage bags 53
Stripping analysis 59
Stripping voltammetry 801
Strong acid 745
Substitution pattern 577
Sulfate ion 25
Sulfonylurea herbicides 107
Supercritical fluid extraction 813
Super-phosphate fertilizer 31
Synchronous-derivative technique 679
- Tape monitor 305
Target factor analysis 189, 539
Terbium complex 77
Terpenes 179
tert-Butylhydroquinone 441
3-tert-Butyl-4-hydroxyanisole 441
Tetrabutylammonium chloride 415
²³⁴Th 851
Thallium 59
Thermal lens spectrometry 813
1,3,4-Thiadiazole-sulfonamides 859
1-(2-Thiazolylazo)-2-naphthol 899
1-2(Thiazolylazo)-2-naphthol 485
Thorin 929
Total proteins 373
Trace 651
Trace metals 869

- Transition metals 467
Transport 603
Triflupromazine 261
Tungsten electrode 639
- Ultra-filtration unit 461
Uniform shell designs 433
Uranium determination as phthalate complex 31
Urban environment 165
UV detection 425
UV-Vis spectroscopy 99
- Vanadium determination 1083
Vapor generation 125
Vegetables 53
- 5-Vinyl-1,3-oxazolidine-2-thione 199
Vitamin C 1023
Voltammetry 703
- Water 393, 703
Water samples 179, 1099
WDXRF 869
Wheat 53
- XPS 717
X-ray fluorescence spectrometry 929
- Zinc 485, 597
Zirconium 47, 937
Zn(II) determination 899